

Haschek and Rousseaux's Handbook of

# TOXICOLOGIC PATHOLOGY

**FOURTH EDITION**

**VOLUME 5**

Toxicologic Pathology of Organ Systems

CARDIOVASCULAR  
RENAL  
LOWER URINARY  
RESPIRATORY  
HEMATOPOIETIC  
IMMUNE  
INTEGUMENTARY  
MAMMARY  
MALE REPRODUCTIVE  
FEMALE REPRODUCTIVE  
EMBRYO, FETUS, AND PLACENTA

Editors

WANDA M. HASCHEK  
COLIN G. ROUSSEAU  
MATTHEW A. WALLIG  
BRAD BOLON

Associate Editors

JEFFREY I. EVERITT  
KAREN S. REGAN

Illustrations Editor

BETH W. MAHLER



# HASCHEK AND ROUSSEAU'S HANDBOOK OF TOXICOLOGIC PATHOLOGY

---

FOURTH EDITION

*Volume V: Toxicologic Pathology of Organ Systems*



This page intentionally left blank

# HASCHEK AND ROUSSEAUX'S HANDBOOK OF TOXICOLOGIC PATHOLOGY

---

FOURTH EDITION

*Volume V: Toxicologic Pathology of Organ Systems*

*Edited by*

WANDA M. HASCHEK

COLIN G. ROUSSEAUX

MATTHEW A. WALLIG

BRAD BOLON

*Associated Editors*

JEFFERY J. EVERITT

KAREN S. REGAN

*Illustrations Editor*

BETH W. MAHLER



**ACADEMIC PRESS**

An imprint of Elsevier

Academic Press is an imprint of Elsevier  
125 London Wall, London EC2Y 5AS, United Kingdom  
525 B Street, Suite 1650, San Diego, CA 92101, United States  
50 Hampshire Street, 5th Floor, Cambridge, MA 02139, United States

Copyright © 2025 Elsevier Inc. All rights are reserved, including those for text and data mining, AI training, and similar technologies.

For accessibility purposes, images in electronic versions of this book are accompanied by alt text descriptions provided by Elsevier. For more information, see <https://www.elsevier.com/about/accessibility>.

Publisher's note: Elsevier takes a neutral position with respect to territorial disputes or jurisdictional claims in its published content, including in maps and institutional affiliations.

No part of this publication may be reproduced or transmitted in any form or by any means, electronic or mechanical, including photocopying, recording, or any information storage and retrieval system, without permission in writing from the publisher. Details on how to seek permission, further information about the Publisher's permissions policies and our arrangements with organizations such as the Copyright Clearance Center and the Copyright Licensing Agency, can be found at our website: [www.elsevier.com/permissions](http://www.elsevier.com/permissions).

This book and the individual contributions contained in it are protected under copyright by the Publisher (other than as may be noted herein).

### Notices

Knowledge and best practice in this field are constantly changing. As new research and experience broaden our understanding, changes in research methods, professional practices, or medical treatment may become necessary.

Practitioners and researchers must always rely on their own experience and knowledge in evaluating and using any information, methods, compounds, or experiments described herein. In using such information or methods they should be mindful of their own safety and the safety of others, including parties for whom they have a professional responsibility.

To the fullest extent of the law, neither the Publisher nor the authors, contributors, or editors, assume any liability for any injury and/or damage to persons or property as a matter of products liability, negligence or otherwise, or from any use or operation of any methods, products, instructions, or ideas contained in the material herein.

ISBN: 978-0-12-821045-1

For information on all Academic Press publications visit our website at  
<https://www.elsevier.com/books-and-journals>

*Publisher:* Stacy Masucci  
*Acquisitions Editor:* Kattie Washington  
*Editorial Project Manager:* Billie Jean Fernandez  
*Production Project Manager:* Maria Bernard  
*Cover Designer:* Matthew Limbert

Typeset by TNQ Technologies



# Dedication

---

To teach is to learn ...

*(Japanese proverb)*

To our families, teachers, colleagues, and friends who have supported us in our journeys through life, encouraged us when needed, mentored us in our learning, challenged us in our teaching, joined us in our passion, followed us in our trailblazing, and inspired us in our scholarly pursuits ...

We are grateful for the opportunities we have enjoyed to advance pathology and toxicology as distinct and blended disciplines, both for our own betterment and in service to our local and global communities.

This page intentionally left blank

# Contents

---

**Contributors**            **xiii**

**About the Editors**        **xv**

**Preface**            **xvii**

## 1. Cardiovascular System

BRIAN R. BERRIDGE, REBECCA A. KOHNKEN  
AND EUGENE H. HERMAN

1. Introduction	2
Part I: Heart	2
2. Structure and Function	3
2.1. Gross and Microscopic Anatomy	3
2.2. Physiology and Functional Considerations	8
2.3. Xenobiotic Exposure	10
3. Evaluation of Toxicity	11
3.1. Bioactivity Screening for Cardiac Toxicity	12
3.2. Functional Evaluation of Toxicity	12
3.3. Morphologic Evaluation of Toxicity	18
3.4. Background Alterations, Artifacts, and Spontaneous and Age-Related Lesions	22
3.5. Biomarkers	24
3.6. Biochemical Evaluation of Toxicity	25
4. Responses to Injury	25
4.1. Developmental Cardiotoxicity	25
4.2. Cardiac Dysfunction as a Manifestation of Toxicity	26
4.3. Changes in Cardiac Mass as a Response to Toxicity	28
4.4. Drug-Induced Cardiomyopathies	29
4.5. Cardiomyocellular Injury	34
4.6. Endocardium	48
4.7. Neoplasia	49
4.8. Valves	49
4.9. Epicardium	50
4.10. Pericardium	50
5. Mechanisms of Toxicity	50
5.1. Mechanisms of Altered Cardiac Function	51

5.2. Mechanisms of Direct Cellular Injury	52
5.3. Mechanisms of Indirect Injury	55
5.4. Cardiotoxicity of Cardiac Drugs	55
5.5. Hypersensitivity Reactions	56
5.6. Xenobiotic Interactions	56
5.7. Modifying Factors in Cardiac Toxicity	57
6. Cardiotoxicity Issues in Drug Development	57
6.1. Cardiovascular-Related Drug Development Attrition	57
6.2. Rodent Progressive Cardiomyopathy	58
6.3. Animal Models of Human Cardiac Disease	58
6.4. Clinical Translation of Nonclinical Cardiotoxicity	59
Part II: Blood Vessels	59
7. Structure and Function	60
7.1. Microscopic Anatomy	60
7.2. Cellular and Extracellular Components of the Vasculature: Biology	61
7.3. Physiology and Functional Considerations	63
8. Evaluation of Toxicity: Vasotoxic Effects	66
8.1. Physiological Methods for Testing	66
8.2. In Vitro Methods for Detecting Vascular Toxicity	67
8.3. Morphologic Evaluation	69
8.4. Background Alterations, Artifacts, Spontaneous and Age-Related Lesions	70
8.5. Use of Animals as Models for Vascular Toxicity	71
8.6. Biomarkers of Vascular Injury	72
9. Responses to Injury	73
9.1. Atherosclerosis Acceleration by Toxic Agents	73
9.2. Medial Proliferation	74
9.3. Intimal Proliferation	74
9.4. Calcification	75
9.5. Aneurysms	76
9.6. Medial Hemorrhagic Necrosis	76
9.7. Fibrinoid Necrosis	77

9.8.	Microangiopathy	77	
9.9.	Immune-Mediated Vascular Inflammation	77	
9.10.	Regeneration and Repair	78	
10.	Vascular Toxicity in Specific Organs	79	
10.1.	Brain	79	
10.2.	Lungs	79	
10.3.	Heart	80	
10.4.	Liver	80	
10.5.	Kidney	81	
10.6.	Stomach	81	
11.	Conclusion	81	
	References	81	

## 2. Kidney

KENDALL S. FRAZIER, MARSHALL S. SCHICCITANO, KATHLEEN HEINZ-TAHENY AND RACHEL E. CIANCIOLO

1.	Introduction	87	
2.	Structure, Function, and Cell Biology	89	
2.1.	Renal Ontogeny	89	
2.2.	Renal Structure	91	
2.3.	Renal Function	100	
2.4.	Renal Cell Biology	109	
3.	Evaluation of Toxicity	113	
3.1.	Physiologic Considerations	113	
3.2.	Biochemical and Biomarker Evaluations	116	
3.3.	Morphologic Evaluation	129	
3.4.	Testing for Renal Carcinogenic Potential	137	
3.5.	In Vitro Techniques	139	
3.6.	Scoring Schemes	145	
3.7.	Computational Pathology	146	
4.	Responses to Injury	147	
4.1.	Physiologic, Molecular, and Biochemical Response	147	
4.2.	Morphologic Response	148	
5.	Mechanisms of Toxicity	157	
5.1.	Nephrotoxicity Classification	159	
5.2.	Mechanisms of Glomerular Toxicity	160	
5.3.	Mechanisms of Interstitial Injury	168	
5.4.	Mechanisms of Proximal Tubular Injury	172	
5.5.	Other Sites of Renal Injury	188	
5.6.	Renal Carcinogenesis	191	
6.	Issues in Drug Development	199	
6.1.	Animal Models	199	
6.2.	Adversity	202	
7.	Conclusion	206	
	Acknowledgments	207	
	References	207	

## 3. Lower Urinary Tract

SAMUEL M. COHEN

1.	Introduction	213	
2.	Structure, Function, and Cell Biology	214	
2.1.	Kidney Pelvis and Papilla	214	
2.2.	Ureters	214	
2.3.	Urinary Bladder	214	
2.4.	Urethra	215	
2.5.	Urothelium	215	
3.	Evaluation of Toxicity	217	
3.1.	Physiologic and Biochemical Evaluation	217	
3.2.	Morphologic Evaluation	218	
3.3.	Techniques for Evaluation	219	
4.	Responses to Injury	221	
4.1.	Acute Injury	221	
4.2.	Chronic Injury	222	
4.3.	Carcinogenesis	223	
4.4.	Morphologic Lesions	226	
5.	Mechanisms of Toxicity	230	
6.	Issues in Drug and Chemical Development	231	
	References	232	

## 4. Respiratory System

MOLLY H. BOYLE, JACK R. HARKEMA, KRISTEN J. NIKULA, RONNIE CHAMANZA, DAVID K. MEYERHOLZ, MARY BETH GENTER AND WANDA M. HASCHEK

1.	Introduction	236	
2.	Structure, Function, and Cell Biology	237	
2.1.	Macroscopic and Microscopic Anatomy	237	
2.2.	The Nose	237	
2.3.	The Pharynx and Larynx	247	
2.4.	The Trachea, Bronchi, and Bronchioles	248	
2.5.	Gas-Exchange Regions of the Lung	257	
3.	Testing for Toxicity	261	
3.1.	Methods of Testing	261	
3.2.	Background Findings	266	
3.3.	Nasopharyngeal and Laryngeal Regions	269	
3.4.	Tracheobronchial Airways and Pulmonary Parenchyma	270	
3.5.	Animal Models	272	
3.6.	Target Liability Assessment and <i>In Vitro</i> Models	278	
3.7.	Quantitative Techniques and Lung Imaging Modalities	281	
4.	Responses to Injury	287	
4.1.	Factors Affecting Toxic Injury and Host Response	287	



4.2. Patterns of Respiratory Tract Injury to Inhaled Toxicants	288	6.5. Altered Blood Cell Function	415
4.3. Cell-specific Versus Nonspecific Injury	288	6.6. Indirect Injury, Secondary Effects, and Modifying Factors	417
4.4. Cell Proliferation, Regeneration, and Repair Processes	288	7. Issues in Drug Development and Regulatory Considerations	418
4.5. Nasal, Nasopharyngeal, and Laryngeal Responses to Injury	290	7.1. Translatability	418
4.6. Tracheobronchial and Pulmonary Responses to Injury	293	7.2. Adversity	419
4.7. Pulmonary Parenchymal Responses to Injury	301	7.3. Regulatory Issues	420
5. Mechanisms of Toxicity	316	8. Conclusion	421
5.1. Direct Toxicity	318	Glossary	421
5.2. Metabolic Activation	319	References	422
5.3. Immune-Mediated Toxicity	321		
5.4. Toxicity and Responses to Inhaled Particles	324	6. Immune System	
5.5. Toxicity and Responses to Inhaled Fibers	326	TRACEY L. PAPENFUSS, DIRK SCHAUDIEN, CHIDOZIE J. AMUZIE AND SUNISH MOHANAN	
5.6. Xenobiotic Interactions	327	1. Introduction and Background	438
5.7. Modifying Factors in Toxicity	327	2. Function	438
5.8. Adversity Considerations	328	2.1. Antigen Presentation and Recognition	441
6. Conclusion	328	2.2. Immune Regulation of the Effector Reactions	441
References	329	2.3. Effector Reactions	443
		2.4. Immunological Memory	443
		2.5. Lymphocyte Trafficking and Homing	444
		2.6. Cooperation with Other Organ Systems	444
5. Hematopoietic System		3. Development, Structure, and Physiology	444
LILA RAMAIAH, TIM ERKENS, MADHU SIRIVELU AND ALLISON VITSKY		3.1. Thymus	446
1. Introduction	337	3.2. Bone Marrow	449
2. Phylogenesis and Ontogenesis	340	3.3. Spleen	449
2.1. Phylogeny	340	3.4. Physiology/Function	452
2.2. Mammalian Ontogeny	344	3.5. Lymph Nodes	453
3. Structure, Function, and Cell Biology	345	3.6. Mucosa-Associated Lymphoid Tissue (MALT)	456
3.1. Anatomy of the Bone Marrow	345	3.7. Tertiary Lymphoid Structures	458
3.2. Hematopoiesis	347	3.8. Immune-specific Components in Select Organs	461
4. Evaluation of Hematototoxicity	360	4. Physiological Influences on the Immune System Throughout the Lifespan	463
4.1. Evaluation of Bone Marrow	362	4.1. Immune Responses to Aging	464
4.2. Evaluation of Peripheral Blood	366	4.2. Immune Responses to Hormones	464
4.3. In Vitro Techniques	371	4.3. Immune Responses to Stress	465
4.4. Animal Models	371	5. Immunomodulation, Immune Systems Responses, and Mechanisms of Toxicity	466
5. Responses to Injury	372	5.1. Defining Immunotoxicology, Immunosuppression, and Immunostimulation	466
5.1. Changes in Peripheral Blood	372	5.2. Biochemical Pathways and Exaggerated Pharmacology in the Immune System	466
5.2. Changes in Bone Marrow	379		
5.3. Myeloproliferative Lesions	386		
5.4. Changes in Secondary Hematopoietic Organs	389		
6. Mechanisms of Hematototoxicity	392		
6.1. Direct Nonimmune Injury to Hematopoietic Cells	392		
6.2. Direct Nonimmune Injury to Circulating Cells	404		
6.3. Immune Injury and Destruction	412		
6.4. Idiosyncratic Reactions	414		

5.3.	Perturbations of the Immune System and Recoverability (Relevance to Adversity)	467
5.4.	Nonantigen-Specific Toxicity	469
5.5.	Antigen-specific Toxicity	472
5.6.	Pathophysiological Changes Associated with Therapies Affecting the Immune System	472
5.7.	Recoverability of the Immune System (Acute vs. Chronic Changes, Reversibility)	475
5.8.	Immune Derangements and Neoplasia	475
6.	Evaluation of Changes and Toxicity	476
6.1.	Interpreting Immune System Changes	476
6.2.	Testing for Toxicity	479
6.3.	Anatomic Pathology	479
6.4.	Organ-specific Histopathology	484
6.5.	Clinical Pathology Evaluation and Considerations	487
6.6.	Immunotoxicology Evaluation and Considerations	487
7.	Responses to Injury	490
7.1.	Immunosuppression	490
7.2.	Immunostimulation	490
8.	Preneoplastic Changes and Neoplasia	495
8.1.	Stromal Tumors: Thymoma	495
8.2.	Tumors of Hematopoietic and Lymphopoietic Cells	496
8.3.	Lymphomas	496
8.4.	Histiocytic Sarcoma	496
9.	Best Practices and Regulatory Considerations on Evaluation of Toxicity and Adversity in the Immune System	497
10.	Conclusion	499
	References	499

## 7. Integument

KELLY L. DIEGEL, LYDIA ANDREWS-JONES AND ZBIGNIEW W. WOJCINSKI

1.	Introduction	506
2.	Structure and Function	506
2.1.	The Epidermis	508
2.2.	Melanocytes	511
2.3.	Merkel Cells	512
2.4.	Langerhans Cells and Dermal Dendritic Cells	512
2.5.	The Dermal–Epidermal Junction and Dermis	513
2.6.	The Subcutis	515
2.7.	The Adnexa	515
2.8.	The Minipig in Dermal Toxicity Assessment	518

2.9.	Physiology and Biochemistry of the Integument	520
2.10.	Percutaneous Absorption	520
2.11.	Metabolism and the Integument	522
3.	Evaluation of Toxicity	523
3.1.	Physiologic and Morphologic Safety Evaluation Strategies and Techniques	523
3.2.	Special Considerations in Design of Topical Dermatologic Studies	527
3.3.	Skin Sample Collection Techniques	528
3.4.	Special Techniques	531
3.5.	Three-Dimensional In Vitro Skin Model Systems	534
4.	Responses to Injury	536
4.1.	General Mechanisms of Response to Injury–Cutaneous Immunity	536
4.2.	Special Considerations–Translational Immunology of Skin	541
4.3.	Wound Healing	543
4.4.	Influence of Skin Microbiome on Adaptive Immune Response	549
4.5.	Specific Cutaneous Morphologic Lesions and Patterns of Injury	550
4.6.	Neoplastic Lesions and Carcinogenesis Models	554
5.	Mechanisms of Toxicity	559
5.1.	Direct Cutaneous Toxicity	559
5.2.	Immune-Mediated Cutaneous Toxicity	565
5.3.	Mechanisms of Toxicity: Photosafety	568
5.4.	Mechanisms of Toxicity: Photoaging	572
5.5.	Mechanisms of Toxicity: Antisense Oligonucleotides	572
5.6.	Mechanisms of Toxicity: Pigmentation	573
5.7.	Mechanisms of Toxicity: Adnexa—General and Specific Toxicities	574
6.	Conclusion	576
	Acknowledgments	577
	References	577

## 8. Mammary Gland

SUZANNE E. FENTON AND SCHANTEL HAYES BOUKNIGHT

1.	Introduction	584
2.	Mammary Gland Structure and Function	585
2.1.	Stages of Development	585

2.2. Variation in Development Across Species	589	4. Responses to Injury	680
2.3. Endocrine and Paracrine Modifiers of Development	597	4.1. Organ Weight Changes	680
2.4. Functional Outcomes	601	4.2. Morphologic Changes (Nonproliferative)	681
3. Evaluation of Mammary Gland Toxicity	603	4.3. Morphologic Changes (Proliferative)	690
3.1. In Vitro Techniques	606	4.4. Recovery and Reversibility of Injury	695
3.2. Commonly Used Animal Models	606	4.5. Immaturity and Peripuberty as Confounding Factors for Identifying Toxicity	696
3.3. Physiologic Outcomes	610	4.6. Background Pathology as a Confounding Factor for Identifying Reproductive Toxicity	701
3.4. Morphological Evaluations	612	4.7. Stress and Body Weight Loss as a Confounding Factor for Identifying Reproductive Toxicity	707
3.5. Biochemical Indicators and Biomarkers	613	5. Mechanisms and Patterns of Toxicity	708
4. Responses to Injury	615	5.1. Molecular and Biochemical	708
4.1. Physiologic Responses	615	5.2. Morphologic Patterns of Response to Different Types of Injury	709
4.2. Molecular and Biochemical Responses	616	5.3. Mechanisms of Developmental Toxicity	725
4.3. Morphological Indicators	616	6. Conclusion	727
5. Mechanisms of Toxicity	621	Acknowledgments	728
6. Conclusion	622	References	728
Appendix: Preparation and Evaluation of Mammary Gland Whole Mounts in Mice and Rats	622		
1. Collection of the Intact Mammary Gland	622		
2. Fixing and Staining Whole Mounts	624		
3. Suggested Evaluation Methods for Mammary Gland Whole Mounts	625		
Acknowledgments	630		
References	630		
<b>9. Male Reproductive System</b>		<b>10. Female Reproductive System</b>	
JUSTIN D. VIDAL, NATASHA CATLIN AND CYNTHIA J. WILLSON		DANIEL G. RUDMANN, JUSTIN D. VIDAL AND ERIC VAN ESCH	
1. Introduction	635	1. Introduction	743
2. Structure, Function, and Cell Biology	636	2. Structure, Function, and Cell Biology	746
2.1. Embryonic Development	636	2.1. The Ovary	747
2.2. Postnatal Development of the Reproductive Tract	637	2.2. The Histology of the Rat Ovary during Prepubertal and Pubertal Development	750
2.3. Structure and Function of the Testis	640	2.3. The Histology of the Rat Female Reproductive Tract during the Estrous Cycle	751
2.4. Spermatogenesis and the Spermatogenic Cycle	648	2.4. The Histology of the Dog Female Reproductive Tract during the Estrous Cycle	756
2.5. Structure and Function of the Rete Testis, Efferent Ducts, Epididymis, and Vas Deferens	651	2.5. The Histology of the Cynomolgus Macaque Female Reproductive Tract during the Menstrual Cycle	759
2.6. Structure and Function of the Accessory Sex Organs	658	2.6. The Histology of the Minipig Female Reproductive Tract during the Estrous Cycle	765
2.7. Hormonal Regulation of Reproductive Function	661	2.7. The Histology of the Rabbit Female Reproductive Tract during the Estrous Cycle	770
3. Evaluation of Toxicity	665	2.8. The Endocrinology of the Estrous and Menstrual Cycles	770
3.1. Physiologic Evaluation	666	2.9. Hormonal Events during a Given Reproductive Cycle	770
3.2. Biochemical and Biomarker Evaluation	671	2.10. Regulation of Hormonal Secretion	773
3.3. Morphologic Evaluation	674		
3.4. Special Techniques	679		

3. Evaluation of Female Reproductive System Toxicity	775	3.5. Histogenesis and Functional Maturation	832
3.1. Spontaneous Changes in the Female Reproductive System	778	4. Structure, Function, and Cell Biology—Placenta	833
4. Responses to Injury	779	4.1. Structure	833
5. Mechanisms of Toxicity in the Female Reproductive System	783	4.2. Cell Biology and Function	835
5.1. Stress and Negative Energy Balance	784	5. Evaluation of Toxicity	838
5.2. Hyperprolactinemia	788	5.1. Toxicity Testing	839
5.3. Altered Activity of Sex Steroid Enzymes and Cholesterol Metabolism	791	5.2. Key Endpoints in Developmental Toxicity Testing	841
5.4. Targeted Cancer Therapies	791	6. Responses to Injury	847
5.5. Modulation of Central Nervous System Biology	792	6.1. Death	848
5.6. Toxicity Induced by Constituents of the HPO Axis and Modulators of Nuclear Hormone Receptors	793	6.2. Malformations	848
5.7. Toxicity due to Vaginal Irritation	796	6.3. Deformations	868
5.8. Study, Interpretative, and Regulatory Issues in Female Reproductive Safety Assessment	796	6.4. Intrauterine Growth Restriction	870
6. Carcinogenesis in the Female Reproductive System	797	6.5. In-Life Functional Alterations	871
6.1. Ovary	798	6.6. Congenital Neoplasia	872
6.2. Uterus	804	7. Mechanisms of Developmental Toxicity	876
6.3. Vagina and Cervix	808	7.1. Excessive Cell Death	876
6.4. Clitoral Glands	809	7.2. Dysregulated Autophagy	877
7. Conclusion	810	7.3. Interference with Programmed Cell Death (Apoptosis)	877
References	811	7.4. Reduced Cell Proliferation	878
		7.5. Failed Cellular Interactions	879
		7.6. Impeded Morphogenetic Movements	879
		7.7. Reduced Biosynthesis of Essential Components	880
		7.8. Inhibition of Angiogenesis	881
		7.9. Endocrine Disruption	881
		7.10. Oxidative Stress	882
		7.11. Mechanical Disruption	882
		7.12. Intracellular pH Alterations	883
		8. Developmental Toxicity Issues in Product Development	883
		8.1. Biological Factors that Modify Developmental Toxicity	883
		8.2. Study Design Considerations	889
		9. Regulatory Considerations	902
		9.1. Managing Risk	902
		10. Conclusion	904
		Glossary	905
		Acknowledgments	908
		References	908
		Index	919

## 11. Embryo, Fetus, and Placenta

BRAD BOLON, SUSAN A. ELMORE, WENDY HALPERN AND COLIN G. ROUSSEAU

1. Introduction	820
2. Fundamentals of Developmental Toxicologic Pathology	821
2.1. Basic Principles	821
2.2. Critical Phases of Development	821
2.3. Incidence of Congenital Defects	823
3. Structure, Function, and Cell Biology—Embryo and Fetus	823
3.1. Fertilization to Blastocyst Formation	824
3.2. Implantation	826
3.3. Gastrulation	827
3.4. Organogenesis	829

# Contributors

---

**Chidozie J. Amuzie** Johnson and Johnson Innovation,  
Toronto, ON, Canada

**Lydia Andrews-Jones** AbbVie, Irvine, CA, United States

**Brian R. Berridge** B2 Pathology Solutions LLC, Cary, NC,  
United States

**Brad Bolon** GEMpath, Inc., Longmont, CO, United States

**Schantel Hayes Bouknight** Charles River Laboratories,  
Durham, NC, United States

**Molly H. Boyle** Labcorp Early Development Labs, Inc.,  
Somerset, NJ, United States

**Natasha Catlin** Pfizer, Inc., Groton, CT, United States

**Ronnie Chamanza** Janssen Pharmaceutical Companies of  
Johnson & Johnson, Buckinghamshire, United Kingdom

**Rachel E. Cianciolo** Zoetis Reference Laboratories,  
Cincinnati, OH, United States

**Samuel M. Cohen** University of Nebraska Medical Center,  
Omaha, NE, United States

**Kelly L. Diegel** GSK, Collegeville, PA, United States

**Susan A. Elmore** ElmorePathology, LLC, Chapel Hill, NC,  
United States

**Tim Erkens** Janssen Research & Development, LLC, a  
Johnson & Johnson Company, Beerse, Belgium

**Suzanne E. Fenton** Center for Human Health and the  
Environment, NC State University, Raleigh, NC, United  
States

**Kendall S. Frazier** Private Consultant, Alligator Point, FL,  
United States

**Mary Beth Genter** University of Cincinnati, Cincinnati, OH,  
United States

**Wendy Halpern** Genentech (a Member of the Roche Group),  
South San Francisco, CA, United States

**Jack R. Harkema** Michigan State University, East Lansing,  
MI, United States

**Wanda M. Haschek** University of Illinois at Urbana-  
Champaign, Urbana, IL, United States

**Kathleen Heinz-Taheny** Eli Lilly, Indianapolis, IN, United  
States

**Eugene H. Herman** National Cancer Institute, Bethesda,  
MD, United States

**Rebecca A. Kohnken** AbbVie Inc., North Chicago, IL,  
United States

**David K. Meyerholz** University of Iowa, Iowa City, IA  
United States

**Sunish Mohanan** Gilead Sciences, Foster City, CA, United  
States

**Kristen J. Nikula** Inotiv, Maryland Heights, MO, United  
States

**Tracey L. Papenfuss** StageBio, General Toxicologic  
Pathology, Mount Jackson, VA, United States

**Lila Ramaiah** Janssen Research & Development, LLC, a  
Johnson & Johnson Company, Spring House, PA, United  
States

**Colin G. Rousseaux** University of Ottawa, Faculty of  
Medicine, Ottawa, ON, Canada

**Daniel G. Rudmann** Charles River Laboratories, Ashland,  
OH, United States; Moderna Therapeutics, Cambridge, MA,  
United States

**Dirk Schaudien** Fraunhofer-Institute for Toxicology and  
Experimental Medicine ITEM, Hannover, Germany

**Marshall S. Schiccitano** IQVIA, Durham, NC, United States

**Madhu Sirivelu** Novartis Pharmaceuticals Corporation,  
East Hanover, NJ, United States

**Eric van Esch** InSight Pathology BV, Oss, the Netherlands

**Justin D. Vidal** Charles River Laboratories, Ashland, OH,  
United States

**Allison Vitsky** Pfizer Inc, San Diego, CA, United States

**Cynthia J. Willson** Inotiv-RTP, Morrisville, NC, United  
States

**Zbigniew W. Wojcinski** Toxicology & Pathology Consulting  
LLC, Hillsborough, NC, United States

This page intentionally left blank



# About the Editors

---

## EDITORS

---

**Wanda M. Haschek-Hock, BVSc, PhD**, is a Diplomate of the American College of Veterinary Pathologists (DACVP), former Diplomate of the American Board of Toxicology (DABT), Fellow of the International Academy of Toxicologic Pathology (FIATP), and Honorary Member of the Latin American Society of Toxicologic Pathology. She is a Professor Emerita at the University of Illinois College of Veterinary Medicine, Department of Pathobiology. Wanda has over 45 years of experience in comparative, respiratory, and toxicologic pathology with a research focus on natural toxins and food safety. She is a former President of the Society of Toxicologic Pathology (STP) and the Society of Toxicology's (SOT) Comparative and Veterinary Specialty Section and has served as an Associate Editor for *Toxicological Sciences* and *Toxicologic Pathology*, as a Councilor of the American College of Veterinary Pathologists (ACVP), and as a Member of the American Board of Toxicology (ABT). She served as an Editor for three editions of the *Fundamentals of Toxicologic Pathology* and *Haschek and Rousseaux's Handbook of Toxicologic Pathology*. She is a recipient of the STP's Lifetime Achievement Award, the SOT Midwest Regional Chapter's Kenneth DuBois Award, and the University of Sydney's Faculty of Veterinary Science Alumni Award for International Achievement.

**Colin G. Rousseaux, BVSc, PhD, DABT, FIATP**, is also a Fellow of the Royal College of Pathology (FRCPath) and a Fellow of the Academy of Toxicological Sciences (FATS). He is a Professor (Adjunct) in the Department of Pathology and Laboratory Medicine, Faculty of Medicine, University of Ottawa, Canada. He has over 35 years of experience in comparative and toxicologic pathology with a research focus on herbal remedies, fetal development and teratology, and environmental pollutants. He has described, investigated, and evaluated numerous toxicologic pathology issues associated with pharmaceuticals, pesticides, and agrochemicals. He has served on the editorial board of *Toxicologic Pathology*. He is a former President of the STP. Colin served as an Editor for three editions of the *Fundamentals of Toxicologic Pathology* and *Haschek and Rousseaux's Handbook of Toxicologic Pathology*.

**Matthew A. Wallig, DVM, PhD, DACVP**, is a Professor Emeritus in the Department of Pathobiology, College of Veterinary Medicine, the Department of Food Science and Human Nutrition, and the Division of Nutritional Sciences at the University of Illinois. His research has focused on the chemoprotective properties and mechanisms of phytochemicals in the diet, in particular, such as those in cruciferous vegetables, soy, and tomatoes. His current interests have expanded to include the defining morphologic parameters for diagnostic quantitative ultrasound in pancreatitis, pancreatic and hepatic neoplasia, metastatic disease, and chronic hepatic diseases, such as metabolic dysfunction-associated liver disease (MASLD) and metabolic dysfunction-associated steatohepatitis (MASH). Matt has served as an Editor for the last two editions of the *Fundamentals of Toxicologic Pathology* and *Haschek and Rousseaux's Handbook of Toxicologic Pathology*.

**Brad Bolon, DVM, MS, PhD, DACVP, DABT, FATS, FIATP, FRCPath**, has worked [sic] as an experimental and toxicologic pathologist in several settings: academia, a contract research organization, pharmaceutical companies (in both biomolecule and traditional small molecule settings), and private consulting. His main professional interests are the pathology of genetically engineered mice (especially embryos, fetuses, and placentas) and toxicologic neuropathology to assess the efficacy and safety of many therapeutic entities (biomolecules, cell and gene therapies, medical devices, and small molecules). He is a former President of the STP and a Member of the American College of Toxicology (ACT), the British Society of Toxicological Pathology (BSTP), and the European Society of Toxicologic Pathology (ESTP). Brad served as an Editor for the third edition of the *Fundamentals of Toxicologic Pathology* and an Associate Editor for the third edition of *Haschek and Rousseaux's Handbook of Toxicologic Pathology*.

## ASSOCIATE EDITORS

---

**Jeffrey I. Everitt, DVM, DACVP, FIATP**, is also a Diplomate of the American College of Laboratory Animal Medicine (ACLAM). He is a Professor (Emeritus) in the Department of Pathology, Duke University School of



Medicine, Durham, North Carolina. He has over 40 years of experience in comparative and toxicologic pathology with a research focus on fiber-induced lung disease. He has described, investigated, and evaluated toxicologic pathology issues associated with pharmaceuticals and agrochemicals while working in the pharmaceutical industry (GlaxoSmithKline) and at the Chemical Industry Institute of Toxicology (CIIT). He served as an Associate Editor of *Toxicologic Pathology*, Councilor of the STP, and on many advisory panels for academic, industry, and government entities.

**Karen S. Regan, DVM, DACVP, DABT**, has worked in various pathology and management roles at contract research organizations and is the President of her independent consultancy. She has over 30 years of experience in the toxicologic pathology of pharmaceuticals, agrochemicals, and medical devices. She has served as the President of the Toxicologic and Exploratory Specialty Section of the Society of Toxicology and as a Counselor for the Society of Toxicologic Pathology. She has been actively engaged in the standardization of the nomenclature for toxicologic pathology and is currently the Chair of the INHAND Male Reproductive Committee and a member of the INHAND Female Reproductive Committee. She has served as an expert pathologist on multiple pathology working groups for

the pharmaceutical and agrochemical industries as well as government entities. Her special interests are reproductive pathology, neuropathology, and ototoxicity.

## ILLUSTRATIONS EDITOR

**Beth W. Mahler** is employed by Experimental Pathology Laboratories, Inc., located at Research Triangle Park, NC, and works as a contractor at the U.S. National Institute of Environmental Health Sciences (NIEHS) in the Comparative and Molecular Pathogenesis Branch under the Division of Translational Toxicology (DTT). She has over 44 years of experience as a certified histologist (HT) in the areas of histology, animal necropsy, embryo collection and sectioning, special techniques, and digital photomicroscopy. Since 2006, she has served as the Illustrations Editor for the journal *Toxicologic Pathology*. Her past illustrative editorship roles include Associate Editor of the *Pathology of the Mouse*, edited by Dr. Robert R. Maronpot, and Illustrations Editor for the previous editions of the *Fundamentals of Toxicologic Pathology* and *Haschek and Rousseaux's Handbook of Toxicologic Pathology*, as well as the *Spontaneous Pathology of the Laboratory Non-human Primate*, edited by Alys Bradley, Jennifer Chilton, and Beth Mahler.

# Preface

---

Since its inception three decades ago, the *Handbook of Toxicologic Pathology* has been a comprehensive resource, covering fundamental knowledge and skills as well as the key technical procedures essential for the proficient practice of toxicologic pathology. This reference has found a home in the libraries of numerous academic, government, and industrial institutions engaged in basic and applied biomedical research around the globe and, in doing so, has become an indispensable reference for many toxicologic pathologists, toxicologists, regulators, physicians, biomedical researchers, and students. Indeed, the *Handbook* has been recognized by many as the most authoritative single source of information in this field due to the breadth and depth of the coverage of the field of toxicologic pathology.

Prior to the publication of the inaugural *Handbook* edition in 1991, information regarding toxicologic pathology had to be gleaned in a piecemeal manner from articles on various toxicology and the few toxicologic pathology journals. The success of this one-volume 1st edition and the expanded roles of toxicologic pathologists over time led, in due course, to the release of updated *Handbook* versions in subsequent years: a two-volume 2nd edition in 2002 and a three-volume 3rd edition in 2013. The many scientific advances, ongoing and extensive collaboration among global societies of toxicologic pathology, and new regulatory guidance that has occurred since the release of the 3rd edition prove that a new edition is necessary to maintain, and indeed enhance, the value of this resource for practitioners of the toxicologic pathology craft. For this reason, the Editors and Associate Editors are pleased to offer this new and expanded *Handbook* to aid your explorations of the toxicologic pathology field.

This 4th edition of *Haschek and Rousseaux's Handbook of Toxicologic Pathology* has been extensively updated to continue its comprehensive coverage. Due to the unrelenting explosion of information in this field, the 4th edition is now five volumes, with important concepts distributed in the following way:

- Volume 1 (released in 2022) covers the *Principles and Practice of Toxicologic Pathology*, including such key topics as basic concepts in biology, pathology, pharmacology, and toxicology as they intersect with the field of toxicologic pathology (Chapters 2–8);
- primary methods in toxicologic pathology (Chapters 9–16); overviews of major models employed in toxicologic research (Chapters 17–24); and essential practices in generating and interpreting toxicologic pathology data (Chapters 25–29). New chapters in Volume 1 address the absorption, distribution, metabolism, and excretion (ADME) principles for biomolecules; toxicologic pathology considerations in developmental and reproductive toxicity (DART) testing; digital pathology; and various animal models, including rodents, rabbits, dogs, nonhuman primates, and alternative models (e.g., in silico, ex vivo, in vitro and in vivo).
- Volume 2 (released in 2023) addresses *Toxicologic Pathology in Safety Assessment*. Safety assessment covers the application of toxicologic pathology in developing specific product classes (Chapters 1–12) and principles of data interpretation (Chapters 13–17). New chapters in this volume consider the fundamental attributes of novel therapeutic classes (nucleic acid- and protein-based pharmaceutical agents, gene therapy and gene editing, stem cell and other cell therapies, medical devices, and vaccines); agricultural and bulk chemicals; and the differentiation of adverse from nonadverse effects. These chapters address both pathology and regulatory issues. Previous chapters on such topics as drug discovery and development, toxicity and carcinogenicity testing, report preparation, and risk assessment and communication have undergone extensive revision that includes an in-depth discussion of new developments in this field.
- Volume 3 (released in 2023) is dedicated to *Environmental Toxicologic Pathology and Selected Toxicant Classes*. This volume covers toxicologic pathology, as it relates to food (Chapter 2), nutrition (Chapter 3), and the selected toxicant classes in the environment that affect human and animal health (Chapters 4–14). New chapters include herbal remedies (Chapter 4) and animal- and bacteria-derived toxins (Chapters 8 and 9); for these chapters, particular attention has been paid to the role of such substances in formulating new therapies (either as the active agent or as important contaminants of the manufacturing process). All previous chapters (e.g.,

endocrine disruptors, heavy metals, nanoparticulates, poisonous plants, and radiation) have been extensively revised and updated. Organ-specific environmental diseases are addressed in Volumes 4 and 5.

- Volumes 4 (released in 2024) and 5, *Toxicologic Pathology of Organ Systems* (this volume), provide a deep and broad treatment of major systems, emphasizing the comparative and correlative aspects of normal biology and toxicant-induced dysfunction, principal methods for toxicologic pathology evaluation, and major mechanisms of toxicity. [Chapters in Volume 4 cover the digestive tract, liver, bones and teeth, muscle and tendon, pancreas, adipose tissue, endocrine system, nervous system, eye, and ear.] Chapters in Volume 5, as in Volume 4, have been extensively updated and expanded, and placenta has been added to the chapter on embryo and fetus. New topics addressed in Volume 4 include the toxicologic pathology of adipose tissue, tendons, and teeth. New guidance regarding product development and regulatory issues has been incorporated in the organ system chapters for both volumes.

The expanded coverage of nonclinical testing principles and practices, the new material on various models of toxicity, and the toxicologic pathology of novel toxicant classes (especially new therapeutic modalities) will be a

particular strength of this new edition and will continue to justify its long-standing reputation for excellence. The Editors do accept that information relevant to toxicity research, hazard identification, and risk assessment and management is ever growing, and they encourage readers to extend their search for up-to-the-minute information in this area.

We would like to thank the dedicated efforts of the Associate Editors—Stacey Fossey and John Vahle (Volume 1), Katie Heinz-Taheny and Dan Rudmann (Volumes 2 and 3), Molly Boyle and Mark Hoenerhoff (Volume 4), and Jeff Everitt and Karen Regan (Volume 5); our Illustrations Editor, Beth Mahler; and the many chapter authors for their outstanding contributions in bringing this book to fruition. In addition, we wish to specifically acknowledge the significant involvement of many leading toxicologic pathologists as essential subject matter experts in contributing to this and the previous editions; many are now retired, and a number are deceased, including our friends and mentors Glenn Cantor, Charles C. Capen, Victor J. Ferrans, Gordon C. Hard, Kevin P. Keenan, Adalbert Koestner, Robert W. Leader, Daniel Morton, John F. Van Vleet, and Hanspeter R. Witschi.

**Wanda M. Haschek**  
**Colin G. Rousseaux**  
**Matthew A. Wallig**  
**Brad Bolon**

# Cardiovascular System

Brian R. Berridge<sup>1</sup>, Rebecca A. Kohnken<sup>2</sup>, Eugene H. Herman<sup>3</sup>

<sup>1</sup>B2 Pathology Solutions LLC, Cary, NC, United States, <sup>2</sup>AbbVie Inc., North Chicago, IL, United States, <sup>3</sup>National Cancer Institute, Bethesda, MD, United States

## OUTLINE

<b>1. Introduction</b>	<b>2</b>	<b>5.6. Xenobiotic Interactions</b>	<b>56</b>
<b>Part I: Heart</b>	<b>2</b>	<b>5.7. Modifying Factors in Cardiac Toxicity</b>	<b>57</b>
<b>2. Structure and Function</b>	<b>3</b>	<b>6. Cardiotoxicity Issues in Drug Development</b>	<b>57</b>
2.1. Gross and Microscopic Anatomy	3	6.1. Cardiovascular-Related Drug Development	
2.2. Physiology and Functional Considerations	8	Attrition	57
2.3. Xenobiotic Exposure	10	6.2. Rodent Progressive Cardiomyopathy	58
<b>3. Evaluation of Toxicity</b>	<b>11</b>	6.3. Animal Models of Human Cardiac Disease	58
3.1. Bioactivity Screening for Cardiac Toxicity	12	6.4. Clinical Translation of Nonclinical	
3.2. Functional Evaluation of Toxicity	12	Cardiotoxicity	59
3.3. Morphologic Evaluation of Toxicity	18	<b>Part II: Blood Vessels</b>	<b>59</b>
3.4. Background Alterations, Artifacts, and		<b>7. Structure and Function</b>	<b>60</b>
Spontaneous and Age-Related Lesions	22	7.1. Microscopic Anatomy	60
3.5. Biomarkers	24	7.2. Cellular and Extracellular Components of	
3.6. Biochemical Evaluation of Toxicity	25	the Vasculature: Biology	61
<b>4. Responses to Injury</b>	<b>25</b>	7.3. Physiology and Functional Considerations	63
4.1. Developmental Cardiotoxicity	25	<b>8. Evaluation of Toxicity: Vasotoxic Effects</b>	<b>66</b>
4.2. Cardiac Dysfunction as a Manifestation of		8.1. Physiological Methods for Testing	66
Toxicity	26	8.2. In Vitro Methods for Detecting Vascular	
4.3. Changes in Cardiac Mass as a Response to		Toxicity	67
Toxicity	28	8.3. Morphologic Evaluation	69
4.4. Drug-Induced Cardiomyopathies	29	8.4. Background Alterations, Artifacts,	
4.5. Cardiomyocellular Injury	34	Spontaneous and Age-Related Lesions	70
4.6. Endocardium	48	8.5. Use of Animals as Models for Vascular	
4.7. Neoplasia	49	Toxicity	71
4.8. Valves	49	8.6. Biomarkers of Vascular Injury	72
4.9. Epicardium	50	<b>9. Responses to Injury</b>	<b>73</b>
4.10. Pericardium	50	9.1. Atherosclerosis Acceleration by Toxic	
<b>5. Mechanisms of Toxicity</b>	<b>50</b>	Agents	73
5.1. Mechanisms of Altered Cardiac Function	51	9.2. Medial Proliferation	74
5.2. Mechanisms of Direct Cellular Injury	52	9.3. Intimal Proliferation	74
5.3. Mechanisms of Indirect Injury	55	9.4. Calcification	75
5.4. Cardiotoxicity of Cardiac Drugs	55	9.5. Aneurysms	76
5.5. Hypersensitivity Reactions	56	9.6. Medial Hemorrhagic Necrosis	76

9.7. Fibrinoid Necrosis	77	10.3. Heart	80
9.8. Microangiopathy	77	10.4. Liver	80
9.9. Immune-Mediated Vascular Inflammation	77	10.5. Kidney	81
9.10. Regeneration and Repair	78	10.6. Stomach	81
<b>10. Vascular Toxicity in Specific Organs</b>	<b>79</b>	<b>11. Conclusion</b>	<b>81</b>
10.1. Brain	79	<b>References</b>	<b>81</b>
10.2. Lungs	79		

## 1. INTRODUCTION

Cardiovascular (CV) disease is common in many Western societies and is increasing in prevalence in developing countries as well. The manifestations of CV disease are varied and can present as developmental cardiac defects (e.g., ventricular or atrial septal defects), heritable cardiomyopathies due to gene mutations, cardio-metabolic disease, coronary artery disease with ischemia, arrhythmias, hypertension, or inflammation of the myocardium or blood vessels due to autoimmune or infectious disease. This prevalence and these varied presentations create significant individual patient susceptibility to additional insult by cardioactive drugs or environmental toxicants and present a challenging context in which to detect those insults. They additionally represent gaps in our usual approach to evaluating CV safety or chemical hazard since our traditional animal models do not have those diseases. In addition, and like most important organs and systems, the CV system has a significant level of functional reserve capacity that allows that function to constantly respond to changing work demands but also complicates our ability to recognize CV disease until it is advanced and potentially irreversible.

The heart and blood vessels that course throughout the mammalian body are anatomically arranged to facilitate their functional role. Accordingly, the structure and function of the heart and blood vessels have an intimate interrelationship such that changes in one often produces adverse changes or, at least, compensatory changes in the other (Hanton, 2007). The significant contribution that the CV system makes to maintaining life leaves little tolerance for xenobiotic-induced injuries from natural toxins, environmental chemicals, or drugs.

Accordingly, the two primary structural and functional components of the integrated “cardiovascular” system—the heart and blood vessels—are discussed together.

## PART I: HEART

The heart, the dynamic center of a vast network of circulatory conduits, is subject to structural and functional alterations from exposure to a long list of potentially toxic xenobiotics. Alterations in cardiac function may result from changes in ion movements, membrane function, autonomic controls, energy-producing systems, or structural injuries. Morphological alterations include changes in cardiac mass (e.g., hypertrophy), injury to cellular elements of the heart, or even “repair” mechanisms (e.g., fibrosis), and may result from direct xenobiotic injury or due to changes in cardiac work or the heart’s ability to do work. In human patients, the presence of naturally occurring preexisting cardiovascular disease may predispose some individuals to xenobiotic-induced cardiac injury and dysfunction.

A wide spectrum of toxicity testing assessments is routinely used to detect and characterize cardiac toxicity. These assessments include sensitive measures of electrophysiology, blood pressure, cardiac contractility, and morphology. This battery of assessments is often used in routine toxicity testing and often mandated by international pharmaceutical regulatory agencies for new drug approvals (Anonymous, 2005, 2009, 2020). Data from toxicity studies must be interpreted with respect to the characteristic anatomic and functional attributes of a given test species. Such features are highly conserved across species, but many subtle differences also exist (Hew and Keller, 2003).



## 2. STRUCTURE AND FUNCTION

### 2.1. Gross and Microscopic Anatomy

The heart is a conical muscular organ that in mammals, birds, and reptiles has evolved to form a four-chambered pump with four valves that ensure unidirectional flow of blood through the organ and circulatory system. The heart lies within a conical fibroserous sac, the pericardium, which normally contains a small amount of clear serous fluid to mitigate friction. The heart is interposed as a pump in the vascular system where the right side supplies the pulmonary circulation and the left side the systemic circulation.

The right atrium of mammals receives systemic venous blood from the cranial (anterior) vena cava, caudal (posterior) vena cava, azygos vein, and coronary sinus. Blood from the right atrium enters the right ventricle by passing through the right atrioventricular (AV) orifice.

The right ventricle consists of an inflow sinus and an outflow conus (or infundibulum) that are separated by a thick muscular ridge, the supra-ventricular crest. Most of the luminal surface is coarsely trabeculated by muscular ridges termed trabeculae carneae. The inflow orifice is circumscribed by the right AV (tricuspid) valve. The valvular leaflets are anchored at their base to the fibrous ring of the AV orifice; the atrial surface of the valve is smooth, whereas the ventricular surface is rough and is the site of attachment for the firm white chordae tendineae. The chordae extend to insert in the three papillary muscles (two septal, one lateral), which project from the luminal surface of the chamber. The outflow orifice into the pulmonary artery at the summit of the conus arteriosus is circumscribed by the pulmonary valve with its three semilunar cusps. Fibrocartilaginous nodules are centrally placed on the free edge of each cusp.

The left atrium has a smooth luminal surface except for the auricle or atrial appendage, which is lined by pectinate muscles. The auricle is a muscular sac extending from the atrium, increasing the capacity of the atrium but with unique structural features (e.g., thinner muscular wall). Blood returning from the lungs enters the left atrium by the pulmonary veins and exits into the left ventricle via the left AV orifice. The left atrial wall is somewhat thicker than that of the right atrium, and the left atrial endocardium is also thicker and more opaque than that found in the right atrium.

The left ventricle has thick muscular walls (both free wall and septum) and is conical in shape (circular on cross-section). The volume of the cavity may be minimal if the heart is fixed in contraction. Generally, the luminal surface has few trabeculae in contrast to the right ventricle. The left AV (mitral) valve circumscribes the AV orifice. The valvular leaflets are larger and thicker than those in the right AV valve. The chordae tendineae are fewer and larger than on the right side and insert into two large papillary muscles (septal [or anterior] and parietal [or posterior]). The left ventricular outflow tract is formed by the upper third of the ventricular septum and the ventricular surface of the septal leaflet of the mitral valve. The aortic orifice is circumscribed by the three semilunar cusps of the aortic valve. The cusps are thicker than those of the pulmonary valve but have similar fibrous nodules in the middle of the free border of the cusps.

The walls of the cardiac chambers consist of three layers: the epicardium, the myocardium, and the endocardium. The epicardium or outer layer of the heart is the visceral layer of the serous pericardium. The entire surface of the pericardial cavity is covered by mesothelium. The subepicardial layer is attached to the myocardium; it contains a thin layer of fibrous connective tissue, adipose tissue, and numerous blood vessels, lymphatic vessels, and nerves.

The myocardium is the dense striated muscular layer of the heart. It is composed of cardiac muscle cells (myocytes or myofibers) attached to each other end-to-end and laterally forming interdigitating fascicles. These sheets of cells are anchored to the four fibrous rings of the fibrous skeleton of the heart, with one ring surrounding and supporting each of the AV and semilunar valves. The fibrous rings of the cardiac skeleton may contain plates of cartilage that undergo metaplasia to bone in older animals, especially in cattle, to form the os cordis. The cardiac skeleton separates the atrial myocardium from the ventricular myocardium except for penetrating fibers of the AV conduction system. The myocardial thickness is related to the pressures present in each chamber; the atria are thin and the ventricles are thick. The thickness of the left ventricular free wall is approximately threefold greater than that of the right ventricular free wall when measured in a transverse section across the middle of the chambers. This is because the pressures are higher in the

systemic circulation (served by the left ventricle) than in the pulmonary circuit (supplied by the right ventricle).

The endocardium is the inner layer of the heart that lines the chambers and extends over projecting structures such as the valves, chordae tendineae, and papillary muscles. The endocardium in the atria is thicker than in the ventricles and normally appears grossly white. The luminal surfaces of the endocardium are lined by endothelium set on a thin layer of connective tissue. The subendocardial layer contains blood vessels, nerves, and connective tissue with Purkinje fibers (cellular elements of the ventricular electrical conduction system) throughout the ventricles.

The arterial supply to the heart consists of left and right coronary arteries that originate from the root of the aorta (at the sinuses of Valsalva behind the left and right cusps of the aortic valve). The arteries tend to form a ring as they encircle the base of the heart in the AV (coronary) groove. They then radiate over the heart in the subepicardium and give off perforating intramyocardial arteries that supply a rich capillary bed throughout the myocardium. Extensive anastomoses occur among the capillaries that tend to run parallel to the cardiac muscle cells. On histologic cross-section, the ratio of capillaries to muscle cells is approximately 1:1. The coronary veins tend to follow the courses of the arteries, and open into the right atrium by the coronary sinus. The lymphatic vessels course in the epicardium and converge into trunks that lie adjacent to the coronary arteries in the coronary groove and eventually exit to reach the tracheobronchial lymph nodes.

The cardiac conduction system is a primary conduit of electrical impulses that stimulate an orchestrated and rhythmic contraction of the myocardium. Components include the sinoatrial (SA) node at the junction of the cranial (anterior) vena cava and the right atrium; the AV node and bundle located beneath the septal leaflet of the right AV (tricuspid) valve and traversing the lower atrial septum onto the upper portion of the muscular ventricular septum; and the right and left bundle branches that descend on each side of the muscular ventricular septum and eventually ramify over the ventricles as the Purkinje fiber network. Normal features of the heart such as the median nodular thickenings of the aortic and pulmonic valve leaflets may occasionally be misinterpreted as lesions.

Cardiac weight (as % body weight) varies greatly among species. Pigs and rats have small hearts (approximately 0.3% of body weight); cows, mice, and guinea pigs have intermediate-sized hearts (approximately 0.5% of body weight); and dogs, cats, and horses have large hearts (from 0.75% of body weight in nonathletic dog breeds to 1.25% in athletic breeds) (Altman and Dittmer, 1971; Ayers and Jones, 1978).

### **2.1.1. Cellular and Extracellular Elements of the Heart**

The atrial and ventricular myocardia are composed of a variety of cells, of which the myocytes are the primary force-generating cells. Cardiomyocytes comprise 80% of the heart mass, but only 25% of the cellular content by number. Myocytes are elongated and joined to one another by intercellular junctions. The latter mediate electrical coupling of the myocytes and render them able to act as a functional syncytium. The myocytes are surrounded by a rich network of blood vessels and capillaries embedded in a thin matrix of interstitial connective tissue. Also present in this matrix are nerves and lymphatics as well as cells such as mast cells, histiocytes, fibroblasts, pericytes, and poorly differentiated mesenchymal cells.

#### **2.1.1.1. VENTRICULAR MYOCYTES**

Ventricular myocytes are approximately cylindrical, but branch freely, and are 80–100  $\mu\text{m}$  in length and 10–20  $\mu\text{m}$  in diameter (Figures 1.1 and 1.2). Myocytes are limited by the sarcolemma, a structure formed by the plasma membrane (plasmalemma) and an external lamina (laminar coat, basement membrane, basal lamina, and glycocalyx).

The T-tubule (transverse tubule) system is a network of tubular invaginations of the sarcolemma into the interior of cardiac myocytes. T-tubules extend from the outer cell surface throughout the cells in a generally transverse direction, coursing around the myofibrils at the levels of the Z bands (which separate adjacent sarcomeres). However, longitudinally oriented branches interconnect adjacent transversely oriented T-tubules. The T-tubule system allows proximate contact between the extracellular environment and the contractile apparatus of the cells. The system functions in facilitating the inward spread of action potentials at the cell surface via ionic exchange with the interstitium and also in the excitation–contraction coupling in the ventricular myocardium.



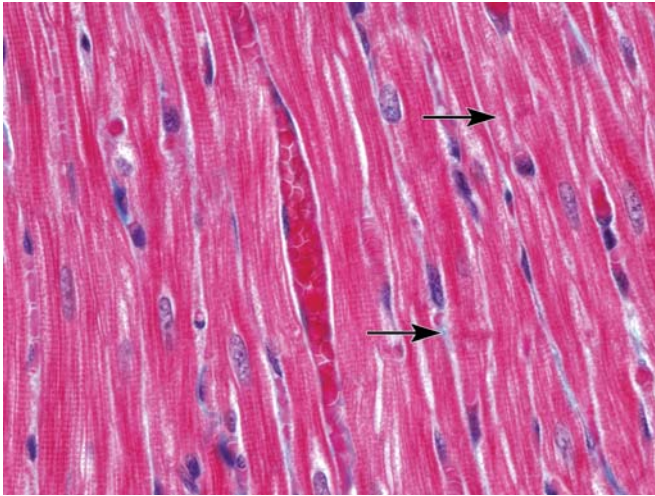


**FIGURE 1.1** Longitudinal section of rat myocardium with numerous, parallel, myocytes abutting a central capillary filled with dark red erythrocytes. Myocytes are characterized by an oval basophilic nuclei and abundant red sarcoplasm with thin dark cross-striations (representing sarcomeres); occasionally, an intercalated disc (*arrows*) may be seen wherein adjacent cells are fused to form a syncytium. Formalin-fixed, paraffin-embedded, Masson's trichrome stain. Original magnification 60 $\times$ . Reproduced from Haschek WM, Rousseaux CG, Wallig MA, editors: *Haschek and Rousseaux's handbook of toxicologic pathology*, ed 3, 2013, Academic Press, Figure 46.1, p. 1571, with permission.

Neighboring myocytes are connected end-to-end and, to a lesser extent, side-to-side by intercellular junctions. These intercellular adhesions permit rapid transmission of the action potentials throughout the entire syncytium, thereby providing coordinated contractile waves that effectively move blood through the heart. The end-to-end junctions are known as intercalated discs, the side-to-side junctions as lateral junctions.

Myocytes contain one or two centrally located oblong nuclei. The nuclear contours are smooth when the cells are relaxed and wrinkled when the cells are contracted. Bundles of myofibrils surround the nucleus, leaving a conical area free of contractile elements but densely packed with other cellular organelles, including the Golgi complex, mitochondria, glycogen, lysosomes, and lipofuscin granules at the nuclear poles.

The contractile elements occupy about 50% of the cytoplasm of myocytes and form a continuous mass of myofilaments that are arranged in bundles of myofibrils separated by the interfibrillar matrix. This matrix contains mitochondria, sarcoplasmic reticulum (SR) and T-tubules, glycogen particles, and other organelles.

Myofibrils are highly ordered arrays of contractile proteins. They exhibit a periodicity that is evident by light microscopy in the form of dark anisotropic A bands and light less-anisotropic I bands. The I bands are bisected by a thick dark Z band. The array of contractile elements between two adjacent Z bands is known as a sarcomere and constitutes the contractile unit of cardiac muscle ([Figure 1.2](#)).

The A band is composed of thick myofilaments composed of myosin aggregates where each myofilament measures 1.5  $\mu\text{m}$  in length and 10–15 nm in diameter. The I band is composed of thin myofilaments that are formed by aggregates of the fibrous form of actin and various other proteins. The thin myofilaments measure 1  $\mu\text{m}$  in length and 4–8 nm in diameter.

The Z bands of adjacent myofibrils tend to be in register. They are connected to each other and to the internal surface of the plasmalemma by bundles of transversely oriented cytoskeletal filaments that average 10 nm in diameter. Because of these connections, the sarcolemma in contracted cells assumes a scalloped appearance, with indentations in register with the Z bands.

The ultrastructural orientation of the SR is closely related to that of the myofibrils and the T-tubule system. An important function of the SR is to actively take up and release calcium ( $\text{Ca}^{2+}$ ) ions during the contraction–relaxation cycle of the myocyte. The SR also functions in the metabolism of glycogen and lipids.

Ventricular myocytes are rich in mitochondria, constituting roughly 35% of the cell volume. Mitochondria are situated between the myofibrils, in subsarcolemmal, interfibrillar, and perinuclear areas. Mitochondria are the sites of oxidative phosphorylation and for synthesizing high-energy phosphates, thus providing the energy needed for muscular contraction and relaxation. Cardiac mitochondria are very sensitive to noxious influences; at the ultrastructural level, they can be drastically changed in structure by even short periods of ischemia.

Lysosomes, phagosomes, and multivesicular bodies are commonly observed in cardiac myocytes, as are residual bodies of lysosomal origin (lipofuscin granules). All of these structures are usually located in the perinuclear region. The Golgi apparatus in ventricular myocytes is usually found in the form of multiple stacks of cisterns and associated vesicles in the perinuclear areas. It is less extensively developed in ventricular myocytes than in their atrial counterparts.

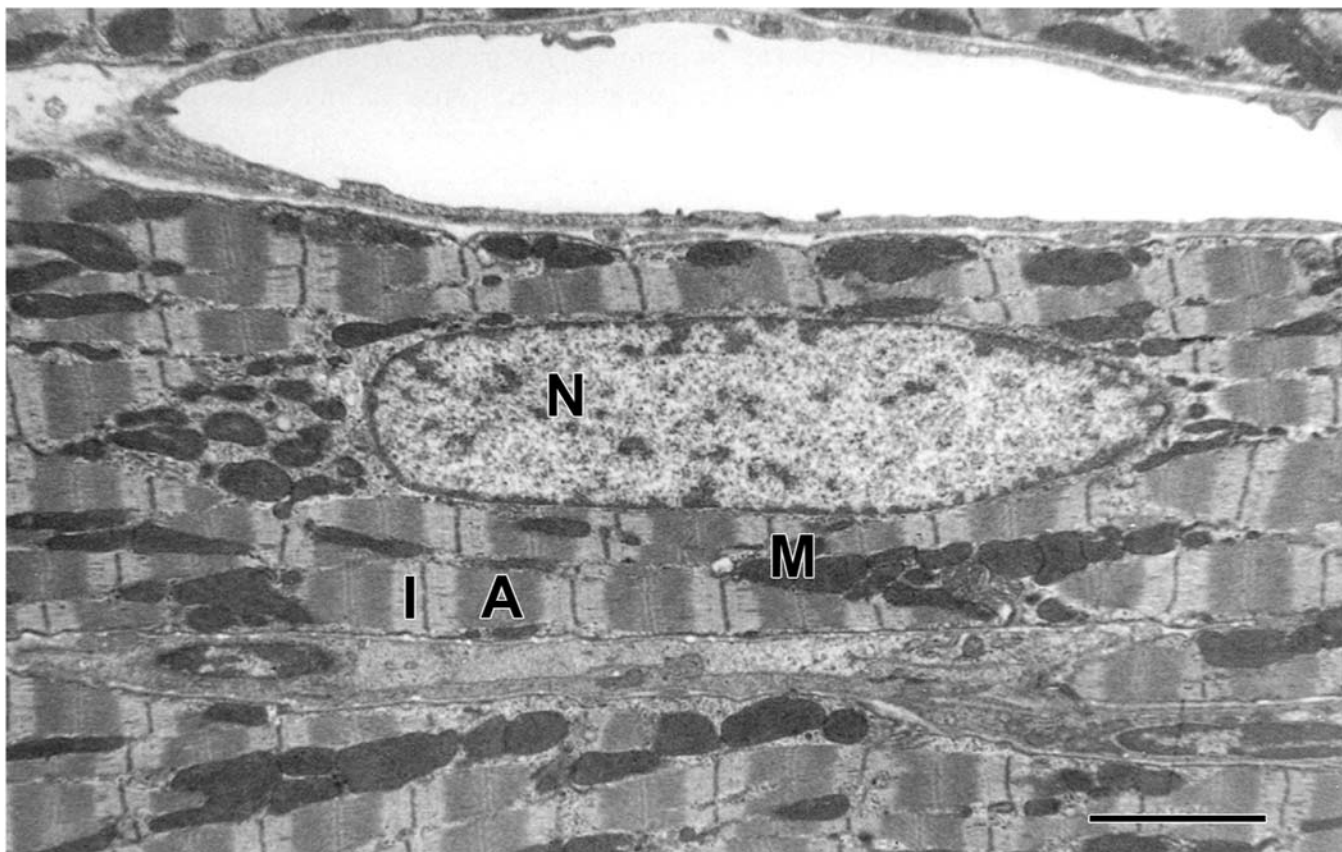


**FIGURE 1.2** Electron micrograph of perfused rat myocardium. Several myocytes lie adjacent to an open capillary (top). Sarcomeres are relaxed and have prominent A (dark) and I (light) bands. The thin dark Z binds that bisect the I bands represent the borders between adjacent sarcomeres. N, nucleus; M, mitochondria. Bar = 5 mm. *Reproduced from Haschek WM, Rousseaux CG, Wallig MA, editors: Handbook of toxicologic pathology, ed 2, 2002, Academic Press, Figure 2, p. 367, with permission.*

Ventricular myocytes contain small amounts of glycogen. This material is found in the beta- or monoparticulate form in the interfibrillar spaces and perinuclear areas, and between the myofilaments.

#### 2.1.1.2. ATRIAL MYOCYTES

The architecture of atrial myocytes resembles that of ventricular myocytes. However, the 2 cell types differ in a number of fine structural features, including the intercellular junctions, the T-tubule system, the SR, the mitochondria, and the presence of “atrial” granules.

The arrangement of atrial myocytes is less regular than that of ventricular myocytes. The cell length is in the same range (80–100  $\mu\text{m}$ ), but the diameter of the atrial myocytes (6–12  $\mu\text{m}$  in humans) is smaller than that of ventricular myocytes (10–20  $\mu\text{m}$ ).

Atrial myocytes contain a population of cytoplasmic organelles termed atrial granules. These structures are round or oval vesicles, limited by

single membranes, and have a moderately dense core that is separated from the surrounding membrane by a less dense zone. These granules are formed in the rather extensive Golgi vesicles of atrial myocytes. The granules are the storage sites for important regulatory hormones, the atrial natriuretic peptides (ANPs). The prohormone pro-ANP is released in response to elevated vascular volume or atrial wall stretch. Natriuresis (increased urinary excretion of sodium [ $\text{Na}^+$ ]) and diuresis (increased urinary excretion of water) are induced by the mature ANP, which acts to increase glomerular filtration rate, renal blood flow, urine volume, and urinary  $\text{Na}^+$  excretion, and to decrease plasma renin activity.

#### 2.1.1.3. ELECTRICAL CONDUCTION SYSTEM

The conduction system of the heart consists of the SA node, the AV node, and the bundle of His. The nodes are aggregates of modified myocytes innervated by autonomic nerves that set the pace for electrical signaling in the heart, while



the bundle of His is a series of modified myocytes (termed Purkinje fibers) that transfers the signals from the AV node to the ventricular myocytes. The bundle of His becomes subdivided into the main left and right branches and their peripheral ramifications. The morphology of the specialized conducting cells shows great variation, not only among different species but also in different components of the conduction system within a given species. For example, the modified cardiomyocytes of the SA node are loosely aggregated around the SA artery of the right atrium, while the AV node is a more circumscribed aggregate of cells at the base of the heart above the AV septum. Similarly the Purkinje fibers of the rodent heart are histologically indistinct while those of the minipig are very prominent (Kawashima and Sasaki, 2011; Skydsgaard et al., 2021).

#### 2.1.1.4. CELLULAR COMPONENTS OF MYOCARDIAL INTERSTITIUM

Fibroblasts are spindle-shaped connective tissue cells with a few cytoplasmic processes that extend in various directions and for varying distances into the surrounding interstitial tissue. Fibroblasts do not have an external lamina or basement membrane, and their surfaces frequently are in direct contact with collagen fibrils. The major function of fibroblasts is the synthesis of connective tissue proteins, particularly collagen.

Myofibroblasts resemble fibroblasts in most of their ultrastructural features but can be distinguished from the latter by their nuclear indentations and the abundance of actin filaments in their cytoplasm. Myofibroblasts are thought to represent a type of intermediate differentiation state between fibroblasts and smooth muscle cells (SMCs). In the heart, myofibroblasts are present in valvular and endocardial connective tissue.

Macrophages (histiocytes) are normally present in small numbers in the myocardial interstitium and in the connective tissue of endocardium and valves. These cells, sometimes accompanied by a few lymphocytes, are present occasionally in mononuclear cell aggregates within the interstitial tissue as an incidental background finding in untreated animals. Mast cells are generally found in small numbers in the myocardial interstitium, usually as isolated cells in perivascular locations and in the endocardium. However, mast cells may be more numerous in some individuals of some species (e.g., mouse).

#### 2.1.1.5. EXTRACELLULAR COMPONENTS OF MYOCARDIAL INTERSTITIUM

The collagen fibrils in the myocardial interstitium have been shown, by scanning electron microscopy (SEM), to have a highly organized tridimensional arrangement. Small bundles of collagen fibrils ("collagen struts") constitute a fibrous scaffold that mechanically interconnects adjacent myocytes and connect myocytes to neighboring capillaries. These struts provide sarcomere alignment from myocyte to myocyte and prevent cell slippage during contraction.

#### 2.1.1.6. CELLULAR COMPONENTS OF THE MYOCARDIAL VASCULATURE

The detailed structure of the various types of vascular cells in the heart is comparable to those of cells in blood vessels generally. These features are presented with the discussion of the vessels (see Part II: Blood Vessels).

#### 2.1.1.7. MYOCARDIAL INNERVATION

Small nerves composed of unmyelinated nerve fibers are commonly found in cardiac muscle, where they course in the proximity of blood vessels. These nerves carry autonomic signals that help regulate blood vessel diameter (and thus myocardial perfusion).

#### 2.1.1.8. PERICARDIUM

The pericardial membrane or sac (i.e., the parietal pericardium) is composed of two layers: the outer serosa and an inner fibrosa (fibrous connective tissue layer). The serosa consists of the surface lining layer of mesothelial cells and of a narrow submesothelial space that separates the serosa from the underlying fibrosa. The smooth surface of the serosa reduces friction between the dynamically moving heart surface and surrounding thoracic structures, while the fibrosa affords strength to maintain pericardial integrity.

The visceral pericardium (i.e., the epicardium) consists of a mesothelial cell layer and a submesothelial layer that varies considerably in composition from one area to another. In some regions, particularly in the atria, it has a layer of elastic tissue and a deeper layer that is rich in collagen fibrils. In contrast, this layer over the ventricles is characterized by a thin layer of mesothelial cells that is continuous with the fibrous epicardium.

#### 2.1.1.9. ENDOCARDIUM

The endocardium is a delicate layer that invests the entire inner surface of the heart. Its structure

and thickness are variable from one chamber to another, and even within different regions of a given heart chamber. The endocardium is thicker in the atria than in the ventricles, in the left-sided compared to the corresponding right-sided chambers, and in the outflow tracts relative to the inflow tracts of the ventricles. The ventricular endocardium is composed of five distinct layers: the endothelial layer, the inner connective tissue layer, the elastic tissue layer, the SMC layer, and the outer connective tissue layer (also called the subendocardial layer). The endothelial surface of the endocardium is continuous with the endothelial lining of the blood vessels that enter and leave the heart. The endocardial connective tissue is continuous with that in the myocardial interstitium and valvular leaflets.

#### 2.1.1.10. CARDIAC VALVES

Cardiac valves ensure unidirectional flow of blood through the four chambers of the heart. Two morphologic subtypes are typical: AV valves and semilunar valves. The AV valves separate atria from ventricles, and semilunar valves ensure unidirectional blood flow out of the heart and into the aorta or pulmonary artery.

The AV valves consist of the mitral (left) and tricuspid (right) valves. The mitral valve consists of the fibrous annulus where the valves meet the subjacent myocardium, the leaflets, the chordae tendineae, and the papillary muscles. The annulus itself is composed of a ring of circumferentially oriented collagen and elastic fibers, with connections that extend into the ventricle and the atrium. The valve leaflets themselves consist of three distinct layers: the fibrosa, the spongiosa, and the ventricularis. The bundles of collagen that constitute the fibrous core of the valve leaflet extend from the annulus, first forming a broad sheet (known as the fibrosa) that shows a basket-weave arrangement throughout the leaflet, then continuing into the chordae tendineae, and finally spreading out into a fibrous connective tissue network that covers the tips of the papillary muscles. The middle spongiosa is composed of loose collagen and abundant glycosaminoglycans, while the thin ventricularis is composed of collagen and elastic fibers. The architecture of the tricuspid valve and the layered arrangement of the tricuspid valve leaflets are generally similar to those in the mitral valve. However, the individual layers of connective tissue are thinner in the tricuspid valve.

The semilunar valves also have a well-defined three-layered structure that differs in some respects from that of the AV valves. Three layers are recognizable in semilunar valves: the fibrosa, the spongiosa, and the ventricularis. These layers are similar in distribution in the aortic and pulmonary valves but are thinner and more delicate in the latter.

## 2.2. Physiology and Functional Considerations

The heart propels blood through the lungs (pulmonary circulation) and throughout the body (systemic circulation), providing oxygen and nutrients to all tissues. The efficiency of the heart and its ability to perform its task depend on the coordinated and rhythmic conduction of electrical impulses coupled with rapid coordinated activation of the contractile apparatus. The functional units of the myocardium are the cylindrically shaped striated cardiomyocytes described earlier, but the function of the organ depends on their integrated action as a syncytium.

### 2.2.1. *Phases of the Cardiac Cycle*

The cardiac cycle is defined by movement of blood through different chambers of the heart and the body as a whole. The cycle reflects sequential pressure changes in various heart chambers with pressures on the left higher than on the right since less force is needed to move blood through the lungs (right side) compared to the remainder of the body (left side). The cardiac valves ensure that movement of blood remains unidirectional. Holes in the heart chamber walls (which are often developmental defects) or incomplete valve closures (due to deformity or disease) reduce the unidirectional flow which can put abnormal pressures on the associated heart chambers with functional and pathologic consequences.

Blood circulation depends on the coordinated cyclic contraction and relaxation of the heart chambers. During the cardiac cycle, the two atria contract before the two ventricles. “Diastole” refers to filling of a chamber (i.e., a period of muscle relaxation), while “systole” indicates blood expulsion from the chamber due to myocardial contraction. Diastole begins with closure of both semilunar valves to prevent blood from leaving the ventricles followed by opening of the AV valves. Next, the atria

contract so that returning blood fills the ventricles (unoxygenated blood from the body to the right ventricle, freshly oxygenated blood from the lungs to the left ventricle). Systole starts when the AV valves close to prevent backflow of ventricular blood into the atria. Thereafter, the semilunar valves open and the ventricles contract to expel blood from the heart (into the lungs from the right ventricle, and out through the aorta and into the systemic circulation from the left ventricle).

### 2.2.2. Resting and Action Potentials of Cardiac Myocytes

Electrical activity in the heart is generated at the level of the individual muscle cells as self-propagating depolarizing and repolarizing action potentials across the cell membrane (Amin et al., 2010; Bers, 2002). The principal diffusible ions responsible for these action potentials are  $\text{Na}^+$ , potassium ( $\text{K}^+$ ),  $\text{Ca}^{2+}$ , and chloride ( $\text{Cl}^-$ ). The time course of de- and repolarization occurs in two basic patterns: slow response and fast response.

Cardiomyocytes have a steady resting membrane potential of approximately  $-90$  mV (inside to outside) (Amin et al., 2010). This potential depends primarily on the differences in concentration of  $\text{K}^+$  and  $\text{Na}^+$  ions across the cell membrane, and the differential permeability of the cell membrane to the ions. When the membrane potential reaches a critical value of  $-60$  to  $-70$  mV (i.e., the threshold potential), the fast  $\text{Na}^+$  channels open and initiate the action potential (phase 0). Conduction velocity is directly related to the rate of rise of phase 0. At the end of phase 0, the cell is completely polarized, with an inside voltage of approximately  $+30$  mV. During phase 1 and early phase 2 of the action potential, the influx of  $\text{Na}^+$  markedly declines and the membrane potential begins to fall. The commencement of repolarization during phase 1 of the fast-type action potential is thought to be due to a transient inflow of negatively charged  $\text{Cl}^-$  ions and an outflow of positively charged  $\text{K}^+$  ions. During the plateau phase (phase 2),  $\text{Ca}^{2+}$  and  $\text{Na}^+$  enter the cell through slow channels. The inflow of  $\text{Ca}^{2+}$  at this time is believed to initiate the excitation-contraction coupling process. During phase 3, the  $\text{K}^+$  permeability increases and the slow  $\text{Na}^+$  and  $\text{Ca}^{2+}$  channels are inactivated. The final result is the repolarization of the membrane and the return of the resting action potential (phase

4). Disease processes and certain drugs and other chemicals that alter membrane properties can affect the rate and duration of the action potential.

There is some variability in the rate of action potential response, with slower responding fibers found in a few specific locations in the heart (e.g., the SA and AV nodes). The resting potential in slow-response cells is near  $-60$  mV. At this level, fast  $\text{Na}^+$  channels are virtually inactive, and thus only slow  $\text{Na}^+$  and slow  $\text{Ca}^{2+}$  channels are functional. The slow channels are activated when the transmembrane potential reaches  $-40$  mV. As a result, depolarization proceeds slowly by diffusion of  $\text{Na}^+$  and  $\text{Ca}^{2+}$  into the cell. Slow-response cells can act as intrinsic cardiac pacemakers in the absence of signals originating from the SA node (i.e., the main cardiac “pacemaker”) because the membrane potential in phase 4 is constantly decreasing in these myocytes. This depolarization is believed to result from a progressive reduction in  $\text{K}^+$  permeability in conjunction with a steady inflow of  $\text{Na}^+$  into the cell. These two effects continue until the transmembrane potential reaches a value sufficient to initiate a new action potential. Some conducting fibers of the right atrium, AV node, and Purkinje fiber system may exhibit pacemaker potentials and can initiate cardiac activity if the SA node is not functioning normally. The SA node normally overrides other pacemaker cells because its rate of depolarization is more rapid than that of other cells in the electrical conduction system and the myocardium. Cellular level depolarization and repolarization coincide with contraction (systole) and relaxation (diastole) at the organ level.

### 2.2.3. Initiation and Conduction of Cardiac Impulses

Rhythmicity in the heart is normally controlled by pacemaker cells in the SA node and conducting tissue. Both slow- and fast-response fibers are involved in this impulse initiation and subsequent conduction to other parts of the heart. The impulse originating in the SA node of the right atrium travels rapidly to all parts of the right and left atria and AV node. Conduction of the impulse through the AV node is slower and limits the frequency with which impulses from the atria can enter the ventricles. Once past the AV node, the impulse is again conducted rapidly through the specialized conducting fibers of the bundle of His. This bundle subdivides into the many branches forming the subendocardial



Purkinje system, which ultimately delivers the impulse to the ventricular muscle cells. The propagation of excitation initiates the coordinated contractile process in both ventricles.

#### 2.2.4. Excitation–Contraction Coupling

Myocellular contraction is initiated by an increase in intracellular  $\text{Ca}^{2+}$  triggered by the opening of membrane  $\text{Ca}^{2+}$  channels during depolarization (Bers, 2002). Inflow of extracellular  $\text{Ca}^{2+}$  also triggers the release of large intracellular  $\text{Ca}^{2+}$  stores from the SR into the sarcoplasm (i.e., cytosol). Rising intracellular concentrations of  $\text{Ca}^{2+}$  in the sarcoplasm stimulate the release of the regulatory proteins, tropomyosin and troponin, on the thin filament to expose sites for myosin binding on the actin proteins of the filament. Myosin ATPase is activated by hydrolyzing adenosine triphosphate (ATP). The energy released by this reaction is used to form cross-bridges between actin and myosin, resulting in “filament sliding” and myofibril and myocyte contraction. The force and velocity of contraction is influenced by the amount of  $\text{Ca}^{2+}$  that reaches the contractile sites. Relaxation of contracted cardiomyocytes results from an ATP-driven process of intracellular reuptake (into the SR) and extracellular extrusion of  $\text{Ca}^{2+}$ .

#### 2.2.5. Myocardial Metabolism

Heart muscle uses chemical energy to initiate and sustain the work of contraction. Most of the energy liberated from fuel substances results from the production of ATP. Energy sources such as lactate, glucose, triglycerides, and fatty acids ultimately enter the tricarboxylic acid (TCA) cycle to generate ATP (Bertero and Maack, 2018). Within the TCA cycle, the carbons from pyruvate are oxidized through intermediate steps to carbon dioxide, and oxidative phosphorylation is initiated in the mitochondria. The energy produced by the reactions is stored in the heart as ATP or creatine phosphate. The process of energy utilization also involves  $\text{Ca}^{2+}$  ions. The action potential allows both externally and internally sequestered  $\text{Ca}^{2+}$  to move into the cytosol of the myocytes. The released  $\text{Ca}^{2+}$  then activates the myofilaments by binding ATP into reactive sites between the myosin and the actin filaments. An ATPase enzyme splits ATP in the presence of magnesium, and the myofilaments slide along each other. This sliding motion results in myofibril and sarcomere contraction.

#### 2.2.6. Innervation of the Heart

Neural control of the heart is mediated by both the parasympathetic and sympathetic divisions of the autonomic nervous system. In general, the parasympathetic division is in control during homeostasis, while the sympathetic division is activated during times of stress (see *Nervous System*, Vol 4, Chap 8).

Parasympathetic fibers from the vagus nerve (cranial nerve X) supply the SA node, atrial muscle fibers, AV node, and, to a limited degree, the ventricular myocardium. The main effects of the vagus nerve, which are mediated by the neurotransmitter acetylcholine, are a decrease in the force of atrial and ventricular contraction, a decrease in conduction velocity through the AV node, and a decrease in heart rate. These actions of acetylcholine result primarily from a decrease in the slope (phase 4) of the pacemaker potential and from the production of a more negative diastolic potential. This hyperpolarization may be caused by an increase in  $\text{K}^+$  permeability.

Sympathetic innervation to the heart is supplied by the cranial sympathetic chain ganglia. The release of the neurotransmitter norepinephrine by sympathetic stimulation increases the slope of diastolic depolarization so that the threshold potential is reached more quickly and the rate of SA nodal discharge is increased (i.e., a positive chronotropic response, where chronotropy is an effect on heart beat rate). This effect is attributed to an augmentation of slow inward  $\text{Ca}^{2+}$  currents. The effects on the AV node and other conducting fibers are similar to those of the SA node. Sympathetic stimulation of myocytes leads to an increase in force of contraction (positive inotropic response, where inotropy is an effect on the force of heart contraction). This action is mediated by cyclic adenosine monophosphate (cAMP, a “second messenger” signaling molecule). cAMP is thought to activate a kinase enzyme that ultimately makes more  $\text{Ca}^{2+}$  available for the contractile proteins.

#### 2.3. Xenobiotic Exposure

The heart and blood vessels are susceptible to injury or dysfunction when exposed to a variety of chemicals and drugs. Some agents exert myocardial effects directly, while many may produce cardiovascular alterations through indirect actions involving other body systems. As with noncardiac organs, blood provides the

primary route by which the heart is exposed. The cardiovascular system's role in circulating blood and xenobiotic metabolites may result in unique and prolonged exposure of the heart and vessels to toxic agents. Consequently, progressive and irreversible effects may occur with repeated exposure. Substances producing myocardial effects may enter the vascular compartment from any exposure route including enteral, dermal, and pulmonary absorption. The intimate association of the cardiovascular and pulmonary systems provides a particularly unique exposure via inhalation. For example, inhaled carbon monoxide (CO) competes with hemoglobin-binding of oxygen (O<sub>2</sub>), leading to decreased O<sub>2</sub> availability, hypoxia, tachycardia, and other electrocardiographic changes (Gandini et al., 2001). Likewise, inhaled low-molecular-weight halogenated alkanes used for industrial purposes as well as volatile anesthetics can cause arrhythmias and sensitize the heart to the injurious effects of sympathoadrenal discharge or to exogenous catecholamines (Benowitz, 1992).

A substance in the blood capable of producing myocardial toxicity need not have a direct effect on cardiovascular function. Chemically induced alterations in other organs such as the kidney may lead to acid-base imbalances and/or electrolyte concentration changes of sufficient magnitude to cause significant alterations in cardiovascular function, which present as altered electrophysiology and clinically detectable arrhythmias.

### 3. EVALUATION OF TOXICITY

Assessment of cardiac liabilities in drug safety or chemical hazard evaluations should be biologically holistic recognizing the important interdependence between structural changes and function in the heart and blood vessels. Assessment of either structure or function in isolation would be incomplete and complicate the ability to infer a pathogenesis for any changes observed, define an effective biomarker strategy for clinical biomonitoring and management, or even understand species specificity. Histopathology is a significant and sensitive contribution to traditional animal toxicity evaluations, but it is not an efficient or popular clinical biomarker in human patients. Accordingly, defining serum biochemical or functional correlates to a structural change enhances our ability to clinically manage and mitigate a putative liability.

Well-characterized methods (in vitro, ex vivo, and in vivo) are available for detecting and characterizing toxicity in the cardiovascular system. Among these are cell cultures, micromass assays, organoids, and tissue slices (see *Alternative Models in Biomedical Research: In Silico, In Vitro, Ex Vivo, and Non-Traditional In Vivo Approaches*, Vol 1, Chap 24). Contemporary drug safety assessment involves a relatively standard battery of evaluations that can be modified or complemented as needed to address specific issues or needs. These evaluations for therapeutic products are often guided by regulatory expectations described in guidances and may include specific expectations for some organ systems like the cardiovascular system (Anonymous, 2005, 2009, 2020). Regulatory expectations for chemical hazard assessment are less specific. In general, the heart is routinely weighed as well as examined grossly and histologically as a component of a general toxicity animal study for pesticides, solvents, and other chemicals.

The ability to accurately predict the human effects of either drugs or environmental exposures from animal studies has challenges. Though the mammalian system exhibits significant anatomic and molecular conservation across species, there are biological differences that can impact the ability to model a toxicity in animals with equal opportunity for a toxicity to occur in animals that is not a risk for human patients, and vice versa. These points of discordance can result in unintended harm to patients and significant challenges for developing safe drugs. An example of an important biological difference that can impact the ability to recognize human risks is that represented by differences in circulating lipoprotein profiles. Most commonly used laboratory animals do not replicate the lipoprotein profile of human patients (Kaabia et al., 2018). Likewise, the rodent cardiac action potential lacks a significant contribution by the hERG (I<sub>Kr</sub> [rapid delayed K<sup>+</sup> rectifier]) ion channel, so rodents are not appropriate species to assess drug-induced QT prolongation risks (Hoffmann and Warner, 2006).

Also, significant differences in disease context exist between human patients and animal models commonly used for safety testing. The animal models most used in toxicity-testing studies are young and healthy. Human patients, on the other hand, have a wide spectrum of morbidities and comorbidities that can have a significant influence on the cardiotoxic and vasculotoxic potentials of many xenobiotics.



Given the variety of ways cardiovascular toxicity can present, a comprehensive approach to evaluation should be considered with assessments of cardiac function and structure. Functional measures should include electrocardiograms (ECGs), contractility, and blood pressure. Morphologic assessments should include organ weight and histologic evaluation of all regions of the heart (e.g., myocardium, valves, atria, ventricles, major vessels) as well as blood vessels in and outside of the heart.

### 3.1. Bioactivity Screening for Cardiac Toxicity

In vitro screening for CV-relevant biological activity that may represent a hazard or toxicity in animal or human studies is increasingly common as an approach to early identification of these liabilities. One approach used by some pharmaceutical companies involves evaluating the ability of an agent to engage and modify activity on a panel of important cellular targets. These targets often include receptors, ion channels, enzymes, and transporters. This assessment is known as a secondary pharmacology screen since it is intended to identify unintended or “secondary” pharmacology from that which is primarily intended. For example, Bowes et al. identified 44 cellular targets including G protein-coupled receptors, ion channels, intracellular enzymes, neurotransmitter transporters, nuclear hormone receptors, and a kinase (Bowes et al., 2012). Many of the targets evaluated have been or are intentionally targeted pharmacologically but could represent liabilities if they occur as unintended side effects. Approximately 2/3 of the Bowes’ targets are recognized to have CV activity. The biological activity identified in these screens may provide early insights into a potential liability that could be investigated prior to definitive nonclinical studies, that may be avoided by influencing selection of a candidate drug to move forward for clinical testing, and that may even provide a mechanistic explanation for effects seen during in vivo studies. These in vitro screens generally have the weakness that they are primarily evaluating parent molecules in the absence of any metabolic or environmental transformation that may occur.

Progress in the development of stable and reproducible human-derived cellular substrates like induced pluripotent stem cells (iPSCs) has

prompted the use of cell-based screening to evaluate general cell health endpoints (e.g., cytotoxicity) as well as cardiac-specific activities (e.g., action potential generation and responses,  $\text{Ca}^{2+}$  transients, mitochondrial function, contractile function, etc.) (Grimm et al., 2020). These screens tend to be slower (lower throughput) and lack the mechanistic specificity of secondary pharmacology screens. They also lack the ability to evaluate effects induced by metabolic byproducts, but the major byproducts can be deliberately synthesized and evaluated independently if the need dictates and the products are known (Grimm et al., 2020). Alternatively, these screens have the potential to identify activities not captured in the simpler secondary pharmacology screens and are more easily related to potential in vivo effects.

### 3.2. Functional Evaluation of Toxicity

#### 3.2.1. Monitoring Myocardial Contractile Function

Mechanical energy in cardiac muscle is reflected in two measurable contractile properties of the muscle: the ability to shorten and the ability to develop force. All indices of the contractile state are based on these two characteristics of muscle contraction or some derivative of them, such as velocity of shortening or force development.

A positive inotropic agent will increase both the extent and velocity of muscle shortening, and the extent and rate of force development. In the intact animal, an increased force can be accompanied by changes in ventricular loading conditions due to effects on arterial blood pressure and ventricular chamber size. The change in ventricular load can influence the degree of muscle shortening and force development.

To accurately quantify a change in myocardial contractility, the influence of changes in muscle loading conditions must either be eliminated or taken into account. The influence of loading conditions on myocardial contractility, whether the experimental model is an isolated cardiac muscle or an intact ventricle, is determined by the preload and afterload. The “preload” (i.e., the degree of cardiomyocyte stretch at the end of diastole) sets the initial resting muscle length and, as a result, the level at which the muscle functions along its length–tension curve. The extent of muscle shortening and the velocity of muscle

shortening both decrease as the afterload increases where the “afterload” is the amount of pressure the heart must work against to eject its ventricular volume.

#### 3.2.1.1. EX VIVO ISOLATED MUSCLE PREPARATIONS

A variety of isolated muscle preparations have been developed for evaluating myocardial contractility. Because there is a complex relationship between inotropism (force of contraction) and chronotropism (rate of contraction), force of contraction measurements are best made in controlled in vitro test systems where the cardiac tissue is electrically stimulated at a constant rate. The papillary muscle, the left atrium, and atrial or ventricular trabeculae from the dog, cat, guinea pig, or rabbit are the most frequently used areas of the heart for this purpose (Wallis et al., 2015). In these types of preparations, contractile force is best determined as isometric tension development (where ‘isometric’ relates to actions in which tension occurs without muscle contraction) and the isotonic force-velocity relation (where “isotonic” denotes development of tension associated with muscle contraction) (Anderson et al., 1976).

#### 3.2.1.2. EX VIVO ISOLATED PERFUSED HEART PREPARATIONS

On many occasions in experiments with intact animals, it is extremely difficult to separate the interaction of one major organ system from another, or to single out the action of any substance on a specific functional unit such as the heart. In an attempt to resolve this problem, Langendorff, in 1895, devised an isolated perfused heart technique in which the intact mammalian heart was isolated from the body and maintained in a viable beating condition (Bell et al., 2011). Subsequently, many modifications have been described, and the hearts of several species have been perfused with blood or a variety of physiological solutions. These isolated heart preparations are useful for toxicity studies for a number of reasons. The isolated heart allows a definitive evaluation of chemical effects directly on the heart without interference or interactions with other tissues and organs present in the body. In addition, it is possible to maintain control over variables, such as perfusion pressure and blood flow, that are likely to change dynamically during the course of an experiment in an intact animal. A key advantage of such isolated organs is that the in vivo

structural composition of the heart is retained in such a system. The principal limitation in using isolated organ preparations is that physiological viability of the organ can be retained for only limited periods of time (up to 4 h).

Studies have shown that the isolated heart can be a useful tool in the identification and characterization of cardiotoxic actions on ventricular contraction, heart rate and rhythm, and coronary vasculature. The isolated rat heart model has provided direct evidence that butylated hydroxytoluene (BHT, an antioxidant added to many foods) depresses myocardial contractility and causes cellular damage as measured by the leakage of creatine phosphate from the myocardium into blood (Gad et al., 1979). Studies in the isolated rabbit heart have shown that the arrhythmogenic activity of tricyclic antidepressants (e.g., amitriptyline, imipramine) is associated with alterations in myocardial automaticity and conductivity (Barth and Muscholl, 1974). In the isolated dog heart, epinephrine causes a brief increase and ellipticine (an antineoplastic agent) a prolonged increase in force of contraction and heart rate (Herman et al., 1971). Daunorubicin (another antineoplastic agent) produces an increase in the tone of the coronary arteries in the isolated dog heart, as evidenced by an increase in coronary perfusion pressure (Vick and Herman, 1971). The ability of the isolated heart to respond to many agents indicates that this preparation is useful in differentiating the actions of substances that may alter cardiac function.

#### 3.2.1.3. IN VIVO INVASIVE PREPARATIONS

A major advantage of ex vivo studies like the Langendorff hanging heart preparation is that determinants of cardiac performance such as heart rate, preload, and afterload may be fixed and maintained or varied as desired. For studies in intact animals, the analysis of drug effects on myocardial contractility is more difficult unless these three functions are carefully controlled. However, studies with intact animals provide information concerning adaptive responses to xenobiotics that cannot be assessed in isolated organs. In a closed-chest anesthetized dog, cat, or pig, indirect assessment of contractility is possible if certain variables such as heart rate, arterial blood pressure, and cardiac output are recorded simultaneously. Methods for detecting changes in myocardial contraction depend on monitoring intravascular and intracardiac pressures and cardiac output. Estimates of the

contractile state can be derived from the rate of intraventricular pressure development. Left ventricular pressures (P) can be obtained by placing a cardiac catheter equipped with a pressure transducer. A widely used measure of cardiac contractility is  $dP/dT_{\max}$ , which represents the maximum change in left ventricular pressure over change in time during the isovolumic phase of ventricular systole (i.e., the short initial phase of heart contraction when pressure rises in the ventricle but is not yet sufficiently high to permit ejection). Measurements in anesthetized animals have the disadvantage of being acute and thus potentially influenced by the presence of anesthetic agents.

The development of surgically implantable and telemetered devices has allowed a broadening use of continuous and sensitive monitoring of cardiovascular function in ambulatory and conscious animals. Such data are well suited for translating findings in animals to predict potential human responses. These devices allow very sensitive measures of parameters like ECG, blood pressure, and even left ventricular pressures (LVPs) in both rodents and nonrodents to be assessed over longer periods of time and without the influence of anesthesia and handling. LVPs allow derivation of  $dP/dT_{\max}$  to assess cardiac contractility, as described above for catheterized animals under anesthesia. Alternatively, the QA interval (period between the onset of the ECG Q wave and aortic pressure signal upstroke) is occasionally used as a measure of contractility when ECG and aortic pressures are available but LVPs are not.

#### 3.2.1.4. IN VIVO NONINVASIVE METHODS

A variety of clinical imaging modalities have been applied for assessing cardiac structure and function in laboratory animal species (see *In Vivo Small Animal Imaging: A Comparison to Gross and Histopathologic Observations in Animal Models*, Vol 1, Chap 13). The most common of these methods is echocardiography using an ultrasound instrument with image-capture rate capabilities appropriate for the beating heart. Standard echocardiography uses high-frequency sound waves to generate images of the heart structure, while Doppler echocardiography assesses such functional attributes as the speed and direction of blood flow by utilizing the Doppler effect. Instruments need to be either adjustable since basal heart rates in rodents are far higher (300<sup>+</sup> beats per minute [bpm]) compared to those of nonrodents (60–120 bpm). Echocardiography is

a staple of human clinical medicine, where it is commonly used to assess both structural and functional changes in the human heart. Echocardiography has been successfully used to detect drug-induced myocardial alterations in dogs and is even now increasingly used in rodents as newer technologies have gained the resolution and image-capture rates necessary to look at these small and rapidly beating hearts (300+ beats per minute in rodents compared to 60 to 120 beats per minute in nonrodents).

Echocardiography permits quantitative and qualitative evaluation of several structural and functional parameters, and it allows sensitive assessment of left ventricular function. Measured and/or derived values include ejection fraction (the proportion of ventricular blood that is pumped out of the heart with each beat), end-diastolic and end-systolic ventricular volumes, stroke volume (amount of blood moved from the left ventricle with each systolic contraction), and cardiac output (quantity of blood pumped by the heart during a given span of time). Ventricular mass can also be quantified using three-dimensional (3D) capabilities or 2D heart slices and an appropriate algorithm that considers the 3D cardiac architecture of the evaluated species. Valve function can also be evaluated using Doppler capabilities common on most instruments.

In addition to echocardiography, magnetic resonance imaging (MRI) and computed tomography (CT) have been applied to laboratory animals to assess cardiac function noninvasively. Both MRI and CT have the advantage of being isotropic (i.e., all regions of the heart are imaged equally) and therefore less limited in their ability to image all regions of the heart, but these modalities also share the disadvantage of requiring special equipment (particularly for examining rodents). Nonetheless, instrumentation with the appropriate resolution for rodent applications is available and has been used to assess heart function in xenobiotic-treated animals.

#### 3.2.2. Monitoring Myocardial Electrical Activity

Cardiac arrhythmias are the most common and generally the easiest drug or chemical-induced adverse cardiovascular response to detect. Xenobiotics can interfere with the formation and conduction of cardiac action potentials, thereby inducing clinically significant arrhythmias including supraventricular and ventricular premature contractions, conduction abnormalities, bradycardia

(decreased heart rate), or tachycardia (increased heart rate). Disturbances of impulse formation may be due to changes in normal automaticity of the specialized conduction tissues or to abnormal autonomic neural signaling generated in any area of the heart. The most important arrhythmogenic actions of xenobiotics can be reproduced and monitored in heart muscle slice preparations, isolated heart preparations, and intact animals.

An arrhythmia of particular concern in drug development is one associated with inhibition or blocking of a key  $K^+$  channel that mediates myocardial repolarization via ion flow through the  $I_{kr}$  (rapid delayed  $K^+$  rectifier) channel (Roden, 2016). Suppression of  $I_{kr}$  function may occur from genetic defects or molecular blockade affecting the Kv11.1 protein, a pore-forming subunit of the  $I_{kr}$  channel encoded by the *hERG* (*human Ether-à-go-go-Related Gene*) gene. Blocking of the  $I_{kr}$  channel manifests as a delay in myocyte repolarization that is reflected as a prolongation of the QT interval (i.e., long QT syndrome) in the ECG. Delayed repolarization is a significant risk factor for a potentially fatal arrhythmia known as Torsades de Pointes (TdP), which is characterized clinically by ventricular tachycardia with dysrhythmia. In terms of small molecule etiologies, QT prolongation has been associated with some common drugs like the antihistamine terfenadine, the antibiotic grepafloxacin, and the gastric prokinetic agent cisapride (all of which have been removed from the US drug market). As a result of this drug liability, specific regulatory (safety pharmacology) testing requirements have been developed (Anonym, 2020).

### 3.2.2.1. EX VIVO HEART MUSCLE PREPARATION

The use of isolated Purkinje fibers to evaluate possible arrhythmic effects of substances can provide significant preliminary information. Purkinje fibers from dogs and sheep are the most frequently used models; however, fibers have also been used from other animals including calves, pigs, goats, and rabbits. The number of useable Purkinje fibers varies with each heart, and in the dog ranges from three to eight. Long-term continuous recording from cardiac Purkinje fibers is possible because these conduction elements contract less vigorously

than atrial or ventricular myocytes dedicated to myocardial contraction.

In contrast to Purkinje fibers, many contractile myocytes suitable for isolated tissue studies can be obtained from each heart for all species. Muscle bundles should be no greater than  $0.6\text{ mm}^2$  in cross-section to ensure adequate oxygenation (which occurs by diffusion). Papillary muscles small enough to ensure adequate oxygenation can be found in cats, guinea pigs, and rabbits. Normally these muscle cells are not spontaneously active and must be electrically stimulated to evoke action potentials. The electrical activity of contractile muscle fibers is often studied concurrently with Purkinje fibers. Alterations in membrane potentials can be used to evaluate arrhythmic activity. While the various phases of the action potential from Purkinje and contractile muscle fibers are the same, the action potentials from these tissues do differ in amplitude, duration, and rate of depolarization. Membrane action potentials result from changes in the ionic permeability of the cell membranes. When evaluating the effects of xenobiotics, it is important to be aware of a variety of factors other than the test article that can alter intracellular electrical potentials. These include bath (culture medium) composition and temperature as well as the rate of stimulation. Recordings of intracellularly measured action potentials reflect changes occurring during the excitation process. For example, decreases in the rate of depolarization are always linked to a slowing of intracardiac conduction velocity.

### 3.2.2.2. IN VITRO CULTURED HEART CELLS

In vitro primary cell culture systems have been used for many years in cardiotoxicity screening and mechanistic assays. The cellular substrates used have varied and include explanted adult rodent cardiomyocytes, explanted neonatal or fetal rat cardiomyocytes, and immortalized cell lines like H9c2 cells (derived from embryonic rat heart). Likewise, the physiologic focus of these studies has varied and includes electrophysiology endpoints, contractility, hypertrophy, viability, and mitochondrial function.

Significant limitations exist for each of these systems with respect to how well they reflect the in vivo state, but meaningful data have been derived. Neonatal or fetal cells continue to beat



and retain some capacity for cell division but are metabolically very different from adult cardiomyocytes since they are more adapted to an anaerobic form of metabolism rather than the oxidative bias of adult cells. By comparison, adult cells may also continue to beat but are challenging to harvest, do undergo some dedifferentiation in vitro, and have limited survival in culture systems. A significant challenge for any explanted culture system is the difficulty in excluding “non-target” cells (e.g., fibroblasts) from the system since the nonmyocyte cells often overgrow the terminally differentiated myocyte population. Embryonic H9c2 cells are immortalized and therefore more straightforward to establish in culture, but they are relatively undifferentiated and may weakly recapitulate the phenotype of differentiated adult cardiomyocytes.

More recently, significant focus has shifted to embryonic stem cell (ESC) and induced pluripotent stem cell (iPSC) systems in efficacy and toxicity testing. Such heart-derived stem cells (see *Stem Cell and Other Cell Therapies*, Vol 2, Chap 10) provide cellular substrates that possess good culture stability, relevant differentiation traits, and can even be of human origin, thus addressing concerns about translatability of animal data to human patients. Significant progress has been made in driving differentiation of stem cells along specific cellular lineages, like cardiomyocytes, through judicious application of appropriately composed culture medium. The iPSC systems allow one to harvest differentiated cells (e.g., fibroblasts) from human donors, dedifferentiate them to a pluripotent state, and then redifferentiate them along varying phenotypic lineages. Additionally, these approaches allow one to model genotypic variability or even disease states in vitro by harvesting source cells from patients with varying genotypic or phenotypic backgrounds. Although this technology is still being refined, it is likely to impact in vitro modeling significantly in the future.

### 3.2.3. Complex In Vitro Modeling Systems

Progress in human-derived ESC and iPSC systems have been complemented by advances in microfabrication presenting opportunities to better replicate in vivo tissue and organ level complexity in vitro (see *Alternative Models in*

*Biomedical Research: In Silico, In Vitro, Ex Vivo, and Non-Traditional In Vivo Approaches*, Vol 1, Chap 24). These systems are generally 3D, may include multiple cell types (e.g., cardiomyocytes, fibroblasts, endothelial cells [ECs]), and may include microfluidic flow of media (Truskey, 2018). They may allow for self-assembly of the cellular constituents (organoids) (Lewis-Israeli et al., 2021) or provide for microfabrication-guided patterning of the cells to mimic the parallel arrangement of cardiomyocytes in vivo allowing for coordinated contraction and replication of action potential distribution across the “tissue.” More sophisticated systems for modeling the heart include the ability to create tension or resistance to either spontaneous or paced cardiomyocyte contractility (Mathur et al., 2016). Cardiac organoids are being used for toxicity testing of antineoplastic drugs and environmental toxicants as a means of assessing exposure–response relationships and mechanisms of action (Truskey, 2018).

#### 3.2.3.1. INTACT ANIMALS

All data regarding the effects of xenobiotics on myocardial electrical action potentials obtained from in vitro and ex vivo studies using isolated cells and tissues should ultimately be correlated with outcomes observed in vivo using whole animal studies. The information from whole animal studies is most often obtained from ECG or His bundle electrography. His-bundle recordings, which emphasize measurements specifically on the electrical conductance circuitry, may provide more reliable information compared to a routine ECG, but the His bundle technique is more difficult.

ECGs in large or small animals can be collected in conscious-restrained, anesthetized, or conscious unrestrained (i.e., instrumented) animals. Use of implanted and telemetered instrumentation for sensitive measures of ECG, blood pressure, and even LVPs has become common in drug development settings (Berridge et al., 2016b; Sarazan, 2014). This instrumentation allows remote monitoring (i.e., from outside the cage) of basic measures of cardiac function for prolonged periods of time (e.g., continuous for 24 h to repeated measures spread over days or weeks) without the influence of handling stress or human interaction.

Significant changes in the ECG following exposure to xenobiotics may result from functional alterations to the myocyte cell membrane and/or structural damage to the myocyte. Drugs or other xenobiotics can alter the transmembrane potential by modifying the electrophysiological properties of the myocardial plasmalemma. Alterations in resting membrane potential, membrane responsiveness, conduction velocity, duration of the action potential duration and refractory period, slope of diastolic depolarization and threshold level (automaticity) curves, and sensitivity to external stimuli (excitability) may be detected.

A major problem with studies examining potential arrhythmogenesis (particularly QT prolongation secondary to block of the hERG channel) is the extrapolation of results obtained from animal studies to humans. To minimize this problem, dogs have been used as the standard animal model for ECG analysis because the cardiac ion channel distribution in canine and human hearts is similar and the larger organ size in dogs exhibits comparable cardiac electrophysiological characteristics compared to rodents (Kaese et al., 2013). Rabbits and minipigs are also used for this purpose (Kaese et al., 2013; Lawrence et al., 2005).

In pharmacology and toxicology studies, it is usual to monitor only one lead of the several used to record an ECG. A single ECG lead usually is sufficient to determine heart rate and to detect grossly abnormal myocardial rhythms. However, a more comprehensive evaluation of electrical alterations and morphological changes has required the development of procedures where recordings are made from 3 (common in nonrodents for diagnostic purposes) to 10 leads (common in humans for diagnostic purposes). Xenobiotics that cause ECG changes are likely to induce alterations in the transmembrane action potentials of myocardial cells, which can vary from subtle to marked alterations in the shape of the ST-T portion of the complexes to pronounced conduction defects and ectopic arrhythmias. Certain xenobiotics induce myocardial cellular degeneration or necrosis, which can produce arrhythmias, conduction disturbances, and observable changes in the shape of the ST segment. Common ECG alterations detected after exposure to cardioactive substances in nonclinical studies include QRS interval prolongation,

lengthening or shortening of QT intervals, characteristic changes in the shape of the ST-T complex, various degrees of AV block, right bundle branch block, left bundle branch block, intraventricular block, increases in P-wave amplitude and duration, and ectopic arrhythmias. Further details for interpreting ECG readouts may be found in a series of scientific statements from the American Heart Association (Kligfield et al., 2007).

#### **3.2.4. Monitoring Arterial Blood Pressure**

The recording of arterial blood pressure in toxicity studies complements electrocardiography by adding a hemodynamic variable to routinely monitored cardiovascular functions. Most of the toxicity studies in which blood pressure is recorded are carried out in dogs and rats. Single and multiple blood pressure measurements have been reported in these and other species using both direct and indirect methods. Most assessments of blood pressure in drug safety studies are short term in duration (up to 24 h) and follow a single dose of a novel drug candidate.

##### **3.2.4.1. DIRECT METHODS TO MONITOR ARTERIAL BLOOD PRESSURE**

Direct blood pressure measurements entail either direct percutaneous puncture or exposure and catheterization of a major artery. Direct puncture of a large artery in an unanesthetized animal requires restraint, a situation which may increase baseline blood pressure due to epinephrine release. Exteriorization of large arteries for direct needle puncture has been reported to reduce the necessity for rigorous restraint. Direct measurement of arterial blood pressure from an arterial cannula is a widely used technique in both anesthetized and conscious rats, dogs, and other animals (Jespersen et al., 2012). However, anesthesia impairs reflex blood pressure regulation, and thus less marked changes in pressure can generally be expected to occur in anesthetized animals. In chronic studies, the implanted catheter needs to remain outside the skin. These indwelling catheters are subject to numerous complications and require daily attention to maintain patency. As mentioned above with methods for evaluating electrical activity in intact animals, surgically implanted telemetered instrumentation that includes a pressure catheter situated in a major artery is common in drug development settings. This

instrumentation allows longitudinal monitoring in conscious and unrestrained animals without the artifactual distraction of human intervention. The instrumentation most often used also allows concurrent measurements of ECG and LVPs.

#### 3.2.4.2. INDIRECT METHODS TO MONITOR ARTERIAL BLOOD PRESSURE

A widely used indirect method to measure systemic arterial blood pressure in the rat is tail cuff sphygmomanometry. This technique necessitates restraint of the animal and heating and immobilization of the tail. It may also require preconditioning of the animal. However, the indirect tail cuff method measures only systolic pressure in rats. A good correlation appears to exist between direct and indirect methods of blood pressure assessment in the rat.

A variety of noninvasive techniques for indirect blood pressure measurements have been evaluated in conscious dogs and pigs. A good correlation between indirect oscillometric-derived blood pressure (where automated “oscillometric” analyses assess fluctuations in blood volume amplitude due to blood flow pressure waves) and that obtained directly by auscultation (where the upper and lower limits of the pressure range are recorded by listening to pulsatile noise [Korotkoff sounds] related to turbulent blood flow through partially occluded vessels) has been observed. However, in studies using the auscultatory technique, diastolic pressure was considerably lower when measured indirectly than when measured directly. Tail cuff techniques are also available for large animals. For example, a tail cuff method using a photoelectric sensor has been described for use in normotensive and hypertensive miniature swine. The values of systolic, diastolic, and mean arterial pressures obtained by this method were comparable to the values of these parameters monitored directly. In the dog, automatic sphygmomanometry allows simultaneous monitoring of systolic, diastolic, and mean arterial pressures and heart rate. A positive correlation was found between blood pressure and heart rate values obtained by this method and those recorded by direct arterial catheterization in both anesthetized and conscious dogs. A major disadvantage to all tail cuff techniques is that it is not possible to record blood pressure readings continuously.

### 3.3. Morphologic Evaluation of Toxicity

Toxic injuries to the heart that result in expression of morphologic alterations are detected by careful gross and microscopic evaluation. In specific instances, further study may be desirable including ultrastructural evaluation, histochemical and/or immunohistochemical (IHC) procedures, and/or morphometric analysis. Special attention must be given to challenges that are common to morphologic evaluations. These include inadequate sampling, presence of post-mortem changes, misinterpretation of tissue artifacts as test article-related findings, and failure to recognize normal biological variations in structure, incidental lesions, and lesions of spontaneous diseases.

#### 3.3.1. Gross Examination

Many thorough descriptions have been published on the methods of gross dissection and examination of the exterior and interior features of the heart at necropsy with the procedure used determined by the species of animal from which the heart was collected ([Constantin and Tăbăran, 2022](#)). Variations in the standard necropsy method may be useful to expose certain lesions (e.g., cardiac valvular lesions) or to optimize the display of various heart features for photography.

An intact heart weight (following removal of any blood remaining in the heart chambers) is a useful measure of changes in heart mass. Such changes may occur due to increased or decreased body mass, compensatory or pathologic hypertrophy, atrophy, or cachexia. Heart weight may be evaluated as an absolute value and/or as a ratio to the body weight (which is variable depending on such factors as diet and exercise), brain weight, or length of the tibia with the latter two relative measures allowing for consideration of changes in the rate of body growth. Midventricular cardiac cross-sections can reveal changes in relative thickness of the ventricular free walls and/or septum, thus providing insights into regional changes in hemodynamics (e.g., right ventricular hypertrophy in the presence of pulmonary hypertension, left ventricular hypertrophy in the presence of systemic hypertension). Changes in heart weight might be accompanied by observable differences in heart size, which may be

proportional or regional. A change in size might be accompanied by a change in shape. Hypertrophic hearts are often more rounded and lack a prominent conical shape and distinct pointed apex. Unfixed and dilated hearts may have flaccid and thinned ventricular free walls.

Cardiac lesions at the gross level may present in various ways. Developmental abnormalities are typically congenital (i.e., present at birth) and may manifest as abnormal placement of the major vessels at the base of the heart, persistent patency of the ductus arteriosus (i.e., a normal fetal artery connecting the aorta and pulmonary artery, which allows blood to bypass the lungs until breathing begins at birth), septal defects in the atria and/or ventricles, or malformation of the heart valves (see *Embryo, Fetus and Placenta*, Vol 5, [Chap 11](#)). Altered cardiac color provides evidence regarding the nature of any tissue changes at the affected site. A pale heart may be evidence of myocardial edema, ischemia, or necrosis, or sometimes severe anemia (reduced circulating red blood cell mass). A pale heart may also be evidence of infiltrative disease such as myocardial amyloidosis, inflammation, or neoplasia like schwannoma (most often regional) or lymphoma (more likely to be diffuse). A heart that is diffusely or regionally dark red-brown may be congested, while bright red patches or streaks on the epicardial and/or endocardial surfaces (including valve leaflets) may be hemorrhage and may be associated with myocardial injury or coagulopathy (i.e., altered clotting). Ventricles, atria, and the lumina of major arteries can be occluded by acute clots (emboli or thrombi) or chronic thrombi.

### 3.3.2. Microscopic Examination

Tissue specimens for microscopic study may be obtained at the time of necropsy (usual for nonclinical studies) or by endomyocardial biopsy from living patients. Endomyocardial biopsies, although used widely now in human medicine, have had limited application in animal studies except for occasional use in dogs and nonhuman primates (usually for research purposes rather than safety assessment).

Samples from hearts acquired during nonclinical studies should be multiple and representative to detect findings that are not diffusely distributed and lesions that are not grossly

apparent. Tissue blocks collected at necropsy should routinely include specimens from both atria (including auricles), both ventricular free walls, ventricular septum, left ventricular papillary muscle, and the coronary arterial tree. In small laboratory animals, a longitudinal section through the heart taken perpendicular to the ventricular septum is often sufficient to evaluate all these features in a single section. If present, any gross lesions should be sampled, including areas spanning the border between the visibly affected and unaffected tissue. Sampling should be increased in regions where lesions are predicted to be produced by a specific test article based on known effects of that agent or recognized “class effects” for similar agents.

The conduction system may be evaluated microscopically by collecting samples from appropriate anatomical sites ([Palate et al., 1995](#)). The SA node is situated at the juncture of the cranial vena cava and the right atrium and can often be captured by a series of cross-sections through that region in nonrodent species or serial histologic sections from single samples in rodents. Sections through the SA node often include the SA artery, which is a common site for both spontaneous and drug-induced vascular injury in both rodents and nonrodents. The AV node is situated at the base of the interventricular septum and may be captured by longitudinal samples perpendicular to the axis of this septum. Purkinje fibers of the bundle of His are present immediately subjacent to the ventricular endocardium in nonrodents and may be recognized by their greater width and paler sarcoplasm compared to contractile striated myofibers.

Tissue fixation is generally performed by immersion of samples (in nonrodents, for slabs approximately 0.5 cm thick for at least one dimension) or the entire heart (rodents and rabbits) in neutral buffered 10% formalin (composition of commercial formulations: 3.7% formaldehyde with ~1% methanol as a stabilizer). Perfusion fixation may be used to optimize fixation quality of cells in deep tissue if ultrastructural studies are to be done. Perfusion is usually performed with 4% methanol-free formaldehyde (MFF [known colloquially as “paraformaldehyde” [PFA]) or mixtures of MFF and glutaraldehyde (GLUT) such as Karnovsky’s fixative (2% MFF, 2.5% GLUT) or



McDowell and Trump's fixative (4% MFF, 1% GLUT).

Fixed cardiac samples are routinely processed and embedded in paraffin, sectioned at 4–5  $\mu\text{m}$ , and stained with hematoxylin and eosin (H&E). Special stains that are often useful to optimally visualize microscopic alterations include phosphotungstic acid hematoxylin (PTAH, to demonstrate contraction bands in myofibers and accumulating fibrin), Masson's trichrome (to highlight collagenous connective tissue), periodic acid-Schiff (PAS, to reveal carbohydrate-rich membranes), and various elastin stains. Application of lipid stains (e.g., oil red O, Sudan black) may be of value, but these stains require frozen (fixed or unfixed) sections. Increasingly, investigators are embedding fixed specimens (approximately 1 mm square) in water-soluble soft plastic (e.g., glycol methacrylate) to permit preparation of semithin sections for light microscopic evaluation. Where ultrastructural evaluation is intended, 1- $\mu\text{m}$ -thick semithin sections of tissue embedded in hard plastic (epoxy) resin (e.g., araldite, epon) are produced to select regions from which thin sections (commonly 800 to 1000 Angstroms-thick) may be prepared for high-resolution study of cellular and subcellular alterations by transmission electron microscopy (TEM).

A variety of enzyme histochemical (e.g., acid phosphatase); IHC (e.g., Factor VIII, vascular endothelial growth factor [VEGF], endothelin, actin, myosin, desmin, collagen); and autoradiography procedures may be useful to characterize findings in myocardial (and vascular) tissue. For example, several stains have been used to demonstrate early ischemic damage to the myocardium (e.g., PTAH). Finally, special procedures are available to demonstrate specific processes, including apoptosis (e.g., cleaved caspase 3 IHC, TUNEL assay), altered vascular and cellular permeability (immunolabeling for cardiac troponin), and induced proliferation of heart cells (endogenous proteins like phosphohistone H3 [PHH3], Ki67, or proliferating cell nuclear antigen [PCNA]).

### 3.3.3. Ultrastructural Examination

Many cardiac lesions of toxic origin have been studied by TEM to detect and characterize organellar changes that may provide insights into the pathogenesis of morphologic damage to

myocytes or organ dysfunction. Mitochondria are a common target of such examinations, but ultrastructural evaluation may also be useful for characterizing lysosomal accumulation, changes in the integrity of the myofilament contractile apparatus, and intracellular accumulations of glycogen or lipid.

It is important that investigators appreciate the limitations and challenges associated with ultrastructural study (see *Special Techniques in Toxicologic Pathology*, Vol 1, Chap 11). For example, fixation should be optimal (preferably by perfusion), and tissue artifacts during processing should be avoided. Hypercontracted myocytes are often seen at the margin of immersion-fixed tissue blocks; therefore, these areas should be avoided in taking samples for ultrastructural study. Extensive sampling may be necessary if the cardiac alterations are not diffusely distributed. Even under optimal conditions, some cardiotoxicities may not have remarkable morphologic findings because death may have occurred rapidly from functional disturbances and structural alterations did not have sufficient time to evolve. A variety of techniques have been adapted for use at the ultrastructural level, including enzyme and immunohistochemistry and autoradiography.

Use of SEM for study of cardiac lesions of toxic origin has had limited application. The technique is best suited to the study of surface lesions, such as valvular and endocardial alterations, which are less commonly target sites for toxic cardiac injuries. On occasion, developmental toxicity affecting the heart may be examined by SEM in rodent embryos, but this approach is more common for mechanistic (hypothesis-driven) studies rather than safety assessment.

### 3.3.4. Quantification of Morphologic Alterations

Routine morphologic evaluations at the gross, microscopic, and ultrastructural levels are mainly directed at identification and, where warranted, accurate and thorough characterization of structural changes. Given the natural variation in normal cell and tissue morphology and the fairly frequent presence of preexisting pathology (i.e., spontaneous background findings) in many individuals of common laboratory animal species, semiquantitative grading of microscopic alterations for severity and/or distribution is

typically important in discriminating toxicity-related changes (Hailey et al., 2017a, b). Where warranted, severity grades can be analyzed statistically to identify potentially consequential differences among treatment groups in a study (see *Experimental Design and Statistical Analysis for Toxicologic Pathologists*, Vol 1, Chap 16).

Fully quantitative measurements (e.g., morphometry, stereology) are occasionally used to evaluate the extent of cardiac damage. These techniques are especially useful for the study of tissues prepared for electron microscopy with optimal fixation and embedding methods to avoid artifacts. Morphometry usually involves linear or areal measurements of particular regions or findings, and generally requires high homology (i.e., consistent sampling at a given site) among sections from all animals; in toxicity studies, morphometric measurements should be acquired from at least six animals per group (or per sex per group if both sexes are being assessed), although greater numbers are preferable. In contrast, stereological analysis using systematic uniform random sampling (SURS) and adequate sample sizes allows determination of various parameters such as volume density, surface density, and numerical density of objects (e.g., cells, organelles, or various subcellular components), and subsequent statistical analysis to detect significant differences among treatment groups. Morphometry is fairly rapid, but bias is possible based on the operator's decisions regarding where to take the measurements. In contrast, stereology takes more time for sample processing (usually several hours per specimen), but SURS eliminates bias in acquiring measurements (Boyce et al., 2010).

### 3.3.5. Artificial Intelligence and Machine Learning

The digitalization of data and rapid increase in computing power and data storage has enabled the parallel development of approaches that can not only mitigate human analytical biases and imprecisions but also make the analysis of data more efficient (e.g., faster, more precise, and less expensive), and even more informative by extracting knowledge not easily discerned by humans. Artificial intelligence (AI) and machine learning (ML) as computer-aided approaches represent two of these novel opportunities (see *Digital Pathology and Tissue Image*

*Analysis*, Vol 1, Chap 12). The definition and scope of these approaches are rapidly evolving but can be reasonably thought of as a broad field of using computers and human-defined algorithms as an aid in data analysis (i.e., AI) that can extend to providing the computers the opportunity to “self-learn” from experience (i.e., ML). Neural networks and deep learning are approaches to ML that attempt to computationally replicate the interconnectivity of human neurons to enable computational “learning” in ways that are invisible to the human operator. That invisibility can be a challenge to traditional analytical approaches when validating novel assays and methods.

In the area of pathology diagnostics and research, AI and ML have been mostly applied to the detection of cancer and tumor differentiation in cytologic and histologic specimens. Even so, a few applications in CV pathology have been explored (Tokarz et al., 2021; Glass et al., 2022).

Endocardial biopsies and histopathologic assessment are occasionally used in clinical medicine to identify morphologic changes that may provide insight into the etiology and severity of myocardial disease-causing clinical heart failure in human patients. These biopsies are generally small, accessible from limited regions of the heart (e.g., ventricular endocardium via cardiac catheterization), and structurally distorted. Accordingly, interobserver variability can be significant, and extrapolating histologic changes to whole organ function or dysfunction can be challenging. Nirschl et al. (2018) developed a computational deep learning approach to predict clinical heart failure from endocardial biopsies of patients. In a series of samples from 209 patients, heart failure or severe pathology could be predicted with high sensitivity and specificity that exceeded the success rates of two expert pathologists who also reviewed the biopsies. Though endocardial biopsies are generally used to characterize heart failure that has already been detected clinically rather than predict it, the approach demonstrates the ability to decrease variability and increase sensitivity using these approaches.

Rodent progressive cardiomyopathy (PCM) is a common spontaneous disease in laboratory rats and mice. As noted below, the lesions of PCM can be confused with or imputed to toxicant-related injury. Accordingly,

identification of a xenobiotic-induced effect in rodent studies can come down to a quantitative difference in prevalence of the disease (where “prevalence” is all preexisting and new cases affecting the population at a given time), incidence of the lesions (where “incidence” represents new cases only), and/or the severity of the lesions. Tokarz et al. developed an automated image analysis approach enhanced by a convolutional neural network/deep learning technique to detect and quantify the PCM in digital image scans of longitudinally oriented sections of rat hearts (Tokarz et al., 2021). Their analysis demonstrated good concordance with the observations of a small group of experienced toxicologic pathologists.

AI and ML-based approaches are not without challenges. Consistent sampling and data generation (e.g., diagnostic nomenclature and grading criteria) are critical for consistency in analysis. Digital images of sufficient resolution to be amenable to image analysis are extremely large, requiring lots of data storage capacity. Novel algorithms have to be written and “trained” with representative samples and ultimately evaluated or validated by the human observers that they are intended to complement or replace. Neural network-based deep learning approaches involve computations that are invisible to the human operator. Those challenges aside, AI and ML are likely to progress in their applications and may in time define the future of safety assessment.

### 3.4. Background Alterations, Artifacts, and Spontaneous and Age-Related Lesions

The cardiovascular system, like any biological system, is host to a number of age-related morphologic changes and is a site of common spontaneous diseases in most if not all of the laboratory animal species used to model xenobiotic toxicity. To prevent attributing toxicologic significance to background lesions in hearts, it is essential to have well-designed studies with suitable numbers of control animals. The frequency of background lesions varies considerably among different species and even for cohorts of animals from the same species but having different genetic backgrounds. For example, foci of mononuclear leukocyte accumulation (diagnosed as “mononuclear cell infiltration” if adjacent

myofibers are not damaged) occasionally occur in the myocardial interstitium in rodents but with some consistency in nonhuman primates. It is not uncommon to occasionally observe mineralized necrotic myofibers (ranging from a few to multiple) that are not treatment-related. Foci of myocardial necrosis and/or fibrosis may be seen in untreated animals. Aged rats may have foci of cartilaginous and/or osseous metaplasia involving the subendocardium and aortic root. Proliferation of the subendocardial connective tissue occurs in rats and may be confused with naturally occurring schwannomas (i.e., a neoplasm of neural crest origin) that can occur in the same location. Atrial thrombosis that partially or completely occludes the lumen can develop with some frequency in aged control mice, rats, and hamsters. Xenobiotic treatment may alter the incidences of these common background changes.

Species-specific variations in the morphology of cardiac muscle cell nuclei can be confusing to inexperienced morphologists. For example, nonhuman primates tend to have multiple myocytes with large prominent nuclei. In young swine, it is common to observe multiple nuclei arranged in rows within myocytes.

Discrimination of artifactually hypercontracted cardiac myocytes from fibers with early coagulative necrosis is important. The finding of hypereosinophilic “shredded” fibers from hypercontraction is often seen in the periphery of blocks of tissue collected soon after death and placed into cold fixatives (Figure 1.3). These

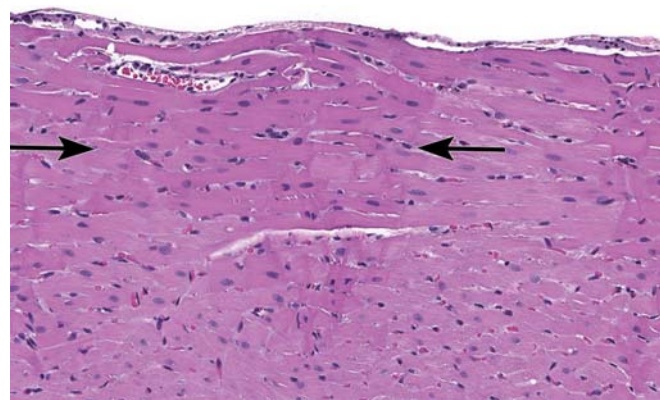


**FIGURE 1.3** Section of heart from a rat with an area of artifactual hypereosinophilic hypercontraction subjacent to the epicardial surface (bracketed by arrows). Formalin-fixed, paraffin-embedded section; H&E stain. Original magnification 20×.



hypercontracted fibers neither show alterations consistent with nuclear damage (e.g., pyknosis [condensation], karyorrhexis [fragmentation], karyolysis [dissolution]) nor incite leukocytic infiltration as is commonly seen with myofiber necrosis.

Vacuoles may occur in the sarcoplasm of cardiomyocytes. It is important to identify true vacuolar alterations affecting organelles from the loss of sarcoplasmic staining due to extensive glycogen loss, which may be seen in samples of myocardium collected sometime after death.

Differentiation of spontaneous cardiac diseases from treatment-induced lesions is important. Probably the greatest challenge of this type occurs in rats affected with rodent PCM. Animals affected by this disease will have scattered foci of acute to subacute, often individual, cardiomyocyte necrosis with associated mononuclear cell infiltration (Figure 1.4). More chronic and larger lesions may heal with fibrosis and sometimes may be associated with local myocyte loss (Figure 1.5). The disease may be recognized in young animals (usually 20 weeks of age or younger) but becomes more prominent as the animals age, often by the increased prominence of fibrosis. The severity of the lesions may be exacerbated by xenobiotic treatment.

Degenerative myocardial lesions are also occasionally seen in untreated cynomolgus macaques which, when present in individual treated animals, could present an interpretive challenge.

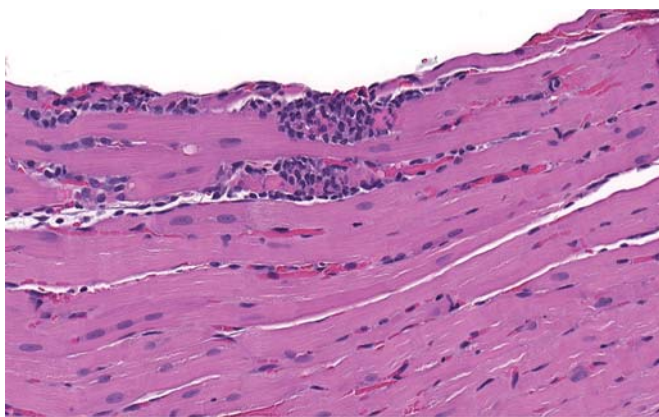


**FIGURE 1.4** Section of heart from a 10-week-old male rat with a focus of cardiomyocyte necrosis and leukocyte infiltrate characteristic of rodent progressive cardiomyopathy, a background disease. Formalin-fixed, paraffin-embedded section; H&E stain. Original magnification 40 $\times$ .

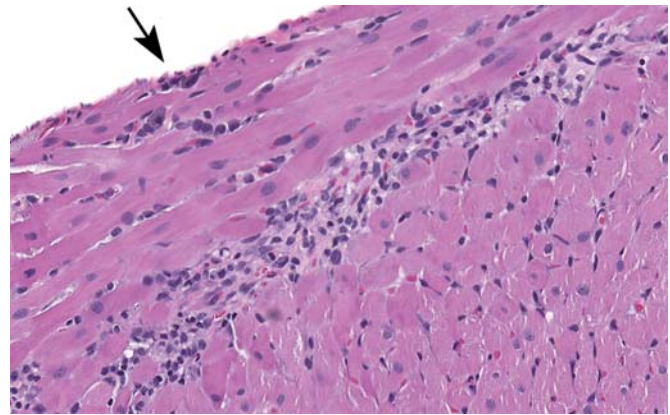


**FIGURE 1.5** Section of heart from a 10-week-old male rat with a linear area of myocardial necrosis, inflammation, and early fibrosis subjacent to the epicardial surface (arrow) of the right ventricular free wall. These larger lesions are less common than the more focal lesions represented in Figure 1.4 but are occasionally seen in untreated control animals and considered within the spectrum for rodent progressive cardiomyopathy. Formalin-fixed, paraffin-embedded section; H&E stain. Original magnification 40 $\times$ .

Acute to chronic changes exhibit hemorrhage, cardiomyocyte necrosis, cardiomyocyte disarray, and fibrosis. These findings occur most commonly in the left ventricle with some predilection for the subendocardial region (Vidal et al., 2010). Minipigs of various strains are increasingly used as a nonrodent species in toxicity testing. Like rodents, these animals can also exhibit a low incidence of minimal focal to multifocal cardiomyocyte necrosis with mixed mononuclear cell infiltration (Helke et al., 2016).

Myocardial and epicardial calcification (cardiac calcinosis) is a frequent finding in some inbred mouse strains and is an occasional finding in guinea pigs and rats. Affected mouse strains include DBA/2, C, C3H, BALB/c, A, CBA, and CHI. The changes often present as raised plaques, and if sufficiently large may be evident grossly as hard, white spots of variable size on the outer heart surface.

Hypertrophic cardiomyopathy has been described as a spontaneous disease in both nonhuman primates and swine. Characterized by concentric hypertrophy of the left ventricle with reduced ventricular volume, this condition can lead to sudden death in affected animals as it does in humans. Etiologies for this disease are varied including heritable gene mutations,

which have been proposed for this condition in both nonhuman primates and swine (Ueda et al., 2021).

Another spontaneous and age-related cardiac disease is valvulopathy of rats and dogs. This finding must be differentiated from treatment-induced valve lesions. Affected valves are irregularly thickened with increased mucopolysaccharide-rich interstitial matrix, which is cell-poor and pale blue on H&E-stained sections. As test animals are usually young, the occurrence of spontaneous valvulopathy would not be expected in most studies.

### 3.5. Biomarkers

Biomarkers are quantifiable biological endpoints used for noninvasive or minimally invasive monitoring of the health of a target organ system. Biomarkers are used commonly in clinical settings to evaluate patient health, diagnose disease, follow disease progression, and assess therapeutic efficacy. Biomarkers are also used in nonclinical toxicity testing to monitor the onset and progression of toxicity in animal models. Ideally, the biomarkers used in nonclinical studies can be “translated” to the clinical setting to aid in managing toxicity (i.e., by early detection) in human patients.

A number of well-characterized biomarkers are available to monitor cardiovascular form and function in the nonclinical and clinical settings. ECGs are a standard biomarker in clinical medicine (both medical and veterinary) for assessing the “electrical” health of the heart and are frequently used to detect alterations in contractile rhythm (i.e., arrhythmias). Though arrhythmias may result from changes in ion concentrations at the cellular or systemic level (refer to discussion above on electrophysiology of the heart in [Section 2.2](#), “Physiology and Functional Considerations”), they can also be seen with structural injuries or infiltrative diseases that can interfere with the orderly propagation of action potentials across the myocardium. QT prolongation as a surrogate risk factor for TdP is a particular focus of ECG analysis in the development of human pharmaceuticals (Roden, 2016). However, as noted previously, rodents are not a relevant model of drug-induced QT prolongation, so dogs are a preferred nonclinical model for evaluating this biomarker. ECGs are readily conducted in both large and

small (rodents) animal models with ready translation of the methods between the nonclinical setting and clinical monitoring strategies.

Imaging methods like echocardiography are also a standard biomonitoring method in clinical medicine and can be readily applied to animal models. Echocardiography allows noninvasive assessment of both cardiac form and function. Cardiac mass, ventricular volumes, and valve morphology can be assessed by the skilled ultrasonographer. Quantifiable measures of cardiac function such as ejection fraction (a clinical standard for assessing contractile function of the heart), fractional shortening (the extent of reduction in the end-diastolic heart diameter [a measure of contractility]), and cardiac output are also routinely collected. Reduced heart contractility related to disease or organ failure typically is reflected in decreases for all three parameters.

Both CT and MRI are applied in the clinical setting for specific applications (e.g., CT angiograms; MRI of infarcts) and have been used in animal models as well. These two imaging methods provide a level of structural resolution that is unattainable with echocardiography. However, imaging consumes more resources and requires expensive equipment with special facilities and so is used more selectively than echocardiography.

In addition to the structure-based biomarkers mentioned above, circulating biochemical markers that are accessible in serum or plasma can “report” cardiomyocellular injury or hemodynamic stress in the heart. Creatine kinase (CK), myoglobin, and troponins are all protein constituents of cardiomyocytes that are readily released from fatally injured cells. Accordingly, their rising activity (for CK) or concentrations in circulation can be evidence of cardiomyocellular injury. Some isoforms of these proteins are also found in other muscle cells, so cardiac selectivity is determined by the specificity of the assay used to measure their concentrations. Assays for cardiac-specific isoforms of troponins (cTnI and cTnT) are currently considered to be the most sensitive and specific and are widely applied in clinical settings (Reagan, 2010). In fact, increases in serum or plasma concentrations of cTns are considered in the clinical diagnostic scheme for myocardial infarctions in human patients. Nonclinical applications of cTnI as a biomarker of cardiomyocyte injury in animal species are growing with the availability

of assays with relevant cross-species reactivity (Apple et al., 2008; Berridge et al., 2009). One limitation that must be considered when measuring cTn as a surrogate marker of cellular injury in the heart is the relatively short half-life of these proteins in circulation. Concentrations of cTn increase quickly in the presence of acute cellular injury but also decline quickly as the acute manifestations of injury wane. Accordingly, a thorough understanding of the pathogenesis of the lesion to be monitored is useful to ensure appropriate sampling strategies.

Natriuretic peptides are hormones synthesized by atrial and ventricular cardiomyocytes that are stored and released in response to cardiac wall stress or stretch. Two structurally related natriuretic peptides are ANP and brain natriuretic peptide (BNP), with predominance in the atria and ventricles, respectively. Ventricular wall stress can also induce the expression of ANP in ventricular cardiomyocytes. ANP and BNP are both released into the systemic circulation in pro-peptide form, which may be readily detected using many commercially available assays; these pro-peptide forms tend to be larger and more stable than the more active cleavage products. The active molecules bind specific receptors present in multiple tissues (e.g., kidney, heart, adipose tissue, blood vessels) with a primary action as inhibitors of the renin–angiotensin system. Natriuresis in the kidney results in net fluid excretion and plasma volume depletion, thereby reducing hemodynamic stress on the heart.

BNP and NT-proBNP (N-terminal pro-BNP) are commonly targeted in human patients as noninvasive biomarkers of congestive heart failure and have demonstrated value as prognostic markers of long-term cardiovascular risk. These markers have also become popular for clinical monitoring of patients treated with cardiotoxic antineoplastic drugs such as anthracyclines. NT-proBNP has also been utilized in nonclinical animal models to characterize hemodynamic stresses that may lead to drug-induced cardiac hypertrophy (Crivellente et al., 2011).

NT-proANP (N-terminal pro-ANP) has also been used in human patients, but less so than BNP. BNP assays that cross-react readily with the rodent peptides have proven elusive. Accordingly, NT-proANP has recently been characterized in the rodent and is demonstrating

characteristics similar to those seen with BNP or NT-proBNP in humans (Colton et al., 2011).

### 3.6. Biochemical Evaluation of Toxicity

Procuring fresh samples of cardiac tissues, especially myocardium, at the time of euthanasia or by biopsy in living animals and human patients allows the use of biochemical analysis to accompany and augment morphologic evaluations. Tissue samples may be assayed for activities of specific molecules (e.g., enzymes) or more broadly as in the case of metabolomics, which typically assesses numerous chemical intermediates or metabolites in a variety of biological substrates including tissue samples. Further discussion of these procedures is beyond the scope of this chapter, but general reviews of the concept and common practices may be explored further in appropriate publications (McGarrah et al., 2018).

## 4. RESPONSES TO INJURY

The heart's response to toxic injury is varied but finite, much like other important target organs. Responses can involve changes in function (rhythmicity or contractility), structure (change in mass, cardiomyocellular injury), or both. As noted previously, changes in cardiac load can lead to structural injuries, and structural injuries to the heart can lead in turn to dysfunction. Accordingly, toxicity assessment strategies for potential cardiovascular effects require methods for assessing cardiovascular function as well as morphology.

### 4.1. Developmental Cardiotoxicity

Abnormal cardiac function in the newborn is usually a consequence of a congenital malformation. Ventricular and atrial septal defects are the most common structural changes (see *Embryo, Fetus and Placenta*, Vol 5, Chap 11) (Yasui et al., 1999). These defects have been associated with maternal exposure during gestation to either diphenylhydantoin (anticonvulsant) or thalidomide (to control nausea [“morning sickness”]) in humans, phenobarbital (anticonvulsant) or caffeine in rats, and acetylsalicylic acid (aspirin) or cortisone in dogs.



Chemicals can also influence the functional development of the heart (Mahler and Butcher, 2011). Central control of cardiovascular reflexes is established prenatally, but the peripheral sympathetic system develops over the first post-natal weeks. Administration of reserpine (antihypertensive) to pregnant rats causes a permanent elevation of sympathetic tone in their offspring, which leads to a persistently elevated heart rate. Neonatal treatment with reserpine or with glucocorticoids slows development of the sympathetic nervous system. Perinatal exposure to ethanol, opiates, or thyroid hormone accelerates development of the sympathetic nervous system in rats, but a deficit in the number of nerve terminals and neurotransmitter receptors occurs, resulting in reduced sensitivity to sympathetic stimulation that persists in adulthood.

Treatment with cardiovascular drugs during pregnancy can cause adverse effects on the cardiovascular function of the fetus or the newborn (Pesco-Koplowitz et al., 2018). For example, a  $\beta$ -adrenergic receptor agonist (“ $\beta$ -agonist”) given as a tocolytic (antilabor) agent can cause arrhythmia, and a  $\beta$ -blocker given as an antihypertensive may cause cardiac depression in the newborn child. Delayed or long-lasting effects have also been demonstrated in animal experiments. Exposure of neonatal rats to low concentrations of lead causes an enhanced response to the arrhythmia-inducing effect of norepinephrine later. These findings indicate the need for specific evaluation of functional effects in nonclinical studies, particularly when the drug is destined for use during pregnancy or administration to neonates.

## 4.2. Cardiac Dysfunction as a Manifestation of Toxicity

The heart’s intrinsic properties of automaticity, excitability, conductivity, and contractility endow it with a variety of drug-sensitive molecular and cellular targets. Consequently, exposure of the heart to certain agents may produce functional changes in rhythm and the force of contraction that might be severe enough to result in death (Table 1.1).

### 4.2.1. Arrhythmias

Arrhythmias are among the most serious immediate cardiac functional abnormalities.

Disturbances of impulse formation and of impulse conduction, either singly or in combination, are the main causes of cardiac arrhythmias. Severe arrhythmias may eventually progress from occasional or intermittent to sustained rate abnormalities, which may be fatal.

A key factor in the occurrence of arrhythmias is the relationship between the resting potential of a cell and the action potential that can be evoked. Since the ability of an action potential to propagate to an adjacent cell is directly related to the rate of rise and the amplitude of the action potential, changes in the membrane potential level also affect conductivity. Normal cardiac function depends on conduction of the impulse over specialized pathways beginning at the SA node, continuing through the AV node, and then spreading in coordinated fashion over the His–Purkinje system to reach ventricular muscle fibers. Exposure to certain agents or ischemic conditions can lower the resting membrane potential of myocytes. These alterations decrease the speed of conduction and favor production of a “heart block” (i.e., disruption of electrical signaling leading to altered rates and rhythms). Paradoxically, the effects of quinidine and other antiarrhythmic agents on the heart may be to initiate rhythm disturbances. This action can occur as a result of a diminution in the activity of fast  $\text{Na}^+$  channels, thereby allowing the development of slow responses. The most common site of conduction disturbance is the AV node, but similar disturbances may occur between the SA node and the atria, in either of the main branches of the bundle of His, or in the more peripheral Purkinje fiber network. Conduction delay and heart block can lead to tachyarrhythmias because an impulse may reenter and excite the heart more than once. A marked reduction in conduction velocity due to depressed  $\text{Na}^+$  current, slow  $\text{Ca}^{2+}$  current, or both is the alteration that permits impulse reentry. Such reentry can occur at many sites in the heart; common examples are the SA node (premature atrial beats), the atrial muscles (atrial flutter or fibrillation), the AV node (paroxysmal supraventricular tachycardia), and the ventricles (premature beats, ventricular tachycardia). Complete (“third degree”) AV block allows the ventricles to escape neural control. In human patients, ventricular control is restored by implantation of a pacemaker.

**TABLE 1.1** Cardiotoxic Agents that Produce Death by Functional Disturbances Without Morphologic Alterations**CARDIOTONIC AGENTS (INCREASE FORCE OF MYOCARDIAL CONTRACTION)****1. Agents that inhibit  $\text{Na}^+/\text{K}^+$  ATPase**

Cardiac glycosides and aglycones: Digitalis (*Digitalis purpurea*), digoxin, digitoxin, ouabain, asclepin (*Asclepias* sp.), oleandrin and neriine (*Nerium oleander*), bufodienolides (*Bufo marinus*)

**2. Agents that increase  $\text{Na}^+$  influx**

Interact with electrogenic  $\text{Na}^+$  channel: Alkaloids (aconitine, veratrum), polypeptides (scorpion venom, anthopleurin-A)

Increase resting membrane permeability to  $\text{Na}^+$ : Grayanotoxin (*Kalmia* sp., *Rhododendron* sp., *Pieris japonica*) batrachotoxin, ciguatoxin

Create artificial  $\text{Na}^+$  channels in sarcolemma: Carboxylic acid ionophores (monensin, salinomycin)

**3. Agents that increase  $\text{Ca}^{2+}$  influx**

Calcium ionophores (X-537A, A23187), fluoride, digitalis, histamine

**MYOCARDIAL DEPRESSANTS****1. Agents that decrease  $\text{Na}^+$  permeability**

Tetrodotoxin, saxitoxin, local anesthetics, antiarrhythmic drugs (quinine), higher alcohols, polyethylene glycol

**2. Agents that replace sarcolemmal  $\text{Ca}^{2+}$  and increase  $\text{Ca}^{2+}$  influx**

Metals (Cd, Mn, Ba)

**3. Agents that alter contractility**

Inhalation anesthetics (enflurane, halothane, isoflurane, methoxyflurane)

Halogenated hydrocarbons used in fire extinguisher compounds, propellants, solvents, refrigerants (chlorinated or fluorinated methane or ethane derivatives)

Cardio-depressant peptides produced during circulatory shock (myocardial depressant factor [MDF])

Reproduced with minor modifications from Haschek WM, Rousseaux CG, and Wallig MA, editors: Handbook of toxicologic pathology, ed 2, 2002, Academic Press, Table II, p. 384, with permission.

Changes in heart rhythm are readily diagnosed by ECG. Alterations in the ECG are infrequent effects seen with antidepressants such as the tricyclic antidepressants, phenothiazine, lithium, and the selective serotonin reuptake inhibitors.

**4.2.2. Changes in Contractility**

Action potential propagation across the cardiomyocyte cell membrane activates voltage-sensitive membrane  $\text{Ca}^{2+}$  channels triggering an influx of extracellular  $\text{Ca}^{2+}$ . The cardiomyocyte SR is a major intracellular store of  $\text{Ca}^{2+}$  modulated by SERCA (sarco/endoplasmic reticulum  $\text{Ca}^{2+}$ -ATPase) that facilitates movement of  $\text{Ca}^{2+}$  from the cytosol into the SR. Catecholamines activate the adenyl cyclase system by stimulating membrane  $\beta$ -adrenergic receptors. The resulting increase in cAMP induces release of intracellular  $\text{Ca}^{2+}$  stores from the SR, which

provides  $\text{Ca}^{2+}$  ions to the contractile proteins. Increasing concentrations of intracellular  $\text{Ca}^{2+}$  stimulate the release of an inhibitory troponin complex associated with actin on the thin myofilament, thus allowing actin and myosin myofibrils to slide along one another to yield cardiomyocyte contraction. The force of the contraction is related to the concentration of intracellular  $\text{Ca}^{2+}$ ; higher  $\text{Ca}^{2+}$  levels lead to stronger contractions. Relaxation of the cardiomyocyte is produced by reducing intracellular  $\text{Ca}^{2+}$  to basal levels by energetically pumping  $\text{Ca}^{2+}$  out of the cell or back into intracellular stores like the SR. By interfering with the actions of norepinephrine,  $\beta$ -adrenergic blocking agents such as propranolol exert negative inotropic and chronotropic effects. Vagal (parasympathetic) impulses or cholinergic substances can also produce negative inotropic and chronotropic effects.



Impaired contractility may be the result of a decrease in cardiac energetics (availability of fuel substrate, oxygen extraction, energy production, or utilization of energy) or impairment of the process of excitation–contraction coupling. These functional disturbances may be unaccompanied by structural effects.

The heart contains an abundance of mitochondria. Since the energy used in the process of excitation–contraction coupling is derived from mitochondrial ATP, agents that affect myocardial oxidative phosphorylation would be expected to indirectly alter cardiac function. A number of agents can interfere with the process of energy liberation, storage, or use. For example, ergot derivatives and vasopressin can all produce coronary vasoconstriction and decrease the myocardial oxygen supply (Jiang et al., 2017; Klotz and McDowell, 2017; Reddy et al., 2020; Yonpam et al., 2021). Some substances may affect oxyhemoglobin association or dissociation, thereby interfering with oxygen delivery. When coronary blood flow or oxygen extraction is reduced, the metabolism and function of the heart can be disrupted at all levels. Agents can alter the energy liberation and supply process by interfering with the rate-limiting steps in the TCA cycle. For example, some anesthetics and several cytotoxins (rotenone, cyanide) interfere with electron transport systems or uncouple phosphorylation in the mitochondria (Jiang et al., 2017).

Cardioactive compounds can alter myocardial contractility by affecting any of the structures or steps involved in the excitation–contraction process. The sarcolemma constitutes the permeability barrier of the cell to extracellular nutrients, substrates, metabolites, and ions. Disturbances in sarcolemmal permeability to ions or alterations in the activity of membrane enzymes (e.g., adenylyl cyclase,  $\text{Na}^+/\text{K}^+$ -ATPase, and  $\text{Ca}^{2+}$ -activated ATPase) can change the action potential and influence myocardial contractile strength. The ATP-dependent  $\text{Na}^+$  pump ( $\text{Na}^+/\text{K}^+$ ATPase) that maintains normal transmembrane gradients of  $\text{Na}^+$  and  $\text{K}^+$  ions is extremely sensitive to cardiac glycosides. Verapamil blocks the slow inward  $\text{Ca}^{2+}$  current and thus reduces intracellular  $\text{Ca}^{2+}$  stores available to release the inhibitory troponin complex.

#### 4.3. Changes in Cardiac Mass as a Response to Toxicity

Cardiac mass can increase or decrease in response to a variety of endogenous and exogenous stimuli. Xenobiotic-induced changes in cardiac mass are usually an *increase* in mass and will be the primary focus of this section. In general, cardiomyocytes respond to energetic and mechanical stresses by increasing mass. Decreases in mass are uncommon but may occur with mechanical unloading or increased muscle catabolism as might occur with cachexia. Decreases in mass should be differentiated from “failure to grow,” which can occur in longitudinal toxicity studies in actively growing animals that would also have a decreased body weight relative to untreated animals.

Cardiac hypertrophy is an increase in the mass of the heart muscle beyond the normal limits for age, sex, and body weight. An increase in heart mass may result from an increase in workload (e.g., increased chronotropy or increased inotropy), an increase in mechanical wall stress (e.g., increased preload or afterload), decreased energy production (i.e., energetic stress), or when primary growth pathways are stimulated in cardiomyocytes (e.g., by anabolic steroids). All these scenarios are potential outcomes of xenobiotic effects. Importantly, changes that are initially compensatory can progress to maladaptive hypertrophy (e.g., cardiomyopathies) with time, progression, and/or persistence of a stressor. An increase in cardiac mass beyond normal limits does represent an independent risk factor for cardiac dysfunction and even sudden cardiac death due to arrhythmia.

Hyperthyroidism, whether experimentally induced or spontaneous, occurs in various animal species including the rat, guinea pig, rabbit, cat, and dog. Cardiac hypertrophy, the result of enhanced protein anabolism, is consistently produced but regresses with restoration of normal thyroid functional status. Cats given *L*-thyroxine (0.75 mg/kg/day for 10 months) have biventricular hypertrophy with weight increases of 86% in the left ventricle and 60% in the right ventricle (Strauer and Scherpe, 1975). Light microscopic and ultrastructural studies have demonstrated hypertrophy of individual cardiac muscle cells and increased

numbers of mitochondria with densely packed cristae in each cell. In rats with thyroid hormone-induced myocardial hypertrophy, angiogenesis of myocardial capillaries precedes ventricular enlargement (Tomanek and Busch, 1998). Presumably, a coincident induction of angiogenesis would more closely mimic the remodeling of the athletic heart, resulting in less opportunity for pathologic outcomes.

In rats implanted with a growth hormone-secreting tumor, cardiomegaly develops with prominent ventricular hypertrophy. Similar cardiac lesions occur in human patients with acromegaly.

Dogs and rats develop myocardial hypertrophy following chronic treatment with oxfenicine, an inhibitor of long chain fatty acid oxidation. Increased cardiac mass in this situation results from “energetic stress,” since an increased reliance on energy production from glucose substrates (i.e., secondary to decreased fatty acid oxidation) is less efficient.

#### 4.4. Drug-Induced Cardiomyopathies

A cardiomyopathic heart is one that is structurally altered (e.g., enlarged, remodeled heart muscle) and dysfunctional. Cardiomyopathies are generally characterized as dilated, hypertrophic, or restricted.

Dilated cardiomyopathies are a heterogeneous group of heart muscle diseases that have congestive heart failure (i.e., systolic pump failure) and dilatation of both ventricular chambers as common features. Mural thrombi and focal endocardial thickening are common in this condition, as are small foci of myocytolysis and myocardial fibrosis. The etiology of the dilated cardiomyopathy remains unknown in many human patients (idiopathic dilated cardiomyopathy). In other patients, dilated cardiomyopathy is associated with chronic alcoholism (alcoholic cardiomyopathy), administration of toxic agents, or viral infection.

##### 4.4.1. Alcoholic Cardiomyopathy

Ethanol has several detrimental effects on myocardial metabolism, but despite this the pathogenic mechanism(s) of alcoholic cardiomyopathy (a dilated cardiomyopathy) remain uncertain. Cardiomyopathy develops only in a small percentage of alcoholic patients. It appears likely that the toxic effect of ethanol on

the myocardium is modified by other factors and that the “alcoholic” cardiomyopathy observed clinically in human patients is a multifactorial disease. A metallothionein-knockout (MT-KO) mouse model fed an ethanol-containing liquid diet for 2 months appears to replicate the cardiac hypertrophy and fibrosis seen in alcoholic cardiomyopathy of humans and may provide a model for understanding this pathogenesis better (Noren et al., 1983).

The anatomic findings in myocardial biopsy specimens from patients with alcohol-induced dilated cardiomyopathy are nonspecific and do not differ significantly among patients with or without a history of chronic alcoholism. Alcoholic cardiomyopathy can be complicated by concomitant deficiency of thiamine or other nutrients and by other toxic materials ingested along with ethanol. The most striking example of this cooperative cardiotoxicity was illustrated by epidemics of severe acute cardiomyopathy with pericardial effusion that developed in chronically malnourished alcoholic patients who had ingested large amounts of beer to which cobalt salts had been added during the manufacturing process (to improve the quality of the foamy head) (Balazs and Herman, 1976; Packer, 2016). Structural findings in these patients include prominent vacuolization, myofibrillar lysis, glycogen accumulation, and edema of the muscle cells. Experiments in animals have shown that protein deficiency is an important factor increasing the absorption of cobalt from the gastrointestinal (GI) tract.

##### 4.4.2. Antimicrobial Cardiomyopathy

Furazolidone (FZ), a nitrofurantolone antibacterial and antiprotozoal that has been used in both animals and humans, causes dilated cardiomyopathy with severe ventricular dilatation and diffuse myofibrillar lysis when administered to young ducks, chickens, and turkeys (Jankus et al., 1972). Supplementation with selenium, vitamin E, and taurine does not protect against FZ-induced cardiomyopathy; however, propranolol (a  $\beta$ -blocker) has been reported to be protective. The biochemical mechanisms mediating this cardiomyopathy remain unknown.

##### 4.4.3. Antineoplastic Cardiomyopathy

Neoplastic disease is a multifaceted syndrome resulting from the acquired ability of cancer cells

to autonomously grow and proliferate by avoiding usual control mechanisms of induced cell death and immune protection. The adverse consequences of cancer cell growth are the result of one or more DNA mutations that allow these cells to circumvent normal protective mechanisms (see *Carcinogenesis: Mechanisms and Evaluation*, Vol 1, Chap 8). Without these restraints, cancer cells can undergo uncontrolled replication, dedifferentiation and loss of function, invasiveness, and metastasis. Cancer chemotherapies are intended to target these abnormal properties. Clinical studies and cumulative therapeutic experience have shown that cancer chemotherapy is effective at targeting and eliminating neoplastic cells in patients. However, these treatments also target pathways essential to normal cell function and thus cause inadvertent adverse effects in tissues such as the heart.

**Anthracyclines:** Historically, the first antineoplastic drugs associated with serious cardiovascular toxicity were the anthracycline antibiotics, which disrupt DNA integrity. Because of inappropriate models, myocardial alterations induced by the anthracyclines were not detected in preclinical studies but instead were initially detected during early clinical trials with daunorubicin and doxorubicin.

Although anthracyclines can produce acute (ventricular arrhythmias and depression of contractility) and subacute (pericarditis and myocarditis) cardiac toxicity, these antineoplastic agents are well known for the distinctive chronic dilated cardiomyopathy that they produce in humans and experimental animals. Gross lesions of doxorubicin-induced cardiotoxicity described in pigs, rabbits, and dogs are hydropericardium, hydrothorax, and ascites (fluid accumulation in the pericardial sac, thoracic cavity, and abdominal cavity, respectively). In pigs, fibrinous pericarditis is occasionally present. The myocardium is often pale and the hearts are dilated when compared with control hearts; however, many animals have no gross evidence of cardiotoxicity at necropsy. Microscopically, two major lesions are observed: cardiomyocyte degeneration characterized by intracellular loss of myofibrils and cytoplasmic vacuolization ([Figures 1.6 and 1.7](#)); the vacuolation is caused by massive dilatation of the SR. These changes can also involve the conduction system of the heart. The microscopic and ultrastructural alterations in the

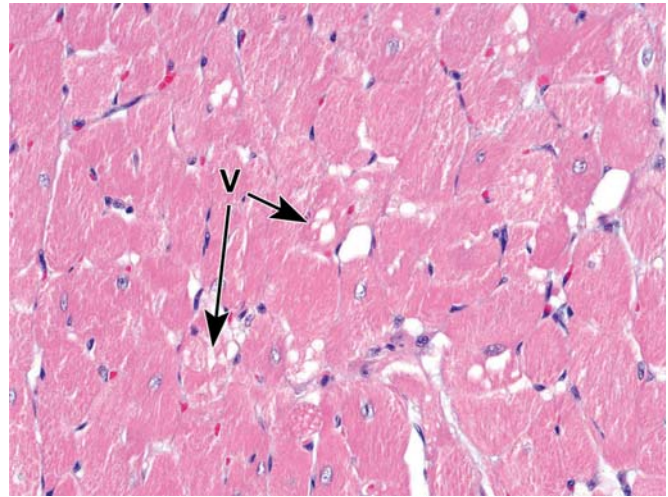


**FIGURE 1.6** Prominent, large, clear intracellular vacuoles in ventricular cardiac myocytes of a rat 6 weeks after administration of a single bolus intravenous dose of doxorubicin. Formalin-fixed, paraffin-embedded section; H&E stain. Original magnification 40 $\times$ . Reproduced from Haschek WM, Rousseaux CG, Wallig MA, editors: *Haschek and Rousseaux's handbook of toxicologic pathology*, ed 3, 2013, Academic Press, Figure 46.3, p. 1591, with permission.

myocardium of pigs, rabbits, and dogs with chronic doxorubicin cardiotoxicity are similar to those in humans and in other species of animals.

The pathogenesis of anthracycline cardiotoxicity, which is generally dose-dependent (usually at least 400 mg/m<sup>2</sup> total cumulative dose) remains uncertain. However, a number of possible mechanisms have been proposed, including drug intercalation into the DNA of cardiac muscle cells, inhibition of several enzyme systems necessary for DNA structural remodeling (e.g., topoisomerase 2 [TOP2]), and promotion of peroxidative damage mediated by free radicals to cell membranes (including those of mitochondria and SR), DNA, and various proteins (most importantly enzymes) ([Ferreira et al., 2008](#)).

Because anthracyclines are clinically useful anti-neoplastics for a variety of neoplasms, considerable efforts have been made to diminish the cardiotoxicity of anthracyclines without compromising their therapeutic effectiveness. Scores of compounds have been investigated with mixed results including angiotensin-converting enzyme (ACE) inhibitors,  $\beta$ -blockers,



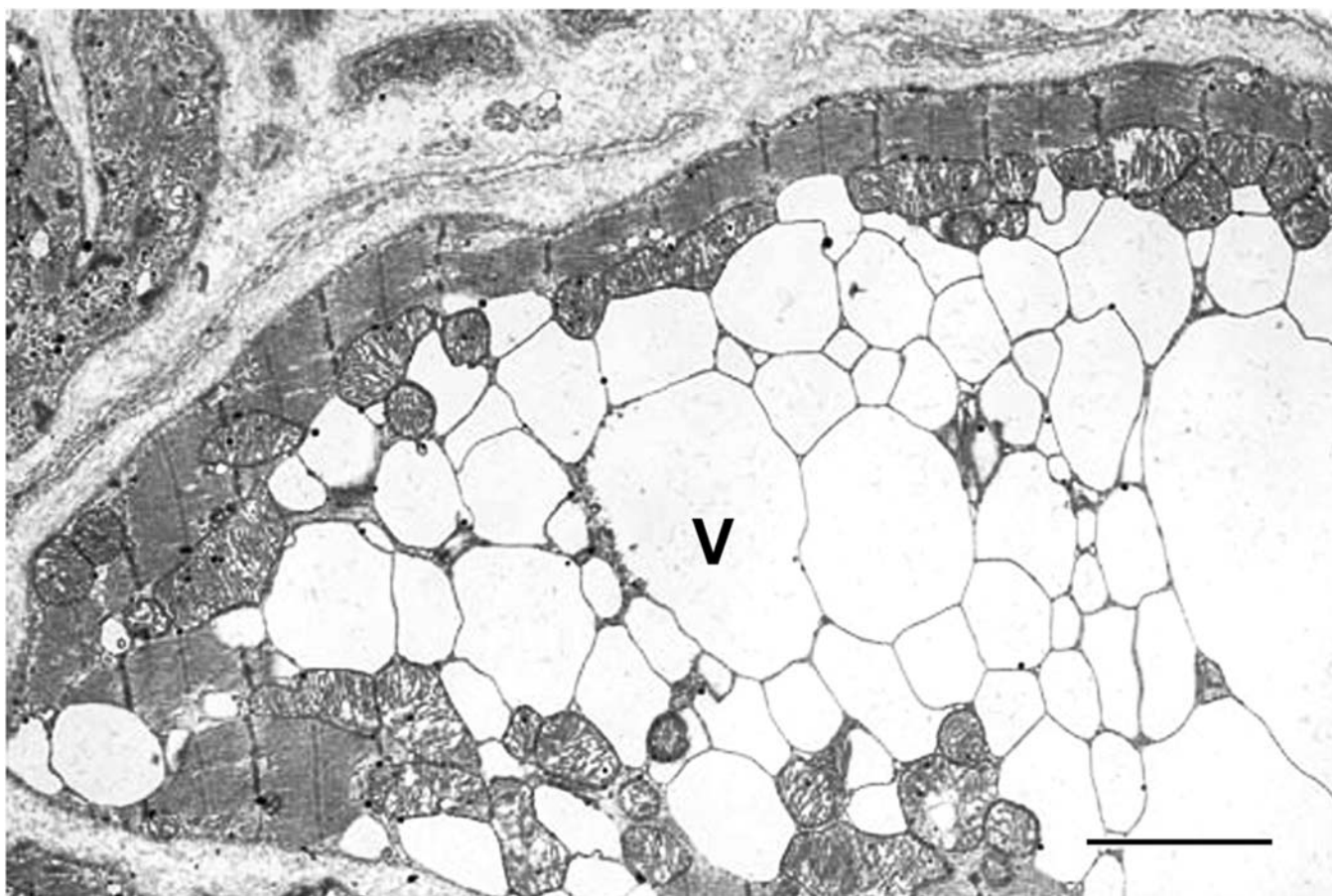


**FIGURE 1.7** Electron micrograph of a cardiac myocyte with vacuolar (V) degeneration from severe distension of the sarcoplasmic reticulum in a dog given 16 mg/kg (total cumulative dose) of doxorubicin over 4 months. Bar = 2  $\mu$ m. Reproduced from Haschek WM, Rousseaux CG, Wallig MA, editors: *Handbook of toxicologic pathology*, ed 2, 2002, Academic Press, Figure 4, p. 388, with permission.

L-carnitine, probucol (a “non-statin” cholesterol-lowering drug), CoQ10 (coenzyme Q10), N-acetylcysteine, vitamin E, phenethylamine (a central nervous system [CNS] stimulant), and deferoxamine (a metal chelator). The most successful results in this regard have been obtained with dexrazoxane (ICRF-187), an agent that probably chelates iron (needed to mediate the peroxidative reactions promoted by anthracyclines). A potential second mechanism of dexrazoxane protection has been reported whereby formation of the tertiary complex Dox-DNA-TOP2B is prevented by inducing TOP2B to assume a closed-clamp conformation (Herman and Ferrans, 1998). When given prior to doxorubicin, dexrazoxane markedly reduces the severity of the cardiomyopathy that develops in rabbits, rats, dogs, and pigs as well as in both adult and pediatric patients. In dogs, the

administration of dexrazoxane has allowed the dose of doxorubicin to be increased fourfold without producing significant chronic cardiomyopathy. Compounds that act as free radical scavengers (e.g., vitamin E, N-acetylcysteine) have been shown to decrease doxorubicin toxicity in acute models but have been much less successful clinically in blocking the chronic cardiotoxic effects of doxorubicin.

Doxorubicin is also known to cause very late, delayed ventricular dysfunction in young adults who have undergone antineoplastic therapy successfully during childhood and survived for 10 years or longer. Cardiac morphologic findings in these patients have not been consistent, and the exact mechanism(s) mediating this greatly delayed cardiotoxicity remain to be determined. It has been suggested that previous therapy with doxorubicin prevents proper growth of the

heart during adolescence. It is thought that the selective cardiotoxicity of anthracyclines is due to the fact that the heart, unlike other organs such as the liver, has very limited defenses (i.e., low levels of antioxidant enzymes such as superoxide dismutase, catalase, and glutathione peroxidase) that protect against peroxidative damage.

Antineoplastic agents other than the anthracyclines are also capable of producing cardiovascular damage. The spectrum of cancer chemotherapies has expanded and now includes several new modalities such as targeted agents and immunotherapies. Unfortunately, these new classes of antineoplastic drugs may also induce various types of cardiovascular toxicity. Some of these therapies elicit a very limited and others a very broad cardiotoxicity profile (Combs and Acosta, 1990; Geiger et al., 2010).

*Alkylating agents:* Alkylating drugs cause cell death, especially in rapidly dividing cells, by adding alkyl groups that crosslink DNA and prevent its replication. Cyclophosphamide is an alkylating nitrogen mustard that can provoke cardiovascular complications (Iqbal et al., 2019). Significant cardiotoxicity noted after treatment with high doses can include fatal hemorrhagic myocarditis. This occurs when patients are treated with high doses in preparation for bone marrow transplantation. Cyclophosphamide-induced cardiotoxicity is thought to be due to the metabolite acrolein which causes cardiomyocyte inflammation, reactive oxygen formation, and reduced activity of nitric oxide synthase (which promotes vasodilation and enhances blood flow, thereby reducing ischemic stress). Treatment with busulfan has been reported to cause endocardial fibrosis, and mitomycin C can induce myocardial fibrosis.

*Antimetabolites:* Antimetabolites interfere with mitosis by substituting for substances that are essential for DNA or RNA synthesis and thus reduce cell viability. 5-Fluorouracil (5-FU), an antimetabolite used to treat certain tumors, also exhibits cardiotoxicity (Alter et al., 2006; Polk et al., 2014). Cardiotoxic manifestations induced by 5-FU include angina pectoris (chest pain due to myocardial ischemia), ventricular tachycardia, myocardial infarction, cardiomyopathy, and heart failure. These alterations are thought to be due to indirect effects on the coronary arteries (leading to altered myocardial

perfusion) and direct effects on cardiomyocytes. 5-FU and its metabolites can induce oxidative stress in coronary vascular smooth muscle that results in vasospasm and thrombosis. 5-FU is also capable of causing direct cardiomyocyte damage by depressing mitochondrial function and activating apoptosis. These effects can occur after the initial dose.

*Antimicrotubular agents:* Microtubule inhibitors such as taxanes (e.g., paclitaxel) and vinca alkaloids (e.g., vinblastine and vincristine) target and interfere with microtubule structure and function, thereby limiting cell separation during cell division and ultimately provoking cell death (Kuncl, 2009; Perotti et al., 2003). Microtubules are engaged in a constant state of polymerization and depolymerization. Paclitaxel binds to tubulin and prevents depolymerization, while the vinca alkaloids thwart polymerization. Antimicrotubular agents cause cardiovascular toxicities such as heart block, hypertension, arrhythmias, myocardial ischemia, and congestive heart failure. The mechanism of microtubule inhibitor-induced cardiovascular toxicity is not completely understood, but alterations in myocyte  $\text{Ca}^{2+}$  handling, changes in the cardiac Purkinje system, or disruption of the autonomic nervous system control of the myocardium have been proposed as potential contributors.

*Cytokine immunotherapy:* Cytokines are released by immune and nonimmune cells as a result of cellular stresses such as infection, inflammation, and tumorigenesis. The released cytokines stimulate the rapid appearance of immune signaling, an action that can produce a powerful and coordinated immune response to target novel ("non-self") antigens such as those expressed by neoplastic cells. Cardiotoxicity has been noted after treatment with various types of cytokines used for cancer immunotherapy (e.g., interleukin 1 [IL-1], IL-2 IL-3, IL-4, and several interferons). The most frequently occurring cardiovascular complication induced by IL-2 is the vascular leak syndrome, which is thought to result from the interaction of IL-2-activated lymphocytes (lymphokine-activated killer [LAK] cells) and endothelial cells (Fujita et al., 1994; Kragel et al., 1990). Vascular leak syndrome is characterized by a widespread increase in vascular permeability leading to fluid retention in tissues and organs (including the heart), peripheral edema, ascites, pleural



effusion, and pulmonary edema. Treatment with an interleukin has also been associated with hypotension, tachycardia, vasodilation, arrhythmia, and myocardial infarction. Reports of cardiomyopathy have been reported following therapy with interferon alpha (INF- $\alpha$ ) and interferon beta (INF- $\beta$ ).

*Platinum-containing agents:* Cisplatin (cis-diammine-dichloroplatinum II) is an alkylating agent that is used to treat a variety of neoplasms. Damage to noncardiac organs is more prevalent than that occurring in the heart. Cisplatin-induced cardiotoxicity varies from hypertension and coronary artery disease to dysrhythmia and heart failure (Demkow and Stelmaszczyk-Emmel, 2013; Oun and Rowan, 2017). The pathogenesis of the toxicity involves direct adverse effects on cardiomyocytes and generation of reactive oxygen radicals that cause inflammation and thrombus formation.

*Nonanthracycline antibiotics:* Bleomycin is a glycopeptide that has been used to treat a variety of neoplasms. The primary mechanism responsible for its antitumor action is oxidative damage to DNA by binding metal ions (including iron). The most common adverse effect of bleomycin is pulmonary toxicity (see *Respiratory System*, Vol 5, Chap 4) (Danson et al., 2005; Rowinsky, 1991). However, bleomycin has also been associated with a low incidence of cardiotoxic effects including peripheral arterial thrombosis, coronary artery disease, and heart failure. A chest pain syndrome has been reported to occur during infusion of bleomycin.

*Proteasome inhibitors:* Three currently available proteasome inhibitors are bortezomib, carfilzomib, and ixazomib. These agents exhibit antineoplastic activity by inhibiting the proteasome, which impairs protein turnover leading to the accumulation of abnormal or dysfunctional proteins which is toxic to the affected cells. The most common cardiovascular toxicity reported after proteasome inhibitor treatment are heart failure, hypertension, and dysrhythmias (Geiger et al., 2010). These cardiotoxic effects are thought to occur because proteasome inhibition alters a number of downstream processes including endoplasmic reticulum stress, protein aggregation, caspase and apoptosis activation, and myocyte hypertrophy.

*mTOR (mammalian target of rapamycin) inhibitors:* The mTOR inhibitors such as everolimus

and sirolimus are agents used to treat a variety of neoplasms. mTOR inhibitors ultimately reduce protein synthesis and cell proliferation by interfering with a kinase complex (mTORC1). These inhibitor compounds also reduce angiogenesis by inhibiting VEGF and hypoxia-inducible factor 1 (HIF-1) expression. Hypertension appears to be the most frequently reported cardiovascular effect, but instances of angina pectoris (chest pain secondary to cardiac ischemia), atrial fibrillation, cardiomyopathy, heart failure, and deep vein thrombosis have also been noted.

*Monoclonal antibodies:* Trastuzumab is a recombinant humanized monoclonal antibody that is used in cancer patients who have elevated expression of the human epidermal growth factor 2 (HER2 [or ErbB2 or HER2/neu]) receptors. Trastuzumab and newer agents such as lapatinib, pertuzumab, and ado-trastuzumab target this receptor, which is involved in the normal functioning of the myocardium. As a result, HER2/neu inhibition alters key pathways that mediate myocyte viability and prevent apoptosis. The spectrum of trastuzumab-induced cardiotoxicity varies from cardiomyopathy and heart failure to peripheral edema, hypertension, and arrhythmias (Barish et al., 2019). The myocardial histopathological lesions induced by trastuzumab differ from those caused by doxorubicin. In trastuzumab-treated rabbits, the main myocardial finding is infiltration of lymphocytes and macrophages. Ultrastructural changes observed in myofibers include edema associated with separation of myofibril bundles and rupture of the sarcomere (Laird-Fick et al., 2020). Some of the cardiotoxic effects induced by trastuzumab in patients may be reversible over time upon cessation of treatment.

*Immune checkpoint inhibitors (ICIs):* Important ICI like ipilimumab, nivolumab, and pembrolizumab exert antineoplastic activity by altering immunoregulatory signaling through inhibition of the immune function-attenuating molecules cytotoxic antigen 4 (CTLA4) or programmed cell death ligand-1 (PD-L1). This action inhibits T cell–cancer cell interactions, an effect that disengages the tumor-mediated “turn-off” functions in the T-cells. As a result, the ICIs stimulate disinhibited immune cells to attack neoplastic cells. This action also has the additional effect of misdirected autoimmune attack toward

normal tissues including cardiomyocytes. This autoimmune action can lead to accelerated atherosclerosis and cardiovascular complications such as stroke, coronary artery disease, and myocardial infarction. Myocarditis is deemed the most severe complication of ICI therapy. The median onset for this adverse effect is 18–39 days after the initial dose.

*Tyrosine kinase inhibitors:* The human genome includes numerous tyrosine kinase (TK) and TK-like genes whose expression is represented in two ways: transmembrane receptors and intracellular nonreceptor kinases. TKs are important proteins whose activation causes phosphorylation of certain substrates necessary for cell viability. The overexpression and/or mutation of a TK induces abnormal cell proliferation and differentiation accompanied by retarded apoptosis. TK inhibitors (TKIs) are small molecule drugs that inhibit phosphate group transfer to the tyrosine component of a protein, which prevents activation of the kinase. The TKIs inhibit a broad spectrum of targets that control growth and angiogenesis in tumor cells. However, because TKs are also widely distributed in nonneoplastic cells, TKIs exert similar inhibitory actions in normal cells including cardiomyocytes.

Clinical experience has determined that most TKIs in use are associated with some type of cardiotoxicity (arrhythmias, hypertension, left ventricular ejection fraction dysfunction, heart failure, and/or myocardial infarction). Some clinically useful TKIs include:

1. Imatinib targets multiple kinases (Bcr-Abl, c-Kit [stem cell factor receptor], and platelet-derived growth factor [PDGFR]). Some patients treated with imatinib experience a decline in left ventricular ejection fraction, which can lead to heart failure. Transmission electron micrographs of biopsies taken from imatinib-treated patients have shown prominent membrane whorls, pleomorphic mitochondria, scattered cytosolic lipid droplets, and vacuoles within cardiomyocytes (Kerkelä et al., 2006).
2. Dasatinib targets Bcr-Abl, cKit, PDGFR, and the Src family of kinases. Peripheral edema is the most common cardiovascular effect. Other reported cardiotoxic alterations include heart failure, QT prolongation, and pericardial effusion. One of the most serious complications of dasatinib treatments is

precapillary pulmonary hypertension (caused by vessel remodeling in the lung leading to increased pulmonary vascular resistance). While severe, this latter condition is reversible.

3. Sunitinib and sorafenib inhibit VEGF receptor (VEGFR), PDGFR, and c-Kit. These agents induce cardiotoxic effects such as decreased left ventricular ejection fraction, hypertension, and congestive heart failure. Sorafenib specifically alters kinases that are necessary for myocyte survival. Inhibition of these kinases leads to increased myocyte apoptosis and interstitial fibrosis.
4. Second- and third-generation TKIs (ponatinib, nilotinib, bosutinib) have been reported to induce arterial hypertension, heart failure, arrhythmias, acute coronary syndromes, pulmonary hypertension, and venous thrombosis. The mechanism of cardiotoxicity linked to these newer TKIs is complex and may be due to decreased capillary density and/or endothelial damage in the myocardium and energy depletion in myofibers.

*Chimeric antigen receptor T-cell (CAR-T) cell therapy:* CAR T-cells are autologous (patient-derived) T-cells that have been engineered ex vivo using lentivirus or retrovirus to target specific antigens expressed by neoplastic cells (e.g., CD19) (see *Gene Therapy and Gene Editing*, Vol 2, Chap 8). One of the most frequent and important side effects of CAR-T therapy is the cytokine release syndrome (CRS, or “cytokine storm”), a systemic acute inflammatory condition in which immune cell stimulation by the CAR T-cells leads to rapid and extensive release of cytokines followed by multiorgan dysfunction. The cardiovascular consequences observed with CRS consist of circulatory shock, hypotension, and possibly multiorgan failure. Cardiotoxicity thought to be directly related to CAR-T therapy (and not just as an indirect consequence of CRS) is reported to include arrhythmias, heart failure, and cardiovascular-related deaths.

#### 4.5. Cardiomyocellular Injury

Xenobiotic-induced cardiomyocellular injury can manifest in a variety of ways depending on the mechanism, pathogenesis, and organellar target of toxicity. These injuries can range from sublethal damage (e.g., degeneration) to cell

death by apoptosis or necrosis. Cardiomyocellular necrosis is often accompanied by an inflammatory reaction and possibly interstitial connective tissue deposition, depending on the magnitude of the lesion. Widely disseminated or cumulative injury resulting in measurable changes in cardiac function may be detectable by assessing conduction (ECG) or contractility (echocardiography).

#### 4.5.1. Vacuolar Degeneration

Vacuolar degeneration is a distinctive microscopic alteration in cardiac myocytes characterized by variably sized, well-delineated, clear, and colorless spaces within the sarcoplasm. This change is best associated with the chronic progressive toxicity of anthracyclines. Vacuoles at the light microscopic level (Figure 1.6) are revealed by TEM to be dilated elements of SR (Figure 1.7). In mildly affected myocytes, the vacuoles vary from 0.1 to 1  $\mu\text{m}$  in diameter,

but in severely affected cells, the vacuoles may be up to 5  $\mu\text{m}$  in diameter. Distortion of sarcomeres and lysis of contractile elements often develops as the injury progresses.

Vacuolation of myocytes must be interpreted with care. Vacuolation that occurs without other evidence of degeneration can be seen in routine histologic sections (including control animals) where the vacuoles may be revealed by TEM to be lipid droplets or swollen mitochondria.

#### 4.5.2. Myofibrillar Degeneration

Myofibrillar degeneration (also termed myocytolysis) is a distinctive sublethal injury of cardiac muscle cells in which affected fibers have pale eosinophilic sarcoplasm and lack cross-striations. Myocyte contours also may be rounded due to cell swelling. Ultrastructurally, degenerating myofibrils exhibit variable degrees of fragmentation (myofibrillar lysis) (Figure 1.8).

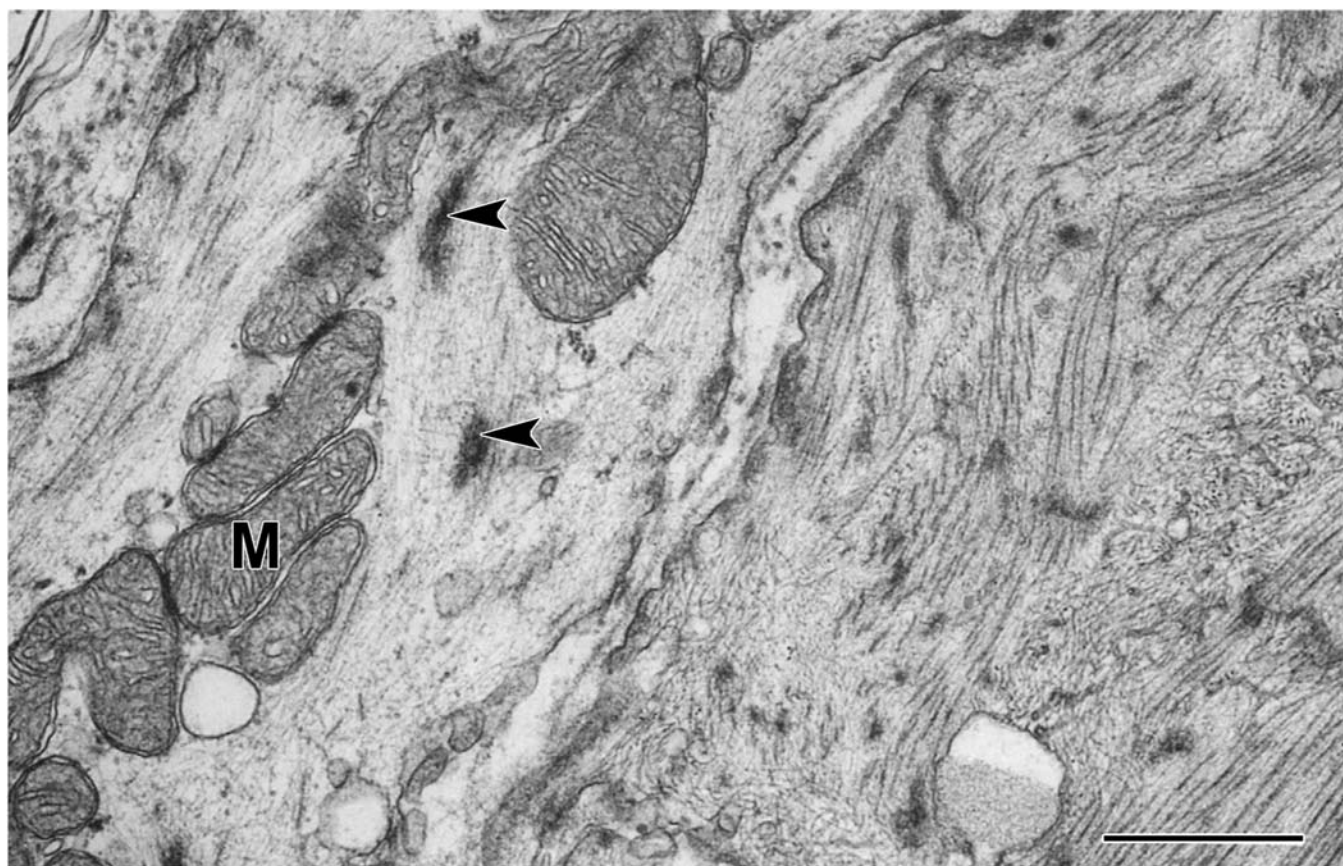


**FIGURE 1.8** Furazolidone toxicosis in a duckling. High magnification view of two myocytes with severe myofibrillar lysis (also called “myocytolysis”) and scattered dense masses of displaced Z band material (arrowheads). The myocyte on the left exhibits nearly complete lysis. The mitochondria (M) have normal contours and display intact and properly organized cristae. Bar = 1  $\mu\text{m}$ . Reproduced from Haschek WM, Rousseaux CG, Wallig MA, editors: *Handbook of toxicologic pathology*, ed 2, 2002, Academic Press, Figure 7, p. 390, with permission.



This cardiac lesion has been described following exposure to anthracyclines in humans, FZ in birds,  $K^+$  deficiency in rats, and plasmocid in rats (Figures 1.9 and 1.10). In anthracycline cardiotoxicosis, degeneration of contractile elements often is accompanied by myocyte vacuolation.

Myofibrolysis is best seen ultrastructurally and can be present in damaged myocytes with or without sarcoplasmic vacuolization. Thick myofilaments are preferentially lysed, and irregular clumps of Z-band material may be present (Figure 1.8). Accumulation of glycogen granules and elements of SR occurs in some myofibers undergoing myofibrillar lysis. Affected myocytes may also have mitochondrial alterations consisting of swelling and disruption of membranes and scattered accumulations of residual bodies, but the myofibrillar lysis may occur in the absence of mitochondrial changes (Figure 1.8).

Congestive cardiomyopathy is produced in turkeys, ducklings, and chickens by excessive

intake of FZ (Figure 1.11). This condition was first reported in 1972 in turkey poultts accidentally exposed to excessive amounts of this antibacterial drug (Jankus et al., 1972). Since then, numerous studies have been reported on the clinical, pathologic, and biochemical alterations of FZ-induced cardiomyopathy. The cardiomyopathy is produced readily by oral administration or feed supplementation of FZ. In ducklings, FZ induces dose-related frequency and severity of clinical disease. Clinical signs include growth retardation, ascites, and death. Ducklings fed 750 mg FZ/kg of feed for 28 days develop a high incidence of cardiomyopathy with low mortality (Van Vleet and Ferrans, 1983b). Cessation of FZ feeding results in the regression of ascites and reversal of the cardiomyopathy. At necropsy, congestive heart failure manifests as severe ascites and hydropericardium with substantial congestion of the lungs and liver. The heart is enlarged, with marked biventricular dilatation ("round heart") and thin ventricular walls. However, light

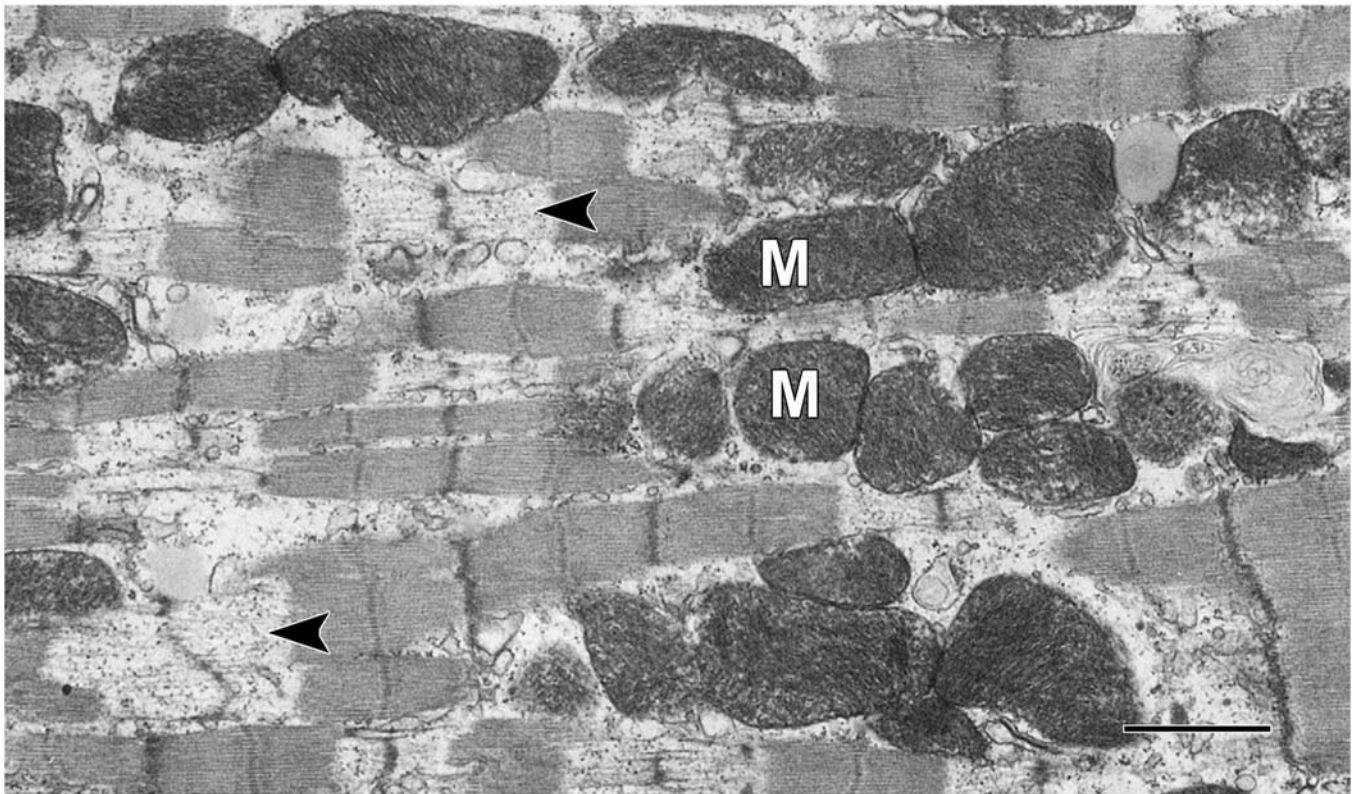


**FIGURE 1.9** Selective disruption and lysis of I bands (arrowheads) in sarcomeres of the left ventricular myocardium of a rat with acute plasmocid toxicity. The mitochondria (M) have normal contours and display intact and properly organized cristae. Bar = 1  $\mu$ m. Reproduced from Haschek WM, Rousseaux CG, Wallig MA, editors: *Handbook of toxicologic pathology*, ed 2, 2002, Academic Press, Figure 8, p. 391, with permission.

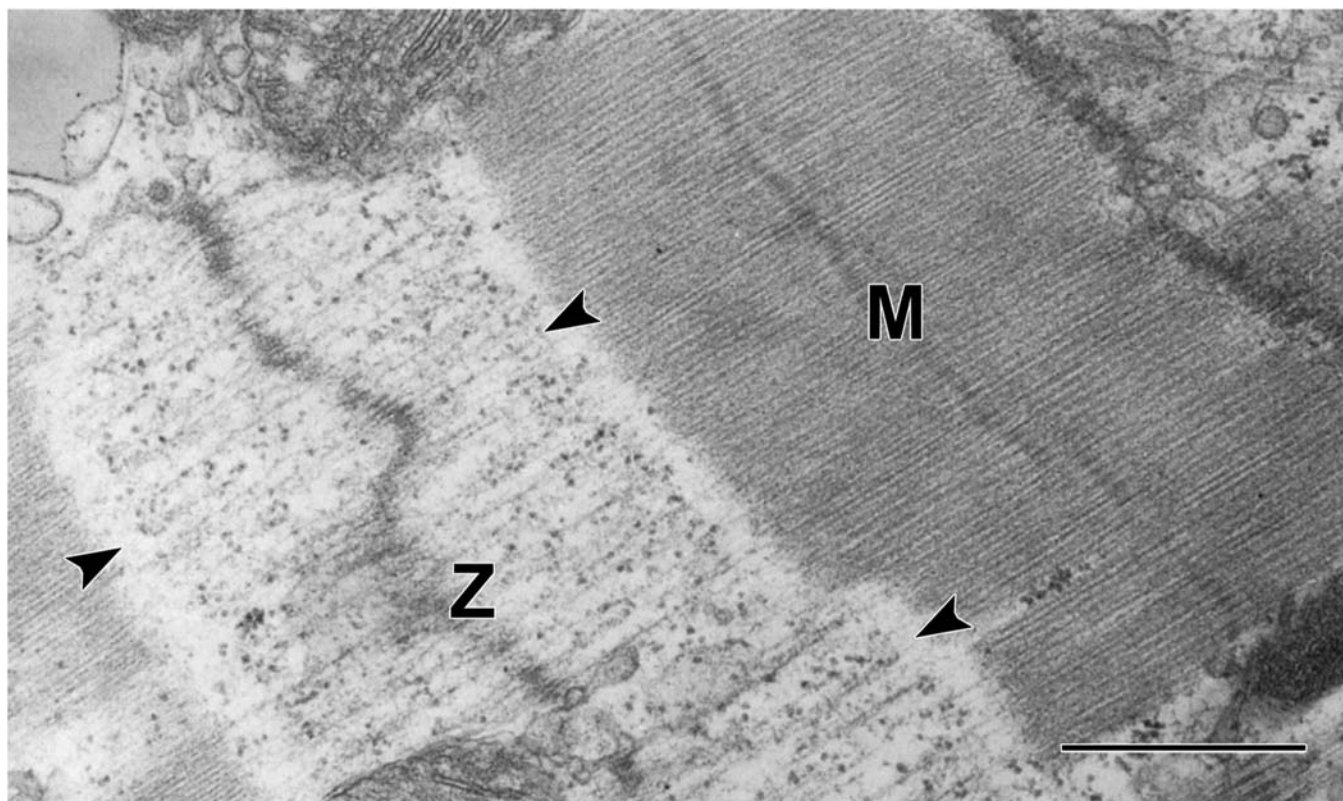


**FIGURE 1.10** Higher magnification of a portion of Figure 1.9 shows lysis of actin filaments and disruption of myofibrils at the junction of A and I bands (arrowheads). M, M-band (center of the A-band); Z, Z-band (border of the sarcomere). Bar = 1  $\mu$ m. Reproduced from Haschek WM, Rousseaux CG, and Wallig MA, editors: *Handbook of toxicologic pathology*, ed 2, 2002, Academic Press, Figure 9, p. 391, with permission.

microscopic study of the myocardium failed to demonstrate necrosis, inflammation, or fibrosis and instead revealed myocytolysis with pale sarcoplasm. Ultrastructurally, the outstanding structural alteration was myofibrillar lysis (Figure 1.8) (Van Vleet and Ferrans, 1983a). Affected myocytes showed a loss of intact myofibrils, with scattered masses of free thick and thin filaments, clumps of Z-band material, and disordered accumulations of cytoskeletal filaments. Numerous polyribosomes were present in the areas of myofibrillar lysis. It is not known whether the myofibrillar lysis results from FZ-induced decreased synthesis, increased degradation, and/or disaggregation of contractile proteins. FZ-induced cardiotoxicity in ducklings offers an attractive model for studies of congestive cardiomyopathy.

#### 4.5.3. Lipofuscinosis

Lipofuscin (so-called 'wear and tear pigment') is a lipid-containing product of lysosomal

digestion. Lipofuscinosis or brown atrophy of the myocardium occurs in healthy aged animals and in animals with severe cachexia, as well as occurring as a hereditary lesion in healthy Ayrshire cattle. Affected hearts appear brown and microscopically have clusters of yellow-brown granules at the nuclear poles of myocytes. These granules ultrastructurally appear as intralysosomal accumulation of membranous and amorphous debris.

#### 4.5.4. Phospholipidosis

Phospholipid accumulation is another lipid-containing degradation product that may be associated with drug-related toxicity in many cells, including those of the cardiovascular system. Ultrastructurally, phospholipidosis appears as concentric lamellar whorls in the cytoplasm of affected cells (which might include cardiomyocytes and endothelial cells). These accumulations have been described in myocytes of rats given Brown FK, a food-coloring agent



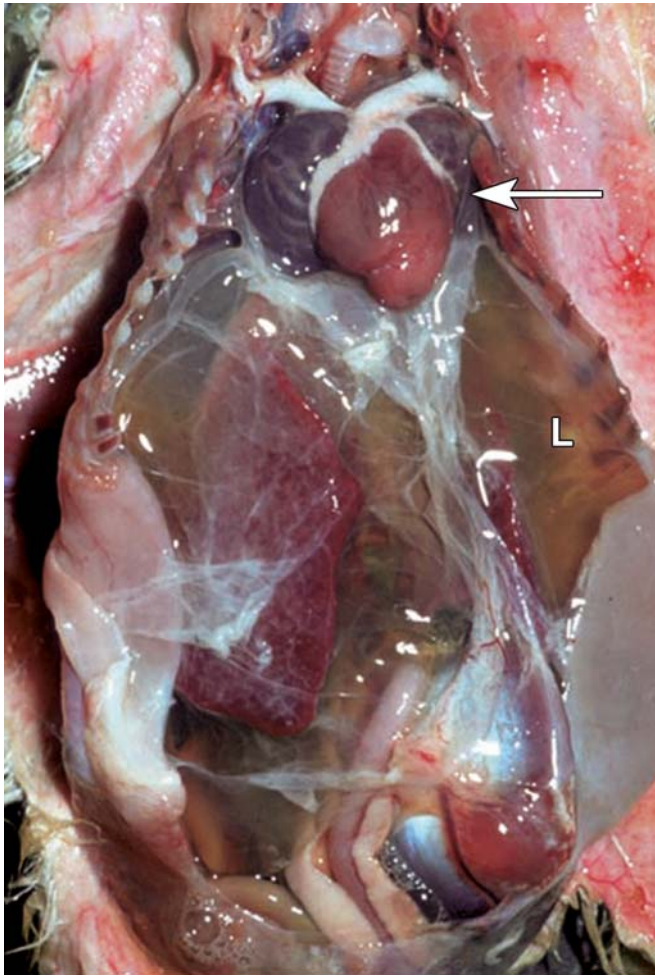


**FIGURE 1.11** Cardiac dilatation (arrow) and congestive heart failure in a duckling associated with furazolidone toxicosis. Serous fluid accumulation is present in the body cavities, and fibrin deposits (i.e., wispy protein strands) are adhered over the liver (L). Reproduced from Van Vleet, Ferrans: *Cardiovascular system*. In McGavin M., Zachary JE, editors: *Pathologic basis of veterinary disease*, ed 4, Mosby Elsevier, 2007, Figs 10–13, p. 566, with permission.

and in rats, mice, and humans given chloroquine (Figure 1.12). Drug-induced phospholipidosis presents a safety assessment challenge since its target organ distribution can be variable as can its association with overt cell or tissue injury. In general, the magnitude of accumulation is dose-related and temporally progressive with continued exposure but also is reversible with discontinuation of exposure.

#### 4.5.5. Cardiomyocyte Necrosis

Xenobiotic-induced cardiomyocyte necrosis or myocardial necrosis (which involves more than

just cardiomyocytes) can occur focally, regionally, or diffusely depending on the pathogenesis, dose, and potency of the agent. Focal to multifocal distributions may need to be distinguished from spontaneous rodent PCM, which presents similarly in younger animals. Regional distributions may provide insights into pathogenesis. For example, myocardial necrosis with a distribution oriented toward the subendocardium and papillary muscles is often associated with ischemia, vascular injury, or energetic dysfunction. Widespread or diffuse necrosis not associated with acute death of the host is often insidiously progressive and involves loss of individual cardiomyocytes, progressive interstitial fibrosis, and compensatory hypertrophy of the remaining intact cardiomyocytes.

Necrosis of cardiac myocytes is generally followed by inflammation and phagocytosis of myofiber debris (mainly sarcoplasm). The result is persistence of sarcolemmal “tubes” of basal lamina surrounded by condensed interstitial stroma and vessels. In lesions with severe disruption of the myocardium, the residual effects may be fibroblast proliferation and collagen deposition to form scar tissue. Regeneration of cardiac myocytes is generally not observed. Rarely, in very young animals and especially in birds, a limited amount of myocyte regeneration may occur as indicated by the presence of cardiomyocyte mitoses. Hyperplasia of myocytes is a normal component of cardiac development in the first several months of life but then ceases. Thereafter, the remainder of cardiac growth is the result of myocyte hypertrophy until normal cell sizes are reached.

Three morphologic forms of cardiac muscle cell necrosis are distinguishable: coagulation, contraction band, and lytic necrosis. These forms depend on the nature and time course of the lesion.

Coagulation necrosis follows sustained disruption of the blood supply. Ischemia of less than 20 min duration produces peracute myocyte damage characterized by glycogen depletion, mitochondrial swelling, mild intracellular edema, and relaxation of sarcomeres (reflecting loss of contractility) (Sage, 1986; Sage and Gavin, 1985). These changes are reversible upon restoration of the blood flow. However, when the period of ischemia exceeds 20 min, irreversible injury begins to develop, and by 60 min most

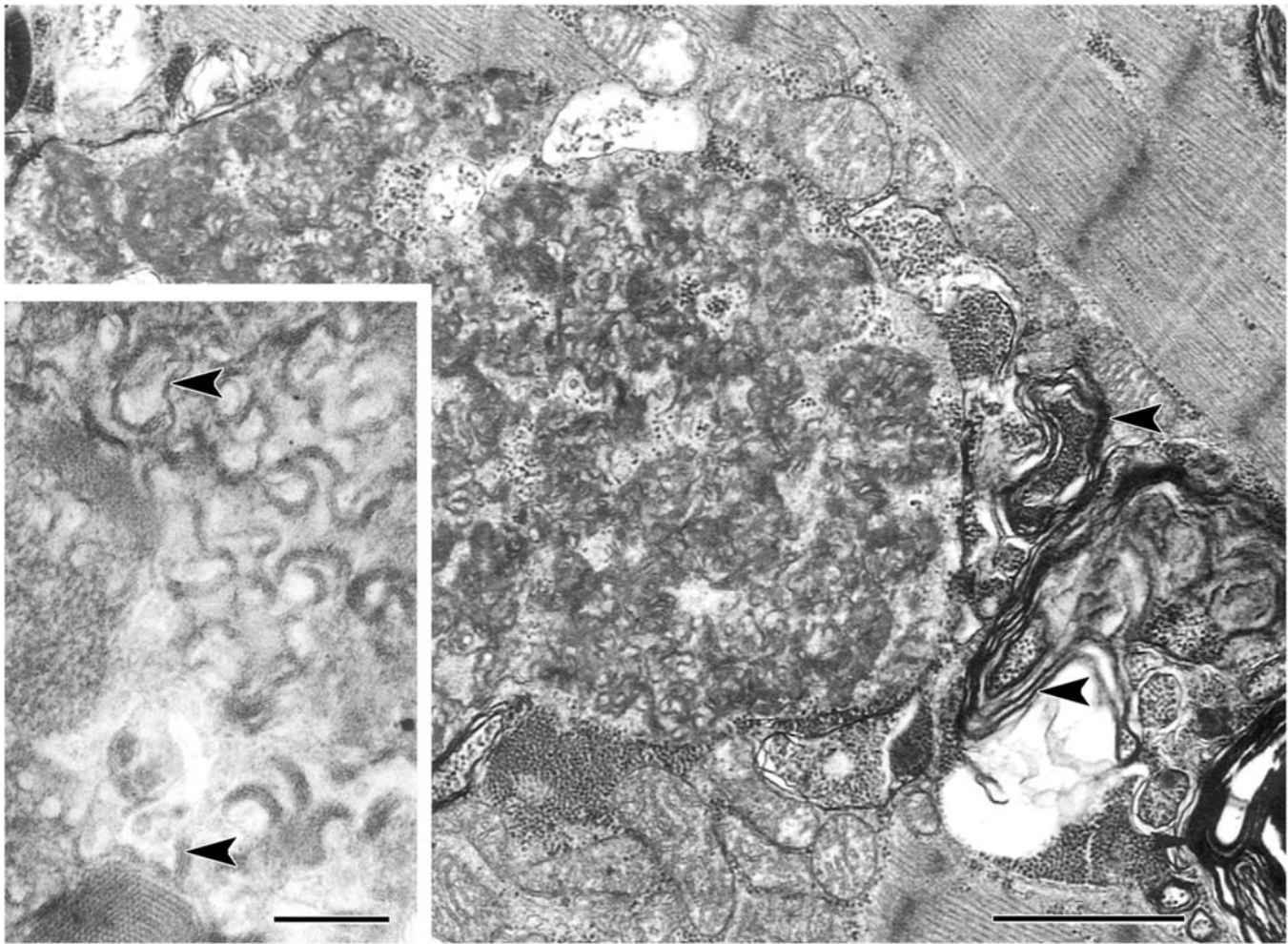


**FIGURE 1.12** Electron micrograph of phospholipidosis in a right ventricular myocardial biopsy from a human patient with cardiomyopathy who had received chloroquine for several years to treat systemic lupus erythematosus. The phospholipid deposits appear as large accumulations of curvilinear bodies (*center*) and membranous lamellae (*arrowhead*). Bar = 1  $\mu$ m. (*Inset*) Higher magnification of curvilinear bodies (*arrowheads*). Bar = 0.2  $\mu$ m. Reproduced from Haschek WM, Rousseaux CG, and Wallig MA, editors: *Handbook of toxicologic pathology*, ed 2, 2002, Academic Press, Figure 11, p. 393, with permission.

of the cells in the ischemic area are irretrievably launched on a path culminating in coagulation necrosis. This form of necrosis is characterized by intramitochondrial flocculent precipitates (thought to be derived from mitochondrial lipids), margination of nuclear chromatin (indicating irreversible nuclear damage), small holes or defects in the plasma membrane (representing loss of its permeability barrier function), relaxed myofibrils with indistinct myofilaments, and various degrees of dissociation of the intercellular junctions. Coagulation necrosis is limited to central areas of myocardial infarcts, in which reflow does not occur following ischemic damage.

Contraction band necrosis develops at the periphery of infarcts. This variant of necrosis is characterized by hypercontraction of myofibrils, intramitochondrial electron-dense calcific deposits, and eventual progression to myocytolysis. The distinctive features of contraction band necrosis are related to the entry of large amounts of  $\text{Ca}^{2+}$  ions, which originate from partial reperfusion of peripheral areas of ischemic lesions, into cells that have been damaged by ischemia. The passage of  $\text{Ca}^{2+}$  through damaged, abnormally permeable plasma membranes is responsible for the hypercontraction since accumulation of the  $\text{Ca}^{2+}$  ions releases the regulatory tropomyosin complex. This passage occurs



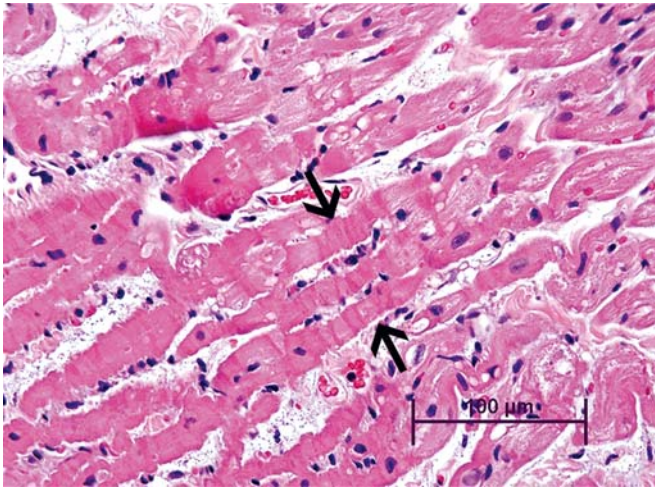


**FIGURE 1.13** Myocardium with contraction band necrosis in a rat. Transverse bands (arrows) of darkly eosinophilic material are separated by pale, sometimes granular or vacuolated sarcoplasm. Formalin-fixed, paraffin-embedded section, H&E stain. *Reproduced from Haschek WM, Rousseaux CG, and Wallig MA, editors: Fundamentals of toxicologic pathology, ed 2, 2010, Academic Press, Figure 12.12, p. 345, with permission.*

either when severely but temporarily ischemic tissue is reperfused with arterial blood or when necrosis develops because of factors not related to a reduction in coronary blood flow. For these reasons, contraction band necrosis is seen in many forms of cardiac toxic injury, including the lesions caused by catecholamines, vasodilating antihypertensive agents, and other cardiotoxic compounds (Figures 1.13 and 1.14).

Lytic necrosis may be a primary finding or a progression from contraction band necrosis. In this variant, myocytolysis is mediated through fragmentation of the myofilaments, a change that results in an empty appearance of the cells. The time-course of this progression is highly variable.

#### 4.5.5.1. PROGRESSION OF MORPHOLOGIC ALTERATIONS FOLLOWING LETHAL CARDIOMYOCYTE INJURY

Grossly, large areas of necrosis generally appear pale initially. Over time, affected regions may progress to prominent yellow to white,

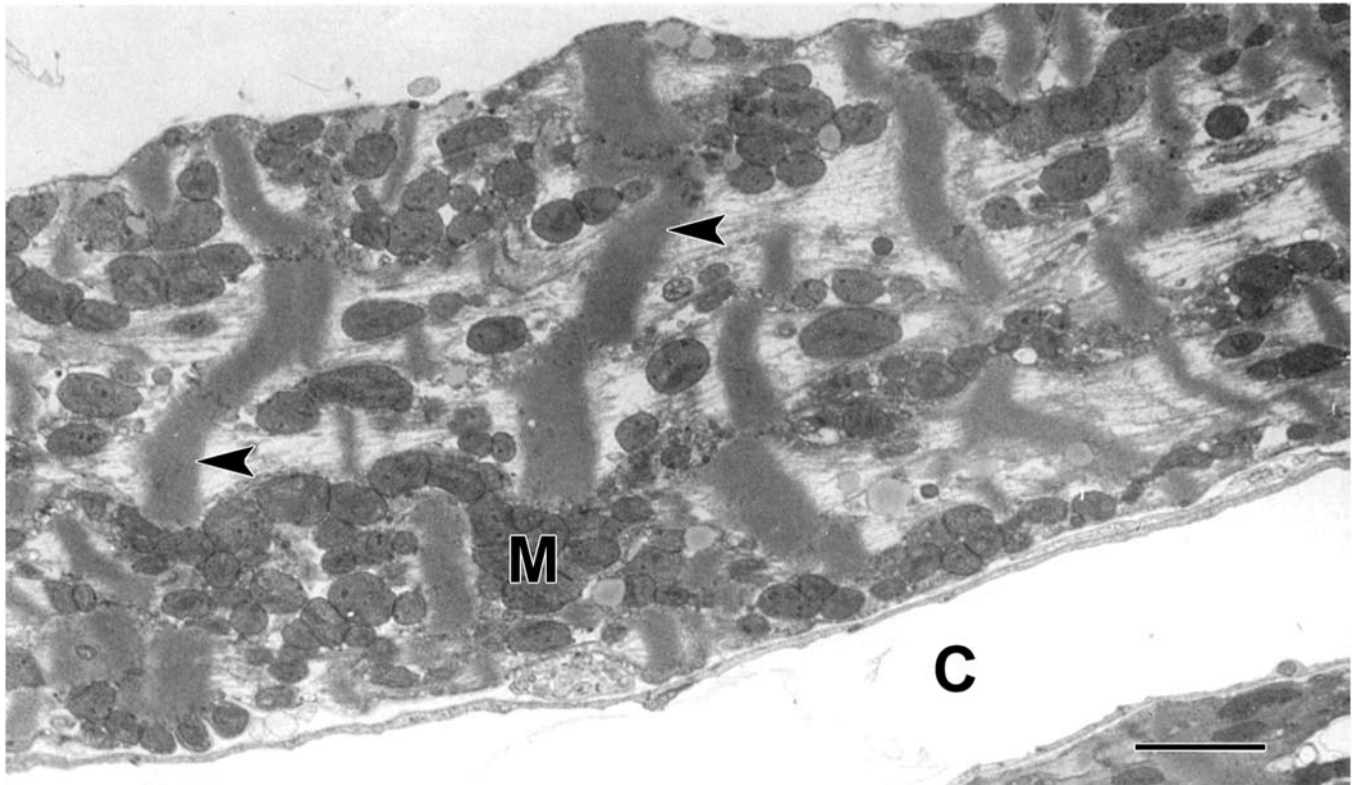


**FIGURE 1.14** Contraction band necrosis in a ventricular myocyte of a rat with acute plasmocid toxicosis. Dense transverse masses of contractile material are prominent (arrowheads). The sarcolemma is intact despite the cell hypercontraction. C, capillary; M, mitochondria. Bar = 2 μm. *Reproduced from Haschek WM, Rousseaux CG, and Wallig MA, editors: Handbook of toxicologic pathology, ed 2, 2002, Academic Press, Figure 15, p. 398, with permission.*

dry, gritty areas with dystrophic mineralization (i.e., calcium salt deposition in degenerating tissue) (Figure 1.15). The lesions may be focal, multifocal, or diffuse. If the lesions are of ischemic origin or produced by an energy-work mismatch (i.e., insufficient energy production for the work demand which often occurs with ischemia or energy production dysfunction), the most frequent sites of focal lesions are the left ventricular papillary muscles and the subendocardial myocardium. These lesions may be overlooked at necropsy unless multiple incisions are made in the ventricular myocardium. Sampling of the left ventricular papillary muscles should be included in any thorough microscopic assessment of the heart. In diseases with diffuse necrosis, such as so-called “white muscle disease” of calves and lambs with selenium–vitamin E deficiency, the pale lesions may be readily observed on the epicardial and endocardial surfaces.

Microscopically, myofibers in areas of recent injury often appear swollen and hypereosinophilic (termed “hyaline degeneration”) (Figure 1.16). Striations are indistinct, and nuclei are pyknotic. Necrotic fibers often have scattered basophilic granules that represent mitochondrial accumulation of calcium salts as confirmed by electron microscopy. Another pattern of necrosis may also be observed when affected myocytes have a “shredded” appearance from

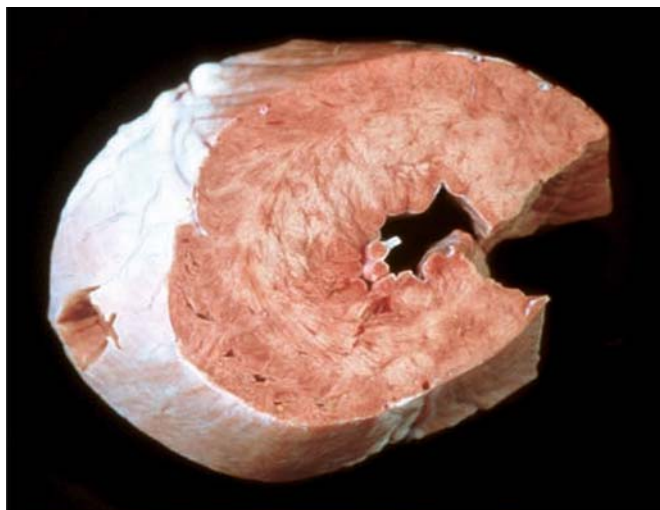


**FIGURE 1.15** Myocardial necrosis (white-mottled areas) in a cross-section of the left ventricle of a calf associated with acute monensin toxicosis. *Reproduced from Haschek WM, Rousseaux CG, and Wallig MA, editors: Fundamentals of toxicologic pathology, ed 3, 2013, Academic Press, Figure 12.10A, p. 1598, with permission.*

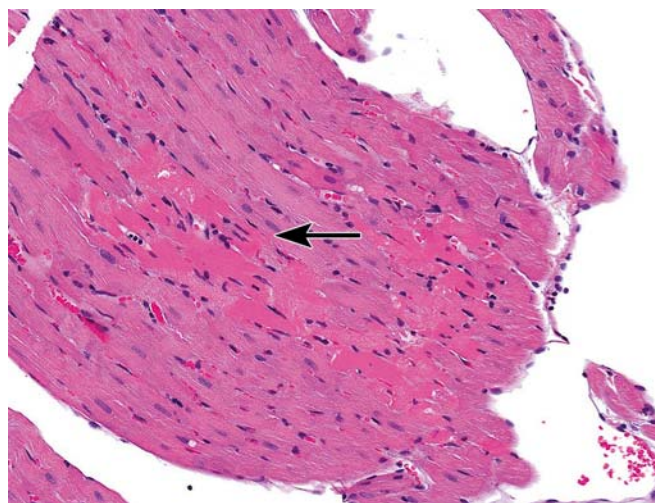


**FIGURE 1.16** Section of myocardium from a rat given a high dose of isoproterenol (an epinephrine analog) 4 h previously. Discrete hypereosinophilia (arrow) involving a subset of cardiomyocytes in the section center represents an early stage of cardiomyocyte necrosis. Formalin-fixed, paraffin-embedded section, H&E stain. Original magnification 20 $\times$ . *Reproduced from Haschek WM, Rousseaux CG, and Wallig MA, editors: Haschek and Rousseaux's handbook of toxicologic pathology, ed 3, 2013, Academic Press, Figure 46.13, p. 1598, with permission.*

hypercontraction and formation of multiple transversely oriented bars of disrupted contractile material (i.e., contraction band necrosis) (Figure 1.13). A third set of features is seen in necrotic myocytes in large areas of ischemic necrosis (infarcts), where fibers undergo coagulation necrosis and thus are relaxed and lack hypercontracted contractile elements.

Areas of necrosis will have infiltration by leukocytes within 24–48 h after injury. These cells are mainly macrophages, with occasional neutrophils, that lyse the necrotic cells and phagocytize the debris (Figure 1.17). In early stages of resolving necrosis, it may be difficult to distinguish the lesions from those produced by some types of fulminant myocarditis with prominent inflammatory cell infiltration. Later lesions of resolving necrosis will have persistent stromal elements (interstitial fibroblasts and collagen deposition, prominent capillaries) and empty “tubes” of basal laminae from necrotic myocytes (Figure 1.18). The healing phase of necrosis is further characterized by proliferation of connective tissue cells (fibroblasts, capillary endothelial cells) and deposition of connective tissue fibers (collagen, elastic tissue) and matrix (e.g., acid mucopolysaccharides)



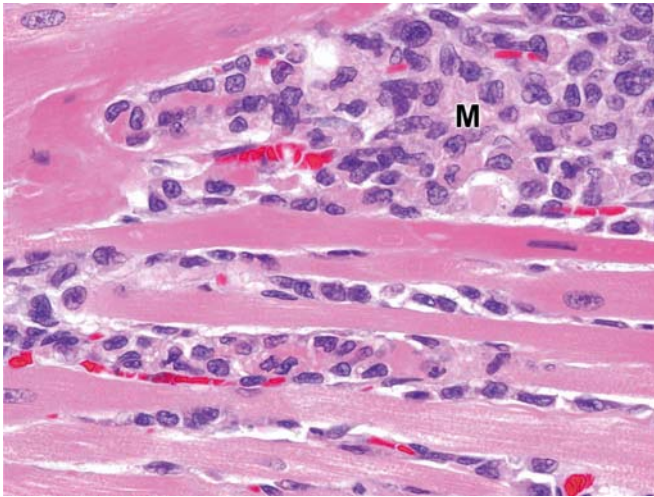


**FIGURE 1.17** Cardiomyocyte necrosis in a rat given a single subcutaneous dose of isoproterenol 24 h previously. Elongated aggregates of macrophages (M) have infiltrated the myocardium and are phagocytizing the fragmented remnants of cardiomyocytes (which appear as clumps of irregular eosinophilic material scattered among the macrophages). This stage of myocardial necrosis follows that illustrated in [Figure 1.16](#). Formalin-fixed, paraffin-embedded section, H&E stain. Original magnification 40 $\times$ . Reproduced from Haschek WM, Rousseaux CG, and Wallig MA, editors: *Haschek and Rousseaux's handbook of toxicologic pathology*, ed 3, 2013, Academic Press, Figure 46.14, p. 1599, with permission.

([Figure 1.19](#)). Grossly, these areas will appear as white scars.

The outcome of cases with myocardial necrosis will vary depending on the extent of the damage. Many animals will die acutely from cardiac contractile failure (leading to inadequate blood flow) if the extent of myocardial damage is extensive. Early deaths from necrosis-related arrhythmias may also occur. Some cases may eventually develop cardiac decompensation (i.e., gradual and often progressive inability to efficiently circulate blood) and die with cardiac dilatation and scarring and lesions typical of chronic congestive failure. Finally, with minimal damage, only microscopically detectable residual myocardial lesions may be found, and death eventually will occur from some other cause.

#### 4.5.5.2. AGENTS THAT PRODUCE MYOCARDIAL NECROSIS

Xenobiotics can cause myocardial injury by direct cellular effects, indirect effects (e.g., by stimulating hyperfunction or secondary to vascular injury), or both resulting in cardiomyocyte damage as well as changes in the myocardial

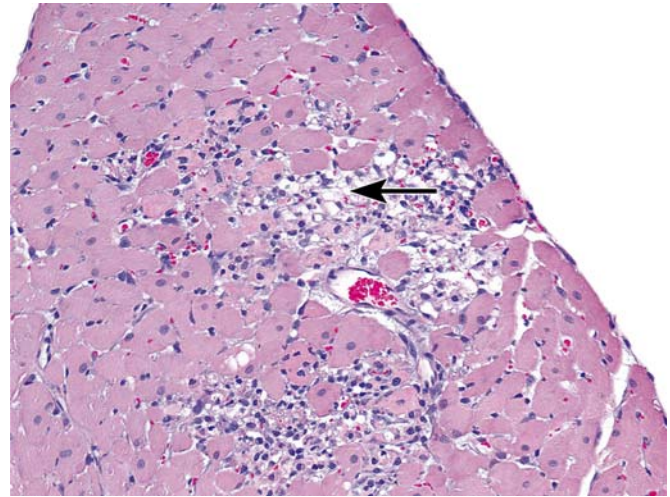


**FIGURE 1.18** Cardiomyocyte necrosis in a rat given a single subcutaneous dose of isoproterenol 48 h previously. Macrophages have removed fragmented cellular material, leaving empty "sarcolemmal tubes" (arrow). This stage of myocardial necrosis follows that illustrated in [Figure 1.17](#). Formalin-fixed, paraffin-embedded section, H&E stain. Original magnification 20 $\times$ . Reproduced from Haschek WM, Rousseaux CG, and Wallig MA, editors: *Haschek and Rousseaux's handbook of toxicologic pathology*, ed 3, 2013, Academic Press, Figure 46.15, p. 1599, with permission.

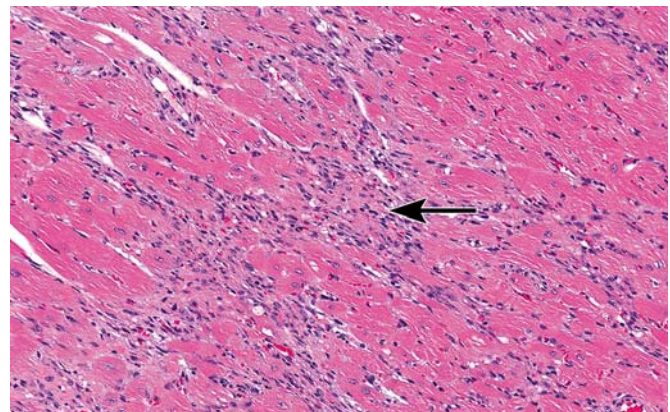


**FIGURE 1.19** Myocardial fibrosis. Substantial areas of cardiomyocyte necrosis are replaced by fibrosis (arrow) in a rat given a single subcutaneous dose of isoproterenol 2 weeks previously. Characteristic features of these scars include increased cell numbers (a mixture of fibroblasts and residual leukocytes, mainly lymphocytes and macrophages) and intersecting bands of pale eosinophilic fibrous connective tissue. These scars lack the conductive and contractile properties of normal myocardium, creating regional areas of altered ventricular wall electrical conduction and motion if the affected regions are large. Formalin-fixed, paraffin-embedded section, H&E stain. Original magnification 20 $\times$ . Reproduced from Haschek WM, Rousseaux CG, and Wallig MA, editors: *Haschek and Rousseaux's handbook of toxicologic pathology*, ed 3, 2013, Academic Press, Figure 46.16, p. 1599, with permission.



interstitium. This type of drug toxicity is dose-related and may present either as acute toxic injury or a more chronic drug-induced cardiomyopathy.

Acute toxic myocardial injuries may exhibit interstitial edema, multifocal areas of cardiac muscle cell necrosis with contraction bands, and/or an inflammatory cell infiltrate consisting of lymphocytes, plasma cells, macrophages, and sometimes polymorphonuclear leukocytes (usually neutrophils). Eosinophils may be present but seldom are prominent. The paucity of eosinophils and the presence of various stages of myofiber death and healing by fibrosis serve to differentiate direct toxic myocardial injury from hypersensitivity myocarditis (which features more eosinophils and little fibrosis). Microthrombi may be present with or without overt evidence of vascular injury. Selected chemicals known to produce myocardial injuries by direct or indirect toxic mechanisms are presented in [Table 1.2](#). It should be remembered that a cellular inflammatory reaction may be poorly developed or totally absent in toxic myocardial injuries that involve immunosuppressive agents.

#### **4.5.6. Myocardial Infarction Associated with Toxic Reactions**

Myocardial infarcts as circumscribed areas of coagulative necrosis are most commonly associated with coronary arterial occlusion in human patients who have unstable atherosclerotic plaques in their coronary arteries. However, myocardial infarction may occur in drug-induced coronary arterial injury (as from amphetamines), fibromuscular intimal proliferation (estrogen- and/or progesterone-containing oral contraceptives), embolization from infective endocarditis (associated with intravenous drug abuse), or in patients with normal coronary arteries following exposure to toxic levels of CO, nitrates, thyroid preparations, methylsergide or ergot derivatives, and certain antineoplastic agents. Large areas of necrosis, not related to obstruction of large extramural coronary arteries, have been produced in experimental animals by the administration of toxic doses of isoproterenol (a sympathomimetic  $\beta$ -adrenergic receptor agonist) though these lesions tend to be hemorrhagic and associated with coagulative and lytic necrosis. It was originally thought that this necrosis resulted from

isoproterenol-induced increases in cardiac rate, contractility, and oxidative metabolism beyond the limits of the oxygen supply system. More recently, however, it has become evident that isoproterenol also produces other highly complex effects, including a marked increase in  $\text{Ca}^{2+}$  uptake, stimulation of the adenylyl cyclase system, aggregation of platelets, and formation of free radicals capable of causing peroxidative damage. Isoproterenol-induced myocardial necrosis has been advocated as a model of human myocardial infarction, but this is probably not supported by differences in pathogenesis. Other sympathomimetic amines (norepinephrine, epinephrine) are capable of inducing lesions of myocardial necrosis, which are small, multifocal, and usually localized in the left ventricular subendocardium.

Catecholamine-induced cardiac lesions in experimental animals occur in conjunction with adrenal pheochromocytomas, tetanus, subarachnoid hemorrhage, and other CNS lesions. In these conditions, release of large amounts of catecholamines can lead to focal cardiac injury. Ischemic cardiac injury can be aggravated by high circulating levels of catecholamines in patients suffering acute myocardial infarction.

#### **4.5.7. Hypersensitivity Myocarditis**

Hypersensitivity myocarditis represents the most common form of drug-induced heart disease in human patients. The clinical criteria for the diagnosis of this disorder are (1) previous use of the drug without incident; (2) the hypersensitivity reaction bears no relationship to the magnitude of the dose of the drug; (3) the reaction is characterized by clinical signs consistent with classic allergy, serum sickness, or infectious disease; (4) immunologic confirmation; and (5) persistence of symptoms until the drug is discontinued. Hypersensitivity myocarditis associated with drug therapy is characterized by infiltration of the heart muscle with numerous eosinophils admixed with mononuclear cells, predominantly lymphocytes and plasma cells. The cellular infiltrate may be focal or diffuse and is associated with foci of myocytolysis. Fibrotic changes are absent in the myocardium, and all lesions are similar in age and appearance. Vascular involvement is frequent and consists of medial necrosis and inflammation affecting small arteries, arterioles, and venules. The inflammatory reaction

TABLE 1.2 Cardiotoxic Agents

Agents	Organ/system effects	Proposed mode of action
<b>SUBSTITUTED ALIPHATIC HYDROCARBONS</b>		
<b>A. Haloalkanes</b>		
1. Chloroform	Arrhythmias	Sensitizes heart to endogenous catecholamines
2. Cyclopropane and diethylether	Arrhythmias	Sensitizes heart to catecholamines
3. Freons (fluorocarbons)	Reduced cardiac output and coronary flow	Reflex increases in sympathetic and parasympathetic impulses to heart via respiratory mucosal irritation
4. Haloanesthetics (halothane, methoflurane, enflurane)	Negative chronotropic, inotropic and dromotropic effects; possible cardiac arrest	Myocardial depression
<b>B. Alcohols and aldehydes</b>		
1. Acetaldehyde	Negative inotropic effects	Release of catecholamines and resulting sympathetic effects
2. Ethanol	Decreased cardiac contraction; arrhythmias, ventricular fibrillation, sudden death	Depression of oxidative phosphorylation in heart mitochondria
<b>HEAVY METALS</b>		
1. Barium	Potent arrhythmogen, ventricular tachycardia	Induces diastolic depolarization
2. Cadmium	Diastolic heart failure	Impaired glucometabolic regulation
3. Cobalt	Dilated cardiomyopathy	Interrupts citric acid cycle; induces oxidative stress; inhibits ATP production
4. Lead	Arrhythmias; negative inotropy	Sensitization to norepinephrine; interference with $\text{Ca}^{2+}$ ; interference with ATP production
<b>GASES</b>		
1. Carbon disulfide	Angina pectoris, development of coronary heart disease	Inhibition of dopamine hydroxylase; disruption of thyroxine metabolism
2. Carbon monoxide	Tachycardia, arrhythmia, angina pectoris	Binds hemoglobin and interferes with myocardial energy metabolism
<b>DRUGS</b>		
<b>A. Cardioactive drugs</b>		
1. Antiarrhythmics		
a. Quinidine and procainamide	Ventricular fibrillation, cardiac arrest	Prolongation of QRS and QT intervals

(Continued)

**TABLE 1.2** Cardiotoxic Agents—cont'd

<b>Agents</b>	<b>Organ/system effects</b>	<b>Proposed mode of action</b>
b. Lidocaine	Sinus bradycardia, depressed inotropy	Blocks voltage-gated Na <sup>+</sup> channels
c. Phenytoin	Cardiac arrest	Suppression of automaticity
<b>2. Adrenergic agonists</b>		
a. Epinephrine and isoproterenol	Positive inotropy and chronotropy	Increased b-adrenergic sympathetic stimulation
<b>3. Adrenergic antagonists as well as reserpine and guanethidine</b>	Decreased inotropy	Decreased b-adrenergic sympathetic stimulation
<b>4. Glycosides of digitalis, strophanthin and oleandrin</b>	Increased inotropy, irritability, and arrhythmias	Inhibits sarcolemmal Na <sup>+</sup> pump with elevation of intracellular Ca <sup>2+</sup>
<b>5. Nicotine</b>	Arrhythmias	Suppresses K <sup>+</sup> conductance
<b>6. Minoxidil</b>	Vasodilation, hypotension	Inhibits K <sup>+</sup> channel
<b>7. Hydralazine</b>	Vasodilation, hypotension	Inhibits Ca <sup>2+</sup> release from sarcoplasmic reticulum
<b>8. Endothelin receptor antagonist</b>	Hypotension, coronary medial necrosis, reflex tachycardia	Antagonizes the vasoconstrictive activity of endothelin
<b>B. Ca<sup>2+</sup> antagonists</b>		
1. Bepridil	Negative chronotropy and inotropy	Decreased intracellular Ca <sup>2+</sup>
2. Papaverine	Negative chronotropy and inotropy	Decreased intracellular Ca <sup>2+</sup>
3. Verapamil, nifedipine	Negative chronotropy and inotropy	Decreased intracellular Ca <sup>2+</sup>
<b>C. CNS active drugs</b>		
1. Imipramine and amitriptyline	Enhance or decrease inotropy (dose-dependent), prolong action potential, arrhythmias	Inhibit catecholamine reuptake
2. Lithium	Ventricular arrhythmias	
3. Monoamine oxidase (MAO) inhibitors	Arrhythmias	Exaggerated sympathomimetic effects
4. Methyldopa	Eosinophilic myocardial inflammation	Hypersensitivity myocarditis
5. Methylsergide	Valvulopathy, endocardial fibrosis	Serotonin receptor (5HT <sub>2B</sub> ) receptor agonism
6. Neuroleptics (e.g., phenothiazines)	Tachycardia, hypotension	α <sub>1</sub> receptor blockade

(Continued)

**TABLE 1.2** Cardiotoxic Agents—cont'd

<b>Agents</b>	<b>Organ/system effects</b>	<b>Proposed mode of action</b>
7. Barbiturates (e.g., Thiopental)	Negative inotropy	Decreased availability of intracellular $\text{Ca}^{2+}$
<b>D. Antimicrobial agents</b>		
1. Anthracyclines (doxorubicin, daunorubicin)	Arrhythmias, dilated cardiomyopathy	Oxidative injury, mitochondrial dysfunction
2. Emetine	Sinus tachycardia, arrhythmias, myocardial necrosis	Conduction disturbances, effects on $\text{K}^+$ movements
3. Ionophores (monensin, lasalocid, narasin, salinomycin, maduramicin)	Myocardial necrosis	Increased intracellular $\text{Na}^+$
4. Penicillin and sulfonamide	Eosinophilic myocardial inflammation	Hypersensitivity myocarditis
<b>E. Growth promoting agents</b>		
1. Anabolic steroids (e.g., Clenbuterol)	Positive inotropy, chronotropy, myocardial hypertrophy	$\beta_2$ adrenergic agonism
<b>F. Cationic amphiphilic drugs</b>		
1. Chloroquine	Cardiomyocyte vacuolation and necrosis	Drug-induced phospholipidosis
<b>G. Appetite suppressants</b>		
1. Fenfluramine-phentermine	Valvulopathy	Serotonin receptor (5HT2B) agonism on valvular interstitial cells
<b>H. Cytokines</b>		
1. Interleukin-2	Myocardial edema, myocyte injury, hemorrhage	Endothelial injury, vascular leak syndrome
2. Interferon	Myocarditis, dilated cardiomyopathy, arrhythmia, microvascular thrombosis	Autoimmune-mediated inflammation, antiangiogenic properties
<b>I. Antiviral agents</b>		
1. Nucleoside reverse transcriptase inhibitors (NRTIs)	Cardiomyopathy	Inhibition of mitochondrial biogenesis
<b>J. Carcinogenic agents</b>		
1. 3-Butadiene and nitrosamines	Hemangiosarcomas in heart and other organs	Chemical mutagenesis
2. Radiofrequency radiation	Myocardial schwannoma	Presumed mutagenesis
<b>K. Teratogenic agents</b>		
1. Dextroamphetamine	Ventricular and atrial septal defects	
2. Ethanol	Ventricular septal defects	

(Continued)



**TABLE 1.2** Cardiotoxic Agents—cont'd

<b>Agents</b>	<b>Organ/system effects</b>	<b>Proposed mode of action</b>
3. Retinoic acid analogs	Transposition of great arteries	Excess retinoic acid signaling
<b>L. Cancer chemotherapeutics</b>		
1. Antimetabolite (5-fluorouracil)	Myocardial ischemia, cardiac arrest, vasospasm and thrombosis	Inhibits mitosis, mitochondrial dysfunction
2. Alkylating agents (cyclophosphamide)	Microvascular thrombosis, pericarditis	Endothelial injury, acrolein as toxic metabolite
3. Antimicrotubular agents (paclitaxel)	Heart block, arrhythmias, hypertension	Possible alterations in calcium handling or disruption of autonomic controls
4. Platinum-containing agents (cisplatin)	Hypertension, coronary artery disease, arrhythmia	Generation of reactive oxygen species
5. Proteasome inhibitors (bortezomib, carfilzomib)	Heart failure, hypertension, arrhythmias	Decreased protein degradation leading to cytotoxicity
6. Tyrosine kinase inhibitors	Heart failure, hypertension, arrhythmias	Targeted or untargeted inhibition of TKIs with implications for cardiomyocyte cell health
<b>NATURAL TOXINS</b>		
1. Batrachotoxin	Arrhythmias, ventricular fibrillation	Sodium channel activation
2. Cobra venom $\beta$ -cardiotoxin	Negative inotropy and lusitropy	Blocks $\beta 1$ and $\beta 2$ adrenergic receptors
3. Endotoxin	Negative inotropy, chronotropy	Depression of $\text{Ca}^{2+}$ ATPase activity; depression of $\text{Ca}^{2+}$ uptake
4. Grayanotoxins	Positive inotropy	Increased $\text{Na}^{+}$ permeability; opens voltage-gated $\text{Na}^{+}$ channels
5. Scorpion neurotoxins	Positive chronotropy, fibrillation	Slows closing of $\text{Na}^{+}$ channel and opening of $\text{K}^{+}$ channels
6. Tetrodotoxin and saxitoxin	Conduction defects, arrhythmia	Blocks fast $\text{Na}^{+}$ channels
7. Ciguatoxin	Bradycardia, AV block, heart failure	Makes sarcoplasmic membrane leaky to $\text{Ca}^{2+}$ ; inhibits mitochondrial $\text{Ca}^{2+}$ storage; increased $\text{Na}^{+}$ permeability
8. Gossypol	Myocardial necrosis/fibrosis; congestive heart failure	$\text{Na}^{+}/\text{K}^{+}$ ATPase inhibition
9. Moniliformin	Bradycardia, myocardial necrosis and sudden death in chicks and Turkey poults	Inhibits mitochondrial function
10. Fumonisin	Left-sided heart failure and pulmonary edema in swine	Altered sphingolipid biosynthesis

Reproduced with minor modifications from Haschek WM, Rousseaux CG, and Wallig MA, editors: Handbook of toxicologic pathology, ed 2, 2002, Academic Press, Table I, p. 374–378, with permission.

may also involve the pericardium but characteristically spares the cardiac valves. The absence of extensive myocardial necrosis or fibrosis distinguishes drug-related hypersensitivity myocarditis from other forms of myocarditis in which eosinophils are prominent. Endocardial fibrosis is not a feature of hypersensitivity myocarditis. Selected drugs associated with hypersensitivity myocarditis are listed in Table 1.3. Some of these drugs have also been associated with hypersensitivity vasculitis. The pathogenesis of drug-induced hypersensitivity myocarditis remains unclear. The condition appears to be immunologically mediated, perhaps as a reaction in which the drug or one of its metabolites acts as a hapten and combines with an endogenous macromolecule; it is this combination that is antigenic. Hypersensitivity myocarditis has also developed after injection of horse serum, tetanus toxoid, and smallpox vaccine.

#### 4.6. Endocardium

Morphologic endocardial alterations are infrequently associated with cardiotoxic agents, but endocardial fibrosis and atrial thrombosis have been described with xenobiotic treatment. Heart valves are not considered with “endocardium” in this discussion and instead are discussed separately below.

##### 4.6.1. Fibrosis

Endocardial mural fibrosis can occur in association with toxic or ischemic myocardial necrosis. Large regions of subendocardial necrosis, as might be seen with high doses of isoproterenol, may be replaced by fibrosis. Morphologically similar lesions may occur with coronary artery occlusions as is seen in human patients with myocardial infarctions. Mural endocardial thickening occurs in the late stages of allylamine cardiotoxicity and in radiation-induced myocardial fibrosis. Endocardial fibrosis may also be a sequela to altered laminar flow of blood in the cardiac chambers. These “jet” lesions are most commonly seen in atria with valvular dysfunction that allows spurts of regurgitating blood flow back into the atria when ventricles contract.

Atrial thrombosis that may result from endocardial/endothelial effects has been reported with a spectrum of chemicals tested by the

**TABLE 1.3** Drugs Associated With Hypersensitivity Myocarditis in Human Patients

Acetazolamide	Allopurinol <sup>a</sup>
Aminophylline	Amitriptyline
Ampicillin	
Carbamazepine <sup>a,b</sup>	Cephalothin
Chloramphenicol <sup>a</sup>	Chlorpropamide <sup>a</sup>
Chlorthalidone <sup>a</sup>	Colchicine <sup>a</sup>
Diclofenac	Digitalis/digoxin
Diphenylhydantoin <sup>a,b</sup>	
Furosemide <sup>a</sup>	
Hydrochlorothiazide	
Indomethacin	Isoniazid <sup>a,b</sup>
Lidocaine	
Methyldopa <sup>b</sup>	
Oxyphenbutazone <sup>a</sup>	
p-Aminosalicylic acid <sup>b</sup>	Penicillin <sup>a</sup>
Phenindione	Phenylbutazone <sup>a,b</sup>
Phenytoin	Procainamide <sup>a,b</sup>
Pyribenzamine	
Quinidine <sup>a</sup>	
Reserpine <sup>b</sup>	
Spironolactone <sup>a</sup>	Streptomycin
Sulfonamides <sup>c</sup>	Sulfadiazine
Sulfamethoxazole	Sulfisoxazole
Sulfonylureas	
Tetracycline <sup>a</sup>	Theophylline
Triamterine	Trimethoprim

<sup>a</sup> Also associated with hypersensitivity non-necrotizing vasculitis.

<sup>b</sup> Also associated with lupus-like syndrome.

<sup>c</sup> Sulfonamides have been associated with toxic necrotizing vasculitis.

Modified from Haschek WM, Rousseaux CG, Wallig MA, editors: *Handbook of toxicologic pathology*, ed 3, 2013, Academic Press, Table IV, p. XXX, with permission.

National Toxicology Program (NTP) of the U.S. National Institute of Environmental Sciences (Yoshizawa et al., 2005). Putative mechanisms for this change include endothelial damage,

altered hemodynamics, aberrant platelet function, and changes in clotting factors.

#### 4.7. Neoplasia

Chemically induced cardiac neoplasms are infrequent but have been described in rats, mice, and hamsters. The agents include carbamates (1,1-diphenyl-2-butynyl-*N*-cyclohexyl carbamate), fluorenylacetamide, urethane, ethylnitrosourea (ENU), methylnitrosourea (MNU), dimethylnitrosamine (DMN), methylnitrosamine, ethyl methanesulfonate (EMS), ethylnitrosobiuret, hydrazine, triazene, diethylnitrosamine (DEN), and 1,3-butadiene. Most of the induced neoplasms are of endocardial origin and mesenchymal in derivation (e.g., schwannomas), but a few arise from the vasculature of the myocardium or pericardium (e.g., hemangiosarcoma) (Figure 1.20).

Cardiac schwannomas are a rare incidental finding in 2-year carcinogenicity studies in rats. An increased incidence of subendocardial and myocardial schwannomas has been reported in rats exposed to radiofrequency radiation at a “dose” designed to approximate the exposure that comes from cell phone use (Falcioni et al., 2018).

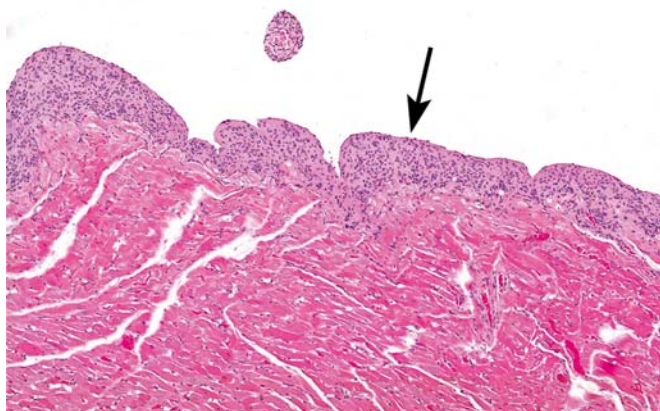


**FIGURE 1.20** Endocardial schwannoma (arrow) in a female F344 rat given methylene blue trihydrate in a 2-year bioassay. The tumor appears as a hypercellular, undulating, pale basophilic zone overlying the eosinophilic myocardium. Formalin-fixed, paraffin-embedded section, H&E stain. Reproduced from Haschek WM, Rousseaux CG, and Wallig MA, editors: *Haschek and Rousseaux's handbook of toxicologic pathology*, ed 3, 2013, Academic Press, Figure 46.17, p. 1609, with permission.

#### 4.8. Valves

Drug-induced heart-valve injury has hampered the development of a few classes of drugs and continues to do so. Valve injury can involve any or all of the cellular elements of the valve leaflets or cusps, and may be proliferative, degenerative, and/or inflammatory. Valve injuries that alter normal valve structure or compliance can lead to a disruption in unidirectional blood flow, creating workload challenges for the heart (e.g., increased preload) and consequential changes in the myocardium like hypertrophy and decreased contractility.

##### 4.8.1. Proliferative Valvulopathies

Valvulopathies are structural changes that distort the shape and function of valve leaflets. Valve lesions may be induced by several causes including age-related degeneration, outflow obstructions (e.g., aortic stenosis), and exposure to some toxic agents. The best-known drug-induced valvulopathy is that which occurs in human patients taking the anorexigenic diet drug combination fenfluramine–phentermine (Connolly et al., 1997). A subset of patients taking this agent for varying periods of time presented with clinical signs of heart failure and/or murmurs. Echocardiography revealed morphologically distorted and dysfunctional AV valves. Microscopic evaluation of a few explanted valves demonstrated valve thickening with stromal proliferation and increased myxomatous matrix. This product was subsequently removed from the market.

Similar valve lesions have been described in patients with naturally occurring carcinoid tumors or who have received ergot alkaloid-derived drugs for migraines or Parkinson's disease (e.g., methylsergide, pergolide). Carcinoid tumors (malignant tumors of the intestinal tract) can produce and secrete high concentrations of serotonin. Similarly, ergot alkaloids and the fenfluramine metabolite norfenfluramine have been demonstrated to be agonists of the 5HT<sub>2B</sub> serotonin receptor, which is expressed on and demonstrated to be mitogenic for valve stromal cells. Accordingly, 5HT<sub>2B</sub> agonism has been implicated as the cause of these natural or xenobiotic-induced valve injuries. However, animal modeling of this effect has been challenging and has met with mixed success, making

it very difficult to discharge this risk in the nonclinical safety assessment setting.

#### **4.8.2. Degenerative/Inflammatory Valvulopathies**

More recently, a more destructive valvulopathy has been described in rats given activin receptor-like kinase 5 (ALK5) inhibitors. ALK5 receptors are type I transforming growth factor beta (TGF- $\beta$ ) receptors targeted for a number of therapeutic indications like cancer, chronic inflammatory disease, and progressive renal disease. Treatment with an ALK5 inhibitor has been shown to quickly induce hemorrhage, inflammation, and stromal cell proliferation in multiple heart valves of rats (Anderton et al., 2011). Similar lesions have been seen but not published by others developing drugs with a similar target. The lesions described with ALK5 inhibitors are distinguished from those described with 5HT2B agonists by their consistent and rapid development in animal models and their more inflammatory and destructive character.

### **4.9. Epicardium**

Epicardial lesions induced by toxic agents are infrequent. Examples include drug-induced epicardial hemorrhage and pericarditis.

#### **4.9.1. Epicardial Hemorrhage**

Minoxidil is a vasodilating antihypertensive drug that is used in human patients with refractory hypertension. In animal safety testing, minoxidil induces hemorrhagic right atrial lesions in dogs given doses as low as 1 mg/kg (Herman et al., 1989). This agent can also produce left ventricular papillary muscle necrosis and superficial endocardial and epicardial hemorrhages in various regions of the heart. The hemorrhagic atrial lesions are associated with fibrinoid necrosis of arterioles, focal myocyte damage, and epicardial inflammation, and they progress eventually to fibrosis. In dogs, protection against minoxidil-induced cardiac lesions is provided by pretreatment for several days with furosemide (a diuretic), but not with propranolol (a  $\beta$ -blocker) or hydrochlorothiazide (another diuretic). The mechanism of this protection is unknown.

In miniature swine, administration of minoxidil (10 mg/kg/day for 2 days) produces tachycardia and hypotension (Herman et al., 1989).

At necropsy 24 h after minoxidil treatment, the cardiac lesions in pigs include diffuse left atrial epicardial hemorrhage and focal myocardial necrosis in the left ventricular papillary muscles.

Other vasodilating antihypertensive drugs, such as hydralazine, diazoxide, and SK&F 24260, produce epicardial and papillary muscle lesions localized to the left ventricle in rats and dogs similar to those produced by minoxidil. However, these agents are not known to produce atrial hemorrhage such as those induced by minoxidil and theobromine. The left ventricular papillary muscle necrosis is thought to result from a decrease in vascular perfusion.

### **4.10. Pericardium**

Pericarditis with or without pericardial effusion has been reported to occur in patients with drug-induced systemic lupus erythematosus. In the majority of these patients, the pericarditis is only one of the many manifestations of the lupus-like syndrome. In many of the reports, the evidence linking drug usage to the lupus-like syndrome is highly circumstantial. The syndromes have been most clearly documented in the case of hydralazine and procainamide.

Drugs that cause toxic myocarditis, hypersensitivity myocarditis, or large areas of myocardial necrosis often also cause pericarditis by extension of the inflammation to the pericardium, particularly the visceral pericardium (i.e., the epicardium). Pericardial hemorrhage can occur as a result of cyclophosphamide toxicity and of therapy with anticoagulants, and also in some patients with uremia who are given heparin during the course of hemodialysis.

## **5. MECHANISMS OF TOXICITY**

Cardiotoxic reactions are potentially life-threatening; for this reason, their detection in nonclinical safety studies of drug candidates or in premarketing hazard assessments of other chemicals is of great importance. The detectability of cardiotoxic reactions in these studies depends greatly on the mechanism of action by which the chemical acts on the heart. Effects that result in acute changes in function or direct cellular injury are readily modeled in laboratory animals. In contrast, effects that are more chronically



progressive, alter a cell or organ's ability to respond to another insult, or exacerbate a preexisting disease process may or may not develop in animals under the experimental conditions of conventional safety studies. Such chronic sequelae, and particularly those reactions that require predisposing factors for their occurrence, are often detected only in clinical trials or with extensive postmarketing use of the product. Nevertheless, many of these reactions can be reproduced in laboratory animals with suitable experimental designs and husbandry conditions, so the identification of appropriate animal models is important in the development of new drugs to ensure their safety. Table 1.2 summarizes known cardiotoxic agents and their effects.

### 5.1. Mechanisms of Altered Cardiac Function

The intrinsic properties of myocardial tissue, such as automaticity, excitability, and conductivity, endow the heart with a variety of chemically and biologically sensitive pathophysiological targets. Disruptions in normal cardiac function can arise from alterations in membrane function, energy production, contractility, vascular tone, or autonomic influences.

#### 5.1.1. Changes in Rate and Rhythm

Changes in heart rate induced by xenobiotics are generally secondary to some shift in autonomic signaling to the pacemaker centers (i.e., ganglia) in the heart (particularly the SA node). That change in signaling can be direct or indirect. Direct effects may result from xenobiotic influences on brain centers that control the activity of the autonomic nervous system peripherally or on receptor activity (e.g.,  $\beta$ -adrenergic receptors) in the heart. Indirect effects result from drug effects that occur outside the heart. For example, drugs that cause vasodilation and decrease blood pressure often have the indirect effect of increasing heart rate as normal cardiovascular compensatory mechanisms are initiated. Increased catecholamine release by the adrenal medulla also increases the heart rate.

Arrhythmias are among the most serious immediate functional cardiac abnormalities. Anomalous action potential formation and/or conduction are primary causes of arrhythmias. Substances can directly influence the initiation or propagation of

the cardiac action potential by altering the ionic gradients and fluxes that are involved in these processes. Ions such as barium and strontium carry current through the slow channels in place of  $\text{Ca}^{2+}$  ions (Shen and Vassalle, 1996). This action initially leads to cardiac stimulation, but subsequently these two ions cause serious arrhythmias followed by cardiac arrest. These latter adverse effects are thought to be due to impaired efflux of  $\text{K}^+$  ions from myocardial cells.

The two types of electrical activity (fast and slow responses) that have been characterized in cardiac tissue have a major role in precipitating arrhythmias. Fast-response myocytes are located in the working atria and ventricles, and in most portions of the electrical conducting system except the SA and AV nodes. Exposure to certain agents or ischemic conditions can reduce the resting membrane potential of the cardiac myocyte. The reduction in membrane potential causes a decrease in the speed of impulse conduction and enhances the chance for a block in conduction of electrical activity. The fast-response myofibers possess a second slow inward current carried by  $\text{Ca}^{2+}$  ions that develops only when the fast  $\text{Na}^+$  depolarizing current has decreased the membrane potential. Sustained partial depolarization of the membrane to about 60 mV by abnormal conditions, such as increased extracellular  $\text{K}^+$  concentration or hypoxia, inactivate the fast  $\text{Na}^+$  channel while leaving the slow  $\text{Ca}^{2+}$  component functional. The initiation and conduction of the slow-response action potential in myofibers that are partially depolarized by damage or hypoxia may provoke abnormalities of cardiac rhythm.

Probably the most studied drug-induced arrhythmia in the past 20 years is that related to drugs that block the cardiomyocyte repolarizing hERG  $\text{K}^+$  channel. Congenital mutations in the *hERG* gene that result in dysfunction of this  $\text{K}^+$  channel cause prolongation of the repolarization phase of the action potential and prolongation of the QT interval on the ECG (long QT syndrome). Patients with this electrophysiologic abnormality are recognized to be predisposed to a fatal form of ventricular arrhythmia called TdP; QT prolongation is a surrogate measure of TdP risk. The recognition that a number of commonly used drugs like terfenadine can induce an acquired form of long QT syndrome with putative risk for fatal

arrhythmia has instigated the inclusion of nonclinical and clinical assays to characterize this risk potential. Currently, a battery of in vitro and in vivo nonclinical and clinical assessments is required for drugs intended for human clinical use (Anonymous, 2005). Since not all QT prolongation induces an inherent risk of TdP and because QT prolongation itself is not injurious to the heart, there is considerable controversy regarding the validity of this surrogate measure and its contribution to drug attrition pre- and postmarketing. More recent efforts have focused on developing an integrated and multiion channel assessment to characterize the true risk of clinical arrhythmia (Vicente et al., 2018).

### 5.1.2. Contractility

Contractile work by the myocardium requires the concerted integration of both structural and biochemical components of the myocardium. Cardiac contractility is most quickly influenced by changes in autonomic adrenergic stimulation, which may be an intended pharmacologic activity of some cardiac-directed drugs but may also occur as an “off-target” effect. Changes in autonomic adrenergic stimulation affect contractile force largely by influencing  $\text{Ca}^{2+}$  flux into and out of the cardiomyocyte. Likewise, xenobiotic inhibition of energy pathways that affect ATP production (e.g., mitochondrial injury, changes in substrate utilization) can also alter  $\text{Ca}^{2+}$  fluxes and change contractility. More chronically, loss of cardiomyocytes through apoptosis or necrosis—with or without replacement by less contractile interstitial fibrosis—will affect contractile function either regionally or for the organ as a whole.

## 5.2. Mechanisms of Direct Cellular Injury

Direct cardiotoxic effects can be the result of selective or random interactions of a xenobiotic with molecules of vital importance in cardiomyocytes. These interactions may be facilitated by metabolic pathways, drug transporters, or physiologic functions unique to the beating heart.

The high energy requirement of the heart predisposes the myocardium to the adverse effects of metabolic poisons. Toxic reactions may involve suppression of an enzyme system. Cyanide, a rapidly fatal poison, binds and inhibits the enzyme cytochrome C oxidase in

the mitochondrial electron transport chain, which essentially shuts down oxidative phosphorylation and aerobic ATP production (Hall et al., 2015). Accordingly, all tissues are susceptible to the deleterious effects of cyanide, but the heart is most particularly susceptible given its constant need for energy.

Adverse myocardial effects may be elicited when a molecule or one of its active metabolites interacts with structural macromolecules in the myocyte. Since myocardial enzymes that metabolize endogenous substances may also use xenobiotics as substrates, biotransformation can occur in the heart. The role of metabolically derived, chemically reactive substances in the initiation of certain myocardial toxicities has been described. For the industrial chemical allylamine, rats develop localized to multifocal myocardial degeneration and necrosis following acute exposure, whereas prolonged dosing leads to more regional myocardial injury with a predilection for the subendocardial region and vascular injury (Boor, 1983). An amine oxidase enzyme found in the heart and blood vessels converts allylamine to acrolein, a highly reactive metabolite that binds macromolecules; this metabolite is responsible for the observed myocardial injuries, possibly by cross-linking DNA strands and inhibiting certain enzymes. Acrolein is conjugated by glutathione and is excreted as a mercapturic acid conjugate. It is likely that the extent of injury, a balance between the extent of acrolein formation, and the availability of glutathione at the site of biotransformation.

The role of reactive chemical species in myocardial toxicity is of considerable consequence in other ways. Two factors of significance regarding the development of reactive metabolite-induced injury include the rate of formation for the reactive products and the availability of protective cellular responses and substrates in sufficient quantity. Some agents can stimulate the formation of reactive oxygen species in the heart and induce oxidative myocyte injury. For example, anthracycline antineoplastic agents such as doxorubicin produce a distinctive type of chronic congestive cardiomyopathy in humans and experimental animals. Two major morphological lesions are found in the myocyte: dilation of the sarcoplasmic reticulum and loss of myofibrils. The pathogenesis of these lesions is believed to be, in part, linked

to the generation of toxic oxygen free radicals (Combs and Acosta, 1990; Ferreira et al., 2008). A key factor in this concept is the finding that doxorubicin can form a complex with iron that is capable of mediating the production of reactive oxygen radicals. This complex can bind to cell membranes and, by reacting with endogenous thiols, is capable of oxidative destruction of structural macromolecules such as those found in the cell membrane. The unique sensitivity of the heart to the cardiotoxic effects of doxorubicin may be secondary to the low cellular concentrations of protective enzymes (e.g., catalase) or the inhibition of antioxidant enzymes (e.g., glutathione peroxidase) that can prevent accumulation of damaging reactive oxygen radicals.

Another mechanism of direct cardiotoxicity is related to small molecule or biologic (e.g., monoclonal antibody) therapeutics that may target mediators of normal cardiomyocyte physiology. TK enzymes modulate a variety of signaling pathways concerned with important cellular functions such as metabolism, cell cycle progression, proliferation, differentiation, and survival. In nonproliferating cells like cardiac myocytes, TK activity is tightly controlled, and it is present only at low levels in normal cells. However, increased TK expression can facilitate the transformation to neoplasia in certain tissues. Tyrosine kinase inhibitors (TKIs) are a relatively new category of small molecule drugs that act intracellularly to interfere with specific pathways influenced by upregulated kinase enzymes. TKI agents target the ATP-binding pocket and thus prevent ATP from binding to the upregulated kinase enzyme. It is this action that attenuates kinase signaling activity in tumor cells. To a certain extent, the selectivity of TKIs is limited because the configuration of the ATP-binding pocket is conserved across most human kinases. Thus, although treatment with TKIs is intended to target overexpressed kinases in certain types of tumor cells, these agents have also been found to exert inhibitory actions against off-target kinases in normal tissues. The experimental and clinical reports of cardiotoxicity following treatment with TKIs indicate that some of these off-target kinases also serve important functions in the heart.

Clinically significant congestive heart failure has been noted in patients treated with the TKI imatinib. Electron microscopic evaluation of

cardiac biopsies from imatinib-treated patients revealed myocyte membrane whorls, pleomorphic mitochondria with effaced cristae, scattered cytoplasmic lipid droplets and vacuoles, and glycogen accumulation (Kerkelä et al., 2006). Similar myocyte alterations have been found in the hearts of mice treated with imatinib. Furthermore, in mice imatinib induces a decrease in the mitochondrial membrane potential, an effect that can lead to changes in mitochondrial structure (cytosolic vacuolization) and, ultimately, cell death. Imatinib produces changes in rat myocardial morphology and viability as indicated by observed increases in the numbers of myocytes undergoing necrosis, apoptosis, and autophagy (Herman et al., 2011). Exposure to imatinib also causes alterations in isolated cardiomyocyte cells, characterized by activation of the SR stress response, loss of myofibrils, disrupted and disorganized alpha-actinin, alterations in mitochondrial structure, increased myocyte apoptosis, and increased release of lactic dehydrogenase (Hasinoff and Patel, 2010). The pathogenesis of imatinib-induced myocardial toxicity is thought to be due in part to inhibition of the BCR-ABL signaling pathway and the resulting induction of the endoplasmic reticulum stress response. A similar pathogenic mechanism would also be applicable to other TKIs, such as dasatinib and nilotinib, which exert analogous cardiotoxic activity.

Sunitinib is a multikinase inhibitor that suppresses TK-mediated tumor cell proliferation and angiogenesis activity. This agent inhibits a variety of growth factor and cytokine receptors whose targets include VEGFRs, PDGFRs, and c-KIT. Sunitinib can interact with more than 50 kinases because it binds relatively nonselectively to the ATP-binding pocket associated with the catalytic site. It is this domain that is highly conserved across receptors. While the nonspecific inhibitory activity elicited by sunitinib may be an advantage for controlling neoplastic cell growth, this action represents a potential liability for the cardiomyocyte. As a result, sunitinib-induced suppression of multiple growth factor pathways can compromise cardiomyocyte cell viability and lead to myocardial toxicity. Clinically, sunitinib has been associated with congestive heart failure, left ventricular dysfunction, and hypertension. Electron micrographs of endomyocardial biopsies obtained from sunitinib-

treated patients that developed cardiovascular symptoms show cardiomyocyte hypertrophy, swollen mitochondria with effaced cristae, and membrane whorls. Examination of myocardial tissue from mice treated with sunitinib reveals similar changes in myocardial morphology (myocyte hypertrophy and mitochondria that were distended and atypically shaped) (Mellor et al., 2011). If hypertension is induced by infusion of phenylephrine, treatment with sunitinib results in a significant increase in myocyte apoptosis. Rat neonatal cardiomyocytes exposed in vitro to high concentrations of sunitinib exhibit release of mitochondrial cytochrome-c, activation of caspase-9, a decrease in mitochondrial membrane potential, and a significant decline in intracellular ATP (Cheng et al., 2011). Alterations have also been noted when human stem cell-derived cardiomyocytes are exposed in vitro to sunitinib (Cohen et al., 2011). In these cells, the major changes include a loss of cellular ATP, an increase in oxidized glutathione, and induction of apoptosis. The cardiotoxic activity exerted by sunitinib has also been observed in a new zebrafish model, where exposure to this TKI leads to cardiomyocyte apoptosis, decreases in total numbers of cardiomyocytes, contractile dysfunction, and ventricular dilatation (Cheng et al., 2011). The pathogenesis of sunitinib-induced cardiotoxicity appears to be complex. Sunitinib causes suppression of AMP-activated protein kinase signaling (an action which affects mitochondrial activity) and PDGFR inhibition (an effect that diminishes myocardial protection against stress-related injury). The inhibitory effects of sunitinib on VEGF may cause decreases in myocardial capillary density and hypoxic signal induction in the myocardium. Sunitinib also influences ribosomal S6 kinase (RSK) activity. Inhibition of RSK activates the pro-apoptotic factor BCL2, an effect that facilitates the release of cytochrome C from mitochondria in injured cells and increases myocyte apoptosis. Sorafenib is a TKI with a molecular target profile that is analogous to sunitinib. This agent exerts a similar spectrum of cardiotoxic effects.

Direct cardiomyocyte toxicants may primarily target specific subcellular organelles leading to whole cell dysfunction and even cell death. The heart easily compensates for individual cell dysfunction and death, but large-scale

cardiomyocyte loss will lead to clinically detectable whole-organ dysfunction and possibly death of the patient. Many subcellular organelles of cardiac myocytes are subject to damage by toxic agents, as noted here.

1. Mitochondria—xenobiotics may interfere with mitochondrial enzymes (e.g., cyanide, thyroid hormone); uncouple oxidative phosphorylation (e.g., dinitrophenol, cobalt, lead, mercury); bind to mitochondrial DNA (e.g., acriflavin); produce mitochondrial mineralization (e.g., dihydrotachysterol, sodium phosphate); or produce selective mitochondrial damage by undetermined mechanisms (e.g., monensin, *Cassia occidentalis*, bis(2-chloroethoxy)methane).
2. Sarcoplasmic reticulum—toxic agents may cause selective dilatation of SR elements (e.g., anthracyclines) and other SR alterations (e.g., guanidine, volvatoxin A) or alter the contractile apparatus by inducing myofibrosis (e.g., sympathomimetic amines, plasmocid, diuretics, or other conditions leading to potassium deficiency, FZ in birds, halothane, corticosteroids).
3. Sarcolemma—agents can selectively affect the sarcolemma (e.g., tetrodotoxin, verapamil, cardiac glycosides).
4. Nucleus/nucleolus—toxicants may selectively damage the nucleic acids and/or proteins engaged in DNA maintenance and replication (e.g., acrolein, anthracyclines).
5. Lysosomes/residual bodies—xenobiotics may cause drug-induced phospholipidosis associated with damage to organellar membranes (e.g., chloroquine).

Organellar injuries may give some insight into the molecular mechanisms of toxicity. Many of the changes in the contractile apparatus, nucleus, or membrane system (plasma membrane, T-tubules, and SR) are associated with complex alterations in the concentrations of  $\text{Ca}^{2+}$ ,  $\text{Mg}^{2+}$ ,  $\text{Na}^+$ , and  $\text{K}^+$ , as well as with changes in the intracellular compartmentalization of these ions. In addition, these changes in combination with shifts in intracellular pH can be associated with activation and intracellular release of lysosomal hydrolytic enzymes, including cathepsin D and other proteases, and phospholipases. This cascade of changes, coupled with alterations in the permeability of plasma membranes,



acts as a determinant of whether or not cellular injury progresses to the point of irreversibility—that is, cellular necrosis.

### 5.3. Mechanisms of Indirect Injury

Some cardiac injuries associated with xenobiotic exposure may occur secondary to effects outside the heart itself and result from changes in the metabolic milieu of circulating plasma or changes in cardiac workload. For example, drug-induced kidney injury may result in altered cardiac function and myocellular injury. Systemic electrolyte imbalances often accompany kidney dysfunction and can lead to arrhythmias. Uremia resulting from severe kidney dysfunction can cause direct cardiomyocyte injury (necrosis and mineralization) or vascular endothelial injury that leads to cardiac ischemia (e.g., secondary to thrombosis).

Drugs that alter vascular tone (i.e., constriction or dilation) change cardiac workloads and may alter blood perfusion of the cardiac muscle. For example, drugs like the  $K^+$  channel inhibitor minoxidil are potent vasodilators, which leads to a drop in blood pressure and initiation of compensatory increases in heart rate and plasma volume secondary to renal fluid retention. Ultimately, the heart sees an increase in work (increased heart rate), an increase in the volume of blood that is pumped (plasma volume expansion), and possibly a decrease in coronary perfusion (decreased systemic vascular resistance). The results may be an increase in cardiac mass and ischemic cardiomyocellular injury.

Drugs like the mixed  $\beta$ -adrenergic agonist isoproterenol have direct effects on the heart as well as effects on the peripheral vascular system that can synergize to cause cardiac injury at toxic doses. Isoproterenol causes an increase in both the rate (chronotropy) and force of cardiac contraction (inotropy), resulting in increased cardiac work. It also causes peripheral vasodilation that decreases coronary perfusion pressures. High doses of isoproterenol classically produce acute, multifocal to regionally extensive myocardial necrosis in animal models (Figures 1.16 and 1.17).

Weight loss herbals containing natural forms of ephedra (*Ma Huang*) and caffeine have been associated with adverse clinical events that ultimately led to their market withdrawal in 2004. Ephedra is a potent sympathomimetic amine

with activity on both  $\alpha$ - and  $\beta$ -adrenergic receptors. Caffeine is a centrally acting stimulant that increases endogenous catecholamine release and causes vasoconstriction. Modeling of these effects with ephedrine/caffeine combinations in laboratory rodents reveals rapid increases in heart rate and blood pressure with secondary myocardial hemorrhage and necrosis (Dunnick et al., 2007). The observation that 14-week-old rats are more sensitive to the effects of this combination than 7-week-old rats is consistent with similar observations for the hyperpharmacologic effects of isoproterenol.

### 5.4. Cardiotoxicity of Cardiac Drugs

Adverse cardiac reactions are common with cardiovascular drugs like digitalis glycosides, antiarrhythmics, and antihypertensives. These reactions are the result of exaggerated pharmacological effects following an overdose or occurring because of an unusual sensitivity in the patient brought about by young or advanced age, comorbidities, or drug interactions. The heart can also be a target of unintended pharmacologic side effects when the drug acts on an organ other than the desired one. Examples of cardiac effects of drugs that act on the CNS are neuroleptic and antidepressant-induced arrhythmias.

If the desired pharmacological effect occurs in a laboratory animal species, it is likely that the exaggerated or “hyper-pharmacologic” effect can also be elicited. Effects of this nature are dose-related and may appear only at doses that are nearly lethal in laboratory animals. However, they may occur at therapeutic doses in humans since several conditions may predispose to their development. Of particular significance are those conditions that are frequently encountered in the greatest users of drugs: the elderly. Altered physiological functions that may potentiate the adverse effects of cardioactive drugs are decreased glomerular filtration rate or preexisting heart disease. For example, the toxicity of digoxin is increased with a reduction in the glomerular filtration rate, and  $\beta$ -adrenergic blocking agents cause potentially fatal effects in patients with congestive heart failure. Life-threatening cardiovascular effects may develop following a therapeutic dose of  $\beta$ -blockers in patients whose cardiac function depends upon the maintenance of sympathetic drive.

Arrhythmias and QT-interval prolongation occur in patients receiving overdoses or even therapeutic doses of tricyclic antidepressants or neuroleptics. However, several conditions sensitize to these effects. Sudden cardiac deaths associated with ventricular fibrillation may develop in patients who have preexisting heart disease and are taking therapeutic doses of these drugs. Thioridazine is one of the most cardiotoxic phenothiazine neuroleptic drugs. One of its metabolites, a ring sulfoxide, appears to be responsible for cardiotoxicity. Patients at risk are those who rapidly metabolize thioridazine to this cardiotoxic metabolite. Neuroleptic-induced electrocardiographic changes may be enhanced by glucose loading, which increases the intracellular to extracellular ratio of  $K^+$  in response to an increase in insulin.

### 5.5. Hypersensitivity Reactions

The heart is also a target of immune-mediated effects of xenobiotics. Allergic skin reactions are occasionally accompanied by subtle electrocardiographic changes and, in rare instances, by hypersensitivity myocarditis. Diagnostic testing for suspected allergens in humans carries some risk of cardiac reaction. In systemic anaphylaxis, mediators such as histamine and leukotrienes cause constriction of coronary arteries and decrease the force of contraction of the heart muscle. Thus, a primary cardiac event occurs and can include arrhythmia or even heart failure.

In addition to anaphylaxis, cytotoxic immune complex-elicited injuries can affect the heart. Methylidopa-induced myocarditis fits into this category. Numerous drugs can cause immune complex-mediated reactions in the coronary vessels (e.g., sulfonamides, penicillin, procainamide, quinidine), and autoimmune mechanisms have been implicated with some of these drugs. Development of the reactions in humans has been associated in some instances with a specific gene haplotype (a set of alleles) of the major histocompatibility complex (MHC). The great polymorphism of the gene product is responsible for variability in the sensitivity to antigens among various human populations and individuals. Animal models are generally not predictive of the potential for hypersensitivity-related cardiotoxicities in human patients.

### 5.6. Xenobiotic Interactions

Drug-drug interactions may play a role in the development of serious cardiotoxic reactions.

The myocardial sensitivity to the arrhythmogenic actions of cardiac glycosides is increased by diuretic agents that deplete  $K^+$  and magnesium through increased urinary excretion. Digitalis glycosides and extracellular  $K^+$  have competitive affinities for the membrane  $Na^+/K^+$ -ATPase enzyme. Exposure to  $K^+$  may simultaneously increase  $Na^+/K^+$ -ATPase activity and decrease the binding of glycosides to this enzyme. A decrease in extracellular  $K^+$  would intensify the inhibitory effect of glycosides on the  $Na^+/K^+$ -ATPase system, resulting in an increase in intracellular  $Na^+$  concentration; as a result, the magnitude of the membrane potential may approach the threshold for initiation of diastolic depolarization and thus initiate serious arrhythmias. Concurrent exposure to cardiovascular agents that have similar effects but which act by different mechanisms can cause potentiation of specific adverse effects. For example, the simultaneous administration of propranolol, a  $\beta$ -adrenergic receptor blocker, and verapamil, a  $Ca^{2+}$  channel antagonist, has caused profound AV block and marked hypotension.

Normally, catecholamine administration causes a predictable series of dose-related myocardial effects. Initially sinus tachycardia occurs, but a variety of arrhythmias are induced as the dose is increased, including ventricular bigeminy (i.e., interruption of the normal heart rhythm by an extra beat), multifocal premature ventricular contractions (PVCs), or ventricular tachycardia. Finally, at high concentrations, ventricular fibrillation ensues in which disordered electrical conduction cause the myocardium to quiver (fibrillate) without pumping blood. Exposure to certain halogenated hydrocarbon chemicals reduces the amount of catecholamines necessary to cause these arrhythmias.

Two additional potential targets for adverse drug-drug interactions in the heart are cytochromes P450 metabolizing enzymes and membrane drug transporters. Several P450 enzymes are known to be expressed in the mammalian heart and have roles in metabolizing endogenous substrates as well as xenobiotics, as they do in other tissues. Though a specific role in facilitating direct cellular toxicity in the heart through generation of a toxic metabolite is speculated, this mechanism is poorly explored in cardiac tissue. In addition, several drug transporters, including the well-characterized transporters P-glycoprotein (ABCB1; endothelial cells) and breast cancer resistance protein

(BCRP, also known as ABCG2), are expressed in the heart. Transmembrane ATP-binding cassette (ABC) proteins are efflux transporters of substrates against a concentration gradient and move materials out of the cell. Normal function of these transporters protects the cellular components of the heart from harmful accumulation of toxic xenobiotics. Alternatively, inhibition of transporters may enhance toxicity. This effect is best exemplified in the observation of enhanced doxorubicin toxicity in mice and rats coadministered the transporter inhibitors verapamil and cyclosporine A (Santostasi et al., 1991).

### 5.7. Modifying Factors in Cardiac Toxicity

Individual responses to cardiotoxic xenobiotics can be variable, particularly in heterogeneous human patient populations. Modifying influences include demographic factors like age, sex, gender, and race; biological factors like genetic polymorphisms in key metabolizing enzymes or transporters; pathobiological factors like preexisting disease in or outside of the cardiovascular system; and coadministration of other xenobiotics (i.e., poly-pharmacy).

The role of some sensitizing factors has been demonstrated in laboratory animals. For example, age- or weight-dependent susceptibility to the cardiotoxicity of  $\beta$ -adrenergic agonists and antihypertensive vasodilating agents occurs in the rat and to some extent in other laboratory animal species. Young, weaned rats are fairly resistant to the cardiotoxicity of isoproterenol (a nonselective  $\beta$ -blocker) (Hanton et al., 1991). The LD<sub>50</sub> (lethal dose in 50% of animals) of subcutaneously (SC) injected isoproterenol is about 1 g/kg in these weanling rats and focal subendocardial necrosis occurs at 100 mg/kg. In contrast, 6-month-old rats, particularly those of the Sprague–Dawley strain that can reach 500–600 g body weight, develop an increased sensitivity to the cardiotoxicity of isoproterenol. The LD<sub>50</sub> of isoproterenol injected SC at this age is about 0.6 mg/kg; death is preceded by ventricular fibrillation, and myocardial necrosis occurs at a dose as low as 50 mg/kg. The mechanism of this difference in the sensitivity of young weanling rats and older heavier rats has not been established. Their sensitivity to the positive chronotropic effect of the drug is similar, and the electrophysiological events in isolated papillary muscles are comparable in both groups before and after isoproterenol treatment. It is conceivable that the

susceptibility to the consequence of isoproterenol treatment—that is, to hypoxia—differs. Hypoxia is most likely responsible for the development of cardiac lesions, and perhaps also for the ventricular fibrillation.

The cardiotoxicity of isoproterenol was overlooked in nonclinical safety studies because the investigators used young weanling rats. The older heavier rats and adult Beagle dogs develop focal subendocardial necrosis after suprapharmacological doses of isoproterenol (and other drugs) that produce tachycardia and hypotension.

## 6. CARDIOTOXICITY ISSUES IN DRUG DEVELOPMENT

### 6.1. Cardiovascular-Related Drug Development Attrition

CV safety liabilities are a common source of both preclinical and clinical drug development attrition and may be structural or functional in origin (Hanton, 2007). In nonclinical testing, structural cardiotoxicities are most often identified in repeat-dose animal studies where morphologic evaluations are usual. Pathologic changes may occur in either the rodent or nonrodent studies or both and can manifest as alterations in heart weight and/or gross and/or microscopic morphology. They may also manifest as an increase in the severity and/or incidence of common background CV lesions in laboratory animal species (e.g., rodent PCM, vascular injury in any species). Functional liabilities are most often identified in single-dose safety pharmacology studies and manifest as changes in heart rhythm, contractility, or blood pressure. CV-related changes in one species and not others often raise the concern that the changes are species-specific and may not represent a hazard of relevance to human patients. Drugs that induce toxicities that result in structural injury or damage to the heart in animals may be difficult to progress to clinical testing in patients without a significant dose-related margin of safety for concerns that the toxicity might cause irreversible structural harm to patients. In contrast, functional changes in nonclinical animal studies are often predictive of functional changes in human patients though the directionality of that change (e.g., increase or decrease) may vary (Bhatt et al., 2019).

Clinically, cardiotoxicity is most often recognized as a change in CV function or a quantitative imbalance in naturally occurring CV events that are common in general populations. Functional changes may manifest as arrhythmia, a change in blood pressure, or even congestive heart failure. Identifying drug-related CV effects that diverge from the usual incidence of CV events expected for a given patient population is a particular challenge since such effects are not modeled in the usual safety assessment paradigm and cannot be recognized until a significant number of patients are exposed during clinical testing or postmarket use.

## 6.2. Rodent Progressive Cardiomyopathy

Rodent PCM is a disease syndrome commonly recognized in laboratory rats and mice. The disease occurs with varying incidence and severity and progresses over time; the etiology is not known. PCM manifests in young animals as widely scattered, usually minimal to mild foci of cardiomyocyte necrosis with attendant mixed inflammatory infiltrates. With age, PCM lesions become more frequent and may be more severe, leading to localized areas of myocardial fibrosis as a myocardial remodeling response. Overt cardiac dysfunction is not generally a feature of this background disease.

The translational or human relevance of treatment-related differences in the incidence and/or severity of PCM is challenging. Responses to direct cardiomyocyte toxic injury (e.g., necrosis, inflammation, fibrosis) may resemble this common background disease. It is also possible that a drug or environmental exposure may exacerbate the pathogenesis of this spontaneous disease. Accordingly, changes in PCM in response to treatment or exposure may indicate a need for more mechanistic investigation to understand better how the treatment may be interacting with this disease process.

## 6.3. Animal Models of Human Cardiac Disease

Though animal studies—both rodent and non-rodent—are commonly used to model xenobiotic effects on the cardiovascular system, the animals in these studies are generally young and

“healthy” and thus not representative of the older human populations who consume the majority of drugs to treat cardiovascular conditions. Moreover, it is widely recognized that most populations of people who are susceptible to the adverse effects of drugs or other environmental exposures also have a moderate incidence of previously existing cardiovascular disease, which is a common predisposing factor in many of the world’s more developed societies today. These existing diseases include hypertension, cardiometabolic diseases like diabetes mellitus and atherosclerotic coronary artery disease, and even subclinical or clinical heart failure. These diseases represent additional susceptibility to xenobiotic-induced adverse effects but may also be the target of xenobiotic-exacerbated health effects. Evaluating the interaction of preexisting cardiac disease and xenobiotic-related cardiotoxicity is a common interest but is challenging given the dearth of animal models that combine these features.

Many experimental animal models of heart failure, hypertension, and cardiometabolic disease have been described. No single animal model will mimic all the features of a particular cardiac disease in human patients. However, use of these models to address specific questions regarding the evaluation of the structural, biochemical, or functional alterations in various types of cardiovascular disease has been of great value. These models have also provided much-needed information on the interaction of etiologic factors, the pathophysiologic alterations, and the efficacy of various therapeutic agents in a variety of cardiovascular disease syndromes. Though some toxicity studies have been conducted, the use of these models for characterizing the interaction of disease and toxicity has many challenges. These include the complexity of the diseases themselves, variability in translation of the disease model to humans, and the complexity and variability of endpoints that should be measured. The study design chosen depends on whether the objective is to measure xenobiotic effects on the onset, the progression, or the severity of disease ([Herman et al., 2011](#)). Accordingly, use of disease models in toxicology is a worthy but challenging endeavor.



## 6.4. Clinical Translation of Nonclinical Cardiotoxicity

As noted above, cardiac toxicity can manifest as structural or morphologic injuries, rhythmic or contractile dysfunction, altered blood pressure, or any combination of the three. Usual repeat-dose nonclinical safety studies generally provide more opportunity to identify morphologic changes in the heart. Functional parameters (e.g., ECG) are routinely assessed in single-dose functional studies in rodents and nonrodents although some functional parameters may be collected in repeat-dose studies. The etiology of test article-related cardiac toxicities is often not elucidated but may occur from disruption of any of the usual cellular and physiological processes that support cardiac health including ion channel function, cellular energetics, organelle injury, disruption of the contractile apparatus, autonomic neural control, or a myriad of other biological targets with important roles in cardiac biology. Structural injuries to the heart other than overt and substantial cardiomyocyte necrosis and without a measurable functional correlate may be difficult to detect clinically (where histologic assessments are much less common).

Clinical cardiac disease is most often recognized initially as contractile or rhythmic dysfunction that may or may not be associated with structural abnormalities in the heart. Cardiac dysfunction is associated with many common, chronic and progressive diseases in many societies across the globe today. The etiology of cardiac disease is varied and may result from developmental abnormalities, genetic mutations, systemic metabolic disease, infectious agents, autoimmune disease, drug-related injury, or even idiopathic effects. Given the significant physiological reserve capacity of the cardiovascular system, clinical cardiac dysfunction may not be recognized until late in the progression of what is often irreversible disease. Therapeutic approaches are often directed at mitigating the dysfunction and managing (typically slowing) the progression. In general, disease reversal and tissue restoration are not feasible with current cardiac therapies, but next-generation products such as stem cell therapies offer the potential for genuine tissue repair (see *Stem Cell and Other Cell Therapies*, Vol 2, Chap 10).

Putative cardiac safety liabilities identified in conventional nonclinical studies may be challenging to progress to clinical testing in human patients without a substantial dose-related margin of safety, understanding of their mechanism or mode of action, and availability of one or more biomarker of early change. Cardiac troponins are sensitive circulating biomarkers of cardiomyocyte injury, but cell damage is generally when troponins can be detected. Natriuretic peptides can report changes in intracardiac and systemic plasma volume pressures associated with cardiac stretch. Functional measurements (e.g., ECG, echocardiography) can provide insights into rhythmic or contractile dysfunction. Most of these biomarkers are not used routinely in clinical biomonitoring in the absence of symptoms, and they may be insensitive at the individual level given the significant variability in CV health among populations. Drug-induced toxicities that manifest as exacerbation of preexisting susceptibility or disease are even more challenging to identify. Accordingly, thorough nonclinical characterization of cardiovascular liabilities is key to effective clinical management.

## PART II: BLOOD VESSELS

Vessels, subdivided into arteries, veins, capillaries, and lymphatics, have remarkable adaptations of their structure to achieve required functions. Xenobiotics may provoke vascular alterations that may be unique to the vessels of a particular organ or have tropism for a particular segment of specific types of vessels. A spectrum of morphologic reactions is induced by vascular toxicoses including accelerated atherosclerosis, medial and intimal proliferation, calcification, aneurysms, medial hemorrhagic necrosis, fibrinoid necrosis, microangiopathy, and vasculitis. The outcome of healing of vascular injuries may be dominated by repair processes rather than regeneration and may be complicated by development of vascular medial sclerosis, thrombosis, aneurysm formation, and vascular rupture. This section briefly reviews basic vascular biology and common vascular responses to toxicants.

## 7. STRUCTURE AND FUNCTION

### 7.1. Microscopic Anatomy

The vascular system is subdivided into blood vessels and lymphatic vessels. Blood vessels contain blood consisting of a complex cellular component (erythrocytes [red blood cells], leukocytes [white blood cells of various classes], and thrombocytes [platelets]) and protein-rich fluid. Details regarding blood and blood-forming elements are available in the companion chapter on the *Hematopoietic System*, (Vol 5, [Chap 5](#)). Lymphatics contain lymph, a clear or cloudy white liquid composed of leukocytes, proteins, and in some cases fats (e.g., chyle in intestinal lymphatics) that is generated by collection of interstitial fluid from tissues. In many organs and tissues, blood vessels and lymphatic vessels run in parallel. Lymphatic vessels are not present in the CNS.

Blood vessels are subdivided into arterial, capillary, and venous segments. The arteries are classified as three types: elastic arteries, muscular arteries, and arterioles. The venous vessels are termed veins and venules. Interposed between the arterial and venous segments are the capillary beds. Some authors prefer to further define a vascular segment, termed the microcirculation, which specifically includes smaller-diameter vessels (arterioles, capillaries, and venules) and serves as the major area of exchange between the circulating blood and the peripheral tissues. The lymphatic vasculature includes larger lymphatic vessels and lymph capillaries.

The overall anatomical arrangement of the blood and lymphatic vessels, with minor differences in the luminal diameter, wall thickness, and the presence of other features such as valves vary between the different segments of the system. The luminal surface of all vessels is lined by longitudinally aligned endothelial cells overlying a basal lamina. Vascular walls (for blood and lymphatic vessels) are divided into three layers: tunica intima, tunica media, and tunica adventitia. However, some or all of the layers may be absent or thinned in some segments of the vascular system, depending on the intravascular pressures. The large elastic arteries, such as the aorta, have an intimal layer composed of endothelium and subendothelial connective tissue; and a very thick medial layer composed

of concentrically arranged layers of smooth muscle cells (SMCs) alternating with fenestrated elastic laminae and small amounts of ground substance. The media is demarcated by the internal and external elastic laminae. The outermost layer, the adventitia, is composed of collagen, elastic fibers, and connective tissue cells with penetrating blood vessels, termed the vasa vasorum, that supply nutrition to the adventitia and the outer half of the media. In muscular arteries and arterioles, the media is largely composed of SMCs arranged in a circumferential pattern ([Figure 1.21](#)), and a vasa vasorum is largely absent. Arterioles are the smallest arterial channels and are generally recognized as vessels of less than 100  $\mu\text{m}$  in diameter surrounded by one to three layers of SMCs.

Capillaries are 5–10  $\mu\text{m}$  in diameter (approximately the diameter of erythrocytes and leukocytes) and thus represent the major site of gas and nutrient exchange in all body organs. Capillary endothelium is arranged in one of three types: continuous (as in the muscle, brain, and

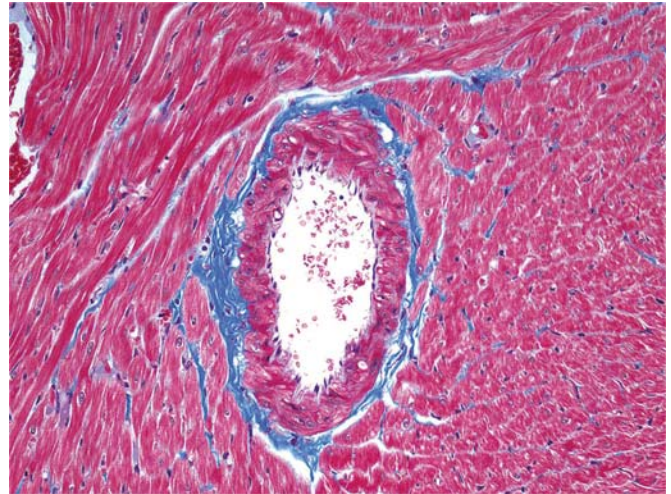


**FIGURE 1.21** Cross-section of a coronary artery (a muscular artery) in a section of myocardium from a rat. The undulating tunica intima lining the luminal surface is surrounded by a thick tunica media composed of concentrically arranged smooth muscle cells. The adventitia (blue-colored connective tissue) separates the tunica media from the adjacent myocardium. Formalin-fixed, paraffin-embedded section, Masson's trichrome stain. Original magnification 20 $\times$ . Reproduced from Haschek WM, Rousseaux CG, and Wallig MA, editors: *Haschek and Rousseaux's handbook of toxicologic pathology*, ed 3, 2013, Academic Press, Figure 46.18, p. 1618, with permission.

lung); fenestrated (as in the endocrine glands or renal glomeruli); or discontinuous (as in the liver and hematopoietic organs). Continuous endothelium is characterized by intercellular coupling by tight junctions, and cells are anchored to a continuous basal lamina. Fenestrated endothelium features multiple transcellular wide pores (50–60 nm in diameter) that are sealed by a 5- to 6-nm-thick diaphragm, and cells are attached to a continuous basal lamina. Discontinuous endothelium has large fenestrations (100–200 nm in diameter) without diaphragms and is associated with a poorly formed basal lamina. Lesions in the endothelium may require electron microscopy to be visualized.

Veins and venules have thin walls in relation to their luminal size when compared with arteries. The reduced wall thickness is because the blood pressures in veins are lower. Accordingly, veins lack an internal elastic lamina, which is present in vessels (arteries and arterioles) that need additional strength to withstand higher pulsatile pressures (Figure 1.22). The adventitia of veins is the thickest layer. Valves are present in veins to prevent retrograde blood flow away from the heart.

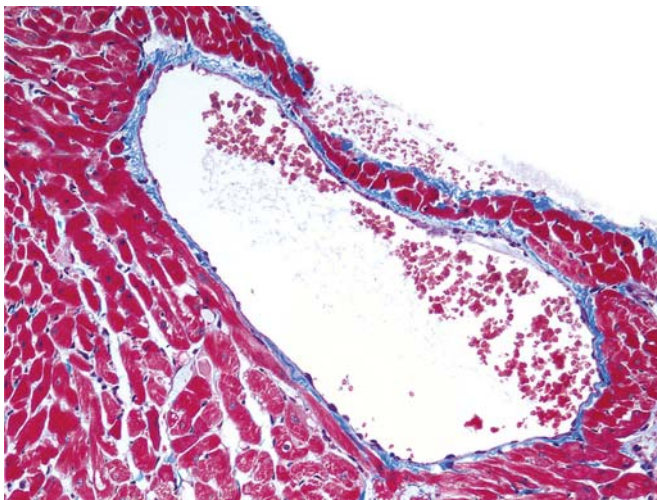


**FIGURE 1.22** Section of a normal coronary vein from the heart of a rat. The venular walls are thin and lined by endothelial cells along the luminal surface, and the adventitia (blue-colored connective tissue) lies immediately beneath it. Formalin-fixed, paraffin-embedded section, Masson's trichrome stain. Original magnification 20 $\times$ . Reproduced from Haschek WM, Rousseaux CG, and Wallig MA, editors: *Haschek and Rousseaux's handbook of toxicologic pathology*, ed 3, 2013, Academic Press, Figure 46.19, p. 1618, with permission.

Pericytes are specialized cells with functions in angiogenesis and endothelial cell regulation that are found intermittently inside the basal lamina along the outer (abluminal) margins of endothelial cells (Hamilton et al., 2010). These cells occur in capillaries, postcapillary venules, and some arterioles.

Lymphatic capillaries lack basal laminae. Large lymphatic vessels appear similar to veins, with such structural features as large lumina, thin walls, and intimal valves.

## 7.2. Cellular and Extracellular Components of the Vasculature: Biology

### 7.2.1. Endothelial Cells

Endothelial cells are flattened and measure  $<3\mu\text{m}$  in thickness in their central part, which contains the nucleus and most of the cellular organelles. Peripheral areas are much thinner and contain only a few organelles. The luminal surfaces are covered with a thin glycocalyx that is demonstrable only by special staining procedures such as cationic ferritin and peroxidase-coupled lectins. Microvilli and filopodia extend from the endothelial surface into the vascular lumen. The numbers of these structures vary considerably from one body region to another. The abluminal surfaces are supported by a well-defined external lamina, rich in types III and IV collagen. The cytoplasm of endothelial cells contains transport vesicles, mitochondria, free ribosomes, cisterns of rough endoplasmic reticulum (RER), the Golgi complex, lysosomes, multivesicular bodies, glycogen particles, cytoskeletal filaments (which may be arranged in bundles), microtubules (which are arranged parallel to the longitudinal axis of the vessel), and Weibel–Palade bodies (not present in all species). By TEM, Weibel–Palade bodies are membrane-bound secretory granules with a dense matrix in which clear tubular spaces 20 nm in diameter are present. These secretory structures contain the clotting factor von Willebrand Factor (Factor VIII) and the adhesion molecule P-selectin, thus providing qualitatively specific cytological markers for endothelial cells.

The endothelium comprises a single layer of cells that acts as a thrombosis-resistant surface



and physical barrier. Alteration of this monolayer may provoke changes in transendothelial permeability, vascular contraction or relaxation, initiation of thrombosis, and recruitment/adhesion/translocation of inflammatory cells from the blood into tissues. The junctions of endothelial cells also play an important role in maintaining the functional integrity of the vascular surface. They can be disrupted by various pharmacologic agents and other toxicants, resulting in leakage of intravascular content. The intercellular junctions are also subject to dynamic changes representing another route of transendothelial transport. The patterns of organization for the junctions of endothelial cells differ in arterioles, capillaries, and venules. These differences account for regional variations in endothelial permeability along the microvascular tree.

### **7.2.2. Smooth Muscle Cells**

SMCs in vessel walls are spindle-shaped and have single elongated nuclei. As in cardiac myocytes, the configuration of the nuclear membranes in vascular SMCs changes during contraction and relaxation. SMCs contain thin (actin) and thick (myosin) contractile filaments as well as cytoskeletal filaments. The thin filaments are the most conspicuous feature of SMCs; they fill most of the cytoplasm, are easily demonstrated in electron microscopic preparations, are 4–8 nm thick, and insert into condensations of electron-dense material (“dense bodies”) located subjacent to the plasma membranes. The external laminae of SMCs are well developed, and transport vesicles are numerous along their surfaces. In the face of vascular injury, SMCs may undergo a phenotypic switch to a dedifferentiated and proliferative cell type that can contribute to formation of neointima (i.e., a new and usually thicker, nonendothelial layer of tissue that lines the lumen of damaged muscular blood vessels) and matrix protein synthesis. Thus, toxicologic injury to SMCs has significant implications for vascular repair (Hamilton et al., 2010).

### **7.2.3. Pericytes and Veil Cells**

Pericytes are perivascular mesenchymal cells that surround capillaries and postcapillary venules and some small arterioles. Pericytes have a cell body with a prominent nucleus and a small amount of cytoplasm with several long cytoplasmic processes that intercalate with the

abluminal endothelial wall of its resident and neighboring capillaries. These cells share a gap junction with endothelial cells and enable direct exchange of small molecules as well as paracrine signaling between these cells. Pericytes maintain hemodynamic stability of capillaries, but also facilitate angiogenesis, support endothelial survival, and have some macrophage-like activities (Bergers and Song, 2005). Pericytes combine with endothelial cells in producing the basal lamina.

Veil cells (also called periadventitial cells) are supportive cells present in the adventitial layers of dermal microvessels (Braverman et al., 1986). Normal vessels are surrounded by a single layer of veil cells. With age, the lateral extensions of veil cells are less prominent so that the vessel surface is covered to a lesser degree. The veil cell layer increases in thickness in some diseases (e.g., diabetes).

### **7.2.4. Connective Tissue**

Connective tissue cells are located in two sites with respect to blood and lymphatic vessels. In all vessels, connective tissue cells are concentrated in the intima as the subendothelial connective tissue. In large vessels, such cells are also found in the adventitia where they surround parallel groups of blood vessels, lymphatics, and nerves.

Elastic fibers allow the resilient rebound of the stretched vessel wall, while collagen fibers provide tensile strength to the vessel wall. The elastic fibers may be isolated but are more often arranged in the walls of elastic arteries in sheets as distinct laminae or layers (internal and external elastic lamina) or as fenestrated lamellae. Collagen fibers are scattered in the intima and media where they are mainly produced by SMCs, and in the adventitia where they are made by fibroblasts. Collagen, mainly type III, is especially abundant in the walls of veins.

The extracellular spaces of the vessel wall contain a ground substance (matrix) rich in glycosaminoglycans such as chondroitin sulfate and dermatan sulfate. Arteries contain higher concentrations of ground substance than veins. The ground substance affects permeability across the wall and contributes to the physical properties of the vessel wall. Furthermore, cellular interaction with the extracellular matrix regulates cell adhesion, migration, and proliferation of leukocytes (Xu and Shi, 2014).



### 7.3. Physiology and Functional Considerations

#### 7.3.1. *Blood Circulation and Tissue Perfusion*

The circulatory system of multicellular organisms has evolved to distribute blood through a closed circuit of branching vessels, with propulsion provided by the muscular heart (a modified portion of the vascular system), delivering nutrients to and removing cell products and wastes from all the cells of the body. Blood is ejected from the heart during systole into large elastic arteries, the aorta and pulmonary arteries, under considerable pressure that causes stretching of elastic tissue in the vessel walls. During diastole, elastic recoil occurs and hydrostatic pressure is maintained to allow blood to be conducted into the muscular (distributing) arteries. The potential volume of the circulatory system is considerably greater than the normal blood volume. To allow distribution to meet the needs of each of the different parts of the body, the muscular arteries and arterioles contract or distend appropriately under the influence of neural stimulation and autoregulation via local metabolic stimuli. Thus, blood is delivered to the capillary beds in necessary amounts but at low pressure where rapid blood–tissue exchanges occur across the endothelial layer (which serves as a thin semipermeable barrier). Blood then enters the venous portion of the circulatory system at low pressure and flows slowly. The veins distend greatly and serve as a blood reservoir; the blood volume in veins is approximately four- to fivefold greater than in the corresponding arteries.

#### 7.3.2. *Endothelial Permeability*

The transvascular exchange of water and solutes represents a large volume of material with net outward movement at the arteriolar end of the capillary and net inflow at the venous end. Most of the exchange occurs by diffusion, and less by filtration–absorption processes. Intravascular forces that govern transcapillary exchanges include hydrostatic pressure, osmotic pressure (of plasma proteins and other solutes), and concentration gradients of molecules. Endothelium has a unique, bidirectional permeability to water and solutes provided by a modulating transport system involving vesicles, channels,

fenestrae, and diaphragms via transcytosis and endocytosis. The extent of transcapillary exchange may vary greatly among various capillary beds. High permeability occurs across beds with fenestrated or discontinuous endothelia. Low permeability occurs in those with continuous endothelium and unique blood–tissue barriers, such as in the brain and eye. Sophisticated studies of endothelial transport mechanisms using various macromolecular tracers have established a complicated regional localization of transport sites over the cell surfaces. For example, fenestrae are primarily associated with permeability to water and solutes, while plasmalemmal vesicles and channels are selectively permeable to anionic proteins.

#### 7.3.3. *Metabolic Activities in Vascular Cells*

The integrity of the endothelium is essential to maintain the normal structure and function of the vessel wall. Exposure of the subendothelial tissues will initiate platelet aggregation and subsequent thrombus formation. In addition to functioning as a semipermeable barrier, the endothelium has a number of metabolic activities that can have both local and systemic ramifications, and which vary according to the location in the body. These include a role in hemostasis and thrombosis by production of procoagulant substances (Factor VIII, plasminogen inhibitor) and anticoagulant substances (prostacyclin, plasminogen inhibitor); a role in the modulation of vascular tone (prostacyclin, angiotensin II, nitric oxide, endothelin); a role in the metabolism of vasoactive substances (ACE; enzymatic degradation of norepinephrine, serotonin and bradykinin); a role in vascular growth and remodeling (TGF- $\beta$ , heparin sulfate, glycosaminoglycans, thrombospondin, VEGF, insulin-like growth factors [IGF]); a role in inflammatory and immune reactions (nitric oxide, prostacyclin, complement regulatory factors, cytokines, chemokines, adhesion molecules, selectins); secretion of type III and IV collagen to form basal lamina; and production of fibronectin, laminin, elastin, glycosaminoglycans, and blood group antigens A and B. In addition, endothelial cells can secrete matrix metalloproteinases (MMPs) and their specific tissue inhibitors (TIMPs) that regulate the turnover of connective tissue proteins and the remodeling of tissues during normal growth and repair of tissue injury.

Endothelial cells are able to contract and possess receptors for compounds such as angiotensin and insulin.

Vascular smooth muscle is similar to the smooth muscle of other organs like the GI tract (i.e., the actin and myosin components are not aligned into a striated configuration resembling that of cardiac myocytes). Vascular SMCs are numerous in the media and less numerous in the normal intima and adventitia. Each SMC is surrounded by basal lamina and often attached by gap junctions. These cells are metabolically active and produce various types of connective tissue fibers (collagen types I and III, elastin) and ground substance (glycosaminoglycans). When stimulated, vascular SMCs may elaborate growth factors and cytokines, proliferate, migrate, and assume phagocytic activity.

Vascular SMCs are usually situated circumferentially around blood vessels and vary in numbers depending on vessel type and circulatory system location. The presence of these SMCs in the medial portion of the vascular walls of arteries, arterioles, and veins provides the means by which changes in vessel tone can occur. The normal functioning of vascular smooth muscle is dependent on a variety of physiological influences. As a result, many factors are responsible for the diverse pharmacologic and toxicologic responses observed in different types of vascular smooth muscle.

#### **7.3.4. Vascular Function**

##### **7.3.4.1. NEURAL INFLUENCES**

Neural control of the vasculature is exerted mainly by the sympathetic division of the autonomic nervous system. Sympathetic fibers innervate most arteries, arterioles, and veins. These are mostly adrenergic fibers, although some vessels receive cholinergic sympathetic fibers. Both  $\alpha$ -adrenergic and  $\beta$ -adrenergic receptors exist in the same vessels and share the same neurotransmitter (norepinephrine). Whether the smooth muscle constricts or dilates depends on the affinity and numbers of the two classes of adrenergic receptors. Muscarinic cholinergic receptors are present on both SMCs and endothelial cells. Receptors for histamine, serotonin, adenosine, and other vasoactive substances are also found in many portions of the vasculature. It has been shown that nerves do not penetrate

the entire thickness of blood vessels. In small arteries, innervation is limited to the adventitia, while in larger arteries, there are nerve-free regions that include the innermost quarter to half of the smooth muscle layer. As a result, there is a significant difference in sensitivity to all common vasoconstrictor substances between those outer portions of the vessel that are innervated and the nerve-free inner layer of muscle. Only the inner layer of muscle is sensitive enough to react to circulating levels of vasoconstrictor hormones (norepinephrine, epinephrine), whereas the outer portion of the vessels requires high concentrations of norepinephrine released by sympathetic nerves to provoke a response. Muscle and skin vasculature are controlled by sympathetic innervation. In other tissues, the role of blood vessel control by the autonomic nervous system is less clear, but some studies suggest that autonomic nerves may exert control in renal, cerebral, and coronary blood vessels. In certain situations, adjustment of vascular tone by the autonomic nervous system is less important than other control systems or mediators. It appears that some vasoconstrictor and vasodilator substances that act directly on vascular SMCs also exert an indirect action by altering the release of norepinephrine from sympathetic nerves. Endogenous substances that appear to act at specific presynaptic receptors and decrease norepinephrine release include acetylcholine, adenosine, histamine, dopamine, prostaglandins of the E series, and norepinephrine itself. Other endogenous substances, such as angiotensin and prostaglandins of the F series, potentiate the release of norepinephrine.

##### **7.3.4.2. LOCAL HUMORAL AND ENVIRONMENTAL INFLUENCES**

Blood vessels are capable of both synthesizing and metabolizing vasoactive hormones, and as a result are not entirely dependent on circulating substances or neurotransmitters for control of vascular tone. The endothelium is the source of many potent endogenous vasoactive substances, including the vasodilator nitric oxide and the vasoconstrictive endothelin-1. Endothelial cells also produce prostacyclin, a substance that causes vasodilation and prevents the adhesion of platelets to the vascular endothelium. In addition, the endothelium may contribute to the local control of vascular tone by secreting other

relaxing and contracting factors, such as angiotensin II and platelet-derived growth factor (PDGF). Angiotensin II is produced in the lungs and also, to a certain extent, in limb vessels themselves. Regardless of the source, angiotensin II reacts directly with resistance vessels (arterioles and smaller arteries) to cause vasoconstriction; resistance vessels are responsible for controlling up to 90% of peripheral vascular resistance. PDGF, in addition to its mitogenic properties, also acts as a smooth muscle contractile agonist. It is likely that local metabolites (e.g.,  $K^+$ , ATP, adenosine, oxygen, carbon dioxide) are also available to act on the vascular smooth muscle.

#### 7.3.4.3. RESPONSES OF BLOOD VESSELS TO VASOACTIVE SUBSTANCES

Blood vessels of different types and from different areas do not react uniformly to the presence of certain drugs and other xenobiotics. Norepinephrine induces uniform contraction of all types of blood vessels, but angiotensin exerts more constrictor activity in the resistance vessels than in the veins. Ergot alkaloids, at low doses, demonstrate preferential constrictor activity in veins with little increase in resistance vessel tone. A selectivity of action is also seen with xenobiotics that dilate vessels. Hydralazine mainly relaxes resistance vessels, while glyceryl trinitrate preferentially exerts this action on veins.

#### 7.3.4.4. ELECTRICAL ACTIVITY AND INTRACELLULAR CALCIUM RESPONSES TO VASOACTIVE SUBSTANCES

Heterogeneity in smooth muscle responses resulting from exposure to xenobiotics relates in part to the varying patterns of cellular electrical activity and to the variety of mechanisms that are involved in the control of the cytoplasmic concentration of  $Ca^{2+}$ . SMCs are characterized by a low resting membrane potential ( $-40$  to  $-60$  mV). The action potential of vascular smooth muscle is mainly driven by an inward flux of  $Ca^{2+}$  ions. Excitation spikes can be detected as  $Ca^{2+}$  enters the cell, and the membrane potential becomes more positive. Some types of smooth muscle display phasic activity, an effect that is associated with the generation of spike action potentials.  $Ca^{2+}$  is also critical to the contractile process. As for cardiac myocytes, the SR appears to be the major cellular compartment for  $Ca^{2+}$  storage in SMCs; both contraction and relaxation are influenced by the levels of  $Ca^{2+}$  in the cytoplasm. Critical levels of cytoplasmic  $Ca^{2+}$  are

achieved by entrance through voltage-dependent membrane channels and through release of the cation from intracellular storage sites. Spontaneous contractile activity resulting from  $Ca^{2+}$  entry in this manner is not present in all smooth muscle; some types develop sustained contractions only in response to agonists such as norepinephrine and angiotensin. Agents that stimulate contraction have the potential to produce greater depolarization and to increase the frequency of spike potentials. However, vascular contractile activity can be induced without membrane depolarization, and in these instances, alterations in membrane permeability are important. Vascular contraction as a result of changes in membrane permeability appears to involve the movement of  $Ca^{2+}$  through a receptor-mediated channel and the subsequent release of additional  $Ca^{2+}$  from intracellular stores. Varying combinations of phasic and sustained contraction are found in the SMCs from different types of vessels. It has been suggested that entrance of  $Ca^{2+}$  through channels may have limited importance, and that agonist-induced contraction may depend entirely on the release of  $Ca^{2+}$  from intracellular storage sites. Dependence of the contractile response on  $Ca^{2+}$  influx appears to vary considerably at different points along the vascular tree. The dependence is least in the aorta, where contractile responses appear to rely almost entirely on the release of  $Ca^{2+}$  from intracellular storage sites. In contrast,  $Ca^{2+}$  influx is essential for contraction of small resistance arteries. Differences in pharmacologic and toxicologic responses are thought to be related to the varying intrinsic smooth muscle properties found in vessels of different types. The primary action of  $Ca^{2+}$  antagonists such as verapamil and nifedipine on resistance vessels may be related to the greater importance of phasic activity associated with entry of  $Ca^{2+}$  through voltage-dependent  $Ca^{2+}$  channels. In contrast, the preferential action of sodium nitroprusside in veins is an indication of the importance of the receptor-operated sustained contraction mechanism.

#### 7.3.4.5. EFFECTS OF ENDOTHELIAL CELL FUNCTION AND DAMAGE ON BLOOD-VESSEL ACTIVITY

Vascular endothelial cells serve as a protective barrier in blood vessel walls and serve as an active source for the synthesis, metabolism, uptake, storage, and degradation of a number of

vasoactive substances. Endothelial cell damage can be a factor in diseases that affect the vasculature. Endothelial cells seem to be directly involved in the decrease of vascular tone noted in certain arteries and veins as a result of exposure to naturally occurring vasodilator substances such as acetylcholine, bradykinin, arachidonic acid, substance P, and ATP. When endothelial cells are destroyed, the vessels lose the ability to relax upon exposure to most of these dilator substances. In addition, the loss of functional endothelial cells seems to transform normal vasodilator responses into potent vasoconstrictor activity. A substance that damages or destroys endothelial cells to the extent that vasodilatory responses are altered could conceivably cause significant decreases in blood flow and subsequent tissue damage in certain organs. Additionally, injured endothelial cells switch from a thrombo-resistant fibrinolytic phenotype to a thrombo-promoting function, thus initiating the clotting cascade. Activated endothelium also recruits inflammatory cells and supports translocation of blood cells into tissues.

## 8. EVALUATION OF TOXICITY: VASOTOXIC EFFECTS

Vascular toxicity may be localized to alterations in vascular function to a particular organ or vascular bed. In vivo and in vitro methods may serve to elucidate potential toxic mechanisms; however, the selection of the method to be used is primarily dependent on the type of vessel affected as well as the location/organ system. In a particular tissue, xenobiotics may affect not only arteries or veins but also arterioles, venules, and capillaries. Furthermore, endothelial and vascular function, and response to injury, may differ by vascular niche.

### 8.1. Physiological Methods for Testing

#### 8.1.1. *Noninvasive Measurements of Blood Flow*

Direct measurement of blood flow can be made by Doppler ultrasound techniques, which provide moment-to-moment phasic flow information without interrupting circulation. This type of information is important in situations

either where the vascular effects of a substance are transient or where changes occur over a period of time. These techniques have been used successfully in monitoring blood flow in large arteries such as the aorta as well as from smaller vessels such as the renal, mesenteric, femoral, carotid, and coronary arteries. Duplex ultrasound and/or color flow imaging are more complex noninvasive procedures that are used clinically in the diagnosis of arterial and venous vascular disease.

A clinically relevant direct measurement of peripheral blood flow is performed by transdermal optical imaging. This technique utilizes subtle skin color changes resulting from reemitted light between hemoglobin and melanin chromophores to detect blood flow pulsation in different areas of the skin (Luo et al., 2019).

#### 8.1.2. *Invasive Measurements of Blood Flow, Vascular Tone, and Microvasculature*

Direct blood flow measurement can be made by electromagnetic flow meters. The probes can be chronically implanted so measurements can be made later without the use of further anesthesia. In general, electromagnetic probes are bulky and at times difficult to zero and calibrate, especially in chronic and “low flow” conditions.

The methods of blood flow measurement described next tend to quantify flow through the major vessels of the organ and may not accurately reflect perfusion of the microcirculation or account for shunting. Other methods such as microspheres, temperature-pulse decay probes, and gamma-emitting macroaggregates of albumin may serve to measure perfusion over time.

Measurements of organ blood flow can be made with the aid of dilution methods utilizing the Fick principle (Cohen et al., 1991). This principle states that oxygen consumption in an organ is equal to the product of the organ’s blood flow and the difference in the levels of an indicator substance in the arterial and venous circulations. Indicator substances may be an inert gas, a natural metabolite, a nondiffusible dye, a radioactive tracer, or more commonly cold saline; the indicator substance is injected into the blood upstream of the organ in which flow is to be measured, and its concentration measured by an appropriate detector at a downstream sampling site. The indicator dilution method is useful for measuring mean organ blood flow if the indicators used are removed from the blood



by these organs. For example, the liver removes bromsulfalein (or bromsulphalein) and the kidneys remove *p*-amino-hippurate, while the brain and heart absorb nitrous oxide. In each instance, arteriovenous differences in indicator concentrations enable flow to be measured. Dilution methods require invasive vascular techniques and provide mean flow data only over limited periods of time (seconds to several minutes). As a result, changes detected from one dilution to another might occur as a result of variations in cardiac output. To allow for clearance, it may also be necessary to limit the number of repetitive administrations of indicator within a given monitoring period.

Direct *in vivo* measurement of blood flow is also possible by using a semiisolated dog or cat biceps muscle preparation. The advantage of this preparation is that the principal components (skeletal muscle, blood vessels, and nerves) are part of a single system. Measurement of blood flow and vascular reactivity in these preparations is most reliable under normal flow conditions. A cat hind limb preparation was developed for situations where blood flow is low. This preparation allows monitoring of the effects of vasoactive substances on the resistance and capacitance vessels (where capacitance vessels [veins] have the ability to increase the blood volume without a large increase in blood pressure) at times when the circulation to the area is compromised. Perfusion of isolated hind limb preparations at a constant rate provides a means of detecting substance-induced alterations in vascular resistance.

Angiography can detect alterations in vascular tone using a suitable contrast medium injected into the vessel. This technique allows for identification of substances that possess vasoactive effects. However, it is not possible to determine whether this activity is due to a direct or indirect effect on the vascular smooth muscle.

Direct microscopic observations of microvascular beds can be achieved in easily transilluminated thin membranes. Studies of this type are usually limited to acute experiments in anesthetized animal preparations such as the hamster cheek pouch, the rat and mouse ear, or mesentery in any species. A transparent chamber for use in the rabbit ear considerably lengthens the period for direct observation of substance effects on blood vessels in unanesthetized animals. Microvascular dimensions can be recorded with the

aid of an image-splitter television microscope. This technique allows measurement of changes in vessel wall thickness, lumen diameter, and total vessel diameter in both isolated tissues (*ex vivo*) and the intact vascular beds (*in vivo*).

## 8.2. In Vitro Methods for Detecting Vascular Toxicity

Once a vascular effect of a xenobiotic is identified, it may be more useful to examine its action on an isolated system rather than on the entire vascular bed. Multiple species and vascular beds have been used in vascular studies. *In vitro* preparations allow a more controlled analysis of the potential toxic vascular effects. However, it should also be noted that results obtained from isolated or even perfused tissues do not always completely recapitulate the action of the xenobiotic on the vasculature in the intact organism, particularly if cellular components of the blood are involved in the activity of the substance.

### 8.2.1. Isolated Vascular Preparations

*In vitro* vascular toxicity studies can be conducted on strips or rings obtained from large arteries of laboratory animals such as rabbits and rats (Wenceslau *et al.*, 2021). The method involves suspending spiral cut strips or transverse rings of vessels, usually aorta, in a physiological solution. The preparation makes it possible to study changes induced in the tone of vascular smooth muscle due to xenobiotics added to the bathing solution (Gonzales *et al.*, 2000). Information concerning the action of substances on microscopic resistance and capacitance vessels has also been obtained from isolated strip and ring preparations. Direct effects of substances on veins can also be detected in isolated venous strip preparations.

The use of *in vitro* vascular preparations has also provided a means for determining the extent to which endothelial-dependent responses are responsible for the activity of vasoactive xenobiotics. Rings of vascular smooth muscle, with and without endothelium, are usually examined in a parallel system so the activity of vasoactive substances can be compared. The endothelial cells are removed from the intimal surface of the blood vessel by gently rubbing the surface with small forceps. Substances have been

identified which interfere with the production, release, or action of endothelium-derived relaxing factors. The potential role of endothelial cells in vascular activity can also be assessed in a perfused preparation that uses a blood vessel ring without endothelial cells. The perfusion of the vessel ring occurs via a steel cannula or through blood vessels with or without endothelial cells. Agents causing the release of vasoactive substances from endothelial cells can be identified by means of this type of bioassay technique.

### **8.2.2. Cellular Electrophysiological Methods**

The actions of some xenobiotics on the vasculature can be mediated by changes in membrane potential, action potential, or contractile activity. Use of an intracellular microelectrode can provide the means for determining the magnitude of the transmembrane potential and whether a substance causes changes in this membrane potential. The intracellular microelectrode technique can also be used to determine cell membrane resistance. Membrane potential-sensing dyes can be employed in cultured vascular SMCs, and alterations in membrane potential can be detected using live cell imaging or plate reader assay formats (Sguilla et al., 2003). Multielectrode array (MEA) plates can be used to measure electrical activity in any excitable cell type, such as cardiomyocytes derived from human induced pluripotent stem cells (see below), to measure the fiber “beat” (contraction) rate, field potential duration, spike amplitude, and other endpoints (Tertoolen et al., 2018). MEAs provide a medium- to high-throughput platform as compared to the low-throughput patch clamp method, with moderate translation to measurement of cardiac action potential. This methodology can be employed to identify drug effects on ion channels through detection of QT and RR interval, for example Sala et al. (2017).

### **8.2.3. Cultured Vascular Smooth Muscle Cells**

Methods similar to those described for cultured cardiac muscle cells have produced cultured reaggregates of endothelial and spontaneously contracting vascular SMCs. Reaggregated cells have been maintained in primary cultures for a number of weeks, and these cells retain both electrical and mechanical properties resembling those of SMCs from intact adult blood vessels. These cultured

cell preparations can be used to examine the electrophysiological and toxicological effects of substances acting directly on endothelial cells and noninnervated vascular SMCs. Primary cultured vascular cells can also be used for simple viability/cytotoxicity assays in cells derived from multiple species as a measure of direct vascular toxicity of xenobiotics. However, a major disadvantage to use of these vascular SMCs is that they are much more difficult to propagate than are cultured heart cells.

### **8.2.4. Human-Derived Induced Pluripotent Stem Cells**

iPSCs can be induced to generate endothelial cells and vascular SMCs that functionally and structurally resemble their primary cells (Tu et al., 2021). While not as widely used as iPSC-derived cardiomyocytes, vascular origin assays have shown promise in preclinical investigations of xenobiotic-induced vascular toxicity. iPSCs are induced to differentiate into mesoderm and subsequently to ECs with a combination of such growth factors as VEGF and fibroblast growth factor 2 (FGF2, also known as basic FGF [bFGF]), and finally sorted for the CD31-positive population (where CD31 is a marker for endothelium). The resultant stem cell-derived endothelial cells (iPSC-ECs) are morphologically similar to primary endothelial cells and can perform endothelial functions such as increasing nitric oxide production in response to vasodilators and other stimuli.

### **8.2.5. Emerging Technologies**

Advances in 2D cell culture, organoids, and organ-on-chip technologies also provide novel platforms to model vascular toxicity. For example, iPSC-ECs cultured in monolayer (2D) respond to chemical stress in a manner consistent with primary endothelial cells and can be used to evaluate cell survival, reactive oxygen species generation, low-density lipoprotein (LDL) uptake, cellular migration, and cytokine generation. This 2D model provides a high-throughput platform to investigate xenobiotic-induced vascular toxicity. 2D cultures of primary endothelial cells can also be used to evaluate passage of substrates or currents as a surrogate for vascular permeability, as with a transwell assay or transendothelial electrical resistance (TEER) determination (Robinson et al., 2018).

3D culture adds an additional layer of complexity compared to 2D cultures by introducing cell–matrix interactions (see *Alternative Models in Biomedical Research: In Silico, In Vitro, Ex Vivo, and Non-Traditional In Vivo Approaches*, Vol 1, Chap 24). Such 3D cultures present a means of assessing diffusion gradients and effects of secreted factors. Spheroids (i.e., 3D aggregates of cultured cells with minimal internal organization) feature a mix of vascular cell types, either iPSC-derived or primary, that form layers which crudely recapitulate the in vivo organization and microenvironment. More complex vascular organoids (i.e., 3D cultures with partial but substantial internal organization resembling the natural organ) can incorporate various extracellular matrix components to produce high-fidelity engineered microvessels. Finally, organ-on-chip (more formally termed “microphysiological systems”) technology incorporates microfluidic perfusion and can be engineered to model arterial narrowing due to formation of atherosclerotic plaques (Kennedy et al., 2021). Fast-moving improvements in this area may provide a powerful tool for exploration of vascular toxicity.

### 8.3. Morphologic Evaluation

#### 8.3.1. Gross Examination

At necropsy, the large blood vessels including the large elastic arteries and great veins near the heart can be examined grossly. Longitudinal incision will expose the intimal surface for inspection and may allow detection of degenerative lesions of the walls (typically seen as discoloration or change in texture) that may be accompanied by mineralization, fibrosis, or lipid deposition. Other grossly apparent lesions include aneurysm formation, thrombosis, and vascular rupture. Indirect evidence of vascular disease may be gained by observation of lesions that accompany vascular damage, including hemorrhage and tissue infarction. However, many vascular lesions will not be detectable by gross examination, and intravenous injection of Monastral blue, Evan’s blue, India ink, or horseradish peroxidase prior to necropsy can be utilized to detect sites of compromised vascular permeability. Subsequent screening of these sites

by microscopic evaluation can determine the extent and type of vascular injury.

Lymphatic vessels typically are not evaluated at necropsy. This choice reflects the fact that large lymphatic vessels are uncommon.

##### 8.3.1.1. PREPARATION OF TISSUES

All isolated vessels, such as aorta, should be sampled by transverse section. Any vessel with gross lesions that suggest either apparent or suspicious vascular damage should be sampled for microscopic evaluation. Microscopic study of the vessels (mainly blood vessels, which are easily identified in H&E-stained sections) in each of the organs routinely sampled at necropsy increases the opportunity to detect vascular changes, particularly in small vessels. Lymphatic vessels typically are examined in association with lymph nodes, although their presence is assured mainly in animals where the nodes may be embedded intact (e.g., rats, mice, and hamsters).

A particular technique to evaluate the mesenteric vasculature in the rat was recently described as this is an important site of both spontaneous and pharmacologic-induced vascular injury in this species. In this method, the entire mesenteric arcade, complete with intestinal tract, is collected and laid flat. The intestines and mesenteric lymph nodes are removed, and the mesentery is rolled up into balls of tissue and placed into a tissue cassette (Pereira Bacares, 2016). Sectioning of the tissue onto a glass slide allows evaluation of multiple cross, longitudinal, and tangential sections of several arteries and their branches.

#### 8.3.2. Microscopic and Biochemical Evaluation

The evaluation procedures described for the heart may also be used for the study of vessels and include light microscopy, electron microscopy, and biochemical analysis. Light microscopic study may include the use of special staining procedures for elastic fibers (Verhoeff’s elastica), collagen (Masson’s trichrome, Movat’s pentachrome), and mucopolysaccharides (PAS). Lipid stains on frozen sections are essential for lesions suspected to contain lipids. IHC methods can be used for both light and transmission electron microscopic study. SEM is especially suited for morphologic evaluation of lesions of the luminal surface.



#### 8.4. Background Alterations, Artifacts, Spontaneous and Age-Related Lesions

Detection of drug-induced coronary artery lesions, such as the hemorrhagic medial necrosis described for minoxidil and other vasoactive compounds, is complicated in the dog by the occurrence of various spontaneous arterial lesions, some of which are poorly characterized. These spontaneous lesions include (1) idiopathic necrotizing arteritis and/or periarteritis, (2) idiopathic extramural coronary arteritis, and (3) various degenerative alterations that include arteriosclerosis of intramural coronary arteries, intimal thickening of extramural coronary arteries, excess mucopolysaccharides, atherosclerosis, amyloidosis, hyalinosis, medial calcification, and arterial necrosis associated with uremia.

Idiopathic necrotizing arteritis and/or polyarteritis ("Beagle pain syndrome" or "idiopathic juvenile polyarteritis") has received considerable attention (Kerns et al., 2001; Snyder et al., 1995). Some but not all dogs with histologically confirmed arterial lesions have a spectrum of distinctive clinical signs that include an altered gait and posture (arched back, lowered head, stiff gait), reluctance to open the mouth, fever, anorexia, and weight loss. The clinical signs are often episodic but tend to be progressive, and affected dogs are generally euthanized for humane reasons. Generally, young dogs are affected, with onset of the clinical disease at 4–9 months of age. The lesions involve small to medium-sized muscular arteries. In some dogs, only the cardiac vessels (particularly the extramural branches of the right coronary artery) are involved, but the spinal and cerebral arteries may be affected in dogs with altered gait and posture. Other sites with affected vessels are the lung, thymus, stomach, thyroid, adrenals, and testis. The microscopic alterations are variable but tend to occur as chronic-active necrotizing arteritis. Fibrinoid necrosis of the arterial walls may be seen with neutrophilic infiltration. However, the inflammatory reaction is usually composed of mononuclear leukocytes and extends from the outer media into the adventitia (Figure 1.23). Intimal thickening and medial fibrosis are present in healing lesions. Secondary degenerative alterations may be present in the

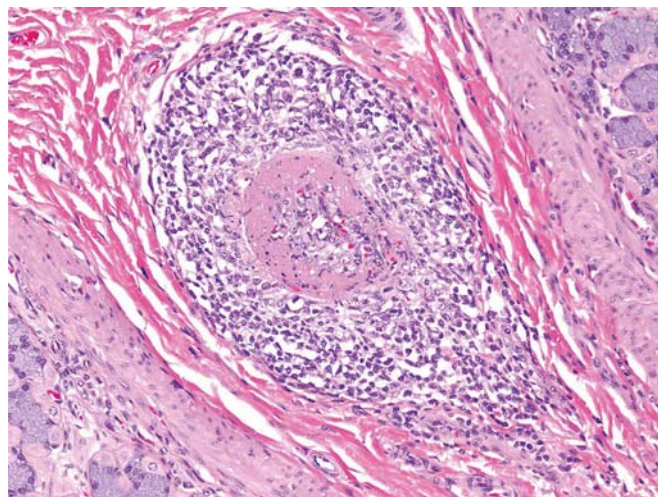


**FIGURE 1.23** Fibrinoid arterial necrosis with perivascular mononuclear cell inflammation as a spontaneous lesion identified in the lamina propria of the stomach of a dog. Formalin-fixed, paraffin-embedded section, H&E stain. Original magnification 20×. Reproduced from Haschek WM, Rousseaux CG, and Wallig MA, editors: *Handbook of toxicologic pathology*, ed 3, 2013, Academic Press, Figure 46.20, p. 1626, with permission.

spinal cord and spinal nerve roots adjacent to affected arteries. The condition is idiopathic although an association with ascariasis (endoparasitism with nematode worms) has been suggested. Immunologically mediated injury also has been suspected, as for Kawasaki disease of children, but has not been confirmed by IHC studies. No evidence of an inherited pattern has been seen. Affected dogs do not show a clinical response to the administration of corticosteroids or antibiotics.

Idiopathic extramural coronary arteritis was observed in 7%–8% of dogs studied by comprehensive sampling of the coronary arteries (Son, 2004). No involvement of extracardiac or intramural myocardial arteries was observed. The lesions were segmental and were found in various portions of the coronary arteries; some dogs had multiple sites of involvement. Microscopic alterations included an extensive adventitial inflammatory reaction with mononuclear or mixed leukocyte infiltration, medial fibrinoid necrosis, and intimal inflammation with fibrosis.

Aged dogs may develop arteriosclerosis (i.e., arterial stiffening) of the intramyocardial arteries, particularly coincident with mitral valve endocardiosis. This arteriosclerosis is



distinguished from arteriosclerosis that may be observed in the intramural coronary arteries of the papillary muscles, even in young dogs (Kohnken and Weber, 2020). Spontaneous degenerative changes may also be observed in the aorta of dogs, including medial mucoid extracellular matrix accumulation (also called cystic medial necrosis) and chondroosseous metaplasia, both of which can occur even in young dogs (Yang and Kohnken, 2021). Medial fibrosis and medial microcalcification are common findings in the aorta of older dogs.

Rodents may have spontaneous focal occurrence of arterial lesions such as mineralization (often at branch points where turbulent blood flow is likely), cartilaginous and/or osseous metaplasia, or medial hypertrophy affecting the walls and perivascular inflammation. These changes are more common in older animals and are not associated with clinical signs.

Aged rats frequently develop polyarteritis nodosa, especially of the mesenteric, pancreaticoduodenal, and testicular arteries although blood vessels in any organ may be affected. Preferred INHAND (International Harmonization of Nomenclature and Diagnostic Criteria) terms for this finding are "Degeneration/necrosis, medial or mural, artery" or else "Necrosis/inflammation, medial or mural, artery," with the choice of term depending on the extent of leukocyte infiltration within the lesion (Berridge et al., 2016a). This lesion is a multisystemic transmural necrotizing vasculitis affecting small or medium-sized muscular arteries. Incidences are often higher in males and vary among strains. Incidences are higher in the spontaneously hypertensive rat, reaching 76.1% in males, and affect numerous vascular beds in this strain (Saito and Kawamura, 1999). The cause in rats is unknown, though a similar disease in juvenile humans is often associated with hepatitis B virus infection. A spontaneous background hepatic artery degeneration and necrosis in young male Sprague–Dawley rats has also been reported with an incidence up to 20%. A medium-sized hepatic artery near the hilus was affected in these cases, featuring mural hemorrhage and fibrinoid necrosis, edema, and inflammatory infiltrates in earlier lesions and with mural fibrosis in more chronic lesions (Carlson and Yee, 2020).

Arteritis is also a common background finding in Göttingen minipigs, and may be observed in a single small- or medium-sized vessel often in the heart, vagina, rectum, epididymis, spinal cord, pancreas, urinary bladder, kidney, or stomach (Dincer et al., 2018; Skydsgaard et al., 2021). The cause in this species is unknown though an immune-mediated etiology has been speculated.

### 8.5. Use of Animals as Models for Vascular Toxicity

Animal models for studies of human vascular disease have mainly centered on research on atherosclerosis and hypertension. Models of atherosclerosis (i.e., arterial stiffening due to intramural deposition of lipid-rich plaques) are numerous and have been developed in birds (pigeon, chicken, turkey, and Japanese quail); zebrafish; nonprimate mammals (rabbit, pig, dog, mouse, and rat); and nonhuman primates (stump-tailed macaque, rhesus monkey, cynomolgus macaque, pigtail macaque, squirrel monkey, baboon, and African Green monkey). None of these models fulfills all of the requirements for an ideal model of human atherosclerosis, including (1) ease in acquiring, maintaining, and manipulating; (2) ability to reproduce in the laboratory; (3) well-defined genetic features; (4) development of lesions similar to those in humans with a similar time course; and (5) development of lesions with consumption of reasonably normal diets. Indeed, the optimal animal model of atherosclerosis should develop various stages of the disease, including fatty streaks, foam cell accumulation, and vulnerable and stable plaques and also develop relevant vascular complications such as calcification, plaque rupture, arterial stenosis, aneurysm, and ideally organ infarcts.

While no animal model is ideally suited to evaluate all of these aspects of a complicated disease, the pig may come closest to a translatable model of atherosclerosis in humans. Pigs have a human-like lipoprotein profile, and when fed a diet high in cholesterol can reach plasma cholesterol levels and develop coronary atherosclerotic lesions that are similar to humans (Getz and Reardon, 2012). The pig is also large enough to allow for noninvasive monitoring of lesion development. Unfortunately, obvious

challenges in terms of cost and husbandry limit the routine use of pigs. Into this gap are emerging transgenic mouse models, combining classical apoE knockout or LDL receptor knockout strains with additional genetic or dietary modifications to allow modeling of particular aspects of atherosclerosis.

Animal models of hypertension can be categorized by the mode of intervention (genetic, renal) or by the key end-organs and mechanisms that drive the hypertension (e.g., enhanced sympathetic nervous system tone, high circulating angiotensin II or aldosterone levels, increases in blood volume). Most models replicate secondary hypertension, as opposed to idiopathic primary hypertension for which the mediators and drivers have largely remained unidentified. Lowering renal blood flow or reducing nephron mass can increase blood pressure by activating the renin-angiotensin-aldosterone system. Genetic models include spontaneously hypertensive rat and Dahl salt-sensitive rat, while minipigs and nonhuman primate models are also emerging. An example is the cross between ApoE<sup>-/-</sup> and fibrillin-1 mutant mice, generating an intriguing model that is characterized by arterial stiffening and atherosclerotic plaque rupture (which is a key clinical concern in human patients) (Van der Donckt et al., 2015).

The Fawn hooded rat develops spontaneous pulmonary hypertension and associated pulmonary vascular alterations (Kuijpers and de Jong, 1986). Increased blood pressure is detectable as early as 5 weeks of age, and steady-state pressures of 80–240 mmHg are reached by 1 year of age. Death results from nephrosclerosis (complicated by the nephrotic syndrome) and/or cardiac failure with chronic pulmonary congestion.

Nonclinical models are also being utilized increasingly in the development of vascular-related medical devices, such as drug-eluting stents, bioresorbable scaffolds, and drug-coated balloons (Perkins and Rippy, 2019). Rodents, rabbits, dogs, sheep, goats, and nonhuman primates have been utilized in these assessments, but in recent years, swine are the most common choice due to the close similarity of their vascular physiology and anatomy compared to humans. These models seek to characterize the performance of the device with regard to its delivery and degradation, the safety and biocompatibility of the device, as well as the efficacy.

## 8.6. Biomarkers of Vascular Injury

Noninvasive biomarker strategies for vascular injury are limited. Measurement of nonspecific biomarkers of inflammation (e.g., erythrocyte sedimentation rate, C-reactive protein, complement assays and circulating immune complexes) has been used in monitoring patients with vasculitis. The diagnostic specificity of these markers is variable. The presence of antineutrophil cytoplasmic antibodies alone also has a low specificity. However, in combination with the presence of antiproteinase-3 or myeloperoxidase antibodies, the sensitivity and specificity for detecting certain types of autoimmune vasculitides is increased. Raised concentrations of cell adhesion molecules such as soluble adhesion molecule-1 (ICAM-1), E-selectin, and vascular cell adhesion molecule-1 (VCAM-1) have been detected in the sera of patients in a variety of vasculitides and other vascular disorders. However, epidemiological studies of these and other proposed vascular biomarkers, including P-selectin, thrombomodulin, thrombopoietin, and glycoprotein IIb/IIIa (GP IIb/IIIa), have yielded poor correlation with clinical disease incidence or outcomes. Therefore, vascular biomarkers are not widely used in nonclinical toxicology research (Pletsch-Borba et al., 2019). Increased amounts of soluble adhesion molecules are thought to reflect endothelial cell activation with upregulation of those substances. Concentrations of von Willebrand Factor (vWF, a marker of endothelial cell damage) have also been examined in relation to vasculitis, as increased vWF levels have been observed in a variety of vascular diseases. However, additional studies are needed to evaluate the role these substances or other biomarkers may play in the diagnosis and assessment of vascular injury.

A study to visualize protease activity associated with vascular remodeling ex vivo in affected vessels has shown that MMP activation and increased vascular leakage correlated well with incidence and severity of reported histopathological findings in rats (Gonzalez et al., 2017). There was also a positive correlation with circulating levels of TIMP 1 and neutrophil gelatinase-associated lipocalin (NGAL). A combined approach to discovery and application of biomarker investigation will likely be needed to make improvements in nonclinical detection and prediction of vascular injury.

## 9. RESPONSES TO INJURY

Vascular injuries may be primary or secondary. Secondary lesions develop as an extension of a disease process in surrounding tissues, while primary vascular diseases result from direct damage to vessels. Primary lesions may be generalized or regional in distribution. Arteries tend to develop significant alterations more frequently than veins, capillaries, and lymphatics. The spectrum of pathologic alterations may include (1) degenerative conditions with accumulation of lipid, mineral deposits or extracellular matrix deposition; (2) degeneration or necrosis of vascular smooth muscle and/or endothelial cells; (3) proliferative lesions of the intima, media, or endothelial basal lamina; and/or (4) inflammation. The etiology of any of these vascular injuries is multifactorial and can be complicated by spontaneous changes and other factors (e.g., aging-related findings). Many of these disorders have a slow progressive course and do not become clinically apparent until a secondary event such as thrombosis and subsequent ischemic injury occurs to destabilize blood flow. However, some of the vascular diseases that are initiated by toxic injury, infectious agents, or immunologically mediated mechanisms develop rapidly and may produce widespread lesions and sometimes clinical signs.

### 9.1. Atherosclerosis Acceleration by Toxic Agents

There is epidemiologic evidence in human patients and direct evidence from studies on animal models of atherosclerosis that exposure to certain chemical agents along with the presence of atherogenic risk factors may enhance the development of atherosclerosis. Chemical substances that have been incriminated include goitrogenic agents, carbon disulfide, benzo[*a*]pyrene, dimethylbenz[*a*]anthracene, homocysteine, CO, fluorocarbons, oral contraceptives (especially those containing mainly progestins), combined hydrochlorothiazide and propranolol therapy, calcium, lead, and soft water.

Morphologic changes of considerable importance are induced by drugs or chemicals that modify atherosclerotic lesions, either by changes in plasma lipids and lipoproteins or by more

direct effects on vascular walls. CO increases capillary permeability and hastens plaque formation in animals fed high-cholesterol diets. The effect of CO might also be due to decreased availability of oxygen since plaque formation is also accelerated in animals exposed to hypoxic conditions. Excessive amounts of homocysteine have been implicated in the pathogenesis of thrombotic and arteriosclerotic vascular disease. Homocysteine can react directly with nitric oxide to form highly reactive S-nitroso-thiol compounds that may mediate potentially harmful secondary biochemical effects. Homocysteine appears to induce a sequence of alterations including platelet adhesion, SMC proliferation, formation of foam cells, and ultimately loss of the endothelial layer at the site of atherogenic lesions. Vascular changes are also attributed to carbon disulfide (CS<sub>2</sub>) as long-term exposure of industrial workers has been associated with a two- to threefold increase in coronary heart disease. CS<sub>2</sub> has been shown to accelerate development of atherosclerosis in rabbits maintained on a high-cholesterol diet. There are at least two mechanisms by which CS<sub>2</sub> might enhance the formation of atherogenic lesions in blood vessels: direct injury to the endothelium, and induction of hypothyroidism with resulting alterations in lipid metabolism. Thiocarbamide, a potent antithyroid substance, is the principal urinary metabolite detected after exposure to CS<sub>2</sub> and may be responsible for the CS<sub>2</sub>-mediated suppression of thyroid glandular activity.

Other toxic substances such as penicillamine and β-aminopropionitrile can cause vascular alterations by inducing changes in connective tissue—an effect that ultimately results in the formation of nonatherosclerotic aneurysms in the aorta and other large arterial vessels. These agents apparently inhibit specific steps in the biosynthetic pathway of connective tissue proteins. Chromium seems to have a significant role in maintaining the integrity of the vasculature. Serum cholesterol levels are elevated and the incidence of atherosclerotic plaques increases when chromium is deficient.

The lesions and sequelae of atherosclerosis are well described. The vessels with the most severe alterations tend to be the muscular and elastic arteries. The pig, rabbit, and chicken are more susceptible compared to the dog, cat, cow, or rat. The initial lesions are fatty streaks (intimal



aggregations of foam cells with vacuolated cytoplasm that are derived from both macrophages and SMCs), which are most readily detected grossly by application of fat stains such as Sudan IV. The hallmark lesion is the raised intimal atheromatous plaque, which develops later. The plaque is composed of lipid deposits together with cells (SMCs, monocytes/macrophages, and a few lymphocytes), connective tissue fibers, and matrix. Atherosclerotic lesions may evolve over time into complicated plaques that may feature mural necrosis with embolism of a component of the plaque, followed by cycles of thrombosis and lumen recanalization at the site of the plaque.

## 9.2. Medial Proliferation

Exposure to certain chemical substances can initiate degenerative or inflammatory alterations in vascular smooth muscle. These toxic effects may occur as a result of excessive pharmacologic activity or by direct reaction of xenobiotics with structural or functional macromolecules in the vascular wall.

Hypertrophy and hyperplasia of SMCs in small muscular arteries and arterioles may result from chronic hypertension, exposure to ergot alkaloids (which cause vasoconstriction) or pyrrolizidine alkaloids (which induce veno-occlusive disease [also termed hepatic sinusoidal obstruction syndrome]), or as an age-related change. In cattle with ergotism and fescue toxicity, the distinctive clinical feature is ischemic necrosis or dry gangrene of the extremities, including the tail, limbs, ears, and nose, due to extended vasoconstriction. These signs are usually present within 10–14 days of initial exposure to fescue pasture. The ergot alkaloids are produced by *Claviceps purpurea*, a fungus that infects rye and other grains and grasses. Tall fescue (*Festuca arundinacea*) parasitized by endophytic fungi such as *Neotyphodium coenophialum* (previously *Epichloe typhina*, *Acremonium coenophialum*) will also produce ergot alkaloids. Arterioles in the ischemic tissue of the extremities will have prominent medial thickening due to proliferated vascular SMCs and may also have fibromuscular intimal proliferation and hyalinization in some peripheral vessels. Vasoconstriction of the distal extremities is also hypothesized to play a role in vascular injury

and leakage produced by vildagliptin, a dipeptidyl peptidase-4 (DPP-4) inhibitor, in cynomolgus monkeys (Hoffmann et al., 2017).

## 9.3. Intimal Proliferation

Intimal proliferative lesions of arteries (characterized by infiltration and proliferation of vascular SMCs, glycosaminoglycan and collagen production, and endothelial hypertrophy) have been observed with use of estrogen- or progesterone-containing oral contraceptives in women (Figure 1.24), chronic administration of ergotamine and methylsergide maleate in human patients, exposure to talc or magnesium silicate exposure in intravenous drug users, and administration of allylamine or phosphodiesterase inhibitors to rats. Fibromuscular intimal proliferation in small and medium-sized arteries

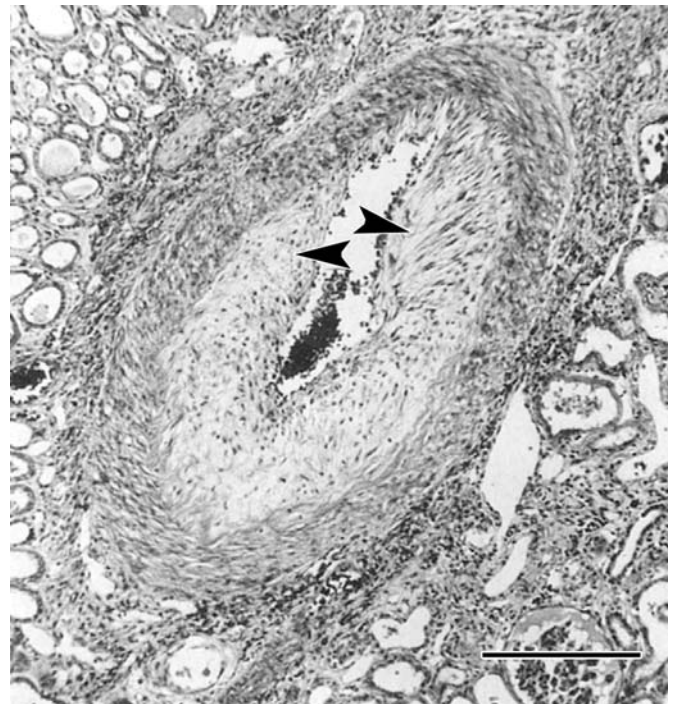


**FIGURE 1.24** Severe fibromuscular intimal proliferation (pale zone [denoted by arrowheads]) separating the endothelium and tunica media) attributed to long-term oral contraceptive use affecting a renal artery of a woman. Formalin-fixed, paraffin-embedded section, Movat pentachrome stain. Bar = 400  $\mu$ m. Courtesy of Dr H.A. McAllister, Jr, St. Luke's Episcopal Hospital, Houston, TX; Reproduced from Haschek WM, Rousseaux CG, and Wallig MA, editors: *Handbook of toxicologic pathology*, ed 2, 2002, Academic Press, Figure 20, p. 420, with permission.



(such as coronary arteries) occurs in rats given allylamine. Metabolism of allylamine yields acrolein, a substance that can denature proteins and disrupt nucleic acid synthesis. This metabolite is thought to be responsible for other more subtle changes, such as medial hypertrophy and proliferation of vascular smooth muscle.

The intimal lesions produced by ergotamine and methylsergide maleate are primarily fibroblastic in elastic and large muscular arteries but involve fibromuscular hyperplasia in medium and small arteries. Similar fibrotic lesions may also occur in cardiac valves and endocardium of affected patients. The pathogenesis of the intimal proliferative lesions is not clear, but it is suggested that these agents directly stimulate fibroblastic proliferation or act indirectly via serotonin mediation of the proliferative response.

#### 9.4. Calcification

Arterial medial calcification is a frequent lesion in animals. The vascular lesions may

involve both elastic and muscular arteries and often occur concurrently with endocardial mineralization. The toxic etiologies for arterial calcification include calcinogenic plant toxicosis and vitamin D toxicosis. Vitamin D toxicosis may occur acutely, as it does in dogs exposed to cholecalciferol-containing rodenticides, or from chronic ingestion of food containing excess vitamin D fortification. Affected arteries appear grossly as solid, dense pipe-like structures or as raised white solid intimal plaques. Microscopically, prominent basophilic granular mineral deposits are present either on elastic fibers of the media of elastic arteries or as a complete ring of mineralization involving the internal elastic lamina and the medial musculature of muscular arteries ([Figure 1.25](#)).

The calcinogenic plants (*Cestrum diurnum*, *Trisetum flavescens*, *Solanum malacoxylon*, *Solanum torvum*) contain the active metabolite of vitamin D<sub>3</sub> (1,25-dihydroxycholecalciferol) or its glycoside. Different names have been given to these plant-induced syndromes in various areas of the world,

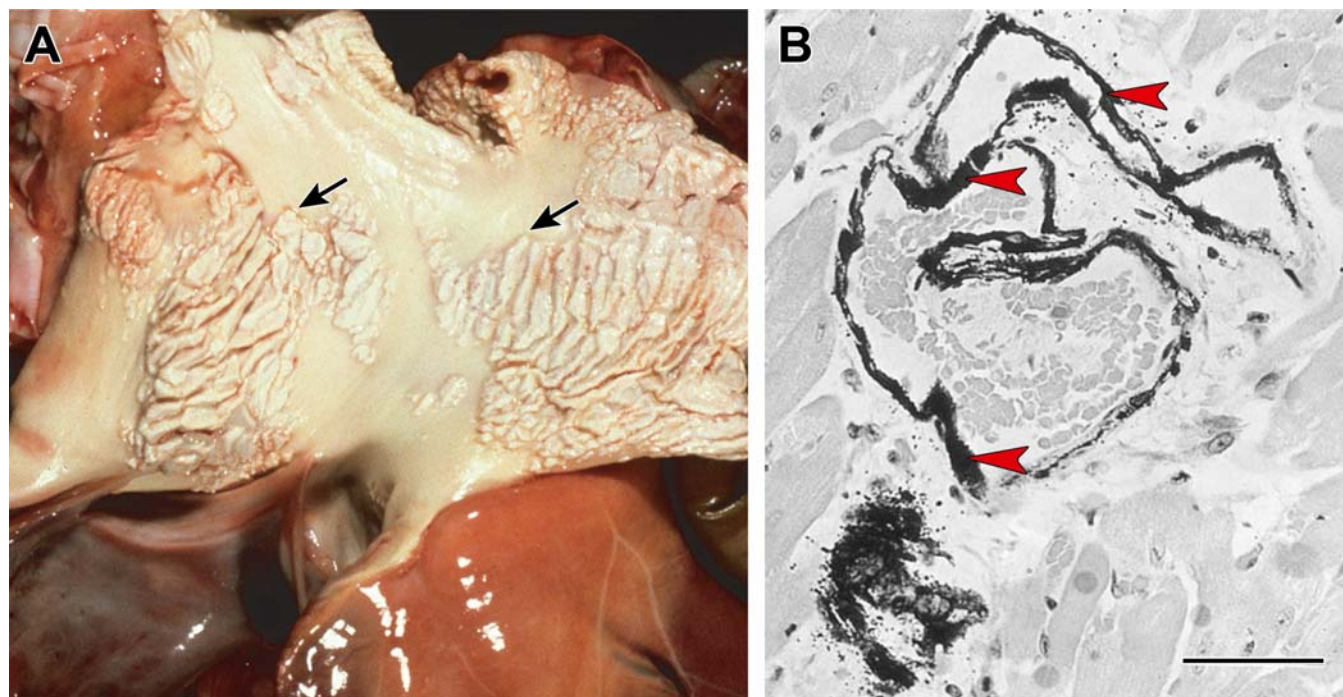


**FIGURE 1.25** (A) Aortic mineralization in a calf. The surface of the aorta has raised, irregular, white plaque-like lesions (*arrows*) scattered over the pale yellow intimal surface due to dystrophic mineralization; the heart is present below the aorta. (B) Medial calcification (*dark material at arrowheads*) and focal myocyte calcification (*bottom left corner*) in the ventricular myocardium of a rat with acute vitamin D toxicosis. Formalin-fixed, paraffin-embedded section, von Kossa stain. Bar = 100 mm. (A) Reproduced from Haschek WM, Rousseaux CG, and Wallig MA, editors: *Fundamentals of toxicologic pathology*, ed 2, 2010, Academic Press, Figure 12.19A, p. 361, with permission; (B) Reproduced from Haschek WM, Rousseaux CG, and Wallig MA, editors: *Handbook of toxicologic pathology*, ed 2, 2002, Academic Press, Figure 21, p. 421, with permission.

including “Manchester wasting disease” in Jamaica, “enzootic calcinosis” in Europe, “naa-helu disease” in Hawaii, “enteque seco” in Argentina, and “espichamento” in Brazil.

### 9.5. Aneurysms

Localized weakening of the wall of large elastic arteries results in formation of aneurysms. The lesion is produced by exposure to *Lathyrus* sp. (termed lathyrism); administration of  $\beta$ -aminopropionitrile (the active principle of *Lathyrus* sp.), penicillamine or aminoacetonitrile (copper chelators); and copper deficiency. Dissecting aneurysms of the aorta are produced in turkeys fed  $\beta$ -aminopropionitrile. The mechanism of lesion production by these agents is inhibition of lysyl oxidase, a copper-containing enzyme involved in crosslinking of collagen and elastin (which are essential ingredients for normal strength of the walls of elastic arteries).

### 9.6. Medial Hemorrhagic Necrosis

Arterial lesions with necrosis of medial smooth muscle and medial hemorrhage have been observed following treatment with a variety of vasoactive substances. Examples are minoxidil, with right atrial vascular damage and hemorrhage in dogs and left atrial hemorrhage in pigs (Figure 1.26); hydralazine and nicorandil, with right atrial hemorrhage and medial necrosis and hemorrhage in muscular arteries in dogs; theobromine, which produces right atrial lesions in dogs; diazoxide, which produces left atrial lesions in pigs; digoxin, which produces right atrial and biventricular lesions in dogs; norepinephrine, which produces small disseminated myocardial necrosis and more diffuse arterial injury involving cardiac, hepatic, and mesenteric vessels in dogs, rabbits, and cats; epinephrine, which produces lesions similar to those of norepinephrine; and phosphodiesterase type III inhibitors such as SK&F 94120

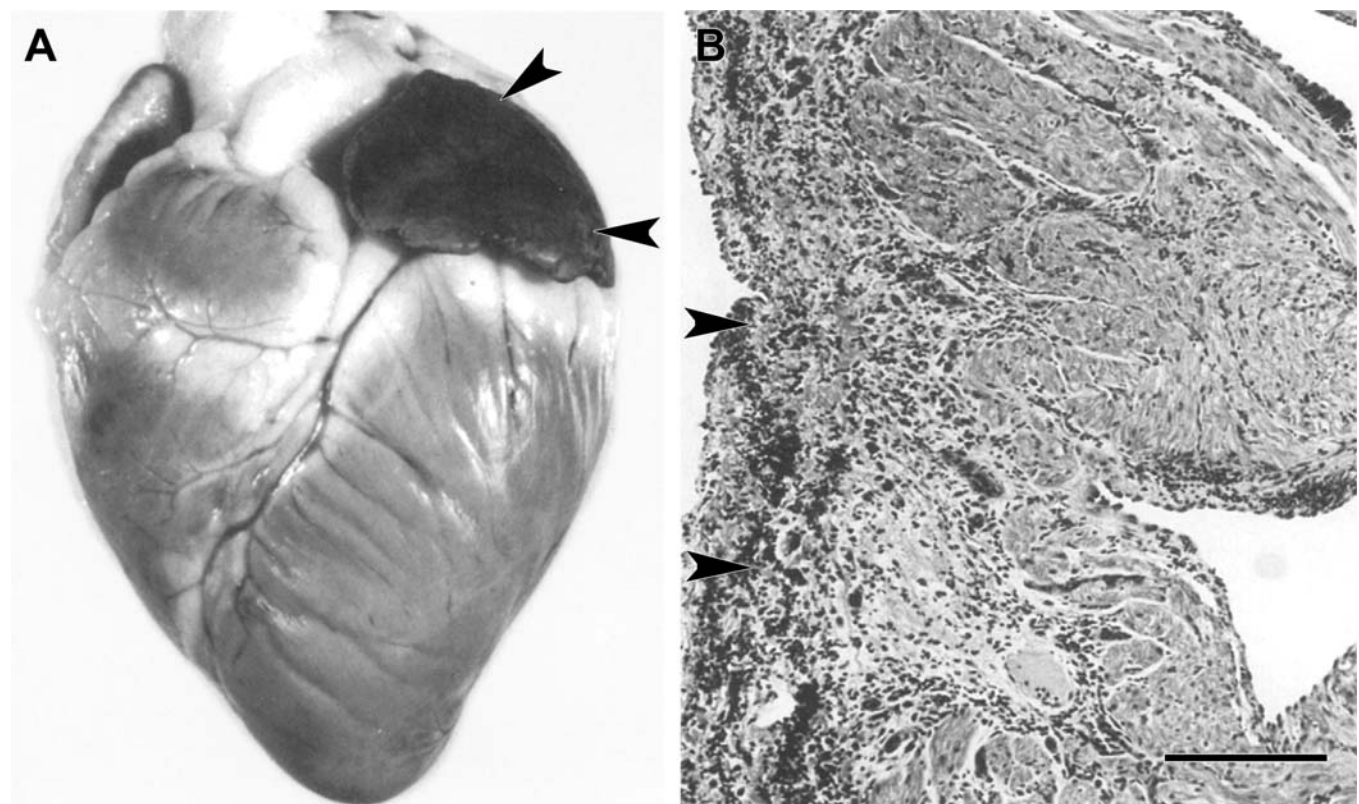


**FIGURE 1.26** Atrial hemorrhage in the left atrium of a pig given minoxidil, a modulator of  $K^+$  channel activity in vascular smooth muscle cells, orally at 10 mg/kg. (A) Gross image of the heart with discolored left atrial appendage (arrowheads). (B) Prominent epicardial and endocardial hemorrhage. Formalin-fixed, paraffin embedded section, H&E stain. Bar = 400  $\mu$ m. Reproduced from Haschek WM, Rousseaux CG, and Wallig MA, editors: *Handbook of toxicologic pathology*, ed 2, 2002, Academic Press, Figures 22 and 23, pp. 421 and 422, with permission.



(5-(4-acetamidophenyl)pyrazin-2(1H)-one), a inotrope/vasodilator drug, high doses of which produce necrotizing arteritis in dogs, most frequently in the right atrium; and CI-930 (4,5-dihydro-6-(4-(1H-imidazole-1-yl)-phenyl)-5-methyl-3(2H)-pyridazinone monohydrochloride) which produces hemorrhages, arterial lesions, and focal myocardial necroses in dogs and monkeys. Medial necrosis of coronary arteries also occurs following administration of an endothelin receptor antagonist to monkeys and dogs, and an antihypertensive adenosine agonist to monkeys.

Arterial mediolysis, a lesion featuring splitting and necrosis of the media with abundant medial hemorrhage, has been described as an idiopathic finding in the kidney of pigs and as a result of racetopamine administration in the splanchnic abdominal arteries of greyhound dogs (Leifsson and Slavin, 2015). The pathogenesis is thought to derive from neuromodulation of the peripheral sympathetic nervous system by this  $\beta_2$  adrenergic agonist, leading to release of norepinephrine that stimulates  $\alpha_1$  receptors at the adventitia-media junction (Slavin and Yaeger, 2012).

### 9.7. Fibrinoid Necrosis

Accumulation of serum proteins and polymerized fibrin in the wall of small arteries following endothelial damage results in a distinctive eosinophilic homogenous appearance of the media of the affected vessels (Figure 1.27). This lesion has been described in cerebral vessels of pigs and guinea pigs with organic mercury toxicosis, and in those of nonhuman primates and dogs with lead toxicosis. Fibrinoid necrosis may also occur as a consequence of acute hypertension, or as a spectrum of changes associated with infectious or immune-mediated injury to endothelial cells.

Fibrinoid necrosis of small veins is considered to be the primary lesion in horses with phenylbutazone toxicosis. This finding appears to be the basis for renal medullary necrosis and oral and GI ulceration. The loss of endothelial cells and formation of thrombi may also occur.

### 9.8. Microangiopathy

Cadmium administration to rats results in hemorrhagic testicular necrosis due to selective

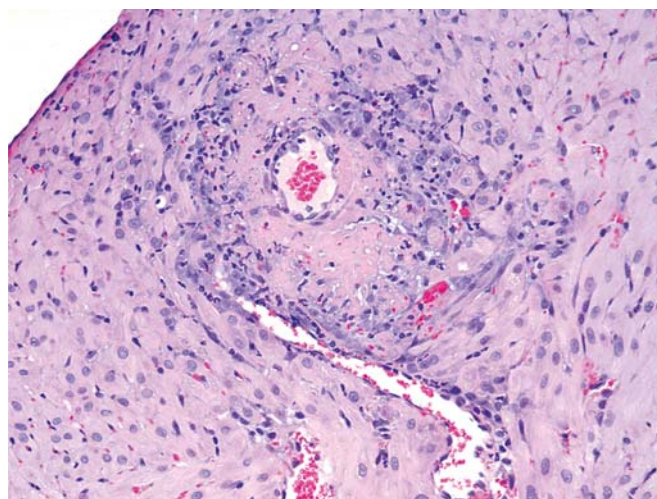


**FIGURE 1.27** Fibrinoid necrosis of a coronary artery in a rat given a vascular endothelial growth factor (VEGF) inhibitor. The wall of the artery is replaced by homogeneous pink material representing deposits of fibrin and plasma proteins. These deposits extend into the perivascular tissues, which exhibit increased numbers of basophilic nuclei due to perivascular inflammation. Formalin-fixed, paraffin embedded section, H&E stain. Original magnification 20 $\times$ . Reproduced from Haschek WM, Rousseaux CG, Wallig MA, editors: *Haschek and Rousseaux's handbook of toxicologic pathology*, ed 3, 2013, Academic Press, Figure 46.24, p. 1631, with permission.

damage to testicular capillary endothelium. Microthrombosis and hemorrhage have been produced in the heart by administration of cyclophosphamide.

### 9.9. Immune-Mediated Vascular Inflammation

Vascular inflammatory lesions associated with drugs are divided into hypersensitivity vasculitis, immune-complex mediated injury, toxic vascular injury, and lupus-like syndromes. Drug-induced vascular injury usually affects all three layers of predominately small-sized vessels (arterioles, venules, and capillaries). Medium-sized muscular arteries, such as coronary arteries, are occasionally involved, but large arteries and veins are usually not targets of drug-induced vasculitis.

Aside from direct toxicity, immune-mediated vasculitis can result from exposure to sensitizing compounds which act as haptens, presumably combining with the host's own proteins and inducing formation of appropriate antibodies.

Predominant components involved in the inflammatory reaction include eosinophils and mononuclear cells. The induction of vasculitis is not dose- or time-dependent and appears to be related to the deposition of soluble immune complexes in the vessel wall and to the activation of the complement system. Penicillin, sulfonamides, methyl-dopa, procainamide, quinidine, and a number of other drugs and chemicals have been implicated in causing this type of reaction in humans.

### 9.9.1. Hypersensitivity Vasculitis

This condition commonly includes the vascular lesions associated with serum sickness, systemic bacterial infections, protozoal infections, reactions to influenza vaccines, and drug-related vasculitides. The lesions are characterized by a predominantly mononuclear leukocytic infiltrate and occasional eosinophils within the outer media, in the absence of fibrinoid necrosis or necrotizing lesions of the vessel wall. The endothelial lining of involved arterial and venous channels is intact and free of thrombi.

Various drugs have been found to induce a hypersensitivity-type vascular injury (ampicillin, procainamide, dextran, hydralazine, penicillin, sulfonamide, tetracycline, propylthiouracil, quinidine, allopurinol, and phenylbutazone). This type of drug-induced vasculitis is neither dose- nor time-dependent. The lack of a dose-dependent response and the clinical presentation suggest that this form of drug-related vasculitis is a delayed hypersensitivity phenomenon and may be related to haptenic binding.

### 9.9.2. Immune Complex-Mediated Vascular Injury

Multiorgan vascular and perivascular inflammation is the most common histologic manifestation of immune complex disease in nonhuman primates exposed to a nonnative protein (such as a humanized or fully human therapeutic antibody) (Vahle, 2018). The kidney is a particularly common site for such findings due to the tortuosity of the capillaries in and around the glomerular tuft, so glomerulonephritis is also a common feature. Biotherapeutics, and in particular monoclonal antibodies, can induce immunogenicity through a variety of mechanisms leading to immune complex formation and type III hypersensitivity reaction (which is characterized by intravascular deposition of insoluble immune complexes, activation of complement, and release of inflammatory mediators that result in the

pathologic finding). Complement-related vascular effects are a key event in the development of vasculitis following administration of biotherapeutics (Frazier et al., 2015). Following complement activation, endothelial cells are activated, leukocytes adhere and translocate across the endothelium, and vascular permeability is increased. C5a and the membrane attack complex (MAC) are key drivers of vascular injury and act by conferring a proinflammatory/procoagulant phenotype to endothelial cells as well as mediating vascular permeability. Complement activation is also implicated in the pathogenesis of antisense oligonucleotide (ASO)-induced vasculitis in the absence of immune complex formation (Engelhardt et al., 2015).

Common sites of vascular inflammation include small- to medium-sized vessels in the serosa or mesentery, gall bladder, pancreas, urogenital tract, ciliary body and uvea of the eye, glomerular capillaries in the kidney, aortic root, and extramural coronary arteries of the heart. Morphologic features include fibromuscular intimal hyperplasia with loss of endothelial cells and disruption of the internal elastic lamina, prominent mural or adventitial lymphocytic infiltrates with occasional neutrophils, and hemorrhage. Medial degeneration and fibrinoid vascular necrosis are uncommon but may occur in advanced lesions. Immunohistochemical evaluation with demonstration of immune complexes and/or complement components may be helpful in confirming the pathogenesis of such lesions.

### 9.9.3. Lupus-Like Syndromes

Considerable evidence now exists that drug-induced lupus occurs not in a random population that develops drug hypersensitivity but among individuals with an intrinsic predisposition to the syndrome. The mechanism by which these drugs cause or unmask the lupus-like syndrome is unknown. It is suggested that the drug either modifies nucleoprotein antigenicity or reinforces the antigenicity of circulating DNA that is normally present in small amounts.

## 9.10. Regeneration and Repair

The consequences of vascular injury are multiple. Most injuries will heal by repair with fibrosis rather than by regeneration to restore normal structure to the affected vessel. Vascular endothelial cells are an exception to this generalization. When the affected area of the vessel is



small, the endothelium is repaired by spreading and migration of neighboring endothelial cells to cover the damage site. If lesions are extensive, cell proliferation is also required in addition to cell migration to replace irreversibly damaged cells and reestablish the continuity of the endothelium. If needed to support reconstitution of the endothelial layer, pluripotent (CD34<sup>+</sup>) stem cells are recruited from the bone marrow and other sites so that they can differentiate into endothelial cells at the site of injury (Jiang et al., 2021).

However, residual damage and cascades of clotting events more often follow vascular injuries. Damage to the endothelial layer and the other layers of arterial walls may initiate thrombosis with subsequent regional ischemic injury of the organ in the circulatory field. Repeated thrombosis and recanalization may ultimately result in substantial stenosis (narrowing) or full occlusion of the affected vessel, requiring neoangiogenesis to produce new satellite blood vessels that can restore perfusion to the affected tissue. Other injuries may result in damage to the integrity of the vascular media with dilatation and potential rupture of the vessel. Some healed lesions will result in only minor structural and functional alterations of the affected vessels and thus will be detected only as incidental lesions by microscopic study.

## 10. VASCULAR TOXICITY IN SPECIFIC ORGANS

There is increasing evidence that blood vessels vary in their pharmacologic and toxicologic responses to chemical substances. It is known that the heterogeneity in responsiveness occurs not only between veins and arteries but also between anatomically similar vessels in different regions of the circulatory system. A similar spectrum of differences is also reported to exist for microvessels. Differential responses may be related to distribution/exposure to the toxic substance, local microenvironment, and unique characteristics of a particular vascular bed. Most vasoactive xenobiotics are widely distributed throughout the vascular tree and are therefore capable of system-wide activity. However, rapid metabolism, such as that of acetylcholine in the blood, or effective removal, such as that of the prostaglandins of the lung, can lead to limited effects of these substances to particular vascular

beds. Likewise, if a significant amount of a xenobiotic is bound to plasma albumin, as occurs with diazoxide, the concentration of the substance reaching the vessel will be less than expected.

Differences in responsiveness may be due to external influences such as innervation and the local humoral environment. Other differences may result from internal cellular differences in the receptor subpopulation and composition, differences in endothelial junctions, and the specific processes responsible for cellular electrical activity and the release and uptake of Ca<sup>2+</sup>. These and other factors are likely to contribute to the variety of vascular toxicities observed in different organs.

### 10.1. Brain

The integrity of the blood-brain barrier (BBB) depends on the metabolic status of the endothelial cells as well as on the effectiveness of their tight junctions (see *Nervous System*, Vol 4, Chap 8). Certain divalent cations, high concentrations of norepinephrine and serotonin, and pentylenetetrazol-induced convulsions disrupt the junctions, leading to increases in cerebrovascular permeability. Hypertonic solutions of various substances (e.g., salt, urea, mannitol) cause shrinking of vascular endothelium and separation of tight junctions, leading to opening of the BBB. In newborn rats exposed to lead, widening of tight junctions, increased permeability, and a significant impairment of the BBB are known to occur. These effects are thought to be due to the avid reaction of lead with sulfhydryl groups in critical cellular proteins. A variety of chemical substances, such as alcohols and other lipid solvents, cobra venom, surfactants, and high concentrations of sulfhydryl reactants, also can increase cerebral vascular permeability. These compounds are disruptive to cell membranes and capillaries. Antineoplastic agents such as cyclophosphamide induce alterations in a number of vascular areas. This substance causes hemorrhagic lesions in both the cerebral and visceral vasculatures. High doses of amphetamine have caused damage to cerebral arteries, possibly as a result of hypertension.

### 10.2. Lungs

Pulmonary edema (abnormal accumulation of fluid in pulmonary alveoli) due to increased permeability of alveolar capillaries can occur following

inhalation of irritant substances, exposure of endothelial cells through intravenous administration of xenobiotics, or excessive intravenous infusion of fluid (see *Respiratory System*, Vol 5, [Chap 4](#)). Most agents induce direct injury to pulmonary capillary walls. Toxicants such as arsenic and  $\alpha$ -naphthylthiourea also affect the vasculature of the lungs, leading to pulmonary edema ([Allison et al., 1989](#)). Exposure to oxygen ( $O_2$ ) causes vascular toxicity in the lungs and eyes of premature or full-term infants. In rats, exposure to 60% oxygen (instead of the normal atmospheric level of 21%) for several days will increase pulmonary capillary volume and thickness leading to perivascular edema. Exposure to higher oxygen pressure (1–4 atm) of short duration (2–4 h) leads to partial or total occlusion of capillaries and morphologic evidence of damage to endothelial cells. Chronic exposure to ozone ( $O_3$ ) causes pulmonary arterial lesions that result in thickening of the arterial walls. Ultrastructural changes in the alveolar capillaries have also been found. Other mechanisms besides direct vascular damage may permit fluid to escape into the airways. Intravenously administered opiates, such as heroin and methadone, may modify central neurogenic influences on pulmonary capillary permeability.

Monocrotaline, a pyrrolizidine alkaloid, causes structural remodeling of pulmonary blood vessels and delayed pulmonary hypertension in rats. The onset of hypertension is preceded by ultrastructural changes such as evagination of vascular SMCs with loss of myofilaments. Bacterial endotoxins adversely affect many vascular beds (see *Bacterial Toxins*, Vol 3, [Chap 9](#)). In the lung, increased vascular permeability and pulmonary hypertension are reported following exposure to endotoxins.

A direct or indirect effect of IL-2 on endothelial cells may damage the vascular endothelium, increase vascular permeability, and induce a vascular leak syndrome in the lungs and other tissues. Clinical features of vascular injury in the lungs may include hemoptysis, cough, shortness of breath, wheezing, and pleurisy.

### 10.3. Heart

Ergonovine and vasopressin cause marked constriction of coronary arteries. ECG signs such as ST segment depression indicate that the resulting coronary spasm may lead to myocardial hypoxia. In chronic animal studies, methylsergide has produced coronary intimal proliferation and

vascular occlusion. The coronary vasculature is a target site for the toxic effects of bacterial endotoxin. Infusion of endotoxin causes severe coronary artery damage, which ultimately results in arterial stenosis rather than luminal restoration. Minoxidil, a long-acting vasodilating drug, induces a hemorrhagic lesion in Beagle dogs and miniature swine that is most consistently present in the atria ([Figure 1.26](#)). The hemorrhages often are associated with lesions that involve small coronary arteries and are characterized by endothelial injury, intramural accumulations of erythrocytes and platelets, perivascular hemorrhage, fibrin deposits, and inflammation. The pathogenesis of the coronary artery lesions produced by minoxidil is not known. Various other vasoactive drugs, such as phosphodiesterase inhibitors and endothelin-1 antagonists, are also capable of inducing coronary artery lesions. The minoxidil-induced vascular lesions conform morphologically to the lesions induced by subcutaneous insertion of sterile inert plastic pellets over the cremaster muscles of rats. This procedure results in arteriolar lesions characterized by focal dilation, endothelial damage, and increased permeability. It has been suggested that the lesion is caused by release of endogenous mediators affecting the vascular smooth muscle or the endothelial cells.

Inflammation and necrosis of the extramural coronary arteries are also commonly featured in juvenile polyarteritis in Beagle dogs. This condition can be exacerbated by xenobiotic exposure. This finding also occurs as a target of immune-complex deposition-mediated vascular injury in nonhuman primates administered a nonnative protein xenobiotic such as a therapeutic antibody.

### 10.4. Liver

Liver toxins such as DMN produce a hemorrhagic necrosis that ultimately leads to complete venous occlusion. Oxaliplatin, pyrrolizidine alkaloids, and other potent small molecules delivered by chemotherapeutic antibody-drug conjugates can cause hepatic sinusoidal obstruction syndrome (previously called veno-occlusive disease) ([Kohnken et al., 2022](#)). This disease is initiated by damage to sinusoidal endothelial cells, ultimately leading to sinusoidal capillarization and remodeling, venous fibrosis, and portal hypertension. The vascular bed of the liver can also be altered by bacterial endotoxins (see *Bacterial Toxins*, Vol 3, [Chap 9](#)). These agents affect the microcirculation by causing swelling of

endothelial cells and adhesion of platelets to sinusoid walls. Certain agents causing chronic hepatitis (oxyphenisatin, nitrofurantoin) or cirrhosis (ethanol, arsenicals, methotrexate) ultimately induce portal hypertension.

### 10.5. Kidney

A number of agents causing renal cellular damage may also affect renal blood vessels (see Kidney, Vol 5, Chap 2). Any xenobiotic that will cause constriction of preglomerular or relaxation of postglomerular vessels will exert a negative effect on glomerular filtration rate. Inorganic lead causes vasoconstriction of the preglomerular vessels and, ultimately, sclerosis of these vessels. Renal toxicity caused by lead, cadmium, and some analgesics is at times associated with increases in systemic arterial pressure because of alterations in the renal blood pressure regulatory systems. Long-term exposure to cadmium in rats has caused thickening of renal arterioles and diffuse fibrosis of capillaries, alterations that may be responsible for the resulting salt and water retention and hyperreninemia seen after exposure to this agent. Vascular lesions are produced in renal and splanchnic arteries of rats given intravenous infusions of the dopaminergic agent fenoldopam mesylate. Hypersensitivity reactions induced by a number of substances (gold salts and D-penicillamine in humans and mercuric chloride in experimental animals) consistently cause immune-complex deposits on the basement membranes of glomerular capillaries. Glomerular capillaries are also a classic site of immune complex deposition secondary to administration of nonnative proteins, which results in fibrinoid vascular necrosis and inflammation within the glomerular tuft and occasionally in efferent/afferent arterioles. Hematuria, renal failure, nephrosis, and hypertension have all been associated with vascular alterations in the kidney.

### 10.6. Stomach

Acetylsalicylic acid given to rats produces early alterations in the basement membrane of the endothelial cells of capillaries and postcapillary venules. These changes subsequently may cause small vessel damage in the gastric mucosa.

## 11. CONCLUSION

The CV system is a dynamic integration of form and function composed of the muscular pump, the valves that ensure unidirectional flow of blood, and the blood vessels that transport that blood. Injury to the components of the cardiovascular system can have serious consequences for the survival of the organism.

Accordingly, evaluations of xenobiotic effects on the CV system should include assessments of both structural morphology and function of the heart and vessels. Like most biological systems, the CV system has a discrete number of ways of responding to injury. Those responses form the focus of the varying ways of evaluating xenobiotic-induced changes, including the morphological assessments that comprise the core of the toxicologic pathology discipline.

A broad spectrum of xenobiotics from heavy metals, industrial chemicals, plant and animal toxins, and drugs have been demonstrated to have the potential to affect the CV system. Our understanding of the mechanisms of those effects is variable. Advances in cell-based and mechanistic modeling technologies will permit us to leverage our growing mechanistic understanding of CV toxicity to provide additional insights to improve safety testing and human risk assessment.

## REFERENCES

- Allison RC, Rippe B, Prasad VR, et al.: Pulmonary vascular permeability and resistance measurements in control and ANTU-injured dog lungs, *Am. J. Physiol.* 256:H1711-H1718, 1989.
- Alter P, Herzum M, Soufi M, et al.: Cardiotoxicity of 5-fluorouracil, *Cardiovasc. Hematol. Agents Med. Chem.* 4:1-5, 2006.
- Altman PL, Dittmer DS: Heart and pumping action. In Altman PL, Dittmer DS, editors: *Respiration and circulation*, 1971, pp 227-356. Bethesda, MD.
- Amin AS, Tan HL, Wilde AAM: Cardiac ion channels in health and disease, *Heart Rhythm* 7:117-126, 2010.
- Anderson PA, Rankin JS, Arentzen CE, et al.: Evaluation of the force-frequency relationship as a descriptor of the inotropic state of canine left ventricular myocardium, *Circ. Res.* 39: 832-839, 1976.
- Anderton MJ, Mellor HR, Bell A, et al.: Induction of heart valve lesions by small-molecule ALK5 inhibitors, *Toxicol. Pathol.* 39:916-924, 2011.

- Anonymous. In Services HAH, editor: *The non-clinical evaluation of the potential for delayed ventricular repolarization (QT interval prolongation) by human pharmaceuticals*, 2005, Food and Drug Administration. <https://www.fda.gov/regulatory-information/searchfda-guidance-documents/s7b-nonclinical-evaluation-potential-delayed-ventricular-repolarization-qt-interval-prolongation>. (Accessed 30 May 2024).
- Anonymous: Guidance on nonclinical safety studies for the conduct of human clinical trials for marketing authorization for pharmaceuticals M3(R2). In *International conference on harmonisation of technical requirements for registration of pharmaceuticals for human use*, 2009.
- Anonymous: Safety pharmacology studies for human pharmaceuticals S7A. In Services HaH, editor: *International conference on harmonisation of technical requirements for registration of pharmaceuticals for human use*, 2020, Food and Drug Administration.
- Apple FS, Murakami MM, Ler R, et al.: Analytical characteristics of commercial cardiac troponin I and T immunoassays in serum from rats, dogs, and monkeys with induced acute myocardial injury, *Clin. Chem.* 54:1982–1989, 2008.
- Ayers KM, Jones SR: The cardiovascular system. In Benirschke K, Garner FM, Jones TC, editors: *Pathology of laboratory animals*, New York, NY, 1978, Springer-Verlag, pp 1–69.
- Balazs T, Herman EH: Toxic cardiomyopathies, *Ann. Clin. Lab. Sci.* 6:467–476, 1976.
- Barish R, Gates E, Barac A: Trastuzumab-induced cardiomyopathy, *Cardiol. Clin.* 37:407–418, 2019.
- Barth N, Muscholl E: The effects of the tricyclic antidepressants desipramine, doxepin and iprindole on the isolated perfused rabbit heart, *Naunyn-Schmiedeberg's Arch. Pharmacol.* 284:215–232, 1974.
- Bell RM, Mocanu MM, Yellon DM: Retrograde heart perfusion: the Langendorff technique of isolated heart perfusion, *J. Mol. Cell. Cardiol.* 50:940–950, 2011.
- Benowitz NL: Cardiotoxicity in the workplace, *Occup. Med. (Phila.)* 7:465–478, 1992.
- Bergers G, Song S: The role of pericytes in blood-vessel formation and maintenance, *Neuro Oncol.* 7:452–464, 2005.
- Berridge BR, Mowat V, Nagai H, et al.: Non-proliferative and proliferative lesions of the cardiovascular system of the rat and mouse, *J. Toxicol. Pathol.* 29:1s–47s, 2016a.
- Berridge BR, Pettit S, Walker DB, et al.: A translational approach to detecting drug-induced cardiac injury with cardiac troponins: consensus and recommendations from the Cardiac Troponins Biomarker Working Group of the Health and Environmental Sciences Institute, *Am. Heart J.* 158:21–29, 2009.
- Berridge BR, Schultze AE, Heyen JR, et al.: Technological advances in cardiovascular safety assessment decrease preclinical animal use and improve clinical relevance, *ILAR J.* 57:120–132, 2016b.
- Bers DM: Cardiac excitation-contraction coupling, *Nature* 415:198–205, 2002.
- Bertero E, Maack C: Metabolic remodelling in heart failure, *Nat. Rev. Cardiol.* 15:457–470, 2018.
- Bhatt S, Northcott C, Wisnialowski T, et al.: Preclinical to clinical translation of hemodynamic effects in cardiovascular safety pharmacology studies, *Toxicol. Sci.* 169:272–279, 2019.
- Boor PJ: Allylamine cardiotoxicity: metabolism and mechanism. In Spitzer J, editor: *Myocardial injury*, New York, NY, 1983, Plenum, pp 533–543.
- Bowes J, Brown AJ, Hamon J, et al.: Reducing safety-related drug attrition: the use of in vitro pharmacological profiling, *Nat. Rev. Drug Discov.* 11:909–922, 2012.
- Boyce JT, Boyce RW, Gundersen HJ: Choice of morphometric methods and consequences in the regulatory environment, *Toxicol. Pathol.* 38:1128–1133, 2010.
- Braverman IM, Sibley J, Keh-Yen A: A study of the veil cells around normal, diabetic, and aged cutaneous microvessels, *J. Invest. Dermatol.* 86:57–62, 1986.
- Carlson T, Yee L: Spontaneous necrotizing hepatic arteriopathy in male Sprague-Dawley rats, *Toxicol. Pathol.* 48:905–908, 2020.
- Cheng H, Kari G, Dicker AP, et al.: A novel preclinical strategy for identifying cardiotoxic kinase inhibitors and mechanisms of cardiotoxicity, *Circ. Res.* 109:1401–1409, 2011.
- Cohen IL, Perkins RJ, Bilen Z, et al.: Continuous hemodynamic monitoring: an integrated invasive-noninvasive approach using the Fick principle, *Appl. Cardiopulm. Pathophysiol.* 3:351–359, 1991.
- Cohen JD, Babiarz JE, Abrams RM, et al.: Use of human stem cell derived cardiomyocytes to examine sunitinib mediated cardiotoxicity and electrophysiological alterations, *Toxicol. Appl. Pharmacol.* 257:74–83, 2011.
- Colton HM, Stokes AH, Yoon LW, et al.: An initial characterization of N-terminal-proatrial natriuretic peptide in serum of Sprague Dawley rats, *Toxicol. Sci.* 120:262–268, 2011.
- Combs AB, Acosta D: Toxic mechanisms of the heart: a review, *Toxicol. Pathol.* 18:583–596, 1990.
- Connolly HM, Crary JL, McGoon MD, et al.: Valvular heart disease associated with fenfluramine phentermine, *N. Engl. J. Med.* 337:581–588, 1997.
- Constantin I, Tăbăran AF: Dissection techniques and histological sampling of the heart in large animal models for cardiovascular diseases, *J. Vis. Exp.* 184, 2022.
- Crivellente F, Tontodonati M, Fasdelli N, et al.: NT-proBNP as a biomarker for the assessment of a potential cardiovascular drug-induced liability in beagle dogs, *Cell Biol. Toxicol.* 27:425–438, 2011.
- Danson S, Blackhall F, Hulse P, et al.: Interstitial lung disease in lung cancer: separating disease progression from treatment effects, *Drug Saf.* 28:103–113, 2005.
- Demkow U, Stelmaszczyk-Emmel A: Cardiotoxicity of cisplatin-based chemotherapy in advanced non-small cell lung cancer patients, *Respir. Physiol. Neurobiol.* 187:64–67, 2013.
- Dincer Z, Piccicuto V, Walker UJ, et al.: Spontaneous and drug-induced arteritis/polyarteritis in the Göttingen minipig-review, *Toxicol. Pathol.* 46:121–130, 2018.
- Dunnick JK, Kissling G, Gerken DK, et al.: Cardiotoxicity of Ma Huang/cafeine or ephedrine/cafeine in a Rodent model system, *Toxicol. Pathol.* 35:657–664, 2007.



- Engelhardt JA, Fant P, Guionaud S, et al.: Scientific and regulatory policy committee points-to-consider paper\*: drug-induced vascular injury associated with nonsmall molecule therapeutics in preclinical development: Part 2. Antisense oligonucleotides, *Toxicol. Pathol.* 43:935–944, 2015.
- Falcioni L, Bua L, Tibaldi E, et al.: Report of final results regarding brain and heart tumors in Sprague-Dawley rats exposed from prenatal life until natural death to mobile phone radiofrequency field representative of a 1.8 GHz GSM base station environmental emission, *Environ. Res.* 165:496–503, 2018.
- Ferreira ALA, Matsubara LS, Matsubara BB: Anthracycline-induced cardiotoxicity, *Cardiovasc. Hematol. Agents Med. Chem.* 6:278–281, 2008.
- Frazier KS, Engelhardt JA, Fant P, et al.: Scientific and regulatory policy committee points-to-consider paper\*: drug-induced vascular injury associated with nonsmall molecule therapeutics in preclinical development: Part I. Biotherapeutics, *Toxicol. Pathol.* 43:915–934, 2015.
- Fujita S, Puri R, Yu ZX, et al.: Interleukin-1 $\alpha$  reduces the severity of the vascular leak syndrome produced by interleukin-2 and interleukin-2 plus interferon- $\alpha$ , *Toxicol. Pathol.* 22:381–397, 1994.
- Gad SC, Leslie SW, Acosta D: Inhibitory actions of butylated hydroxytoluene on isolated ileal, atrial, and perfused heart preparations, *Toxicol. Appl. Pharmacol.* 49:45–52, 1979.
- Gandini C, Castoldi AF, Candura SM, et al.: Carbon monoxide cardiotoxicity, *J. Toxicol. Clin. Toxicol.* 39:35–44, 2001.
- Geiger S, Lange V, Suhl P, et al.: Anticancer therapy induced cardiotoxicity: review of the literature, *Anti Cancer Drugs* 21:578–590, 2010.
- Getz GS, Reardon CA: Animal models of atherosclerosis, *Arterioscler. Thromb. Vasc. Biol.* 32:1104–1115, 2012.
- Glass C, Lafata KJ, Jeck W, et al.: The role of machine learning in cardiovascular pathology, *Can. J. Cardiol.* 38:234–245, 2022.
- Gonzales RJ, Carter RW, Kanagy NL: Laboratory demonstration of vascular smooth muscle function using rat aortic ring segments, *Adv. Physiol. Educ.* 24:13–21, 2000.
- Gonzalez RJ, Lin SA, Bednar B, et al.: Vascular imaging of matrix metalloproteinase activity as an informative preclinical biomarker of drug-induced vascular injury, *Toxicol. Pathol.* 45:633–648, 2017.
- Grimm FA, Klaren WD, Li X, et al.: Cardiovascular effects of polychlorinated biphenyls and their major metabolites, *Environ. Health Perspect.* 128:77008, 2020.
- Hailey JR, Maleeff BE, Thomas HC, et al.: A diagnostic approach for rodent progressive cardiomyopathy and like lesions in toxicology studies up to 28 days in the Sprague Dawley rat (Part 1 of 2), *Toxicol. Pathol.* 45:1043–1054, 2017a.
- Hailey JR, Maleeff BE, Thomas HC, et al.: A diagnostic approach for rodent progressive cardiomyopathy and like lesions in toxicology studies up to 28 days in the Sprague Dawley rat (Part 2 of 2), *Toxicol. Pathol.* 45:1055–1066, 2017b.
- Hall AH, Isom GE, Rockwood GA: *Toxicology of cyanides and cyanogens: experimental, applied and clinical aspects*, 2015, John Wiley & Sons.
- Hamilton NB, Attwell D, Hall CN: Pericyte-mediated regulation of capillary diameter: a component of neurovascular coupling in health and disease, *Front. Neuroenergetics* 2, 2010.
- Hanton G: Preclinical cardiac safety assessment of drugs, *Drugs R D* 8:213–228, 2007.
- Hanton G, Longeart L, Lodola A: Cardiotoxicity of hydralazine and minoxidil in the rat. Influence of age, *Res. Commun. Chem. Pathol. Pharmacol.* 71:231–234, 1991.
- Hasinoff BB, Patel D: The lack of target specificity of small molecule anticancer kinase inhibitors is correlated with their ability to damage myocytes in vitro, *Toxicol. Appl. Pharmacol.* 249:132–139, 2010.
- Helke KL, Nelson KN, Sargeant AM, et al.: Background pathological changes in minipigs: a comparison of the incidence and nature among different breeds and populations of minipigs, *Toxicol. Pathol.* 44:325–337, 2016.
- Herman E, Vick J, Burka B: The cardiovascular actions of ellipticine, *Toxicol. Appl. Pharmacol.* 18:743–751, 1971.
- Herman EH, Ferrans VJ: Preclinical animal models of cardiac protection from anthracycline-induced cardiotoxicity, *Semin. Oncol.* 25:15–21, 1998.
- Herman EH, Ferrans VJ, Young RSK, et al.: A comparative study of minoxidil-induced myocardial lesions in beagle dogs and miniature swine, *Toxicol. Pathol.* 17:182–192, 1989.
- Herman EH, Knapton A, Rosen E, et al.: A multifaceted evaluation of imatinib-induced cardiotoxicity in the rat, *Toxicol. Pathol.* 39:1091–1106, 2011.
- Hew KW, Keller KA: Postnatal anatomical and functional development of the heart: a species comparison, *Birth Defects Res. B Dev. Reprod. Toxicol.* 68:309–320, 2003.
- Hoffmann P, Martin L, Keselica M, et al.: Acute toxicity of vildagliptin, *Toxicol. Pathol.* 45:76–83, 2017.
- Hoffmann P, Warner B: Are hERG channel inhibition and QT interval prolongation all there is in drug-induced torsadogenesis? A review of emerging trends, *J. Pharmacol. Toxicol. Methods* 53:87–105, 2006.
- Iqbal A, Iqbal MK, Sharma S, et al.: Molecular mechanism involved in cyclophosphamide-induced cardiotoxicity: old drug with a new vision, *Life Sci.* 218:112–131, 2019.
- Jankus EF, Noren GR, Staley NA: Furazolidone-induced cardiac dilatation in turkeys, *Avian Dis.* 16:958–961, 1972.
- Jespersen B, Knupp L, Northcott CA: Femoral arterial and venous catheterization for blood sampling, drug administration and conscious blood pressure and heart rate measurements, *J. Vis. Exp.* 59, 2012.
- Jiang C, Qian H, Luo S, et al.: Vasopressors induce passive pulmonary hypertension by blood redistribution from systemic to pulmonary circulation, *Basic Res. Cardiol.* 112: 21, 2017.
- Jiang L, Chen T, Sun S, et al.: Nonbone marrow CD34(+) cells are crucial for endothelial repair of injured artery, *Circ. Res.* 129:e146–e165, 2021.
- Kaabia Z, Poirier J, Moughaizel M, et al.: Plasma lipidomic analysis reveals strong similarities between lipid fingerprints in human, hamster and mouse compared to other animal species, *Sci. Rep.* 8:15893, 2018.

- Kaese S, Frommeyer G, Verheule S, et al.: The ECG in cardiovascular-relevant animal models of electrophysiology, *Herzschrittmachertherap. Elektrophysiol.* 24:84–91, 2013.
- Kawashima T, Sasaki H: Gross anatomy of the human cardiac conduction system with comparative morphological and developmental implications for human application, *Ann. Anat.* 193:1–12, 2011.
- Kennedy CC, Brown EE, Abutaleb NO, et al.: Development and application of endothelial cells derived from pluripotent stem cells in microphysiological systems models, *Front. Cardiovasc. Med.* 8:625016, 2021.
- Kerkelä R, Grazette L, Yacobi R, et al.: Cardiotoxicity of the cancer therapeutic agent imatinib mesylate, *Nat. Med.* 12: 908–916, 2006.
- Kerns WD, Roth L, Hosokawa S: Idiopathic canine polyarteritis. In Mohr U, Carlton W, Dungworth D, et al., editors: *Pathobiology of the aging dog*, Ames, IA, 2001, Iowa State University Press, pp 118–126.
- Kligfield P, Gettes LS, Bailey JJ, et al.: Recommendations for the standardization and interpretation of the electrocardiogram: part I: the electrocardiogram and its technology: a scientific statement from the American heart association electrocardiography and arrhythmias committee, council on clinical cardiology; the American college of cardiology foundation; and the heart rhythm society: endorsed by the international society for computerized electrocardiology, *Circulation* 115:1306–1324, 2007.
- Klotz JL, McDowell KJ: Tall fescue ergot alkaloids are vasoactive in equine vasculature, *J. Anim. Sci.* 95:5151–5160, 2017.
- Kohnken R, Falahatpisheh H, Janardhan KS, et al.: Anatomic and clinical pathology characterization of drug-induced sinusoidal obstruction syndrome (Veno-Occlusive disease) in cynomolgus macaques, *Toxicol. Pathol.* 50:13–22, 2022.
- Kohnken R, Weber A: Characterization of spontaneous vascular findings in the papillary muscles of beagle dogs, *Toxicol. Pathol.* 48:899–904, 2020.
- Kragel AH, Travis WD, Feinberg L, et al.: Pathologic findings associated with interleukin-2-Based immunotherapy for cancer: a postmortem study of 19 patients, *Hum. Pathol.* 21: 493–502, 1990.
- Kuijpers MH, de Jong W: Spontaneous hypertension in the fawn-hooded rat: a cardiovascular disease model, *J. Hypertens. Suppl.* 4:S41–S44, 1986.
- Kuncl RW: Agents and mechanisms of toxic myopathy, *Curr. Opin. Neurol.* 22:506–515, 2009.
- Laird-Fick HS, Tokala H, Kandola S, et al.: Early morphological changes in cardiac mitochondria after subcutaneous administration of trastuzumab in rabbits: possible prevention with oral selenium supplementation, *Cardiovasc. Pathol.* 44:107159, 2020.
- Lawrence CL, Pollard CE, Hammond TG, et al.: Nonclinical proarrhythmia models: predicting Torsades de Pointes, *J. Pharmacol. Toxicol. Methods* 52:46–59, 2005.
- Leifsson PS, Slavin RE: Segmental arterial mediolysis in pigs presenting with renal infarcts, *Vet. Pathol.* 52:1157–1162, 2015.
- Lewis-Israeli YR, Wasserman AH, Gabalski MA, et al.: Self-assembling human heart organoids for the modeling of cardiac development and congenital heart disease, *Nat. Commun.* 12:5142, 2021.
- Luo H, Yang D, Barszczyk A, et al.: Smartphone-based blood pressure measurement using transdermal optical imaging technology, *Circ. Cardiovasc. Imaging* 12:e008857, 2019.
- Mahler GJ, Butcher JT: Cardiac developmental toxicity. In *Birth defects res C embryo today*, vol 93, pp 291–297.
- Mathur A, Ma Z, Loskill P, et al.: In vitro cardiac tissue models: current status and future prospects, *Adv. Drug Deliv. Rev.* 96:203–213, 2016.
- McGarrah RW, Crown SB, Zhang GF, et al.: Cardiovascular metabolomics, *Circ. Res.* 122:1238–1258, 2018.
- Mellor HR, Bell AR, Valentin JP, et al.: Cardiotoxicity associated with targeting kinase pathways in cancer, *Toxicol. Sci.* 120:14–32, 2011.
- Nirschl JJ, Janowczyk A, Peyster EG, et al.: A deep-learning classifier identifies patients with clinical heart failure using whole-slide images of H&E tissue, *PLoS One* 13: e0192726, 2018.
- Noren GR, Staley NA, Einzig S, et al.: Alcohol-induced congestive cardiomyopathy: an animal model, *Cardiovasc. Res.* 17:81–87, 1983.
- Oun R, Rowan E: Cisplatin induced arrhythmia; electrolyte imbalance or disturbance of the SA node? *Eur. J. Pharmacol.* 811:125–128, 2017.
- Packer M: Cobalt cardiomyopathy, circulation: heart failure, *Circulation* 9:e003604, 2016.
- Palate BM, Denoël SR, Roba JL: A simple method for performing routine histopathological examination of the cardiac conduction tissue in the dog, *Toxicol. Pathol.* 23:56–62, 1995.
- Pereira Bacares ME: Sampling the rat mesenteric artery: a simple technique, *Toxicol. Pathol.* 44:1166–1169, 2016.
- Perkins LEL, Rippey MK: Balloons and stents and scaffolds: preclinical evaluation of interventional devices for occlusive arterial disease, *Toxicol. Pathol.* 47:297–310, 2019.
- Perotti A, Cresta S, Grasselli G, et al.: Cardiotoxic effects of anthracycline-taxane combinations, *Expert Opin. Drug Saf.* 2:59–71, 2003.
- Pesco-Koplowitz L, Gintant G, Ward R, et al.: Drug-induced cardiac abnormalities in premature infants and neonates, *Am. Heart J.* 195:14–38, 2018.
- Pletsch-Borba L, Grafetstätter M, Hüsing A, et al.: Biomarkers of vascular injury in relation to myocardial infarction risk: a population-based study, *Sci. Rep.* 9:3004, 2019.
- Polk A, Vistisen K, Vaage-Nilsen M, et al.: A systematic review of the pathophysiology of 5-fluorouracil-induced cardiotoxicity, *BMC Pharmacol. Toxicol.* 15:47, 2014.
- Reagan WJ: Troponin as a biomarker of cardiac toxicity: past, present, and future, *Toxicol. Pathol.* 38:1134–1137, 2010.

- Reddy P, Hemsworth J, Guthridge KM, et al.: Ergot alkaloid mycotoxins: physiological effects, metabolism and distribution of the residual toxin in mice, *Sci. Rep.* 10:9714, 2020.
- Robinson BD, Shaji CA, Lomas A, et al.: Measurement of microvascular endothelial barrier dysfunction and hyperpermeability in vitro, *Methods Mol. Biol.* 1717:237–242, 2018.
- Roden DM: Predicting drug-induced QT prolongation and torsades de pointes, *J. Physiol.* 594:2459–2468, 2016.
- Rowinsky EK: Current developments in antitumor antibiotics, epipodophyllotoxins, and vinca alkaloids, *Curr. Opin. Oncol.* 3:1060–1069, 1991.
- Sage MD: Ultrastructural alterations to myocytes and associated microvascular functional changes at lateral margins of developing experimental myocardial infarcts, *J. Mol. Cell. Cardiol.* 18(Suppl 4):17–21, 1986.
- Sage MD, Gavin JB: The development and progression of myocyte injury at the margins of experimental myocardial infarcts, *Pathology* 17:617–622, 1985.
- Saito N, Kawamura H: The incidence and development of periarteritis nodosa in testicular arterioles and mesenteric arteries of spontaneously hypertensive rats, *Hypertens. Res.* 22:105–112, 1999.
- Sala L, Ward-van Oostwaard D, Tertoolen LGJ, et al.: Electrophysiological analysis of human pluripotent stem cell-derived cardiomyocytes (hPSC-CMs) using multi-electrode arrays (MEAs), *J. Vis. Exp.* 123, 2017.
- Santostasi G, Kuttu RK, Krishna G: Increased toxicity of anthracycline antibiotics induced by calcium entry blockers in cultured cardiomyocytes, *Toxicol. Appl. Pharmacol.* 108: 140–149, 1991.
- Sarazan RD: Cardiovascular pressure measurement in safety assessment studies: technology requirements and potential errors, *J. Pharmacol. Toxicol. Methods* 70:210–223, 2014.
- Sguilla FS, Tedesco AC, Bendhack LM: A membrane potential-sensitive dye for vascular smooth muscle cells assays, *Biochem. Biophys. Res. Commun.* 301:113–118, 2003.
- Shen J-B, Vassalle M: Barium-induced diastolic depolarization and controlling mechanisms in Guinea pig ventricular muscle, *J. Cardiovasc. Pharmacol.* 28:385–396, 1996.
- Skydsgaard M, Dincer Z, Haschek WM, et al.: International harmonization of nomenclature and diagnostic criteria (INHAND): nonproliferative and proliferative lesions of the minipig, *Toxicol. Pathol.* 49:110–228, 2021.
- Slavin RE, Yaeger MJ: Segmental arterial mediolysis—an iatrogenic vascular disorder induced by ractopamine, *Cardiovasc. Pathol.* 21:334–338, 2012.
- Snyder PW, Kazacos EA, Hogenesch H, et al.: Pathologic features of naturally occurring juvenile polyarteritis in beagle dogs, *Vet. Pathol.* 32:337–345, 1995.
- Son WC: Idiopathic canine polyarteritis in control beagle dogs from toxicity studies, *J. Vet. Sci.* 5:147–150, 2004.
- Strauer BE, Scherpe A: Experimental hyperthyroidism II. Mechanics of contraction and relaxation of isolated ventricular myocardium, *Basic Res. Cardiol.* 70:131–141, 1975.
- Tertoolen LGJ, Braam SR, van Meer BJ, et al.: Interpretation of field potentials measured on a multi electrode array in pharmacological toxicity screening on primary and human pluripotent stem cell-derived cardiomyocytes, *Biochem. Biophys. Res. Commun.* 497:1135–1141, 2018.
- Tokarz DA, Steinbach TJ, Lokhande A, et al.: Using artificial intelligence to detect, classify, and objectively score severity of rodent cardiomyopathy, *Toxicol. Pathol.* 49:888–896, 2021.
- Tomanek RJ, Busch TL: Coordinated capillary and myocardial growth in response to thyroxine treatment, *Anat. Rec.* 251: 44–49, 1998.
- Truskey GA: Human microphysiological systems and organoids as in vitro models for toxicological studies, *Front. Public Health* 6:185, 2018.
- Tu C, Cunningham NJ, Zhang M, et al.: Human induced pluripotent stem cells as a screening platform for drug-induced vascular toxicity, *Front. Pharmacol.* 12:613837, 2021.
- Ueda Y, Kovacs S, Reader R, et al.: Heritability and pedigree analyses of hypertrophic cardiomyopathy in rhesus macaques (*Macaca Mulatta*), *Front. Vet. Sci.* 8:540493, 2021.
- Vahle JL: Immunogenicity and immune complex disease in preclinical safety studies, *Toxicol. Pathol.* 46:1013–1019, 2018.
- Van der Donckt C, Van Herck JL, Schrijvers DM, et al.: Elastin fragmentation in atherosclerotic mice leads to intraplaque neovascularization, plaque rupture, myocardial infarction, stroke, and sudden death, *Eur. Heart J.* 36:1049–1058, 2015.
- Van Vleet JF, Ferrans VJ: Furazolidone-induced congestive cardiomyopathy in ducklings: myocardial ultrastructural alterations, *Am. J. Vet. Res.* 44:1014–1023, 1983a.
- Van Vleet JF, Ferrans VJ: Furazolidone-induced congestive cardiomyopathy in ducklings: regression of cardiac lesions after cessation of furazolidone ingestion, *Am. J. Vet. Res.* 44: 1007–1013, 1983b.
- Vicente J, Zusterzeel R, Johannesen L, et al.: Mechanistic model-informed proarrhythmic risk assessment of drugs: review of the “CiPA” initiative and design of a prospective clinical validation study, *Clin. Pharmacol. Ther.* 103:54–66, 2018.
- Vick JA, Herman EH: An isolated dog or monkey heart preparation for studying cardioactive compounds, *Pharmacology* 6:290–299, 1971.
- Vidal JD, Drobatz LS, Holliday DF, et al.: Spontaneous findings in the heart of Mauritian-origin cynomolgus macaques (*Macaca fascicularis*), *Toxicol. Pathol.* 38:297–302, 2010.
- Wallis R, Gharanei M, Maddock H: Predictivity of in vitro non-clinical cardiac contractility assays for inotropic effects in humans—A literature search, *J. Pharmacol. Toxicol. Methods* 75:62–69, 2015.
- Wenceslau CF, McCarthy CG, Earley S, et al.: Guidelines for the measurement of vascular function and structure in isolated arteries and veins, *Am. J. Physiol. Heart Circ. Physiol.* 321:H77–H111, 2021.
- Xu J, Shi GP: Vascular wall extracellular matrix proteins and vascular diseases, *Biochim. Biophys. Acta* 1842:2106–2119, 2014.
- Yang C, Kohnken R: Age-related changes in the canine aorta, *Vet. Pathol.* 58:376–383, 2021.

Yasui H, Morishima M, Nakazawa M, et al.: Developmental spectrum of cardiac outflow tract anomalies encompassing transposition of the great arteries and dextroposition of the aorta: pathogenic effect of extrinsic retinoic acid in the mouse embryo, *Anat. Rec.* 254:253–260, 1999.

Yonpam R, Gobbet J, Jadhav A, et al.: Vasoactive effects of acute ergot exposure in sheep, *Toxins* 13, 2021.

Yoshizawa K, Kissling GE, Johnson JA, et al.: Chemical-induced atrial thrombosis in NTP rodent studies, *Toxicol. Pathol.* 33:517–532, 2005.



# Kidney

Kendall S. Frazier<sup>1</sup>, Marshall S. Schiccitano<sup>2</sup>, Kathleen Heinz-Taheny<sup>3</sup>,  
Rachel E. Cianciolo<sup>4</sup>

<sup>1</sup>Private Consultant, Alligator Point, FL, United States, <sup>2</sup>IQVIA, Durham, NC, United States, <sup>3</sup>Eli Lilly, Indianapolis, IN, United States, <sup>4</sup>Zoetis Reference Laboratories, Cincinnati, OH, United States

## OUTLINE

1. Introduction	87	4.2. Morphologic Response	148
2. Structure, Function, and Cell Biology	89	5. Mechanisms of Toxicity	157
2.1. Renal Ontogeny	89	5.1. Nephrotoxicity Classification	159
2.2. Renal Structure	91	5.2. Mechanisms of Glomerular Toxicity	160
2.3. Renal Function	100	5.3. Mechanisms of Interstitial Injury	168
2.4. Renal Cell Biology	109	5.4. Mechanisms of Proximal Tubular Injury	172
3. Evaluation of Toxicity	113	5.5. Other Sites of Renal Injury	188
3.1. Physiologic Considerations	113	5.6. Renal Carcinogenesis	191
3.2. Biochemical and Biomarker Evaluations	116	6. Issues in Drug Development	199
3.3. Morphologic Evaluation	129	6.1. Animal Models	199
3.4. Testing for Renal Carcinogenic Potential	137	6.2. Adversity	202
3.5. In Vitro Techniques	139	7. Conclusion	206
3.6. Scoring Schemes	145	Acknowledgments	207
3.7. Computational Pathology	146	References	207
4. Responses to Injury	147		
4.1. Physiologic, Molecular, and Biochemical Response	147		

## 1. INTRODUCTION

Kidneys perform many important physiological functions to maintain normal homeostasis in the body, including excretion of waste products of metabolism, regulation of body water and salt, maintenance of extracellular fluid volume and

acid–base balance, and elimination of waste substances such as drugs and chemicals and their breakdown products. The kidney is a very common toxicologic target organ for pharmaceutical therapeutic agents, chemicals, and environmental toxins, and lesions of the upper urinary tract are therefore frequently encountered in

preclinical toxicologic studies. The kidney is particularly susceptible because of the high blood flow to this organ relative to its mass, and proportionally high renal excretion associated with many drugs and chemicals. In addition, the unique propensity of renal tubule epithelium in concentrating urine and its constituents results in higher local concentration and compound exposure than other organs or tissues. The kidney is further susceptible to injury because of inherent high metabolic activity and high oxygen consumption of renal epithelium (especially when high local concentrations are achieved in toxicity studies), and the significant transporter activity of renal tubule epithelium resulting in cell-specific uptake of metabolites from both urinary and blood interfaces. Drug–drug interactions, when agents are administered in combination, may further complicate and promulgate toxicologic injury. The specific pattern of renal injury is dependent on the nature of the drug, its toxicokinetic properties, clearance profile, and particular metabolic attributes, and ultimately on the local tissue concentration of the agent and length of time of exposure. Renal injury may occur as a result of direct effects on tubules or glomeruli or indirectly via altered hemodynamics. In toxicology, refinement of risk assessment requires specific knowledge of the molecular, biochemical, and structural effects of drugs and chemicals at the cellular and subcellular levels which can enable the toxicologic pathologist to suggest potential mechanisms of action for nephrotoxics. Drug- and chemical-associated renal injury represents a very important cause of morbidity in humans, and may occur in both acute and chronic forms. About 20%–30% of intensive care unit patients and 2%–5% of hospitalized patients will develop drug-induced acute renal insufficiency. A myriad of therapeutic agents are injurious to the kidney of humans including anti-cancer agents such as cisplatin, antifungal agents, antibiotics such as gentamicin or other aminoglycosides, proton pump inhibitors (PPIs), contrast agents, and, most commonly, with analgesic nonsteroidal antiinflammatory drugs. The eventual outcome of drug intoxications can result in dialysis dependency and/or necessitate kidney transplantation. In the last decade, there has been an increasing incidence of immune-mediated glomerular injury in patients related to the growing use of biologic therapies and immunomodulating drugs. Unfortunately, nephrotoxicity is often identified late in drug development

programs, with only about 2% of drug attrition occurring during preclinical studies. However, 19% of drug attrition during phase 3 studies is attributable to renal injury. Medical nephrology has advanced markedly in the past 2 decades, and renal pathology has mirrored this progress, with the advent of digital imaging, routine immunofluorescent and ultrastructural analysis of biopsies, individualized medicine based on cellular/molecular characterization of renal insults, and computational pathologic approaches to disease diagnosis. Nonclinical toxicologic pathology has been slower to accept and incorporate these new approaches routinely into toxicity studies, but nephropathologists across academia and in industry have made significant strides in applying novel renal biomarkers, molecular mechanistic investigative studies, pharmacokinetic modeling of kidney, state-of-the-art imaging approaches, and computational pathologic analysis to more fully understand nephrotoxicity in nonclinical studies at the mechanistic level and therefore to better apply findings for clinical translation of risk.

In the safety assessment of new molecular entities, multiple separate analyses comparing nonclinical and clinical data have demonstrated the strong concordance in response to xenobiotics when rodent and nonrodent toxicity study data are applied in combination to clinical risk assessment ([Anderson et al., 2009](#)). For example, a study in 2018, spanning 70 years and over 3000 drugs, indicated there is a high concordance for predictivity of kidney toxicity in rats as compared to human which strongly supports the rat as good choice for toxicity model of clinical renal hazard ([Clark and Steger-Hartmann, 2018](#)). However, there are some important exceptions including immune-mediated drug injury in humans, and xenobiotic-associated alpha<sub>2</sub>-globulin nephropathy in rats. Safety assessment based on data from otherwise normal laboratory animals can be challenging compared with the many complicating factors in human drug-induced renal injury, such as age-associated variability in renal structure and function, or concomitant conditions affecting renal functions, such as hydration status, hypertension, heart failure, or cirrhosis. The toxic effect exposures or human safety margins are therefore difficult to extrapolate precisely from laboratory animals to humans because of these variable risk factors for renal toxicity. This chapter emphasizes the

structural and biochemical changes that occur in nephrotoxicity and the potential mechanisms involved. Gross, microscopic, and ultrastructural anatomy is presented, followed by physiologic considerations, notable species, sex- and age-related differences in susceptibility to nephrotoxicity, and occurrence of common spontaneous renal diseases in laboratory animals that may complicate interpretation of renal findings. Screening strategies for new chemicals, potential mechanisms of renal injury, and newer methods to characterize these mechanisms are reviewed using specific drug and chemical examples for illustration.

## 2. STRUCTURE, FUNCTION, AND CELL BIOLOGY

### 2.1. Renal Ontogeny

There are two embryonic kidney precursors, the pronephros and mesonephros, which ultimately undergo regression; any interruption in their growth could result in renal aplasia or agenesis. In mammals, the embryological development of the permanent kidney (metanephros) begins when the tip of the mesonephric duct, known as the ureteric bud, invades the undifferentiated mesenchyme. The ureteric bud and metanephric mesenchyme undergo complex interactions during renal development. During development, several discrete steps generate the kidney's three-dimensional (3D) pattern, including specific branch types, regional differential growth of stems, the specific axes of growth (corticomedullary, dorsoventral, and rostrocaudal), and the temporal progression of the pattern. Branching tubulogenesis of the ureteric bud is critically important for proper kidney morphology. When the ureteric bud of the metanephros interacts with loose mesenchymal cells and begins growing, branching, and differentiating, mesenchymal cells simultaneously condense around elongating metanephric buds forming the basis for nephrogenesis, and eventually resulting in the formation of tubules and glomeruli. Just after regression of the pronephros, excretory tubules of the mesonephros first appear, lengthen rapidly, form first comma-shaped structures, then S-shaped loops. Most early mesonephric structures regress via apoptosis, and do

not persist in the metanephros. S-shaped bodies are reformed in the metanephros from elongating tubules. These S-shaped bodies eventually form elongated structures which differentiate into both proximal and distal tubules in the metanephric kidney, as well as eventually into glomeruli. Endothelial cells are situated or trapped in the curves of these S-shaped bodies and result in the formation of capillary loops. S-shaped bodies curl around a tuft of capillaries that together will form a glomerulus at their medial extremity. Primitive structures subsequently fold in on each other, and with the simultaneous incorporation of developing vascular tufts, develop into mature glomeruli (Owen and Heywood, 1986; McMahon, 2016; Al-Awqati and Goldberg, 1998). Continuous lengthening of the excretory tubule results in formation of the proximal convoluted tubule (PCT), loop of Henle, and distal convoluted tubule (DCT). The ureteric bud forms branching tubules that eventually differentiate into the collecting ducts and the ureter down to its insertion in the bladder trigone. Concomitantly, the cells of the metanephric mesenchyme differentiate into epithelial cells (through a process of epithelial-mesenchymal transition [EMT]) that will eventually develop into remaining components of the nephron. The kidney therefore develops from two sources—metanephric mesoderm, which forms excretory units, and the ureteric bud, which forms the collecting ducts, pelvis, and ureter (McMahon, 2016). In mammals, the kidney initially develops in the pelvic region before ascending into the abdomen. Various growth factors are intimately involved in this process and are precisely timed to induce epithelial proliferation, migration, and folding, including epidermal growth factor (EGF), fibroblast growth factors, insulin-like growth factors (IGFs), vascular endothelial growth factor (VEGF), and particularly the transforming growth factor-beta family members, among several others. The WT1, PAX 2/8, and BCL2 genes have been identified as being especially important in regulating normal branching morphogenesis and nephron differentiation during nephrogenesis. Both the ureteric bud and the metanephric blastema progenitor cells require canonical Wnt/ $\beta$ -catenin signaling for normal morphogenesis. Derangement in gene expression induced by genetic mutations, environmental factors, or prenatal

xenobiotic renal exposure can result in congenital abnormalities of the kidney. The neonatal kidney in all species is smaller than the adult kidney, but will increase in mass during the pediatric growth period in a species-specific manner. However, the number of glomeruli remains constant between birth and maturity, with increased kidney volume mainly due to increased tubule mass. Development of the human kidney begins with the formation of the pronephros as early as gestational week (GW) 3, followed by the mesonephros at 4 weeks and the metanephros at 5 weeks of gestation. At 9 weeks, the first glomeruli appear, and nephrogenesis is complete by GW 36 in humans. In mice, the ureteric bud forms from the mesonephric duct at gestational day (GD) 9, nephron induction begins at GD 10, the first glomeruli appear around GD 14, and nephrogenesis continues for a few days after birth. Nephrogenesis is completed postnatally before PND 28 (with tubulogenesis finished between PND 11–15) in rats, by PND 16–18 days in dogs, and by the third week in pigs and rabbits (Table 2.1). Nephrogenesis is completed prior to birth in humans and by GW 24 in monkeys (McMahon, 2016; Frazier, 2017, 2021; Bueters et al., 2020; Cappon and Hurtt, 2010; Zoetis and Hurtt, 2003). However, postnatal maturation of nephrons and tubule elongation continues until about 1 year of age in human infants, and for up to 5 months in rhesus or cynomolgus monkeys. Maturation occurs in a proximal to distal hierarchy with distal tubule and collecting duct structures forming after proximal tubules during kidney development. Hence, it is more common to find medullary architecture disturbed in congenital lesions (Obert et al., 2020). After

completion of nephrogenesis, renal growth occurs by as much as a 235%–300% increase in tubular volume and a 33% increase in glomerular volume. In dogs, changes in glomerular and tubular growth are essentially complete by approximately 6 months of age. In concert with nephrogenesis, human renal vasculogenesis is completed by week 36 of gestation. In monkey, kidneys vascular maturation is also completed at birth, but in dogs, it is not completed until 6 weeks of age. In rats, renal vasculogenesis is not completed until PND 17–19, while in mice, it is completed by PND 7.

Teratogenic effects in the fetal kidney due to drug or chemical exposure in utero are dependent on toxicant delivery to the fetal circulation. Cross-placental transfer of a toxicant depends on its lipid solubility, size, and the concentration gradient that exists between maternal and fetal circulations. In humans, congenital anomalies of the kidney and urinary tract (CAKUT) comprise a broad spectrum of renal and lower urinary tract, structural and functional malformations that include renal agenesis, aplasia, hypoplasia, dysplasia, supernumerary kidneys, ectopic/fused kidneys, ureteropelvic junction obstruction, and several other conditions. Aplasia may result from early regression of the ureteric bud, altered metanephric differentiation, or defects in communication between the branching ureteric duct and undifferentiated metanephric blastema (Obert et al., 2020; Frazier, 2021). Renal dysplasia (also referred to as renal maldevelopment), characterized by disorganized development of parenchyma due to asynchronous differentiation, is also thought to be caused by disrupted signaling growth factor interactions between the ureteric bud and metanephric blastema. Histologically, dysplasia is characterized by the persistence of abnormal, undifferentiated or embryonic structures and abnormal patterning of renal tissues. Agents potentially teratogenic to the early developing kidney are numerous and include allopurinol, retinol, mercuric chloride, and colchicine (Frazier, 2021).

Renal malformations arising from early in utero exposure to nephrotoxic agents tend to result in severe anatomic defects such as renal agenesis or aplasia when exposure occurs prior to metanephros formation, but other morphologic and structural effects are seen if exposure occurs later during embryonic growth. Prenatal exposure to a nephrotoxicant can also result in

**TABLE 2.1** Timing of Completion of Nephrogenesis Across Species

Human	Gestational week 36
Monkey	Gestational week 24
Mouse	Postnatal day 2–4
Dog	Postnatal day 16–18
Rat	Postnatal week 2–3
Pig	Postnatal week 3
Rabbit	Postnatal week 3



degeneration or necrosis of the developing nephron instead of aplasia or other CAKUT lesions. This can lead to abortion if damage is severe. Fetal renal necrosis has been reported with gestational exposure to a variety of antineoplastic agents. When less severe, or damage is focal, nephrotoxic lesions due to late embryonic exposure may be noted in perinatal juvenile animals in toxicity studies as increased incidence of cysts, infarcts, hydronephrosis, and/or dysplasia (see *The Role of Pathology in Evaluation of Reproductive, Developmental, and Juvenile Toxicity*, Vol 1, Chap 7). Toxicologic lesions may occur in the kidney unexpectedly in juvenile toxicity studies even when no renal lesions are noted in adults of the same species, strain and gender at similar doses. The predisposing reasons for this disconnect can be due to a variety of factors including altered toxicokinetic profiles related to developing transporters, differences in perfusion or excretion, or differing critical windows of organ development (Frazier, 2017, 2021). Basic familiarity with renal development, function, and structure enables the toxicologist and pathologist to understand the relevance of the nephrotoxic response and to put the findings in the proper clinical perspective. Site localization of injury forms the initial basis for understanding potential pathogenesis and predicting the functional consequences of a lesion. Additionally, subcellular localization of the primary xenobiotic effect (site of earliest and most sensitive alteration) is a prerequisite step for establishing an intracellular organellar target in mechanistic studies.

Understanding comparative development schemes can be critically important in determining the clinical significance of toxicologic findings in juvenile toxicity studies in laboratory animal species and the potential timing of critical windows of toxicologic risk to human infants or pediatric patients. As noted in Table 2.1, nephrogenesis (as well as vasculogenesis and overall renal morphologic and functional development) occurs at specific timepoints across species and not necessarily in the same sequence or order. A critical event such as tubule maturation may occur before birth in one species but only postnatally in others. This difference in timing could be the basis for a postnatal risk of juvenile toxicity in a rodent, but an embryologic risk to a pregnant mother in a human patient. As an example,

exposure of humans or nonhuman primates to a variety of angiotensin-converting enzyme (ACE) inhibitors during gestation will result in marked renal tubular dysgenesis, characterized by distorted tubules, acute tubular necrosis (ATN), and immature glomeruli. Similar lesions occur in rats, but at different times in renal development, from the last 5 days of gestation to approximately PND 15. However, when the same ACE inhibitors, such as enalapril, are given to juvenile rats after PND 21 or to adult rats, similar lesions are not noted in the kidneys, and no renal lesions are noted in human infants when given after birth. These renal abnormalities are a result of pronounced toxic effects on renal morphogenesis that occur in humans particularly when ACE inhibitors are given in the last few weeks of pregnancy (Cappon and Hurtt, 2010). Of note, ACE inhibitors are routinely given to infants older than 1 year of age for hypertension without any adverse effects. Susceptibility of these nephrotoxic/teratogenic effects therefore vary markedly by species/age and generally correlate with the critical period for nephrogenesis, tubular growth, and differentiation. As stated earlier, nephrogenesis occurs in humans during gestation but continues into the postnatal period in rats. The mechanism for nephrotoxic teratogenic effects by the ACEi class during pregnancy has been elucidated and involves tubule dysmorphogenesis, but ACE inhibitors may also induce fetal hypotension, decrease renal blood flow (RBF), and disrupt the maternal and fetal renin-angiotensin axis. Angiotensin II (ATII) receptor activity is required for multiple steps of renal morphogenesis, and mutations in this gene have been associated with congenital renal abnormalities (Rigoli et al., 2004). Thus, the molecular basis for pathogenesis of ACE inhibitor teratogenesis in humans and for neonatal rat nephrotoxicosis both depend on interruption and interference with tubule development, leading to a reduced number of nephrons and simultaneously hemodynamic compromise (Frazier, 2017).

## 2.2. Renal Structure

### 2.2.1. Gross and Subgross Anatomy

Since the rat is the most common species utilized in preclinical toxicity studies and is particularly well-suited for clinical safety

prediction, it will be the focus of the anatomical section and only important differences in other species will be highlighted. The kidney of the mature rat is bean-shaped and weighs approximately 0.51%–1.08% (with a mean of 0.65%) of the body weight, varying with age and sex. The kidneys are located retroperitoneally, ventrolateral to the vertebral column. The right kidney is located cranially to the left. It has basic unipapillary architecture, the simplest type of mammalian kidney. Other types can be regarded as adaptations to larger body sizes. In transverse section, the cortex and outer stripe of the outer medulla (OSOM) can be differentiated from the inner stripe of the outer medulla (ISOM) and the inner medulla with the papilla extending into the renal pelvis. Furthermore, the arcuate vessels are readily visualized in section (Figures 2.1 and 2.2). The renal pelvis represents a dilatation of the ureter.

### 2.2.2. Vasculature and Innervations

The processes that assemble vasculature during embryonic development, in the kidney and in other tissues, are distinguished by the presence or absence of contiguous preexisting vessels, termed angiogenesis or vasculogenesis, respectively. Growth factor receptor tyrosine kinases on vascular cells are important mediators of these processes in the kidney. Basic fibroblast growth factor (bFGF), hepatocyte growth factor (HGF), and VEGF promote endothelial cell proliferation, migration, or morphogenesis, whereas platelet-derived growth factor (PDGF)- $\beta$  receptors and PDGF- $\beta$  ligand are shown to play important roles in glomerular development (Hammerman et al., 1993). In the adult kidney, the renal artery branches in the hilus into 6–10 interlobar arteries, giving rise in turn to arcuate arteries coursing parallel to the capsule along the corticomedullary junction. Interlobular

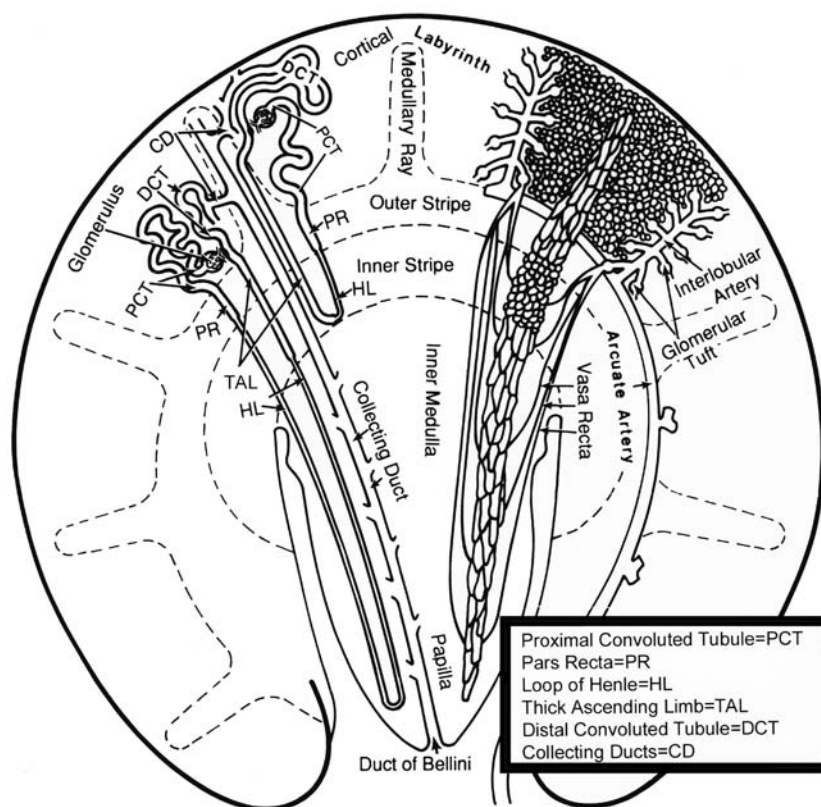


**FIGURE 2.1** Schematic drawing of the nephron and vasculature, denoting subtopographical anatomic relationships. Reproduced from Haschek WM, Rousseaux CG, Wallig MA, editors: *Handbook of toxicologic pathology*, ed 2, 2002, Academic Press, Figure 18, p. 203, with permission.

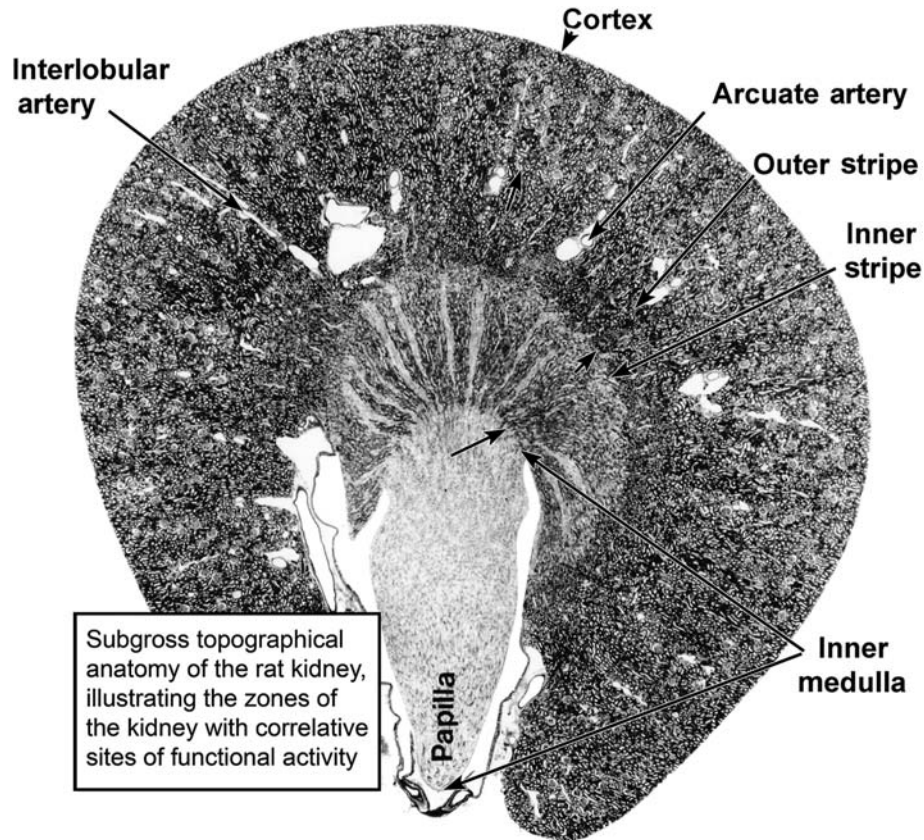


**FIGURE 2.2** Subgross topographical anatomy of the rat kidney, illustrating the zones of the kidney and correlative sites of functional activity. Reproduced from Haschek WM, Rousseaux CG, Wallig MA, editors: *Handbook of toxicologic pathology*, ed 2, 2002, Academic Press, Figure 2, p. 258, with permission.

arteries arise from the arcuates, coursing perpendicular to the capsule, each supplying a cortical labyrinth. Each interlobular artery gives rise to 6–11 afferent arterioles. All renal artery branches are end arteries without significant collateral supply. The renal circulation is a portal system since glomerular capillary beds reunite into an efferent arteriole, running for a varying distance before again forming a capillary bed surrounding portions of the lower nephron. All circulation to the medulla is of postglomerular capillary derivation. Veins run parallel to the main arterial and arcuate system. Lymphatics run parallel only to the cortical vasculature. Efferent arterioles of subcapsular nephrons are long, breaking into capillary beds that supply the same nephron, then subsequently coalescing to form an interlobular vein. Efferent arterioles of midcortical and juxtamedullary nephrons, in contrast, give rise to descending vasa recta which break up into capillary plexuses, forming the blood supply to the

medulla. Capillary plexuses reunite, forming ascending vasa recta. Capillary plexuses are dense in the inner stripe, but sparse in the outer stripe and inner medulla (Seely, 2017). Ascending vasa recta join the arcuate veins at the corticomedullary junction. Except for dendritic cells, the interstitial compartments of cortex and medulla are not functionally contiguous. Dendritic cells are present in the renal interstitium, forming a contiguous network throughout the entire kidney, playing an immune surveillance role for this organ.

Parenchymal oxygenation is not homogenous in the kidney as physiologic medullary hypoxia exists because of limited local oxygen supply. Medullary hypoxia is caused by a unique regional microcirculation associated with a countercurrent oxygen exchange in the vasa recta that marginally matches oxygen demand for high levels of tubular reabsorptive capacity. Ambient partial pressure of oxygen normally declines at the corticomedullary junction and outer stripe to 20–30 mmHg and



hypoxic tubular injury predominantly occurs among tubular segments in this region. Mammalian kidneys are richly innervated with postganglionic sympathetic fibers to the afferent and efferent renal arterioles, juxtaglomerular apparatus (JGA), proximal tubule, loop of Henle, and distal tubule. In the rat, the ganglia of origin of the sympathetic efferent innervation include T13 and L1 ipsilateral and contralateral paravertebral ganglia and the prevertebral superior mesenteric and celiac ganglia. The sensory afferent innervation presents a different segmental distribution of the dorsal root ganglia for the right and the left kidney. For the left kidney, the corresponding ganglia extend from T8 to L2 with the greatest numbers in T12 and T13, whereas ganglia as high as T6 and as low as L2 harbor neurons innervating the right kidney. The sensory nerve fibers contain substance-P and calcitonin gene-related peptide (CGRP). Activation of these sensory nerves plays an important role in the renal regulation of body fluid and sodium homeostasis. Accordingly, the efferent renal sympathetic nerves can affect the control of renal vascular resistance (RVR) and increase renin release; they have also been shown to regulate sodium and water excretion both by arteriolar vasoconstriction, resulting in a change in intrarenal hemodynamics, and by a direct effect on proximal tubular sodium reabsorption and on ascending portions of the cortical loop of Henle sodium and chloride reabsorption. Nerves that are associated with intrarenal arterioles have been noted to have ramifications in the afferent and efferent arterioles as well as in the JGA. These nerve fibers are monoaminergic with norepinephrine and dopamine activity.

### 2.2.3. Microscopic and Ultrastructural Functional Anatomy

Histologic and ultrastructural cytologic characteristics of the following nephron subunits are important in toxicologic pathology: glomerulus, PCT, pars recta (PR), loop of Henle, thick ascending limb (TAL), JGA (Figure 2.3), DCT, collecting ducts, and renal interstitium (Kriz and Kaissling, 2000; Al-Awqati and Goldberg, 1998; Owen and Heywood, 1986).

### 2.2.4. Glomerulus

The glomerulus is composed of a capillary network lined by a thin layer of endothelial cells;

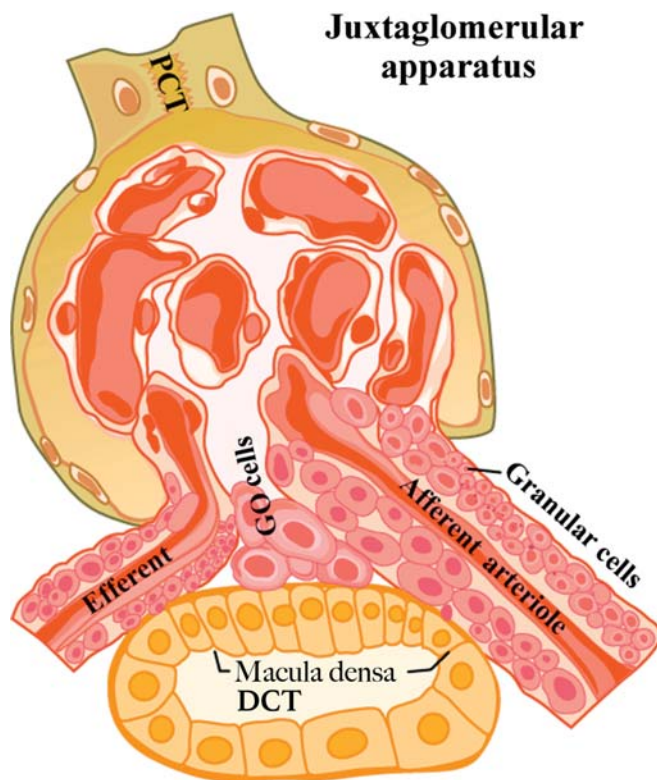


**FIGURE 2.3** Drawing of juxtaglomerular apparatus (JGA). Proximal convoluted tubule (PCT), distal convoluted tubule (DCT), and Goormaghtigh cell (GO). Reproduced from Haschek WM, Rousseaux CG, Wallig MA, editors: *Handbook of toxicologic pathology*, ed 2, 2002, Academic Press, Figure 3, p. 260, with permission.

a central region of mesangial cells and mesangial matrix; the visceral epithelial cells (VECs) or podocytes, and parietal epithelial cells (PECs) of Bowman's capsule and the associated basement membranes. The filtering membrane of the glomerulus consists of fenestrated capillary endothelial cells, a glomerular basement membrane (GBM), and podocytes (Figure 2.4). The ratio of endothelial to mesangial to podocytes in the glomerular tuft is 3:2:1. Podocytes are postmitotic highly differentiated cells that include a cell body, major processes, and foot processes (pedicels) bridged by slit diaphragms. Mutations in genes controlling podocyte components are associated with hereditary renal diseases. Podocyte disorders also play a crucial role in a broad spectrum of acquired glomerular diseases, including xenobiotic-mediated podocytopathies. The PECs of Bowman's capsule and its basement membrane are continuous



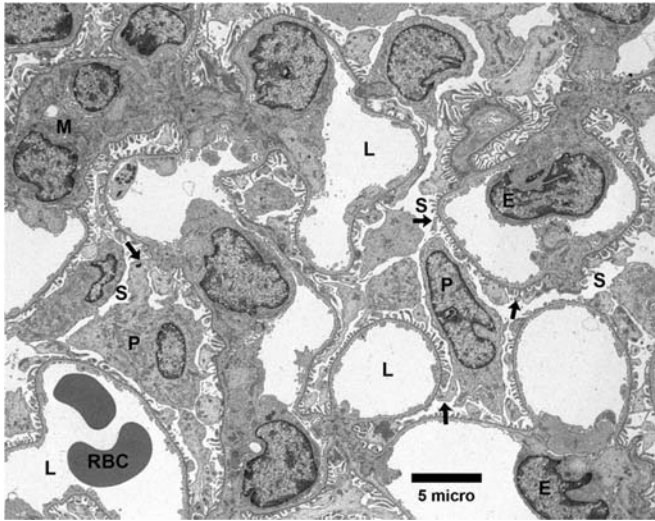


**FIGURE 2.4** Ultrastructure of the rat glomerulus, illustrating podocytes (P) and their foot processes (arrows) adjacent to the basement membrane, endothelial cells (E) of capillary loops (L), red blood cells (RBCs), and glomerular filtration space (S). *Reproduced from Haschek WM, Rousseaux CG, Wallig MA, Bolon B, editors: Haschek and Rousseaux's handbook of toxicologic pathology, ed 3, 2013, Academic Press, Figure 47.4, p. 1673, with permission.*

with the PCT. Frequently in the normal mature male mouse, and occasionally in the mature male rat, the PCT epithelial cells extend into Bowman's capsule, surrounding the glomerular tuft. These cells may suffer the same toxicologic fate as those in the PCT. Endothelial cells of glomeruli are unique both in location and in anatomy compared to most other endothelial cells in the body. Even within the kidney, endothelial cells in different renal compartments show differential chemokine expression profiles. The absence of a diaphragm with retention of a basement membrane and fenestrations enables the filtration function of glomeruli. These cells are covered by a dense glycocalyx, the dissolution of which can result in abnormal glomerular filtration. Interaction with the podocytes and mesangial cells, as well as with circulating and infiltrating inflammatory cells, contributes to maintenance of body fluid homeostasis and modulation of disease. The GBM principally consists of Type IV collagen and polyanionic proteoglycans, particularly heparan sulfate. The mesangium forms the supporting framework through which the glomerular tuft capillaries ramify. The mesangium includes an extracellular

matrix (ECM) composed of Type IV collagen, proteoglycans, and other proteins, and two cell types. The mesangial stellate cell is contractile, responding to vasoactive hormones such as Angiotensin II. This stellate cell synthesizes and secretes the mesangial matrix. The second mesangial cell is phagocytic, secretes paracrine growth factors, and participates in local immune reactions. Mesangial uptake lags behind the systemic reticuloendothelial system with respect to the appearance as well as the disappearance of antigen. The lymphatic system receives the end products of mesangial phagocytic cell processing. Each adult rat kidney contains roughly 30,000–35,000 nephrons (as compared to an average of 900,000 to 1,000,000 in humans and 14,000 in mice). Glomeruli of short-looped nephrons are ~20% smaller in cross-sectional diameter than those of long-looped (juxtamedullary) nephrons (discussed below). The average diameter of the glomerulus is approximately 120  $\mu$ m, 130  $\mu$ m, and 200  $\mu$ m in the kidney of rat, Beagle dog, and human, respectively. In the developing dog kidney, glomerular size increases approximately 40% during the first 2 months and reaches its mature size by 6 months of age (Figure 2.5).

### 2.2.5. Proximal Convoluted Tubule

The proximal tubule begins at the urinary pole of the glomerulus and consists of an initial convoluted portion, the PCT, which is composed of the S<sub>1</sub> and S<sub>2</sub> segments, and is a direct continuation of the parietal epithelium of the Bowman's capsule, and a straight portion, the pars recta, which is located in the outer stripe. Three segments (S<sub>1</sub>, S<sub>2</sub>, and S<sub>3</sub>) are identifiable in several animal species, including rat, rabbit, mouse, and the cynomolgus monkey, but these divisions are not readily visible in the human kidney. The S<sub>1</sub> segment is short, connecting with the glomerular filtration space. The cells of this segment have the highest rate of oxidative metabolism in the kidney. The S<sub>2</sub> segment represents the vast majority of the PCT and extends a short distance into the pars recta. The vast majority of pars recta consists of the S<sub>3</sub> segment. In the rabbit, a well-defined neck segment is shown to be present between the parietal epithelium of Bowman's capsule and the PCT. This segment is not present in the rat or human. The proximal tubule is approximately 8 mm, 10 mm, and 14 mm long in

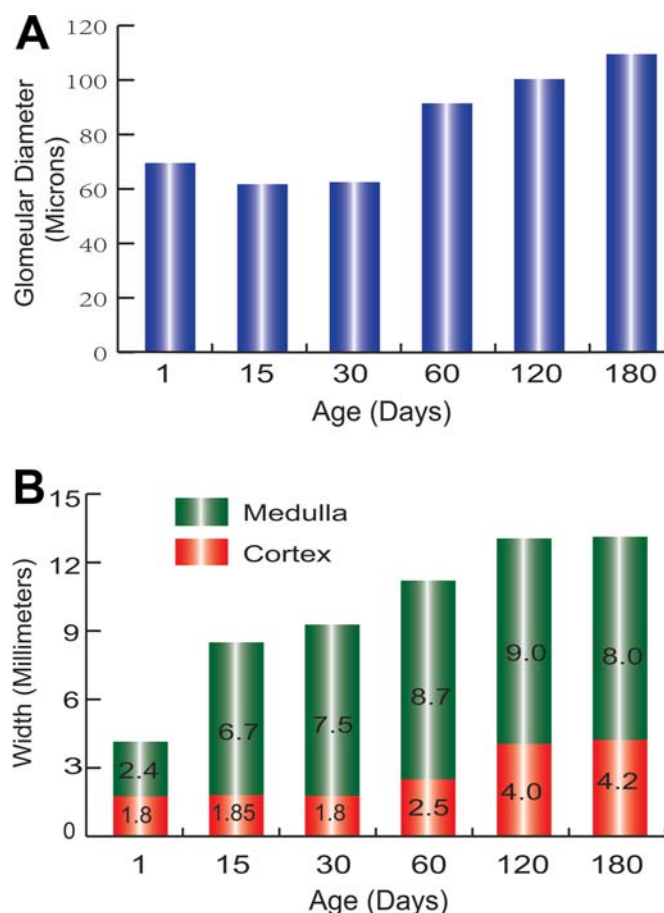


**FIGURE 2.5** Age-related changes in glomerulus diameter and cortical and medullary width in beagle dogs. Reproduced from Haschek WM, Rousseaux CG, Wallig MA, editors: *Handbook of toxicologic pathology*, ed 2, 2002, Academic Press, Figure 5, p. 261, with permission.

the rat, rabbit, and human, respectively. The PCTs, as well as the pars recta, are qualitatively differentiated from the remainder of the nephron and collecting duct by their luminal brush border, recognized in hematoxylin and eosin (H&E) sections, in electron micrographs (microvilli), and by using special stains such as periodic acid-Schiff (PAS) or alkaline phosphatase. These cells are cuboidal, with eosinophilic cytoplasm and a central large, round nucleus. Ultrastructurally, endocytotic vesicles, lysosomes, phagolysosomes, endoplasmic reticulum (predominantly smooth), Golgi apparatus, and many basally localized mitochondria are prominent (Verlander, 1998). Peroxisomes and lipid vacuoles also occur in PCTs.

### 2.2.6. Pars Recta

The pars recta, the straight portion of the proximal tubule of the juxtamedullary nephron, is located in the OSOM (Figure 2.6). Pars recta of short-looped (subcapsular) nephrons is found within the medullary rays or within the outer stripe. The ratio of long- to short-looped nephrons is approximately 1:2. Histologically and ultrastructurally, the pars recta is similar to the PCTs, with two exceptions: phagolysosomal proteinic reabsorption droplets are much less prominent in the pars recta, and the brush border in the rat is the highest and most developed in the pars recta. Differentiation between PCT and pars recta has significant functional and toxicologic relevance as the segments have differences in relative transporter abundance, metabolizing enzymes, and oxygen demands.

### 2.2.7. Thin Limbs of the Loop of Henle

The transition from the proximal tubule to the thin descending limb of the loop of Henle is abrupt, and marks the boundary between the outer and the inner stripes of the outer medulla. Four epithelial cell types are described in the thin descending and the thin ascending limbs of the loop of Henle; each, however, is histologically flattened and has amphophilic cytoplasm. Ultrastructurally, cell types vary from nonspecialized cells without interdigitation to cells with interdigitation and specialization (Verlander, 1998). Specialization is evidenced by increased numbers of mitochondria and intramembranous particles, and sparse surface microvilli. The length of loop of Henle varies, with subcapsular nephrons having a very short loop extending only into the outer stripe. Nephrons arising in midcortex have loops extending midway through the inner medulla. Juxtamedullary nephrons (long-looped nephrons) extend deep into the papilla (Figure 2.1). However, only about 250 nephrons reach the last millimeter of the tip of the papilla. The transition from the pars recta to the descending loop of Henle results in reduction in the outside diameter with only a slight change in luminal diameter. The inner stripe of the outer zone of the medulla consists of loops of Henle, TALs, and collecting ducts (Figure 2.6). The inner zone of the medulla consists of thin descending and ascending limbs of loop of Henle and collecting ducts.



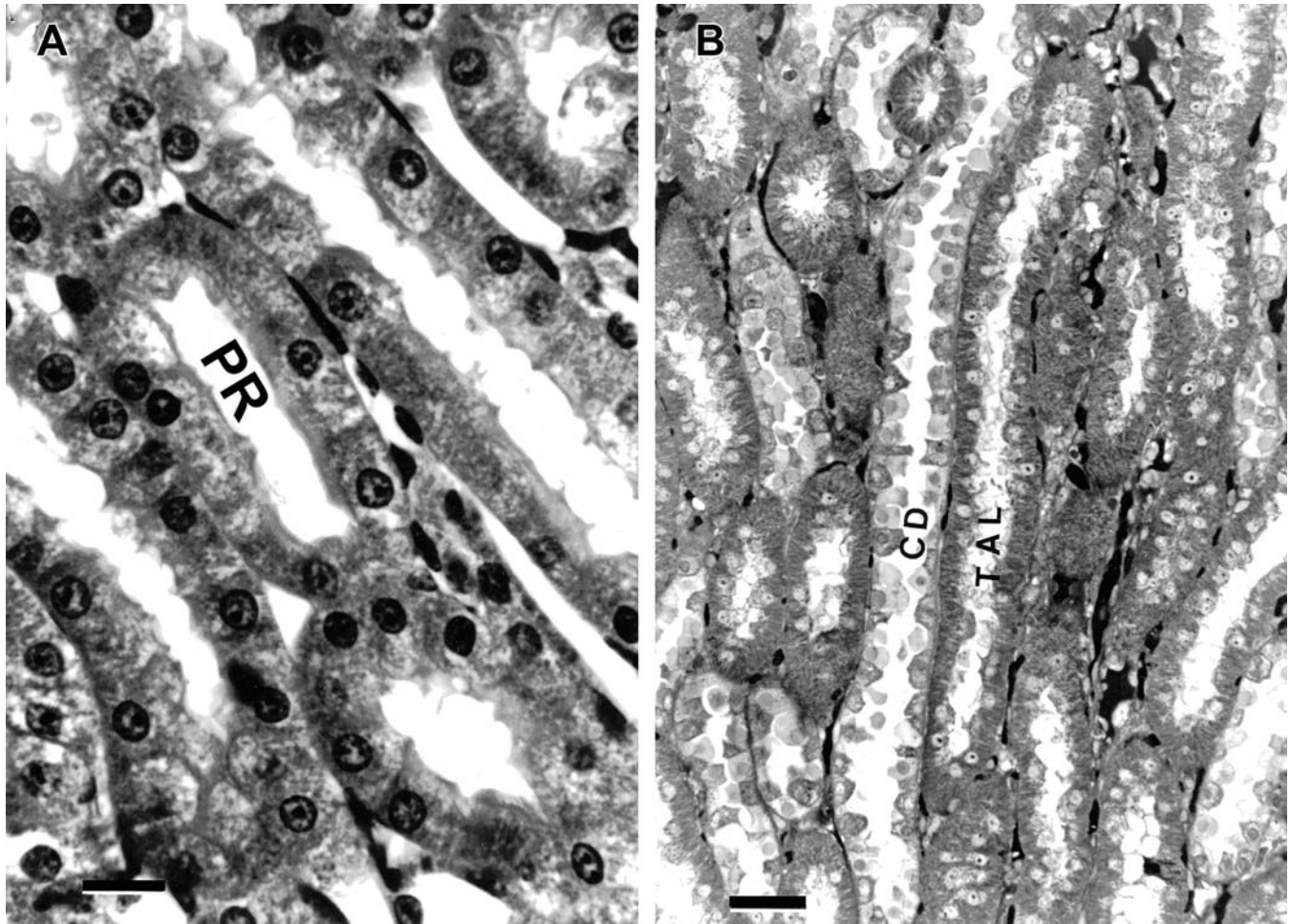


**FIGURE 2.6** Light micrograph of a rat kidney. (A) Outer stripe illustrating normal pars recta (PR) or straight portion of the proximal tubule. Bar = 20 mm. (B) Inner stripe illustrating normal thick ascending tubule (TAT) and collecting duct (CD). Plastic-embedded section (2 mm) stained with Lee's hematoxylin. Bar = 50 mm. *Reproduced from Haschek WM, Rousseaux CG, Wallig MA, editors: Handbook of toxicologic pathology, ed 2, 2002, Academic Press, Figure 7, p. 263, with permission.*

### 2.2.8. Thick Ascending Limb and Distal Tubule

The distal tubule comprises three structurally distinct segments: the TAL of the loop of Henle, the macula densa, and the DCT. The TAL is found in the outer zone of the medulla and in the cortex, ending near its own glomerulus, just past the macula densa. In the rat and rabbit, the cortical TAL extends beyond the vicinity of the macula densa and forms an abrupt transition with the DCT. Cells lining the TAL are cuboidal with eosinophilic cytoplasm and round central nucleus. TAL cells are smaller than PCT and pars recta cells. Thus, in the tubule cross-section of the TAL, several more cells are found than in the PCT or pars recta tubules.

Ultrastructurally, cells of the TAL have prominent mitochondria and rough endoplasmic reticulum (Verlander, 1998). Glycogen or lipid droplets and phagolysosomes also may be found in the cytoplasm. Tamm-Horsfall protein covers the luminal surface of the cells lining the TAL.

### 2.2.9. Juxtaglomerular Apparatus

The JGA is located at the vascular pole of the glomerulus, where a portion of the distal nephron comes into contact with its parent glomerulus. The main components of the JGA are the macula densa of the TAL, the renin-producing granular cells of the afferent arteriole, and the extraglomerular mesangial cell (laci cell; Figure 2.3). The macula densa is a specialized region of the TAL

adjacent to the hilum of the glomerulus. The cells of macula densa are low columnar and exhibit an apically placed nucleus. With electron microscopy, the macula densa cell base is seen to interdigitate with the adjacent lacinia cells to form a complex relationship.

#### **2.2.10. Distal Convoluted Tubule**

The DCT is approximately 1 mm in length and begins at a variable distance beyond the macula densa, extending to the connecting tubule that connects the nephron with the collecting duct. The connecting tubule is well defined in the rabbit kidney but not well delineated from the other distal segments in the rat, mouse, or human kidney and is derived from the ureteric bud. Cytologically, the DCT cells are taller but otherwise similar to those of the TAL of loop of Henle. However, Tamm–Horsfall protein is not found covering the luminal cell membrane. Calbindin D28K immunohistochemical stains can be utilized to specifically label DCTs in mice, rats, dogs, and monkeys, although small sections of connecting segment may also stain positively.

#### **2.2.11. Collecting Ducts**

The collecting ducts extend from the connecting segment in the cortex through the outer and the inner medulla to the tip of the papilla, and can arbitrarily be subdivided into three regions based on their location in the kidney. These include the cortical collecting ducts, the outer medullary collecting ducts, and the inner medullary collecting ducts. The cells lining the collecting duct are low cuboidal in the cortex, increasing in height to low columnar in the papilla. Two cell types occur: the intercalated cell (a dark cell), and the principal cell with amphophilic or clear cytoplasm. The intercalated cells are further divided into two types that play a role in acid base balance. Type A intercalated cells mediate acid secretion and bicarbonate reabsorption. Type B intercalated cells mediate bicarbonate secretion and acid reabsorption. In the inner medulla, the intercalated cell is absent. Collecting ducts progressively anastomose from cortex to papilla. In the papilla, collecting ducts form the ducts of Bellini, which empty into the pelvis.

#### **2.2.12. Interstitium**

The cortex in the rat consists of 7% interstitium by volume, of which only 3% represents the interstitial cells. By contrast, in the medulla, the

amount of interstitium continuously increases toward the tip of the papilla, reaching up to 29% by volume. The interstitium of the papilla consists of mucopolysaccharides and 3 cell types: stellate cells, monocytes, and pericytes. The stellate cell synthesizes prostaglandins (PGs). The stellate cells are interconnected and subcompartmentalize the interstitium, forming a barrier to axial diffusion of solutes. The corticomedullary junction connective tissue and outer stripe serve to isolate the increasingly hypertonic medullary interstitium from the cortex. The proportion of interstitium in the inner medulla increases with age and ischemia.

#### **2.2.13. Comparative Considerations—Age, Sex, and Species**

Interspecies differences in renal structure and function are summarized in [Table 2.2](#). The dog kidney is unipapillary, with fusion of renal pyramids into a crest-like papilla, including pyramidal vestiges recognized as recesses or invaginations of the renal pelvis. These renal recesses are separated by interlobar artery branches of the renal artery. The five or six interlobar artery branches form the arcuate arteries at the corticomedullary junction. Dogs have venous drainage (without parallel arteries) of subcapsular parenchyma, with veins grossly visible on the surface.

The minipig kidney is multilobular with a wide cortex, short papilla, and simple type vascular bundles. Short-looped nephrons predominate over long-looped nephrons. Pig and human kidneys are anatomically quite similar, both being characterized as multilobular and multipapillary and with many similarities in anatomical relationships between intrarenal arteries and the collecting duct system. A unique feature of minipig papillary collecting duct cells is the presence of electron-dense granules in the basal cytoplasm which appear to be secreted into the lateral intercellular spaces. The frequent occurrence of a single renal artery in pigs is also different from humans, in which multiple renal arteries exist. In both humans and pigs, an elaborate system of interlobar and segmental arteries is present to supply the numerous kidney lobes, whereas in dogs and rodents, these segmental arteries are unnecessary because of the lack of multiple medullary pyramids. As in the human kidney, there are free anastomoses between the intrarenal veins in the pig. Therefore, the human comparability of renal architecture, physiology, and immune



**TABLE 2.2** Comparative Renal Structure and Functional Characteristics to Aid in Understanding and Interpretation of Responses to Nephrotoxicants

Parameter	Rat	Monkey <sup>a</sup>	Dog	Pig	Human
Body weight (kg)	0.24	3.8	9.1	46	70
Single kidney weight (g)	0.75	9	31	77	157
Nephrons (per g body weight)	128	49	45	26	16
Number of nephrons (000s)	30	103–123	340–490	400–1196	300–1100
Glomeruli radius (m)	61	83	90	83	100
Proximal tubule length (mm)	12	NA	20	NA	16
Tubule radius (m)	29	NA	33	NA	36
Long loops (%)	28	NA	100	3	14
Medullary thickness (relative)	5.8	NA	4.3	1.6	3.0
Maximum osmolality (mOsmol/kg)	2610	1900	2610	1080	1400
Inulin clearance (mL/minute/kg)	6.0	1.9	4.3	NA	2.0
Maximal GFR (mL/minute/m <sup>2</sup> )	35	70	104	72	75
Renal organization	Unipapillary	Unipapillary	Unipapillary	Multilobular	Multilobular
Medullary structure	Complex	Simple	Simple	Simple	Simple

<sup>a</sup> *Cynomolgus monkey kidney is unipapillary while Rhesus monkey kidney is multilobular.*

NA, data not available.

*Modified from Haschek WM, Rousseaux CG, Wallig MA, Bolon B, editors: Haschek and Rousseaux's handbook of toxicologic pathology, ed 3, 2013, Academic Press, Table 47.3, p. 1678, with permission.*

systems makes the minipig a suitable model of human kidney disease. *Cynomolgus* monkey kidneys are unipapillary with fusion of renal pyramids into relatively short crest-like papilla. In mice, the glomerular size relative to total kidney weight is smaller than in other species, including rat. Glomerular size tends to increase with age and can vary widely among strains of rodents.

The rat has the most prominent OSOM visible subgrossly, constituting one-third of the medulla by volume. The outer stripe in human kidney is thin, whereas in the dog, it is virtually absent. This forms the basis of the frequent misrecognition, in the rat, of the junction of the inner and the outer stripes as the corticomedullary junction. The dog has primarily long-looped nephrons, in contrast to rat and human. In the dog, the pars

recta occurs only in medullary rays and joins loops of Henle near the corticomedullary junction; thus, all loops of Henle have a 180-degree turn in the inner medulla. The development of the inner medulla varies proportionately with urine-concentrating capacity of the species. The concentrating capacity of the kidney depends on the medullary depth. Greater relative size of the medulla indicates greater ability to concentrate urine to a greater osmolality. The relative medullary thicknesses for various species are 3 for humans, 5.8 for rats, 1.6 for pigs, and 4.3 for dogs. The organization of renal parenchyma at the cellular level is basically comparable among the commonly studied laboratory animal species. However, in the PCT of the male rat, there are unique large, crystalloid alpha-2μ-globulin cytoplasmic phagolysosomal inclusions recognized

as hyaline droplets by high-magnification light microscopy (Figure 2.7A, discussed later). Intraglomerular cellular reflux occurs in the dog in hyperthermia or as a postmortem artifact, and in humans as an ischemic or toxicologic change in acute kidney injury (AKI). This detachment and upward displacement of the proximal convoluted tubular epithelium into Bowman's filtration space contrasts with the occasional normal appearance of PCT cells lining the parietal layer of Bowman's capsule in the male mouse and rat. Tamm–Horsfall, a protein of relevance in cast formation in humans, lines the luminal

membrane of cells of the DCT in humans but not in rats, but it lines the luminal surface of cells in the TAL in both species. Immunohistochemical stains for Tamm–Horsfall stains can therefore aid in the identification of these segments given knowledge of species differences (Bauchet et al., 2011).

## 2.3. Renal Function

The primary functions of kidneys can be divided into four major categories: (1) control of the body's fluid and electrolytes, (2) production of hormones, (3) excretion of the waste products of metabolism, and (4) selected metabolic activities. Most importantly, nitrogenous waste products consisting of urea, creatinine, and ammonia ion are excreted in the urine. Any significant alterations in renal function are manifested as retention of waste products.

### 2.3.1. Control of Body Water and Electrolytes

The kidneys play a major role in the control of fluid and electrolyte composition of the body. The size of the body fluid compartment and total body water are kept remarkably constant by maintaining fluid osmolality through control of thirst centers and renal sodium and water excretion. Sodium and its attendant anions contribute 90%–95% of the osmotic activity of the body fluid osmolality. Renal activity in electrolyte and fluid balance are mediated by the modulation of glomerular filtration rate (GFR), adrenergic nerve activity, antidiuretic hormone (ADH), aldosterone, and natriuretic hormones. The kidneys typically receive 25% of the cardiac output, but only about 10% of oxygen consumption occurs in the kidneys. Approximately 85% of RBF is associated with cortex, 14% with outer medulla, and 1% with inner medulla, reflecting heterogeneity in intrarenal blood distribution and perfusion. Filtration is the basic determinant in urine formation and a key measurement of kidney function. Vascular resistance varies within the kidney, so RBF remains constant (autoregulation) over a wide range of systolic pressures from 90 to 220 mmHg. Neural regulation of RBF is minimal in the normal steady state. The proximal tubule represents the site of reabsorption of the most sodium without regard to body requirements. Obligatory water

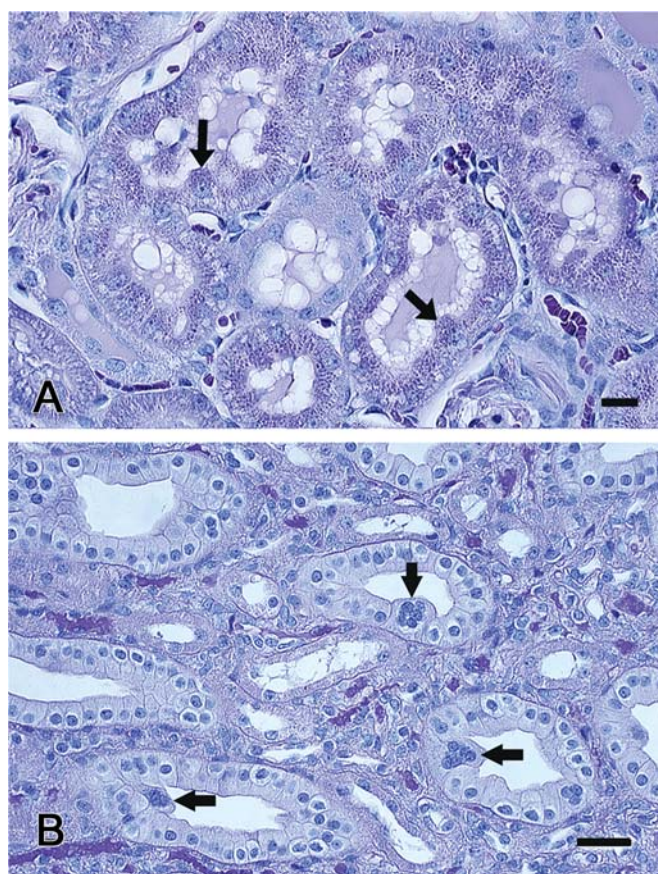


**FIGURE 2.7** (A) Light micrograph of the young sexually mature male rat renal cortex, illustrating spontaneous hyaline droplets (arrows). Bar = 30 mm. (B) The renal medulla of a young male cynomolgus monkey illustrates spontaneous syncytial cells (arrows) in the collecting tubules. Bar = 25 mm. Courtesy of Dr Xiantang Li, Drug Safety R&D, Pfizer, Groton, CT; Reproduced from Haschek WM, Rousseaux CG, Wallig MA, Bolon B, editors: *Haschek and Rousseaux's handbook of toxicologic pathology*, ed 3, 2013, Academic Press, Figure 47.10, p. 1679, with permission.

reabsorption occurs, also regardless of body needs. This water reabsorption is passive, accompanying active reabsorption of solutes. Secondary active transport of sodium is mediated by  $\text{Na}^+/\text{K}^+$  ATPase in the basolateral cell surface membranes. This creates a low concentration of intracellular sodium, such that it is passively transported down its concentration gradient from the lumen into the epithelial cell (described in detail below). Importantly, many apical  $\text{Na}^+$  transporters are actually cotransporters; therefore, other important molecules such as glucose enter the cell together with sodium. A widespread correlative ultrastructural feature of salt-transporting epithelia across species is the presence of basolateral cell-process interdigitations and tight junctions. An osmotic gradient is established and maintained by selective permeability in the loops of Henle and passive diffusion in the vasa recta. The ability of the kidneys to concentrate urine is dependent on the gradient of increasing interstitial osmolality running from the outer medulla to the tip of the papilla created by the countercurrent system. Salt and water transport in the loop of Henle is passive. Permeability is high to water but low to salt in the descending limb. By contrast, in the ascending limb, sodium permeability is high, but water permeability is low. As filtrate passes down the loop of Henle, osmolality increases as a result of osmosis of water into the hypertonic interstitium. The interstitium is rich in osmotically active urea because of reabsorption by the collecting ducts. Sodium is transported passively in the TAL but actively elsewhere in the distal nephron and is dependent on body requirements with responsiveness to aldosterone. By contrast, chloride is actively transported in the TAL. Facultative reabsorption of water occurs, regulated according to body needs by ADH in collecting duct epithelium. Permeability to water is low in the absence of ADH in the distal nephron.

### 2.3.2. Potassium

The kidney is responsible for controlling potassium concentration in the body. A marked decrease in urinary potassium clearance does not occur until body potassium stores are depleted by 20%–40%. Reabsorption occurs primarily through paracellular diffusion between tubule epithelium, but also through an

apical membrane  $\text{Na}^+/\text{K}^+/\text{Cl}^-$  cotransporter. The proximal tubule accounts for 70% of potassium reabsorption with further reabsorption in the loop of Henle, with less than 10% reaching the distal nephron. However, aldosterone control of potassium excretion occurs in the distal nephron. Potassium secretion begins in the early DCT and progressively increases along the distal tubules into the cortical collecting duct. Under conditions of potassium depletion, reabsorption occurs in the collecting duct through a process mediated by upregulation of  $\text{H}^+/\text{K}^+$ -ATPase (Palmer, 2015).

### 2.3.3. Calcium and Phosphate

Calcium and phosphate balance is profoundly influenced by active transport in the proximal tubule. The glomerular filtrate concentration of calcium is 50%–75% of the plasma level. Calcium is 99% reabsorbed, 60% in the PCT by a paracellular mechanism. Calcium absorption also occurs in the TAL, DCT, and collecting tubule. PTH, activated vitamin D, and estrogen enhance calcium reabsorption. Acidosis contributes to hypercalciuria by reducing calcium reabsorption in tubules, and alkalosis results in decreased urine calcium. The phosphate glomerular filtrate concentration is 90% of the plasma level. Within the nephron, approximately 85% of phosphate reabsorption occurs within the proximal tubule, whereas the remainder is typically cleared in the urine. Three renal sodium phosphate cotransporters, positioned within proximal tubule apical brush border, cotransport sodium down its gradient to move inorganic phosphate from the urine filtrate into the tubule cell.

### 2.3.4. Magnesium

Of plasma magnesium, 75% is filterable. Over 80% of filtered magnesium is reabsorbed, predominantly in the loop of Henle and to a lesser degree in proximal tubules.

*Excretion of Waste Products:* Nitrogenous waste products consisting of urea, creatinine, and ammonia ion are excreted in the urine. Kidney has remarkable functional reserves as excretion of these nitrogenous waste products is unaffected until at least 60% reductions have occurred in GFR, depending on the species. Beyond this, urea levels are dependent on both GFR and its production, affected by protein intake and tissue catabolism. Creatinine is



cleared primarily via glomerular filtration with proximal tubular secretion accounting for around 15% of total renal clearance, and with little reabsorption, creatinine clearance (Cl<sub>cr</sub>) is often used as a surrogate for GFR. Creatinine is a better guide to GFR than urea as it is less dependent on diet, but it can be influenced by a number of factors including age, sex, hemodynamic changes, and muscle mass. Creatinine is transported into renal epithelium from blood by basolateral high capacity SLC type transporters and then into urine via other SLC efflux apical transporters. Importantly, drugs such as dolutegravir and cobicistat inhibit creatinine transport into the urine filtrate and thus increase plasma levels without any associated nephron damage. The majority of renal ammonia excretion derives from production within the kidney, not from glomerular filtration, and renal ammoniogenesis predominantly results from glutamine metabolism within proximal tubules. In contrast to historical dogma, there is actually only limited plasma membrane NH<sub>3</sub> permeability and secretion in the kidney, with the majority of ammonium transport resulting through specific active transporters within proximal tubule epithelial cells. Ammonia production and transport are regulated by a variety of factors, including extracellular pH and potassium levels, mineralocorticoids, glucocorticoids, and ATII (Weiner and Verlander, 2013).

### **2.3.5. Elaboration of Hormones and Regulatory Peptides**

The kidney is involved in the elaboration of critical hormones and growth factors including erythropoietin (EPO), renin, and PGs. In addition, the kidney is a site of degradation of hormones, such as insulin and aldosterone. The kidneys are also responsible for the production of the active form of Vitamin D derived from Vitamin D<sub>3</sub> under the influence of parathyroid hormone.

### **2.3.6. Erythropoietin**

EPO is largely produced by renal peritubular interstitial cells. Plasma levels of EPO are controlled by recruitment of additional peritubular cells rather than increased production by individual cells. EPO regulates the formation of red blood cells by stimulating bone marrow, but also prevents erythrocyte destruction in the

circulation and has other functions including antiapoptosis, antiinflammatory, antioxidant, angiogenesis, cell proliferation, and antitumor effects. Renal hypoxia and androgens cause increased EPO secretion. Some of the intracellular pathways involved in EPO effects include JAK-2, Akt (protein kinase) phosphorylation, and NF- $\kappa$ B. Administration of synthetic EPO or EPO agonists at supraphysiologic doses to normal rodents in toxicity studies results in a stereotypical array of findings related to erythrocyte hemoconcentration and sludging related to elevated hematocrits in these animals (Adams et al., 2020).

### **2.3.7. Renin**

Renin is produced within JG cells after processing and cleavage of prorenin, which is produced in the liver. The primary stimuli for renin release from JG cells include reduction of renal perfusion pressure and hyponatremia. Renin release is also influenced by the sympathetic nervous system and by endocrine influences, including AII, ADH, endothelin (ET), and PGs. Renin activates AII, which causes secretion of aldosterone by the adrenal cortical zona glomerulosa. The net effect is systemic vasoconstriction, intrarenal vasoconstriction, and increased aldosterone release. The effect of aldosterone is predominantly on the distal tubules, affecting an increase in sodium reabsorption in exchange for potassium. However, there are also vasodilatory effects based on fragments of AII, so the downstream effects depend on specific receptor binding and other local factors.

### **2.3.8. Prostaglandins**

The kidney secretes PGs and thromboxanes from arachidonic acid by the cyclooxygenase enzyme system. This enzyme system is present in various renal cell types, including vascular, glomerular, tubular, and interstitial cells throughout the kidney. The predominant cyclooxygenase enzyme activity metabolites are prostacyclin (PGI<sub>2</sub>) and prostaglandin E<sub>2</sub> (PGE<sub>2</sub>) which play important roles in regulating the physiological action of other hormones on renal vascular tone, mesangial contractility, and tubular processing of salt and water. Local interstitial PG effects play a major role in the distal medulla in protection from ischemia and papillary necrosis (described in detail later in the chapter).



### 2.3.8.1. RENAL TRANSPORTERS

**2.3.8.1.1. COTRANSPORTERS (SECONDARY ACTIVE TRANSPORT)** Secondary active transport is defined as the situation when two substances interact with one specific carrier in the cell membrane and both substances are translocated across the membrane. The energy stored in concentration gradients is used in osmo-osmotic coupling (co- or countertransport) for concentrative transport of other solutes. The metabolic energy for secondary active transport of  $\text{Na}^+$  at the luminal membrane in the proximal tubule comes from  $\text{Na}^+/\text{K}^+$  ATPase, which transports  $\text{Na}^+$  out of the cell across the basolateral membrane and maintains a favorable electrochemical gradient for the entry of  $\text{Na}^+$  at the luminal membrane. Many other ions use similar cotransport in the kidney.

### 2.3.9. Glucose Transporters

Two different families of proteins are responsible for sugar transport in cells: the glucose transporter (GLUT) family, and the sodium/glucose transporter (SGLT) family. In the mammalian kidney, the major site for glucose reabsorption is the early S1 segment of the PCT with approximately 90% of filtered glucose reabsorbed in S1 and proximal S2 segments, and only a small fraction reaching the S3 segment. In the kidney, SGLT2 and SGLT1 account for more than 90% and approximately 3%, respectively, of glucose reabsorption from the glomerular filtrate. SGLT expression is heavily regulated and involves a wide array of interconnected signal transduction pathways including insulin, leptin, cyclic AMP/protein kinase A, protein kinase C, glucagon-like peptide 2, STAT3, PI3K/Akt, MAPKs, and NF- $\kappa$ B. In vivo rodent models of diabetes have demonstrated increased expression of SGLT1, SGLT2, and/or GLUT2 in the proximal tubule brush border accompanied by increased SGLT- and GLUT-mediated glucose uptake. These transporters have therefore become a staple target of antidiabetic (insulin-resistant) drug therapy.

### 2.3.10. Xenobiotic Renal Transporters

Some of the most important transporter classes in kidney for drug transport include the ATP-binding cassette (ABC) and solute carrier (SLC) families. ABC transporters use energy generated by the hydrolysis of ATP to transport molecules

across cell membranes, while the SLCs generally transport substances either down their concentration gradient or against their concentration gradient, via coupling and cotransport to a second substance down its own concentration gradient. In general, drugs with molecular weight below 400 Da are substrates for kidney transporters. The process of secreting organic anions and cations through the tubular epithelium is achieved through unidirectional transcellular transport, involving the uptake of organic ions into the cells from the blood across the basolateral membrane followed by extrusion across the brush-border membrane into the proximal tubular fluid. Proximal tubules contain several cellular uptake transporters within the SLC transporter family, including organic anion transporters (OATs), organic cation transporters (OCTs), the organic cation/carnitine transporters (OCTNs), and the organic anion transporting polypeptides (OATPs). The OAT family consists of multiple isoforms (OAT 1–4), urate transporter 1 (URAT), and rodent OAT5)) representing mainly the renal secretory and reabsorptive pathway for organic anions (Table 2.3). Subsequent studies have shown that while OAT1 and OAT3 preferentially transport organic anions (e.g., nonsteroidal antiinflammatory

**TABLE 2.3** Xenobiotic Transporters in the Kidney

Transporter	Location	Direction	Type
PgP	Apical	Efflux	ABC
OAT1	Basolateral	Uptake	SLC
OAT3	Basolateral	Uptake	SLC
OCT1/2	Basolateral	Uptake	SLC
MRP1	Basolateral	Efflux	ABC
MRP2/4	Apical	Efflux	ABC
URAT1	Basolateral	Uptake	SLC
MATE1/2	Apical	Efflux	SLC
OCTN	Apical	Uptake	SLC
OATP	Apical	Uptake	SLC
PEPT2	Apical	Uptake	SLC
BCRP	Apical	Efflux	ABC
MATE1/2-K	Apical	Efflux	SLC

drugs [NSAIDs] and urate), they are also capable of transporting organic cations (e.g., cimetidine) and organic zwitterions (e.g., carnitine). The OAT family is also involved in the distribution of organic anions in the body, drug–drug interactions, and toxicity of anionic substances such as nephrotoxic drugs and uremic toxins. These substrates generally tend to be transported by OAT1, OAT3, and OATP4 on the basolateral side of PCTs, and multidrug resistance protein MRP 2, MRP4, OATP1A2, and breast cancer resistance protein (BCRP) on the apical side. Other specific proteins in the SLC superfamily found in the kidney include OCT1, OCT2, OCTn1, OCTn2, multidrug and toxin extrusion protein 1 (MATE1), and peptide transporter 2 (PEPT2). The PEPT system transports penicillin, cephalosporins, and ACE inhibitors from the urine filtrate into proximal tubules. Organic cations are moved across membranes by OCT2 on the basolateral side, and MATE1, MATE2/2-K, P-glycoprotein (Pgp), organic cation and carnitine transporter (OCTN) 1 and OCTN2 on the apical side. MRPs are members of the ABC superfamily of efflux transporters, which transport a wide variety of anionic and cationic chemicals, drugs, and metabolites across renal membranes. BCRP is present within renal proximal tubules on the apical border. There are several other transporters found in the kidney, including the sodium-phosphate cotransporters (NPT1, NPT2a, NPT2b, and NPT2c) and the equilibrative nucleoside transporters (ENTs) 1, ENT2, and ENT3 (Bueters et al., 2020; Shen et al., 2019; Ivanyuk et al., 2017).

### 2.3.11. Uptake Transporters

Uptake transporters occur on both apical and basolateral surfaces and result in the accumulation of substances within PCTs from the urinary filtrate or blood, respectively. Drug–drug interactions at the level of basolateral transporters typically decrease the clearance of an affected drug, causing higher systemic exposure and potentially increased toxicity. In contrast, interactions at the apical surface can also lower drug clearance, but may be associated with even higher renal toxicity, due to intracellular accumulation. Human OAT1–3 are largely found on the basolateral membrane of PCTs although OAT2 is also present on the apical surface of human and rat proximal tubules. OATs are responsible for the uptake of anionic xenobiotics, such as beta-

lactam antibiotics and NSAIDs. These transporters show similar expression patterns at the transcriptional level in rodents, but there are several important species differences in renal transporter expression and differences can be noted due to both age and gender. For instance, while OAT4 is found on the apical surface of human PCTs, it is replaced largely by OAT5 in rat renal proximal tubules. Endogenous dicarboxylate anions (such as alpha-ketoglutarate) are considered to be the critical factor for organic anion exchange. Because renal OATs are important contributors to the excretion of many drugs and their metabolites, their pharmacokinetics, and resulting toxicity can be influenced greatly following coadministration of other drugs affecting the transporter. For example, the half-life of penicillin G is significantly prolonged when combined with probenecid, an inhibitor of OAT-mediated uptake. The tubular secretion and resulting elimination of methotrexate is severely reduced when coadministered with acidic drugs such as NSAIDs, antiviral agents, or  $\beta$ -lactam antibiotics due to competition for the transporter. Cidofovir, a substrate for OATs, has been associated with dose-limiting nephrotoxicity, but when combined with probenecid, the prevalence of nephrotoxicity is diminished. Similarly, OAT1-mediated accumulation of cephaloridine and related cephalosporin antibiotics have been linked to proximal tubule cytotoxicity, but nephrotoxicity in proximal tubules can be completely prevented by coadministration of probenecid. This response can be utilized rather straightforwardly in investigative studies to help define mechanism of toxicity. P-aminohippurate (PAH) secretion is often used as a surrogate for OAT1 secretion in investigative experiments and drug interaction studies. Cephaloridine antibiotics, ochratoxin A, and a variety of other agents can be demonstrated to inhibit PAH transport in basolateral membrane vesicles and are thus considered to be transported by the proximal tubular epithelium in part via the PAH/OAT1 transporter system (George et al., 2017; Frazier, 2021).

Enhanced nephrotoxicity related to transporter activity is not limited to the OAT class. Cisplatin cellular entry into PCT is facilitated by a number of transporters including OCT2 and the mechanism of cytotoxicity is highly dependent on cellular transport. Metformin is

also a substrate for OCT2, and hence drug–drug interactions at this transporter are critical to metformin pharmacokinetics and therefore its toxicity. Among OCTs, human kidneys have abundant OCT2 on the basolateral surface of PCTs, whereas rodent kidneys have two isoforms (OCT1 and OCT2) in this location, apparently with overlapping functions. OCT3 is also present in human kidneys and transports cation, but its role in renal toxicity has not been determined. OCTN1 and OCTN2 are both localized to the apical side of rodent and human PCTs. In addition to carnitine, OCTN1 and OCTN2 transport cationic agents such as valproic acid. OATP4 is highly expressed on the basolateral surface membranes of proximal tubules in humans, but other isoforms are present in rodents, especially mice. Cardiac glycosides and anticholesterol statin drugs are substrates for OATP4 (George et al., 2017; Ivanyuk et al., 2017).

### 2.3.12. Efflux Transporters

Renal efflux transporters move waste products into the urinary filtrate from the PCT across the apical surface. As noted previously, when this efflux transporter function is disturbed, compounds can accumulate in tubules and result in toxicity. Pgp plays an important role in drug interactions in multiple organs, including kidney. Pgp, along with MRP2, MRP4, BCRP, and OATP1A are found on the apical surface on the urinary filtrate interface of PCTs. Pgp is localized to the apical membrane of both rodent and human proximal tubules and actively exports a wide variety of drugs and chemicals, including chemotherapy drugs, steroids, and immunosuppressive agents. MRP2 and MRP4 extrude organic anions, including  $\beta$ -lactam antibiotics, or glucuronide—and glutathione (GSH) —conjugated drugs like acetaminophen or arsenic, respectively, into urine. Of the eight mice MRPs, six MRPs (MRP1–6) are significantly expressed in the kidney. In humans, MRP3 and 4 are expressed at much higher levels in female than male kidneys and are also under hormonal influence in mice and rats (Maher et al., 2006). Tenofovir is primarily a substrate of OAT1 and, to a smaller degree of OAT3, but together they transport the drug from blood into PCTs via uptake transporters. However, tenofovir is subsequently transported from PTC into urine by MRP4. The nephrotoxicity of tenofovir is

enhanced when combined with another antiviral agent, Ritonavir, which inhibits multiple renal transporters, including MRP4. In kidney, BCRP transports anionic substances including anticancer drugs and sulfa antibiotics. BCRP is found on the apical surface of PCTs in rodents at much higher levels than in humans. It is one of the major uric acid efflux transporters in the kidney, but also functions to excrete drugs and toxins. MATE1 and its cousin MATE2-K are efflux transporters that are substrates for drugs such as cimetidine and metformin. Rat PCT apical membranes contain MATE1 transporters, while human apical membranes contain both MATE1 and MATE2-K. The  $\text{Na}^+$ -dependent phosphate transporter 4 (NPT4) is an efflux transporter of urate and involved in the pathogenesis of gout, but also transports other organic anions (George et al., 2017; Radi, 2020).

In general, kidney transporters are largely immature at birth in humans and laboratory animals, but in rats and mice mature by approximately 3–6 weeks after birth, depending on transporter class (Frazier, 2021). Lack of maturation of uptake transporters can thus diminish toxicity of agents that utilize these transporters in neonates, but may enhance the toxicity of xenobiotic agents that require efflux transporter maturation to be secreted from PCTs into urinary filtrate. The major effect of transporter maturation in juvenile toxicity studies is on the pharmacokinetics of a drug or chemical, and therefore on the systemic and local drug concentrations at a given dose. Hepatocyte nuclear factors 1a and 4a regulate the expression of many or most transporters during gestational and later development and into adulthood. PXR regulatory factor plays a major role in maturation of metabolic enzymes, but it also regulates some kidney transporter genes, especially during development. In addition to the basolateral and brush-border membranes, transport across intracellular membranes such as the mitochondrial inner membrane is also considered a critical determinant of metabolite distribution.

### 2.3.13. Protein and Amino Acid Transport

Filtered proteins bind to the brush border and are taken up by endocytosis. Endocytotic vacuoles then fuse with lysosomes, forming proteinic phagolysosomes, where catabolism occurs.

Transport of proteins is affected by size, charge, and configuration. For example, cationic albumin is reabsorbed in a fivefold greater amount than anionic albumin. Sex differences in protein handling do occur. For example, the female rat reabsorbs more labeled protein and then degrades the reabsorbed protein more rapidly than the male in the same unit of time. The endopeptidase and exopeptidase activities of the proximal tubular cell are greater in the female than in the male rat. The endocytic receptors megalin and cubilin have been identified as essential receptors responsible for the reabsorption of proteins (Nielsen et al., 2016). Megalin is a 600-kDa glycosylated receptor containing a single transmembrane domain and a longer C-terminus tail extending into the cytoplasm of predominantly apical PCTs that regulates receptor trafficking and endocytosis. Cubilin is a 460-kDa glycosylated extracellular protein that interacts with other peptides involved in endocytosis. In proximal tubules, cubilin interacts with megalin, forming a multireceptor complex, driving internalization of the complex and bound ligand. This has been supported by in vitro uptake studies of the cubilin ligands transferrin and apolipoprotein A-I showing that the uptake was inhibited by antimegalin antibodies and megalin antisense nucleotides (Nielsen et al., 2016). It has been shown that cubilin also depends on transmembrane proteins, such as amnionless, for membrane localization and proper functional endocytosis. Once the proteins are reabsorbed, they are subsequently degraded in lysosomes. Once released from the phagolysosome, free amino acids are transported across the basolateral membrane by amino acid transporters back into blood. Reabsorption of filtered proteins in the proximal tubule is an important physiologic function by regulating biologically important substances like vitamins, hormones, enzymes, and others. Urinary filtrate containing excessive protein will initiate a cascade of degenerative events leading to tubular injury, interstitial inflammation, and fibrosis.

Fractional excretion of most amino acids is between 0.2% and 2.5%, although this proportion may increase in various pathologic conditions. Of the amino acids in the glomerular filtrate, 99% are actively reabsorbed in animals and humans, in a low-specificity process.

Reabsorption of amino acids occurs within the first millimeter of the PCT past the glomerulus in the dog and human. Different transport systems are responsible for the transport of neutral, acidic, and glycine-shared amino acids. Kidneys are also considered important in the interorgan metabolism of amino acids, which may have both qualitative and quantitative significance. Because urinary amino acid excretion is quantitatively negligible compared with amino acid reabsorption, it is reasonable to disregard urinary excretion in studies of renal amino acid flux. Fanconi syndrome, which causes impaired reabsorption of filtered molecules, including amino acids, small proteins, and glucose, is a disorder of the proximal tubules. It has more recently been termed proximal tubulopathy in human literature, and has multiple etiologies (Hall et al., 2014). In humans, it is often associated with tyrosinemia, but in Shiba Inu dogs, it has been associated with abnormal lipid rafts that misdirect the transporters at the apical membrane. There are several drugs and toxic agents such as valproic acid, tetracycline, and inhaled glue that have been implicated in acquired renal Fanconi syndrome (Hall et al., 2014). Proteins of up to 70 kDa (or slightly larger than albumin) enter urine in the glomerular filtrate. Hemoglobin, though of similar size to albumin, enters urine more readily because of its shape. The absence of hemoglobin in normal urine is predicated on hemoglobin binding to the large protein, haptoglobin.

### **2.3.14. Control of Acid-Base Balance**

The kidney plays a very important role in the regulation of acid-base balance. Endogenous acid production comes from incomplete metabolism of fats and carbohydrates, from oxidation of sulfur-containing amino acids, and from oxidation and hydrolysis of phosphoprotein residues. The kidneys regulate hydrogen ion concentration by three mechanisms: reabsorption of filtered bicarbonate, secretion of titratable acid, and secretion of ammonia. In the dog, 85% of bicarbonate reabsorption takes place in the proximal tubule. In tubule epithelium, hydrogen ions are produced by hydration of carbon dioxide. Hydrogen ions are then secreted into the tubular lumen in exchange for a sodium ion, leaving sodium and bicarbonate ions behind within the cell. Buffers in the tubular lumen (predominantly



monohydrogen phosphate) accept the hydrogen ion, passing down the nephron as a titratable acid. Renal tubule cells synthesize ammonia by enzymatic deamination of amino acids. Ammonia diffuses down its concentration gradient into the tubular fluid where it acts as an acceptor of hydrogen ions, forming ammonium ions. The ammonium ion is lipid insoluble; thus, it is trapped in the tubule lumen and excreted in the urine via active transport.

### **2.3.15. Insulin Metabolism**

The kidney plays a central role in the metabolism of insulin, which is freely filtered through the glomerulus. Of the total renal insulin clearance, approximately 60% occurs by glomerular filtration and 40% by extraction from the peritubular vessels. Insulin in the tubular lumen enters proximal tubular cells by carrier-mediated endocytosis and is then transported into lysosomes, where it is metabolized to amino acids. The net effect is that less than 1% of filtered insulin appears in voided urine. The renal clearance of insulin in humans is 200 mL/minute, significantly exceeding the normal GFR of 120 mL/minute and is due to tubular secretion. This results in 6–8 units of insulin degraded by the kidney each day, and accounts for approximately 25% of the daily pancreatic production. The contribution of renal metabolism increases further in diabetic subjects receiving exogenous insulin, since injected insulin enters the systemic circulation directly without first passing through the liver. After nephrectomy in rats, the removal rate of insulin from the circulation is reduced by approximately 65%. Insulin is reported to directly influence calcium conservation by the kidney.

### **2.3.16. Fatty Acid Utilization**

The kidney extracts, and utilizes, glucose, lactate, palmitate, citrate, glutamine, and other fatty acids from plasma for energy metabolism. The rate of respiration in the kidney parallels the rate of active transport. The proximal tubule accounts for 70% of all reabsorptive activity in the kidney. Lactate is one of the main metabolic substrates oxidized by the proximal tubules.

### **2.3.17. Cholesterol Control**

Hepatic cholesterol synthesis is controlled by negative feedback of the cholesterol precursor mevalonic acid. The kidney plays a dominant

role in metabolizing mevalonate by a nonsterol shunt pathway. Thus, renal disease may cause hypercholesterolemia, but there are no known examples of xenobiotic inhibition of these processes in the kidney. The female rat metabolizes mevalonate at twice the male rate; thus, the male converts more mevalonate to cholesterol than does the female.

### **2.3.18. Renal Xenobiotic Metabolism**

The kidney plays an important role in the metabolism of hormones, drugs, chemicals, and other waste products. The kidney generally metabolizes endogenous and exogenous substances to molecules with reduced biological activity; however, there are instances in which metabolism produces a toxic metabolite that may result in mutagenesis or cell necrosis. In some cases (e.g., glycation of benzoic acid), biotransformation is shown to occur at a faster rate in the kidney than in the liver. Numerous enzymes play a role in the metabolism and clearance of compounds in the kidney, including cytochrome P450 (CYP450) enzymes, as well as non-P450 enzymes such as uridine-diphosphate-glucuronosyltransferases (UGTs), esterases, glutathione-S-transferases, sulfotransferases, and others. Renal tubules can participate in a diverse array of metabolic reactions, such as oxidation, reduction, hydrolysis, and conjugation, facilitating elimination of many drugs. The CYP450-dependent mixed-function oxidases (MFOs) are heme proteins catalyzing many phase I chemical reactions, and is the most studied xenobiotic-metabolizing enzyme system in the kidney. Tissue enzyme activity and immunohistochemistry have been widely employed to measure xenobiotic-metabolizing enzymes in the kidney. The major activity is present in the cytoplasm of proximal tubules, and specifically within microsomes (Table 2.4).

In proximal tubules, MFO activity occurs primarily in pars recta (S3) in the rat. CYP450 content of the kidney is only 10%–20% of liver content. However, at the cellular level, the cells of the pars recta are comparable with hepatocytes in concentration of P450 enzymes. Rat MFOs in kidney, however, are not induced by phenobarbital as they are in the liver. The most prominent P450 enzymes in kidney include CYP2B6, CYP3A5, CYP4A11, CYP4F2, CYP4F8, CYP4F11, CYP4F12, although there are species differences in prevalence (Racine et al., 2014;

**TABLE 2.4** Renal Distribution of Xenobiotic Metabolizing Enzymes

Enzyme	Proximal tubule	Distal tubule	Loop of henle	Collecting ducts
Cytochrome P450	+			
Alcohol dehydrogenase	+			
N-acetyltransferase	+	+		
N-methyltransferase		+		
Aldehyde reductase	+			+
Aldose reductase	+		+	
Carboxylesterase	+			
Cysteine conjugate $\beta$ -lyase	+			
Epoxide hydrolyase	+			+
Glutathione S-transferase	+	+		
Ketone reductase	+			
NADPH-cytochrome c reductase	+			
Steroid 21 hydroxylase		+		+
Sulfotransferase	+			
UDP-guloronyltransferase	+			

Modified from Haschek WM, Rousseaux CG, Wallig MA, Bolon B, editors: Haschek and Rousseaux's handbook of toxicologic pathology, ed 3, 2013, Academic Press, Table 47.6, p. 1685, with permission.

[Frazier, 2021](#)). Polycyclic aromatic hydrocarbons are inducers of rat renal P450 microsomal enzymes. In the rabbit, both phenobarbital and polycyclic aromatic hydrocarbons induce renal MFO activity. Microsomal P450 activity in the rabbit is highest in the S2 segment of the proximal tubule. Fatty acid hydroxylation is greater in the kidney than in liver in rabbits and humans. Induction of metabolizing enzymes in the kidney can lead to elevations in absolute kidney weights but rarely in tubule hypertrophy ([Hard, 2018b](#)).

Metabolic biotransformation in the kidney is noted with several compounds. While reactions may result in decreased toxic potential, the identical mechanism can lead to the formation of reactive species in other drugs, resulting in enhanced nephrotoxicity. For instance, cisplatin causes nephrotoxic effects in multiple species. Inhibition of  $\gamma$  glutamyltransferase (GGT) prevents cisplatin induced kidney toxicity in both rats and mice, indicating that metabolism through this enzyme plays a critical role in the toxic principle.

Acyclovir-associated nephrotoxicity is dependent on the formation of an acyclovir aldehyde renal metabolite via alcohol dehydrogenase. 3,4,5-Trichloroaniline (TCA) is an industrial chemical that results in renal tubule necrosis upon exposure. When rodents are pretreated with the CYP450 inhibitor piperonyl butoxide, the cyclooxygenase inhibitor indomethacin, or peroxidase inhibitor mercaptosuccinate, renal lesions with TCA are significantly reduced. However, no effect is seen after pretreatment with flavin-containing monooxygenase (FMO) inhibitors, indicating that bioactivation of TCA to toxic metabolites by P450s, cyclooxygenase, and/or peroxidase (but not FMOs) contributes to the nephrotoxicity ([Racine et al., 2014](#); [Frazier, 2021](#)).

### 2.3.19. Renal Clearance and Toxicity

Detoxification of a xenobiotic compound may result solely from excretion and renal clearance rather than metabolism. In instances of renal impairment, the clearance of a drug can be compromised, resulting in increased systemic

levels with continuing administration. Due to decreased excretion into urine, compounds may accumulate in the renal epithelium or in other organs and subsequently achieve toxic levels. This is a major contributor to drug toxicity in hospitalized patients with preexisting renal pathology. Physiochemical properties of the drug correlate with effective renal clearance. Compounds with low molecular weights (LMWs), low lipophilicity, and preferentially ionic at pH 7.4 are eliminated effectively. Substances with high molecular weight, protein binding, and lipophilicity, or those almost completely nonionic, will be ineffectively cleared in the urine.

## 2.4. Renal Cell Biology

As noted in the section on embryogenesis, growth factors and their cell surface receptors are important regulators of growth and development via their effects in the inductive events related to nephrogenesis. These growth factors act preferentially on glomeruli (FGFs, PDGF, TGF $\beta$ , VEGF), interstitial cells (TGF $\beta$ , CTGF, PDGF), or on tubules (EGF, TGF- $\alpha$ , HGF). These may regulate cellular proliferation, transformation, morphogenesis, fibrosis, regeneration, and differentiation in the kidney. For example, in experimental models, infusion of EGF, IGF-1, or HGF in the regenerating phase of ATN accelerates renal tubular recovery. Growth factor expression in the kidney may increase after a reduction in renal mass or after significant tubule damage; this expression is suggested to trigger the compensatory growth of remaining nephrons. The overexpression of growth factors plays a role in the severity of renal lesions as these peptides participate in various other processes, such as control of cellular hypertrophy, hyperplasia, regulation of matrix synthesis and degradation, and stimulation of immune-inflammatory responses. For example, growth factors such as TGF $\beta$ , PDGF, and CTGF are stimulated during chronic kidney disease (CKD) and are critical factors in inducing fibrosis via fibroblast mitogenesis, EMT, enhanced collagen production by these fibroblasts, and inhibition of matrix degradation (Frazier et al., 2000) (Figure 2.8).

Proto-oncogenes are involved in the regulation of cellular proliferation; they trigger the expression of growth-related genes and participate in the transduction pathway that mediates the mitogenic effect of polypeptide growth factors.

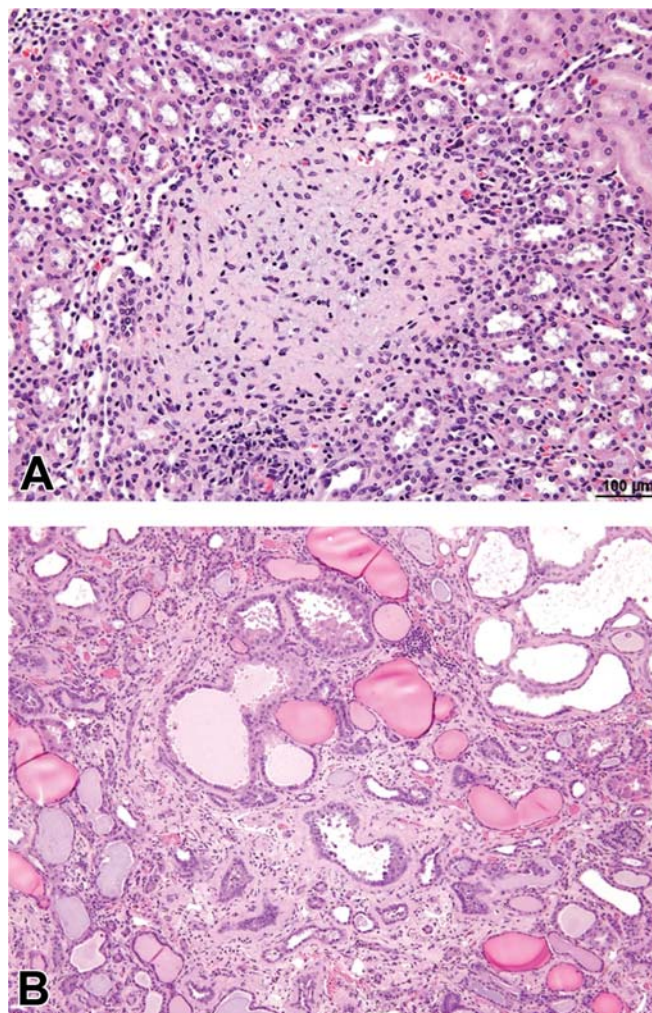


**FIGURE 2.8** A. Renal fibrosis in the medulla of a Sprague–Dawley rat due to focal infarction after thrombosis in an arcuate vessel. Note circumscribed area of fibrosis and loss of collecting ducts, surrounded by normal renal parenchyma. B. Renal fibrosis due to CPN in the cortex and medulla of an aged Han Wistar rat. Dilated and hyperplastic tubules filled with hyaline casts are separated by abundant mature interstitial collagen. Many tubules are atrophic and there is no differentiation between cortex or medulla. Inflammation is present but not prominent. *Courtesy of John Seely and the National Toxicology Program archive with permission.*

Activation of several proto-oncogenes (c-myc, c-fos, c-jun, c-H-ras, and c-K-ras) has been found in conditions with marked renal tubular epithelial proliferation, such as with folic acid-induced nephropathy or ischemia–reperfusion-induced tubular necrosis. Molecular targets (e.g., EGF and VEGF) of new antineoplastic therapies are



also expressed in the kidney, explaining some of the nephrotoxicities observed with these agents. For instance, glomerular lesions have been noted in humans and juvenile rats when given anti-VEGF therapies and AKI, and tubule necrosis is associated with several anti-EGF therapies used as anticancer agents (Frazier, 2022). In both cases, the molecular targets have been localized to specific parts of the nephron where their activity is important for renal function. The chemokines (e.g., RANTES [regulated on activation, normal T-cell expressed and secreted] and MCP-1 [macrophage chemoattractant protein-1]) belong to the family of proinflammatory chemotactic cytokines that help direct the emigration of inflammatory cells into the interstitium. In addition to their chemoattractant properties, chemokines mediate a myriad of other activities including modulation of the synthesis of TNF- $\alpha$  and IL-1 by macrophages, the regulation of TGF- $\beta$  production, and the effects on the Th1/Th2 balance during T-cell maturation. They play an important physiologic role in many forms of progressive renal injury; for example, RANTES and macrophage chemoattractant protein-1 are upregulated in nephrotoxic serum nephritis temporarily with a role in interstitial infiltrates. In situ production of the chemokine eotaxin is observed in diabetic nephropathy (DN) and showed that it may have an important role in the progression of interstitial inflammation and in eGFR decrease in these patients (Araújo et al., 2020). Recently, the CX3CL1-CX3CR1 axis has been shown to contribute to both detrimental and protective effects in various kidney diseases and could represent a novel therapeutic target after a further understanding of how the expression and function of CX3CL1 are regulated (Zhuang et al., 2017). In addition, CXCL10 was recently shown to be involved in the development of renal diseases through the chemoattraction of inflammatory cells and facilitation of cell growth and angiostatic effects (Gao et al., 2020).

Heat shock proteins (HSPs) prevent inappropriate peptide interactions and are important for protection against cell stress and injury (Sreedharan and Van Why, 2016). In the kidney, however, HSPs can be specific antigenic targets for immunological injury (Rao, 2016). For example, HSP-70 participates in antigen presentation and can be detected on the cell surface. Many patients with systemic lupus

erythematosus (SLE) have autoantibodies to HSP-70, HSP-90, or ubiquitin. Cells in the renal medulla are unique among mammalian cells in that they are routinely challenged with 10-fold variations in extracellular osmolarity (lethal to most cells). One mechanism of protection against osmotic stress in the renal medulla is intracellular accumulation of osmolytes. It is now recognized that stress protein induction complements the cytoprotection provided by organic osmolytes such as betaine, inositol, sorbitol, and glycerol-phosphorylcholine and can provide protection when organic osmolyte regulation is insufficient. The collecting duct contains novel osmotic stress proteins in the HSP-70 superfamily. Protein chaperone induction by one stress does not provide universal protection to all other potential injurious influences. The kidney is a major site of PG synthesis. In contrast to picomolar circulating concentrations of PG, urinary PG excretion is in the nanomolar range, indicating high intrarenal synthesis. Cyclooxygenase (PG endoperoxide synthase) catalyzes the committed step in PG biosynthesis. Mammalian cells contain two related but unique isozymes, cyclooxygenase-1 (COX-1) and cyclooxygenase-2 (COX-2). COX-1 is primarily expressed constitutively and is involved in the production of PGs which modulate normal physiologic functions in several organ systems, including the kidneys, gastrointestinal (GI) tract, and platelets. COX-2 expression is inducible by bacterial endotoxins, cytokines, and growth factors, and is involved in the production of PGs which modulate physiological events in development, ovulation, cell growth, and inflammation. In contrast to COX-1 knockout mice, COX-2 knockout mice have kidney development abnormalities and early death. Within the kidneys, PGs act as vasodilators, increasing renal perfusion. The main mechanism of NSAID action is COX enzyme inhibition and this inhibition can lead to AKI especially in the elderly (Lucas et al., 2019). It is thought that the main form of AKI caused by NSAIDs is hemodynamically mediated. Recent experiments have demonstrated an important but unexpected role for macrophage COX-2 signaling which lessens progression of diabetic kidney disease (DKD), unlike the pathogenic effects of increased COX-2 expression in intrinsic renal cells. Although increased COX-2 expression in macrophages is often cited as



a characteristic of a proinflammatory phenotype, studies indicate that COX-2 expression may actually mitigate detrimental effects in DN (Wang et al., 2017).

Nitric oxide (NO) is a small gaseous molecule with multiple pathophysiological effects in the body, including neurotransmission, vasodilation, and host cell defense; leukocyte recruitment at inflammatory sites; salt-sensitive hypertension; and progression of renal insufficiency. NO has a very short half-life (in seconds) and acts in a paracrine manner on cells in proximity to where it is produced. NO is synthesized from the amino acid L-arginine by NO synthases (NOSs), a family of isozymes with distinct functional, biochemical, and regulatory properties. These isozymes include endothelial NOS (eNOS), neuronal NOS (nNOS), and inducible NOS (iNOS); eNOS and nNOS are constitutively expressed in the body, whereas iNOS is produced primarily from macrophages following cytokine activation (e.g., tumor necrosis factor- $\alpha$  and interferon- $\gamma$ ). In the kidney, NO is considered to play an important role in the regulation of renal hemodynamics, renin release, and tubuloglomerular feedback. Immunohistochemical, *in situ* hybridization, and rt-PCR studies show that all three isoforms are constitutively expressed in the kidney. nNOS is the most abundant isoform localized primarily in the macula densa and in smaller amounts in glomeruli, vasculature, collecting ducts, and the inner medullary thin limb of Henle. In rats, nNOS expression in the macula densa is inversely regulated by salt intake. The blood vessels throughout the kidney, including arcuate and interlobular arteries and afferent and efferent arterioles, express eNOS. The expression of eNOS is higher in efferent arterioles than in afferent arterioles. Low levels of iNOS are expressed throughout the kidney and are upregulated by treatment with lipopolysaccharide (LPS). In the normal rat, iNOS is expressed in the tubular epithelium in various segments including TALs and collecting ducts. LPS-treated rats express iNOS in mesangial cells and in medullary interstitial cells. In addition, iNOS may be present in the smooth muscle and granular cells of afferent arterioles. The expression of iNOS increases in glomerular infiltrating macrophages or mesangial cells of nephrotoxic nephritis, immune complex glomerulonephritis, and anti-Thy-1 nephritis. Distribution and physiological functions of NOS isoforms in the kidney suggest that specific or nonspecific inhibition of any or all

NOS isoforms by candidate therapeutics may result in renal effects. Drugs such as N-monomethyl-L-arginine (L-NMA) and nitro-L-arginine methylester (L-NAME) are nonselective NOS inhibitors, whereas glucocorticoids and aminoguanidine preferentially inhibit iNOS. The acute and repeated dose studies with NOS inhibitors have shown renal toxicity in laboratory animals. Blockade of endogenous NO with L-NMA causes a significant rise in mean arterial blood pressure in association with glomerular arteriolar vasoconstriction and glomerular hypoperfusion. Dogs given L-NMA exhibit reductions in RBF, urine output, and urinary sodium excretion; rats develop marked renal vasoconstriction and hypoperfusion with decrease in GFR and an increase in filtration fraction. The prolonged inhibition of NOS by L-NMA causes widespread arteriolar constriction, focal arteriolar obliteration, and segmental fibrinoid necrosis in glomeruli. The NO, soluble guanylyl cyclase (sGC), and cyclic guanosine monophosphate (cGMP) signaling pathways play a pivotal role for the regulation of kidney function by the regulation of kidney blood flow as well as by protective effects on glomerular and tubular compartments with numerous preclinical studies demonstrating that targeting the NO/sGC/cGMP signaling cascade and increasing cGMP production are beneficial in various kidney pathologies (Krishnan et al., 2018). In patients undergoing multiple valve replacement and cardiopulmonary bypass, administration of NO decreased the incidence of AKI, transition to stage 3 CKD, and major adverse kidney events (Lei et al., 2018).

The ETs are 21-amino acid peptides derived from the proteolysis cleavage of preproendothelin and proendothelin. In the kidney, ETs (mainly ET-1 and ET-3) have been detected in the cortex, medulla, and papilla with primary localization at the small blood vessels (arcuate and interlobular arteries) and glomerular capillaries. In the kidney, ET receptors are localized to endothelial cells of glomerular and peritubular capillaries, the vasa recta, papillary interstitial cells, and collecting duct epithelial cells. In the kidney, ETs constrict glomerular mesangial cells and both afferent and efferent arterioles. The basal levels of ETs are not considered to be a modulator of systemic or renal hemodynamics under normal physiological conditions. ET production is accelerated in response to physical stimuli (e.g., increased shear stress or vascular stretch) and

cytokines (e.g., TGF- $\beta$ , TNF- $\alpha$ , and TXA<sub>2</sub>). ET-1 administration in humans significantly reduces RBF, GFR, and urine volume. The ET-1 system is also involved in salt and water reabsorption, acid–base balance, and promotion of mesangial cell growth, and in the pathophysiology of acute renal injury, in chronic renal failure, and in renal remodeling. ET-1 transgenic mice develop glomerulosclerosis, interstitial fibrosis, and reduced renal function. Plasma ET-1 levels are shown to correlate with the severity of chronic renal failure, and increased ET-1 and ET receptor upregulation has been reported in animal models of acute renal injury and in humans with chronic renal failure. Increased production of ETs has also been reported following treatment with certain drugs, including cyclosporine, L-NMA (NOS inhibitor), and radiocontrast media. Cyclosporine is a widely used immunosuppressive agent with nephrotoxicity as the major cause of morbidity. In humans and animals, cyclosporine therapy leads to renal vasoconstriction with a reduction in GFR and systemic hypertension. Renal effects of cyclosporine are possibly mediated by ET. ET-1 and ET-2 expression is significantly upregulated in CKD patients (Hsu et al., 2021). ET is known to induce ER stress and the NLRP3 inflammasome in human kidney cells. Clinically, ETs or ET-converting enzymes are a potential target for the development of new renoprotective treatments for CKD progression. ET has an important role in rat renal postnatal development. Pharmacological inhibition with a dual ET receptor antagonist during the early postnatal period decreases the number of glomeruli, the juxtamedullary filtration surface area, the GFR and increases proteinuria (Borghese et al., 2016).

Matrix metalloproteinases (MMPs) are enzymes with metal ion-dependent activity that degrade ECM glycoproteins. These enzymes play a vital role in embryogenesis, tissue remodeling, angiogenesis, and wound healing. Mammalian nephrogenesis comprises a series of intricate events characterized by a sustained remodeling and turnover of ECM, suggesting a role of MMPs in renal development. MMPs have also been shown to be expressed constitutively in glomeruli. All eight members of the MMP family are secreted in a latent form and require proteolysis cleavage for activation. They are regulated at the transcriptional level by a variety of growth factors and genes and at the

protein level by the tissue inhibitors of metalloproteinases (TIMPs). Aberrant expression of MMPs and TIMPs in renal pathophysiology has long been recognized, and with the recent generation of specific knockout mice, the mechanistic role of several MMPs and TIMPs is becoming better understood and has revealed both pathogenic and protective roles (Parrish, 2017). MMP-9 activation of Notch signaling in glomerular endothelial cells is downstream of TGF- $\beta$ 1 and supports a profibrotic role for MMP-9 by promoting epithelial–mesenchymal transition of tubular epithelial cells, endothelial–mesenchymal transition of peritubular endothelial cells, and endothelial–mesenchymal transition of glomerular endothelial cells, thereby, leading to kidney fibrosis in both tubulointerstitial and glomeruli compartments. MMPs and TIMPs are also involved in the development and progression of DN (Garcia-Fernandez et al., 2020). The equilibrium between MMPs and TIMPs is altered in DN.

Circadian variations in renal function are well characterized. In addition to a role for the kidney in maintaining day- and night-time blood pressure rhythms, renal function oscillates in a circadian manner with daily fluctuations in RBF and GFR and the excretion of sodium, potassium, phosphate, magnesium, and acid. The underlying molecular mechanisms for these oscillations are unclear. Recently, many clock-controlled genes have been identified in the kidney through gene expression profiling and candidate gene approaches. These genes encode products that range from transcription regulators to cell junction proteins. Discerning the role of the circadian clock in the kidney has important implications for the design of novel therapies and improvement of existing treatments for renal disease. A study was conducted in rats to identify molecules responsible for blood pressure circadian rhythm formation under the control of the kidney biological clock in hypertension. Phosphoribosyl pyrophosphate amidotransferase (Ppat) and fragile X mental retardation, autosomal homolog 1 (Fxr1) showed circadian rhythm expression and represent potential pivotal molecules in the control of blood pressure circadian rhythm by the kidney in hypertension (Murata et al., 2020). Total RBF and excretion of electrolytes and nitrogenous waste products also display profound circadian variations (Eckerbom et al., 2020). The kidney plays a critical role in these rhythmic processes

through the coordinated, timed regulation of channels and transporters responsible for sodium reabsorption (Solocinski and Gumz, 2015).

MicroRNAs (miRNAs) are endogenously produced, short RNAs of 21–25 nucleotides. These are important regulators of gene expression at the posttranscriptional level. miRNAs are known to have a high specific tissue expression distribution, with many kidney-specific miRNAs identified, and therefore have been shown to have great potential as biomarkers of nephrotoxicity (Nassirpour et al., 2015; Chorley et al., 2021). In kidney, miRNAs are indispensable for development and homeostasis and important in the regulation of blood pressure, hormone, water, and ion balance. Investigating the roles of miRNAs in the regulation of renal development and pathology has thus emerged as an important area of kidney research. Dicer is the enzyme responsible for the processing of pre-miRNAs into mature, functional miRNAs. Conditional Dicer ablation from podocytes results in proteinuria, tubulointerstitial fibrosis, glomerulosclerosis, and foot process effacement within weeks after birth, progressing to end-stage kidney disease and mortality within 2 months. Similarly, renal histology of mice with Dicer deletion in the renin-secreting JGA cells shows prominent multifocal interstitial fibrosis and vascular abnormalities. miR-26a was recently found as a versatile regulator of renal biology and disease, and is involved in the maintenance of podocyte homeostasis and the actin cytoskeleton. It is also able to modulate the homeostasis and function of mesangial cells. In addition, miR-26a affects the expansion of regulatory T cells in the context of ischemia-reperfusion injury and autoimmune diabetes and thus protects the renal system from immune attack (Li et al., 2019). Key miRNAs are highly expressed within specific cells of the kidney and can act as effectors of TGF- $\beta$  factors and high glucose in DN (Kato et al., 2009). They can alter MC and podocyte functions and lead to ECM accumulation, podocyte dysfunction, albuminuria, and EMT. Emerging evidence has further pinpointed the pathogenic roles played by miRNAs in other renal diseases including AKI, chronic fibrosis, renal hypertension, renal carcinoma, and polycystic kidney disease (PKD) (Chandrasekaran et al., 2012).

### 3. EVALUATION OF TOXICITY

The basis of clinical safety assessment is to be able to predict nephrotoxicity based on findings highlighted in preclinical toxicology studies and to monitor for these potential adverse effects in clinical trials. The importance of this endeavor is emphasized by retrospective studies demonstrating many cases of renal failure in humans are related to drug toxicity, and further that renal toxicity can be an important cause of candidate attrition during drug development. In toxicology, routine methodologies comprising standard biomarkers in blood and urine followed by gross and microscopic pathology are considered appropriately sensitive in standard preclinical testing to identify kidney as a potential target organ. Once nephrotoxicity potential is recognized, additional *in vitro*, *ex vivo*, or specialized *in vivo* investigative studies can be performed in a tiered approach to gain further understanding on mechanisms of toxicity, or to screen a library of test articles if availability of test material limits assessment in standard toxicology studies (Ennulat et al., 2018). Clinical chemistry screens with blood urea nitrogen (BUN), creatinine, and electrolytes, urinary excretion of protein and electrolytes, and routine urinalysis (with volume, specific gravity, and microscopic sediment evaluations) supplemented with kidney weights and histology provide adequate information on the physiologic status of the kidney or any significant perturbations in renal functions in a well-designed routine toxicology study. In situations where regulatory authorities or clinicians need further information on the nephrotoxic potential or mechanism of an observed drug-induced kidney injury (DIKI), additional renal biomarkers can be added. This can be done prospectively as additional end points on toxicity studies or in clinical trials to provide additional evidence that early changes in renal function are detectable prior to onset of more significant renal injury (discussed in 3b below).

#### 3.1. Physiologic Considerations

The physiologic status of the test animal and understanding of the age, sex, and interspecies differences in renal anatomy and physiology

are important in assessing the renal response to drugs and chemicals. Anatomical features of the nephron result in differences in susceptibility to toxicants. For instance, the distal tubule is characterized by epithelium with high electrical resistance and corresponding rigorous interepithelial tight junctions, whereas the proximal tubule has a rather leakier epithelium, which therefore is more susceptible to flux or freer passage of compounds into proximal tubular cells. Various nephron segments are prone to different toxic insults. For instance, cisplatin principally damages S3 segments, whereas pigment nephropathy induced by hemoglobin or myoglobin additionally involves S2 segments of the proximal tubule. Distribution of xenobiotic accumulation related to selective sites of tubular reabsorption may contribute to this variation. Age, gender, and species-related differences in anatomy and physiology should be thoroughly considered in translating preclinical toxicity data for humans.

### **3.1.1. Glomerular Filtration Rate Estimation**

In human clinical practice, GFR is most often estimated (eGFR), rather than using direct measurement, via the Cockcroft-Gault (CG) equation, Chronic Kidney Disease Epidemiology (CKD-Epi) Collaboration equation, the Modification of Diet in Renal Disease (MDRD) equation, the Schwartz equation (in children), or other formulas. The CG is an older method which has lost favor in clinical nephrology practice for a variety of reasons. The MDRD and CDK-EPI equations use variables that adjust eGFR to account for differences in age, sex, and ethnicity. All estimating equations have errors relative to measured GFR. There have been attempts to adapt human eGFR equations for use in laboratory animal species, but these have largely been unsuccessful, and no widely accepted eGFR formulas for preclinical species are utilized routinely in toxicologic studies, especially in regulatory studies (Obert et al., 2021). One of the measured parameters that are included in the estimation of eGFR in both animals and humans has historically been creatinine; therefore, Cl<sub>cr</sub> is a major determinant of eGFR. However, many factors unrelated to renal function can influence creatinine levels. While the majority of creatinine is filtered directly through the glomerulus, as much as 15%–40% may be secreted via renal transporters, depending on species, and tubule

transport may be altered by chemicals or drugs such as dolutegravir. Estimated GFR is absolutely critical to assess humans with CKD, but due to logistical concerns and the relative unavailability of technology or complex mobile instrumentation, currently direct measurement of GFR is impractical to institute in nonclinical safety assessment studies. Since eGFR calculations and interpretation in laboratory animals are not well established and still being refined, surrogate markers of GFR are utilized. Actual GFR measurement in toxicity studies is rarely performed and in practice, has generally been limited to the dog.

### **3.1.2. Considerations in Pediatric or Neonatal Kidneys**

Over the last 2 decades, pediatric drug research has expanded greatly, leading to enhanced pediatric drug labeling, but over 50% of the drugs used in the pediatric population are unlicensed or prescribed off-label. Drug response differences in children are common, often leading to challenges in optimizing dosages and duration. Renal functional differences based on age will also often result in vastly different toxicologic responses. For example, developmental changes in renal function can dramatically alter the plasma clearance of compounds with extensive renal elimination. Renal absorption, distribution, metabolism, and excretion (ADME) of drugs vary depending on age and maturation, which will lead to differences in toxicity and efficacy in the kidney. When neonatal or juvenile laboratory animal studies are designed, a thorough knowledge of the differences in comparative kidney development between neonatal children and juvenile laboratory animals is essential (Frazier, 2021). The juvenile animal data can best be utilized to inform human pediatric populations if evaluated in the most appropriate species at the most relevant age, considering comparability of the specific organ system development in question coupled with the disease indication, and likely route of human exposure. Factors in the neonatal kidney that influence ADME properties of drugs and chemicals include RBF, GFR, tubule mass, and immaturity. Functional and morphologic maturation will further impact tubular secretion, acid-base balance, and urine concentrating ability. Developmental ontogeny of metabolizing enzymes, transporters, and other factors involved in renal



clearance will all have an impact on the severity and timing of kidney toxicity (Bueters et al., 2020; Frazier, 2017, 2021; Zoetis and Hurtt, 2003; McMahon, 2016). In humans before 34 weeks of gestational age, the functional demands on the fetal kidney are minimal, but these increase dramatically in the last part of the third trimester and with birth. While the adult kidney receives 20%–25% of the cardiac output, the human fetal kidney receives only 4%, which increases to 10% by the end of the first postnatal week. Renal function in neonates remains different from that of adults, and GFR corrected for body size is not comparable to adult values until the child is 12 months old. In humans, GFR remains relatively low during gestation but rises rapidly shortly after birth, increasing steadily until it reaches adult levels near 2 years of age. After birth, the rise in GFR is attributed to increased RBF, higher capillary pressure, decreased RVR, and increased cardiac output.

In Beagle dogs, there is a gradual increase in GFR in the first 3 weeks postnatally. This increase in GFR is primarily the result of continuing glomerular differentiation in the outer cortical region. In adult dogs, as in other species, normal GFR values depend greatly on the methodology utilized to measure it, but generally agreed upon values are under 1 mL/minute per kilogram at postnatal day (PND) 1 versus 3.7–4.3 mL/minute per kilogram at adulthood. In rats, GFR has been demonstrated to be only slightly lower than adult values at PND 28 and data indicate that maturation is not totally completed in the rat until PND 42. For minipigs, age-based comparisons are problematic due to dramatically increased weight over time. GFR values of approximately 50 mL/minute have been noted in minipigs at 4 weeks of age, corresponding to approximately 4.5–5 mL/minute per kilogram. By week 15, GFR has increased to over 100 mL/minute, but due to increased size, GFR values actually decrease to 3–4 mL/minute per kilogram, which is roughly similar to the dog on a body weight basis. Because of logistical problems in obtaining values in neonatal mice, standard ranges are not available for mice younger than 2 weeks (Bueters et al., 2020).

Changes in tubular function, similar to GFR, occur with age and are important in age-dependent differences in susceptibility to nephrotoxicity. Fetuses and early neonates have

inefficient urine concentrating ability as a result of short proximal tubules and inefficient salt gradients. Tubular function in human kidney does not reach adult capacity until 18–24 months of age and in rat kidney until about 6 weeks of age (Frazier, 2017; Seely, 2017). In humans, fetal urine formation starts during the first trimester and urine production increases steadily during gestation, whereas paradoxically bladder storage interval remains unchanged. RBF progressively increases during gestation and achieves full-term levels by GW 32–35 in humans. Human kidneys undergo a striking transition at birth characterized physiologically by an increase in RBF and a marked increase in glomerular filtration pressure, resulting in a rapid rise in GFR. In contrast, urinary sodium output drops so that sodium, and therefore water are retained. In rats, measurements from a variety of methodologies have shown that RBF is at its maximum capacity by PND 20. In CD-1 mice, RBF reaches maximal levels at PND 13, while in other mice strains, this occurs between PND 16 and 22. In dogs, RBF more than doubles between PND 1 and 30. Experiments in pigs aged 6 h to 45 days showed mean RBF increased from 43 to 760 mL/minute per square meter due largely to rapid growth when normalized to body surface area (Bueters et al., 2020). In rhesus monkeys, RBF increases twofold from birth to adulthood, but in cynomolgus monkeys, this difference is reportedly minimal (Bueters et al., 2020). Reduced RBF results in decreased local renal drug exposure and therefore potentially decreased toxicity in infants. The neonatal renal tubular function for the transport of organic ions is also low and thus accumulation of nephrotoxic substances in proximal tubular epithelial cells may also be diminished in infants. There may also be immature metabolic activity which can reduce the formation of reactive metabolites in the kidney. Therefore, in many cases, neonates may be less prone to have drug-induced nephrotoxicity. Examples of agents in which adults have a much higher risk of nephrotoxicity than neonates include aminoglycosides, vancomycin, cadmium, cisplatin, and acetaminophen. In contrast, there are also a host of agents in which kidney toxicity is enhanced in juvenile animals due to susceptibility of renal structures undergoing growth and maturation, including VEGF inhibitors, doxorubicin, and many other antineoplastic agents (Frazier, 2017).

### 3.1.3. *Changes in Aged Kidneys*

After the age of 40 in humans, there is a progressive decrease in renal function, which is primarily the result of progressive loss of renal mass and a decline in nephron number. Age-related renal damage contributes significantly to abnormalities in GFR and tubular function resulting in different susceptibility of the aged population to nephrotoxic response as compared to neonates, juveniles, and young adults. Similarly, in rats, GFR gradually decreases with age, and by 18 months, GFR is decreased to approximately 68% of its rate compared to young adult rats. These age-related changes are manifested in increased serum levels of urea, creatinine, sodium, and chloride, decreased serum levels of albumin, decreased Clcr, decreased urine output and sodium excretion, and proteinuria. Proteinuria along with urinary loss of albumin is evident as early as 6 months of age. These changes are even more pronounced in those rat strains susceptible to chronic progressive nephropathy (CPN). With progressive nephron loss in older dogs, there are decreases in GFR, similar to those in rats and humans. In humans, tubular transport efficiency is greatly reduced in the aged kidney as a result of progressive nephron loss, decreased mitochondrial function, and reduced numbers of proximal tubule ion transporters. Defects in tubular transport with increasing age are demonstrated by decreases in PAH uptake by proximal tubular cells. Rats also develop age-related changes in normal tubular transport function. This is characterized by progressive decreases in urinary concentrating ability, and decreased chloride, calcium, and potassium retention. Changes in tubule transport function are evidenced by a 5%–10% decrease in urine osmolality in rats as early as 6 months of age, and between the ages of 12 and 27 months, there is a 40% decrease in active renal tubular transport in rats. Renal tubular function in dogs does not reach adult levels until after 1–2 months of age, as evidenced by reduced renal amino acid reabsorption. With age, dogs develop reductions in both tubular transport and urinary concentrating capacity, similar to rats and humans (Sellers et al., 2005).

### 3.1.4. *Hypertrophy*

The kidney adapts to altered demands by functional and structural changes. Compensatory

hypertrophy occurs in the kidney after extirpation of the contralateral kidney. Hypertrophy is recognized by an increase in the volume of the cortex (primarily involving PCTs), without an increase in nephron number but with some increase in glomerular volume. Measurement of the cross-sectional area of PCTs parallels functional adaptation measurements more precisely than does organ weight. The PCT response primarily represents hypertrophy with only slight hyperplasia. The quantitative contribution of each kidney to the GFR in a rat with an implanted third kidney can be assessed using (99m) Tc-diethylenetriaminepentaacetic acid (Tc-DTPA) scanning. Total GFR is unaltered because of compensatory atrophy with 15% reduction in weight and 30%–40% reduction of GFR, with no change in glomerular numbers in each of the native kidneys. The implanted kidney loses 20% of its nephrons as a consequence of surgery; thus, GFR is 20% less than that of the native kidneys. Several stimuli are recognized as the causes of renal hypertrophy, including administration of increased protein, amino acids, urea, or NaCl. Testosterone treatment, ACTH-mediated hyperadrenocorticism, and diabetes mellitus also cause renal hypertrophy. Potassium depletion results in an increase in luminal membrane area and altered mitochondrial content of collecting duct intercalated cells. Chronic furosemide treatment results in increased sodium loss, with a persistent need for increased sodium reabsorption in the DCT to compensate. Xenobiotics metabolized by the kidney can cause renal enlargement, presumably through adaptive increase in metabolizing-enzyme synthesis activity. Cyclosporine A treatment is associated with renal enlargement and glomerular hyperfiltration in rats. Decalin, a propellant, results in renal hypertrophy across species and sexes. Biochemically, compensatory hypertrophy leads to an increase in the RNA:DNA ratio. By contrast, this change in the RNA:DNA ratio apparently does not occur in renal parenchyma undergoing tissue repair.

## 3.2. Biochemical and Biomarker Evaluations

In preclinical toxicology studies, microscopic evaluation of kidney remains the gold standard for clinical predictivity, but its limitation is that it cannot be monitored effectively in clinical investigations. A safety biomarker is defined as

**TABLE 2.5** Renal Biomarkers in Urine of Value in Determining Nephrotoxicity

Biomarker	Rat	Dog	Minipig	Monkey	Human
NAG	+	+	NA	+	+
KIM1	+	+/-	+	+	+
NGAL	+	+	NA	+	+
Albumin	+	+	+	+	+
Glucose	+	+	+	+	+
aGST	+/-	+/-	NA	NA	+/-
B2Microglob.	+	+/-	NA	NA	+
Clusterin	+	+	NA	+	NA
CysC (and serum)	+	+	+	+	+
SDMA (serum)	+	+	NA	NA	+
DKK3	+/-	NA	NA	NA	+
RPA-1	±	—	—	—	—

NA = insufficient data available.

any analyte that can be quantified to indicate an adverse response to a test agent. Sensitive and specific biomarkers of renal injury are useful, not only because they can permit repetitious monitoring but also because practical matrices for monitoring renal injury in humans are generally limited to blood and urine. The utility of reliable biomarkers extends beyond the context of toxicity testing of chemicals in general, for it has important application in a cross-sectional sense regarding human kidney disease. Thus, it is equally important to develop biomarkers to diagnose and predict clinical outcomes in diverse clinical settings. The application of different renal biomarkers to predict location of renal injury is summarized in [Table 2.5](#). Baseline renal function values for various ages of Sprague–Dawley (SD) rats and of young adult Beagle dogs are summarized in ([Tables 2.6 and 2.7](#)). Development and utilization of some of the main traditional and novel biomarkers of renal injury prediction are discussed below (also see *Clinical Pathology in Nonclinical Toxicity Testing*, Vol 1, Chap 10; *Biomarkers: Discovery, Qualification and Application*, Vol 1, Chap 14).

### 3.2.1. Evaluation of Traditional Biomarkers

Traditional biomarkers of renal injury used for many years in laboratory animals and humans

have included serum creatinine (sCr), urea (UN), glucose, and leakage of enzymes including urinary N-Acetyl- $\beta$ -(D)-glucosaminidase (NAG) and glutathione S transferases (GSTs), total urinary protein and albumin, or LMW proteins such as  $\beta$ 2-microglobulin ( $\beta$ 2-M). These analytes can be evaluated in routinely collected serum and urine samples, but of these, only UN, sCr, urinary protein, urinary albumin, and glucose are routinely utilized in clinical practice and laboratory animal toxicity studies, with the others largely replaced by newer generation analytes. There are a variety of highly sensitive biomarkers of renal toxicity that can be additionally incorporated into subsequent toxicology studies if kidney is considered to be a potential target organ. For robust assessments of urinary biomarkers, it is essential to collect urine specimens of good quality (e.g., in metabolism cages) over a 12- to 16-hour period and to consider the age of animals being evaluated. In rats, the urinalysis results may become more variable because of the development of spontaneous age-related renal diseases—for example, increased urinary excretion of protein and calcium, and decreased urinary excretion of sodium, chloride and N-acetyl- $\beta$ -D glucosaminidase (NAG) related to CPN.

**TABLE 2.6** Baseline Renal/Function Parameters Over the Lifespan of Sprague Dawley Rats

Parameter	Age (months)			
	≤2	6	12	≥18
Kidney weight (g)	2.13 ± 0.23	3.46 ± 0.35	3.97 ± 0.36	5.22 ± 2.12
Body weight (g)	115 ± 6.0	645 ± 38	773 ± 109	914 ± 88
Urine output (mL/ 22 hours)	26 ± 9.5	23 ± 8.5	26 ± 6.8	21 ± 9.8
Urine osmolality (mOsm/kg)	853 ± 328	791 ± 468	745 ± 332	816 ± 329
Sodium excretion (mmol/22 hours)	0.58 ± 0.2	0.6 ± 0.3	0.37 ± 0.2	0.33 ± 0.2
Potassium excretion (mmol/22 hours)	1.6 ± 0.3	1.9 ± 0.3	2.0 ± 0.2	1.9 ± 0.6
Chloride excretion (mmol/22 hours)	0.61 ± 0.2	0.7 ± 0.2	0.63 ± 0.2	0.42 ± 0.3
Calcium excretion (mg/22 hours)	0.6 ± 0.2	1.6 ± 0.9	1.8 ± 0.9	2.5 ± 1.3
Phosphorus excretion (mg/ 22 hours)	17 ± 4.2	18 ± 3	17 ± 4.8	18 ± 5.4
Protein excretion (mg/22 hours)	7.3 ± 1.9	9.4 ± 2.4	18.5 ± 8.9	103.4 ± 122
Creatinine clearance (ml/minute/100 g body weight)	0.383 ± 0.07	0.367 ± 0.07	0.331 ± 0.07	0.26 ± 0.10
Urinary NAG (U/L)	10.1 ± 3	14.6 ± 4	16.3 ± 4	22.6 ± 12
Urinary alkaline phosphatase (U/L)	3 ± 4	1 ± 1	2 ± 3	4 ± 7
Serum urea (mg/dL)	19 ± 1	17.3 ± 1	16.9 ± 1	22 ± 13
Serum creatinine (mg/dL)	0.6 ± 0.03	0.7 ± 0.06	0.7 ± 0.07	1 ± 0.6
Serum total protein (mg/dL)	6.2 ± 0.3	6.4 ± 0.1	6.5 ± 0.2	6.1 ± 0.2
Serum albumin (mg/ dL)	4.6 ± 0.2	4.2 ± 0.2	4.3 ± 0.2	3.7 ± 0.4
Serum sodium (mmol/L)	144 ± 1.6	146 ± 1.2	148 ± 1.8	148 ± 1
Serum potassium (mmol/L)	6.4 ± 0.5	5.9 ± 0.7	5.5 ± 0.3	6.2 ± 0.7
Serum chloride (mmol/L)	102 ± 1.8	106 ± 0.9	107 ± 1.9	108 ± 2.5
Serum calcium (mg/dL)	11.3 ± 0.5	10.2 ± 0.3	10.6 ± 0.4	10.7 ± 0.6
Serum phosphorus (mg/dL)	11.1 ± 0.8	8.3 ± 1.7	12 ± 2.6	11.6 ± 2.1

*Reproduced from Haschek WM, Rousseaux CG, Wallig MA, Bolon B. editors: Haschek and Rousseaux's handbook of toxicologic pathology, ed 3, 2013, Academic Press, Table 47.8, p. 1695, with permission.*



**TABLE 2.7** Baseline Renal Function Values in Young Adult Beagle Dogs

Parameter	Mean SD
Urine output (mL/18 hours)	235 ± 58
Urine flow rate (mL/minute)	0.9 ± 0.25
Urine osmolality (mOsm/kg)	541 ± 52
Plasma osmolality (mOsm/kg)	308 ± 15
Sodium excretion (mmol/18 hours)	35 ± 12
Potassium excretion (mmol/18 hours)	14 ± 4.7
Chloride excretion (mmol/18 hours)	25 ± 7.7
Calcium excretion (mg/18 hours)	17 ± 6.1
Phosphorus excretion (mg/18 hours)	59 ± 33.8
Protein excretion (mg/18 hours)	20 ± 11.5
Creatinine clearance mL/minute/100 g BW	3.5 ± 0.4
N-acetyl-β-D glucosaminidase (U/L)	1.1 ± 2.65
β-2 microglobulin (mg/18 hours)	6.3 ± 2.6
Renal blood flow (mL/minute)	104 ± 17.1
Renal vascular resistance (vru)	68 ± 16
Filtration fraction	0.20 ± 0.06

*Reproduced from Haschek WM, Rousseaux CG, Wallig MA Bolon B. editors: Haschek and Rousseaux's handbook of toxicologic pathology, ed 3, 2013, Academic Press, Table 47.9, p. 1696, with permission.*

### 3.2.2. Serum Creatinine and Urea Nitrogen

In both humans and laboratory animals, the traditional biomarkers sCr and urea nitrogen (UN) have been utilized for decades to monitor renal function. The advantage of these two biomarkers is that they progressively increase in both acute and chronic renal toxicity and the magnitude of response correlates with decreases

in renal function as assessed by GFR. Unfortunately, they are late indicators of renal injury and do not become significantly elevated until at least 60% or more of the kidney mass has been injured, depending on the species. While sCr and UN are often elevated in the acute stages of injury in short-term toxicology testing of laboratory animals, recent investigations have shown these elevations are overwhelmingly related to extrarenal factors related to moribundity, hemoconcentration, or diuresis and not to the existence of concomitant renal injury. It has been recognized for over 75 years that there are a host of extrarenal factors that affect UN, including dehydration, nutritional status, and systemic hemodynamic changes. Creatinine can be affected by diet, muscle mass, housing, circadian variation, hydration status, physical activity, and age. In addition, several drugs can compete or interfere with the renal creatinine transporter system resulting in spurious changes. In addition, sCr and UN do not provide any indication concerning the region of kidney affected. The normal sCr and UN values in the presence of chronic renal injury reflect the functional reserve of the kidney. For these reasons, routine use of terminal urea and sCr measurements in nonclinical toxicology studies do not provide a sensitive indicator of renal function. This is in stark contrast to the clinical benefit derived from serial creatinine monitoring used in clinical human and veterinary medical practice. While UN and sCr are still very useful in detecting significant renal injury and their utilization in clinical chemistry panels in toxicity studies remain essential, diagnosis and interpretation of changes in either analyte should be based on the totality of clinical pathology information available. This should include but not be limited to other renal parameters such as serum phosphorus, urine protein/albumin, or urine glucose levels in either clinical trial patients or in animals enrolled in nonclinical toxicity studies. When and where necessary, more sensitive and selective novel renal biomarkers may also be included as discussed below.

### 3.2.3. Proteinuria and Albuminuria

As a locally produced biofluid in the kidney, urine offers an advantage over serum by increasing marker specificity for monitoring of renal injury. The classical paradigm of glomerular capillary leakage as the primary cause of proteinuria/albuminuria is currently challenged by increasing recognition that glomerular filtration of proteins such as albumin have been significantly underestimated in the past. Beyond the glomerulus, albumin is efficiently retrieved through megalin and/or cubilin binding into proximal tubule cells where the protein is catabolized to small peptides, some of which may then be secreted back into the urine. Thus, increase in albumin in the urine can signal impairment of the degradation pathway when there is proximal tubule injury. Consequently, proteinuria should be regarded as a reflection of 3 separate mechanisms: (1) abnormal transglomerular passage of large proteins due to glomerular dysfunction, (2) abnormal reuptake into proximal tubules due to tubular dysfunction, or (3) overflow proteinuria associated with increased production or circulation of large quantities of proteins in disease states (e.g., light chains in multiple myeloma, myoglobin in rhabdomyolysis) that as in tubular dysfunction, exceed the reabsorption capacity of the proximal tubule. Notably these three mechanisms are not mutually exclusive. Both urine total protein and urine albumin are presented in data form as concentrations and, like other urine analytes, may be subsequently normalized to creatinine as a ratio. In humans, spot urine samples are usually taken from a first morning void, but in nonclinical studies in animals, urine is collected in a metabolism cage and the total volume collected over a specific period—usually 12–18 h depending on species and the relevant experimental design. Changes in urinary protein levels remain the most reliable method for monitoring the progression of glomerular disease in human patients and animals. Urinary protein levels can fluctuate considerably in both acute and chronic renal failure and may vary considerably even in human patients or animals with

relatively normal renal function (Carter et al., 2016). With the exception of the rat, urinary albumin levels tend to parallel changes in urinary total protein in most species. Rat urine is heavily protein-laden with large quantities of alpha<sub>2</sub>μ-globulin, especially in males. Albumin absorption is distributed almost equally across the three segments of the proximal tubule and is present in urinary filtrate in fragmented (>98%) and intact (1%–2%) forms. Interestingly, not all urinary albumin is completely resorbed into the blood stream. Plasma albumin levels can decrease over time with chronic loss, and with a higher percentage of renal uptake, changes in urinary albumin may be overshadowed by large protein spillage in glomerular disease. Hence, while monitoring changes in urinary albumin and protein is of clear benefit, and considered predictive in both acute and chronic renal toxicity, urine protein levels may not detect progressive renal damage or dysfunction in very acute toxicosis or with advanced chronic renal disease (Obert et al., 2021). In some cases, xenobiotic-associated increases in urine protein may reflect physiologic, rather than toxicologic alterations in the renal tubules. For example, administration of antisense oligonucleotides (ASOs) can result in ASO binding to LMW proteins in the urinary filtrate and interfere with the megalin/cubilin transporter, resulting in transient, low-grade proteinuria in multiple species including mice, rats, monkeys, and humans (Janssen et al., 2019; Frazier and Seely, 2019; Frazier and Obert, 2018). This interaction does not reflect in any damage to the proximal tubules and minimal proteinuria that occurs shortly after ASO administration should not be interpreted as kidney injury. However, many ASOs may also induce direct tubule degeneration at high doses in animals, so accurate interpretation of urine protein with ASOs requires analysis of other analytes and concomitant histopathologic data (Frazier, 2022).

### 3.2.4. Urinary N-acetyl = β-(D)-Glucosaminidase

NAG is a lysosomal brush-border enzyme of 140 kDa present mainly in the proximal tubule

cells. It is the most active glycosidase in proximal tubule cell lysosomes and tends to be concentrated in the S2 segment. As NAG is too large to be filtered through glomeruli, its urinary excretion reflects increased lysosomal activity and tubule cell injury, and it has proved to be a sensitive biomarker of renal insult. The advantages of NAG pertain to its sensitivity and to its ease of measurement. First, subtle alterations in proximal tubule cells such as brush-border damage lead to shedding of NAG into the urine as a reflection of the amount of tubule damage. Secondly, the analyte is easily and reproducibly measured and quantified colorimetrically by spectrophotometer. However, NAG may lack the specificity required for a reliable subtopographical marker of tubule necrosis. It can be a more sensitive and specific (and hence more effective) marker of tubule injury than other analytes when there are perturbations of lysosomal turnover. Conditions such as hyaline droplet accumulation in rats, albumin overload with albumin-conjugated antibodies or ASO accumulation within proximal tubules represent renal changes related to lysosome function. In these situations, elevations in urine NAG appear to result from amplified endolysosomal release, shedding of NAG from the brush border, and impairment of lysosomal reuptake. Other markers such as KIM1 or NGAL that rely on overt tubule injury (degeneration) for release into urine are less specific in such cases.

### 3.2.5. Urinary Glutathione S Transferases

GSTs are cytosolic dimeric enzymes involved in detoxification of xenobiotic compounds through addition of glutathione. Several isoforms exist, but in the kidney, there are two main classes, GST- $\alpha$  and GST- $\pi$ . GST- $\alpha$  is highly expressed in proximal tubule cells, whereas GST- $\pi$  is localized to the DCT, thin limbs of Henle, and the collecting ducts. Therefore, application of these parameters raises the possibility of discriminating between damage to the proximal tubules and damage to the distal nephron and collecting system. In a cross-sectional study of human patients with proteinuria, the highest

levels of urinary GST- $\alpha$  were in patients still in an early phase of their proteinuric renal disease, whereas the highest levels of GST- $\pi$  increased permeability of the glomerular capillary wall, and/or the subsequent impaired resorption of proteins by epithelial cells of the PCTs. Unfortunately, neither GST- $\alpha$  or GST- $\pi$  have proven reliable enough for routine incorporation into preclinical toxicity studies and their current utilization has been limited to use in large biomarker panels in investigative studies.

### 3.2.6. Evaluation of Novel Biomarkers (See also Biomarkers: Discovery, Qualification, and Application, Vol 1, Chap 14)

Traditional markers of renal toxicity primarily indicate impaired kidney function rather than tissue injury, thus do not fulfill the requirements for an efficient safety biomarker in the clinic that will predict acute or progressive renal injury in an accurate and timely fashion. Over the past 2 decades, there has been a concerted effort to identify and develop new biomarkers of kidney injury in both humans and laboratory animal species. These efforts led to the assessment of several biomarkers, including kidney injury molecule-1 (KIM-1), clusterin, trefoil factor 3 (TFF3), renal papillary antigen 1 (RPA-1), neutrophil gelatinase-associated lipocalin (NGAL), beta2 microglobulin (B2M), and osteopontin (OPN) for DIKI and additionally other serum analytes such as cystatin C (CysC), symmetrical dimethyl arginine (SDMA), and dickkopf 3 (DKK3) which have found utility in chronic animal studies and CKD (Ennulat et al., 2018; Ozer et al., 2010; Han et al., 2008; Obert et al., 2021). As of this writing, urinary KIM-1, albumin, total protein, clusterin, B2M, cystatin-C, and renal papillary antigen have all been applied successfully in renal investigative studies and have been qualified by the Food and Drug Administration (FDA) for defined use in rat preclinical studies (Phillips et al., 2016; Ennulat et al., 2018). In addition, urinary NGAL and OPN have also received a letter of support by the FDA for further evaluation in rat preclinical studies. Development and

utilization of some of the main novel biomarkers of renal injury prediction are discussed below. Newly qualified urine biomarkers are not and should not be routinely included on all nonclinical toxicity studies, but rather reserved for select prospective use only upon identification of drug-induced renal microscopic lesions in initial nonclinical toxicity screening when their use may provide information for clinical risk assessment (Ennulat et al., 2018; Frazier et al., 2019; Frazier, 2019). Urinary biomarker evaluation should not be indicated when renal effects are limited to those above the maximum tolerated dose (MTD) or related to moribundity or mortality. Instead, use should be reserved for specific cases where nonclinical lesions are near expected or measured exposures at proposed clinical doses, where there is regulatory concern (e.g., novel presentation or mechanism) or where drug indications include populations with potential renal impairment (in which case similar biomarkers might be included in subsequent clinical trials). It is also critical to analyze these novel renal biomarker data as an exploratory analyte, comparing individual data to predose baselines rather than as group means, and to use a defined threshold (e.g.,  $4\times$  increase from predose) rather than simply identifying or highlighting analytes that increase slightly as potential drug-related findings. Magnitude of change is critically important in understanding what is a real and significant xenobiotic-induced change. Alterations in a few animals of KIM1, NGAL, or clusterin of less than fourfold are unlikely to represent renal injury on their own, especially without concomitant histopathologic evidence. Sponsors have often used additional thresholds to indicate a renal signal in either nonclinical or clinical studies (such as increases in more than one marker on two consecutive timepoints) in an attempt to distinguish false positive renal signals.

Although urinary biomarkers have established their utility in nonclinical toxicity studies, they should not be relied upon to establish or support adversity arguments (Ennulat et al., 2018; Frazier et al., 2019).

### 3.2.7. Kidney Injury Molecule-1

KIM-1 is a type 1 transmembrane glycoprotein with an immunoglobulin ectodomain that serves

as a scavenger receptor for oxidized low-density lipoproteins and phosphatidylserine-mediated phagocytosis of apoptotic cells. KIM-1 is not detectable in normal kidney tissue, but increases substantially in kidney following injury. It has a central role in the renal tubule repair process by removing dying cells and cell debris from the injured tubule. It is expressed at very high levels in dedifferentiated proximal tubule cells in animal and human kidneys after toxic or ischemic renal insult. Upon injury to proximal tubule cells, the ectodomain of KIM-1 is proteolytically cleaved by metalloproteinases from damaged cells and released into urine. In multiple rat studies, KIM-1 was tested under conditions of nephrotoxicity induced by gentamicin, inorganic mercury, chromium, adriamycin, cisplatin, ochratoxin, and a variety of other nephrotoxic drugs and chemicals (Chiu-solo et al., 2010; Han et al., 2008; Obert et al., 2021). KIM-1 proved to be more sensitive than other analytes in detecting proximal tubule damage regardless of whether it affected cortical or outer medullary proximal tubules, was more rapidly elevated than NAG, and much more sensitive and selective than sCr or UN. Elevated KIM-1 levels persist during regeneration phases following dosing with gentamicin and carbapenem, and suggest ongoing tubule repair. While numerous rodent toxicity studies have demonstrated the utility of urinary KIM-1 for the detection of AKI, performance of urinary KIM-1 in nonrodent species has been less consistent. Early increases in urine KIM-1 were noted in some, but not all, monkey studies with drug-induced AKI, and it has been utilized to monitor for acute DIKI in the minipig, but performance varies with the nephrotoxic agent. In the dog, there is significant variability among individuals and conflicting data between studies resulting in questionable single analyte assay performance in canines. For this reason, it is seldom utilized in veterinary clinical practice, but urine KIM-1 has been shown to be increased in AKI and in conditions such as canine babesiosis or Lyme disease. In the clinical setting, urinary KIM-1 has been shown to be a good predictor of acute renal injury prior to detectable changes in eGFR in humans, and it has begun to be used in CKD to follow disease progression. Clinical studies have indicated that KIM-1 is most efficient at distinguishing ATN from other types



of renal injury, such as CKD. In addition to its role in acute tubular damage, glomerular KIM-1 expression has shown to be increased in parallel with proteinuria and podocytopenia in diabetic animal models supporting its use as a potential biomarker for glomerular injury in proteinuric kidney disease. In addition to urinary KIM1, KIM1 can be analyzed in serum. In diabetic patients, serum KIM-1 changes correlated with renal decline and onset of later stage CKD and in separate studies was found to be elevated in patients with CKD of various etiologies. Because of the direct translatability of urinary KIM1 from nonclinical to clinical studies and good predictability, sensitivity, and selectivity, it has become a staple for inclusion in toxicity studies once nephrotoxicity of a xenobiotic has been established in initial studies, but it is best utilized in a panel with other renal biomarkers (Ennulat et al., 2018; Obert et al., 2021).

#### **3.2.8. Neutrophil Gelatinase-Associated Lipocalin**

NGAL is an iron-carrying glycoprotein of the lipocalin family that is bound to MMP-9 in human neutrophils and is involved in the transport of substances through membranes. NGAL is a 25-kDa polypeptide chain (in its monomeric form) that is secreted in a bound state with gelatinases from neutrophils, macrophages, and other cells involved in inflammation, and is also involved in early stages of nephron development. It is widely expressed in adult tissues, but expression is most prominent in leukocytes and kidney, including loop of Henle and collecting ducts. Tubule cells process the NGAL-iron complex leading to increased cytoplasmic iron concentrations, activation of iron-dependent cellular processes, and reduced oxidative stress. Because NGAL was rapidly induced in mouse kidney urine after acute cisplatin tubule necrosis, it is considered a promising candidate biomarker for PCT injury (Phillips et al., 2016). It is one of the earliest and most upregulated genes in rodent tubular necrosis and ischemic renal injury models, especially in the distal nephron, but has also demonstrated utility as a biomarker of tubule injury in dogs and minipigs in AKI. NGAL increased continuously during the AKI-CKD transition (from day 3 to day 28 postinjury) in a mouse ischemic kidney

model, whereas KIM-1 declined gradually in the chronic phase suggesting that NGAL may be able to dynamically monitor AKI-CKD progression. Similarly, in rat renal models, urinary NGAL levels tend to increase during the AKI phase and remain elevated for several weeks in CKD phases. Subsequently it has been investigated in a series of studies covering a wide spectrum of human renal disease and has been shown to be a good predictor of renal injury and an excellent prognostic biomarker of AKI prior to detectable changes in eGFR. In CKD patients, increased urine NGAL reflects residual renal function and is directly correlated with sCr and proteinuria, and inversely with GFR until late in disease progression when advanced stages of CKD and renal atrophy result in diminished renal reserve. For these reasons, NGAL has become an important tool in the clinical nephrologists' arsenal and along with KIM-1, has also become incorporated into clinical protocols in trials to monitor for drug-induced renal injury in humans. NGAL, however, is not specific for kidney, as serum levels are also raised in the presence of liver injury, acute bacterial infections, and chronic obstructive pulmonary disease, among other conditions. Because of potential nonrenal sources of serum NGAL related to systemic inflammation, urine NGAL changes should be compared to serum values and/or interpreted in the context of other renal biomarkers and with consideration of effects potentially related to other concurrent disease. Urinary NGAL to creatinine ratios have been quite successful in detecting DIKI in a variety of animals including mice, rats, dogs, and nonhuman primates. In dogs, NGAL has demonstrated promise as a predictive biomarker of progression of AKI, and to a lesser extent, CKD, and has generally outperformed KIM-1 or sCr in this species. However, in monkeys, NGAL was shown to be inferior in detecting minimal kidney lesions when compared to KIM-1 or clusterin. While NGAL is very sensitive for renal tubule toxicity in rodents, it was the most nonspecific biomarker evaluated in a series of rat studies comparing renal and nonrenal toxins, and increased urine/plasma NGAL was observed in a variety of different toxicities in the absence of renal lesions. Nevertheless, NGAL is considered to have successfully passed through the

preclinical, assay improvement, and clinical testing stages of the biomarker development process. Because of its sensitivity, early onset of change and direct clinical translation/predictivity, it has become increasingly utilized in preclinical toxicity or investigative studies. It should be utilized as a component of a renal biomarker urinary panel to explore and monitor for DIKI once the nephrotoxic potential of a compound has been established in initial drug development studies (Rouse et al., 2011; Frazier et al., 2019; Obert et al., 2021).

### 3.2.9. Clusterin

Clusterin is a 75- to 80-kDa disulfide-linked heterodimeric glycoprotein. It is involved in the clearance of cellular debris and apoptosis. Clusterin is expressed in most mammalian tissues and appears to be associated with a range of conditions in humans. It is elevated in the kidney and urine of rats, dogs, and primates in association with acute injury induced by ischemia/reperfusion, nephrotoxics, and other causes of renal damage. In a rat model of unilateral ureteral obstruction, clusterin- $\alpha$  elevation in urine and strong positivity for clusterin- $\beta$  in tubule epithelium are shown as early changes of tubule injury. Like KIM-1, it is expressed on dedifferentiated cells after injury, and thus appears to have some utility in being able to detect tubule regeneration after injury, at least in rodents. In comparison studies with 11 other urinary biomarkers, clusterin performed as well as KIM1 and albumin as the most sensitive and specific markers of drug-induced tubular injury, but poorly in the detection of glomerular injury. Clusterin demonstrated a significant increase when measured in urine in animal models of renal ischemia and PKD. In these models, there is a significant increase in proteinuria with correlative increases in urinary excretion of clusterin. In rats given cisplatin, gentamicin, or N-phenylanthranilic acid (NPAA), clusterin correlated well with injury to the proximal tubule, distal tubule, and collecting duct, particularly when tubular regeneration was present. In addition to rat and mouse, where studies have demonstrated its utility in detecting renal injury in various other models of diabetes or DIKI, it also has performed reasonably well in dog and cynomolgus monkeys, but so far there is little or no information for how it works in

minipig (Ennulat et al., 2018; Griffin et al., 2019; Wagoner et al., 2017). Human clinical data are also sparse with clusterin as a marker, as nearly all data have been derived from animal models and in nonclinical toxicity studies. Thus, its clinical translatability at the time of writing is still in question.

### 3.2.10. Trefoil Factor 3

TFF3 is a member of a family of small secretory proteins characterized by three intrachain disulfide bonds constituting the trefoil motif. The synthesis of these proteins has been reported particularly in mucin-producing cells of the GI tract and respiratory epithelia. Marked reduction of TFF3 protein levels occur following treatment with renal toxicants, including cisplatin, gentamicin, and carbapenem. In situ hybridization studies localize TFF3 expression to tubules and/or collecting ducts of the outer stripe of outer medulla and medullary rays, but its physiological function within the kidney is not known. In human CKD patients, TFF3 levels are increased significantly in both urine and serum and in a separate study urinary elevations in patients with heart disease were associated with coexistent kidney disease at the time of death. In contrast, in studies of DIKI in rodents, urinary TFF3 *decreased* rather than increased, and in two other separate studies, one using cisplatin and another using various nephrotoxics covering different areas of injury along the nephron, TFF3 urinary levels were also markedly reduced. In the rare studies performed prospectively in humans, paradoxically increased TFF3 was observed in urine, mirroring changes noted in CKD patients. The reason for the discrepancy in TFF3 effects in humans and rodents is unknown, but based on lack of clinical translatability and variability in performance in mice and nonrodents, TFF3 has fallen out of favor and its use in nonclinical toxicity studies has largely been replaced by urinary KIM1, NGAL, and albumin (Griffin et al., 2019; Frazier et al., 2019).

### 3.2.11. Urinary Beta2-Microglobulin

B2M is a single polypeptide chain of ~12 kDa with a structure consisting of two disulfide-linked beta sheets and a tertiary structure similar to the constant domain of immunoglobulins. It associates with the major

histocompatibility complex I (MHC-I)/human leukocyte antigen I (HLA-I) on the surface of all nucleated cells. The interaction between B2M with the alpha chain of the HLA-I is essential for antigen presentation. B2M is freely filtered through the glomerulus, and almost entirely reabsorbed and catabolized in the PCTs. In rats, urine B2M is sensitive to functional alterations of the proximal tubules and an increase in its urinary excretion has been considered to reflect impairment of the PCTs' resorption process, and thus tubule injury. While B2M accumulates in the serum when GFR is impaired, B2M concentrations may be increased in several conditions unrelated to primary renal disease such as neoplasia or extrarenal inflammatory conditions (Obert et al., 2021). Numerous human clinical studies have demonstrated large correlations between measures of renal function and serum levels of B2M once values have been normalized/transformed, and hence B2M has been utilized in equations to estimate GFR similar to creatinine or cystatin. In the majority of these studies however, B2M did not improve upon cystatin in sensitivity or precision. The usefulness of this polypeptide as a biomarker is further limited by its instability in pathological urine due to pH-dependent enzymic degradation. Therefore, great care must be taken to collect urine in an ice-cold, adequately buffered environment with the addition of stabilizers to preserve B2M levels during the period of collection and in storage. B2M is highly species-specific, and its assays may not be readily available for all laboratory animal species. B2M use as a renal biomarker has therefore been largely supplanted by more recent novel biomarkers in nonclinical toxicity studies.

### 3.2.12. Renal Papillary Antigen

Few biomarkers have been discovered capable of detecting damage to the distal collecting system of the kidney. In particular, it is critical to detect any potential of a newly developed drug for causing renal papillary necrosis (RPN), a specific type of kidney injury that has been well documented in humans as a drug-induced entity. Papillary necrosis risk is effectively identified in routine toxicology testing, but in humans, severe degrees of papillary injury can occur without detection. Monoclonal antibodies to rat renal papillary tissue, termed RPA-1 and RPA-

2, have been used as a diagnostic tool for identifying toxic damage to the rat papilla. The amount of RPA-1 is increased in rat urine following exposure to classical papillotoxins, including single doses of 2-bromoethanamine (2-BEA) or propyleneimine, and single or repeated doses of indomethacin. The exact molecular identity of RPA-1 has not yet been determined, but it is known to be predominantly a high molecular weight (in the mega-Dalton range) membrane-bound glycoprotein. RPA-1 is normally present in rat urine, presumably through physiological membrane shedding from collecting ducts. RPN is a relatively common form of toxicity encountered in preclinical safety testing, and (encompassed under the term analgesic nephropathy) has been a problem in humans habitually consuming NSAIDs, particularly those containing phenacetin. Unfortunately, the human ortholog of RPA has not been successfully identified, nor a similar antigen in a form that is easily translatable from rodent to human, so this assay has not been successfully transferred into the clinic. It still has utility in nonclinical studies in localizing injury to the distal medulla and is useful in panels of biomarkers or in investigative rodent studies.

Other potential biomarkers of acute renal injury include interleukin-18 (IL-18), and OPN. IL-18 has been shown to be an early indicator of ATN and predictive of human mortality in certain renal disease states. In a cross-sectional comparison of 204 patients with or without AKI, urinary IL-18 had a sensitivity of 68% and specificity of 95% (Parikh et al., 2004). While there is ongoing research into the utility of this marker, it has thus far gained little traction for use in animal toxicity studies. OPN is a proinflammatory molecule detectable in serum and renal tissue. It is found in kidneys in the TAL of the loop of Henle and in distal nephrons and is excreted in urine. Elevated urine OPN levels have been noted in DN patients, hypertensive renal disease, transplant nephropathies, and patients with lupus. It has been shown to be sensitive and selective for tubule injury and in prospective studies with a host of known nephrotoxics, OPN outperformed UN and sCr in monitoring DIKI in rodents and significantly improved accurate diagnosis of renal tubule degeneration in the rat. Urine OPN was much less effective in detecting tubule regeneration

or glomerular injury. Given this evidence, it has been qualified as a renal biomarker by the FDA in rodents, and is under active exploration as a renal biomarker in humans. However, it is present in many tissues, so there is a possibility for increases in urinary OPN due to extrarenal injury. It has been successfully used as a renal injury marker in a few selected prospective studies with dogs, minipigs, and nonhuman primates in animal toxicity studies, but to-date there is insufficient published data to provide a sound basis for routine use in nonclinical drug development (especially in nonrodents), and at present OPN is best utilized in a panel with other more established parameters like KIM-1, NGAL, and urinary albumin.

### **3.2.13. Alternative Biomarkers for Chronic Duration Nonclinical Safety Studies**

While most of the established analytes and novel renal biomarkers listed above have been utilized in animal toxicity studies, they are best suited for use in shorter term situations where they can prospectively detect the onset and progression of acute DIKI. This is because these biomarkers were largely developed and evaluated for detection and monitoring of renal dysfunction in the setting of AKI. They also have the advantage of providing nephron segment injury localization in animals with DIKI. Of these, KIM-1, albumin, and NGAL have demonstrated the most translational applicability and have gained the most widespread use in the pharmaceutical safety assessment arena in acute or subacute nonclinical studies, but even they have proved inadequate in chronic studies where subtle renal changes occur over time due to drug or chemical exposure (Obert et al., 2021). This has led to the investigation of other potential analytes that may be useful in detecting chronic renal injury or to monitor the progression of CKD. The following biomarkers will be discussed in this context, although they also show some utility in the acute setting of DIKI.

### **3.2.14. Cystatin C**

CysC is produced by all nucleated cells in the body, and, unlike sCr, it is not influenced by factors unrelated to kidney function and has proven to be an important analyte for estimating GFR. After glomerular filtration, the vast majority of CysC is reabsorbed and catabolized

by the proximal tubules in rats. Therefore, urinary CysC has been proposed as a marker of renal tubule impairment and serum CysC to complement the widely used estimate of GFR based on Cl<sub>cr</sub>. This change in preference is because, in contrast to creatinine, CysC has no dependence on muscle mass, diet, or tubular secretion. However, the accuracy of serum CysC assays are affected by thyroid disease or glucocorticoid coadministration. Urinary CysC has also been shown to be an early biomarker of ischemic AKI and nephrotoxicity in humans, including multiple studies with cisplatin, amphotericin B, methotrexate, and aminoglycosides among others (Griffin et al., 2019; Togashi et al., 2012). Due to its effectiveness to diagnose clinical AKI induced by a variety of agents, CysC has become an important tool for regulatory decision making in drug development, but it is just beginning to be utilized in chronic studies in animals, and is one of the promising new analytes that may make the transition from AKI to CKD biomarker. Serum CysC correlated more strongly with measured GFR than creatinine and better predicted mortality in CKD patients. While in humans eGFR calculations with CysC in blood and urine are replacing creatinine, eGFR calculations in general have not been utilized in veterinary practice or in animal toxicity studies for a variety of reasons. This has not limited the utilization of CysC in investigative toxicity studies. In rats, serum CysC was more sensitive and reliable than sCr and was able to detect DIKI lesions in various segments of the nephron regardless of mechanism, often earlier than other analytes. In dogs with renal dysfunction, CysC was more sensitive than sCr for detecting decreased GFR. In a rat model of colistin nephrotoxicity, serum CysC correlated better with histologic evidence of tubular injury than creatinine. In monkeys, it has been successfully utilized to detect AKI due to gentamicin nephrotoxicity. CysC outperformed other analytes in detection of early CKD in dogs, and has been utilized to detect the progression of chronic renal changes in rodents (Togashi et al., 2012). As CysC analysis becomes more common in nonclinical studies, it may achieve its place as a chronic marker of renal dysfunction in animals, but more nonclinical data are required before it will be routinely utilized in investigational toxicologic studies.



### 3.2.15. Symmetrical Dimethyl Arginine

SDMA is another promising candidate for a chronic renal biomarker. SDMA and its isomer asymmetrical dimethyl arginine (ADMA) are released into cytoplasm from mitochondria after arginine is metabolized, then transported into the systemic circulation where SDMA is excreted through the kidney in a process entirely dependent on glomerular filtration. Serum SDMA levels have risen progressively with increased renal dysfunction or injury and especially in chronic renal disease, but independently of other nonrenal factors associated with other diseases. Human CKD patients show significant, progressive increases in SDMA compared to normal subjects and there is a strong correlation between SDMA and measured or estimated GFR. SDMA has been utilized routinely in veterinary clinical practice for over a decade in dogs and cats with great success in detecting and monitoring renal function in glomerulotubular diseases. However, SDMA as a single measurement is not recommended as a screening tool, and instead serial monitoring and critical difference (CD) is preferred practice. Recently, the assay has been successfully utilized in rodents. In renal ischemia models in rats and mice, as well as in nephrectomized rat models, serum SDMA levels increased progressively as renal mass was reduced. SDMA has only recently begun to be incorporated in target animal safety studies and safety assessment investigative studies, but it appears to have utility as a renal biomarker, especially in studies of chronic duration where other markers may wane, or in those involving the dog, where normal and dynamic ranges have been firmly established (Obert et al., 2021).

### 3.2.16. Dickkopf Homolog 3

*Dickkopf homolog 3* (DKK3) is another surrogate biomarker for GFR that has recently been suggested for use in chronic toxicity studies to detect and monitor the progression of renal dysfunction. DKK3 is a stress-induced, profibrotic glycoprotein that modulates the Wnt signaling pathway. It can detect tubular injury and progressive tubulointerstitial fibrosis in animals and humans. DKK3 is expressed in developing kidneys, but expression is suppressed in adults. It is reexpressed in renal tubules undergoing degeneration or disease, and especially those eliciting a profibrotic T-cell response. DKK3 has been shown to be an

effective biomarker of renal tubular stress, and to predict AKI and kidney function loss in post-surgical cardiac patients. DKK3 has been used to monitor CKD progression in humans, as urinary and plasma DKK3 levels are significantly higher in patients with CKD than in the control population and DKK3 increases correlate with GFR and with the extent of renal fibrosis. DKK3 may also be important in progression of renal disease in animals. Renal tubule injury and fibrosis were attenuated in models of chronic kidney injury and findings were confirmed with antibody-mediated DKK3 blockade (Zewinger et al., 2018; Obert et al., 2021). DKK3 expression was upregulated in renal tubules in a mouse adriamycin nephropathy model, and in rat kidney injury models elevated DKK3 correlated with both acute tubular injury and chronic renal disease. Although it is too early for definitive assessment, the use of DKK3 in rodent and non-rodent toxicology may hold promise as a biomarker of chronic renal injury as a surrogate for GFR.

In summing up the position of this field of intense research activity over the past 2 decades, the most practical outcome will not be reliance on a single utilitarian biomarker of renal tubule damage, but assembly of a battery of reliably predictive markers for use in monitoring DIKI in clinical medicine. At least for the detection of postoperative or DIKI in human patients, urinary KIM-1, NGAL, and albumin appear to be among the candidates for this combination approach. Their combined use has become established in subsequent nonclinical toxicity investigative studies once nephrotoxicity has been established by histopathologic evidence in routine GLP studies in animals. Clusterin and OPN may join this list and become part of a more in-depth renal tubule injury panel once more performance data are accumulated. In order to cover the possibility of papillary necrosis, inclusion of RPA-1 might be considered in this context in rodents. Urinary protein levels remain the staple of detection for drug-induced glomerular injury. In order to monitor for subtle renal changes occurring in chronic studies or in CKD patients, the use of CysC, SDMA, or DKK3 may be incorporated in the future. Just as in the case of individual biomarkers, the efficacy of combining multiple biomarkers will necessitate rigorous validation, which is ongoing in both the nonclinical and clinical arenas.

**TABLE 2.8** Suggested Descriptive Nomenclature for Reporting Common Nonproliferative Lesions in Kidney**Congenital lesions**

Renal aplasia  
 Renal hypoplasia  
 Polycystic kidney  
 Hydronephrosis  
 Renal dysplasia

**Disturbances of cell growth/differentiation**

Atrophy, glomerulus  
 Atrophy tubule  
 Hypertrophy, tubule  
 Regeneration, tubule  
 Karyomegaly  
 Bowman's capsule metaplasia/hyperplasia  
 Squamous cell metaplasia of pelvic epithelium  
 Osseous metaplasia  
 Mesangial hyperplasia

**Inflammatory changes**

Glomerulonephritis  
 Pyelonephritis  
 Inflammatory infiltrate  
 Interstitial nephritis  
 fibrosis

**Miscellaneous changes**

Basophilia, tubule  
 Extramedullary hematopoiesis  
 Basophilic granules

**Cell death**

Single cell necrosis  
 Necrosis, tubule  
 Papillary necrosis  
 Infarcts

**TABLE 2.8** Suggested Descriptive Nomenclature for Reporting Common Nonproliferative Lesions in Kidney—cont'd**Degenerative changes**

Degeneration, tubule  
 Vacuolation, tubule  
 Hyaline droplets  
 Cysts, tubule  
 Pigmentation  
 Dilation, tubule  
 Casts (hyaline or granular)  
 Crystals or calculi  
 Mineralization (tubule, vascular, or pelvis)  
 Amyloid  
 Glomerulosclerosis  
 Glomerulonephritis  
 Glomerulopathy

**Vascular changes**

Thrombosis  
 Infarct  
 Periarteritis,  
 Necrosis, medial

**Special disease processes**

Chronic progressive nephropathy (CPN)  
 Alpha<sub>2</sub>μ-globulin nephropathy  
 Obstructive nephropathy  
 Retrograde nephropathy

Severity modifiers: Minimal (<1%); Mild (1%–10%); Moderate (10%–25%); Severe (25%–75%); Very Severe (>75%). Duration modifiers: Acute, subacute, or chronic; Distribution modifiers: Focal, multifocal/segmental, or diffuse/global.  
 Modified from Haschek WM, Rousseaux CG, Wallig MA, editors: *Handbook of toxicologic pathology*, ed 2, 2002, Academic Press, Table X!V, p. 325, with permission.

(Continued)

### 3.3. Morphologic Evaluation

Histopathology is recognized as the single most appropriate screen for evidence of renal injury in animal toxicity studies. For routine microscopic examination, immersion fixation in 10% neutral-buffered formalin of a single longitudinal section of the left and transverse section of the right kidney represents a practical approach in allowing thorough examination of all elements within the kidney. Perfusion fixation optimally prepares the kidney for the examination of luminal surfaces, or for EM evaluation. Perfusion fixation can induce cytoplasmic vacuolar artifacts, which may be difficult to differentiate from hydropic phagolysosomal swelling. Additionally, glutaraldehyde can interfere with special stains such as the Mallory-Heidenhain stain and many IHC stains, which often require specific handling and pretreatment. Specimens for ultrastructural evaluation to determine the organellar target should be selected to include one or two affected animals from the earliest time point and lowest affected dose group and one or two animals from the next time point, in addition to appropriate controls rather than examples from the most affected animals where secondary necrosis or severe degeneration may obscure lesions directly related to mechanism of insult. When examining glomerular lesions, silver stains and/or PAS stains are necessary to delineate basement membranes, and EM evaluation is more critical than in cases of tubule toxicity. IHC may be especially helpful in detecting the presence of antidrug antibodies (ADAs) or autoantibodies in nonhuman primates. Immunofluorescence is helpful in specific instances, and especially for detecting complement deposition in glomerular tufts.

The classification of renal disease varies among pathologists and, over time, by the same pathologist. An evaluation strategy should include standardized nomenclature established for toxicologic purposes that have been published for the kidney (INHAND and SEND) that utilize unambiguous descriptive terminology and that is easily understood by regulatory reviewers and other pathologists (Frazier et al., 2012) available at [toxpath.org](http://toxpath.org) (Table 2.8). These established schemes include subtopographical anatomy, description of the basic pathologic process, modifiers, and quantitative measure of lesion distribution/extent in pathology data and reports. There are other specific scoring schemes utilized for investigative renal studies in rodents and rodent kidney models and these are discussed later in Section 3.

#### 3.3.1. Spontaneous Renal Diseases

Familiarity with spontaneous diseases occurring in animal models is essential for the establishment of the nature and cause of morbidity or mortality in an individual animal. For optimizing hazard identification, including the statistical analyses of tumor incidences in carcinogenicity bioassays, cause of death is pivotal. In acute toxicity studies, recognition that death from renal toxicity with renal failure typically takes 3 days in the rat is important. Death within 24–48 h of initial treatment probably cannot be attributed to nephrotoxicity with renal failure as the primary mechanism. Spontaneous disease may mask or mimic a toxicologic response, or the most minimal expression of nephrotoxicity may present as slight exacerbation of the severity of a spontaneously occurring lesion. A majority of rats in chronic and carcinogenicity studies exhibit several age-related inflammatory, degenerative, and proliferative lesions in the kidney, predominated by CPN. In standard 2- to 13-week toxicology studies, approximately 50%–60% of SD rats exhibit histologic changes in the kidney. The incidence of CPN is higher in males (~30%) than in females (~20%). Incidence of CPN in 4- to 5-month-old male F344 rats is 100%. In addition to CPN, other microscopic changes include mineral deposits, and interstitial mononuclear cell infiltrates (Figure 2.9). Renal parenchymal mineralization is more frequent in females, and incidence and severity increase with age. Less common (<2%) microscopic changes in SD rat kidney include intratubular casts, increased hyaline droplet accumulation (alpha<sub>2</sub>μ-globulin nephropathy), focal tubular dilation, focal interstitial fibrosis, tubular epithelial vacuolation, glomerular lipodosis, focal infarcts, renal pelvic dilation (hydronephrosis), and karyomegaly (Figure 2.9).

The background incidence of microscopic changes in Wistar-Han rats is significantly lower than that of SD rats due primarily to the lower incidence of CPN. Approximately 35%–45% of Wistar-Han rats in standard 2- to 13-week toxicology studies exhibit histologic changes in the kidney. Simple tubular epithelial hyperplasia, atypical hyperplasia, adenoma, and carcinoma are seen in longer-term rat studies (Figure 2.10). With the exception of the familial renal amphophilic vacuolar (A-V) adenomas of rats, which appear to be universally of spontaneous origin, other renal tubular neoplasms occurring as



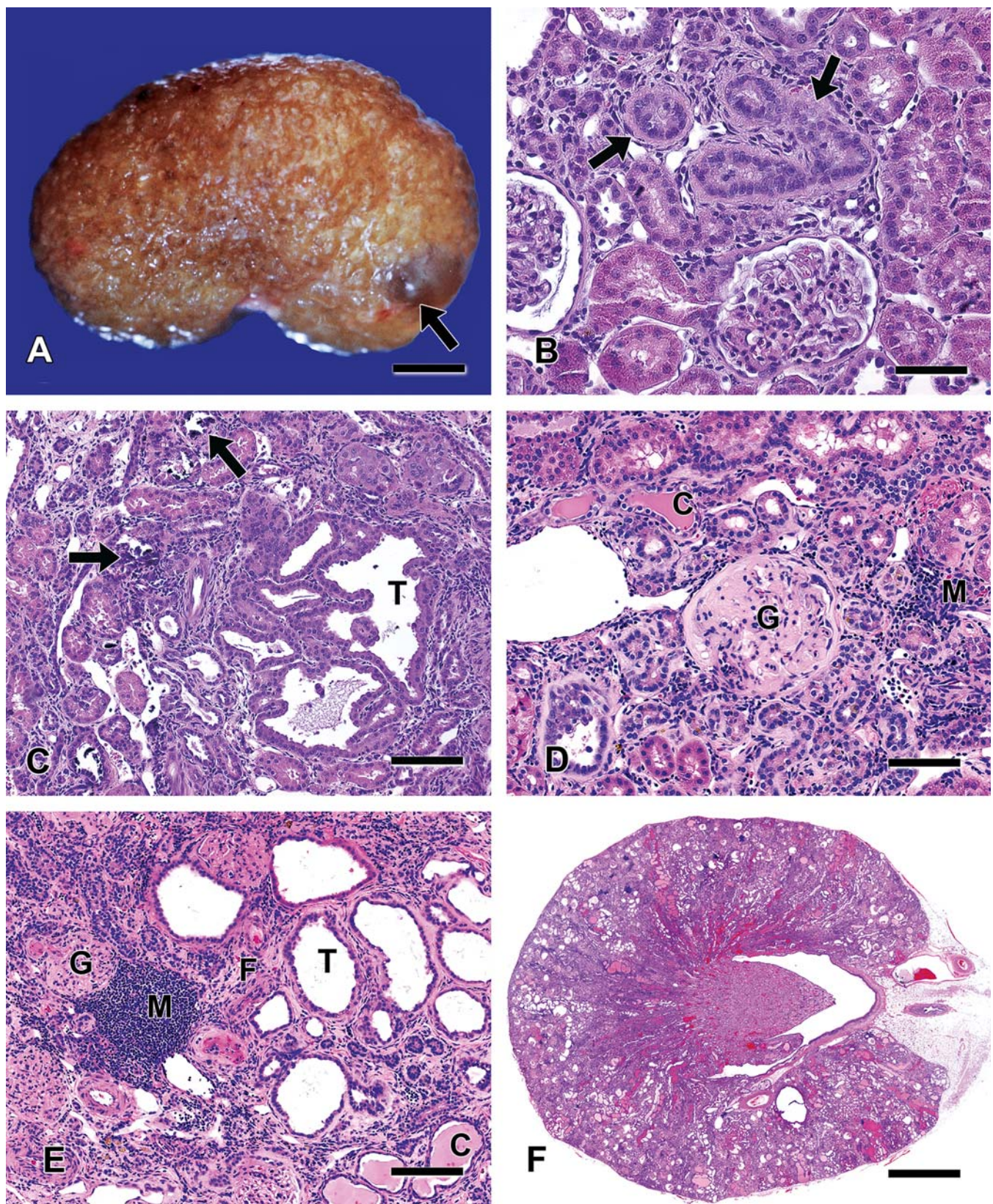


**FIGURE 2.9** CPN in Sprague-Dawley rats. Gross photograph (A) illustrates the cystic or granular surface of a kidney in late stage of CPN. Bar = 3 mm. Light micrographs (B–F) illustrate the hallmarks of CPN. (B) Illustrating tubular epithelial hyperplasia and thickened basement membrane (arrows). Bar = 45 mm. (C) Illustrating tubular and interstitial mineralization (arrows) and tubular dilation and hyperplasia (T). Bar = 55 mm. (D) Illustrating glomerular sclerosis (G), interstitial mononuclear or inflammatory cell infiltration (M), and tubular casts (C). Bar = 55 mm. (E) Illustrating glomerular sclerosis (G), interstitial fibrosis (F), mononuclear or inflammatory cell infiltration (M), and tubular dilation (T) and casts (C). Bar = 110 mm. (F) Subgross micrograph shows the late stage of CPN of a 2-year-old Sprague-Dawley rat. Bar = 1 mm. Courtesy of Dr Xiantang Li, Drug Safety R&D, Pfizer, Groton CT; Reproduced from Haschek WM, Rousseaux CG, Wallig MA, Bolon B, editors: Haschek and Rousseaux's handbook of toxicologic pathology, ed 3, 2013, Academic Press, Figure 47.14, p. 1702, with permission.



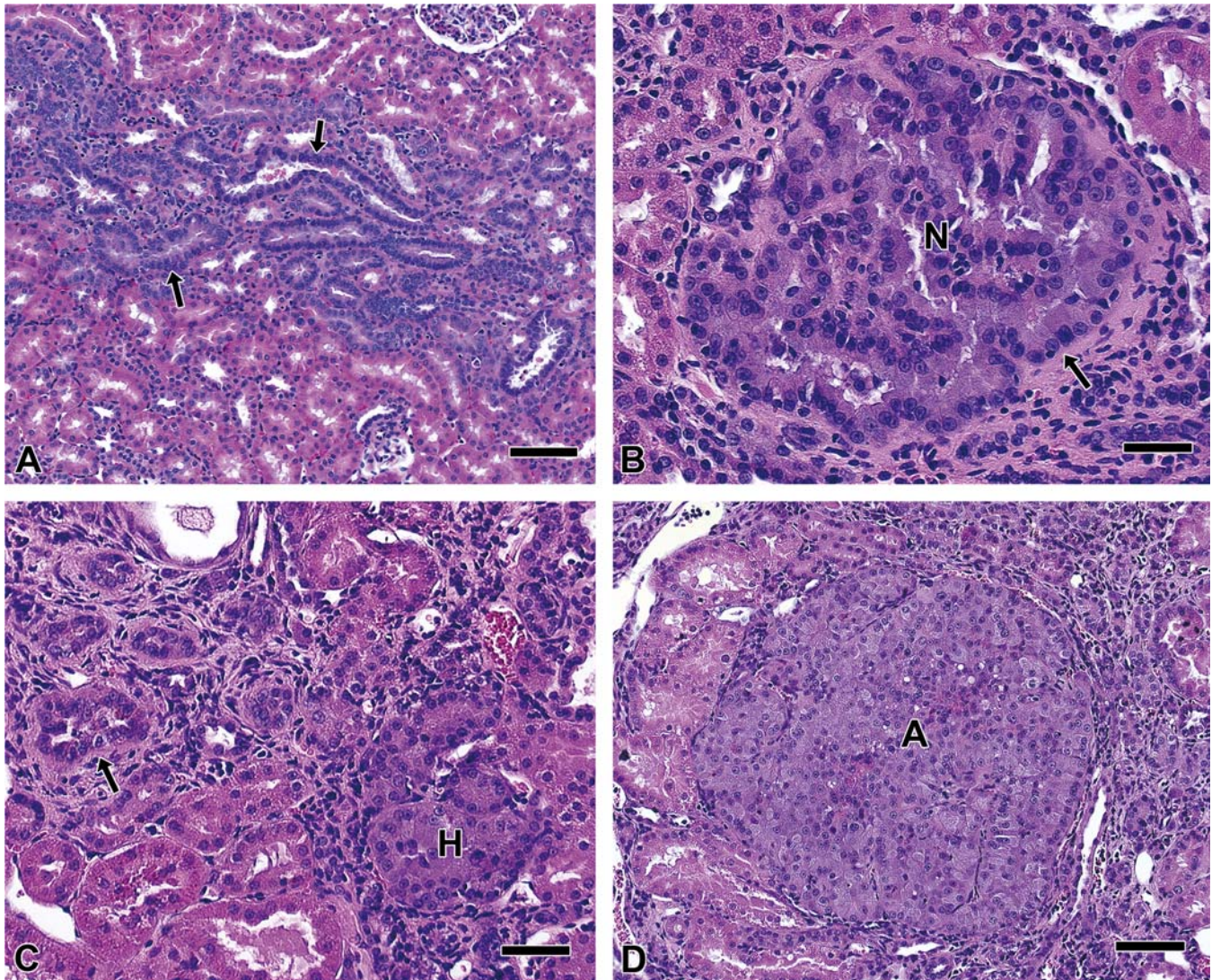


**FIGURE 2.10** Proximal tubule proliferation and neoplasia. (A) Focal tubular epithelial cell hyperplasia with variable luminal dilation (arrows). Bar = 70  $\mu$ m. (B) Atypical tubular epithelial cell hyperplasia (H) and basement membrane thickening (arrow). Bar = 55  $\mu$ m. (C) Adenomatous or papillary nodular hyperplasia (N) with cellular basophilia and basement membrane thickening (arrow). Bar = 35  $\mu$ m. (D) tubular adenoma (A) with cellular proliferation and loss of the tubular lumen and basement membrane. Bar = 50  $\mu$ m. *Reproduced from Haschek WM, Rousseaux CG, Wallig MA, Bolon B, editors: Haschek and Rousseaux's handbook of toxicologic pathology, ed 3, 2013, Academic Press, Figure 47.16, p. 1704, with permission.*

a result of xenobiotic exposure cannot be morphologically differentiated from spontaneously occurring tubular tumors. The cytoplasm of A-V adenomas tends to be eosinophilic to amphophilic and vacuolated, giving the name to these lesions, and they generally do not metastasize (Figure 2.11). Eker rats have a genetically based renal tubular neoplasm that is also distinctive from renal tumors in the stocks and strains used in toxicity studies such as SD, Wistar-Han, and F344 rats. Renal mesenchymal tumor (RMT), which tends to be highly

malignant, occurs in young rats associated with genotoxic insult at an immature age. The predominant cell type is a fibroblastic spindle cell, with predisposition to encircle sequestered preexisting tubules. Nephroblastoma is a tumor of the young rat, rarely occurring spontaneously but inducible with specific in utero genotoxic xenobiotic insult. This tumor consists of islands of densely packed blastema-like basophilic cells with scant cytoplasm and ill-defined cytoplasmic margins, often with a tubular structure at their center. Glomeruloid bodies are found



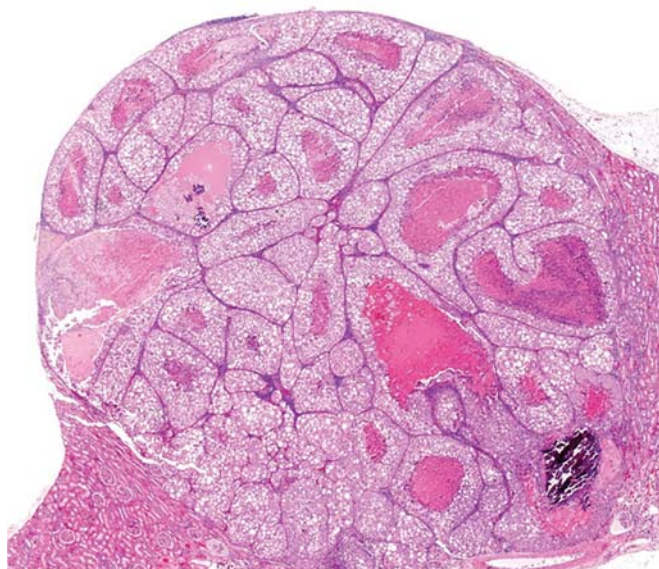


**FIGURE 2.11** Amphiphilic vacuolar adenoma from a rat kidney. A large circumscribed, expansile mass is present in the cortex which is composed of clusters of large cells with multiple vacuoles surrounding necrotic centers and interspersed with a fibrovascular stroma around nodules. This tumor has a genetic basis in rodents and thus has no clinical relevance when noted in increased numbers in a carcinogenicity study.

in about 50% of cases. Polyoma virus injected into rats can cause a renal sarcoma, with rather uniform histologic appearance. Lipomatous tumors (Figure 2.12) are spontaneous tumors that are slow growing and usually appear in old animals, appearing to arise at the corticomedullary junction. Urothelial carcinomas can occur in the pelvis and ureters.

### 3.3.2. Chronic Progressive Nephropathy

CPN is a spontaneous disease of laboratory rats that represents a significant confounder for interpretation of renal histopathology in toxicology studies. The hallmark features in rats include clusters of basophilic tubules, nuclear crowding, thickened basement membranes, tubule casts, and glomerulosclerosis (Figure 2.9) (Hard and Khan, 2004; Hard and Seely, 2006). The disease progresses relentlessly from a solitary affected tubule in the earliest stage, to formation of multiple foci, ultimately involving the whole kidney and sometimes leading to death through chronic renal failure in rats typically over 18 months of age. Male gender is a primary risk factor for developing CPN, and this

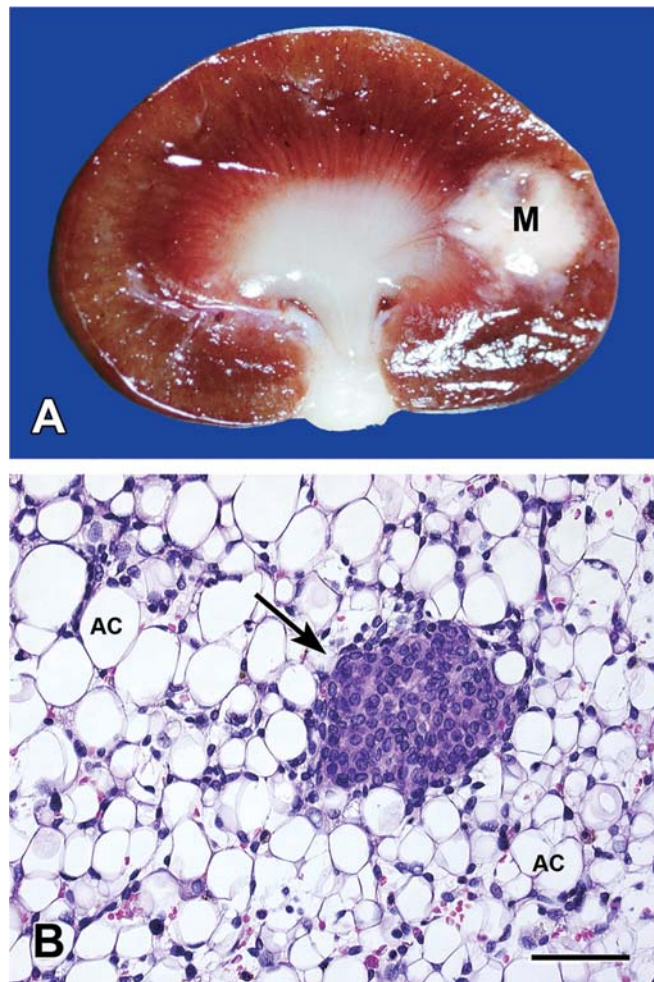


**FIGURE 2.12** Lipomatous tumor in the kidney of a rat. (A) A well-demarcated pale mass (M) in the renal cortex with infiltration into medulla. (B). Well-differentiated mature adipose cells (AC) with entrapped renal epithelial cells (arrow). Bar = 60 mm. Reproduced from Haschek WM, Rousseaux CG, Wallig MA, Bolon B, editors: *Haschek and Rousseaux's handbook of toxicologic pathology*, ed 3, 2013, Academic Press, Figure 47.17, p. 1705, with permission.

predisposition has been linked to the presence of androgen rather than to an absence of estrogen. CPN is an age-related disease modulated by numerous extrinsic factors such as diet and chemical exposures. Among these, restriction of caloric intake and specifically protein is the most effective method for inhibiting the disease process. Although the underlying etiology of the condition is believed to involve genetic, epigenetic, and/or environmental initiating factors, the mechanistic pathogenesis of CPN is extremely complex. The molecular and

biochemical pathways of the degenerative phases of the disease have recently been described in detail, involving the essential interactions of five key and interrelated proteins—renin, angiotensin II (Ang II), hypoxia-inducible factor 1 $\alpha$  (HIF-1 $\alpha$ ), transforming growth factor- $\beta$ 1 (TGF $\beta$ 1), and NO (Obert and Frazier, 2019). Once the renin–angiotensin system within the renal interstitium is activated in these initial phases of the disease, a cascade of events occurs which ultimately results in the later phases of CPN, characterized by regenerative and proliferative pathways in renal tubules, paralleling degeneration and atrophy associated with end-stage renal disease (ESRD) (Hard and Seely, 2006). Many chemicals are known to exacerbate the severity of CPN to an advanced stage, and this interaction between chemical and CPN can result in a small increase in the incidence of renal adenomas in 2-year carcinogenicity bioassays. Because CPN is a rodent-specific entity, the finding of a small, statistically significant increase in renal tubule tumors, linked to exacerbation of CPN by a test article in a preclinical study for carcinogenicity, can be regarded as having no relevance for extrapolation in human risk assessment (Hard and Khan, 2004; Hard et al., 2009a, 2009b). However, concordance of renal tumors and CPN of significant severity needs to be made in individual animals to make this assignment. Microscopic lesions of CPN can be seen in rats as early as 2 months of age and may present only as basophilic tubules and can be confused with other similar drug-induced degenerative lesions. Because CPN is a complex of a number of individual structural lesions, including tubule basophilia, simple tubule hyperplasia, hyaline casts, glomerulosclerosis, and hyperplasia of the papilla lining, it is recommended that study pathologists recognize the complex as a single entity, and record it as such under the term CPN rather than recording diagnoses separately (Frazier et al., 2012). However, if tubule basophilia, hyperplasia, casts, or glomerular change occurs in the rat kidney unrelated to CPN disease, changes must be reported as unique findings.

### 3.3.3. Common Spontaneous Lesions in Beagle Dogs

Most laboratory Beagle at less than 3 years of age have healthy kidneys. Immature glomeruli especially in outer cortex can occur in dogs up

to 6 months of age. Approximately 50%–60% of Beagle dogs in standard toxicology studies exhibit histologic findings in the kidney. Most common (>2%) microscopic changes include focal tubule basophilia (Figure 2.13), mineral deposits in medullary collecting ducts, interstitial mononuclear cell infiltrates, and focal pigment deposition (Woicke et al., 2021). Less common microscopic changes include focal tubular dilation, focal hyaline casts, focal interstitial or capsular fibrosis, tubular epithelial vacuolation, glomerular lipidosis, focal hemorrhages, granulomas, and transitional cell hyperplasia of renal pelvis. Glomerular lipidosis is a lesion characterized by segmental distortion of glomerular capillaries by lipid-laden and/or ceroid-laden macrophages. It can be associated with transient or mild proteinuria when widespread, but there is not an analogous lesion in humans. Mineralization is more common in females, and can be seen in as many as 60% of animals in a given study. None of the above lesions have clinical significance.

### 3.3.4. Common Spontaneous Lesions in Monkeys

Background histologic changes have been reported in kidneys at an incidence of 75% of

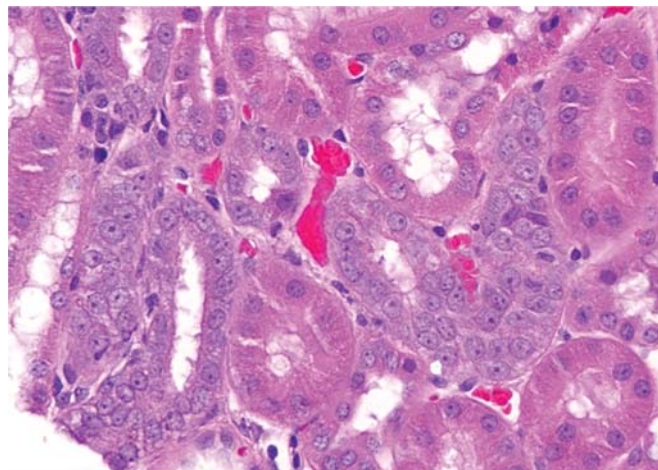


**FIGURE 2.13** Focal tubule basophilia from a control beagle dog. This focus of adjacent proximal tubules has increased nuclear to cytoplasmic ratio, basophilic cytoplasm, and increased mitoses representing a regenerative process. This is an extremely common background finding in beagle dogs and is usually graded as minimal, but when more severe can represent a xenobiotic-induced lesion.



control cynomolgus monkeys in toxicology studies. The most common microscopic changes include interstitial mononuclear cell infiltrates, segmental glomerulosclerosis, focal vasculopathy, mineralization, and tubule degeneration and regeneration (Colman et al., 2021). Focal vasculopathy is characterized by mononuclear cell infiltrates surrounding blood vessels with rare vessel wall hyalinosis or medial degeneration. Less common microscopic changes in cynomolgus monkey kidney include hypercellular immature glomeruli, focal tubule dilation, focal interstitial fibrosis, tubule vacuolation, granulomas, chronic infarcts, and, rarely, unilateral atrophy. Multifocal segmental to global glomerulosclerosis is often noted in marmosets, and can be seen in kidneys of cynomolgus monkeys as young as 3 years old. Incidence and severity increase significantly with advanced age (Frazier and Obert, 2018). Marmosets also have chronic interstitial nephritis as a common spontaneous finding in addition to glomerular lesions related to IgM accumulation due to immunologic mechanisms (Brack, 1988). Eosinophilic intracytoplasmic inclusions affect urothelium of approximately 10% of rhesus monkeys, and should not be confused with viral inclusions. Incidence of background changes in cynomolgus monkeys can vary markedly based on monkey site of origin/strain. Both vasculopathy and glomerulonephritis can occur in monkeys given biologic therapies, especially humanized antibodies, due to immune-mediated ADAs, but they generally will occur in more than one individual on study and can be further investigated by immunohistochemistry to distinguish from more rare spontaneous cases.

### 3.3.5. Common Spontaneous Lesions in Minipigs

Porcine kidneys have multireniculate and multipapillate structure similar to that of humans. Common spontaneous lesions in normal minipigs include tubule basophilia, mineralization, casts, interstitial inflammatory infiltrates, interstitial fibrosis, scattered individual glomeruli with sclerosis, and cysts (Skydsgaard et al., 2021). Tubule basophilia often occurs as a spontaneous aging lesion near the corticomedullary junction in minipigs, associated with thickened basement membranes or peritubule fibrosis, and appears to

be similar to CPN in rodent kidneys, but the pathogenesis is unknown in the pig. Less common spontaneous lesions include glomerulonephritis, most frequently of membranous or membranoproliferative type. In many cases, this has been associated with previous or current bouts of the hemorrhagic syndrome in minipigs (Vezzali et al., 2011). Spontaneous lesions have to be established as definitively separated from similar drug- or chemical-induced renal pathology and may be problematic. Tubule basophilia is an extremely common manifestation of mild nephrotoxicity in the minipig and often occurs without vacuolation, necrosis, or other aspects of degeneration that are commonly noted concurrently in the kidneys of other species with DIKI (Skydsgaard et al., 2021). Tubule basophilia may be accompanied by mitoses or cellular hypertrophy, which in other species would suggest regeneration, but other signs of regeneration are usually lacking in minipig kidneys. With more severe tubule injury, basophilia may progress to tubule dilation and/or necrosis. The minipig kidney seems especially prone to collagen formation and fibrosis after injury, but in contrast to humans where renal fibrosis is progressive and often carries a negative prognosis, in the pig it can remain static or even regress over time (Figure 2.14). Glomerulonephritis may occur as a function of DIKI, particularly with humanized antibodies, and as in the monkey, with biologic therapies is usually related to immune-mediated ADAs without clinical relevance. In other cases, direct injury to the glomeruli have been produced by drugs or chemicals. In such cases, interpretation of a drug effect is best determined by finding multiple animals affected and a clear dose response.

### 3.3.6. Common Spontaneous Lesions in Mice and Other Species

Common nonneoplastic lesions in the kidney of the CD-1 mouse (Table 2.9) include amyloidosis (Figure 2.15), interstitial mononuclear cell infiltrates, CPN, tubule dilation, mineralization, and, rarely, cytoplasmic vacuolation (Frazier, 2021; Burek et al., 1988) (Figure 2.15B). CPN in mice shares many features with the rat, and is characterized by basophilic regenerative tubules, thickened basement membranes, and interstitial mononuclear cell infiltrates. Occasionally, tubular protein casts and focal glomerulosclerosis with dilated Bowman's space is seen in older animals.

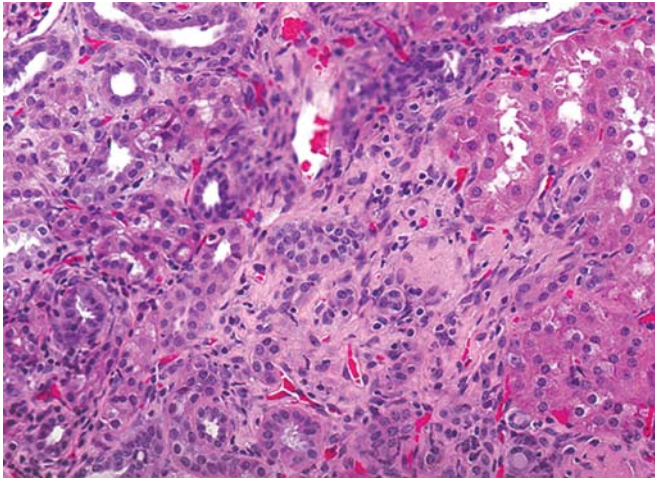


**FIGURE 2.14** Interstitial fibrosis in a kidney from a Gottengen minipig administered a nephrotoxic xenobiotic. Note that the renal tubules in the center of the photomicrograph are surrounded and separated by thick mature collagen which has resulted in atrophy of some of the tubules. There is a minimal inflammatory infiltrate and karyorrhectic debris mixed in the fibrotic areas. Fibrotic responses are a common finding in xenobiotic-induced nephrotoxic lesions in this species.

The incidence is higher in males than females. The severity of renal involvement and extrarenal secondary effects is modest compared with that seen in rats. Both amyloidosis and glomerular changes from CPN can be noted in the same animals within glomeruli in carcinogenicity studies complicating descriptive terminology. Tubule dilation associated with distal obstruction from mouse urologic syndrome (MUS) is also commonly encountered in chronic studies. MUS can be a common source of mortality in male mice. The proliferative lesions reported in the mouse kidney include tubular epithelial cell hyperplasia, tubular adenoma (Figure 2.16A), carcinoma, nephroblastoma (Figure 2.16B), histiocytoma, and urothelial carcinoma of renal pelvis.

The most common disease of Syrian hamsters is amyloidosis. The kidney is typically involved, with incidence at 2 years usually over 50% in both sexes. In Syrian hamsters, ESRD is usually the major cause of death. Typically, renal amyloidosis is causative while nonamyloid-related ESRD can also be important. Cellular infiltration of the kidney, nephropathy, and mineralization represents the other common

**TABLE 2.9** Pattern of Occurrence of Common Age-related Kidney Lesions in Control CD-1 Mice

Age (weeks)	1–13	14–26	27–39	40–52	53–65	66–79	80–91	92–104	>104
Number of mice	167	117	43	43	95	320	559	1259	120
<b>AMYLOIDOSIS (%)</b>									
Male	0	0	0	12	13	77	79	55	100
Female	0	2	0	8	32	58	70	54	93
<b>CELLULAR INFILTRATION (%)</b>									
Male	0	15	15	0	23	32	31	44	44
Female	1	4	13	19	27	29	25	42	12
<b>CHRONIC NEPHROPATHY (CPN) (%)</b>									
Male	0	0	0	0	7	14	18	11	74
Female	0	0	4	4	3	9	13	9	29
<b>MINERALIZATION (%)</b>									
Male	0	2	0	0	2	4	5	13	0
Female	1	0	9	0	0	2	4	5	0

Modified from Haschek WM, Rousseaux CG, Wallig MA, editors: *Handbook of toxicologic pathology*, ed 2, 2002, Academic Press, Table XVII, p. 329, with permission.



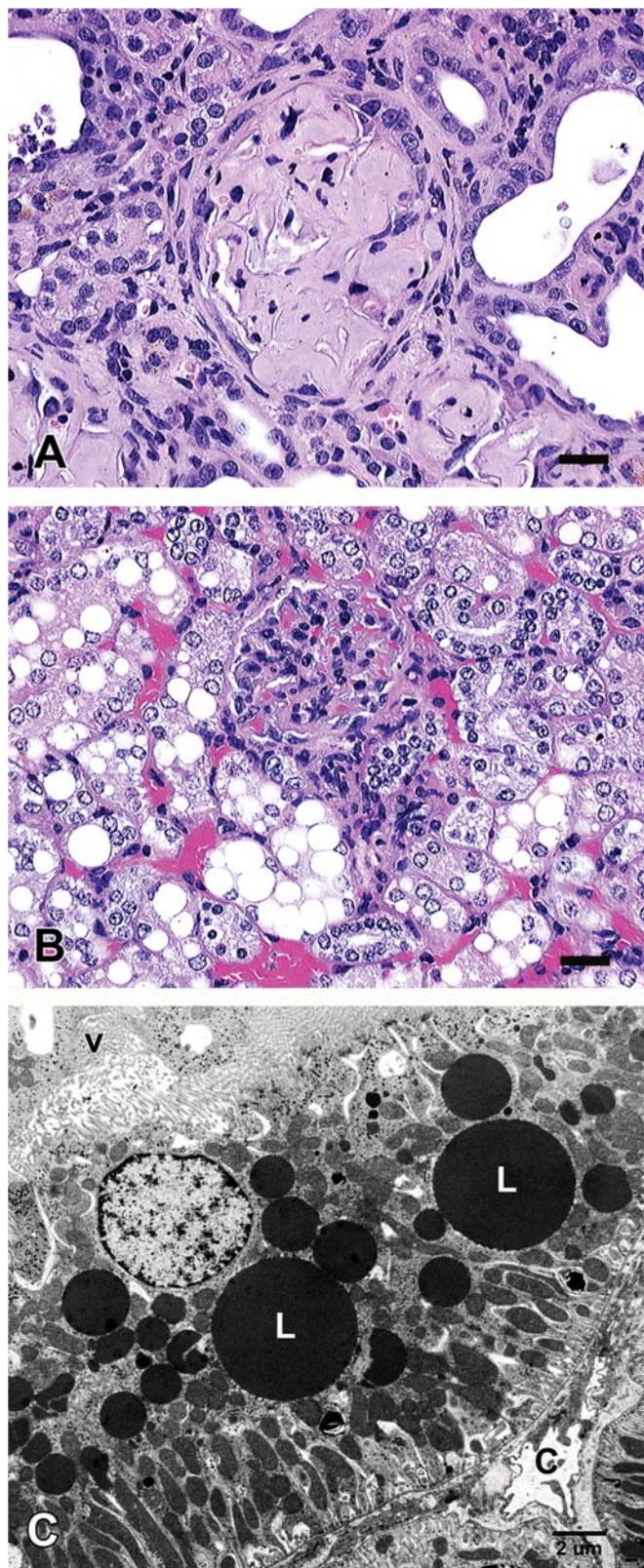


**FIGURE 2.15** (A) Light photomicrograph illustrating renal amyloidosis in a 2-year-old CD-1 mouse kidney. Bar = 20 mm. (B) Light photomicrograph illustrating

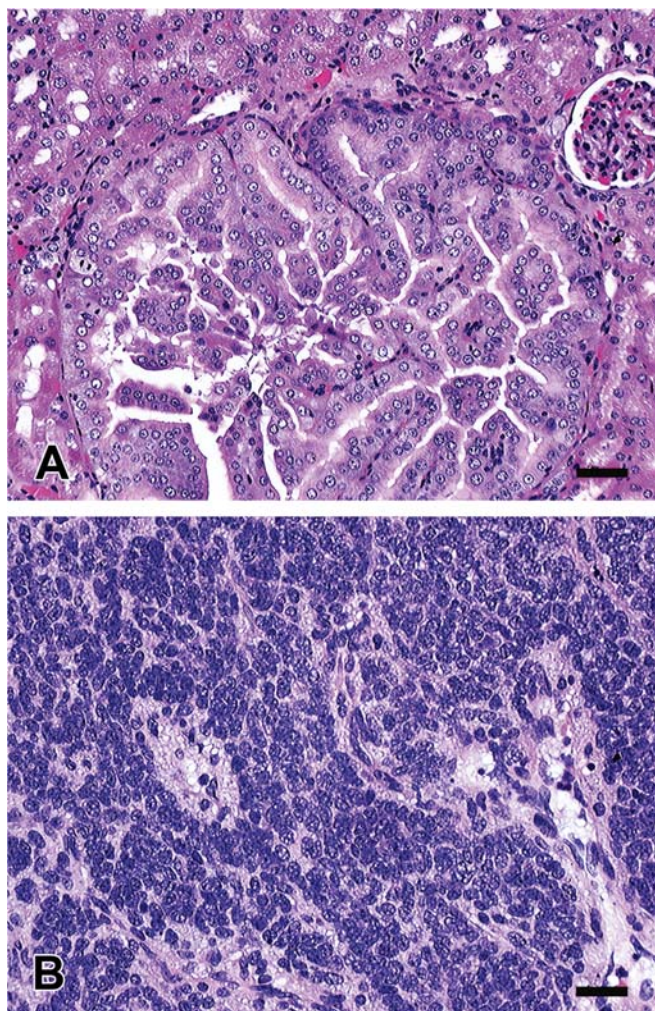


**FIGURE 2.16** (A) Light photomicrograph illustrating a tubular adenoma in an old CD-1 mouse kidney. Bar = 40 mm. (B) Light photomicrograph illustrating nephroblastoma in an old CD-1 mouse kidney. Bar = 20 mm. Reproduced from Haschek WM, Rousseaux CG, Wallig MA, editors: *Handbook of toxicologic pathology*, ed 2, 2002, Academic Press, Figure 35, with permission.

renal lipodosis in a 2-year-old CD1 mouse kidney. Bar = 20 mm. (C) Electron micrograph illustrating intracytoplasmic lipid droplets (L) in a proximal renal tubular epithelial cell of a Wistar rat. Note microvilli (V) projecting into the tubular lumen and a capillary (C) subjacent to the basement membrane. Reproduced from Haschek WM, Rousseaux CG, Wallig MA, Bolon B, editors: *Haschek and Rousseaux's handbook of toxicologic pathology*, ed 3, 2013, Academic Press, Figure 47.19, p. 1708, with permission.



age-related lesions found in the hamster kidney. In New Zealand white rabbits, granulomatous nephritis caused by *Encephalitozoon cuniculi* can be frequent, even in young rabbits, with a reported incidence of 20% at ages under 1 year. Mineralization also occurs commonly in young rabbits, with higher incidence in females than in males. Nephroblastoma is noted in the rabbit kidney more frequently than other common laboratory species.

### 3.4. Testing for Renal Carcinogenic Potential

The 2-year chronic bioassay conducted in rats and mice has historically been utilized for determining the carcinogenic potential of drugs, industrial chemicals, agrochemicals, and food-related substances for over 4 decades, though most pharmaceutical companies today have eliminated the 2-year mouse bioassay in favor of the rasH2 transgenic alternative when possible. Equivocal findings consume significant resources in the toxicology and pathology communities to try to resolve conclusions with incidences that the power of the current bioassay cannot resolve. Published experiences of background incidences for tumors for a given strain within the laboratory, and published literature reviews help put findings in context. The universal criterion of malignancy evidenced by metastasis is an uncommon feature of renal tubular carcinomas, but exceptions exist such as some DNA-damaging chemicals or tumors induced by ochratoxin, fumonisin B<sub>1</sub>, and DMN. Because criteria are somewhat arbitrary and since progression can occur from benign to malignant, little merit exists in the differentiation of benign and malignant renal epithelial tumors. Thus, benign and malignant neoplasm should be added together in the reporting activity for risk assessment, with the exception of renal A-V tumors which are considered spontaneous and should always be grouped separately. Urothelial tumors are also of different embryonic derivation and of different etiopathogenesis from renal tubule neoplasms and should also be assessed separately.

Rat models of renal tumor development, regardless of mechanism, demonstrate a dose-responsive increase in hyperplastic tubules, representing a continuum of change up to and

including neoplasia. When studying tumorigenic events and especially in instances of low tumor incidence, it may be helpful to distinguish simple hyperplasia from atypical tubule hyperplasia, the latter of which is considered preneoplastic (Table 2.10). Cytologic features, lesion size, and loss of membrane integrity all help differentiate hyperplasia from benign neoplasia, and benign neoplasia from malignancy. High incidence of atypical hyperplasia without evidence of repair or regeneration (e.g., no CPN) occurs with agents like nitrilotriacetic acid, and suggests carcinogenic potential. A definitive increase in tumor incidence ( $\geq 10\%$  difference) and all types of hyperplasia including borderline lesions in a group also forms a basis for probable occurrence of a tumorigenic process.

Karyomegaly or cytomegaly, especially associated with genotoxic xenobiotics or heavy metals observed in subchronic or chronic toxicology studies should lead to prediction that lifetime studies may yield tubular tumors, although there are exceptions such as lysinoalanine (which is not considered a carcinogen). Multiple mechanisms exist for induction of karyomegaly and cytomegaly and these changes alone do not represent a preneoplastic lesion. Karyomegaly is likely due to nuclear divisions without associated cytokinesis, resulting in increased nuclear size. It is noted with chemical exposure most often in rats, but enlarged nuclei or multinucleated cells may occasionally be noted in the medullary ducts of control rhesus and cynomolgus monkeys as a normal finding (Frazier and Seely, 2019). Karyomegaly occurs commonly in renal tubules of rats given chemotherapeutic antibody-drug conjugates (ADCs) containing auristatins (MMAE or MMAF) which disrupt microtubule formation in the nucleus.

Approximately 25% of chemicals tested by the National Toxicology Program (NTP) are recorded as nephrotoxic, whereas only a relatively small number of these have produced renal tubule tumors in 2-year bioassays. The two classes of agents identified with high potential for nephrotoxicity were organohalides and less often, aromatic amines. The organohalides are generally considered as genotoxic as well as cytotoxic in the proximal tubule. Specific subchronic lesions of alpha<sub>2</sub>μ-globulin nephropathy suggest a potential for renal tumorigenesis. Thirteen chemicals, administered for at least 1 year with sacrifice after

**TABLE 2.10** Classification of Renal Tubular Proliferative Lesions in Rodents

Designation	Subclass	Criteria
Tubular regeneration		Tubule lined by cells with basophilic cytoplasm and often increased numbers but without increase in size of the tubule
Simple tubular hyperplasia	Predominantly basophilic, also eosinophilic, clear, or oncocytic	Definite increase in cross-sectional diameter of the tubule and increase in number of cells lining the tubule in a single layer <sup>a</sup>
Atypical tubular hyperplasia	Predominantly basophilic, also eosinophilic, clear, oncocytic, or amphophilic Cystic or solid	Tubules increased in size because of increase in cell number with multiple layers and orderly growth in relation to nephron basement membrane; cellular atypia may occur <sup>a</sup>
Adenoma	Cell type is basophilic, eosinophilic, clear, oncocytic, or amphophilic predominant growth pattern is tubular, lobular, or solid	Unequivocal loss of continuity with original nephron unit, often with compression of adjacent parenchyma; synthesis of new basement membrane; frequent cellular atypia; typically greater in cross-sectional diameter than twice a normal glomerular tuft
Adenocarcinoma	Cell type is predominantly basophilic, also eosinophilic, clear, or amphophilic; predominant growth is tubular; usually marked cellular atypia and pleomorphism; distinct formation of tubules), lobular (nests of cells separated by scanty connective tissue), or solid (continuous sheets of cells)	Scirrhous response (prominent dense fibrous connective tissue proliferation) Disorderly basement membrane synthesis and invasiveness or growth without regard to limiting basement membranes; frequently necrosis; neovascularization; size typically greater than 3 mm in diameter;
Amphophilic-vacuolar tumor	Solid, well circumscribed, and lobulated; delicate fibrovascular stroma; unilateral or bilateral; grows to large size; cystic or necrotic centers within amphophilic lobules	Familial; never drug-related; rarely, if ever metastasizes but may extend to and invade adjacent tissue; benign or malignant

<sup>a</sup> Regenerative, simple, and atypical hyperplasia occurs on a nephron basis as several adjacent affected tubules typically are noted in cross-section with perpendicular orientation to the medulla. Neoplasm and atypical hyperplasia are enumerated, whereas simple hyperplasia is graded.

Modified from Haschek WM, Rousseaux CG, Wallig MA, Bolon B, editors: Haschek and Rousseaux's handbook of toxicologic pathology, ed 3, 2013, Academic Press, Table 47.13, p. 1709, with permission.

2 years of age which induced specific sub-chronic lesions were all associated with renal tumors. Thus, nephrotoxicity per se does not necessarily predict a renal neoplastic response, but a lack of toxicity does not absolutely

preclude the possibility of renal tumors either, particularly in the case of genotoxins. Conversely, nongenotoxic renal tumorigens that have been reported all have consistently caused tubule toxicity in short-term studies.

Critical tools for the development and efficacy testing of renal cancer drug therapies are rodent renal cancer models that recapitulate the human disease. Xenograft (cell line or patient derived, heterotopic or orthotopic), chemically induced, genetically engineered, and syngeneic models of human renal cancer have provided experimental systems for testing the effectiveness of new chemotherapeutic or biological modifying agents for tumor treatment. Two forms of renal cancer, renal cell carcinoma (RCC) and nephroblastoma are the most frequently modeled. A few are described below. For an extensive review of renal cancer models, see [Sobczuk et al. \(2020\)](#).

Renal cancer is among the top 10 most common cancers and RCC, derived from renal tubule epithelial cells is the most prevalent type and accounts for most renal malignancies. The major subtype of carcinoma is clear cell RCC (ccRCC) which is named based on the vast accumulation of cytoplasmic lipids and glycogen. A multitude of RCC cell lines are commercially available for research. An orthotopic model of RCC utilizes murine renal adenocarcinoma cells, or RENCA, orthotopically implanted into the kidney. RENCA cells may also be administered intraperitoneally or intravascularly to mimic a metastatic state. Streptozotocin-induced renal carcinomas, described in both rats and mice and developed as a mouse model by Hard, have notable morphologic differences as compared to human RCC ([Hard, 1985](#)). A high percentage (60%–70%) of human RCCs are associated with mutations or hypermethylation and subsequent inactivation of the von Hippel-Lindau (*VHL*) tumor suppressor gene. Development of a transgenic mouse model of renal cell cancer by inactivation of the *VHL* gene therefore seemed plausible, but this modification alone resulted in the production of renal cysts only, and not ccRCC. Current ccRCC models utilize combined deletions of *VHL* with other RCC-related genes including polybromo-1 (*PBRM1*), breast cancer gene (*BRCA*) associate protein-1 (*BAP1*), retinoblastoma (*Rb1*), and transformation related protein 53 (*Trp53*) that produce tumors with similarities in genetics, histology, and response to therapeutics as in human ccRCC ([Harlander et al., 2017](#); [Hou and Ji, 2018](#); [Sobczuk et al., 2020](#)). In addition to mouse models, the Eker rat, heterozygous for a mutation in the tuberous sclerosis (*Tsc2*)

locus, provides a good model in which to study the development of renal cancer. The *TSC2* gene is a tumor suppressor gene thought to be specifically involved in the pathogenesis of RCC in humans as well as in rats. *TSC2*<sup>+/–</sup> Eker rats develop multifocal and bilateral RCC with 100% incidence by a year of age. The polypeptide growth factor TGF- $\beta$  is constitutively overexpressed in Eker rat cell tumors and serves as a biomarker for preneoplastic proliferative lesions.

Nephroblastoma, or Wilms tumor, is the most common malignant embryonal abdominal tumor in children, arising from nephrogenic blastema and has a mixed, triphasic histology consisting of blastemal, epithelial, and stromal components ([Tian et al., 2014](#)). Initial work on developing nephroblastoma models proved challenging. Early cell line work in SK-NEP-1 cells, thought to represent anaplastic Wilms tumor, was later found to contain the EWS-FLI1 gene fusion transcripts characteristic of Ewing sarcoma and not a relevant disease model. Other cell lines failed to reproduce the triphasic histologic elements. Transgenic mouse models knocking down Wilms tumor 1 gene (*WT1*) alone were embryonically lethal in homozygotes and tumors did not develop in heterozygotes. Mutational analysis of human tumors showed multifactorial up- and down-regulation of several key genes leading to combined *WT1* ablation with *IGF2* upregulation in addition to other key genes eventually creating cell lines and mouse models with histologic (triphasic elements) and molecular (gene expression patterns) similarities to the human condition ([Brandt et al., 2016](#); [Sobczuk et al., 2020](#)).

### 3.5. In Vitro Techniques

#### 3.5.1. In Vitro/Ex Vivo Assay Platforms

The kidney is highly complex, composed of a filter unit and a tubular segment, together containing over 20 different cell types. In vitro models that recapitulate critical aspects of kidney physiologic function, response to injury, and repair will accelerate drug discovery and development. Further implementation of newer technologies such as organ-on-a-chip, emphasizing the 3 Rs of toxicology (reduce, refine, replace), will make a positive impact by potentially



reducing the overall number of animal safety studies, by reducing the usage of only relevant species for predictive toxicity testing, and advancing the very lofty goal of 1 day potentially replacing animals in preclinical safety assessment (see *Alternative Models in Biomedical Research: In Silico, In Vitro, Ex Vivo, and Non-Traditional In Vivo Approaches*, Vol 1, Chap 24). Because the proximal tubule is one of the main sites of reabsorption, DIKI is often caused by accumulation of drugs in the renal cortex with resulting tubular damage and tubular cell cytotoxicity. Recapitulating this complex structure and function of the kidney in vitro is very challenging (Khoshel-Rad et al., 2022). It is difficult for in vitro assays to adequately predict in vivo observed effects, predominantly due to an inadequate preservation of the organs' microenvironment in the models used. Historical methods to detect potential DIKI using in vitro high-throughput cytotoxicity screens have primarily relied upon using 2D monolayers of either primary kidney cells or kidney cell lines derived from proximal tubules, such as HK-2. Sensitivity, specificity, and robustness of potential mechanisms and biomarkers of toxicity should all be easily quantifiable in an ideal in vitro cell culture system. In vitro studies are also important to gain additional insight into pathophysiological mechanisms and to validate observations in isolated cells and organs prior to confirmation in more complex models. The advantages of using in vitro renal models include the ability to examine direct effects of chemicals at the cellular level, ease of use, low cost, and the capability for automation/high throughput. However, in vitro to in vivo correlation is a major limitation of current kidney models, and several questions need to be addressed before their selection and use.

Recently there have been remarkable advances in refinement of in vitro and ex vivo models of cell/organ cultures and utilization of genomics, proteomics, and metabolomics in developing predictable models of renal cell responses to toxic insults. To date, there is no single ideal kidney-based in vitro model for the study of nephrotoxicity; however, many advanced in vitro culture systems include several characteristics that are important for the successful toxicologic assessment of drug candidates, including 3D architectural features, ECM components,

fluid flow, and multiple cell types in combination. The two main requirements of efficient in vitro and in vivo models to predict DIKI in humans are the ability to generate detectable levels of relevant renal injury biomarkers and the ability to discern nephrotoxicity from general cytotoxicity. There are many kidney-based in vitro models available, each with advantages and disadvantages that need to be carefully considered before beginning a mechanistic investigation and examples are described in (Table 2.11).

### 3.5.2. Two-dimensional Models

Immortalized kidney epithelial cell lines frequently used for nephrotoxicity studies represent two-dimensional (2D) models and are derived from human embryonic kidney (HEK-293), human proximal tubular cell (HK-2), pig kidney (LLC-PK1), dog kidney (MDCK and MDBK), rat kidney transformed cell line (TRKE-1), rhesus monkey (LLC-MK-2), and African green monkey (Vero). Although cell lines are readily available, they do not fully express all the differentiated functions found in their in vivo counterparts due to loss of polar architecture and changes in drug transporter expression. Primary proximal tubular epithelial cells are considered more toxicologically relevant with respect to kidney physiology and best for drug transporter studies. Drug concentration is generally highest in the proximal tubule owing to filtration, and most drugs undergo transporter-mediated active secretion, reabsorption, and metabolism in this segment (Choudhury and Ahmed, 2006; Bens and Vandewalle, 2008). Human renal epithelial cells (HREs) are composed of cells from the cortex and glomerular region. Human renal cortical cells (HRCCs) are from proximal and distal tubules. Human mesangial cells (HMCs) are isolated from the renal glomerulus and modified smooth muscle cells between capillaries. While primary cells better mimic the physiological state of cells in vivo, they have a limited growth capacity and tend to lose their phenotype over time. Conventional 2D cell models (adherent immortalized or primary cells) are limited in their abilities to accurately predict clinical toxicity since they lack the fundamental complexity of in vivo tissue environments. In a recent review of in vitro platforms, it was concluded that difficulty in maintaining

**TABLE 2.11** In Vitro Models for Studying Renal Toxicity

Model	Advantages	Disadvantages
2D culture (cell lines)	<ul style="list-style-type: none"> <li>- Highly proliferative, and easier to culture.</li> <li>- Inexpensive, established and easy cell observations and measurements.</li> </ul>	<ul style="list-style-type: none"> <li>- Expression profiles for key proteins of interest like injury markers, transporters and enzymes can be very different than in normal cells.</li> <li>- Lack critical microenvironmental stimuli to effectively mimic in vivo conditions.</li> <li>- Functional changes may occur during passaging.</li> </ul>
2D culture (primary cultures)	<ul style="list-style-type: none"> <li>- Retain most properties of in vivo kidney cells such as polarity, tight junctions, and expression of multiple drug transporters.</li> </ul>	<ul style="list-style-type: none"> <li>- Have a finite lifespan and limited expansion capacity.</li> <li>- Often require additional nutrients not included in classical media.</li> </ul>
3D culture (organoids)	<ul style="list-style-type: none"> <li>- More physiologically relevant cell model.</li> <li>- Ability to mimic the interactions between multiple cell types.</li> <li>- Mimic the complexity of the human body in a more natural way.</li> </ul>	<ul style="list-style-type: none"> <li>- Low throughput.</li> <li>- Not extensively characterized.</li> <li>- Challenges in microscopy and measurement.</li> </ul>
Microphysiological systems (organ-on-a-chip)	<ul style="list-style-type: none"> <li>- Allows for the integration of liquid flow dynamics and interactions with cultured cells.</li> <li>- More physiologically relevant than static cell systems and good at replicating the physical microenvironment of living organs.</li> </ul>	<ul style="list-style-type: none"> <li>- Low throughput.</li> <li>- Not extensively characterized.</li> <li>- Require validation and optimization.</li> <li>- Engineered man-made system.</li> </ul>

transporter and metabolic function in primary cells and cell lines, and in reaching levels of transporter function comparable to those observed in vivo, are an expected deficiency of the use of static 2D culture formats (Soo et al., 2018). As a result, efforts are being directed toward more sophisticated cell models with the potential for improved in vitro to in vivo correlation, including immortalized 2D cell lines, pluripotent stem cell-derived renal cells, organoids, and kidney-on-a-chip.

### 3.5.3. Three-dimensional Models

Because of the limitations of 2D cell culture, industry-wide initiatives have driven the development of 3D human tissue models and these are thought to better recapitulate the human in vivo response to drugs. In vitro 3D cell culture systems provide robust, predictable in vitro

models of the proximal tubule that can assess both kidney tubular secretion and the potential for tubular injury. 3D organized structures, known as organoids, are 3D multicellular cultures that resemble the structure, physiology, and diseases of their organ of origin. These cultures are generated from either pluripotent stem cells or adult stem or progenitor cells (de Souza, 2018). Kidney organoids are derived from embryonic stem cells or induced pluripotent stem cells and contain many renal cell types like proximal tubule, distal tubule, collecting duct, Henle's loop, endothelial cells, podocytes, interstitial and stromal cells in early developmental form (Morizane et al., 2015; Takasato et al., 2015; Combes et al., 2019). Organoids display a higher degree of organization, specialization, and maturation compared to their 2D culture counterparts. Examples of other 3D

culture systems include RPTEC/TERT1 and Nki-2 cells that, when cultured in Matrigel or Matrigel mixed with collagen I, respectively, are able to further mature and form tubular structures as seen in vivo. There are important defects in the cell composition of lab-grown organoids compared to normal kidney. Organoids lack vasculature which means that they are limited in terms of how much they can grow without incurring cell death. Current cell differentiation protocols need further refinement to generate organoids with more mature adult-like cell types.

Alternatively, adult stem cell tubuloids recapitulate renewal and repair in the adult kidney tubule and give rise to long-term expandable and genetically stable cultures that consist of adult proximal tubule, loop of Henle, distal tubule, and collecting duct epithelium. These 3D multicellular structures also more accurately resemble the complex architecture and composition of the functional intact kidney when compared to 2D models using cell lines. Both organoid types have the potential to better reflect human physiology and disease compared to animal models and allow for high-throughput drug screening. While these newer systems are an improvement, organoids and tubuloids still lack accessible inlets and outlets, limiting their usefulness and static 3D culture models lack natural flow dynamics necessary for the development of cell polarity and function. Recent attention has therefore been directed to integrating microfluidic technology into 3D models. Options for 3D models include not only organoids and but also kidney microphysiological systems (MPSs) (organ-on-a chip) that can recreate fluidic characteristics found in vivo and have shown increased sensitivity to known nephrotoxic drugs when compared to 2D cultures (DesRochers et al., 2013; Secker et al., 2017; Gijzen et al., 2021). 3D kidney models recently have begun to utilize transwell membrane culture systems and have expanded into microtissue development. Proximal tubular cells grown on transwell membrane culture systems allow the formation of epithelial barriers and recapitulate the apical and basolateral uptake of compounds in vitro. Immortalized human renal cortical epithelial cells in a transwell dish permitted long-term culture of human derived kidney cells with in vivo-like epithelial barriers and this transwell format improved

translatability and enhanced sensitivity, as compared with conventional 2D kidney cell culture.

#### **3.5.4. Microphysiological Systems (Organ-on-a Chip)**

To overcome the limitation of 2D cell culture models lacking flow-dependent tubular actions, MPSs have recently gained favor. The kidney can be effectively modeled using organ-on-a-chip technology, and this is an extremely effective approach for reproducing in vivo tissue structure and function. Kidney-on-a-chip-based systems are widely available, but constantly being refined, due to technical and biological constraints on the recreation of the proper anatomical architecture. The ideal future microfluidic device may have the ability to seed all the nephron cell types on the same chip and also be able to interact with the vasculature. Some of the more popular commercial MPS models have been tested for their ability to predict DIKI with a large number of nephrotoxic compounds in addition to exemplar toxicants like gentamicin, cyclosporin, or cisplatin (Cohen et al., 2021). Multiple cell types and functional units comprise the human kidney and to be considered physiologically relevant, a biomimetic kidney-on-a-chip must integrate cell-cell interactions, such as the tight junctions between epithelia. More difficult interactions, like those that exist between glomerular vascular endothelial cells and podocytes have been harder to develop. The integration of these components in the development of a true kidney-on-a-chip has yet to be achieved but glomerulus on-a-chip, proximal tubules on-a-chip, distal tubule-/collecting duct-on-a-chip have been developed and have the potential to provide key in vivo predictive data. However, MPS technologies for testing distal tubular drug toxicities (e.g., amphotericin toxicity), tubular obstruction (e.g., acyclovir toxicity), or interstitial nephritis (e.g., cyclosporines or cephalosporins) remain limited. The advantage of the kidney-on-a chip technology is that the flow of the cell culture medium is in contact with cells allowing recapitulation of hemodynamic conditions related to urine flow in the nephron and blood flow in the surrounding capillaries.

Combining the 3D culture of organs or tissues with microfluidic chip technology can provide



a more suitable differentiation and culture environment and improve tissue function and sensitivity to stimulation (Cong et al., 2020; Kulkarni, 2021). The MPS model allows more accurate adjustment of environmental conditions according to the type of cells in culture. Flow culture can control the supply of nutrients and remove accumulated cellular waste or secondary metabolites from the culture medium. Also, the oxygenation level can be regulated, shear stress guarantees the barrier integrity of the cell layer, and cell migration can be controlled and monitored. Immortalized kidney cell lines were originally used in developing kidney organ-on-a chip systems, but these cell lines do not fully recapitulate the primary cell phenotype, nor do they display complete functional differentiation (Ashammakhi et al., 2018). Primary human cells, such as human proximal tubule (PT) epithelial cells (hPTECs), can circumvent many of these problems and are often used. However, it can be difficult to obtain and maintain sufficient numbers of primary cells that have a limited number of population doublings. Recently, human transformed cell lines (with added transporters) have been incorporated into MPS platforms and multiple separate cell layers (including endothelial coculture) have been added in tubule channels (Jang et al., 2013; Petrosyan et al., 2019; Yin et al., 2020). The complexity of these systems varies with the type and manufacturer, but many have demonstrated applicability in drug and chemical testing as described below.

### 3.5.5. Application of In Vitro Assays

Any of the MPS platforms generally are more sensitive to drug insult than 2D systems when toxicity is assessed (Maass et al., 2019). However, even the best in vitro screens for nephrotoxicity are currently only moderately predictive of toxicity in humans (despite using human cells), and generally poorly predictive for very subtle nephrotoxics. This is because current in vitro cellular models still do not exactly replicate the combined morphology and function of kidney tubules, but they are improving year by year. Advances in recent protocols to enable the directed differentiation of pluripotent stem cells into multiple renal cell types and the development of microfluidic and 3D culture systems have opened a range of potential new options

for evaluating drug nephrotoxicity. Many kidney-on-chip systems have been well characterized for the expression and function of transporters, enzymes, and other functional proteins that are expressed by the kidney (Bajaj et al., 2018). Primary human proximal tubular epithelial cells (HPTECs) possess characteristics of differentiated epithelial cells rendering them desirable to use in such in vitro systems and have been routinely used as a platform to screen nephrotoxic compounds in vitro by pharmaceutical companies (Adler et al., 2016). A rapid 1-step protocol for the differentiation of human induce pluripotent stem cells (hiPSCs) into proximal tubular-like cells has been developed (Kandasamy et al., 2015). Proximal tubular-like cells could be directly applied for compound screening and along with machine learning methods, allowed for the prediction of drug-induced proximal tubular toxicity in humans with high accuracy. Injury mechanisms and drug-induced cellular pathways were reliably identified by using automated cellular imaging techniques. Mixed immortalized cell lines have been used to generate functional and mature kidney spheroids containing multiple renal lineages, such as the proximal tubule, loop of Henle, distal tubules, and podocytes, using ECM and physiological force (Kang et al., 2019). These cells expressed all apical and basolateral transporters that are important for drug metabolism and displayed key functional aspects of the proximal tubule. Following exposure to cisplatin and cyclosporin A, cells fluxed and took up drugs via specific apical or basolateral transporters and displayed increased cell death and expression of renal injury markers. Kidney organoids have begun use in toxicological screening of both tubular and glomerular structures (Romero-Guevara et al., 2020). As an example, kidney organoids were shown to respond to cisplatin by increasing the expression of KIM-1 (Morizane et al., 2015).

In addition to increasingly complex 3D model systems, many new analytes have been added to compound screening activities. Endpoints such as cell viability, apoptosis, mitotic block, nuclear area, nuclear roundness, mitochondrial mass, mitochondrial membrane potential, kidney biomarker measurements (RNA and protein), image-based phenotypic endpoints, and other functional endpoints can be incorporated when

using primary and immortalized cell lines, organoids, and kidney-on-a-chip formats. Implemented at the right stage of drug discovery and development and coupled to high-content evaluation techniques, these in vitro models have the potential to reduce attrition and aid the selection of candidate drugs with an appropriate safety profile and to choose the most appropriate monitoring strategy. In a study involving renal analyte evaluation, primary human kidney cells were used in an applied systems biology approach combining multidimensional datasets and machine learning to identify biomarkers and predicted nephrotoxic compounds (Ramm et al., 2019). These techniques can be even more effective in renal toxicity evaluation when MPS fluid dynamic systems are utilized. A high throughput, 3D microfluidic platform consisting of human renal proximal tubules on a chip (nephroscreen) for the detection of DIKI has been developed and marketed (Vormann et al., 2021). This microfluidic organ-on-a-chip system coupled with a multiparametric biomarker analysis was able to identify many potential nephrotoxins and was considered a reliable medium throughput, standardized, automatable system that proved sensitive and provided insights into modes of toxicity. Significant increases of renal injury signals have been observed in many published studies with this and other competing marketed MPS platforms including KIM-1, NGAL, NAG, CLU, OPN, and a panel of injury-associated miRNAs (Weber et al., 2018). Another of the recent emerging in vitro microfluidics platforms utilizing the human proximal tubule epithelial cell line (ciPTEC-OAT1) cultured on a three-lane OrganoPlate has been successfully tested against over 25 toxins with demonstrated changes in three miRNAs, KIM-1, NAG, LDH, and GGT, among other analytes (Wilmer et al., 2016; Suter-Dick et al., 2018).

In vitro technologies are also being used to study the mechanisms of kidney toxicity and for constructing adverse outcome pathways (Soares et al., 2020). Although broad, open-ended, mechanistic investigations are often discouraged, it is realistic to obtain mechanistic data for nephrotoxicity so that investigative teams know which specific questions to pursue. In this type of in vitro work, it is critical to maintain a focus on clinical relevance of any observed findings.

Assays that are predictive of at least some compound-induced mechanisms leading to renal damage have great utility in providing early feedback to minimize these liabilities during the development of new drugs (Huang et al., 2015; Ramm et al., 2019). Phenotypic imaging data are used for network analyses to identify similarities between compounds with known and unknown mechanisms of toxicity. Compounds flagged by this in vitro screening can then be triaged for further testing in lower throughput repeat-dose in vitro studies, 3D or organ-on-a chip systems, or preclinical in vivo studies. To predict biotransformation (liver) and elimination (kidney) in humans is a rather difficult task to achieve using normal 2D cultures (Chang et al., 2016); however, metabolizing enzymes may be added in MPS, or alternatively, in a combination of liver and kidney organ-on-a-chip platform to account for metabolism effects on toxicity. For example, in a study using 72-hour drug exposure, no nephrotoxic effects were observed in kidney-only chip devices, but cells in a multiorgan liver and kidney device exhibited renal cell death, and an increased release of intracellular calcium indicating cell distress related to toxic metabolites.

### 3.5.6. 3D Bioprinting

A significant challenge to the methods described above is the difficulty to accurately recreate the geometric and architectural complexity of the kidney in vivo (Wragg et al., 2019). The thought is that better reproduction of the anatomical complexity of the kidney will allow for more instructive modeling of physiological and pathophysiological events. Emerging additive manufacturing or “three-dimensional (3D) printing” techniques could provide a promising alternative to conventional methodologies (Fransen et al., 2021; Sochol et al., 2016). This promising strategy precisely controls the spatial distribution and layer-by-layer assembly of cells, ECMs, and other biomaterials. 3D printing technology allows for the creation of precisely controlled 3D tissue or organ models through localization of cells, biomolecules, and materials precisely similar to tissue specific microenvironments with the development of fabrication methods (Dey and Ozbolat, 2020). The 3D printed in vitro kidney model can be utilized to study the complex human physiology in

tissue and organ contexts, which could potentially be used as a substitute for animals and applied in drug development and toxicology testing (Jang et al., 2016). A bioprinting method for creating 3D proximal tubules on chip that are fully embedded within an ECM and housed in perfusable tissue chips have been developed, allowing them to be maintained for greater than 2 months. Investigators demonstrated that after exposure to cyclosporine, the epithelial barrier was disrupted in a dose-dependent manner (Homan et al., 2016). Although individual 3D printing techniques each provide distinct benefits for recreating finite units of physiologic structures and/or functions, no singular method yet encompasses the full array of capabilities required to accurately recapitulate in vivo kidney physiology. Nonetheless, current micro/nanoscale 3D printing approaches offer numerous advantages over traditional microfabrication methodologies.

### 3.6. Scoring Schemes

In regulatory toxicologic pathology, standardized scoring schemes are utilized which have been previously described in this chapter and throughout this textbook volume. Individual lesions are graded from 0 (normal) and the most subtle (1) up to a maximum of 5, with minimal (slight), mild, moderate, severe, and very severe descriptive terms corresponding to the level of injury and taking into account distribution (Frazier and Seely, 2019; Frazier, 2019). Very severe lesions are, by definition, those expected to result in impending mortality or at least significant morbidity. Each separate diagnosis is graded based on its own attributes. In regulatory toxicity studies, every separate lesion may have its own diagnosis. For instance, a single animal in a study may have diagnoses for tubule vacuolation, tubule necrosis, interstitial inflammation, and glomerulosclerosis all listed and graded separately. In efficacy studies, investigative studies, or with animal models of kidney injury, the same general scoring applies, but in some cases, a system of grading from 0 to 10 is assigned to allow for greater differentiation. In practice, there appears to be little gained from using the expanded severity scale. Importantly, it is critical to lump diagnoses together when trying to quantify renal

lesions in efficacy or investigative studies. Separating scores for degenerative and necrotic lesions and assigning multiple diagnoses for kidney pathology with similar pathogenesis will invariably confuse interpretation. Instead, early lesions such as tubule basophilia or vacuolation can be lumped with later more severe lesions such as tubule dilation, necrosis, or cell sloughing, but with the former graded lower than the latter (Seely and Frazier, 2015). Grading schemes based on localization within the kidney are also commonly utilized by nephropathologists in these types of efficacy studies. Hence, there may be separate grading of overall pathologic change in the glomeruli, tubules, renal vasculature, and interstitium, or alternatively using separate scores for glomeruli, cortex, medulla, and papilla/pelvis. When describing and scoring models of CKD, fibrosis is generally scored separately, and can be assessed using special stains (Masson's trichrome or Sirius Red) and morphometry, or by direct measurement such as prolyl hydroxylase biochemistry (Frazier et al., 2019; Ennulat et al., 2018). Pattern of lesions can also be useful. For example, in dogs, bands of fibrosis radiating from the corticomedullary junction to the cortex suggest vascular-mediated disease (ischemia), whereas fibrosis that involves the renal medulla and papilla would be more suggestive of scarring from previous pyelonephritis. When scoring lesions within a cohort of animals, observation of the pattern of injury helps the nephropathologist identify outliers if there is an individual with an unusual pathogenesis compared to others in the group. When assessing rodent models of PKD, the number and size of cysts within a region of kidney can be quantified in section. Since cysts in PKD are generally rather homogenous throughout the kidney, a direct comparison between animals can be made and correct interpretations may be assumed on only one or a few renal histopathologic sections. However, for the most accurate quantification of renal lesions, stereologic principles of histomorphometry can be applied to reasonably assess and draw conclusions from lesions throughout the entire kidney. In diabetic kidney models, stereology has been used to quantify the severity of glomerular lesions. Rodent models of DN rarely recapitulate the type of injury seen in humans, likely because the time frame required to cause histologically identifiable injury is at least 10 years



of poor glucose control. However, stereology and morphometry can demonstrate mesangial expansion and GBM thickening, which are early lesions in humans (Gunderen et al., 2013).

### 3.7. Computational Pathology

Computational pathology refers to the application of computational analysis to the study and diagnosis of disease and in respect to toxicologic pathology, it refers to the “big-data” approach to pathology, where multiple sources of information including pathology image data and meta-data are combined to extract patterns and analyze features, and includes digital imagery, morphometry, computer-aided diagnosis, and artificial intelligence-mediated (AI-machine learning and deep learning) analyses. Increasing utilization of whole slide images from tissue sections has allowed an ever-expanding resource of data derived from these images that can provide the pathologist with a host of biologic information to enhance efficacy models or strengthen clinical safety assessment. The widespread applicability of computational pathology methodology has begun to transform regulatory renal pathology as it has other fields. In human renal pathology, regular diagnosis is often performed based solely on digital images of H&E-stained sections, with morphometric quantitation of immunofluorescence, ultrastructural or immunohistochemical photomicrographs (see *Digital Pathology and Tissue Image Analysis*, Vol 1, Chap 12). However, at the time of this writing, digital image capture is performed primarily for peer review and for individual kidney mechanistic research projects in the realm of nonclinical toxicologic nephrology. The progressive implementation of digital pathology and computer-aided algorithms into clinical trials is transforming the practice of nephrology and it is only a matter of time before these advancements make their way into nonclinical studies. For instance, digital pathology-based clinical trial results have been published, including evaluation of globotriaosylceramide inclusions in Fabry’s disease in patients receiving a chaperone, enzyme replacement therapy in kidney disease, and for assessing lupus nephritis in patients treated with antitumor necrosis factor-like mAb (Barisoni and Hodgin, 2017). Regulatory acceptance has

been a greater hurdle than technology to date for nonclinical studies. One of the major regulatory concerns with AI approaches to toxicologic pathology cases is lack of transparency, explainability, or provability for how an algorithm generates reliable results or the so-called “black box” surrounding generated conclusions. Therefore, it is critical for the pathologist to provide and clarify information about the histopathologic features used by the algorithm to generate traceable conclusions. A rigorous approach toward separating training data (“training set”) from data that are used to measure the predictive performance (“test set”) has also been recommended. Rather than tuning parameters of a classifier, repeatedly assessing the performance on a test set, and then reporting the outcome of only the most successful experiment, a separate “validation” data set can provide better confidence in data outcomes.

There are several general categories where computational pathology can be applied: (1) abnormality detection, (2) decision support, (3) tissue lesion screening, (4) diagnostic scoring simplification, (5) counting automation, and (6) object quantification, and most of these are relevant to renal toxicology as it evolves in the next several years. Applications of computational pathology in nonclinical kidney toxicology to-date have included morphometrically assessing median and mean size of glomeruli, average tubule lumen diameters, immunohistochemical scores (e.g., for fibrosis), and mitotic scores, but there are a whole host of other parameters that are open to AI-assisted analyses. For instance, in clinical research applications, machine learning-assisted analysis demonstrated strong correlation between tubulointerstitial mRNA gene expression signatures and morphologic changes of fibrosis and inflammation, which validated the authors’ hypothesis (Barisoni and Hodgin, 2017). In toxicologic pathology research in animals, AI-assisted learning has been applied to retinal measurements, evaluation of hepatic vacuolation and rat cardiomyopathy diagnosis and scoring, among many others (Turner et al., 2021). Similar nephrotoxicology applications are currently underway in assessing and scoring rodent PKD models with drug candidates, standardizing CPN scoring in chronic studies, and defining and scoring overlapping lesions in CKD models. This field will undoubtedly expand/explode in the upcoming decade.

## 4. RESPONSES TO INJURY

### 4.1. Physiologic, Molecular, and Biochemical Response

Drugs and chemicals can have direct toxic effects on cells of the renal vasculature, tubules, and glomeruli, and/or induce inflammation of the renal interstitium. A major concept in toxicologic pathology of the kidney is the propensity for the nephron to respond to injury as a unit rather than respond only at the subtopographical site of injury. The nonspecific hallmark of the nephron response to injury (cell degeneration) is the alteration of the tinctorial characteristics of the proximal tubular cell cytoplasm from the normal functional eosinophilia to the basophilia of a cell undergoing rapid protein synthesis. Changes are present in continuous segments of a single nephron and histologically observed in several tubules in cross-section. Many xenobiotic agents may induce morphologically characteristic primary injury in a specific location along the nephron, based on the cellular or subcellular organelle target site. Responses to injury should therefore be considered on a subtopographical basis.

Degeneration refers to a spectrum of cellular insults and morphologic changes in tubule epithelial cells, including vacuolation, attenuation, and tinctorial changes such as basophilia. These may represent reversible injury to the renal epithelium or early manifestations of irreversible changes leading to necrosis. Tubule basophilia is the most common toxic injury in preclinical toxicity studies and represents some of the initial and earliest morphologic changes of nephron injury. It is a hallmark feature of spontaneous CPN in rodents; a component of obstructive nephropathy and phospholipidosis; and may also represent regenerative responses. In humans, the term simplification is used when the apical brush border is lost from proximal tubular epithelial cells. This can maintain the viability of the cells, which require less energy since their brush border and associated enzymes have been shed. In fact, sloughed apical cell fragments can be observed in human urine samples as “muddy brown casts” because the

CYP450 enzymes give a slight brown tinge to the debris.

With further damage, degeneration leads to necrosis, apoptosis, anoikis, or hyperplasia (also see *Morphologic Manifestations of Toxic Cell Injury*, Vol 1, Chap 6). In necrosis, swelling of plasma and organelle membranes leads to rupture and dissolution of organized cell structure. Necrotic cells are typically enlarged and are generally more intensely eosinophilic than normal. However, with time, they may lose staining and appear much lighter than surrounding cells. Necrotic cells will lose their attachments and drop off of the lining of the tubule into the lumina, potentially forming cellular aggregates or debris. Necrotic cells may induce local inflammation and/or hemorrhage.

In apoptosis, condensation of the cytoplasm and nuclei is followed by cell fragmentation and formation of apoptotic bodies. Increased apoptosis can be recognized in histology sections by increased tissue replication rate by terminal deoxynucleotidyl transferase (TdT) nick end-labeling (TUNEL) or by demonstration of increased apoptotic cells in urine or uriniferous spaces. In addition, expression levels of messenger RNA (mRNA) and protein of apoptosis-related genes such as bax, Bcl-2, cytochrome *c*, caspase-9, and caspase-3 can be used in nephrotoxicity assessment. Apoptosis is initiated via an intrinsic pathway that involves changes in subcellular organelles including mitochondria, lysosomes, or endoplasmic reticulum, or it can be initiated via an extrinsic pathway, also called the death receptor pathway, that involves the activation of death receptors in response to ligand binding. Both the pathways lead to the activation of specific proteases called the executioner caspases (caspase-3 and -7), which results in the characteristic morphological signs of membrane blebbing, cell shrinkage, and DNA fragmentation (Servais et al., 2008). Nephrotoxic drugs are said to act mainly through the intrinsic pathway. The role of proapoptotic Bcl-2 like proteins in drug-induced apoptosis in renal cells is well documented for gentamicin and cyclosporine A (Xiao et al., 2011). At least four pathways are shown to be involved in renal cell apoptosis induced by cyclosporine A, and

caspases are thought to be the final common pathway. In addition to Bcl-2, integrins, signal transducers, for example, protein kinases and transcription factors such as NF- $\kappa$ B and p53 are shown to regulate cell survival. The histomorphologic presentation of apoptosis in the kidney is termed single cell necrosis. Unlike other organs, single cell necrosis in the kidney is considered to represent a combination of apoptosis and solitary oncotic necrosis, as demonstrated by early cisplatin toxicosis in the outer stripe. Drugs and toxic agents with apoptotic potential are summarized in Table 2.12. Accelerated apoptosis has been defined as a pivotal feature in renal toxicity such as observed in fumonisin-induced injury in rats. Numerous toxicants have been implicated to trigger or block the intracellular processes resulting in abnormal regulation of apoptosis with resulting pathologic consequences ranging from renal agenesis to neoplasia. Autophagy has not received as much attention as apoptosis in the kidney, but studies have shown that antibiotics and antifungal agents can induce autophagy and this is implicated in the pathogenesis of renal injury (Decuypere et al., 2015; Kimura et al., 2017). Many of these same studies also suggest that autophagy may be renal-protective.

Anoikis is a common manner of cell loss in the kidney (Yin et al., 2021). This process occurs when tubular epithelial cells detach from the basement membrane but remain viable. Many cells will die via intrinsic apoptosis as they travel along in the tubular lumens with the urinary filtrate; however, some cells can remain viable and can even be harvested from urine samples and grown in culture. Interestingly, cells that do not have the morphologic features of apoptosis or necrosis can be seen in tubules of canines with experimental ischemia reperfusion injury (IRI) and in spontaneous renal disease, even with excellent tissue preparation. These may represent cells undergoing anoikis as opposed to being artifactual sloughing.

## 4.2. Morphologic Response

### 4.2.1. Glomerulus

Any process that interferes with the structural integrity of the glomerulus can result in

**TABLE 2.12** Drugs and Toxicants with the Potential to Induce Apoptosis in the Kidney

Inducing agent	Chemical/drug class
Acetaminophen	Analgesic
Adriamycin	Anthracycline antineoplastic
<i>Alternaria alternata</i> lycopersici toxin	Mycotoxin
Aminoglycosides	Antibiotic
Amphotericin	Antifungal
Cadmium	Heavy metal
Ceramide	Sphingolipid metabolite
Cidofovir	Antiviral
Cisplatin	Antineoplastic drug
Curcumin	Dietary pigment/spice
Cyclophosphamide	Antineoplastic drug
Cyclosporin A	Immunosuppressant
Diclofenac	NSAID
Doxorubicin	Antineoplastic drug
Dithiothreitol	Reducing agent
Endotoxin	Bacterial toxin
Fumonisin B <sub>1</sub>	Mycotoxin
Gliotoxin	Mycotoxin
Hygromycin	Antibiotic
Hydrochlorothiazide	Thiazide diuretic
Melphalan	Antineoplastic drug
Mercuric chloride	Heavy metal
Metolazone	Thiazide diuretic
Microcystin LR	Cyanobacterial toxin
Ochratoxin A	Mycotoxin
Okadaic acid	Polyether fatty acid
Ricin	Plant toxin (ribosome inactivating protein)
s-(1,2-dichlorovinyl)-L-cysteine	Reducing agent
Verocytotoxin	<i>E. coli</i> enterotoxin
Zolendronate	Bisphosphonate

Modified from Haschek WM, Rousseaux CG, Wallig MA, editors: *Handbook of toxicologic pathology*, ed 2, 2002, Academic Press, Table XI, p. 313, with permission.



abnormal loss of protein in the urine, predominantly albumin. Microscopically, glomeruli should be evaluated for cellularity, patency of capillary lumen, changes in GBM, and the mesangium, as the microscopic lesions of nephrotoxicity in the glomerulus can simply manifest as thickening of GBM (Figure 2.17) or can include inflammatory cell infiltrates. It is important to note that, unlike humans, renal glomerular GBM thickening by itself in nonhuman primates does not necessarily imply an evidence of induced glomerular disease state. Approximately 10% of cynomolgus monkeys exhibit spontaneous occurrence of GBM thickening of varying severity under the light microscope. Ultrastructurally, about 20% of control cynomolgus monkeys may exhibit electron-dense deposits (subendothelial, intramembranous, subepithelial, or mesangial) and occasionally separation of podocytes from GBM and podocyte foot process fusion. These changes have been seen more frequently in Chinese-origin cynomolgus macaques than those from Mauritius. Glomerular injury can be inflammatory or noninflammatory. A combination of histologic, immunohistochemical, immunofluorescence, and ultrastructural evaluations provides valuable information in distinguishing between spontaneous and induced lesions, and between inflammatory and noninflammatory processes. The relevant ultrastructural observations may include the presence or absence of electron-dense deposits and their location, presence or absence of fibrils (e.g., amyloid), thickened or abnormal contouration of the GBM, podocyte hypertrophy as defined by increased cytoplasm and/or formation of microvilli, podocyte foot process effacement, increased podocyte densities and vacuolation, curvilinear bodies (hyaline glomerulopathy), and tubuloreticular inclusions in the capillary endothelial cells.

#### 4.2.2. Noninflammatory Glomerular Injury

Podocyte injury underlies most forms of proteinuric glomerular diseases of the kidney. A noninflammatory glomerular injury of potential importance in toxicologic pathology is designated “focal segmental glomerulosclerosis” (FSGS), described below. It can be both

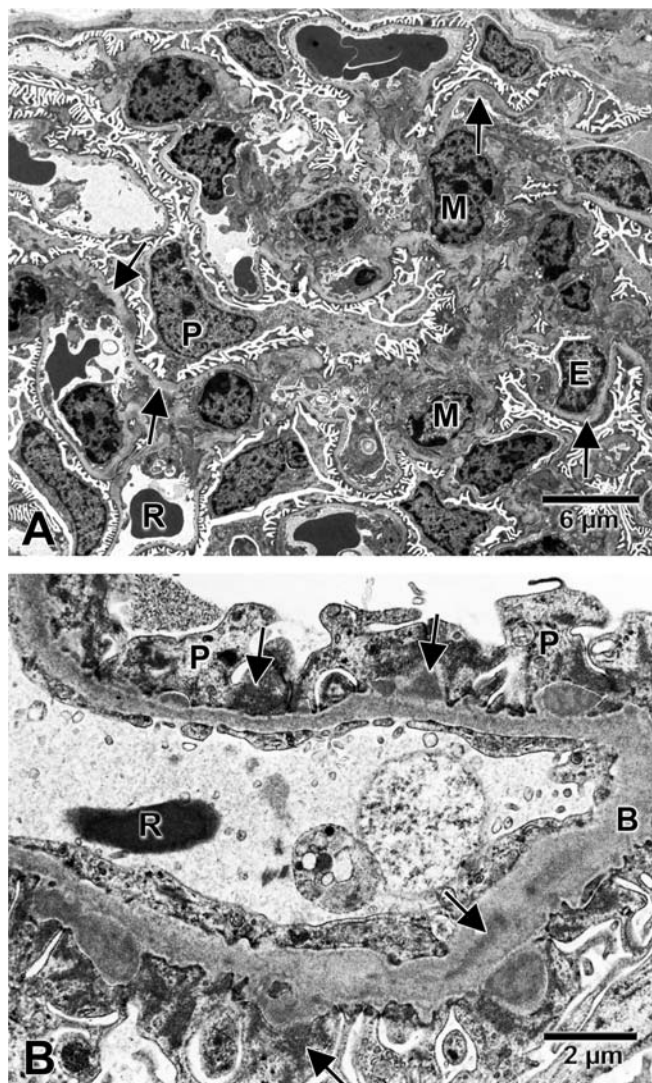


**FIGURE 2.17** Ultrastructural glomerular lesions in a monkey treated with a protein therapeutic. (A) Increased mesangial cells (M), podocyte hypertrophy (P), and thickened basement membrane (arrows). Note endothelial cells (E) and erythrocytes (R) in the capillary loops. (B) Thickened basement membrane, 1000 $\times$  (B) swelling and fusion of podocyte foot processes (P) with multifocal electron-dense deposits of presumably immune complexes (arrows), 10000 $\times$ . Courtesy of Dr Tom Brown, Drug Safety R&D, Pfizer, Groton, CT; Reproduced from Haschek WM, Rousseaux CG, Wallig MA, Bolon B, editors: *Haschek and Rousseaux's handbook of toxicologic pathology*, ed 3, 2013, Academic Press, Figure 47.22, p. 1720, with permission.

a spontaneous and induced lesion and has many etiologies, but the common final pathway to induce FSGS is podocyte injury, detachment, and loss.

### 4.2.3. Podocyte Injury

A classification of podocyte diseases in 2013 included four major types of podocytopathies, all of which are associated with variable degrees of foot process effacement: (1) minimal change nephropathy (MCN), with normal morphology by light microscopy and preserved podocyte number; (2) FSGS, characterized by segmental scarring of the tuft, occasionally accompanied by hyalinosis, adhesions to the Bowman capsule, and decreased number of podocytes; and rarely (3) collapsing glomerulopathy, characterized by glomerular damage with substantially increased podocyte number and pseudocrescent formation.

### 4.2.4. Focal Glomerulosclerosis

“Focal” denotes the absence of involvement of all nephrons, in contrast to diffuse involvement. The term “segmental” denotes involvement of only part of an individual glomerulus, in contrast to global involvement. Therefore, FSGS is a histologic pattern of glomerular diseases in which a portion of the glomeruli have sclerosis (or scarring) of a portion of their capillary tufts. The underlying cause of the sclerosis is podocyte injury and detachment. If enough podocytes covering a segment of the glomerular tuft are lost, the segment of glomerulus will scar and the capillary lumens in that segment will be compressed and/or replaced by ECM. Importantly, the matrix will consist of normal constituents of the glomerular mesangium and GBM; it will not be fibrillary collagen produced by fibroblasts. As such, the term glomerular fibrosis should not be used to describe this lesion. Furthermore, even though only segments of some of the tufts are sclerotic based on histologic evaluation, the podocyte injury, as evidenced by foot process effacement and microvillus transformation, could be widespread when examined ultrastructurally. The time course of podocyte damage and detachment can be prolonged. If the insult (e.g., toxicant exposure, hypertensive episode, viral infection) is removed, then some podocytes can recover and restore their foot processes. Therefore, histologic evaluation of FSGS cases often only reveal the tip of the iceberg of podocyte injury. Some causes of FSGS cannot be removed. For examples FSGS develops in animals that have renal maldevelopment/dysplasia because they have fewer

functioning nephrons than normal. The remaining nephrons have to undergo hypertrophy to compensate for the decreased number. This results in enlargement of the glomerular tuft and stretching of the podocytes, thereby inducing cell stress and eventually cell death. Those cases will have progressive FSGS, with many glomeruli passing through a stage of segmental sclerosis and eventually becoming globally sclerotic.

Aminonucleoside toxicity is an example of induced FSGS. Light microscopically, increased PAS-positive staining occurs in the affected tuft with increased silver staining of the thickened basement membrane. Ultimately the tuft becomes sclerotic or scarred (>3 weeks) and may stain positively with Masson’s trichrome for collagen. Occasionally, immune-complex trapping can be demonstrated, but this is considered secondary. Doxorubicin nephropathy in rats is characterized by podocyte injury (minimal change disease), but at high enough doses, it can cause FSGS. In mice, doxorubicin nephropathy is strain dependent and recently, the pathogenesis was elucidated. A single nucleotide polymorphism (SNP) in the DNA repair gene, PKCs, is associated with susceptibility to doxorubicin. Another required step is that following doxorubicin administration, plasminogen has to bind to the glomerulus. Interestingly, plasminogen KO in susceptible strains is protected from developing podocyte injury. Therefore, murine doxorubicin nephropathy is a 2-hit process and interestingly, some types of FSGS in humans also require two insults. For example, in humans, there are genetic variants of podocyte structural proteins such as nephrin, podocin, and CD2-associated protein (CD2AP) which can be more susceptible to cell stress and injury. Insults that might be sublethal to podocytes of other humans can result in cell death (and eventual FSGS) in humans with susceptible genetic variants.

### 4.2.5. Membranous Nephropathy

Membranous nephropathy is associated with immune complex deposition in the glomerular tuft and should be appropriately investigated to differentiate it from background lesions, especially in monkeys (Figure 2.17). Repeated (chronic) injection of soluble antigens or biotherapeutic products can cause this lesion,

characterized by immune-complex (IgG and C3) deposition on the abluminal (subpodocytic) aspect of the capillary walls. This location is referred to as “subepithelial” because the podocytes are epithelial cells (in contrast to the mesenchymal endothelial and mesangial cells). Membranous nephropathy is recognized light microscopically with the Jones methenamine silver stain, as spikes of argyrophilic material on the epithelial surface of the basement membrane. Rarely, aggregates of intravenously administered biotherapeutic products may lodge in glomeruli without the typical antigen–antibody complexes and initiate in situ immune-mediated glomerular injury. In routine H&E-stained sections, the capillary walls of the glomeruli can be thickened. In early stages, the thickening can be subtle and might only be appreciable with EM evaluation. In late stages, the walls will be thickened and remodeled. Importantly, the subepithelial immune complexes can cause podocyte injury and glomerulosclerosis can be secondary to membranous nephropathy. This should not be confused with FSGS, however, because that diagnosis is reserved for patients that have nonimmune-mediated glomerular disease. Instead, the diagnosis of “immune complex mediated membranous nephropathy with secondary segmental sclerosis” is preferred.

#### 4.2.6. Amyloidosis

Amyloidosis is a spontaneous disease characterized by the extracellular deposition of polypeptide fragments of serum proteins appearing in routine section as a lightly eosinophilic amorphous material within glomerular tufts (Figure 2.15A). Confirmation of the deposits as amyloid can be accomplished with light microscopy using, for example, Congo Red (CR) stains. Amyloid appears peach colored when the CR slide is viewed with bright field microscopy but changes to a birefringent apple green when the slide is view with polarized light. Many proteins and protein fragments can form amyloid fibrils. Serum amyloid A (SAA) is a common protein precursor in humans and dogs. This protein is synthesized by the liver in states of systemic inflammation as an acute phase protein. It undergoes fibrillogenesis in glomeruli, renal vasculature and interstitium. First, SAA will become an amyloid precursor protein which has high  $\beta$ -pleated sheet content

and then it will self-aggregate with other SAA precursors. It will then be stabilized with glycoaminoglycans (GAGs) and serum amyloid P (SAP) protein. These stable aggregates are difficult to degrade and, once present in a glomerulus, will be a nidus for additional amyloid fibrils to join. Importantly, however, many proteins can become amyloid fibrils. In humans, light chain fragments of immunoglobulins are common sources of amyloid fibrils. Other proteins including fibrinogen A $\alpha$ , transthyretin, and  $\beta$ 2-microglobulin are also sources of amyloid. There are rodent models of these less common causes of amyloidosis, but most spontaneous amyloidosis cases in laboratory animals are due to SAA amyloid. The diagnosis of amyloid in mouse carcinogenicity studies may be complicated by the concomitant presence of glomerular fibrosis due to murine CPN by 2 years of age.

#### 4.2.7. Inflammatory Glomerular Injury

Hypercellularity is the hallmark of an inflamed glomerulus, termed glomerulonephritis. If the proliferating cell is mesangial, the process is designated “mesangioproliferative glomerulonephritis.” When there are increased numbers of nuclei in the capillary lumens, the terms “endocapillary hypercellularity” or “endocapillary proliferation” are used. Notably, mesangial hypercellularity and endocapillary hypercellularity are not mutually exclusive, and they can occur in the same glomerulus. If neutrophils are increased within the tuft, the process can be designated as exudative glomerulonephritis. Postinfectious glomerulonephritis (e.g., poststreptococcal glomerulonephritis) is an example of exudative glomerulonephritis in humans which can stem from an immunomodulatory phenomenon.

Severe tuft inflammation may lead to the formation of “crescents” which is when Bowman’s space has increased cellularity. In normal glomeruli, there should only be two layers of cells in Bowman’s space: the podocytes lining the capillary tuft and the PECs lining Bowman’s capsule. However, if glomerular damage is severe enough to rupture a glomerular capillary loop or segmentally rupture Bowman’s capsule, inflammatory cells will flood into Bowman’s space. These crescents are accumulation of many cell types including leukocytes,



fibroblasts, red blood cells, and injured/hypertrophied podocytes and PECs. There is often also fibrin in early crescents and fibrosis in late-stage crescents. Crescent formation is an important lesion in human nephropathology and is sometimes diagnosed as crescentic glomerulonephritis. It can be experimentally induced in rodents by injection of autoantibodies against the GBM. Crescents can occur in pigs with glomerulonephritis, but it is uncommon in dogs. The reason behind the species variation in ability to form crescents is unknown.

Similar to FSGS, the term membranoproliferative glomerulonephritis (MPGN) describes a pattern in which the glomerular tufts are hypercellular (usually in both the endocapillary and mesangial) and the GBM is thickened. This pattern often has a primary immunologic etiology in humans, although there are some diseases which are not immune-mediated. Similarly in dogs, MPGN is usually secondary to immune complex deposition. As opposed to immune deposition seen in membranous nephropathy, however, the deposits are located between the endothelial cell and the GBM. The immune deposits activate the complement pathway and their proximity to the glomerular capillary lumens will attract inflammatory cells when the anaphylatoxins are formed. This inflammatory cell recruitment explains the endocapillary hypercellularity that is typical of the MPGN pattern. The GBM thickening is also different than that observed with membranous nephropathy. In MPGN, the endothelial cells create new basement membrane material to form a barrier between the cell and the deposits which are beneath them. When these cases are stained with Jones methenamine silver, there is a double contoured appearance of the GBM that consists of new basement membrane material (black), nonstaining layer that represents the immune deposits and then the original GBM (outer black layer). Although many cases of MPGN in humans and most of the spontaneous cases of MPGN in dogs are due to immune complex deposition, other diseases can have a similar histologic pattern. For example, in humans, there can be mutations in the proteins of the complement system which can result in overactivation of complement pathway. Mild infections can trigger the pathway which will overreact. Complement proteins deposited or

trapped in the glomerular capillary walls can increase their thickness and recruit inflammatory cells to the glomerulus. These diseases are called often called C3 glomerulonephritides because it is easy to demonstrate the presence of C3 (and complete absence or limited amounts of immunoglobulins). Importantly, however, the genetic alteration might actually represent a mutation that knocks out a complement pathway inhibitor or makes a more effective complement pathway promoter. C3-mediated diseases have been rarely reported in dogs as breed-related glomerulonephropathies, but the specific complement protein driving the cases in these rare reports has not been elucidated. In Norwegian pigs, spontaneous complement factor H deficiency was associated with an MPGN pattern and EM revealed dense deposits in the glomerulus. This lineage of affected pigs has been maintained as an animal model for human MPGN. C3 glomerulonephropathy has been experimentally modeled in mice by knockout of complement factor inhibitors; however, spontaneous C3-associated glomerular disease in rodents is not reported.

Another glomerular disease that can have an MPGN pattern in humans, dogs, and rodents is due to direct glomerular endothelial cell injury. The lesion that can develop is known as thrombotic microangiopathy (TMA). It too can have a wide variety of causes, ranging from bacterial toxins (e.g., Shiga toxin) to malignant range hypertension, and especially related to drug exposure due to chemotherapeutic agents. The endothelial cell damage causes endothelial cell swelling, recruitment of inflammatory cells, and GBM thickening when plasma travels into the wall and mesangial zones because the endothelial layer is severely damaged. Glomeruli can have fibrinoid vascular necrosis and there can also be fibrin thrombi in glomerular capillaries. Often, the afferent/efferent arterioles are also involved in TMA cases, and there can be fibrinoid vascular necrosis at the hilus. Ultrastructurally, there is loss of endothelial cell fenestrae and the GBM often has an electron lucent expansion beneath endothelial cells. The glomerular lesions described above are relevant in nonclinical toxicologic pathology, and have counterparts in human nephropathology. Routine use of advanced diagnostic tools will broaden the acceptance of refined glomerular categorization systems in toxicologic pathology of all domestic

species, including those utilized in toxicologic studies. Hopefully, this will enable easier recognition of subtle glomerular lesions and classification of the type of glomerular injury.

#### 4.2.8. Tubule Injury

##### 4.2.8.1. NECROSIS AND DEGENERATION

Injury to proximal tubular epithelium, induced by xenobiotics in the human and laboratory animals and referred to collectively as DIKI, can lead to ATN ([Figure 2.18](#)). Several patterns of specific alterations occur, depending on the inciting agent, dose, and the mechanism. Various nephron segments differ in their capacity to withstand hypoxic insults. The pathophysiology of renal tubular damage is often multifactorial, but mechanisms include direct cytotoxic effect (doxorubicin, cisplatin), hypoxic damage induced by altered medullary microcirculation or enhanced metabolic requirements (NSAIDs, radiocontrast agents, cyclosporine), and injury caused by free-radical generation (heme pigments and chemotherapeutic agents) ([Figure 2.19](#)). These mechanisms are not mutually exclusive. Amphotericin B illustrates the multifactorial nature of injury as it directly injures tubular cell membranes, induces hypoxic

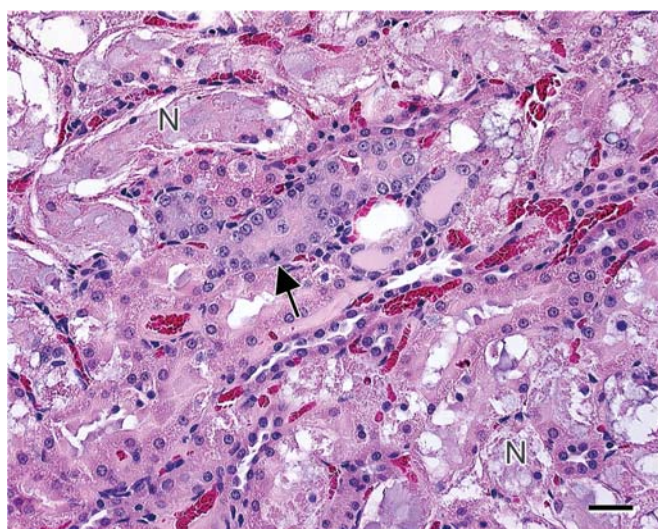


**FIGURE 2.18** Multifocal acute tubular necrosis (N) and regeneration (arrow) in a rat treated repeatedly with nanoparticles of a small molecule candidate. Courtesy of Dr Xiantang Li, Drug Safety R&D, Pfizer, Groton, CT. Reproduced from Haschek WM, Rousseaux CG, Wallig MA, Bolon B, editors: *Haschek and Rousseaux's handbook of toxicologic pathology*, ed 3, 2013, Academic Press, Figure 47.24, p. 1721, with permission.

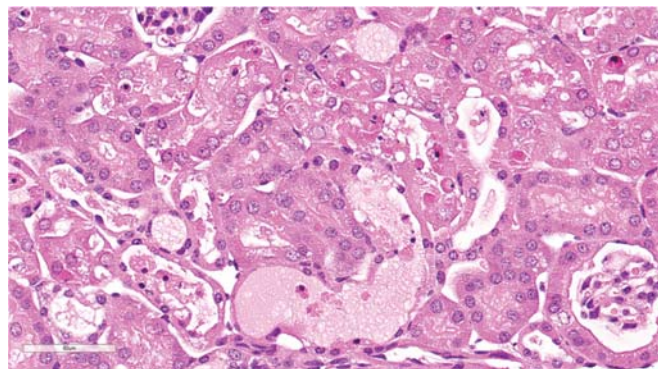


**FIGURE 2.19** Necrosis of tubules in kidney of Sprague-Dawley rat given cisplatin for 7 days. There is loss of virtually all cells lining the basement membrane in a few of the proximal tubules with only sloughed epithelium and debris filling the lumina. Remaining epithelium is attenuated in an attempt to cover the exposed basement membrane. A few surrounding tubules exhibit vacuolation and/or single cell necrosis.

tubular damage by profound renal vasoconstriction, and enhances oxygen consumption to maintain the cellular transmembrane electrolyte gradient.

There is an exhaustive list of agents which result in direct cytotoxicity to tubule epithelium. Injury can come from the blood via the basolateral surface or from the urine filtrate through the apical brush border. The proximal tubule is the most frequent site of direct toxic injury, as it has greater permeability to ions and chemical flux than the distal tubule (due to the tight intracellular junctions and high electrical resistance found in distal tubules). The proximal tubules are also the site of most of the membrane-bound active transport activity within the kidney ([Frazier and Seely, 2019](#)). However, with more severe insult or longer duration of exposure, the area of injury expands to include more proximal and distal segments of the affected nephron due to the tendency of the nephron to respond as a unit. Heavy metals such as mercury and xenobiotics requiring metabolic transformation to exert their toxic potential all typically induce tubule necrosis in the pars recta. Cell respiration and metabolic transformation both occur in the pars recta. Other heavy metals, such as lead, and xenobiotics bound to circulating proteins and xenobiotics requiring transport, such as organic acids or bases, preferentially injure the PCT because protein reabsorption activity predominates in this part of the nephron. Many



agents that induce proximal tubule necrosis at higher doses typically induce single cell necrosis at lower doses. For example, gentamicin and mercury cause replicative and apoptotic rate increases in PCT. Cisplatin renal injury is limited to scattered single cell necrosis at low doses but severe tubule necrosis of entire zones of the corticomedullary areas at higher doses. Single cell necrosis refers to the loss of one or a few individual epithelial cells within a tubule profile due to either apoptosis or oncotic processes. In contrast, tubule necrosis refers to the loss of a majority of cells within a profile and has much more severe consequences for tubule function, with greater potential for effects on absorption, secretion, or urine flow dynamics.

#### 4.2.9. Vacuolation

Vacuolation of tubules is a generally reversible type of degeneration associated with renal exposure to many xenobiotic agents. It can lead to necrosis, but more often accompanies specific types of tubule injury involving intracellular accumulation of lipids, glycogen, or fluids. Vacuolation can result from intracellular accumulation of excipients or vehicles such as cyclodextrins and is a feature of phospholipidosis and gentamicin toxicity. Drug-induced vacuolation is characterized by clear, variably sized spaces within pale or granular, swollen cytoplasm. Diffuse cytoplasmic vacuolation of tubular epithelium is seen with biologic therapeutics containing polyethylene glycol of various molecular weights, especially in rodents (Figure 2.20). Osmotic vacuolation occurs in rats and dogs after exposure to osmotically active agents such as mannitol and sucrose. Microscopically, the change is diffuse in PCTs and is characterized by cytoplasmic vacuolation and rarefaction.

Phospholipidosis in the kidney is associated with the administration of cationic amphophilic compounds. Light microscopically, proximal tubule cells may have subtly increased cytoplasmic lucency. Specific immunohistochemical stains can be used to positively identify phospholipid. In toluidine blue-stained plastic sections, cytoplasmic bodies are readily visible by light microscopy. Ultrastructurally, the hallmark of phospholipidosis is the presence of concentric multilaminated phospholipid membrane whorls in the phagolysosome,

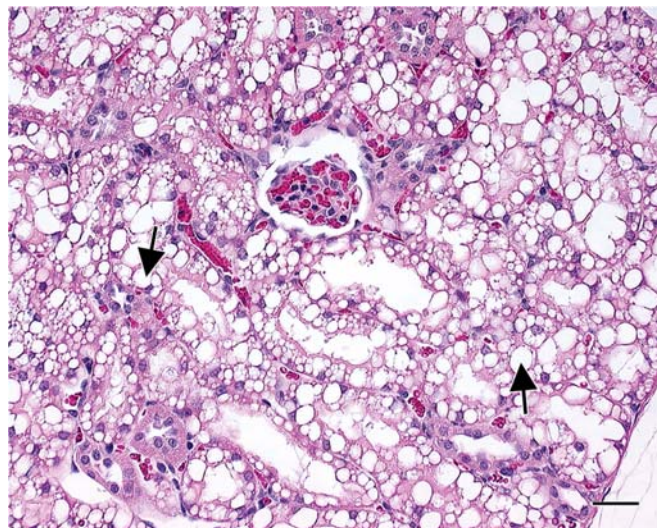


**FIGURE 2.20** Renal tubular epithelial cell vacuolation (arrows) in a rat treated with pegylated monoclonal antibody therapeutic. Bar = 40 mm. Courtesy of Dr Xiantang Li, Drug Safety R&D, Pfizer, Groton, CT; Reproduced from Haschek WM, Rousseaux CG, Wallig MA, Bolon B, editors: *Haschek and Rousseaux's handbook of toxicologic pathology*, ed 3, 2013, Academic Press, Figure 47.26, p. 1722, with permission.

designated myelin figures. Renal phospholipidosis is generally accompanied by its presence in other vulnerable organs.

Lipidosis of proximal tubular epithelium occurs spontaneously in the rat and the mouse but can also be induced by xenobiotic administration such as decalin or corn oil (Figures 2.15B–C). These cytoplasmic fat droplets can be confirmed by oil red-O staining of frozen sections.

#### 4.2.10. Tubule Dilation and Cysts

Nephrotoxics can commonly induce dilation of the tubular luminal diameter, as a consequence of necrosis or loss of individual tubule epithelial cells and loss of the brush border (Figure 2.21). The resulting thinning of the apical region of the proximal tubular epithelial cells also often makes the lumen appear empty and therefore can be mistaken for tubular dilation. Hyperfiltration can result in greater intratubular pressures and when combined with thinning of tubule walls due to epithelial loss, true tubule dilation can progress, resulting in cysts. The developing kidney in neonatal rodents in juvenile toxicity studies is particularly sensitive to these changes due to immaturity of the structural



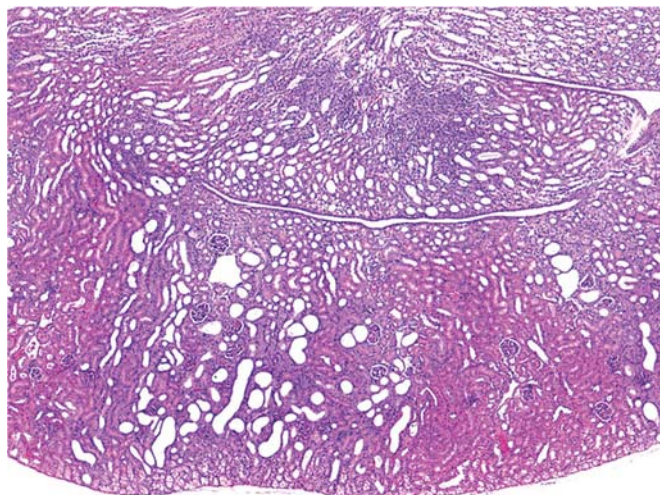


**FIGURE 2.21** Tubule dilation associated with xenobiotic administration in a Sprague-Dawley rat kidney given a nephrotoxic drug for 14 days. Note the large luminal spaces in tubules throughout the cortex and medulla. This lesion can occur due to obstruction but may also represent sequelae to degeneration and necrosis of renal tubule epithelium due to other mechanisms.

scaffold of the tubule and thin interstitium. Dilated tubules are often clustered together representing tubules along the same or adjacent nephron segments. In other cases, the pattern may be zonary with dilation limited to the corticomedullary junction or subcapsular areas. There may be hyaline or granular casts filling lumina. Dilation also frequently accompanies pyelonephritis, with lumina containing neutrophils and lymphocytes. Tubule dilation may be associated with increases in UN, sCR, and novel urine biomarkers. While tubule dilation most often accompanies other forms of renal degeneration, it can occur as a primary toxic response to a variety of xenobiotic agents, including corticosteroids, lithium, and ACE inhibitors (Frazier et al., 2012). Cystic tubules are found commonly in end-stage kidney disease and in later stages of rodent CPN but are most often encountered in preclinical studies in kidneys as solitary congenital cysts unrelated to drug treatment. Rarely, multiple large cysts are noted in kidneys, with atrophy of surrounding cortical tubules as a consequence of congenitally acquired PKD, which has been noted in rodents, dogs, cats, and humans and is genetically determined (Figure 2.22). A few xenobiotic agents will also

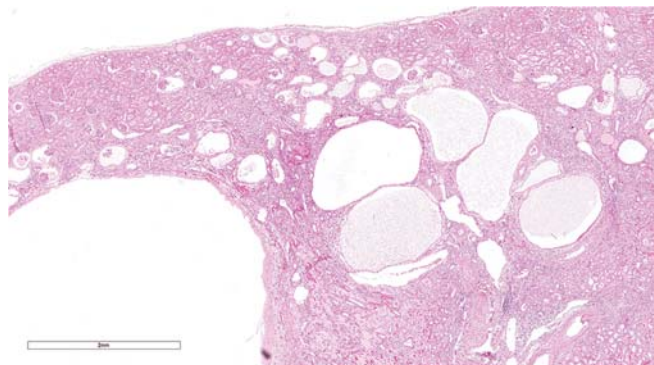


**FIGURE 2.22** Polycystic kidney in a not otherwise specified nonhuman primate. The kidney is distorted by variably sized dilated/cystic tubules throughout the cortex and medulla. These are lined by attenuated to occasionally hyperplastic epithelium and filled with pale to deeply eosinophilic proteinaceous material. There is significant interstitial fibrosis and chronic inflammation with occasional interspersed functional nephrons. The subcapsular surface is irregular due to the expansion of the cystic tubules and contraction of the interstitial fibrosis.

induce PKD in rodents and nonrodents, and many of these target ciliary functions in the tubules. In humans, “polycystic” is used for cases where the genetic mutation in PKD1 or PKD2 is proven; if there are multiple cysts but no mutations, then the term “multicystic” is utilized. However, in regulatory toxicity studies where genetic mutation can only be inferred, the morphologic diagnosis of polycystic kidney should be reserved for kidneys that have at least six or more cysts, are primary cystic diseases and not a result or function of an overlying degenerative process such as CPN, and where cysts are not simply the end result of tubule dilations related to other necrotic toxicities in a few animals. A few cysts in a kidney are best diagnosed simply as kidney, cyst (multiple). Several mouse and rat strains have been derived as models to study PKD and to test efficacy of pharmaceuticals targeting this disease in humans.

#### 4.2.11. Other Types of Tubule Injury

Hyaline droplet change represents phagolysosomal protein overload. Increased protein in the glomerular filtrate protein due to glomerular disease primarily represents albumin and typically stains positive with PAS. By contrast, the protein overload associated with  $\alpha$ 2 $\mu$ -

globulin nephropathy in male rats results in hyaline droplets that are PAS-negative, but Mallory's Heidenhain-positive (Figure 2.23). Mallory's stain is not specific for alpha<sub>2</sub>μ-globulin, but is specific to the biochemical attributes of this and other proteins.

Poorly soluble sulfonamides can crystallize in the tubules and cause direct toxicity to the tubular epithelium via mechanical means. Crystals are usually detected on gross but not histological examination, since they dissolve with tissue processing. Proximal tubular degeneration occurs with oxalate crystalluria, which can be induced by ingestion of ethylene glycol or oxalate-containing plants or vegetables. Pale yellow, birefringent, calcium oxalate crystals are present in the tubular lumina, and sometimes also in the tubular epithelium and interstitium, and can be readily identified with polarized light. Distal tubular necrosis is reported in cats and dogs following ingestion of pet food contaminated by melamine and cyanuric acid. Crystals are pinwheel-shaped and granular, and are readily visualized without the need for polarized light

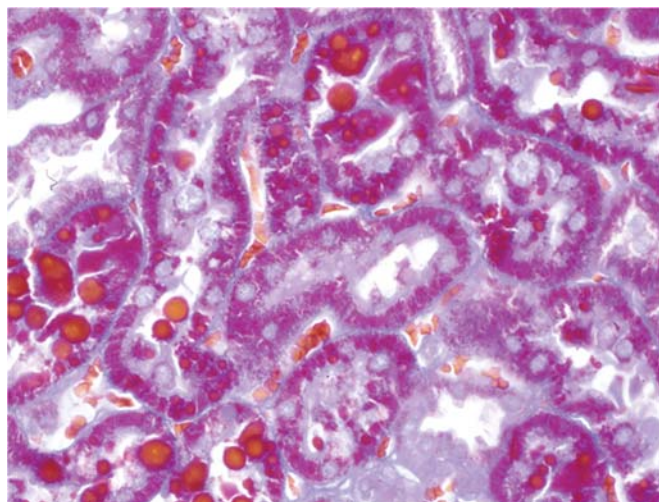


**FIGURE 2.23** Alpha-2μ-globulin nephropathy in a male rat kidney with hyaline droplets demonstrated by Mallory-Heidenhain stain. Note variably sized, bright red clusters of droplets within the cytoplasm of proximal tubules representing accumulation of alpha-2μ-globulin within lysosomes. The large red droplets in the lumen are an artifact of the staining procedure. In this case, the incidence of hyaline droplets within renal epithelium was increased in incidence in a dose-responsive manner in association with drug treatment, but this is a male rat-specific phenomenon.

(Figure 2.24) (Hard et al., 2009a, 2009b). In rodents, changes associated with melamine cyanurate result in characteristic lesions diagnosed as retrograde nephropathy (described later in Section 5).

Xenobiotics exerting a vitamin D-type activity at sufficiently high doses cause tubule and vascular mineralization of renal basement membranes. A commercially available rodenticide contains cholecalciferol and has this potential for rodents, as well as domestic animals, when consumed. Perturbation of calcium:phosphorus ratios through the use of certain commercially available synthetic rodent diets (AIN 76) may also result in severe tubular luminal mineralization, predominantly restricted to the pars recta. As calcium salt precipitation may be difficult to detect in routine tissue sections, special stains, such as Alizarin Red S or Von Kossa's, can be used for better demonstration of mineralization.

#### 4.2.12. Papillary Injury

Nephrotoxicity can manifest as medullary collecting duct injury that extends to complete RPN. The least severe and earliest morphologic change observed following treatment with most papillo-toxic agents is decreased alcian blue staining of the interstitial matrix due to loss of

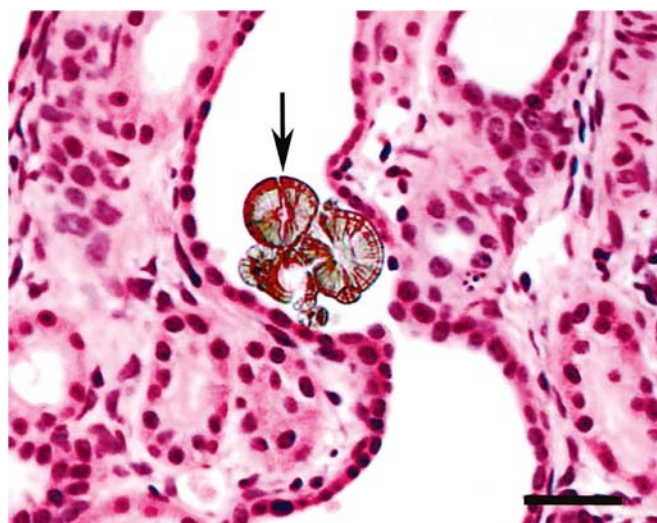


**FIGURE 2.24** Dilated distal tubule containing a cluster of crystals with radiating spokes and concentric striations (arrow) from a cat with pet food toxicity. H&E stain. Bar = 45 mm. Reproduced from Brown CA, Jeong KS, Poppenga RH, et al.: Outbreaks of renal failure associated with melamine and cyanuric acid in dogs and cats in 2004 and 2007. *J. Vet. Diagn. Invest.* 19:525–531, 2007, with permission.



glycosaminoglycans followed by degeneration and coagulative necrosis of interstitial cells. This change probably represents a precursor lesion without evidence of necrosis in other elements of the renal papilla. With progression, vascular congestion and degeneration of capillary endothelia become apparent, followed by degeneration and necrosis of the epithelial cells of the loops of Henle, collecting ducts, and urothelium. These changes start at the tip of the papilla and involve increasing proportions of the papilla, reflecting increasing severity. Severe cases of RPN are visible grossly as pale areas involving the tip of or the entire papilla (Figure 2.25). The urothelial lining of the papilla may be intact or focally disrupted. With further injury, confluent necrosis can extend proximally to the base of the papilla. In the most severe cases, necrosis extends into the outer medulla. The necrotic papilla may become mineralized, or the mineralization may be restricted to a transverse band (the abscission zone) at the junction with viable medulla. Sloughing of the necrotic papilla into the renal pelvis may occur, followed by reepithelization over the remaining viable medulla. Secondary cortical changes develop as a consequence of nephron obstruction.

#### 4.2.13. Interstitial Injury

Disorders that affect the tubules can cause injury in the interstitium, and vice versa, leading to the clinical term of tubulointerstitial disease. Molecular studies in the past few years have elucidated the importance of the renal interstitium in a whole host of kidney diseases and syndromes without apparent morphologic change. Mild tubulointerstitial injury sensitizes glomeruli to subsequent podocyte-specific injury, and glomerular dysfunction results in intrinsic toxicity to proximal tubules and is a key factor in renal disease progression. Excessive protein reabsorption activates inflammatory profibrotic pathways within the interstitium (Obert and Frazier, 2019). There are species differences in how the kidney interstitium responds to injury. For instance, the interstitium plays a key role in the pathogenesis of CPN, via activation of the local intrarenal interstitial renin-angiotensin-aldosterone system (RAAS) in mice and rats. CPN exacerbation represents the most minimal expression of renal toxicity in the rat. While inflammatory infiltrates frequently occur in interstitium of rats, these are usually of limited severity or

distribution and drug-related responses involving diffuse renal interstitial inflammation are rare. In contrast, interstitial disease in humans or dogs may be represented by a progressive and florid inflammatory response termed interstitial nephritis. This species difference in interstitial response is further exemplified by comparison of chronic renal effects of a diphosphonate drug at high dosages in the dog and the rat. The dog response is that of chronic interstitial nephritis, whereas the rat response is characterized as increased incidence and severity of CPN. Chronic interstitial nephritis is characterized across species by interstitial fibrosis, interstitial inflammatory infiltrates, tubular atrophy, and glomerular sclerosis. If interstitial inflammation occurs in nonclinical species without evidence of tubular injury, is severe and appears early in the process, has abundant eosinophils or neutrophils, or occurs with peritubular immune complex deposition, the process may be regarded as a primary interstitial nephritis. Renal fibrosis is encountered with some frequency in animal toxicity studies, and is more prominent in some species than others. For instance, the minipig is particularly prone to fibrotic responses in the interstitium with comparatively mild renal injury, and monkeys and dogs are both prone to glomerulosclerosis characterized by florid collagen deposition. Fibroblasts are naturally present within the interstitium but additionally are recruited to the site by growth factors and can also be stimulated to become myofibroblasts. Tubules undergoing injury release TGF $\beta$ 1 in a paracrine signal to the surrounding interstitium, resulting in myofibroblast conversion and synthesis of downstream profibrotic growth factors such as PDGF and connective tissue growth factor (CTGF), which enhance collagen production by these cells. If tubule damage is severe enough to result in exposure of the basement membrane and disruption of laminar adhesion molecules attached to tubule cells, the same growth factors may also promote EMT, resulting in the generation of more local myofibroblasts and further fibrosis (Frazier et al., 2000).

## 5. MECHANISMS OF TOXICITY

Xenobiotic-associated kidney injury typically depends on a sufficient concentration of the toxic moiety present in the target cell or



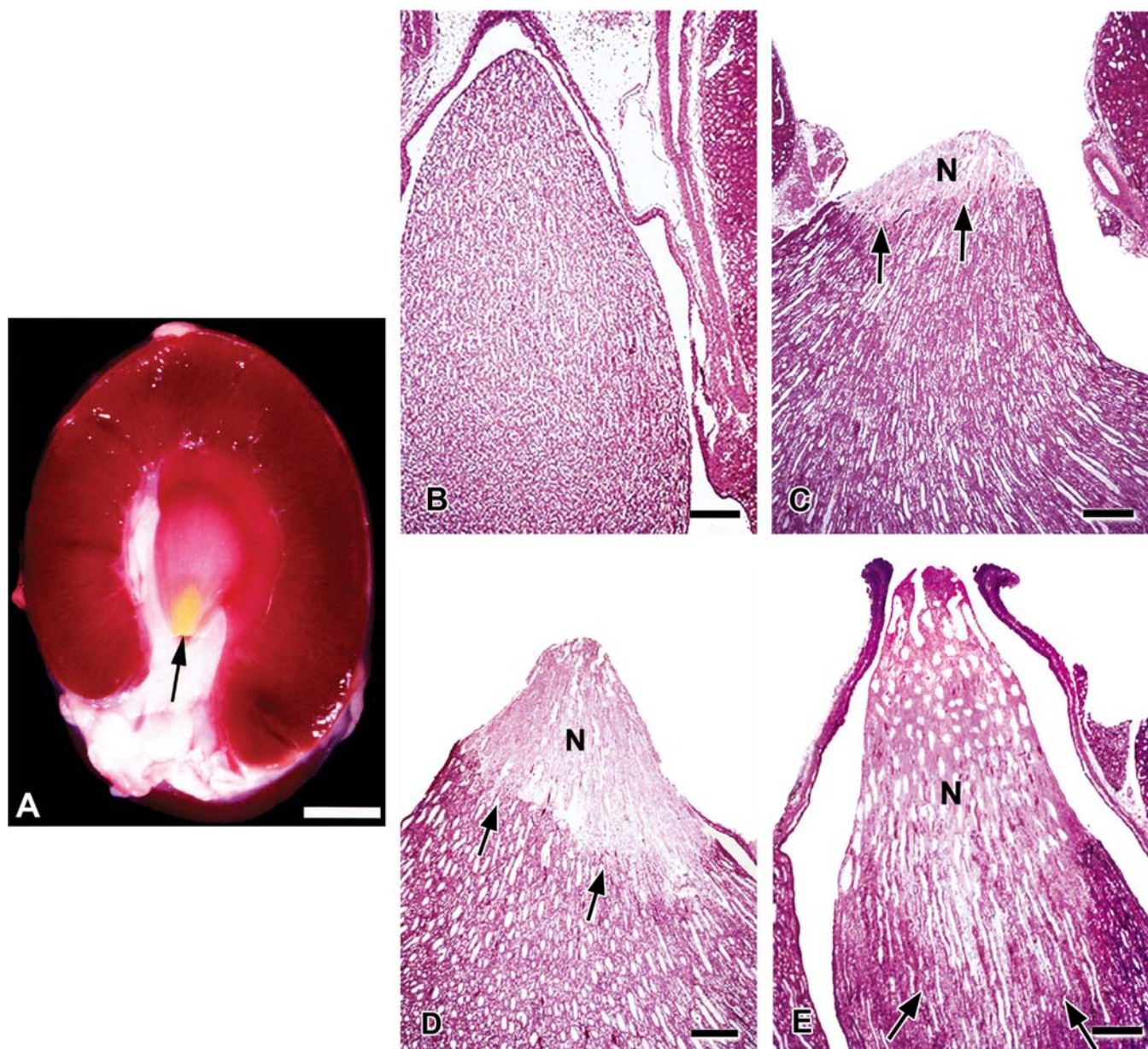


**FIGURE 2.25** Nonsteroidal antiinflammatory drug-induced renal papillary lesions. (A) Gross appearance of renal papillary necrosis (arrow). Bar = 5 mm. Photomicrographs show the normal renal papillae (B), and grade I (C), II (D), and III (E) renal papillary necrosis (N and arrows). Bars = 350 mm. *Reproduced from Haschek WM, Rousseaux CG, Wallig MA, editors: Handbook of toxicologic pathology, ed 2, 2002, Academic Press, Figure 29, with permission.*

subcellular organelle per given time to elicit cellular damage. The magnitude of blood flow per gram of renal parenchyma is higher than for any other tissue, predisposing renal parenchyma to toxic insult. Glomerular filtration with tubular reabsorption serves to further concentrate potentially toxic moieties. Tubular transport occurs via protein binding and

subsequent endocytosis, through active or passive links with ATP hydrolysis-dependent transport such as the sodium pump, or through specific ABC or SLC renal transporters on the basolateral and apical membranes. The kidney has the capacity to dissociate protein-bound toxins, a capability lacking in other organs. Protein binding may protect extrarenal tissues

from a potentially injurious agent. The kidney also has the capability to alter the pH of tubular fluid, which can serve to transform solutes into reactive forms or to result in the precipitation and potential crystallization of compounds which can cause luminal obstruction. Finally, the kidney participates in the metabolism of xenobiotics. Renal metabolism with derivation of reactive electrophilic intermediates causes injury following covalent or peroxidatic reactions with the target cell macromolecules.

In order to protect against covalent binding, cells possess high concentrations of thiols, primarily glutathione. However, these thiols can become depleted, leading to covalent bonding to critical biomacromolecules. Free radicals may be derived by reduction or oxidation of various xenobiotics. Free radicals can donate a free electron to molecular oxygen to form a superoxide anion radical. The superoxide anion radical is generally converted to hydrogen peroxide by superoxide dismutase. The ferrous ion can catalyze the Fenton reaction, involving conversion of hydrogen peroxide to a hydroxyl radical and a hydroxide anion. The hydroxyl radical also binds covalently to critical cellular macromolecules. Lipid peroxidation, oxidative stress, and genetic mutation can be the consequence of free radicals and electrophiles derived by xenobiotic metabolism. The generation of excess free oxygen radicals and reactive oxygen species (ROS) can affect proinflammatory and profibrotic pathways that promote impairment in insulin metabolic signaling, reduced endothelial-mediated vasorelaxation, and associated cardiovascular and renal structural and functional abnormalities. Labile iron is necessary for the catalysis of superoxide anion and hydrogen peroxide, and the generation of the injurious hydroxyl radical. Acute hypoxia and cellular damage can liberate larger amounts of cytosolic and extracellular iron that is poorly liganded; thus, large increases in the generation of oxygen-free radicals are possible, causing tissue damage. Lipid peroxidation is implicated in the toxicity of several xenobiotics, such as glutathione-depleting agents, ethanol, and mercuric chloride. However, inhibition of renal redox cycle enzymes appears not to be an important determinant of the increased lipid peroxidation associated with mercuric chloride nephrotoxicity.

Predisposing risk factors contribute significantly to the incidence and severity of drug-induced AKI in patients, including age, genetic background, hydration status, sepsis, hypotension, previous or comedications, and preexisting renal disease such as diabetes. These factors tend to amplify the toxic potential of drug or chemical exposure. DIKI can potentially progress from AKI to CKD and end-stage renal failure through a series of secondary pathophysiologic processes triggered by the initial injury. The underlying mechanisms which result in transition from AKI to CKD in humans are not well understood. Renal dysfunction may occur gradually with chronic exposure to a variety of NSAIDs, analgesics, antibiotics, anticancer agents, or a variety of other agents. With significant nephron damage, adaptive increases in glomerular pressures ensue that result in an increase in single-nephron GFR of remaining surrounding nephrons, and this can eventually result in hyperfiltration phenomenon and progressive nephron atrophy and fibrosis. The nephrons that are collapsing will be associated with glomerulosclerosis which will further perpetuate the vicious cycle of hemodynamic disturbance in adjacent nephrons, leading to end-stage failure. Other biochemical processes involved in CKD pathogenesis include glomerular shear stress, alterations in mesangial matrix, transcapillary flux, ischemia pathway perturbations, tubuloglomerular feedback, intrarenal RAS alterations in the interstitium, nitrous oxide and ROS interactions, and paracrine profibrotic growth factor interactions (Obert and Frazier, 2019).

## 5.1. Nephrotoxicity Classification

Nephrotoxicity can be categorized according to functional and structural characteristics of compounds, morphologic presentation of lesions, mechanism of renal damage, and subtopographical location of injury (Table 2.13).

### 5.1.1. Functional and Structural Characteristics of Molecules

Nephrotoxics can be classified on the intrinsic structural or functional characteristics of the xenobiotic. As members of each class often act through similar mechanisms, the



**TABLE 2.13** List of the Basis for Classification of Nephrotoxics

---

Functional/structural characteristics of the xenobiotic
Morphologic presentation of lesions
Subtopographical location of target or injury
Mechanism of injury:
Direct perturbation of cell or subcellular organelle function
Perturbation of renal hemodynamics and/or GFR
Immune-mediated injury to glomeruli or interstitium
Direct effects on molecular targets and growth factors
Injury via metabolic activation
Injury related to renal transport functions
Perturbation of endogenous or nutritive substrate
Injury due to ischemia and tissue hypoxia
Exacerbation of spontaneous age-related chronic progressive nephropathy
Obstructive nephropathy

---

*Modified from Haschek WM, Rousseaux CG, Wallig MA, Bolon B, editors: Haschek and Rousseaux's handbook of toxicologic pathology, ed 3, 2013, Academic Press, Table 47.21, p. 1726, with permission.*

classification helps organize our comprehension of the exhaustive numbers of individual nephrotoxics. The xenobiotics or agents for which kidney injury occurs as a major toxic host response are listed in [Tables 2.14 and 2.15](#). Obscure chemicals or chemicals that cause functional perturbation without overt evidence of morphologic alteration are excluded. This listing emphasizes experimental and domestic animal nephrotoxics, although most agents induce comparable injury in all laboratory and higher species. Notable exceptions are addressed in subsequent sections.

### 5.1.2. Subtopographical Targets

Nephrotoxics can be categorized by their subtopographical or subcellular organelle target site ([Table 2.14](#)). Localization of subtopographical and subcellular organelle predilection is an integral step in investigative pathogenesis studies, requiring time-course sequence assessment with

light- and/or electron-microscopic evaluation. Identifying the target site for a xenobiotic does not necessarily identify the mechanism of injury, but it provides important clues based on physiologic aspects of the specific target cell or structure. Target site identification is a prerequisite in understanding functional impact, clinical relevance, and in choosing the most effective clinical monitoring strategy.

### 5.1.3. Mechanisms of Renal Injury

Mechanisms with which xenobiotics can elicit renal injury are summarized in [Table 2.13](#) and are further discussed below. Consideration of these potential mechanisms can help identify appropriate in vivo and in vitro tools and selection of relevant biomarkers in refining the risk assessment or in monitoring the progression of nephrotoxicity. In the following sections, well-characterized nephrotoxics will be discussed to exemplify specific mechanisms of injury in different segments of nephron.

## 5.2. Mechanisms of Glomerular Toxicity

### 5.2.1. Glomerular Podocyte Injury

Podocyte injury is an essential feature of progressive glomerular diseases, including direct damage by infectious agents such as human immunodeficiency virus (HIV) and drugs such as adriamycin (doxorubicin). In podocytopathies, many molecules/proteins are involved in the cross-talk between different glomerular cells during disease progression. Initial local podocyte damage can spread to induce injury in otherwise healthy podocytes and further affect both glomerular endothelial and mesangial cells, implying that even limited podocyte injury might initiate a vicious cycle of progressive glomerular damage. Injured podocytes may have foot process effacement and slit diaphragm alterations as an early manifestation of injury, and subsequently undergo detachment, apoptosis, and dedifferentiation.

A reclassification of podocyte diseases into four major types of podocytopathies including collapsing glomerulopathy (CG) was discussed in the previous section. CG is a proliferative



disease defined by segmental or global wrinkling of the GBMs associated with proliferation of podocytes and PECs, pseudocrescent formation, and sometime tubulointerstitial injury. Podocyte injury results in a dedifferentiated phenotype, reflected by the loss of expression of maturity markers and reexpression of proliferative markers, dysregulation of the phenotype reflected by loss of expression of WT-1, and transdifferentiation toward a macrophage-like phenotype. While there is genetic predisposition in some populations, especially African Americans, CG has been observed in immunocompromised states in association with HIV, autoimmune diseases, or following treatment with bisphosphonates, interferon-alpha, or valproic acid. Although the exact mechanism of CG is not known, disruption of mitochondrial functionality in general may represent a common pathophysiological mechanism (e.g., pamidronate). The mechanism of podocyte injury following HIV or other viral infections may be a direct cytopathic effect, with intracellular expression of viral genome or proteins, and/or indirect effect mediated by release of cytokines by inflammatory cells in the circulation or in the renal parenchyma. Other mechanisms include dysregulation of VEGF expression and acute ischemic processes, such as TMA after therapy with calcineurin inhibitors.

Adriamycin is a well-known inducer of renal injury in rodents, which mirrors that seen in human CKD due to primary FSGS. Adriamycin induces injury by direct toxic damage to the glomerulus with subsequent tubulointerstitial injury. Changes occur in the glomerular filtration barrier, including podocytes, glomerular endothelial cells, glycocalyx, and GBM. Changes are characterized by reduced thickness of glycocalyx, increased size of glomerular endothelial cell pores, reduced glomerular charge selectivity, and effaced podocyte foot processes. These changes are associated with reductions in glomerular cell production of proteoglycans and glycosaminoglycans contained within the glycocalyx.

The target site for puromycin aminonucleoside nephropathy has been critically examined with detailed sequential ultrastructural evaluation of glomeruli in a daily low-dose rat model. The earliest change occurs as effacement of podocytic foot processes by broad expanses of

epithelial cytoplasm, followed by proteinuria. With persistent proteinuria, puromycin induces FSGS characterized by podocytopenia, focal sclerosis of the tuft, and adhesions to Bowman's capsule. Bisphosphonates including pamidronate, alendronate, and zoledronate have been associated with nephrotoxicity, the spectrum of which includes collapsing and noncollapsing forms of FSGS, minimal change disease, and acute interstitial nephritis (AIN). Morphologically, there is an increased podocyte proliferation index and decreased expression of synaptopodin, suggesting a mechanism of direct podocyte toxicity. Mitochondrial perturbations in podocytes with pamidronate and iron overload with other bisphosphonates have also been reported.

Osborne-Mendel (OM) rats are obesity-prone when fed a high-fat diet. In addition to obesity, they demonstrate several metabolic abnormalities, including cardiac and renal hypertrophy, hyperglycemia, and hyperinsulinemia. Male OM rats develop age-dependent changes in podocytes characterized by cytoplasmic vacuolation and hyaline droplets, podocytopenia, effacement of foot processes, reduced numbers of filtration slits, and rearrangement of the actin cytoskeleton.

In nonclinical toxicity studies, monkeys may be especially susceptible to glomerular lesions similar to FSGS because of the presence of background subclinical infections and concomitantly administered immunomodulatory therapeutic agents (Figure 2.17). Loss of podocytes (viable and apoptotic cells) in the urine precedes proteinuria; thus, podocyturia can serve as the first noninvasive marker of active glomerular damage. In addition to light-microscopic and ultrastructural evaluations, immunohistochemical methods can be used to characterize podocyte toxicity including markers of podocyte plasma membrane proteins (podocalyxin, glomerular epithelial protein-1, GLEPP-1), slit-diaphragm-associated protein (nephrin), cytoskeleton-associated pedicel protein (synaptopodin), protein synthesized by podocytes (VEGF), PEC markers (paired box gene 2, PAX2), transcription factors (Wilms tumor protein-1, WT-1) and cytoskeleton intermediate filaments. In FSGS, a progressive loss of podocyte markers

**TABLE 2.14** Nephrotoxicity Classification Based on the Functional Characteristics of the Specific Potentially Injurious Agent

Functional characteristics of the inducing xenobiotic	Specific potentially injurious agent
Hemodynamic and prerenal factors	Angiotensin-converting enzyme inhibitors, hypertension, hydropenia
Inotropic and vasodilator cardiotonics	Digoxin, isoproterenol, ischemia, shock
Proteins and amino acids	Albumin, alpha <sub>2</sub> μ-globulin, Bence-Jones, D-serine, dietary protein, hemoglobin, lysinoalanine, lysozyme, maleic acid, myoglobin, rapeseed
Naturally occurring organic toxins	Aflatoxin, aristolochic acids, bacterial toxins, broom weed, Chinese tallow tree, citrinin, furan derivatives, greasewood, halogeton, <i>Lantana camara</i> , monocrotaline, mushroom, pigweed ( <i>Amaranthus retroflexus</i> ), rhubarb
Synthetic biological toxicants	Fumigants/nematocides, 1,2-dibromomethane, 1,2-dibromethane-3-chloropropane, n-succinimide
Germicides	O-Benzyl-p-chlorophenol
Herbicides	Bipyridium compounds
Insecticides	Chlorinated hydrocarbons, hexachlorocyclohexane, organophosphorous compounds, toxaphene
Normal endogenous substrates	ACTH, bilirubin, calcium, fluoride, glucose, iron, magnesium, phosphate, potassium, sodium, serotonin, vesicourethral reflux, vitamin D <sub>2</sub> , zinc
Physical agents	Electrical shock, heat stroke, radiation
Metals	Aluminum, antimony, arsenic, beryllium, bismuth, cadmium, copper, gold, lead, lithium, mercuric chloride, nickel, rubidium, trimethyltin, uranium
Glycols	Diethylene glycol, diethylene glycol monoethyl, ethylene dichloride, ethylene glycol, ethylene glycol dinitrite, propylene glycol
Industrial chemicals involved in plastics and resins manufacture	Acrylonitrile, hexachloro-1, 3-butadiene, organonitriles
Chelators	Diphosphonates (Cl <sub>2</sub> MDP, EHDP), bisphosphonates, ethylenediamine tetraacetic acid (EDTA), nitrilotriacetic acid (NTA)
Anesthetics and anticonvulsants	Halothane, methoxyflurane
Antibiotics/antifungals/antimalarials	Amikacin, ampicillin, amphotericin B, bacitracin, beta-lactam compounds, cephaloridine, chloroquine, colistin, gentamicin, kanamycin, methicillin, neomycin, netilmicin, polymixins, streptomycin, sulfonamides, tobramycin, vancomycin
Immunomodulatory agents	Adalimumab, basiliximab, calcineurin inhibitors (cyclosporin, tacrolimus), cyclophosphamide, dactinomycin, daclizumab, etanercept, infliximab, methotrexate, sirolimus

(Continued)

**TABLE 2.14** Nephrotoxicity Classification Based on the Functional Characteristics of the Specific Potentially Injurious Agent—cont'd

Functional characteristics of the inducing xenobiotic	Specific potentially injurious agent
Osmotic agents and diuretics	Carbonic anhydrase inhibitors, dextran, ethacrynic acid, furosemide, mannitol, sucrose, thiazides, torasemide
Organic solvents	Carbon tetrachloride, chloroform, halogenated aliphatics, toluene, trichlorethylene, trihalomethanes
Cancer therapeutics	Alemtuzumab, adriamycin, bevacizumab, capecitabine, cetuximab, cisplatin, crizotinib, dasatinib, gemtuzumab, imatinib, interferon alfa, isotretinoin, lapatinib, letrozole, melphalan, ofatumumab, paclitaxel, puromycin mononucleoside, rituximab, sorafenib, streptozotocin, sunitinib, tamoxifen, trastuzumab, vincristine
Diagnostic agents	Diatrizoate iodide
Hyperuricacidemia therapeutics	Allopurinol
Male antifertility agents	$\alpha$ -Chlorohydrin
Nonsteroidal antiinflammatories	Acetaminophen, celecoxib, diclofenac, diflunisol, ibuprofen, indomethacin, ketoprofen, meloxicam, nabumetone, naproxen, oxaprozin, paracetamol, paracoxib, peroxicam, phenacetin, rofecoxib, salicylates, sulindac, valdecoxib
Miscellaneous agents	Melamine, raisins, grapes, interferon, IV $\gamma$ -globulin, acyclovir, cimetidine, foscarnet, probenecid, captopril, clofibrate, propranolol, isoniazid, methyl dopa, azathioprine, ACTH, bilirubin, calcium, fluoride, glucose, iron, lithium, magnesium, phosphate, potassium, sodium, serotonin, zinc

Modified from Haschek WM, Rousseaux CG, Wallig MA, editors: *Handbook of toxicologic pathology*, ed 2, 2002, Academic Press, Table IV, p. 279, with permission.

(synaptopodin, podocalyxin, GLEPP-1, and VEGF) is noted, while PAX2 and cytokeratin in PECs may exhibit an increase in staining intensity. WT-1 staining is shown to be variable, but usually parallels PAX2 staining in PECs.

### 5.2.2. Glomerular Endothelial Cell Injury

Glomerular endothelial cells are a component of the normal glomerular permeability barrier, modulating adhesion and infiltration of circulating cells, and producing factors that regulate intraglomerular hemodynamics and hemostasis. The glomerular endothelial cell is both a target in injury and a contributor to perpetuation of injury. These cells closely interact with podocytes and mesangial cells, and are modulated by key angiogenic factors derived from these cells. Therefore, indirect glomerular endothelial injury

is observed when podocytes are severely injured, resulting in loss of key angiogenic factors necessary for maintenance of endothelial cell survival and function. Endothelial cells respond to injury by elaboration of increased prothrombotic substances, including plasminogen activator inhibitor-1 (PAI-1). Markers of endothelial dysfunction include elevated serum levels of von Willebrand factor (vWF). Specific disease states where glomerular endothelial cell injury directly or indirectly contributes to disease pathogenesis include hemolytic uremic syndrome (HUS), DN, obesity, transplant glomerulopathy, and immune complex/crescentic glomerulonephritis.

Mesangiolytic, capillary endothelial cell loss, capillary fibrin deposits, and glomerular capillary cysts (aneurysms) occur as acute phase



**TABLE 2.15** Nephrotoxicant Classification Based on Subtopographical Site of Injury or the Functional Effect Causing Injury in the Kidney

Target/functional activity	Associated nephrotoxics or inducing agent
<b>GLOMERULUS</b>	
Direct effects on podocytes	Puromycin, bisphosphonates, interferon- $\alpha$ , valproic acid
Direct effect on glomerular endothelium	VEGF and VEGF-R inhibitors
Oxidative activation	Adriamycin
Increased GFR	Hypertension, aldosterone, high-protein diet
Decreased GFR (via efferent arteriole constriction)	Cyclosporin, tacrolimus, amphotericin B, radiocontrast media, NSAIDs
Decreased GFR (via systemic effects)	ACE inhibitors, inotropic and vasodilator cardiotonics
Proximal convoluted tubule	
Sodium pump-linked transport	Phosphate, lithium
Endocytosis, pinocytosis, protein-linked uptake	Aminoglycosides, $\alpha_2$ m globulin, Bence-Jones protein, hemoglobin, myoglobin, lead, cadmium, bismuth, sucrose, manitol, nitrilotriacetic acid
Obstructive nephropathy	Folic acid, ethylene glycol, glycolic acid, oxalic acid, methotrexate, sulfonamides, peptide mimetics (e.g., integrins receptor antagonists)
<b>PARS RECTA</b>	
Oxidative stress	Chloroform, acetaminophen, acetamide, paracetamol, p-aminophenol, 1,1-dichloroethylene, bromobenzene, epichlorhydrin, 1,2-dichloropropane, n-succinimide
Activation by glutathione system	1,2-Dibromomethane, trisphosphate, 1,2-dibromo-3-chloropropane, 1,2-dichloroethane
B-lyase-mediated bioactivation	Trichlorethylene, hexachlorobutadiene, trichloroethane, tetrachloroethane, chlorinated and fluorinated olefins
Organic acid transport (with metabolism to reactive intermediate)	Carbapenems, cephalosporin, citrinin, procainamide, methotrexate
Organic base transport (with oxidative activation)	Cisplatin
Cell respiration	Mercury salts, ischemia/hypoxia reperfusion injury
Distal nephron	Fluoride, methoxyflurane, 5-azacytidine, furosemide (thick ascending tubule), thiazide-like diuretics (distal convoluted tubule), amiloride (cortical collecting ducts)
<b>RENAL PAPILLA</b>	
Interstitial concentration via countercurrent exchanger and oxidative activation via endoperoxide synthase	NSAIDs, phenacetin, 2-bromoethylamine, 5-nitrofurans

Modified from Haschek WM, Rousseaux CG, Wallig MA, editors: *Handbook of toxicologic pathology*, ed 2, 2002, Academic Press, Table I, p. 259, with permission.

responses to snake bites, croton oil, glomerular ischemia, hypertension, HUS, TMA, thrombotic thrombocytopenic purpura (TTP), transplant rejection, radiation, and immune-mediated glomerulonephritis (see [Figure 2.26](#) for examples). Mesangial cells generate their own ECM and together they constitute the central stalk of the glomerulus. In close partnership with endothelial cells and podocytes, they form the functional glomerular unit and are in continuity

with the extraglomerular mesangium and the JGA. Mesangial cell injury directly or indirectly contributes to a wide variety of glomerular diseases. Mesangioproliferative diseases are typically associated with mesangial Ig deposition and comprise primary diseases such as IgA nephropathy, mesangioproliferative glomerulonephritis, and systemic diseases such as lupus nephritis. Mesangial matrix expansion with diffuse or nodular glomerulosclerosis is

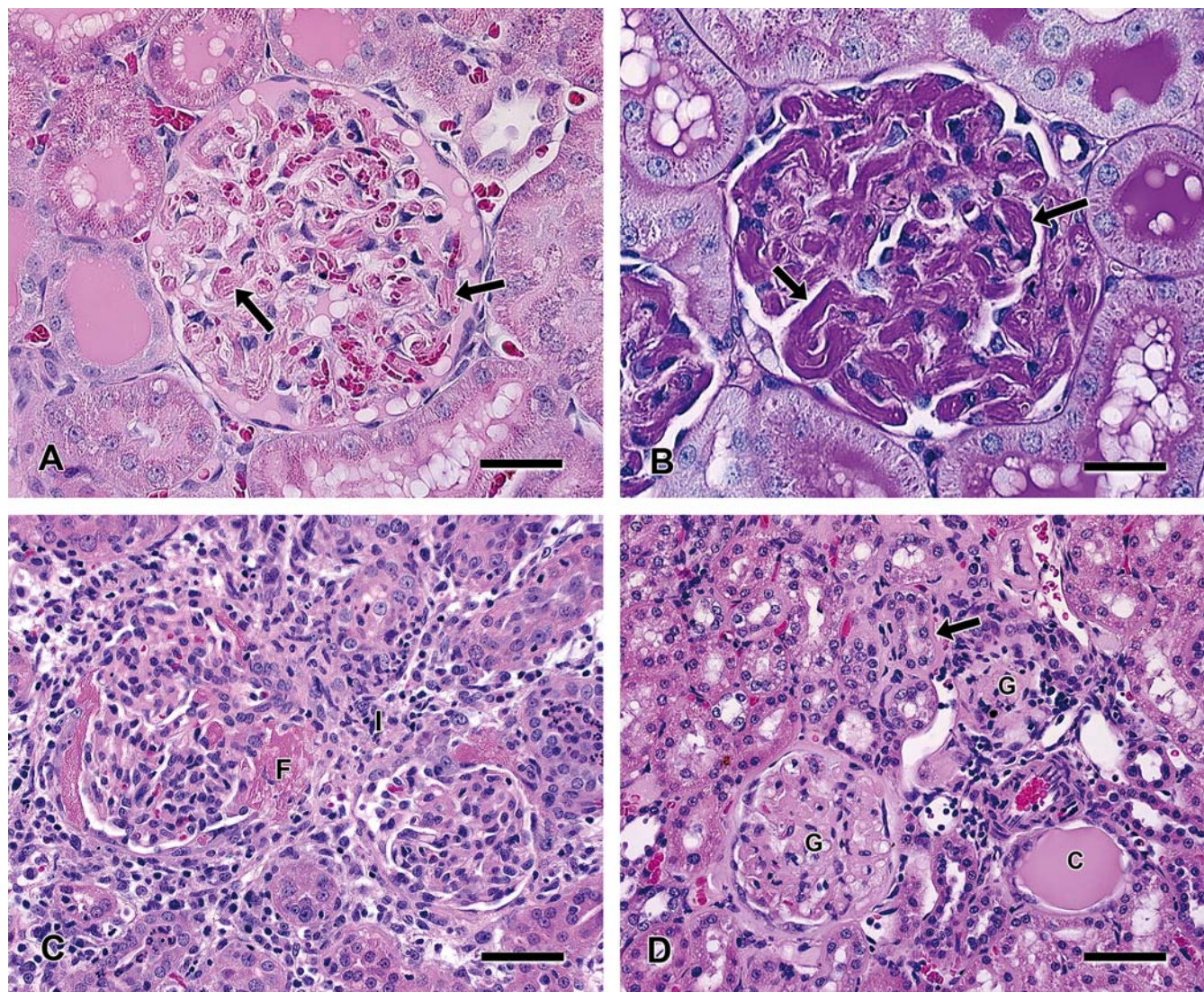


**FIGURE 2.26** Thrombotic glomerulopathy in a rat treated with a nanoparticle formulation illustrates fibrinous thrombi in the capillary loops (arrows) stained with H&E (A) and PAS (B), respectively. Bar = 30 mm. (C) Glomerulonephritis in a monkey treated with a protein therapeutic illustrates effacement of glomeruli by inflammatory cells and fibrin deposition. Bar = 55 mm. (D) Glomerulosclerosis in a young spontaneously hypertensive rat fed a high salt diet, which accelerated glomerular sclerosis (G) and nephropathy processes such as tubular regeneration (arrow) and casts (C). Bar = 60 mm. Courtesy of Dr Xiantang Li, Drug Safety R&D, Pfizer, Groton, CT; Reproduced from Haschek WM, Rousseaux CG, Wallig MA, Bolon B, editors: *Haschek and Rousseaux's handbook of toxicologic pathology*, ed 3, 2013, Academic Press, Figure 47.30, p. 1733, with permission.



a typical feature of DN. The induction of HUS by bevacizumab, an antibody against VEGF, in the treatment of patients with cancer is associated with proteinuria, mesangiolysis, glomerular endothelial damage, and basement membrane duplication. Mesangiolysis occurs following an acute insult such as with toxins (e.g., Habu snake venom) or directly through destruction of mesangial cells by antibodies directed against a mesangial antigen (Thy 1.1. in rats). The resultant pathology is characterized by mesangiolysis and severe capillary aneurysmal dilation, similar to the congenital defects observed in knockouts for endothelial PDGF-B or mesangial PDGFR- $\beta$ .

Hemolytic uremia syndrome represents a serious complication of bacterial endotoxemia. The increased susceptibility of children with diarrhea-positive HUS has been proposed to be due to increased glomerular expression of globotriaosylceramide (Gb3). This receptor binds shiga toxin and is preferentially expressed on glomerular endothelium. Hemolytic uremia can be produced in the rabbit by injection of *Shigella* endotoxin and prevented by pretreatment with busulfan (causing leukopenia). Hemolytic uremia is characterized by leukocyte-mediated intravascular fibrin deposition in, and occlusion of, glomerular capillaries with resultant renal cortical necrosis (generalized Schwartzman reaction model). Medications such as cyclosporin, mitomycin-C, and estrogen-containing contraceptives have been associated as risk factors for hemolytic uremia in humans.

Direct injury to the glomerular endothelium is observed in immune complex disease with subendothelial deposits where activation of complement and membrane attack complex occurs in the subendothelial space. TNF- $\alpha$  is increased in a variety of inflammatory conditions and causes increases in endothelial cell adhesion molecule expression and expression of IL-6. TNF- $\alpha$  disrupts the glycocalyx and also directly increases endothelial permeability.

Reflux nephropathy arising as mesangial injury occurs in humans with vesicoureteral reflux. The mechanism of injury is not well defined but does not require infection. Early factors include expansion of mesangial matrix, possibly because of tubular secretory antigenic proteins, normally restricted to uriniferous space, reaching the mesangial matrix or interstitial space because of back pressure, with subsequent immune-

mediated tissue injury. Laboratory rats can have reflux upon micturition, evident by retrograde flow of dye placed in the urinary bladder under physiologic pressure. The pathologic consequence of reflux is not defined in the rat. Retrograde nephropathy characterized by tubular dilation extending from the papilla to the cortex has been reported in rats treated with melamine. This is thought to be due to melamine precipitation in the lower urinary tract creating pressure effects through transient obstruction. Histologically, distal nephron injury was characterized by tubular dilation, epithelial tubular degeneration and necrosis, and intratubular crystal deposition. Dilated nephrons extended proximally from the medulla in a radial pattern involving clusters of adjacent nephrons. Unique striated, gold to brown crystals were present in distal tubules and collecting ducts (Figure 2.24). Crystals dissolve over time in neutral buffered formalin. Inflammation, fibrosis, and, sometimes, granulomatous lesions may be present. These renal changes are similar to human reflux nephropathy of early childhood when urinary tract infection is superimposed on congenital vesiculoureteral reflux. Microscopic changes of human reflux nephropathy primarily involve the tubules and interstitium and are characterized by tubular atrophy and dilation, and corticomedullary scarring.

### **5.2.3. Changes in Polyanionic Binding Sites in the Glomerular Filtration Barrier**

Protamine (a) heparin antagonist induces charge reduction in the glomerular filtration barrier followed by functional evidence of injury, manifested as proteinuria. Fixed polyanionic binding sites in the filtration barrier serve to retain anionic plasma proteins such as albumin in the circulation. Otherwise nontoxic doses of circulating polycationic agents such as protamine cause protein leakage, which secondarily induces morphologic lesions. Podocyte injury in this model is a consequence of albuminuric or protein overload.

### **5.2.4. Interference in Formation of Crosslinks in Glomerular Basement Membrane Collagen**

D-penicillamine affects GBM directly in rats, possibly by interfering with collagen crosslink formation. Adverse effects of the drug, which



is used in the treatment of rheumatoid arthritis, include development of membranous glomerulonephritis as an apparent consequence of defective basement membrane synthesis.

#### **5.2.5. Perturbation of Renal Hemodynamics**

Persistent elevation of glomerular capillary flow causes glomerular injury, characterized by mesangial expansion and proteinuria, progressing to FSGS. Two interrelated but potentially independently acting hemodynamic functional alterations causing injury include increase in single nephron glomerular filtration rate (SNGFR) and increase in glomerular capillary hydraulic pressure (GCHP). Increased SNGFR and GCHP can be induced by deoxycorticosterone injection and by saline as the drinking water source, which is a model for inducing hypertension. Prednisone treatment in humans for 2 weeks is associated with increased GFR. Methylprednisolone in dogs results in increased GFR and RPF and decreased filtration fraction. It is also associated with reduced RVR after short-term exposures and increased RVR after long-term exposures in dogs. The morphologic changes in kidneys following subchronic and chronic administration of glucocorticoid agonists can therefore be attributed to alterations in local hemodynamics or effects on insulin metabolism. These could mimic early stages of DN. Dogs, following chronic glucocorticoid agonist treatment, show increased size of kidneys and individual glomeruli. Histologically, glomerular lesions may be composed of glomerulosclerosis, accumulation of eosinophilic material within Bowman's capsule, eosinophilic material within capillaries, glomerular synechia, parietal cell hyperplasia, and arteriolosclerosis. Renal lesions are less prominent in rats with glucocorticoid agonists and may include increased kidney weights, basophilic tubules, and tubule vacuolation. A decrease in dietary protein in the normal rat leads to decreased SNGFR and GCHP. Dietary protein plays an important role in the development and progression of kidney injury. An increase in dietary protein can cause an increase in kidney size and GFR, with subsequent glomerular injury, accumulation of mesangial deposits, and, eventually, glomerulosclerosis. Overnutrition in the laboratory rat is not only a modifying factor but also presumably a causal factor in the occurrence of spontaneous CPN (described in detail later). Reduction

in renal mass also results in an increase in SNGFR and GCHP in renal parenchyma as a compensatory response to maintain renal function. The increased SNGFR and GCHP can occur even with insufficient loss of renal mass for development of reduced GFR and acute renal failure, indicating that GFR values do not necessarily reflect SNGFR. Hormones such as glucagon and PGs are suspected as mediators of these intrarenal hemodynamic changes. Reduction in renal mass results in nephron injury morphologically similar to that associated with hypertension and protein overnutrition. Reduction of dietary protein significantly reduces the severity and rate of progression of disease in the remnant parenchyma. Reduced renal mass with individual nephron hyperfiltration, subsequent mesangial expansion, and sclerosis with further nephron loss thus represents the final common pathway to progressive renal failure regardless of the primary injury mechanism.

#### **5.2.6. Other Mechanisms of Glomerular Injury**

Reactive oxygen intermediates (ROIs) have been implicated in the pathogenesis of inflammatory, immune, and toxic insults in glomerular injury. ROIs mediate inactivation of NO and modify the metabolism of PGs. Diabetic hyperglycemia is associated with glomerular and mesangial basement membrane thickening, characteristics of diabetic glomerulopathy. Glycosylation of basement membrane protein proportional to the level of glucose in the local environment has been hypothesized as a mechanism of the basement membrane injury. Xenobiotics perturbing glucose levels could thus potentially act through this mechanism.

Renal injury caused by ionizing radiation is increasing in incidence paralleling the increased frequency of bone marrow transplants following whole body irradiation (see *Radiation and Physical Agents*, Vol 3, Chap 14). Two forms of injury are recognized: an acute form noticed within 1 year of irradiation and manifested as hypertension, edema, and anemia; and a chronic form that occurs more insidiously with diminished GFR, hypertension, and occasionally proteinuria. Interstitial fibrosis is the common pathologic finding in patients with chronic radiation nephritis. Experimental studies indicate ultrastructural glomerular endothelial disruption as

an early event, with subsequent tubular degeneration and atrophy.

### 5.3. Mechanisms of Interstitial Injury

Connections to the basement membrane result in functional interactions between tubules and interstitium. As such, the tubulointerstitial region can be considered one compartment. Epithelial cell replacement in tubules is dependent on intimate communication with PDGF- $\beta$  receptor-positive interstitial cells (Schuessl et al., 2018). The RAAS plays a key role in crosstalk between TAL, afferent and efferent arterioles, and juxtaglomerular cells, resulting in tubuloglomerular feedback that maintains proper renal function. However, the interstitium can also have an effect on the nature of glomerular injury.

#### 5.3.1. Immune-Mediated Interstitial and Glomerular Injury (Biologic Induced Autoimmune Renal Disorders)

A number of drugs have been associated with immune-mediated renal injury in humans. As noted above in the section on glomerular mechanisms of injury, immune-mediated kidney injury accounts for many forms of primary glomerular disease in humans, whereas drug-associated immune-mediated tubulointerstitial injury represents an equally important form of renal disease. Drug-induced immune-mediated renal toxicity often is represented by florid interstitial inflammation with pyuria and/or white blood cell casts, hematuria, and proteinuria. This response, usually defined clinically as AIN, has been associated with a variety of drugs, including penicillin, methicillin, ampicillin, rifampin, sulfonamides, thiazides, cimetidine, phenytoin, allopurinol, cephalosporins, cytosine arabinoside, furosemide, interferon, ciprofloxacin, clarithromycin, telithromycin, pantoprazole, omeprazole, and atazanavir. The process most commonly producing this pattern of renal injury in humans is hypersensitivity to drugs such as NSAIDs and PPIs. In fact, considering an exhaustive list of drugs identified as injurious to human kidneys, interstitial nephritis is the most common presentation or mechanism. The condition typically has a delayed onset and is not dose-responsive. Proinflammatory biologic anticancer drugs which activate the immune system have resulted in lesions in

rodents compatible with interstitial nephritis. Florid inflammatory lesions also sometimes occur in the renal interstitium of mice and monkeys with administration of some ASO therapies, but the lesions tend to be centered around vessels and distinct from interstitial nephritis cases in other species (Engelhardt et al., 2015). Mercurials and drugs with a sulfhydryl group, such as gold salts, penicillamine, and captopril, are associated with membranous glomerulopathy. NSAIDs and lithium are responsible for the nephrotic syndrome with minimal glomerular change considered a T cell-mediated disease, but a large number of drugs have been implicated in immunologically mediated AIN without nephrotic syndrome. Drug-associated immune-mediated kidney injury in humans depends on host factor variability for expression, as well as interaction with preexisting disease. The etiopathogenesis can vary depending on the specific agent but involves deposition of systemically circulating immune complexes or immune complexes formed in situ. Surprisingly, interstitial nephritis is much less common in animal toxicity studies, with the exception of biologic therapeutic administration (especially humanized antibodies) in rodents and monkeys.

#### 5.3.2. Antidrug Antibodies in Animals and Human Patients

ADAs resulting from immune reactions to foreign proteins result in perivascular and intravascular inflammation in the kidneys and other organs, especially in monkeys given biologic therapy. Different Ig classes have varying capacities for activating classical or alternative complement pathways which can affect immune complex deposition within renal vessels or interstitium. Large immune complexes directly activate the classical complement pathway resulting in the attachment of C3b to the Fc region of antibody within the complex. This mediates binding to the complement receptor 1 (CR1) on erythrocytes. If erythrocyte CR1 clearance mechanisms are saturated, clearance can occur through macrophage phagocytosis via binding to platelet Fc $\gamma$ RII, but when FcR- or complement-mediated clearance is further saturated, large complexes may deposit in tissues and capillaries (Frazier and Obert, 2018). In monkeys with ADA-related immunogenicity, one third of cases involve glomerular lesions,

one third involve only vascular or perivascular lesions in organs, and one third include both glomerular and organ vascular lesions (Frazier and Obert, 2018). Immunohistochemical demonstration of granular or linear deposits within the vascular walls at branch points, using immunolabeled antibodies directed against endogenous IgG, IgM, or drug are characteristic for the condition, as is immunofluorescent staining of glomeruli for complement (Rojko et al., 2014). The presence of high ADA titers provides further confirmation, particularly if high titers correspond with a reduction in drug plasma exposure. Nonclinical ADA-related renal injury generally does not correlate with any injury to humans as immunogenicity is not clinically predictive, and ADA-related immune complex formation in the kidneys of monkeys is therefore not a translatable toxicity, except in rare instances. Not all of the cases in animal toxicity studies are a result of ADAs, as the more proinflammatory molecules can cause this reaction exclusive of ADA. For instance, immune checkpoint inhibitor anticancer agents that target PD-1 or CTL-4, or those that stimulate STING pathways have resulted in lesions indistinguishable from interstitial nephritis, and drugs that strongly induce TNF $\alpha$  can produce a similar reaction in rodents when administered. Other cases which may also be exclusive of ADA include the presence of precipitated or aggregated drug material in tissues and in situ complexing of a biotherapeutic. Nonendogenous IgG aggregates can simulate immune complexes causing local hypersensitivity reactions. Aggregates can form during drug production, formulation, or repackaging that can further enhance complex number and size during later manufacturing processes (Leach et al., 2014). For instance, a CCL20 biotherapeutic resulted in intravascular aggregates, with a clear dose response and high incidence of vascular inflammation but with a low incidence of ADA (Laffan et al., 2020). The drug complexes, which spontaneously formed in situ, fixed complement and were considered to have potentially greater clinical significance resulting in termination of the program. In cases of immunomodulating drugs, the lack of ADA and pronounced cytokine stimulation profiles in affected animals have provided clues of innate immune activation as a mechanism and are also indicative of potential

clinical translatability of the toxicity (Frazier et al., 2015). In contrast, ASOs of certain backbones have been especially proinflammatory and have resulted in large inflammatory nodules in the kidneys and other organs of both rodents and monkeys. This has been shown to be related to specific activation of the alternative complement cascade in monkeys, and to species sensitivity of pattern recognition receptors in mice, and to have little clinical relevance to man in either case (Engelhardt et al., 2015).

Immune-mediated reactions do occur in the kidneys of human patients given biotherapeutic drugs (see *Protein Therapeutics*, Vol 2, Chap 6), but these reactions are not predicted by animal studies because, as a rule, different pathogenic factors are involved. As recombinant peptides, antibodies and multimeric complex biologics have been given to larger and larger numbers of patients, specific kidney conditions, termed “biologics-induced autoimmune renal disorders” (BAIRD) have been recognized with greater frequency (Piga et al., 2014; Frazier, 2021). BAIRD cases are classified in humans as: glomerulonephritis associated with systemic vasculitis; glomerulonephritis in lupus-like syndrome; or as isolated autoimmune renal disorders (Piga et al., 2014). Biologic therapies that target common proinflammatory signaling pathways (especially TNF $\alpha$ ) such as Etanercept, Adalimumab, Infliximab, Tocilizumab, and Abatacept have had a greater tendency to form immune reactions than more recent humanized antibody therapies which target ever more selective immune pathways. This suggests that proinflammatory immunomodulation in human patients is equally important in pathogenesis as compared to immunogenicity of the protein, but this varies with the agent. Infliximab is considered especially immunogenic with high ADA titers in patients. Other biologics like rituximab may have both immunogenic and immunomodulatory pathogenic factors that result in BAIRD (Frazier, 2022).

### **5.3.3. Antisense Oligonucleotide Nephropathy and Glomerulonephritis**

ASO-based therapeutics are designed to bind to RNA through Watson–Crick hybridization (see *Nucleic Acid Pharmaceutical Agents*, Vol 2, Chap 7). The kidney is frequently a target organ because of their preferential accumulation within



PCTs in rodents and monkeys after being filtered through the glomerulus. ASO accumulation is visualized easily in tissue sections as basophilic granules, but the tinctorial qualities of the granules varies substantially between species and with the specific ASO (Figure 2.27). Ultrastructural evaluations demonstrate the presence of granular material generally contained within vesicles or vacuoles. At high doses in animals, degeneration characterized by cellular swelling and cytoplasmic vacuolation may occur, but this does not appear to be a problem in humans taking the drugs, and changes do not affect clinicopathologic parameters (Frazier, 2015; Frazier and Obert, 2018). As noted above, some classes of ASOs with specific 2-O-methyl and less frequently 2-O-methoxyethyl phosphorothioate structure have innate proinflammatory potential that is related to both their backbone and their base sequence. This can result in inflammatory infiltrates in multiple organs including kidney. The mechanism is different in monkeys and mice. In monkeys, the specific pathophysiologic

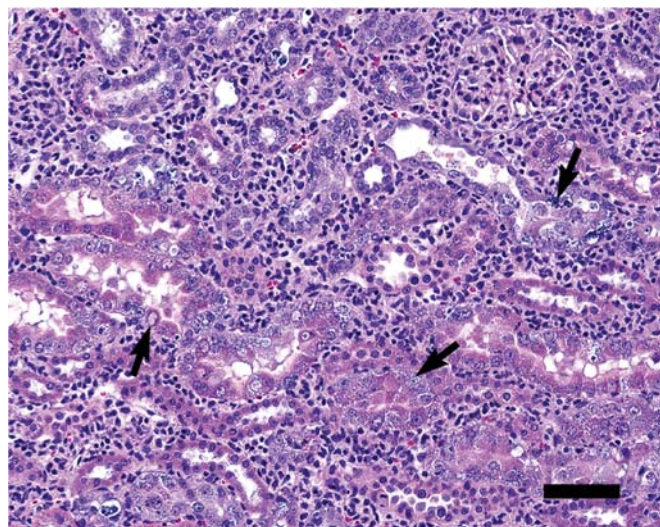


**FIGURE 2.27** Antisense oligonucleotide nephropathy in a rat kidney; note accumulation of basophilic material (arrows) within tubular epithelial cells, intranuclear accumulation of eosinophilic homogeneous material within proximal tubular epithelial cells, and interstitial infiltration of predominantly mononuclear cells. Bar = 50  $\mu$ m. Courtesy of Dr Xiantang Li, Drug Safety R&D, Pfizer, Groton, CT; Reproduced from Haschek WM, Rousseaux CG, Wallig MA, Bolon B, editors: *Haschek and Rousseaux's handbook of toxicologic pathology*, ed 3, 2013, Academic Press, Figure 47.32, p. 1741, with permission.

mechanism of the inflammatory response is related to inhibition of negative regulators of the alternative pathway of the complement cascade, including factor H, by many ASOs. This is of limited clinical relevance since human complement activation occurs at much higher doses than in monkey (Engelhardt et al., 2015; Frazier, 2015). In mice, activation of the innate immune system and local cytokines through toll-like receptors as well as other pattern recognition receptor cascades such as the RIG-like receptors occurs (Frazier and Obert, 2018). The mouse appears to be particularly hypersensitive as compared to humans. Some other ASOs (a few specific examples of locked nucleic acids (LNAs), silencing RNAs (siRNAs), and rarely phosphorothioate ASOs) have been associated with overt tubule nephrotoxicity, and this is unrelated to proximal tubule accumulation. The mechanism appears to be associated with aptameric binding to kidney epithelial proteins. Evidence indicates liver toxicity with ASOs is associated with binding to paraspeckle proteins in nucleoli, and therefore it is suspected that the same aptameric pair may be responsible for these cases of severe tubule nephrotoxicity by the same mechanism. Proteinuria has occurred both preclinically and clinically with many ASO therapies, but appears to be transient, rapidly reversible and due to competitive binding interactions with the megalin/cubilin transporter resulting in increased filtrate concentration and urine excretion. Glomerulonephritis has been noted in both mice and monkeys with the more proinflammatory 2-methoxyethyl and especially 2-O-methyl phosphorothioate ASOs, particularly at high doses. The pathogenesis and morphology again differ markedly between species, and there does not appear to necessarily be a connection between these findings and clinical risk. Glomerular alterations in mice are distinctly fibrillary with immune fragment deposition (hyaline glomerulopathy) and amyloidosis. In contrast, MPGN with immune complexes centered on basement membranes is the predominant morphologic pattern in monkeys (Frazier and Obert, 2018). Although much less common than the incidence of perivascular inflammation, the mechanism of glomerular injury in each species is similar to that already described, involving complement activation in monkey and pattern recognition receptor activation in mice. However,

a more serious renal complication of ASO therapy has been noted in very rare human patients given a few specific ASO compounds, involving rapidly progressive glomerulonephritis of immune-mediated etiology. The pathogenesis and predisposing factors are poorly understood, but preexisting renal pathology may be a factor (Frazier and Obert, 2018). Unfortunately, neither mice nor monkeys have been predictive for this serious clinical toxicity, so frequent monitoring of urine protein is standard practice in clinical trials for many of these agents. ASOs conjugated to a trivalent *N*-acetylgalactosamine (GalNAc) ligand are being evaluated in investigational clinical studies for a variety of indications. These preferentially bind to the asialoglycoprotein receptor in the liver for selective hepatic uptake. As such their nephrotoxic potential has been dramatically diminished and their clinical safety profile improved.

#### **5.3.4. Renal Safety of Other Novel or Alternative Therapies**

In addition to ASO therapies such as the phosphorothioate class, there has been a resurgence of interest in RNA interference therapies in the last decade. Rather than relying on mRNA degradation through RNase H activity, these 20–25-nucleotide-long duplexes load into the RNA-induced silencing complex (RISC), which result in destabilization and cleavage of selective mRNAs. While unbound or unconjugated siRNAs are rapidly cleared through the urine and can result in significant renal tubule accumulation in a manner similar to ASOs, siRNA therapies with chemical modifications have been conjugated to lipid nanoparticles (LNPs) to prolong their half-life and vastly increase their target potency. This has reduced their potential nephrotoxicity, but accumulation in the kidney still occurs resulting in basophilic granule accumulation and vacuolation or degeneration at high doses. LNPs are rapidly transported into various cellular compartments via scavenger receptors, particularly phagocytic cells such as macrophages. Hence, macrophage accumulation has been reported for LNP-conjugated siRNAs in many tissues, including kidney interstitium. This should not be confused with inflammation and is considered an expected and nonadverse finding. Many of the recent siRNA candidates, including the marketed patisiran, involve GalNAc-

conjugated siRNAs that (like ASO-GalNAc) demonstrate improved safety profiles with no apparent nephrotoxicity.

Silver nanoparticles (AgNPs) are utilized in a variety of cosmetic, textile, and healthcare (antibiotic) applications (see *Nanoparticulates*, Vol 3, Chap 13). AgNPs induce a dose-, size-, and time-dependent cytotoxicity, particularly for particles with sizes  $\leq 10$  nm and accumulate in rodent organs following intravenous, intraperitoneal, and intratracheal routes of administration including liver, kidney, lung, and brain. AgNPs have the potential to interact with proteins, lipids, and DNA through effects on cellular respiratory enzymes and generating ROS that induce oxidative stress and subcellular damage. AgNPs can also release silver ions, potentially inducing cell damage by interacting with thiol groups. Although less sensitive than liver, lung, or spleen, the kidney can undergo necrosis and degeneration of proximal tubules and degenerative changes in the glomerulus in rodent toxicity studies. Hemolysis, a frequent complication of AgNPs can also further damage the proximal and distal tubules. Silver ion accumulation can be demonstrated in the renal tubules under these circumstances. Kidney-excretable nanoparticles have also been produced as a diagnostic entity for renal disease, as part of the new field of nanomedicine as an imaging aid for X-ray, MRI, and other modalities. Nanoparticle glomerular filtration is regulated by size, with filtration generally limited to  $<5$ – $6$  nm. Long or tubular structures such as carbon filament nanofibers can pass lengthwise through the glomerulus, but negative charged molecules will pass with greater difficulty than those positively charged. In trials for some of these imaging applications, nonclinical renal tubule toxicity similar to that noted with AgNPs has been noted. As the field develops, nephrotoxicity is expected to be diminished.

Chimeric antigen receptor T-cell (CAR-T) therapies using engineered cytotoxic T cells target cancers such as lymphoma, and are represented by drugs such as axicabtagene, ciloleucel, and tisagenlecleucel. CARs are genetically engineered surface receptors consisting of an extracellular antigen-binding domain recognizing specific tumor antigens and intracellular T-cell signaling domains incorporated on autologous T cells Frazier (2022). The most common adverse

reaction is cytokine release syndrome (CRS), but there is also a risk for AKI with this class. Incidence of AKI has been reported as high as 30% after 100 days, but in general cases are mild and most patients recover. Decreased kidney perfusion and ATN have also been reported with CAR-T.

#### **5.4. Mechanisms of Proximal Tubular Injury**

Proximal tubular toxicants frequently affect both convoluted and straight segments, although these segments may be differentially affected. The unique portal circulation plays a role in proximal tubule susceptibility to nephrotoxics. There is a marked cortical medullary gradient with relative hypoxia in the outer medulla. This is related to the lower medullary blood flow, the countercurrent exchange of oxygen, and the high metabolic requirements of the TAL and pars recta. Blood flow to the outer stripe is via postglomerular capillary venous efferent vessels. The number of mitochondria is significantly lower in the S3 segment compared to that in the S1 and S2 segments. The outer stripe is hence the most sensitive in the rat kidney to hypoxia and is a site for synergism between toxicity and hypoperfusion. Such synergism also occurs clinically, as the majority of cases of human drug-induced nephrotoxicity occur in the presence of compromised renal perfusion. The proximal tubule, and specifically the S3 segments of the pars recta at or near the corticomedullary junction, will therefore be a primary site of toxicity for agents affecting RBF, cellular ATP, or mitochondrial function. As has been noted previously, proximal tubules are also susceptible to injury because of their preferential xenobiotic transporter activity, and because they contain the largest amount of metabolic capability within the kidney, including CYP450 and beta-lyase activity. Thus, the S3 PCT segments are especially prone to injury when metabolic activation results in toxic or reactive intermediates.

##### **5.4.1. Direct Perturbation of Cell or Subcellular Organelle Function**

Nephrotoxicity due to direct perturbation of cellular or subcellular organelle function occurs

most commonly in the highly metabolically active proximal tubules and less so in the distal tubules and collecting ducts. The injury can be related to accumulation of xenobiotics or their metabolites in subcellular organelles (e.g., aminoglycoside antibiotic lysosomal overload). Heavy metals usually accumulate in the kidney, liver, bone, and brain (see *Metals*, Vol 3, Chap 10). The injury in the kidney typically involves the pars recta. Common examples of heavy metals resulting in direct cellular toxicity in the kidney include cadmium, mercury, manganese, and lead. Specific examples and their precise etiopathogenesis of injury are described below.

##### **5.4.2. Antibiotic Nephrotoxicity**

As a paradigm of drug-induced renal tubule injury, administration of the major classes of antibiotics are commonly a source of nephrotoxicity. The frequency of occurrence of antibiotic-induced nephrotoxicity varies greatly and depends upon the class of antibiotic, the properties of particular derivatives within one antibiotic class, and the physiological status of the patient. Several anatomically and functionally distinct kidney sites are susceptible targets for the adverse effects of antibiotics, and antibiotic-induced nephrotoxicity may be indirectly or directly mediated ([Seale and Rennert, 1982](#)). With the possible exception of the loop of Henle, each region of the nephron can be damaged by one or more antibiotic classes. The proximal tubule, site of the quantitatively most significant resorptive functions, is particularly vulnerable. Different manifestations of antimicrobial-induced nephrotoxicity include ATN, AIN, and obstructive nephropathy. Antimicrobials known to elicit AKI and ATN in a dose-dependent manner include aminoglycosides, cephalosporins, bacitracin, and vancomycin ([Morales-Alvarez, 2020](#)).

##### **5.4.3. Aminoglycoside Toxicity**

Aminoglycoside-induced kidney injury occurs when the drug accumulates within the proximal tubule epithelial cells of the renal cortex, leading to direct cytotoxicity. This class of antibiotics includes gentamicin, amikacin, kanamycin, streptomycin, and tobramycin, among others, and all share some nephrotoxic potential. The toxicity of aminoglycosides is related to their concentrative uptake by proximal tubular cells



and their capacity to interact with critical intracellular targets. Concentrative uptake is mediated by adsorptive endocytosis across the apical membrane followed by sequestration within lysosomes. The fundamental mechanism underlying the toxicity of these organic polycations is their capacity to interact electrostatically with and disrupt the metabolism of anionic phospholipids, especially the phosphoinositides. Polyaspartic acid, a polyanionic peptide, protects against aminoglycoside nephrotoxicity by forming electrostatic complexes with these drugs and inhibiting their interaction with critical intracellular targets. The aminoglycoside enters the cytosol and accumulates in organelles such as the mitochondria, Golgi complex, and the nucleus. This mechanism explains the disruption in protein synthesis and mitochondrial dysfunction observed in aminoglycoside nephrotoxicity (Nagai and Takano, 2004). Propensity for binding phospholipids, charge, and toxic potential are strongly correlated when comparing different aminoglycoside antibiotics. Gentamicin, as the prototypic and most studied drug in this class, has a LMW, binds only weakly to plasma proteins, and is freely cleared into the glomerular filtrate as the primary route of excretion. Within minutes of administration, specific, receptor-mediated binding of drug to the proximal tubule brush border can be demonstrated. A charge interaction exists between cationic sites on the gentamicin molecule and anionic sites on the brush border. After binding, gentamicin is taken into the cell by endocytosis, followed by fusion of the endocytic vesicles with phagosomes. Within the phagolysosome, gentamicin inhibits phospholipases and sphingomyelinase responsible for the degradation of phospholipid-rich cell membranes. Thus, the drug and phospholipid membranes are sequestered and accumulate in the phagolysosome, especially in S1 and S2 segments. This phenomenon is reflected ultrastructurally by the appearance of myeloid bodies occurring in all levels of the proximal tubule but with a predilection for the PCT. Calcium competes with gentamicin for binding sites; thus, calcium loading ameliorates gentamicin toxicity. Because of phagolysosomal sequestration, renal cortical half-life of gentamicin is 109 h. Gentamicin administered to rats at 1 mg/kg body weight daily induces

myeloid bodies, but no tubular necrosis by light microscopy. At 10 mg/kg/day, focal tubular necrosis and functional deficit occurs; at 40 mg/kg/day, tubular necrosis is widespread. Lysosomal overload of gentamicin and phospholipid membranes results in compromised lysosomal membrane integrity. Lysosomal enzyme leakage occurs as a consequence, and possibly explains cell necrosis as the overt manifestation of toxicity. Lesions are not limited to the proximal tubules, and other mechanisms of toxicity occur. Polyuria is frequently encountered with aminoglycoside nephrotoxicity and is considered to be due to the inhibition of chloride transport in the TAL. In addition, because of their polycationic nature, aminoglycosides such as gentamicin also interact with anionic sites on glomerular capillary endothelial cells, which can result in direct glomerular injury and functionally decrease GFR. GFR reduction is also likely the result of other mechanisms within the kidney, including tubular glomerular feedback, direct mesangial and vascular contraction, and indirect mesangial and vascular contraction produced by inflammation and paracrine mediators. There is also evidence for oxidative stress in gentamicin-induced tubular injury. Thus, gentamicin-induced nephrotoxicity involves multiple causes: (1) direct tubular cytotoxicity, (2) phospholipidosis, (3) glomerular injury, (4) vascular toxicity, and (5) induction of oxidative stress with the production of ROS in mitochondria. Gentamicin injury is followed within 7 days by replicative rate increase in proximal tubules. The chronic effect of gentamicin toxicity in the absence of overt tubular necrosis consists of increased incidence and severity of lesions of chronic CPN compared with controls. Females, including rats and humans, may be more severely affected than males at comparable tissue levels of the drug. Specific risk factors, such as volume depletion and comedications, predisposing to gentamicin injury have been identified clinically (Petejova et al., 2019).

#### 5.4.4. Cephalosporin

Cephalosporins and other unrelated  $\beta$ -lactam antibiotics cause proximal tubular necrosis in humans and laboratory animals. When assessing nephrotoxicity, the tubule transporter system,

which allows transport of the drug from the blood to the urine via the tubules, is particularly important, as noted in other sections of this chapter. Antibiotic-induced kidney damage is determined via the tubular reabsorption mechanism (aminoglycosides, amphotericin B, cisplatin) and via the tubular secretion mechanism (cephalosporins, vancomycin). Drug transport to the tubule epithelium is the first fundamental stage in the onset of the nephrotoxic process and transporters are involved in many antibiotic-mediated nephrotoxic mechanisms (Pazhayattil and Shirali, 2014). The selective toxicity of  $\beta$ -lactams (e.g., penicillins, cephalosporins, carbapenems, and monobactams) on renal proximal tubular cells is related to their uptake and high intracellular concentrations achieved by active transport through OAT1 and PEPT transporters. Cephaloridine, as a model cephalosporin, is metabolized in PCTs and at sufficiently high concentrations, induces lipid peroxidation-type injury to membranes. Evidence for oxidative stress as a mechanism of injury includes: (1) inhibition of injury by superoxide dismutase, by catalase, by the hydroxyl radical scavenger mannitol, and by the singlet oxygen scavenger histidine; (2) increase in malondialdehyde production in vitro; (3) superoxide anion generation in vitro; (4) glutathione depletion of renal cortex from treated animals; and (5) potentiation of injury by pretreatment with antioxidant-deficient diets (vitamin E and selenium). Importance of metabolism and generation of reactive intermediates is indicated by demonstration of covalent binding of renal cortex-homogenate microsomal fraction by cephalosporin in a quantity proportional to their toxic potential. Additionally, piperonyl butoxide, a well-known inhibitor of renal MFOs, reduces cephalosporin nephrotoxicity. Predictably, species-, strain-, sex-, and age-related differences in the toxic potential of cephalosporins occur as they do for other xenobiotics requiring metabolism for induction of injury. Species differences in transport have also been demonstrated as the explanation for differences in injury potential. Depressed mitochondrial respiration secondary to acylation of the mitochondrial transporter for succinate has been implicated in the pathogenesis of toxicity caused by other cephalosporins and carbapenems. Among possible

mechanisms of injury, transport into the tubular cell, acylation of target proteins, and lipid peroxidation are most commonly seen among the class (Morales-Alvarez, 2020). Many cephalosporins also result in hyaline droplet formation within proximal tubules based on drug-protein complexes that are visible with light microscopy in rodents and nonrodents.

#### **5.4.5. Nephrotoxicity of Other Antibiotics**

Polymyxins (e.g., colistin and polymyxin B) belong to the glycopeptide antibiotic group. Colistin is a nephrotoxic antibiotic, and the mechanism of nephrotoxicity occurs due to an increase in tubular epithelial cell membrane permeability, which results in cation, anion, and water influx leading to cell swelling and cell lysis. There are also some oxidative and inflammatory pathways that may be involved in colistin nephrotoxicity (Javan et al., 2015). Renal toxicity of polymyxins is a complex process and appears to induce renal vasoconstriction, sensitizing proximal tubule cells to direct cytotoxic effects of the drug. Drug accumulation in proximal tubule cells is potentially driven by apical reabsorption at the brush border membrane via megalin-mediated endocytosis; oxidative stress subsequently plays an important role in the development of renal toxicity. Ultimately, drug accumulation within cells leads to organelle damage, increased membrane permeability, cell lysis, and ATN (Spapen et al., 2011). Vancomycin is a glycopeptide antibiotic and also associated with nephrotoxicity concern. The underlying pathophysiological basis of vancomycin toxicity in proximal tubule cells involves induction of depolarization of the mitochondrial membrane with production of mitochondrial ROS and peroxidation of mitochondrial phospholipid cardiolipin. The activation of caspase-9 and caspase-3/7 is accompanied by vancomycin-induced apoptotic cell death (Petejova et al., 2019). Many antibiotics result in obstructive nephropathy (discussed in detail later in the section).

#### **5.4.6. Heavy Metals (See also Metals, Vol 3, Chap 10)**

Heavy metals typically are injurious to the proximal tubule and nervous system. They tend to accumulate in the kidney, liver, bone, and brain. The spectrum of heavy metal renal effects, as well as pathogenesis, can be appreciated by considering the effects of cadmium, mercury,

manganese, and lead. Other heavy metals are less studied but share features of injury with one or more of these chemicals.

#### 5.4.7. Cadmium

Cadmium ( $\text{Cd}^{2+}$ ) is a widespread environmental and occupational contaminant. Upon uptake from digestive or respiratory portals of entry, cadmium binds to albumin and other high molecular weight proteins, and then is taken up by the liver. In the liver, cadmium is bound to the LMW metal transport protein metallothionein and released into the blood stream. Plasma levels of cadmium bound to metallothionein (6500 Da) remain low since this complex passes freely into the glomerular filtrate. The complex is reabsorbed, as are many LMW proteins, in the proximal tubules by endocytosis. Metallothionein is hydrolyzed in the phagolysosome, releasing cadmium, which stimulates metallothionein synthesis *de novo*. Cadmium ( $\text{Cd}^{2+}$ ) rapidly binds newly synthesized or reabsorbed metallothionein. The renal toxicity of cadmium occurs upon the intralysosomal release of free ligand, which also may interact with proteins other than metallothionein (Zalups and Diamond, 2005). Cadmium accumulates in the kidney, bound to metallothionein in a time- and dose-responsive manner. The biological half-life in humans is approximately 10 years. Threshold levels of cadmium must accumulate prior to induction of overt tubular injury. The threshold varies widely in experimental animals from 10 to 200  $\mu\text{g Cd}^{2+}/\text{g}$  wet weight because of variations in dose rate, route, and form of cadmium administered. Nephrotoxicity may occur in humans when  $\text{Cd}^{2+}$  concentrations exceed 50  $\mu\text{g}/\text{g}$  kidney wet weight. The earliest ultrastructural alteration of cadmium toxicity occurs as phagolysosomal change. Tubular necrosis, primarily affecting S1 and S2 segments of the proximal tubule, or with less intense exposure, changes limited to increased incidence or severity of CPN are common morphologic changes with cadmium injury in the rat. The mechanism of tubule injury involves free radical damage. Renal damage is not exclusive to tubules. Cadmium also accumulates within mesangial cells causing them to proliferate, with increased size and number (Xiao et al., 2009). Chronic interstitial nephritis has also developed clinically with long-term exposure.

#### 5.4.8. Mercury

As with cadmium, the toxic potential of mercury depends on dose rate, form, and route of administration. Toxicity of the inorganic salts is quantitatively different from organic mercurials because of differential solubility. Mercurial nephrotoxicity in humans today is almost always a consequence of chronic occupational exposure. Acute mercury poisoning represents the classical cause of proximal tubular cell necrosis. This response preferentially occurs in the pars recta, but with increased time and dose can affect all segments. Cellular uptake of  $\text{Hg}^{2+}$  into the proximal tubule occurs via cotransport with other ligands such as glutathione or albumin (Zalups and Diamond, 2005; Diamond and Zalups, 1998). Both apical transport on the brush border and basolateral transport through OATs occur. The mechanism of proximal tubular cell injury traditionally has centered on uncoupling of oxidative phosphorylation in mitochondria. Mercury does inhibit mitochondrial enzymes. Furthermore, this mechanism is consistent with subtopographical localization in the pars recta, the site of predilection for hypoxic injury. As with other heavy metals, mercury reacts with free sulfhydryl groups and thus leads to further depletion of glutathione and subsequent oxidative stress to perpetuate tubule injury. Male rats are significantly more sensitive to mercury-induced renal injury; this is associated with correlative sex differences in renal levels of sulfhydryl groups. Mercuric chloride-induced nephrotoxicity has been used as a model to suggest that toxicologic evaluations conducted only at the end of a subchronic study may significantly underestimate nephrotoxic potential. In the acute phase of treatment, overt tubular necrosis and functional evidence of renal failure occur. In subchronic exposures (20–90 days), functional indices may return to normal. However, histopathologic evidence of regeneration and repair persists, so the antecedent injury may go unrecognized. Chronic exposure of rat to mercury results in increased incidence and severity of lesions of CPN. Chronic mercury poisoning has been reported to involve immune-mediated mechanisms of injury, including membranous glomerulonephritis related to deposition of anti-basement membrane antibodies (Zalups and Diamond, 2005).



#### 5.4.9. Lead

Rapid and selective accumulation of lead occurs in the kidney, initially isolated to the cytosolic fraction of proximal tubular epithelium. Lead is highly reactive with the sulfhydryl group of two cytosolic proteins having molecular weights of 11,500 and 63,000 Da accounting for the accumulation. These high-affinity lead-binding proteins regulate the bioavailability of lead, as well as transport into the nucleus. Lead pretreatment results in a 30%–40% decrease in binding of lead to renal mitochondria. Through specific cytosolic protein binding, the renal toxicity of this metal is reduced. Acute or subchronic lead nephrotoxicity is characterized by the presence of intranuclear inclusions visible by special stains in proximal tubular epithelial cells in most species. In the kidney, 80%–90% of lead is concentrated in nuclei, suggesting that the intranuclear inclusions represent a storage site. Extrusion of the nuclear inclusion into the cytoplasm and increasing tubular lysosomal activity may represent a sequence of lead metabolism by the proximal tubule. Cytoplasmic lead can bind to mitochondria, inhibiting mitochondrial respiration, with resultant mitochondrial swelling as a potential mechanism of injury. Acute lead exposure is also characterized by increased apoptotic necrosis and proximal tubular cell replication, evidenced by [ $^3\text{H}$ ] thymidine incorporation into DNA of dividing cells. Karyomegaly occurs frequently with lead toxicity in rats (especially males) and is a sensitive morphologic indicator. Chronic lead exposure may lead to increased incidence/severity of CPN in rats, but is associated with tubule atrophy and renal fibrosis in humans. Chronic exposure at dosages which show cytomegaly and karyomegaly is associated with renal tubule tumor formation in rats. However, lead exposure does not appear to represent a risk for renal tumorigenesis in humans.

#### 5.4.10. Anticancer Drug-Induced Nephrotoxicity

Nephrotoxicity is an inherent adverse effect of certain anticancer drugs in humans and animals. Chemotherapeutics typically have no margin of safety, and often are used in patients with altered or diminished function of drug metabolism and clearance systems. Patients often have renal abnormalities necessitating pretreatment

screening and monitoring of kidney function, and sometimes dose modulation based on findings. Renal toxicity can be manifest by primarily tubular-limited dysfunction, glomerular injury with proteinuria, full-blown AKI, and long-term chronic kidney injury. In humans, renal pathologic alterations in most cases develop from direct cytotoxicity of the chemotherapeutic agents, but underlying host risk factors and the renal handling of drugs can increase the likelihood and severity of nephrotoxicity. A survey compared toxicity prediction for 12 platinum analogs that had both preclinical (mice, rats, and/or dogs) and clinical data from matching drug administration schedules. Nephrotoxicity was observed in human Phase I clinical trials for 3 of 12 drugs. Corresponding nephrotoxicity was seen for all human nephrotoxic drugs in dogs and for two of three in rats. Nephrotoxicity was seen for another four drugs in rats and five drugs in dogs without any corresponding nephrotoxicity signal in humans. Therefore, predicting nephrotoxicity potential based on nonclinical toxicology studies in animals for humans can be challenging because of overt sensitivity of animals and use of relatively high doses in nonclinical studies. Additionally, prophylactic measures can be used in humans to prevent nephrotoxicity (e.g., hydration and forced diuresis), whereas toxicology studies in experimental animals are devoid of such measures. Mechanisms of chemotherapy-induced nephrotoxicity generally include cytotoxic damage to nephron components or renal vasculature, HUS, or prerenal perfusion deficits.

#### 5.4.11. Cisplatin

Cisplatin (and to a lesser degree carboplatin) therapy may be associated with AKI, increased azotemia, renal magnesium wasting, progression to CKD, and, rarely, HUS. Renal effects with cisplatin encompass tubule damage, glomerular injury, vascular damage, and even interstitial injury. In the rat, the pars recta (S3) is preferentially affected, but in humans, all of the proximal tubules, DCTs, and collecting ducts may also be affected. Early lesions with low doses occur within 48 h in rats and result in single cell necrosis of the S3 segments, which progress to confluent necrosis and epithelial loss with increased dose or longer duration of dosing. Other areas of the nephron may then be affected secondarily proximally and distally due to

dysfunction. Cisplatin is transported into proximal tubules using multiple transporters, but preferentially OCT2 from the basolateral border, where it accumulates in the pars recta. Cisplatin–glutathione conjugates may also be important in renal targeting (Townsend and Hanigan, 2002). The mechanism of cisplatin toxicity is complex, but likely depends on its metabolism via hydrolysis to a reactive intermediate, as inhibition of  $\gamma$  GGT prevents cisplatin-induced renal toxicity in both rats and mice. Once it is internalized and metabolized, cisplatin affects a wide variety of critical cellular functions including inducing DNA cross-links as well as deleterious effects on protein synthesis, glucose transport, and  $\text{Na}^+/\text{K}^+$ -ATPase activity. Alterations in glomeruli and the interstitium appear to be due to selective vasoconstriction.

Other chemotherapeutic agents also result in direct cellular damage. Ifosfamide therapy is linked to proximal tubular damage, urinary loss of electrolytes, glucose, and amino acids (Fanconi syndrome), rickets, and osteomalacia. Azacitidine renal effects are characterized by tubular acidosis, polyuria, and urinary loss of electrolytes, glucose, and amino acids. AKI and HUS are reported following high doses of methotrexate.

#### **5.4.12. Molecular Targeted Anticancer Therapies**

Nephrotoxicity with molecular-targeted anticancer therapies can be directly related to perturbation of targets expressed in the normal kidney. VEGF and VEGFR inhibitors, including sunitinib, pazopanib, sorafenib, axitinib, and bevacizumab, among others, most commonly are associated with TMA, proteinuria, and hypertension in patients, but glomerulonephritis and AIN may also occur (Abbas et al., 2015). The mechanism of renal changes is multifactorial. Hypertension is a common accompaniment to anti-VEGF therapy, and this can result in typical alterations associated with stimulation of the intrarenal RAAS axis, including degenerative effects on tubules and the stimulation of interstitial fibrosis with long-term therapy if left unchecked. However, hypertension and proteinuria commonly regress with drug cessation in humans. NO pathway inhibition appears to be important in the molecular pathogenesis of hypertension-mediated renal injury. Decreased nitrous oxide leads to endothelial dysfunction

and capillary rarefaction, and is associated with pressure natriuresis and volume overload. Oxidative stress may also be important in other kidney lesions. Glomerular histologic changes have been noted in rodents (especially in juvenile animals), and appear to result from the incorporation of drug into mesangial cells, podocytes, and endothelial cells. Osmiophilic inclusion bodies are noted ultrastructurally. VEGF is normally expressed in podocytes in the glomerulus, and VEGF receptors are present on endothelial, mesangial, and peritubular capillary cells. Glomerular injury may develop from loss of VEGF effects on maintaining the filtration barrier, by down-regulation of tight junction proteins (Jhaveri et al., 2017; Abbas et al., 2015). It should be noted that many of the VEGFR inhibitors also inhibit several other tyrosine kinases and therefore not all kidney effects in this class of anticancer agents are solely related to VEGF inhibition.

Other similar targeted chemotherapeutics also result in nephrotoxicity. EGFR inhibitors produce proteinuria, IgA nephropathy, and ATN. Cetuximab and panitumumab, both antibody therapies targeting EGFR, also cause electrolyte imbalances including hypomagnesemia and hypokalemia due to direct toxic effects on renal epithelium. Hypomagnesemia is due to the inhibition of ion channel transport functions located on the apical surface of the TAL and the distal tubule, where filtered magnesium is reabsorbed and where abundant renal EGFR is localized. EGFR is expressed in collecting ducts, and glomerular mesangial and PECs. EGF is involved in maintaining tubular integrity and is a potent mitogen for cultured mesangial cells and EGFR inhibitors have rarely been associated with glomerulonephritis and nephrotic syndrome clinically (Jhaveri et al., 2017). Cetuximab may also result in renal tubular acidosis and AKI related to direct cytotoxicity.

c-kit inhibitors produce TMA, glomerulonephritis, proteinuria, and hypertension. Both imatinib and dasatinib can result in acute or chronic renal failure and the mechanism is proposed to be direct cytotoxicity related to high renal clearance. Ibrutinib, another tyrosine kinase inhibitor used to treat leukemia, and rituximab, an anti-CD20 monoclonal antibody, share the potential for acute renal failure due to tumor lysis syndrome (Abbas et al., 2015). In dogs, cKIT

inhibitors administered to treat mast cell tumors were associated with podocytopathy (minimal change disease) and proteinuria. In some cases, the proteinuria resolved following cessation of therapy. Vemurafenib, a BRAf inhibitor targeting melanoma, induces increased plasma creatinine by two separate mechanisms: inhibition of creatinine tubular secretion and mild renal functional impairment (Jhaveri et al., 2017). However, other BRAf inhibitors such as dabrafenib did not show similar high incidences of creatinine increases or clinical nephrotoxicity, suggesting this is not a target-mediated effect. In juvenile rats, dabrafenib administration prior to weaning has been shown to induce degeneration and mineral deposits in the collecting ducts (Groseclose et al., 2015). However, similar renal lesions were not found in adult rats and the toxicity was demonstrated to be related to a metabolite that was both age- and species specific.

#### 5.4.13. Immune Checkpoint Inhibitors

Nivolumab and pembrolizumab represent a new class of anticancer drugs (immune checkpoint inhibitors) which block PD-1, a molecule expressed in mononuclear cells and which can be induced in renal epithelium in cancer patients. These drugs have been associated with AKI in approximately 2% of patients, and many of these cases have been associated with AIN (Frazier, 2022). The mechanism is presumably immune-mediated, but the specific pathogenesis is poorly understood. Ipilimumab is a monoclonal antibody that is also considered an immune checkpoint inhibitor. It has antitumor activity by targeting and antagonizing the actions of CTLA-4 and thus activating the immune system. It can cause migration of activated T cells into the kidney, leading to AKI and AIN. Cell-mediated immune activation results in the accumulation of interstitial mixed inflammatory cell infiltrates, sometimes causing local granulomas. Glomerulonephritis may rarely occur in patients. Similar renal lesions occur in rodents with high dose chronic therapy.

#### 5.4.14. Antibody-Drug Conjugates

ADCs are a class of cancer therapeutics composed of a chemically linked engineered antibody and a cytotoxic drug. Commonly used cytotoxic moieties are derived from maytansinoids such as emtansine or mertansine and

auristatins such as mono-methyl auristatin E (MMAE) or mono-methyl auristatin F (MMAF). They induce cell necrosis in tumors via microtubule depolymerization. In recent years, multiple ADCs have been successfully approved for use, making them an important class of agents in oncology, but they have historically had the potential for kidney toxicity (along with ocular and hepatic toxicity). Microtubule effects result in characteristic karyomegaly in renal tubule epithelium in rodents and nonrodents, which can be associated with degeneration and necrosis with inflammation at high doses (Figure 2.28). However, newer generation ADCs such as belantamab mafodotin have MMAF linkages which do not cleave extracellularly, and this appears to have markedly reduced the nephrotoxic potential of the recent class of ADC anticancer agents clinically, although karyomegalic renal tubule cells are still noted in preclinical studies (Frazier, 2022).

#### 5.4.15. Xenobiotics that Cause Renal Injury via Metabolic Activation

A xenobiotic may be metabolized in the kidney to a reactive intermediate (Table 2.16). Cells of the pars recta contain a much greater proportion of smooth endoplasmic reticulum than any other portion of the nephron; thus, the outer stripe is typically the primary site of injury for xenobiotics, mediated by metabolic activation. It is in these cells that CYP450 and other MFOs catalyze reactions to produce

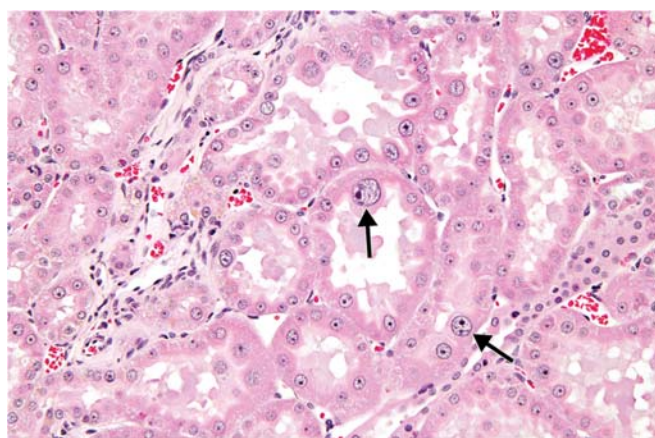


**FIGURE 2.28** Kidney from an F344/N rat from a chronic study demonstrating tubules with hypertrophic cytoplasm and karyomegalic nuclei of proximal tubule epithelium (arrows). Courtesy of the Division of Translational Toxicology, NIEHS.



**TABLE 2.16** Experimental Manipulation of the Rat for Implicating Renal P-450 Microsomal Metabolism with Derivation of a Reactive Intermediate as the Mechanism of Toxicity

Pretreatment modulating factor	Influence
Butathione/sulfoximine	Inhibits glutathione synthesis
Diethyl maleate	Depletes renal glutathione
Cysteine	Increases renal glutathione
Polybrominated biphenyl	Stimulates renal metabolism
Piperonyl butoxide	Blocks renal metabolism
Phenobarbital	Stimulates hepatic metabolism
Cobalt	Blocks hepatic metabolism

Modified from Haschek WM, Rousseaux CG, Wallig MA, editors: *Handbook of toxicologic pathology*, ed 2, 2002, Academic Press, Figure 19, p. 291, with permission.

a more readily excretable form of the parent xenobiotic. Phase II metabolism reactions involving conjugation with glutathione typically decreases the reactivity of metabolic intermediates, correspondingly reducing toxicity potential. However, some xenobiotics that are metabolized to sulfur-containing metabolites conjugated with glutathione can be further metabolized to cysteine S-conjugates, and then metabolized by cysteine conjugate beta-lyases to reactive thiols. Xenobiotic injury via the beta-lyase pathway is preferentially expressed in the outer stripe. Metabolism to cysteine conjugates may sometimes occur in the liver, with subsequent transport to and uptake by the pars recta, with its high concentration of beta-lyases. Hexachloro-1, 3-butadiene, tetrafluoroethylene (TFE), chlorotrifluoroethylene, trichlorethylene (TCE), and dichlorovinyl cysteine all produce nephrotoxic effects via the beta-lyase pathway mechanism, and correspondingly produce selective necrosis in the pars recta (Figure 2.29). As an example, TCE is primarily metabolized by CYP450s to trichloroethanol and its glucuronide metabolite which eventually get metabolized to dichlorovinyl-L-cysteine, which is further metabolized by the beta-lyase system to a highly reactive thiol electrophile, injurious to renal epithelium (Lock and Reed, 2006). Electrophiles

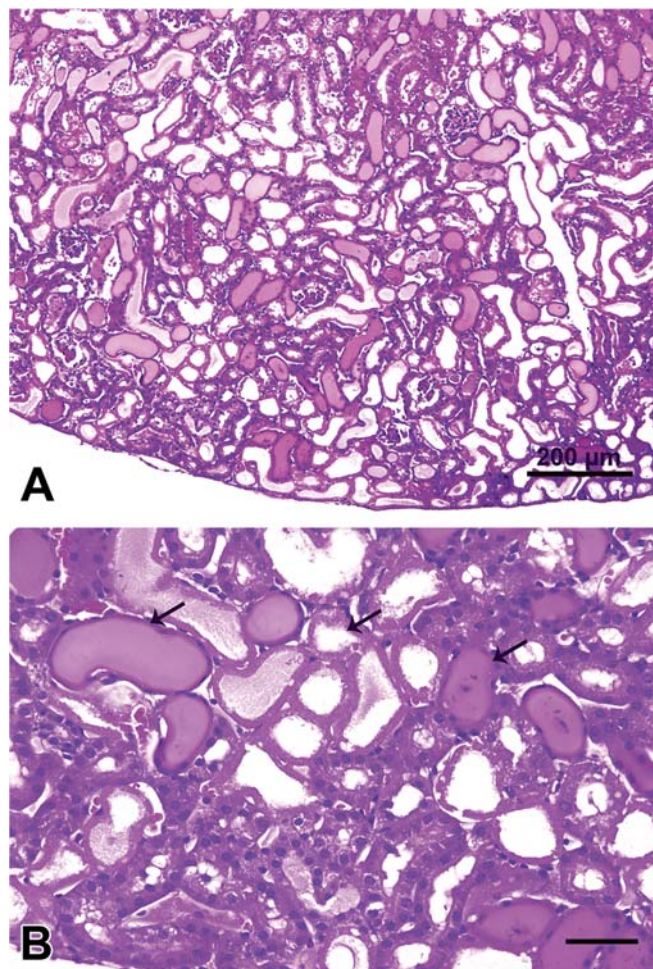


**FIGURE 2.29** Necrosis of pars recta in a male mouse kidney treated with a single dose of carbon tetrachloride (0.25 mL/kg) and sacrificed hours later. (A) Low magnification showing diffuse tubular dilatation and intratubular protein casts. (B) High magnification showing pars recta necrosis (arrows). Bar = 30 mm. Reproduced from Haschek WM, Rousseaux CG, Wallig MA, editors: *Fundamentals of toxicologic pathology*, ed 2, 2013, Academic Press, Figure 11.11, p. 288, with permission.

may bind covalently and cause irreversible inactivation of protein, DNA, RNA, and/or lipid macromolecules.

#### 5.4.16. Organohalides

Organohalides form a class bridging three functional categories: synthetic biologic toxins, organic solvents, and chemicals involved in plastics and resin manufacturing. The kidney is a primary target organ for toxic organohalides. A significant portion of the United States population is chronically exposed to small

amounts of these chemicals in water. The acute necrotizing effects, as well as teratogenic and carcinogenic effects at high doses in the laboratory animal, are dependent on the conversion of the parent compound to toxic metabolites. Species, sex, and tissue differences in susceptibility to injury are expected, related to differences in the pharmacokinetic behavior of each specific chemical.

Chlorine disinfection of drinking water results in the formation of trihalomethanes, primarily chloroform. Chloroform is considered a prototypical organohalide; its mechanism of injury has been extensively studied and involves cytotoxic action on renal epithelium. Nephrotoxicity produced by chloroform requires its metabolism by renal CYP450 and the formation of a reactive intermediate that binds covalently to nucleophilic groups on cellular macromolecules (Liu et al., 2013). Intrarenal CYP450 biotransforms chloroform to trichloromethanol, which is unstable, after which HCl is released to form phosgene. Prerequisite renal metabolism can be demonstrated by enhanced toxicity following pretreatment with drugs such as polybrominated biphenyls, known to stimulate renal MFOs. Phenobarbital, the classical CYP450 stimulator in liver, does not induce rat renal MFOs and thus does not enhance rat chloroform nephrotoxicity. Pretreatment with inhibitors of renal metabolism, specifically piperonyl butoxide, reduces chloroform nephrotoxicity. In the mouse, renal toxicity may occur in the absence of hepatotoxicity, further suggesting intrarenal metabolic activation. Furthermore, subcutaneous administration of chloroform causes greater renal toxicity than oral dosing at comparable levels of systemic absorption, presumably because the liver "first-pass effect" is avoided. Species, strain, and sex susceptibility to chloroform nephrotoxicity are proportional to renal MFO activity. The location and distribution of radiolabeled chloroform are also proportional to the extent of nephrotoxicity. Mature male mouse kidneys have significantly higher MFO activity than females or neutered males. The intact male DBA/2J mouse is significantly more susceptible than the C57BL/6J mouse and other species, correlating with increased capacity of the kidney to metabolize chloroform. Irreversible binding, measured by covalent

adduct quantitation, correlates with the severity of tissue injury. The putative chloroform metabolite phosgene depletes renal glutathione, subsequently initiating an autocatalytic peroxidative degradation of membranes. Glutathione conjugation with the injurious chloroform metabolite reduces or prevents covalent binding with tissue macromolecules. Thus, pretreatment with diethylmaleate, which reduces renal glutathione, significantly enhances chloroform nephrotoxicity.

TFE is another example of a nephrotoxic organohalide that has a similar toxicologic mechanism to TCE. TFE is metabolized in the liver to a GSH conjugate, and is then degraded into a cysteine-S conjugate and cleared by the kidney and transported into renal epithelium. Alternatively, TFE can be GSH conjugated along the renal brush border and immediately transported into the tubule. Kidney toxicity produced by this haloalkene is characterized morphologically by necrosis of proximal tubules, particularly in the S3 segments. Metabolism by the beta-lyase system in the pars recta results in the production of a reactive thiol that is capable of binding covalently to cellular macromolecules and causing degenerative effects, with an emphasis on mitochondria. Lipid peroxidation may be involved in the pathogenesis since pretreatment with antioxidants can ameliorate renal damage (Groves et al., 1993).

#### **5.4.17. Organic Acid/Base Transport as a Mechanism for Renal Toxicity**

As noted in earlier sections of this chapter, organic acid transport systems may be important components of the mechanism of uptake and intracellular accumulation of some nephrotoxics such as antibiotics, cidofovir/antiviral agents, cisplatin, metformin, citrinin, and cysteine conjugates (e.g., TCE). While uptake of a drug or chemical into proximal tubule epithelium may be responsible for accumulation, toxicity also depends on whether efflux transporters fail to secrete it from the cell before injury ensues. In this regard, drug-drug interactions are responsible for most transporter-based nephrotoxicities. More importantly, intracellular accumulation and drug concentration within a cell does not necessarily equate with the toxic potential of a compound. Rank order of nephrotoxicity

of individual agents within a drug class rarely corresponds to actual measured drug concentrations within kidney, but instead is more dependent upon the intrinsic reactivity of the individual drug with subcellular or organellar targets.

Uptake of anionic compounds through the OAT1 transporter on the basolateral surface of proximal tubules (as represented by para-aminohippurate-PAH) can be inhibited by coadministration of competing organic anions such as probenecid and penicillin. PAH and probenecid have been demonstrated to reduce toxicity of drugs requiring transport as an organic anion in mechanistic studies. Conversely, mepiperphenidol, quinine, and quinidine have been used as inhibitors of organic base transport through OCT1 and 2 competitive inhibition.

#### **5.4.18. Mycotoxins (See also Mycotoxins, Vol 3, Chap 6)**

Mycotoxins represent an important class of xenobiotics that cause renal injury in humans and food animals. Ochratoxin A, the cause of Danish porcine nephropathy, is an organic anion and results in proximal tubular injury which first appears as cytoplasmic vacuolation with phagolysosomal hydropic swelling followed by tubular necrosis. Ochratoxin A was also thought to be the cause of Balkan endemic nephropathy, an important urologic syndrome of humans in Eastern Europe, although the etiologic agent is now believed to be aristolochic acid. Ochratoxin A is actively transported via the OAT, resulting in tubular accumulation. Blocking transport with probenecid modulates toxicity. Ochratoxin A is probably metabolized to a reactive intermediate as the mechanism of injury. Ochratoxin A or its metabolite inhibit mitochondrial ATP production and stimulate lipid peroxidation in tubules. Balkan endemic nephropathy is associated with an increased incidence of renal pelvic cancer, but in laboratory rodents, ochratoxin induces only renal tubule tumors (Grollman and Jelakovic, 2007). Fumonsin-B<sub>1</sub> causes renal injury in several species, and cancer in rats. The most sensitive target tissue in rats, the pars recta, develops accelerated apoptosis in subchronic studies and tubular neoplasms in chronic studies. Fumonsin perturbs renal sphingolipid profiles.

Deoxynivalenol is a toxin produced by the fungus *Fusarium graminearum* in the heads of small grains. Experimentally, this mycotoxin has been shown to produce IgA nephropathy.

#### **5.4.19. Xenobiotics Perturbing Endogenous or Nutritive Substrates**

Examples of nephrotoxicity from perturbation of an endogenous or nutritive substrate include toxicity related to overload of iron or phosphate, osmotic vacuolation, oxalate crystalluria and other causes of obstructive nephropathy, alpha<sub>2</sub>-globulin nephropathy, hemoglobin or myoglobin nephropathies, amino acid toxicity, and toxicities associated with some synthetic diets.

#### **5.4.20. Iron Toxicity**

Bisphosphonates chelate cations and are used to inhibit bone resorption through physicochemical and intracellular effects, including direct binding to calcium phosphate crystals within bone matrix, but are known to be potentially nephrotoxic. A prototype, chloromethane diphosphonate (Cl<sub>2</sub>MDP), preferentially sequesters iron. Cl<sub>2</sub>MDP perturbation of iron at the subcellular level may be associated with the nephrotoxic response, specifically through peroxidative processes. Cl<sub>2</sub>MDP causes proximal tubular necrosis with quantitative predilection for pars recta. Cl<sub>2</sub>MDP is not metabolized, but does accumulate in renal cortex and outer stripe (as well as in bone). The spectrum of toxicity induced by bisphosphonates (for e.g., pamidronate, alendronate, and zoledronate) includes MCN, collapsing and noncollapsing forms of FSGS, and tubulointerstitial nephritis. Morphologically, there is an increased podocyte proliferation index and decreased expression of synaptopodin, suggesting a mechanism of direct podocyte toxicity. Mitochondrial perturbations in podocytes with pamidronate and iron overload with other bisphosphonates have also been reported.

#### **5.4.21. Osmotic Vacuolation**

Osmotic vacuolation (historically referred to as osmotic nephrosis) refers to a nonspecific histopathologic and clinical finding characterized by vacuolation and swelling of renal proximal tubular cells. Glucose and sucrose are reabsorbed by pinocytosis, leading to vacuolation of the



cytoplasm and specifically hydropic swelling of the phagolysosome (Figure 2.25). Hence, agents that produce abundant glucosuria and/or promote systemic diabetes may result in this type of tubule injury, but most of the pathogenesis of injury related to DN is completely separate from vacuolar effects on tubule epithelium. Mannitol, hydroxyethyl starch, dextran, high levels of zinc, and contrast media also induce tubule vacuolation via absorption of compounds that draw fluid into the lysosomal compartment. The functional impact of this change is minimal, and vacuolation actually may represent a transient adaptive response. AKI and CKD have been reported in rare cases—for example, after surgical placement of an antiadhesive barrier of macromolecular polysaccharides in the peritoneal cavity.

#### **5.4.22. Obstructive Nephropathy**

Obstructive nephropathy is a relatively common cause of renal injury in both laboratory animals and humans related to crystalluria. Risk factors for xenobiotic or endogenous crystal precipitation within the kidney tubules include effective intravascular volume depletion, underlying kidney disease, and certain metabolic disturbances that promote changes in urinary pH favoring crystal precipitation. Intrarenal obstruction occurs secondarily to accumulation of compounds with low solubility and high renal clearance within the tubules, such as following high dosages of xemilofiban, naproxen, methotrexate, acyclovir, sulfonamides, and triamterene that precipitate out of solution within lumina (Yarlagadda and Perazella, 2008; Frazier et al., 2012; Frazier and Seely, 2019). Antibiotics that induce crystals and obstructive nephropathy in humans and/or animals include quinolone antibiotics (norfloxacin, ciprofloxacin), ampicillin, and sulfonamides (Radi, 2019). The likelihood of crystal precipitation depends on the concentration of the drug in the urine and the urinary pH (Naughton, 2008). NSAIDs and analgesics can lead to ureteral obstruction as a result of papillary necrosis. Uric acid crystal deposition can occur with acid urine usually after cancer chemotherapy with alkylating agents; the risk of its development is related directly to plasma uric acid concentrations. In domestic animals, causes include oxalate crystalluria from ethylene glycol and melamine-related retrograde nephropathy (both discussed

below). Obstruction can occur anywhere from the level of renal tubules to the urethral meatus. In the adult human kidney, approximately 2 L of urine flows through the renal papilla daily. Mild episodes of polyuria may alternate with periods of oliguria or, occasionally, anuria. A complete obstruction of short duration results in profound alterations in renal hemodynamics and glomerular filtration with minimal anatomic changes. Apoptotic signals and increased ROS contribute to necrosis and loss of nephrons. Injury is perpetuated by chemokine-mediated inflammatory recruitment and stimulation of paracrine growth factor-mediated fibrosis (Chevalier, 2006).

#### **5.4.23. Oxalate Crystalluria**

Ethylene glycol is a prototype for chemicals causing oxalate crystalluria. Reduced renal function may occur in acute exposure without oxalate deposition. A metabolic derivative of ethylene glycol oxidized via alcohol dehydrogenase is oxalic acid. Oxalic acid in the renal tubular lumen sequesters calcium, precipitates, and the resulting crystals obstruct the nephron, leading to renal injury. The consistent finding in the fatal cases of acute ethylene glycol poisoning in animals with renal failure is marked oxalate deposition (Figure 2.30).

#### **5.4.24. Melamine-Related Retrograde Nephropathy**

Melamine, 1,3,5-triazine-2,4,6-triamine, is used primarily for manufacturing melamine resins used in the production of a wide variety of products. The addition of melamine to food constituents in order to boost the apparent protein content has been a widespread practice in China. In 2007, an outbreak of renal failure in domestic cats and dogs associated with renal tubule crystalluria resulted in a major recall of pet food in North America. Analysis of the pet food demonstrated the presence of triazine compounds, primarily melamine and cyanuric acid. Experimentally, a mixture of melamine and cyanuric acid produced melamine cyanurate crystalluria and acute renal toxicity in cats, fish, and rodents. Cyanuric acid complexing with melamine was critical for the precipitation of crystals in the kidney (Figure 2.24). A similar outbreak in Asia in 2004 resulted in deaths of approximately 6000 dogs and fewer cats due to renal failure.

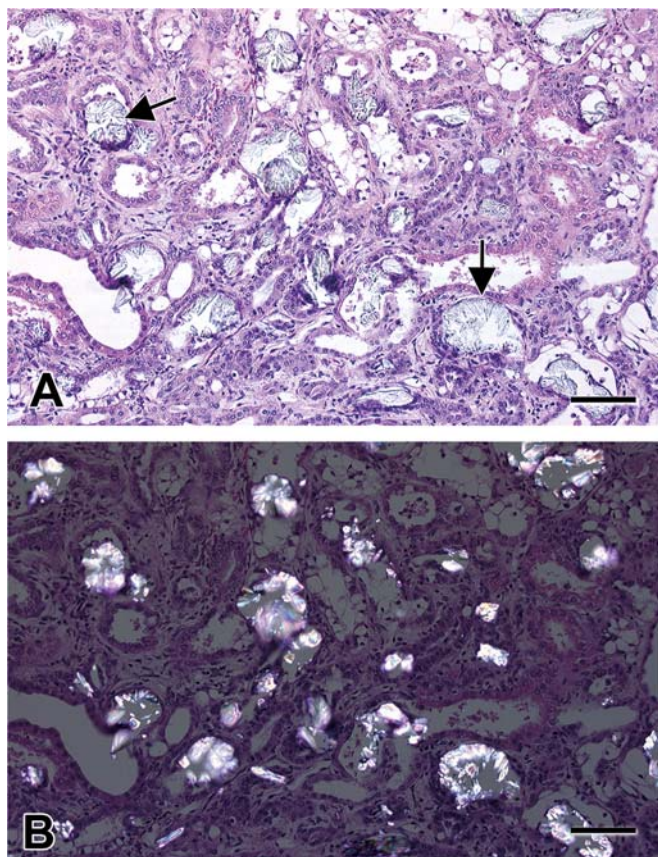


**FIGURE 2.30** Kidney of a pig with ethylene glycol (antifreeze) toxicity. (A) Tubular dilation and epithelial regeneration with prominent refractile oxalate crystals in the lumen of proximal tubules (arrows). (B) Prominent refractile oxalate crystals in the lumen of proximal tubules under the polaroid light. Bar = 75 mm. *Courtesy of Dr Xiantang Li, Drug Safety R&D, Pfizer, Groton, CT 258; Reproduced from Haschek WM, Rousseaux CG, Wallig MA, Bolon B, editors: Haschek and Rousseaux's handbook of toxicologic pathology, ed 3, 2013, Academic Press, Figure 47.36, p. 1748, with permission.*

#### 5.4.25. Alpha<sub>2</sub>μ-Globulin Nephropathy and Hyaline Droplet Nephropathy

Normal mature male rats spontaneously develop hyaline droplets in PCT epithelial cell cytoplasm, observable by light microscopy (Figure 2.7A). Ultrastructurally, these hyaline bodies represent phagolysosomal proteinic reabsorption droplets, and biochemically they consist of alpha<sub>2</sub>μ-globulin. Hyaline droplets reflect the normal glomerular filtration, uptake and proximal tubule cytoplasmic accumulation of this poorly hydrolysable LMW protein. The mature male rat synthesizes abundant alpha<sub>2</sub>μ-

globulin in the liver, secreting approximately 50 mg per day, which is rapidly cleared in the glomerular filtrate. Approximately 15–20 mg of alpha<sub>2</sub>μ-globulin is lost in the urine each day in the normal mature male rat, creating a physiologic proteinuria. Humans do not excrete significant levels of proteins similar to alpha<sub>2</sub>μ-globulin. The male mouse also is physiologically proteinuric because of mouse urinary protein (MUP), which has similar electrophoretic characteristics but is not reabsorbed by the proximal tubule. Exacerbated hyaline droplet accumulation was reported to be one of the most common renal findings in a histopathological survey of 42 ninety-day toxicity studies in rats conducted by the NTP (Hard et al., 1993). Several drugs and chemicals of societal importance affect the male rat through perturbation of alpha<sub>2</sub>μ-globulin, including D-limonene and unleaded gasoline. In addition to characteristic apically located, eosinophilic, ovoid droplets, there may be minimal to mild secondary tubule degeneration in severe cases (Frazier et al., 2012). Granular casts are also recognized as a hallmark feature of alpha<sub>2</sub>μ-globulin nephropathy and occur at the junction of the OSOM and ISOM, representing collection of cellular debris where the lumen of the S3 tubule narrows into the thin descending limb of the loop of Henle (Figure 2.31). Granular casts are composed of exfoliated cortical cells engorged with protein resulting in marked dilation of solitary tubules. The lining tubular epithelium is flattened and the basement membrane slightly thickened. A third pathognomonic lesion for this syndrome, albeit less common, is linear mineral deposits in the descending limb of Henle, representing fragments of the granular casts that lodge in the prebend segment. The most important factor in the development of drug- or chemical-exacerbated alpha<sub>2</sub>μ-globulin nephropathy is reversible, noncovalent binding of the agent to the protein. The resulting bound complex in rat proximal tubules is more resistant to hydrolytic degradation in the lysosomal compartment than the native protein and therefore persists. While the binding site in rats forms a large cavity, the lack of homologous LMW urinary proteins with similar binding pockets in other species do not readily accommodate ligand binding with xenobiotic agents in kidneys of other animals or humans (Chaudhuri et al.,



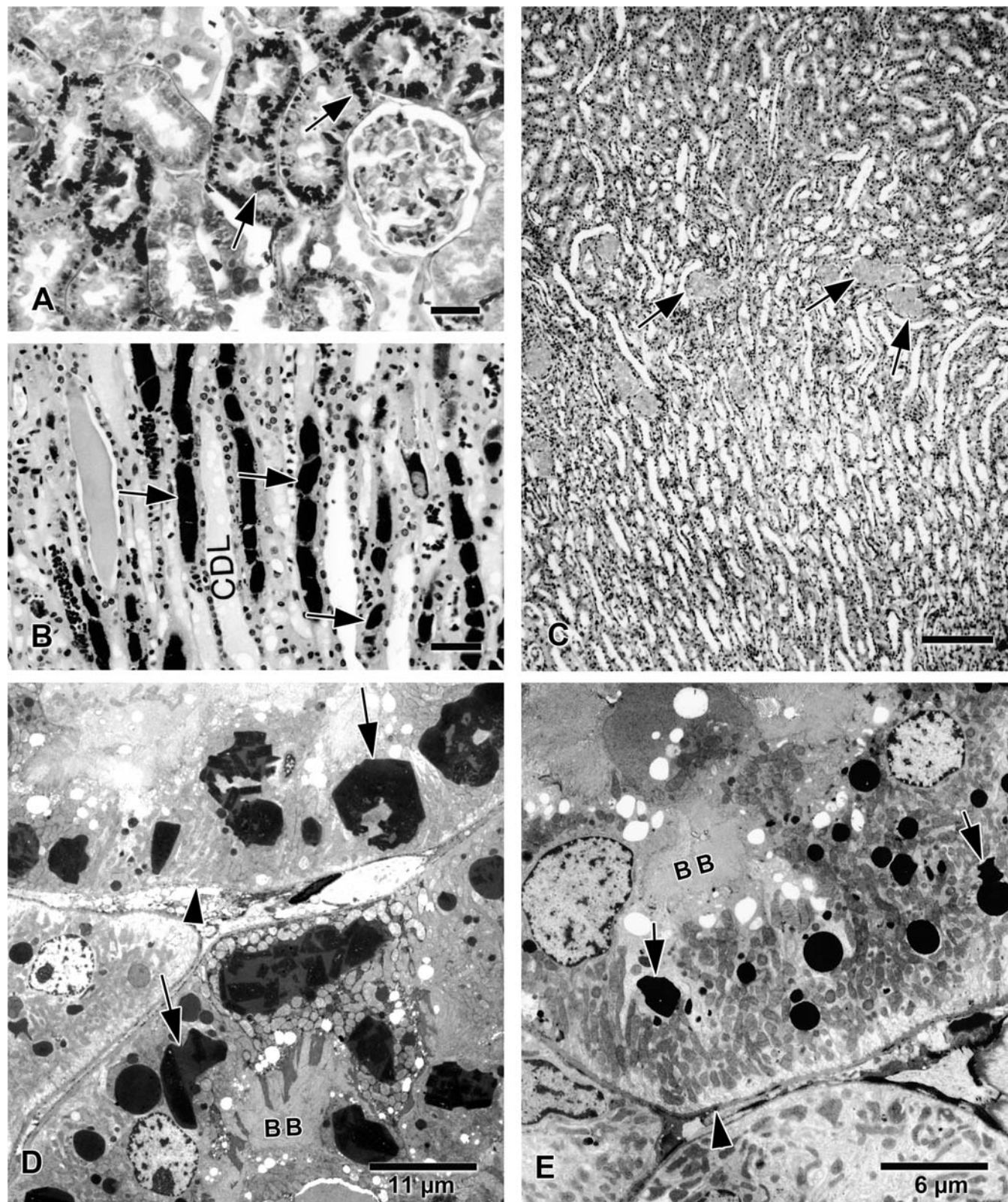


**FIGURE 2.31** Inducible male rat  $\alpha_2\mu$ -globulin nephropathy in male rats. (A) Exacerbated hyaline droplet formation in the cytoplasm of the proximal convoluted tubular cells (arrows) as a consequence of decalin treatment. Mallory's Heidenhain stain. Bar = 30 mm. (B) Linear mineral deposits (arrows) in the prebend segment of the loops of Henle, considered a consistent characteristic feature of the chronic changes (> 3 months treatment) in this



1999). Alpha<sub>2</sub>μ-globulin nephropathy is often associated with an increased incidence or severity of CPN. The agents causing alpha<sub>2</sub>μ-globulin nephropathy in the male rat over a life-time cause renal tubular tumors in male rats but not in female rats or mice of either sex (Table 2.17). The alpha<sub>2</sub>μ-globulin epithelial cell overload results in cell loss with a replicative response persisting through the first year of treatment of the male rat. This replicative response has been demonstrated to be linked with the subsequent tubular tumor development. The alpha<sub>2</sub>u-protein considered alone is injurious, and has been demonstrated to injure the kidney upon infusion in female rats and also to cause cell transformation in the Syrian hamster embryo test system. Because abundant liver synthesis of alpha<sub>2</sub>μ-globulin is specific to the male rat, this response is not considered predictive for humans. The recognition of male-rat specificity of this nephropathy resulted in the FDA and EPA not exerting regulatory restrictions relative to the unique male rat tumorigenic response to D-limonene and unleaded gasoline.

Not all hyaline droplets represent alpha<sub>2</sub>μ-globulin. Intralysosomal hyaline droplets may consist of other LMW proteins or of drug-protein complexes. Hyaline droplets occur commonly in the renal proximal tubules of rats with systemic histiocytic sarcoma or occasionally with renal lymphoma and are composed of lysozyme (Frazier and Seely, 2019). Mallory Heidenhain stains are generally negative in these alternative cases and differentiation can be inferred from unusual presentation such as high incidence in females, presence in species other than rats, or unusual shape (e.g., acicular or hexagonal). Clinical significance of hyaline droplets unrelated to alpha<sub>2</sub>μ-globulin depends on their composition. For instance, hyaline droplets have been associated with some cephalosporin antibiotics in rodents and nonrodents, but are not thought to contribute significantly to their nephrotoxicity.

**TABLE 2.17** Examples of Xenobiotics which Produce alpha<sub>2</sub>μ-globulin Nephropathy in Male Rats

β-Myrcene
Dimethyl methylphosphonate
Ethyl and methyl tert-butyl alcohol
Hexachloroethane
Hexachlorobenzene
Jet fuels: JP-4, JP-TS, JP-7, RJ-5, JP-10
Nitrotoluene
Isophorone
D-Limonene
Lindane
Paradichlorobenzene
Pentachloroethane
Tert-butyl alcohol
Unleaded gasoline

*Modified from Haschek WM, Rousseaux CG, Wallig MA, editors: Handbook of toxicologic pathology, ed 2, 2002, Academic Press, Table VII, p. 299, with permission.*

#### 5.4.26. Myoglobin and Hemoglobin

Myoglobin can induce acute renal failure as a result of myoglobinuria and pigmented cast nephropathy secondary to rhabdomyolysis. Toxic causes of rhabdomyolysis include snake or spider venom, caustic intramuscular injections, several marine biotoxins, and with myotoxins such as high doses of statin drugs (see *Animal Toxins*, Vol 3, Chap 8). Hemoglobin can also induce a morphologically comparable pigmented cast nephropathy. Hemoglobin excess occurs at injurious levels in glomerular filtrate after intravascular hemolysis. Causes of intravascular hemolysis include exogenous chemicals, such as phenothiazine, as well as snake venom. The concentration of hemoglobin

syndrome. Collecting duct lumen (CDL). Bar = 50 μm. (C) Granular casts (arrows) entrapped at the junction of inner and outer stripe, considered a subchronic pathognomonic lesion of this syndrome. Bar = 250 μm. (D) Decalin-treated and (E) control animals: Ultrastructural correlate of the hyaline droplets observed by light microscopy. Note the increased size and propensity for crystalloid change of phagolysosomes (arrows) with decalin treatment. Basement membrane of the proximal tubules (arrowhead); brush border (BB), Bar = 50 mm. *Modified from Haschek WM, Rousseaux CG, Wallig MA, editors: Handbook of toxicologic pathology, ed 2, 2002, Academic Press, Figure 24, p. 1297–1299, with permission.*

sufficient to injure the kidney typically is associated with red discoloration of plasma. By contrast, in myoglobinuria, because of smaller molecular weight, renal clearance is sufficiently high to maintain normal colored plasma. The urine is darkly discolored in either syndrome. The mechanism of renal injury is not defined, but may include nephron obstruction as well as proximal tubular phagolysosomal overload and generation of intracellular ROS.

#### **5.4.27. Amino Acid Toxicity**

Lysinoalanine, an amino acid formed during alkali treatment of protein, may be found in processed foods for human consumption. Lysinoalanine induces cytomegaly and/or karyomegaly in the pars recta of rat and mouse, but this effect has not been observed in hamsters, monkeys, or rabbits. The change seems largely reversible and long-term studies with lysinoalanine have not led to renal tumor formation or any other adverse change. Lysine, a component of some parenteral nutrition therapies, and D-serine injection in the rat induce necrosis of the proximal tubule. In the case of D-serine, the induced necrosis is restricted to the pars recta. Serine is also normally synthesized *in vivo* in the rat as well as in the human kidney.

#### **5.4.28. Synthetic Diet-induced Nephrocalcinosis**

Within a few weeks of feeding certain commercially available semipurified diets to rats (e.g., AIN 76), intratubular mineral deposits consisting of calcium and phosphate salts become marked in the pars recta. The alteration primarily affects the female rat. Changing dietary calcium and phosphorus ratios by increasing calcium or by adding magnesium to the diet decreases or prevents this mineral precipitation. Altering water load and intratubular pH also affects mineral deposition in the kidney.

#### **5.4.29. Xenobiotics Inducing Ischemia and/or Hypoxia**

Renal ischemia and hypoxia is a mechanism of toxicity with several xenobiotic agents, and is involved in the generation of multiple rodent models of kidney disease such as the spontaneous hypertensive rat (SHR) or renal arterial clamp models. In the rat kidney subjected to

ischemia and then reperfused, necrosis occurs in the proximal tubule, invariably accompanied by medullary congestion, which is most marked in the outer stripe (Figure 2.32). This tubule injury appears in periods of ischemia as short as 15 min. The shorter the period of ischemia, the longer the reperfusion interval required before necrotic cells can be visualized. With slightly longer periods of ischemia (45–60 min) and reperfusion (up to 24 h), necrosis also appears in PCTs, although the pars recta is the most prominently affected segment. Distribution of proximal tubule necrosis in ischemia–reflow injury has features in common with a pattern produced by hypoxia, as well as by mitochondrial toxicants such as mercury. Four interrelated mechanistic explanations for the irreversible cell injury are: (1) impaired mitochondrial oxygen uptake, with anaerobic ATP depletion then oxidative stress upon reperfusion; (2) generation of free radicals perpetuating cellular damage; (3) precipitous calcium influx from the extracellular to intracellular compartment, with activation of calcium-dependent catabolic processes; and (4) release of cytotoxic lysosomal enzymes into the cytosol. Interestingly, ischemic proximal tubule damage is more severe in old rats than in young rats.

Proximal tubules have little capacity for anaerobic glycolysis; hence, they are particularly sensitive to impaired RBF and oxygen delivery, as occurs in the model of transient clamping of the renal artery. Although medullary TALs have

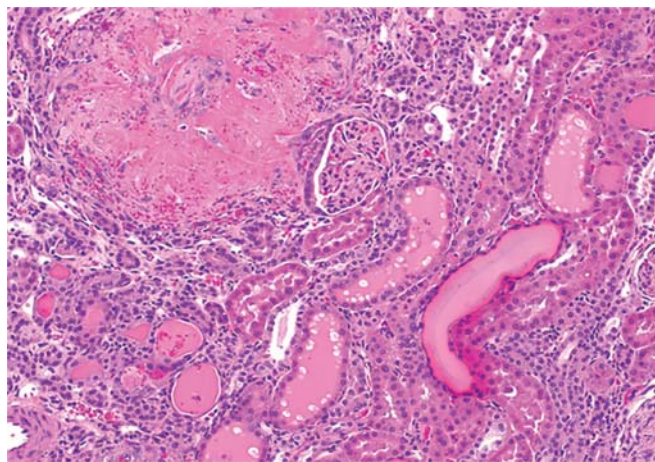


**FIGURE 2.32** Vascular degeneration and resulting parenchymal necrosis (top left) with tubule dilation and casts in a kidney from a spontaneously hypertensive rat given a high salt diet.

a greater capacity to generate ATP by glycolysis, hypoxic injury may be enhanced based on their location in the kidney, high resorptive capacity and blood flow. Hence it is quite common to see hypoxic injury show the most significant lesions in the area of the corticomedullary junction where both TAL and pars recta are localized. Endothelial cells within the interstitial microcapillaries in the outer stripe of the medulla undergo activation after ischemic insult, resulting in loss of vascular patency and upregulation of leukocyte adhesion molecules, as well as activation of multiple proinflammatory pathways. Rapid accumulation of neutrophils and monocytes in injured kidney is an essential feature of the innate immune response induced by ischemia–reperfusion injury. Tubule epithelial cells within the pars recta are particularly sensitive to ischemia and with Ang II stimulation, release a variety of chemokines, including the CXCL subfamily, (IL-8/CXCL8, Gro- $\alpha$ /CXCL1, and MIP-2/Gro- $\beta$ /CXCL2) that acts primarily on neutrophils, the CCL subfamily (MCP-1/CCL2), the CX3CL subfamily (fractalkine/CX3CL1) that has specific effects on monocytes and monocyte-derived lineages, and RANTES/CCL5 that operates more broadly to attract monocytes and lymphocytes. Many cellular responses to hypoxia are controlled by HIF genes. Downstream genes are then stimulated or upregulated to protect from hypoxic injury by promoting neovascularization (VEGF), erythropoiesis (EPO), glycolysis (glucose transporter 1), and decreasing oxidative stress (heme oxygenase). With renal hypoxia, HIF-1 $\alpha$  accumulates in tubules and in papillary interstitial cells, whereas HIF-2 $\alpha$  is induced in peritubular endothelial cells and fibroblasts ([Rosenberger et al., 2005](#)). HIF-1 $\alpha$  can be stabilized by several factors including NO, TNF $\alpha$ , Ang II, interleukin-1, insulin, and IGFs,

ROS and free radicals can be generated throughout damaged kidneys. Pericytes surrounding the vasa recta in the renal medulla are Ang II responsive and, under intrarenal RAAS activation, result in vasoconstriction leading to ischemic generation of free radicals by damaged tubules ([Obert and Frazier, 2019](#)). There is intercellular communication between the TAL and the vasa recta pericytes which involve scavenging of ROS and NO which helps modulate injury from oxidative stress.

NO is an important second messenger in a wide variety of critical physiologic pathways, but in the presence of oxidative stress, NO can be converted into reactive nitrogen species that contribute to renal injury. In the presence of superoxide anion, NO is capable of forming the powerful oxidant peroxynitrite (ONOO $^-$ ), which damages proteins and lipid membranes. Ang II mediates these deleterious effects through release of vascular superoxide radicals generated by stimulation of nicotinamide adenine dinucleotide/NAD phosphate oxidase that inactivates NO.

Mitochondrial dysfunction caused by ATP depletion associated with reduced oxygen availability is supported by demonstration of beneficial effects of ATP treatment following ischemic injury in the rat. ATP has been shown to be catabolized in tissues during hypoxia to yield increased levels of hypoxanthine. Normally, xanthine oxidase acts quickly on hypoxanthine, oxidizing it to xanthine. During ischemia, with reduced oxygen availability, xanthine oxidase is converted to a form capable of producing superoxide. Upon reperfusion, a sudden increase in available oxygen in the presence of accumulated reduced substrate results in rapid formation of active oxygen species and oxidative stress. Allopurinol, a drug used to treat hyperuricacidemia (gout) in humans, inhibits xanthine oxidase activity and reduces lipid peroxidation in the ischemic injury model, further supporting a relationship between ATP catabolism and oxidative stress. Ischemic cell injury is associated with a precipitous influx of calcium from the extracellular to the intracellular compartment which activates calcium-dependent phospholipase and cysteine proteases (calpains), resulting in breakdown of cell membranes with production of toxic free fatty acids and lysophospholipids. The calcium channel blocker verapamil provides partial protection from the irreversible cell injury of ischemia, confirming involvement of this mechanism in ischemic injury. There is also an important role for the intercellular adhesion molecule-1 (ICAM-1) in reperfusion injury as a monoclonal antibody against ICAM-1 prevented injury in a rat model of renal ischemia. In both humans and pigs, an elaborate and similar system of interlobar and segmental arteries is present to supply the numerous kidney lobes, whereas in dogs and rodents,



segmental arteries are bypassed due to the lack of multiple medullary pyramids. As in the human kidney, there are free anastomoses between the intrarenal veins in the pig. Temporary clamping of the renal artery in pigs results in cortical infarction, whereas occlusion of the venous return results in medullary infarction. Obstruction of an arcuate artery also results in wedge-shaped infarction.

#### **5.4.30. Cyclosporine**

Cyclosporine, an immunosuppressive agent used to prevent graft rejection that inhibits calcineurin and T-cell activation, has a high rate of nephrotoxicity associated with its use in patients. Cyclosporine markedly augments the glomerular vasoconstrictor response to vasoactive hormones. Thus, cyclosporine induces an unfavorable perturbation in transmembrane signaling response, serving as a prototype for a transmembrane signaling disorder. Cyclosporine causes intensive renal vasoconstriction, resulting in decreases in RBF and GFR related to induction of renal PGs, thromboxane, and activation of intrarenal renin-angiotensin system. ET activation is considered to be critically involved in this process since coadministration of ET receptor antagonists or anti-ET antibodies inhibit cyclosporine-induced vasoconstriction. Humans receiving solid organ transplantation and cyclosporine have shown elevated levels of ET. Similarly, rats receiving short-term cyclosporine therapy show marked elevations in ET. These rats also develop elevated mean arterial pressure and reduction in glomerular blood flow due to constriction of renal vasculature that is reversed by anti-ET therapy. Acute nephropathy is characterized by pronounced apoptosis of proximal tubules that becomes overt tubule necrosis with increasing dose. Chronic treatment of cyclosporine in rats and humans is associated with glomerulosclerosis, interstitial fibrosis, and tubule atrophy, without significant AKI as an initiating lesion. The mechanism is believed to involve both local vasoconstriction and oxidative stress caused by repetitive episodes of acute vascular constriction resulting in a chronic form of tubulointerstitial disease. Interstitial fibrosis and tubular atrophy are accompanied by efferent arteriopathy, beginning in the outer medulla with extension into the medullary rays. Glomerular injury is further enhanced via stimulation of cellular immunity pathways. In Gottingen

minipigs, acute cyclosporine exposure is associated with glomerular hyperfiltration, whereas chronic treatment results in patchy interstitial fibrosis, glomerulosclerosis, and renal enlargement of the cortex.

### **5.5. Other Sites of Renal Injury**

#### **5.5.1. Distal Nephron**

Primary xenobiotic injury to the distal segments of the nephron, including the thin loop of Henle, TAL, DCTs, and collecting ducts, is much more uncommon than injury to the proximal tubules. Previously mentioned examples include obstructive nephropathies from crystalluria, retrograde nephropathy associated with melamine and cyanuric acid, and agents which result in glucosuria that predispose the papilla to pyelonephritis secondary to bacterial infection. Examples of glucosuric agents include metformin, SGLT inhibitors, and even some anticancer agents such as AKT inhibitors. Examples of drugs for which there is evidence of primary injury to distal segments include methoxyflurane, tilorone, and amphotericin B. Tilorone is an interferon inducer and causes phospholipidosis in the DCT. Functional abnormalities in the distal segments generally present as derangements in concentrating ability or acidification. Amphotericin B and methoxyflurane both result in an ADH-resistant polyuria. The mechanism of amphotericin B toxicity involves binding and interfering with cholesterol, resulting in the formation of transmembrane pores which disrupt cell membrane permeability and cause the distal tubules and collecting ducts to be more freely permeable to fluid and ions. Amphotericin B may also affect the distal nephron due to cell swelling driven by increased cation permeability in disrupted tubule cell membranes as well as hypoxic epithelial damage via renal vasoconstriction. The mechanism of methoxyflurane renal toxicity is a result of one of its fluoride metabolites inhibiting sodium chloride (and hence water) reabsorption in the TAL by damaging the function of adenylate cyclase-mediated solute transport channels.

#### **5.5.2. 2-Amino-4,5-diphenyl Thiazole HCl-related Medullary Cysts**

2-Amino-4,5-diphenyl thiazole HCl is of interest as a model for the induction of PKD

because it may help to clarify factors prerequisite for cyst development in the absence of tubular obstruction and in the presence of a normal transtubular pressure gradient. Specifically, this chemical causes a structural defect of the basement membrane as an integral step in the pathogenesis. The primary site of basement membrane injury is in the collecting duct of the outer medulla. Tubular basement membrane is principally responsible for limiting distensibility of the renal tubule.

### 5.5.3. Renal Papillary Injury

Renal papillary injury can occur under various conditions that affect medullary blood flow or solute concentration, for example, amyloidosis, DN, dehydration, and treatment with various chemicals and drugs. Among drugs, renal papillary injury is widely recognized following treatment with NSAIDs in both animals and humans (see [Section 5.5.4](#)). Chemically induced papillary necrosis has also been associated with other agents, including cyclophosphamide, dapsone, radiocontrast media, 2-BEA hydrobromide, ethyleneimine, and jet fuel petroleum in laboratory animals. 2-BEA-treated rats provide a good model for studying the morphologic changes associated with papillary insult. Reduced urine flow and increased interstitial medullary solute concentration are associated with increased drug concentration and decreased blood flow in the papilla. Correspondingly, depletion of effective plasma volume or increased solute load increases the propensity for occurrence. Decreased flow may be mediated by renin release. Drugs and metabolites often reach their highest concentrations within the filtrate of the papilla predisposing this region to injury. Both pyelonephritis and obstruction due to crystalluria are important factors in the development of spontaneous papillary necrosis ([Figure 2.33](#)). Many xenobiotics can specifically target PG pathways in the papillary interstitium, but multiple molecular mechanisms for papillary injury exist. Drug or chemical-induced lesions in the papilla of mild or subtle severity need to be distinguished from similar artifactual changes that may arise in the same region ([Seely et al., 2019](#)). Neoplasia may ultimately develop from this hyperplastic urothelium if the rat survives into old age. Neoplasia occurring secondary to RPN is of

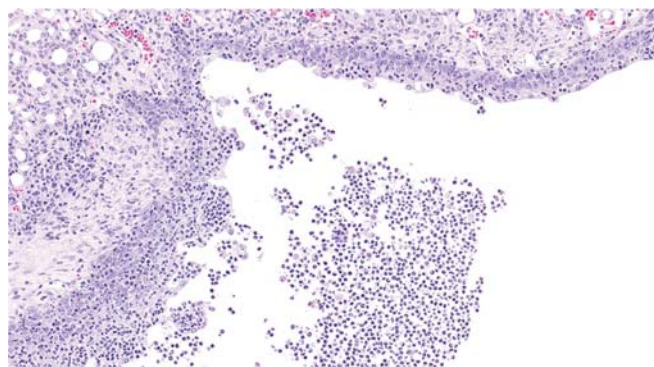


**FIGURE 2.33** Pyelonephritis and dilation of the renal pelvis in the renal papilla of a rat kidney demonstrating clusters and casts of neutrophils which extend into the lining epithelium of the papilla and expand the medullary and papillary interstitium.

limited relevance in risk assessment, since RPN is uncommon in humans and is typically linked with analgesic abuse, particularly phenacetin.

Additional tubular factors contributing to renal dysfunction include loss of tubular cell polarity, reflux of tubular fluids, and inflammatory processes, which lead to compromised renal microvasculature. The ultimate indicator of renal dysfunction, reduced GFR, may reflect primarily altered glomerular hemodynamics, as occurs during hypovolemic shock or endotoxemia, or with extremely high doses of gentamicin which alters the charge of the glomerular filter barrier. Obstruction of the tubule lumen causes increased intratubular pressures and activation of tubuloglomerular feedback that also leads to GFR decreases and eventually nephron collapse. Chemical warfare agents such as organophosphates can produce acute renal damage. Nonlethal acute exposure to sarin has been associated with significant reduction in GFR, oliguria, retention of electrolytes, hematuria, and glucosuria.

### 5.5.4. NSAID-Related Nephrotoxicity

As noted above, NSAIDs have been associated with RPN in both humans and animals ([Figure 2.34](#)). In addition to renal papillary injury, other renal effects of NSAIDs include AKI, fluid and electrolyte disturbances in humans, monkeys, rats, and dogs; nephrotic syndrome, AIN in humans; and outer cortical atrophy with interstitial fibrosis in dogs, monkeys, and human infants. Conditions that result in plasma volume contraction (e.g.,



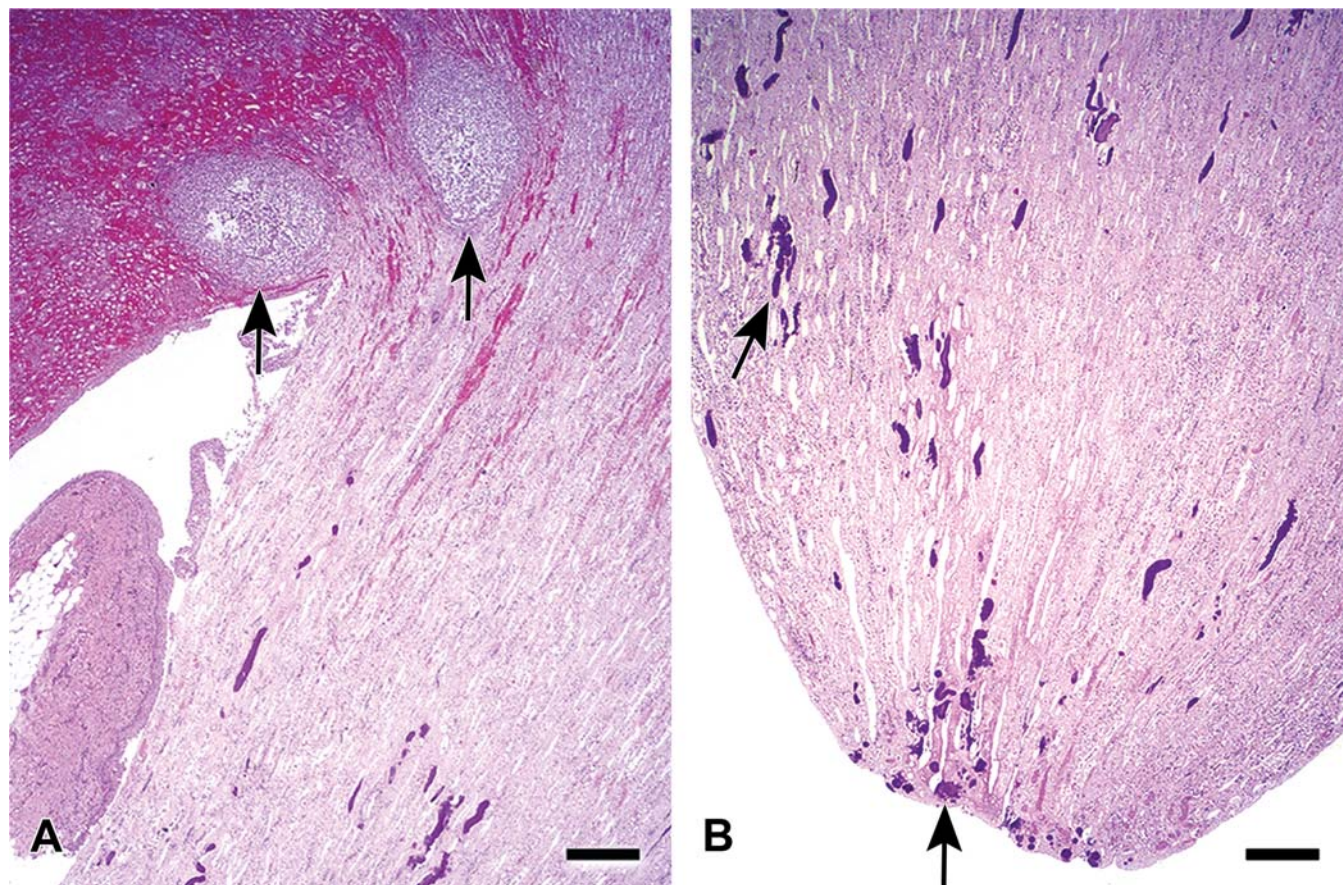


**FIGURE 2.34** Kidney from a dog treated with an antiinflammatory drug resulting in gastrointestinal ulceration and secondary septicemia. (A) Note corticomedullary thrombosis (arrows) and perivascular hemorrhages secondary to septicemia. (B) Note diffuse acute necrosis involving the papilla along with multifocal bacterial colonies (arrows). Bar = 450 mm. Reproduced from Haschek WM, Rousseaux CG, Wallig MA, Bolon B, editors: *Haschek and Rousseaux's handbook of toxicologic pathology*, ed 3, 2013, Academic Press, Figure 47.40, p. 1758, with permission.

hemorrhage, salt loss, hypoalbuminemia), congestive heart failure, cirrhosis, and ascites cause a homeostatic increase in vasoconstrictors including norepinephrine and angiotensin-II. Vasodilatory effects of PGs at the afferent arteriole counterbalance this vasoconstrictor effect to maintain GFR and renal perfusion. NSAIDs importantly selectively inhibit COX-2 or alternatively nonselectively inhibit both COX-1 and COX-2 isoforms which results in the inhibition of prostacyclin production without the inhibition of thromboxane production. Loss of PGs by NSAID inhibition of COX (especially at the afferent arteriole) results in pronounced vasoconstriction and a decrease in glomerular capillary pressure resulting in a decline of GFR. AKI in humans associated with NSAID treatment is caused by this hemodynamic effect as a result of loss of counter-regulatory PGs. These

PGs exert modulatory influences on many ion transport sites along the nephrons and are important in sodium and water homeostasis in the kidney. Thus, NSAID inhibition of renal PGs interferes with PG-mediated sodium chloride transport, ADH, and distribution of blood flow from cortical to juxtamedullary nephrons. The sodium and water retention manifests clinically as edema. PGs also regulate renin release and thus indirectly affect aldosterone production. NSAID treatment may result in hyporeninemic hypoaldosteronism. Aldosterone is important in potassium excretion from the DCTs and collecting ducts. The combination of loss of vasodilatory PGs, loss of PG effects on platelets, accumulation of drug in the papilla at higher concentrations, and production of reactive metabolites are considered responsible for papillary necrosis. Papillary injury occurs with



structurally dissimilar compounds that share the ability to inhibit PG synthesis, suggesting that redistribution of PG-dependent medullary blood flow may contribute to the development of papillary injury due to prolonged medullary ischemia. No remarkable changes in renal functions occur if lesions are localized to the tip of the papilla.

In experimental studies, papillary necrosis is produced readily in rats, occasionally in rabbits and dogs, and rarely in monkeys. As a chronic consequence of papillary injury, rats develop urothelial neoplasia. The pig appears to be refractory to NSAID papillary necrosis and has not been shown to develop the lesion at levels substantially above those causing it in rats (1 g/kg/day of salicylate in the pig for 10 months with no effect vs. 250 mg/kg as a single dose in rats resulting in papillary necrosis). Several morphologic features in rats likely predispose them to papillary injury including a well-developed inner medulla, unipapillary kidney, higher urine-concentrating capacity, exclusive postglomerular tuft blood supply to the papilla, and increased NSAID or metabolite papilla concentration on a mg drug/kg body weight basis. Along with these factors, interspecies differences in COX isoform distribution may explain the enhanced susceptibility of rats as compared to other species. Both COX isoforms are expressed in the kidneys of laboratory animal species, but localization and level of basal expression may differ. While regional localization of COX-1 appears similar across species, significant interspecies differences exist in COX-2 localization (Khan et al., 2002). COX-1 is expressed at high levels in the collecting ducts, papillary interstitial cells, and renal vasculature of all species. Basal levels of COX-2 are present in the macula densa, TALs, and papillary interstitial cells in adult rats, dogs, and mice and in other species only under conditions of elevated renin such as hypertension, DN, and congestive heart failure (Khan et al., 2002). Due to wide distribution of COX-2, rats, dogs, and mice are likely more sensitive to the consequences of COX-2 inhibition in kidney as renal medulla and papilla are the major sites of PG production.

COX-2 expression in the macula densa and TAL of immature and developing nephrons of fetal and newborn kidneys is significantly higher

than in the mature kidney, and declining to negligible levels by 2 months after birth. Because of the high expression levels, COX-2 in immature kidney is considered to play a role in nephron development via cell differentiation and by maintaining RBF to individual nephrons in counterbalance to the renin-angiotensin system. COX-2 knockout mice and human infants born from mothers given NSAIDs in the third trimester are shown to exhibit renal abnormalities considered to be associated with the inhibition of COX-2. Microscopically, these lesions are similar to those seen with chronic hypoperfusion of the kidney primarily in the outer cortex (Figure 2.35) and include glomerular tuft atrophy with dilatation of Bowman's spaces (atubular glomeruli), accumulation of proteinaceous fluid within Bowman's spaces and tubules, persistence of immature glomeruli, tubular atrophy and loss, interstitial fibrosis, and thickened arteriolar walls (Khan et al., 2002).

The mechanism for interstitial nephritis with NSAIDs is unknown, but up to 5% of renal lesions in humans are attributed to conventional NSAIDs. AIN, sometimes accompanied by nephrotic syndrome may follow chronic NSAID treatment. Ultrastructurally, patients with nephrotic syndrome show minimal change glomerulopathy with marked podocyte foot-process effacement.

## 5.6. Renal Carcinogenesis

Renal cell cancer is important in humans; approximately 3% of all malignancies in humans arise in the kidney. Of these, 80%–90% arise in the PCT and are designated RCCs. RCCs usually arise after 40 years of age, with a peak incidence in the sixth and seventh decades of life. Males are affected approximately two to three times as frequently as females. Renal adenomas are much more frequent, with incidence as high as 20% in randomly autopsied patients. Over 85% of these adenomas occurred in kidneys with glomerulosclerosis. Epidemiologic studies indicate that renal cancer appears to be increasing in incidence on a global basis. This increase is associated with both the more widespread use of diagnostic imaging and increasing prevalence of established risk factors such as cigarette smoking, obesity, and hypertension. Association

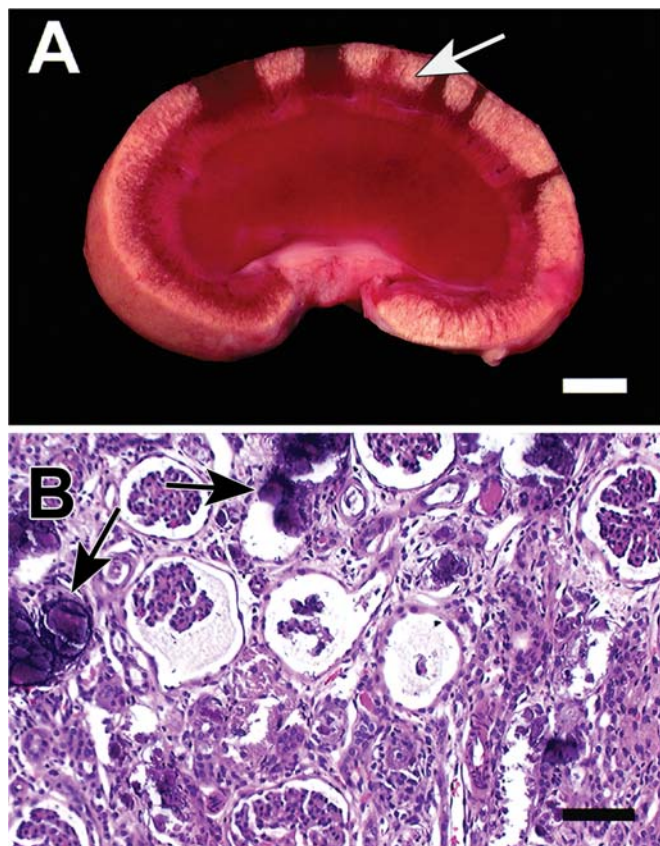


**FIGURE 2.35** Ischemic lesions are present in the outer cortex of a dog kidney secondary to reduced renal perfusion from renal artery constriction. Note presence of necrosis in (A) the outer cortex (arrow) and sparing of inner cortex, medulla, and papilla. Bar = 5 mm. (B) Photomicrograph from same kidney showing tubular epithelial necrosis, tubular mineralization (arrows), and glomerular tuft atrophy. Bar = 50 mm. Reproduced from Haschek WM, Rousseaux CG, Wallig MA, editors: *Handbook of toxicologic pathology*, ed 2, 2002, Academic Press, Figure 28, with permission.

with other factors such as caffeine, carbonated soft drinks, hydrocarbon solvents, and gasoline has not been substantiated. Nephrotoxicity due to drugs and chemicals can manifest itself as a proliferative lesion. The renal tumor that is the most relevant to humans with respect to risk assessment is of tubule origin, termed renal tubule tumor in rodents and RCC in humans. Nephroblastoma has been induced in rats by genotoxic chemicals (such as streptozotocin) and direct-acting nitrosoureas administered transplacentally. The first successful *WT1* mutant mouse tumor model was published in 2011; however,

a newer transgenic mouse model has been developed, the  $Wt1^{-/f}H19^{+/-m}Cre^{ERTM}$  mouse, which develops tumors earlier, and with histologic and genetic features as well as response to anticancer therapeutics similar to the human (Sobczuk et al., 2020).

Understanding of the potential mechanisms underlying the development of chemically associated cancer has increased markedly over the years, often stimulated by carcinogenicity bioassay results. In particular, there has been the accumulation of knowledge on key, often histopathologic, events occurring on a causal pathway leading to cancer in target organs during subchronic phases of study, which are now referred to as modes of action. In the rat kidney, modes of action can include evidence of cytotoxicity, increased cell proliferation, and hyaline droplet nephropathy due to chemical binding to the protein alpha<sub>2</sub>μ-globulin. The latter mode of action (MoA) is rat-specific and has been judged not relevant to humans by regulatory and authoritative bodies. Prior to the addendum to International Council for Harmonisation (ICH, 2021) S1B(R1), carcinogenicity testing guidelines required a lifetime (2-year) rodent bioassay, usually conducted in the rat, and an additional lifetime or shorter-term assay in a second species, typically the mouse. The utility of the 2-year rodent bioassay has been called into question and retrospective analyses suggest that the lifetime rat bioassay does not always provide further value to cancer hazard identification or risk assessment (Benfenati et al., 2009). Rather an integrated, weight-of-evidence-based approach is recommended. For information on mechanisms of carcinogenicity and the ICH S1 proposed addendum, see *Carcinogenesis: Mechanisms and Evaluation*, Vol 1, Chap 8 and *Carcinogenicity Assessment*, Vol 2, Chap 5.

A retrospective analysis of the NTP 2-year rodent bioassay database showed approximately 10% of the almost 600 chemicals assessed having some or clear evidence of carcinogenicity for the rodent kidney, typically resulting in renal tubule tumors (rarely urothelial tumors of the renal pelvis or ureter). None of the chemicals in the NTP series induced nephroblastoma, RMT, or lipomatous tumor (Hard, 2018a, 2018b). Renal tumors are rarely reported in the 26-week transgenic rasH2 carcinogenicity model and, to date, only one publication identified spontaneous

occurrence of renal tubule tumors similar to the familial amphophilic–vacuolar phenotypic variant that occur in SD, Wistar and Fischer 344 rats. The authors traced the lineage of the affected mice and did not find evidence of a familial association (Paranjpe et al., 2016). A retrospective analysis of chemicals that had been tested for both carcinogenicity and subchronic toxicity by the NTP, focusing on three organ systems, including kidney, showed that five of the 16 chemicals produced renal tubule tumors in the 2-year studies and four of these were associated with histopathologic alterations in the respective 13-week toxicity studies. The histologic findings included hyaline droplet accumulation (anthraquinone, decalin), apoptosis (fumonisin B<sub>1</sub>), regeneration (benzophenone, decalin, fumonisin B<sub>1</sub>), or exacerbated CPN (anthraquinone). In addition, all five chemicals cited above, including methyleugenol, were associated with the nonspecific finding of increased kidney weight, both absolute and relative, at 13 weeks. The combination of kidney weight and histopathologic change at 13 weeks for this series of chemicals identified all of the renal carcinogens. However, there were also false positives in this analysis, as some chemicals that did not produce renal tumors after 2 years were associated with renal lesions or organ weight increase at 13 weeks. These analyses led to the conclusion that 13-week studies using conventional endpoints were not adequate to identify all nongenotoxic chemicals with the potential to produce tumors by 2 years in rats (Hard, 2018a, 2018b). Additional endpoints, such as bromodeoxyuridine (BrdU) labeling for cell turnover or a measure of apoptosis, were suggested as possible complements to the routine evaluation. However, these assessments do not address the utility of this strategy in predicting for human carcinogenesis. Traditional lifetime rodent bioassays are recognized to have a substantive false negative rate and an egregious false positive rate in predicting for human pharmaceutical cancer risk.

On the basis of the evidence accumulating from studies with chemical agents, a list of mechanisms is proposed by which chemicals are believed to produce, or be associated with, an increase in renal tumors in the rodent. This mechanistic approach has been used to analyze and categorize the chemicals in the NTP

database. The possible mechanisms of xenobiotic-induced carcinogenesis are summarized in Table 2.18. These mechanisms include direct or indirect DNA reactivity, multiphase bioactivation usually involving glutathione conjugation in liver and subsequent enzymatic activation in kidney, mitotic disruption, direct or indirect cell damage stimulating a sustained regenerative response (from direct cytotoxicity or disruption of a physiologic process), exaggerated pharmacologic response, species-dominant metabolic pathway, or exacerbation of CPN. Renal carcinogenesis associated with direct or indirect cytotoxicity, exaggerated pharmacologic response, species-dominant metabolic pathway, and CPN involves nongenotoxic chemicals.

### 5.6.1. Genotoxic Xenobiotics

Current knowledge of chemical renal carcinogenesis has its foundations in early work in developing chemical induction models of renal cancer and studying tumor pathogenesis. For renal tubule tumors, these earlier models employed genotoxic carcinogens such as N-nitrosomorpholine, N-nitrosodimethylamine, N-(4'-fluoro-4-biphenyl)acetamide, and N-ethyl-N-hydroxyethyl nitrosamine. These various studies provided evidence that renal tubule tumor is preceded by a stage of tubule alteration involving hyperplasia of the lining epithelium. It is now generally accepted that this alteration, known as atypical tubule hyperplasia, is a precursor of, and on a continuum with, renal tubule adenoma and carcinoma. It has also been shown recently that atypical tubule hyperplasia has the morphological characteristics of an expansive lesion. Foci are surrounded peripherally, at least partially, by attenuated fibroblasts and/or capillaries, and they have a high DNA synthesis labeling rate, indicating that the lesion is expanding in size, and on the pathway to becoming an adenoma. Consequently, induction of foci of atypical tubule hyperplasia by a chemical in a truncated bioassay predicts that the test chemical is a renal carcinogen, when administered over a lifetime.

Many chemicals require metabolic conversion to exert their genotoxic and consequent carcinogenic potential. Resultant electrophilic intermediates covalently bind renal macromolecules, including nucleic acids. Aflatoxin B<sub>1</sub>, dimethylnitrosamine, daunomycin, and 2-aminofluorene



**TABLE 2.18** Examples of Agents Illustrating Main Mechanisms of Renal Tubule Tumor Formation in Rodent Models with or without Relevance for Human Risk Assessment

Mechanism	Example agent(s)	Notes
Direct DNA reactivity	Dimethylnitrosamine, N-nitrosomorpholine, N-ethyl-N-hydroxyethylnitrosamine, and N-(4'-fluoro-4-biphenyl)acetamide	While some genotoxic compounds can induce tumor formation without metabolic activation, most genotoxic compounds require metabolism to a reactive intermediate
Indirect DNA reactivity through free radical formation	Ferric nitrilotriacetate, potassium bromate	Indirect genotoxicity is mediated by oxidative stress with free radical formation and through electron imbalance producing cytotoxicity and DNA damage
Multiphase bioactivation involving glutathione + A31one (GSH) conjugation	Hexachlorobutadiene, chlorothalonil, trichlorethylene, and some quinones	Transformation into nephrotoxic GSH S-conjugates resulting in generation of biologically reactive intermediates
Mitotic disruption	Ochratoxin A	Histologically, degeneration and single cell necrosis of renal tubule epithelium in pars recta, sustained tubule cell proliferation, and karyomegaly (increased ploidy). Chronically, formation of hyperplastic foci consistent with the precursor of RTTs
Sustained cell proliferation from direct cytotoxicity	Fumonisin B <sub>1</sub>	Sustained nephrotoxicity with PCT cell degeneration/regeneration, and simple tubule hyperplasia; renal tumor development may be an outcome of continued cell loss and compensatory regeneration. <b>Some agents such as fumonisin B<sub>1</sub> may not be relevant mechanisms for human risk assessment</b>
Sustained cell proliferation by disruption of a physiologic process (i.e., $\alpha$ 2 $\mu$ -globulin nephropathy)	Unleaded gasoline, 1,4-dichlorobenzene, D-limonene and decalin	Noncovalent, reversible binding of the chemical or its metabolite to $\alpha$ 2 $\mu$ -globulin. Histologically, hyaline droplets within the PCT cytoplasm and lumen with tubular degeneration/regeneration and dilatation and interstitial inflammation. Sustained cell loss and compensatory regeneration is hypothesized to be the stimulus leading to development of RTT; <b>male rat-specific process not relevant for human risk assessment</b>
Exaggerated pharmacologic response	Alpha-glucosidase inhibitors (acarbose)	Hypothesized that RTT developed due to exaggerated pharmacologic response of glucose deprivation resulting in extreme malnutrition. <b>Not considered relevant for human risk assessment</b>

(Continued)

**TABLE 2.18** Examples of Agents Illustrating Main Mechanisms of Renal Tubule Tumor Formation in Rodent Models with or without Relevance for Human Risk Assessment—cont'd

Mechanism	Example agent(s)	Notes
Species-dominant metabolic pathway	SGLT2 inhibitor with male mouse specific metabolite generation	Nongenotoxic mode-of-action for rodent RTT induction involving species- and sex-specific metabolism by the male mouse. <b>Not relevant for human risk assessment</b>
Chemical exacerbation of CPN	Hydroquinone, ethyl benzene, quercetin, coumarin, and primidone	Lesions low grade but increased incidence of atypical tubule hyperplasia (precursor to RTTs), adenoma, and RTTs in rats with most severe CPN. <b>Not relevant for human risk assessment</b>

alpha 2μ-globulin = α2u-g; CPN = chronic progressive nephropathy; GSH = glutathione; PCT = proximal convoluted tubule; RTT = renal tubule tumor (Hard, 2018a, 2018b)

exemplify this concept. Genotoxic renal carcinogens share the propensity to exert their biologic effect in multiple species, strains, sexes, and tissues. Tissue site, strain, sex, and species differences in response to exposure parallel the capability of the target site to accumulate and metabolize the xenobiotic, as shown with nitridazole and dimethylnitrosamine. Furthermore, genotoxic renal carcinogens typically induce tumors rapidly, in high incidence, and with minimal duration of exposure. Rodent experiments with bleomycin sulfate, 1,2-dimethylhydrazine, ENU (N-ethyl-N-nitrosourea), azoxymethane, and dimethylnitrosamine demonstrate this potential. Some genotoxic renal carcinogens (ENU), when administered in utero, induce nephroblastoma, which is a counterpart of Wilm's tumor in juvenile humans. Other genotoxic chemicals administered prenatally (during renal immaturity) typically induce RMTs in the rat. By contrast, after onset of sexual maturity, agents inducing RMT during immaturity primarily induce tubule neoplasia. Dimethylnitrosamine is a model agent for this age of exposure factor.

Xenobiotics inducing renal tumors in multiple species and both sexes suggest the presence of human renal carcinogenic potential (e.g., ochratoxin A) if comparable exposures are achieved in humans. Variations in tumor response can be quantitative, based on varying levels of metabolic conversion and adduct formation at the target cell level. Species and sex variability frequently exists in metabolism of xenobiotics. Correlative differences in sensitivity to the toxic

and carcinogenic effect of xenobiotics causing injury following derivation of reactive metabolites can be observed. Genotoxic renal carcinogens are nephrotoxic; however, the cytotoxic event and associated repair processes usually are not considered essential factors in the eventual tumor development. The cytotoxic responses typically include proximal tubular cell necrosis, and sometimes karyomegaly of proximal tubular epithelium. These genotoxic xenobiotics also can cause increased relative kidney weight in animals upon repetitive exposure. This is presumably associated with stimulated renal MFO activity.

### 5.6.2. Heavy Metal Carcinogens

Several heavy metals share structural and functional renal effects in the rodent species. Metals that have been carefully scrutinized, including chromium, mercury, nickel, and lead, induce genetic injury and may interact or bind directly with DNA. Several metals are carcinogenic in rodent kidneys—for example, lead, nickel, gold, chromium, and mercury (organic). The carcinogenic response typically is not species or strain specific. The accumulation of the metal at the tissue target site is prerequisite to the carcinogenic response. The solubility of the metal complex, the vehicle for the metal, and the dose level and duration of treatment all influence the metal's carcinogenic potential in rodents. Each of these latter factors presumably influences the critical target tissue level. Similarly, the chemical form of the metal influences its carcinogenic potential.

Carcinogenic heavy metals have nephrotoxic potential, characterized by ATN if administered at sufficiently high levels. Increased tubular replicative rate occurs, even at doses failing to induce oncotic cell necrosis, presumably associated with increased apoptotic necrosis. In subchronic and chronic studies at carcinogenic levels, these metals induce karyomegaly and cytomegaly in proximal tubular epithelium. The karyomegalic cell has not been demonstrated as a precursor cell (preneoplastic change) in the cancer response. Nonetheless, karyomegaly may represent a useful short-term marker of renal events occurring relevant to the carcinogenic process. Heavy metals that induce nephrotoxicity, interact with DNA, or accumulate in the nucleus, and that are nephrotoxic (with karyomegaly) in subchronic studies can be predicted to be rodent renal carcinogens if tested in lifetime studies at doses inducing these short-term effects. The relevance of this rodent response for higher species, including humans, has not been demonstrated. In part, this may be because the high levels required to induce precursor lesions are unlikely to be encountered outside the laboratory setting.

### **5.6.3. Mechanisms of Nongenotoxic Rodent Renal Carcinogenesis**

Several chemicals exert a nephrotoxic response which apparently forms a prerequisite event in the tumorigenic process. The toxic injury is manifest by increased apoptosis, replicative rate increase, and hyperplastic response in tubular epithelium (Table 2.15). Exposure must occur over the majority of the rodent's lifespan and tumors appear late, usually well after 1 year of treatment. Tumor incidence often is low and toxic tubular tumorigens typically do not interact directly with DNA and are not considered genotoxic, as evaluated in short-term assays. However, several chemicals tested in rodent cancer bioassays have not been demonstrated to cause tumors despite the presence of chronic toxic injury, possibly because of the limitations of the bioassay to detect weak tumorigens. The tumor potential of nephrotoxic antibiotics such as netilmicin and gentamicin has not been assessed with the duration criterion for chemicals in this mechanistic class.

### **5.6.4. Lysosomal Enzyme Release**

Several mechanisms by which toxicity occurs can be conceptually linked to cancer induction. For example, lysosomal overload may destabilize lysosomal enzymes, resulting in release into the cytosol and opportunity to interact with nucleic acid. Lysosomal enzymes RNase and DNase have been demonstrated to have genotoxic potential. This enzyme leakage may not only be relevant in tumorigenesis but also represents a potential toxicity mechanism wherein the cell undergoes necrosis. Two models of extensively studied rodent toxic tubular tumorigens include the inducible alpha<sub>2</sub>μ-globulin nephropathy syndrome and the NTA-treated rodent. In both of these syndromes, phagolysosomal swelling occurs. In the alpha<sub>2</sub>μ-globulin nephropathy syndrome, the swelling occurs because of alpha<sub>2</sub>μ-globulin accumulation. In the NTA model, the swelling is osmotic in nature, associated with zinc overload. In both models, the chronic toxicologic response has been demonstrated to be inexorably linked with the tumor response (Figure 2.36).

### **5.6.5. Oxidative Stress/Chronic Inflammation**

Oxidative stress can be mediated chemically and has been linked to genetic injury. Active oxygen species clearly have the potential to interact with nucleic acid or any protein in their milieu. ROS derived in oxidative stress bind covalently with DNA, creating promutagenic DNA modifications with 8-hydroxy-2-deoxyguanosine (8-OHdG) as an example. Increased levels of oxidative stress can be quantified by determining 8-OHdG levels in the urine. A potential model for this mechanism is the rodent treated with xenobiotics inducing peroxisomal proliferation, potassium bromide, and the ferrous salt of NTA administered parenterally. NO and its derivatives produced in inflamed tissues can contribute to carcinogenesis. Following reaction of NO with oxygen and superoxide, electrophiles are formed. Specifically, peroxynitrite-induced adducts and single-strand breaks of DNA can result from increased tissue NO concentration. Chronic inflammation in the kidney can clearly be linked with increased risk for renal cancer.



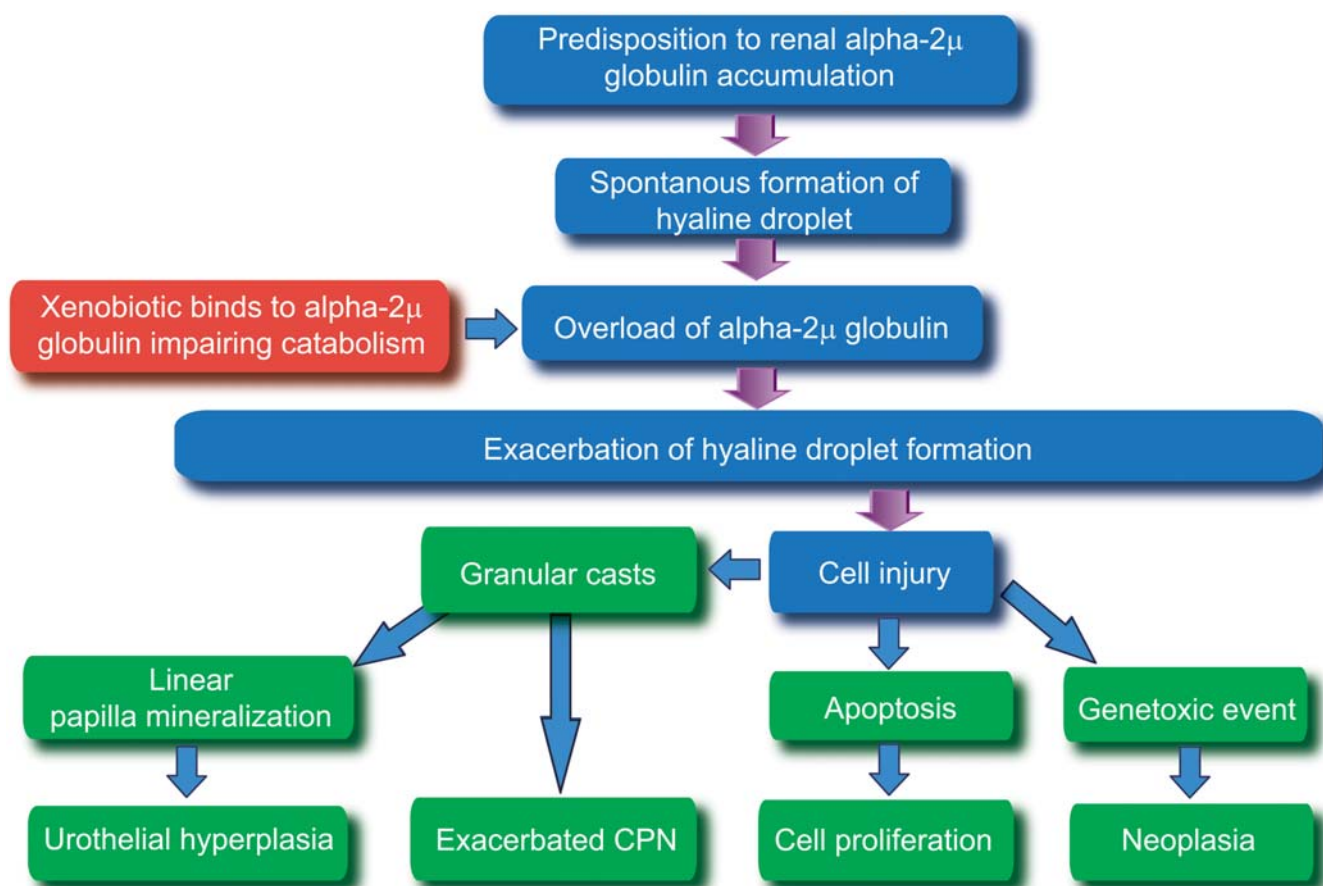


**FIGURE 2.36** Schematic pathogenesis of the specific lesions occurring in inducible male rat alpha2μ-globulin nephropathy syndrome. Reproduced from Haschek WM, Rousseaux CG, Wallig MA, Bolon B, editors: Haschek and Rousseaux's handbook of toxicologic pathology, ed 3, 2013, Academic Press, Figure 47.38, p. 1752, with permission.

#### 5.6.6. Sustained Increase of Replicative Rate and Apoptosis

Sustained replicative rate increase, as well as perturbed rate of apoptotic necrosis, have been suggested as risk factors for carcinogenesis in the kidney. Chronic toxicity can be presumed to be associated with a persistent replicative increase and perturbed apoptotic rate. Examples include β-cyclodextrin, folic acid, agents inducing the male rat-specific alpha2μ-globulin nephropathy and fumonsin-B<sub>1</sub>.

#### 5.6.7. Heritable Change without Direct Xenobiotic Effect on DNA

Alternative mechanisms to direct injury of DNA for heritable genetic change have been identified. One example of an alternative mechanism involves the alteration of DNA methylation. DNA methylation plays a role in the regulation of gene activity. Hypomethylated

genes possess an increased potential for expression as compared to a hypermethylated gene. Changes in the methylation status of a gene via xenobiotic exposure provide a mechanism by which its potential for expression can be altered in a heritable but epigenetic manner. A second example of an alternative mechanism is the selective loss of the p53 gene reported to occur via intensive selection pressure associated with persistently unregulated apoptotic necrosis. Although the specific molecular pathways explaining nongenotoxic agent carcinogenesis are unknown, it remains certain that heritable genetic change is a prerequisite in carcinogenesis.

#### 5.6.8. Exacerbation of CPN and Renal Tumors

Recent work has shown that advanced CPN in control rats is a risk factor for developing renal

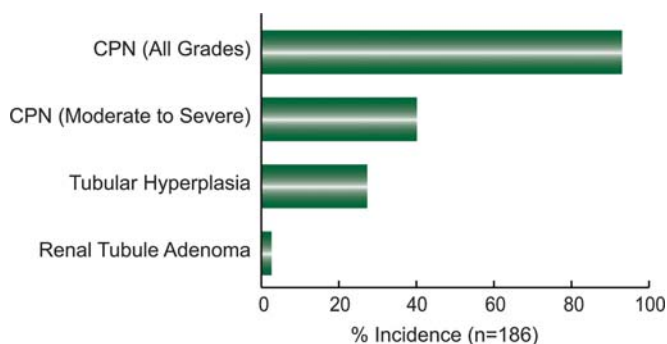


**FIGURE 2.37** Close association between severe chronic progressive nephropathy, hyperplasia, and neoplasia in male control Sprague–Dawley rats in a 2-year carcinogenicity study. *Reproduced from Haschek WM, Rousseaux CG, Wallig MA, Bolon B, editors: Haschek and Rousseaux's handbook of toxicologic pathology, ed 3, 2013, Academic Press, Figure 47.41, p. 1763, with permission.*

tubule tumors (strictly adenomas) and their precursors, foci of atypical tubule hyperplasia (Figure 2.37). This may be because of the high rate of cell turnover that characterizes some of the CPN-affected tubules throughout its progression. In the F344 male rat with end-stage CPN, the incidence of these precursor and neoplastic lesions combined can exceed 20%. In cases where chemicals exacerbate this spontaneous process to advanced stages (including end-stage kidney), there may be a dose-related increase in renal tubule tumors in the 2-year carcinogenicity bioassay. In an investigation assessing the predictiveness of CPN exacerbation in NTP studies, there was a statistically significant increase in renal tubule tumors at 2 years, where CPN had been exacerbated by the chemical at 13 weeks, and early CPN exacerbation had predicted renal tumor outcome with 100% sensitivity and 88% specificity. Such a finding does not necessarily indicate that the chemical is a renal carcinogen, as the risk for spontaneous development of adenomas will increase with increasing exacerbation of the severity of CPN. As a potential MoA in rodents, CPN exacerbation is unlikely to be relevant for species extrapolation in risk assessment.

### 5.6.9. Modifying Factors in Renal Tumorigenesis

Initiation promotion concepts have been widely studied in the skin, urinary bladder, liver,

lung, intestine, and thyroid. In comparison, renal tumor promotion models are not as well defined. Xenobiotics that significantly enhance the carcinogenic potential of an initiator but that do not independently induce nephrotoxicity or renal cancer are usefully considered in this mechanistic category. The only reasonably well-defined renal tumor promoters are nicotinamide and peroxisomal proliferators. Nicotinamide apparently is metabolized within the kidney and increases kidney size as a presumed consequence of adaptive increase of microsomal enzyme synthesis in subchronic exposures. The mechanism of promotion is unknown, although stimulation of increased oxidative stress has been proposed. In additional support of this promoter concept, peroxisomal proliferators have been demonstrated to promote renal tubular tumors. Initiators used in renal tumor promotion studies typically include N-ethyl-N-hydroxyethylnitrosamine or diethylnitrosamine.

### 5.6.10. Nutritional Factors

Dimethylnitrosamine is a potent single-dose carcinogen for rat kidney, if administered with preconditioning by a high-carbohydrate no-protein diet. This protein starvation reduces liver microsomal enzyme activity, permitting a sufficient quantity of unmetabolized carcinogen to reach the kidney for metabolic transformation. Furthermore, complex interrelationships exist among divalent cations in the biologic system. For example, iron–NTA complexes administered parenterally induce renal tumors, whereas the aluminum salt, similarly administered, does not.

### 5.6.11. Hormonal Influence on Renal Carcinogenesis

Estrogens induce a high incidence of renal tubular cancer in male Syrian hamsters. However, the carcinogenic potential cannot be correlated with the estrogenic hormonal potency. Estrogen has been demonstrated to accumulate in renal cortex, to be metabolized to a reactive intermediate, and to form covalent DNA adducts at the tumor target cell site. Furthermore, short-term tests have demonstrated genotoxic potential for estrogen. The mechanism of estrogen carcinogenicity in the hamster kidney remains uncertain, despite these observations. Hormonal status also clearly can influence the carcinogenic response

of other genotoxic chemicals. For example, the renal tumor response to dimethylnitrosamine and chloroform can be abolished by castration of male mice. The influence of hormones on chemical carcinogenesis probably can occur for multiple reasons. The latter example may be explained by sex-hormone influence on metabolizing-enzyme activity in the proximal tubule.

#### 5.6.12. Aging

The rate of tubular cell proliferation tends to decrease and cell cycle time tends to increase with age in rodent kidneys. Additionally, a reduction of drug metabolism activity in tubular epithelium occurs with age. Correspondingly, the older rat is more resistant to renal tumor induction with genotoxic agents such as N-methyl-N-nitrosourea or irradiation than the young rat. The relationship between these aging changes and carcinogenesis is biologically complex. A spontaneous increase in chromosome alterations occurs with age in rats; this may potentially, in part, explain the increase in spontaneous renal tumor incidence with age. When exploring the relationship of the common endemic age-associated lesions of the laboratory rat, CPN, and tubular tumorigenesis, two factors are of note. First, despite the renal parenchymal decline of replicative rate, there is an increase in replicative rate on a nephron basis associated with progression of CPN. Tubules lined by cells with cytoplasmic basophilia exhibit increased replicative rates compared with tubules lined by epithelial cells with the normal eosinophilic tinctorial appearance. Because of the importance of growth stimulation in tumorigenesis, this individual nephron replicative rate increase may have significance when considered in association with age-associated chromosome alterations in spontaneous tumorigenesis. Second, toxic renal tumorigens typically increase incidence or severity of CPN, which clearly increases the number of nephrons with increased mitotic activity.

## 6. ISSUES IN DRUG DEVELOPMENT

### 6.1. Animal Models

Animal models of human renal disease have been explored to understand the molecular

mechanistic complexity and pathogenesis of renal disease to discover and validate therapeutic targets, demonstrate efficacy of novel drug candidates, and explore potential new renal safety and efficacy biomarkers. Mice and rats are by far the most common animal models employed due to their wide availability, ease of breeding and housing, and our ability to modify their genomes (see *Animal and Alternative Models in Toxicologic Research*, Vol 1, Part 3). Models include spontaneous and inbred strains, genetically engineered rodents (see *Genetically Engineered Animal Models in Toxicologic Research*, Vol 1, Chap 23), and surgical, and chemically induced models. Common models of acute and chronic kidney injury will be briefly reviewed here. For renal cancer models, please refer to [Section 3.4](#).

Awareness of strain genetics and gender differences will direct the investigator to appropriate model selection. For example, C57BL/6 mice do not develop significant proteinuria, glomerulosclerosis, interstitial fibrosis, and hypertension when used in multiple renal disease models and this needs to be considered if C57BL/6 is the background strain in the transgenic or knockout model. C57BL/6 are also refractory to adriamycin (doxorubicin) nephrotoxicity and streptozotocin-induced DN. Mouse strains with only a single renin gene (such as C57BL/6) have decreased RAAS activity leading to resistance in development of renal fibrosis of the remnant kidney in the subtotal nephrectomy model (as compared to the preferred strain with two active renin genes, the 129Sv). Nude mice strains have high background incidences of hyaline glomerulopathy. Sex also influences outcome of many models. Male rodents are more sensitive to age-dependent glomerular injury, ischemic renal injury, progression of PKD (androgens enhance more rapid cyst formation), and streptozotocin-induced nephropathy (17 $\beta$ -estradiol protects pancreatic  $\beta$  cells from oxidative injury in females). Male rodents also have higher CYP450 activity in PCTs which can be many fold higher than females.

#### 6.1.1. Acute Kidney Injury Models

The hallmark of AKI is the sudden loss of renal excretory function which can trigger a cascade of multiorgan failure and mortality as well as development of CKD. Causes of AKI include:



(1) reduced blood flow to the kidneys (prerenal) leading to reduced GFR such as from low blood pressure or a hypovolemic state; (2) direct renal injury (intrinsic) culminating in acute tubule necrosis from ischemia or nephrotoxicity such as infarction events from blood clots or certain medications; or (3) obstruction (postrenal) from kidney stones, cancer, or an enlarged prostate in men. Prerenal and intrinsic injury often occur as a continuum. Animal models of AKI must encompass the main pathophysiological occurrences in the human patient including vasoconstriction and endothelial dysfunction, tubule epithelial cell injury and death, and immune cell infiltration. Current models of AKI attempt to replicate these conditions and examples include IRI model (prerenal), direct renal injury in chemically induced or sepsis models, and obstructive insult such as the unilateral ureteral obstructive (UUO) model. Hospitalized patients are particularly susceptible to AKI due to underlying issues, risk factors, and medical treatments such as hypovolemic state, heart disease, sepsis, diabetes mellitus, hypertension, cardiac surgery, rhabdomyolysis, and use of nephrotoxic drugs.

#### **6.1.2. Ischemia Reperfusion Injury Models**

Renal ischemic events are the most common causes of clinical AKI. The IRI model is the most utilized rodent model of AKI but also can be applied to large animals such as dogs or pigs. Generally, this model employs bilateral ischemia as this is considered most relevant to clinical presentation. Histologically, tubule degeneration/necrosis with dilatation and loss of brush border occurs most severely at the S3 segment of the proximal tubules along the outer stripe of the medulla. Cellular or granular eosinophilic casts and proteinaceous fluid within tubules are also frequent features in this model.

#### **6.1.3. Chemically induced Renal Injury Models**

Many chemically induced models were born from clinical experience and therefore highly relevant for use in drug testing and biomarker discovery. These include cisplatin (chemotherapeutic agent), gentamicin (aminoglycoside antibiotic), and nonsteroidal antiinflammatories (acetaminophen in particular) as well as many

others. Cisplatin induces direct proximal tubule toxicity typified by epithelial cell necrosis/apoptosis/autophagy and inflammation, renal vasoconstriction, and oxidative stress in both rodents and humans. Gentamicin, as well as other aminoglycoside antibiotics, is toxic to proximal tubule epithelium through necrosis or induction of apoptosis following receptor-mediated uptake and lysosomal accumulation, phospholipidosis, and eventual cellular dysfunction. NSAIDs (acetaminophen in particular) cause different types of nephrotoxicity through inhibition of the cyclooxygenase enzyme which blocks conversion of arachidonic acid into PGs. In the kidney, PGs maintain vasodilation and renal hemodynamics. The main form of NSAID renal injury is hemodynamically mediated AKI with ATN but electrolyte and acid-base disorders, oxidative stress, AIN, and papillary necrosis can also occur. Finally, radiocontrast media AKI is a common clinical condition following imaging studies. Animal models are helping to elucidate the pathophysiology of renal injury caused by these agents. Current theories from models suggest renal vasoconstriction leading to medullary hypoxia and formation of free radicals, direct renal tubule epithelial cell toxicity, and IRI.

AKI from rhabdomyolysis is thought to occur through a combination of hypovolemia, myoglobinuria, and metabolic acidosis. Myoglobin nephrotoxicity is a result of the combination of renal vasoconstriction and intratubular casts formation as well as direct toxicity of myoglobin to kidney tubular cells. Rhabdomyolysis-associated AKI is replicated through bilateral intramuscular injection of glycerol in male mice since female mice lack enough muscle mass for technical feasibility. Other models in either rats or mice include exercise induced or heat stress-related myopathy.

#### **6.1.4. Sepsis-associated Renal Models**

There are multiple animal models of sepsis which include LPS intraperitoneal (most common) or intravenous injection, intestinal leakage (host-barrier disruption models, e.g., cecal ligation and puncture [CLP] or colon ascends stent peritonitis [CASP]), and bacterial infusion which has also been conducted in large

animals such as dogs. Clinically, sepsis is defined by two phases. The first phase is termed warm shock or the hyperdynamic phase and characterized by low systemic vascular resistance and increased cardiac output. As the condition persists, cardiac output declines while systemic vascular resistance does not change resulting in the hypodynamic phase or cold shock. Animal models of sepsis are judged on their ability to mimic the changes in hemodynamics. Two areas in which the models have been heavily critiqued are the much more rapid time course of induction to multiorgan failure in rodent models and the lack of supportive care and/or comorbidities in these models that are features of the human condition. Other criticisms include differences in the nature of the initiating agent, relative lack of sensitivity to endotoxemia in rodents as compared to humans, and young age of mice on study (compared to older sepsis patients). Histologically, both clinically and in animal models, acute tubule necrosis and AKI are inconsistently produced. As compared to IRI, sepsis results in reversibly injured renal tubular epithelial cells due to an adaptive response during the inflammatory process and microvascular dysfunction. The models do offer insight into pathophysiology and molecular pathways in immune response in sepsis induction through progression. Current thinking suggests employing a systematic multiple-model approach and increasing the complexity of the models in use specifically to address the clinical setting of human patients (such as adding supportive care and antibiotics) to aid in the evaluation of new therapies.

#### **6.1.5. Obstructive Uropathy Models**

The UUO model (postrenal, obstructive) involves unilateral ligation of a ureter which may be irreversible or reversible (ligation removed at a designated timepoint). Male rodents are typically used as female reproductive organs can unnecessarily complicate the surgical procedure. In the obstructed kidney, backpressure from accumulating urine dilates collecting ducts first and then progresses to the distal and proximal tubules which reduces GFR and causes pressure necrosis in tubule epithelial cells. Initially, RBF increases in the immediate hours following ligation but drops leading to ischemia

and activation of the RAAS, compounding blood flow through additional renal vasoconstriction. Histologic changes include tubule dilation with overall loss of tubule mass, hydronephrosis, infiltration of leukocytes, and tubule epithelial cell death through apoptosis and oxidative stress. The interstitial space is expanded by ECM and inflammation leading to progressive renal tubulointerstitial fibrosis. This model is especially utilized in exploring treatments for renal fibrosis which is a critical process in the transition of AKI to CKD and finally, ESRD. One major limitation of this model is the ability of the contralateral, unobstructed kidney to compensate overall renal function in the animals on study (Bao et al., 2018; Pabla et al., 2021; Singh et al., 2012).

#### **6.1.6. Chronic Kidney Disease Models**

The main causes of CKD are diabetes and hypertension. In both situations, the sustained hyperglycemia or elevation in blood pressure (or the comorbidity of both) leads to injury of the delicate capillary network of the glomeruli leading to glomerular injury and sclerosis. It is estimated that approximately 15% of adults in the United States have CKD, with hypertension and diabetes accounting for three of four newly diagnosed cases. Other causes of CKD include SLE (lupus nephritis), FSGS, Alport syndrome, IgA nephropathy, human immunodeficiency virus-associated nephropathy (HIVAN), and PKD. CKD models cover the array of human conditions, but much of the research focuses on representation of diabetic and/or hypertensive nephropathy, glomerular injury, PKD, renal fibrosis, and chronic tubulointerstitial nephritis (Bao et al., 2018; Yang et al., 2010).

#### **6.1.7. Diabetic Kidney Disease Models**

In the United States, diabetes mellitus (both types 1 and 2) is the leading cause of glomerular disease and ESRD. It is estimated that one-third of people living with diabetes will develop DKD and thus represents a large unmet medical need. Glomerular hyperfiltration, glomerular and tubule epithelial hypertrophy, and microalbuminuria occur early in disease with progression to thickening of GBMs, mesangial and interstitial ECM accumulation, albuminuria, glomerulosclerosis, and eventual loss of renal function. In 2001, the Animal Models of Diabetic

Complication Consortium (AMDCC) was formed to identify the features of animal models that reproduce human diabetic complications and the criteria include (Brosius et al., 2009):

- Progressive renal insufficiency in the setting of hyperglycemia (>50% decline in GFR),
- Albuminuria (>10-fold increase compared with age-, gender-, and strain-matched controls), and
- Histologic changes of
  - Mesangial matrix expansion (with or without mesangiolysis or nodular sclerosis),
  - Arteriolar hyalinosis,
  - Tubulointerstitial fibrosis, and
  - Glomerular basement membrane thickening.

Rodent models of type 1 diabetes used in DKD research include streptozotocin-induced ( $\beta$ -islet toxin) in mice or rats and Akita mice (*Ins2*+/*C96Y* mutation) whose insulin 2 mutation leads to  $\beta$ -cell failure. Rodent models of type 2 diabetes include *db/db* mice (autosomal recessive point mutation of the leptin receptor, *Lepr<sup>db</sup>*, often enhanced with surgical manipulation such as uninephrectomy or genetically modified to overexpress renin), *ob/ob* mice (autosomal recessive point mutation of the leptin gene, *Lep<sup>ob</sup>*), KK-Ay mice (heterozygous agouti yellow or Ay mutation conferring insulin resistance), and Zucker diabetic fatty rats (autosomal recessive missense mutation in the leptin receptor, *Lepr<sup>fa</sup>*) as examples. These models display hyperglycemia, microalbuminuria, azotemia, and many also are hypertensive. Those models with concurrent hypertension have the most profound histologic changes in the kidney. Histologically, mesangial matrix expansion  $\pm$  nodular glomerulosclerosis, proteinaceous casts, interstitial inflammation and fibrosis, and arteriolar hyalinosis are consistent features. Mesangiolysis and microaneurysms are much less commonly observed other than in the double knockout strain, C57BLKS eNOS $-/-$  *db/db*, in which the moderate, persistent hypertension likely contributes to development of these changes. Kimmelstiel–Wilson nodules, the histologic hallmark of human DKD characterized by nodular glomerular sclerosis with a central region of acellularity surrounded by palisading cells, are difficult to observe in these rodent models and may be due to the accelerated nature of the rodent models as compared to

the chronic nature of human DKD. Importantly, these models show response to standard of care and are an important tool in DKD drug discovery (Heinz-Taheny et al., 2018).

### 6.1.8. Hypertensive Kidney Models

Hypertension is the second major cause of renal failure in humans, often occurring as a comorbidity with diabetes mellitus. High blood pressure injures the delicate capillary networks of glomeruli and confounds the microvascular injury already occurring in the hyperglycemic state of a patient with diabetes. There are many spontaneous, manipulated, or genetically modified hypertensive models (+/– hyperglycemic state) including spontaneously hypertensive rats (+/– uninephrectomy), AII infusion, eNOS $-/-$  mice, deoxycorticosterone acetate (DOCA)–salt mice or rats, Dahl salt-sensitive rats, NG-Nitro-L-arginine-methyl ester (L-NAME)–induced hypertensive-rats, and renal mass reduction (such as 5/6 nephrectomy) models as examples. Glomerulosclerosis, interstitial fibrosis, and arterial lesions (medial and intimal thickening, hyalinosis, and/or perivascular fibrosis) are hallmarks of both rodent models and humans. The TGR (mREN2)27 rat is a transgenic model containing the murine Ren-2 gene which develops severe hypertension and homozygotes will die from cardiovascular complications such as heart or kidney failure or stroke. Other models of CKD are briefly described in Table 2.19.

## 6.2. Adversity

Unlike many other organs, adversity calls in the kidney are relatively straightforward. For criteria and further information on how adversity is applied in toxicologic studies, readers are referred to the chapter on adversity in volume two of this Handbook. The assessment of adversity should always be based on the findings in the particular study involved (rather than inferences on progression in future longer duration studies) and on the impact of changes on the animal's overall health status. Therefore, histologic findings should be evaluated in conjunction with clinical pathology data. Significant elevations in UN, sCr, phosphorus, or urine protein or urine glucose in association with moderate to severe renal histologic



changes should be indicative of adversity (Kerlin et al., 2016). However, minimal renal lesions in the face of such clinicopathologic alterations might indicate extrarenal etiology that may or may not relate to adverse toxicology. Since the presence of inflammatory infiltrates within the renal interstitium are commonly noted as spontaneous background findings in multiple species, they are generally considered nonadverse, especially when minimal or mild in severity, or when localized in distribution. In cases of interstitial nephritis, where there is relatively severe inflammation with wide distribution and a lack of perivascular localization (such as may occur with immunomodulatory therapies (such as CTL-4 antagonists or PD-1 inhibitors), infiltrates may be considered adverse (Frazier et al., 2012; Frazier, 2015; Frazier and Obert, 2018). Inflammation in the kidney is also generally considered adverse when intravascular in distribution and accompanied by medial necrosis or other evidence of arteriolar degeneration. Glomerular lesions are almost universally considered adverse in animals, including inflammatory or degenerative changes. Background findings such as random obsolescent glomeruli or focal glomerulolipidosis should be disregarded in this assessment. Significant glomerular lesions are commonly noted with biologic (e.g., humanized antibody or peptide) therapies when administered in nonhuman primates and rodents that have no clinical relevance (Frazier and Obert, 2018). Despite the lack of toxicologic relevance in humans, the lesions are still categorized as adverse. It is important to recognize that spontaneous background changes, such as glomerulosclerosis in monkeys or glomerulonephritis syndrome in minipigs, are exempt from adversity calls.

Tubule toxicity may be either adverse or nonadverse, depending on severity, distribution, and concordance with clinicopathologic data. In general, tubule necrosis and/or tubule dilation should be considered adverse in the kidney, while tinctorial changes (such as tubule basophilia) or vacuolation should be considered nonadverse except in the more severe cases. Single cell necrosis should be assessed on a case-by-case basis with consideration of the changes on overall renal function and homeostasis. When single cell necrosis is limited to

minimal or mild severity, it is generally considered nonadverse because adjacent epithelial cells rapidly replace the defect induced by individual sloughed cells, and there is no effect on nephron absorption, secretion, or hemodynamics. When graded moderate or severe, the lesion may result in either focal exposure to the naked basement membrane or clusters of cells obstructing urine flow through the tubule. In such cases the change is more appropriately diagnosed as tubule necrosis since the majority of cells within a tubule profile are affected. "Single cell necrosis" as a diagnosis therefore needs to be differentiated from tubule necrosis by the toxicologic pathologist, as unlike the latter, single cell necrosis is considered nonadverse and does not significantly affect tubule or nephron physiologic function. The use of "tubule necrosis" as a diagnosis is also problematic for any minimal, nonadverse renal lesion since in clinical medicine it is easily confused with "Acute Tubule Necrosis," an older synonym for AKI in human patients, and thus incorrectly assumed as adverse by regulatory reviewers or clinicians (Frazier et al., 2012). In such case, more benign overarching diagnostic nomenclature such as "degeneration" may more clearly represent nonadversity in reports. Obstructive nephropathy is considered adverse, especially when there is secondary degeneration, necrosis, or dilation proximal to crystallization. Tubule dilation in such cases represents disruption of nephron flow, which should signify an adverse response. Because mineralization of individual tubule segments is commonly noted in rodents spontaneously, the presence of focal mineral deposits or tubule crystals are not considered adverse. Hyaline droplets or alpha-2 $\mu$ -globulin nephropathy, related to accumulation of proteinic material within lysosomes in the PCTs, has been thoroughly investigated and discussed by a large body of toxicologic pathologists with a consensus that such lesions should be universally considered nonadverse (Palazzi et al., 2016). Similarly, basophilic granules associated with administration of ASOs should be considered a nonadverse change, even when of severe grade, since this change only represents accumulation of drug material within endolysosomes (Frazier, 2015).

**TABLE 2.19** Alternative Rodent Models of Chronic Kidney Disease (CKD)

Disease model	Mechanism	Animal model(s)	Features	Comments
Systemic lupus erythematosus (SLE) nephritis	Systemic autoantibodies directed against nuclear elements with immune complex-induced intrarenal inflammation	NZB/NZW F1 (New Zealand black x New Zealand white) mice, MRL <sup>lpr</sup> (Murphy Roths large, lymphoproliferation) and CD95 mutants; Pristane-induced; BAFF-transgenic mouse strains	Mesangial matrix expansion and hypercellularity with proliferation of endothelial and mesangial cells; thickening of the glomerular basement membrane with wire-loop capillaries; glomerular crescent formation (less common in MRL <sup>lpr</sup> ); mesangial and subendothelial IgG and C3 deposition; mononuclear cell infiltrates	Most of these models have limitations due to the broad spectrum of clinical disease and genetics in humans. For example, NZB/NZW F1 mice do not show other clinical presentations of lupus such as rash or arthritis and the lpr mutation in the MRL <sup>lpr</sup> differs from the genetics in human lupus
Alport syndrome	Inherited defect in type IV collagen leading to defects in the collagen scaffold of the glomerular basement membrane	COL4A3 <sup>-/-</sup> and COL4A5 G5X mutant mouse (model of X-linked alport syndrome)	Mesangial proliferation with segmental to global glomerulosclerosis; ultrastructural glomerular basement membrane lamellation and splitting and podocyte effacement; microhematuria and proteinuria	Samoyed (X-linked), English cocker spaniels (autosomal recessive), and bull terrier (autosomal dominant) inherited canine models exist
Focal segmental glomerulosclerosis (FSGS)	Podocyte injury	Adriamycin (doxorubicin)- (rat, BALBc mice) and puromycin- (rat) induced models	Sclerosis of glomerular segments with alterations of the mesangial cellularity and/or electron microscopic effacement of podocyte foot processes with absence of immune complexes	No primary models available
Human immunodeficiency virus-associated nephropathy (HIVAN)	Virus-induced FSGS by direct infection of the podocyte or cytokine release that injures podocytes	Transgenic 26 or Tg26 heterozygote mouse (uses a replication-deficient version of HIV as the integrated transgene); HIV Δgag/pol transgenic Sprague–Dawley rat	Severe disease in Tg26 including diffuse segmental to global glomerulosclerosis of the collapsing variant of FSGS with microcystic tubular changes, monocytic interstitial infiltrate, protein casts, and ultrastructural podocyte effacement; proteinuria, ascites, hypoalbuminemia. And increased blood urea nitrogen	Viral models in cats (feline immunodeficiency virus) and nonhuman primates (simian immunodeficiency virus) exist

(Continued)

**TABLE 2.19** Alternative Rodent Models of Chronic Kidney Disease (CKD)—cont'd

Disease model	Mechanism	Animal model(s)	Features	Comments
IgA nephropathy	Immune-mediated glomerulonephritis	ddY mice and the derived high IgA mouse (HIGA); human IgA1 knock-in ( $\alpha$ 1KI)-CD89 transgenic mice	Mesangial cell proliferation and matrix expansion associated with granular mesangial immunodeposits of IgA and complement 3 with variable IgG and/or IgM codeposits	IgA nephropathy is the most common cause of primary glomerulonephritis worldwide
Polycystic kidney disease	Autosomal dominant or recessive disorder resulting in multiplicity of progressive and adverse renal cyst formation	Transgenic mouse models utilize conditional knockout, deletions or silencing of polycystic kidney disease 1 or 2 (PKD1 or PKD2) genes (among others)	Tubular and glomerular cysts, the hallmark of the human condition, with renal insufficiency and death from renal failure	Homozygous PKD1 or PKD2 knockout results in embryonic lethality; also develop extrarenal lesions: Hepatic fibrosis, intrahepatic biliary cysts, pancreatic cysts, and cardiac anomalies

### 6.2.1. Regulatory Issues

Since the kidney is so often a toxicologic target organ in nonclinical studies, and because drug-induced renal injury also may result in serious adverse events in clinical trial patients, it is not surprising that nephrotoxicity is a frequent topic of discussion between regulatory agencies and pharmaceutical sponsors. Nephrotoxicity has also been a common cause of clinical hold letters. There is no fast rule for an appropriate clinical margin of safety in the clinic once nephrotoxic signals are identified in nonclinical studies. This will depend greatly on the indication, health status of the clinical population (e.g., healthy volunteers vs. aged patients with severe comorbidities), and the specific nature of the renal hazard in animals. Adverse changes such as tubule necrosis are likely to be more concerning than tubule vacuolation, phospholipidosis, tubule basophilia, or other lesions considered nonadverse. As noted in the section on adversity, regulatory confusion has arisen related to the distinction between single cell necrosis and tubule necrosis, which has resulted in differences in opinions in adversity characterization of lesions between agencies and sponsors, and the unfortunate application of clinical holds. For these reasons, it is imperative that broad

terminology such as “necrosis” be avoided when describing less severe, nonadverse lesions such as degeneration or single cell necrosis at lower doses, even when overt tubule necrosis is present at high doses in the same study. Even degeneration of minimal or mild severity in submission packages has been (incorrectly) labeled as an adverse lesion in rodent renal tubules by some overzealous regulatory reviewers even when toxicologic pathologists have agreed on nonadversity for such lesions. Glomerulonephritis, when not associated with ADA, is going to draw much more regulatory concern and result in a much more conservative approach to dose escalation and starting/stopping criteria than other renal changers in animals. While ADA-related glomerulonephritis in monkeys with biologic therapies usually does not result in any developmental hurdles, inadequate documentation or demonstration of ADA-related immunogenicity in monkeys or humans can result in significant developmental delays (Rojko et al., 2014). Without substantiation of ADA mechanism, there is a risk for regulatory demands for investigational studies including reversibility arms to establish lack of clinical relevance of nonclinical findings in order to reinstitute clinical dosing. BAIRD or other



causes of immune-mediated responses in a small percentage of human patients given biologic therapies is an expected consequence of these medications, but consistently elevated ADA in clinical patients or multiple cases of renal autoimmune disorders will raise significant concerns in clinical trials of biotherapeutic agents.

Rapidly progressive glomerulonephritis has also occurred in rare patients given ASO therapies. This resulted in the lack of approval and eventual termination of one agent (drisapersen). However, another ASO causing glomerular lesions (inotersen) was given approval for marketing based on the favorable risk:benefit profile and thorough investigative work regarding potential mechanism, clinical risk, and subsequent preventative measures added to the trial and postmarketing plan. After regulatory discussions, careful and more frequent monitoring programs and additional screening were instituted to ensure patient safety.

In the authors' combined experience, regulatory concern with nephrotoxicity most often involves unexpected clinical, rather than nonclinical kidney disorders, but fortunately these tend to be uncommon. While the kidney is generally identified as a target organ by nonclinical studies, renal adverse events may occur in patients at doses below where they are modeled or predicted based on nonclinical findings. Urine protein/creatinine ratios are frequently included in clinical trial screens as a mechanism for monitoring for DIKI. However, in humans, as well as in animals, proteinuria can occur due to a wide variety of causes unrelated to tubule injury, even including menstruation (Obert et al., 2021). Regulatory questions have therefore frequently arisen over the interpretation of low-grade urine protein clinical events and resulted in greater scrutiny of both clinical and nonclinical urine results. This is especially true with the ASO class of agents which can induce proteinuria due to both physiologic transporter interactions and toxicologic injury to tubules (Frazier and Seely, 2019; Janssen et al., 2019). Additional investigative studies have occasionally been requested by authorities, a more frequent avenue for enhancing the development plan has involved the addition of exploratory renal biomarkers for patients in the clinic. The addition of urinary KIM1, NGAL, and/or albumin (as well as other parameters)

on a weekly, biweekly, or monthly basis with interim evaluations and real-time analysis (along with nephrology consult where indicated) has provided a significant and effective safety precaution for early monitoring for drug-induced renal injury. Strict entrance and stopping criteria in trials may also provide further comfort that renal injury will be prevented or that it can be identified early enough to prevent catastrophic renal insult (e.g., dialysis dependency). When nonclinical renal lesions are unusual or unprecedented, there is heightened regulatory concern. In this regard, kidney changes such as interstitial nephritis identified in animals and their potential translation to clinical trial patients are of special concern. These types of lesions have occurred as a hypersensitivity response to antibiotics and immunomodulatory drug candidates. Since the lesion may be progressive in patients, a conservative approach to further development is often suggested. Although incidents of clinical interstitial nephritis may not terminate a program, they may be a cause of dose pause or delay of a cohort until it is established further cases are not identified.

The last area of nephrotoxicity representing frequent communication with regulatory authorities involves the potential translation of risk of renal findings from juvenile toxicity studies to human pediatric patients (see also *The Role of Pathology in Evaluation of Reproductive, Developmental, and Juvenile Toxicity*, Vol 1, Chap 7). Because maturation of anatomical and functional renal parameters do not necessarily follow the same sequence or order in rodents and humans, and because many structural developmental milestones in rats occur postnatally, kidney findings in juvenile rat studies may prompt in-depth discussions with agencies and key opinion leaders to determine what ages or stage of development in human pediatric patients are most vulnerable to an agent and to ensure proper labeling once this information is established.

## 7. CONCLUSION

The kidney is recognized as one of the most common target organs of toxicity of drugs and chemicals. It is particularly susceptible because of the high blood flow relative to its mass and

the unique property of renal tubule epithelium in concentrating urine and its constituents, including drugs, chemicals, and metabolites. The gold standard method for identification of the renal toxicity potential of new products remains light microscopic examination of the kidney, but additional renal functional assays, imaging modalities, and biochemical biomarkers of renal injury are becoming increasingly important in diagnosis and monitoring of nephrotoxicity. Purposely designed time-course studies that utilize ultrastructural pathology, immunohistochemical and immunofluorescent stains also play a pivotal role in the continued development of products exhibiting nephrotoxic potential. To refine the risk assessment, establishment of cellular and subcellular organelle targets of xenobiotic injury by the pathologist forms a cornerstone in expanding the understanding of the mechanisms and processes involved in renal injury. Demonstration of the pathogenesis of the full spectrum of toxic lesions enables the definition of primary or secondary changes and reversible, irreversible, or progressive processes. Localization of lesions provides the best opportunity to identify sensitive biomarkers to monitor for toxicity.

## Acknowledgments

The authors owe an immense debt of gratitude to Dr. Nasir Khan, Dr. Carl Alden, and the late Dr. Gordon Hard, who cowrote the first three editions of this chapter, and which provides the strong basis for this update and without whose valuable contributions this edition would not be possible.

## REFERENCES

- Abbas A, Mirza MM, Ganti AK, et al.: Renal toxicities of targeted therapies, *Targeted Oncol.* 10:487–499, 2015.
- Adams DF, Watkins MS, Durette L, et al.: Carcinogenicity assessment of daprodustat (GSK1278863), a hypoxia inducible factor (HIF)-prolyl hydroxylase inhibitor, *Toxicol. Pathol.* 48:362–378, 2020.
- Adler M, Ramm S, Hafner M, et al.: A quantitative approach to screen for nephrotoxic compounds in vitro, *J. Am. Soc. Nephrol.* 27:1015–1028, 2016.
- Al-Awqati A, Goldberg MR: Architectural patterns in branching morphogenesis in the kidney, *Kidney Int.* 54: 1832–1842, 1998.
- Anderson TD, Khan KN, Tassinari MS, et al.: Comparative juvenile safety testing of new therapeutic candidates: relevance of laboratory animal data to children, *J. Toxicol. Sci.* 34(Special Issue II):SP209–SP215, 2009.
- Araújo LS, Torquato BGS, da Silva CA, et al.: Renal expression of cytokines and chemokines in diabetic nephropathy, *BMC Nephrol.* 21:308–328, 2020.
- Ashammakhi N, Wesseling-Perry K, Hasan A, et al.: Kidney-on-a-chip: untapped opportunities, *Kidney Int.* 94(6):1073–1086, 2018.
- Bajaj P, Chowdhury SK, Yucha R, et al.: Emerging kidney models to investigate metabolism, transport, and toxicity of drugs and xenobiotics, *Drug Metab. Dispos.* 46(11):1692–1702, 2018.
- Bao YW, Yuan Y, Chen JH, Lin WQ: Kidney disease models: tools to identify mechanisms and potential therapeutic targets, *Zool. Res.* 39:72–86, 2018.
- Barisoni L, Hodgin JB: Digital pathology in nephrology clinical trials, research, and pathology practice, *Curr. Opin. Nephrol. Hypertens.* 26:450–459, 2017.
- Bauchet A, Masson R, Guffroy M, et al.: Immunohistochemical identification of kidney nephron segments in the dog, rat, mouse, and cynomolgus monkey, *Toxicol. Pathol.* 39:1115–1128, 2011.
- Benfenati E, Benigni R, Demarini DM, et al.: Predictive models for carcinogenicity and mutagenicity: frameworks, state-of-the-art, and perspectives, *J. Environ. Sci. Health C Environ. Carcinog. Ecotoxicol. Rev.* 27:57–90, 2009.
- Bens M, Vandewalle A: Cell models for studying renal physiology, *Pflügers Archiv* 457:1–15, 2008.
- Brandt A, Löhers K, Beier M, et al.: Establishment of a conditionally immortalized Wilms tumor cell line with a homozygous WT1 deletion within a heterozygous 11p13 deletion and UPD limited to 11p15, *PLoS One* 11, 2016.
- Borghese MFA, Ortiz MC, Balonga S, et al.: The role of endothelin system in renal structure and function during the postnatal development of the rat kidney, *PLoS One* 11(2):e0148866, 2016. <https://doi.org/10.1371/journal.pone.0148866>.
- Brack M: IgM-mesangial nephropathy in callithricids, *Toxicol. Pathol.* 25:270–276, 1988.
- Brosius 3rd FC, Alpers CE, Bottinger EP, et al.: Animal Models of Diabetic Complications Consortium: Mouse models of diabetic nephropathy, *J. Am. Soc. Nephrol.* 20(12):2503–2512, 2009, <https://doi.org/10.1681/ASN.2009070721>.
- Bueters R, Bael A, Gasthuys E, et al.: Ontogeny and cross species comparison of pathways involved in drug absorption, distribution, metabolism, and excretion in neonates (Review): kidney, *Drug Metabol. Dispos.* 48:353–367, 2020.
- Burek JD, Duprat P, Owen R, et al.: Spontaneous renal disease in laboratory animals, *Int. Rev. Exp. Pathol.* 30:231–319, 1988.
- Cappon GD, Hurtt ME: Developmental toxicity of the kidney, *Reprod. Toxicol.* 3:193–204, 2010.
- Carter JL, Parker CT, Stevens PE, et al.: Biological variation of plasma and urinary markers of acute kidney injury in patients with chronic kidney disease, *Clin. Chem.* 62:876–883, 2016.
- Chandrasekaran K, Karolina DS, Sepramaniam S, et al.: Role of microRNAs in kidney homeostasis and disease, *Kidney Int.* 81:617–627, 2012.

- Chang SY, Weber EJ, Ness KV, et al.: Liver and kidney on chips: microphysiological models to understand transporter function, *Clin. Pharmacol. Ther.* 100:464–478, 2016.
- Chaudhuri BN, Kleywegt GJ, Bjorkman J, et al.: The structures of alpha 2μ-globulin and its complex with a hyaline droplet inducer, *Acta Crystallogr. D Biol. Crystallogr.* 55:753–762, 1999.
- Chevalier R: Pathogenesis of renal injury in obstructive uropathy, *Curr. Op. Pediatr.* 18:153–160, 2006.
- Chiusolo A, Defazio R, Zanetti E, et al.: Kidney injury molecule-1 expression in rat proximal tubule after treatment with segment-specific nephrotoxics: a tool for early screening of potential kidney toxicity, *Toxicol. Pathol.* 38:338–345, 2010.
- Chorley BN, Ellinger-Ziegelbauer H, Tackett M, et al.: Urinary miRNA biomarkers of drug-induced kidney injury and their site specificity within the nephron, *Toxicol. Sci.* 180:1–16, 2021.
- Choudhury D, Ahmed Z: Drug-associated renal dysfunction and injury, *Nat. Clin. Pract. Nephrol.* 2:80–91, 2006.
- Clark M, Steger-Hartmann T: A big data approach to the concordance of the toxicity of pharmaceuticals in animals and humans, *Regul. Toxicol. Pharmacol.* 96:94–105, 2018.
- Cohen A, Ioannidis K, Ehrlich A, et al.: Mechanism and reversal of drug-induced nephrotoxicity on a chip, *Sci. Transl. Med.* 13(582), 2021.
- Combes AN, Zappia L, Er PX, et al.: Single-cell analysis reveals congruence between kidney organoids and human fetal kidney, *Genome Med.* 11:3, 2019.
- Colman K, Andrews RN, Atkins H, et al.: International harmonization of nomenclature and diagnostic criteria (INHAND): non-proliferative and proliferative lesions of the non-human primate (*M. fascicularis*), *J. Toxicol. Pathol.* 34(3 suppl):1S–18S, 2021.
- Cong Y, Han X, Wang Y, et al.: Drug toxicity evaluation based on organ-on-a-chip technology: a review, *Micromachines* 11: 381, 2020.
- Decuypere JP, Ceulemans LJ, Agostinis P, et al.: Autophagy and the Kidney: implications for ischemia-reperfusion injury and therapy, *Am. J. Kidney Dis.* 66:699–709, 2015.
- de Souza N: Organoids, *Nat. Methods* 15:23–24, 2018.
- DesRochers TM, Suter L, Roth A, Kaplan DL: Bioengineered 3D human kidney tissue, a platform for the determination of nephrotoxicity, *PLoS One* 8(3):e59219, 2013.
- Dey M, Ozbolat IT: 3D bioprinting of cells, tissues and organs, *Sci. Rep.* 10(1):14023, 2020.
- Diamond GL, Zalups RK: Understanding renal toxicity of heavy metals, *Toxicol. Pathol.* 26:92–103, 1998.
- Eckerbom P, Hansell P, Cox E, et al.: Circadian variation in renal blood flow and kidney function in healthy volunteers monitored with noninvasive magnetic resonance imaging, *Am. J. Physiol. Ren. Physiol.* 319:F966–F978, 2020.
- Engelhardt J, Fant P, Guionaud S, et al.: Scientific and Regulatory Policy Committee Points to-consider paper\*: drug Induced Vascular Injury associated with non-small molecule therapeutics in preclinical development. Part II. antisense oligonucleotides, *Toxicol. Pathol.* 43:935–944, 2015.
- Ennulat D, Ringenberg M, Frazier KS: Regulatory Forum Opinion Piece: recommendations for a tiered approach to mechanistic toxicology studies of preclinical renal toxicity, *Toxicol. Pathol.* 46:636–646, 2018.
- Frazier KS: Antisense Oligonucleotides: the promise and the challenges from the toxicologic pathologist's perspective, *Toxicol. Pathol.* 43:7–19, 2015.
- Frazier KS: Species differences in renal development and associated developmental nephrotoxicity, *Birth Defects Res.* 109:1243–1256, 2017.
- Frazier KS: Urinary system. In Steinbach TJ, Patrick DJ, Cozenza ME, editors: *Toxicologic pathology for non-pathologists*, New York, 2019, Springer Nature/Humana Press, pp 201–250.
- Frazier KS: The impact of functional and structural maturation of the kidney on susceptibility to drug and chemical toxicity in neonatal rodents, *Toxicol. Pathol.* 49:1377–1388, 2021.
- Frazier KS: Kidney effects by alternative classes of medicines in patients and relationship to effects in nonclinical toxicity studies, *Toxicol. Pathol.* 50(4):408–414, 2022.
- Frazier KS, Engelhardt J, Fant P, et al.: Scientific and Regulatory Policy Committee Points-to-consider paper\*: drug induced vascular injury associated with non-small molecule therapeutics in preclinical development. Part I. biotherapeutics, *Toxicol. Pathol.* 43:915–934, 2015.
- Frazier KS, Obert LA: Drug-induced glomerulonephritis: the spectre of biotherapeutic and antisense oligonucleotide immune activation in the kidney, *Toxicol. Pathol.* 46:904–917, 2018.
- Frazier KS, Paredes A, Dube P, et al.: Connective tissue growth factor expression in the rat remnant kidney model and association with tubular epithelial cells undergoing transdifferentiation, *Vet. Pathol.* 37:328–335, 2000.
- Frazier KS, Ryan AM, Peterson RA, Obert LA: Kidney pathology and investigative nephrotoxicology strategies across species, *Semin. Nephrol.* 39:190–201, 2019.
- Frazier KS, Seely JC: Urinary system. In Sahota PS, Popp JA, Hardisty JF, Gopinath C, editors: *Toxicologic pathology: preclinical safety assessment*, 2nd Ed., 2019, CRC Press/Taylor Francis, FL, pp 569–638.
- Frazier KS, Seely JC, Hard GC, et al.: Proliferative and non-proliferative lesions in the rodent urinary system, *Toxicol. Pathol.* 40(4SI):14–86, 2012.
- Fransen MFJ, Addario G, Bouten CVC, et al.: Bioprinting of kidney in vitro models: cells, biomaterials, and manufacturing techniques, *Essays Biochem.* 65(3):587–602, 2021.
- Gao J, Wu L, Wang S, Chen X: Role of chemokine (C-X-C Motif) ligand 10 (CXCL10) in renal diseases, *Mediat. Inflamm.* 6194864, 2020.
- Garcia-Fernandez N, Jacobs-Cachá C, Mora-Gutiérrez JM, et al.: Matrix metalloproteinases in diabetic kidney disease, *J. Clin. Med.* 9:472, 2020.
- George B, You D, Joy MS, Aleksunes LM: Xenobiotic transporters and kidney injury, *Adv. Drug Deliv. Rev.* 116:73–91, 2017.



- Gijzen L, Yengej FAY, Schutgens R, et al.: Culture and analysis of kidney tubuloids and perfused tubuloid cells-on-a-chip, *Nat. Protoc.* 6(4):2023–2050, 2021.
- Griffin BR, Faubel S, Edelstein CL: Biomarkers of drug-induced kidney toxicity, *Ther. Drug Monit.* 41:213–226, 2019.
- Grollman AP, Jelakovic B: Role of environmental toxins in endemic (Balkan) nephropathy, *J. Am. Soc. Nephrol.* 18: 2817–2823, 2007.
- Groseclose MR, Laffan S, Frazier KS, et al.: Imaging MS: an investigation of juvenile rat nephrotoxicity associated with dabrafenib administration, *J. Am. Soc. Mass Spectrom.* 6:887–898, 2015.
- Groves CE, Hayden PJ, Lock EA, Schnellmann RG: Differential cellular effects in the toxicity of haloalkene and haloalkane cysteine conjugates to rabbit renal proximal tubules, *J. Biochem. Toxicol.* 8:49–56, 1993.
- Gunderen HJG, et al. In Haschek WM, Rousseaux CG, Wallig MA, editors: *Haschek and Rousseaux's handbook of toxicologic pathology*, 3rd Ed, Vol 1, 2013, Academic Press, pp 215–286. chap 8.
- Hall AM, Bass P, Unwin RJ: Drug-induced renal Fanconi syndrome, *QJM* 107:261–269, 2014.
- Hammerman MR, Rogers SA, Ryan G: Growth factors and kidney development, *Pediatr. Nephrol.* 7:616–620, 1993.
- Han WK, Waikar SS, Johnson AM, et al.: Urinary biomarkers in the early detection of acute kidney injury, *Kidney Int.* 73: 863–869, 2008.
- Hard GC: Identification of a high-frequency model for renal carcinoma by the induction of renal tumors in the mouse with a single dose of streptozotocin, *Cancer Res.* 45:703–708, 1985.
- Hard GC: Critical review of renal tubule karyomegaly in non-clinical safety evaluation studies and its significance for human risk assessment, *Crit. Rev. Toxicol.* 48:575–595, 2018a.
- Hard GC: Mechanisms of rodent renal carcinogenesis revisited, *Toxicol. Pathol.* 46(8):956–969, 2018b.
- Hard GC, Flake GP, Sills RC: Re-evaluation of kidney histopathology from 13-week toxicity and two-year carcinogenicity studies of melamine in the F344 rat: morphologic evidence of retrograde nephropathy, *Vet. Pathol.* 46:1248–1257, 2009a.
- Hard GC, Johnson KJ, Cohen SM: A comparison of rat chronic progressive nephropathy with human renal disease-implications for human risk assessment, *Crit. Rev. Toxicol.* 39(4):332–334, 2009b.
- Hard G, Khan KN: A contemporary overview of chronic progressive nephropathy in the laboratory rat and its significance for human risk assessment, *Toxicol. Pathol.* 32: 171–180, 2004.
- Hard GC, Rodgers IS, Baetcke KP, et al.: Hazard evaluation of chemicals that cause accumulation of alpha 2μ-globulin, hyaline droplet nephropathy, and tubule neoplasia in the kidneys of male rats, *Environ. Health Perspect.* 99:313–349, 1993.
- Hard GC, Seely JC: Histological investigation of diagnostically challenging tubule profiles in advanced chronic progressive nephropathy (CPN) in the Fischer 344 rat, *Toxicol. Pathol.* 34:941–948, 2006.
- Harlander S, Schönenberger D, Toussaint N, et al.: Combined mutation in Vhl, Trp53 and Rb1 causes clear cell renal cell carcinoma in mice, *Nat. Med.* 23:869–877, 2017.
- Heinz-Taheny KM, Harlan SM, Qi Z, Heuer JG: Synopsis of sweet! Mouse models of diabetic kidney disease, *Toxicol. Pathol.* 46:970–975, 2018.
- Homan KA, Kolesky DB, Skylar-Scott MA, et al.: Bioprinting of 3D convoluted renal proximal tubules on perfusable chips, *Sci. Rep.* 6:34845, 2016.
- Hou W, Ji Z: Generation of autochthonous mouse models of clear cell renal cell carcinoma: mouse models of renal cell carcinoma, *Exp. Mol. Med.* 50:1–10, 2018.
- Hsu YH, Zheng CM, Chou CL, et al.: Therapeutic effect of endothelin-converting enzyme inhibitor on chronic kidney disease through the inhibition of endoplasmic reticulum stress and the NLRP3 inflammasome, *Biomedicines* 9:398–407, 2021.
- Huang JX, Kaeslin G, Ranall MV, et al.: Evaluation of biomarkers for in vitro prediction of drug-induced nephrotoxicity: comparison of HK-2, immortalized human proximal tubule epithelial, and primary cultures of human proximal tubular cells, *Pharmacol. Res. Perspect.* 3:e00148, 2015.
- ICH (International Council for Harmonisation of Technical Requirements for Pharmaceuticals for Human Use): ICH Guidelines, 2021. [https://database.ich.org/sites/default/files/ICH\\_S1BR1\\_Step2\\_DraftGuideline\\_2021\\_0510.pdf](https://database.ich.org/sites/default/files/ICH_S1BR1_Step2_DraftGuideline_2021_0510.pdf). Accessed July 22 2024.
- Ivanyuk A, Livio F, Biollaz J, Buclin T: Renal drug transporters and drug interactions, *Clin. Pharmacokinet.* 56:825–892, 2017.
- Jang J, Yi HG, Cho DW: 3D printed tissue models: present and future, *ACS Biomater. Sci. Eng.* 2:1722–1731, 2016.
- Jang KJ, Mehr AP, Hamilton GA, et al.: Human kidney proximal tubule-on-a-chip for drug transport and nephrotoxicity assessment, *Integr. Biol.* 5:1119–1129, 2013.
- Janssen MJ, Nieskens TTG, Steevens TAM, et al.: Therapy with 2'ome antisense oligonucleotides causes reversible proteinuria by inhibiting renal protein reabsorption, *Mol. Ther. Nucleic Acids* 18:298–307, 2019.
- Javan AO, Shokouhi S, Sahraei Z: A review on colistin nephrotoxicity, *Eur. J. Clin. Pharmacol.* 7:801–810, 2015.
- Jhaveri KD, Wanchoo R, Sakhiya V, et al.: Adverse renal effects of novel molecular oncologic targeted therapies: a narrative review, *Kidney Int. Rep.* 2:108–123, 2017.
- Kandasamy K, Chuah JKC, Su R, et al.: Prediction of drug-induced nephrotoxicity and injury mechanisms with human induced pluripotent stem cell-derived cells and machine learning methods, *Sci. Rep.* 27(5):12337, 2015, <https://doi.org/10.1038/srep12337>.

- Kang HM, Lim JH, Noh KH, et al.: Effective reconstruction of functional organotypic kidney spheroid for in vitro nephrotoxicity studies, *Sci. Rep.* 9:17610, 2019.
- Kato M, Arce L, Natarajan R: MicroRNAs and their role in progressive kidney diseases, *Clin. J. Am. Soc. Nephrol.* 4: 1255–1266, 2009.
- Kerlin R, Bolon B, Burkhardt J, et al.: Scientific and regulatory policy committee: recommended (“best”) practices paper for determining, communicating and using adverse effect data from nonclinical studies, *Toxicol. Pathol.* 44:147–162, 2016.
- Khan KNM, Paulson SK, Verburg K, et al.: Pharmacology of cyclooxygenase-2 inhibition in the kidney, *Kidney Int.* 61: 1210–1219, 2002.
- Khoshel-Rad N, Ahmadi A, Moghadasali R: Kidney organoids: current knowledge and future directions, *Cell Tissue Res.* 387(2):207–224, 2022.
- Kimura T, Isaka Y, Yoshimori T: Autophagy and kidney inflammation, *Autophagy* 13:997–1003, 2017.
- Krishnan SM, Kraehling JR, Eitner F, et al.: The impact of the nitric oxide (NO)/soluble guanylyl cyclase (sGC) signaling cascade on kidney health and disease: a Preclinical Perspective, *Int. J. Mol. Sci.* 19:1712–1730, 2018.
- Kriz W, Kaissling B: Structural organization of the mammalian kidney. In Seldin DW, Giebisch G, editors: *The kidney: physiology and pathophysiology, third ed vol 1*, Philadelphia, 2000, Lippincott Williams and Wilkins, pp 587–654.
- Kulkarni P: Prediction of drug-induced kidney injury in drug discovery, *Drug Metab. Rev.* 53:234–244, 2021.
- Laffan SB, Thomson AS, Mai S, et al.: Immune complex disease in a chronic monkey study with a humanised, therapeutic antibody against CCL20 is associated with complement-containing drug aggregates, *PLoS One* 15:e0231655, 2020.
- Leach MW, Rottman JB, Hock MB, et al.: Immunogenicity/hypersensitivity of biologics, *Toxicol. Pathol.* 42:293–300, 2014.
- Lei C, Berra L, Rezoagli E, et al.: Nitric oxide decreases acute kidney injury and stage 3 chronic kidney disease after cardiac surgery, *Am. J. Respir. Crit. Care Med.* 198:1279–1287, 2018.
- Li X, Pan X, Fu X, et al.: MicroRNA-26a: an emerging regulator of renal biology and disease, *Kidney Blood Press. Res.* 44:287–297, 2019.
- Liu S, Yao Y, Lu S, et al.: The role of renal proximal tubule P450 enzymes in chloroform-induced nephrotoxicity: utility of renal specific P450 reductase knockout mouse models, *Toxicol. Appl. Pharmacol.* 272:230–237, 2013.
- Lock EA, Reed CJ: Trichloroethylene: mechanisms of renal toxicity and renal cancer and relevance to risk assessment, *Toxicol. Sci.* 91:313–331, 2006.
- Lucas GNC, Leitão ACC, Alencar RL, et al.: Pathophysiological aspects of nephropathy caused by non-steroidal anti-inflammatory drugs, *J. Bras. Nefrol.* 41:124–130, 2019.
- Maass C, Sorensen NB, Himmelfarb J, et al.: Translational assessment of drug-induced proximal tubule injury using a kidney microphysiological system, *CPT Pharmacometrics Syst. Pharmacol.* 8:316–325, 2019.
- Maher JM, Cheng X, Tanaka Y, et al.: Hormonal regulation of renal multidrug resistance-associated proteins 3 and 4 (Mrp3 and Mrp4) in mice, *Biochem. Pharmacol.* 71:470–478, 2006.
- McMahon AP: Development of the mammalian kidney, *Curr. Top. Dev. Biol.* 117:31–64, 2016.
- Morales-Alvarez MC: Nephrotoxicity of antimicrobials and antibiotics, *Adv. Chron. Kidney Dis.* 7:31–37, 2020.
- Morizane R, Lam AQ, Freedman BS, et al.: Nephron organoids derived from human pluripotent stem cells model kidney development and injury, *Nat. Biotechnol.* 33:1193–1200, 2015.
- Murata Y, Ueno T, Tanaka S, et al.: Identification of clock genes related to hypertension in kidney from spontaneously hypertensive rats, *Am. J. Hypertens.* 33:1136–1145, 2020.
- Nagai J, Takano M: Molecular aspects of renal handling of aminoglycosides and strategies for preventing the nephrotoxicity, *Drug Metabol. Pharmacokinet.* 19:159–170, 2004.
- Nassirpour R, Homer BL, Mathur S, et al.: Identification of promising urinary microRNA biomarkers in two rat models of glomerular injury, *Toxicol. Sci.* 148:35–47, 2015.
- Naughton CA: Drug-induced nephrotoxicity, *Am. Fam. Physician* 78:743–750, 2008.
- Nielsen R, Christensen EI, Birn H: Megalin and cubilin in proximal tubule protein reabsorption: from experimental models to human disease, *Kidney Int.* 89:58–67, 2016.
- Obert LA, Suttie AW, Abdi M, et al.: Spontaneous unilateral renal aplasia in a cynomolgus monkey (*Macaca fascicularis*) with potential pathogenesis, *Toxicol. Pathol.* 48:766–783, 2020.
- Obert LA, Elmore SA, Ennulat D, Frazier KS: Review of specific biomarkers of chronic renal injury and their potential utilization in nonclinical safety studies, *Toxicol. Pathol.* 49:1–28, 2021.
- Obert LA, Frazier KS: Intrarenal renin-angiotensin system involvement in the pathogenesis of Chronic Progressive Nephropathy—bridging the informational gap between disciplines, *Toxicol. Pathol.* 47:799–816, 2019.
- Owen RA, Heywood R: Age-related variations in renal structure and function in Sprague-Dawley rats, *Toxicol. Pathol.* 14:158–167, 1986.
- Ozer JS, Dieterle F, Troth S, et al.: A panel of urinary biomarkers to monitor reversibility of renal injury and a serum marker with improved potential to assess renal function, *Nat. Biotechnol.* 28:486–494, 2010.
- Pabla N, Scindia Y, Gigliotti J, Bajwa A: *Mouse models of acute kidney injury in animal models in medicine and biology*, 2021, IntechOpen. Available from, <https://www.intechopen.com/online-first/76410>. (Accessed July 22 2024).
- Palazzi X, Burkhardt JE, Caplain H, et al.: Characterizing “adversity” of pathology findings in nonclinical toxicity studies: results from the 4<sup>th</sup> ESTP international expert workshop, *Toxicol. Pathol.* 44:820–824, 2016.
- Palmer BF: Regulation of potassium homeostasis, *Clin. J. Am. Soc. Nephrol.* 10:1050–1060, 2015.

- Paranjpe MG, Belich JL, McKeon ME, et al.: Renal tumors in 26-week Tg.Rash2 mice carcinogenicity studies, *Toxicol. Pathol.* 44:633–635, 2016.
- Parikh CR, Jani A, Melnikov VY, et al.: Urinary interleukin-18 is a marker of human acute tubular necrosis, *Am. J. Kidney Dis.* 43:405–414, 2004.
- Parrish AR: Matrix metalloproteinases in kidney disease: role in pathogenesis and potential as a therapeutic target, *Prog. Mol. Biol. Transl. Sci.* 148:31–65, 2017.
- Pazhayattil GS, Shirali AC: Drug-induced impairment of renal function, *Int. J. Nephrol. Renovascular Dis.* 7:457–468, 2014.
- Petejova N, Martinek A, Zadrazil J, Teplan V: Acute toxic kidney injury, *Ren. Fail.* 41:576–594, 2019.
- Petrosyan A, Cravedi P, Villani V, et al.: A glomerulus-on-a-chip to recapitulate the human glomerular filtration barrier, *Nat. Commun.* 10:3656, 2019.
- Phillips JA, Holder DJ, Ennulat D, et al.: Rat urinary osteopontin and neutrophil gelatinase-associated lipocalin improve certainty of detecting drug-induced kidney injury, *Toxicol. Sci.* 151:214–223, 2016.
- Piga M, Chessa E, Ibba V, et al.: Biologics-induced autoimmune renal disorders in chronic inflammatory rheumatic diseases: systematic literature review and analysis of a monocentric cohort, *Autoimmun. Rev.* 13:873–879, 2014.
- Racine C, Ward D, Anestis DK, et al.: 3,4,5-Trichloroaniline nephrotoxicity *in vitro*: potential role of free radicals and renal biotransformation, *Int. J. Mol. Sci.* 15(11):20900–20912, 2014.
- Radi ZA: Kidney pathophysiology, toxicology, and drug-induced injury in drug development, *Int. J. Toxicol.* 8:215–227, 2019.
- Radi ZA: Kidney transporters and drug-induced injury in drug development, *Toxicol. Pathol.* 48:721–724, 2020.
- Ramm S, Todorov P, Chandrasekaran V, et al.: A systems toxicology approach for the prediction of kidney toxicity and its mechanisms *in vitro*, *Toxicol. Sci.* 169:54–69, 2019.
- Rao SN: The role of heat shock proteins in kidney disease, *J Transl Int Med* 4:114–117, 2016.
- Rigoli L, Chimenz R, di Bella C, et al.: Angiotensin-converting enzyme and angiotensin type 2 receptor gene genotype distributions in Italian children with congenital uropathies, *Pediatr. Res.* 56:988–993, 2004.
- Rojko JL, Evans M, Price SA, et al.: Formation, clearance, deposition, pathogenicity, and identification of biopharmaceutical-related immune complexes: review and case studies, *Toxicol. Pathol.* 42:725–764, 2014.
- Romero-Guevara R, Ioannides A, Xinaris C: Kidney organoids as disease models: strengths, weaknesses and perspectives, *Front. Physiol.* 11:e563981, 2020.
- Rosenberger C, Heyman SN, Rosen S, et al.: Up-regulation of HIF in experimental acute renal failure: evidence for a protective transcriptional response to hypoxia, *Kidney Int.* 67:531–542, 2005.
- Rouse RL, Zhang J, Stewart SR, et al.: Comparative profile of commercially available urinary biomarkers in preclinical drug-induced kidney injury and recovery in rats, *Kidney Int.* 79:1186–1197, 2011.
- Schiessl IM, Grill A, Fremter K, et al.: Renal interstitial platelet-derived growth factor receptor-beta cells support proximal tubular regeneration, *J. Am. Soc. Nephrol.* 29:1383–1396, 2018.
- Seale TW, Rennert OM: Mechanisms of antibiotic-induced nephrotoxicity, *Ann. Clin. Lab. Sci.* 12:1–10, 1982.
- Secker PF, Luks L, Schlichenmaier N, Dietrich DR: RPTEC/TERT1 cells form highly differentiated tubules when cultured in a 3D matrix, *ALTEX* 35:223–234, 2017.
- Seely JC, Frazier KS: Regulatory forum opinion piece: dispelling confusing pathology terminology; recognition and interpretation of selected rodent renal tubule lesions, *Toxicol. Pathol.* 43:457–463, 2015.
- Seely JC: A brief review of kidney development, maturation, developmental abnormalities, and drug toxicity: juvenile animal relevancy, *J. Toxicol. Pathol.* 30:125–133, 2017.
- Seely JC, Francke S, Mog S, et al.: Renal papillary rarefaction: an artifact mimicking papillary necrosis, *Toxicol. Pathol.* 47:645–648, 2019.
- Sellers RS, Senese PB, Khan KNM: Interspecies differences in the nephrotoxic response to cyclooxygenase inhibition, *Drug Chem. Toxicol.* 27:111–122, 2005.
- Servais H, Ortiz A, Devuyst O, et al.: Renal cell apoptosis induced by nephrotoxic drugs: cellular and molecular mechanisms and potential approaches to modulation, *Apoptosis* 13:11–32, 2008.
- Shen H, Scialis RJ, Lehman-McKeeman L: Xenobiotic transporters in the kidney: function and role in toxicity, *Semin. Nephrol.* 39:159–175, 2019.
- Singh AP, Junemann A, Muthuraman A, et al.: Animal models of acute renal failure, *Pharmacol. Rep.* 64:31–44, 2012.
- Skydsgaard M, Dincer Z, Haschek WM, et al.: International harmonization of nomenclature and diagnostic criteria (INHAND): nonproliferative and proliferative lesions of the minipig, *Toxicol. Pathol.* 49:110–228, 2021.
- Soares S, Souza L, Cronin MT, et al.: Biomarkers and *in vitro* strategies for nephrotoxicity and renal disease assessment, *Nephrol. Renal. Dis.* 5:1–14, 2020.
- Sobczuk P, Brodziak A, Khan MI, et al.: Choosing the right animal model for renal cancer research, *Transl. Oncol.* 13:e100745, 2020.
- Sochol RD, Gupta NR, Bonventre JV: A role for 3D printing in kidney-on-a-chip platforms, *Curr. Transplant Rep.* 3:82–92, 2016.
- Solocinski K, Gumz M: The circadian clock in the regulation of renal rhythms, *J. Biol. Rhythm.* 30:470–486, 2015.
- Soo JY, Jansen J, Masereeuw R, Little MH: Advances in predictive *in vitro* models of drug-induced nephrotoxicity, *Nat. Rev. Nephrol.* 14:378–393, 2018.
- Spapen H, Jacobs R, Van Gorp V, et al.: Renal and neurological side effects of colistin in critically ill patients, *Ann. Intensive Care* 1:14–21, 2011.
- Sreedharan R, Van Why SK: Heat shock proteins in the kidney, *Pediatr. Nephrol.* 31:1561–1570, 2016.



- Suter-Dick L, Mauch L, Ramp D, et al.: Combining extracellular miRNA determination with microfluidic 3D cell cultures for the assessment of nephrotoxicity: a proof of concept study, *AAPS J.* 20(86), 2018.
- Takasato M, Er PX, Chiu HS, et al.: Kidney organoids from human iPS cells contain multiple lineages and model human nephrogenesis, *Nature* 526(7574):564–568, 2015.
- Tian F, Yourek G, Shi X, et al.: The development of Wilms tumor: from WT1 and microRNA to animal models, *Biochim. Biophys. Acta, Rev. Cancer* 1846:180–187, 2014.
- Togashi Y, Sakaguchi Y, Miyamoto M, Miyamoto Y: Urinary cystatin C as a biomarker for acute kidney injury and its immunohistochemical localization in kidney in the CDDP-treated rats, *Exp. Toxicol. Pathol.* 64:797–805, 2012.
- Townsend DM, Hanigan MH: Inhibition of  $\gamma$  glutamyl transpeptidase or cysteine S-conjugate  $\beta$ -lyase activity blocks the nephrotoxicity of cisplatin in mice, *J. Pharmacol. Exp. Therapeut.* 300:42–48, 2002.
- Turner OC, Knight B, Zuraw A, et al.: Mini review: the last mile—opportunities and challenges for machine learning in digital toxicologic pathology, *Toxicol. Pathol.* 49:714–719, 2021.
- Verlander JW: Normal ultrastructure of the kidney and lower urinary tract, *Toxicol. Pathol.* 26:1–17, 1998.
- Vezzali E, Manno RA, Salerno D, et al.: Spontaneous glomerulonephritis in Gottingen minipigs, *Toxicol. Pathol.* 39:700–705, 2011.
- Vormann MK, Vriend J, Lanz HL, et al.: Implementation of a human renal proximal tubule on a chip for nephrotoxicity and drug interaction studies, *J. Pharmaceut. Sci.* 110:1601–1614, 2021.
- Wagoner MP, Yang Y, McDuffie JE, et al.: Evaluation of temporal changes in urine-based metabolomic and kidney injury markers to detect compound induced acute kidney tubular toxicity in beagle dogs, *Curr. Top. Med. Chem.* 17: 2767–2780, 2017.
- Wang X, Yao B, Wang Y, et al.: Macrophage cyclooxygenase-2 protects against development of diabetic nephropathy, *Diabetes* 66:494–504, 2017.
- Weber EJ, Lidberg KA, Wang L, et al.: Human kidney on a chip assessment of polymyxin antibiotic nephrotoxicity, *JCI Insight* 3:e123673, 2018.
- Weiner D, Verlander JW: Renal ammonia metabolism and transport, *Compr. Physiol.* 3:201–220, 2013.
- Wilmer MJ, Ng CP, Lanz HL, et al.: Kidney-on-a-chip technology for drug-induced nephrotoxicity screening, *Trends Biotechnol.* 34:156–170, 2016.
- Woicke J, Al-Haddawi MM, Bienvenu J-G, et al.: International harmonization of nomenclature and diagnostic criteria (INHAND): nonproliferative and proliferative lesions of the dog, *Toxicol. Pathol.* 49(1 Suppl):5–109, 2021.
- Wragg NM, Burke L, Wilson SL: A critical review of current progress in 3D kidney biomanufacturing: advances, challenges, and recommendations, *Ren. Replace Ther.* 5(18), 2019.
- Xiao W, Liu Y, Templeton DM: Pleiotropic effects of cadmium in mesangial cells, *Toxicol. Appl. Pharmacol.* 238:315–326, 2009.
- Xiao Z, Li C, Shan J, et al.: Mechanisms of renal cell apoptosis induced by cyclosporine A: a schematic review of in vitro studies, *Am. J. Nephrol.* 33:558–566, 2011.
- Yang HC, Zuo Y, Fogo AB: Models of chronic kidney disease, *Drug Discov. Today Dis. Model.* 7:13–19, 2010.
- Yarlagadda SG, Perazella MA: Drug-induced crystal nephropathy: an update, *Expert Opin. Drug Saf.* 7:147–158, 2008.
- Yin L, Du G, Zhang B: Efficient drug screening and nephrotoxicity assessment on co-culture microfluidic kidney chip, *Sci. Rep.* 10:6568, 2020.
- Yin L, Yu L, He JC, Chen A: Controversies in podocyte loss: death or detachment? *Front. Cell Dev. Biol.* 9:771931, 2021.
- Zalups RK, Diamond GL: Nephrotoxicology of metal. In Tarloff JB, Lash LH, editors: *Toxicology of the kidney*, 3rd ed., Boca Raton, 2005, CRC Press, pp 937–994.
- Zewinger S, Rauen T, Rudnicki M, et al.: Dickkopf-3 (DKK3) in urine identifies patients with short-term risk of eGFR Loss, *J. Am. Soc. Nephrol.* 29:2722–2733, 2018.
- Zhuang Q, Cheng K, Ming Y: CX3CL1/CX3CR1 axis, as the therapeutic potential in renal diseases: friend or foe? *Curr. Gene Ther.* 17:442–452, 2017.
- Zoetis T, Hurtt ME: Species comparison of anatomical and functional renal development, *Birth Defects Res. B Dev. Reprod. Toxicol.* 68:111–120, 2003.

# Lower Urinary Tract

Samuel M. Cohen

University of Nebraska Medical Center, Omaha, NE, United States

## OUTLINE

1. Introduction	213	4. Responses to Injury	221
2. Structure, Function, and Cell Biology	214	4.1. Acute Injury	221
2.1. Kidney Pelvis and Papilla	214	4.2. Chronic Injury	222
2.2. Ureters	214	4.3. Carcinogenesis	223
2.3. Urinary Bladder	214	4.4. Morphologic Lesions	226
2.4. Urethra	215	5. Mechanisms of Toxicity	230
2.5. Urothelium	215	6. Issues in Drug and Chemical Development	231
3. Evaluation of Toxicity	217	References	232
3.1. Physiologic and Biochemical Evaluation	217		
3.2. Morphologic Evaluation	218		
3.3. Techniques for Evaluation	219		

## 1. INTRODUCTION

The lower urinary tract extends from the kidney pelvis bilaterally through the ureters leading into the urinary bladder, with the final output through the urethra. It functions as a conduit for urine formed in the kidneys to be stored in the urinary bladder before final excretion through the urethra. The structure and function of the lower urinary tract is similar in all mammals, including the structure of the unique lining of the epithelium, the urothelium (formerly referred to as transitional cell epithelium). During fetal organ development, the urothelium is a relatively rapidly proliferating tissue, but the mitotic rate decreases rapidly following birth such that the adult animal has a low mitotic rate (0.1–0.4 mitoses/1000 cells/

hour), with a turnover rate estimated at 100–200 days (Ellwein and Cohen, 1988). Many chemicals or their metabolites are excreted in the urine, thus coming into contact with the urothelium, particularly in the urinary bladder. Urothelial toxicity predominantly occurs due to urinary exposure rather than blood-borne exposure.

Considerable information has been gained during the past several decades regarding toxic effects of chemicals and other agents on the lower urinary tract in humans, including carcinogenicity. This has been due to identification in clinical settings, occupations, and the environment of specific agents that affect the lower urinary tract, with subsequent development of animal models. Since urine is the route of excretion of numerous chemicals, it is not surprising

that the urothelium is a frequent target for toxicity, especially since many of these agents are concentrated in the urine compared to systemic exposure. Furthermore, many agents alter urinary composition, which can also produce toxicity, such as the formation of urinary calculi or increased susceptibility to bacterial infection.

## 2. STRUCTURE, FUNCTION, AND CELL BIOLOGY

### 2.1. Kidney Pelvis and Papilla

The kidney pelvis acts like a funnel, collecting the urine produced in the kidney and leading to a central “stem,” the ureter. The epithelial lining of the kidney pelvis is an urothelium, beginning as a single cell layer at the fornices and expanding to three to 6 cell layers when it reaches the ureter (Souza et al., 2018). The lining epithelium of the kidney papilla is a flattened to cuboidal epithelium which does not have the differentiation characteristics of the urothelium. As a consequence, proliferative changes of the lining papilla, such as commonly occur in chronic progressive nephropathy (CPN), should not be referred to as kidney pelvis or urothelial hyperplasia, but rather should be referred to as hyperplasia of the lining epithelium of the papilla (Souza et al., 2018). Mouse and rat kidneys each have a single papilla projecting into the lumen of the pelvis. Larger mammals, including humans, have multiple papillae.

### 2.2. Ureters

The ureters are a continuation of the kidney pelvis, extending bilaterally from the kidney pelvis to their entrance dorsolaterally in the wall of the urinary bladder. They extend a short distance through the muscular wall of the urinary bladder before emptying into the trigone area of the bladder posteriorly and laterally. Its presence in the wall of the bladder serves as a barrier to the reflux of the urine from the bladder lumen. Points of constriction in the course of the ureter occur in all species at the ureteropelvic junction and at the entrance of the ureter into the bladder wall. In larger animals, especially those that are upright such as

nonhuman primates and humans, there is also narrowing where the ureter crosses over the pelvic brim. These sites of narrowing are the most common for obstruction to normal urine flow by urinary calculi. The muscle wall of the ureters has an inner circular and outer longitudinal layer of smooth muscle fibers with an adventitial covering. In sections where they traverse the bladder, care must be taken identifying the ureters so that they are not mistaken for diverticuli or invasive carcinoma (Figure 3.1).

### 2.3. Urinary Bladder

The urinary bladder is located in the posterior abdominal cavity and the pelvis, ventral to the colon. In rodents, the most anterior part of the bladder is referred to as the dome, and the most posterior portion, formed by a triangle-like area where the ureters enter and the urethra exits the bladder, is referred to as the trigone. The bladder can become convoluted when empty, but smoother as it stretches to fill with urine, since the bladder is a highly distensible organ. Urinary volumes in rats and mice typically range up to 1 mL, but even greater volumes can occur under selected circumstances, such as when there is urethral obstruction, calculi or tumors present, or a diuretic is administered.

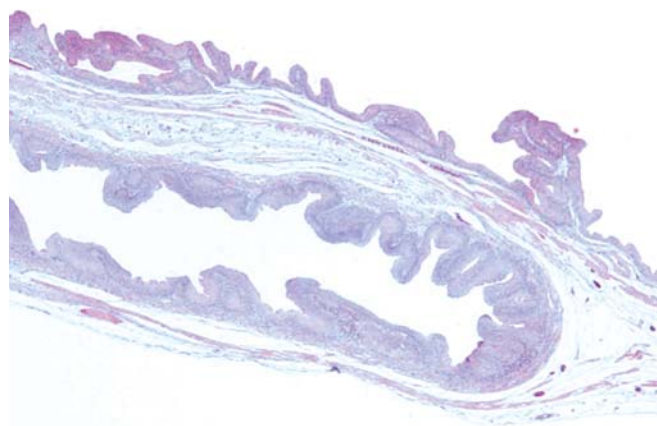


**FIGURE 3.1** Ureter in the wall of the rat urinary bladder. Papillomatosis present on the urothelial surface of the bladder (upper portion of photograph) and in the ureter. Reproduced from Haschek WM, Rousseaux CG, Wallig MA, editors: *Haschek and Rousseaux's handbook of toxicologic pathology*, ed 3, 2013, Academic Press, Figure 48.1, p. 1776, with permission.



The urinary lumen of the bladder is lined by the urothelium. In rodents, this normally is 3 cell layers thick, and occasionally four, especially in mice (Figures 3.2 and 3.3). Care must be taken in examining sections to prevent tangential sections across the urothelium being misinterpreted as hyperplasia. The urothelium rests on a thin basement membrane separating the epithelium from the underlying loose connective tissue, which contains an interwoven plexus of small capillaries. This subepithelial connective tissue has been referred to as a submucosa, although this is argued because of the frequent lack of a distinct muscularis mucosa. However, studies have provided considerable evidence that there is truly a muscular mucosa present, although it is incomplete. The subepithelial connective tissue is surrounded by layers of a smooth muscle coat, connective tissue, and adventitia. Mast cells are common in the subepithelial connective tissue, particularly around blood vessels, and these increase in number when there is epithelial proliferation. Unless care is taken, these are frequently degranulated and can be difficult if not impossible to detect in routine histologic sections. Lymphocytes and histiocytes are commonly present in small numbers in the subepithelial tissues of the mouse urinary bladder, but usually not in the rat. They are always present in monkey subepithelial connective tissue.

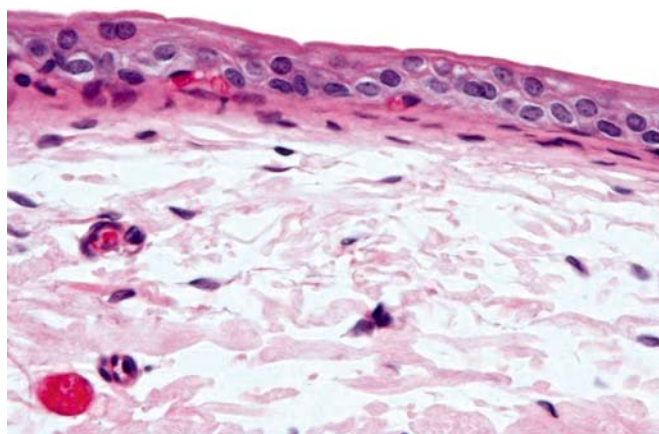


**FIGURE 3.2** Normal rat urinary bladder epithelium, nearly always 3 cell layers thick with a thin superficial layer. Reproduced from Haschek WM, Rousseaux CG, Wallig MA, editors: *Haschek and Rousseaux's handbook of toxicologic pathology*, ed 3, 2013, Academic Press, Figure 48.2, p. 1777, with permission.

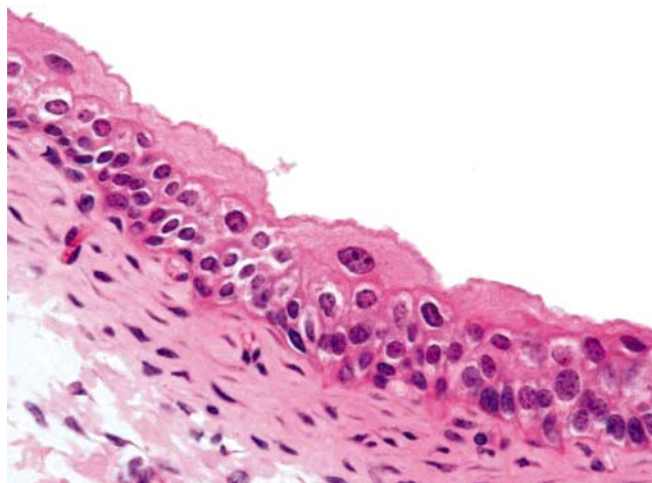


**FIGURE 3.3** Normal mouse urinary bladder urothelium, frequently 4 cell layers thick rather than three, and with a thicker superficial cell layer than in rats. Reproduced from Haschek WM, Rousseaux CG, Wallig MA, editors: *Haschek and Rousseaux's handbook of toxicologic pathology*, ed 3, 2013, Academic Press, Figure 48.3, p. 1777, with permission.

## 2.4. Urethra

The urethra of the female is short, slightly flattened dorsoventrally, and extends from the urinary bladder to the clitoral fossa just anterior to the vaginal orifice. The short urethra in females is amenable to canulization for intravesical administration of substances, whereas the long, more complex urethra in males does not permit such maneuvers easily. The urethra of the male is considerably longer, extending from the bladder through the pelvic girdle (membranous urethra) and continuing to the penis as the penile urethra, opening at the tip of the penis. The urethra of the male and female is generally lined by urothelium, but squamous epithelium can also be present at various portions, particularly near the external orifice. Squamous epithelium is common in females, although it is less frequent in rodents than in primates.

## 2.5. Urothelium

The urothelium is a unique, highly specialized epithelium lining the lower urinary tract. It has a variable number of cell layers, but in the rodent urinary bladder, it is usually 3 cell layers thick in the urinary bladder and more in the ureter. In larger mammals, such as dogs, monkeys, and

humans, the urothelium frequently can have more than three layers, occasionally up to 10 or more (Figure 3.3).

There are distinct cell types in the urothelium, with the basal cell layer composed of cuboidal cells resting on a basement membrane attached via hemidesmosomes. Intermediate cells tend to be somewhat larger, and if the urothelium has more than 3 cell layers, it is because of multiple layers of intermediate cells. The superficial cells are large, covering multiple underlying intermediate cells. Differentiation of the urothelium appears to occur secondary to PPAR $\gamma$  activation (Varley et al., 2004).

The urothelium of the nonhuman primate (Figure 3.4) is somewhat different than that of humans and other species, including dogs and rodents (Hardisty et al., 2008). Like humans, the urothelium can have more than 3 cell layers and still not be considered hyperplastic, as there is extensive variability depending on a number of variables. An explanation for the variability in number of cell layers has not been ascertained. Nonhuman primate urothelium has distinguishing factors. Keratohyaline granules are present in the urothelium, mostly toward the surface, which are not seen in other species. This suggests a tendency toward squamous differentiation, although the urothelium stains positive for uroplakin, indicative of the true urothelial differentiation that these cells have. Another distinguishing feature of the nonhuman primate urothelium is the presence of lymphocytes and macrophages within the urothelium. In other species, these would be considered indicative of a chronic inflammatory response, but they are normally present in the nonhuman primate. Whether these represent a response to an unidentified infection, possibly of viral origin, has yet to be defined.

The superficial cell layer is composed of large, flat, polygonal cells (greater than 100 microns in their greatest dimension) with a scalloped surface. By transmission electron microscopy, intracytoplasmic fusiform vesicles are plentiful, more so in the contracted bladder (Figure 3.5). The plasma membrane of the luminal surface of the fusiform vesicles and the luminal surface of the superficial cells is unique, consisting of an asymmetric unit membrane, so named because the outer leaflet of the membrane is thicker than the inner cytoplasmic leaflet when

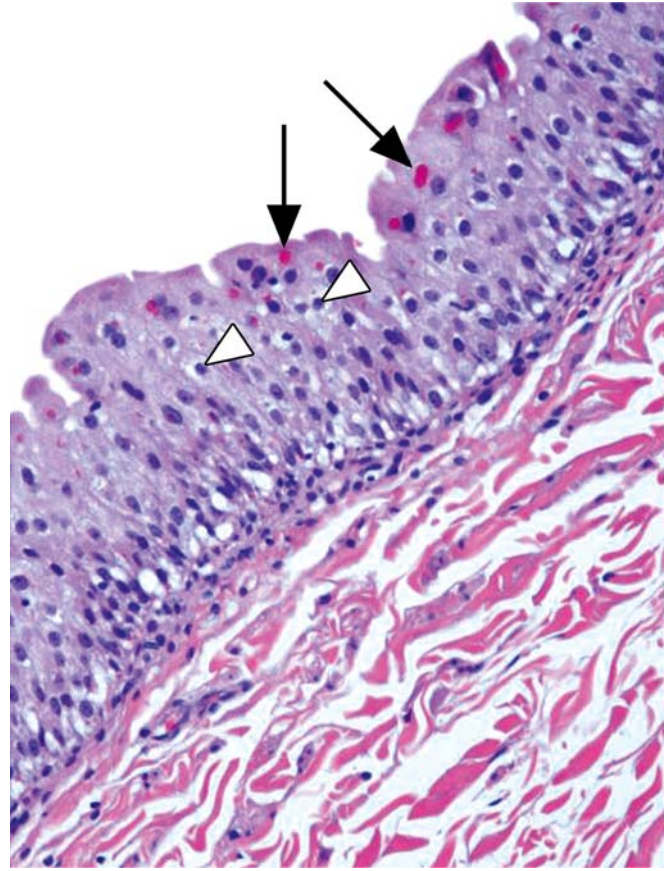


**FIGURE 3.4** Monkey, urinary bladder, normal. Basal vacuolation represents autolytic change. Eosinophilic granules (arrows) in the superficial layer represent keratohyaline. Intraepithelial lymphocytes and macrophages (arrowheads) are plentiful. *Reproduced from Haschek WM, Rousseaux CG, Wallig MA, editors: Haschek and Rousseaux's handbook of toxicologic pathology, ed 3, 2013, Academic Press, Figure 48.4, p. 1778, with permission.*

viewed by electron microscopy. This membrane is composed of plaques consisting of a hexagonal array of subunits (Yu et al., 1994). The particles of the subunits consist of four distinctive proteins, the uroplakins, representing the terminal differentiation of the urothelium. These proteins are unique to the urothelium, although minute amounts can be present in other cell types. The fusiform vesicles can be connected to the luminal surface and are believed to represent foldings in the luminal membrane for expansion and contraction of the urinary bladder. The lining epithelium also serves a barrier function to the absorption of urine. Contributing to the barrier function of the urothelium is a circumferential band of tight



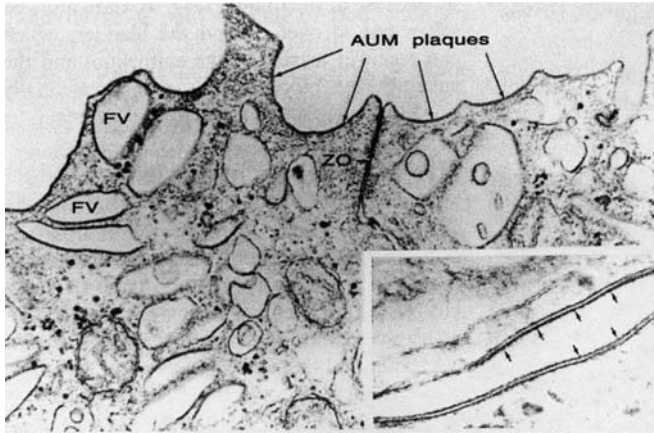


**FIGURE 3.5** Luminal surface of two superficial cells of the urinary bladder, joined by zonular occludens intercellular junction (ZO) (tight junction). The luminal membrane has a scalloped appearance due to the presence of rigid, curved, asymmetric unit membrane (AUM) plaques alternating with short segments of symmetric membrane, which serve as “hinge” areas. Intracytoplasmic fusiform vesicles (FV) are lined by AUM plaques. Inset: The thicker leaflets of the AUM plaque of fusiform vesicles face inward, lining the intravesicular space. This leaflet contains particulate membrane components (arrows). Transmission electron microscopy. *Reproduced from Haschek WM, Rousseaux CG, Wallig MA, editors: Haschek and Rousseaux’s handbook of toxicologic pathology, ed 2, 2002, Academic Press, Figure 1, p. 339, with permission.; Originally from Alroy J: Ultrastructure of canine urinary bladder carcinoma, Vet. Path., 16(6):693–701, 1979.*

junctions between superficial cells. Using scanning electron microscopy (SEM), the luminal surface of the bladder is seen as being composed of hexagonal, large, flattened cells, with an interwoven microridge system (Jacobs et al., 1983) (Figure 3.6).

### 3. EVALUATION OF TOXICITY

#### 3.1. Physiologic and Biochemical Evaluation

There are limited pathogenic mechanisms for producing toxicity of the urothelium. These include direct mitogenesis, cytotoxicity and regeneration, and absorption of materials from the urine with accumulation in the urothelium (Cohen, 2018). Cell death can be due to necrosis (most common) or apoptosis (Vogel et al., 2009).

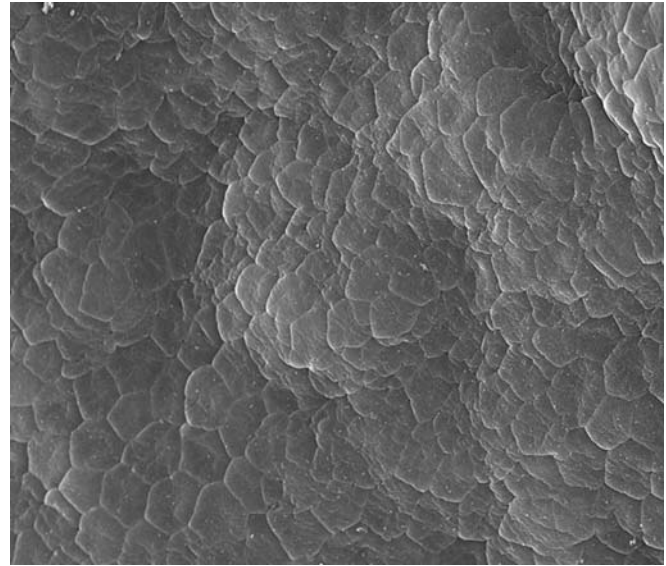


**FIGURE 3.6** Luminal surface of the rat urinary bladder epithelium showing the relatively flat, hexagonal superficial cells tightly adherent to each other. Scanning electron micrograph. *Reproduced from Haschek WM, Rousseaux CG, Wallig MA, editors: Haschek and Rousseaux’s handbook of toxicologic pathology, ed 3, 2013, Academic Press, Figure 48.6, p. 1779, with permission.*

If the full thickness of the urothelium and basement membrane is damaged, an inflammatory reaction and hemorrhage occurs with consequent regeneration and repair.

It has become apparent that alterations in the normal constituents in the urine can significantly influence toxicity, at least in rodents, in addition to the actual effects of the administered chemicals (Cohen, 1995; Cohen et al., 2007). In turn, the composition of the urine can be influenced considerably by the type of diet that is administered and by the amount of water consumed.

Urinary composition has a diurnal variation which is dependent on the time of day or night that the animal eats (Cohen, 1995; Fisher et al., 1989). Since rodents normally are nocturnal animals, the volume of urine and concentration of the components increase while they are eating at night, and decrease during the day while they are asleep. The opposite occurs if the animals are diet restricted, since the animals become acclimated to the regimen and frequently eat and drink in the morning when food becomes available. This leads to increased urinary volume and concentration of most components during the day, not night.



A major influence on urinary toxicity is pH (Cohen, 1995; Cohen et al., 2007; Roberts et al., 2021). The pH of rodent urine generally varies between 5.0 and 9.0, but occasionally can be higher. pH is influenced considerably by diet. Many rodent diets result in a urine that is approximately neutral at night and becomes acidic during the day when the animal stops eating. However, certain diets will produce an acidic urine routinely, such as the semisynthetic casein-based diet, AIN-76a, or an alkaline urine, with a diet such as Altromin 1321.

Urinary pH has considerable influence on the solubility of various constituents of the urine, such as calcium, magnesium, and phosphate, but also greatly influences the ionization of chemicals that have such potential. By altering urinary pH, the toxicity of various chemicals can be significantly modified, even for genotoxic carcinogens such as the aromatic amines.

A major difference between rodent and human urine is the overall osmolality (Cohen, 1995). Rodent urine is usually highly concentrated, with osmolality ranging from 1200 to 3000 mosmol/L. This is largely due to extremely high concentrations of urea ( $>1$  M), as well as high concentrations of several electrolytes, protein, and mucopolysaccharides. In contrast, human urine usually has an osmolality of 50–400 mosmol/L, even if dehydrated. It has been estimated that the highest osmolality theoretically attainable in humans is 1000–1200 mosmol/L, but such levels have not been observed. Male mouse and male rat urine have exceedingly high concentrations of protein, primarily because of  $\alpha$ 2u-globulin in rats and mouse urinary protein (MUP) in mice.  $\alpha$ 2u-Globulin protein has been of considerable importance in the toxicity and carcinogenicity of several chemicals affecting the kidney and urinary bladder of rats (Swenberg and Lehman-McKeeman, 1999). Since there is no comparable protein in humans, such findings in the male rat are not relevant to humans. Furthermore, rodents have a gradual increase in urinary proteinuria with age because of increased albumin excretion associated with the development of CPN, especially in the rat and particularly in males.

Differences in the concentration of calcium, phosphate, and magnesium can influence the toxicity and carcinogenicity of various chemicals, largely due to their involvement in the formation

of various urinary solids. Calcium frequently precipitates in rodent urine as the phosphate salt, whereas in monkeys and humans, it more frequently precipitates as calcium oxalate. Calcium is maintained in a supersaturated soluble state primarily because of its binding to various chelating substances in the urine, especially citrate, but also various proteins and, possibly, mucopolysaccharides. Urinary silicate levels can reach substantial concentrations in certain species, depending on dietary sources, which can lead to formation of silicate crystals and calculi (Okamura et al., 1992). This is particularly true in sheep and some other domesticated mammals. Urinary calcium, phosphate, and magnesium are present at considerably higher concentrations in rats than in mice, which is the likely explanation of the greater susceptibility of rats to formation of urinary solids than mice.

### 3.2. Morphologic Evaluation

Chemicals administered by various routes are frequently excreted by the kidney (see *Kidney*, Vol 5, Chap 2) into the urine, and usually are more concentrated than in systemic blood. If the concentration in the urine reaches a sufficiently high level, a cytotoxic response can be induced. This can be due directly to the administered chemical, or, more frequently, to one or more metabolites. Morphologic evaluation of the bladder is best performed on the bladder inflated with fixative, prior to removal from the body with the animal anesthetized (Cohen et al., 2007). It is particularly important that inflation of the bladder with fixative occurs, while the animal is under anesthesia rather than after the animal's death, since electron microscopic changes can occur within 1 minute of the time the animal dies. These autolytic changes can be similar to treatment-related changes. The foldings normally present in the empty bladder can make it difficult to distinguish subtle degrees of hyperplasia from tangential sectioning that occurs readily because of the folding. Care must be taken not to overdistend the bladder, which can result in tearing of the epithelium and the subepithelial blood vessels, occasionally producing artifactual subepithelial spaces.

Histopathologic evaluation is routinely accomplished by light microscopy of hematoxylin and eosin-stained sections. However, superficial cytotoxicity is difficult to definitively identify by light microscopy because of the thinness of the superficial cells, the focal nature of the changes, and tearing artifacts that occur during collection and processing of the tissue (Cohen et al., 2007). Changes in the urothelium occur in response to exposure to urinary solids or directly by chemicals that are cytotoxic to the urothelial cells. If the effect is mild, the toxicity involves only the superficial and possibly the intermediate cell layers, and is not associated with hematuria or inflammation. It is only if there is damage to the full thickness of the urothelium and breach of the basement membrane (ulceration) that an inflammatory response will occur. Immunohistochemical stains can be helpful in identifying poorly differentiated neoplasms. Stains for uroplakins or cytokeratin 7 can be useful in defining urothelial differentiation, and stain for p40 can be useful for identifying squamous differentiation. Smooth muscle markers, such as smooth muscle actin (SMA) or smooth muscle myosin (SMM), can help in distinguishing the mouse submucosal mesenchymal lesion from invasive carcinoma, with carcinomas having positive staining for keratin.

The nomenclature for the various lesions in the lower urinary tract has evolved over the past several years, with standardization having been achieved through the efforts of the INHAND program (Frazier et al., 2012). This nomenclature is used in this chapter.

### 3.3. Techniques for Evaluation

#### 3.3.1. Urinalysis

An extensive description of methods for collection and examination of urine and the lower urinary tract tissues is presented in Cohen et al. (2007). (See also *Clinical Pathology in Non-Clinical Toxicology Testing*, Vol 1, Chap 10).

It is essential in examining urine that the animals not be fasted, since there are marked changes in urinary composition within 1–2 h after eating stops. We recommend fresh void urine collection with immediate processing to avoid artifactual changes that can occur over time or with changes in temperature.

Formation of urinary solids is a major source of toxicity, particularly in rats (Cohen, 2018). Microcrystals are normally present in the urine in small amounts, usually in the form of magnesium ammonium phosphate (struvite) crystals. As long as these are present in relatively small numbers and concentrations, they are not a source of toxicity. Other solids present in the urine include cells, cellular debris, casts, and, in males, occasional seminal plugs (Frazier et al., 2012). Collectively, this material is referred to as the urinary sediment and is usually not toxic to the lining urothelium.

Examination of urine for solids can be routinely performed by the usual analysis after centrifugation of urinary sediment by light microscopy. However, more sensitive and precise analyses can be accomplished by processing the resuspended centrifuged urine through a 0.22  $\mu$  nitrocellulose filter and examining by SEM with attached energy dispersive spectroscopy (Cohen et al., 2007). By using X-ray analysis, elemental identification of any crystals can be accomplished.

Solids can form and collect in the urine, ranging in size from small (amorphous precipitate) to microscopic (crystals) to macroscopic (calculi) material. Distinguishing between crystals and calculi is somewhat arbitrary, but has been variously defined as solids greater than 100–300  $\mu$ m in diameter. Frequently, calculi form around a protein or other organic nidus. Rarely, protein can form a calculus by itself. These solids produce a variable degree of toxicity to the surface of the urothelium, depending on their toxic nature and on the size and coarseness of the material.

Solids can form secondary to high concentrations of the administered chemical or its metabolites, or they can be produced by excess concentrations of normal constituents of the urine leading to precipitation. Numerous factors affecting the composition of the urine contribute to the formation of these solids, including urinary pH, calcium, citrate, magnesium, phosphate, protein, and other variables, including osmolality.

Formation of solids from normal urinary constituents occurs as a consequence of marked alterations in normal urinary physiology and composition. For example, excess uric acid

production leads to high concentrations of urates in the urine and to the production of urate calculi. This can occur, for example, by the surgical formation of a portacaval shunt, leading ultimately to the formation of urate calculi. Similarly, any treatment resulting in the excess excretion of calcium and phosphate in the urine, or decreased citrate, will lead to calcium phosphate lithiasis.

With precipitates and crystals, the extent of the damage frequently is limited to the superficial cell layer and occasionally the intermediate cell layer, and is often focal in nature. If superficial, it can be difficult to detect by light microscopy or to distinguish from the tearing that commonly occurs during processing of tissues for histopathology. Examination of the luminal surface by SEM provides a more extensive sampling and greater sensitivity for definitively detecting changes of necrosis and other aspects of toxicity (Figure 3.7).

It is only if there is penetration of the full thickness of the urothelium and penetration through the basement membrane (ulceration) that an inflammatory response and hematuria will

occur. As long as the damage to the urothelium is confined to the urothelium, an inflammatory response does not occur. Thus, although inflammation is a helpful sign that there has been toxicity to the urothelium, its absence is not evidence against the occurrence of superficial necrosis.

Cell death occurs in the urothelium primarily due to necrosis. This can be preceded by precursor changes such as cytoplasmic and nuclear swelling (Figure 3.8), similar to that seen in hepatocytes, and has been referred to as oncocytosis. Also, cell death can occur by apoptosis. Apoptosis normally occurs in the urothelium to a very limited extent (<3 per 1000 cells), but has been described as a major cause of urothelial cell death in S1P knockout mice (Vogel et al., 2009).

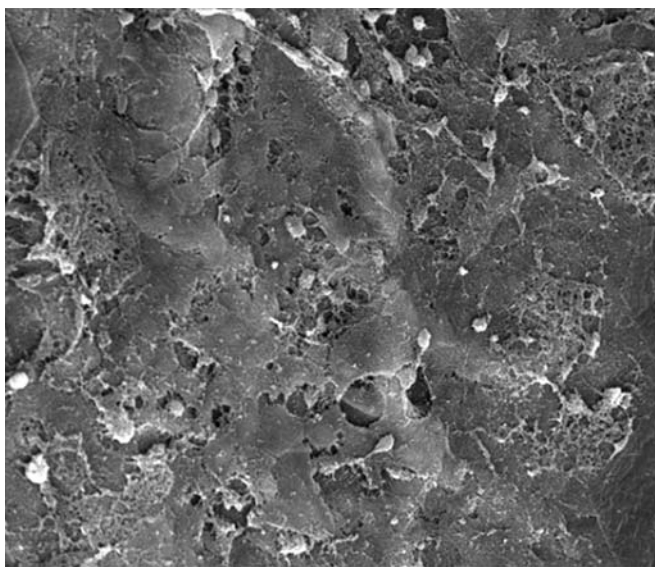


**FIGURE 3.7** Scanning electron micrograph of rat urinary bladder urothelium illustrating severe superficial cell necrosis, with widening intercellular spaces and deterioration of the superficial cells. *Reproduced from Haschek WM, Rousseaux CG, Wallig MA, editors: Haschek and Rousseaux's handbook of toxicologic pathology, ed 3, 2013, Academic Press, Figure 48.7, p. 1781, with permission.*

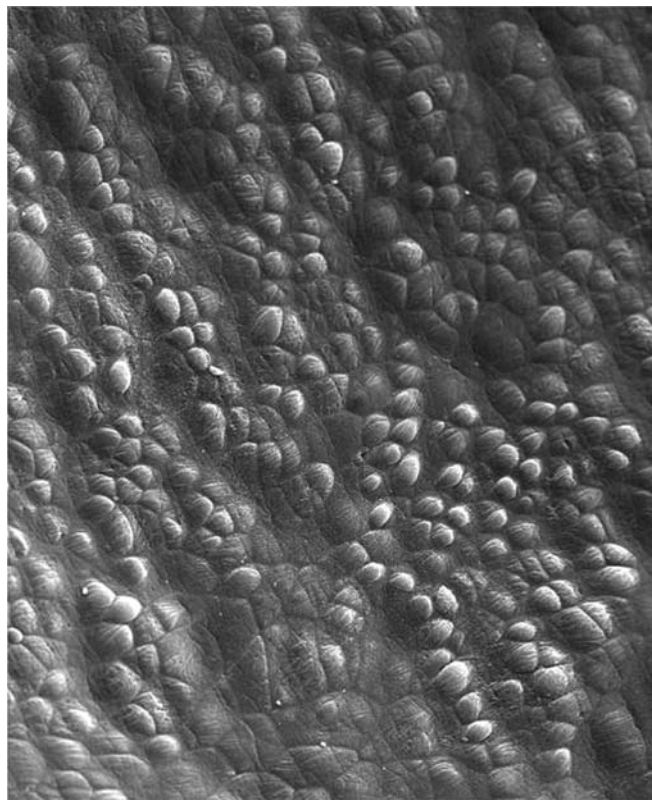


**FIGURE 3.8** Scanning electron micrograph of rat urinary bladder urothelium illustrating swelling of the superficial urothelial cells. This process can be reversible or progress to necrosis. *Reproduced from Haschek WM, Rousseaux CG, Wallig MA, editors: Haschek and Rousseaux's handbook of toxicologic pathology, ed 3, 2013, Academic Press, Figure 48.8, p. 1782, with permission.*



### 3.3.1.1. SPECIAL TECHNIQUES

It has become apparent that increased cell proliferation is a common precursor to the development of bladder tumors in rodents, and can readily be used as a screening mechanism for detecting potential bladder carcinogens. Although this usually includes the presence of hyperplasia, it is occasionally more limited, being detectable only by an increase in DNA replication. Cell proliferation in the urinary bladder is normally low, so that an increase in the amount of proliferation frequently requires examination of a large number of urothelial cells to obtain statistical significance. Furthermore, since rodents are horizontal quadrupeds, urine can settle in the ventral dome of the bladder. As a consequence, it is important that sections of the bladder examined for histopathology and DNA replication be taken through the ventral portion of the bladder, especially including both the dome and the trigone.

Increased DNA replication can be detected by a variety of labeling indices (Wood et al., 2015) (see also *Special Techniques in Toxicologic Pathology*, Vol 1, Chap 11). Most reliable is incorporation of a substance into the replicating DNA, such as tritiated thymidine (rarely used any longer) detected with autoradiography, or bromodeoxyuridine (BrdU) with immunohistochemical detection. These require administration of chemicals used for assessing DNA replication prior to the animal's death. It is best to use a 1- to 2-hour pulse of the agent rather than longer periods through an osmotic minipump. Stress to the rodent, such as excessive handling or implantation of a minipump, leads to urinary changes and increased urothelial proliferation. An estimate can also be made of cell proliferation on paraffin-embedded tissue utilizing proliferation cell nuclear antigen (PCNA) or Ki-67 antigen detected by immunohistochemistry. If using these latter antigens, care must be taken to standardize the preservation and processing of the tissue, especially paying attention to the time that the tissue is in fixative and in the paraffin block.

Cytotoxicity of specific chemicals or metabolites can be readily assessed utilizing well-characterized immortalized but nonmalignant urothelial cell lines from rats and humans or primary cell cultures from mice, rats, or humans.

Comparing the LC<sub>50</sub> in vitro to the urinary concentration following administration of the chemical provides an excellent means of assessing relevancy and of putting into perspective the dose response (de Rocha et al., 2012, 2014). Cytotoxicity in vitro will generally occur at lower concentrations than in vivo because the cells in culture are not fully differentiated. They do not have the protective superficial cell layer. Methods have been developed for inducing terminal differentiation of urothelial cells in culture, but it is unclear yet if such systems can be used for toxicity assessments.

## 4. RESPONSES TO INJURY

### 4.1. Acute Injury

If the full thickness of the urothelium is damaged and the basement membrane is breached, the result is an ulcer of the urothelium (Cohen et al., 2007; Fukushima et al., 1981). The ulcer induces a typical acute inflammatory response, beginning with necrosis of the epithelium and underlying connective tissues, accompanied by hemorrhage and an acute inflammatory infiltrate. Eventually, regeneration of the epithelium occurs with healing of the ulcer, and the inflammatory response gradually subsides and changes to a chronic inflammation infiltrate and granulation tissue formation. If the extent of the damage is not extensive, the lesion can heal completely without evident residual effect, such as chronic inflammation or scar formation. However, if the damage is more extensive, chronic inflammation can persist and scar formation occurs. In the rat and mouse, the time-course of this process is consistent regardless of the inciting stimulus, whether chemical or physical. The ulceration usually is present within hours to a few days of the inciting stimulus, with a peak proliferative and inflammatory response within 5–7 days. Usually, the lesion is repaired within approximately 3 weeks after the removal of the initiating agent, with the bladder returning to normal within 3–5 weeks. Complete resolution of the damage is dependent on removal of the inciting stimulus, the overall condition of the animal, and the composition of the urine. Vacuolation of the

epithelium is a frequent initial change in the epithelium before there is clear evidence of necrosis. Vacuolation related to toxicity frequently occurs initially in the superficial and intermediate cell layers, whereas autolysis usually begins with vacuolation of the basal layer. However, to clearly distinguish these, immediate fixation is necessary.

If the inciting stimulus produces only superficial damage, the extent of the proliferative response of the epithelium is usually mild simple hyperplasia (Cohen et al., 2007) (Figure 3.9). However, if the damage involves ulceration, particularly if it continues for an extended period of time, there is a prominent proliferative response of the urothelium resulting in formation of nodular (Figure 3.10) and papillary (Figure 3.11) hyperplasia, and even extensive formation of papillomas, referred to as papillomatosis (Figure 3.12) (Shirai et al., 1989).

The epithelial proliferative responses are accompanied by a proliferation of the underlying capillary network. This capillary proliferation reverses upon reversion of the epithelial proliferation (Cohen et al., 1980). These urothelial proliferative responses are completely reversed upon withdrawal of the inciting stimulus, even the extensive papillomatosis.

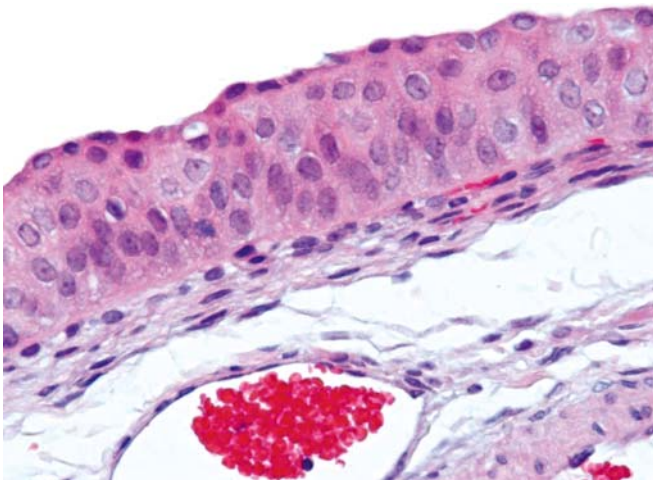


**FIGURE 3.9** Mild simple hyperplasia of the rat urinary bladder urothelium. There is no atypia, mitoses are rare, and the superficial cells remain. Reproduced from Haschek WM, Rousseaux CG, Wallig MA, editors: *Haschek and Rousseaux's handbook of toxicologic pathology*, ed 3, 2013, Academic Press, Figure 48.9, p. 1783, with permission.

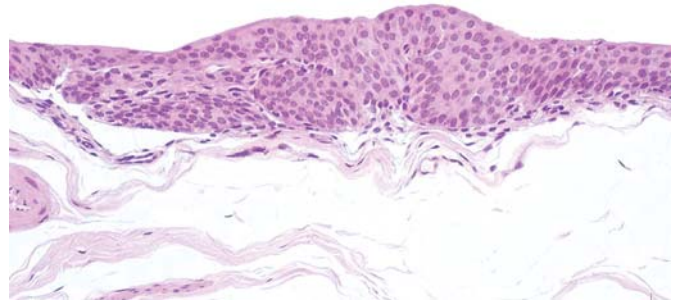


**FIGURE 3.10** Nodular hyperplasia of the rat urinary bladder urothelium. The nodules which appear to be in the submucosa are actually attached to the overlying epithelium. Reproduced from Haschek WM, Rousseaux CG, Wallig MA, editors: *Haschek and Rousseaux's handbook of toxicologic pathology*, ed 3, 2013, Academic Press, Figure 48.10, p. 1783, with permission.

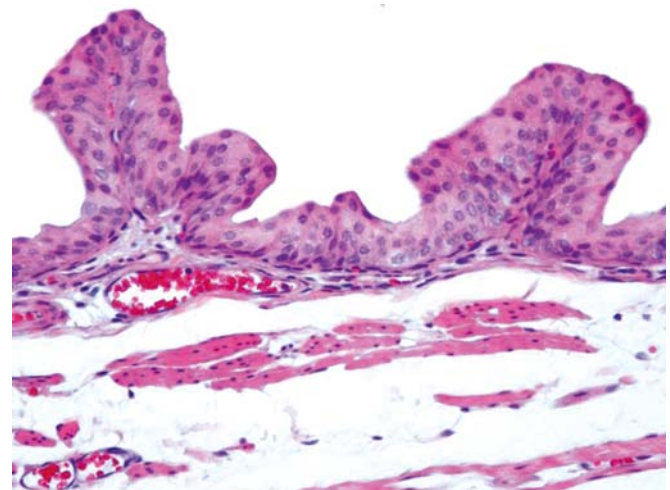


**FIGURE 3.11** Papillary hyperplasia of the rat urinary bladder urothelium with distinct fibrovascular core. Reproduced from Haschek WM, Rousseaux CG, Wallig MA, editors: *Haschek and Rousseaux's handbook of toxicologic pathology*, ed 3, 2013, Academic Press, Figure 48.11, p. 1784, with permission.

#### 4.2. Chronic Injury

Many strains of rats frequently show calcification of the fornix of the kidney pelvis, usually accompanied by chronic inflammation, urothelial hyperplasia, and hyperplasia of the lining of the papilla (Tomonari et al., 2016). A chronic inflammatory infiltrate can be present in the submucosa of the urinary tract, particularly if the toxic stimulus produces full-thickness damage to the epithelium. In mice, the lymphocytic infiltrate must be distinguished from



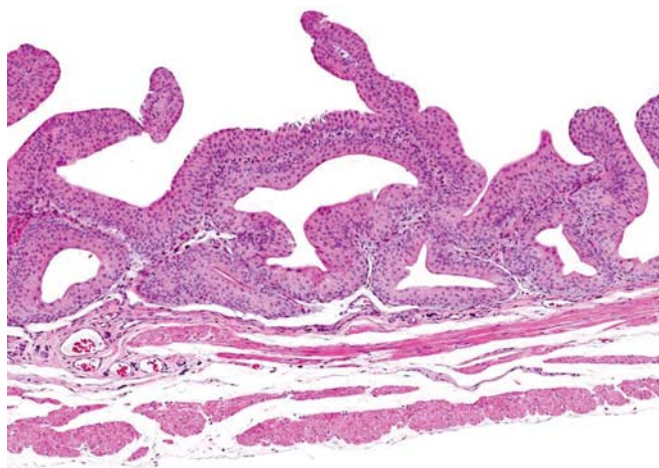


**FIGURE 3.12** Papillomatosis of the rat urinary bladder urothelium. Although these lesions have branching and thus could be considered true papillomas, they are completely reversible if the inciting agent is removed. There is no atypia, and the epithelial lining over the fibrovascular core is three to 5 cell layers thick. Reproduced from Haschek WM, Rousseaux CG, Wallig MA, editors: *Haschek and Rousseaux's handbook of toxicologic pathology*, ed 3, 2013, Academic Press, Figure 48.12, p. 1784, with permission.

a lymphomatous/leukemic infiltrate which is commonly present in many strains of mice. Fibrosis and scar tissue formation is infrequent but has been reported in association with extensive and severe toxicity to the urothelium and underlying connective tissue. Granulomatous inflammation is infrequent and usually associated with crystalline material becoming embedded into the tissue. Association with various infectious organisms can also occur.

### 4.3. Carcinogenesis

Cancer of the urinary bladder occurs uncommonly in untreated rats or mice, except for certain strains that either have a high background incidence of spontaneous calculus formation (e.g., Brown Norway rat) or are infected chronically with the rat bladder nematode (*Trichosomoides crassicauda*), rarely present in rat strains over the past 30 years since the advent and availability of specific pathogen-free animals.

Urothelial tumors occur most frequently in the urinary bladder, but are seen occasionally in the kidney pelvis and much less commonly in

the ureter. However, certain strains of rats (SD/cShi) and mice (NON-Shi) develop high incidences of hydronephrosis and spontaneously have a significantly higher incidence of tumors of the upper urinary tract rather than in the urinary bladder (Mori et al., 1994; Murai et al., 1994).

Urothelial neoplasms can be induced in most species by either DNA-reactive chemicals or chemicals that act by increasing cell proliferation (Cohen, 2018) (see *Carcinogenesis: Mechanisms and Evaluation*, Vol 1, Chap 8). Animal models of urinary bladder cancer have been extensively used because of the identification of numerous chemicals and mixtures that produce bladder cancer in humans, including aromatic amines, cigarette smoking, cyclophosphamide, and inorganic arsenic. Aromatic amines are present in relatively high concentrations ( $\sim 100 \mu\text{g}$ ) in each cigarette, and are likely a major contributor to the carcinogenicity of cigarette smoke for the urothelium.

Many aromatic amines, such as 2-acetylaminofluorene (2-AAF), administered to rodents produce tumors of other tissues in addition to bladder, particularly the liver and the mammary gland. However, several urinary bladder-specific carcinogens have been identified and animal models have been developed, particularly utilizing N-butyl-N-(4-hydroxybutyl) nitrosamine (BBN) administered in the drinking water or by gavage (Ito et al., 1984). The DNA-reactive chemicals are positive in a variety of genotoxic screening tests, such as the Ames assay, and have identifiable structural alerts in various computerized programs for mutagenicity and carcinogenicity. They are activated metabolically to reactive metabolites that bind covalently to DNA, leading to mutations and, ultimately, the formation of cancer. DNA adducts are identifiable by a variety of assays.

In general, these DNA-reactive chemicals also are cytotoxic at high doses and induce a regenerative proliferative response. Often, they produce a detectable incidence of tumors in a 2-year bioassay only if administered at cytotoxic concentrations, with the associated consequent regenerative hyperplasia. However, exposure to genotoxic chemicals at noncytotoxic levels but in combination with nongenotoxic chemicals that increase urothelial cell proliferation, such



as with cigarette smoking, can lead to increased cancer risk (Cohen et al., 2006). The offending nongenotoxic chemicals in cigarette smoke are possibly nicotine and/or its metabolites (Suzuki et al., 2018).

In contrast, a large number of chemicals produce bladder tumors in rodents by a mode of action involving increased cell proliferation rather than direct interaction with DNA (Cohen, 2018). The increased cell proliferation can be induced by direct mitogenesis (only one example known for the bladder: propoxur, although it has also been suggested for RAF inhibitors in rodents (Wisler et al., 2011).) or by cytotoxicity and regenerative proliferation secondary to the formation of urinary solids or by the presence of cytotoxic chemicals in the urine. Urinary solids can form from constituents normally present in urine, such as calcium, urate, or magnesium, or they can form from the administered chemical (or metabolite) excreted at high concentrations in the urine, for example, melamine. Formation of urinary solids is a high-dose effect, based on the physical chemical property of solubility, representing the clearest example of a threshold effect in toxicity and carcinogenicity. A process unique to rats is the formation of large amounts of calcium phosphate-containing precipitate secondary to administration of extremely high doses (2.5% of the diet) of various sodium or potassium salts, including saccharin, ascorbate, phosphate, chloride, bicarbonate, citrate, and others. The reason for lack of formation in mouse urine is the much lower concentrations of calcium and phosphate compared to rats. Lack of effect in nonhuman primates and in humans is due to the much lower osmolality and protein levels compared to rats (IARC, 1999).

Crystals and calculi can form in the urine of most species, but the consequences can be dramatically different (Cohen, et al., 2010; Dominick et al., 2006). Crystals and calculi can form following administration of numerous chemicals, and the crystals can be toxic to the urothelium in rodents, whereas crystals are not toxic in humans (Dominick et al., 2006). They can have no effect in humans, can be an indicator of systemic disease (e.g., urate crystals and gout), or can indicate the possibility of calculus formation, which is toxic. In rodents, calculi can be

present for long periods of time, resulting in urothelial tumors. Long retention times are achieved because of the horizontal posture of quadrupeds, the calculi accumulating in the dome of the bladder. In contrast, calculi in humans lead to obstruction and severe pain, leading to their immediate removal—spontaneously, medically, or surgically. Numerous chemicals have been associated with the production of urinary calculi in rodents and humans (Table 3.1). In humans, long-term retention of calculi can occur in the presence of diverticuli or neurogenic bladder. In such circumstances, there usually is an associated bacterial cystitis, a known risk factor for urinary tract cancer.

Similarities and differences between rodents and humans in their inflammatory and proliferative response to calculi were illustrated in the episode involving adulteration of baby formula

**TABLE 3.1** Substances Producing Urinary Calculi When Administered to Rodents And/Or Humans

Urate	Melamine
Homocysteine	Silicates
Cystine	Oxamide
Oxalates	Terephthalic acid
Calcium phosphate	Dimethylterephthate
Diethylene glycol	Polyoxyethylene-8-stearate
Acetazolamide	Glycine
Sulfonamides	Sulfosulfuron
Uracil	Triamterene
Thymine	Ampicillin
Xanthine	Amoxicillin
Orotic acid	Bisacodyl
Indinavir	Nitrolotriacetate
Glafenic acid	Salicylazosulfapyridine
Nelfinavir	Disperse Blue 1
Tosufloxacin	Hydroxyanthraquinone
Efavirenz	Fosetyl-al
Pyroxasulfone	Biphenyl

*Modified from Haschek WM, Rousseaux CG, Wallig MA, editors: Handbook of toxicologic pathology, ed 2, 2002, Academic Press, Table I, p. 342, with permission.*

with melamine (Guan et al., 2009). In the 1980s, melamine at high concentrations in the diet was shown to produce urinary tract calculi and urothelial tumors in rats (Meek et al., 2003). This occurred at levels four or five orders of magnitude greater than environmental human exposures. However, adulteration of baby formula at levels producing similarly high exposures in infants as achieved in the rat studies led to formation of urinary tract calculi and consequent toxicity. Although a few individuals died from the acute obstructive effects, most recovered and the toxicity was reversible.

Usually, an increase in urothelial cell proliferation secondary to chemical administration in rodents is detectable within 4 weeks of administration of an agent, but occasionally 13 weeks are required. Rather than proceeding to a full 2-year bioassay, more information can be gathered by screening for urothelial proliferation in a 90-

day study with detailed examination of the urinary bladder for hyperplasia and/or increased cell proliferation by one of the DNA replication indices (Cohen, 2018) (Figure 3.13). If negative in such a screen, it is highly unlikely that the agent will induce urothelial tumors in a 2-year bioassay. Short-term studies (1–13 weeks, depending on the type of agent) can then be performed, with collection of the urine for examination of variations in urinary composition, especially for the detection of urinary solids, and the identification of cytotoxicity and regeneration can be specifically evaluated. Assessment of the DNA reactivity of the compound is readily accomplished utilizing a combination of structure–activity relationships and the Ames assay. Utilizing such an approach, one can quickly identify a potential mode of action for the increase in proliferation as either DNA-reactive proliferation or non-DNA-

### Screening and Evaluation of Rodent Urinary Tract Toxicity

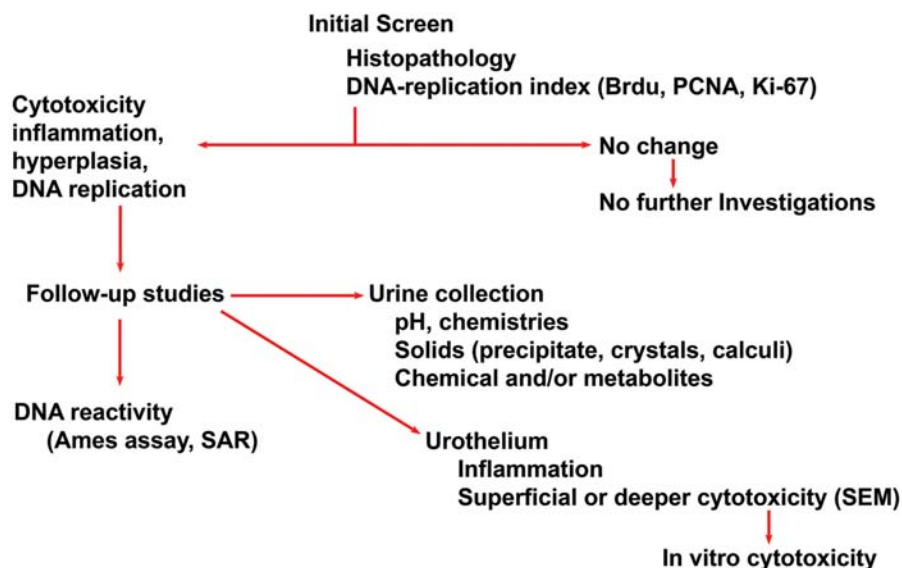


**FIGURE 3.13** A proposed system for evaluating rodent urinary tract toxicity. An initial screen is performed in a 90-day study incorporating histopathology and a measure of DNA replication. If no changes are detected in this initial screen, no further investigations are required regarding the lower urinary tract. If there is evidence of cytotoxicity, inflammation, hyperplasia, or increased DNA replication, follow-up studies are required, including an evaluation for DNA reactivity, urinary composition for solids and chemistry, and an examination of the urothelium for the presence or absence of cytotoxicity or proliferation. A more detailed evaluation approach is presented in Cohen (2018). Reproduced from Haschek WM, Rousseaux CG, Wallig MA, editors: Haschek and Rousseaux's handbook of toxicologic pathology, ed 3, 2013, Academic Press, Figure 48.13, p. 1786, with permission.

reactive proliferation due to mitogenesis or cytotoxicity and regeneration. Cytotoxicity and regeneration will be due either to the formation of urinary solids or to the presence of cytotoxic chemicals and/or metabolites in the urine.

#### 4.4. Morphologic Lesions

##### 4.4.1. Nonneoplastic Lesions

Nonneoplastic lesions include cytotoxicity, hyperplasia, diverticuli, calcification, and inclusions.

###### 4.4.1.1. CYTOTOXICITY

Cytotoxicity and necrosis limited to the superficial cell layer are difficult to detect by light microscopy, but are readily evident by SEM (Cohen et al., 2007) (Figure 3.7). The earliest manifestation of cytotoxicity by light microscopy is frequently vacuolization of the cytoplasm. Unfortunately, this is the same change that occurs with autolysis (Figure 3.3). Severe toxicity is seen with complete ulceration of the epithelium and destruction of the basement membrane, resulting in hemorrhage, acute inflammatory reaction, and granulation tissue formation.

A unique vacuolation involving superficial cells occurs in nonhuman primates secondary to administration of PPAR $\gamma$  and dual agonists (Hardisty et al., 2008) and recently reported with anti-HIV noncatalytic site integrase inhibitors (Roberts et al., 2021). Such vacuoles are uncommonly observed in untreated nonhuman primates. The mechanism for their formation has not been identified nor their relevance to potential human toxicity.

###### 4.4.1.2. HYPERPLASIA AND METAPLASIA

Hyperplasia can be either focal or diffuse. Simple hyperplasia is defined as an increase in the number of cell layers normally present (Figure 3.9), without formation of nodules or papillary projections into the lumen. This can be semiquantitatively graded as minimal, mild, moderate, or severe, depending on the number of cell layers present. An inflammatory reaction may or may not be present. Urothelial hypertrophy is usually associated with the hyperplasia and may actually be evident

histologically before the appearance of hyperplasia (Oleksiewicz et al., 2005).

Nodular hyperplasia (Figure 3.10) represents an endophytic growth of epithelial cells accumulating in what appears to be the subepithelial connective tissue. This is similar to Brunn's nests in nonhuman primate and human pathology. Although these frequently do not appear to be connected to the overlying epithelium, serial sections usually can demonstrate a connection. This must be distinguished from an invasive lesion, which occasionally can be difficult. However, lack of cellular atypia, few mitoses, and lack of individual cell invasion or tentacular invasion is strong evidence that it is hyperplasia and not a malignancy.

Papillary hyperplasia (Figure 3.11) is an exophytic growth that occurs more commonly in rats than in mice, and consists of fronds of well-differentiated epithelial cells layered on a central fibrovascular core. The lining epithelium is usually three to five layers thick, but occasionally will have more cell layers. Nodular and papillary hyperplasia frequently occur together. They may be accompanied by chronic inflammation, but not necessarily. Distinguishing between papillary hyperplasia and papillomas can be difficult, with size being used as one criterion and branching as another. However, this becomes particularly problematic when there are numerous such lesions in an entity referred to as papillomatosis (Shirai et al., 1989) (Figure 3.12). Nevertheless, the lesions in papillomatosis, which individually appear to be papillomas, are readily reversible on cessation of the inciting stimulus. Whether urothelial papillomas are reversible lesions or not remains controversial, but the reversibility of papillomatosis and other reported examples suggests that papillomas can be reversible, similar to such lesions in rodent skin.

Squamous metaplasia of the urothelium can be produced by chronic inflammation, administration of bladder toxicants or carcinogens, or vitamin A deficiency. The metaplasia is usually nonkeratinizing, but keratinization can occur (Figure 3.14). Squamous metaplasia is frequently accompanied by chronic inflammation, and can be reversible. It is thought that pure squamous cell carcinomas arise from areas of squamous metaplasia, but this has not been proven.



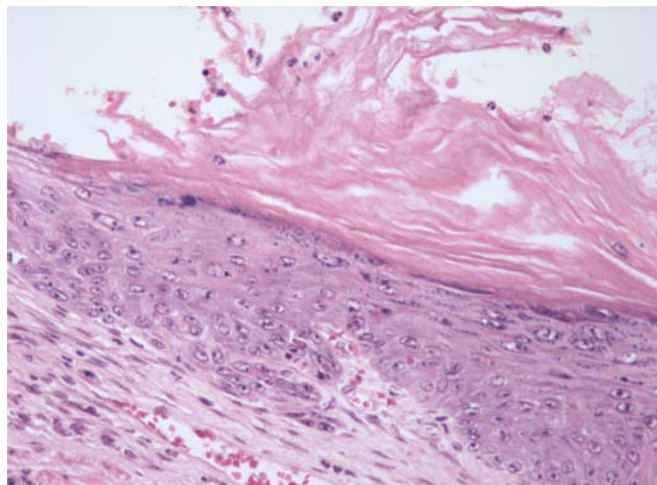


**FIGURE 3.14** Squamous metaplasia with keratinization of the rat urinary bladder urothelium. This is usually accompanied by a chronic inflammatory reaction.

Glandular metaplasia can also occur, either of the colonic type or the cervical type.

#### 4.4.1.3. DIVERTICULI

Diverticuli have been reported in mice and rats and other species, including humans, and consist of an invagination of the mucosa through the muscle wall into the surrounding fibroadipose tissue. The diverticuli can be lined by normal epithelium, simple hyperplasia, papillary and nodular hyperplasia, or papillomatosis, and may show squamous metaplasia. It is important to distinguish diverticuli from invasive carcinoma. This distinction relies mostly on the lack of cellular atypia in diverticuli. Occasionally, diverticuli will contain a true neoplasm.

#### 4.4.1.4. CALCIFICATION

Calcification of the lower urinary tract is commonly seen at the fornix of the kidney pelvis, and is usually accompanied by chronic inflammation and epithelial hyperplasia (Tomonari et al., 2016). Calcification can also be seen in other portions of the lower urinary tract, frequently associated with the presence of calculi. The presence of mineralization in the urothelium in association with proliferative and neoplastic lesions can be used as evidence for the presence of urinary calculi or crystals. Remnants of calcification can also be seen in the lumen associated with neoplastic lesions,

even if calculi are not obvious. Enhanced visualization of calcification can be achieved with special stains, such as Von Kossa. Calculi composed of substances other than calcium, especially those composed of organic chemicals, may not be detectable by histologic analysis because they may be lost during fixation, embedding, or staining.

#### 4.4.1.5. INCLUSIONS

Intracytoplasmic eosinophilic granules are occasionally observed in urothelial cells, particularly in mice (Figure 3.15). They usually are not associated with an inflammatory reaction or a hyperplastic response. In some instances, it appears that they are an accumulation of the test chemical and/or metabolites. They have been reported most commonly in mice treated with various arsenicals, with the granules shown to represent intramitochondrial inclusions containing inorganic arsenic bound to a yet to be identified substance. Intracytoplasmic urothelial granules are believed to be due to an abnormal processing of the asymmetric unit membrane by the cells (Liao et al., 2019). Cytoplasmic granules associated with fragments of red blood cells secondary to erythrophagocytosis have been reported in rats (Lensen et al., 2021).

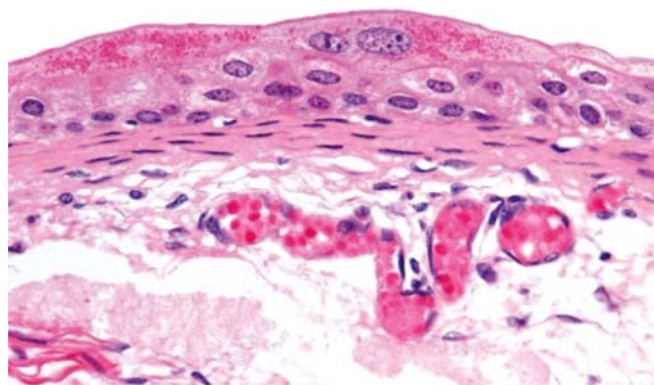


**FIGURE 3.15** Intracytoplasmic eosinophilic granules in the superficial cells of the mouse urinary bladder urothelium after treatment with inorganic arsenic. The granules appear to be related to abnormal processing of the asymmetric membrane plaques leading to accumulation in mitochondria (Liao et al., 2019). Reproduced from Haschek WM, Rousseaux CG, Wallig MA, editors: *Haschek and Rousseaux's handbook of toxicologic pathology*, ed 3, 2013, Academic Press, Figure 48.15, p. 1788, with permission.

#### 4.4.2. Proteinaceous Plug

A unique lesion in certain strains of male mice is the presence of proteinaceous plugs at the bladder neck and proximal urethra producing obstructive uropathy of mice (also referred to as mouse urologic syndrome or obstructive syndrome of mice) (Frazier et al., 2012). The plugs are composed of protein and can contain sperm, frequently have bacteria, and occasionally calcified material. They produce distention of the bladder and rapid death without warning signs or symptoms. Their cause is not specifically known but are considered to possibly be due to fighting, bacterial infection, hormonal effects, or a combination of these. The protein is thought to come from seminal fluids and possibly also from urine. Smaller proteinaceous plugs without bladder distention are thought to represent an agonal event.

#### 4.4.3. Neoplastic Lesions

Most neoplasms of the lower urinary tract are epithelial in origin, and the majority show urothelial differentiation.

##### 4.4.3.1. PAPILLOMA

Papillomas are benign epithelial lesions of the urothelium that project into the lumen as polypoid formations. In rodents, these frequently have the appearance of inverted papillomas. There is no cellular or nuclear pleomorphism or anaplasia, and they can have a narrow or broad base. Mitoses are uncommon, and the epithelial lining of the papillary fronds and nodules is generally limited to three to five cell layers in thickness. Focal areas of atypia, mitotic activity, increased basophilia, and invasiveness of the underlying connective tissue are indicators of a transition to carcinoma. Nodularity in the underlying connective tissue with smooth, rounded borders needs to be distinguished from invasiveness, since these nodules are usually still connected with the overlying epithelium and do not represent invasive carcinoma.

##### 4.4.3.2. CARCINOMA

It is apparent, based on morphologic evidence, clinical course, and molecular investigations, that urothelial carcinoma in humans represents two distinct diseases, although they can both

occur in the same patient (Wu, 2005). The more common disorder consists of low-grade papillary neoplasms that do not invade or metastasize, but have a propensity to recur. These tumors frequently have mutations or derangements of fibroblast growth factor receptor 3 (FGFR3) and other molecular changes. In contrast, the second disease is usually nonpapillary but always high grade, and frequently presents as an invasive lesion that commonly metastasizes. This type of disease begins as a dysplastic abnormality of the epithelium, either as a high-grade papillary lesion or as flat carcinoma in situ (CIS), with eventual invasion of the underlying connective tissue. These tumors usually have abnormalities in *p53* and frequently the retinoblastoma (*Rb*) gene.

These two diseases are represented to a considerable degree in rodents. In rats, the lesions nearly always begin as simple hyperplasia, progressing to nodular and papillary hyperplasia, papilloma formation, and, ultimately, papillary carcinoma (Cohen, 1983). In contrast to humans, these low-grade papillary carcinomas can evolve into invasive lesions, although they rarely metastasize. In mice, this same type of progression can occur, but more commonly there is induction of flat dysplasia, CIS (Figure 3.16), and invasive high-grade carcinoma (Figure 3.17) that can metastasize (Becci et al., 1981). This has been investigated extensively with N-butyl-N-(4-hydroxybutyl)-nitrosamine (BBN) administered either in the drinking water or by intragastric gavage. The two distinctive types of lesions (low-grade noninvasive papillary and high-grade CIS progressing to invasive carcinoma) have been produced utilizing transgenic mice with a uroplakin promoter attached to specific genes, specifically targeting the urothelium.

The degree of differentiation of urothelial carcinomas has been used in grading these tumors, usually utilizing a three-grade system, but more recently only distinguishing low versus high grade. Staging has also been utilized, with noninvasive versus invasive, and the extent of invasion classified as into subepithelial connective tissue, into the muscle layer, or into adjoining fibroadipose tissue and adjacent structures. Many urothelial carcinomas in rodents also have areas of squamous differentiation and/or glandular



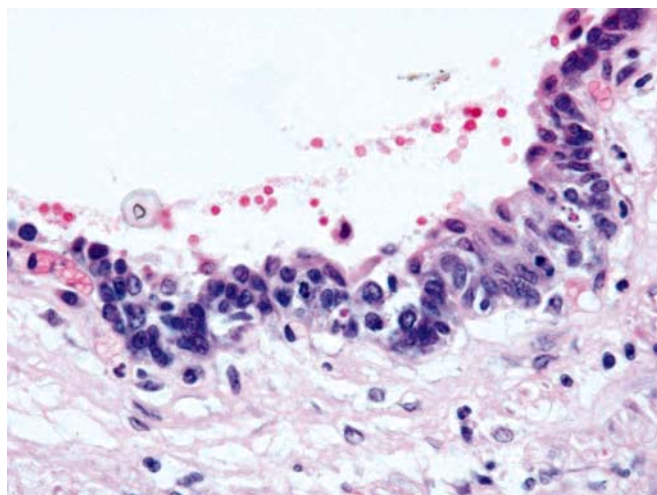


**FIGURE 3.16** Carcinoma in situ (high-grade dysplasia) of the mouse urinary bladder urothelium. Marked anaplasia is present in the urothelium, with occasional mitoses. The superficial urothelial cells are loosely adherent, frequently exfoliating into the lumen. Accompanying hematuria is evident. This may also be accompanied by a chronic inflammatory reaction. *Reproduced from Haschek WM, Rousseaux CG, Wallig MA, editors: Haschek and Rousseaux's handbook of toxicologic pathology, ed 3, 2013, Academic Press, Figure 48.16, p. 1789, with permission.*

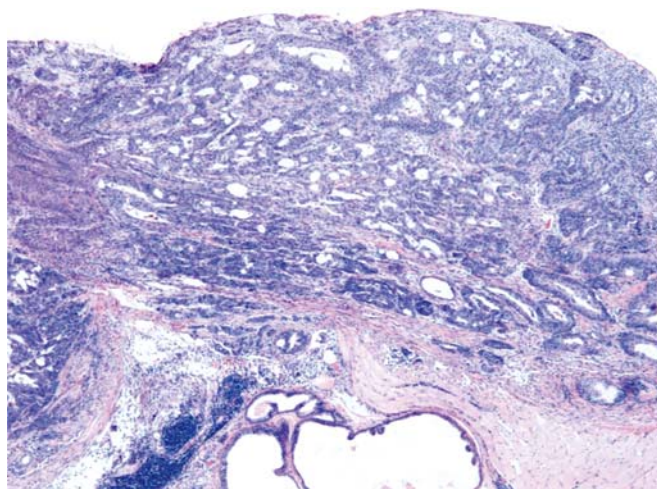


**FIGURE 3.17** Invasive urothelial carcinoma in a mouse urinary bladder extending into the adjoining prostate (bottom). Many of the urothelial clusters show a space which can be mistaken for glandular differentiation. This has been referred to as a pseudoglandular appearance. *Reproduced from Haschek WM, Rousseaux CG, Wallig MA, editors: Haschek and Rousseaux's handbook of toxicologic pathology, ed 3, 2013, Academic Press, Figure 48.17, p. 1789, with permission.*

differentiation. Occasionally, because of central necrosis, urothelial carcinoma can have a pseudoglandular appearance (Figure 3.17). In mice, the tumors frequently can be pure squamous cell carcinomas without true evidence of urothelial differentiation (Figure 3.18). A distinction between urothelial and squamous differentiation, particularly in high-grade lesions, can be difficult, but can be accomplished to some extent by the utilization of immunohistochemistry for uroplakins. Adenocarcinomas of the lower urinary tract are rare in rodents, as are undifferentiated carcinomas. The latter can be small cell, large cell, or spindle cell variants, and occasionally will have multinucleated giant cells present.

Tumors of the lower urinary tract in dogs or nonhuman primates have rarely been observed spontaneously, and few chemicals have been shown to induce such tumors since more than a year of chemical administration is usually required. However, recent publications regarding an integrin  $\alpha v \beta 6$  inhibitor and certain TGF $\beta$  kinase inhibitors have reported high-grade invasive urothelial carcinomas of the urinary bladder and kidney pelvis in nonhuman primates in as short as 4 weeks (Guffroy et al., 2023).

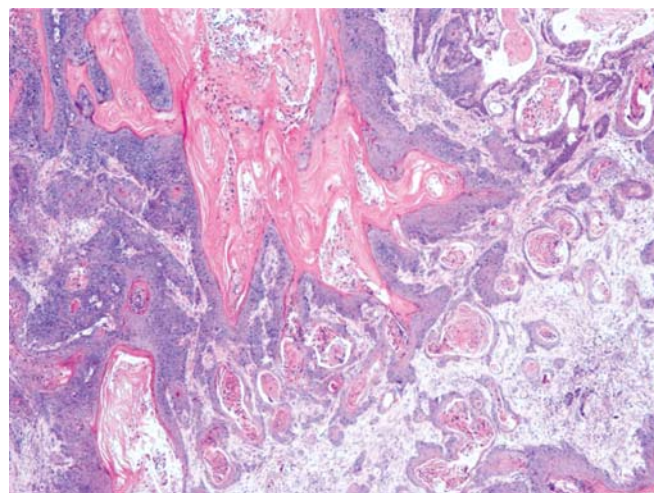


**FIGURE 3.18** Invasive squamous cell carcinoma with keratinization in a mouse urinary bladder. Squamous cell carcinomas can also occur without keratinization and are classified as high grade. *Reproduced from Haschek WM, Rousseaux CG, Wallig MA, editors: Haschek and Rousseaux's handbook of toxicologic pathology, ed 3, 2013, Academic Press, Figure 48.18, p. 1790, with permission.*



#### 4.4.3.3. MESENCHYMAL TUMORS

Mesenchymal tumors of the rat and mouse are uncommon, but most types of benign mesenchymal tumors have been reported at least once. Most common are smooth muscle tumors, such as leiomyomas and leiomyosarcomas. These are generally rare, although they have been shown to be induced in rats by administration of Disperse Blue associated in animals with urinary calculi (NTP, 1986). Vascular tumors, including hemangiomas and hemangiosarcomas, have been reported, although they are uncommon. In the rat, occasionally the large polypoid masses representing papillomas will have malignant transformation of the underlying stroma. These have been classified variably as malignant fibrous histiocytomas or fibrosarcomas.

Spontaneously occurring leukemic and lymphomatous infiltrates are common in many strains of mice. The specific cellular composition is that of the primary leukemia or malignant lymphoma, the lower urinary tract simply representing another area of malignant infiltration. Primary lymphoid neoplasms of the lower urinary tract are rare.

In certain strains of mice, subepithelial nodules composed of large epithelioid cells and small spindle cells and admixed with lymphocytes (Figure 3.19) have been reported (Butler et al., 1997). These were originally referred to as epithelial vegetative bodies, but it has become clear that they are of mesenchymal origin, with no connection to the overlying epithelium. Controversy remains as to whether these are reactive or neoplastic lesions, but the accepted term has become "mouse urinary bladder submucosal mesenchymal proliferative lesion." By electron microscopy, they show smooth muscle differentiation and evidence of vascular origin, possibly associated with a pericytic origin. They are nearly always confined to subepithelial connective tissue, but occasional lesions penetrate the muscle wall following the connective tissue bands normally present in the wall. Invasion of the overlying epithelium has not been reported nor have metastases.

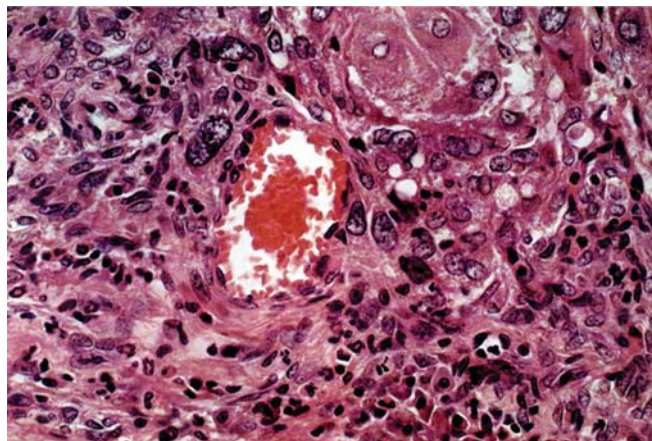


**FIGURE 3.19** Mouse urinary bladder submucosal mesenchymal proliferative lesion consisting of vascular spaces, large epithelioid cells (upper portion of figure) and small spindle cells admixed with an inflammatory infiltrate. Reproduced from Butler WH, Cohen SM, Squire RA: Mesenchymal tumors of the mouse urinary bladder with vascular and smooth muscle differentiation, *Toxicol. Pathol.*, 25:268–274, 1997, Figure 3, p. 270, with permission.

## 5. MECHANISMS OF TOXICITY

There are limited mechanisms for producing toxicity of the urothelium (Cohen, 2018). These include genotoxicity, direct mitogenicity, or cytotoxicity (due to the chemical or formation of urinary solids). Chemicals (or metabolites) can directly interact with the urothelium or induce alterations in the composition of the urine, producing an indirect effect on the urothelium. A key to evaluating lower urinary tract toxicity is focusing on urinary levels of the administered chemicals rather than on blood levels. This is particularly critical in assessing mode of action and interspecies comparisons. For direct effects on the urothelium by the chemical or its metabolites, the interaction can be with DNA, protein, or cell membranes. Interaction with DNA is the basis for the formation of DNA adducts, some of which can produce mutations. Interactions with proteins or cell membranes can lead to necrosis or apoptosis, leading to cell death, exfoliation, and regenerative proliferation. If this toxicity is superficial, there usually is no inflammation. If deeper, the reaction involves the

typical sequence of acute inflammation, chronic inflammation, and ultimately repair or fibrosis; granulomatous inflammation occasionally occurs. If the epithelium proliferates, there is a concomitant proliferation of the submucosal capillary network. Indirect effects of chemicals leading to changes in urinary composition usually produce toxicity by the production of urinary solids (precipitate, crystals, calculi). Obstruction of the urinary tract can be caused by calculi, tumors, severe inflammation, or proteinaceous plugs (in mice) leading to hydronephrosis and hydroureter with associated inflammatory and proliferative changes. Strains of mice and rats have been discovered which spontaneously develop hydronephrosis and hydroureter. Obstructive signs have also been reported secondary to neurogenic mechanisms.

Evaluating the lower urinary tract for toxicity requires examination of the histopathology of these organs and a detailed evaluation of the urine (Cohen et al., 2007). Many of the changes that occur in the urothelium can be transient, so that standardization of the time of collection is essential. It is also necessary that the animals are sacrificed shortly after the final administration of the test agent.

A detailed description of methods for collection, processing, and examination of these tissues and of the urine have been described (Cohen et al., 2007). Some basic principles need to be followed when evaluating the lower urinary tract for evidence of toxicity and possible modes of action. Most importantly, the urine needs to be collected from the animals without fasting. Since the presence of urinary changes, including solids, is an essential part of the examination, fasting will rapidly negate the effect, since the change is transient. Crystals will be rapidly excreted because of their small size. Many of the calculi will actually dissolve and also be excreted if the stimulus is not continued. Frequently, multiple times of the day are necessary for examining the composition of the urine because of the marked variability in the urine due to diurnal variations. Fresh void specimens are preferable to longer collections for examination for urinary solids and normal urinary constituents. Presence and concentrations of administered chemical or metabolites may require larger volumes than are routinely available in fresh void specimens.

A combination of light microscopy, a method for assessing DNA replication (BrdU, PCNA, Ki-67), combined with SEM provides a useful combination of methods for narrowing of the possible modes of action involved with nearly any type of toxicity (Cohen, 2018). More detailed investigations for specific changes can be implemented following these initial screening procedures.

A scheme for evaluating agents for possible lower urinary tract toxicity is presented in Figure 3.13. For screening, routine histopathology and DNA replication labeling index are adequate to detect any possible toxicity. More detailed studies include examination of the urine for composition and the presence or absence of solids, and a more detailed evaluation of the urothelium for the presence or absence of cytotoxicity, especially utilizing SEM for superficial cytotoxicity.

If an effect is identified in the lower urinary tract, the first step is to exclude the possibility of DNA reactivity. This frequently has already been established before the chemical is evaluated in animals.

If cytotoxicity is identified and urinary solids are eliminated as a possible cause, collection of urine for the identification of the administered chemical and metabolites and their concentrations can be performed. This can then be combined with in vitro cytotoxicity assays utilizing urothelial cell lines to investigate possible specific agents that are causing the cytotoxicity, and to identify quantitatively the concentrations necessary for cytotoxicity to occur.

## 6. ISSUES IN DRUG AND CHEMICAL DEVELOPMENT

Utilizing these methods, one can quickly screen for the presence of lower urinary tract toxicity and identify the mode of action that is involved. Furthermore, a quantitative dose response can be established.

Since many chemicals are metabolized and excreted in the urine, the lower urinary tract is frequently the site of toxicity. The toxic effects can be secondary to the chemical (and/or metabolite) itself or due to alterations in normal urinary constituents. Evaluation for lower urinary tract toxicity involves screening for

morphologic effects such as urothelial hyper trophy, hyperplasia, and inflammation, plus an evaluation of a cell replication labeling index. If the screen shows an effect on the lower urinary tract, the mode of action and dose response can be evaluated, including assessment for genotoxicity, formation of urinary solids, or cytotoxic effects of the chemical and metabolites. A critical factor is urinary concentrations rather than blood levels. Specific methods are required to properly assess evaluation of the urine, urothelium, and overall structure of the lower urinary tract. A comparison of effects between species is then performed to assess the potential relevance for possible human toxicity.

## REFERENCES

- Alroy J: Ultrastructure of canine urinary bladder carcinoma, *Vet. Path.* 16(6):693–701, 1979.
- Becci PJ, Thompson HJ, Strum JM, et al.: N-butyl-N- (4-hydroxybutyl) nitrosamine-induced urinary bladder cancer in C57BL/6 X DBA/2 F1 mice as a useful model for study of chemoprevention of cancer with retinoids, *Cancer Res.* 41(3):927–932, 1981.
- Butler WH, Cohen SM, Squire RA: Mesenchymal tumors of the mouse urinary bladder with vascular and smooth muscle differentiation, *Toxicol. Pathol.* 25:268–274, 1997.
- Cohen SM: Pathology of experimental bladder cancer in rodents. In Bryan GT, Cohen SM, editors: *The pathology of bladder cancer*, Boca Raton, 1983, CRC Press, Inc, pp 1–40.
- Cohen SM: The role of urinary physiology and chemistry in bladder carcinogenesis, *Food Chem. Toxicol.* 33:715–730, 1995.
- Cohen SM, Boobis AR, Meek ME, et al.: 4-Aminobiphenyl and DNA reactivity: case study within the context of the 2006 IPCS human relevance framework for analysis of a cancer mode of action for humans, *Crit. Rev. Toxicol.* 36(10):803–819, 2006.
- Cohen SM: Screening for human urinary bladder carcinogens: two-year bioassay is unnecessary, *Toxicol. Res.* 7(4):565–575, 2018.
- Cohen SM, Tatematsu M, Shinohara Y, et al.: Neo-vascularization in rats during urinary bladder carcinogenesis induced by N-[4-(5-nitro-2-furyl)-2-thiazolyl] formamide, *J. Natl. Cancer Inst.* 65(1):145–148, 1980.
- Cohen SM, Ohnishi T, Clark NM, et al.: Investigations of rodent urinary bladder carcinogens: collection, processing, and evaluation of urine and bladders, *Toxicol. Pathol.* 35(3): 337–347, 2007.
- Cohen SM, Arnold LL, Suzuki S: Urinary tract calculi and bladder tumors. In Hsu C-H, Stedeford T, editors: *Cancer risk assessment. Chemical carcinogenesis, hazard evaluation, and risk qualification*, Hoboken, NJ, 2010, John Wiley & Sons, Inc, pp 501–514.
- Da Rocha MS, Dodmane PR, Arnold LL, et al.: Mode of action of pulegone on the urinary bladder of F344 rats, *Toxicol. Sci.* 128(1):1–8, 2012.
- Da Rocha MS, Arnold LL, De Oliveira MLCS, et al.: Diuron-induced rat urinary bladder carcinogenesis: mode of action and human relevance evaluations using the International Programme on Chemical Safety framework, *Crit. Rev. Toxicol.* 44(5):393–406, 2014.
- Dominick MA, White MR, Sanderson TP, et al.: Urothelial carcinogenesis in the urinary bladder of male rats treated with muraglitazar, a PPAR  $\alpha/\gamma$  agonist: evidence for urolithiasis as the inciting event in the mode of action, *Toxicol. Pathol.* 34:903–920, 2006.
- Ellwein LB, Cohen SM: A cellular dynamics model of experimental bladder cancer: analysis of sodium saccharin in the rat, *Risk Anal.* 8(2):215–221, 1988.
- Fisher MJ, Sakata T, Tibbels TS, et al.: Effect of sodium saccharin and calcium saccharin on urinary parameters in rats fed Prolab 3200 or AIN-76 diet, *Food Chem. Toxicol.* 27:1–9, 1989.
- Frazier KS, Seely JC, Hard GC, et al.: Proliferative and non-proliferative lesions of the rat and mouse urinary system, *Toxicol. Pathol.* 40(4 Suppl.):14S–86S, 2012.
- Fukushima S, Cohen SM, Arai M, et al.: Scanning electron microscopic examination of reversible hyperplasia of the rat urinary bladder, *Am. J. Pathol.* 102(3):373–380, 1981.
- Guan N, Fan Q, Ding J, et al.: Melamine-contaminated powdered formula and urolithiasis in young children, *N. Engl. J. Med.* 260(11):1067–1074, 2009.
- Guffroy M, Trela B, Kambara T, et al.: Selective inhibition of integrin  $\alpha\beta6$  leads to rapid induction of urinary bladder tumors in cynomolgus macaques, *Toxicol. Sci.* 191(2):400–413, 2023.
- Hardisty JF, Anderson DC, Brodie S, et al.: Histopathology of the urinary bladders of cynomolgus monkeys treated with PPAR agonists, *Toxicol. Pathol.* 36(6):769–776, 2008.
- IARC Working Group: *Consensus Report* 147. 1999, IARC Scientific Publications, pp 1–32.
- Ito N, Shirai T, Fukushima S, et al.: Dose-response study of urinary bladder carcinogenesis in rats by N-butyl-N- (4-hydroxybutyl) nitrosamine, *J. Cancer Res. Clin. Oncol.* 108(1): 169–173, 1984.
- Jacobs JB, Cohen SM, Friedell GH: Scanning electron microscopy of the lower urinary tract. In Cohen SM, Bryan GT, editors: *The Pathology of bladder cancer*, Boca Raton, FL, 1983, CRC Press, pp 141–181.
- Lensen JFM, Hytttila-Hopponen M, Karlsson S, Kuosmanen T, Lehtimäki J, Leino T: Characterization of urothelial inclusions in male Wistar Han rats treated orally with the novel  $\alpha2A$ -adrenoceptor agonist tasipimidine, *Toxicol. Pathol.* 49(7):1232–1242, 2021, <https://doi.org/10.1177/01926233211027471>.
- Liao Y, Tham DKL, Liang F, et al.: Mitochondrial lipid droplet formation as a detoxification mechanism to sequester and degrade excessive urothelial membranes, *Mol. Biol. Cell* 30: 2969–2984, 2019.



- Meek ME, Bucher JR, Cohen SM, et al.: A framework for human relevance analysis of information on carcinogenic modes of action, *Crit. Rev. Toxicol.* 33(6):591–653, 2003.
- Mori S, Hosono M, Machino S, et al.: Induction of the renal pelvic and ureteral carcinomas by N-butyl-N (4-hydroxybutyl) nitrosamine in SD/cShi rats with spontaneous hydronephrosis, *Toxicol. Pathol.* 22(4):373–380, 1994.
- Murai T, Mori S, Hosono M, et al.: Effect of phenacetin pretreatment on renal pelvic carcinogenesis by N-butyl-N (4-hydroxybutyl) nitrosamine in NON/Shi mice of both sexes, *Teratog. Carcinog. Mutagen.* 14(4):193–201, 1994.
- NTP: NTP technical report on toxicology and carcinogenesis studies of CI disperse blue 1 in F344/N rats and B6C3F1 mice, *Natl. Toxicol. Program Tech. Rep. Ser.* 299:1–241, 1986.
- Okamura T, Garland EM, Johnson LS, et al.: Acute urinary tract toxicity of tetraethylorthosilicate in rats, *Fund. Appl. Toxicol.* 18(3):425–441, 1992.
- Oleksiewicz MB, Thorup I, Nielsen S, et al.: Generalized cellular hypertrophy is induced by dual-acting PPAR agonist in rat urinary bladder urothelium in vivo, *Toxicol. Pathol.* 33(5):552–560, 2005.
- Roberts RA, Campbell RA, Sikakana P, et al.: Species-specific urothelial toxicity with an anti-HIV noncatalytic site integrase inhibitor (NCINI) is related to unusual pH-dependent physicochemical changes, *Toxicol. Sci.* 183(1):105–116, 2021.
- Shirai T, Fukushima S, Tagawa Y, et al.: Cell proliferation induced by uracil-calculi and subsequent development of reversible papillomatosis in the rat urinary bladder, *Cancer Res.* 49(2):378–383, 1989.
- Souza NP, Hard GC, Arnold LL, et al.: Epithelium lining rat renal papilla: nomenclature and association with chronic progressive nephropathy (CPN), *Toxicol. Pathol.* 46:266–272, 2018.
- Suzuki S, Cohen SM, Fuji S, et al.: Orally administered nicotine effects on rat urinary bladder proliferation and carcinogenesis, *Toxicology* 398–399:31–40, 2018.
- Swenberg JA, Lehman-McKeeman LD:  $\alpha$ 2-Urinary globulin associated nephropathy as a mechanism of renal tubule cell carcinogenesis in male rats, *IARC (Int. Agency Res. Cancer) Sci. Publ.* 147:95–118, 1999.
- Tomonari Y, Kurotaki T, Sato J, et al.: Spontaneous age-related lesions of the kidney fornices in Sprague-Dawley rats, *Toxicol. Pathol.* 44(2):226–232, 2016.
- Varley CL, Stahlschmidt J, Lee W-C, et al.: Role of PPAR $\gamma$  and EGFR signalling in the urothelial terminal differentiation programme, *J. Cell Sci.* 117(Pt 10):2029–2036, 2004.
- Vogel P, Donoviel MS, Read R, et al.: Incomplete inhibition of sphingosine 1-phosphate lyase modulates immune system function yet prevents early lethality and non-lymphoid lesions, *PLoS One* 4(1):e4112, 2009.
- Wisler JA, Afshari C, Fielden M, et al.: Raf inhibition causes extensive multiple tissue hyperplasia and urinary bladder neoplasia in the rat, *Toxicol. Pathol.* 39(5):809–822, 2011.
- Wood CE, Hukkanen RR, Sura R, et al.: Scientific and regulatory policy committee (SRPC) review: interpretation and use of cell proliferation data in cancer risk assessment, *Toxicol. Pathol.* 43(6):760–775, 2015.
- Wu X-R: Urothelial tumorigenesis: a tale of divergent pathways, *Nat. Rev. Cancer* 5(9):713–725, 2005.
- Yu J, Lin JH, Wu XR, et al.: Uroplakins Ia and Ib, two major differentiation products of bladder epithelium, belong to a family of four transmembrane domain (4TM) proteins, *J. Cell Biol.* 125(1):171–182, 1994.

This page intentionally left blank

# Respiratory System

Molly H. Boyle<sup>1</sup>, Jack R. Harkema<sup>2</sup>, Kristen J. Nikula<sup>3</sup>, Ronnie Chamanza<sup>4</sup>,  
David K. Meyerholz<sup>5</sup>, Mary Beth Genter<sup>6</sup>, Wanda M. Haschek<sup>7</sup>

<sup>1</sup>Labcorp Early Development Labs, Inc., Somerset, NJ, United States, <sup>2</sup>Michigan State University, East Lansing, MI, United States, <sup>3</sup>Inotiv, Maryland Heights, MO, United States, <sup>4</sup>Janssen Pharmaceutical Companies of Johnson & Johnson, Buckinghamshire, United Kingdom, <sup>5</sup>University of Iowa, Iowa City, IA United States, <sup>6</sup>University of Cincinnati, Cincinnati, OH, United States, <sup>7</sup>University of Illinois at Urbana-Champaign, Urbana, IL, United States

## OUTLINE

<b>1. Introduction</b>	<b>236</b>	4.2. Patterns of Respiratory Tract Injury to Inhaled Toxicants	288
<b>2. Structure, Function, and Cell Biology</b>	<b>237</b>	4.3. Cell-specific Versus Nonspecific Injury	288
2.1. Macroscopic and Microscopic Anatomy	237	4.4. Cell Proliferation, Regeneration, and Repair Processes	288
2.2. The Nose	237	4.5. Nasal, Nasopharyngeal, and Laryngeal Responses to Injury	290
2.3. The Pharynx and Larynx	247	4.6. Tracheobronchial and Pulmonary Responses to Injury	293
2.4. The Trachea, Bronchi, and Bronchioles	248	4.7. Pulmonary Parenchymal Responses to Injury	301
2.5. Gas-Exchange Regions of the Lung	257	<b>5. Mechanisms of Toxicity</b>	<b>316</b>
<b>3. Testing for Toxicity</b>	<b>261</b>	5.1. Direct Toxicity	318
3.1. Methods of Testing	261	5.2. Metabolic Activation	319
3.2. Background Findings	266	5.3. Immune-Mediated Toxicity	321
3.3. Nasopharyngeal and Laryngeal Regions	269	5.4. Toxicity and Responses to Inhaled Particles	324
3.4. Tracheobronchial Airways and Pulmonary Parenchyma	270	5.5. Toxicity and Responses to Inhaled Fibers	326
3.5. Animal Models	272	5.6. Xenobiotic Interactions	327
3.6. Target Liability Assessment and In Vitro Models	278	5.7. Modifying Factors in Toxicity	327
3.7. Quantitative Techniques and Lung Imaging Modalities	281	5.8. Adversity Considerations	328
<b>4. Responses to Injury</b>	<b>287</b>	<b>6. Conclusion</b>	<b>328</b>
4.1. Factors Affecting Toxic Injury and Host Response	287	<b>References</b>	<b>329</b>



## 1. INTRODUCTION

The mammalian respiratory system is susceptible to injury caused by either air- or blood-borne toxicants. Susceptibility of the lung to injury caused by inhaled toxicants is due in large part to the extensive interface between the airway epithelia and inspired air. Likewise, the extensive interface between the alveolar capillary surface area and circulating blood makes the lung susceptible to blood-borne toxicants.

The respiratory tract comprises the largest mucosal surface of the body, with an internal surface area that is 25 times greater than the external surface of the body covered by skin. In contrast to other mucosa-lined organs found in the digestive and reproductive tracts that are only periodically exposed to the external environment, the respiratory organs are constantly in contact with large amounts of inhaled air that may contain airborne xenobiotic compounds, such as gaseous and particulate air pollutants (Thomas and Zelikoff, 1999). At rest, the adult human takes in 10,000–15,000 L of ambient air through the nasal passages each day. The pulmonary circulation receives the total cardiac output from the heart's right ventricle, making the lung also vulnerable to blood-borne toxic agents. Targeted toxicity of air- or blood-borne toxicants within the upper or lower respiratory tract is dependent on numerous factors, but most importantly, the physical and chemical character of the chemical agent, site-specific tissue dosimetry and sensitivity, and host-dependent factors such as health status, the respiratory system microbiome, sex, and age (Miller, 2000).

The respiratory system is a structurally complex arrangement of organs designed principally for the intake of oxygen and the elimination of carbon dioxide, that is, respiratory gas exchange or "respiration." Though its main function is gas exchange, the respiratory tract is composed of specialized tissues and cells that have other important functions, such as the production of glycoproteins (e.g., mucus) and phospholipids (e.g., surfactant), activation and inactivation of circulating hormones, and metabolism of xenobiotic compounds entering the body through inhalation or other routes of administration. Another important function, especially of the upper respiratory tract, is host

defense against exposure to inhaled infectious agents (e.g., viruses and bacteria) and noxious chemical agents (e.g., respirable dusts and gaseous pollutants). In addition, parts of the nasal airways are lined by a unique neurosensory olfactory epithelium (OE) that connects directly to the brain, allowing the detection of odors (e.g., sense of smell or olfaction), but also providing an alternative route for some airborne agents (e.g., viruses, metals, nanoparticles, pharmaceuticals) to enter the brain, bypassing the blood–brain barrier.

Exposure to respiratory toxicants can occur in occupational settings (e.g., silica, asbestos, chronic acid fumes); during medical treatment (e.g., bleomycin, cyclophosphamide, X-rays); in self-inflicted injury (e.g., cigarette smoking and cocaine use); and during the course of everyday activities, such as inhalation exposure to common air pollutants (e.g., ozone, particulate matter, smoke from wildland fires) or ingestion of toxic agents in food and medications (e.g., toxic rapeseed oil, pyrrolizidine alkaloids, methimazole). Pulmonary diseases linked to chemical injury range from acute reversible diseases (e.g., metal fume fever following inhalation of zinc) to chronic irreversible diseases (e.g., fibrosis following chronic inhalation of silica, lung cancer caused by cigarette smoking). A variety of defense mechanisms, such as the mucociliary apparatus in the conducting airways and alveolar macrophages (AMs) in the pulmonary parenchyma, can prevent contact of the injurious agent with vulnerable alveolar epithelial cells in the deep lung. Unfortunately, sometimes these defenses are inadequate, and toxic lung injury occurs.

The location and type of injury is the result of complex interactions between the agent and the host. Determining factors are the physicochemical characteristics of the agent, the severity of insult (dose), and the metabolic capabilities present in the cellular components of the host respiratory tissue. Characteristics of the host response and severity of insult will determine whether the injury is reversible or irreversible, and whether long-term health effects will occur.

Potential anatomic communications between the gut and lung and complex pathways involving their respective microbiota have supported the existence of a gut–lung axis which involves host–microbe as well as microbe–

microbe interactions, shaping immune responses, and interfering with the course of respiratory diseases. While the vast majority of studies have focused on the bacterial component of the microbiota in healthy and pathological conditions, others have highlighted the contribution of fungal and viral kingdoms in both digestive and respiratory systems (Enaud et al., 2020).

## 2. STRUCTURE, FUNCTION, AND CELL BIOLOGY

### 2.1. Macroscopic and Microscopic Anatomy

Although there is considerable variation among mammalian species in the macroscopic and microscopic anatomy of the respiratory tract (Tables 4.1 and 4.2), the general principles involved in gas exchange are identical. The respiratory tract can be divided into two portions based on gross anatomy and physiology: (1) the proximal conducting (nonrespiratory) airways that include the nose, pharynx, larynx, and tracheobronchial airways (trachea, bronchi, and bronchioles); and (2) the distal respiratory portion comprised of the respiratory bronchioles, alveolar ducts, and alveolar sacs

(Figure 4.1). The conducting portion of the respiratory system serves not only as a conduit moving air in and out of the lungs but also to warm, moisten, and filter the inspired air. Additionally, the conducting airways provide an antimicrobial environment through a mechanical barrier (e.g., mucociliary clearance) and antimicrobial secretions (e.g., lactoferrin, defensins). For consistency in translational terminology, bronchi are morphologically defined as intrapulmonary airways with cartilage and submucosal glands, while bronchioles are smaller airways that lack cartilage and submucosal glands (Renne et al., 2009). Gas exchange between air and blood is restricted to the latter respiratory portion located in the delicate alveolar parenchyma of the lung. The upper conducting airways must be sufficiently open to the distal alveolar regions for the system to function properly, allowing adequate delivery of oxygen to the lungs, red blood cells, and the rest of the body to sustain life.

### 2.2. The Nose

In both humans and laboratory animals, the nose is the primary portal of entry for the respiratory system. Besides serving as the major

**TABLE 4.1** Interspecies Comparison of Pulmonary Anatomy

Anatomical Characteristics	Mouse, Rat, Hamster	Dog, Cat, Rhesus, Monkey	Minipig	Human
Pleura	Thin	Thin	Thick	Thick
Secondary lobulation	Absent	Absent	Present	Incomplete
Pulmonary veins	Cardiac muscle in media	Thin, mainly fibrous wall	Thick, smooth muscle in intima	Thin, mainly fibrous wall
Intrapulmonary bronchi (airways with cartilage and submucosal glands)	Absent	Present	Present	Present
Intrapulmonary bronchioles (airways without cartilage or submucosal glands)	Present	Present	Present	Present
Respiratory bronchioles	None/minimal	Extensive	None-minimal	Present

Modified from Haschek WM, Rousseaux CG, Wallig MA, editors: *Handbook of toxicologic pathology*, ed 2, 2002, Academic Press, Vol. 2, Table II, p. 13, with permission.

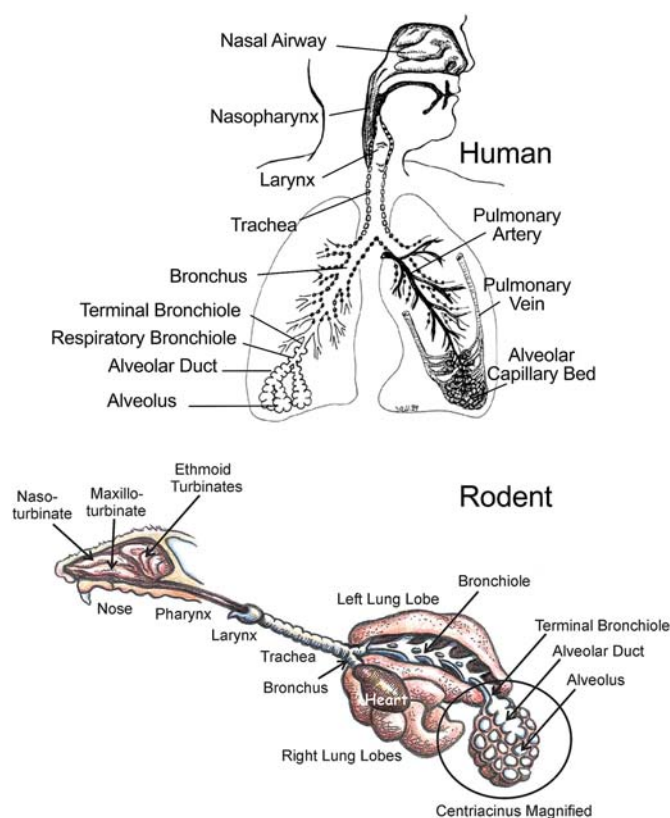


**FIGURE 4.1** Diagrammatic representation of the human and rodent respiratory tracts. Dots along the laryngeal and tracheobronchial airways indicate intramural cartilage. Modified from Haschek WM, Rousseaux CG, Wallig MA, editors: *Handbook of toxicologic pathology*, ed 3, 2013, Academic Press, Figure 51.1, p. 1937, with permission.

sensory organ for smell, the nose also functions as an air conditioner and a defender of the lower respiratory tract by filtering, humidifying, and heating the inhaled air. In addition, it protects the delicate gas-exchange regions of the lung by absorbing water-soluble and reactive gases and vapors, trapping inhaled particles, and metabolizing airborne xenobiotics (Harkema et al., 2006).

Many diseases related to microbial infections (e.g., severe acute respiratory syndrome coronavirus 2 [SARS-CoV-2], the causal agent of coronavirus disease 2019 [COVID-19]), allergic reactions (e.g., ragweed-induced asthma), or

natural aging (e.g., loss of olfactory epithelium) may affect nasal airways and associated paranasal sinuses (Harding and Pinkerton, 2014). Exposure to toxic agents may also cause or exacerbate these nasal diseases. Major scientific advances have been made in the field of nasal toxicology by using laboratory animals in short- and long-term inhalation studies, or in experimental intranasal (IN) delivery of vaccines. This field of toxicology has grown exponentially since the first published reports in the early 1980s indicating that long-term inhalation exposures to high concentrations of formaldehyde caused nasal tumors in laboratory rodents. Recently, the loss of smell and taste as well as the high viral load of SARS-CoV2 in nasal tissues of patients with COVID-19 also highlighted the importance of the nose in respiratory health and disease. The preferential targeting and infection of olfactory epithelium, particularly sustentacular cells, by the SARS-CoV-2 virus is now believed to be the main cause of olfactory dysfunction and anosmia in COVID-19 patients. In response to SARS-CoV-2 infection, immune cells are recruited to the site of infection, resulting in release of many signaling molecules, including sphingolipid metabolites. Sphingosine nasal spray has been proposed for inhibiting entry of SARS-CoV-2 into cells, and modulation of sphingosine-1-phosphate receptors is under investigation in the context of SARS-CoV-2 infection (Meyerholz and Reznikov, 2022; Edwards et al., 2020).

The human nasal cavity, like that of laboratory animals, is divided into two main air passages by the nasal septum. Each nasal passage extends from the nostrils to the nasopharynx. The nasopharynx is defined as the airway posterior to the termination of the nasal septum and proximal to the termination of the soft palate. Inhaled air flows through the nostrils, or nares, into the vestibule, a slight dilatation just inside the nares before it enters the main chamber of the nose. Unlike the more distal main chamber, which is surrounded by bone, the nasal vestibule is surrounded by flexible cartilage. The luminal surface is lined by a squamous epithelium (SE) similar to that of skin. In humans, unlike



laboratory animals, the nasal vestibule also contains varying numbers of hair follicles near the nostrils.

After passing through the nasal vestibule, inhaled air courses through the narrowest part of the entire respiratory tract, the nasal valve, and then into the main nasal chamber. A lateral wall, septal wall, roof, and floor define each nasal passage of the main chamber. The lumen of the main chamber is lined by well-vascularized and innervated mucous membranes (nasal mucosa) that are covered by an epithelial lining fluid containing a continuous surface layer of mucus. The nasal mucous layer is moved distally, by the synchronous beating of motile cilia, to the oropharynx, where it is swallowed into the esophagus.

Turbinates, bony structures lined by the well-vascularized mucosal tissue, project into the airway lumen from the lateral walls into the main chamber of the nose. Turbinates increase the inner surface area of the nose, which is important in the conditioning of the inhaled air. The relative surface area (i.e., surface area/volume) of the nasal cavity is approximately five times greater in the laboratory mouse than in humans, due principally to the greater complexity of its nasal turbinates (Herbert et al., 2015a, 2015b).

Though there are some general similarities among the nasal passages of laboratory rodents, nonhuman primates, and humans, there are also striking species differences in nasal architecture (Figure 4.2A). From a comparative viewpoint, humans have relatively simple noses with breathing as the primary function (microsomatic), while rats, mice, and dogs have more complex noses with olfaction as the primary function (macrosomatic). In addition, the nasal and oral cavities of humans, and most nonhuman primates, are arranged in a manner to allow for both nasal and oral breathing (Plopper and Harkema, 2005). In contrast, laboratory rodents, including rats and mice, are obligate nose breathers, due to the close apposition of the epiglottis to the soft palate. As a result, nasal pathology in a rodent can cause significant breathing complications and even death.

Marked differences in nasal airflow patterns between mammalian species are primarily due to the species-specific variation in number and shape of the nasal turbinates. The human nose has three turbinates: the superior, middle, and inferior (Figure 4.2A). These structures are relatively simple in shape compared to turbinates of laboratory animals (e.g., rats, mice, rabbits, and dogs) that have complex folding and branching patterns. In laboratory rodents, rabbits, and dogs, evolutionary pressures concerned chiefly with olfactory function and dentition have defined the shape of the turbinates and the type and distribution of the cells lining these structures. In the proximal nasal airway, the complex naso- and maxilloturbinates of mice are thought to provide better protection of the lower respiratory tract due to enhanced filtration, absorption, and disposal of airborne particles and gases, as compared to the simple structure of the middle and inferior turbinates in the human nose. The highly complex shape of the ethmoid turbinates lined predominantly by olfactory neuroepithelium in the distal half of the nasal cavity of laboratory animals is suitably designed for acute olfaction. Differences in the complexity of the gross turbinate structure throughout the nasal airway of the adult laboratory mouse are illustrated in Figure 4.2B.

Luminal surfaces of the nasal mucosa, except for the most proximal regions of the nasal vestibule, are lined by a watery, sticky material called mucus that is secreted from mucous cells in surface epithelium and from underlying glands in the lamina propria. Its physical and chemical properties are well suited for its role in upper airway defense by trapping inhaled particles and scrubbing out certain reactive gases. The synchronized beating of airway surface cilia propels the nasal mucus at different speeds and directions depending on the IN location. Mucus covering the olfactory mucosa moves very slowly, with a turnover time of several days. In contrast, the mucus covering the respiratory mucosa is driven along rapidly by synchronized beating of cilia, with an estimated turnover time of about 10 min in the laboratory rat.

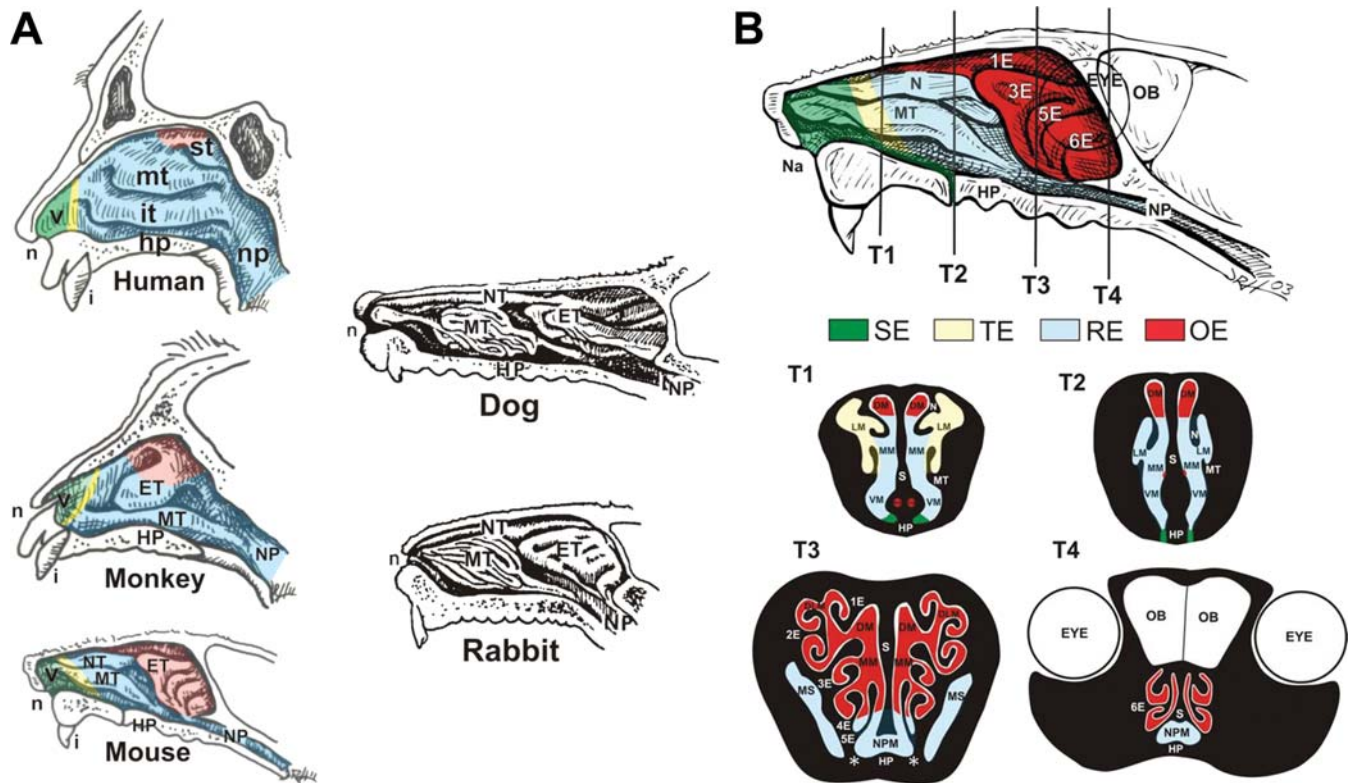


**FIGURE 4.2** (A) schematic drawings of the right nasal passages from the human, monkey, mouse, rabbit, and dog. The septum has been removed to expose the lateral wall. Colors in the human, monkey, and mouse represent the intranasal distribution of surface epithelial populations—green, squamous epithelium (SE); yellow, transitional epithelium (TE); blue, respiratory epithelium (RE); red, olfactory epithelium (OE). V, nasal vestibule; st, superior turbinate; it, inferior turbinate; hp, hard palate; i, incisor tooth; n, naris; NP, nasopharynx; ET, ethmoid turbinate; MT, maxilloturbinate. (B) Right nasal passage of the mouse with transverse sections (T1–T4) taken at different levels of the nasal passage. Ethmoid turbinates are labeled 1E–6E. (T1–4) Rostral surfaces of the transverse sections identifying the different intranasal airways (VM, ventral meatus; MM, middle medial meatus; LM, lateral meatus; DM, dorsal meatus; DLM; dorsal lateral meatus; MS, maxillary sinus; NPM, nasopharyngeal meatus) and location of other anatomic structures (S, septum; VNO, vomeronasal organ; OB, olfactory bulb of the brain; \*, nasal associated lymphoid tissue). Reproduced from Treuting PM, Dintzis SM, editors: *Comparative anatomy and histology: a mouse and human atlas*, 2012, Academic Press, with permission.

Nasal mucus containing entrapped materials is ultimately propelled by beating cilia to the naso- and oropharynx, and then swallowed into the esophagus and cleared through the digestive tract. The nasal mucociliary apparatus (i.e., mucus and cilia) exhibits a range of responses to inhaled xenobiotic agents and can be a sensitive indicator of toxicity. Since this upper airway apparatus is one of the first lines of defense against inhaled pathogens, dusts, and irritant gases, toxicant-induced compromises in its defense capabilities can lead to increased nasal infections and increased

susceptibility to lower respiratory tract diseases (e.g., viral or bacterial pneumonias).

### 2.2.1. Nasal Epithelium

Besides differences in the gross architecture of the nose between laboratory animals and humans, there are also species differences in the surface epithelial cell populations lining the nasal passages. These differences among species are found in the distribution of nasal epithelial populations and in the types of nasal cells within these populations. There are, however, four distinct nasal epithelial

populations in both animals and humans. These include the SE, which is primarily restricted to the nasal vestibule; ciliated, pseudostratified, cuboidal/columnar epithelium, or respiratory epithelium (RE), in the main chamber and nasopharynx; poorly ciliated cuboidal/columnar epithelium, or often termed transitional epithelium (TE), lying between SE and RE in the proximal aspect of the main chamber; and OE, located in the dorsal or dorsoposterior aspect of the nasal cavity. [Figures 4.2A and B](#) illustrate the distribution of nasal epithelia in the nasal cavity of the mouse, monkey, and human. [Figure 4.2B](#) shows the transverse sections (T1–T4) that are commonly used to evaluate the nasal passages in laboratory rats and mice (Treuting and Dintzis, 2012).

The nasal vestibule in both animals and humans is completely lined by SE. This region of the nasal mucosa probably functions similarly to the epidermis of skin, to protect the underlying tissues from potentially harmful environmental agents. Though the cellular composition is similar among rodent and primate species, SE is much thicker in primates.

Distal to the stratified SE and proximal to the ciliated respiratory epithelium is a narrow zone of poorly or nonciliated, microvilli-covered cuboidal/columnar surface epithelium, which has been referred to as nasal nonciliated or scantily ciliated respiratory epithelium, or nasal TE ([Figure 4.3](#)). Common, distinctive features of TE in mice, monkeys, and humans include: (1) an anatomical location in the proximal aspect of the nasal cavity between the SE and the respiratory epithelium; (2) the presence of numerous nonciliated cuboidal or columnar surface cells and basal cells; (3) few ciliated cells and a scarcity of mucous (goblet) cells; and (4) an abrupt morphological border with SE but a less abrupt border with respiratory epithelium. In the T1 transverse tissue section of mice, the TE lines the luminal surfaces of the lateral wall, maxilloturbinate, and medial aspect of the nasoturbinate. These epithelial surfaces border the lateral meatus in the proximal nasal airways. Murine TE is thin (one to two cells thick), pseudostratified, and composed of three nonciliated cell types (basal, columnar, and cuboidal) and scattered ciliated cells. In contrast, the TE of primates is thick (four to five cells), stratified, and composed of at least five different epithelial cell types, including mucous cells.

Luminal, nonciliated cells in the TE of mice rarely contain secretory granules, but do have abundant smooth/agranular endoplasmic reticulum (SER) in their apices. SER is an important intracellular site for xenobiotic-metabolizing enzymes, including cytochromes P450 mixed function oxidases. The prominent presence of this organelle in these cells, as well as in the sustentacular cells of olfactory epithelium, suggests metabolizing capability for certain inhaled and noninhaled xenobiotics.

In both animals and humans, the lamina propria beneath the TE and respiratory epithelium, described below, is a highly vascularized and innervated loose fibroelastic connective tissue containing serous and seromucous secretory glands. Cavernous venous plexuses, sometimes referred to as “swell bodies,” are also present in the lamina propria of the nasal mucosa and located in distinct regions along the nasal airway. Dilation of these vessels is thought to alter nasal airflow by thickening the mucosa, narrowing air passages, and diverting inhaled air. Prominent swell bodies in the mouse are found in the maxilloturbinates and lateral wall in the proximal nasal passage.

The majority of nonolfactory nasal epithelium of mice, monkeys, and humans is RE, morphologically defined as a pseudostratified, cuboidal/columnar, ciliated epithelium ([Figure 4.3](#)). Most of the nasal cavity in humans and nonhuman primates is lined by RE. In laboratory rodents, however, less than half of the nasal cavity is covered by respiratory epithelium. In both rodent and primate species, the maxillary sinus is also lined by RE. Like SE, RE in primates is much thicker than that of rodents.

RE in the nasal cavity of the mouse is composed of morphologically distinct cell types that include numerous ciliated (most abundant), mucous, and basal cells, and lesser numbers of nonciliated columnar/cuboidal cells, including solitary chemoreceptor and brush cells that have distinctive apical microvilli. In both primate and rodent RE, the thickness and number of ciliated and mucous cells varies according to IN location. In mice, for example, mucous goblet cells are conspicuous in the respiratory epithelium lining the proximal, mid, and ventral septum (T1; [Figure 4.3C](#)) and the nasopharyngeal meatus (T4). Mucous cells, however, are scarce in RE lining the more distal midseptum, lateral wall,



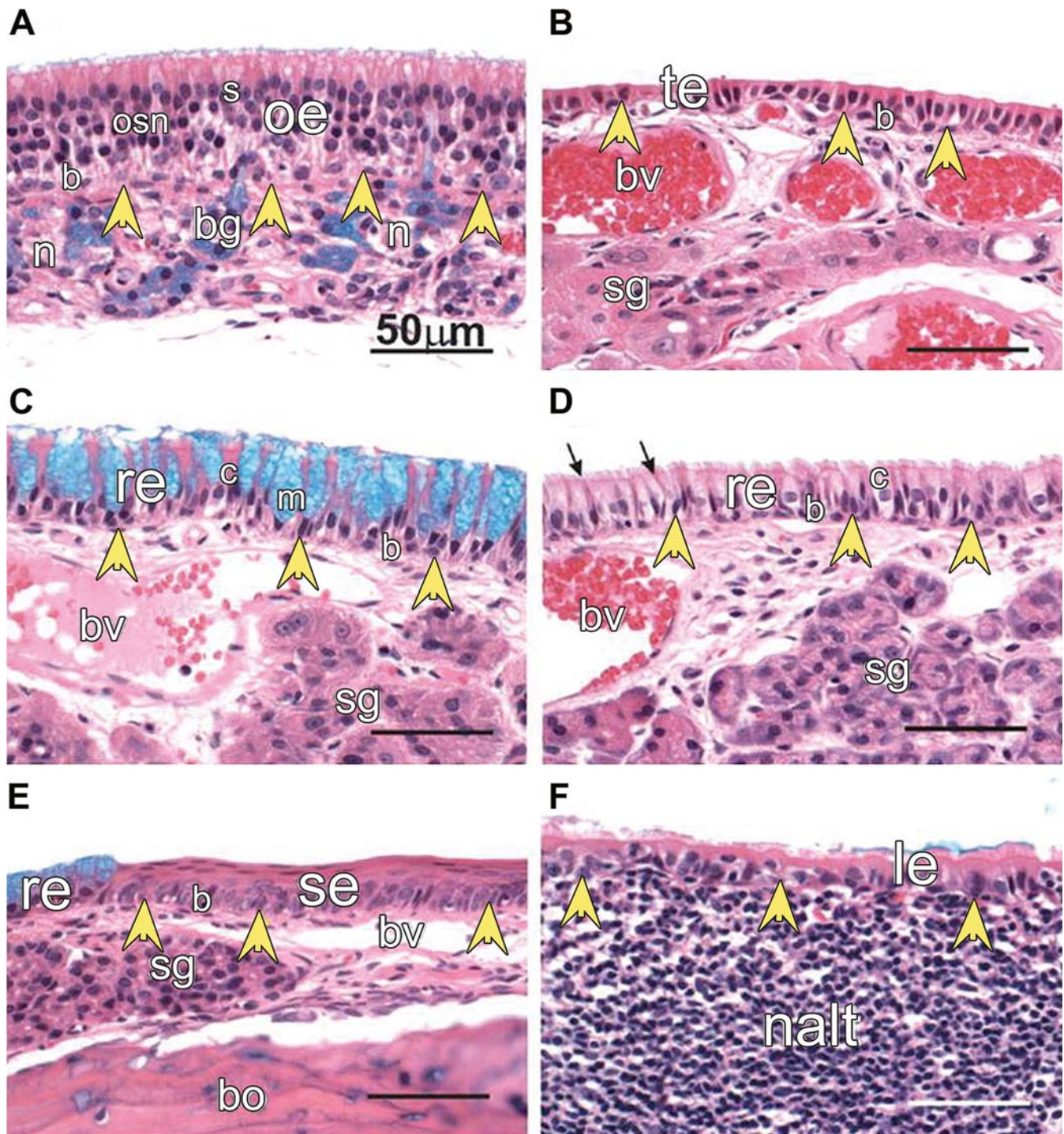


**FIGURE 4.3** Light photomicrographs of the rat's nasal mucosa containing (A) olfactory epithelium (oe), (B) transitional epithelium (te), (C) respiratory epithelium (e) with numerous mucous cells (m), (D) respiratory epithelium with serous cells, (E) squamous epithelium (se), and (F) lymphoepithelium overlying nasal associated lymphoid tissue (NALT). Arrows, identifying the basal lamina between surface epithelium and underlying lamina propria; n, nerve bundles; bg, Bowman's gland; s, sustentacular cell nuclei; OSN, nuclei of olfactory sensory neurons; b, basal cells; bv, blood vessels; sg, secretory glands in lamina propria; bo, bone; H&E/Alcian blue stain. Reproduced from Harkema JR, Carey SA, Wagner JG: *The nose revisited: a brief review of the comparative structure, function, and toxicologic pathology of the nasal epithelium*, *Toxicol. Pathol.* 34:252–269, 2006, with permission.

nasoturbinate and maxilloturbinate in T2, and the maxillary sinus in T3 (Figure 4.3D). In the RE of human and nonhuman-primates, there is a gradual anterior to posterior increase in mucous goblet cell density along both the nasal septal and lateral walls.

Numerous secretory glands, containing serous and/or mucous cells, are located in the lamina propria beneath RE predominantly in the proximal septum and lateral walls of mice. The largest nasal secretory gland in the mouse and rat is the bilateral lateral nasal gland (LNG), also referred to as Steno's gland, which surrounds the maxillary sinus located in the lateral wall adjacent to each nasal passage (T3; Figure 4.2B). Similar nasal glands are also found in the primate nose, including that of humans.

Secretory contents of the LNG drain into the nasal vestibule. This nasal gland is a major site for the synthesis and secretion of odorant-binding proteins that are odorant carriers in nasal mucus. It also synthesizes large amounts of immunoglobulin A (IgA), which is important for immune defense of the upper respiratory tract, and testosterone and salivary androgen-binding proteins, which are likely important in olfaction and reproductive behavior. Because of its high metabolic capacity, it is also a potential target site for chemical toxicity caused by secondary metabolites of inhaled or ingested xenobiotic compounds (e.g., tobacco-specific carcinogen 4-[N-methyl-N-nitrosamino]-1-[3-pyridyl]-1-butanone; also, some chemotherapeutic compounds and the antihyperthyroid drug, methimazole).

The most prominent difference in nasal epithelium between laboratory animals and humans is the amount of the main nasal airway chamber that is lined by OE (Figure 4.3A). OE lines a greater percentage of the nasal cavity of mice, which have an acute sense of smell, as compared to that of monkeys or humans, whose sense of smell is not as well developed. Approximately 50% of the nasal cavity of rats and mice is lined by this unique sensory neuroepithelium. OE of humans is limited to a small area of 500 mm<sup>2</sup> in the middorsal nasal passages, which is only 3% of the total surface area of the nasal cavity. In contrast, OE lines most of the ethmoid turbinates, roof, lateral wall, and septum in the

distal nasal airways of mice (T2, T3, and T4; Figure 4.2B). These anatomic disparities may result in increased nasal deposition in the rodent when compared to larger nonclinical species and humans.

In both animals and humans, OE is a pseudostriated, columnar neuroepithelium containing three principal epithelial cell types. These are the olfactory sensory neurons (OSNs), sustentacular cells, and basal cells. OSNs are bipolar neuronal cells interposed among the sustentacular cells. Mature OSNs immunohistochemically express olfactory marker protein (OMP) that is used for light-microscopic detection of these unique neuroepithelial cells found in both rodents and primates, including humans. The cellular composition and epithelial thickness are remarkably similar among primate and rodent species.

Dendritic portions of the OSN extend above the epithelial surface and terminate in a bulbous olfactory knob from which protrude 10–15 immotile cilia. These long and thin cilia, about 50  $\mu$ m in length and 0.1–0.3  $\mu$ m in diameter, are enmeshed with each other and with microvilli in the surface fluid, and provide an extensive surface area for reception of odorants. The ciliary membranes of the OSN contain the odorant receptors (ORs) responsible for the chemical interaction with, and initial detection of inhaled odors. ORs are G protein-coupled, seven-transmembrane membrane proteins that are encoded by the largest gene families known to exist in the animal genome. It is estimated that there are 500–1000 OR genes in the mouse, and ~1000 sequences in humans, residing in multiple clusters spread throughout the genome, with more than half being pseudogenes. A single OR gene is expressed in a minute subset of OSNs with the current belief that each OSN expresses only a single OR (one receptor–one neuron rule). Interestingly, mouse OR genes are expressed in OSNs within one of four even-sized, distinct topographical zones in the OE lining the nasal cavity. OSNs expressing a given OR are distributed in a random punctate manner within a zone. There are approximately two million OSNs within the nasal cavity of a mouse.

The axon of the OSN originates from the base of the cell and passes through the basal lamina



to join axons from other OSNs forming unmyelinated nerve fascicles, or bundles, in the lamina propria. These olfactory nerves penetrate the bony cribriform plate that separates the nasal cavity from the brain and form the outer olfactory nerve layer of the olfactory bulb. Axons of OSNs that express the same OR gene converge with extreme precision on ~2000 signal-processing modules called “glomeruli” that reside in distinct locations within olfactory bulb. “Glomeruli” are relatively large spherical neuropils (100–200  $\mu\text{m}$  in diameter) in which the axons of OSNs form synaptic connections on the dendrites of mitral and tufted cells, the output neurons of the olfactory bulb. Transmission of olfactory information is further sent through the axons of the mitral and tufted cells to the olfactory cortex (Figure 4.4).

OE also contains two types of basal cells: horizontal (HBCs) and globose (GBCs). HBCs are thin cells located along the basal lamina and share many of the same morphologic and histochemical features as the basal cells of nasal respiratory epithelium (e.g., contain keratins). In contrast, GBCs are morphologically more round or oval and are located above the HBCs. These cells have a more electron-lucent cytoplasm than the HBCs and are not immunohistochemically reactive for keratin. Some of the GBCs are the progenitor cells for OSNs, while the HBCs give rise to GBCs. Multipotent basal cells within the OE or in Bowman’s gland (BG) ducts are the likely progenitors for sustentacular cells, which are described below.

Sustentacular (supporting) cells are columnar epithelial cells that span the entire thickness of the OE from the airway surface to the basal lamina. The distinct oval nuclei of the sustentacular cells are aligned in a single row along the apical aspect of the OE and are the most apically located epithelial nuclei within the mammalian OE (Figure 4.3A). The supranuclear portion of the cell is broad while the portion of the cell below the nucleus tapers to a thin foot-like process that attaches to the basal lamina. These supporting cells surround the OSNs, making multiple contacts with OSNs through fine cellular extensions. The apical surfaces of sustentacular cells are lined by numerous long microvilli that intermingle with the thin cilia of

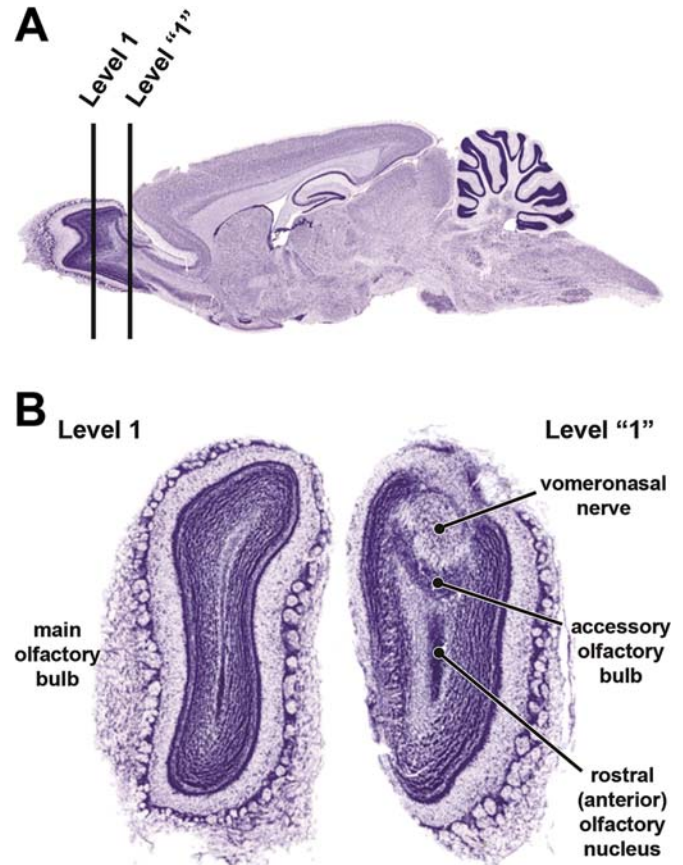


**FIGURE 4.4** Panel A. Sagittal section of rat brain, with two sections indicated through the olfactory bulb (sections 1 and 1'). Panel B. Coronal (cross)-sectional images of sections 1 and 1' shown in Panel A. Image 1 indicates the main olfactory bulb, whereas Image 1' represents the accessory olfactory bulb. Key features indicated in the accessory olfactory bulb include the vomeronasal nerve, which conducts chemosensory/pheromone-related information from the vomeronasal organ in the nasal cavity in rodents ([Hernandez-Clavijo et al., 2021](#)), and the anterior olfactory nucleus, involved in odorant signal processing ([Brunjes et al., 2005](#)). Image credits: Dr. Robert C. Switzer III (NeuroScience Associates, Knoxville, TN)/NSALabs.com with Dr. Brad Bolon (GEM-path, Inc.); labeled according to [Kruger et al. \(1995\)](#).

the OSNs along the surface of the airway lumen. Sustentacular cells in the OE are a site of ACE2 expression, which serves as a cellular receptor for some viruses (e.g., SARS-CoV2) to allow cellular invasion and may result in OE necrosis, anosmia, and/or viral entry to the brain (Figure 4.5).



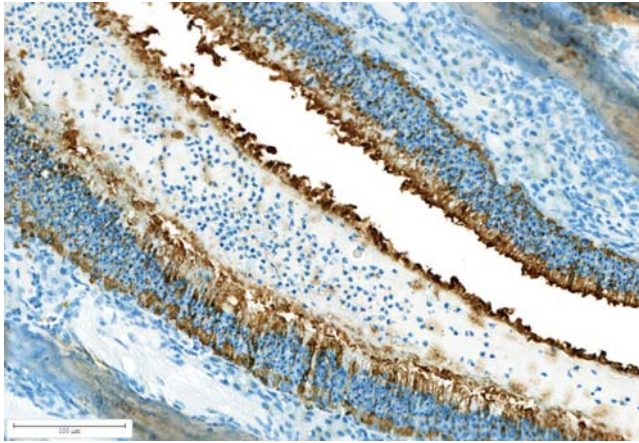


**FIGURE 4.5** Light photomicrograph of the nose of a hamster experimentally infected with SARS-CoV2. The apical surfaces of sustentacular cells are lined by numerous long microvilli that intermingle with the thin cilia of the OSNs along the surface of the airway lumen. Sustentacular cells in the OE are a site of ACE2 expression, which serves as cellular receptor for some viruses (e.g., SARS-CoV2) to allow cellular invasion and may result in OE necrosis, anosmia and/or viral entry to the brain.

The supranuclear cytoplasm of sustentacular cells also has abundant SER and xenobiotic-metabolizing enzymes (e.g., cytochrome P450, flavin-containing monooxygenases, N-acetyltransferases). The metabolism in these cells may be important in detoxification of inhaled xenobiotics and in the function of smell (Ding et al., 2018). Sustentacular cells are thought to contribute to the regulation of the ionic composition of the overlying mucous layer that undoubtedly affects the chemical interactions between odors and their ORs. Mammalian sustentacular cells do not contain mucin glycoproteins characteristics of the columnar mucus-secreting epithelial cells in the nasal respiratory epithelium (e.g., mucous goblet cells).

In addition to these principal epithelial cells in the OE, there are substantial numbers of different types of apically located microvillous cells whose function(s) is/are not fully understood. One subgroup of microvillous cells in OE has a morphology like microvillous sensory neurons of the vomeronasal organ (VNO) (described below), with an axonal component projecting to the olfactory bulb. These cells also express the

transient receptor potential (TRP) channels. The TRP ion channel superfamily functions as diverse cellular sensors. It has been suggested that these cells interface with peptidergic nerve fibers with neuropeptides (e.g., substance P), suggesting that these solitary chemosensory cells may transmit sensation of chemical irritants via the trigeminal nerve.

The production and secretion of mucus covering the luminal surface of OE is restricted to the subepithelial BGs (Figure 4.3A). These distinct mucus-producing secretory glands are located in the underlying lamina propria and interspersed among the olfactory nerve bundles. They are simple tubular-type glands composed of small compact acini. Ducts from these nasal glands transverse the basal lamina at regular intervals and extend through the OE to the luminal surface. BGs contain copious amounts of neutral and acidic mucosubstances that contribute to the mucous layer covering the luminal surface of the OE. Like the sustentacular cells, both the acinar and duct cells of BG also contain many xenobiotic-metabolizing enzymes.

Besides the OE in the main nasal chamber described above, there are three accessory olfactory organs found in the nasal airways of mice, but not well developed or functional in the human nose. These include the VNO, the septal organ of Masera (SOM), and the septal organ of Grüneberg (SOG). The VNO, also referred to as the organ of Jacobson, is a paired tubular diverticulum located in the ventral portion of the proximal septum (tissue section T1) of the mouse and rat. The lateral wall of each diverticulum is lined by a thick nonsensory columnar epithelium, while the medial wall is lined by a neuroepithelium. The sensory nerves in the VNO have long microvilli but lack the cilia found in OSNs of the OE (i.e., neuronal microvillus cells described above). Like OSNs in the main nasal chamber of the mouse, these olfactory neurons express OMP (Harkema et al., 2018).

The axonal portions of OE in the VNO synapse with glomeruli located in the accessory olfactory bulb rather than those in the olfactory bulb. A small duct extends from each diverticulum to the proximal nasal airway lumen near the nasal opening of the nasopalatine canal that connects

the nasal cavity with the oral cavity. A primary function of the VNO is to detect pheromones, airborne chemical messages or signals sent between individual rodents and essential for normal reproductive physiology and behavior. Initial pheromone detection in the VNO is triggered by its binding to G protein-coupled receptors followed by the activation of TRP. Another small, but distinct chemosensory structure found in the noses of rodents, including mice, is the SOM. The SOM is a small patch of olfactory neuroepithelium with OMP-positive OSNs surrounded by RE and lying bilaterally in the ventral nasal septum near the entrances of the nasopalatine ducts (T2; [Figure 4.2B](#)). It constitutes approximately 1% of the OE in the main chamber of the murine nose.

Neuronal projections from the SOM connect to distinct regions in the main olfactory bulb. The SOM has not been identified in the human nose. It has been suggested that the SOM may have an alerting function by sensing airborne odors during quiet breathing when IN airflows do not reach the main OE in the more dorsal regions of the nasal cavity in rodents. Considering the anatomical location of the SOM near the IN opening of the nasopalatine duct connecting the oral and nasal cavities, it may also detect odors from the mouth and act as a chemosensory surveyor of foods.

A third accessory population of OMP-expressing sensory neurons is the SOG. The SOG is located bilaterally in a discrete area of the dorsorostral tip of the nasal septum in the mouse and rat. Since it is located rostral to the routine T1 nasal section, this accessory olfactory organ would not be examined with the routine tissue sectioning of the mouse nasal cavity for light microscopy.

Like the SOM, the axons of the SOG project to a distinct subset of glomeruli in the main olfactory bulb. Unlike OSNs of the MOE, VNO, and SOM that are all part of a luminal surface epithelium, the OSNs of the SOG are arranged in clusters in the lamina propria beneath OMP-negative surface epithelium. Though the function of SOG is unknown, its rostral location suggests that it may have a special function for early detection of distinct odorants.

### **2.2.2. Nasal-Associated Lymphoid Tissue**

In addition to the four principal nasal epithelia already described, there is another specialized epithelium, lymphoepithelium (LE), in the nasal airways of rodents, which covers discrete focal aggregates of nasal-associated lymphoid tissue (NALT) in the underlying lamina propria ([Figure 4.3F](#)). In rats and mice, NALT with associated LE is restricted to the ventral aspects of the lateral walls at the opening of the nasopharyngeal duct (T3). The overlying LE is composed of cuboidal ciliated cells, a few mucous cells, and numerous nonciliated, cuboidal cells with luminal microvilli (so-called membranous or M cells), similar to those in the gut- and bronchus-associated lymphoid tissues (GALT and BALT) in the intestinal and lower respiratory tracts, respectively (see Immune System, Vol 4, Chap 6). M cells are thought to be involved in the uptake and translocation of inhaled antigen from the nasal lumen to the underlying lymphoid structures.

NALT, with its specialized lymphoepithelium, has also been described in the nasopharyngeal airways of nonhuman primates, but these lymphoid structures with LE are more numerous and are located on both the lateral and septal walls of the proximal nasopharynx of the monkey. The correlate of NALT in humans is Waldeyer's ring, the oropharyngeal lymphoid tissues composed of the adenoid, and the bilateral tubal, palatine, and lingual tonsils ([Chamanza et al., 2016](#)).

The location of NALT at the entrance of the nasopharyngeal duct is a strategic position, as most of the nasal secretions and inhaled air, both presumably laden with antigenic material, flow over this area. Though the function of NALT and its place in the general mucosal-associated lymphoid system are not fully understood, these mucosal lymphoid tissues may have an important function in regional immune defense of the upper airways.

### **2.2.3. Nasal Nerves and Blood Vessels**

Inhaled chemicals may neurogenically stimulate the OE in the main chamber and accessory olfactory organs, and also chemoreceptors of nasal trigeminal nerves, which are part of the somatic

sensory system for the eyes, nose, and mouth. Trigeminal chemoreceptors are present throughout the nasal epithelium lining the murine and human nasal cavities. Stimulation of trigeminal nerve fibers produces sensations described as irritating, painful, burning, cooling, tingling, stinging, or pungent. Chemical stimulation of these sensory nerves may also result in protective reflexes such as sneezing, increased secretions (e.g., nasal mucus), decreased respiration rate (e.g., apnea), and reduction in the nasal airway volume due to vascular congestion and mucosal swelling. Nasal trigeminal nerve fibers that respond to irritants release neuropeptides, such as substance P and calcitonin gene-related peptides (CGRPs), and are presumably polymodal nociceptors.

Nasal trigeminal nerve fibers ramify repeatedly in the nasal mucosa, and their intraepithelial nerve endings extend close to the airway surface, just below the apical tight junctions connecting epithelial cells. Interestingly, some of these trigeminal nerve fibers in the murine nasal epithelium, predominantly in the RE lining the proximal nasal airways, synapse with solitary chemoreceptive cells (SCCs), distinct nonciliated epithelial cells with loose apical microvilli. These epithelial cells are morphologically distinct from brush cells, also found in the RE, that have a stiff tuft of apical microvilli. SCCs express elements of the taste transduction cascade, including Tas1R and Tas2 receptor molecules,  $\alpha$ -gustducin, PLC $\beta$ 2, and TrpM5. They detect inhaled irritants and other xenobiotic substances that trigger trigeminal mediated airway reflexes. SCCs in mice are located in the nasal, laryngeal, and tracheobronchial airways, but only in the nasal epithelium due to synapses with trigeminal nerve fibers. In contrast to the nasal SCCs that rely on taste receptors, the free trigeminal nerve endings in the nasal epithelium mediate irritant responses through TRP cation channels (TRP: e.g., TrpV1, TrpA1), and other ion channels. Therefore, free trigeminal nerve fibers and SCCs respond to different chemical agents.

The subepithelial lamina propria of the nasal mucosa has a rich and complex network of blood vessels, with each of the epithelial regions receiving blood from a separate arterial supply.

A unique feature of the nasal vasculature is the large venous sinusoids (i.e., capacitance vessels, venous erectile tissue, or “swell bodies”) that are distributed throughout the mucosa. These blood vessels are well developed in specific sites of the anterior or proximal aspects of the nasal passages. Capacitance vessels have dense adrenergic innervations, and the congestion and constriction of these vascular structures are regulated by the sympathetic nerve supply to the nose. Congestion of blood in these vessels can change mucosal thickness, resulting in nasal airflow pattern alterations and increased nasal resistance.

### 2.3. The Pharynx and Larynx

The pharynx connects the nasal and oral airways to the laryngeal airway ([Figure 4.1](#)). In humans and nonhuman primates, the pharynx is situated posterior to the nasal cavity, mouth, and larynx. In many other laboratory animal species (e.g., dogs, rats, mice), the pharynx is distal to most of the nasal airway and dorsal to the oral cavity and larynx. The pharynx is a musculomembranous tube that is anatomically divided into nasal, oral, and laryngeal regions. The nasopharynx is lined with ciliated respiratory epithelium with mucous goblet cells, while the oropharynx and laryngopharynx are lined by nonkeratinized SE.

One of the more conspicuous anatomical differences in the pharyngeal region of the upper airway among mammalian species is the angle of the dorsoventral bend in the nasopharynx ([Figure 4.1](#)). Rodent and canine species have a slight nasopharyngeal bend (e.g., 15 and 45 degrees in rats and dogs, respectively), while primates have a marked bend (e.g., 80 and 90 degrees in Rhesus monkeys and humans, respectively) due to their more erect stature. The degree of this bend in the upper airway impacts the regional dosimetry of some inhaled agents. Interestingly, this site is where mucosal lymphoid tissues are found and where streams of mucus lining the nasal airways converge before being swallowed.



The larynx is the part of the upper respiratory tract between the pharynx and trachea (Figure 4.1). It is a bilaterally symmetrical structure that is framed by cartilages and bound by ligaments and muscles. It functions as (1) a pathway for inhaled and exhaled air during breathing; (2) a valve, with the epiglottis, to prevent swallowed food from being aspirated into the lungs; and (3) a tone-producing vocal structure for phonation. Anatomically, the larynx is the first site of constriction in the respiratory tract (Herbert and Leininger, 1999). The airway lumen of the human larynx is lined, for the most part, by pseudostratified ciliated respiratory epithelium, except for a small area on the vocal folds where it is stratified SE. In laboratory rats and mice, a transitional zone of nonciliated epithelium extends between the squamous and ciliated respiratory epithelia. This transitional zone, located at the base of the epiglottis, is a common site of injury from inhaled aerosols due to both enhanced deposition and the susceptibility of the thin TE (Kaufmann et al., 2009). In general, even the thickest epithelial areas in the rodent larynx are appreciably thinner than the thinnest epithelial lining in the primate or dog.

As in the nasal airways, there are species-specific differences in the structure and functions of the larynx. For example, rodents have a ventral pouch caudal to the base of the epiglottis that is a common site of inhaled irritant injury (Renne and Gideon, 2006; Renne et al., 2007). This structure, however, is absent in humans. In terms of inhalation toxicology, the larynx is a major resistive element to airflow and a potential site for inhaled particle deposition. The rapid expansion and contraction of this organ of phonation creates turbulence and inspiratory air jets that may lead to additional particle impaction on the wall of the trachea. In the rodent, the larynx and trachea form a nearly straight line from the nasal turbinates and the cranial laryngeal surface is directly targeted by incoming airflow. This, along with the rapid respiratory rate of the obligate nose-breathing rodent, enhances the impaction of aerosols on the anterior surface where lesions are commonly seen (Mowat et al., 2017). In contrast, the larynx of nonrodents, including humans, is more sharply angled, just about 90° to the oronasal cavity, and respiration occurs through

both oral and nasal cavities as was already discussed. Therefore, there is a reduced amount of aerosol impaction on the anterior surface of the larynx in nonrodents.

## 2.4. The Trachea, Bronchi, and Bronchioles

The trachea is continuous with the larynx in the neck and extends distally into the thoracic cavity to the carina, where it bifurcates to form two primary or mainstem bronchi (Figure 4.1). The trachea lies close to the ventral or anterior aspect of the neck where the surrounding tissue gives little structural support. The tracheal airway remains patent on inspiration due to C-shaped cartilaginous rings that lie within the ventral and lateral walls. In humans, the posterior wall of the trachea is composed of flexible fibroelastic and smooth muscle tissue.

The airway wall of the trachea and more distal conducting airways (bronchi and larger bronchioles) is composed of three distinct layers: the mucosa, submucosa, and adventitia. The mucosa lining the airway lumen is lined by pseudostratified, ciliated epithelium and a thin subepithelial lamina propria, compared to the thick lamina propria in the nasal mucosa. A fine smooth muscle layer divides the mucosa from the submucosa. These conducting airways are connected to the surrounding tissue by a loose connective tissue, the adventitia.

The distal end of the trachea divides into two extrapulmonary mainstem bronchi at the carina within the thoracic cavity (Figure 4.1). The carina is another site susceptible to aerosol injury, particularly in laboratory rats and mice, due to enhanced deposition (impaction) and the thinness of the epithelium lining the carina at the tip of the tracheal bifurcation (Gopinath and Mowat, 2014; Mowat et al., 2017). The efficiency of the mucociliary transport mechanism in vivo is reduced at airway branching, further increasing the sensitivity of the site. The rodent carina is more frequently affected than that of the nonrodent due to the disparity in mucosal thickness at this site, with the epithelium of the rodent being approximately 3–4 times thinner than that of the nonrodent. Therefore, the typical

lesions seen in the rat carina have a similar etiology to those seen in the larynx and can be regarded similarly when assessing potential clinical implications of an inhaled pharmaceutical.

Within the lungs, airways with cartilage or submucosal glands are called bronchi and airways without cartilage or submucosal glands are called bronchioles. In the larger laboratory animals and humans, the intrapulmonary bronchi divide into smaller diameter airways within the lung, and there is a point (airway diameter of  $\sim 1$  mm in humans) where intramural cartilage and submucosal glands are no longer present. These airways are called bronchioles. The presence of intramural cartilage and submucosal glands distinguishes bronchi (with large airway diameters) from bronchioles (with smaller airway diameters) in the lungs of dogs, cats, nonhuman primates, and humans. In contrast, laboratory rodents (mice, rats) lack bronchi and have conducting airways solely composed of bronchioles (Meyerholz et al., 2018).

The human respiratory tract contains several generations of nonrespiratory bronchioles (i.e., no alveolar outpocketings along the bronchiolar airway). Considerably fewer generations of these intrapulmonary airways are present in other mammalian species, such as the dog, cat, and monkey. The number of generations of nonrespiratory bronchioles in rodents and rabbits is similar to that in humans (Pereira et al., 2011).

The most distal nonrespiratory bronchiole is defined as the terminal bronchiole. The distal end of this conducting airway connects to alveolarized (respiratory) airways. This junction, where conducting and respiratory airways join, is called the centriacinus. It is a common site of injury from inhaled gases and particles that reach the lung. In humans and some laboratory mammals (e.g., dogs, cats, monkeys), the terminal bronchioles end into several generations of respiratory bronchioles containing widely scattered intramural alveoli, often referred to as alveolar outpocketings. In contrast, the terminal bronchioles in smaller laboratory animals, like rats, mice, hamsters, and rabbits, end directly into one short segment of

respiratory bronchioles or into small air passages completely lined by alveoli and designated as alveolar ducts (Figures 4.6 and 4.8).

#### **2.4.1. Epithelial Cells Lining Tracheobronchial Airways**

The respiratory epithelium lining the tracheobronchial airways varies from a tall columnar ciliated epithelium in the proximal trachea to a low cuboidal epithelium in the distal bronchioles, and a simple SE (i.e., alveolar type I epithelial cells) lining the alveolar outpocketings of the respiratory bronchioles (Figures 4.6, 4.7 and 4.8). Surface epithelial cell type and abundance varies among species and airway generations (Table 4.2). Species differences in the composition of the airway surface epithelium exist not only in the amount of lining tissue but also in the density of its specific cell phenotypes, for example, mucous, ciliated, basal cells (Figure 4.6). For example, the thickness of the epithelium lining the trachea of humans is three times thicker than that in monkeys and 10 times thicker than that of laboratory mice or rats. A substantial percentage of the tracheal and bronchial epithelium in primates and dogs is occupied by mucus cells, but these secretory epithelial cells are generally not found to the same extent in healthy, pathogen-free laboratory mice and rats. Serous cells are the main secretory cells lining the conducting airways from the trachea to the proximal bronchioles in rats, with club cells becoming abundant distally. Club cells are the main secretory cells throughout the tracheobronchial airways of mice (Tepper et al., 2016) and discussed in more detail below. The proportion of ciliated cells in the respiratory epithelium is relatively similar among species, but the proportion of basal cells varies among species. In the rodent, basal cells are confined to the trachea, where they are interspersed among the ciliated, secretory, and neuroendocrine cells. In the human lung, however, basal cells are present throughout the airways, including small bronchioles (Rock et al., 2009).

##### **2.4.1.1. CILIATED CELLS**

Ciliated cells are one of the most abundant epithelial cells that line the conducting airways

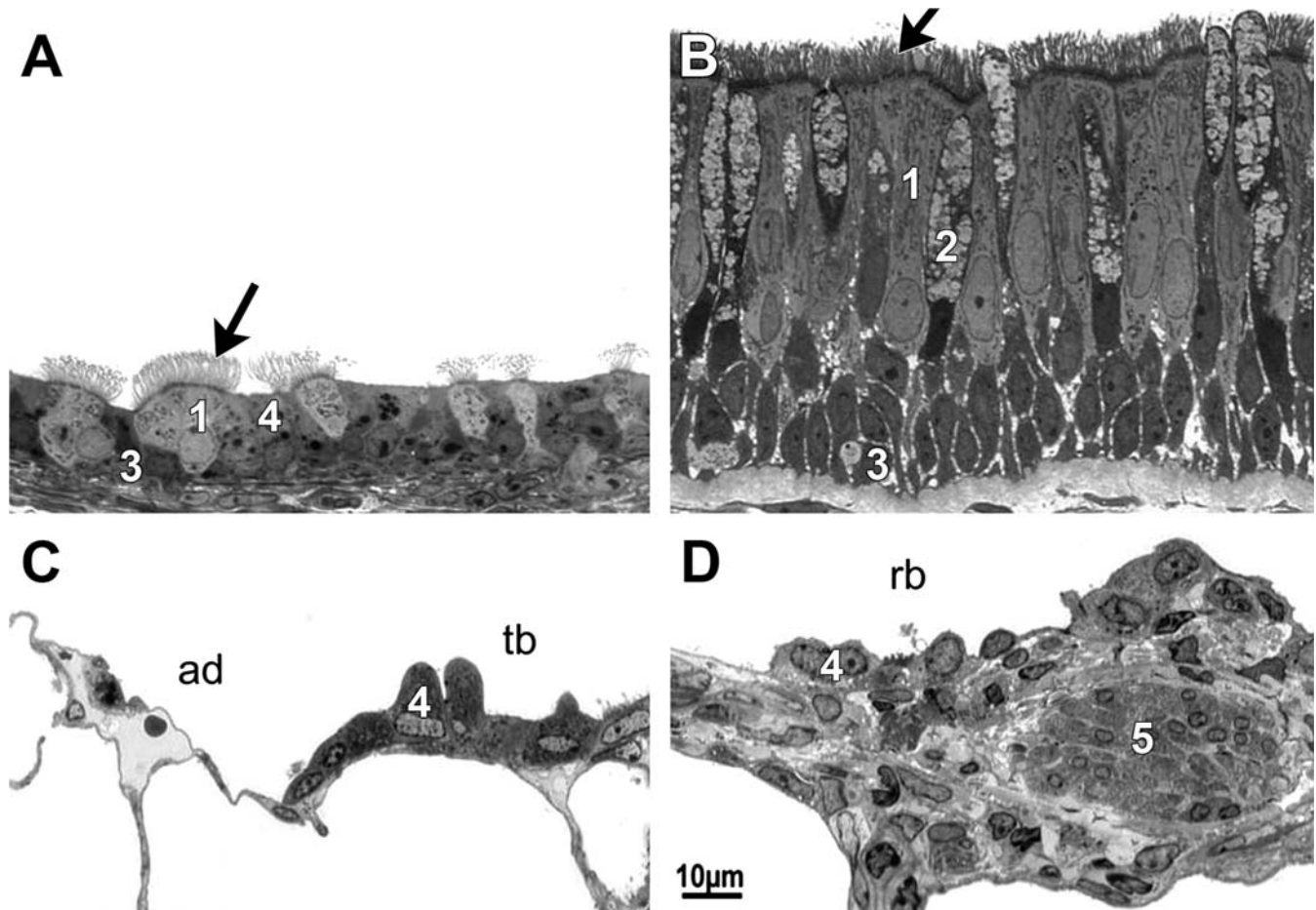


**FIGURE 4.6** Transmission electron photomicrographs of the surface epithelium lining tracheal (A, B) and distal bronchiolar (C, D) airway in the mouse (A, C) and rhesus monkey (B, D). 1, ciliated cells; 2, mucous cells; 3, basal cells; 4, nonciliated club cells; 5, intramural smooth muscle; arrows, cilia; ad, alveolar duct; tb, airway of terminal bronchiole; rb, airway of respiratory bronchiole. Modified from Wolfe-Coote, editor: *The laboratory primate: the handbook of experimental animals*, ed 1, 2005, Academic Press, pp. 503–506, with permission.

of the respiratory tract in most mammalian species. Along with airway secretory cells, they comprise the cellular components of the mucociliary defense apparatus that is important in clearing various inhaled foreign agents (e.g., dust, bacteria) which deposit on a moving layer of mucus that lines the luminal surfaces. The primary function of ciliated cells is to generate the flow of airway mucus with synchronized beating of numerous motile cilia that extend from the apical aspects of these dynamic cells. Cilia beat at a high frequency of 12–15 beats/second. The synchronous beating of cilia along the airway moves the mucous in a specified direction depending on the location in the

respiratory tract. Nasopharyngeal mucus is moved distally toward the orifice of the esophagus, where it is constantly swallowed. In the tracheobronchial tract, mucus flows proximally up the airways toward the esophageal opening where it is swallowed into the gastrointestinal tract as well.

There are roughly 200–300 cilia per ciliated cell. The shaft of each cilium contains a characteristic arrangement of longitudinal microtubules, the axoneme. It is composed of a central pair of singlet tubules surrounded by nine doublet tubules, with a complex of fine radial spokes binding them together. In the outer doublets, the microtubules have two extensions, or “arms,” composed of



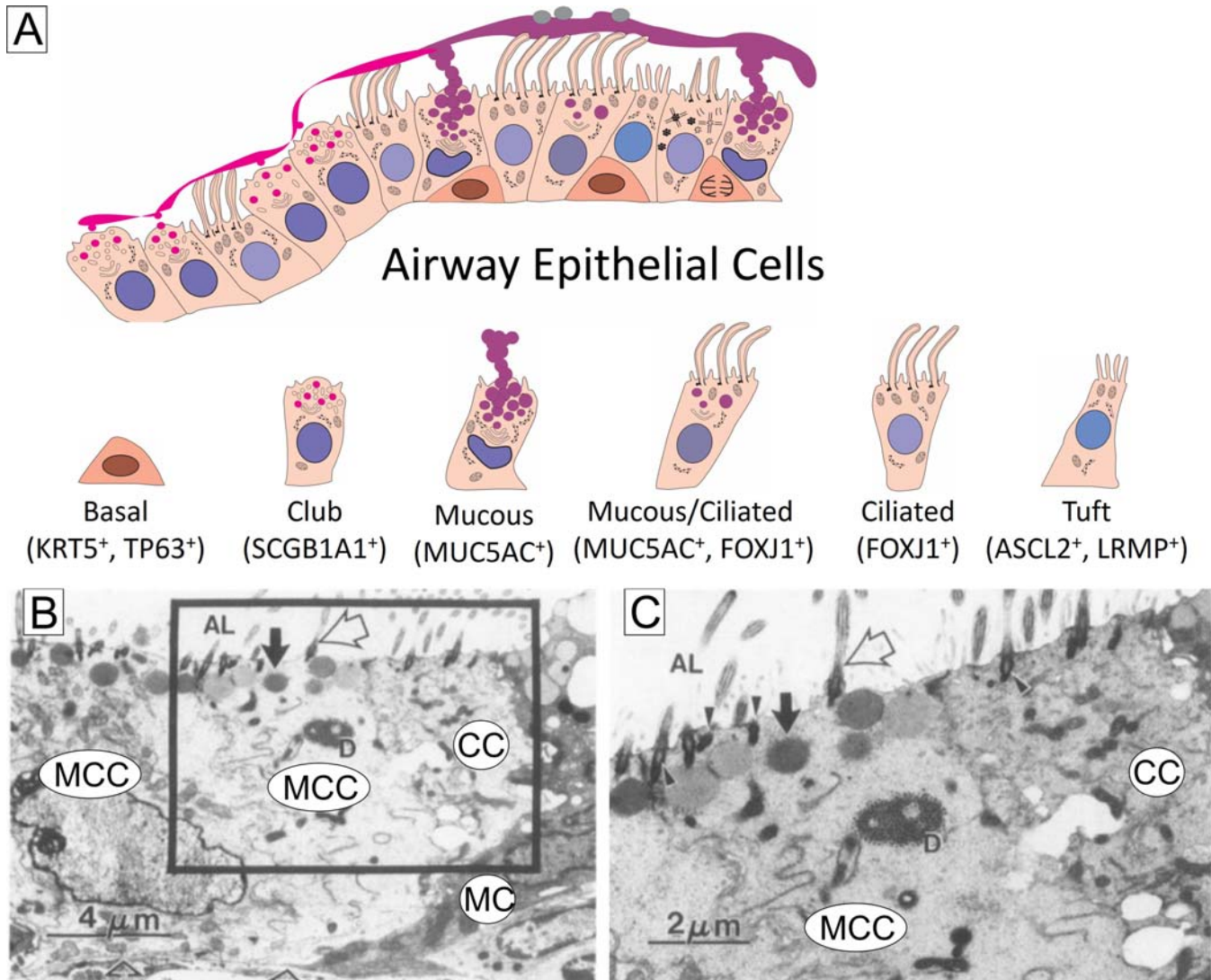


**FIGURE 4.7** (A) Cartoon of airway epithelial cell types with specific protein cell markers in bronchiolar epithelium. (B) Transmission electron photomicrograph of bronchiolar epithelial cells lining main axial airway in right caudal lobe of an F344/N rat 2 days after three daily instillations of bacterial endotoxin (gram-negative lipopolysaccharide from *E. coli*). (C) Higher magnification of area within the box in (B). MCC, mucous/ciliated cell with both apical cilia (open arrow) and cytoplasmic secretory granules (closed arrows); AL, airway lumen; D, large deuterosome; open arrowhead, basal lamina; closed arrowhead, basal body. (B & C) Modified figures from Harkema JR, Hotchkiss JA: *In vivo* effects of endotoxin on intraepithelial mucosubstances in rat pulmonary airways. *Quantitative histochemistry, Am J Pathol.* 141(2):307–317, 1992.

dynein protein that contains ATPase generating the energy for motility of the cilium. Expression of FOXJ1, a transcriptional factor that is essential for organization of the apical ciliary apparatus, is used as genetic marker for ciliated cells in

single-cell RNA sequencing (scRNA-seq) and cellular lineage tracing in airway epithelium (Treutlein et al., 2014).

In general, ciliated cells are terminally differentiated or “end-stage” cells with limited

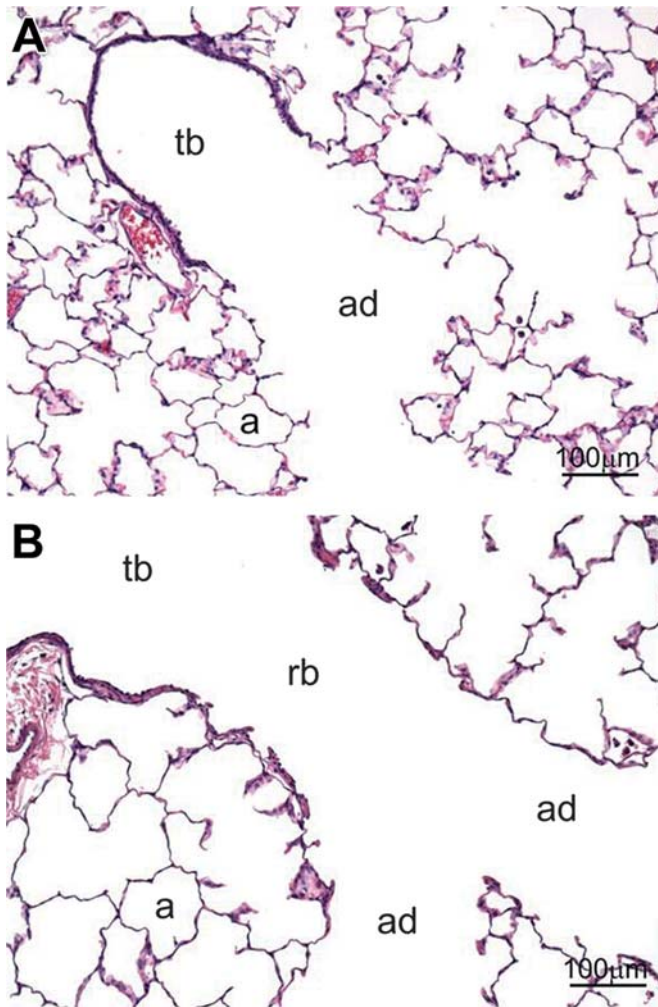


**FIGURE 4.8** Light photomicrographs of the centriacinar region in the laboratory rat (A) and rhesus monkey (B). Respiratory bronchioles (rb) are present in the monkey, but not the rat. tb, terminal bronchiole; ad, alveolar duct; a, alveolus; H&E stain. *Reproduced from Haschek WM, Rousseaux CG, Wallig MA, editors: Handbook of toxicologic pathology, ed 3, 2013, Academic Press, Vol. 3, Figure 51.5, p. 1948, with permission.*

capacity to divide and proliferate. They originate from progenitor basal or secretory cells (e.g., club cells) (Konkimalla et al., 2022; Rock and Hogan, 2011). Ciliated cells are particularly sensitive to injury from inhaled chemical irritants, such as chlorine, nitrogen dioxide, sulfur dioxide, ozone, and tobacco smoke. Toxicant-induced injury to ciliated epithelial cells may be manifested as ciliostasis (loss of

motility), detachment or resorption of cilia, or cell death with exfoliation (Figure 4.9). The end result is impairment of mucociliary clearance, which can be reversible, or lead to potentially life-threatening situations such as secondary bacterial bronchitis and bronchopneumonia.

#### 2.4.1.2. MUCOUS CELLS

Secretory epithelial cells are interspersed among the ciliated cells in the surface epithelium of conducting airways. The three principal secretory cells in respiratory epithelium lining the tracheobronchial airways are the mucous (goblet) cells, club cells (formerly known as Clara cells), and serous cells discussed earlier. The cytoplasm of all these cells contains unique, spherical, membrane-bound secretory granules in the apical portion of the cell or “theca.” Secreted materials from these surface epithelial cells, and those from the secretory cells in submucosal glands, provide the air–tissue interface with a moisturizing, lubricating, and protective fluid layer, often referred to as epithelial lining fluid.

Mucous cells are an important secretory cell type in the tracheobronchial airways of humans, monkeys, and dogs. In healthy pathogen-free laboratory rats and mice, mucous cells are restricted primarily to the trachea and extrapulmonary bronchi, and normally absent in the more distal intrapulmonary bronchioles. Mucous cells secrete mucus, a hydrated sticky gel made up primarily of water but also containing distinctive carbohydrate-rich glycoproteins or “mucins,” lipids, proteins, salts, and other small dialyzable components. Airway mucous cells often have expanded theca filled with large numbers of individual or coalescing secretory granules and a narrow basal portion that together give them a classical “goblet” shape. Ultrastructurally, the secretory granules vary in electron density and often coalesce near the apex of the cell. Histochemically, the secretory granules stain with Alcian blue (pH 2.5) and periodic acid Schiff (AB/PAS), indicating the presence of both acidic and neutral mucosubstances.

**TABLE 4.2** Simplified Comparison of Epithelial Classification and Major Cell Types in Respiratory Structures of Select Species

Respiratory structure <sup>a</sup> (Epithelial Classification)	Mouse	Rat	Dog	Human, Monkey
Trachea (Pseudostratified)	<sup>b</sup> Club, ciliated and basal cells	Ciliated, serous and basal cells	Ciliated, mucous and basal cells	Ciliated, basal and mucous cells
Bronchi (Pseudostratified)	Club and ciliated cells	Ciliated, serous and basal cells	Ciliated and mucous cells	Ciliated and mucous cells
Bronchioles (Simple columnar)	Club and ciliated cells	Club and ciliated cells	Club cells	Ciliated and club cells
Alveoli (Simple squamous)	Type 1 and type 2 pneumocytes	Type 1 and type 2 pneumocytes	Type 1 and type 2 pneumocytes	Type 1 and type 2 pneumocytes

<sup>a</sup> Airway epithelial height is proportional to airway caliber in most species.

<sup>b</sup> Major cell types are generally listed according to highest frequency.

Production and secretion of the airway mucus is important for maintaining the mucociliary defense apparatus of the conducting airways. Inhalation exposure to chemical and physical irritants, like inhaled cigarette smoke, ozone, chlorine, and particulate matter, often causes hypersecretion of mucosubstances resulting in excess airway mucus. In chronic respiratory disease states like allergic asthma and chronic bronchitis, the combination of excess luminal mucus and exaggerated constriction of bronchial airways (hypersensitivity) can result in impeded airflow to the distal lung and thus compromise oxygen delivery to respiratory portions of the lung. Repeated exposures to these irritating agents may also result in an abnormal increase in the number of these airway secretory cells in areas with normally few or no mucous cells (i.e., mucous cell hyperplasia and metaplasia, respectively). Airway mucous cells differentiate from either basal cells or club cells. Mucous cells express mucin genes (e.g., MUC5B, MUC5AC) and Sam-pointed domain Ets-like factor (SPDEF; essential for mucous cell differentiation) that identify these secretory cells in scRNA-seq assays of airway epithelium (Treutlein et al., 2014).

#### 2.4.1.3. CLUB CELLS

Club cells are nonciliated, nonmucous, secretory cells in respiratory epithelium. These

epithelial cells secrete several distinctive proteins, including club cell secretory protein (CC16) that is encoded by SCGB3A1. By light microscopy, club cells are morphologically columnar to cuboidal with a distinctive dome-shaped luminal surface and contain small PAS-positive secretory granules. In laboratory mice, the club cell is the principal secretory cell type throughout the conducting airways. In contrast, club cells are most predominant in the terminal and respiratory bronchioles of humans and monkeys.

Ultrastructurally, the club cell in most laboratory rodents is a distinctly polarized epithelial cell with a basally located nucleus, a prominent apical projection toward the airway lumen containing electron-dense secretory granules, and abundant cytoplasmic SER. Greater than 40% of the cytoplasmic volume of the club cells in the mouse is occupied by SER. In humans and other primates, club cells are low cuboidal cells with only a slight apical projection, and less cytoplasmic SER as compared to the rodent club cells. Interestingly, dogs and cats have large amounts of cytoplasmic glycogen in their club cells.

The primary functions of club cells are: (1) to secrete surfactants (surfactant proteins A, B, and D) and the antiinflammatory secretoglobulin (SCGB1A1 CC16) that contribute to the airway epithelial lining fluid; (2) to serve as progenitor cells for ciliated and secretory epithelial cells;



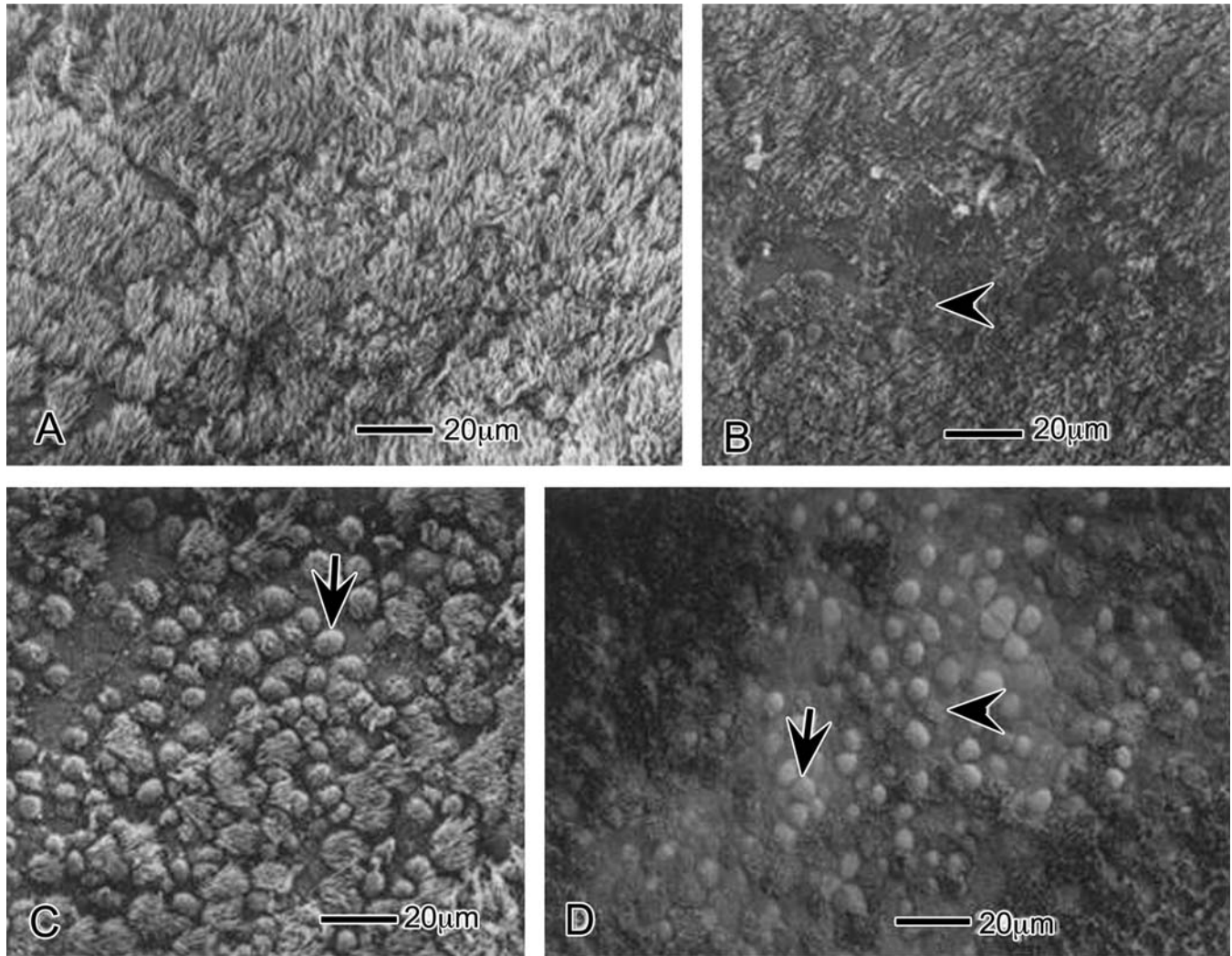


**FIGURE 4.9** Scanning electron photomicrographs of the ciliated epithelial surfaces lining the proximal nasal septum of macaque monkeys exposed to 0 ppm ozone (A; filtered air control), 0.15 ppm ozone for 6 or 90 days (B and C, respectively) or 0.30 ppm for 90 days. Surfaces exposed to ozone had loss of cilia (arrow heads) and proliferation of mucous cells (arrows, domed apical surfaces of mucous cells). *Reproduced from Harkema JR, Plopper CG, Hyde DM, St George JA, Wilson DW, Dungworth DL: Response of the macaque nasal epithelium to ambient levels of ozone. A morphologic and morphometric study of the transitional and respiratory epithelium, Am. J. Pathol. 128:29–44, 1987, with permission.*

and (3) to metabolize xenobiotic compounds (e.g., naphthalene) through P450 cytochrome-dependent mixed-function oxygenases associated with the SER. Through the latter metabolizing process, certain inhaled or ingested xenobiotic agents, like naphthalene, 3-methylindole (3MI), acetaminophen, and 4-

ipomeanol, generate toxic metabolites that can damage the club cell, causing degeneration and necrosis.

Though SCGB1A1+, KRT5lo, and MUC5AC- are generally used as the signature gene profile for club cells, identification of other gene expression clusters via scRNA-seq has suggested

subcategories of club cells including progenitor, proliferating, and effector club cells in nonsmokers and healthy cigarette smokers. Progenitor club cells express higher levels of mitochondrial, ribosomal proteins, and KRT5 relative to other club cell subpopulations. The smaller proliferating population express cyclins and proliferation markers. Effector club cells express genes related to host defense, xenobiotic metabolism, and barrier function.

#### 2.4.1.4. SEROUS CELLS

Serous cells are secretory cells in the respiratory epithelium that are phenotypically distinct from mucous and club cells. They are the predominant secretory cells in the trachea, extrapulmonary bronchi, and proximal intrapulmonary bronchioles of laboratory rats. Serous cells are also present in some subepithelial lateral and septal glands in the nasal airways of rats and mice, and submucosal glands in human airways. Small populations of serous cells are also present in the airway epithelium lining bronchioles and small bronchi of humans. In human submucosal glands, serous cells express high levels of LTF, LYZ, and PIP. In contrast, mucous cells in these glands express high levels of MUC5B, but not MUC5AC.

Distinct, electron-dense, membrane-bound granules are present in the apical cytoplasm of serous cells and contain histochemically PAS-positive, neutral mucosubstances. In contrast to club cells, these secretory cells have abundant amounts of rough (granular) endoplasmic reticulum, rather than smooth (agranular) endoplasmic reticulum. Besides the neutral mucosubstances, these secretory cells have been found to contain calcitonin gene-related protein and antibacterial agents, lysozyme, and lactoferrin. Like club cells, serous cells can produce seromucous or mucous granules after exposure to certain inhaled irritating or allergic agents (e.g., bacterial endotoxin, ovalbumin), thus differentiating into mucous cells without cell division.

#### 2.4.1.5. BASAL CELLS

Basal cells are the primary support cells in the respiratory epithelium. These epithelial cells are small, flattened cells that are closely attached to the basal lamina and do not extend to the airway lumen. It is the presence of these epithelial cells located in the larger conducting airways that accounts for the pseudostratified classification given to respiratory epithelium. Basal cells have a small cytoplasm to nucleus ratio, and organelle-poor cytoplasm that is filled primarily with intermediate filaments. Numerous desmosomes attach the basal cell to the surrounding epithelial cells. Cytoskeletal, junctional, and adhesive proteins of these cells help to anchor the epithelium to its underlying connective tissue stroma.

Basal cells are a population of multipotent stem cells that are important in regeneration and homeostasis of the respiratory epithelial cell population. In humans, the pseudostratified respiratory epithelium containing basal cells extends from the upper conducting airways (nose and trachea) distally to the terminal bronchioles that are approximately 0.5 mm in diameter, and only the respiratory bronchioles are lined by a simple cuboidal epithelium lacking basal cells and relying on club cells as primary progenitor cells. In contrast, basal cells, like mucous cells, are few in the conducting airways of laboratory rodents. In mice and rats, basal cells are mainly restricted to the respiratory epithelium lining the trachea and mainstem bronchi, and absent in the epithelium lining the intrapulmonary bronchiolar airways.

Selective markers of airway basal cells include TP63 transcription factor, keratins 5 and 14 (KRT5 and KRT14), podoplanin (PDPN), nerve growth factor receptor (NGFR), galectin 1 (LGALS1), integrins  $\alpha 6$  and  $\beta 4$  (ITGA6 and ITGB4), laminins  $\alpha 3$  and  $\beta 3$  (LAMA3 and LAMB3). A pool of basal cells expressing c-myc differentiates into ciliated epithelial cells, while Notch activation drives another pool of airway basal cells to differentiate into secretory cells. Interestingly, results of single cell RNA analysis

and lineage tracing studies suggest that airway basal cells might first differentiate into club cells (SCGB1A1) and then ciliated cells (DEUP1, FOXJ1) and mucous cells (MUC5AC); or in some diseased states, less frequent mucous-ciliated cells (FOXJ1, MUC5AC).

#### 2.4.1.6. NEUROENDOCRINE CELLS

Compared to other airway epithelial cells, neuroendocrine cells are relatively sparse in mammalian species. Gene expression markers for these cells are CGRP and CHGA. Neuroendocrine cells occur individually or in small clusters called neuroepithelial bodies. They display endocrine, paracrine, and secretory mechanisms, and are often associated with intraepithelial nerve fibers. The cytoplasm of these distinct epithelial cells contains distinctive dense-cored secretory granules that store bioactive substances, including calcitonin-gene related peptide, and bombesin-like peptides (e.g., gastrin-releasing peptide). These cells have been reported to increase in number from mainstem bronchi to bronchioles but are absent from more distal terminal bronchioles. In the lungs of adult mice, neuroepithelial bodies are often located at airway bifurcations. Naphthalene-induced necrosis of club cells in mice is often followed by epithelial regeneration at airway branch points and associated with hyperplasia of neuroepithelial bodies.

Neuroendocrine cells and neuroepithelial bodies have multiple proposed physiological functional roles, including modulation of early lung development and airway chemoreceptors. Neuroepithelial bodies may be sensors for hypoxia. Another novel role for these cells, as guardians of lung stem cell niches, has recently emerged. It has been suggested that pulmonary neuroendocrine cells foster a microenvironment, or niche, which is resistant to destruction by environmental agents and promotes stem cell renewal. This has implications for injury and repair mechanisms as well as carcinogenesis. Exposure of laboratory rodents to chemical carcinogens such as tobacco-specific

nitrosamines often lead to marked, albeit reversible, neuroendocrine cell hyperplasia, and non-neuroendocrine adenomas and nonsmall cell lung carcinomas ([El-Hashash, 2021](#)).

#### 2.4.1.7. BRUSH/TUFT CELLS AND IONOCYTES

A rare epithelial cell in the conducting airways is the brush/tuft cell. Brush/tuft cells, as the name implies, have conspicuously long microvilli on their apical surface. These microvilli are unusually long,  $\sim 2 \mu\text{m}$ , and have axial filaments that continue into the cell without ending in a terminal web. Gene signature markers for these rare airway epithelial cells are ASCL2 and LRMP. Brush/tuft cells are found in the respiratory epithelium lining both nasal and tracheobronchial airways. Some of these cells are solitary chemosensory cells that utilize the chemoreceptive transduction cascade first described in taste buds. They too have basolateral contacts with nerve fibers, suggesting their role as sensory elements. Intraepithelial chemosensitive free nerve endings and the solitary chemosensory brush cells have different receptors and therefore are responsive to different inhaled chemical irritants. The sensory nerve endings use various TRP channels, for example, TrpV1 or TrpA1, and other chemosensitive ion channels. Solitary chemosensory cells, however, rely on taste receptors and their downstream signaling cascade, involving G protein,  $\alpha$ -gustducin, the phospholipase C beta2, and TrpM5, for its sensory activation.

Another rare cell type is the ionocyte (formerly called a chloride cell), present in most species, and making up less than 1%–3% of airway epithelial cells in the human respiratory tract. These are nonciliated cells located in both nasal and pulmonary airways, with greater abundance in the nasal epithelium. Ionocytes express high levels of CFTR, the Cl-channel that is defective in cystic fibrosis, and the transcriptional factor Forkhead BoxI1 (FOX I1, the signature gene for this airway epithelial cell). CFTR, however, is not restricted to ionocytes, but is common in serous cells of submucosal glands and is also seen in airway



secretory cells (e.g., club cells, mucous cells) and basal cells ([Livraghi and Randell, 2007](#)).

#### **2.4.2. Bronchus-Associated Lymphoid Tissues**

Some, but not all, mammalian species contain BALT, well-organized, and densely packed aggregates of lymphoid tissue, in the bronchial mucosa. Like NALT, BALT belongs to the body's mucosa-associated lymphoid tissue (MALT) system (see *Immune System*, Vol 5, [Chap 6](#)). Morphologically it resembles NALT in the upper respiratory tract or Peyer's patches in the intestinal tract ([Elmore, 2006](#)).

BALT is a prominent airway tissue in laboratory rats and rabbits, although it is absent in the lung of healthy laboratory mice. BALT is also absent from the pulmonary airways of healthy dogs, cats, nonhuman primates, and humans. In these species, though BALT is not constitutively expressed, antigenic stimulation or airway inflammation can induce its formation in the bronchial airways. Inducible BALT (iBALT) or tertiary (ectopic) lymphoid organs are typically found in the interstitial tissue adjacent to pulmonary airways, arteries, or veins (perivascular and peribronchial/bronchiolar lymphoid cuffing). The perivascular interstitial space becomes densely packed with T and B lymphoid cells, and plasma cells in laboratory animals with experimentally triggered infectious, allergic, or autoimmune airway diseases. BALT reactions are not exclusively initiated or maintained by an immune response, as inflammation can initiate BALT hyperplasia. Once induced, BALT may persist for months and participate in immune responses ([Hall et al., 2021](#)). Follicular dendritic cells help to organize lymphoid cells to form germinal centers like those in secondary lymphoid organs (e.g., lymph nodes).

Morphologically, the classically defined BALT is covered by a specialized lymphoepithelium that is composed of nonciliated, cuboidal epithelial cells that are interspersed with lymphocytes. This lymphoepithelium is devoid of ciliated or mucous epithelial cells. The absence of

a mucociliary barrier facilitates the transport and presentation of inhaled antigenic agents to the underlying BALT, providing immune surveillance of the inhaled air.

BALT is organized as a dome-like aggregate of tightly packed lymphoid cells underlying the luminal lymphoepithelium. A follicular region dominated by B cells lies directly beneath the airway epithelium. T cell-dominated parafollicular regions make up the abluminal periphery of this subepithelial lymphoid tissue.

BALT's follicular region is the most prominent feature of BALT and is composed mainly of IgD<sup>hi</sup>IgM<sup>lo</sup> mature B lymphocytes. Follicular regions may also have antigen-induced germinal centers and B cells with alternative isotypes, such as IgG, IgA, or IgE, as well as scattered dendritic cells. In addition, follicles contain CD4 T cells, but rarely contain CD8 T cells. Parafollicular regions of BALT are the primary home for T cells, dendritic cells, reticular cells, macrophages, and plasma cells. These regions also contain an extensive network of blood vessels and, most notably, high endothelial venules through which bloodborne lymphocytes enter the BALT.

### **2.5. Gas-Exchange Regions of the Lung**

Lobation of the lung varies greatly among species. The human has two lobes on the left and three on the right; the monkey and cat have three left lobes and four right lobes; the dog has two on the left (cranial lung lobe that is subdivided into a cranial portion and a caudal portion and a left caudal lung lobe) and four on the right; and the mouse, rat, and hamster have a single left lobe and four right lobes. Depending on species, lobes may be divided into bronchopulmonary segments, subsegments, and lobules by interlobular tissue ([Table 4.1](#)). The lobule consists of a lobular bronchiole with its branches and associated structures.

Visceral pleura covers the outer surfaces of the lung lobes, and the parietal pleura covers the walls of the thoracic cavity. Communication between the two pleural cavities (right and left)

and pleural thickness (Table 4.1) are species-dependent. Vessels (pulmonary artery and veins, bronchial artery, and lymph vessels) and nerves enter the lungs with the bronchi at the hilus; the tracheobronchial lymph nodes are also found in this area (Dixon et al., 1999; Herbert et al., 2015a, 2015b).

### 2.5.1. Respiratory Bronchioles

Bronchioles that have a few alveolar outpockets arising from their walls are defined as respiratory bronchioles. These poorly alveolarized bronchioles are the transitional airways between the conducting (nonrespiratory) bronchioles and alveolarized ducts that are completely lined by alveolar outpockets. As previously mentioned, several generations of respiratory bronchioles are present in the lungs of humans, dogs, cats, and monkeys. In the lungs of mice, rats, guinea pigs, and rabbits, respiratory bronchioles are absent or only a short, single generation. In these small laboratory animals, there is an abrupt transition from the nonrespiratory terminal bronchial to the alveolar duct (Figure 4.8). The luminal surface of the nonalveolarized portion of respiratory bronchioles is lined by ciliated cells and club cells, but normally lacks mucous cells and basal cells. The cellular and acellular structures of the alveolarized outpocketing of the respiratory bronchiole resemble those of alveolar ducts and alveoli that are described below.

### 2.5.2. Alveolar Parenchyma of the Lung

The basic unit of ventilation in the mammalian lung consists of alveoli and alveolar ducts distal to the transition from one bronchiole to an alveolar duct system. Alveoli and alveolar ducts of these “ventilator units” occur in a highly interconnected pattern which forms distinct subdivisions of the alveolar parenchyma that do not overlap. The ventilator unit is functionally important because it is the smallest common denominator in determining the distribution of inspired air to the gas-exchange surfaces of the lung. Though there are distinctive species-related differences in the branching patterns of the small airways and in the presence or absence

of respiratory bronchioles, all mammalian species have the interconnected terminal bronchiole to alveolar duct junctions that serve as the portals of entry for distinct ventilator units where gas-exchange occurs.

The “pulmonary acinus” consists of all the gas-exchange structures distal to a single terminal bronchiole, which is composed of two or more ventilator units. The human lung contains 30,000–40,000 terminal bronchioles and therefore, by definition, an equal number of pulmonary acini. The average number of alveoli per acinus is relatively constant among mammalian species. The ventilator unit size and the size of an individual alveolus are directly proportional to the size of the animal species (e.g., human alveolus > mouse alveolus). For example, human lungs have approximately 50-fold greater numbers of acini, a 17-fold greater acinar volume, and a sevenfold greater acinar diameter compared to acini in the lungs of mice.

The pulmonary parenchyma (gas-exchange region of the lung) comprises 90% of the total volume of the mammalian lung. The most prominent structures in the lung parenchyma are the alveolar ducts and alveoli. Alveolar ducts arise from the most distal (terminal) bronchiolar airways, that is, respiratory or nonrespiratory bronchioles, depending on the species. The walls of alveolar ducts are composed of a linearized arrangement of alveoli (Figure 4.8). The proximal alveolar duct branches into secondary alveolar ducts, each of which ends in a blind outpouching composed of two or more small clusters of alveoli called alveolar sacs.

The alveoli are the primary functional and structural units of the lung parenchyma where a very thin tissue barrier separates the surface of the airspace from the luminal surface of capillaries (Figure 4.10). There are approximately 500 million alveoli in the human lung, with a total surface area of 100 square meters. The ratio of capillary surface area to the surface area of the alveolar air space is close to 1. The mean distance between the surface of the alveolar air space and blood surface of the capillaries in the alveolar septal wall is only 0.4  $\mu\text{m}$  in the

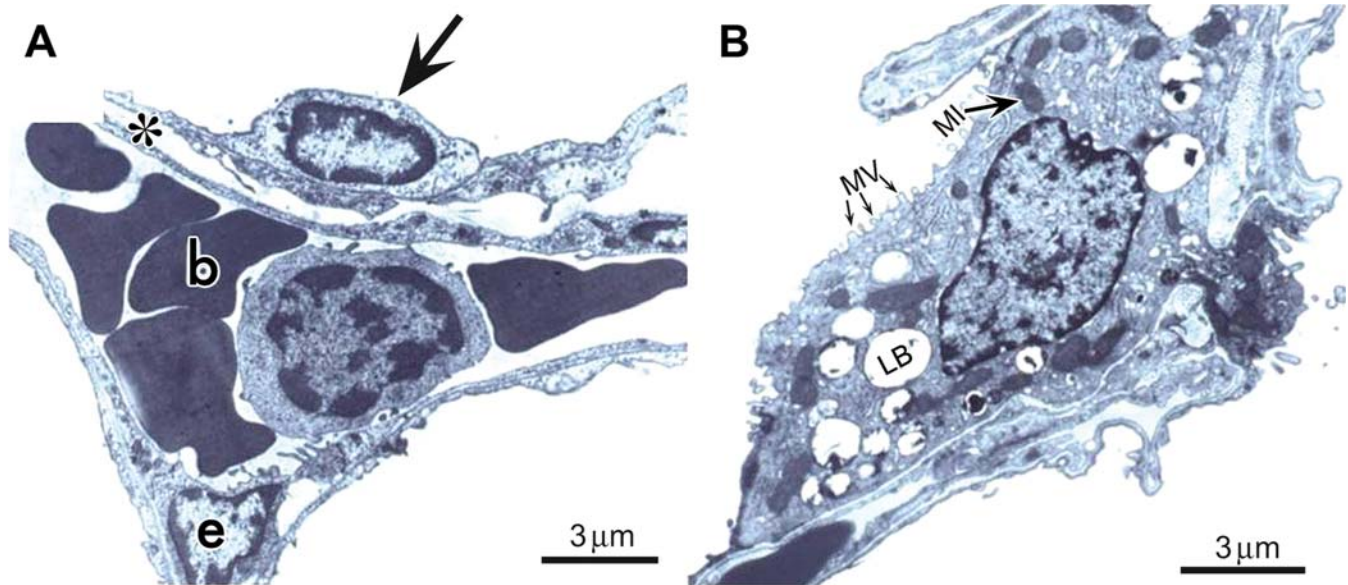


**FIGURE 4.10** Transmission electron photomicrographs of the alveolar septum. Alveolar airspaces are lined by type 1 and 2 epithelial cells (A and B, respectively). b, red blood cells in the alveolar capillary; e, endothelial cell lining the capillary lumen; mv, microvilli on apical surface of the type 2 cell; LB, cytoplasmic lamellar bodies in type 2 cell. Reproduced from Cohen M, Zelijoff J, Schlesinger R, editors: *Pulmonary immunotoxicology*, 2001, Springer, with permission.

rat and  $0.6\ \mu\text{m}$  in the human. This extremely thin air–blood barrier in mammalian lungs allows for efficient gas transfer between the inspired air and the circulating blood.

The interconnected capillaries within the alveolar wall form a single vascular bed that is separated from the alveolar air space by a thin structural barrier of epithelial, interstitial, and endothelial tissues. The integrity of the alveolar septa is maintained by interstitial connective tissues composed of collagen and elastin fibers that interweave around the capillaries, forming what are called “thick” and “thin” regions within the wall. The thick regions of the septa contain the extracellular matrix (ECM) of collagen and elastin fibers intermixed with interstitial cells (e.g., fibroblasts, myofibroblasts), all of which lie between the epithelial lining of the alveolar air space and the endothelial lining of the capillary lumen. The thin portions of the septa represent the air–blood barrier and are formed by epithelial and endothelial single cell layers that are separated only by a thin single basement membrane.

### 2.5.3. Epithelial Cells of the Alveolus

Alveoli arise from the respiratory bronchioles and the alveolar ducts. The alveolar septum or wall consists of three components: epithelium (which lines the alveolus or air space), interstitium, and capillary endothelium. Gas exchange occurs in the alveoli across the thin epithelial lining and adjacent endothelium (air–blood barrier).

The major alveolar cell types are the epithelial type I and type II cells, the pulmonary endothelial cells, interstitial cells, and macrophages. Type I cells constitute 8%–11% of all cells found in the alveolar region, and type II epithelial cells constitute 13%–16%. Tight junctions are present between epithelial cells. Epithelial cells lie on a continuous basement membrane, as do endothelial cells. In many places, the basement membrane of both cell types is fused, forming an extremely thin air–blood barrier. In other areas, the cells are separated by interstitium that consists of scant connective and elastic tissue and resident interstitial cells, macrophages, lymphocytes, plasma cells, and mast cells.



There are only two types of alveolar epithelial cells: type I and type II cells or pneumocytes (Figure 4.10). Type I cells are large, flat (less than  $0.2\ \mu\text{m}$  thick) simple squamous cells with a central ovoid nucleus. These epithelial cells function primarily as a gas-permeable membrane that lines approximately 95% of the alveolar air space. Alveolar type I epithelial cells are attenuated, highly differentiated cells that do not divide; they cover approximately 90%–95% of the alveolar surface. Since these cells have a large surface area, they are highly susceptible to injury. The main function of the type I cell is the maintenance of a barrier to prevent leakage of fluid and proteins across the alveolar wall into the air spaces, while allowing gases to cross the air–blood barrier freely.

Alveolar type II epithelial cells are cuboidal in shape, located in corners or niches between capillaries, and contain lamellar bodies in which surfactant is stored. The functions of type II cells include the synthesis, storage, and secretion of pulmonary surface-active material; the reepithelialization of the alveolar wall after lung injury; and transepithelial solute transport to limit the volume of and perhaps regulate the composition of alveolar fluid. To regenerate lost epithelial cells, alveolar type II cells can serve as progenitor cells and proliferate to create new alveolar type II cells that then differentiate into alveolar type I cells (Aspal and Zemans, 2020).

Capillaries, lined by endothelial cells (30%–42% of all cells), are of the closed type without openings or fenestrations. Intercellular junctions between endothelial cells are characterized by *zonulae occludens* but are less tight than the epithelial junctions. Therefore, unlike other tissues, the major permeability barrier in the lung is the alveolar epithelium.

Macrophages have been identified in three distinct locations in the lung: the interstitium, alveoli, and capillary lumen. Macrophages present in the alveolar interstitium are derived from bone marrow, can divide, and can either phagocytize particulate material that crosses the alveolar walls or move into the alveolar compartment to become alveolar macrophages. Another macrophage-like cell in the interstitium

is the dendritic cell, which is specialized for antigen presentation and accessory function.

AMs are derived from the interstitial compartment; however, they do divide and are a self-renewing population of cells. The intravascular macrophage (IVM) is present in humans, nonhuman primates, pigs, cats, horses, ruminants, and marine mammals, but not in rodents or dogs. It is a fixed macrophage of the capillary bed, has specialized junctional complexes with adjacent endothelial cells, and is morphologically and, presumably, functionally similar to hepatic Kupffer cells. IVMs function similarly to AMs. IVMs account for some of the species differences that occur in response to pulmonary injury.

Fibroblasts are the major cell type present in the interstitium. Apart from maintaining the structural integrity of the lung and production of collagen and other matrix components, such as fibronectin, fibroblasts produce a variety of enzymes, including collagenase, and other factors, such as prostaglandins and plasminogen activator that may modulate the function of other cell types. Fibroblasts play a major role in disease processes that result in fibrosis.

#### **2.5.4. Pulmonary Blood Vessels, Lymphatics, and Nerves**

Blood reaches the lungs through two separate systems, the pulmonary vessels and the bronchial vessels. The pulmonary arterial system differs from other organs in that it is derived from the low-pressure pulmonary arteries, supplying blood for gas exchange in the pulmonary capillaries. It carries high volumes of venous blood from the right heart, and supplies the distal portion of the respiratory bronchioles, the alveolar ducts, alveoli, and pleura. The bronchial system is a high-pressure arterial system derived from the aorta that carries oxygenated blood to meet the metabolic needs of the larger airways, visceral pleura, and large pulmonary vessels.

The pulmonary arteries differ morphologically from the smaller muscular bronchial arteries. However, because of the reduced pressure, pulmonary arteries and veins may resemble each other fairly closely, especially in large

animals. The muscular layer of the pulmonary arteries and veins varies with species (Table 4.1). In rodents, pulmonary veins extending from the left atrium into the lung tissue have an adventitial coating of cardiomyocytes.

Lymphatics are confined to the extraalveolar interstitium, that is, peribronchial, interlobular, and pleural interstitium. Lymph flows centripetally through a subpleural network that is joined by perivascular and peribronchial lymphatics at the hilus. Afferent lymphatic vessels from the lungs drain into the lymph nodes, and then into the thoracic, right, and left lymphatic ducts, and the bloodstream.

The sympathetic and parasympathetic divisions of the autonomic nervous system provide motor (efferent) innervation to the lungs, including bronchial smooth muscle, blood vessels, submucosal glands, and lymphatics. Sensory (afferent) innervation is maintained by way of several types of chemo- and mechanoreceptors that respond to inhaled irritants and other stresses.

### 3. TESTING FOR TOXICITY

Evaluation of pulmonary function, imaging techniques, cytology of lavage fluid or sputum, and morphologic examination of respiratory tissues (biopsy) are common tests conducted in a clinical setting. Experimentally, respiratory toxicity can be evaluated *in vivo*, *in vitro*, or in combined *in vivo-in vitro* systems (Mohr et al., 1996). An understanding of the strengths and weaknesses of the various systems or models is critical to this selection. Consideration for whole animal studies includes selection of the appropriate routes of xenobiotic exposure, species differences in xenobiotic metabolism or respiratory tract anatomy, and cell susceptibility to toxic injury.

There are many ways in which injury and the response to injury can be characterized and quantified. A combination of morphology, physiology, biochemistry, and molecular biology is often the most useful way to evaluate toxic lung injury. *In vivo*, acute and chronic

respiratory damage can be evaluated by noninvasive and nondestructive respiratory function tests; by morphological methods such as histology, quantitative morphometry, cell kinetics, and immunohistochemistry (IHC); and by biochemical techniques such as analysis of bronchoalveolar lavage (BAL) fluid and lung collagen content (Henderson, 2005). Similar biochemical and morphological evaluations can be performed in some *in vitro* systems. Qualitative observations are useful for the characterization of the type and severity of response, while quantitative data allow statistical analyses and descriptive modeling that can be used to extrapolate results across studies and species.

#### 3.1. Methods of Testing

##### 3.1.1. Whole Animal Exposure

Replication and study of lung damage caused by bloodborne agents in appropriate animal models usually does not present technical difficulties, except where there are marked species differences in metabolism. Duplicating human inhalation exposure to xenobiotics is more challenging, and requires special techniques and equipment. Furthermore, most small rodents are obligatory nose-breathers, and many aerosolized noxious agents are deposited and filtered in the upper respiratory passages. When exposed to irritants, rodents may reduce minute ventilation or simply bury their nose in their fur, if exposed in whole-body chambers, thus decreasing the inhaled dose. Despite these potential complications regarding regional deposition and dosimetry, inhalation studies are usually the best means to study responses to materials that people may inhale intentionally or unintentionally, especially when exposures are repeated.

As a general rule across all mammals including humans, air velocity slows and airflow's directional change becomes less abrupt deeper in the respiratory tract. Particle characteristics (e.g., mass median aerodynamic diameter [MMAD], shape, density, electrical charge, hygroscopicity) and formulation characteristics (pH, tonicity, viscosity, solubility, and the physical/chemical characteristics of the drug and

any added excipients); as well as physiologic properties of the animal or patient including regional anatomy, breathing mode (nasal breathers vs. oronasal breathers), local metabolism usually by respiratory or olfactory epithelium in the nose and club cells in the lung, and biological variability all contribute to the disposition of a xenobiotic in the respiratory tract (Tepper et al., 2016). Usually, the alveoli are the optimal region for absorption, but they can be challenging to reach because of airway branching.

### 3.1.2. Inhalation Exposure

The lung is the only tissue receiving 100% of the cardiac output. Delivery via inhalation has a potential for rapid onset of action, increased potency, and longer duration of action, which may be highly desirable for therapeutic areas requiring instantaneous efficacy (e.g., asthma; epilepsy; even anxiety). Pulmonary delivery may also be a viable alternative for compounds that are poorly bioavailable via the oral route since pulmonary delivery avoids intestinal and hepatic metabolism. Because it is injection-free, pulmonary delivery is more amenable to self-administration with improved patient compliance compared to injectable therapies.

Although inhalation is often the most appropriate way to expose experimental animals to airborne toxicants, it is also technically the most demanding. Generation of gases and aerosols, measuring exposure concentrations and particle sizes or numbers, maintaining adequate chamber concentration and homogeneity of the exposure materials, and avoiding accumulation of ammonia, carbon dioxide, and heat requires investments in equipment and trained personnel.

Inhalation studies may be conducted in a static mode, where the test article is introduced into an inhalation chamber only once, at the beginning of the experiment. Though not common, the static mode is used when the amount of test article available is extremely limited.

Various losses (due to device inefficiency; inhaled volume fraction; impaction, sedimentation, or diffusion; bioavailability; reaching target tissue) occur from the time a drug is added to

a device until it deposits in the lung or enters the systemic circulation (Tepper et al., 2016). Most inhalation studies are conducted in a dynamic mode. In a dynamic system, the test article is mixed with the air that flows through the inhalation chamber and a constant concentration of the agent within the chamber is maintained throughout the experiment. Exposure to test article may occur via whole-body chambers, nose-only chambers (rodents), or by using oral-nasal facemasks or helmets (dogs and primates). These methods most closely mimic the way humans are exposed to inhaled materials (Pauluhn, 2005).

In an inhalation toxicology study, the delivered and deposited dose are those typically of interest (Tepper et al., 2016). The delivered dose is also sometimes reported as the inhaled, presented, or nominal dose. Dose estimation is an important consideration for extrapolation of findings from experimental animals to humans and for setting the maximum allowable dose for clinical trials of inhaled drugs. Pulmonary deposited dose is calculated:

$$\text{Dose (mg / kg / day)} = (C \times T \times \text{RMV} \times \text{FD}) / \text{BW},$$

where:

C = drug concentration (mg/L),

T = duration of exposure (min/day),

RMV = respiratory minute volume (L/minute),

DF = pulmonary deposition factor, and

BW = body weight (kg).

Substitution of lung weight (g) for body weight gives the dose in mg/g lung. C, T, and BW are directly measured, RMV can be observed but is usually estimated (Alexander et al., 2008), and DF is estimated based on particle size. For safety studies of drug candidates, particles should have an MMAD of 1–4  $\mu\text{m}$  to allow for pulmonary deposition.

Deposition occurs through three mechanisms: inertial impaction, sedimentation, and diffusion based on particle size, although other properties (e.g., particle shape and electrostatic charge) also influence these mechanics. Drugs can be bio-engineered to target specific regions of the lung



with greater accuracy. Particles with MMADs between 1 and 5  $\mu\text{m}$  tend to deposit by sedimentation in this region of the lung due to lower flow velocities therein (Hall et al., 2021).

Regulatory authorities, such as the U.S. Food and Drug Administration, generally take a conservative approach and consider the pulmonary deposition fraction, that is, the nominal inhaled dose deposited in the lung, for particles less than 5  $\mu\text{m}$  to be 0.1 (10%) for rodents, 0.25 (25%) for dogs and nonhuman primates, and 1 (100%) for humans. The maximum allowable dose in a clinical trial conducted in the US is typically based on the estimated pulmonary deposited dose at the No Adverse Effect Level in the most sensitive species, using these estimated deposition fractions and additional safety margins of 10 for rodents, six for dogs, and five for nonhuman primates. The assumption of a 100% deposition in humans plus an additional safety margin may limit the ability to dose-escalate in the clinic to efficacious levels and highlights the importance of differentiating adverse from nonadverse findings in nonclinical species.

In the clinic, drug delivery to the lung from aerosol inhalers can be quantified by planar gamma scintigraphy (Newman, 1993). Other methods for estimating clinical drug delivery to evaluate bioequivalence of products or to compare inhalation devices include pharmacokinetic studies, pharmacodynamic safety and efficacy studies, and in vitro particle size determination. The fine particle dose (FPD) is the dose of particles less than 5  $\mu\text{m}$  MMAD. This value is derived from measurements of the emitted dose from the proposed human device (e.g., a nebulizer or dry powder inhaler), and multiplying that dose by a fine particle fraction (FPF), which is measured using impingers or cascade impactors. FPD has been proposed by some toxicologists as an alternative to using a 100% deposition fraction for estimating human dose, although it consistently overestimates human deposited lung dose (Newman, 1998), perhaps providing a safety margin in calculations.

### 3.1.3. Instillation and Aspiration Exposures

Intratracheal instillation and pharyngeal aspiration are acceptable alternate routes of exposure in some cases. The major disadvantages are that

the test article, delivered at a high dose rate, becomes unevenly distributed, and animals must be individually and repeatedly treated. The dose rate to the lung is several orders of magnitude greater than that achieved in experimental, occupational, or environmental inhalation exposures, which greatly confounds interpretation of lung responses. Intratracheal spray devices may distribute the test article more evenly than intratracheal instillation, but these devices do not overcome the other disadvantages of instillation. Aspiration of test material droplets placed on the nares of rodents and use of nasal sprays in dogs are standard methods for studying nasal effects of pharmaceutical agents intended for delivery by nasal spray.

IN drug delivery is increasing in human medicine for treatment of local conditions (e.g., antihistamines for asthma), and also for central nervous system and systemic conditions. Delivery to extranasal locations is believed to be dependent on both uptake through the nasal vasculature, and also through penetration across the olfactory epithelium to access the brain. The latter process may occur via transporters expressed on the olfactory epithelium, between cells of the OE (paracellular transport), and/or by direct transport from the nasal cavity to the brain along mature olfactory neurons. Various devices and formulations have been and are being developed to improve delivery of IN drug formulations (Keller et al., 2021).

IN-administered drugs to treat nervous system disorders include ketamine and esketamine as treatments for depression; dihydroergotamine mesylate for treatment of migraines; Narcan nasal (naloxone HCl) as a treatment for presumed or actual opioid overdoses; various drugs, such as perillyl alcohol, and drug combinations, for the treatment of refractory glioblastoma multiforme brain tumors; and insulin for the treatment of patients with Alzheimer's disease (Faria et al., 2020).

IN-administered drugs are similarly showing effectiveness for systemic delivery of drugs for various nonnervous system disorders. These include aqueous 17- $\beta$ -estradiol for menopausal symptoms; nasal sprays containing salmon calcitonin to treat osteoporosis; desmopressin as an antidiuretic hormone to treat diabetes insipidus and enuresis, as well as mild hemophilia A and von Willebrand's disease (type I); and

gonadotropin-releasing hormone analogs such as buserelin and nafarelin to reduce the testosterone and estrogen levels in patients being treated for prostate cancer and endometriosis (Lethagen et al., 1990).

Development of IN vaccines was rationalized because of the abundant nasal lymphoid tissues present in humans. Among these, a live attenuated influenza vaccine (LAIV), nasal flu vaccine (Brand name: FluMist Quadrivalent) is approved for persons aged 2–49 years of age. In response to the unprecedented need for vaccines to combat the COVID-19 pandemic, various groups are working to develop IN vaccines, which, while promising, have not been approved in the United States for use as of the writing of this work. Similarly, beneficial effects have been reported in mice administered an IN vaccine targeting amyloid plaques as a possible treatment for Alzheimer's disease.

### **3.1.4. Isolated Perfused Lung**

Uses of the isolated perfused lung include study of the metabolic fate of foreign chemicals processed by the lung, characterization of effects on lung function, characterization of the interactions between lung toxicants and circulating inflammatory cells, and evaluation of the distribution and extent of toxicant-induced cellular perturbations. Lungs from such diverse species as rabbits, rats, mice, and guinea pigs can be used. The toxicant under study can be administered by either the circulatory or the ventilatory route.

Major advantages of this system over other *in vitro* systems include the minimal amount of damage caused during preparation, and the maintenance of structural and functional integrity of the lung. Disadvantages include the comparatively short viability of the preparation (about 5 hours) and the complexity of the methodology. It is not well suited for examining the effects of toxic agents upon lung structure and function.

### **3.1.5. Tissue Sections and Organ Cultures**

Whole lung tissue slices, airway rings, isolated or microdissected airways, and arterial rings or strips have all been used to maintain a degree of structural or organizational integrity of targeted respiratory components. Maintenance of

normal cellular relationships is the major advantage of organ or explant culture over isolated cell culture systems. Short-term viability of the tissue sections and technical issues related to tissue maintenance, including the loss of normal means of cell nutrition, gaseous diffusion, and waste excretion, have limited the usefulness of organ cultures, particularly those derived from adult animals. Despite these issues, these systems have been used to study metabolic activity and biochemical response to toxicants. Embryonic and fetal lung organ cultures have been used extensively in the study of embryonic and fetal development of the lung, and effects of toxicants on gene expression and airway branching morphogenesis.

### **3.1.6. Isolated Cells and Cell Culture Systems**

Isolated cells provide a powerful approach to the understanding of the biology of individual cell types. Cultures of individual cell types, including type I and II cells, various airway epithelial cells, fibroblasts, endothelial cells, and macrophages, have been used to determine cell composition, biochemical activity, control mechanisms, and responses to toxicants. These cells may be cultured in isolation or as cocultures. Epithelial cells require maintenance at the air-medium interface to preserve polarity and differentiation. Numerous commercially available cell lines provide alternatives to harvesting and primary culture.

### **3.1.7. Pulmonary Function**

Pulmonary function tests, which are easy to use and noninvasive, are applied in epidemiological studies of air pollution effects, in some workplace exposure monitoring programs, and in clinical studies of inhaled pharmaceutical agents. Vital capacity, functional reserve volume, tidal volume, airway resistance, maximum flow, and forced expiratory volume are readily measured in humans. Physiological measurements provide useful information in intact animals regarding adverse health effects, especially in relation to ventilatory function or gas exchange (Labiris and Dolovich, 2003). In humans and laboratory animals, these tests are advantageous because they are noninvasive, may not interfere with other toxicologic tests,

and can be repeated on the same subject. Many of the same parameters are measured in humans and animals, which aids cross-species comparisons and extrapolations. Murine models of airway disease have limitations that should be considered when extrapolating findings from the animal model to the human disease (Glaab and Braun, 2021). The disadvantage is that handling, stress, and other factors may affect the results. Therefore, sham-treated or sham-exposed animals should be included in the test groups. In small laboratory animals, some of these tests are performed in anesthetized animals, as terminal procedures, or using excised lungs. Pulmonary function tests assess the mechanical characteristics of ventilation in relation to pressures, airflow, and air volume within the lung; the presence and magnitude of functional impairment can be determined. In nonclinical species, respiratory frequency and tidal volume are used to differentiate upper respiratory tract irritation (slow, deep breathing) from pulmonary irritation (rapid, shallow breathing). Compliance, assessed by volume–pressure curves, provides an alternative means of assessing structural changes that affect function. In addition, pulmonary function tests may detect functional changes in cases where there is no alteration in structure, for instance, in bronchoconstriction.

### 3.1.8. Bronchoalveolar Lavage

BAL can be used to evaluate toxicant-induced alterations in pulmonary epithelial integrity, cell damage, inflammatory infiltrates and cytokines, and surface release of cellular secretory products. It is also a convenient way to recover macrophages and other cells for *in vitro* studies. If the animal is large enough, BAL can be performed in the living animal, either as a single test or sequentially to monitor changes. In smaller animals, such as the rat and mouse, BAL is usually performed in the lung *in situ* or following excision after euthanasia.

The aspirated fluid can be analyzed for its cellular profile, protein content, enzymes, cytokines and chemokines, and lipids. Increased activity of marker enzymes such as lactate dehydrogenase, alkaline or acid phosphatase, and/or angiotensin-converting enzyme can be indicators of cell damage, and increased serum albumin is

indicative of pulmonary edema. Similar changes are not detectable in the serum, unless there is a significant inflammatory process within the lung tissue, in which case there may be a systemic leukocytosis and increases in serum chemistry biomarkers such as C-reactive protein and fibrinogen. BAL can also be used to monitor subcellular changes in cells recovered from BAL fluid (Maygarden *et al.*, 2001), as is the case with foamy macrophages containing lamellar bodies, indicating drug-induced phospholipidosis.

The advantages of BAL include the relative simplicity of the procedure, the rapidity with which results can be obtained, the ability to sample the whole or large portions of the lungs, and, in larger animals, the ability to perform sequential evaluations. In general, constituents of BAL fluid correlate well with morphological changes. However, at times, increases in BAL components are seen at exposure levels that do not induce histopathological changes and the thresholds at which increases in various BAL components become toxicologically meaningful have not been established. Disadvantages include that BAL is a terminal procedure in smaller experimental animals and that only the surface of the alveoli and airways are sampled. The BAL sampling process can also produce artifacts on histological sections if the entire lung is lavaged, such as alveolar flooding by proteinaceous fluid that resembles edema (Poitout-Belissent *et al.*, 2021). Additionally, the collection and analysis of BAL can present hurdles when using infectious agents (e.g., SARS-CoV-2) that require BSL3 or BSL4 barrier facilities. Lavage of the nasal cavity may be useful for the detection of toxicant-induced changes in this region of humans or experimental animals.

### 3.1.9. Biochemical Evaluation

The biochemistry of lung cells, lining fluid, and matrix has been extensively studied with methods ranging from analysis of whole homogenized lung tissue to defined lung cell types *in vitro*. Data can be expressed on a whole-lung or unit-weight basis. In most cases, expression per lung or lobe basis is preferred, as lung weight may be altered by components other than those being examined. Metabolism of foreign chemicals by lung tissue can be examined in isolated perfused lung preparations.



Advantages of biochemical measurements are that they are quantitative and may provide mechanistic information (Hsia et al., 2010). A major disadvantage is the difficulty of localizing or relating specific biochemical events to a defined cell population.

### 3.1.10. Morphological Evaluation

Morphological evaluation of the respiratory tract can be performed by a variety of methods, depending on factors such as the objectives of the study, species used, suspected site or type of injury, other evaluations to be performed, cost, and facilities available. Animals are usually anesthetized and then exsanguinated. Evaluation begins at the macroscopic level and can proceed through to the light microscopic and ultrastructural levels. Each of these assessments is important; for instance, it is easy to miss focal lesions if samples are taken for ultrastructural studies without prior localization of changes. Outline drawings of the respiratory tract may be useful to record the location of lesions. Fixation for histologic and ultrastructural evaluation is discussed below.

## 3.2. Background Findings

Incidental background findings occur frequently in experimental animals, and awareness of these findings is necessary to avoid incorrect association of findings with test article exposure. The International Harmonization of Nomenclature and Diagnostic Criteria (INHAND) publications (available at [toxpath.org](http://toxpath.org)) list many of these findings and provide diagnostic criteria; and several other references are also available (Chamanza, 2012; Colman et al., 2021; Cooper et al., 2022; Helke et al., 2021; McInnes, 2012; Mukaratirwa et al., 2016; Scudamore, 2012; Taylor, 2012; Woicke et al., 2021). Pulmonary vasculitis, thrombosis, and interstitial inflammation may occur in animals of any species exposed by continuous or repeated intravenous infusion. Hair- or skin-fragment emboli and granulomas are frequently found in the lungs of animals that receive intravenous injections.

Background findings are common in the upper respiratory tract and lung of rats and mice and other experimental species and these can be exacerbated by inhalation exposure to test articles. Eosinophilic globules are frequently observed

in the respiratory epithelium, olfactory epithelium, and nasal mucosal glands and ducts of aging rats and mice. This hyaline material, which is immunohistochemically positive for a chitinase like-3 (Chil-3 or aka Ym1), is usually located within nonciliated cells, but also occurs extracellularly, and the amount or extent of eosinophilic globules is increased by exposure to some irritants.

Hyaline material commonly accumulates subepithelially in the nasal septum of mice, whereas corpora amylacea, lymphoid aggregates in the nasal mucosa, and folding of the nasal respiratory epithelium, which may resemble gland formation, can be observed in control rats. Mucous cell hyperplasia/hypertrophy is occasionally seen in the nasal respiratory epithelium of control rats. Globule leukocytes in the laryngeal mucosa are common incidental findings in rats and focal epithelial alteration or low-grade squamous metaplasia may be seen in the laryngeal epithelium at the base of the epiglottis as a spontaneous change in control rats. Foreign bodies, inflammation, and epithelial hyperplasia may be observed in the laryngeal ventral pouch of mice and rats and eosinophilic material may accumulate in the lumens of laryngeal and tracheal glands of control animals in these species. Loss of cilia, sometimes with attenuation of the respiratory epithelium, is occasionally seen at the carina in control rats. In mice, eosinophilic globules may be seen in tracheal and bronchial epithelial cells, whereas eosinophilic inclusions are seen sporadically in club cells in rat bronchioles. Another common finding in rat bronchioles is focal neuroendocrine cell hyperplasia. Within the lung, foci of alveolar hemorrhage occur as an agonal event in mice and rats. Similar foci with pigmented macrophages or with eosinophilic crystals and inflammation are common in rats that have been anesthetized during the study period, and can occur as incidental, spontaneous events.

Eosinophilic crystalline pneumonia (ECP) (Figure 4.11) occurs as an idiopathic change in the mouse lung with an incidence and severity that is influenced by strain and genotype. It is especially common and severe in C57BL/6, 129, and 129S4/SvJae strains. ECP is characterized by coalescing infiltrates of macrophages with eosinophilic foamy to granular cytoplasm, extracellular crystals in alveoli, lymphoplasmacytic cuffing of airways and vasculature, and

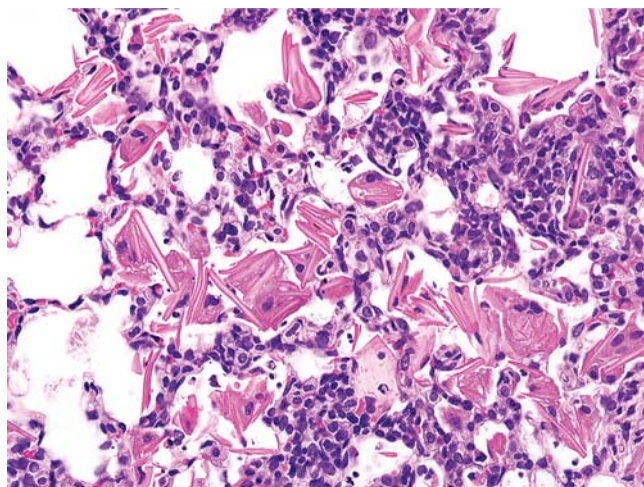


**FIGURE 4.11** Lung from a Nicotinamide dinucleotide phosphate oxidase-deficient ( $p47^{phox-/-}$ ) mouse with eosinophilic crystalline pneumonia. Inflammation is characterized by intraalveolar macrophages that are distended by large amounts of intracytoplasmic eosinophilic crystalline material. H&E stain, 400 $\times$  Photograph courtesy of Dr Jerrold Ward. Reproduced from Haschek WM, Rousseaux CG, Wallig MA, editors: *Handbook of toxicologic pathology*, ed 3, 2013, Academic Press, Vol. 3, Figure 51.8, p. 1960, with permission.

hyperplasia of type II cells and bronchiolar epithelium (Hoenerhoff et al., 2006). One of the most common background findings in the lung of young and old rats and aging mice is multifocal aggregates of vacuolated alveolar macrophages, which was historically called alveolar histiocytosis (Nikula et al., 2014). The macrophage aggregates are typically subpleural, in the peripheral lung, or in alveoli near branch points of bronchioles where alveolar ventilation is reduced. Inflammation, alveolar epithelial hyperplasia, and fibrosis may occur in conjunction with the macrophage aggregates. Eosinophilic or eosinophilic and lymphocytic perivascular infiltrates are another common finding in lung of young and old rats, as is alveolar osseous metaplasia.

Since 2003, the Tg.rasH2 mouse model has been accepted by regulatory agencies worldwide for 26-week short-term carcinogenicity assays as an alternative to the standard 2-year assays in conventional mice (Paranjpe et al., 2013). Since then, the number of short- and long-term studies conducted with alternative mouse models has grown substantially. The incidence of

submucosal inflammation in the nose is high in both male and female mice and almost close to 50% in each sex. This finding is not detected grossly and is mostly observed microscopically at minimal to mild/slight severity. The submucosal glands usually contain inspissated material with necrotic debris and few degenerate neutrophils. The area surrounding these glands may contain mixed inflammatory cells, particularly neutrophils and lymphocytes. Few of the adjacent submucosal glands may contain hypertrophied epithelial cells with eosinophilic inclusions. Occasionally, eosinophilic crystals may be seen in the glands and the mucosal epithelium may be minimally hyperplastic. Not all features, however, are noted simultaneously (Figure 4.12) (Paranjpe et al., 2013).

In control dogs, nasal mucosal infiltrates, particularly mononuclear cell infiltrates, are commonly seen. Minimal inflammation, atrophy, mucous cell hyperplasia/metaplasia, and squamous metaplasia of nasal respiratory epithelium are occasionally seen. In the larynx and trachea, ectasia of submucosal glands and minimal inflammatory cell infiltrates are common. SE is a normal finding in the dorsal trachea near the junction between the membranous and cartilaginous portion of the trachea. Fibrosis/epithelial hyperplasia (formerly called fibrosing alveolitis) is a background finding in the lungs of Beagle dogs used in research and usually located subpleurally and in a wedge-shaped distribution. This finding is characterized by septal fibrosis, alveolar epithelial hyperplasia, and variable amounts of inflammatory cell infiltrates. Focal accumulations of vacuolated macrophages, similar to alveolar histiocytosis in rodents, are commonly observed in dogs. Focal osseous metaplasia also occurs spontaneously in canine pulmonary parenchyma. Granulomas secondary to aspiration of foreign material are commonly noted as well.

Lung lesions in control dogs can be spontaneous or related to dosing procedures or inhalation of vehicle/excipient in inhalation studies. Common lung findings in control dogs in both gavage and inhalation studies include perivascular and/or peribronchiolar mononuclear cell infiltrates, mixed cell infiltrates, and bronchioalveolar mixed cell inflammation. Centriacinar mixed cell infiltrate is more common in inhalation studies and may be associated with an

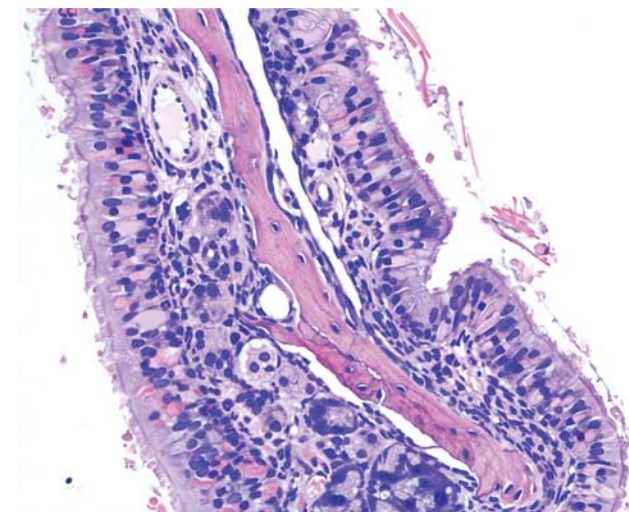


**FIGURE 4.12** Nasal turbinate from a Tg.rasH2 mouse, submucosal inflammation. There is a 50% background incidence of low grade (minimal to mild/slight) submucosal inflammation in those nose/nasal turbinates of male and female Tg.rasH2 mice. The finding is not detected grossly and is characterized by ectatic submucosal glands with inspissated material, hyperplastic epithelium, eosinophilic droplet inclusions within hypertrophic respiratory epithelium, inflammatory cells within the submucosa, and/or eosinophilic crystals within meatuses. Not all features may be noted simultaneously. H&E stain, 200 $\times$ .

irritant effect of vehicle, whereas bronchiolar mixed cell inflammation is more common in gavage studies, potentially due to gavage-related reflux or gavage error. Foci of fibrosis or epithelial hyperplasia may be present concomitant with inflammation or may persist after inflammatory cell infiltrates have resolved. Granulomatous inflammation or granulomas with foreign bodies are seen in control dogs from both oral gavage and inhalation studies (Mukaratirwa et al., 2016; Woicke et al., 2021).

In dogs, aspiration bronchopneumonia to varying degrees often presents as a locally extensive usually anteroventral pneumonia, with a propensity for the right middle lobe (Dear, 2020). Foreign material derived from gastric contents may not be visible in lung sections despite microscopically extensive lung damage. Improper administration of material intended for gavage may result in a similar bronchopneumonia in any species, although the lobe(s)

involved will vary by the site of improper administration. The type of tissue response depends on the nature and amount of the material aspirated.

In control nonhuman primates, nasal mucosal infiltrates, foci of inflammation, or foci of erosion, degeneration/regeneration, or atrophy may occur, and foci of mucous cell or squamous cell hyperplasia/metaplasia are occasionally observed. Common lung findings in nonhuman primates include anthracosis; pleural adhesions and focal subacute or chronic pleuritis; perivascular and peribronchiolar lymphoplasmacytic infiltrates; focal increases in alveolar macrophages; foci of fibrosis and/or interstitial inflammation; and minimal to slight/mild chronic interstitial pneumonia. Interstitial inflammation is typically located in the subpleural parenchyma, and consists of increased numbers of alveolar macrophages, septal fibrosis, and hyperplasia of the bronchiolar and alveolar epithelium. Focal granulomatous pneumonia or granulomas due to inhalation or aspiration of foreign material, often food or plant material, is sometimes noted. Less common background lesions include vascular or perivascular inflammation, thrombi, and arteriosclerosis (Colman et al., 2021) (see *Cardiovascular System*, Vol 5, Chap 1).

Aspiration of small amounts of material, such as from the tip of a gavage tube or secondary to reflux, may result in centriacinar accumulations of vacuolated macrophages and variable concomitant inflammatory or hyperplastic findings in any laboratory species (Figure 4.13). Reflux of gavage dosing material and stomach contents with retrograde aspiration has been reported to cause nasal lesions in rodents, especially rats and rasH2 transgenic mice (Paranjpe et al., 2017; Damsch et al., 2011). The identification of reflux problems after gavage dosing is important, because in some cases, it can be mitigated by reducing gavage volume and/or fasting 4 hours prior to dosing. The occurrence of gavage-related reflux is difficult to prove and therefore often remains speculative if only the lungs are examined. Examination of the nasal cavity is therefore important, as it may provide strong evidence for reflux-related pathology, especially in rodents that die before scheduled euthanasia.



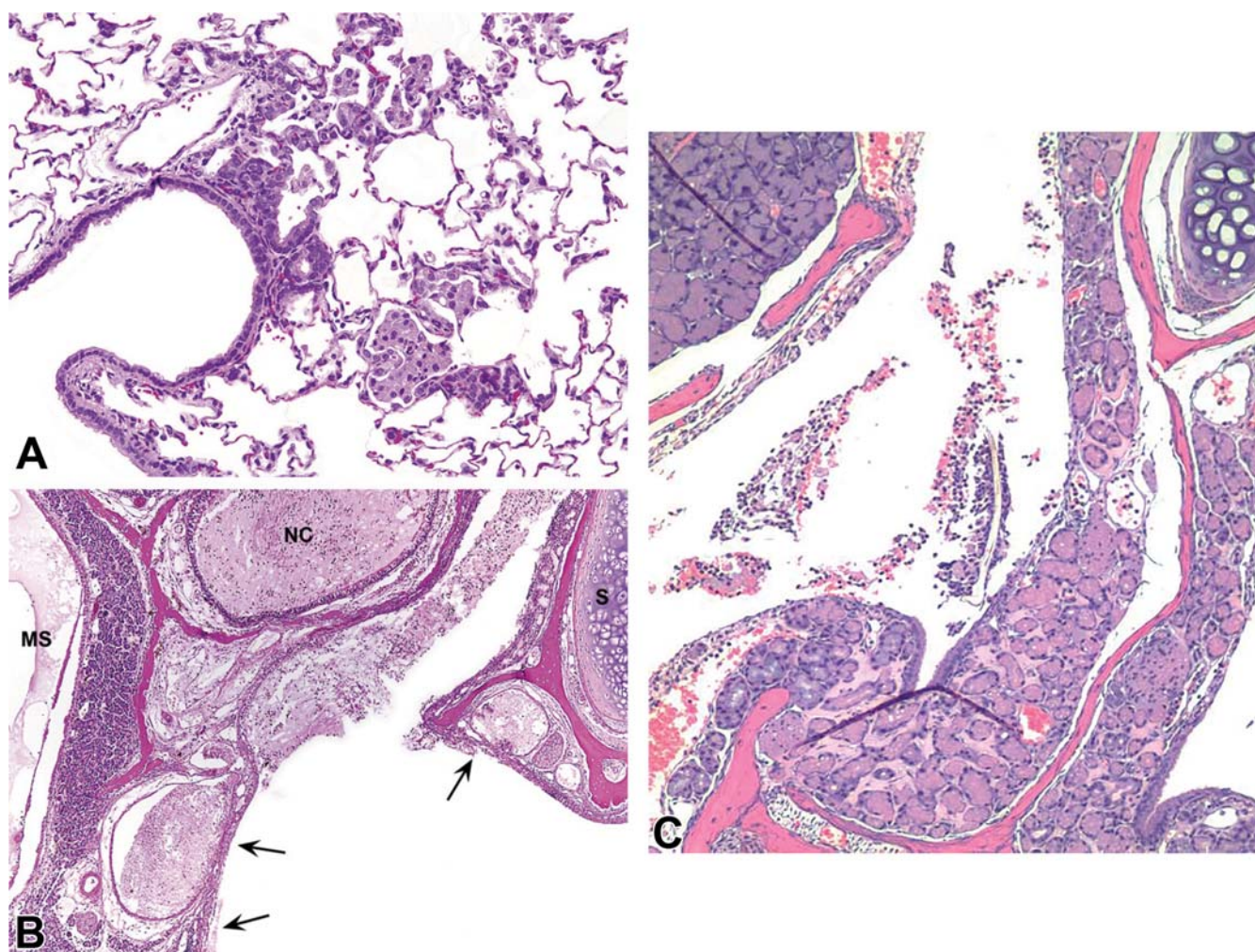


**FIGURE 4.13** (A) lung from a control rat that aspirated vehicle administered by gavage. There is a centriacinar accumulation of vacuolated alveolar macrophages. Lesser numbers of neutrophils, bronchiolar metaplasia of alveolar epithelium, and alveolar epithelial hyperplasia are also present, H&E stain. (B) Nasal cavity from a rat following gastric reflux and nasal aspiration. The epithelium lining the anterior nasopharyngeal duct is necrotic (arrows) as is the epithelium lining the septum (S). There are inflammatory exudates in the nasal cavity (NC) and maxillary sinus (MS). H&E stain. (C) Nasal turbinates, Tg.rasH2 mouse, reflux-induced inflammation with intralesional foreign material. Nasal cavity from a Tg.rasH2 mouse following gastric reflux and nasal aspiration. The epithelium lining the turbinates of the posterior nose is denuded and remaining respiratory epithelium has undergone squamous metaplasia. There are inflammatory exudates and foreign material in the meatus. The Tg.rasH2 mice are generally much smaller than the conventional 2-year mice as well as rats and their small esophageal size may play a role in causing rapid and repeated gastric reflux in gavage studies. Irritant properties such as low pH and/or viscosity of the vehicle or test article exacerbate the severity of microscopic lesions observed in the nose. (A) Courtesy of Dr Torrie Crabbs and the National Toxicology Program. (A) and (B) Reproduced from Haschek WM, Rousseaux CG, Wallig MA, editors: *Handbook of toxicologic pathology*, ed 3, 2013, Academic Press, Vol. 3, Figure 51.9, p. 1961, with permission.

### 3.3. Nasopharyngeal and Laryngeal Regions

In smaller laboratory animals, gross examination of the nose is usually limited to the exterior,

with internal examination performed on histologic sections. Nasopharyngeal structures of small and large laboratory animals are generally

fixed in situ with the rest of the nose and a portion of the skull in 10% buffered formalin solution. Optimal fixation is achieved using retrograde flushing of the nasal cavity with the fixative through the nasopharyngeal orifice. In larger animals, dissection and trimming of the nasal cavity prior to fixation is possible and allows for gross examination of internal structures. If dissection is performed prior to fixation, appropriate sections are fixed by immersion. Decalcification, preferably using the slow formic acid–sodium citrate method, follows. For ultrastructural studies, a glutaraldehyde-formaldehyde fixative is preferred, as is demineralization in 10% ethylenediaminetetraacetic acid in 0.1-M cacodylate buffer.

For light microscopic examination, standard cross-sections from decalcified tissue should be made with a razor. Because of the diverse epithelium and particular distribution within the nasal cavity, it is imperative to examine sections from exactly the same location in both control and treated animals (see [Section 2.2](#) and [Figure 4.2A and B](#)). Mapping of the location, type, and severity of lesions may be useful, especially in rodents, because the nasal passage is very complex, and lesions may occur in small but distinct regions. This method allows identification of the susceptible site and cell type. For larger animals, standardized sections from proximal and distal regions of the nasal cavity, pharynx, and larynx should be selected.

The larynx is also an important target site for inhaled materials. In rodents, the major target site is located on the ventral floor near the base of the epiglottis, cranial to the ventral laryngeal diverticulum (ventral pouch). Epithelial alteration of respiratory epithelium and squamous metaplasia frequently occur along the base of the epiglottis within the anterior (level I) larynx in inhalation studies. Epithelial alteration, a premetaplastic finding, is characterized by focal loss of cilia and epithelial flattening that does not fulfill the criteria of squamous metaplasia. An expert international workshop on laryngeal squamous metaplasia in rodents concluded that epithelial alteration

and minimal squamous metaplasia should be considered nonadverse as dysfunction of the larynx would not be expected ([Kaufmann et al., 2009](#)).

### 3.4. Tracheobronchial Airways and Pulmonary Parenchyma

Macroscopic examination determines the topographic distribution of abnormalities and may guide sample selection. The lungs are examined and palpation may be appropriate in larger species, though care must be taken to not induce artifactual changes that interfere with morphological and ultrastructural examination. The pleural cavity should be examined for the presence of fluid or surface abnormalities of the pleura. Determination of lesion distribution can be useful in differentiating toxicant-induced findings from spontaneous disease, aspiration, or procedural accident.

Lung weight, a useful parameter for initial determination of whether or not the test article causes a pulmonary effect, is determined prior to fixation. Both wet and dry weight information may be useful because lung weight may be increased by edema, inflammation, fibrosis, or neoplasia. If dry lung weights are to be measured, a separate subset of animals or weighing of individual lobes is required.

Buffered formalin is the usual fixative for light microscopy, while formaldehyde-glutaraldehyde fixatives are preferable for combined light and electron microscopic studies ([Renne et al., 2001](#)). The lungs from laboratory animals should generally be fixed by intraairway instillation. Intravascular fixation may be the method of choice for ultrastructural examination of pulmonary vasculature, or in situations when it is critical to immobilize lung lining fluid, intraairspace cells (e.g., inflammatory cells), or particles. Fixation by immersion may be used when lung tissue is no longer aerated, as with severe edema (see [Section 4](#) and [Figure 4.25A](#), below).

Fixation by airway instillation is the best method when lung tissue is still aerated. The

quality of fixation is high, and alveoli are open, allowing detection of subtle lesions. Airway fixation can be done simply with a syringe and blunt needle inserted into the trachea in small animals, or into a selected lobar bronchus in larger animals if only a portion of lung is to be fixed. The fixative is instilled at a relatively constant rate and pressure, until the periphery of the lobes is uncurled and the visceral pleura is smooth. The airway should be ligated after fixative instillation to maintain inflation. This method is highly reproducible and satisfactory for routine light microscopic examination. For morphometric studies, fixation at a constant pressure (20–30 cm of hydrostatic pressure depending on species) is required. The final volume of intratracheally fixed lungs should be measured as a prelude to most stereological studies. Fixed lung volume depends on the fixative, initial flow rates, final pressure, and whether the lungs are fixed in situ or after excision. Lung volume should be measured only after good fixation is achieved. Lung volume can be determined by gravimetric or volumetric measurement of fluid displaced by the immersed lung, or by the Cavalieri principle ([Gundersen et al., 2013](#)). Appropriate sampling is essential in quantitative and stereological studies.

The protocol for sampling lung tissue for microscopic evaluation is of critical importance. Lesions may be focal rather than diffuse, and may affect airways, parenchyma, or both. In addition, the sections examined represent a very small portion of the total lung. Sampling must be standardized for each study. For inhalation studies, the proximal trachea, tracheobronchial bifurcation (carina), and tracheobronchial lymph nodes are examined in addition to the lung. In small animals, for simple qualitative morphological examination in inhalation studies, the lung lobes should be separated at trimming and longitudinal sections trimmed parallel to the axis of the main bronchus of the left and right caudal lung lobes. These sections should include the bronchus and major vessels. Transverse sections are obtained from the remaining lobes. For large animals, multiple samples are required to adequately sample central and peripheral airways, multiple

alveolar regions, and the pleura. In many studies, lung samples are divided for biochemical analyses, gene expression, and morphological examination.

The dissection approach to pulmonary airway morphologic studies provides specimens of precisely defined branching history, generation number, and anatomic position within regions of the lung and within specific segments. This allows studies that compare: (1) different airway generations in the same pathway, (2) bifurcation points and the airway segments between them, (3) terminal airways of differing pathway lengths and numbers of branching, (4) terminal airways of different regions of same lobe, (5) same airway generations in different lobes, and (6) same airway generations from animal to animal and species to species ([Plopper et al., 1983](#)).

Paraffin sections, approximately 5  $\mu\text{m}$  thick, are sufficient for routine hematoxylin & eosin (H&E) histopathology. For greater resolution, 1- $\mu\text{m}$  thick sections impregnated with resin are preferred. A variety of special histological and immunohistochemical staining techniques, and in situ hybridization, are available to evaluate connective tissue components, mucopolysaccharides, specific secretory products or protein markers, enzymes, and inflammatory or immunological mediators. Useful histological stains that are readily available in most laboratories include those used to evaluate collagen (Sirius red or trichrome stains), elastin (Verhoeff-hematoxylin, resorcin-fuchsin, and orcein), reticulin (silver stains), mucosubstances in secretory cells (AB/PAS), and basement membrane (Gomori's methenamine silver, PAS). These stains may be combined with immunohistochemical techniques, such as use of  $\alpha$ -smooth muscle actin and Verhoeff-hematoxylin to evaluate pulmonary arterioles ([Figure 4.14](#)).

Transmission electron microscopy (TEM) is used for ultrastructural examination of lung cells, many morphometric studies, and unequivocal identification of some cell types, such as individual cells in the alveolar wall ([Figures 4.6 and 4.9](#)). Scanning electron microscopy and confocal microscopy are useful for special



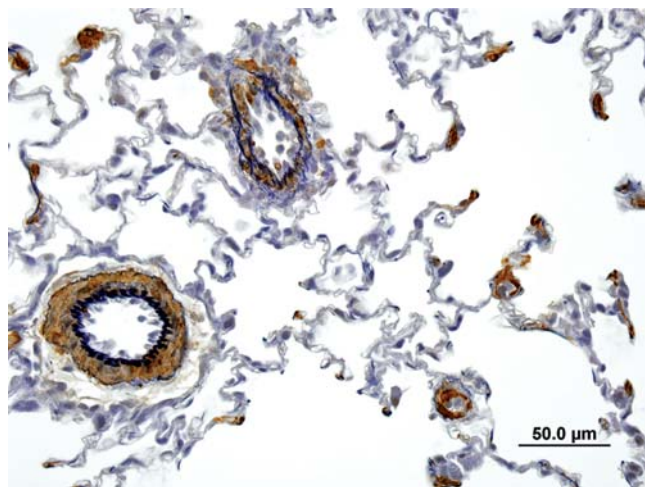


**FIGURE 4.14** Remodeling of pulmonary arterioles in the lung of a rat injected with monocrotaline is illustrated by immunostaining with an antibody to  $\alpha$ -smooth muscle actin and counterstaining with Verhoeff-hematoxylin to demonstrate hypertrophy of arteriolar smooth muscle and reduplication of elastin layers, respectively. Reproduced from Haschek WM, Rousseaux CG, Wallig MA, editors: *Handbook of toxicologic pathology*, ed 3, 2013, Academic Press, Vol. 3, Figure 51.10, p. 1963, with permission.

studies, such as changes in airway surfaces (see [Section 4](#) and [Figure 4.19C–E](#), below) or cell populations, and for three-dimensional (3D) localization of cells labeled with fluorescent markers, respectively.

### 3.5. Animal Models

Models of human disease are developed in laboratory animals to study the mechanisms involved in the initiation and progression of the disease as well as to test potential treatments (see *Animal and Alternative Models in Toxicologic Research*, Vol 1, Part 3). In addition, mouse strains with differing disease phenotypes are used to study the genetic bases of differential responses. To test potential treatments, the choice of disease or mechanistic model is determined by similarity to the pathophysiology of the human disease of interest, expression of the drug target, and ability to translate findings from animals to humans (see *Animal and Alternative Models in Toxicologic Research*, Vol 1, Chap 3).

The choice of animal species for the testing of compounds potentially toxic to the respiratory

tract may be made on the basis of species similarity to humans and the type of response anticipated. However, nonclinical safety assessment inhalation studies are conducted using two species, a rodent and a nonrodent. Similarities across species include the diversity of cell types, cell size of major alveolar cell types, the allometry of lung volume and alveolar surface area to body mass, and thickness of air to blood-tissue barrier. Species differences include nasal cavity morphology, airway branching patterns, airway composition, epithelial cell distribution, club cell composition and metabolic function, transition from airways to alveolar duct; and alveolar number, surface area, and size. Other criteria for species selection include existence of a large or appropriate database, as well as cost and ease of animal handling.

The NHP lung most closely resembles the human lung in structure, physiology, and mucosal immune mechanisms and its use in a variety of research studying inhaled microbes, pollutants, and allergens has been pivotal in defining pathogenesis and discovering treatments ([Miller et al., 2017](#)).

Animal models of lung disease include asthma, chronic obstructive pulmonary disease (COPD), acute lung injury, pulmonary fibrosis, and pulmonary arterial hypertension (PAH). Infectious disease models are also important. Asthma models typically use sensitization and challenge with ovalbumin, *Aspergillus*, or dust mite antigen to study the cells and mediators responsible for development of hyperreactive airways. Mice are often used in these studies, though compared to humans, mice have less airway innervation, thinner airway epithelium and no bronchial mucus glands, and less airway smooth muscle. Therefore, it is not surprising that airway hyperresponsiveness tends to be less severe in mice versus humans.

Animal models of COPD have used cigarette smoke, proteases, cadmium chloride, agents that induce apoptosis, and transgenic animals to induce disease ([Coggins, 2010](#)). COPD induced by cigarette smoke is likely the most relevant model for many studies because cigarette smoke is the main cause of human COPD and exposure of animals to cigarette smoke induces inflammation, mucous metaplasia, airway fibrosis in some species/strains, and

airspace enlargement with alveolar septal destruction in some species/strains. A major disadvantage to cigarette smoke models of COPD is the time required to induce emphysema and the complexity of the exposure systems (Wong, 2007).

Acute lung injury has been induced using endotoxin, bleomycin, hyperoxia, acid aspiration, and intravenous oleic acid. These agents induce injury to type I and type II alveolar epithelial cells and endothelial cells, resulting in pulmonary edema. The amount of inflammation and the subsequent course after acute injury varies according to the provoking agent.

Intratracheal bleomycin administration also induces pulmonary fibrosis. However, unlike idiopathic pulmonary fibrosis (IPF) in humans, the bleomycin model is partially reversible and does not induce progressive fibroproliferation. The inadequacy of the intratracheal bleomycin model of IPF may be explained in part by the reliance of this model on inflammation rather than epithelial-mesenchymal signaling failure and abnormal tissue repair, the basis for the human disease (Mortaz et al., 2012).

PAH animal models examine the mechanism of angioproliferation of plexiform lesions, in which the role of increased pulmonary blood flow is considered as an important trigger in the development of pulmonary vascular remodeling. One of the most promising rodent models of increased pulmonary flow is the unilateral left pneumonectomy combined with a “second hit” of monocrotaline (MCT) or Su5416. MCT is a macrocyclic pyrrolizidine alkaloid that causes pulmonary vascular syndrome in rats characterized by proliferative pulmonary vasculitis, pulmonary hypertension, and *cor pulmonale*. Su5416 is a vascular endothelial growth factor inhibitor. Other PAH rat models, such as chronic hypoxia-induced PAH and MCT lung injury model, do not develop vascular obliteration of the small vessels, neointimal and plexiform lesions, and high pulmonary arterial and right ventricular pressures, therefore insufficiently producing increased pulmonary blood flow and the neointimal pattern of remodeling as described in patients (Katz et al., 2019; Maarmann et al., 2013). In both animal models and in

human disease, p38 MAPK signaling through IL-6 provides a link between vascular remodeling and inflammation. Newly developed animal models have begun to address better recapitulation of PAH manifestations in humans (Carman et al., 2019).

The increasing density of the human population and unlimited capacity for global travel pose a great risk for respiratory pathogens to impose catastrophic disease on a global scale. Such a scenario was realized with the SARS-COV-2 virus, the causal agent for the COVID-19 pandemic. The COVID-19 pandemic has shown that on a global scale, pathogens that target the respiratory system are of particular concern to human health due to the possibility of airborne transmission, leading to rapid dissemination of infection via domestic and international travel (McCormick et al., 2022). This has increased the demand for biomedical research to develop vaccines and novel therapeutics against respiratory pathogens. The development of human vaccines against respiratory infections relies on the use of appropriate animal models (see *Vaccines*, Vol 2, Chap 9). Animal models for vaccine research have different applications, which include:

- a) analysis of route of infection, transmission of disease, and disease pathogenesis;
- b) understanding the host immune responses to natural infection and vaccination characterization;
- c) vaccine safety and assessment of the potential to induce vaccine-associated enhancement of respiratory disease (VAERD);
- d) analysis of the onset and durability of vaccine-induced immunity; and
- e) novel strategies for vaccine delivery and formulation; and novel vaccination concepts.

Thus, an appropriate animal model for vaccine research is one that ideally shares modes of infection and disease progression similar to those in humans, including the induction of the immune response following vaccination, the route of infection of the pathogen, the infective dose, correlates of protection, and disease progression and pathogenesis. Although NHP are often a better model due to the similarities in immune

mechanisms and lung physiology and anatomy to humans, their use is challenging due to financial, supply chain, technical, and ethical considerations. In addition, for some respiratory diseases such as the respiratory syncytial virus (RSV), SARS-Cov-2, or influenza, the laboratory NHP may not be the best model due to their failure to fully recapitulate the clinical disease observed in humans. In fact, some rodent species may result in a more clinically relevant disease. As a result, several rodent and other small animal models of respiratory infections and vaccine efficacy studies such as mice, the cotton rat, hamsters, and ferrets are still used for respiratory diseases that pose global public health problems (Herati and Wherry, 2018; Gerdtz et al., 2015).

The human RSV is a pneumovirus that causes severe lower respiratory tract infections in young children and the elderly. It is the leading respiratory cause of hospitalization and mortality in infants. In May 2023, the Food and Drug Administration announced the approval of the first RSV vaccine approved for use in the United States in individuals 60 years of age and older. The development of safe and effective vaccines against RSV has been a challenging task, mostly due to the lack of animal models that fully recapitulate the pathogenesis of RSV infection in humans. Development of vaccines against RSV is also associated with the assumed or theoretical risk of developing vaccine-associated enhanced respiratory disease (VAERD), since the first report of VAERD in young children, more than 50 years ago, was associated with a formalin-inactivated RSV (FI-RSV) vaccine. In that case, infants that received FI-RSV vaccine during early infancy developed more serious lower-respiratory-tract disease when infected with the virus than did unvaccinated individuals or those who received formalin-inactivated parainfluenza virus vaccine.

Animal models of RSV include those in which human RSV is used to infect other mammalian hosts such as NHP, cotton rats, mice, and lambs; and those in which nonhuman pneumoviruses are studied in their natural host, such as bovine RSV in calves and pneumonia virus of mice (PVM). However, animal models such as laboratory NHPs, cotton rats, mice, and ferrets are only semipermissive for human RSV replication, and

experimental infection with large doses of virus results in mild lung histopathology with little or no clinical signs. Therefore, these models' ability to predict vaccine efficacy is doubtful and several RSV vaccine candidates that were completely protective in rodent models have proven to be poorly effective clinically. In contrast, experimental infection of calves with bovine RSV or mice with PVM result in clinical disease and extensive pulmonary pathology, which means that studies of nonhuman pneumoviruses in their native hosts more likely reflect the pathogenesis of natural human RSV infection. These animal models have been of great value in studies on mechanisms of immunity and the pathogenesis of pneumovirus infections; and evaluation of human RSV vaccine concepts. Mice and cotton rats have provided valuable insight into the pathogenesis and mechanisms of immunity to RSV, and in the development of monoclonal antibody prophylaxis for infants at high risk of severe RSV infection. Apart from vaccine efficacy studies, cotton rats, mice, and NHPs have also been used as models of RSV-induced VAERD (Taylor, 2017).

The standard protocol for testing RSV vaccine efficacy in the cotton rat model illustrates the general procedures and format for the testing of vaccines for respiratory viruses, and the role of the discovery pathologist in vaccine efficacy studies for infectious respiratory disease. In a typical vaccine efficacy study in the cotton rat model, animals are immunized with a candidate vaccine on day 0, boosted three to four weeks later and inoculated intranasally (or intratracheally) with RSV, 3 weeks after boosting. Several doses (dose down) may be used in order to evaluate the potential contribution of antibody-dependent enhancement (ADE) to the severity of RSV disease, since one proposed hypothesis for VAERD is that low avidity antibodies associated with suboptimal doses contribute to respiratory disease enhancement. Necropsy and terminal sampling are performed at the time of maximal viral replication and pulmonary pathology, 4–6 days postinfection (dpi) for this particular virus and model. Endpoints may include viral replication in the lung and nose, lung histopathology; and lung IHC for viral nuclear proteins, quantitative



polymerase chain reaction (qPCR) for virus detection, and/or cytokine gene expression. The pathologist provides lung scores for each individual lung (or lung lobes), animal, and the treatment group. Knowledge of the viral pathogenesis in the animal model and characteristic lesions helps guide the pathologist in preparing a lesion scoring system detecting potential VAERD. For instance, in the cotton rat model, RSV replicates in the ciliated airway epithelium and alveolar pneumocytes, and the disease is characterized by bronchitis and bronchiolitis with intraluminal cellular debris, as well as interstitial pneumonia, peribronchial and perivascular mononuclear infiltrates, and occasional syncytial cells. In this model, a disproportionate increase in alveolitis with increased neutrophils or eosinophils and increased viral load in vaccinated animals (compared to the unvaccinated groups); and/or evidence of a dysregulation of cytokine responses with enhanced expression of Th2-type cytokines, particularly evident within hours of RSV challenge, may represent VAERD ([Boukhvalova et al., 2018](#); [Fuentes et al., 2017](#)).

VAERD refers to any severe lower respiratory tract disease following infection in vaccinated individuals, as a result of nonprotective immune responses against the respective wild-type viruses. Because the enhanced respiratory disease is triggered by failed attempts to control the infecting virus, VAERD typically presents with symptoms in the target organ, in this case the lung. RSV, measles, influenza, MERS, and SARS-Cov-2 may be associated with VAERD. The first case of VAERD occurred after vaccination with an inactivated RSV vaccine. In 1966, a formalin-inactivated vaccine against RSV (FI-RSV) was administered to infants and children in four studies in the United States. When the vaccinated children were exposed to RSV in the community, those children who were seronegative for the virus before vaccination experienced a significant increase in the frequency and severity of RSV-associated pneumonia. This enhanced form of RSV disease presented with severe respiratory disease, characterized by prolonged fever and wheezing, and pathological findings of increased areas of lung consolidation, moderate to severe bronchiointerstitial pneumonia, and necrotizing bronchiolitis, leading to hospitalization and mortality. The resulting

enhancement of the lower respiratory tract infection in vaccinated children was termed enhanced RSV disease (ERD), or VAERD. Since this incident, VAERD has generally been associated with formalin-inactivated vaccines, but the risk of developing VAERD has been extended to all novel vaccines, particularly those against lung disease. Although the mechanisms that result in VAERD remain unknown, the pathogenesis appears to be immune-mediated. Animal models of VAERD have been developed by immunizing animals with FI-RSV and then challenging them with human RSV so that the lung histopathology of unvaccinated challenged animals can be compared. The animal models (cotton rat, mice, rabbits, and NHPs) have shown that enhancement of the pulmonary disease is associated with a T helper 2-like cytokine pattern (IL-4, IL-5, and IL-10), a high ratio of CD4<sup>+</sup> to CD8<sup>+</sup> T cells and other cellular infiltrates, the presence of poorly neutralizing antibodies, immune-complex formation, and/or ADE. In particular, the presence of poorly or nonneutralizing low avidity antibodies (such as those caused by the mismatched challenge strain) capable of activating the complement cascade and cytokine dysregulation has been associated with VAERD in animals ([Ebenig et al., 2022](#)). The presence of poorly neutralizing antibodies in VAERD is also considered to be associated with suboptimal dosing or very low doses of vaccines, hence dose-de-escalation or dose down studies are performed during vaccine development to assess this risk ([Bigay et al., 2022](#)).

In order to recognize VAERD, it is necessary to have a clear understanding of the clinical presentation, pathology, and usual course of the natural disease. Morphologically, VAERD is characterized by a different and more severe pathological presentation in vaccinated animals compared to those in unvaccinated groups. In VAERD models, granulocytic infiltrates, particularly eosinophils, in the alveolar or peribronchial areas have been described. In the VAERD FI-RSV vaccinated cotton rat model, infection was characterized by increased infiltration of neutrophils in the alveoli and peribronchial areas. In the BALB/c mouse model, VAERD was associated with bronchiolar or polymorphonuclear infiltrates characterized by abundant eosinophils, or perivascular lymphocytic infiltrates. In macaques, respiratory disease enhancement was characterized by

peribronchiolar and perivascular accumulations of macrophages, lymphocytes, neutrophils, and eosinophils, as well as alveolitis and interstitial pneumonia (Munoz et al., 2021).

Apart from histopathology, the theoretical risk of VAERD in animal models is assessed by measurement of cytokines associated with a Th1- (interferon gamma) and Th2- (IL-4, IL-5, IL-10 or IL13) type response, viral load, and clinical signs. Vaccine-enhanced pulmonary pathology in cynomolgus macaques vaccinated with FI-RSV and challenged with human RSV was associated with increased lung eosinophils and a Th2 type response (IL-13, IL-5). Therefore, in VAERD models, an increased lung virus load and a Th2 polarization are considered supporting evidence of VAERD, particularly in low dose groups with break through infections. Although VAERD has not been reported clinically following current vaccines against respiratory pathogens, including SARS-Cov-2, there is theoretical concern, especially given the history with other respiratory viruses in general. This potential risk drives study designs and investigations in early vaccine development. For the pathologist, diligent evaluation of the lungs, careful recording, knowledgeable interpretation of cellular infiltrates (particularly eosinophils and neutrophils), and accurate and consistent recording of severity grades is key in identifying this syndrome (Munoz et al., 2021).

Influenza virus infection in humans is primarily an upper respiratory tract disease with systemic symptoms that may lead to pulmonary complications including primary viral pneumonia and secondary bacterial pneumonia. The disease ranges in severity from subclinical to viral pneumonia that may be associated with mortality. Systemic symptoms include fever and chills, headache, myalgia, lethargy, and anorexia, and develop early in the course of illness. Respiratory symptoms include dry cough, pharyngeal pain, and nasal congestion and discharge.

Human influenza viruses are initiated when hemagglutinin (HA) binds to host cell sialic acid (also known as N-acetylneuraminic acid) linked to galactose by either  $\alpha$ -2,3 or  $\alpha$ -2,6 linkages. Human influenza virus strains preferentially bind  $\alpha$ -2,6-linked sialic acid, which predominates in the upper respiratory tract. In contrast, the human lower respiratory tract

epithelium predominantly expresses  $\alpha$ -2,3-linked sialic acid, as do epithelial cells of birds, the natural reservoirs for most influenza viruses. Animal influenza viruses that gain the ability to bind  $\alpha$ -2,6-linked sialic acid can more efficiently transmit from human to human; and animals with respiratory tract sialic acid expression profiles similar to humans are likely to be better models for human influenza (Kumlin et al., 2008).

The most commonly used animal models for human influenza viral research are ferrets and mice, although hamsters, guinea pigs, and cotton rats have also been used. Ferrets are the most ideal influenza model because unlike mice, (1) they are naturally susceptible to human influenza A (including the H1N1 strain) and B viruses without the need for adaptation, (2) they have a similar clinical course of disease to humans and develop symptoms that replicate many of the features of influenza in humans, and (3) they have physical features, including airway morphology and sneeze response, that make them amenable for characterizing important aspects of disease. In addition, ferrets and humans have similar anatomical expression of sialic acid receptors (Zhao and Pu, 2022). Following IN infection with seasonal influenza strains, ferrets develop an upper respiratory tract infection like humans, with the lower respiratory tract decreasingly affected. Clinical observations include fever, sneezing, and a runny nose, and are often used as important endpoints in assessing antiviral therapeutic or vaccine efficacy in preventing influenza disease. Other measured endpoints include virus shedding reduction in the nares, decreased febrile response, inflammatory markers, histopathology, and, in the case of high-pathogenicity avian viruses, improved survival of ferrets inoculated with a lethal dose. The main disadvantages of ferrets, compared to mice, are their size, expense, and husbandry requirements (Kiros et al., 2012).

Mice have been frequently utilized in influenza research and are considered an attractive influenza model due to their availability, relatively low cost, availability of immunologic reagents, and the variety of genetic backgrounds and available targeted defects. However, mice do not particularly replicate the typical disease course of human influenza, and most unadapted

influenza viruses do not replicate in mice. The susceptibility of mice to influenza depends on the strain of influenza and strain of mouse. Influenza that has been adapted to mice through serial passage and other highly pathogenic avian strains can cause disease and replicate in the respiratory tract and extrapulmonary sites of mice. Due to the lack of expression of a critical antiviral functional protein (Mx1), inbred laboratory mice are highly susceptible to adapted influenza strains. In contrast, wild mice are resistant. In particular, DBA/2J and A/J mice are known to be more susceptible to disease, even with viral isolates not adapted to mice. Depending on the strain of virus used, mice may show clinical signs such as lethargy, anorexia, piloerection, neurological symptoms, or mortality. Unlike humans and ferrets, mice become hypothermic, rather than mounting a febrile response. Importantly, influenza in mice typically manifests as a primary viral pneumonia associated with labored breathing, cyanosis, and severe pulmonary histopathology. Apart from lung pathology scores, other endpoints commonly used to evaluate influenza viral pathogenicity in mice are body weight loss and mortality, viral titers, lung weights, oxygen saturation in the blood, and gross motor-activity levels ([Bouvier and Lowen, 2010](#)).

For influenza virus subtypes handled under Biosafety Level 2 (BSL-2) conditions, the standard protocols for both ferrets and mice influenza models largely follow that described for the RSV virus in the cotton rat model. However, for the influenza model, earlier necropsy time points such as 1, 3, and 6 dpi are generally implemented due to the acute nature of the disease. Additionally, the histopathology evaluation and scoring system is usually extended beyond the lungs, to include the nasal cavity, trachea, and/or some other extrapulmonary tissues. Histopathology and severity vary according to the host (species, strain, age), the inoculum, and dose. In most models, variably severe rhinitis is first observed at 3 dpi and peaks in severity at 6 dpi. Rhinitis is characterized by respiratory epithelial necrosis, sloughing, and luminal neutrophilic and necrotic cellular debris. In the lung, viral infection is characterized by necrotizing bronchitis and interstitial pneumonia with edema, hyaline membranes, and fibrin ([Barnard, 2009](#)).

SARS-CoV-2, the causal agent of the COVID-19 pandemic in humans, is a novel enveloped  $\beta$ -coronavirus with high nucleotide identity to SARS-CoV-1 (80%) and to SARS-related coronaviruses that have been detected in horseshoe bats (96.2%). The COVID-19 disease has spread across the world with devastating global effects on healthcare systems and economies. In humans, SARS-CoV-2 causes mild to severe lung disease that ranges in severity from asymptomatic to fatal outcomes. Age, gender, genetics; and risk factors such as immune status, diabetes, obesity, and other concurrent conditions are factors believed to influence disease severity. Hamsters, mice, and laboratory NHPs (rhesus macaques especially) have been used in the development of currently available vaccines and therapeutics. In addition, and as with most vaccine programs, rabbits and rats have been used in GLP safety studies ([Martin, 2022](#)).

The rhesus macaque is a nonlethal challenge model that exhibits mild disease, often unassociated with clinical symptoms, but having microscopic lung findings consistent with mild human disease and detectable viral replication, predominantly in the upper respiratory tract and lungs. Generally, animals are inoculated by a SARS-CoV-2 strain intranasally and intratracheally and necropsied 7 or 14 dpi. Primary vaccine efficacy readouts are viral load in BAL and nasal swab samples (attained regularly after inoculation), clinical scoring for body temperature, and gross and microscopic pathology. Despite comparable viral replication patterns, the hamster challenge model shows more severe clinical disease than NHPs, more aligned with severe human clinical disease ([Heydemann et al., 2023](#)).

Our current understanding is that the SARS-Cov-2 virus replicates in the URT and LRT, and lesions tend to follow regions of virus replication and/or where the virus can be identified on IHC. Host cell binding to the host cell receptor and entry is mediated by Spike (S), a glycoprotein that coats the envelope. The S1 subunit of the S protein contains the receptor-binding domain that binds to the peptidase domain of angiotensin-converting enzyme 2 (ACE 2). In SARS-CoV-2, the S2 subunit is highly preserved and is considered a potential antiviral target. The distribution of ACE 2 receptors in different tissues may explain the sites of infection and species susceptibility. For instance, in humans,



many ACE2 receptors are known to be localized in the apical surface of Krt18+ sustentacular cells in the olfactory neuroepithelium and the distribution of ACE2 protein is similar to that reported in bat nasal epithelium. This could explain the characteristic confinement of olfactory nasal lesions in the caudodorsal regions of the hamster nose and immunostaining pattern for SARS-CoV-2 nuclear protein (Figure 4.5). Histopathology in both the hamster and rhesus macaque model is characterized by a patchy or multifocal to coalescing interstitial pneumonia centered around bronchioles and terminal bronchioles. The interstitial pneumonia is characterized by perivascular mononuclear infiltrates that progress into a perivascularitis in more severe lesions as well as alveolar septal thickening with alveolar and/or bronchiolar macrophage infiltrates. Consolidation, fibrosis, and alveolar type II pneumocyte hyperplasia predominate in more severe lesions commonly present in hamsters and elderly macaques. In both models, SARS-Cov-2 lesions tend to affect mostly the cranial lung lobes. In rhesus macaques, a tendency toward more severe lesions in males and aged animals has been reported (Choudhary et al., 2022). A lung lesion scoring system for the rhesus macaque model (Table 4.3) shows that alveolar septal thickening, perivascular mononuclear infiltrates, alveolar macrophages, edema, and intrabronchial macrophages are the most common observations.

Despite the close homology between NHP and human lung anatomy, physiology, and immunology, the global NHP shortage and prolonged nature of chronic respiratory diseases present hurdles for future research. In vitro models, experimental design limiting animal number, enhanced use of historical control data, digital databases, and expanded use of new world monkey species with accelerated lifespans (e.g., marmosets) may be viable options in circumventing logistical challenges related to supply and condition mimicry (Chamanza et al., 2022).

### 3.6. Target Liability Assessment and In Vitro Models

For targeted therapies that are highly specific, on-target toxicity is a major contributor to

attrition in both nonclinical and clinical drug development. For cancer monoclonal antibody biopharmaceuticals, such as CD3 redirectors, an early assessment of the potential liabilities associated with on-target, off-tumor target engagement, due to low levels of expression of tumor antigens in healthy tissues, including the lung, is essential. This is particularly true for epithelial tumor antigens which are frequently targeted in solid tumor indications (Barber and Ganti, 2011).

Although pulmonary toxicities are relatively infrequent with most targeted therapies when compared to other organ system such as the liver, central nervous, and cardiovascular systems, life-threatening respiratory side effects may occur and have been reported. In addition, targets expressed in the lung are generally more accessible to most modalities. Therefore, the characterization of both the intended and unintended target engagement, and their respective desired pharmacological and potential adverse outcomes forms a major component of early hazard identification and risk assessment. This generally involves composing a comprehensive target safety assessment (TSA) or target liability assessment (TLA) that identifies and defines the target distribution and expression profile in the normal lung and other tissues (Brennan, 2017). A major objective of the TLA is to identify relevant and susceptible tissues for safety evaluation and facilitate the creation of a prospective testing strategy and risk mitigation plan. A tissue and cell-based target expression profile also allows the drug development team to monitor any safety questions identified through the nonclinical and clinical stages of development. The first step in generating TSA or TLA reports involves a literature search on target gene and protein expression analysis. It is important to realize that these may not be very reliable, and often need to be confirmed with in-house studies in cynomolgus monkey and human tissues. Since toxicity is driven by the level and localization of target expression, quantification of the observed target expression levels is essential for CD3-bispecific molecules (Kamperschroer et al., 2020). Therefore, a target expression analysis that leverages multiple tools for mRNA analysis such as RNA-sequencing, in situ hybridization, and quantitative PCR, as well as tools for protein analysis such as western blot, IHC, and mass

**TABLE 4.3** Lung Lesions Scoring System for SARS-Cov-2

<b>Lung Lesion</b>	<b>Description (All Lesions Graded 1–5 Based on the Severity and Extent of Lesion in Each Lung Section)</b>
Inflammation, interstitial/septal thickening	Expansion of alveolar septa with congestion, inflammatory infiltrates, fibrin, or fibrosis
Infiltrate, macrophage, alveolar	Focal to multifocal accumulation of macrophages within the alveolar space
Infiltrate, mononuclear, perivascular	Focal to multifocal infiltration or cuffing of perivascular space by mononuclear cells, mostly lymphocytes. If inflammation was present (perivascularitis/periarteritis), a higher grade was given
Infiltrates, macrophage, bronchiolar	Focal to multifocal accumulation of macrophages, including multinuclear cells within the bronchiolar lumen
Type II pneumocyte hyperplasia	Focal to multifocal proliferation of type II pneumocytes, or occasionally, bronchiolar epithelium (high cuboidal cells).
Inflammation, bronchiolar/bronchial	Degeneration, attenuation, or necrosis of bronchial/bronchiolar epithelium associated with intraepithelial inflammatory infiltrates
Infiltrate, granulocyte, peri-bronchiolar/bronchial	Focal to multifocal granulocytic infiltrates in the alveoli
Alveolar edema/flooding	Diffuse accumulation of eosinophilic/proteinaceous material in alveolar space, including hyaline membranes or their remnants in recovered animals
BALT hyperplasia	Increased size, number, and cellularity of BALT with prominent germinal centers

BALT = bronchus-associated lymphoid tissue

spectrometry, is generally used. In addition, study of the target gene of interest, including the presence of gene orthologs, splice variants, corresponding protein variant alleles, and oncogenic mutations may be executed. To gain a proper understanding of the target localization and cellular expression in the lung (e.g., expression in parenchymal, stromal, or immune cells), additional methods such as scRNA-seq or IHC multiplexing are often needed in various tissues and across species. For example, folate receptor 1 (FOLR1) expression in the normal lung has been associated with clinical manifestations of cytokine release and lung damage in the cynomolgus monkey. Based on IHC with commercial anti-FOLR1 antibodies, it was shown that cynomolgus monkeys and humans share expression of FOLR1 on pneumocytes (Singh et al., 2021).

It is also essential to understand that normal target expression in the lung or other tissues may change under disease conditions. For example, an upregulation of the target by tissue injury and/or under proinflammatory conditions can increase the risk of toxicity in an organ that, under normal conditions has low expression levels of the target. Most target protein expression profile IHC work is generally carried out on FFPE, cryosections, or tissue microarrays (TMAs), but gene expression analysis may be successfully executed on in vitro systems, such as the lung organ on a chip platform. For example, alveolus lung organ on-chip was successfully used to recapitulate FOLR1 CD3 bispecific molecule-mediated lung toxicities observed in cynomolgus monkeys, and then leveraged to drive the design of a second-generation molecule, whose favorable lung

safety profile predicted by the chip model was verified in vivo (Kerns et al., 2021).

### 3.6.1. *In Vitro Methods*

In vitro studies are indispensable tools for characterizing and understanding respiratory tract toxicology. In vitro models facilitate the precise application of toxicants, quantification of pathways and kinetics of toxicant interactions, generation of data from specific cells or anatomic compartments, and integration of studies performed at different organizational levels (Allen, 2005).

In recent times, lung biology and lung disease research have benefited immensely from the vast amount of information gleaned from transcriptomics conducted on tissues composed of millions of cells (bulk sample), initially with hybridization-based microarrays, and later with next-generation sequencing (NGS) techniques, often referred to as RNA-seq. RNA-seq is a genomic approach for the detection and quantitative analysis of messenger RNA molecules in a biological sample and is useful for studying cellular responses. While RNA-seq has greatly advanced the understanding of lung biology, the averaging of transcripts that occurs in pooling large numbers of cells does not allow for detailed assessment of the transcriptome at the cell or nucleus level. scRNA-seq allows for the description of RNA molecules in individual cells, with high resolution and permits comparison of the transcriptomes of different individual cells, thereby allowing the assessment of transcriptional similarities and differences within a population of cells (heterogeneity) (Paananen and Fortino, 2019).

In lung biology and disease research, scRNA-seq has not only revealed previously unappreciated levels of heterogeneity that led to the discoveries of previously unknown cell populations, including the identification of ionocytes in airway epithelium and the characterization of profibrotic macrophages and aberrant basaloid cells in IPF. It has allowed for the development of comprehensive molecular cell atlases for the human and mouse lung, identifying biochemical functions of lung cells and the transcription factors and markers for identifying and monitoring them. A molecular atlas for the lung has also been used to define the cell targets of circulating

hormones and predicting local signaling interactions and immune cell homing; as well as identifying cell types that are directly affected by lung disease genes and respiratory viruses (Travaglini et al., 2020).

A few limitations of scRNA-seq include the need for fresh samples, loss or death of cells or inadequate dissociation, and transcriptional stress responses induced during tissue digestion. Single-nucleus RNA sequencing (snRNA-seq), an emerging alternative to scRNA-seq that generates transcriptomic information from isolated nuclei, has been touted to address these deficiencies in the lung and other tissues (Koenitzer et al., 2020).

Lung organoids are 3D tissue-engineered miniature or microscale lungs that accurately replicate the histological and physiological aspects of the native lung. They are generally composed of multiple cell types with proximal airway epithelium, distal alveolar epithelium, and mesenchymal lineages. The culture process of lung organoids differs from that of a traditional cell culture in that lung organoids can simulate the developmental process of the lung, as well as recapitulate lung function and the 3D organizational structure, such as alveoli, airways, and lung buds. Recent advances in isolating lung epithelial progenitor cells from human-induced pluripotent stem cells (hiPSCs) and stromal cells, as well as defining stem cell niche factors important for lung development, have led to the establishment of these complex 3D culture systems (Kong et al., 2021; Leibel et al., 2020; Liao and Li, 2020).

As with other tissue organoids, generation of lung organoids is an alterable and controllable process related to the starting cell types and culture microenvironments, including culture media and culture systems, and the addition of regulators of cell signaling pathways. The starting cells for lung organoids are pulmonary pluripotent stem/progenitor cells, adult stem cells, and embryonic stem cells. Lung differentiation occurs in 3D culture systems, usually on Matrigel, an extract of a natural basement membrane which contains a complex ECM to provide cells with a support framework and promote growth and differentiation. Another culture system, the air-liquid interface (ALI) culture, is considered to be more closely related to respiratory physiology, and preferentially



recapitulates the pseudostratified mucociliary epithelial structure of airways. To obtain lung organoids of realistic structure and function, these two systems—Matrigel and ALI—are now frequently combined as a “3D-ALI” system (Kong et al., 2021).

Lung organoids have been used to help decipher normal and aberrant human lung development, study pulmonary disease; and in drug discovery, test the efficacy or toxicity of drug candidates. In fact, there are conditions in which therapeutic efficacy has only been proven using lung organoids. For instance, the viral vector-mediated genetic correction of the lethal inborn error of surfactant B production (due to a deletion mutation in the surfactant B gene) could only be demonstrated in lung organoids, due to the generation of a robust alveolar type II phenotypic configuration (Cooney et al., 2022). Most recently, lung organoids have been used to assess the pathophysiology of environmental toxicants and SARS-COV 2. Additionally, since lung organoids can be derived from hiPSCs generated from a wide spectrum of individuals with diverse backgrounds, “patient-specific lung organoids” can also be generated. Such lung organoids may be used to help explain age, sex, or racial background-related disparities in disease susceptibility, such as response to infection with viruses such as SARS-CoV-2 (Peng et al., 2022).

### 3.7. Quantitative Techniques and Lung Imaging Modalities

Quantitative information on changes in structure of the respiratory tract may be obtained by morphometric techniques. Measurements made from two-dimensional sections can be used to quantify structures as they exist in greater dimensions (see *Digital Pathology and Tissue Image Analysis*, Vol 1, Chap 12 and *In Vivo Small Animal Imaging: A Comparison to Gross and Histo-pathologic Observations in Animal Models*, Vol 1, Chap 13). Standardized inflation and fixation, unbiased sampling techniques, strategies to account for nonrandom orientation of some structures, and appropriate resolution are required (Hyde et al., 2007). Light microscopy provides sufficient resolution to estimate volume of mucosubstances per unit length of

airway, volumes of major tissue structures and air, proportional volumes of airways and parenchyma, alveolar surface area, and total number of alveoli by stereological techniques. TEM is used to determine numerical densities of cells and volumes of specific cell types within the lung, to analyze subcellular compartments, and to estimate the thickness of the air–blood barrier.

Autoradiography may be used to localize inhaled radioactive particles or radiolabeled molecules within the respiratory tract. If radiolabeled compounds are not covalently bound, frozen sections must be used. Whole-body frozen sections have been used to determine the macroscopic distribution of radiolabeled compounds in tissues such as the nasal epithelium, trachea, bronchi, and pulmonary parenchyma.

Cell turnover and cell kinetics have been studied by autoradiographic and immunohistochemical techniques. Regardless of method, it is not possible to clearly differentiate type I cells from interstitial cells using standard 4–5- $\mu$ m paraffin sections. Thinner (usually 1- $\mu$ m) sections of lung embedded in resin such as methacrylate are used when differentiation of cell types is required. Animals may be given a single injection or a constant infusion (using a minipump) of [ $^3$ H] thymidine or the thymidine analog 5-bromo-2'-deoxyuridine (BrdU). Radiolabeled thymidine or BrdU is incorporated into DNA and is detected in tissue sections using autoradiography or a specific antibody to bromodeoxyuridine (Figure 4.15C and D). Endogenous markers of cell proliferation, such as proliferating cell nuclear antigen (PCNA) or Ki67, can also be used to identify proliferating cells. These markers are particularly useful for evaluating proliferation in archived tissues. Proliferative activity can be expressed as labeling index; that is, number of labeled cells within a defined cell population (e.g., type II alveolar cells) or within the overall cell population (e.g., number of labeled terminal bronchiolar epithelial cells per total number of terminal bronchiolar epithelial cells counted or number of alveolar cells labeled per total number of cells counted in the alveolar zone).

In nonclinical and translational research, invasive and noninvasive imaging of the lung can be an indispensable tool for studying animal models of lung disease. Lung imaging provides a unique

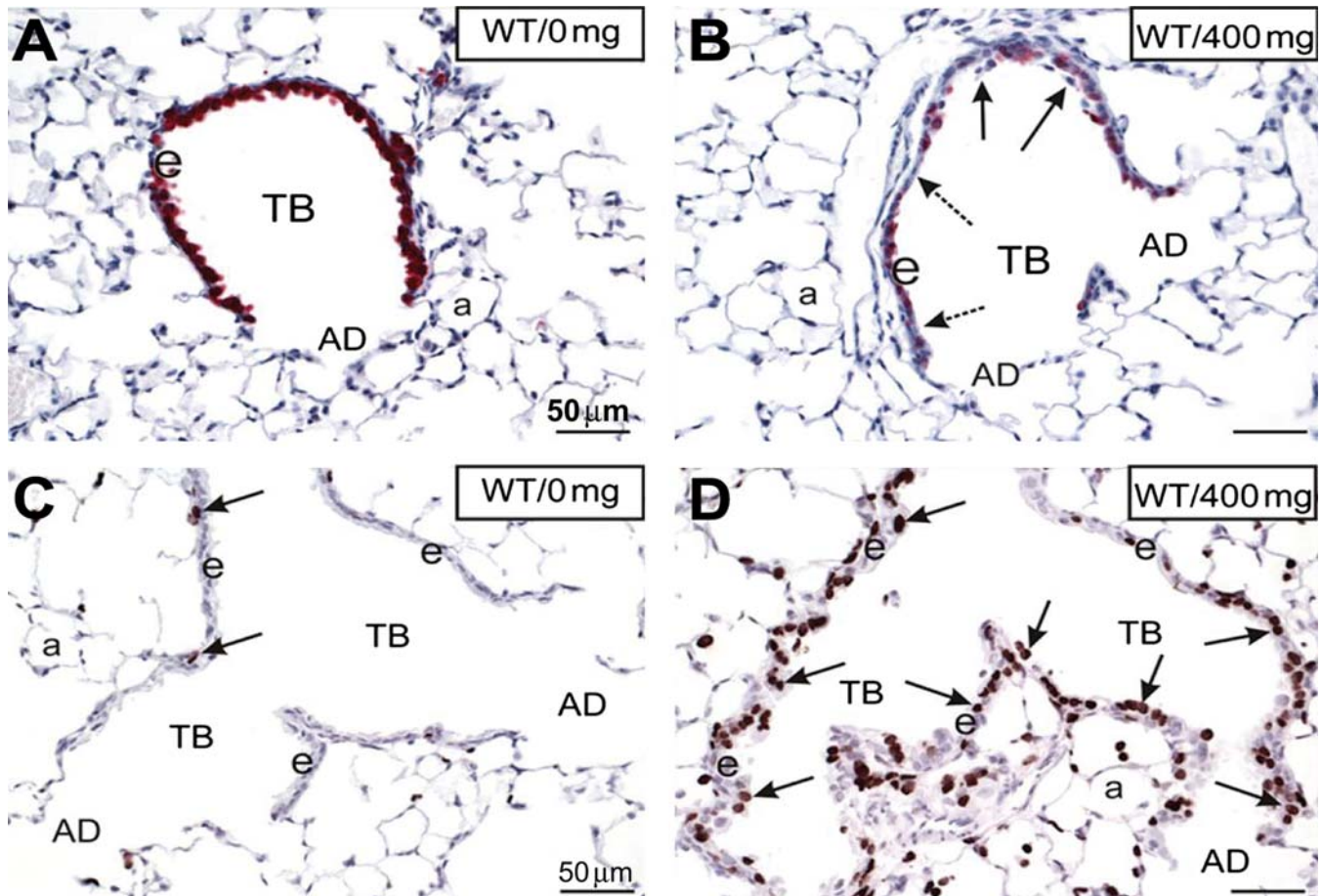


**FIGURE 4.15** Light photomicrographs of terminal bronchioles (TB) from male mice administered 0 mg/kg bw (corn oil-control mice; A, C) or 400 mg/kg bw (B, D) styrene by gavage. Degeneration, necrosis, and exfoliation (arrows) of airway epithelium (e) is restricted to TB of mice that received styrene (B, D). Tissue sections were immunohistochemically stained for club cell-specific protein (CCSP) (A, B; red-stained club cells) or nuclear incorporation of bromodeoxyuridine (brown stain; proliferating cells undergoing DNA synthesis; C, D). Compared to respective corn oil-control mice (A), there is marked loss of CCSP-staining (stippled arrows) in (B). Compared to respective corn oil-control mice (C), large numbers of BrdU-positive nuclei (cells in S phase of cell cycle undergoing DNA synthesis) are present in (D). AD, alveolar ducts; a, alveolus. Tissue sections were counter-stained with hematoxylin. *Figures reproduced from Cruzan G, Bus J, Hotchkiss J, Harkema J, Banton M, Sarang S: CYP2F2-generated metabolites, not styrene oxide, are a key event mediating the mode of action of styrene-induced mouse lung tumors, Regul. Toxicol. Pharmacol. 62(1):214–220, 2012, with permission.*

adjunct to histopathology and permits longitudinal evaluation of functional and morphological changes at high spatial resolution, thereby providing valuable information on lesion progression or recovery. Imaging provides for the study of lung function such as the flow of gases into the lungs or gas exchange across the blood–gas barrier, which can be combined with and correlated to a high-quality anatomical image. Noninvasive techniques can assist in monitoring for disease development, or response

to a specific course of treatment in efficacy studies. In addition, lung imaging may also provide important quantitative information on lesion size and volume, both unattainable by conventional pathology evaluation. Optical imaging techniques that enable in situ and label-free visualization of cellular processes on a microscopic level. For example, ex vivo imaging of fresh and fixed specimens allows spatially resolved and label-free detection of thousands of molecules. Although imaging has been used

historically to study animal models of lung disease (emphysema, pulmonary hypertension, acute lung injury, pulmonary fibrosis, conventional toxicity and carcinogenicity studies), it is more recently most widely utilized in murine oncology research (Maronpot et al., 2017; Pinar and Jones, 2018; Vanherp et al., 2018). In nonclinical oncology research, imaging offers morphological and functional insights in addition to 2D, 3D, and 4D quantitative data on progression and regression of tumor xenografts.

The use of noninvasive imaging modalities used in pulmonary research has increased in recent years. Such modalities include ultrasound, chest radiography, optical imaging, micro-positron emission tomography (micro-PET), single photon emission computed tomography (SPECT), video microscopy, micro-computed tomography (micro-CT), magnetic resonance imaging (MRI) and magnetic resonance microscopy (MRM), optical imaging, and molecular markers such as bioluminescence imaging (BLI). Invasive imaging techniques include confocal microscopy and photon microscopy, while tissue-based platforms include the matrix-assisted laser desorption ionization mass spectrometry imaging (MALDI-MSI), which enables label-free imaging to detect and identify molecules in lung sections and map their spatial distribution (Aichler et al., 2018).

Micro-CT imaging provides quantitative longitudinal information on dynamic disease processes in rodent models of lung disease (Vande et al., 2016) and allows for the quantitative monitoring of progression or regression of lung disease following therapeutic intervention. In rodent models of lung emphysema and pulmonary fibrosis, micro-CT and postacquisition image analysis algorithms can detect changes in lung density over the respiratory cycle, as well as over days to weeks from the induction of lung lesions. Advantages of micro-CT imaging include high resolution, quantitative 3D reconstructions of lung anatomy, and the ability to perform inspiratory and expiratory scans to determine air trapping and density assessments that correlate well with disease severity. Lung micro-CT delivers translationally relevant data about the whole lung, including regional differences with high resolution and sensitivity to provide insight into lung anatomy, function, and pathology. Limitations

of micro-CT imaging include the relatively poor soft-tissue contrast, cardiac and respiratory motion artifact, and a potential adverse impact of repeated radiation exposure in some susceptible strains of mice. Besides their use in rodent models of respiratory disease, CT images can also be used in large animals such as primates for quantification of lung abnormalities using volume or radiodensity. Micro-CT uses a cone-beam X-ray source and two-dimensional detector with the source and detector rotated through 360 degrees. Compared to clinical CT scanners, micro-CT scanners are more sensitive to X-ray energy because they have a much smaller field of view (typically 1–5 cm wide vs. 30–40 cm wide) (du Plessis et al., 2017).

Micro-PET and SPECT imaging are mostly used in oncology research for the detection of lung tumor metastases and tumor growth kinetics and/or tumor inhibition in lung implanted xenograft tumors in mice. They have also been used in other models of lung disease, particularly for glucose uptake measurements in a model of acute lung injury. PET and SPECT utilize radionuclides to study molecular target biochemical changes, and metabolic information on in vivo processes. First, a target-specific radiolabeled imaging agent is identified. A small amount of the radiolabeled agent is injected intravenously, and its lung distribution is traced using a PET camera. PET and SPECT can detect biochemical and molecular changes that precede anatomical changes. Moreover, continuous longitudinal data can be acquired using a radionuclide-labeled experimental substance. For instance, tumor uptake of a specific radiolabeled antibody drug conjugate can be attained at multiple time points. SPECT imaging has also been used to estimate ventilation/perfusion ratios with some success (Parakh et al., 2022).

In vivo MRI and MRM of the small animal lung have become valuable research tools for studying morphologic and functional changes in rodent models of lung diseases (Drieuhyuys and Hedlund, 2007). They offer noninvasive tools for longitudinal imaging at high spatial resolution, particularly to demonstrate ventilation and quantitative perfusion. MRI uses a powerful magnet and radio frequency energy to image atomic nuclei within the body. As the most abundant atomic nucleus in the body, the hydrogen proton is the most commonly used



MRI nucleus. However, adaptations can be made for less abundant atomic nuclei, including  $^{31}\text{P}$ ,  $^{13}\text{C}$ ,  $^{23}\text{Na}$ ,  $^{19}\text{F}$ , and  $^{17}\text{O}_2$ , as well as hyperpolarized nuclei such as He. Direct imaging of pulmonary gas spaces can be obtained using breathable gases such as helium and xenon. In using hyperpolarized helium, gas distribution and dynamics can be followed; and airway constrictions and obstructions can be detected. Imaging of the lung can be hampered by relatively low tissue density (and therefore low water content), limiting signal-to-noise; and variations in magnetic “susceptibility,” associated with the many air–tissue interfaces of the alveoli and bronchioles, creating local magnetic field heterogeneities (field gradients) that can lead to image degradation. As a result, researchers can use very fast imaging sequences with short imaging times combined with respiratory synchronization for small species with high respiratory and cardiac rates, and the inability to breath-hold during procedures (Dothager and Piwnica-Worms, 2009; Fox et al., 2012).

### 3.7.1. Molecular Markers

Molecular imaging of lung disease refers to the noninvasive measurement and characterization of specific molecules, molecular processes, and molecular events over time and space in the living animal. While conventional imaging modalities such as chest X-rays and CT scans offer high spatial resolution, and provide anatomical and structural information of the lungs, they are unable to differentiate between lung diseases with overlapping pathophysiology or allow identification of the etiology, pathogenesis, or the immune response and the field of molecular imaging is of great interest as a result. Using a molecular targeting probe to carry a dye- or gamma photon-based isotope, target expression can be visualized. Current nonclinical and clinical molecular imaging approaches primarily use PET- or SPECT-based techniques. CT and MRI have also been used successfully with specific or nonspecific radiopharmaceutical agents. The diseased lung demonstrates low background signals compared to healthy lung tissue. Tumors and inflammatory processes can be readily visualized using a variety of molecular markers. Molecular markers can be divided into two

general categories: direct imaging of endogenous targets and indirect imaging using reporter genes that generate a detectable signal to monitor endogenous processes. Direct imaging detects elevated levels of receptors, enzymes, and kinases at the target tissue. For example, using micro-PET, elevated expression of glucose transporters and hexokinases with subsequent increased phosphorylation and retention of  $^{18}\text{F}$ -fluorodeoxyglucose ( $^{18}\text{F}$ -FDG) in metabolically active tumor cells or activated immune cells can be detected during infection and inflammation. Molecular probes for endogenous targets are amenable to clinical translation (Dimastromatteo et al., 2018).

Optical imaging for noninvasive tissue visualization is a technique that analyzes functional and molecular events using *in vivo* staining and reporter gene approaches. It is an important tool in the study of “-omics” fields, which allows monitoring of lung function in its natural structural context. The lungs are a challenging environment for optical imaging due to the structure of the airways and alveoli. The presence of many overlapping and highly curved air/liquid interfaces causes significant scattering of light while imaging the lung, compared with imaging homogenous tissue. Probes and biomarkers developed and validated in other areas of the body will often require reoptimization when tested in the lung, even at equivalent tissue depths (Gammon et al., 2014).

The two broad categories of optical imaging are (BLI) and fluorescence imaging. BLI relies on the sensitive detection of visible light produced when a reporter enzyme oxidizes its luciferin substrate. The oxidation transiently converts the luciferin to a higher energy state, and when it settles back to the ground state, a photon is released. BLI has been widely adopted by the cancer community to track metastatic lesions in the lung. BLI, in combination with nuclear imaging (PET and SPECT), has also been successfully used to study pulmonary inflammation. Because it can be executed with ease and results are straightforwardly quantified and interpreted, BLI has many applications in nonclinical research including effective gene delivery in cystic fibrosis. In this area, researchers have used luciferase gene expression to optimize the efficiency of viral and nanoparticle delivery and stable integration of genes in

the lung (Gammon et al., 2014). In studying pulmonary inflammation and NF- $\kappa$ B (implicated in ARDS) activation, transgenic mice expressing Photinus luciferase cDNA under the control of an NF- $\kappa$ B-dependent promoter were developed. In this model, NF- $\kappa$ B-dependent luciferase production after treatment with LPS or other systemic or lung toxicants reflects NF- $\kappa$ B activity over time and allows a more detailed analysis of the role of NF- $\kappa$ B activation in regulating inflammatory events (Blackwell et al., 2000). In oncology research, BLI can be used with lung cancer cell lines and bacteria expressing luciferase to track tumor growth or responses to therapies (tumor growth inhibition) in efficacy studies (Zhu et al., 2018).

In fluorescence imaging, the signal is generated by exciting a molecule with filtered light, as opposed to a chemical reaction in BLI, and a longer wavelength of light is emitted from the excited state. In vivo imaging of fluorescence provides for the study of biomolecules in both living and fixed cells at macroscopic and microscopic levels. There are many fluorescent proteins, dyes, and probes for gene expression, protein structure/localization, cell signaling, growth, and apoptosis research. Biomolecular processes of interest can be assayed directly (i.e., activated probes) or indirectly (i.e., reporter gene). Delivering the compound into the lungs (i.e., via minimally invasive nasal aspiration or direct tracheal instillation into the lungs) and keeping the probe biologically active and not immediately cleared by the mucociliary escalator (which is able to filter out particles between 2 and 10  $\mu$ m) are the main challenges in using fluorescent probes to image the lung. These hurdles actually apply to any imaging modality requiring contrast probe or tracer administration. Delivery of reporter compounds via direct tracheal instillation using dosages that are several folds higher than the effective concentration applied in vitro has been reported to help circumvent these challenges (Gammon et al., 2014; Ntziachristos, 2009).

Intravital microscopy is an invasive optical imaging technique that enables in situ visualization of cellular processes on a microscopic level, based on detection of fluorescent signals. Since access to the lungs is a prerequisite for the microscopy, different types of approaches have been developed over the years. The most common involves the implantation of a thoracic optical

window which can be combined with a variety of microscopic techniques. However, the implantation approach is challenging since it only allows examination of superficial lung structures. The alternative approach, fibered confocal fluorescence microscopy (FCFM), uses flexible optical fibers inserted into the lung to enable imaging of deeper tissues (Liu et al., 2019). Bronchoscopy FCFM is an emerging optical imaging technique that allows for real-time detection of fluorescently labeled cells within live animals, thereby bridging the gap between in vivo whole-body imaging methods and traditional histological examinations. Unlike traditional FCFM that requires invasive procedures to access lungs, the bronchoscopic FCFM approach is minimally invasive, allowing longitudinal monitoring of lung lesions in free-breathing animals. Invasive techniques have a high microscopic resolution of  $<1.0$  mm, providing unique information unobtainable by noninvasive imaging modalities, and thereby bridging the gap between in vivo imaging techniques and standard ex vivo histopathology. These modalities have facilitated elegant and detailed studies of alveolar epithelial-endothelial interactions, immune cell migration, and intercellular dynamics in the lungs of live mice, by using either a thoracic window or isolated blood-perfused lungs. They do not, however, provide global read-outs of the lung function or responses to treatment (Ahookhosh et al., 2023).

### 3.7.2. Imaging of Ex Vivo Lung Tissue

MALDI-MSI is a powerful technique that combines mass spectrometry molecular analysis with histopathology and IHC, enabling spatially resolved and label-free detection of hundreds to thousands of molecules within a single tissue section. MALDI-MSI is used in animal models of lung disease for biomarker discovery, drug distribution, and disease characterization. For the bleomycin-induced fibrosis mouse model, for example, MALDI enables a direct molecular comparison of patient-derived tissue (e.g., IPF) to the corresponding mouse model. The FFPE tissue from mice and human patients can be analyzed simultaneously on TMAs, and validated with IHC and H&E slides, ultimately identifying comparative human diseases and corresponding animal model characteristics. Statistically derived numbers of specific or

shared molecular clusters in the human and murine fibrotic tissues can then be determined. MALDI can therefore be used to validate or determine animal model translatability. A broad range of analytes can be investigated in the lung fibrosis model including proteoglycan deposition, glycosaminoglycans, or chondroitin/dermatan sulfates, as well as the distribution and concentration of drugs within a tissue section. Of the currently available modalities used for tissue-based research, MALDI has unique advantages that include high sensitivity, wide range of molecules, molecular specificity, and the flexibility to identify numerous and varied analytes on a single platform. In general, mass spectrometry imaging makes possible the detection/identification of molecules for which the IHC antibodies are not available, or for which other imaging methods are not suitable. Furthermore, MALDI-MSI is commonly applied for the detection and identification of smaller proteins (usually with molecular weights not exceeding 30 kDa), peptides, lipids, or oligosaccharides (Ryan et al., 2019).

### **3.7.3. Imaging in Animal Models of SARS-CoV-2**

In NHP COVID-19 vaccine efficacy studies, imaging has been used to characterize lung abnormalities with longitudinal quantitative comparison of vaccinated versus unvaccinated animals. Noninvasive longitudinal imaging of NHP SARS-CoV-2 infection allows more effective characterization of the lung disease pathogenesis and in vivo vaccine efficacy. Serial imaging of pretrial baselines and postchallenge enables longitudinal data collection through frequent examination using a limited number of animals. Limited data can be obtained from lung radiography findings in SARS-CoV-2-infected NHPs with mild or no clinical signs. Compared to radiography, PET-CT combines high-resolution anatomical information attained from CT with quantitative functional assessments from PET. When PET-CT is coupled with the metabolic radiotracer fluoro-2-deoxyglucose (FFDG), a glucose analog that is internalized but not metabolized by inflammatory cells, heightened metabolic activity can be quantified as a proxy for COVID-induced pulmonary and regional lymph node inflammation. Because animals are imaged using the same modalities

and scanners, readouts of SARS-CoV-2-exposed NHPs are highly translational to patients. The spectrum of COVID-related lung imaging characteristics includes alveolar, interstitial, pleural, and vascular abnormalities. Alveolar ground glass opacities (GGOs) are often noted with septal interstitial thickening (crazy-paving pattern) in a bilateral, multilobar, and peripheral distribution. Lung abnormalities detected by CT tend to correlate with gross and microscopic pathology (Finch et al., 2020).

### **3.7.4. Lung Injury Caused by Antibody-Based Therapeutics for Targeted Therapy**

Monoclonal antibodies (mAbs) and other derivatives of the monoclonal antibody format, including bispecific or trispecific antibodies, antibody-drug conjugates (ADCs), and antibody fragments such as fragment antigen binding (Fab), single-chain fragment variable (scFv), or single-domain antibody, are now established as targeted therapies for cancer, transplant rejection, conditioning for bone marrow transplant, or autoimmune disease (Hansel et al., 2010). In nonclinical toxicity studies, organ toxicity associated with antibody-based therapeutic modalities is usually related to the target and associated exaggerated pharmacology, which in most cases, is predictable. Similarly, with antibody-based immuno-oncology biotherapeutics in particular, the majority of organ toxicities in animals are related to the target expression levels in normal tissues; and induce predictable “on target/off tumor” lesions, resulting from a direct attack on normal tissues that have the shared expression of the targeted antigen (Weaver and Valentin, 2018). Therefore, lung pathology can occur if the target antigen is also expressed at sufficient levels in normal lung tissue. An example is mesothelin, a 40-kDa glycosylphosphatidylinositol-anchored membrane glycoprotein normally expressed on mesothelial cells lining the peritoneum, pericardium, and pleura. Mesothelin is an attractive surface target for immunotherapy since it is significantly overexpressed in a number of malignancies, including mesothelioma, ovarian cancer, pancreatic cancer, cervical cancer, NSCLC, and lung adenocarcinoma, in which it is associated with aggressive phenotypes and a poor prognosis. In normal tissue, mesothelin is normally only present in limited amounts on the cell surface of mesothelial cells. Certain



antibody-based therapeutics, including bispecifics and ADCs (the clinical candidate or their surrogate molecules) targeting mesothelin, have been associated with pleuritis, adhesions, and subpleural lung inflammation in NHP, as on target/off tumor effects. However, mesothelin-targeted therapeutic modalities are relatively safe at therapeutically effective doses due to limited expression in normal tissues and high expression levels in cancers (Hassan and Ho, 2008; Rashdan et al., 2018).

Another example is folate-receptor 1 (FOLR1), a glycosylphosphatidylinositol-linked protein known to be overexpressed in various epithelial malignancies including ovarian, breast, renal, and lung cancers, but also expressed at lower levels in normal epithelial cells in the lung and kidneys. The risk of on target/off tumor toxicity is considered low and FOLR1 is an attractive target candidate, as it is only expressed on the apical surfaces of polarized noncancerous epithelial cells, and is not exposed to the bloodstream (Thomas et al., 2013). However, in nonclinical studies with an anti-FOLR1 bispecific T cell engager, severe on-target toxicity in the NHP lung was observed. Cynomolgus monkeys administered the highest dose developed adverse respiratory symptoms, resulting in euthanasia at 24 hours postdose and associated lung lesions of edema, congestion, and acute inflammation. Further immunohistochemical investigation with commercial anti-FOLR1 antibodies demonstrated shared cynomolgus monkey and human expression of pneumocyte FOLR1 (Kamperschroer et al., 2020).

Pulmonary toxicities from infusion reactions resulting in cytokine release syndrome and/or complement activation; immune reactions such as acute anaphylaxis; immunogenicity and anti-drug antibody (ADA)-mediated immune reactions; or infections secondary to immunomodulation are more common than target-related pulmonary toxicity with biotherapeutic administration in nonclinical settings. Alveolar edema associated with cytokine release may be observed soon after dosing, while lung blood vessels are a common target for immune complex deposition and immune-mediated vasculitis. With immunomodulatory biotherapeutic administration in NHPs, secondary lung inflammation may occur from

infection with pathogens including cytomegaloviruses, *Pneumocystis*, measles, or adenoviruses. Molecular localization techniques such as IHC, ISH, NGS, PCR, or simple histochemical methods can help in diagnosing and differentiating secondary immunomodulatory effects from primary, target-related effects. In human patients, pulmonary toxicity manifesting as interstitial lung disease or interstitial pneumonitis has been reported with anticancer immunotherapies, most notably, immune-checkpoint inhibitors (ICIs). These findings, like other ICI-associated immune-related adverse events (irAEs), are rarely replicated in laboratory animal species, including NHP (Ramos-Casals et al., 2020).

## 4. RESPONSES TO INJURY

### 4.1. Factors Affecting Toxic Injury and Host Response

Responses of the respiratory tract to air- and bloodborne toxicants depend primarily on the nature, dose, and exposure duration or dose regimen of the xenobiotic agent. Host factors such as age, genotype, gender, epigenetics, nutrition, and previous exposure history will also influence the airway and alveolar responses to toxicant-induced injury. The pattern, distribution, and severity of respiratory tract lesions depend to a large measure on the interplay of local dosimetry and tissue sensitivity at various anatomic sites along the respiratory tract (Sells et al., 2007). As noted previously, anatomic, physiologic, cellular, and biochemical species differences within the respiratory system may result in response differences to toxicant injury and prove difficult the estimation of human health risk from such studies (Salem and Katz, 2015).

Inhaled highly water-soluble chemicals and large particles (mean aerodynamic diameters  $>2.5$ – $10\text{ }\mu\text{m}$ ) such as coarse ambient particulate matter [ $\text{PM}_{10}$ ] will generally cause toxicity to the upper respiratory tract. Poorly soluble chemicals and small particles ( $\leq 2.5\text{ }\mu\text{m}$ —fine ambient particulate matter [ $\text{PM}_{2.5}$ ]) will target the lower respiratory tract and/or alveolar parenchyma. Once defense mechanisms at specific airway

sites are overwhelmed by toxic insult, injury ensues followed closely by acute inflammatory and epithelial responses to repair the damage.

#### 4.2. Patterns of Respiratory Tract Injury to Inhaled Toxicants

Two principal gradients of damage are often observed in the respiratory tract upon exposure to inhaled toxicants. At each site, the gradient is a proximal to distal decrease in lesion severity. The physicochemical nature of the airborne toxicant and the inhalation exposure conditions dictate whether one or both gradients of airway toxicity occur, as well as the severity and distribution of the injury (and response to injury) within each site. The first gradient is in the upper respiratory tract extending from the nasopharyngeal passages through the tracheobronchial airways. The second is in the lower respiratory tract and extends from the terminal bronchioles (proximal centriacinus) to the alveolar ducts and adjacent alveoli (distal centriacinus) in the pulmonary parenchyma. The gradient in the upper airways occurs most often with inhalation exposure to highly water-soluble chemicals (e.g., sulfur dioxide) or large particles (e.g., PM<sub>10</sub>), while the second gradient of injury in the centriacinar region of the lung is caused by inhaled poorly soluble chemicals (e.g., nitrogen dioxide) and small particles (e.g., PM<sub>2.5</sub>).

Gases or aerosolized chemicals that are of low water solubility but highly reactive (e.g., ozone, chlorine), as well as certain nanoparticles (e.g.,  $\leq 20$  nm carbon black nanoparticles), cause gradient injury at both upper and lower respiratory sites with repeated long-term exposures in laboratory rodents. Interestingly, both the nasal and centriacinar sites of injury are also predicted dosimetric "hot spots" for ozone and nanoparticles, based on computational deposition modeling.

An exception to these two site-specific gradients of damage is airway injury caused by inhaled toxicants for which xenobiotic metabolism (metabolic activation or deactivation) is a crucial step in the lesion pathogenesis. For example, inhaled acetaldehyde toxicity causes marked injury to the nasal olfactory epithelium devoid of the detoxifying enzyme aldehyde dehydrogenase, and minimal injury to adjacent

enzyme (aldehyde dehydrogenase)-rich respiratory epithelium.

#### 4.3. Cell-specific Versus Nonspecific Injury

Respiratory tract exposure to a wide variety of agents results in epithelial cell injury and death. Injury to individual cells may be reversible, such as altered mucus production or loss of cilia, or irreversible, leading to cell death. Chemical agents may nonspecifically affect all epithelial cells within a region or may selectively injure a single cell type (Table 4.4).

In general, the most vulnerable cells to toxic injury are the ciliated cells of the respiratory epithelium lining the conducting airways, and the alveolar type I epithelial and capillary endothelial cells of the alveolar gas-exchange region in the deep lung. Because of their functional and morphological characteristics (the large surface area of alveolar type I epithelial cells and endothelial cells presented to air- and blood-borne toxicants, respectively), these cells are damaged nonselectively by toxicants. Nonspecific injury may also occur when agents are so toxic that all cells in contact with the agent are injured. An example of this is aspiration of a caustic solution or exposure to high airborne concentrations of a warfare/terrorist agent such as chlorine or mustard gas causing diffuse necrotic damage with exfoliation of airway and alveolar epithelium.

As mentioned previously, susceptibility of other cell types to injury is dependent on the nature of the toxicant and its interaction with a unique function of the cell. For example, olfactory sustentacular cells and bronchiolar club cells contain high concentrations of cytochrome P450 enzymes and are susceptible to injury by toxicants which require metabolic activation (e.g., 3-methylfuran, acetaminophen, styrene, naphthalene, and 4-ipomeanol) (Ding and Kaminsky, 2003).

#### 4.4. Cell Proliferation, Regeneration, and Repair Processes

Irrespective of the mechanism of toxicity and cell type affected, relatively stereotyped repair processes that include proliferation of stem cells and inflammation follow initial damage. Proliferation of resident cells generally occurs as a regenerative response following cell necrosis. This is an

**TABLE 4.4** Specificity of Cell Damage by Selected Compounds Which Undergo In Situ Metabolic Activation Within the Respiratory Tract

Compound	Primary Cell Type Affected	Species	Route
Acetaminophen	Olfactory mucosa, transitional epithelium, club cell	Rat, mouse	Oral, ip
Bromobenzene	Club cell	Rat, mouse	ip
Butylated hydroxytoluene (BHT)	Type I epithelial cell, capillary endothelial cell	Mouse (not rat)	ip
Carbon tetrachloride	Club cell	Guinea pig Rat	Inhalation ip
Coumarin	Club cell	Rat, mouse	Inhalation
4-Ipomeanol	Club cell (also causes pulmonary edema)	Rat, mouse	ip
3-Methylfuran	Olfactory mucosa, club cell	Mouse, rat, hamster	Inhalation
Naphthalene	Club cell, olfactory epithelium	Mouse, rat	ip, inhalation
Alpha-naphthylthiourea (ANTU)	Capillary endothelial cell	Rat	Oral
Trialkyl phosphorothioates	Type I epithelial cell, club cell	Rat	Oral, ip
Phenacetin	Olfactory mucosa	Rat	Oral

ip, intraperitoneal.

Modified from Haschek WM, Rousseaux CG, Wallig MA, editors: *Handbook of toxicologic pathology*, ed 2, 2002, Academic Press, Vol. 2, Table VI, p. 32, with permission.

acceleration of the normal cell renewal process by which tissue integrity is maintained. In some situations, cell proliferation can be initiated by the migration of inflammatory cells into the lung. In addition to repair processes, cell proliferation is also associated with lung growth and neoplasia.

Chemical damage to the nasal olfactory epithelium can be repaired by regeneration if sufficient basal cells survive to initiate this repair process. If injury occurs to the ciliated respiratory epithelium, surviving cells spread to cover the denuded basal lamina. This is accompanied by proliferation of surviving immature secretory cells or basal cells. These cells may divide and differentiate into ciliated cells, resulting in a restoration of the surface epithelium. In the smaller bronchiolar airways, the club cell is the progenitor cell responsible for reparative regeneration in response to toxicant-induced bronchiolar injury. Proliferating club cells may differentiate into either mature club cells or ciliated cells.

Injury to the alveolar epithelium is followed by proliferation of type II epithelial cells whose

normal function is surfactant secretion. Newly divided type II cells can differentiate into end-stage type I cells, which are incapable of division, or mature type II cells. Proliferation of type II cells may also follow migration of inflammatory cells from the capillary bed into the alveoli. Injury to capillary endothelium within the lung is repaired by proliferation of remaining endothelial cells or by circulating stem cells. Alveolar macrophage increases are also commonly noted. Alveolar macrophages are ultimately derived from bone marrow monocyte precursors. Monocytes migrate directly from the circulation to the alveolar lumen where they differentiate to alveolar macrophages, whereas other monocytes migrate from the circulation to the interstitium where they take up residence and provide a local population that continues to divide and can migrate into alveoli to replenish the alveolar macrophage pool. Additionally, macrophages in alveolar lumens can divide. In response to injury, mediators are released that result in an influx of polymorphonuclear cells and monocytes into the



lung. Under conditions of high demand for phagocytes, alveolar macrophages originate both from circulating monocytes and from mitotic activity and migration of interstitial monocytes. These monocytes, originating from either pool, differentiate into alveolar macrophages, replenishing and augmenting the alveolar macrophage population. A common response to pulmonary toxicant exposure is an accumulation of proinflammatory/cytotoxic M1 macrophages at sites of tissue injury, followed by the appearance of antiinflammatory/wound repair M2 macrophages. It is thought that the outcome of the pathogenic responses to toxicants depends on the balance in the activity of these macrophage subpopulations (Laskin et al., 2019).

Proliferation of fibroblasts located in the walls of the airways and in the pulmonary interstitium frequently follows injury. This proliferation is usually not due to direct injury to the fibroblast but related to the loss of overlying epithelium and basement membrane, as well as to the production of mediators and growth factors by alveolar macrophages and inflammatory cells. Excessive fibroblast proliferation and collagen production can lead to fibrosis or “scarring,” which compromises normal pulmonary elasticity or compliance and gaseous diffusion.

Under most conditions of acute injury, proliferation of epithelial cells begins within the first day of injury and peaks over the next few days. Proliferation of other cell types occurs at later times. Inhibition of epithelial cell proliferation can delay or inhibit normal repair, resulting in chronic damage or secondary bacterial infections. Remodeling of tissue may occur with chronic injury if repair mechanisms are unable to keep pace. This structural remodeling may be beneficial or have adverse consequences (Redente et al., 2021). In addition, inhibition of cell differentiation (e.g., under conditions of chronic exposure) can result in large numbers of undifferentiated cells. These cells may be less susceptible to the original injury and tolerance may develop. These cells may also play a role in the development of neoplasia (Beers and Morrissey, 2011).

Thus, mild epithelial or endothelial injury without basement membrane damage, severe inflammation, or persistence of the inciting agent may be resolved by simple cellular regeneration. With more severe damage, a significant inflammatory component may be elicited which may

be followed by tissue destruction or fibrosis. In some cases, persistence of the inciting agent within the tissue may lead to the development of granulomatous disease, as observed with inhalation exposure to crystalline silica or carbon nanotubes (Donaldson et al., 2006).

#### 4.5. Nasal, Nasopharyngeal, and Laryngeal Responses to Injury

As the portal of entry for inhaled air, the nasal cavity is susceptible to injury from airborne xenobiotic agents due to its anatomic location. Important factors in the pathogenesis of toxicant-induced nasal lesions include airflow, absorption, tissue susceptibility, mucociliary apparatus, and metabolism. The distribution of damage is dependent on regional deposition of inhaled chemicals and on tissue or cell susceptibility to individual agents. Regional deposition of inhaled chemicals is dependent on airflow; and in the case of particles, characteristics such as size and aerodynamic shape. Species differences in regional airflow play a role in lesion distribution. Nasal uptake of gases is dependent on the partition coefficient of the gas and, in the case of reactive gases, on the rate of reaction. For example, in the dog, nasal uptake is 100% for formaldehyde, 40%–70% for ozone, and 1% for carbon monoxide. Distribution of nasal lesions is also dependent on cell or tissue susceptibility. For example, olfactory epithelium is damaged by xenobiotics that require metabolic activation, such as methyl bromide, 3-methylfuran, 3MI, carbon tetrachloride, naphthalene, methimazole, and acetaminophen. This usually occurs irrespective of the route of administration. On the other hand, ciliated cells and perhaps mucous cells are the targets of toxicity caused by other nasal toxicants such as formaldehyde.

Substances affecting nasal function may impair mucociliary flow, change nasal airflow resistance, and irritate or damage the nasal mucosa. Damage to the OSNs of the olfactory epithelium can result in anosmia (loss of smell). Chemically induced nasal epithelial lesions fall into one or more of the following categories: degeneration and necrosis, inflammation, repair, adaptation, and proliferative lesions, including neoplasia (Table 4.5).

Degeneration and necrosis are usually followed by inflammation and cell proliferation to

**TABLE 4.5** Classification of Nonneoplastic Alterations to the Respiratory System

Alteration	Xenobiotic
<b>NASAL CAVITY AND AIRWAYS</b>	
Degeneration/ necrosis	Acetaminophen, 3-methylfuran
Inflammation	Acetaldehyde, formaldehyde, cigarette smoke, ammonia
Metaplasia/ hyperplasia	Acetaldehyde, formaldehyde, cigarette smoke, ammonia
Fibrosis	NO <sub>2</sub> , methyl isocyanate
Chronic bronchitis	Chronic exposure to cigarette smoke, irritant gases
<b>PULMONARY PARENCHYMA</b>	
Edema	Phosgene, $\alpha$ -naphthothiourea, endotoxin
Inflammation	Hyperoxia, radiation, bleomycin, paraquat, silica
Fibrosis	Hyperoxia, radiation, bleomycin, paraquat, silica
Emphysema	Smoking, CdCl <sub>2</sub>

Reproduced from Haschek WM, Rousseaux CG, Wallig MA, editors: *Handbook of toxicologic pathology*, ed 2, 2010, Elsevier, Table 6.6, p. 110, with permission.

repair damaged epithelium. Excessive proliferation can result in epithelial hyperplasia. Increased cell turnover can potentially predispose to carcinogenesis since increased DNA synthesis will increase the probability of mutation. Continued low-level toxic exposure may result in adaptive responses such as squamous or mucous cell metaplasia, or mucous cell hyperplasia/hypertrophy. The presence of exudate in the nasal cavity is a valuable indication of nasal toxicity and is readily detected by light

microscopy at low magnification. However, nasal exudate is also a hallmark of microbial infections caused by mycoplasma and Sendai virus. The relatively stereotyped nature of the response of tissues to injury, independent of etiology, needs to be reemphasized.

In the larynx, the transitional zone between the stratified SE cranially and the respiratory epithelium caudally is the most sensitive site for inhaled xenobiotic-induced injury resulting in epithelial alteration, degeneration, squamous metaplasia, or hyperplasia. Xenobiotics affecting the larynx include tobacco smoke and cobalt sulfate. These lesions must be differentiated from aging changes, thus emphasizing the need for age-matched controls in evaluating xenobiotic-induced changes.

#### 4.5.1. Nonneoplastic Lesions

##### 4.5.1.1. ACUTE LESIONS

In the nasal epithelium, the mildest change may be loss of motile cilia from ciliated cells, or immotile cilia from OSNs, with little change in the underlying or adjacent cells. Similarly, loss of OSNs may occur without apparent disruption of the overall structure of the olfactory epithelium. Acute necrosis and loss of olfactory epithelium may be seen following inhalation or bloodborne exposure to toxicants requiring metabolic activation by the P450 system, such as 3-methylfuran and acetaminophen, respectively. Once the basement membrane is exposed, cytokines are released and inflammation ensues (Dolinay et al., 2012). Acetaminophen also causes selective necrosis of nasal olfactory epithelium.

More severe nasal epithelial lesions, such as segmental loss of basal lamina or ulceration, cause damage to the underlying lamina propria and even the bone or cartilage. This can lead to turbinate atrophy or perforation of the nasal septum. With extensive nasal epithelial damage, the affected area may be covered by an exudate indicating marked rhinitis. Repair may take place, or if repeated exposure occurs, squamous metaplasia of respiratory or even olfactory regions may result, occasionally with extensive keratinization.

#### 4.5.2. Subacute/Chronic Lesions

Subacute/chronic nonneoplastic changes of the olfactory mucosa following inhalation of irritant

substances such as acrolein, formaldehyde, acetaldehyde, and cigarette smoke may include atrophy of the olfactory epithelium or even loss of the entire olfactory mucosa, including nerve bundles and BGs in the lamina propria. In the latter case, the olfactory mucosa may be replaced by squamous or respiratory metaplasia (Figure 4.16). The dorsomedial region of the nasal cavity appears the most vulnerable to these changes. Cessation of

exposure may lead to recovery, but the regenerated olfactory epithelium may still appear disorganized and relatively thin.

Common changes of the transitional and respiratory epithelium following inhalation of irritant substances such as acetaldehyde, formaldehyde, and cigarette smoke are epithelial hyperplasia and/or squamous metaplasia of the nasal in the proximal nasal airways. Mucous cell metaplasia

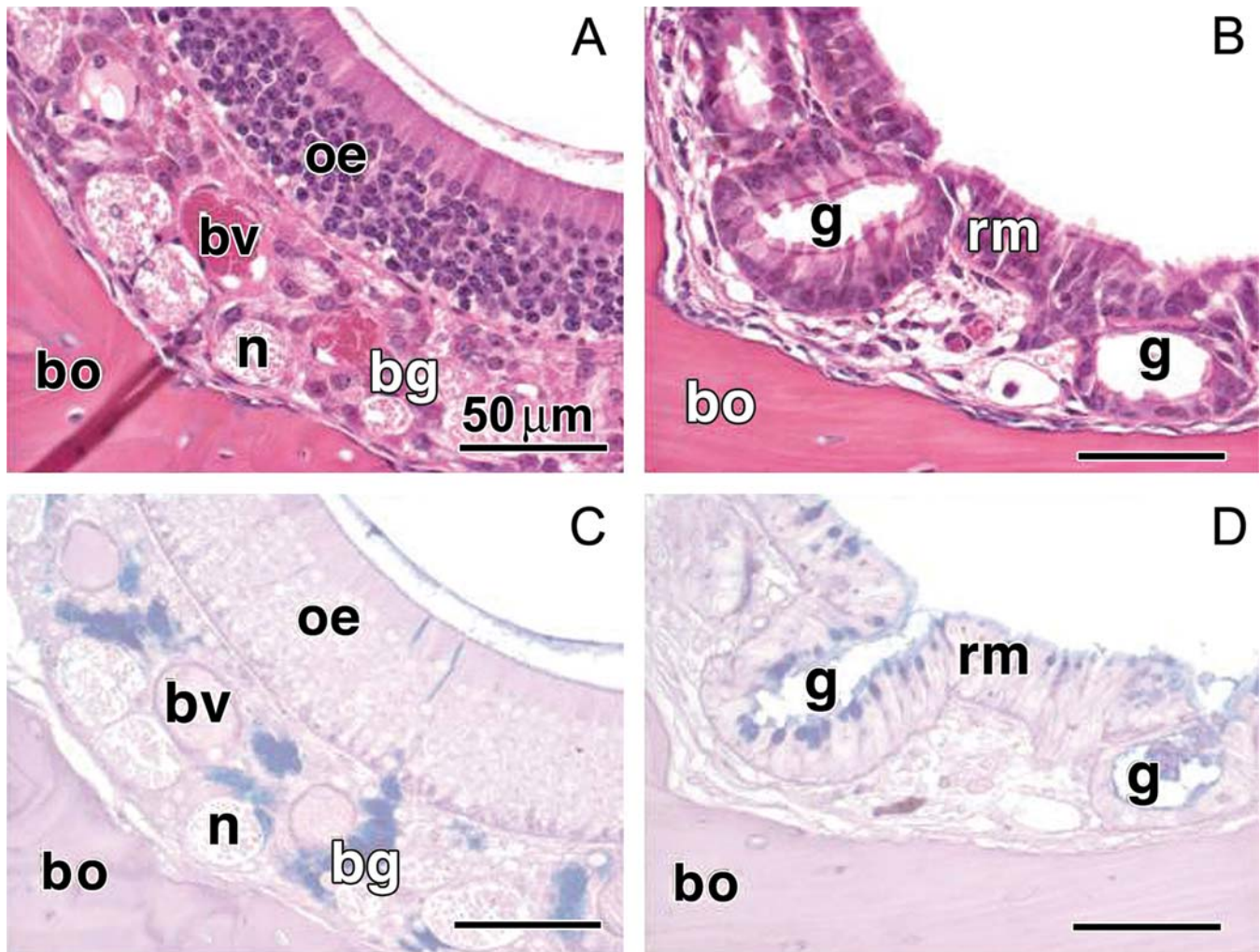


**FIGURE 4.16** Light photomicrographs of nasal epithelium lining the dorsomedial meatus in the proximal nasal airway (T1) of mice chronically exposed only to filtered air (A, C) or to an inhaled toxicant (B, D). Tissues in (A) and (B) were stained with hematoxylin and eosin, while tissues in (C) and (D) were stained with Alcian blue (pH 2.4) and periodic acid schiff (AB/PAS) to identify cells containing acidic and neutral mucosubstances. There is a marked loss of olfactory epithelium (oe) and Bowman's glands (bg) in the nasal mucosa from the mouse exposed to the inhaled toxicant (B). Olfactory epithelium is replaced by respiratory epithelium and subepithelial glands (g), indicating respiratory metaplasia (rm) of the oe. Notice that the AB/PAS-stained mucosubstances are normally restricted to the Bowman's glands (bg) and associated transepithelial ducts (C), but in rm the AB/PAS-stained mucosubstances are present in the mucous cells of the metaplastic glands and surface epithelium. *Reproduced from Harkema JR, Carey SA, Wagner JG: The nose revisited: a brief review of the comparative structure, function, and toxicologic pathology of the nasal epithelium, Toxicol. Pathol. 34:252–269, 2006, with permission.*



or hyperplasia/hypertrophy may also occur. Repeated ozone exposures cause epithelial hyperplasia followed by mucous cell metaplasia/hyperplasia in the proximal nasal airways of both monkeys and rats (Figures 4.9 and 14.16C) (Harkema et al., 1987). The mucus produced by these cells may have an increased concentration of acidic mucous glycoproteins, resulting in altered viscoelastic properties that modify mucous flow, thus affecting airway clearance mechanisms.

Stratified squamous metaplasia, with or without keratinization, is also frequently observed and may interfere with mucociliary clearance (Figure 4.17D). This metaplastic change is often reversible following cessation of exposure. If normal epithelial adaptive or repair processes cannot take place because of severe injury with complete loss of epithelial cells, including progenitor cells, excessive fibrin will accumulate in the nasal exudates, followed by intraluminal fibrosis. In rodents, excessive hyperkeratosis, severe inflammatory exudation, or fibrosis may lead to obstruction of the nasal cavity and even death of these obligate nasal breathers.

In summary, chemically induced injury of the nasal epithelium may be followed by regenerative hyperplasia or metaplastic changes such as respiratory metaplasia of the olfactory epithelium and mucous or squamous cell metaplasia of the transitional and respiratory epithelium. Severe hyperplastic and squamous metaplastic changes from persistent mucosal injury may be a prelude to nasal neoplasia.

#### 4.5.3. Nasal Neoplasia

In spite of the rare occurrence of spontaneous nasal tumors in rodents, the nasal cavity is highly sensitive to environmental carcinogens, irrespective of the route of administration, and thus should be examined in all carcinogenicity studies. Grossly, these neoplasms appear as gray white to yellowish infiltrative masses partially occluding the nasal cavity, often with necrotic areas and with destruction of adjacent tissue. These may occasionally extend into the brain or metastasize to other organs. The larynx is also a target site for xenobiotics, and should therefore be routinely examined.

Nasal tumors have been induced experimentally in rodents following inhalation of a variety of important industrial chemicals such as formaldehyde, acrolein, acetaldehyde, alachlor, bis(chloromethyl) ether,

hexamethylphosphoramide, and vinyl chloride. Obligate nasal breathing and complexity of the nasal turbinates may explain why tumors develop in rodents but have not been reported in association with exposure to these chemicals in humans. Tumors have also been induced following parenterally administered chemicals such as nitrosamines. Malignant nasal neoplasms are rare in humans, except for six occupational groups: those that work with chromate, nickel, mustard gas, isopropyl alcohol, wooden furniture, and boot and shoes. In addition, welders, flame cutters, and solderers have an increased risk of nasal cancer. Animal studies have incriminated certain hexavalent chromium compounds and metallic nickel as carcinogenic agents (Feron et al., 2001).

Tumors of the rat nasal cavity have been classified as adenomas, squamous cell papillomas, adenocarcinomas and carcinomas of squamous cell, adenosquamous and neuroepithelial (also called olfactory neuroblastoma and esthesioneuroblastoma) types (Renne et al., 2009). These mainly arise from the lining epithelium, or less commonly, the submucosal glands. Squamous cell carcinomas and adenocarcinomas have also been reported in the larynx of rats and hamsters.

In humans, squamous cell carcinoma is the most common spontaneous nasal tumor (75%), while adenocarcinomas and undifferentiated tumors are less common (10% each). Nonmalignant nasal polyps can obstruct nasal airflow and may be attributed to severe allergic responses and asthma. In the dog, adenocarcinoma, squamous cell carcinoma, and undifferentiated carcinoma are equally prevalent.

#### 4.6. Tracheobronchial and Pulmonary Responses to Injury

As in the upper airways, toxic injury to the lower respiratory tract may nonspecifically affect most epithelial cells or be limited to a single cell type. Injury may be mild and reversible, with minimal inflammation and complete repair by epithelial regeneration. More severe injury, with nonspecific necrosis or following chronic toxicant exposure, can induce high-grade inflammation and fibrosis, which is irreversible. The epithelial lining of the bronchiolar region is exquisitely susceptible to injury by oxidant gases ( $\text{NO}_2$ ,  $\text{SO}_2$ , and  $\text{O}_3$ ) and toxicants (3MI).

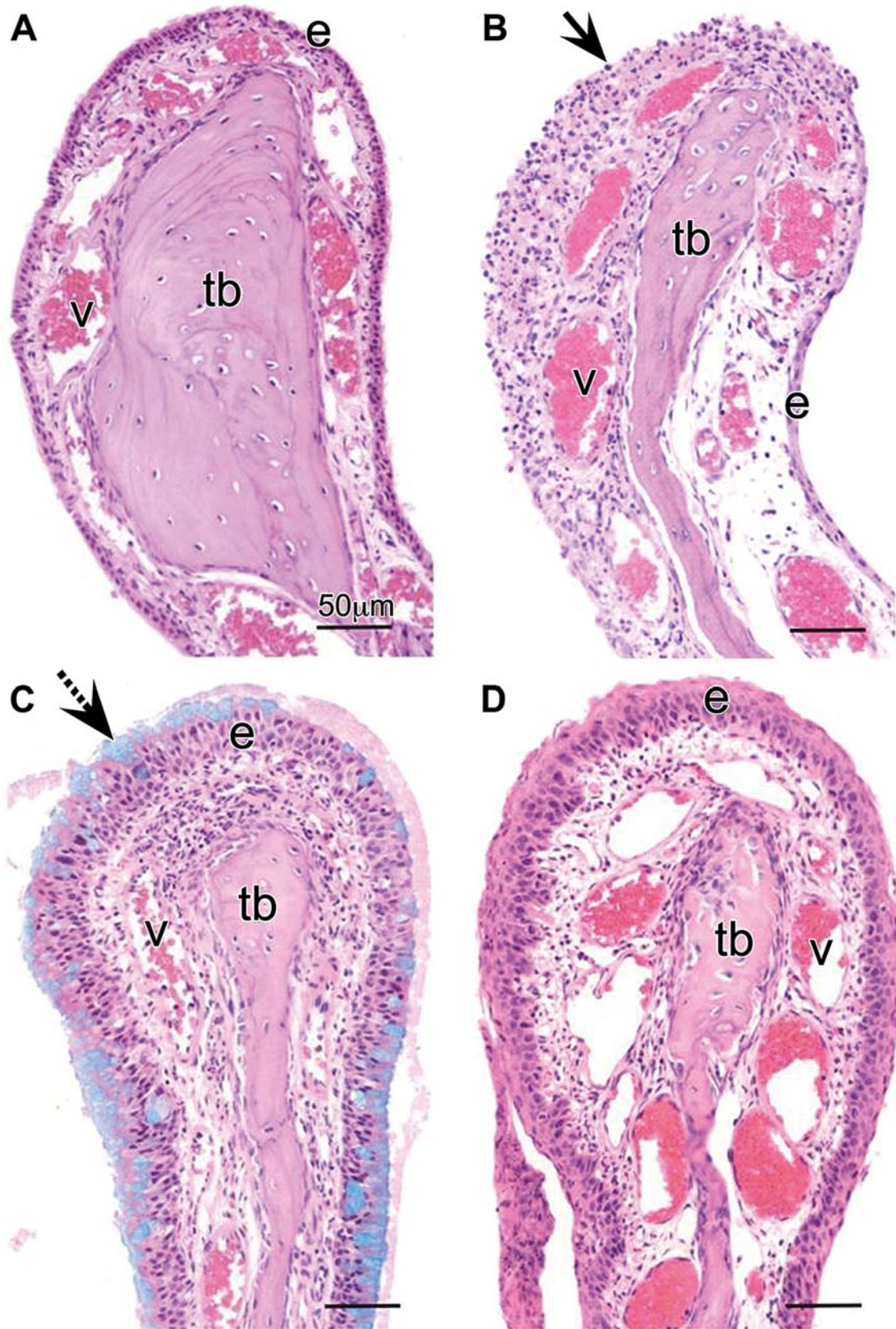


**FIGURE 4.17** Light photomicrographs of the maxilloturbinates in the proximal nasal airways of rats that were exposed to either filtered air alone (A; controls), short-term inhalation exposure to a high concentration of mainstream



Injury to airway epithelium invariably impairs mucociliary clearance due to alterations in mucus or to injury of ciliated cells. Changes in ciliated cells may range from ciliostasis or ciliary loss to cell death. An increased rate or amount of mucus secretion is a common response to inhaled toxicants such as SO<sub>2</sub>, O<sub>3</sub>, NO<sub>2</sub>, and NH<sub>3</sub>. Mucus hypersecretion from surface epithelial cells may be stimulated by direct irritation. Hypersecretion and an increase in glycoprotein content from submucosal glands may follow parasympathetic stimulation or parasympathomimetic drugs such as acetylcholine and pilocarpine. A change in the glycoprotein fraction affects the viscosity of mucus. Excess mucus has an irritant effect on sensory nerve endings, often triggering the cough reflex. Release of acetylcholine from irritated synapses of the autonomic innervation present in the bronchiolar epithelium causes bronchiolar constriction and mucus secretion. Mast cell mediators, as well as prostaglandins and lipoxygenase products, also appear to stimulate mucus secretion.

Morphologically, mucus may be readily observed in airways of affected animals, whereas in normal animals, it is not. In some cases of chronic exposure, increased numbers/size of mucous cells (hyperplasia/hypertrophy, respectively) or abnormally located mucous cells (mucous cell metaplasia) may be observed. If these changes persist, they can result in blockage of mucus-producing glands and ducts, airway obstruction, and/or alveolar injury. Debris can accumulate and incite an inflammatory response. Inflammation, if present, may be confined to the airway wall or extend into the lumen. Neutrophils predominate in the early stages of inflammation, whereas mononuclear cells are

prominent in later stages. Eosinophils may be associated with allergic conditions.

Injury to epithelium may result in epithelial degeneration, detachment, and exfoliation of cells. This loss is normally followed by inflammation and repair. If the basement membrane is not damaged and the injurious agent does not persist, the epithelium will regenerate within a few days by proliferation of immature secretory stem cells or club cells in the small airways. Differentiation of these cells is followed by recovery. If the basement membrane is damaged, fibroblast precursors may migrate from the ulcerated airway wall into the lumen, particularly when a fibrinous exudate is present. Organization can occur within 7–10 days, resulting in intraluminal fibrosis (bronchiolitis obliterans; [Figure 4.18](#)). This type of lesion has been reported with highly reactive volatile chemicals such as methyl isocyanate (MIC), with NO<sub>2</sub> in silo filler's disease, and with diacetyl in microwave-popcorn factory workers. Fibroblast proliferation may also occur in the lamina propria or peri-airway. If severe inflammation is present, in addition to basement membrane damage, bronchiectasis (destruction of airway wall with dilation) or abscess formation, following infection, may occur.

If clearance is sufficiently impaired and spontaneous resolution does not take place, obstruction of airways with concomitant bronchoconstriction and hypoxic vasoconstriction may occur and lead to death from hypoxia, or alveolar injury and emphysema. In the event of continued irritation, squamous metaplasia may occur. Both squamous metaplasia and uncontrolled cell proliferation may potentially be followed by neoplasia.

cigarette smoke (B), or long-term exposures to a high concentration of ozone or cigarette smoke (C and D, respectively). Tissues were stained with hematoxylin and eosin, and Alcian blue (AB). The transitional epithelium (e) lining the maxilloturbinate in (B) has exfoliated (arrow) and a conspicuous acute inflammatory cell influx is present in the lamina propria. The ozone-exposed maxilloturbinate (C) is remarkably thickened due to epithelial hyperplasia and mucous cell metaplasia (stippled arrow, mucous cells with AB-stained mucosubstances). Numerous inflammatory cells are also present in the underlying lamina propria. Long-term cigarette exposure (D) caused squamous metaplasia of the transitional epithelium along with inflammation in the lamina propria. The turbinate bones (tb) are atrophic in the maxilloturbinate of the rats exposed to these inhaled toxicants (B, C, D). v, blood vessels. (A & C) Reproduced from Harkema JR, Carey SA, Wagner JG: *The nose revisited: a brief review of the comparative structure, function, and toxicologic pathology of the nasal epithelium*, *Toxicol. Pathol.* 34:252–269, 2006, with permission. (B & D) Reproduced from Haschek, Rousseaux, Wallig, editors: *Handbook of toxicologic pathology*, ed 3, 2013, Academic Press, vol. 3, figure 51.13, p. 1972.



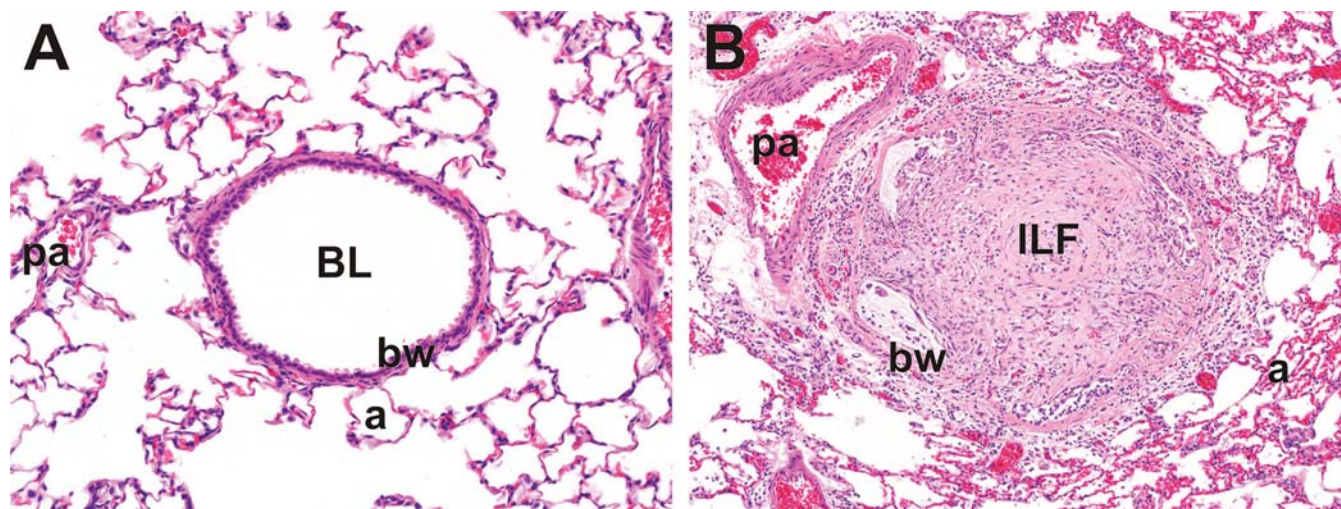


**FIGURE 4.18** Light photomicrographs of small diameter, preterminal bronchioles in the lungs of mice that received repeated, daily inhalation exposures to either filtered air (A; control) or a butter flavoring agent, 2,3 pentanedone (B). The bronchiolar lumen (BL) in (B) is almost completely obliterated by fibrotic tissue (intraluminal fibrosis; ILF), the distinguishing histologic feature of bronchiolitis obliterans. Tissue sections were stained with hematoxylin and eosin. bw, bronchiolar wall; a, alveolar parenchyma; pa, pulmonary artery. *Courtesy of Drs Crystal Johnson, Gordon Flake, and Daniel Morgan at the National Toxicology Program, National Institute of Environmental Health Sciences, Research Triangle Park, NC, USA. Reproduced from Haschek WM, Rousseaux CG, Wallig MA, editors: Handbook toxicologic pathology, ed 3, 2013, Academic Press, Vol. 3, Figure 51.14, p. 1974, with permission.*

#### 4.6.1. Cell-Specific Injury

Ciliated cells lining the tracheobronchial airways may be selectively damaged by inhaled toxicants (e.g., loss of cilia is a stereotyped response to inhalation of acidogenic gases such as SO<sub>2</sub> and NO<sub>2</sub>, while cigarette smoke slows ciliary beat frequency). Ozone selectively damages ciliated cells in the terminal and respiratory bronchioles, causing loss of cilia or cell death. This is followed by conspicuous hyperplasia of club cells in both rodents and monkeys (Figure 4.19).

As mentioned previously, selective toxicity to the club cell is induced by agents that require metabolic activation to their putative toxin by the cytochrome P450 enzymes (Table 4.4). Damage may be limited to club cells, or may be followed by more extensive pulmonary injury, depending on the specific compound, dose, and species. Examples of selective club cell toxins are 4-ipomeanol, naphthalene, 3-methylfuran, CCl<sub>4</sub>, styrene, and acetaminophen. Movement of remaining bronchiolar cells to cover the denuded basement membrane follows necrosis of club cells and rapid proliferation of remaining club cells to regenerate normal epithelium.

Selective damage to club cells, unrelated to their cytochrome P450 content, has also been reported. This selectivity is presumably related to other unique features of the cell. For instance, methylcyclopentadienyl manganese tricarbonyl (MMT), which is detoxified in the liver by the cytochrome P450 enzymes, causes mitochondrial damage in club cells, likely due to the high oxidative enzyme content of these cells. In addition, some PCB congeners affect club-cell secretory functions.

#### 4.6.2. Hyperreactive Airway Disease

Hyperresponsive airways are a possible sequel to bronchiolar injury. Hyperactive airway disease can develop following transient and seemingly innocuous viral infections, from exposure to certain allergens, or from exposure to inhaled or ingested respiratory toxicants. Sustained inhalation of dust particles may play a role by upregulating the production of cytokines (interleukin 8, IL-8) and monokine-inducible protein (MIP-2) by alveolar macrophages, attracting neutrophils into the bronchoalveolar region, and ultimately causing secondary bronchiolar injury. Airway hyperresponsiveness is

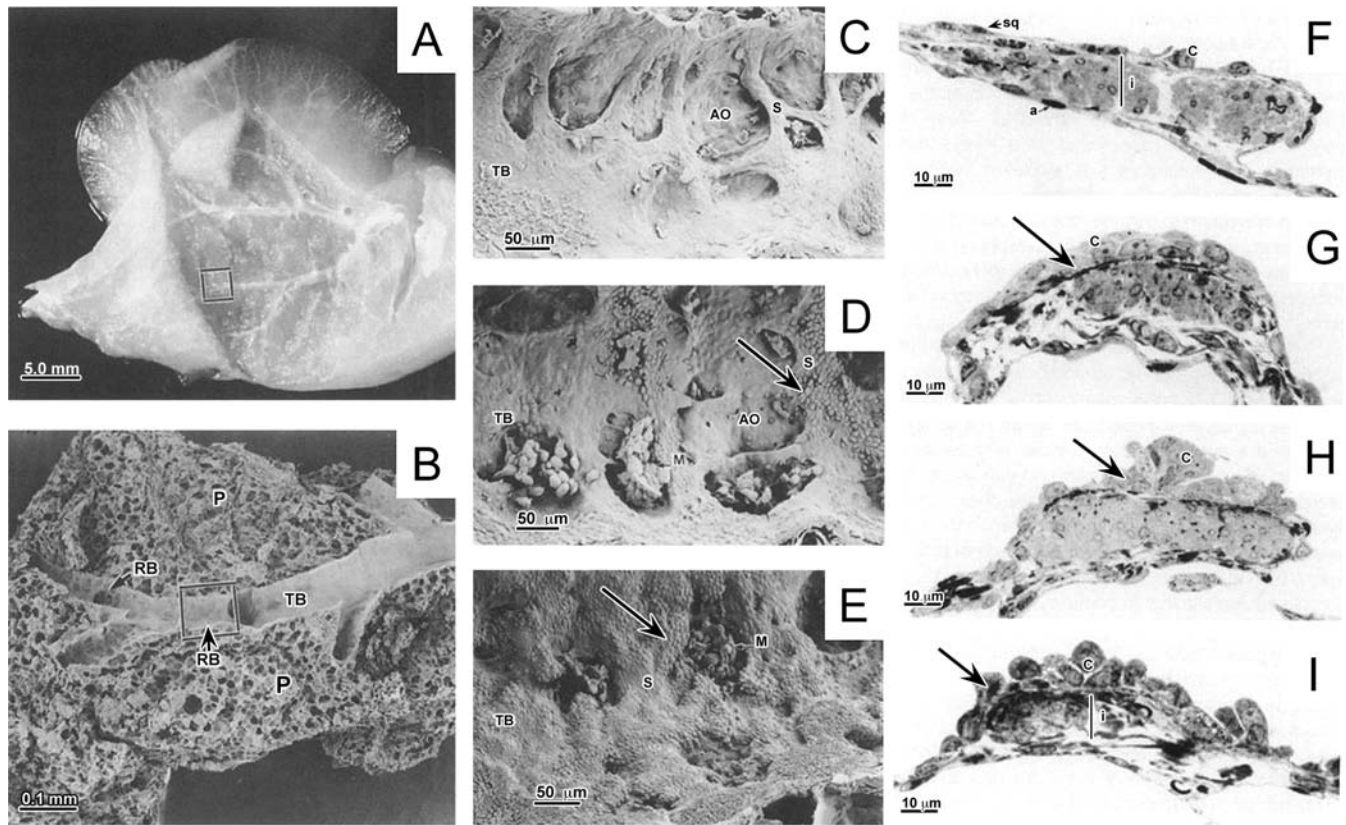


**FIGURE 4.19** Ozone-induced remodeling of the respiratory bronchioles in nonhuman primates. (A) Photograph of the dissected left cranial lung lobe from a macaque monkey with exposed axial airways. Box in (A) outlines the centriacinar region that was excised for scanning electron microscopy. (B) Scanning electron photomicrograph of the selected centriacinar region. Box in (B) identifies the location of proximal respiratory bronchioles that were further examined by both light and scanning electron microscopy. Scanning electron photomicrographs of first-generation respiratory bronchioles from monkeys exposed to 0 ppm ozone for 90 days (C), 0.15 ppm ozone for 90 days (D), or 0.30 ppm for 90 days (E). TB, distal end of terminal bronchiole; AO, alveolar outpockets; S, inter-alveolar septa; M, alveolar macrophages. Note the greater accumulation of macrophages in alveolar outpockets and nonciliated club cells (arrows) in ozone-exposed airways (D, E). Light photomicrographs of interalveolar septa of respiratory bronchioles from monkeys exposed to 0 ppm ozone for 90 days (F), 0.15 ppm ozone for 6 days (G), 0.15 ppm ozone for 90 days, or 0.30 ppm ozone for 90 days. Epithelial hyperplasia due to an increase in club cells (arrows) is present in (G), (H), and (I). Reproduced from Harkema et al.: Response of macaque bronchiolar epithelium to ambient concentrations of ozone, *Am. J. Pathol.* 143(3):857–866, 1993, with permission.

characterized by exaggerated bronchoconstriction following exposure to mild stimuli such as cold air. Typically, increased numbers of mast cells, eosinophils, and T lymphocytes are present in the airway mucosa.

#### 4.6.3. Chronic Obstructive Pulmonary Disease

Chronic bronchitis, emphysema, and asthma comprise the clinical entity known as COPD. Asthma can be clinically differentiated from chronic bronchitis and emphysema because the obstruction is reversible. Chronic bronchitis

and emphysema are difficult to distinguish clinically, but they are distinguished postmortem based on morphologic criteria. A distinction is often made between disease of the larger airways (chronic bronchitis) and disease of bronchioles (bronchiolitis or small airways disease). However, most patients with chronic obstructive lung disease show evidence of both conditions because the etiologic agents, such as cigarette smoke, affect the lung at all airway levels. Emphysema also frequently accompanies chronic bronchitis and contributes to small airway obstruction.



#### 4.6.4. Asthma

Asthma is recognized clinically as episodic, reversible airway bronchoconstriction. Pathologically, it is a chronic inflammatory disease of airways. Episodic acute inflammation corresponds to clinical exacerbations of asthma. In asthmatics, the control of airway muscle shortening is abnormal. It is thought that chronic inflammation causes the airways of asthmatics to narrow when stimulated in ways that have minimal effects on nonasthmatics.

Asthma is generally categorized as being intrinsic (idiosyncratic) or extrinsic. Intrinsic asthma is initiated by nonimmune mechanisms and is seen in some patients after ingestion of aspirin, pulmonary (usually viral) infections, cold, inhaled irritants, stress, and exercise. Extrinsic asthma starts as a type I hypersensitivity reaction to an extrinsic antigen and includes atopic (allergic) and occupational asthma. Allergic or atopic asthma, which is an IgE-mediated sensitivity primarily to inhaled antigens (allergens) and resulting in bronchoconstriction, is the most common form. Examples of antigens include dusts, pollens, animal dander, and certain foods. Initial sensitization (priming) by the antigen induces T-helper lymphocytes that produce interleukin-4 and interleukin-5 (Figure 4.20).

These cytokines support Th2 immunity characterized by the production of IgE by B lymphocytes, increased numbers of mast cells with antigen-specific IgE bound to their receptors, and recruitment of eosinophils. Subsequent exposure to antigen results in an acute response (immediate phase, minutes) and a late-phase (hours) reaction. On reexposure to inhaled antigen, antigen-induced crosslinking of IgE bound to mast cells on the airway surface causes release of preformed mediators that open tight junctions between epithelial cells. Antigen then enters the mucosa and activates mucosal and submucosal mast cells and eosinophils that release additional mediators. These mediators, either directly or indirectly through neural reflexes, induce bronchospasm, increased vascular permeability and edema, mucus production, and recruitment of additional inflammatory cells from the blood. The recruitment of neutrophils, eosinophils, basophils, lymphocytes, and monocytes marks the start of the late phase. During the late phase, there is additional mediator release from leukocytes, endothelial cells, and epithelial cells. Endothelins from endothelial and epithelial cells are potent bronchoconstrictors and inducers of airway smooth muscle cell proliferation

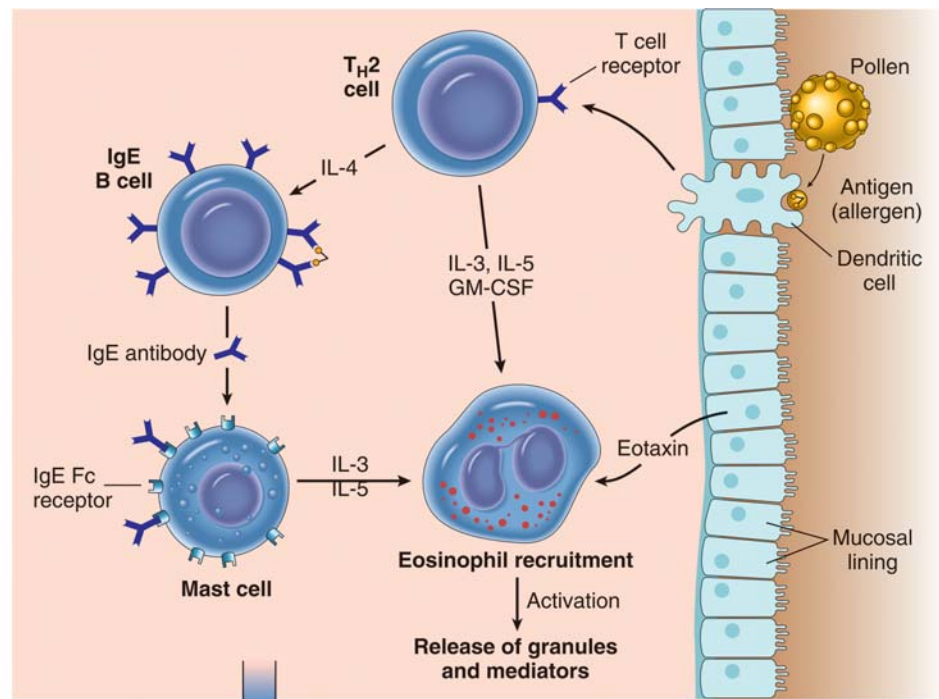
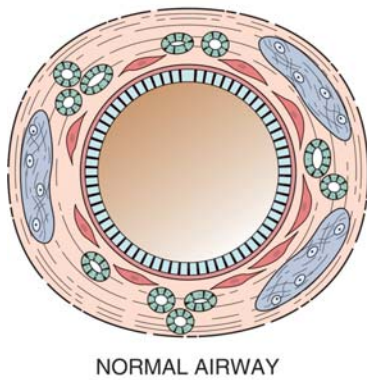
and fibrosis. Release of eotaxin from airway epithelial cells results in eosinophil recruitment and activation. During this phase, eosinophilic cationic protein and major basic protein released from eosinophils damage the epithelium and cause bronchoconstriction. Ambient air pollutants, such as ozone and particulate matter, are now thought not only to cause exacerbation of preexisting asthmatic conditions but also to act as adjuvants during initial sensitization to enhance the development of this common airway disease.

Occupational asthma has been associated with exposure to fumes such as epoxy resins, organic and inorganic dusts such as wood, cotton, and platinum, and gases such as toluene diisocyanate and formaldehyde. The mechanisms underlying occupational asthma may vary according to the stimulus. Occupational asthma due to low molecular weight antigens such as toluene diisocyanate appears to be IgE-independent and most likely mediated by CD8<sup>+</sup> T cells, IL-5 secretion, and eosinophils.

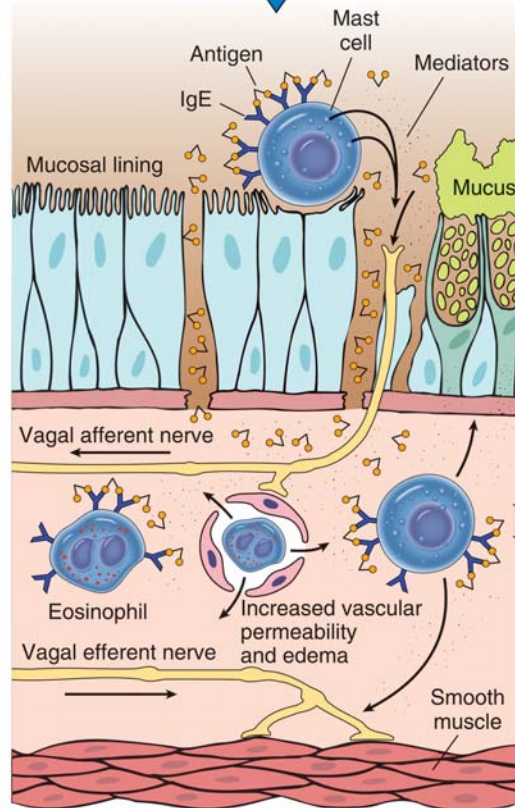
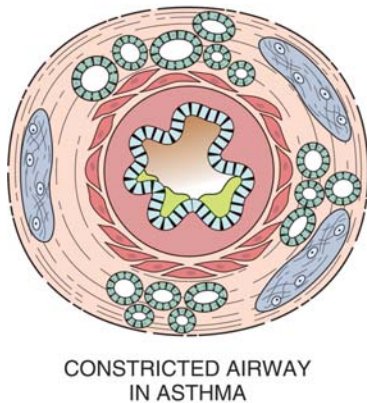
The morphologic features of asthma include excess mucus and eosinophils in the bronchial lumen, goblet cell metaplasia/hyperplasia of the surface epithelium, epithelial desquamation, hypertrophy and hyperplasia of the submucosal mucous glands, congestion and edema of the bronchial mucosa, chronic airway inflammation, basement membrane thickening, structural remodeling of airway longitudinal elastic bundles, and hypertrophy/hyperplasia of smooth muscle. The smooth muscle thickening is seen throughout the bronchial tree, which is most pronounced in the segmental airways and terminal bronchioles. The inflammatory cells in the airway walls include eosinophils, lymphocytes, neutrophils, macrophages, and mast cells. Eosinophils are prominent and may comprise 5%–50% of the infiltrating cells. This characteristic eosinophilic infiltrate differentiates asthma from other chronic inflammatory conditions of the airway. Most laboratory rodent models of allergic asthma, using experimental allergens like egg protein, ovalbumin, or house dust mite antigen, recapitulate some, but not all of, the pathologic and immunologic features of human asthma (Figure 4.21) (Haspeslagh et al., 2017). Similar experimental protocols using nonhuman primates result in additional facets of allergic airway disease (e.g., basement membrane thickening and airway interstitial remodeling) that are often seen in the human condition but are not commonly found in rat or mice models (Finkelman and Willis-Karp, 2008).



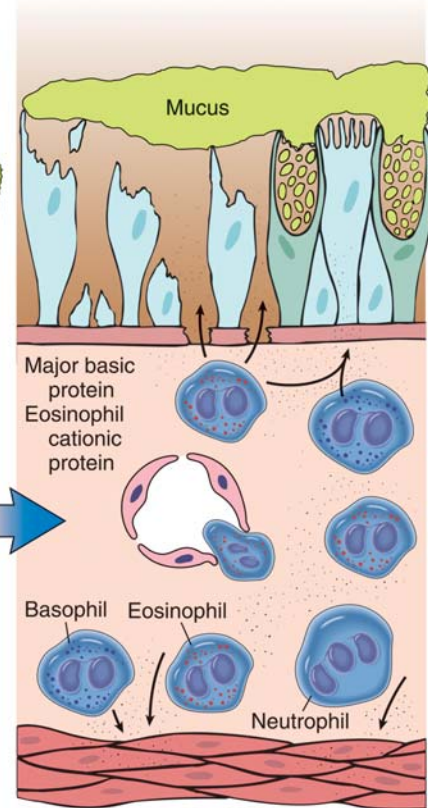
## A SENSITIZATION TO ALLERGEN



## B ALLERGEN-TRIGGERED ASTHMA



IMMEDIATE PHASE (MINUTES)



C LATE PHASE (HOURS)

**FIGURE 4.20** Allergic asthma. (A) Inhaled allergens (antigen) elicit a T<sub>H</sub>2-dominated response favoring IgE production and eosinophil recruitment (priming or sensitization). (B) On reexposure to antigen (Ag), the immediate reaction is triggered by Ag-induced crosslinking of IgE bound to IgE receptors on mast cells in the airways. These cells release preformed mediators that open tight junctions between epithelial cells. Antigen can then enter the mucosa to activate mucosal mast cells and eosinophils, which in turn release additional mediators. Collectively, either directly or via neuronal reflexes, the mediators induce bronchospasm, increased vascular permeability, and mucus production, and recruit additional mediator-releasing cells from the blood. (C) The arrival of recruited leukocytes signals the initiation of the late phase of asthma and a fresh round of mediator release from leukocytes, endothelium, and epithelial cells. Factors, particularly from eosinophils (e.g., major basic protein, eosinophilic cationic protein), also damage the epithelium. *Reproduced from Husain and Kumar: The lung. In Kumar V, Abbas AK, Fausto N, editors: Robbins and Cotran pathologic basis of disease, ed 7, 2005, Elsevier Saunders, Figure 15-11, p. 725, with permission.*



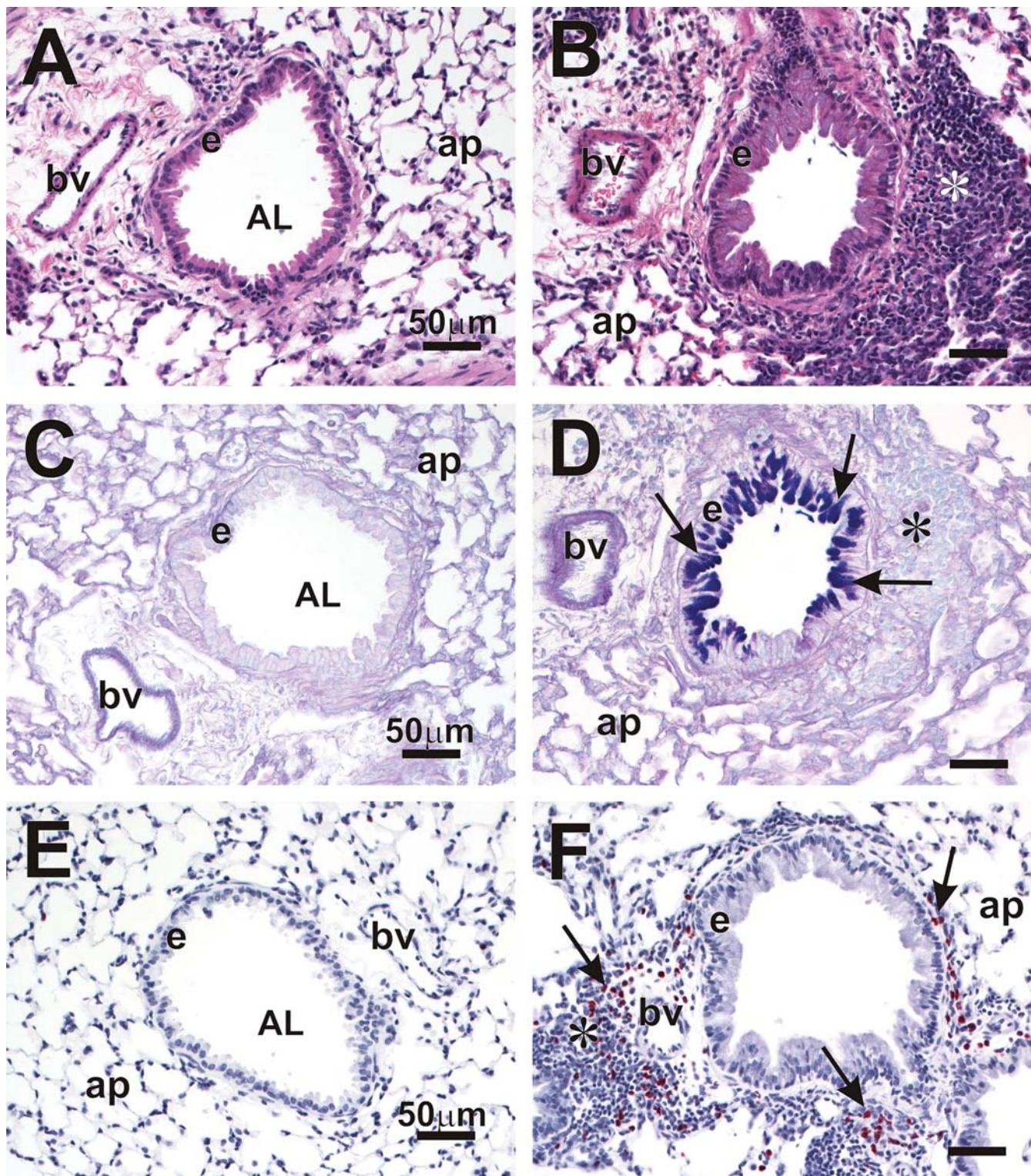


**FIGURE 4.21** Light photomicrographs of preterminal bronchioles from saline-instilled control mice (A, C, E) and mice that were sensitized and challenged with the experimental allergen, ovalbumin (B, D, F). Tissues sectioned were histochemically stained with hematoxylin (A, B) and with Alcian blue/periodic acid (AB/PAS) for intraepithelial mucosubstances (C, D), and immunohistochemically stained for eosinophil-specific major basic protein (E, F). Asterisks identify peribronchiolar mixed inflammatory cell infiltrate composed of lymphocytes, plasma, cells and eosinophils. Arrows in (F) depict eosinophils containing major basic protein. Ovalbumin treatment induced peribronchial mononuclear inflammatory cell influx (asterisk) with eosinophils and mucous cell metaplasia with large amounts of intraepithelial mucosubstances (B, D, F). From Li N, Wang M, Bramble LA, Schmitz DA, Schauer JJ, Sioutas C, Harkema JR, Nel AE: The adjuvant effect of ambient particulate matter is closely reflected by the particulate oxidant potential, *Environ. Health Perspect.* 117:116–123, 2009, with permission.



#### 4.6.5. Proliferative Lesions

Squamous metaplasia and hyperplastic lesions occur in the rat trachea, most frequently at the carina, and in the larynx, particularly along the ventral surface at the base of the epiglottis, the medial aspects of the arytenoid cartilages, and the dorsal surface at the level of the arytenoid cartilages. The rat larynx appears to be uniquely sensitive to induction of epithelial alteration, squamous cell hyperplasia, and squamous metaplasia by various industrial chemicals, pharmaceuticals, and propellants (Kaufmann et al., 2009; Osimitz et al., 2007). Papillomas are the main spontaneous neoplasms reported within the airways of rats. Benign neuroendocrine tumors, though uncommon, must be considered when papilloma-like tumors are found.

#### 4.7. Pulmonary Parenchymal Responses to Injury

Although it would be of great diagnostic convenience if specific agents elicited a characteristic response, the lung responds in a similar way to a wide variety of infectious and toxic agents. Viral and chemical agents frequently incite a comparable type of interstitial pneumonia, and both need to be considered as differentials for diffuse spontaneous pulmonary diseases. Particulates such as silica may incite a granulomatous response similar to that induced by tuberculosis and some mycotic agents. Occasionally, the etiologic agent can be identified, although methods other than the routine H&E-stained paraffin sections are usually required for detection. The response does vary to some degree, depending on the nature of the agent and on the severity and persistence of injury, as well as on the particular cell type affected and the reparative processes initiated by the injury.

Endothelial and type I epithelial cells are especially susceptible to toxic injury. When endothelial cells are injured or die, there is an increase in vascular permeability. Platelets may adhere to the exposed basement membrane, resulting in release of vasoactive agents. Complement activation, coagulation, and fibrinolysis may also occur before the basement membrane is repopulated. Increased vascular permeability allows the leakage of fluid into interstitial spaces and lymphatics, and eventually into alveolar spaces. If damage is more severe, edema may be followed by interstitial inflammation.

Epithelial damage is accompanied by the acute exudative phase of inflammation characterized by fibrin, neutrophils, and edema. Type II cells start to proliferate within 12–24 hours and, after a few days, may line alveoli; by light microscopy, this appears as a cuboidal epithelial lining. With time, the inflammatory component will consist of increased numbers of mononuclear cells and macrophages. If damage is not too severe and the basement membrane is intact, resolution may occur by transformation of type II cells into type I cells and subsidence of the inflammatory component. However, if alveolar epithelium has been denuded and the basement membrane has been damaged, fibroblast precursors move rapidly into the alveolar space and, particularly in the presence of fibrin, will result in intraalveolar fibrosis. Similarly, fibrosis may be a consequence of severe endothelial cell damage and fibrin deposition. Interstitial fibrosis may occur after distortion of the normal cell–cell contacts by inflammation or edema. Fibroblast proliferation can be noted within 72 hours of initial injury, and fibrosis may be evident in as little as 7 days. Atypical type II cells may persist in these areas.

Continued inflammation of the alveolar wall implies persistence of the causative agent or injurious mechanisms, which is an important feature of chronic interstitial pneumonia. The characteristic components of chronic alveolar irritation are proliferation and persistence of type II epithelial cells, interstitial thickening due to fibrosis, and accumulation of mononuclear cells. An intraalveolar exudate largely composed of macrophages may be present. Sustained or recurrent injury to capillary endothelium can lead to progressive vascular remodeling and chronic pulmonary hypertension (see *Cardiovascular System*, Vol 5 Chap 1). Pulmonary hypertension has been reported after ingestion of certain plants or medicines, including the leguminous plant *Crotalaria spectabilis*, indigenous to the tropics and used medicinally in “bush tea” and the appetite depressant agent aminorex.

Macrophage reactions are among the most common findings seen in inhalations studies (Forbes et al., 2014). Alveolar macrophages are efficient at removing foreign agents from the lung. They remove soluble pharmaceuticals by pinocytosis, and poorly soluble drugs by phagocytosis. As previously discussed, there are considerable species differences in particle-



dependent clearance rates and microanatomy varying according to species. It is important, though sometimes challenging, to distinguish adaptive versus adverse responses, especially since it is currently not possible to monitor and characterize potential macrophage accumulation in man due to the absence of clinical measurement techniques and discriminatory biomarkers. Macrophage reactions display a phenotypic continuum from a simple minor increase in numbers or aggregates, to colocalization with inflammatory changes involving other cell types, to granulomas with fibrosis.

In the alveoli, resident macrophages patrol the surface epithelium and phagocytose insoluble or poorly soluble particles as well as endocytose more soluble particles. Macrophages have impressive ability to consume particles up to 30  $\mu\text{m}$  diameter. Overload may ensue if macrophage capacity becomes overwhelmed due to size and/or solubility, for example. In rats, the threshold for overload is crossed when the volume of ingested particles exceeds 6% of their normal cytoplasmic volume. High concentrations of inhaled (insoluble) particles are microscopically characterized by inflammation containing macrophages with foamy or granulated cytoplasm and neutrophils; accompanied by parenchymal changes which may include fibrosis (Hall et al., 2021).

#### 4.7.1. Phospholipidosis

Alveolar macrophage phospholipidosis occurs when there is excessive accumulation of phospholipids in lysosomal lamellar bodies resulting in a foamy phenotype (Figure 4.22) (Lenz et al., 2018). Classically, phospholipidosis has been associated with the administration of compounds with a cationic amphophilic structure. The route of administration may be intravascular, oral, or by inhalation. When the route is intravascular or oral, the response typically is not restricted to alveolar macrophages. Often, however, the alveolar macrophage is the most sensitive cell type affected, readily manifesting the foamy morphology microscopically. Phospholipidosis can be seen in surfactant protein D-deficient mice and in response to infections such as tuberculosis and human immunodeficiency virus (Forbes et al., 2014).

Phospholipidosis was first recognized in the literature in 1971. Since then, over 50 drugs known

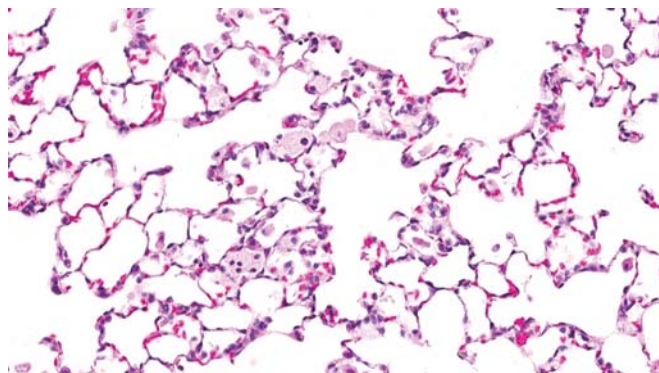


**FIGURE 4.22** Phospholipidosis. Alveolar macrophage phospholipidosis occurs when there is excessive accumulation of phospholipids in lysosomal lamellar bodies resulting in a foamy phenotype. Classically, phospholipidosis has been associated with administration of compounds with a cationic amphophilic structure. The route of administration may be intravascular, oral, or by inhalation. When the route is intravascular or oral, the response typically is not restricted to alveolar macrophages. Often, however, the alveolar macrophage is the most sensitive cell type affected, readily manifesting the foamy morphology microscopically.

to cause phospholipidosis in animals have gone to market. Phospholipidosis is often not associated with degenerative or inflammatory changes, but in some cases can cause widespread tissue destruction characterized by coalescing abscesses. There is debate as to whether associated inflammatory changes are directly due to phospholipidosis or some other mechanism such as lysosomal fragility and proteolytic enzyme leakage from compound-phospholipid complexes that have exceeded a certain concentration.

In its mildest form, phospholipidosis is usually reversible, but recovery may take time due to suppression of macrophage clearance. Phospholipidosis has also been shown to accelerate the accumulation of other pneumophilic coadministered drugs. The significance of phospholipidosis in terms of adversity is complex. While it is considered an adaptive process, there may be concomitant toxicological changes in-life and/or microscopically that are clearly adverse. It is suggested that each phospholipidosis study be approached individually with respect to adversity and consideration of its effect on homeostatic functions.

Foamy alveolar macrophages have other etiologic origins. Excessive salivation may lead to

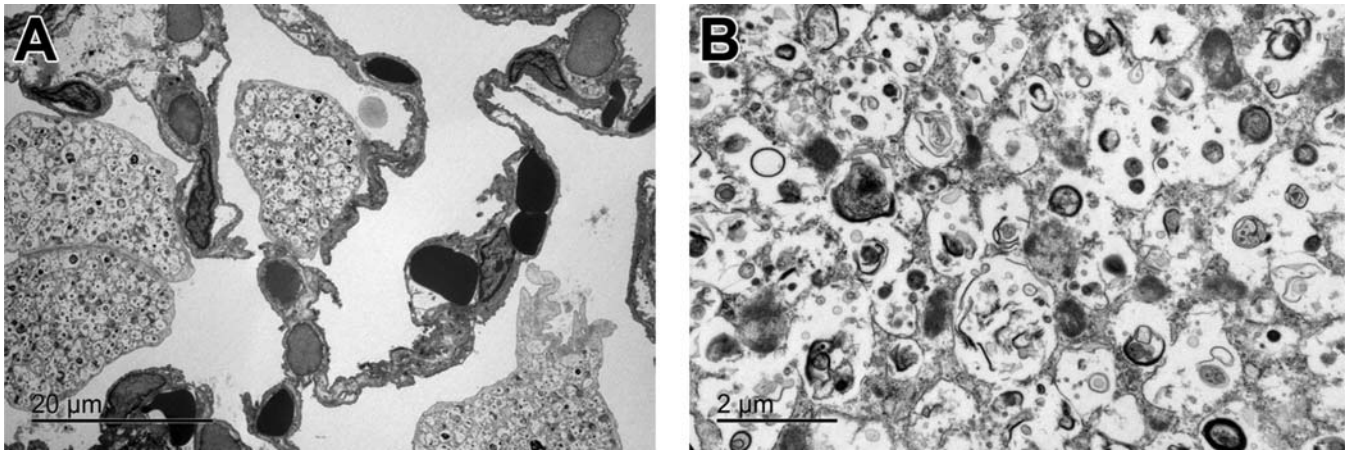


**FIGURE 4.23** Lung, rat, TEM, phospholipidosis, midpower (A). Multiple septal walls containing low numbers of endothelial cells, capillaries with erythrocytes, and type I pneumocytes. Adjacent to the septal walls are four markedly enlarged alveolar macrophages. The macrophages contained numerous, small electron dense bodies (lamellar bodies) separated by clear space. Lung, rat, TEM, phospholipidosis, high power (B). There are numerous variably sized electron dense bodies separated by clear space. Electron dense bodies form a whorled or onion-skin pattern which multifocally sloughed or separated from the larger bodies. These are lysosomal lamellar bodies.

accidental inhalation of saliva and laryngospasm or even paralysis, known to occur with barbiturates. Diets with high fat content can result in foamy alveolar macrophages due to foamy transformation of blood monocytes and migration into alveoli. Liposomal delivery vehicles such as methylcellulose can result in foamy morphology as well.

Examination of macrophage contents via TEM assists in revealing distinctive features such as insoluble compound, crystalline formations (related to drug crystals), multilamellar bodies (suggestive of phospholipidosis), or amorphous material and myelin-like multilamellar bodies in proteinosis (Figure 4.23). Additionally, if there is a strong suspicion of phospholipidosis, immunohistochemical staining for LAMP-2 (a lysosome-associated protein) and adipophilin (a protein that forms the membrane around non-lysosomal lipid droplets) can be used to differentiate phospholipidosis and lipidosis (Obert et al., 2007; Asaoka et al., 2013). IHC is less precise than TEM, but also less resource-intensive and costly.

Pulmonary alveolar proteinosis (PAP) (see below) often resembles phospholipidosis histologically, but the eosinophilic intraalveolar material is more prominent and proteinosis is typically associated with noncationic

amphophilic drugs. ECM is eosinophilic with an H&E stain, stains positively for PAS and is diastase resistant, and both amorphous material and myelin-like multilamellar bodies are seen via TEM. Staining for neutral fats via oil red O or adipophilin IHC can help differentiate proteinosis from phospholipidosis, as proteinosis tends to stain strongly for neutral lipids while phospholipidosis does not.

#### 4.7.2. Pulmonary Alveolar Proteinosis

PAP or alveolar lipoproteinosis is caused by disordered production or clearance of surfactant (Seymour and Presneill, 2002). Granulocyte-macrophage colony-stimulating factor (GM-CSF) regulates clearance of surfactant by alveolar macrophages and autoimmune PAP in adults is caused by the development of GM-CSF antibodies, whereas hereditary PAP is due to gene mutations resulting in dysfunctional GM-CSF receptor. In these forms of “primary” PAP, there is accumulation of acellular, lipoproteinaceous material in alveoli. PAP may also be seen with hematologic neoplasms. Occupationally and in animal toxicity studies, PAP has been caused by particle inhalation, either due to particle overload with relatively inert particles or due to inhalation of more toxic particles at lower doses. Titanium, aluminum, indium, tin

oxide, soluble and insoluble nickel compounds, metal oxide nanoparticles, silica, cement dust, coal dust, and talc are examples of particles that have induced PAP in animals or humans (Cho et al., 2012; Bomhard, 2017). PAP due to impairment of macrophage-mediated clearance (overload) is caused by disturbance of the normal balance between production of surfactant by type II cells, and clearance and recycling of surfactant by macrophages and type II cells. Morphologically, type II cell hyperplasia and increased macrophages with degeneration and necrosis of macrophages may be evident along with variable amounts of inflammation (usually granulomatous) and fibrosis.

The accumulated material in PAP is eosinophilic in an H&E stain and PAS positive. PAS positivity, particularly with diastase resistance, is considered definitive for a diagnosis of PAP. Amorphous material and myelin-like, multilamellar bodies are visible by TEM (Bomhard, 2017).

#### 4.7.3. Pulmonary Edema

Pulmonary edema can occur as a result of altered hemodynamics or increased permeability of the air–blood barrier. Altered hemodynamics can result from increased capillary hydrostatic pressure due to cardiac failure, acute injury to the nervous system (neurogenic pulmonary edema), or decreased plasma oncotic levels due to decreased plasma protein levels.

The constituents of the lung that are important in fluid homeostasis are the vascular bed, endothelial barrier, interstitial space, lymphatics, alveolar epithelial barrier, and alveolar surface tension (Figure 4.24). Altered hemodynamics or increased endothelial permeability will result in fluid loss through the moderately leaky endothelium into the adjacent interstitium. Interstitial fluid normally percolates along the interstitium until it reaches the lymphatics that are located adjacent to airways and associated vessels, within interlobular septa (in species that have these) and beneath the pleura. Alveolar fluid clearance across the alveolar epithelium is also a mechanism of fluid removal from the lung. Dilated lymphatics and increased lymph flow are good early indicators of edema. If lymphatic capacity is overwhelmed, interstitial edema will occur. When the capacity of the interstitium is inundated, or if there is damage to alveolar

epithelial cells, fluid will leak into the alveoli causing alveolar edema, which interferes with diffusion of gases and results in impaired gas exchange. Because of their tight junctions, alveolar epithelial cells provide a tighter barrier to exudation of fluid than do endothelial cells. Depending on the extent of increased permeability, fibrin and low molecular weight proteins such as albumin, will accompany the fluid loss. Pleural effusion is a common feature of pulmonary edema in rodents; interstitial fluid passes from the subpleural interstitium into the pleural cavity through stomata in their very thin pleural mesothelium.

The edematous lung is larger and firmer than normal and does not collapse. Fluid oozes from the cut section. The pleura and interlobular septa are thickened by clear fluid, and pleural effusion (hydrothorax) may be present. Froth in the airways without other findings may be due to agonal change. These changes are easy to detect in large animals, but more difficult to identify in rodents. Lung wet weight and, more specifically, the wet-to-dry-weight ratio are useful in determining the presence of edema. More sensitive and specific techniques for measuring pulmonary edema are available in order to discriminate between simple edema and increased blood content (congestion or hemorrhage) or cellular components. On microscopic examination, early/mild edema is characterized by dilated lymphatics, widening and separation of interstitial tissue (especially perivascularly); and if alveoli are affected, expansion of the alveolar lumen. This should not be confused with artifacts induced by intratracheal fixation. If the fluid contains protein, it will have a homogeneous eosinophilic appearance on H&E-stained sections (Figure 4.25). Fixation in Zenker's solution precipitates protein and increases the staining of proteinaceous edema. If fibrin is present, this will appear as pink fibrillary material. Special stains to confirm the presence of fibrin, such as phosphotungstic acid hematoxylin (PTAH), can be used.

Permeability edema occurs when there is excessive opening of endothelial gaps or damage to the air–blood barrier (type I epithelial cells or endothelial cells). Changes in capillary permeability may be due directly to endothelial cell injury or cellular or humoral “mediators” of inflammation. Numerous inhaled or circulating



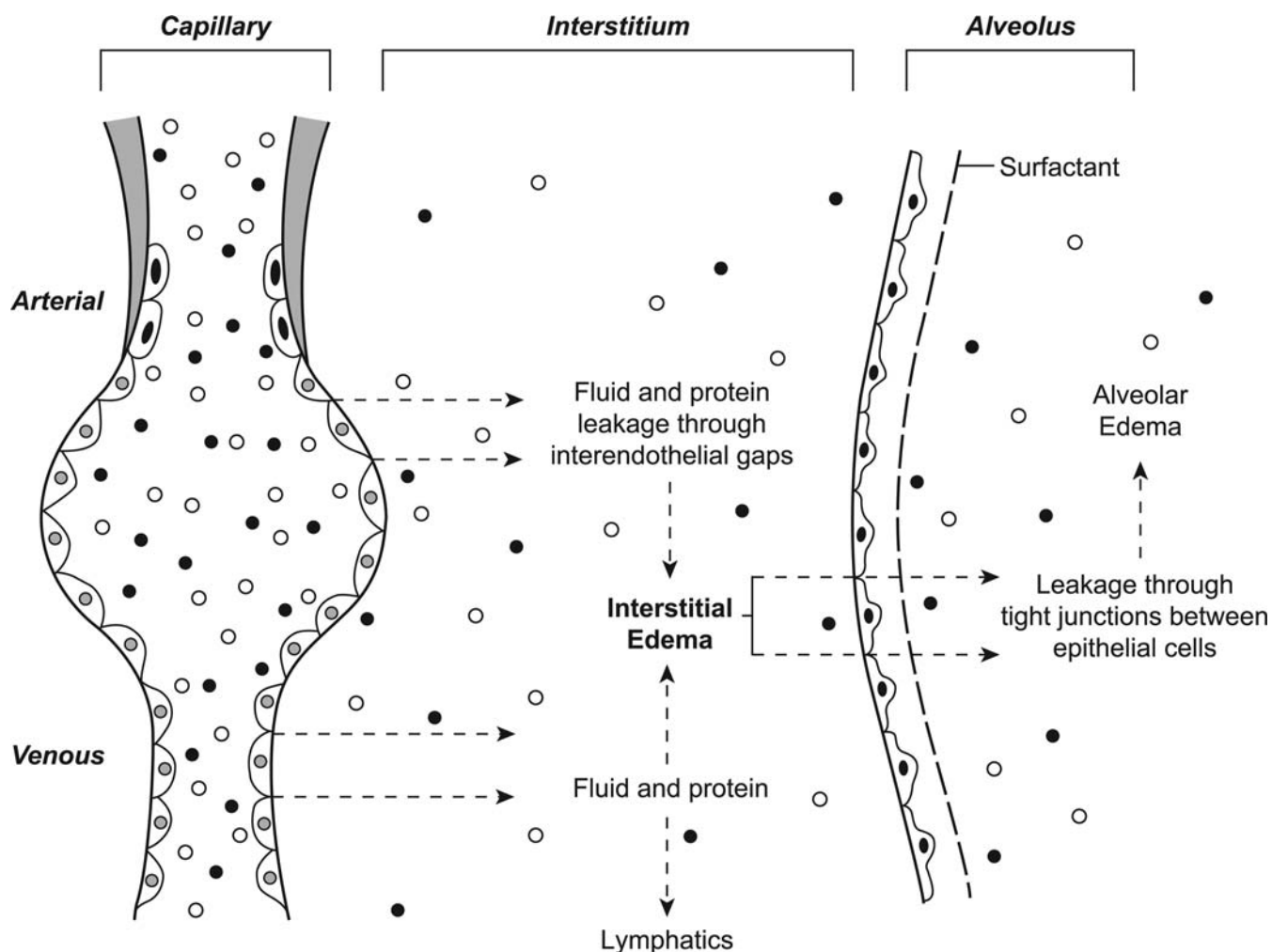


**FIGURE 4.24** Pulmonary edema. Interstitial edema occurs when excess fluid enters the interstitium from the pulmonary vasculature. Alveolar edema occurs when interstitial fluid enters the alveolar lumen either following direct alveolar epithelial damage or following a build-up of interstitial fluid. *Reproduced from Haschek WM, Rousseaux CG, Wallig MA, editors: Handbook of toxicologic pathology, ed 2, 2002, Academic Press, Vol. 2, Figure 20, p. 53, with permission.*

toxicants, bacterial toxins, anaphylactic shock, and drugs are believed to cause pulmonary edema by a direct effect on the endothelium or type I epithelial cells. Mediators that alter endothelial permeability may be released from mast cells (histamine) during allergic responses, from aggregated platelets, and from phagocytic cells as they migrate through the endothelium. Since type I epithelial cells are highly vulnerable to toxicants such as  $\text{NO}_2$ ,  $\text{SO}_2$ ,  $\text{H}_2\text{S}$ , and 3MI, as well as to free radicals, alveolar edema accompanies many toxic pulmonary diseases.

Pulmonary edema interferes with the respiratory gas-exchange function of the lung. With mild injury, repair processes can result in a return to

normal; however, with severe or prolonged injury, inflammation and eventually fibrosis may follow.

The classic example of toxicant-induced pulmonary edema is that induced by  $\alpha$ -naphthylthiourea (ANTU), a rodenticide. The rat is extremely sensitive to ANTU; massive pulmonary edema and pleural effusion occur as a consequence of endothelial damage to capillaries and venules. Inflammation does not occur. In animals that survive, edema is resolved by 48 hours, without permanent lung damage. Although the mechanism by which ANTU damages the lung is not known, it appears that ANTU is metabolically activated to a toxic oxidative species.

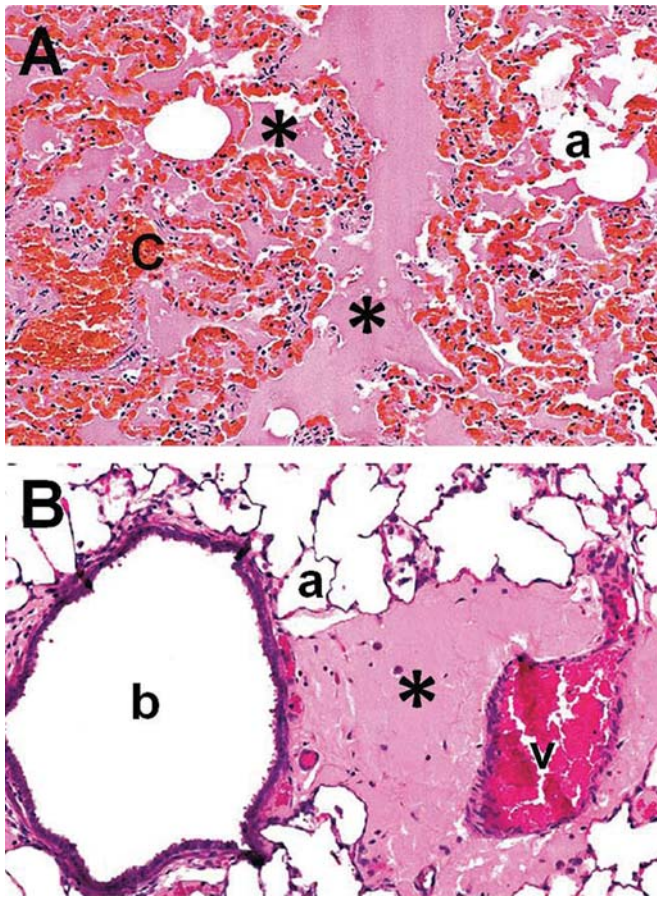


**FIGURE 4.25** Light photomicrographs of pulmonary edema located in bronchiolar and alveolar airspaces (asterisk in A) along with congestion (C) of capillaries in the septal wall, and in the perivascular interstitial spaces (asterisk in B) of the rat; H&E stain. Reproduced from Renne R, Brix A, Harkema J, Herbert R, Kittel B, Lewis D, March T, Nagano K, Pino M, Rittinghausen S, Rosenbruch M, Tellier P, Wohrmann T: Proliferative and non-proliferative lesions of the rat and mouse respiratory tract, *Toxicol. Pathol.* 37 (Suppl. 7):5S–73S. 2009, (Figures 99 and 100), with permission.

Many other toxicants also cause edema. These include bacterial endotoxin, which injures endothelial cells; paraquat, which damages epithelial cells (both type I and II); oxygen, which damages both endothelial and epithelial cells; and 4-ipomeanol, which damages club cells. In most cases, pulmonary edema occurs as an acute response with resolution or a successive inflammatory response. In the case of phosgene and smoke inhalation, edema is characteristically delayed for 1–2 days. Delayed edema is also produced by intravenously administered

opiates, such as heroin and methadone. These opiates may act through the central nervous system. Delayed onset of severe proteinaceous edema, the “exudative phase” of radiation pneumonitis, occurs after ionizing radiation exposure. Many cardiovascular toxicants ultimately cause pulmonary edema, which may be lethal (see *Cardiovascular System*, Vol 4, Chap 1). Permeability edema due to epithelial and endothelial or microvascular damage is seen with several gases, including smoke from fires, endotoxemia, drugs, and chemicals such as paraquat. The lung is the target organ for anaphylactic shock in most domestic animals (those with IVMs); however, the portal-mesenteric vasculature is the primary target in dogs and rodents.

Diffuse endothelial and alveolar damage leading to fulminating edema is termed acute respiratory distress syndrome (ARDS). It is an important condition in humans, characterized by intravascular aggregation of neutrophils, diffuse alveolar damage (DAD), permeability edema, and formation of hyaline membranes (Figure 4.26). DAD results from systemic diseases as well as direct injury to the lung, where macrophages generate overwhelming amounts of cytokines (mainly  $\text{TNF-}\alpha$ ) and neutrophils aggregated in capillaries release destructive enzymes and toxic oxygen metabolites. DAD, characterized by edema, hyaline membranes, epithelial injury, and inflammation, is a common pathological feature of severe infections (viral, bacterial, fungal) in humans and some animal models. ARDS can occur due to direct lung injury caused by oxygen toxicity, radiation therapy, inhalation of toxicants and other irritants, such as smoke; or by systemic conditions resulting from shock, pancreatitis, narcotic overdose, and other drug reactions. ARDS is difficult to treat and is frequently fatal. This type of lesion also occurs in domestic animals and is considered to be a very early stage and severe form of interstitial pneumonia. An ARDS-type lesion may occur in laboratory dogs following aspiration or inhalation of stomach acid or vomitus (Ware and Matthay, 2000).

#### 4.7.4. Pulmonary Inflammation

Inflammation, also referred to as alveolitis or interstitial pneumonia, results from diffuse or patchy damage to alveolar septa caused by bloodborne or inhaled toxicants; in humans,



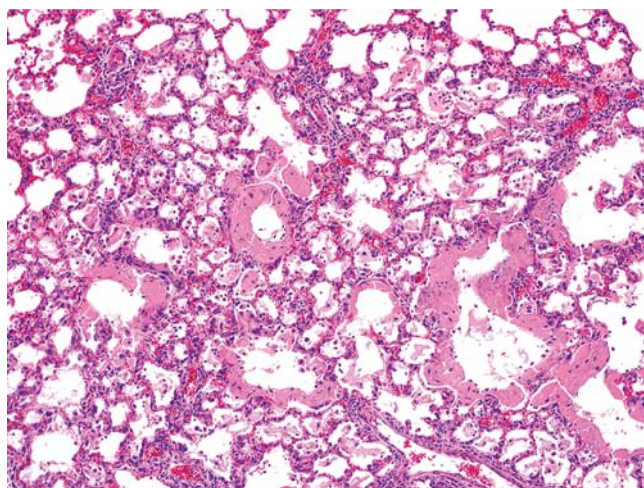


**FIGURE 4.26** Light photomicrograph of the lung from a mouse that received repeated, daily inhalation exposure to the butter flavoring agent, 2,3-pentanedione. Airspaces of alveolar ducts and alveoli are lined by hyaline membranes, H&E stain. *Courtesy of Drs Crystal Johnson, Gordon Flake, and Daniel Morgan at the National Toxicology Program, National Institute of Environmental Health Sciences, Research Triangle Park, NC, USA. Reproduced from Haschek WM, Rousseaux CG, Wallig MA, editors: Handbook of toxicologic pathology, ed 3, 2013, Academic Press, Vol. 3, Figure 51.20, p. 1982, with permission.*

the etiology in most cases of interstitial pneumonia is unknown. Inflammation is also a component of pneumoconiosis and other granulomatous diseases; however, once the disease is well established, the fibrotic component is most prominent.

Pulmonary inflammation is a highly regulated process that involves a complex interaction of leukocytes that arrive via the circulation, and resident leukocytes and pulmonary cells ([Figure 4.27](#)). Once in the lung, imported leukocytes communicate with pulmonary and vascular cells through adhesion and other inflammatory molecules such as the complement system (C3a, C3b, C5a), coagulation factors (factors V and VII), arachidonic acid metabolites (interleukins, monokines, chemokines), adhesion molecules, enzymes and enzyme inhibitors (elastase, antitrypsin), oxygen metabolites ( $O_2$ , OH,  $H_2O_2$ ), antioxidants (glutathione [GSH]), and nitric oxide. These and other molecules can initiate, maintain, and resolve the inflammatory process. Pulmonary macrophages are the single most important effector cell and source of cytokines

for all stages of pulmonary inflammation. They modulate the recruitment and tracking of circulatory leukocytes in the lung through the secretion of chemokines. Nitric oxide regulates the vascular and bronchial tissue and modulates the production of cytokines and the recruitment and trafficking of neutrophils in the lung. Uncontrolled production and release of cytokines can result in ARDS, pulmonary fibrosis, and/or asthma.

#### 4.7.5. Interstitial Pneumonia

Infectious and chemical agents can cause interstitial pneumonia which may occur following hyperoxia, ingestion of paraquat, administration of chemotherapeutic drugs such as bleomycin and busulfan, and radiation exposure that damages epithelial and/or endothelial cells, or the basement membrane. Pulmonary hypersensitivity reactions can manifest as interstitial pneumonia. Since interstitial pneumonia is a diffuse lesion, it can be difficult to identify on gross examination, especially in smaller animals. Failure to collapse to the extent of a normal lung (best identified prior to removal from the thoracic cavity) and firmness on palpation are the key gross features. In most cases, it is impossible to determine the causative agent from the histological changes in the lung; however, in a small percentage of cases, identifying features may be present ([Hakkinen et al., 1982](#)).

In the acute phase, the capillary endothelial and alveolar epithelial cells are injured, with subsequent flooding of alveoli with serofibrinous exudate. Occasionally, if injury is especially severe, hyaline membranes form from serum proteins and components of surfactant that line the airspaces. They have a hyaline appearance (eosinophilic, homogenous, amorphous) on microscopic examination ([Figure 4.26](#)). This is followed by leukocytic infiltration of both alveolar lumina and interstitium. In human medicine, this stage of the disease is frequently referred to as the ARDS ([Ballard-Croft et al., 2012](#)).

Inhalation of manure (“pit”) gases such as  $H_2S$  and  $NH_3$ , inhalation of  $NO_2$  from silos, and ingestion of paraquat can cause similar injury in humans and animals. Resolution of acute injury occurs by proliferation of stem cells to replace damaged endothelium and epithelium,



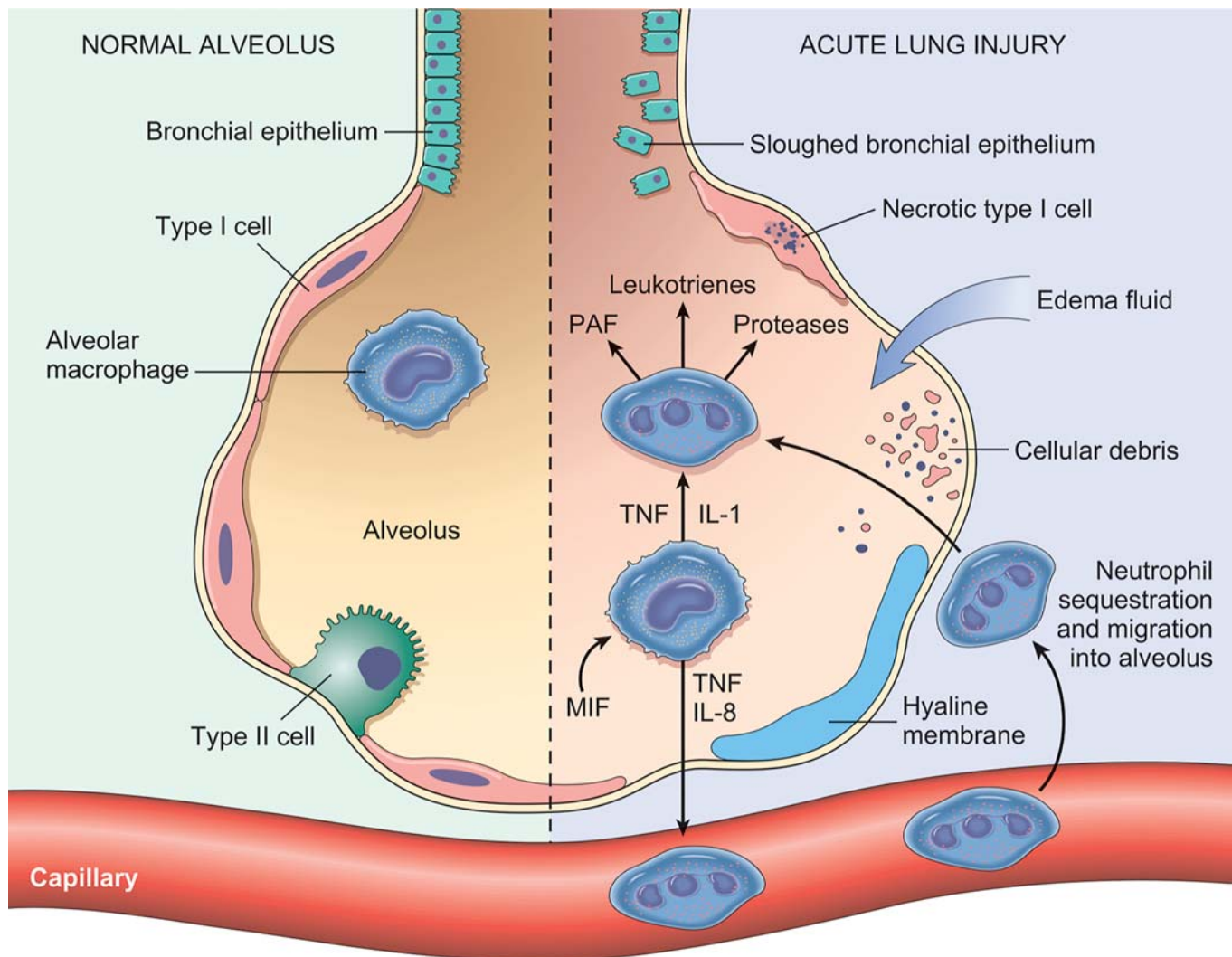


**FIGURE 4.27** Normal alveolus (left side) compared with injured alveolus in the early phase of acute lung injury and ARDS. Proinflammatory cytokines, such as interleukin 8 (IL-8), interleukin 1 (IL-1), and tumor necrosis factor (TNF) (released by macrophages), cause neutrophils to adhere to pulmonary capillaries and extravasate into the alveolar spaces, where they undergo activation. Activated neutrophils release a variety of factors, such as leukotrienes, oxidants, proteases, and platelet activating factor (PAF), which contribute to local tissue damage, accumulation of edema fluid in the airspaces, surfactant inactivation, and hyaline membrane formation. Macrophage migration inhibitory factor (MIF) released into the local milieu sustains the proinflammatory response. Subsequently, the release of macrophage-derived fibrogenic cytokines such as transforming growth factor  $\beta$  (TGF- $\beta$ ) and platelet-derived growth factor (PDGF) stimulate fibroblast growth and collagen deposition associated with the healing phase of injury. *Modified from Ware LB, Matthay MA: The acute respiratory distress syndrome, N. Engl. J. Med. 342:1234, 2000; Reproduced from Husain: The lung. In Kumar V, Abbas AK, Fuasto N, editors: Robbins and Cotran pathologic basis of disease, ed 8, 2010, Elsevier Saunders, Figure 15-4, p. 682, with permission.*

and by resolution of the inflammatory component. This proliferative stage is characterized by type II cell hyperplasia with thickening of the alveolar wall.

If injury is more severe or consists of multiple episodes or chronic exposure, inflammation persists, and normal regeneration is inhibited.

The chronic phase is characterized by intraalveolar accumulation of various mononuclear cells (mostly macrophages), proliferation and persistence of increased numbers of alveolar type II cells, and interstitial thickening due to accumulations of lymphoid cells, fibroblast proliferation, and collagen deposition. Examples of toxicants

causing chronic interstitial pneumonia include paraquat, some chemotherapeutic drugs like bleomycin, and radiation. Once established, fibrosis is irreversible and frequently progressive. Extensive tissue destruction may also occur, resulting in so-called “honeycomb” lung. Honeycomb lung is the result of severe chronic interstitial lung disease, with both fibrosis and cicatricial (“scar”) emphysema as major components.

Environmental exposures to agents such as cigarette smoke, e-cigarettes, and wildfires can predispose to development of ARDS (Wick and Matthay, 2021). A national US outbreak of acute to subacute lung injury associated with vaping preceded the onset of COVID-19 and was termed EVALI (e-cigarette, or vaping, product use-associated lung injury). The Centers for Disease Control and Prevention (CDC) Lung Injury Response Pathology Working Group described the main pathology findings on biopsy or autopsy as DAD or organizing pneumonia (Reagan-Steiner et al., 2020). Lipoid pneumonia and acute fibrinous pneumonia were also reported. EVALI was found to be most commonly associated with the use of cannabis-based vaping products, especially obtained from informal sources, within 90 days prior to onset of clinical signs. Vitamin E acetate, illicitly used as a diluent, was identified as the main potential causative agent and similar histopathology to that of EVALI was observed following exposure to vitamin E acetate in a mouse model in which direct, dose-dependent alveolar type 2 epithelial toxicity was noted (Cherian et al., 2020; Wick and Matthay, 2021). Cases of EVALI continue to be reported. An array of other harmful chemicals, including flavorings and elevated concentrations of metals, have been detected in e-cigarette aerosols (Holden and Hines, 2016).

#### 4.7.6. Pulmonary Fibrosis

The definition of fibrosis is difficult, but for all practical purposes, relates to one or more of the following: an increased amount of collagen, an abnormal location of the deposited collagen, and/or an abnormality in the nature of the collagen itself. Morphologically, fibrosis is defined as an increase in observable connective tissue at the microscopic level; special stains may be required to demonstrate its presence. Biochemically, fibrosis is defined as an increased

amount of collagen, which can be estimated from the hydroxyproline content of the lung, or differences in relative concentration of the different collagen types. Fibrosis can be distributed diffusely or focally throughout the lungs. Functionally, there is a reduction in compliance and an impairment of gaseous diffusion.

Fibrotic lung disease in humans is a heterogeneous group of chronic lung disorders that may be produced by a variety of toxic agents, including inhaled silica, asbestos, and beryllium; ingested paraquat; and chemotherapeutic drugs or thoracic irradiation. Fibrosis may also be produced in infectious and immune-mediated disorders; in many cases, the fibrosis is idiopathic (idiopathic pulmonary fibrosis, IPF). It is possible that IPF is toxic in origin, or the result of interaction between several toxicants or between infectious and toxic agents.

Fibrosis may occur following DAD, as in interstitial pneumonia, in which collagen is distributed relatively uniformly throughout the lungs. Collagen is deposited within the interstitium of the alveolar walls and may also be present within the alveolar lumen. Grossly, if the lung is severely affected, it will not collapse when the thoracic cavity is opened, and will be paler and firmer than normal. It is difficult to induce severe pulmonary fibrosis in laboratory animal models (Khalil et al., 2007).

Fibrosis is also a major component of pneumoconiotic diseases such as silicosis and asbestosis in which collagen is distributed multifocally throughout the lung as a component of the chronic inflammatory response to inhaled particles (Figure 4.28). In the affected human lung, multiple firm nodules, sometimes coalescing, develop in severe cases (Figure 4.29). At autopsy, these may be noted on visual examination but may be more evident on palpation. Pigment may be associated with the lesions, such as in coal miners’ pneumoconiosis. The presence of silica in dust inhaled by coal miners is the major cause of the pneumoconiosis.

The development of fibrosis is a very complex process that has been studied extensively both in vivo and in vitro in numerous experimental animal models, as well as in humans. Pulmonary fibrosis can occur if there is disruption of the normal repair mechanism following interstitial injury. Such interstitial injury can result from

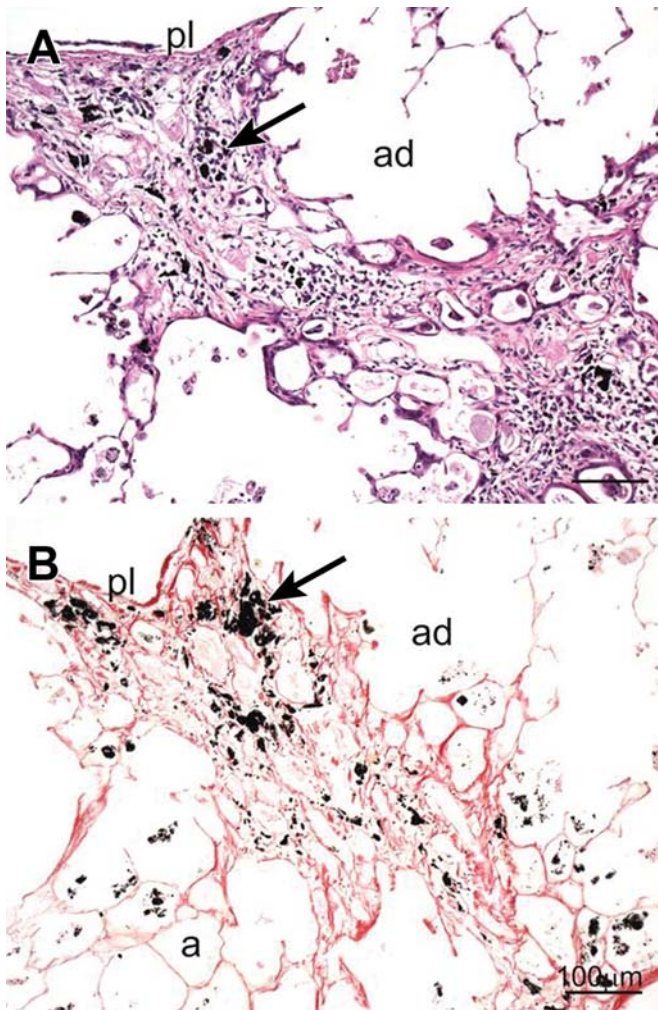


**FIGURE 4.28** Light photomicrographs of an area of pulmonary fibrosis in the lungs of a rat subchronically exposed by inhalation to a large concentration of carbon black particles. One section was stained with hematoxylin and eosin (A) and the other was histochemically stained with picrosirius red for collagen (B). The scarred areas have effaced a large area of the alveolar parenchyma and caused enlargement of adjacent air spaces of alveolar ducts (ad). Large and small aggregates of the inhaled particles (arrows) are embedded in the fibrotic tissue. pl, pleural surface of the lung lobe. *Reproduced from Haschek WM, Rousseaux CG, Wallig MA, editors: Handbook of toxicologic pathology, ed 3, 2013, Academic Press, Vol. 3, Figure 51.22, p. 1985, with permission.*

one or more of the following: alteration in number, properties, and/or differentiation of parenchymal cells; inflammatory and immune

responses; modification of connective tissue destruction; or acellular expansion of interstitium by edema fluid. GM-CSF is recently postulated to orchestrate the pulmonary response to infection including fibrosis ([McCormick et al., 2022](#)).

Most forms of fibrosis are biologically complex and can be mediated through effector cells of the inflammatory and immune systems, platelets, the complement cascade, and in situ factors. Interaction of these components is exceedingly complex. The macrophage appears to play a central role, although neutrophils, eosinophils, and mast cells may also be involved ([Laskin et al., 2019](#)). However, both neutrophils and macrophages can stimulate as well as suppress the fibrotic response, and both contain collagenases.

Immunostimulation is recognized and recently studied as an important contribution in lung fibrosis in some animal models and patient subsets. Available data indicate that pulmonary fibrosis includes diverse and discrete immunoregulating populations involving regulatory lymphocytes (T and B regs) and myeloid cells (immunosuppressive macrophages and myeloid-derived suppressive cells; MDSCs). They are initially recruited to limit the establishment of deleterious inflammation but participate in the development of lung fibrosis by producing immunoregulatory mediators (mainly TGF- $\beta$ 1 and IL-10) that directly or indirectly stimulate fibroblasts and matrix protein deposition. This is considered a silent immunoregulatory environment that sustains an alternative mechanism of fibrosis explaining why, in some conditions, neither proinflammatory cytokine deficiency nor steroid and immunosuppressive therapies limit lung fibrosis. As such, sustained immunoregulation should be considered in therapeutical strategies for lung fibrotic disorders under presumed nonimmunostimulatory circumstances ([Huaux, 2021](#)).

Experimentally, pulmonary fibrosis has been studied following administration of silica, hyperoxia, radiation, bleomycin, and combinations of agents such as butylated hydroxytoluene (BHT) or bleomycin with oxygen. Ozone, endotoxin, and particulate matter induce parenchymal inflammation that can also be followed by



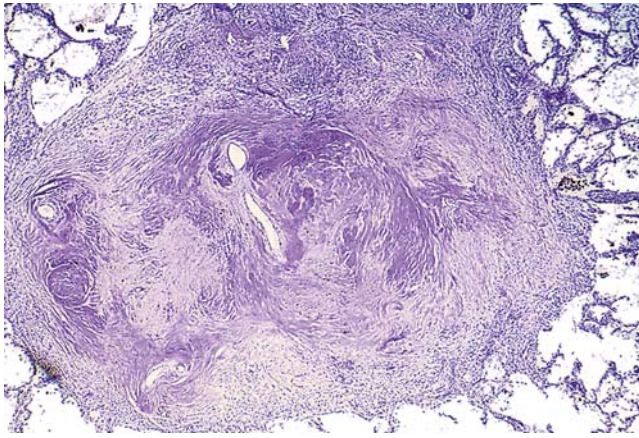


**FIGURE 4.29** Several coalescent collagenous silicotic nodules. Courtesy of Dr John Godleski, Brigham and Women's Hospital, Boston, MA; Reproduced from Husain: *The lung*. In Kumar V, Abbas AK, Fausto N, editors: *Robbins and Cotran pathologic basis of disease*, ed 8, 2010, Elsevier Saunders, Figure 15-19, p. 682, with permission.

fibrosis. In general, however, rodents are not considered good models for human pulmonary fibrosis.

As previously mentioned, fibrosis is also an important component of the pneumoconiosis (occupational lung disease caused by inhaling dust particles), at least those caused following occupational exposure to mineral dusts such as asbestos, silica, and beryllium. Inhalation of dust containing crystalline-free silica leads to a progressive pulmonary disease characterized by extensive formation of granulomatous lesions and fibrosis throughout the lung parenchyma. Silicosis is mostly an occupational disease found in rock miners, sandblasters, stonecutters, and foundry workers, and generally presents decades after exposure. A recent Californian outbreak in countertop workers reported a median (interquartile range) work tenure of 10–20 years (Fazio et al., 2023). Silica particles that reach the deep lung are phagocytized by alveolar macrophages and taken up into phagolysosomes. Contrary to many other dusts, which may remain within the phagolysosomes, silica has the potential to destroy lysosomal membranes, resulting in release of digestive enzymes and chemical mediators. These mediators, and other products of destroyed cells,

stimulate the migration of additional macrophages to the lesion and may incite fibroblasts to proliferate and to synthesize increased amounts of collagen. Silica also causes activation and release of mediators by viable macrophages, including interleukin-1, tumor necrosis factor (TNF), fibronectin, lipid mediators, oxygen derived free radicals, and fibrogenic cytokines. The developing silicotic nodules may eventually undergo hyaline degeneration, enlarge slowly, and coalesce into larger lesions (Figure 4.29). In humans, the disease is often associated with tuberculosis.

Coal worker's pneumoconiosis ("black lung") results from deposition of coal particles in the deep lung. The simple form of the disease (accumulation of pigment with macrophage infiltration) usually does not produce serious symptoms, although the inhaled coal dust may produce chronic bronchitis. The disease usually does not progress once exposure has ceased. Coal miners' pneumoconiosis may become more severe if large amounts of dust are inhaled or if silica is present in the inhaled coal dust. Improved underground mining technology and newer mining methods thought to decrease the size of silica particles in dust may be increasing the amounts of coal dust and silica inhaled by miners, resulting in increased severity of disease at exposure concentrations (limits) that were formerly considered protective from coal miners' pneumoconiosis. Anthracosis, the simple accumulation of carbon pigment without a cellular response, is present in coal miners and urban dwellers.

Inhalation of asbestos fibers in mining, milling, and manufacturing operations as well as in the construction industry is another occupational health hazard that may lead to the development of chronic interstitial lung disease (asbestosis). Initially, inflammation develops at the bronchiolar-alveolar duct junction, a preferred site for deposition of inhaled asbestos fibers. Eventually, diffuse interstitial fibrosis develops. Deposition of iron on deposited fibers gives rise to asbestos bodies, a marker of asbestos exposure. The more important risk following exposure to asbestos is the development of cancer, either from the bronchial epithelium (bronchogenic carcinoma) or

from the pleura (malignant mesothelioma). There is a synergistic interaction between asbestos and cigarette smoking in the development of bronchogenic carcinoma, but not malignant mesothelioma.

Several metals, such as cadmium and beryllium, also may produce interstitial lung disease (see *Metals*, Vol 3, Chap 10). Acute beryllium disease is characterized by acute interstitial pneumonia and is usually associated with accidental exposure to high concentrations of beryllium. Although comparatively rare, it may be rapidly progressive and has been fatal in 10%–15% of cases. Chronic beryllium disease is caused by induction of cell-mediated immunity and is characterized by multiple granulomas in the pulmonary parenchyma. Modern industrial hygiene methods have been successful in eliminating acute but not chronic beryllium disease. Beryllium is a known human carcinogen, and beryllium compounds are carcinogenic in rats and monkeys after inhalation or intratracheal instillation. Preliminary studies of materials developed for new technologies, such as carbon nanotubes and microspheres, suggest that they may induce granulomatous inflammation and fibrosis (see *Nanoparticulates*, Vol 3, Chap 13).

#### 4.7.7. Pulmonary Emphysema

Pulmonary emphysema is defined as abnormal permanent enlargement of air spaces distal to the terminal bronchiole, accompanied by destruction of air space walls. Emphysema is one of the causes of COPD (see [Section 4.6](#), Tracheobronchial and Pulmonary Response to Injury). There are two main reasons for airflow obstruction: destruction of parenchyma decreasing the elastic recoil that is normally used for expiration, and lost structural support and radial tension imparted by normal parenchyma collapse prematurely during expiration of small airway lumens. While pressure–volume curves document decreased elastic recoil and increased compliance, a definitive diagnosis of emphysema requires morphologic assessment.

At autopsy or necropsy, the emphysematous lung is larger than normal and often does not collapse completely when the thoracic cavity is opened. Air space wall destruction is recognized microscopically by an increase in the number and size of fenestrations in the alveolar septa,

with the alveolar septa appearing as isolated detached segments in later stages ([Figure 4.30](#)). Fibrosis is not a component of emphysema, but is often present in emphysematous lungs because cigarette smoking, the most common cause of emphysema in humans, also causes bronchiolitis with fibrosis of respiratory bronchioles.

There are two main anatomic types of emphysema, classified according to the distribution of air space enlargement within the acinus: panacinar emphysema, and centrilobular (sometimes called proximal acinar) emphysema. In panacinar emphysema, the enlargement of airspaces is distributed throughout the acinus and involves the respiratory bronchioles, alveolar ducts, and alveolar sacs. In centrilobular emphysema, the air space enlargement primarily involves respiratory bronchioles, with lesser involvement of the alveolar ducts and relative sparing of the alveolar sacs. In humans, approximately 95% of symptomatic emphysema cases are centrilobular. Irregular emphysema is primarily associated with fibrous scars and is sometimes called cicatricial emphysema ([Figure 4.28](#)). Distal acinar emphysema, also called paraseptal emphysema, spares the alveolar ducts. The latter two types, irregular and paraseptal emphysema, are not associated with airflow obstruction.

The pathogenesis of emphysema is summarized by the protease/antiprotease hypothesis, which states that the susceptibility of the lung parenchyma to proteolytic degradation is determined by the relative balance between elastases and other proteases and their inhibitors ([Figure 4.31](#)). The principal protease activities are derived from inflammatory cells. The principal antiprotease activity in serum and interstitial tissue is  $\alpha_1$ -protease inhibitor (PI), but secretory leukoprotease inhibitor in bronchial mucus and  $\alpha_1$ -macroglobulin in serum may also be important to lung protection. Lung destruction occurs when protease activity predominates due to excessive proteases or inhibition of antiproteases. Evidence supporting this theory comes from observations of severe emphysema in patients with  $\alpha_1$ -PI deficiency and experimental models that use inhaled or intratracheally instilled proteases to induce emphysema, or animals with antiprotease deficiencies.

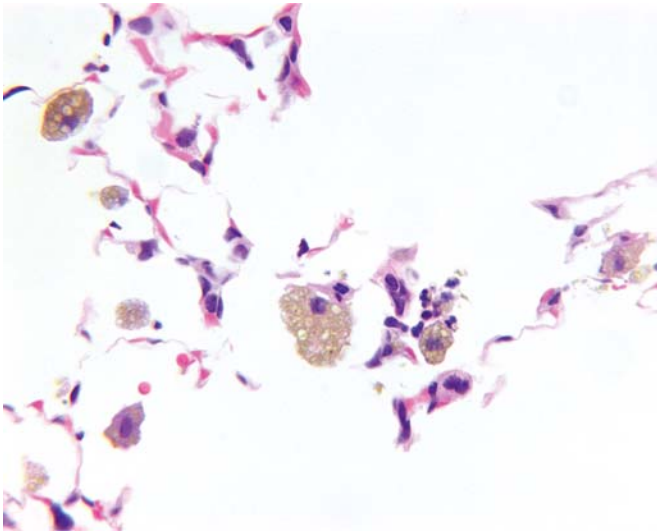


**FIGURE 4.30** Alveolar parenchyma from a cigarette smoke-exposed mouse. Pigmented macrophages, inflammation, and septal breaks and fragments, which are features of emphysema, are illustrated. Courtesy of Dr Thomas March. Reproduced from Haschek WM, Rousseaux CG, Wallig MA, editors: *Handbook of toxicologic pathology*, ed 3, 2013, Academic Press, Vol. 3, Figure 51.24, p. 1987, with permission.

Genetic and environmental factors determine the risk for developing COPD including emphysema (Green et al., 2007; Wick and Matthay, 2021). Genetic deficiency of  $\alpha_1$ -PI is associated with an increased risk for emphysema. Other genes may also influence risk for COPD. Cigarette smoking is the most important risk factor for developing emphysema. Smokers have increased numbers of neutrophils and macrophages in their lungs, and smoking stimulates release of elastase from neutrophils and enhances elastolytic protease activity in macrophages. There is also decreased antielastase activity in the lungs of smokers. Another risk factor for emphysema is occupational exposure to a dusty environment, such as in underground coal- or goldmining, or exposure to cadmium oxide fumes (Rushton, 2007).

#### 4.7.8. Pulmonary Neoplasia

Lung cancer was a rare disease at the turn of the century, but its incidence increased after World War I. By the end of the 20th century, it had become the leading cause of cancerous death

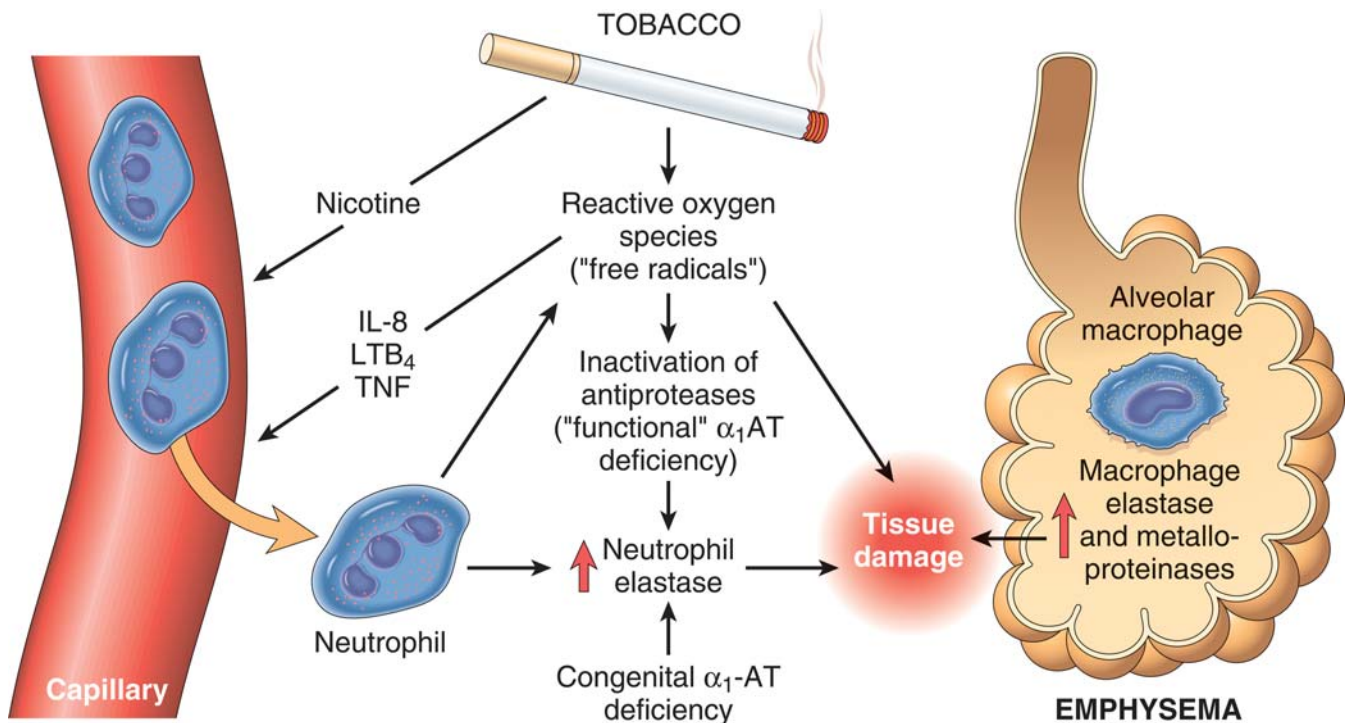


**FIGURE 4.31** Pathogenesis of emphysema. Excessive protease activity and ROS are additive in their effects and contribute to tissue damage.  $\alpha_1$ -antitrypsin ( $\alpha_1$ -AT) deficiency can be either congenital or "functional" as a result of oxidative inactivation. See text for details. IL-8, interleukin 8; LTB<sub>4</sub>, leukotriene B<sub>4</sub>; TNF, tumor necrosis factor. Reproduced from Husain: *The lung*. In Kumar V, Abbas AK, Fausto N, editors: *Robbins and Cotran pathologic basis of disease*, ed 8, 2010, Elsevier Saunders, Figure 15-8, p. 682, with permission.



in both men and women. The most important risk factor in lung cancer is smoking cigarettes and other inhaled tobacco or plant products. Tobacco use may be responsible for approximately 85%–90% of all lung cancers. Lung cancer and other tobacco smoke-induced diseases (cardiac disease, pulmonary disease) constitute a public health problem of major proportions.

Lung cancer also occurs in nonsmokers. One possible risk factor is exposure to environmental tobacco smoke (ETS), a mixture of smoke emanating from the lit end of a cigarette and the smoke exhaled into the surrounding air by active smokers. An additional risk factor is air pollution in urban areas. Inhalation of common air pollutants, particularly small particles emanating from the combustion of fossil fuels and loaded with carcinogens such as polycyclic aromatic hydrocarbons and nitroarenes, is also a risk factor. Radon gas exposure (a radioactive gas formed from radioactive decay of uranium) is the leading cause of lung cancer in nonsmokers, especially in some geographic regions.

Recently, it was proposed that environmental particulate matter measuring  $\leq 2.5 \mu\text{m}$  known to be associated with lung cancer risk, promotes lung cancer by acting on cells that harbor preexisting oncogenic mutations in healthy lung tissue. Focusing on EGFR-driven lung cancer, which is more common in never-smokers or light smokers, the researchers found a significant association between particulate matter measuring  $\leq 2.5 \mu\text{m}$  and the incidence of lung cancer for 32,957 EGFR-driven lung cancer cases. Functional mouse models revealed that air pollutants cause an influx of macrophages into the lung and release of interleukin-1 $\beta$ , resulting in a progenitor-like cell state within EGFR mutant lung alveolar type II epithelial cells that fuel tumorigenesis. Ultradeep mutational profiling of histologically normal lung tissue from 295 individuals revealed oncogenic EGFR and KRAS driver mutations in 18% and 53% of healthy tissue samples, respectively (Hill et al., 2023).

In humans, there are four major lung tumor types: squamous cell carcinoma (about 30% of all lung cancers), adenocarcinoma (just over

30%), small cell carcinoma (20%–25%), and large cell carcinoma (poorly differentiated carcinomas that do not have features of the three other types). Lung cancer continues to have a notoriously poor prognosis. Most tumors appear to originate from the bronchial epithelium, often referred to as “bronchial cancer.” In laboratory rodents, intratracheal instillation of polycyclic aromatic hydrocarbons has produced such tumors, while inhalation exposure gives rise to lung tumors located more peripherally and resembling human bronchioloalveolar tumors, rather than bronchogenic carcinoma. With the increasing use of molecular techniques, it has come to light that many peripherally located adenomas and adenocarcinomas in animals might represent useful models for human lung cancer. NSCLC and small cell lung cancer (SCLC) mouse models have been developed to study human lung cancer. Chemically induced or spontaneous lung cancer in susceptible inbred strains has been widely used, but genetically engineered somatic mouse models better recapitulate the genotype–phenotype correlations found in human lung cancer. Furthermore, orthotopic transplantation of primary human cancer tissue fragments or cells into lungs of immune-compromised mice can be constructive models for nonclinical research (Safari and Meuwissen, 2015).

Rodent models of malignant mesothelioma help facilitate the understanding of the biology and potential treatments. Introducing the same genetic lesions as found in human mesothelioma in mice results in tumors that show close resemblance with the human tumorous counterpart, including the sometimes fulminant inflammatory responses that accompany human malignant mesothelioma. The quick development of mesothelioma in mice given the appropriate combination of stimuli, with or without exposure to asbestos, makes the autochthonous models particularly useful for testing new treatment strategies in an immunocompetent setting. On the other hand, patient-derived xenograft models are particularly useful to assess effects of inter- and intratumor heterogeneity and human-specific features of mesothelioma (Testa and Berns, 2020). Spontaneous lung cancers in

animals are rare, although certain mouse strains may have a comparatively high lung tumor rate. An international project (INHAND) to develop standardized diagnostic criteria and nomenclature for lesions has proposed the following classification for lung neoplasms located in alveoli and terminal bronchioles in mice and rats: bronchioloalveolar adenoma, carcinoma (bronchioloalveolar, acinar [mice only], adenosquamous, squamous cell), and epithelioma (rat only; cystic, keratinizing, and nonkeratinizing). Tumors in bronchioles are listed as: papilloma, adenocarcinoma, squamous cell carcinoma, and neuroendocrine tumor (benign and malignant) (Renne et al., 2009). Most lung tumors found in rodents are found peripherally, originating from the lung parenchyma, including terminal bronchioles, differentiating some form of lung tumors in rodents from human lung cancer. Furthermore, while human lung cancer frequently metastasizes to organs such as liver, bone, and brain, distant metastasis is much less frequent in rodent lung cancers, although they can invade adjacent tissues, lymphatics, and blood vessels. Two rodent lung tumors are described in more detail below due to their toxicological significance.

#### 4.7.9. Lung Tumors in Mice

The most common spontaneous lung tumor in mice is the adenoma which originates from either the type II alveolar epithelial cells or the bronchiolar club cells in the peripheral lung. A/J mice or Swiss-Webster mice have high spontaneous incidence, with exposure to carcinogens greatly increasing the number of lung tumors per animal. Other strains are more resistant, rarely developing lung tumors. B6C3F1 and CD1 mice, two strains commonly used in carcinogenicity studies, have a fairly high spontaneous incidence of bronchioloalveolar adenomas and carcinomas. In both strains, adenomas are more common than carcinomas and the incidence of neoplasms is higher in male versus female mice.

Many gene mutations found in human lung adenocarcinoma, particularly in the *ras* family of oncogenes, also occur with high frequency in mouse lung tumors. Alterations in signal transduction pathways and other biochemical

parameters in human and mouse tumors are also similar, thereby assisting in research efforts on the carcinogenic process from hyperplasia to adenoma to carcinoma in situ, stages practically inaccessible in man (Figure 4.32).

Rats exposed by inhalation to high concentrations of diesel exhaust, oil shale dust, talc, titanium dioxide, or carbon black develop bronchioloalveolar adenomas, bronchioloalveolar carcinomas, squamous cell carcinomas, or adenosquamous carcinomas in the peripheral lung (Figure 4.33). In addition, lesions labeled as keratin cysts and cystic epithelioma (keratinizing and nonkeratinizing) originate from foci of bronchioloalveolar metaplasia. Keratinizing cystic epitheliomas are more common than nonkeratinizing epitheliomas and consist of whorled keratin masses surrounded by well-differentiated layers of stratified SE. They often arise adjacent to fibrotic foci, and a large bronchiole with hyperplastic epithelium often opens into the lesion. These tumors only develop when the macrophage-mediated clearance mechanism of the lung is overwhelmed and there is excessive retention of particles in the alveoli ("particle overload"). Excess particulate matter may lead to secondary inflammatory and proliferative lesions, eventually leading to tumors by nongenotoxic mechanisms.

Dogs have been used widely in inhalation studies due to their convenient size, cooperative temperament, and similarity to the human in respect to bronchiolar structure and pulmonary deposition of inhaled aerosols. However, they are rarely used in laboratory carcinogenicity studies due to the long timespan before tumors arise. In one study, however, Beagle dogs that inhaled radon or beta-emitting radionuclides developed sinus and nasal cancers. Both carcinomas and hemangiosarcomas were induced in the lung by beta-emitting radionuclides (see *Radiation and Other Physical Agents*, Vol 3, Chap 14, p. 890–891). Dogs are companion animals, and by default, exposed to a similar environment as humans. In dogs, bronchioloalveolar carcinomas are the most prevalent type of pulmonary neoplasm. Unlike in humans, bronchogenic carcinomas and anaplastic small and large cell carcinomas are infrequent. *K-ras*



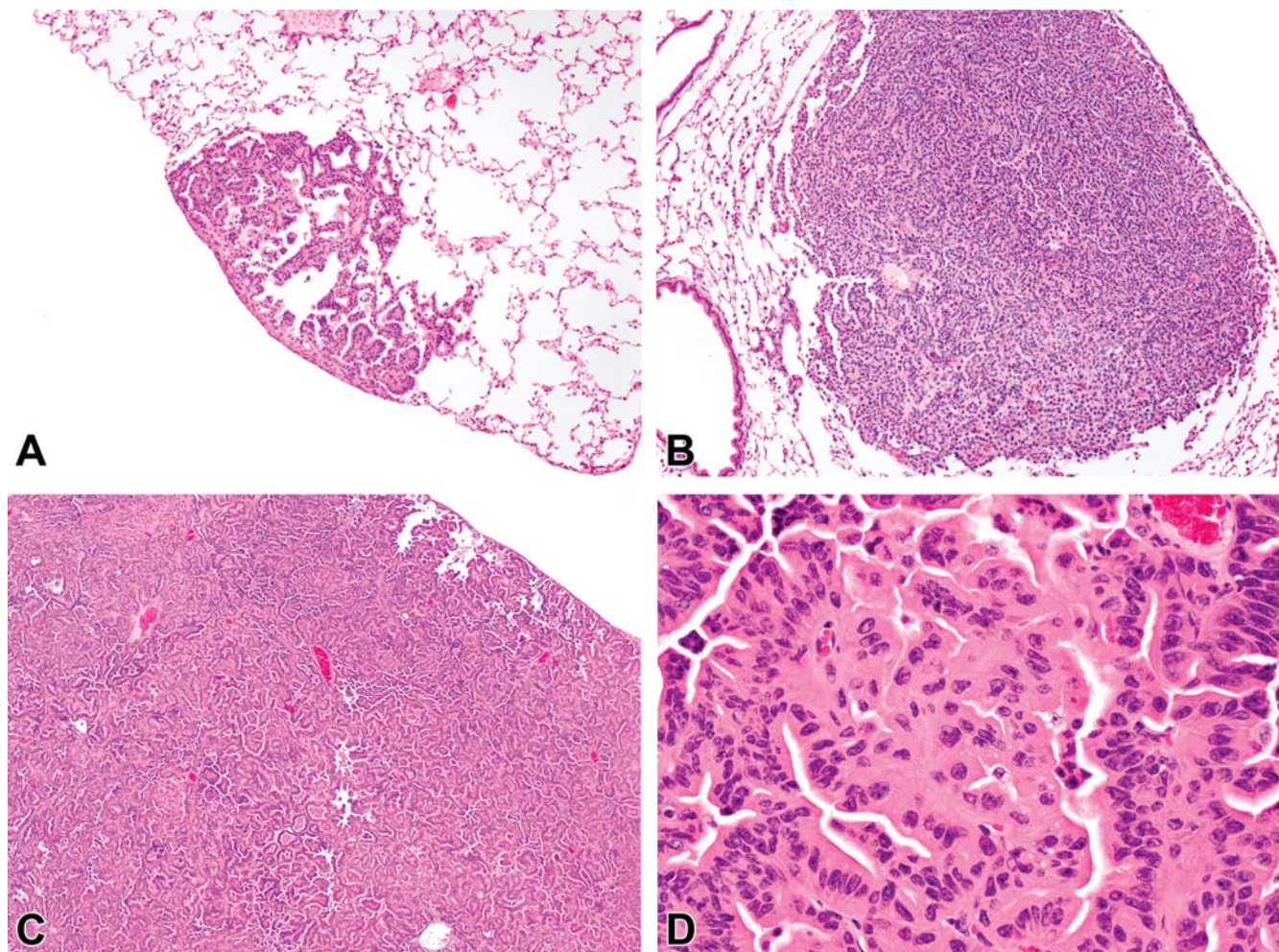


**FIGURE 4.32** Light photomicrographs of hyperplastic and neoplastic lesions in mice exposed to cigarette smoke. Focal bronchiolar-alveolar hyperplasia, which forms a wedge shape but does not obscure the alveolar architecture (A). Bronchioloalveolar adenoma showing typical features including small size, high cell density that obscures the alveolar architecture, sharp demarcation from the surrounding lung, and convex border (B). Bronchioloalveolar carcinoma illustrating typical large size and architectural distortion (C). Higher magnification of the carcinoma showing nuclear atypia and lack of polarity (D). H&E stain. *Courtesy of Dr Julie Hutt. Reproduced from Haschek WM, Rousseaux CG, Wallig MA, editors: Handbook of toxicologic pathology, ed 3, 2013, Academic Press, Vol. 3, Figure 51.26, p. 1990, with permission.*

mutations (GGT to GGA transitions at codon 12) have been detected both in spontaneously occurring and in  $^{239}\text{PuO}_2$ -induced malignant canine lung tumors. More recently, it has been realized that some naturally occurring primary canine lung cancers share clinicopathologic features with human lung cancers in never-smokers. Researchers charted the genomic landscape of canine lung cancer and performed functional characterization of novel, recurrent *HER2*

(*ERBB2*) mutations occurring in canine pulmonary adenocarcinoma (Lorch et al., 2019).

## 5. MECHANISMS OF TOXICITY

Toxic lung damage is an exceedingly complicated series of interdependent events. Primary lung injury may be initiated by mechanisms such as osmotic or cytolytic membrane injury,



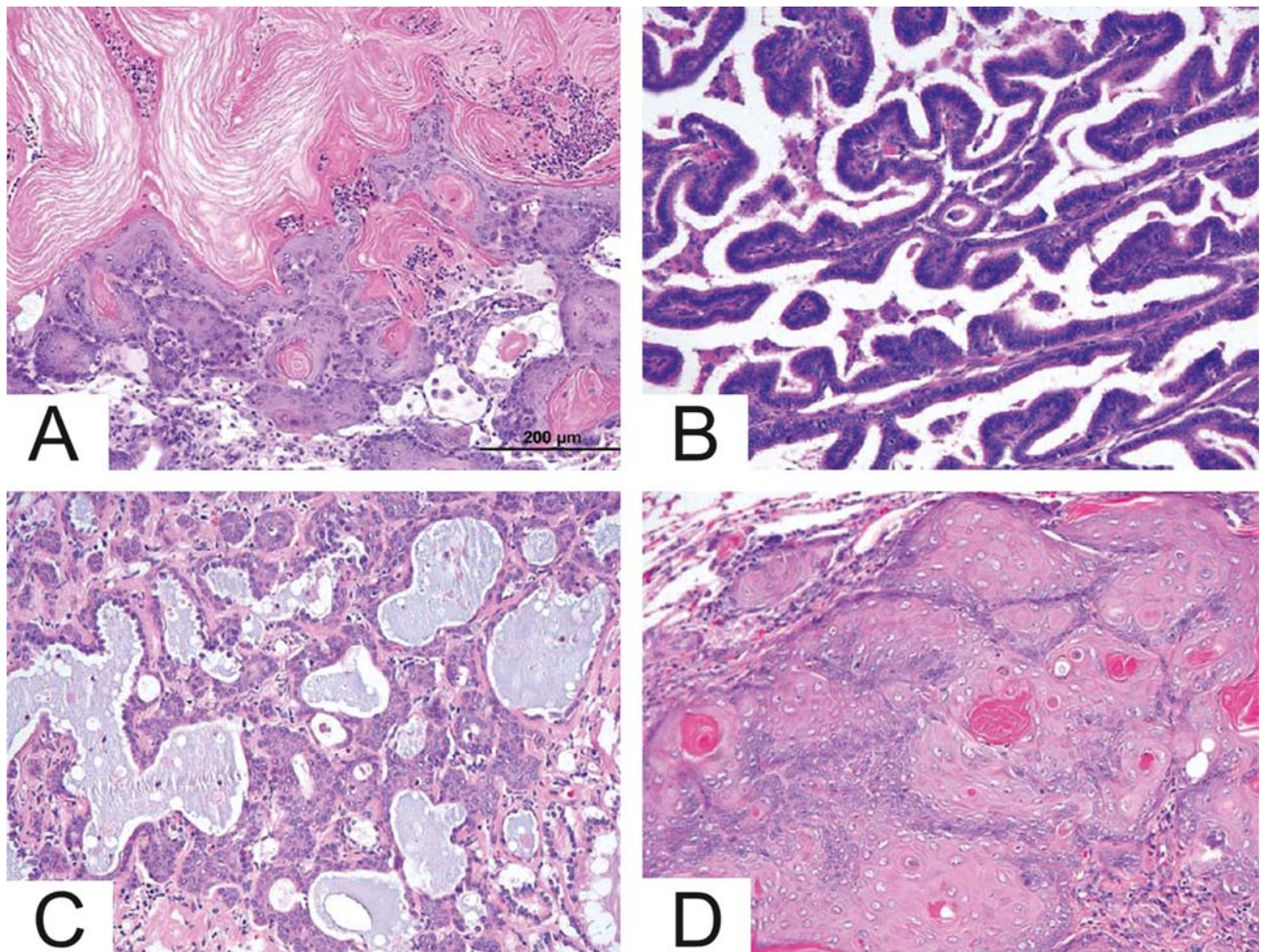


**FIGURE 4.33** Light photomicrographs of a cystic keratinizing epithelioma (A), bronchioloalveolar carcinoma (B), adenosquamous carcinoma (C), and squamous cell carcinoma (D) in the lungs of rats; H&E stain. *Reproduced from Renne R, Brix A, Harkema J, Herbert R, Kittel B, Lewis D, March T, Nagano K, Pino M, Rittinghausen S, Rosenbruch M, Tellier P, Wohrmann T: Proliferative and nonproliferative lesions of the rat and mouse respiratory tract, Toxicol. Pathol. 37 (Suppl. 7):5S–73S, 2009 (Figures 113, 115, 117, and 118), with permission.*

oxidative damage to cell constituents mediated through the formation of reactive oxygen species (ROS), or metabolism of foreign chemicals to reactive intermediates that are potentially able to interact with intracellular targets (Table 4.6).

Primary lung injury is often amplified through secondary events such as formation and release of mediators (for example, vasoactive amines and leukotrienes), activation of the kinin and complement cascades, release of lysosomal enzymes, release of cytokines, and activation of

inflammatory cells. Activation of phagocytes results in the release of ROS, which contributes to an imbalance of the oxidant/antioxidant defenses and further amplifies the cascade, leading to injury. M1 macrophages, which are activated by interferon- $\gamma$ , are important for phagocytosis, antigen presentation, and production of T-helper cytokines. In contrast, alternatively activated macrophages, which are activated by stimuli such as IL-4 and IL-13, may have an antiinflammatory role or play

**TABLE 4.6** Mechanisms of Toxicity to the Respiratory System With Selected Examples

Mechanism	Xenobiotic
<i>Direct toxicity</i>	Oxygen, ozone, phosgene, hydrochloric acid, other fumes and gases
<b>METABOLIC ACTIVATION</b>	
In situ metabolic activation	Acetaminophen, bromobenzene, butylated hydroxytoluene, carbon tetrachloride, coumarin, 4-ipomeanol, 3-methylfuran, naphthalene, methimazole
Activation outside the lung	Pyrrolizidine alkaloids (e.g., monocrotaline)
Cyclic reduction/oxidation with production of ROS	Paraquat, nitrofurantoin
<b>IMMUNE-MEDIATED</b>	
Hypersensitivity reaction:	
Type I hypersensitivity	Toluene, diisocyanates, trimellitic anhydride, ozone
Type II hypersensitivity	Trimellitic anhydride, mercury, organic dusts, beryllium
Immune suppression	Oxidant gases, asbestos, tobacco smoke, benzene, toluene, cadmium, zinc, lead
<i>Nonimmune secretion of inflammatory mediators can cause hyperreactive airway syndrome</i>	Isocyanates, formaldehyde, trimellitic anhydride, ozone
<i>Xenobiotic interactions through simultaneous or sequential exposure</i>	Oxygen enhances toxicity of paraquat, bleomycin, butylated hydroxytoluene, CdCl <sub>2</sub>

*Reproduced from Haschek WM, Rousseaux CG, Wallig MA, editors: Handbook of toxicologic pathology, ed 2, 2002, Academic Press, Vol. 2, Table V, p. 29, with permission.*

a major role in chronic airway diseases, including COPD and asthma (Byers and Holtzman, 2011). Toxicity may also be directly related to the physicochemical properties of inhaled agents or their ability to induce immune-mediated responses (Husain, 2021).

5.1. Direct Toxicity

Many agents produce respiratory injury by a direct interaction of the reactive molecule with its respiratory tract target. Examples include oxidant and irritant gases such as oxygen, ozone, chlorine, phosgene, ammonia, hydrochloric acid, and many other fumes and gases. These gases and many acidic or alkaline irritants may produce cytolytic changes directly at their site of primary interaction, the exposed

cell membrane, or increase the generation and accumulation of ROS and thus trigger cell injury. See Section 4.2 for a discussion of gradients of injury due to inhaled toxicants. Direct injury may also occur by systemically administered or inhaled biopharmaceuticals.

Injury mediated by ROS appears to be an important mechanism in toxic respiratory damage for oxygen, ionizing radiation, and bleomycin. Ozone is so highly reactive that it likely produces aldehydes and hydroxyperoxides through ozonolysis of substances in the airway and lung lining fluid, as well as ROS from free radical reactions. These reaction products damage cells.

As a consequence of either direct or indirect cell injury, inflammatory cells, particularly macrophages and polymorphonuclear leukocytes, may be recruited into the lung



parenchyma. Upon appropriate stimulation, these cells can undergo activation and produce a burst of ROS, especially hydrogen peroxide, which in turn may also damage respiratory cells (Figure 4.27). Platelet aggregates localized to sites of pulmonary microvascular injury may also generate active oxygen species.

Common consequences of exposure to toxicants that directly injure the upper respiratory tract are damage to ciliated cells, inflammation, and mucus cell hyperplasia/hypertrophy. Inhaled direct toxicants that reach the alveolar region at high concentrations may induce acute or delayed pulmonary edema due to necrosis of type I or endothelial cells. Following inhalation of phosgene, hydrochloric acid, ammonia, or smoke, a latent period of several hours may occur prior to the appearance of lung damage. Fatal pulmonary edema may then develop, even in the absence of further exposure to the offending agent.

## 5.2. Metabolic Activation

A great deal of information is now available describing the role of metabolic activation of xenobiotics in respiratory toxicity (see Section 4 for cell-specific injury). Three different mechanisms may be involved. In the first scenario, the parent compound itself reaches the respiratory tract, either through the blood following systemic administration or as an inhalant. The compound then undergoes metabolic activation to the proximate toxin (Figure 4.34).

Interaction with the target is often manifested as covalent binding of the reactive metabolite to cell macromolecules. Activation by microsomal mixed-function oxidases, especially the cytochrome P450 enzymes, is a key element in the process; on the other hand, protective systems, such as intracellular levels of GSH and enzymes involved in maintaining reducing equivalents within the cell, are crucial components in protection. Cell types that contain high concentrations of cytochrome P450s are particularly important in the detoxification of xenobiotics; however, these cells are vulnerable to injury caused by the reactive metabolites they form. Examples of chemicals that cause respiratory damage

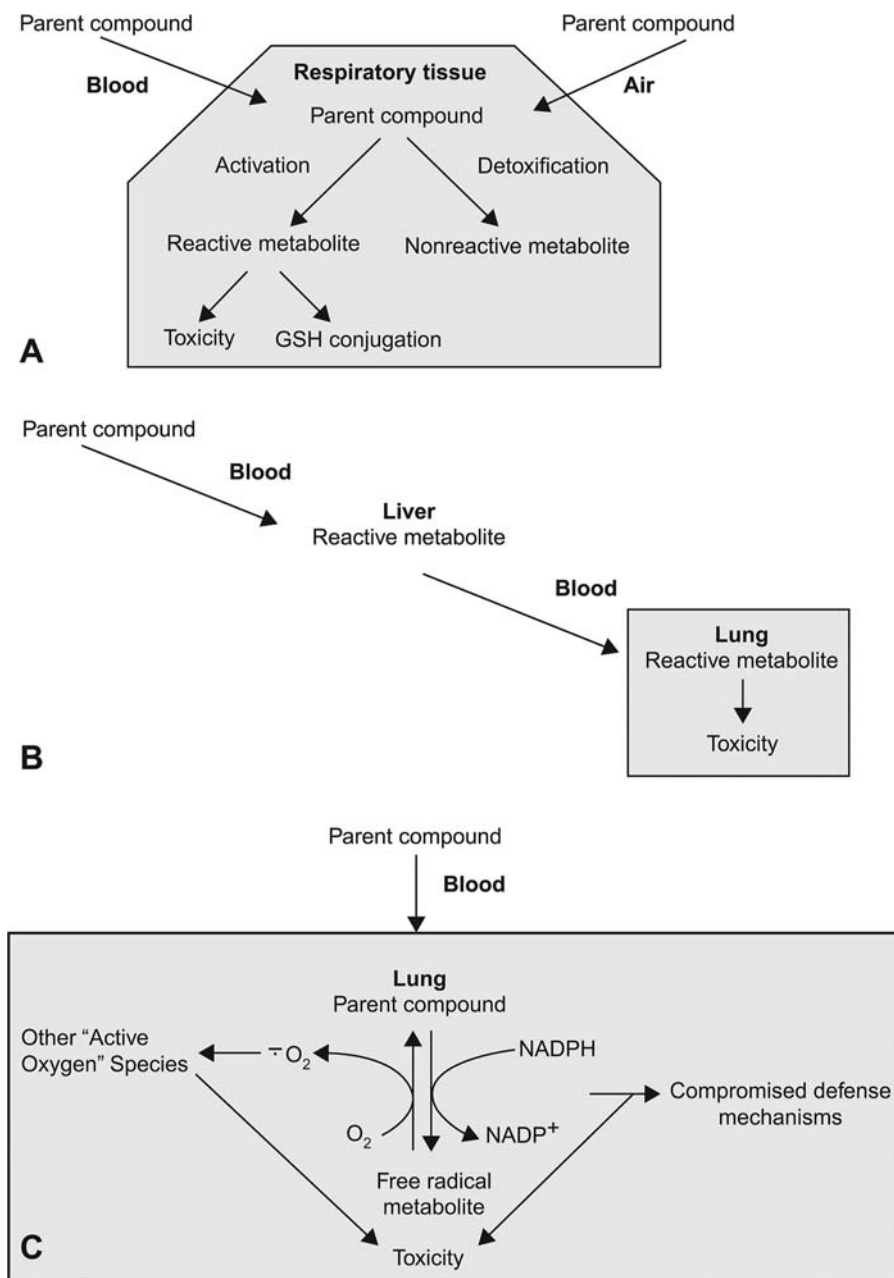
following in situ metabolic activation include phenacetin, bromobenzene, coumarin, 4-ipomeanol, BHT, CCl<sub>4</sub>, 3MI, acetaminophen, and 3-methylfuran (Tables 4.4 and 4.6). 3MI is formed in ruminants by bacterial degradation of tryptophan in the rumen. It is present in cigarette smoke and in the human intestinal tract. 3MI is absorbed into the circulation, taken up by the lung, and metabolized by the cytochrome P450 enzymes, resulting in toxicity. In cattle, severe damage to alveolar cells results in an acute interstitial pneumonia, which is identical to that caused by the ingestion of moldy sweet potatoes containing 4-ipomeanol. In mice, both 3MI and 4-ipomeanol cause club cell necrosis; 3MI also causes necrosis of olfactory epithelium.

The second mechanism of metabolic activation of xenobiotics in respiratory toxicity involves uptake of a systemically administered foreign compound by the liver, or any other organ, where the agent is metabolized to a highly reactive and toxic metabolite(s) (Figure 4.34B). This metabolite(s) may cause liver injury, but also escape into the circulation via the hepatic veins and inferior vena cava. The next capillary bed encountered is in the lung, and widespread damage may occur. The best studied examples of chemicals causing this form of lung damage are the pyrrolizidine alkaloids.

The pyrrolizidine alkaloid MCT is found in the plant *C. spectabilis*. Human toxicity has occurred from consuming contaminated grain or herbal teas made from such plants, whereas animal toxicity can occur following grazing on such plants. At high doses, MCT rapidly causes severe liver injury and death. At lower doses, it produces mild liver injury and delayed pulmonary injury characterized by pulmonary hypertension. MCT is bioactivated in the liver to pyrrolic metabolites by the cytochrome P450 enzyme system. The “putative” reactive metabolite dehydromonocrotaline (MCTP) is toxic to both liver and lung. It is stable enough to reach the lung, which is itself incapable of the bioactivation of MCT. The target cell in the lung is the endothelial cell. Injury is delayed and progressive, both in vivo and in vitro. The first phase is characterized by vessel leakage; the later hypertensive phase is characterized by vessel



**FIGURE 4.34** Mechanisms of respiratory injury involving metabolic activation. (A) In situ metabolic activation of parent compound. (B) Activation of parent compound in liver; metabolite produces toxicity in lung. (C) Parent compound undergoes cyclic reduction/oxidation, indirectly inducing toxicity. Reproduced from Haschek WM, Rousseaux CG, Wallig MA, editors: *Handbook of toxicologic pathology*, ed 2, 2002, Academic Press, Vol. 2, Figure 11, p. 31, with permission.



smooth muscle hypertrophy and perivascular fibrosis, elevated vascular pressure, and hypertrophy of the right heart. In vitro, MCTP results in delayed and progressive injury to endothelial cells and a decrease in their proliferative capability. In vivo MCTP, in addition to causing

endothelial cell injury, prevents normal repair processes; thus, progressive injury takes place.

The third mechanism of metabolic activation of xenobiotics in respiratory toxicity involves what has been called "futile redox cycling" (Figure 4.34C). It is best exemplified by the

pulmonary toxicity of the herbicide paraquat. Paraquat is selectively taken up by alveolar epithelial cells via an energy-dependent transport system. It is not metabolized but undergoes cyclic oxidation and reduction with concomitant production of ROS such as superoxide anion, hydrogen peroxide, and hydroxyl free radicals. Paraquat's lung toxicity is exacerbated by the administration of oxygen, so a clear history to determine why a patient is in pulmonary distress is needed before administering oxygen to a paraquat-poisoned patient. Direct evidence for the formation of lipid peroxides in paraquat toxicity remains more elusive. The pulmonary antioxidant defense mechanisms, including Vitamins C and E, make it difficult to obtain reliable measurements of peroxidative processes. A second event in paraquat toxicity is excessive oxidation, GSH oxidation, and eventual depletion of cellular reducing equivalents, particularly of NADPH. The extent to which this mechanism contributes to the development of toxic lung damage is unknown. Acute pulmonary edema may occur within a few hours of ingestion of paraquat, and pulmonary fibrosis and death typically occurs 1–3 weeks after ingestion of lethal amounts of paraquat.

Bleomycin, nitrofurantoin, and disulfiram are examples of drugs that likely cause toxicity by oxidative mechanisms. Bleomycin, a chemotherapeutic drug, reaches the lung via the circulation where DNA–bleomycin– $\text{Fe}^{2+}$  complexes are formed. These complexes have oxidase-like activity and produce superoxide anion. DNA breaks are caused by free radical reactions. Lung is particularly susceptible to bleomycin-induced injury because the activity of bleomycin hydrolase is low in the lung. Similarly, metabolism of nitrofurantoin and disulfiram produces hydroxyl radicals or superoxide. The oxygen radicals overcome the normal protective effects of antioxidants such as superoxide dismutase, glutathione peroxidase, and alpha-tocopherol, resulting in cell damage, inflammation, and fibrosis. Cyclophosphamide and 1,3 bis (2-chloroethyl)-1-nitrosourea (BCNU) are two chemotherapeutic agents whose mechanism of toxicity is not completely known, but there is evidence that they both lead to production of

oxidant species and/or imbalance of the oxidant/antioxidant defense system. The mechanism is important with respect to patient management because administration of oxygen increases the toxicity of all of these compounds. Also, radiation treatment combined with chemotherapy may synergize the toxicity (Forman and Zhang, 2021).

### 5.3. Immune-Mediated Toxicity

Both physical and immunological mechanisms are important in the pulmonary defense against chemical and infectious agents. However, the immune response may result in an adverse effect if hypersensitivity reactions, immune suppression, or nonimmunological enzymatic injury occur (Table 4.6). Hypersensitivity diseases or allergies are the most common types of immune-mediated respiratory disease caused by inhaled agents. The four types of hypersensitivity reactions are discussed (*Immune System*, Vol 4, Chap 6). Type I (anaphylactic), Type II (cytotoxic), and Type III (Arthus type) are antibody-mediated reactions, whereas Type IV (delayed hypersensitivity) is a cell-mediated reaction.

The most common types of hypersensitivity reactions documented in the respiratory tract are Types I and III. Exposure to pulmonary sensitizers, either foreign proteins or simple chemicals that act as haptens, at sufficiently high concentrations induces the formation of specific antibodies. Type I hypersensitivity is primarily manifested as rhinitis (inflammation of the nasal mucosa) or asthma (bronchoconstriction; see Asthma, in Section 4.6), although life-threatening bronchospasm and edema can occur in severe anaphylaxis. Initial exposure to the allergen or sensitizer induces production of IgE antibodies, which bind to mast cells and basophils. Subsequent exposure to the allergen cross-links the cell-bound IgE and triggers mast cell degranulation with release of vasoactive amines and other mediators (Figure 4.20). Platelet activation factor causes platelet aggregation and release of histamine, heparin, and vasoactive amines, thus further amplifying the response. Eosinophils and neutrophils, attracted by eosinophil chemotactic factor of anaphylaxis

and neutrophil chemotactic factors, release hydrolytic enzymes that cause tissue necrosis. Chemicals that produce a Type I reaction include toluene diisocyanates, trimellitic anhydride, and platinum salts. However, the Type I reactions due to small chemical molecules may be mediated by CD8<sup>+</sup> T cells, IL-5 secretion, and eosinophils through an IgE-independent mechanism. Numerous pharmaceutical agents have been implicated in Type I reactions, but  $\beta$ -lactam antibiotics and sulfa-containing drugs are the most common causes of drug-induced Type I reactions (Bhadra and Suratt, 2009). Penicillin is thought to cause approximately 75% of fatal anaphylactic reactions in the United States.

Type III hypersensitivity is manifested as hypersensitivity pneumonitis, also called “extrinsic allergic alveolitis,” and results from deposition of antigen–antibody complexes plus complement in the lungs, which in turn causes inflammation. Chemicals that produce Type III hypersensitivity include trimellitic anhydride and mercury. Organic dusts containing spores of thermophilic bacteria, true fungi, or animal proteins are the most common cause of hypersensitivity pneumonitis in people. Examples such as farmer’s lung, humidifier lung, mushroom picker’s lung, and pigeon breeder’s lung are termed for the settings in which the antigens are encountered. The initial alveolitis may progress to chronic fibrotic lung disease with granulomas. Type IV hypersensitivity is likely involved, along with the Type III response, in the formation of granulomas. Type IV hypersensitivity occurs when sensitized T lymphocytes induce a cell-mediated response after a latent period. An example of a primary Type IV response is the granulomatous reaction induced by beryllium in dogs and people. In rats, however, the granulomas induced by beryllium are considered foreign-body type granulomas and beryllium-specific T cells are not found.

Immune suppression due to inhaled air pollutants has been documented in humans through epidemiological studies and in experimental animals, primarily through bacterial infectivity models, for agents that include oxidant gases such as ozone, nitrogen dioxide, and sulfur dioxide (see *Immune System*, Vol 5, Chap 6),

tobacco smoke, benzene, toluene, and metals such as arsenic, cadmium, nickel, zinc, and lead. Effects on the physical and innate (nonspecific) lung defense mechanisms frequently cannot be separated, but various studies have demonstrated adverse effects on the mucociliary apparatus, pulmonary surfactant, and macrophage function. As an underlying potential mechanism for immune suppression, decreased macrophage function, including phagocytosis and antigen presentation, has been the most studied and documented suppressive effect on the immune system of experimental animals exposed to oxidant gases, aerosols, and particulate air pollutants. Effects on the adaptive immune system have been documented less frequently, but immunosuppression in experimental animals exposed to dioxin has resulted in decreased cell-mediated immune responses and depressed antibody production in response to T-dependent antigens.

Certain chemicals may induce nonimmune-mediated pulmonary disease that mimics immune-mediated disease. Agents may trigger mast cell degranulation without allergen binding to IgE. Although the ensuing response is not a hypersensitivity reaction, the cascades and signs produced akin to those in Type I hypersensitivity. Pharmaceutical compounds known to produce this type of response include calcium ionophores and codeine. Chemicals that stimulate epithelial irritant receptors may cause secretion of inflammatory mediators without antibody involvement, resulting in a pseudoallergic reaction that resembles immediate or Type I hypersensitivity. Such nonspecific airway irritation is called hyperreactive airway syndrome, and can be stimulated by chemicals such as isocyanates, formaldehyde, trimellitic anhydride, and ozone. The hyperreactive airway syndrome has been defined as an increased bronchial responsiveness to an inhaled substance that can, depending on dose, produce airway obstruction. Hyperreactive airways are frequently used as an index of occupational asthma. It should be noted that viruses and physical stimuli, such as cold air and exercise, can also induce bronchial hyperreactivity. Interaction of multiple factors may be important in the induction of airway reactivity in any single individual (Figure 4.20).



### 5.3.1. Inhaled Therapeutic Biologics

Inhaled biologics in therapeutic development are increasing (see *Protein Therapeutics*, Vol 2, Chap 6). Biologics comprise a broad variety of complex macromolecules with unique physicochemical characteristics. A key requirement for successful delivery is stability and avoiding physicochemical degradation by mechanisms such as denaturation, aggregation, deamidation, oxidation, and glycation. Physicochemical degradation can lead to inactivation or safety issues such as immunogenicity caused by degradation products or impaired clearance. In contrast, agglomeration, when particles congeal, can also occur. Agglomeration might lead to larger particles with more upper respiratory tract deposition.

The drug needs to maintain its structural integrity and bioactivity throughout the formulation process and subsequent storage. Drying techniques and excipients may be used to enhance stability, but such methods, especially excipient addition, can exacerbate or induce toxicity. This is why second control groups receiving excipients only may be incorporated into study design. PEGylation involving the attachment of high molecular weight polyethylene glycol is an approach that offers increased stability, prolonged systemic half-life, and reduction of proteolysis, and/or renal excretion.

Further, the formulated drug will have to withstand forces related to the delivery device so that deep lung deposition can be achieved. The choice between delivery via nebulized aerosol or dry powder will depend on the indication, the formulation, as well as the breathing capabilities and preferences of the target patient population.

Once in the lung, it will be important for the drug to avoid excessive clearance mechanisms. Macrophages can clear macromolecules from the lungs within 24–48 hours; and naturally occurring pulmonary proteases can degrade delivered proteins. There are several methods that have been used to avoid clearance mechanisms and increase absorption. Chemical enhancers can act via a variety of different mechanisms including alteration of the mucus layer, protection against enzymatic degradation, tight junction opening, and formation of micelles which facilitate protein transcellular transport. Liposomes enhance drug absorption by

accelerating the surfactant recycling process in alveolar cells. Protein fusion uses the approach of joining proteins of interest with another protein that specifically binds to a receptor on lung epithelium to improve transcytosis by directing a deliverable through a specific active uptake pathway. PIs block naturally occurring pulmonary enzymes from degrading delivered drugs. Size and shape modification and permeation enhancement through mucus commonly utilizes nanotechnology. Nanobodies (discussed in *Toxicity and Responses to Inhaled Particles below*) are particularly suited for inhalation delivery as they are small, simple, and robust with high thermal stability (Depreter et al., 2013).

Immunogenicity may occur when ADAs are produced as a result of the host's immune response against a large molecule's foreign epitopes. Such reactions are often not dose dependent and may manifest microscopically as vascular changes producing edema, microthrombi, and inflammation. The most common findings across NHP inhalation studies of inhaled biologics include macrophage accumulation and perivascular and/or peribronchiolar (BALT) mononuclear cell inflammatory infiltration in the lungs and sometimes related increased (tracheobronchial and/or mediastinal) lymph node cellularity. Lymphoid infiltrates represent a local immune response to inhaled foreign proteins or nucleic acids that are apparent histologically after about 2 weeks of treatment. However, BALT reactions are not exclusively initiated or maintained by an immune response. Inflammatory reactions can also give rise to BALT hyperplasia and immune stimulation and inflammation serve to enhance the function of each other; inflammation increasing the exposure of the immune system to antigens, and injured cells release proinflammatory molecules and danger signals that further stimulate inflammation and activate dendritic cells to induce an immune response. Once induced, iBALT may persist for months (Hall et al., 2021).

Safety concerns from immune complex disease (ICD) are relatively infrequent but may result in microscopic changes characterized by multiorgan vasculitis and glomerulonephritis. In the lung, this may present as thrombosis and vascular/perivascular inflammation. ICD may present in any dose group

with a tendency to show an inverse correlation with dose (i.e., occur more frequently in the mid- and low-dose groups) and affect a single animal or multiple animals. The clinicopathological response can vary significantly between animals even within the same dose group. Diagnosis is a weight of evidence approach based upon clinical signs (ranging from none to death), clinical pathology, IHC, and/or drug exposure data including ADA titers (Hall et al., 2021).

#### 5.4. Toxicity and Responses to Inhaled Particles

As previously discussed, pulmonary toxicity and responses to inhaled particles are influenced by the dose of material, the size and surface area of the particles, the chemical composition of the particles, and the dynamics of their deposition, retention, and clearance in the lung. For inhaled drugs in particle form, the pharmacology of the drug may modulate the expression of toxicity. Responses to inhaled particles may include adaptive, nonadverse physiological responses and/or inflammatory and immune-mediated responses; cell injury; and/or repair. Dose, or the amount of material in the lung, is usually considered in terms of mass or, particularly for nanomaterials, particle numbers. For particulate chemicals, metabolism also affects toxicity. Highly soluble particles leave the lung rapidly and the dose is delivered in a pattern that is similar to inhaled gases. In contrast, poorly soluble particles persist in the lung after cessation of exposure, thus delivering a protracted dose to the lung.

After a single inhalation exposure to particles, the amount of particulate material in the lung decreases with time due to dissolution and/or mechanical clearance. Dissolution is the major route of clearance of soluble particles. Phagocytosis by macrophages and clearance via the mucociliary escalator or lymphatics is a major mechanism for removal of poorly soluble particles, other than nanomaterials, from the lung. However, this mechanism may be abrogated by highly toxic particles. Silica particles, for example, are toxic to macrophages and, as part of the cytotoxic response, macrophages release cytokines that stimulate fibroblasts to replicate and synthesize collagen. In addition, silica also

causes activation and release of mediators by viable macrophages, including interleukin-1, TNF, fibronectin, lipid mediators, oxygen derived free radicals, and fibrogenic cytokines. The macrophage cytotoxicity and ensuing inflammatory and fibrotic responses retard particle clearance (Leikauf, 2018).

Although in some cases brief exposure results in significant lesions with time, most particulate materials must be inhaled repeatedly to induce lesions in experimental animals. Examples of particles that are generally considered toxic but that require repeated inhalation exposures to induce significant lesions in experimental animals include nickel subsulfide, asbestos, and diesel soot.

Depending on the physicochemical properties of the particle, concentration, duration of exposure, and species exposed, nonneoplastic parenchymal responses to particles may include infiltrates of alveolar macrophages, alveolar type bronchioloalveolar hyperplasia (Figure 4.35), inflammation, bronchiolar type bronchioloalveolar hyperplasia (bronchiolization), proteinosis, and fibrosis (Figure 4.28). After cessation of exposure, lesions may regress, persist, or progress.

Numerous studies in rats using inert, insoluble, fine particles, particularly titanium dioxide and carbon black, have led to a consensus that, for these nonfibrous particles, the quantity of material in the lung is the key determinant of the lung pathology (Bermudez et al., 2002). Furthermore, evaluation of data across multiple studies indicates that a lung burden of approximately 0.1 mg/g lung is required for findings to be detectable in histologic sections by light microscopy. When that burden is achieved in rats, increased numbers of alveolar macrophages are observed. Chronic and reversibility studies have shown that with exposures resulting in lung burdens of these relatively “inert” particles below approximately 1 mg/g lung, the adaptive increase in alveolar macrophages does not progress to more complicated lesions, and is reversible. When lung burdens exceed approximately 1 mg/g lung, inflammation, bronchioloalveolar hyperplasia, and fibrosis are observed and these findings may persist or progress after cessation of exposure. Very large lung burdens, approximately 50–100 mg/g lung, result in “lung overload” (previously discussed in multiple sections) in which macrophage-mediated

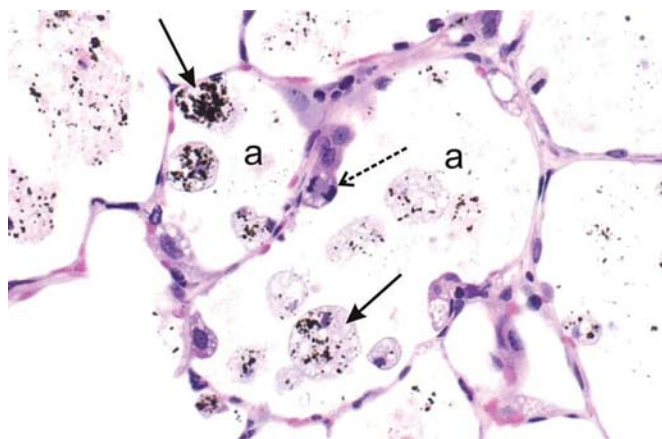


**FIGURE 4.35** Light photomicrograph of the alveolar parenchyma from a rat exposed to a large airborne concentration of carbon black particles for 90 days. Numerous enlarged, particle-laden alveolar macrophages (solid arrows) are present in the alveolar airspaces (a). Type 2 cell hyperplasia is present along the alveolar septa with a mitotic figure (stippled arrow) in one of these epithelial cells, indicating cell proliferation. H&E stain. *Reproduced from Haschek WM, Rousseaux CG, Wallig MA, editors: Handbook of toxicologic pathology, ed 3, 2013, Academic Press, Vol. 3, Figure 51.29, p. 1997, with permission.*

clearance is reduced and lung lesions typically progress after cessation of exposure.

The recognition of increased alveolar macrophages as an adaptive, nonadverse response (Nikula et al., 2014) to inhaled poorly soluble materials has become important as pharmaceutical drug candidates with low solubility are developed for delivery as dry powder formulations to maximize lung efficacy and minimize systemic effects. The increase in alveolar macrophages is a normal defense mechanism to inhaled “dusts,” and is independent of the chemistry or pharmacologic mechanism of the drug particles (Jones and Neef, 2011). Findings complicated by inflammation and epithelial hyperplasia indicate that the threshold for a nonadverse response has been exceeded. The adverse response may be due to drug chemistry, pharmacology, and/or the burden of insoluble drug material.

There are several nongenotoxic, poorly soluble particles, such as titanium dioxide, talc, and carbon black, which induce lesions in rats that are exposed under conditions resulting in overload of macrophage-mediated clearance. Chronic

inhalation of these poorly soluble particles by rats can result in pulmonary inflammation, proteinosis, fibrosis, bronchioloalveolar hyperplasia, squamous metaplasia, and/or squamous cysts. Neoplastic lesions that occur late in life (usually between 24 and 32 months of age) include squamous epitheliomas, bronchioloalveolar adenomas, squamous cell carcinomas, and bronchiolar-alveolar adenocarcinomas. In contrast to rats, mice and hamsters develop less severe lesions and do not develop lung tumors even though the particle lung burdens are similar to the rat. These findings have raised questions concerning the appropriate use of data from rats, exposed under conditions resulting in clearance overload, for hazard identification in humans.

The preceding discussion of particle toxicity applies to particles greater than 100 nm in size. Particles with at least one dimension in the nanoscale (less than 100 nm) are referred to as nanomaterials if they are engineered, man-made materials; and as ultrafine particles if they are air pollutants. The majority of ultrafine particles are produced by incomplete fuel combustion in engines and industrial furnaces; however, natural sources include volcanic activity and sandstorms. Concern for the potential toxicity of nanoparticles initially came from epidemiological data showing a relationship between exposure to ultrafine particulate air pollution and increased cardiovascular and respiratory morbidity and mortality in sensitive populations. Subsequent studies in animals using air pollution condensates, as well as several in vivo and in vitro studies using manufactured nanoparticles, have helped describe potential mechanisms of nanoparticle-related toxicity (see *Nanoparticulates*, Vol 2, Chap 30) (Hubbs et al., 2011; BeruBe et al., 2007).

Inhalation is the major route of entry into the body for nanoparticles. Nanoparticles have a high surface area per unit mass and thus have a large catalytic surface for formation of free radicals that drive oxidative stress, which is especially important for nanoparticles with bound transition metals and metal-based nanoparticles (e.g., silver and cadmium nanoparticles) which can be highly toxic. Additionally, the large surface per unit mass of nanoparticles may lead to adsorption of organic toxicants in air pollution and increase their interaction with cells. Soluble



metals and aromatic hydrocarbons on the surface of nanoparticles may interact with lung lining fluid and undergo cyclic redox reactions that produce ROS. Inhaled nanoparticles may agglomerate in the lung lining fluid or become coated by opsonins. Agglomerated or opsonized nanoparticles are phagocytosed by macrophages, which may induce oxidative stress and inflammatory processes similar to those induced by other respirable particles (Thorley et al., 2014). Nanoparticles that are not phagocytosed by alveolar macrophages efficiently enter lung epithelial cells and fibroblasts in the interstitium as well as cross the alveolar–capillary barrier to enter the circulation, whereby they are distributed to other organs. Nanoparticles deposited on the olfactory mucosa may translocate to the brain through sensory nerves and the olfactory bulb. When nanoparticles gain entrance to cells, they may induce oxidative stress and cause protein, DNA, and membrane injury, as well as activate inflammatory and growth factor cascades and the oxidant-induced transcription factor nuclear factor- $\kappa$ B. Such processes potentially lead to inflammation and fibrosis. Inflammation and oxidative stress in the lung indirectly promote atherothrombosis and atherosclerosis through effects on the endothelium, cardiac blood flow, platelet activation, and coagulation. An area of active research is in understanding the risk for nanoparticle-induced genotoxicity and carcinogenesis (Li et al., 2010).

### 5.5. Toxicity and Responses to Inhaled Fibers

Fibers are a special type of particle defined as having a length to diameter ratio greater than 3:1. The fibers of toxicological concern are asbestos (chrysotile, crocidolite, anthophyllite, amosite, actinolite, and tremolite), synthetic vitreous fibers (SVFs; glasses and ceramics in fibrous form), fibrous erionite (Weissman and Kiefer, 2011), and more recently, nanotubes. Epidemiological studies and studies in experimental animals using asbestos and SVF have led to general agreement that four interrelated factors—dose, particle dimensions, surface

properties, and biopersistence—largely determine the toxicity of inhaled fibers. Iron ions on amphibole types of asbestos react with lung lining fluid and generate ROS that induce toxicity, and oxidant stress may lead to DNA damage. There is a direct relationship between biopersistence (determined by fiber length and chemical composition) and toxicity. Longer, thinner fibers are more toxic because they are not cleared by alveolar macrophages and persist in the lung. Fibers longer than approximately 15  $\mu$ m are particularly toxic and bioactive. They are not completely engulfed by macrophages, leading to the release of lysosomal contents, cytotoxicity, oxidant stress, and stimulation of inflammatory and growth factor pathways (Mossman et al., 2007).

Inhaled asbestos causes asbestosis, which is a fatal interstitial fibrosis, lung cancer, and pleural disease consisting of pleural fibrosis, plaques, and mesothelioma, as previously discussed. Fibers must be thinner than 0.5  $\mu$ m to translocate to the pleural surface. Inhaled asbestos and erionite, which is a nonasbestos, long fiber, are the only known causes of mesothelioma in humans.

Inhaled asbestos fibers activate complement in the lung lining fluid, leading to chemotaxis of inflammatory cells and upregulation of TNF- $\alpha$ , PDGF, TGF- $\alpha$ , and TGF- $\beta$ . These potent growth factors are key to the development of asbestosis. The mechanistic pathways leading to asbestos-induced lung cancer and mesothelioma are not clear. In vitro assays have demonstrated that these fibers can be directly genotoxic and clastogenic. As described above, asbestos fibers induce chronic inflammation, release of ROS, and upregulation and activation of growth factors, which may indirectly lead to cancer. Several in vitro and in vivo experiments have indicated a role for oxidant-dependent stimulation of signaling pathways leading to cell proliferation and transformation.

Nanofibers are a diverse group of materials. Their potential for toxicity will likely be determined by dimensions, surface properties, bioactivity, and biopersistence. Carbon nanotubes are among the most commonly manufactured nanomaterials. Inhaled carbon nanotubes have been shown to penetrate alveolar

macrophages, the alveolar wall, and the pleura in mouse studies. They induced an inflammatory response, oxidant stress, granulomatous pneumonia, and interstitial fibrosis. In vitro experiments have shown that carbon nanotubes can induce mitotic disruption (see *Nanoparticulates*, Vol 3, Chap 13).

## 5.6. Xenobiotic Interactions

Toxicological interactions may play a role in the pathogenesis of lung injury. Inhalation of two different aerosols, simultaneously or in sequence, may produce more or less severe lesions than anticipated from the known toxicity of either aerosol alone. It is well known that combination of SO<sub>2</sub> with certain salt aerosols will act synergistically to adversely affect pulmonary function. Concomitant exposure to acidic aerosols and to ozone (at specific exposure levels and exposure times) enhances the development of pulmonary fibrosis over that occurring following exposure to either inhalant alone. Of particular importance is the observation that such interactions occur at pollutant levels approximating conditions encountered in the environment. On the other hand, interactions between inhalants occasionally may mitigate toxicity—for example, ammonia neutralizes acidic fumes.

Simultaneous exposure to a bloodborne pulmonary toxin and to an inhalant may also greatly enhance the development of untoward effects in the lung. Previously mentioned examples are enhancement of paraquat, bleomycin, or BHT toxicity by oxygen species. Additionally, compared to the normal lung, a damaged lung is often much more vulnerable to toxic effects of a second agent. In experimental animals, primary lung injury caused by toxic agents, such as inhaled CdCl<sub>2</sub>, can be greatly amplified by subsequent inhalation of oxygen at a concentration (50%–70% in the inhaled air) that otherwise would produce little, if any, harmful effect in a normal lung. In humans with DAD (acute respiratory distress syndrome), oxygen therapy, although necessary, may enhance the later development of fibrotic changes. Finally, the risk for lung cancer in uranium miners or asbestos workers is greatly increased by cigarette smoking.

## 5.7. Modifying Factors in Toxicity

Factors affecting susceptibility to nonneoplastic and neoplastic pulmonary disease include genetic factors, species differences, age, and nutrition, as well as preexisting disease such as asthma. For example, newborn and young rats are usually more resistant to oxygen toxicity than adults. This correlates with their ability to induce superoxide dismutase, catalase, and glutathione peroxidase on exposure to a high concentration of oxygen. In adults, tolerance can be induced by prior exposure to oxygen, which induces the activity of superoxide dismutase. Tolerance cannot be induced in adult hamsters or mice, and they show little increase in superoxide dismutase activity. In addition, a vitamin E-deficient diet can enhance the susceptibility to oxygen toxicity (Frank, 1980).

Species differences in response to sensory irritants can result in large differences in the actual dose delivered to the respiratory tract. This has been thoroughly studied with formaldehyde. Mice and rats exposed to 15 ppm formaldehyde for 6 hours, following a similar 4-day pretreatment, had an immediate decrease in respiratory rate and minute volume, but no change in tidal volume. The minute volume of mice was decreased to 50% of preexposure values, whereas that of rats showed only a 15% decrease. Thus, the nasal cavity of rats received a significantly higher dose of formaldehyde—approximately 75% greater—than that of mice. Histological lesions and cell proliferation were greater in rats than in mice, thus correlating with the difference in dose received between mice and rats.

Recent research characterizing the respiratory microbiome has provided invaluable knowledge about the function of microbial species that inhabit the various organ systems. The lungs, previously thought to be sterile, are now known to harbor a unique microbiota and, additionally, to be influenced by microbial signals from distal body sites, such as the intestine. In healthy lungs, the microbial biomass is low, containing 10<sup>3</sup> to 10<sup>5</sup> bacteria per gram of tissue (for comparison, the large intestine reaches a density of 10<sup>11</sup> to 10<sup>12</sup> bacteria per gram). The source and maintenance of the airway microbiota is thought to be determined by the balance between microbial immigration from the upper respiratory tract

(e.g., via microaspiration of microorganism-seeded saliva) and microbial elimination by host defense mechanisms (e.g., clearance by alveolar macrophages and mucociliary transport), with relatively little contribution from the local reproduction of the microbes themselves (Wypych et al., 2019).

## 5.8. Adversity Considerations

There are a few induced findings for which adversity determinations are defined. Epithelial alteration and minimal to mild/slight squamous metaplasia of the larynx in rodents is regarded as nonadverse. Similarly, increased alveolar macrophages are not considered adverse at low levels, since organ function is not meaningfully compromised. Additionally, eosinophilic globules in nasal mucosae; and low grade nasal mucous cell hyperplasia/hypertrophy in the anterior nose and cilia loss/epithelial attenuation in the tracheal bifurcation are generally considered nonadverse and regarded as adaptive changes due to nonspecific irritation and flow dynamics, respectively.

Unlike some systems, most respiratory organs have capacity for self-renewal and considerable functional reserve. However, opinion differences between pathologists, toxicologists, and regulators exist on how a morphologic lesion might impact the health status of an animal (i.e., as harmful or not). There is no universal standard to assess adversity and various opinions exist as to whether lung inflammation, inflammatory cell infiltrates, and other common findings are adverse, and if so, at what severity (Hall et al., 2021). It is important to note that a low-grade finding in a healthy caged nonclinical species may be deemed nonadverse in the absence of meaningful detrimental effects on lung function as inferred from microscopic changes and other supporting study data. However, this same change may be adverse in patients with significantly reduced lung function and comorbidities. Ultimately, adversity determinations should be made using weight of evidence approach pertaining to the specific study and species in which the findings have occurred. Risk and adversity in humans relate to risk assessment and should integrate all the uncertainties associated with lesion progression and patient vulnerability. One should not confuse hazard identification

and risk assessment when making a call of adversity nor call something adverse in the nonclinical species based on an anticipated adverse effect extrapolated to a vulnerable human population.

## 6. CONCLUSION

In summary, the respiratory tract is a complex organ system both macroscopically and microscopically, with many different functions and cell types localized throughout the nasopharyngeal, tracheobronchial, and pulmonary segments. Exposure to xenobiotics occurs via inhalation and via the blood following ingestion, dermal exposure, or parenteral administration. Xenobiotics vary from particles of variable size and solubility to gases and to plant toxins, thus dosimetry and site of injury are critical in interpreting the response to injury. In addition, species differences must be considered in interpretation of data to be used in risk assessment.

In naturally occurring disease, because the pulmonary response to injury is often nonspecific, it is important to consider the gross distribution of pulmonary lesions and to use detailed history and ancillary test results in conjunction with histological evaluation to determine potential etiologic agents.

Inhalation studies are used globally to test drugs, chemicals, and environmental pollutants for potential toxicity and carcinogenicity. In drug development, inhalation is an increasingly explored route of nonparenteral drug administration for biologics and small molecules (Gregori et al., 2021). Depending upon the therapeutic area, inhalation may be chosen as the optimal route of delivery to target the site of drug action and achieve higher bioavailability compared to alternative routes. The lungs represent a source of xenobiotic metabolizing enzymes that may significantly influence the pharmacokinetics of inhaled drugs, with implications for drug efficacy and safety. Examination of the respiratory tract in nonclinical studies may reveal manifestations of systemic toxicity, occurrence of local metabolism, or insight into toxicities within other organ systems.



## REFERENCES

- Ahookhosh K, Vanoirbeek J, Vande Velde G: Lung function measurements in preclinical research: what has been done and where is it headed? *Front. Physiol.* 14:1130096, 2023 Mar 22.
- Aichler M, Kunzke T, Buck A, et al.: Molecular similarities and differences from human pulmonary fibrosis and corresponding mouse model: MALDI imaging mass spectrometry in comparative medicine, *Lab. Invest.* 98(1):141–149, Jan 2018.
- Alexander DJ, Collins CJ, Coombs DW, Gilkison IS, Hardy CJ, Karantabias G, Johnson N, Karlsson A, Kilgor JD, McDonald P: Association of Inhalation Toxicologists (AIT) working party recommendation for standard delivered dose calculation and expression in nonclinical aerosol inhalation toxicology studies with pharmaceuticals, *Inhal. Tox.* 20:1179–1189, 2008.
- Allen CB: In vitro models for lung toxicology. In Gardner DE, editor: *Toxicology of the lung*, Boca Raton, FL, 2005, CRC Press, Taylor and Francis, pp 107–150.
- Asaoka Y, Togashi Y, Imura N, Sai T, Miyoshi T, Miyamoto Y: Immunohistochemistry of LAMP-2 and adipophilin for phospholipidosis in liver and kidney in ketoconazole-treated mice, *Exp. Toxicol. Pathol.* 65(6):817–823, 2013 Sep.
- Aspal M, Zemans RL: Mechanisms of ATII-to-ATI cell differentiation during lung regeneration, *Int. J. Mol. Sci.* 21(9): 3188, 2020 Apr 30.
- Ballard-Croft C, Wang D, Sumpter LR, Zhou X, Zwischenberger JB: Large-animal models of acute respiratory distress syndrome, *Ann. Thorac. Surg.* 93:1331–1339, 2012.
- Barber NA, Ganti AK: Pulmonary toxicities from targeted therapies: a review, *Targeted Oncol.* 6(4):235–243, Dec 2011.
- Barnard DL: Animal models for the study of influenza pathogenesis and therapy, *Antivir. Res.* 82(2):A110–A122, 2009 May.
- Beers MF, Morrissey EE: The three R's of lung health and disease: repair, remodeling, and regeneration, *J. Clin. Invest.* 121:2065–2073, 2011.
- Bermudez E, Mangum JB, Asgharian B, Wong BA, Reverdy EE, Janszen DB, Hext PM, Warheit DB, Everitt JI: Long-term pulmonary responses of three laboratory rodent species to subchronic inhalation of pigmentary titanium dioxide particles, *Toxicol. Sci.* 70:86–97, 2002.
- Berube K, Balharry D, Sexton K, Koshy L, Jones T: Combustion-derived nanoparticles: mechanisms of pulmonary toxicity, *Clin. Exp. Pharmacol. Physiol.* 34:1044–1050, 2007.
- Bhadra K, Suratt BT: Drug-induced lung diseases: a state-of-the-art review, *J. Respir. Dis.* 30:1–10, 2009.
- Bigay J, Le Grand R, Martinon F, Maisonnasse P: Vaccine-associated enhanced disease in humans and animal models: lessons and challenges for vaccine development, *Front. Microbiol.* 13:932408, 2022 Aug 10.
- Blackwell TS, Yull FE, Chen CL, et al.: Multiorgan nuclear factor kappa B activation in a transgenic mouse model of systemic inflammation, *Am. J. Respir. Crit. Care Med.* 162(3 Pt 1):1095–1101, Sep 2000.
- Bomhard E: Particle-induced pulmonary alveolar proteinosis and subsequent inflammation and fibrosis: a toxicologic and pathologic review, *Toxicol. Pathol.* 45(3):389–401, 2017.
- Boukhvalova MS, Yim KC, Blanco J: Cotton rat model for testing vaccines and antivirals against respiratory syncytial virus, *Antivir. Chem. Chemother.* 26, 2018 Jan-Dec.
- Bouvier NM, Lowen AC: Animal models for influenza virus pathogenesis and transmission, *Viruses* 2(8):1530–1563, 2010.
- Brennan RJ: Target safety assessment: strategies and resources, *Methods Mol. Biol.* 1641:213–228, 2017.
- Brunjes PC, Illig KR, Meyer EA: A field guide to the anterior olfactory nucleus (cortex), *Brain Res. Rev.* 50(2):305–335, 2005.
- Byers DE, Holtzman MJ: Alternatively activated macrophages and airway disease. *Chest* 140, 768–774.
- Carman BL, Predescu DN, Machado R, Predescu SA: Plexiform arteriopathy in rodent models of pulmonary arterial hypertension, *Am. J. Pathol.* 189(6):1133–1144, 2019 Jun.
- Chamanza R: Non-human Primates: cynomolgus (*Macaca fascicularis*), and rhesus (*Macaca mulatta*) macaques and the common marmoset (*Callithrix jacchus*). In McInnes EF, editor: *Background lesions in laboratory animals a color atlas*, 2012, Elsevier Ltd, pp 1–16.
- Chamanza R, Amuzie CJ, Chilton J, Engelhardt JA: Special issue on the pathobiology of laboratory nonhuman primates: a review of species, substrain, geographical origin, age, and modality-related factors, *Toxicol. Pathol.* 50(5):548–551, 2022.
- Chamanza R, Taylor I, Gregori M, Hill C, Swan M, Goodchild J, Goodchild K, Schofield J, Aldous M, Mowat V: Normal anatomy, histology, and spontaneous pathology of the nasal cavity of the cynomolgus monkey (*Macaca fascicularis*), *Toxicol. Pathol.* 44(5):636–654, 2016 Jul.
- Cherian SV, Kumar A, Estrada-Y-Martin RM: E-Cigarette or vaping product-associated lung injury: a review, *Am. J. Med.* 133(6):657–663, 2020 Jun.
- Cho W-S, Duffin R, Bradley M, Megson IL, MacNee W, Howie SEM, Donaldson K: NiO and Co3O4 nanoparticles induce lung DTH-like responses and alveolar lipoproteinosis, *Eur. Respir. J.* 39:546–557, 2012.
- Choudhary S, Kanevsky I, Yildiz S, Sellers RS, Swanson KA, Franks T, Rathnasinghe R, Munoz-Moreno R, Jangra S, Gonzalez O, Meade P, Coskran T, Qian J, Lanz TA, Johnson JG, Tierney CA, Smith JD, Tompkins K, Illenberger A, Corts P, Ciolino T, Dormitzer PR, Dick Jr EJ, Shivanna V, Hall-Ursone S, Cole J, Kaushal D, Fontenot JA, Martinez-Romero C, McMahon M, Krammer F, Schotsaert M, García-Sastre A: Modeling SARS-CoV-2: comparative pathology in rhesus macaque and golden

- Syrian hamster models, *Toxicol. Pathol.* 50(3):280–293, 2022 Apr, <https://doi.org/10.1177/01926233211072767>.
- Coggins CR: A further review of inhalation studies with cigarette smoke and lung cancer in experimental animals, including transgenic mice, *Inhal. Toxicol.* 22:974–983, 2010.
- Cohen M, Zelikoff J, Schlesinger R, editors: *Pulmonary immunotoxicology*, 2001, Springer.
- Colman K, Andrews RN, Atkins H, Boulineau T, Bradley A, Braendli-Baiocco A, Capobianco R, Caudell D, Cline M, Doi T, Ernst R, van Esch E, Everitt J, Fant P, Gruebbel MM, Mecklenburg L, Miller AD, Nikula KJ, Satake S, Schwartz J, Sharma A, Shimoi A, Sobry C, Taylor I, Vemireddi V, Vidal J, Wood C, Vahle JL: International harmonization of nomenclature and diagnostic criteria (INHAND): non-proliferative and proliferative lesions of the non-human primate (*M. fascicularis*), *J. Toxicol. Pathol.* 34(3 Suppl):1S–182S, 2021.
- Cooper TK, Meyerholz DK, Beck AP, Delaney MA, Piersigilli A, Southard TL, Brayton CF: Research-relevant conditions and pathology of laboratory mice, rats, gerbils, Guinea pigs, hamsters, naked mole rats, and rabbits, *ILAR J.* 62:77–132, 2022 Jan 4.
- Cooney AL, Wambach JA, Sinn PL, McCray Jr PB: Gene therapy potential for genetic disorders of surfactant dysfunction, *Front. Genome* 3:785829, 2022 Jan 14.
- Cruzan G, Bus J, Hotchkiss J, Harkema J, Banton M, Sarang S: CYP2F2-generated metabolites, not styrene oxide, are a key event mediating the mode of action of styrene-induced mouse lung tumors, *Regul. Toxicol. Pharmacol.* 62(1):214–220, 2012.
- Damsch S, Eichenbaum G, Tonelli A, Lammens L, Van den Bulck K, Feyen B, Vandenbergh J, Megens A, Knight E, Kelley M: Gavage-related reflux in rats: identification, pathogenesis, and toxicological implications (review), *Toxicol. Pathol.* 39:348–360, 2011.
- Dear JD: Bacterial pneumonia in dogs and cats: an update, *Vet. Clin. North Am. Small Anim. Pract.* 50(2):447–465, 2020 Mar.
- Depreter F, Pilcer G, Amighi K: Inhaled proteins: challenges and perspectives, *Int. J. Pharm.* 447(1–2):24–80, 2013 Apr 15.
- Dimastromatteo J, Charles EJ, Laubach VE: Molecular imaging of pulmonary diseases, *Respir. Res.* 19(1):17, 2018 Jan 24.
- Ding X, Kaminsky LS: Human extrahepatic cytochromes P450: function in xenobiotic metabolism and tissue-selective chemical toxicity in the respiratory and gastrointestinal tracts, *Annu. Rev. Pharmacol. Toxicol.* 43:149–173, 2003.
- Ding X, Li L, Van Winkle LS, Zhang QY: Biochemical function of the respiratory tract: metabolism of xenobiotics. In McQueen CA, editor: *Comprehensive toxicology*, vol. 15, *Respiratory toxicology*, Oxford, UK, 2018, Elsevier Science, pp 171–193.
- Dixon D, Herbert RA, Sills RC, Boorman GA: Lungs, pleura, and mediastinum. In Maronpot RR, editor: *Pathology of the mouse*, Saint Louis, MO, 1999, Cache River Press, pp 293–332.
- Dolinay T, Kim YS, Howrylak J, Hunninghake GM, An CH, Fredenburgh L, Massaro AF, Rogers A, Gazourian L, Nakahira K, Haspel JA, Landazury R, Eppanapally S, Christie JD, Meyer NJ, Ware LB, Christiani DC, Ryter SW, Baron RM, Choi AM: Inflammasome-regulated cytokines are critical mediators of acute lung injury, *Am. J. Respir. Crit. Care Med.* 185(11):1225–1234, 2012.
- Donaldson K, Aitken R, Tran L, Stone V, Duffin R, Forrester G, Alexander A: Carbon nanotubes: a review of their properties in relation to pulmonary toxicology and workplace safety, *Toxicol. Sci.* 92:5–22, 2006.
- Dothager RS, Piwnica-Worms D: Molecular imaging of pulmonary disease in vivo, *Proc. Am. Thorac. Soc.* 6(5):403–410, 2009 Aug 15.
- Driehuys B, Hedlund LW: Imaging techniques for small animal models of pulmonary disease: MR microscopy, *Toxicol. Pathol.* 35(1):49–58, 2007.
- du Plessis A, Broeckhoven C, Guelpa A, le Roux SG: Laboratory x-ray micro-computed tomography: a user guideline for biological samples, *GigaScience* 6(6):1–11, 2017 Jun 1.
- Ebenig A, Muraleedharan S, Kazmierski J, Todt D, Auste A, Anzaghe M, Gömer A, Postmus D, Gogesch P, Niles M, Plesker R, Miskey C, Gellhorn Serra M, Breithaupt A, Hörner C, Kruip C, Ehmann R, Ivics Z, Waibler Z, Pfaender S, Wyler E, Landthaler M, Kupke A, Nouailles G, Goffinet C, Brown RJP, Mühlebach MD: Vaccine-associated enhanced respiratory pathology in COVID-19 hamsters after TH2-biased immunization, *Cell Rep.* 40(7):111214, 2022 Aug 16.
- Edwards MJ, Becker KA, Gripp B, Hoffmann M, Keitsch S, Wilker B, Soddemann M, Gulbins A, Carpinteiro E, Patel SH, Wilson GC, Pöhlmann S, Walter S, Fassbender K, Ahmad SA, Carpinteiro A, Gulbins E: Sphingosine prevents binding of SARS-CoV-2 spike to its cellular receptor ACE2, *J. Biol. Chem.* 295(45):1474–1482, 2020 Nov 6.
- El-Hashash AHK: *Stem cell innovation in health and disease volume 1: the lung*, San Diego, CA, USA, 2021, Academic Press.
- Elmore SA: Enhanced histopathology of mucosa-associated lymphoid tissue, *Toxicol. Pathol.* 34:687–696, 2006.
- Enaud R, Prevel R, Ciarlo E, Beaufils F, Wieërs G, Guery B, Delhaes L: The gut-lung axis in health and respiratory diseases: a place for inter-organ and inter-kingdom crosstalks, *Front. Cell. Infect. Microbiol.* 10:9, 2020 Feb 19.
- Faria GM, Soares IDP, D'Alincourt Salazar M, Amorim MR, Pessoa BL, da Fonseca CO, Quirico-Santos T: Intranasal perillyl alcohol therapy improves survival of patients with recurrent glioblastoma harboring mutant variant for MTHFR rs1801133 polymorphism, *BMC Cancer* 20(1):294, 2020 Apr 7.
- Fazio JC, Gandhi SA, Flattery J, et al.: Silicosis among immigrant engineered stone (quartz) countertop fabrication workers in California, *JAMA Intern. Med.* 183:991–998, 2023.
- Feron VJ, Arts JH, Kuper CF, Slootweg PJ, Woutersen RA: Health risks associated with inhaled nasal toxicants, *Crit. Rev. Toxicol.* 31(3):313–347, 2001 May.
- Finch CL, Crozier I, Lee JH, et al.: Characteristic and quantifiable COVID-19-like abnormalities in CT- and PET/CT-imaged lungs of SARS-CoV-2-infected crab-eating macaques (*Macaca fascicularis*), *bioRxiv*, 2020 May 14.

- Finkelman FD, Willis-Karp M: Usefulness and optimization of mouse models of allergic airway disease, *J. Allergy Clin. Immunol.* 121:603–606, 2008.
- Forbes B, O'Lone R, Allen PP, Cahn A, Clarke C, Collinge M, Dailey LA, Donnelly LE, Dybowski J, Hassall D, Hildebrand D, Jones R, Kilgour J, Klapwijk J, Maier CC, McGovern T, Nikula K, Parry JD, Reed MD, Robinson I, Tomlinson L, Wolfreys A: Challenges for inhaled drug discovery and development: induced alveolar macrophage responses, *Adv. Drug Deliv. Rev.* 71:15–33, 2014 May.
- Forman HJ, Zhang H: Targeting oxidative stress in disease: promise and limitations of antioxidant therapy, *Nat. Rev. Drug Discov.* 20(9):689–709, 2021 Sep.
- Fox MS, Welch I, Hobson D, Santyr GE: A novel intubation technique for minimally invasive longitudinal studies of rat lungs using hyperpolarized  $^3\text{He}$  magnetic resonance imaging, *Lab. Anim* 46(4):311–317, 2012 Oct.
- Frank L: Oxygen toxicity. In , New York, NY, 1980, Pergamon Elsevier Science, Inc., pp 275–302. Sipes IG, McQueen CA, Gandolfi JA, editors: *Comprehensive toxicology*, vol. 8. New York, NY, 1980, Pergamon Elsevier Science, Inc., pp 275–302.
- Fuentes S, Klenow L, Golding H, Khurana S: Nonclinical evaluation of bacterially produced RSV-G protein vaccine: strong protection against RSV challenge in cotton rat model, *Sci. Rep.* 7:42428, 2017 Feb 10.
- Gammon ST, Foje N, Brewer EM, et al.: Preclinical anatomical, molecular, and functional imaging of the lung with multiple modalities, *Am. J. Physiol. Lung Cell Mol. Physiol.* 306(10):L897–L914, 2014 May 15.
- Gerdts V, Wilson HL, Meurens F, et al.: Large animal models for vaccine development and testing, *ILAR J.* 56(1):53–62, 2015.
- Glaab T, Braun A: Noninvasive measurement of pulmonary function in experimental mouse models of airway disease, *Lung* 199(3):255–261, 2021 Jun.
- Gopinath C, Mowat V: The respiratory system. In Gopinath C, Mowat V, editors: *Atlas of toxicological pathology*, New York, 2014, Springer, pp 19–45.
- Green FH, Vallyathan V, Hahn FF: Comparative pathology of environmental lung disease: an overview, *Toxicol. Pathol.* 35:136–147, 2007.
- Gregori M, Naylor SW, Freke MC, Chamanza R, Piaia A, Hall P: Multisite analysis of lesions in the respiratory tract of the rat and nonhuman primate (cynomolgus monkey) exposed to air, vehicle, and inhaled small molecule compounds, *Toxicol. Pathol.* 49(2):349–369, 2021.
- Gundersen HJG, Mirable R, Brown D, Boyce RW. In Haschek WM, Rousseaux CG, Wallig MA, editors: *Stereological principles and sampling procedures for toxicologic pathologists, Handbook of Toxicologic Pathology*, 3rd ed., 2013, Academic Press, pp 215–286.
- Hakkinen PJ, Whitely JW, Witschi HH: Hyperoxia, but not thoracic X-irradiation, potentiates bleomycin- and cyclophosphamide-induced lung damage in mice, *Am. Rev. Respir. Dis.* 126:281–285, 1982.
- Hall AP, Tepper JS, Boyle MH, et al.: BSTP review of 12 case studies discussing the challenges, pathology, immunogenicity, and mechanisms of inhaled biologics, *Toxicol. Pathol.* 49(2):235–260, 2021 Feb.
- Hansel TT, Kropshofer H, Singer T, Mitchell JA, George AJT: The safety and side effects of monoclonal antibodies, *Nat. Rev. Drug Discov.* 9(4):325–338, 2010.
- Harding R, Pinkerton KE: *The lung: development, aging and the environment*, 2nd ed. San Diego, CA, USA, 2014, Academic Press.
- Harkema JR, Carey SA, Wagner JG: The nose revisited: a brief review of the comparative structure, function, and toxicologic pathology of the nasal epithelium, *Toxicol. Pathol.* 34: 252–269, 2006.
- Harkema JR, Carey SA, Wagner JG, Dintzis SM, Liggitt D: Nose, sinus, pharynx, and larynx. In Treuting PM, Dintzis SM, editors: *Comparative anatomy and histology: a mouse and human atlas*, Amsterdam, The Netherlands, 2018, Academic Press, pp 89–114.
- Harkema JR, Plopper CG, Hyde DM, St George JA, Wilson DW, Dungworth DL: Response of the macaque nasal epithelium to ambient levels of ozone. A morphologic and morphometric study of the transitional and respiratory epithelium, *Am. J. Pathol.* 128:29–44, 1987.
- Haspeslagh E, Debeuf N, Hammad H, Lambrecht BN: Murine models of allergic asthma, *Methods Mol. Biol.* 1559:121–136, 2017.
- Hassan R, Ho M: Mesothelin targeted cancer immunotherapy, *Eur. J. Cancer* 44(1):46–53, 2008.
- Helke KL, Meyerholz DK, Beck AP, Burrough ER, Derscheid RJ, Löhr C, McInnes EF, Scudamore CL, Brayton CF: Research relevant background lesions and conditions: ferrets, dogs, swine, sheep, and goats, *ILAR J.* 62:133–168, 2021.
- Henderson RF: Use of bronchoalveolar lavage to detect respiratory tract toxicity of inhaled material, *Exp. Toxicol. Pathol.* 57(Suppl. 1):155–159, 2005.
- Herati RS, Wherry EJ: What is the predictive value of animal models for vaccine efficacy in humans? Consideration of strategies to improve the value of animal models, *Cold Spring Harbor Perspect. Biol.* 10(4):a031583, 2018 Apr 2.
- Herbert RA, Janardhan KS, Pandiri AR, Cesta MF, Chen V, Miller RA: Lung, pleura and mediastinum. In Suttie AW, editor: *Boorman's pathology of the rat: reference and atlas*, 2nd edn., San Diego, CA, 2015a, Academic Press, Inc, pp 437–466.
- Herbert RA, Janardhan KS, Pandiri AR, Cesta MF, Chen V, Miller RA: Nose, larynx, and trachea. In Suttie AW, editor: *Boorman's pathology of the rat: reference and atlas*, 2nd edn., San Diego, CA, 2015b, Academic Press, Inc, pp 391–435.
- Herbert RA, Leininger JR: Nose, larynx, and trachea. In Maronpot RR, editor: *Pathology of the mouse*, Saint Louis, MO, 1999, Cache River Press, pp 259–292.
- Hernandez-Clavijo A, Sarno N, Gonzalez-Velandia KY, Degen R, Fleck D, Rock JR, Spehr M, Menini A, Pifferi S: TMEM16A and TMEM16B modulate pheromone-evoked



- action potential firing in mouse vomeronasal sensory neurons, *eNeuro* 8(5), 2021 Sep 15.
- Heydemann L, Ciurkiewicz M, Beythien G, Becker K, Schughart K, Stanelle-Bertram S, Schaumburg B, Mounogou-Kouassi N, Beck S, Zickler M, Kühnel M, Gabriel G, Beineke A, Baumgärtner W, Armando F: Hamster model for post-COVID-19 alveolar regeneration offers an opportunity to understand post-acute sequelae of SARS-CoV-2, *Nat. Commun.* 14(1):3267, 2023 Jun 5.
- Hill W, Lim EL, Weeden CE, Lee C, Augustine M, Chen K, Kuan FC, Marongiu F, Evans Jr EJ, Moore DA, Rodrigues FS, Pich O, Bakker B, Cha H, Myers R, van Maldegem F, Boumelha J, Veeriah S, Rowan A, Naceur-Lombardelli C, Karasaki T, Sivakumar M, De S, Caswell DR, Nagano A, Black JRM, Martínez-Ruiz C, Ryu MH, Huff RD, Li S, Favé MJ, Magness A, Suárez-Bonnet A, Priestnall SL, Lüchtenborg M, Lavelle K, Pethick J, Hardy S, McDonald FE, Lin MH, Troccoli CI, Ghosh M, Miller YE, Merrick DT, Keith RL, Al Bakir M, Bailey C, Hill MS, Saal LH, Chen Y, George AM, Abbosh C, Kanu N, Lee SH, McGranahan N, Berg CD, Sasieni P, Houlston R, Turnbull C, Lam S, Awadalla P, Grönroos E, Downward J, Jacks T, Carlsten C, Malanchi I, Hackshaw A, Litchfield K, Tracerx C, DeGregori J, Jamal-Hanjani M, Swanton C: Lung adenocarcinoma promotion by air pollutants, *Nature* 616(7955):159–167, 2023 Apr.
- Hoenerhoff MJ, Starost ME, Ward JM: Eosinophilic crystalline pneumonia as a major cause of death in 129S4/SvJae mice, *Vet. Pathol.* 43:682–688, 2006.
- Holden VK, Hines SE: Update on flavoring-induced lung disease, *Curr. Opin. Pulm. Med.* 22(2):158–164, 2016 Mar.
- Hsia CCW, Hyde DM, Ochs M, Weibel ER: An official research policy statement of the American thoracic society/European respiratory society: standards for quantitative assessment of lung structure, *Am. J. Respir. Crit. Care Med.* 181:394–418, 2010.
- Huax F: Interpreting immunoregulation in lung fibrosis: a new branch of the immune model, *Front. Immunol.* 12: 690375, 2021 Aug 20.
- Hubbs AF, Mercer RR, Benkovic SA, Harkema J, Sriram K, Schwegler-Berry D, Goravanahally MP, Nurkiewicz TR, Castranova V, Sargent LM: Nanotoxicology – a pathologist's perspective, *Toxicol. Pathol.* 39:301–324, 2011.
- Husain AN: The lung. In Kumar V, Abbas AK, Aster JC, editors: *Robbins & cotran pathologic basis of disease*, 10th edn., New York, NY, 2021, Elsevier Saunders.
- Hyde DM, Tyler NK, Plopper CG: Morphometry of the respiratory tract: avoiding the sampling, size, orientation, and reference traps, *Toxicol. Pathol.* 35:41–48, 2007.
- Jones RM, Neef N: Interpretation and prediction of inhaled drug particle accumulation in the lung and its associated toxicity, *Xenobiotica* 42(1):86–93, 2011.
- Kamperschroer C, Shenton J, Lebrec H, Leighton JK, Moore PA, Thomas O: Summary of a workshop on nonclinical and translational safety assessment of CD3 bispecifics, *J. Immunot.* 17(1):67–85, 2020.
- Katz MG, Fargnoli AS, Gubara SM, et al.: The left pneumonectomy combined with monocrotaline or sugen as a model of pulmonary hypertension in rats, *J. Vis. Exp.*, 2019:145, 2019, <https://doi.org/10.3791/59050>.
- Kaufmann W, Bader R, Ernst H, et al.: 1st international ESTP expert workshop: “larynx squamous metaplasia”. A reconsideration of morphologic and diagnostic approaches in rodent studies and its relevance for human assessment, *Exp. Toxicol. Pathol.* 61(6):591–603, 2009.
- Keller LA, Merkel O, Popp A: Intranasal drug delivery: opportunities and toxicologic challenges during drug development, *Drug Deliv. Transl. Res.*, 2021 Jan 25:1–23, 2021 Jan 25.
- Kerns SJ, Belgur C, Petropolis D, et al.: Human immunocompetent Organ-on-Chip platforms allow safety profiling of tumor-targeted T-cell bispecific antibodies, *Elife* 10: e67106, 2021.
- Khalil N, Churg A, Muller N, O'Connor R: Environmental, inhaled and ingested causes of pulmonary fibrosis, *Toxicol. Pathol.* 35:86–96, 2007.
- Kiros TG, Levast B, Auray G, Strom S, van Kessel J, Gerdts V: *The importance of animal models in the development of vaccines. Innovation in vaccinology*, 29, pp 251–264.
- Kruger L, Saporta S, Swanson LW: *Photographic atlas of the rat brain*, Cambridge, 1995, Cambridge University Press.
- Koenitzer JR, Wu H, Atkinson JJ, Brody SL, Humphreys BD: Single-nucleus RNA-sequencing profiling of mouse lung. Reduced dissociation bias and improved rare cell-type detection compared with single-cell RNA sequencing, *Am. J. Respir. Cell Mol. Biol.* 63(6):739–747, 2020 Dec.
- Kong J, Wen S, Cao W, Yue P, Xu X, Zhang Y, Luo L, Chen T, Li L, Wang F, Tao J, Zhou G, Luo S, Liu A, Bao F: Lung organoids, useful tools for investigating epithelial repair after lung injury, *Stem Cell Res. Ther.* 12(1):95, 2021 Jan 30.
- Konkimalla A, Tata A, Tata PR: Lung regeneration: cells, models, and mechanisms, *Cold Spring Harbor Perspect. Biol.* 14(10):a040873, 2022 Oct 3.
- Kumlin U, Olofsson S, Dimock K, Arnberg N: Sialic acid tissue distribution and influenza virus tropism, *Influenza Other Respir. Viruses* 2(5):147–154, 2008 Sep.
- Labiris NR, Dolovich MB: Pulmonary drug delivery. Part I: physiological factors affecting therapeutic effectiveness of aerosolized medications, *Br. J. Clin. Pharmacol.* 56(6):588–599, 2003.
- Laskin DL, Malaviya R, Laskin JD: Role of macrophages in acute lung injury and chronic fibrosis induced by pulmonary toxicants, *Toxicol. Sci.* 168(2):287–301, 2019.
- Leibel SL, McVicar RN, Winquist AM, Niles WD, Snyder EY: Generation of complete multi-cell type lung organoids from human embryonic and patient-specific induced pluripotent stem cells for infectious disease modeling and therapeutics validation, *Curr. Protoc. Stem Cell Biol.* 54(1): e118, Sep 2020.

- Leikauf GD: Toxic responses of the respiratory system. In Klaassen CD, editor: *Casarett and Doull's toxicology: the basic science of poisons*, 9th Edn., New York, NY, 2018, McGraw Hill, pp 793–838.
- Lenz B, Braendli-Baiocco A, Engelhardt J, Fant P, Fischer H, Francke S, Fukuda R, Gröters S, Harada T, Harleman H, Kaufmann W, Kustermann S, Nolte T, Palazzi X, Pohlmeyer-Esch G, Popp A, Romeike A, Schulte A, Lima BS, Tomlinson L, Willard J, Wood CE, Yoshida M: Characterizing adversity of lysosomal accumulation in nonclinical toxicity studies: results from the 5th ESTP international expert workshop, *Toxicol. Pathol.* 46(2):224–246, 2018 Feb.
- Lethagen S, Harris AS, Nilsson IM: Intranasal desmopressin (DDAVP) by spray in mild hemophilia A and von Willebrand's disease type I, *Blut* 60(3):187–191, 1990 Mar.
- Li JJ, Muralikrishnan S, Ng C-T, Yung L-YL, Bay B-H: Nanoparticle-induced pulmonary toxicity, *Exp. Biol. Med.* 235:1025–1033, 2010.
- Li N, Wang M, Bramble LA, Schmitz DA, Schauer JJ, Sioutas C, Harkema JR, Nel AE: The adjuvant effect of ambient particulate matter is closely reflected by the particulate oxidant potential, *Environ. Health Perspect.* 117: 116–123, 2009.
- Liao D, Li H: Dissecting the niche for alveolar type II cells with alveolar organoids, *Front. Cell Dev. Biol.* 8:419, 2020.
- Liu A, Xiao W, Li R, Liu L, Chen L: Comparison of optical projection tomography and light-sheet fluorescence microscopy, *J. Microsc.* 275(1):3–10, 2019 Jul.
- Livraghi A, Randell SH: Cystic fibrosis and other respiratory diseases of impaired mucus clearance, *Toxicol. Pathol.* 35: 116–129, 2007.
- Lorch G, Sivaprakasam K, Zismann V, Perdignes N, Contente-Cuomo T, Nazareno A, Facista S, Wong S, Drenner K, Liang WS, Amann JM, Sinicropi-Yao SL, Koenig MJ, La Perle K, Whitsett TG, Murtaza M, Trent JM, Carbone DP, Hendricks WPD: Identification of recurrent activating HER2 mutations in primary canine pulmonary adenocarcinoma, *Clin. Cancer Res.* 25(19):5866–5877, 2019 Oct 1.
- Maarman G, Lecour S, Butrous G, Thienemann F, Sliwa K: A comprehensive review: the evolution of animal models in pulmonary hypertension research; are we there yet? *Pulm. Circ.* 3(4):739–756, 2013.
- Maronpot RR, Nyska A, Troth SP, Gabrielson K, Sysa-Shah P, Kalchenko V, Kuznetsov Y, Harmelin A, Schiffenbauer YS, Bonnel D, Stauber J, Ramot Y: Regulatory forum opinion piece\*: imaging applications in toxicologic pathology-recommendations for use in regulated nonclinical toxicity studies, *Toxicol. Pathol.* 45(4):444–471, 2017.
- Martin TR: Lung injury and repair in coronavirus disease 2019-related acute lung injury, *Am. J. Pathol.* 192(3):406–409, 2022 Mar.
- Maygarden SJ, Iacocca MV, Funkhouser WK, Novotny DB: Pulmonary alveolar proteinosis: a spectrum of cytologic, histochemical, and ultrastructural findings in bronchoalveolar lavage fluid, *Diagn. Cytopathol.* 24:389–395, 2001.
- McCormick TS, Hejal RB, Leal LO, Ghannoum MA: GM-CSF: orchestrating the pulmonary response to infection, *Front. Pharmacol.* 12:735443, 2022.
- McInnes EF: Wistar and sprague-dawley rats. In McInnes EF, editor: *Background lesions in laboratory animals a color atlas*, 2012, Elsevier Ltd, pp 17–36.
- Meyerholz DK, Reznikov LR: Influence of SARS-CoV-2 on airway mucus production: a review and proposed model, *Vet. Pathol.* 59:578–585, 2022.
- Meyerholz DK, Suarez CJ, Dintzis SM, Frevert CW: Respiratory system. In *Comparative anatomy and histology: a mouse, rat and human atlas*, 2018, Academic Press, pp 147–162.
- Miller F: Dosimetry of particles in laboratory animals and humans. In Gardner DE, Crapo JD, McClellan RO, editors: *Toxicology of the lung*, Philadelphia, PA, 2000, Taylor and Francis, pp 43–555.
- Miller LA, Royer CM, Pinkerton KE, Schelegle ES: Nonhuman primate models of respiratory disease: past, present, and future, *ILAR J.* 58(2):269–280, 2017.
- Mohr U, Adler K, Dungworth D, Harris C, Plopper C, Saracci R, editors: *Correlations between in vitro and in vivo investigations in inhalation toxicology*, Washington, DC, 1996, ILSI Press.
- Mortaz E, Masjedi MR, Allameh A, Adcock IM: Inflammation signaling in pathogenesis of lung diseases, *Curr. Pharmaceut. Des.* 18(16):2320–2328, 2012.
- Mossman BT, Borm PJ, Castranova V, Costa DL, Donaldson K, Kleeberger SR: Mechanisms of action of inhaled fibers, particles and nanoparticles in lung and cardiovascular diseases, *Part. Fibre Toxicol.* 4:4–14, 2007.
- Mowat V, Alexander DJ, Pilling AM: A comparison of rodent and nonrodent laryngeal and tracheal bifurcation sensitivities in inhalation toxicity studies and their relevance for human exposure, *Toxicol. Pathol.* 45(1):216–222, 2017.
- Mukaratirwa S, Garcia B, Isobe K, Perrerrino C, Bradley A: Spontaneous and dosing route-related lung lesions in Beagle dogs from oral gavage and inhalation toxicity studies: differentiation from compound-induced lesions, *Toxicol. Pathol.* 44(7):962–973, 2016.
- Munoz FM, Cramer JP, Dekker CL, Dudley MZ, Graham BS, Gurwith M, Law B, Perlman S, Polack FP, Spergel JM, Van Braeckel E, Ward BJ, Didierlaurent AM, Lambert PH, Brighton Collaboration Vaccine-associated Enhanced Disease Working Group: Vaccine-associated enhanced disease: case definition and guidelines for data collection, analysis, and presentation of immunization safety data, *Vaccine* 39(22):3053–3066, 2021 May 21.
- Newman SP: How well do in vitro particle size measurements predict drug delivery in vivo? *J. Aerosol Med.* 11(Supl. 1): S97–S104, 1998.
- Newman SP: Scintigraphic assessment of therapeutic aerosols, *Crit. Rev. Ther. Drug Carrier Syst.* 10:65–109, 1993.
- Nikula KJ, McCartney JE, McGovern T, Miller GK, Odin M, Pino MV, Reed MD: STP position paper: interpreting the

- significance of increased alveolar macrophages in rodents following inhalation of pharmaceutical materials, *Toxicol. Pathol.* 42:472–486, 2014.
- Ntziachristos V: Optical imaging of molecular signatures in pulmonary inflammation, *Proc. Am. Thorac. Soc.* 6(5):416–418, 2009 Aug 15.
- Obert LA, Sobocinski GP, Bobrowski WF, Metz AL, Rolsma MD, Altrogge DM, Dunstan RW: An immunohistochemical approach to differentiate hepatic lipidosis from hepatic phospholipidosis in rats, *Toxicol. Pathol.* 35(5):728–734, 2007 Aug.
- Osimitz TG, Droege W, Finch JM: Toxicologic significance of histologic change in the larynx of the rat following inhalation exposure: a critical review, *Toxicol. Appl. Pharmacol.* 225:229–237, 2007.
- Paananen J, Fortino V: An omics perspective on drug target discovery platforms, *Briefings Bioinf.* 21(6):1937–1953, 2019.
- Parakh S, Lee ST, Gan HK, Scott AM: Radiolabeled antibodies for cancer imaging and therapy, *Cancers* 14(6):1454, 2022 Mar 11.
- Paranjpe MG, Belich JL, Richardson DR, Vidmar T, Mann PC, McKeon ME, Elbekai RH, Brown C: Exudative inflammatory lesions in the nasal cavities of the 26-week Tg.rasH2 mice oral gavage carcinogenicity studies, *Int. J. Toxicol.* 36(1):21–28, 2017.
- Paranjpe MG, Shah SA, Denton MD, Elbekai RH: Incidence of spontaneous non-neoplastic lesions in transgenic CBYB6F1-Tg(HRAS)2Jic mice, *Toxicol. Pathol.* 41(8):1137–1145, 2013.
- Pauluhn J: Overview of inhalation exposure techniques: strengths and weaknesses, *Exp. Toxicol. Pathol.* 57(Suppl. 1): 111–128, 2005.
- Peng L, Gao L, Wu X, Fan Y, Liu M, Chen J, Song J, Kong J, Dong Y, Li B, Liu A, Bao F: Lung organoids as model to study SARS-CoV-2 infection, *Cells* 11(17):2758, 2022 Sep 4.
- Pereira ME, Macri NP, Creasy DM: Evaluation of the rabbit nasal cavity in inhalation studies and a comparison with other common laboratory species and man, *Toxicol. Pathol.* 39:893–900, 2011.
- Pinar IP, Jones HD: Novel imaging approaches for small animal models of lung disease (2017 Grover Conference series), *Pulm. Circ.* 8(2), Apr-Jun 2018.
- Plopper CG, Mariassy AT, Lollini LO: Structure as revealed by airway dissection. A comparison of mammalian lungs, *Am. Rev. Respir. Dis.* 128(2 Pt 2):S4–S7, 1983 Aug.
- Plopper CG, Harkema JR: The respiratory system and its use in research. In Wolfe-Coote S, editor: *The laboratory primate: the handbook of experimental animals*, Amsterdam, The Netherlands, 2005, Academic Press, pp 503–506.
- Poitout-Belissent F, Grant SN, Tepper JS: Aspiration and inspiration: using bronchoalveolar lavage for toxicity assessment, *Toxicol. Pathol.* 49(2):386–396, 2021 Feb.
- Ramos-Casals M, Brahmer JR, Callahan MK, Flores-Chávez A, Keegan N, Khamashta MA, Lambotte O, Mariette X, Prat A, Suárez-Almazor ME: Immune-related adverse events of checkpoint inhibitors, *Nat. Rev. Dis. Prim.* 6(1):38, 2020 May 7.
- Rashdan S, Minna JD, Gerber DE: Diagnosis and management of pulmonary toxicity associated with cancer immunotherapy, *Lancet Respir. Med.* 6(6):472–478, 2018.
- Reagan-Steiner S, Gary J, Matkovic E, Ritter JM, Shieh W-J, Martines RB, Werner AK, Lynfield R, Holzbauer S, Bullock H, Denison AM, Bhatnagar J, Bollweg BC, Patel M, Evans ME, King BA, Rose DA, Baldwin GT, Jones CM, Zaki SR: Pathological findings in suspected cases of e-cigarette, or vaping, product use-associated lung injury (EVALI): a case series. The Lancet, *Respir. Med.* 8(12):1219–1232, 2020.
- Redente EF, Black BP, Backos DS, Bahadur AN, Humphries SM, Lynch DA, Tudor RM, Zemans RL, Riches DWH: Persistent, progressive pulmonary fibrosis and epithelial remodeling in mice, *Am. J. Respir. Cell Mol. Biol.* 64(6):669–676, 2021 Jun.
- Renne R, Brix A, Harkema J, Herbert R, Kittel B, Lewis D, March T, Nagano K, Pino M, Rittinghausen S, Rosenbruch M, Tellier P, Wohrmann T: Proliferative and nonproliferative lesions of the rat and mouse respiratory tract, *Toxicol. Pathol.* 37(Suppl. 7):S5–S73S, 2009.
- Renne R, Fouillet X, Maurer J, Assaad A, Morgan K, Ha F, Nikula K, Gillet N, Copley M: Recommendation of optimal method for formalin fixation of rodent lungs in routine toxicology studies, *Toxicol. Pathol.* 29:587–589, 2001.
- Renne RA, Gideon KM: Types and patterns of response in the larynx following inhalation, *Toxicol. Pathol.* 34:281–285, 2006.
- Renne RA, Gideon KM, Harbo SJ, Staska LM, Grumbein SL: Upper respiratory tract lesions in inhalation toxicology, *Toxicol. Pathol.* 35(1):163–169, 2007.
- Rock JR, Hogan BL: Epithelial progenitor cells in lung development, maintenance, repair, and disease, *Annu. Rev. Cell Dev. Biol.* 27:493–542, 2011.
- Rock JR, Rawlins E, Onaitis M, Hogan B: Basal cells as stem cells of the mouse trachea and human conducting airways, *Dev. Biol.* 331, 2009.
- Rushton L: Occupational causes of chronic obstructive pulmonary disease, *Rev. Environ. Health* 22(3):195–212, 2007 Jul-Sep.
- Ryan DJ, Spraggins JM, Caprioli RM: Protein identification strategies in MALDI imaging mass spectrometry: a brief review, *Curr. Opin. Chem. Biol.* 48:64–72, 2019 Feb.
- Safari R, Meuwissen R: Practical use of advanced mouse models for lung cancer, *Methods Mol. Biol.* 1267:93–124, 2015.
- Salem H, Katz SA, editors: *Inhalation toxicology*, third ed., Boca Raton, FL, 2015, CRC Taylor & Francis.



- Scudamore C: Beagle dog. In McInnes EF, editor: *Background lesions in laboratory animals a color atlas*, 2012, Elsevier Ltd, pp 37–44.
- Sells DM, Brix AE, Nyska A, Jokinen MP, Orzech DP, Walker NJ: Respiratory tract lesions in noninhalation studies, *Toxicol. Pathol.* 35:170–177, 2007.
- Seymour JF, Presneill JJ: Pulmonary alveolar proteinosis: progress in the first 44 years, *Am. J. Respir. Crit. Care Med.* 166:215–235, 2002.
- Singh A, Dees S, Grewal IS: Overcoming the challenges associated with CD3+ T-cell redirection in cancer, *Br. J. Cancer* 124(6):1037–1048, 2021 Mar.
- Taylor I: Chapter 4. Mouse. In McInnes EF, editor: *Background lesions in laboratory animals a color atlas*, 2012, Elsevier Ltd, pp 45–72.
- Taylor G: Animal models of respiratory syncytial virus infection, *Vaccine* 35(3):469–480, 2017 Jan 11.
- Tepper JS, Kuehl PJ, Cracknell S, Nikula KJ, Pei L, Blanchard JD: Symposium summary: “breathe in, breathe out, its easy: what you need to know about developing inhaled drugs”, *Int. J. Toxicol.* 35(4):376–392, 2016 Jul.
- Testa JR, Berns A: Preclinical models of malignant mesothelioma, *Front. Oncol.* 10:101, 2020 Feb 11, <https://doi.org/10.3389/fonc.2020.10.1016/j.lungcan.2012.12.021>.
- Thomas A, Maltzman J, Hassan R: Farletuzumab in lung cancer, *Lung Cancer* 80(1):15–18, 2013 Apr. <https://doi.org/10.1016/j.lungcan.2012.12.021>.
- Thomas PT, Zelikoff JT: Air pollutants: modulators of pulmonary host resistance against infection. In Holgate SA, Samet JM, Koren HS, Maynard R, editors: *Air pollution and health*, San Diego, CA, 1999, Academic Press, pp 357–380.
- Thorley AJ, Ruenaroengsak P, Potter TE, Tetley TD: Critical determinants of uptake and translocation of nanoparticles by the human pulmonary alveolar epithelium, *ACS Nano* 8(11):11778–11789, 2014 Nov 25.
- Travaglini KJ, Nabhan AN, Penland L, Sinha R, Gillich A, Sit RV, Chang S, Conley SD, Mori Y, Seita J, Berry GJ, Shrager JB, Metzger RJ, Kuo CS, Neff N, Weissman IL, Quake SR, Krasnow MA: A molecular cell atlas of the human lung from single-cell RNA sequencing, *Nature* 587(7835):619–625, 2020 Nov.
- Treuting PM, Dintzis SM, editors: *Comparative anatomy and histology: a mouse and human atlas*, 2012, Academic Press, with permission.
- Treutlein B, Brownfield DG, Wu AR, Neff NF, Mantalas GL, Espinoza FH, Desai TJ, Krasnow MA, Quake SR: Reconstructing lineage hierarchies of the distal lung epithelium using single-cell RNA-seq, *Nature* 509(7500):371–375, 2014.
- Vande VG, Poelmans J, De Langhe E, et al.: Longitudinal micro-CT provides biomarkers of lung disease that can be used to assess the effect of therapy in nonclinical mouse models, and reveal compensatory changes in lung volume, *Dis. Model. Mech.* 9(1):91–98, 2016.
- Vanherp L, Poelmans J, Hillen A, et al.: Bronchoscopic fibered confocal fluorescence microscopy for longitudinal in vivo assessment of pulmonary fungal infections in free-breathing mice, *Sci. Rep.* 8(1):3009, 2018.
- Ware LB, Matthay MA: The acute respiratory distress syndrome, *N. Engl. J. Med.* 342:1234, 2000.
- Weaver RJ, Valentin JP: Today’s challenges to de-risk and predict drug safety in human “mind-the-gap”, *Toxicol. Sci.* 167(2):307–321, 2018.
- Weissman D, Kiefer M: Erionite: an emerging north american hazard, *NIOSH Science Blog*, 2011.
- Wick KD, Matthay MA: Environmental factors, *Crit. Care Clin.* 37(4):717–732, 2021 Oct, <https://doi.org/10.1016/j.ccc.2021.05.002>.
- Woicke J, Al-Haddawi MM, Bienvenu JG, Caverly Rae JM, Chanut FJ, Colman K, Cullen JM, Davis W, Fukuda R, Huisinga M, Walker UJ, Kai K, Kovi RC, Macri NP, Marxfeld HA, Nikula KJ, Pardo ID, Rosol TJ, Sharma AK, Singh BP, Tamura K, Thibodeau MS, Vezzali E, Vidal JD, Meseck EK: International harmonization of nomenclature and diagnostic criteria (INHAND): nonproliferative and proliferative lesions of the dog, *Toxicol. Pathol.* 49(1):5–109, 2021 Jan.
- Wolfe-Coote. In *The laboratory primate: the handbook of experimental animals*, 2005, Academic Press, pp 503–506.
- Wong BA: Inhalation exposure systems: design, methods and operation, *Toxicol. Pathol.* 35:3–13, 2007.
- Wypych TP, Wickramasinghe LC, Marsland BJ: The influence of the microbiome on respiratory health, *Nat. Immunol.* 20(10):1279–1290, 2019 Oct.
- Zhao C, Pu J: Influence of host sialic acid receptors structure on the host specificity of influenza viruses, *Viruses* 14(10):2141, 2022 Sep 28.
- Zhu H, Kauffman ME, Trush MA, Jia Z, Li YR: A simple bioluminescence imaging method for studying cancer cell growth and metastasis after subcutaneous injection of lewis lung carcinoma cells in syngeneic C57BL/6 mice, *React. Oxyg. Species (Apex)*. 5(14):118–125, 2018 Mar.

This page intentionally left blank

# Hematopoietic System

Lila Ramaiah<sup>1</sup>, Tim Erkens<sup>2</sup>, Madhu Sirivelu<sup>3</sup>, Allison Vitsky<sup>4</sup>

<sup>1</sup>Janssen Research & Development, LLC, a Johnson & Johnson Company, Spring House, PA, United States, <sup>2</sup>Janssen Research & Development, LLC, a Johnson & Johnson Company, Beerse, Belgium, <sup>3</sup>Novartis Pharmaceuticals Corporation, East Hanover, NJ, United States, <sup>4</sup>Pfizer Inc, San Diego, CA, United States

## OUTLINE

1. Introduction	337	6. Mechanisms of Hematotoxicity	392
2. Phylogenesis and Ontogenesis	340	6.1. Direct Nonimmune Injury to Hematopoietic Cells	392
2.1. Phylogeny	340	6.2. Direct Nonimmune Injury to Circulating Cells	404
2.2. Mammalian Ontogeny	344	6.3. Immune Injury and Destruction	412
3. Structure, Function, and Cell Biology	345	6.4. Idiosyncratic Reactions	414
3.1. Anatomy of the Bone Marrow	345	6.5. Altered Blood Cell Function	415
3.2. Hematopoiesis	347	6.6. Indirect Injury, Secondary Effects, and Modifying Factors	417
4. Evaluation of Hematotoxicity	360	7. Issues in Drug Development and Regulatory Considerations	418
4.1. Evaluation of Bone Marrow	362	7.1. Translatability	418
4.2. Evaluation of Peripheral Blood	366	7.2. Adversity	419
4.3. In Vitro Techniques	371	7.3. Regulatory Issues	420
4.4. Animal Models	371	8. Conclusion	421
5. Responses to Injury	372	Glossary	421
5.1. Changes in Peripheral Blood	372	References	422
5.2. Changes in Bone Marrow	379		
5.3. Myeloproliferative Lesions	386		
5.4. Changes in Secondary Hematopoietic Organs	389		

## 1. INTRODUCTION

The **hematopoietic system** (sometimes referred to as the hemopoietic system) is composed of all blood-forming tissues and circulating blood cells and is one of the largest organs in the body. Its primary function is hematopoiesis, the continuous production of highly

specialized mature circulating blood cells responsible for respiratory (hemoglobin in erythrocytes), immune (leukocytes), and hemostatic (thrombocytes/platelets) processes. This system is uniquely susceptible to toxic insults and ranks alongside the liver and kidney as one of the most important target organs of toxicity. Circulating blood cells perform many



vital functions, and even mild injury can impair tissue oxygenation, immune function, or hemostatic function. The rapid rate of proliferation required to support systemic demands for blood cells also makes hematopoietic tissue particularly sensitive to toxic injury (e.g., radiation or cytoreductive and antimitotic agents). Finally, hematopoiesis is a tightly regulated, complex and dynamic process that may be susceptible to disruption by xenobiotics.

**Hematotoxicity** is defined as the adverse effect of an agent on blood cells or blood-forming tissues. It may occur via direct injury or indirectly through injury to other body systems, with consequences that can span the entire spectrum of hematologic cell types, including bone marrow precursors, erythrocytes (red blood cells [RBCs]), leukocytes (white blood cells [WBCs]), and platelets (PLTs). Therefore, bone marrow and peripheral blood are assessed in a functional precursor-product relationship, respectively, and interpreted considering changes occurring in other tissues.

Identifying and interpreting toxic effects on the hematopoietic system requires an understanding of normal hematopoiesis (development, homeostatic physiology, and anatomy), mechanisms of hematotoxicity, and responses and pathologic syndromes manifested by injured hematopoietic tissues. The goal of this chapter is to provide a functional, mechanistic, and morphologic background for understanding the broad range of toxic effects on the hematopoietic system, and to demonstrate how patterns of alterations in blood and blood-forming tissues can point to potential causes and mechanisms. It is not intended to be comprehensive of all xenobiotic-induced hematologic toxicities. This chapter focuses on the myeloid, erythroid, and megakaryocytic/platelet compartments of the bone marrow. For the evaluation of the lymphoid compartment, the reader is referred to *Immune System*, Vol 5, [Chap 6](#) and to published literature ([Haley, 2017](#)). For the evaluation and interpretation of hematology and hemostasis, the reader is referred to *Interpretation of Clinical Pathology Results in Nonclinical Toxicity Testing*, Vol 2, Chap 14 and to *Clinical Pathology in Nonclinical Toxicity Testing*, Vol 1, Chap 10. Abbreviations used in this chapter are listed in [Table 5.1](#).

**TABLE 5.1** Abbreviations

ALAS	Aminolevulinic Acid Synthase
AhR	Aryl hydrocarbon receptor
AIHA	Autoimmune hemolytic anemia
AITP	Autoimmune thrombocytopenia
AML	Acute myeloid leukemia
AML1	Acute myeloid leukemia transcription factor 1
ANG	Angiopoietin
ATP	Adenosine triphosphate
AGM	Aorta-gonad-mesonephros
ATP	Adenosine triphosphate
AZT	Azidothymidine
BCR	B cell receptor
BFU-E	Blast-forming units—Erythroid
BM	Bone marrow
BMP	Bone morphogenetic protein
Btk	Bruton's tyrosine kinase
CD	Cluster of differentiation
CDK	Cyclin-dependent kinase
Cfba2	Core-binding factor subunit alpha-2
CFU-E	Colony-forming units—Erythroid
CLP	Common lymphoid progenitor
CMP	Common myeloid progenitor
COX	Cyclooxygenase
CSF	Colony-stimulating factor
DDT	Dichlorodiphenyltrichloroethane
DIC	Disseminated intravascular coagulation
DMBA	Dimethylbenz[a]anthracene
DMS	Demarcation membrane system
DNA	Deoxyribonucleic acid
DPG	Diphosphoglycerate
EDTA	Ethylenediaminetetraacetic acid
EKLF	Erythroid Krüppel-like factor
EMH	Extramedullary hematopoiesis

(Continued)

TABLE 5.1 Abbreviations—cont'd

EPC	Endothelial precursor cells
EPO	Erythropoietin
FGF	Fibroblast growth factor
FLT3	Fms-like tyrosine kinase 3
FLVCR	Feline leukemia virus, subgroup C, receptor
EMP	Erythroblast macrophage protein
G6PD	Glucose-6-phosphate dehydrogenase
G-CSF	Granulocyte colony-stimulating factor
GMP	Granulocyte/Monocyte progenitor
GMT	Gelatinous marrow transformation
GM-CSF	Granulocyte/Monocyte colony-stimulating factor
HCK	Hemopoietic cell kinase
HDAC	Histone deacetylase
Hgb	Hemoglobin
HIF	Hypoxia-inducible factor
HO-1	Heme oxygenase 1
HSC	Hematopoietic stem cell
HSP	Hemoglobin stabilizing proteins
ICAM	Intercellular adhesion molecule
IGF	Insulin-like growth factor
IL	Interleukin
IMHA	Immune-mediated hemolytic anemia
ITP	Immune-mediated thrombocytopenia
JAK	Janus kinase
KLF1	Krüppel-like factor 1
LYVE-1	lymphatic vessel endothelial hyaluronan receptor-1
LUC	Large unstained cells
M-CSF	Macrophage colony-stimulating factor
MDSC	Myeloid-derived suppressor cells
M:E	Myeloid to erythroid ratio
MEP	Megakaryocytic/Erythroid progenitor
MGDF	Megakaryocyte growth and development factor
MK	Megakaryocyte
MPL	Myeloproliferative leukemia (virus oncogene)

(Continued)

TABLE 5.1 Abbreviations—cont'd

MPP	Multipotent progenitor
MSC	Mesenchymal stem cell
NHP	Nonhuman primates
NK	Natural killer
NRTI	Nucleoside reverse transcriptase inhibitor
PCV	Packed cell volume
PDE	Phosphodiesterase
PDGF(R)	Platelet-derived growth factor (receptor)
PGE	Prostaglandin E
PHD	Prolyl-4-hydroxylase domain
PLT	Platelet
PTP	Protein tyrosine phosphatase
O	Oxygen
Rb	Retinoblastoma
RBC	Red blood cell
REPOS	Renal erythropoietin-producing and oxygen-Sensing
RNA	Ribonucleic acid
ROS	Reactive oxygen species
SCF	Stem cell factor
SCL/TAL1	Stem cell leukemia/T-cell acute leukemia 1
SDF	Stromal cell-derived factor
SERPIN	Serine protease inhibitor
SOD	Superoxide dismutase
TCDD	Tetrachlorodibenzo-p-dioxin
TGF	Transforming growth factor
TIMP	Tissue inhibitors of metalloproteinases
TNF	Tumor necrosis factor
TPO	Thrombopoietin
TRAIL	TNF-related apoptosis-inducing ligand
UTS	Untranslated sequence
VEGF(R)	Vascular endothelial growth factor (receptor)
VLA	Very late antigen
vWF	Von Willebrand factor
WBC	White blood cell

Adapted from Haschek WM, Rousseaux CG, Wallig MA, editors: Haschek and Rousseaux's handbook of toxicologic pathology, ed 3, 2013, Academic Press, Table 50.1, p. 1866–67, with permission.

## 2. PHYLOGENESIS AND ONTOGENESIS

**Phylogenesis** refers to the evolutionary origin of an organ or organ system through the timeline of the developmental history of organisms in a taxon. **Ontogenesis** refers to the embryonic origin and postembryonic development of an organ or organ system of individual organisms. Phylogeny and ontogeny tend to parallel one another such that hematopoiesis during embryo-fetal development for individual mammalian species (ontogeny) recapitulates conserved phylogenetic events in the evolution of the hematopoietic system in mammals in general (Galindez and Aggio, 1997; Serb and Oakley, 2005).

### 2.1. Phylogeny

Gas transport in aqueous solutions by metalloproteins (e.g., tissue protoheme, hemoglobin, myoglobin, chlorocruorin, hemocyanin, and hemerythrin) is an ancient, fundamental form of respiration that is present in all aerobic organisms, including unicellular organisms and plants (Glomski and Tamburlin, 1989). Specialized hematopoietic cells can be identified in all multicellular organisms (metazoans). In acoelomates (e.g., sponges, coelenterates and platyhelminths), primitive hematopoietic cells (variously termed amebocytes, interstitial cells, and neoblasts) exist individually within a matrix located between the ectoderm and the endoderm (mesoglea or mesodermal parenchyma). In coelomates (phylogenetically higher invertebrates and vertebrates), hematopoietic cells (variously termed hemocytes, hemangioblasts/angioblasts, and hematopoietic stem cells [HSCs]) aggregate into organized structures and tissues, marking the emergence of the hematopoietic system, concomitant with the coelom and circulatory system (Table 5.2) (Glomski and Tamburlin, 1990; Ramaiah et al., 2013). Hematopoietic organs are specialized clusters of developing hematopoietic cells framed in a hemopoietic-promoting stroma (splanchnopleure) (Galindez and Aggio, 1997).

#### 2.1.1. Respiratory Systems

Nonvertebrate functional hemoglobins range from single chain, truncated or chimeric globins

(found in prokaryotes, eukaryotic algae, protozoa, and plants) to large, multisubunit, multidomain hemoglobins (in nematodes, mollusks, and crustaceans) and giant hemoglobins composed of globin and nonglobin subunits (in annelid and vestimentiferan worms) (Terwilliger, 1998; Weber and Vinogradov, 2001). The heme moiety of the molecule, responsible for the reversible binding of oxygen, is evolutionarily and ontogenically stable. In contrast, the globin moiety, responsible for kinetics of gas binding and release, is structurally variable throughout evolution and ontogenesis.

The hemolymph of invertebrates contains freely circulating respiratory pigments or intracellular hemoglobins present as monomers or dimers (Terwilliger, 1998). Vertebrates (except for jawless fish) have heterogeneous, tetrameric hemoglobins composed of pairs of two dissimilar globin chains ( $\alpha$  and  $\beta$ ). This allows for reversible cooperative oxygen binding and sigmoid-shaped oxygen-hemoglobin dissociation curves, as opposed to the hyperbolic curves of monomeric hemoglobins such as myoglobin (Brunori and Miele, 2023; Pillai et al., 2020; Terwilliger, 1998). Oxygen-hemoglobin dissociation curves plot oxyhemoglobin (% saturation) against oxygen tension ( $PO_2$  mmHg) to express hemoglobin's oxygen affinity at different oxygen pressures/saturations. In other words, the curves show how readily hemoglobin binds to or releases oxygen from or into surrounding tissues, respectively. A sigmoidal oxygen-hemoglobin dissociation curve reflects cooperative among hemoglobin tetramers, in which the binding of oxygen to one hemoglobin subunit induces conformational changes that increase the oxygen affinity of other subunits. Deoxyhemoglobin has a relatively low oxygen affinity, but when one oxygen molecule binds to a single subunit, the oxygen affinity increases, allowing the second molecule to bind more easily, and the third and fourth even more easily. The oxygen affinity of 3-oxy-hemoglobin is  $\sim 300$  times greater than that of deoxyhemoglobin. Conversely, the release of oxygen from one hemoglobin subunit induces conformational changes that decrease the oxygen affinity of other subunits, resulting in amplified release of oxygen into tissues. The ability for hemoglobin to release oxygen increases as fewer oxygen molecules are bound. Ultimately, the



**TABLE 5.2** Phylogenesis of Hematopoietic Tissues in Metazoans

<b>Multicellular Organisms (Metazoa)</b>						
<b>Invertebrates</b>				<b>Vertebrates</b>		
	<b>Acoelomates</b>	<b>Lower Coelomates</b>	<b>Higher Coelomates</b>	<b>Lower Vertebrates and Ectotherms</b>	<b>Birds</b>	<b>Mammals</b>
<b>Gas transport</b>	Hgb/Cgb	O <sub>2</sub> -binding metalloproteins circulating freely or within hyaline hemocytes		Nucleated erythrocytes	Nucleated erythrocytes	Nucleated erythrocytes (during development); anucleated erythrocytes (in adulthood)
<b>Blood clotting</b>		Hemocytes or coelomocytes and primitive coagulation factors		Nucleated thrombocytes	Nucleated thrombocytes	Anucleated platelets
<b>Immunity</b>	Amebocytes, interstitial cells or neoblasts	Hemocytes or coelomocytes		Leukocytes	Leukocytes	Leukocytes
<b>Hematopoietic organs</b>		Specialized vascularized domains within mesothelium, behind vascular or visceral walls	Lymphoid glands attached to the coelomic wall or large blood vessels	<b>Primitive:</b> Lateral mesoderm <b>Definitive:</b> Hemopoietic foci in mesodermal tissues	<b>Primitive:</b> Blood islands in yolk sac <b>Definitive:</b> BM	<b>Primitive:</b> Blood islands in yolk sac <b>Definitive:</b> BM (with notable exception of spleen as an additional site in rodents)

BM: bone marrow; Cgb: cyanoglobin; Hgb: hemoglobin

*Adapted from Haschek WM, Rousseaux CG, Wallig MA, editors: Haschek and Rousseaux's handbook of toxicologic pathology, ed 3, 2013, Academic Press, Table 50.2, p. 1868, with permission.*

physiological role of vertebrate hemoglobin, to bind oxygen in the lungs or gills and to release it in peripheral tissues, is possible because hemoglobin subunits act cooperatively to maximize oxygen binding where oxygen tension is high and to release it where oxygen tension is low.

In vertebrates, hemoglobin is sequestered in specialized circulating cells (erythrocytes), conferring respiratory efficiency and protective advantages (Nunomura et al., 2015). The intracellular packaging of hemoglobin allows for transport of higher concentrations of osmotically active hemoglobin molecules in the blood than would be physiologically feasible if the proteins were free in solution. Erythrocytes have a different ionic and molecular composition when compared with plasma, including lower pH and decreased levels of organic phosphate constituents such as diphosphoglycerate (DPG) and adenosine triphosphate (ATP). These characteristics promote the respiratory functions of hemoglobin and shelter it from irreversible oxidation. The intracellular sequestration of hemoglobin extends its half-life by avoiding degradation in the plasma, thereby preventing its loss through phagocytic and renal tubular activity, and by colocalization with appropriate protective intracellular enzymes (Glomski and Tamburlin, 1989). Nonmammalian RBCs are nucleated ellipsoid cells that can bend, have a high surface-to-volume ratio, and can easily traverse through the walls of capillaries. In mammals, evolutionary modifications including regression of tubulin marginal bands (which maintain the flat discoid shape of red cells), nuclear loss, and DPG production instead of ATP produced in mitochondria or by anaerobic respiration have further enhanced the red cell's circulatory and respiratory capabilities. Loss of the nucleus reduces oxygen consumption and cell volume without changing the surface area. This conformation results in cells shaped as radially symmetrical, biconcave discs that have low inertial forces in circulation, while the high surface-to-volume ratio provides deformability and easy migration through capillaries.

In camelids (mammals living in arid habitats), erythrocytes are anucleate but elliptical, thin and flat with very little volume due to retention of marginal tubulin bands (Cohen and Terwilliger, 1979). This cell structure doubles their surface-

to-volume ratio but results in a very low packed cell volume (PCV) (and high plasma volume) in whole blood. Camelid erythrocytes can contain the same amount of hemoglobin (i.e., same O<sub>2</sub>-carrying capacity) but hold much less water, which makes them resistant to changes in plasma osmotic pressure that occur with severe dehydration (Bogner et al., 2005). Furthermore, because of the low PCV, blood flows normally without changes in viscosity even when the tissues are dehydrated (Yagil et al., 1974a, b).

### 2.1.2. Hemostatic Systems

Hemostatic functions and coagulation factors arose alongside the hematopoietic and circulatory systems. The hemocytes of invertebrates serve both respiratory and hemostatic functions. In contrast, in vertebrates, thrombocytes/platelets maintain hemostasis while leaving respiratory functions to erythrocytes (Jenne et al., 2013).

### 2.1.3. Immunologic Systems

Mechanisms for the recognition and elimination of pathogens exist in all living organisms (including unicellular organisms) and form the foundations for innate immunity. Recognition is based on the discrimination of "self" and "non-self" components using pathogen-recognizing receptors encoded in the genome (see *Immune System*, Vol 5, Chap 6). Bacteria protect themselves against bacteriophage (viral) infection by recognizing and eliminating viral nucleic acids (Hemmi et al., 2000). Deoxyribonucleic acid (DNA) viruses are recognized and eliminated by bacterial restriction enzymes (restriction/modification [R-M] system) that can distinguish self-DNA from viral DNA (Dupuis et al., 2013). RNA interference is another highly conserved mechanism for the elimination or silencing of foreign nucleic acids, such as double-stranded viral ribonucleic acid (RNA) (Hamilton and Baulcombe, 1999; Li et al., 2002). Evolutionarily conserved antimicrobial peptides (e.g., amoebapores, mammalian granulolysins, defensins) have an amphipathic structure composed of hydrophobic and cationic amino acids organized in discrete clusters (Machado and Ottolini, 2015; Zasloff, 2002). These compounds target charged molecules on the outer membranes of foreign microbial cells. Prokaryotes and eukaryotes may also kill pathogens by altruistic death of infected cells (abortive infection in prokaryotes

and phagocytosis, and complement-mediated and programmed cell death in eukaryotes) (Koonin and Krupovic, 2019; Koonin and Zhang, 2017). Innate immune responses are further enhanced by programmed hypervariability at genetic loci involved in immunity. These generate diversity at a higher rate than random point mutation and allow organisms to quickly adapt to pathogens (diversity-generating retroelements and phase variation mechanisms in bacteria) (Labrie et al., 2010; Meselson and Yuan, 1968). The transition to multicellularity necessitated recognition of “non-self” as well as compromised or altered “self” cells (e.g., cancer cells). Multicellular organisms evolved a more complex self/nonself recognition mechanism (e.g., pathogen markers and missing “self” molecules). Receptors for conserved microbial patterns such as macrophage mannose-binding receptors that recognize gram-positive and gram-negative bacteria and fungi are preserved in evolution, including phagotrophic amoebae (Ezekowitz et al., 1989). Missing “self” recognition is based on specific expression of “self” molecules and destruction of cells without this “self” marker. Peptides that destroy cell membranes emerged in lower invertebrates and evolved to a complex, highly regulated complement cascade of about 30 proteins in mammals (Litman et al., 2005).

Specialized immune cells arose in the earliest multicellular organisms as dedicated phagocytes that used reactive oxygen species (ROS) to kill pathogens, while higher metazoans developed multiple phagocytic cell types. Coelomate immunocytes can be subdivided into four major blood cell types: prohemocytes, hyaline hemocytes, granular hemocytes, and eleocytes (Schulenburg et al., 2004). Prohemocytes form only a small percentage of the blood cells in the peripheral blood/hemolymph of mature invertebrates. They are immature blood cell progenitor cells that differentiate into most of the other blood cell types. Morphologically, prohemocytes are small, round cells with a large nucleus and scant cytoplasm, resembling blood progenitors in vertebrates (Chiang et al., 1988). Hyaline hemocytes (plasmotocytes or monocytes) are the most prevalent. These phagocytic cells (macrophages) are involved in the removal of apoptotic cells during development as well as in the ingestion or encapsulation of pathogens (innate

immune response) (Liu et al., 2020). They contain oxygen-binding proteins in annelids, sipunculids, lophophorates, and echinoderms. Granular hemocytes are composed of three types (neutrophilic, eosinophilic, and basophilic). They are densely packed with regularly sized granules, which are ultrastructurally electron-dense, enzyme-filled lysosomes. These primitive granulocytes are involved in developmental and metabolic functions as well as in immune functions, including wound healing, blood clotting, phagocytosis, and encapsulation of pathogens (Medzhitov and Janeway, 2002).

Primitive forms of adaptive immune recognition exist in bacteria and archaea. The incorporation of short bacteriophage DNA sequences into bacterial genome between Clustered Regularly Interspaced Short Palindromic Repeats provides bacteria with a virus-specific and sequence-specific memory of past exposures and adaptive immune response (Arroyo-Olarte et al., 2021; Sampson et al., 2013) (see *Gene Therapy and Gene Editing*, Vol 2, Chap 8). Intracellular recognition systems are present in prokaryotes, but specific antibody defenses associated with T and B lymphocyte differentiation in vertebrates are not found in invertebrates (Bartl et al., 2003; Litman et al., 2005). Vertebrates developed a more sophisticated mechanism for adaptive pathogen recognition based on the creation of unlimited variability of immune receptors and on clonal expansion of cells bearing a specific receptor in response to an antigen/pathogen challenge.

#### 2.1.4. Hematopoietic Organs

In phylogenetically lower coelomates, hemocytes associate with one another as clusters in specialized vascularized domains (termed “hematopoietic clusters”) within the mesothelium (splanchnopleure), in close association with vascular or visceral walls. In higher coelomates, hemocytes cluster into bilayer structures within an indistinct stroma; these clusters are attached to the coelomic wall or large blood vessels. These primitive hematopoietic organs are composed of an inner layer of proliferating prohemocytes surrounded by an outer layer of differentiated plasmocytes (phagocytic cells). With the emergence of primitive and definitive hematopoiesis in vertebrates came the development of true hematopoietic organs (Galindez and Aggio, 1997).



In lower vertebrates, primitive hematopoiesis takes place in the lateral mesoderm, whereas in birds and mammals, it occurs in blood islands present in the yolk sac before shifting to the bone marrow later in embryonic development. Definitive hematopoiesis in bone marrow is a late development in phylogeny. Lower vertebrates and ectotherms have hematopoietic foci in mesodermal tissues (diffuse gut-associated tissue in agnathes and the Leydig's organ or epigonal organ in cartilaginous fish), kidney (pronephron in teleosts), or spleen. In lower vertebrates, lymphopoiesis and myelopoiesis are anatomically associated within these foci. Bony fish have rudimentary bone marrow, whereas amphibians, reptiles, birds, and mammals have separate organs for lymphopoiesis (thymus) and myelopoiesis (bone marrow). Permanent separation between lymphoid and myeloid tissues is first observed in birds (Galin-dez and Aggio, 1997). Similarly, birds exhibit the first distinct segregation of lymphocyte development at different sites, with lymphoid nodules (in all bird species) and lymph nodes (in some aquatic bird species) producing T lymphocytes and the bursa of Fabricius generating B lymphocytes (Cross, 1989).

## 2.2. Mammalian Ontogeny

The development of the hematopoietic system in mammalian species has been classically described as occurring in two distinct phases

(primitive hematopoiesis and definitive hematopoiesis) (Boyd and Bolon, 2010), though recent evidence indicates that it is more appropriately described as overlapping waves (Lacaud and Kouskoff, 2017; Orkin and Zon, 2008; Palis, 2014). **Primitive hematopoiesis** supports blood cell production early in gestation during embryogenesis, whereas **definitive hematopoiesis** generates committed hematopoietic progenitors necessary to foster all lineages observed in the fetus, neonate, and adult animal (Table 5.3) (Crane et al., 2017; Ramaiah et al., 2013). Cell adhesion factors ( $\beta_1$ - and  $\beta_4$ -integrins), growth factors (e.g., fibroblast growth factor [FGF], bone morphogenetic protein [BMP], vascular endothelial growth factor [VEGF], erythropoietin [EPO], thrombopoietin [TPO], interleukin [IL]-3 [IL-3], IL-6, Sonic hedgehog [Shh], Indian hedgehog [Ihh], stem cell factor [SCF], angiopoietin [Ang]), and transcription factors (e.g., GATA-binding proteins GATA-1, -2, -4; stem cell leukemia/T-cell acute leukemia 1 [Scl/Tal-1; PU.1, acute myeloid leukemia transcription factor 1 [AML1, also known as RUNX1], core-binding factor subunit alpha-2 [Cfba2]) regulate primitive and definitive hematopoiesis, although the response to different factors differs between the two stages (Ogawa et al., 2001; Yumine et al., 2017; Zambidis et al., 2005).

Primitive hematopoiesis begins in early embryogenesis, at the primitive streak stage. In vertebrates and invertebrates, a common

**TABLE 5.3** Ontogenesis: Primitive Versus Definitive Hematopoiesis in Mammals

Primitive Hematopoiesis	Definitive Hematopoiesis
In yolk sac (RBC, MK, macrophages) during early gestation	In liver, then spleen and bone marrow during late gestation and in postnatal life
RBCs: nucleated in midstage embryo, shed nucleus in late-stage embryo, and remain large until P5	Begin to be released between days E10-E18
RBC: ~6x larger and ~6x more Hgb	
Have a higher affinity for oxygen (cats excepted) due to a lower concentration of 2,3-diphosphoglycerate (2,3-DPG)	
MK: Fewer nuclei, lower ploidy, ½ the size of definitive MK	
Macrophages: Lack some enzyme activities, capable of division, longer half-life; source of many tissue macrophages	Macrophages are the source of circulating monocytes and resident macrophages

E: embryonic day; Hgb: hemoglobin; MK: megakaryocyte; P: postnatal day; RBC: red blood cells

Adapted from Haschek WM, Rousseaux CG, Wallig MA, editors: Haschek and Rousseaux's handbook of toxicologic pathology, ed 3, 2013, Academic Press, Table 50.3, p. 2870, with permission.

progenitor cell of mesothelial origin gives rise to both vascular (endothelial) progenitors and hemocyte progenitors (hemocytoblasts) (Ramaiiah et al., 2013). Hemangioblasts, arising in the inner layer of the visceral yolk sac, are the committed precursors of HSCs. Within the yolk sac, these primitive cells aggregate into blood islands composed of a central core of hematopoietic progenitors surrounded by an outer rim of endothelial progenitors. Most cells produced during primitive hematopoiesis are of the erythroid lineage. Hematopoietic progenitors first differentiate into erythroid colony-forming cells, and then into primitive erythroblasts. With the development of circulation, the blood islands are linked to the vascular system, and fully differentiated primitive (nucleated) erythroid cells enter the blood. Colony-forming cells eventually regress in the blood islands, leaving primitive erythroblasts as the sole source of erythrocytes until definitive hematopoiesis takes hold (in late-stage embryos). Consequently, anemia observed during midstage embryogenesis is due to a defect in primitive erythropoiesis. Other hematopoietic lineages encountered during primitive hematopoiesis include megakaryocytes (MKs) and macrophages (Golub and Cumano, 2013).

Definitive hematopoiesis begins in midstage embryogenesis. Cytopenia occurring in late-stage embryos, fetuses, and neonates is due to a defect in either colonization of sites supporting definitive hematopoiesis and/or failure of the definitive hematopoiesis process. Definitive HSCs (hemogenic endothelial cells) arise de novo primarily from the mesoderm (splanchnopleura) of the aorta-gonad-mesonephros (AGM) region, although some may also arise from the various extraembryonic membranes (e.g., allantois, chorion, definitive placenta, and yolk sac) and umbilical arteries (Nelson et al., 2021; Wu and Hirschi, 2021). The AGM-derived HSCs contribute to all major hematopoietic cell lineages, whereas HSCs from the placenta support the development of erythroid, myeloid, and lymphoid lineages and those from the yolk sac are limited to lymphoid and myeloid cells. Pluripotent cells migrate to sites of definitive hematopoiesis that contain hematopoietic stromal cell niches (liver and various lymphoid organs initially before shifting mainly to bone marrow thereafter) (Boyd and Bolon, 2010). At

these sites, pluripotent HSCs commit to a more limited range of lineage options (e.g., erythroid, myeloid or myelolymphoid progenitors).

For definitive hematopoiesis, HSCs first populate the embryonic liver (Crane et al., 2017). During late embryogenesis, the liver sinusoids are the primary site of definitive hematopoiesis. From the liver, HSCs migrate to embryonic thymus (lymphoid); fetal spleen (erythroid, then lymphoid); lymph nodes (lymphoid); or bone marrow (erythroid, myeloid, lymphoid, and megakaryocyte/platelet). The bone marrow is first colonized early in fetal life and becomes the primary site for hematopoiesis soon after birth. Foci of hematopoiesis are still present in the liver of pigs and rodents at birth, and persist in the spleen of mice, and to a lesser extent rats, throughout life. In other mammals, hematopoiesis may return to the spleen or occasionally liver under conditions of prolonged demand for increased blood cell (usually erythroid or myeloid) production.

Globin gene expression switches during development. The 5' members of both globin loci are expressed in the embryo, while 3' members are expressed in the adult humans, coinciding temporally with the transition from primitive to definitive red cells (Kingsley et al., 2006). Five functional human  $\beta$ -globin genes undergo two major transitions in expression during ontogeny, first from embryonic ( $\epsilon$ ) to fetal ( $G\gamma, A\gamma$ ) globins and thereafter to adult ( $\delta, \beta$ ) globins. In mice, no fetal-to-adult hemoglobin switch occurs. Instead, all of the globin genes in the  $\alpha$ -globin and  $\beta$ -globin ( $\epsilon\gamma$ - $\beta H1$ - $\beta1$ - $\beta2$ ) clusters are expressed in primitive red cells, whereas only the adult ( $\alpha1, \alpha2, \beta1, \beta2$ ) globin genes are expressed in definitive red cells (Trimborn et al., 1999). Fetal hemoglobin has a high affinity for oxygen to supply the developing fetus with sufficient oxygen from the mother's blood.

### 3. STRUCTURE, FUNCTION, AND CELL BIOLOGY

#### 3.1. Anatomy of the Bone Marrow

The bone marrow is the major site of hematopoiesis in the body and is the largest primary lymphoid tissue. Following severe toxic insult to the marrow, the regenerative capacity of the

blood and most peripheral lymphoid organs will depend on the survival of pluripotent stem cells, which give rise to all cells of the blood and the immune system including lymphocytes, plasma cells, erythrocytes, platelets, granulocytes, monocytes, and natural killer (NK) cells. Conversely, systemic effects such as inflammatory reactions or hemorrhage may also be reflected in the bone marrow in response to increased demand for blood cells.

Evaluation of the bone marrow is a key component of any toxicity study (Reagan et al., 2011; Rebar, 1993), and to evaluate the bone marrow an understanding of its normal structure (Elmore, 2006a) and function is crucial. This section discusses the anatomy of bone marrow, whereas histomorphology of the individual cellular components is discussed later in this chapter (Section 4.1. *Evaluation of the bone marrow*). Foci of hematopoiesis may normally be present within secondary hematopoietic organs such as the liver and the splenic red pulp, and these foci may increase in response to physiological need. The structure and function of these ancillary hematopoietic organs are discussed in chapters on *Liver and Gallbladder*, Vol 4, Chap 2 and the *Immune System*, Vol 5, Chap 6.

The intertrabecular spaces of axial, other appendicular, and long bones are filled with marrow, a highly vascular, loose connective tissue stroma that contains precursors of mature blood cells at various stages of their development. The predominance of mature erythrocytes confers a deep red color to active marrow. This hematopoietically active “red marrow” is commonly found in young animals, but with time marrow will become less active and is slowly replaced by adipocytes, thus becoming yellow in color. Therefore, over time, cellular organization of the marrow changes as tissue remodeling occurs.

When considering its anatomical structure, bone marrow can be subdivided into three components: a vascular compartment, stroma, and the hematopoietic cell compartment. The vascular compartment is well organized and complex (Figure 5.1). The nutrient (marrow cavity-penetrating) and periosteal arteries supply the highly vascular marrow. The larger nutrient artery traverses through the cortical bone via the nutrient canal (located midshaft in

long bones) and then branches in both directions to run parallel to the long axis in the central part of the marrow cavity. This artery further divides into branches called radial arteries, which produce a system of capillaries that permeate the marrow. Smaller periosteal arteries, derived from arteries in surrounding skeletal muscles, also traverse the cortical bone to form capillaries that anastomose with the vessels derived from the nutrient artery, thus forming a venous sinusoidal plexus throughout the marrow cavity. Blood from the sinusoidal plexus subsequently drains into the large central vein and exits the bone as the nutrient vein via the nutrient canal. This provides a circular pattern of blood flow, with blood moving from the center of the marrow cavity toward the periphery, then back toward the center. Lymphatic circulation does not appear to play a role in normal bone marrow fluid drainage, and lymphatic vessels are only observed in connective tissue overlying the periosteum. Though the thin-walled vessels of the bone marrow appear morphologically similar to lymphatic capillaries, immunohistochemical (IHC) staining with specific lymphatic endothelial cell markers (e.g., lymphatic vessel endothelial hyaluronan receptor-1 [LYVE-1]/podoplanin) indicates that lymphatic capillaries are absent from bone and bone marrow (Ramiah et al., 2013).

The stroma supporting the vasculature and hematopoietic cells consists of adventitial reticular/barrier cells (fibroblasts), adipocytes, macrophages, nerves, and components of the extracellular matrix such as reticulin fibers, collagens, laminin, fibronectin, hemonection, and proteoglycans. The reticular cells produce the argyrophilic reticulin fibers that crosslink to form a fine meshwork. The reticulin meshwork acts as a highly ordered physical support system for the marrow. Adipocytes in the marrow are thought to originate from adipogenic reticular stromal cells (Matsushita et al., 2022).

The hematopoietic compartment is the site of blood cell generation in the marrow. The main elements that occupy this domain are cells of the erythroid, myeloid, and megakaryocytic lineages, but lymphoid precursors also are present and can expand substantially if physiological stimuli induce this lineage. Hematopoiesis is an extravascular process, and the hematopoietic compartment is separated from



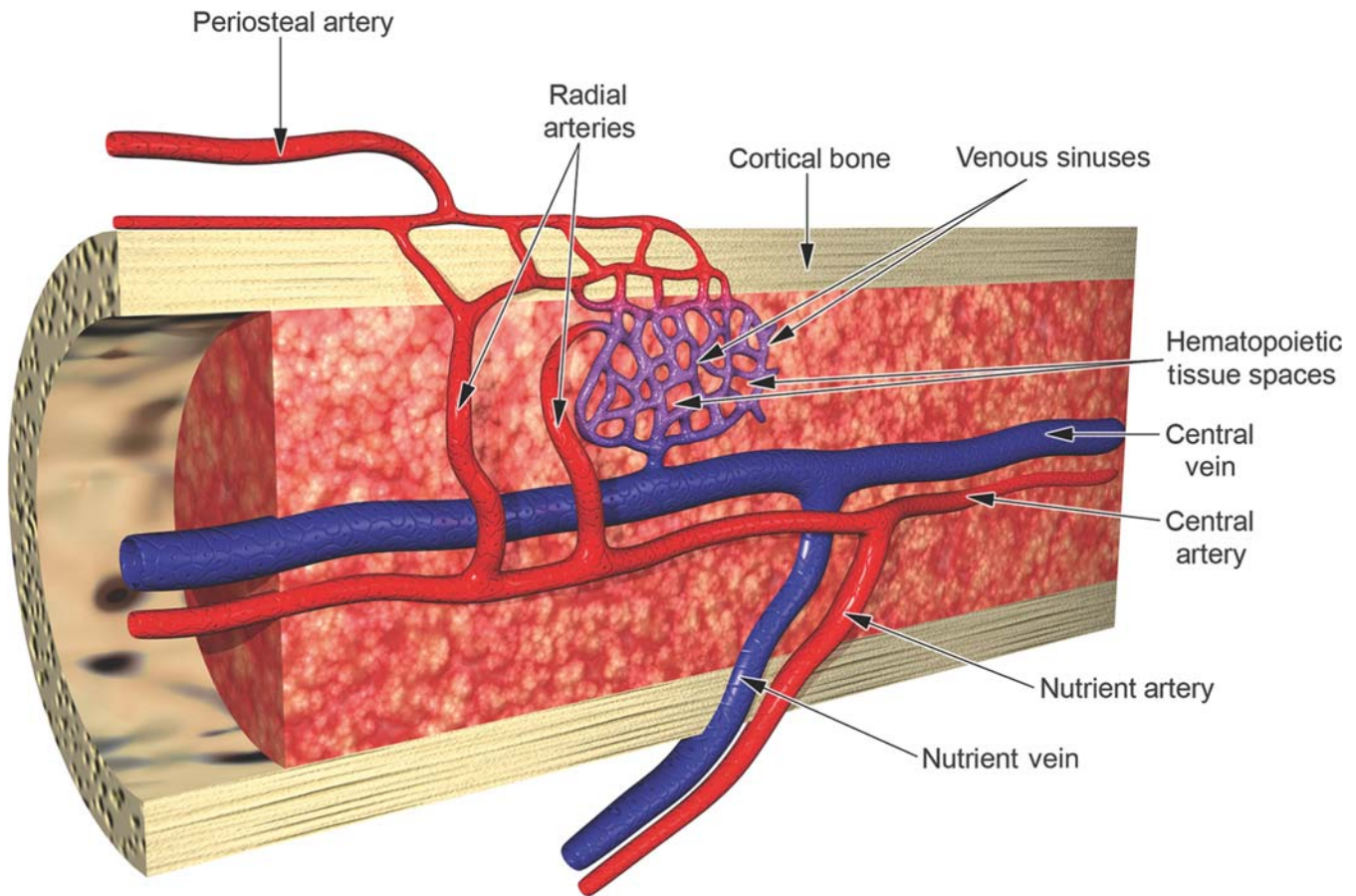


**FIGURE 5.1** Diagrammatic representation of the bone marrow vascular supply. Drawing prepared by David Sabio and reproduced from Travlos GS: Normal structure, function, and histology of bone marrow, *Toxicol. Pathol.* 34, 548–565, Figure 5, 2006. Adapted from: Abboud CN, Lichtman MA: Structure of the marrow and the hematopoietic microenvironment. In *Williams Hematology*, ed 6, 2001. McGraw-Hill. (Used with permission from Sage Publications.)

the circulation by vascular sinus endothelium, basement membrane, and adventitia. Both myelinated and nonmyelinated nerves can also be found adjacent to the arterioles. These nerves serve the smooth muscle of the vessel walls, and occasionally can be observed within the hematopoietic tissue.

### 3.2. Hematopoiesis

#### 3.2.1. The Hematopoietic Microenvironment

The hematopoietic microenvironment is a highly organized three-dimensional space that regulates the life cycle, maturation, and migration of hematopoietic cells (Butler et al., 2018; Gulei et al., 2020; Kokkaliaris, 2020; Lucas, 2017; 2021; Wei and Frenette, 2018; Wilson and Trumpp, 2006; Wu et al., 2021). It is composed

of a structural framework (bone, cartilage, fat, fibrous connective tissue); extracellular matrix (fibronectin, laminin, collagen, hemonection, tenascin-C, thrombospondin, hyaluronate); stromal cells (osteoblasts, osteoclasts, macrophages, fibroblasts, adipocytes, neurons); sinusoidal endothelial cells; and soluble factors (cytokines, chemokines). Stromal cells promote the self-renewal and multipotent state of quiescent stem cell pools while orchestrating the proliferation and lineage determination of proliferating and differentiating pools. Stromal cells influence cell signaling pathways and gene expression and direct the movement of hematopoietic precursors through specialized hematopoietic niche systems. Influences occur through direct cell–cell interactions, paracrine interactions, and the elaboration of the extracellular matrix. Reciprocal molecular interactions

via receptors and integrins are regulated by growth factors, cytokines, and transcription factors elaborated by stromal and hematopoietic cells. As hematopoietic cells terminally differentiate, marrow adhesion factors are either deactivated (cleaved) or not expressed, allowing the cells to exit the marrow microenvironment and enter circulation. Protease inhibitors (SERPINS [SERine Proteinase INhibitors] and TIMPs [tissue inhibitors of metalloproteinases]) regulate the mobilization of mature or neoplastic cells. Terminally differentiated cells entering the circulation via capillaries must transmigrate through the outer adventitial layer, basement membrane layer, and endothelial cell layer via diaphragm fenestrae (mural windows or pores with a thin [diaphragm-like] membrane).

**Hematopoietic niches** are highly specialized, integrated, microanatomical units within local hematopoietic microenvironments (Fröbel et al., 2021). They provide the physical matrix and chemical medium that protects, supports, and nurtures hematopoiesis. Conceptually, HSCs and progenitors localize to specific niches according to their differentiation stage, though these niches are not always observable microscopically (Pinho and Frenette, 2019; Tikhonova et al., 2019). Best characterized are the subendosteal/osteoblastic stem cell niche, the vascular stem cell niche, and the erythroblastic island (see Section 3.2.3 Life Cycle of Blood Cells) (He et al., 2014; Kaushansky and Zhan, 2018; Wilson and Trumpp, 2006; Yeo et al., 2019). The maturation and migration of HSCs through these niches is described below and in Sections 3.2.2 and 3.2.3.

The subendosteal or osteoblastic niche is located in the outer region of the bone marrow, in close proximity to osteoblasts lining the endosteum (Cordeiro-Spinetti et al., 2015). It sustains and regulates multipotent HSCs and progenitor cells to ensure their long-term survival in a quiescent state with low-level self-renewal. As such, almost 75% of HSCs in the osteoblastic niche are quiescent. The subendosteal niche is composed of and maintained by specialized osteoblasts that display ligands that facilitate HSC homing and regulate the speed of cycling and mobilization (Arai et al., 2005). HSCs in the subendosteal niche eventually migrate to the perisinusoidal vascular niche, where they maintain direct contact with the stromal

reticular cells on the abluminal side of endothelial sinuses. The increased perfusion by sinusoidal blood provides the nutrients and oxygen required to maintain this proliferating perivascular pool of hematopoietic cells.

The subendosteal niche in which quiescent HSCs reside is at the lowest end of an oxygen gradient arising from capillaries in the vascular niche (characterized by ~1% O<sub>2</sub> tension in subendosteum to ~20% O<sub>2</sub> tension near sinuses) (Cipolleschi et al., 1993; Itkin et al., 2016). HSCs in the subendosteal niche remain quiescent thanks to low oxygen tension and low levels of ROS (Jang and Sharkis, 2007; Pinho and Frenette, 2019). ROS function as tightly regulated intracellular signaling molecules that control gene expression by activation of redox-sensitive transcription factors. In response to mitogenic stimuli, NADPH (nicotinamide adenine dinucleotide phosphate) oxidase transiently produces ROS, resulting in maintained G<sub>1</sub> phase cyclin D1 expression. ROS fluctuate in a cell cycle-dependent manner to regulate stem cell fate determination, quiescence, and self-renewal potential of HSCs. Low ROS levels suppress proliferation, differentiation, and mobilization, and direct HSCs to divide symmetrically, thereby promoting HSC maintenance and preventing premature differentiation. In contrast, HSCs rapidly proliferate in the well-oxygenated vascular niche.

Hypoxia-inducible factor 1 $\alpha$  (HIF-1 $\alpha$ ) is a transcription factor that is central to promotion of stem cell quiescence in the hypoxic environment (Eliasson and Jonsson, 2010; Eliasson et al., 2010). HIF-1 $\alpha$  is present in all nucleated cells of all metazoan species, whereas HIF-2 $\alpha$  expression is restricted to certain cell types within vertebrate species and plays a key role in both erythropoiesis and vascularization. The hypoxic microenvironment of the endosteal niche constitutively expresses HIF-1 $\alpha$ , which drives expression of cell-cycle inhibitors (p16<sup>Ink4a</sup>/p19<sup>Arf</sup>) to prevent cell cycle entry. Other gene regulatory factors including ATM (ataxia telangiectasia mutated), BMI-1 (B lymphoma Mo-MLV [Moloney murine leukemia virus] insertion region 1 homolog), and FOXO (Forkhead O) also modulate ROS at the stem cell level to promote self-renewal and long-term stem cell maintenance. In the stem cell niche, growth factor stimulation induces a rapid increase in ROS that activates

p28 MAPK (mitogen-activated protein kinase), stimulating quiescent HSCs to enter the cell cycle, and undergo asymmetric division and differentiation (Geest and Coffey, 2009). Some studies also suggest that ROS may also directly modify cell-cycle regulatory proteins to promote progression from the G<sub>1</sub> phase through to the S phase.

### 3.2.2. Stem Cell Biology

Adult bone marrow contains multipotent stem cells that give rise to expanding populations of committed progenitors. Pluripotent cells can follow many differentiation pathways and thus can produce cells of nearly all cell lineages of the body, while multipotent cells follow a more limited number of differentiation pathways and thus generate cells of related cell lineages (see *Stem Cell and Other Cell Therapies*, Vol 2, Chap 10). Pluripotent stem cells (e.g., hemangioblasts) have unlimited self-regenerative capacity, while multipotent stem cells have reduced self-regenerative capacity but can maintain a population of undifferentiated cells within the stem cell pool for months to years through symmetric division. Multipotent stem cells can also generate committed progenitor cells by asymmetric division, whereby one daughter cell begins to differentiate along a specific lineage while the other remains as an undifferentiated stem cell (Hofer and Rodewald, 2018).

As multipotent stem cells differentiate into oligopotent and unipotent stem cells (capable of following a few [oligo-] or single [uni-] differentiation pathways), the partially differentiated stem cells become more numerous, progressively lose their capacity for self-renewal, and increase lineage-specific gene expression to become increasingly committed to their differentiated lineage. Multipotent stem cells replenish HSCs, supportive stroma mesenchymal stem cells (MSCs), and vasculature endothelial precursor cells (EPCs). The most differentiated stem cells, unipotent stem cells, are lineage-committed progenitors with limited self-renewal capacity. Mature, terminally differentiated blood cells have limited or no capacity for self-renewal.

HSCs are the earliest precursors to erythrocytes, leukocytes (of all classes), and thrombocytes (platelets). HSCs can be loosely subdivided into three pools: (1) the quiescent stem cell pool (multipotent and oligopotent), (2) the mitotic pool (oligopotent and unipotent),

and (3) the postmitotic pool. The quiescent stem cell pool comprises a small number of nondividing or slowly dividing “long-term repopulating” cells (12–14 symmetric divisions per week in mice) that maintain their stem cell activities and prevent premature stem cell exhaustion. Some quiescent cells divide asymmetrically to generate “short-term repopulating” cells that maintain rapid cycling ( $\geq 5$  divisions in 7 weeks). Quiescent HSCs are located in the subendosteal niche, while dividing HSCs are located closer to the central vascular niche, which promotes differentiation and mobilization of mature blood cells into the circulation (see Section 3.2.1 The Hematopoietic Microenvironment) (Wilson et al., 2007; Yahata et al., 2008). Small numbers of HSCs circulate in blood and lymphatic vessels ( $\sim 0.0125\%$  of leukocytes) and contribute to the restoration of hematopoiesis in peripheral tissues (Massberg and von Andrian, 2009). HSCs appear cytologically similar to small lymphocytes but can be identified by flow cytometry based on cell surface marker expression. All but the most primitive HSCs express the markers CD34, c-Kit, CD133, and Sca-1 (Hofer and Rodewald, 2018). HSCs also express a unique set of transcription factors, including Oct-4, Nanog, and Sox-2 (Wognum et al., 2003).

Under the classic view of hematopoiesis, HSCs become progressively lineage-restricted through a succession of asymmetric divisions. The model is hierarchical, branching, and linear (Figure 5.2). The hematopoietic lineage begins with HSCs that differentiate into multipotent progenitors (MPPs), followed by primitive common lymphoid (CLP) or myeloid (CMP) progenitors (Takizawa et al., 2012). The CMP further divides into a megakaryocytic/erythroid progenitor (MEP) giving rise to erythrocytes and platelets and a granulocyte/monocyte progenitor (GMP) giving rise to monocytes/macrophages, granulocytes, and mast cells. Although this system is elegant and valid in most instances, it is not universal or immutable. Hierarchical relationships exhibit plasticity and vary among species, model systems, and cell types (Laurenti and Gottgens, 2018; Smith, 2003). For example, mice have a CMP/CLP, while strict division of lineage-specific myeloid and lymphoid progenitors is observed in humans. In addition, expression of surface antigens at each developmental stage differs among species (e.g., human but



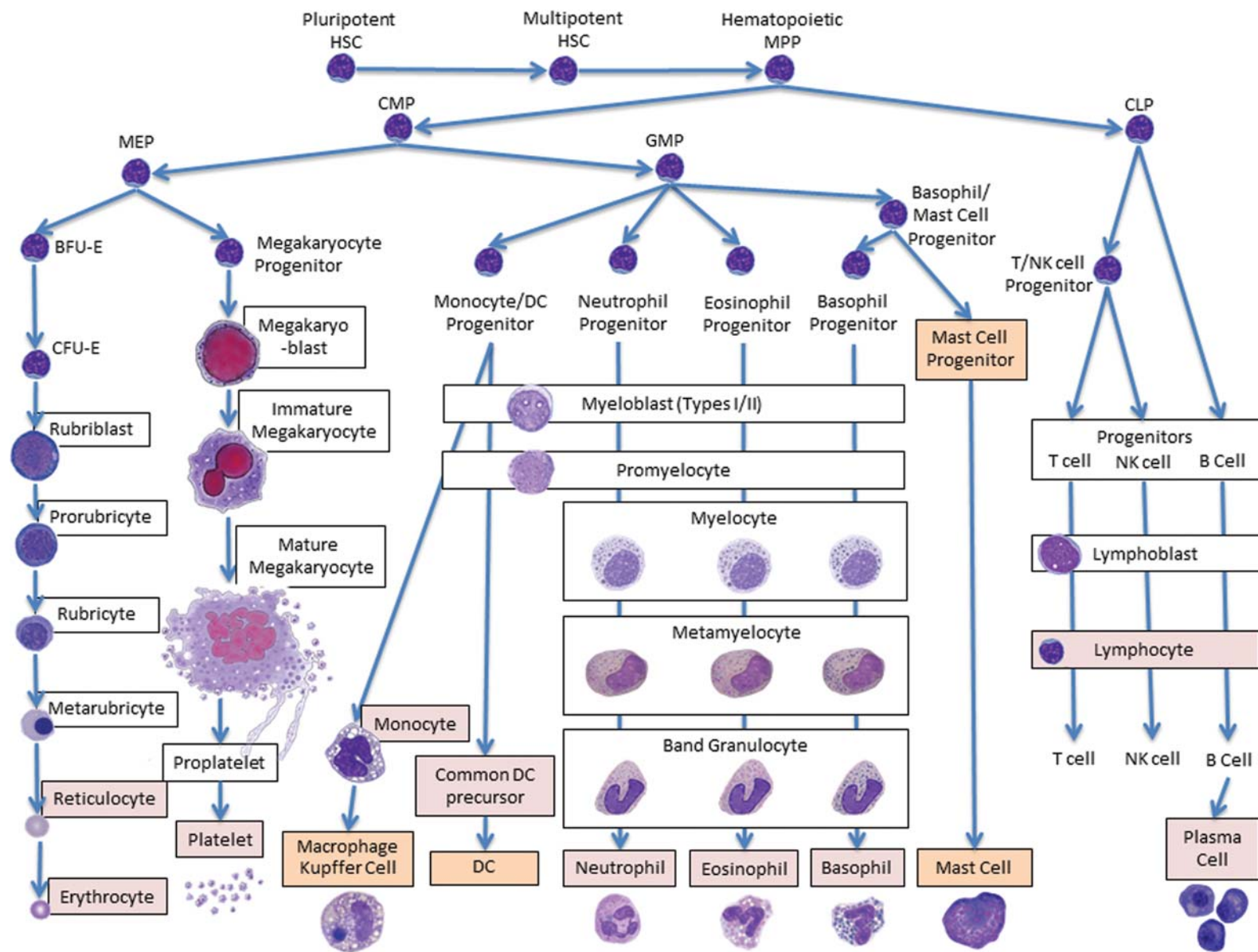


**FIGURE 5.2** Schematic of the conventional model for hematopoiesis. Lineage differentiation varies with the species and is more plastic than this linear model implies. Multipotent cells (capable of following multiple differentiation pathways): HSC and MPP; oligopotent cells (able to follow a few differentiation pathways): CMP, MEP, GMP and CLP; unipotent (capable of producing cells of a single lineage): BFU and progenitors. Cell types shown in boxes can be recognized in bone marrow by light microscopic evaluation at high magnification (images are representative of cytologic appearance), whereas those not in boxes are not distinguishable; orange box: tissue cell; pink box: circulating cell. Abbreviations: *BFU-E*, blast-forming unit - erythroid; *CFU-E*, Colony Forming Unit - erythroid; *CLP*, common lymphoid progenitor; *CMP*, common myeloid progenitor; *DC*, dendritic cells; *Eos*, eosinophils; *Ery*, erythrocytes; *GMP*, granulocyte/macrophage progenitor; *HSC*, hematopoietic stem cell; *MEP*, megakaryocyte/erythroid progenitor; *MPP*, multipotent progenitor cell; *NK*, natural killer cells. Adapted from Ramaiah L, Bounous DI, Elmore SA: Chapter 50—hematopoietic system. In Haschek WM, Rousseaux CG, Wallig MA, editors: *Haschek and Rousseaux's handbook of toxicologic pathology*, ed 3, Boston, 2013, Academic Press, Fig. 50.2, pp. 1863–1933.

not murine HSCs express *fms*-like tyrosine kinase 3 [FLT3]) (Parekh and Crooks, 2013). Macrophages, dendritic cells (DCs), lymphocytes, and mast cells have proliferative capacity while they reside in extramedullary tissues (tissues outside bone marrow). Furthermore, some classes of cells such as DCs and mast cells follow a graded lineage commitment model, where cells arise from progenitors of varying differentiation stage and lineage (Naik, 2020). Finally, seemingly committed cells can be induced in some situations to convert into cells of another lineage (i.e., lineage reprogramming or transdifferentiation) (Orkin and Zon, 2008) or to dedifferentiate into stem or regenerating cells (Rodriguez-Fraticelli et al., 2018; Wei et al., 2020).

Lineage programming and the balance between self-renewal and differentiation are regulated by factors both external and intrinsic to the stem cell, including cytokines, niche interactions, cell surface marker and receptor expression, metabolic factors, signal transduction regulators, transcription factors, epigenetic regulators, and microRNAs (Bujko et al., 2019; Dahariya et al., 2019; Hajishengallis et al., 2021; Hu and Shilatifard, 2016; Kaushansky and Zhan, 2018; Pouzolles et al., 2016). This coordinated program induces lineage-restricted factors and suppresses factors promoting other lineages, resulting in expression of appropriate sets of lineage-specific factors and receptors. The list of these factors is long and ever-expanding, and their thorough review is beyond the scope of this chapter. Interested readers are directed to selected references on the topic (Metcalf, 2008; Murphy, 1993; Rieger et al., 2009; Robb, 2007; Rodrigues et al., 2021; Zhu and Emerson, 2002).

### 3.2.3. Life Cycles of Blood Cells

#### 3.2.3.1. ERYTHROPOIESIS

Erythropoiesis takes place within distinct anatomical units called erythroblastic islands (Figure 5.3) (Manwani and Bieker, 2008). Erythroblastic islands are located throughout the marrow near venous sinuses and may also be observed in the fetal liver and fetal spleen of all species, and often in the splenic red pulp of mature rodents. This unique developmental niche contains single macrophages that support the maturation of surrounding erythroid cells (Figure 5.4). Central macrophages are surrounded by a ring of 10–30 developing erythroid cells of varying levels of maturity, from

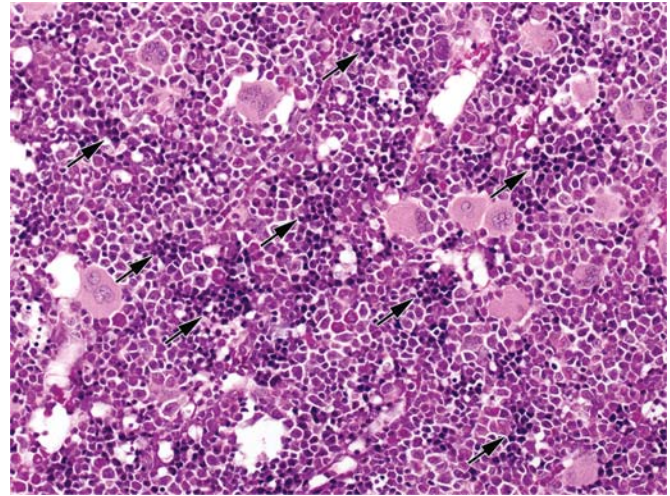


**FIGURE 5.3** Erythropoietic islands are identified in bone marrow at low magnification as clusters of small, round, deeply basophilic cells with scant cytoplasm (arrows). H&E. Adapted from Haschek WM, Rousseaux CG, Wallig MA, editors: Haschek and Rousseaux's handbook of toxicologic pathology, ed 3, 2013, Academic Press, Figure 50.3, p. 1876, with permission.

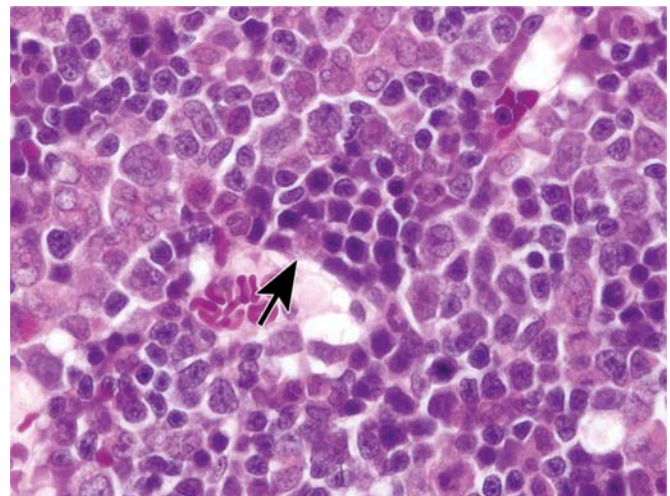


**FIGURE 5.4** Erythropoietic island at higher magnification. This unique developmental niche consists of a cluster of maturing erythroid cells (darker cells) whose development is supported by a single centrally located macrophage (arrow). Every erythroblastic island has a macrophage associated with it, although it is often located out of the plane of the tissue section. H&E. Reproduced from Haschek WM, Rousseaux CG, Wallig MA, editors: Haschek and Rousseaux's handbook of toxicologic pathology, ed 3, 2013, Academic Press, Figure 50.4, p. 1876, with permission.

erythroid colony-forming units (CFU-E) to reticulocytes. These specialized macrophages express elevated levels of F4/80 and Forssman



glycosphingolipid, are highly adhesive, have high endocytic activity, and do not function as phagocytes (i.e., cannot generate a respiratory burst to produce ROS) (Manwani and Bieker, 2008; Yeo et al., 2019). Erythroid cells adhere to macrophage cytoplasmic processes via erythroblast macrophage protein (EMP), VLA-4 (very late antigen-4, also known as *integrin*  $\alpha_4\beta_1$ ), and ICAM-4 (intercellular adhesion molecule 4). Macrophages elaborate several factors that stimulate (ferritin, IGF-1 [insulin-like growth factor 1]) or inhibit (TNF- $\alpha$  [tumor necrosis factor alpha], TRAIL [TNF-related apoptosis-inducing ligand], IL-6 [interleukin 6], TGF- $\beta$  [transforming growth factor beta]) erythropoiesis (Battaller et al., 2019). As erythroid cells terminally differentiate, macrophages are essential for iron transfer and phagocytosis of extruded nuclei and defective erythrocytes.

In erythropoiesis, each HSC undergoes a series of divisions and differentiation steps to produce millions of mature RBCs (erythrocytes) (Beutler, 2005). Over a period of months, multipotent hematopoietic progenitors differentiate into MEPs, followed by erythroid blast-forming units (BFU-E) and CFU-E. In culture, BFU-E take 7–9 days to develop into CFU-E, which take 3–5 days to develop into rubriblasts (Finch et al., 1977). Over a period of approximately five days and five mitotic divisions, rubriblasts differentiate sequentially into prorubricytes, polychromatophilic rubricytes, metarubricytes, and reticulocytes (Harvey, 2008). In humans, there are normally about 50 rubricytes and 113 reticulocytes for every rubriblast (Finch et al., 1977). In most species, reticulocytes spend 2–3 days maturing in bone marrow before being released into circulation.

Later stages of erythropoiesis can be discriminated by cytological evaluation of stage-specific features in bone marrow smears at high magnification (Figure 5.4). The first stage of erythroid development that is recognizable by light microscopy is the rubriblast, which is distinguished from more differentiated stages by its prominent nucleolus (Reagan et al., 2019). As erythroid cells progressively divide and differentiate, they become more numerous, decrease in size, condense their nuclear chromatin, and increase in cytoplasmic hemoglobin concentration. Immature cells have high nuclear to cytoplasmic ratios, and this ratio decreases as cells progressively differentiate. At the polychromatophilic rubricyte stage, the beginning of hemoglobin accumulation

is observable by light microscopy (using a Romanowsky stain like Wright or Wright-Giemsa) as a shift in cytoplasmic color from blue to a mixed pale blue/light pink tint. Metarubricytes (blue-pink to orange) have a nearly full content of hemoglobin and are ready to extrude their nucleus (which is condensed and dark blue). Nuclear expulsion yields a polychromatophilic erythrocyte (reticulocyte on vital stains) that has excess surface area and lacks 20%–30% of its maximal hemoglobin content. Reticulocytes still harbor residual mitochondria, Golgi membranes, microtubule components, ribosomes, and RNA, components required for hemoglobin synthesis, so their size is slightly larger and their cytoplasm is slightly blue relative to mature erythrocytes.

EPO is the principal erythropoietic hormone. It is an evolutionarily well-conserved glycoprotein hormone that shares structural homology with growth hormones and other hematopoietic class 1 cytokines. In response to anemia or hypoxic stress, EPO stimulates survival and proliferation of erythroid cells and regulates the kinetics of maturation and hemoglobinization of developing cells, resulting in increased circulating RBCs and oxygen-carrying capacity. During fetal development, EPO produced by hepatocytes supports erythropoiesis in the fetal liver (Shih et al., 2018). After birth, specialized renal erythropoietin-producing and oxygen-sensing (REPOS) cells become the primary source for EPO production (Wenger and Hoogewijs, 2010). REPOS cells are peritubular, interstitial, fibroblast-like cells that survey the corticomedullary oxygen gradient in the juxtamedullary cortex of the kidney (see *Kidney*, Vol 5, Chap 2). These specialized cells induce a 150-fold–1000-fold increase in EPO production when they detect decreased regional blood oxygen levels (Fu et al., 1993).

Oxygen levels are sensed by prolyl-4-hydroxylase domain (PHD) enzymes, which covalently modify hypoxia-inducible transcription factor-1/2 $\alpha$  (HIF-1/2 $\alpha$ ) subunits into an intrinsic reduction-oxidation (redox) reaction (PHD-HIF-von Hippel-Lindau system) (Wenger and Hoogewijs, 2010). Oxygen-dependent HIF-1/2 $\alpha$  hydroxylation results in polyubiquitination and proteasome degradation of this protein. Decreased regional oxygenation stabilizes HIF- $\alpha$ , allowing it to heterodimerize with HIF- $\beta$  and become transcriptionally active. This dimer results in transcriptional activation of EPO as well as other genes involved in the



adaptive response to decreased oxygen supply. Hypoxia also induces proliferation of REPOS cells and leads to EPO mRNA stabilization. In adult rodents and at times of severe hypoxia in adults of other species, the liver can contribute to EPO production in response to tissue hypoxia (up to 50% of total EPO in rodents). Interestingly, REPOS cells of the kidney respond to hypoxia in an all-or-nothing fashion, whereas hepatocytes respond in a graded fashion. EPO mRNA is also detectable in the brain, spleen, lung, and testes, though these organs are not able to produce sufficient EPO levels to support erythropoiesis (Marti et al., 1996; Tan et al., 1991).

The EPO receptor is expressed at low levels on early erythroid progenitors (BFU-E) and at elevated levels in late progenitors (CFU-E) and early committed erythroid cells, thereby protecting these cells against apoptosis (Bresnick et al., 2018). The receptor is then down-regulated as cells become increasingly differentiated. Binding by EPO up-regulates the expression of EPO receptor and erythroid-specific transcription factors (e.g., GATA-1, SCL/TAL1, and EKLF [erythroid Krüppel-like factor, also termed KLF1]). EPO receptors are also expressed on endothelial, neural, muscle, cardiovascular, and renal tissues, where EPO acts as a cytoprotectant and/or growth hormone (Suresh et al., 2020a, b; Suresh et al., 2019). Therefore, EPO may improve oxygen delivery and protect against tissue ischemia by promoting vasoconstriction and stimulating angiogenesis (i.e., formation of new blood vessels from preexisting vessels) and nerve regeneration in nonhematopoietic tissues.

The strength and duration of EPO pulses, EPO receptor expression, and the activities of kinases and phosphatases all regulate the kinetics of RBC maturation. Kinases and phosphatases act at specific sites on the EPO receptor and its downstream signaling molecules to dictate whether cells should proliferate or differentiate. High kinase (JAK2 [Janus kinase 2]) activity relative to phosphatase (SH-containing phosphatases 1 and 2 [SHP1 and SHP2], CD45, and PTP-1B [protein tyrosine phosphatase 1B]) activity tends to delay maturation of erythroid precursors, resulting in enhanced proliferation (larger reticulocytes) and suppressed differentiation (less hemoglobin) (Fibach, 2011).

Terminal differentiation in erythroid cells requires tight regulation of DNA synthesis,

nuclear division, cytokinesis (cell division), chromatin condensation, organelle loss, and cytoplasmic hemoglobinization (i.e., hemoglobin accumulation) to maintain maturation synchrony (Ramaiah et al., 2013). Factors regulating terminal differentiation are only beginning to be elucidated, but they include reduced KLF1 transcription factor expression, inhibition of PU.1 transcription factor expression, sensitivity to DNase I digestion, hypomethylation (which permits enhanced expression) of the  $\beta$ -globin locus, altered availability of cell cycle control molecules (Rb protein, p27), and induction of cytoplasmic, cytoskeletal, and membrane maturation (Hsieh et al., 2000; Sankaran et al., 2008). KLF1 induces gene expression of globins and their molecular chaperones and also coordinates the production of iron-bound heme (e.g., mitoferrin, ferritin, transferrin receptor and erythroid aminolevulinic acid synthase [ALAS-E/ALAS-2]) (Hodge et al., 2006). This network of proteins ensures successful acquisition of iron, biogenesis of iron sulfur (Fe-S) clusters (which participate in heme synthesis), and maximal hemoglobin accumulation while avoiding iron or heme overload. Terminally differentiated erythroid cells accumulate heme earlier and faster than globin (in a molar excess of 2- to 10-fold). Excess free heme can induce ROS and thus is either rapidly degraded by heme oxygenase to prevent cytotoxicity or is exported by transporters such as FLVCR (feline leukemia virus, subgroup C receptor) (Iolascon et al., 2009; Munoz et al., 2009). The pace of cell division and chromatin maturation generally follows that of hemoglobin synthesis such that as hemoglobin accumulates, cells progressively become smaller, and transcriptional activity diminishes. Heme regulates its own synthesis as well as that of globin (Koury and Ponka, 2004; Nunomura et al., 2015). It is still unclear what causes nuclear extrusion (Stevens-Hernandez and Bruce, 2022). However, observations suggest that when a specified level of nonhemoglobin-associated heme is reached and a significant fraction of the free heme is localized in the cell nucleus, iron uptake and cell division are halted, and the nucleus is extruded (Alsaker, 1977; Menon and Ghaffari, 2021).

Following nuclear extrusion, the successful protracted synthesis of hemoglobin relies on the persistence of globin mRNA and on the stabilization of free globin chains (Peixeiro et al., 2011;

Ross and Sullivan, 1985; Waggoner and Liebhaver, 2003). Globin mRNA continues to be translated to protein for as long as a week following nuclear extrusion, and the half-life of these mRNAs has been estimated to range from 10 to 60 h depending on the species (Ross and Sullivan, 1985; van Zalen et al., 2012). Globin mRNAs are stabilized and protected from degradation by mRNP (messenger ribonucleoprotein) complexes. These are composed of mRNA-binding proteins (*trans*-acting elements) and 5' and 3' elements (UTS [untranslated sequences], cap structures, poly (A) tails) that are encoded within the mRNA (*cis*-acting elements). Hemoglobin stabilizing proteins ( $\alpha$ -HSP) play a key role in hemoglobin assembly and stabilization. They form stable but reversible complexes with free globin chains prior to heterodimerization and hemoglobin formation. This promotes proper folding and limits chemical reactivity, ROS production, aggregation, and precipitation.

Reticulocyte maturation occurs within the bone marrow as well as in circulation and the red pulp of the spleen. As reticulocytes mature, they continue to synthesize hemoglobin and lose organelles, membrane surface area, and cell surface proteins by exosome formation and membrane blebbing (Stevens-Hernandez and Bruce, 2022). Young reticulocytes have a high metabolic rate and synthetic function. Moreover, young reticulocytes are quite fragile due to their low membrane stability and deformability, which is 90% lower than that of late-stage reticulocytes (Li et al., 2018). During maturation, reticulocyte membranes are remodeled, and cytoskeleton is stabilized (Liu et al., 2010). In reticulocytes, hemoglobin synthesis persists at a low rate for 3–4 days until it reaches a finite maximal concentration. At this time, the cell membranes and cytoskeleton become stable, cell surface area is lower, and remnant organelles are degraded, yielding a mature erythrocyte (Minetti et al., 2020).

The release of reticulocytes from bone marrow into circulation is a consequence of the loss of surface adhesion molecules, heightened cell deformability, pressure gradients along the bone marrow sinus wall, and the opening of endothelial pores that permit mature cells to enter the vessel lumen (Alsaker, 1977; Harvey, 2008). As reticulocytes mature, they become

smaller and more flexible, and the size of the endothelial pores becomes a key determinant to their release. With stimulated erythropoiesis, EPO increases the number and size of the pores to facilitate the release of larger (less mature) reticulocytes. Therefore, in addition to its stimulation of erythroid proliferation and differentiation, EPO increases oxygen-carrying capacity by inducing a rapid release of immature reticulocytes from the bone marrow into circulation.

The maturity of reticulocytes and erythrocytes released from the bone marrow varies among species and with age (Harvey, 2008). During basal erythropoiesis in humans (i.e., baseline conditions during health), most late-stage erythroid cells released into circulation are reticulocytes. Dogs release immature “aggregate”-type reticulocytes, whereas cats release mature “punctate”-type reticulocytes under basal conditions and aggregate reticulocytes in response to an erythropoietic stimulus. Aggregate reticulocytes are characterized by a dark blue interlacing network of cytoplasmic precipitate, while punctate reticulocytes lack the reticular pattern of cytoplasmic staining but contain a few scattered, variably sized, dark blue cytoplasmic granules. In ruminants and horses, late-stage erythroid cells are released as mature erythrocytes. Ruminants release reticulocytes into circulation in response to an erythropoietic stimulus. Horses do not release reticulocytes into circulation even with a regenerative response but instead release large erythrocytes. During basal erythropoiesis, which replaces naturally senescent RBCs to maintain normal red cell mass, reticulocytes have a relatively short lifespan (~24 hours in humans, 7–10 days for punctate reticulocytes in cats). However, under conditions of erythropoietic stimulation (“demand-adapted” or “stress” erythropoiesis), reticulocytes released from the bone marrow are less mature and consequently have a longer circulating lifespan (two- to four-fold longer). Therefore, reticulocyte counts reflect differences in production as well as reticulocyte lifespan. In rats, basal reticulocyte counts are high in neonates (40%–90% of all circulating erythrocytes), lower in young rats (10%–20%), and lowest in aged rats (2%–5%) (Kojima et al., 1999; Turton et al., 1989). Reticulocyte responses are robust in mice and rats. Dramatic age-related changes in reticulocyte counts can be observed in pigs including

minipigs. In this species, reticulocyte counts rapidly increase at 3–7 days of age, decrease at approximately 3 weeks of age, increase again at 8 weeks, and finally decrease at approximately 3 months of age (Miller et al., 1961). It is common to observe abrupt changes in reticulocyte numbers even in 6-month-old minipigs (Glerup et al., 2013).

The lifespan of mature circulating erythrocytes is determined by senescence-based clearance, damage-based clearance, and eryptosis (i.e., red cell apoptosis), and varies among species according to basal metabolic rate, species longevity, and body mass (Table 5.4) (Christian, 2010; Kaestner and Minetti, 2017). Clearance of senescent or damaged erythrocytes is carried out by macrophages of the reticuloendothelial system. Injuries accumulated over the lifespan of erythrocytes produce a variety of recognition ligands on the external cell surface that stimulate specific phagocytic receptors on macrophages. These include unmasked antigens and carbohydrate epitopes, exteriorization of phosphatidylserine, loss of self-recognition due to alterations in CD47, band 3 clustering (IgG opsonization and complement binding, binding by oxidized hemoglobin), lipid peroxidation, and

transmembrane signaling resulting from cytoskeletal injury (Franco et al., 2012). Erythrocyte senescence involves receptor-mediated removal of aged or damaged erythrocytes by splenic and bone marrow macrophages and hepatic Kupffer cells. The rate of senescence-based clearance due to the accumulation of oxidative injury to cell surface molecules and intracellular enzymes is highly dependent on the cell's antioxidant status. The oxidation of proteins causes hemoglobin-spectrin crosslinking, resulting in increased membrane rigidity, decreased deformability, and/or stimulation of membrane proteolysis. Age-related decreases in antioxidant status result in 0%–60% shorter lifespan in old rodents when compared to young rodents.

After erythrocyte phagocytosis by macrophages, hemoglobin is catabolized into separate globin and heme proteins. Globin is further degraded into its constituent amino acids. Heme is degraded to produce iron, biliverdin, and carbon monoxide in a reaction catalyzed by heme oxygenase-1 (HO-1). Iron may be stored within macrophages while bound to ferritin, where it can remain to contribute to the hemoglobinization of newly forming RBCs. Alternatively, iron may be exported via ferroportin to circulate

**TABLE 5.4** Normal Erythrocyte Lifespan in Selected Mammalian Species

Species	Erythrocyte Lifespan (days)	References
Mice	30–52	Bolliger and Everds (2012); Agar and Board (1983); Weiss and Wardrop (2011)
Rats	56–69	Derelanko (1987); Edmondson and Wyburn (1963); Van Putten (1958)
Guinea pigs	60–80	Edmondson and Wyburn (1963); Everett and Yoffey (1959)
Hamsters	50–70	Meyerstein et al. (1975); Toffelmire and Boegman (1980)
Rabbits	60–70	Dale and Daniels (1991)
Cats	66–78	Christian (2010)
Dogs	110–115	Christian (2010)
Goats and sheep	115	Christian (2010); Kaestner and Minetti (2017)
Cattle and horses	130–150	Christian (2010)
Nonhuman primates	86–105	Fonseca et al. (2018); Valeri and Ragno (2006)
Humans	115–120	Franco (2012); Kaestner and Minetti (2017); Kurtin (2012)

*Adapted from Haschek WM, Rousseaux CG, Wallig MA, editors: Haschek and Rousseaux's handbook of toxicologic pathology, ed 3, 2013, Academic Press, Table 50.4, p. 1879, with permission.*



while bound to transferrin. Within the macrophage, biliverdin is converted to bilirubin. Bilirubin then noncovalently binds to albumin for improved solubility while circulating. Albumin-bound bilirubin is taken up by hepatocytes and conjugated to enhance its water-solubility and excretion via bile into the gastrointestinal tract. Gastrointestinal bilirubin is converted to urobilinogen by gastrointestinal bacteria and may be either reabsorbed and then reexcreted into the intestinal tract or converted to stercobilinogen prior to fecal excretion (Ramaiah et al., 2013). Reabsorbed urobilinogen may continue to circulate in the hepatobiliary-gastrointestinal circuit or may be excreted in the urine (Stockham and Scott, 2008).

A more recently described mechanism of erythrocyte death is eryptosis. This process represents a specialized form of RBC apoptosis. Eryptosis occurs before the erythrocyte has had a chance to be naturally removed from the circulation at the end of its lifespan (Repsold and Joubert, 2018). Affected cells are characterized by cell shrinkage, blebbing, phospholipid scrambling of the cell membrane, and surface expression of phosphatidylserine (Lang et al., 2012).

### 3.2.3.2. MEGAKARYOPOIESIS AND THROMBOPOIESIS

Megakaryopoiesis, the development of MKs from HSCs, begins in the subendosteal niche of the bone marrow. Migration of MKs to the vascular niche and exposure to elevated oxygen tension promotes terminal differentiation and production of proplatelets that allow platelet release into the bloodstream (thrombopoiesis). Extracellular matrix elements in specific sites regulate MK maturation and migration (Malara et al., 2011). In the low oxygen subendosteal niche, type I collagen and fibronectin promote MK spreading and inhibit proplatelet production. The increased oxygen tension of the vascular niche promotes fibrinogen and von Willebrand Factor (vWF) expression, which supports MK maturation and proplatelet production. Platelet-producing MK are also present in other high oxygen compartments such as spleen (red pulp) and lung capillaries.

Thrombopoiesis occurs adjacent to the sinus endothelium, which allows for the direct release of mature platelets into the blood via proplatelet penetration of sinus walls (Stegner et al., 2017). Within the subendosteal niche, TPO (also termed

Mpl ligand) and platelet-derived growth factor (PDGF) induce MEPs to differentiate into lineage-committed MK progenitors. MK progenitors undergo a highly specialized form of division called endomitosis in which there is no true cell division from the progenitor stage (promegakaryoblast) to the MK stage (Mazzi et al., 2018). This facilitates the synthesis of massive quantities of cytoskeletal, cytoplasmic, and membrane components necessary for platelet production. Endomitosis is a form of thwarted mitosis in which DNA synthesis, prophase, prometaphase, and metaphase occur, but there is a failure of anaphase, telophase, and cytokinesis due to an altered mitotic spindle. This process results in progressive polyploidy (i.e., more than two complete sets of chromosomes) and yields giant cells with multilobulated nuclei and abundant pale pink cytoplasm (Figure 5.5). Diploid promegakaryoblasts differentiate into tetraploid megakaryoblasts, polyploid promegakaryocytes, and finally megakaryocytes. As they mature, MKs

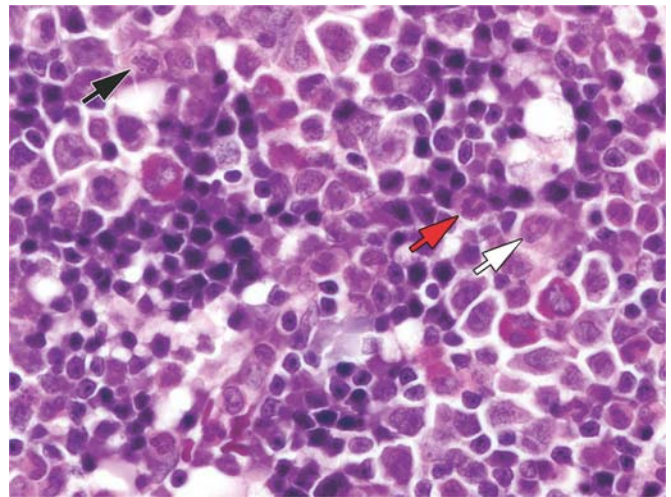


**FIGURE 5.5** Rat bone marrow. Granulocytes, particularly those of the neutrophilic series, can be identified on high magnification as cells with pale cytoplasm and noncircular nuclei. Black arrow: mature, segmented neutrophil with multilobulated nucleus; red arrow: immature, nonsegmented band neutrophil with horseshoe-shaped nucleus; white arrow: immature, nonsegmented neutrophil with ring-shaped nucleus. H&E. Reproduced from Haschek WM, Rousseaux CG, Wallig MA, editors: *Haschek and Rousseaux's handbook of toxicologic pathology*, ed 3, 2013, Academic Press, Figure 50.5, p. 1884, with permission.

become progressively larger (up to 200 microns in diameter) and lose this DNA proliferative capacity. After multiple rounds of endomitosis (occurring over approximately 2 days) have been completed, MK ploidy may range from 16N (mice and humans) to 32N (dogs and rabbits), and even up to 32–64N (cats and cattle) (Ebbe and Boudreaux, 1998; Kuter et al., 1994; Mazzi et al., 2018; Topp et al., 1990). The number of divisions an MK undergoes determines the final ploidy and cytoplasmic volume.

Polypliodization of MK precursors is followed by cytoplasmic maturation, which takes place over approximately two more days. This involves production of membrane receptors (CD41/61, CD42 and glycoprotein V),  $\alpha$ -granules and dense granules, protein synthetic apparatus (spliceosomes and pre-mRNAs), and an internal demarcation membrane system (DMS) (Mazzi et al., 2018). The DMS is an elaborate membrane network of tubular invaginations that extend from the plasma membrane to fill the MK cytoplasm, except for a narrow band at the periphery of the cell. The DMS provides a reservoir for the formation and extension of proplatelet processes.

After completion of endomitosis and cytoplasmic maturation, stromal cell-derived factor-1 $\alpha$  (SDF-1 $\alpha$ ) initiates MK migration to the vascular-rich niche for terminal differentiation and thrombopoiesis (Noetzli et al., 2019). Within the vascular niche, mature MKs bind to endothelial cells and begin elaborating multiple pseudopod membrane projections called proplatelets. The elongation of proplatelet processes and organelle transport to the distal tips of proplatelet processes is driven by microtubules (French, 2013). Platelets are shed into venous sinusoids by proplatelet fragmentation (Eckly et al., 2020). As they are shed, they take with them a full complement of membranes, organelles, granules, and soluble macromolecules, thereby consuming MK cytoplasm (Potts et al., 2020). Newly released, younger platelets (referred to as ‘reticulated platelets’) have higher cytoplasmic RNA content and are analogous to reticulocytes. Each megakaryocyte produces 1000–3000 platelets before the residual nucleus is degraded by macrophages (Moujalled et al., 2021).

TPO is a highly conserved protein that serves as the primary megakaryopoietic and thrombopoietic cytokine. The TPO receptors (designated

c-Mpl) are expressed on platelets, megakaryocytes, megakaryocyte precursors, and endothelial cells (Nakamura-Ishizu and Suda, 2020). TPO stimulates proliferation and differentiation of MEP (MEPs), controls the endomitosis and maturation of MKs, and regulates proplatelet formation (Nakamura-Ishizu and Suda, 2020). Stimulation of MEPs, the common MEPs, also results in stimulation of erythroid proliferation and differentiation; interestingly, the sequence of TPO is fairly homologous to EPO. TPO also acts with several cytokines to promote the growth of primitive stem cells and GMPs and induces splenic extramedullary hematopoiesis (EMH). TPO is primarily made in the liver but also is produced in kidney, striated muscle, bone marrow stromal cells, spleen, testis, and brain. Its synthesis is enhanced by inflammation, particularly by IL-6. TPO cleavage by thrombin generates polypeptides and truncated TPO forms with varying activity (Ramaiah et al., 2013). Circulating levels of TPO are regulated by receptor-mediated uptake and degradation (Varghese et al., 2017). Internalization and degradation of TPO by platelets serves to clear it from circulation, thereby regulating megakaryopoiesis and thrombopoiesis (Hitchcock et al., 2021). Megakaryopoiesis is inhibited by platelet factor 4 (PF4), which is produced by platelets (in  $\alpha$ -granules).

The connections between megakaryocyte ploidy, effectiveness of platelet formation, and platelet volume have been the subject of abundant investigation. Apart from specifically evaluated circumstances, correlations are debated and not well understood (Corash, 1989; Corash and Levin, 1990; Machlus and Italiano, 2013).

### 3.2.3.3. MYELOPOIESIS

**Myelopoiesis** is defined as the development of nonlymphoid leukocytes. The stages of myelopoiesis are variable among species, cell types, and model systems. Monocytes/macrophages, granulocytes, and mast cells arise from a CMP (humans) or a common myeloid/lymphoid progenitor (mice), which differentiate into a GMP (Luc et al., 2012). These common progenitors then differentiate into lineage-committed (i.e., unipotent) monocyte, neutrophil, eosinophil, basophil, and mast cell progenitors. In a synchronous sequence of divisions and maturation steps, cells acquire lineage-specific

cytoplasmic granules and nuclear conformations as they differentiate into their respective mature forms. This process is controlled by the coordinated up-regulation and/or down-regulation of transcription factors such as GATA-1, GATA-2, PU.1, and C/EBP- $\alpha$  at specific stages of maturation, as well as by myelopoietic cytokines (SCF, TPO, IL-3, GM-CSF [granulocyte/macrophage colony-stimulating factor, also termed CSF2], IL-6) (Friedman, 2007; Lawrence et al., 2018). The monocytic/macrophage lineage is the default pathway for myeloid progenitors; the expression of specific cytokines and transcription factors can direct cells toward a granulocyte or mast cell differentiation pathway (Mitroulis et al., 2018; Schultze et al., 2019).

**Granulopoiesis** describes the development of granulated leukocytes (neutrophils, eosinophils, basophils) with the exception of mast cells, because mast cell maturation is extramedullary (Malengier-Devlies et al., 2021). Like erythropoiesis, granulopoiesis also occurs within anatomical units in the marrow, although the foci are less distinct. Committed neutrophil, eosinophil, and basophil precursors undergo a similar maturation sequence that can be followed by light microscopy.

Developing granulocytes can be subdivided into mitotic (proliferating), maturing, and storage pools. The proliferating pool constitutes 10%–30% of bone marrow granulocytes and is composed of dividing cells (myeloblasts, promyelocytes and myelocytes). Myeloblasts have a round nucleus with a nucleolus and a high nuclear to cytoplasmic ratio. As myeloblasts mature from Type I to Type II, they begin to acquire primary granules in the cytoplasm. The promyelocyte is characterized by a round nucleus that lacks a nucleolus and primary granules, although secondary granules may begin to appear in the cytoplasm. At the myelocyte stage (the last dividing stage), secondary granules are prominent. The appearance (specifically color) of the secondary granules defines the granulocyte lineage as neutrophilic, eosinophilic, or basophilic. The maturation and storage pools constitute 65%–90% of bone marrow granulocytes. The maturation pool is composed of metamyelocytes and band granulocytes. Each myeloblast produces 16–32 metamyelocytes, which mature into band granulocytes. Metamyelocytes (characterized by a slightly indented

nucleus) and band granulocytes (which exhibit a horseshoe-shaped nucleus) no longer divide but undergo further nuclear maturation (chromatin condensation and nuclear segmentation) (Ramaiah et al., 2013).

The degree of nuclear segmentation varies with the granulocyte lineage and species. The storage pool is composed of band granulocytes and segmented granulocytes residing within the marrow. Granulocyte maturation from myeloblast to segmented granulocyte takes approximately 6 days. In some species, neutrophils are released in a cyclic or pulsatile fashion (~every 3 days in mice, ~14 days in dogs, and ~20 days in humans) (Mackey, 2020). Under conditions of increased demand for neutrophils, cytokines such as G-CSF (granulocyte colony-stimulating factor, also known as CSF3) stimulate granulopoiesis, shorten neutrophil precursor maturation time and bone marrow transit time (from 6 days to 2–3 days), stimulate the release of neutrophils from bone marrow, and prevent neutrophil apoptosis (Hidalgo et al., 2019; Schultze et al., 2019). Basophils, which also express high-affinity immunoglobulin E (IgE) receptors, may arise from a common basophil/mast cell progenitor. However, basophils mature in the bone marrow. Transcription factor CCAAT/CEBP $\alpha$  directs cells toward the basophil lineage and away from a mast cell lineage (Arinobu et al., 2005; Chen et al., 2005; Schneider et al., 2010; Wanet et al., 2021).

As cytokine concentrations increase, progressively more immature myeloid cells are released into circulation. Generally speaking, granulocyte lifespan in circulation is short (neutrophils: 6–8 hours; basophils: <6 hours; eosinophils: <1 hour) (McCracken and Allen, 2014; Simon and Kim, 2010; Summers et al., 2010; Tak et al., 2013). Under normal homeostatic conditions, the estimated lifespan of neutrophils is ~12 hours in mice and ~5.7 hours in rats (Casanova-Acebes et al., 2013; Gerecke et al., 1973; Rosales, 2018). As granulocytes circulate, nuclear maturation continues, resulting in increased nuclear condensation and segmentation. Granulocytes that exit the blood vascular system do not reenter circulation but are utilized and removed in situ (Hidalgo et al., 2019). If not utilized in tissues, neutrophils migrate back to the bone marrow for elimination (Casanova-Acebes et al., 2013; Lawrence et al., 2020).



Mast cell hematopoiesis is not fully understood. Lineage-committed progenitors to this unique cell type may be derived directly from MPPs instead of the CMP. Mast cell progenitors leave the bone marrow, enter circulation, and migrate to peripheral tissues including skin, heart, lung, and gastrointestinal submucosa. Within these tissues, the progenitors undergo proliferation, differentiation, and maturation. Mature mast cells distinguish themselves by expression of high affinity IgE receptors (FcεRI), c-Kit, and characteristic large, purple cytoplasmic secretory granules.

The lineage-committed monocyte/dendritic cell progenitor (MDP) is the precursor to a heterogeneous group of mononuclear cells, phagocytes, and antigen-presenting cells (APCs) including monocytes, most macrophages, DC subsets, and osteoclasts. Like mast cells, these cells all have the capacity to proliferate at extramedullary sites. Within the bone marrow, MDPs differentiate to monocytes and to the common DC precursors (CDPs) (Collin and Bigley, 2016). The CDPs differentiate into plasmacytoid DCs or pre-DCs in the bone marrow (Guernonprez et al., 2019). Pre-DCs then exit to the circulation to eventually mature into classical DCs in the spleen and lymph nodes, or mucosal DCs in the lamina propria of mucosal tissues such as the intestinal tract. Regulatory T cells, Flt3, and the lymphotoxin-β receptor all work together to control pre-DC proliferation and maturation in lymphoid organs. Classical DCs have a short lifespan and are rapidly replaced by bone marrow precursors. Some DCs arise directly from HSCs, CMPs, and CLPs. Langerhans cells (epidermal DCs) are unique in that they do not originate from the bone marrow. Instead, they appear to originate from a precursor that colonizes the skin during embryogenesis, differentiates in situ, and then proliferates during the first week of life and continues to divide in situ during adulthood (Collin and Milne, 2016).

Differentiation of MDPs into monocytes is poorly understood, and differentiation stages in the bone marrow are not readily identified (Cane et al., 2019). Monocytes may be viewed as circulating precursor cells that give rise to tissue macrophages (M-CSF [macrophage colony-stimulating factor, also known as CSF1]), inflammatory DCs (GM-CSF and Flt3L), and osteoclasts (M-CSF and RANKL

[receptor activator of nuclear factor-κB (NF-κB) ligand, also known as TNFSF11]). Monocytes remain in circulation for approximately 1 day. Macrophages have a long lifespan (years) and may divide at a slow rate while in tissues. Inflammatory cytokines stimulate (“activate”) resident tissue macrophages to differentiate into a variety of inflammatory effector cells including tissue macrophages, multinucleated giant cells, syncytial cells, and epithelioid macrophages. Inflammatory DCs have a lifespan of 3–5 days.

Not all tissue macrophages originate from monocytes. Tissue-specific macrophages such as hepatic sinusoidal macrophages (Kupffer cells), microglia in the central nervous system, dermal macrophages, splenic marginal zone macrophages, and splenic metallophilic macrophages establish themselves during embryogenesis and maintain steady state numbers in tissue by local replication. When activated, these resident macrophages typically enlarge and can proliferate at a faster pace.

CMPs also give rise to a population of phenotypically heterogeneous myeloid-derived suppressor cells (MDSCs) (Varga et al., 2008). These cells, which resemble immature monocytes/granulocytes, proliferate in response to factors that promote myelopoiesis but inhibit differentiation into mature myeloid cells. Factors such as glucocorticoids, VEGF, PGE<sub>2</sub> (prostaglandin E<sub>2</sub>), GM-CSF, TGF-β, IL-1β, IL-10, IL-6, and M-CSF promote the accumulation and activation of circulating immature myeloid cells at local sites of inflammation or neoplasia. MDSCs at local sites suppress immune responses by inhibiting T cell proliferation and proinflammatory cytokine production, thus diminishing inflammation during acute or chronic infections, trauma, sepsis, autoimmune disease, and graft responses while promoting immune evasion by tumor cells.

### 3.2.3.4. LYMPHOPOIESIS

As previously discussed, the “classic” model describes hematopoiesis as occurring in distinct branches, with the CLP being the primitive lymphoid progenitor from which B cells, T cells, and NK cells arise (Kondo, 2010). From the CLP, cells go through progressive lymphoid lineage specification. B cells are generated in the bone marrow, while MPPs and CLPs migrate

from the bone marrow to the thymus to support T cell proliferation. The development of NK cells is still under investigation, but the process includes generation within the bone marrow and maturation within the bone marrow and secondary lymphoid organs.

Differentiation into pro-B cells involves genetic rearrangements (specifically V(D)J recombination) and enhanced proliferation in response to IL-7 (Ramaiah et al., 2013). Pre-B cells express pre-B cell receptors (BCRs) and undergo further rearrangement of immunoglobulin loci, differentiating into immature B cells. Functional BCRs promote egress of immature and mature B cells to peripheral lymphoid organs where tonic BCR signaling prevents cell death until final differentiation into memory and antigen-producing cells.

Lymphocytes circulating in peripheral blood consist primarily of T cells. Lymphocyte lifespan is highly variable, ranging from short-lived cell populations with high proliferation and high death rates (such as occurs in germinal centers) to long-lived memory cells, which may live for years.

#### 4. EVALUATION OF HEMATOTOXICITY

Bone marrow and peripheral blood findings must be evaluated concurrently in a functional precursor-product relationship. A high degree of concordance between hematology and bone marrow histopathology is expected for hematotoxicity, though correlates might not be present if “drug” (e.g., biologics or small molecules) effects are acute, focal, or functional. In addition, hematopoietic tissues cooperate with and respond to changes in other organs (e.g., kidney, lung) and systems (e.g., cardiovascular, hemostatic, immune) to maintain homeostasis. Interpretations regarding potential hematotoxic changes are made considering known exposures, the timing of toxicant effects, the kinetics of hematopoietic responses, lifespan of circulating blood cells, changes in other tissues, and clinical observations.

Hematology changes can be broadly classified as being due to altered production, redistribution/sequestration, or destruction/loss/

consumption. When considering hematology findings, examination of the bone marrow helps to determine if changes are due to altered production (Table 5.5). Similarly, histopathologic evaluation of bone marrow may place cell and tissue abnormalities into context by considering their impact on peripheral blood. Specific responses to xenobiotics are described later in this chapter (Section 5. Responses to Injury).

For veterinary clinical diagnosis, evaluation of the hematopoietic system usually begins with identification of morphologic or numerical abnormalities in circulating peripheral blood cells. Changes in peripheral blood that could be due to altered production (as opposed to loss, sequestration, destruction, or consumption) may prompt evaluation of bone marrow (bone marrow cytology and biopsy/histopathology), particularly if changes are unexplained or inappropriate.

In the nonclinical toxicology setting, concurrent hematology and bone marrow histopathology are evaluated routinely and constitute first-tier screening tools for evaluation of the hematopoietic system (Table 5.6). Hematology and bone marrow histopathology provide critical information about general body homeostasis and organ function and/or injury and are part of the core test panels recommended for nonclinical toxicity studies. In most instances, hematology and bone marrow histopathology are sufficient to understand test article-related effects on the hematopoietic system. Hematology consists of a complete blood count (CBC) that examines circulating populations of RBCs, WBCs, and platelets. Histopathology of bone marrow assesses overall tissue architecture, cellularity, focal lesions, and megakaryocyte cellularity and provides an estimate of myeloid to erythroid (M:E) ratio. In contrast, bone marrow cytology assesses lineage maturation, cytomorphology, M:E ratio, and lineage-specific cell numbers (differential counts). Other organs that have a lymphoid or hematopoietic component should also be evaluated histologically; these include the lymph nodes, mucosa- or gut-associated lymphoid tissue, thymus, liver and spleen. Histologic examination of the spleen is particularly important in rodents because of their robust splenic extramedullary hematopoietic responses during health at all stages of life. Because hematotoxicity may also occur

**TABLE 5.5** General Examples of Responses to Injury in Blood and Bone Marrow

Change in Peripheral Blood	Change in Bone Marrow	Causes
Increased cell count	None	Relative change (resulting from altered hemodynamics or distribution), functional defect
	Increased cellularity	Increased demand, stimulation of hematopoiesis
	Decreased cellularity	Decreased loss, destruction, or consumption (increased lifespan) (rare)
Decreased cell count	None	Relative change (resulting from altered hemodynamics or distribution)
	Increased cellularity (regenerative)	Increased loss, destruction, consumption, and/or ineffective bone marrow response
	Decreased cellularity (nonregenerative)	Injury to hematopoietic precursors or microenvironment, suppression of hematopoiesis, factor deficiency, abnormal hematopoiesis, and/or bone marrow infiltration/replacement by nonhematopoietic elements

**TABLE 5.6** Standard and Nonstandard Assays for Evaluation of the Hematopoietic System

Standard Assessment (Tier 1)	Nonstandard and Specialized Techniques (Tier 2 and 3)
<p>Hematology (complete blood count), consisting of:</p> <ul style="list-style-type: none"> <li>• Red blood cell count (RBC)</li> <li>• Hemoglobin concentration (Hgb)</li> <li>• Hematocrit (Hct)</li> <li>• Mean cell volume (MCV)</li> <li>• Mean cell hemoglobin (MCH)</li> <li>• Mean cell hemoglobin concentration (MCHC)</li> <li>• Red cell distribution width (RDW)</li> <li>• Reticulocyte count (Retic [absolute])</li> <li>• Platelet count (plt)</li> <li>• Total white blood cell count (WBC)</li> <li>• White blood cell differential, reported as absolute counts of:               <ul style="list-style-type: none"> <li>• Neutrophils</li> <li>• Lymphocytes</li> <li>• Monocytes</li> <li>• Eosinophils</li> <li>• Basophils</li> <li>• Large unstained cells (LUCs) (automated only)</li> </ul> </li> </ul> <p>Peripheral blood smear preparation and evaluation</p> <p>Bone marrow smear preparation</p> <p>Histopathology of bone marrow and other hematopoietic tissues (e.g., spleen, thymus, and sometimes liver and lymph nodes)</p>	<p>Peripheral blood:</p> <ul style="list-style-type: none"> <li>• Research indices on automated hematology analyzers</li> <li>• Categorization of reticulocytes</li> <li>• Neutrophil and platelet function tests</li> <li>• Osmotic fragility</li> <li>• Hemolytic potential</li> <li>• Percent methemoglobin</li> <li>• Special morphologic assessments and cytochemistry</li> <li>• Heinz body evaluation</li> <li>• Direct and indirect antiglobulin tests</li> <li>• Transmission electron microscopy</li> </ul> <p>Bone marrow:</p> <ul style="list-style-type: none"> <li>• Cytology</li> <li>• Flow cytometry</li> <li>• Immunohistochemistry</li> <li>• Transmission electron microscopy</li> </ul> <p>In vitro and in vivo cell culture and clonogenic assays</p> <p>Specialized animal models</p>

From Ramai L: *The hematopoietic system: Evaluation and data interpretation in nonclinical safety studies*. In McQueen CA, editors: *Comprehensive toxicology*, ed 3, 2018, Oxford, Table 1, Elsevier, p. 400, with permission.



indirectly through injury to other organ systems or metabolic pathways, consideration must be given to all other organ systems as well as the general condition of the animal when evaluating potential effects on the hematopoietic system.

Nonstandard second-tier and third-tier assessments performed to assess one or more blood cell lineages on a case-by-case basis may help to further characterize unexplained or inappropriate effects. These upper-tier assessments include specialized hematologic tests (e.g., categorization of reticulocytes, neutrophil and platelet function, osmotic fragility, hemolytic potential, percent methemoglobin, special morphologic assessments, Heinz body counts, Coombs testing); bone marrow smear cytology; bone marrow flow cytometry; in vitro culture; in vivo culture (stem cell transplantation, spleen-forming units in lethally irradiated mice); animal models (genetically modified mice); retroviral-mediated gene transfer and gene therapy; immunohistochemistry; and electron microscopy (Tripathi et al., 2014; Tomlinson et al., 2013). Flow cytometry allows for high-throughput and precise quantitative evaluation of the M:E ratio and potential hematopoietic lineages in some species. In toxicity studies, bone marrow cytology or flow cytometry may be performed to further characterize effects on different lineages.

#### 4.1. Evaluation of Bone Marrow

##### 4.1.1. Histopathology

The hematopoietic system is a common target of chemical exposure, so careful evaluation of the bone marrow is a critical component of hematotoxicity assessment. Since the bone marrow is a site of erythroid, myeloid, megakaryocytic and lymphoid lineages, any alteration in cellularity should include identification of the cell type(s) affected. Other organs that have a lymphoid or hematopoietic component might also be affected, so histopathologic evaluation is also warranted for the lymph nodes, mucosa-associated lymphoid tissues, thymus, liver and spleen. For the evaluation of the lymphoid compartment, the reader is referred to the *Immune System*, Vol 5, [Chap 6](#) and to other relevant publications (Elmore, 2006a, b, c, d, e; Haley, 2017; Maronpot, 2006).

Bone marrow responses to chemical exposure may also occur indirectly through injury to other organ systems or metabolic pathways. Therefore, bone marrow assessments should take into consideration the histopathologic findings in all organ systems as well as general health status, stress, diet, and body weight changes. Age is also an important consideration since marrow tends to be replaced with adipose tissue over time due to decreased demand. Another consideration is the species since small animals such as rodents have less adipose tissue (relative to hematopoietic tissue) at a given site compared to large animals like dogs and monkeys. The amount of hematopoietic tissue may also vary by site. The recommended sites for histologic evaluation of bone marrow in the rodent are the distal femur and sternum (Reagan et al., 2011). For drug safety assessment, in-life findings, dose-response relationships, and careful comparison of tissue structure using sections from the same anatomic location in age- and sex-matched concurrent controls are important considerations.

Histologic examination of the bone marrow is performed in conjunction with a CBC and, in some situations, in conjunction with cytological evaluation of blood and/or bone marrow smears; flow cytometry of bone marrow, peripheral blood, or other hematopoietic organs; and/or other assessment techniques (see [Table 5.6](#)). Importantly, bone marrow intended for histologic evaluation must be placed in fixative as soon as possible following sampling or death as leakage of enzymes from myeloid cells combined with the possibility of diminished exposure to fixative due to the presence of intact (i.e., relatively impermeable) bone within sections can lead to a higher susceptibility of cells to autolytic changes (Travlos, 2006). Histologic evaluation of the bone marrow is generally performed on H&E-stained sections and should begin at low magnification with an overall assessment of tissue architecture (bone, endosteum, hematopoietic tissue, interstitium, and vasculature) and cellularity. Higher magnification is needed for identification and evaluation of cell lineages (erythroid, myeloid, megakaryocytic); estimation of M:E ratio; vasculature (venous sinuses, radial arteries, nutrient vein, nutrient artery); iron stores (hemosiderin-laden macrophages); and other features such as

neoplasia, inflammation, infectious agents, etc. Unless proliferation is evident, the marrow stromal cells are not assessed quantitatively using routine H&E-stained sections. Microscopic findings are identified and recorded, preferably using a semiquantitative scoring system and/or one that incorporates descriptive terminology (Biddle, 2022; Gibson-Corley et al., 2013; Reagan et al., 2011). Detailed information on lesions and accepted terminology is available in recent publications, including both International Harmonization of Nomenclature and Diagnostic Criteria (INHAND) and National Toxicology Program documents (Cora and Travlos, 2014; Willard-Mack et al., 2019).

The marrow cells that can be identified with H&E include the maturing stages of erythroid, myeloid, and megakaryocytic cells as well as adipocytes, hemosiderin-laden macrophages, and mast cells. Cytologic examination is necessary to identify proliferating stages of myeloid and erythroid cells, lymphoid cells, and changes in maturation or morphology (Figure 5.2). Alterations in maturation sequence are most readily identified by cytologic evaluation though severe disturbances may be seen histologically in the marrow as changes in the ratio of proliferating cells to maturing cells (which is generally 1:4 in rodents).

Erythroblastic islands may be evaluated histologically, though they are not always readily apparent without the aid of immunohistochemistry. They are not commonly observed cytologically because they are readily disrupted during smear preparation. Mature erythroid cells within erythroblastic islands are small and hyperchromatic, with round, dense, and deeply basophilic nuclei (Figures 5.3 and 5.4). The cytoplasm is basophilic in immature erythroid cells and becomes increasingly eosinophilic as cell maturation proceeds. Granulopoiesis is also compartmentalized, but the foci are less distinct. Histologically, immature myeloid cells are large, with bean-shaped nuclei and finely granular, vesicular chromatin. Segmented and band neutrophils can be easily identified (Figure 5.5). Megakaryocytes are frequently located adjacent to sinus endothelium to facilitate release of platelets into the circulation. These are the largest and thus easiest cells to identify due to their abundant pale eosinophilic cytoplasm and prominent multilobulated nuclei (Figure 5.6).

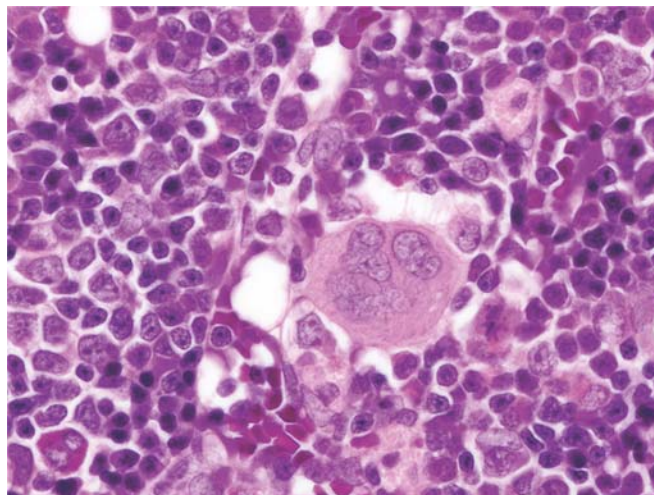


**FIGURE 5.6** Megakaryocytes are easily identified as very large cells with multilobulated nuclei and abundant eosinophilic cytoplasm. They are frequently found adjacent to venous sinusoids where they release platelets directly into circulation. H&E. *Reproduced from Haschek WM, Rousseaux CG, Wallig MA, editors: Haschek and Rousseaux's handbook of toxicologic pathology, ed 3, 2013, Academic Press, Figure 50.6, p. 1885, with permission.*

Lesions identified in H&E-stained sections of bone marrow typically represent changes in hematopoietic cell lineages (erythroid or myeloid), megakaryocytes and/or stromal cells. Lesions in the lymphoid lineage are less commonly observed because definitive identification of lymphoid cells is difficult, except in cases of lymphoma. IHC stains for B and T cells may be necessary for a more complete evaluation of marrow lesions involving the lymphoid lineage. Noteworthy changes in hematopoietic cells including lymphoid cells can be identified in Romanowsky-stained (e.g., Wright or Wright-Giemsa) bone marrow aspirates and cytological smears. Relative increases or decreases in hematopoietic cells may be identified by estimating the percentages of the marrow cavity containing fat versus hematopoietic cells and comparing these percentages to those seen in concurrent control animals. Cell numbers and maturation sequence may also be estimated as the M:E ratio and the presence/predominance of immature cell types. However, histology should still be considered a screening tool, and cytologic evaluation would be needed for a complete evaluation of lineage-specific changes.

Assessment of the potential for recovery may also be important in the histologic assessment

of the bone marrow, especially for some nonclinical toxicity studies. In most cases, bone marrow is considered to have a high likelihood of recovery as the hematopoietic tissue is labile and quite responsive to pro-hematopoietic stimuli under usual conditions. Even in situations where tissue injury has included fibrosis, recovery has often been observed (Lotiun et al., 2005; Perry et al., 2013).

4.1.2. Cytology

Bone marrow cytology should be performed when there is an inappropriate or unexplained change in bone marrow cellularity (by histopathology) or an inappropriate or unexplained change in peripheral blood count or morphology (Bolliger, 2004; Reagan et al., 2011). Cytology is particularly useful to assess lineage proportions, maturation synchrony, and completeness and morphologic changes within individual cells. Examples of situations in which cytologic evaluation of bone marrow may be indicated are listed in Table 5.7.

Evaluation of bone marrow cytology is not indicated in many cases. It rarely adds useful information when there is an appropriate bone marrow response to peripheral demand, such as an appropriate increase in peripheral blood cell count, reticulocytes, and/or bone marrow cellularity. Changes that can be explained also do not warrant cytologic evaluation (e.g., bone marrow suppression due to substantial decreases in food consumption or exposure to substances with known antiproliferative or cytotoxic effects). Bone marrow cytology is not useful to investigate dysfunction of granulocytes or platelets and is rarely useful in cases of lymphocyte count decreases. Cytology cannot be used to assess marrow architecture (e.g., myelofibrosis) or cellularity since tissue features are lost in smears.

In toxicity studies, bone marrow smears may be collected at necropsy and stored for future evaluation as needed on a case-by-case basis. Bone marrow smears should be prepared in a manner that optimizes hematopoietic cellularity and cell preservation and minimizes blood contamination (Reagan et al., 2011). Smears should have sufficient numbers of cells spread into a flattened monolayer to allow for discrimination of fine structural details in individual

TABLE 5.7 Examples of Situations in Which Cytologic Evaluation of Bone Marrow May Be Indicated

Unexplained Peripheral Cytopenias (Blood Samples)
Nonregenerative Anemia Not due to Decreased Food Consumption
Reticulocytopenia during Anemia
Neutropenia without Inflammation
Thrombocytopenia without Coagulopathy
Bicytopenia or Pancytopenia
Presence of atypical cells in circulation (blood samples)
Nucleated red blood cells without regenerative anemia
Immature circulating cells of unknown origin or cause, or requiring classification among leukemias, confirmation of bone marrow origin or differentiation from other neoplasias including histiocytic neoplasia and multiple myeloma
Dysplastic erythrocytes, leukocytes, or platelets suggestive of abnormal maturation (e.g., megaloblasts, hypersegmentation or hyposegmentation)
Marked, persistent and unexplained increases in erythrocyte, leukocyte, or platelet number (blood samples)
Altered hematopoietic lineage maturation or morphology observed histologically

cells as well as quantification of sufficient cells (usually between 200 and 500) to ensure that the sample is representative of the bone marrow. Acceptable techniques for cytologic evaluation of marrow include pull or push smears, paintbrush smears, and cytocentrifuge preparations. Specimens may be mixed with albumin/serum to optimize cellular preservation and should be prepared in an area prepared to avoid exposure to formalin fumes (which alter cell staining properties). Slides should be air-dried for several hours or overnight to avoid structural artifacts caused by moisture retention (Reagan et al., 2011).

Cytologic bone marrow examination should follow a tiered approach based on peripheral blood and histologic findings. An initial qualitative assessment confirms the presence or absence of abnormalities and determines the nature of those abnormalities. Normal hematopoietic



constituents (megakaryocytes, myeloid and erythroid lineages, and lymphoid cells) are examined for abnormalities in morphology and maturation. The M:E ratio and megakaryocyte numbers can be visually approximated. In some cases, the qualitative assessment is sufficient to explain peripheral or histologic findings. A qualitative assessment is also ideal when morphologic changes preclude definitive cell classification.

Cytologic findings of altered lineage proportions or maturation sequence may require further characterization by differential counting of hematopoietic subtypes (e.g., myeloid vs. erythroid, proliferating vs. maturing) or specific precursors (Figure 5.2). Megakaryocytes are not included in differential counts but are evaluated for appropriate maturation. Manual differential counts performed on bone marrow cytologic preparations should be interpreted with caution since they have wide normal ranges and are highly dependent on sampling technique, sampling site, species, cellularity, and specimen quality. In addition, in some species (e.g., rats and mice) regenerative responses are more robust in the spleen than in the bone marrow (Schubert et al., 2008; Suttie, 2006). Stem cells, progenitor cells, and small lymphocytes, normally present in high proportions in rodents, are indistinguishable cytomorphologically though they may be included in differential counts, particularly if they have an atypical appearance. Other components of bone marrow that may be evaluated cytomorphologically include iron stores; approximation of relative megakaryocyte cellularity; relative hematopoietic cellularity associated with bone spicules; increased macrophages, mast cells or plasma cells; atypical hematopoietic and nonhematopoietic cells; and infectious agents.

#### **4.1.3. Quantitative Bone Marrow Assessment**

The biggest limitation to differential counting of cytologic specimens is that relatively few cells are counted, usually between 200 and 500. Assessments by flow cytometry or automated hematology analysis (e.g., Sysmex XT2000iV) represent potential alternatives when accurate quantitative data on major hematopoietic lineages is required (myeloid vs. erythroid; mitotic

vs. postmitotic) (Kozlowski et al., 2018b; Kurata et al., 2007). Large numbers of cells (10,000–35,000) can be rapidly counted and classified, thus improving accuracy and reproducibility. In mice and rats, the near entirety of a long bone's marrow can be harvested to provide absolute cell counts.

Bone marrow specimens destined for flow cytometry may be collected by fine needle aspiration or core biopsy for survival procedures in rabbits, dogs and larger animals, or at necropsy for rodents and larger animals. Collection and processing protocols vary with the study purpose and analytical method but generally involve suspension of cells in isotonic ethylenediaminetetraacetic acid (EDTA) or phosphate-buffered saline (PBS) containing a suitable fixative for the marker and cell type (formaldehyde, TransFix, Cyto-Chex, and serum-containing media) (Sedek et al., 2020), and either bovine serum albumin (BSA) or fetal bovine serum (FBS). In contrast to cytologic specimens, which persist for decades once air-dried, flow cytometry cell suspensions must be analyzed within 24–48 hours to retain viability and antigen expression.

In nonclinical safety assessment, flow cytometry is generally limited to quantification of myeloid, erythroid, and lymphoid cells, and proliferating versus mature cells. It cannot be used to obtain a complete differential count and thus cannot replace cytologic assessment. Because flow cytometry cannot assess cytomorphology or provide a full differential count (which includes specific precursors), concurrent cytopspin preparations of cell suspensions should always be prepared in case cell morphology needs to be evaluated. Due to lack of relevant reagents and antibodies for animal species and variability in methods, platforms, and investigative goals, flow cytometry is not widely implemented as a standard screening tool in routine toxicologic investigations. However, it represents a viable investigative approach for discovery toxicology. Note that flow cytometry can also be applied to other hemolymphatic tissues including peripheral blood as well as dissociated lymphoid organs (e.g., lymph node, spleen). A common use for flow cytometry is to assess *in vivo* genotoxicity/clastogenicity using a modified flow cytometric micronucleus assay (Criswell et al., 2003).

Platelet, granulocyte, and macrophage function and activation can also be evaluated using flow cytometry. Additional applications of flow cytometry to hematotoxicity testing include detection of chromosomes and other subcellular particles such as microspheres as well as isolation and enrichment of cell subpopulations for in vitro applications. In the research and clinical setting, flow cytometry has been employed to obtain detailed characterization of cell populations using forward/side-angle light-scatter properties and fluorochrome or antibody labeling.

Cells can be distinguished and characterized according to a multitude of criteria. Key features include cell size, nuclear complexity, DNA and RNA content, myeloperoxidase staining, and surface marker expression. Megakaryocyte maturation can be evaluated using ploidy and expression of specific membrane proteins (e.g., vWF). DNA content can serve as an indicator of proliferative activity. Flow cytometry has also been used to characterize myelodysplasia and clonal disorders in humans and dogs. It can identify aberrant expression of antigens, altered granularity of maturing myeloid cells, asynchronous expression of maturation-associated markers, inappropriate expression of lymphoid-related antigens, and either lack or decreased reactivity for myeloid-associated antigens that may be associated with myelodysplastic diseases.

The validation of the Sysmex XT2000iV hematology analyzer to produce bone marrow differential counts in Wistar rats, CD-1 mice, beagle dogs, and cynomolgus monkeys has recently been described (Criswell et al., 2014a, b). This automated approach utilizes a bone marrow cell suspension and applies a two-step process of magnetic cell-sorting (MACS) of lymphocytes followed by application of customized gating to produce a 5-part bone marrow differential count (proliferating and maturing counts for myeloid and erythroid cells as well as a lymphocyte cell count) comparable to those provided by cytologic evaluation of bone marrow smears. Like flow cytometry, this technique must be used in combination with a cytologic evaluation of a cytopspin preparation to evaluate for the presence of megakaryocytes and evaluate cell morphology (Criswell et al., 2018, 2014a, b; Pernecker et al., 2017).

## 4.2. Evaluation of Peripheral Blood

### 4.2.1. Routine Hematology

The basic components of standard hematology evaluation include numerical data from an automated analyzer and microscopic examination of peripheral blood films. The broad principles underlying cell counting by hematology analyzers include impedance-based techniques (e.g., Abbott CELL-DYN 3500, Heska Element HT-5) and flow cytometry-based methods (e.g., Siemens Advia 120/2120, Sysmex XT or XN-V series). In an impedance-based cell counter, when a cell passes through an aperture between two electrodes, it changes the impedance (electrical resistance and reactance) of the flowing sample. This change in impedance is proportional to cell volume, resulting in both a cell count and a measure of volume. This component of the analyzer provides total cell counts for WBCs (all principal classes), RBCs, and platelets. However, discrimination of leukocyte subtypes is limited with this method. In flow cytometry-based methods, when a cell passes through a laser beam in a fluidic compartment, the absorbance and scatter of light are measured at multiple angles to determine the cell's volume (forward scatter), internal complexity including granularity (side scatter) with or without additional staining by fluorescent reagents, which helps distinguish various leukocyte subtypes as well as reticulocytes and reticulated platelets (see [Section 4.2.2 Emerging/Advanced Technologies and Biomarkers](#)). Standard lists of parameters obtained from common hematology analyzers are presented in Tier 1 of [Table 5.6](#).

The two major hematology analyzers used in the nonclinical setting are the Siemens Advia (Advia 120 or Advia 2120i) and Sysmex (XT or XN-V series) systems ([Table 5.8](#)). These analyzers use a combination of methods that are predominantly flow cytometry-based. The Advia analyzer determines total WBC counts, differential WBC counts (neutrophils, lymphocytes, monocytes, eosinophils, basophils, and large unstained cells [LUCs; large cells with low or no peroxidase activity typically considered to be monocytes, immature/reactive lymphocytes, or atypical/neoplastic cells]), RBC parameters including reticulocytes, and platelets (Harris et al., 2005). The Advia components include (1)

a peroxidase channel, where leukocytes are classified based on their peroxidase activity and size (eosinophils, neutrophils, monocytes, lymphocytes, and LUC); (2) a basophil channel, where erythrocytes and leukocytes are lysed and nucleated cells are classified based on their nuclear density/lobularity; and (3) an RBC channel that uses a special diluent which renders erythrocytes as isovolumetric spheres that can be classified based on their size and refractive index upon passing through a laser beam. Oxazine 750, a nucleic acid dye, is used with the Advia system to differentiate reticulocytes from mature RBCs. In contrast, Sysmex analyzers combine a similar ensemble of cell-specific lyses with fluorescent dyes and flow cytometry (Grebert et al., 2021). The Sysmex components include (1) the WNR (WBC and nucleated RBC) channel where fluorescent flow cytometry using polymethine dye differentiates nucleated RBCs from WBCs and enumerates both; (2) the WDF (white cell differential by fluorescence) channel where fluorescent flow cytometry and shape recognition algorithms provide a WBC differential count (neutrophils, lymphocytes, monocytes and eosinophils); (3) the platelet-F channel that provides a platelet count and immature platelet fraction (IPF); and (4) the reticulocyte channel that assesses the reticulocyte count, immature reticulocyte fraction, and reticulocyte hemoglobin.

Automated hematology analyzers generate reproducible data, providing leukocyte differentials based on evaluating approximately 10,000–20,000 cells per sample that are highly accurate. Despite this degree of sophisticated analysis, there have been case studies detailing erroneous results from automated hematology analyzers. Jordan et al. (2014) describe a wide variety of analyzer artifacts, including erroneous platelet counts due to microcytic hypochromic RBCs and RBC fragments in a nonclinical safety study in cynomolgus monkeys, atypical RBC cytoforms in Wistar Han rats due to glutaraldehyde reagent-induced RBC agglutination, and inaccurate neutrophil counts in a myeloperoxidase knockout mouse model. Pseudoreticulocytosis caused by high RBC burden of *Plasmodium* spp. has been reported in cynomolgus monkeys (Sharma et al., 2022). Notably, basophils are not accurately detected in most nonclinical species using automated hematology analyzers (Lilliehook and Tvedten, 2011).

In addition to quantitative data from an automated hematology analyzer, microscopic examination of a stained blood film is an essential component of hematology analysis. Typical steps in nonclinical toxicity studies include preparation of a blood film in which cells are evenly distributed, staining the air-dried blood film using a Romanowsky-type stain (Wright or Wright-Giemsa), and retention of the slides for possible later examination under a microscope. At low magnification (4× or 10× objectives), blood films should be scanned for leukocyte aggregates, erythrocyte agglutination, platelet clumps, or any large/abnormal cells starting at the feathered edge and moving toward the body of the blood film. Additionally, blood films should be assessed for erythrocyte and leukocyte densities. A manual differential leukocyte count is performed by evaluating 100–200 consecutive leukocytes using a 40× or 50× objective. Morphologic evaluation of erythrocytes (abnormal shapes, sizes, color, inclusions); leukocytes (e.g., toxic change in neutrophils, hypersegmented neutrophils, reactive lymphocytes, inclusions); and platelets (e.g., large or hypogranular platelets as well as assessment of platelet density) is performed using a 100× objective.

The approach to interpreting changes in hematology parameters is detailed in Section 5 Responses to Injury. For the evaluation and interpretation of hematology and hemostasis in nonclinical toxicity studies, the reader is referred to *Interpretation of Clinical Pathology Results in Nonclinical Toxicity Testing*, Vol 2, Chap 14 and to *Clinical Pathology in Nonclinical Toxicity Testing*, Vol 1, Chap 10.

#### 4.2.2. Emerging/Advanced Technologies and Biomarkers

**Reticulated platelets:** Newly released, younger platelets (referred to as “reticulated platelets” [RPs]) have higher cytoplasmic RNA content and are analogous to reticulocytes. Increased numbers of RPs in circulation have been suggested as a sensitive and early indication of increased thrombopoiesis (Ault et al., 1992). The principle of detecting RP is based on labeling platelet RNA with nucleic acid-staining dyes and subsequently distinguishing RP that have taken up the dye (in contrast to mature platelets, which do not). The two broad approaches to enumerate RP include traditional flow cytometry and automated methods using



**TABLE 5.8** Nonstandard or “Research Use Only” Parameters Reported by Automated Hematology Analyzers

	Description	References
<i>SIEMENS ADVIA (120/2120I)</i>		
Mean platelet component (MPC)	Measure of platelet internal complexity (refractive index), which decreases with platelet activation or swelling	Boos et al. (2007); Vagdatli et al. (2010)
Plateletcrit (PCT)	Percentage of blood volume occupied by platelets, reflecting circulating platelet mass	Budak et al. (2016)
Platelet volume distribution width (PDW)	Reflects range of platelet size variability, which increases with accelerated production or platelet activation	Vagdatli et al. (2010); Wang et al. (2017)
Platelet component concentration distribution width (PCDW)	Measure of variability of platelet internal complexity (refractive index)	Boos et al. (2007); Kim et al. (2008)
Mean platelet (dry) mass (MPM)	Calculated based on mean platelet volume and mean platelet component (MPC); increases with platelet activation	Boos et al. (2007); Phillips et al. (2022)
Platelet dry mass distribution width (PMDW)	Measure of variability in platelet dry mass; increases with platelet activation	Kim et al. (2008)
Mean cell volume of all gated red cells (MCVg)	Mean cell volume of the combined population of mature RBC and reticulocytes	Harris et al. (2005)
Mean cell volume of reticulocytes (MCVr)	Mean cell volume of the reticulocyte population; may decrease with iron deficiency or increase with certain types of anemia	Butthep et al. (2000); Brugnara (2000); Fry and Kirk (2006)
Red cell distribution width of all gated RBC (RDWg)	Indicator of the range of RBC volumes or volume variability within the combined population of mature RBC and reticulocytes	Siemens (2016)
Red cell distribution width of reticulocytes (RDWr)	Indicator of the range of volumes or volume variability within the reticulocyte population; may be affected by anemias	Brugnara (2000); Oustamanolakis et al. (2011)
Hemoglobin concentration mean of all gated red cells (CHCMg)	Mean hemoglobin concentration of the combined population of mature RBC and reticulocytes	Harris et al. (2005)
Hemoglobin concentration mean of reticulocytes (CHCMr)	Mean hemoglobin concentration of reticulocytes; may decrease with increased erythropoiesis or iron deficiency	Brugnara (2000); Ceylan et al. (2007)
Immature reticulocyte fraction-high absorption reticulocytes (IRF-H)	Percentage of reticulocytes that are the most immature based on RNA concentration measured by fluorescence; reflects erythropoietic activity	Brugnara (2000); Jung et al. (2023)
Myeloperoxidase intracellular index (MPXI)	Mean neutrophil myeloperoxidase staining intensity; may decrease with inflammation	Celliers et al. (2020); Chu and Stokol (2021)

(Continued)

**TABLE 5.8** Nonstandard or “Research Use Only” Parameters Reported by Automated Hematology Analyzers—cont’d

	Description	References
<i>SYSMEX (XT/XN SERIES)</i>		
Impedance, optical and fluorescence platelet counts (PLT-I, PLT-O, PLT-F)	Alternative platelet counting methods based on impedance (PLT-I), laser light flow cytometry (PLT-O) and fluorescence flow cytometry (PLT-F). PLT-O and PLT-F may be less susceptible to interferences and more accurate for lower counts compared with PLT-I.	Schoorl et al. (2013); Tantanate et al. (2017); Wada et al. (2015)
Plateletcrit (PCT)	Percentage of blood volume occupied by platelets; reflects circulating platelet mass	Ali et al. (2019)
Platelet volume distribution width (PDW)	Reflects range of platelet sizes or variability, which increases with platelet activation or increased production	Ali et al. (2019)
Platelet large cell ratio (P-LCR)	Percentage of platelets >12 fL; increases may be indicative of immature platelets, platelet activation or disorders	Ali et al. (2019); Hong et al. (2014); Kaito et al. (2005)
Immature platelet fraction (IPF)	Percentage of immature platelets; increases may reflect thrombopoiesis or thrombopoietic disorders, while decreases may indicate bone marrow suppression	Hong et al. (2014)
Immature reticulocyte fraction (IRF)	Percentage of immature reticulocytes to total number of reticulocytes; indicator of ongoing/recent erythropoiesis	Chang and Kass (1997); Schapkaitz (2018)
Reticulocyte hemoglobin equivalent (RET-He)	Hemoglobin content of reticulocytes, used to monitor changes in hemoglobin and iron status	Auerbach et al. (2021); Brugnara et al. (2006); Toki et al. (2017)
Mature red blood cell (RBC) hemoglobin equivalent (RBC-He)	Hemoglobin content of mature RBC, used to monitor changes in hemoglobin and iron status	Brugnara et al. (2006)
Nucleated red blood cell count (NRBC)	Number of nucleated RBC in peripheral blood	Buoro et al. (2015); Hwang et al. (2016)

hematology analyzers. In the traditional flow cytometry methods, platelets are labeled with thiazole orange or similar nucleic acid dyes and “positive” platelets are identified either based on forward/side scatter-based gating on platelets or by including a platelet-identifying antibody (e.g., anti-CD41 or anti-CD61) to discriminate platelets from noise and other cells (Smith and Thomas, 2002). Sysmex hematology analyzers (e.g., XE series in human, XN-1000V for nonclinical species) have developed an automated method to quantify RP, expressed as IPF. In this method, IPF is identified by the use of nucleic acid dyes such as polymethine and oxazine (Briggs et al., 2004) in the reticulocyte/optical platelet channel or in a dedicated platelet

channel using optical fluorescence. Both RP and IPF are expressed as a proportion of total platelets, and both values are supposed to reflect the rate of platelet production. RP evaluation has been described in a number of nonclinical species including dogs (Smith and Thomas, 2002; Wilkerson et al., 2001), rats (Pankraz et al., 2008), mice (Robinson et al., 2000), and nonhuman primates (Sirivelu, 2018). IPF has been investigated in mice (Davenport et al., 2021). Although there is much variation in reference ranges among laboratories and among methods employed for these parameters, there is value in assessing RP or IPF as a marker of thrombopoiesis. An increase in RP or IPF in animals with thrombocytopenia shows that the

underlying mechanism is likely not a failure in bone marrow production of platelets but rather an alternate mechanism like increased platelet destruction/consumption in peripheral tissues.

*Platelet function testing:* There are several testing methods to assess platelet function including aggregometry, flow cytometry-based platelet activation, and use of benchtop analyzers such as platelet function analyzers (PFAs). It is particularly important to consider preanalytical variables (e.g., anticoagulant used, needle size, sample tubes, time to analysis, temperature of storage, transport, method of blood collection) before performing any tests of platelet function. Platelets are a challenging cell type to handle; hence, care must be taken to minimize the effect of preanalytical variables so that the results of functional testing can be interpreted accurately. Detailed descriptions of the methods and their merits are beyond the scope of this chapter, so interested readers may refer to other publications on this subject (Hvas and Grove, 2017; Paniccia et al., 2015).

Platelet aggregometry is performed either on platelet-rich plasma (PRP; obtained by centrifugation of anticoagulated whole blood at low g-force) or whole blood. Using PRP, light transmission aggregometry (LTA) is considered to be the gold standard of platelet function testing. Briefly, platelet aggregation is measured by the analysis of light transmission through a sample of PRP: at baseline, PRP significantly reduces light transmission owing to its turbid nature. Upon addition of a platelet agonist, formation of aggregates reduces the turbidity of the suspension, resulting in increased light transmission. The results are expressed as % of light transmitted (Hvas and Favaloro, 2017; Koltai et al., 2017). Whole blood aggregometry (WBA) is helpful in studying platelet function in anticoagulated whole blood without any additional sample processing. This test measures change in resistance or impedance between two electrodes as platelets form aggregates onto the electrodes in response to platelet agonists. The tracings from a typical WBA plot include resistance (ohms) on the Y-axis and time (minutes) on the X-axis (Fritsma and McGlasson, 2017; McGlasson and Fritsma, 2009).

*Flow cytometry-based testing:* Several functional endpoints such as platelet surface activation markers, platelet-leukocyte aggregates (Finsterbusch et al., 2018), platelet-derived extracellular vesicles (Nolan and Jones, 2017), etc., can be assessed using flow cytometry. A typical

workflow includes the following steps (Michelson, 2009; van Velzen et al., 2012): diluting anticoagulated whole blood, labeling platelets and/or leukocytes with appropriate antibodies under nonstimulating and stimulating conditions (e.g., ADP, thrombin, collagen as platelet agonists), and subsequent fixation and dilution of samples. The samples are then analyzed by flow cytometry using a well-defined gating strategy. Antibody panels include platelet identifiers (anti-CD41 or anti-CD61); platelet activation markers (e.g., P-selectin [CD62P], CD40L); and leukocyte markers (e.g., CD14, CD16, CD42a). The results are expressed as % positive events and/or median fluorescence intensity (MFI). Xenobiotic-induced effects on neutrophil function are rare, and neutrophil function testing is rarely performed in a nonclinical setting.

*Neutrophil function testing:* In vitro testing for neutrophil activity is an upper-tier test to assess a principal element of the innate immune system. Common assays include impaired integrin or selectin adhesion (CD11/CD18), impaired chemotaxis or phagocytosis, impaired bacterial killing effect or defects in respiratory burst (Dinauer, 2014; Haynes and Fletcher, 1990).

*Automated image analysis:* Automated image analysis approaches for quantifying bone marrow cellularity on H&E-stained slides have recently been described (Kozłowski et al., 2018a, b; Smith et al., 2021). Slides are scanned with a whole slide scanner, and then software algorithms developed specifically for this purpose are applied to the scanned images. In many situations, the automated methods have been able to detect changes in cellularity to a level consistent with manual scoring performed by an experienced pathologist. Other quantitative assessments, such as the M:E ratio, M:E to lymphoid ratio (helpful for discerning between mononuclear hematopoietic populations and lymphoid populations within the marrow), and megakaryocyte density, have also been included in some cases. Although this technology is still emerging, the application of automation and use of conventionally prepared tissue sections mounted on slides (as opposed to reliance on specialized sample collection, as is required for quantitative bone marrow assessment by flow cytometry or Sysmex XT, 2000iV) is intriguing. Early results suggest that this approach will be useful as a screening tool for some hematopoietic cellularity assessments and to support the development of more advanced marrow quantification applications in the future.



### 4.3. In Vitro Techniques

Several *ex vivo* and *in vitro* methods can be used to evaluate the hematotoxicity of drugs, chemicals, and other agents. The main limitation of *in vitro* methods is that they are not always predictive of *in vivo* outcomes (see *Alternative Models in Biomedical Research: In Silico, In Vitro, Ex Vivo, and Non-Traditional In Vivo Approaches*, Vol 1, Chap 24). While conditions in the living body cannot be completely reproduced *in vitro*, the appeal of these applications is their potential to significantly reduce and refine animal use in toxicity testing by providing cell-based data for translation of results between species and test articles as well as for dose setting and predicting the maximum tolerated dose (MTD). *In vitro* assays are also useful to investigate mechanisms of hematotoxicity and to screen agents in early discovery toxicology. The acquisition of chromosomal aberrations (additions, deletions, or rearrangements) can be evaluated by cytogenetic analysis to investigate genotoxicity, clastogenesis, myelodysplasia, and leukemogenesis.

Clonogenic assays evaluate the ability of stem and progenitor cells to proliferate and differentiate into colonies (colony-forming units [CFUs]) in selective media (containing appropriate cell type-specific cytokines and growth factors) when exposed to potential toxicants (Pessina et al., 2005). *In vitro* CFU assays currently used for hematotoxicity testing include CFU-MK (megakaryocyte), CFU-GM (granulocyte-macrophage), and BFU-E/CFU-E (erythrocyte) (Goto et al., 2017). These assays have the advantage that they can be performed on cryopreserved bone marrow cells. However, there are disadvantages to these assays: primary human cells are limited in quantity and suffer from batch-to-batch variation, cells of different species may differ in their sensitivities, and immortalized cells do not adequately predict hematotoxicity of nonneoplastic cells. In addition, colony-forming assays are time-consuming to perform and rely on the subjective and technically demanding manual enumeration of colonies.

Automated nonclonogenic fluorometric microculture cytotoxicity assays (FMCAs) are promising approaches for more reproducible, high-throughput bone marrow assessment. FMCAs use 384-well microplate formats, fluorescein labeling, and flow cytometric detection to provide high-throughput hematotoxicity screening (Haglund et al., 2010). Quantification of intracellular ATP concentration, which varies

proportionately with the rate of cell proliferation, has been described as a high-throughput approach, with limited implementation to date (Haglund et al., 2013). Although it is becoming increasingly evident that injury to MSCs may result in hematotoxicity, *in vitro* assays evaluating these cells are currently not well developed.

An important limitation of conventional clonogenic assays is the inability to detect hematotoxicity that arises as a consequence of effects that influence hematopoiesis of specific cell types, such as those of the hematopoietic niche. Coculture of hematopoietic progenitors with bone marrow stromal cells such as fibroblasts, adipocytes, endothelial cells, and macrophages allows for long-term bone marrow culture (up to several months) (Jing et al., 2010). Coculture with stromal or “feeder” cells is used to enhance hematopoietic cell growth and to investigate hematopoietic-mesenchymal interactions involved in hematopoiesis. Many fresh primary target cells from bone marrow (hematopoietic or mesenchymal) are now available commercially. More recently, microphysiological systems (MPSs) have been developed to replicate the hematopoietic microenvironment with greater fidelity. These *in vitro* organ models make use of three-dimensional culturing techniques, specific extracellular matrix components or scaffolds, and microfluidic perfusion to successfully screen for hematotoxic drugs (Dehne et al., 2019).

### 4.4. Animal Models

Animal models of hematotoxicity have historically relied on naturally occurring susceptibilities in specific species or strains and breeds, or exposure to classic hematotoxicants, where the pathogenesis and course of injury were determined to be similar to a human condition (Chen, 2005). Examples include busulfan-induced chronic latent aplasia in CBA, C3H, or BALB/c mice. In contrast, administration of chloramphenicol to C3H/He and BALB/c mice, Wistar Hanover rats, and guinea pigs induces reversible anemia but fails to produce irreversible aplastic anemia and leukemia as seen in humans (Chen, 2005).

Immune-mediated bone marrow failure can be modeled in mice by transplanting lymphocytes from 1 mouse strain into the bone marrow of a different strain (Neschadim and Branch, 2016; Risitano, 2005). This transfer results in destruction of normal host cells with oligoclonal expansion of

donor T cells in recipient bone marrow and restriction of T cell receptor  $\beta$  variable region expression. In vivo clonogenic assays measure the capacity of transplanted hematopoietic cells to form large splenic foci of hematopoiesis (i.e., spleen colony-forming assay) in lethally irradiated mice.

A number of specialized animal models exist for the investigation of drug-induced bone marrow toxicity. IL-21-induced anemia has been investigated in monkeys (Overgaard et al., 2007). Using a nonlinear mixed-effects model that separates drug effects from phlebotomy and stress effects, investigators proposed that IL-21-associated anemia was a consequence of erythrocyte removal rather than decreased bone marrow production. A modified regimen of busulfan in a model of aplastic anemia in CD-1 or BALB/c mice produced chronic bone marrow hypoplasia and increased serum concentrations of FLT3 ligand (Molyneux, 2008). Studies of cephalosporin-induced blood dyscrasias in beagle dogs have demonstrated that antibody-mediated blood cell destruction contributes to pancytopenia (Bloom et al., 1988). Accelerated hematopoiesis in gene null mutant ("knock-out") mice has been used to investigate the effects of drugs that do not alter basal hematopoiesis (Wolf, 2013).

Humanized mice (i.e., engineered to express human genes or harbor engrafted human cells; see *Genetically Engineered Animal Models in Toxicologic Research*, Vol 1, Chap 23) have shown promise as models for drug-induced hematotoxicity. In one model, temozolomide treatment in NSG mice (formal designation: NOD.Cg-Prkd<sup>scid</sup> Il2rg<sup>tm1Wjl</sup>/SzJ) whose bone marrow has been reconstituted with human CD34<sup>+</sup> cells produced loss of human-derived bone marrow hematopoietic cells (Cai et al., 2011). In a model of drug-induced immune thrombocytopenia, clearance of platelets in NOD/scid mice (formal designation: NOD.Cg-Prkd<sup>scid</sup>/J) infused with human platelets was shown to be mediated by drug-dependent antiplatelet antibodies (Bougie et al., 2010; Liang et al., 2010).

A wide variety of mutant mice exist, including hypotransferrinemic mice, EPO-deficient mice, thalassemic mice, hemojuvelin and hepcidin knock-out mice (Chattopadhyay et al., 2015; Molyneux, 2008). Myeloproliferative neoplasia has been investigated in mice with a single nucleotide polymorphism in the JAK2 kinase (KAJ2V617F). Transgenic and targeted knock-in mice expressing mutated mouse or human genes

have facilitated the investigation of the molecular pathogenesis of hematopoietic disease.

Hematopoiesis and drug-induced hematotoxicity can also be studied in zebrafish (*Danio rerio*) (Martin et al., 2011). Zebrafish embryos are amenable to high-throughput screening since they can be housed in 96-well plates. In addition, they are permeable to water-soluble chemicals and easy to manipulate genetically. However, in contrast to in vitro colony-forming assays, zebrafish better replicate mammalian hematopoietic microenvironment and circulatory system. Zebrafish have kidney marrows, which are functionally equivalent to the bone marrow niche of mammals (Kapp et al., 2018; Phillips et al., 1999). As such, they can better predict drug toxicity and off-target effects. They can also be used to screen for new regulators of hematopoiesis and to investigate developmental hematopoiesis.

## 5. RESPONSES TO INJURY

This section describes basic principles for interpreting xenobiotic/drug-induced hematologic and hematopoietic alterations. Relevant information on pathophysiology that should be taken into consideration when interpreting changes includes normal hematopoiesis, mechanisms of hematotoxicity, functional hematopoietic responses, and the relationship of blood and blood-forming tissues to other organ systems. Such considerations are particularly important when investigating drugs that target cellular pathways related to hematopoiesis. Interpretation also requires consideration for potential sources of preanalytical variability, analytical imprecision, and postanalytical errors.

### 5.1. Changes in Peripheral Blood

Confirmation of normal (physiologic) hematologic function requires ensuring that the bone marrow is appropriately responding to a systemic insult. Examples include reticulocytosis in response to anemia (i.e., "regenerative" anemia), leukocytosis and a left shift (i.e., increased ratio of nonsegmented [immature] to segmented neutrophils in the blood) in response to tissue inflammation, thrombocytosis in response to blood loss, and polycythemia (i.e., increased RBC numbers in the blood) in response to tissue hypoxia. For example, after an acute peripheral loss of erythrocytes (i.e., hemorrhage), it takes approximately 3–5 days to

see increased circulating reticulocytes arising from enhanced bone marrow production. An inappropriate bone marrow response to a change in peripheral blood cell counts may indicate toxicity to, dysfunction of, or some other primary abnormality affecting the hematopoietic system (e.g., pancytopenia due to irradiation-induced depletion of HSCs in bone marrow). When evaluating bone marrow responses, it is essential to bear in mind the rate of injury, cellular lifespan, and kinetics of bone marrow production for the species in question and to confirm that sufficient time has elapsed to observe the appropriate response (Table 5.9).

Cellular changes in blood can be classified as being due to redistribution/sequestration, altered destruction/loss/consumption, or altered production. The bone marrow generally does not respond to small-magnitude changes in circulating blood cells or transient changes due to redistribution or sequestration. Destruction, consumption, or loss of circulating cells should elicit cell proliferation as a physiologic bone marrow response, reflecting normal hematopoietic function. Decreased production resulting in cytopenia (e.g., “non-regenerative” anemia) indicates abnormal hematopoietic function. Myeloproliferative disorders such as myelodysplastic syndromes and leukemias are due to dysregulated blood cell production. Myelodysplastic neoplasms are uncommon consequences of hematotoxicity in nonclinical studies but have been reported in animals and humans as clinical conditions resulting from toxicant exposure.

The number and variety of bone marrow responses are numerous. The literature in humans, and to a lesser degree experimentally in rodents and other laboratory animal species, is vast. Clinically, however, the number of hematotoxic agents clearly associated with bone marrow suppression is much smaller. Some specific responses are discussed below and presented in Table 5.10 (Ramaiah et al., 2013).

#### **5.1.1. Redistribution, Sequestration and Demargination/Margination**

In nonclinical species, circulating counts of RBCs, reticulocytes, and platelets may transiently increase secondary to splenic contraction associated with a physiological stimulus (e.g., exercise, stress in dogs and monkeys, physical restraint in rodents). Redistribution of platelets into tissue vasculature (mostly the red pulp of the spleen, less commonly small vessels in the liver and rarely

lung) leads to a transient decrease in circulating platelet counts. Since this does not decrease total platelet mass, thrombopoiesis is not stimulated. Marked, acute, reversible thrombocytopenia with no increase in TPO was due to sequestration of platelets in the liver following liver-specific endothelial injury (characterized by loss of sinusoidal endothelial cells and marked platelet accumulation in sinusoids) (Guffroy et al., 2017). Antisense oligonucleotides have also been associated with moderate thrombocytopenia due to splenic and liver sequestration of platelets, with no effect on platelet growth factors (Narayanan et al., 2018). In dogs, transient sequestration of erythrocytes in the splenic vasculature leading to moderate splenomegaly (organ enlargement) occurs with barbiturates (Hahn et al., 1943).

Neutrophil increases in the blood occur under some conditions due to **demargination** (i.e., redistribution of neutrophils from the marginated neutrophil pool [temporarily adhered to endothelial cells] to the circulating neutrophil pool [free flowing in blood and thus collected in blood samples]). Physiological changes leading to demargination include stress (due to glucocorticoid release) and excitement (due to epinephrine [also called adrenaline] release). A number of xenobiotics (e.g., ethanol, colchicine, and adrenergic agonists) alter granulocyte adherence to vascular endothelium and are known to markedly alter the equilibrium between the circulating and marginated compartments of the leukocyte pool. In contrast to inflammation, demargination typically does not cause marked leukocytosis or a left shift. Histamine, iron oxide, and dextran produce an apparent granulocytopenia by increasing the size of the marginated pool. Lymphocytes continuously recirculate between blood, lymph nodes, and secondary lymphoid organs. Detailed descriptions of this phenomenon are beyond the scope of this chapter but may be found elsewhere (Bimczok and Rothkötter, 2006). Lymphocyte recirculation kinetics depend on the type of lymphocyte (T cell or B cell), its functional role (naïve, memory or effector), and cytokine signals.

#### **5.1.2. Hemolytic Anemia**

Acquired hemolytic anemia is among the most frequently reported drug reactions in humans, though it is usually of minor severity. Decreased lifespan of circulating erythrocytes defines hemolytic anemias. This type of anemia can



**TABLE 5.9** Reported Species-Specific Cellular Lifespans and Kinetics of Response to Injury in Bone Marrow and Blood

Cell	Species	Cell Lifespan in Circulation (Days Unless Otherwise Noted)	Acute Injury to/Loss of Bone Marrow Hematopoietic Cells <sup>a</sup>		Acute Injury to/Loss of Circulating Cells
			<i>Time to peripheral cell decreases (days unless otherwise noted)</i>	<i>Time to peripheral cell recovery (onset or more extensive recovery) (days unless otherwise noted)</i>	<i>Time to onset of regenerative response (days)<sup>b</sup></i>
Platelet	Mouse	4 (Odell and Mc, 1961)	6–10 (McElroy et al., 2015; Thomas et al., 1996)	~11–21 (Farese et al., 2015; Yeager et al., 1983)	
	Rat	4 (Hjort and Paputchis, 1960)			
	Dog	5–7 (Moroni et al., 2011; Tanaka et al., 2002)	9–20 (Escobar et al., 2012; Lelieveld et al., 1987; Moroni et al., 2011)	15–22 (Lelieveld et al., 1987; Moroni et al., 2011)	
	NHP	5.5–8 (Corash et al., 1984; Harker et al., 1997; Moroni et al., 2011)	11–15 (Moroni et al., 2011)	15–18 (Moroni et al., 2011)	
	Human	8–12 (Harker et al., 2000; Kurtin, 2012; Moroni et al., 2011)	8–15 (approx.) (Fanucchi et al., 1997)	23–25 – 5+ weeks (Moroni et al., 2011; Vadhan-Raj et al., 2000)	4–5 (Kurtin, 2012; Latimer, 2011)
RBC	Mouse	30–52 (Bolliger and Everds, 2012; Agar and Board, 1983; Weiss and Wardrop, 2011)	9–12 (RBC) 2 (Retics) (McElroy et al., 2015)	~24–28 (Retic and/or RBC) <sup>c</sup> (McElroy et al., 2015)	
	Rat	56–69 days (Derelanko, 1987; Edmondson and Wyburn, 1963; Van Putten, 1958)	~15–20		2–4 (Retics) <sup>c</sup> (Wichmann et al., 1989)
	Dog	110–115 days (Christian, 2010)	2–3 months		3–4 (Retics) <sup>c</sup> (Latimer, 2011; Stockham and Scott, 2008)

<b>Neutrophil</b>	NHP	86–105 days (Fonseca et al., 2018; Valeri and Ragno, 2006)	2–3 months		
	Human	115–120 (Franco, 2012; Kurtin, 2012)	3 months		5 days (Retics <sup>c</sup> ) (Latimer, 2011)
	Mouse	6–14 hours (Basu et al., 2002)	4–7 (McElroy et al., 2015; Moore and Warren, 1987)	14–20 (McElroy et al., 2015; Moore and Warren, 1987)	
	Rat	5–7 hours (Gerecke et al., 1973)	4 (Wang et al., 2020)		
	Dog	10 hours (Latimer, 2011)	14–21 (Escobar et al., 2012; Moroni et al., 2011)	17–22 (Moroni et al., 2011)	3–5 (Deubelbeiss et al., 1975)
	NHP	1.63 (He et al., 2018)	5.5 (nadir at 11–15) (Harker et al., 1997; Moroni et al., 2011)	17–22 (Harker et al., 1997; Moroni et al., 2011)	
	Human	10 hours (Athens et al., 1961; Kurtin, 2012)	~5–8 (depending on cause) (Crawford et al., 1991; Fanucchi et al., 1997; Kondo et al., 1999)	~16–20 – 4+ weeks (Crawford et al., 1991; Moroni et al., 2011)	3–5 (Latimer, 2011)

<sup>a</sup> Postirradiation and/or administration of cytotoxic compound.

<sup>b</sup> Assumes ability to regenerate appropriately.

<sup>c</sup> Reticulocyte (Retic) maturation into erythrocytes (red blood cells [RBC]) takes 4–5 days and proceeds in bone marrow and peripheral blood (Riley et al., 2001).

NHP, nonhuman primate; RBC, red blood cells; Retics, reticulocytes; Recovery time is proportional to severity and may vary depending on the mechanism of initial insult. Detailed myelotoxicity-related erythrocyte data are difficult to find, due to longer lifespan of these cells.

**TABLE 5.10** Responses to Injury in Blood and Bone Marrow

Change in Blood	Change in Bone Marrow	Cause	Examples
Increased RBCs	None	Relative erythrocytosis	Reduced water intake (fasted mice); fluid loss; splenic contraction (dogs)
Increased platelets		Relative thrombocytosis	Muscular activity; excitement
Increased neutrophils and lymphocytes		Physiologic leukocytosis	Excitement in dogs and macaques (epinephrine-induced shift within blood vessels from the marginal pool to the circulating pool)
Increased neutrophils		Neutrophil demargination	Glucocorticoids (stress); ethanol, colchicine, epinephrine (excitement)
Increased RBC	Increased erythroid cellularity $\pm$ left shift	Physiologic (appropriate) erythrocytosis due to tissue hypoxia	Decreased tissue oxygenation (abnormal Hgb: Met-Hgb); systemic hypoxia due to lung disease; systemic alkalosis (increased hemoglobin affinity for oxygen)
	Increased erythroid cellularity	Secondary inappropriate erythrocytosis	Erythropoietin excess; activation of erythropoietin receptors; endocrinopathy (cortisol, androgen, thyroxine, and growth hormone)
	(Inappropriate) Increased erythroid cellularity, dyserythropoiesis	Primary erythrocytosis due to myeloproliferative disease	Polycythemia vera
Increased platelets	Increased MK cellularity	General bone marrow stimulation	Blood loss, iron deficiency, hemolytic anemia, inflammation, growth factors, reactive thrombocytosis
Leukocytosis with band neutrophils	Increased myeloid cellularity $\pm$ left shift	Stimulation of myelopoiesis	Inflammation; growth factors or cytokines (GM-CSF)
Decreased RBCs and/or platelets	None	Splenic congestion	Barbiturate-induced splenic congestion (nonrodents) Reversible thrombocytopenia due to antisense oligonucleotide (ASO) therapy (mice, monkeys, and humans)
Decreased neutrophils		Margination	Histamine, iron oxide, dextran



Decreased RBCs	Increased erythroid cellularity	External blood loss	Repeated or excessive blood collection (common); external hemorrhage
		Intravascular hemolysis	Complement-mediated lysis; direct contact (saponin, phenylhydrazine, arsine, naphthalene); oxidative injury; copper toxicity; inhibition of mitochondrial function or glucose metabolism; excess dietary cholesterol (Guinea pigs)
		Extravascular hemolysis	Antibody-mediated (autoimmunity, hapten-induced, large granular lymphocytic [LGL] leukemia of F344 rats); erythrocyte fragmentation (microangiopathy, disseminated intravascular coagulopathy); oxidative and structural damage; internal hemorrhage
Decreased platelets	Increased megakaryocyte cellularity	Loss/destruction	Acute blood loss Immune-mediated consumptive coagulopathy
Neutropenia $\pm$ band neutrophils	Increased myeloid cellularity $\pm$ left shift	Inflammation	
Decreased erythrocytes	Decreased erythroid cellularity	Myelosuppression	>20% decrease in food consumption, stress, decreased oxygen demand
		Absolute iron deficiency	Dietary iron deficiency, prolonged hemorrhage
		Functional iron deficiency	Chronic inflammation, hepcidin overexpression, ferroportin suppression
		Chronic disease	Chronic kidney or liver failure
		Dyserythropoiesis	Altered nucleic acid synthesis
Pancytopenia	Decreased erythroid and myeloid cellularity	Direct injury to hematopoietic precursors	Ionizing radiation, benzene, chemotherapy
		Bone marrow infiltration (myelophthisis)	Leukemia, myelofibrosis

GM-CSF = granulocyte/macrophage colony-stimulating factor; Hgb = hemoglobin; MK = megakaryocyte; RBC = red blood cells

Modified from Haschek WM, Rousseaux CG, Wallig MA, editors: *Haschek and Rousseaux's handbook of toxicologic pathology*, ed 3, 2013, Academic Press, Table 50.9, p. 1916–17, with permission.

range from subtle erythrocyte membrane changes resulting in premature removal from the circulation (extravascular hemolysis) to severe life-threatening hemolysis.

Hemolytic anemias are often accompanied by a regenerative response manifested by increased erythroid cellularity of the bone marrow and increased numbers of circulating reticulocytes. Higher reticulocyte numbers in the blood may increase the mean cell volume (MCV) since reticulocytes are larger than mature erythrocytes. The peripheral blood smear may show morphologic evidence of erythrocyte destruction (indicative of intravascular or extravascular hemolysis) including schistocytes (RBC fragments) and spherocytes (RBCs lacking biconcave shape and central pallor), and occasionally Heinz bodies (aggregates of denatured hemoglobin) and other forms of poikilocytosis (abnormally shaped RBCs) (Figure 5.7) depending on the pathogenesis of the anemia. A regenerative response (i.e., reticulocytosis) may not be present if the disease rapidly progresses to death, as is frequently the case with acute intravascular hemolysis. A rapid decline in hematocrit in the absence of overt hemorrhage is compatible with hemolytic anemia.

Intravascular hemolysis is dramatic and often life-threatening due to the precipitous drop in hematocrit and oxygen-carrying capacity of the blood as well as the release of cell contents. This variant of hemolysis is typified by hemoglobinemia, hemoglobinuria, and hyperbilirubinemia. Intravascular hemolysis associated with toxicity is most

often immune-mediated in origin, typically due to a type II (antibody-mediated) reaction with fixation by complement (i.e., assembly of a membrane attack complex) and lytic pore formation.

Extravascular hemolysis, on the other hand, is often less dramatic and more insidious in its presentation. As with intravascular hemolysis, this type of reaction can be immune-mediated. These reactions may be type II in mechanism, with nonlytic fixation of complement, or type III in nature, with immune complex formation and removal of the antibody-coated erythrocytes by the mononuclear phagocytic cells in the spleen, liver, and lymph nodes. Erythrocytes damaged directly by hematotoxic agents without assistance from the immune system are removed in a similar fashion by these phagocytic cells. Since affected erythrocytes are not lysed within the vascular space, hemoglobinemia and hemoglobinuria are not observed, and hyperbilirubinemia is variable, depending on the rate of hemolysis. Splenomegaly is frequently encountered in chronic hemolytic anemia because damaged erythrocytes are sequestered by fixed macrophages within the red pulp. These cells can become quite large and prominent (i.e., hypertrophy), giving the spleen a solid “meaty” appearance grossly. Widespread and marked EMH along with pronounced increases in the numbers of hemosiderin-laden macrophages (siderophages) is also common, especially in the splenic red pulp.

### 5.1.3. Blood Loss Anemia

Loss of blood via hemorrhage is an infrequent test article-related finding in toxicity studies. This type of anemia, in the context of toxicologic pathology, is typically the result of impaired hemostasis leading to uncontrolled hemorrhage. This can be due to impairment of platelet production in the marrow, impaired platelet function by the action of the toxic agent, or by alterations in the function of coagulation factors. Among the agents affecting coagulation, those most commonly encountered by humans and animals include warfarin and related chemicals (bromadiolone, brodifacoum, chlorophacinone, diphacinone, pindone); dicoumarol (in moldy sweet clover hay); and coumarol (Ramaiah et al., 2013). These vitamin K antagonists inhibit the actions of clotting factors II, VII, IX, and X, leading to impaired hemostasis. Severe thrombocytopenia may be associated with clinical observations including petechiae, ecchymoses, melena, and prolonged bleeding from small

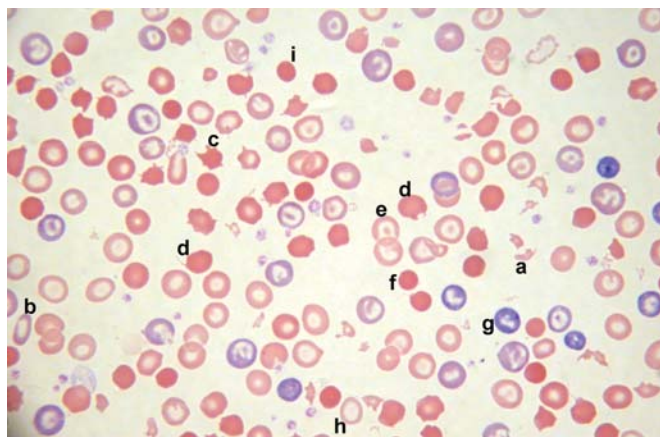


**FIGURE 5.7** Severe drug-induced poikilocytosis (abnormally shaped red blood cells) in a peripheral blood smear from a male Sprague-Dawley rat. Wright-Giemsa-stained blood smear ( $\times 500$ ). a, Schistocyte; b, elliptocyte; c, acanthocyte; d, keratocyte; e, codocyte (target cell); f, pyknocyte; g, polychromatophil; h, hypochromic cell.

wounds (e.g., venipuncture). When these clinical manifestations are observed in the absence of decreased platelet counts, altered platelet function may be involved.

#### **5.1.4. Inflammation**

Inflammation in toxicity studies is most commonly incidental (e.g., spontaneous abscesses) or secondary to the pharmacologic action of an agent (vaccines and immunoncology drugs) or procedure-related effects (infection of catheterization site). The leukogram or pattern of WBC changes in blood, including the cells affected as well as the direction and magnitude of change, depends on the mechanism of action, inciting agent, site of inflammation, and chronicity (Takizawa et al., 2012). Inflammation stimulates myelopoiesis and thrombopoiesis and suppresses erythropoiesis. This combination of effects may result in one or more of the following hematologic changes: increased M:E ratio in the bone marrow, decreased circulating reticulocytes, and increased circulating platelets.

### **5.2. Changes in Bone Marrow**

#### **5.2.1. Changes in Hematopoietic Cells**

A variety of lesions have been observed in bone marrow, including those resulting from disturbances in growth, degenerative changes, inflammatory changes, and neoplasia. For practical purposes, these may be divided into physiologic proliferation, nonproliferative lesions, clonal diseases, and proliferative lesions.

In nonclinical toxicity studies, the most frequently observed bone marrow changes are physiologic responses to changes/lesions elsewhere in the body. These are characterized by the appropriate release of cells stored in the bone marrow into circulation, with peripheral increases in the affected cell type. Less frequent are primary hematologic diseases due to bone marrow dysfunction. These are characterized by inappropriate responses to peripheral cytopenia (nonregenerative anemia, thrombocytopenia, leukopenia); inappropriate cytosis (polycythemia vera, essential thrombocytosis, leukemia); and/or qualitative changes (i.e., abnormalities in function and/or morphology).

#### **5.2.2. Physiologic Responses**

A physiologic response to increased cell demand (e.g., anemia or infection) may result in increased

nucleated cells in the bone marrow. The ratio of hematopoietic cells to fat in bone marrow increases with the need for more blood cells (in contrast to situations with decreased peripheral demand, in which the ratio of fat to hematopoietic cells is increased). Hematopoietic cell increases may involve all or individual cell lineages and may exhibit a left shift (an increase in immature cells relative to mature cells), but cell morphology and synchrony of maturation is unaffected in these homeostatic processes. If only 1 cell lineage (e.g., erythroid or myeloid) is affected, then the affected lineage should be indicated.

Increases in erythropoietic cells indicate demand-adapted erythropoiesis in response to anemia (e.g., early blood loss or hemolytic anemia) or increased blood EPO levels (e.g., hypoxia, administration of exogenous recombinant human EPO). In the case of anemias, the development of erythroid hyperplasia in the bone marrow will depend on the type, duration, and severity of the anemia and also on the age of the animal. Similar increases may be seen in the spleen and the liver, especially in the mouse. Rubricytes and metarubricytes predominate, but there may also be an increase in rubriblasts and prorubricytes. If the increase involves the erythroid lineage but not the myeloid lineage, the M:E ratio in the bone marrow may be decreased.

Likewise, if the increase involves the myeloid lineage, then the M:E ratio in the bone marrow may be increased. Greater numbers of granulopoietic cells are frequently associated with inflammation and systemic exposure to molecular signals that induce immune responses (e.g., damage [DAMP]- and pathogen [PAMP]-associated molecular patterns). The nature and severity of the bone marrow response will depend on cytokines and whether the infectious agents or molecular patterns are in circulation and can reach bone marrow hematopoietic cells (Takizawa et al., 2012). Although there will be an increase in all immature granulocytic forms, the metamyelocytes as well as band and segmented granulocytes will predominate. If the response is acute, segmented neutrophils may be decreased due to increased release from the marrow storage pool. However, with a typical “leukemoid reaction” (i.e., a very high WBC count composed of nonneoplastic cells), myeloid hyperplasia (Figure 5.8) with a normal distribution of granulocytes is the key feature distinguishing it from leukemia (i.e., a high



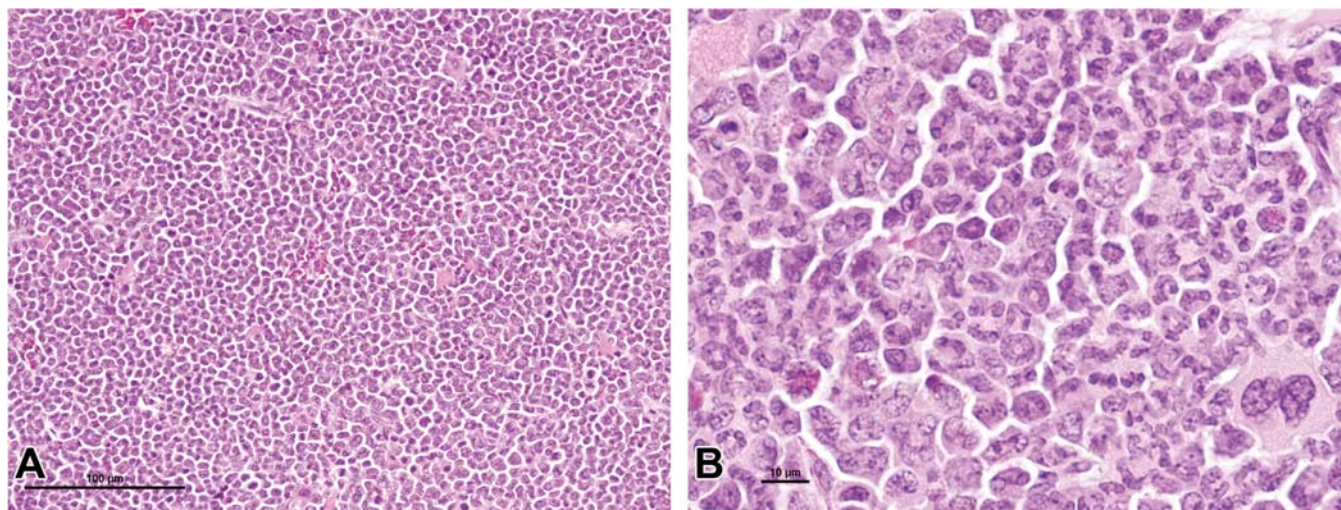


**FIGURE 5.8** Increased myeloid (neutrophil) cellularity of the bone marrow. (A) Low magnification. (B) High magnification. Proliferation of granulocytes (including many ring and band [immature] forms as well as prominent mitotic figures) has displaced erythroid islands (as shown in Figures 3 and 4), resulting in pallor of the marrow and a markedly elevated myeloid-to-erythroid (M:E) Ratio. H&E. *Reproduced from Haschek WM, Rousseaux CG, Wallig MA, editors: Haschek and Rousseaux's handbook of toxicologic pathology, ed 3, 2013, Academic Press, Figure 50.8, p. 1920, with permission.*

WBC count due to neoplasia). Increases in mast cells in the marrow, and rarely in circulation, may be observed with inflammation, particularly with parasitic infections secondary to immunosuppression.

Increased megakaryopoietic cellularity in the marrow is often associated with conditions that increase the consumption or destruction of platelets, although some responsive anemias may also result in increased MKs. Increased megakaryocyte ploidy may occur with increased MK cellularity, but cytomorphology is otherwise normal. Although the M:E ratio will not be affected, more MKs may be detected in tissue sections, and an increased percentage may be detected in bone marrow differential counts. A few MKs may be observed in the spleen of rodents under normal conditions, but their number may be increased if MK production is higher in the marrow.

### 5.2.3. Nonproliferative Bone Marrow Lesions

Reductions in the number of circulating platelets, granulocytes, or reticulocytes are the most common manifestations of bone marrow suppression. Persistent granulocytopenia is one of the most sensitive indicators of myelotoxicity. Because of the short lifespan of neutrophils in the circulation, neutropenia is usually the earliest detectable sign of myelotoxicity in the peripheral

blood, occurring early (1–3 days after exposure) if high doses of alkylating agents are administered but later (7–14 days) with lower doses of alkylating agents and other agents. Decreased reticulocyte numbers may be detected as early as 2–3 days. Thrombocytopenia may be observed after 9–14 days. Effects on red cell mass may not be seen except during more chronic studies because of the long lifespan of erythrocytes.

Decreased numbers of neutrophils must be interpreted with caution since minimal to mild fluctuations in granulocyte numbers frequently occur in experimental animals as a consequence of demargination related to excitement during necropsy rather than drug-induced bone marrow suppression (Ramaiah et al., 2013). Nonspecific stresses or systemic chemical toxicity can transiently alter cell cycle kinetics in proliferating bone marrow populations, thus producing wide fluctuations in circulating granulocyte numbers. Rodents and rabbits are especially susceptible to stress-induced leukopenia. Decreases in reticulocytes can also occur with nonspecific myelosuppression secondary to inflammation or chronic disease.

Decreases in marrow cellularity are characterized by reductions in its hematopoietic area and cellular density with relative increases in adipose tissue (Willard-Mack et al., 2019). These decreases must be distinguished from age-



related changes in all species and from spontaneous atrophy in rats (Travlos, 2006). Decreases in bone marrow nucleated cells may involve all lineages or individual cell lineages. If the decrease involves the erythroid lineage (erythroid hypoplasia), then the M:E ratio may be increased. Conversely, if the decrease involves the myeloid lineage (myeloid hypoplasia), then the M:E ratio may be decreased. If only the megakaryopoietic cells are affected

(megakaryocytic hypoplasia), MK numbers and ploidy are reduced but the M:E ratio is unchanged.

If all hematopoietic cell lineages are affected, then there may be an associated peripheral blood pancytopenia (dependent upon the chronicity of the marrow lesion) and a prominent replacement of the hematopoietic tissue in the marrow cavity with adipose tissue (Figure 5.9). It is also important to note that if normal cellularity or

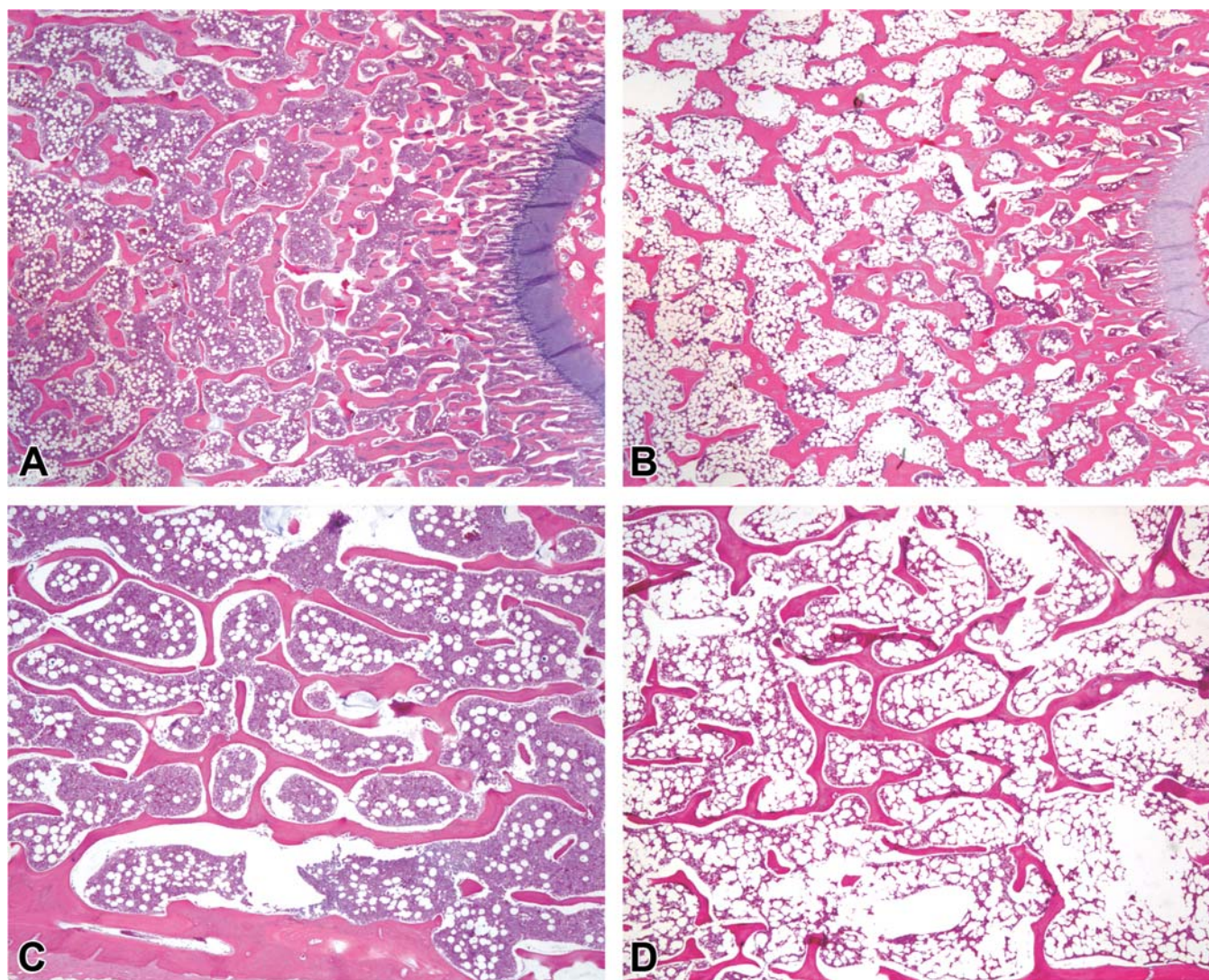


**FIGURE 5.9** Decreased hematopoietic cellularity in the bone marrow of beagle dogs. A&C: Control. B&D: Bone marrow hematopoietic hypocellularity and replacement by adipocytes following exposure to a corticotropin releasing factor-2 receptor (CRFR2) agonist. This marrow change was accompanied by mild decreases in reticulocyte counts and red cell mass in the hemogram along with decreased food consumption, body weight loss, decreased thymus weight, and thymic lymphoid depletion. H&E. *Reproduced from Haschek WM, Rousseaux CG, Wallig MA, editors: Haschek and Rousseaux's handbook of toxicologic pathology, ed 3, 2013, Academic Press, Figure 50.9, p. 1921, with permission.*

increased cellularity is observed in bone marrow tissue sections, there may still be a decrease in 1 cell line with a concurrent increase in another. Asynchronous maturation may be observed histologically but should be confirmed by cytologic evaluation.

Decreased numbers of myelopoietic cells are uncommon but occur with exposure to some agents such as chemotherapeutics, antibiotics, and antihypertensives. If severe enough, the M:E ratio may also be decreased. Decreased MK cellularity is a less common solitary finding; it is mostly associated with overall bone marrow suppression.

Decreased numbers of erythropoietic cells may be associated with a CBC that shows a nonregenerative or poorly regenerative anemia. Such decreases may be due to a direct drug effect (e.g., estrogen, antivirals, chemotherapeutics, etc.) or to an indirect effect (e.g., TNF, hypothyroidism, emaciation, inflammation, neoplasia, chronic renal or liver disease, etc.). Morphologically, bone marrow sections may appear hypocellular, the M:E ratio may be increased, and there may be a shift in the maturation sequence to the later, more mature stages of cell development.

Iron stores in the marrow are typically visible as golden-brown pigment granules with H&E stain and blue granules with Prussian blue stain (Figure 5.10). The evaluation of iron stores may be useful, along with marrow cellularity and morphology, in differentiating the mechanisms of some anemias. For example, *anemia of chronic inflammation* is characterized by normal marrow cellularity and cell morphology with increased iron, *iron deficiency anemia* presents with decreased iron, and *anemia of chronic renal disease* is indicated by normal to decreased cellularity of the erythroid components of the marrow with normal iron stores.

Severe stress, malnutrition, inanition, or cachexia may lead to **gelatinous marrow transformation** (GMT), a diffuse or focal atrophy of marrow adipocytes. A gelatinous material composed of hyaluronic acid-rich mucopolysaccharide without reticulin fibers replaces adipocytes and hematopoietic tissue. The fat atrophy is thought to result in part from inadequate trophic stimulation from the altered bone marrow microenvironment. Lesions are reversible upon return to adequate nutritional status.

Similar conditions have been reported in male Göttingen minipigs and rabbits as well as miniature horses, ruminants, reindeer, and cats, and in calves after fluoride intoxication of the dam (Alonso et al., 2021; Beeler-Marfisi et al., 2011; Bollen and Skydsgaard, 2006; Long et al., 2020).

Bone marrow necrosis, usually coagulation-type, may occur with severe injury caused by chemotherapeutic agents (Kojima et al., 2009). Necrosis may also occur with vascular occlusion (infarction) or thrombotic occlusion. In addition, bone marrow necrosis affecting one or more hematopoietic lineages can result from severe malnutrition or feed restriction in some species, particularly rats and dogs (Miyata et al., 2009; Takamatsu et al., 2015). Bone marrow necrosis is usually accompanied by refractory anemia with or without leukopenia and thrombocytopenia. Necrotic areas of bone marrow have an eosinophilic tint (due in part to loss of nucleic acids in disintegrating cells) and indistinct cellular margins. Degenerating hematopoietic and stromal cells may be vacuolated or frankly necrotic, with nuclear pyknosis (condensation) and karyorrhexis (fragmentation). Vacuolated macrophages phagocytizing cellular debris and containing ceroid or lipofuscin granules may be increased in number. There may be extensive replacement of normal stroma by necrotic debris and hemorrhage, with or without blue foci of mineralization depending on the severity and chronicity of the injury. If coagulative necrosis is present, only the eosinophilic outline of the marrow cells and structure may remain (Figure 5.11, Panels E and F). Note that care must be taken to differentiate necrosis from autolytic change, which can occur either if marrow is not placed into fixative quickly enough following sampling or if inadequate tissue fixation occurs through intact cortical bone. Certain autolytic findings can mimic features of degeneration or necrosis such as the appearance of condensation in MK nuclei, which can strongly resemble an early degenerative change (MacKenzie and Eustis, 1990; Travlos, 2006).

Pure red cell aplasia is a clinical syndrome characterized by normocytic (i.e., fewer RBCs but each containing normal hemoglobin content) anemia, reticulocytopenia, normal leukocyte and platelet counts, and absence of mature marrow erythroid progenitors (Means, 2016a, b). Since



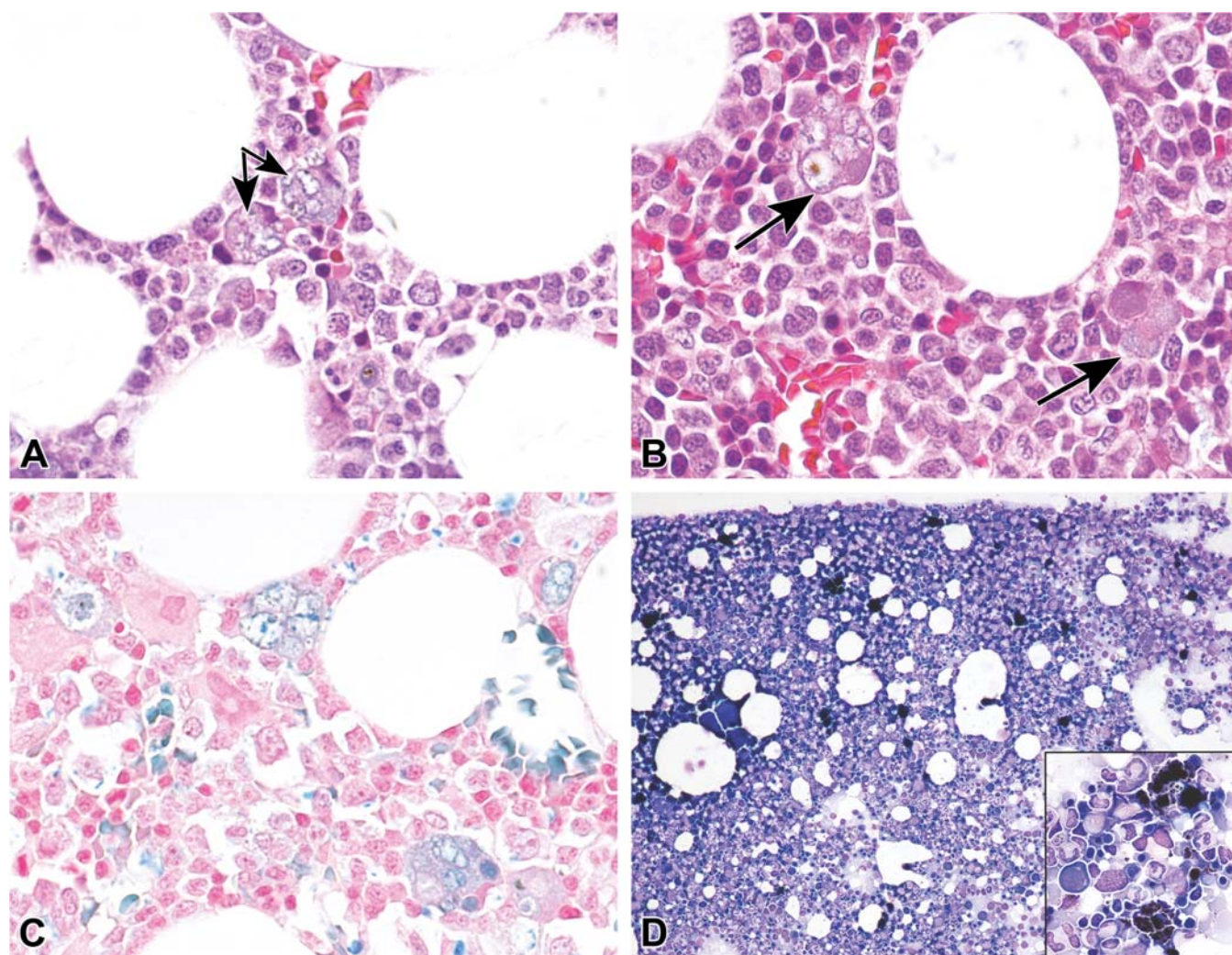


**FIGURE 5.10** Iron overload in the bone marrow. A&B: Minimally increased iron pigment (pale brown-gray cytoplasmic deposits [with color altered due to decalcification]) in macrophages (arrows) (H&E). C: Visible iron accumulation (as ferric  $[\text{Fe}^{3+}]$  ions) by Prussian blue staining. D: Cytological smear shows increased intracellular and extracellular iron stores in the absence of increased erythrophagocytosis by Wright's stain. Inset: Extracellular iron pigment is visible in large clumps and scattered as small granules (Wright's stain). *Reproduced from Haschek WM, Rousseaux CG, Wallig MA, editors: Haschek and Rousseaux's handbook of toxicologic pathology, ed 3, 2013, Academic Press, Figure 50.10, p. 1922, with permission.*

the granulocytes and MKs are not affected, the overall marrow cellularity may not be dramatically altered. The M:E ratio would be markedly increased, and hemosiderin-laden macrophages may be increased as well. Pure red cell aplasia is a persistent (chronic), refractory anemia that tends to develop after prolonged exposure to recombinant EPO as well as with a variety of drugs including immunosuppressants (azathioprine, FK506, antithymocyte globulin); antibiotics (linezolid, isoniazid, rifampin, chloramphenicol); antivirals (interferon- $\alpha$ ,

lamivudine, zidovudine); and anticonvulsants (diphenylhydantoin, carbamazepine, valproic acid) as well as chloroquine, allopurinol, fludarabine, ribavirin and gold.

Aplastic anemia (or more appropriately aplastic pancytopenia) is a clinical syndrome associated with bone marrow failure. This condition is characterized by pancytopenia and generalized, severe decreased bone marrow cellularity (Shallis et al., 2018; Wang and Liu, 2019; Young, 2018). This condition should not be confused with pure red cell aplasia, which involves



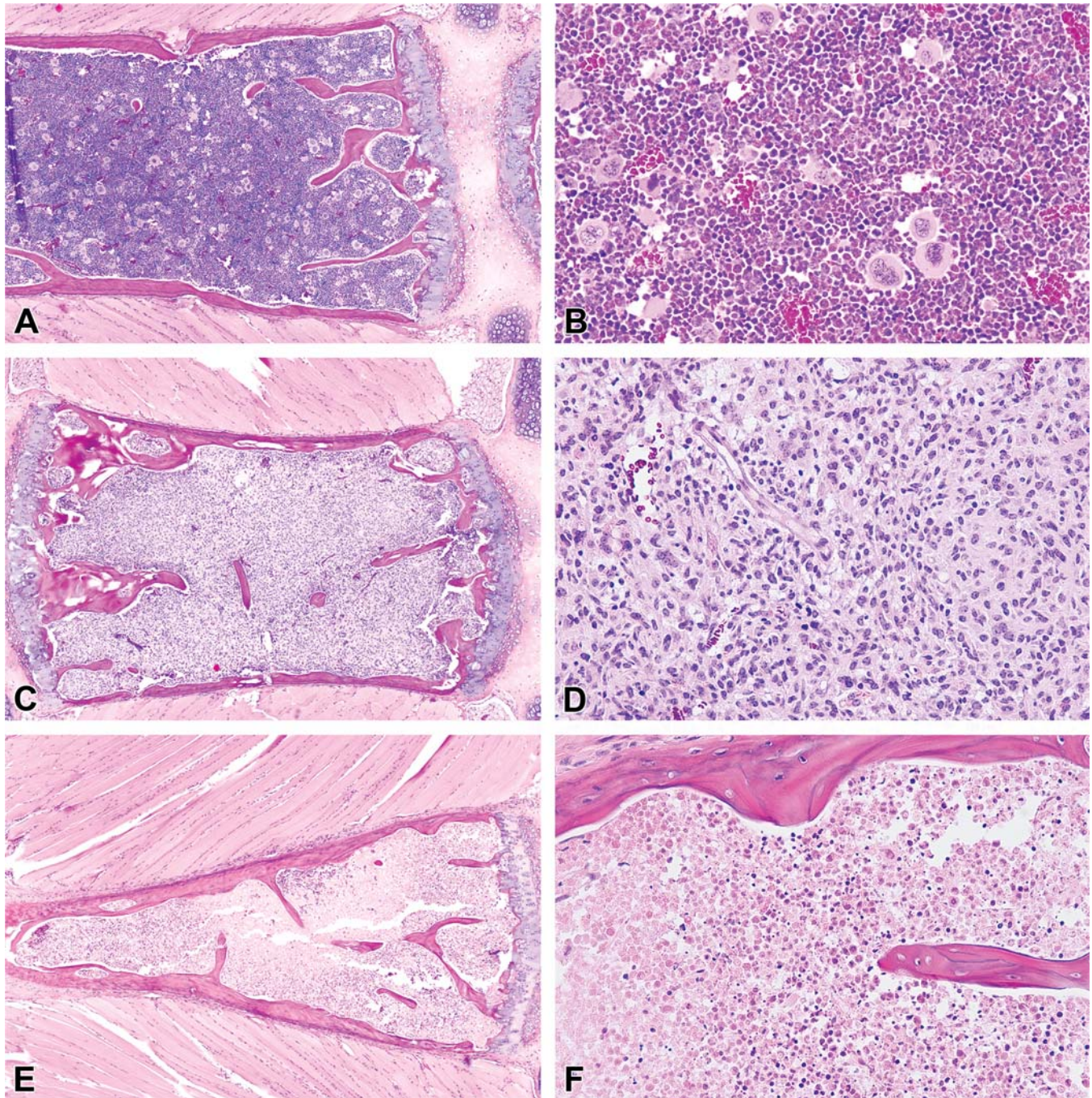


**FIGURE 5.11** Drug-induced severe stromal hyperplasia and bone marrow necrosis in mice. A&B: Control. C&D: Stromal hyperplasia with severe hematopoietic cell depletion; note the lack of associated collagen. E&F: Bone marrow necrosis. H&E. Reproduced from Haschek WM, Rousseaux CG, Wallig MA, editors: *Haschek and Rousseaux's handbook of toxicologic pathology*, ed 3, 2013, Academic Press, Figure 50.11, p. 1923, with permission.

decreased production of only the erythropoietic cell lineage. Aplastic pancytopenia is distinguished from other diseases producing pancytopenia (such as leukemia, infiltrating malignancies, or myeloproliferative disease) by

histologic examination of the bone marrow. The marrow may be completely devoid of hematopoietic cells, with only adipose tissue, fibrous stromal cells, and vascular sinuses remaining. There may be small, isolated islands of



hematopoietic cells or other cells scattered about the marrow, such as lymphocytes, plasma cells, macrophages, and mast cells. Aplastic pancytopenia is a disorder of stem cell regulation in which stem cells, either through exhaustion of numbers or a defect in differentiation, are unable to generate blood cells. Stromal cell defects and immune-mediated destruction of stem cells may also play a significant role in chronic bone marrow failure. In some of these cases, there is evidence to support a clonal origin for aplastic anemia. The syndrome carries a grave prognosis because in the absence of successful bone marrow transplantation, approximately 40% of all affected humans die within 6 months of diagnosis. Aplastic anemias arising secondarily to chemotherapy or xenobiotic exposure carry an even more dismal prognosis.

Aplastic pancytopenia is rare in domestic animals. It has been reported with exposure to antimicrobials (dogs and cats), chemotherapeutics (dogs and cats), phenylbutazone (horses and dogs), estrogen (cats), bracken fern (cattle and sheep), and aflatoxin B<sub>1</sub> (horses, cattle, dogs, pigs) (Brazzell and Weiss, 2006; Kelly et al., 2020; Weiss, 2003). Xenobiotic-associated aplastic pancytopenia is usually acute, with severe neutropenia seen within 1 week and severe thrombocytopenia within 2 weeks. These predispose to infection and hemorrhage, respectively. The development of anemia depends on the RBC lifespan for the species of interest.

Animal models of aplastic pancytopenia are relatively few and have been largely restricted to those induced by viruses, busulfan, ionizing radiation, or benzene (Chen, 2005). The bone marrow has long been recognized as particularly susceptible to radiation-induced decreases in hematopoietic cellularity leading to aplastic pancytopenia in many species, including dogs, monkeys, and mice. Dogs have been used as models for radiation-induced aplastic anemia, and are commonly used in bone marrow transplantation research.

Radiation produces both transient and prolonged bone marrow suppression, depending on the dose, dose rate, and exposure conditions (Fliedner et al., 2002). Local irradiation of rats with 2000 rad results in a transient decrease in hematopoietic cellularity and recovery. This pattern of suppression followed by regeneration is also present in other species. Twice the dose

results in a transient decrease in hematopoietic cellularity with a latent period, followed by a prolonged decrease in hematopoietic cellularity. Aplastic anemia resulting from either busulfan treatment or irradiation is characterized by a marked reduction in most proliferating cell populations in mice.

#### 5.2.3.1. CLONAL HEMOPATHIES

Erythrocytes are not often subject to alterations in peripheral counts resulting from interference with hematopoiesis since they have a long lifespan relative to leukocytes. Therefore, frank anemia is usually a late manifestation of bone marrow suppression, even though erythropoiesis per se may be more sensitive to chemical disruption than granulopoiesis. Bone marrow suppression-related decreases in RBC counts are usually clonal disorders of erythropoiesis accompanied by morphologic changes suggestive of maturational alterations. They may initially manifest in circulating cells only as megaloblastic, sideroblastic, or hemolytic anemias, but they can also eventually progress to myelodysplasia (in which immature blood cells do not mature normally) and secondary acute leukemia.

Xenobiotics that interfere with RNA or DNA synthesis or produce disturbances in cell division or maturation frequently produce a megaloblastic anemia (characterized by very large RBCs). Such agents include folate antagonists (methotrexate), inhibitors of purine or pyrimidine synthesis (6-mercaptopurine and 5-fluorouracil), pentose sugar analogs such as cytosine arabinoside, antiviral agents, and alkylating agents (Ramaiah et al., 2013). In humans, megaloblastic anemia has been associated with xenobiotics that interfere with vitamin B<sub>12</sub> or folate metabolism (trimethoprim and pyrimethamine) or absorption (ethanol, *p*-aminosalicylic acid and colchicine) or that decrease cobalamin levels (histamine 2-receptor antagonists and proton pump inhibitors). This condition is characterized by macrocytic erythrocytes in circulation and a hypercellular bone marrow with large, abnormal hematopoietic progenitor cells ("megaloblasts"). Leukopenia and/or thrombocytopenia may also occur. Lead can also cause anemia, but this anemia is typically microcytic (i.e., smaller RBCs) in nature.



Sideroblastic anemia is a clonal disorder of erythropoiesis caused by altered RBC iron utilization (e.g., heme synthesis and/or precipitation of iron and ferritin in mitochondria) in maturing erythroid cells. It is characterized by ringed sideroblasts (rubricytes containing iron-positive cytoplasmic granules surrounding the nucleus) in the bone marrow and peripheral microcytosis. Xenobiotics that have been associated with sideroblastic anemia in humans include ethanol, isoniazid, pyrazinamide, cycloserine, chloramphenicol, copper chelation/deficiency, zinc, lead, trichlorethylene, linezolid, penicillamine, triethylene tetramine dihydrochloride, and gallium arsenide (Tehranchi et al., 2005; Weiss and Lulich, 1999).

Paroxysmal nocturnal hemoglobinuria is a clonal HSC disease reported only in humans and some animal models (calves and mice) (Rosti, 2002; Shimizu et al., 1979). It results in episodic or chronic, complement-induced, intravascular hemolytic anemia, hemoglobinuria, and thrombosis. The disease is hypothesized to be due to the clonal expansion of a mutated HSC that lacks a membrane-localized glycosylphosphatidyl-inositol (GPI) anchor protein (Bocconi et al., 2000). Affected cells consequently have a cell surface deficiency of all proteins that use the GPI anchor for attachment to the cell membrane, including proteins that prevent complement-mediated lysis, such as decay-accelerating factor (DAF or CD55), which disrupts C3 convertase formation, and protectin (CD59), which binds the membrane attack complex and prevents C9 binding to the cell (Merrill and Brodsky, 2018). Binding by complement also causes platelet dysfunction and thrombosis. Paroxysmal nocturnal hemoglobinuria has been associated with exposure to benzene, vitamin C, and antithymocyte globulin, and may also be observed with aplastic anemia and myelodysplasia.

### 5.3. Myeloproliferative Lesions

Myelofibrosis involves bone marrow fibroblast proliferation and deposition of reticulin (Figure 5.12, Panels C & D). Primary myelofibrosis is a myeloproliferative (neoplastic) disease that is mostly observed in humans although it has also been reported in dogs (Knight et al., 2011). The pathogenesis of

myelofibrosis appears to be intimately linked with MK proliferation and differentiation. Proliferating MKs secrete growth factors such as TGF- $\beta$ , PDGF, and FGF that induce fibroplasia and reticulin deposition (Bataller et al., 2019). Secondary myelofibrosis, also referred to simply as fibrosis, is a more frequently reported non-neoplastic change. This finding often occurs as a result of marrow necrosis followed by replacement with fibrous connective tissue (i.e., “scar tissue”).

Excessive TPO agonism by second-generation thrombopoietic agents bearing no sequence homology to TPO (e.g., romiplostim, eltrombopag) results in reversible myelofibrosis, hyperostosis and increased bone marrow reticulin. This sequence of changes represent an example of adverse exaggerated “on target” pharmacology rather than toxicity per se. Moreover, they may even produce thromboembolic complications, myeloblast proliferation, and even malignant transformation of hematopoietic cells (Kim et al., 2019; Nieto et al., 2011).

Initially, actively proliferating fibroblasts fill marrow spaces and deposit substantial amounts of reticulin. This reaction may become progressive, resulting over time in virtual total replacement of hematopoietic cells with inactive fibrous tissue, probably as a result of interference with the bone marrow blood supply. Fibrosis/secondary myelofibrosis may be associated with chronic renal disease (e.g., rats with fibrous osteodystrophy), immune-mediated hemolytic anemia (IMHA), inflammation, dysmegakaryopoiesis, neoplasia, and long-term treatment with drugs causing bone marrow necrosis (Ramiah et al., 2013).

Hematologic findings vary considerably, depending on the species and the severity of the lesion. However, EMH in tissues such as spleen, liver, and lung is sometimes observed in association with myelofibrosis. Fibrosis/secondary myelofibrosis associated with drug or toxicant exposure has been most frequently reported in the dog, with agents that frequently produce generalized myelosuppression (e.g., estrogen) being implicated most often (Figure 5.13).

Myelodysplastic syndromes (MDS, alternatively “dysmyelopoiesis” or more recently “myelodysplastic neoplasm”) are clinically heterogeneous clonal HSC disorders. These

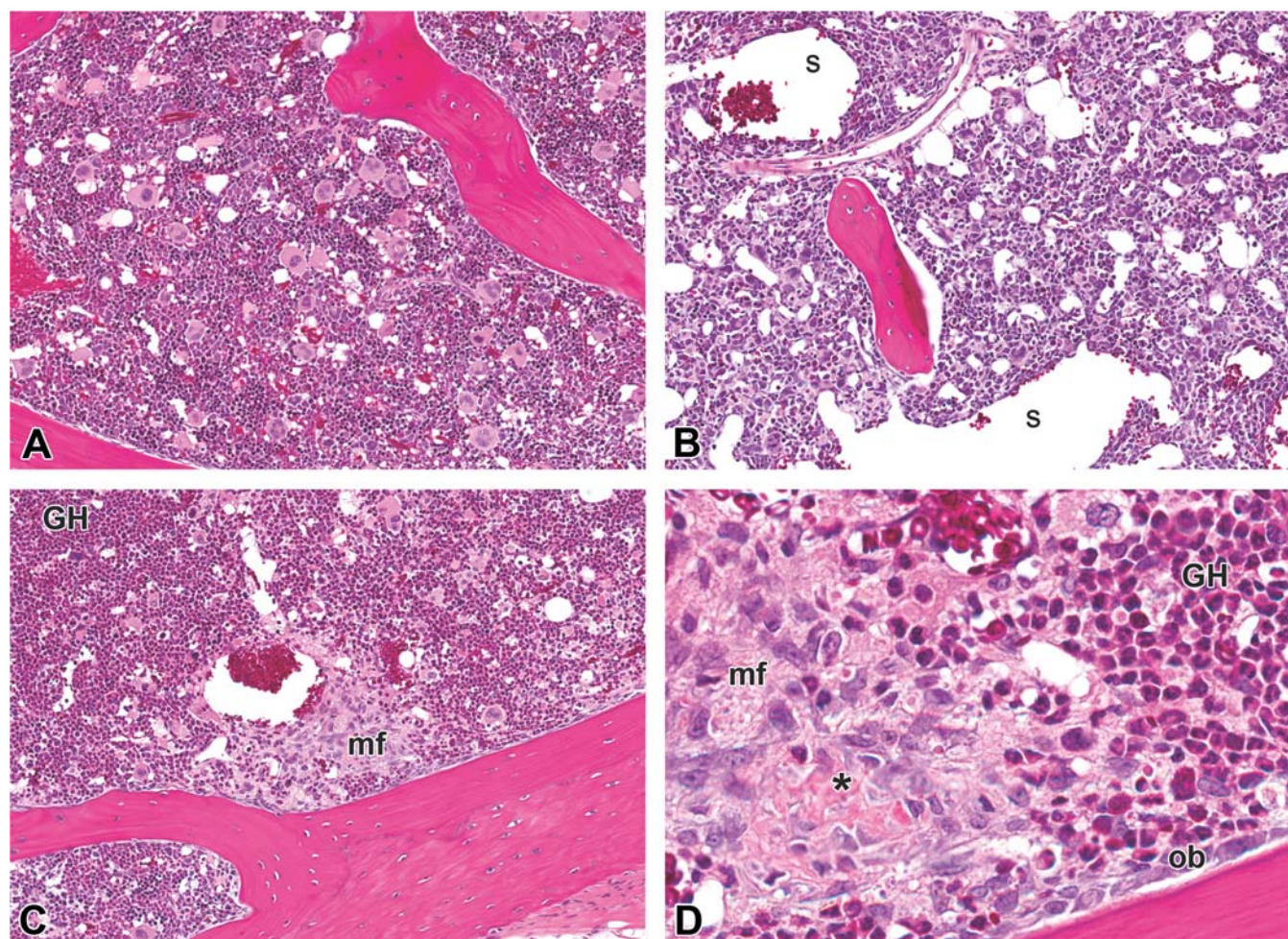


**FIGURE 5.12** Drug-induced decreased megakaryocyte (MK) cellularity with secondary fibrosis in rats. A: Control. B: Mild generalized decreased hematopoietic cellularity with severely decreased MK cellularity and slight dilation of medullary sinusoids (s) (end of dosing for 7 days). C&D: Focal fibrosis (mf) and increased myeloid (granulocytic) cellularity (GH) with a predominance of late-stage granulocytes (end of 7-day recovery). Fibrosis was characterized by activation and extension of osteoblasts (ob) into areas of fibrosis and the formation of new woven bone (\*). Fibrosis and woven bone formation were secondary to induction of thrombopoietin (TPO) production and prolonged bone marrow megakaryopoiesis. H&E. *Reproduced from Haschek WM, Rousseaux CG, Wallig MA, editors: Haschek and Rousseaux's handbook of toxicologic pathology, ed 3, 2013, Academic Press, Figure 50.12, p. 1926, with permission.*

conditions are characterized by ineffective hematopoiesis (failure to mature or impaired differentiation) of one or more nonlymphoid lineages associated with peripheral cytopenia(s), bone marrow dysplasia, and risk for progression to acute myeloid leukemia (Gondek and DeZern, 2020). They have been described in dogs, cats, and humans. Myelodysplastic syndrome is most commonly associated with varying degrees of anemia, sometimes accompanied by macrocytosis, with leukopenia and/or thrombocytopenia. Histologically, the bone marrow

typically is hypercellular with a predominance of immature cells of one or more lineages, though hypocellularity with an excessive proliferation of one or more cell lineages or mature blood cells with shortened lifespans can be observed instead. Dysplasias may involve one or several cell lineages, resulting in dyserythropoiesis, dysgranulopoiesis, dysmegakaryopoiesis, or multilineage MDS. Immature forms or blast cells may be increased in numbers but represent less than 20% of nucleated cells. Diagnosis requires qualitative and quantitative



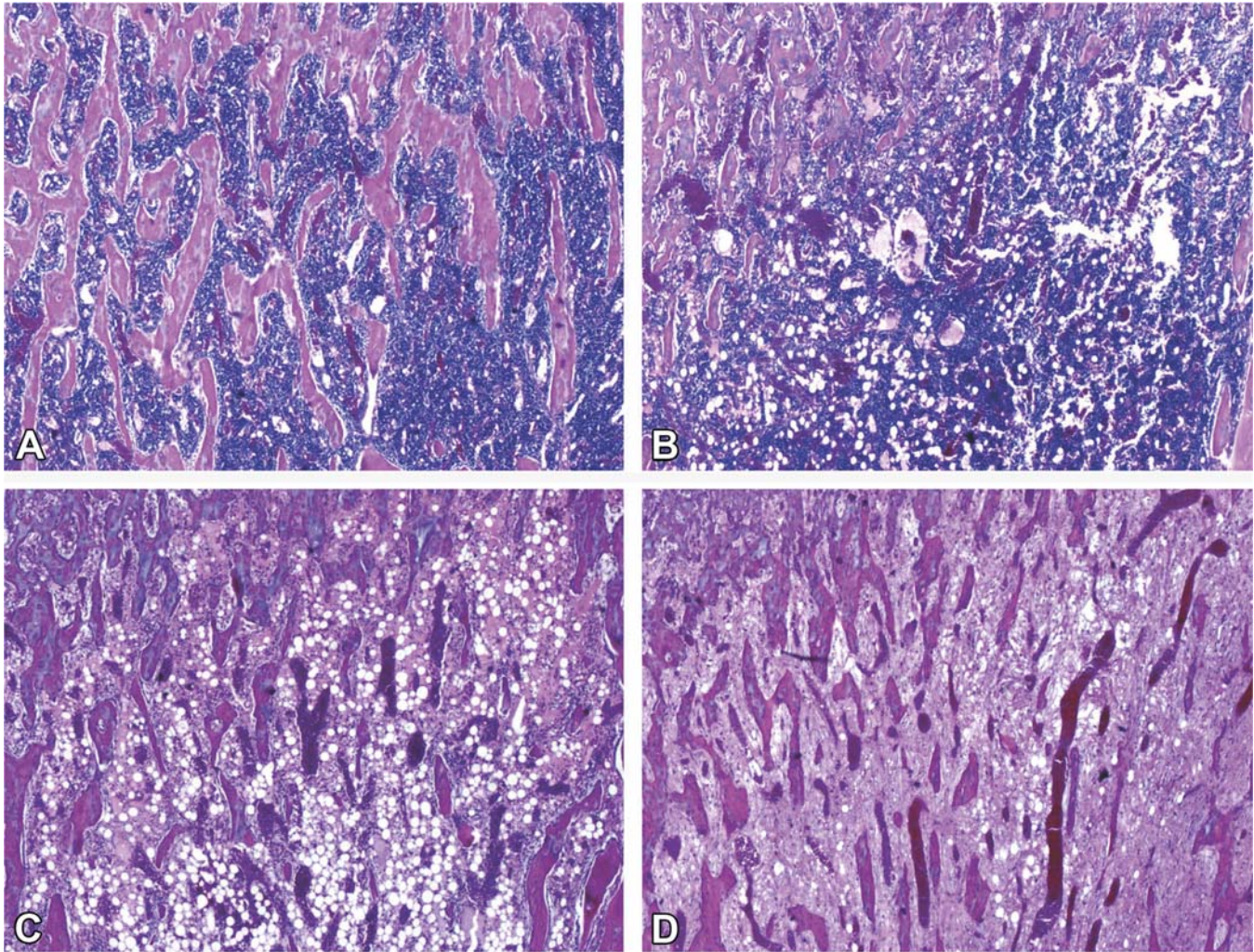


**FIGURE 5.13** Drug-induced decreased hematopoietic cellularity in the bone marrow of a dog given an anticancer agent (p53 enhancer) for 2 weeks. A: 0 mg/kg (control); B: 25 mg/kg (mildly decreased hematopoietic cellularity); C: 75 mg/kg (moderately decreased hematopoietic cellularity); D: 150 mg/kg (severely decreased hematopoietic cellularity with marrow replacement by fibrosis). H&E. Reproduced from Haschek WM, Rousseaux CG, Wallig MA, editors: *Haschek and Rousseaux's handbook of toxicologic pathology*, ed 3, 2013, Academic Press, Figure 50.13, p. 1927, with permission.

evaluation of cytological preparations from bone marrow aspirates.

Myelodysplastic syndrome may be classified as leukemia if >20% of nucleated hematopoietic marrow cells are immature forms or blasts and/or if there is observation of these cells in the peripheral blood, often but not always with associated cell accumulation in nonhematopoietic tissues (Ramaiah et al., 2013). Leukemia, primarily AML, is often preceded by a "preleukemic" or prodromal state of chronic bone marrow insufficiency. This phenomenon occurs with high frequency in leukemias

arising secondary to previous cancer therapy. The rate of progression from MDS to frank leukemia in humans appears to be particularly high in cases associated with previous radiation therapy or chemotherapy or with repeated benzene exposure. Studies using cytogenetic or biochemical markers to identify the clonal origins of abnormal cell populations have revealed that clonal abnormalities may be present for years prior to the clinical onset of leukemia. Myelodysplastic syndrome carries a grave prognosis, with reported mortalities of 30%–84%.



Leukemias are among the most widely recognized and feared malignancies in humans. Derived from bone marrow, the neoplastic cells are usually disseminated via the blood at some time during their development. In general, leukemias can arise as abnormal cell populations from any cell lineage, although there is some predisposition to one or more cell types, depending on the method of induction and the species or strain studied. Leukemias in humans that are associated with chemical or drug exposure are predominantly of the acute myeloid (usually granulocytic) type. Although there are exceptions, leukemias consisting predominantly of immature or blast cells tend to proliferate rapidly and invade aggressively, whereas those in which a more differentiated cell phenotype prevails tend to take a more protracted course. Reports that clearly link treatment with drugs to induction of leukemias in domestic animals are exceedingly rare, although myelodysplasias have been reported with more frequency (see above).

A common feature of hematologic malignancies in both experimental animals and humans is their clonal nature. That is, these neoplasms are derived from a single cell. Leukemogenesis is a multifactorial process that cannot be modeled or simulated as a function of an uni- or bimolecular event. Therefore, it is not surprising that no initiation/promotion paradigms have been established for chemical leukemogenesis in experimental animals.

Variable numbers of lymphoid cells are normally observed in bone marrow, with higher proportions of lymphocytes observed in young rodents (Ramaiah et al., 2013). In lymphoid hyperplasia, there may be focal or diffuse increases in lymphocytes. Small mature lymphocytes predominate, although lymphoblasts and prolymphocytes may be increased. In common laboratory animal species, lymphoid cells account for <30% of nucleated hematopoietic cells in marrow of both common nonclinical species (especially rodents, with mice more affected than rats) and humans. When lymphoid cells account for >30% of nucleated hematopoietic cells, lymphoma or leukemia are more likely (Martin et al., 1992; Parmentier et al., 2020).

The distinction between lymphoma, a malignancy involving primarily the thymus, lymph nodes, or splenic white pulp, and leukemia, a malignancy involving primarily the bone

marrow, spleen, or blood is often difficult. Neoplastic cells in hematopoietic tissues tend to be present in focal aggregates with lymphoma or in sheets with leukemia. Mouse lymphoid neoplasms form space-occupying lesions in tissues, yet spread in a leukemoid manner in the blood, rendering the distinction difficult (Figures 5.14 and 5.15) (Ramaiah et al., 2013).

#### 5.4. Changes in Secondary Hematopoietic Organs

Any physiological demand for additional hematopoietic cells that results in increased cell production in the bone marrow may also result in EMH in tissues other than the bone marrow (Johns and Christopher, 2012). Most cases of physiological EMH involving RBC, myeloid, and occasionally MK lineages involve the spleen and liver, although EMH also may develop in other tissues (e.g., adrenal gland, choroid plexus of the brain, fat, lung, and lymph nodes) with some frequency, particularly in rodents. In contrast, lymphoid nodules incorporating B and/or T cell lineages typically evolve as new (tertiary) lymphoid organs at sites of chronic, ongoing inflammation (see *Immune System*, Vol 5, Chap 6).

Increased EMH may be seen as a reaction to local changes in the bone marrow, such as hematotoxic insult or injuries to hematopoietic cells, or to systemic conditions that cause anemia, such as infections or chronic diseases (e.g., neoplasms). The spleen and liver are most often involved, especially in rodents since they normally have foci of EMH in these organs throughout adulthood, and this can increase hematopoietic cell production when needed. However, other organs may also be involved following hematogenous spread of multipotential stem cells from the bone marrow with eventual tissue infiltration (Ramaiah et al., 2013).

In all organs that support EMH, the hematopoietic cells are composed of varying numbers of erythroid, myeloid, or megakaryocytic cells (Figure 5.16). One or more cell types may predominate, depending on the inciting cause and/or specific demand. For example, diagnoses of erythropoiesis or erythroid hyperplasia may be used when the most prominent component is erythroid cells, while granulopoiesis or

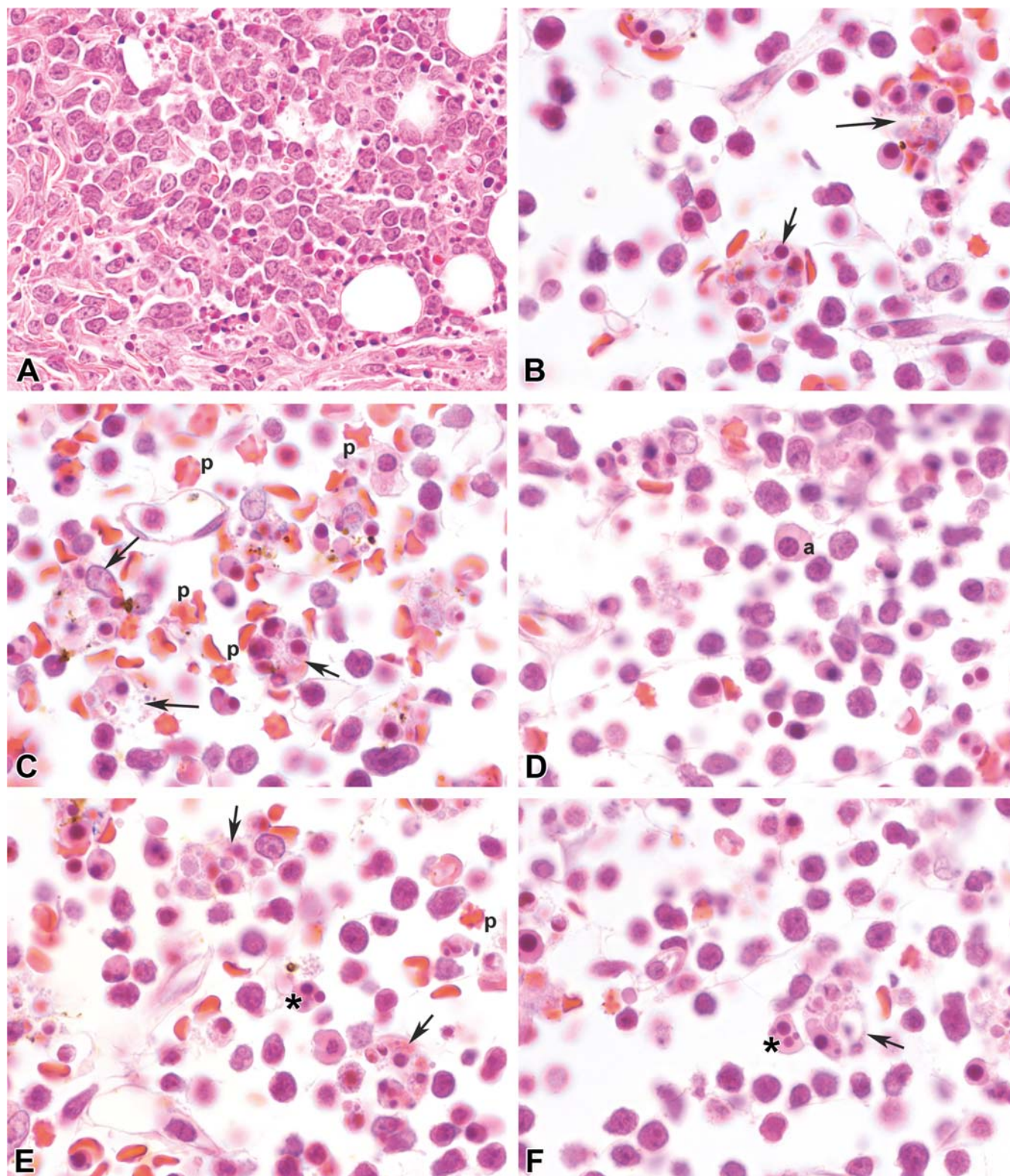


**FIGURE 5.14** Spontaneous lymphoma invading into skeletal muscle (A) with bone marrow dyserythropoiesis and erythrophagocytosis (B–F) in a 16-month-old female rat. Distinct features seen in the marrow (B–F) include increased hemophagocytic macrophages (erythrophagocytosis [black arrows] with pyknotic cells and cellular debris), asynchronous erythroid maturation (a), multinucleated erythroid cells (\*), and poikilocytic (abnormally shaped) erythrocytes (p). H&E. *Reproduced from Haschek WM, Rousseaux CG, Wallig MA, editors: Haschek and Rousseaux's handbook of toxicologic pathology, ed 3, 2013, Academic Press, Figure 50.14, p. 1928, with permission.*



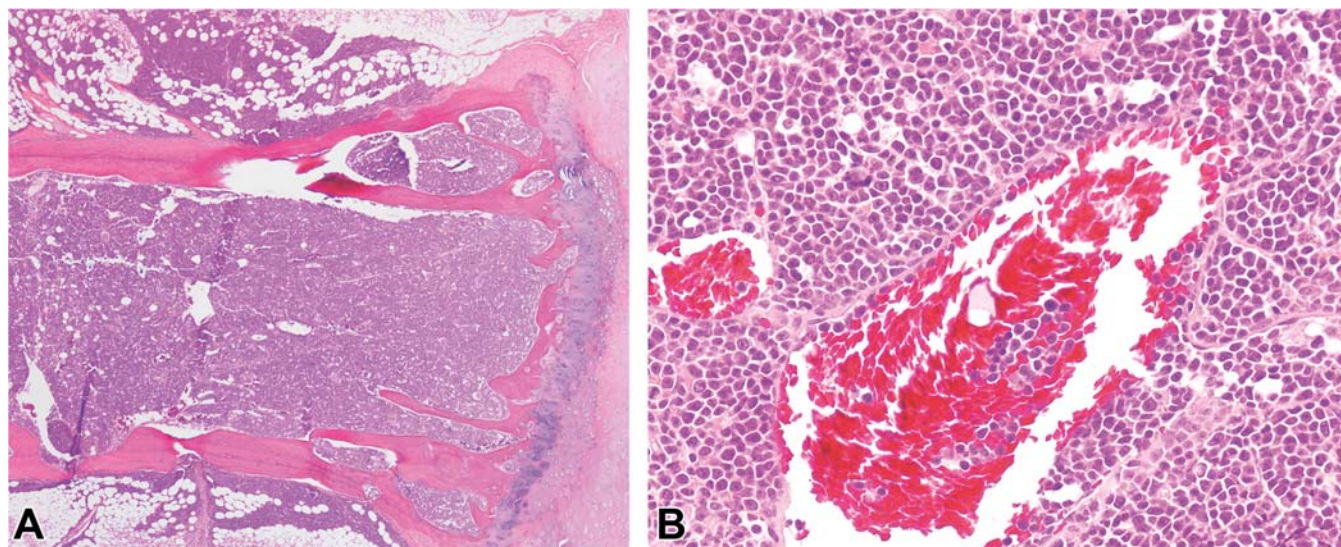


**FIGURE 5.15** Spontaneous lymphoma with lymphoid leukemia in a 19-month-old male rat. (A) Higher magnification (B) to illustrate cell and tissue detail including the presence of numerous neoplastic cells in the bone marrow and blood vessels. H&E. Reproduced from Haschek WM, Rousseaux CG, Wallig MA, editors: *Haschek and Rousseaux's handbook of toxicologic pathology*, ed 3, 2013, Academic Press, Figure 50.15, p. 1929, with permission.

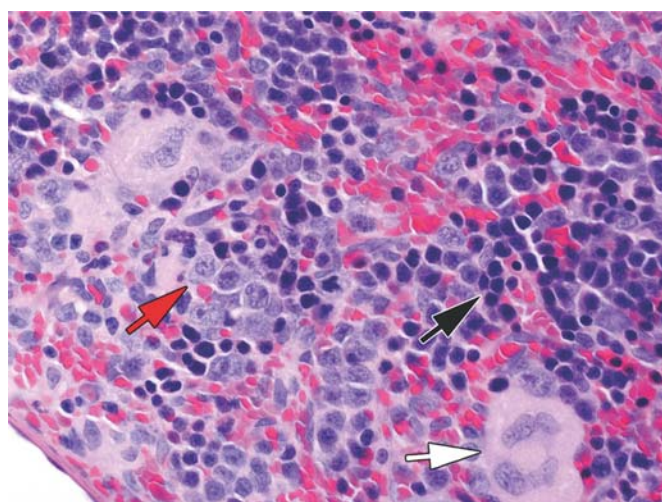


**FIGURE 5.16** Extramedullary hematopoiesis (EMH) in the spleen. EMH generally consists of erythropoiesis (cells with dark cytoplasm and nuclei [black arrow]), myelopoiesis (cells with pale basophilic cytoplasm and nuclei [red arrow]), and megakaryopoiesis (giant cells with abundant eosinophilic cytoplasm and multi-lobulated nuclei [white arrow]). Careful comparison of organ structure to that of concurrent controls is required to identify xenobiotic-induced effects since EMH is a normal component of the splenic red pulp in rodents. H&E. Reproduced from Haschek WM, Rousseaux CG, Wallig MA, editors: *Haschek and Rousseaux's handbook of toxicologic pathology*, ed 3, 2013, Academic Press, Figure 50.16, p. 1930, with permission.

myeloid or granulocytic hyperplasia may be used if the major component is granulocytic cells. The erythroid component may predominate secondary to hemorrhage or erythrocyte destruction, and the myeloid component may predominate secondary to inflammatory or immunoproliferative conditions. If 1 cell lineage predominates, one or more other cell lineages may also be affected since they share a common progenitor cell.

The diagnosis of EMH should always be made after careful comparison of the organ structure with tissue features evident in concurrent controls since some degree of EMH is normally present in the livers and spleens of rodents. Marked EMH with a predominant myeloid component (as in response to severe inflammation) shares some histological similarities with granulocytic leukemia, so this diagnosis should be made after careful evaluation of other tissues and organs for a potential focus of infection or other inflammatory stimulus. In general, immunohistochemistry is needed to identify increases in the lymphocyte component within foci of EMH.

In the spleen, EMH is characterized by varying numbers of MKs as well as clusters of myeloid and erythroid precursors throughout the red pulp. In severe cases, the entire red pulp may be occupied by erythroid precursors, or less



commonly myeloid precursors. The presence of basophilic and polychromatic erythroblasts can usually be discerned on routine histologic sections. Extensive splenic EMH occurs in many species secondary to anemia, blood loss, or hypoxia. In the spleen, background levels of EMH are more common in mice, more common in young compared to aged rodents, and more common in females compared to males. EMH as a response to injury may be seen as an increase in the number and/or size of foci of hematopoiesis or as a diffuse (nonneoplastic) hyperplasia of the red pulp (Suttie, 2006). EMH is distinct from ectopic bone marrow, which may form between bony trabeculae within foci of osseous metaplasia that develop in the spleen of mice with longstanding pro-hematopoietic influences.

EMH is abundant in the fetal and neonatal liver, but small, scattered foci still exist in the adult. In such cases, EMH is typically found within the sinusoids, around central veins, and around portal blood vessels. In response to injury, liver foci of EMH may increase in size and/or number.

## 6. MECHANISMS OF HEMATOTOXICITY

Adverse xenobiotic-induced hematotoxic reactions can be classified as Type A or Type B responses. Most reactions (~80%) are type A reactions. These are predictable and dose-dependent effects that usually result from the direct effect of a xenobiotic or its metabolite on hematopoietic or circulating blood cells. Type B reactions are infrequent to rare, unpredictable and nondose-related events that are attributable to immune-mediated hypersensitivity or are idiosyncratic (Weiss, 2012).

Xenobiotics may injure blood cells by a single or multiple mechanisms, and mechanisms of injury overlap between agents. Depending on the mechanism involved, they may target cells of a specific type (erythroid, myeloid, platelet) and stage of maturity (stem cell, progenitor, maturing, circulating) or they may target a broad spectrum of blood cells. Xenobiotics also impact the hematopoietic system indirectly through their systemic toxicities and effects on other organs and organ systems. Importantly, there is

much overlap in mechanisms of injury among species including humans, and hematopoietic toxicity in animals holds high concordance with human toxicity (Olson et al., 2000). Thus, examination of the blood and bone marrow are standard procedures to assess dose-response effects utilizing laboratory species as well as in human and animal clinical situations where systemic toxicities are the suspected cause of disease.

### 6.1. Direct Nonimmune Injury to Hematopoietic Cells

Xenobiotics can injure blood and bone marrow cells in many ways. Known mechanisms of direct hematotoxicity include altering molecular bonds (frank breaks, alkylation, crosslinking, and oxidation of nucleic acids, proteins, carbohydrates, and lipids); disrupting membrane integrity, inducing apoptosis, and inhibiting essential cellular functions (e.g., quiescence, division, differentiation, motility, mitochondrial function, and cytoskeletal function) in hematopoietic cells (Ramaiah et al., 2013). Injury to the extracellular matrix, supportive stromal cells, and/or vasculature of the marrow is an important indirect contributor to hematopoietic toxicity.

In contrast to mature peripheral blood cells, which are prone to direct injury from high exposures to circulating xenobiotics, bone marrow cells are somewhat more sequestered from toxicants, and thus less prone to direct damage, due to the supportive functions of stromal cells. However, the hematopoietic system is sensitive to a wide variety of injurious agents owing to its rapid metabolic and proliferative rate, extensive vascularization, local metabolism of xenobiotics, and life-long reliance on a limited pool of self-renewing stem cells. Although the susceptibility of hematopoietic cells is attributed to the rapid rate of division of the mitotic pool, xenobiotics can injure cells at all stages of maturity, from quiescent stem cells and proliferating cells to maturing and fully differentiated circulating cells, depending on the inciting agent.

Some agents show specificity for self-renewing stem cell populations. Phase-specific agents such as potent alkylating chemicals target resting pluripotent stem cells as well as proliferating cells, thereby leading to severe and prolonged bone marrow damage with delayed recovery.

Other alkylating agents preferentially affect stem cells with low self-renewal potential and high proliferative activity. Cycle-specific agents target proliferating cells of any type, and they typically produce a dose-dependent, less prolonged and severe bone marrow suppression that is often followed by protracted recovery (Ramaiah et al., 2013).

For cycle- or phase-specific agents, the frequency and duration of exposure can be an important factor in determining toxicity. Altering the timing of exposure relative to the cell cycle (i.e., varying the interval between doses) can lead to synchronization of the cell cycle, with subsequent alteration of the number of cells susceptible to toxicity at any given time. For example, a single therapeutic dose of cyclophosphamide can result in a transient depression in circulating leukocytes, whereas repeated dosing at 2-week intervals may result in severe leukopenia, aplastic anemia, and death (Ramaiah et al., 2013). Species differences also modulate hematotoxic effects (Goto et al., 2017).

Bone marrow toxicity is most often manifested as myelosuppression (Weiss, 2012). Rapidly proliferating bone marrow cells demonstrate unique susceptibility to certain cytotoxic agents compared with their nonproliferating counterparts. Although many agents are selectively toxic to rapidly dividing cell populations, there can be considerable variation in the response of proliferating precursor, progenitor, and stem cell populations to a toxic agent. Injury to uncommitted stem cells will generally produce aplastic pancytopenia (“aplastic anemia”), while injury to committed myeloid or erythroid progenitors will produce agranulocytosis or pure red cell aplasia, respectively. Injury to the mitotic pool results in generalized bone marrow hypoplasia or aplasia, with recovery supported by surviving quiescent stem cells. Death of maturing cells may produce maturation arrest and/or increased proportions of immature cells. Altered nuclear or cytoplasmic maturation usually leads to dysplasia; altered nuclear maturation due to interference with DNA synthesis or mitosis results in atypical mitotic figures, nuclear fragmentation, and bi/multinucleation. When protein synthesis is spared and cytoplasmic maturation can proceed (e.g., accumulation of hemoglobin or secondary granules, loss of RNA), altered nuclear maturation produces

macrocytosis, megalocytosis, and/or granulocyte hypersegmentation.

Agents that inhibit hemoglobin production, assembly, or stability result in altered cytoplasmic maturation in erythroid cells. Nuclear maturation proceeds (characterized by appropriate chromatin condensation and loss of RNA) and cells continue to divide, but cytoplasm does not expand and mature. This disconnect leads to microcytosis with hypochromasia (poor hemoglobinization), retention of cytoplasmic RNA (slight basophilia), and indistinct or scalloped plasma membranes. Agents that inhibit heme synthesis cause iron and ferritin to precipitate in mitochondria of maturing erythroid cells, producing siderocytes.

Injury to circulating cells produces peripheral cytopenia with the appropriate bone marrow hyperplastic response. Classes of common hematotoxic agents include antineoplastic, antimicrobial, and immunosuppressive chemotherapeutics (e.g., alkylating agents, purine/pyrimidine antagonists, topoisomerase inhibitors); kinase inhibitors; other antimicrobials (antibiotics, antiretrovirals, antifungals/parasitocides); hormones (e.g., estrogen); hormone antagonists (e.g., aromatase inhibitors, mitotane); cytokines (e.g., interferons); environmental contaminants (chlorinated polycyclic aromatic hydrocarbons, benzene, pesticides); physical injury (ionizing radiation, oxidants, burns, hyperthermia); heavy metals (arsenic, lead); and some natural toxins (mycotoxins and plant toxins [e.g., bracken fern]) (Table 5.11) (Ramaiah et al., 2013).

### 6.1.1. Injury to Hematopoietic Progenitors

Benzene and its derivatives are among the most studied hematotoxicants (Dewi et al., 2019). These chlorinated polycyclic aromatic hydrocarbons are genotoxic, mutagenic, and cytotoxic to pluripotent stem cells and progenitor cells (Travis et al., 1994; Wang et al., 2012). Benzene is hematotoxic even at low doses (<1 ppm, the current occupational standard), causing a variety of hematologic disorders including aplastic pancytopenia, myelodysplastic syndrome, and leukemia (Cox et al., 2021; Guo et al., 2019). The toxic effect of benzene is primarily due to its multiple reactive intermediates and metabolites (hydroquinone, *p*-benzoquinone, catechol, and muconaldehyde). Benzene derivatives and metabolites induce

**TABLE 5.11** Classes of Agents Causing Injury to Hematopoietic Cells

Class		Examples	Mechanism of Action	Hematotoxicity
Cytotoxic agents	Alkylating agents	Nitrogen mustards: Mechlorethamine, cyclophosphamide, ifosfamide, melphalan, chlorambucil	DNA crosslinking	Myelosuppression with neutropenia and thrombocytopenia; chromosomal aberrations, aneuploidy, poikilocytosis, macrocytosis, hypersegmentation; myelodysplastic syndrome, leukemia
		Methylhydrazine derivatives: Procarbazine		
		Alkyl sulfonate (busulfan)		
		Nitrosureas: Carmustine (bcnu), streptozotocin, bendamustine		
		Triazenes: Dacarbazine (CTIC), temozolomide		
		Platinum coordination complexes (platinum analogs): Cisplatin, carboplatin, oxaliplatin		
	Vinka alkaloids	Mitomycin C	Bioreductive alkylation; DNA crosslinking	
		Vinblastine, vinorelbine, vincristine	Inhibit microtubule function	
		Taxanes		
		Paclitaxel, docetaxel		
	Topoisomerase inhibitors and DNA intercalators	Epipodophyllotoxins: Etoposide, teniposide, actinomycin D; acridines (pyrazoloacridine)	Intercalate DNA; inhibit topoisomerase	
		Fluoroquinolone, camptothecin, topotecan, irinotecan	Inhibit topoisomerase	
		Anthracyclines: Daunorubicin, doxorubicin, idarubicin	Inhibit topoisomerase; intercalate DNA; oxidative injury	
		Hydroxyurea	Intercalate DNA; inhibit ribonucleotide reductase; inhibit topoisomerase; increases synthesis of $\gamma$ -globin chains (fetal globin), increasing oxygen affinity	



	Radiomimetics	Anthracenediones: Mitoxantrone Bleomycin Eneidiynes Ecteinasidin	Inhibit topoisomerase; intercalate DNA Oxygen-mediated DNA double strand breaks	
Nucleoside/ nucleotide antagonists	Folic acid analogs/ antagonists	Methotrexate (amethopterin), pemetrexed	Inhibit DNA synthesis	
	Pyrimidine analogs	Fluorouracil, cytarabine (cytosine arabinoside), gemcitabine, fludarabine, 2-chlorodeoxy- adenosine, clofarabine, capecitabine, gemcitabine, 5-aza-cytidine, deoxy-5- aza-cytidine, flucytosine		
	Purine analogs and related inhibitors	Mercaptopurine, pentostatin, flurabine, clofarabine, nelarabine, azathioprine		
	Nucleoside reverse transcriptase inhibitors (NRTI)	Ribavirin, zidovudine (AZT)	Inhibit cellular and mitochondrial DNA polymerase	
Antibiotics	Sulfonamides	Sulfanilamide, sulfadiazine, sulfamethoxazole, sulfisoxazole, sulfacetamide	Immune-mediated	Agranulocytosis, aplastic anemia; acute hemolytic anemia
	Chloramphenicol	Chloramphenicol	Inhibit synthesis of mitochondrial proteins critical for aerobic metabolism and incorporation of iron into heme.	Bone marrow suppression (type A): Anemia, reticulocytopenia, leukemia; aplastic anemia (type B): Immune- mediated; dogs: ringed sideroblasts
	Oxazolidinones	Linezolid, eperezolid	Inhibit protein synthesis	Myelosuppression: Pancytopenia, thrombocytopenia; dogs: megakaryocyte hypersegmentation
	Cephalosporins	Cefonicid, cefazedone	Mitochondrial injury; immune-mediated	Myelosuppression and maturation arrest

(Continued)

**TABLE 5.11** Classes of Agents Causing Injury to Hematopoietic Cells—cont'd

Class		Examples	Mechanism of Action	Hematotoxicity
Antifungals		Fluconazole, itraconazole, voriconazole	Reduce ergosterol synthesis by inhibiting fungal cytochrome P450 enzymes	Myelosuppression, leukopenia, thrombocytopenia
		Terbinafine	Reduce ergosterol synthesis by inhibiting the fungal enzyme squalene epoxidase	Myelosuppression, leukopenia, thrombocytopenia
		Griseofulvin	Inhibit cell wall synthesis	Myelosuppression (cats)
Antivirals		Ganciclovir	Inhibit viral DNA synthesis	Myelosuppression: neutropenia, thrombocytopenia
		Interferons	Inhibit paracrine production of hematopoietic growth factors; immune-mediated	Myelosuppression: neutropenia, thrombocytopenia
Antiparasitics		Levamisole, albendazole, metronidazole, fenbendazole, thiacetarsamide	Levamisole: Immune-mediated in humans idiosyncratic	Agranulocytosis; pancytopenia, BM hypoplasia
Hormones and hormone antagonists	Adrenocortical suppressants	Mitotane		BM necrosis
	Estrogens	Diethylstilbestrol, ethinyl estradiol, esters of estradiol (benzoate, cypionate, propionate, valerate, enanthate and undeclylate)	Induction of a thymic factor that suppresses hematopoiesis.	Anemia (rats); fatal pancytopenia (dogs and ferrets)
Differentiating agents		Histone deacetylase inhibitors	Decrease the transactivation function of GATA-1, inhibiting GATA binding protein-1 (GATA-1) gene expression in megakaryocytes leading to a delay in megakaryocyte maturation	Thrombocytopenia

Agents directed at specific molecular targets	Tyrosine kinase inhibitors	Pazopanib, lestaurtinib, imatinib (Gleevec), nilotinib Sunitinib, sorafenib Dasatinib	Inhibits kinase signaling by erythropoietin/thrombopoietin receptor	Myelosuppression with neutropenia, thrombocytopenia, anemia, macrocytosis and lymphopenia
			Inhibits kinases expressed in megakaryocytes	Thrombocytopenia
	TPO agonists	First generation	Immune-mediated	Thrombocytopenia
		Second generation: Romiplostim and eltrombopag	Excessive stimulation of megakaryocytes and platelet-derived growth factor/transforming growth factor- $\beta$ -induced stimulation of fibroplasia	Fibrosis/myelofibrosis and hyperostosis
CNS drugs	Anticonvulsants	Phenytoin, primidone, phenobarbital,	Phenytoin in humans: Binds and inhibits intestinal conjugase, which converts monoglutamates into folic acid; phenobarbital/phenytoin in dogs: destroy mature granulocytes	Phenytoin in humans: aplastic anemia, neutropenia, thrombocytopenia, macrocytosis, neutrophil hypersegmentation; phenobarbital/phenytoin in dogs: aplastic anemia, neutropenia, thrombocytopenia, myelonecrosis/fibrosis
	Atypical antipsychotics	Clozapine	Oxidative injury: Bioactivation to a chemically reactive nitrenium ion	Agranulocytosis
Ionizing radiation			DNA damage (strand breaks, crosslinks, mutagenesis), oxidative injury	Myelosuppression with neutropenia and thrombocytopenia; chromosomal aberrations; myelodysplastic syndrome; leukemia.
Plant and fungal toxins	Mycotoxins	Trichothecenes: Nonmacrocytic (e.g., T-2 toxin, diacetoxyscirpenol, vomitoxin) and macrocytic (e.g., from <i>Stachybotrys chartarum</i> ).	Radiomimetic: selective targeting of rapidly dividing cells	Aplastic anemia

(Continued)



**TABLE 5.11** Classes of Agents Causing Injury to Hematopoietic Cells—cont'd

Class		Examples	Mechanism of Action	Hematotoxicity
	Bracken fern	Ptaquiloside from <i>Pteridium aquilinum</i>	Thiamine deficiency due to thiaminase DNA adduct formation	Myelosuppression, pancytopenia, leukemia
Environmental contaminants	Chlorinated polycyclic aromatic hydrocarbons	Benzene, benzene derivatives (chlorophenothane (DDT), lindane, pentachlorophenol), carbon tetrachloride, hexachlorophene, chlordane, chlorobenzene, chlorinated dioxins, trichlorethylene, DMBA, benzopyrene, TCDD	Mutagenic; aryl hydrocarbon receptor agonism; oxidative injury; protein alkylation; initiation of redox cycling; immune dysfunction; growth factor inhibition	Aplastic anemia; dysmyelopoiesis; myelodysplastic syndrome, acute myeloid leukemia
		Trichlorethylene	Inhibit heme synthesis (inhibit delta-aminolevulinate dehydratase) in rats	Dyserythropoiesis, metarubricytosis, microcytosis, hypochromasia, basophilic stippling
	Heavy metals	Lead	Inhibit heme synthesis ( $\gamma$ -ALA dehydratase and ferrochelatase) and RNA depolymerization (pyrimidine 5'-nucleotidase)	
	Inorganic arsenic		Oxidative injury DNA damage, lipid peroxidation; induced release of heme from hemoglobin	Aplastic pancytopenia, dyserythropoiesis with karyorrhexis, megaloblastosis and multinucleation; hemolytic anemia

DMBA: Dimethylbenz(a)anthracene; TCDD: benzopyrene, tetrachlorodibenzo-p-dioxin; TPO: thrombopoietin

Modified from Haschek WM, Rousseaux CG, Wallig MA, editors: Haschek and Rousseaux's handbook of toxicologic pathology, ed 3, 2013, Academic Press, Table 50.6, p. 1891–95, with permission.

myelosuppression by direct interaction with DNA and proteins, initiation of redox cycling, protein alkylation (tubulin, histones, topoisomerases), induction of chromosomal aberrations, aryl hydrocarbon receptor (AhR) agonism, immune dysfunction (TNF- $\alpha$ , interferon [IFN]- $\gamma$ ), and growth factor inhibition.

Hepatic metabolites of benzene (phenol, catechol, and hydroquinone) are oxidized by peroxidases in the bone marrow (myeloperoxidase primarily) and converted to several biologically reactive quinones. In addition, benzene metabolism by cytochromes p450 enzymes (e.g., CYP2E1 and CYP1B1) expressed in bone marrow produces toxic metabolites locally in hematopoietic tissues. Peroxidase and/or phenoxy-mediated oxidation of benzene metabolites (hydroquinone) initiate redox cycling, glutathione conjugation, and formation of 1,4-benzoquinone, a reactive electrophile considered to be one of the ultimate hematotoxic metabolites of benzene (Abernethy, 2004; Duval et al., 2019; Wollin and Dieter, 2005).

The production of ROS near the DNA strand results in DNA backbone cleavage and cell cycle arrest in an attempt to repair DNA. This arrest is seen as an initial increase, followed shortly by a decrease in bone marrow cell turnover, suggesting a defect in the maturation of precursor cells. Benzene metabolites also indirectly suppress hematopoiesis via injury to the kidney and EPO-producing juxtaglomerular cells. In addition, benzene injures the microenvironment and triggers a sustained stress response that alters paracrine regulation of hematopoietic progenitors, activates quiescent cells, and depletes the stem cell pool (Dewi et al., 2020).

A recently identified mechanism of myelosuppression induced by polycyclic hydrocarbons (primarily dioxins and benzene) is agonism of the AhR (Yang et al., 2019). This ligand-activated cytoplasmic transcription factor expressed in HSCs prevents premature exhaustion of the quiescent stem cell pool by regulating cell cycle entry. AhR also regulates the expression of enzymes involved in xenobiotic activation and the responses to altered microenvironment, hypoxia, redox states, and circadian rhythms. The significance of AhR activation in benzene-induced hematotoxicity is highlighted in AhR knockout mice, which fail to develop benzene hematotoxicity (Gasiewicz et al., 2010).

### 6.1.2. Injury to the Mitotic Pool—Inhibition of DNA Synthesis and Cell Division

Myelotoxicity is a well-recognized dose-limiting side effect of antineoplastic and antimicrobial chemotherapeutic agents. These agents have direct, predictable, and dose-related cytoreductive effects leading to myelosuppression. Reversible neutropenia and thrombocytopenia may be observed initially, with aplastic pancytopenia, myelodysplastic syndrome, myelofibrosis, and/or leukemia occurring with prolonged exposure. Because chemotherapeutics inhibit DNA replication, their greatest impact is on the rapidly dividing cells of the mitotic pool, whereas quiescent cells and postmitotic cells are relatively resistant. However, the deleterious effects of a single exposure can induce quiescent cells to enter the cell cycle, rendering them susceptible to subsequent exposures. The inhibition of DNA synthesis can result in macrocytosis with or without nuclear hypersegmentation. Because myelotoxicity secondary to ionizing radiation or cytotoxic chemicals is a consequence of injury to rapidly dividing cells, it is usually accompanied by toxicity directed against rapidly dividing cells in lymphoid organs (see *Immune System*, Vol 5, Chap 6), gastrointestinal mucosa (see *Digestive Tract*, Vol 4, Chap 1), and testicular tubules (see *Male Reproductive Tract*, Vol 5, Chap 9). Therefore, it is incumbent on the toxicologic pathologist to examine these organ systems as well to determine if the toxic effect is specifically hematopoietic in nature or more generalized in its antiproliferative effects.

Cytotoxic antineoplastic agents are varied in structure and mechanism of cellular injury. Alkylating agents and ionizing radiation cause DNA interstrand crosslinks and strand breaks that induce cell cycle arrest (to repair DNA) and inhibit replication. If the DNA damage is complex and difficult to repair, injured cells undergo apoptosis. Topoisomerase-targeting antineoplastic agents inhibit DNA unwinding, causing DNA strand breaks. Some topoisomerase inhibitors are nonintercalative, while others can intercalate themselves within DNA to also inhibit DNA replication and RNA synthesis. In addition to intercalating DNA and inhibiting topoisomerase, hydroxyurea inhibits ribonucleotide reductase, an enzyme necessary for the conversion of ribonucleotides into

deoxynucleotides. Bleomycin, ecteinascidin, and enediynes are radiomimetic agents that cause DNA double-strand breaks in the presence of oxygen (Povirk, 1996).

Vinca alkaloids, taxanes, and colchicine impede cell division through inhibition of microtubule assembly and mitotic spindle formation. This results in an arrest at G<sub>2</sub>/M, so susceptibility is confined to cells in late S and early G<sub>2</sub> phases at the time of exposure. Since only a proportion of asynchronously dividing marrow cells are in this part of the cycle at any given time, increasing the dose of a phase-specific cytotoxic agent beyond an effective threshold does not increase the number of affected cells. These agents target cells in a specific phase of the cell cycle and produce a plateau-type dose-response curve (Ramaiah et al., 2013).

Antimetabolite analogs of folic acid, pyrimidines, and purines block DNA replication and cell division by inhibiting the synthesis of nucleotides and nucleosides (Chan et al., 1992). Because these compounds impact nucleic acid synthesis while sparing protein synthesis, asynchronous maturation of nuclei relative to cytoplasm may be observed (macrocytosis, hypersegmentation). In humans, drugs that contribute to vitamin B<sub>12</sub> deficiency (paraminosalicylic acid, colchicine, neomycin, ethanol, omeprazole, zidovudine) or folate deficiency (phenytoin, primidone, carbamazepine, phenobarbital, sulfasalazine, cholestyramine, triamterene) reduce thymidine synthesis, resulting in suppression of DNA synthesis and megaloblastic anemia affecting all lineages.

Ingestion of bracken fern (*Pteridium aquilinum*) causes aplastic pancytopenia in cattle, sheep, pigs, horses, rats, and mice (Ramaiah et al., 2013; Schacham et al., 1970). Bracken fern contains a variety of toxic agents including thiaminases and ptaquiloside. Hematotoxicity is partly attributed to thiaminases that degrade thiamine to produce a thiamine deficiency. This deficiency produces pathological changes in other systems as well (e.g., polioencephalomalacia in ruminants, beriberi in nonruminants); however, all suffer some degree of myelosuppression leading to pancytopenia. The sesquiterpenoid toxin ptaquiloside found in bracken fern has been linked to pancytopenia and is presumed to be responsible for the cancer-causing effects of bracken fern. The hydrolysis

of ptaquiloside results in the formation of a dienon intermediate that can produce DNA adducts. As an alkylating agent, ptaquiloside has effects like other alkylating agents known to cause myelosuppression, pancytopenia, and leukemia. The highly water-soluble DNA-damaging toxin can contaminate water, milk, and meat, thus leading to chronic exposures responsible for alimentary tract and other cancers in humans and animals.

Zearalenone is a nonsteroidal estrogenic mycotoxin produced by *Fusarium* fungi that contaminates different components of the food chain (Taranu et al., 2011). Injury to hematopoietic cells occurs due to its genotoxic effects, which include chromosomal aberrations and DNA fragmentation (see *Mycotoxins*, Vol 3, Chap 6).

### 6.1.3. Injury to the Maturing Pool—Inhibition of Protein Synthesis

Inhibition of protein synthesis is a common mechanism of action for xenobiotics. Conceptually, committed hematopoietic cells of the maturing pool are most susceptible since these are actively synthesizing an abundance of cytoplasmic constituents. Mammalian erythropoietic cells are particularly sensitive to the inhibitory effects of chloramphenicol (an antibiotic) on protein synthesis (Yunis, 1973). Chloramphenicol inhibits synthesis of proteins in the inner mitochondrial membrane critical for aerobic metabolism and incorporation of iron into heme. Chloramphenicol (and thiamphenicol) suppresses erythropoiesis resulting in a dose-related, reversible anemia and reticulocytopenia. Inbred mice are more susceptible when compared to outbred mice, and outbred mice are more susceptible than rats. Neutropenia and thrombocytopenia may also be observed in mice, rabbits, dogs, and cats.

Oxazolidinone antibiotics are inhibitors of protein synthesis that block the initiation step of mRNA translation. Linezolid induces mild, reversible, duration-dependent, and dose-related myelosuppression characterized by anemia and thrombocytopenia with or without neutropenia (Taketani et al., 2009). As for many antibiotics, the mechanism of linezolid-induced myelosuppression is hypothesized to involve inhibition of mitochondrial protein synthesis. In dogs, eperezolid increases MK numbers and



MK mitoses, leading to nuclear hypersegmentation and multiple separate or satellite nuclei, and decreases circulating platelet numbers. These effects may be due to altered regulation of MK endomitosis in dogs.

Trichothecenes are a chemically related group of mycotoxic metabolites present in food products contaminated with some filamentous fungi including *Fusarium* and *Stachybotrys* (Lautraite et al., 1997). The ingestion of moldy food containing trichothecenes produces mycotoxicosis in both humans and animals. Trichothecene mycotoxins are directly toxic without metabolic activation, allowing for rapid effect on rapidly proliferating tissues of the gastrointestinal tract, lymph nodes, skin, thymus, spleen, and bone marrow. Consequences of exposure include feed refusal, vomiting, dermatitis, immunosuppression, and hematologic disturbances (hemorrhage, leukopenia, and in some cases aplastic pancytopenia). Trichothecenes produce toxicity by inhibiting eukaryotic and mitochondrial protein synthesis and by preventing peptide bond formation. Trichothecenes also inhibit DNA and RNA synthesis, cell division and mitochondrial function, and disrupt membrane integrity, though it is not clear if these outcomes are secondary to inhibition of protein translation. Trichothecenes also induce both oxidative and ribotoxic stress (i.e., where the ribotoxic response reflects interference with the function of ribosomal RNA), contributing to DNA and membrane damage and to their radiomimetic and hemolytic properties. Finally, these mycotoxins have been shown to cause immunosuppression by interacting with protein sulfhydryl groups required for immune cell interactions.

Lead disrupts erythropoiesis by interfering with several enzymes. For instance, lead impacts heme synthesis by inhibiting  $\gamma$ - and  $\delta$ -aminolevulinate dehydratase and ferrochelatase (Siha et al., 2019). The lack of proper hemoglobinization results in failure of nuclear extrusion. Lead also inhibits pyrimidine 5'-nucleotidase, which is involved in depolymerization of reticulocyte ribosomal RNA, leading to retention of RNA. Lead toxicity is characterized by dyserythropoiesis and an increased M:E ratio in the bone marrow with microcytosis, hypochromasia, metarubricytosis, and basophilic stippling (retained cytoplasmic RNA) in circulation.

#### 6.1.3.1. AGENTS DIRECTED AT SPECIFIC MOLECULAR TARGETS

Recent advances in our understanding of molecular and cellular pathobiology have enabled the development of a variety of novel agents (small molecules and biologics) directed at specific molecular targets, thus providing enhanced efficacy and reduced toxicity. These novel therapeutics have been targeted to growth factor receptors, intracellular signaling pathways, epigenetic processes, angiogenesis, DNA repair, and apoptotic pathways. However, biotherapeutics have the potential to produce adverse hematologic drug effects despite their exquisite target selectivity (Everds and Tarrant, 2013). Biotherapeutics have immediate, direct, and prolonged access to blood cells and are more likely to cause infusion-like reactions due to their parenteral route of administration. In addition, blood cells have complex interactions with targeted immune system proteins (soluble or cell-surface). Neutrophils, monocytes, and platelets are readily activated by interaction of biotherapeutics with cell surface receptors and are primed for activation, release of mediators, redistribution, or destruction. Mechanisms of biotherapeutic-induced hematotoxicity have been reviewed (Everds et al., 2013; Everds and Tarrant, 2013). Briefly, they include infusion reactions (cytokine release or Type III [antigen-antibody complex-mediated] hypersensitivity), complement activation or complement-dependent extravascular hemolysis, decreased hematopoiesis (cytokine-mediated dysregulation of hematopoiesis or antidrug antibodies [ADAs] that cross-react with endogenous growth factors such as EPO), and antibody binding (direct binding of the therapeutic antibody to blood cells, de novo generation of anti-blood cell antibodies, monoclonal antibodies with enhanced effector function, or multimeric protein complexes localized to platelets).

Small molecule tyrosine kinase inhibitors all competitively inhibit ATP at the catalytic binding site of the tyrosine kinase. Because of structural homology among protein kinases, kinase inhibitors are not always as selective for a specific target kinase as predicted or intended, and may have off-target inhibitory effects on various kinases in hematopoietic cells (Simon et al., 2020). Therefore, myelotoxicity and myelodysplasia occur and are

potentially severe consequences of some kinase inhibitors. However, kinase inhibitors differ from one another in the spectrum of targeted kinases, pharmacokinetics, and adverse effects. For example, tyrosine kinase inhibitors of the VEGF receptor (VEGFR) like sorafenib and sunitinib commonly induce myelosuppression of varying frequency and severity through off-target inhibition of Flt3 and c-Kit. Dasatinib, an inhibitor targeted to the oncogenic Bcr-Abl (breakpoint cluster region–Abelson) tyrosine kinase, nonspecifically inhibits Src kinases expressed in MKs. This prevents MK migration along the SDF-1 $\alpha$  gradient from the proliferative osteoblastic niche to the vascular niche, resulting in decreased proplatelet formation and thrombocytopenia. Target selectivity has improved hematopoietic (and other) safety issues in some circumstances. For instance, cyclin-dependent kinases (CDKs) are serine/threonine kinases that partner with cyclin proteins to regulate the progression of the cell cycle, making them attractive therapeutic targets. Early, broad-spectrum CDK inhibitors have been limited in part by toxicity, including hematotoxicity. This has led to the pursuit of more targeted agents such as selective CDK 4,6 inhibitors (palbociclib, abemaciclib, ribociclib), which are designed to specifically block the G<sub>1</sub>/S transition of the cell cycle, resulting in temporary cell cycle arrest as opposed to cell death (Bonelli et al., 2019; Zhang et al., 2021).

Second-generation thrombopoietic agents (romiplostim and eltrombopag) designed to bear no homology to TPO and thus not induce immune-mediated thrombocytopenia are associated with hematologic toxicity related to their exaggerated pharmacologic effects (Everds and Tarrant, 2013). Excessive stimulation of MKs by these agents results in reversible myelofibrosis and hyperostosis and increased bone marrow reticulins (see Section 5.3 *Myeloproliferative Lesions*). It is hypothesized that induction of megakaryopoiesis and thrombopoiesis by TPO agonists results in increased production of fibrogenic growth factors (PDGF and TGF- $\beta$ ) and osteoprotegerin (a soluble RANKL receptor involved in osteoclast differentiation) by MKs and platelets. PDGF stimulates fibroblast proliferation, and TGF- $\beta$  also has stimulatory effects on fibroblasts and osteoblasts (Bataller et al., 2019). The excessive proliferation of fibroblasts and

mesenchymal cells results in myelofibrosis and osseous metaplasia. In rats given RWJ-800,088, a PEGylated peptide agonist for mpl (myeloproliferative leukemia virus oncogene), greater than threefold increases in platelet counts were associated with myelofibrosis and hyperostosis (Knight et al., 2011). Other consequences of TPO agonism include thromboembolic complications, myeloblast proliferation, and malignant transformation of hematopoietic cells. Non-PEGylated agents may produce severe rebound thrombocytopenia upon cessation of treatment due to rapid TPO clearance by the numerous circulating platelets.

#### 6.1.3.2. OXIDATIVE INJURY TO HEMATOPOIETIC CELLS

ROS are among the major determinants of cellular senescence, cytotoxicity, and genotoxicity, and play a primary role in the development of myelofibrosis, myelodysplastic syndrome, and leukemia. All cells including marrow hematopoietic cells and circulating blood cells are continuously exposed to ROS. Thus, ROS constitute a heterogeneous group of inorganic molecules and free radicals with a wide spectrum of lifespans and reactivities, including superoxide (O<sub>2</sub><sup>-</sup>), hydrogen peroxide (H<sub>2</sub>O<sub>2</sub>), singlet oxygen (<sup>1</sup>O<sub>2</sub>), nitric oxide (NO), peroxynitrite (ONOO<sup>-</sup>), and hydroxyl radical (\*OH) (Roberts et al., 2009).

ROS are endogenously produced at low levels as products of aerobic respiration and are also important cell signaling intermediates that govern the redox states of signaling proteins. Endogenous sources of ROS include mitochondria, peroxisomes, cytochromes p450 in endoplasmic reticulum, NADPH oxidase within the plasma membrane and cytosol, and other cytosolic enzymes (xanthine oxidase, cyclooxygenases, nitric oxide synthase, lipoxygenase). The major source for ROS in hematopoietic cells is superoxide from the mitochondrial electron transport chain and from a variety of oxidases expressed throughout hematopoietic development. Superoxide is short-lived but can dismutate to hydrogen peroxide, a long-lived species from which all other physiologic ROS molecules are derived. Maturing erythroid precursors also generate ROS when incorporating iron into heme in mitochondria. In this process, hydrogen peroxide is spontaneously converted by ferrous (Fe<sup>2+</sup>) iron ions (Fenton reaction) to the highly reactive hydroxyl radical (Moldogazieva et al., 2020).

Oxidative stress, defined as an excess of ROS, can be caused by increased ROS production, disturbances in cellular redox cycling of signaling intermediates, or antioxidant depletion/inhibition. Oxidative stress in hematopoietic tissues induces a variety of disease states ranging from bone marrow failure to leukemia (Tower, 2012). To minimize the deleterious effects of oxidative stress, most cells including hematopoietic cells have developed several mechanisms to regulate ROS production and assuage ROS-induced damage. ROS-generating systems are often coupled to a complex network of antioxidant systems and functionally organized redox circuits that serve to compartmentalize and scavenge ROS. Antioxidants that regulate ROS levels and/or mediate signal transduction by ROS include reducing enzymes (superoxide dismutase, catalase, glutathione peroxidase, thioredoxin, peroxiredoxin); nonenzymatic small molecule scavengers (ascorbic acid [vitamin C], uric acid, bilirubin, glutathione [GSH], zinc, selenium, tocopherols [vitamin E],  $\beta$ -carotene, ubiquinol-10 [coenzyme Q], lycopene); and proteins (albumin, haptoglobin, ferritin, ceruloplasmin) (Semenza, 2011).

Oxidative injury caused by ROS is an important mechanism of blood cell and hematopoietic toxicity associated with a wide variety of exogenous agents that have ROS-generating electron transfer functionalities (Lenaz and Strocchi, 2011). Exposure to these agents generates ROS of varying severity and in a variety of tissues depending on their reactivity, metabolism, and site of exposure. Oxidants with a propensity for hematopoietic cells include physical agents (ionizing radiation, ultraviolet light); drugs and their metabolites (especially chemotherapeutics, 5-fluorouracil, adriamycin, barbiturates, phorbol esters, peroxisome-proliferating compounds, captopril); pollutants (cigarette smoke, ozone); and environmental and industrial chemicals (arsenic, benzene, chlorinated compounds, acrylonitrile, butoxyethanol) (Rizzo, 2012). Chemical drug classes include quinones (or phenolic precursors), metal ions and metal complexes (or complexors), aromatic nitro compounds (or reduced derivatives), and conjugated imines or iminium species.

HSCs of the bone marrow and other hematopoietic organs are vulnerable to injury by ROS (Knight et al., 2011; Shao et al., 2008). ROS exert

their damaging effects by directly modifying cellular or extracellular macromolecules and by altering the redox state of factors involved in signal transduction. They are capable of reacting with and altering the structure and function of all biological molecules, including nucleic acids, proteins, carbohydrates, and lipids. Lipid peroxidation severely damages cell membranes, causing alterations in membrane fluidity, cell shape, enzyme systems, receptors, and ion channels. Increased permeability to calcium and other ions resulting from lipid peroxidation may initiate inflammation and apoptosis. ROS also denature critical proteins such as hemoglobin and thiol-dependent enzymes. Injury to mitochondria reduces ATP production and disrupts normal cell function. The spectrum of DNA lesions caused by oxidative stress is similar to that for ionizing radiation (base modifications, apurinic/apyrimidinic sites, protein-DNA crosslinks, single and double strand breaks).

In the quiescent pool, DNA damage from ROS buildup drives HSCs out of quiescence and activates cellular proliferation, which is essential for repair of complex DNA damage (Hole et al., 2010; Ludin et al., 2014). These abnormalities may lead to accelerated aging of HSCs, apoptosis, or mutagenesis. In the proliferating pool, the cellular response to ROS-induced DNA damage is to arrest the cell cycle and repair the damage. Failure of DNA repair results in apoptosis or chromosomal instability, mutagenesis, altered gene expression, and initiation, promotion, and progression of carcinogenesis (Ghaffari, 2008). As such, ROS-generating agents constitute an important class of carcinogen implicated in all steps of carcinogenesis (complete carcinogens).

The consequences of oxidative injury therefore range from hemolytic anemia, with or without neutropenia and thrombocytopenia, to myelodysplasia and leukemia. The deleterious effects of oxidative stress are not limited to cytotoxicity caused by direct damage to cellular molecules. Oxidative stress also disrupts homeostatic redox cycling in hematopoietic cells, resulting in activation of quiescent cells and premature stem cell exhaustion. Indeed, in some cases the mitogenic effects of chemical carcinogens are due to induction of ROS rather than receptor binding or cytotoxicity (Hole et al., 2011).



Several mechanisms exist to limit oxidative stress to the mammalian HSCs (Jang and Sharkis, 2007). The hypoxic subendosteal niche in which quiescent HSCs reside serves to reduce ROS and protect stem cells from oxidative stress. HSCs in the low-oxygen marrow microenvironment generate ATP via anaerobic glycolysis instead of mitochondrial oxidative phosphorylation to further limit the production of ROS. FoxO (Forkhead Box O) transcription factors are essential for resistance to oxidative stress in pluripotent HSCs and committed erythroid stem cells because they maintain HSC quiescence and induce expression of proteins involved in cellular responses to oxidative stress (such as SOD [superoxide dismutase], catalase and GADD45 [Growth Arrest and DNA Damage]) (Tothova et al., 2007). The critical role of FoxO in maintenance of HSC self-renewal and hematopoietic homeostasis is highlighted in FoxO knockout mice. HSCs (but not committed progenitors) isolated from FoxO<sup>-/-</sup> mice have increased levels of ROS and cell cycle abnormalities.

At noncytotoxic doses, an agent may induce subtle increases in ROS that are relevant to organ function. Many ROS, such as hydrogen peroxide, are membrane-permeable such that production affects not only the cells generating them but also neighboring cells and the microenvironment (bystander effect) (Lisanti et al., 2010). The shift in redox signaling induced by oxidative stress recapitulates the rapid increases in ROS that are observed with growth factor stimulation.

Chronically elevated ROS effectively limit the lifespan of HSCs, resulting in premature exhaustion of HSCs, hematopoietic dysfunction, and eventual myelodysplastic syndrome. Since many of the conserved pathways regulating stem cell self-renewal and differentiation are also stress-response pathways, activation of stress response pathways by oxidative stress alters regulation of cell fate. The repeated activation of quiescent stem cells over a life span can have cumulative cell-autonomous effects including epigenetic dysregulation, mutations, and telomere erosion. Disruption of HSC quiescence prematurely exhausts the stem cell pool and causes hematologic failure under various stresses, such as oxidative stress, cell cycling, and aging (Ludin et al., 2014).

## 6.2. Direct Nonimmune Injury to Circulating Cells

Peripheral blood cells are commonly subjected to direct injury since they come into direct contact with circulating xenobiotics (Table 5.12) (Ramaiah et al., 2013). RBCs are most sensitive; being anucleate, they have no regenerative capacity and limited capacity for damage repair, and once their defense systems are damaged or overwhelmed, their ability to compensate is virtually zero. Similarly, platelets have no regenerative capacity and are highly susceptible to functional alteration or activation by xenobiotics. Nucleated cells tend to be much more resistant to direct injury. Lymphocytes have self-regenerative capacity but are susceptible to immunomodulation and predisposed to apoptosis when exposed to stressors. Granulocytes are in a better position to resist damage, having abundant cytoplasm that is well stocked with organelles. Monocytes and macrophages tend to be the most resistant to the direct action of cytotoxic agents thanks in part to their robust self-regenerative capacity, although there are numerous agents that can significantly alter their functions in inflammation and immunity.

Injury to circulating RBCs results in hemolysis that may be intravascular or extravascular, depending on the mechanism, severity, and rapidity of the injury. Acute exposures to agents that are highly reactive or that interfere with ATP production can rapidly cause intravascular hemolysis while the slow, unchecked accumulation of less extensive RBC injury tends to cause extravascular hemolysis (erythrophagocytic destruction), eryptosis, and shortened erythrocyte life span. The most common causes of premature erythrocyte destruction or death are oxidative injury, non-oxidative chemical injury, and immune-mediated destruction (discussed in Section 6.3 *Immune-Mediated Destruction*) (Shander et al., 2011).

Acute or severe RBC injury leading to intravascular hemolysis is viewed as a pathological state due to the vasoactive and redox-active properties of hemoglobin (Hgb) (Rother et al., 2005). As such, there are numerous protective mechanisms in place to degrade or sequester free Hgb and its dissociation products. Hgb dimers derived from the dissociation of normal Hgb tetramers are bound in the circulation by

haptoglobin. This limits the potential tissue damage caused by propagation of the free radicals generated within the heme-containing globin chains. CD163 receptors on monocytes/macrophages also clear free Hgb. Heme is degraded by heme oxygenase, and the resulting free iron is bound by ferritin or transferrin.

The heme groups and free radicals released from Hgb are cleared from the blood by  $\alpha_1$ -microglobulin, a heme- and radical-binding protein. However, during hemolysis, normal plasma and cellular binding capacities are exceeded. Free Hgb may irreversibly bind NO, resulting in vasoconstriction and vascular dysfunction. The heme moiety of free Hgb dimers is toxic to cells and can induce injury through formation of ROS. Heme-mediated oxidative side effects include hemoglobinuric nephrosis, acute renal failure, hepatic necrosis, and blood-brain barrier disruption (Butt, 2011). Ferric ( $\text{Fe}^{3+}$ ) iron may react with chloride to form hemin, a hydrophobic molecule that intercalates into the membranes of RBCs. Hemin in normally limited quantities is removed from RBC membranes by interaction with albumin, hemopexin, and haptoglobin. However, hemin accumulation causes rapid lysis of the RBC. Hemin also promotes lipid peroxidation and mitochondrial dysfunction, and can lead to vasculitis, phlebitis, and coagulopathy (Schaer et al., 2013).

The accumulation of erythrocyte injury can reduce the cell lifespan in circulation. Macrophages may remove altered RBC membrane to produce spherocytes or may destroy the erythrocyte outright. In addition, antibody binding to opsonized band 3 clusters may cause RBC autoagglutination. Excessive eryptosis is triggered by osmotic shock, oxidative stress, energy depletion, hyperthermia, and a number of small molecules and is also observed with lead or mercury intoxication. Small molecules trigger eryptosis by increasing cytosolic calcium ( $\text{Ca}^{2+}$ ) stores, stimulating ceramide formation, depleting ATP, causing oxidative stress, and/or activating caspase-3 (a master enzyme that mediates the common final steps of the apoptosis cascade; see *Morphologic Manifestations of Toxic Cell Injury*, Vol 1, Chap 6).

### 6.2.1. Oxidative Injury to Circulating Cells

Circulating erythrocytes experience some of the highest levels of oxidative stress in the

body. This is both because they carry large quantities of oxygen and because they are exposed to exogenous oxidizing agents in plasma. In mature erythrocytes, endogenous ROS arise primarily from the spontaneous conversion of oxyhemoglobin to methemoglobin and from anaerobic glycolysis (glucose-6-phosphate [G6P] from the Embden–Meyerhof pathway). In maturing erythroid cells and reticulocytes, ROS are also produced as a consequence of iron incorporation into heme, which produces the highly reactive hydroxyl ( $\text{OH}^+$ ) radical. ROS also increase during many diseases (diabetes, inflammation, hyperthyroidism, neoplasia, parasitemia, intense exercise, ischemia/reperfusion) in amounts sufficient to decrease RBC lifespans, although they may not be associated with anemia. There are numerous exogenous sources of oxidants, including foods, chemicals, drugs, and environmental contaminants.

Oxidative stress in erythrocytes results from the combined effects of increased ROS production and antioxidant inhibition/depletion. Oxidoreductive enzymes (methemoglobin reductase, copper/zinc-superoxide dismutase, catalase, glutathione peroxidase, thioredoxin reductase, thioredoxin, and peroxiredoxins) and nonenzymatic scavengers (GSH, vitamin E, ascorbic acid, and carotenoids) protect erythrocytes against oxygen radicals. The pentose phosphate pathway generates NADPH, which is the major source of reducing equivalents needed for catalase function and for maintenance of the reduced states of glutathione and thioredoxin. Glucose-6-phosphate dehydrogenase (G6PD), the first and rate-limiting enzyme of the pentose phosphate pathway, is induced by oxidative stress to increase NADPH synthesis. G6PD levels normally decrease as erythrocytes age so that older erythrocytes are most susceptible to hemolysis (Arese et al., 2012). In ruminants, the rumen's reducing environment also confers resistance to ingested oxidants.

Oxidants may damage hemoglobin, enzymes, iron, cytoskeleton, and membranes, resulting in abnormal oxygen-carrying capacity, cell shape, and membrane fluidity as well as hemolysis. Oxidative stress also triggers eryptosis by different but converging pathways: (1) caspase activation; (2) formation of  $\text{PGE}_2$ , leading to activation of  $\text{Ca}^{2+}$ -permeable channels; and (3) phospholipase  $\text{A}_2$ -mediated release of platelet-activating factor

TABLE 5.12 Agents Causing Direct (Nonimmune) Injury to Circulating Blood Cells

Mechanism		Cell	Xenobiotic
Oxidative injury	Methemoglobinemia (oxidation of heme iron)	Erythrocytes	Aliphatic esters of nitrous acid (n-hydroxylamines), aliphatic esters of nitric acid (glyceryl trinitrate), amyl and butyl nitrite, local anesthetics (e.g., lidocaine, benzocaine, prilocaine), nitrate- contaminated water, nitrites, nitroaromatics (nitrobenzene, phenylhydroxylamine, dinitrotoluene), plants (brassicaceae, capeweed, pigweed, sorghums, <i>Tribulus</i> sp., variegated thistle), potassium chlorate, aminophenols, anilines, sulfonamides, chlorine dioxide
	Heinz bodies (oxidation of globin)		Aspirin, phenacetin, phenylhydramine, phenylhydrazine, phenothiazine, phenazopyridine, primaquine, propofol, ecabapide, benzocaine, dapsone, menadione, methylene blue, crude oil (marine birds), naphthalene. Plants (onions, garlic, <i>Brassica</i> sp., <i>Acer rubrum</i> ) Acetaminophen (cats, dogs); propylene glycol (cats); zinc (dogs); copper (ruminants, Bedlington terriers)
	Sulfhemoglobin		Acetaminophen, acetanilide, aniline, chlorate salts, hydroxylamine, dimethyl disulfide, methylene blue (in G6PD deficient individuals), naphthalene, nitrobenzenes, phenols, primaquine, sulfites, sulfonamides, onions and garlic (dogs and cats), sulfanilamide, phenazopyridine, propylene glycol, phenothiazine (horses), red maple ( <i>Acer rubrum</i> ) (horses), brassica spp. rye grass (ruminants)
	Membrane damage		Acetaminophen, arsine, copper, dapsone, primaquine, ribavirin, snake venom (vipers)
	Induced apoptosis	Leukocytes	Clozapine
Direct lysis	Membrane damage	Erythrocytes	Insect and snake venoms; 1-tryptophan and indoles; arsine
		Platelets	IL-2, valproate, phenytoin, GM-CSF, snake venom
	Complement-mediated destruction	Neutrophils	Clozapine, rituximab, 5-azacytidine, propylthiouracil
		Erythrocytes	Benzene, vitamin C, antithymocyte globulin
Altered function	Enzyme inhibition	Erythrocytes	Lead, zinc (pennies, metallic hardware), chromium, copper, mercury
	Altered cooperative binding of globin units		Methemoglobinemia, carbon monoxide, clofibrilic acid, bezafibrate, aromatic benzaldehydes, hydroxyurea.
	Inhibition of serotonin reuptake	Platelets	Fluoxetine, some tricyclic antidepressants
	Inhibition of thromboxane		COX-1 inhibitors

(Continued)



**TABLE 5.12** Agents Causing Direct (Nonimmune) Injury to Circulating Blood Cells—cont'd

Mechanism	Cell	Xenobiotic
synthesis (antithrombotic) Inhibition of prostaglandin synthesis (prothrombotic)		COX-2 inhibitors
Membrane receptor antagonism		$\beta$ -lactam containing antibiotics (e.g., penicillin, ampicillin, cephalosporins)
Calcium channel antagonism		$\beta$ -blocker cardiac drugs (e.g., propranolol), $\beta$ -lactam antibiotics
Risk of thrombosis		Clopidogrel, antiglycoprotein iib/iiia inhibitors; antiestrogens (tamoxifen, toremifene); progestins (hydroxyprogesterone caproate, medroxyprogesterone acetate, megestrol acetate); aromatase inhibitors (anastrozole, letrozole, exemestane); EPO
Altered adherence and motility	Neutrophils	Colchicine, dextran, ethanol, glucocorticoids, iron oxide, rifampicin, macrolide antibiotics
Impaired superoxide production		Methadone
Inhibits kinase signaling		Dasatinib
Impaired phagocytosis		Ethanol, glucocorticoids

COX, cyclooxygenase; EPO, erythropoietin; G6PD, glucose-6-phosphate dehydrogenase; GM-CSF, granulocyte/macrophage colony-stimulating factor; IL-2, interleukin-2

Modified from Haschek WM, Rousseaux CG, Wallig MA, editors: *Haschek and Rousseaux's handbook of toxicologic pathology*, ed 3, 2013, Academic Press, Table 50.7, p. 1902–03, with permission.

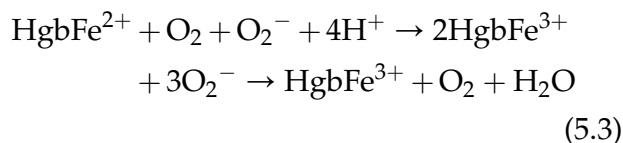
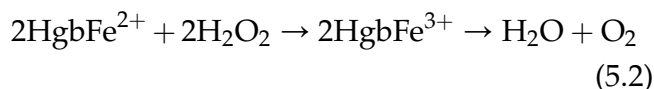
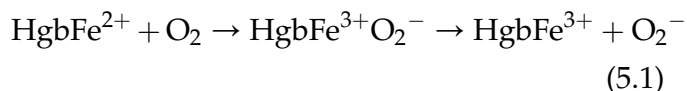
(PAF), which activates a sphingomyelinase and leads to formation of the membrane-scrambling molecule ceramide (Dreischer et al., 2022; Lang et al., 2017). Activation of  $\text{Ca}^{2+}$ -permeable cation channels increases cytoplasmic  $\text{Ca}^{2+}$  concentrations. Increased cytosolic  $\text{Ca}^{2+}$  induces phosphatidylserine externalization (“membrane flipping”), which marks cells for phagocytosis and clearance.  $\text{Ca}^{2+}$  also activates  $\text{Ca}^{2+}$ -sensitive potassium ( $\text{K}^+$ ) channels, leading to efflux of  $\text{K}^+$  and chloride ( $\text{Cl}^-$ ) ions, hyperpolarization of the cell membrane, and cell shrinkage. These intracellular ionic shifts activate calpain, a cysteine protease that degrades cytoskeletal proteins, causing cell membrane blebbing and impacting the cell's ability to sustain its usual discoid conformation and deformability.

Clozapine-induced neutropenia results from the drug's oxidation in activated neutrophils and bone marrow cells to a reactive nitrenium ion by the action of myeloperoxidase (Williams et al., 2000; Yang, 2011). The accumulation of this reactive metabolite depletes GSH, rendering neutrophils and their precursors highly susceptible to oxidant-induced apoptosis.

### 6.2.2. Oxidation of Iron in Hemoglobin: Methemoglobin

The spontaneous but reversible oxidation of the iron moiety of Hgb from ferrous iron ( $\text{Fe}^{+2}$ ) to ferric iron ( $\text{Fe}^{+3}$ ) results in the formation of methemoglobin (Met-Hgb) and superoxide (Equation 5.1). A direct interaction of reduced Hgb with hydrogen peroxide, the reduction

product of superoxide, also results in Met-Hgb formation (Equation 5.2). The rate of iron oxidation is enhanced by increased temperature, decreased pH, organic phosphate, metal ions, partial oxygenation of Hgb, and superoxide anions (Equation 5.3). Nitrites interact with heme to facilitate oxidation of heme iron.



Met-Hgb is normally maintained below 1% of total Hgb by cytochrome *b*<sub>5</sub> Met-Hgb reductase (NADH dehydrogenase) and its cofactor flavin adenine dinucleotide (FAD). However, oxidizing agents can facilitate the oxidation of heme to met-heme, and increase Met-Hgb concentrations.

Met-Hgb cannot bind oxygen but increases the oxygen affinity of other Hgb molecules within the tetramer, thus impairing oxygen delivery to tissues. Met-Hgb levels of less than 10% are asymptomatic, while levels greater than 10%–20% (>1.5 g/dL) are clinically relevant and may be associated with anoxia, cyanosis, reduced oxygen saturation, lethargy, and brown-colored arterial blood even though arterial pO<sub>2</sub> values are normal (Coleman and Coleman, 1996; Skold and Klein, 2013). Levels >70% are life-threatening. Met-Hgb is a reactive molecule that further increases oxidative stress and causes osmotic fragility and intravascular hemolysis.

Oxidation of Met-Hgb and Hgb can also produce hemichromes, which alter the proteins' tertiary structure (Lutz, 2012). Hemichrome formation may be reversible, such that it can be converted back to Met-Hgb and reduced Hgb. However, when irreversible, hemichromes facilitate heme dissociation from globin to produce precipitated hemichromes and heme-

free globin. Precipitated hemichromes interact with erythrocyte membranes to induce membrane protein band 3 clustering, resulting in opsonization of band 3 clusters and recognition by phagocytic macrophages.

In domestic animals, specifically grazing animals, high nitrites and nitrates in water supplies are prime causes of methemoglobinemia (Bruning-Fann and Kaneene, 1993; Wollin and Dieter, 2005). However, plants that contain variable but sometimes high concentrations of nitrates may also be causal, such as those of the Brassicaceae family (mustards, kales, turnips, cabbages, etc.), sorghum, variegated thistle (*Silybum*), pigweed (*Amaranthus*), cape-weed (*Cryptostemma*), and *Tribulus*. Cattle are more susceptible than sheep and horses. Potassium chlorate, an herbicide, can also cause methemoglobinemia in grazing animals that ingest contaminated plants. Methemoglobinemia due to ingestion of red maple (*Acer rubrum*) has been reported in horses and other species including alpacas and zebras. Methemoglobinemia has also been reported in a dog exposed to skunk spray.

Various therapeutic drugs and environmental chemicals have also been shown to induce Met-Hgb formation following natural or experimental exposures. Therapeutic agents that induce methemoglobinemia in humans include amyl nitrate, nitroglycerine, primaquine, NO, metoclopramide, flutamide, and quinones (Bowman, 2005). Local anesthetics (e.g., lidocaine, benzocaine, prilocaine), acetanilide, phenacetin, primaquine and phenazopyridine, dapsone, sulfonamides, silver nitrate, methylene blue, vitamin K antagonists, DL-methionine, and nitroglycerine can also induce methemoglobinemia in a variety of species (Hejtmancik et al., 2002). Environmental agents associated with methemoglobinemia include nitrites, nitrates, nitrobenzenes, aniline dyes and aniline derivatives, butyl nitrite, potassium chlorate, gasoline additives, aminobenzenes, nitrotoluenes, nitroethane, *o*-toluidine, paratoluidine,  $\beta$ -naphthol disulfonate, and cyclohexanone oxime (Shander et al., 2011).

The oxidation of ferric iron by hydrogen sulfide (H<sub>2</sub>S) irreversibly produces

sulfhemoglobin, a denatured, nonfunctional form of the parent Hgb molecule containing a sulfur atom in one or more of the porphyrin rings. Most of the chemical agents that cause methemoglobinemia can also cause sulfhemoglobinemia. In humans, sulfhemoglobinemia has been reported with exposure to sulfate, sulfonamides, phenazopyridine, acetanilide, phenacetin, nitrates, trinitrotoluene, and sulfasalazine (Gopalachar et al., 2005).

### 6.2.3. Oxidation of Globin

In addition to oxidation of iron at the heme core of Hgb, oxidants can damage the protein (globin) moiety of the Hgb molecule. Oxidation of sulfhydryl groups on the globin moiety of Hgb results in cross-linking between Hgb molecules as well as oxidative denaturation of globin with dissociation from heme. Aggregation and precipitation of denatured Hgb, often near the cell membrane, results in Heinz body formation and premature RBC phagocytosis. Removal of Heinz bodies (oxidized Hgb) by the reticuloendothelial system in organs such as spleen can lead to abnormally shaped erythrocytes, including pseudospherocytes and degmacytes (in which RBC surfaces have irregular semicircular indentations) ["bite cells"] or vesicles ["blister cells"], mainly associated with removal of Heinz bodies and cytoplasm.

Heinz body anemia secondary to oxidative damage to Hgb has been identified in domestic animals in association with a wide variety of plants, drugs, chemicals, and diseases (Table 5.13) (Ramaiah et al., 2013). Agents frequently associated with oxidative injury to erythrocytes include acetaminophen, aspirin, phenacetin, phenylhydramine, phenylhydrazine, phenothiazine, phenazopyridine, primaquine, propofol, ecabapide, benzocaine, dapson, menadione, methylene blue, crude oil (marine birds), and naphthalene (Hedayati and Jahanbakhshi, 2013). The presence of Heinz bodies has also been reported in association with several diseases including *diabetes mellitus*, hyperthyroidism, lymphoma, and hepatic disease (particularly in cats). Species differences in xenobiotic metabolism and antioxidant defenses account for variations in susceptibility to oxidative injury and Heinz body formation. More Heinz bodies are observed in cats (up to 5% in healthy animals) because the spleen does not efficiently

remove damaged RBCs and because feline Hgb has eight reactive sulfhydryl groups per Hgb tetramer, as compared with four in dogs and two in humans and most other species (McMichael, 2007; Weiss, 1988). In contrast, rodents (rat, mouse and guinea pig) are less susceptible to glutathione depletion because they have more reactive cysteine residues per Hgb tetramer when compared to other species. These reactive cysteine residues compete and cooperate with GSH, acting as a sink for ROS to reduce oxidative stress. Allelic variations in the  $\beta$  globin gene complex, resulting in variations in the number of reactive cysteines, have been described in some strains of mice that are more sensitive than rats to the formation of Heinz bodies.

#### 6.2.3.1. OXIDATION OF CYTOSKELETON AND MEMBRANE PROTEINS AND LIPIDS

Hemoglobin is not the only molecule susceptible to damage by oxidants. The erythrocyte cytoskeleton and membranes are also prone to injury. Erythrocytes with damaged membranes may be removed by splenic macrophages if damage is slowly evolving or may lyse within the bloodstream if membrane damage is severe and fulminating. Lipid peroxidation and cytoskeletal injury results in phospholipids cross-linking, membrane "stiffening," and decreased cell deformability. This hinders flow through narrow capillary beds and enhances fragility, resulting in RBC fragmentation (keratocytes and schistocytes). Restricting erythrocyte transit through the splenic red pulp also increases their exposure to resident macrophages. In dogs and horses, oxidative injury to cytoskeleton and membranes frequently causes adhesion of opposing bilayers to form eccentrocytes (RBCs with the Hgb shifted to one side of the cell) and pyknocytes (small, dark, often misshapen RBCs lacking central pallor) (Caldin et al., 2005).

Membrane lipid peroxidation alters membrane permeability to  $K^+$  and altered  $Na^+/K^+$  gradients. Severe membrane damage may lead to impaired ability to maintain intracellular ion gradients, leading to swelling and even bursting of the damaged erythrocyte within blood vessels (intravascular hemolysis). Copper is notoriously damaging to erythrocyte membranes, especially in sheep, which are extremely sensitive to damage by this element



**TABLE 5.13** Agents Causing Heinz Body Anemia in Animals

Class	Agent	Mechanism	Species	Outcome
Plants	Allium family (onions, garlic)	Aliphatic sulfides decrease glucose-6-phosphate dehydrogenase activity	Most domestic species; Shiba Inu dogs	Heinz body hemolytic anemia
	<i>Brassica</i> sp. (cabbage, kale, rape)	1. S-methyl-L-cysteine sulfoxide metabolized to dimethyl sulfide (oxidant) by rumenal bacteria 2. High sulfur content reduces copper availability 3. Low copper and zinc content	Ruminants	Heinz body hemolytic anemia
	<i>Acer rubrum</i> (wilted red maple leaves)	Rapid glutathione depletion	Horses and zebras	Eccentrocytosis with or without heinz bodies, methemoglobinemia
Drugs/ Chemicals	Acetaminophen	Low acetaminophen UDP-glucuronosyltransferase activity in cats results in increased levels of oxidant acetaminophen metabolites	Cats Dogs	Heinz body hemolytic anemia
	Propylene glycol (food additive)		Cats	Heinz body hemolytic anemia
	Zinc (pennies, hardware, ointments)	Band 3 clustering	Dogs	Spherocytosis Heinz body hemolytic anemia
	Copper (subterranean clover, copper plumbing)	Acute release from liver	Ruminants (esp. sheep); Bedlington terriers	Intravascular hemolysis, heinz bodies, methemoglobinemia

Modified from Haschek WM, Rousseaux CG, Wallig MA, editors: Haschek and Rousseaux's handbook of toxicologic pathology, ed 3, 2013, Academic Press, Table 50.8, p. 1906, with permission.

(Mendel et al., 2007; Roney et al., 2011; Vertiz et al., 2014). Snake venom, especially from the viper group, also causes RBC membrane damage (see *Animal Toxins*, Vol 3, Chap 8), as does arsine (arsenic hydride), a byproduct of certain industrial processes, and the aniline-based drugs, dapsone and primaquine (Bordin, 2010; Bowman et al., 2005; Fernandez et al., 2018). The antiviral drug ribavirin has been

shown to cause Met-Hgb formation and promote hemolysis via oxidative membrane damage and ATP depletion, leading to decreased  $\text{Na}^+/\text{K}^+$  membrane pump function (De Franceschi et al., 2000).

#### 6.2.3.2. NONOXIDATIVE INJURY

Exposure to some xenobiotics is associated with hemolysis without significant oxidative

injury. Often, the cause of injury is unknown or unclear. For example, arsenic hydride (arsine) gas, which may be inhaled when arsenic-contaminated metals are treated with strong acids (metal mining, paint, herbicides) can result in severe intravascular hemolysis with anemia, jaundice, and hemoglobinuria. Although arsine is a strong reducing agent, its hemolytic potential is hypothesized to result from a direct interaction with Hgb, resulting in heme release from globin. Arsine may also interact with sulfhydryl groups of  $\text{Na}^+/\text{K}^+$  pumps, which result in disruption of ion homeostasis and osmotic hemolysis (Rael, 2005; Rael et al., 2006, 2000).

Metals such as lead, zinc (pennies, metallic hardware), chromium, copper, and mercury inhibit enzymes required for RBC maturation and function (Roney et al., 2011). While some effects may be observed in maturing cells of the bone marrow, peripheral destruction is also observed. The damaging effects of lead are multiple but result in reduced RBC lifespan, dyserythropoiesis, and an increased bone marrow M:E ratio. Ringed sideroblasts can be observed in the bone marrow as rubricytes containing iron-positive granules (siderotic inclusions ["Pappenheimer bodies"]) around the nucleus. Sideroblastic anemia is common in lead and zinc toxicity and has also been associated with isoniazid, chloramphenicol, linezolid, penicillamine, triethylene, and tetramine dihydrochloride as well as with chemotherapy-related myelodysplasia (Broun et al., 1990; Fiske et al., 1994; Latimer et al., 1989; Luttgen et al., 1990). Lead interferes with enzymes involved in heme synthesis ( $\gamma$ -aminolevulinic acid [ALA] dehydratase and ferrochelatase), resulting in a nonregenerative, sideroblastic, hypochromic, microcytic anemia with metarubricytosis due to failure of nuclear expulsion. Lead also inhibits pyrimidine 5'-nucleotidase (involved in depolymerization of reticulocyte ribosomal RNA) leading to retention of RNA in reticulocytes and basophilic stippling. It also promotes oxidative stress by inhibiting antioxidants (superoxide dismutase, catalase, glutathione peroxidase, G6PD, and GSH). Common sources of lead include lead-containing paints (dogs and cats), batteries (cattle), industrial contaminants in pastures (cattle), and lead shot (waterfowl and raptors) (Piomelli, 1981; Valentine et al., 1976).

Copper toxicity causes acute intravascular hemolytic anemia, icterus, and hemoglobinuric nephrosis in sheep, goats, and calves due to inhibition of enzymes involved in the hexose monophosphate shunt and Embden–Meyerhof pathway (Johns and Heller, 2021; Lin et al., 2017; Mendel et al., 2007; Nederbragt et al., 1984; Söli, 1980). Pyrrolizidine alkaloid hepatotoxicity is associated with excessive release of hepatic copper stores into circulation and secondary hemolytic crisis. Ingestion of excess chromium may also result in a hemolytic anemia and thrombocytopenia, although the mechanism is not known (Ray, 2016). Mercury and methylmercury intoxication is most common in fish, waterfowl, and shore birds since they are at greatest risk of exposure to this environmental contaminant. Mercury inhibits glutathione reductase, G6PD, and acetylcholinesterase, and is also associated with idiosyncratic IMHA and immunotoxicity. Hematologic findings associated with mercury toxicity include anemia, dysmyelopoiesis, and increased bone marrow cellularity (Vianna et al., 2019).

Hemolysin toxins found in insect and snake venoms can cause hemolysis, either by direct (polypeptidic "direct lytic factor") or indirect (phospholipase) action on RBC membranes (Fernandez et al., 2018) (see *Animal Toxins*, Vol 3, Chap 8). ATPases contained in snake venoms deplete ATP resulting in the inhibition of ion pumps, an influx of water, RBC swelling and hemolysis. Phospholipase A<sub>2</sub> (PLA<sub>2</sub>) promotes lysolecithin incorporation in the outer layer of the RBC membrane, causing a disproportionate expansion of the outer layer and formation of echinocytes (RBCs with multiple small, evenly spaced projections from the cell surface) and spherocytosis. Similarly, 1-tryptophan and indoles are readily incorporated into RBC membranes due to their lipophilic properties, resulting in acute hemolytic anemia and hemoglobinuria.

Thrombocytopenia due to direct cytotoxicity and/or increased clearance by the reticuloendothelial system has been reported in association with IL-2, valproate, phenytoin, GM-CSF, and snake venom. Drug-induced neutropenia can occur in association with clozapine; rituximab; 5-azacytidine, which causes hypomethylation-induced apoptosis; and propylthiouracil, which causes complement-mediated destruction of

neutrophils. Clozapine is metabolized in neutrophils by myeloperoxidase to a reactive nitrenium ion metabolite that appears to initiate an immune response and accelerate neutrophil apoptosis (Ramaiah et al., 2013).

### 6.3. Immune Injury and Destruction

Type B drug reactions are unpredictable and lack a distinct dose–response relationship (Baldo and Pham, 2021). These include immune-mediated hypersensitivity reactions, nonimmune hypersensitivities, and idiosyncratic reactions. Immune-mediated hypersensitivity occurs through antibody-mediated mechanisms. Antibody binding can trigger direct complement-mediated lysis or sequestration and phagocytosis of cells coated by complement C3 and immunoglobulin by elements of the reticuloendothelial system. Immune-mediated hypersensitivities are typically classified as Type I (immediate, IgE-mediated), Type II (IgG- or IgM-mediated), Type III (IgG/IgM immune complex-mediated), and Type IV (delayed-type or cell-mediated) (Maker et al., 2019). Nonimmune hypersensitivities (pseudoallergies) arise as a consequence of activation of the complement system (C activation-related pseudoallergy [CARPA]) in the absence of antibodies, though they resemble allergic reactions clinically (Szebeni, 2005, 2014). Idiosyncratic reactions are rare, unpredictable responses that are not attributable to a single mechanism. Instead, they are hypothesized to occur due to the combined contribution of immune-mediated, genetic, and environmental factors.

Drug-induced immune-mediated hematologic disorders are most commonly due to Type II hypersensitivity. These conditions are associated with four types of antibodies: hapten (neoantigen)-dependent antibodies, drug-dependent antibodies, drug-induced (drug-independent) autoantibodies, and drug-specific antibodies (Greinacher et al., 2001).

Hapten-dependent antibodies recognize drug-protein adducts on membranes of erythrocytes or platelets, resulting in anemia or thrombocytopenia, respectively. In vitro demonstration of hapten-dependent antibodies requires that cells be pretreated with the suspect drug, resulting in a positive indirect antiglobulin test when serum is mixed with pretreated cells. In animals

and humans, hapten-dependent drug-induced hemolytic anemia is associated with penicillins, cephalosporins, levamisole, sulfonamides, vaccination, and heparin (horses).

Drug-dependent antibodies require the presence of soluble drug to bind their cellular targets. In contrast to hapten-dependent antibodies, drug-dependent antibodies do not recognize drug-coated cells, and high concentrations of soluble drug do not inhibit antibody binding. Rather, the drug promotes interaction of the Fab (fragment antigen-binding) region of the antibody to its target (typically a cell surface molecule) without linking covalently to either of the reacting macromolecules. Antibody binding immobilizes the drug such that it becomes trapped at the site of the target molecule. Cytopenia is usually drug-specific and resolves after withdrawal of the drug. In humans, drug-dependent antibodies have been associated with IMHA due to cefotetan, ceftriaxone, ceftizoxime, tolmetin, etodolac, chlorpropamide, carboplatin, cisplatin, ibuprofen, oxaliplatin, piperacillin, probenecid, quinine, quinidine methyl dopa, and fludarabine, and with immune-mediated thrombocytopenia due to quinine, many antibiotics, nonsteroidal antiinflammatory drugs (NSAIDs), anticonvulsants, and ocreotide.

Drug-induced (drug-independent) autoantibodies are responsible for the classic, true autoimmune disorders of autoimmune hemolytic anemia (AIHA) and autoimmune thrombocytopenia (AITP). In these cases, the drug induces antibodies that react with cells in the absence of drug. These antibodies can be detected in vitro and will bind to their “self” target in the absence of exogenous drug (positive antiglobulin test). Drugs associated with AIHA or AITP include  $\alpha$ -methyl dopa, levodopa, procainamide, piperacillin, cefotetan, ceftriaxone, penicillamine, sulfamethoxazole, and gold salts. With drug-independent autoantibodies, AIHA can persist even after the drug is withdrawn. Drug-dependent antibodies require the presence of drug alone but are not reactive to cells (e.g., quinine-induced thrombocytopenia).

Type III hypersensitivity (immune complex disease) leading to platelet aggregation and consumption via thrombosis can occur in patients treated for prolonged periods with heparin. Heparin-induced thrombocytopenia is



a unique disorder associated with binding and activation of platelets by drug-antibody complexes. In this common form of drug-induced immune thrombocytopenia, heparin binds to PF4 (a component of platelet  $\alpha$ -granules) and induces antibodies specific for heparin-PF4 complexes (Tardy et al., 2020). The immune complex binds to and activates platelets via Fc receptors, in contrast to drug-dependent antibodies that bind their targets via the antibody Fab domain. Although the resultant thrombocytopenia is usually not severe enough to cause bleeding, immune complex-mediated platelet activation and aggregation may result in thrombosis (Patel et al., 2021).

Blood cells are uniquely susceptible to immune-mediated destruction because they are directly exposed to both xenobiotics and antibodies, and because the normal removal of aged or damaged cells requires antibody-mediated identification and removal by phagocytes of the reticuloendothelial system. Drug-induced opsonization by antibodies also leads to increased clearance of the coated cells by reticuloendothelial macrophages. Immune-mediated destruction usually involves removal of circulating blood cells, producing disorders such as immune-mediated anemia, immune-mediated thrombocytopenia, and immune-mediated neutropenia. However, antibody-mediated destruction can extend to hematopoietic cells of the bone marrow, resulting in pure red cell aplasia, agranulocytosis, or aplastic pancytopenia (Lucidi et al., 2017). The list of drugs and the mechanisms by which they induce immune-mediated destruction as well as their resultant hematologic disorders is highly variable, and it is suspected the genetic and environmental factors play important roles with respect to such variability. Specific drugs may cause different types of hypersensitivity reactions in different individuals, and multiple mechanisms may operate in a single individual. In addition, temporal associations of exposure and onset of immune-mediated hematologic disorders are not always consistent. In general, there is a delay between exposure and the onset of the adverse reaction. Amnestic immune responses, characterized by rapid onset of hypersensitivity after a rechallenge, confirm that the effect is immune-mediated. However, immune-mediated hypersensitivities may not have an

amnestic response if the hypersensitivity has a strong autoimmune component that results in deletion of autoimmune memory cells after drug withdrawal.

Drug-induced IMHA is characterized by destruction of RBCs by antibodies acting against antigens on the erythrocyte membrane. Antibody-mediated erythrocyte destruction produces a decreased hematocrit (with or without hyperbilirubinemia and a positive Coombs test [indicating the presence of anti-RBC antibodies in the blood]) and an inflammatory leukogram. Reticulocytosis is observed if bone marrow erythroid cells are unaffected (Garden et al., 2019). Onset is abrupt, and frequently the hematocrit plunges precipitously. In the dog, for example, if the hematocrit declines by 50% or more in 30 days or less and there is no evidence of hemorrhage, hemolytic anemia is present since the normal 120-day lifespan of the erythrocyte in the dog has been reduced to one quarter of normal. Spherocytosis and RBC agglutination may be observed if the blood sample is obtained soon after onset, when cells are rapidly being removed from the circulation. The reticulocyte count is normal to increased, and the direct antiglobulin test may be positive. Erythropoiesis is normal or increased in bone marrow if sufficient time for a regenerative response (i.e., 4–7 days) has elapsed. Erythrophagocytosis may also be prominent in the spleen, bone marrow, and liver. The absence of one or more of these laboratory features does not preclude the diagnosis of immune-mediated anemia, especially if erythropoiesis is normal or increased in the marrow. The list of drugs that have been reported on a sporadic basis to produce IMHA is very long indeed, and these reactions can often be difficult, if not impossible, to distinguish clinically from idiosyncratic reactions. However, some classes of drugs produce these reactions on a somewhat more consistent basis. Drugs most often associated with IMHA in multiple species, especially humans, dogs, and horses, include the penicillins, cephalosporins, and sulfonamides. Propylthiouracil-induced IMHA occurs in cats being treated for hyperthyroidism, while phenacetin, quinidine, and  $\alpha$ -methyldopa, among numerous others, have been reported to cause IMHA in humans.

In immune-mediated thrombocytopenia, platelet destruction occurs as antibodies bind to platelets, thus leading to their clearance by the

reticuloendothelial system (Narayanan et al., 2019; Vayne et al., 2020). Platelet production may also be decreased due to immune-mediated suppression of MKs and proplatelets. Thrombocytopenia is typically observed 6–8 days after exposure and may be asymptomatic or accompanied by purpura (i.e., purple discolorations indicative of hemorrhage) on mucosal and skin surfaces (Arnold et al., 2013). Thrombocytopenia is coupled with normal to increased thrombocytopoiesis in the bone marrow, normal CFU-Meg (megakaryocyte) cloning activity in *in vitro* cell culture, and rapid return of platelet counts to normal upon the withdrawal of drug. Laboratory confirmation, utilizing the platelet-associated immunoglobulin test, gives inconsistent results. Classical causes include quinine and quinine-like drugs; antimicrobials (vancomycin, rifampin, linezolid, sulfonamides, and penicillins); antiinflammatory drugs; antineoplastics; antidepressants; benzodiazepines; and anticonvulsants (carbamazepine, phenytoin, valproic acid) as well as cardiac and antihypertensive drugs (Curtis, 2014b; George and Aster, 2009). The most common mechanism is binding of drug-dependent antibodies to platelet membrane glycoproteins IIB/IIIa or Ib/IX. Abciximab (a chimeric Fab fragment) and fibans (i.e., RGD mimetic inhibitors such as eptifibatide and tirofiban) are antithrombotic agents that impair platelet function through the inhibition of GPIIb/IIIa-fibrinogen interaction. These agents induce a conformational change in GPIIb/IIIa that is recognized by drug-dependent antibodies and results in severe thrombocytopenia in humans. First-generation TPO receptor (mpl) agonists (e.g., pegylated recombinant human megakaryocyte growth and development factor [MGDF] and recombinant human TPO) designed to treat thrombocytopenia instead produced paradoxical thrombocytopenia due to immune-mediated production of anti-TPO antibodies and inhibition of binding to mpl, the TPO receptor. Drug-induced immune-mediated thrombocytopenia has also been reported in a dog after amiodarone administration. Thrombocytopenia that is compound-related should be distinguished from pseudothrombocytopenia, a spurious finding that occurs when the EDTA anticoagulant exposes neoantigens on platelet membranes as blood samples cool in the laboratory prior to analysis.

Drug-induced immune-mediated neutropenia is a rare disorder caused by hapten-dependent, drug-dependent, and autoantibodies against neutrophil-specific glycoproteins (Fc $\gamma$ III, CD177, GP70-95, CD11a, CD11b). This condition results in acute and profound neutropenia or agranulocytosis associated with infection and possible mortality. Drugs most often associated with agranulocytosis are antithyroidals, antibacterials, and anticonvulsants (Curtis, 2014a). In drug-induced neutropenia, the onset is abrupt, and frequently the neutrophil counts plunge precipitously. In toxicity studies, in most cases a single dog is affected, a graded dose-response is absent, neutrophil counts are decreased markedly, a neutrophil “left shift” is not present (unless infection supervenes), and the bone marrow is normo- or hypercellular at the nadir of the neutropenia (McManus et al., 1999; Vargo et al., 2007). Neutrophil counts rapidly return to normal following cessation of drug treatment, and there is no decrease in CFU-GM cloning activity in bone marrow cell cultures, indicating intact neutrophil stem cell proliferative capacity. Laboratory evidence for the immune-mediated destruction of neutrophils is difficult to provide. Ideally, specific laboratory confirmation requires the demonstration of either a drug-dependent antineutrophil antibody test or a similar drug-dependent test for immune complexes. Such tests are available, but they are technically complex and frequently provide false negative results. The demonstration of leukoagglutinin has also been considered as evidence for the immune-mediated destruction of neutrophils, but the test lacks specificity. Therefore, the diagnosis is made based on the clinical and hematologic features described earlier.

#### 6.4. Idiosyncratic Reactions

Drug-induced idiosyncratic toxicities comprise a complex group of rare, unpredictable, nondose-related adverse events that are not expected based on an inciting agent’s pharmacology (Patton and Duffull, 1994). Due to their infrequent occurrence both in humans and animals, animal models are not predictive and evidence for mechanisms is primarily based on epidemiologic studies.

The pathogenesis of idiosyncratic drug reactions is hypothesized to involve the combined effects of hypersensitivity, immunomodulation, reactive metabolites, oxidative stress, and genetic predisposition (Sernoskie et al., 2021). Many cases are believed to be immune-mediated based on a delay between the initial exposure and the onset of the adverse reaction as well as on the rapid onset upon rechallenge (amnestic response), although the presence of antibodies is not always documented (Zhang et al., 2011).

The “hapten hypothesis” proposes as causal the induction of a neoantigen (i.e., hapten) by the interaction of the drug with the cell membrane of the affected cell, although formation of drug-dependent antibodies and/or immune complexes has also been implicated. Most drugs associated with idiosyncratic reactions form reactive metabolites that are hypothesized to covalently bind cellular proteins to form immunogenic conjugates. The reactive metabolite is often formed in the target organ of toxicity. Drugs oxidized to reactive metabolites by myeloperoxidase may thus induce immune-mediated neutropenia.

The “danger hypothesis” proposes that reactive metabolites or their covalent binding to proteins induce stress and cellular expression of danger signals (DAMPs) that trigger an immune response. The “pharmaceutical interaction” hypothesis proposes that the drug directly targets immunoregulatory mechanisms by up-regulating costimulatory signals in APCs that activate helper T cells. Drug-dependent antibodies may also play a role when less reactive metabolites enter the circulation and induce hypersensitivity.

Idiosyncratic hematologic toxicity is characterized by a sudden, severe decrease in circulating blood cells that may also rarely involve the marrow. It usually affects one or two animals in a study or population and occurs most often in dogs. It involves neutrophils, erythrocytes, or platelets, singly or in combination, with 1 cell type often being much more affected than other cell types in a given individual. The phenomenon is named after the cell that is most affected (e.g., idiosyncratic neutropenia, idiosyncratic thrombocytopenia, or idiosyncratic aplastic pancytopenia); if red cells are affected, the syndrome would be referred to as idiosyncratic hemolytic anemia. Idiosyncratic cytopenias

have many of the characteristics of an immune-mediated process, such as rapid clearance or premature removal of affected cells from the circulation, rapid recovery when the drug is withdrawn, shortening of induction time upon reexposure to the drug, and, in many instances, reinduction of the cytopenia with a lower dose than the original inciting dose. The clinical characteristics of idiosyncratic anemia, thrombocytopenia, and neutropenia are similar to those of immune-mediated disorders. Onset is abrupt, and frequently the cell count plunges precipitously in a single or a few treated animals.

### 6.5. Altered Blood Cell Function

Xenobiotics can induce their toxic and/or adverse effects by altering essential functions of blood cells. In erythrocytes, altered respiratory function is due to effects on cooperative binding of globin units and Hgb oxygen affinity. In animals and humans, this may occur secondary to methemoglobinemia, carbon monoxide, clofibrate, bezafibrate, aromatic benzaldehydes, changes in pH, 2,3-BPG (bisphosphoglyceric acid) concentrations, and body temperature, or induced expression of fetal globins (hydroxyurea).

Many drugs can affect platelet function directly (Hassan, 2005; Kao et al., 2022). Severity of platelet effects by these drugs is highly variable, and not only species-dependent but also very dependent on individual susceptibility to the drug. Drug classes that interfere with platelet function include NSAIDs, thienopyridines (clopidogrel), peroxisome proliferator-activated receptor (PPAR) agonists/antagonists,  $\beta$ -lactam antibiotics, cardiovascular drugs ( $\beta$ -blockers), psychotropic drugs, anesthetics, antihistamines, and chemotherapeutics. Cyclooxygenase-1 (COX-1)-inhibiting NSAIDs are the best-known class of drugs to affect platelet function. They exert their effects by reversibly (nonaspirin NSAIDs) or irreversibly (aspirin or acetylsalicylic acid) inhibiting acetylation of COX-1, resulting in inhibition of thromboxane A<sub>2</sub> (TXA<sub>2</sub>) synthesis, vital for proper platelet function. In contrast, COX-2 inhibitors have pro-thrombotic effects since they inhibit production of prostacyclin, which inhibits platelet function.



A number of prescription drugs used to prevent thrombosis act by inhibiting platelet activation. Although their *in vitro* effects are potent, they are rarely associated with exaggerated pharmacologic effects of clinical bleeding. Epoprostenol (synthetic prostacyclin) activates platelet membrane G-proteins to produce cyclic adenosine monophosphate (cAMP), which inhibits platelet activation and counteracts any increase in cytosolic calcium levels that would result from TXA<sub>2</sub> binding. Cilostazol is a selective inhibitor of phosphodiesterase 3 (PDE<sub>3</sub>) that is used to prevent thrombus formation (Ito et al., 2012). PDE<sub>3</sub> regulates cAMP turnover to restrain platelet activation. cAMP is continuously produced in platelets and is induced by platelet agonists. By increasing cAMP, PDE<sub>3</sub> inhibitors suppress thrombin-induced Ca<sup>2+</sup> responses and integrin  $\alpha$ IIb $\beta$ 3 affinity regulation.

*In vitro*, PDE<sub>3</sub> inhibition blocks platelet aggregation, integrin activation, secretion, and thrombin generation. Its effects extend to all major processes in thrombus formation: assembly of platelets into aggregates, secretion of autocrine products, and procoagulant activity. The *in vitro* inhibitory effects of PDE<sub>5</sub> inhibitors (sildenafil and zaprinast) on platelet function are postulated to result from cyclic guanosine monophosphate (cGMP)-mediated effects on cAMP and from inhibition of thrombin-induced serotonin release (Kouvelas et al., 2009). Statins are hypothesized to inhibit platelet function through their inhibition of NF- $\kappa$ B, though this effect may be associated with their antiinflammatory effects (Nenna et al., 2021).

Some antithrombotic drugs interfere with membrane receptors essential for platelet activation. Thienopyridines (clopidogrel and ticlopidine) act by specifically and irreversibly inhibiting adenosine diphosphate (ADP) receptors (P2Y<sub>12</sub>) required for platelet activation by ADP (von Kügelgen, 2021). Platelet GPIIb/IIIa receptor antagonists (abciximab, tirofiban, snake venom disintegrin, barbourin) prevent binding by fibrinogen and vWF. Some snake venoms also contain acidic phospholipase that have potent inhibitory effects on platelet aggregation. Selective serotonin reuptake inhibitor (SSRI) drugs (e.g., fluoxetine) block the uptake of serotonin into platelets, leading to platelet serotonin depletion and impaired platelet aggregation (Little et al., 2006).

Calcium channel blockers and  $\beta$ -lactam antibiotics inhibit platelet function by interfering with agonist-stimulated Ca<sup>2+</sup> release from endoplasmic reticulum necessary for platelet aggregation. The inhibitory effect of penicillin is also postulated to involve irreversible attachment of the drug to the platelet surface, causing impairment of agonist (ADP, collagen, thrombin) binding to platelet receptors. Residual impairment of receptor function may be observed even after the antibiotic is discontinued. The clinical effect is most severe with hypoalbuminemia because higher levels of unbound drug are available to interact with the platelet surface.

Agents that inhibit platelet function generally do not cause clinical bleeding unless there is a coexisting hemostatic defect such as uremia, marked thrombocytopenia, von Willebrand's disease, or vitamin K deficiency. Other indirect causes in altered platelet function include hyperglobulinemia, increased fibrin degradation products (due to disseminated intravascular coagulation [DIC] or liver failure), uremia, and colloidal plasma expanders. Clinically, defects in platelet function produce prolonged bleeding times and gastrointestinal bleeding but may not be associated with alterations in platelet count or morphology or overt bleeding.

Thrombotic microangiopathies (e.g., thrombotic thrombocytopenic purpura [TTP] and hemolytic-uremic syndrome [HUS]) occur secondary to excessive platelet activation (whether direct, immune-mediated, or related to endothelial injury) (Chatzikonstantinou et al., 2020). They are associated with thrombocytopenia, microangiopathic hemolytic anemia, and symptoms of microvascular occlusion. Drugs associated with thrombotic microangiopathy in humans include cyclosporine, mitomycin-C, gemcitabine, cisplatin,  $\alpha$ -interferon, tacrolimus, thienopyridines, ticlopidine, clopidogrel quinine, and adeno-associated virus (AAV) gene therapies (Chand et al., 2021).

Numerous agents have been associated with or linked to impaired neutrophil function, but only a few have clear-cut and consistent associations. Among these are glucocorticoids in virtually all species, while the antipsychotic clozapine, opiates (especially heroin), radiocontrast agents (e.g., ioxaglate), aminopyrine, iron oxide, rifampicin, colchicine, dextran, chlordane, mercuric chloride, methylmercuric chloride, and

zinc salts (acne medication) have been implicated in humans (Boujbiha et al., 2012). Some agents have been shown to impair superoxide production (methadone). Other agents, such as macrolide antibiotics, suppress expression of integrins and receptors to alter neutrophil adherence, mobility, and/or chemotaxis. Dasatinib, a potent tyrosine kinase inhibitor chemotherapeutic, inhibits neutrophil activation by blocking Src family kinases and inhibiting integrin-dependent and Fc-receptor-dependent neutrophil activation and downstream signaling (Futosi et al., 2012). Functional consequences of dasatinib include decreased spreading, adhesion, and exocytosis of secondary granules. Impaired neutrophil phagocytosis is associated with ethanol and glucocorticoids. Altered function leads to premature neutrophil death, neutropenia, and susceptibility to infection. Enhanced neutrophil function has been reported in humans in association with sodium sulfite, mercuric chloride, chlordane, and toxaphene.

## 6.6. Indirect Injury, Secondary Effects, and Modifying Factors

The toxic effect of xenobiotics on bone marrow and circulating blood cells can result from direct injury, immune-mediated damage, or as a consequence of indirect effects on other tissues. Xenobiotic-related indirect effects on the hematopoietic system are exceedingly common, and they often reflect the systemic consequences and homeostatic responses to the effects of xenobiotics. Indirect effects can be broadly classified as causing suppression of hematopoiesis, injury to the bone marrow microenvironment, and/or decreased cell survival in circulation.

### 6.6.1. Suppression of Hematopoiesis

Suppression of hematopoiesis is commonly observed secondary to decreased food consumption, iron deficiency, chronic disease (especially neoplasia), and inflammation (Giulietti et al., 1991; Markovic et al., 2007; Miyata et al., 2009; Morita et al., 2017; Radakovich et al., 2015). Causes of iron deficiency include repeated phlebotomy, chronic blood loss, rapid growth (e.g., piglets fed mainly or solely with milk, which contains low levels of iron), and copper deficiency in ruminants. Inflammation and

disorders of hepcidin, a peptide hormone that regulates iron use, lead to decreases in iron availability for Hgb synthesis and are associated with cytokines that also suppress hematopoiesis (IL-12, interferon- $\gamma$ ).

Estrogen indirectly causes myelosuppression by inducing production of a myelopoiesis-inhibitory factor by thymic stromal cells (Horiguchi et al., 2013). Natural and synthetic estrogens can cause fatal pancytopenia (dogs and ferrets) and anemia (rats) at therapeutic doses. Some drugs suppress hematopoiesis via exaggerated pharmacology (IL-12) or off-target suppression (nonselective kinase inhibitors).

Chronic treatment with recombinant human EPO induces production of anti-EPO antibodies that neutralize exogenous and endogenous EPO, resulting in profound erythroid hypoplasia and nonregenerative anemia. In dogs, anemia is observed 2–3 months after initiation of treatment and does not resolve with administration of canine EPO. Antibody-mediated pure red cell aplasia has also been reported in patients receiving EPO due to the formation of anti-EPO antibodies (in humans and mice) after exposure to rubber leachates from prefilled Eprex syringes with uncoated rubber stoppers (Boven et al., 2005). Bone marrow suppression of thrombopoiesis has been reported after treatment with histone deacetylase (HDAC) inhibitors (Ali et al., 2013; Bishton et al., 2011).

### 6.6.2. Damage to the Bone Marrow Microenvironment

Damage to the bone marrow microenvironment and microvasculature also suppresses hematopoiesis (Ramaiah et al., 2013). Mechanisms include disruption of blood supply, disruption of nurse cell functions and cytokine expression (which can yield injury to adipocytes, macrophages, osteoblasts and osteoclasts), disruption of interactions between matrix and cellular adhesion molecules, and displacement of hematopoietic cells by nonhematopoietic cells (e.g., stromal hyperplasia; Figure 5.11) or extracellular matrix. Acute microvascular injury and sinusoidal endothelial cell degeneration increases vascular permeability, resulting in sinusoidal dilatation, interstitial edema, hemorrhage with fibrin exudation and infiltration by neutrophils, inflammation, and ischemia. Chronic injury leads to necrosis (ischemic/

coagulation-type necrosis [Figure 5.11] or individual cell necrosis) and myelofibrosis (Figure 5.13D). Other stromal lesions include serous fat atrophy, myelophthisis (marrow replacement by nonhemopoietic tissue), fibrous osteodystrophy (excessive bone resorption with replacement by fibrous connective tissue), osteosclerosis (thickening of bony trabeculae that impinges on the marrow), and microangiopathy (capillary wall thickening and fragility leading to disturbed regional blood flow).

Causes of acute marrow stromal injury in dogs and/or cats include inflammatory diseases (IMHA, immune-mediated thrombocytopenia, systemic lupus erythematosus, and infectious diseases), DIC, leukemia/lymphoma, and drugs (cyclophosphamide, carprofen, metronidazole and fenbendazole). Serous fat atrophy is associated with prolonged anorexia. As seen with aging, expansion of adipocytes in the marrow is associated with the suppression of hematopoiesis.

In many cases, agents and metabolites that injure HSCs also injure bone marrow stromal stem cells, their progeny, and surrounding extracellular matrix through direct and bystander effects. Ionizing radiation disruption of endosteal niche homeostasis is characterized by transient expansion of the osteoblasts followed by expansion of adipocytes. It is hypothesized that aplastic pancytopenia induced by benzene may result from damage to the microenvironment since benzene-treated lethally irradiated marrow is not reconstituted by transplantation of normal marrow. In dogs, drug-related stromal injury is more often associated with coagulation-type necrosis than vascular injury or acute inflammation. IL-6 antagonists (tocilizumab, siltuximab) decrease myelopoiesis, resulting in transient neutropenia due to the critical role of IL-6 in regulation of stromal function. It is constitutively expressed by and required for proliferation of bone marrow stromal cells and is essential for the production of extracellular matrix that induces osteoblastic differentiation of MSCs. Alterations in the microenvironment also contribute to stem cell aging, myelodysplasia, malignant transformation, and metastasis.

### 6.6.3. Decreased Cell Lifespan

Decreased erythrocyte survival due to increased senescence occurs secondary to

accumulating damage over the cell's lifespan, such as oxidative injury, microangiopathy (due to physical disruption of membranes of circulating erythrocytes), membrane lipid changes, decreased deformability, mitochondrial dysfunction (lack of ATP to maintain  $\text{Na}^+/\text{K}^+$  gradients and repair mechanisms), and band 3 clustering (IgG opsonization and complement binding). Alterations in membrane lipid profiles may occur as a consequence of alterations in plasma lipids (e.g., hypercholesterolemia and low triglycerides) and are observed with liver disease and lipid-modulating therapeutics. Neoplasia and inflammation may, in rare instances, induce excessive erythrophagocytosis secondary to cytokine-induced nonneoplastic proliferation of macrophages (i.e., hemophagocytic syndrome).

Other factors that indirectly affect circulating cell counts include redistribution and indirect induction of lysis. Redistribution of circulating blood cells affects peripheral cell counts but not total body counts. Demargination of neutrophils induced by glucocorticosteroids increases circulating cell counts as does the release of reticulocytes and platelets from splenic pools. Inhibition of leukocyte extravasation by antiinflammatory agents such as inhibitors of leukocyte adhesion molecules (linomide, enlimomab) also produces increased WBC counts. In humans, splenic sequestration of platelets with organ enlargement and thrombocytopenia has been associated with portal hypertension secondary to oxaliplatin-induced liver sinusoidal injury (Jardim et al., 2012). Indirect causes of intravascular hemolysis include hypophosphatemia (cattle), acute hyponatremia (water intoxication), and rapid administration of 40% dimethyl sulfoxide (DMSO, in horses). Species with small erythrocytes appear to be most susceptible to hypotonicity-induced hemolysis.

## 7. ISSUES IN DRUG DEVELOPMENT AND REGULATORY CONSIDERATIONS

### 7.1. Translatability

The evaluation of hematotoxicity is a valuable element of nonclinical safety assessment given that (1) animal studies are generally predictive



of hematotoxicity in humans and that (2) bone marrow toxicity can be readily monitored in peripheral blood. In an International Life Sciences Institute (ILSI) report examining the concordance between animal toxicity and target organ toxicities in humans for a wide variety of new pharmaceuticals, human hematological toxicities (as well as gastrointestinal and cardiovascular) held the highest incidence of overall concordance with animal toxicity (Olson et al., 2000). This was partly attributable to certain therapeutic classes that are prone to hematotoxicity (e.g., due to the expected effects of cytotoxic anticancer agents on rapidly dividing cells of the hematopoietic system) (Greaves et al., 2004). However, other drug classes can also exhibit hematotoxicity through a variety of mechanisms including bone marrow suppression, immune-mediated destruction, blood loss, dysmyelopoiesis, oxidative injury, and hemolysis. Importantly, a blinded analysis of the IQ Consortium nonclinical to clinical (Phase 1) translational database indicated that animal studies were strongly predictive of the absence of clinical adverse hematologic effects (negative predictive value 88% in monkeys, 92% in rodents and 93% in dogs) (Monticello et al., 2017).

## 7.2. Adversity

In the context of nonclinical toxicity studies, adversity has been defined as “a test item-related change in the morphology, physiology, growth, development, reproduction or life span of the animal model that likely results in an impairment of functional capacity to maintain homeostasis and/or an impairment of the capacity to respond to an additional challenge” (see *Assigning Adversity to Toxicologic Outcomes*, Vol 2, Chap 15) (Kerlin et al., 2016; Palazzi et al., 2016). The determination of adversity is therefore based on potential detrimental effects to the entire organism (test animal) rather than changes in individual parameters as well as on the functional integration of effects and responses among multiple organs. The adversity determination for hematotoxicity has been extensively described (Ramaiah et al., 2017). Most commonly, adverse hematologic toxicities consist of a constellation of related findings in peripheral blood and bone marrow, possibly with secondary effects in other tissues and

impacts on clinical condition. An isolated hematology finding should be considered adverse only if it is clearly linked to a clinical outcome in the study animals or if it is associated with a high risk for an adverse clinical consequence. Changes that are not clearly adverse but raise concern for the potential for adversity may help build a weight of evidence for establishing the no observed adverse effect level (NOAEL).

In nonclinical studies, drug-induced hematologic abnormalities are identified based on the recognition of differences (often dose-dependent) in animals administered a test article relative to values in control animals (or individual animal baseline values). When multiple animals are evaluated at each dose, even minimal changes are often readily identified. One of the most challenging aspects of hematologic evaluation then becomes placing minimal changes into proper context. Minimal hematologic changes arising secondary to effects impacting nonhematopoietic organs and tissues are quite common. These hematologic effects often pose no risk to human safety and must be distinguished from direct effects that target the hematopoietic system. This determination is made based on consideration of relationships among all relevant study findings.

Suppression of erythropoiesis by cytotoxic anticancer agents may be accompanied by evidence of toxicity to multiple hematopoietic cell lines as well as other rapidly proliferating tissues, such as gastrointestinal epithelium. Due to individual cell line kinetics and relative life-spans, thrombocytopenia, neutropenia, and adverse clinical sequelae related to substantial reductions of other rapidly dividing cell populations may be observed prior to the development of anemia.

Profoundly low circulating platelet counts may potentiate hemorrhage, which is most often characterized clinically by the presence of petechiae (small subcutaneous hemorrhages) and ecchymoses (larger subcutaneous hemorrhages). Other clinical findings may include mucosal bleeding, hematuria (blood in the urine), hyphema (blood in the anterior chamber of the eye), and prolonged bleeding after venipuncture. Widespread platelet activation can also reduce mean arterial pressure, causing transient loss of consciousness due to the release of serotonin from platelets.

Platelet counts  $<50,000/\text{mL}$  are associated with an increased bleeding risk and may be considered adverse even in the absence of clinical evidence of bleeding. The determination of adversity is further supported by the consistency and/or time course of thrombocytopenia and/or concurrent maturational changes in bone marrow megakaryocytes. Conversely, thrombocytosis may increase the susceptibility to inflammation and risk for thrombosis, and greater than three-fold increases in platelet counts may be associated with myelofibrosis and hyperostosis (increased growth of bone).

Risk of infection or susceptibility to pathogen challenge increases when neutrophil counts are markedly to severely decreased, though the determination differs depending on the species ( $1000/\mu\text{L}$  to  $200/\mu\text{L}$  in dogs,  $<500/\mu\text{L}$  in monkeys, and  $<50/\mu\text{L}$  in rats). The determination of adversity is based on the severity of the neutrophil decrease (absolute values, consistency, and/or time course) and increased risk of infection, regardless of the presence of an active infection (as infections rarely occur in neutropenic animals because the laboratory environment controls exposure to pathogens). Concurrently decreased bone marrow myeloid cellularity, fever, and/or other evidence of infection may add to the weight of evidence needed for the adversity determination.

RBC mass (Hgb, RBC, and hematocrit [HCT]) is strongly associated with potential adverse effects on animal survival due to its essential role in tissue oxygenation. However, assigning adversity to red cell mass decreases is not only based on the magnitude of change or hemoglobin concentration. It requires consideration of the rapidity of decreases, the ability of the animal to sufficiently compensate for the decrease, the persistence or exacerbation with repeated dosing, and any intercurrent findings and effects (potential or observed) on tissue oxygenation. Rapid, severe decreases in red cell mass may be associated with immediate adverse consequences such as weakness, fainting, or death, whereas clinical signs associated with slowly progressing changes of similar magnitude could be limited to mild lethargy. The adversity of decreased red cell mass may be compounded by functional deficits. Methemoglobin impairs oxygen release and delivery to tissues. Methemoglobinemia combined with decreased red cell

mass may reduce thresholds for adversity determinations.

Drug effects are commonly magnified by issues unrelated to the drug, such as blood loss due to repeated phlebotomy or menstruation in female monkeys, requiring that such confounders be integrated in the overall assessment of adversity (Perigard et al., 2016). When nonregenerative decreases in red cell mass are secondary to generalized illness or nonhematopoietic organ toxicity, bone marrow histologic findings are generally limited to diffuse decreases in hematopoietic cellularity. Therefore, bone marrow smear evaluation does not provide additional benefit. In these cases, the focus of adversity determinations should be based on the primary toxic effects rather than on secondary nonregenerative red cell mass decreases.

### 7.3. Regulatory Issues

With respect to nonclinical safety evaluation of the hematopoietic system, few detailed instructions have been provided by various regulatory agencies responsible for assessing human health products or environmental concerns. However, the importance of hematopoietic system evaluation is emphasized within several individual documents. Specific information regarding individual agency guidelines have been compiled by Reagan et al. in *Best practices for evaluation of bone marrow in nonclinical toxicity studies* (Reagan et al., 2011), though guidelines for various modalities are fluid and updated regularly. In one pharmaceutical company's analysis of 1-month toxicity studies for a wide spectrum of candidate drugs, the bone marrow was among the six most frequently affected organs, accompanied by the liver, thymus, adrenal glands, kidney, and spleen (Horner et al., 2013).

Hematopoietic toxicity can result in life-threatening clinical outcomes, and some hematologic endpoints may be reportable to regulatory authorities when they reach critical levels in patients enrolled in clinical trials (NCI, 2017). Given the high likelihood of transability of hematotoxicity between nonclinical investigations and the clinic, an appropriate evaluation of the hematopoietic system is a critical component of nonclinical toxicologic evaluation (Olson et al., 2000).

## 8. CONCLUSION

The hematopoietic system is composed of all blood-forming tissues and all circulating blood cells and is one of the largest organs in the body. Its primary function is hematopoiesis, the continuous production of highly specialized circulating blood cells responsible for respiratory (hemoglobin in erythrocytes), immune (leukocytes), and hemostatic (thrombocytes/platelets) functions vital to survival. This system is exquisitely susceptible to toxic insults due to its high metabolic and proliferative rates as well as its high exposure to xenobiotics in circulation. It ranks alongside the liver, thymus, adrenal glands, kidney, and spleen as one of the most important and commonly affected target organs of toxicity (Horner et al., 2013). Hematotoxicity, defined as the adverse effect of an agent on blood cells or blood-forming tissues, can result in life-threatening clinical outcomes and may be reportable to regulatory authorities when observed in clinical trials (NCI, 2017). In nonclinical studies, hematotoxicity is a rare class of clinical pathology findings that can be considered adverse in isolation based on threshold values based on the critical role of blood cells in oxygen transport, hemostasis, and immunity. The evaluation of hematotoxicity is a valuable element of nonclinical safety assessment given that (1) animal studies are generally predictive of hematotoxicity in humans (Olson et al., 2000) and that (2) bone marrow toxicity can be readily monitored in peripheral blood. Thus, blood and bone marrow are routinely assessed in nonclinical toxicity studies.

Evaluation of the hematopoietic system involves microscopic identification of morphologic abnormalities in circulating peripheral blood cells and/or bone marrow (biopsy and/or cytology) as well as an assessment of peripheral blood and bone marrow in a functional precursor-product relationship. This requires an understanding of normal bone marrow structure and function including the bone marrow microenvironment, normal blood cell morphology (both immature and mature stages), mechanisms of hematotoxicity, hematopoietic tissue responses to injury, and the relationship of blood and blood-forming tissues to other organ systems. Hematotoxicity may occur via direct injury or indirectly through injury to other body systems, with consequences that can span

the entire spectrum of hematologic cell types including bone marrow precursors, erythrocytes, leukocytes, and platelets. Interpretations are made based on known exposures, the timing of toxicant effects, the kinetics of hematopoietic responses, blood cell life cycles, changes in other tissues, and clinical observations. Interpretation also requires consideration for potential sources of artifact, preanalytical variability, analytical imprecision, and postanalytical errors. This chapter provides a thorough functional, mechanistic, and morphologic background for understanding the broad range of toxic effects on the hematopoietic system, with focus on the myeloid, erythroid, and megakaryocytic/platelet compartments of the bone marrow.

## GLOSSARY

- Bone marrow** A highly vascular, loose connective tissue stroma within the medullary cavities of bones that contains precursors of mature blood cells at various stages of their development; this tissue is the major site of hematopoiesis in the body and the largest primary lymphoid tissue
- Common lymphoid progenitor (CLP)** Multipotent stem cells that can differentiate into all lymphocyte lineages (B cells, NK cells, and T cells)
- Common myeloid progenitor (CMP)** Multipotent stem cells that can differentiate into all nonlymphoid cell types, giving rise to **common megakaryocytic/erythroid progenitors** (MEPs, the precursor for erythrocytes and thrombocytes) and **common granulocyte/monocyte progenitors** (GMPs, for granulocytes, mast cells, and monocytes/macrophages)
- Definitive hematopoiesis** Generation of committed hematopoietic progenitors necessary during late gestation (fetal and postnatal periods, including adulthood)
- Demargination** Redistribution of cells from the marginated pool (temporarily adhered to endothelial cells) to the circulating pool (free flowing in blood and thus collected in blood samples)
- Endomitosis** A physiological form of thwarted mitosis in megakaryocytes in which DNA synthesis is not followed by cell division, leading to progressive polyploidy (multiple complete sets of chromosomes) in giant cells with multilobulated nuclei
- Eryptosis** Premature erythrocyte death through a specialized form of apoptosis
- Erythroblastic island** Developmental niche consisting of a single central macrophage surrounded by and supporting the maturation of 10–30 erythroid cells
- Erythrocyte** Red blood cell
- Erythropoiesis** The production of erythrocytes, the circulating blood cell lineage responsible for transporting hemoglobin-bound gases (oxygen and carbon dioxide) between body tissues and the lungs
- Granulocyte** Leukocyte lineages (neutrophils, eosinophils, basophils) in which mature cells contain one or more types of cytoplasmic granules containing various bioactive molecules (adhesion molecules, antibacterial proteins, binding proteins, enzymes, etc.)
- Granulopoiesis** The production of leukocyte lineages with intracytoplasmic granules (neutrophils, eosinophils, basophils) that are involved in innate immunity



**Hematopoiesis** Production of mature circulating blood cells responsible for respiratory (hemoglobin in erythrocytes), immune (leukocytes), and hemostatic (thrombocytes/platelets) processes

**Hematopoietic niche** Specialized, integrated microanatomical units in the bone marrow that support the growth and proliferation of pluripotent hematopoietic stem cells and multipotent (partially committed) lineage-specific hematopoietic precursors

**Hematopoietic system (alternatively hemopoietic system)** All blood-forming tissues and circulating blood cells

**Hematotoxicity** The adverse effect of an agent on blood cells or blood-forming tissues

**Heme** A porphyrin ring complexed with ferrous ( $\text{Fe}^{2+}$ ) iron and protoporphyrin IX, which forms the essential prosthetic group in hemoglobin that is responsible for the reversible binding of oxygen

**Hemolysis** Destruction of erythrocytes (red blood cells) outside ("extravascular") or inside ("intravascular") blood vessels

**Leukocyte** Any of several white blood cell lineages (e.g., granulocytes, lymphocytes, monocytes) that serve as specialized circulating immune cells participating in the innate and/or acquired immune responses

**Lymphocyte** The leukocyte lineage that functions chiefly to control and carry out various roles related to acquired immunity

**Lymphopoiesis** Production of lymphocytes

**Megakaryopoiesis** Production of megakaryocytes (MKs), the progenitor cells from which thrombocytes (platelets) are derived

**Monocyte** A large phagocytic white blood cell in circulation, which has the capacity to migrate into tissues to become a resident phagocytic cell (i.e., a macrophage)

**Multipotent stem cells** Progenitor cells that can develop into a limited number of cell types in a particular lineage or related lineages. These cells have the capacity for long-term self-renewal through symmetrical mitotic division

**Myelopoiesis** Production of mature circulating nonlymphoid leukocytes (granulocytes and monocytes) from hematopoietic stem cells

**Ontogenesis (alternatively ontogeny)** Embryonic origin and post-embryonic development of an organ or organ system in an individual organism

**Phylogenesis (alternatively phylogeny)** Evolutionary origin of an organ or organ system an entire taxon of related organisms

**Pluripotent stem cells** Progenitor cells that can give rise to nearly all cell types of the body (but not the placenta)

**Primitive hematopoiesis** Process of generating blood cells during embryogenesis (early gestation)

**Thrombocyte** Tiny, disc-shaped cell fragments ("platelets") extruded by megakaryocytes that circulate in blood until recruited during coagulation to help stabilize clots needed to stop bleeding

**Thrombopoiesis** Production of platelets (thrombocytes), the key cellular component in hemostasis, by megakaryocytes

**Totipotent stem cells** Progenitor cells that can give rise to all cell types found in an embryo as well as all cell types in extraembryonic (placenta) tissues

## REFERENCES

Abernethy DJ: Human CD34+ hematopoietic progenitor cells are sensitive targets for toxicity induced by 1,4-benzoquinone, *Toxicol. Sci.* 79(82–89), 2004.

Agar NS, Board PG, editors: *Red blood cells of domestic mammals*, Amsterdam & New York, 1983, Elsevier Science Publishers B.V. 1983.

Ali A, Bluteau O, Messaoudi K, et al.: Thrombocytopenia induced by the histone deacetylase inhibitor abexinostat

involves p53-dependent and -independent mechanisms, *Cell Death Dis.* 4, 2013.

Ali U, Gibbs R, Knight G, et al.: Sex-divided reference intervals for mean platelet volume, platelet large cell ratio and plateletcrit using the Sysmex XN-10 automated haematology analyzer in a UK population, *Hematol. Transfus. Cell Ther.* 41:153–157, 2019.

Alonso FH, Tarbert DK, Wu B, et al.: Gelatinous transformation of bone marrow in a rabbit, *J. Vet. Diagn. Invest.* 33:1183–1187, 2021.

Alsaker RD: The formation, emergence, and maturation of the reticulocyte: a review, *Vet. Clin. Pathol.* 6:7–12, 1977.

Arai F, Hirao A, Suda T: Regulation of hematopoiesis and its interaction with stem cell niches, *Int. J. Hematol.* 82:371–376, 2005.

Arese P, Gallo V, Pantaleo A, et al.: Life and death of glucose-6-phosphate dehydrogenase (G6PD) deficient erythrocytes – role of redox stress and band 3 modifications, *Transfus. Med. Hemotherapy* 39:328–334, 2012.

Arinobu Y, Iwasaki H, Gurish MF, et al.: Developmental checkpoints of the basophil/mast cell lineages in adult murine hematopoiesis, *Proc. Natl. Acad. Sci. U.S.A.* 102: 18105–18110, 2005.

Arnold DM, Nazi I, Warkentin TE, et al.: Approach to the diagnosis and management of drug-induced immune thrombocytopenia, *Transfus. Med. Rev.* 27:137–145, 2013.

Arroyo-Olarte RD, Bravo Rodriguez R, Morales-Rios E: Genome editing in bacteria: CRISPR-Cas and beyond, *Microorganisms* 9, 2021.

Athens JW, Haab OP, Raab SO, et al.: Leukokinetic studies. IV. The total blood, circulating and marginal granulocyte pools and the granulocyte turnover rate in normal subjects, *J. Clin. Invest.* 40:989–995, 1961.

Auerbach M, Staffa SJ, Brugnara C: Using reticulocyte hemoglobin equivalent as a marker for iron deficiency and responsiveness to iron therapy, *Mayo Clin. Proc.* 96:1510–1519, 2021.

Ault KA, Rinder HM, Mitchell J, et al.: The significance of platelets with increased RNA content (reticulated platelets). A measure of the rate of thrombopoiesis, *Am. J. Clin. Pathol.* 98:637–646, 1992.

Baldo BA, Pham NH: Classification and descriptions of allergic reactions to drugs. In *Drug allergy: clinical aspects, diagnosis, mechanisms, structure-activity relationships*, ed 2, 2021, Springer, pp 17–57.

Bartl S, Baish M, Weissman IL, et al.: Did the molecules of adaptive immunity evolve from the innate immune system? *Integr. Comp. Biol.* 43:338–346, 2003.

Basu S, Hodgson G, Katz M, et al.: Evaluation of role of G-CSF in the production, survival, and release of neutrophils from bone marrow into circulation, *Blood* 100:854–861, 2002.

Bataller A, Montalban-Bravo G, Soltysiak KA, et al.: The role of TGFbeta in hematopoiesis and myeloid disorders, *Leukemia* 33:1076–1089, 2019.

Beeler-Marfisi J, Menoyo AG, Beck A, et al.: Gelatinous marrow transformation and hematopoietic atrophy in a miniature horse stallion, *Vet. Pathol.* 48:451–455, 2011.

- Beutler E: Production and destruction of erythrocytes. In Beutler EL, Marshall A, Collier BS, editors: *William's hematology*, New York, NY, 2005, McGraw Hill, pp 355–368.
- Biddle KE: Opinion on the optimal histologic evaluation of the bone marrow in nonclinical toxicity studies, *Toxicol. Pathol.* 50:266–273, 2022.
- Bimczok D, Rothkötter HJ: Lymphocyte migration studies, *Vet. Res.* 37:325–338, 2006.
- Bishton MJ, Harrison SJ, Martin BP, et al.: Deciphering the molecular and biologic processes that mediate histone deacetylase inhibitor-induced thrombocytopenia, *Blood* 117:3658–3668, 2011.
- Bloom JC, Thiem PA, Sellers TS, et al.: Cephalosporin-induced immune cytopenia in the dog: demonstration of erythrocyte-, neutrophil-, and platelet-associated IgG following treatment with cefazedone, *Am. J. Hematol.* 28:71–78, 1988.
- Boccuni P, Del Vecchio L, Di Noto R, et al.: Glycosyl phosphatidylinositol (GPI)-anchored molecules and the pathogenesis of paroxysmal nocturnal hemoglobinuria, *Crit. Rev. Oncol. Hematol.* 33:25–43, 2000.
- Bogner P, Miseta A, Berente Z, et al.: Osmotic and diffusive properties of intracellular water in camel erythrocytes: effect of hemoglobin crowdedness, *Cell Biol. Int.* 29:731–736, 2005.
- Bollen P, Skydsgaard M: Restricted feeding may induce serous fat atrophy in male Göttingen minipigs, *Exp. Toxicol. Pathol.* 57:347–349, 2006.
- Bolliger AP: Cytologic evaluation of bone marrow in rats: indications, methods, and normal morphology, *Vet. Clin. Pathol.* 33:58–67, 2004.
- Bolliger AP, Everds NE: Chapter 2.9 -Haematology of the mouse. In *The laboratory mouse*, ed 2, 2012, Academic Press, pp 331–347.
- Bonelli M, La Monica S, Fumarola C, et al.: Multiple effects of CDK4/6 inhibition in cancer: from cell cycle arrest to immunomodulation, *Biochem. Pharmacol.* 170:113676, 2019.
- Boos CJ, Beevers GD, Lip GY: Assessment of platelet activation indices using the ADVIATM 120 amongst 'high-risk' patients with hypertension, *Ann. Med.* 39:72–78, 2007.
- Bordin L: Dapsone hydroxylamine induces premature removal of human erythrocytes by membrane reorganization and antibody binding, *Br. J. Pharmacol.* 161:1186, 2010.
- Bougie DW, Nayak D, Boylan B, et al.: Drug-dependent clearance of human platelets in the NOD/scid mouse by antibodies from patients with drug-induced immune thrombocytopenia, *Blood* 116:3033–3038, 2010.
- Boujbiha MA, Salah GB, Feleh AB, et al.: Hematotoxicity and genotoxicity of mercuric chloride following subchronic exposure through drinking water in male rats, *Biol. Trace Elem. Res.* 148:76–82, 2012.
- Boven K, Stryker S, Knight J, et al.: The increased incidence of pure red cell aplasia with an Eprex formulation in uncoated rubber stopper syringes, *Kidney Int.* 67:2346–2353, 2005.
- Bowman ZS: Primaquine-induced hemolytic anemia: role of membrane lipid peroxidation and cytoskeletal protein alterations in the hemotoxicity of 5-hydroxyprimaquine, *J. Pharmacol. Exp. Therapeut.* 314:838–845, 2005.
- Bowman ZS, Morrow JD, Jollow DJ, et al.: Primaquine-induced hemolytic anemia: role of membrane lipid peroxidation and cytoskeletal protein alterations in the hemotoxicity of 5-hydroxyprimaquine, *J. Pharmacol. Exp. Therapeut.* 314:838–845, 2005.
- Boyd KL, Bolon B: Embryonic and fetal hematopoiesis. In Weiss DJ, Wardrop KJ, editors: *Schalm's veterinary hematology*, Ames, IA, 2010, Wiley-Blackwell, pp 3–7.
- Brazzell JL, Weiss DJ: A retrospective study of aplastic pancytopenia in the dog: 9 cases (1996–2003), *Vet Clin Path* 35:413–417, 2006.
- Bresnick EH, Hewitt KJ, Mehta C, et al.: Mechanisms of erythrocyte development and regeneration: implications for regenerative medicine and beyond, *Development* 145, 2018.
- Briggs C, Kunka S, Hart D, et al.: Assessment of an immature platelet fraction (IPF) in peripheral thrombocytopenia, *Br. J. Haematol.* 126:93–99, 2004.
- Broun ER, Greist A, Tricot G, et al.: Excessive zinc ingestion. A reversible cause of sideroblastic anemia and bone marrow depression, *JAMA* 264:1441–1443, 1990.
- Brugnara C: Reticulocyte cellular indices: a new approach in the diagnosis of anemias and monitoring of erythropoietic function, *Crit. Rev. Clin. Lab Sci.* 37:93–130, 2000.
- Brugnara C, Schiller B, Moran J: Reticulocyte hemoglobin equivalent (Ret He) and assessment of iron-deficient states, *Clin. Lab. Haematol.* 28:303–308, 2006.
- Bruning-Fann CS, Kaneene JB: The effects of nitrate, nitrite, and N-nitroso compounds on animal health, *Vet. Hum. Toxicol.* 35:237–253, 1993.
- Brunori M, Miele AE: Modulation of allosteric control and evolution of hemoglobin, *Biomolecules* 13, 2023.
- Budak YU, Polat M, Huysal K: The use of platelet indices, plateletcrit, mean platelet volume and platelet distribution width in emergency non-traumatic abdominal surgery: a systematic review, *Biochem. Med.* 26:178–193, 2016.
- Bujko K, Cymer M, Adamiak M, et al.: An overview of novel unconventional mechanisms of hematopoietic development and regulators of hematopoiesis—a roadmap for future investigations, *Stem Cell Rev. Rep.* 15:785–794, 2019.
- Buoro S, Vavassori M, Pipitone S, et al.: Evaluation of nucleated red blood cell count by Sysmex XE-2100 in patients with thalassaemia or sickle cell anaemia and in neonates, *Blood Transfus.* 13:588–594, 2015.
- Butler JT, Abdelhamed S, Kurre P: Extracellular vesicles in the hematopoietic microenvironment, *Haematologica* 103:382–394, 2018.
- Butt OI: Blood-brain barrier disruption and oxidative stress in Guinea pig after systemic exposure to modified cell-free hemoglobin, *Am. J. Pathol.* 178:1316–1328, 2011.
- Butthep P, Wisedpanichkij R, Jindadamrongwech S, et al.: Reticulocyte analysis in iron deficiency anemia and hemolytic anemia, *J. Med. Assoc. Thai.* 83(Suppl 1):S114–S122, 2000.

- Cai S, Wang H, Bailey B, et al.: Humanized bone marrow mouse model as a preclinical tool to assess therapy-mediated hematotoxicity, *Clin. Cancer Res.* 17:2195–2206, 2011.
- Caldin M, Carli E, Furlanello T, et al.: A retrospective study of 60 cases of eccentrocytosis in the dog, *Vet. Clin. Pathol.* 34: 224–231, 2005.
- Cane S, Ugel S, Trovato R, et al.: The endless saga of monocyte diversity, *Front. Immunol.* 10:1786, 2019.
- Casanova-Acebes M, Pitaval C, Weiss LA, et al.: Rhythmic modulation of the hematopoietic niche through neutrophil clearance, *Cell* 153:1025–1035, 2013.
- Celliers A, Rautenbach Y, Hooijberg E, et al.: Neutrophil myeloperoxidase index in dogs with babesiosis caused by babesia rossi, *Front. Vet. Sci.* 7(72), 2020.
- Ceylan C, Miskioğlu M, Colak H, et al.: Evaluation of reticulocyte parameters in iron deficiency, vitamin B(12) deficiency and beta-thalassemia minor patients, *Int. J. Lab. Hematol.* 29:327–334, 2007.
- Chan TC, Boon GD, Shaffer L, et al.: Antiviral nucleoside toxicity in canine bone marrow progenitor cells and its relationship to drug permeation, *Eur. J. Haematol.* 49:71–76, 1992.
- Chand DH, Zaidman C, Arya K, et al.: Thrombotic microangiopathy following onasemnogene abeparvovec for spinal muscular atrophy: a case series, *J. Pediatr.* 231:265–268, 2021.
- Chang CC, Kass L: Clinical significance of immature reticulocyte fraction determined by automated reticulocyte counting, *Am. J. Clin. Pathol.* 108:69–73, 1997.
- Chattopadhyay S, Chatterjee R, Law S: Noncanonical Wnt5a-Ca(2+) -NFAT signaling axis in pesticide induced bone marrow aplasia mouse model: a study to explore the novel mechanism of pesticide toxicity, *Environ. Toxicol.* 31:1163–1175, 2015.
- Chatzikonstantinou T, Gavrilaki M, Anagnostopoulos A, et al.: An update in drug-induced thrombotic microangiopathy, *Front. Med.* 7(212), 2020.
- Chen CC, Grimbaldeston MA, Tsai M, et al.: Identification of mast cell progenitors in adult mice, *Proc. Natl. Acad. Sci. U.S.A.* 102:11408–11413, 2005.
- Chen J: Animal models for acquired bone marrow failure syndromes, *Clin. Med. Res.* 3:102–108, 2005.
- Chiang AS, Gupta AP, Han SS: Arthropod immune system: I. Comparative light and electron microscopic accounts of immunocytes and other hemocytes of *Blattella germanica* (Dictyoptera: Blattellidae), *J. Morphol.* 198:257–267, 1988.
- Christian J: Erythrokinetics and erythrocyte destruction. In Weiss DJ, Wardrop KJ, editors: *Schalm's veterinary hematology*, Ames, Iowa, 2010, Blackwell Publishing, pp 136–143.
- Chu SAA, Stokol T: Assay variability and storage stability of the myeloperoxidase index of the ADVIA 2120i hematology analyzer in canine and equine whole blood samples, *Vet. Clin. Pathol.* 50:28–36, 2021.
- Cipolleschi MG, Dello Sbarba P, Olivetto M: The role of hypoxia in the maintenance of hematopoietic stem cells, *Blood* 82:2031–2037, 1993.
- Cohen WD, Terwilliger NB: Marginal bands in camel erythrocytes, *J. Cell Sci.* 36:97–107, 1979.
- Coleman MD, Coleman NA: Drug-induced methaemoglobinaemia. Treatment issues, *Drug Saf.* 14:394–405, 1996.
- Collin M, Bigley V: Monocyte, macrophage, and dendritic cell development: the human perspective, *Microbiol. Spectr.* 4, 2016.
- Collin M, Milne P: Langerhans cell origin and regulation, *Curr. Opin. Hematol.* 23:28–35, 2016.
- Cora M, Travlos G: Bone marrow. In Cesta M, Herbert RA, Brix A, Malarkey DE, Sills RC, editors: *National toxicology program nonneoplastic lesion atlas*. <https://ntp.niehs.nih.gov/atlas/nnl/hematopoietic-system/bone-marrow>. (Accessed 15 July 2024).
- Corash L: The relationship between megakaryocyte ploidy and platelet volume, *Blood Cell* 15:81–107, 1989.
- Corash L, Costa JL, Shafer B, et al.: Heterogeneity of human whole blood platelet subpopulations. III. Density-dependent differences in subcellular constituents, *Blood* 64:185–193, 1984.
- Corash L, Levin J: The relationship between megakaryocyte ploidy and platelet volume in normal and thrombocytopenic C3H mice, *Exp. Hematol.* 18:985–989, 1990.
- Cordeiro-Spinetti E, Taichman RS, Balduino A: The bone marrow endosteal niche: how far from the surface? *J. Cell. Biochem.* 116:6–11, 2015.
- Cox Jr LA, Ketelslegers HB, Lewis RJ: The shape of low-concentration dose-response functions for benzene: implications for human health risk assessment, *Crit. Rev. Toxicol.* 51:95–116, 2021.
- Crane GM, Jeffery E, Morrison SJ: Adult haematopoietic stem cell niches, *Nat. Rev. Immunol.* 17:573–590, 2017.
- Crawford J, Ozer H, Stoller R, et al.: Reduction by granulocyte colony-stimulating factor of fever and neutropenia induced by chemotherapy in patients with small-cell lung cancer, *N. Engl. J. Med.* 325:164–170, 1991.
- Criswell KA, Bock JH, Johnson K, et al.: Validation of Sysmex XT-2000iV analyzer-generated quantitative bone marrow differential counts in cynomolgus monkeys, Beagle dogs, and CD-1 mice, *Vet. Clin. Pathol.* 47:539–555, 2018.
- Criswell KA, Bock JH, Wildeboer SE, et al.: Comparison of the Sysmex XT-2000iV and microscopic bone marrow differential counts in Wistar rats treated with cyclophosphamide, erythropoietin, or serial phlebotomy, *Vet. Clin. Pathol.* 43: 137–153, 2014a.
- Criswell KA, Bock JH, Wildeboer SE, et al.: Validation of Sysmex XT-2000iV generated quantitative bone marrow differential counts in untreated Wistar rats, *Vet. Clin. Pathol.* 43:125–136, 2014b.
- Criswell KA, Krishna G, Zielinski D, et al.: Validation of a flow cytometric acridine orange micronuclei methodology in rats, *Mutat. Res.* 528:1–18, 2003.



- Cross GM: The avian lymphatic system. In *Cage bird medicine and surgery*, Camden NSW, 1989, AAVAC University of Sydney, pp 225–231.
- Curtis BR: Drug-induced immune neutropenia/agranulocytosis, *Immunohematol* 30:95–101, 2014a.
- Curtis BR: Drug-induced immune thrombocytopenia: incidence, clinical features, laboratory testing, and pathogenic mechanisms, *Immunohematol. Am. Red Cross* 30:55–65, 2014b.
- Dahariya S, Paddibhatla I, Kumar S, et al.: Long non-coding RNA: classification, biogenesis and functions in blood cells, *Mol. Immunol.* 112:82–92, 2019.
- Dale GL, Daniels RB: Quantitation of immunoglobulin associated with senescent erythrocytes from the rabbit, *Blood* 77: 1096–1099, 1991.
- Davenport P, Lorenz V, Liu ZJ, et al.: Development of gates to measure the immature platelet fraction in C57BL/6J mice using the Sysmex XN-V series multispecies hematology analyzer, *J. Vet. Diagn. Invest.* 33:913–919, 2021.
- De Franceschi L, Fattovich G, Turrini F, et al.: Hemolytic anemia induced by ribavirin therapy in patients with chronic hepatitis C virus infection: role of membrane oxidative damage, *Hepatology* 31:997–1004, 2000.
- Dehne E-M, Winter A, Marx U: Microphysiological systems in the evaluation of hematotoxicities during drug development, *Curr. Opin. Toxicol.* 17:18–22, 2019.
- Derelanko MJ: Determination of erythrocyte life span in F-344, Wistar, and Sprague-Dawley rats using a modification of the [<sup>3</sup>H]diisopropylfluorophosphate ([<sup>3</sup>H]DFP) method, *Fund. Appl. Toxicol.* 9:271–276, 1987.
- Deubelbeiss KA, Dancy JT, Harker LA, et al.: Neutrophil kinetics in the dog, *J. Clin. Invest.* 55:833–839, 1975.
- Dewi R, Hamid ZA, Rajab NF, et al.: Genetic, epigenetic, and lineage-directed mechanisms in benzene-induced malignancies and hematotoxicity targeting hematopoietic stem cells niche, *Hum. Exp. Toxicol.* 39:577–595, 2019.
- Dewi R, Hamid ZA, Rajab NF, et al.: Genetic, epigenetic, and lineage-directed mechanisms in benzene-induced malignancies and hematotoxicity targeting hematopoietic stem cells niche, *Hum. Exp. Toxicol.* 39:577–595, 2020.
- Dinauer MC: Disorders of neutrophil function: an overview, *Methods Mol. Biol.* 1124:501–515, 2014.
- Dreischer P, Duszenko M, Stein J, et al.: Eryptosis: programmed death of nucleus-free, iron-filled blood cells, *Cells* 11, 2022.
- Dupuis ME, Villion M, Magadan AH, et al.: CRISPR-Cas and restriction-modification systems are compatible and increase phage resistance, *Nat. Commun.* 4:2087, 2013.
- Duval R, Bui L-C, Mathieu C, et al.: Benzoquinone, a leukemogenic metabolite of benzene, catalytically inhibits the protein tyrosine phosphatase PTPN2 and alters STAT1 signaling, *J. Biol. Chem.* 294:12483–12494, 2019.
- Ebbe S, Boudreaux MK: Relationship of megakaryocyte ploidy with platelet number and size in cats, dogs, rabbits and mice, *Comp. Haematol. Int.* 8:21–25, 1998.
- Eckly A, Scandola C, Oprea A, et al.: Megakaryocytes use in vivo podosome-like structures working collectively to penetrate the endothelial barrier of bone marrow sinusoids, *J. Thromb. Haemostasis* 18:2987–3001, 2020.
- Edmondson PW, Wyburn JR: The erythrocyte life-span, red cell mass and plasma volume of normal Guinea-pigs as determined by the use of <sup>51</sup>Chromium, <sup>32</sup>Phosphorus labelled di-isopropyl fluorophosphonate and <sup>131</sup>Iodine labelled human serum albumin, *Br. J. Exp. Pathol.* 44:72–80, 1963.
- Eliasson P, Jonsson JI: The hematopoietic stem cell niche: low in oxygen but a nice place to be, *J. Cell. Physiol.* 222:17–22, 2010.
- Eliasson P, Rehn M, Hammar P, et al.: Hypoxia mediates low cell-cycle activity and increases the proportion of long-term-reconstituting hematopoietic stem cells during in vitro culture, *Exp. Hematol.* 38:301–310, 2010.
- Elmore S: Enhanced histopathology of the bone marrow, *Toxicol. Pathol.* 34:666–686, 2006a.
- Elmore SA: Enhanced histopathology of mucosa-associated lymphoid tissue, *Toxicol. Pathol.* 34:687–696, 2006b.
- Elmore SA: Enhanced histopathology of the lymph nodes, *Toxicol. Pathol.* 34:634–647, 2006c.
- Elmore SA: Enhanced histopathology of the spleen, *Toxicol. Pathol.* 34:648–655, 2006d.
- Elmore SA: Enhanced histopathology of the thymus, *Toxicol. Pathol.* 34:656–665, 2006e.
- Escobar C, Grindem C, Neel J, et al.: Hematologic changes after total body irradiation and autologous transplantation of hematopoietic peripheral blood progenitor cells in dogs with lymphoma, *Veterinary Pathology* 49:341–343, 2012.
- Everds N, Li N, Bailey K, et al.: Unexpected thrombocytopenia and anemia in cynomolgus monkeys induced by a therapeutic human monoclonal antibody, *Toxicol. Pathol.* 41:951–969, 2013.
- Everds NE, Tarrant JM: Unexpected hematologic effects of biotherapeutics in nonclinical species and in humans, *Toxicol. Pathol.* 41:280–302, 2013.
- Everett NB, Yoffey JM: Life of Guinea pig circulating erythrocyte and its relation to erythrocyte population of bone marrow, *Proc. Soc. Exp. Biol. Med.* 101:318–319, 1959.
- Ezekowitz RA, Kuhlman M, Groopman JE, et al.: A human serum mannose-binding protein inhibits in vitro infection by the human immunodeficiency virus, *J. Exp. Med.* 169: 185–196, 1989.
- Fanucchi M, Glaspy J, Crawford J, et al.: Effects of polyethylene glycol-conjugated recombinant human megakaryocyte growth and development factor on platelet counts after chemotherapy for lung cancer, *N. Engl. J. Med.* 336: 404–409, 1997.
- Farese AM, Hankey KG, Cohen MV, et al.: Lymphoid and myeloid recovery in Rhesus macaques following total body X-irradiation, *Health Phys.* 109:414–426, 2015.
- Fernandez ML, Quartino PY, Arce-Bejarano R, et al.: Intravascular hemolysis induced by phospholipases A2 from the venom of the Eastern coral snake, *Micrurus fulvius*:

- functional profiles of hemolytic and non-hemolytic isoforms, *Toxicol. Lett.* 286:39–47, 2018.
- Fibach E: Involvement of phosphatases in proliferation, maturation, and hemoglobinization of developing erythroid cells, *J. Signal Transduct.*, 2011:860985.
- Finch CA, Harker LA, Cook JD: Kinetics of the formed elements of human blood, *Blood* 50:699–707, 1977.
- Finsterbusch M, Schrottmaier WC, Kral-Pointner JB, et al.: Measuring and interpreting platelet-leukocyte aggregates, *Platelets* 29:677–685, 2018.
- Fiske DN, McCoy 3rd HE, Kitchens CS: Zinc-induced sideroblastic anemia: report of a case, review of the literature, and description of the hematologic syndrome, *Am. J. Hematol.* 46:147–150, 1994.
- Fliedner TM, Graessle D, Paulsen C, et al.: Structure and function of bone marrow hemopoiesis: mechanisms of response to ionizing radiation exposure, *Cancer Biother. Rad.* 17:405–426, 2002.
- Fonseca LL, Joyner CJ, Saney CL, et al.: Analysis of erythrocyte dynamics in Rhesus macaque monkeys during infection with *Plasmodium cynomolgi*, *Malar. J.* 17:410, 2018.
- Franco RS: Measurement of red cell lifespan and aging, *Transfus. Med. Hemotherapy* 39:302–307, 2012.
- Franco RS, Puchulu-Campanella ME, Barber LA, et al.: Changes in the properties of normal human red blood cells during in vivo aging, *Am. J. Hematol.* 88:44–51, 2012.
- French DL: Megakaryocytes put a foot through the door, *Blood* 121:2379–2380, 2013.
- Friedman AD: Transcriptional control of granulocyte and monocyte development, *Oncogene* 26:6816–6828, 2007.
- Fritsma GA, McGlasson DL: Whole blood platelet aggregometry, *Methods Mol. Biol.* 1646:333–347, 2017.
- Fröbel J, Landspersky T, Percin G, et al.: The hematopoietic bone marrow niche ecosystem, *Front. Cell Dev. Biol.* 9:705410, 2021.
- Fry MM, Kirk CA: Reticulocyte indices in a canine model of nutritional iron deficiency, *Vet. Clin. Pathol.* 35:172–181, 2006.
- Fu P, Evans B, Lim GB, et al.: The sheep erythropoietin gene: molecular cloning and effect of hemorrhage on plasma erythropoietin and renal/liver messenger RNA in adult sheep, *Mol. Cell. Endocrinol.* 93:107–116, 1993.
- Futosi K, Németh T, Pick R, et al.: Dasatinib inhibits proinflammatory functions of mature human neutrophils, *Blood* 119:4981–4991, 2012.
- Galindez EJ, Aggio MC: The hemopoietic system: a phylogenetic approach, *Histol. Histopathol.* 12:823–826, 1997.
- Garden OA, Kidd L, Mexas AM, et al.: ACVIM consensus statement on the diagnosis of immune-mediated hemolytic anemia in dogs and cats, *J. Vet. Intern. Med.* 33:313–334, 2019.
- Gasiewicz TA, Singh KP, Casado FL: The aryl hydrocarbon receptor has an important role in the regulation of hematopoiesis: implications for benzene-induced hematopoietic toxicity, *Chem. Biol. Interact.* 184:246–251, 2010.
- Geest CR, Coffey PJ: MAPK signaling pathways in the regulation of hematopoiesis, *J. Leukoc. Biol.* 86:237–250, 2009.
- George JN, Aster RH: Drug-induced thrombocytopenia: pathogenesis, evaluation, and management, *Ash Educ. Program Book*, 2009:153–158, 2009.
- Gerecke D, Schultze B, Maurer W: Kinetics of neutrophilic granulocytes in the blood of rats, *Cell Tissue Kinet.* 6:369–378, 1973.
- Ghaffari S: Oxidative stress in the regulation of normal and neoplastic hematopoiesis, *Antioxid. Redox Signal.* 10:1923–1940, 2008.
- Gibson-Corley KN, Olivier AK, Meyerholz DK: Principles for valid histopathologic scoring in research, *Vet. Pathol.* 50:1007–1015, 2013.
- Giulietti M, La Torre R, Pace M, et al.: Reference blood values of iron metabolism in cynomolgus macaques, *Lab. Anim. Sci.* 41:606–608, 1991.
- Glerup P, Grand N, Skydsgaard M: Chapter 13 - the use of minipigs in non-clinical research. In Haschek WM, Rousseaux CG, Wallig MA, editors: *Haschek and Rousseaux's handbook of toxicologic pathology*, Third Edition, Boston, 2013, Academic Press, pp 461–475.
- Glomski CA, Tamburlin J: The phylogenetic odyssey of the erythrocyte. I. Hemoglobin: the universal respiratory pigment, *Histol. Histopathol.* 4:509–514, 1989.
- Glomski CA, Tamburlin J: The phylogenetic odyssey of the erythrocyte. II. The early or invertebrate prototypes, *Histol. Histopathol.* 5:513–525, 1990.
- Golub R, Cumano A: Embryonic hematopoiesis, *Blood Cells Mol. Dis.* 51:226–231, 2013.
- Gondek LP, DeZern AE: Assessing clonal haematopoiesis: clinical burdens and benefits of diagnosing myelodysplastic syndrome precursor states, *Lancet Haematol.* 7:e73–e81, 2020.
- Gopalachar AS, Bowie VL, Bharadwaj P: Phenazopyridine-induced sulfhemoglobinemia, *Ann. Pharmacother.* 39:1128–1130, 2005.
- Goto K, Goto M, Ando-Imaoka M, et al.: Evaluation of drug-induced hematotoxicity using novel in vitro monkey CFU-GM and BFU-E colony assays, *J. Toxicol. Sci.* 42:397–405, 2017.
- Greaves P, Williams A, Eve M: First dose of potential new medicines to humans: how animals help, *Nat. Rev. Drug Discov.* 3:226–236, 2004.
- Grebert M, Granat F, Braun JP, et al.: Validation of the Sysmex XN-V hematology analyzer for canine specimens, *Vet. Clin. Pathol.* 50:184–197, 2021.
- Greinacher A, Eichler P, Lubenow N, et al.: Drug-induced and drug-dependent immune thrombocytopenias, *Rev. Clin. Exp. Hematol.* 5:166–200, 2001.
- Guermontprez P, Gerber-Ferder Y, Vaivode K, et al.: Origin and development of classical dendritic cells, *Int. Rev. Cell Mol. Biol.* 349:1–54, 2019.
- Guffroy M, Falahatpisheh H, Biddle K, et al.: Liver microvascular injury and thrombocytopenia of antibody-

- calicheamicin conjugates in cynomolgus monkeys—mechanism and monitoring, *Clin. Cancer Res.* 23:1760–1770, 2017.
- Gulei D, Tomuleasa C, Qian L, et al.: Editorial: novel drugs targeting the microenvironment and the epigenetic changes in hematopoietic malignancies, *Front. Pharmacol.* 11:614614, 2020.
- Guo X, Zhong W, Chen Y, et al.: Benzene metabolites trigger pyroptosis and contribute to haematotoxicity via TET2 directly regulating the Aim2/Casp1 pathway, *EBioMedicine* 47:578–589, 2019.
- Haglund C, Aleskog A, Hakansson LD, et al.: The FMCA-GM assays, high throughput non-clonogenic alternatives to CFU-GM in preclinical hematotoxicity testing, *Toxicol. Lett.* 194:102–107, 2010.
- Haglund C, Larsson R, Höglund M: *High-throughput screening methods in toxicity testing*, 2013, Wiley, pp 421–429.
- Hahn PF, Bale WF, Bonner JF: Removal of red cells from active circulation by sodium pentobarbital, *Am. J. Physiol.* 138: 415–420, 1943.
- Hajishengallis G, Li X, Chavakis T: Immunometabolic control of hematopoiesis, *Mol. Aspect. Med.* 77:100923, 2021.
- Haley PJ: The lymphoid system: a review of species differences, *J. Toxicol. Pathol.* 30:111–123, 2017.
- Hamilton AJ, Baulcombe DC: A species of small antisense RNA in posttranscriptional gene silencing in plants, *Science* 286:950–952, 1999.
- Harker LA, Marzec UM, Kelly AB, et al.: Prevention of thrombocytopenia and neutropenia in a nonhuman primate model of marrow suppressive chemotherapy by combining pegylated recombinant human megakaryocyte growth and development factor and recombinant human granulocyte colony-stimulating factor, *Blood* 89:155–165, 1997.
- Harker LA, Roskos LK, Marzec UM, et al.: Effects of megakaryocyte growth and development factor on platelet production, platelet life span, and platelet function in healthy human volunteers, *Blood* 95:2514–2522, 2000.
- Harris N, Kunicka J, Kratz A: The ADVIA 2120 hematology system: flow cytometry-based analysis of blood and body fluids in the routine hematology laboratory, *Lab. Hematol.* 11:47–61, 2005.
- Harvey JW: Chapter 7 - The erythrocyte: physiology, metabolism, and biochemical disorders. In Kaneko JJ, Harvey JW, Bruss ML, editors: *Clinical biochemistry of domestic animals*, ed 6, 2008, Academic Press, pp 173–240.
- Hassan AA: Acquired disorders of platelet function, *Ash Educ. Program Book*, 2005:403–408, 2005.
- Haynes AP, Fletcher J: Neutrophil function tests, *Baillieres Clin. Haematol.* 3:871–887, 1990.
- He N, Zhang L, Cui J, et al.: Bone marrow vascular niche: home for hematopoietic stem cells, *Bone Marrow Res.* 128436:2014, 2014.
- He Z, Allers C, Sugimoto C, et al.: Rapid turnover and high production rate of myeloid cells in adult Rhesus macaques with compensations during aging, *J. Immunol.* 200:4059–4067, 2018.
- Hedayati A, Jahanbakhshi A: Hematotoxic effects of direct infusion of crude diesel oil on juvenile great sturgeon *Huso huso*, *Comp. Clin. Pathol.* 22:1117–1122, 2013.
- Hejtmančík MR, Ryan MJ, Toft JD, et al.: Hematological effects in F344 rats and B6C3F1 mice during the 13-week gavage toxicity study of methylene blue trihydrate, *Toxicol. Sci.* 65: 126–134, 2002.
- Hemmi H, Takeuchi O, Kawai T, et al.: A Toll-like receptor recognizes bacterial DNA, *Nature* 408:740–745, 2000.
- Hidalgo A, Chilvers ER, Summers C, et al.: The neutrophil life cycle, *Trends Immunol.* 40:584–597, 2019.
- Hitchcock IS, Hafer M, Sangkhae V, et al.: The thrombopoietin receptor: revisiting the master regulator of platelet production, *Platelets* 32:770–778, 2021.
- Hjort PF, Paputichis H: Platelet life span in normal, splenectomized and hypersplenic rats, *Blood* 15:45–51, 1960.
- Hodge D, Coghill E, Keys J, et al.: A global role for EKLF in definitive and primitive erythropoiesis, *Blood* 107:3359–3370, 2006.
- Hofer T, Rodewald HR: Differentiation-based model of hematopoietic stem cell functions and lineage pathways, *Blood* 132:1106–1113, 2018.
- Hole PS, Darley RL, Tonks A: Do reactive oxygen species play a role in myeloid leukemias? *Blood* 117:5816–5826, 2011.
- Hole PS, Pearn L, Tonks AJ, et al.: Ras-induced reactive oxygen species promote growth factor-independent proliferation in human CD34+ hematopoietic progenitor cells, *Blood* 115:1238–1246, 2010.
- Hong H, Xiao W, Maitta RW: Steady increment of immature platelet fraction is suppressed by irradiation in single-donor platelet components during storage, *PLoS One* 9: e85465, 2014.
- Horiguchi H, Oguma E, Sakamoto T, et al.: Suppression of erythropoietin induction by diethylstilbestrol in rats, *Arch. Toxicol.* 88:137–144, 2013.
- Horner S, Ryan D, Robinson S, et al.: Target organ toxicities in studies conducted to support first time in man dosing: an analysis across species and therapy areas, *Regul. Toxicol. Pharmacol.* 65:1–10, 2013.
- Hsieh FF, Barnett LA, Green WF, et al.: Cell cycle exit during terminal erythroid differentiation is associated with accumulation of p27(Kip1) and inactivation of cdk2 kinase, *Blood* 96:2746–2754, 2000.
- Hu D, Shilatifard A: Epigenetics of hematopoiesis and hematological malignancies, *Genes Dev.* 30:2021–2041, 2016.
- Hvas AM, Favaloro EJ: Platelet function analyzed by light transmission aggregometry, *Methods Mol. Biol.* 1646:321–331, 2017.
- Hvas AM, Grove EL: Platelet function tests: preanalytical variables, clinical utility, advantages, and disadvantages, *Methods Mol. Biol.* 1646:305–320, 2017.
- Hwang DH, Dorfman DM, Hwang DG, et al.: Automated nucleated RBC measurement using the Sysmex XE-5000



- hematology analyzer: frequency and clinical significance of the nucleated RBCs, *Am. J. Clin. Pathol.* 145:379–384, 2016.
- Iolascon A, De Falco L, Beaumont C: Molecular basis of inherited microcytic anemia due to defects in iron acquisition or heme synthesis, *Haematologica* 94:395–408, 2009.
- Itkin T, Gur-Cohen S, Spencer JA, et al.: Distinct bone marrow blood vessels differentially regulate haematopoiesis, *Nature* 532:323–328, 2016.
- Ito H, Uehara K, Matsumoto Y, et al.: Cilostazol inhibits accumulation of triglyceride in aorta and platelet aggregation in cholesterol-fed rabbits, *PLoS One* 7:e39374, 2012.
- Jang Y-Y, Sharkis SJ: A low level of reactive oxygen species selects for primitive hematopoietic stem cells that may reside in the low-oxygenic niche, *Blood* 110:3056–3063, 2007.
- Jardim DL, Rodrigues CA, Novis YAS, et al.: Oxaliplatin-related thrombocytopenia, *Ann. Oncol.* 23, 2012.
- Jenne CN, Urrutia R, Kubes P: Platelets: bridging hemostasis, inflammation, and immunity, *Int. J. Lab. Hematol.* 35:254–261, 2013.
- Jing D, Fonseca AV, Alakel N, et al.: Hematopoietic stem cells in co-culture with mesenchymal stromal cells—modeling the niche compartments in vitro, *Haematologica* 95:542–550, 2010.
- Johns J, Heller M: Hematologic conditions of small ruminants, *Vet. Clin. North Am. Food Anim. Pract.* 37:183–197, 2021.
- Johns JL, Christopher MM: Extramedullary hematopoiesis: a new look at the underlying stem cell niche, theories of development, and occurrence in animals, *Vet. Pathol.* 49: 508–523, 2012.
- Jordan HL, Register TC, Tripathi NK, et al.: Nontraditional applications in clinical pathology, *Toxicol. Pathol.* 42:1058–1068, 2014.
- Jung JH, Yang Y, Seo D, et al.: Clinical utility of immature reticulocyte fraction for identifying early red blood cell regeneration in anemic dogs, *J. Vet. Intern. Med.* 37:484–489, 2023.
- Kaestner L, Minetti G: The potential of erythrocytes as cellular aging models, *Cell Death Differ.* 24:1475–1477, 2017.
- Kaito K, Otsubo H, Usui N, et al.: Platelet size deviation width, platelet large cell ratio, and mean platelet volume have sufficient sensitivity and specificity in the diagnosis of immune thrombocytopenia, *Br. J. Haematol.* 128:698–702, 2005.
- Kao DS, Zhang SW, Vap AR: A systematic review on the effect of common medications on platelet count and function: which medications should be stopped before getting a platelet-rich plasma injection? *Orthop. J. Sports Med.* 10, 2022.
- Kapp FG, Perlin JR, Hagedorn EJ, et al.: Protection from UV light is an evolutionarily conserved feature of the haematopoietic niche, *Nature* 558:445–448, 2018.
- Kaushansky K, Zhan H: The regulation of normal and neoplastic hematopoiesis is dependent on microenvironmental cells, *Adv. Biol. Regul.* 69:11–15, 2018.
- Kelly D, Lamb V, Juvet F: Eltrombopag treatment of a dog with idiopathic aplastic pancytopenia, *J. Vet. Intern. Med.* 34:890–892, 2020.
- Kerlin R, Bolon B, Burkhardt J, et al.: Scientific and regulatory policy committee: recommended (“Best”) practices for determining, communicating, and using adverse effect data from nonclinical studies, *Toxicol. Pathol.* 44:147–162, 2016.
- Kim H-Y, Park SW, Kim JH, et al.: Romiplostim-related myelofibrosis in refractory primary immune thrombocytopenia: a Case report, *Medicine* 98, 2019.
- Kim HK, Kim JE, Ham CK, et al.: Prognostic value of platelet indices as determined by ADVIA 120 in patients suspected of having disseminated intravascular coagulation, *Int. J. Lab. Hematol.* 30:117–123, 2008.
- Kingsley PD, Malik J, Emerson RL, et al.: “Maturation” globin switching in primary primitive erythroid cells, *Blood* 107:1665–1672, 2006.
- Knight E, Eichenbaum G, Hillsamer V, et al.: Nonclinical safety assessment of a synthetic peptide thrombopoietin agonist: effects on platelets, bone homeostasis, and immunogenicity and the implications for clinical safety monitoring of adverse bone effects, *Int. J. Toxicol.* 30:385–404, 2011.
- Kojima S, Haruta J, Enomoto A, et al.: Age-related hematological changes in normal F344 rats: during the neonatal period, *Exp. Anim.* 48:153–159, 1999.
- Kojima S, Sasaki J, Tomita M, et al.: Multiple organ toxicity, including hypochromic anemia, following repeated dose oral administration of phenobarbital (PB) in rats, *J. Toxicol. Sci.* 34:527–539, 2009.
- Kokkalis KD: Dissecting the spatial bone marrow microenvironment of hematopoietic stem cells, *Curr. Opin. Oncol.* 32:154–161, 2020.
- Koltai K, Kesmarky G, Feher G, et al.: Platelet aggregometry testing: molecular mechanisms, techniques and clinical implications, *Int. J. Mol. Sci.* 18, 2017.
- Kondo M: Lymphoid and myeloid lineage commitment in multipotent hematopoietic progenitors, *Immunol. Rev.* 238: 37–46, 2010.
- Kondo M, Oshita F, Kato Y, et al.: Early monocytopenia after chemotherapy as a risk factor for neutropenia, *Am. J. Clin. Oncol.* 22:103–105, 1999.
- Koonin EV, Krupovic M: Origin of programmed cell death from antiviral defense? *Proc. Natl. Acad. Sci. U.S.A.* 116: 16167–16169, 2019.
- Koonin EV, Zhang F: Coupling immunity and programmed cell suicide in prokaryotes: life-or-death choices, *Bioessays* 39:1–9, 2017.
- Koury MJ, Ponka P: New insights into erythropoiesis: the roles of folate, vitamin B12, and iron, *Annu. Rev. Nutr.* 24:105–131, 2004.
- Kouvelas D, Goulas A, Papazisis G, et al.: PDE5 inhibitors: in vitro and in vivo pharmacological profile, *Curr. Pharmaceut. Des.* 15:3464–3475, 2009.
- Kozlowski C, Brumm J, Cain G: An automated image analysis method to quantify veterinary bone marrow cellularity on H&E sections, *Toxicol. Pathol.* 46:324–335, 2018a.

- Kozlowski C, Fullerton A, Cain G, et al.: Proof of concept for an automated image analysis method to quantify rat bone marrow hematopoietic lineages on H&E sections, *Toxicol. Pathol.* 46:336–347, 2018b.
- Kurata M, Iidaka T, Hamada Y, et al.: Simultaneous measurement of nucleated cell counts and cellular differentials in rat bone marrow examination using flow cytometer, *J. Toxicol. Sci.* 32:289–299, 2007.
- Kurtin SJ: Myeloid toxicity of cancer treatment, *J. Oncol. Pract.* 3:209, 2012.
- Kuter DJ, Beeler DL, Rosenberg RD: The purification of megapoietin: a physiological regulator of megakaryocyte growth and platelet production, *Proc. Natl. Acad. Sci. U.S.A.* 91:11104–11108, 1994.
- Labrie SJ, Samson JE, Moineau S: Bacteriophage resistance mechanisms, *Nat. Rev. Microbiol.* 8:317–327, 2010.
- Lacaud G, Kouskoff V: Hemangioblast, hemogenic endothelium, and primitive versus definitive hematopoiesis, *Exp. Hematol.* 49:19–24, 2017.
- Lang F, Bissinger R, Abed M, et al.: Eryptosis—the neglected cause of anemia in end stage renal disease, *Kidney Blood Press. Res.* 42:749–760, 2017.
- Lang F, Lang E, Föller M: Physiology and pathophysiology of eryptosis, *Transfus. Med. Hemotherapy* 39:308–314, 2012.
- Latimer KS. *Duncan and Prasse's veterinary laboratory medicine: clinical pathology*, ed 5, 2011, John Wiley & Sons.
- Latimer KS, Jain AV, Inglesby HB, et al.: Zinc-induced hemolytic anemia caused by ingestion of pennies by a pup, *J. Am. Vet. Med. Assoc.* 195:77–80, 1989.
- Laurenti E, Gottgens B: From haematopoietic stem cells to complex differentiation landscapes, *Nature* 553:418–426, 2018.
- Lautraite S, Parent-Massin D, Rio B, et al.: In vitro toxicity induced by deoxynivalenol (DON) on human and rat granulomonocytic progenitors, *Cell Biol. Toxicol.* 13:175–183, 1997.
- Lawrence SM, Corriden R, Nizet V: The ontogeny of a neutrophil: mechanisms of granulopoiesis and homeostasis, *Microbiol. Mol. Biol. Rev.* 82, 2018.
- Lawrence SM, Corriden R, Nizet V: How neutrophils meet their end, *Trends Immunol.* 41:531–544, 2020.
- Lelieveld P, van der Vijgh WJ, van Velzen D, et al.: Preclinical toxicology of platinum analogues in dogs, *J. Cancer Res. Clin. Oncol.* 23:1147–1154, 1987.
- Lenaz G, Strocchi P: Reactive oxygen species in the induction of toxicity. In *General and applied systems toxicology*, 2011, Wiley, pp 1–44.
- Li H, Li WX, Ding SW: Induction and suppression of RNA silencing by an animal virus, *Science* 296:1319–1321, 2002.
- Li H, Yang J, Chu TT, et al.: Cytoskeleton remodeling induces membrane stiffness and stability changes of maturing reticulocytes, *Biophys. J.* 114:2014–2023, 2018.
- Liang SX, Pinkevych M, Khachigian LM, et al.: Drug-induced thrombocytopenia: development of a novel NOD/SCID mouse model to evaluate clearance of circulating platelets by drug-dependent antibodies and the efficacy of IVIG, *Blood* 116:1958–1960, 2010.
- Lilliehook I, Tvedten HW: Errors in basophil enumeration with 3 veterinary hematology systems and observations on occurrence of basophils in dogs, *Vet. Clin. Pathol.* 40:450–458, 2011.
- Lin Y-J, Ling M-P, Chen S-C, et al.: Mixture risk assessment due to ingestion of arsenic, copper, and zinc from milkfish farmed in contaminated coastal areas, *Environ. Sci. Pollut. Res.* 24:14616–14626, 2017.
- Lisanti MP, Martinez-Outschoorn UE, Chiavarina B, et al.: Understanding the “lethal” drivers of tumor-stroma co-evolution: emerging role(s) for hypoxia, oxidative stress and autophagy/mitophagy in the tumor micro-environment, *Cancer Biol. Ther.* 10:537–542, 2010.
- Litman GW, Cannon JP, Dishaw LJ: Reconstructing immune phylogeny: new perspectives, *Nat. Rev. Immunol.* 5:866–879, 2005.
- Little KY, Zhang L, Cook E: Fluoxetine-induced alterations in human platelet serotonin transporter expression: serotonin transporter polymorphism effects, *J. Psychiatry Neurosci.* 31: 333–339, 2006.
- Liu J, Guo X, Mohandas N, et al.: Membrane remodeling during reticulocyte maturation, *Blood* 115:2021–2027, 2010.
- Liu S, Zheng SC, Li YL, et al.: Hemocyte-mediated phagocytosis in Crustaceans, *Front. Immunol.* 11:268, 2020.
- Long ME, Mustonen AM, Zitzer NC, et al.: Persistent non-regenerative anemia in a 4-year-old cat, *Vet. Clin. Pathol.* 49: 11–16, 2020.
- Lotinun S, Sibonga JD, Turner RT: Evidence that the cells responsible for marrow fibrosis in a rat model for hyperparathyroidism are preosteoblasts, *Endocrinology* 146:4074–4081, 2005.
- Luc S, Luis TC, Boukarabila H, et al.: The earliest thymic T cell progenitors sustain B cell and myeloid lineage potential, *Nat. Immunol.* 13:412–419, 2012.
- Lucas D: The bone marrow microenvironment for hematopoietic stem cells, *Adv. Exp. Med. Biol.* 1041:5–18, 2017.
- Lucas D: Structural organization of the bone marrow and its role in hematopoiesis, *Curr. Opin. Hematol.* 28:36–42, 2021.
- Lucidi CA, de Rezende CLE, Jutkowitz LA, et al.: Histologic and cytologic bone marrow findings in dogs with suspected precursor-targeted immune-mediated anemia and associated phagocytosis of erythroid precursors, *Vet. Clin. Pathol.* 46:401–415, 2017.
- Ludin A, Gur-Cohen S, Golan K, et al.: Reactive oxygen species regulate hematopoietic stem cell self-renewal, migration and development, as well as their bone marrow microenvironment, *Antioxid. Redox Signal.* 21:1605–1619, 2014.
- Luttgen PJ, Whitney MS, Wolf AM, et al.: Heinz body hemolytic anemia associated with high plasma zinc concentration in a dog, *J. Am. Vet. Med. Assoc.* 197:1347–1350, 1990.
- Lutz HU: Naturally occurring anti-band 3 antibodies in clearance of senescent and oxidatively stressed human red blood cells, *Transfus. Med. Hemother.* 39:321–327, 2012.

- Machado LR, Ottolini B: An evolutionary history of defensins: a role for copy number variation in maximizing host innate and adaptive immune responses, *Front. Immunol.* 6:115, 2015.
- Machlus KR, Italiano Jr JE: The incredible journey: from megakaryocyte development to platelet formation, *J. Cell Biol.* 201:785–796, 2013.
- MacKenzie WF, Eustis SL: Bone marrow. In Boorman GA, Elistis SL, Elwell MR, Montgomery CA, Mackenzie WF, editors: *Pathology of the fisher rat - reference and atlas*, San Diego, 1990, Academic Press, pp 315–337.
- Mackey MC: Periodic hematological disorders: quintessential examples of dynamical diseases, *Chaos* 30:063123, 2020.
- Maker JH, Stroup CM, Huang V, et al.: Antibiotic hypersensitivity mechanisms, *Pharm. Times* 7:122, 2019.
- Malara A, Gruppi C, Rebuzzini P, et al.: Megakaryocyte-matrix interaction within bone marrow: new roles for fibronectin and factor XIII-A, *Blood* 117:2476–2483, 2011.
- Malengier-Devlies B, Metzemaekers M, Wouters C, et al.: Neutrophil homeostasis and emergency granulopoiesis: the example of systemic juvenile idiopathic arthritis, *Front. Immunol.* 12:766620, 2021.
- Manwani D, Bieker JJ: The erythroblastic island, *Curr. Top. Dev. Biol.* 82:23–53, 2008.
- Markovic M, Majkic-Singh N, Ignjatovic S, et al.: Reticulocyte haemoglobin content vs. soluble transferrin receptor and ferritin index in iron deficiency anaemia accompanied with inflammation, *Int. J. Lab. Hematol.* 29:341–346, 2007.
- Maronpot RR: Enhanced histopathology of lymphoid tissues, *Toxicol. Pathol.* 34:631–633, 2006.
- Marti HH, Wenger RH, Rivas LA, et al.: Erythropoietin gene expression in human, monkey and murine brain, *Eur. J. Neurosci.* 8:666–676, 1996.
- Martin CS, Moriyama A, Zon LI: Hematopoietic stem cells, hematopoiesis and disease: lessons from the zebrafish model, *Genome Med.* 3:83, 2011.
- Martin RA, Brott DA, Zandee JC, et al.: Differential analysis of animal bone marrow by flow cytometry, *Cytometry* 13:638–643, 1992.
- Massberg S, von Andrian UH: Novel trafficking routes for hematopoietic stem and progenitor cells, *Ann. N. Y. Acad. Sci.* 1176:87–93, 2009.
- Matsushita Y, Ono W, Ono N: Toward marrow adipocytes: adipogenic trajectory of the bone marrow stromal cell lineage, *Front. Endocrinol.* 13:882297, 2022.
- Mazzi S, Lordier L, Debili N, et al.: Megakaryocyte and polyploidization, *Exp. Hematol.* 57:1–13, 2018.
- McCracken JM, Allen LA: Regulation of human neutrophil apoptosis and lifespan in health and disease, *J. Cell Death* 7: 15–23, 2014.
- McElroy PL, Wei P, Buck K, et al.: Romiplostim promotes platelet recovery in a mouse model of multicycle chemotherapy-induced thrombocytopenia, *Exp. Hematol.* 43:479–487, 2015.
- McGlasson DL, Fritsma GA: Whole blood platelet aggregation and platelet function testing, *Semin. Thromb. Hemost.* 35:168–180, 2009.
- McManus PM, Litwin C, Barber L: Immune-mediated neutropenia in 2 dogs, *J. Vet. Intern. Med.* 13:372–374, 1999.
- McMichael MA: Oxidative stress, antioxidants, and assessment of oxidative stress in dogs and cats, *J. Am. Vet. Med. Assoc.* 231:714–720, 2007.
- Means Jr RT: Pure red cell aplasia, *Hematol. Am. Soc. Hematol. Educ. Program* 2016:51–56, 2016a.
- Means Jr RT: Pure red cell aplasia, *Blood* 128:2504–2509, 2016b.
- Medzhitov R, Janeway Jr CA: Decoding the patterns of self and nonself by the innate immune system, *Science* 296:298–300, 2002.
- Mendel M, Chłopecka M, Dziekan N: Haemolytic crisis in sheep as a result of chronic exposure to copper, *Pol. J. Vet. Sci.* 10:51–56, 2007.
- Menon V, Ghaffari S: Erythroid enucleation: a gateway into a “bloody” world, *Exp. Hematol.* 95:13–22, 2021.
- Merrill SA, Brodsky RA: Complement-driven anemia: more than just paroxysmal nocturnal hemoglobinuria, *Hematology* 2018:371–376, 2018.
- Meselson M, Yuan R: DNA restriction enzyme from *E. coli*, *Nature* 217:1110–1114, 1968.
- Metcalf D: Hematopoietic cytokines, *Blood* 111:485–491, 2008.
- Meyerstein N, Yagil R, Sod-Moriah UA: Red cell survival in heat-exposed hamsters, *Comp. Biochem. Physiol. A Comp. Physiol.* 50:691–694, 1975.
- Michelson AD: Methods for the measurement of platelet function, *Am. J. Cardiol.* 103:20A–26A, 2009.
- Miller ER, Ullrey DE, Ackermann I, et al.: Swine hematology from birth to maturity. II. Erythrocyte population, size and hemoglobin concentration, *J. Anim. Sci.* 20:890–897, 1961.
- Minetti G, Bernecker C, Dorn I, et al.: Membrane rearrangements in the maturation of circulating human reticulocytes, *Front. Physiol.* 11:215, 2020.
- Mitroulis I, Ruppova K, Wang B, et al.: Modulation of myelopoiesis progenitors is an integral component of trained immunity, *Cell* 172:147–161, 2018.
- Miyata H, Asanuma F, Iwaki Y, et al.: Evaluation of myelotoxicity in dietary restricted rats, *J. Toxicol. Pathol.* 22:53–63, 2009.
- Moldogazieva NT, Mokhosoev IM, Mel’nikova TI, et al.: Dual character of reactive oxygen, nitrogen, and halogen species: endogenous sources, interconversions and neutralization, *Biochemistry (Mosc.)* 85:S56–S78, 2020.
- Molyneux G: Serum FLT-3 ligand in a busulphan-induced model of chronic bone marrow hypoplasia in the female CD-1 mouse, *Int. J. Exp. Pathol.* 89:159, 2008.
- Monticello TM, Jones TW, Dambach DM, et al.: Current nonclinical testing paradigm enables safe entry to First-In-Human clinical trials: the IQ consortium nonclinical to clinical translational database, *Toxicol. Appl. Pharmacol.* 334: 100–109, 2017.



- Moore M, Warren DJ: Synergy of interleukin 1 and granulocyte colony-stimulating factor: in vivo stimulation of stem-cell recovery and hematopoietic regeneration following 5-fluorouracil treatment of mice, *Proc. Natl. Acad. Sci. U.S.A.* 84:7134–7138, 1987.
- Morita J, Izumi T, Ogawa B, et al.: Effects of reduced food intake for 4 weeks on physiological parameters in toxicity studies in dogs, *J. Toxicol. Sci.* 42:31–42, 2017.
- Moroni M, Lombardini E, Salber R, et al.: Hematological changes as prognostic indicators of survival: similarities between Gottingen minipigs, humans, and other large animal models, *PLoS One* 6:e25210, 2011.
- Moujalled D, Gangatirkar P, Kauppi M, et al.: The necroptotic cell death pathway operates in megakaryocytes, but not in platelet synthesis, *Cell Death Dis.* 12:133, 2021.
- Munoz M, Villar I, Garcia-Erce JA: An update on iron physiology, *World J. Gastroenterol.* 15:4617–4626, 2009.
- Murphy Jr MJ: The hematopoietic cytokines: an overview, *Toxicol. Pathol.* 21:229–230, 1993.
- Naik SH: Dendritic cell development at a clonal level within a revised ‘continuous’ model of haematopoiesis, *Mol. Immunol.* 124:190–197, 2020.
- Nakamura-Ishizu A, Suda T: Multifaceted roles of thrombopoietin in hematopoietic stem cell regulation, *Ann. N. Y. Acad. Sci.* 1466:51–58, 2020.
- Narayanan P, Shen L, Curtis BR, et al.: Investigation into the mechanism(s) that leads to platelet decreases in cynomolgus monkeys during administration of ISIS 104838, a 2'-MOE-modified antisense oligonucleotide, *Toxicol. Sci.* 164:613–626, 2018.
- Narayanan PK, Henry S, Li N: Drug-induced thrombocytopenia: mechanisms and relevance in preclinical safety assessment, *Curr. Opin. Toxicol.* 17:23–30, 2019.
- NCI. In Services UDOHAH, editor: *Common terminology criteria for adverse events (CTCAE)*, Version 5.0, 2017, National Institutes of Health, National Cancer Institute.
- Nederbragt H, van den Ingh TS, Wensvoort P: Pathobiology of copper toxicity, *Vet. Q.* 6:179–185, 1984.
- Nelson EA, Qiu J, Chavkin NW, et al.: Directed differentiation of hemogenic endothelial cells from human pluripotent stem cells, *J. Vis. Exp.* 169, 2021.
- Nenna A, Nappi F, Lusini M, et al.: Effect of statins on platelet activation and function: from molecular pathways to clinical effects, *BioMed Res. Int.*, 2021:6661847.
- Neschadim A, Branch DR: Mouse models for immune-mediated platelet destruction or immune thrombocytopenia (ITP), *Curr. Protoc. Im.* 113:15–30, 2016.
- Nieto M, Calvo G, Hudson I, et al.: The European Medicines Agency review of eltrombopag (Revolade) for the treatment of adult chronic immune (idiopathic) thrombocytopenic purpura: summary of the scientific assessment of the Committee for Medicinal Products for Human Use, *Haematologica* 96:e33–e40, 2011.
- Noetzli LJ, French SL, Machlus KR: New insights into the differentiation of megakaryocytes from hematopoietic progenitors, *Arterioscler. Thromb. Vasc. Biol.* 39:1288–1300, 2019.
- Nolan JP, Jones JC: Detection of platelet vesicles by flow cytometry, *Platelets* 28:256–262, 2017.
- Nunomura W, Cianciarullo AM, Kato T, et al.: Phylogeny and ontogeny of erythropoiesis, *BioMed Res. Int.* 136270:2015, 2015.
- Odell Jr TT, Mc DT: Life span of mouse blood platelets, *Proc. Soc. Exp. Biol. Med.* 106:107–108, 1961.
- Ogawa M, Fraser S, Fujimoto T, et al.: Origin of hematopoietic progenitors during embryogenesis, *Int. Rev. Immunol.* 20: 21–44, 2001.
- Olson H, Betton G, Robinson D, et al.: Concordance of the toxicity of pharmaceuticals in humans and in animals, *Regul. Toxicol. Pharmacol.* 32:56–67, 2000.
- Orkin SH, Zon LI: Hematopoiesis: an evolving paradigm for stem cell biology, *Cell* 132:631–644, 2008.
- Oustamanolakis P, Koutroubakis IE, Messaritakis I, et al.: Measurement of reticulocyte and red blood cell indices in the evaluation of anemia in inflammatory bowel disease, *J. Crohns Colitis* 5:295–300, 2011.
- Overgaard RV, Karlsson M, Ingwersen SH: Pharmacodynamic model of interleukin-21 effects on red blood cells in cynomolgus monkeys, *J. Pharmacokinet. Pharmacodyn.* 34:559–574, 2007.
- Palazzi X, Burkhardt JE, Caplain H, et al.: Characterizing “adversity” of pathology findings in nonclinical toxicity studies: results from the 4th ESTP international expert workshop, *Toxicol. Pathol.* 44:1–15, 2016.
- Palis J: Primitive and definitive erythropoiesis in mammals, *Front. Physiol.* 5:3, 2014.
- Paniccia R, Priora R, Liotta AA, et al.: Platelet function tests: a comparative review, *Vasc. Health Risk Manag.* 11:133–148, 2015.
- Pankraz A, Ledieu D, Pralet D, et al.: Detection of reticulated platelets in whole blood of rats using flow cytometry, *Exp. Toxicol. Pathol.* 60:443–448, 2008.
- Parekh C, Crooks GM: Critical differences in hematopoiesis and lymphoid development between humans and mice, *J. Clin. Immunol.* 33:711–715, 2013.
- Parmentier S, Kramer M, Weller S, et al.: Reevaluation of reference values for bone marrow differential counts in 236 healthy bone marrow donors, *Ann. Hematol.* 99:2723–2729, 2020.
- Patel P, Michael JV, Naik UP, et al.: Platelet FcγRIIA in immunity and thrombosis: adaptive immunothrombosis, *J. Thromb. Haemostasis* 19:1149–1160, 2021.
- Patton WN, Duffull SB: Idiosyncratic drug-induced haematological abnormalities. Incidence, pathogenesis, management and avoidance, *Drug Saf.* 11:445–462, 1994.
- Peixeiro I, Silva AL, Romao L: Control of human beta-globin mRNA stability and its impact on beta-thalassemia phenotype, *Haematologica* 96:905–913, 2011.
- Perigard CJ, Parrula MCM, Larkin MH, et al.: Impact of menstruation on select hematology and clinical chemistry variables in cynomolgus macaques, *Vet. Clin. Pathol.* 45: 232–243, 2016.

- Pernecker I, Bauer NB, Johannes S, et al.: Comparison of the Sysmex XT-2000iV with microscopic differential counts of canine bone marrow, *J. Vet. Diagn. Invest.* 29:148–153, 2017.
- Perry R, Farris G, Bienvenu JG, et al.: Society of Toxicologic Pathology position paper on best practices on recovery studies: the role of the anatomic pathologist, *Toxicol. Pathol.* 41:1159–1169, 2013.
- Pessina A, Malerba I, Gribaldo L: Hematotoxicity testing by cell clonogenic assay in drug development and preclinical trials, *Curr. Pharmaceut. Des.* 11:1055–1065, 2005.
- Phillips C, Naskou MC, Spangler E: Investigation of platelet measurands in dogs with hematologic neoplasia, *Vet. Clin. Pathol.* 51:216–224, 2022.
- Phillips TJ, Hen R, Crabbe JC: Complications associated with genetic background effects in research using knockout mice, *Psychopharmacology* 147:5–7, 1999.
- Pillai AS, Chandler SA, Liu Y, et al.: Origin of complexity in haemoglobin evolution, *Nature* 581:480–485, 2020.
- Pinho S, Frenette PS: Haematopoietic stem cell activity and interactions with the niche, *Nat. Rev. Mol. Cell Biol.* 20:303–320, 2019.
- Piomelli S: Chemical toxicity of red cells, *Environ. Health Perspect.* 39:65–70, 1981.
- Potts KS, Farley A, Dawson CA, et al.: Membrane budding is a major mechanism of in vivo platelet biogenesis, *J. Exp. Med.* 217, 2020.
- Pouzolles M, Oburoglu L, Taylor N, et al.: Hematopoietic stem cell lineage specification, *Curr. Opin. Hematol.* 23:311–317, 2016.
- Povirk LF: DNA damage and mutagenesis by radiomimetic DNA-cleaving agents: bleomycin, neocarzinostatin and other enediynes, *Mutat. Res.* 355:71–89, 1996.
- Radakovich LB, Santangelo KS, Olver CS: Reticulocyte hemoglobin content does not differentiate true from functional iron deficiency in dogs, *Vet. Clin. Pathol.* 44:511–518, 2015.
- Rael LT: Interaction of arsine with hemoglobin in arsine-induced hemolysis, *Toxicol. Sci.* 90:142–148, 2005.
- Rael LT, Ayala-Fierro F, Bar-Or R, et al.: Interaction of arsine with hemoglobin in arsine-induced hemolysis, *Toxicol. Sci.* 90:142–148, 2006.
- Rael LT, Ayala-Fierro F, Carter DE: The effects of sulfur, thiol, and thiol inhibitor compounds on arsine-induced toxicity in the human erythrocyte membrane, *Toxicol. Sci.* 55:468–477, 2000.
- Ramaiah L, Bounous DI, Elmore SA: Chapter 50—Hematopoietic system. In Haschek WM, Rousseaux CG, Wallig MA, editors: *Haschek and Rousseaux's handbook of toxicologic pathology*, Third Edition, Boston, 2013, Academic Press, pp 1863–1933.
- Ramaiah L, Tomlinson L, Tripathi NK, et al.: Principles for assessing adversity in toxicologic clinical pathology, *Toxicol. Pathol.* 45(2):260–266, 2017.
- Ray RR: Adverse hematological effects of hexavalent chromium: an overview, *Interdiscipl. Toxicol.* 9:55–65, 2016.
- Reagan WJ, Irizarry-Rovira A, Poitout-Belissent F, et al.: Best practices for evaluation of bone marrow in nonclinical toxicity studies, *Toxicol. Pathol.* 39:435–448, 2011.
- Reagan WJ, Irizarry Rovira AR, DeNicola DB: Hematopoiesis. In *Veterinary hematology: atlas of common domestic and non-domestic species*, ed 3, 2019, Wiley.
- Rebar AH: General responses of the bone marrow to injury, *Toxicol. Pathol.* 21:118–129, 1993.
- Repsold L, Joubert AM: Eryptosis: an erythrocyte's suicidal type of cell death, *BioMed Res. Int.*, 2018:9405617.
- Rieger MA, Hoppe PS, Smejkal BM, et al.: Hematopoietic cytokines can instruct lineage choice, *Science* 325:217–218, 2009.
- Riley RS, Ben-Ezra JM, Goel R, et al.: Reticulocytes and reticulocyte enumeration, *J. Clin. Lab. Anal.* 15:267–294, 2001.
- Risitano AM: New challenges to developing animal models for human immune-mediated marrow failure, *Clin. Med. Res.* 3:63–64, 2005.
- Rizzo AM: Effects of long-term space flight on erythrocytes and oxidative stress of rodents, *PLoS One* 7:e32361, 2012.
- Robb L: Cytokine receptors and hematopoietic differentiation, *Oncogene* 26:6715–6723, 2007.
- Roberts RA, Laskin DL, Smith CV, et al.: Nitrate and oxidative stress in toxicology and disease, *Toxicol. Sci.* 112: 4–16, 2009.
- Robinson M, MacHin S, Mackie I, et al.: In vivo biotinylation studies: specificity of labelling of reticulated platelets by thiazole orange and mepacrine, *Br. J. Haematol.* 108:859–864, 2000.
- Rodrigues CP, Shvedunova M, Akhtar A: Epigenetic regulators as the gatekeepers of hematopoiesis, *Trends Genet.* 37: 125–142, 2021.
- Rodriguez-Fraticelli AE, Wolock SL, Weinreb CS, et al.: Clonal analysis of lineage fate in native haematopoiesis, *Nature* 553:212–216, 2018.
- Roney N, Abadin HG, Fowler B, et al.: Metal ions affecting the hematological system, *Met. Ions Life Sci.* 8:143–155, 2011.
- Rosales C: Neutrophil: a cell with many roles in inflammation or several cell types? *Front. Physiol.* 9:113, 2018.
- Ross J, Sullivan TD: Half-lives of beta and gamma globin messenger RNAs and of protein synthetic capacity in cultured human reticulocytes, *Blood* 66:1149–1154, 1985.
- Rosti V: Murine models of paroxysmal nocturnal hemoglobinuria, *Ann. N. Y. Acad. Sci.* 963:290–296, 2002.
- Rother RP, Bell L, Hillmen P, et al.: The clinical sequelae of intravascular hemolysis and extracellular plasma hemoglobin: a novel mechanism of human disease, *JAMA* 293: 1653–1662, 2005.
- Sampson TR, Saroj SD, Llewellyn AC, et al.: A CRISPR/Cas system mediates bacterial innate immune evasion and virulence, *Nature* 497:254–257, 2013.
- Sankaran VG, Orkin SH, Walkley CR: Rb intrinsically promotes erythropoiesis by coupling cell cycle exit with mitochondrial biogenesis, *Genes Dev.* 22:463–475, 2008.

- Schacham P, Philp RB, Gowdey CW: Antihematopoietic and carcinogenic effects of bracken fern (*Pteridium aquilinum*) in rats, *Am. J. Vet. Res.* 31:191–197, 1970.
- Schaer DJ, Buehler PW, Alayash AI, et al.: Hemolysis and free hemoglobin revisited: exploring hemoglobin and hemin scavengers as a novel class of therapeutic proteins, *Blood* 121:1276–1284, 2013.
- Schapkaitz E: Stability of new erythrocyte and reticulocyte parameters in testing for anemia on the Sysmex XN 9000, *Lab. Med.* 49:219–225, 2018.
- Schneider E, Thieblemont N, De Moraes ML, et al.: Basophils: new players in the cytokine network, *Eur. Cytokine Netw.* 21:142–153, 2010.
- Schoorl M, Schoorl M, Oomes J, et al.: New fluorescent method (PLT-F) on Sysmex XN2000 hematology analyzer achieved higher accuracy in low platelet counting, *Am. J. Clin. Pathol.* 140:495–499, 2013.
- Schubert TE, Obermaier F, Ugocsai P, et al.: Murine models of anaemia of inflammation: extramedullary haematopoiesis represents a species specific difference to human anaemia of inflammation that can be eliminated by splenectomy, *Int. J. Immunopathol. Pharmacol.* 21:577–584, 2008.
- Schulenburg H, Kurz CL, Ewbank JJ: Evolution of the innate immune system: the worm perspective, *Immunol. Rev.* 198: 36–58, 2004.
- Schultze JL, Mass E, Schlitzer A: Emerging principles in myelopoiesis at homeostasis and during infection and inflammation, *Immunity* 50:288–301, 2019.
- Sedek Ł, Kulis JAN, SŁota Ł, et al.: The influence of fixation of biological samples on cell count and marker expression stability in flow cytometric analyses, *Cent. Eur. J. Immunol.* 45:206–213, 2020.
- Semenza GL: Oxygen sensing, homeostasis, and disease, *N. Engl. J. Med.* 365:537–547, 2011.
- Serb JM, Oakley TH: Hierarchical phylogenetics as a quantitative analytical framework for evolutionary developmental biology, *Bioessays* 27:1158–1166, 2005.
- Sernoskie SC, Jee A, Uetrecht JP: The emerging role of the innate immune response in idiosyncratic drug reactions, *Pharmacol. Rev.* 73:861–896, 2021.
- Shallis RM, Ahmad R, Zeidan AM: Aplastic anemia: etiology, molecular pathogenesis, and emerging concepts, *Eur. J. Haematol.* 101:711–720, 2018.
- Shander A, Javidroozi M, Ashton ME: Drug-induced anemia and other red cell disorders: a guide in the age of polypharmacy, *Curr. Clin. Pharmacol.* 6:295–303, 2011.
- Shao J, White CC, Dabrowski MJ, et al.: The role of mitochondrial and oxidative injury in BDE 47 toxicity to human fetal liver hematopoietic stem cells, *Toxicol. Sci.* 101:81–90, 2008.
- Sharma D, Priest H, Wilcox A: Pseudoreticulocytosis by the ADVIA 2120 hematology analyzer and other hematologic changes in a cynomolgus macaque (*Macaca fascicularis*) with malaria, *Toxicol. Pathol.* 50:684–692, 2022.
- Shih HM, Wu CJ, Lin SL: Physiology and pathophysiology of renal erythropoietin-producing cells, *J. Formos. Med. Assoc.* 117:955–963, 2018.
- Shimizu Y, Naito Y, Murakami D: The experimental study on the mechanism of hemolysis on paroxysmal hemoglobinemia and hemoglobinuria in calves due to excessive water intake, *Nihon Juigaku Zasshi* 41:583–592, 1979.
- Siemens: ADVIA® 120/2120/2120i hematology systems supplemental information research use only (RUO). In 2016, Siemens. Ireland, <https://doclib.siemens-healthineers.com/rest/v1/view?document-id=344126>. (Accessed 14 July 2024).
- Siha MS, Shaker DA-H, Teleb HS, et al.: Effects of delta-aminolevulinic acid dehydratase gene polymorphism on hematological parameters and kidney function of lead-exposed workers, *Int. J. Occup. Environ. Med.* 10:1689–1693, 2019.
- Simon F, Borrega JG, Bröckelmann PJ: Toxicities of novel therapies for hematologic malignancies, *Expert Rev. Hematol.* 13:1–17, 2020.
- Simon SI, Kim MH: A day (or 5) in a neutrophil's life, *Blood* 116:511–512, 2010.
- Sirivelu M: Validation of flow cytometry-based quantitation of reticulated platelets in cynomolgus monkeys and wistar rats. In *STP 37th annual symposium, Abstract no. 18*, 2018, p 15. [https://www.toxpath.org/AM2018/docs/STP-AM18\\_Posters-Abstract-Index.pdf](https://www.toxpath.org/AM2018/docs/STP-AM18_Posters-Abstract-Index.pdf) (toxpath.org). Accessed July 15, 2024.
- Skold A, Klein R: Symptomatic-low grade methemoglobinemia because of dapsone: a multiple hit hypothesis, *Am. J. Therapeut.* 20:e729–e732, 2013.
- Smith C: Hematopoietic stem cells and hematopoiesis, *Cancer Control* 10:9–16, 2003.
- Smith MA, Westerling-Bui T, Wilcox A, et al.: Screening for bone marrow cellularity changes in cynomolgus macaques in toxicology safety studies using artificial intelligence models, *Toxicol. Pathol.* 49:905–911, 2021.
- Smith 3rd R, Thomas JS: Quantitation of reticulated platelets in healthy dogs and in nonthrombocytopenic dogs with clinical disease, *Vet. Clin. Pathol.* 31:26–32, 2002.
- Søli NE: Chronic copper poisoning in sheep. A review of the literature, *Nord Vet. Med.* 32:75–89, 1980.
- Stegner D, vanEeuwijk JMM, Angay O, et al.: Thrombopoiesis is spatially regulated by the bone marrow vasculature, *Nat. Commun.* 8:127, 2017.
- Stevens-Hernandez CJ, Bruce LJ: Reticulocyte maturation, *Membranes* 12, 2022.
- Stockham SL, Scott MA: *Fundamentals of veterinary clinical pathology*, ed 2nd, Ames, 2008, Blackwell Publishing.
- Summers C, Rankin SM, Condliffe AM, et al.: Neutrophil kinetics in health and disease, *Trends Immunol.* 31:318–324, 2010.
- Suresh S, Lee J, Noguchi CT: Effects of erythropoietin in white adipose tissue and bone microenvironment, *Front. Cell Dev. Biol.* 8:584696, 2020a.
- Suresh S, Lee J, Noguchi CT: Erythropoietin signaling in osteoblasts is required for normal bone formation and for bone loss during erythropoietin-stimulated erythropoiesis, *Faseb. J.* 34:11685–11697, 2020b.



- Suresh S, Rajvanshi PK, Noguchi CT: The many facets of erythropoietin physiologic and metabolic response, *Front. Physiol.* 10:1534, 2019.
- Suttie AW: Histopathology of the spleen, *Toxicol. Pathol.* 34: 466–503, 2006.
- Szebeni J: Complement activation-related pseudoallergy: a new class of drug-induced acute immune toxicity, *Toxicology* 216:106–121, 2005.
- Szebeni J: Complement activation-related pseudoallergy: a stress reaction in blood triggered by nanomedicines and biologicals, *Mol. Immunol.* 61:163–173, 2014.
- Tak T, Tesselaar K, Pillay J, et al.: What's your age again? Determination of human neutrophil half-lives revisited, *J. Leukoc. Biol.* 94:595–601, 2013.
- Takamatsu K, Yamashita H, Satake S, et al.: Effects of four-week feed restriction on toxicological parameters in beagle dogs, *Exp. Anim.* 64:269–280, 2015.
- Taketani T, Kanai R, Fukuda S, et al.: Pure red cell precursor toxicity by linezolid in a pediatric case, *J. Pediatr. Hematol. Oncol.* 31:684–686, 2009.
- Takizawa H, Boettcher S, Manz MG: Demand-adapted regulation of early hematopoiesis in infection and inflammation, *Blood* 119:2991–3002, 2012.
- Tan CC, Eckardt KU, Ratcliffe PJ: Organ distribution of erythropoietin messenger RNA in normal and uremic rats, *Kidney Int.* 40:69–76, 1991.
- Tanaka R, Murota A, Nagashima Y, et al.: Changes in platelet life span in dogs with mitral valve regurgitation, *J. Vet. Intern. Med.* 16:446–451, 2002.
- Tantanate C, Khowawisetsut L, Pattanapanyasat K: Performance evaluation of automated impedance and optical fluorescence platelet counts compared with international reference method in patients with thalassemia, *Arch. Pathol. Lab Med.* 141:830–836, 2017.
- Taranu I, Marin DE, Manda G, et al.: Assessment of the potential of a boron-fructose additive in counteracting the toxic effect of fusarium mycotoxins, *Br. J. Nutr.* 106:398–407, 2011.
- Tardy B, Lecompte T, Mullier F, et al.: Detection of platelet-activating antibodies associated with heparin-induced thrombocytopenia, *J. Clin. Med.* 9, 2020.
- Tehranchi R, Invernizzi R, Grandien A, et al.: Aberrant mitochondrial iron distribution and maturation arrest characterize early erythroid precursors in low-risk myelodysplastic syndromes, *Blood* 106:247–253, 2005.
- Terwilliger NB: Functional adaptations of oxygen-transport proteins, *J. Exp. Biol.* 201:1085–1098, 1998.
- Thomas GR, Thibodeaux H, Errett CJ, et al.: In vivo biological effects of various forms of thrombopoietin in a murine model of transient pancytopenia, *Stem Cells* 14:246–255, 1996.
- Tikhonova AN, Dolgalev I, Hu H, et al.: The bone marrow microenvironment at single-cell resolution, *Nature* 569:222–228, 2019.
- Toffelmire EB, Boegman RJ: Erythrocyte life-span in dystrophic hamsters, *Can. J. Physiol. Pharmacol.* 58:1245–1247, 1980.
- Toki Y, Ikuta K, Kawahara Y, et al.: Reticulocyte hemoglobin equivalent as a potential marker for diagnosis of iron deficiency, *Int. J. Hematol.* 106:116–125, 2017.
- Tomlinson L, Boone LI, Ramaiah L, et al.: Best practices for veterinary toxicologic clinical pathology, with emphasis on the pharmaceutical and biotechnology industries, *Vet. Clin. Pathol.* 42:252–269, 2013.
- Topp KS, Tablin F, Levin J: Culture of isolated bovine megakaryocytes on reconstituted basement membrane matrix leads to proplatelet process formation, *Blood* 76:912–924, 1990.
- Tothova Z, Kollipara R, Huntly BJ, et al.: FoxOs are critical mediators of hematopoietic stem cell resistance to physiologic oxidative stress, *Cell* 128:325–339, 2007.
- Tower J: Stress and stem cells, *Wiley Interdiscip. Rev. Dev. Biol.* 1, 2012.
- Travis LB, Li CY, Zhang ZN, et al.: Hematopoietic malignancies and related disorders among benzene-exposed workers in China, *Leuk. Lymphoma* 14:91–102, 1994.
- Travlos GS: Histopathology of bone marrow, *Toxicol. Pathol.* 34: 566–598, 2006.
- Trimborn T, Gribnau J, Grosveld F, et al.: Mechanisms of developmental control of transcription in the murine alpha- and beta-globin loci, *Genes Dev.* 13:112–124, 1999.
- Tripathi NK, Ramaiah L, Everds N: Clinical pathology. In *The role of the study director in nonclinical studies*, 2014, Wiley, pp 225–243.
- Turton JA, Hawkey CM, Hart MG, et al.: Age-related changes in the haematology of female F344 rats, *Lab. Anim* 23:295–301, 1989.
- Vadhan-Raj S, Verschraegen CF, Bueso-Ramos C, et al.: Recombinant human thrombopoietin attenuates carboplatin-induced severe thrombocytopenia and the need for platelet transfusions in patients with gynecologic cancer, *Ann. Intern. Med.* 132:364–368, 2000.
- Vagdatli E, Gounari E, Lazaridou E, et al.: Platelet distribution width: a simple, practical and specific marker of activation of coagulation, *Hippokratia* 14:28–32, 2010.
- Valentine WN, Paglia DE, Fink K, et al.: Lead poisoning: association with hemolytic anemia, basophilic stippling, erythrocyte pyrimidine 5'-nucleotidase deficiency, and intraerythrocytic accumulation of pyrimidines, *J. Clin. Invest.* 58:926–932, 1976.
- Valeri CR, Ragno G: The survival and function of baboon red blood cells, platelets, and plasma proteins: a review of the experience from 1972 to 2002 at the Naval Blood Research Laboratory, Boston, Massachusetts, *Transfusion* 46:1S–42S, 2006.
- Van Putten LM: The life span of red cells in the rat and the mouse as determined by labeling with DFP32 in vivo, *Blood* 13:789–794, 1958.
- van Velzen JF, Laros-van Gorkom BA, Pop GA, et al.: Multicolor flow cytometry for evaluation of platelet surface antigens and activation markers, *Thromb. Res.* 130:92–98, 2012.

- van Zalen S, Jeschke GR, Hexner EO, et al.: AUF-1 and YB-1 are critical determinants of beta-globin mRNA expression in erythroid cells, *Blood* 119:1045–1053, 2012.
- Varga G, Ehrchen J, Tsianakas A, et al.: Glucocorticoids induce an activated, anti-inflammatory monocyte subset in mice that resembles myeloid-derived suppressor cells, *J. Leukoc. Biol.* 84:644–650, 2008.
- Varghese LN, Defour JP, Pecquet C, et al.: The thrombopoietin receptor: structural basis of traffic and activation by ligand, mutations, agonists, and mutated calreticulin, *Front. Endocrinol.* 8:59, 2017.
- Vargo CL, Taylor SM, Haines DM: Immune mediated neutropenia and thrombocytopenia in 3 giant schnauzers, *Can. Vet. J.* 48:1159–1163, 2007.
- Wayne C, Guéry E-A, Rollin J, et al.: Pathophysiology and diagnosis of drug-induced immune thrombocytopenia, *J. Clin. Med.* 9:2212, 2020.
- Vertiz G, Garcia-Ortuno LE, Bernal JP, et al.: Pharmacokinetics and hematotoxicity of a novel copper-based anticancer agent: casiopeina III-Ea, after a single intravenous dose in rats, *Fundam. Clin. Pharmacol.* 28:78–87, 2014.
- Vianna ADS, Matos EP, Jesus IM, et al.: Human exposure to mercury and its hematological effects: a systematic review, *Cad. Saúde Pública* 35:e00091618, 2019.
- von Kügelgen I: Molecular pharmacology of P2Y receptor subtypes, *Biochem. Pharmacol.* 187:114361, 2021.
- Wada A, Takagi Y, Kono M, et al.: Accuracy of a new platelet count system (PLT-F) depends on the staining property of its reagents, *PLoS One* 10:e0141311, 2015.
- Waggoner SA, Liebhaber SA: Regulation of alpha-globin mRNA stability, *Exp. Biol. Med.* 228:387–395, 2003.
- Wanet A, Bassal MA, Patel SB, et al.: E-cadherin is regulated by GATA-2 and marks the early commitment of mouse hematopoietic progenitors to the basophil and mast cell fates, *Sci. Immunol.* 6(56), 2021.
- Wang F, Meng Z, Li S, et al.: Platelet distribution width levels can be a predictor in the diagnosis of persistent organ failure in acute pancreatitis, *Gastroenterol. Res. Pract.* 2017: 8374215, 2017.
- Wang L, He X, Bi Y, et al.: Stem cell and benzene-induced malignancy and hematotoxicity, *Chem. Res. Toxicol.* 25: 1303–1315, 2012.
- Wang L, Liu H: Pathogenesis of aplastic anemia, *Hematology* 24:559–566, 2019.
- Wang W, Luo D, Chen J, et al.: Amelioration of cyclophosphamide-induced myelosuppression during treatment to rats with breast cancer through low-intensity pulsed ultrasound, *Biosci. Rep.* 40, 2020.
- Weber RE, Vinogradov SN: Nonvertebrate hemoglobins: functions and molecular adaptations, *Physiol. Rev.* 81:569–628, 2001.
- Wei C, Yu P, Cheng L: Hematopoietic reprogramming entangles with hematopoiesis, *Trends Cell Biol.* 30:752–763, 2020.
- Wei Q, Frenette PS: Niches for hematopoietic stem cells and their progeny, *Immunity* 48:632–648, 2018.
- Weiss DJ: Susceptibility of canine, feline and human erythrocytes to oxidant-mediated injury, *Vet. Clin. Pathol.* 17:75–78, 1988.
- Weiss DJ: New insights into the physiology and treatment of acquired myelodysplastic syndromes and aplastic pancytopenia, *Vet. Clin. North Am. Small Anim. Pract.* 33: 1317–1334, 2003.
- Weiss DJ: Drug-associated blood cell dyscrasias, *Compendium* 34:E1–E8, 2012.
- Weiss DJ, Lulich J: Myelodysplastic syndrome with sideroblastic differentiation in a dog, *Vet. Clin. Pathol.* 28:59–63, 1999.
- Weiss DJ, Wardrop KJ: Erythrokinetics and erythrocyte destruction. In *Schalm's veterinary hematology*, 2011, John Wiley & Sons, pp 136–143.
- Wenger RH, Hoogewijs D: Regulated oxygen sensing by protein hydroxylation in renal erythropoietin-producing cells, *Am. J. Physiol. Ren. Physiol.* 298:F1287–F1296, 2010.
- Wichmann HE, Loeffler M, Pantel K, et al.: A mathematical model of erythropoiesis in mice and rats. Part 2: stimulated erythropoiesis, *Cell Tissue Kinet.* 22:31–49, 1989.
- Wilkerson MJ, Shuman W, Swist S, et al.: Platelet size, platelet surface-associated IgG, and reticulated platelets in dogs with immune-mediated thrombocytopenia, *Vet. Clin. Pathol.* 30:141–149, 2001.
- Willard-Mack CL, Elmore SA, Hall WC, et al.: Non-proliferative and proliferative lesions of the rat and mouse hemolymphoid system, *Toxicol. Pathol.* 47:665–783, 2019.
- Williams DP, Pirmohamed M, Naisbitt DJ, et al.: Induction of metabolism-dependent and -independent neutrophil apoptosis by clozapine, *Mol. Pharmacol.* 58:207–216, 2000.
- Wilson A, Oser GM, Jaworski M, et al.: Dormant and self-renewing hematopoietic stem cells and their niches, *Ann. N. Y. Acad. Sci.* 1106:64–75, 2007.
- Wilson A, Trumpp A: Bone-marrow haematopoietic-stem-cell niches, *Nat. Rev. Immunol.* 6:93–106, 2006.
- Wognum AW, Eaves AC, Thomas TE: Identification and isolation of hematopoietic stem cells, *Arch. Med. Res.* 34: 461–475, 2003.
- Wolf JC: Chapter 14 - Alternative animal models. *Haschek and Rousseaux's handbook of toxicologic pathology*, ed 3. 2013, Academic Press, pp 477–518.
- Wollin KM, Dieter HH: Toxicological guidelines for monocyclic nitro-, amino- and aminonitroaromatics, nitramines, and nitrate esters in drinking water, *Arch. Environ. Con. Tox.* 49:18–26, 2005.
- Wu Q, Zhang J, Lucas D: Anatomy of hematopoiesis and local microenvironments in the bone marrow. Where to? *Front. Immunol.* 12:768439, 2021.
- Wu Y, Hirschi KK: Regulation of hemogenic endothelial cell development and function, *Annu. Rev. Physiol.* 83:17–37, 2021.
- Yagil R, Sod-Moriah UA, Meyerstein N: Dehydration and camel blood. 3. Osmotic fragility, specific gravity, and osmolality, *Am. J. Physiol.* 226:305–308, 1974a.

- Yagil R, Sod-Moriah UA, Meyerstein N: Dehydration and camel blood. II. Shape, size, and concentration of red blood cells, *Am. J. Physiol.* 226:301–304, 1974b.
- Yahata T, Muguruma Y, Yumino S, et al.: Quiescent human hematopoietic stem cells in the bone marrow niches organize the hierarchical structure of hematopoiesis, *Stem Cell.* 26:3228–3236, 2008.
- Yang L: Exploring off-targets and off-systems for adverse drug reactions via chemical-protein interactome—clozapine-induced agranulocytosis as a case study, *PLoS Comput. Biol.* 7, 2011.
- Yang S-H, Kang M-G, Kim H-R, et al.: Fluoranthene-induced cytotoxicity and direct effect of aryl hydrocarbon receptor antagonist on hematopoietic stem cell differentiation, *Ann. Lab. Med.* 39:580–583, 2019.
- Yeager AM, Levin J, Levin FJEH: The effects of 5-fluorouracil on hematopoiesis: studies of murine megakaryocyte-CFC, granulocyte-macrophage-CFC, and peripheral blood cell levels, *Exp. Hematol.* 11:944–952, 1983.
- Yeo JH, Lam YW, Fraser ST: Cellular dynamics of mammalian red blood cell production in the erythroblastic island niche, *Biophys. Rev.* 11:873–894, 2019.
- Young NS: Aplastic anemia, *N. Engl. J. Med.* 379:1643–1656, 2018.
- Yumine A, Fraser ST, Sugiyama D: Regulation of the embryonic erythropoietic niche: a future perspective, *Blood Res.* 52:10–17, 2017.
- Yunis AA: Chloramphenicol-induced bone marrow suppression, *Semin. Hematol.* 10:225–234, 1973.
- Zambidis ET, Peault B, Park TS, et al.: Hematopoietic differentiation of human embryonic stem cells progresses through sequential hematoendothelial, primitive, and definitive stages resembling human yolk sac development, *Blood* 106:860–870, 2005.
- Zaslloff M: Antimicrobial peptides of multicellular organisms, *Nature* 415:389–395, 2002.
- Zhang M, Zhang L, Hei R, et al.: CDK inhibitors in cancer therapy, an overview of recent development, *Am. J. Cancer Res.* 11:1913–1935, 2021.
- Zhang X, Liu F, Chen X, et al.: Involvement of the immune system in idiosyncratic drug reactions, *Drug Metabol. Pharmacokinet.* 26:47–59, 2011.
- Zhu J, Emerson SG: Hematopoietic cytokines, transcription factors and lineage commitment, *Oncogene* 21:3295–3313, 2002.



# Immune System

Tracey L. Papenfuss<sup>1</sup>, Dirk Schaudien<sup>2</sup>, Chidozie J. Amuzie<sup>3</sup>,  
Sunish Mohanan<sup>4</sup>

<sup>1</sup>StageBio, General Toxicologic Pathology, Mount Jackson, VA, United States, <sup>2</sup>Fraunhofer-Institute for Toxicology and Experimental Medicine ITEM, Hannover, Germany, <sup>3</sup>Johnson and Johnson Innovation, Toronto, ON, Canada, <sup>4</sup>Gilead Sciences, Foster City, CA, United States

## OUTLINE

<b>1. Introduction and Background</b>	<b>438</b>	<b>5.3. Perturbations of the Immune System and Recoverability (Relevance to Adversity)</b>	<b>467</b>
<b>2. Function</b>	<b>438</b>	<b>5.4. Nonantigen-Specific Toxicity</b>	<b>469</b>
2.1. Antigen Presentation and Recognition	441	<b>5.5. Antigen-specific Toxicity</b>	<b>472</b>
2.2. Immune Regulation of the Effector Reactions	441	<b>5.6. Pathophysiological Changes Associated with Therapies Affecting the Immune System</b>	<b>472</b>
2.3. Effector Reactions	443	<b>5.7. Recoverability of the Immune System (Acute vs. Chronic Changes, Reversibility)</b>	<b>475</b>
2.4. Immunological Memory	443	<b>5.8. Immune Derangements and Neoplasia</b>	<b>475</b>
2.5. Lymphocyte Trafficking and Homing	444	<b>6. Evaluation of Changes and Toxicity</b>	<b>476</b>
2.6. Cooperation with Other Organ Systems	444	6.1. Interpreting Immune System Changes	476
<b>3. Development, Structure, and Physiology</b>	<b>444</b>	6.2. Testing for Toxicity	479
3.1. Thymus	446	6.3. Anatomic Pathology	479
3.2. Bone Marrow	449	6.4. Organ-specific Histopathology	484
3.3. Spleen	449	6.5. Clinical Pathology Evaluation and Considerations	487
3.4. Physiology/Function	452	6.6. Immunotoxicology Evaluation and Considerations	487
3.5. Lymph Nodes	453	<b>7. Responses to Injury</b>	<b>490</b>
3.6. Mucosa-Associated Lymphoid Tissue (MALT)	456	7.1. Immunosuppression	490
3.7. Tertiary Lymphoid Structures	458	7.2. Immunostimulation	490
3.8. Immune-specific Components in Select Organs	461	<b>8. Preneoplastic Changes and Neoplasia</b>	<b>495</b>
<b>4. Physiological Influences on the Immune System Throughout the Lifespan</b>	<b>463</b>	8.1. Stromal Tumors: Thymoma	495
4.1. Immune Responses to Aging	464	8.2. Tumors of Hematopoietic and Lymphopoietic Cells	496
4.2. Immune Responses to Hormones	464	8.3. Lymphomas	496
4.3. Immune Responses to Stress	465	8.4. Histiocytic Sarcoma	496
<b>5. Immunomodulation, Immune Systems Responses, and Mechanisms of Toxicity</b>	<b>466</b>		
5.1. Defining Immunotoxicology, Immunosuppression, and Immunostimulation	466		
5.2. Biochemical Pathways and Exaggerated Pharmacology in the Immune System	466		

9. Best Practices and Regulatory Considerations on Evaluation of Toxicity and Adversity in the Immune System	497	10. Conclusion	499
		References	499

1. INTRODUCTION AND BACKGROUND

The immune system is composed of specialized cells, tissues, and organs scattered throughout the body. This complex system has numerous specialized cellular interactions, cell signaling pathways, and elaborated soluble factors that responds to potential insults and is context-dependent. Immune responses vary between individuals, populations, and species and change over time. They are influenced by endogenous factors including gender, hormones, genetics, and comorbidities/disease states. Exogenous factors, such as drugs, therapies, chemicals, and medical devices, can further alter immune system form and function.

Given the dynamic nature of immune responses, it can be difficult to define what effects or changes are “toxic” or abnormal. Immunotoxicology is the discipline that evaluates the toxic effects of xenobiotics (e.g., chemicals, drugs, etc.) on the immune system. Until recently, immune suppression was the most commonly recognized toxic effect of concern—hypersensitivities, allergies, and autoimmune diseases being less commonly recognized. However, within the last decade, the emergence and exponential growth of therapies specifically designed to modulate the immune system (i.e., immunotherapies) have challenged the traditional definition of what is a “toxic” effect. An evolving approach of evaluating and understanding the nature and type of immune system changes, rather than defining a change as toxic or not, has developed. The term immunosafety is increasingly being applied to describe an integrated approach to understanding the myriad of effects, toxic or otherwise, within the immune system.

The intent of this chapter is to present structure and function of immune cells, tissues, and organs, and to provide concepts to consider when evaluating immune system changes. In particular, the impact and changes associated with the expanding development of immunomodulatory

therapies and the associated regulatory challenges to evaluating immune system changes. The first section of this chapter focuses on the anatomy, histophysiology, and compartments of the thymus, spleen, lymph nodes, mucosa-associated lymphoid tissue (MALT), and tertiary lymphoid tissues, as well as lymphoid cells and tissues (Table 6.1) throughout the body in non-lymphoid organs. For the blood and bone marrow, the reader is referred to *Hematopoietic System*, Vol 5, Chap 6. The next sections review the basic mechanisms of immune system responses to injury and exogenous substances, approaches to evaluating these changes, and factors to consider regarding immunomodulatory effects. The remainder of the chapter will identify and discuss unique scientific and regulatory considerations and challenges that are relevant to evaluating immune system pathology.

2. FUNCTION

The immune system is a complex network of cells, tissues, organs, proteins, soluble factors, and numerous molecular signaling pathways that work cooperatively to respond to a wide array of stimuli and maintains health and homeostasis in an individual (Snyder, 2012; Kumar, 2021a, 2021b, 2021c; Abbas et al., 2022a, 2022b). There is a normal range of immune responses in any individual based on genetic factors and previous immune system education and challenges. The innate and adaptive arms of the immune response work cooperatively to maintain homeostasis through a coordinated communication via cells and signaling pathways.

The immunological defense of the body is aimed against pathogens from the environment and the elimination of senescent or altered (tumor) cells. This defense mechanism can be divided into antigen-specific (adaptive) and antigen-nonspecific (innate) immunity whereby the innate responses are rapid, nonspecific, and do not

**TABLE 6.1** Compartments, Cells, and Functions of Lymphoid Tissues

Organs and compartments	Cells	Functions
<b>Bone marrow</b>	Hematopoietic cells organized as islands within adipose tissue; mature leukocytes; plasma cells	Differentiation of stem cells into cells of the different lineages; erythroid, myeloid, megakaryocytic, and lymphoid
<b>Thymus cortex</b>	Fine reticular epithelium; macrophages; immature T cells/thymocytes	Generation of T cell competence; T cell receptor rearrangement; positive and negative selection of thymocytes; autoreactive cells; phenotypic changes; hormone synthesis
<b>Thymus medulla</b>	Plump reticular epithelium; macrophages; dendritic cells (DCs); T lymphocytes/thymocytes	T cell competence generation; thymic hormone synthesis; antigen presentation
<b>Thymus corticomedullary zone</b>	Immature and mature lymphocytes	Entrance of bone marrow-derived stem cells; exit of T cells that have undergone intrathymic maturation
<b>Thymus epithelial-free areas</b>	Immature T cells, macrophages, no or incomplete capsule (laminin-negative)	T cell proliferation; depot of T cells and/or route for double positive T cells into periphery (postulated)
<b>Thymus perivascular spaces</b>	Mature B and T cells; no CD4 <sup>+</sup> CD8 <sup>+</sup> (double positive; DP) cells; capsule; age-related collagen deposition	Little-understood pathway of thymocyte/mature T cell migration
<b>Lymph node paracortex and spleen inner PALS</b>	Interdigitating cells; T cells	Lymphocyte entry through the high endothelial venules (HEVs) in the lymph node or central arteriole in the spleen; antigen presentation to T cells; T cell proliferation-differentiation-regulation
<b>Lymph node and spleen primary follicles</b>	DCs; macrophages; B cells; few T cells	Immunologically quiescent; storage of virgin/memory B cells, recirculating B cells (surface IgM + IgD <sup>+</sup> B cells)
<b>Lymph node and spleen germinal centers</b>	Follicular DCs; tingible-body macrophages; B cells; few T cells	B-cell maturation; antigen presentation in the form of immune complexes
<b>Lymph node medulla</b>	Plasma cells; T effector cells; reticular mesenchymal cells	Antibody synthesis; reactions of delayed hypersensitivity; cytotoxic T cells
<b>Spleen white pulp</b>	Provides immune function of spleen; subcompartments with various populations of T cells, B cells, macrophages, DCs, NK cells, and supporting cells	T cell-independent B cell proliferation-differentiation; B memory cells (surface IgM + IgD <sup>+</sup> )
<b>Spleen Periarteriolar lymphoid sheaths (PALS)</b>	Primarily T cells, surround central arteries; DCs, macrophages	T cell-independent B cell proliferation-differentiation; B memory cells (surface IgM + IgD <sup>+</sup> )
<b>Spleen marginal zone</b>	Marginal zone macrophages, marginal metallophilic cells/macrophages; marginal zone B cells	T cell-independent B cell proliferation-differentiation; B memory cells (surface IgM + IgD <sup>+</sup> )

(Continued)



**TABLE 6.1** Compartments, Cells, and Functions of Lymphoid Tissues—cont'd

Organs and compartments	Cells	Functions
<b>Spleen red pulp</b>	Sinuses with blood; parenchyma with macrophages, lymphocytes, natural killer cells, plasma cells	Blood filtering, phagocytosis, and extramedullary hematopoiesis
<b>MALT follicles</b>	See lymph node and spleen follicles	See lymph node and spleen follicles
<b>MALT interfollicular areas</b>	Mainly small T cells; interdigitating cells	Lymphocyte entry through HEVs, antigen presentation to T cells
<b>MALT lymphoepithelium</b>	M (microfold) cells; intraepithelial lymphocytes and macrophages	Uptake of exogenous substances, mainly particulates; initiation of immune responses including IgA production
<b>MALT epithelial mucosal cells</b>	T cells; NK cells; epithelial cells	First line of defense; extrathymic maturation of T cells; secretory component by epithelium and transport of IgA and IgM to lumen via epithelium
<b>MALT lamina propria cells</b>	T and B cells; plasma cells; macrophages	Synthesis of IgA antibody; phagocytosis and killing
<b>Immune cells in nonimmune organs/tertiary immune organs</b>	Macrophages, B and T cells, DCs, NK cells; may form follicles, germinal centers; may resemble lymph nodes	Development of immune responses often secondary to immune stimulation/inflammation; immunological defense; tissue repair

Modified from Haschek WM, Rousseaux CG, Wallig MA, editors: *Handbook of toxicologic pathology*, ed 2, 2002, Academic Press. Table I, p 595, with permission.

generate a memory response, while adaptive responses are typically antigen-specific, take time to be initiated, and generate a memory response.

The innate immune system is the body's first line of defense against pathogens or other insults where cells respond in an antigen-nonspecific manner to the offending agent. The response is rapid and there is no memory response. Innate immune cells and responses can help instruct the more specific and memory-based adaptive arm of the immune response. The adaptive immune response involves immune cells and soluble factors that comprise the cell-mediated and humoral responses that destroy foreign invaders or tumors and help prevent future disease. The adaptive immune response is typically antigen-specific, takes time to be initiated, and generates a memory response.

The innate immune response provides an initial defense mechanism that is always present and ready to combat any offending agent (Abbas et al., 2022a). It is composed of physical barriers, soluble factors, and cells present throughout the body. Mechanical or physical barriers such as epithelia of the skin and mucosa prevent

microbes from entering the body. The mucociliary apparatus can prevent microbes from attaching at mucosal sites, while the lipids and tight junctions of the skin epithelium provide a physical barrier to microbial invasion. These and other physical or physiological components (e.g., body temperature, pH, etc.) all contribute to innate immune defenses. If these barriers or mechanisms are damaged or dysfunctional, subsequent immune responses are then activated. Innate immune cells involved in this process include granulocytes (basophils, eosinophils, neutrophils), natural killer cells, macrophages, dendritic cells (DCs), mast cells, and other innate lymphoid cells. Many of these cells can specifically phagocytose, damage, and kill invaders or, in the case of DCs and macrophages, serve as antigen-presenting cells (APCs) to instruct and influence the development of appropriate adaptive immune responses. In addition to cells, there are numerous specific sensors or receptors (e.g., toll-like receptors, inflammasomes, retinoic acid-inducible gene (RIG-I)-like receptors (RLRs), signaling pathways (e.g., NF- $\kappa$ B, Fas,

RANK, AKT, etc.), and soluble factors (e.g., cytokines, chemokines, defensins, complement, antimicrobial peptides, lysozyme, DNases, RNases, antiproteases, acute phase proteins, etc.) that provide an immediate defense to eliminate pathogens and damaged cells, promote and regulate resultant innate and adaptive immune responses, initiate tissue repair, and restore homeostasis.

The adaptive immune response is more specific than the innate immune response and provides a catered response to insults. Both cell-mediated and humoral responses form a complicated system that responds to both intracellular and extracellular pathogens and other pathological dysfunctions. Cell-mediated immune responses involve the activation and promotion of cell processes where the protective function is primarily cell-associated, while humoral immunity involves factors that are primarily located in the extracellular “humoral” fluids (Weaver and Murphy, 2007; Leung et al., 2010; Kumar, 2021a; Abbas et al., 2022a). Cell-mediated immunity involves the activation of phagocytes, cytotoxic T cells, and cytokines, while humoral immunity involves macromolecules such as antibodies, complement proteins, and antimicrobial peptides.

### 2.1. Antigen Presentation and Recognition

The first defense upon entry of a pathogen/antigen into the body (mostly through mucosae and skin) includes inactivation in a nonspecific way—for example, by natural killer cells, granulocytic leukocytes, and cells of the mononuclear phagocyte system (MPS). It also includes the initiation of an antigen-specific immune response (Figure 6.1), which requires adequate captivation, presentation, and recognition of the pathogen or antigen. The antigen is ingested and degraded by immature antigen-presenting (dendritic) cells, which reside in the targeted tissue. The antigen is then carried to local/drainage lymph nodes, where the DCs mature and the antigen is presented to T lymphocytes. After antigen presentation, various effector reactions (responses) are possible that enable the optimal destruction or inactivation of the antigen/pathogen and return to homeostasis.

Professional APCs include DCs, macrophages, and B cells are the primary drivers of developing

immune responses due to their ability to provide the necessary receptors, costimulatory molecules, and other factors and interactions with T cells. Although all nucleated cells have the potential to serve as nonprofessional APCs, they are limited to expressing only major histocompatibility complex (MHC) class I molecules. It is a combination of the type of APC, nature of the antigen being presented, the presence of costimulatory molecule expression, and the local environment (including cytokines, tissue factors, and interaction with other cells) that ultimately affect the nature and characteristics of the resultant overall immune response. DCs have a particularly important role in driving naïve helper T cell differentiation into effector T cell populations with specific functionality. Transcription factor pathways (e.g., T-bet, STAT4, STAT6, GATA3, STAT3, ROR $\gamma$ T, and FoxP3) drive the development and differentiation of these effector T cells and generate Th1, Th2, Th17, regulatory T cells, and a host of other helper T cell subpopulations that produce the cell-mediated and humoral responses of the adaptive immune response (Abbas et al., 2022c).

### 2.2. Immune Regulation of the Effector Reactions

After antigen presentation and activation of T cells, a choice of effector reactions (response) is possible to enable the optimal destruction or inactivation (“immune elimination” and “immune exclusion”) of the antigen/pathogen. The process involves a delicate and intricate interaction of cells and cell products (cytokines). In the antibody (immunoglobulin)-mediated reaction, also called the humoral reaction, activated T cells induce B cells to become antibody-producing plasma cells. In the cellular effector reaction, T cells activate cytotoxic (T<sub>c</sub>) cells and other effector T cells. The immune response needs to be downregulated properly, to prevent unnecessary tissue and organ destruction. The immune system aims at a continuous state of homeostatic balance, whereas the introduction of an antigen/pathogen disturbs this balance due to the activation of antigen-specific T- and B-lymphocyte clones. The system not only allows the proliferation and amplification of relevant clones to cope with the antigen but

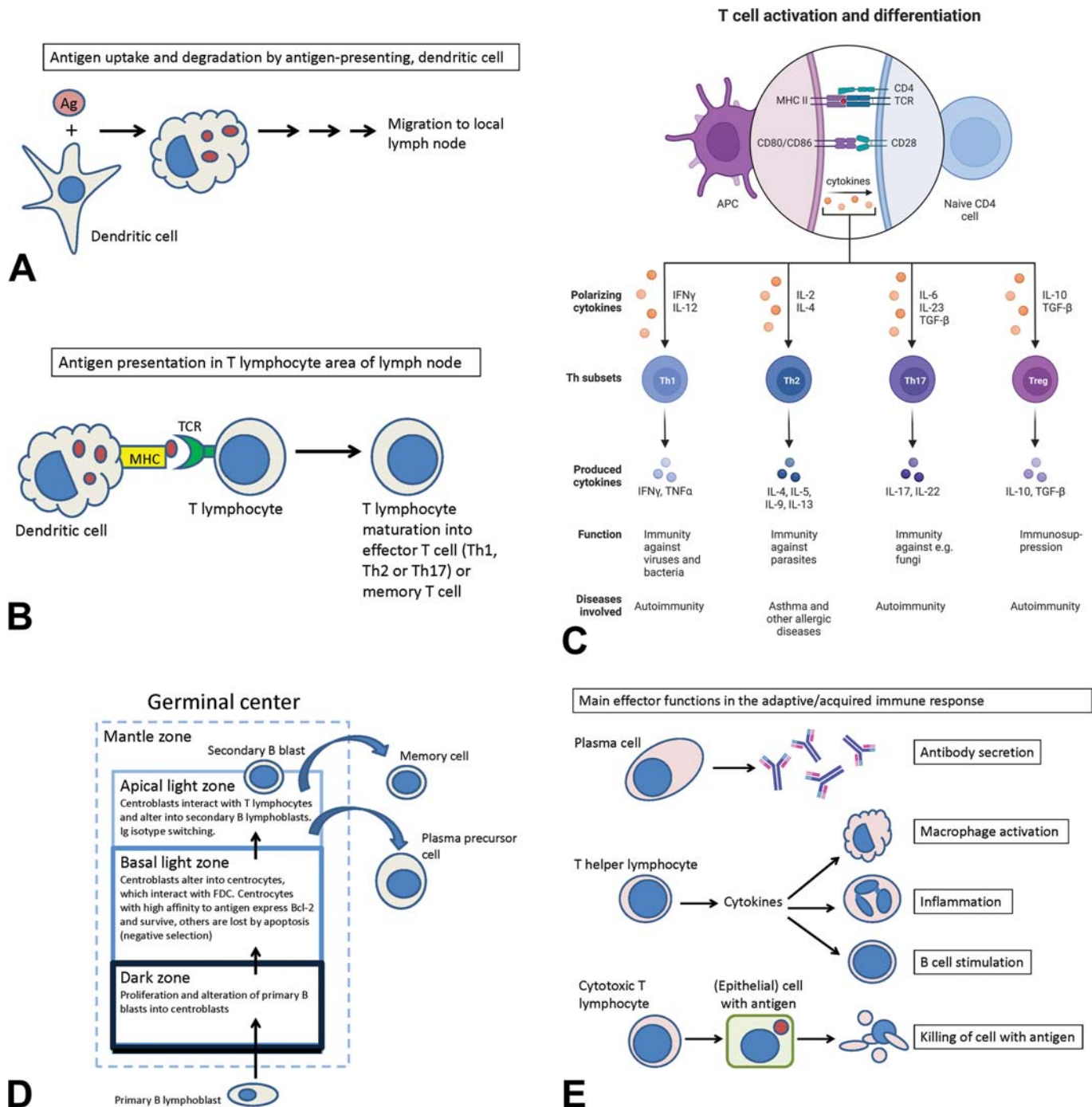


**FIGURE 6.1** Schematic presentation of the generation of antigen-specific local and systemic immune responses via mucosal epithelium: Overview and detailed figures. (A) Soluble antigens preferentially enter via the normal epithelium, whereas particulate antigen preferentially is taken up by microfold or M cells. Dendritic cells (DCs) ingest and partially degrade antigens/pathogens. (B) Subsequently the DCs migrate and present the modified antigen to T cells. T cells can recognize antigens only when presented on major histocompatibility (MHC) molecules (also known in humans as HLA; human leukocyte antigen). Antigens processed by endocytosis are presented predominantly on MHC class II molecules, whereas endogenous antigens (viral antigens, self-peptides) are predominantly presented on MHC class I molecules. B cells can directly recognize antigen. As a result of contact with an antigen, antibodies can be produced by plasma cells, via maturation of immature B lymphoblasts into plasma cell precursors. (C) Naïve CD4<sup>+</sup> T cells differentiate into a number of subpopulations, some of which are indicated (i.e., Th1, Th2, Th17, and Treg cells). (D) The maturation of B blasts takes place in germinal centers, which develop in a primary or resting follicle. (E) Finally, effector reactions are generated, including secretion of specific antibodies (secretory Ig) into the lumen, to bind to antigen and exclude it. *Modified from Figure 49.1 p. 1798 in Haschek WM, Rousseaux CG, Wallig MA, editors: Haschek and Rousseaux's handbook of toxicologic pathology, ed 3, 2013, Academic Press with permission. Created with BioRender.com*



also searches for (and reaches) a state of newly defined homeostasis.

### 2.3. Effector Reactions

The effector arm is the part of the immune system that actually eliminates or inactivates antigens/pathogens (Figure 3C-4th edition, 49.1D-third edition). In general, helper T cells (Th) promote the appropriate responses, while antibodies are primary effectors of humoral immune responses and cytotoxic T cells being primary mediators of cell-mediated or cytotoxic responses.

Helper T cells are activated and differentiate into specific subpopulations that promote the appropriate immune responses to eliminate or inactive antigens/pathogens. Some of the more commonly identified populations and associated characteristics are listed below:

- Th1 cells that promote immunity against viruses and bacteria but if dysregulated, may contribute to the development of autoimmune disease.
- Th2 cells that promote immunity against parasites but if dysregulated, may contribute to the development of asthma, allergic diseases, and some autoimmune diseases
- Th17 cells that promote immunity against fungal infections but if dysregulated, may contribute to the development of autoimmunity.
- Treg cells that provide immunosuppression or immune regulation but if dysregulated, may contribute to the development of autoimmune diseases.

Antibodies, a key mediator of humoral immunity, effectuate the reaction in a number of ways:

1. They activate the complement system and induce complement-mediated lysis or phagocytosis of the antigen by macrophages and neutrophils. In addition, attraction of granulocytes is promoted.
2. They bind to the antigen/pathogen and prevent infection of tissues by the pathogen.
3. They coat (opsonize) antigen/pathogen to enable its phagocytosis.
4. They form a bridge between killer cell and targeted antigen/infected cell, leading to

destruction of the infected cell (antibody-dependent cellular cytotoxicity or ADCC)

5. They bind to antigens and exclude them via special antibodies, like immunoglobulin A, that are secreted at the mucosal sites.

The effector reaction to most antigens/pathogens is mediated by T (helper) lymphocytes; however, some reactions do not involve the activation of T lymphocytes. An example is the T cell independent activation of B cells against antigens that consist of repeated polysaccharide units as present on the bacteria *Escherichia coli* and *Pneumococcus*. Activated cytotoxic T cell (Tc) cells directly attack the antigen, by killing the cells which are infected by the antigen/pathogen. Other activated T cells produce and release their cytokines. This induces macrophages to kill their ingested antigen and induces the extravasation of granulocytes to the targeted tissue (inflammation).

Unresponsiveness of the immune system (tolerance) to an antigen can occur by silencing of certain lymphocytes. Self-tolerance (against the body's own antigens) takes place during lymphocyte development, in both the thymus and bone marrow, by negative selection of those lymphocytes that recognize self-antigens (central tolerance). It can also take place in the periphery of the body, by the induction of anergy of the lymphocytes upon inappropriate presentation of antigen; by activation-induced apoptosis of the autoreactive lymphocytes; or by suppressive action of regulatory T lymphocytes (peripheral tolerance). Tolerance can also be acquired for antigens that otherwise would induce an immune response. This occurs in pregnancy, when the fetus is tolerated by the maternal immune system. It can also be induced by repeated exposure to very large or very low doses of antigen, as during desensitization protocols against allergens. The power to induce peripheral tolerance is a typical feature of the MALTs.

### 2.4. Immunological Memory

A special feature of the adaptive immune response is the generation of memory after initial contact with the antigen (Figure 49.1C). The first immune response to an antigen includes activation and amplification of antigen-specific T or B cells in exerting effector reactions. The second contact with the antigen causes recruitment of

more antigen-specific cells. This recruitment gives a higher signal, a more efficient elimination of the antigen or pathogen, and the response is faster than the initial response.

Lymphocytes are the cells of immunologic memory. The memory for the humoral (antibody) arm is evident by isotype switching of B cells between primary and secondary immune responses. The first contact generates IgM-class antibody, whereas antibodies of other immunoglobulin classes (especially IgG) are generated after subsequent contacts. T cells demonstrate a rearranged isoform of the leukocyte common antigen CD45 upon antigen contact. They lose the expression of CD45RA, while the expression of CD45R0 becomes detectable. Simultaneously, the expression of the lymphocyte homing receptor CD44 is increased. T- and B-cell memory can be long-lasting, and might persist without repeated exposure to the pathogen. The generation of memory is the basis for vaccination, performed to prevent contracting infectious disease by an initial contact with the pathogen in attenuated nonpathogenic form.

### 2.5. Lymphocyte Trafficking and Homing

Lymphocytes travel via the blood to their appropriate compartments of the lymphoid organs. Subsets of lymphocytes continuously circulate via the blood and lymph and pass through the lymphoid tissues and organs. The cells of the mucosal and skin immune system migrate upon contact with antigen and join the circulation, where they contact cells from the systemic immune system. Thereafter, they may migrate back to the mucosal surfaces. The antigen message received at one distinct site can thus be shared with the systemic immune system. After antigen presentation in the gastrointestinal tract, effector cells (e.g., cytotoxic T cells and plasma cells) can be found at the site of stimulation and at other secretory sites (e.g., the respiratory tract). This traveling and homing to the lymphoid organ compartments is regulated by, among others, adhesion molecules (IgSF CAMs, integrins, cadherins, selectins) that are responsible for adhesion of lymphocytes to the specialized high endothelial venules (HEVs) or to activated endothelium at effector sites.

### 2.6. Cooperation with Other Organ Systems

The communication with other homeostatic mechanisms in the body is an important aspect of immunoregulation. Immune cells travel continuously and in vast quantities throughout the body, contacting cells of other organ systems. In addition, mediators of the immune response have their effect on systems outside of the immune system. Communication and cooperation of the immune system with the neural and endocrine systems is particularly important. Their interaction is mediated by a network of hormones, cytokines, and receptors (Figure 6.2; Taub, 2008; Kau et al., 2011; Klein, 2021). For example, IL-1, generated by APCs, affects the temperature regulatory center (induction of fever) and sleep regulatory center (induction of slow-wave sleep) in the hypothalamus. In addition, there is increasing recognition of the contribution of the gut microbes (microbiome) significantly contribute to innate and adaptive arms of the immune system (Kau et al., 2011). Xenobiotics (toxicants and drugs), diet, and physical/psychological stressors can alter the adaptive as well as the innate immunity. The immune system may be especially sensitive during immune development, as in the fetus and neonate, but also in adult life during pregnancy, glucocorticoid-related stress, and aging. Additional information regarding the influence of aging, hormones, and stress are discussed later in this chapter.

A more detailed discussion of the numerous cells, pathways, and components of immune responses is beyond the scope of this chapter. However, understanding the potential mechanisms and immune pathways involved or affected by any given therapy or xenobiotic is a necessary component when evaluating and understanding immune system changes and determining immune system toxicity.

## 3. DEVELOPMENT, STRUCTURE, AND PHYSIOLOGY

Components of the immune system are present throughout the body. The lymphoid (or immune) organs can be divided into primary (or central), secondary (or peripheral), and

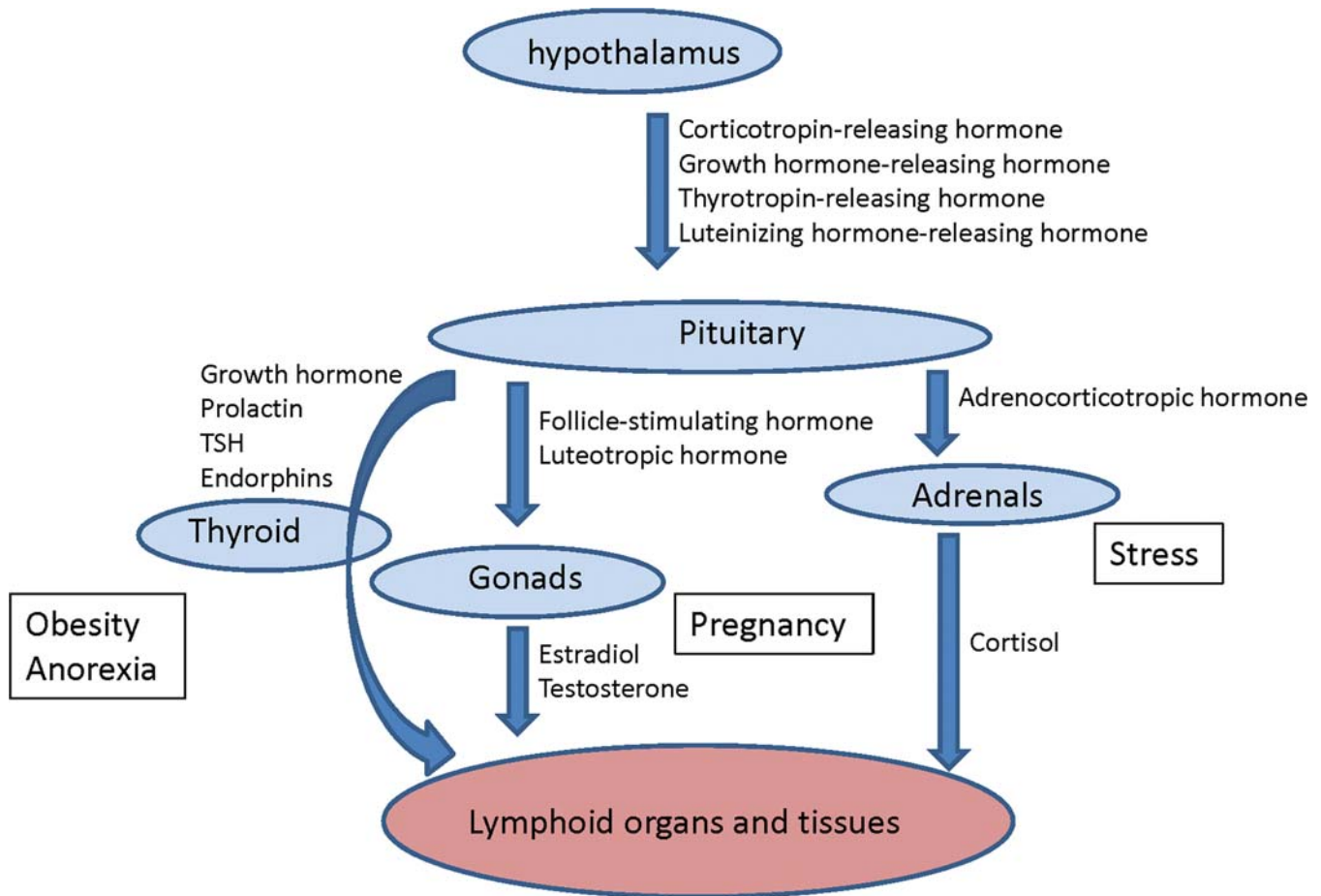


**FIGURE 6.2** The influence of the neuroendocrine system on the immune system. Copied from Figure 49.2 p. 1801 in Haschek WM, Rousseaux CG, Wallig MA, editors: *Haschek and Rousseaux's handbook of toxicologic pathology*, ed 3, 2013, Academic Press.

tertiary lymphoid organs or tissues (Abbas et al., 2022a, 2022b) (Gago da Graça et al., 2021). The bone marrow and the thymus are primary lymphoid organs responsible for lymphocyte generation from progenitor or stem cells but with some ability to function as a secondary organ. Secondary lymphoid organs are the spleen, lymph nodes, and MALTs as well as other sites where naïve T and B lymphocytes develop, mature, and are activated under the influence of antigen, APCs, and local environment. Tertiary lymphoid tissues are de novo organizations of lymphoid tissue that are found upon antigenic exposure in nonlymphoid organs. Their presence is uncommon and often reversible (Abbas et al., 2022a, 2022b).

Although specific lymphoid organs are commonly recognized, the immune system is present in the circulation and distributed

throughout the body, through lymphatics that are in close association with blood vessels. Thus, the classification of organs and tissues into lymphoid and nonlymphoid organs/tissues is somewhat artificial. Each organ has its population of both resident and circulating immune cells that provide organ specific immune responses and some organs have well defined roles in immune system development or function. For example, the skin and mucosal sites are organs that play important roles in immune function by serving as a barrier to the exterior environment and housing immune competent cells, APCs, and specialized T and B lymphocytes that are critical to the development of appropriate protective immune responses at these sites. The liver plays important roles in lymphopoiesis in the fetus, the clearance of immune complexes by Kupffer cells (KCs), IgA transport,



acute phase protein synthesis, and regulation of immune responses in the intestines (see *Liver and Gall Bladder*, Vol 4, Chap 2). Extrathymic pathways to T cell differentiation exist in the liver and intestine and may represent a primitive immune system that plays a pivotal role in immune reactions during aging, pregnancy, bacterial infections, malignancies, and autoimmune disease (Abo, 2001). Although there are numerous examples of various organs contributing specific aspects to the immune response, in this chapter the traditional classification into lymphoid and nonlymphoid organs and tissues is maintained. For an excellent overview of the functional aspects of the immune system, the reader should consult immunology texts (Kumar, 2021a; Abbas et al., 2022a).

### 3.1. Thymus

#### 3.1.1. Development

The thymus develops from the third and fourth pharyngeal pouches and migrates caudally along with the thyroid and parathyroid glands. The thymus reaches its final destination in the thorax at approximately gestation day (GD) 15 in the mouse and is in close proximity to the thoracic cavity by GD15 in the rat. Thymic remnants in rats and mice may remain in the neck, where they are commonly encountered in histologic sections of the thyroid glands (Pearse, 2006). The thymus in most species can be located predominantly within the region of the thoracic inlet of the neck or upper chest (thorax) with the location of the thymus of nonhuman primates more prominently located within the thoracic cavity in front of and/or above the heart, similar to humans. The primordial epithelial components of the thymus receive T cell progenitor cells that originate in the aorta–gonad–mesonephros (AGM) region at approximately GD10 in the mouse. Thereafter, a codependent development of epithelial and lymphoid elements results in the final lymphoid organ. The thymus reaches a histomorphologic stage of maturity in advance of other lymphoid organs and has well-developed microscopic features at the time of birth. It quickly matures to a morphology with a highly cellular cortex and less densely cellular medulla (Figure 6.3). A progressive reduction in weight and size with corresponding decreases in

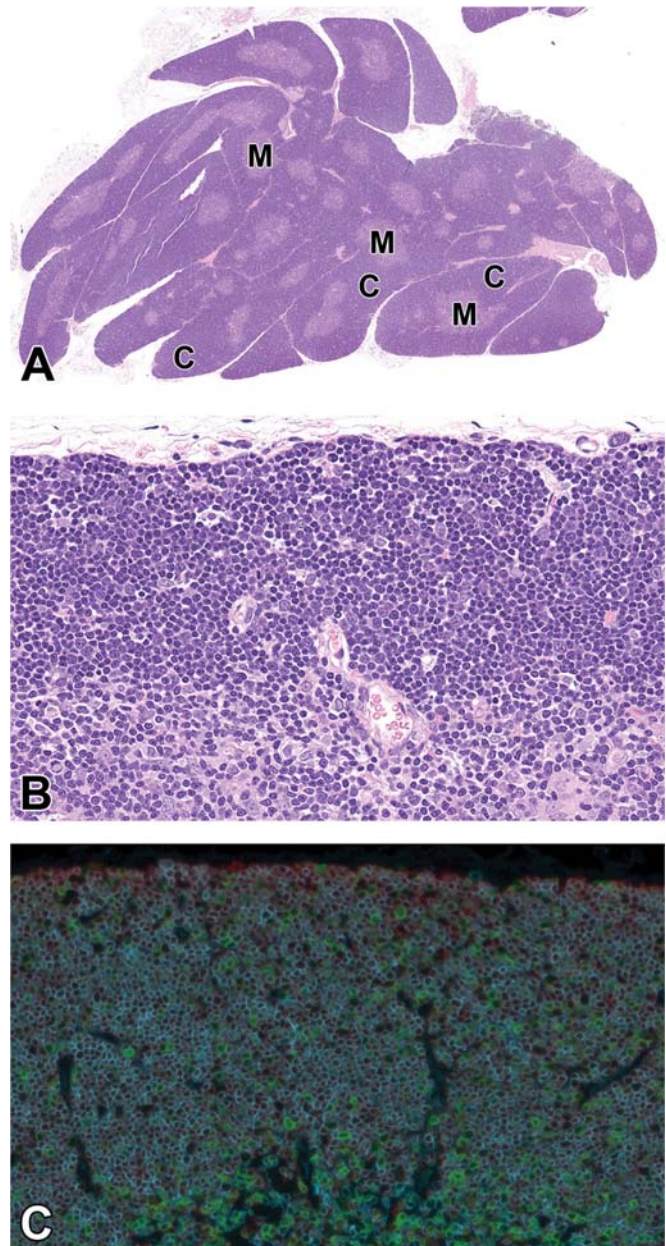


**FIGURE 6.3** (A) Thymus from 5-month-old Wistar rat showing two major lobes with a highly cellular cortex (C), distinct corticomedullary boundaries and less cellular medulla (M). Hematoxylin and eosin (H&E) stain, original magnification 20 $\times$ . (B) Higher magnification of the same thymus, H&E stain, original magnification 400 $\times$ . (C) Thymus from a 4-week-old mouse. Immunohistochemistry showing CD8<sup>+</sup> cells (red, few in number) and CD4<sup>+</sup> cells (blue) and CD3<sup>+</sup> cells (green), original magnification 400 $\times$ .

the ability to delineate cortex from medulla and replacement by univacuolar adipocytes occurs as animals age. The most pronounced changes

are seen during normal physiological thymic involution during puberty. The thymic cortex of young animals has a high level of cellular proliferation that is most pronounced in the subcortical zone and it is this proliferation that may be primarily responsible for the increased weight, size, and cellularity that occurs following (and in response to) therapeutic depletion of the thymic cortex (Nishino et al., 2006; Kuper et al., 2013).

### 3.1.2. Structure/Anatomy

In most mammals, the thymus is a bilobed organ surrounded by a thin connective tissue capsule dividing each lobe further into multiple lobules, each with a histologically distinct outer cortex and inner medulla (Haley, 2003). Mice do not have such lobular separation. The organ consists of a framework of epithelial cells that contain primarily T lymphocytes but also a small number of B lymphocytes, plasma cells, antigen-presenting cells, and other neuroendocrine cells. The distinct thymic regions have different functional activities that occur during T cell development. The cortex, corticomedullary junction, and medulla each have distinct populations of immune cells and functional attributes that are reflective of the role of the thymus as a primary site of T cell development and production.

The adult thymic cortex typically consists of a sheet of mature lymphocytes with a sparse background population of epithelial, dendritic and stromal cells, and macrophages. Thymic epithelial cells in the outer cortex, called “nurse cells,” have long membrane extensions that surround as many as 50 lymphocytes. In active thymuses of several species, including humans, areas free of epithelium (EFAs) are observed as a normal finding in the outer cortex (Elmore, 2006d). The EFAs areas house lymphocytes and macrophages, and the proliferative activity is high. Within the cortex, there are more numerous, densely packed, smaller lymphocytes than those located within the medulla resulting in the darker staining characteristic of cortex versus the medulla. There is a degree of variation in cortical lymphocyte populations associated with developmental processes, with populations of larger mitotically active cells often present in the subcapsular region and deep cortex. The rapidly dividing lymphocytes are often short-lived and undergo apoptosis.

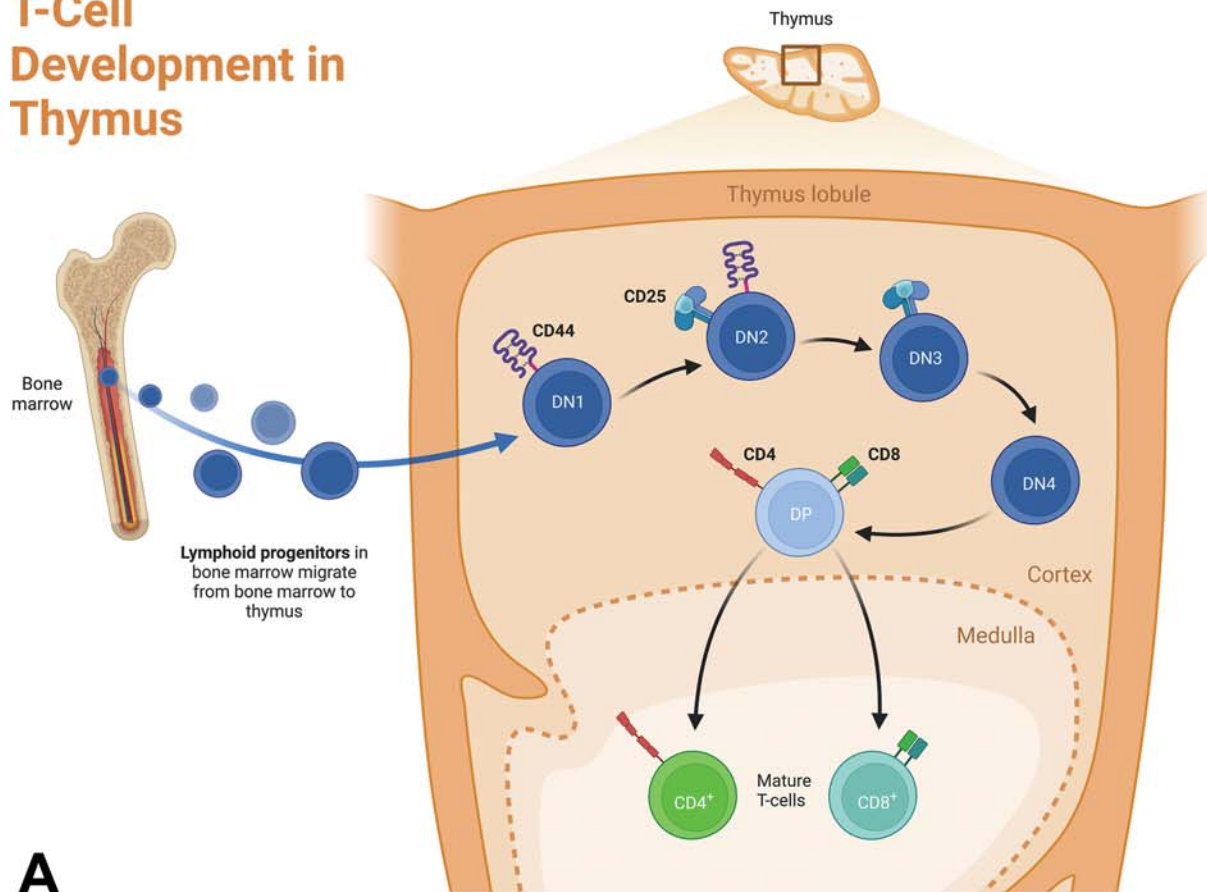
Apoptotic bodies and the macrophages that phagocytize these apoptotic bodies (i.e., tingible body macrophages) can be prominent and a normal background finding, but careful consideration should be given to the potential impact of xenobiotics on apoptosis in toxicity studies. The corticomedullary junction has a mixture of mature and immature cells, many blood vessels, DCs, and perivascular B cells, and plasma cells. The medulla is less densely cellular and contains more mature T cells with more cytoplasm than cortical lymphocytes, resulting in the characteristic paler staining of the medulla. Hassall’s corpuscles epithelial cells are commonly observed in the thymic medulla. These generally have a large nucleus, degenerate cytoplasm, and cytoplasmic keratinization in some species. Although Hassall’s corpuscles are readily recognized structures, they are less commonly noted in rodents and dogs compared to humans and nonhuman primates. The number of Hassall’s corpuscles may increase in the presence of lymphocyte destruction. Within the thymus, there are additional epithelial cell types that can be differentiated from Hassall’s corpuscle based on IHC staining characteristics, differences in their antigenic expression, ultrastructural characteristics, and ability to synthesize thymic hormones (Pearse, 2006). Interdigitating DCs located at the corticomedullary junction have long extensions that interact with developing thymic lymphocytes. Epithelial cords and tubules are found in or close to the interlobular septa, especially at the corticomedullary junction. Cells lining the tubules may show cilia and signs of secretory activity. In addition to the expected population of maturing T lymphocytes and supporting elements, the thymic medulla of some animals contains B cell nodules and clusters of plasma cells. Thorough examination of the thymus of young Beagle dogs from a toxicology laboratory revealed a 70% incidence of medullary B cell follicles (Ploemen et al., 2003).

### 3.1.3. Physiology/Function

Prior to thymic senescence, T cell progenitors are formed in the bone marrow, and then migrate to the thymic cortex (Figure 6.4A). Within the thymus, these cells undergo extensive proliferation and selection processes, which result in survival of single positive CD4<sup>+</sup>CD8<sup>-</sup> and

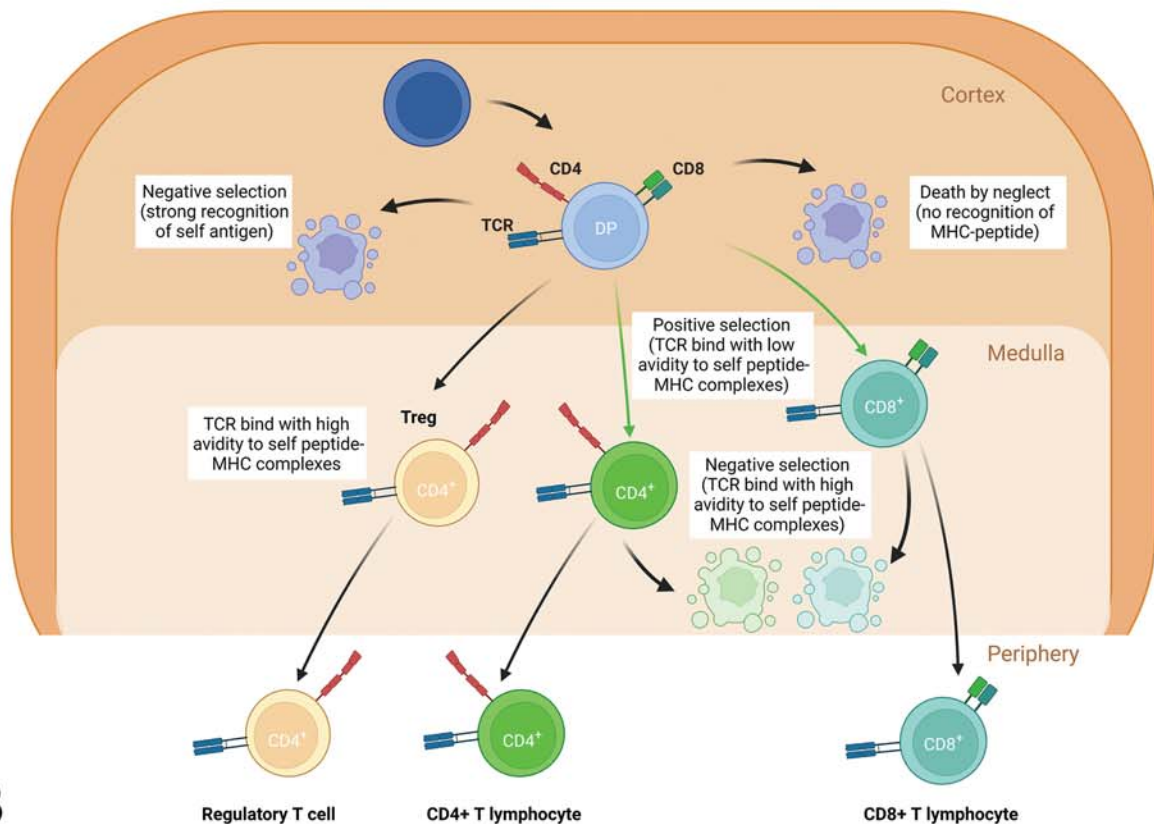


# T-Cell Development in Thymus



A

## T-Cell Selection in Thymus



B



CD4<sup>+</sup> CD8<sup>+</sup> T cells (Figure 6.4B). Cells that fail to recognize self-MHC or have an excessively high affinity with self-MHC, and cells that have an affinity for self-antigens, are eliminated by apoptosis. MHC, composed of both Class I and Class II molecules, consists of gene clusters that encode a set of cell membrane proteins called the MHC molecule. In humans, these are also referred to as human leukocyte antigens (HLAs). MHC regulates many cell–cell interactions in the immune response and is a target in transplant rejection. It is estimated that 95%–99% of immature T lymphocytes undergo apoptosis as a result of selection. The minor population that survives the selection process migrates to the medulla, where maturation continues. Maturation of T cells involves an orchestrated movement of cells from the entry point of corticomedullary postcapillary venules, outward to the subcapsular region, and subsequently reverse migration to an exit that probably involves both venules and lymphatic capillaries in the medulla (Pearse, 2006). The mature T cells are able to recognize foreign antigens in the context of MHC. The size and cellularity of the thymus decreases as an animal ages with the most prominent decrease (atrophy) noted during and after sexual maturity. At that time, most T cells have matured within the thymus and therefore, the functionality of the thymus will decrease. This normal physiological involution will result in a thymus with low lymphocyte cellularity and replacement with adipose tissue.

### 3.2. Bone Marrow

For detailed information of the bone marrow, the reader is referred to *Hematopoietic System*, Vol 5, Chap 6. The bone marrow is not only the major hematopoietic organ but also a primary

lymphoid organ. Both lymphocytic and myelomonocytic lineages can be found in the bone marrow with common myelomonocytic progenitor cells giving rise to monocytes and granulocytes which play primary roles in innate immune responses. Lymphopoiesis takes place in the fetal liver and the microenvironment of the adult bone marrow (Figure 6.5) (Allen and Dexter, 1984; Nagasawa, 2006). The multipotential lymphoid stem cell in the bone marrow develops into B lymphocytes and T lymphocytes/NK progenitor cells, with B lymphopoiesis continuing in the bone marrow (in mammals), and T lymphocyte progenitor cells migrating to the thymus (Figure 6.4A and B lymphocytes develop within the bone marrow in multiple steps to immature B cells exiting the bone marrow) (LeBien and Tedder, 2008).

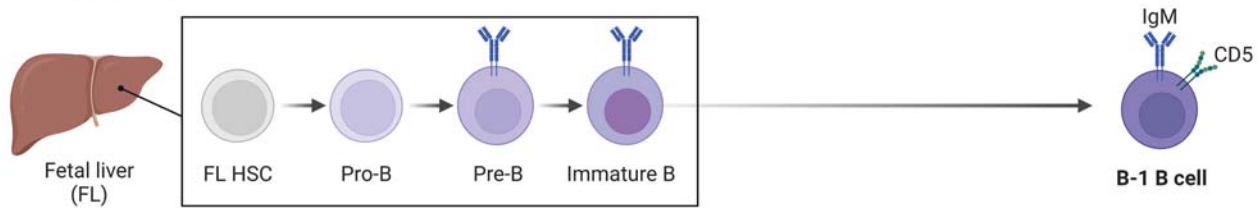
### 3.3. Spleen

#### 3.3.1. Development

The spleen starts to develop as a collection of primitive reticular cells in the dorsal mesogastrium. The first cells to appear are hematopoietic and are an important site of hematopoiesis in the fetus. This function is maintained in rats and mice throughout adulthood, but in other species, it is resumed only in certain diseases. In the mouse, splenic tissue can first be identified at GD 12.5 and the first hematopoietic cells can be seen at GD 15.5 (Cesta, 2006b; Seymour et al., 2006) and at GD 17 in the rat (Losco, 1992; Cesta, 2006b). Rodent spleen contains little or no white pulp (see below) at birth, whereas in the dog, lymphocytes first appear in the spleen at GD 52 (Van Rees et al., 1996; HoganEsch and Hahn, 2001). The first lymphocytes to appear in the spleen of rats are T cells that accumulate in the PALS regions (Losco, 1992; Van Rees

**FIGURE 6.4** (A) T cell maturation in the thymus. Progenitor cells from the bone marrow enter the thymus through blood vessels in the cortico-medullary zone and after maturation and selection leave the thymus as mature T cells. The progression of CD4<sup>+</sup> CD8<sup>+</sup> double negative (DN) cells is shown where these progress through DN1 through DN4 stages of maturation to become CD4<sup>+</sup> CD8<sup>+</sup> double positive (DP) cells. The DN1 cells are CD44<sup>+</sup> CD25<sup>+</sup>, have recently arrived from the bone marrow, and are located at the cortico-medullary junction. The DN2 cells are CD44<sup>+</sup> CD25<sup>+</sup> and present within the mid-cortex, the DN3 cells CD44<sup>+</sup> CD25<sup>+</sup> cells, while the DN4 cells are intermediate between DN3 and DP cells and develop into DP cells. (B) T cell selection in the thymus. The DP cells are present in the cortex and are eliminated if they strongly recognize self-antigen (negative selection) or do not recognize histocompatibility complex (MHC; death by neglect). Cells whose T cell receptor (TCR) binds self peptide-MHC with low avidity are stimulated to survive (positive selection) and within the medulla, differentiate into single positive (SP) CD4<sup>+</sup> or CD8<sup>+</sup> cells. Surviving cells, whose TCR binds with high avidity to self-peptide MHC are eliminated (negative selection) or differentiate into regulatory T cells (Treg). Created with BioRender.com.

### B-1 cell development



### B-2 cell development

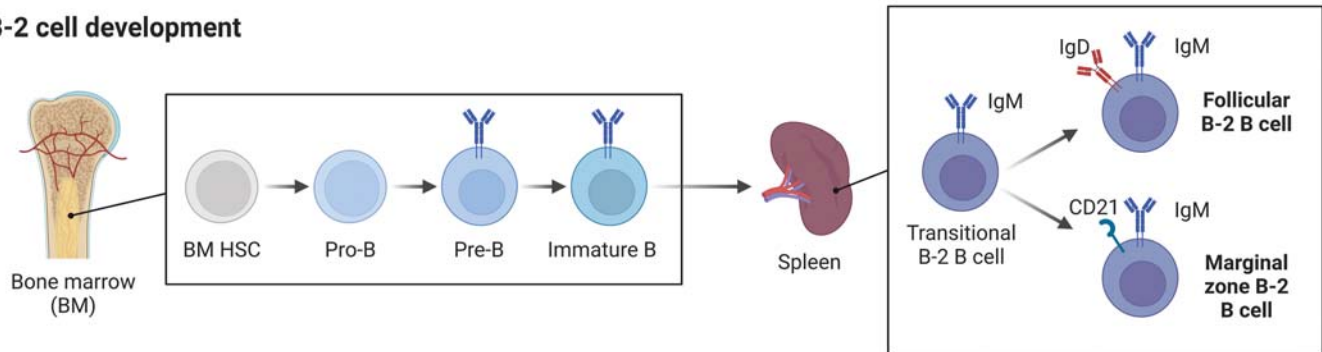


**FIGURE 6.5** B cells in the periphery are of two different subtypes that evolve from different progenitors. B-1 cells are a distinct lineage that develops from fetal liver (FL)-derived hematopoietic stem cell (HSC). B cells that arise from bone marrow (BM) HSC after birth are also called B-2 cells. One B-2 cell subset, called follicular B-2 B cells, represents the majority of circulating cells. Another subset is called marginal zone B-2 B cell, which is abundant in rodent spleens. *Created with BioRender.com.*

et al., 1996; Parker, 2016). In rats, this process starts two days postpartum. Five days postpartum, DC precursors appear, after which B cell follicles begin to develop. Immunologic function starts at 14 days of age with cell-to-cell contact of antigen-presenting DCs (Losco, 1992). The spleen reaches peak development at puberty in rats, followed by gradual decrease in size (involution) over time, although immune stimulation and development of immune responses can influence splenic size throughout life (Losco, 1992).

#### 3.3.2. Structure/Anatomy

The gross appearance and size of the spleen are variable and depend on the species and the degree of distension. Histologically, there are distinct interspecies differences and classification of spleens including defense (few trabeculae and smooth muscle fibers) and storage (many trabeculae and smooth muscle fibers) spleens (Figure 6.5), but in general, the spleen consists of two main compartments, the red pulp and the white pulp (Cesta, 2006b; Elmore, 2006c; Papenfuss, 2017b). The red pulp consists of

venous sinuses lined by incomplete endothelium. The parenchyma between the sinuses contains macrophages, lymphocytes, plasma cells, and also many natural killer cells. Most of these parenchymal cells are cells from the blood that have left the capillaries and have not yet reached the sinuses. Only a small portion of the cells from the blood do not go directly to the sinuses but enter the parenchyma directly.

Most splenic lymphocytes reside in the anatomic compartments of the white pulp, each of which contains functionally distinct cellular populations (Figure 6.6). The white pulp consists of a central arteriole surrounded by the periarteriolar lymphocyte sheath (PALS; T cell area), an outer PALS (B cell area), and a zone around the PALS and follicles called the marginal zone (MZ; B cell area). Compartments in the spleen are similar to those in the lymph nodes with comparable immune responses occurring in these sites, although splenic white pulp lacks HEVs seen in lymph nodes (Papenfuss, 2017b). Specifically, the PALS have a mesenchymal reticular network and lymphocyte content that is similar to that of the lymph node paracortex,

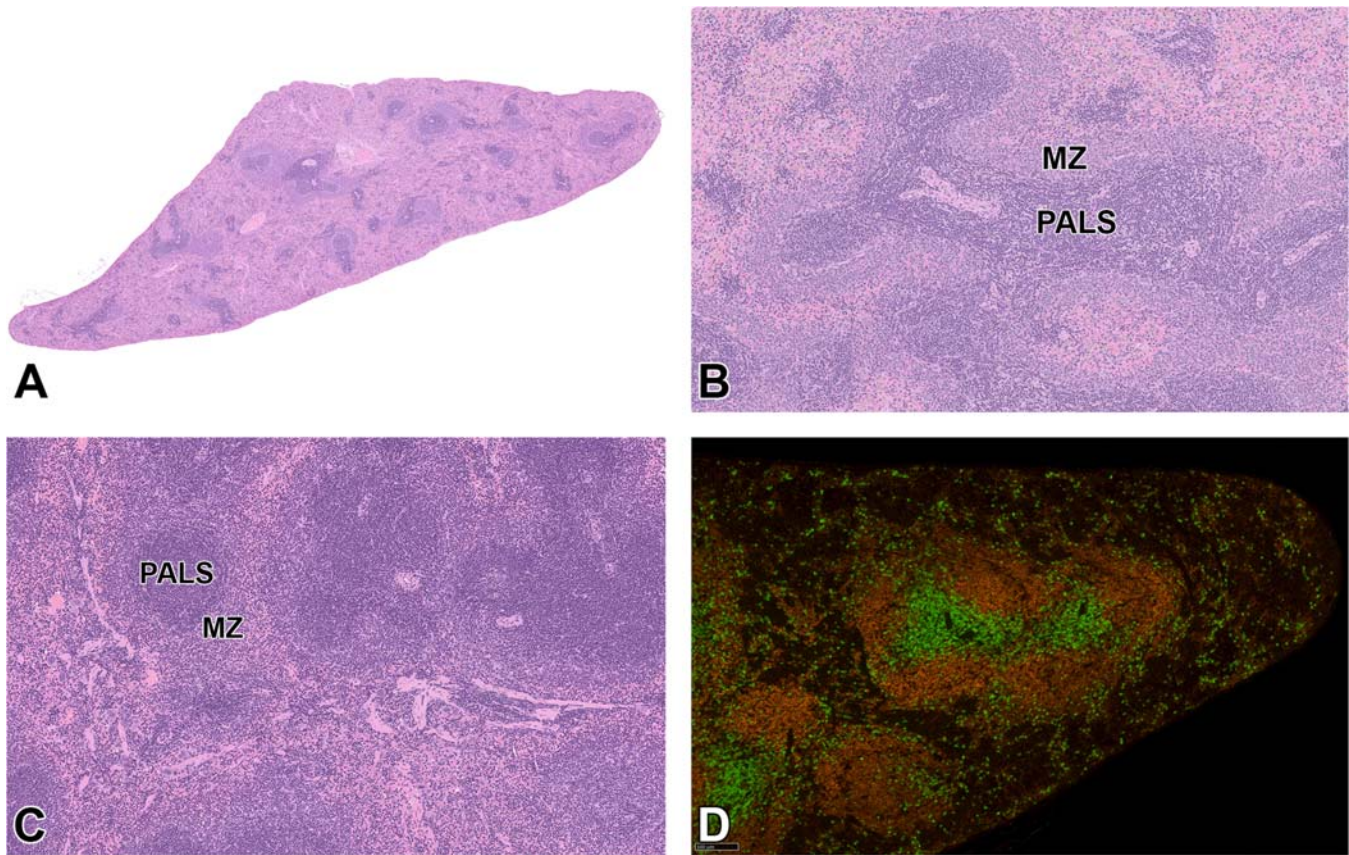


**FIGURE 6.6** Spleen, of a normal rat (A); at low magnification (20 $\times$ ) and (B) higher magnification (200 $\times$ ) where the densely populated intensely basophilic periarteriolar lymphoid sheaths (PALS) surrounded by the paler basophilic less cellular marginal zone (MZ) can be visualized. The spleen of a normal 4-week old mouse (C) has a less apparent marginal zone (MC) compared to the rat (magnification 200 $\times$ ). (D): Immunohistochemistry (IHC) staining of a mouse spleen showing T cells (CD3<sup>+</sup>, green) in the central PALS surrounded by B cells (CD19<sup>+</sup>, red) in the marginal zone (magnification 200 $\times$ ).

while the splenic follicles are similar to lymph node follicles. Although an MZ can technically be described in lymph nodes, the term marginal zone is largely reserved for describing the region present between the red and white pulp unique to the spleen.

The PALS are identified by the central arteriole surrounded by lymphocytes (primarily T cells) and contain inner and outer regions (Figure 6.6). The inner PALS, surrounding the central arterioles, is dense and contains mostly CD4<sup>+</sup> and some CD8<sup>+</sup> T cells, with fewer DCs, macrophages, and B cells. These cells, along with flattened reticular cells and reticular fibers, form concentric layers as they surround the central arterioles. The outer PALS houses mainly small and medium-sized B cells with some T cells, macrophages, and, when exposed to antigen,

plasma cells. The differences between inner and outer PALS may require immunohistochemistry (IHC) for critical evaluation. The PALS has a mesenchymal reticular network and lymphocyte content similar to that of the lymph node paracortex (see below). The PALS are continuous with the follicles which are composed of primarily B cells but some follicular DCs and CD4<sup>+</sup> T cells (Cesta, 2006b; Papenfuss, 2017b). The splenic follicles are similar to lymph node follicles and are generally present at central arteriole bifurcation sites. The follicles contain an inner (central) region with larger lymphocytes and an outer (corona or mantle zone) region with smaller lymphocytes. Follicles contain numerous B cells with fewer CD4<sup>+</sup> T cells and follicular DCs. Upon antigenic stimulation, follicles can develop germinal centers (GCs)



containing not only lymphocytes but also apoptotic cells and tingible body macrophages.

The MZ is located between the red and white pulp and consists of a mixture of B cells, macrophage populations, and other immune and supporting cells. It has a unique microenvironment with special macrophage types, namely the MZ macrophages and marginal metallophilic macrophages (Cesta, 2006b). Marginal metallophilic macrophages are located along the border of the marginal sinus and can be stained by silver impregnation (hence “metallophilic”). The B cells at the MZ are of medium size and have a special phenotypic expression (surface IgM + IgD-). The supporting framework of this zone consists of reticular fibroblasts. The junction between the MZ and red pulp is not always distinct since the supporting framework of this zone consists of reticular fibroblasts that are continuous with the reticular fibroblasts in the red pulp. The location of the MZ is ideally situated to survey the blood since splenic circulation allows arterial blood to enter the marginal sinus and percolates in a low-flow manner through the MZ into the red pulp to interact with MZ B cells, specialized macrophage populations (e.g., MZ and marginal metallophilic), and DCs. MZ B cells are of medium size, have a special phenotypic expression (surface IgM + IgD-) compared to follicular B cells, and are well-equipped to detect blood-borne antigens and function as APCs to play roles in T cell-dependent and T cell-independent responses. Macrophages in the MZ are particularly adept at surveying the blood for pathogens. The presence of numerous APC populations (B cells, macrophages, and DCs) in this region are important contributors to inducing immune responses that result in the differentiation of B cells into plasma cells and memory cells and facilitate the migration of MZ B cells into B cell follicles within the MZ.

A capsule composed of dense fibrous connective tissue, elastic fibers, and smooth muscle, with mesothelial cells comprising the outermost layer, surrounds the spleen. The muscular component allows for splenic contraction and infusion of additional blood into the systemic circulation which varies by species. Trabeculae composed of smooth muscle, fibroelastic tissue, blood vessels, lymph vessels, and nerves extend from the capsule into the splenic parenchyma. Rats, mice, and humans have a thin capsule

and trabeculae, and ample lymphoid tissue. Minipigs have a thicker capsule and trabeculae, and less lymphoid tissue than rodents and man. Dogs have an even thicker capsule than pigs, and trabeculae with well-developed smooth muscle, but sparse lymphoid tissue. Canine spleens can store a large amount of circulating blood in the sinusoids of the red pulp, which can be rapidly emptied.

### 3.4. Physiology/Function

The spleen is a large blood-filtering and blood-forming organ. Its main immunological function is to guard the body's vascular compartment by generating, among others, T cell-independent IgM antibody responses to bacterial polysaccharides (in the white pulp), and by exerting an enormous phagocytic power (mainly red pulp). Key functions of the splenic red pulp include filtering blood to remove effete erythrocytes and platelets, playing a role in iron storage and turnover, hematopoiesis, and as a potential reservoir for platelets and erythrocytes. The primary immune function of the red pulp is to survey the blood for blood-borne pathogens. There is direct contact between phagocytic cells and bloodborne particles in the red pulp that is unobstructed by blood vessels and where blood supply is large (estimated at about 5% of the total blood volume per minute). Splenic macrophages not only perform a major function in blood cell clearance (e.g., ingestion of senescent red blood cells), but also ingest nonopsonized particles/pathogens. Thus, the red pulp plays a role in the early stage of bacteremia, before specific antibody formation and subsequent opsonization. Together with the hepatic phagocytic system, splenic macrophages also play an important role in synthesizing the majority of complement components involved in the complement cascade.

The primary site of initiation and propagation of immune responses in the spleen occurs within the white pulp. Circulating T cells enter the spleen through arterioles in the red pulp and MZ, interact with APCs, and are ultimately directed to the T cell zones in the white pulp, where they interact with other immune cells, including B cells, to direct subsequent immune responses, including the differentiation of plasma cells. Being located at the interface

between red and white pulp, the MZ is ideally situated to survey the blood. Numerous APC populations present in the MZ monitor the blood, capture and present antigens to T lymphocytes, and interact with T and B lymphocytes of the adaptive immune response to initiate and propagate appropriate immune responses.

### 3.5. Lymph Nodes

#### 3.5.1. Development

A lymph node is essentially a discrete mass of fibrovascular tissue enclosed within a dilated lymphatic vessel with lymphocytes as transient residents (Willard-Mack, 2006). This intimate juxtaposition of the vascular and lymphatic systems begins during development when a mesenchymal bud invaginates into a lymphatic sac and compresses the sac lumen against the opposite wall (Bailey and Weiss, 1975; Eikelenboom et al., 1978; Mebius, 2003). The mesenchymal bud doesn't penetrate the lymphatic endothelium that lines the sac (and later the sinuses that arise from it), and instead becomes covered by the endothelial cells as it expands. The sac wall becomes the capsule, and the point of mesenchymal invagination becomes the hilus. The mesenchymal tissue differentiates into lobules and the sac lumen develops into a system of sinuses that surround the lobules. Lymph flows through the sinuses and around the lobules. Lymphoid lobules are thus positioned right in the middle of the "information super-highway" where they can sample inflammatory mediators and collect DCs carried in the lymph stream and bring them into direct contact with lymphocytes imported from the circulation (Willard-Mack, 2006).

The lymph nodes of mice are relatively few (approximately 22) compared to other species and are organized into simple chains (Dunn, 1954). In larger species, the number of lymph nodes is higher (approximately 450 in humans) and are organized in more complex chains that drain parts of organs. This is accompanied by a higher number of anastomoses of afferent lymphatic vessels in larger species compared to smaller ones. This high number of anastomoses leads to a mixing of lymph from a specific site that culminates in lymph nodes that have a more uniform drainage pattern, whereas in small animals, the

relative lack of anastomosis leads to translocation of small amounts of material to subportions of the node rather than to the entire node (Haley, 2017). There is high interspecies variability in lymph nodes as well as between individual animals of the same species, strain, and age.

#### 3.5.2. Structure/Anatomy

Lymph nodes are widely distributed throughout the mammalian body and are typically located at points where there is confluence of lymphatic vessels from a major anatomic area such as a limb. Figure 6.7 shows some of the basic lymph nodes (and other immune organs) of the rat. They have a basic filtering function, but, more importantly, provide a structural matrix and physiologic system that allows the immune system to interrogate and, when appropriate, respond to incoming pathogens and antigenic epitopes.

Histologically, lymph nodes are composed of a variable number of contiguous lymphoid lobules, each of which consists of a cortex, paracortex, and medulla (Figure 6.8A). The superficial cortex is a predominantly B cell zone that consists of primary lymphoid follicles, macrophages, follicular DCs, and diffuse interfollicular cortex (Figure 6.8B). Following antigenic stimulation, the primary follicles enlarge to form larger secondary follicles containing GCs composed of proliferating cells (Figure 6.8C). The classical orientation of the GCs consists of a basal zone of large, densely packed centroblasts, and an apical population of smaller, less densely packed centrocytes. The paracortex is a zone that is populated mostly by T cells and interdigitating DCs (Figure 6.8B). Each lobule of the lymph node drains a specific region, and therefore different lobules within a lymph node commonly exhibit different levels of reactivity. This is particularly noticeable in mesenteric lymph nodes of rodents, which form a long chain of contiguous lymphoid lobules, often with striking variation in histomorphology. The histologic structure of lymph nodes is highly dependent on (local) antigenic stimulation. Normally, mesenteric lymph nodes and superficial lymph nodes such as the cervical and submandibular lymph nodes are in a state of chronic stimulation (draining the antigen-rich gastrointestinal tract and oronasopharynx, respectively). In the nonimmunized animal, they may be

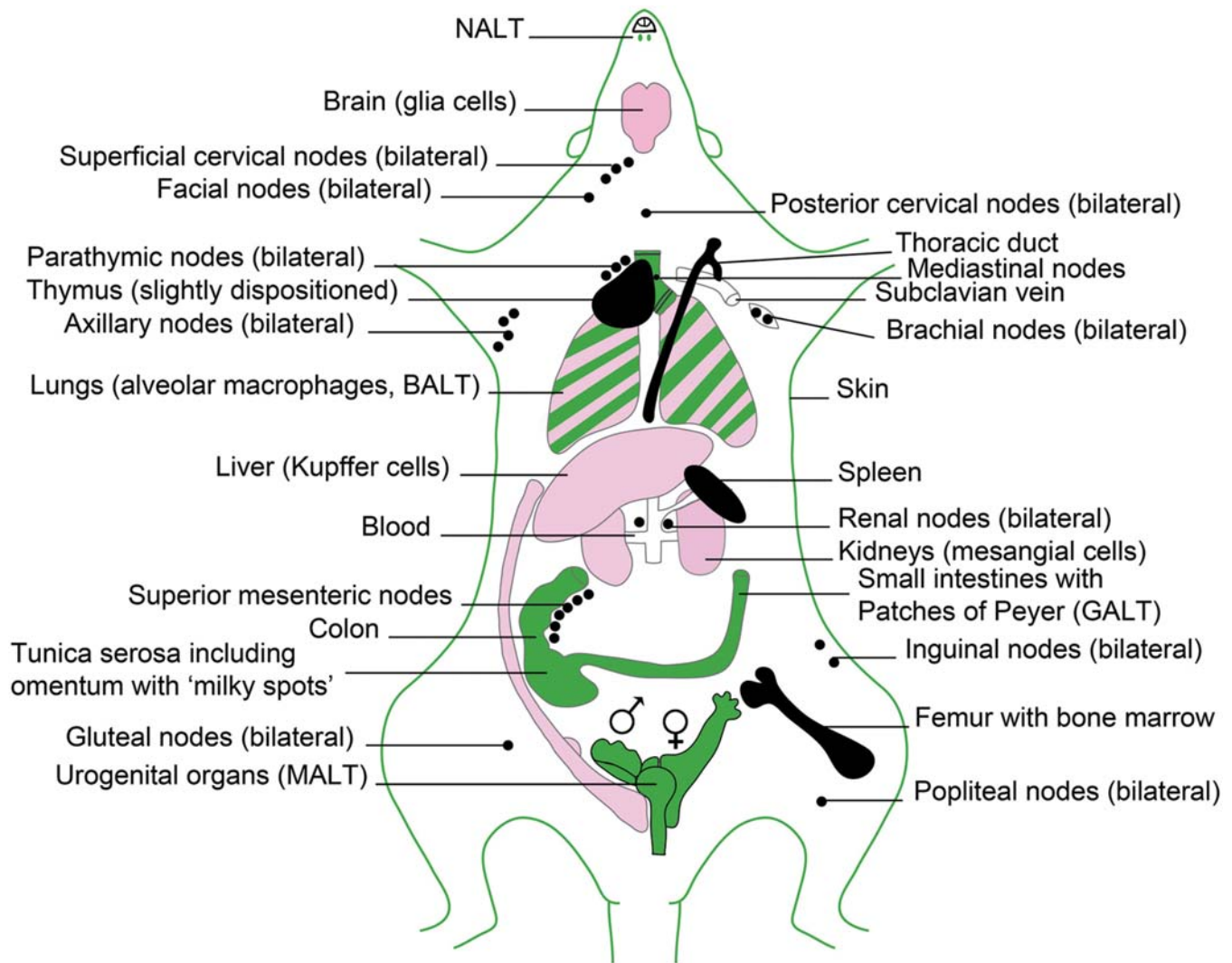


**FIGURE 6.7** Lymphoid (immune) organs and tissues in the rat. Classic lymphoid organs (bone marrow, thymus, spleen and lymph nodes) are in black; mucosae and skin are in green; special mononuclear systems are in pink. Data on lymph nodes that drain the genital tract in the rat are unknown. In mice, the lumbar/ilic/audal/para-aortic lymph nodes drain the uterus. *Figure reproduced courtesy of World Health Organization, EHC no. 180, 1996, with permission.*

quiescent, or they may contain prominent secondary follicles with GCs, well developed paracortex, considerable numbers of macrophages in the sinuses and paracortex, and plasma cells (Figure 6.8D) in the medullary cords. Minipigs, as pigs in general, have an anatomic reversal of the classical cortical and medullary components in lymph nodes with medullary sinusoids and cords located peripherally and the paracortical T cell-dependent areas and lymphoid follicles located more centrally (Haley, 2003; Haley, 2017; Skydsgaard et al., 2021).

Lymph node components are supported by a reticular meshwork composed of fibroblastic reticular cells (FRCs). The reticular meshwork is organized such that lymphocytes percolate freely through the lymph node but maintain close contact with FRCs (Willard-Mack, 2006). Flattened FRCs line sinuses and the border of lobules and are coated with molecules that facilitate lymphocyte adhesion and migration. The nutritive vascular supply enters the lymph node hilus and ramifies throughout the node. The vascular ramifications are surrounded by a “pericytic” FRC meshwork containing



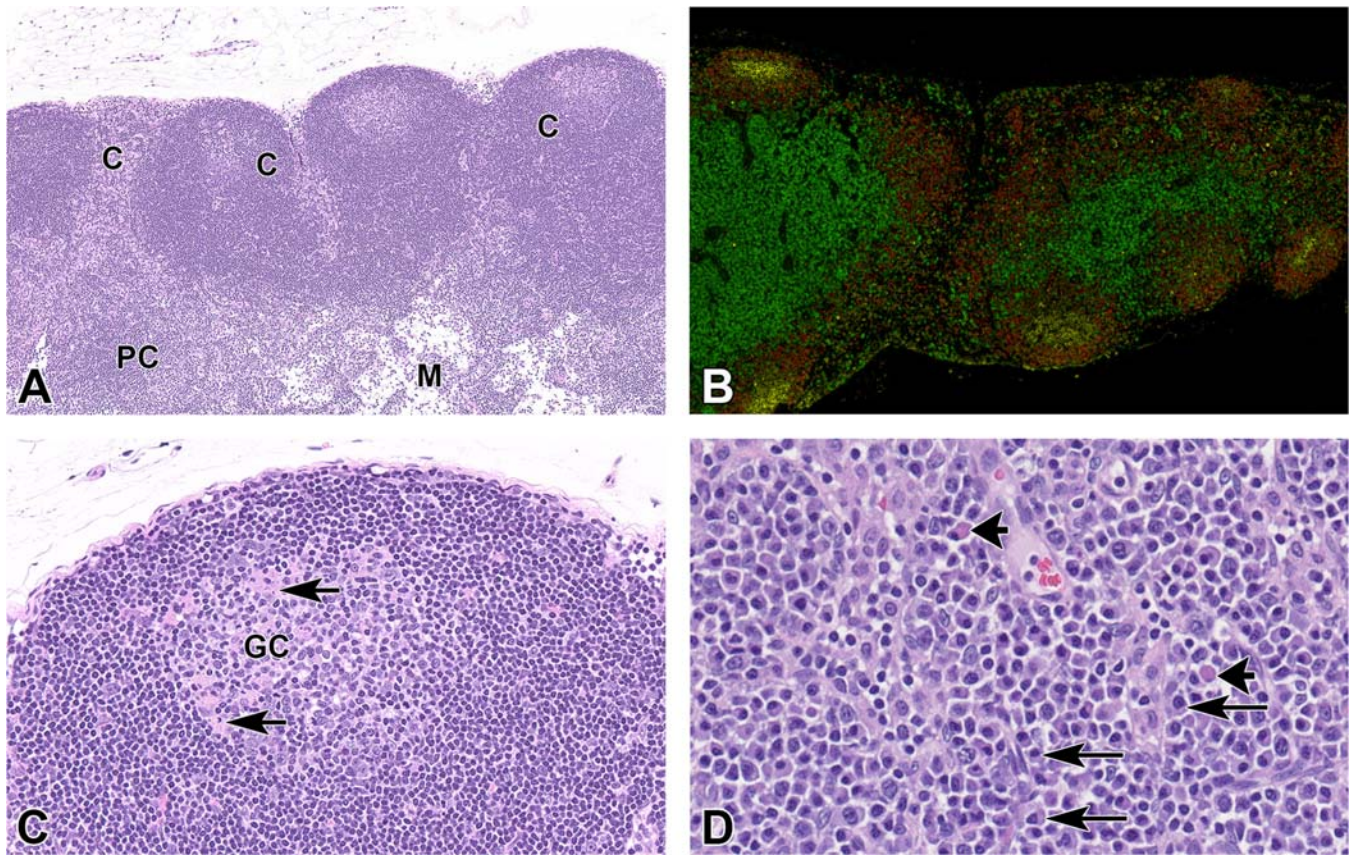


**FIGURE 6.8** (A) Mesenteric lymph node from adult Wistar rat. Lymph nodes are composed of a variable number of contiguous lymphoid lobules, each of which consists of a cortex (C), paracortex (PC), and medulla (M). Here prominent cortical follicles and an expanded hypercellular paracortex in one lobule are shown (hematoxylin and eosin (H&E) stain, magnification 100 $\times$ ). Mesenteric lymph node from 4-week-old mouse. (B) Immunohistochemistry (IHC) showing predominantly B cell zone (CD19<sup>+</sup>, red) in the superficial cortex with developing secondary lymphoid follicles (here with IgM-positive central cells, yellow) and CD3<sup>+</sup> cells (green) in the paracortical region. (C) The paracortex consists of a single deep cortical unit that is populated by mostly T cells and interdigitating dendritic cells. Following antigenic stimulation, the primary follicles enlarge to form secondary follicles containing germinal centers (GC) with intense proliferation and apoptosis of cells (arrows) hematoxylin and eosin (H&E) stain, magnification 400 $\times$ . (D) Mandibular lymph node from PND42 Sprague Dawley rat showing medullary cords that contain a large number of plasma cells (long arrows) seen as round to ovoid cells containing abundant cytoplasm, eccentrically placed nuclei, and a pale perinuclear area with occasional Mott cells (short arrows) which are plasma cells containing a cytoplasm filled with brightly eosinophilic inclusions composed of immunoglobulin. Plasma cell precursors migrate to medullary cords where they produce antibody that is secreted into the efferent lymph. Hematoxylin and eosin, magnification 400 $\times$ . (D) Reproduced from Figure 49.16 p. 1814 in Haschek WM, Rousseaux CG, Wallig MA, editors: *Haschek and Rousseaux's handbook of toxicologic pathology*, ed 3, 2013, Academic Press, with permission.

numerous recirculating lymphocytes forming highly cellular cords, especially in the medulla. Medullary cords are generally easily discernible due to contrast in cellularity with surrounding sparsely cellular medullary sinuses. Cords within the paracortex and diffuse superficial cortex are less distinctive due to the high cellularity of surrounding structures (Willard-Mack, 2006).

Subcapsular sinuses are located immediately beneath the thin fibrous capsule, and in most species receive incoming lymph via afferent lymphatic vessels. These sinuses communicate via transverse sinuses with the deep medullary sinuses, which coalesce to form efferent lymphatic vessels that exit the lymph node at the hilus. In pigs, the lymph flows into the node centrally and leaves it through efferent

vessels in the capsular surface. In all other animals, paracortical sinuses originate as blind sacs that lie parallel to cords in the peripheral zone of the paracortex. Paracortical sinuses receive lymphocytes produced by expansion of T cell populations in the paracortex and deliver those lymphocytes to the medullary sinuses, and thereby to the efferent lymph. HEVs are specialized postcapillary venous swellings (venules) in secondary lymphoid organs (except the spleen) that are the site of lymphocyte migration from the blood. In the lymph nodes, the HEVs are in the interfollicular zone of the superficial cortex and peripheral zone of the deep cortical units. The endothelium of HEVs has a cuboidal morphology and contains various receptors and cell adhesion molecules that interact with leukocytes. The HEV adhesion molecules assist in the movement of naive lymphocytes that regularly enter the lymph nodes via the HEVs. These lymphocytes also scan APCs for foreign antigens. Therefore, lymphocytes can be seen frequently between these specialized endothelial cells. As a result of local proliferation within the lymph node and introduction of blood-borne lymphocytes via HEVs, lymph exiting the lymph node has a 50-fold increase in lymphocyte population as compared to the lymph that enters the node. It is estimated that 25% of lymphocytes exiting a nonstimulated lymph node originate via migration from blood through the HEVs. Lymphocytic migration from blood into stimulated lymph nodes can increase lymphocyte exiting 10-fold over that seen with nonstimulated lymph nodes. The increase in lymph node cellularity due to local lymphocytic proliferation and increased lymphocyte migration from the blood results in the “reactive” lymph nodes that are common in association with inflammatory lesions.

### 3.5.3. Physiology/Function

Lymph nodes filter lymph for soluble antigens and DC-associated antigens that traffic from other locations such as the skin. Soluble antigens that enter the subcapsular sinus are sorted by molecular size and delivered to DCs, macrophages, and follicular DCs to initiate T and B cell response. DCs assimilate local antigens in peripheral tissues and travel in lymph to the subcapsular sinuses of regional lymph nodes.

Maturing DCs traveling in blood or lymph lose their ability to assimilate antigen and acquire augmented ability to serve as APCs. After delivery to the subcapsular sinuses of lymph nodes, DCs home to the paracortex, where they reside and serve as APCs to activate different T cell populations. Activated  $CD4^+$  or  $CD8^+$  T cells exit the lymph node as effector cells. A fraction of the activated  $CD4^+$  T cells migrate into follicles to help B cells. These helper T cells are called T follicular helper cells. B cells home to primary follicles and “search” for follicular DCs bearing a specific antigen. When the specific antigen is encountered, the B lymphocytes undergo clonal expansion, forming a secondary follicle with a GC. Selective processes result in apoptosis of a large percentage of the proliferating cells. Surviving antigen-specific cells form memory B cells and plasma cells. Plasma cell precursors migrate to medullary cords, where they produce high-affinity antibodies that are secreted into the efferent lymph [Figure 6.8D](#).

## 3.6. Mucosa-Associated Lymphoid Tissue (MALT)

### 3.6.1. Development

About half the lymphocytes of the immune system are in the MALT. Mucosal tissues are important sites at the interface with the external environment. MALT is situated along the surfaces of all mucosal tissues and often named according to location. The most well-known representatives of MALT are gut-associated lymphoid tissue (GALT), nasopharynx-associated lymphoid tissue (NALT), and bronchus-associated lymphoid tissue (BALT); however, conjunctiva-associated lymphoid tissue (CALT), lacrimal duct-associated (LDALT), larynx-associated (LALT), salivary duct-associated lymphoid tissue (DALT), and other site-specific MALT tissues have also been described (see also *Digestive System*, Vol 4, Chap 1, *Respiratory System*, Vol 5, Chap 4 and *Eye*, Vol 4, Chap 9) ([Cesta, 2006a](#)). In general, MALT is relatively undeveloped at birth with low cellularity. Exposure to environmental antigens after birth, especially from the developing gut microflora, results in stimulation that results in T cell areas becoming fully populated and



then expanding to form follicular GCs. The development (ontogeny) and structure of MALTs differ depending on the nature or location of the MALT and with age and species (Cesta, 2006a). Figure 6.9A shows NALT of rat and minipig and Figure 6.9B shows the various types of MALT lymphocytes within the intestines (Figure 6.10). Species differences exist in the development and structure of MALT. For example, MALT in the oronasal region in man, domestic animals, and minipig is quite extensive and forms a “ring” of various lymphoid tissues, called together the Waldeyer’s ring among which are tonsils, large lymphoid nodules in the pharyngeal region. The NALT in nonhuman primates is more numerous and present on the lateral and septal walls of the nasopharynx,

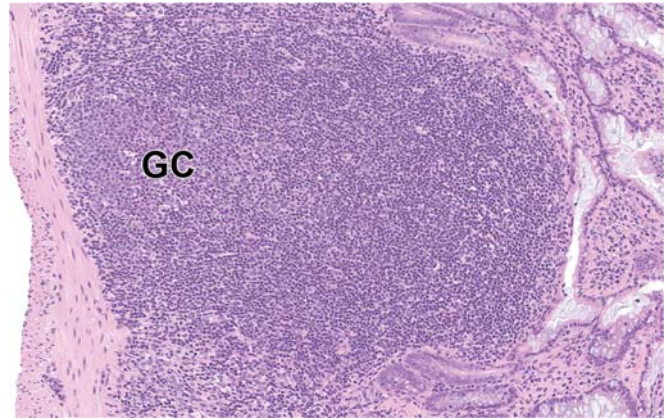


**FIGURE 6.10** Gut-associated lymphoid tissue (GALT) of the ileum (also called Peyer’s patch) of a rat with germinal center (GC). Hematoxylin and eosin (H&E) stain, original magnification 200 $\times$ .

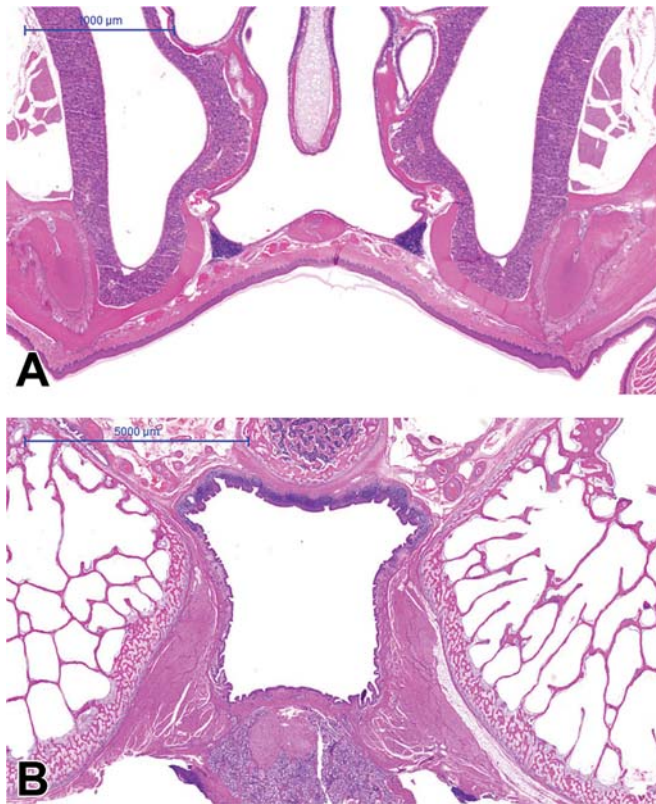


**FIGURE 6.9** (A) Nasopharynx-associated lymphoid tissue (NALT) of rat and (B) minipig. NALT in rat is a paired organ, located at the base of the nasopharynx; in the minipig NALT is a single organ (as in man) at the roof of the nasopharynx. Hematoxylin and eosin (H&E) stain; magnification 20 $\times$ . Reproduced from Figure 49.18 p. 1816 in Haschek WM, Rousseaux CG, Wallig MA, editors: *Haschek and Rousseaux’s handbook of toxicologic pathology*, ed 3, 2013, Academic Press, with permission.

while in the mouse and rat, MALT in the oronasal region is limited to NALT without the presence of defined tonsils (Haley, 2003). In addition, LALT and BALT are commonly observed in rats, but in other species, like mice and man, BALT is minimal and present especially or only when stimulated or induced (iBALT).

### 3.6.2. Structure/Anatomy

The organization of MALT is similar to that of lymph nodes with both follicular and interfollicular areas being present (Figure 6.10). Given that pathogens can enter the tissue from the lumen through the covering epithelial layer, afferent lymph vessels are lacking (Cesta, 2006a). The covering epithelium contains specialized epithelial cells (M or microfold cells). Medulla-like areas are absent in MALT although stimulated MALT tissues often have similar features of prominent follicles with GCs like lymph nodes. These changes are commonly observed in Peyer’s patches (PPs) and other small intestinal GALT sites, as well as other MALT tissues (e.g., tonsils in humans) that have high antigenic exposure. The MALT provides an important line of defense and IgA is an important antibody produced at mucosal sites and in mucosal secretions. MALT contains precursors of IgA-antibody plasma cells and populations of T cells capable of promoting the B cell immunoglobulin class (isotype) switch into IgA-producing B cells/plasma cells. Numerous single T lymphocytes are disseminated in the



covering epithelium (intraepithelial lymphocytes or IELs) and lamina propria (lamina propria lymphocytes or LPLs) of the gastrointestinal tract and actually form the body's largest single T lymphocyte pool. The epithelium of the gastrointestinal tract has lymphocyte-maturing capacity, analogous in some ways to the thymus epithelium.

### 3.6.3. Physiology/Function

The epithelial surfaces of the body form the major route of entry for antigens. Upon antigen contact, an immune response is generated in MALT, which is passed on to the draining lymph nodes, such as mesenteric lymph nodes of the gastrointestinal tract.

The immune response in MALT differs from that at other sites of the body, being primarily an IgA-antibody response. B cell differentiation into IgA-producing plasma cells after local antigen presentation is accompanied by lymphocyte traffic and specific homing. The B cells move via draining lymph nodes into the blood circulation and from there to the mucosa, where they lodge as IgA plasma cells in the lamina propria. Two IgA monomers are linked together and this dimeric IgA is called secretory IgA (sIgA). This sIgA is secreted into luminal fluids such as saliva and gastrointestinal secretions (Abbas et al., 2022d). The main function of IgA is to prevent the entry of potentially pathogenic substances into the body. Histologic assessment of MALT such as gut-, bronchus-, nose-, larynx-, skin-, vascular-, and eye-associated lymphoid tissue gives information concerning the secretory immune system and the first line of defense that the body uses to protect itself from pathogens entering (Cesta, 2006a; Elmore, 2006a; Kuper et al., 2013).

Precise knowledge of the region drained by individual lymph nodes is critical in many areas of pathology, particularly surgical pathology, but also essential to accurately assess potential xenobiotic damage to the lymphoid system and regional drainage for medical device toxicologic pathology (Haley, 2017; Wancket, 2019). However, it should be noted that the lymphatic drainage can greatly vary between animals of the same species, strain, and age. Patterns of lymphatic drainage in the laboratory mouse and rat have been systematically investigated

(Tilney, 1971; Koornstra et al., 1991; Van den Broeck et al., 2006) (Table 6.2, Figure 6.7).

## 3.7. Tertiary Lymphoid Structures

### 3.7.1. Development

Whereas lymphoid organs and tissues arise in a strict temporal and spatial manner, tertiary lymphoid tissues can form at any time and lack site specificity (Figure 6.11). Tertiary lymphoid structures (TLSs) result from lymphoid neogenesis in the course of chronic inflammation or antigenic stimulation, often developing under the influences of persistent microbial infection, autoimmune disease, or response to an allograft. It is likely that this lymphoid neogenesis involves many of the same signaling pathways that regulate the organogenesis of lymph nodes, spleen, and MALT. In contrast to secondary lymphoid organs such as lymph nodes, TLSs refer to structures with varying organization. The pancreas and thyroid are examples of organs tending to form organized lymphoid structures with GCs in chronic inflammation. In contrast, TLS does not commonly develop in the brain and skin, even with extensive lymphocyte inflammation.

### 3.7.2. Structure/Anatomy

TLSs are ectopic organized lymphoid structures that typically consist of follicles, often containing GCs, surrounded by T cell aggregates with HEVs. The microarchitecture of the tertiary GCs resembles that of GCs in lymph nodes and spleen (Figure 6.12), but atypical GC structures have been found as well. TLS can be simple lymphocyte aggregates or more organized structures. In some GCs, the basal light zone contains only a few apoptotic bodies. In addition, the venules do not always acquire a HEV phenotype. Like MALT, TLSs are not supplied by afferent lymph vessels and are not encapsulated, indicating that they are directly exposed to antigens from the surrounding environment.

### 3.7.3. Physiology/Function

Once TLSs have formed, cytokines and chemokines are produced along with antibodies directed against specific antigens in the inflamed tissue. It is not known whether tertiary lymphoid tissues have the same functional properties as

**TABLE 6.2** Areas Drained by Lymph Nodes in Rodents

<b>Lymph node (group) Rat<sup>a</sup>/ Mouse<sup>b</sup></b>	<b>Areas drained</b>	<b>Efferent drainage</b>
<b>HEAD AND NECK</b>		
Superficial cervical/(accessory) mandibular	Tongue, nasolabial lymphatic plexus, brain <sup>b</sup>	Posterior cervical lymph nodes
Facial/Superficial parotid	Head: Ventral aspect and sides of neck	Posterior cervical lymph nodes
Internal jugular	Pharynx, larynx, proximal part of esophagus	Posterior cervical lymph nodes
Posterior cervical/Cranial deep cervical	Superficial cervical, facial, and internal jugular nodes, pharynx, larynx, proximal part of esophagus, NALT <sup>c</sup>	Cervical duct
<b>UPPER AND LOWER EXTREMITY, TRUNK</b>		
Brachial/Proper axillary	Upper extremities, shoulders, chest	Axillary nodes
Axillary/Accessory axillary	Upper extremities, trunk, brachial nodes	Subclavian duct
Inguinal/Subiliac	Thigh, flanks, scrotum, lateral tail	Axillary nodes
Popliteal/Popliteal	Foot, hind leg	Lumbar, inguinal nodes
Gluteal/External iliac	Tail	Caudal, lumbar, inguinal, and popliteal nodes
<b>THORAX</b>		
Parathymic/Cranial mediastinal	Peritoneal cavity, liver, pericardium, thymus, lung	Mediastinal duct
Posterior mediastinal/Tracheobronchial; caudal mediastinal	Thoracic viscera, pleural space, pericardium, thymus	Mediastinal duct
Paravertebral	Diaphragm, thoracic viscera	Posterior mediastinal nodes
<b>PELVIS AND RETROPERITONEUM</b>		
Caudal	Ventral tail, anus, rectum, gluteal nodes	Iliac nodes
Iliac/Medial iliac	Pelvic viscera, popliteal, gluteal, caudal nodes	Renal nodes
Para-aortic/Lateral iliac; lumbar aortic	Pelvic viscera, popliteal, gluteal, caudal nodes	Renal nodes
Renal/Renal	Kidney, suprarenal, lumbar lymphatics	Renal duct to cistern chyli
External lumbar	Fat pad, psoas muscles, pelvic viscera	Lumbar lymphatics
<b>ABDOMEN</b>		
Splenic	Splenic capsule and trabeculae	Posterior gastric nodes

(Continued)

**TABLE 6.2** Areas Drained by Lymph Nodes in Rodents—cont'd

Lymph node (group) Rat <sup>a</sup> / Mouse <sup>b</sup>	Areas drained	Efferent drainage
Posterior gastric/Gastric	Distal esophagus, stomach, pancreas, splenic node	Portal nodes
Portal	Liver, splenic, posterior, gastric nodes	Portal duct to cistern chyli
Superior mesenteric/Jejunal	Duodenum, small bowel, cecum, ascending and transverse colon, Peyer's patches	Superior mesenteric duct to cisterna
Inferior mesenteric/Colic	Descending and sigmoid colon	Inferior mesenteric duct to cisterna

<sup>a</sup> Nomenclature according to *Tilney (1971)*.

<sup>b</sup> Nomenclature according to *Van den Broeck et al. (2006)*.

<sup>c</sup> *Koornstra et al. (1991)*, *Hameleers et al. (1990)*.

Modified from Haschek WM, Rousseaux CG, Wallig MA, editors: *Haschek and Rousseaux's handbook of toxicologic pathology*, ed 3, 2013, Academic Press, Table 49.2, p 1808–1809, with permission.

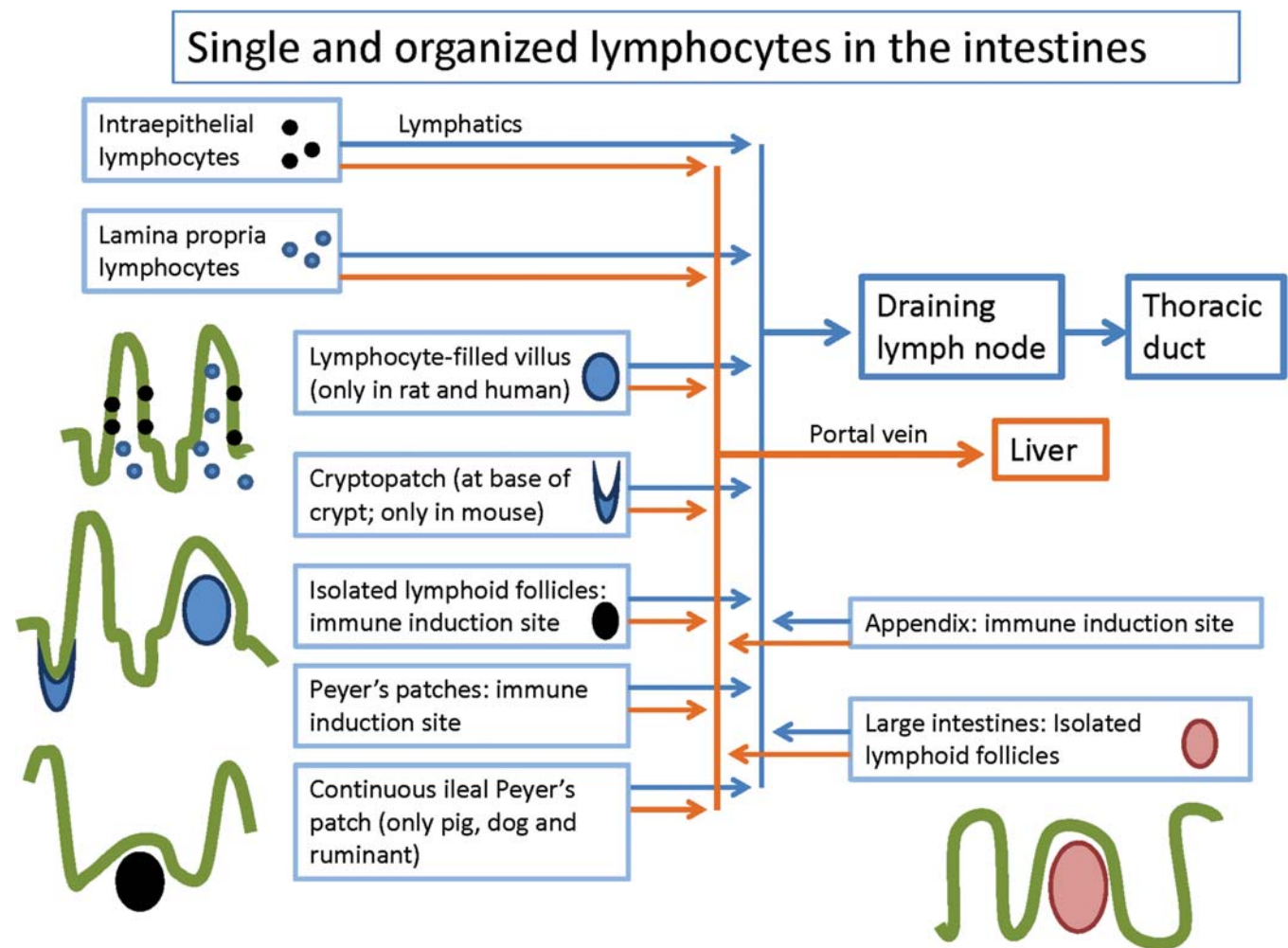


**FIGURE 6.11** Scheme of mucosa-associated lymphoid tissue (MALT) in the gastrointestinal tract. After Brandtzaeg and Pabst (2004); *Let's go mucosal: communication on slippery ground*. *Trends Immunol.* 25, 570–577, with permission.



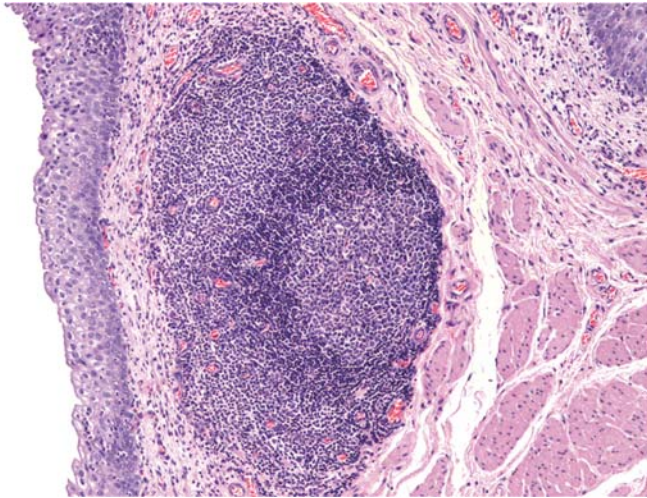


**FIGURE 6.12** Tertiary lymphoid tissue in the urinary bladder mucosa of a dog with chronic inflammation: The mucosa of the lower urinary tract is prone to the development of lymph follicles during ascending chronic inflammation. In this case, a diffuse infiltrate is present in the transitional epithelium and organized lymphoid tissue resembling a secondary follicle with germinal center formation in the propria mucosae. (Hematoxylin and eosin (H&E) stain, original magnification 100 $\times$ ). Reproduced from Figure 49.19 p. 1816 in Haschek WM, Rousseaux CG, Wallig MA, editors: *Haschek and Rousseaux's handbook of toxicologic pathology*, ed 3, 2013, Academic Press., with permission.

secondary lymphoid organs. Lymphoid structures can keep a chronic infection in check, but in autoimmunity, they can exacerbate deleterious inflammatory changes and can facilitate neoplastic growth. In some instances, they may possess antitumor activity. B cell lymphomas are reported to originate from TLSs in humans as a consequence of continuous B lymphocyte proliferation. In conclusion, TLSs can help resolve chronic inflammation, thereby being beneficial to the organism, or can contribute directly to the disease process (Munoz-Erazo et al., 2020).

### 3.8. Immune-specific Components in Select Organs

#### 3.8.1. Skin

In addition to the MALT, specialized immunity at epithelial barriers is also present in the skin (see *Integument*, Vol 5, Chap 7).

Keratinocytes can produce antimicrobial peptides and cytokines, which promote and regulate subsequent immune responses (Abbas et al., 2022a). Specific DCs or Langerhans cells are found in the epidermis. They are related to tissue-resident macrophages, arising from embryonic fetal liver and yolk sac precursors. Pathogens that reach the dermis initiate an immune response by macrophages, mast cells, and innate lymphoid cells. Cutaneous DCs transport the antigens to draining lymph nodes, where they initiate T cell responses. T cells, activated in the skin-draining lymph nodes, express chemokine receptors and adhesion molecules that favor their homing back to the skin (Abbas et al., 2022a). CD4<sup>+</sup> and CD8<sup>+</sup> effector memory cells that are produced in response to cutaneous lesions migrate to the dermis and epidermis and stay there for long periods (Abbas et al., 2022a).

#### 3.8.2. Liver (See also Liver and Gallbladder, Vol 4, Chap 2)

The liver contains a substantial population of immunologically active cells, including T and B lymphocytes, KCs, liver adapted NK cells (pit cells), NKT cells, stellate cells, and DCs (Robinson et al., 2016). Histomorphologic observations are consistent with the liver being the primary

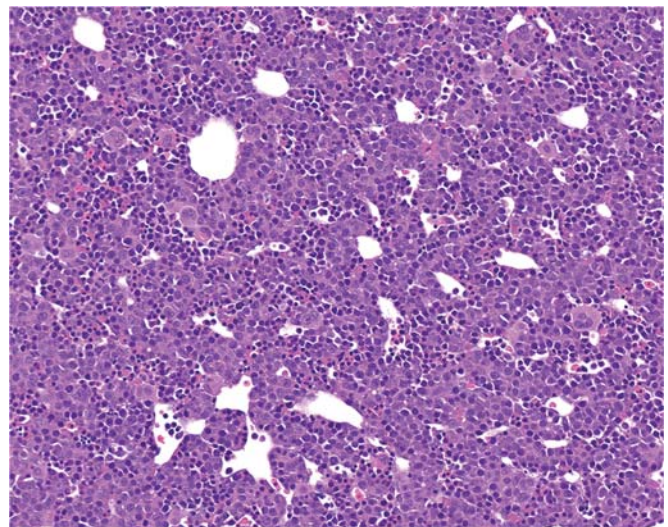


**FIGURE 6.13** Liver from gestation day (GD) 15 Sprague-Dawley rat. Note diffuse hematopoietic activity. Hematoxylin and eosin (H&E) stain, original magnification 200 $\times$ . Reproduced from Figures 49.20 p. 1817 in Haschek WM, Rousseaux CG, Wallig MA, editors: *Haschek and Rousseaux's handbook of toxicologic pathology*, ed 3, 2013, Academic Press, with permission.

hematopoietic organ of the rat at GD15 (Figure 6.13). Functionally, hepatic T cells are phenotypically different from T cells in blood, lymph nodes, or spleen and KCs are distributed differently across the different zones of the liver zones 1 (periportal), 2 (midzonal), and 3 (perivenous), with the highest number of T cells present in zone 1 and decreasing across zones 2 and 3. Additionally, KCs differ across zones, with periportal KCs being larger and having a higher lysosomal enzyme content and phagocytic activity compared to KCs in other zones. This suggests that these highly active periportal KCs are the first point of contact for incoming potentially pathogenic microorganisms (Nguyen-Lefebvre and Horuzsko, 2015). Nonspecific phagocytosis in the liver is mediated primarily by KCs, which constitute the largest population of tissue macrophages in the body. KCs also play an important role in elimination of immunoglobulin complexes, defective circulating erythrocytes, and bacterial endotoxin derived from the gastrointestinal tract. Hepatic sinusoidal endothelial cells (SECs) express collagen, mannose, Fc, and scavenger/hyaluronan receptors that recognize a broad array of molecules that must be cleared from the circulation to prevent immune reactions. Liver SECs can also take up antigen, process the antigen, and present it to T cells (Bhandari et al., 2021). Hepatocytes may also function as APCs, but the uptake of antigens by such nonprofessional APCs contribute to tolerance induction rather than immunity, likely due to the lack of input from helper T cells (Grakoui and Crispe, 2016). This mechanism prevents a reaction to the wide spectrum of potentially antigenic molecules assimilated from the gastrointestinal tract. Antigen presentation via hepatocytes may also result in premature T cell death, which is suspected to be an example of death by neglect, resulting from absence of an effective costimulatory signal.

### 3.8.3. Immune-privileged organs

Immune-privileged organs represent tissues in which immune responses are not readily initiated and foreign antigens are often tolerated (Abbas et al., 2022a). The central nervous system (CNS), eye, and testes/ovaries belong to this group (see *Nervous System*, Vol 4, Chap 8, *Eye*, Vol 4 Chap 9, and *Male and Female Reproductive*

*Systems*, Vol 5, Chaps 9 and 10). Immune privilege is achieved through a variety of mechanisms, including tight junctions of endothelial cell in blood vessels, local production of immunosuppressive cytokines, and expression of cell surface molecules that inactivate or kill lymphocytes. However, if antigens of these tissues are released due to trauma or other events that may disrupt immune privilege, recognition of normally sequestered self-antigens and ultimately prolonged tissue inflammation or autoimmune responses may be initiated. Of note, immune privilege is not simply immunosuppression but rather a controlled regulation of immune responses. For example, although the CNS is considered immune-privileged, there is evidence that immune surveillance does occur (Forrester et al., 2018; Negi and Das, 2018). The frequency of opportunistic infections within the brain increases in immunosuppressed patients suggesting that T cell or monocytes traffic into the brain to mediate immune responses (Negi and Das, 2018).

### 3.8.4. Serosa-Associated Lymphoid Cluster

Serosa-associated lymphoid cluster (SALC) or fat-associated lymphoid cluster (FALC, see *Adipose Tissue*, Vol 4 Chap 6) are aggregates of leukocytes associated with the serosa (Kuper et al., 2018). They are positioned around a central vessel or at vascular crossroads. Numbers of SALCs increase in the mediastinal fat of mice between the 3 and 12 months of age (Elewa et al., 2016). Distinct T and B compartments seem to be absent and follicular DCs have not been found in SALCs. Therefore, GC-like formations seem to be absent or more primitive. SALCs are involved in the induction of the adaptive immune responses. The immune responses appear independent of spleen, lymph nodes, and PPs, since the response occurs even in the absence of these lymphoid organs (e.g., “SLP” mice; Jackson-Jones et al., 2016). The SALCs are involved in the surveillance of serous cavities against foreign material including infectious agents and nanomaterials (Kuper et al., 2018; Jackson-Jones and Bénézech, 2020). The SALCs seem to coordinate the activation of innate lymphocytes in early, acute immune responses and identifiable SALC can increase in numbers in this process (Bénézech et al., 2015).

#### 4. PHYSIOLOGICAL INFLUENCES ON THE IMMUNE SYSTEM THROUGHOUT THE LIFESPAN

There are numerous physiological factors that can influence the immune system throughout the life of an animal. Factors such as age, sex, diet,

nutritional status, stress, and numerous others can all impact the health and function of an immune response. A detailed account of how these various factors influence the immune system is beyond the scope of this chapter, but the select influences of the most common factors affecting immune responses in toxicology studies are provided below and in [Table 6.3](#).

**TABLE 6.3** Effects of Stress, Feed, and Aging on Organ Weights, Immune Functions, and Histology of Lymphoid Organs

	Species	Organ weights	Immune cells/functions	Histology
<b>Stress</b>	Rat	Spleen and thymus ↓ (along with deteriorated condition or reduced body weight gain)	Granulocytes ↑	Spleen: Cellularity of B cell areas and marginal zones ↓ Thymus: Cortical atrophy with ↑ apoptosis/cortical starry sky macrophages
	Mouse	Spleen and thymus ↓ (along with deteriorated condition or reduced body weight gain)	Granulocytes ↑, lymphocytes (T: CD4 <sup>+</sup> and CD8 <sup>+</sup> ) ↓, B cells expressing MHC class II protein (most sensitive parameter) ↓, spleen cell # ↓	Thymus: Cortical atrophy with ↑ apoptosis/cortical starry sky macrophages
<b>Hypocaloric status/ Feed restriction</b>	Rat	Spleen ↓	Proliferative response to mitogens ↑, IL-2 receptors on splenic T cells ↓, white blood cells/granulocytes ↓	Large granular lymphocytic (LGL) leukemia incidence in the F344 strain of rat ↓
	Mouse	Spleen ↓	NK cell function ↑, B cell subpopulations ↑, T precursor cell ↑	Lymphoma incidence ↓, autoimmunity-related lesions in susceptible strains ↓
<b>Aging</b>	Rat	Thymus ↓, Spleen ↑	Proliferative response to mitogens ↓, lymphokine production ↓	Spleen: White pulp ↓, red pulp ↑, pigment deposits (red pulp) ↑ Thymus: Involution Lymphoma incidence ↑
	Mouse	Thymus ↓, Spleen ↑	B cells: Proliferation response to mitogens ↓, affinity response ↓, monoclonal gammopathies/autoantibodies ↑ T cells: Age-related shift of subsets depending on strain, bone marrow production of pro-T cells ↑, NK cell function ↑	Spleen: Lymphoid hyperplasia ↑, macrophages ↑, hemopoiesis ↑, pigment ↑ Thymus: Involution Lymphoma incidence ↑

Modified from Haschek WM, Rousseaux CG, Wallig MA, editors: Haschek and Rousseaux's handbook of toxicologic pathology, ed 3, 2013, Academic Press, Table 49.9, p 1815, with permission.



### 4.1. Immune Responses to Aging

During embryogenesis, the immune system forms the various immune organs that are present at birth. For a detailed description of immune system development during embryogenesis and postnatally, the reader is referred to additional references (Holsapple, 2003; Figueredo et al., 2016; Parker, 2016; Skaggs et al., 2019). The function of the neonatal immune system differs from that of an adult and can differ substantially in the postnatal period depending on species. Differences of placentation type, transfer of maternal antibodies (e.g., contributions via colostrum or transplacental transfer), and the degree of immune system development that occurs postnatally (e.g., precocial vs. altricial young, etc.) can all affect the degree of protection the neonate has immediately following birth. The immune system of the neonate can be affected by factors occurring during gestation or immediately following birth. Immune responses in immature animals may vary from those of adult animals, with or without concomitant morphologic differences in immune system organs, and these should be taken into consideration when evaluating neonatal animals (Simon et al., 2015; Tsafaras et al., 2020). The field of developmental immunotoxicology evaluates such influences and can be a component of toxicity evaluations for developmental and reproductive toxicology (DART) studies (Holsapple et al., 2003).

Puberty is a time of significant hormonal changes that can impact immune organs, most notably the thymus. Age-related physiological involution of the thymus is a normal process that is most markedly observed during puberty, which can interfere with the critical evaluation of the thymus since morphologic changes are similar to stress or test article-related changes (Elmore, 2006d; Elmore, 2012). Additional discussion of the contributions of stress to evaluation of the thymus and other immune organs is provided in later sections. As an organism ages, the immune system undergoes immune senescence that, over time, can lead to diminished immune responses, vulnerability to infections, and increases in certain types of inflammation (Simon et al., 2015). Such inflammation is considered to contribute to the increased diseases of the elderly, such as infections, cancer, and both autoimmune and chronic inflammatory diseases (Fulop et al.,

2017; Nikolich-Zugich, 2018). For the toxicologic pathologist evaluating immune tissues, aging changes begin at the time of puberty and continue throughout life. These changes are typically recognized in the thymus and manifest as a progressive reduction in organ weight and size and decreased delineation between cortex and medulla. Proliferative areas in the outer cortex vanish and the lymphocyte populations are replaced by univacuolar adipocytes. In old animals, often only remnants of thymic tissue or replacement by adipocytes remain. Although the release of T lymphocytes from the thymus is markedly reduced, secondary lymphoid organs do not undergo related involution, but instead a functional shift from naive to memory T cells takes place. The age-related increase in thymic epithelial cords and tubules depends on sex and strain. Generally, these structures are more prominent in females than in males. Lymph nodes, particularly unstimulated ones such as the popliteal lymph nodes, often become very small and may be difficult to find at necropsy in aged animals. In these inactive nodes, reduced lymphocyte content, reduced HEVs, and increased medullary lipomatosis can be observed. The bone marrow gradually releases increased numbers of myeloid cells at the expense of B lymphocytes and hematopoietic tissue is commonly replaced with adipocytes over time.

### 4.2. Immune Responses to Hormones

The immune system can be significantly affected by hormones, including sex and stress hormones. Differences in sex hormones contribute to the sexual dimorphism between male and female responses and the changes seen during puberty and pregnancy (Klein and Flanagan, 2016; Skaggs et al., 2019). During puberty, sex hormones can significantly impact immune function with physiologic thymic involution being the most prominent change. For the pathologist, differentiating this normal physiological process from stress- or xenobiotic-induced changes can be one of the more challenging aspects of thymic evaluation given that most toxicology studies utilize animals of peripubertal age. During pregnancy, radical but reversible changes are caused by the natural alteration of sex hormone balance with changes in thymic weights, lymphocyte cellularity, and increases in CD4<sup>+</sup>CD25<sup>+</sup>

regulatory cells (Skaggs et al., 2019). Aspects of stress related responses are discussed in further detail in the following section.

### 4.3. Immune Responses to Stress

Stress influences neural and neuroendocrine pathways and results in hormonal changes (e.g., increased glucocorticosteroids) and adaptive responses in a variety of organs. Stress, and its associated effects, are a common feature of many toxicity studies, either through direct test article toxicity, secondary effects from experimental procedures, or a combination of these contributing to lymphoid (and other) organ changes. Many factors can induce stress responses (e.g., including, transportation, housing, handling, diet, exercise, sex, or other experimental procedures), so the use of age-matched control groups experiencing similar conditions, as well as the evaluation of additional stress-related parameters can be helpful when attempting to identify test article-related effects. Changes in thymus and adrenal weights, circulating leukocyte counts, and lymphocyte subsets can be the most sensitive indicators of stress. Stress may also result in changes in food consumption, body and other organ weights, behavior or activity, reproductive parameters, and both clinical and histopathology changes. A weight-of-evidence (WOE) approach incorporating a variety of these changes can help determine potential stress-related effects.

In general, the hallmarks of the stress response can include decreases in body and immune organ weights, activity, and food consumption and alterations in circulating leukocytes and reproductive function and increased adrenal gland weights (Everds et al., 2013). Moribund animals of multiple species can have significant changes, particularly lymphocyte depletion. Acute stress commonly presents with both clinical pathology and histological changes of sensitive immune cell populations, while chronic stress and associated habituation more commonly impacts total body or organ weights (e.g., thymus, spleen, adrenal glands, and sex organs). Acute and chronic stressors can have differential effects on acute phase proteins, cytokines, and various aspects of immune function with physiological and morphologic effects most commonly observed in the blood, thymus, spleen, and bone marrow. The thymus is typically the most

sensitive indicator of stress given the predominance of immature lymphocytes that are particularly sensitive to glucocorticoid-related effects resulting in lymphocyte depletion (Figure 6.14A). Stress-related changes in the thymus typically include decreased organ weight and decreased cortical cellularity that may have increased tingible body macrophages and cellular debris (starry sky appearance). The response to acute stressors is rapid (within hours to days). Histological cortical changes in the thymus progress from increased apoptosis of cortical thymocytes with increased numbers of tingible body macrophages to lymphocyte depletion, which can be such that a reversed pattern of lymphocyte density is observed in the medulla. Stress-related changes in the spleen may include variable morphology, particularly of the B lymphocyte areas due to the redistribution of B lymphocytes from the bone marrow to the spleen. In moribund animals, the splenic red and white pulp can become severely atrophic (Figure 6.14B).

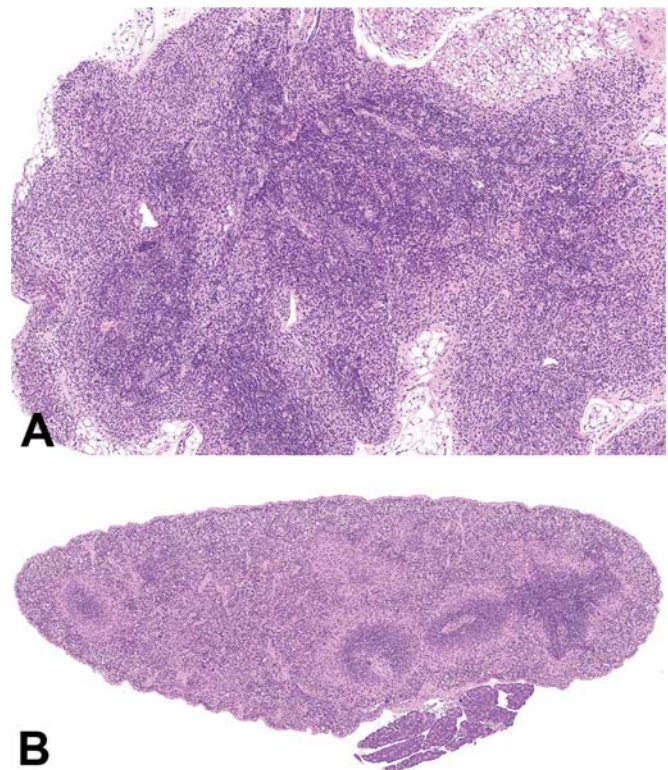


**FIGURE 6.14** Tissue from a moribund mouse showing significant lymphocyte depletion in the thymus (A) and spleen (B). In the spleen cells of the red pulp are significantly depleted. Hematoxylin and eosin (H&E) stain; magnification 20 $\times$ .

Stress-related changes in clinical chemistry or hematology parameters can also be seen with circulating leukocytes being the most sensitive indicator of stress (Everds et al., 2013). Increased total and differential leukocyte counts are typically seen immediately following a stress due to epinephrine effects. Increases in neutrophils and decreases in lymphocytes and eosinophils, often referred to as a stress leukogram, are seen minutes to hours after the stressor and are mediated by glucocorticoids. Stress can influence hematopoiesis and both red and white blood cell (WBC) populations. Although stress can alter serum/plasma glucose concentrations, glucose levels are a relatively insensitive indicator of stress, as are platelet levels.

Stress effects on the adrenal gland differs between acute and chronic stress. Acute stress can cause decreased vacuolation within the adrenal cortex and chromaffin cell degranulation within the medulla, while chronic stress can cause increased adrenal gland weights and associated hypertrophy/hyperplasia of the cortex and medulla. Although acute and chronic stress don't necessarily cause changes in thyroid gland weights or microscopic findings, changes in thyroid hormone (T3 and T4) concentrations can occur and are often decreased in both acute and chronic stress. Stress can affect other nonimmune parameters and include decreases in body weights or body weight gain, food consumption, and size and function of reproductive organs, as well as gastric ulceration. Concluding that immune changes are related to stress is often a WOE that considers changes both in immune organs and stress parameters and other nonimmune organs (Everds et al., 2013).

## 5. IMMUNOMODULATION, IMMUNE SYSTEMS RESPONSES, AND MECHANISMS OF TOXICITY

### 5.1. Defining Immunotoxicology, Immunosuppression, and Immunostimulation

While immunosuppressive effects have long been appreciated as indicative of toxicity, the evaluation of immune system changes due to xenobiotics has significantly evolved to include

dimensions beyond immunosuppression. This has been largely due to the significant expansion of immunotherapies that have complex and nuanced immunomodulatory effects, ranging from immunosuppression (often of selective immune system components) to immunostimulation. With such immunomodulatory compounds, intended pharmacology can become potentially immunotoxic when exaggerated pharmacology/on-target effects occur. For example, a compound that suppresses aspects of an immune response may increase the risk of reactivation of latent pathogens or may increase the susceptibility to infectious or autoimmune diseases or malignancies. Examples may include cyclosporine, sirolimus, leflunomide, and various immunomodulators that increase the risk of infections and others that may increase the risk of malignancies depending on their mode of action/immunosuppression (e.g., cyclosporine, etanercept, and adalimumab with associated TNF-alpha inhibition, rituximab that targets CD20, and many others) (Lebrec et al., 2016; Hussain and Khan, 2022). In contrast, a compound that stimulates aspects of an immune response may increase the risk of inflammatory or autoimmune diseases with potential serious sequelae (e.g., cytokine storms, hypersensitivities, or anaphylaxis). While immediate immune effects can often be readily identified, there may be risks to patients resulting from long-term immunomodulation that likely require monitoring of patient data over a longer period.

### 5.2. Biochemical Pathways and Exaggerated Pharmacology in the Immune System

Many xenobiotics have the potential to influence various cell types and cell signaling or molecular pathways important for appropriate development of innate and adaptive immune responses. Although descriptions of the numerous pathways involved in the development and production of immune responses are beyond the scope of this chapter, it is important to be familiar with general immune function and pathways relevant to potential changes seen or expected during evaluation. Understanding immune pathways involved with any xenobiotic a priori can help inform and predict



potential changes indicative of immune system effects that may be seen in studies and is particularly helpful when evaluating immunotherapies designed to target the immune system (e.g., cell-based, small molecules, or biologics including vaccines, antibody-based targeted therapies, and oncolytic viruses, see *Vaccines*, Vol 2, Chap 9). [Table 6.4](#) outlines some common immune targets for compounds, agents, or therapies.

Determining immune-related effects may not be difficult, however, but evaluating efficacy versus exaggerated pharmacology and reporting on what constitutes toxicity can be a particular challenge with immunotherapies. Such therapies are designed during development to modulate the immune system, often with a specific therapeutic indication and patient population in mind. These factors, along with an individual's range of immune responses and recoverability can vary significantly. Determining what effects are outside the range of "normal" variability to ultimately constitute "toxicity" and how to report on the whether a finding is adverse or adaptive can be challenging and opinions and approaches may vary ([Kimber and Dearman, 2002](#); [Pandiri et al., 2017](#)).

### 5.3. Perturbations of the Immune System and Recoverability (Relevance to Adversity)

When the immune response is directed against a xenobiotic, particularly one designed for therapeutic applications, there can be desired and undesired effects that can vary in clinical impact. Many immunotherapies (biologics) have components that may be recognized as foreign in a given test species, and the generation of an immune response may have minimal to no clinical relevance or may affect therapeutic efficacy or result in toxicity. Immunogenicity is a term used to describe the ability of an agent to incite an immune response and although immunogenicity can and does occur, particularly with biologics, the effects can range from being clinically relevant to being of limited to no clinical significance and not predictive of immunogenicity in humans ([Bugelski and Treacy, 2004](#); [Leach et al., 2014](#)). Antibodies can be generated against the drug (e.g., antidrug antibodies; ADAs) that can have effects on therapeutic efficacy, immune function,

**TABLE 6.4** Select Immune Pathways and Effects of Targeting

Immune component targeted	Effector functions and effects of targeting
<i>IMMUNE ORGANS</i>	
Lymph nodes, mucosal sites	Receptors can promote homing/delivery to specific organs
<i>INNATE IMMUNE CELLS</i>	
DCs or other APCs	Phagocytic, influence antigen processing, presentation, and immune response
NK cells	Cytotoxicity, influences removal of NK targets (tumors)
Granulocytes	Influences defense against specific pathogens
<i>ADAPTIVE IMMUNE CELLS</i>	
T cells-helper	Can influence humoral, cell-mediated, or regulatory immune response
T cells-cytotoxic	Influences destruction of infected/target cells
B cells, plasma cells	Influences production of antibodies; (protective against pathogen, may promote autoimmune/inflammatory responses)
Immune cell interactions	Numerous effects via receptors, soluble mediators, etc. (proinflammatory, antiinflammatory, regulatory)
<i>SOLUBLE FACTORS</i>	
Antibodies	Numerous potential effects (proinflammatory, antiinflammatory, regulatory)
Complement	Facilitates uptake and destruction of pathogens by phagocytic cells
Defensins, other molecules	Proinflammatory/defense
Cytokines	Numerous effects (stimulatory, inhibitory); promote specific immune responses, homeostasis

(Continued)

**TABLE 6.4** Select Immune Pathways and Effects of Targeting—cont’d

Immune component targeted	Effector functions and effects of targeting
Hormones	Numerous effects, depends on hormones (sex and thyroid hormones have significant effects)
<b>SIGNALING PATHWAYS</b>	
Inflammatory pathways	Promote inflammatory/immune response; defense against pathogens
Inflammasome, innate receptors	Receptors/sensors that induce inflammation in response to pathogens/infectious microbes
Immune signaling	Innate and innate-adaptive signaling pathways/influence immune response  T cell and B cell receptor signaling  Cytokine and other pathways signaling
Development	Development of specific immune cells
Differentiation	Numerous transcription factors and differentiation pathways for various immune cells; have numerous effects and promote numerous different immune responses
Regulation	Immune regulatory pathways
<b>OTHER ORGANS</b>	
Microbiome (Gut)	Influences immune response, brain-gut-immune axis
Liver	Promotes immune tolerance/regulation
Endocrine system	Sex hormones, thyroid hormones

or result in toxicity. The generation of ADAs often lead to morphological signs of immune activation, namely increased GC formation, lymphocyte proliferation, and increased immune tissue compartment sizes. Neutralizing ADAs can have an undesired effect on efficacy,

but that may not be regarded as toxic per se. While ADAs may have neutralizing effects that impact efficacy, other antibodies/ADAs may contribute to a variety of immune effects, including hypersensitivity and the formation of immune complexes (Figure 6.15). Such immune complexes, although potentially impactful in a test species, may not have relevance to the human patient population. The relevance and potential “toxicity” of such changes may be equivocal with variable relevance in translating between animal studies and humans but are important considerations in understanding the effects on the immune system and potential clinical significance.

Potential toxicity in the immune system following xenobiotic exposure can result from direct effects and indirect effects and these can be nonantigen- or antigen-specific (See

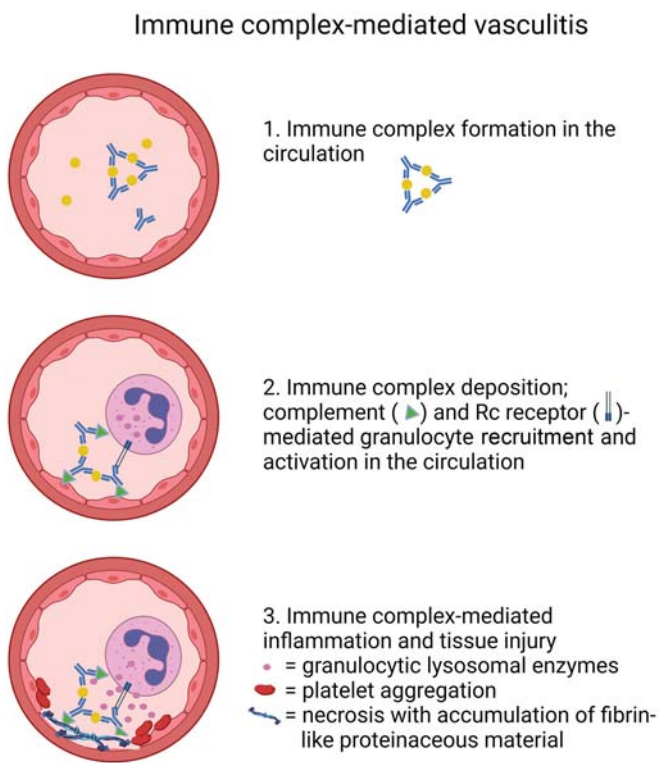


**FIGURE 6.15** Immune complex-mediated vasculitis (type III hypersensitivity). The morphologic manifestation is necrotizing vasculitis, with necrosis of the vessel wall and neutrophilic inflammation. The necrotic tissue, immune complex deposits, complement and plasma protein lead to an eosinophilic deposit. The micro-anatomy of the vessel is thus obscured, and the phenomenon is designated fibrinoid necrosis. Created with BioRender.com.

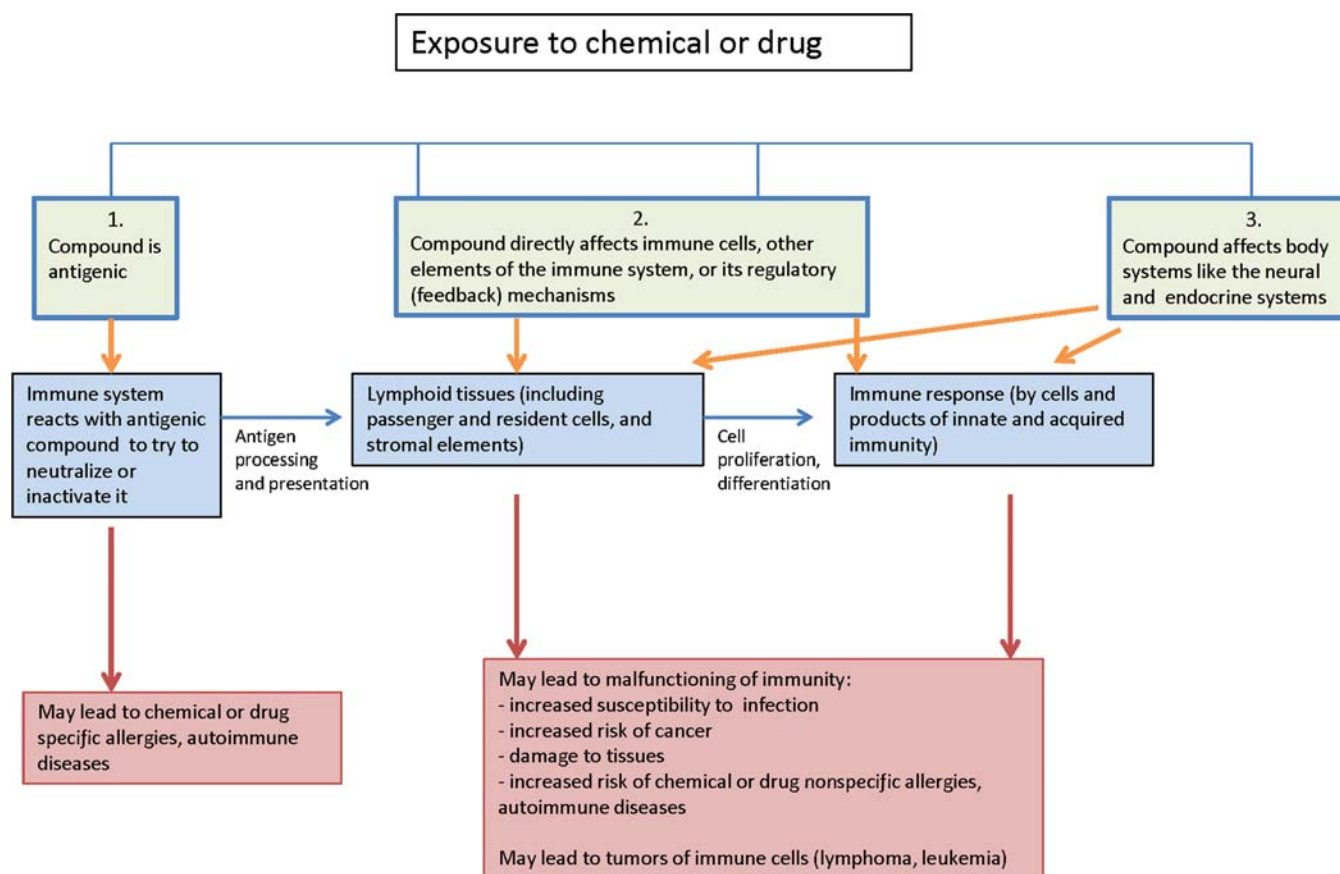


**FIGURE 6.16** Mechanisms of immune toxicity. Reproduced from Figure 49.24 p. 1823 in Haschek WM, Rousseaux CG, Wallig MA, editors: *Haschek and Rousseaux's handbook of toxicologic pathology*, ed 3, 2013, Academic Press, with permission.

Figure 6.16 and Table 6.4). Effects can include effects on immune cell populations, viability, and phenotype that ultimately impact immune cell function. Nonantigen-specific effects are most commonly due to direct toxic effects (e.g., resulting in immune cell death) although indirect effects in other organ systems, namely the neural and endocrine systems, can lead to malfunctioning of the immune system. Nonantigen-specific effects can also include certain types of hypersensitivities or infusion reactions or inflammatory responses that stimulate the nonspecific components of the immune system (e.g., activation of complement and/or other innate immune responses). Antigen-specific effects occur when a xenobiotic or component of it is recognized as foreign (e.g., antigen) by the immune system and the immune response is specific to that antigen (Figure 6.16). In induced immunostimulation, small molecules act as haptens, whereas large biotechnology-

derived molecules can be directly immunogenic in experimental animals. Antigen-specific effects can represent a range of possible responses including hypersensitivities (that are directed against a specific recognized antigen), inflammatory responses, allergies, and autoimmune diseases. Table 6.5 outlines some common examples of compounds, agents, or therapies that influence immune effects.

#### 5.4. Nonantigen-Specific Toxicity

The role of the immune system in generating immune cells via proliferation of precursors or immune cell populations renders it especially vulnerable to toxic compounds. Xenobiotics can demonstrate direct toxicity to lymphocytes and their precursors with the bone marrow and thymus being most sensitive, although effects on the proliferation or survival of immune cells can be observed in other immune organs.



**TABLE 6.5** Examples of Compounds and Agents that can Affect the Immune System

	Compounds or agents	Immune effects
<b>Immunosuppression</b>	Dexamethasone or other steroids (immunosuppressant)	Targets lymphocytes (causes apoptosis), complex effects on inflammatory immune pathways, reduced immune cell function, activity, migration
	Cyclosporin A (immunosuppressant)	Inhibits immune system function; reduces lymphocyte activity
	Azathioprine (cytostatic)	Inhibits DNA, RNA and protein synthesis (is antagonist of purine metabolism)
	NO <sub>2</sub> , SO <sub>2</sub> , O <sub>3</sub> air pollution	Associated with increased susceptibility to airway infection
	Irradiation	Antiproliferative effect; death of lymphocytes, immunomodulation
	UV-B light	Immunomodulation; induction of immunosuppressive effects
	Nerve pain/antiseizure medication (pregabalin)	Modulates immune responses following injury/ with neuropathic pain; decreases NK cell activity/impacted neuropathic pain
<b>Hypersensitivities</b>	Penicillin and related antibiotics	Hypersensitivity reactions, Types I-IV
	Infusion reactions	Hypersensitivity reactions typically
	Antibiotics containing sulfonamides (sulfa drugs)	Hypersensitivity reactions, primarily type I
	Aspirin, ibuprofen, and other NSAIDs	Hypersensitivity reactions, typically type IV
	Insulin	Hypersensitivities, most commonly type I
	Muscle relaxers (intravenous) atracurium, succinylcholine, vecuronium	Hypersensitivity reactions, especially type I
	HIV drugs (abacavir, nevirapine, etc.)	Hypersensitivity reactions, changes in immune tolerance
	Nickel ions	Hypersensitivity reactions/contact dermatitis
<b>Inflammatory reactions</b>	Agents that cause tissue damage/necrosis	Increased inflammatory response in response to necrosis (danger) signals
	Anticonvulsants (phenobarbital, carbamazepine, lamotrigine, phenytoin)	Antiepileptic hypersensitivity syndrome, (idiosyncratic mechanism ill-defined)
	Chemotherapy drugs (paclitaxel, docetaxel, procarbazine, cytarabine, L-asparaginase, cisplatin; platinum salts, taxanes, procarbazine epipodophyllotoxins)	Hypersensitivity reactions, typically acute type I, II, can be I-IV (especially for platinum-containing antineoplastics)
	Therapeutic proteins, monoclonal therapy (ceuximab, rituximab)	Potential immunogenicity (drug-specific antibodies, hypersensitivities, etc.)
	Osteoporosis medication (bisphosphonates)	Enhances humoral immunity, complex immune effects
	Mercury chloride	Glomerulonephritis in Brown Norway rats

(Continued)

**TABLE 6.5** Examples of Compounds and Agents that can Affect the Immune System—cont'd

	Compounds or agents	Immune effects
<b>Autoimmune disease</b>	Crystalline silica (quartz)	Associated with increased autoimmune disease (scleroderma, RA, SLE)
	Propylthiouracil	Systemic lupus erythematosus (SLE), Wegener's disease
	Sulfadiazine, hydralazine, chlorpromazine, procainamide, propylthiouracil	Drug-induced liver injury (DILI), SLE, autoimmune/immune activation
	Methyldopa	Can cause autoimmune hemolytic anemia/thrombocytopenia, immune activation (hepatitis, hyperglobulinemia)
	Quinidine	Immune-mediated thrombocytopenia (antibody-mediated)
<b>Mixed effects</b>	Heavy metals	Complex immunomodulatory effects (suppressive/stimulation)
	Polychlorinated dibenzo-p-dioxins, dibenzofurans, biphenyls	Complex effects, can cause immunosuppression, induce autoimmune disease; affects immune cell numbers, function; mycotoxins inhibit signaling pathways, resulting in immunosuppression
	Asthma inhalers	Decrease inflammation therapeutically; may have mild immunosuppressive
	Minocycline	Mixed effects; immunosuppression early, immune activation later
	Isoniazid	Induces immune cell autophagy
	Antibiotics (levofloxacin)	Varied effects, decreased inflammatory cytokines, may cause tendonitis/rupture
	Acne treatment (isotretinoin)	Multiple immune effects; may increase some autoimmune disease, downregulate other immune responses
	Breast cancer medications (anastrozole, exemestane, letrozole)	Often complex estrogenic activities/conflicting reports of immune effects
	Chlorinate hydrocarbons; zearalenone (myotoxin), 9-tetrahydrocannabinol; diethylstilbestrol (DES)	All have estrogenic activity which affect immune system responses; primarily immunosuppressive effects; DES cause offspring to develop immune-related diseases/cancer
	Cholesterol-lowering medications (statins)	Antiinflammatory, immunosuppressive effects, autoimmunity (myopathy) is rare

DES = diethylstilbestrol, RA = rheumatoid arthritis; SLE = systemic lupus erythematosus.

Immature T cells (thymocytes) are susceptible to toxic compounds due to the fragile composition of these cells and to their delicate dynamic processes associated with gene amplification, transcription, and translation associated with

their development. The disappearance of lymphoid cells from blood and tissue is often the first sign of this type of toxicity. Associated cells within the thymus and thymic stroma (e.g., tissue macrophages, interdigitating cells,

etc.) may respond to this disappearance by degeneration, ending in atrophy and fibrosis. In a similar fashion, direct toxicity of numerous hematopoietic constituents can occur within the bone marrow. Often multiple lineages can be affected so changes in both myeloid and erythrocyte lineages should be thoroughly evaluated. When toxicity is directed against pluripotent hematopoietic progenitors, the effects can be quite significant. Monitoring of clinical pathology parameters, histopathologic findings, and bone marrow smears is ideal and can be particularly helpful in understanding both acute effects and the ability of the bone marrow to recover over time (see *Hematopoietic System*, Vol 5, Chap 5). Direct toxicity seen in secondary immune organs or other immune sites typically manifests as degeneration, necrosis, or loss at these sites although other morphologic changes of immune cells may also be appreciated.

The immune system is especially sensitive to imbalances in the endocrine and neural systems, because these three systems are so closely intertwined. This is exemplified by the profound influence of sex and stress hormones on immune reactivity. For example, autoimmune diseases are linked to sex steroid hormone balance, occurring more frequently in females (Klein and Flanagan, 2016). The influence of glucocorticoids and other stress-related hormones is well known and covered in a previous section. Compounds can also have an indirect toxic effect on the immune system via effects on other organ systems. For example, liver damage seen in cirrhosis (e.g., potential causes of pyrrolizidine alkaloids, chronic alcohol consumption, amiodarone, etc.) can contribute to numerous effects on the immune system including immunodeficiency, increased susceptibility to bacterial infection, and system inflammation due to the homeostatic role that the liver contributes to the system immune response (Albillos et al., 2014; Racanelli and Rehmann, 2006).

### 5.5. Antigen-specific Toxicity

Antigen-specific toxicity can affect immune cell populations resulting in functional changes of immunostimulation or immunosuppression. Adverse responses such as hypersensitivities to xenobiotics are common consequences of inadvertent sensitization or stimulation of the immune

system in response to antigens. The classification system of Gell and Coombs distinguishes four types of hypersensitivities (Table 6.6), although in practice, the distinction is often less strict than suggested. New classifications for drug allergies that do not easily fit into one of the traditional four categories have been described, including pseudoallergic reactions (e.g., complement activation-related pseudoallergy; CARPA), primarily antibody-mediated reactions, and cell-mediated reactions (Szebeni, 2014).

The elicitation of an immune reaction against low molecular weight chemicals strongly depends on the capacity of the chemical to form immunogenic hapten-carrier conjugates with endogenous proteins. This conjugate formation involves either the parent molecule itself or a reactive metabolite. The clinical findings can vary depending on the type of hypersensitivity and can be severe to life-threatening, but also can present with few to no pathologic (clinical or anatomic) changes. For example, urticaria in the skin may be caused by “irritants” like drugs (e.g., codeine); physical stimuli (e.g., cold and heat); and other agents (e.g., plasma protein products, gelatin, starch, and dextran via direct mast cell degranulation or complement activation). This type of irritant-induced reaction or “pseudoallergy” in the skin is clinically quite similar to the IgE-dependent, antigen-specific Type I reactions.

### 5.6. Pathophysiological Changes Associated with Therapies Affecting the Immune System

Toxicologic pathology can provide important information regarding immune system changes that occur following administration of therapies that, whether by design or inadvertent, affect the immune system (Figure 6.17). The following section provides some observed pathologic changes that can be seen in the context of immunosuppression or immunostimulation. It is important to note that there may be immunotherapies that are designed to either inhibit or stimulate a specific component of the immune system but whose composite effect is a combination of effects. In such cases, the use of the term “immunomodulatory” to describe effects with an associated description of the immune system effects may be most appropriate. Checkpoint



**TABLE 6.6** Classification of Hypersensitivity Reactions and Representative Diseases

Type of hypersensitivity	Mechanisms	Pathology	Examples of diseases
Type I immediate	IgE antibody production; binding of IgE to IgE receptor on, e.g., mast cells leads to release of vasoactive amines (e.g., histamine) and other mediators from the mast cells	Vascular dilatation; edema; mucus production; smooth muscle contraction; inflammation, tissue injury	Anaphylaxis; hay fever; atopic asthma; hives
Type II cytotoxic (antibody)	Production of IgM, IgG antibodies; antibody binding to antigen on target cell or tissue leading to phagocytosis or target cell lysis; complement activation; leukocyte infiltration	Generally, inflammation is organ-specific; see phagocytosis and cell lysis; inflammation	Autoimmune hemolytic anemia; Goodpasture syndrome; Grave's disease
Type III immune complex	Deposition of antigen-antibody complexes; often complement activation; leukocyte infiltration; release of enzymes	Generally, inflammation is not organ-specific; see necrotizing vasculitis/fibrinoid necrosis	Systemic lupus erythematosus; rheumatoid arthritis; types of glomerulonephritis; Arthus reaction
Type IV delayed, cell-mediated	T cell activation leading to release of cytokines or to cytotoxicity; inflammation and macrophage activation	Perivascular lymphocytic infiltrate; edema; granulomatous or lymphocytic inflammation; cell necrosis	Granulomatous diseases like tuberculosis; delayed skin reactions/allergic; contact dermatitis; allergic alveolitis (hypersensitivity pneumonitis; type I diabetes; rheumatoid arthritis; chronic asthma)
Anaphylactoid hypersensitivity (drug-related)	Complement mediated	Vascular dilatation; edema; immediate versus delayed	Infusion reaction, in animals, often lack complete evidence to prove drug-related anaphylactoid

*Modified from Table 49.7, Haschek WM, Rousseaux CG, Wallig MA, editors: Haschek and Rousseaux's handbook of toxicologic pathology, ed 3, 2013, Academic Press, with permission.*

inhibitors, a type of cancer immunotherapy, are one such example in that they inhibit the function of checkpoints, but the net effect is to increase an antitumor immune response (Fessas et al., 2020; Waldman et al., 2020). Ipilimumab, a human IgG1k anti-CTLA4 mAb is one such example whereby it inhibits the inhibitory CTLA4 receptor to promote antitumor immune responses (Waldman et al., 2020).

### 5.6.1. Immunosuppression

Immunosuppression occurs when any aspect of the immune system is decreased in its ability to perform a normal functional role. Historically, immunosuppression has largely been considered toxic and often adverse, depending on the degree of severity and recoverability. Immunosuppression may allow activation of latent pathogens, promote harmful increases in normally nonpathogenic commensal flora (e.g., demodicosis), or

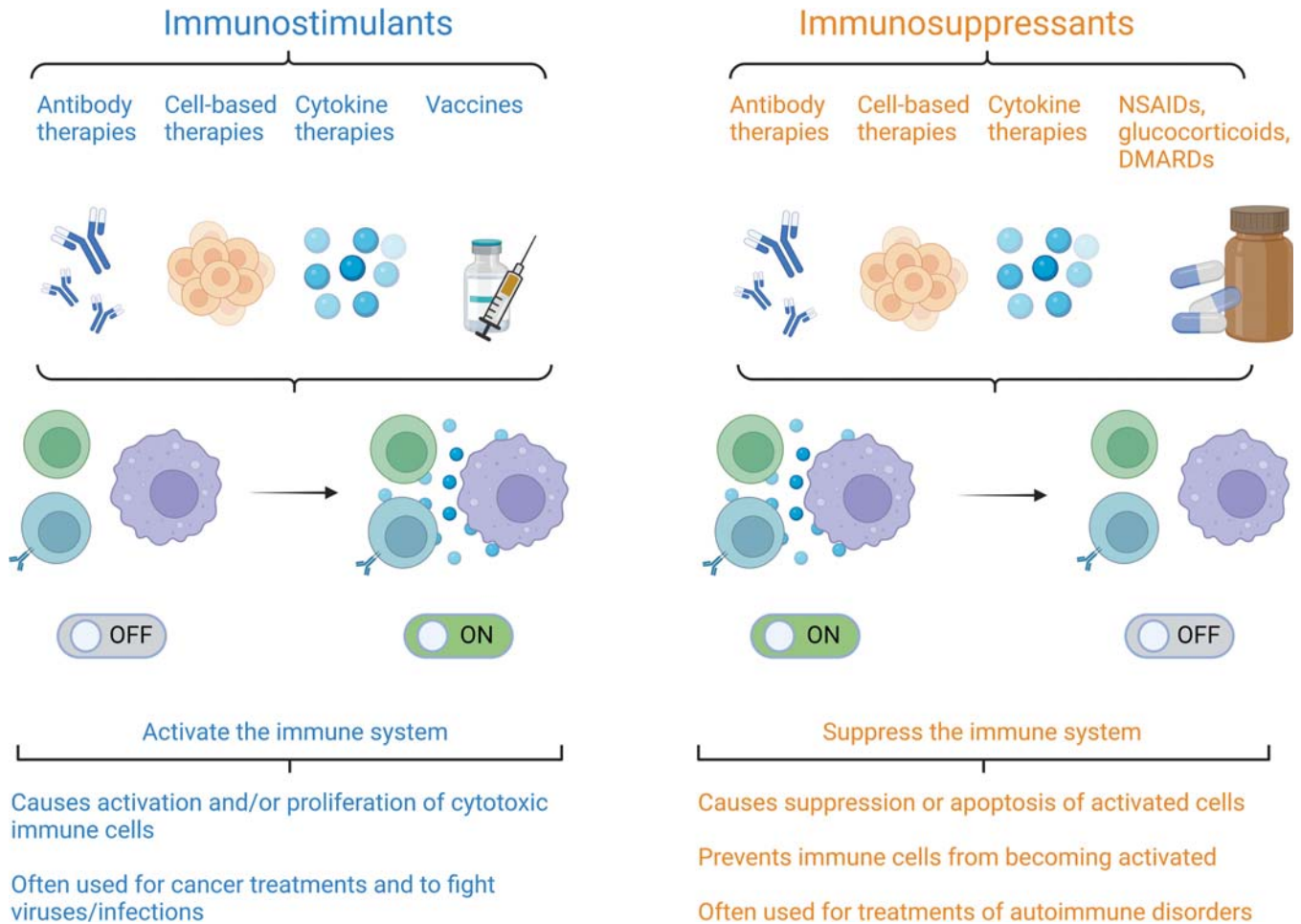


**FIGURE 6.17** Overview of immunomodulators. Whereas immunostimulants activate the immune system, immunosuppressants suppress it with different intended outcomes. Created with [BioRender.com](https://www.biorender.com).

enhance pathogenic processes such as opportunistic infections or lymphoproliferative diseases. Knowledge about background incidences of disease in a colony, treatments utilized for disease control, determination of specific immune functions, and histopathology findings may give clues to distinguish spontaneous disease from disease secondary to immunosuppression or drug-related toxicities.

### 5.6.2. Immunostimulation

Immunostimulation occurs when any aspect or response of the immune system increases its ability to perform a normal functional role. Immunostimulation can occur in both an antigen-specific or nonspecific manner and can contribute to effects ranging from inflammation to autoimmunity. Adjuvants are an example of nonspecific enhancement of the immune system

that are used in vaccines to help generate a protective immune response, and checkpoint inhibitors are designed to stimulate antitumor immune responses. However, immune stimulation can also be unintended and harmful. For example, induced polyclonal B cell activation, via overproduction of cytokines, can lead to antibody deposition in joints and in renal glomeruli which can damage these tissues (Rojko et al., 2014). Additionally, compounds that induce aberrant production of inflammatory mediators or those that disrupt normal regulatory mechanisms can result in damage. Perhaps one of the most life-threatening and concerning immunostimulatory effects is that of cytokine release syndrome (CRS). Such CRS, or cytokine storm, responses are an acute systemic inflammatory syndrome characterized by the activation of large numbers of immune cells and the release

of numerous inflammatory cytokines which results in a variety of symptoms including fever, rash, cardiovascular, pulmonary, and neurological effects, and potentially multiple organ dysfunction and death (Suntharalingam et al., 2006). Infusion reactions can result in CRS and are not uncommon with immune therapy administration. For example, the first dose reaction observed in the Phase 1 clinical trial of a humanized anti-CD28 superagonist (TGN 1412; TeGenero) resulted in adverse events in all, previously healthy, volunteers due to effects related to CRS. These included metabolic acidosis, respiratory distress, and multiple abnormalities in hemodynamics, coagulation, and pulmonary function, resulting in multisystemic organ dysfunction and the need for critical ICU support (Suntharalingam et al., 2006).

### 5.6.3. Immunomodulation

Immunomodulation perhaps best describes the complex composite of functional immune effects that can occur with immunotherapies. Although such immunotherapies may be designed to impact a particular component or pathway of the immune system, the net effect represents the impact of the immunotherapy within the context of a complex immune system response (e.g., activation, regulation, or some combination thereof) (Waldman et al., 2020).

Immune checkpoint inhibitors (ICIs) are a key example demonstrating such mixed effects, since immune enhancement of antitumor immune responses results from the inhibition of specific (inhibitor) immune pathways (Fessas et al., 2020). While this has the obvious benefit of increasing antitumor immune responses, the activation of T cells within normal tissues can be a common finding of T cell overexpression and increased immune reactivity. Additionally, potential hyperactivation of specific T cells, high levels of CD4 T-helper cytokines, and increased migration of cytolytic CD8 T cells can occur within normal tissues and result in tissue injury and immunotoxicity in specific organs. Clinical use of ICIs is associated with a series of specific adverse events caused by the activation of the immune response (immune-related adverse events—irAEs), which can affect many organ systems, including the skin, gastrointestinal tract, endocrine system, lung, liver, pancreas, kidney, neurologic system, kidney,

joints, hematologic system, the skeletal muscle, and heart (Michot et al., 2016; Genova et al., 2017; Shannon, 2017). In such situations, changes in nonimmune organs can indicate immune system changes or potential toxicity that may not be apparent with the evaluation of immune cells or tissues. A full discussion of the benefits and potential irAEs for immunomodulatory therapies is beyond the scope of this text (Badran et al., 2020; Conroy and Naidoo, 2022).

### 5.7. Recoverability of the Immune System (Acute vs. Chronic Changes, Reversibility)

It is important to note that the immune system is extraordinarily dynamic and responsive with an enormous capacity of immune cells to proliferate, expand, and regenerate. Thus, toxic insults can have significant effects in the short-term but can quickly and often completely resolve over time. For example, after exposure to glucocorticosteroids with resultant lymphocyte loss, regeneration and reconstitution can occur within 2 weeks and the original architecture (e.g., of the thymus) may be restored within 3–4 weeks following the initial stress-associated decrease in cellularity. It is important to remember the profound ability of the immune system to recover when assessing immune changes, particularly assessments that occur in a single point in time.

### 5.8. Immune Derangements and Neoplasia

The immune system plays an important role in monitoring for malignancy in a process termed “immune surveillance” whereby the immune system eliminates potentially neoplastic cells (Kumar, 2021a; Abbas et al., 2022a). Increases in cancer incidence or risk can be seen with changes in immune function whether due to effects on antitumor immunity or due to increases in infectious agents or inflammatory responses that may secondarily contribute to tumor development (Ponce et al., 2014; Lebrech et al., 2016; Gonçalves et al., 2017). For example, the association between immune deficiencies and increased tumor incidence is well known in HIV-associated Kaposi sarcomas (Gonçalves et al., 2017). Some viruses are associated with carcinogenesis. For example, cytomegalovirus can manifest oncogenic potential in some



situations and Epstein–Barr virus produces polyclonal B cell activation that shifts from polyclonal into oligoclonal and monoclonal B cell malignancies. Although inflammation can often stimulate immune responses that might limit tumor growth, chronic inflammation can contribute to the development of neoplasia by contributing to malignant transformation or supporting tumor growth, invasion, and metastatic spread (Multhoff et al., 2011; Lebrech et al., 2016). Given that there is a complex interplay between overall immune responses (i.e., immunosuppression vs. inflammation) and the development of tumors, immunomodulatory therapies with differing effects on immune function can have variable effects on cancer risk (Lebrech et al., 2016). Immunosuppression is associated with an increased cancer risk yet chronic inflammation can contribute to tumor development. Tumors themselves can contribute to alterations in antitumor responses whereby there is disruption of hematopoiesis and expansion of immature (immunosuppressive) neutrophils, monocytes, and other immune cells. Cancer immunotherapies commonly focus on promoting antitumor immune responses but depending on the mechanisms involved, can impact the balance between inflammation, immunosurveillance, antitumor immunity, and tumor development (Lebrech et al., 2016).

## 6. EVALUATION OF CHANGES AND TOXICITY

### 6.1. Interpreting Immune System Changes

The determination of how various xenobiotics impact the immune system involves the integration of numerous data endpoints by pathologists, immunologists, and multiple other scientists. A WOE approach incorporating these various data end points are ultimately what is used to determine the effects (e.g., immunosuppression, immunostimulation, hypersensitivity, autoimmunity, etc.) and potential toxicity, adversity, and risk assessment of any given molecule on the immune system (U. S. Food and Drug Administration; Center for Drug Evaluation and Research; Center for Biologics Evaluation and Research, 1997; ICHHT Guideline, 2005; U. S. Food and Drug Administration (FDA), 2023;

Haley, 2005; Descotes, 2006; European Medicines Agency, 2006; Rooney et al., 2012; Gallucci and Yucesory, 2020).

Compound-induced immunotoxicity is generally assessed in the framework of standard guideline-driven toxicity studies. Immunotoxicologic evaluation includes evaluating immune system changes in tissues, immune cell population numbers, and immune system functionality. Hematology, clinical chemistry (globulin and albumin/globulin ratios), gross pathology, organ weights, and histology of immune tissues, as well as, numerous immunotoxicologic data endpoints (e.g., immunophenotyping and functional immune assays) are important parameters included during the evaluation of the immune system (U. S. Food and Drug Administration; Center for Drug Evaluation and Research; Center for Biologics Evaluation and Research, 1997; Haley, 2005; ICHHT Guideline, 2005; Descotes, 2006; European Medicines Agency, 2006; Rooney et al., 2012; Gallucci and Yucesory, 2020; U. S. Food and Drug Administration (FDA), 2023). More advanced evaluation or immunophenotyping of cell populations numbers, phenotype, and potential function from cells in circulation or from specific immune organs can be accomplished using flow cytometry and such evaluation is often employed alongside clinical pathology evaluations or within clinical pathology laboratories (Papenfuss, 2017a). While a detailed discussion of immunotoxicology testing is beyond the scope of this chapter, a brief list of some of the more commonly used immunotoxicology assays is provided in Table 6.7. The following sections highlight considerations for the toxicologic pathologist when evaluating immune system changes. Specifically, macroscopic observations, organ weights, histopathologic changes, and clinical pathology findings supportive of immune system effects are provided. More specialized techniques for interrogating and interpreting pathology-related changes (in the immune system and elsewhere) are available, more commonly in discovery and academic environments but increasingly being employed in drug development, particularly for immunomodulatory therapies. For additional information on such specialized approaches, the reader is directed to *Special Techniques in Toxicologic Pathology*, Vol 1, Chap 11 and *Digital Pathology and Digital Analysis*, Vol 1, Chap 12.

TABLE 6.7 Immunotoxicology Assays

Immunotoxicology	Assay	Description
General assays	Hematology/serum chemistry (standard toxicity study findings)	Evaluates changes in circulating cell populations indicative of immune system changes (e.g., granulocytes, lymphocytes, globulin levels)
	Bone marrow cellularity	Evaluates changes that may reflect effects on hematopoiesis
	Immunophenotyping (flow cytometry, Immunohistochemistry; HC)	Evaluates cell populations based on phenotypic markers or functional capabilities (body fluids or tissues)
	Histopathology (standard toxicity study findings)	Evaluates anatomic pathology changes in immune organs and other tissues throughout the body indicating immune system changes
	Lymphoid organ weights (standard toxicity study findings)	Evaluates organ weight changes (most typically of thymus and spleen)
	T cell-dependent antibody response (TDAR)	Measures immune function that is dependent upon the effectiveness of multiple immune processes, including antigen uptake and presentation, T cell help, B cell activation, and antibody production.
	T cell-independent antibody response (TIDAR)	Measures immune function elicited by mitogenic stimuli (e.g., lipopolysaccharide-LPS, CpG oligonucleotides, or polyinosinic polycytidylic acid-poly-IC) that elicit polyclonal B cell activation via toll-like receptors (TLRs) or polysaccharides that engage the B cell receptor (marginal zone B cell model)
	Cytokine release assay (CRA)	Evaluates the activation of T cells stimulated with cells presenting the candidate peptide (target cells).
	Cytokine assays/detection	Assays assessing blood, tissue, or fluid levels of cytokines (both unstimulated and stimulated samples)
	Cell-specific functional assays	Assays assessing cell-specific function, effects of stimulation, activation, costimulation, etc.; various endpoints
	Phagocytosis/respiratory burst	Measure of innate immune cell function (phagocytosis/engulfment and rapid release of reactive oxygen species, respectively)
	Macrophage/neutrophil function	Measures functionality of these innate immune cells (e.g., cytokine production, bactericidal activity, killing, chemotaxis, phagocytosis, degranulation, migration, macrophage polarization into M1/M2 subpopulations, etc.)
	Natural kill (NK) cell activity	Measures NK parameters (cytolytic activity against tumors, intracellular levels of perforin, granzymes, granulysin, etc.)
	Host resistance assays	Evaluates immune system changes (resultant effects from toxin/therapeutic) by evaluating immune clearance or response to an infectious challenge agent

(Continued)

TABLE 6.7 Immunotoxicology Assays—cont'd

Immunotoxicology	Assay	Description
<b>Hypersensitivity-Focused</b>	Miscellaneous	A variety of advanced molecular techniques to evaluate genotype and phenotype
	CARPA (complement activation-related pseudoallergy)	Evaluates the acute and reversible immune reaction (i.e., infusion, anaphylactic/anaphylactoid or idiosyncratic reaction) of nonimmune allergy resulting from complement activation (typically by nanocarriers) that activates a complex response
	Complement activation	Evaluates complement components (e.g., C3a, C5a, SC5b-9, CH50) to determine complement activation
	Local lymph node assay (LLNA)	Evaluates skin sensitization to chemicals (i.e., lymphocyte proliferation in the draining lymph nodes; murine model)
	Histamine and tryptase degranulation assays	Evaluates the degranulation in mast cells and basophils (for histamine and tryptase) as indicative of hypersensitivity/allergy
<b>Drug-specific response-Focused</b>	Delayed type hypersensitivity (DTH)	Measures antigen-specific T cell response, indicator of cell-mediated (T helper 1; Th1) response, typically skin sensitization with antigen
	IgE (serum) levels	Measures IgE levels (antigen-specific) as an indicator of hypersensitivity/allergy
	Immunogenicity	Measures antibodies (e.g., antidrug antibodies) that can be used to determine potential impacts of antibodies on efficacy, safety, and immunologically related adverse clinical events
	Immune complex detection	Evaluates deposition of immune complexes (ICs) by routine H&E or IHC staining to detect drug, immunoglobulin, and/or complement components in the affected tissues
	Tissue cross-reactivity	Screening assays that are used to identify the nonspecific and specific binding of test biologics, such as antibodies or antibody-like proteins in different types of human or animal tissues
	Receptor occupancy	Measures the degree to which the test drug occupies its target receptor in the tissue or animal. Receptor occupancy is determined by measuring the ability of a dose of the test drug to compete with binding of a radiotracer to the receptor.
	Fc-gamma receptor binding	Evaluates binding of Fc-gamma receptor, particularly to therapeutic monoclonal antibodies
	Antigen-specific T cell responses/T cell polarization	Assays evaluating antigen-specific T cell responses and that can identify the nature of the T cell (i.e., Th1, Th2, Th17, etc.) responses (e.g., enzyme-linked immunosorbent assay (ELISA) or immunosorbent spot (ELISPOT))



## 6.2. Testing for Toxicity

Many changes that can occur normally in immune cells or organs are also indicators of toxicity. The ability to understand and recognize potential toxic effects or pathologic changes in the immune system requires knowledge of the histophysiology, background, and incidental findings for the specific species and strain (Haley, 2003; Haley, 2017). Additionally, understanding the normal roles and function of immune cells, the immune response, and the respective anatomic compartments of immune tissues is also very helpful to both identify changes and evaluate the pathophysiologic importance of immune system changes (Snyder, 2012). Thus, discerning the induced effects and potential immunotoxicity can be challenging and often requires a WOE approach with multiple data endpoints, to determine the potential effects and toxicity on the immune system. The challenge for the toxicologic pathologist is to evaluate changes in the immune system in to discern what changes are considered outside the realm of normal versus what is toxic and potentially adverse. When feasible, providing correlations between the various anatomic and clinical pathology findings and immunotoxicology data endpoints will be most helpful when determining toxicity and assigning adversity. Table 6.8 outlines specific types of immune findings potentially encountered by the pathologist that may demonstrate correlations for several common examples.

Ideally, immune system evaluation would include both pathology endpoints (organ weights, gross and microscopic changes, clinical pathology data), as well as, additional data sets including but not limited to clinical observations and immunotoxicologic endpoints. The inclusion of multiple data sets can provide (1) the most robust understanding of pathologic changes, (2) rationale to determine the adversity of the changes, and (3) the WOE used by regulatory agencies and for assigning risk. There are several references available that provide recommendations, highlight the approach, and provide terminology useful in evaluating and reporting immune system findings (Bregman et al., 2003; Haley, 2005; Greaves, 2012; Kuper et al., 2013; Papenfuss et al., 2019; Willard-Mack et al., 2019). The STP position paper and INHAND

guidance document specifically provide practical guidance and preferred terminology for evaluation of the immune system, particularly for toxicology studies (Haley, 2005; Willard-Mack et al., 2019). Some of the approaches to evaluating pathologic and toxicologic changes in the immune system are outlined in the following sections, and although there is a focus on approaches applied in toxicology studies, the concepts are applicable across multiple other situations.

## 6.3. Anatomic Pathology

### 6.3.1. Gross Observations

Gross observations at necropsy include evaluation of changes in color, consistency, and size of lymphoid organs. Lymphoid organs, with the exception of the spleen, are typically pale with a consistency more compact than surrounding adipose tissue. The lymphocyte-rich tissue of the splenic white pulp can be appreciated as pale structures against a dark red pulp background and changes of overall prominence in the white pulp may be appreciated. In lymph nodes, it is much more likely that alterations in lymph node size or contour would indicate some degree of immune responsiveness. However, lymph node, and to a lesser degree spleen, size can vary widely between individuals due to a variety of factors including age, species, and immunologic challenge history. In general, a decrease in thymic size is the most common and consistent change noted and is most commonly due to thymic involution, atrophy, or a combination of these. An involuted/atrophic thymus is characterized by diminished size and variable consistency, either due to a higher proportion of fibrovascular stroma (firm) or replacement by adipose tissue (soft). Red thymic discoloration can occur as perimortem agonal change due to acute petechial hemorrhage or exsanguination-related alteration and should not be confused with toxicity. Hyperplastic and neoplastic splenic and other lymphoid tissues often have increased pallor and size. Lymph nodes may change their color after capture of pigments such as those draining the skin of tattooed animals or the lung following inhalation of pigmented dusts. The spleen can take up

**TABLE 6.8** Effects of Stress, Immune Suppression, Immune Stimulation, and Hypersensitivity on Pathology and Immunotoxicology Findings in Immune Organs

Type of immuno-modulation	Organ weights	Gross findings	Histopathology	Clinical pathology	Immunotoxicology findings
Stress	± Decreases in ≥1 of: <ul style="list-style-type: none"> <li>• Body weight</li> <li>• Thymus</li> <li>• Spleen</li> <li>• Reproductive organs</li> </ul> ± Increases in <ul style="list-style-type: none"> <li>• Adrenal glands</li> </ul>	Changes in size correlating with body or organ weight changes	<ul style="list-style-type: none"> <li>• Thymus, spleen (other lymphoid organs) ± ↓ cellularity, apoptosis</li> <li>• Adrenal cortex + hypertrophy/hyperplasia</li> <li>• Reproductive organs + possible atrophy, inactive</li> <li>• Stomach + gastric ulceration</li> </ul>	<p><i>Acute stress:</i></p> <ul style="list-style-type: none"> <li>• ↑ lymphocytes, ↑ neutrophils</li> <li>• ↑ RBC mass/reticulocytes</li> <li>• ↑↓ glucose, ↑ liver enzymes (e.g., CK, LDH, AST, ALT) and acute phase proteins</li> </ul> <p><i>Chronic stress:</i></p> <ul style="list-style-type: none"> <li>• ↓ lymphocytes, ↔ ↓ eosinophils, ↑ neutrophils</li> <li>• ↓ RBC mass/reticulocytes</li> <li>• ↓ triglycerides, ± ↑ acute phase response, ALP (dogs)</li> </ul>	<p><i>Immunophenotyping:</i></p> <ul style="list-style-type: none"> <li>• ↓ lymphocytes (B cells &gt; T cells)</li> <li>• ↑ CD4<sup>+</sup> and CD8<sup>+</sup> T cells (CD4<sup>+</sup> &gt; CD8<sup>+</sup>)</li> <li>• Redistribution of B cells (↑ in spleen, ↓ in bone marrow)</li> <li>• ↓ survival of immature T cells (thymic)</li> </ul> <p><i>Functional evaluation:</i> Limited/Not routinely performed</p> <ul style="list-style-type: none"> <li>• ↑ inflammatory cytokines (IL-1, IL-6, ± TNF-alpha)</li> <li>• ↑ glucocorticoids and/or epinephrine, activation of HPA axis</li> </ul>
Immune suppression	Thymus and Spleen <ul style="list-style-type: none"> <li>• Decreased</li> <li>• None</li> <li>• Variable</li> </ul>	± Immune organ subcompartment changes ± Evidence of immune suppression (e.g., secondary infections)	Lymphoid organs ± ↓ cellularity ± apoptosis/necrosis of immune cells ± evidence of secondary infection	↔ ↓ lymphocytes (or other affected immune cell) ± myelosuppression	Changes correlate to immune component affected <i>Immunophenotyping:</i> ↓ #s, %, activation markers <i>Functional evaluation:</i> <ul style="list-style-type: none"> <li>• ↓ innate (macrophage, neutrophils, NK cell) functionality</li> <li>• ↓ cytokine profile, activation markers, etc.</li> <li>• ↓ TDAR (evaluates T &amp; B cell compartments) (↓ IgG)</li> </ul>

Immune stimulation	Thymus and Spleen • None • Variable	None to enlarged immune organs, immune organ subcompartments	Lymphoid organs/ subcompartment ± ↑ cellularity ± hypertrophy/ hyperplasia of immune cells	↔ ↑ lymphocytes (or other affected immune cell)	Changes correlate to immune component affected <i>Immunophenotyping</i> : ↑ #s, %, activation markers <i>Functional evaluation</i> : ↑ innate (macrophage, neutrophils, NK cells) functionality ↑ cytokine profile, activation markers, etc. ↑ TDAR (evaluates T & B cell compartments)
Hypersensitivity	None	<i>Most often none</i> Findings depend on hypersensitivity type and clinical signs <sup>a</sup> ± petechiation, erythema, edema, mucus ± evidence of inflammation, immune cell infiltrates (e.g., vasculitis, dermatitis) ± findings consistent with clinical signs (e.g., emesis, pallor, etc.)	<i>Often none</i> : Varies (depends on type of hypersensitivity) <sup>a</sup> ± may see evidence of systemic inflammation ± mast cell degranulation, edema, inflammation (if not a rapid response) ± infiltrate/immune complexes in kidneys, vessels, serosa, multiple organs; detectable by H&E, IHC, etc.	Variable ± thrombocytopenia, decreased rbc mass, neutrophilia + Complement activation, circulating ADAs + thrombocytopenia, decreased rbc mass, neutrophilia	May see complement activation, ADAs, infiltrates/inflammation Cytokines - may see increased inflammatory cytokines/cytokine release syndrome

<sup>a</sup> Clinical signs may be include variable to no clinical signs (e.g., excessive salivation, facial erythema, pruritus often seen with anaphylaxis/anaphylactoid reactions) and a range of inflammatory infiltrates and/or immune complex hypersensitivity findings that may manifest as hemolytic anemia, vasculitis, dermatitis, rhinitis, etc.

ADAs, Anti-drug antibodies; ALT, alanine transaminase; AST, aspartate aminotransferase; CD, creatine kinase; H&E, hematoxylin and eosin stain; HPA, hypothalamic-pituitary-adrenal axis; IHC, immunohistochemical; IL, interleukin; LDH, lactate dehydrogenase; RBCs, red blood cells; TDAR, T cell dependent antibody response assay.

Compiled from Everds NE, Snyder PW, Bailey KL, et al.: *Interpreting stress responses during routine toxicity studies: a review of the biology, impact, and assessment*, *Toxicol. Pathol.* 41(4):560–614, 2013; Leach MW, Rottman JB, Hock MB, et al.: *Immunogenicity/hypersensitivity of biologics*, *Toxicol. Pathol.* 42(1):293–300, 2014, Mease KM, Kimzey AL, Lansita JA: *Biomarkers for nonclinical infusion reactions in marketed biotherapeutics and considerations for study design*. *Curr. Opin. Toxicol.* 1–15, 2017 Jun 4, <https://doi.org/10.1016/j.cotox.2017.03.005>. Gwaltney-Brant S: *Immunotoxicity biomarkers*, *Biomark. Toxicol.* 413–425, 2019.



pigmented materials from the blood, can be a repository for lipofuscin pigment in old animals, or can accumulate hemosiderin pigment as a sequel of increased erythrocyte turnover. Alterations occur in the size of immune organs or anatomic subcompartments within organs (particularly for the spleen) that can correlate with organ weight and/or histopathological findings. Less commonly, gross findings in nonlymphoid tissues can support immune system changes. For example, alterations in adrenal glands may support stress as a contributor to decreased thymic size, weight, or cellularity or the presence of skin infections may provide evidence of altered (compromised) immune function.

Gross observations consistent with immunosuppression may include decreased size of lymphoid tissues or subcompartments of organs most significantly involved in immune function and color changes may reflect immune cell necrosis or loss. Gross observations consistent with immunostimulation may range from an increased size and/or prominence of lymphoid tissues. Occasionally, clinically significant immunostimulation might manifest as redness of skin in very sick animals, with or without other cardiovascular events such as increased heart rate or decreased blood pressure. Red, purple, or blue skin discoloration might also be observed with anaphylactoid responses associated with immune complex depositions and/or vascular occlusion. Immune complex-related skin gross lesions tend to occur in extremities that depend on small vessels such as pinna of the ear, as well as distal fore- and hindlimbs. The red skin associated with cytokine and chemokine-related immunostimulation is usually bright to deep red and may be seen on skin from any region of the body including the trunk, face, limbs, or elsewhere on the body, and often reflect a degree of vasodilation. While gross observations in immune organs may be suggestive of changes in immune function, often there are no macroscopic findings that are pathognomonic for either immunosuppression or immunostimulation.

### 6.3.2. Organ Weights

Organ weights are traditionally collected for the thymus and spleen but not for other immune organs due to either size limitations (especially for small animals) or marked biological

variability. At necropsy, spleen and especially thymus weights (and associated size) can give a first indication of possible immunotoxicity or immune system alterations and are a more reliable indicator than organ weight changes in lymph nodes (Haley, 2005). Xenobiotic-induced weight decreases may indicate immunotoxicity or a sequel to stress-related toxic effects such as hypocaloric status or toxicity to nonlymphoid organs (Table 6.3). Although less common, weight increases may indicate xenobiotic-related effects reflective of immune stimulation or effects on immune cell trafficking. Lymph node weights are not typically collected due to significant normal interindividual variability and species-specific limitations of lymph node size, particularly in smaller laboratory species. Organ weights of the bone marrow and MALT are not logistically feasible due to anatomic- and collection-specific challenges. The evaluation of organ weight changes should be correlated with both gross findings (if present) and histopathological evaluation whenever possible (Sellers et al., 2007).

Thymus weight changes can often be the only organ weight change noted within a study with the most common finding being that of lower thymic weights. Interpretation of thymic weight changes needs to be performed cautiously since changes may represent xenobiotic-related effects, stress-related effects, normal physiological involution (or rebound hyperplasia), or a combination of these.

Spleen weight changes can be quite variable and are related either to alterations of the white pulp or, more often, to hematopoietic or other changes in the red pulp. Increased spleen weights may represent increases in immune cell populations, increased trafficking of cells to the spleen, or increases in (extramedullary) hematopoiesis, depending on the species. Weight changes in defense-type spleens (predominately lymphocytes in spleen) found in rodents and nonhuman primates are more likely to reflect changes in immune state, after biological variation and physiological factors like age and stress have been accounted for. In contrast, weight changes in the storage-type spleens of dogs and to a lesser degree, pigs, are sensitive to pooling of blood during euthanasia and might be less indicative of immune effects. The use of age-matched and historical controls and an

understanding of species-specific considerations can be helpful to interpret spleen weight data. Since spleen weights do not allow the discrimination of white pulp (lymphoid portion) and red pulp (hematopoietic portion) components, microscopic evaluation is helpful to interpret the contribution of specific cells or compartments.

Although not routinely recorded, lymph node weights are taken on occasion and changes in organ weights may correlate with changes in lymphoid cellularity observed microscopically. If lymph nodes are collected, accurate preparation and isolation from the surrounding tissue is a prerequisite to receiving meaningful results. Additionally, anatomic location and variability in antigenic exposure, stimulation, and lymphatic drainage patterns can all influence lymph node weights. For example, cervical/mandibular lymph nodes drain the orofacial region and are continually exposed to a variety of antigen stimuli (via air and oral uptake) so weights can vary substantially. Mesenteric lymph nodes drain the small and large intestines and generally have a consistent grade of background stimulation, while popliteal or iliac lymph nodes usually are unstimulated with little organ weight variation unless they drain a region of substance administration.

### 6.3.3. Microscopic Findings

Microscopic evaluation of the immune system should be approached in a systematic way with an understanding of background, incidental or normal range of findings, and application of consistent terminology that best reflects the changes observed. Typical immersion fixation of tissues in 10% neutral buffered formalin, followed by paraffin embedding and staining of sections with hematoxylin and eosin (H&E) is the standard technique and is typically sufficient for the evaluation of immune system components. Immunohistochemical and specialty staining and/or immunophenotyping approaches are uncommonly performed during routine evaluation and are typically reserved to answer specific research questions.

The classification of organs and tissues into immune and nonimmune organs/tissues is a somewhat artificial, but useful way to categorize immune compartments, and provides a systematic approach to ensure evaluation of

immune system changes. Several references that describe normal structure, function, and histology of lymphoid organs and best practices for routine pathology evaluation of the immune system are available (Haley, 2005; Cesta, 2006a, 2006b; Pearse, 2006; Travlos, 2006; Willard-Mack, 2006). Given that immune cells are distributed throughout the body, the evaluation of nonimmune organs provides information on changes occurring within the immune system. Organs that interface with the external environment (e.g., skin and mucosal sites) have significant populations of immune cells, including antigen-presenting cells and specialized T and B cell lymphocytes that work to both initiate and propagate immune responses so changes at these sites may provide insight or supportive evidence of immune system effects. Microscopic evaluation may include specifically identifying changes within the compartments or microenvironments within each lymphoid organ when appropriate (Haley, 2005). These compartments and function may differ between lymphoid organs necessitating the ability to identify these compartments and develop an understanding of immune activities that occur within each compartment. Evaluation of these various compartments and the interactions and impact of changes within the immune system are effectively evaluated in routine safety studies. An augmented examination termed “enhanced histopathology” was coined in response to published guidelines for the evaluation of lymphoid tissues in immunotoxicity studies. These guidelines outlined the following three points: (1) each lymphoid organ has separate compartments that support specific immune functions, (2) these compartments should be evaluated individually, and (3) semiquantitative descriptive rather than interpretive terminology should be used to describe those changes. Given that many immune changes can be appreciated during routine systematic evaluation of immune and nonimmune organs, the “enhanced histopathology” approach is uncommonly performed. It is typically warranted if findings indicate a complex immunomodulatory effect or when applied as a component of a tiered immunotoxicology approach (Luster et al., 1988; Elmore, 2012; Elmore, 2018).

The recognition of pathologic changes indicative of immune system alterations requires an

understanding of normal or background findings specific for the age, sex, and species being evaluated. Inclusion of age-matched controls is an important and a required aspect of study design that allows the toxicologic pathologist to determine the range of normal, set a threshold of background or incidental findings, and assess the relative importance of pathologic (or toxic) changes present within the study (Haley, 2005). Terminology describing changes can vary widely between pathologists and the toxicologic pathologist is encouraged to utilize INHAND and SEND-compliant terminology, which is descriptive rather than interpretative, in order to provide consistency in diagnoses and terminology between pathologists, and clarity and consistency to nonpathologists (Haley, 2005; Willard-Mack et al., 2019; <https://www.cdisc.org/standards/foundational/send>). An example of a descriptive approach would be. “inflammation, neutrophilic with necrosis, fibrosis, increased macrophages, and presence of foreign material” that would describe a more interpretative finding of an “abscess” or even of chronic suppurative inflammation.

#### 6.4. Organ-specific Histopathology

Microscopic immune system findings can occur in one or more tissues. A common xenobiotic-induced lymphoid change is lymphocyte cell death resulting in decreased cellularity. Cell death can occur via apoptosis (selective, energy-dependent programmed cell death) or necrosis (nonselective, passive cell death) with a distinction between the two processes potentially requiring specific staining (e.g., activated caspase 3 for identification of apoptotic cells). However, cell necrosis is more commonly associated with inflammatory cell infiltration, hemorrhage, and/or cellular debris (Elmore et al., 2016). Although lymphocyte death, whether via apoptosis or necrosis, is the most common lymphoid finding, there can be additional changes of increased cell number, differentiation, or activation of various immune cells. Increases in lymphocyte numbers, with possible concomitant alterations in immune organ sub-anatomical compartments, can be particularly prominent with immune activation, such as seen with differentiation of B cells into plasma cells. Primary and secondary immune organs

can have different microscopic findings and specific responses to xenobiotics, some of which are outlined below.

##### 6.4.1. Thymus

Physiologically, the thymus of the juvenile animal has the highest lymphoid cellularity that then decreases over time with only remnants of thymic tissue present in most aged animals. The thymus is often the first organ to be affected by immunomodulating compounds (Figure 6.18A–C). Sensitivity of cortical thymocytes to immunomodulating compounds differs between the stages of T lymphocyte development in the thymus with immature thymocytes of the thymic cortex being very susceptible to toxic injury and prone to apoptotic cell death. Administration of numerous xenobiotics, particularly hormones (e.g., xenoestrogens such as diethylstilbestrol, genistein, or methoxychlor), causes lymphocyte depletion of the thymic cortex (See *New Frontiers in Endocrine Disruptor Research*, Vol 3, Chap 12). Changes in thymic cellularity, cortical to medullary ratios, adipose deposition, and lipofuscin accumulation can be recognized responses following xenobiotic administration or in response to stress and can be similar to age-related changes. Microscopic findings within the thymus often have associated changes in organ size and weight and may affect circulating lymphocyte numbers. Following depletion of cortical lymphocytes, a rebound hyperplasia is occasionally seen with increased numbers of cortical lymphocytes and associated increases in organ size and/or weight. Depletion of cortical lymphocytes can result in an apparent high cellularity of the thymic medulla and “inverse” appearance of the thymus (Figure 6.18B) where the cortex has fewer lymphocytes than the medulla.

##### 6.4.2. Bone Marrow

The bone marrow is both a major hematopoietic and lymphoid organ that can be a target organ indicating toxicity (see *Hematopoietic System*, Vol 5, Chap 5). The most common means of evaluation of bone marrow include histopathologic examination of bone marrow (with adjacent bone) or assessment of bone marrow smears. Findings are often used in conjunction with the complete blood count (CBC) to provide insight regarding changes that may otherwise be missed by examining a single parameter.



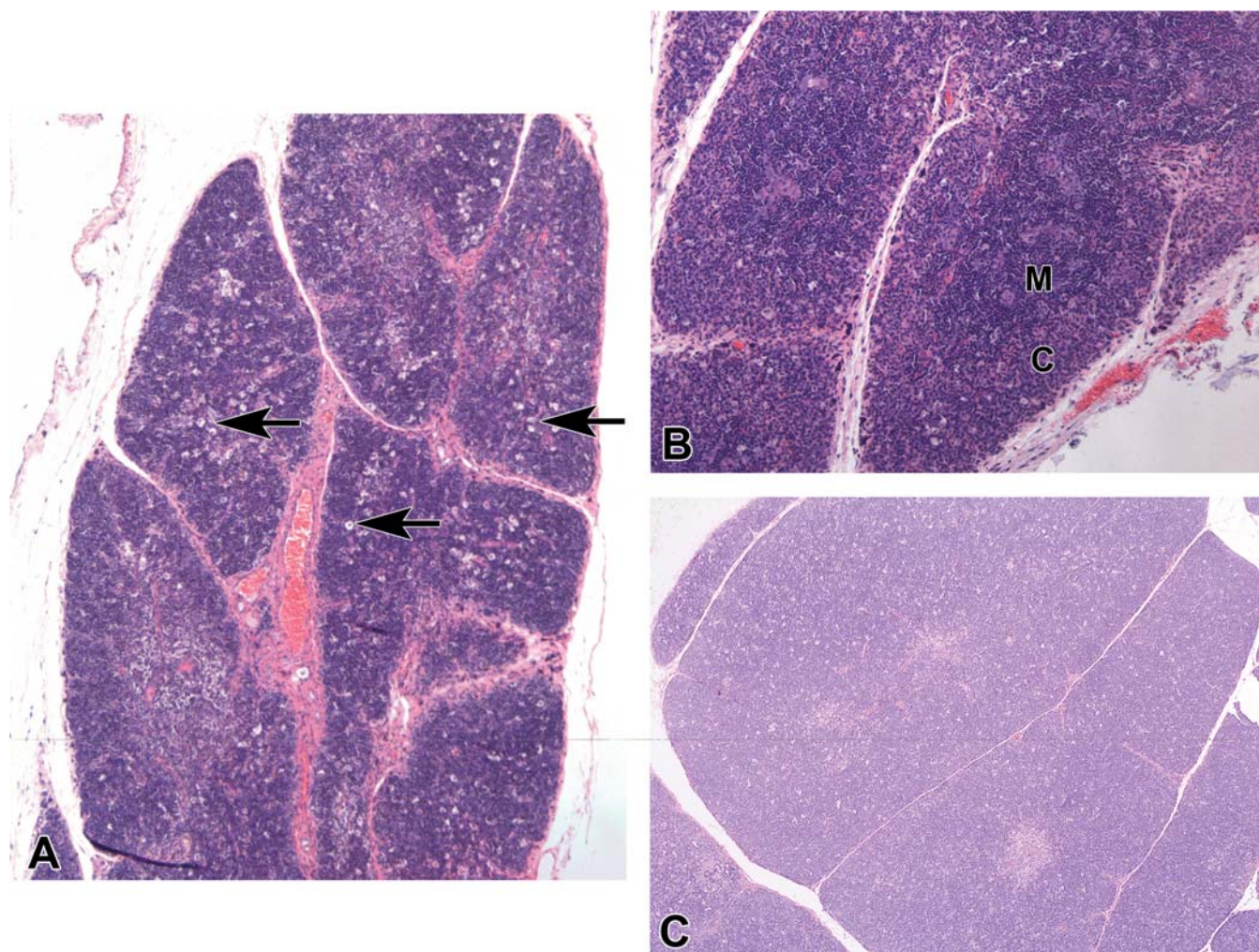


**FIGURE 6.18** (A) Thymus after 28 days of treatment with 150 mg/kg Benzo[a]pyrene with reduced cortex size and numerous starry sky macrophages (arrows); hematoxylin and eosin (H&E) stain; magnification 40 $\times$ . (B) Chemically induced thymic atrophy can lead to an inversed density of cortex (C) and medulla (M). Whereas the cortex is depleted, the medulla is hypercellular; hematoxylin and eosin (H&E) stain; magnification 100 $\times$ . (C) Increased ratio of cortex to medulla is a rare finding since generally cortical thymocytes are most susceptible to induced apoptosis. Cyclosporine treatment can induce this, which can lead to subsequent depletion of splenic PALS due to reduced lymphocyte egress from the thymus. Hematoxylin and eosin, 10 $\times$ . *Reproduced from Figure 49.28 p. 1841 in Haschek WM, Rousseaux CG, Wallig MA, editors: Haschek and Rousseaux's handbook of toxicologic pathology, ed 3, 2013, Academic Press, with permission.*

Cellular density and the myeloid to erythroid (M:E) ratio are most commonly assessed during routine histopathologic evaluation, whereas immunophenotypic evaluation or determination of a maturation index are less commonly applied (Elmore, 2006b; Travlos, 2006).

Bone marrow cellularity can be affected by xenobiotics with increases or decreases appreciable in one or several lineages. Alterations in the myeloid or erythroid lineages can impact cellular numbers, composition, M:E ratio, and

related CBC parameters. Although the cellular morphology and changes in the M:E ratio may be appreciated during histopathologic evaluation of H&E-stained sections, bone marrow smears or cytocentrifuge preparations are often necessary for accurate determination of the M:E ratio and synchrony of maturation. Effects on specific cell lineages should be individually described whenever possible to give an overall understanding of the effects on bone marrow constituents. Given the significant variability in

cellularity that can be seen depending on the age, collection site, species, and between individuals, it is important to have proper controls. Bone marrow cellularity is highest in young animals and decreases with age as marrow constituents are replaced with adipocytes over time.

Decreases in bone marrow cellularity can be a common finding in toxicology studies. It is important to determine the cell lineages affected and correlate changes with CBC and other tissue findings and determine how these changes evolve over time. Decreased cellularity can occur through decreased production or loss via apoptosis or necrosis and may be observed in a single lineage, across multiple lineages, and in various precursor populations. Significant decreases in bone marrow cellularity can be appreciated in severely debilitated animals although definitive serous fluid accumulation (serous atrophy of fat) is uncommonly seen. Ideally, evaluating these changes over time can provide insight regarding reversibility of these changes and potential long-term effects on bone marrow cell populations.

Increased bone marrow cellularity is a less common finding in toxicology studies with increases in the erythroid population being more common than nonerythroid populations. Increases in the erythroid lineage are most commonly noted in response to anemia, and often seen in association with changes in hemoglobin, hematocrit, and erythron parameters (e.g., mean corpuscular volume, mean corpuscular hemoglobin concentration, etc.). In rodents, extramedullary hematopoiesis (EMH) in the spleen, and potentially the liver, can be relatively common, and increased cellularity within the bone marrow is typically increased as well. Increased cellularity in the granulocytic lineages is the most common contributor to increases in the myeloid cell populations and is often a result of increased demand as during an inflammatory response, but also in response to altered trafficking or neoplastic processes. Increases in the megakaryocyte population is less common and seen with changes in platelet parameters and/or associated coagulation profiles.

#### **6.4.3. Peripheral Lymphoid Organs: Spleen, Lymph Nodes, and MALT**

Lymphocytes and other immune cells generated in the primary lymphoid organs of the

thymus and bone marrow typically mature, enter the circulation, and emigrate into peripheral lymphoid organs. These circulating immune cells are composed of both newly generated and recirculating cells. The spleen has the highest frequency of lymphocyte recirculation, so reduced lymphocyte cellularity secondary to reduced lymphocyte output from the thymus is commonly seen in splenic white pulp. In lymph nodes that have generally lower rates of lymphocyte recirculation, reduced cellularity of the T cell regions can be less pronounced or even absent. Compounds associated with suppression of T lymphocytes can cause, as a secondary effect, morphological changes in B cell areas. Histological findings in secondary immune organs related to immunosuppression are decreased lymphoid cellularity of splenic white pulp follicles and MZs, lymph node cortex and medullary cords, and follicles of PPs. Often the development of secondary follicles with active GCs from primary follicles is decreased, although at very low doses GC development can be increased. This may be due to an early effect on T suppressor cells, which leads to an overall stimulation of the immune response. Specific changes in B cell populations, such as direct targeting with immunotherapies, can present as depletion of MZs in the spleen or have effects on GC size and appearance. Changes in cellularity of various immune cell populations (T and B lymphocytes, plasma cells, macrophages, granulocytes, and other immune, nonimmune, and supporting cells) can occur in various compartments within the peripheral lymphoid organs. Such changes can provide important information regarding which immune cell populations may be affected by a given xenobiotic. It is often most helpful to consider the composite changes seen in peripheral lymphoid organs as indicative of immune changes rather than being prescriptive about findings and changes in one lymph node compared to another since changes may not be consistent across every lymph node.

Reports about chemically induced changes of MALT are scarce when compared to changes of thymus, spleen, and lymph nodes. This is remarkable, since the GALT contains a significant proportion of the body's immune cells and has a particularly complex structure consisting of diffuse and organized lymphoid tissues. The cause of this discrepancy is likely the



predominance of tolerance induction in MALT; however, MALT is also more difficult to examine critically. This applies especially to the single intraepithelial and lamina propria lymphocytes that make up a large proportion of MALT. The different MALT tissues share structural and functional features, but differences in cellular composition regarding the T cell/B cell ratio and CD4<sup>+</sup>/CD8<sup>+</sup> T cell ratio are present in these different organs with such differences likely reflective of functional roles in these locations but being relatively undefined. The intestinal PPs of the GALT are the most commonly evaluated mucosal immune site. BALT hyperplasia is a common observation subsequent to chronic inflammatory stimuli. BALT increase, especially in subacute and subchronic studies, can be a physiological response or represent evidence of immunotoxicity. The evaluation of a physiological response depends on study type. With vaccines, BALT hyperplasia may be expected, whereas in other cases, it can point to unwanted antigenicity. BALT enlargement can occur due to macrophages accumulating particulate test compound. Investigation of the regional lymph node at the lung hilus is helpful to evaluate BALT increase. Since lymphocytes from MALT migrate to their draining lymph nodes, these nodes (GALT: mesenteric; NALT and BALT: cervical and lung hilus lymph nodes) should be evaluated together with MALT. Immunotoxic effects in the MALT are commonly seen in association with similar changes in other secondary (or primary) lymphoid organs, with MALT-related changes being most consistently appreciable in the PP or other prominent GALT.

### 6.5. Clinical Pathology Evaluation and Considerations

Clinical pathology parameters can provide valuable information regarding changes relating to immune cell populations, immunophenotyping endpoints, and various biomarkers, and provide information that help determine relative toxicity (Tomlinson et al., 2013; Tomlinson et al., 2016; Ramaiah et al., 2017). Clinical pathology data can provide useful information regarding immune cells (granulocytes, lymphocytes, and monocytes) and responses (e.g., globulin levels and albumin/globulin ratios) in the circulation and immune organs (see *Clinical Pathology in*

*Nonclinical Toxicity Testing*, Vol 1, Chap 10, and *Interpretation of Clinical Pathology Results in Nonclinical Toxicity Testing*, Vol 2, Chap 14). Numerous biomarkers (e.g., complement, histamine, specific and ADA levels, etc.) and immunophenotyping parameters are commonly included as part of a clinical pathology evaluation which can provide information on specific immune cell populations and responses, kinetics of the response, correlate with histopathology findings and contribute to an understanding of pathophysiological changes in the immune system. Numerous hematology, coagulation, urinalysis, and serum chemistry values are included in routine toxicology studies in multiple species (Tomlinson et al., 2013). The ICH S8 guidelines from 2006 outlined some recommended immune-specific clinical pathology parameters including the WBC count, total differential counts, blood and bone marrow smears, globulin levels, and albumin/globulin ratio. Additional parameters and biomarkers are commonly included, particularly with studies involving immunomodulatory therapies (European Medicines Agency, 2006). Stress-related changes can be seen in the WBC, RBC mass parameters, reticulocyte counts, bone marrow cellularity, and glucose concentration that may assist in evaluation of immune tissue effects (Everds et al., 2013).

### 6.6. Immunotoxicology Evaluation and Considerations

Immunotoxicology evaluation includes both pathology endpoints and other immunotoxicology assays that evaluate immune cell populations and function. The results of these assays, particularly in conjunction with pathology findings, can provide a better understanding of immune system changes and can also serve as potential prognostic indicators. It is important for the toxicologic pathologist to be familiar with some of the more commonly used assays and terms employed with immunotoxicologic evaluation. Table 6.7 outlines some of the assays involved in overall immunotoxicology evaluation and these will be briefly discussed below.

#### 6.6.1. Immune Cell Evaluation

The evaluation and measurement of cell numbers, cell function, anatomic changes to



immune tissue subcompartments, and numerous other factors help provide a better understanding of how specific xenobiotics affect the immune system. While standard anatomic pathology evaluation can demonstrate some changes (e.g., tissue morphology, changes in cell number, apoptosis, necrosis, inflammation, and neoplasia), traditional tissue-based pathologic changes are less sensitive or unable to provide specific information regarding quantification of cell numbers, changes in immune cell populations, or functional changes. IHC staining of tissues can provide additional information concerning various cell populations in situ, but these are uncommonly applied in toxicity safety studies. Rather, clinical pathology data of lymphocytes, granulocyte, and myelomonocytic cell populations and immunophenotyping by flow cytometry is more commonly employed and provides information regarding immune cells in tissues or the circulation.

Phenotypic analysis, or analysis of immune cells by specifically expressed markers (proteins or antigens expressed on the surface or intracellularly), is most commonly performed by IHC/immunofluorescence in situ or by flow cytometry (Papenfuss, 2017a; Aeffner et al., 2022). In these techniques, the cell-specific markers are detected using antibodies specific to the marker and detection of the antibody (by enzymatic or fluorescent) methods are captured and evaluated. Table 6.9 provides some examples of markers that may be used for immunophenotyping in various species. One of the benefits of in situ detection by IHC or IF is that anatomic localization of various cell populations is preserved. However, although many IHC markers are available, there may be difficulties using formalin-fixed paraffin embedded (FFPE) tissues and specific specialized handling, storage, and equipment are considerations when utilizing IHC and IF in tissue sections. In these circumstances, in situ hybridization (ISH), especially multiplex ISH techniques, might be utilized.

Immunophenotyping of immune cell populations is primarily performed using flow cytometry. Flow cytometry interrogates cell suspensions (from blood, fluid, tissues, cell cultures, etc.) that have been labeled with fluorescent markers of interest. Numerous markers can be evaluated simultaneously providing detailed information

on populations and subpopulations. However, flow cytometry does require specialized instrumentation and highly trained personnel with familiarity on the specifics of sample collection, preparation, analysis, data interpretation, and equipment use. For many of these specialized techniques, it is important to have a thorough understanding of the sample collection, handling, fixation, preparation methodologies, characteristics of the tissue, staining procedure, and antibody-specific criteria required for each technique, as these factors can be critical. For example, FFPE tissues may be useful for some antibodies, but frozen sections may be superior due to formal denaturing of some antigens. Additionally, thoughtful consideration of study design and coordination of sample collection and processing is necessary to ensure sufficient and appropriate samples are available when multiple specialized techniques are desired. For additional information, the reader is referred to handbooks on immunology, reviews, and the *Special Techniques in Toxicologic Pathology*, Vol 1, Chap 11 to select cell markers identifying specific immune cell populations.

### 6.6.2. Immune Function Evaluation

For the anatomic pathologist, microscopic changes that reflect changes in immune function are often not apparent, may be difficult to appreciate, and typically provide only an indirect suggestion of altered function. Although pathology is a component of immunotoxicologic evaluation, numerous additional in vitro, ex vivo, and in vivo studies are available that can provide a more robust understanding of immune system changes and alterations in immune function. However, such functional data may or may not be available to the toxicologic pathologist. Immune function tests are helpful and typically needed to contextualize and correlate information observed during histopathology evaluation. Immune function tests are generally used as a follow-up (second tier) to a general toxicity study (first tier). Such a tiered approach has been designed for chemicals as well as drugs. Some of the assays that evaluate immune function disturbances, such as T cell-dependent antibody response (TDAR), host resistance assays, and phagocytosis and cytotoxicity assays, are listed in Table 6.7.

**TABLE 6.9** Select Immunophenotyping Markers

Immune cell(s) <sup>a</sup>	Mouse/rat	Non-human primates	Humans	Dogs	MiniPig
<b>T cells</b>	CD3 <sup>+</sup>	CD3 <sup>+</sup>	CD3 <sup>+</sup>	CD3 <sup>+</sup>	CD3 <sup>+</sup>
<b>Helper T cells</b>	CD3 <sup>+</sup> CD4 <sup>+</sup>	CD3 <sup>+</sup> CD4 <sup>+</sup> CD8 <sup>-</sup>	CD3 <sup>+</sup> CD4 <sup>+</sup>	CD3 <sup>+</sup> CD4 <sup>+</sup>	CD3 <sup>+</sup> CD4 <sup>+</sup> Cd8lo
<b>Regulatory T cells</b>	CD45RCloCD45 +CD25+FoxP3+	CD4 <sup>+</sup> CD25+Fox3+	CD3 <sup>+</sup> CD4 <sup>+</sup> CD25+FoxP3+	CD45RCloCD45 +CD25+FoxP3+	
<b>Cytotoxic T cells</b>	CD3 <sup>+</sup> CD8 <sup>+</sup>	CD3 <sup>+</sup> CD4 <sup>-</sup> CD8 <sup>+</sup>	CD3 <sup>+</sup> CD8 <sup>+</sup>	CD3 <sup>+</sup> CD8 <sup>+</sup>	CD45 <sup>+</sup> CD8hi
<b>B cells</b>	CD3 <sup>-</sup> CD45RA+	CD3 <sup>-</sup> CD20 <sup>+</sup> CD8+/ -CD1c ±	CD3 <sup>-</sup> CD20 <sup>+</sup>	CD3 <sup>-</sup> CD45RA+	IgM + CD21 <sup>-</sup> CD11RA+/ -CD14+/-CD11c ±
<b>NK cells</b>	CD3 <sup>-</sup> CD161a+	CD3 <sup>-</sup> CD16+/ -CD8 <sup>+</sup> CD20-/dim	CD3 <sup>-</sup> CD16+/ dimCD56bright/dim	CD3 <sup>-</sup> CD161a+	Ig-CD2 <sup>+</sup> CD11b + CD16+ perforin + CD3 <sup>-</sup> CD4 <sup>-</sup>
<b>NK-T cells</b>	CD3 <sup>+</sup> CD161a+	CD3 <sup>+</sup> CD16 <sup>+</sup>	CD161+CD94 <sup>+</sup> CD3 <sup>+</sup> CD56dim	CD3 <sup>+</sup> CD161a+	CD3 <sup>+</sup> CD4 <sup>-</sup> CD8 ±
<b>Monocytes</b>	CD4 <sup>+</sup> CD43 <sup>+</sup> CD172a + CD161a+	CD3 <sup>-</sup> CD14+/ -HLA-DR + CD16 ±	CD14++CD16 <sup>-</sup> (classical), CD14 <sup>+</sup> CD16++ (non-classical)	CD3 <sup>+</sup> CD161a+?	CD172a + CD14 <sup>+</sup> CD16+MHC II low
<b>Macrophages</b>	CD11b/c + MHCII + CD68 <sup>+</sup> CD163+CD172a	CD68 <sup>+</sup> CD163+	CD68+HLA-DR+ (M1), CD206+CD204+ CD163+ (M2)	CD11b/ c + MHCII + CD68 <sup>+</sup> CD172a	CD172a + CD14+/ -CD16+MHC IIlo
<b>Dendritic cells (DCs)</b>	CD11c + MHCII + CD172a+	CD11c+/-CD16 -CD205+CD141 ±	CD8a+/ -CD14 <sup>+</sup> ,CD163+/ -SIRPA+	CD11c + MHCII + CD172+	CD172a + CD1 <sup>+</sup> CD14+/ loCD16+MHC II + CD80/ CD86+
<b>Plasmacytoid DCs (pDCs)</b>	CD11b-MHCII+	CD123+pDC+	B220+CD209 +SiglecH + IFN-a+	CD11b-MHCII+	CD4+MHC II + CD172-/ loCD16 ±

<sup>a</sup> Markers are primarily for flow cytometry applications, are not a comprehensive list and may not be appropriate for all cell populations. The reader is directed to most recent publications and data sheets for specific applications.

### 6.6.3. Biomarkers and Integration of Immune Data

Biomarkers are indicators that can be objectively measured to indicate organ injury, disease, or response (or exposure) to a xenobiotic. They help in the extrapolation of data from experimental animals to humans, and to monitor human exposure and test human immune reactions to biopharmaceuticals or other xenobiotics which have high species specificity. Immune biomarkers provide an indication of change to any component of the immune system which could range from expression of particular cell surface markers, alterations in cell fractions or cell functional state, production of soluble factors (e.g., cytokines), alterations in immune cell trafficking or infiltration, changes in inter- and intra-cellular immune cell networks, and changes in immune cell (e.g., T cell receptor) repertoires and populations ([Lapuente-Santana and Eduati, 2020](#)).

There is no defined list of immune system biomarkers. Appropriate biomarkers are selected based on a combination of factors related to the specifics of the therapy, its MOA, and immune system indicators demonstrating effects on efficacy or safety in a disease or model system. Biomarkers that can provide information about immune system effects (whether on immune organs, cell populations, or functionality) may include cell counts, organ weights, clinical pathology, histopathology, antibody assays, T-dependent antibody responses, delayed-type hypersensitivity (DTH) responses, lymphocyte phenotyping, NK activity, phagocytosis and chemotaxis, proliferation tests, cytokine profiling, and other soluble mediators (e.g., local lymph node assay or IgE levels) ([Willis and Lord, 2015](#); [Llibre and Duffy, 2018](#); [Gwaltney-Brant, 2019](#)). In the clinical setting, biomarkers are also commonly utilized to evaluate efficacy of treatment, monitoring for toxicity, and as prognostic indicators. For example, various biomarkers can be used to identify responders to immune checkpoint therapy which include tumor microenvironment, microbiome, DNA repair pathway defects, high mutational burden, tumor neoantigen load, immune cell infiltration, PD-1, PDL, 1CTLA-4 expression, and alterations in immune cell signaling pathways ([Liebl and Hofmann, 2019](#); [Gwaltney-Brant, 2019](#); [Sacdalan and](#)

[Lucero, 2021](#)). Alternatively, when evaluating inflammatory markers, changes in hematology dynamics, acute-phase proteins, complement factors, and cytokines can be evaluated but may lack specificity to identify the offending cause ([Germolec et al., 2018](#)). Biomarkers are an integral component of immunotoxicologic evaluation and include both pathologic and immunologic changes indicative of immune system effects. Ideally, integration of all data endpoints relevant to the immune system (from discovery to the patient population) ultimately will provide the most accurate picture of immune system effects.

## 7. RESPONSES TO INJURY

### 7.1. Immunosuppression

Pathologic findings present in response to immunosuppression are primarily limited to decreases in size and cellularity of lymphoid organs, particularly the thymus, spleen, and lymph nodes. Clinical pathology and immunophenotyping can identify and evaluate the kinetics of immune cell populations over time. Classic examples of immunosuppressants include dexamethasone (and other glucocorticosteroids), Cyclosporine A, and azathioprine ([Kuper et al., 2013](#)). These lymphoid changes often return to normal after a period of clearance of the initiating drug or stimuli and can demonstrate a potential rebound hyperplasia. Of note, in situations where specific cellular components of the immune system are suppressed or decreased, it is uncommon to see any microscopic changes in the tissues. Although functional changes may not be determined from microscopic examination, other evidence of functional alterations indicative of immunosuppression may be apparent. These may include evidence of reactivation of latent viruses with associated viral-related effects and viral inclusions, the presence of opportunistic infections, or rarely, neoplasms.

### 7.2. Immunostimulation

While the historical focus has been on identifying changes supportive of immunosuppression, signs of immunostimulation and



hypersensitivity reactions are increasingly being identified in the nonclinical and clinical context of studies with biologics and cancer immunotherapies. In the context of immunostimulation, in addition to effects noted in immune organs, numerous other systems can be affected, including the cardiovascular, hepatobiliary, endocrine, cutaneous, nervous, and urinary systems. Selected examples of some of the changes seen in these organs are included below and in [Table 6.10](#). For completeness, stereotypical responses of some of these systems will be discussed briefly under responses to injury.

### 7.2.1. Tissue-specific Responses

#### 7.2.1.1. CARDIOVASCULAR

A spectrum of vascular changes that are functionally/morphologically similar may be elicited by a broad range of immunostimulatory therapies across modalities (see *Cardiovascular System*, Vol 5, Chap 1). Significant hemodynamic changes may occur either following the first (usually innate immune system) or subsequent (likely adaptive immune system) doses, within hours of treatment with some immunostimulatory biopharmaceuticals. The drivers of these vascular changes are related to the activation of the innate and/or adaptive immune system and can involve complement fixation, cytokine release, and/or secondary thrombosis. Commonly, these immune-mediated pathophysiological processes integrate at downstream pathways that drive endothelial dysfunction, such as increased production of nitric oxide in vascular endothelium ([Tobin et al., 2014](#)). Morphologically, these types of injury might have discernible impact on capillary beds, veins and arteries in the short term, particularly if tissues are collected and examined within the first 72 h. When short-term changes are present, they are mostly endothelial and/or intimal and might include plump hypertrophied endothelial cells with prominent nucleoli. The extent of vascular leakage associated with cytokine release or other infusion reactions can be assessed by using the accumulation of Evans Blue dye in tissues ([Wick et al., 2018](#)). Hemodynamic changes in relation to immunotherapies can be common and may be life-threatening. Often, a cytokine-related pathogenesis is consistent with clinical experience and may ultimately

result in the recommendation (by the FDA) to include vasopressors or other cardiovascular-related precautions in managing the hemodynamic effects of CRS ([U. S. Food and Drug Administration, 2006](#); [Lee et al., 2014](#); [U. S. Food and Drug Administration \(FDA\), 2023](#)). Over time, therapies that alter immune tolerance and/or activate complement might drive thickening of vascular intima, endothelial loss, and disruption of internal elastic lamina ([Frazier et al., 2015](#)). Mixed or predominately lymphocytic inflammatory infiltrates may be seen in the vascular wall or surrounding adventitia. Intimal hyperplasia may be present, and these often form foci for thrombi formation. The communication of immunostimulation-related vascular alterations in nonclinical toxicology study reports needs to carefully consider the underlying pathophysiology and delineate the affected organ system(s). For example, a pathologist might separate injury to the vascular beds of the heart and testes into different potential etiopathogeneses that might require different risk management approaches. The communication of these different interpretations could define whether findings are considered to be more consistent with disseminated or multiorgan arteritis representing disseminated vascular response to immune stimulation of changes to immune tolerance versus other responses that might be more local/regional. Immune-related cardiac toxicity in nonclinical models is much less common but allows insights into potential pathogenesis, diagnostic strategy, and choice of drug combinations. When present, such cardiac toxicity can be life-threatening.

#### 7.2.1.2. HEPATOBILIARY

In the liver, changes of sinusoidal leukocytosis, concurrent with KC hypertrophy, may be seen in conjunction with immunostimulation (see *Liver and Gallbladder*, Vol 4, Chap 2). In nonclinical species, these findings may be associated with single cell necrosis and transient elevation of liver enzymes (e.g., alanine transaminase; ALT and aspartate transaminase; AST) indicating that susceptible hepatocytes are more likely to die during periods of immunostimulation. Histopathological evaluations of monkeys treated with an immunostimulatory biopharmaceutical indicate that an acute pattern

**TABLE 6.10** Nonlymphoid Tissue Changes Associated with Immunostimulation

Organ systems	Tissue injury	Examples <sup>a</sup>	Comments	References
Cardiovascular	Mononuclear infiltrate/ inflammation (perivascular or mural), multiorgan arteritis, intimal hyperplasia ± endothelial hypertrophy, myocarditis	PD-1/PD-L1, CD3 bispecific Abs	In some instances, extensive myocarditis can be concurrent with extensive arteritis which can be difficult to differentiate. Arteritis is found to be reversible after 3 months in NHP toxicologic studies	<a href="#">Kamperschroer et al. (2020)</a> ; <a href="#">Frazier et al. (2015)</a> ; <a href="#">Saber et al. (2017)</a> ; <a href="#">Ji et al. (2019)</a> ; FDA, CDER (2016)
Hepatobiliary	Mononuclear infiltrate/ inflammation, Kupffer cell hypertrophy	PD-1/PD-L1, CD3 bispecific Abs	Infiltrate/ inflammation is mostly periportal	<a href="#">Cattley et al. (2019)</a>
Renal	Mononuclear infiltrate/ inflammation, degeneration/ regeneration of proximal tubular epithelium, tubular attenuation, cell sloughing, interstitial nephritis, lupus-like glomerulonephritis	CTLA-4 and PD-1/ PDL1; CD3 bispecific Abs	Kidney tubular changes are more common at doses of immunotherapies eliciting higher levels of circulating cytokines	<a href="#">Kamperschroer et al. (2020)</a> ; <a href="#">Seethapathy et al. (2021)</a> ; <a href="#">Yang and Hu (2019)</a>
Pulmonary	Perivascular and alveolar mononuclear infiltrate/ inflammation, alveolar edema	CTLA-4 and PD-1/ PDL1; CD3 bispecific Abs	Lung findings such as pulmonary edema are more common in higher less tolerated doses of immunotherapy	<a href="#">Kamperschroer et al. (2020)</a> ; <a href="#">Sunthralingam et al. (2006)</a>
Gastrointestinal	Mononuclear infiltrate/ inflammation in lamina propria and submucosa (predominantly perivascular)	CTLA-4 and PD-1/ PDL1; CD3 bi/tri-specific Abs	Mainly observed in colon, but all segments of intestines could be affected	<a href="#">Saber et al. (2017)</a>
Endocrine	Mononuclear infiltrate/ inflammation mainly in pituitary, adrenal, thyroid, pancreas	CTLA-4 and PD-1/ PDL1; CD3 bispecific Abs	In the adrenal, maybe associated with neutrophilic infiltrate in the cortex and transitions to mononuclear infiltrate in the medulla in longer duration studies	<a href="#">Tsoli et al. (2000)</a> ; <a href="#">Gao et al. (2021)</a> ; <a href="#">Peterson et al. (2019)</a>

(Continued)

**TABLE 6.10** Nonlymphoid Tissue Changes Associated with Immunostimulation—cont'd

Organ systems	Tissue injury	Examples <sup>a</sup>	Comments	References
Cutaneous	Mononuclear infiltrate/ inflammation of dermis, epidermal degeneration/single cell necrosis	Trastuzumab (anti-HER2)?	Individual cell necrosis often observed in basal epithelium where adjacent cells can be normal and often associated with lymphocytic infiltrate	<a href="#">Wojcinski et al. (2019)</a>
Neurologic	Perivascular mononuclear infiltrate/ inflammation of the choroid plexus and meninges, neuropil, and spinal cord	Opdualag, CD3 bispecific Abs	Mononuclear cellularity infiltrate (MNCI) often dense can be found deeper in the brain parenchyma and neuropil, extending into cervical spinal cord compared to the background minimal MNCI which is often limited to meninges; brain MNCI did not typically present with any neurologic symptoms	<a href="#">Danish and Santomaso (2021)</a> ; <a href="#">Taraseviciute et al. (2018)</a> ; <a href="#">Kamperschroer et al. (2020)</a> ; <a href="#">Yang and Hu (2019)</a> ; FDA, CDER (2021)

<sup>a</sup> The example list is not exhaustive for all the immunostimulatory approved compounds.

of neutrophil infiltration and sinusoidal leukocytosis are common morphologic components often seen in association with marked cytokine elevation ([Frazier et al., 2015](#); ([Brott et al., 2018](#))). Another common response of the liver to immunostimulation is perivascular infiltration of mononuclear to mixed inflammatory cell infiltrates. This observation is predominately periportal around the medium caliber arteries in cynomolgus macaques and is not often associated with significant tissue damage in the areas of accumulation.

#### 7.2.1.3. RENAL

As in the liver, immunostimulatory therapies induce a range of acute and chronic responses in the kidney (see *Kidney*, Vol 5, Chap 2). Most of these observations are in cynomolgus monkeys treated with immune cell redirector therapies ([Kamperschroer et al., 2020](#)). The acute histopathologic findings tend to be minimal to mild, focal to multifocal, and predominately tubular. They range from degeneration to

regeneration of proximal tubular epithelial cells, tubular attenuation, cell sloughing, and occasional hyaline to mineral casts in the tubular lumen. There may be mononuclear infiltrates around the affected tubules. When clinical pathology is available within the few days of histopathology finding occurrence, elevations in blood urea nitrogen (BUN) and creatinine might be observed. One unique feature of immunostimulation-related changes in the kidney is that BUN and creatinine tend to be elevated but with minimal focal tubular injury challenging the popular notion that 50%–75% of the nephron needs to be damaged before changes in renal markers can be seen. A prerenal mechanism might contribute to this phenomenon. With the extent of vasodilation in these animals, the possible renal contribution to BUN and creatinine elevation needs to be considered with a more likely hemodynamic component driven by cytokines and chemokines. Inflammation is reported to alter kidney function and elevate BUN and creatinine ([Harirforoosh](#)



et al., 2013). Other kinds of proinflammatory states such as sepsis are associated similar renal findings suggesting a mechanistic link between acute inflammation and renal function. In the context of immunostimulation-related peripheral vasodilation, an alteration to the patency of the glomeruli can increase protein concentration of glomerular filtrate and increase the tubular resorption workload for tubular epithelial cells. The altered filtration apparatus and effects on epithelial workload can impact the health of more susceptible tubular cells, manifesting as focal to multifocal epithelial cell death with sloughing of susceptible epithelial cells and/or concurrent multifocal proteinaceous cast formation.

#### 7.2.1.4. ENDOCRINE

Hypophysitis, thyroid disorders, diabetes mellitus, and adrenal insufficiency have been reported with immunomodulatory therapies such as checkpoint inhibitors (e.g., PD-1/PD-L1 and CTLA-4 checkpoint inhibitor therapies) (Fessas et al., 2020). Proinflammatory and Th1 cytokines such as IFN- $\gamma$ , IL-6, or TNF- $\alpha$  alter endocrine systems in a way that drives the pathogenesis of autoimmune endocrinopathies (Tsoli et al., 2000). Multiorgan infiltrates, predominantly lymphocytes of T cell lineages, are commonly observed in multiple organs, including endocrine organs. These infiltrates increase with repeated dosing of biotherapeutics and it is thought that the proinflammatory and Th1 cytokines such as IFN- $\gamma$ , IL-6, or TNF- $\alpha$  alter endocrine systems in a way that drives the pathogenesis of autoimmune endocrinopathies (Tsoli et al., 2000). Recent studies using compounds that inhibit CTLA-4 in graft versus host disease mice support the hypothesis that multiorgan infiltrates observed in the context of inflammation and immunostimulation can be ameliorated by reversing the biology of checkpoint blockade (Gao et al., 2021). It is unclear whether the autoimmunity seen in these organs is due to circulating self-antigens that are lodged in these well-vascularized endocrine organs or a higher propensity of endocrine proteins to trigger autoimmunity. Regardless of the initiating factor, it should be recognized that endocrine organs tend respond to immunostimulatory agents with dense infiltrates (see *Endocrine System*, Vol 4, Chap 7).

#### 7.2.1.5. NEUROLOGICAL

Proinflammatory cytokines, such as IL-1b, IL-6, TNF- $\alpha$ , and others, can have a significant influence on the CNS, and result in pyrexia, somnolence, and an overall sickness response (Faggioni et al., 1995). Recent evidence from immunostimulatory anticancer agents have identified immune cell-associated neurotoxicity syndrome (ICANS) as a clinical and neuropsychiatric syndrome that can occur in the days to weeks following CAR T cell and other T cell-engaging therapies (Danish and Santomasso, 2021). Some of these T cell engaging therapies cause mononuclear infiltrates in the CNS of nonhuman primates (Taraseviciute et al., 2018; Kamperschroer et al., 2020). The nervous system morphology in these cases tends to be perivascular and ranges from mononuclear cell infiltration around vessels to perivascular edema in severe cases (see *Nervous System*, Vol 4, Chap 8). The pathogenesis is not well understood, but several lines of evidence implicate elevated cytokines, altered blood-brain barrier (BBB), and activated microglia (Morris et al., 2022). Recognizing different patterns of infiltrates in relation to vessels, highly vascularized areas, or areas with weak BBB and application of molecular pathology tools may help provide some insight into the mechanism drivers of immunostimulation-related pathology in the CNS.

#### 7.2.1.6. PULMONARY

Immunostimulatory therapies often result in dense perivascular mononuclear infiltrates in the lung with increased probability for regional to disseminated alveolar edema, depending on the extent and duration of systemic effects of immunostimulation (see *Respiratory Tract*, Vol 5, Chap 4). The mechanisms responsible for pneumonitis in people are not yet fully understood. The effector and regulatory T cell dysregulation along with highly activated CD4 and CD8 T cell infiltration and increased inflammatory cytokine levels may ultimately lead to lung injury. Similar mechanisms likely underly pneumonitis and changes seen in other organs. For example, concomitant irAEs can be seen in other organ systems (e.g., skin, gastrointestinal, and musculoskeletal) in more than 50% of patients with pneumonitis. Additionally, the lung responses appear to be related to the degree of

immunostimulation since increased pneumonitis is often present when combination therapies of immunostimulatory agents occur compared to a single (e.g., checkpoint inhibitor) therapy.

### 7.2.2. Hypersensitivity and Autoimmunity Changes

Antigen-specific derangement processes like allergy and autoimmune disease can lead to tissue damage, protein (immune) complex deposits, and/or inflammatory cell infiltrates, and changes in immune cell populations and composition in both lymphoid and nonlymphoid target organs. Such changes in lymphoid organs can alert the pathologist to potential immune system alterations. Changes indicating immune system effects can also be present in nonimmune organs. Well-known targets are vasculature, kidneys, synovial membranes, thyroid skin, liver, and lungs. The morphological hallmark of allergy and autoimmune (-like) disease is cellular infiltration and/or inflammation. Unfortunately, there are at present no morphological criteria to identify antigen-specific inflammatory responses. Antigen-specific inflammation in non-lymphoid organs includes changes such as granulocytic and lymphocytic cell infiltrates, granulomas, necrosis, and fibrosis. These infiltrates are also common in nonspecific inflammation, and therefore their interpretation is difficult.

Typical changes like vasculitis, inflammation at dermal-epidermal interfaces, fibrinoid necrosis, and expansion of extracellular matrix are suggestive of an allergic- or autoimmune-related inflammation. In subacute and subchronic toxicity studies, symptoms of full-blown autoimmune diseases are rarely encountered, because the time of exposure is too short, the number of animals per group is often small, and species- or strain-specific differences in sensitivities often are present. Therefore, in most cases, only early indicators of such a disease may be present, such as lymphocytic infiltrates in the pancreatic islets as a prodromal symptom of early diabetes.

The histology of clinically manifest, antigen-specific inflammatory reactions depends on the type of immune reaction. Hypersensitivities are a response of concern with several types being described and of clinical concern with immunostimulation. Hypersensitivities can be categorized

according to the Gell and Coombs classification although different types of hypersensitivities can be induced (e.g., complement-mediated induced hypersensitivity/pseudoallergic reactions, etc.) and can contribute to the pathogenesis of life-threatening infusion reactions and adverse clinical events (Table 6.6). It should be kept in mind that an antigen often induces more than one type of reaction which can be reflected by the morphology of the inflammation. However, many hypersensitivity reactions may have limited to no pathological findings, and it is difficult to predict when such events may occur.

## 8. PRENEOPLASTIC CHANGES AND NEOPLASIA

In the lymphoid organs and tissues, mobile and fixed/stromal cells have to be considered separately. The incidence of tumors derived from resident mesenchymal and vascular cells of lymphoid and hematopoietic tissues is generally low in rodents, but unanticipated increases may be seen depending on genetic background. Reactive proliferations involving the stromal and vascular compartments of lymphoid organs or bone marrow and blood are more common and often related to circulatory disorders in aging rodents. For more information about the classification of neoplasia of the immune system in rodents, the reader is referred to the INHAND nomenclature (Willard-Mack et al., 2019) and the goRENI webpage (<https://www.goreni.org/>) with a select number of examples provided below.

### 8.1. Stromal Tumors: Thymoma

Hyperplasia and neoplasia of thymic epithelial cells have a strong interconnection with the proliferation, maturation, and release of lymphoid cells from the thymus (Figure 6.19). The spectrum of thymomas ranges from cases with low proportions of proliferating epithelial cells and high number of thymocytes, thus resembling T cell lymphoma, to purely epithelial tumors resembling squamous cell carcinoma. Thymomas with high numbers of lymphocytes often lead to concomitantly increased lymphoid cellularity in secondary lymphoid organs. As a differential diagnosis, epithelial hyperplasia

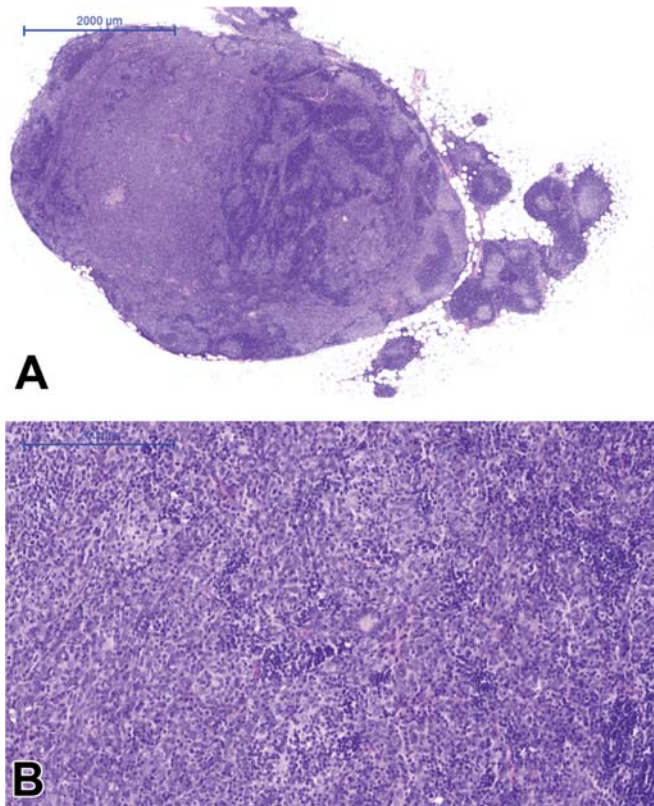


**FIGURE 6.19** Thymomas are epithelial tumors, in some cases with massive involvement of lymphocytes. (A) Thymoma in one lobe of the thymus of an aged Wistar rat. (B) In a higher magnification image of the tumor, neoplastic epithelial cells are slightly spindle-shaped. Hematoxylin and eosin (H&E) stain; Magnification of 20 $\times$  and 400 $\times$ . *Figures 49.31 p. 1847 in Haschek WM, Rousseaux CG, Wallig MA, editors: Haschek and Rousseaux's handbook of toxicologic pathology, ed 3, 2013, Academic Press.*

of branchial remnants forming tubules, cords, and cysts should be taken into account. These epithelial hyperplasias do not influence the lymphoid compartment and are common in both (aging) rats and mice and are more frequent in females.

## 8.2. Tumors of Hematopoietic and Lymphopoietic Cells

Hematopoietic cell tumors include leukemia, lymphoma, and histiocytic sarcoma (see *Hematopoietic System*, Vol 5, Chap 5). They represent frequent spontaneous and induced tumor entities in rodents but are less common in other species. The spontaneous background

incidences of these tumor entities are highly interstudy comparability and validity of historical data. The diagnoses are mainly based on morphological criteria, using formalin-fixed tissues and H&E staining. To further differentiate these tumors, the use of IHC is recommended. The interpretation of immunohistochemical results may be challenging due to issues such as varying fixation periods, variations in the expression of markers, coincidence of systemic tumors, and mixtures of neoplastic and nonneoplastic cells in certain tumor entities.

## 8.3. Lymphomas

In lymphomas, typical gross findings represent enlargement of thymus, spleen, and lymph nodes. In advanced cases, tumor infiltrates involve the mesentery and nonlymphoid organs such as liver, lungs, and kidneys, which then exhibit nodular changes or enlargement. At necropsy, collection of smears or imprints for cytological investigations or frozen specimens for IHC can be useful for later investigations beyond the options offered by formalin-fixed material. Histopathological hallmarks of lymphoma in lymphoid organs include unexplained increased lymphoid cellularity and disruption of compartment structure and/or organ boundaries by the putative neoplastic cell growth. Cytological criteria consistent with neoplastic transformation include monomorphic appearance of the suspected neoplastic cells, atypical cytological details, and increased (and atypical) mitotic figures. Although the genesis of lymphomas has not been systematically investigated in rodents, nonmalignant clonal expansion of lymphocytes is known as a cause of, and may precede, lymphoma. Initial sites of clonal expansion of autonomously growing neoplastic cells can involve both primary and secondary lymphoid organs. In aged mice with lymphoid hyperplasia of “antigen-experienced” B cell clones in peripheral lymphoid organs, it is sometimes difficult to distinguish these nonneoplastic proliferations from lymphoma (Figure 6.20).

## 8.4. Histiocytic Sarcoma

Histiocytic sarcomas are derived from “histiocytic” cells (monocytes, macrophages, DCs).



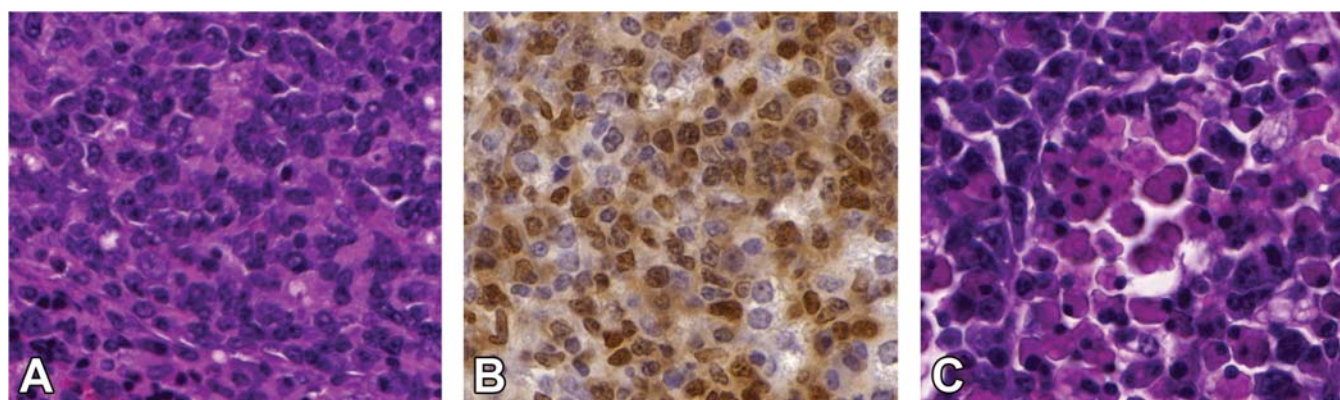


**FIGURE 6.20** (A) Pleomorphic lymphoma arising in the splenic white pulp of a CD-1 mouse from a 2-year carcinogenicity study, showing cohesive cells with variable morphology. (B) Neoplastic cells are positive by immunohistochemistry (IHC) for the B cell marker PAX-5. (C) Plasmacytic lymphoma from a CD-1 mouse with prominent Russell bodies. *Reproduced from Figure 49.34 p. 1854 and Figure 49.35 p. 1855 in Haschek WM, Rousseaux CG, Wallig MA, editors: Haschek and Rousseaux's handbook of toxicologic pathology, ed 3, 2013, Academic Press, with permission.*

They are common in rodents. In mice, they often originate from liver or uterus but may also be seen in other organs. In the liver, the cells can form irregular sinusoidal aggregates or nodules. In the uterus of mice, often one large nodule is present. In the lungs, tumor cells often fill or ensheath small blood vessels. In H&E-stained sections, histiocytic sarcomas can display similarities to pleomorphic lymphoma. Typical features of histiocytic sarcoma are monomorphic cell population with pleomorphic or indented nuclei and eosinophilic cytoplasm, occurrence of multinucleated cells, and signs of phagocytosis. Immunohistochemically, the cells are positive for macrophage markers and lysozyme. Hyaline droplets in the renal proximal tubules staining positive for lysozyme are often seen in affected animals presents induced hematopoietic tumors in rat and mouse, and their relevance to humans (Figure 6.21).

## 9. BEST PRACTICES AND REGULATORY CONSIDERATIONS ON EVALUATION OF TOXICITY AND ADVERSITY IN THE IMMUNE SYSTEM

As described throughout this chapter, the immune system is extraordinarily complex with a wide range of responses normally and in response to internal and external factors and significant variability in responses between

individuals and across populations. This variability presents a challenge to determine whether a specific change of the immune system is within the range of normal, is adaptive or reversible, or may represent toxicity. Evaluating the toxic change is further complicated when evaluating changes in the context of immunomodulatory therapies designed to modify the immune system. Yet, even in light of these challenges, the evaluation of toxic changes and assignment of adversity is an important activity of toxicologic pathologists. Several publications provide guidance on assigning adversity to preclinical safety studies, but the practical application in determining what is a harmful or adverse change in the immune system may be particularly challenging (see *Assigning Adversity to Toxicologic Outcomes*, Vol 2, Chap 15). There continues to be an emphasis that adversity determination should remain flexible, context-dependent, and incorporate a WOE approach (Kerlin et al., 2016; Palazzi et al., 2016; Ramaiah et al., 2017; Papenfuss et al., 2023).

It can be challenging for the toxicologic pathologist to assess risk for immune system changes and there is much discussion and many approaches, philosophies, and current opinions on determining adversity. It is a complicated arena for pathologists who evaluate a highly dynamic and responsive immune system with a significant biological variability and wide range of “normal” responses for the individual

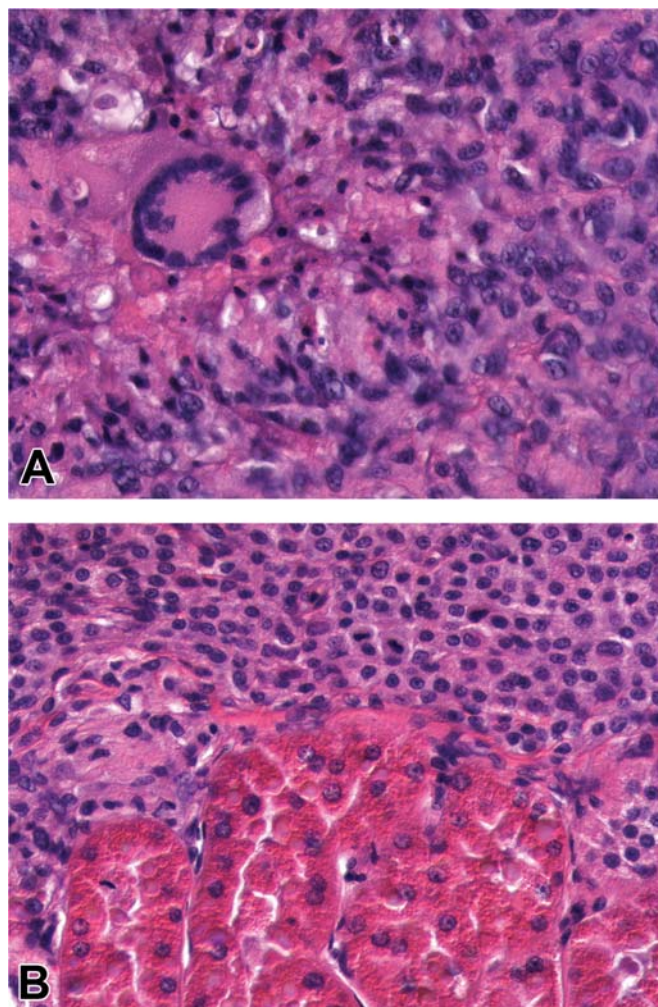


**FIGURE 6.21** (A) Histiocytic sarcoma, Wistar rat, exhibiting multinucleated giant cells. Observation of giant cells is helpful for diagnosis in unclear cases. (B) Histiocytic sarcoma, Wistar rat. Half of the image shows a tumor infiltrate in the kidney, which is very typical. The infiltrate is a monomorphic infiltrate of small cells with eosinophilic cytoplasm. Renal proximal tubules with abundant hyaline droplets are visible; this is often observed with histiocytic sarcoma infiltration, even if it occurs elsewhere in the body. *H&E stain, Reproduced from Figure 49.36 p. 1856 in Haschek WM, Rousseaux CG, Wallig MA, editors: Haschek and Rousseaux's handbook of toxicologic pathology, ed 3, 2013, Academic Press, with permission.*

and population. Therapies themselves affect the immune system (often by design). Interpretations and conclusions made by the pathologist may differ depending on the context of a particular project, the role of the pathologist within the pipeline of therapy development, and when

intended pharmacology moves from exaggerated pharmacology and toxicity. For example, at what point does a therapy designed to decrease lymphocyte populations that results in decreased lymphocytes in lymphoid organs and the circulation move to being “efficacious” consistent with its intended pharmacology, to “toxic” from exaggerated pharmacology? Can this determination be made without data to support evidence of immune system dysfunction? Ideally, integration of pathology and other immunology and immunotoxicology endpoints would provide the best WOE approach to understand the potential toxicity and associated adversity within the immune system (Papenfuss et al., 2023). It is not uncommon, however, that data sets and study endpoints may not be available at the time of pathology evaluation and the pathologist and associated scientists should be aware that this may limit the ability to definitively identify toxic effects or adversity on pathology findings alone.

Practically speaking, it may be most helpful to identify when immune findings are nonadverse or adaptive. Nonadverse findings include those that are of limited severity, are transient, represent an adaptive response, lack a functional correlate, are isolated or independent, or are secondary/indirect effects (Kerlin et al., 2016). Unless there is overt evidence or additional data that changes in the immune system are not transient, adaptive, or of sufficient severity to connote adversity, many immune findings would likely be considered nonadverse. This is particularly true given that immunological functional alterations are typically not discernible based on gross, organ weight, clinical pathology, or microscopic changes alone. Additional data sets, including clinical pathology parameters, clinical observations, and a variety of phenotypic and functional immunotoxicology endpoints, along with a tiered approach to immunotoxicity evaluation, can be very helpful to provide a WOE when elevating changes to those indicative of toxicity and when assigning adversity to immune system changes (European Medicines Agency, 2006; De Jong and Van Loveren, 2007; Papenfuss et al., 2023). Numerous organizations, such as, the ICH (the International Conference on Harmonisation of Technical Requirements for Registration of Pharmaceuticals for Human Use), US FDA



(American Food and Drug Administration), EU CPMP (European Committee for Proprietary Medicinal Products), OECD (Organisation for Economic Co-operation and Development, EPA (Environmental Protection Agency), and others provide guidance documents specific to the therapeutic and audience of interest that may be relevant and applicable to the pathologist evaluating and assessing immune system changes. A full list of such resource material is beyond the scope of this chapter and readers should identify resources and develop a library of references relevant to their needs (Papenfuss et al., 2023).

## 10. CONCLUSION

Toxicologic pathologists play a critical role in identifying immune system changes and immunosafety determination. It continues to be the pathologist's role to identify changes, interpret and contextualize these changes and potential toxicity, and communicate the nature and significance of these changes. Although immunomodulatory therapies have changed the landscape and interpretive context of what defines toxicity for immune system changes, the responsibilities of the pathologist remain the same, regardless of their role, activities, and pathogenic process being considered.

## REFERENCES

- Abbas AK, Lichtman AH, Pillai S: Properties and overview of immune responses. In Lichtman AK, Abbas AH, Pillai S, editors: *Cellular and molecular immunology*, Philadelphia, PA, 2022a, Elsevier, pp 1–11.
- Abbas AK, Lichtman AH, Pillai S: Cells and tissues of the immune system. In L. AK, Abbas AH, Pillai S, editors: *Cellular and molecular immunology*, Philadelphia, PA, 2022b, Elsevier, pp 13–14.
- Abbas AK, Lichtman AH, Pillai S: Differentiation and functions of CD4+ effector T cells. In Lichtman AK, Abbas AH, Pillai S, editors: *Cellular and molecular immunology*, Philadelphia, PA, 2022c, Elsevier, pp 233–250.
- Abbas AK, Lichtman AH, Pillai S: Specialized immunity at epithelial barriers and immune privileged tissues. In Lichtman AK, Abbas AH, Pillai S, editors: *Cellular and molecular immunology*, Philadelphia, PA, 2022d, Elsevier, pp 251–260.
- Abo T: Extrathymic pathways of T-cell differentiation and immunomodulation, *Int. Immunopharm.* 1(7):1261–1273, 2001.
- Aeffner F, Forest T, Schumacher V, Zarella M, Bradley A: Digital pathology and tissue image analysis. In Haschek WM, Rousseaux CG, Wallig MA, Bolon B, editors: *Haschek and Rousseaux's handbook of toxicologic pathology: Principles and practice of toxicologic pathology* (vol. 1), 2022, pp. 395–421.
- Albillos A, Lario M, Alvarez-Mon M: Cirrhosis-associated immune dysfunction: distinctive features and clinical relevance, *J. Hepatol.* 61(6):1385–1396, 2014.
- Allen TD, Dexter TM: The essential cells of the hemopoietic microenvironment, *Exp. Hematol.* 12(7):517–521, 1984.
- Badran YR, Leet DE, Dougan M: Immune-related adverse events: what we've learned and where we're heading, *Expert Rev. Anticancer Ther.* 20(9):727–730, 2020.
- Bailey RP, Weiss L: Ontogeny of human fetal lymph nodes, *Am. J. Anat.* 142(1):15–27, 1975.
- Bénézech C, Luu NT, Walker JA, et al.: Inflammation-induced formation of fat-associated lymphoid clusters, *Nat. Immunol.* 16(8):819–828, 2015.
- Bhandari S, Larsen AK, McCourt P, et al.: The scavenger function of liver sinusoidal endothelial cells in health and disease, *Front. Physiol.* 12:757469, 2021.
- Bregman CL, Adler RR, Morton DG, et al.: Recommended tissue list for histopathologic examination in repeat-dose toxicity and carcinogenicity studies: a proposal of the Society of Toxicologic Pathology (STP), *Toxicol. Pathol.* 31(2): 252–253, 2003.
- Brott D, Amuzie CJ, Chamanza R, et al.: Cardiovascular system. In Sahota PS, Popp JA, Hardisty JF, Gopinath C, editors: *Toxicologic pathology: nonclinical safety assessment*, ed 2, Boca Raton, 2018, Taylor & Francis group.
- Bugelski PJ, Treacy G: Predictive power of preclinical studies in animals for the immunogenicity of recombinant therapeutic proteins in humans, *Curr. Opin. Mol. Therapeut.* 6(1): 10–16, 2004.
- Cattley RC, Popp JA, Vonderfecht SL: Chapter 12: Liver, gallbladder, and exocrine pancreas. In Sahota PS, Popp JA, Hardisty JF, Gopinath C, Bouchard P, editors: *Toxicologic pathology: nonclinical safety assessment*, ed 2, Boca Raton, 2019, CRC Press, pp 451–514.
- Cesta MF: Normal structure, function, and histology of mucosa-associated lymphoid tissue, *Toxicol. Pathol.* 34(5): 599–608, 2006a.
- Cesta MF: Normal structure, function, and histology of the spleen, *Toxicol. Pathol.* 34(5):455–465, 2006b.
- Conroy M, Naidoo J: Immune-related adverse events and the balancing act of immunotherapy, *Nat. Commun.* 13(1):392, 2022.
- Danish H, Santomaso BD: Neurotoxicity biology and management, *Cancer J.* 27(2):126–133, 2021.
- De Jong WH, Van Loveren H: Screening of xenobiotics for direct immunotoxicity in an animal study, *Methods* 41(1):3–8, 2007.
- Descotes J: Methods of evaluating immunotoxicity, *Expert Opin. Drug Metabol. Toxicol.* 2(2):249–259, 2006.



- Dunn TB: Normal and pathologic anatomy of the reticular tissue in laboratory mice, with a classification and discussion of neoplasms, *J. Natl. Cancer Inst.* 14(6):1281–1433, 1954.
- Eikelenboom P, Nassy JJ, Post J, et al.: The histogenesis of lymph nodes in rat and rabbit, *Anat. Rec.* 190(2):201–215, 1978.
- Elewa YH, Ichii O, Kon Y: Comparative analysis of mediastinal fat-associated lymphoid cluster development and lung cellular infiltration in murine autoimmune disease models and the corresponding normal control strains, *Immunology* 147(1):30–40, 2016.
- Elmore SA: Enhanced histopathology of mucosa-associated lymphoid tissue, *Toxicol. Pathol.* 34(5):687–696, 2006a.
- Elmore SA: Enhanced histopathology of the bone marrow, *Toxicol. Pathol.* 34(5):666–686, 2006b.
- Elmore SA: Enhanced histopathology of the spleen, *Toxicol. Pathol.* 34(5):648–655, 2006c.
- Elmore SA: Enhanced histopathology of the thymus, *Toxicol. Pathol.* 34(5):656–665, 2006d.
- Elmore SA: Enhanced histopathology of the immune system: a review and update, *Toxicol. Pathol.* 40(2):148–156, 2012.
- Elmore SA: Enhanced histopathology evaluation of lymphoid organs, *Methods Mol. Biol.* 1803:147–168, 2018.
- Elmore SA, Dixon D, Hailey JR, et al.: Recommendations from the INHAND apoptosis/necrosis working group, *Toxicol. Pathol.* 44(2):173–188, 2016.
- European Medicines Agency: ICH S8 Immunotoxicity studies for human pharmaceuticals—scientific guideline, 2006, European Medicines Agency. Retrieved July 3, 2024, from, [https://www.ema.europa.eu/en/documents/scientific-guideline/ich-s-8-immunotoxicity-studies-human-pharmaceuticals-step-5\\_en.pdf](https://www.ema.europa.eu/en/documents/scientific-guideline/ich-s-8-immunotoxicity-studies-human-pharmaceuticals-step-5_en.pdf).
- Everds NE, Snyder PW, Bailey KL, et al.: Interpreting stress responses during routine toxicity studies: a review of the biology, impact, and assessment, *Toxicol. Pathol.* 41(4):560–614, 2013.
- Faggioni R, Benigni F, Ghezzi P: Proinflammatory cytokines as pathogenetic mediators in the central nervous system: brain-periphery connections, *Neuroimmunomodulation* 2(1): 2–15, 1995.
- Fessas P, Possamai LA, Clark J, et al.: Immunotoxicity from checkpoint inhibitor therapy: clinical features and underlying mechanisms, *Immunology* 159(2):167–177, 2020.
- Figueredo JM, Papenfuss T: Hematopoietic system. In Parker GA, editor: *Atlas of histology of the juvenile rat*, San Diego, CA, 2016, Elsevier, pp 349–371.
- Food and Drug Administration: Center for Drug Evaluation and Research Application: Application Number 761034Orig1s000. Pharmacology Review(s) (BLA 761034) Tecentriq (atezolizumab), 2016, April 27. [https://www.accessdata.fda.gov/drugsatfda\\_docs/nda/2016/761034Orig1s000PharmR.pdf](https://www.accessdata.fda.gov/drugsatfda_docs/nda/2016/761034Orig1s000PharmR.pdf).
- Food and Drug Administration: Center for Drug Evaluation and Research Application: Application Number 761234Orig1s000. NDA/BLA Multi-disciplinary Review and Evaluation (BLA 761234) Opdivo (nivolumab and relatlimab-rmbw), 2021, July 19. [https://www.accessdata.fda.gov/drugsatfda\\_docs/nda/2022/761234Orig1s000MultidisciplineR.pdf](https://www.accessdata.fda.gov/drugsatfda_docs/nda/2022/761234Orig1s000MultidisciplineR.pdf).
- Forrester JV, McMenamin PG, Dando SJ: CNS infection and immune privilege, *Nat. Rev. Neurosci.* 19(11):655–671, 2018.
- Frazier KS, Engelhardt JA, Fant P, et al.: Scientific and regulatory policy committee points-to-consider paper\*: drug-induced vascular injury associated with nonsmall molecule therapeutics in preclinical development: Part I. Biotherapeutics, *Toxicol. Pathol.* 43(7):915–934, 2015.
- Fulop T, Larbi A, Dupuis G, et al.: Immunosenescence and inflamm-aging as two sides of the same coin: friends or foes? *Front. Immunol.* 8:1960, 2017.
- Gago da Graça C, van Baarsen LGM, Mebius RE: Tertiary lymphoid structures: diversity in their development, composition, and role, *J. Immunol.* 206(2):273–281, 2021.
- Gallucci RL, Yucesory B: Immunotoxicology. In *An introduction to interdisciplinary toxicology, from molecules to man*, 2020, pp 233–244.
- Gao C, Gardner D, Theobalds MC, et al.: Cytotoxic T lymphocyte antigen-4 regulates development of xenogenic graft versus host disease in mice via modulation of host immune responses induced by changes in human T cell engraftment and gene expression, *Clin. Exp. Immunol.* 206(3):422–438, 2021.
- Genova C, Rossi G, Rijavec E, et al.: Releasing the brake: safety profile of immune check-point inhibitors in non-small cell lung cancer, *Expert Opin. Drug Saf.* 16(5):573–585, 2017.
- Germolec DR, Shipkowski KA, Frawley RP, et al.: Markers of inflammation, *Methods Mol. Biol.* 1803:57–79, 2018.
- Gonçalves PH, Uldrick TS, Yarchoan R: HIV-associated Kaposi sarcoma and related diseases, *Aids* 31(14):1903–1916, 2017.
- Grakoui A, Crispe IN: Presentation of hepatocellular antigens, *Cell. Mol. Immunol.* 13(3):293–300, 2016.
- Greaves P: *Hemopoietic and lymphatic systems in histopathology of preclinical toxicity studies: interpretation and relevance in drug safety evaluation*, San Diego, 2012, Academic Press.
- Gwaltney-Brant S: Immunotoxicity biomarkers, *Biomark. Toxicol.*, 2019:413–425, 2019.
- Haley PJ: Species differences in the structure and function of the immune system, *Toxicology* 188(1):49–71, 2003.
- Haley PJ: The role of histopathology in the identification of immunotoxicity, *J. Immunot.* 2(4):181–183, 2005.
- Haley PJ: The lymphoid system: a review of species differences, *J. Toxicol. Pathol.* 30(2):111–123, 2017.
- Hameleers DM, van der Ven I, Sminia T, Biewenga J: Anti-TNP-forming cells in rats after different routes of priming with TNP-LPS followed by intranasal boosting with the same antigen, *Res. Immunol.* 141(6):515–528, 1990 Jul-Aug, [https://doi.org/10.1016/0923-2494\(90\)90020-y](https://doi.org/10.1016/0923-2494(90)90020-y).
- Hariforoosh S, Asghar W, Jamali F: Adverse effects of nonsteroidal antiinflammatory drugs: an update of gastrointestinal, cardiovascular and renal complications, *J. Pharm. Pharmaceut. Sci.* 16(5):821–847, 2013.
- HoganEsch HH, Hahn FF: The lymphoid organs: anatomy, development, and age-related changes. In Mohr UC, Dungworth WW, Capen DL, Ames CC, editors:

- Pathobiology of the aging dog*, 2001, Iowa State University Press, pp 127–135.
- Holsapple MP: Developmental immunotoxicity testing: a review, *Toxicology* 185(3):193–203, 2003.
- Holsapple MP, West LJ, Landreth KS: Species comparison of anatomical and functional immune system development, *Birth Defects Res. B Dev. Reprod. Toxicol.* 68(4):321–334, 2003.
- Hussain Y, Khan H: *Immunosuppressive drugs*. *Encyclopedia of infection and immunity*, 2022, pp 726–740.
- ICHHT Guideline: ICH harmonised tripartite guideline: immunotoxicity studies for human pharmaceuticals, *Current Step 4 Version*, 2005:1–15, 2005.
- Jackson-Jones LH, Bénézech C: FALC stromal cells define a unique immunological niche for the surveillance of serous cavities, *Curr. Opin. Immunol.* 64:42–49, 2020.
- Jackson-Jones LH, Duncan SM, Magalhaes MS, et al.: Fat-associated lymphoid clusters control local IgM secretion during pleural infection and lung inflammation, *Nat. Commun.* 7:12651, 2016.
- Ji C, Roy D, Goals J, et al.: Myocarditis in cynomolgus monkeys following treatment with immune checkpoint inhibitors, *Clin. Cancer Res.* 25(15):4735–4748, 2019, <https://doi.org/10.1158/1078-0432.CCR-18-4083>.
- Kamperschroer C, Shenton J, Lebrech H, Leighton JK, Moore PA, Thomas O: Summary of a workshop on preclinical and translational safety assessment of CD3 bispecifics, *J. Immunotoxicol.* 17(1):67–85, 2020.
- Kau AL, Ahern PP, Griffin NW, et al.: Human nutrition, the gut microbiome and the immune system, *Nature* 474(7351): 327–336, 2011.
- Kerlin R, Bolon B, Burkhardt J, et al.: Scientific and regulatory policy committee: recommended (“Best”) practices for determining, communicating, and using adverse effect data from nonclinical studies, *Toxicol. Pathol.* 44(2):147–162, 2016.
- Kimber I, Dearman RJ: Immune responses: adverse versus non-adverse effects, *Toxicol. Pathol.* 30(1):54–58, 2002.
- Klein JR: Dynamic interactions between the immune system and the neuroendocrine system in health and disease, *Front. Endocrinol.* 12:655982, 2021.
- Klein SL, Flanagan KL: Sex differences in immune responses, *Nat. Rev. Immunol.* 16(10):626–638, 2016.
- Koornstra PJ, de Jong FI, Vlek LF, et al.: The Waldeyer ring equivalent in the rat. A model for analysis of oronasopharyngeal immune responses, *Acta Otolaryngol.* 111(3): 591–599, 1991.
- Kumar V, Abbas AK, Aster JC: The cell as a unit of health and disease. In Kumar V, Abbas AK, Aster JC, editors: *Robbins and Cotran pathologic basis of disease*, Philadelphia, PA, 2021a, Elsevier, pp 1–31.
- Kumar V, Abbas AK, Aster JC: Cell injury, cell death, and adaptations. In Kumar V, Abbas AK, Aster JC, editors: *Robbins and Cotran pathologic basis of disease*, 2021b, Elsevier, pp 33–69.
- Kumar V, Abbas AK, Aster JC: Diseases of the immune system. In Kumar V, Abbas AK, Aster JC, editors: *Robbins & Cotran pathologic basis of disease*, Philadelphia, PA, 2021c, Elsevier, pp 189–266.
- Kuper CF, van Bilsen J, Wijnands MVW: The serosal immune system of the thorax in toxicology, *Toxicol. Sci.* 164(1):31–38, 2018.
- Kuper CF, Elmore SA, Parker GA: Immune system in toxicologic pathology. In Haschek CG, M. W, Rousseaux, editors: *Haschek and Rousseaux’s handbook of toxicologic pathology*, San Diego, 2013, Academic Press, pp 1795–1862.
- Lapuente-Santana O, Eduati F: Toward systems biomarkers of response to immune checkpoint blockers, *Front. Oncol.* 10: 1027, 2020.
- Leach MW, Rottman JB, Hock MB, et al.: Immunogenicity/hypersensitivity of biologics, *Toxicol. Pathol.* 42(1):293–300, 2014.
- LeBien TW, Tedder TF: B lymphocytes: how they develop and function, *Blood* 112(5):1570–1580, 2008.
- Lebrech H, Brennan FR, Haggerty H, et al.: HESI/FDA workshop on immunomodulators and cancer risk assessment: building blocks for a weight-of-evidence approach, *Regul. Toxicol. Pharmacol.* 75:72–80, 2016.
- Lee DW, Gardner R, Porter DL, et al.: Current concepts in the diagnosis and management of cytokine release syndrome, *Blood* 124(2):188–195, 2014.
- Leung S, Liu X, Fang L, et al.: The cytokine milieu in the interplay of pathogenic Th1/Th17 cells and regulatory T cells in autoimmune disease, *Cell. Mol. Immunol.* 7(3):182–189, 2010.
- Liebl MC, Hofmann TG: Identification of responders to immune checkpoint therapy: which biomarkers have the highest value? *J. Eur. Acad. Dermatol. Venereol.* 33(Suppl 8): 52–56, 2019.
- Llibre A, Duffy D: Immune response biomarkers in human and veterinary research, *Comp. Immunol. Microbiol. Infect. Dis.* 59:57–62, 2018.
- Losco P: Normal development, growth, and aging of the spleen. In Mohr UD, L., Capen CC, editors: *Pathobiology of the aging rat*, Washington, DC, 1992, ILSI Press, pp 75–94.
- Luster MI, Munson AE, Thomas PT, et al.: Development of a testing battery to assess chemical-induced immunotoxicity: national Toxicology Program’s guidelines for immunotoxicity evaluation in mice, *Fund. Appl. Toxicol.* 10(1):2–19, 1988.
- Mease KM, Kimzey AL, Lansita JA: Biomarkers for nonclinical infusion reactions in marketed biotherapeutics and considerations for study design, *Curr. Opin. Toxicol.*, 2017:1–15, 2017, <https://doi.org/10.1016/j.cotox.2017.03.005>.
- Mebius RE: Organogenesis of lymphoid tissues, *Nat. Rev. Immunol.* 3(4):292–303, 2003.
- Michot JM, Bigenwald C, Champiat S, et al.: Immune-related adverse events with immune checkpoint blockade: a comprehensive review, *Eur. J. Cancer* 54:139–148, 2016.
- Morris EC, Neelapu SS, Giavridis T, et al.: Cytokine release syndrome and associated neurotoxicity in cancer immunotherapy, *Nat. Rev. Immunol.* 22(2):85–96, 2022.

- Multhoff G, Molls M, Radons J: Chronic inflammation in cancer development, *Front. Immunol.* 2:98, 2011.
- Munoz-Erazo L, Rhodes JL, Marion VC, et al.: Tertiary lymphoid structures in cancer—considerations for patient prognosis, *Cell. Mol. Immunol.* 17(6):570–575, 2020.
- Nagasawa T: Microenvironmental niches in the bone marrow required for B-cell development, *Nat. Rev. Immunol.* 6(2): 107–116, 2006.
- Negi N, Das BK: CNS: not an immunoprivileged site anymore but a virtual secondary lymphoid organ, *Int. Rev. Immunol.* 37(1):57–68, 2018.
- Nguyen-Lefebvre AT, Horuzsko A: Kupffer cell metabolism and function, *J. Enzymol. Metabol.* 1(1), 2015.
- Nikolich-Zugich J: The twilight of immunity: emerging concepts in aging of the immune system, *Nat. Immunol.* 19(1):10–19, 2018.
- Nishino M, Ashiku SK, Kocher ON, et al.: The thymus: a comprehensive review, *Radiographics* 26(2):335–348, 2006.
- Palazzi X, Burkhardt JE, Caplain H, et al.: Characterizing "adversity" of pathology findings in nonclinical toxicity studies: results from the 4th ESTP international expert workshop, *Toxicol. Pathol.* 44(6):810–824, 2016.
- Pandiri AR, Kerlin RL, Mann PC, et al.: Is it adverse, non-adverse, adaptive, or artifact? *Toxicol. Pathol.* 45(1):238–247, 2017.
- Papenfuss TL: Flow cytometry and immunophenotyping in drug development in Immunopathology in toxicology and drug development. In Parker GA, editor: *Immunopathology in toxicology and drug development*, Switzerland, 2017a, Springer International Publishing, pp 343–371.
- Papenfuss TL, Himmel L, Kuper CF, et al.: Toxicologic pathology forum: considerations regarding determination of adversity for immunopathology findings in nonclinical toxicology studies with immune-modulating therapeutics, *Toxicol. Pathol.* 51:205–215, 2023.
- Papenfuss TLC: In Parker GA, editor: *Spleen. Immunopathology in Toxicologic Drug Development* (vol. 2). 2017b, Springer International Publishing, pp 37–58.
- Papenfuss TL, Rebellato MC, Bolon B: Pathology of the lymphoid system. In Steinbach TJ, Patrick DJ, Cosenza ME, editors: *Toxicologic pathology for non-pathologists*, New York, 2019, Humana Press, pp 355–395.
- Parker GP: Immune system. In *Atlas of histology of the juvenile rat*, San Diego, CA, 2016, Elsevier, pp 293–347.
- Pearse G: Normal structure, function and histology of the thymus, *Toxicol. Pathol.* 34(5):504–514, 2006.
- Peterson RA, Chandra S, Hoenerhoff MJ: Chapter 19: Endocrine glands. In Sahota PS, Popp JA, Hardisty JF, Gopinath C, Bouchard P, editors: *Toxicologic pathology: nonclinical safety assessment*, ed 2, Boca Raton, 2019, CRC Press, pp 827–888.
- Ploemen JP, Ravesloot WT, van Esch E: The incidence of thymic B lymphoid follicles in healthy beagle dogs, *Toxicol. Pathol.* 31(2):214–219, 2003.
- Ponce RA, Gelzleichter T, Haggerty HG, et al.: Immunomodulation and lymphoma in humans, *J. Immunot.* 11(1):1–12, 2014.
- Racanelli V, Rehermann B: The liver as an immunological organ, *Hepatology* 43(2 Suppl 1):S54–S62, 2006.
- Ramaiah L, Tomlinson L, Tripathi NK, et al.: Principles for assessing adversity in toxicologic clinical pathology, *Toxicol. Pathol.* 45(2):260–266, 2017.
- Robinson MW, Harmon C, O'Farrelly C: Liver immunology and its role in inflammation and homeostasis, *Cell. Mol. Immunol.* 13(3):267–276, 2016.
- Rojko JL, Evans MG, Price SA, et al.: Formation, clearance, deposition, pathogenicity, and identification of biopharmaceutical-related immune complexes: review and case studies, *Toxicol. Pathol.* 42(4):725–764, 2014.
- Rooney AA, Luebke RW, Selgrade MK, et al.: Immunotoxicology and its application in risk assessment, *Exper. Suppl. (Basel)* 101:251–287, 2012.
- Saber H, Del Valle P, Ricks TK, Leighton JK: An FDA oncology analysis of CD3 bispecific constructs and first-in-human dose selection, *Regul. Toxicol. Pharmacol.* 90:144–152, 2017, <https://doi.org/10.1016/j.yrtph.2017.09.001>. Epub 2017 Sep5. PMID: 28887049.
- Sacalan DB, Lucero JA: The association between inflammation and immunosuppression: implications for ICI biomarker development, *OncoTargets Ther.* 14:2053–2064, 2021.
- Seethapathy H, Herrmann AM, Sise ME: Immune checkpoint inhibitors and kidney toxicity: advances in diagnosis and management, *Kidney Med.* 3(6):1074–1081, 2021, <https://doi.org/10.1016/j.xkme.2021.08.008>. PMID: 34939017; PMCID:PMC8664750.
- Sellers RS, Morton D, Michael B, et al.: Society of Toxicologic Pathology position paper: organ weight recommendations for toxicology studies, *Toxicol. Pathol.* 35(5):751–755, 2007.
- Seymour R, Sundberg JP, Hogenesch H: Abnormal lymphoid organ development in immunodeficient mutant mice, *Vet. Pathol.* 43(4):401–423, 2006.
- Shannon VR: Pneumotoxicity associated with immune checkpoint inhibitor therapies, *Curr. Opin. Pulm. Med.* 23(4): 305–316, 2017.
- Simon AK, Hollander GA, McMichael A: Evolution of the immune system in humans from infancy to old age, *Proc. Biol. Sci.* 282(1821):20143085, 2015.
- Skaggs H, Chellman GJ, Collinge M, et al.: Comparison of immune system development in nonclinical species and humans: closing information gaps for immunotoxicity testing and human translatability, *Reprod. Toxicol.* 89:178–188, 2019.
- Skydsgaard M, Dincer Z, Haschek WM, et al.: International harmonization of nomenclature and diagnostic criteria (INHAND): nonproliferative and proliferative lesions of the minipig, *Toxicol. Pathol.* 49(1):110–228, 2021.
- Snyder PW: Immunology for the toxicologic pathologist, *Toxicol. Pathol.* 40(2):143–147, 2012.



- Suntharalingam G, Perry MR, Ward S, et al.: Cytokine storm in a phase 1 trial of the anti-CD28 monoclonal antibody TGN1412, *N. Engl. J. Med.* 355(10):1018–1028, 2006.
- Szebeni J: Complement activation-related pseudoallergy: a stress reaction in blood triggered by nanomedicines and biologicals, *Mol. Immunol.* 61(2):163–173, 2014.
- Taraseviciute A, Tkachev V, Ponce R, et al.: Chimeric antigen receptor T cell-mediated neurotoxicity in nonhuman primates, *Cancer Discov.* 8(6):750–763, 2018.
- Taub DD: Neuroendocrine interactions in the immune system, *Cell. Immunol.* 252(1–2):1–6, 2008.
- Tilney NL: Patterns of lymphatic drainage in the adult laboratory rat, *J. Anat.* 109(Pt 3):369–383, 1971.
- Tobin GA, Zhang J, Goodwin D, et al.: The role of eNOS phosphorylation in causing drug-induced vascular injury, *Toxicol. Pathol.* 42(4):709–724, 2014.
- Tomlinson L, Boone LI, Ramaiah L, et al.: Best practices for veterinary toxicologic clinical pathology, with emphasis on the pharmaceutical and biotechnology industries, *Vet. Clin. Pathol.* 42(3):252–269, 2013.
- Tomlinson L, Ramaiah L, Tripathi NK, et al.: STP best practices for evaluating clinical pathology in pharmaceutical recovery studies, *Toxicol. Pathol.* 44(2):163–172, 2016.
- Travlos GS: Histopathology of bone marrow, *Toxicol. Pathol.* 34(5):566–598, 2006.
- Tsafaras GP, Ntontsi P, Xanthou G: Advantages and limitations of the neonatal immune system, *Front. Pediatr.* 8:5, 2020.
- Tsoli M, Boutzios G, Kaltsas G: *Immune system effects on the endocrine system*, South Dartmouth (MA), 2000, MDText.com, Inc.
- U. S. Food and Drug Administration: *S8 immunotoxicity studies for human pharmaceuticals*. Retrieved from July 3, 2024, <https://www.fda.gov/regulatory-information/search-fda-guidance-documents/s8-immunotoxicity-studies-human-pharmaceuticals>.
- U. S. Food and Drug Administration (FDA). Nonclinical evaluation of the immunotoxic potential for pharmaceuticals, 2023. Retrieved from July 3, 2024, <https://www.fda.gov/media/169117/download>.
- U. S. Food and Drug Administration; Center for Drug Evaluation and Research; Center for Biologics Evaluation and Research: *Guidance for industry: S6 Preclinical safety evaluation of biotechnology-derived pharmaceuticals*. Retrieved from July 3, 2024, <https://www.fda.gov/media/72028/download>.
- Van den Broeck W, Derore A, Simoens P: Anatomy and nomenclature of murine lymph nodes: descriptive study and nomenclatory standardization in BALB/cAnNCrl mice, *J. Immunol. Methods* 312(1–2):12–19, 2006.
- Van Rees EP, Siminia T, Dijkstra CD: Structure and development of the lymphoid organs. In Mohr UD, Capen CC, Dungworth DL, Sundberg WW, Ward JP, M J, editors: *Pathobiology of the aging mouse*, Washington, DC, 1996, ILSI Press, pp 173–187.
- Waldman AD, Fritz JM, Lenardo MJ: A guide to cancer immunotherapy: from T cell basic science to clinical practice, *Nat. Rev. Immunol.* 20(11):651–668, 2020.
- Wancket LM: Regional draining lymph nodes: considerations for medical device studies, *Toxicol. Pathol.* 47(3):339–343, 2019.
- Weaver CT, Murphy KM: T-cell subsets: the more the merrier, *Curr. Biol.* 17(2):R61–R63, 2007.
- Wick MJ, Harral JW, Loomis ZL, et al.: An optimized Evans blue protocol to assess vascular leak in the mouse, *J. Vis. Exp.* 139, 2018.
- Willard-Mack CL: Normal structure, function, and histology of lymph nodes, *Toxicol. Pathol.* 34(5):409–424, 2006.
- Willard-Mack CL, Elmore SA, Hall WC, et al.: Non-proliferative and proliferative lesions of the rat and mouse hemolymphoid system, *Toxicol. Pathol.* 47(6):665–783, 2019.
- Willis JC, Lord GM: Immune biomarkers: the promises and pitfalls of personalized medicine, *Nat. Rev. Immunol.* 15(5): 323–329, 2015.
- Wojcinski ZW, Andrews-Jones L, Aibo DI, Kikkawa R, Dunstan R: Chapter 21: Skin. In Sahota PS, Popp JA, Hardisty JF, Gopinath C, Bouchard P, editors: *Toxicologic pathology: nonclinical safety assessment*, ed 2, Boca Raton, 2019, CRC Press, pp 1021–1092.
- Yang J, Hu L: Immunomodulators targeting the PD-1/PD-L1 protein-protein interaction: from antibodies to small molecules, *Med. Res. Rev.* 39(1):265–301, 2019.

This page intentionally left blank

# Integument

Kelly L. Diegel<sup>1</sup>, Lydia Andrews-Jones<sup>2</sup>, Zbigniew W. Wojcinski<sup>3</sup>

<sup>1</sup>GSK, Collegeville, PA, United States, <sup>2</sup>AbbVie, Irvine, CA, United States, <sup>3</sup>Toxicology & Pathology Consulting LLC, Hillsborough, NC, United States

## OUTLINE

<b>1. Introduction</b>	<b>506</b>	<b>4. Responses to Injury</b>	<b>536</b>
<b>2. Structure and Function</b>	<b>506</b>	4.1. General Mechanisms of Response to Injury-Cutaneous Immunity	536
2.1. The Epidermis	508	4.2. Special Considerations-Translational Immunology of Skin	541
2.2. Melanocytes	511	4.3. Wound Healing	543
2.3. Merkel Cells	512	4.4. Influence of Skin Microbiome on Adaptive Immune Response	549
2.4. Langerhans Cells and Dermal Dendritic Cells	512	4.5. Specific Cutaneous Morphologic Lesions and Patterns of Injury	550
2.5. The Dermal-Epidermal Junction and Dermis	513	4.6. Neoplastic Lesions and Carcinogenesis Models	554
2.6. The Subcutis	515	<b>5. Mechanisms of Toxicity</b>	<b>559</b>
2.7. The Adnexa	515	5.1. Direct Cutaneous Toxicity	559
2.8. The Minipig in Dermal Toxicity Assessment	518	5.2. Immune-Mediated Cutaneous Toxicity	565
2.9. Physiology and Biochemistry of the Integument	520	5.3. Mechanisms of Toxicity: Photosafety	568
2.10. Percutaneous Absorption	520	5.4. Mechanisms of Toxicity: Photoaging	572
2.11. Metabolism and the Integument	522	5.5. Mechanisms of Toxicity: Antisense Oligonucleotides	572
<b>3. Evaluation of Toxicity</b>	<b>523</b>	5.6. Mechanisms of Toxicity: Pigmentation	573
3.1. Physiologic and Morphologic Safety Evaluation Strategies and Techniques	523	5.7. Mechanisms of Toxicity: Adnexa—General and Specific Toxicities	574
3.2. Special Considerations in Design of Topical Dermatologic Studies	527	<b>6. Conclusion</b>	<b>576</b>
3.3. Skin Sample Collection Techniques	528	<b>Acknowledgments</b>	<b>577</b>
3.4. Special Techniques	531	<b>References</b>	<b>577</b>
3.5. Three-Dimensional In Vitro Skin Model Systems	534		



## 1. INTRODUCTION

The integument is one of the most dynamic and important of organs. The skin has a unique role as a first-line defense against numerous environmental insults (e.g., physical trauma, temperature fluctuations, infectious and chemical agents, UV radiation), thus the health of the skin impacts and reflects the health of the organism. Beyond barrier function, the skin is also important as a neurosensory organ, acts as an endocrine organ, is an essential component of the immune system, aids in locomotion, and has essential psychologic/behavioral functions in many species. In toxicologic pathology, the skin may represent a target organ for those compounds that make direct contact with it via topical or systemic exposure, or as an indirect target of dysfunction of other organ systems such as the endocrine or immune systems. The skin may also reflect changes in other internal organs (e.g., jaundice), and serves as an external reflection of various internal pathophysiologic conditions.

Because the skin is often the first organ exposed to exogenous chemicals and environmental conditions, it is not surprising that skin disease is one of the most common concerns in occupational health. Skin toxicity in the workplace is most-commonly encountered as contact dermatitis (contact or allergic) in response to chemical exposure. In the United States, the economic impact of occupational contact dermatitis alone is estimated to be over \$1.5 billion per annum (Milam et al., 2020). Workers in industries such as manufacturing are historically considered most at risk for these exposures, but during the COVID-19 pandemic, increased incidences of occupationally induced dermatoses in healthcare workers was also reported in response to the use of sanitizing agents and even personal protective equipment (Sawada, 2023). Careers that involve exposure to radiation or any number of physical conditions (sun, heat, cold, moisture) may also result in skin disease. Beyond contact dermatoses, workplace skin toxicity may manifest as wounds or burns, infections, and even cancer (Peate, 2002).

In drug development, adverse skin reactions are also a significant clinical concern. Drug eruptions in the clinical setting range from those of limited severity (erythematous and urticarial) to life-threatening (Stevens–Johnson syndrome [SJS] and toxic epidermal necrolysis). Unique

immunologically related presentations of skin toxicity have become more commonly recognized with the industry's increased focus on biologic or "large molecule" drugs. Acneiform rash is reported with epidermal growth factor receptor (EGFR) inhibitors, injection or infusion site reaction and psoriasiform or lichenoid dermatoses with tumor necrosis alpha antagonists (Pasadyn et al., 2020) and a full spectrum of cutaneous and even systemic side effects for immune checkpoint inhibitors (Tattersall and Leventhal, 2020). Both treatments and prophylactic agents can be implemented in cutaneous adverse events. Most recent is the example of urticaria and "COVID arm" following vaccination and more serious immunologically driven cutaneous angiopathy that is also reported.

## 2. STRUCTURE AND FUNCTION

The structure of the integument varies depending on the species. The skin of each of these species is unique, with adaptations reflecting the environment in which it lives. The following overview focuses on the essential elements of the skin common to animal models used in toxicity studies and humans: the epidermis, dermis, subcutis, and adnexa. For a further review of the anatomy, structure, and function of the skin, the reader is referred to Ali and Oehme (1992), Diegel et al. (2018), Welle and Linder (2022), Lazar and Murphy (2020), Proksch et al. (2008).

Although there are aspects of the morphology of the integument that are unique to a given species, there are several aspects common to all species discussed and are the basis of comparative dermatology. For example, the thicker the hair coat, the thinner the skin. Since hair is in part protective, the need for a thick epidermis in furred animals is not as great as it is in sparsely haired animals, for example, pigs and humans. The latter tend to have compensatory thick epidermal layers for additional protection in the absence of thick fur. The hair follicle density of the rat is more than 30 times that of the human, while the epidermis of the rat is less than one-fourth the thickness of human epidermis. It also follows that a thicker epidermis needs a thicker dermis for support. As epidermal thickness increases, so too does the dermal contribution to overall skin thickness (Table 7.1).

**TABLE 7.1** Comparison of Features of Skin from Major Laboratory Animal Species and Human

Species	Hair follicle density (per cm <sup>2</sup> )	Skin-full thickness (μM)	Epidermal thickness (μM)	Stratum corneum thickness (μM)
Human	Body 14–32, Forehead 292 <sup>a</sup> Sparse, 11 <sup>b</sup>	2000–3000 <sup>b</sup>	50–120 <sup>b,c</sup>	8–20 <sup>b</sup>
Pig	Sparse, 11–31 <sup>b</sup>	1500–2000 <sup>b</sup>	30–140 (compiled <sup>b,c,d,e,h</sup> )	10–26 (compiled <sup>b,c,d,e,h</sup> )
Beagle dog	96	2477	21–29 <sup>e</sup>	5–9 <sup>e</sup>
Hamster	402	619	13.8	2–9
Haired Guinea pig (Hartley)	154 <sup>h</sup>	2418 <sup>h</sup>	63 <sup>h</sup>	29 <sup>h</sup>
Hairless Guinea pig	194 <sup>h,i</sup>	1731 <sup>f,g</sup>	115 <sup>h</sup>	36 <sup>h</sup>
Rabbit	229	2311	11–18 <sup>c,e</sup>	3–15 <sup>c,e</sup>
Rat, strain not specified	Thick, 289 <sup>b</sup>	1000–2000 <sup>b</sup>	22 <sup>b</sup>	5 <sup>b</sup>
Sprague–Dawley rat	342	1242	15	4
F-344 rat	219 <sup>h</sup>	1138 <sup>h</sup>	33 <sup>h</sup>	11 <sup>h</sup>
Mouse, strain not specified	658 <sup>b</sup>	400–1000 <sup>b</sup>	9–13 <sup>b</sup>	3 <sup>b</sup>
B6C3F1 haired mouse	384 <sup>h</sup>	518 <sup>h</sup>	21 <sup>h</sup>	6 <sup>h</sup>
SKH1 hairless mouse	79 <sup>h,i</sup>	475 <sup>h</sup>	47 <sup>h</sup>	10 <sup>h</sup>
Rhesus monkey	56 <sup>h</sup>	1492 <sup>h</sup>	35 <sup>h</sup>	4 <sup>h</sup>

<sup>a</sup> From *Otberg et al. (2004)*; with comparison in text to other publications<sup>b</sup> *Grambow et al. (2021)*.<sup>c</sup> *Uhm et al. (2023)*.<sup>d</sup> *Summerfield et al. (2015)*.<sup>e</sup> *Monteiro-Riviere et al. (1990)*.<sup>f</sup> *Sueki et al. (2000)*.<sup>g</sup> *Barbero and Frasch (2009)*.<sup>h</sup> *Grabau et al.*, skin full thickness calculated from sum dermal thickness and epidermal thickness, as reported.<sup>i</sup> Note that hairlessness caused by abnormal hair follicles, please see section on hairless animal models.

Except as noted, reprinted from Haschek WM, Rousseaux CG, Wallig MA, editors: Haschek and Rousseaux's Handbook of Toxicologic Pathology, ed 3, 2013, Academic Press, Table 55.1, p. 2220, with permission. It is acknowledged that skin thickness and hair follicle density varies with region of body, species, strain, age and gender of animals so values shown are approximations for comparative purposes. This information is compiled from multiple publications so experimental conditions were not constant. Values in publications rounded to whole numbers.

The thicker the epidermis, the more vascular the upper (papillary) dermis. This increased vasculature provides nutrients and flushes waste products from the avascular overlying epidermal layer. Since human skin has a thick epidermis relative to other species, it has a rich superficial vascular plexus in the papillary dermis. The abundant superficial dermal vascular network leads to an increased potential for systemic exposure to any material or xenobiotic, that can cross through the epidermis into the dermis. This ability to cross the epidermis is key to dermal exposure, as the epidermis is a primary barrier between internal systems and the environment. Therefore, individuals that have a thin epidermis or areas on the body with a relatively thin epidermis (e.g., facial skin) may also experience increased absorption of xenobiotics from the skin. Gender differences exist in skin thickness, for example, in female C57BL5 mice the epidermis is approximately 40% thicker and the subcutis is approximately 11-fold thicker as compared to male mice. In contrast, the entirety of the dermis is 190% thicker in male than in female C57BL5 mice ([Azzi et al., 2005](#)).

### 2.1. The Epidermis

The epidermis is the outermost layer of the skin, and is the main barrier to external insults. Morphologically, the epidermis is divided into layers named for positional and microscopic/submicroscopic features of cells in each layer: the stratum basale (SB), stratum spinosum (SS), stratum granulosum (SG), stratum lucidum (SL), and stratum corneum (SC) ([Figure 7.1](#)).

The SB is the deepest layer of the epidermis and is composed of progenitor cells that respond to continual cell turnover in more superficial layers. These cells mature to replace constantly shedding, anucleate squamous cells in the outer SC. Keratinocytes in the SB are attached to the basement membrane (dermal–epidermal junction [DEJ]) by hemidesmosomes.

The phospholipid content of the epidermis is highest in the SB, and gradually diminishes as keratinocytes differentiate. The SB also contains the interfollicular epidermal stem cell compartment. The molecular characterization of these cells includes p63 expression in the nucleus (i.e., a tumor suppressor that increases DNA repair, arrests the cell cycle, and induces

apoptosis of badly damaged keratinocytes), and high concentrations of  $\beta 1$  (i.e., mediators of adhesion to the extracellular matrix and regulators of initiation of terminal differentiation) and  $\alpha 6$  integrins (i.e., regulators of keratinocyte chemotaxis).

An additional subset in the SB is a group of slow-cycling basal cells with an ability to retain electrophiles that bind to DNA; thus, they have been termed carcinogen-retaining cells. These cells may play a role in the initiation phase of chemical carcinogenesis. Another group of cells located in the SB is morphologically distinguishable by their hyperbasophilic cytoplasm and condensed nuclear chromatin. They have been described in hyperplastic epithelia and especially in phorbol ester-treated epidermis ([Klein-Szanto et al., 1980](#)). These cells, known as dark basal keratinocytes, or simply dark cells, seem to be associated with epidermal hyperplasia and preneoplasia.

The desmosomes join neighboring cells of the next layer (SS) and give rise to artifactual spine-like formations between cells in fixed tissues, thus giving the layer its name. In the SS, synthesis of a number of proteins important to the differentiating keratinocyte begins, including involucrin, profilaggrin, and filaggrin.

In the next layer (SG), profilaggrin and filaggrin are present in the keratohyalin granules that give this layer its name. The granules appear as deep blue structures present in the cytoplasm in hematoxylin-and-eosin (H&E)-stained tissue sections. Profilaggrin is key to the coalescence and crosslinking of the keratin proteins that will become essential for lending strength to the corneocytes (i.e., keratinocytes that have completed their differentiation cycle) of the SC. Filaggrin is a precursor protein to natural moisturizing factor (NMF), an important amino acid component in the intercellular compartment of SC that helps maintain skin hydration and health.

Lamellar bodies are present in the SG and in the most superficial part of the SS. These are organelles, best classified as secretory lysosomes, that contain lipids released to form the lipid portion of the intercellular “mortar” of the corneocyte “bricks” of the SC. The lamellar bodies also contain hydrolytic enzymes such as acid protease, which aids in the process of desquamation, and proteins (e.g., defensins) that



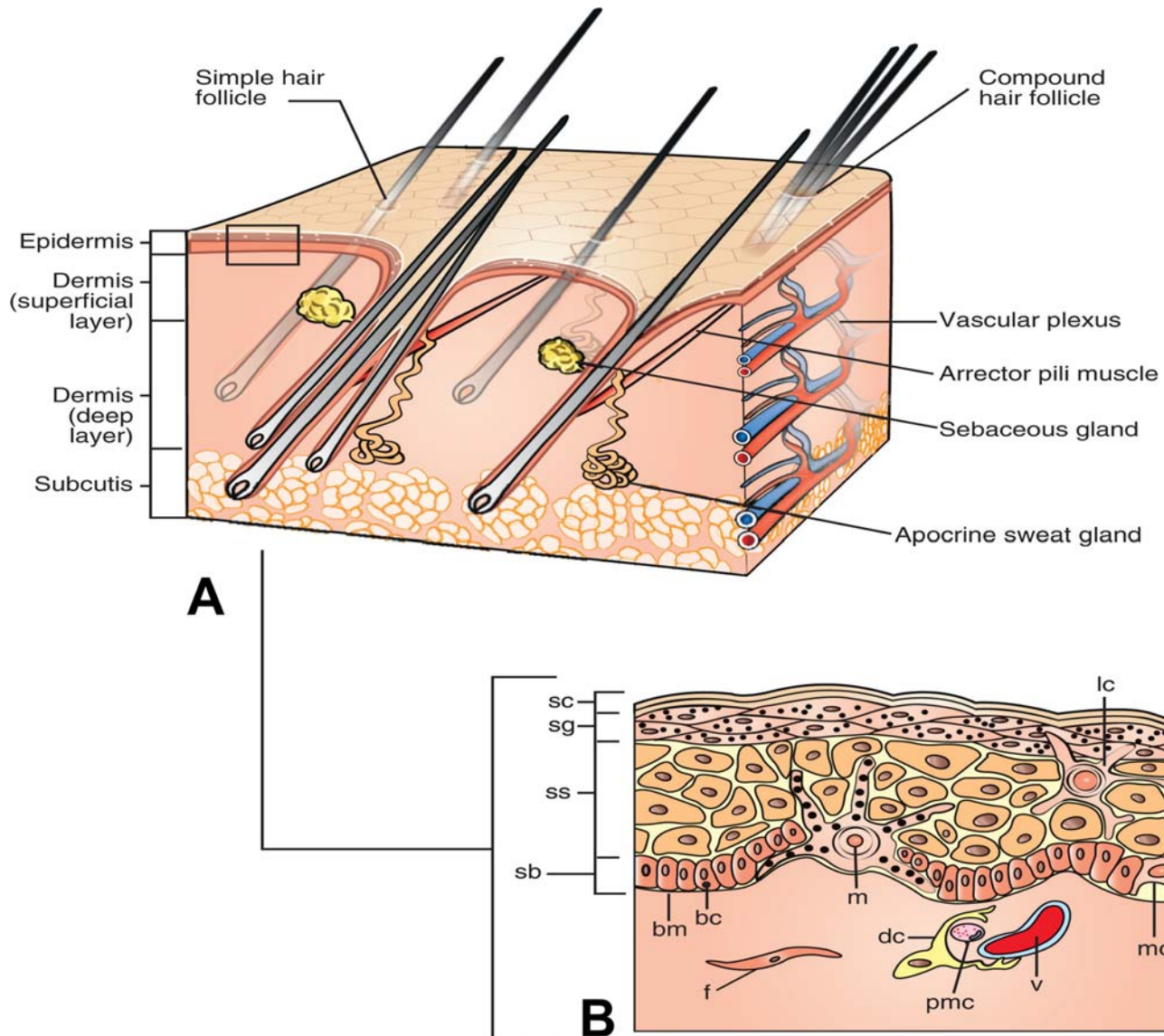


**FIGURE 7.1** Microanatomy of the skin. (A) Skin and its appendages. Note that hair follicles can be compound (more than 1 hair shaft) or simple (a single shaft). Dogs have compound follicles, rats have simple follicles, and humans have both types. (B) Epidermis: Basement membrane (bm), basal cells (bc), stratum basale (sb), stratum spinosum (ss), stratum granulosum (sg), stratum corneum (sc), melanocytes (m), Langerhans cells (lc), Merkel cells (mc). Dermis: Vessels (v), fibroblasts (f), perivascular mast cells (pmc), dermal dendritic cells (dc). *Reproduced from Welle MM, Linder DJ: The integument. In: Zachary JF, editor: Pathologic basis of veterinary disease, ed 7, 2022, Mosby Elsevier, Figure 17-1, p. 1096, with permission.*

contribute to barrier defense against pathogens. As the contents of the lamellar bodies are extruded and the nucleus and organelles of the keratinocyte are lost, the corneocyte is formed (Ishida-Yamamoto et al., 2004).

The SL is present only in specialized, thickened areas of skin (e.g., palmoplantar in humans; foot pads and nasal planum of dogs) and lies just beneath the SC. Microscopically, these cells

appear to have lightened or cleared areas of cytoplasm which represent specialized protein-bound lipid contents. The SL provides an extra layer of cornified cell “padding” to those areas exposed to repetitive friction, impact, or trauma.

Corneocytes are an important part of cutaneous barrier function and are tightly bound within the SC. Keratin intermediate filaments in the SC have high glycine, glutamic acid, and serine

concentrations, and they are crosslinked via disulfide linkages to form insoluble fibers during the process of differentiation. In a typical keratin fiber, a smaller acidic Type I fiber is linked to a larger neutral or basic Type II fiber. Combined pairs of keratin fibers are specific to types and subregions of epithelia. In stratified epithelia such as the skin, acidic fiber K14 forms a heterodimer with basic fiber K5 in the SB. Suprabasal layer cells of the epidermis are characterized by K1 in combination with K10. Molecular detection of expression of these keratin subtypes can be useful in determining cell origin in both healthy and disease states (Bragulla and Homberger, 2009).

Pathologic conditions of skin such as psoriasis or preneoplasia may alter the pattern of distribution of keratin filaments. For example, keratins 6, 16, and 17 are variably expressed in disease conditions marked by high epidermal turnover rates such as wound healing, psoriasis (Figure 7.2), and some skin cancers, but absent in healthy human adult skin. In experimental models, loss of high molecular weight keratins in epidermal cells is a marker of premalignancy (Moll et al., 2008; Zhang, 2018). Basal expression of K18/K8 is seen in some human squamous cell tumors (Zhang, 2018).

During the process of cornification, involucrin crosslinks with loricrin to help form the tough cornified cell envelope of the corneocyte with other proteins (i.e., trichohyalin and small proline-rich proteins, facilitated by transglutaminases), resulting in the outermost protective layer of the skin.

The process of cornification requires complex cell–cell communication and adhesion. The cytoskeleton of the epidermal keratinocytes has complex networks of proteins that include microtubules, actin filaments, and intermediate filaments (i.e., keratin). Synthesis of keratin in any of its forms is an almost exclusive characteristic of epithelial cells.

Cell–cell adhesion in any epithelial tissue is provided by specialized cell–cell junctions, primarily adherens junctions, desmosomes, and tight junctions. These cell–cell junctions not only form physical connections between cells but also function in the organization and regulation of cytoskeletal elements and signaling pathways that serve to regulate the “whole tissue” development, healing, structure, and physiology (reviewed by Sumigray and Lechler, 2015). Adherens junctions

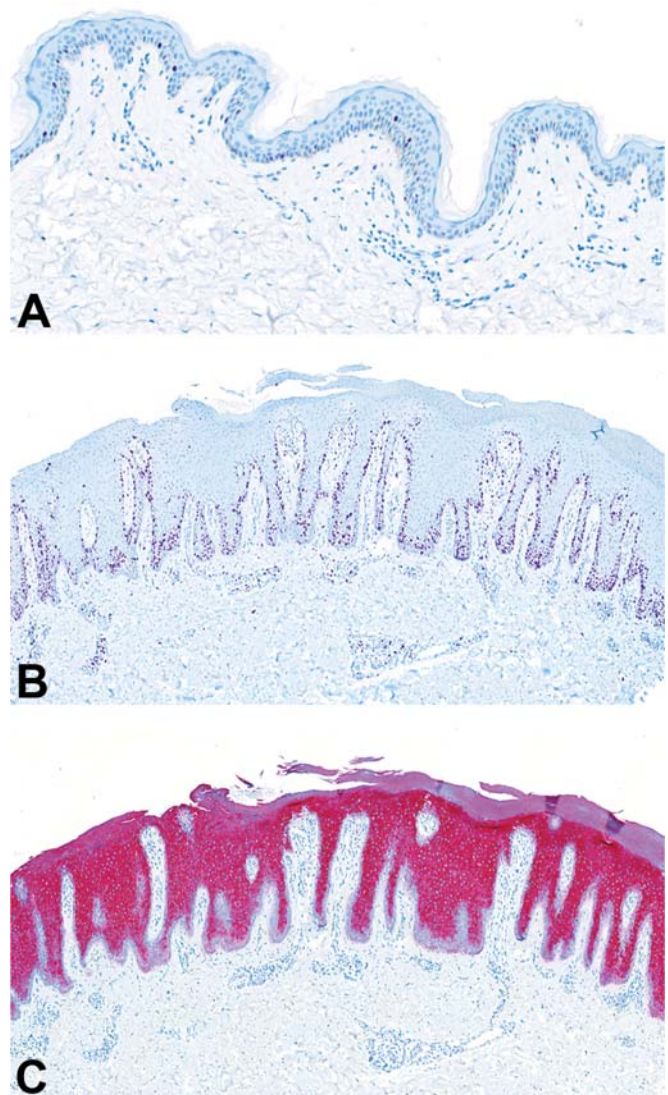


**FIGURE 7.2** Immunohistochemical staining of normal and psoriatic human skin. (A) Normal Ki67 expression (purple chromagen) in basal layer of healthy human skin. (B) Increased Ki67 expression (purple chromagen) in proliferative basal cells in skin from psoriasis patient. (C) Keratin 16 expression in suprabasilar epidermis (red chromagen) characteristic of increased turnover/hyperproliferative state of psoriatic skin. Keratin 16 expression is limited or absent in the epidermis of normal adult human skin, 4 $\times$ .

and desmosomes are found on the lateral apical membranes of basal cells and on all surfaces of suprabasal cells. Adherens junctions are cadherin-based that link the actin cytoskeleton to the plasma membrane and form physical linkages between adjacent cells. Adherens junctions contribute to cell motility and shape via links to



internal cytoskeletal components such as actin, and intracellular actin-binding  $\alpha$ -catenin. Transmembrane E-cadherin is the primary cadherin in interfollicular epidermis, and P-cadherin is expressed in both interfollicular and follicular epidermis. Desmosomes also form around transmembrane cadherin molecules, largely desmogleins and desmocollins. They represent the primary means of cell–cell adhesion in nucleated epidermal layers, and provide the majority of adhesive strength and resistance to mechanical stress. Autoantibodies to desmoglein 2 and 1 are the root cause of pemphigus vulgaris, and pemphigus foliaceus, respectively. Tight junctions, unlike adherens junctions and desmosomes, are not cadherin-based adhesion structures, but instead used claudins and occludins with varying expression patterns within different layers of the epidermis. Tight junctions are important for barrier function and preventing loss of fluids.

Intercellular cement composed of ceramides, cholesterol, cholesterol esters, and free fatty acids preserves water in deeper layers of the skin. Secretions from sebaceous glands and sweat glands (particularly in humans) form a water-oil emulsion film superficially in the SC, with antimicrobial properties and additional protection from cutaneous water loss. Equally important in barrier function is the cutaneous microbiome that resides within the superficial epidermis (Braff and Gallo, 2006; Seweryn, 2018; Grice and Segre, 2011). A balance between these “healthy” bacteria, fungi, and even arthropods such as *Demodex* spp. mites is essential in maintaining homeostasis in the skin. Environmental factors or disease can exacerbate pathogenic processes in the skin via alteration of the skin microbiome.

The keratinocyte life cycle as described above ranges from 5 to 30 days, depending on the anatomic site and state of health of the skin (reviewed by Houben et al., 2007). A few specialized cell types present in the skin deserve special mention with respect to the function of the skin as an organ.

## 2.2. Melanocytes

For a review of melanocytes and their function, the reader is referred to reviews by Park et al. (2009), Plonka et al. (2009), Sulaimon and Kitchell (2003).

Melanocytes are dendritic cells (DCs) derived from the neural crest and generate pigment in membrane-bound melanosomes. Melanocytes are located in the basilar epidermis in humans, but largely absent from interfollicular epidermis in most laboratory animal species/furred mammals. Melanocytes are also found in the eye, the cochlea of the ear, the brain/meninges, lung, and the heart of some species. Melanin in melanocytes provides a means by which the skin can defend against the potential genotoxic effects of harmful UV radiation. Melanin can also bind certain potentially harmful compounds such as cations and metals. Sparsely haired species, such as humans, rely largely on epidermal melanogenesis for protection from UV damage to the skin. By contrast, furred species have reduced or absent interfollicular epidermal melanogenesis (the process of melanin production), because their hair coat protects against UV absorption. However, in furred or feathered species, melanocytes provide pigmentation to the skin or fur that is necessary for behavioral aspects of survival, such as camouflage or sexual display in certain species.

Melanocytes can express class II MHC in response to various antigens and cytokines, and, like keratinocytes, are actively phagocytic antigen-presenting cells (APCs) that act as one of many cell types in the innate immune system of the skin. Melanocytes also express pattern recognition receptors (PRRs) and toll-like receptors (TLRs) and produce a number of cytokines (such as IL-1), type-I interferons, and a number of chemokines (Gasque and Jaffar-Bandjee, 2015).

Melanin contained in melanosomes is a tyrosine-based molecule important for protecting the skin against UV radiation. Melanogenesis is driven by a number of stimuli in the skin, the most important of which are signals from keratinocytes (including proopiomelanocortin precursors, nitric oxide, growth factors, endothelin 1, and various cytokines) and UV radiation exposure. Melanocyte function and survival are linked, in part, to their counterpart fibroblasts in the dermis. Dermal fibroblasts drive melanocyte function through eicosanoid and neurotrophin production (Archambault et al., 1995). Each melanocyte “serves” about 30–40 keratinocytes in the basal layers of the epidermis. Melanosomes are organelles derived from the



endoplasmic reticulum of melanocytes and serve as packages for transfer of melanin. Although the number of melanocytes remains constant, the production and transfer of melanosomes to keratinocytes can be up- or downregulated. Melanosomes form a cap overlying the nucleus of the recipient keratinocyte, thus protecting the nuclear DNA from harmful UV radiation.

The color imparted to follicular and epidermal keratinocytes depends on the ratios of melanin subtypes present in the melanosomes injected into their cytoplasm by melanocyte dendritic projections. The process is largely driven by keratinocyte “cross-talk” with melanocytes. Eumelanin is brown to black and is produced when agonists such as  $\alpha$ -MSH and ACTH engage melanocortin-1 receptors on melanocytes. The melanocortin receptor (MC1-R) agonist,  $\alpha$ -MSH, also acts as a skin protective agent, suppressing inflammation and stimulating DNA repair in addition to stimulating eumelanin synthesis. Pheomelanin is red to yellow and is regulated through melanocortin-1 receptor antagonism by agouti signaling protein (ASP) (reviewed by [Schaffer and Bolognia, 2001](#)).

Both melanin subtypes are dependent on tyrosinase (TYR) and TYR-related proteins for formation. Eumelanin is more photostable, insoluble, and better equipped to control the formation of potentially dangerous reactive metabolites. Pheomelanin is the soluble form of melanin, and its products include such reactive oxygen species, potentially leading to cell damage rather than protection. Genetic factors favoring a higher pheomelanin:eumelanin ratio in hair and keratinocytes, such as MC1-R mutations, are linked to greater risks for skin damage and neoplasia.

Pigmentation of the skin is not only important to mammalian species. Lower vertebrates, including many species of fish, reptiles, and amphibians, also have melanin-containing cells known as melanophores ([Kelsh, 2004](#)). Melanophores represent one of at least six known types of chromatophores in the skin of these species, many of which display an array of colorful skin phenotypes. Chromatophores may impart color to the cells in the skin by variable pigments that they can produce and the appearance of these pigments under white light. Melanophores (brown to black), xanthophores (yellow),

erythrophores (red), and cyanophores (blue) are examples of these types of cells. Also derived from neural crest cells, iridophores and leucophores are chromatophores that have the unique ability to move an array of crystals in response to neurosensory stimuli. Depending on the wavelengths of light reflected by shifts in the crystals, the color of the skin changes. The ability to shift granule positioning in the skin and underlying tissues allows species with such chromatophores to adjust skin pigment quickly, reacting to and reflecting their surroundings (reviewed by [Salim and Ali, 2011](#)).

### 2.3. Merkel Cells

Arranged along the base of the epidermis and outer hair follicle, Merkel cells are a nonneuronal mechanosensory cell involved with the sensation of touch (reviewed by [Bataille et al., 2022](#)). They represent a cell type unique to the skin and oral mucosa that are mechanoreceptors with dense granules containing neurotransmitter-like mediators (e.g., synaptophysin, met-enkephalin, vasoactive intestinal peptide, neuron-specific enolase, acetylcholine, calcitonin gene-related peptide, and chromogranin A). They also contain cytokeratins (e.g., K20 is specific for Merkel cells in the skin, although it may also be present in cells of other organs, including the small intestine, colon, urothelium, and uterus), providing evidence for an epithelial origin. These cells form complexes with somatosensory nerve fibers. The dendrites of the Merkel cells contact unmyelinated axons in the epidermis where they function together as a unit (tylotrich pads) to signal adnexal secretions (sweat), changes in blood flow, and tactile sensation, and possibly serve in a paracrine function along with other cells of the skin.

### 2.4. Langerhans Cells and Dermal Dendritic Cells

Langerhans cells (LCs) and dermal dendritic cells (DDCs) are bone marrow monocyte-lineage derived cells that are key components of adaptive and innate immune defense in the epidermis and dermis, respectively. LCs are the primary epidermal DC populations and are spaced regularly throughout the suprabasilar

epidermal layers. LCs adhere to keratinocytes, through desmosomal and tight junction attachments. They represent 1%–3% of the total epidermal cell count, varying dependent upon the anatomic location. LCs are characterized by CD45 expression. Also characteristic of LCs is CD1a expression and the presence of the c-type lectin langerin (CD207) held in ultrastructurally visible, racquet-shaped organelles called Birbeck granules. In healthy skin, these cells are relatively inactive but may attenuate an inflammatory response. They are able to preferentially respond to specific or severe foreign antigens, thereby preventing continual upregulation of inflammatory mediators whenever foreign antigens are sensed, which is nearly constant in the skin.

LCs interact with other DC populations in the skin. Generally, similar to LCs, DDCs are important in cutaneous innate and adaptive immunity. The combined efforts of LCs and DDCs in the skin result in immune defense responses unique to the skin and harnessing these responses has been the science that drives new innovation in vaccine delivery, among other therapeutic modalities. More detailed information on the role of LCs, DDCs, and other cutaneous DC populations important in cutaneous immunity and response to injury is presented below in [Section 4](#), Response to Injury. Please also refer to reviews by [Zhou et al. \(2022\)](#) and [Scheib et al. \(2022\)](#).

## 2.5. The Dermal–Epidermal Junction and Dermis

The DEJ aids in barrier function (both from and into epidermis), allows for firm attachment of epidermis to dermis, aligns cells of the epidermis, and serves as a base for reepithelialization in wound healing. The outermost DEJ is formed largely by basal keratinocyte plasma membranes and their attachments, hemidesmosomes ([Figure 7.3](#)). These link to the lamina lucida, the weakest zone of the DEJ, and are composed of fibronectin, nidogen, laminin/integrin subunits, and bullous pemphigoid antigens. Elements of the lamina lucida are attached to the underlying lamina densa, a strong collagenous layer derived from collagens IV and V and crosslinking elements. Collagens that attach the DEJ to the dermis include anchoring fibrils

(Type VII collagen) of the sublamina densa. This area contains a number of collagens, procollagens, and early elastic fiber components (oxytalan).

The dermis gives the skin tensile strength through collagen, contributes to movement by allowing stretch through elastic fibers, has immune regulatory capabilities, contains vascular and neurologic elements important for communication with the epidermis and environment, and forms the matrix for adnexa. The dermis largely determines the thickness of skin and is contiguous. Subregions of the dermis in humans are termed papillary and reticular. In most lab animal species, epidermal rete ridges are not present so these subregions are usually simply described as superficial and deep, respectively. The primary components of the dermis are collagens and elastins that confer tensile strength, and proteoglycans, glycosaminoglycans, and hyaluronans that help dissipate pressure forces.

The superficial dermis contains small collagen fibers and numerous small elastic fibers or elastic fiber precursors arranged in a loose meshwork. Fibroblasts are also present superficially and deep, and produce important dermal matrix components. The deep dermis has larger bundles of both collagen and a few mature elastic fibers arranged in parallel to the epidermis. Dermal collagen is primarily Type I, with Types III and V present in smaller amounts.

Nerves in the skin are both sensory and motor. Many sensory nerve endings interact with specialized corpuscular units (mechanoreceptors such as Merkel cells and Pacinian or Meissner's corpuscles, nociceptors, thermoreceptors) responsible for pressure, sensing movement, itch/pain, and temperature. The hair follicles are also surrounded by sensory axons. Motor innervation is from sympathetic autonomic nerves and responds to either cholinergic or adrenergic stimuli. Cholinergic activity in the skin induces responses like vasodilation. Adrenergic responses include vasoconstriction, apocrine gland secretion, and hair follicle positioning. Eccrine sweat glands are under cholinergic control; however, these glands are largely absent in most areas of nonhuman mammalian skin.

Dermal vasculature is rich and complex. Superficial, middle, and deep vasculature

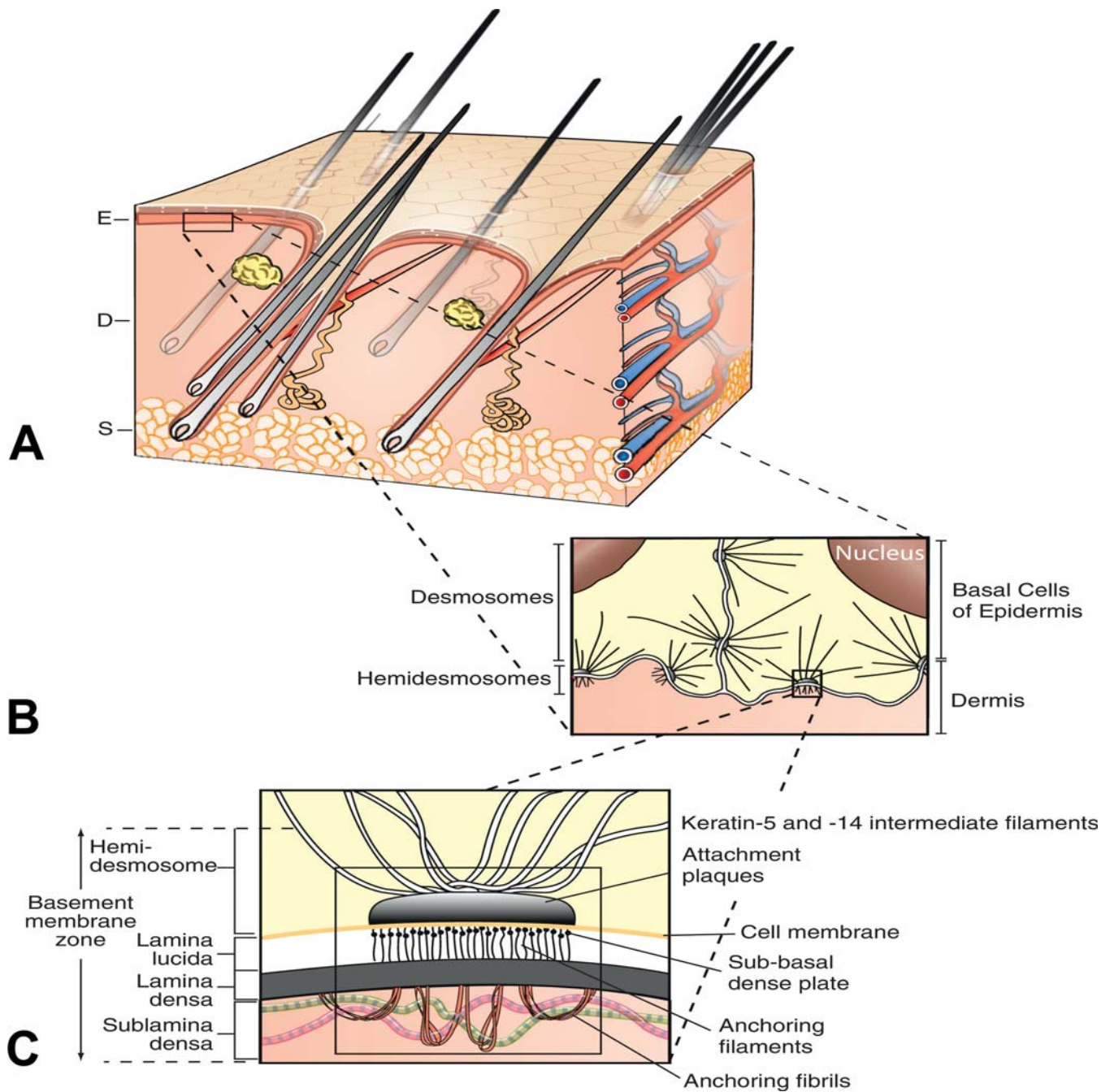


**FIGURE 7.3** Detailed structure of the dermo-epidermal junction. A. Skin epidermis (E), dermis (D), and subcutis (S). B. Detail of basal layer of stratum corneum with desmosomes attaching keratinocytes and hemidesmosomes attaching keratinocytes to basement membrane. C. Detail of basement membrane attaching to basal keratinocyte via hemidesmosome. Modified from Welle MM, Linder DJ: *The integument*. In: Zachary JF, editor: *Pathologic basis of veterinary disease*, ed 7, 2022, Mosby Elsevier, Figure 17-4, p. 1099, with permission

plexuses supply corresponding layers of the skin. Arteriovenous anastomoses are common in the skin of the extremities in particular and are necessary for frequent changes in temperature and blood pressure. These junctions respond

to vasoconstrictors and vasodilators such as epinephrine and histamine. Many vessels of the skin have relatively thick walls compared to those of similar size in internal organs, which protects the skin against shear and pressure



forces. Also present in the dermis are the fibroblast-like veil cells that define spaces for vessels within the dermis, and create a perivascular space.

Cutaneous lymphatics arise as capillaries in the superficial dermis, but deep to the most superficial blood capillaries. Gaps within the lymphatic vessels form channels by linking with the dermal matrix, and channel fluids from the dermis into the lymphatic system. Lacking smooth muscle and pericytes, lymphatics of the dermis rely on subcutaneous muscle contraction, pressure of the surrounding matrix, and associated blood vessel movements to initiate flow of immunologic, waste, and even degraded pathogenic and xenobiotic materials away from the dermal interstitium. In the deeper subcutis, lymphatics have smooth muscle walls and are actively contractile, directly directing the flow of lymph to and from the skin.

## 2.6. The Subcutis

The subcutis is the adipose-rich tissue beneath the dermis responsible for attachment to underlying muscle, fascia, or periosteum. Connective tissue septa present throughout the subcutis facilitate movement and support dense vessel and nerve networks in the tissue. This layer also serves to absorb shock to underlying structures, shape the external features of the organism, and regulate temperature. The rich triglyceride stores of the subcutis can be utilized as an energy store and also serve to protect underlying tissues from temperature extremes. Visceral and subcutaneous adipose stores are also important in the secretion and targeting of various hormones and cytokines. In contrast to visceral adipose stores, it appears that the adipose tissue of the subcutis is better equipped for efficient lipolysis and less apt to secrete inflammatory cytokines, making it a compelling target for metabolic disease therapies (Gil et al., 2011).

An important component of the subcutis of most laboratory animal species is the panniculus carnosus skeletal muscle layer, which allows for skin “twitch” movement. This layer is largely absent (present only as vestigial remnants) in humans and is present only in restricted anatomic sites in the minipig. This component of the hypodermis should be considered when

designing studies and interpreting findings in injection sites in laboratory animals, as the muscle layer can limit distribution of injected materials and may be involved in adverse injection site reactions (e.g., myocyte degeneration/regeneration, inflammation, etc.).

## 2.7. The Adnexa

The cutaneous adnexal unit refers to a hair follicle, the associated arrector pili muscle, and associated glands. The hair follicle itself is essentially a downgrowth of the epidermis (Figures 7.4 and 7.5). The arrector pili muscle attaches to the hair follicle and has roles in piloerection and gland secretion that are under cholinergic control. The hair shaft is composed of an inner medulla, a surrounding cortex, and an outer cuticle. The hair follicle has subanatomic regions known as the infundibulum (from the surface epidermis to the sebaceous gland duct entrance to the hair follicle), the isthmus (just below the infundibulum, from the sebaceous duct to the arrector pili muscle insertion), and the inferior segment (from the isthmus deep to the dermal papilla). The external root sheath that contains the hair is contiguous with the surface epidermis.

The internal root sheath is attached to the cuticle of the hair and is distinguishable in tissue sections by the presence of eosinophilic cytoplasmic trichohyalin granules. The dermal papilla is at the base of the follicle. It is a connective tissue-based appendage of the dermis itself that is covered by mitotically active epithelial cells that contribute to hair growth, the hair matrix. In humans and mice, a structure known as the “bulge” is attached to the outer root sheath near the insertion of the arrector pili muscle. The bulge is charged with supplying the adnexal unit and, in some instances, the surface epidermis (e.g., wound healing) with pluripotent stem cells for regeneration (Review by Charruyer and Ghadially, 2011). The bulge area may be absent in other species, with stem cells being present in infundibular and isthmus regions of the follicle itself, although some research does support bulge cell presence in the dog (Kobayashi et al., 2010).

Hair follicles can be simple, with a single hair shaft in each follicle, or compound, with multiple shafts in each follicle. Most lab animal species

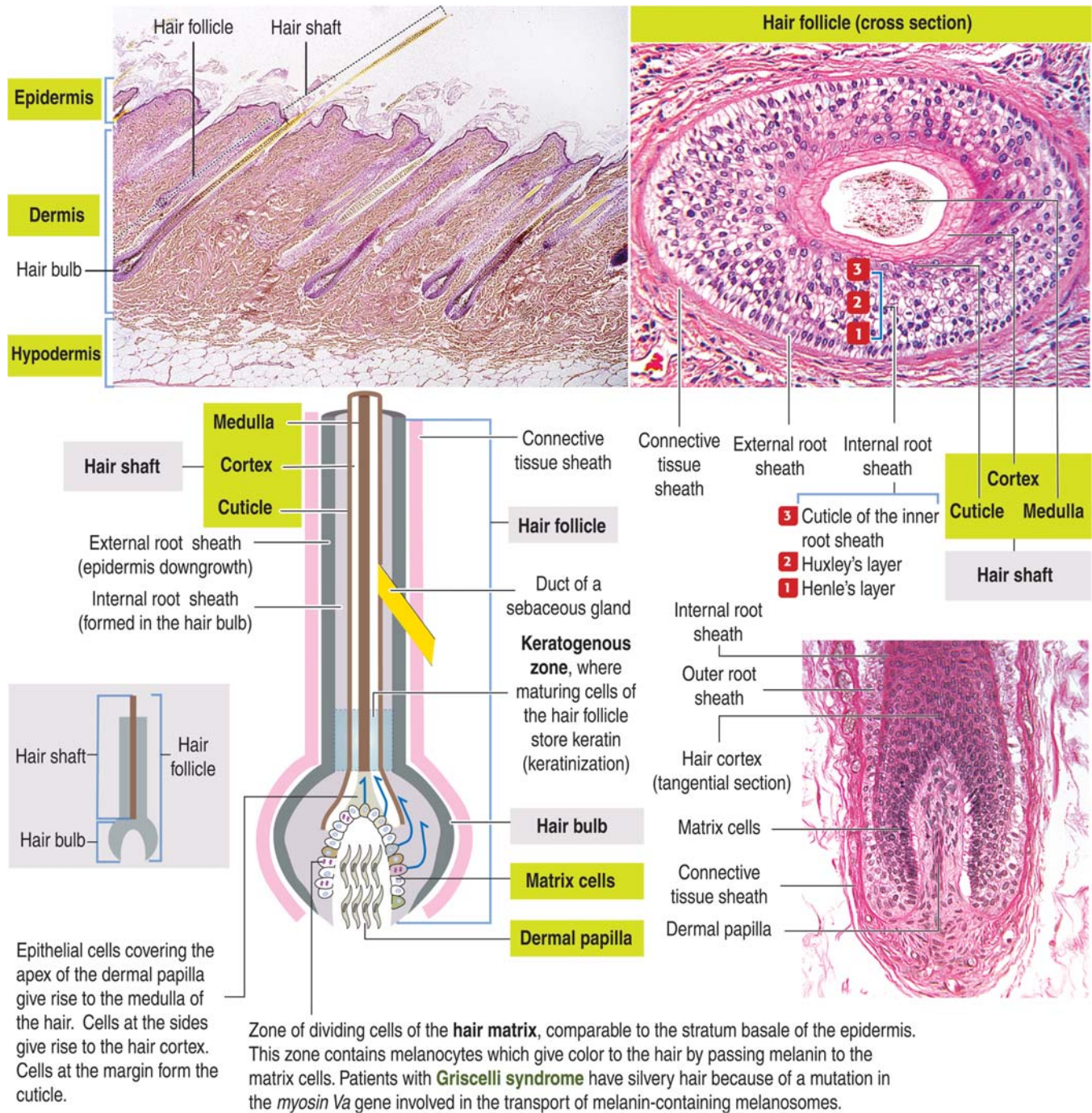


**FIGURE 7.4** Structure of the hair follicle. From Kierszenbaum L, Tres L: *Histology and cell biology: An introduction to pathology*, ed 5, 2019, Saunders Elsevier, Figures 11–16, p. 410, with permission.

have simple follicles, apart from dogs and rabbits. Humans, sheep, and goats have both simple and compound follicles. Simple follicles can be further classified as primary (guard) hairs and secondary (wool/undercoat) hairs. Primary follicles are larger and cover the fur layer formed

by secondary hairs in many furred species. Dogs may have both hair types in a single follicle (Welle and Wiener, 2016; Welle, 2023).

Hair growth is divided into stages: anagen (active growth), catagen (transition phase), telogen (resting stage), and exogen (shedding).



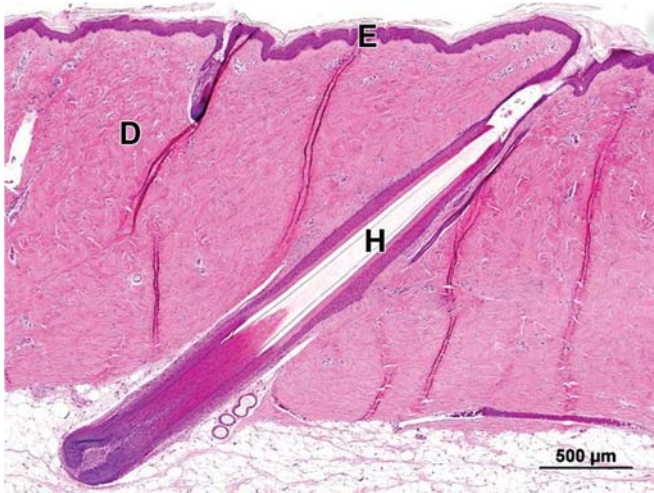


**FIGURE 7.5** Simple hair follicle in the skin of a Göttingen minipig. E, epidermis; D, dermis; H, hair follicle. H&E.

During hair growth, an ordered array of keratinized cells is gradually pushed upward in the form of hair shafts. These cells give rise to hair by a process of terminal differentiation, analogous to but more complicated than the process described for epidermal cornification. Keratinization of hair follicle cells is of four morphologic subtypes: infundibular (like the surface epidermis, featuring keratohyalin), trichilemmal (important in identification of catagen hairs, dense eosinophilic keratin “flames”), trichogenic/matrical (“ghost cell” keratinization), and medullary/inner root sheath (with deeply eosinophilic trichohyalin granules). Hair follicles renew from the dermal papilla, which regresses but does not disappear as the hair follicle proceeds through the hair cycle. As the hair follicle enters anagen once again, the dermal papilla becomes active and begins to grow, leading to generation of a new hair shaft (Figure 7.6) (Schneider et al., 2009). Following exogen, a small subset of follicles may enter a stage known as kenogen, which is also called hairless telogen. Although kenogen is normally followed by anagen in health, larger numbers of kenogen hairs that do not transition into telogen and instead undergo atrophy are present in some nonscarring alopecias (Welle, 2023). Atrophy and subsequent loss of the dermal papilla leads to permanent loss of the hair follicle, as is seen with certain types of alopecia

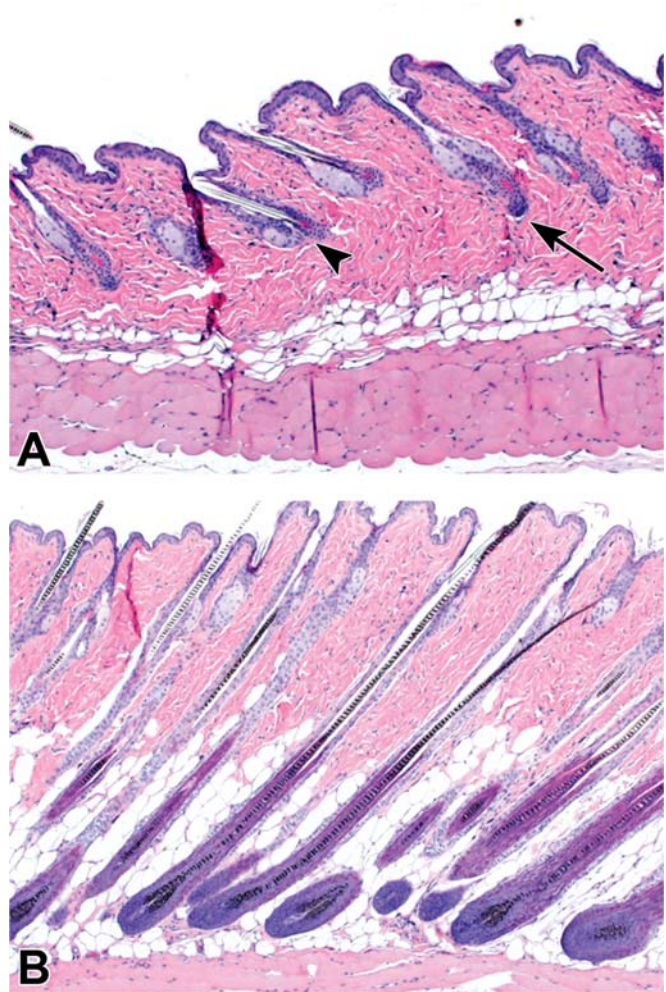


**FIGURE 7.6** Skin from C57Bl6 mice. (A) Telogen (resting phase) hair follicles to left, with early anagen/catagen hair follicles to right. Note lack of dermal papilla in telogen follicles (arrowhead) but beginning growth of dermal papillae (arrow) in transitioning hair follicles. Also note the thickening of overall dermis in area of beginning growth, and that the entirety of hair follicles remains within the dermis and does not extend into adipose layer. (B) Anagen phase hair follicles with large prominent dermal papillae extending down into adipose layer with thick hair follicles and hair shafts. H&E, 40 $\times$ .

including “male pattern baldness” (androgenic alopecia).

Of note, when shaved, normally haired mice regrow their hair coat in “waves” so that abrupt transitions occur between areas of actively growing anagen follicles, and resting telogen phase follicles (Figure 7.7) (Plikus and Chuong,



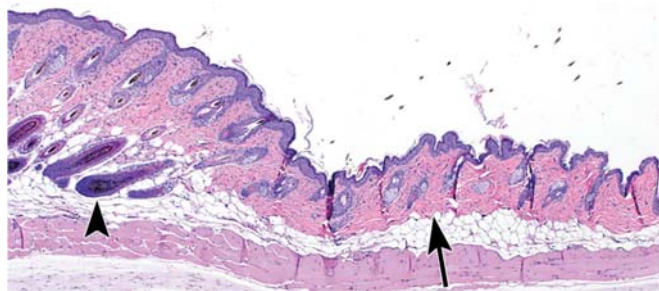


**FIGURE 7.7** Margin of hair growth “wave” in normal C57Bl6 mouse after shaving (left side). Arrowhead, area of active growth; arrow, area of resting follicles. H&E, 40 $\times$ .

2008). This is normal for mice and should not be mistaken for a test article-related effect.

Two types of sweat glands, eccrine and apocrine, have been described in mammals. Eccrine glands participate in thermoregulation by secreting water and salts directly to the epidermal surface. Although abundant throughout the skin in great apes and humans, eccrine sweat glands in domestic and laboratory animals are largely limited to the foot pads in dogs and the nasal planum and carpus of pigs. These are merocrine glands (secreting by vesicular exocytosis) that are composed of a long coiled secretory tubule and a connecting long excretory duct which ends in the epidermis separate from the hair follicle; the epithelium lining both is simple columnar. The apocrine glands, which generally empty into the hair follicle at the level of the sebaceous gland, secrete a proteinaceous material (also in a merocrine fashion despite the nomenclature) that originates from the glandular epithelial cells. Their function is likely multifactorial, but they are related to accessory scent glands (e.g., porcine mental organ, eyelid/external ear glands, glands of the anal sac in dogs, etc.) that produce attractant odors in some species. While distributed generally over the skin of most species, apocrine glands in humans are limited to the armpits, groin, and nipples. Mammary glands are also modified apocrine glands specialized to produce milk.

Sebaceous glands develop from the neck or infundibulum of hair follicles and are composed of large polyhedral lipid-laden cells that undergo holocrine secretion after they are sloughed into the short duct to form sebum, composed of wax esters, squalene, free fatty acids, and

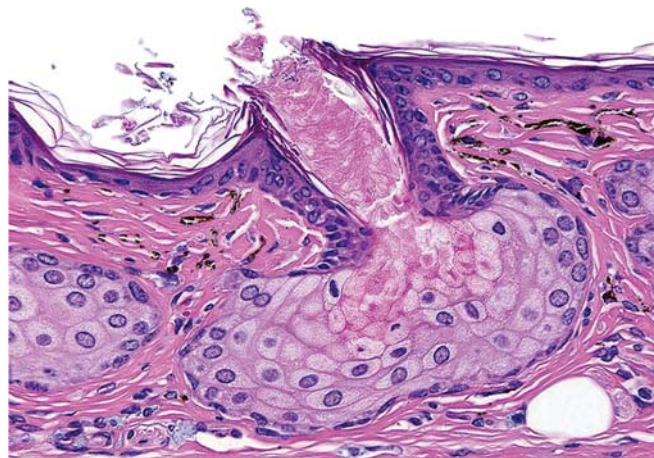


**FIGURE 7.8** Sebaceous glands in the ear of a normal male hamster: The large size makes the hamster an attractive model for studies of sebaceous gland physiology/targeting. H&E, 40 $\times$ . Reproduced from Haschek WM, Rousseaux CG, Wallig MA, editors: *Haschek and Rousseaux's handbook of toxicologic pathology*, ed 3, 2013, Academic Press, Figure 55.4, p. 2228, with permission.

triglycerides. Sebum is discharged into the infundibulum of the hair follicles and spreads to the epidermal surface, where it helps to keep the SC moist and has antimicrobial function derived from free fatty acids. There are large sebaceous glands in some species (e.g., chin glands in cats, tail glands in dogs, etc.) that also likely have scent marking, tactile, or pheromonal roles. Male hamsters have large aural sebaceous glands, making the hamster a popular animal model for testing compounds targeting sebaceous gland activity (Figure 7.8).

## 2.8. The Minipig in Dermal Toxicity Assessment

Unlike many other major organs, there are very distinct differences in skin structure among laboratory animal species and between these species and humans. Consequently, comparative evaluation of skin toxicity can be difficult to assess. Most species used commonly in toxicity evaluations (mice, rabbits, rats, guinea pigs, dogs, and nonhuman primates) have relatively dense fur covering much of their bodies, and as such, their skin serves as a poor comparator to human skin. The sparse hair covering of the laboratory minipig and the associated thicker

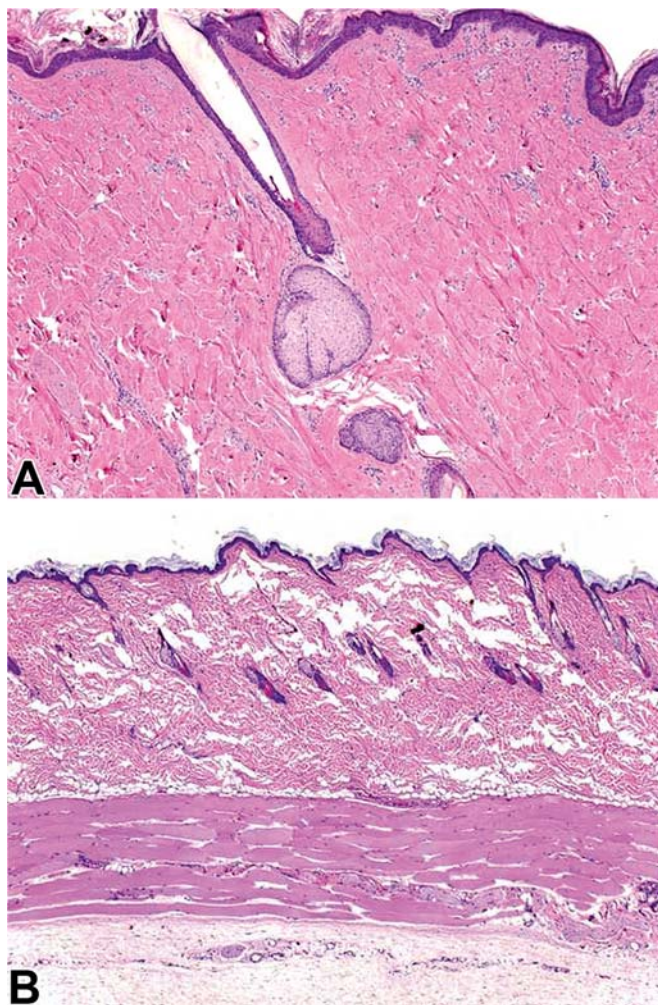


**FIGURE 7.9** Comparative photomicrographs of minipig (A) and rat (B) skin, taken at the same magnification. Note the difference in epidermal and dermal thickness, and adnexal distribution. Compare with [Figure 7.10](#). Reproduced from Haschek WM, Rousseaux CG, Wallig MA, editors: *Haschek and Rousseaux's handbook of toxicologic pathology*, ed 3, 2013, Academic Press, Figure 55.5, p. 2229, with permission.

epidermis most closely mimics the human skin, making it an attractive model in topical toxicity assessment ([Figures 7.9 and 7.10](#)).

There are several breeds of laboratory minipig, but one of the most commonly utilized for regulatory toxicology is the Göttingen, based on its small size (about 45 kg as an adult). (See *Animal Models in Toxicologic Research: Pig*, Vol 1, Chap 20). Like humans, the minipig has a papillary dermis with epidermal rete ridges. The cellular composition of the dermis and subcutis is also similar. Both humans and pigs have a relatively

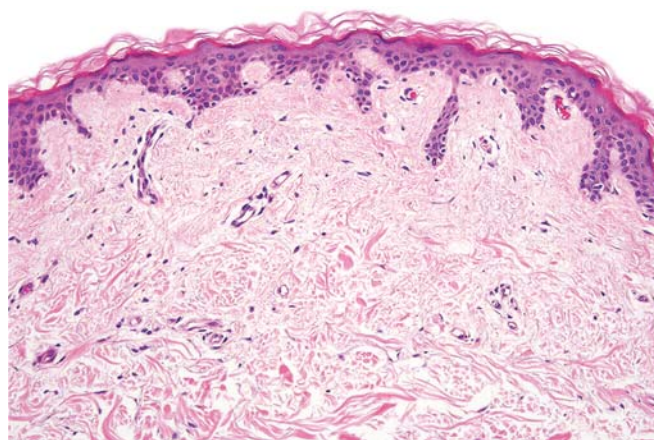


**FIGURE 7.10** Normal human skin: note similarities to minipig skin ([Figure 7.9](#)). Used with permission, Courtesy of Dr Phillip McKee. Reproduced from Haschek WM, Rousseaux CG, Wallig MA, editors: *Haschek and Rousseaux's handbook of toxicologic pathology*, ed 3, 2013, Academic Press, Figure 55.6, p. 2229, with permission.

thick dermis with a large elastic fiber component. The dermis tightly adheres to the underlying subcutis and musculature, and the dermal and subcutaneous vasculature and lymphatics are rich and similarly distributed. Also similar to humans, minipig skin thickens and has increased permeability with reduced effectiveness of wound healing with age. Enzymatic properties and drug metabolism in the epidermis and some adnexa also are comparable, as are lipid composition of the epidermis and sebum. Skin pH is slightly higher in the minipig (pH 6–7) compared to humans (pH 5–6).

There are even spontaneous models of human skin disease such as melanoma and bullous pemphigoid that exist in minipig strains (the Sinclair and Yucatan, respectively). Yet the thicker SC and increased subcutaneous fat deposition in minipigs are points of dissimilarity with humans. There are also some differences in the enzymatic profile of the skin, in the distribution of eccrine and apocrine sweat glands, and in the regulation of exogen (seasonal shedding phase of the hair growth cycle, as one example) as well. Still, the minipig appears to be the species best suited for comparative toxicology of the skin ([Meyer et al., 1978](#); [Simon and Mai-bach, 2000](#); [Swindle et al., 2012](#); [Mahl et al., 2006](#); [Makinen et al., 1997](#)).



## 2.9. Physiology and Biochemistry of the Integument

Of particular importance for epidermal homeostasis are the mechanisms that control epidermal growth and differentiation so that a steady state in epidermal thickness is maintained. Adenyl cyclase and cyclic nucleotide phosphodiesterase are active in the epidermis, and incremental increases in the cellular levels of cyclic AMP (c-AMP) inhibit proliferation of keratinocytes. In the epidermis, c-AMP levels appear to be regulated by autocrine factors (chalones) produced within the epidermis. Beta-adrenergic receptors, prostaglandins, histamine, and c-AMP may play a role in proliferative diseases, such as psoriasis, and in tumor promotion. In addition to the c-AMP-dependent protein kinase, it has been shown that protein kinase C (PKC) is also important in homeostasis of the skin, with expression in both keratinocytes and fibroblasts (Mitev and Miteva, 1999).

PKC is physiologically activated by diacylglycerol (DAG). DAG is released from the cell membrane along with inositol phosphate by phospholipase C. Inositol phosphate regulates intracellular calcium in epidermal cells. In tissue cultures, low levels of calcium (0–0.05 nM) in the medium maintain epidermal cells in a proliferative state, whereas higher calcium concentrations induce terminal differentiation. Calcium also is required for the activation of PKC. PKC can also be activated by phorbol esters and is believed to play a central role in tumor promotion. Many other mechanisms have also been implicated in epidermal regulation. For example, transforming growth factor-beta (TGF- $\beta$ ) appears to be an important negative growth factor.

Growth factors, including epidermal growth factor (EGF) and related ligands for the EGF receptor, fibroblast growth factor (FGF) family members, and insulin-like growth factor (IGF) contribute to the hyperproliferative response in chronic inflammatory conditions and in other hyperproliferative diseases. More recently, there is mounting evidence indicating that T cell-derived cytokines, including members of the IL-20 and IL-6 families such as IL-22 and oncostatin M, play a significant role in the regulation of epidermal growth and regeneration (Huguier et al., 2019; Boniface et al., 2005).

Because terminal differentiation is typically the major regulatory mechanism of cell elimination in the skin, the frequency of apoptosis is relatively low in normal epidermis. More important than its potential role in regulating epidermal thickness may be the role of apoptosis in elimination of genetically damaged cells. By eliminating cells that can no longer successfully repair their damaged DNA, apoptosis appears to have a significant role in prevention of skin cancer. An example of this role is the high rate of apoptosis in epidermal cells that have been exposed to UV radiation (i.e., sunburn cells). In this case, apoptosis is a p53-mediated phenomenon that also involves the FAS/Fas-L complex. In contrast, cornification of the epidermis is in essence a programmed cell death distinct from apoptosis and is controlled by caspase 14.

## 2.10. Percutaneous Absorption

Skin is the largest organ but is often overlooked as a route of exposure in drug development. Skin can be exposed to a compound or metabolite via systemic routes like any other compound but is often also exposed directly via percutaneous absorption. This may occur unintentionally (i.e., grooming behavior with compounds that are fed, or excreted in urine or feces) or intentionally via direct application to the skin. With percutaneous absorption, there are several main routes by which a compound can gain entry via the skin. The intercellular route involves movement between the cells, while the intracellular route involves movement through the cells. Compounds can also gain entry via adnexa such as hair follicles, or glandular structures. There are multiple recent textbooks available that are dedicated to the science of transdermal drug delivery and not all details can be covered here. The intention is to provide an overview. *Please refer also to Volume 1, Chapter 3. ADME Principles in Small Molecule Drug Discovery and Development.*

The intercellular route is the primary means by which compounds gain entry through the epidermis. Molecular weight limits entry, so that compounds greater than around 500 Da (Da) will not diffuse easily through the intercellular lipid matrix. In formulating compounds to pass between (intercellular) or through (transcellular) cells of the follicular or interfollicular



epidermis, lipophilicity becomes another important consideration. The “bricks” (i.e., corneocytes) of the epidermis are hydrophilic, yet the “mortar” (i.e., intercellular substance) is lipophilic, composed primarily of ceramides, free fatty acids, and cholesterol.

Relative lipophilicity of any drug applied topically, then, may determine whether the drug can pass through the epidermis, or whether it will remain in the lipid-rich intercellular layer. The arrangement of the corneocytes in the epidermal layer can also play a role. Ease of penetration is enhanced when these cells are stacked on top of each other, as in rodent skin, but penetration becomes more difficult when the intercellular path is more tortuous, such as in humans. Regional variations in permeability at different body locations will affect absorption. This is dependent on differences in the thickness of the SC—for instance, scrotal skin, where the SC is one of the thinnest, is very permeable. Physical integrity of the SC plays an integral role in absorption, since in most skin diseases, the barrier function is notably diminished (e.g., psoriatic skin) even though the epidermis may be thickened.

Size of molecules is also important. Advances in ultrafine particle (e.g., nanoparticles, those less than 100 nm in diameter) formulation technology and research have led to a better understanding of dermal delivery of drugs. For instance, although compounds/particles may be small enough to follow the intercellular pathway between keratinocytes, it has been shown that these some particles tend to travel preferentially along the epithelium of hair follicles (Gu et al., 2022). In follicles, compounds may leach slowly into the adnexal unit (hair follicle and associated glands), and consequently act as a kind of reservoir for sustained activity against targets in the adnexal unit. Alternatively, formulations may allow delivery through the follicle wall into the surrounding dermis, targeting dermal components or even entering the circulation for systemic delivery. If the hair follicle is a factor in dermal absorption, then hair follicle density may become important with animal models and translation to the human patient. In particular, consideration should be made regarding where the intended site of application will be on the human patient for a number of factors, including hair follicle

density, relative thickness of the epidermis, and the regional activity of adnexa, enzymes, and microbiome. The epidermis itself also has some capability to act as a drug depot. This has been demonstrated in the SC with steroids, for example (Sitruk-Ware, 1989).

Ions may bind or form complexes with collagen in the dermis, thus remaining there for long periods of time with the potential to exert their toxicologic properties (e.g., chromium and ferric ions). The ionization state of the penetrant also affects the rate of diffusion; electrolytes in aqueous solution have poor penetrability, and the ionization of a weak electrolyte notably reduces its permeability (e.g., salicylic acid as opposed to sodium salicylate). Ions such as sodium, potassium, aluminum, and bromide penetrate very slowly. Simple polar substances appear to penetrate the SC at approximately the same rate as water. The addition of methylene groups onto a simple polar nonelectrolyte increases the lipid solubility of the molecule.

The physicochemical properties of the vehicle or excipients are also very important in influencing the rate of percutaneous absorption, since they will regulate the vehicle/SC partition coefficient. Hydration of the SC increases the permeability of both water- and lipid-soluble compounds; thus, occlusive dressings of materials such as polyethylene, which increases the humidity at the skin surface, are used in the transdermal delivery of drugs (e.g., corticosteroids). Skin occlusion also raises the local temperature, which is another important factor that enhances permeability.

Other substances that increase permeability may act via skin damage. These include organic solvents such as methanol, acetone, hexane, and ether. They produce delipidization of the skin, and generate interstices in the tissue, so it behaves like a nonselective porous membrane. The SC is also damaged by anionic and cationic surfactants (soaps, detergents), even at low concentrations. Surfactants are used in cosmetics and topical pharmaceutical compounds to increase permeability, as they can alter the composition of lipids between keratinocytes. Because such alterations can lead to changes in skin pH, increased water loss, and an altered cutaneous microbiome, surfactants should be used with caution as excipients in topically applied products.

When substances reach the living layers of the epidermis, they are exposed to the metabolic machinery of epidermal cells, which can inactivate or activate certain chemicals. Metabolic viability is a major factor affecting the in vitro permeation of certain chemicals (e.g., benzo[*a*]pyrene). Once chemicals have passed through the epidermis, which is an avascular tissue, they enter the dermis and are cleared by blood and lymphatic vessels. Under physiological conditions, dermal blood flow is not a rate-limiting factor for percutaneous absorption, but it may play a role under certain conditions such as hyperemia. Finally, with topical delivery to most lab animal species, enhanced unintended exposure via the oral route via grooming (animal to which compound is applied or cage mates, etc.) should be considered, as should unintended aerosol exposure to control animals housed in the same area as treated animals.

### 2.11. Metabolism and the Integument

The integument serves to protect the body from exogenous insults as a physical barrier, but the importance of the skin as an active metabolic organ must also be recognized. Metabolic products of the skin may protect the organism, signal beneficial local or systemic physiologic changes, and in some instances even lead to disease. The epidermis should be viewed as a tissue in steady-state growth that is not metabolically inert, but, rather, very active in sustaining itself and in regulating the body's interrelation with the environment. Extensive injury of the skin will affect the general homeostasis of the body (e.g., extensive burns). The opposite is also true, since general metabolic diseases (e.g., diabetes) will affect skin responses to injury.

The skin is involved in many endocrine-related responses and consequently, can be considered a type of endocrine organ as well (see *Endocrine System*, Vol 4, Chap 7). Enzymes important for the metabolism of steroid hormones such as androgens, estrogens, progesterone, and glucocorticoids are known to be present in the skin. For example, testosterone is a glucocorticoid derivative that is metabolized to more potent forms in the skin via cytochrome P450-mediated 5 $\alpha$  hydroxylation. Testosterone and its derivatives are responsible for

stimulating sebum secretion and modulating hair growth. Estrogens and progesterone are also metabolized in the skin. The skin is also an important organ in the synthesis of vitamin D.

In the spinous layer of the epidermis, UV light photolyzes provitamin D<sub>3</sub> (7-dehydrocholesterol) to previtamin D<sub>3</sub>; this in turn can be isomerized to form vitamin D<sub>3</sub> (cholecalciferol), which enters the circulation for further metabolism by liver and kidney into active vitamin D. Epidermal cells have receptors for 1,25-dihydroxy vitamin D<sub>3</sub>, which may regulate epidermal differentiation.

The presence and induction of a variety of cytochrome P450 (CYP) enzymes, as well as other oxygen and NADP(H)-dependent oxidases and the mixed function oxidase (MFO), have been demonstrated in skin. Modification of substances by CYPs to metabolites (often polar) is Phase I metabolism. Phase II metabolism "detoxifies" these metabolites to make them water soluble, and able to be excreted in aqueous form. These enzymes play a fundamental role in the oxidative metabolism of endogenous substances such as steroids, prostaglandins, fatty acids, and leukotrienes, but may also play a more sinister role when they come in contact with and metabolize xenobiotics. Cutaneous CYP enzymes play a critical role in the metabolism of certain xenobiotics; in most cases, this metabolism results in detoxification (see *Principles of Pharmacodynamics and Toxicodynamics*, Vol 1, Chap 5; reviewed by [Kazem et al., 2019](#)) There are situations, however, where relatively innocuous but highly lipid-soluble xenobiotics are "activated." For example, benzo[*a*]pyrene, or B[*a*]P, (a member of the polycyclic aromatic hydrocarbon (PAH) family of xenobiotics associated with overcooking food or with burning of carbonaceous material in general), can be metabolized by the CYP-dependent aryl hydrocarbon hydroxylase (AHH) system, resulting in a variety of mostly nontoxic metabolites. There is, however, at least one "active" metabolite, a particular diol epoxide that is very reactive and capable of binding to nucleic acids and proteins.

The epoxide spontaneously forms covalent bonds with DNA bases to produce bulky adducts which ultimately produce mutations when the affected DNA segment is replicated. Adduct

formation is believed to be the first step of cancer induction by this type of compound. Metabolic activation of other members of the PAH family also occurs. For example, several oxygenated reactive metabolites of 3-methylcholanthrene and benz[*a*]anthracene are active carcinogens in the mouse skin bioassay. Therefore, phase I metabolism by skin may not be very efficient or may even have a counterproductive effect, transforming relatively weak carcinogens into strong carcinogens and mutagens (see *Carcinogenesis: Mechanisms and Evaluation*, Vol 1, Chap 8).

Another phase I enzyme often expressed along with the CYPs, epoxide hydrolase, is also active in animal and human skin. This enzyme converts epoxides that are often generated by CYPs to dihydrodiol metabolites, which in turn are further metabolized by AHH into the highly reactive diol epoxides.

Phase II enzyme reactions, which involve conjugating enzyme systems such as the glucuronosyl transferases, sulfotransferases, and glutathione S-transferases, also occur in skin and constitute an additional detoxification pathway for the reactive epoxide intermediates. Conjugation with endogenous substrates such as glucuronic acid, sulfate, and glutathione results in the formation of water-soluble metabolites that are readily eliminated from the cells.

### 3. EVALUATION OF TOXICITY

#### 3.1. Physiologic and Morphologic Safety Evaluation Strategies and Techniques

##### 3.1.1. Traditional Test Systems

Evaluation of cutaneous toxicity is essential for any therapeutic agents intended for use by topical administration. Additionally, evaluation of potential adverse effects on the skin is necessary for therapeutic compounds that unintentionally come into contact with the skin (e.g., oral medications) and those that expose the skin systemically (i.e., distribution of systemically circulating drugs to the skin), and for nontherapeutic agents (i.e., cosmetics) that are applied to skin. Numerous global regulatory guidances (e.g., Food and Drug Administration (FDA) [<https://www.fda.gov/regulatory-information/search-fda-guidance-do>

[cuments](#)], International council for Harmonisation (ICH) [<https://www.ich.org/page/ich-guidelines>], European Medicines Agency (EMA) [<https://www.ema.europa.eu/en/human-regulatory/research-development/scientific-guidelines>], Organisation for Economic Co-operation and Development (OECD) [<https://mneguidelines.oecd.org/guidelines/>]) are available to provide guidance for the type of toxicity testing recommended for the different types of compounds under investigation. These guidances also extend to the various excipients used in preparation of formulations. Although there is not yet a guidance specific to topical drugs, ICH M3(2) Guidance for Industry (2010) provides recommendations for international standards and harmonization of nonclinical studies in support of initiation of clinical trials and registration for drugs in various therapeutic areas with respect to type, timing, and duration of nonclinical studies. In conjunction with the ICH M3(R2) guidance, ICH S10 (2015) provides additional guidance for photosafety testing that is of particular value in the development of topical drugs.

For compounds intended for topical application, there have been numerous initiatives to reduce animal use in topical toxicity testing (see. *Issues in Laboratory Animal Science that Impact Toxicologic Pathology*, Vol 1, Chap 29). Many of these initiatives involve newer and more sophisticated in vitro technologies that are gaining regulatory acceptance internationally (OECD Test No. 431, 2019a). Topical exposure of mouse skin organ cultures to a toxic substance, such as dinitrochlorobenzene, demonstrated similar morphologic changes to mouse skin in vivo, and in addition was associated with enzyme leakage allowing for detection of sublethal cell injury which may not be seen during histopathological evaluation of tissues (Helman et al., 1986). Similarly, methyl green-pyronine staining of porcine or human skin explant cultures has been shown to be a useful tool for assessing chemical irritancy through evaluation of keratinocyte cytotoxicity as measured by a decrease in keratinocyte RNA (Jacobs et al., 2002).

For cosmetics, animal testing has recently been banned by European regulatory agencies and is only allowed by exemption where there are significant concerns over toxicity or fertility effects. In Europe, the cosmetics industry has



actively participated in the development and legal adoption of the new REACH system (i.e., [European Union Registration, Evaluation, Authorisation and Restriction of Chemicals](#); European Union Regulation No. 1907/2006) for the registration and management of chemicals in Europe. This regulation combines previous directives and regulations to identify and control the risks and possible hazards of all chemical substances available on the European market.

In vivo topical toxicity testing methods have focused on assessing skin irritation, cutaneous sensitization, ocular toxicity, and photosafety testing in various animal species and strains. The animal model selected and type of protocol used will depend on the objective of toxicity testing.

The rabbit has been used for many years as the animal model of choice for evaluation of topical irritation potential. Although an extensive historical database exists for dermal irritation in the rabbit, this animal model has been shown to be more sensitive to primary irritants than human skin. More recently, the minipig has become the animal model of choice for assessing dermal irritation and tolerability of topical compounds, on the basis of the greater similarity of morphologic and physiologic characteristics of pig skin to human skin. Additionally, porcine models, in particular the Duroc/Yorkshire model, are considered the best animal models of recreating human wounds based on the collagen structure which is remarkably similar to that in humans. The guinea pig is the animal model of choice for assessing the allergic contact dermatitis potential of chemicals ([OECD Test No. 406, 2022](#)).

The route of administration selected in assessing the safety of topically applied compounds will depend on the endpoint of the assessment. Similar to therapeutic agents intended for oral or parenteral administration, in vivo topical toxicity testing should be evaluated in both rodent and nonrodent species. The rat is the rodent species of choice for evaluation of potential systemic toxicity of topical compounds, whereas the minipig is recommended as the nonrodent species. For topical therapeutic agents, there is also an expectation from regulatory agencies that both topical toleration and potential adverse systemic effects will be evaluated.

### 3.1.2. Draize Scale

Evaluation of the irritation potential of topically applied compounds has utilized animal models of skin irritation. The Draize scale technique has been commonly utilized for quantitatively determining the degree of irritation caused by topical application of compounds and providing a quantitative measure of comparison and differentiation of the irritation potential of various compounds (e.g., minor irritants vs. major irritants). This technique was adapted in the USA by the Code of Federal Regulations ([CFR, 2023](#)) and is legislated under provisions of the *Federal Hazardous Substances Act* ([FHSA, 2023](#)). The Draize scale evaluates the degree of redness (i.e., erythema), crust or scab formation (i.e., eschar), and edema.

For evaluation of dermal irritancy potential, the Draize technique involves application of the test substance to a defined area on the skin of rabbits, guinea pigs, or other animal models (e.g., minipigs). Solutions may be applied directly to the skin surface, whereas solid substances are first dissolved in an appropriate solvent or moistened before application. The application site is covered by a semioclusive dressing such as gauze. The test typically involves six animals, each with four to six defined patch-test areas. Testing is conducted on intact skin but may be adapted for abraded skin if dictated by the indication of use (e.g., wound healing). Observations of skin reactions are made at 4, 24, and 72 h after application and rated according to the Draize scale ([Table 7.2](#)). Histopathologic evaluations are not required in skin irritation evaluations using the Draize scale technique, but still form a critical component in repeat-dose dermal toxicity testing.

Human skin irritancy assessment is often required to complement animal irritancy testing in order to understand human risk more precisely ([Table 7.3](#)).

### 3.1.3. Photosafety Testing

Chemicals or drugs that absorb light in the UVA (320–400 nm), UVB (290–320 nm), or visible range (400–700 nm) are photoreactive. Photoactivation of a chemical may result in adverse effects, termed photosensitivity reactions, that may manifest as phototoxicity (photoirritation;

**TABLE 7.2** The Draize Scale—Grading Values for skin Reactions Following Topical Application of Potential Irritants

Skin reaction	Value
<i>Erythema and eschar (crust or scab) formation:</i>	
No erythema	0
Very slight erythema (barely perceptible)	1
Well-defined erythema	2
Moderate to severe erythema	3
<i>Edema formation:</i>	
No edema (barely perceptible)	0
Very slight edema (raised edges of area well-defined)	1
Slight edema	2
Moderate edema	3
Severe edema (raised more than 1 mm and extending beyond the area of exposure)	4

Modified from National Academy of Sciences Committee for the Revision of NAS Publication 1138: Principles and procedures for evaluating the toxicity of household substances, Washington, DC, 1977, National Academy of Science, pp 23–59. Reprinted from Haschek WM, Rousseaux CG, Wallig MA, editors: Haschek and Rousseaux's handbook of toxicologic pathology, ed 3, 2013, Academic Press, Table 55.2, p. 2233, with permission.

**TABLE 7.3** Grading Scale in Human Skin Patch Test

Grade	Lesion
0	No response
0.5	Indistinct erythema
1	Well-defined erythema
2	Erythema and edema
3	Vesicles and/or papules
4	Bulla or other severe reaction

Modified from National Academy of Sciences Committee for the Revision of NAS Publication 1138: Principles and procedures for evaluating the toxicity of household substances, Washington, DC, 1977, National Academy of Science, pp 23–59. Reprinted from Haschek WM, Rousseaux CG, Wallig MA, editors: Haschek and Rousseaux's handbook of toxicologic pathology, ed 3, 2013, Academic Press, Table 55.3, p. 2234, with permission.

chemically induced skin irritation, requiring light that does not involve the immune system; Repetto et al., 2008), photoallergy (an immunologic reaction to a chemical that is activated by light; Ibottson, 2014), photogenotoxicity (a genotoxic response observed after exposure to a chemical photoactivated by UV or visible light; Struwe et al., 2008), and photocarcinogenicity (Stern, 1998).

Photosafety testing is intended to identify agents with photosensitivity potential. Both in vitro and in vivo assays have been developed to assess the photosensitivity potential of photo-reactive chemicals. Regulatory guidances have been developed internationally for assessment of drugs intended for human use by topical administration (Table 7.4).

Key considerations in the assessment of photosensitivity potential in these guidances are photoirritation, photoallergenicity, photogenotoxicity, photocarcinogenicity, and photocarcinogenicity (see Section 5.3 in this chapter for discussion of these changes). The data supporting recommendations in the regulatory guidances are still evolving; however, ICH S10 (2015) is the current international standard.

Photosafety testing begins with a determination of the ability of a chemical to absorb UV/visible radiation, since a chemical that does not absorb light will not be photoreactive and therefore will not require further photosafety testing. UV/visible light absorbance is determined by a spectroscopic scan (measures wavelengths of light in the 180–400 nm range which included UVA, UVB, UVC, or visible light), which determines that wavelength of light that is absorbed and the degree of absorbance. Absorbance is measured as the molar extinction coefficient (MEC), expressed as  $\text{Mol}^{-1}\text{L}^{-1}$ . The threshold for photoreactivity of a chemical that may be associated with a biological effect has been a subject of much debate, and, based on data accumulated over recent years, compounds with an MEC <1000 are not considered to be associated with biologically adverse effects and therefore, do not require photosafety testing (ICH S10, FDA, 2015).

For photoreactive chemicals that absorb light in the UVA/visible light range, the 3T3 NRU assay is a validated in vitro assay for photoirritation potential (OECD Test No. 432, 2019b). In this assay, different concentrations of test substance

**TABLE 7.4** Regulatory Agency Guidances for Nonclinical Development of Topical Agents

Regulatory Agency	Guidance	Year of Implementation or Version
ICH/EMA/FDA	M3(R2) nonclinical safety studies for the conduct of human clinical trials for pharmaceuticals	ICH 2009 EMA 2013 FDA 2010
ICH/EMA/FDA	S10 photosafety evaluation of pharmaceuticals	ICH 2013 EMA 2014 FDA 2015
EMA	Guideline on nonclinical local tolerance testing of medicinal products	2015

EMA, European Medicines Agency; FDA, U.S. Food and Drug Administration; ICH, International Council for Harmonisation of Technical Requirements for Pharmaceuticals for Human Use.

**TABLE 7.5** Assessment of Phototoxic Potential based on Photoirritancy Factor and Mean Photo Effect

Photoirritancy factor (PIF)	Mean photo effect (MPE)	Phototoxic potential
<2	<0.1	Nonphototoxic
>2 and <5	>0.1 and < 0.15	Probably phototoxic
>5	>0.15	Phototoxic

Reprinted from Haschek WM, Rousseaux CG, Wallig MA, editors: *Haschek and Rousseaux's handbook of toxicologic pathology*, ed 3, 2013, Academic Press, Table 55.4, p. 2234, with permission.

are incubated with Balb/c 3T3 cells and either exposed to solar simulated light or maintained in the dark. Cell viability is assessed after 24 h by measuring optical density using a vital dye (neutral red). The phototoxic potential of the test substance is determined by comparison of the IC<sub>50</sub> (i.e., the concentration of test substance which reduces cell viability by 50%) with and without exposure to solar-simulated light, and is expressed as the photoirritancy factor (PIF) as in the following Eq. (7.1):

$$PIF = \frac{IC_{50}(-UVA)}{IC_{50}(+UVA)} \quad (7.1)$$

In cases where two equally effective (IC<sub>50</sub>) concentrations in dark (−UVA) and light (+UVA) cannot be determined, the mean photo effect (MPE), defined as the weighted average across a representative set of photo effect values, can be calculated from comparison of the concentration–response curves.

The phototoxicity potential of the test substance is interpreted as in Table 7.5.

Unfortunately, the 3T3 NRU assay will not work with strictly UVB-absorbing chemicals, since UVB irradiation is cytotoxic to 3T3 cells and, as such, will require in vivo testing. Human epidermis models (e.g., EpiDerm, EpiSkin, and SkinEthic) are being investigated as alternate in vitro models for utility in phototoxicity testing for these types of chemicals (Lynch and Wilcox, 2011).

In vivo phototoxicity testing may be conducted in guinea pigs, rabbits, hairless mice, or hairless guinea pigs (Sueki et al., 2000). In this assay, the application site on the test species is exposed to UV irradiation from a solar simulator. After a period of time to allow for absorption of the test article, the Draize scale is used to determine the phototoxic response by grading of irritation potential at 24, 48, and 72 h. In a review of concordance of toxicity of pharmaceuticals in humans and animals, phototoxicity response in



guinea pigs correlated well with that in humans (Lovell and Sanders, 1992).

Photoallergenicity is typically evaluated in vivo in guinea pigs. The Buehler Guinea Pig Sensitization assay (with exposure to simulated light) is preferred over the Guinea Pig Maximization assay, which, although considered more sensitive than the Buehler assay, is associated with subcutaneous reactions attributed to the use of adjuvant in this assay. It should be noted that nonclinical photoallergenicity testing is not recommended as the predictivity for photoallergy tests is unknown (ICH S10, 2015).

It is now generally accepted by regulatory agencies that photogenotoxicity testing should not be conducted because there are too many false positives, even with compounds that are not photoreactive (ICH S10, 2015).

Photocarcinogenicity testing may be required for topical compounds that are used chronically, are phototoxic, and are topically applied, or if there is indication for concern based on the class of compound (ICH S10, 2015, ICH M3(R2), 2010). However, photocarcinogenicity testing may not be needed for compounds that are photoirritants if a warning is provided in patient information. Photocarcinogenic potential must also be taken into consideration for chemicals that may not be photoreactive but may influence carcinogenicity through immunosuppressive effects (e.g., cyclophosphamide) or altering the optical properties of the skin (e.g., certain emollients). SKH-1 hairless mice are used as models of UVR-induced carcinogenesis and develop skin tumors that are considered relevant to the study of human skin cancer.

### 3.2. Special Considerations in Design of Topical Dermatologic Studies

When a compound is delivered systemically and skin is a target, then additional sections of skin may be evaluated, and particular attention is paid to gross lesions involving the skin. However, when a compound is delivered topically to the skin, there are several considerations for study design.

#### 3.2.1. Addition of a Sham Control Group

Since laboratory animals typically have dense hair coats (see section on hairless skin models),

it is typically necessary to shave and/or depilate the skin to expose the test site. Hair removal or other study procedures can introduce some trauma and/or irritation to the area, and therefore inclusion of two control groups (a vehicle control and a sham treated control) is strongly recommended. The sham treated control group receives all study procedures such as shaving on the same schedule as the most intensely treated group. Since vehicles that are designed to enhance skin penetration can themselves produce some changes in the epidermis, or be irritating to the skin, the sham control group can differentiate between vehicle effects and procedural effects.

#### 3.2.2. Prevention of Oral Ingestion and Cross Contamination

Since laboratory animals groom themselves, especially where their hair coat or skin may feel abnormal to them (e.g., the application site), it is necessary to take some precautions to prevent accidental oral ingestion of a test substance designed to be applied topically. Since some study designs involve applying different test substances to different parts of the body of a test subject (e.g., vehicle to one side of the back and test article to the other side), it is also important to take precautions to prevent cross-contamination of test application areas. It is beyond the scope of this chapter to cover all the various needs of laboratory animals used for topical toxicity testing, but laboratory animal veterinarians should always be consulted for the best methods to prevent accidental ingestion of the test substance and/or cross-contamination while providing for the comfort of the test subjects and allowing normal eating, drinking, socialization, and grooming appropriate for the species.

The application of Elizabethan-type collars for prolonged periods of time can interfere with the ability to eat or drink and can cause procedural trauma to the animals. Therefore, if collars are used, the number of hours collars are in place should be limited to allow normal eating, drinking, socialization, and grooming behavior. It is important to know the pharmacokinetic (PK) properties of the test compound and/or vehicle before designing longer term studies so that adequate application times are built into the study design, without excessive times for

test animals to wear collars or other methods to prevent ingestion.

Vests and/or occlusive dressings can be applied to protect the application area. Care must be taken while removing and reapplying the dressings to prevent cross-contamination of application sites, and special attention must be paid to equipment, and surfaces (such as restraint devices) that may come into contact with the test material when changing dressings. Occlusive dressings themselves can be irritating to the skin so skilled technicians should be employed to change the dressings and pay attention to the condition of the skin during dressing changes. This is another reason to include a sham control group.

Many laboratory animals, especially minipigs, like to scratch, particularly if their skin feels unusual to them, and may use things like enrichment devices and water spigots to scratch. These things can become contaminated and themselves be sources of accidental oral ingestion, cross-contamination, and trauma to the skin.

### **3.2.3. Application of More than One Test Substance to Same Subject**

Topical studies allow for the potential for multiple application sites on the same animal which can provide for internal controls and reduced animal usage. These methods are especially useful with large animals such as minipigs (Willard-Mack et al., 2016). If systemic PK data are a study endpoint, then only one pharmacologically active test article can be applied per animal; however, it is still possible to have another application site that serves as a sham or vehicle control site on that same animal. If a study is designed with more than one test substance per animal, prevention of cross-contamination is critically important. Histopathology should include the application sites and untreated skin. Consideration should be given to regional differences in the skin in different anatomic areas (i.e., the normal thickness of the epidermis and adipose layers of the skin of all species varies in different areas of the body) when trying to evaluate any potential test article-related changes. For this reason, a common study design may be to apply test substance to one side of the animals' back, while the other side serves as a sham, untreated, or vehicle control, or all three.

Hairless animal models are especially attractive for topical dermatologic application studies because this removes the need for shaving and/or depilation of the haircoat and allows easier visualization of the test sites. However, hairlessness is not normal in laboratory animal species, so there is always an underlying reason for the hairless coat condition. Also of note, actual fractional area of hair follicles and other adnexae like sebaceous glands may be actually increased in hairless models (rats, guinea pigs, mice) when compared to their background strains, so hairlessness is something of a misnomer (Grabau et al, 1995).

For these reasons, if a hairless animal model is used, it is important to understand the underlying reason for the hairlessness to be sure the abnormal pathology producing the hairless condition will not interfere with interpretation and evaluation of study endpoints. An example of this is the SKH1-*Hr<sup>hr</sup>* hairless mouse. This mouse is an immunocompetent (as opposed to the athymic nude mouse which is also hairless) hairless mouse that is popular in dermatologic research. The first haircoat in these mice develops normally but by 3 weeks old the mice have lost all hair except their vibrissae (whiskers) (Benavides et al., 2009). These mice have a dysregulation of the regression of catagen hair, which results in the formation of dermal cysts that are not connected to the epidermis. Many of their hair shafts grow parallel to the skin surface, which results in the formation of "foreign body" granulomas and cysts (Figure 7.11).

## **3.3. Skin Sample Collection Techniques**

### **3.3.1. Preferred Necropsy Collection and Considerations for Sampling Site Selection**

Similar to other tissues in the body, care must be taken during the collection, handling, and processing of skin samples at necropsy. Orientation of skin sections is critical for haired animals in order to obtain a good cross-section of the entire hair follicle and associated glands, as opposed to a tangential section, which may fail to include potential target areas of toxicity.

Skin samples are typically sectioned parallel to the longitudinal cranio-caudal axis of the animal to provide the appropriate orientation of hair

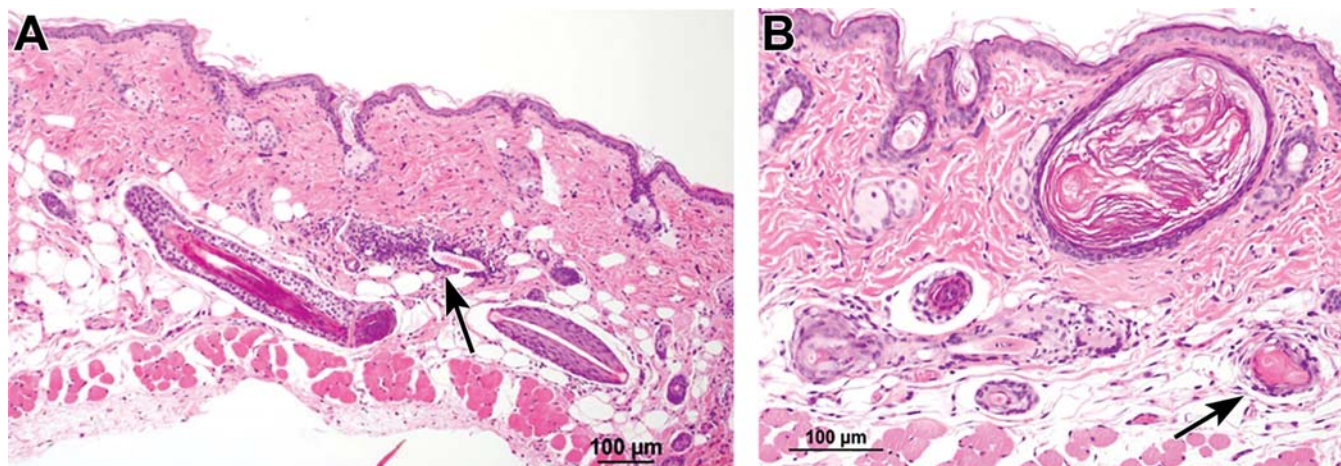


**FIGURE 7.11** Skin from untreated SK1 hr/hr hairless mice. Note abnormal hair shafts growing parallel to skin surface but failing to penetrate the skin surface. Foreign body type granulomas have formed around degenerating hair shafts (arrows in A and B). In B, a large, keratin-filled dermal cyst is present.

follicles. Skin samples collected at necropsy should be placed flat on a piece of cardboard with subcutis down to prevent curling or folding during fixation. Ten percent neutral-buffered formalin (NBF) is the preferred multipurpose fixative, and skin samples are typically fixed for ~24 h. Frozen tissues or alternate fixatives may be considered for special purposes (e.g., glutaraldehyde for electron microscopy [EM] or Michel's fixative for immunofluorescence). Care must be taken during histologic sectioning to obtain a representative area of the lesion, and in some cases, step-sectioning (e.g., 50–75 µm) may be warranted to ensure full evaluation of the lesion and all skin structures. Ancillary diagnostic procedures may include immunohistochemistry (e.g., PCNA labeling), image analysis, stereology, and morphometry (see *Special Techniques in Toxicologic Pathology*, Vol 1, Chap 11 and *Digital Pathology and Tissue Image Analysis*, Vol 1, Chap 12).

In addition to the importance of how to collect and fix skin samples, it is important to consider where to sample, and how this meets the objectives of study design or diagnostic considerations, and desired endpoints. Skin varies in thickness and degree of “tightness” over different parts of the body, as does haircoat, and adnexa, and the microbiome, all of which can influence local exposure and potential for toxicity. Translatability to the human patient may also be of consideration when considering where to apply a locally administered

therapeutic (i.e., topical, sustained release) and subsequently where to sample. Additionally with systemically administered therapeutics, regional anatomic variation in skin morphology could influence local exposure and thus response to the therapeutic.

In general, skin in laboratory animals is thickest over the back, and becomes thinner on the flanks of the limbs, and thinnest on the abdomen. Hair density generally follows a similar pattern. If there are considerations for skin thickness or hair density in the study endpoints, then these variations in thickness may become important. For example, in a PK study with a topically applied compound, the variation in skin thickness at the application site could influence PK endpoints, and it is important to keep sampling sites consistent so that comparisons between dosage groups are accurate. Humans also have varying skin thickness so the relevant area for topical application and/or sampling in laboratory animals should be considered in study design to optimize translatability to human patients. For example, skin on the human face is much thinner than on the trunk or limbs. If the therapeutic under study is intended to be applied to the face, then study design with animal models should consider this factor in translation of PK, local response, etc.

Adnexa varies with location on the body; examples include mammary glands present in abdominal skin, or vibrissae (whiskers) present on facial skin. In swine, a commonly



used nonrodent species in dermal studies, the thickness of the skin over the back is greatest around the neck and shoulders, and becomes thinner toward the haunches. This is more pronounced in older males compared to females, or younger males. Mature swine develop wrinkles with sometimes abundant sebaceous secretions especially around the dorsal neck, and more prominent in males. Therefore, this can influence PK from the point of view of general thickness but also pooling in wrinkles or interaction with sebum or associated microbiota on the skin surface. All of these factors should be considered in study design.

For loose skinned animals like rodents, or dogs, it is easy to displace the skin from the location where it generally lies, especially in an animal that has been euthanized or is anesthetized. Therefore, it is important to maintain anatomic landmarks when sampling skin in these species and it is recommended that administration and/or sampling sites in any species be marked with either tattoos, marker, or other method to identify landmarks.

The physical characteristics of a formulation can also affect the appropriate sampling site. For example, if a watery formulation is applied to the dorsal back, it is likely to run down the side of the animal, and therefore exposure may be greatest on the sides or ventrum, rather than the dorsum. If the formulation causes the experimental animal to experience sensations such as tingling or pruritis, the animal may rub, scratch, or lick at the application site which can have significant effects on PK or distribution of the compound.

When lesions are present, sampling sites become especially important in order to obtain diagnostic samples. Ulceration is the end result of many different pathophysiological processes in skin (i.e., vesicles, pustules, corrosion, trauma, scratching, etc.), and additionally, ulcerated areas commonly develop secondary bacterial contamination in the exposed wound bed, with predictable healing processes. Ulcerated areas are the most visible skin lesion, and therefore the easiest and most obvious areas to sample. However, since ulceration is an end stage lesion, skin samples from these areas often do not yield adequate information to diagnose the underlying cause.

For this reason, it is important to try to identify and sample lesions that are at an earlier stage of development. Careful examination of skin is important for any study, but especially for those with skin lesions or symptoms so that early lesions can be identified, or possible elucidating information. Early lesions may appear discolored (i.e., reddened, or pale), have altered texture (firmer than surrounding skin, or softer), have altered contour (raised or depressed) or may be swollen (edema), or have blisters (vesicles), but the skin is not yet broken. These are ideal lesions to sample to provide diagnostic information. Additionally, it is important to sample the edge of lesions, rather than the center since the edge usually has the initial pathologic process. Excisional biopsies that sample the edge of the lesion plus wider margins with adjacent normal appearing skin provide the most useful information, but this may not be possible with punch biopsies. For this reason, in the case of necropsy, collection of large pieces of skin with wide margins is much preferred over small samples or biopsies. It is recommended to collect samples of multiple lesions if present to provide the best opportunity for samples to be diagnostically elucidating.

### **3.3.2. Skin Biopsy as a Companion Diagnostic Technique**

Skin biopsy samples may provide a rapid method for diagnosis of neoplastic or other serious skin conditions, such as nonhealing ulcers. However, care must be taken during collection to ensure optimal sampling. Excisional biopsy samples are preferred over punch biopsies to facilitate examination of the entire lesion, for deeper sampling, and to avoid damage to smaller lesions by the biopsy process. However, excisional biopsies are much more invasive than are punch biopsies in live animals. Site selection is critical, and should include representative lesions such as rashes, crust (i.e., acantholytic epidermis), vesicles, ulcers, alopecic areas, abnormal pigmentation, and nodules. Prior to biopsy, the site must be carefully prepared to avoid damaging the epidermis or overlying crust or exudate. Hair may be clipped with care.

Punch biopsy instruments vary in size (e.g., 2–10 mm) and purpose; punch biopsies less than 3 mm provide too small a sample for

histopathologic evaluation and should be avoided. Typically, 4-mm punch biopsy instruments are used for paws or periorcular skin areas, whereas 6- to 8-mm punch biopsy tools are used for haired skin. For excisional biopsies, a sample should include some normal skin adjacent to the lesion. Marking the area to be sampled with an indelible or surgical marker can facilitate accurate collection. Tissue samples are gently handled with small-toothed tissue forceps by grasping nonaffected areas of the skin sample or subcutis. Similar to necropsy procedures, biopsy skin samples are placed on a piece of cardboard with subcutis side down prior to fixation to prevent curling or folding.

Most commonly, skin samples are fixed in 10% NBF (10 times volume of formalin relative to the volume of the skin sample) and fixed for up to 24 h with gentle agitation. Formalin-fixed tissues may be used for immunohistochemical staining by immunoperoxidase techniques; however, for immunostaining, an alternate fixative such as Michel's medium or use of frozen tissue samples may be considered. Skin samples for EM are typically fixed in glutaraldehyde.

### 3.4. Special Techniques

#### 3.4.1. Genetic Toxicity Profiling

The study of genetically determined responses to drugs in humans and animal models is variably termed pharmacogenetics and pharmacogenomics. Pharmacogenetics refers to the clinical study of the differing responses of individuals to drugs related to genetic variation; pharmacogenomics is the application of genomic technologies for characterization of drugs. Pharmacogenetics may help to explain diverse responses to drugs in relation to efficacy, metabolism, and toxicity (i.e., adverse drug reactions). For example, although the pathogenesis of psoriasis is relatively well defined, there are still many individuals that do not respond to treatment.

Individual responses to drugs are associated with nucleotide polymorphisms in genes that code for liver enzymes responsible for drug metabolism and consequent PK/toxicokinetics (TK) profiles. Pharmacogenetics has provided an understanding of why azathioprine, which is widely used in dermatology, is associated with myelosuppression, through a mechanism

attributed to low thiopurine methyltransferase activity in certain individuals. Identification of genetic markers through pharmacogenomic platforms is considered superior to traditional biomarkers (e.g., markers of inflammation), and can assist in identifying high-risk individuals in order to provide effective and timely treatment while reducing the risk of adverse drug reactions from pharmacotherapy. Please see *Biomarkers Discovery Qualification and Application*, Vol 1, Chap 14.

#### 3.4.2. Plucked Hair Assessment

Plucked hair follicles are considered useful surrogate biomarkers for measuring response to drug treatment based on their sensitive and rapid response (i.e., within hours) to drug exposure. This technique can provide a measurement of pharmacodynamic response that is noninvasive and allows for repeated sampling without unduly stressing the subject. Hair follicles may be evaluated by immunohistochemical techniques to identify specific antigens (e.g., Ki-67, EGFR, phospho-p27, phosphor-histone H3, phosphor-MAPK, phosph-Rb) and subjected to image analysis of labeled cells for quantification of treatment-related changes.

#### 3.4.3. In Vivo Microscopy

Recent advances in innovative technologies have allowed for visualization and quantification of cells noninvasively by in vivo microscopy. In vivo imaging techniques include dermoscopy, confocal laser scanning microscopy, magnetic resonance imaging (MRI), multiphoton microscopy, terahertz imaging, and optical coherence tomography (OCT).

In vivo microscopy provides a means of studying aspects of dynamic biology not allowed by traditional histopathologic techniques (i.e., in fixed tissues). In vivo imaging techniques may allow the monitoring of cellular responses to therapy in animal models of disease. For example, the effect of antiangiogenic agents on neovascularization in tissues or tumors may be used to determine the quality of response to new therapeutic agents or various treatment paradigms. The progression of disease and its response to treatment may be studied temporally or longitudinally without the need to euthanize animals at multiple time points and consequently allow for the reduction in the number

of animals needed for study. The imaging technology that is typically used is scanning laser confocal and multiphoton excitation microscopy, which utilizes high-speed scanning image acquisition and is able to detect specific labeled molecular markers (e.g., fluorescent and bioluminescent markers) in vivo with a high level of sensitivity.

In vivo microscopy technologies allow directed visualization of lesions in situ. The combination of various technologies such as MRI, PET (positron emission tomography), or CT (computed tomography) with metabolic biomarkers can facilitate detecting diseases, tracking specific cell types, predicting disease process outcomes, and monitoring the effectiveness of various therapies (see *In Vivo Small Animal Imaging: A Comparison to Gross and Histopathologic Observations in Animal Models*, Vol 1, Chap 13). For example, infrared fluorescent dyes linked to specific biomarkers may be used in combination with OCT imaging to provide enhanced in vivo molecular imaging.

In vivo microscopy technologies may use indexing of lesions, which is stratification of a lesion into cohorts, as a statistical technique for predicting outcomes of disease (see *Experimental Design and Statistical Analysis for Toxicologic Pathologists*, Vol 1, Chap 16).

In vivo imaging of pigmented skin lesions with different wavelengths allows for comparison of the multispectral signature with signatures of known lesions, thereby providing a means of allowing determination of whether or not to biopsy the lesion. Skin color can be assessed objectively using a tristimulus chromameter that measures skin reflectance and color saturation (red to green and yellow to blue scales) providing a good correlation with total epidermal melanin. High-resolution laser Doppler imaging provides a two-dimensional image of skin perfusion, whereby vasodilation as part of an inflammatory response can be utilized for assessment of skin irritation typing and grading (Fullerton et al., 2002; Monteiro-Riviere et al., 1990).

#### 3.4.4. Label-free Optical Imaging of Skin

Several novel label-free optical imaging technologies that can be used for visualizing skin anatomy and function with unprecedented

details have emerged over the last 2 decades with the progress in laser technology and fiber optics. These optical imaging techniques enable real-time, noninvasive visualization of micro-morphological features in skin in vivo up to a depth of 200 microns. Some of the promising optical imaging techniques for dermatological applications include multiphoton microscopy (Koehler et al., 2010; Masters and So, 2001), fluorescence lifetime imaging microscopy, Coherent anti-Stokes Raman scattering microscopy, and photoacoustic microscopy. These techniques can be utilized for preclinical as well as clinical studies to obtain complimentary information regarding the skin structure and function.

In multiphoton microscopy, endogenous fluorophores in skin such as nicotinamide adenine dinucleotide (phosphate) (NAD(P)H), flavins, porphyrins, elastin, keratin, and melanin allow label-free visualization of cellular and subcellular features of various skin layers. An example of a recent study using a commercially available multiphoton imaging system (MPTflex, JenLab GmbH, Germany) for imaging minipig skin in vivo is shown in Figure 7.12. 3D reconstruction imaging of skin in vivo is made possible by multiphoton imaging as well (Alex et al., 2020).

#### 3.4.5. Confocal Microscopy

Confocal microscopy allows for visualization of tissue morphology and architecture at the cellular and molecular levels, thereby providing additional data beyond those obtainable by traditional histological methods, including volumetric and time/flow data. Confocal laser microscopy (CLM) provides horizontal optical sections for evaluation, rather than the traditional vertical sections in histology sections. Cellular images of epidermis obtained in vivo correlate well with histologic observations from vertical sections. Clinical use of confocal devices is becoming increasingly common in dermatology practice (González et al., 2003; Masters and So, 2001; Levine and Markowitz, 2018). Stereological measurements provide a mechanism for the evaluation of nucleus size and total cell counts, as well as subfractions of reactive and nonresponsive cells, which can then be correlated to treatment effects. CLM enables capture of images that are in focus across an entire plane using wavelengths of ~400–1000 nm, which allows for submicron resolution.



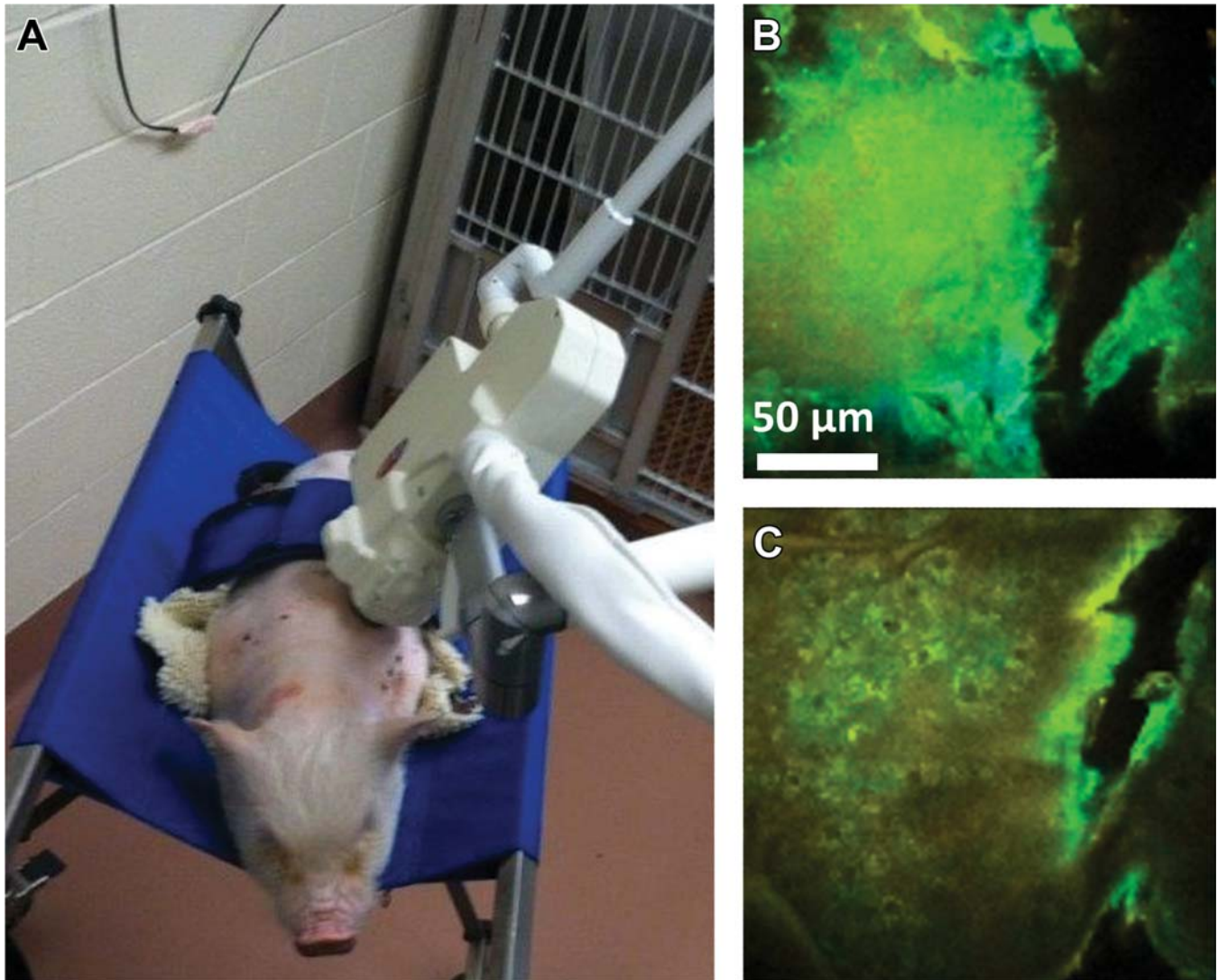


**FIGURE 7.12** Imaging minipig skin in situ using a commercially available multiphoton imaging microscope, MPTflex CARS (JenLab GmbH, Germany). (A) Photograph of a sedated minipig coupled to the articulated arm of the imaging system. (B and C) Representative label-free multiphoton images obtained from the skin surface and 40  $\mu\text{m}$  deep, respectively. The contrast in these images is generated by auto-fluorescent endogenous components in skin such as NAD(P)H, FAD and keratin. Stratum corneum features are visible in B and epidermal cellular features are visible in C. The images are false color coded based on the fluorescence intensity at each pixel. Obtained using 40x, 1.05 numerical aperture oil-immersion objective and scale bar is 50  $\mu\text{m}$ . Alex A, Chaney EJ, Žurauskas M, et al.: *In vivo* characterization of minipig skin as a model for dermatological research using multiphoton microscopy. *Exp. Dermatol.* 29:953–960, 2020, Figure 1. p. 955, with permission.

For skin, this technology acquires images one layer at a time (SC, SS, SB, etc.) rather than a cross-section of the entire skin when cut from a paraffin-embedded section (Corcuff et al., 1993). The level of detail of the image may be modified with refinement of contrast media; molecular imaging and three-dimensional reconstruction may be used to provide additional

data. Confocal laser scanning microscopy in combination with Fourier analysis has been shown to be a reliable method for assessing dermal collagen bundle orientation. Confocal microscopy can be used with ultrasound evaluation to visualize variable depths of the layers of the skin for enhanced recording of morphometric changes in the skin (Nouveau-Richard et al., 2004).

### **3.4.6. Optical Coherence Tomography**

OCT utilizes low-coherence interferometric technology (i.e., infrared wavelengths) to acquire reflectance/backscatter data. Comparison of tissue reflectance to reference light allows for construction of cross-sectional images. OCT resolution is almost comparable to high magnification optical microscopy with an imaging capability of 1–3 mm depth within tissues, thereby allowing generation of volumetric data (e.g., epidermal thickness) at microscopic resolution (Morgensen et al., 2008). OCT volumetric data allow for three-dimensional construction of tissues, providing a greater understanding of histomorphologic changes than otherwise provided by two-dimensional histology images. OCT can also be used to acquire serial images over time or live-motion images allowing evaluation of progression or regression of a lesion in response to therapeutic intervention. Additionally, OCT can be utilized to identify areas for biopsy, or to provide an alternative diagnostic technology to areas not amenable to biopsy (Gambichler et al., 2006).

### **3.4.7. Other Useful In Vivo Tools for Enhanced Physiologic Assessment of Skin**

Various other noninvasive techniques can also be used to evaluate skin qualities, depending on the desired endpoints of the study. These measurements can be made serially over time to monitor either progression of a condition or response to treatment and have good translatability to human patients. Conditions of measurement must be kept constant, including operators and the type/brand of instrument used. One such tool is that which measures TEWL, or transepidermal water loss. Increases in TEWL are indicative of compromised barrier function in the skin. Consequently, TEWL is very useful and often applied in in vivo translational models of human skin diseases like atopic dermatitis and psoriasis. Hydration status of the skin at a given point in time can be measured via electromagnetic penetrance using a moisture meter. A cutometer is a device that uses suction pressure to sense changes in viscoelasticity properties of the skin, changes which may reflect pathologic states in both dermis and epidermis.

### **3.4.8. Electron Microscopy**

Transmission (TEM) and scanning electron microscopy (SEM) of skin can provide useful information regarding changes occurring on the surface of the skin or at subcellular levels, and mechanistic characterization of changes in the skin observed clinically or by light microscopy. For example, TEM may allow visualization of degenerative changes in mitochondria and damage to the epidermal basement membrane or provide a means of identification of particular cell types by the presence of cell-specific organelles (e.g., Birbeck granules in LCs or melanosomes in melanocytes).

Typical fixatives for preservation of skin for optimal ultrastructural evaluation include glutaraldehyde, paraformaldehyde, and osmium tetroxide. Skin samples are sectioned into thin (~1 mm wide) strips prior to immersion fixation to allow orientation of the various layers of the epidermis. Postfixation, orientation may be maintained during embedding by placement of the long axis of the skin section parallel to the long axis of the capsule and keeping the capsule horizontal during polymerization. Orientation of skin sections is confirmed by examination of ultrathin (~1 micron) sections stained with Toluidine blue prior to further sectioning for EM. Similarly for SEM, tissue samples are fixed in glutaraldehyde, subjected to critical point drying, mounted on SEM stubs, and shadowed by 60/40 gold/palladium in a vacuum coating unit.

## **3.5. Three-Dimensional In Vitro Skin Model Systems**

Three-dimensional in vitro human skin model systems have been increasingly used in recent years both for toxicologic applications as well as for basic pathophysiologic research. These models have also recently gained increased acceptance for the toxicologic evaluation of topical irritation and corrosion (OCED test guideline 431 and 404), as well as cutaneous permeability/transport and phototoxicity.

These in vitro models have also been increasingly used for the assessment of cutaneous toxicity and biology from systemically administered agents. The most commonly utilized

three-dimensional human skin models are EpiDerm, EpiSkin, and SkinEthic. All three are reconstituted human epidermal (RHE) models which are composed of normal human epidermal keratinocytes that form a three-dimensional reconstitution of normal human epidermis containing all viable and nonviable cell layers (SB, SS, SG, and SC). All models are metabolically and mitotically active, have a lipid and ceramide profile very similar to normal human epidermis, and express normal epidermal differentiation markers such as keratin 1/10, pro-filaggrin, and involucrin. They are all grown in serum-free media system and are highly reproducible.

These RHE models have been extensively evaluated for their ability to correctly predict topical skin irritation/corrosion and have all demonstrated very good accuracy and reproducibility in their ability to accurately predict skin corrosion (90+%) (Pedrosa et al., 2017). Their ability to predict skin permeability/transport and phototoxicity has been less extensively evaluated, but they have also gained acceptance for those uses as well.

One specific alteration that is thought to increase the predictive ability of RHE models for the evaluation of cutaneous permeability/transport, as well as enabling their use for additional assessments, such as for cutaneous wound healing, is the addition of a dermal layer to the RHE model, since all of the RHE models are composed solely of viable and nonviable cell layers. Two such three-dimensional in vitro models that have added dermis to the reconstituted epidermal keratinocytes are EpiDermFT and Apligraf, although these epidermal/dermal models have yet to be validated for the purposes of permeability/transport evaluation.

In addition to the evaluation of topically applied substances, RHE models have also been used for the evaluation of skin toxicity from systemically administered substances, the biologic/physiologic effects of a variety of cytokines and growth factors, as well as investigations into the pathophysiology of the cutaneous diseases such as psoriasis. For example, the EGFR inhibitors cetuximab and erlotinib have a clinical dose-limiting toxicity of rash. In the EpiDerm RHE model, both EGFR inhibitors induced a decrease in epidermal thickness with the presence of occasional necrotic keratinocytes, and also induced

a marked decrease in the expression of phosphoS6, a Ser/Thr protein kinase that is activated/phosphorylated in response to EGFR activation (Figure 7.13).

As an example of the use of the RHE model in pathophysiologic investigation, the IL-10 cytokine family members IL-19, IL-20, IL-22, and IL-24 were all found to induce morphologic, biochemical, and molecular changes consistent with some of the features found in psoriatic epidermis. IL-22 in particular, which is involved in the regulation of host defense responses and repair processes, but importantly in the induction or exacerbation of inflammation, elicited many of the same features in the EpiDerm RHE model that are found in psoriatic epidermis. Some of the morphologic and differentiation features that IL-22 induces in RHE, such as hypogranulosis and upregulation in expression of the hyperproliferative cytokeratin 6, the antimicrobial peptide S100A7, and activation/phosphorylation of the nuclear transcription factor Stat3, are features shared by psoriatic epidermis, in contrast to those elicited by EGF, a recognized growth factor with effects on numerous epithelia, including epidermis (Figure 7.14). The IL-22 pathway has demonstrated in vitro to in vivo and cross-species translatability through conservation across species (Lee et al., 2018). As such, the IL-22 pathway is of therapeutic interest in treatment of infectious or inflammatory diseases, as well as repair of the epithelial barrier. Additionally, safety risks identified nonclinically translate well to clinical use.

The ability of cytokines such as IL-22 and oncostatin M to induce morphologic and differentiation features in keratinocytes that mimic those found in psoriatic epidermis, as well as activate keratinocytes to upregulate many of the same genes known to be upregulated in psoriatic skin in the absence of blood vessels and leukocytes, is remarkable, and reinforces the hypothesis that epidermal keratinocytes are central to the initiation of cutaneous inflammation as well as the initiation of cutaneous response to injury, infection, and toxicity. IL-22 induced similar changes in a reconstituted human epidermal-dermal model, EpiDermFT, with the additional finding of epidermal down-growth of rete ridges into the dermal collagen, much as is seen in psoriatic lesions.



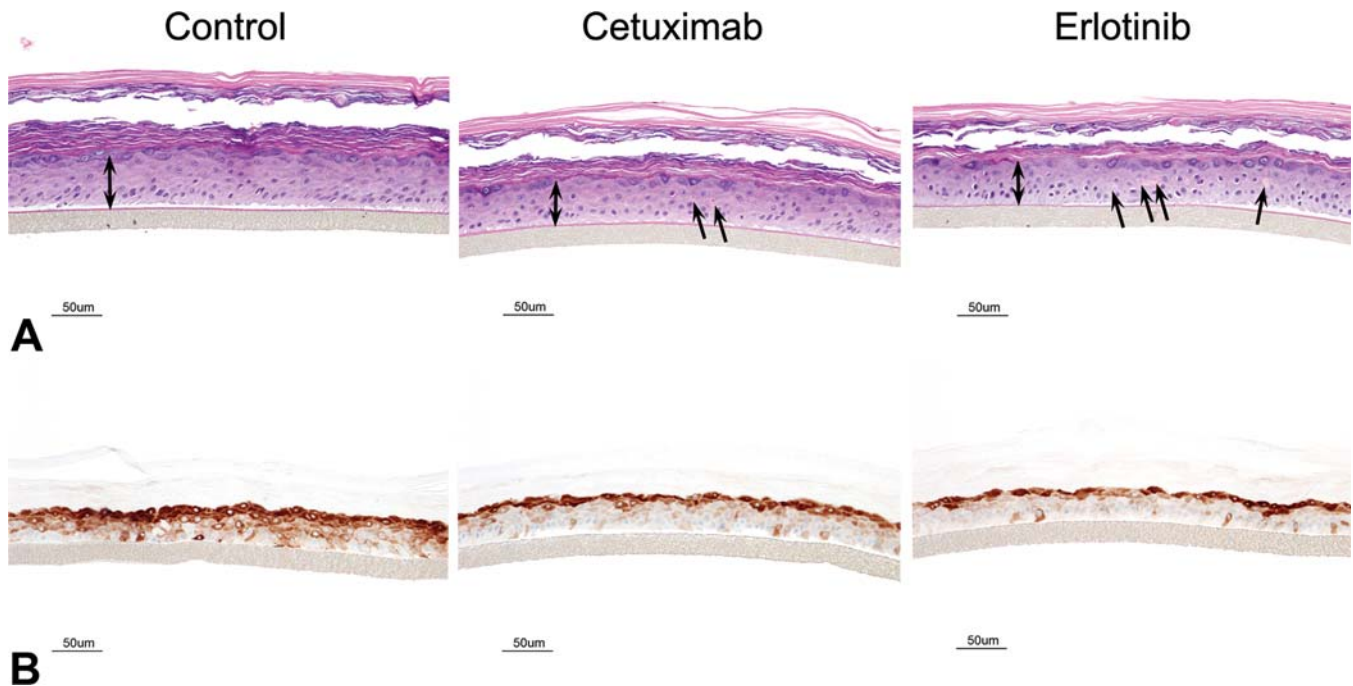


**FIGURE 7.13** Sections of reconstituted human epidermis (EpiDerm©) stained with H&E (A) and IHC stained for phosphoS6 protein (B) illustrating a reduction in the viable epidermal thickness in EpiDerm© sections treated with the EGFR inhibitors cetuximab and erlotinib (as denoted by a decreased length of the double-headed arrows compared to the untreated control). The decrease in epidermal thickness in sections treated with EGFR inhibitors is accompanied by epidermal keratinocyte single cell necrosis (arrows) as well as decreased staining for phosphoS6 (B), an intracytoplasmic effector protein downstream of EGFR. *Reproduced from Haschek WM, Rousseaux CG, Wallig MA, editors: Haschek and Rousseaux's handbook of toxicologic pathology, ed 3, 2013, Academic Press, Figure 55.5, p. 2239, with permission.*

## 4. RESPONSES TO INJURY

### 4.1. General Mechanisms of Response to Injury-Cutaneous Immunity

The skin, like other organ systems, has a relatively stereotypic response to injury, regardless of the specific mechanism underlying the insult. Despite the limited range of response, there is still a great deal that can be ascertained from the different morphologic, physiologic, and molecular alterations that arise in response to injury.

One of the skin's primary functions is to serve as a physical and physiologic protective barrier against injury from the external environment and from loss of water and solutes from the body. When the skin is exposed to irritants, such as xenobiotics, infectious agents, or ultraviolet (UV) radiation that may damage or disrupt this barrier, it mounts an inflammatory and proliferative response in order to prevent further

damage and to restore a morphologically and physiologically functioning barrier.

This barrier disruption manifests in the form of both morphologic and physiologic alterations that will vary depending on the degree of barrier damage and, to some extent, on the specific irritant, although most pathophysiologic responses are generalized and independent of the specific initiating factor(s). A core premise underlying the skin's response to injurious stimuli is that the epidermis, and particularly epidermal keratinocytes and DCs, including LCs, are central to the initiation of the skin's response to injury.

The hypothesis that the epidermal keratinocyte is a primary initiator of the skin's response to noxious stimuli has gained widespread acceptance. Epidermal keratinocytes can recognize pathogen-associated molecular patterns (PAMPs) of microbial origin and danger-associated molecular patterns (DAMPs), such as xenobiotics and other irritants, through TLRs, including TLR-1, TLR-2, TLR-4, TLR-5,

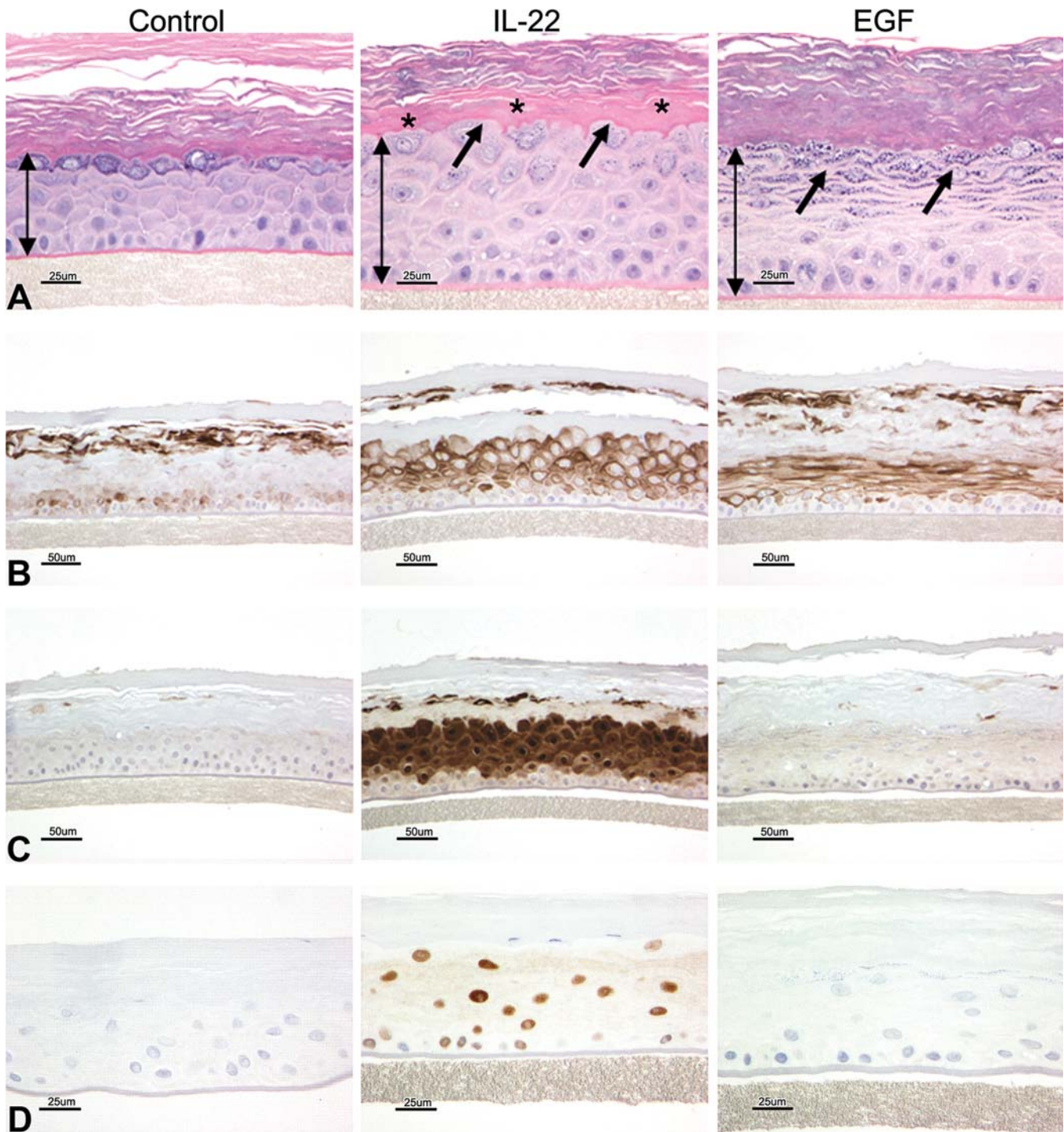


**FIGURE 7.14** Effects of IL-22 on epidermal differentiation in reconstituted human epidermis. Images in (A) demonstrate that IL-22 induces epidermal hyperplasia, as denoted by the increased length of the double-headed arrows compared to the untreated control. In addition, IL-22 also uniquely altered normal epidermal differentiation as demonstrated by hypogranulosis, or a decrease in the granular cell layer (arrows), as well as hyalinization of the lower stratum corneum (asterisks\*). In contrast, EGF also induced epidermal hyperplasia, but induced hypergranulosis in contrast to hypogranulosis seen with IL-22 treatment (arrows). Similarly, images in (B), stained for cytokeratin 16, images in (C), stained for psoriasin (S100A7), and images in (D), stained for pSTAT3, all demonstrate that IL-22 alters epidermal differentiation and activates pSTAT3 as compared to EGF. These effects of IL-22 on reconstituted human epidermis are very similar to those seen in psoriatic epidermis. *Modified from Sa SM, Valdez PA, Wu J et al.: The effects of IL-20 subfamily cytokines on reconstituted human epidermis suggest potential roles in cutaneous innate defense and pathogenic adaptive immunity in psoriasis. J Immunol 178:2229–40, 2007, Figure 3, with permission.*



and TLR-6 on their surface and TLR-3 and TLR-9 in their endosome. These receptors trigger an inflammatory cascade leading to the generation of antimicrobial peptides such as  $\beta$ -defensins, cathelicidins and S100 family proteins, pro-inflammatory chemokines such as IL-8, CXCL9, CXCL10, CXCL11, CCL27, and CCL20, and pro-inflammatory cytokines such as IL-1 $\beta$ , TNF, IL-6, and IL-18.

These chemokines and cytokines recruit and activate leukocytes and convert the initial innate immune response to an adaptive immune response. In addition, keratinocytes express nucleotide-binding domain, leucine-rich repeat-containing (NLR) proteins that recognize cytoplasmic PAMPs, DAMPs, and UV radiation. When engaged, NLRs trigger a pro-inflammatory signaling pathway through a large multiprotein complex, termed an inflammasome, formed by an NLR, an adapter protein termed ASC, and pro-caspase 1. Inflammasome assembly activates caspase-1, which in turn cleaves pro-IL-1 $\beta$  to active IL-1 $\beta$  (Figure 7.15).

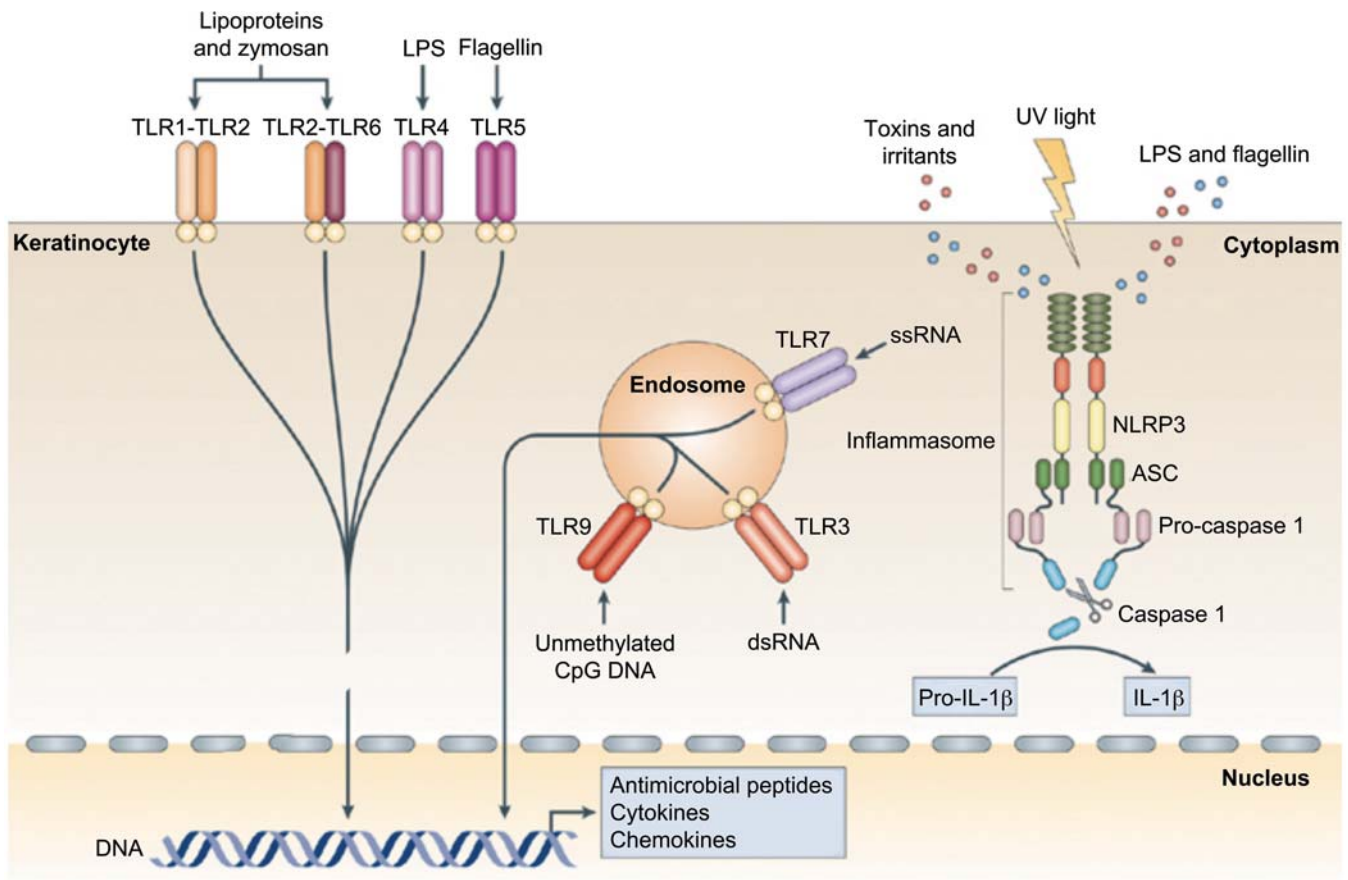
The immune response triggered by keratinocyte activation is believed to be central to the skin's response to a wide range of stimuli and leads to the stereotypic morphologic response(s). Even the immune-mediated/autoimmune disease psoriasis is now believed to be, at least partially, caused by inappropriate or poorly regulated activation of epidermal keratinocytes, which in turn leads to inflammation and the hallmark morphologic changes associated with this condition. The ability of cytokines such as IL-22 and oncostatin M to induce morphologic and differentiation features in keratinocytes that mimic those found in psoriatic epidermis in three-dimensional RHE skin models in the absence of blood vessels and leukocytes reinforces the hypothesis that epidermal keratinocytes are central to the initiation of cutaneous inflammation as well as the initiation of cutaneous response to injury, infection, and toxicity.

Skin-resident DCs, which are bone marrow-derived, have also been implicated as playing an important role in the initiation of the cutaneous inflammatory response to various noxious stimuli. DCs in general are immune cells that can initiate antigen-specific immunity and tolerance in a variety of tissues and are currently separated into three main groups; conventional DCs (cDCs), monocyte-derived DCs (moDCs), and

plasmacytoid DCs (pDCs; possibly to be renamed in near future) with phenotypic markers defined in human and other species. Continually evolving detailed information on DC subtypes and functions is out of the scope of this chapter; Recent reviews by [Park et al. \(2023\)](#), [Hornero and Idoyaga \(2023\)](#) have more information. Skin resident DCs exist in a DC network with immature cells that take up and process antigens, and mature cells that are dedicated to identifying and stimulating T-cells and secondary lymphoid organs (reviewed by [Clausen and Stoitzner, 2015](#)). Immature DCs continually probe their environment for invading pathogens as well as sampling self and environmental antigens. Once mature, DCs migrate to skin-draining lymph nodes with upregulation of surface expression of MHC/peptide complexes to recognize and interact with antigen-specific naïve T cells. Once in the T cell area of the lymph node, DCs can induce both inflammation or tolerance. DCs are defined by their location (epidermal vs. dermal), their cell surface antigen expression, and, most importantly, by their functionality with continually evolving understanding of the functional implications of their phenotypes (reviewed by [Clausen and Stoitzner, 2015](#)). Conventionally, the primary immature DCs in the epidermis were called LCs, with dermal DCs considered a second phenotype. Recent advances have shown that immature langerin + DCs (CD207 +; used to identify LCs) are also present in the dermis and so this subdivision is not absolute.

LCs (primarily epidermal DC population), as previously described, express CD1a and the c-type lectin, langerin (DC207), which is expressed in association with ultrastructurally visible racquet-shaped organelles called Birbeck granules. LC precursors expressing CD14 and langerin migrate from blood vessels in the dermis into the epidermis, where expression of e-cadherin, CXCL14, TGF- $\beta$ 1, CCL20, IL-15, and GM-CSF is typical of immature LCs. Immature LCs are the immune sentinel cells in the epidermis equipped for antigen capture via TLR and c-type lectins such as langerin. Upon antigen capture and activation, these cells become mature LCs (express major histocompatibility class (MHC) I and MHC II and costimulatory molecules important in the adaptive





Nature Reviews | Immunology

**FIGURE 7.15** Keratinocytes as sensors of danger. Keratinocytes are central skin sentinels and can recognize foreign and dangerous agents, for example pathogen-associated molecular patterns (PAMPs) of microbial origin and danger-associated molecular pattern (DAMPs), such as irritants and toxins, through toll-like receptors (TLRs) and the inflammasome. TLRs are transmembrane receptors that are present on the cell surface or on the surface of endosomal compartments. Lipopolysaccharide (LPS) stimulates TLR4; bacterial lipoproteins and fungal zymosan stimulate TLR1–TLR2 and the TLR2–TLR6 heterodimers; bacterial flagellin activates TLR5. PAMP recognition by TLRs leads to activation of host cell signaling pathways and subsequent innate and adaptive immune responses with antimicrobial peptide, cytokine, and chemokine production. Keratinocytes also express nucleotide-binding domain, leucine rich repeat-containing (NLR) family, pyrin domain containing 3 (NLRP3), which belongs to the newly identified class of proteins encoded by the NLR gene family. These proteins can recognize PAMPs that are in the cytoplasm (such as LPS and flagellin), DAMPs, and ultraviolet (UV) light, and activate the inflammasome complex. This multimeric complex is formed by an NLR, an adapter protein termed ASC (apoptosis-associated speck-like protein containing a caspase recruitment domain) and pro-caspase 1, and its assembly leads to the activation of caspase 1, which processes prointerleukin-1b (pro-IL-1b) into biologically active IL-1b. CpG, cytosine-phosphate-guanine 5' to 3'. Reprinted from Nestle FO, Di Meglio P, Qin JZ et al.: Skin immune sentinels in health and disease. *Nat. Rev. Immunol.* 9:679–691, 2009, Figure 2, p. 22, with permission from Macmillan Publishers Limited.

immune response) and migrate to the inner paracortex of draining lymph nodes to present antigens to T cells.

Because of their role in cutaneous antigen presentation, LCs are believed to be important

in the initiation of cutaneous cell-mediated immune responses, such as those responsible for allergic contact dermatitis. More recently, data from mice deficient in LCs suggest that LCs may decrease rather than enhance inflammation,

leading to the hypothesis that LCs may be involved in the generation of tolerance rather than in the initiation of inflammation ([Otsuka et al., 2018](#)).

It appears likely that CD103<sup>+</sup> ( $\alpha$ E integrin) langerin<sup>+</sup> DCs are the antigen-presenting DCs most important in the initiation of the skin immune response. These CD103<sup>+</sup> DCs most likely reside in the dermis rather than in the epidermis. A third skin DC population important in the cutaneous response to injury comprises the inflammatory dendritic epidermal cells (IDECs), which, unlike LCs, express CD206, CD1b, and CD36, do not express langerin, and in particular, overexpress high-affinity Fc receptors for IgE (Fc $\epsilon$ RI), making them reactive to specific IgE-bound allergens. IDECs are believed to reside in both the epidermis and dermis, respond particularly to CCR5 and CCR6 chemokines, and are believed to be important in the pathogenesis of allergic contact dermatitis as well as atopic dermatitis.

Immature DCs within the dermis express CD1c and CD206 but have only low expression of CD1a. Dermal DC activation is also believed to be central to the initiation of the cutaneous inflammatory response, regardless of the initiating stimulus. Dermal DCs, like keratinocytes, also express pathogen recognition receptors such as TLR1, TLR4, and CD206. Upon activation, dermal DCs become “inflammatory dermal DCs,” acquire CD11c expression, and secrete pro-inflammatory chemokines and cytokines, including iNOS and TNF. In addition, because of their close proximity to the vasculature in the dermis and lack of e-cadherin attachments to keratinocytes, dermal DCs have the ability to deliver antigenic signals very quickly to draining lymph nodes, where they home to the outer paracortical region to contribute to B-cell responses as well as to T-cell activation.

A specific type of dermal DC, the pDC (reviewed by [Hornero and Idoyaga, 2023](#); [Guiducci et al., 2010](#)), is rare in normal skin but increases in number during cutaneous inflammation. pDCs express CD45RA, CD123, and CD303, and secrete abundant type I interferons (IFN- $\alpha$ ) in response to the recognition of nucleic acids via TLR7 and TLR9. pDCs may play a role in the pathogenesis of psoriasis and systemic lupus erythematosus (SLE).

A third set of cells implicated in the initiation of the cutaneous immune response comprises skin-resident T lymphocytes, found both within the epidermis as well as in the dermis. Epidermal resident T cells are primarily CD8<sup>+</sup>  $\alpha\beta$  memory T cells and are often found in close proximity to LCs. Dermal resident T cells are also mostly memory cells but are roughly equally distributed between CD4<sup>+</sup> and CD8<sup>+</sup> T cells. Dermal resident T cells express cutaneous lymphocyte-associated antigen (CLA) and gain skin-homing properties after contact with resident DCs.

In addition to cutaneous resident T cells, all three major types of CD4<sup>+</sup> helper T lymphocytes, Th1, Th2, and Th17 cells, have been found in the skin during various inflammatory conditions. Initially, Th1 helper T cells, driven by IL-12 and producing IFN- $\gamma$  and related cytokines, were believed to be the primary T cells involved in the cutaneous immune response and cutaneous response to injury. More recently, IL-23-driven Th17 cells have been recognized as being essential in host immune defense against many bacterial and fungal pathogens at both cutaneous and mucosal surfaces. IL-17 and IL-22, cytokines produced by Th17 cells, upregulate keratinocyte production of antimicrobial peptides ([Nogroles et al., 2008](#); [Sonnenberg et al., 2011](#)). Thus, Th17 cells and their cytokines link the adaptive immune response to the innate immune response of keratinocytes in order to optimize the host immune response to cutaneous pathogens.

Another T cell subtype that appears to span innate and adaptive responses is present in larger numbers at mucosal sites like skin is the MAIT cell, or mucosal-associated invariant T cell. These cells appear to be widely conserved across species but have different interspecies distribution patterns in mucosal organs like gut, lung, skin, and even liver ([Corbett et al., 2020](#)). MAIT cells recognize antigen specifically presented on MR1 (MHC-related protein 1), an antigen-presenting molecule that is specific to riboflavin moieties. These vitamin B analogue sequences were originally thought to activate MAIT cells specifically in instances of bacterial infection, but focused MAIT research has shown the importance of the MAIT-MR1 axis in viral response, cancer, tissue repair, and even drug-related tissue injury. Still, the contribution of

these cells to the maintenance of the cutaneous microbiome is an area of increasing interest (Jabeen and Hinks, 2023).

MAIT and other skin-resident T cells are believed to play a major role in skin immune homeostasis and surveillance and have also been implicated in the pathogenesis of psoriasis and atopic dermatitis. A specific subset of skin-homing T cells that produce IL-22 but not IL-17 or IFN- $\gamma$ , termed Th22 cells (reviewed by Fujita, 2013; Ahn et al., 2020), has been recently identified in the skin of patients with atopic dermatitis. IL-22 production and Th22 polarization is driven by pDC production of IL-6 and TNF, thus linking up these 2 cell types in cutaneous and mucosal immune homeostasis and defense. Th22 cell production of the epithelial-specific cytokine IL-22, which induces keratinocyte proliferation, differentiation, and production of antimicrobial peptides such as  $\beta$ -defensins and S100 family proteins, pro-inflammatory chemokines such as IL-8, CXCL1, and CXCL7, and cytokines and growth factors involved in epidermal regeneration such as IL-20 and vascular endothelial growth factor (VEGF), provides further evidence for the cross-talk between the adaptive immune system and the innate immune system, particularly in epidermal keratinocytes.

Thus, the current model for the cutaneous response to injury, regardless of the specific type or etiology of the injury, is initiated by epidermal keratinocyte recognition of PAMP or DAMPs via engagement of TLRs and/or NLRs, thus triggering pro-inflammatory signaling pathways, an inflammatory cascade that leads to the generation of antimicrobial peptides such as  $\beta$ -defensins and cathelicidins, pro-inflammatory chemokines such as IL-8, CXCL1, CXCL9, CXCL10, and CXCL11, and cytokines such as IL-1 $\beta$ , TNF, IL-6, and IL-18. These keratinocyte-derived chemokines and cytokines further recruit and activate DCs and other leukocytes to elaborate additional cytokines and chemokines, such as IFN- $\alpha$  from pDCs and IL-12 and IL-23 from dermal DCs, which further recruit and activate T lymphocytes of both the Th1 and particularly the Th17/Th22 lineage to release pro-inflammatory cytokines such as IFN- $\gamma$ , IL-17, and IL-22, thus converting the initial innate immune response to an adaptive immune response, and providing cross-talk between the

two arms of the immune system (Figure 7.16). This immune response is believed to be central to the skin's response to a wide range of injurious stimuli and leads to the morphologic responses that are described in this chapter.

## 4.2. Special Considerations-Translational Immunology of Skin

Mice are the primary pharmacologic models of many human conditions and diseases. Because of size, relative ease of genetic manipulation in the current research milieu, short gestation time with large litter size, and known strains that mimic aspects of human disease, they are useful in both efficacy and toxicology studies (see. *Animal Models in Toxicologic Research: Rodents*, Vol 1, Chap 17). However, from a translational point of view, when using mice as comparative models, there are some key differences in murine immunology in comparison to humans. With the advent of technologies like single cell RNAseq, even more diversity in cutaneous lymphocyte type and function is continually being discovered (Kobayashi and Moro, 2022), and the translational aspects of these discoveries (largely in rodent models) to humans must always be ascertained. The following are some examples of known differences between murine and human cutaneous immunology. Cutaneous lymphocytes in mice are largely  $\gamma\delta$  type [also called dendritic epidermal T cells (DETCs); considered to be at transition from innate to adaptive immunity and of importance in wound healing] (Hu et al., 2022; Chen et al., 2021) and these are the main source of IL-17A, IFN $\gamma$ , and growth factors; while in humans, cutaneous lymphocytes are primarily  $\alpha\beta$  type. Macrophage expression (constitutive or induced) of iNOS and arginase has been reported to be different in mouse and human. At the most basic level of immunity, the largest circulating WBC population in mice are lymphocytes, whereas in humans, this is neutrophils. This may point to the overall immune strategy between species being one of tolerance (mice) versus activation (human). TLRs differ considerably in both expression and function in mice. Of particular importance, when using information from mouse models to study the roles of various pharmaceutical interventions in allergic dermatoses,



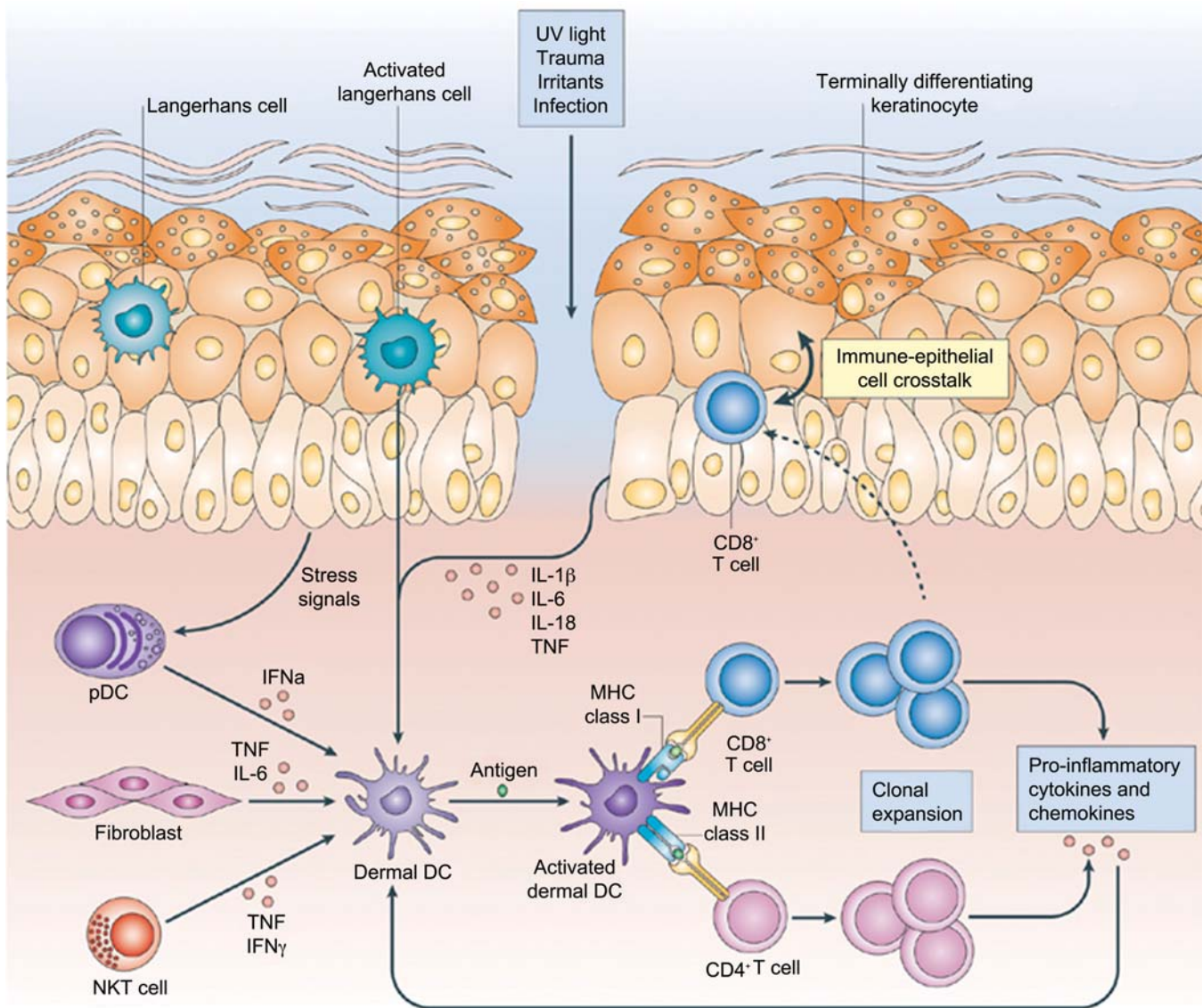


**FIGURE 7.16** Skin-resident immune sentinels. Ultraviolet (UV) light, trauma, irritants, or infection (essentially any type of barrier disruption) triggers a coordinated immune response to maintain skin homeostasis. Skin resident immune cells are key sentinels for restoring homeostasis but can also be effector cells during cutaneous injury. Epidermal Langerhans cells (LCs) are key immunological sentinels. Keratinocytes sense and react to noxious stimuli by producing pro-inflammatory cytokines such as interleukin-1 $\beta$  (IL-1 $\beta$ ), IL-6, IL-18, and tumor necrosis factor (TNF), which in turn activate dermal DCs (dendritic cells). Innate immune cells, such as plasmacytoid dendritic cells (pDCs), activated by stress signals derived from keratinocytes, can also contribute to dermal DC activation by releasing interferon- $\alpha$  (IFN- $\alpha$ ). Fibroblasts can produce TNF and IL-6, and natural killer T (NKT) cells can produce TNF and IFN- $\gamma$ , thereby contributing to the local inflammatory response. Dermal DCs activate and promote the clonal expansion of skin-resident memory CD4 $^{+}$  or CD8 $^{+}$  T cells. T cell-derived proinflammatory cytokines and chemokines in turn can further stimulate epithelial and mesenchymal cells, including keratinocytes and fibroblasts, thus forming an amplifying feedback loop for the inflammatory reaction. Moreover, skin-resident T cells can migrate into the epidermis, engaging in cross-talk between immune cells and keratinocytes. *Reprinted from Nestle FO, Di Meglio P, Qin JZ et al.: Skin immune sentinels in health and disease. Nat. Rev. Immunol. 9:679–691, 2009, Figure 3, p. 23, with permission from Macmillan Publishers Limited.*

mast cell granule contents differ in mouse and man, with serotonin being a key component in mice. Likewise, neutrophil granule contents also differ in mice. Granule constituents like defensins, lysozyme, and alkaline phosphatase that are important in human neutrophils are generally poorly expressed or absent in mice. Basophils (circulating cell) are related to mast cells (tissue resident cell) and can participate in IgE-dependent and IgE-independent allergic responses (reviewed by [Miyake and Karsuyama, 2017](#)) in a variety of tissues in mice and humans, including skin. When mice are used to study human allergic skin disease, the role of basophils in induced allergic skin diseases of mice has been difficult to discern. Originally, these cells were thought to be largely absent in chronic allergic conditions in mice, but this position has recently been debated ([Mestas and Hughes, 2004](#); [Zschaler et al., 2014](#)).

Human melanocytes are present diffusely rather than largely restricted to hair follicles in haired areas as they are in mice. Since melanocytes have immunologic properties, the paucity of these cells superficially may directly impact immune responses in the epidermis. Melanophages have a defined role in cutaneous physiology (melanomas, pigmented nevi, melasma), but understanding of these cells remains elusive in mice.

### 4.3. Wound Healing

Wound healing is an important focus in toxicologic pathology, not only as it relates to interventions to expedite the process and reduce complication like excessive scarring, but also because there are many drugs being developed for systemic indications (oncology, immunology, etc.) that may involve modulation or inhibition of some of the key molecular mediators in the complex sequence of events that is required to heal cutaneous defects. The complex process of wound healing is often presented as occurring in sequential stages, however these stages are physiologically overlapping and intricately linked. The very detailed molecular processes involved in these steps are beyond the scope of this chapter but are reviewed comprehensively in several recent publications ([Peña and Martin, 2024](#), [Rodrigues et al., 2019](#)). There are two primary types of wound healing; first intention

when the edges of the wounds are closely opposed either by suturing or by the type of wound (e.g., a scratch), and second intention where the wound bed is left open and heals by contraction, granulation tissue formation, and/or re-epithelialization. Adverse effects on the ability of a wound to heal are a potential concern for many therapeutics or toxicants, especially if these affect the processes of inflammation, neo-vascularization, or remodeling of connective tissue. A review of some of the most essential of these processes follows with a focus primarily on second intention healing.

In general, when a wound is created in the skin, the first defenses of the body are those of vasoconstriction and hemostasis to prevent fluid loss and to provide immediate barrier protection at the wound site ([Figure 7.17](#)). The coagulation cascade is activated to form a clot containing fibrin and platelets that release important mediators for subsequent stages of wound resolution ([Rittié, 2016](#)). These mediators include growth factors, such as PDGF, TGF- $\beta$ , VEGF, EGF, and IGF, that contribute to the healing process ([Peña and Martin, 2024](#); [Rodrigues et al., 2019](#)). Although platelets are an important source of effectors during this early stage of wound healing, it has been shown that thrombocytopenic mice are competent in growth factor production and resultant cell proliferation within the wound. So, additional cell types, for example lymphocytes and macrophages, that increase in number at the wound site in thrombocytopenic animals also have a clear effector role ([Rodrigues et al., 2019](#)).

Inflammation at the wound site occurs early in the healing cascade and is driven by and complements the hemostatic process. Neutrophils populate the wound by extravasation from damaged vessels and through attraction to chemokines and molecular pattern signals (pathogen-associated, PAMPs; damage-associated, DAMPs). Tissue-resident macrophages and circulating monocytes are recruited by neutrophils. Macrophages clear cell debris at the wound site and begin the process of modeling and deposition of the wound matrix. Deposition of structural components of the wound, including fibrin and collagen, provide the scaffold for new blood vessels to grow into the wound site (granulation) and provide the bed upon which keratinocytes can begin to form a new skin barrier over the wound (re-epithelialization).



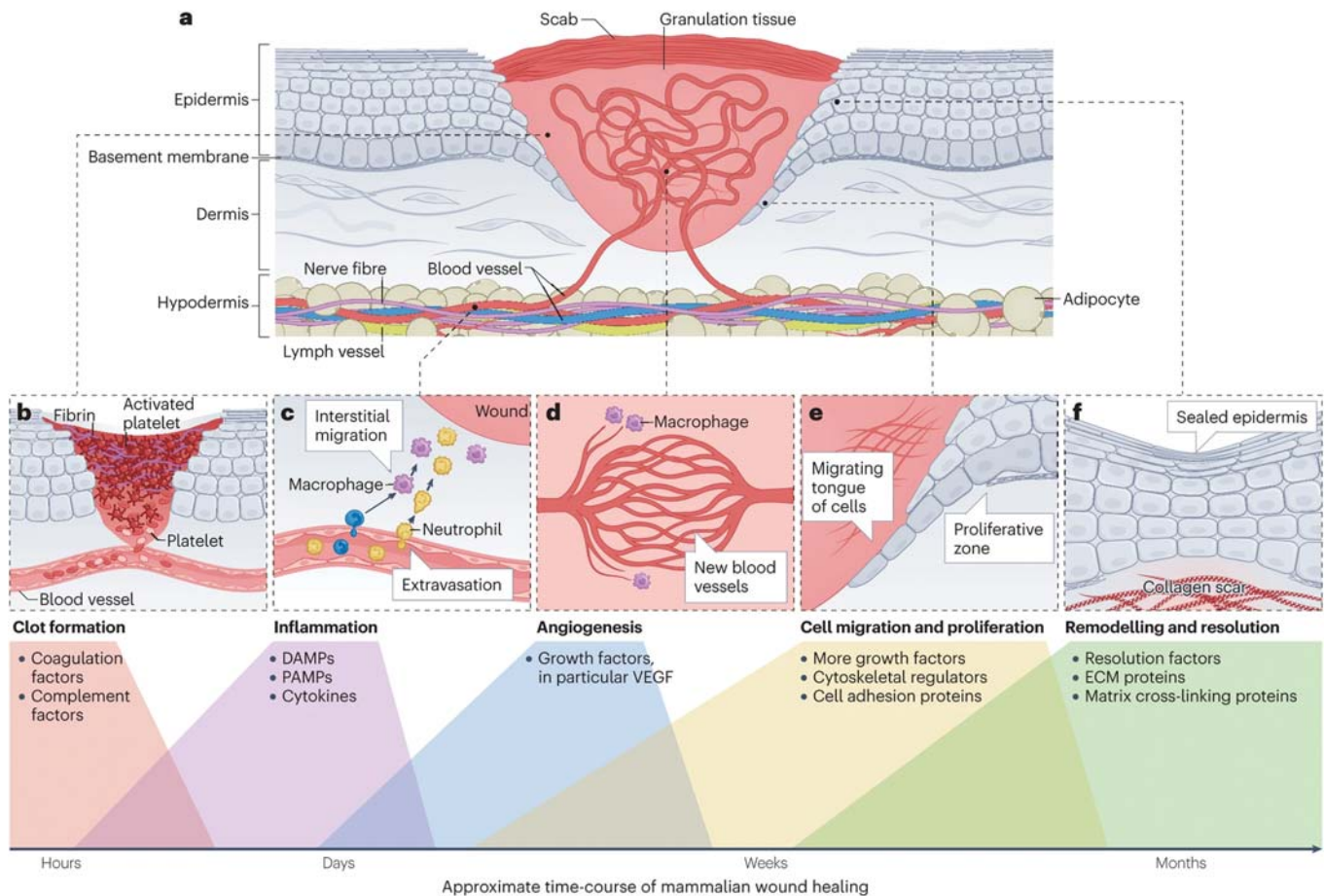


**FIGURE 7.17** (A) Schematic of a skin wound as it closes to illustrate the various phases and contributing cell players. (B) Immediately upon tissue damage, a clot forms to temporarily plug the wound gap. (C) Soon after this, the wound inflammatory response kicks in, with innate immune cells, neutrophils and macrophages drawn from local resident populations and through recruitment by extravasation from nearby vessels before migrating into the wound. (D) These inflammatory cells, particularly macrophages, orchestrate the formation of granulation tissue to replace the missing connective tissue, which entails wound angiogenesis, fibroblast migration and deposition of a new collagen matrix. (E) As the granulation tissue is being laid down, resurfacing is driven by re-epithelialization, which involves both epidermal migration and cell division to restore barrier integrity. (F) Finally, these episodes cease as the wound edges confront one another and the wound has healed; however, the various cells and tissues have not resolved and remodeled, which they now do to varying degrees, generally leaving a wound scar. DAMPs, damage-associated molecular patterns; ECM, extracellular matrix; PAMPs, pathogen-associated molecular patterns; VEGF, vascular endothelial growth factor. Reproduced from Peña OA, Martin P. Cellular and molecular mechanisms of skin wound healing, *Nat. Rev. Mol. Cell. Biol.* 25:599–616, 2024. <https://doi.org/10.1038/s41580-024-00715-1>, Fig 1, p 601, with permission.

The skin has an incredibly diverse resident T cell population (see sections 4.1 and 4.2). In humans and mice, both  $\alpha\beta$  and  $\gamma\delta$  T cells are present, but the contribution of each in the process of wound healing is less well-defined in humans than in mice. In mice,  $\gamma\delta$  T cells are enriched in the epidermis (i.e., DETCs, dendritic epidermal T cells so named because of dendritic morphology in mice that does not

translate to human  $\gamma\delta$  T cells) and central to barrier surveillance and signaling (via FGFs and IGF1) to keratinocytes, and therefore figure prominently in the wound healing process (Peña and Martin, 2024, Rodrigues et al., 2019).  $\alpha\beta$  T cell subsets in the skin include  $CD4^+$ ,  $CD8^+$ ,  $T_{reg}$ s, and NK cells. B cells and innate lymphoid cells (ILCs) in the skin are additional lymphoid cells important in the



healing process (Peña and Martin, 2024; Rodrigues et al., 2019).

Mast cells are recruited to wounds early in the inflammatory process via complement cascade signaling. The contribution of mast cells to the wound healing process, however, is not clear. It is well-documented that mast cells play a role in conditions associated with excessive connective tissue deposition, such as hypertrophic scarring and scleroderma, but some studies show that mice with reduced mast cell function show relatively normal wound healing (Peña and Martin, 2024; Rodrigues et al., 2019).

Some non-immune cell types also figure prominently in wound healing. These include fibroblasts, pericytes, and endothelial cells that contribute to granulation tissue; keratinocytes that cover the wound area and provide essential cell signaling functions; and a number of additional cell types that are not as well-studied but nonetheless important. Nerve fibers at wound sites have a role in myofibroblast activity. Associated glial cells and Schwann cells have also been shown to be important in wound healing (Peña and Martin, 2024). Melanocytes may be necessary for skin damage repair as they are dendritic in nature, interact with fibroblasts and macrophages during wound healing, and clearly respond to damage signals in conditions such as keloid. The hypothesis that hyperpigmentation is a protective response in some instances is compelling (Peña and Martin, 2024; Rodrigues et al., 2019). Adipocytes in the hypodermis have also been shown to be pivotal in providing signals for cell trophism and antimicrobial defenses at wound sites. Clearly, there are myriad cell-to-cell interactions during wound healing which remain to be fully elucidated.

As inflammation continues and new tissue begins to fill the wound bed, re-epithelialization begins on the surface. The degree to which this process occurs is different in humans compared to that of many species used in nonclinical investigations (Table 7.6). Humans and pigs have tight skin which is adherent to the underlying muscle and fascia and is not readily moved from its natural position. Loose skin in many laboratory animal species has a flexible attachment to underlying tissues, including a panniculus carnosus muscle, allowing it to move readily (Grada et al., 2018). Wounds in tight-skinned animals heal by re-epithelialization early in the

process, whereas loose-skinned animals heal with contraction of the wound site by myofibroblasts thereby bringing the wound edges in closer apposition. Contraction also occurs in tight-skinned animals, but as part of the final remodeling stage. The type of wound created can also contribute to the phases of the healing process. For example, superficial (partial-thickness) wounds in humans (e.g., surgical incisional wounds) may largely heal by re-epithelialization, whereas larger, excisional, full-thickness (deep to the dermis) wounds will necessitate granulation tissue formation prior to the re-epithelialization stage (Rittié, 2016).

During the re-epithelialization process, surface keratinocytes cover the wound defect by proliferation and migration of cells from the spinous layer. New keratinocytes are not only derived from the interfollicular compartment, but also from adnexa. In fact, in partial-thickness wounds, initial re-epithelialization is largely accomplished by progenitor cells from hair follicles and sweat glands (Rittié, 2016). Regeneration of adnexa following wounding will depend on presence of stem cells, so complete loss of pilosebaceous units from full-thickness wounds is likely to result in a permanently hairless scar.

The normal process of wound healing progresses through acute hemostasis, inflammation, and regeneration within days to weeks, but the final stage of remodeling (increasing tensile strength and flexibility) will take weeks to months (Rittié, 2016). Chronic wounds, i.e., those that fail to heal within this time frame, are a continued focus in development of drugs and other therapeutic interventions. Chronic wounds can result from aberrations in any stage of the healing process. Chronic wounds associated with diabetes, for instance, are associated with localized, persistent inflammatory signals (e.g., TNF-alpha, IL-1, IL-6), infection and biofilm alteration; neutrophil infiltration and associated tissue necrosis; impaired angiogenesis and nerve function; and systemic effects that can result in sustained impaired cell defense mechanisms (Grada et al., 2018; Masson-Meyers et al., 2020; Grambow et al., 2021; Zindle et al., 2021).

Because chronic wound conditions are so multifaceted in pathophysiology, they can be very difficult to model in vitro. There have been great recent advances in complex in vitro

TABLE 7.6 Characteristics of Skin in Human and Animal Species Commonly Used in Wound Healing Assessment

Species	Skin attachment type <sup>a</sup>	Primary wound closure <sup>a,b,e</sup>	Wound healing time frame <sup>a,c,e,f</sup>	Specific model examples <sup>a,c,d,e,g,k</sup>	Model advantages <sup>a,c,d,e,g,h,j</sup>	Model disadvantages <sup>a,c,d,e,g,h,j</sup>
Human	Tight	R/G	7–14 days	N/A	- Main species of interest	- Ethical considerations
Pig	Tight	R/G (primary) or C (some full-thickness wounds)	12–14 days	<ul style="list-style-type: none"> <li>- Keloid/hypertrophic scar</li> <li>- Infected wound model</li> <li>- Ischemic ulcer model</li> <li>- Diabetic/metabolic models</li> </ul>	<ul style="list-style-type: none"> <li>- Similarities to human skin (see also Animal Models in Toxicologic Research: Pig, Vol 1, Chap 20), considered most translationally relevant for most aspects</li> <li>- Large size for studying multiple wound replicates</li> </ul>	<ul style="list-style-type: none"> <li>- Husbandry and cost</li> <li>- Not easily genetically engineered</li> <li>- Biologic agent cross-reactivity may be low compared to humans (generally true of all species other than nonhuman primate)</li> <li>- Ethical considerations may be greater for non-rodent models</li> </ul>
Rabbit	Loose	C (primary) or R/G (some models)	13–16 days	<ul style="list-style-type: none"> <li>- Ischemic ear model</li> <li>- Hypertrophic scarring</li> <li>- Diabetic models</li> </ul>	<ul style="list-style-type: none"> <li>- Partial thickness (ear) wounding can be used for studying re-epithelialization</li> <li>- Ear model allows for internal control (topicals) and has large surface area</li> </ul>	<ul style="list-style-type: none"> <li>- Husbandry and surgical methodology for wound models</li> <li>- Ethical considerations</li> </ul>
Rat	Loose	C	5–7 days	<ul style="list-style-type: none"> <li>- Wound splinting</li> <li>- Pressure ulcer</li> <li>- Ischemic flap</li> <li>- Tail (hypertrophic scarring)</li> </ul>	<ul style="list-style-type: none"> <li>- Larger than mice</li> <li>- Ease of husbandry/training</li> <li>- Diabetic models available</li> <li>- Abundant literature</li> </ul>	<ul style="list-style-type: none"> <li>- Few similarities to human skin</li> <li>- Full thickness wounds in most models</li> <li>- Hair cycle may influence healing speed</li> <li>- Differences in male and female skin thickness</li> </ul>
Guinea pig	Loose	C	12 days <sup>g</sup>	- General models <sup>i</sup>	<ul style="list-style-type: none"> <li>- Size and cost</li> <li>- Pigmentation studies</li> <li>- Vitamin C requirements allow mechanistic studies on collagen (similar to humans)<sup>j</sup></li> </ul>	<ul style="list-style-type: none"> <li>- Not as widely used or reported on</li> <li>- No genetic tractability</li> <li>- Few similarities to human skin</li> </ul>

Mouse	Loose	C	5–7 days	<ul style="list-style-type: none"> <li>- Diabetic mice</li> <li>- Wound splinting</li> <li>- Xenografts</li> <li>- Dorsal skin chamber</li> <li>- Ischemic flap</li> <li>- Pressure ulcer</li> <li>- Biomechanical load</li> </ul>	<ul style="list-style-type: none"> <li>- Size and cost</li> <li>- Ease of genetic alteration(s)</li> <li>- Well-documented diabetic models</li> <li>- Abundant public databases</li> <li>- Splinted models will better translate to human wounds</li> </ul>	<ul style="list-style-type: none"> <li>- Few similarities to human skin</li> <li>- Documented disparities in translational immune responses</li> <li>- Full thickness wounds in most models</li> <li>- Hair cycle may influence healing speed</li> <li>- Differences in male and female skin thickness</li> </ul>
Zebrafish	N/A	R/G	Re-epithelialization is complete in less than 24 h; complete regeneration of all skin and scale by 28 days	<ul style="list-style-type: none"> <li>- General models<sup>i</sup></li> </ul>	<ul style="list-style-type: none"> <li>- Fewer ethical considerations</li> <li>- Well-documented embryology</li> <li>- In vivo imaging methods routine and less complicated</li> </ul>	<ul style="list-style-type: none"> <li>- Non-mammalian</li> <li>- Compatibility with therapeutic agents intended for human physiology unknown</li> </ul>

<sup>a</sup> Grada et al. (2018).

<sup>b</sup> R/G = re-epithelialization/granulation; C = contraction.

<sup>c</sup> Grambow et al. (2021).

<sup>d</sup> Zindle et al. (2021).

<sup>e</sup> Richardson et al. (2013).

<sup>f</sup> Wound healing times are generally expressed as a minimum time to initial closure, but can vary significantly depending on wound type and size.

<sup>g</sup> Gupta et al. (2023); There is evidence for acceleration of wound healing in pigmented guinea pigs compared to non-pigmented guinea pigs.

<sup>h</sup> Flynn et al. (2023).

<sup>i</sup> General models that are applied across species include incisional, excisional, and burn models (see text).

<sup>j</sup> Schencke et al. (2016).

<sup>k</sup> Wong et al. (2011).



modeling of the skin (microfluidic systems, skin equivalents, bioprinting, etc.; [Sarian et al., 2023](#); [Flynn et al., 2023](#)), but these tend to be fit-for-purpose in interrogating specific molecular mechanisms or wound features. In vivo models are still the most translationally relevant, even though they are also sometimes limited in scope, particularly as applied to chronic wound healing.

[Table 7.6](#) summarizes the major features of the most commonly used laboratory species used in wound healing studies and provides references for additional detail. There is a wide array of human conditions modeled in these species. The most simple studies are incisional wounds, usually used to study post-surgical healing, with apposed wound edges and first intention healing. Incisional wounds can be partial or full-thickness, but the former are difficult to model in rodents because of the relatively thin combined dermal and epidermal thickness in these species. Partial thickness wounding in rodents can be achieved through tape-stripping (removing only the surface layers of the epidermis), abrasive brushing (to remove most of the epidermis) or blistering (to separate epidermis from dermis) ([Flynn et al., 2023](#)). Rodents are more routinely utilized in full-thickness wound models including excisional, burn, and ischemic models (amongst others; [Zindle et al., 2021](#); [Grada et al., 2018](#); [Flynn et al., 2023](#)). Excisional wounds are used to model more chronic stages of healing such as those present with ulcerated skin. Simple excisional wounds can be created via punch biopsy. Multiple punches can be made on the dorsal skin of rodent and pig models, or ears of the rabbit. The rabbit ear model has the advantage of mimicking human healing by re-epithelialization and granulation. Rodent models can also be modified to delay initial contraction by splinting excisional wounds, so that they more closely resemble chronic wounds in humans.

Chronic wounds with complicated secondary infections can be modeled through inoculation of excisional wounds with bacteria. Wound healing in diabetic animal models has been studied with many of the described wound types. Rodent (and some nonrodent) animal models that are genetically or chemically modified to have features of diabetes or metabolic disease are employed for many of these studies ([Rai et al.,](#)

[2022](#)). Ischemic wounds are another common area of chronic wound investigation. These models include pressure ulcers (“bedsores”) that can be induced by placement of magnets resulting in localized tissue necrosis (with or without including a reperfusion injury stage), suturing of vessels to replicate localized loss of vascular integrity (rabbit ear vasculature lends itself well to this model), and skin flap models that are variably attached at the base to study not only circulatory loss, but also revascularization ([Sami et al., 2019](#)).

Burn models include full- or partial thickness wounds, depending on method of wound induction (air, wax, metal, etc.), and may occasionally include secondary bacterial infection (see also *Radiation and Other Physical Agents*, Vol 3, Chap 14) ([Sami et al., 2019](#)). Radiation burns are another area of interest, particularly in oncology. Radiation burn studies usually involve irradiating the skin prior to wound creation ([Sami et al., 2019](#)). Pigs, rabbits, and rodents have all been used as models of burn and radiation injury, with each having important advantages and disadvantages (similarities to human skin, size, cost, husbandry, difficulty of performing procedures, etc.). Species selection is an important consideration for use of any of these models as each will have unique translational mechanistic features.

Complications during wound healing and remodelling can result in excessive scarring, called hypertrophic scarring when limited to the wound area, or keloid when scar tissue extends beyond the zone of wound repair. There are many factors that contribute to the degree of scarring including size and depth of the wound, location of wound (wounds over joints may have increased movement and therefore likelihood of hypertrophic scar for instance), adequacy of blood supply, type of healing, wound infection, and intrinsic factors to the patient such as age, genetics, other health conditions (especially diabetes or chemotherapy), smoker or non-smoker, environment, nutritional status, and of course wound care. Pharmaceutical interventions aimed at reducing scarring must first allow the wound to heal, and so timing becomes critical in this type of intervention. Scarring is a difficult area to study because the process of scarring is not complete until remodelling is complete which may take months to even years after wounding,

and there are factors throughout the phases of wound healing that will influence the ultimate degree of scarring. Rodent models of scarring, considered less translationally relevant because of the differences in skin anatomy when compared to humans, include genetically altered animals, human tissue graft models, and models with biomechanical forces applied to wounds to stimulate scar formation. Rabbit ear scar models are popular, since the skin of the ear is tightly adherent to underlying cartilage and can form a hypertrophic scar with post-wounding intervention (Mistry et al., 2022). Several pig models are validated for studying scarring. The Red Duroc pig, a full-sized breed of farm pig, is considered a highly translationally relevant model for human hypertrophic scar formation. The Red Duroc fibroproliferative scar model has characteristic macroscopic (i.e., firm, thick, hairless, and hypo- or hyperpigmented scars) and microscopic (i.e., whorl-like pattern of disorganized collagen bundles, high numbers of myofibroblasts, mast cells, and collagen nodules) features and similar immunohistochemical staining patterns (i.e., IGF-1, TGF- $\beta$ 1, versican, and decorin) (Seaton et al., 2015) to human hypertrophic scars. (See also *Animal Models in Toxicologic Research: Pig*, Vol 1, Chap 20).

#### 4.4. Influence of Skin Microbiome on Adaptive Immune Response

Any discussion of skin immune response needs to also consider the interaction of the skin microbiome with the innate and adaptive immune responses of the skin. The skin is populated by a wide range of commensal microbial organisms including bacteria, fungi, viruses, and ectoparasites (Belkaid and Segre, 2014; Grice and Segre, 2011) that vary by region of body, time of year, environmental exposure, between individuals, and by healthy versus diseased states (Kloepfer et al., 2022). The skin commensal microbiome is greatly influenced by multiple factors in our modern environment including such things as environmental temperature controls (heating or air conditioning), degree and frequency of bathing, climate, sun exposure, pollution, antimicrobial use, and lifestyle choices such as nature relatedness, nutrition, sleep, exercise, smoking, and beauty routine (choice of

cosmetic products and frequency of application) (Khmaladze et al., 2020), and of special concern, choices made around the time of birth and infancy (Prescott et al., 2017). This has led to the concept of an “interactome” which is the end result of interactions between the sum total of our genome, microbiome, and exposome (Khmaladze et al., 2020). In addition, emerging evidence shows links (crosstalk) between skin and gut microbiome that influences the development of chronic skin diseases in patients (systemic sclerosis—Russo et al., 2023; atopic dermatitis—Han et al., 2022; psoriasis—Thye et al., 2022; reviewed by Widhiati et al., 2022). The gut microbiome is discussed in *Digestive Tract*, Vol 4.

There is a symbiotic relationship between the microbiome that normally inhabits the skin and the development of adaptive immunity; disruption of this symbiotic relationship leads to dysbiosis and contributes to the development of autoimmune and chronic inflammatory diseases (Lee and Mazmanian, 2010). Of great concern is that the skin microbiome is yet another environmental ecosystem that is losing biodiversity, and that this loss of biodiversity is a risk factor for the development of chronic inflammatory diseases. Early life is a critical period for establishment of the microbiome, and our adaptive immune responses, with long-term implications for health (Prescott et al., 2017). Antenatal events can include diet, environmental exposure to pollutants and toxins, and nature relatedness. Perinatal events can include the maternal microbiota, the method of birth (caesarian section vs. vaginal), early bathing, and the choice of soaps and detergents. Postnatal influences are most important in the first year of life and include diet, family, animal and social contact, outdoor play, and nature exposure. All of these factors help to establish the microbiome and influence the subsequent interactions between the adaptive immune response and pathogenic or commensal environmental exposures later in life. There are numerous excellent review papers on these interactions; suggested reading includes Belkaid and Segre (2014), Lee and Mazmanian (2010), Khmaladze et al. (2020), Prescott et al. (2017), Gallo and Nakatsuji (2011).

The microbiome of laboratory housed research animals is not subject to the wide variety of environmental exposures and genetic variations of our human patients. At the time of this

publication, not much research is focused on the microbiome of laboratory animals and its influence on experimental results in toxicologic pathology. However, the microbiome is yet another factor to consider with differences in experimental results, species differences, immune responses, and translation to our human patients, both in health and disease (see *Issues in Laboratory Animal Science that Impact Toxicologic Pathology*, Vol 1, Chap 29).

#### 4.5. Specific Cutaneous Morphologic Lesions and Patterns of Injury

The histopathologic interpretation of lesions in the integument is based on the basic morphologic reaction patterns in the integument, as much and perhaps more so than in other organ systems. Pattern recognition for the diagnosis of inflammatory conditions in the skin was pioneered by A. Bernard Ackerman ([Ackerman et al., 2005](#)) in his seminal book *Histologic Diagnosis of Inflammatory Skin Diseases: A Method Based on Pattern* and has been extensively used for the recognition and diagnosis of dermatitides in both human and veterinary pathology since.

These basic morphologic reaction patterns serve as a very useful device for the recognition of specific cutaneous morphologic responses to injury. In this section, the standardized International Harmonization of Nomenclature and Diagnostic Criteria for Lesions in Rats and Mice (INHAND) nomenclature is followed here, with any updates (and additional information) available at <http://www.goreni.org>. This information is also available on the Society of Toxicologic Pathology (STP) Website ([www.toxpath.org](http://www.toxpath.org)) (also see *Nomenclature and Diagnostic Resources in Anatomic Toxicologic Pathology*, Vol 1, Chap 25). The specific publication for the INHAND nomenclature for the skin in rodents is [Mecklenburg et al. \(2013\)](#). Species-specific nomenclature for other species is covered in manuscripts dedicated to those species and is also available at [www.toxpath.org](http://www.toxpath.org), and on [goreni.org](http://goreni.org) Website.

##### 4.5.1. Nonproliferative Lesions of the Epidermis

*Atrophy, epidermis* is characterized by thinning of all noncornified epidermal layers with

a corresponding decrease in nucleated keratinocytes, such that the distinction between SB, SS, and SG may no longer be apparent. Substances that decrease normal keratinocyte proliferation and metabolic activity, such as topical corticosteroids, are a common cause of epidermal atrophy.

*Erosion/ulcer* of the epidermis is characterized by loss of superficial epidermal layers (erosion) or complete loss of the epidermis with disruption of the epidermal basement membrane (ulceration). Erosions are always due to superficial epidermal trauma and are most commonly associated with trauma from scratching. Ulceration is also often caused by superficial epidermal trauma (e.g., fighting among cage mates), but may also be the result of toxicity or a necrotizing dermatitis. Ulceration due to toxicity needs to be differentiated from ulcerative dermatitis, which occurs spontaneously in certain strains of mice and rats, most commonly in the C57BL/6 mouse ([Kastenmayer et al., 2006](#); [Hampton et al., 2012](#)).

*Necrosis, epidermis* can be classified as either single cell or full thickness necrosis. Epidermal necrosis is a hallmark feature of drug hypersensitivity reactions or drug eruptions, where it can occur as single cell necrosis, and is termed erythema multiforme, or as full thickness epidermal necrosis, where it is termed toxic epidermal necrolysis (TEN) ([Harr and French, 2010](#)). Single cell necrosis of keratinocytes may be further subdivided into apoptosis, or programmed cell death, and dyskeratosis, which is the occurrence of terminal keratinization of individual keratinocytes that has not occurred as part of the orderly process of epidermal keratinization; apoptosis cannot be differentiated from dyskeratosis on H&E-stained sections. Apoptotic keratinocytes in UV light-exposed epidermis are often referred to as “sunburn cells.”

*Edema, epidermis, intracellular* (also called *vesicular change, hydropic degeneration, vacuolar degeneration, ballooning degeneration, reticular degeneration*) refers to intracellular edema of keratinocytes, and is characterized by increased size and pallor of keratinocytes with peripheral displacement of the nucleus. In the SB, synonyms are hydropic degeneration and vacuolar degeneration, while in the suprabasal epidermis, it is often referred to as ballooning degeneration. If vesicular change is severe, keratinocytes may rupture and form intraepidermal vesicles.



In contrast to intracellular edema, *edema, epidermis, intercellular* (also called *spongiosis*) refers to intercellular edema between epidermal keratinocytes and is characterized by widened intercellular spaces with accentuation of desmosomes. Severe epidermal spongiosis may lead to rupture of intercellular desmosomes and the formation of intraepidermal vesicles. Spongiosis is a common feature of skin inflammation.

A *vesicle* is an intra- or subepidermal cavity or cleft filled with fluid and is also referred to as a *bulla*. It occurs following loss of cohesion between epidermal keratinocytes or between epidermis and dermis, resulting in the formation of a fluid-filled cavity. Vesicles can result from immune-mediated injury or as a result of epidermal or dermal edema as a consequence of poxvirus infection, frictional trauma, or burns. Intraepidermal vesicles may develop secondary to severe spongiosis and/or severe vesicular change with rupture of keratinocytes and are also termed *reticular degeneration*. Vesicles that are located between the SB and the underlying mesenchyme are termed *clefts*.

A *pustule*, also referred to as a *microabscess*, is a focal intraepidermal accumulation of leukocytes, and is commonly found as a feature of generalized skin inflammation. Pustules may be further classified according to the predominant leukocyte population (neutrophilic, eosinophilic, or lymphocytic). Pustules that are filled with isolated rounded keratinocytes with a normal nucleus are referred to as *acantholytic pustules*. A predominantly neutrophilic pustule in a CD45RB<sup>Hi</sup> SCID mouse model of psoriasis is illustrated in Figure 7.18.

*Hyperkeratosis, epidermis* refers to an increase in the thickness of the SC, and is classified as either orthokeratotic, composed of normal anucleate corneocytes, or parakeratotic, composed of nucleated corneocytes. Hyperkeratosis frequently accompanies epidermal hyperplasia and is often associated with chronic epidermal irritation. When the hyperkeratotic SC contains leukocytes or a proteinaceous exudate, it is commonly referred to as a *crust*.

A *cyst, squamous* is an intradermal cyst lined by a wall composed of orderly stratified squamous epithelium with a lumen filled by concentrically arranged lamellar keratin. Squamous cysts can spontaneously occur in mice, particularly in the B6C3F1 strain.

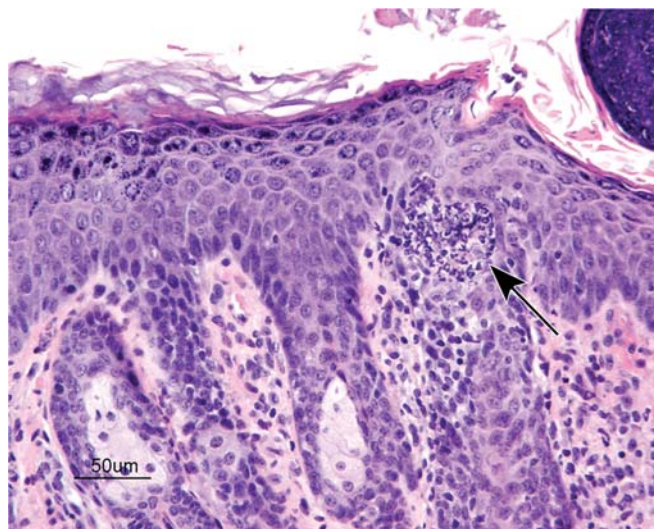


**FIGURE 7.18** A predominantly neutrophilic pustule (arrow) within the hyperplastic epidermis of a CD45RB<sup>Hi</sup> SCID mouse model of psoriasis. Reproduced from Haschek WM, Rousseaux CG, Wallig MA, editors: Haschek and Rousseaux's handbook of toxicologic pathology, ed 3, 2013, Academic Press, Figure 55.11, p. 2246, with permission.

Nonproliferative lesions of the dermis are primarily included in terminology in the soft tissue section of <http://www.goreni.org>. An example of a unique dermal change in skin is that of *calcinosis circumscripta*. This lesion is characterized by mineral deposits in the dermis surrounded by variable granulomatous inflammation and fibrosis. The usual pathogenesis involves repetitive trauma to the involved skin, most notably in extremities/paws of lab animals. Calcinosis circumscripta is further described as dystrophic (not associated with elevated serum calcium levels) or metastatic (associated with elevated serum calcium levels) (Figure 7.19).

*Elastosis* (also called *solar elastosis*, *actinic elastosis*, or *elastosis senilis*) is another unique change in the dermis after long term, excessive exposure to UV light that is part of photoaging, and so is primarily seen in lightly haired, lightly pigmented regions with sun exposure, making it primarily an issue in humans. However, there is great interest in developing animal models of photoaging, including elastosis (See Section 5.4—Mechanisms of Toxicity: Photoaging for more information.). *Elastosis* is characterized by lack of eosin staining in the upper dermis due

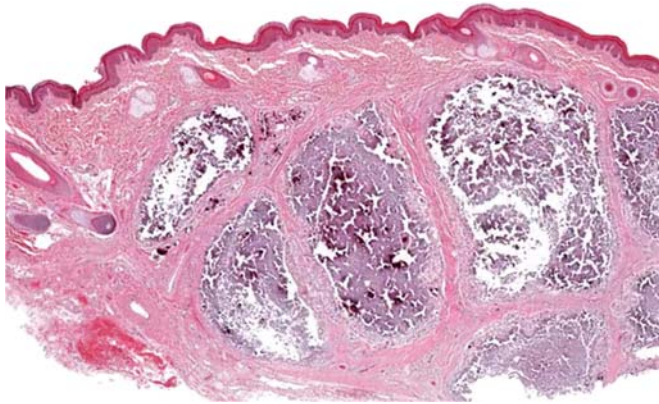


**FIGURE 7.19** Photomicrograph of skin from the paw of a nonhuman primate with dystrophic calcinosis circumscripta. The lesion is characterized by multiple to coalescing, large, dermal, basophilic to amphophilic mineral deposits surrounded by macrophages and fibroblasts, H&E.

to accumulation of lightly basophilic, tangled masses of thickened elastic fibers with generally parallel orientation to the surface of the skin. Elastic fibers are produced by dermal fibroblasts, and must be differentiated from fibrosis, which is the production of collagen fibers. A histologic stain for elastic fibers is the Orcein stain. Histologic images of solar elastosis are available on the internet.

#### 4.5.2. Nonproliferative Lesions of the Cutaneous Adnexa

Many of the lesions found in cutaneous adnexa have been described in the previous section on the epidermis; hence, only features unique to the adnexal condition will be covered in this section.

*Atrophy, adnexa* is defined by a marked reduction in follicular and sebaceous gland size and cell number well beyond that found physiologically during the normal telogen stage of the hair cycle. It is characterized by small remnants of follicles and sebaceous glands appearing as strands of keratinocytes surrounded by a thickened connective tissue sheath. Most follicles have lost their hair shaft, and dermal atrophy or scarring may be present. Hair follicles lose cells when they undergo regression in the catagen stage of the hair cycle. Therefore, hair follicle atrophy must be distinguished from the catagen and telogen stages of the hair cycle. Hair follicle atrophy (also called *alopecia*) can be caused by

a number of different compound classes, such as antiproliferatives and steroid hormones.

*Adnexal dysplasia* (also called *follicular dysplasia* when referring specifically to hair follicles) is an abnormality in the shape of the hair follicle and/or the hair shaft with no evident reduction in size. While for the epidermis, dysplasia usually denotes a preneoplastic proliferative change, in cutaneous adnexa, it primarily describes a malformation of the adnexal structure. Many genetically modified mice, including mice null for growth factors and their receptors such as EGFR (termed Waved-2), transforming growth factor- $\alpha$  (termed Waved-1), fibroblast growth factor-5 (termed Angora), and keratinocyte growth factor (termed Rough), have been described that exhibit various forms of congenital hair follicle malformation. The loss of pigment from hair follicles may also be classified as a dysplasia.

*Necrosis, adnexa* (also called *follicular necrosis* when referring specifically to hair follicles) is similar to epidermal necrosis, and is characterized by degeneration of follicular keratinocytes, either as single cells (single cell type) or as multiple cells (diffuse type). Chemotherapeutic agents such as paclitaxel and doxorubicin induce follicular necrosis of the single cell type, and thus alopecia. Follicular keratinocyte single cell necrosis in a Lewis rat given a kinase inhibitor systemically is illustrated in [Figure 7.20](#). Hair follicle dystrophy can be classified as a form of necrosis, as follicular keratinocytes undergo uncoordinated vacuolar degeneration or apoptosis.

*Hyperkeratosis, adnexa* (also called *follicular hyperkeratosis* when referring specifically to hair follicles) is similar to epidermal hyperkeratosis and is characterized by increased keratin within follicles that may be cystic or dilated. Follicles and/or adnexal ducts may become obstructed by keratin, leading to retained hair shafts and/or secretory products.

*Inflammation, adnexa* (also called *follicular inflammation* when referring specifically to hair follicles) is classified according to its pattern or location (perifollicular, intrafollicular, luminal, mural), similar to inflammation affecting the dermis. Inflammation can also be subcategorized according to its character (lymphocytic, plasmocytic, neutrophilic, eosinophilic, granulomatous). The terms “interface folliculitis” or “furunculosis” can be found in the literature



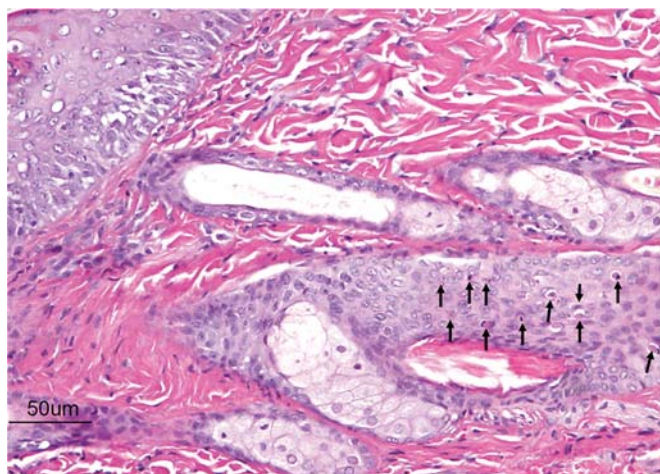


**FIGURE 7.20** Keratinocyte single cell necrosis (arrows) within the hair follicle epithelium of a Lewis rat given a kinase inhibitor systemically, H&E. Reproduced from Haschek WM, Rousseaux CG, Wallig MA, editors: *Haschek and Rousseaux's handbook of toxicologic pathology*, ed 3, 2013, Academic Press, Figure 55.12, p. 2247, with permission.

but are not INHAND terms. “Interface folliculitis” refers to perifollicular and mural inflammation that is generally associated with distinct necrosis of follicular keratinocytes. “Furunculosis” refers to follicular inflammation that has penetrated through the follicular wall leading to follicular rupture and marked inflammation in the surrounding dermis and connective tissue due to a foreign body inflammatory response to the hair shaft and follicular keratins. Both of these should be diagnosed as inflammation, adnexa in consideration of INHAND harmonization. Inflammation of the cutaneous adnexa in rodents can occur spontaneously due to dermatophytosis, or as a consequence of topical or systemic treatment with toxic agents.

#### 4.5.3. Proliferative Nonneoplastic Lesions of the Epidermis

*Hyperplasia, epidermis* (also referred to as *squamous cell hyperplasia* or *acanthosis*) is characterized by increased thickness of the nonkeratinized layers of the epidermis (primarily in the SS and SG), due to an increased number of epidermal keratinocytes (primarily in the SS). As mentioned earlier, hyperplasia is frequently accompanied by hyperkeratosis. Additionally, rete ridge formation is often present, but the epidermal basement membrane

remains intact. In the dysplastic type of hyperplasia, epidermis, the nonkeratinized layers of the epidermis are irregularly thickened and differentiation between SB, SS, and SG is lost. Cellular atypia is not present, and the epidermal basement membrane still remains intact. The dysplastic type of squamous cell hyperplasia is often specifically considered as a precursor to neoplasia and is frequently found in these mice following treatment with topical carcinogens such as 7,12-dimethylbenz[*a*]anthracene (DMBA) or tetradecanoyl phorbol acetate (TPA).

Hyperplasia, epidermis typically occurs as a response to a variety of insults including inflammation, toxic irritation, repeated abrasion of the superficial SC, or prolonged exposure to UV light. Direct induction of epidermal keratinocyte proliferation by chemicals such as is TPA is commonly used for tumor initiation in cutaneous two-step carcinogenesis (initiation/promotion) studies. Three mouse models have typically been used in cutaneous carcinogenesis studies: the Tg.AC and rasH2 transgenic mouse models, and the SENCAR mouse strain. In all three models, cutaneous irritation, inflammation, and keratinocyte proliferation with epidermal squamous cell hyperplasia were found to be very sensitive predictors of a later tumorigenic response—namely, the development of cutaneous papillomas upon carcinogen treatment. These preneoplastic changes were also found to be at least somewhat predictive of carcinogenic potential in humans, although currently none of these models are accepted by regulatory agencies for use in stand-alone studies for evaluation of cutaneous carcinogenicity.

#### 4.5.4. Proliferative Nonneoplastic Lesions of the Adnexa

*Hyperplasia, adnexa* (with modifier of *sebaceous gland*) is characterized by enlargement of sebaceous glands with maintenance of the normal glandular architecture. Enlarged sebaceous gland acini contain increased cells that are primarily mature, sebum-containing cells. Sebaceous cell hyperplasia frequently accompanies squamous cell hyperplasia, and both are commonly seen with chronic inflammation.

*Hyperplasia, adnexa* (with modifier of *hair follicle*) is characterized by enlargement or density of hair follicles with otherwise normal morphology. This must be differentiated from



normal anagen phase of the hair cycle, and compared to sham and vehicle controls.

#### **4.5.5. Proliferative Nonneoplastic Lesions of the Dermis**

*Melanocyte hyperplasia* (may also be called *pigment cell hyperplasia*) is an accumulation of pigmented melanocytes within the dermis between hair follicles and sebaceous glands. Melanocyte hyperplasia has been observed in some initiation-promotion and skin painting studies in mice. It can also occur during chronic dermal inflammation, where it needs to be distinguished from the dermal accumulation of pigment-laden macrophages, or melanophages, that are macrophages that have engulfed melanin pigment.

### **4.6. Neoplastic Lesions and Carcinogenesis Models**

#### **4.6.1. Carcinogenesis Models**

The multistage model of mouse skin carcinogenesis is a very well-established model that has greatly aided in the identification of the underlying cellular, biochemical, and molecular mechanisms associated with the various stages of epithelial carcinogenesis. In this model, tumor development occurs via three distinct stages: initiation, promotion, and progression. Tumor initiation involves induction of a mutation of a critical gene or genes and can occur following a single topical administration of a genotoxic carcinogen, such as 7,12-DMBA at a subcarcinogenic dose. At the initiation stage, there are no demonstrable histopathologic alternations present. The *Ha-ras* gene appears to be a primary target gene for the initiation stage in this carcinogenesis model and becomes mutated following exposure to DMBA. Following initiation, tumor promotion occurs by repeatedly applying a non-mutagenic tumor promoter, such as 12-O-tetradecanoylphorbol-13-acetate (TPA). Tumor promoters increased expression of growth regulatory genes and stimulates epidermal keratinocyte proliferation and hyperplasia by causing the cell to produce and maintain chronic squamous cell epidermal hyperplasia that is characterized by sustained proliferation of epidermal keratinocytes. These changes are believed to result from epigenetic mechanisms such as activation of the cellular receptor, PKC.

Tumor promoters upregulate genes that encode growth regulatory molecules transcriptionally, by posttranslational modification, or in some cases by direct stimulation of enzymatic activities. Some of the growth regulatory pathways upregulated by tumor promoters involve several different tyrosine kinase growth factor receptor families and their ligands, including the EGFR family and its ligands, such as transforming growth factor (TGF) $\alpha$ , the insulin-like growth factor-1 receptor (IGF-1R) family, and the c-met family. In addition, signaling molecules downstream of these growth factor receptors, including Src, Stat3, PI3K/Akt, mTOR, and MAPK, are also upregulated during tumor promotion.

During the promotion stage, initiated cells undergo clonal expansion, resulting in the development of squamous cell papillomas. These squamous cell papillomas have been shown to overexpress a variety of genes, many similar to those upregulated during tumor promotion, which contribute to their ability to grow in the absence of further external stimuli. The third and final stage in the multistage model of skin carcinogenesis is the progression stage, which involves malignant transformation of the squamous cell papillomas to malignant squamous cell carcinomas; again, this stage is driven by upregulation of many of the same genes upregulated in the tumor promotion stage.

Three mouse models have been commonly used for cutaneous carcinogenesis evaluation, although, as stated earlier, none are currently approved for stand-alone cutaneous carcinogenicity assessment by regulatory agencies: the Tg.AC (v-Ha-ras) transgenic mouse, the rasH2 transgenic mouse, and the SENCAR mouse. The Tg.AC and rasH2 mouse models are both *rasHa* transgenic lines. Tg.AC mice are hemizygous for a mutant *v-Ha-ras* transgene.

The Tg.AC model was developed using an inducible  $\zeta$ -globin promoter to drive the expression of a mutated *v-Ha-ras* oncogene and is regarded as a genetically initiated model. The transgene is transcriptionally silent until activated by full-thickness wounding, UV irradiation, or topical application of specific carcinogens to the shaved dorsal surface of these mice. This will induce epidermal squamous cell papillomas or carcinomas, which is the reporter phenotype that defines the activity of the carcinogen.

The *rasH2* mouse, also known as *Tg.rasH2*, was created by insertion of a human *c-rasHa* transgene driven by its own promoter. Hemizygous *rasH2* mice respond with greater sensitivity to carcinogens than nontransgenic mice and are similarly recommended for genotoxic and non-genotoxic carcinogen identification.

SENCAR mice are not genetically engineered; rather, the line was selected over eight generations for increased skin tumor multiplicity and decreased tumor latency in response to DMBA and TPA treatment. SENCAR mice have an approximately 10- to 20-fold increase in sensitivity to DMBA initiation and a two- to threefold increase in sensitivity to TPA promotion compared to the parental CD-1 stock. The SENCAR mouse is a commonly used short-term model system for evaluating the promoting or initiating activity of test items for two-stage skin carcinogenesis in mice. These mice respond rapidly and sensitively with skin tumors following topical application of a single low dose of an initiating agent, typically a mutagenic carcinogen, followed by multiple applications of a tumor promoting agent.

When evaluated for sensitivity and predictability of mouse skin models for carcinogenic hazard identification, all of the 3 mouse models respond similarly (with mild inflammation and epidermal squamous cell proliferation and hyperplasia) to several weeks of treatment with topical carcinogens. All 3 mouse models were also similar in their development of the reporter phenotype; the development of squamous cell papillomas following extended carcinogen treatment and has been shown to be fairly predictive of carcinogenic potential in humans. Thus, the very early endpoints of cutaneous inflammation and epidermal squamous cell proliferation and hyperplasia may be used as predictors of cutaneous tumorigenesis in these 3 mouse skin carcinogenesis models, and all 3 mouse models had similar responses and sensitivities to topical carcinogenesis.

Cutaneous tumors, particularly those derived from the epidermis and cutaneous adnexa, are not uncommon spontaneous findings in rodents, so attention must be paid to the potential occurrence of spontaneous tumors in the commonly used mouse models of skin carcinogenesis. In these mouse models, the typical carcinogen-induced tumors are squamous cell papilloma

with malignant progression to squamous cell carcinoma. It is essential to differentiate these epidermal keratinocyte-derived epithelial tumors from other spontaneously occurring tumors derived from epidermal keratinocytes (e.g., benign and malignant basal cell tumors) as well as tumors derived from cutaneous adnexal epithelia (e.g., sebaceous gland adenomas and carcinomas, keratoacanthomas, and benign hair follicle tumors).

#### **4.6.2. Neoplastic Proliferative Lesions of the Epidermis**

Squamous cell neoplasms are the typical tumors that occur in all mouse skin tumor models and arise first as squamous cell hyperplasia (described above) followed by the development of squamous papillomas (described here) and, finally, malignant squamous cell carcinomas.

*Papilloma, squamous cell* are benign neoplasms that are derived from epidermal keratinocytes, and are the earliest neoplastic lesion induced by carcinogens in the mouse models of skin carcinogenesis. They can be further characterized into four types: exophytic, endophytic, with cellular atypia, and nonkeratinizing. The exophytic type has a stalk at its base and is also often referred to as a pedunculated papilloma. The endophytic type has no stalk, but instead is contiguous with the adjacent epidermis and invaginates to form a depression (Figure 7.21). The cellular atypia type contains atypical squamous cells with large hyperchromatic nuclei that are found primarily in the basal and suprabasal layer of the epidermis. The nonkeratinizing type of papilloma, as the name suggests, lacks typical keratinization.

Regardless of type, all papillomas are well-circumscribed papilliform exophytic or endophytic masses with no compression of the surrounding tissue and no capsule. They are composed of keratinizing squamous cells overlying a well-vascularized stroma. Mitotic figures are common. Individual suprabasal cells may show premature keratinization or dyskeratosis, and there is a variable degree of parakeratotic hyperkeratosis. Ulceration and inflammation may be present, particularly in larger papillomas.

*Carcinoma, squamous cell*, also referred to as *epidermoid carcinomas*, are malignant neoplasms

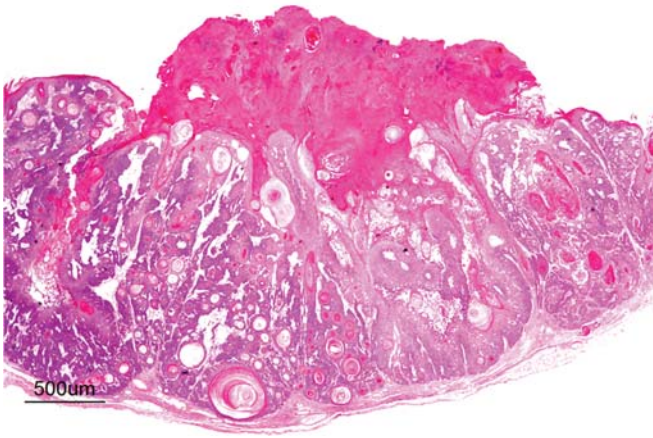


**FIGURE 7.21** An endophytic squamous papilloma in a mouse. The endophytic type does not have a stalk but is instead contiguous with the adjacent epidermis with dermal invagination to form a depression. The invaginated surface is covered by a serocellular crust. *From slide Courtesy of Oded Foreman, Genentech. Reproduced from Haschek WM, Rousseaux CG, Wallig MA, editors: Haschek and Rousseaux's handbook of toxicologic pathology, ed 3, 2013, Academic Press, Figure 55.13, p. 2250, with permission.*

derived from epidermal keratinocytes. Squamous cell carcinomas are poorly demarcated, generally mostly endophytic, and show no compression of the surrounding mesenchyme, although some tumors elicit a desmoplastic reaction in the surrounding dermis. The tumor is composed of islands or cords of cells that penetrate the basal lamina and invade the dermis, with the neoplastic cells sometimes invading the underlying subcutis or subcutaneous muscle. There is generally some evidence of squamous differentiation (Figure 7.22), although its extent is variable. Centrally located concentric layers of keratin that are often termed *keratin pearls*, *cancer pearls*, or *horn pearls* are also frequently present. Some neoplastic cords may show a central lumen containing individualized (acantholytic) keratinocytes that are surrounded by several layers of neoplastic epithelial cells ("pseudo-glandular pattern"). Abnormal keratinization (dyskeratosis) of single cells occurs sporadically, and intercellular bridges are generally present except in very poorly differentiated tumors. Ulceration and inflammation are often present, particularly in larger and/or more invasive tumors.

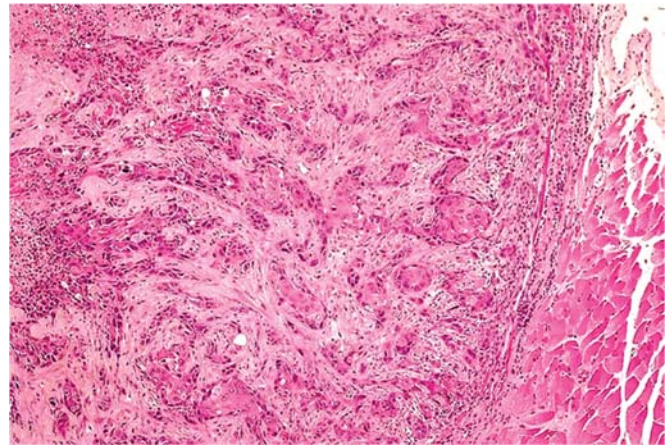


**FIGURE 7.22** Cutaneous squamous cell carcinoma in a mouse. The tumor arises from an ulcerated epidermal surface and is composed of islands or cords of cells that invade the dermis, with an accompanying inflammatory and fibroblastic response in the adjacent dermis (desmoplasia). Neoplastic cells demonstrate variable evidence of squamous differentiation and keratinization. *From slide courtesy of Oded Foreman, Genentech. Reproduced from Haschek WM, Rousseaux CG, Wallig MA, editors: Haschek and Rousseaux's handbook of toxicologic pathology, ed 3, 2013, Academic Press, Figure 55.14, p. 2250, with permission.*

*Tumor, basal cell, benign* are derived from stem cells within hair follicles (especially hair follicle bulge) and are classified into three distinct types: basosquamous, trichoblastoma, and granular. All basal cell tumors are fairly well circumscribed and multilobulated with some association to the epidermis. Neoplastic basal cells may be arranged in cords or fine ribbons that may become cystic. There is no invasion of the basement membrane and no compression or desmoplasia of the surrounding dermal mesenchyme. The neoplasm is composed of uniform lobules, islands, or cords of closely packed cells that are supported by a variable degree of fibrovascular stroma. Tumor cells generally resemble normal epidermal basal cells without intercellular bridges, and palisade at the periphery of lobules. Foci of squamous cell differentiation may occur, and sebaceous cells may also be present. Central cystic degeneration and melanin pigment may be present. In the basosquamous type of basal cell tumor, foci of keratinization are present. In the trichoblastoma type, small foci of sebaceous cells and/or



trichogenesis are present. In the granular type, basal cells containing PAS-positive granules are present similar to those found in anagen hair follicles.

*Carcinoma, basal cell* also referred to as *carcinoma malignant basal cell tumor* (subtype *basosquamous type*), is a malignant tumor derived from stem cells within hair follicles and/or the inter-follicular epidermis. Basal cell carcinomas are poorly circumscribed dermal tumors with some association to the epidermis or adnexa and local invasion. They are composed of lobules and cords of closely packed cells that are supported by a variable degree of fibrovascular stroma. Tumor cells generally resemble normal epidermal basal cells without intercellular bridges, and palisade at the periphery of lobules. Central necrosis in tumor lobules may be present; these necrotic areas are referred to as *pseudocysts*. In pigmented strains, melanin pigmentation is commonly found, desmoplasia in the surrounding mesenchyme is common, and extensive local invasion may be present.

Benign and malignant basal cell tumor development has been very convincingly linked to upregulated hedgehog (Hh) signaling via several lines of evidence, including genetic mutation analyses, mouse models of basal cell tumors, and the successful treatment of malignant basal cell tumors in the clinic using Hh signaling inhibitors (Epstein, 2008). In addition, many if not all basal cell tumors are believed to derive from hair follicle stem cells, as both basal cell tumors and follicular stem cells express keratin 15, and Hh signaling has been shown to be critical for normal hair follicle developmental morphogenesis (Grachtchouk et al., 2011; Youssef et al., 2010).

In humans, the vast majority of basal cell tumors have identifiable mutations in at least one allele of patched 1 (*PTCH1*), a tumor suppressor gene that encodes an Hh signaling receptor. In addition, some basal cell tumors have activating mutations in smoothened (*SMO*), a positive regulator of Hh signaling. Hh signaling occurs when Hh ligands bind to *PTCH1*, specifically through *SMO*, and relieve inhibition of the Hh pathway leading to activation of the Gli family of transcription factors and cellular proliferation. A basal cell tumor from a *PTCH1* heterozygous null C57BL/6 mouse is illustrated in Figure 7.23.

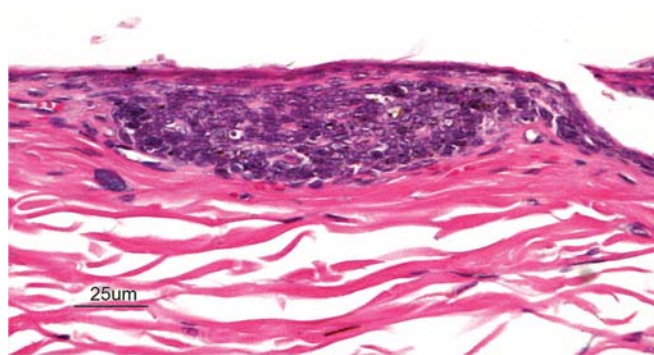


**FIGURE 7.23** An early benign cutaneous basal cell tumor arising from the epidermal surface of a patched 1 (*PTCH1*) heterozygous null C57BL/6 mouse demonstrates that the majority of basal cell tumors have identifiable mutations in at least one allele of *PTCH1*, a tumor suppressor gene that encodes a Hh signaling receptor. This early benign basal cell tumor is a very well circumscribed lobule that is connected to the overlying epidermis and demonstrates no invasion of the basement membrane and no compression or desmoplasia of the surrounding dermis. Tumor cells resemble normal epidermal basal cells without any evidence of intercellular bridges. From slide courtesy of Oded Foreman, Genentech. Reproduced from Haschek WM, Rousseaux CG, Wallig MA, editors: Haschek and Rousseaux's handbook of toxicologic pathology, ed 3, 2013, Academic Press, Figure 55.15, p. 2251, with permission.

#### 4.6.3. Adnexal Neoplastic Lesions

*Adenoma, sebaceous cell* is derived from the reserve cells that line the periphery of gland lobules. In contrast to sebaceous gland hyperplasia, in a sebaceous cell adenoma, the normal glandular architecture has become distorted, but the tumor is still composed of lobules and acini and is well demarcated from the surrounding tissue. Squamous differentiation and keratinization may be present, and mitoses are often seen at the lobular periphery.

*Carcinoma, sebaceous cell* is less differentiated than adenomas and poorly delineated from surrounding tissue, with frequent deep dermal invasive growth. The tumor is composed of lobules and acini containing polygonal cells of variable size, and variable amounts of intracytoplasmic lipid vacuoles. There is high mitotic activity with numerous atypical mitotic figures. Squamous differentiation and individual cell necrosis, cystic degeneration with the presence of amorphous cellular debris, and melanin

pigmentation may be present. Both sebaceous gland adenomas and carcinomas are rare spontaneous tumors in rodents.

*Keratoacanthomas* arise from squamous epithelial keratinocytes derived from the infundibulum of the hair follicle. They are very well-demarcated but generally unencapsulated masses that occur in the superficial dermis and connect to the overlying epidermis, sometimes containing a pore to the skin's surface (Figure 7.24A). The tumor is composed of one to several lobules containing a prominent central cavity filled with concentric whorls of keratin. The cavities are lined by well-differentiated squamous epithelium that sometimes contains epithelial whorls with central foci of keratinization (Figure 7.24B). Mitotic figures are uncommon. Experimentally induced keratoacanthomas in mice have been reported to undergo spontaneous regression, possibly correlated to the normal hair follicle growth and regression cycle.

*Benign hair follicle tumors* have four distinct types: trichoepithelioma, trichofolliculoma, pilomatricoma, and tricholemmoma. All four types are derived from the hair follicle matrix, and all are well delineated but unencapsulated with no invasion. All have multiple lobules consisting of different stages of follicular trichogenic differentiation, often with one or multiple cysts. Malignant hair follicle tumors as they occur in man (e.g., malignant pilomatricoma, malignant trichilemmoma) have not been described in rodents (Mecklenburg et al., 2013).

The trichoepithelioma type is derived from the hair follicle matrix epithelium that gives rise to the inner root sheath and hair shafts. They have a fine mesenchymal matrix that resembles the hair follicle dermal papilla and manifests as focal invaginations of the basement membrane.

In contrast to basal cell neoplasms, the epithelium of trichoepitheliomas does not differentiate into sebaceous cells. The trichofolliculoma type is a large cystic neoplasm that has a large central cystic lumen containing keratin and hair shaft that is lined by squamous epithelium which gives rise to well-differentiated hair follicles that radiate from the cystic center. The pilomatricoma type consists of multiple nodules of hair matrix and hair cortex epithelial cells that

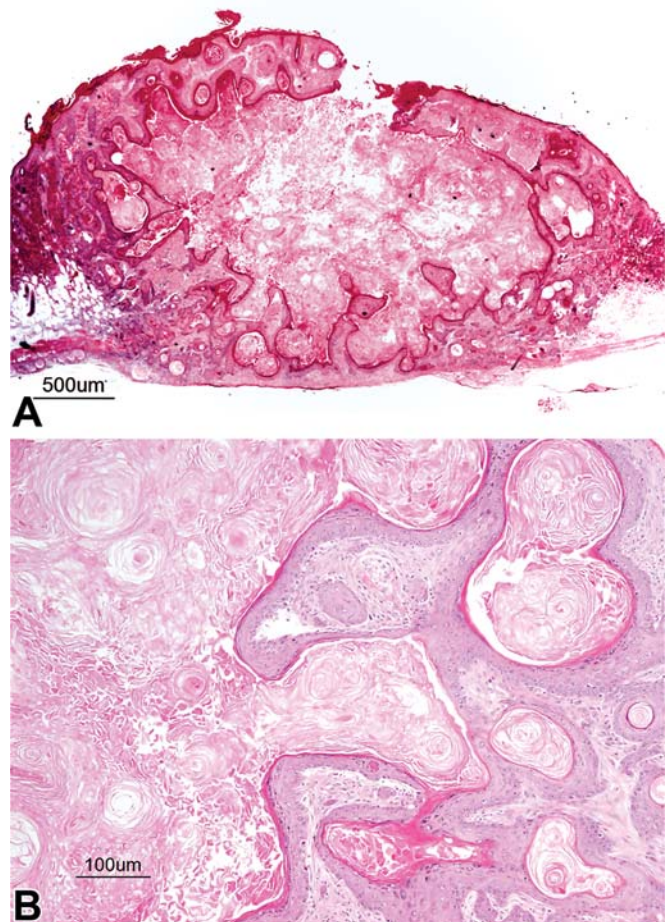


**FIGURE 7.24** (A) A low-magnification image of a cutaneous keratoacanthoma in a mouse demonstrating that the tumor is a very well-demarcated mass in the superficial dermis with a prominent pore to the skin's surface. (B) A higher magnification of a keratoacanthoma illustrating the central cavity filled with concentric whorls of keratin (left side of image) lined by well-differentiated squamous epithelium that contains epithelial whorls with central foci of keratinization and resembles the epithelium of the follicular infundibulum. From slide courtesy of Oded Foreman, Genentech. Reproduced from Haschek WM, Rousseaux CG, Wallig MA, editors: *Haschek and Rousseaux's handbook of toxicologic pathology*, ed 3, 2013, Academic Press, Figure 55.16, p. 2252, with permission.

abruptly keratinize without the presence of keratohyalin granules to a central lumen that contains keratin and keratinized ghost or shadow cells (Figure 7.25). They can differentiate into and are characterized by ghost or shadow cells that are entrapped by an abruptly



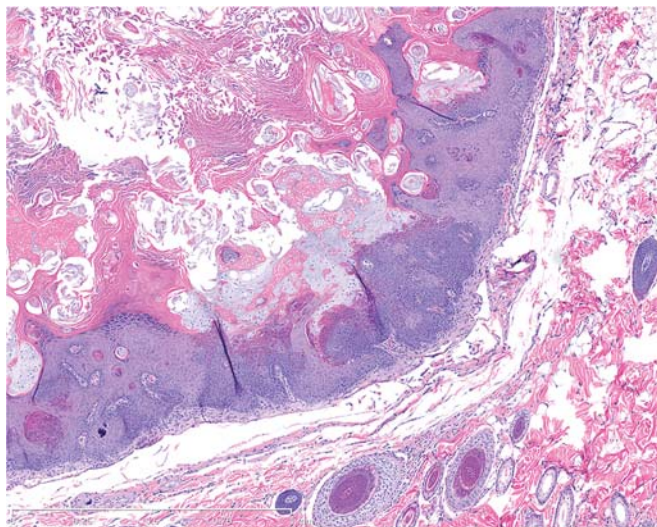


**FIGURE 7.25** A pilomatricoma type of benign hair follicle tumor from a rat. The tumor consists of multiple nodules of hair matrix and hair cortex epithelial cells that abruptly keratinize without the presence of keratohyalin granules to a central lumen that contains keratin and keratinized ghost or shadow cells. *Courtesy of Melissa Schutten, Genentech. Reproduced from Haschek WM, Rousseaux CG, Wallig MA, editors: Haschek and Rousseaux's handbook of toxicologic pathology, ed 3, 2013, Academic Press, Figure 55.17, p. 2253, with permission.*

keratinizing epithelium. The tricholemmoma type is a neoplasm derived from the outer root sheath epithelium, and thus consists of small epithelial nests lined by a prominent basal membrane.

Cells at the periphery of nests are basaloid and palisading, while the more differentiated suprabasal cells contain PAS-positive glycogen granules similar to those in the external outer root sheath epithelium of normal anagen hair follicles. Suprabasal cells at the center of nests often demonstrate tricholemmal keratinization characterized by very hyaline amorphous keratin.

#### 4.6.4. Dermal Neoplastic Lesions

*Benign melanoma* is derived from epidermal and/or adnexal melanocytes and is characterized by a dense nodular accumulation of pigmented cells within the dermis with or without an epidermal connection. Neoplastic

melanocytes are polygonal, epithelioid, or spindle-shaped, with variable degrees of intracytoplasmic melanin pigment granules.

*Malignant melanoma* is also characterized by a dense nodular accumulation of cells within the dermis with or without an epidermal connection, but there is invasive growth, and the neoplastic cells are more pleomorphic in size and shape and may or may not contain melanin pigment. When they lack pigmentation, they are referred to as amelanotic malignant melanomas. Both benign and malignant melanomas are very rare spontaneous incidental tumors in rats and mice. Amelanotic melanomas in rats occur most frequently in the pinna, eyelid, scrotum, and perianal region.

## 5. MECHANISMS OF TOXICITY

### 5.1. Direct Cutaneous Toxicity

Because of its unique role as a first-line barrier defense against a number of environmental insults, the skin is exposed to a wide variety of toxic agents. These toxic agents can harm the skin directly, causing irritation or corrosion, or can induce systemic and cutaneous immune-mediated toxic effects that manifest as cutaneous toxicity (Table 7.7).

Direct cutaneous toxicity is caused by direct damage to the skin from any number of external irritants, such as chemical agents, xenobiotics, infectious agents, thermal injury, or UV radiation that damage or disrupt the skin's barrier function. When this occurs, the skin mounts an inflammatory and proliferative response in order to prevent further damage and to restore a morphologically and physiologically functioning barrier.

Differentiating direct cutaneous toxicity due to injection of a drug from trauma induced by the needle itself can be difficult. Histopathologic changes associated with subcutaneous injection of normal (0.9% NaCl) saline at 1.77 mL/kg using a 26.5-gauge needle were investigated in Sprague-Dawley rats (Ramot et al., 2019a, 2019b). Microscopic examination of injection sites 24-hour after subcutaneous injection



**TABLE 7.7** Mechanisms of Cutaneous Toxicity

Type of toxicity	Lesion	Mechanism	Xenobiotic/causative agent
<i>DIRECT TOXICITY</i>			
Irritation	Hyperkeratosis (parakeratotic and orthokeratotic types)	Primary as in seborrhea, or secondary to trauma, inflammation, metabolic, or nutritional disorders	Chlorinated naphthalenes, iodine, mercury, sun exposure
	Primary inflammation (e.g., pustules, vesicles, acantholysis, edema)	Disruption of intercellular junctions	Acids, alkalis, organic solvents (mineral spirits, pine oils, essential oils, turpentine), phenol, oxidizing/reducing agents, keratolytic agents
	Secondary inflammation (e.g., dermal or pannicular nodules; sterile pyogranuloma)	Foreign body reaction; injection site reactions	Strong acids, caustic (alkali) agents, oxidizing/reducing agents, foreign bodies, immune reaction
	Epidermal degeneration, necrosis, apoptosis	Direct cellular toxicity, physical injury (e.g., thermal burns), radiation	Acids, alkalis, oxidizing/reducing agents, organic solvents, keratolytic agents, thermal injury, UV and ionizing radiation
Corrosion/necrosis	Epidermal necrosis, erosion, ulceration, vesiculation	Chemical burn, physical injury (e.g., laceration, thermal burns), radiation	Strong acids, caustic (alkali) agents, oxidizing/reducing agents, bleomycin, thermal injury, sulfur mustard, inorganic mercury salts, inorganic arsenic salts, UV and ionizing radiation
		Vasoactive agents, ischemia, infarction, vasculitis, thromboembolism	Ergot alkaloids
Proliferation	Epidermal hyperplasia (acanthosis, dyskeratosis), dysplasia, or carcinogenicity (e.g., adenoma, carcinoma)	Chronic irritation or factors altering epidermal growth/differentiation (e.g., cytokines and growth factors) or genotoxicity	UV radiation, inorganic arsenic, sulfur mustard, T-2 toxin, toxic organic agents/metabolites (e.g., polyaromatic hydrocarbons, polyhalogenated hydrocarbons)
Atrophy	Epidermal atrophy	Hormonal imbalances, partial ischemia, malnutrition	Corticosteroids
Immune-mediated toxicity	Acantholysis, toxic epidermal necrolysis (10), Stevens-Johnson syndrome, erythema multiforme	Direct activation of immune effectors, disruption of intercellular junctions	Polymyxin B, DMSO, aspirin, phorbol esters, biogenic amines
		IgE-dependent (Type I hypersensitivity)	Therapeutic agents (e.g., penicillin), foods (urticaria)
		Immune-complex mediated	Penicillin, aminosalicic acid, streptomycin
		T-lymphocyte mediated (Type IV hypersensitivity; contact allergens)	Ethyl aminobenzoate, neomycin, metal (e.g., nickel, chromium), metal derivatives (e.g., oligomercurial), plant toxins (e.g., poison ivy)

**TABLE 7.7** Mechanisms of Cutaneous Toxicity—cont'd

Type of toxicity	Lesion	Mechanism	Xenobiotic/causative agent
Phototoxicity		Primary phototoxicity	Tetracyclines, sulfonamides, chlorpromazine, nalidixic acid, phenothiazines, acridine, anthracene, phenanthrenes, fluorocoumarins, fagopyrin, hypericin
		Secondary phototoxicity (e.g., hepatotoxicity mediated by phylloerythrin)	Hexachlorobenzene, lead, pyrrolizidines, pyrrolizidine alkaloids, hepatotoxic plants, lantadines A and B, furanosesquiterpenoids, oxalates, mycotoxins, mycrocystin
Photoallergy		Delayed Type IV hypersensitivity (light activated)	Sulfonamides, phenothiazides, coumarin derivatives, glyceryl p-aminobenzoic acid
<b>PIGMENTATION DISORDERS</b>			
	Hyperpigmentation	Increased amount of melanin or melanocytes due to chronic inflammation, endocrine disorders	Corticotrophin, oral contraceptive drugs, cancer chemotherapeutics (e.g., bleomycin), hydantoins
	Hypopigmentation	Lack of melanocytes or melanin transfer	Fluphenazine, corticosteroids, chloroquine, copper deficiency
<b>ADNEXAL DAMAGE</b>			
	Hair follicle atrophy	Interference with anagen (rapid growth phase)	Doxorubicin, vincristine, methotrexate, cyclophosphamide, phenylglycidyl ether, dixyrazine, colchicine
	Hair follicle atrophy	Interference with telogen (stationary growth phase)	Chlorinated naphthalenes, propranolol, triparanol, heparin, coumarin, oral contraceptives, phenylglycidyl ether, dixyrazine, thallium, selenium, inorganic arsenic, inorganic mercury, iodine, mimosine
	Alopecia	Loss of hair due to chemical toxicity or hormonal effects	Depilatory agents (e.g., eflornithine), retinoids, androgens, progesterone—estrogen combinations
Acneiform lesions	Hyperkeratinization, chloracne	Comedone formation	Polyhalogenated hydrocarbons (e.g., dioxins)
Anhidrosis	Damage/loss of sweat glands, neutrophilic eccrine hidradenitis	Direct cytotoxicity	Cytotoxic agents (e.g., cytarabine, bleomycin), formaldehyde, arsenic, thallium, lead, fluorine

Reprinted from Haschek WM, Rousseaux CG, Wallig MA, editors: *Haschek and Rousseaux's handbook of toxicologic pathology*, ed 3, 2013, Academic Press, Table 55.5, p. 2254–55, with permission.

consisted of hemorrhage, inflammation, necrosis, and epidermal epithelial crusts and/or parakeratosis.

Reversible damage to the skin by direct contact with toxic agents is referred to as irritation, and results in activation of mast cells, complement, and/or prostaglandin synthesis. Irritation generally occurs within 4 h following topical application of the irritating substance. Histopathologically, skin irritation is characterized by epidermal hyperkeratosis and hyperplasia with dermal inflammation and is frequently associated with a variety of other epidermal changes such as erosion/ulceration, necrosis, or vesicular change. Corrosion is necrosing (irreversible) skin damage induced by direct contact with the initiating agent. Corrosion (necrosis) is characterized by full thickness necrosis of the epidermis leading to ulceration with penetration into the underlying dermis and involvement of the cutaneous adnexa and even the underlying subcutaneous tissue.

When chemical substances or xenobiotics are applied directly to the skin, their effect is determined not only by their primary mode of toxicity but also by the processes of cutaneous absorption and metabolism of the substance. The outer surface of the skin is coated by the lipid sebum which is secreted from the sebaceous glands and forms a barrier against polar water-soluble compounds.

Lipophilic nonpolar compounds can more readily pass through the epidermal surface and the intercellular spaces and can also enter through the hair follicles and sebaceous glands. Absorption is further affected by the integrity and thickness of the epidermis and dermal vascularization. Microsomal enzymes in keratinocytes are able to metabolize topically applied chemicals, thus rendering them inactive or active. For instance, DMBA becomes a potent skin carcinogen after metabolic activation by keratinocytes.

A specific example of direct cutaneous toxicity is direct thermal injury, also referred to as a burn. Burns have classically been classified into three categories: first-, second-, and third-degree burns. First-degree burns have lesions that are limited to the epidermis, and resemble those induced by slight UV irradiation, with the formation of individually

necrotic epidermal keratinocytes, or “sunburn cells.” First-degree burns are often accompanied by mild dermal erythema and edema.

Second-degree burns show epidermal necrosis with epidermal–dermal separation leading to cleft formation, but again with only mild dermal lesions of erythema, edema, and sometimes mild leukocytic infiltration. Third-degree burns are characterized by both epidermal and dermal necrosis. While these classic descriptions are still in common usage, clinical practice and experimental studies frequently use the alternative classification of full and partial thickness burns.

Partial thickness burns are further classified as superficial, which are roughly equivalent to first- and mild second-degree burns, and deep, which are roughly equivalent to severe second-degree burns or less severe third-degree burns. Deep partial thickness burns are characterized by full thickness epidermal necrosis with necrosis of superficial cutaneous adnexa and dermal vessels but sparing of deep cutaneous adnexa and vessels. They can be distinguished from full thickness burns, which exhibit complete epidermal and dermal necrosis, including necrosis of all cutaneous adnexa and dermal vessels, by staining for the presence of proliferation markers, such as PCNA, which will be present in partial but not full thickness burns, and/or staining for intact collagen with stains such as Masson’s trichrome, which will demonstrate the depth to which dermal collagen fibers have undergone coagulation (Figure 7.26).

Histologically, mild thermal injury to the epidermis is characterized by nuclear and cytoplasmic swelling, generally of epidermal keratinocytes in superficial burns, with later development of individual necrotic keratinocytes (sunburn cells). More severe thermal injury to the epidermis will have entire layers of the superficial epidermis with nuclear rupture, pyknosis, and necrosis of epidermal keratinocytes that exhibit brightly eosinophilic cytoplasm which cannot be morphologically distinguished from premature keratinization, or dyskeratosis. If the entire epidermis undergoes necrosis there may also be subepidermal vesicle formation and separation from the underlying dermis (Figure 7.27).



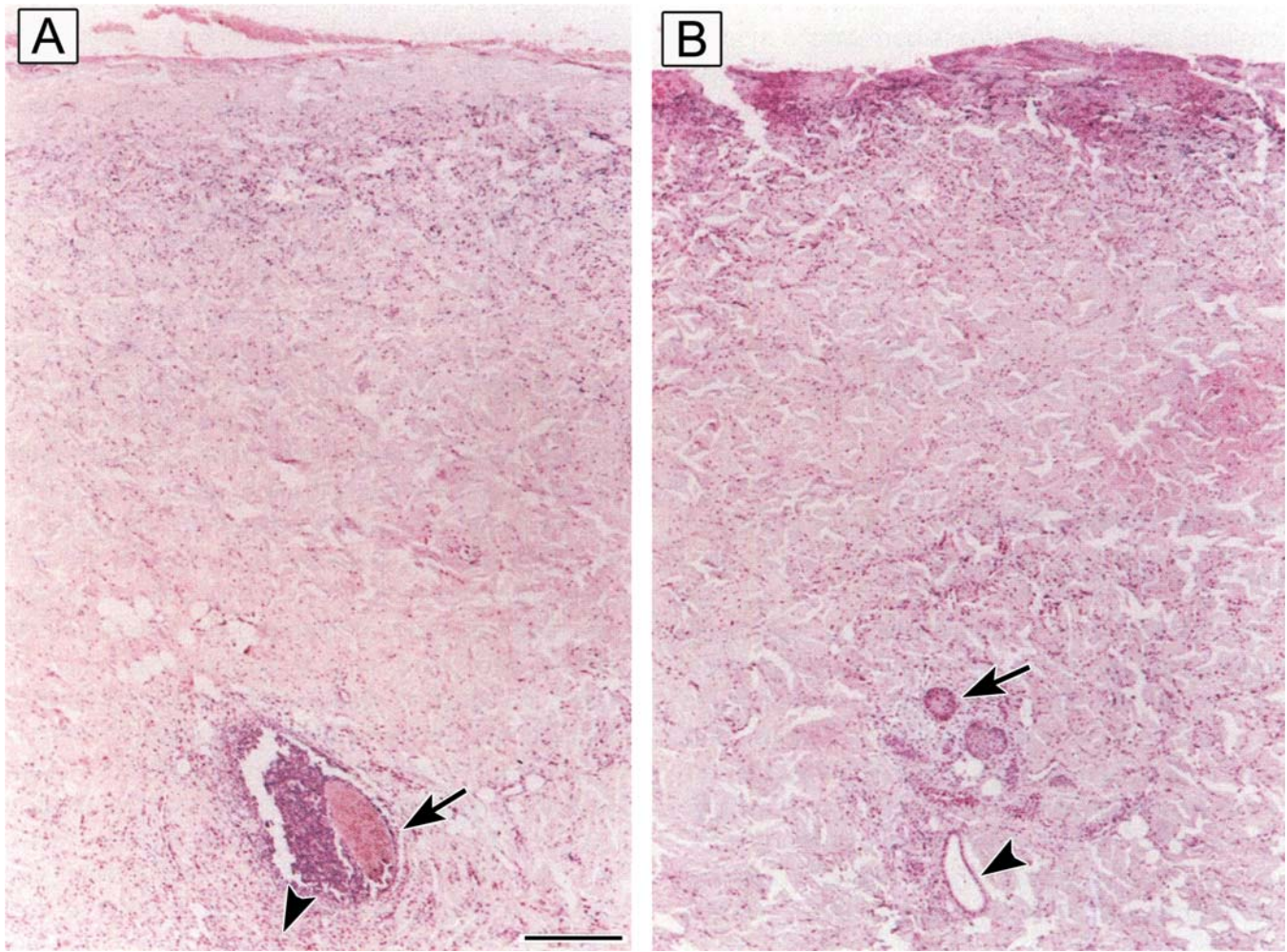


**FIGURE 7.26** Representative sections of full (A) and deep partial (B) thickness burns from Yucatan minipigs harvested 4 days postburn and stained for PCNA expression in order to illustrate the depth of cutaneous damage. Both burn sections lack epidermis (the epidermis was fully necrotic and was removed). The full thickness burn section (A) illustrates a completely necrotic hair follicle deep in the section (arrow) with a few PCNA-positive dermal fibroblasts (arrowhead) beneath the necrotic follicle. The deep partial thickness burn section (B) contains PCNA-positive proliferating remnants of a hair follicle (arrow) as well as an eccrine sweat gland duct (arrowhead). Bar is 250 mm. Reprinted from Danilenko DM, Ring BD, Tarpley J, et al.: *Growth factors in porcine full and partial thickness burn repair*. *Am. J. Pathol.* 147: 1261–1277, 1995, Figure 1, p. 1264, with permission from the American Society of Investigative Pathology.

Following initial severe thermal damage to the epidermis, adnexa, and dermis, a marked inflammatory reaction generally follows, characterized initially by an infiltration of neutrophils (Figure 7.28), followed subsequently by mononuclear inflammatory cells, including macrophages and lymphocytes.

Another example of direct cutaneous toxic injury is that induced by the T-2 trichothecene mycotoxin, produced by any one of a number of different fungi of the genus *Fusarium*. T-2 toxicity manifests as degeneration and necrosis of epidermal basal cell layer keratinocytes with progression to full thickness epidermal necrosis





**FIGURE 7.27** Full thickness epidermal necrosis with subepidermal vesicle and cleft formation (\*) due to separation of the epidermis and dermis in the skin of a horse with a full thickness burn. Necrotic cellular debris and neutrophils are present both within the subepidermal vesicles and overlying the necrotic epidermis. *Reproduced from Haschek WM, Rousseaux CG, Wallig MA, editors: Fundamentals of toxicologic pathology, ed 2, 2010, Academic Press, Figure 7.11, p. 50, with permission.*

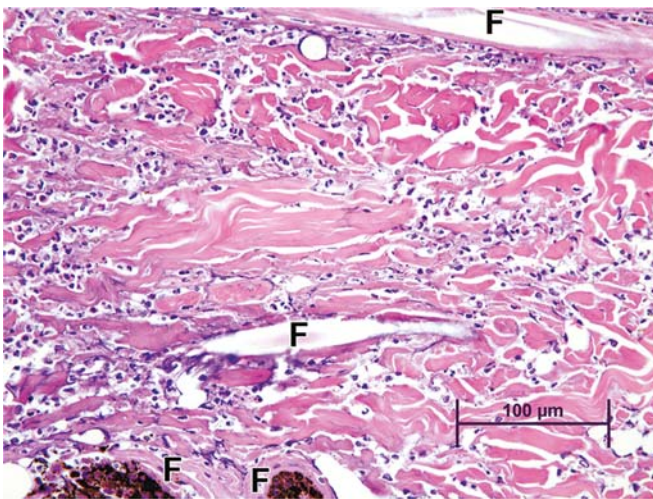


**FIGURE 7.28** Full thickness burn in the skin of a dog illustrating the secondary neutrophilic inflammatory infiltration in the dermis. Hair follicles exhibiting epithelial necrosis (F) are present in the affected dermis. *Reproduced from Haschek WM, Rousseaux CG, Wallig MA, editors: Fundamentals of toxicologic pathology, ed 2, 2010, Academic Press, Figure 7.3, p. 143, with permission.*

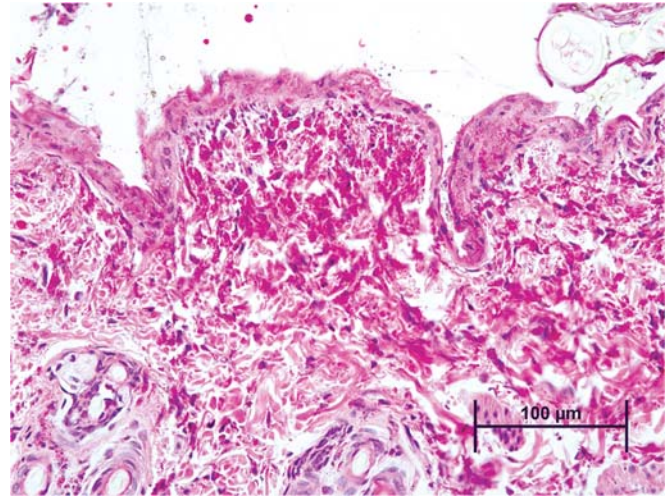


**FIGURE 7.29** T-2 mycotoxicosis in a rabbit characterized by full thickness epidermal necrosis as well as necrosis with coagulation of collagen in the superficial dermis. *Reproduced from Haschek WM, Rousseaux CG, Wallig MA, editors: Fundamentals of toxicologic pathology, ed 2, 2010, Academic Press, Figure 7.10, p. 150, with permission.*

and ulceration. Necrosis of the dermis is also frequently seen (Figure 7.29). The specific mechanism of T-2 toxicity is unknown, although this is still under study with recent studies suggesting that the toxin may cause direct damage to cell membranes, with little or no effect on DNA (Iwahashi et al., 2009), as well as inducing oxidative stress, activation of myeloperoxidase, MMP activity, increase in inflammatory cytokines, activation of p38 MAPK leading to apoptosis of epidermal cells (Agrawal et al., 2012).

A special example of direct cutaneous toxicity is genotoxic injury due to interaction of the toxic agent with DNA. Epidermal keratinocytes exhibit a high rate of proliferation and turnover, and therefore are particularly susceptible to this type of toxic damage. The initial damage caused by genotoxic agents occurs in the basal layer of the epidermis, where the toxic agent can interact with DNA by a variety of mechanisms such as alkylation, DNA breaks, chromosomal breaks, and adduct formation. This results in an increased rate of mutation. At lower doses, the only obvious effect may be the induction of

neoplasia, but epidermal necrosis may occur at higher doses. The observation may be secondary regenerative epidermal hyperplasia when surviving keratinocytes proliferate in order to replace the cells lost by necrosis due to damage by the mutagen.

In extreme cases, the action of the mutagen impairs the cell renewal process itself, resulting in ulceration since replacement of cells lost to differentiation as well as damaged cells is not possible. This mechanism of toxicity is thought to be the cause of the necrotizing lesions associated with sulfur mustard (mustard gas), which selectively targets basal keratinocytes, causing extensive alkylation of DNA to the point of cell death, leading to necrosis of individual epidermal keratinocytes and epidermal vesicular change, often accompanied by a secondary dermal inflammatory response (Figure 7.30).

Testing of topically applied chemicals for acute dermal irritation/corrosion was historically performed in rabbits (OECD, Test number 404, 2015). However, as outlined in the supplement to the OCED Test Guideline 404 on dermal

irritation/corrosion testing (OECD, Test number 404, 2015), consideration of existing data, structure–activity relationships, physiochemical properties of the test item, and testing in validated in vitro and ex vivo systems are recommended before an in vivo study is conducted. Several in vitro testing methods for skin corrosion have been validated, including transcutaneous electrical resistance, evaluation in a human skin model, and evaluation in a RHE model. Acute and chronic toxicity of topically applied substances has typically been evaluated in rats, rabbits, or guinea pigs. However, due to the high degree of morphological and physiological similarity between minipig skin and human skin, minipigs have now gained widespread acceptance as the most appropriate model for dermal toxicity and are being used as the model of choice with increasing frequency.

## 5.2. Immune-Mediated Cutaneous Toxicity

Cutaneous toxicity that occurs as the result of immune-mediated mechanisms falls into the same categories as systemic immune-mediated diseases. Type I hypersensitivity is acute, and classically manifests cutaneously as urticaria (hives = round red welts, often with swelling, that are frequently intensely pruritic). This is mediated by IgE specific to the antigen binding to mast cells and basophils, with subsequent degranulation of these cells with release of vasoactive mediators such as histamine, prostaglandins, and leukotrienes. The key to the diagnosis of true urticaria is that the lesions, which consist of raised pruritic erythematous wheals, typically demonstrate the brightest erythema at the outer edge of lesions with rapid paling toward the middle.

Histopathologically, urticaria is characterized by dermal angioedema, often with congestion of dermal vessels. The key difference between drug-induced and nondrug-induced urticaria is that in nondrug-induced urticaria there is often little else to see histologically, while drug-induced urticaria is characterized by a presence of a mononuclear infiltrate, with or without eosinophils, which is often perivascular. The mononuclear cells are T cells, typically with

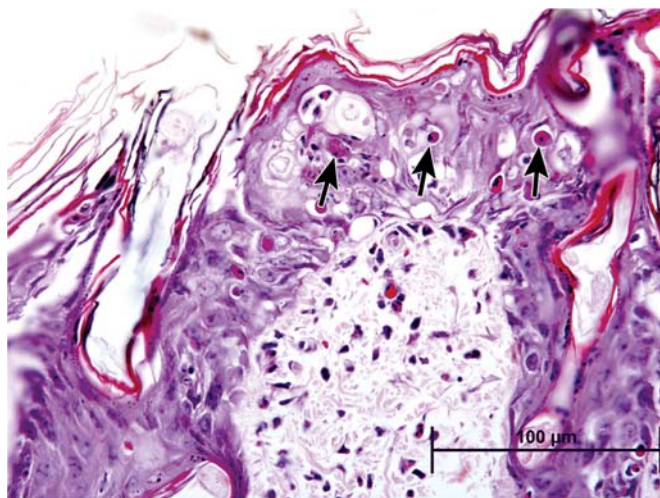


**FIGURE 7.30** Skin from a Guinea pig exposed to sulfur mustard or mustard gas, illustrating single cell necrosis of epidermal keratinocytes (arrows) with secondary inflammation and edema in the underlying superficial dermis. Reproduced from Haschek WM, Rousseaux CG, Wallig MA, editors: *Fundamentals of toxicologic pathology*, ed 2, 2010, Academic Press, Figure 7.4, p. 144, with permission.



CD8<sup>+</sup> cells in the epidermis and CD4<sup>+</sup> cells forming the superficial dermal infiltrate. In some cases, lesions of vasculitis may be present; this is referred to as urticarial vasculitis.

Type II hypersensitivity is cytotoxicity induced by IgG or IgM antibodies with complement activation. The various forms of pemphigus are an example of cutaneous Type II hypersensitivity, with autoantibodies directed against keratinocyte antigens that result in loss of adhesion between keratinocytes due to disruption of desmosomes, with formation of intraepidermal blisters. The hallmark loss of keratinocyte adhesion is the result of autoantibody binding to various antigens on the keratinocyte cell surface. In pemphigus vulgaris, autoantibodies mostly bind to desmoglein 3, while in pemphigus foliaceus, they bind primarily to desmoglein 1, the main desmosomal adhesion glycoprotein (Maruani et al., 2008; Refer also to Section 2.1, The Epidermis). In many cases of pemphigus, an etiologic factor such as drugs or other environmental factors is known or suspected. Drugs may be involved in as many as 10% of pemphigus cases. A number of drugs have been causally linked to the development of pemphigus, particularly those containing thiol groups, such as D-penicillamine and captopril. Other drugs that have been linked to pemphigus include penicillin, cephalosporins, piroxicam, rifampicin, phenobarbital, and propranolol.

The specific lesions of pemphigus are dependent on where the intraepidermal disruption of keratinocytes occurs, but all are characterized by intra- or subepidermal separation of keratinocytes (acantholysis) with the formation of intraepidermal or subepidermal cleft, often containing rounded-up epidermal keratinocytes (acantholytic cells) and variable degrees of inflammatory leukocytes, particularly neutrophils (Figure 7.31).

Type III hypersensitivity is mediated by IgG or IgM antigen–antibody immune complex deposition. Cutaneous vasculitis and cutaneous lupus erythematosus (LE) are examples of Type III hypersensitivity. Vasculitis is characterized by inflammation of small cutaneous vessels with

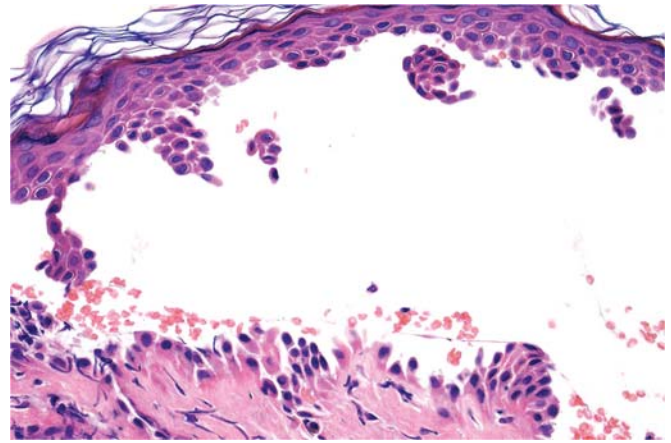


**FIGURE 7.31** Skin from a human with pemphigus vulgaris illustrating subepidermal separation of epidermal keratinocytes from the underlying dermis (acantholysis) with the resultant formation of a subepidermal cleft containing rounded-up epidermal keratinocytes (acantholytic cells) and occasional red blood cells. Courtesy of Richard Carr, MD., Department of Histology, Warwick Hospital, United Kingdom. Reproduced from Haschek WM, Rousseaux CG, Wallig MA, editors: *Haschek and Rousseaux's handbook of toxicologic pathology*, ed 3, 2013, Academic Press, Figure 55.23, p. 2260, with permission.

or without vascular necrosis and/or thrombosis. Cutaneous lupus can have a variety of histologic presentations but is often characterized by an interface dermatitis consisting of a lichenoid inflammatory cellular infiltrate at the dermal–epidermal interface. Lichenoid drug eruptions have a very similar histopathologic appearance. Approximately 20%–30% of cutaneous vasculitides are drug-induced, generally arising 7–10 days following administration of the inducing drug substance. Cutaneous vasculitis manifests as pruritic, palpable purpura with a maculopapular eruption. Certain drugs are associated with specific typical histopathologic findings. For example, leukocytoclastic vasculitides are mostly commonly associated with allopurinol, erythromycin, penicillin, sulfonamides, and thiazide diuretics, while polyarteritis nodosa-like vasculitides are most commonly associated with aspirin, phenytoin, potassium, quinidine, and thiouracil. Although eosinophils

are not present in all cases of drug-induced vasculitis, when they are present, they serve as a valuable clue to the drug-related nature of the vasculitis (reviewed by [Ramdial and Naidoo, 2009](#); [Friedmann et al., 2010](#)).

Drug-induced cutaneous LE is another example of a cutaneous toxicity due to a Type III hypersensitivity reaction. The cutaneous histological and immunofluorescence findings of drug-induced LE are indistinguishable from those of idiopathic LE. Histopathologically, findings range from an interface dermatitis to a dense lichenoid infiltrate with lymphocytes, macrophages, and eosinophils. Individually necrotic keratinocytes may be present, as may dermal edema and vasodilatation.

The drugs most commonly implicated in drug-induced LE are carbamazepine, chlorpromazine, hydralazine, isoniazid, methyldopa, minocycline, penicillamine, procainamide, quinidine, terbinafine, omeprazole, and the TNF- $\alpha$  inhibitors infliximab and etanercept, both of which are biologics. The exact pathogenesis of drug-induced LE is unknown, but reactive drug metabolites are implicated for those induced by xenobiotics (reviewed by [Ramdial and Naidoo, 2009](#), [Friedmann et al., 2010](#)).

It has been hypothesized that cutaneous autoimmune inflammation as exemplified in cutaneous lupus is dependent on pDC activation by nucleic acid antigen via the innate immune receptors TLR7 and TLR9 ([Williams et al., 2009](#)). In the specific case of cutaneous lupus induced by the TNF- $\alpha$  inhibitor biologics, nucleic acid antigens termed nucleosomes become detectable in the plasma of rheumatoid arthritis (RA) patients after the start of TNF- $\alpha$  inhibitor therapy, suggesting that this rise in plasma nucleosome levels might contribute to a break of tolerance and thereby induce autoantibodies in susceptible individuals. This hypothesis is supported by the finding that antinucleosome antibodies correlated strongly with the presence of antinuclear antibodies, a hallmark of systemic LE in anti-TNF- $\alpha$  treated RA patients ([Guiducci et al., 2010](#)).

Type IV hypersensitivity is often a local reaction, and in the skin is referred to as allergic contact dermatitis. Type IV hypersensitivity is a cell-mediated (T cells) rather than an

antibody-mediated reaction to the inciting allergen and is typically delayed in onset. Upon contact with the antigen, sensitized T-cells recruit additional cells and release cytokines resulting in an inflammatory reaction. Examples of Type IV hypersensitivity mediated dermatitis include the reaction to poison ivy, certain drugs, and the tuberculin reaction.

Different toxic agents can induce more than one immune-mediated mechanism. As an example, penicillin, which is often cited as the classic example of a drug acting as a hapten, can cause both an IgE-mediated Type I hypersensitivity reaction manifesting as urticaria, as well as non-IgE-mediated reactions that manifest as variable degrees of epidermal keratinocyte necrosis, ranging from erythema multiforme to TEN and SJS—severe conditions with widespread full thickness epidermal necrosis and detachment from the underlying dermis.

The pathogenesis of immune-mediated cutaneous toxicity is not completely understood, although current understanding suggests involvement of both the adaptive and innate immune systems. It had long been surmised that drugs and other xenobiotics acted as haptens, as described for penicillin, and when conjugated to proteins became presented to the immune system and elicited an immune response. More recently, the involvement of the innate immune system has come to the forefront. As described earlier in this chapter, keratinocytes sense DAMPs through their TLRs ([Guiducci et al., 2010](#)), which triggers the release of antimicrobial peptides such as S100A8/S100A9 complexes, cytokines, and chemokines that in turn recruit and activate leukocytes. Completing the loop, leukocytes that are recruited to the epidermis then release cytotoxic factors such as perforin and granzysin from CD8<sup>+</sup> cytotoxic cells and NK cells, as well as TWEAK, TRAIL, Fas ligand, and other TNF family members, from macrophages and DCs, that in turn induce the keratinocyte death that underlies drug-induced blistering syndromes such as erythema multiforme and TEN.

Erythema multiforme, TEN, and SJS (reviewed by [High, 2023](#)) represent a continuum of lesions whose hallmark histological finding is epidermal necrosis ranging from the single cell

type in erythema multiforme to the full-thickness type in SJS (less than 10% of skin involved) to TEN (>30% of skin involved). Inflammatory cellular infiltration may be present, particularly adjacent to individually necrotic keratinocytes in erythema multiforme. Often there is no or minimal inflammatory cellular infiltration during the early stages of TEN or SJS, conditions that exhibit full thickness epidermal necrosis with epidermal lifting and cleft formation (Figure 7.32). These types of reactions are rarely seen in experimental animals but have been described (personal observations of one of the authors).

The pathogenesis of these conditions is not completely understood but is believed to be immune-mediated, as rechallenging an individual with the same drug can result in rapid recurrence of the condition. The clinical, histopathological, and immunological findings in these conditions support the currently prevalent

hypothesis that they are specific Type IV drug hypersensitivity reactions in which cytotoxic CD8+T lymphocytes play an important role in the initial pathogenesis of lesions.

Gene expression analysis of cells from the blister fluid of patients with TEN and SJS has also recently identified secretory granulysin, a cationic cytolytic protein secreted by cytotoxic T cells, NK cells, and NKT cells, as a key molecule responsible for the induction of keratinocyte death (Harr and French, 2010). Blister fluid cells express high levels of granulysin mRNA; the protein is found in increased concentrations in blister fluid, and when injected intradermally into mice, granulysin induces keratinocyte necrosis and histopathologic lesions similar to those of SJS and TEN. Recent evidence suggests that granulysin alone is insufficient to induce cytotoxic T cell-mediated cell death, and that the simultaneous release of perforin is also required to fully induce single cell necrosis.

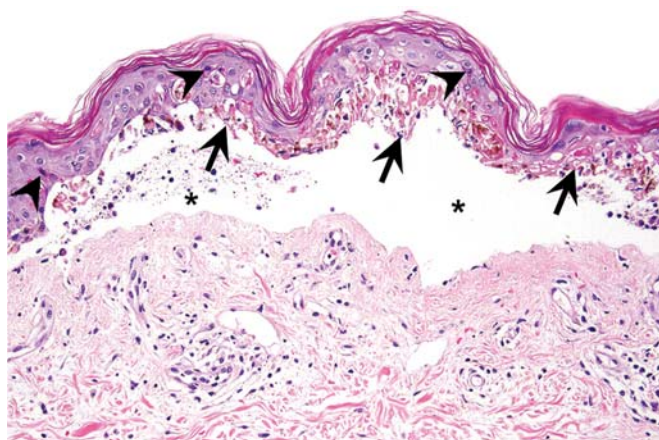


**FIGURE 7.32** Skin from a human with toxic epidermal necrolysis (TEN) illustrating widespread necrosis of the entire basal layer of the epidermis (arrows) with scattered necrosis of suprabasal keratinocytes (arrowheads) and epidermal-dermal separation and cleft formation (asterisks). The cleft is filled with a small amount of cellular debris and amorphous material. There is little or no associated inflammatory reaction in either the epidermis or dermis. *Courtesy of Dr Phillip McKee. Reproduced from Haschek WM, Rousseaux CG, Wallig MA, editors: Haschek and Rousseaux's handbook of toxicologic pathology, ed 3, 2013, Academic Press, Figure 55.24, p. 2261, with permission.*

### 5.3. Mechanisms of Toxicity: Photosafety

#### 5.3.1. Photosensitivity

Many exogenous chemicals and drugs may absorb UV or visible light. Interaction of a particular wavelength of light with a compound that may absorb UV/visible radiation may lead to an enhanced excitement state for electrons, or the release of free electrons. As electrons return to the less excited state, there is a release of energy which may lead to the generation of free radicals or highly reactive singlet oxygen species, which in turn may react and damage lipid membranes, proteins, and nucleic acids, causing cell injury and death.

Photoactivation of chemicals may involve different areas of the electromagnetic spectrum including UVA (320–400 nm), UVB (290–320 nm), or the visible range (400–700 nm). Although highly cytotoxic, UVC (200–290 nm) is typically filtered out in the atmosphere and consequently is not considered a significant risk in vivo. Most photoreactions in vivo are caused by less energetic UVA radiation, whereas more energetic UVB radiation is involved in fewer photoreactions in vivo since the shorter UVB wavelengths penetrate skin less deeply



than the longer UVA wavelengths. Visible light may also induce photoreactions, but these are rarely observed. Acute effects of UV irradiation on skin include direct damage to DNA, cell growth arrest, single cell necrosis, and stimulation of melanogenesis, whereas chronic effects may include photoaging or photocarcinogenesis.

Chemicals or drugs that absorb light are termed photoreactive, and light-induced chemical reactions are termed photosensitivity reactions. Photosensitivity reactions may involve several different mechanisms, and are classified as phototoxicity (photoirritation), photoallergy, photogenotoxicity, and photocarcinogenicity (including photocarcinogenicity). Phototoxic reactions are nonimmunologically mediated, whereas photoallergic reactions are immunologically mediated.

Photosensitivity reactions may result from direct contact with the skin, both intentional (i.e., topically applied drugs) and unintentional (i.e., exogenous environmental toxins), or from systemic exposure due to distribution of the photoreactant chemical (e.g., endogenous chromophores such as flavins or porphyrins or xenobiotic compounds) by the circulation to the skin (Figure 7.33).

Photosensitivity may also be caused by endogenous substances through the liberation of photoreactive metabolic by-products into circulation. Porphyria is associated with a disturbance in the metabolism of porphyrins resulting in an overproduction of porphyrin intermediates of heme synthesis, most notably protoporphyrin. Porphyria may be hereditary or secondary to

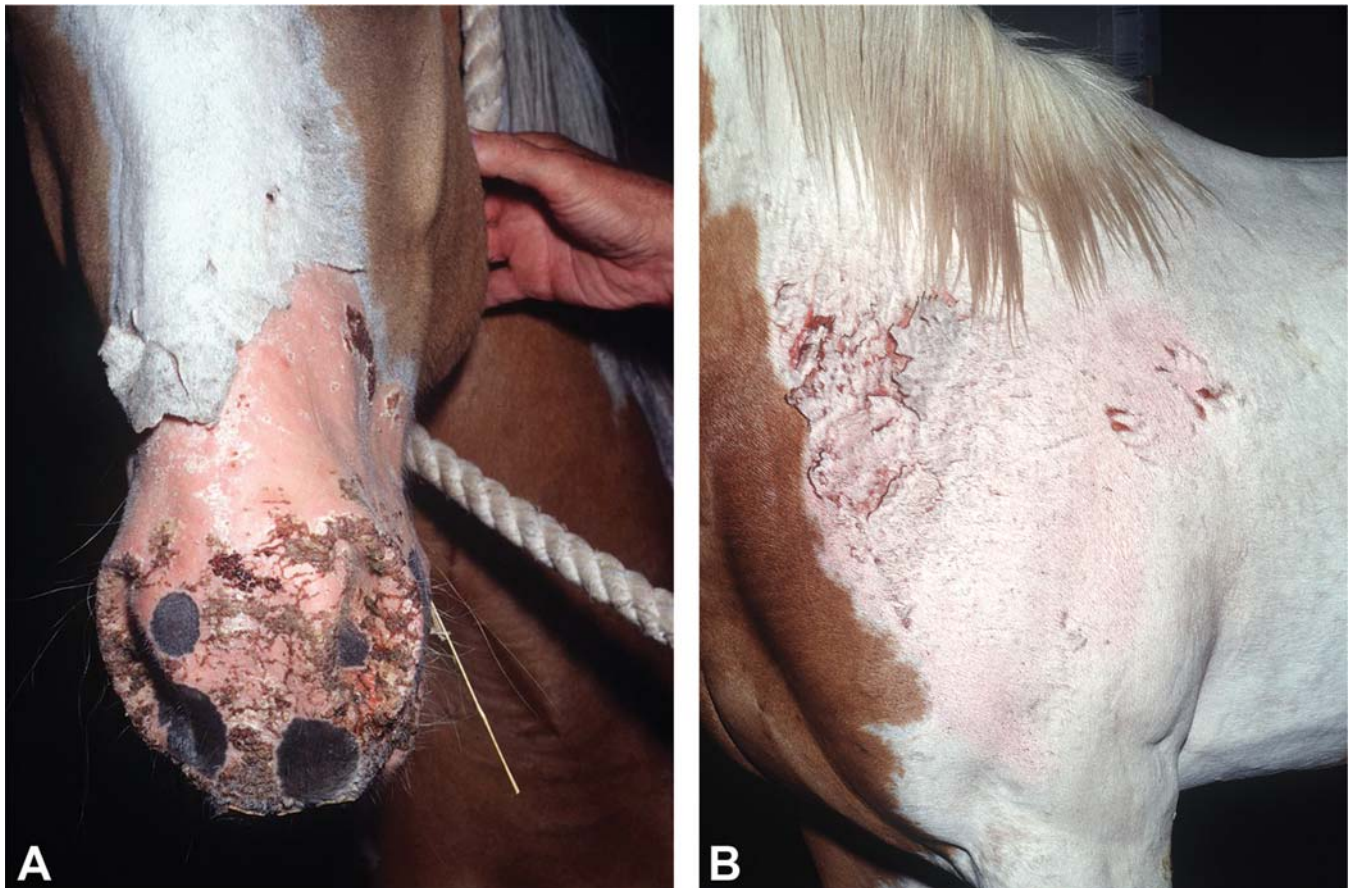


**FIGURE 7.33** Primary photosensitization in a horse linked to a plant phototoxicant in alfalfa hay feed. A: Confluent epidermal necrosis with sloughing and crusting of the muzzle. B: Ulceration, fissuring and crusting in skin over shoulder. Note that distribution of lesions is largely restricted to nonpigmented skin. *Courtesy of Dr. Stephen D. White, University of California, Davis, with permission.*

hepatotoxicity from exposure to various chemicals, including polychlorinated compounds (e.g., hexachlorobenzene), alcohol, or lead. Distribution of porphyrin to the skin and consequent exposure to light results in a photoactivation of porphyrin, generation of free radicals, and skin lesions.

Compounds that induce photosensitizing reactions include naturally occurring plant derivatives, environmental toxins, and numerous classes of drugs. Furocoumarins constitute an important class of naturally occurring plant photosensitizing agents such as psoralens that are synthesized by common rue, bergamot, fennel, and dill. One such derivative, 8-methoxypsoralen (8-MOPS), also known as xanthotoxin, is used in photodynamic therapy (PUVA) to treat skin conditions such as vitiligo and psoriasis. Coal-tar derivatives are well-known causes of phototoxicity and photodermatitis in industrial and road workers.

Numerous classes of drugs have been implicated in photosensitizing reactions (Ferguson, 2002; Hofmann and Weber, 2021), including cardiac antiarrhythmic drugs (e.g., amiodarone), phenothiazines (e.g., chlorpromazine), antimalarials (e.g., quinine, quinidine), thiazide diuretics, tetracyclines (e.g., doxycycline, chlortetracycline), fluoroquinolone antibiotics (e.g., enoxacin, sparflaxacin), antimicrobials (e.g., sulfonamides), fibric acid derivatives (e.g., fenofibrate, gemfibrozil), psychiatric medications (e.g., tricyclics, carbamazepine, benzodiazepines), nonsteroidal antiinflammatory drugs (NSAIDs, e.g., naproxen, tenoxicam), and miscellaneous others (e.g., amantadine, dapsone, nifedipine, isotretinoin). Herbal medications (e.g., St John's wort), sunscreen ingredients (e.g., para-aminobenzoic acid [PABA]), tattoo dyes (e.g., cadmium sulfide), and vitamins (e.g., B6, pyridoxine hydrochloride) have also been associated with photosensitizing reactions.

### 5.3.2. Phototoxicity

Phototoxic reactions, also referred to as photoirritation, are characterized by an acute (minutes to hours), nonimmunologic skin reaction occurring in UV radiation or sun-exposed skin areas, typically resembling exaggerated sunburn. Skin temperature is increased at the site of phototoxicity, and in addition to erythema (redness), there may be edema, vesiculation, desquamation, and, chronically, hyperpigmentation.

Histopathologically, in affected areas of skin, phototoxic reactions are characterized by epidermal keratinocyte single cell necrosis (may be called "sunburn cells"), oncotic necrosis, dyskeratosis, and vacuolation with dermal edema, vascular changes, suppurative inflammation, and/or mononuclear cell infiltrates. Administration of 8-MOPS by gavage to hairless mice followed by exposure to UVA irradiation (Langner et al., 1977) resulted in dose-related skin reactions ranging from an erythematous phototoxic reaction without subsequent skin lesions to severe burning with subsequent scarring (Figure 7.34). Similarly, oral administration of quinolone antimicrobial drugs to albino Balb/c mice and UVA irradiation in combination but not separately caused a cutaneous phototoxic reaction characterized by auricular degeneration of basal epidermal cells and fibroblasts, edema, and dermal neutrophilic infiltration (Makinen et al., 1997; Shimoda et al., 1993).

### 5.3.3. Photoallergy

In contrast to phototoxic reactions, photoallergic reactions are uncommon, and are

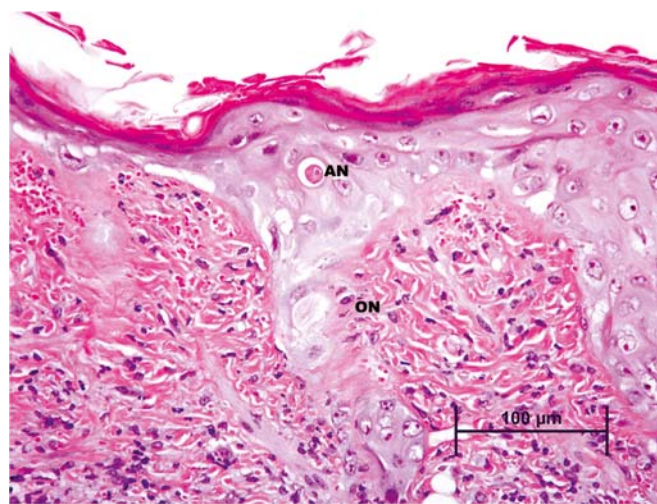


**FIGURE 7.34** Primary photosensitization in the skin of a mouse exposed to the phytochemical psoralens followed by UV light exposure. Apoptotic necrosis (AN) and oncotic necrosis (ON) are evident in the epidermis and there is a secondary inflammation in the underlying superficial dermis. *Reproduced from Haschek WM, Rousseaux CG, Wallig MA, editors: Fundamentals of toxicologic pathology, ed 2, 2010, Academic Press, Figure 7.7, p. 146, with permission.*



immunologic reactions requiring previous sensitization and manifesting 24–72 h after exposure. Photoallergic reactions are considered delayed-type hypersensitivity (Type IV) that involves two phases: an induction phase and a challenge phase. Most chemicals involved in photoallergic reactions are of small molecular weight, which allows penetration of skin, but often too small to elicit an immune response, but by definition must be photoactivated to induce an immune response (reviewed by [Ibottson, 2014](#)). Combination of the photoactivated chemical (hapten) with a protein carrier results in the formation of hapten–carrier adducts which are processed by LCs in the skin and transported via lymphatics to regional lymph nodes, where a T-cell response is triggered. Subsequent exposure to the same chemical triggers a Type IV hypersensitivity reaction in UV radiation-exposed areas as well as on unexposed areas of skin. The skin reaction generally recurs upon repeat exposure to UV radiation even after intake of the initiating agent has stopped. Photoallergic reactions are characterized by dermatitis and pruritus and may extend beyond sun-exposed areas of skin. Histopathologic changes are typical of allergic contact dermatitis, including epidermal keratinocyte necrosis, epidermal spongiosis, perivascular lymphoid cuffs, and lichenoid infiltrates of lymphocytes with or without neutrophils.

#### **5.3.4. Photogenotoxicity**

Numerous chemicals, including psoralens, fluoroquinolones, and phenothiazines, have been identified as having photogenotoxic potential that may be associated with an increased risk of developing skin cancer. Photogenotoxicity may occur as the result of direct DNA damage from UV radiation (primarily UVB, rarely UVA) or following photoactivation of chemicals by UV irradiation resulting in generation of DNA-damaging free radical oxygen species. Administration of 8-MOPS in combination with suberythemagenic doses of UVA irradiation is a well-recognized potent mutagen that forms psoralen–DNA adducts. Factors that may influence photogenotoxicity outcome include binding

and retention time of the chemical in different layers of the skin, DNA repair mechanisms, and antioxidant status ([Struwe et al., 2008](#)).

#### **5.3.5. Photocarcinogenicity**

Prolonged and repeated exposure to UV radiation is well established as the primary factor responsible for the majority of skin cancers in humans. UV radiation induces direct DNA damage, but also induces indirect effects on DNA, proteins, and lipids through the generation of reactive oxygen intermediates and chronic inflammation. For example, 8-MOPS administered to mice exposed to suberythemagenic doses of UVA irradiation rapidly develop cutaneous squamous cell carcinomas. UV radiation can mutate a number of genes that are involved in tumor initiation, promotion, and progression. Many of these genes are tumor suppressors and include mutated p53 in squamous cell carcinomas and basal cell carcinomas, mutated p16 in malignant melanomas, and mutated PTCH-1 leading to unregulated Hh signaling in basal cell carcinomas and some squamous cell carcinomas ([Hussein, 2005](#)).

Hairless p53 heterozygote knockout mice exposed to UVB radiation developed squamous cell carcinomas faster and of a more malignant, poorly differentiated variety than in wild-type mice ([van Kranen et al., 2005](#)), supporting the important role of point mutations of p53 genes in skin carcinogenesis. UV radiation also induces growth arrest and DNA damage-inducible genes such as GADD45, a p53-regulated gene that suppresses cell growth, in keratinocytes and melanocytes. GADD45 is a key protective factor in UV-induced carcinogenesis, as UV-irradiated GADD45 null mice had reduced single cell necrosis of epidermal keratinocytes but an increase in tumors compared to wild-type mice.

Certain chemicals that may not be photoreactive may influence cutaneous carcinogenicity through immunosuppressive effects (e.g., cyclophosphamide) or altering the optical properties of the skin (e.g., certain emollients). This reaction is termed photoco-carcinogenicity and should be considered for drugs that are intended for chronic administration.



#### 5.4. Mechanisms of Toxicity: Photoaging

Aging is a normal, unavoidable consequence of advancing years. Photoaging by contrast is aging of human skin due to exposure to UV radiation. It is also called photodamage, solar damage, or sun damage. Photoaging can begin as early as our teen years, but the repercussions are not seen for years. These include pigmentary changes, deep coarse wrinkles, loss of skin tone and elasticity, and degeneration of dermal elastin (solar elastosis). Means to study and combat photoaging are of increasing importance to our aging population. Since photoaging is a chronic toxicity that takes years to develop, this is difficult to study in the laboratory setting, especially in a high throughput testing paradigm. Studies on mechanisms are focused on the effects of UV radiation on the skin, and it is known that different wavelengths of light have differing effects on skin. In brief, UVB rays (280–315 nm; ~5% of UV radiation to reach earth's surface) penetrate the epidermis and are directly damaging to DNA, thus increasing the chance for development of various epidermal skin cancers. UVA rays (315–400 nm; ~95% of UV radiation to reach earth's surface) penetrate much more deeply to the level of the dermis causing damage to collagen and elastin and are therefore more responsible for the damage leading to photoaging. The primary mechanism of toxicity of UVA rays is the production of reactive oxygen species, which ultimately lead to breakdown of collagen in the dermis. A good review is Gilchrest, *Photoaging, Milestones Cutaneous Biology* (2013) (see also *Radiation and Other Physical Agents*, Vol 3, Chap 14; [Yaar and Gilchrest, 1998](#)).

Treatments for photoaging include preventative measures such as sunscreens or clothing that block UVA rays, and a variety of retinols, cosmetic products, moisturizers, fillers, and other devices, leading to an industry of cosmetics. These compounds or devices require studies of efficacy and safety, thus involving the toxicologic pathologist.

#### 5.5. Mechanisms of Toxicity: Antisense Oligonucleotides

Recently, there has been great interest in antisense oligonucleotide (ASO) therapeutics in the

treatment of a variety of disease including inflammation (e.g., allergy, autoimmunity), cancer, neuromuscular disorders (e.g., Duchenne muscular dystrophy, amyotrophic lateral sclerosis, Huntington's disease, Alzheimer's disease), metabolic diseases (diabetes, hypercholesterolemia), viral diseases (e.g., Hepatitis B virus), and wound healing (e.g., ASO to type I collagen to prevent scarring) via mRNA knockdown. ASOs are single-stranded, synthetic deoxy- or ribonucleotide sequences that bind to specific, complementary mRNA sequences to inhibit their expression. Toxicities associated with ASOs are due to proinflammatory mechanisms, accumulation, or aptameric interactions (i.e., ASO binding to extracellular, cell-surface, or intracellular proteins; with accumulation the most commonly observed in nonclinical toxicity studies) ([Frazier, 2015](#)). Cytoplasmic accumulation of ASOs has been referred to as "basophilic granules" in renal or hepatocellular epithelial cells and ultrastructurally, are considered to be ASO material. A second type of cytoplasmic change has been described in tissue macrophages as weakly staining granules and finely vacuolated cytoplasm. The appearance of ASO accumulation in macrophages is attributed to cellular activation and cytokine production from the proinflammatory effects of ASOs rather than the accumulation of ASOs in epithelial cells. Granular/vacuolated macrophages have been noted in skin following subcutaneous injection of ASOs in mice occurring in the hypodermal and adventitial layers of the subcutis but also in the dermis interspersed among the reticular fibers near the site of injection. Subcutaneous injection of ASOs is also associated with varying degrees of subcutaneous inflammation or mixed inflammatory cell infiltrates, as well as degeneration, inflammatory cell infiltration, and/or regeneration of the panniculus carnosus. This reaction may, in part, be associated with the trauma of needle penetration and thus, evaluation of vehicle control animals is important for differentiating test article-related effects from procedural effects. Sham controls that receive all procedures but no vehicle or drug are of additional benefit for differentiating vehicle effects from procedural effects.

## 5.6. Mechanisms of Toxicity: Pigmentation

Skin and hair color may be influenced by the presence of hemoglobin and carotenoids but is primarily attributed to the presence of melanocytes that synthesize melanin pigments. There are two primary types of melanin that influence skin color: eumelanin, which is brown-black, and pheomelanin, which confers red-yellow pigmentation. Melanocytes export melanin in melanosomes (melanin-containing granules) to adjacent keratinocytes for distribution to the upper layers of the skin, or from the hair bulb to the hair shaft. The number, size, composition, density, and distribution of melanosomes are primarily responsible for variations in pigmentation, whereas the number of melanocytes remains relatively constant. Numerous intrinsic factors may also influence skin pigmentation by acting on melanocytes. These include genetic factors and epigenetic factors derived from keratinocytes (e.g., bFGF,  $\alpha$ -MSH, PAR2), dermal fibroblasts (e.g., DKK1, TGF- $\beta$ 1, bFGF, HGF, SCF), endocrine and neural factors (e.g., nitric oxide,  $\alpha$ -MSH), and systemic inflammation (e.g., prostaglandins, leukotrienes, thromboxanes, IL1, IL6).

Studies on mouse coat color mutants have identified more than 300 genes that may influence skin and hair color. Melanocortin-1 receptor (MC1R) is considered the major determinant of pigment phenotype. Alpha-melanocyte-stimulating hormone ( $\alpha$ -MSH) and adrenocorticotrophic hormone (ACTH) are the principal agonists of MC1R that act to increase eumelanin via elevation of cAMP levels. Melanin synthesis is controlled by TYR enzymes that initiate melanin synthesis by catalyzing oxidation of L-tyrosine. TYR activity is mediated principally by TYR-related protein 1 (TRP1) and dopachrome tautomerase (TRP2).

Skin pigmentation may also be influenced by extrinsic factors such as ultraviolet radiation (UVR). The skin is the main barrier to environmental stresses and noxious stimuli, and the melanocytes' ability to absorb UVR provides a significant contribution to the protective mechanisms of skin. UVA (315–400 nm) and particularly UVB (280–315 nm) are able to penetrate skin and stimulate melanin pigmentation. Hence, the degree of pigmentation, which reflects degree

of photoprotection afforded, is termed skin "phototype" and may be used as a predictor of photoaging and photocarcinogenesis where lighter-skinned individuals are at higher risk.

Disorders of pigmentation may be classified as hyperpigmentation or hypopigmentation, which may or may not involve alterations in melanocyte numbers. In the extreme, complete lack of pigmentation, termed albinism, is the result of genetic mutations. More often, however, pigmentation changes are associated with variations in the amount of melanin in skin or hair (i.e., described clinically as normochromia, hyperchromia, and hypochromia), although drug or metal deposits may occasionally be involved.

Drug-induced cutaneous pigmentation disorders that may account for 10%–20% of acquired cases of hyperpigmentation in humans are of particular interest to the toxicologic pathologists. Numerous drugs have been implicated in pigmentation disorders, including NSAIDs, antimalarial agents (e.g., chloroquine, quinine), antipsychotic drugs (e.g., chlorpromazine, phenothiazine), anti-convulsants (e.g., phenytoin), amiodarone, tetracyclines, cytotoxic drugs (e.g., cyclophosphamide, busulfan, bleomycin, adriamycin), and heavy metals. The mechanisms involved in pigmentation disorders vary with the type of agent involved. For example, some drugs may react with melanin to form drug-pigment complexes, which may be exacerbated by sunlight stimulation of melanin synthesis. Acute or chronic inflammatory processes may result in nonspecific postinflammatory hypopigmentation or hyperpigmentation through the release of numerous mediators, including cytokines and growth factors, which may cause aberrant melanogenesis.

The exact mechanisms involved in postinflammatory hypopigmentation are not clearly understood but are thought to be the result of inhibition of melanogenesis rather than overt destruction of melanocytes (although in some instances severe inflammation may result in destruction and loss of melanocytes with permanent pigment change). Heavy metals, on the other hand, may be deposited in the dermis, contributing to a pigmentation change by a mechanism other than one involving melanin (see *Metals*, Vol 3, Chap 40).

Nonclinical toxicity studies are conducted to determine the toxicologic potential of drug candidates prior to administration to humans in order to assess and mitigate potential adverse clinical effects. Observance of pigmentation disorders may manifest fortuitously in routine toxicity studies or from development of specific animal models. For example, based on studies in pigmented and nonpigmented (albino) rats, chloroquine has demonstrated a distinct affinity for ocular melanin involving reversible hydrophobic or electrostatic interactions (Ono et al., 2003). Administration of an experimental platelet aggregation inhibitor, PD-89454, caused an unintended loss of color in normally pigmented areas of the nose, lips, eyelids, and oral mucosa of Beagle dogs (Walsh and Gough, 1989). Decreased melanin was demonstrated in melanocytes and keratinocytes by Fontana–Masson staining, and ultrastructurally, melanocytes appeared round or globoid, with fewer and smaller dendritic processes, and fewer, incompletely pigmented melanosomes.

In addition to unintended adverse effects of systemic drugs, many drug development efforts have purposefully pursued hypopigmentation for cosmetic skin lightening. Numerous mechanisms have been targeted for decreasing pigmentation, including TYR, TRP1, and TRP2 inhibition (via microphthalmia-associated transcription factor downregulation), increased TYR ubiquitination, decrease of MC1R activity, cAMP inhibition (antiinflammatory agents), interference with melanosome transfer or maturation, and liberation of toxic melanin synthesis intermediates.

Methimazole (MMI) is an antithyroid agent that is an inhibitor of TYR and may serve to inhibit melanogenesis. Topical application of MMI to the ear skin of brown guinea pigs resulted in depigmentation characterized morphologically by altered shape and larger size of melanocytes, loss of dendrites, increased thickness of remaining dendrites, and, in some areas, a reduction in the number of melanocytes (Kasraee, 2002). Similarly, 4-*n*-butylresorcinol (BR; Rucinol) has been shown to be a reversible inhibitor of melanin production in B16 mouse melanoma cells without producing cytotoxicity, through potent inhibition of TYR and TRP1, and shows promise as a whitening agent in the

clinical treatment of liver spots (Katagiri et al., 2001). Administration of 4-S-cysteaminy phenol to C57BL/6J black mice or black guinea pigs caused depigmentation through a mechanism of selective cytotoxicity involving a reduction in the number of functioning melanocytes, a decrease in the number of melanosomes produced and transferred to keratinocytes, and destruction of membranous organelles of melanocytes (Ito and Jimbow, 1987; Ito et al., 1987).

### 5.7. Mechanisms of Toxicity: Adnexa—General and Specific Toxicities

Toxicity of the cutaneous adnexa can be generally categorized into that which affects the hair shaft (follicular atrophy and alopecia), the sweat glands (anhidrosis, hypo- or hyperhidrosis), or the sebaceous glands (xerosis). These changes can occur individually or in combination, depending on the target of the toxicant.

Alopecia is a common cutaneous toxicity secondary to systemically administered drugs, particularly to chemotherapeutic agents (Trüeb, 2009) that have an effect on disrupting the cell cycle in actively dividing cells, such as those in the hair matrix during hair shaft generation in the anagen phase of the hair cycle. A large number of chemotherapeutic agents can induce alopecia, with four major classes of agents that are classified based on their mechanism of inducing alopecia. Microtubule inhibitors, such as paclitaxel, induce the highest incidence of alopecia at > 80% followed by topoisomerase inhibitors such as doxorubicin at 60%–100%, nucleic acid alkylators such as cyclophosphamide at 60%, and 10%–50% for antimetabolites that only damage cells during the S phase, when they are actively synthesizing DNA, such as 5-fluorouracil plus leucovorin or methotrexate.

Combinations of two or more chemotherapeutic agents usually induce a greater incidence and more severe alopecia than single-agent chemotherapy does. Regardless of the specific agent that induces the alopecia, the histopathologic appearance of lesions is similar, with single cell necrosis or apoptosis of follicular keratinocytes, particularly those in the hair bulb and/or hair matrix epithelium. Toxic effects to the sebaceous glands have also been described for



chemotherapeutic agents, and may be associated with, or a contributing cause of, alopecia since sebum is an essential component for normal hair growth.

There are two commonly used animal models for modeling chemotherapy induced alopecia. The first is neonatal rats that have follicles synchronized in anagen shortly after birth, and the second is depilation of adult mice in order to synchronize the hair follicles in anagen. These models have allowed investigation of mechanisms underlying the development of chemotherapy-induced alopecia, as well as the evaluation of agents for the potential prevention and/or therapy of alopecia. A number of agents have been tested for their ability to prevent alopecia in these models, including cyclosporin A, minoxidil, antioxidants, apoptosis inhibitors, and a variety of cytokines and growth factors, all with variable degrees of effectiveness.

In the mouse depilation model, p53 is essential for triggering cyclophosphamide-induced apoptotic cell death in hair follicle keratinocytes. In addition, loss of p53 results in complete protection of murine hair follicles against cyclophosphamide-induced alopecia. *Fas* signaling mediated by p53 is an important pathway mediating apoptosis induced by cyclophosphamide in follicular keratinocytes, as both *Fas* and *Fas* ligand are upregulated in hair follicles following cyclophosphamide treatment, and mice treated with anti-*Fas* ligand antibody as well as *Fas* knockout mice both showed significantly reduced cyclophosphamide-induced alopecia and follicular atrophy along with markedly reduced apoptosis of follicular keratinocytes.

Chloracne is one of the more distinctive nonimmunologic cutaneous manifestations of systemic toxicity. Chloracne is induced following systemic exposure to 2,3,7,8-tetrachlorodibenzo-p-dioxin (TCDD, commonly referred to as dioxin) and related environmental contaminant compounds. Acneiform lesions that tend to form on the face/head and trunk but generally not on the extremities are typical of the condition. Histopathologically, comedones consist of cystically dilated hair follicles without substantive associated inflammation. As lesions advance, hyperkeratinization and sebaceous gland atrophy mark the pilosebaceous unit. Outbreaks of chloracne have been described in several populations accidentally exposed to dioxin.

Rabbits, monkeys, rhino mice, and hairless mice (*hr/hr* mutants) have all been used as models for the development of chloracne-like lesions after exposure to dioxin. It was believed that in mice, hairlessness was required for the development of lesions. More recently, however, haired B6C3F1 mice have also been shown to develop chloracne-like lesions following exposure to dioxin-like compounds. Histopathologically, the characteristic lesions of chloracne are similar to those in humans: a cystic dilation of hair follicles with flattening of the lining epithelium and accompanying atrophy of sebaceous glands (Figure 7.35). Inflammation is not a prominent feature, although it is sometimes present.

Many effects of TCDD are mediated by its specific binding to the Ah receptor (AhR), a cytosolic ligand-activated transcription factor. Binding of dioxin to AhR leads to nuclear translocation of the protein complex, and upregulation of the dioxin-AhR complex to dioxin responsive genes. Although this process is well understood, the mechanism by which it leads to chloracne and related skin lesions is not.

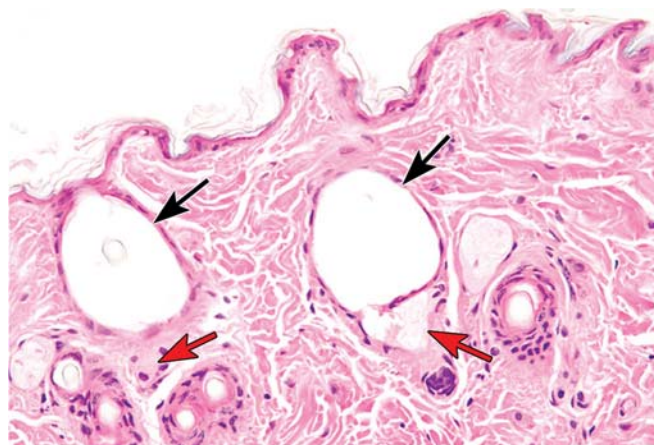


**FIGURE 7.35** Histological section from male B6C3F1 mouse treated for 2 years with 30 mg/kg 3,3',4,4'-tetrachloroazobenzene. Note dilation of hair follicles, flattening of lining epithelium and atrophy of adjacent sebaceous glands. No infiltration of inflammatory cells can be discerned. Black arrows indicate hair follicles. Red arrows indicate sebaceous glands. Reprinted from Ramot Y, Nyska A, Lieuallen W, Maly A, Flake G, Kissling GE, Brix A, Malarkey DE, Hooth MJ: Inflammatory and chloracne-like skin lesions in B6C3F1 mice exposed to 3,3',4,4'-tetrachloroazobenzene for 2 years. *Toxicology* 265:1–9, 2009, Figure 3F, p 6, with permission from Elsevier.

Another class of compounds frequently clinically associated with acneiform rash is that of the EGFR inhibitors. The rash associated with use of these compounds is pruritic, and may be accompanied by xerosis, and hair and nail changes. Because skin lesions do not occur in all patients responding to treatment, a direct pharmacologic effect of these drugs on the skin is suspected, but exact mechanisms are not entirely understood. Apparent associations with skin lesion development and increasing dose of compound or positive correlation with antitumor effect also suggest direct receptor-mediated pathogenesis. Since EGFRs are present in basilar and proliferative epidermal cells, the lesions most reasonably stem from perturbations in normal proliferation and subsequently in barrier function. Sebaceous glands and hair follicles also express EGFRs and are known targets in some cases of toxicity. Histopathologic lesions include hyperkeratosis and folliculitis with perifollicular inflammation, with or without sebaceous gland or dermal vascular changes. EGFR mutant mouse models are all characterized with phenotypic skin changes, and although knockout models are generally lethal, skin of surviving early postnatal knockout mice has also been described as having multiple abnormalities (Mascia et al., 2013).

Drug-induced changes in eccrine and/or apocrine glands of the skin can be direct or indirect. Indirectly, many neurogenic compounds may lead to suppression or stimulation of sweat gland function through activity on sympathetic innervation of the glands, or by effects on myoepithelial cells also important for sweat production. For instance, anticholinergic and antihistamines may be associated with hypohidrosis via an antimuscarinic pathway. Anticholinesterases cause the opposite effect: increased sweat production or hyperhidrosis. Certain drugs, such as opioids and some antidepressants, can be associated with either increased or decreased sweating, depending on which receptor subtypes are being engaged and on thermoregulatory pathway involvement.

Direct toxicity to sweat glands is described for several chemotherapeutic compounds. It is postulated that tendency toward secretion of these compounds in sweat may be at least partially responsible for the targeted gland effect, but a direct toxicity to gland and duct epithelium

may also be causative. The change, known as neutrophilic eccrine hidradenitis, features histologic degeneration or necrosis of eccrine and/or apocrine glands, sometimes with squamous metaplasia of duct epithelium with or without suppurative inflammation. The most commonly implicated drugs are cytarabine and others that are used to treat acute myelogenous leukemia.

Sebum is rich in lipids, so disruption of lipid synthesis pathways can affect sebum production. The spontaneously occurring *asebia* mutant mouse is characteristic. This model has defective stearyl-coA desaturase, an enzyme important in the production of monounsaturated fatty acids. Histopathologically, sebaceous glands are hypoplastic and hair follicles are malformed as a result. Sebaceous glands are also rich in nuclear hormone receptors (estrogens, androgen, and progesterone receptors). Testosterone induces sebocyte proliferation and sebum production. Estrogen can also apparently increase sebum, through modulation of the IGF-1 receptor. Beyond hormones, a myriad of receptor subtypes including retinoid/retinoic acid, growth factors, and neurotransmitters characterize sebocytes. This diverse receptor expression suggests the physiologic importance of the sebaceous gland in a number of biologically important pathways.

## 6. CONCLUSION

The integument has a unique role as a first-line defense against numerous environmental insults (e.g., physical trauma, temperature fluctuations, infectious and chemical agents, UV radiation), thus the health of the skin impacts and reflects the health of the organism. Beyond barrier function, the skin is also important as a neurosensory organ, acts as an endocrine organ, is an essential component of the immune system, aids in locomotion, and has essential psychologic/behavioral functions in many species. In toxicologic pathology, the skin may represent a target organ for those compounds that make direct contact with it via topical or systemic exposure, or as an indirect target of dysfunction of other organ systems such as the endocrine or immune systems. This chapter has reviewed:

- Structure and function of the various cell types and adnexa,

- Methods of toxicity evaluation unique to the skin including study design and special considerations,
- Skin immunology,
- Skin microbiome and its influence on adaptive immunity,
- Morphology of skin lesions and appropriate toxicologic nomenclature,
- Skin carcinogenesis and neoplasms,
- Direct cutaneous toxicity,
- Immune-mediated cutaneous toxicity including hypersensitivity reactions,
- UV exposure-related toxicity and aging,
- Pigmentation-related toxicity,
- Toxicity of adnexa including hair follicles.

## Acknowledgments

We gratefully acknowledge contributions from Aneesh Alex and Professor Stephen Boppart (Biophotonics Imaging Laboratory, University of Illinois Urbana-Champaign) for multiphoton imaging text and photos. Thank you to the Cellular Biomarkers Laboratory at GSK US for providing psoriasis scans for imaging. A large portion of the text included is modified from Haschek WM, Rousseaux CG, Wallig MA, editors: *Haschek and Rousseaux's handbook of toxicologic pathology*, ed 3, 2013, Academic Press (*Integument* Chapter 55).

## REFERENCES

- Ackerman AB, Boer A, Bennin B, et al.: *Histologic diagnosis of inflammatory skin diseases: an algorithmic method based on pattern analysis*, third ed., New York, NY, January 1, 2005, Ardor Scribendi, 13 978-1893357259.
- Agrawal M, Yadav P, Lomash V, et al.: T-2 toxin induced skin inflammation and cutaneous injury in mice, *Toxicology* 302: 255–265, 2012.
- Ahn K, Kim BE, Kim J, et al.: Recent advances in atopic dermatitis, *Curr. Opin. Immunol.* 66:14–21, 2020, <https://doi.org/10.1016/j.coi.2020.02.007>.
- Alex A, Chaney EJ, Žurauskas M, et al.: In vivo characterization of minipig skin as a model for dermatological research using multiphoton microscopy, *Exp. Dermatol.* 29: 953–960, 2020, <https://doi.org/10.1111/exd.14152>.
- Ali N, Oehme FW: A literature review of dermatotoxicity, *Vet. Hum. Toxicol.* 34(5):428–437, 1992 Oct.
- Archambault M, Yaar M, Gilchrist BA: Keratinocytes and fibroblasts in a human skin equivalent model enhance melanocyte survival and melanin synthesis after ultraviolet irradiation, *J. Invest. Dermatol.* 104(5):859–867, 1995.
- Azzi L, El-Alfy M, Martel C, et al.: Gender differences in mouse skin morphology and specific effects of sex steroids and dehydroepiandrosterone, *J. Invest. Dermatol.* 124(1):22–27, 2005.
- Barbero AM, Frasch HF: Pig and guinea pig skin as surrogates for human *in vitro* penetration studies: a quantitative review, *Toxicol. In Vitro* 23(1):1–13, 2009.
- Bataille A, Le Gall C, Misery L, et al.: Merkel cells are multimodal sensory cells, a review of study methods, *Cells* 11: 3827, 2022. <https://doi.org/10.3390/cells11233827>.
- Belkaid Y, Segre JA: Dialogue between skin microbiota and immunity, *Science* 346(6212):954–959, 2014.
- Benavides F, Oberyzy TM, et al.: The hairless mouse in skin research, *J. Dermatol. Sci.* 53:10–18, 2009.
- Boniface K, Bernard FX, Garcia M, et al.: IL-22 inhibits epidermal differentiation and induces proinflammatory gene expression and migration of human keratinocytes, *J. Immunol.* 174:3695–3702, 2005.
- Braff MH, Gallo RL: Antimicrobial peptides: an essential component of the skin defensive barrier, *Curr. Top. Microbiol. Immunol.* 306:91–110, 2006.
- Bragulla HH, Homberger DG: Structure and functions of keratin proteins in simple, stratified, keratinized and cornified epithelia, *J. Anat.* 214(4):516–559, 2009.
- CFR (Code of Federal Regulations) (last accessed July 2023), <https://www.ecfr.gov/current/title-40/chapter-I/subchapter-R/part-798>, 2023.
- Charruyer A, Ghadially R: What's new in dermatology: epidermal stem cells, *G Ital. Dermatol. Venereol.* 146(1):57–67, 2011.
- Chen C, Meng Z, Ren H, et al.: The molecular mechanisms supporting the homeostasis and activation of dendritic epidermal T cell and its role in promoting wound healing, *Burns Trauma* 9, 2021 Jun 23. <https://doi.org/10.1093/burnst/tkab009>.
- Clausen BE, Stoitzner P: Functional specialization of skin dendritic cell subsets in regulating T cell responses, *Front. Immunol.* 6:534, 2015, <https://doi.org/10.3389/fimmu.2015.00534>.
- Corbett AJ, Awad W, Wang H, et al.: Antigen recognition by MR1-reactive T cells; MAIT cells, metabolites, and remaining mysteries, *Front. Immunol.* 11:1–18, 2020, <https://doi.org/10.3389/fimmu.2020.01961>.
- Corcuff P, Bertrand C, Leveque JL: Morphometry of human epidermis *in vivo* by real-time confocal microscopy, *Arch. Dermatol. Res.* 285:475–481, 1993.
- Danilenko DM, Ring BD, Tarpley JE, et al.: Growth factors in porcine full and partial thickness burn repair, *Am. J. Pathol.* 147:1261–1277, 1995.
- Diegel KL, Danilenko DM, Wojcinski ZW. In Wallig MA, Haschek WM, Rousseaux CG, Bolon B, Mahler BW, editors: *Fundamentals of toxicologic pathology*, Third Edition, San Diego, 2018, Academic Press, pp 791–822.
- EMA (European Medicines Agency) <https://www.ema.europa.eu/en/human-regulatory/research-development/scientific-guidelines> (last accessed February 26, 2024).
- Epstein EH: Basal cell carcinomas: attack of the hedgehog, *Nat. Rev. Cancer* 8:743–754, 2008.
- European Union Registration, Evaluation, authorisation and restriction of chemicals; European Union Regulation No. 1907/2006 <https://echa.europa.eu/regulations/reach/legislation> Last accessed February 25, 2024.
- FDA (Food and Drug Administration) [<https://www.fda.gov/regulatory-information/search-fda-guidance-documents>]. Last access February 25, 2024.



- Ferguson J: Photosensitivity due to drugs, *Photodermatol. Photoimmunol. Photomed.* 18:262–269, 2002.
- FHSA (Federal Hazardous Substances Act), 2023. <https://www.ecfr.gov/current/title-16/chapter-II/subchapter-C/part-1500>. last accessed February 25, 2024.
- Flynn K, Mahmoud NN, Sharifi S, et al.: Chronic wound healing models, *ACS Pharmacol. Transl. Sci.* 6(5):783–801, 2023, <https://doi.org/10.1021/acspsci.3c00030>.
- Frazier KS: Antisense oligonucleotide therapies: the promise and the challenges from a toxicologic pathologist's perspective, *Toxicol. Pathol.* 43:78–89, 2015.
- Friedmann PS, Pickard C, Arden-Jones M, et al.: Drug-induced exanthemata: a source of clinical and intellectual confusion, *Eur. J. Dermatol.* 20:255–259, 2010.
- Fujita H: The role of IL-22 and Th22 cells in human skin disease, *J. Dermatol. Sci.* 72(1):3–8, 2013, <https://doi.org/10.1016/j.jdermsci.2013.04.028>.
- Fullerton A, Rode B, Serup J: Skin irritation typing and grading based on laser Doppler perfusion imaging, *Skin Res. Technol.* 8:23–31, 2002.
- Gallo RL, Nakatsuji T: Microbial symbiosis with the innate immune defense system of the skin, *J. Invest. Dermatol.* 131: 1974–1980, 2011.
- Gambichler T, Boms S, Stucker M, et al.: Epidermal thickness assessed by optical coherence tomography and routine histology: preliminary results of method comparison, *J. Eur. Acad. Dermatol. Venereol.* 20:791–795, 2006.
- Gasque P, Jaffar-Bandjee MC: The immunology and inflammatory responses of human melanocytes in infectious diseases, *J. Infect.* 71(4):413–421, 2015, <https://doi.org/10.1016/j.jinf.2015.06.006>.
- Gil A, Olza J, Gil-Campos M, et al.: Is adipose tissue metabolically different at different sites? *Int. J. Pediatr. Obes.* 6(Suppl. 1):13–20, 2011 Sep.
- Gilchrist BA: Photoaging, *J. Invest. Dermatol.* 133(E1):E2–E6, 2013 Jul 1, <https://doi.org/10.1038/skinbio.2013.176>.
- González S, Swindells K, Rajadhyaksha M: Torres A. Changing paradigms in dermatology: confocal microscopy in clinical and surgical dermatology, *Clin. Dermatol.* 21(5):359–369, 2003.
- goRENI. <https://www.goreni.org/>. last accessed February 26, 2024.
- Grabau JH, Dong L, Mattie DR, et al.: Comparison of anatomical characteristics of the skin for several laboratory animals. *United States Airforce Armstrong Laboratory Document AL/OE-TR-1995-0066*, 1995.
- Grachtchouk M, Pero J, Yang SH, et al.: Basal cell carcinomas in mice arise from hair follicle stem cells and multiple epithelial progenitor populations, *J. Clin. Invest.* 121:1768–1781, 2011.
- Grada A, Mervis J, Falanga V: Research techniques made simple: animal models of wound healing, *J. Invest. Dermatol.* 138(10):2095–2105, 2018.
- Grambow E, Sorg H, Sorg C, et al.: Experimental models to study skin wound healing with a focus on angiogenesis, *Med. Sci.* 9:55, 2021, <https://doi.org/10.3390/medsci9030055>.
- Grice EA, Segre JA: The skin microbiome, *Nat. Rev. Microbiol.* 9(4):244–253, 2011.
- Gu Y, Bian Q, Zhou Y, et al.: Hair follicle-targeting drug delivery strategies for the management of hair follicle-associated disorders, *Asian J. Pharm. Sci.* 17(3):333–352, 2022, <https://doi.org/10.1016/j.ajps.2022.04.003>.
- Guiducci C, Tripodo C, Gong M, et al.: Autoimmune skin inflammation is dependent on plasmacytoid dendritic cell activation by nucleic acids via TLR7 and TLR9, *J. Exp. Med.* 207:2931–2942, 2010.
- Gupta R, Priya A, Chowdhary M, et al.: Pigmented skin exhibits accelerated wound healing compared to the non-pigmented skin in Guinea pig model, *iScience* 26(11): 108159, 2023. <https://doi.org/10.1016/j.isci.2023.108159>.
- Hampton AL, Hish GA, Aslam MN, et al.: Progression of ulcerative dermatitis lesions in C57BL/6Cr1 mice and the development of a scoring system for dermatitis lesions, *J Am Assoc Lab Anim Sci* 51(5):586–593, 2012.
- Han C-Y, Kwon S-K, Yeom M, et al.: Exploring the differences in the gut microbiome in atopic dermatitis according to the presence of gastrointestinal symptoms, *J. Clin. Med.* 11(13), 2022, <https://doi.org/10.3390/jcm11133690>.
- Harr T, French LE: Toxic epidermal necrolysis and Stevens-Johnson syndrome, *Orphanet J. Rare Dis.* 5:39, 2010.
- Helman RG, Hall JW, Kao JY: Acute dermal toxicity: *in vivo* and *in vitro* comparisons in mice, *Fund. Appl. Toxicol.* 7:94–100, 1986.
- High WA. <https://www.uptodate.com/contents/stevens-johnson-syndrome-and-toxic-epidermal-necrolysis-pathogenesis-clinical-manifestations-and-diagnosis>. (Accessed 25 February 2024), 2023.
- Hofmann GA, Weber B: Drug-induced photosensitivity: culprit drugs, potential mechanisms and clinical consequences, *J. Dtsch Dermatol. Ges.* 19(1):19–29, 2021 Jan, <https://doi.org/10.1111/ddg.14314>.
- Hornero RA, Idoyaga J: Plasmacytoid dendritic cells: a dendritic cell in disguise, *Mol. Immunol.* 159:38–45, 2023, <https://doi.org/10.1016/j.molimm.2023.05.007>.
- Houben E, De Paepe K, Rogiers V: A keratinocyte's course of life, *Skin Pharmacol. Physiol.* 20(3):122–132, 2007.
- Hu W, Shang R, Yang J, et al.: Skin  $\gamma\delta$  T cells and their function in wound healing (review), *Front. Immunol.*, 2022:13, 2022.
- Huguier V, Giot JP, Simonneau M, et al.: Oncostatin M exerts a protective effect against excessive scarring by counteracting the inductive effect of TGF $\beta$ 1 on fibrosis markers, *Sci. Rep.* 9: 2113, 2019, <https://doi.org/10.1038/s41598-019-38572-0>.
- Hussein MR: Ultraviolet radiation and skin cancer: molecular mechanisms, *J. Cutan. Pathol.* 32:191–205, 2005.
- Ibbotson SH: Photoallergic contact dermatitis, clinical aspects, *Appl. Dermatotoxicol.*, 2014:85–114, 2014, <https://doi.org/10.1016/B978-0-12-420130-9.00005-0>.
- ICH: M3(R2) *Non-clinical safety studies for the conduct of human clinical trials and marketing authorization for pharmaceuticals*,

2010. <https://www.fda.gov/regulatory-information/search-fda-guidance-documents/m3r2-nonclinical-safety-studies-conduct-human-clinical-trials-and-marketing-authorization>. (Accessed 25 February 2024).
- ICH 2015 S10 Photosafety evaluation of pharmaceuticals - Scientific guideline <https://www.ema.europa.eu/en/ich-s10-photosafety-evaluation-pharmaceuticals-scientific-guideline> (last accessed February 25, 2024).
- Ishida-Yamamoto A, Simon M, Kishibe M, et al.: Epidermal lamellar granules transport different cargoes as distinct aggregates, *J. Invest. Dermatol.* 122(5):1137–1144, 2004.
- Ito Y, Jimbow K: Selective cytotoxicity of 4-S-cysteaminylphenol on follicular melanocytes of the black mouse: rational basis for its application to melanoma chemotherapy, *Cancer Res.* 47:3278–3284, 1987.
- Ito Y, Jimbow K, Ito S: Depigmentation of black Guinea pig skin by topical application of cysteaminyphenol, cysteinylphenol, and related compounds, *J. Invest. Dermatol.* 88:77–82, 1987.
- Iwahashi Y, Kitagawa E, Iwahashi H: Analysis of mechanisms of T-2 toxicity using yeast DNA microarrays, *Int. J. Mol. Sci.* 9:2585–2600, 2009.
- Jabeen MF, Hinks TSC: MAIT cells and the microbiome, *Front. Immunol.* 23:1–17, 2023, <https://doi.org/10.7150/ijbs.39016>.
- Jacobs JJ, Lehe C, Cammans KD, et al.: An in vitro model for detecting skin irritants: methyl green-pyronine staining of human skin explant cultures, *Toxicol. In Vitro* (16):581–588, 2002.
- Kasraee B: Depigmentation of brown Guinea pig skin by topical application of methimazole, *J. Invest. Dermatol.* 118: 205–207, 2002.
- Kastenmayer RJ, Fain MA, Perdue KA: A retrospective study of idiopathic ulcerative dermatitis in mice with a C57BL/6 background, *JAALAS* 45(6):8–12, 2006.
- Katagiri T, Okubo T, Oyobikawa M, et al.: Inhibitory action of 4-n-butylresorcinol (Rucinol) on melanogenesis and its skin whitening effects, *J. Soc. Cosmet. Chem. Jpn.* 35:42–49, 2001.
- Kazem S, Linssen EC, Gibbs S: Skin metabolism phase I and phase II enzymes in native and reconstructed human skin: a short review, *Drug Discov. Today* 24(9):1899–1910, 2019. <https://doi.org/10.1016/j.drudis.2019.06.002>.
- Kelsh RN: Genetics and evolution of pigment patterns in fish, *Pigm. Cell Res.* 17(4):326–336, 2004.
- Khmaladze I, Leonardi M, Fabre S, et al.: The skin Interactome: a holistic “Genome-Microbiome-Exposome” approach to understand and modulate skin health and aging, *Clin. Cosmet. Invest. Dermatol.* 13:1021–1040, 2020.
- Klein-Szanto AJ, Major SK, Slaga TJ: Induction of dark keratinocytes by 12-O-tetradecanoylphorbol-13-acetate and mezerein as an indicator of tumor-promoting efficiency, *Carcinogenesis* 1(5):399–406, 1980. <https://doi.org/10.1093/carcin/1.5.399>.
- Kloepfer K, McCauley KM, Kirjavainen KE, et al.: The microbiome as a gateway to prevention of allergic disease development, *J. Allergy Clin. Immunol.* 10(9):2195–2204, 2022, <https://doi.org/10.1016/j.jaip.2022.05.033>.
- Kobayashi T, Iwasaki T, Amagai M, et al.: Canine follicle stem cell candidates reside in the bulge and share characteristic features with human bulge cells, *J. Invest. Dermatol.* 130(8): 1988–1995, 2010.
- Kobayashi T, Moro K: Tissue-specific diversity of group 2 innate lymphoid cells in the skin, *Frontiers in Immunology* 13:1–8, 2022.
- Koehler MJ, Vogel T, Elsner P, et al.: In vivo measurement of the human epidermal thickness in different localizations by multiphoton laser tomography. *Skin, Respir. Technol.* 16: 259–264, 2010.
- Langner A, Wolska H, Marzulli FN, et al.: Dermal toxicity of 8-methoxypsoralen administered (by gavage) to hairless mice irradiated with long-wave ultraviolet light, *J. Invest. Dermatol.* 69:451–457, 1977.
- Lazar AJF, Murphy GF: The skin. In Robbins SL, Kumar V, Cotran RS, editors: *Robbins and cotran pathologic basis of disease*, Philadelphia, PA, 2020, Saunders Elsevier, pp 1165–1204.
- Lee DA, Zhong S, Pai R, et al.: Nonclinical safety assessment of a human interleukin-22FC IG fusion protein demonstrates in vitro to in vivo and cross-species translatability, *Pharm. Res. Perspect.* 6(6):e00434, 2018, <https://doi.org/10.1002/prp2.434>.
- Lee YK, Mazmanian SK: Has the microbiota played a critical role in the evolution of the adaptive immune system? *Science* 330(6012):1768–1773, 2010.
- Levine A, Markowitz O: Introduction to reflectance confocal microscopy and its use in clinical practice, *JAAD Case Rep.* 4(10):1014–1023, 2018, <https://doi.org/10.1016/j.jidcr.2018.09.019>.
- Lovell WW, Sanders DJ: Phototoxicity testing in Guinea-pigs, *Food Chem. Toxicol.* 30:155–160, 1992.
- Lynch AM, Wilcox P: Review of the performance of the 3T3 NRU in vitro phototoxicity assay in the pharmaceutical industry, *Exp. Toxicol. Pathol.* 63:209–214, 2011.
- Mahl JA, Vogel BE, Court M, et al.: The minipig in dermatotoxicology: methods and challenges, *Exp. Toxicol. Pathol.* 57: 341–345, 2006.
- Makinen M, Forbes PD, Stenback F: Quinolone antibacterials: a new class of photochemical carcinogens, *J. Photochem. Photobiol. B* 37:182–187, 1997.
- Maruani A, Machet M-C, Carlotti A, et al.: Immunostaining with antibodies to desmoglein provides the diagnosis of drug-induced pemphigus and allows and prediction of outcome, *Am. J. Clin. Pathol.* 130:369–374, 2008.
- Mascia F, Lam G, Keith C, et al.: Genetic ablation of epidermal EGFR reveals the dynamic origin of adverse effects of anti-EGFR therapy, *Sci. Transl. Med.* 199:1–12, 2013, <https://doi.org/10.1126/scitranslmed.3005773>.

- Masson-Meyers DS, Andrade TAM, Caetano GF, et al.: Experimental models and methods for cutaneous wound healing assessment, *Int. J. Exp. Pathol.* 101(1–2):21–37, 2020.
- Masters BR, So P: Confocal microscopy and multi-photon excitation microscopy of human skin in vivo, *Opt. Express* 8:2–10, 2001.
- Mecklenburg L, Kusewitt D, Kolly C, et al.: Proliferative and non-proliferative lesions of the rat and mouse integument, *J. Toxicol. Pathol.* 26(3 Suppl):27S–57S, 2013.
- Mestas J, Hughes CCW: Of mice and not men: differences between mouse and human immunology, *J. Immunol.* 172: 2731–2738, 2004, <https://doi.org/10.4049/jimmunol.172.5.2731>.
- Meyer W, Schwarz R, Neurand K: The skin of domestic mammals as a model for the human skin, with special reference to the domestic pig, *Curr. Probl. Dermatol.* 7:39–52, 1978.
- Milam EC, Nassau S, Banta E, et al.: Occupational contact dermatitis: an update, *J. Allerg. Clin. Immunol. In Practice* 8(10):3283–3293, 2020.
- Mistry R, Veres M, Issa F: A systematic review comparing animal and human scarring models, *Front. Surg.* 9:711094, 2022, <https://doi.org/10.3389/fsurg.2022.711094>.
- Mitev V, Miteva L: Signal transduction in keratinocytes, *Exp. Dermatol.* 8:96–108, 1999, <https://doi.org/10.1111/j.1600-0625.1999.tb00355>.
- Miyake K, Karasuyama H: Emerging roles of basophils in allergic inflammation, *Allergol. Int.* 66:382–391, 2017, <https://doi.org/10.1016/j.alit.2017.04.007>.
- Morgensen M, Morsy HA, Thrane L, et al.: Morphology and epidermal thickness of normal skin imaged by optical coherence tomography, *Dermatology* 217:14–20, 2008.
- Moll R, Divo M, Langbein L: Review. The human keratins: biology and pathology, *Histochem. Cell Biol.* 129:705–733, 2008.
- Monteiro-Riviere NA, Bristol DG, Manning TO, et al.: Inter-species and interregional analysis of the comparative histologic thickness and laser Doppler blood flow measurements at five cutaneous sites in nine species, *J. Invest. Dermatol.* 95(5):82–586, 1990 Nov.
- National Academy of Sciences Committee for the Revision of NAS Publication 1138. *Principles and procedures for evaluating the toxicity of household substances*, Washington, DC, 1977, National Academy of Science, pp 23–59.
- Nestle FO, Di Meglio P, Qin J-Z, et al.: Skin immune sentinels in health and disease, *Nat. Rev. Immunol.* 9:679–691, 2009.
- Nogales KE, Zaba LC, Guttman E, et al.: Th17 cytokines interleukin (IL)-17 and IL-22 modulate distinct inflammatory and keratinocyte-response pathways, *Br. J. Dermatol.* 159:1092–1102, 2008.
- Nouveau-Richard S, Monot M, Bastien P, et al.: In vivo epidermal thickness measurement: ultrasound vs. confocal imaging, *Skin Res. Technol.* 10:136–140, 2004.
- OECD: Test No. 404: acute dermal irritation/corrosion. In *OECD guidelines for the testing of chemicals, section 4*, Paris, 2015, OECD Publishing, <https://doi.org/10.1787/9789264242678-en>. (Accessed 25 February 2024).
- OECD: Test No. 406: skin sensitisation, *OECD guidelines for the testing of chemicals, section 4*, Paris, 2022, OECD Publishing, <https://doi.org/10.1787/9789264070660-en>. (Accessed 25 February 2024).
- OECD: Test No. 431: in vitro skin corrosion, reconstructed human epidermis (RHE) test method, <https://doi.org/10.1787/9789264264618-en>, 2019a. (Accessed 25 February 2024). [https://www.oecd-ilibrary.org/environment/test-no-431-in-vitro-skin-corrosion-reconstructed-human-epidermis-rhe-test-method\\_9789264264618-en](https://www.oecd-ilibrary.org/environment/test-no-431-in-vitro-skin-corrosion-reconstructed-human-epidermis-rhe-test-method_9789264264618-en).
- OECD: Test No. 432: in vitro 3T3 NRU phototoxicity test. In *OECD guidelines for the testing of chemicals, section 4*, Paris, 2019b, OECD Publishing, <https://doi.org/10.1787/9789264071162-en>. (Accessed 25 February 2024).
- Ono C, Yamada M, Tanaka M: Absorption, distribution and excretion of <sup>14</sup>C-chloroquine after single oral administration in albino and pigmented rats: binding characteristics of chloroquine-related radioactivity to melanin in vivo, *J. Pharm. Pharmacol.* 55:1647–1654, 2003.
- Otberg N, Richter H, Schaefer H, et al.: Variation of hair follicle size and distribution in different body sites, *J. Invest. Dermatol.* 122:14–19, 2004.
- Otsuka M, Egawa G, Kabashima K: Uncovering the mysteries of Langerhans cells, inflammatory dendritic epidermal cells, and monocyte-derived Langerhans cell-like cells in the epidermis, *Front. Immunol.* 9:1768, 2018 Jul 30, <https://doi.org/10.3389/fimmu.2018.01768>.
- Park HY, Ashayerippanah M, Chopin M: Harnessing dendritic cell diversity in cancer immunotherapy, *Curr. Opin. Immunol.* 83:102341, 2023, <https://doi.org/10.1016/j.coi.2023.102341>.
- Park HY, Kosmadaki M, Yaar M, et al.: Cellular mechanisms regulating human melanogenesis, *Cell. Mol. Life Sci.* 66(9): 1493–1506, 2009.
- Pasady SR, Knabel D, Fernandez AP, et al.: Cutaneous adverse effects of biologic medications, *Cleveland Clin J Med* 87(5):288–299, 2020. <https://doi.org/10.3949/cjcm.87a.19119>.
- Peate WF: *Am. Fam. Physician* 66(6):1025–1033, 2002.
- Pedrosa TDN, Catarino CM, Pennacchi PC, et al.: A new reconstructed human epidermis for in vitro skin irritation testing, *Toxicol. Vitro* 42(Aug):31–37, 2017. <https://doi.org/10.1016/j.tiv.2017.03.010>.
- Peña OA, Martin P: Cellular and molecular mechanisms of skin wound healing, *Nat. Rev. Mol. Cell. Biol.*, 25:599–616, 2024, <https://doi.org/10.1038/s41580-024-00715-1>.
- Plikus MV, Chuong C-M: Complex hair cycle domain patterns and regenerative hair waves in living rodents, *J. Invest. Dermatol.* 128(5):1071–1080, 2008, <https://doi.org/10.1038/sj.jid.5701180>.
- Plonka PM, Passeron T, Brenner M, et al.: What are melanocytes really doing all day long, *Exp. Dermatol.* 18(9):799–819, 2009.
- Prescott SL, Larcombe D-L, Logan AC, et al.: The skin microbiome: impact of modern environments on skin ecology, barrier integrity and systemic immune programming, *World Aff. J.* 10:29, 2017.



- Proksch E, Brandner JM, Jensen JM: The skin: an indispensable barrier, *Exp. Dermatol.* 17(12):1063–1072, 2008 Dec.
- Rai V, Moellmer R, Agrawal DK: Clinically relevant experimental rodent models of diabetic foot ulcer, *Mol. Cell Biochem.* 477(4):1239–1247, 2022, <https://doi.org/10.1007/s11010-022-04372-w>. Epub 2022 Jan 28.
- Ramdial PK, Naidoo DK: Drug-induced cutaneous pathology, *J. Clin. Pathol.* 62(6):493–504, 2009 Jun.
- Ramot Y, Kannan K, Reddy R, et al.: Acute histopathologic findings related to needle puncture trauma during subcutaneous injection in the Sprague-Dawley rat model, *Toxicol. Pathol.* 47(1):93–96, 2019a.
- Ramot Y, Nyska A, Lieuallen W, et al.: Inflammatory and chloracne-like skin lesions in B6C3F1 mice exposed to 3,3',4,4'-tetrachloroazobenzene for 2 years, *Toxicology* 265:1–9, 2009b.
- Repetto G, del Peso A, Zurita J: Neutral red uptake assay for the estimation of cell viability/cytotoxicity, *Nat. Protoc.* 3: 1125–1131, 2008, <https://doi.org/10.1038/nprot.2008.75>.
- Richardson R, Slanchev K, Kraus C, et al.: Adult zebrafish as a model system for cutaneous wound-healing research, *J. Invest. Dermatol.* 133(6):1655–1665, 2013.
- Rittié L: Cellular mechanisms of skin repair in humans and other mammals, *J. Cell Commun. Signal.* 10(2):103–120, 2016.
- Rodrigues M, Kosaric N, Bonham CA, Gurtner GC: Wound healing: a cellular perspective, *Physiol. Rev.* 99(1):665–706, 2019.
- Russo E, Bellando-Randone S, Carboni D, et al.: The differential crosstalk of skin-gut microbiome axis as a new emerging actor in systemic sclerosis, *Rheumatology*, 2023:1–9, 2023. <https://doi.org/10.1093/rheumatology/kead208>.
- Salim S, Ali SA: Vertebrate melanophores as potential model for drug discovery and development: a review, *Cell. Mol. Biol. Lett.* 16(1):162–200, 2011.
- Sami DG, Heiba HH, Abdellatif A: Wound healing models: a systematic review of animal and non-animal models, *Wound Med.* 24(1):8–17, 2019, <https://doi.org/10.1016/j.wndm.2018.12.001>. ISSN 2213-9095.
- Sarian MN, Zulkefli N, Che Zain MS, et al.: A review with updated perspectives on in vitro and in vivo wound healing models, *Turk. J. Biol.* 47(4):236–246, 2023.
- Sawada Y: Occupational skin dermatitis among healthcare workers associated with the COVID-19 pandemic: a review of the literature, *Int. J. Mol. Sci.* 24(3):2989, 2023, <https://doi.org/10.3390/ijms24032989>.
- Schaffer JV, Bolognia JL: The melanocortin-1 receptor: red hair and beyond, *Arch. Dermatol.* 137(11):1477–1485, 2001.
- Scheib N, Tiemann J, Becker C, et al.: The dendritic cell dilemma in the skin. Between tolerance and immunity, *Front. Immunol.* 13:929000, 2022, <https://doi.org/10.3389/fimmu.2022.929000>.
- Schencke C, Vasconcellos A, Sandoval C, et al.: Morphometric evaluation of wound healing in burns treated with Ulmo (*Eucryphia cordifolia*) honey alone and supplemented with ascorbic acid in guinea pig (*Cavia porcellus*), *Burns Trauma* 4: 25, 2016. <https://doi.org/10.1186/s41038-016-0050-z>.
- Schneider MR, Schmidt-Ullrich R, Paus R: The hair follicle as a dynamic miniorgan, *Curr. Biol.* 19(3):R132–R142, 2009.
- Seaton M, Hocking A, Gibran NS: Porcine models of cutaneous wound healing, *ILAR J.* 56(1):127–138, 2015.
- Seweryn A: Interactions between surfactants and the skin – theory and practice, *Adv. Colloid Interface Sci.* 256:242–255, 2018, <https://doi.org/10.1016/j.cis.2018.04.002>.
- Shimoda K, Yoshida M, Wagai N, et al.: Phototoxic lesions induced by quinolone antibacterial agents in auricular skin and retina of albino mice, *Toxicol. Pathol.* 21:554–561, 1993.
- Simon GA, Maibach HI: The pig as an experimental animal model of percutaneous permeation in man: qualitative and quantitative observations—an overview, *Skin Pharmacol. Appl. Skin Physiol.* 13:229–234, 2000.
- Sitruk-Ware R: Transdermal delivery of steroids, *Contraception* 39(1):1–20, 1989. [https://doi.org/10.1016/0010-7824\(89\)90012-7](https://doi.org/10.1016/0010-7824(89)90012-7).
- Sonnenberg F, Fouser LA, Artis D: Border patrol: regulation of immunity, inflammation and tissue homeostasis at barrier surfaces by IL-22, *Nat. Immunol.* 12:383–390, 2011.
- Stern RS: Photocarcinogenicity of drugs, *Toxicol. Lett.* 102–103: 389–392, 1998.
- Struwe M, Greulich KO, Junker U, et al.: Detection of photogenotoxicity in skin and eye in rat with the photo comet assay, *Photochem. Photobiol. Sci.* 7:240–249, 2008.
- Sueki H, Gammal C, Kudoh K, et al.: Hairless Guinea pig skin: anatomical basis for studies of cutaneous biology, *Eur. J. Dermatol.* 10:357–364, 2000.
- Sulaimon SS, Kitchell BE: The biology of melanocytes, *Vet. Dermatol.* 14(2):57–65, 2003.
- Sumigraý KD, Lechler T: Cell adhesion in epidermal development and barrier formation, *Curr. Top. Dev. Biol.* 112:383–414, 2015, <https://doi.org/10.1016/bs.ctdb.2014.11.027>.
- Summerfield A, Meurens F, Ricklin M: The immunology of porcine skin and its value as a model for human skin, *Mol. Immunol.* 66(1):14–21, 2015, <https://doi.org/10.1016/j.molimm.2014.10.023>.
- Swindle MM, Makin A, Herron AJ, et al.: Swine as models in biomedical research and toxicology testing, *Vet. Pathol.* 49: 344–356, 2012.
- Tattersall IW, Leventhal JS: Cutaneous toxicities of immune checkpoint inhibitors: the role of the dermatologist, *Yale J. Biol. Med.* 93(1):123–132, 2020.
- Thye AY-K, Bah Y-R, Law JW-F, et al.: Gut-Skin Axis: unravelling the connection between the gut microbiome and psoriasis, *Biomedicines* 10(5), 2022. <https://doi.org/10.3390/biomedicines10051037>.
- Trüeb RM: Chemotherapy-induced alopecia, *Semin. Cutan. Med. Surg.* 28:11–14, 2009.
- van Kranen HJ, Westerman A, Berg RJ, et al.: Dose-dependent effects of UVB-induced skin carcinogenesis in hairless p53 knockout mice, *Mutat. Res.* 571:81–90, 2005.
- Uhm C, Jeong H, Lee SH, et al.: Comparison of structural characteristics and molecular markers of rabbit skin, pig skin, and reconstructed human epidermis for an ex vivo

- human skin model, *Toxicol. Res.* 39:477–484, 2023, <https://doi.org/10.1007/s43188-023-00185-1>.
- Walsh KM, Gough AW: Hypopigmentation in dogs treated with an inhibitor of platelet aggregation, *Toxicol. Pathol.* 17: 549–553, 1989.
- Welle MM: Basic principles of hair follicle structure, morphogenesis, and regeneration, *Vet. Pathol.* 60:732–747, 2023, <https://doi.org/10.1177/03009858231176561>.
- Welle MM, Wiener DJ: The hair follicle: a comparative review of canine hair follicle anatomy and physiology, *Toxicol. Pathol.* 44(4):564–574, 2016, <https://doi.org/10.1177/0192623316631843>.
- Welle MM, Linder KE: The integument. In Zachary JF, editor: *Pathologic basis of veterinary disease*, 7th ed., St. Louis, MO, 2022, Elsevier, pp 1095–1262.
- Widhiati S, Purnomosari D, Wibawa T, et al.: The role of gut microbiome in inflammatory skin disorders: a systematic review, *Dermatol. Rep.* 14(1):9188, 2022, <https://doi.org/10.4081/dr.2022.9188>.
- Willard-Mack C, Ramani T, Auletta C: Dermatotoxicology: safety evaluation of topical products in minipigs: study designs and practical considerations, *Toxicol. Pathol.* 44(3): 382–390, 2016, <https://doi.org/10.1177/0192623315622585>.
- Williams EL, Gadola S, Edwards CJ: Anti-TNF-induced lupus, *Rheumatology* 48:716–720, 2009.
- Wong VW, Sorkin M, Glotzbach JP, et al.: Surgical approaches to create murine models of human wound healing, *J. Biomed. Biotechnol.*, 2011, <https://doi.org/10.1155/2011/969618>, 969618.2011. Epub 2010 Dec 1.
- Yaar M, Gilchrest BA: Aging versus photoaging: postulated mechanisms and effectors, *J. Invest. Dermatol. Symp. Proc.* 3(1):47–51, 1998.
- Youssef KK, Van Keymeulen A, Lapouge G, et al.: Identification of the cell lineage at the origin of basal cell carcinoma, *Nat. Cell Biol.* 12:299–305, 2010.
- Zhang LJ. In Blumenberg M, editor: *Keratins in skin epidermal development and diseases in keratin*, 2018, <https://doi.org/10.5772/intechopen.79050>.
- Zhou L, Jiang A, Veenstra J, et al.: The roles of skin Langerhans cells in immune tolerance and cancer immunity, *Vaccines* 10(9):1380, 2022. <https://doi.org/10.3390/vaccines10091380>.
- Zindle JK, Wolinsky E, Bogie KM: A review of animal models from 2015 to 2020 for preclinical chronic wounds relevant to human health, *J. Tissue Viability* 30(3):291–300, 2021.
- Zschaler J, Schlorke D, Arnhold J: Difference in innate immune response between man and mouse, *Crit. Rev. Immunol.* 34:433–454, 2014, <https://doi.org/10.1615/CritRevImmunol.2014011600>.

# Mammary Gland

Suzanne E. Fenton<sup>1</sup>, Schantel Hayes Bouknight<sup>2</sup>

<sup>1</sup>Center for Human Health and the Environment, NC State University, Raleigh, NC, United States, <sup>2</sup>Charles River Laboratories, Durham, NC, United States

## OUTLINE

<b>1. Introduction</b>	<b>584</b>	<i>4.2. Molecular and Biochemical Responses</i>	616
<b>2. Mammary Gland Structure and Function</b>	<b>585</b>	<i>4.3. Morphological Indicators</i>	616
2.1. Stages of Development	585	<b>5. Mechanisms of Toxicity</b>	<b>621</b>
2.2. Variation in Development Across Species	589	<b>6. Conclusion</b>	<b>622</b>
2.3. Endocrine and Paracrine Modifiers of Development	597	<b>Appendix: Preparation and Evaluation of Mammary Gland Whole Mounts in Mice and Rats</b>	<b>622</b>
2.4. Functional Outcomes	601	1. Collection of the Intact Mammary Gland	622
<b>3. Evaluation of Mammary Gland Toxicity</b>	<b>603</b>	2. Fixing and Staining Whole Mounts	624
3.1. In Vitro Techniques	606	3. Suggested Evaluation Methods for Mammary Gland Whole Mounts	625
3.2. Commonly Used Animal Models	606	<b>Acknowledgments</b>	<b>630</b>
3.3. Physiologic Outcomes	610	<b>References</b>	<b>630</b>
3.4. Morphological Evaluations	612		
3.5. Biochemical Indicators and Biomarkers	613		
<b>4. Responses to Injury</b>	<b>615</b>		
4.1. Physiologic Responses	615		



## Abbreviations

3D 3-dimensional

AhR aryl hydrocarbon receptor

AR androgen receptor

ATSDR Agency for Toxic Substances and Disease Registry

BPA bisphenol A

CDER Center for Drug Evaluation and Research

CRISPR clustered regularly interspaced short palindromic repeats

DART developmental and reproductive toxicology

DCIS ductal carcinoma in situ

DMBA 1,2-dimethylbenz[a]anthracene

EGF epidermal growth factor

EGFR epidermal growth factor receptor

EOGRTS Extended One-Generation Reproductive Toxicity Study

EPA U.S. Environmental Protection Agency

ER- $\alpha$  estrogen receptor-alpha

ERBB/Her-2 erythroblastic leukemia viral oncogene (tyrosine kinase receptor superfamily)

FDA U.S. Food and Drug Administration

GEM Genetically Engineered Mice

GH growth hormone

H&E hematoxylin and eosin

HPG hypothalamic-pituitary-gonadal

ICH International Council for Harmonisation

IGF insulin-like growth factor

INHAND International Harmonization of Nomenclature and Diagnostic

IRIS Integrated Risk Information System

LEF/TCF lymphoid enhancer-binding factor/T-cell factor

LOEL lowest observable effect level

MMP matrix metalloproteinase

MMTV mouse mammary tumor virus

MOG modified one-generation

MSX estrogen-regulated homeobox transcription factor

NHP nonhuman primate

NMU N-nitrosomethylurea

NTP National Toxicology Program

OECD Organisation for Economic Co-operation and Development

PCNA proliferating cell nuclear antigen

PFOA perfluorooctanoic acid

PhiP 2-amino-1-methyl-6-phenylimidazo[4,5-b]pyridine

PR progesterone receptor

PTHrP parathyroid hormone-related protein

TBX T-box transcription factor

TEB terminal end buds

TGF transforming growth factor

US United States

VDR vitamin D receptor

WNT wingless-related integration site/*Beta*-catenin

## 1. INTRODUCTION

The mammary gland is a unique organ system in that it begins development in utero and does not complete its development until adulthood, which can be a span of 14–20 years in women or longer when lactation and involution are considered (Russo and Russo, 2004; Macias and Hinck, 2012). Because of this long developmental period, the mammary gland is at increased risk for perturbations from environmental, pharmaceutical, nutritional, consumer product- and stress-related modifiers compared to other organs which are mature at birth or soon thereafter. Historically, adverse outcomes of the breast have focused strictly on cancer (particularly as it relates to incidence in aged populations), but in recent decades, a shift toward significantly earlier timing of breast development during puberty (thelarche), associations of environmental contaminant exposure with insufficient lactation, and a steady increase in incidence of breast disease in *young* women have been reported (Kay et al., 2022).

The breast is the most common site of invasive cancer and the leading global cause of cancer-related mortality in women (Sung et al., 2021; Lima et al., 2021), and in the United States

(US), when considering women under age 50, breast cancer is the leading cancer diagnosis and cause of death (Ward et al., 2019; Siegel et al., 2022). Between 2000 and 2018, there was a significant 0.6% increase per year in breast cancer incidence in US women under 40 years of age. As such, there is a growing concern about the potential causes and risk factors, including those from environmental exposures, drugs, consumer product use, or diet that may contribute to the development or progression of this deadly disease. Lifetime exposure to estrogens (i.e., early age of menarche, older age at menopause, nulliparity, unopposed estrogen) and genetics (family history of breast/ovarian cancer) are known factors that increase risk for breast cancer, and early age of first pregnancy (<22 years-old) is associated with decreased risk (IBCERCC, 2013). Other biological indices, such as obesity and breast density, are highly correlated with risk of breast cancer and may also be affected by environmental factors.

The interplay of reproductive and hormonal influences on mammary gland cancer risk generally holds across species. For example, mammary cancer is the most common malignant cancer in intact female dogs greater than 6 years old. Spaying (i.e., performing ovariectomy)

prior to first estrus essentially negates the risk, while risk increases when spaying occurs after consecutive cycles (Antuofermo et al., 2007). In macaques, the role of reproductive status is not clearly defined, but mammary gland biology and breast cancer development are generally comparable to that in women. In a population of captive macaques, the lifetime risk for breast cancer was estimated to be about 6% and considered comparable to women (1 in every 8 women, or 12%). The types of cancer, intraductal carcinomas and invasive and metastatic cancers, are also morphologically similar to those in women (Wood et al., 2006; Beck et al., 2014). The role of estrogens and progestins in mammary proliferation are also comparable in macaques and women. In experimental studies in castrated cynomolgus and rhesus macaques, estrogen treatments alone stimulated epithelial proliferation, progesterone treatments alone had negligible effects, while both estrogen and progesterone treatment together stimulated proliferation exceeding that of estrogen alone (Cline et al., 1996).

In rodents, hormonal and reproductive status and genetics have significant effects on the development of mammary cancer (more details in Russo and Russo, 1996; Shepel and Gould, 1999; Planas-Silva et al., 2008). Mammary cancer can be induced with estrogen treatment in both rats and mice (to varying degrees depending on the strain) and incidence of mammary cancer increases with age in many strains of rats. In rats, as in women, pregnancy in early adulthood is protective, although pregnancy does not have the same protective effect in all strains of mice. Mice also deviate from rats, monkeys, and women in that the most common types of mammary cancer in mice are lobuloalveolar, noninvasive, and not metastatic. In contrast, mammary cancers in women, female monkeys, dogs, and rats are ductular, derived from the stem-derived cells of the terminal ductal units, and are invasive and malignant (Alvarado et al., 2017; Ferreira et al., 2023).

Animal studies have determined that there are “windows of susceptibility” during mammary gland development during which external influences may enhance the predisposition to cancer later in life (Fenton, 2006). These same periods of development may be responsible for environmental modification of thelarche timing, lactational sufficiency, as well as mammary density or fibrosity, all of which modify risk of cancer

in the mammary gland. Consequently, methods in safety assessment and hazard identification using animal models should be designed to assess developmental and young adult mammary abnormalities, as well as preneoplastic and neoplastic changes in adults. The purpose of this chapter is to provide an overview of mammary gland biology of different species with relevance to humans, and review models, methods, mechanisms and definitions of mammary gland toxicity and carcinogenicity.

## 2. MAMMARY GLAND STRUCTURE AND FUNCTION

While there are marked anatomical differences in the mammary gland across and within species, its development and function in the female—resulting in the production of milk for nourishment of offspring—is generally recapitulated across all mammals. Mammary glands are a complex organ composed of epithelial lined ducts and alveoli within an adipose-based fat pad and surrounded by fibroblasts, immune/inflammatory cells, and lymphatics and blood vessels (nutrient/oxygen supply). The epithelium is a bilayer of luminal cells and basal myoepithelial cells arranged on a basement membrane. The luminal cells are secretory, and the basal myoepithelial cells have multiple functions including contraction, adhesion, and structural formation of the ducts. Mammary development resembles that of epidermal appendage sweat glands (see *Integument*, Vol 5, Chap 7) but is under control of pituitary and gonadal hormones in addition to the influences of hormones produced by other cells of the mammary fat pad (see *Adipose Tissues*, Vol 4, Chap 6). These hormonal influences (Hannan et al., 2023) transition the gland through numerous phases of growth, differentiation, involution, and atrophy, and have varied effects on males and females.

### 2.1. Stages of Development

While differences are observed in the morphology and hormonal controls of mammary gland development across species, there are fundamental similarities that are important to initially define. Mammary gland development has distinct anatomical and functional changes during embryogenesis and prepuberty that include bud formation and early ductal tree



formation, and during postpuberty and pregnancy that include ductal elongation, lobuloalveolar differentiation, pregnancy and lactation.

**Bud and ductal tree formation:** Gland formation begins early during embryogenesis with the development of linear bilateral ectodermal thickenings, referred to as the mammary line or ridge, which overlie a specialized mesoderm. The ectodermal cells of the ridge migrate and aggregate, forming “mammary epithelial buds” at the location of the future mammary gland. These solid ectodermal cords grow into the underlying mesenchyme, followed by limited epithelial branching and canalization, to form mammary sprouts. Support structures, including adipose tissue, which later forms the fat pad containing blood vessels, lymphatics, and connective tissue, develop from mesenchyme coincidental with mammary bud development. Myoepithelial cells that eventually surround epithelial structures (ectoderm) and nerves (neuroectoderm) differentiate separately, but simultaneously, with the mammary buds. There are some species differences in the number and complexity of sprouts prior to birth as sprouts form the papillary ducts of each gland. Each sprout also communicates externally with epithelium that will form the teat/nipple. Some species have collecting ducts that drain multiple primary ducts into a teat (mice, cows), whereas the human has numerous ducts that drain directly into the nipple.

**Ductal elongation:** Initial growth of the gland occurs through linear ductal elongation promoted by a distinct bulbous structure at the distal end of the duct called the “terminal end bud” (TEB) (Figure 8.1). TEBs are composed of three to six layers of medium-sized epithelial cells with scant cytoplasm and oval nuclei, and myoepithelial cells line the basement membrane and interact closely with the surrounding mesenchymal stroma of the fat pad to determine length and patterning of the gland. The leading portion of the TEB is covered by a distinct layer of “cap cells” overlying more numerous layers of “body cells” (evident in TEB cross-section in Figure 8.1C), each containing stem cells with the capacity to form ductal or luminal alveolar cell types. TEBs are discernible from terminal ends of the duct both due to their dense staining and size ( $\geq 100\ \mu\text{m}$ ; see Figure 8.1B). Canalization occurs at the trailing end of the duct to form a single layer of luminal cuboidal epithelial cells and basally located myoepithelial cells supported by a distinct basement membrane. A continuous basement membrane is principally

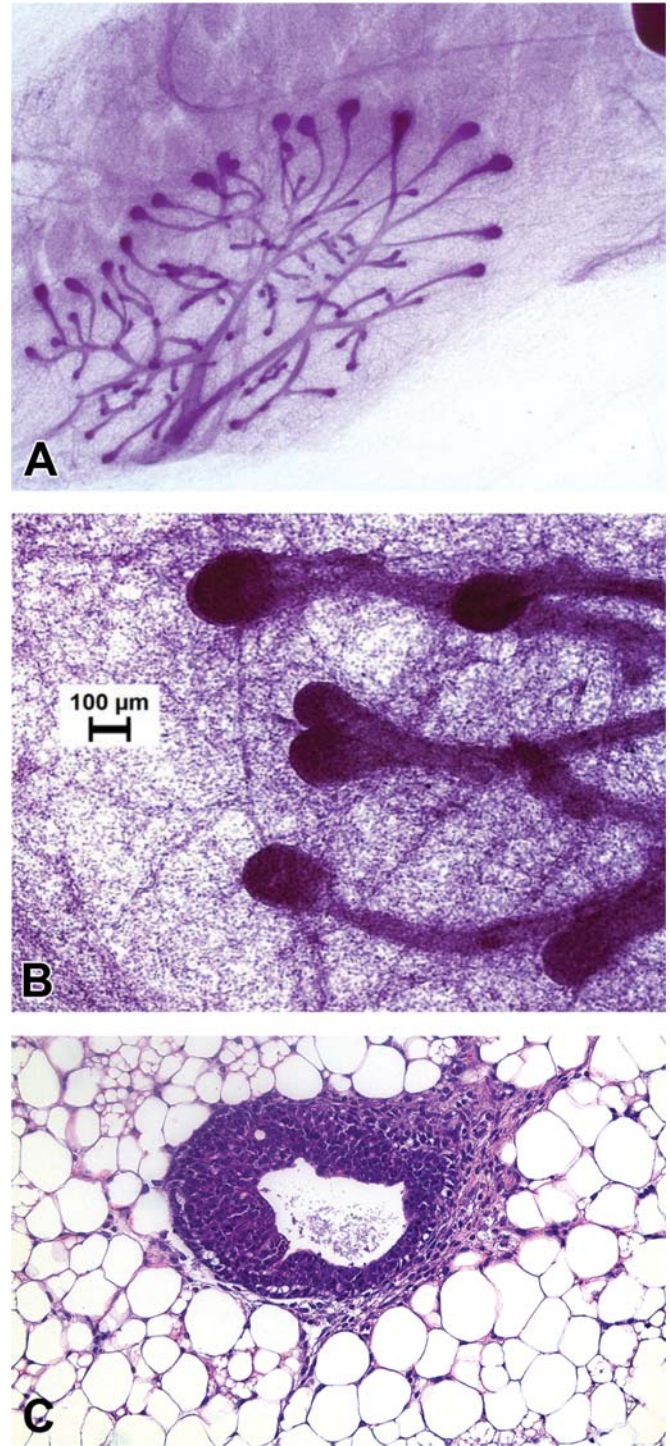


**FIGURE 8.1** Peripubertal mouse female mammary gland showing terminal end bud (TEB) and duct morphology. (A) Carmine alum-stained whole mount of mammary gland with many TEBs at leading edges filling the surrounding fat pad. (B) Higher magnification of the TEBs showing bulbous end and bifurcation. (C) Hematoxylin and eosin-stained paraffin section of a TEB showing the single layer of TEB cap cells (outer ring) and multilayered preluminal body cells. The cap cells often seem artifactually separate from the body cells during processing. There is also often an increased stromal cellularity (inflammatory cells and fibroblasts) along the neck. TEBs should not be confused with foci of hyperplasia in young animals.



composed of type IV collagen, laminin, nidogen, and heparin sulfate proteoglycan. Both luminal epithelial and myoepithelial cells produce laminin1 subunit chains, distinguished by type: epithelial cells deposit  $\alpha 3$  and  $\alpha 5$  chains, and myoepithelial cells deposit  $\alpha 1$  chains. The stroma surrounding the ducts consists of fibroblasts, adipocytes, macrophages, and eosinophils. The stromal cells support ductal elongation and branching. Functionally and microscopically, mammary gland morphology and duct elongation is characterized as both a proliferative and an apoptotic process. Cell sorting and single cell sequencing techniques have been utilized to develop common and novel markers for shared cell types in mammary gland tissue across species (Virtanen et al., 2021; Henry et al., 2021).

**Lobuloalveolar differentiation:** In all species, there is extensive growth of the mammary gland and branching of TEBs into lobular structures during adolescence. Although there are species differences in specific ages and rates of growth, in all species, exponential mammary epithelial growth and development is ignited just prior to other outward signs of puberty and is coincident with a relative burst of ovarian hormones. In most species, including humans, rapid mammary development occurs prior to cycling, suggesting that more than just ovarian hormones control this process. In the young female adult rat, mammary epithelium is arranged into “lobules” of compound branched alveolar sacs, separated by dense interlobular connective tissue and fat (Figure 8.2). Lobules are arranged into distinct lobes with its own excretory duct, also called the lactiferous duct (shown in cross-section; Figure 8.2C), which has its own opening on the teat or nipple via the papillary duct. Cuboidal basal and superficial columnar epithelial cells line the lactiferous duct. The secretory units of lactation are alveoli, which respond to hormonal signals, and begin to develop during pregnancy. An alveolus is lined by secretory cuboidal or columnar epithelium and an outer layer of myoepithelial cells that lie between the epithelium and the basement membrane.

In all mentioned species, changes in the extent of lobule formation may vary with the stage of the estrous/menstrual cycle. In young adult rodents with 4–5 day estrous cycles, there are only subtle changes in mammary gland morphology but as rodents age or experience periods of progesterone-prominent pseudopregnancy, glands will have more extensive budding and lobular formation. In female dogs that have longer estrogen and progesterone-influenced estrous

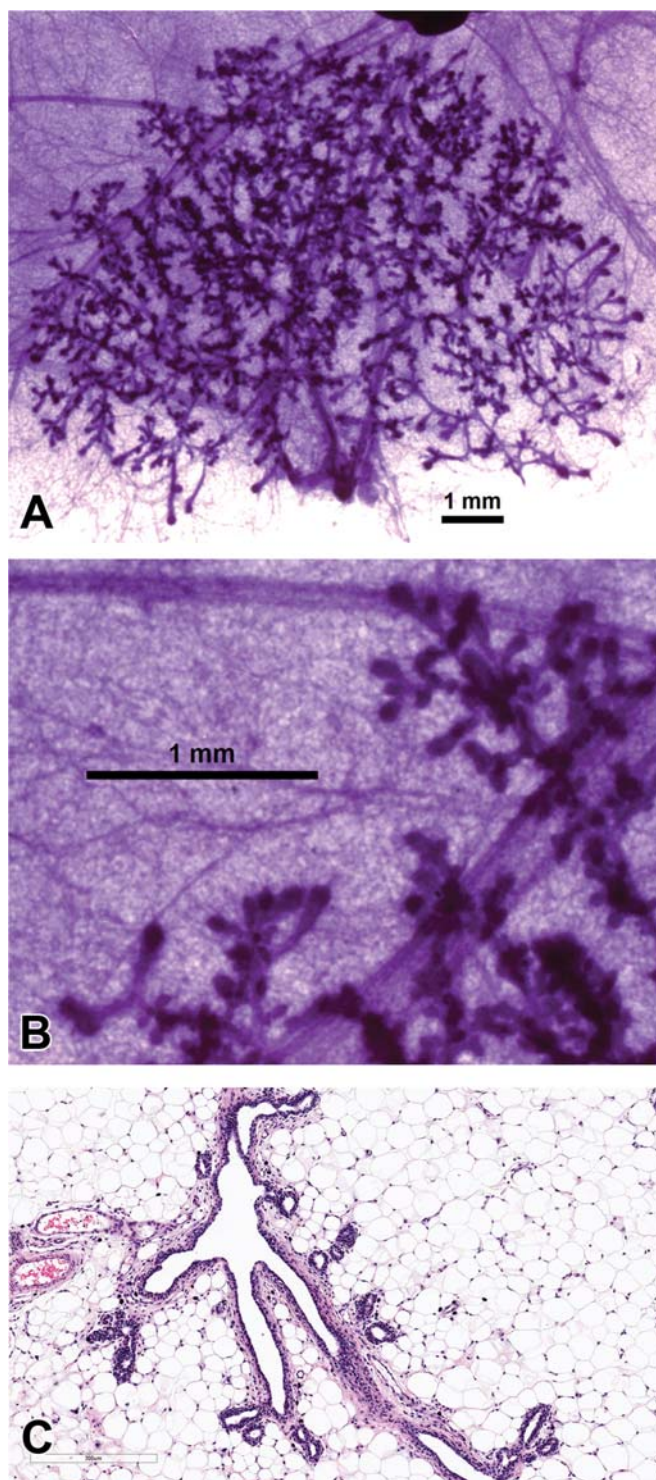


**FIGURE 8.2** Female rat mammary gland at 3 weeks of age showing alveolar buds and duct morphology. (A) Carmine alum-stained whole mount of mammary gland with many branching ducts and alveolar buds filling the fat pad. (B) Higher magnification of branching ducts with alveolar buds. (C) H&E-stained paraffin section of lactiferous duct showing a single layer of cuboidal epithelial cells along the lumen, supported by stromal fibroblasts and myoepithelial cells in an organized fat pad. Panels A and B reproduced from Haschek WM, Rousseaux CG, Wallig MA, editors: Haschek and Rousseaux's handbook of toxicologic pathology, ed 3, 2013, Academic Press, Figure 61.2, p. 2668, with permission.



cycles, mammary gland morphology can vary dramatically from a ductular proliferative state during proestrus and estrus to an alveolar secretory state in diestrus. Because of this, experiments with cycling females should always be conducted with consideration for cycle stage at necropsy.

*Pregnancy and lactation:* Marked epithelial development and differentiation continues through pregnancy and lactation (rat and mouse shown in [Figure 8.3](#)). During pregnancy, extensive epithelial growth and lobular complexity occurs, forming mature alveoli that are required

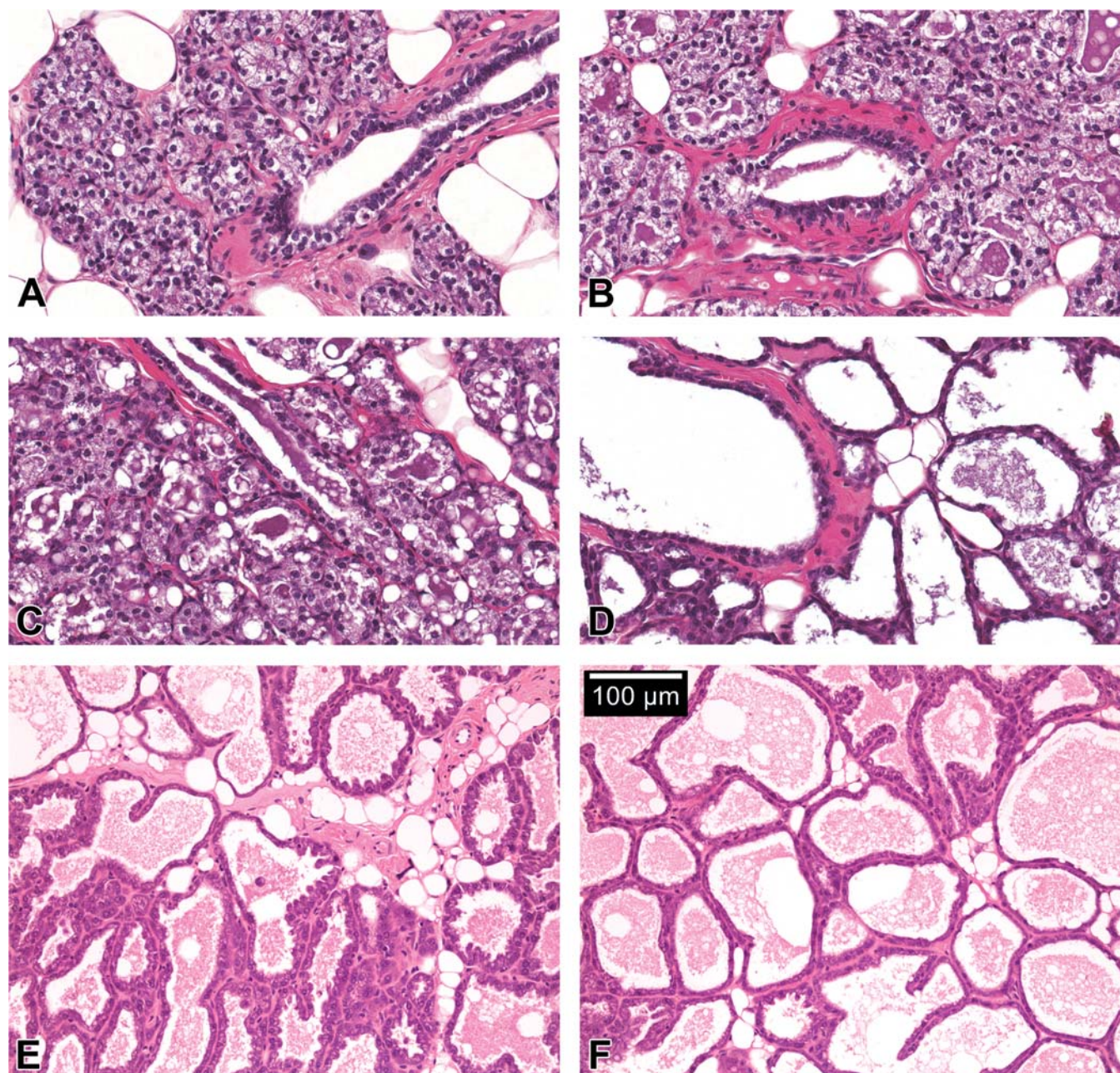


**FIGURE 8.3** (A–D) The pregnant and lactating rodent mammary gland. Harlan Sprague–Dawley (HSD) rat mammary gland H&E-stained paraffin section representing (A) pregnancy day 15, (B) pregnancy day 17, (C) the day of parturition (21 days pregnant), and (D) the fourth day of lactation (40×). Note increasing epithelium and secretory lipids and proteins as time passes. Alveoli become lined by low cuboidal epithelium, surrounded by a layer of myoepithelial cells, a basement membrane and a network of capillaries and lymphatics. (E–F) Lactating CD-1 mouse mammary gland at postnatal day (PND) 10 from (E) 1 mg/kg body weight PFOA-exposed and (F) control dams (40×). Adapted from Filgo AJ, Foley JF, Puvanesarajah S et al.: Mammary gland evaluation in juvenile toxicity studies: temporal developmental patterns in the male and female Harlan Sprague–Dawley rat. *Toxicol Pathol.* 44(7): 1034–1058, 2016, Figure 7, with permission; (E and F) Reproduced from White SS, Stanko JP, Kato K, et al.: Gestational and chronic low-dose PFOA exposures and mammary gland growth and differentiation in three generations of CD-1 mice. *Environ. Health Perspect.* 119(8):1070–1076, 2011, Figure 2, with permission.



to produce milk. With growth of the gland, there is a concurrent reduction in the amount of intra- and interlobular connective tissue (compare [Figure 8.3 A–D](#)). The secretory alveoli become lined by cuboidal epithelium, surrounded by a layer of myoepithelial cells, basement membrane, and an intimate network of capillaries and lymphatics providing nutrients, hormones, and immune components. The continued growth of the mammary gland during the second half of pregnancy is due to increases in the height of epithelial cells and an expansion of the lumen of the alveoli. The cuboidal epithelial cells produce and secrete milk components ([Figure 8.3C](#)), which are expelled from lobuloalveolar units by contraction of myoepithelial cells. During peak lactation ([Figure 8.3D \[rat\]](#), [F \[mouse\]](#)), adipocytes are rarely observed in rodent mammary gland sections. After weaning or end of suckling, the mammary gland undergoes an apoptotic process called involution by which remaining milk is phagocytized and epithelial cells degenerate. The few remaining alveoli are lined by low cuboidal, nonsecretory epithelial cells and prominent myoepithelial cells. The fraction of the gland composed of stromal cells, adipocytes, and interstitial and connective tissue is increased as involution proceeds. Corpora amylacea, which are small concretions of protein, may be found in alveoli, ducts, or interstitial areas in addition to increased mammary epithelial cell apoptosis ([Davis and Fenton, 2013](#)).

## 2.2. Variation in Development Across Species

Species differences exist primarily in the relative timing of development, the extent and complexities of the ductal and lobuloalveolar development, and in male mammary characteristics ([Ferreira et al., 2023](#)). In females, the primitive state of the epithelial ductal tree and the presence of TEBs in the gland just before and well beyond the activation of the ovarian hormones of puberty are strikingly similar phenotypes across species. As demonstrated in [Figure 8.4](#), one of the most dramatic species differences is found in the extent of postpubertal development and glandular complexities; lobule development starts just after puberty in

adolescent girls and rats but is not apparent in mice until adulthood. [Figure 8.4](#) summarizes and allows for a comparison (described here) of developmental landmarks between female mice, rats, and humans. Understanding these species variations are critical in choosing an appropriate research model and in interpreting the effects of test articles. Such interpretations must also consider the morphologic changes that occur during puberty, estrous cycles, pregnancy, lactation, involution, and aging.

*Rodents:* In the mouse, mammary gland development begins about embryonic day 10.5 with the appearance of the five placode sets on the mammary ridge. Further development occurs along each of the mammary lines from embryonic day 11.5 to day 13.5. The mesenchyme adjacent to the mammary epithelium becomes dense and begins to regulate elongation of the mammary buds. Epithelial cords are formed and continue to elongate as epithelial ends form and grow into the developing fat pad through fetal days 15–16.5. Ductal branches and a lumen form just prior to birth. The adult mouse demonstrates a simple branched epithelial structure in adulthood, with increasing numbers of buds, branches, and simple lobules with successive estrous cycles.

The rat differs from the mouse in that mammary bud development begins about embryonic day 12.5, with six sets of mammary buds present by embryonic day 15.5 that develop into a more complex branched pattern around the time of parturition. Both male and female offspring demonstrate the branched pattern and lumens that are present at the time of birth. Prior to vaginal opening, ductal budding is apparent, and the TEBs begin to cleave into clusters of three to five smaller alveolar buds each with a centrally located lumen surrounded by a layer of cuboidal epithelial cells. Thus, histologically, the mammary gland of the prepubertal female rat is characterized by scattered ducts lined by a single or double layer of cuboidal epithelium, which, after branching several times, becomes multilayered to form the TEBs.

Growth and branching of the mammary structure in rodents continue after birth reaching peak growth rate from 21 to 55 days of age. With each successive estrous cycle, the alveolar buds form complex lobules of smaller diameter with a distinct lumen lined by a single layer of low



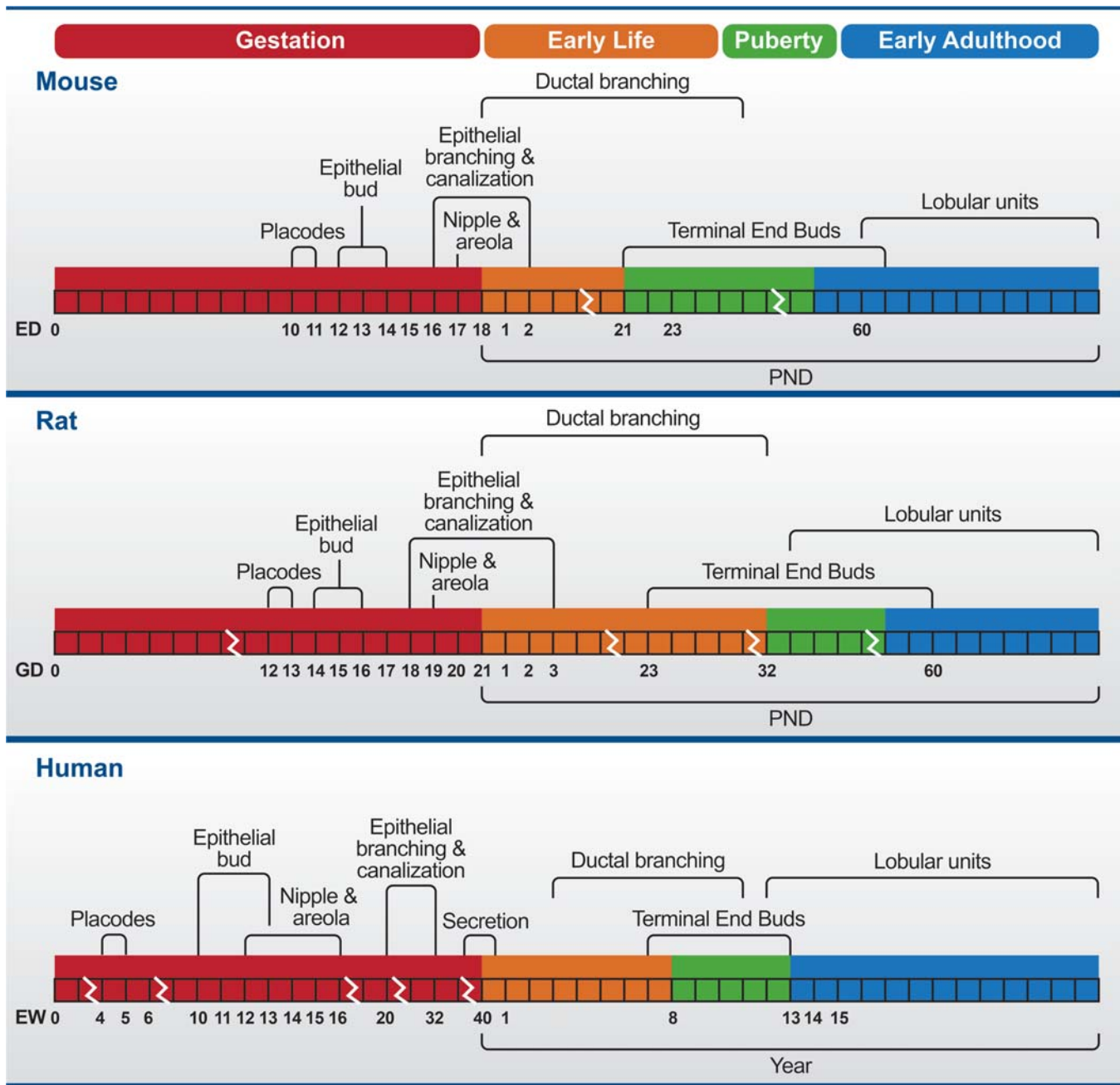


**FIGURE 8.4** Schematic representation of important stages of mammary gland development in female mouse, rat, and human. There are many similarities in the timing and morphological progression across species, especially regarding development of the fetal mammary gland. Epithelial branching occurs between birth and adulthood, with isometric growth (growing at the same pace as the body) prior to puberty and exponential ductal proliferation (growth occurring at a faster pace than the body) during peripuberty and young adulthood. *ED*, embryonic day; *EW*, embryonic week; *GD*, gestation day; *PND*, postnatal day. Modified from Haschek WM, Rousseaux CG, Wallig MA, editors: Haschek and Rousseaux's handbook of toxicologic pathology, ed 3, 2013, Academic Press, Figure 61.3, p. 2670, with permission.

cuboidal epithelium (see examples in Figure 8.2B and C). The glands of mature, virgin female rats are tubuloalveolar, characterized by abundant branching, narrower ducts, and numerous alveolar buds and lobules. As rodents age or experience periods of prolactin and

progesterone-prominent pseudopregnancy, glands will have more extensive budding and lobular formation. There are also slight changes in budding/lobule formation depending on the estrous cycle stage; therefore, stage of cycle should be determined when evaluating

mammary tissue for effects of test articles (see *New Frontiers in Endocrine Disruptor Research*, Vol 3, Chap 12 and *Endocrine System*, Vol 4, Chap 7).

There are some developmental differences between the epithelial structures of the human and rat mammary glands. While there is a constant growth of the female rat ductal and lobular epithelium into the fat pad, in the human, the ductal epithelium grows along connective tissue septa, and rarely do the lobular structures grow into fat tissue. This difference should be considered when test articles influence the effects of parenchyma/stroma in one species or the other. Another difference between these species is that in female rats, the epithelia closest to the nipple is most developed compared to the distal aspects of the gland (last to differentiate). However, in women, development is “labyrinthic,” with differing degrees of development observed in different portions of the breast (Russo, 2015).

When some strains of rats (e.g., Charles River Sprague Dawley or Fischer 344) become middle aged (from 8 to 14 months of age) and reproductive senescence ensues, prolactin levels increase leading to the development of several morphologic changes including inappropriate secretory activity, ectasia of ducts, formation of cysts or galactoceles, epithelial hyperplasia, and periductal fibrosis. The nulliparous female rat mammary gland has considerably less lobular development than in female dogs or primates and is more like the lobular development in the human breast than the simple branched structure of the adult mouse. These similarities and differences are evident in Figure 8.5, showing whole mount preparations of the mouse, rat, and human mammary gland across the life stages.

A major difference across species is noted in male mammary epithelial outgrowth and nipple/areola development. Although the mammary gland becomes a vestigial organ in the male, in general, breast cancer has been reported in male nonhuman primates (NHPs) and dogs on rare occasion, and has also been reported in men, with a lifetime risk of male breast cancer in about 1 in 726 men (American Cancer Society, 2024). In the rodent, the mammary epithelial stalk may be more susceptible to endocrine modulation during development and

retains the capacity to develop cancer in the adult. In male mice, the mammary epithelial rudiment degenerates on or near gestational day 14 in response to condensation of the surrounding mammary mesenchyme, primarily due to a rise in fetal androgen levels. This process leaves only a small remaining stalk of epithelium, but its branching and budding may be affected by estrogenic compounds (see Kay et al., 2022 for summary). There is no nipple or areola formed in either male mice or rats, unlike male dogs, monkeys, and humans. However, prior to puberty (shown at 4 and 21 days of age in Figure 8.6), the mammary gland in male rats is histologically difficult to distinguish from female glands, but there is considerable sexual dimorphism in adulthood (shown at 70 days of age in Figure 8.6). Compared to the tubuloalveolar glands in the adult female rat, the adult male has lobuloalveolar glands lined by a single layer of cuboidal vacuolated epithelial cells, and pseudostratified or stratified epithelium (compare Figure 8.6E and F). The male rat mammary gland epithelium remains smaller in area than the female but is responsive to endogenous and exogenous hormone agonists and antagonists throughout its life (Szabo and Vandenberg, 2021).

**Dogs:** When dogs are used in safety assessment studies, they are usually young and sexually immature, which limits the assessment of reproductive toxicity. Prior to puberty, females have rudimentary glands composed of large interlobular ducts with few laterally projecting TEBs within a dense connective tissue stroma and often cannot be discernible in the dermis. Like other species, marked proliferation of TEBs, linear growth, and tertiary branching into lobes occurs with the onset of puberty, which requires the influence of estrogens and progestins.

In cycling female dogs, the gland of proestrus is essentially quiescent and mostly composed of inactive ducts. Hemosiderin pigment and apoptosis can be observed at this stage. The entire complex of skin and gland is relatively thin when collected and compared during diestrus. Mammary gland morphology varies very little during the next phase (estrus). In some females, very slight/stromal periductal edema and early proliferative changes can be observed (Chandra et al., 2010). During diestrus, there is

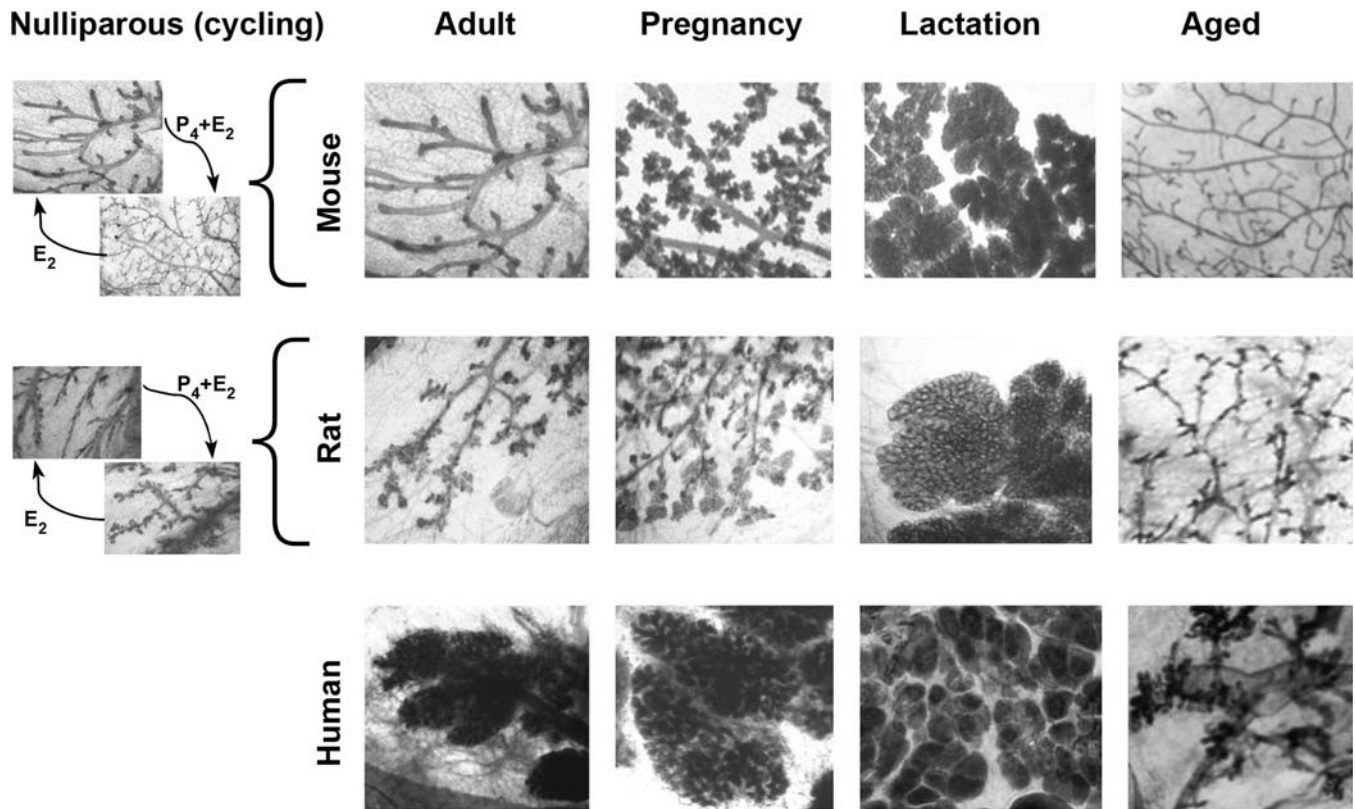


**FIGURE 8.5** Comparison of female mouse, rat, and human mammary gland morphology in critical periods of development. In this comparison of rodent mammary gland and human breast whole mounts over the lifetime, mouse and rat tissues are magnified 1.8 times and human tissue is magnified 2.5 times. Evaluation of similar life stages demonstrates the similarities and differences between the rat and mouse mammary glands and the human breast. In childhood, puberty, and adulthood, the mouse demonstrates a simpler ductal morphology than the rat and human. During adult life, all species demonstrate morphological changes in lobule development characteristics that are reflective of differences in cycle-dependent ovarian hormone levels (E2, estradiol; P4, progesterone). This figure does not show the cyclic changes in the human breast. Numerous morphological similarities are evident across species during pregnancy and lactation. Regression of the mammary ducts and lobules to a static state is seen late in life in all species. Adapted from IBCERCC, 2013. Interagency breast cancer and environmental research coordinating committee (IBCERCC). Breast cancer and the environment: prioritizing prevention. National Institute of Environmental Health Sciences; 2013. [https://www.niehs.nih.gov/sites/default/files/about/assets/docs/breast\\_cancer\\_and\\_the\\_environment\\_prioritizing\\_prevention\\_508.pdf](https://www.niehs.nih.gov/sites/default/files/about/assets/docs/breast_cancer_and_the_environment_prioritizing_prevention_508.pdf) (Last accessed March 1, 2024), Chap 5, Figure 5.1, with permission. Male tissues are not shown due to the lack of representative data in the literature.

marked intralobular ductal epithelial proliferation and formation of many small ductules lined by a multilayered epithelium within loose connective tissue. By default, in the female dog, corpora luteal (CL) function is maintained by prolactin and luteinizing hormone (LH) during the 2 months (approximately 60 days) postovulation regardless of whether the female is pregnant or not (see *Female Reproductive System*, Vol 5, Chap 10). Based on the distinct histological features of the mammary gland during diestrus, Chandra et al. (2010) classified

diestrus into four subphases (diestrus I, II, III, IV). Mammary gland development during phase 1 or the early half of this period (early diestrus if not pregnant, or early pregnancy) is characterized by exuberant stromal proliferation composed of plump fibroblasts arranged in a loose, swirling pattern around basophilic ductular structures. The stroma becomes mucinous and is often accompanied by extravasated erythrocytes and lymphocytic infiltrates. Relative to the stroma, there is glandular tissue composed primarily of plump basophilic, stratified



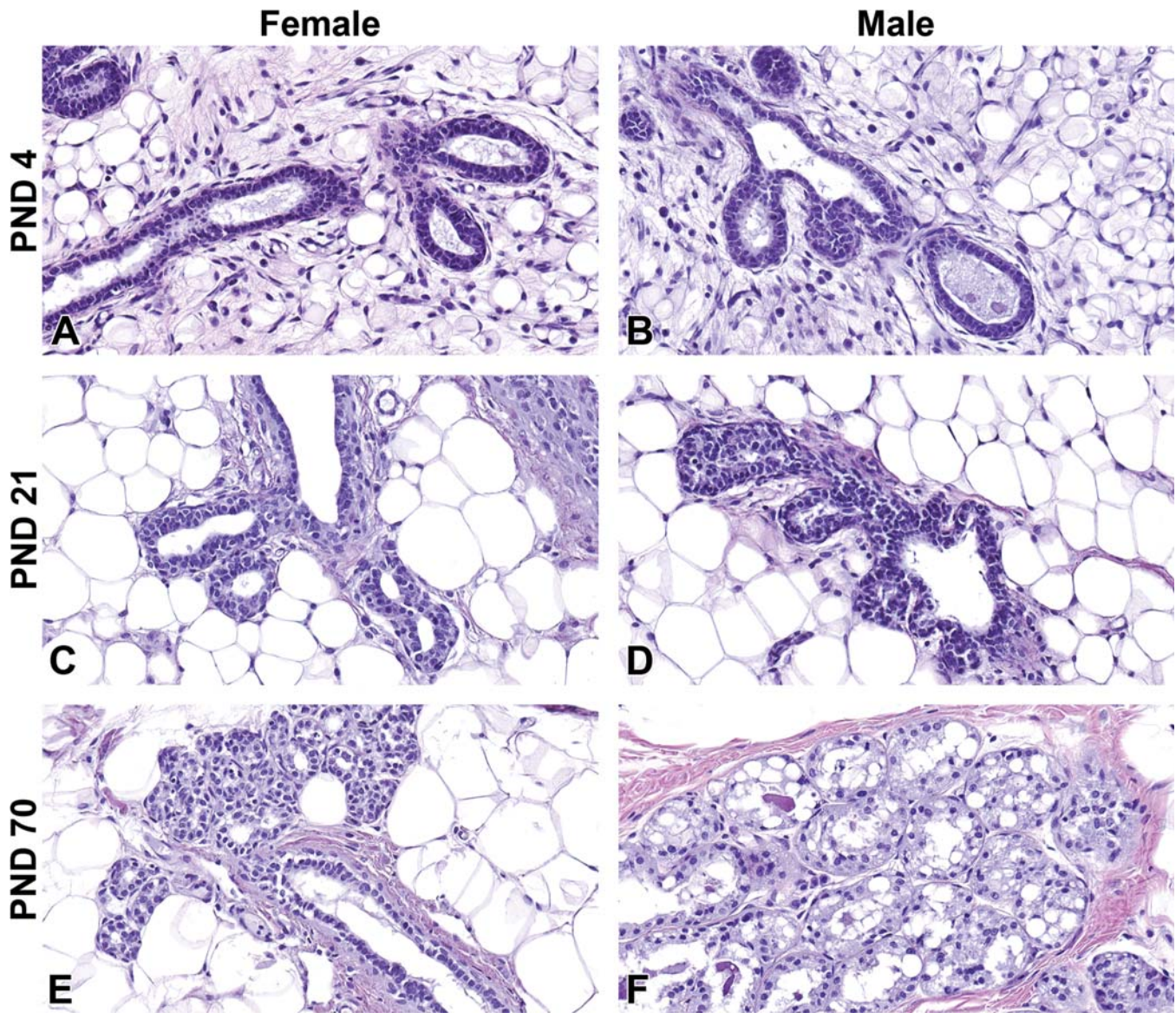


**FIGURE 8.6** Comparison of developing rat mammary gland histology. Images of H&E-stained paraffin sections of female and male mammary gland development in HSD rat offspring from just after birth to sexual maturity. (A) Female and (B) male; at PND 4, mammary gland ducts are lined by a single or double layer of cuboidal epithelial cells 40 $\times$ . (C) Female and (D) male; at PND 21, there is early branching of the mammary epithelium. 40 $\times$ . (E) PND 70 female tubuloalveolar mammary gland, with terminal ductal lobular unit (TDLU) forming, 40 $\times$ . The lobule is composed primarily of ducts and clusters of three to five alveolar buds each with a centrally located lumen surrounded by a layer of cuboidal epithelial cells. (F) By PND 70, the male mammary gland is predominantly lobuloalveolar. Alveoli are prominent and ducts are infrequent. Alveoli and ducts are lined by stratified epithelium that consists of tall vacuolated cuboidal to short columnar epithelial cells. 40 $\times$ . *Reproduced from Filgo AJ, Foley JF, Puvanesarajah S et al.: Mammary gland evaluation in juvenile toxicity studies: temporal developmental patterns in the male and female Harlan Sprague–Dawley rat. Toxicol Pathol. 44(7):1034–1058, 2016, Figures 5 and 6, with permission.*

epithelial cells forming immature ducts and structures that resemble TEB. Increased mitotic activity of epithelial cells is often observed. Mammary glands of pubertal dogs in their first

cycle have similar morphologic features as those observed in diestrus 1. Mammary glands of dogs that have not cycled previously have multiple, discrete foci of undifferentiated, branching ducts

surrounded by faint swirls of basophilic myxomatous stroma. The presence of distended ducts containing eosinophilic secretions (from the previous cycle), a feature lacking in pubertal dogs, and the presence of multiple clusters of dermal adipocytes entrapped in the newly expanding stroma amid the island of newly forming ducts in pubertal dogs are two distinguishing features that can aid in differentiation. During phase II and III, secretory alveoli begin to develop. Alveoli are filled with bright eosinophilic proteinaceous material (milk) and lined by cuboidal to flattened cells and elongated or stellate myoepithelial cells, all supported by minimal intralobular stroma. Stroma is less cellular (mature) and remains prominent around the ducts. Rare mitotic figures and apoptosis can be observed. Morphology of the mammary gland during phase IV can be quite variable in the same dog and between different female dogs. In some dogs, a dual morphology, resembling phase III and early atrophy, can be observed in the same histologic section. If pregnant, the mammary gland is hormonally stimulated by oxytocin and prolactin and becomes secretory. If not pregnant, the mammary gland involutes (anestrus). Involution is characterized by reduction and shrinkage of the alveoli with vacuolated and apoptotic epithelium. In late anestrus, with completely regressed CL, the lobular architecture of the glandular tissue is barely evident as the mammary gland is composed primarily of abundant connective tissue and collapsed ducts. Each of the unique stages are also characterized by distinct estrogen receptor- $\alpha$  (ER- $\alpha$ ) staining of the epithelium (Rehm et al., 2007; Chandra et al., 2010; shown in Figure 8.7). Because of such variations, evaluations of cycling females should always be conducted with consideration for cycle stage.

*Nonhuman primates:* As in female rodents, dogs, and humans, a rudimentary ductal tree is formed early in life in the mammary gland of NHPs. TEBs form the leading epithelial edge, surrounded by myxoid stroma. Most mammary gland development occurs during puberty. In macaques, puberty occurs between 3- and 4-year of age. TEBs contain epithelial cells that are surrounded by myoepithelium and stromal support consisting of fibroblasts and adipocytes. Most of the developing gland is composed of adipose and fibrous connective tissue. The

lactiferous ducts are lined by stratified squamous epithelium as they approach the surface of the nipple, and in the nonlactating animal, they are typically plugged by keratin. As the mammary gland continues to develop, there is rapid elongation and branching of major ducts to form a dense gland of arborized lobuloalveolar units. Thus, even early in puberty with the onset of menstruation, there may be well-differentiated, densely branched lobuloalveolar units lined with secretory epithelial cells, a situation which differs slightly from humans and other species (the others are less developed; Cline and Wood, 2008).

Using nomenclature developed by the Russo's (Russo and Russo, 2004), lobuloalveolar or lobule units in macaque mammary gland can be categorized into types 1, 2, and 3 which consist of up to 11, 47, and 80 ductules per unit, respectively. Generally, the immature lobule type 1 can be formed as early as 2 years before menarche in macaques. The more differentiated lobule type 2 is typically formed closer to menarche. The complexity of the lobuloalveolar units further increases with recurrent menstrual cycles. By early adulthood, the macaque mammary gland is primarily composed of types 1 and 2 lobules. Type 3 lobules can be found in lower numbers but are the predominant type when pregnant or lactating.

Toxicology studies in NHP often employ only a few animals, which may be juveniles just entering puberty. Because the mammary gland of macaques grows so rapidly and invasively at the onset of puberty, care must be taken to avoid erroneously interpreting normal mammary gland development as hyperplasia or neoplasia. Furthermore, there is a high degree of individual variation in the pace of mammary gland development, making animal to animal comparisons difficult if not impossible during this period. Menstrual cycle-related changes are subtle and compartmental; ductal proliferation occurs during the luteal phase of the cycle and alveolar proliferation occurs during the follicular phase, much like estrous cycle variability in rodents (see Figure 8.8). During pregnancy and lactation, extensive alveolar maturation and differentiation to a milk-producing phenotype occurs. Additionally, some macaque species are seasonal breeders (rhesus macaques), and others



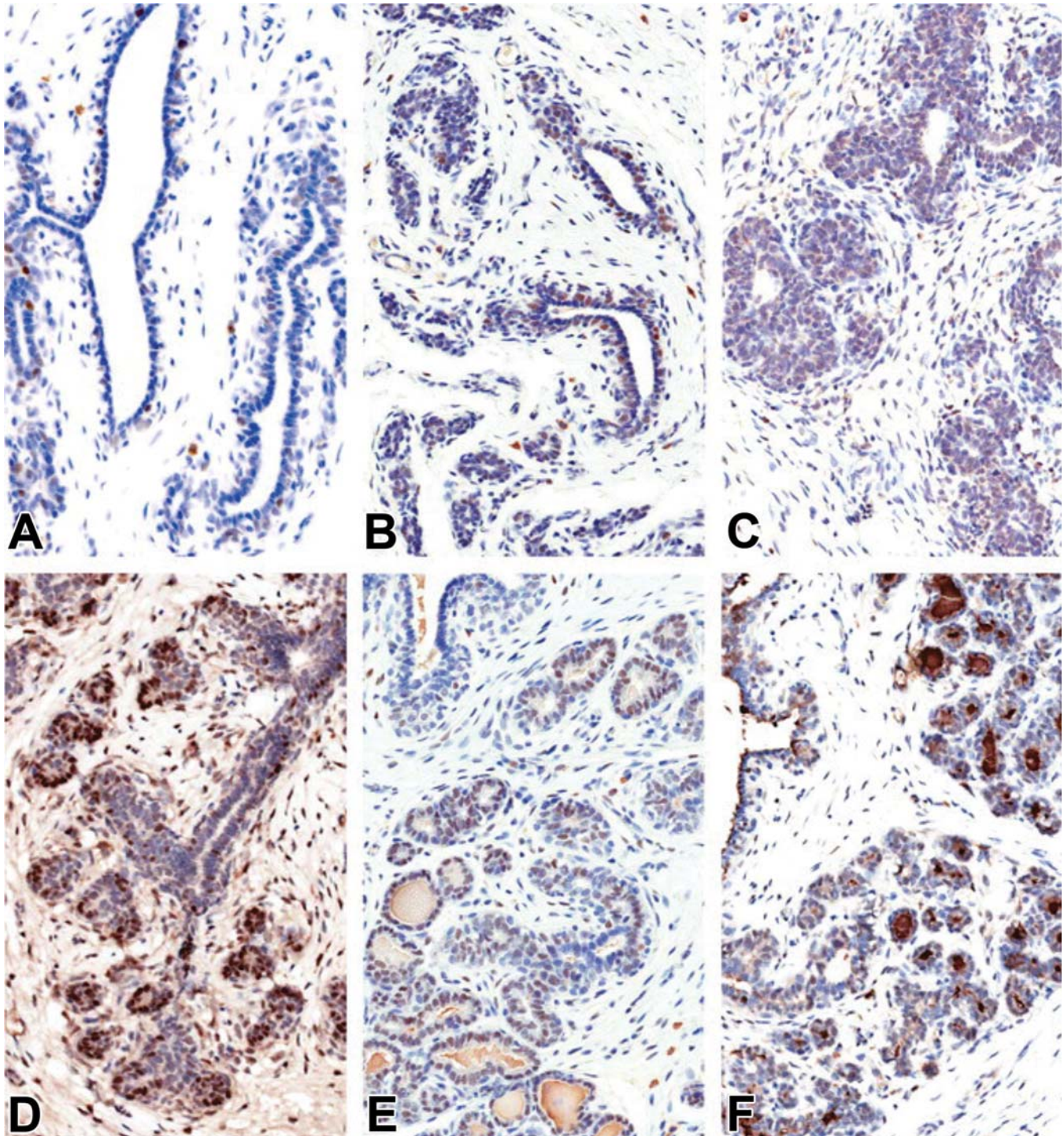


**FIGURE 8.7** Dog mammary gland demonstrating changes over the estrous cycle. Estrogen receptor  $\alpha$  (ER $\alpha$ ) expression in mammary gland of Beagles in anestrus (A), estrus (B), diestrus I (C), diestrus II (D), diestrus III (E), and diestrus IV (F). Note: ER- $\alpha$  was observed in estrus and all four phases of diestrus in both the acinar and ductal epithelial cells, with strongest expression noted in diestrus II. Magnification 40 $\times$ . *Reproduced from Chandra SA, Cline JM, Adler RR: Cyclic morphological changes in the beagle mammary gland. Toxicol Pathol. 38:969–83, 2010, Figure 5, with permission.*



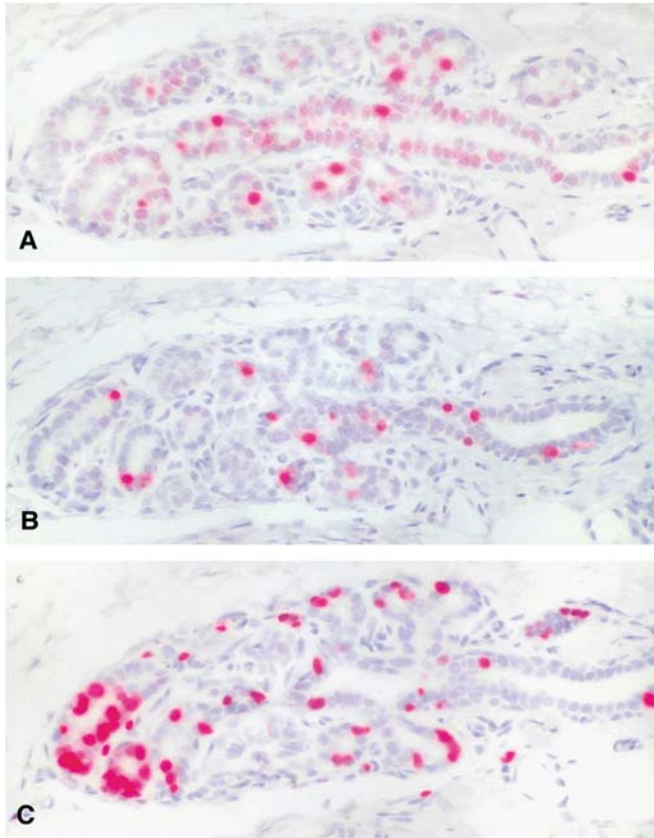


**FIGURE 8.8** Sex steroid receptor expression in a single lobule at the margin of an immature female macaque mammary gland. The cynomolgus macaque mammary gland expresses estrogen receptors  $\alpha$  and  $\beta$  and progesterone receptors (PR) A and B. The receptors are expressed primarily in the lobular and ductal epithelium, most abundant in terminal intralobular ducts. Estrogen receptor  $\alpha$  and PR coexpress in the same cells but are mutually exclusive from cells that are proliferating. Immunohistochemical stain; magnification 40 $\times$ . (A) Estrogen receptor alpha; (B) progesterone receptor A + B; (C) Ki-67 stain for proliferating cells. *Reproduced from Cline, JM: Assessing the mammary gland of nonhuman primates: Effects of endogenous hormones and exogenous hormonal agents and growth factors. Birth Defects Research (Part B) 80:126–146, 2007, Figure. 5, with permission.*

are not (cynomolgus macaques). This difference is important when considering differences in breeding patterns and hormones at certain seasons. Involution is typically extensive with regression of alveoli to a nulliparous state.

Experimental studies have shown that during aging and menopause, or with surgical castration, the mammary gland regresses into a ductal network with marked lobular atrophy and little

proliferative activity. Atrophic ducts maintain estrogen and progesterone receptors and respond to exogenous steroids for some time. Marmosets do not undergo menopause, so older females will maintain more developed glands over their lifetime, while rhesus macaques reach menopause at about 22–24 years-old, accompanied by atrophic changes in the mammary gland.

**Humans:** Mammary milk lines develop in the embryo as early as 4–5 weeks of gestation and form one pair of mammary placodes. The primary ectoderm bud is present by 12 weeks of gestation (the first trimester, which differs significantly from the timing in mice and rats; see [Figure 8.4](#) for comparison) and small ductal outgrowths as a primitive gland are present at birth (similar to female rodents, dogs, NHPs). Also, rather than forming a single ductal tree, each human anlagen forms several trees initiating at the nipple. Before birth, the specified mammary epithelium grows from the nipple into the fat pad to form a small, branched ductal network. The advancing margins of undifferentiated TEBs are surrounded by a loose myxomatous connective tissue matrix. TEBs express both estrogen receptors by gestational week 30 and progesterone receptors at birth, evidence of the role that steroid hormones play in normal breast development. Of course, this also implies that exposure to endocrine-disrupting compounds that may trigger those receptors during gestation may extend potential deleterious influences on the breast later in life. During childhood and adolescence, breast growth keeps pace with overall body growth until greatly accelerating at puberty.

The age at which girls begin breast development during puberty (thelarche), but not the first menstrual period (menarche), has significantly decreased across continents ([Eckert-Lind et al., 2020](#)), with genetics, nutrition, or increased exposure to natural and synthetic estrogenic compounds all implicated as potential causes. Pubertal development is classified in 5 Tanner stages, which describe breast and pubic hair growth prior to the onset of menarche. Appearance of the breast bud is the first indicator of puberty onset in 90% of girls (Tanner stage B (breast) 2) ([Bruserud et al., 2020](#)). According to median Tanner stages over time, breast development has been reported to occur up to 1–2 years

earlier than it did decades ago across various large cohort studies. Thus, breast development is not only significantly advancing in the human population, but there is also a dissociation between the pubertal hormonal control of the larche and menarche.

### 2.3. Endocrine and Paracrine Modifiers of Development

The complex cellular interactions of mammary gland growth, differentiation, and involution are

initiated by stem cell developmental programs, mediated by paracrine signaling between the epithelium and mesothelium of the fat pad early in development, and further orchestrated by hormones from numerous endocrine systems (Seachrist et al., 2018; Hannan et al., 2023; Figure 8.9 also see *Adipose Tissues*, Vol 4, Chap 6, and *Endocrine System*, Vol 4, Chap 7). Much of our fundamental knowledge of these interactions is defined by studies in mice in response to various hormone treatments and in the use of transgenic, knock out, and clustered

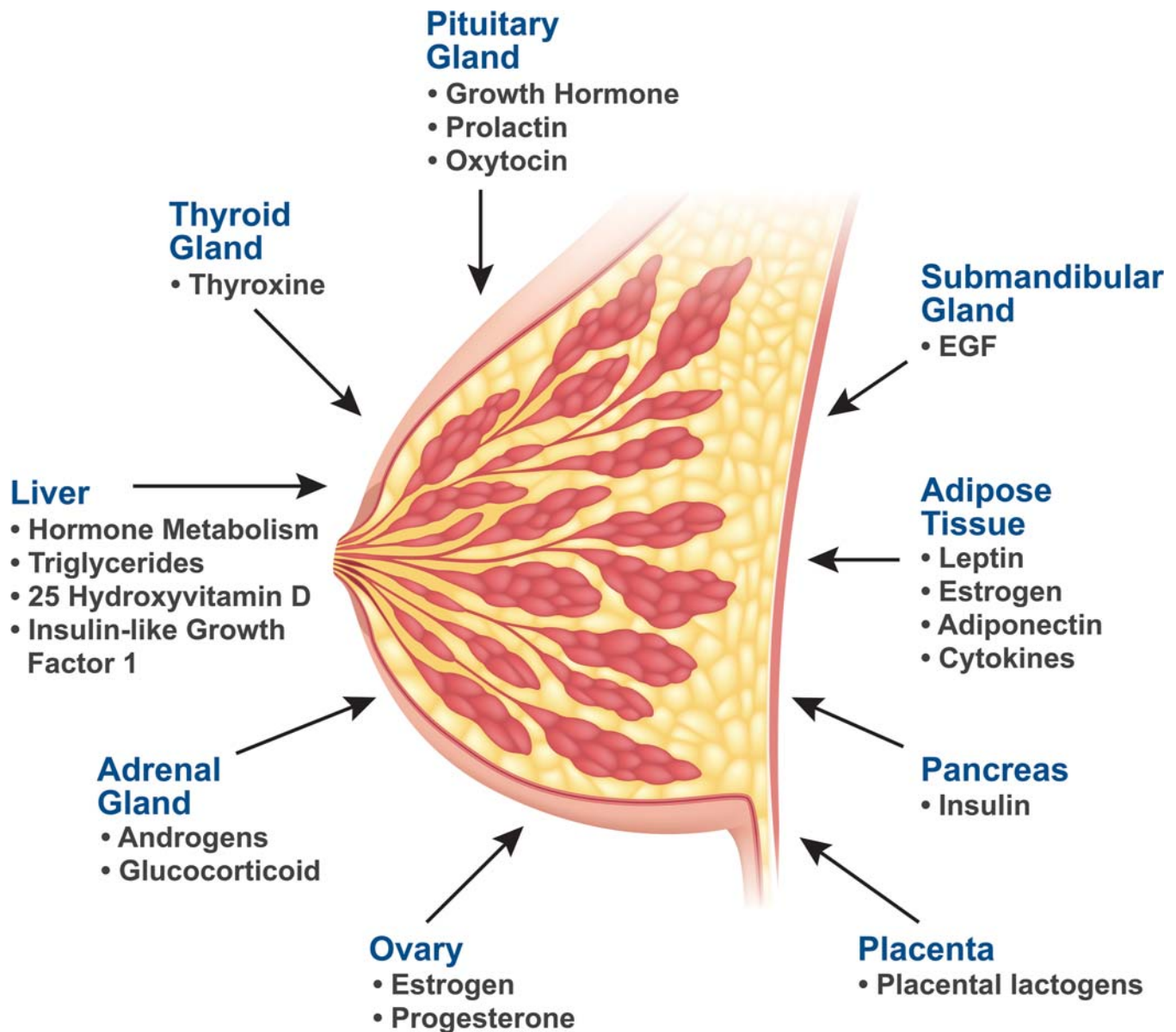


**FIGURE 8.9** Endocrine tissues and their corresponding secreted hormones that influence female breast growth or function through receptor binding or by acting as a precursor to hormones/growth factors produced in mammary tissue. *EGF*, epidermal growth factor.

regularly interspaced short palindromic repeats (CRISPR)-modified mouse models, but there are some species-specific variations in the specific factors, particularly the reproductive hormones, that play major roles in determining the development of this gland. Numerous

studies with hormone receptor deficient (knock-out) or transgenic (gene-modified) mice reveal critical roles for receptor-mediated pathways in mammary gland development and have defined specific mechanistic pathways of effect (see [Table 8.1](#)).

**TABLE 8.1** Mammary Gland Phenotypes in Female Mice Associated With Selected Receptor Deficient/Altered Modifications

Genotype	Null/Defective—Phenotype	Enhanced/Transgenic—Phenotype
ER $\alpha$	Vestigial ducts at nipple; failure of ductal tree to expand	Induces mammary adenocarcinomas
ER $\beta$	No significant pathology	May reduce lesion progression
AR	Overall smaller glands; enlarged/dilated ducts in older adults ( <a href="#">Yeh et al., 2003</a> )	Inhibition of ductal side-branching, dilated primary ducts; promotes luminal phenotype ( <a href="#">Tarulli et al., 2019</a> )
EGFR/HER2-neu	Deficient TEB, deficient ductal growth	Enhanced epithelial proliferation, hyperplastic ducts, metastatic properties
Amphiregulin/TGF- $\beta$ /ErbB2,3,4	Persistent TEB/Deficient lobuloalveolar differentiation and lactation dysfunction	Hyperplastic glands and metastatic focal carcinomas/ErbB4 may deter lesions
Insulin, IGF/IGF-R	Abnormal and decreased branching during early development	Increased mammary tumor risk ( <a href="#">Hadsell and Bonnette, 2000</a> )
PR	Defective ductal side branching in virgin adult; deficient transition from ductular to lobuloalveolar differentiation in pregnancy	PR-A increased side branching, multilayered ducts, loss of basement membrane integrity, altered matrix metalloproteinase activation; PR-B had limited ductal growth but retained the ability to differentiate during pregnancy ( <a href="#">Sampayo et al., 2013</a> )
Prl/Prl-R	Lack of lobular formations in virgin adult/Decreased ductal outgrowth during pregnancy ( <a href="#">Ormandy et al., 2003</a> )	Lactation defects, pup mortality
PTHrP	Failure of the initial round of branching growth that is responsible for transforming the mammary bud into the rudimentary mammary duct system ( <a href="#">Wysolmerski et al., 1998</a> )	Impaired branching morphogenesis during sexual maturity and early pregnancy
GH	Decreased ductal outgrowth during pregnancy	Mammary hyperplasia; intraductal ( <a href="#">Kleinberg et al., 2009</a> )

AR, androgen receptor; EGFR, epidermal growth factor receptor [HER2-neu = human homolog]; ER, estrogen receptor; ErbB, erythroblastosis B (EGFR homologs); GH, growth hormone; IGF, Insulin-like growth factor; IGF-R, Insulin-like growth factor receptor; PR, progesterone receptor; Prl, prolactin; Prl-R, Prolactin receptor; PTHrP, parathyroid hormone related peptide; TEB, terminal end bud; TGF, transforming growth factor.

Modified from Haschek and Rousseaux's *Handbook of Toxicologic Pathology*, third ed. W. M. Haschek, C. G. Rousseaux and M. A. Wallig, eds. (2013) Academic Press, Table 61.1, p. 2674, with permission. Information herein was reported in *Transgenics in Endocrinology* (2001); Palmer CA, Neville MC, Anderson SM, McManaman JL: Analysis of lactation defects in transgenic mice. *J. Mammary Gland Biol. Neoplasia*. 11(3–4):269–282, 2006. doi: [10.1007/s10911-006-9023-3](#). PMID: 17136614; Morato A, Accornero P, Hovey RC: ERBB Receptors and their ligands in the developing mammary glands of different species: fifteen characters in search of an author. *J. Mammary Gland Biol. Neoplasia*. 23;28(1):10, 2023.



*Formation of the rudimentary buds and nipples:* Studies in mice have elegantly demonstrated the coincidental and necessary localization and activation of the canonical Wntless-related integration site/*Beta*-catenin (WNT/ $\beta$ -catenin) signaling pathway in the embryonic mammary placodes to direct stem cells in the surface epithelium toward appendage formation (rather than stratified epidermis differentiation; Hiremath et al., 2012). The canonical WNT pathway involves binding of the WNT ligand to Frizzled receptors and obligate low density lipoprotein receptor-related protein coreceptors. This binding leads to inactivation of the multiprotein axin complex A proteins that function to degrade cytoplasmic  $\beta$ -catenin. As a result of the inhibition,  $\beta$ -catenin accumulates, moves from the cytoplasm to the nucleus, and forms active transcriptional complexes with  $\beta$ -catenin-T-cell factor/lymphoid enhancer-binding factor (LEF/TCF) family members. In the formation of mammary sprouts, WNT gene signaling interacts with several other genes including members of the fibroblast growth factor family, T-box transcription factor TBX3, and estrogen-regulated homeobox transcription factors MSX1 and MSX2. WNT-mediated transcription is also important later in the development of alveolar buds that sprout from the branching TEBs. There is extensive experimental and clinical evidence that dysregulation of WNT signaling is a key feature of mammary cancers.

Nipple formation occurs after formation of the mammary bud epithelium and is an example of one of the earliest mediators of epithelial-mesenchymal cross-talk in mammary gland development. The mammary bud epithelium produces parathyroid hormone-related protein (PTHrP), which is an androgen-regulated protein. Its receptor, PTHR1, is on adjacent mesenchymal cells and activation of this pathway triggers sex-specific development of the nipple/areolae in rodents. The interaction of these molecules is also required for forming the mammary-specific mesenchyme, which in turn is required to form a rudimentary ductal tree (Wysolmerski et al., 1998). In male mice and rats, the fetal androgen surge, which occurs around embryonic day 13–15, respectively, causes the mesenchyme to condense and inhibits the formation of nipples/areolae. In male mice, the androgen surge also causes regression of

the epithelial sprout so that male mice of some strains have no mammary tissue. Several strains (e.g., CD-1 mice) have remaining epithelial stalks with varied numbers of branched ducts and are responsive to estrogenic cues. However, the male rat does form a ductal tree and the male rat mammary gland remains responsive to endogenous and exogenous hormone agonists and antagonists throughout its life (Latendresse et al., 2009; Vandenberg et al., 2013).

In the female, the ductal tree continues to form through androgen and estrogen mediated signaling. Androgens in the female serve as the precursor hormone and are converted to estrogens. Mammary glands of female mice deficient in ER- $\alpha$  develop only rudimentary ductal trees and thus demonstrate the critical role for estrogen-mediated signaling through ER- $\alpha$  in early mammary gland development (Dupont et al., 2000; Gagniac et al., 2020). Mice lacking aromatase, the enzyme necessary for endogenous estradiol production, fail to develop mature glands during puberty (Fisher et al., 1998). Recently, activation of Snail pathway, which controls aromatase expression, has also been implicated in ductal growth and thus provides a mechanism to support estrogen production from androgens within the mammary compartment (Côme et al., 2004).

*Duct elongation and branching:* Epithelial-mesenchymal interactions are equally important in the formation of ductal elongation and branching patterns. Ultimately, the length and complexity of the ducts and the extent of lobuloalveolar proliferation is controlled by the fat pad. The fat pad produces regulatory molecules that promote growth, while inhibiting ducts from overlapping or penetrating adjacent fields by contact inhibition. Among the molecules defined in these interactions, LEF-1, hepatocyte growth factor, keratinocyte growth factor, and neuregulin are factors produced in the mesenchyme that interact with receptors on the epithelial cells to influence mammary epithelial growth. Considerable evidence also indicates that transforming growth factor (TGF)- $\beta$ 1 acts as a key negative regulator of mammary branching by limiting epithelial proliferation and by stimulating extracellular matrix production. Both inhibin and activin growth factors are also involved in epithelial-mesenchymal signaling in mammary gland development. These growth factors are produced

in the stroma to modulate epithelial development, but it is the inhibin beta B subunit signaling that is required for epithelial ductal growth, as well as later alveolar development. Further, the aryl hydrocarbon receptor (AhR)-null and conditionally Arnt-null (targeted during puberty) mice demonstrate retarded mammary proliferation and TEB development, and present with lactational deficits (Le Provost et al., 2002); these effects are also present in dams and offspring when pregnant rats are exposed to dioxin (2,3,7,8-tetrachlorodibenzo-*p*-dioxin) during late gestation (Fenton et al., 2002). Transplant studies suggest an important role of the AhR and Arnt in the stromal component of the mammary gland. However, AhR and Arnt-null animals were also infertile, demonstrating further evidence of the connectivity between the mammary gland and other endocrine systems.

*Lobuloalveolar development:* The bulk of growth of the mammary gland occurs during the post-pubertal period thus highlighting the critical role of ovarian and pituitary-derived hormones. TEBs express both estrogen receptors and progesterone receptors and are primed for response to steroid hormones at the onset of puberty and through the reproductive cycle. Estrogens and progesterone are major controllers of lobuloalveolar development of the mammary gland through receptor-mediated interactions with each other and in the stimulation of and interaction with growth factors. Estrogen mediates its effects through ER- $\alpha$  located in both epithelial and stromal cells in rodents, although it appears to be epithelial specific in humans. Progesterone mediates its effects through both progesterone receptors A and B (PRA and PRB) interspersed on some, but not all epithelial cells. Most of the progesterone receptor expressing epithelial cells in the developing gland also coexpress estrogen receptor. These steroid receptor-positive epithelial cells do not colocalize within the proliferative pool of epithelial cells themselves but regulate growth and lobuloalveolar differentiation through paracrine effects on adjacent steroid receptor-negative cells. This paracrine interaction appears to involve WNT signaling (Timmermans-Sprang et al., 2017). The decrease in progesterone at the time of parturition and increases in oxytocin and prolactin are stimulatory for milk production.

Although there are species differences, protein hormones including growth hormone (GH), prolactin, epidermal growth factor (EGF) receptor (EGFR) ligands, and insulin-like growth factor (IGF)-1 also play roles in growth and development. In mice, and likely most species, prolactin and GH are critical for lobuloalveolar development because this development is deficient and impaired in mice lacking prolactin or GH receptors. In young rodents, prolactin and GH can, with high enough levels, stimulate some growth without steroids. The EGFR family, consisting of four receptors (ERBB 1–4) and many ligands, is important in development of the mammary ductal structure in many species (Earp et al., 1995; Morato et al., 2023). ERBB1, ERBB2, and ERBB3 are functionally active in mouse mammary tissue at puberty, and elimination of ERBB2 (also known as HER2) in the virgin mammary gland resulted in structural alterations in the TEBs and delayed ductal growth during puberty and adolescence (Jackson-Fisher et al., 2004). In eight-week-old mice, ERBB2 is especially prominent in the luminal epithelium and reduced in the stroma, whereas ERBB1 is localized to the stroma. One of the EGFR ligands, amphiregulin is specifically isolated to the TEB cells and modulates the function of the ER- $\alpha$  during pubertal development (Ciarloni et al., 2007).

In NHP, the sex steroid receptor expression profile in the adult macaque mammary gland is similar to humans. Androgen receptor (AR) is also expressed in macaque mammary tissue and in the skin and nipple. In this species, morphological studies have demonstrated that ER- $\alpha$  and progesterone receptors often coexpress in the same cells, but do not coexpress with the proliferation marker Ki67, findings also observed in the mouse. Prolactin is not an obligate component of mammary growth and development in macaques but is required for lactation.

There are numerous other factors that interact and affect the cell biology of the mammary gland. Interestingly, the vitamin D receptor (VDR) serves as a negative growth regulator during mammary gland development via suppression of branching morphogenesis during puberty and modulation of differentiation and apoptosis during pregnancy, lactation, and involution (Welsh et al., 2003). The many matrix metalloproteinases (MMPs) and cell adhesion

molecules also help modulate both ductal outgrowth and involution of the senescent gland. For example, during puberty and pregnancy, MMP-2 is necessary for normal terminal end and lateral ductal branching and extensive branching in midpregnancy, while MMP-3 is required for secondary and tertiary lateral branching of ducts.

## 2.4. Functional Outcomes

Observed trends in human cohorts for advanced thelarche that is not paralleled by changes in early menarche underscore the enhanced sensitivity of the mammary gland to genetic and environmental influences compared to other reproductive tissues (see *Female Reproductive System*, Vol 5, [Chap 10](#)). Importantly, the advancement of breast development increases the overall time that TEBs remain as susceptible targets for endocrine disruptors or carcinogenic compounds in the breast, which in turn, increases the risk for development of cancer. Indeed, earlier age of menarche and later age of menopause are known risk factors for breast cancers ([IBCERCC, 2013](#)). Thus, assessing the maturation of the mammary gland in rodent toxicology studies provides an important means to assess physiological alterations of the gland and identification of potential human health hazards. The hallmark responses of exponential growth and rapid differentiation of the mammary gland at puberty and during pregnancy in preparation for lactation demonstrate that this tissue continues to respond to hormones and remains flexible in its differentiation potential. Thus, critical windows for breast development extend from the prenatal period, continuing through peripubertal years and into adult life ([Fenton, 2006](#); [Rudel et al., 2011](#); summary in [Figure 8.10](#)).

**Mammary gland cancer:** As reviewed in [Section 1](#), there are strong associations reported between breast cancer risk in women and family history of breast disease, age, environmental/pharmaceutical exposures, lifetime exposure to estrogens, and genetics (race/ethnicity, heritable traits). This is also true in many other species ([Edmunds et al., 2023](#)). There are some key aspects concerning mammary cancer in animal models that need to be understood in reference to mammary gland development and cell biology that are particularly relevant to

toxicologists. As in women, hormonal and reproductive status, environmental contaminant exposures, diet, and genetics have significant effects on the development of mammary cancer in rodents. Mammary cancer can be induced with estrogen treatment in both rats and mice and incidence of mammary cancer increases with increasing age in many strains of rats. Rising circulating prolactin levels in aging rats have been associated with both increases in fibroadenomas and adenocarcinomas through biological mechanisms thought to be irrelevant to mechanisms of breast cancer in women. However, recent studies show a greater importance of prolactin in promoting breast cancer in women and therapies currently developed to inhibit prolactin-mediating signaling pathways show some efficacy. In rats and women, early life pregnancy is protective, although pregnancy does not have the same potency of protection in mice. Mammary tumors may form in the duct, alveolar, or terminal ductal lobular unit regions of the mammary gland in most species. Mice deviate from rats, monkeys, and women in that spontaneous mammary tumors in mice are mostly noninvasive and not metastatic. However, mammary gland tumors are prevalent in genetically engineered models ([Cardiff et al., 2000](#)) and mouse mammary tumor virus (MMTV)-infected mice ([Russo and Russo, 1996](#)), and are characterized by tumor type. In contrast, mammary tumors in monkeys, dogs, and rats are derived from the epithelial cells of the terminal ductal lobular units, may be invasive, and are seldom metastatic ( $\leq 10\%$ ). Fibroadenomas are common in rats; the mean incidence of fibroadenoma in females of most rat strains varies from approximately 20% to more than 40% ([Luzhna et al., 2015](#); [Russo, 2015](#)). Fibroadenomas occur more commonly in Sprague–Dawley rats than in other strains, with values as high as 70% ([Brix et al., 2005](#); [Kaspereit and Rittinghausen, 1999](#)). Women also develop fibroadenoma, especially in early life. In women, the cells in which tumors form may vary widely, with lesion types associating with lobule complexity ([Russo, 2015](#)).

Most female rat mammary tumors have a counterpart in human pathology (including benign, precancerous, and malignant lesions) ([Russo and Russo, 1996](#)), but there are some specific lesions in humans (e.g., infiltrating



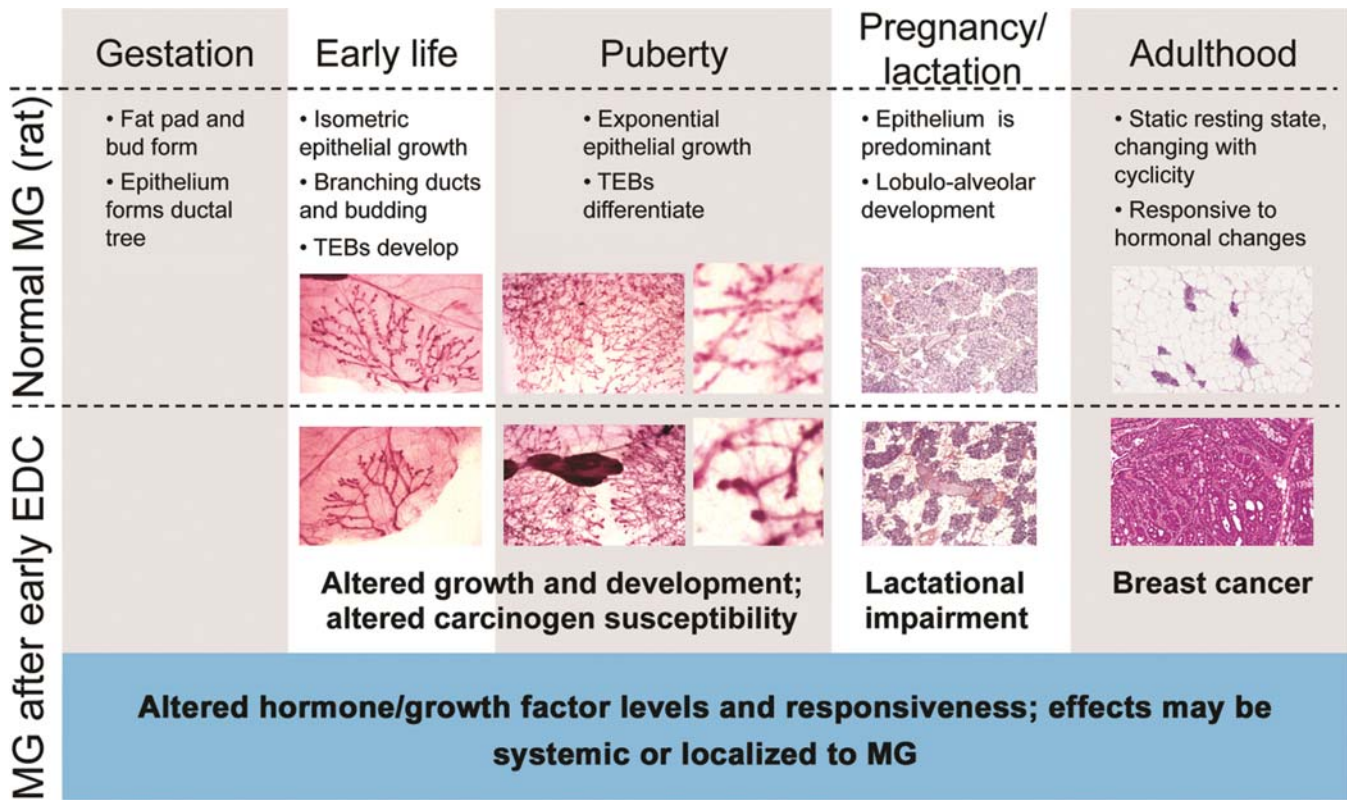


**FIGURE 8.10** Stages of mammary gland development in the female rat; normal (top) and altered (bottom) carmine-stained whole mounts. Numerous examples of early life endocrine disruptor effects on mammary gland development have been associated with later life adverse outcomes such as delayed breast developmental timing (early life [weaning] and puberty column), impaired lactation (pregnancy/lactation column) or increased risk for mammary tumors (adulthood column). Chemicals associated with adverse rodent mammary gland effects, and the susceptible exposure windows, are detailed in [Kay et al. \(2022\)](#). EDC, endocrine-disrupting chemicals; MG, mammary gland; TEB, terminal end bud. Adapted from Rudel RA, Fenton SE, Ackerman JM, et al.: *Environmental exposures and mammary gland development: state of the science, public health implications, and research recommendations*. *Environ. Health Perspect.* 119(8):1053–1061, 2011, Figure 1, with permission.

ductal carcinoma, lobular carcinoma in situ or invasive, and medullary lesions) that have not been reported in the rat ([Russo, 2015](#)). However, mice are reported to develop intraductal hyperplasia, similar in appearance to that of ductal carcinoma in situ (DCIS) in women (see [Figure 8.11](#); [Vandenberg et al., 2008](#)). Mice also develop papillary adenomas, which are not diagnosed in women ([Cardiff et al., 2000](#)). In carcinogen-induced rat models, initiation occurs primarily in the epithelium of TEBs while they are developing into alveolar buds/terminal ducts. Also, the thoracic glands, thought to retain TEBs longest, have the highest incidence of carcinogen-induced tumors.

*Lactation deficiency:* Studies evaluating lactational aspects following a pregnancy have

recently reported that a significant percentage of women abandon breastfeeding due to insufficient milk supply, concern about insufficient nutrition of the infant (losing weight), or pain ([Lechosa-Muñiz et al., 2021](#)). Associations between chemical exposures and impairments in lactogenesis have been reported in tobacco smokers, and in women in pesticide- and per-fluorinated chemical-contaminated communities ([Timmermann et al., 2023](#)) and could partially explain why breastfeeding rates in women in high income countries are lower than recommended by global health organizations.

In rodent models, there is increasing experimental evidence that environmental exposures and some drugs decrease offspring weight gain during the perinatal period and that those deficits

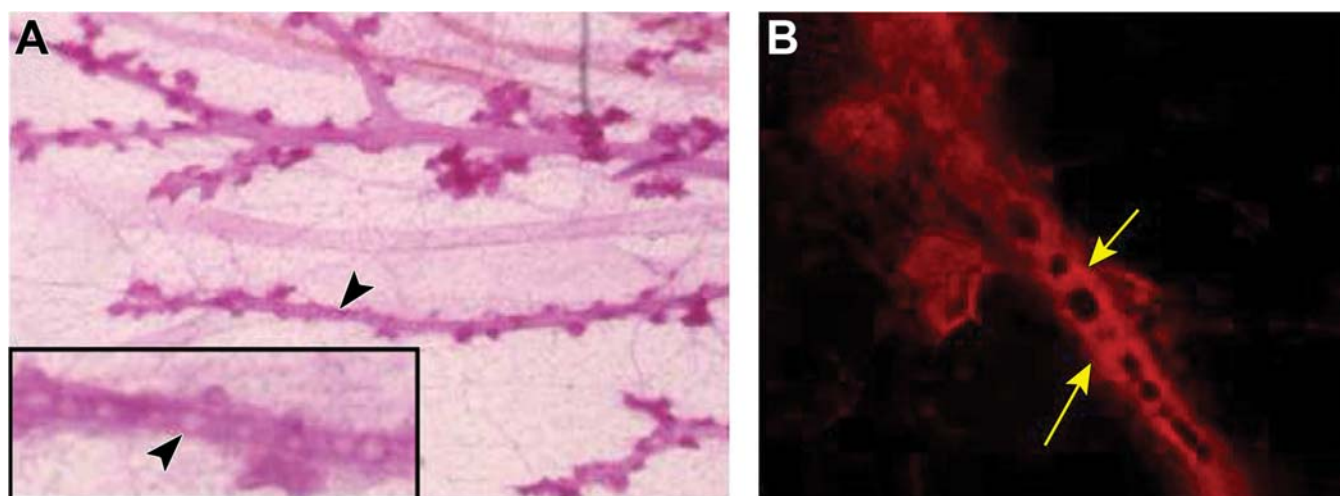


**FIGURE 8.11** Beaded ducts demonstrating hypertrophy/hyperplasia of the duct in whole-mounted mammary gland from bisphenol A (BPA)-exposed CD-1 mouse offspring. Glands from 9-month-old females exposed to BPA during perinatal development displayed beads in several ducts (A). Beads are marked by arrowheads. Inset illustrates a higher magnification of a beaded duct. 32× magnification (B) Confocal images of beaded ducts in BPA-exposed females demonstrate the presence of cells inside the ductal lumen. Areas with cells bridging across the ductal lumen are marked by yellow arrows, 200× magnification. All pictured mammary glands were stained with carmine. *Reproduced from Vandenberg LN, Maffini MV, Schaeberle CM, et al.: Perinatal exposure to the xenoestrogen bisphenol-A induces mammary intraductal hyperplasias in adult CD-1 mice. Reprod. Toxicol. 26(3–4):210–219, 2008, Figure 2, with permission.*

are linked to impaired lactogenesis in the dam (Kay et al., 2022). Chemical exposures may affect lactation output or milk quality by impairing proliferation and differentiation of mammary epithelial cells during pregnancy or disrupting the hormonal processes responsible for breast milk production (including prolactin secretion and signaling and milk protein expression) (Rayner et al., 2005; White et al., 2009; LaPlante et al., 2017). Lack of weight gain in offspring may be caused by maternal toxicity or hormonal effects of test articles, and effects on the lactating glands may be evident histologically. Conventional safety studies, conducted in accordance with the U.S. Food and Drug Administration (FDA), Environmental Protection Agency (EPA), or National Toxicology Program (NTP) guidance, or International Council for Harmonisation (ICH) or the Organisation for Economic Co-operation and Development (OECD) guidelines, that are designed to screen for potential toxicity in multiple organs and organ systems, may prioritize mammary collection and evaluation to evaluate histological sections for lactation deficiencies. In cases when mammary gland toxicity is suspected or if additional information

is needed, the mammary gland may be more thoroughly evaluated in investigational studies specifically designed to look for test item-related changes in the mammary gland by using special techniques such as immunohistochemistry, mammary gland whole mounts, and/or histomorphometry (Matouskova, et al., 2022). Using these supplemental techniques, abnormalities such as delayed or subtle differences in differentiation/lactogenesis may be noted (see Figure 8.3E and F).

### 3. EVALUATION OF MAMMARY GLAND TOXICITY

Studies conducted in rodent models have been the primary method of screening for potential toxicity/hazard for both developmental/reproductive toxicity (DART) studies (see *The Role of Pathology in Evaluation of Reproductive, Developmental, and Juvenile Toxicity*, Vol 1, Chap 7) and carcinogenicity testing (see *Carcinogenicity Assessment*, Vol 2, Chap 5) for decades. As part of a regulatory submission package or in

chemical toxicity testing, these studies are conducted according to various regulatory guidance set forth, for example, by the Center for Drug Evaluation and Research (CDER) branch of FDA (Guidance for Industry); U.S. EPA Code of Federal Regulations, Title 40, Chapter 1, Subchapter R, Part 798—Health Effects Testing Guidelines; ICH Harmonised Tripartite Safety Guidelines; and OECD Guidelines for Testing of Chemicals, Section 4, Health Effects. Test guidance/guidelines are a set of standardized testing methods used in regulatory safety or chemical toxicity testing by government, industry, contract research organizations, and academic researchers to characterize test chemicals or drugs for potential toxicity on various organ systems. While protocols are derived from guidance, they are not proscriptive and there is the ability to make changes to the guidance for specific studies. For instance, if the mammary gland is suspected of being a target organ, then changes to the study protocol can be made to assure that the mammary gland is specifically evaluated. Guidelines are more specifically defined; commonly referenced test guidelines are those of the [OECD \(2018a\)](#). In published guidance/guidelines, the mammary gland may be included for evaluation in rodent and nonrodent short-term and long-term studies that include histopathological evaluation of tissues.

Collection procedures specifically for the rodent mammary gland at necropsy and trimming methods for transverse sections of the mammary gland have been published ([Ruehl-Fehlert et al., 2003](#)) and are available online. These procedures are typical for mammary gland screening in regulatory-type studies. However, if test chemicals are suspected of being endocrine disruptors, alternative collection of the entire fourth and fifth gland (young animals) or the fourth mammary gland may be warranted, along with longitudinal (sagittal) sectioning (see [Figure 8.12](#)). The OECD Test Guideline 443 states, “Research has shown the mammary gland, especially in early life mammary gland development, to be a sensitive endpoint for estrogen action. It is recommended that endpoints involving pup mammary glands of both sexes be included in this Test Guideline, when validated” ([OECD, 2018a](#)).

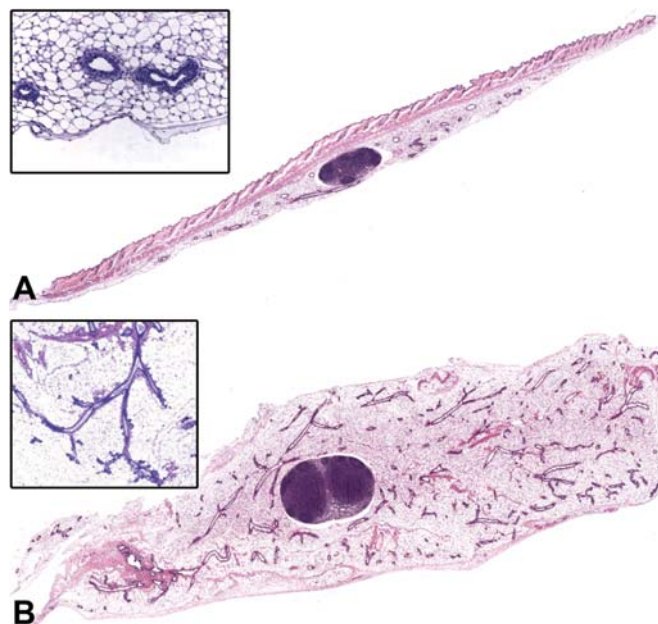


**FIGURE 8.12** Mammary gland, female rat, H&E-stained paraffin sections. (A) Cross- or transverse section and (B) longitudinal (sagittal) section. Longitudinal sections may afford longer lengths of ducts such that ductal bridging or ductular hyperplasia would be apparent; should be used to compare to whole mount preparations of the tissue from the contralateral gland for appropriate comparison. *Courtesy of J. R. Latendresse, Toxicologic Pathology Associates, National Center for Toxicological Research, Jefferson, Arkansas, USA. Reproduced from Haschek WM, Rousseaux CG, Wallig MA, editors: Haschek and Rousseaux's handbook of toxicologic pathology, ed 3, 2013, Academic Press, Figure 61.5, p. 2677, with permission.*

For studies in which mammary gland will be evaluated, knowledge of normal mammary gland development and differentiation is imperative. The use of a mammary gland atlas is advised for familiarity ([Masso-Welch et al., 2000](#); [Filgo et al., 2016](#)). The timeline of development may vary by rat or mouse strain ([Stanko et al., 2016](#)), so familiarity with developmental timing in the strain used within a given study is critical for interpretation of results. Similarly, interpretation of a carcinogenic effect can be complicated by the high incidence of spontaneous mammary tumors in some strains typically used (see [Section 3.2](#)). Also important is evaluation of other endocrine organs/reproductive tissues, alongside the mammary gland, to adequately interpret endocrine-related effects.



Toxicity mediated by decreased endocrine support of the male reproductive system requires an integrated evaluation of the entire reproductive tract, because changes can be present in the testis, epididymis, accessory sex organs, mammary gland (nipple or areola retention), and/or pituitary.

Regulatory-type studies designed to screen for test compound toxicity in animals dosed or exposed as adults have limitations with respect to detection of mammary gland toxicants or carcinogens. Windows of mammary gland susceptibility or sensitivity for some effects begin in utero (Kay et al., 2022), so if chemical exposure starts in adult nulliparous rodents, it is possible that mammary gland toxicants and carcinogens that have their effects during these windows of susceptibility may be missed, or a true lowest observable effect level (LOEL) would not be reached. In these cases, and when there is suspicion or evidence of an effect on the mammary gland (such as for endocrine-disrupting chemicals), a second-tier approach should be considered. Additional studies, such as one-generation toxicity studies, are specifically designed to address these concerns. For example, the main objective of the Extended One-Generation Reproductive Toxicity Study (EOGRTS) is “to evaluate specific life stages not covered by other types of toxicity studies and test for effects that may occur as a result of pre- and postnatal chemical exposure” (OECD, 2018a). The OECD Health Effects Test Guideline 443 (OECD, 2018b) and the NTP Modified One-Generation protocol (MOG; NTP, 2023) include developmental exposure and follow health endpoints of the parental generation and at least one generation of offspring. Additionally, the NTP has recently included developmental exposure in their 90-day chronic exposure and 2-yr bioassays. Currently, the EOGRTS and MOG suggest collection of the mammary gland and evaluation by histopathology (as in Figure 8.12A).

A second constraint of test guidelines is that they may not be optimized for tissue collection for each organ during specific periods of susceptibility. Because the regulatory-type safety studies conducted in adult animals are designed as multiorgan screening studies rather than comprehensive assessments of toxicity for

particular organs, they aim to collect information on many organs and systems in one study; accordingly, standard toxicity studies are not designed around an optimal time point for collection that specifically evaluates toxicity of the mammary glands. For example, in 2-yr bioassays, there is one time point in most cases (study end), so tissue samples that may provide mechanistic information on initiation, progression, hallmarks, and early biomarkers of disease are not available. However, much information can be gathered from collection and evaluation of weanling or 90-day old mammary tissues.

Third, there has always been concern that use of maximum-tolerated dose-based exposures may not be a relevant testing condition or produce results in rodents that are relevant to real-world exposure scenarios for humans. With high exposures, confounding reductions in body weight decrease the propensity for mammary tumor induction. Additionally, in long-term follow-up studies that have considered the mammary gland windows of susceptibility in the study design, endocrine-disrupting chemicals with environmentally relevant exposures may have a stronger effect at the lowest doses versus the highest. This point was clear in studies of bisphenol A (BPA) that were coordinated between academic and government researchers (NTP, 2018, 2021; Howdeshell et al., 2023).

Finally, regarding test guidance/guideline requirements for the mammary gland, there is vague and incomplete guidance for when/how often to collect, assess, and evaluate mammary glands from all animals in the study (Roberts and Stout, 2023; NTP, 2023). For instance, it is required to collect mammary tissue in some cases (EOGRTS), but it is not required to evaluate it histopathologically; in other cases (MOG), mammary tissue may or may not be collected (decided by the study team), and the OECD chronic toxicity and carcinogenicity test guidelines require collection of female and male mammary glands if possible. Therefore, following collection protocols like those indicated here (Ruehl-Fehlert et al., 2003; Matouskova et al., 2022; OECD, 2018a) followed by evaluation of at least a single section of each tissue at each dose is recommended. It is difficult to get early life indicators of mammary

toxicity if not evaluated in developmental and reproductive studies and to date, testing chemicals in fully developed mammary glands has provided little in the way of evidence for environmental influences on mammary cancer. In 2022, the OECD has adopted a project to consider the inclusion of the mammary gland whole mount in the EOGRTS Test Guideline 443 (OECD, 2018b), along with other enhanced guidance for mammary gland assessment. A whole mount of mammary tissue allows for evaluation of the entire gland of mice of all ages and weanling to young adult rats, and protocols for collection, processing, evaluation, and interpretation of whole mounts is provided in the [Appendix](#). Therefore, it is prudent to understand the several options for evaluating mammary gland development, function, and disease.

### 3.1. In Vitro Techniques

Although they lack a modifiable endocrine system, a variety of in vitro mammary cell culture techniques are useful for screening test articles for specific endpoints, as well as in mechanistic studies. Screening assays are used to quickly identify chemicals that may have endocrine active characteristics, to prioritize chemicals in large families, and to identify cytotoxic dose ranges. The idea that chemicals can be screened for estrogenic activity in vitro was validated (Soto et al., 1995) when the E-SCREEN assay was developed. This commonly used assay takes advantage of endogenous estrogen receptor-mediated events in human breast epithelial cancer MCF7/BUS cells (Payne et al., 2000). These specific cells were derived from a woman with breast cancer, and express ER- $\alpha$ . An “A-screen” has been similarly developed for assessing androgen receptor activity using prostate carcinoma or MCF7 cells transfected with AR. Yeast-based steroid hormone receptor gene transcription assays and in silico ligand-dependent reporter assays are also used in drug screening, drug development, and toxicology studies. Compounds showing activity in these screening assays should be considered as potential mammary gland toxicants and second tier testing considered.

Cell culture experiments have provided important mechanistic knowledge of mammary gland biology and cancer. Neoplastic MCF7 and nonneoplastic MCF10 cells (human-derived “normal” breast cells that do not express estrogen receptors or undergo terminal differentiation or senescence) have been widely used, although there are many well-characterized mammary epithelial cells available including cells derived from human breast. Another important and increasingly popular in vitro system is the 3D mammary gland culture or mammospheres. 3D cultures use some type of mammary epithelial cell, suspended in medium in an extracellular matrix or plated on a solid layer of Matrigel to recapitulate some of the intact gland activity. When mammary epithelial cells (such as MCF10A cells) are cultured on laminin-rich extracellular matrix, they produce a basement membrane and arrange themselves in spherical acini with a centrally located lumen and some groups have developed the ability to make mammospheres branch and elongate. Modulation of genes or stromal elements can affect the formation of the acini. Microfluidic and bioengineered paper-based platforms, where more than 1 cell type may be cultured on either side of a permeable membrane from one another, are also becoming popular. In these models, fluid stress may be applied (like blood flow in the body), and signals transfer from one cell type to another due to that flow. As such, these models may provide more realistic information on cell-cell communication and mechanistic pathways. Regardless of these capabilities, there is no developmental model for the mammary gland in which early origins of disease or malformation may be identified, and to date no in vitro model system forms TEBs, the critical cells regulating epithelial outgrowth. However, there are in vitro lactation models (Kobayashi, 2023) that allow for mechanistic understanding of hormonal cues modulating milk protein production.

### 3.2. Commonly Used Animal Models

Although there are developmental and biological differences between mammary glands of various species of animals and humans,

modeling effects of chemicals in animals has proved necessary and critical to advance our understanding of mammary gland biology, response to injury and cancer. The use of animal models (especially rodents) has demonstrated that sensitive life stages (especially fetal development, puberty, and pregnancy) impart a unique sensitivity to some chemical exposures leading to later life disease risk and that toxicants can act by mechanisms other than as frank carcinogens (i.e., as endocrine disruptors) to confer an increased risk of cancer or other late life effect, such as insufficient lactation (as in [Figure 8.10](#)).

*Spontaneous rodent animal models:* Test guideline studies have historically relied on specific strains of inbred rats and mice exposed to maximally tolerated doses of single chemicals from sexual maturity (6–8 weeks old) up to 2 years. For several reasons, one of which being the high background of spontaneous tumors in some strains (Fischer 344/N; [Dinse et al., 2010](#)), the NTP has changed to the Hsd:Sprague Dawley or Wistar Han outbred rat strains. However, industry-sponsored studies more often use outbred CD-1 mice and CD Sprague–Dawley rats, the Agency for Toxic Substances and Disease Registry (ATSDR) and Ramazzini Institute (Italy) have their own strains of Sprague–Dawley rat that are not commercially available, and OECD (and European testing entities) prefers use of the Wistar rat. These different strains of animals have different sensitivities and tumor susceptibilities, which should be considered in study design and interpretation. For example, when the incidences of mammary gland neoplastic lesions were evaluated in non-treated controls in 17 carcinogenicity studies ( $n > 1300$  females), they were the most common spontaneous tumor (~31% of all recorded neoplasms) in female CD Sprague–Dawley rats ([Chandra et al., 1992](#)), and 61% of those tumors were fibroadenomas. In 24-month-old Hsd:Sprague–Dawley female rats, 76% exhibited mammary tumors, with the majority being fibroadenomas ([Kaspereit and Rittinghausen, 1999](#)). Similarly, the NTP reported 71% fibroadenoma incidence in Hsd:Sprague–Dawley females ([Brix et al., 2005](#)). In more recent evaluations ([Luzhna et al., 2015](#)) of HanWistar female rats, ~29% developed mammary fibroadenomas and between 4% and 10% developed adenocarcinomas, while other Wistar strains

demonstrated a slightly lower (~19%) rate of fibroadenoma development (and similar rate of adenocarcinoma). In the same evaluation ([Luzhna et al., 2015](#)), ~13% of Fischer 344/N females demonstrated fibroadenomas (1% adenocarcinomas) and 53%–56% of female Sprague–Dawley formed fibroadenomas, with 10%–11% adenocarcinoma incidence. Female Fischer 344/N rats have reported mammary fibroadenoma incidences up to 44% ([Brix et al., 2005](#)). Fibroadenomas are not considered a premalignant lesion in humans nor are rat mammary fibroadenomas considered predictive of carcinoma in women ([Rudmann et al., 2012](#)). Spontaneous mammary adenocarcinomas, which are considered relevant to women, are more common in Sprague–Dawley rats, with reported incidences of 10%–11% in multiple strains of Sprague–Dawley and Wistar rats ([Chandra et al., 1992](#); [Brix et al., 2005](#); [Luzhna et al., 2015](#)). Mice vary widely by strain in their background incidence of mammary tumors, with those carrying MMTV having high incidence (FVB, C3H/He) and those lacking or having minimal MMTV insertion (Balb/C and C57Bl/6) demonstrating low incidence ([Outzen et al., 1985](#); [Davie et al., 2007](#); [Zhou et al., 2023](#)). In fact, C57BL/6, one preferred genetic background for gene-targeting experiments, confers resistance to MMTV infection and MMTV-induced mammary tumors, and when crossed with another preferred strain for gene-targeting studies, the FVB background, resulted in altered tumor incidence in MMTV-driven transgenic lines ([Rowse et al., 1998](#)).

Following an NTP-sponsored expert panel workshop, and with the accumulation of data linking early exposures with later life mammary gland lesions, NTP carcinogenicity studies have incorporated early life or multigenerational exposures in some cases. Morphologic evaluation of the mammary gland may include whole mounts and advanced sectioning techniques such as those demonstrated in [Figure 8.13](#), which were instrumental in identifying a significantly increased number of lesions compared to a single hematoxylin and eosin (H&E)-stained section following developmental bisphenol analogue exposures ([Tucker et al., 2016, 2018](#)). European studies have also modified their EOGRTS test guidelines in 2012 to include optional mammary gland evaluation of males and females. In



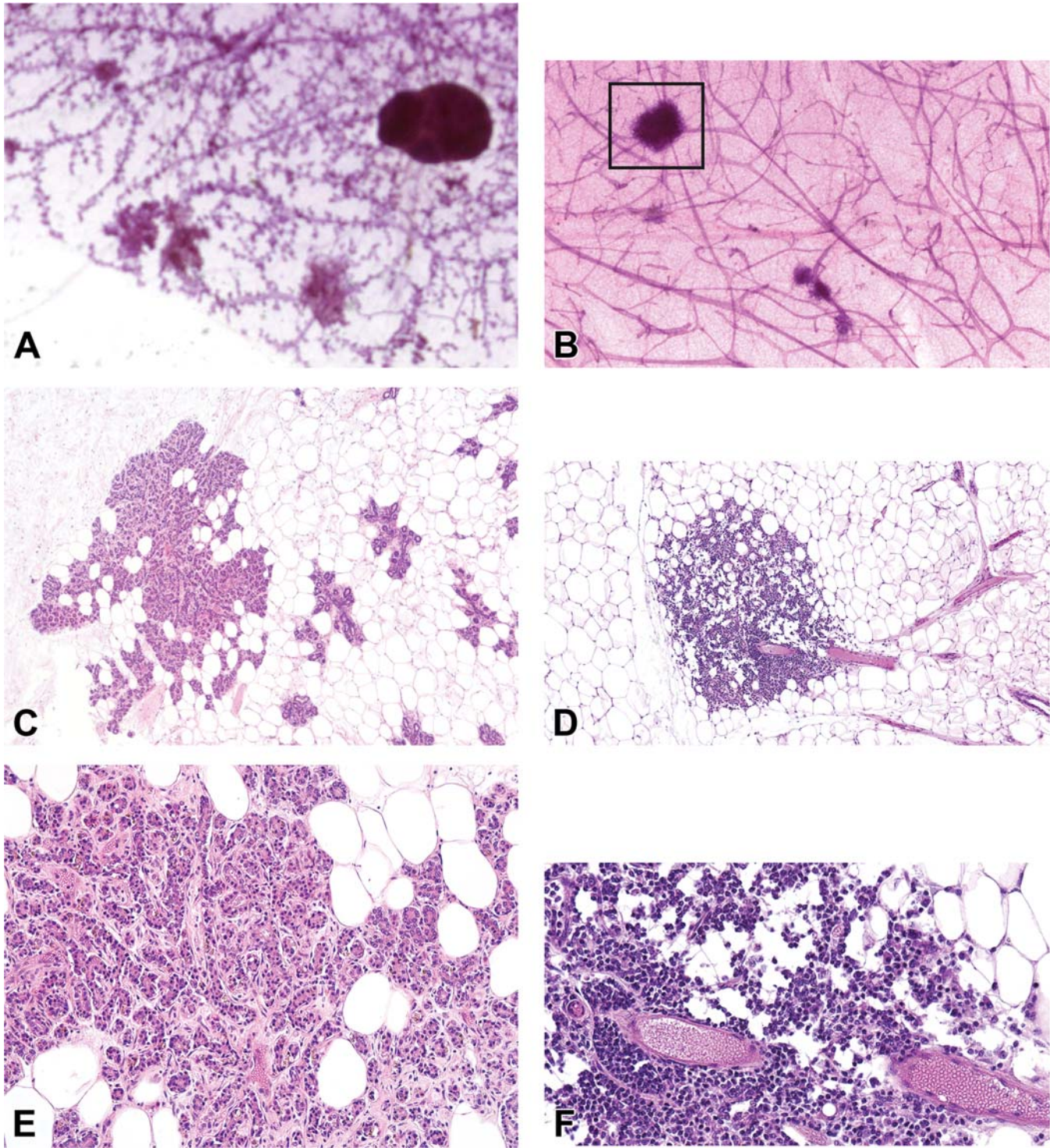


**FIGURE 8.13** Identification of lesions by sectioning of mammary whole mounts of 14-month-old female CD-1 mice. (A) Mammary gland whole mount preparation indicated intensely stained areas of concern near the outer edge of the gland; carmine-stained, 2× magnification; (B) increased opacity around ducts and stromal structures (box) in the contralateral carmine-stained mammary whole mount, 2×. Whole mount in (A) and (B) were removed from slide and sectioned/H&E stained as in [Tucker et al. \(2016\)](#). (C) The lesion in (A) was diagnosed as periductal fibrosis, 10×. (D) In the mammary gland H&E-stained section from (B) there were clusters of mononuclear cells around the blood vessels and extending into the adjacent adipose tissue, 20×; (E) 40× magnification of periductular fibrosis; (F) higher magnification (40×) of (D) illustrated that the inflammation was composed of perivascular lymphocytes. *Reproduced from Tucker DK, Foley JF, Hayes-Bouknight SA, et al.: Preparation of high-quality hematoxylin and eosin-stained sections from rodent mammary gland whole mounts for histopathologic review. Toxicol. Pathol. 44(7):1059–1064, 2016, Figure 2, with permission; (C and E) Reproduced from Haschek W, Rousseaux C, Wallig M, Bolon B, editors: Fundamentals of toxicologic pathology, ed 3, 2018, Academic Press, Figure 19.5, p. 554, with permission.*

addition to morphological evaluation of the mammary gland in all species tested, careful evaluation of serum hormones, and other hormone-related end points in multigeneration studies such as timing of gonadal control of puberty (vaginal opening, heat [dog], first estrus, etc.), cyclicity patterns, retention of nipples/areolae in males, and possibly anogenital distance measurements are important to aid in identification of potential mammary gland toxicants or carcinogens in rodents. Guidance on methods for these complementary endpoints are published ([Roberts and Stout, 2023](#); [OECD, 2018a](#)). Finally, a greater emphasis is now being placed on using “environmentally relevant doses”, instead of maximum tolerated doses, in toxicity studies with our increased understanding of how endocrine-disrupting compounds mediate their effects.

*Chemical carcinogenesis in spontaneous rodent models:* The coadministration of cancer-inducing agents with a test article of interest is a commonly used and well-accepted method in toxicology studies to identify potential mammary carcinogens in rodents. For example, spontaneous mammary gland cancers in rats, generally adenocarcinomas, can be enhanced with treatment with genotoxic carcinogens like 1,2-dimethylbenz[*a*]anthracene (DMBA), *N*-nitrosomethylurea (NMU) and *N*-ethyl-*N*-nitrosourea, or irradiation. DMBA is most effective when administered after puberty. Part of the age-susceptibility pattern to DMBA is attributed to the development of the enzymes necessary to metabolize DMBA to its carcinogenic form after puberty. In contrast, NMU is most effective when administered before puberty due to a deficiency of a DNA repair enzyme in the immature rat gland and the induction of *H-ras* mutations in the mammary epithelial cells. Irradiation is most effective when done in the postpubertal period and enhanced by short-term estrogen treatment during this time. Another consideration for susceptibility to these carcinogens is the relative abundance of TEBs in the gland at the time of administration. The TEBs contain stem cells and have high mitotic indices, thus are susceptible to damage from these chemicals. The relative difference in TEB populations between exposed and control groups should be known at time of carcinogen administration to aid in study interpretation.

*Genetically engineered mice (GEM):* Mice, which tend to have lower incidence of spontaneous mammary cancers that rarely are malignant, have nonetheless been exploited as models for breast cancer. Historically, it was discovered that infection with lactationally transmitted MMTV caused hyperplastic lesions and mammary tumors through activation of WNT, fibroblast growth factor and notch signaling pathways that are also critical in early mammary gland morphogenesis. Hyperplastic lesions and spontaneous tumors that develop in naturally MMTV-infected mice are characteristic of well-differentiated hyperplastic alveolar nodules and alveolar tumors. Some have promoted these lesions to represent preneoplastic lesions comparable to such lesions in women’s breast tissue, but others maintain that the biology and morphology of the hyperplasia and benign tumors are features that should be considered mouse specific. Nonetheless, MMTV has also been exploited in the development of many GEM models of mammary cancer by targeting and driving gene expression using MMTV as a promoter. Other commonly used mammary-specific promoters include the whey acidic protein (commonly known as WAP) and keratin promoters, and have been used more recently to create mammary-targeted expression or deletion of genes using CRISPR technology ([Bu et al., 2023](#)).

A tremendous effort has gone into characterizing GEMs to bridge morphologic and genotypic variations of mouse mammary cancer to breast cancers in women (see review, [Borowsky and Cardiff, 2022](#)). Models have been classified or categorized according to (1) lesions that resemble spontaneous mouse mammary tumors, (2) lesions that are unique and specific for the transgene, and (3) lesions that resemble human breast lesions. However, for most models and transgenes tested, there is limited evidence that these show malignant characteristics and they are not transplantable or immortal. Nonetheless, these models remain informative and recent characterizations further support their importance in understanding mammary gland biology and cancer. The efforts that have generated diversified outbred mice ([Jacob et al., 2023](#)), genetically unique lines of mice, will help to identify susceptible subpopulations and allow linking of genetic underpinnings to disease.



Phenotypic understanding of their mammary tumor susceptibility is in its infancy, but these may prove to be valuable in testing certain pharmaceuticals/xenobiotics for effect on the mammary gland in the future.

*Nonhuman primates (NHPs) as models in breast cancer studies:* The NHP is the most human relevant model to understand pleiotropic effects of toxicants or drugs on mammary gland development as well as carcinogenic potential. Similar to other animal models such as rats and mice, NHP models recapitulate spontaneous/chemically induced disease, and mimic human morphological phenotypes/genotypes, but should not be a primary model to assess breast cancer risk. Several Old World Monkey species (cynomolgus, rhesus, and baboons) and recently New World monkeys (common marmosets) have been used in various breast cancer and breast developmental studies. Cynomolgus and rhesus macaques show spontaneous mammary ductal hyperplastic and neoplastic lesions in older captive animals. The lesions are morphologically similar to lesions observed in humans, allowing for categorization of neoplasia using human terminology and have been shown to progress to metastatic disease. Spontaneous mammary gland carcinomas in rhesus macaques have potential reported etiologies such as viruses, hormones, and irradiation (Dewi and Cline, 2021). Chemically induced breast cancers have been reported in NHP models; however, they are generally considered impractical as induced tumors would likely develop across a period of years and tumor incidence is rare. The majority of macaque studies on the mammary gland have been related to risk instead of incidence. The Hormone Replacement Therapy Study in cynomolgus macaques (Cline et al., 1996) is one of the landmark examples of the translational importance of monkey breast studies. This study suggested higher risk of breast cancer with treatment of estrogen plus progestin, a finding that was later proven to be true in Women's Health Initiative Study and resulted in the termination of the trial (Chlebowski et al., 2020). In addition, macaques have been used in studying exposure to various dietary compounds and endocrine-disrupting chemicals during various life stages (in utero, puberty, and adulthood) to evaluate the effects on breast development and subsequent breast cancer risk (Dewi and Cline, 2021).

In summary, the use of animal models (especially rodents) has demonstrated three critical factors that would have taken decades to discern in humans. First, that sensitive life stages (especially fetal development, puberty, and pregnancy) impart a unique sensitivity to some chemical exposures leading to later life disease risk (Figure 8.10). Second, that toxicants can act by mechanisms other than as frank carcinogens (i.e., as endocrine disruptors; Figure 8.9) to confer an increased risk of cancer or other late life effect, such as insufficient lactation. Third, the use of transgenic, knock-out, and other gene modified rodents (primarily mice) have identified highly important details of mechanisms in disease development (Table 8.1) and progression. Although mice remain the most used model in breast cancer due to genetic manipulation, ability to study mechanisms and availability, NHP (macaques) serve as a unique resource for translational research and testing in the field of breast cancer research. However, increased ethical standards, availability and/or cost, and an increasing expectation to improve strategies to replace, reduce, and refine their use limit their consideration.

### 3.3. Physiologic Outcomes

The most common mammary gland toxicities have their foundation in alterations of the normal physiology of the mammary gland, linking malformations to functional outcomes and cancer. Strong experimental data (summarized in Kay et al., 2022, Table 1) suggest that chemicals (e.g., dioxin, atrazine, benzophenones, bisphenols, perfluorinated substances), drugs (diethylstilbestrol, ethynyl estradiol), and dietary substances (genistein, 2-amino-1-methyl-6-phenylimidazo[4,5-*b*]pyridine [PhiP], mycotoxins [see *Mycotoxins*, Vol 3, Chap 6], high fat diets) can interfere with branching and differentiation of mammary glands, resulting in either delayed or accelerated maturation (examples in Figure 8.14), and transiently or permanently altering the gland morphology.

Chemicals causing developmental abnormalities that are persistent or permanent, or result in functional changes, should be considered teratogenic (see *Embryo, Fetus and Placenta*, Vol 5, Chap 11). Teratogenic effects are defined in the US EPA Integrated Risk Information System



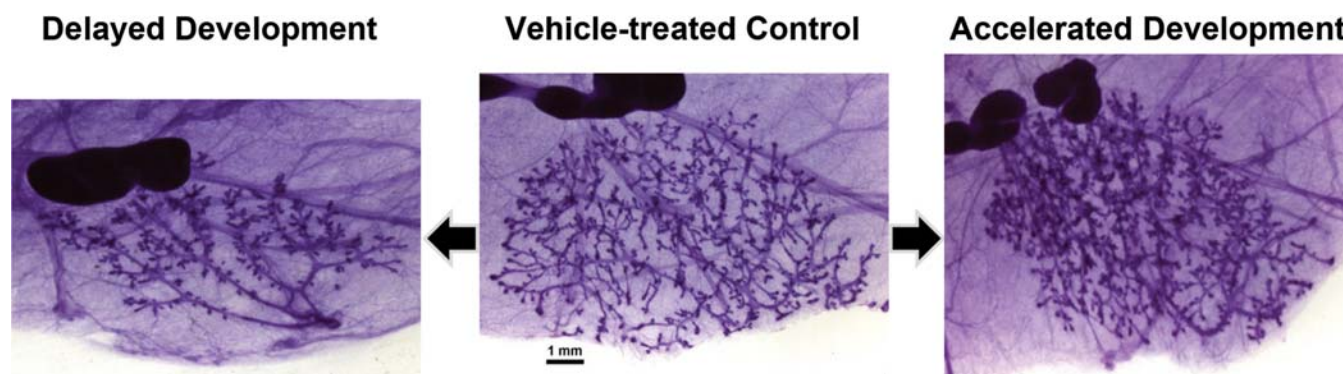


**FIGURE 8.14** Examples of accelerated development (right) and delayed development (left) compared to a representative vehicle-treated control mammary gland at the time of weaning in the female Long Evans rat. Carmine-stained whole mount mammary gland. Specific examples of endocrine-disrupting hormones (EDCs) effects reported. Macon MB, Fenton SE: *Endocrine disruptors and the breast: Early life effects and later life disease*. *J Mammary Gland Biol Neoplasia*. 18(1):43–61, 2013, Figure 3, with permission.

(IRIS) Glossary (EPA, 2023) as “structural developmental defects due to exposure to a chemical agent during formation of individual organs.” Another important developmental target is the TEBs. There is strong evidence demonstrating that the cells within TEBs are the most susceptible or vulnerable to toxic or carcinogenic insult in the mammary gland (Russo and Russo, 1978). Thus, conditions which alter the development and timing of maturation of TEBs may have a substantial impact on the health of the gland in adulthood (Stanko et al., 2016). In dogs and rodents, the susceptibility of the mammary gland to toxicants and carcinogens that perturb the hormonal milieu or that interfere with the cellular responses to hormones begets careful evaluation of serum hormones, and other hormone-related end points such as timing of gonadal control of puberty (vaginal opening, heat, first estrus, etc.), cyclicity patterns, retention of nipples/areolae in males, and possibly anogenital distance measurements. If alterations in any of these measured parameters are observed in studies, the mammary gland should be recognized as a potential target organ. Equally important is that recognition of toxicity mediated by decreased endocrine support of the male or female reproductive system requires an integrated evaluation of the entire reproductive tract, because changes can be present in the gonads, accessory sex organs, mammary gland, and/or pituitary (see *Male Reproductive System*, Vol 5, Chap 9, and *Female Reproductive System*, Vol 5, Chap 10).

Several chemicals are known to interfere with the full development and function of the lactating mammary gland in rats and mice (e.g., dioxin, atrazine, perfluorooctanoic acid [PFOA]; see Kay et al., 2022; White et al., 2011). Such effects should be investigated in reproductive studies reporting decreased postnatal survival, decreased litter weights, or altered growth curves in nursing pups. Nursing pups should have stomachs full of milk. When lactation deficiencies are suspected, functional assessments (often referred to as a “lactational challenge”) of dam-pup interactions should be made. Such evaluations incorporate timed nursing experiments in which dams are separated from pups from 2 to 4 h. Immediately prior to reunion, the litter is weighed, the dam is reintroduced for a fixed amount of time (15–30 min), nursing behavior is assessed, and postnursing litter weights are measured. The difference in pre- and postnursing litter weights serves as a surrogate for milk volume. Histological examination of the dams’ mammary glands is essential to help differentiate underlying morphological alterations (as in Figure 8.3E and F) versus functional alterations (or both). Milk protein measurements from collected milk samples (collected at more than a single time, if possible) may provide valuable biomarkers of effect without having to euthanize the animal. Lipid profiles, protein content, and other nutritional information may be collected using expressed milk samples (Matouskova et al., 2022).

### 3.4. Morphological Evaluations

Thorough morphological evaluation of mammary glands incorporates routine assessment in histological H&E sections (Figure 8.12) as currently practiced for chemical toxicity and regulatory-type safety studies and as warranted, advanced methods such as quantitative morphometric analysis (Stanko and Fenton, 2017) and morphological evaluation of whole mounted mammary glands (see Appendix for protocols and Matouskova et al., 2022). To date there does not seem to be a standard statistically based analysis of the number of histological sections that need to be evaluated or number of objects that need to be counted per slide for special assessments, thus those calculations are required on an individual study basis.

*Histological assessment:* In rodent regulatory-type studies, all gross lesions are collected, and historically mammary gland from the inguinal region is dissected with skin from the same side in both sexes, to include nipple if possible (Ruehl-Fehlert et al., 2003). Sections from this inguinal sample are to be taken transversely or in cross-section (Figure 8.12A). Alternatively, for special assessments, Figure 8.12B demonstrates the major advantage of collecting the fat pad of the fourth and fifth gland of the rodent, cut in longitudinal sections, as it allows a greater chance of detecting a lesion if it exists in the mammary tissue. The contralateral fourth and fifth glands should be isolated for mammary gland whole mounts (see Appendix). Male rats and CD-1 mice retain mammary epithelium, thus could also be evaluated, especially when nipple/areolae retention is noted early in life. Sampling in female or male dogs usually includes one of the inguinal glands and should include the nipple, the duct, and surrounding glandular tissue. More extensive collection is needed for NHPs as mammary epithelial growth extends far into the fat. Glands are placed flat in a histocassette or are flattened onto fiberboard or index card and processed through 48-hour maximum formalin fixation (so not to create brittle adipocyte membranes that may shatter upon sectioning) to a 5-micron section on a charged glass slide and stained with H&E. Temporal biopsies in NHP add the power of analyzing changes over time without the need for euthanasia. Assessment of the mammary

gland should always be done in concert with histologic and/or hormonal evaluation of the hypothalamic–pituitary–gonadal (HPG) axis (hypothalamus, pituitary gland, and gonads), the adrenal gland and other organs such as the prostate and the preputial glands in the male. Evaluation includes examination of a representative section for nonproliferative and proliferative lesions. Diagnostic criteria and nomenclature are summarized in Section 4.

*Morphometric analysis:* Increasingly, tiered approaches to evaluation of mammary tissue are being employed. In addition to an H&E-stained slide evaluation for lesions, sectioned mammary tissue may also receive qualitative assessments, coupled with semiquantitative morphometric analysis, especially when evaluating mammary tissue for developmental delays or precocious development (seen in whole mounts in Figure 8.14). These types of measurements are most useful in weanling or young adult rats, or in mice of any age, and may be performed in sectioned or whole mounted tissues. Useful parameters measured include length of the ductal tree along the longitudinal axis, total area occupied by epithelial ducts, branching density, and total number and size of TEBs, all relative to the total area of mammary epithelium and total area of the fat pad. These parameters can be measured using image analysis software systems (Stanko and Fenton, 2017) or with a dissecting scope, and new software systems are testing artificial intelligence algorithms to quantitate fibrosis and other end points (Hamilton et al., 2022). These measurements on H&E sections are of course limited to the section(s) processed and may not be representative of the gland, depending on the number and location of sections. Immunohistochemistry endpoints including cell proliferation and apoptosis measurements are similarly quantified with respect to location of cells (epithelial, myoepithelial, mesenchymal, ductal, bud, alveoli, and fat pad) and total number of cells evaluated. These endpoints could be measured in tissues of animals of all ages. Increases in epithelial density and cell proliferation in early development have been correlated with the development of cancers later in life in both rodents and NHP (BPA as an example; Acevedo et al., 2013; Tharp et al., 2012). Thus, morphometric analysis of glands, coupled with immunohistochemical staining with proliferating

cell nuclear antigen (PCNA) or Ki67 cell proliferation markers, provide excellent markers of mammary gland changes (see *Special Techniques in Toxicologic Pathology*, Vol 1, Chap 11 and *Digital Pathology and Tissue Image Analysis*, Vol 1, Chap 12).

**Whole mount preparations:** While histologists and pathologists are well-versed in light microscopic techniques and evaluation, whole mount preparation or “wet mounts” (the entire fourth and fifth gland mounted onto a slide), and evaluation is not a routine procedure in all laboratories. However, evaluation of mammary gland morphology in whole mounts allows for a whole gland and potentially more sensitive assessment of the branching complexities and glandular densities. Whole mounts are also more amenable to quantitative assessments of TEBs, alveolar buds, duct and branching development, and growth into the fat pad, because the entire gland is represented. Whole mount preparations are especially useful in mice (any age) and young rats (from birth to 45 days of age) to establish effects of endocrine-disrupting compounds. This technique is currently optional in both the NTP MOG and OECD EOGRTS test guidelines that test in utero exposure to chemicals on developmental/reproductive endpoints. Methods for whole mount preparation and assessment based on previously published peer-reviewed manuscripts are provided (Matouskova et al., 2022). Processing mammary gland for whole mounts is inexpensive but requires careful removal of the fourth and/or fifth gland from the skin and some specialized reagents, detailed in the Appendix. The whole mount should consistently be prepared from the contralateral gland processed for standard H&E slide examination and the H&E section should be cut in the same plane as the whole mount for direct comparison (see Figure 8.12B). Developmental scoring guidelines are provided in Table 8.2 and briefly described below. Note that masses or questionable lesions observed in whole mounts can be evaluated histologically by removing whole mounts from slides, paraffin embedding, sectioning, and H&E staining (Tucker et al., 2017, Figure 8.13).

**Developmental assessment:** As in all assessments of the mammary gland, important factors to consider are the expected (control) developmental maturity of the gland at the various

ages considered (Harlan Sprague–Dawley is shown in Filgo et al., 2016), the species, strain, and the stage of cycle, pregnancy, lactation, or involution. Suggested age-specific factors to use in the evaluation of developing rat mammary tissues are listed in Table 8.2. Glands should be examined under a dissecting microscope first from control animals examined as a group, to establish base-line morphology, such as is customarily done in scoring histopathological lesion severity. Then in blinded fashion, mammary glands can be scored according to the criterion detailed in Table 8.2. If a chemical is known to have an estrogen-like effect in other tissues or cell studies, a 50–500 ng/kg body weight/day ethinyl estradiol positive control may be used, but often the effects of a test compound on the gland are not known and effects opposite of estrogens may be detected (e.g., developmental delays such as those reported by dioxin or PFOA; see Kay et al., 2022 for chart of chemicals and effects).

As detailed in Table 8.2, key parameters to evaluate in the developing mammary gland include: (1) the number of TEBs relative to the number of duct ends and the morphology of the TEBs; TEB in a rat are end structures greater than 100  $\mu\text{m}$  wide while typically in the mouse, TEB are denoted as ends measuring greater than or equal to twice the duct width; (2) the degree of duct branching and amount of mammary epithelium present including the degree of lateral (side) branching and/or budding (branch density) and the number of primary ducts growing from the nipple (particularly in 4 day old animals; this may not be possible in older animals); (3) the degree (relative amount compared to control samples) of alveolar bud and lobule formation; (4) growth of the gland, both length- and width-wise.

### 3.5. Biochemical Indicators and Biomarkers

Measurements of serum protein and steroid hormones involved in reproduction are often used as biomarkers in assessing toxicity in the female. However, use of these as biomarkers specifically in relation to potential mammary gland toxicity may not be informative without correlative morphologic evaluation and, in the postpubertal female, comparison within the same stage of the estrous cycle. Moreover,



**TABLE 8.2** Developmental Scoring System Used for Morphological Assessment of Mammary Gland Whole Mounts Following Early Life Chemical Exposures

Score <sup>a</sup>	Developmental criteria <sup>b</sup>
<b>PND 4</b>	
1	Large lateral branches off primary branches only, few ductal buds from lateral branches, undersized, one or few primary ducts, primary ducts lack buds
2	Small buds formed on primary branches and lateral branches, few branches, more than 1 primary duct with few buds
3	Good growth pattern with score of 1 and 2 surpassed, small terminal buds, moderate branching with moderate budding on both lateral and primary ducts
4	Growth exceeding the above criteria is evident, distended terminal ends and abundant branching pattern, extensive budding on primary and secondary ducts, excellent growth
<b>PND 22–28</b>	
1	Poor structure, clearly underdeveloped, no terminal end buds (TEBs) present (only terminal ducts), few branches off lateral ducts
2	Normal structure, few buds, few lateral branches, TEBs distended, many lateral branches on terminal ducts, but sparse in appearance (larger ducts may have few lateral branches)
3	Good branching, buds present throughout, large TEBs on all ducts and branches, all TEBs and terminal ducts distended
4	Generous branching, buds and TEBs on ducts, excellent migration and gland size, lobule formation starting throughout gland
<b>PND 33</b>	
1	TEBs remain on all sides, 2 glands not grown together, growth pattern and differentiation impaired, no or few lobules apparent
2	TEBs on 2–3 sides, glands close together, growth impaired and sparse branching, lobule buds barely evident
3	Glands close together or touching, TEBs only on distal ends, branching sparse, one gland w/lobules, one not, or half and half
4	Glands grown together, few TEBs remain, dense branching, lobules visible-multi-unit
<b>PND 40–45</b>	
1	TEBs on both ends, sparse branching, limited growth pattern, glands not touching
2	TEBs on both ends, moderate growth, limited lobule development
3	TEBs on long end (MG#4), dense and large, lobules apparent throughout
4	Few to no TEBs remain, very large, dense branching, multiunit lobules developed
<b>PND 67–90</b>	
1	TEBs still present, epithelium doesn't fill fat pad, sparse branching throughout, lobules evident
2	No TEBs evident, sparsely branched with many large lobuloalveolar units, may not fill fat pad
3	Moderate size, moderate filling and branching, some areas beginning to differentiate into static state, moderate lobules
4	Few complex lobules, dense branching throughout gland with extensive buds on ducts

<sup>a</sup> A score of 4 represents a gland that is most well developed, while a score of 1 represents few of the necessary developmental criteria.

<sup>b</sup> The scoring criteria presented in the table above are for female Long Evans rats of the indicated ages. The criteria may be used to detect delayed development following chemical exposures early in life. They may be used for other rat strains, mice, or males of any age, species, or strain with some modifications. As mice have limited lobular development, those young adult criteria (PND45–90) would need moderate adjustment.

Modified from Haschek WM, Rousseaux CG, Wallig MA, editors: Haschek and Rousseaux's handbook of toxicologic pathology, ed 3, 2013, Academic Press, Table 60.2, p. 2681, with permission.

significant morphologic changes can occur in the gland early in development which may not be associated with altered circulating hormones in the adult.

In tissues, measurements of cellular receptor levels, activation of receptors and their signaling pathways, and cell proliferation markers are typically regarded as sensitive biomarkers of toxicity. However, due to the complexity of the mammary tissue, it is often helpful or required to know the cell type that is conferring the noted change in the biomarker. For example, increases in epithelial density and cell proliferation in early development has been correlated with development of cancers later in life in both rodents and NHPs. Thus, morphometric analysis of glands, coupled with immunohistochemical staining with bromo-2'-deoxyuridine, PCNA, or Ki67 cell proliferation markers, provide accurate and sensitive markers of mammary gland changes (Hvid et al., 2021). Receptor levels or pathway activation can also be evaluated through immunohistochemical markers or molecular techniques, using the whole gland. Further analyses can be performed on digested and cell-type-sorted samples (using flow cytometry), with increased time and cost investment. The increased use of single-cell sequencing, and other single cell molecular evaluation techniques are also advancing the ability to determine cell-type specific outcomes.

Lactational effects can be measured through surrogate evaluation of pups or analysis of mammary gland sections of the exposed dam. Milk protein measurements from collected milk samples (collected at more than one time point, if possible) may provide valuable biomarkers of effect without having to sacrifice the animal. Lipid profiles, protein content, and other nutritional information may be collected using expressed milk samples (Matouskova et al., 2022).

## 4. RESPONSES TO INJURY

### 4.1. Physiologic Responses

Especially in developing offspring and young adult rodents, the most recent emphasis in toxicology has been placed on understanding the direct or modifying effects of endocrine-disrupting compounds (Gore et al., 2015; see

*New Frontiers in Endocrine Disruptor Research*, Vol 3, Chap 12 and *Endocrine System*, Vol 4, Chap 7). These compounds are often reported as causing either accelerated maturation or delayed differentiation of the gland in females (Figure 8.14), or in altering glands in the male from a lobular phenotype to a more female-like tubuloalveolar morphology (Figure 8.6E and F). Retained nipples in male rodents are also characteristic of antiandrogen effects. Accelerated mammary growth in females may be characterized as increased TEB formation at early life timepoints (weanlings) and decreased TEB numbers at later time periods (postvaginal opening). Delayed maturation may be characterized by the presence of TEBs until much later in development, extending the window of time that these carcinogen-sensitive structures are present in the gland. Inhibition of development may also be reflected as a decrease density of the gland, as well as an overall decrease in total TEBs formed.

Ductular hyperplasia and dysplasia, evident in both whole mounts (Figure 8.11) and H&E-stained sections, can be induced with various estrogen like compounds, but as mentioned previously, many of these effects depend on timing of exposure and the extent of mammary gland development within the animal of interest. For example, exposure to estrogenic compounds through the perinatal period in rats, when TEBs are developing, is associated with hyperplasia of the buds, while exposure during the peripubertal period, when ducts are developing, is associated with ductal hyperplasia. Neonatal exposure to estrogen, progesterone, or both in mice causes irreversible effects in adults, including secretory stimulation, dilated ducts, and abnormal lobuloalveolar development (Rudel et al., 2011). Phytoestrogens, such as genistein and resveratrol, and the mycoestrogen zearalenone act similarly to estrogen agonists in their effects on the gland. Changes include delayed development, ductal hyperplasia, alveolar hypoplasia, reduced apoptosis in TEBs, increased or decreased numbers of terminal ducts or lobules, and accelerated alveolar differentiation, again depending on time of exposure.

Altered mammary gland development following perinatal exposure has also been observed for other endocrine-disrupting compounds, including atrazine, BPA and its analogs, dibutylphthalate, dioxin, methoxychlor,

nonylphenol, polybrominated diphenyl ethers, PFOA, and others. Some of these compounds such as methoxychlor act as estrogen agonists, but most of these compounds have pleomorphic effects on hormone receptors or hormone signaling in many tissues, and thus correlating a specific physiological and morphological response to classes or specific compounds is complex.

Systemic hormonal changes and correlative mammary morphologies related to spontaneous aging and testing of pharmaceutical-based hormone receptor agonists and antagonists have been nicely characterized in rats (see [Lucas et al., 2007](#)). Common changes in the aging adult male rat include a tubular alveolar pattern with formation of central lumens (lobular atrophy) and is attributed to increased prolactin and GH levels but was reported in male rat mammary tissue exposed to diethylstilbestrol in utero ([Filgo et al., 2016](#)). Because these hormones increase in aging rats, and particularly in strains with high incidence of pituitary tumors, such changes in male rat morphology can be an indirect effect of a treatment as well as represent an adverse effect of endocrine disruption, so careful comparison to untreated controls is critical. In the adult female rat mammary gland, lobuloalveolar hyperplasia with or without ductal ectasia and secretory activity are associated with increased levels of circulating prolactin, GH, or estrogen levels and often associated with endocrine disruptor exposures. Lobular hypertrophy/hyperplasia in the female gland occurs with androgen stimulation or higher levels of circulating testosterone. However, an increase in lobuloalveolar density is also present in early pregnancy, and in response to changes in prolactin levels. Thus, when such morphologies are observed in the mammary gland of rats in study, careful consideration should be given to life stage and determining hormonal effects versus potential direct effects on mammary gland development.

#### 4.2. Molecular and Biochemical Responses

At the biochemical and molecular levels, complex and varied responses occur after injury. Molecular signaling through hormone and growth factor receptors is altered by changes in hormone receptor expression, receptor levels,

receptor affinity to ligands, or receptor localization. These are further altered by the production of local growth factors and hormones as well as genetic mutations that result from injury.

Gene expression profiles from chemically induced mammary gland cancers in Sprague-Dawley rats show distinct differences from spontaneous mammary tumors ([Hoenerhoff et al., 2009](#)). Compared to spontaneous carcinomas, carcinomas induced by either PhiP, DMBA, 2-amino-3,8-dimethylimidazo[4,5-f]quinoxaline, NMU, or 4-aminobiphenyl show higher expression of genes associated with mammary epithelial cell growth and proliferation, such as cyclin D1, platelet-derived growth factor- $\alpha$ , and relatively lower expression of differentiation marker genes, such as  $\beta$ -casein, whey acidic protein, and transferrin. Additionally, several components of the prolactin/prolactin receptor/Stat5a/cyclin D1 signaling pathways are found in the chemically induced rat mammary gland carcinomas. Tissues from mammary cancer in DMBA-treated FVB mice have elevated expression of the AhR, c-myc, cyclin D1, and hyperphosphorylated retinoblastoma protein compared to normal mammary gland tissue. Mammary cancer associated with benzene and ethylene oxide exposure to mice had increased mutations in Tp53 protein and H-ras mutations in a chemically related pattern distinguishable from spontaneous mutations ([Houle et al., 2006](#)). However, for most of the compounds associated with mammary gland injury and dysmorphogenesis, the molecular pathways remain to be defined.

Exciting technologies such as isolating cell free DNA and noncoding RNAs from extracellular vesicles shed from damaged or diseased tissue into the circulation (from blood or milk or urine) has the potential to open many possibilities in terms of predictive biomarkers of disease or exposure (see [Schwarzenbach 2013](#)). These approaches and others are being used to associate environmental chemical exposure with preeclampsia risk and other diseases.

#### 4.3. Morphological Indicators

The response of the mammary gland to injury recapitulates a wide spectrum of nonproliferative and proliferative changes. Standardized nomenclature provides consistency of diagnoses



across studies and captures patterns of lesions that represent xenobiotic effects with biological significance. International Harmonization of Nomenclature and Diagnostic (INHAND) has established rodent and nonrodent working groups to standardize the nomenclature summarized in this chapter for rodents, dogs, and cynomolgus monkeys (*Macaca fascicularis*) (Rudmann et al., 2012; Woicke et al., 2021; Colman et al., 2021). An important note is that the various strains of mice and rats will have their own extent of background lesions beyond which an effect of chemical needs to be evaluated. Historical background incidences from various studies are often available from the animal supplier or study site.

**Rodents:** Nonproliferative changes manifest as degenerative (degeneration, single-cell necrosis, necrosis), inflammatory (infiltrate, inflammation, and fibrosis), and vascular or, in relation to alterations in growth, manifest as atrophy or hypertrophy. Degenerative changes affecting the epithelial and myoepithelial cells of the ducts and alveoli are mostly associated with aging or occasionally observed as a test-article effect. The changes are characterized by epithelial swelling and vacuolization, loss of cell layers and ductal dilation with accumulation of proteinaceous material. Single-cell necrosis/apoptosis of the ductular/alveolar epithelium is characterized by shrunken cells with distinct cell membranes, membrane budding with condensed nuclei, and rare inflammatory infiltrates. Cellular necrosis within the mammary gland is rarely observed, but fat necrosis with inflammation occurs as incidental findings. Regeneration is usually observed in areas of degeneration and necrosis as they typically present together in repeated mammary gland injury.

Inflammatory changes and infiltrates in rodent mammary glands are usually limited to small numbers of lymphocytes, neutrophils, and macrophages and/or plasma cells into the lamina propria of the lobule and associated tissues and should be differentiated from the lymphocytic and eosinophilic infiltrates that accompany normal ductular morphogenesis. The term infiltrate is recommended if other signs of inflammation are not present. The term infiltrate or inflammation should be followed by the predominant cell type or “mixed” if no

predominant cell type is observed. The exception is granulomatous inflammation, which is discussed below.

Inflammation can be categorized temporally as acute, chronic, or chronic active. Inflammation may be observed in mammary gland whole mounts, and sectioned and stained tissue, as shown in mouse tissue in Figure 8.13D and F. Granulomatous inflammation is a special type of chronic inflammation that may suggest an etiologic agent (fungi mycobacteria or foreign body) but is most often observed in rats with rupture of a dilated duct. Granulomatous inflammation consists predominantly of plump macrophages (epithelioid cells) that may form interlacing bundles and may be accompanied by lymphocytes, plasma cells, and fibrosis/fibroplasia. Granulomatous inflammation may be accompanied by regenerative, hyperplastic, and/or metaplastic changes in the epithelium.

Fibrosis, most often periductular, is a common age-related change in rats (Durando et al., 2007) and has been associated with EGF and bisphenol treatment in mice (Figure 8.13C and E). Recent studies have also demonstrated the increasing incidence of toxicants affecting the stromal and adipose-rich areas of the mammary gland, specifically, enhanced macrophage infiltration, stromal hyperplasia, and altered fat cell size or number have been noted (see *Adipose Tissues*, Vol 4, Chap 6; White et al., 2009). Vascular changes such as congestion, edema, hemorrhage, angiectasis, and thrombosis occur rarely in the mammary gland and its vasculature, the mammary fat pad, or surrounding tissues.

Dilation of ducts or alveoli with or without epithelial hypertrophy or hyperplasia occur as an age-related change. However, dilation with alveolar epithelial hypertrophy and hyperplasia has been observed as a test-article related effect in younger animals (White et al., 2009). These lesions occurring at a primary target (mammary gland) or secondary to perturbation of the HPG axis should be considered potential test article related changes.

Alterations in growth are commonly associated with age as well as observed as a test-article related effect in younger animals. For example, ER- $\alpha$  agonists cause hypertrophy/hyperplasia of the alveolar and/or ductal epithelium (Figure 8.15) and secretory activity in female rats and lobular atrophy of the mammary

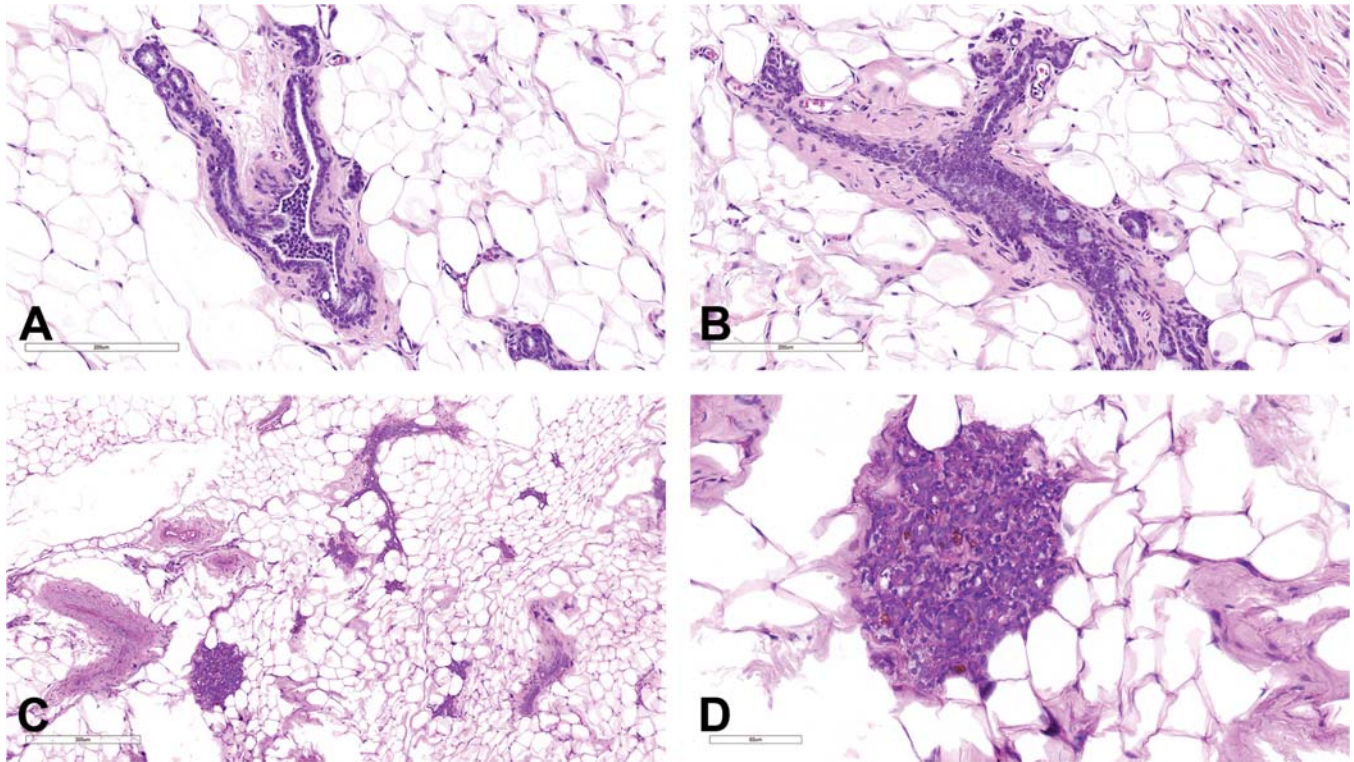


**FIGURE 8.15** Mammary gland: Treatment-induced hypertrophy and hyperplasia, alveolar and ductal epithelium, female Sprague-Dawley 9-month-old rat. H&E stain. (A) Minimal hypertrophy and hyperplasia, ductal epithelium with piling of epithelial cells filling lumen (10× magnification). (B) Mild hypertrophy and hyperplasia, ductal epithelium with ductular closure (10× magnification). (C) Low magnification of a nodule (2× magnification) that at higher magnification in (D) shows hypertrophy and hyperplasia of the alveolar epithelium (10× magnification). Reproduced from Haschek W, Rousseaux C, Wallig M, Bolon B, editors: *Fundamentals of toxicologic pathology*, ed 3, 2018, Academic Press, Figure 19.7, p. 560, with permission.

gland in male rats. Hypertrophy/hyperplasia of the alveolar and/or ducts is characterized by an increased predominance of irregular nests of alveolar cells often not associated with a clear duct, increased alveolar cell size and cytoplasm. Alveolar and ductal epithelium may have a pseudostratified appearance. AR agonists have no effect in the male mammary epithelial structures but may induce increased secretion and accelerated ductal branching the female rat. In contrast, AR antagonists cause atrophy of the male rat mammary gland and areola and/or nipple retention (Schwartz et al., 2021), with no effect on the female rat mammary gland. Progesterone receptor antagonists cause hypertrophy/hyperplasia of the alveolar and/or ductal epithelium and secretions in female rat mammary glands but have no effect on male rat mammary gland, as the male mammary gland does not express these receptors (see Filgo

et al., 2016). Hypertrophy/hyperplasia of the ductal epithelium is increasingly being recognized particularly in studies of rats exposed to chemical carcinogens or endocrine disruptors during development (Crist et al., 1992; Vandenberg et al., 2008). Similar to postnatal exposure, lesions are characterized by a disruption of the epithelial bilayer and disorganized masses of cells bridging across or filling the ductal lumens. The basement membrane remains intact (Figure 8.11).

Lobuloalveolar hyperplasia can be diffuse, focal, focal with atypia, or focal with fibrous proliferation and should be distinguished from hypertrophy/hyperplasia of the alveolar and/or ductal epithelium (described above). Diagnostic distinguishing characteristics of lobuloalveolar hyperplasia include the retention of the regular architecture (distinct tubuloalveolar architecture of the female is maintained), normal



relationship between ductal and alveolar epithelial cells and associated ducts, and little to no cellular (alveolar and ductal cells) pleomorphism. In addition, alveoli and ducts may be distended with eosinophilic material as evidence of secretory activity. Diffuse hyperplasia is usually physiologic and is prominent in late gestation and during lactation. Importantly, dopamine receptor antagonists, which stimulate prolactin secretion, will cause lobular alveolar hyperplasia in females—an effect often seen in aging female rats with elevated prolactin levels.

In rodents, benign neoplasms include adenomas, fibroadenomas (of mixed origin), adenomyoepithelioma, and benign tumors of mixed origin (epithelial and mesenchymal) (Rudmann et al., 2012). In the chemical carcinogen-treated rat model, benign tumors arise from alveolar buds and lobules, while carcinomas arise from epithelial cells in less differentiated TEBs and terminal ducts. Adenomas are usually detected in routine

sectioning of the mammary gland and may be visible as nodules. Histologically they are characterized as well-demarcated, sometimes encapsulated, and expansive masses that compress surrounding normal tissue. They are composed of cysts, alveoli, or papillary fronds of single or multiple layers of epithelial cells aligned on a fine fibrovascular stroma. The epithelial cells are cuboidal, well differentiated, and may show secretory activity. Focal areas of squamous metaplasia may occur. Although there are morphological subtypes, it is not standard to subclassify tumors in toxicity studies (unlike humans, where that is standard practice).

Fibroadenomas are a proliferation of glandular epithelium surrounded by layers of proliferated fibrous tissue. Fibroadenomas are lobular, well-demarcated, and expansile with varying proportions of well-differentiated epithelial tubules or glands and dense fibrous stroma. Small areas of atypia and/or pleomorphism may be present (Figure 8.16A). Mitotic activity is low, and these

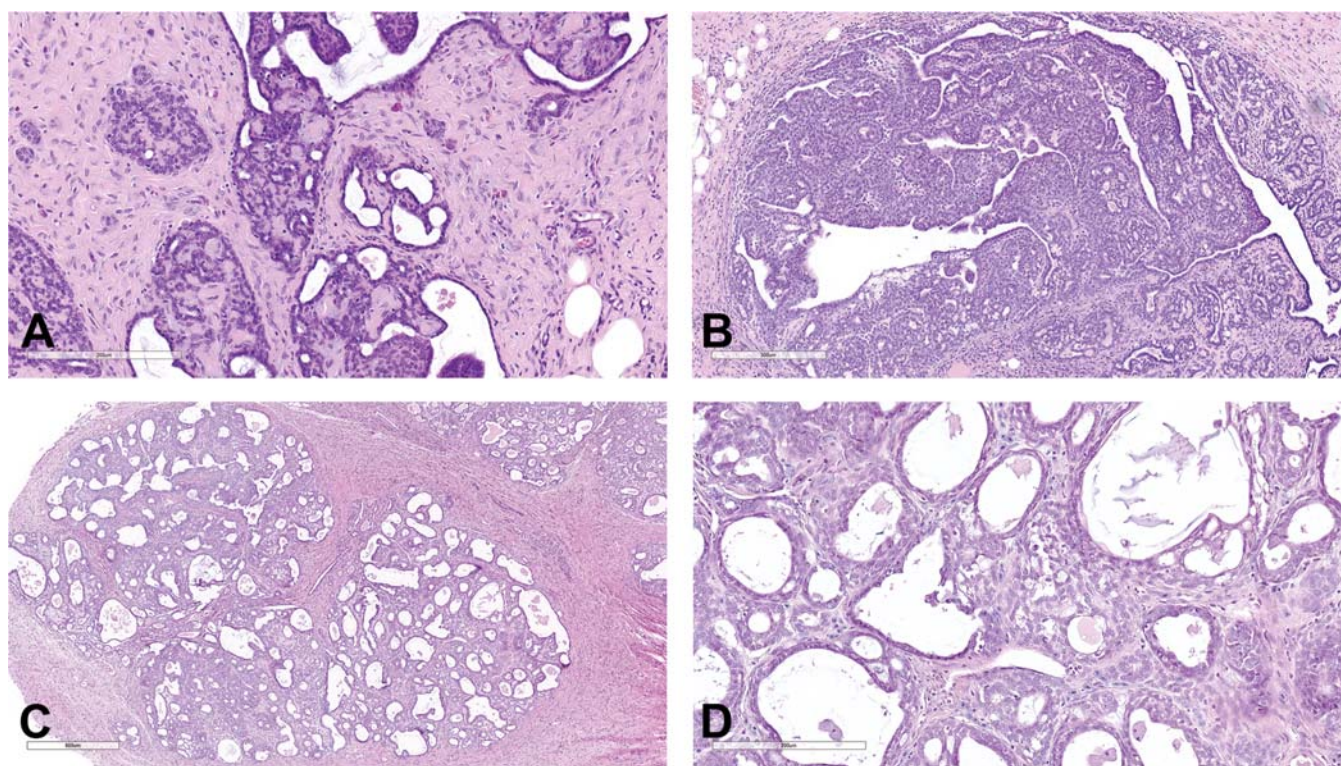


**FIGURE 8.16** Treatment-induced mammary gland tumors, female 9-month-old Sprague-Dawley rat. H&E stain. (A) Fibroadenoma with epithelia atypia. The predominant component is fibrous matrix (4× magnification). (B) Adenocarcinoma. The predominant component is pleomorphic epithelium (4× magnification). (C) Adenocarcinoma arising in fibroadenoma (4× magnification). (D) higher magnification of (C) showing epithelial proliferation and disorganization within fibrous matrix (20× magnification). Reproduced from Haschek W, Rousseaux C, Wallig M, Bolon B, editors: *Fundamentals of toxicologic pathology*, ed 3, 2018, Academic Press, Figure 19.8, p. 561, with permission.



lesions do not express ER- $\alpha$  or PR. Rarely, carcinomas can arise within fibroadenomas and should be diagnosed appropriately as “adenocarcinoma arising in fibroadenoma” (Figures 8.16C, D and 8.17). Whether this is a strain specific lesion is unknown.

Adenomyoepitheliomas are complex mammary gland neoplastic lesions composed of both epithelial and myoepithelial origins described in many species (humans, dogs, rats) and rarely in mice (Bauchet et al., 2008). Histologically, acinar structures are separated by abundant stroma with smooth muscle actin spindle cells. Benign mixed tumors are rare in rodents but are the most common spontaneous tumor in domestic female dogs (Dantas et al., 2012). These mammary tumors are neoplastic proliferations of both epithelial and mesenchymal cells with differentiation of the latter into islands of cartilage, bone, or adipose tissue, and diagnostically classified differently from fibroadenomas because benign mixed tumors do not have a predominant fibrous component. The distinction between benign and malignant

mixed tumors is based on the extent of invasion of the surrounding tissues.

Malignant tumors include adenocarcinomas, adenocarcinomas arising in fibroadenomas, and malignant mixed tumors. Adenocarcinomas (Figure 8.16B) are malignant proliferations of pleomorphic columnar or cuboidal epithelial cells arranged in papillary, cystic, tubular, solid, or cribriform or comedo patterns. There may be complete loss of lobular-alveolar structures and acini may become cystic or blood-filled. Adenocarcinomas express ER- $\alpha$  and PR (Figure 8.17) and can induce a marked scirrhous response. These cancers can be locally invasive and metastatic. In mice, if more than about 25% of the tumor has squamous differentiation, then it should be diagnosed as an adenosquamous carcinoma.

*NHP:* Nonneoplastic lesions manifest as dilation of lobules and ducts, and apocrine metaplasia with alveolar dilation, infiltrates, inflammation and secretory changes resembling apocrine sweat glands. These are generally incidental, related to aging and reproductive status.

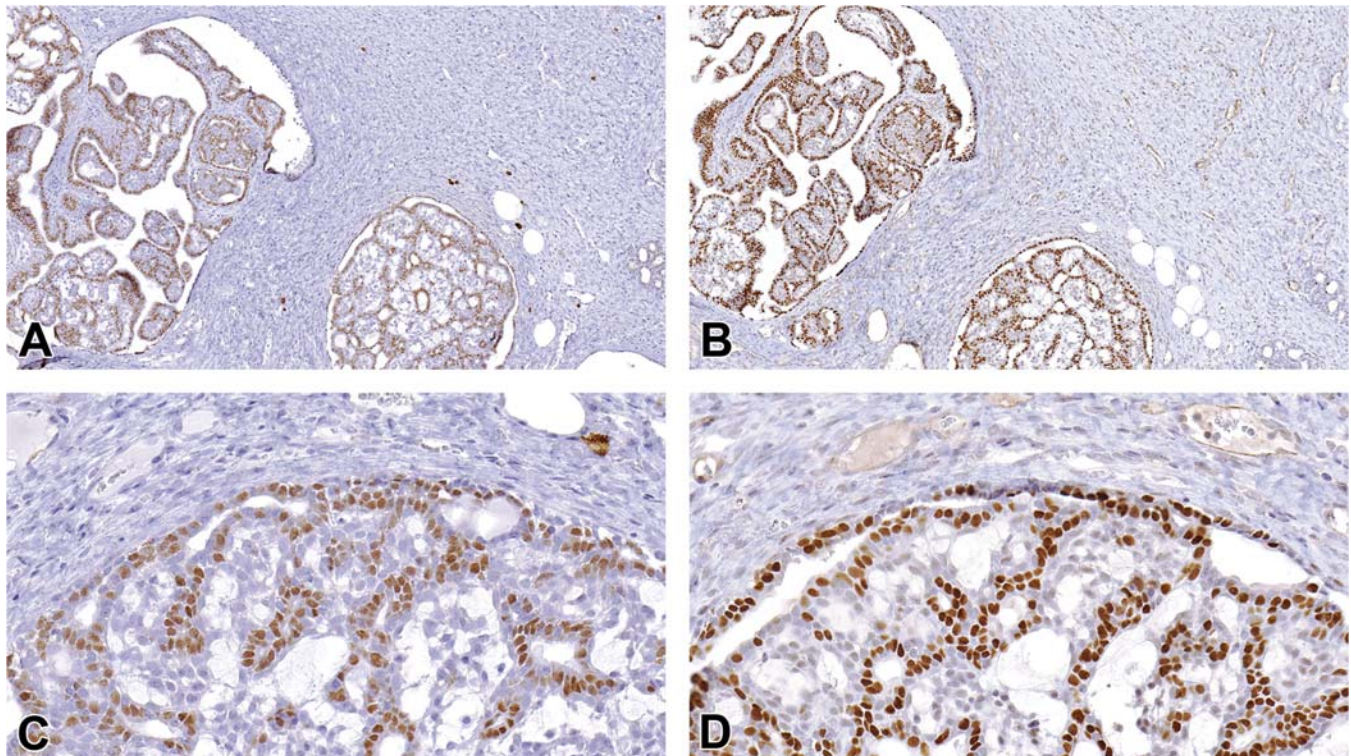


**FIGURE 8.17** Treatment-induced mammary gland adenocarcinoma arising in fibroadenoma, Sprague-Dawley female rat. (A-B) 10 $\times$  and (C-D) 40 $\times$  magnification of serial sections demonstrating (A, C) estrogen receptor- $\alpha$  and (B, D) progesterone receptor staining in the adenocarcinoma only.

Hyperplastic changes can affect lobuloalveolar, lactiferous duct, or intralobular (terminal) duct epithelium and present focal and multifocal lobular proliferations seen in older rhesus, pigtail, and cynomolgus macaques (Wood et al., 2006). The lesions are characterized as enlarged or distinct nodules of well-differentiated alveoli and may proliferate independently of hormonal stimulation. Ductal hyperplasia is characterized by focal increased epithelial cells into two to three layers, with maintenance of polarity and size. These are common spontaneous lesions in intact middle-aged rhesus macaques. Hypertrophy and hyperplasia of the mammary gland components (lobuloalveolar, lactiferous duct, or intralobular duct epithelium) can be observed in male macaques secondary to long-term estrogen and progesterone treatment.

DCIS is distinguished from ductular hyperplasia by increased layers of disorganized, pleomorphic epithelial cells that bridge and occlude the lumens of tubules. The basement membrane remains intact. Loss of basement membrane is diagnostic of carcinomas/adenocarcinomas, which can be invasive and metastatic. DCIS occur commonly in mammary gland of cynomolgus and rhesus macaques, but development of larger carcinomas is not common (Roberts et al., 2014).

*Dog:* In cycling females, mammary gland changes such as fibrosis, apoptosis (single-cell necrosis), and pigment accumulation may be observed as a part of the normal estrous cycle. A detailed description of estrous cycle-related changes in the canine female reproductive tract including the mammary gland is provided (Rehm et al., 2007).

Dogs used in routine toxicology studies are usually young, in excellent condition and only on study for a relatively short period of time. For these reasons, the incidence of mammary neoplasia in this population is different from those in domestic animals. As mentioned above, benign mixed tumors are the most common spontaneous tumor in domestic female dogs (Dantas et al., 2012). For detailed descriptions and diagnostic criteria of canine neoplasms, refer to the "International Histological Classification of Tumors of Domestic Animals: Mammary Tumors of the Dog and Cat," published by the Armed Forces Institute of Pathology in conjunction with the American

Registry of Pathology and the World Health Organization (Misdorp et al., 1999), "Tumors of Domestic Animals" (Goldschmidt et al., 2020), and other relevant literature.

## 5. MECHANISMS OF TOXICITY

Mammary gland toxicity and carcinogenicity have been observed in animal models exposed to a wide variety of agents including estrogens, androgens, antiandrogens, thyroid-active chemicals, and AhR agonists, genotoxic compounds, and mutagens (Kay et al., 2024). However, the mechanisms of toxicity and carcinogenicity are generally unknown. Several of the rodent mammary gland carcinogens are epoxides or epoxide metabolites. These include such chemicals as 1,3-butadiene and related chloroprene and isoprene which are metabolized to epoxides. These epoxides are mutagens and associated with *K-ras* mutations in rodents. Isoprene and 1,3-butadiene also cause chromosomal aberrations in rodent bone marrow cells. Although the mechanisms related to epoxide-induced mammary cancer is unknown, one hypothesis is that the mammary gland is efficient in metabolizing the chemicals to their epoxides. Brominated species are also associated with rodent mammary cancers. Chemicals such as 2,2-bis(bromomethyl)-1,3-propanediol are proposed to act either through oxidative damage or formation of DNA adducts and then DNA damage. Many of these chemicals also induce cytochrome P450 metabolizing enzymes, which, like DMBA, can activate chemical reactivity or be metabolized to electrophilic oxygenated species that bind DNA. It has been proposed that halogenated mammary gland carcinogens, which tend to be lipophilic, accumulate in breast fat resulting in exposures for prolonged periods of time. Atrazine, brominated diphenyl ethers, PFOA, and dioxin, all have been shown to induce delayed mammary gland development following neonatal exposures, presumably through interactions with hormone responses. At the molecular level, in utero exposure of mice to diethylstilbestrol, BPA, and other bisphenol analogs with estrogenic activities increased protein expression and functional activity of the histone methyltransferases, which have been linked to breast cancer risk and epigenetic



regulation of tumorigenesis. It is also possible for endocrine-disrupting compounds to act via indirect mechanisms in rodents to induce persistent morphologic effects in mammary tissue (White et al., 2009; Su et al., 2022). Furthermore, a wealth of data (DeVaux and Herschkowitz, 2018; Ivanova et al., 2021) suggest that epigenetic mechanisms—those changes to DNA that cause a heritable modification without changing the DNA code—may have important roles in mammary and many other cancers over the lifetime.

## 6. CONCLUSION

There are numerous public health reasons for a heightened understanding of environmental contaminants and drugs adversely affecting the mammary gland. The high incidence of breast cancer in young women, precocious breast development during puberty, and evidence of chemicals associated with shortened breastfeeding duration has brought attention to the need for appropriate and sensitive methodologies to prioritize mammary gland evaluation in animal model test guideline and fit-for-purpose studies. We now have a substantial number of genetically modified and spontaneously occurring mice and rat mammary cancer models to employ and various approaches to assess gland morphology. Of the lessons learned, we know that hormonal perturbations including chemicals that act as endocrine disruptors pose a significant risk and that such risk may be increased when exposures occur during development. Given this information, animal studies designed for hazard identification should incorporate exposures during development and, as appropriate, enhanced methods for structural evaluation of mammary gland such as whole mount evaluations and/or morphometry when mammary gland toxicity is suspected or endocrine disruption activity is present. As well, *in vitro* screens should continue to serve as important tools for identifying potential hazards and supporting mechanistic understanding of effects. Indeed, discovering genetic and environmental causes of breast cancer goes hand-in-hand with strategies to prevent and discoveries to treat breast cancer.

## APPENDIX: PREPARATION AND EVALUATION OF MAMMARY GLAND WHOLE MOUNTS IN MICE AND RATS

In this procedure, the entire fourth and fifth mammary gland can be removed from rodents as a single tissue. The tissue is slide-mounted, fixed, stained with carmine alum, and made transparent to allow for evaluation of three-dimensional epithelial structures. The whole mount procedure enables determination of accelerated or delayed mammary gland development due to early life endocrine disruptor exposures. One pup per dam (minimum) should be evaluated if developmental exposure was conducted.

### 1. Collection of the Intact Mammary Gland

#### A. Equipment and Supplies

1. Fine curved scissors
2. Dissection board
3. Straight scissors with one blunt end
4. Holding pins
5. Fine curved forceps
6. Charged slides; use 2 × 3" slides for PND 70 or older rats; standard sized slides may be used for mice and young rats
7. Curved, serrated forceps
8. 70% ethanol
9. Extra nonfrosted/charged glass microscope slides
10. Parafilm (cut into 2 × 3 in. rectangles)
11. Baking or cafeteria style trays for stacking slides
12. 50 mL conical tubes filled with water and capped, or another object with a flat surface that weighs the same, such as 3-D printed materials—50–60 gm equivalent.

#### B. Procedure

1. Prelabel all slides using a xylene-proof method. Pencil works and should be covered with mounting solution at the end to preserve the label.
2. Euthanize animals as designated in the study protocol.
3. Lay the animal on its back on a dissecting board.
4. Stretch the rear feet into an inverted V and pin feet down (holding pins or small gauge needles work well).



5. Wet the animal's abdomen and rear legs with 70% ethanol (to reduce hair in the gland preparation) and wipe down with a small Kim-wipe.
6. With the straight scissors, make a skin incision from the pubis to the rib cage, being careful not to cut through the internal abdominal wall (see [Figure A8.1](#)), and using as few cuts as possible.
7. Make an incision from the origin of the first incision (at the pubis) along the

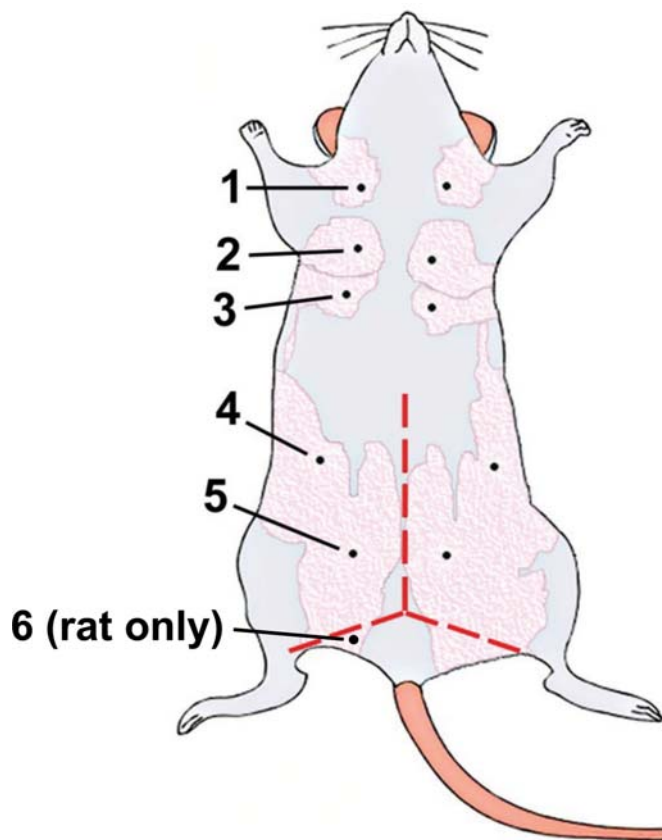


**FIGURE A8.1** Schematic drawing of a mouse showing the five mammary glands and the locations of the nipples. In rats, there is a sixth mammary gland and nipple caudal to the fifth. The dashed line indicates the inverted-Y incision line for removal of the mammary gland fat pad. In the actual procedure, the limbs will be stretched out and down, and the incisions will extend farther down the medial aspect of the hind limbs. Adapted from Honvo-Houéto E, Truchet S: *Indirect Immunofluorescence on Frozen Sections of Mouse Mammary Gland*. *J. Vis. Exp.* (106):53179, 2015. doi:10.3791/53179. Figure 4, with permission.

- medial aspect of each rear limb, forming an inverted Y (see [Figure A8.1](#)).
8. Carefully grasp the skin (and not the gland attached to it) with the curved backside of a serrated forceps at the center of the inverted Y (i.e., at the origin of the incisions at the pubis).
9. Peel the skin back and allow the mammary fat pad to stay attached to the skin, cutting the fat pad away near the pubis if necessary. Be careful not to cut the femoral artery. Pin the skin, but not the fat pad, to the dissection board (or other flat surface such as a cooler top). This exposes the fourth and fifth mammary glands (and sixth in the rat). In the rat, the fifth and sixth glands may need to be separated by cutting through the gland at the leg.
10. Using the back side of the fine curved forceps (not the tips), gently separate the fat pad containing the fourth and fifth glands (leave the sixth gland in rats) from the skin at the point where the skin is pinned and lift it away from the skin (lateral point), cutting the attachments to the skin underneath the fat pad (with fine scissors). Keeping the tips down, and flat against the skin, use long, smooth cuts rather than short snips to prevent alteration of the gland morphology and the formation of air bubbles on the slides. The forceps may need to be repositioned further down the fat pad, or roll the gland up onto itself, to prevent the gland from tearing. Be sure to lift, not pull up on the fat pad. It will tear.
11. When the entire fat pad (to the back of the animal) containing the fourth and fifth mammary glands has been separated from the skin, make a straight (dorsomedial) cut parallel to the animal's body and detach the fat pad/mammary glands.
12. Lay the mammary tissue on a dry labeled slide, with the side that was adjacent to the skin next to the glass, and with the dorsomedial end positioned at the frosted end of the slide. Using the backside of the forceps, completely spread out one fat pad/mammary gland set (glands 4/5 as a single unit) per slide. Try to keep the gland the

same size as it was in the animal. The thickest part of the gland should be adjacent to the slide label and the lymph node should be near the center of the slide.

13. Once the mammary tissue has been spread onto slide and is still wet, press gently on the tissue with your gloved fingers to remove bubbles that may be under the tissue. Place a 2 × 3 inch rectangle of Parafilm on the gland and again gently press on the Parafilm to make sure there are no bubbles. Cover with another glass slide to make a sandwich. Move it to the tray and place an inverted 50 mL conical tube filled with water (or another object weighing 50–60 g) on the mammary tissue/glass slide sandwich.
14. Allow the mammary sandwich to sit at room temp for 30–45 minutes or in a refrigerator for up to 1.5–2 hours. Depending on its thickness, PND 70 or older rat tissues may require as much as 2 hours. This step is to make sure that the gland has adhered to the slide and will not come off when the sandwich is dismembered.

### C. Helpful Hints

1. Removing the intact fourth and fifth gland in one piece is the most difficult part of the process—lift gently without squeezing hard or pulling up. Be sure to use the back side of the curved forceps and not the pointed ends to work with the tissue. The gland may be rolled onto itself to prevent tearing. If you do this, unroll as you put it onto the slide.
2. Make sure to get the tissue adjacent to the animal's dorsum (back), as that is a glandular area in adult animals.
3. Remove as much of the fat pad as possible, width-wise, to ensure that the nipple region of the fourth gland is included. There will typically be plenty of tissue length-wise. To do this, insert the tip of the scissors adjacent to the skin and under the fat pad, and open them, separating the fat pad from the skin.
4. Making small snips at the mammary tissue will result in a poor whole mount. Practice long, smooth cuts to lift the mammary fat pad off the skin. Snipping makes holes for air bubbles.

## 2. Fixing and Staining Whole Mounts

### A. Equipment and Supplies

#### 1. Carnoy's Fixative:

- a. Six parts 100% ethanol
- b. Three parts chloroform
- c. One part glacial acetic acid

This fixative can be made immediately before use—swirl to mix.

#### 2. Carmine Alum Stain:

- a. 1 g carmine (Sigma C1022)
- b. 2.5 g aluminum potassium sulfate (Sigma A7167)
- c. Fill to 500 mL with distilled water
- d. Boil for 20 minutes to get into solution
- e. Adjust final volume to 500 mL with distilled water
- f. Filter (to remove residues) into a dark or foil-wrapped bottle (media filter works)
- g. A small amount (1 crystal) of thymol may be added as a preservative
- h. Refrigerate

Make this 2–5 days before needed. Expiration date is approximately 4 months (6 months with thymol) from date of preparation. With weekly use or use on glands with dense epithelia (adult male or female tissues), it may expire more quickly. Discard if the stain becomes light pink. Carmine can be removed from glassware with 100% ethanol.

#### 3. Glass slide staining dishes

#### 4. 70% and 95% ethanol

#### 5. Xylene

#### 6. Permount (Fisher Scientific)

#### 7. Plastic disposable pipets

#### 8. Cover slips (appropriate size for glands removed—will vary with animal age)

#### 9. Cafeteria style trays covered in bench paper; plastic side up/absorbent side down.

### B. Procedure

1. Remove the 50 mL conical tube and the top glass slide and peel the Parafilm back from the far end, straight toward your body, not up. Be extra careful to not loosen the gland from the slide. The gland needs to be flattened to the slide and stuck in place. If not completely stuck to slide, let it dry out in the air for a few minutes. Place the slides in a glass staining tray. Add Carnoy's Fixative to the staining jar, being

careful to not pour the fixative directly onto the mammary tissue (it will cause them to come off the slides) and leave them there for 4–48 h, depending on thickness, at room temperature. Cover the staining jars tightly so that the fixative doesn't evaporate. May need to wrap lid with parafilm. Most mammary tissue from mice or PND 32–45 rats and smaller can be fixed for 24 h. Tissue from PND 45 or older rats may require more time. If white areas are present in the mammary tissue after fixing (more opaque than rest of gland), change the fixative and allow those glands to fix for an additional 24 h. If gland feels soft, not moderately firm, fix longer. If rats were fed high calorie/high fat chow, they may also need to fix for a longer period of time to clear the fat of lipid content. If in doubt, change fixative and let the glands fix one more day.

2. Pour off fixative and dispose of properly. Soak fixed tissues in 70% ethanol for 15–30 min. Larger tissues, longer soak times.
3. Change gradually to water. (Pour out 1/3, add water, let sit 5 min, repeat 3 times).
4. Equilibrate in water for 5 min.
5. Immerse slides in chilled Carmine alum stain for 12–48 h, depending on thickness (longer does not hurt it, but be consistent for all tissues of same age). Cover the containers in foil as this stain is light sensitive. The stain is reusable.
6. Rinse in water for 30–60 s.
7. Soak in 70% ethanol for 15–30 min.
8. Soak in 95% ethanol for 15–30 min.
9. Soak in 100% ethanol for 20–30 min.
10. Clear in xylene for 8–72 h, depending on the thickness of gland. The gland should be translucent after clearing. If any opaque (whitish) areas remain, place those slides in larger containers with xylene until translucent (clear). Do not proceed to Step 11 if there are nontranslucent areas. (see Helpful Hints below).
11. Once cleared, lay one slide at a time on the trays covered in bench paper and pipet enough Permount onto the tissue to cover the specimen and place a cover slip on top, being careful to avoid air bubbles. If bubbles form, lift the cover slip, pop the bubbles with the edge of a slide, and reapply the cover slip (additional

Permount may be necessary). Check the slides every 4–8 hours as the mounting solution will evaporate leaving gaps under the coverslip in some places. Fill these pockets as soon as possible.

12. After slides have dried, clean excess Permount from the outside of the slide with 100% EtOH or xylene on a cotton swab and let dry in a ventilated area (hood) for a few days before placing on the dissecting microscope.

### C. Helpful Hints

In the early stages of this procedure, be especially careful to:

1. Allow adequate time for the mammary tissue to flatten. It must stick to the slide when the Parafilm is removed. If it doesn't, it will have to be reflattened, as the slides will be on their side in the staining dish.
2. Never pour washes or fixative directly onto the mammary tissue or it may come off the slide. In this event, the gland cannot be reattached. Slides should soak in the solutions, without further agitation.
3. Do not proceed to staining if the gland is not properly fixed in its center.
4. If you get to the final xylene soak and there are opaque areas in the glands, go through the process in reverse and try fixing the tissue for longer period of time. It is possible this process will not work on very thick glands (rats older than 100 days or from obese animals).
5. Once cover-slipped, check the slides to see if you need to add more mounting media. Air gaps under the cover slip are difficult to resolve and will interfere with photography/scanning, etc.
6. Alternate methods for storage of large or thick glands are available ([Matouskova et al., 2022](#)).

### 3. Suggested Evaluation Methods for Mammary Gland Whole Mounts

Note: The study lead may modify for test article specific outcomes of interest.

#### A. Background Information

The objective of preparing whole mounted mammary tissue is to assess or evaluate the effects of a test chemical on development and differentiation of the gland compared to a concurrent control group. Aberrations in



either growth or maturity of the gland may be indicative of later life disease susceptibility or ability to lactate (Fenton, 2006; Rudel et al., 2011). Whole mounts of mammary tissue from male and female mice and rats can be evaluated by following these guidelines, and/or other quantitative methods described herein that may be requested by the COTR. The evaluator must be familiar with the normal structures of the mammary gland: primary and secondary ducts, lateral buds, alveolar buds, lobules, alveoli, TEBs, terminal ducts, and the lymph node (see Figures A8.2 and A8.3). The evaluator must also be familiar with the normal morphology of mammary glands at different ages (Filgo et al., 2016). Mammary epithelial development begins to invade the underlying fat pad just prior to birth in the rodent and progresses at the same rate as body growth,

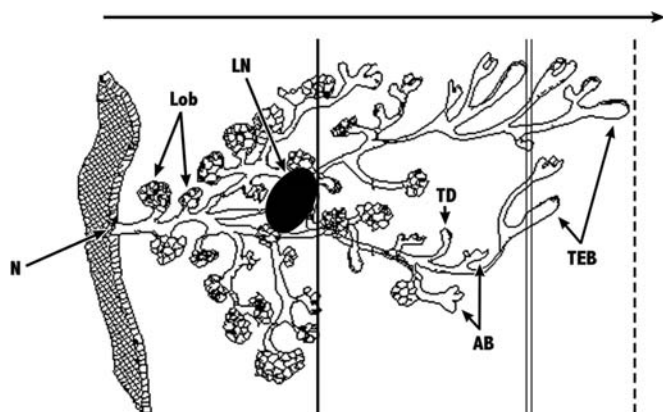


**FIGURE A8.2** Schematic drawing of the microscopic anatomy of the rat mammary gland. The thick, solid line indicates the edge of the lymph node away from the nipple and the dotted line indicates the leading edge of gland growth (i.e., the most distal point of longitudinal growth). The arrow along the top of the figure indicates the direction of longitudinal growth. Longitudinal growth in an adult rat is measured from the thick, solid line to the dotted line. The thin double lines indicate the area two-thirds of the distance from the lymph node to the leading edge of gland growth where the degree of lateral branching is to be quantified, though the thin double lines would follow the curve of the leading edge of growth which cannot be depicted here. AB, alveolar bud; LN, lymph node; Lob, lobule; N, nipple; TD, terminal duct; TEB, terminal end bud. Adapted from Russo IH, Russo J: *Mammary gland neoplasia in long-term rodent studies*. *Environ. Health Perspect.* 104(9):938–967, 1996. Figure 2, with permission.

until puberty. Just prior to vaginal opening, the rate of epithelial outgrowth become exponential and quickly the fourth and fifth glands grow together. TEBs are the rapidly dividing terminal ends that lead the progression to the edges of the fat pad, where contact inhibition takes place. Once this occurs, differentiation of the gland (transition from terminal ducts and TEBs to buds and lobules) takes place, and eventually results in a fat pad filled with branched epithelium containing few residual structures, until such time the animal becomes pregnant.

The morphology of the mammary gland differs by species and may vary slightly between strains of rats or mice (Stanko et al., 2016). Mice have a simple mammary epithelial branching pattern, primarily lacking lateral or alveolar buds until adulthood. Male CD-1 mice have a mammary epithelial stalk, and male rats develop mammary glands filled with epithelium. When screening for chemical effect on the morphology of the glands, the following features are evaluated relative to the control animals (preferably at more than one timepoint):

1. The number of TEBs relative to the number of duct ends and the morphology of the TEBs
  2. The degree of branching and amount of mammary tissue present (e.g., does the tissue fill the fat pad, or does the tissue appear sparse?). Some specific structures to look for include:
    - a. The degree of lateral (side) branching and/or budding (branch density)
    - b. The number of primary ducts growing from the nipple (particularly in PND4 animals; this may not be possible in older animals)
  3. The degree (relative amount compared to control samples) of alveolar bud and lobule formation
  4. Growth of the gland, both length- and width-wise.
- B. Initial Morphological Assessment (Developmental Scoring):**  
The glands are scored in a semiquantitative manner as described below. Samples should be compared within an age group and across doses, as mammary development varies

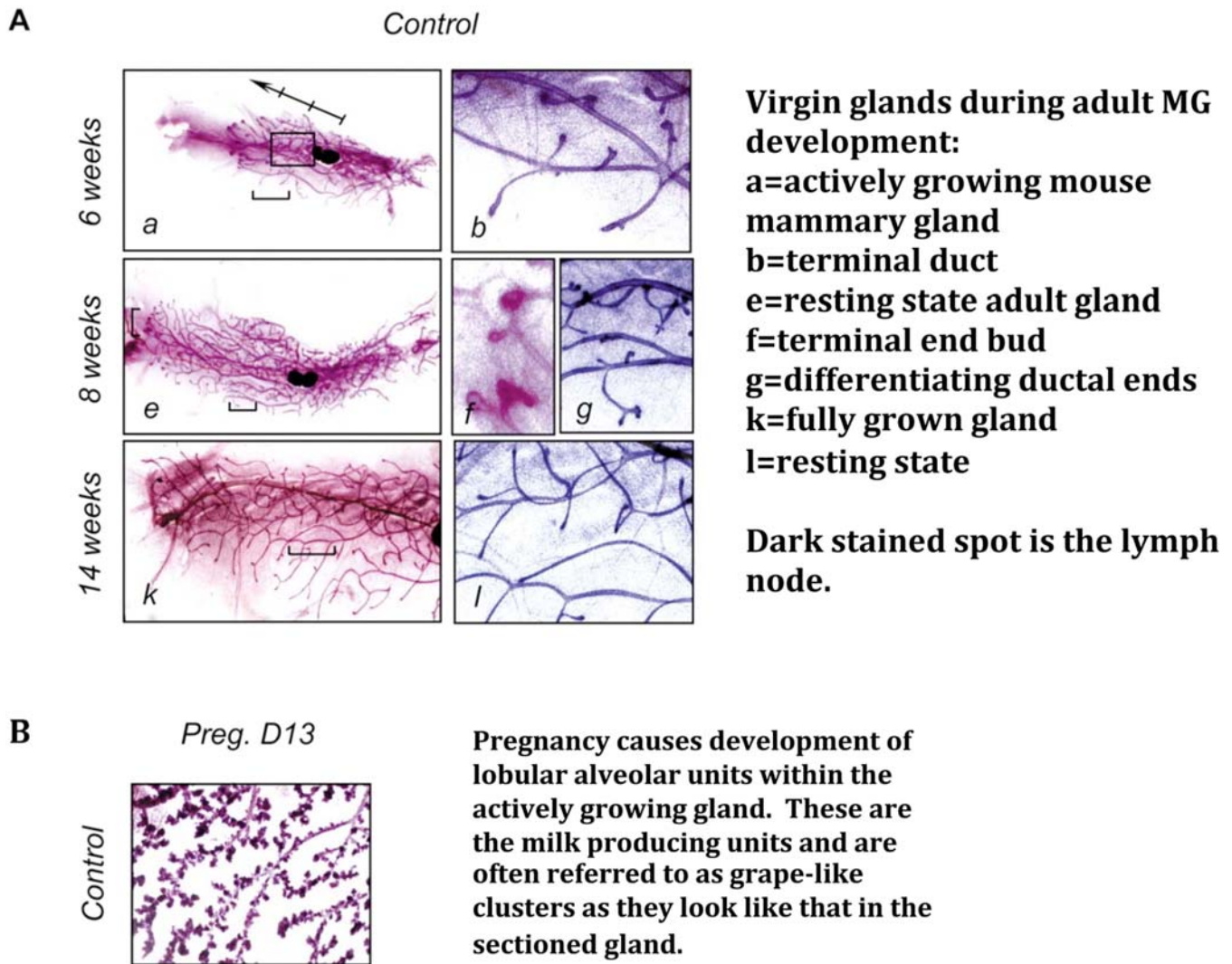


**FIGURE A8.3** Control mammary gland whole mounts—mouse. Adapted from Li G, Robinson GW, Lesche R, et al.: Conditional loss of PTEN leads to precocious development and neoplasia in the mammary gland. *Development* 129(17):4162, 2002. Figure 2, with permission.

considerably between birth and 45 days of age. Suggested age-specific factors to use in the evaluation are listed in [Table 8.1](#).

However, if these criteria are not followed due to variability in animal strain, dose-response, or age, the evaluator should devise and report criteria for scoring. In some cases, a more quantitative evaluation of the glands may be needed to determine if a test effect is present. Suggested methods are described below in section C.

1. Within a single age group, separate the slides according to dose group. Using a dissecting microscope, study the control and highest dose group (or positive

controls) to determine the range of differences in morphology that are expected within the study slides.

2. In a blinded evaluation, using the scoring criteria in [Table 8.2](#) below, assign a developmental score to each mammary gland sample (Scores of 1–4, including half numbers when the mammary gland has characteristics of two adjacent scores—use a 7-point scale). Stack the slides by score.
3. Review the mammary glands within each score a second time and possibly third time to ensure the scores were assigned in a consistent manner over the course of the evaluation time. (This step may be skipped

if the study lead plans to review slides in a Pathology QA evaluation.) Record developmental scores for each slide. Writing notes on why you gave some of the slides the score you assigned them helps when there is not agreement on a score from independent technical assessments.

### C. Quantitative Mammary Developmental Measurements

A more detailed evaluation of the mammary glands may be helpful in determining the presence or absence of a test effect (e.g., if the results of the subjective scoring are equivocal or suggest a specific effect). One or more of the following measurements may further elucidate/confirm results from the initial morphological assessment:

1. TEB ratio (from weaning age until about 10 weeks of age): reported as the ratio of TEBs to the total number of duct ends in 10 random 4× fields at the leading edge of gland growth. TEB are defined as ends  $\geq 100 \mu\text{m}$ .
2. Number of primary ducts growing from nipple (particularly in PND4 animals; this may not be possible in older animals)
3. Degree of lobule formation (from weaning age to adult): A subjective assessment based on comparison to control animals that may be reported on a scale of 0–4 (0—no lobule formation, 4—abundant lobule formation, comparable to controls). Lobules are defined as clusters of three or more bud-like structures.
4. Degree of lateral branching (all ages): Enumerate the total number of branch points in 10 random 40× fields along a band that is two-thirds of the distance from the lymph node to the leading edge of gland growth (see [Figure A8.2](#)).
5. Measure gland growth (measure to the nearest mm)

Note: In the event that the mammary tissue is folded onto itself, the folded epithelium should be measured and added to the length recorded for the lateral or longitudinal growth. Any slides considered to be of such poor quality that a score or measurement cannot be reliably

determined should be omitted from the evaluation.

#### a. Longitudinal growth

- 1) Birth until PND67 days old or until glands have grown together: Measure the length from the collecting duct at the nipple to the farthest point of longitudinal growth, avoiding single abnormal outlier ducts (growth toward the lymph node or dorsum).
- 2) PND 67—Adult: Measure the length from the edge of the lymph node away from the nipple (i.e., the edge closest to the leading edge of gland growth) to the most distal point of longitudinal growth (i.e., at the leading edge of growth, farthest from the lymph node, toward the end of the fat pad).

- b. Lateral growth—Measure the greatest lateral length of the gland, perpendicular to the nipple–lymph node–leading edge axis (the leading edge is toward the dorsum of the animal).
- c. Numerous other methods are suggested in [Matouskouva et al. \(2022\)](#).

### 6. Reporting

- a. Record the morphology scores and growth measurements for all mammary glands.
- b. For both the Initial Morphological Assessment (developmental scoring) and the Quantitative Measurements, criteria for reported measures should be described, as well as the reasoning behind those criteria.

### 7. Interpretation

- A. Statistical analyses of the collected data are required, and the methods may differ if developmental exposures were involved, and pups were sampled. In all cases the exposed animal (dam or adult individual) is the unit of measurement.
  1. For continuous data with normal distributions, an ANOVA with Dunnett's multiple comparisons may be applied to quantitative endpoints.
  2. The Mann–Whitney test may be used to compare chemical dose group to control for Sholl analysis



- ([Stanko and Fenton, 2017](#)) and mammary gland quantitative measurements when the data are not ordinal (nonparametric).
3. One-sided Jonckheere's test may be performed to determine dose-related trends.
  4. When multiple pups per dam are evaluated in the same analysis of quantitative endpoints, which may be common for timing of VO and first estrus, mixed effects analysis of variance (ANOVA) with Dunnett's test may be used to account for potential litter effects.
  5. Other noncontinuous data, such as TEB counts, developmental scores, mean severity scores, or lesion incidence, may be evaluated using a one-sided Fisher's exact test to compare each dose group with the vehicle control group. Cochran–Armitage tests may be used to analyze for trends across dose groups.
- B. Determine direction of effect (development)**
1. Once data are analyzed, the means/standard errors should be plotted, and mean values used to find samples within a dose group for representative photos.
  2. Low developmental scores (lower than control) suggest developmental delays, while higher than control indicate precocious or accelerated development of mammary epithelium.
  3. TEB number should be considered in regard to total number of ducts ends and are most accurately interpreted by incorporating at least two necropsy time points in the study design. A lower than control TEB number may support a developmental delay, if the total number of ends are also lower than control. However, a lower than control TEB number may also indicate precocious/rapid development (because the TEB have differentiated faster than normal) if the total number of ends are more than or equal to control. Alternatively, a higher-than-normal number of TEB at a single time point may not indicate accelerated development—it may in fact point to a developmental delay if TEBs developed later than usual and remain undifferentiated, whereas control TEB have already become terminal ends.
  4. Number of duct branch points within a constant area, epithelial area, and alveolar budding are also good indicators of precocious or delayed development.
- C. Use of whole mount to compare to/compliment histological section**
1. When there is a suggestion that the test chemical is an endocrine disruptor ([Fenton, 2006](#)), in addition to the collection of the gland for histologic evaluation, the contralateral gland should be collected as a whole mount according to the procedures above and stored as permounted slides or in sealed bags with methylsalicylate (in [Matouskova et al., 2022](#)). The histological section should be collected from the entire fourth mammary gland, with the skin removed, and longitudinally sectioned with some of the lymph node present in the section for optimal comparison with whole mounts.
  2. While waiting for histological sections to be trimmed, cut, stained, and evaluated, examine the whole mounts for areas that may indicate a lesion or nodule, and conduct developmental scoring, and any quantitative measures that may aid in interpretation.
  3. If lesion/nodules are apparent, the entire whole mount or just the affected area of the whole mount may be removed and sectioned following procedures outlined in [Tucker et al. \(2016\)](#). Additionally, this may indicate the need to evaluate more than one slide per gland histologically.

## Acknowledgments

We would like to acknowledge our appreciation to Dr. Darlene Dixon (Mechanistic Toxicology Branch, NIEHS) for her advisement and encouragement on the content of this chapter. Also, a huge thank you to Beth Mahler and Paul Cacioppo (NIEHS contractors) for excellence in their assistance with chapter figures. This work was supported in part by the National Institute of Environmental Health Sciences under Award Number P30ES025128.

## REFERENCES

- Acevedo N, Davis B, Schaeberle CM, et al.: Perinatally administered bisphenol a as a potential mammary gland carcinogen in rats, *Environ. Health Perspect.* 121(9):1040–1046, 2013.
- Alvarado A, Faustino-Rocha AI, Colaço B, et al.: Experimental mammary carcinogenesis—rat models, *Life Sci.* 173:116–134, 2017.
- American Cancer Society. <https://www.cancer.org/cancer/types/breast-cancer-in-men/about/key-statistics.html>. (Accessed 29 February 2024), 2024.
- Antuofermo E, Miller MA, Pirino S, et al.: Spontaneous mammary intraepithelial lesions in dogs—a model of breast cancer, *Cancer Epidemiol. Biomarkers Prev.* 16(11):2247–2256, 2007.
- Bauchet AL, Elies L, Maliver P, et al.: A mammary gland adenomyoepithelioma in a C57Bl/6 mouse, *Experimental. Toxicol. Pathol.* 60(4–5):307–311, 2008.
- Beck AP, Brooks A, Zeiss CJ: Invasive ductular carcinoma in 2 rhesus macaques (*Macaca mulatta*), *Comp. Med.* 64(4):314–322, 2014.
- Borowsky A, Cardiff R: Mammary gland. In Vogel P, Sundberg JP, Ward JM, editors: *Pathology of genetically engineered and other mutant mice*, Hoboken, NJ, 2022, John Wiley & Sons, Inc., pp 213–236.
- Brix AE, Nyska A, Haseman JK, et al.: Incidences of selected lesions in control female Harlan Sprague-Dawley rats from two-year studies performed by the National Toxicology Program, *Toxicol. Pathol.* 33(4):477–483, 2005.
- Bruserud IS, Roelants M, Oehme NHB, et al.: References for ultrasound staging of breast maturation, tanner breast staging, pubic hair, and menarche in Norwegian girls, *J. Clin. Endocrinol. Metab.* 105(5):1599–1607, 2020.
- Bu W, Creighton CJ, Heavener KS, et al.: Efficient cancer modeling through CRISPR-Cas9/HDR-based somatic precision gene editing in mice, *Sci. Adv.* 9(19):eade0059, 2023.
- Cardiff RD, Anver MR, Gusterson BA, et al.: The mammary pathology of genetically engineered mice: the consensus report and recommendations from the Annapolis meeting, *Oncogene* 19(8):968–988, 2000.
- Chandra SA, Cline JM, Adler RR: Cyclic morphological changes in the beagle mammary gland, *Toxicol. Pathol.* 38(6):969–983, 2010.
- Chandra M, Riley MGI, Johnson DE: Spontaneous neoplasms in aged Sprague-Dawley rats, *Arch. Toxicol.* 66:496–502, 1992.
- Chlebowski RT, Anderson GL, Aragaki AK, et al.: Association of menopausal hormone therapy with breast cancer incidence and mortality during long-term follow-up of the women's health initiative randomized clinical trials, *JAMA* 324(4):369–380, 2020.
- Ciarloni L, Mallepell S, Briskin C: Amphiregulin is an essential mediator of estrogen receptor alpha function in mammary gland development, *Proc. Natl. Acad. Sci. U.S.A.* 104(13):5455–5460, 2007.
- Cline JM, Soderqvist G, von Schoultz E, et al.: Effects of hormone replacement therapy on mammary gland of surgically post menopausal cynomolgus macaques, *Am J Obstet Gynecol* 174:93–100, 1996.
- Cline JM, Wood CE: The mammary glands of macaques, *Toxicol. Pathol.* 36(7 suppl):130S–141S, 2008.
- CLARITY-BPA Research Program: *NTP research report on the consortium linking academic and regulatory insights on bisphenol a toxicity (CLARITY-BPA): a compendium of published findings: Research Report 18 [Internet]*, Research Triangle Park (NC), 2021, National Toxicology Program, 2021.
- Colman K, Andrews R, Atkins H, et al.: International harmonization of nomenclature and diagnostic criteria (INHAND): non-proliferative and proliferative lesions of the non-human primate (*M. fascicularis*), *J. Toxicol. Pathol.* 34(3 Suppl):1S–182S, 2021.
- Côme C, Arnoux V, Bibeau F, et al.: Roles of the transcription factors snail and slug during mammary morphogenesis and breast carcinoma progression, *J. Mammary Gland Biol. Neoplasia* 9(2):183–193, 2004.
- Crist KA, Chaudhuri B, Shivaram S, et al.: Ductal carcinoma in situ in rat mammary gland, *J. Surg. Res.* 52(3):205–208, 1992.
- Dantas CG, Cavalheiro Bertagnolli A, Ferreira E, et al.: Canine mammary mixed tumours: a review, *Vet. Med. Int.*, 2012: 274608, 2012.
- Davie SA, Maglione JE, Manner CK, et al.: Effects of FVB/NJ and C57Bl/6J strain backgrounds on mammary tumor phenotype in inducible nitric oxide synthase deficient mice, *Transgenic Res.* 16(2):193–201, 2007.
- Davis BJ, Fenton SE: Mammary gland. In Haschek WM, Rousseaux CG, Wallig MA, editors: *Haschek and Rousseaux's Handbook of toxicologic pathology*, 3rd Ed., 2013, Academic Press, pp 2665–2694. Chap 19.
- DeVaux RS, Herschkowitz JI: Beyond DNA: the role of epigenetics in the premalignant progression of breast cancer, *J. Mammary Gland Biol. Neoplasia* 23(4):223–235, 2018.
- Dewi FN, Cline JM: Nonhuman primate model in mammary gland biology and neoplasia research, *Lab Anim. Res.* 37(1): 3, 2021.
- Dinse GE, Peddada SD, Harris SF, et al.: Comparison of NTP historical control tumor incidence rates in female Harlan Sprague Dawley and Fischer 344/N Rats, *Toxicol. Pathol.* 38(5):765–775, 2010.

- Dupont S, Krust A, Gansmuller A, et al.: Effect of single and compound knockouts of estrogen receptors alpha (ERalpha) and beta (ERbeta) on mouse reproductive phenotypes, *Development* 127(19):4277–4291, 2000.
- Durando M, Kass L, Piva J, et al.: Prenatal bisphenol A exposure induces preneoplastic lesions in the mammary gland in Wistar rats, *Environ. Health Perspect.* 115(1):80–86, 2007.
- Earp HS, Dawson TL, Li X, et al.: Heterodimerization and functional interaction between EGF receptor family members: a new signaling paradigm with implications for breast cancer research, *Breast Cancer Res. Tr.* 35:115–132, 1995.
- Eckert-Lind C, Busch AS, Petersen JH, Biro FM, Butler G, Bräuner EV, Juul A: Worldwide secular trends in age at pubertal onset assessed by breast development among girls: a systematic review and meta-analysis, *JAMA Pediatr.* 174(4):e195881, 2020.
- Edmunds G, Beck S, Kale KU, et al.: Associations between dog breed and clinical features of mammary epithelial neoplasia in bitches: an epidemiological study of submissions to a single diagnostic pathology centre between 2008–2021, *J. Mammary Gland Biol. Neoplasia* 28(1):6, 2023.
- EPA: United States environmental protection agency: integrated risk information system (IRIS) glossary, 2023. <https://www.epa.gov/iris/iris-glossary>. (Accessed 1 March 2024).
- Fenton SE, Hamm JT, Birnbaum LS, et al.: Persistent abnormalities in the rat mammary gland following gestational and lactational exposure to 2,3,7,8-tetrachlorodibenzo-p-dioxin (TCDD), *Toxicol. Sci.* 67(1):63–74, 2002.
- Fenton SE: Endocrine-disrupting compounds and mammary gland development: early exposure and later life consequences, *Endocrinology* 147(6 Suppl):S18–S24, 2006.
- Ferreira T, Gama A, Seixas F, et al.: Mammary glands of women, female dogs and female rats: similarities and differences to be considered in breast cancer research, *Vet. Sci.* 10(6):379, 2023, <https://doi.org/10.3390/vetsci10060379>. PMID: 37368765. PMCID: PMC10303014.
- Filgo AJ, Foley JF, Puvanesarajah S, et al.: Mammary gland evaluation in juvenile toxicity studies: temporal developmental patterns in the male and female Harlan Sprague-Dawley Rat, *Toxicol. Pathol.* 44(7):1034–1058, 2016.
- Fisher CR, Graves KH, Parlow AF, et al.: Characterization of mice deficient in aromatase (ArKO) because of targeted disruption of the cyp19 gene, *Proc. Natl. Acad. Sci. U.S.A.* 95(12):6965–6970, 1998.
- Gagniac L, Rusidzé M, Boudou F, et al.: Membrane expression of the estrogen receptor ER $\alpha$  is required for intercellular communications in the mammary epithelium, *Development* 147(5):dev182303, 2020.
- Goldschmidt MH, Penã L, Zappulli V: Tumors of the mammary gland. In Meuten DJ, editor: *Tumors in domestic animals*, 5th ed., 2020, Wiley-Blackwell, pp 723–765. Chap 17.
- Gore AC, Chappell VA, Fenton SE, et al.: EDC-2: the Endocrine Society's second scientific statement on endocrine-disrupting chemicals, *Endocr. Rev.* 36(6):E1–E150, 2015.
- Hadsell DL, Bonnette SG: IGF and insulin action in the mammary gland: lessons from transgenic and knockout models, *J. Mammary Gland Biol. Neoplasia* 5(1):19–30, 2000. <https://doi.org/10.1023/a:1009559014703>. PMID: 10791765.
- Hamilton AM, Olsson LT, Midkiff BR, et al.: Toward a digital analysis of environmental impacts on rodent mammary gland density during critical developmental windows, *Reprod. Toxicol.* 111:184–193, 2022.
- Hannan FM, Elajnaf T, Vandenberg LN, et al.: Hormonal regulation of mammary gland development and lactation, *Nat. Rev. Endocrinol.* 19:46–61, 2023.
- Henry S, Trousdell MC, Cyrill SL, et al.: Characterization of gene expression signatures for the identification of cellular heterogeneity in the developing mammary gland, *J. Mammary Gland Biol. Neoplasia* 26(1):43–66, 2021.
- Hiremath M, Dann P, Fischer J, et al.: Parathyroid hormone-related protein activates Wnt signaling to specify the embryonic mammary mesenchyme, *Development* 139(22):4239–4249, 2012.
- Hoenerhoff MJ, Hong HH, Ton TV, et al.: A review of the molecular mechanisms of chemically induced neoplasia in rat and mouse models in National Toxicology Program bioassays and their relevance to human cancer, *Toxicol. Pathol.* 37(7):835–848, 2009.
- Honvo-Houéto E, Truchet S: Indirect immunofluorescence on frozen sections of mouse mammary gland, *J. Vis. Exp.* (106):53179.
- Houle CD, Ton TV, Clayton N, et al.: Frequent p53 and H-ras mutations in benzene- and ethylene oxide-induced mammary gland carcinomas from B6C3F1 mice, *Toxicol. Pathol.* 34(6):752–762, 2006.
- Howdeshell KL, Beverly BEJ, Blain RB, et al.: Evaluating endocrine disrupting chemicals: a perspective on the novel assessments in CLARITY-BPA, *Birth Defects Res.* 115(15):1345–1397, 2023.
- Hvid H, Skydsgaard M, Jensen NK, et al.: Artificial intelligence-based quantification of epithelial proliferation in mammary glands of rats and oviducts of Göttingen Minipigs, *Toxicol. Pathol.* 49(4):912–927, 2021.
- IBCERCC: Interagency breast cancer and environmental research coordinating committee (IBCERCC). *Breast cancer and the environment: prioritizing prevention*, 2013, National Institute of Environmental Health Sciences. [https://bcerp.org/wp-content/uploads/2\\_summary\\_of\\_recs\\_508.pdf](https://bcerp.org/wp-content/uploads/2_summary_of_recs_508.pdf). (Accessed 12 July 2024).
- Ivanova E, Le Guillou S, Hue-Beauvais C, et al.: Epigenetics: new insights into mammary gland biology, *Genes* 12(2):231, 2021.
- Jackson-Fisher AJ, Bellinger G, Ramabhadran R, et al.: Erbb2 is required for ductal morphogenesis of the mammary gland, *Proc. Natl. Acad. Sci. U.S.A.* 101(49):17138–17143, 2004.
- Jacob JB, Wei KC, Bepler G, et al.: Identification of actionable targets for breast cancer intervention using a diversity outbred mouse model, *iScience* 26(4):106320, 2023.



- Kay JE, Brody JG, Schwarzman M, et al.: Application of the key characteristics framework to identify potential breast carcinogens using publicly available in vivo, in vitro, and in silico data, *Environ. Health Perspect.* 132(1):17002, 2024.
- Kay JE, Cardona B, Rudel RA, et al.: Chemical effects on breast development, function, and cancer risk: existing knowledge and new opportunities, *Curr. Environ. Health Rep.* 9(4): 535–562, 2022.
- Kaspereit J, Rittinghausen S: Spontaneous neoplastic lesions in Harlan Sprague-Dawley rats, *Exp. Toxicol. Pathol.* 51(1):105–107, 1999.
- Kleinberg DL, Wood TL, Furth PA, et al.: Growth hormone and insulin-like growth factor-I in the transition from normal mammary development to preneoplastic mammary lesions, *Endocr. Rev.* 30(1):51–74, 2009, <https://doi.org/10.1210/er.2008-0022>. Erratum in: *Endocr Rev.* 2012 Dec;33(6):1038. PMID: 19075184; PMCID: PMC5393153.
- Kobayashi K: Culture models to investigate mechanisms of milk production and blood-milk barrier in mammary epithelial cells: a review and a protocol, *J. Mammary Gland Biol. Neoplasia* 28(1):8, 2023.
- LaPlante CD, Catanese MC, Bansal R, et al.: Bisphenol S alters the lactating mammary gland and nursing behaviors in mice exposed during pregnancy and lactation, *Endocrinology* 158(10):3448–3461, 2017.
- Latendresse JR, Bucci TJ, Olson G, et al.: Genistein and ethinyl estradiol dietary exposure in multigenerational and chronic studies induce similar proliferative lesions in mammary gland of male Sprague-Dawley rats, *Reprod. Toxicol.* 28(3):342–353, 2009.
- Le Provost F, Riedlinger G, Hee Yim S, et al.: The aryl hydrocarbon receptor (AhR) and its nuclear translocator (Arnt) are dispensable for normal mammary gland development but are required for fertility, *Genesis* 32(3):231–239, 2002.
- Lechosa-Muñoz C, Paz-Zulueta M, Cayón-De Las Cuevas J, et al.: Declared reasons for cessation of breastfeeding during the first year of life: an analysis based on a cohort study in Northern Spain, *Int. J. Environ. Res. Publ. Health* 18(16):8414, 2021.
- Li G, Robinson GW, Lesche R, et al.: Conditional loss of PTEN leads to precocious development and neoplasia in the mammary gland, *Development* 129(17):4159–4170, 2002.
- Lima SM, Kehm RD, Terry MB: Global breast cancer incidence and mortality trends by region, age-groups, and fertility patterns, *EclinicalMedicine* 38:100985, 2021.
- Lucas JN, Rudmann DG, Credille KM, et al.: The rat mammary gland: morphologic changes as an indicator of systemic hormonal perturbations induced by xenobiotics, *Toxicol. Pathol.* 35(2):199–207, 2007.
- Luzhna L, Kutanzi K, Kovalchuk O: Gene expression and epigenetic profiles of mammary gland tissue: insight into the differential predisposition of four rat strains to mammary gland cancer, *Mutat. Res. Genet. Toxicol. Environ. Mutagen* 779:39–56, 2015.
- Macias H, Hinck L: Mammary gland development, *Wiley Interdiscip. Rev. Dev. Biol.* 1(4):533–557, 2012.
- Masso-Welch P, Darcy K, Stangle-Castor N, et al.: A developmental atlas of rat mammary gland histology, *J. Mammary Gland Biol. Neoplasia* 5(2):165–185, 2000.
- Matouskova K, Szabo GK, Daum J, et al.: Best practices to quantify the impact of reproductive toxicants on development, function, and diseases of the rodent mammary gland, *Reprod. Toxicol.* 112:51–67, 2022.
- Misdorp W, Else RW, Hellmen E, et al.: *Histological classification of mammary tumors of the dog and the cat*, 1999, Armed Forces Institute of Pathology, p 7.
- Morato A, Accornero P, Hovey RC: ERBB Receptors and their ligands in the developing mammary glands of different species: fifteen characters in search of an author, *J. Mammary Gland Biol. Neoplasia* 28(1):10, 2023.
- NTP: NTP research report on the CLARITY-BPA core study: a perinatal and chronic extended-dose-range study of Bisphenol A in rats: research report 9, Research Triangle Park NC: National Toxicology Program. Available from: <https://www.ncbi.nlm.nih.gov/books/NBK543883/>. (Accessed 29 February 2024).
- NTP: Developmental and reproductive toxicity, 2023. <https://ntp.niehs.nih.gov/whatwestudy/testpgm/devrepro#MOG>. (Accessed 29 February 2024).
- OECD: OECD revised guidance document 150 on standardised test guidelines for evaluating chemicals for endocrine disruption. OECD series on testing and assessment, no. 150, Paris, 2018a, OECD Publishing, <https://doi.org/10.1787/9789264304741-en>.
- OECD: Extended one-generation reproductive toxicity study (EOGRS) (OECD TG 443). In *Revised guidance document 150 on standardised test guidelines for evaluating chemicals for endocrine disruption*, Paris, 2018b, OECD Publishing, <https://doi.org/10.1787/9789264304741-34-en>.
- Ormandy CJ, Naylor M, Harris J, et al.: Investigation of the transcriptional changes underlying functional defects in the mammary glands of prolactin receptor knockout mice, *Recent Prog. Horm. Res.* 58:297–323, 2003, <https://doi.org/10.1210/rp.58.1.297>. PMID: 12795425.
- Outzen HC, Corrow D, Shultz LD: Attenuation of exogenous murine mammary tumor virus virulence in the C3H/HeJ mouse substrain bearing the Lps mutation, *J. Natl. Cancer Inst.* 75(5):917–923, 1985 Nov.
- Payne J, Jones C, Lakhani S, et al.: Improving the reproducibility of the MCF-7 cell proliferation assay for the detection of xenoestrogens, *Sci. Total Environ.* 248(1):51–923, 2000 Mar 29.
- Planas-Silva MD, Rutherford TM, Stone MC: Prevention of age-related spontaneous mammary tumors in outbred rats by late ovariectomy, *Cancer Detect. Prev.* 32(1):65–71, 2008.
- Rayner JL, Enoch RR, Fenton SE: Adverse effects of prenatal exposure to atrazine during a critical period of mammary gland growth, *Toxicol. Sci.* 87(1):255–266, 2005.

- Rehm S, Stanislaus DJ, Williams AM: Estrous cycle-dependent histology and review of sex steroid receptor expression in dog reproductive tissues and mammary gland and associated hormone levels, *Birth Defects Res. B Dev. Reprod. Toxicol.* 80(3):233–245, 2007.
- Roberts BM, Chumpolkulwong K, Tayamun S, et al.: Mammary carcinoma in a male rhesus macaque (*Macaca mulatta*): histopathology and immunohistochemistry of ductal carcinoma in situ, *J. Med. Primatol.* 43(3):213–216, 2014.
- Roberts GK, Stout MD, editors: *Specifications for the conduct of toxicity studies by the division of translational toxicology*, Research Triangle Park, NC, 2023, National Institute of Environmental Health Sciences.
- Rowse GJ, Ritland SR, Gendler SJ: Genetic modulation of neu proto-oncogene-induced mammary tumorigenesis, *Cancer Res.* 58(12):2675–2679, 1998.
- Rudel RA, Fenton SE, Ackerman JM, et al.: Environmental exposures and mammary gland development: state of the science, public health implications, and research recommendations, *Environ. Health Perspect.* 119(8):1053–1061, 2011.
- Rudmann D, Cardiff R, Chouinard L, et al.: Proliferative and nonproliferative lesions of the rat and mouse mammary, zymbal's, preputial, and clitoral glands, *Toxicol. Pathol.* 40(6):7S–39S, 2012.
- Ruehl-Fehlert C, Kittel B, Morawietz G, et al.: Revised guides for organ sampling and trimming in rats and mice—part 1, *Exp. Toxicol. Pathol.* 55(2–3):91–106, 2003.
- Russo IH, Russo J: Mammary gland neoplasia in long-term rodent studies, *Environ. Health Perspect.* 104(9):938–967, 1996.
- Russo J, Russo IH: Development of the human breast, *Maturitas* 49(1):2–15, 2004.
- Russo J: Significance of rat mammary tumors for human risk assessment, *Toxicol. Pathol.* 43(2):145–170, 2015.
- Russo IH, Russo J: Developmental stage of the rat mammary gland as determinant of its susceptibility to 7,12-dimethylbenz[a]anthracene, *J. Natl. Cancer Inst.* 61(6):1439–1449, 1978.
- Sampayo R, Recouvreux S, Simian M: The hyperplastic phenotype in PR-A and PR-B transgenic mice: lessons on the role of estrogen and progesterone receptors in the mouse mammary gland and breast cancer, *Vitam. Horm.* 93:185–201, 2013, <https://doi.org/10.1016/B978-0-12-416673-8.00012-5>. PMID: 23810007.
- Schwartz CL, Christiansen S, Hass U, et al.: On the use and interpretation of areola/nipple retention as a biomarker for anti-androgenic effects in rat toxicity studies, *Front. Toxicol.* 3:730752, 2021.
- Schwarzenbach H: Circulating nucleic acids as biomarkers in breast cancer, *Breast Cancer Res.* 15(5):211, 2013.
- Seachrist D, Donaubaue E, Keri R: Hypothalamic–pituitary–mammary gland (HPM) axis. In Skinner MK, editor: *Encyclopedia of reproduction*, 2nd ed., 2018, Academic Press, Elsevier, pp 798–807.
- Shepel LA, Gould MN: The genetic components of susceptibility to breast cancer in the rat, *Prog. Exp. Tumor Res.* 35:158–169, 1999.
- Siegel RL, Miller KD, Fuchs HE, et al.: Cancer statistics, 2022, *CA A Cancer J. Clin.* 72(1):7–33, 2022.
- Soto AM, Sonnenschein C, Chung KL, et al.: The E-SCREEN assay as a tool to identify estrogens: an update on estrogenic environmental pollutants, *Environ. Health Perspect.* 103(Suppl 7):113–122, 1995.
- Stanko JP, Fenton SE: Quantifying branching density in rat mammary gland whole-mounts using the Sholl analysis method, *J. Vis. Exp.* (125):55789, 2017, <https://doi.org/10.3791/55789>. PMID: 28745626; PMCID: PMC5612270.
- Stanko JP, Kissling GE, Chappell VA, et al.: Differences in the rate of in situ mammary gland development and other developmental endpoints in three strains of female rat commonly used in mammary carcinogenesis studies: implications for timing of carcinogen exposure, *Toxicol. Pathol.* 44(7):1021–1033, 2016.
- Su Y, Santucci-Pereira J, Dang NM, et al.: Effects of pubertal exposure to butyl benzyl phthalate, perfluorooctanoic acid, and zeranol on mammary gland development and tumorigenesis in rats, *Int. J. Mol. Sci.* 23(3):1398, 2022.
- Sung H, Ferlay J, Siegel RL, et al.: Global cancer statistics 2020: GLOBOCAN estimates of incidence and mortality worldwide for 36 cancers in 185 countries, *CA A Cancer J. Clin.* 71(3):209–249, 2021.
- Szabo GK, Vandenberg LN: Reproductive Toxicology: the male mammary gland: a novel target of endocrine-disrupting chemicals, *Reproduction* 162(5):F79–F89, 2021.
- Tarulli GA, Laven-Law G, Shehata M, et al.: Androgen receptor signalling promotes a luminal phenotype in mammary epithelial cells, *J. Mammary Gland Biol. Neoplasia* 24(1):99–108, 2019. <https://doi.org/10.1007/s10911-018-9406-2>. Epub 2018 Aug 12. PMID: 30099649.
- Tharp AP, Maffini MV, Hunt PA, et al.: Bisphenol A alters the development of the rhesus monkey mammary gland, *Proc. Natl. Acad. Sci. U.S.A.* 109(21):8190–8195, 2012.
- Timmermann A, Avenbuan ON, Romano ME, et al.: Per- and polyfluoroalkyl substances and breastfeeding as a vulnerable function: a systematic review of epidemiological studies, *Toxics* 11(4):325, 2023.
- Timmermans-Sprang EPM, Gracanin A, Mol JA: Molecular signaling of progesterone, growth hormone, Wnt, and HER in mammary glands of dogs, rodents, and humans: new treatment target identification, *Front. Vet. Sci.* 4:53, 2017.
- Tucker DK, Foley JF, Hayes-Bouknight SA, et al.: Preparation of high-quality hematoxylin and eosin-stained sections from rodent mammary gland whole mounts for histopathologic review, *Toxicol. Pathol.* 44(7):1059–1064, 2016.
- Tucker DK, Foley JF, Bouknight SA, et al.: Sectioning mammary gland whole mounts for lesion identification, *J. Vis. Exp.* (125):55796.
- Tucker DK, Hayes-Bouknight S, Brar SS, et al.: Evaluation of prenatal exposure to bisphenol analogues on development

- and long-term health of the mammary gland in female mice, *Environ. Health Perspect.* 126(8):087003, 2018.
- Vandenberg LN, Maffini MV, Schaeberle CM, et al.: Perinatal exposure to the xenoestrogen bisphenol-A induces mammary intraductal hyperplasias in adult CD-1 mice, *Reprod. Toxicol.* 26(3–4):210–219, 2008.
- Vandenberg LN, Schaeberle CM, Rubin BS, et al.: The male mammary gland: a target for the xenoestrogen bisphenol A, *Reprod. Toxicol.* 37:15–23, 2013.
- Virtanen S, Schulte R, Stingl J, et al.: High-throughput surface marker screen on primary human breast tissues reveals further cellular heterogeneity, *Breast Cancer Res.* 23(1):66, 2021.
- Ward EM, Sherman RL, Henley SJ, et al.: Annual report to the nation on the status of cancer, featuring cancer in men and women age 20–49 years, *J. Natl. Cancer Inst.* 111(12):1279–1297, 2019.
- Welsh J, Wietzke JA, Zinser GM, et al.: Vitamin D-3 receptor as a target for breast cancer prevention, *J. Nutr.* 133(7 Suppl): 2425S–2433S, 2003.
- White SS, Kato K, Jia LT, et al.: Effects of perfluorooctanoic acid on mouse mammary gland development and differentiation resulting from cross-foster and restricted gestational exposures, *Reprod. Toxicol.* 27(3–4):289–298, 2009.
- White SS, Stanko JP, Kato K, et al.: Gestational and chronic low-dose PFOA exposures and mammary gland growth and differentiation in three generations of CD-1 mice, *Environ. Health Perspect.* 119(8):1070–1076, 2011.
- Woicke J, Al-Haddawi MM, Bienvenu JG, et al.: International harmonization of nomenclature and diagnostic criteria (INHAND): nonproliferative and proliferative lesions of the dog, *Toxicol. Pathol.* 49(1):5–109, 2021.
- Wood CE, Usborne AL, Starost MF, et al.: Hyperplastic and neoplastic lesions of the mammary gland in macaques, *Vet. Pathol.* 43(4):471–483, 2006.
- Wysolmerski JJ, Philbrick WM, Dunbar ME, et al.: Rescue of the parathyroid hormone-related protein knockout mouse demonstrates that parathyroid hormone-related protein is essential for mammary gland development, *Development* 125(7):1285–1294, 1998.
- Yeh S, Hu YC, Wang PH, et al.: Abnormal mammary gland development and growth retardation in female mice and MCF7 breast cancer cells lacking androgen receptor, *J. Exp. Med.* 198(12):1899–1908, 2003, <https://doi.org/10.1084/jem.20031233>. PMID: 14676301; PMCID: PMC2194158.
- Zhou Y, Xia J, Xu S, et al.: Experimental mouse models for translational human cancer research, *Front. Immunol.* 14: 1095388, 2023.



# Male Reproductive System

Justin D. Vidal<sup>1</sup>, Natasha Catlin<sup>2</sup>, Cynthia J. Willson<sup>3</sup>

<sup>1</sup>Charles River Laboratories, Ashland, OH, United States, <sup>2</sup>Pfizer, Inc., Groton, CT, United States, <sup>3</sup>Inotiv-RTP, Morrisville, NC, United States

## OUTLINE

<b>1. Introduction</b>	<b>635</b>	4.2. Morphologic Changes (Nonproliferative)	681
<b>2. Structure, Function, and Cell Biology</b>	<b>636</b>	4.3. Morphologic Changes (Proliferative)	690
2.1. Embryonic Development	636	4.4. Recovery and Reversibility of Injury	695
2.2. Postnatal Development of the Reproductive Tract	637	4.5. Immaturity and Peripuberty as Confounding Factors for Identifying Toxicity	696
2.3. Structure and Function of the Testis	640	4.6. Background Pathology as a Confounding Factor for Identifying Reproductive Toxicity	701
2.4. Spermatogenesis and the Spermatogenic Cycle	648	4.7. Stress and Body Weight Loss as a Confounding Factor for Identifying Reproductive Toxicity	707
2.5. Structure and Function of the Rete Testis, Efferent Ducts, Epididymis, and Vas Deferens	651	<b>5. Mechanisms and Patterns of Toxicity</b>	<b>708</b>
2.6. Structure and Function of the Accessory Sex Organs	658	5.1. Molecular and Biochemical	708
2.7. Hormonal Regulation of Reproductive Function	661	5.2. Morphologic Patterns of Response to Different Types of Injury	709
<b>3. Evaluation of Toxicity</b>	<b>665</b>	5.3. Mechanisms of Developmental Toxicity	725
3.1. Physiologic Evaluation	666	<b>6. Conclusion</b>	<b>727</b>
3.2. Biochemical and Biomarker Evaluation	671	<b>Acknowledgments</b>	<b>728</b>
3.3. Morphologic Evaluation	674	<b>References</b>	<b>728</b>
3.4. Special Techniques	679		
<b>4. Response to Injury</b>	<b>680</b>		
4.1. Organ Weight Changes	680		

## 1. INTRODUCTION

Recent concerns about declining semen quality in men and impact of environmental chemicals affecting the reproductive health of human and wildlife populations have increased public awareness for environmental contaminants, occupational exposures, and therapeutic drugs to pose a potential risk to male fertility (Bernanke and Köhler, 2009; Levine et al., 2017;

Mann et al., 2020; Semet et al., 2017; Swan et al., 2000; Virtanen et al., 2017). As a result, test article-related effects on the male reproductive system in nonclinical toxicity studies often create concern for potential human effects when evaluating chemicals and pharmaceuticals in development. As with other organ systems, a thorough understanding of normal physiology, common patterns of spontaneous and induced lesions, and species differences is critical to the

evaluation of reproduction and formulation of a robust risk assessment. However, the male reproductive system has several unique features that differ from other organ systems, including the spermatogenic cycle, hormonal regulation, developmental changes during puberty, and evaluation occurring in the context of both repeated-dose general toxicology studies and stand-alone developmental and reproductive toxicology (DART) studies. This requires a broad integration of toxicology and pathology with knowledge of reproductive endocrinology, development, and comparative biology throughout the assessment and development of the chemical/compound.

Effects on the male reproductive system are often first encountered in repeated-dose general toxicology studies. In pharmaceutical development, the approach and importance of thorough evaluation of the male reproductive system in repeated-dose general toxicity studies is described in several International Conference on Harmonization of Technical Requirements for Registration of Pharmaceuticals for Human Use (ICH) guidelines (ICH, 2009, 2011, 2020). In ICH Guidance on Nonclinical Safety Studies for the Conduct of Human Clinical Trials and Marketing Authorization for Pharmaceuticals M3(R2), it states “Men can be included in Phase I and II trials before the conduct of the male fertility study since an evaluation of the male reproductive organs is performed in the repeated-dose toxicity studies” with the assumption that male fertility studies “should be completed before the initiation of large scale or long duration clinical trials (e.g., Phase III trials).” In chemical toxicity testing, EPA and OECD Guidelines also include language detailing the importance of the microscopic assessment of the testis (EPA, 1998; OECD, 2016). As such, prior to conducting DART studies, the organ weight and microscopic data generated by the study pathologist are often the only available information about potential effects of a test article on the male reproductive system as there are limited clinical signs and no currently available routine clinical pathology endpoints in standard general toxicology studies. For a full description of regulatory guidelines related to the reproductive system, see *The Role of Pathology in Evaluation of Reproductive, Developmental and Juvenile Toxicity*, Vol 1, Chap. 7.

This chapter provides an overview of the normal structure and function of the male reproductive system, details common methods for evaluation, describes patterns of spontaneous and induced injury, and reviews current regulatory and translational issues in order to provide a guide for both new and experienced pathologists tasked with evaluating this complicated organ system.

## 2. STRUCTURE, FUNCTION, AND CELL BIOLOGY

### 2.1. Embryonic Development

The early gonad is composed of proliferating coelomic and mesenchymal cells, primordial germ cells, and endothelial cells (Hutson et al., 2009). As the gonad emerges in the genital ridge of the embryo, it has the precursors of both male (Wolffian) and female (Müllerian) reproductive tracts and has the potential to differentiate into either sex (Wilson and Davies, 2007). Development of the male reproductive system is controlled by expression of the sex-determining gene (Sry), which in turn leads to testis formation and regression of the Müllerian duct (Barsoum and Yao, 2006; Gilbert, 2006; Koopman et al., 1991). The differentiation of the Wolffian duct into the excurrent duct system (rete testis, efferent ducts, epididymis, and vas deferens) is maintained through testosterone secreted by Leydig cells, while Müllerian-inhibiting substance (MIS, also referred to as anti-Müllerian hormone, AMH) produced by the pre-Sertoli cells of the early testis causes the regression of the Müllerian ducts (Barsoum and Yao, 2006; Capel, 2000; Hannema and Hughes, 2007). The seminal vesicles develop from lateral buds of the Wolffian duct. However, the prostate and bulbourethral glands, along with the urethra and external genitalia, have a different embryologic origin; these tissues develop from the urogenital sinus under the influence of dihydrotestosterone (DHT), the testosterone metabolite produced locally by 5- $\alpha$  reductase (Creasy, 2001; Klonisch et al., 2004; Wilson and Davies, 2007). The basic developmental processes are quite similar between species, but the timing of certain events show significant species differences.

## 2.2. Postnatal Development of the Reproductive Tract

The rate of development and maturation of the reproductive tissues varies greatly between species, and for nonrodents, between breeds or genetic background within species (Picut et al., 2018). In rodents, the initiation of spermatogenesis, the process in which spermatozoa develop from spermatogonia in the testis, begins immediately at birth and is slightly accelerated compared with the adult, so that sperm are starting to be released from the testis by 6–7 weeks of age in the rat and 4–5 weeks of age in the mouse (Picut and Remick, 2016; Picut et al., 2014; Vergouwen et al., 1993). In contrast, larger animals such as the dog (laboratory beagle dog unless otherwise stated), nonhuman primate (NHP; cynomolgus macaque unless otherwise stated), and human go through a period of dormancy before spermatogenesis begins. The testes will not begin spermatogenesis prior to 5 months of age in the beagle dog or 3 years of age in the NHP (Haruyama et al., 2012; James and Heywood, 1979; Kawakami et al., 1991). Even though this is the age at which sperm start to be produced, it should be appreciated that the efficiency of spermatogenesis and therefore the number of sperm and size of the reproductive organs will continue to increase over a longer period of time. In rats, for example, the first appearance of sperm in the epididymis could be 8 weeks, but full attainment of final organ weight and epididymal sperm count may not be achieved until 12 weeks (Campion et al., 2013). In general, maturation follows a very consistent and predictable timeline in rodents, with most animals reaching sexual maturity at the same age  $\pm 1$  week, but there is significant individual and/or source variation in the rate of maturation in dogs, minipigs, and NHP. In dogs, the age of sexual maturation can be anywhere between 8 and 12 months of age with dogs sourced from Harlan France maturing earlier than dogs sourced from Marshall Farms, USA (Dorso et al., 2008; Kawakami et al., 1991); in minipigs, spermatogenesis is reported to be present from as early as 2 months old in Göttingen to about 4.4 months old in Yucatan boars (Howroyd and Peter, 2016; Taberner et al., 2016), and in NHPs, it can be anywhere between 3.5 and 5.0 years of age with Mauritian NHPs

reaching sexual maturity almost 2 years earlier than Asian mainland animals (Haruyama et al., 2012; Luetjens and Weinbauer, 2012). This has very important implications when attempting to evaluate the effects of test materials on sexual development and maturation with the small group sizes used for large animal studies. Table 9.1 provides an approximate timing for some major postnatal maturational changes in the testis of the rat, dog, minipig, NHP, and human. For details of postnatal development in rats, see Picut et al. (2015) and Whitney (2012), for dogs, see Kawakami et al. (1991), for minipigs, see Kangawa et al. (2016a, 2016b), for NHPs, see Haruyama et al. (2012), and for comparative aspects of the male reproductive system, see Picut et al. (2018) and Vidal et al. (2021).

In all species, Sertoli cells have a limited period in which they divide. In the rat, division starts prenatally, increasing from gestation day (GD) 16 to GD 20, and continues postnatally, ceasing (in vivo and in vitro) by postnatal day (PND) 15 (Orth, 1982; Steinberger and Steinberger, 1971) or PND 18 (Picut et al., 2018). In the rat, the period of rapid proliferation for Sertoli cells and gonocytes at GD 16 renders the late prenatal period a sensitive time for exposure to mitotic inhibitors or radiation (Picut et al., 2018). This period of Sertoli cell division is critical, because the final sperm output is a function of the number of Sertoli cells in the testis (Orth et al., 1988). If division ceases too soon (due to juvenile or maternal hyperthyroidism, for example), it can result in smaller testes and reduced sperm output (Sharpe et al., 2003). Sertoli cell proliferation can also be reduced by too much estrogen, insufficient testosterone, and insufficient follicle-stimulating hormone (FSH). On the other hand, hypothyroidism delays the cessation of Sertoli divisions, which cascades into enlarged adult testis size and increased overall sperm output (Hess et al., 1993). For a review of comparative pre- and postnatal development of the male reproductive system, the reader is referred to Picut et al. (2018).

### 2.2.1. Leydig Cells

Fetal Leydig cells regress and are replaced by a different generation of adult Leydig cells, which also differentiate from interstitial mesenchymal cells. In the rat, these begin to appear



**TABLE 9.1** Approximate Timelines and Hormonal Control for the Development of the Male Reproductive Organs in Rats, Dogs, Minipigs, Nonhuman Primates, and Humans

	Rat	Dog	Minipig	NHP	Human
Gestation length	21 days	63 days	112–115 days	164 days	39 weeks
Testicular descent complete	~PND 21	5–6 weeks	At birth	~36 months <sup>a</sup>	GW 24–36
Preputial separation	PND 39–45	~7 weeks	ND	2.5 years (rhesus)	9 months–3 years
Mini-puberty	0–6 h	ND	<6 weeks	<4 months	3–6 months
Initial spermatogonial proliferation	PND 4–12	16 weeks	<4 weeks	~3 years	9–11 years
BTB formation	PND 15–20	20 weeks	ND	~3 years	12–13 years
Maturation of the testis	Diffuse	Diffuse	Diffuse	Lobule by lobule	Lobule by lobule
Mature spermatids present	~PND 46	8–12 months	As early as 8 weeks	~3.5–5 years	11.8–14 years
Total duration of spermatogenesis (days)	51.6	54.4	35–40	42 (36–48)	64

<sup>a</sup> Transient descent at birth, then move near inguinal ring shortly after birth, with complete descent at puberty.

BTB, blood–testis barrier; GW, gestation week; ND, not determined; NHP, nonhuman primate (cynomolgus macaque unless stated otherwise); PND, postnatal day.

From Taberner E, Navratil N, Jasmin B, et al.: Pubertal age based on testicular and epididymal histology in Gottingen minipigs, *Theriogenology* 86:2091–2095, 2016; Picut CA, Ziejewski MK, and Stanislaus D: Comparative aspects of pre- and postnatal development of the male reproductive system, *Birth Defects Res.* 110:190–227, 2018; Vidal JD, Colman K, Bhaskaran M, et al.: Scientific and regulatory policy committee best practices: documentation of sexual maturity by microscopic evaluation in nonclinical safety studies, *Toxicol. Pathol.* 49:977–989, 2021 and Modified from Haschek WM, Rousseaux CG, Wallig MA, editors: *Haschek and Rousseaux's handbook of toxicologic pathology*, ed 3, 2013, Academic Press, Table 59.1, p. 2498, with permission.

around PND10 and increase in number up to the end of puberty (Ariyaratne and Chamindrani Mendis-Handagama, 2000). In the adult, new Leydig cells are also formed by the differentiation of primitive mesenchymal cells and fibroblast-like cells derived from the peritubular cells; there is very limited proliferation of existing cells (Lejeune et al., 1998).

### 2.2.2. Testicular Descent

Although testicular descent occurs prior to birth in man, it is a postnatal event in the rat (~ PND 21), mouse (~PND 19), rabbit (12–16 weeks), dog (5–6 weeks), minipig (at birth), and NHP (transiently descended at birth but moves near the inguinal ring shortly after birth with complete descent at ~ 3 years) (Picut et al., 2018; Vidal et al., 2021). The passage of the testis through the inguinal ring is controlled

by the genitoinguinal ligament, or “gubernaculum,” which connects the lower pole of the testis and epididymis to the inguinal abdominal wall at what will develop into the inguinal canal (Hutson et al., 2009). Insulin-like hormone 3 (Insl3), secreted by Leydig cells, the main hormone responsible for transabdominal testicular descent, stimulates swelling of the gubernaculum (Hutson et al., 2009). The swelling and migration of the gubernaculum through the inguinal canal precede the testis descent and force open the inguinal ring, allowing the testis to move passively into the scrotum during the second or inguinoscrotal phase of testicular descent, which is under the control of androgens. Once this function is served, the gubernaculum regresses under the control of androgens. Cryptorchidism, or undescended testis, is the failure of one or both testes to descend into the scrotal sac,

and if this occurs, spermatogenesis is blocked by the elevated body temperatures in the peritoneal cavity. Testosterone production is also decreased. Both can be prevented if the abdominal testis is cooled. A variety of risk factors have been proposed to be associated with cryptorchidism in humans, including maternal smoking during pregnancy, low birth weight/prematurity, family history, and maternal or paternal exposure to endocrine-disrupting chemicals (Gurney et al., 2017). The spermatic cord, comprising the internal cremaster muscle, the vessels and nerves that supply the testis and the vas deferens, links the testis to the abdominal cavity. In most species, the inguinal ring closes substantially after descent, but in rodents, it stays open, allowing the animal to voluntarily retract the testes into the abdominal cavity. Care must be taken not to mistake voluntary retraction of the testis as cryptorchidism.

### 2.2.3. Morphologic Appearance of the Developing Postnatal Testis

The histopathological appearance of the testis changes rapidly during postnatal development. It is most well defined in the rat, where there is consistency in morphology across the developing seminiferous tubules and has been reviewed (Picut et al., 2015). At birth the seminiferous tubules of the rat are lined by mitotically active Sertoli cells with elongated nuclei that form a dense basal ring in a single layer. In the center of the tubule are a few (typically five or six in a cross-section) gonocytes with large pale-staining nuclei (Figure 9.1). The Leydig cells form small aggregates of cells within a meshwork of loose connective tissue. Beginning on PND 3, the gonocytes migrate from the center to the base of the tubule where they either degenerate or differentiate into small, type A spermatogonia; gonocytes are no longer apparent by PND 10 (Picut et al., 2014). From PND 8, there is rapid expansion of Sertoli cells and spermatogonia, with differentiation into type A, intermediate, and type B spermatogonia (Picut et al., 2014). From PND 15–18, Sertoli cells cease dividing, and preleptotene, leptotene, and zygotene spermatocytes (with apoptosis) become evident (Picut et al., 2014). As the Sertoli cells commence fluid secretion, a lumen appears in the center of the tubule by PND 18, and vacuoles frequently appear within the Sertoli cell

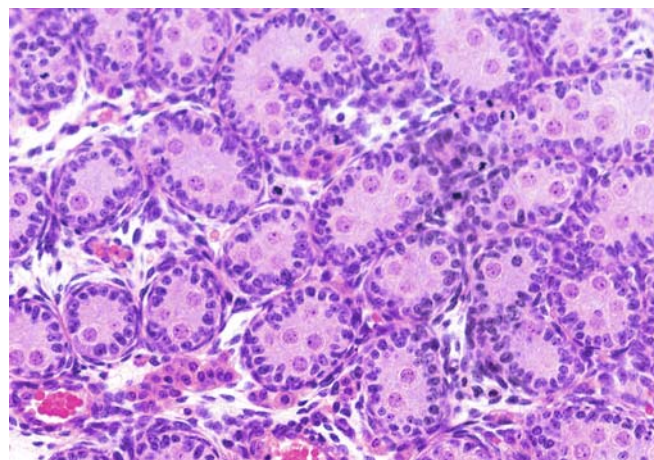


**FIGURE 9.1** Neonatal testis (postnatal day [PND] 2). Seminiferous tubules are lined by closely packed Sertoli cell nuclei. Centrally located gonocytes with large, pale-staining nuclei. Fetal Leydig cells occur singly or form small clusters between the tubules. Rat, H&E,  $\times 20$ . Reproduced from Haschek WM, Rousseaux CG, Wallig MA, editors: *Haschek and Rousseaux's handbook of toxicologic pathology*, ed 3, 2013, Academic Press, Figure 59.3, p. 2500, with permission.

layer. These vacuoles will disappear as the seminiferous epithelium becomes fully populated with germ cells, and so they should not be misinterpreted as evidence of Sertoli cell toxicity when seen in prepubertal, test article-treated animals in a toxicity study. A notable microscopic feature of the developing testis in the rat is a double-layered rosette from PND 18 to 20, with an outer layer of spermatogonia surrounding an inner layer of Sertoli cells (Picut et al., 2014). The blood–testis barrier is complete by  $\sim$  PND 20. Round spermatids appear at PND 26 (Figure 9.2), stage VII tubules with mature, step 19 spermatids at the lumen are apparent by PND 46, sperm are present in the epididymis at PND 52, and the tubular diameter markedly increases between PND 20 and 70, when sexual maturity is nearly complete (Picut et al., 2014). The developing testis is susceptible to toxicity; a review of toxicologic lesions during postnatal development is found in Picut et al. (2018).

In most species, the development of spermatogenesis progresses at a similar rate in all tubules, but in NHPs, it is common for some groups of tubules to be significantly more or less advanced than others (Creasy, 2012) and there is large interanimal, interspecies, and genetic source variability (Figure 9.3) (Luetjens and Weinbauer,



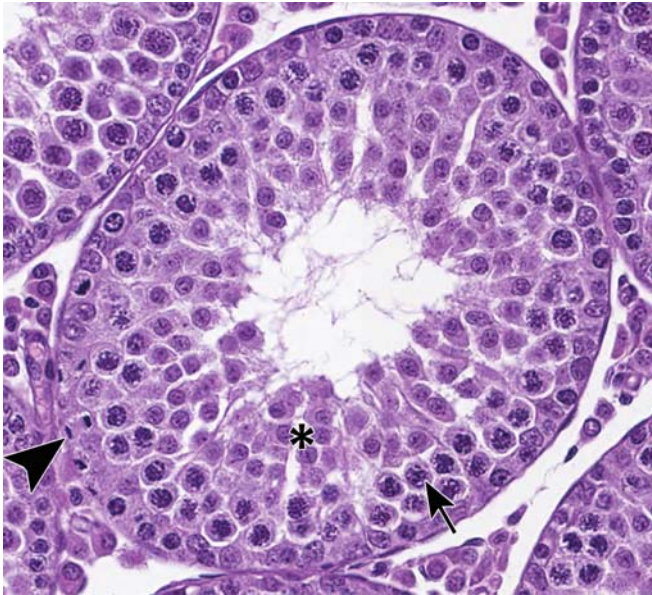


**FIGURE 9.2** Seminiferous tubule from the testis of a 32-day-old rat. This seminiferous tubule contains spermatogonia with mitotic figures (arrowhead), spermatocytes (arrow), and round spermatids (\*). However, there are no elongated spermatids overlying the round spermatids. Rat, H&E,  $\times 40$ .

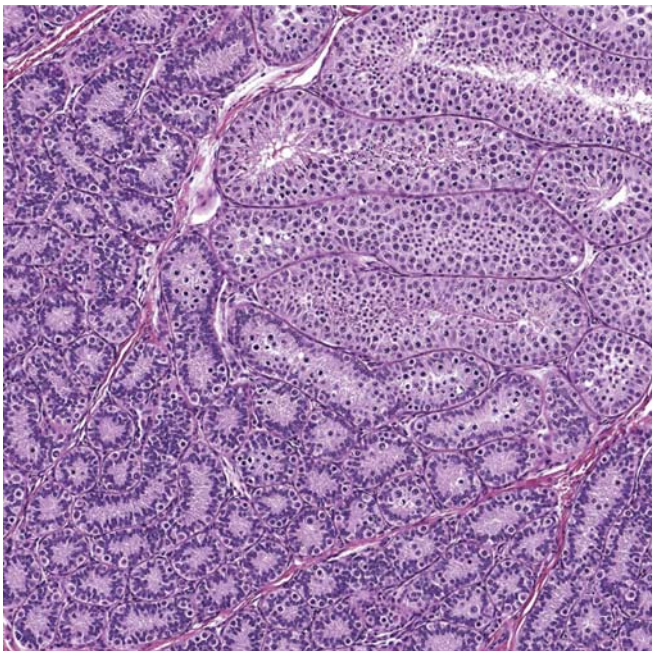


**FIGURE 9.3** Testis from an early peripubertal cynomolgus macaque with a focal area of tubules (top right corner) that have begun spermatogenesis while neighboring tubules are still immature. NHP, H&E,  $\times 10$ .

2012). The testes of NHPs have a quiescent period, like humans (O'Shaughnessy, 2015). A developmental scheme of grade 1 (immature) to grade 6 (adult) has been developed for the microscopic evaluation of the testis in NHPs (Haruyama et al., 2012), but while helpful for understanding the onset and progression of spermatogenesis, is likely too detailed for routine assessment and documentation in toxicity studies (Vidal et al., 2021). As with NHPs, there is wide interanimal and genetic source variability in postnatal testicular development in dogs and minipigs (Dorso et al., 2008; Howroyd and Peter, 2016; Kawakami et al., 1991; Taberner et al., 2016).

In all species, the first wave of spermatogenesis is accompanied by a higher than normal level of germ cell apoptosis (Jahnukainen et al., 2004) and sloughing of some germ cells into the lumen, probably because the Sertoli cell is still undergoing maturation and has not reached maximal efficiency in its ability to support spermatogenesis. This results in some sloughed germ cells in the contracted lumens of the epididymal ducts.

## 2.3. Structure and Function of the Testis

### 2.3.1. Capsule and Vasculature

The testicular parenchyma is composed of convoluted seminiferous tubules separated by interstitial tissue and enclosed in a capsule that has three layers: the outer tunica vaginalis (continuous with the visceral peritoneum), the middle tunica albuginea, which contains collagen and smooth muscle cells or myofibroblasts, and the innermost layer, the tunica vasculosa, which contains blood vessels embedded in a loose connective tissue. Apart from enclosing and confining the seminiferous tubules within the testis, the capsule is thought to play an active role in control of testicular blood flow, presumably because the testicular artery runs within the testicular capsule for much of its length before it enters the testicular parenchyma. The testis is supplied by the internal spermatic artery, a highly coiled tortuous vessel that originates as a branch of the abdominal aorta and runs through the spermatic cord surrounded by the veins of the



pampiniform plexus (Chubb and Desjardins, 1982). The spermatic artery gives off the superior and inferior epididymal branches, which supply parts of the epididymis, and continues as the testicular artery to supply the testis. As the spermatic artery arrives at the testis, it courses within the capsule in a straight line down the epididymal border before taking a sharp turn at the caudal pole to meander within the capsule, via a series of looping reversals, to the site of the rete testis, where it finally dives into the parenchyma of the testis and divides into radiate arteries, which in turn give rise to intertubular arterioles. These supply the network of intertubular and peritubular capillaries that run parallel to, or circumferentially around, the seminiferous tubules, respectively. The capillary endothelium is nonfenestrated and is surrounded by perivascular cells.

The lymphatics form a labyrinth of channels between the Leydig cells and the peritubular cells of the seminiferous tubules in the rat, or form discrete vessels in the dog, NHP, and human (Fawcett et al., 1973). In the rat, dog, and NHP, the capillaries are located within the interstitial tissue, but in the human testis, they enter the peritubular layer of myoepithelial cells. The veins leaving the testis divide as they enter the spermatic cord to form a venous plexus, called the pampiniform plexus, that closely surrounds the incoming spermatic artery and acts as an efficient countercurrent heat exchange system to maintain the testes a few degrees below body temperature, which is necessary for optimal spermatogenesis. Arteriovenous anastomoses have been demonstrated in many species between the incoming arterial supply and venous return in the pampiniform plexus. These anastomoses result in significant interchange of substances and hormones as well as the potential for modification of the overall blood flow to the testis.

### 2.3.2. Interstitium

The seminiferous tubules are enmeshed in interstitial tissue containing Leydig cells, vasculature, macrophages, peritubular myoid cells, varying amounts of supporting connective tissue, and a protein- and testosterone-rich ultrafiltrate that, depending on the species, is contained within lymphatics or is present in the interstitial

space (Fawcett et al., 1973). The anatomic structure and amount of the interstitial tissue varies widely between species.

Leydig cells form loose clusters around the interstitial vasculature in rodents and the remaining space serves as lymphatic sinuses that carry the interstitial ultrafiltrate into the draining lymphatics that exit the testis through the spermatic cord (Fawcett et al., 1973). In the rat, the lymphatic channels are “lined” by a discontinuous endothelium that adheres to the Leydig cells, peritubular cells, and the tunica of the blood vessels. This is very different from man, NHPs, and dogs, where the connective tissue is more plentiful and discrete lymphatic vessels exist.

In response to luteinizing hormone (LH), Leydig cells synthesize testosterone, which enters the interstitial filtrate and reaches the systemic circulation via the spermatic vein or crosses peritubular myoid cells to reach the spermatogonia and Sertoli cells. The size and number of Leydig cells varies considerably among species (Fawcett et al., 1973; Franca et al., 2005). Mice have more and larger Leydig cells than rats (Creasy, 2012). The rat and mouse have a relatively small volume of Leydig cells in the testis (1%–5%) and most of the interstitium is composed of lymphatic sinusoids; in NHPs and humans, clusters of Leydig cells are scattered in loose connective tissue drained by lymphatic vessels, and in the minipig Leydig cells make up a large component of the testis volume and nearly fill the interstitial area (Fawcett et al., 1973; Franca et al., 2005) (Figure 9.4).

Testicular macrophages are a unique subset of the mononuclear phagocyte system comprising a resident population of macrophages that have close physical and functional interactions with the Leydig cells and participate in paracrine regulation, steroidogenesis, Leydig cell proliferation and differentiation, and in the immune-endocrinology of the testis (Hales, 2002). Testicular macrophages secrete a number of proinflammatory cytokines, such as interleukin-1 and tumor necrosis factor, which appear to act as potent inhibitors of Leydig cell steroidogenesis at the transcriptional level (Hales, 2002). Testicular macrophages make up about 25% of the cells in the interstitium in rats (Niemi et al., 1986).



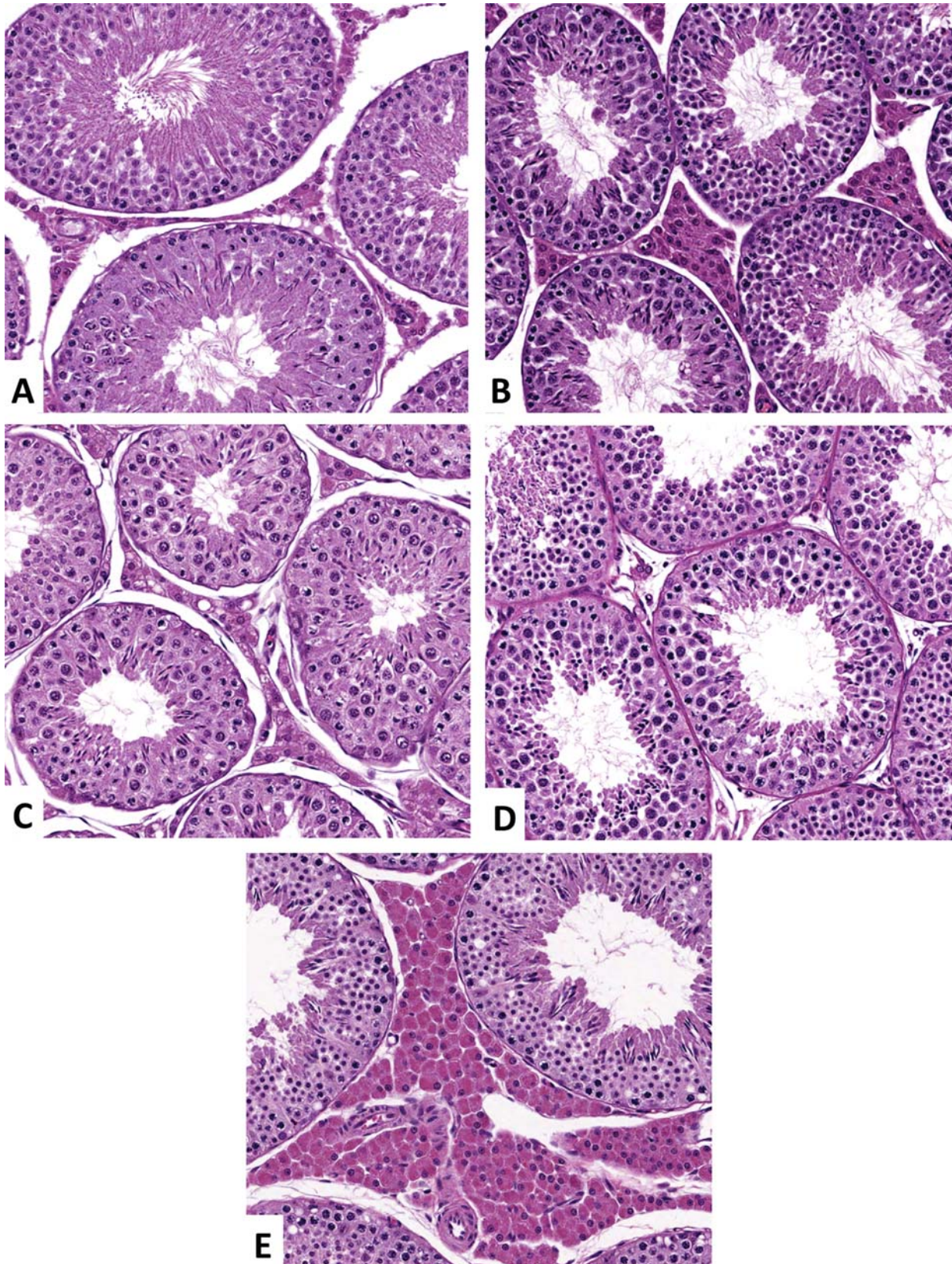


**FIGURE 9.4** Sections of testis demonstrating the relative size and abundance of Leydig cells across species. (A) Rat, (B) mouse, (C) dog, (D) NHP, (E) minipig. H&E,  $\times 20$ .



The tubules are surrounded by an interdigitating layer of peritubular myoid cells which have numerous functions, including forming a very loose part of the blood–testis barrier via intercellular gap junctions, paracrine regulation of Sertoli cells and Leydig cells, and providing contractile properties to the seminiferous tubules for the propulsive movement of the mature, but not yet motile, sperm and fluid toward the rete testis (Maekawa et al., 1996). Between the base of the Sertoli cells and the peritubular cells is a basement membrane which is secreted by both cell types (Hadley and Dym, 1987). Peritubular myoid cells, like Sertoli cells, express androgen receptors (ARs) and thus are testosterone responsive.

### 2.3.3. Seminiferous Tubules

The seminiferous tubules are long, highly convoluted tubes, and in the rat, there are approximately 28 separate tubules, folded to form about 20 m per testis (12 m/g), and approximately 12 separate tubules per testis in mice (Nakata et al., 2021; Wing and Christensen, 1982). It should be recognized then that a single cross-section of a testis containing hundreds of tubular profiles in fact represents less than 30 individual seminiferous tubules in rodents. In rodents, regular convolutions of each tubule are arranged in a transverse circumferential organization, with each end emptying into the sac-like reservoir of the subcapsular rete testis located at the cranial pole of the testis (Nakata et al., 2015). Sometimes each tubule has more than one connection point to the rete testis. In the dog, NHP, and human, the seminiferous tubules are grouped into lobules separated by connective tissue, and individual convoluted tubules are arranged within one lobule with the tubule ends emptying into the more centrally located rete testis that is located within the fibrous mediastinum testis (Figure 9.5). This difference in tubular spatial arrangement between rodents and most other mammals has an impact on the pattern of tubular degeneration and atrophy seen when an individual tubule is affected. In the rodent, the injured tubular profiles will appear scattered throughout the testis often in a circumferential pattern, whereas in the dog and NHP, the affected tubule will be restricted to a single lobule.

### 2.3.3.1. REGULATION OF BLOOD FLOW AND INTERSTITIAL FLUID

Interstitial fluid has a very specific composition, compared with plasma, and is responsible for providing the oxygen and nutrients required by the metabolically active Sertoli and germ cells, which are otherwise located in an avascular environment. Interstitial fluid is thought to be produced as a result of rhythmic alterations in arteriolar blood flow (vasomotion), which brings about movement of fluids from the blood through the unfenestrated capillaries into the interstitial space.

### 2.3.4. Sertoli Cells

#### 2.3.4.1. STRUCTURE

Sertoli cells are large, postmitotic somatic cells that provide the supporting framework for the germ cells (Weber et al., 1983). The germ cells are embedded into apical or lateral invaginations of the Sertoli cells such that many of the germ cells are located between adjacent Sertoli cells (Figure 9.6). The Sertoli cell has a prominent tripartite nucleolus, but its size and shape are not discernible by typical light microscopy. The Sertoli cell is irregularly columnar, with its basal aspect attached to the basement membrane by hemidesmosomes and apical aspect defining the lumen. Sertoli cells have numerous functions: regulation of spermatogenesis, structural and metabolic support of the germ cells, sperm release, phagocytosis of residual bodies and apoptotic germ cells (Gondos and Berndtson, 1993), secretion of tubular fluid for sperm transport, and maintenance of a permeability barrier between interstitial and tubular compartments. Disturbance of any of these functions is likely to impair the process of spermatogenesis and, in turn, sperm production.

#### 2.3.4.2. ROLE IN STRUCTURAL SUPPORT AND GERM CELL TRANSLOCATION

The structural support and movement of germ cells is central to the process of spermatogenesis. Adjacent Sertoli cells are joined at their basolateral aspect by specialized occluding junctions, forming the major component of the blood–testis barrier (Franca et al., 2012). These junctions between Sertoli cells form basal (containing spermatogonia, which are exposed to blood-borne nutrients and toxicants) and adluminal compartments. As spermatogonia in the basal compartment develop into spermatocytes, the Sertoli cells disassemble the junctional complexes on their luminal side,



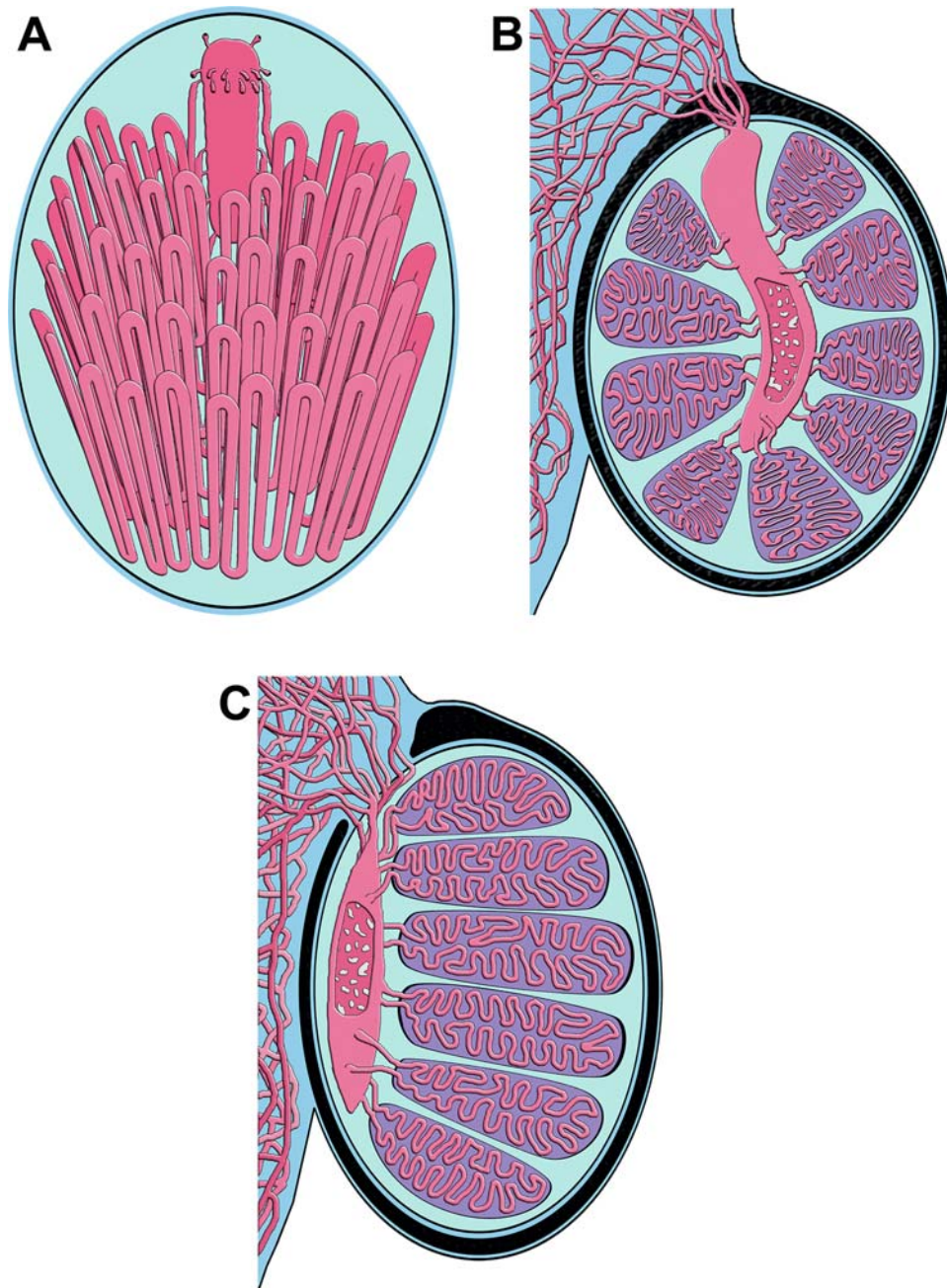


**FIGURE 9.5** The organization of tubules and the position of the rete testis varies with species. This has an impact on the distribution pattern of individual degenerate/atrophic tubules in a section of testis. (A) In the rat, the rete is positioned in a subcapsular position at the cranial pole of the testis and the tubules are arranged circumferentially around the testis. Each end of a tubule empties into the rete. There are no fibrous septae. (B) In the dog, the rete is located centrally and exits to a subcapsular position running within the fibrous mediastinum testis. The tubules are arranged within lobules that are separated from one another by connective tissue septae. (C) In the NHP, the rete is located along the lateral aspect of the testis, adjacent to the epididymis. The tubules are arranged in a lobular pattern separated by fibrous septae. *Reproduced from Haschek WM, Rousseaux CG, Wallig MA, editors: Haschek and Rousseaux's handbook of toxicologic pathology, ed 3, 2013, Academic Press, Figure 59.6, p. 2502, with permission.*

and create new complexes beneath them, thus facilitating the movement of the developing germ cell up into the adluminal compartment (Russell, 1977). As spermatocytes develop into

round and then elongating spermatids over the course of 3 weeks, they are gradually moved up to the luminal surface, and then, as elongating spermatids, they are pulled back down toward

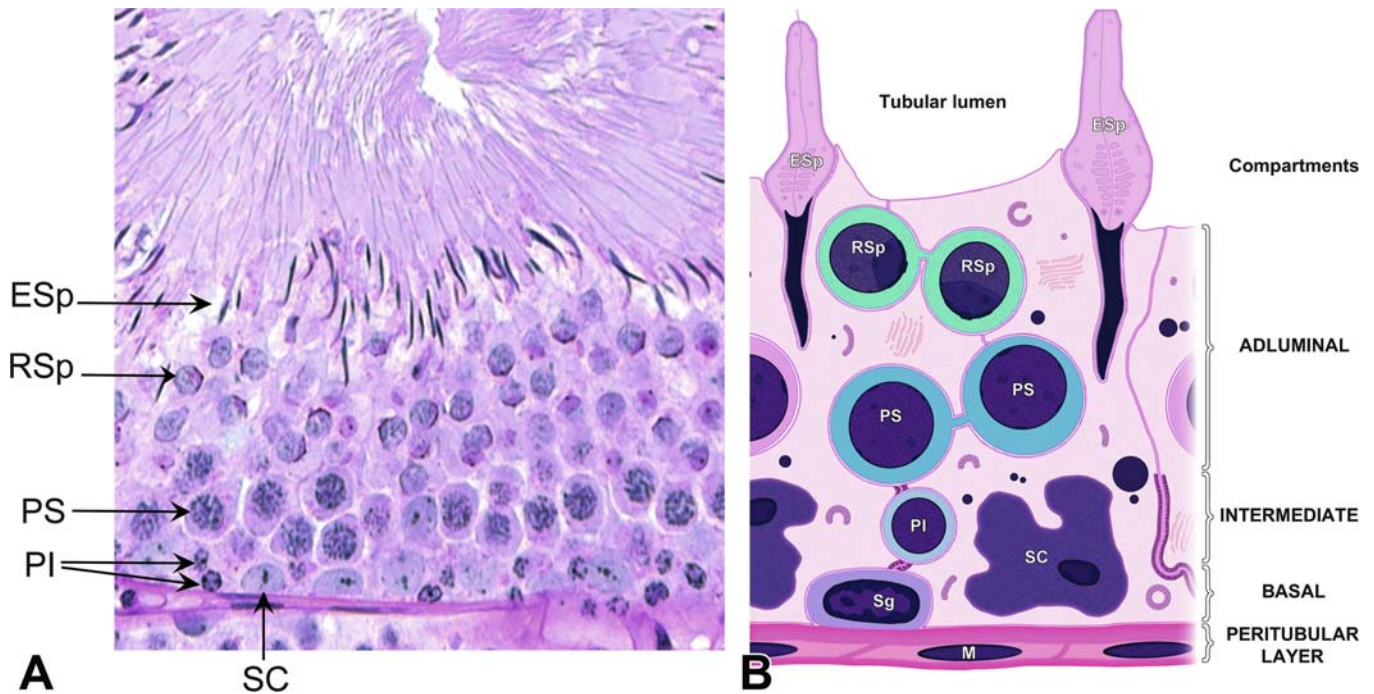


**FIGURE 9.6** Organization and compartmentalization of the seminiferous tubule in the rat. (A) Section of a tubule in stage VII of the spermatogenic cycle (methacrylate embedded, periodic acid Schiff-hematoxylin (PAS-H),  $\times 40$ ). (B) Labeled representation of the same stage tubule, showing the relationship of the compartments and cell types to one another. The tubule is surrounded by myoepithelial peritubular cells (M); Sertoli cell nuclei (SC) lie on the basement membrane interspersed with type A spermatogonia (Sg). There are very few of these in a stage VII tubule, and they cannot be seen in the histological section on the left. Tight junctions between adjacent Sertoli cells form the blood–testis barrier separating the basal from the adluminal compartment. An intermediate compartment is formed when the developing preleptotene spermatocytes (PI) move through the tight junction during this stage. Pachytene spermatocytes (PS) and round spermatids (RSp) form layers of germ cells within the adluminal compartment. Maturation phase elongating spermatids (ESp) are embedded within luminal Sertoli cell cytoplasmic processes while their tails project into the luminal compartment. It is important to recognize that details represented in a methacrylate embedded PAS-H-stained section and in the corresponding diagram may not be readily observed in routinely processed material in general toxicity studies. *Reproduced from Haschek WM, Rousseaux CG, Wallig MA, editors: Haschek and Rousseaux's handbook of toxicologic pathology, ed 3, 2013, Academic Press, Figure 59.7, p. 2504, with permission.*

the Sertoli cell nucleus before returning to the surface to be released. This translocation process appears to be mediated by the well-developed and active cytoskeleton of the Sertoli cell and the specialized junctions between the Sertoli and germ cells (Russell et al., 1989; Vogl et al., 2008). Sertoli cell injury in the form of disruption of the cytoskeletal filaments and retraction of the lateral processes that surround germ cells is associated with premature exfoliation of germ cells into the lumen (Johnson, 2014) (see Section 5.2.1.4 below).

#### 2.3.4.3. ROLE IN METABOLIC SUPPORT OF GERM CELLS AND FLUID PRODUCTION

Germ cells in the adluminal compartment rely entirely on the Sertoli cell for their supply of nutrients and oxygen (Oliveira and Alves,

2015). This relationship is clearly manifest by the location of the germ cell mitochondria, which are arranged immediately under the cell membrane, as close as possible to the incoming energy substrates from the Sertoli cells. As mentioned, a dense and thick network of protein-secreting SER and Golgi surrounds the cluster of elongating spermatid nuclei embedded in Sertoli invaginations. In addition, the Sertoli cells secrete fluid which forms the lumen and carries the immotile mature-and-released sperm to the epididymis for their acquisition of motility.

#### 2.3.4.4. ROLE IN PHAGOCYTOSIS

Phagocytosis is another important function of the Sertoli cell (Penberthy et al., 2018). The Sertoli cell is connected to the germ cells by a variety



of cell junctions, some of which are unique to this cell type. The heads of the elongating spermatids are held within recesses of the Sertoli cell cytoplasm by ectoplasmic specializations termed tubulobulbar complexes, which are phagocytosed prior to sperm release (Russell et al., 1990). During spermatid development (spermiogenesis), the cytoplasmic volume of the spermatid is reduced by up to 70% and a large proportion of its organelles are discarded. This is accomplished by formation of the residual body, which contains redundant organelles, nucleic acids (various RNA species), and cytoplasm. At spermiation, the process by which mature spermatids are released from the Sertoli cells into the seminiferous tubule lumen, the residual body is shed and left behind. The residual body is then phagocytized by the Sertoli cell and merged with lysosomes while being moved down to the basal Sertoli cell cytoplasm, where digestion is completed. The autophagic vacuoles containing residual bodies are readily apparent by light microscopy in all stage IX–XI tubules and, because the compacted RNA stains with hematoxylin, can be easily confused with degenerating germ cells. Apoptotic germ cells, which are a normal feature of spermatogenesis as well as a result of toxic injury, are also removed rapidly by phagocytosis.

#### 2.3.4.5. ROLE IN BLOOD–TESTIS BARRIER FORMATION

Spermatogenesis occurs in a specialized and protected environment that is maintained by the blood–testis barrier in the adluminal compartment of the seminiferous epithelium (Cheng and Mruk, 2012; Franca et al., 2012; Mital et al., 2011). Capillary endothelial cells and peritubular myoid cells are partial barriers (Dym and Fawcett, 1970), but the main exclusion barrier is formed by the basolateral occluding cell junctions between adjacent Sertoli cells that are situated at a level above the spermatogonia and below the spermatocytes (Mruk and Cheng, 2015). By virtue of the peritubular cell layer and the inter-Sertoli cell tight junctions, the testis can be divided into physiologic and toxicologic compartments: the interstitial, the basal, and the adluminal compartments (Figure 9.6) (Dym and Fawcett, 1970). The interstitial compartment is exposed to all substances transported through the capillary endothelium, including toxicants. Although the peritubular cells may exclude some very large molecules, the basal compartment, which contains the

spermatogonia, is also readily accessible to virtually all bloodborne substances. In contrast, the adluminal compartment, which contains all meiotic and postmeiotic cells, is only exposed to bloodborne substances that have been transported through the Sertoli cell. There are a many types of drug transporters present at the level of the blood–testis barrier (Su et al., 2011). This barrier provides some protection against genetic damage or death of the gamete by toxicants.

#### 2.3.5. Spermatogonia

Spermatogonia are the diploid stem cell population of the germ cells that reside basally within the tubule, outside the blood–testis barrier. There are three classes of spermatogonia: stem cell, proliferative, and differentiating. Stem cell spermatogonia are relatively resistant to insult and often survive when other germ cells do not (de Rooij, 2017). Stem cell and proliferative spermatogonia are responsible for renewing their own cell number and producing a pool of spermatogonia that are committed to differentiation. Spermatogonia are present in all tubular cross-sections, but in variable numbers, and range from inconspicuous to forming a nearly contiguous layer in the stages approaching spermiation (Russell et al., 1990). Spermatogonia are classified morphologically based on their chromatin using either light or electron microscopy: For most species, Type A have a pale-staining nucleus that is often flattened basally with indistinct chromatin, Type B have a rounded to slightly oval nucleus with dense clumps of peripheral chromatin, and intermediate spermatogonia have an appearance somewhere between the two (Russell et al., 1990). Type A may be stem, proliferative, or differentiating, and type B and intermediate are differentiating spermatogonia (Hess, 2008; Russell et al., 1990). Spermatogonia classifications and proliferation kinetics differ across species (Clermont, 1972). As the cells undergo mitosis, cytokinesis is incomplete, leaving the descendant population of spermatocytes linked together in a syncytial arrangement via intercellular bridges. These bridges are maintained throughout spermatogenesis and are believed to enable the synchronized development and differentiation of the individual populations of cells. This also underlies the formation of multinucleated giant cells after treatment with toxicants, as described later.



### 2.3.6. Spermatocytes

The final mitotic division of the type B spermatogonia yields preleptotene spermatocytes, which are the most common cells seen in the basal layer at spermiogenesis. Preleptotene spermatocytes produced by the dividing B spermatogonia are almost identical to their parent cell, but preleptotene spermatocytes are approximately 30% smaller (Russell et al., 1990). During preleptotene, DNA synthesis (S phase) occurs, and the cells move away from the basement membrane. These spermatocytes then enter a 3-week long prophase of the first meiotic division, passing through the stages defined by nuclear and cell size changes (leptotene, zygotene, pachytene, and diplotene spermatocyte stages), diakinesis, and the first meiotic division to produce transient, secondary spermatocytes. The rapidly following second meiotic division produces the haploid spermatid. As the spermatocytes pass through meiotic prophase, they become progressively larger and the appearance of the nuclear chromatin alters, reflecting the condensation and movement of the chromosomes as they prepare for meiotic division. During leptotene, spermatocytes move through the tight junctional complex between the Sertoli cells, reaching the adluminal layer (Mruk and Cheng, 2015) and the chromosomes condense, coming together in zygotene as homologous pairs that form characteristic structures in the nucleus called synaptonemal complexes. These are where crossing over occurs, providing the exchange of chromosomal material that contributes to genetic heterogeneity and confers foreign antigenicity to this and all later stages of germ cells, including the sperm that are released into the epididymis. During the pachytene phase, the chromosomes become shorter and thicker and split into two chromatids joined by the centromere. Pachytene is a lengthy phase, typically lasting 1.5–2 weeks, with a fixed duration in a given species, and as a result, pachytene spermatocytes are present in the majority of tubular cross-sections (Russell et al., 1990). During this time, there is a marked increase in cellular and nuclear volume. As the spermatocytes enter the short diplotene phase, the spermatocytes reach their largest size and the chromosomes begin to separate and condense further while synaptonemal complexes disappear. Diakinesis and the two meiotic divisions occur in rapid succession; a single cross-section of tubule undergoing meiotic division will often contain a mix of diplotene spermatocytes, spermatocytes in the first and

second stages of division, secondary spermatocytes (from the first division), and/or the newly formed spermatids from the second division.

### 2.3.7. Spermatids

The second meiotic division of the spermatocytes results in the formation of the haploid spermatid, which is similar in appearance to the transiently observed secondary spermatocyte, but the nuclear diameter is slightly reduced. During the course of differentiation into a spermatozoon, or spermiogenesis, which takes about 3 weeks in the rat, the nucleus and cytoplasm undergo extremely complex morphological modifications (Clermont, 1972; Russell et al., 1990). After about a week in a round shape, the spermatid nucleus undergoes a profound shape change and condensation in preparation for movement through fluids in search of the egg. Beginning early in the round stage, an acrosome (visible in periodic acid Schiff [PAS] stained histological sections of rodents, minipigs, and primates, but not in dogs) develops and spreads over about half the nucleus (Dreef et al., 2007; Kangawa et al., 2016a; Russell et al., 1990). The acrosome is required for the sperm to penetrate and fertilize the oocyte. During and after elongation, the acrosome is retained and develops further over the highly condensed inactive nucleus, while the cytoplasm and mitochondria are totally rearranged to form a motile tail section. To some extent, these changes are species-specific, but the general features are similar across species.

During spermiogenesis, the nucleus is oriented to face the base of the tubule and the nucleus elongates and condenses to form the head of the spermatid. The cytoplasm of the cell is redistributed to the luminal pole of the cell, away from the nucleus, thus forming an elongated cell with the nucleus at one end and cytoplasmic tail and growing flagellum at the other. The flagellum forms the neck and tail regions of the spermatid. In the final maturation phase of spermiogenesis immediately before release from the epithelium, the cytoplasmic volume of the spermatid is greatly reduced by the condensation and expulsion of the spermatid cytoplasm. There is relatively little alteration in the structure of the nucleus during this phase, but cellular remodeling of the spermatid results in many of the redundant organelles and mRNA being deposited in the residual body, which is shed at the time of spermiogenesis and

subsequently phagocytosed by the Sertoli cell. The final shape and morphology of the spermatid is highly species specific (Gu et al., 2019).

## 2.4. Spermatogenesis and the Spermatogenic Cycle

Spermatogenesis is the lengthy process in which stem cell spermatogonia develop to form highly specialized motile spermatozoa. This sequential

development of germ cells from spermatogonia, to spermatocytes, to spermatids begins at the basement membrane and progresses toward the lumen in an orderly and predictable process (Figure 9.7). Multiple generations of germ cells, each of differing maturity, develop simultaneously in a synchronous manner within the seminiferous epithelium. Sertoli cells maintain this vertical array of germ cell associations which form specific sets of cell layers with distinctive patterns in

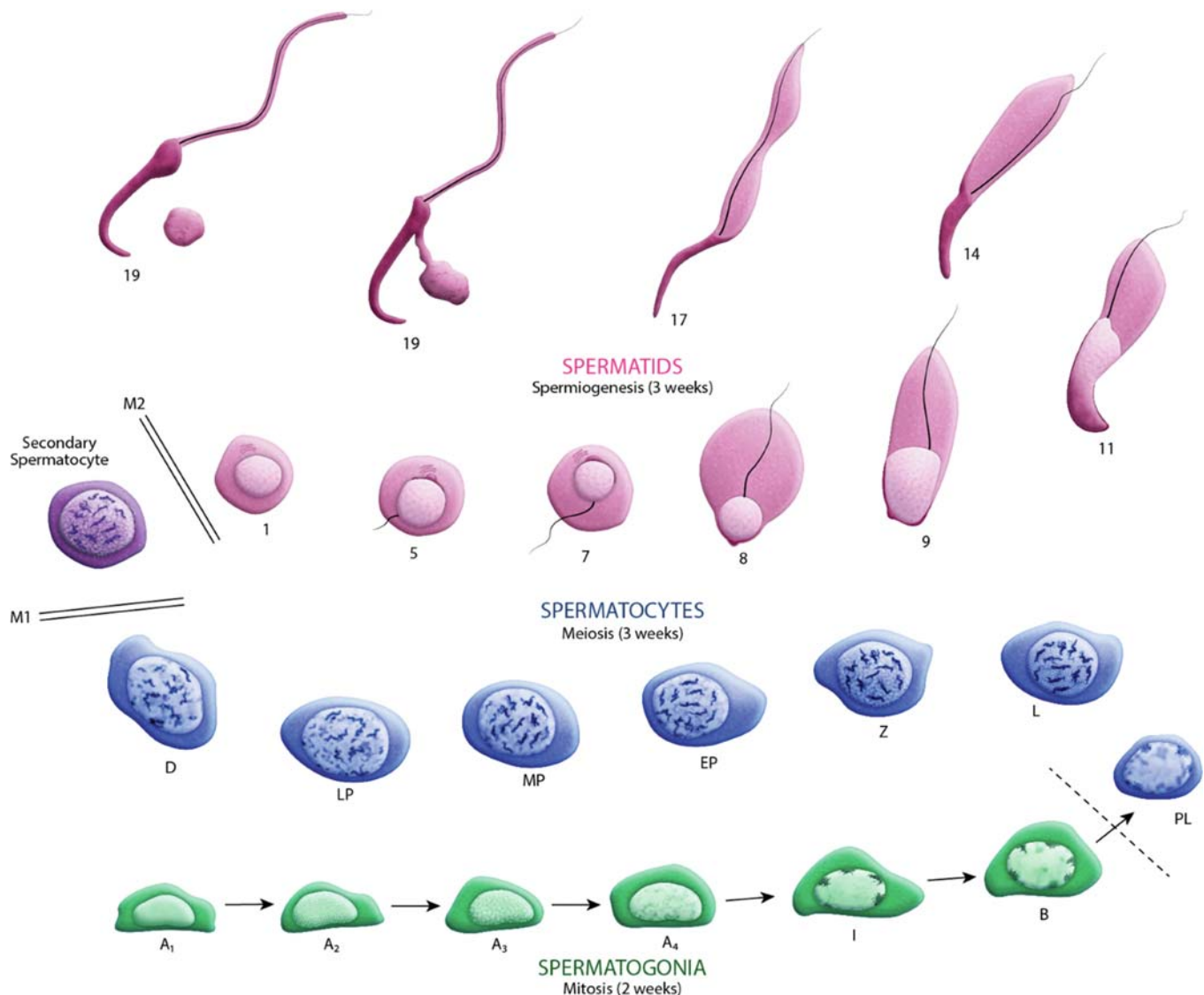


**FIGURE 9.7** Spermatogenesis involves multiple mitotic divisions of spermatogonia, beginning with type A spermatogonia (A) through intermediate (I) spermatogonia and finishing with type B spermatogonia (B). Division of type B spermatogonia produces spermatocytes (dashed line). This consists of preleptotene (PL), leptotene (L), zygotene (Z), and pachytene (P) phases. Pachytene is a long phase that can be split into early (EP), middle (MP), and late (LP). This is followed by diplotene (D) and then a reduction division, (M1) producing transient secondary spermatocytes and the second division (M2) producing haploid spermatids. Spermatids then undergo morphological transformation from a regular round cell into a sperm with an elongated head made up of condensed chromatin and a tail comprising a flagellum surrounded by mitochondria. In the rat, the transformation takes approximately 8 weeks and has been divided into 19 steps of spermiogenesis based on the development of the acrosome and the shape of the developing spermatid (only a few are illustrated here). *Courtesy of David Sabio.*

tubular cross-sections. These patterns of cellular associations are often referred to as “stages” (Hess, 2008; Russell et al., 1990). The time it takes to pass through all stages of development at a given point within the seminiferous tubule and return back to the original grouping of cells is often referred to as one cycle. With each cycle, a given germ cell cohort moves closer to the lumen and it takes multiple cycles to complete the full duration of spermatogenesis. The process is occurring vertically at a given point within the seminiferous tubules, but development is staggered along the length of the tubule with consecutive regions being slightly behind or ahead in development. This creates a progressive wave-like pattern along the long axis of a seminiferous tubule and ensures a steady release of spermatids (Perey et al., 1961).

Since the germ cell associations in cross-sections of seminiferous tubules have predictable and repeating patterns, these groupings or stages can be named and classified (Russell et al., 1990). Historically, most of the literature has focused on the rat and a variety of classification schemes are available (Leblond and Clermont, 1952; Regaud, 1901; Roosen-Runge and Giesel, 1950; Russell et al., 1990). The number of stages into which the cycle is divided is arbitrary and depends on the methods and classification criteria used by the originator of the particular scheme. The most commonly used scheme was developed by Leblond and Clermont in 1952 and divides the rat spermatogenic cycle into 14 stages largely based on the developing morphology of the spermatid acrosome when visualized using PAS stain (Figure 9.8) (Leblond and Clermont, 1952). While all species go through a generally similar overall process of germ cell maturation, the morphologic appearance, efficiency, and timing differ, and descriptions and classification schemes are available for each species (Amann and Howards, 1980; Amann et al., 1976; Clermont, 1972; Dreef et al., 2007; Foote et al., 1972; Kangawa et al., 2016a; Oakberg, 1956; Olar et al., 1983; Russell et al., 1990; Soares et al., 2009; Swierstra and Foote, 1963). It is important to note that these descriptions and classification schemes have been adapted for use in toxicologic pathology and were often developed by anatomists and physiologists using techniques and materials not routinely employed in nonclinical toxicity testing. As such, some of the features and stages described may not be readily observed or appreciated. This can create confusion and frustration for

toxicologic pathologists as many of the readily available “staging maps” do not depict what is observed on routinely processed H&E-stained slides. This often requires the pathologist to combine stages together as features used to separate the stages based on electron microscopy or plastic embedded sections are not present. Even when a PAS stain is employed, the staining is often not optimized for testis and lacks detail in depicting the extent of acrosomal development, and thus offers only limited help in separating stages beyond what can already be assessed using H&E (Figures 9.9 and 9.10). For toxicologic pathologists, attempting to separate stages in detail and memorizing the different schemes across multiple species is onerous and offers limited utility in routine hazard identification. An alternate approach is to focus on basic patterns and key groupings of cells, rather than species-specific details in spermatid morphology. A simplified staging scheme using four main phases has been described by Setchell (1982), and a modified version for use by the toxicologic pathologist is described here (Figures 9.11–9.13). The broad classifications used include 4 phases: maturation, prerelease (spermiation), elongation, and meiotic division. These phases each describe features that are easy to observe in routinely processed material, do not require special staining, and can be applied to any of the common mammalian species used in toxicity testing. This approach allows the pathologist to focus on cell types and progression of spermatogenesis rather than small details in acrosomal morphology. Additional staining with PAS and/or a more detailed assessment (i.e., peer review by a pathologist with expertise in evaluation of the reproductive system) can be added for cause. When evaluating groupings of cell types in the seminiferous epithelium, regardless of the staging scheme used, cross-sections of tubules are generally easier to orient. This is because, in the rat, mouse, dog, minipig, and most NHPs, tubular cross-sections only contain a single cell association, allowing identification of the stage of spermatogenesis, whereas in humans and marmosets, multiple cell associations are present within the tubule, making staging more complex (Hess, 2008; Luetjens et al., 2005; Russell et al., 1990; Wistuba et al., 2003).

In all species, the entire process from spermatogonium to spermatid release (Figure 9.14) spans approximately four cycles (depending on how/when the start of spermatogenesis is defined). As each cycle is completed and the mature



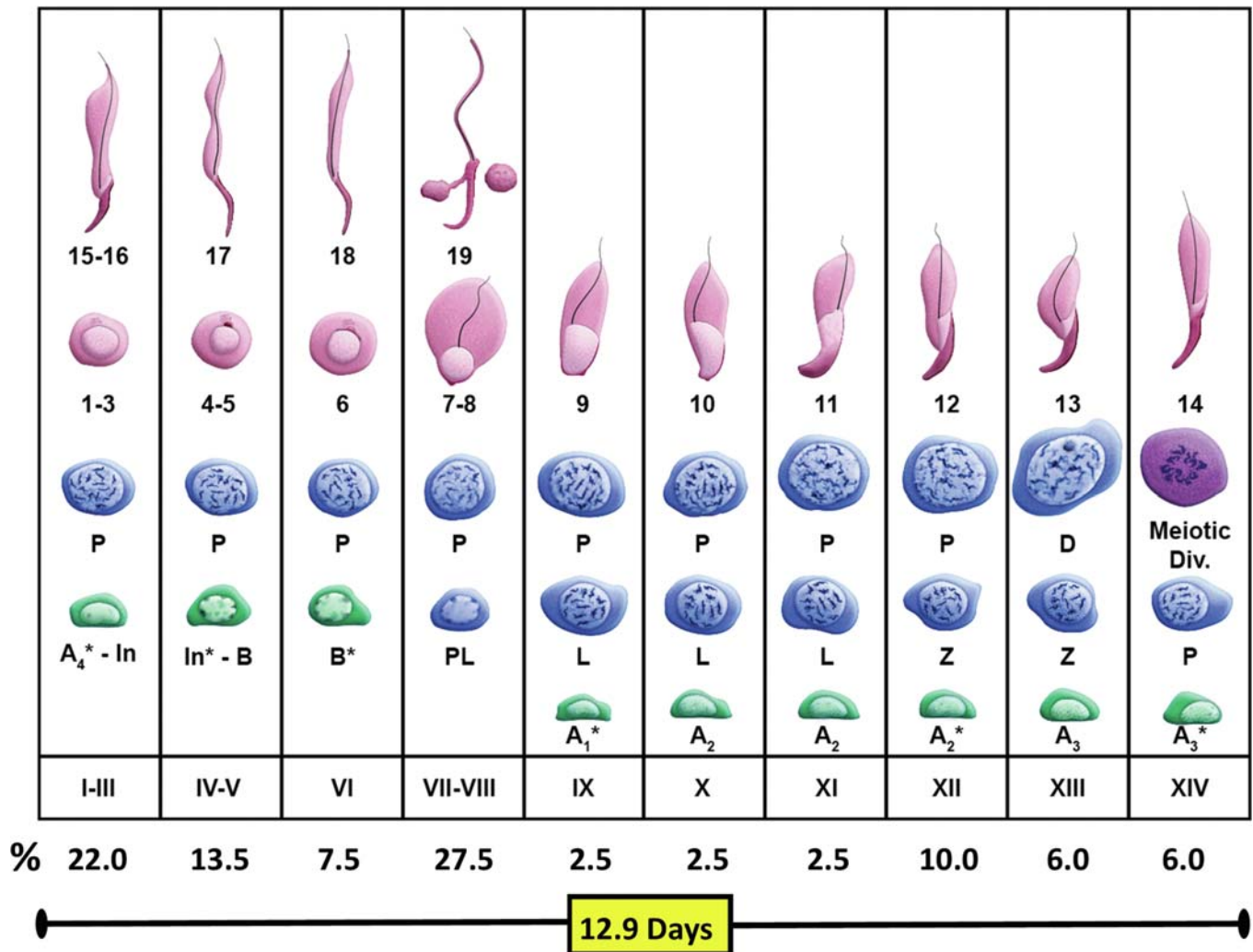


**FIGURE 9.8** Diagram illustrating the cellular composition of the 14 stages of the spermatogenic cycle in the rat. The columns represent stages (I–XIV), which are defined primarily by the morphological characteristics of the accompanying spermatid. Spermatid development is divided into 19 steps (1–19), the first 14 of which are in numerical agreement with stages I–XIV. In stages I–VIII, the detailed morphology of the spermatid acrosome is used when stained with periodic acid Schiff stain with hematoxylin counterstain (PAS/H) to distinguish between stages. Some stages can have overlap or are difficult to definitively separate in routinely processed paraffin-embedded materials and as a result stages I–III, IV–V, and VII–VIII are displayed as grouped stages. In stages IX–XIV, the shape of the elongating spermatid nucleus is used to separate stages. In a given location in any tubule, the cellular associations (stages) will succeed one another over time, proceeding from the left to the right of the diagram. Stage XIV is followed by stage I to begin another cycle. One complete sequence of the 14 cellular associations represents one complete “cycle of the seminiferous epithelium,” whereas the developmental sequence from spermatogonia through to step 19 spermatid represents the full process of spermatogenesis. As the diagram is read from the bottom and from left to right, the spermatogonia go through a number of mitotic (m) divisions developing through type A (A<sub>1–4</sub>), intermediate (I), and type B (B) spermatogonia. It is important to note that undifferentiated type A spermatogonia are present in small numbers in all tubules, but the diagram begins with a type A<sub>1</sub> spermatogonia that is committed to differentiate. Spermatogonial divisions give rise to spermatocytes, which proceed through meiotic prophase, including preleptotene (Pl), leptotene (l), zygotene (z), pachytene (P), and diplotene (D), and through two meiotic divisions (meiotic div). The haploid spermatids produced from the meiotic division undergo the morphological progression through the 19 steps of spermiogenesis (1–19). As the cells develop from spermatogonia to spermatids, they gradually move up through the epithelium. As mature spermatids are released during stage VIII, another generation of spermatogonia becomes committed to spermatogenesis from the slowly dividing pool of stem cells. The relative frequency for each stage or grouping of stages is included. This is important for pathologists to understand as some stages (e.g., IX, X, or XI) are short lived and only represent a small proportion of the tubules examined in a section of testis. *Courtesy of David Sabio.*

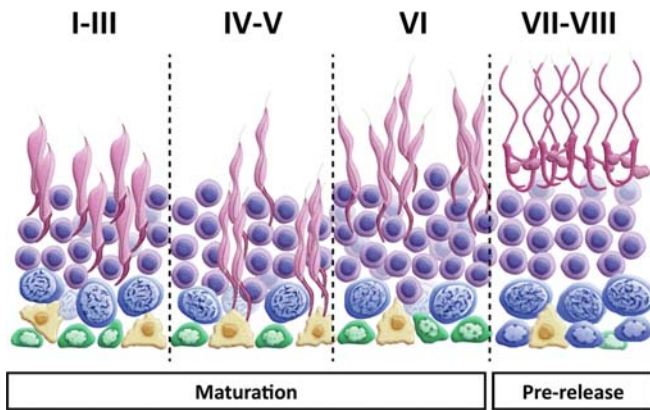


**FIGURE 9.9** Approximate staging of the maturation phase (stages I–VI) and pre-release phase (stages VII–VIII) of the spermatogenic cycle can be easily conducted in H&E-stained sections by using the shape and position of the elongating spermatids in the epithelium rather than the detailed acrosome morphology of the round spermatids in a PAS-H section. In general, this is the most commonly used approach for routine screening of testes for spermatogenic disturbances. When lesions are present, a PAS-H-stained section can be performed to further characterize the cell types affected. *Courtesy of David Sabio.*

spermatozoa are released, another generation of spermatogonia divides and becomes committed to maturation (Figure 9.8). The duration of the cycle and thus of spermatogenesis is fairly constant for a given species and strain of animal (Table 9.2). The more detailed staging schemes described above are very useful when considering the kinetics of spermatogenesis. The duration of a particular stage can be estimated as it is generally proportional to the frequency with which that stage occurs in cross-sections of tubules, that is, the more frequently tubules in a given stage are encountered, the longer that stage must last (Figure 9.8). The duration of each stage can be calculated by dividing the duration of the complete cycle by the % frequency of each stage, and this is remarkably constant between individual rats within a given strain and for each species (Russell et al., 1990).

## 2.5. Structure and Function of the Rete Testis, Efferent Ducts, Epididymis, and Vas Deferens

When sperm are released into the lumen of the seminiferous tubule, they are transported rapidly into a common collecting area within the testis, termed the rete testis (Figure 9.15). Sperm then

pass into a network of efferent ducts, and these in turn lead into a single highly coiled duct that forms the epididymis (Figure 9.16).

When sperm leave the testis, they are incapable of fertilization and have limited to no motility. They are transported out of the testis in seminiferous tubular fluid (STF) that is secreted by the Sertoli cell. Most of the fluid (up to 96%) and many of the proteins in the STF are reabsorbed by the rete testis, efferent ducts, and the initial segment of the epididymis. During their passage through the epididymis, the sperm mature and acquire progressive forward motility and the ability to undergo capacitation and fertilize an oocyte. Maturation involves extensive remodeling of the sperm plasma membrane with the binding and incorporation of proteins synthesized by the epididymal epithelium. In addition, the maturing sperm sheds additional redundant cytoplasm in the form of a cytoplasmic droplet into the ductal lumen. Once in the tail of the epididymis, the sperm are stored for days (humans) or weeks (rodents) prior to being released by ejaculation through the vas deferens into the penile urethra.

### 2.5.1. Rete Testis

The rete testis comprises a single or series of interconnected channels, lined by simple cuboidal or columnar epithelium, into which the seminiferous tubules open and which leads into the efferent ducts. Each end of a given seminiferous tubule connects to the rete testis, and as the tubule transitions to the rete, there is a small portion lined only by Sertoli cells. This region, often termed the tubuli recti, has phagocytic activity and serves a valve-like function (Dym, 1974; Nykänen, 1979) and can sometimes be mistaken for atrophic tubules (Creasy, 2012; Foley, 2001) (Figure 9.15). In the rat and mouse, the rete is situated in an eccentric subcapsular position at the cranial pole of the testis, but in the dog, rabbit, minipig, and NHP, it forms a series of ducts running through the center of the testis (Dym, 1976; Hess et al., 2018; Stoffel and Friess, 1997). The rete testis serves as a collecting reservoir for sperm within the testis. It is also the site of inhibin reabsorption from the testis into the circulation, and the first site of STF reabsorption (Maddocks and Sharpe, 1989; Turner et al., 1984).

### 2.5.2. Efferent Ducts

The efferent ducts (ductuli efferentes) are a series of convoluted tubules that, depending



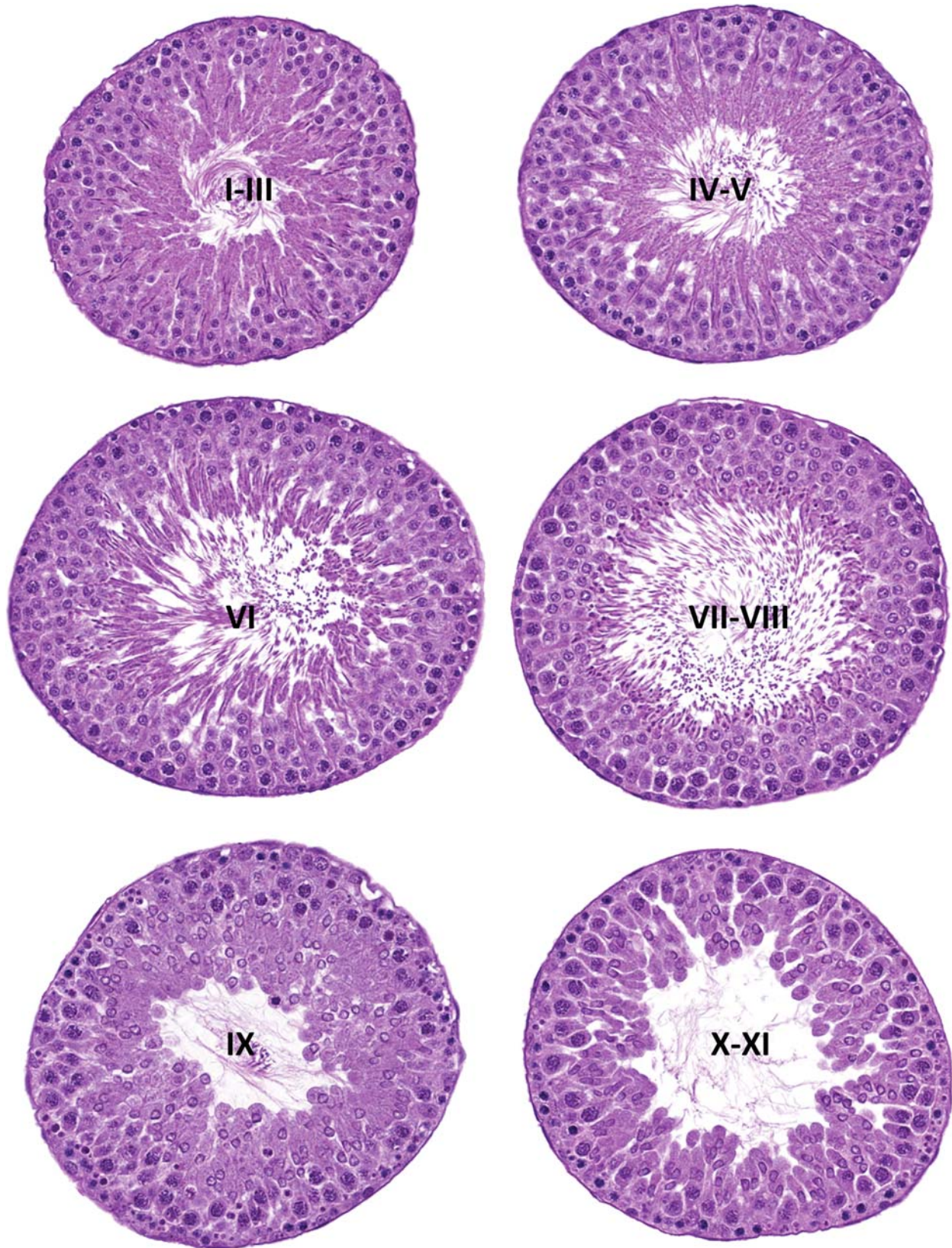


**FIGURE 9.10** Individual cross-sections of seminiferous tubules from a rat demonstrating the key groupings of stages that can readily be observed on H&E-stained sections in routinely processed materials. Rat, H&E,  $\times 30$ .



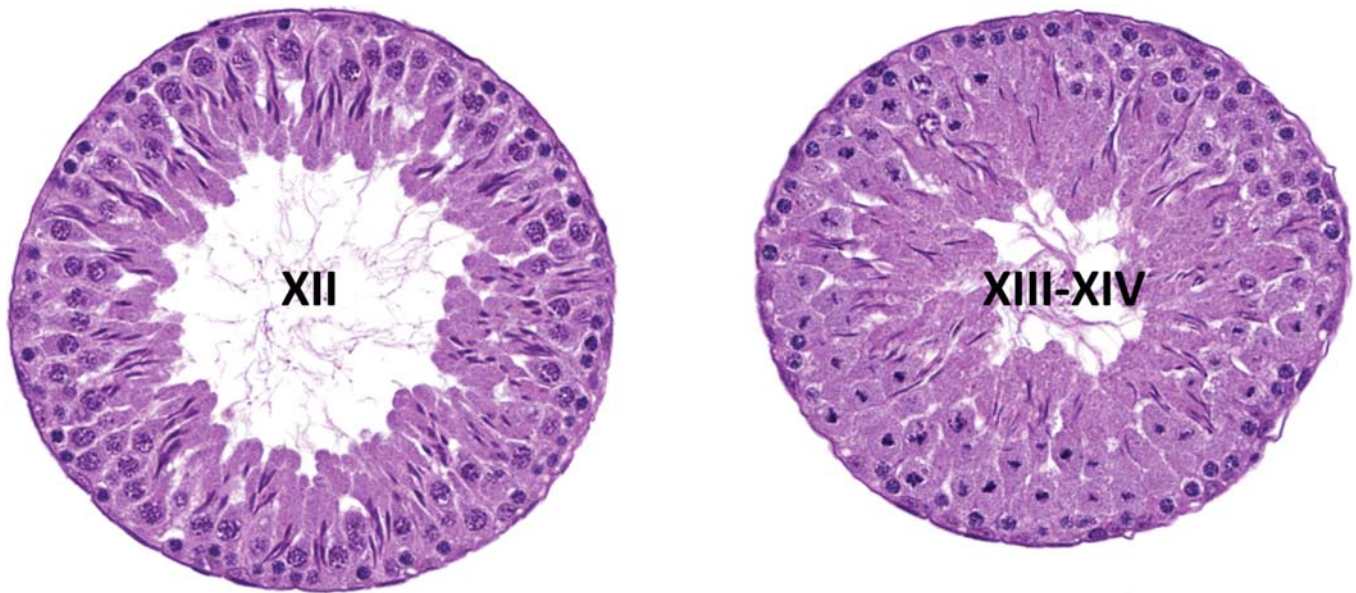


FIGURE 9.10 Cont'd

on the species, either merge into a single distal common duct before emptying into the initial segment (rats and mice) or empty via multiple entry points into the initial segment of the epididymis (dog, NHP, man) (Hess, 2002). In the rodent, almost all of the long and tortuous efferent ducts are located within the epididymal fat pad (Figure 9.16A). Since the epididymal fat is often discarded at necropsy, the efferent ducts in rodents need to be collected prospectively and will not be evident in routine sections of testis or epididymis (La et al., 2012). The final distal portion of the common duct is located within the connective tissue capsule of the head of the epididymis, and may occasionally be seen in standard sections of the rodent epididymis (Foley, 2001) (Figure 9.16B). In contrast, the efferent ducts in nonrodents are much shorter; they are almost entirely located within the head of the epididymis and form a large proportion of the epididymal head. Thus they are often present in routine samples of the epididymis (Ilio and Hess, 1994) (Figure 9.16C).

The main function of the efferent ducts is to transport sperm from the rete testis to the epididymis and to concentrate them by reabsorbing most of the fluid and the proteins from the accompanying STF (Hess, 2002; Ilio and Hess, 1994; Turner et al., 1984). The efferent ducts are derived embryologically from the mesonephric tubules (Omotehara et al., 2022), and share many structural and physiological similarities with the proximal tubule of the kidney. Estrogen, rather than androgen, appears to be the major regulator for the fluid reabsorption.

Estrogen interacts with ER- $\alpha$  receptors that are located in high density within the epithelium (Hess, 2000; Lee et al., 2000).

In addition, endothelin 1 and its receptor are present in the ciliated cells of the efferent ducts and are also thought to play an important role in fluid reabsorption (Harneit et al., 1997). Active transport of water out of the lumen is accomplished in a similar manner to reabsorption of water from the renal nephron. It involves the transport/exchange of  $\text{Na}^+$ ,  $\text{K}^+$ ,  $\text{Cl}^-$ ,  $\text{H}^+$ , and  $\text{HCO}_3^-$  ions across the basal membranes of the epithelium utilizing  $\text{Na}^+/\text{K}^+$ -ATPase,  $\text{Na}^+/\text{HCO}_3^-$ , and  $\text{Na}^+/\text{K}^+/\text{2Cl}^-$  as cotransporters (Ilio and Hess, 1992). This is accompanied by transcellular and paracellular fluid movement from the lumen through aquaporin 1 channels along the apical border, and probably also through the leaky tight junctions between adjacent epithelial cells. Carbonic anhydrase is also present in large quantity in the efferent ducts to supply the  $\text{HCO}_3^-$  needed for the  $\text{HCO}_3^-/\text{Cl}^-$  exchanger (Karhumaa et al., 2001). Endocytosis appears to be the major mechanism through which protein reabsorption is mediated (Oliveira et al., 2009).

### 2.5.3. Epididymis

The epididymis is attached to the testis and has three major regions called the head (caput) which also includes the initial segment; body (corpus); and tail (cauda). Superficially, the epididymis appears to be a histologically simple tissue comprising a series of epithelial lined ducts that carry sperm from the testis to the vas deferens. In reality, it is surprisingly complex, both in the structural diversity of its epithelial



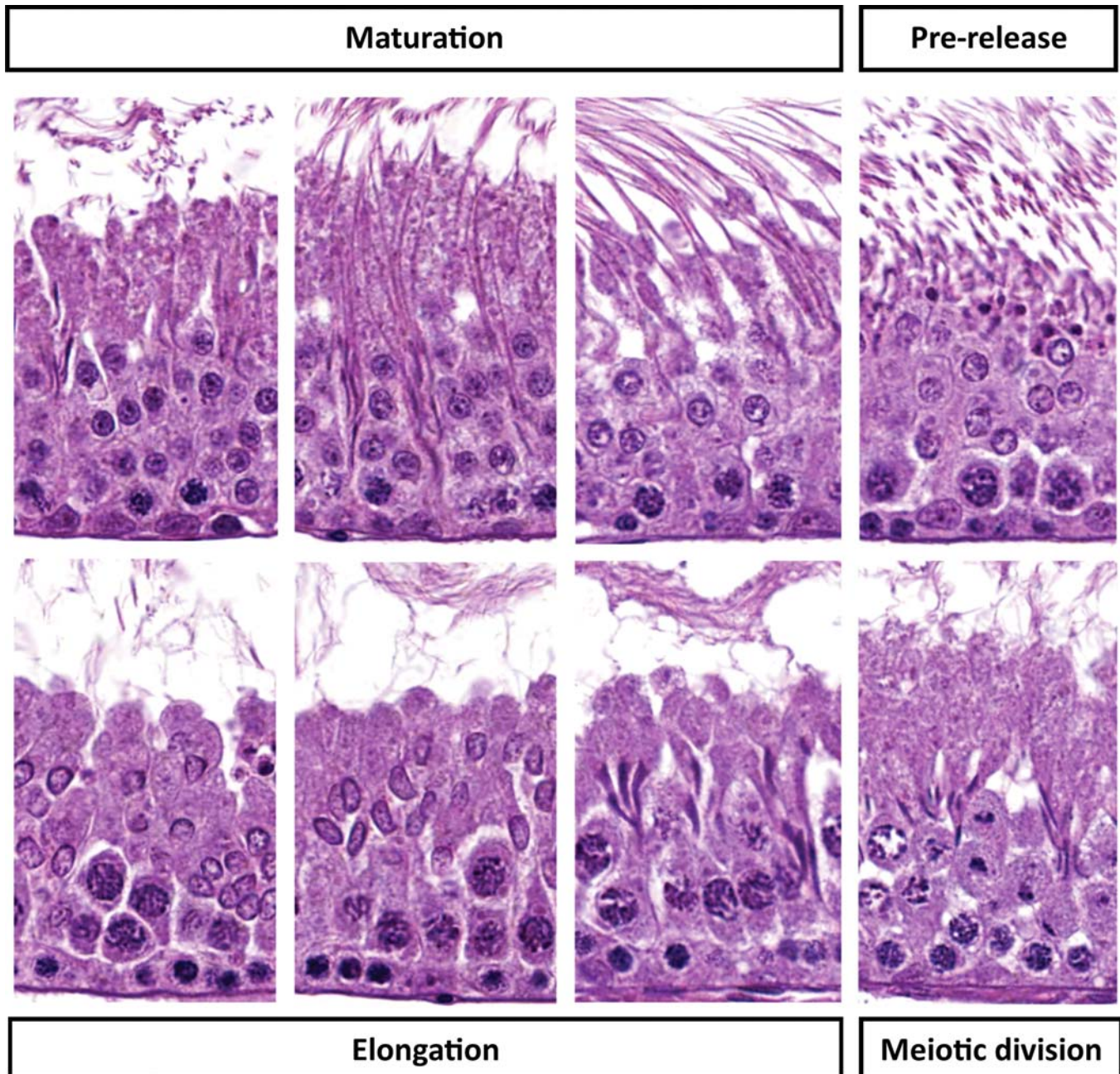


**FIGURE 9.11** High magnification of seminiferous tubules from a rat demonstrating the features and cellular arrangements in the maturation, prerelease, elongation, and meiotic division phases. Compare the location of the elongating spermatids in the maturation phase examples to [Figure 9.9](#). The cell types in each phase are further detailed in [Figure 9.13](#). Rat, H&E,  $\times 40$ .

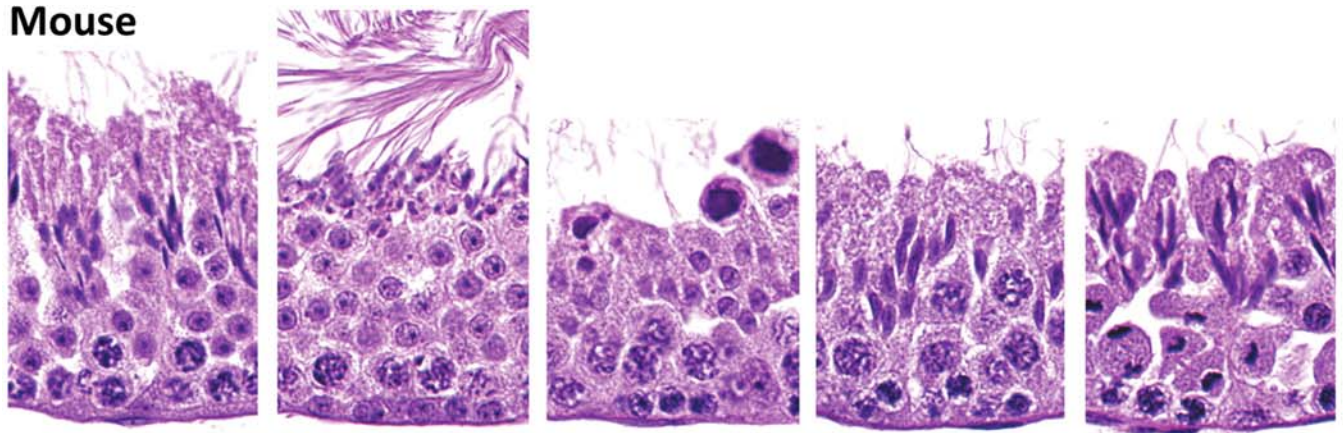
cell types and in the number of critical functions it performs in the maturation and transport of sperm ([Hermo and Robaire, 2002](#); [Reid and Cleland, 1957](#); [Robaire et al., 2006](#)). Cell types that are present throughout the epididymis include principal cells with apical stereocilia (the predominant cell type), basal cells, and halo cells (a subset of T lymphocytes and monocytes). In addition, the initial segment contains apical cells and narrow cells, while clear cells are also

present in the head, body, and tail. The principal cells vary in height and subcellular composition, depending on the epididymal region: they are tall columnar in the head diminishing to cuboidal in the tail ([Figure 9.17](#)).

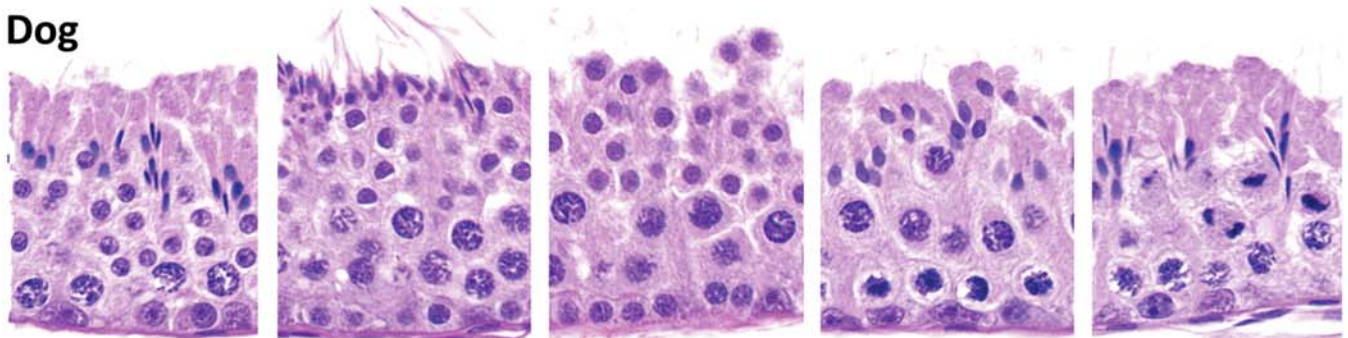
Functions of the epididymal epithelium include the synthesis and secretion of a wide range of proteins, and the transport of ions and small organic molecules across the epithelium to create a slightly basic luminal environment



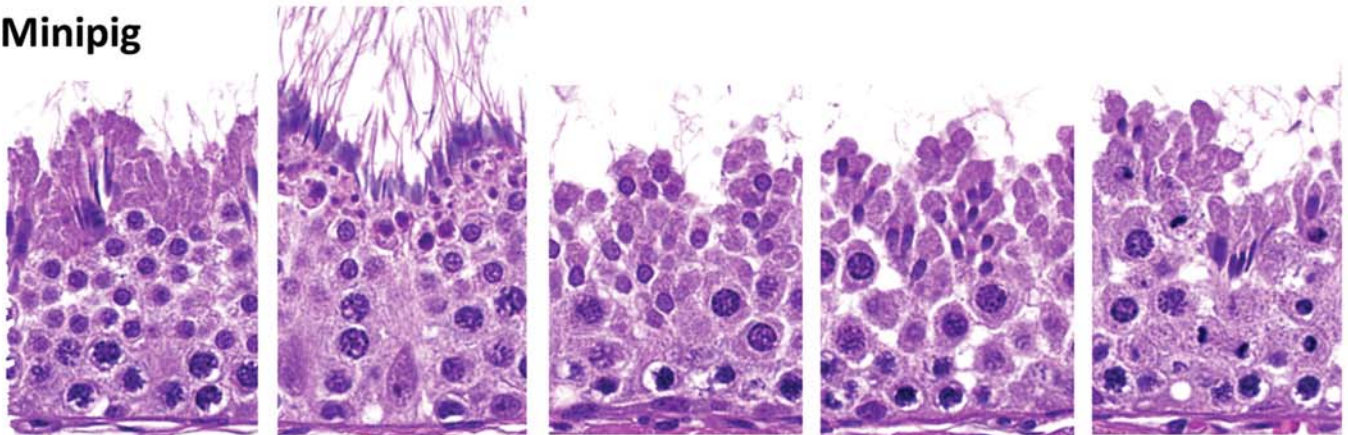
## Mouse



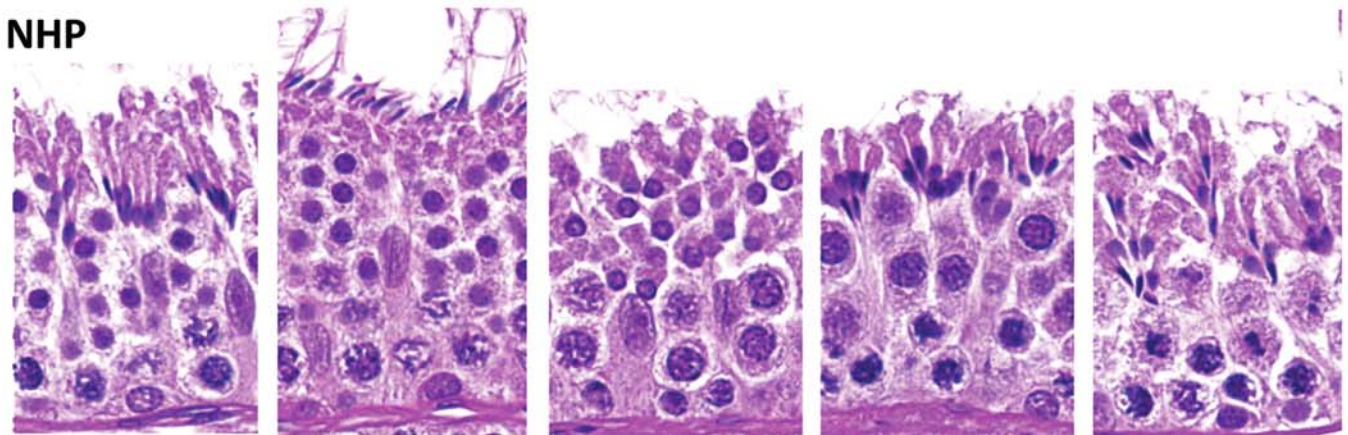
## Dog



## Minipig



## NHP



**Maturation**

**Pre-release**

**Elongation**

**Meiotic division**

**FIGURE 9.12** High magnification of seminiferous tubules from nonrodents and mouse demonstrating the features and cellular arrangements in the maturation, prerelease, elongation, and meiotic division phases. While classical staging schemes use different numbers of stages across species, this simplified four-group system allows for easy comparison across species. Mouse, dog, minipig, and NHP, H&E,  $\times 40$ .



				Mature Spermatids						
	Elongating Spermatids			Round Spermatids		Elongating Spermatids				
	Round Spermatids			Pachytene Spermatocytes				Meiotic Div.		
	Pachytene Spermatocytes			Early Spermatocytes						
	MATURATION			PRE-RELEASE		ELONGATION			MEIOTIC DIV.	
Rat	I-III	IV-V	VI	VII-VIII		IX	X	XI	XII	XIII-XIV
Mouse	I-III	IV-V	VI	VII-VIII		IX		X		XI-XII
Dog	I-II		III	IV		V		VI		VII-VIII
Pig	I-VI			VII		VIII		IX		X-XI
NHP	I-IV			V-VI*		VII-VIII		IX	X	XI-XII

**FIGURE 9.13** Diagram comparing the classical staging schedules across species with the 4-group system of maturation, prerelease, elongation, and meiotic division phases. This 4-group system allows for grouping of basic cell types across species and provides a more simplified approach to evaluating the testis in routine nonclinical toxicity studies.

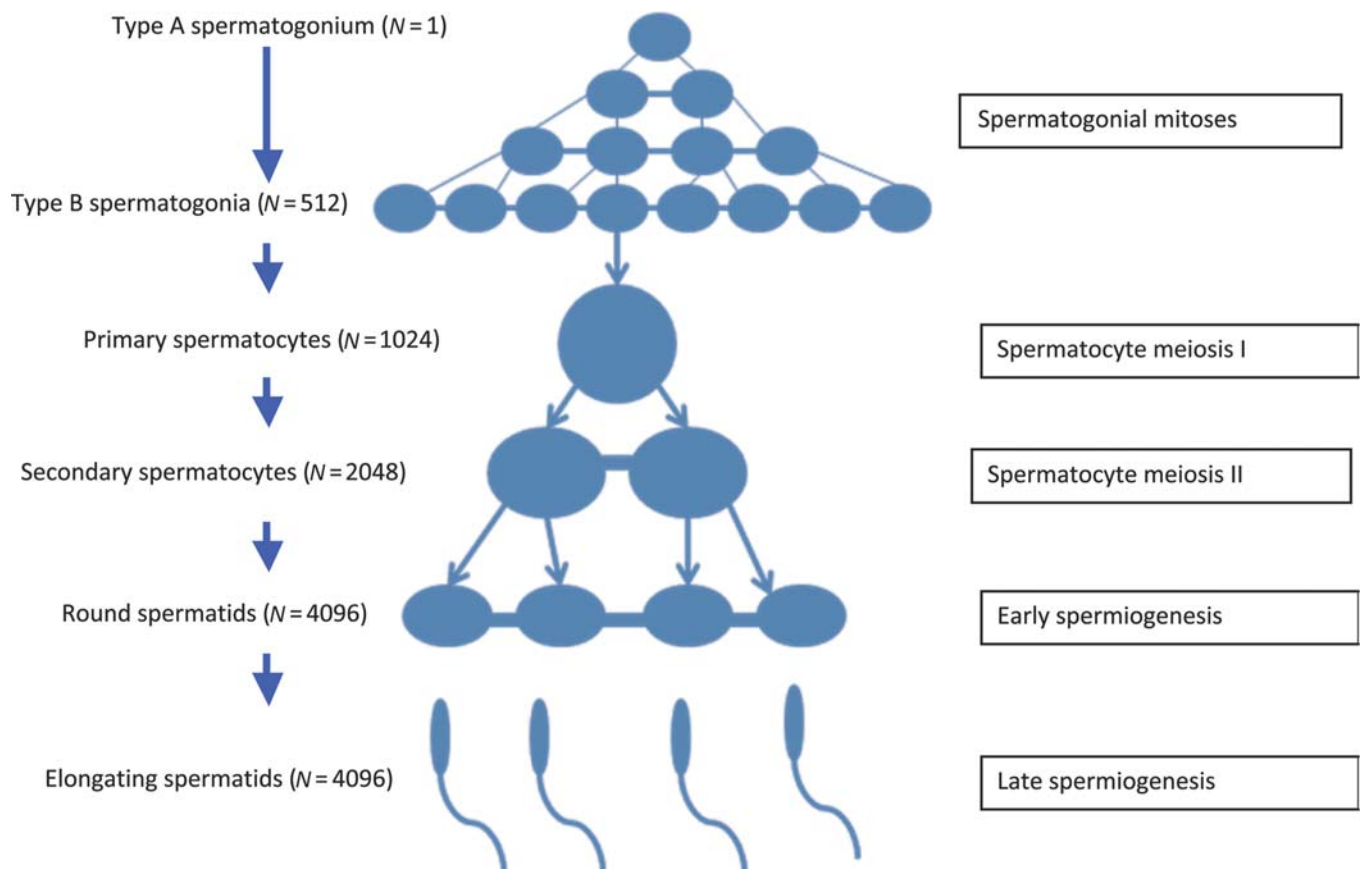


**FIGURE 9.14** The Sertoli cell supports the clonal expansion of a single type A differentiating spermatogonium. Following the multiple mitotic and meiotic divisions, this would amount to over 4000 spermatids. However, regulatory processes induce apoptotic cell death and maintain the actual number at a level that can be supported by each Sertoli cell. The progeny of the germ cell divisions remains in contact with one another through cytoplasmic bridges. Reproduced from Haschek WM, Rousseaux CG, Wallig MA, editors: *Haschek and Rousseaux's handbook of toxicologic pathology*, ed 3, 2013, Academic Press, Figure 59.11, p. 2513, with permission.

**TABLE 9.2** Species Comparison of Spermatogenesis, Epididymal Transit Time, and Sperm Abnormalities

Species	Number of stages <sup>b</sup>	Cycle length (days)	Total duration of spermatogenesis (days)	DSP (millions)	Epididymal transit time (days)	Abnormal sperm (%)
Rat	14	12.9	51.6	17–24	8–11	<5
Mouse	12	8.6	34.5	40–54	5	<5
Dog	8	13.6	54.4	11–16	10	≥50
Pig <sup>a</sup>	8 or 11	8.6–9.1	35–41	23–27	9–11	<20
NHP	12	10.5	42	23 <sup>c</sup>	11	<25
Human	6	16	64	4.0–4.5	6	≥50

<sup>a</sup> based on minipigs and domestic swine.<sup>b</sup> based on classic anatomic and physiologic descriptions.<sup>c</sup> based on rhesus macaque.

DSP, Daily sperm production per gram of testis; NHP, nonhuman primate (cynomolgus macaque).

From Russell LD, Ettlin RA, Sinha Hakim AP, et al: Histological and histopathological evaluation of the testis, Clearwater, Florida, 1990, Cache River Press, pp 1–286; Picut CA, Ziejewski MK, Stanislaus D: Comparative aspects of pre- and postnatal development of the male reproductive system, Birth Defects Res. 110:190–227, 2018; Franca LR, Avelar GF, Almeida FF: Spermatogenesis and sperm transit through the epididymis in mammals with emphasis on pigs, Theriogenology 63:300–318, 2005; Fouquet JP, Dadoune JP: Renewal of spermatogonia in the monkey (*Macaca fascicularis*), Biol. Reprod. 35:199–207, 1986; Dreef HC, van Esch E, De Rijk EPCT: Spermatogenesis in the cynomolgus monkey (*Macaca fascicularis*): a practical guide for routine morphological staging, Toxicol. Pathol. 35:395–404, 2007; Amann RP, Johnson L, Thompson DL, et al.: Daily spermatozoal production, epididymal spermatozoal reserves and transit time of spermatozoa through the epididymis of the rhesus monkey, Biol. Reprod. 15:586–592, 1976; Amann RP, Howards SS: Daily spermatozoal production and epididymal spermatozoal reserves of the human male, J. Urol. 124:211–215, 1980; Clermont Y: Kinetics of spermatogenesis in mammals: seminiferous epithelium cycle and spermatogonial renewal, Physiol. Rev. 52:198–236, 1972; Dostal LA, Juneau P, Rothwell CE: Repeated analysis of semen parameters in beagle dogs during a 2-year study with the HMG-CoA reductase inhibitor, atorvastatin, Toxicol. Sci. 61:128–134, 2001; Foote RH, Swierstra EE, Hunt WL: Spermatogenesis in the dog, Anat. Rec. 173:341–351, 1972; Kangawa A, Otake M, Enya S, et al.: Spermatogenesis in the Microminipig, Toxicol. Pathol. 44:974–986, 2016a; Leblond CP, Clermont Y: Definition of the stages of the cycle of the seminiferous epithelium in the rat, Ann. NY Acad. Sci. 55:548–573, 1952; Luetjens CM, Weinbauer GF, Wistuba J: Primate spermatogenesis: new insights into comparative testicular organisation, spermatogenic efficiency and endocrine control, Biol. Rev. Camb. Philos. Soc. 80:475–488, 2005; Oakberg EF: A description of spermiogenesis in the mouse and its use in analysis of the cycle of the seminiferous epithelium and germ cell renewal, Am. J. Anat. 99:391–413, 1956; Olar TT, Amann RP, Pickett BW: Relationships among testicular size, daily production and output of spermatozoa, and extragonadal spermatozoal reserves of the dog, Biol. Reprod. 29:1114–1120, 1983; Sharpe R, Kerr J, McKinnell C, et al.: Temporal relationship between androgen-dependent changes in the volume of seminiferous tubule fluid, lumen size and seminiferous tubule protein secretion in rats, J. Reprod. Fertil. 101:193–198, 1994 and Modified from Haschek WM, Rousseaux CG, Wallig MA, editors: Haschek and Rousseaux's handbook of toxicologic pathology, ed 3, 2013, Academic Press, Table 59.2, p. 2512, with permission.

which is conducive to protein uptake into the sperm membranes. After early secretion into the lumen of the head, the body is where the sperm incubate in the specialized luminal environment, followed by the selective absorption of luminal contents in the distal body and tail. Thus, the epididymis provides the specialized environment required for the progressive maturation of sperm as they pass from the initial segment to the tail of the epididymis (Robaire et al., 2006; Turner, 1995). During the passage of sperm through the epididymis, changes in sperm morphology and metabolism occur. Excess cytoplasm in the form of the residual cytoplasmic droplet is shed from the sperm, changes occur in the structure of the acrosome

and midpiece, and different surface antigens appear. Associated with these events is the acquisition of the ability to fuse with and fertilize an oocyte. Newly motile sperm must then be maintained in a quiescent state by the caudal secretion of immobilin, which prevents sperm from swimming in the epididymis (Turner and Reich, 1987; Usselman, 1983). This thick glycoprotein is stripped off the sperm by the process of ejaculation and the mixing with the proteases in the accessory organ secretions, resulting in ejaculated sperm which are motile.

Sperm storage prior to ejaculation is also an important function of the tail of the epididymis. Depending on the species and the frequency of ejaculation, sperm reach the tail 1–2 weeks after

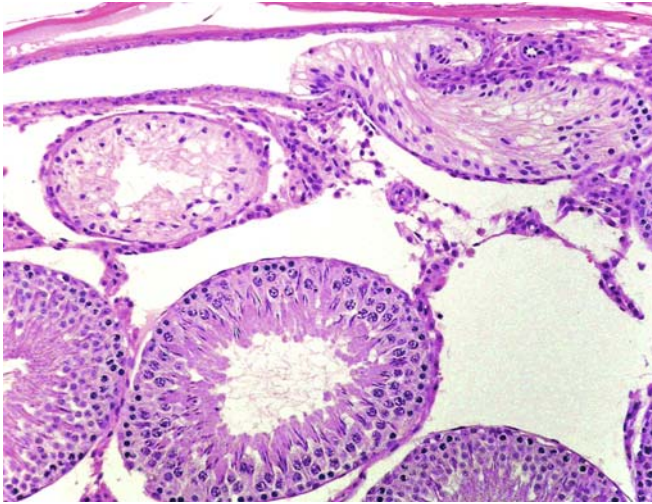


**FIGURE 9.15** Tubulus rectus is the transitional part of the seminiferous tubule as it enters the rete testis. It is lined only by Sertoli cells and can be mistaken for an atrophic tubule in cross-section. The cytoplasmic protrusion into the rete also acts as a one-way valve for sperm and fluid coming out of the tubule. Rat, H&E,  $\times 10$ . Reproduced from Haschek WM, Rousseaux CG, Wallig MA, editors: *Haschek and Rousseaux's handbook of toxicologic pathology*, ed 3, 2013, Academic Press, Figure 59.12, p. 2513, with permission.

release from the seminiferous tubule (Franca et al., 2005). Sperm production is a continuous process; if the stored sperm are not removed by frequent ejaculation, they are voided in the urine.

Many of these functions are regulated by androgens, including the energy-dependent movement of  $\text{Na}^+$  across the epithelium, epithelial inositol secretion into the lumen, and epithelial carnitine uptake from the lumen, as well as the activity of the detoxification enzymes glutathione S transferase and gamma glutathione transferase (Bohmer and Hansson, 1975; Joseph et al., 2011; Pholpramool et al., 1982; Robaire and Hales, 1982; Robaire and Hamzeh, 2011).

#### 2.5.4. Vas Deferens

The vas deferens (ductus deferens) is a thick-walled convoluted tube that is continuous with the tail of the epididymis and connects it to the prostatic urethra (Robaire and Hermo, 1988). In some species, the final part of this tube is dilated to form the ampulla, which joins the duct of the seminal vesicle to become the ejaculatory duct. The histologic transition between the epididymis and the vas deferens is abrupt; this is

largely due to the development of a thick smooth muscle coat around the latter. The epithelium is pseudostratified with long microvilli (stereocilia) on the apical surface. The vas deferens transfers the sperm, which have been stored in the epididymis, to the urethra, where additional secretions are added to produce the semen. The very thick fibromuscular coat that surrounds the duct is innervated by the sympathetic nervous system, and, when stimulated, contracts along with the perineal striated musculature to provide rapid propulsion of the sperm along the tract during ejaculation.

#### 2.5.5. Vasculature

There are two main blood supplies to the epididymis. The head, body, and proximal tail are supplied by the epididymal arteries, arising as two branches of the spermatic artery before entering the pampiniform plexus. The tail of the epididymis is also supplied by the deferential artery, which is a branch of the iliac (hypogastric artery), and which also supplies the vas deferens (Chubb and Desjardins, 1982; Harrison, 1952). The organization of the capillary networks varies in different parts of the epididymis, with a dense network of capillaries with fenestrated endothelium surrounding the initial segment and a simpler arrangement of nonfenestrated capillaries surrounding the remainder of the epididymal ducts (Abe et al., 1984). There is also a substantially greater blood flow to the initial segment than to the rest of the epididymis.

### 2.6. Structure and Function of the Accessory Sex Organs

The accessory sex organs are composed of multiple glands and structures, including the ampullary gland (enlarged end of the vas deferens), prostate gland, coagulating gland, seminal vesicles, bulbourethral gland, preputial gland, and/or preputial diverticulum. There are marked species differences in the types of organs present (Table 9.3) and in the gross and microscopic appearance (Dyce et al., 1987; Greer et al., 1968; Holtz and Foote, 1978; Knoblauch et al., 2018; Lee and Holland, 1987; Lewis et al., 1981; Mubiru et al., 2008; Nath et al., 2018; Skonieczna et al., 2019; Yuan et al., 1987). The



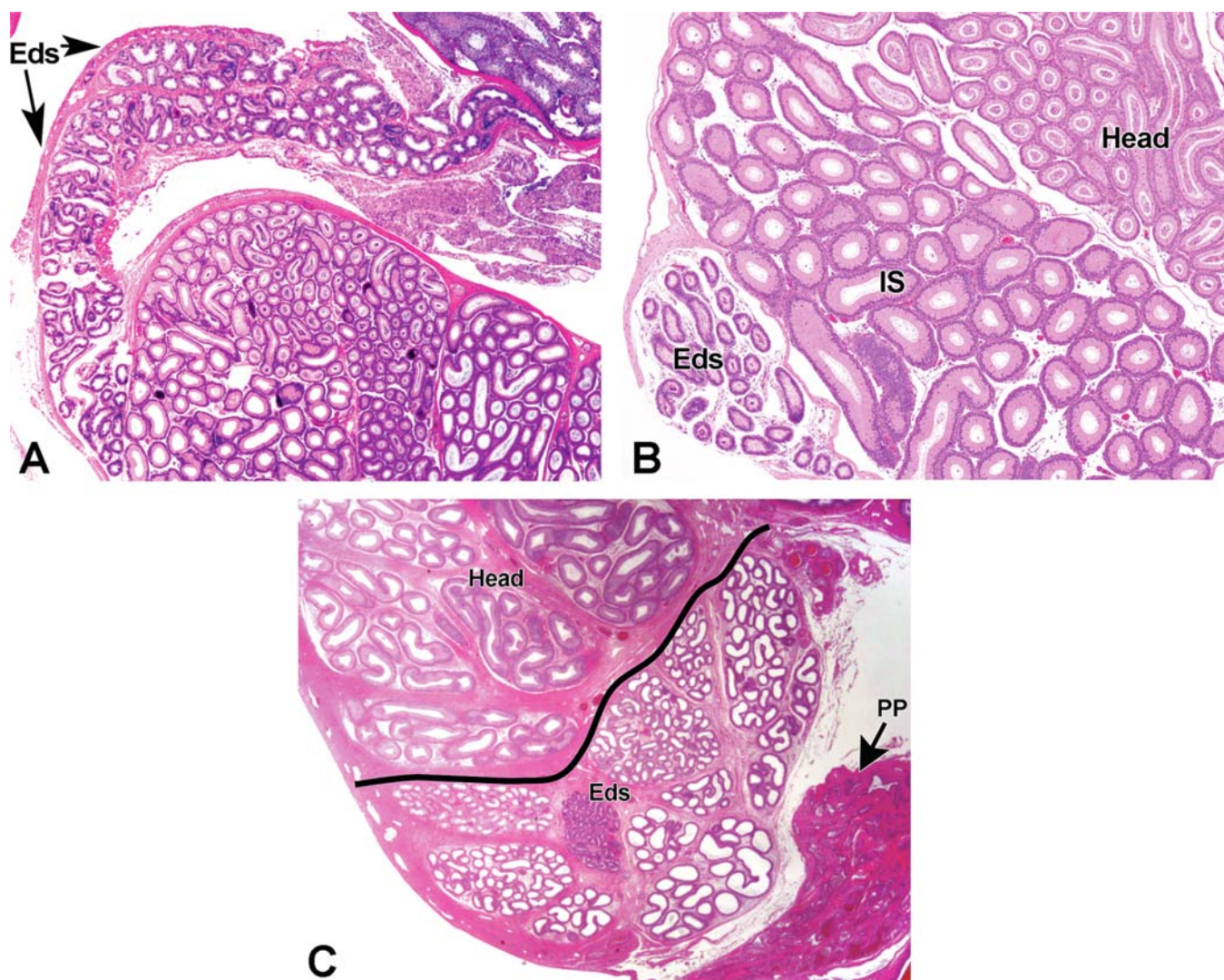


**FIGURE 9.16** (A) The efferent ducts (Eds) join the rete testis to the initial segment of the epididymis. In rodents, they take a tortuous route through the epididymal fat pad and are rarely sampled except by design. They can be the site of sperm granulomas, which can obstruct fluid flow and result in testicular lesions. Mouse, H&E,  $\times 2$ . (B) Difference in histology between the efferent ducts (Eds), initial segment (IS), and head of the epididymis in the mouse. The distal part of the efferent ducts is sometimes sampled with the epididymis. Mouse, H&E,  $\times 4$ . (C) Dog efferent ducts (Eds) are embedded within the head of the epididymis and are often present in a routine longitudinal section. In this section the pampiniform plexus (PP) can also be seen. Dog, H&E,  $\times 2$ . *Reproduced from Haschek WM, Rousseaux CG, Wallig MA, editors: Haschek and Rousseaux's handbook of toxicologic pathology, ed 3, 2013, Academic Press, Figure 59.13, p. 2514, with permission.*

prostate gland and seminal vesicles are the most commonly evaluated in nonclinical toxicity testing. Because the secretory activity of the accessory sex glands is extremely sensitive to androgen levels, weight change and altered cellular activity in the prostate and seminal vesicles can be used as a good and relatively rapid indicator of altered circulating androgen levels.

### 2.6.1. Prostate

The prostate is a compound tubuloalveolar gland that secretes a colorless serous fluid into the urethra through a number of ducts. In the rodent, a discrete pair of ventral lobes and smaller dorsal and lateral lobes are situated around the neck of the bladder (Knoblaugh et al., 2018). Also in rodents, a pair of anterior



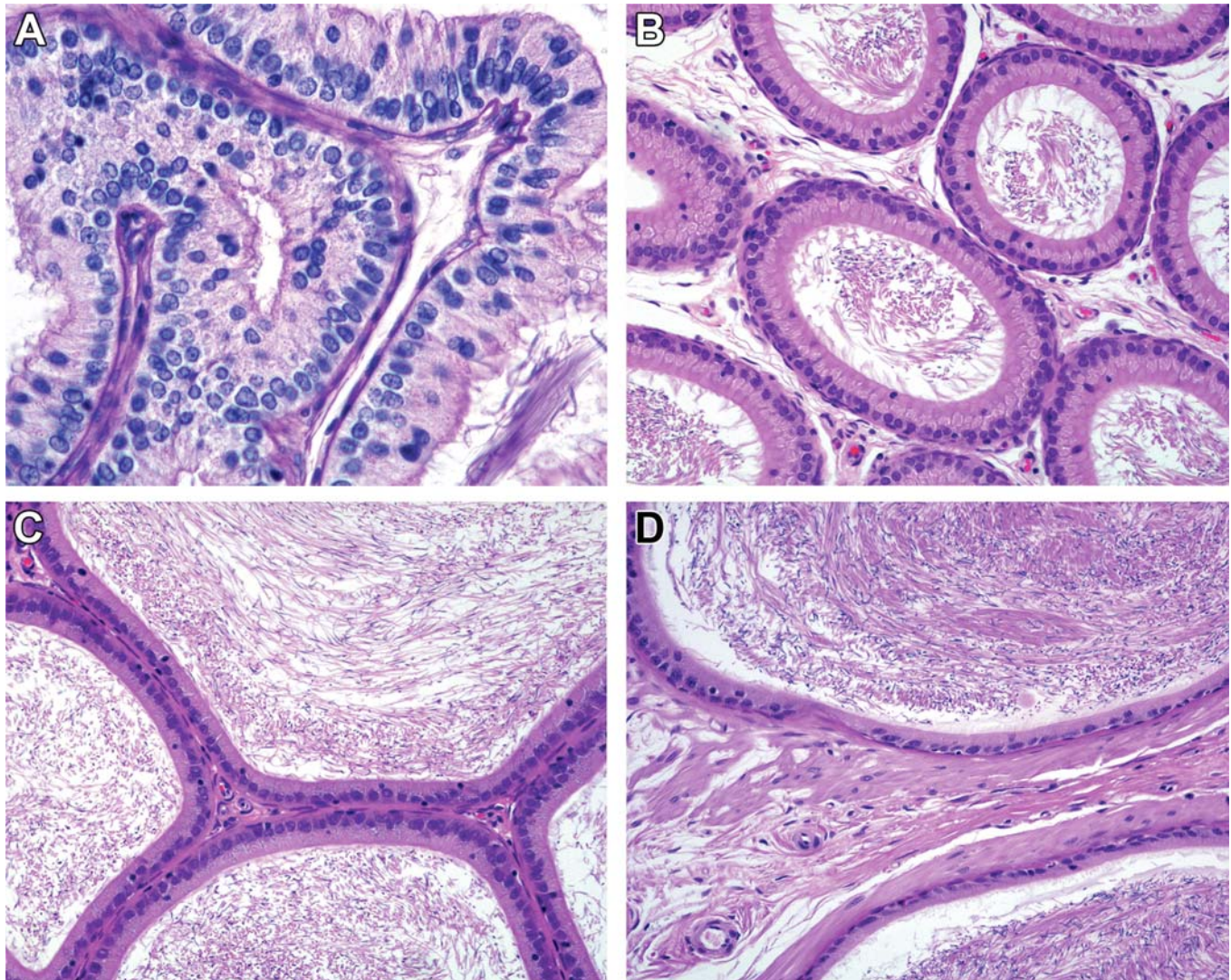


**FIGURE 9.17** (A) Proximal efferent ducts. Pale-staining tall columnar epithelium with ciliated luminal surface. Rat, PAS,  $\times 40$ . (B) Initial segment of the epididymis. Columnar cells with microvilli and prominent supranuclear Golgi and SER. Rat, H&E,  $\times 20$ . (C) Head of the epididymis with lower, cuboidal epithelium. Rat, H&E,  $\times 20$ . (D) Tail of the epididymis with low cuboidal epithelium and surrounded by smooth muscle fibers. Rat, H&E,  $\times 20$ . Reproduced from Haschek WM, Rousseaux CG, Wallig MA, editors: *Haschek and Rousseaux's handbook of toxicologic pathology*, ed 3, 2013, Academic Press, Figure 59.14, p. 2516, with permission.

lobes, often termed the coagulating glands, is situated along the inner curvature of the seminal vesicle (Lee and Holland, 1987). The glandular acini are lined by a simple columnar epithelium and produce a fluid rich in proteolytic enzymes (e.g., acid phosphatase). The fluid also contains relatively high levels of zinc, inositol, transferrin, and citric acid. In the dog, the prostate is large and fully encircles the urethra (Robaire et al., 2006). Rabbits have a complicated arrangement with a prostate gland and separate glandular

structures termed the proprostate and paraprostate (Holtz and Foote, 1978; Skonieczna et al., 2019). In the NHP, there are distinct cranial and caudal lobes of the prostate and the prostatic tissue does not fully encircle the urethra (Lewis et al., 1981). The cranial lobe serves a coagulating gland-like function (Greer et al., 1968).

### 2.6.2. Seminal Vesicles

The seminal vesicles are paired elongated hollow organs filled with a yellowish-white

**TABLE 9.3** Species-Specificity of Male Accessory Sex Organs

Accessory sex organ	Rodent	Rabbit	Dog	Minipig	NHP
Prostate	+	+	+	+	+
Coagulating gland	+	–	–	–	+/– <sup>a</sup>
Seminal vesicles	+	+	–	+	+
Bulbourethral gland	+	+	–	+	+
Ampullary gland	+	+	+	–	–
Preputial gland	+	+/– <sup>b</sup>	–	–	–
Preputial diverticulum	–	–	–	+	–

<sup>a</sup> Macaques have cranial and caudal lobes of the prostate and the cranial lobe serves a coagulating gland-like function.

<sup>b</sup> Rabbits have small inconspicuous preputial glands that can appear microscopically as enlarged sebaceous glands.

NHP: nonhuman primate (cynomolgus macaque)

Modified from Haschek WM, Rousseaux CG, Wallig MA, editors: Haschek and Rousseaux's handbook of toxicologic pathology, ed 3, 2013, Academic Press, Table 59.3, p. 2518, with permission.

viscous fluid. They are situated distal to the vas deferens, and empty via the ejaculatory duct into the urethra. The mucosa has a honeycombed structure formed by complex folding to produce irregular anastomosing channels that communicate with the central cavity; thin primary folds of the mucosa also extend out into the lumen (Knoblaugh et al., 2018). The seminal vesicle fluid is a viscous secretion and major contributor to the total volume of the ejaculate. The fluid is alkaline and contains fructose and lactoferrin (Lilja et al., 1987; Prins and Lindgren, 2015). In rodents, fluid from the coagulation gland, secreted immediately after ejaculation, mixes with vesicular fluid to form the copulatory plug within the vagina. This prevents loss of sperm and further copulation.

### 2.6.3. Bulbourethral Glands

Bulbourethral glands (Cowper's glands) are paired compound tubuloalveolar glands that secrete a mucoid material into the penile urethra. The epithelial cells are pyramidal to columnar with a microvillous surface and finely vacuolated, foamy appearing cytoplasm (Knoblaugh

et al., 2018). The bulbourethral glands secrete a small quantity of clear, viscous fluid, which, in rodents, is secreted immediately before ejaculation of the sperm to clear the urethra of urine and provide lubrication, and may contribute to semen coagulation (Beil and Hart, 1973). In swine, the bulbourethral glands are large, contributing to the relatively large volume of ejaculate in these species and allowing for coagulation of semen in the sow (Badia et al., 2006).

### 2.6.4. Preputial Glands

Preputial glands are paired sebaceous glands located in the subcutaneous tissue of rodents (Knoblaugh et al., 2018). They are near the tip of the penis in the mouse and along the ventral midline in the inguinal region of the rat. Ducts leading from the sebaceous acini are lined by squamous epithelium. The gland is a holocrine gland releasing its secretion by rupture of the acinar cells. The ductular secretion and the intracellular secretory granules are intensely eosinophilic, resembling keratin in appearance. Secretion from the preputial gland contains pheromones (aliphatic alcohols) and glucuronidase.

## 2.7. Hormonal Regulation of Reproductive Function

Overall hormonal control of the testis is maintained by the hypothalamic–pituitary axis and is mediated by gonadotropin-releasing hormone (GnRH) secreted by the hypothalamus, which regulates secretion of the gonadotropins, LH and FSH, by the pituitary (Figure 9.18). The activity of these major hormones are influenced by paracrine, autocrine, and intracrine control mechanisms, which “fine tune” or modulate the endocrine effects (Rudolph et al., 2016; Wu et al., 2020). A basic overview of male reproductive endocrinology is provided here to serve as a basis for understanding endocrine-mediated toxicity in the male. Additional detail is beyond the scope of this chapter and the topic has been extensively reviewed elsewhere (Huhtaniemi, 2018; Kumar et al., 2018; McLachlan et al., 2002; O'Donnell et al., 2001, 2006; Oduwole et al., 2018, 2021; Ramaswamy and Weinbauer, 2014; Smith and Walker, 2015; Sofikitis et al., 2008; Walker, 2021).



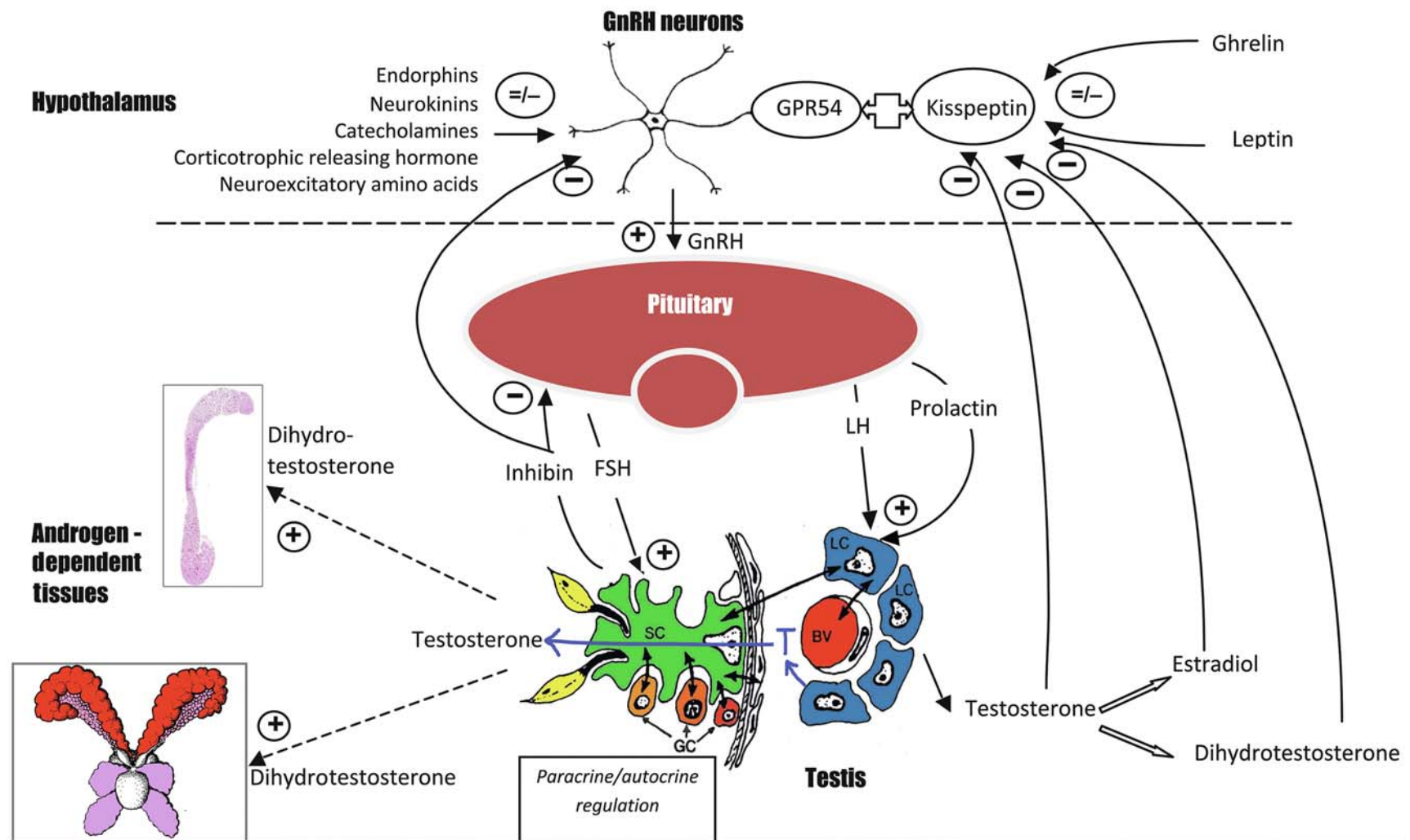


**FIGURE 9.18** Endocrine and paracrine regulation of the testis. Gonadotropin-releasing hormone (GnRH) secreted from the hypothalamus stimulates secretion of follicle stimulating hormone (FSH) and luteinizing hormone (LH) from the pituitary. LH stimulates testosterone (T) production from the Leydig cell (LC), and FSH acts on the Sertoli cell (SC), regulating a number of cellular processes, including inhibin B secretion, which negatively feeds back to the hypothalamus and pituitary to control GnRH and FSH release. Prolactin secreted from the pituitary increases LH receptor sensitivity on the Leydig cell. Testosterone, secreted by the Leydig cell, is important for spermatogenesis within the testis, but is also transported into the peripheral circulation and into the seminiferous tubule fluid, where it is further metabolized to dihydrotestosterone by 5 $\alpha$ -reductase, and to estradiol by aromatase. Estradiol has important regulatory functions, particularly in the efferent ducts and epididymis, while dihydrotestosterone is the main androgen regulating epididymal and accessory sex organ function. Testosterone and its metabolites regulate GnRH and LH secretion through negative feedback to the hypothalamus. GnRH is secreted from neurons within the paraventricular nucleus of the hypothalamus and its secretion is modified and regulated by many different chemicals, including those involved in energy balance and stress responses. The GPR54 receptor and its ligand, kisspeptin, form the critical gateway that modulates the actions of leptin and ghrelin and circulating steroids on the GnRH neurons. Overlaid on this endocrine regulation is a complex autocrine and paracrine regulation, where a multitude of factors are secreted by Sertoli cells, peritubular cells, Leydig cells, germ cells (GCs), and blood vessel (BV) endothelial cells to provide local signaling and regulation to neighboring cells. *Reproduced from Haschek WM, Rousseaux CG, Wallig MA, editors: Haschek and Rousseaux's handbook of toxicologic pathology, ed 3, 2013, Academic Press, Figure 59.15, p. 2520, with permission.*

### 2.7.1. Gonadotropin-Releasing Hormone

GnRH, which is secreted in a pulsatile manner by the GnRH neurons located within the paraventricular nucleus of the hypothalamus, orchestrates the entire endocrine regulation of reproductive function by controlling gonadotropin (FSH and LH) secretion from the pituitary, which in turn regulates secretion of testosterone from the Leydig cells. Secretion of GnRH is regulated not only by negative feedback of the sex steroids but also by a myriad of other chemicals, many of which are involved in other pathways such as maintenance of energy status and regulation of the stress response. The major regulator controlling GnRH secretion is the kisspeptin/GPR54 ligand–receptor complex, which is present in multiple hypothalamic nuclei adjacent to the GnRH-secreting neurons (García-Galiano et al., 2012; Padma et al., 2021). Kisspeptin/GPR54 also mediates the feedback of circulating sex steroids on the GnRH neurons (Beltramo et al., 2014) and has recently been shown to be pivotal in the timing of pubertal onset in many species (Terasawa, 2022).

### 2.7.2. Follicle-Stimulating Hormone

FSH is produced and exported from the pituitary to act principally on the Sertoli cells, although interstitial testicular macrophages may also respond. FSH is a glycoprotein hormone containing two subunits. It is secreted in a pulsatile manner in response to GnRH from the hypothalamus. Inhibin B, secreted by the Sertoli cell, is believed to be involved in a feedback loop from the testis to the pituitary to inhibit FSH production (de Kretser et al., 2000). FSH is believed to exert the majority of its effects via a G protein-coupled membrane receptor on the Sertoli cells, which induces a classical cAMP second-messenger intracellular response. The action of FSH on immature and mature animals is profoundly different. FSH is often considered to be the hormone of puberty, as rising levels of FSH act as a trigger for testicular growth, junction formation between adjacent Sertoli cells, and androgen-binding protein (ABP) secretion from the Sertoli cells, and generally initiates spermatogenesis and the expansion of the seminiferous tubules.

In the adult, the role of FSH varies across species (Ramaswamy and Weinbauer, 2014). The primary impact and effects of FSH in the adult are not fully understood, although its importance seems to vary between species. Suppression of

FSH in the adult rat has a negligible effect on spermatogenesis and appears to modify the number of differentiated spermatogonia entering meiosis but has little effect on the mitotic expansion of the undifferentiated and differentiating population. As a result, spermatogenesis is maintained, although at a lower level (Kumar et al., 1997). In contrast, suppression of FSH in NHPs results in considerable suppression of spermatogenesis and sperm output (Ramaswamy and Weinbauer, 2014) and appears to be important in the regulation of the expansion of undifferentiated stem cell spermatogonia, and so disturbances can have a much greater impact on spermatogenesis (Luetjens et al., 2005).

### 2.7.3. Inhibins and Activins

Inhibins are proteins of the transforming growth factor- $\beta$  (TGF- $\beta$ ) superfamily of growth and differentiation factors. They are secreted by both testis and ovary, and inhibin B decreases FSH but not LH secretion by pituitary cells. Inhibins are formed as dimer composed of one  $\alpha$  subunit and one of two different  $\beta$  subunits (A and B). In the male, inhibin B is secreted by Sertoli cells and appears to have both endocrine (via its effect on the pituitary) and paracrine (other effects on cells within the testis) properties (de Kretser et al., 2000). During the isolation of inhibin, a number of new proteins were found that possess FSH-stimulating activity in pituitary cells. These compounds, now termed activins, appear to be similar in structure to inhibin, but are dimers with two  $\beta$  subunits (Risbridger and Cancilla, 2000; Wijayarathna and de Kretser, 2016). At least three different forms of activins with varying biological activity have been described. As well as regulation of FSH, dual opposing roles for activin and inhibin have been demonstrated for the regulation of steroidogenesis in the Leydig cell. The main source of circulating inhibin is the gonads, but activins are synthesized in a broad range of tissues. Although circulating activin has FSH-modulating abilities, the main role for activin is now considered to be as a paracrine rather than an endocrine regulator of reproductive function. Follistatins, as well as inhibin, are major regulators of activin; most of the circulating activin is bound to follistatins and is inactive (de Kretser et al., 2004).

### 2.7.4. Luteinizing Hormone

LH, like FSH, is a glycoprotein hormone secreted in a pulsatile fashion by the pituitary under GnRH control. In rats, it acts on Leydig

cells in the testis and is the primary regulator of testosterone secretion, which is also secreted in a pulsatile manner (LH pulses occur prior to testosterone pulses). Circulating plasma testosterone (or its metabolites) complete the feedback loop via the kisspeptin/GPR54 complex, to modulate LH secretion through GnRH. The Leydig cell response to the binding of LH to its receptor is mediated through a number of transducing systems, including a cAMP cascade, a phosphoinositol–diacylglycerol mechanism, and an arachidonic acid–prostaglandin mechanism. Modification of LH action can impact the overall function of the Leydig cell. In the rat, prolactin permits LH-stimulated testosterone secretion by increasing the number of LH receptors on the Leydig cell (Purvis et al., 1979). The Leydig cells of other species do not appear to possess prolactin receptors, which has important implications with regard to species-specificity/sensitivity to chemically induced Leydig cell tumors (Cook et al., 1999).

Pulses of LH increase at puberty, both in amplitude and in frequency. LH is involved in the control of Leydig cell development, as differentiation of Leydig cells fails to occur in the absence of LH (Lejeune et al., 1998).

#### 2.7.5. Testosterone

Cholesterol is the obligatory precursor in the synthesis of testosterone and is supplied to the Leydig cell either by receptor-mediated endocytosis of lipoprotein or by *de novo* synthesis from acetate. The rate-limiting step in testosterone synthesis is the metabolism of cholesterol to pregnenolone by the side chain cleavage enzyme complex. This is a cytochrome P450-containing enzyme located in the mitochondria. The remainder of the process occurs outside the mitochondrion, principally on the smooth endoplasmic reticulum, and again is mediated by dedicated cytochrome P450s. From pregnenolone, two metabolic routes, termed  $\Delta^4$  and  $\Delta^5$  pathways, are thought to operate depending on the species. Irrespective of the pathways predominating in any given species, all of the intermediates have been isolated from testicular tissue of all species. Following secretion from the Leydig cell and circulation in the blood, testosterone is metabolized further in the liver, androgen-dependent tissues (e.g., epididymis, seminal vesicles, prostate), and a variety of peripheral tissues.

The major androgenic steroid in males, testosterone, is synthesized primarily in the Leydig cells

and has both intratesticular effects (on spermatogenesis) and peripheral effects (on accessory sex organs as well as nonreproductive organs such as brain, muscle, bone, and skin). There is also significant testosterone metabolism in many peripheral tissues, including conversion to DHT or estradiol. The concentration of testosterone within the testis is very much greater than in the systemic circulation, such that levels of the steroid in the testicular interstitial fluid can be up to 100-fold higher than in the plasma, and the concentrations in the two compartments are not directly proportional to one another (Coviello et al., 2004; Turner et al., 1984). The reasons for the high intratesticular levels are not entirely understood, since qualitatively normal spermatogenesis can be maintained with relatively low levels of testosterone (Zirkin et al., 1989). The high intratesticular testosterone levels may be required to maintain quantitatively maximum spermatogenic potential. Testosterone is not stored within the Leydig cell but is secreted into the interstitial fluid as it is synthesized. From here it is either (1) taken up by the Sertoli cells and bound to ABP, which is then secreted by the Sertoli cell and transported through the seminiferous epithelium into the STF and on into the epididymis; or (2) diffuses into the interstitial capillaries, where it binds quickly to steroid hormone-binding globulin (SHBG) or other plasma proteins for transport through the body, where it has wide-ranging effects on all other tissues of the body. ABP is synthesized by the Sertoli cell, whereas SHBG is synthesized in the liver, although rodents do not express SHBG postnatally (Laurent et al., 2016).

The major stimulus for testosterone production comes from blood levels of LH from the pituitary. In most species, a pulse of LH is followed closely by a pulse of testosterone; however, in rats, this connection is much less predictable, and several LH pulses may elicit no rise in testosterone, or there may be a significant delay before a testosterone pulse occurs (Coquelin and Desjardins, 1982; DePalatis et al., 1978; Ellis and Desjardins, 1982; Lapwood and Florcruz, 1978; Steiner et al., 1980).

Feedback inhibition of LH and hypothalamic GnRH is mediated through circulating levels of testosterone and its metabolites, DHT or estradiol. Conversion of testosterone to DHT or estradiol occurs locally in the brain, but the relative importance of the various molecules is species dependent. In the rat and mouse, DHT is thought to be the major regulator, while estradiol is more



important in the dog, NHP, and human (D'Agata et al., 1981; Prahalada et al., 1994; Turner et al., 2000; Winter et al., 1983).

The main known effects of testosterone in supporting spermatogenesis are to stimulate STF production by the Sertoli cell, to regulate release of the mature spermatids from the Sertoli cell (spermiogenesis), and to support the development of pachytene spermatocytes and later germ cell types. In the rat, ARs are present on Sertoli cells during stages V–VIII and on all peritubular cells with a generally similar pattern observed in humans (Bremner et al., 1994; Suárez-Quian et al., 1999).

#### 2.7.6. Estrogen

Estrogen is an important metabolite of testosterone that plays a role in spermatogenesis and in fluid reabsorption in the efferent ducts (Cooke et al., 2017). Aromatase, which irreversibly converts testosterone to estradiol, is primarily expressed in Leydig cells and germ cells, with the highest functional activity being present in spermatids, where it is localized within the cytoplasmic droplet. Estrogen receptors are also expressed in germ cells, Sertoli cells, and Leydig cells (Cooke et al., 2017). Aromatase activity/estrogen has been shown to contribute to spermiogenesis and sperm motility (Carreau and Hess, 2010).

Estrogen is a major regulator of fluid reabsorption in the efferent ducts, with high concentrations of estrogen present in the epididymal fluid and high concentrations of estrogen receptor- $\alpha$  in the efferent ducts (Hess et al., 2011). Estrogen interacts with receptors expressed in the efferent ductular epithelium to stimulate fluid resorption.

Local conversion of testosterone to estradiol also occurs in the brain and plays an important role in male reproductive behavior. In addition, local conversion to estradiol facilitates the negative feedback effects of testosterone in the dog, NHP, and human.

#### 2.7.7. Dihydrotestosterone

The major regulatory androgen in the epididymis and in the accessory sex organs is not testosterone but the more potent 5-hydroxy metabolite, DHT, which is synthesized within the epididymal epithelium by 5 $\alpha$ -reductase and binds to the AR with higher affinity than

testosterone. 5 $\alpha$ -reductase exists as two different isozymes and is present in the nuclear and, to a lesser extent, the microsomal fraction of the epithelium. Nuclear activity of 5 $\alpha$ -reductase is much higher in the initial segment of the epididymis and then declines as one moves distally, whereas microsomal activity is similar throughout the epididymis, but there is less of it (Azzouni et al., 2012). 5 $\alpha$ -reductase is also expressed in the brain, and local conversion of testosterone to DHT plays an important role in negative feedback regulation in the rodent (Torres and Ortega, 2003; Turner et al., 2000).

#### 2.7.8. Autocrine/Paracrine Regulation of Testicular Function

As already discussed, testosterone is the major regulatory hormone within the testis, but it is important to note that a large variety of factors are also produced locally, which include glycoprotein and steroid hormones, peptide growth factors, cytokines, proopiomelanocortin (POMC) derivatives, neuropeptides, and structural proteins (Cheng and Mruk, 2010; Huleihel and Lunenfeld, 2004). Although their physiological function and significance are unknown in many cases, the production of such a variety of pharmacologically potent molecules within the testis has obvious potential for being toxicologically important.

### 3. EVALUATION OF TOXICITY

The effects of toxicants on male reproductive function can occur through disturbances at one or more tissue sites, including the hypothalamus, pituitary, testis, efferent ducts, epididymis, accessory sex organs, or penis. In many cases, effects at one site will cause secondary changes at other sites; therefore, in general, the more endpoints examined, the better the chance of detecting toxicity and distinguishing the primary cause of toxicity versus the secondary consequences of toxicity. However, with increased number of endpoints, there is a greater chance of detecting a single random change occurring in isolation with no biological consequence.

Effects on the male reproductive system are often first encountered by the study pathologist in repeated-dose general toxicology studies.

These studies generally employ adult animals without breeding endpoints, although nonrodents may have immature, peripubertal, and/or sexually mature animals depending on the length of the study and species (see [Section 4.5](#)). Traditionally, fertility parameters are the major endpoints under evaluation in regulatory fertility studies, and histopathology has not been a standard endpoint because morphological effects on the paternal reproductive tissues should have been detected in the preceding routine 4- and/or 13-week repeat dose studies. In addition, effects on the developing reproductive system may be explored in juvenile toxicity studies and multigenerational assessments. It is important to consider the age and time of exposure along with the age of the animals when evaluation is performed.

### 3.1. Physiologic Evaluation

#### 3.1.1. Organ Weights

Organ weights of the testis, epididymis, prostate, and seminal vesicles can provide unique and mechanistically important information. These organs are commonly weighed in routine general ([Sellers et al., 2007](#)) and reproductive toxicity studies ([Parker, 2012](#)), and a more expanded list of tissues can be employed in dedicated studies ([Gray et al., 2005](#)). When measuring testis and epididymal weights in rodents, it is important to use absolute rather than relative weight since these tissues are conserved despite decreased body weight gain. Generally, decreased body weight gains result in increased relative testis weight. Decreased absolute testis weight is generally due to decreased germ cell content and/or decreased fluid content. Increased absolute testis weight is generally due to increased STF content ([Table 9.4](#)). Accessory organ weights are androgen-dependent, and changes in seminal vesicle and prostate (including secretions) weights can be a much more sensitive indicator of androgen status compared to a single hormone assessment. Depending on the lab, these tissues can be weighed together, individually, or in some cases, the prostate is the only tissue weighed. Regardless of the method employed, it is critical to ensure that all of the luminal secretions are included as part of the

accessory sex organ weight in rodents. The epididymis is also an androgen-dependent tissue, but nearly 50% of its weight reflects sperm content, which is a function of the efficiency of spermatogenesis. These basic concepts apply to nonrodents as well but are generally less sensitive due to the high interanimal variability and relatively small group sizes used in nonclinical toxicity testing.

#### 3.1.2. Sperm Analysis and Spermatid Head Count

Sperm assessment is not a regulatory requirement in pharmaceutical development, but it is a required component of most regulatory submissions for environmental chemical exposure. It is performed most often at the end of the study, and after a mating trial which assesses functional male fertility. Whether or not there is a regulatory requirement, measurement of sperm parameters (count, motility, and morphology of epididymal sperm, and a count of testicular spermatid heads) can provide important information which can also add to mechanistic interpretations, detection of posttesticular sperm abnormalities, and/or can confirm/support the morphologic findings identified in the testis ([Table 9.5](#)).

Collection and evaluation of sperm is one of the few readily available direct biomarkers of reproductive health that can be used in the clinic or in epidemiologic studies of environmental exposure. The usefulness of the measurements and the problems associated with their predictivity of toxicity are discussed in [Section 3.2](#). Measuring the number, motility, and morphology of sperm in the epididymis or vas deferens provides an integrated readout of the efficiency and overall health of testicular spermatogenesis as well as epididymal maturation and transport.

In rodents, sperm measurement is a terminal procedure conducted at necropsy, but since it is possible to collect ejaculates from most other species, there is the potential for examining longitudinal samples, including predose, during dosing, and during recovery, thus providing regular monitoring of any significant effects on spermatogenesis and reversibility. For large animals (rabbits, dogs, pigs, and NHPs), sperm evaluation is also a useful hallmark of sexual maturity.

**TABLE 9.4** Rapid Reference Guide for Evaluation and Interpretation of Weight Changes in the Male Reproductive Tract

Finding/observation	What to look for	Possible causes
Increased testis weight	Seminiferous tubular lumen dilatation	Increased seminiferous tubule fluid which may be due to obstruction of outflow, decreased emptying of tubules, decreased resorption of fluid by rete/epididymis, increased production by Sertoli cell
	Increased interstitial fluid (interstitial edema)	Altered hemodynamics, injury to vascular endothelium, reduced lymphatic drainage
Decreased testis weight	Germ cell depletion	Disruption of spermatogenesis through effects on germ cells, Sertoli cells, hormonal disturbance or blood supply
	Seminiferous tubule lumen contraction	Decreased production of seminiferous tubule fluid which may result from loss of elongating spermatids and/or decreased testosterone production
Increased epididymal weight	Increased interstitial fluid	Altered hemodynamics, injury to vascular endothelium, reduced lymphatic drainage
	Increased ductular fluid	Decreased resorption of fluid by rete, efferent ducts, and/or epithelium (head)
	Sperm granulomas	May be spontaneous, but may be induced by any agent causing inflammation or damage to the epididymal epithelial lining
Decreased epididymal weight	Reduced sperm content and contraction of ductular lumen size	Disruption of spermatogenesis resulting in reduced sperm production or release from the testis
Decreased weight of seminal vesicles and/or prostate	Atrophic changes in the secretory epithelium and decreased secretory product	Reduced levels of circulating testosterone, inhibition of 5 $\alpha$ -reductase or disruption of androgen receptor binding
Increased weight of seminal vesicles and/or prostate	Increased secretory product	Androgenic activity of a treatment; hyperprolactinemia

*Reproduced from Haschek WM, Rousseaux CG, Wallig MA, editors: Haschek and Rousseaux's handbook of toxicologic pathology, ed 3, 2013, Academic Press, Table 59.5, p. 2526, with permission.*

### 3.1.2.1. SPERM COUNT

In rodents, sperm count is generally taken from the tail of the epididymis (based on the landmark of where the vas deferens separates from the epididymis), where sperm are stored. Because the size of the tail varies widely across animals, it is necessary to weigh the tail and express the sperm number per milligram of tissue. Since the function of the tail is mostly to store sperm, this count reflects both sperm production by the testis and also the storage function of the epididymis. Reduced sperm count is generally due to reduced

production (Vidal and Whitney, 2014) but rarely can also be caused by decreased transit time in the epididymis (i.e., the sperm move through more quickly, for example, with TCDD exposure and some estrogenic compounds) (Foster et al., 2010; Meistrich et al., 1975). Sperm counts can be collected at necropsy in nonrodents as well, but with high interanimal variability and relatively small sample size, repeat measures in semen are often employed (see Section 3.2) (Capon et al., 2013; Dostal et al., 2001; Williams et al., 1990).



**TABLE 9.5** Rapid Reference Guide for Evaluation and Interpretation of Sperm Parameters in the Reproductive Tract

Finding/observation	What to look for	Possible causes
Decreased epididymal sperm count	Is there any evidence of testicular injury? Is there a similar decrease in testicular homogenization resistant spermatid (HRS) head count? Is there any decrease in accessory sex organ (ASO) weight? Are the other sperm parameters normal?	If there is no testicular injury and no decrease in HRS, the epididymis may be the primary site of toxicity. If other sperm parameters are normal, decreased count may be due to reduced (quicker) epididymal transit time. If ASO weight is decreased, low sperm count may be due to low testosterone (T). Also consider age and sexual maturity status.
Increased epididymal sperm count	Is there evidence of increased size of the epididymal lumen or evidence of outflow obstruction?	Alterations in epididymal transit time, decreased smooth muscle contraction in the tail of the epididymis.
Decreased testicular HRS count	Are there abnormalities in epididymal sperm parameters? Can you see degeneration/reduction in spermatogenesis or in the number of spermatids? Is there any decrease in ASO weight?	Decreased numbers of HRS means reduced testicular spermatogenesis and should be accompanied by reduced epididymal sperm count. Any spermatogenic disturbance will usually result in decreased HRS. If ASO weight is decreased, low T could be the cause.
Increased testicular HRS count	Is there evidence of spermatid retention? Is this correlated with a decrease in epididymal sperm count or changes in motility or morphology?	An increased count for HRS can only be caused by spermatid retention because spermatogenesis cannot increase its output of sperm. There may be a decrease in epididymal sperm count (but this may be less sensitive). Spermatid retention is usually associated with an increase in abnormal sperm and decreased motility.
Decreased motility	Is there any evidence of testicular injury or changes in HRS? Is there a decrease in ASO weight? Are the other sperm parameters normal?	Decreased motility can be caused by testicular or epididymal toxicity. If it is associated with changes in other sperm parameters, it is likely of testicular origin. Frequently accompanies spermatid retention.
Increased numbers of abnormal sperm	Is there any evidence of testicular injury or changes in HRS? Is there any decrease in ASO weight? Are the other sperm parameters normal?	An increase in the number of morphologically abnormal sperm is usually due to spermatogenic disturbance. It is a very sensitive indicator in the rat.

ASO, accessory sex organs; HRS, homogenization resistant spermatids; T, testosterone.

Reproduced from Haschek WM, Rousseaux CG, Wallig MA, editors: *Haschek and Rousseaux's handbook of toxicologic pathology*, ed 3, 2013, Academic Press, Table 59.6, p. 2527, with permission.

### 3.1.2.2. SPERM MOTILITY

Sperm motility is a functional measurement of the sperm. Sperm are sampled either from the tail of the epididymis or the vas deferens, and assessed for motility either manually or by computer-assisted sperm analyzer (CASA) (Parker, 2012). In rats, motility is generally high and fairly consistent between animals: the normal range for percent motile varies between different laboratories. Sperm motility can be

assessed on sperm collected at necropsy or in a semen sample (nonrodents), and there is an extensive literature on the methodologic requirements for measuring motility and obtaining acceptable values (Seed et al., 1996).

Sperm motility can be affected by disturbances in testicular spermatogenesis or by effects on the epididymis. The necessary components for motility are developed in the testis and these are further modified by the epididymis to allow

for motile sperm. Thus, in a laboratory study in rodents, if normal numbers of well-formed sperm were immotile in the absence of testis pathology, one might reasonably suspect a treatment effect on the epididymis.

#### 3.1.2.3. SPERM MORPHOLOGY

Sperm morphology consists of the basic features of the head or nucleus, midpiece, and tail and reflects the integrity and quality of the sperm. The number of abnormal sperm produced spontaneously varies dramatically with species ([Parker, 2012](#)). Increases in the number of abnormal sperm reflect disturbances in testicular spermatogenesis.

#### 3.1.2.4. TESTICULAR SPERMATID HEAD COUNT

Testicular spermatid head count (or homogenization resistant spermatid head count) is an additional measurement that provides an indication of testicular sperm production ([Meistrich, 1989](#)). Contrast this with caudal epididymal sperm count, which reflects both the production and storage of sperm. Integration of this measurement with that of epididymal sperm count provides powerful insight into the site of an effect, and an integrated view of the toxicity of a treatment ([Table 9.5](#)). Testicular spermatid head count is a convenient way of quantifying spermatogenesis in the testis, which can be measured using CASA. It is much less labor-intensive than manual counting of testicular germ cells using a microscope. One testis is homogenized to the point where only the highly condensed, most mature heads of the elongating spermatid population (steps 16–19 in rats) are left. This is a defined cell population that represents the final days of spermatid development prior to release. It can therefore be used to provide a value for daily sperm production or the number of spermatid heads per gram of tissue. Spermatid head count will decrease in response to anything that decreases spermatogenic efficiency (as long as the injury has had time to work through to the mature elongating spermatids). Note that compounds which prevent the release of mature spermatids at the end of spermatogenesis will increase this number (i.e., with low testosterone), while decreases reflect only downregulations of spermatogenesis. Thus, both an increase and

a decrease from the control value are meaningful.

#### 3.1.3. Fertility Assessment

A detailed review of fertility testing and evaluation of fertility endpoints is outside the scope of this chapter, but it is important to appreciate the basic concepts and the fact that fertility is an important endpoint for consideration by the toxicologic pathologist. Fertility is the final, integrated endpoint of the successful functioning of the male and female reproductive processes.

While there can be many study designs to answer specific questions or to explore specific effects, the general default design for rat studies is, at least conceptually, fairly straightforward. The parental animals are treated for a certain period prior to the period of cohabitation, and the dosing period is based on the kinetics of gamete production. For environmental compounds, the premating exposure period for males is roughly equal to the length of time it takes to produce mature sperm from spermatogonia, that is, about 60 days. For pharmaceuticals, the premating exposure period for males may be as short as 2 weeks, but this requires that testicular histopathology has already been conducted and found to be normal in prior general toxicity studies, and that the class of compound has not previously been associated with testicular toxicity. In this situation, the rationale for the 2-week premating dosing period is to identify any effects on fertility resulting from abnormalities in epididymal sperm (which take approximately 2 weeks to transit and accumulate in the tail of the epididymis), whereas histopathology in the 4- to 13-week general toxicity studies is considered the most sensitive method to identify any abnormalities in the testicular phase of sperm production. Therefore, this places additional importance on the ability of the pathologist to conduct a sensitive and stage-aware morphological evaluation in the general toxicity studies, because a fertility study with a 2-week premating dosing period will not identify any changes due to testicular toxicity. The premating exposure time for females varies depending on whether it is a combination (male and female) or stand-alone fertility study but is approximately 3 weeks. The animals are then cohabited for 1–2 weeks while still being exposed. The females are examined for evidence

of copulation (vaginal sperm upon lavage, or presence of a copulatory plug). Those showing evidence of mating are removed, and either euthanized on GD 13–15 (standard fertility study) or allowed to deliver their litters (multigenerational or continuous breeding study; see *The Role of Pathology in Evaluation of Reproductive, Developmental and Juvenile Toxicity*, Vol 1, Chap. 7).

For pharmaceutical compounds which are not tested through multiple generations, the dams are euthanized in midgestation (GD 13–15) and their uterine content is evaluated for live/dead status and number of embryos. If male fertility is being evaluated, the females will be naïve to treatment; in a female fertility study, the males will be untreated. In both cases, the output is the number of live offspring and some measure of their normalcy. In a male fertility study, the males will then be necropsied and reproductive parameters assessed (principally organ weights and sperm measures if warranted, since histological changes will have been evaluated in earlier studies).

Fertility can be impacted by morphological or biochemical injury in any of the reproductive tissues, by hormonal disturbances anywhere in the HPG axis, or by neurobehavioral alterations in sexual behavior. In general, due to the massive reserve capacity of spermatogenesis in rodents, fertility is relatively insensitive for identifying testicular toxicity, particularly when compared with morphology or sperm parameters. Even though they may remain fertile, other fertility endpoints, such as total litter size or time to pregnancy, can show significant alterations. In comparison with rodents, humans have vastly less reserve to maintain fertility when reproductive function is compromised. The fact that rodents have such high fecundity means that fertility (number of pregnant females per group) may remain high or unaffected in a group of 20 females, despite detectable histopathological changes or changes in sperm parameters. Aggregate data from many multigenerational studies have shown, however, a remarkably good correlation between overall fertility and sperm count and motility (Mangelsdorf et al., 2003); even modest reductions in sperm count (e.g., 10%) in rodents will translate into reduced fertility in a *population* of rodents. Note that this may not be seen in a small group of 20 animals.

### 3.1.4. Testing for Developmental Toxicity

Many of the critical developmental events in the formation of the male reproductive tract occur relatively late in gestation (Marty et al., 2003), and thus it is important that the dam (and pups) are exposed to xenobiotics during this critical period if developmental toxicity is being investigated (Sharpe, 2020). For regulatory requirements and testing endpoints related to male and female developmental reproductive toxicity, see *The Role of Pathology in Evaluation of Reproductive, Developmental and Juvenile Toxicity*, Vol 1, Chap. 7.

Multigenerational studies are able to detect potential effects of endocrine-active chemicals on male reproductive development because the critical period of exposure is covered. Most breeding protocols would give an indication of male fertility, litter size, and sex ratio, but it is only recently that endpoints sensitive to hormonal status have been incorporated into these testing protocols. Endpoints such as anogenital distance (AGD), retention of areolae/nipples, and preputial separation—all key indicators of pre- and postnatal androgen status that are sensitive to the potential effects of exogenous endocrine active agents—have now been included as indicators of normal male reproductive development for multigenerational studies of environmental chemicals. In normal reproduction studies, the sexing of rat pups is accomplished by observing the distance between the sex papilla and the anus. In males, this distance is approximately twice that of females and is a function of the androgenic signaling status of the animals (Schwartz et al., 2019). In the normal male rodent pup, the anlagen of the nipples will regress under the influence of DHT (Imperato-McGinley et al., 1986). Examination of pups before the hair begins to grow (usually around PND 14), and counting the number of areolae or nipples again provides an indication of the hormonal status of the animals. Thus, for example, the classical antiandrogen flutamide will result in a female phenotype for male pups with the presence of nipples (Foster and Harris, 2005). In male rodents, an index of puberty is provided by preputial separation, when the prepuce separates from the glans penis following androgen-induced apoptosis. This normally occurs around PND 40–44, about the time the



first sperm leave the testis and is concurrent with a surge in testosterone (Picut et al., 2018). Significant delays or advances in the timing of this event indicate a change in the androgen status of the animals, and it is an endpoint that is relatively insensitive to body weight changes.

#### 3.1.4.1. MORPHOLOGIC EVALUATION OF THE DEVELOPING REPRODUCTIVE TRACT

Most routine developmental toxicity studies do not involve histopathologic examination of the reproductive tissues. The endpoints that are usually evaluated include gross morphology of the reproductive tract, and measured parameters such as anogenital distance or time of preputial separation. With the recent interest and concern over the potential role of endocrine-disrupting xenobiotics causing developmental abnormalities, particularly in the male reproductive tract, histopathologic evaluation of the neonatal testis has become an important part of some developmental studies. Since juvenile toxicity studies can also involve histopathologic evaluation of the reproductive tissues prior to maturation, it is important for the pathologist to be familiar with the normal developmental sequence (both morphology and timing) as well as being aware of the nature of the morphological changes that might be expected from endocrine disruption during development (Picut et al., 2014; Whitney, 2012). These changes are very different from the changes that are seen in the adult reproductive tract exposed to the same endocrine-disrupting agents (See Section 5.3.5 below).

#### 3.1.5. *Measuring Xenobiotic or Metabolite Access and Accumulation in the Testis*

When determining the levels of a putative toxicant in the testis, the highly compartmental nature of this tissue must be recognized. The fenestrated characteristics of the interstitial vasculature allow small molecules to pass into the interstitial fluid with relative ease. However, the basolateral tight junctions of the Sertoli cells form a blood–tubule barrier, which effectively segregates the majority of the germ cells that are undergoing spermatogenesis from any toxicant in the interstitial compartment. Techniques such as whole-body autoradiography or whole tissue concentrations can assess overall levels of a xenobiotic and/or metabolite(s) in the testis as compared to plasma and other tissues, but

do not account for or have the resolution to assess whether there is presence within the seminiferous tubules. Additional techniques utilizing tissue-based mass spectrometry may allow for visualization at a level to assess compartmentalization of xenobiotics and/or metabolites (Granborg et al., 2022; Lagarrigue et al., 2011).

#### 3.1.5.1. TRANSPORTER-MEDIATED ACCESS

Both testis and epididymis have drug transporters and efflux pumps associated with the epithelium including P-glycoprotein, breast cancer resistance protein, multidrug resistance-associated proteins, and several organic anion transporting polypeptides (Klein and Cherrington, 2014; Klein et al., 2017; Miller and Cherrington, 2018). Compared to other organs (e.g., intestines, kidney, liver) relatively few of these efflux proteins are expressed, but for those that are they occur at relatively high concentration and show significant species differences.

#### 3.1.5.2. METABOLIZING ENZYMES AND ACTIVITY IN THE TESTIS AND EPIDIDYMIS

The majority of the cytochrome P450 enzymes in the testis are highly specialized for androgen production, but there are additional nonsteroidogenic P450s and drug-metabolizing enzymes present in the testis (Chiao and Van Thiel, 1986; Gilibili et al., 2014; Messiha, 1981, 1983). These enzymes often have differential expression across specific compartments and cell types and may differ from hepatic counterparts.

The epididymis can also metabolically activate compounds. For example, trichlorethylene is metabolized and activated to a greater extent in the epididymis than the testis, with consequent production of histologic damage in the epididymis (Forkert et al., 2002).

### 3.2. Biochemical and Biomarker Evaluation

Progressing new therapeutics into the clinic or conducting a public health screening program to detect toxicity arising from environmental exposures to putative toxicants generally relies on appropriate biomarkers for translation of findings from nonclinical species to humans. This is particularly important in the case of male reproductive toxicants where relatively small declines in spermatogenic function in humans may render a proportion of individuals infertile.

Another fact that underlines the need for a biomarker of testicular injury in men is the frequent discordances between species with regard to specific toxicities. Testicular damage caused in rats and not dogs by a drug candidate could be rat-specific, such that the compound would be without toxicity in humans. A sensitive biomarker to monitor for injury would provide confidence to proceed into the clinic; however, the search for a circulating marker of the activity of the seminiferous epithelium has a long and frustrating history. Currently, the two typically employed clinical biomarkers of testicular function include semen analysis and serum hormone concentrations (FDA, 2018).

### 3.2.1. Semen Analysis

Semen analysis represents the only clinical biomarker of spermatogenesis and can be used in nonrodents in nonclinical toxicity studies. Serial collection of semen allows for a repeated assessment over time, which can be useful for studies with longer recovery periods. Sperm counts in semen samples vary widely between subjects and repeat samples taken from dogs, rabbits, NHPs, and humans are also variable within an individual over time (Dostal et al., 2001; Jarow et al., 2013; Kholkute et al., 2000; Meyer et al., 2006; Redmon et al., 2013; Williams et al., 1990). Consequently, in clinical trials, this variability often drives a study design wherein multiple samples (often two semen specimens collected several days apart) are collected from each individual at each time interval (e.g., pretreatment, interim, and end of study) and the values averaged (FDA, 2018; Jarow et al., 2013). In addition, since ejaculation frequency impacts sperm count, subjects are asked to abstain from ejaculating for at least 48 h and a maximum of 7 days before collection (FDA, 2018; Frank et al., 1986; Mayorga-Torres et al., 2015). The percent motile sperm and the number of morphologically normal sperm are also included as part of a conventional sperm assessment.

When considering the use of sperm endpoints in the clinic, it is critical to remember that in addition to the variability between subjects and within subjects, there is an inherent time lag between the initial effect in the seminiferous epithelium and when that effect can be detected in a semen sample. This latency period can

vary depending on the initial cell type affected. These features mean that by the time a change in ejaculated sperm count is detected in a clinical trial (i.e., by the time that counts are depressed sufficiently to be confident that the decrease is not simply variability), the damage in the testis has already progressed. Because the variability is so high, these studies require a large number of men, several samples per man, and a large difference (typically 50%) between groups to be confident that a change has really occurred (FDA, 2018). Given this complexity and the requirements for extra sampling, it is easy to appreciate why such studies are usually performed as stand-alone studies rather than simply added on to a “regular” clinical trial.

### 3.2.2. Hormones

Measurement of serum hormone concentrations in nonclinical toxicity studies is often considered when characterizing possible hormonally mediated mechanisms of toxicity or when exploring potential biomarkers for use in clinical trials. The primary hormones measured in circulation are LH, testosterone, and FSH, but inhibin B will occasionally be included. Any attempt at measuring these hormones in a nonclinical study should be done with careful study design due to the pulsatile nature and species differences in patterns of release (Chapin and Creasy, 2012).

In rats, LH and testosterone secretion do not follow a diurnal or regular pattern and there is considerable variability in both the intra- and interanimal timing of release (Ellis and Desjardins, 1982). Importantly, testosterone peaks do not always follow LH peaks and often several closely spaced LH peaks are required to yield a single peak of testosterone. Due to this considerable variability, when measuring LH and testosterone as single time-point measurements in rats, groups sizes of 10–20 are recommended for LH and as many as 30 for testosterone (Chapin and Creasy, 2012). In addition, it is important to measure both hormones together in the same study as effects in one should influence the other and serve as a degree of biological plausibility when interpreting potential effects. The necessary group size often exceeds most repeated dose toxicity study designs and limits the utility of adding these endpoints onto routine studies, especially retrospectively. When exploring the

possibility of an endocrine-mediated effect, often prostate and seminal vesicle weights along with stage-specific findings in the testes serve as surrogates to infer potential effects on androgen status. When measurements of these hormones are needed, they are best done prospectively in carefully controlled investigative studies.

In dogs, pigs, and NHPs, LH and testosterone are both pulsatile, but in contrast to the rat, they occur at more regular intervals with an LH pulse once every 1–3 h (species and age dependent) and testosterone pulse following approximately 1 h later (Bonneau et al., 1987; Mialot et al., 1988; Steiner et al., 1980). Single time-point measurements in these species still face similar challenges as in the rat due to the pulsatile nature of these hormones. However, in nonrodents, there is a potential to collect multiple samples over a period of several hours and with the more regular pattern of secretion, this collection scheme maximizes the chance to assess both an LH and testosterone peak (Chapin and Creasy, 2012). This can be performed to establish a baseline and then collected during/after treatment and during/after recovery. Careful study design is critical with appropriate number and spacing of samples based on the age and species. As a result, these measurements are best done prospectively. Dogs and pigs do not demonstrate diurnal variability, but NHPs have a pronounced circadian rhythm where the highest serum hormone pulsatile activity and levels occur in the late evening/night (Steiner et al., 1980). In addition, when NHPs are group housed, social hierarchy can impact reproductive function. Lower ranking males can have marked decreases in serum testosterone levels and decreases in testicular volume (Czoty et al., 2009; Niehoff et al., 2010). These effects are most pronounced after changes in housing. When evaluating these hormones in NHPs, these additional factors need to be considered and careful planning and study design is required to ensure robust data are collected.

FSH varies less than LH over time, and so the number of animals needed to power an experiment sufficiently for LH will be more than sufficient for FSH (Chapin and Creasy, 2012). While the main feedback regulator of LH is testosterone, the feedback partner for FSH is inhibin

B, a hormone whose response to toxicity is much less certain. Often FSH will be increased when there is substantial damage in the testis (Reader et al., 1991), but rarely is it a leading or concurrent indicator and is much more often a trailing marker of damage. The rodent testis can function quite well on very low levels of FSH, but FSH appears to have a much more important role in the supporting spermatogenesis in the nonrodent (Ramaswamy and Weinbauer, 2014). Therefore, species differences would be expected in response to treatments that suppress FSH levels.

Inhibin B has been explored as a potential circulating biomarker for monitoring the status of the seminiferous epithelium since it is synthesized by the Sertoli cell and provides feedback regulation of FSH secretion from the pituitary. Inhibin B has been used clinically to help segregate male infertility patients into treatment categories and assess broad responses, but it is not a sensitive predictor of the overall health of the seminiferous epithelium in humans (McNeilly, 2012). A recent Health and Environmental Sciences Institute (HESI) project showed that circulating levels of inhibin B seem to decline concurrently with first appearance of testicular lesions for about half of the toxicants examined, but for the rest, effects on inhibin B trailed the appearance of the lesion (Chapin et al., 2013). Given the inconsistent and often lagging response to testicular insult, inhibin B is not regularly measured in nonclinical studies.

### 3.2.3. Messenger RNA

Another possible biomarker is testis messenger RNA (mRNA) in serum, as demonstrated by a few studies showing an association between sperm mRNA levels and men with infertility issues (Aoki et al., 2006; Steger et al., 2007). Tissue-specific mRNAs (i.e., kidney, liver) appear to be released for different toxicants, adding a useful layer of information. To date, studies producing a variety of lesions in the seminiferous epithelium have found no appreciable or consistent increase in testis-specific mRNA in the blood of those animals, suggesting either that mRNA was not being released from the damaged cells, or that the blood–tubule barrier was sufficiently intact to prevent the leakage of the released mRNAs into the blood (Dere et al., 2017).



### 3.2.4. miRNA

MicroRNAs provide the most recent focus for investigative attempts to find a biomarker for testicular toxicity. These are small noncoding RNAs which can be secreted from apparently any cell type in the body and taken up by any other. They can selectively suppress the expression of mRNAs in a sequence-specific manner, and are stable in the circulation, and therefore provide the possibility that they could be a secreted marker of seminiferous epithelium function that does not depend on treatment-induced barrier breakdown. Investigations are ongoing to identify testis-specific miRNAs and temporal and severity relationships between tubular damage and the serum miRNA profile (Fukushima et al., 2011; Sakurai et al., 2015; Shing et al., 2021; Stermer et al., 2019) and will be needed before an assessment of the value of miRNA as a true biomarker can be made. Another potential advantage of miRNAs is their presence in ejaculated sperm which can be collected and utilized as a direct read out of any damage that they incurred during spermatogenesis. Because of the delay between damage in the testis and availability for collection after traversing the epididymis, miRNAs would not be useful as an early biomarker for drug safety clinical trials, but they could be used for patient or public health monitoring of chronic exposures using a point-in-time assessment of different populations.

### 3.2.5. Toxicogenomics

(See also *The Application of Toxicogenomics to the Interpretation of Toxicologic Pathology*, Vol 1, Chap 11).

Testicular toxicogenomics has been used to characterize the response to testicular toxicants with the objective to identify early disturbances in biochemical pathways and possible mechanisms of toxicity, and to explore genomic responses to doses which were too low to produce detectable pathology (Matsuyama et al., 2011; Yuan et al., 2011). Microarray-based toxicogenomics, such as hybridization-based arrays, excel at finding a broad array of mRNA species. As such, they are poor tools for fine quantitation, and very insensitive for low-abundance transcripts. In this context, it might be expected that they would readily pick up

genes being expressed in Sertoli or Leydig cells or spermatocytes or spermatids—all cell types which are abundant in a testis. But these hybridization-based arrays will almost certainly miss even large-fold changes in genes in the stem cell spermatogonia, if only because those cells comprise such a small part of the testis. Laser-capture microscopy could be used to selectively capture specific cell types or areas of a tubule, but it is important to be aware that finding changes in a small subpopulation of cells in this complex tissue is extremely unlikely.

A second challenge for toxicogenomic investigations in the testis is when to sample. The time course of lesion development is different for all the known testis toxicants, ranging from hours to weeks until the first appearance of pathology. Considering this, any single time point will be a small snapshot of the constantly changing processes occurring within the tubule.

## 3.3. Morphologic Evaluation

Histopathology is often cited as being the most sensitive method for detecting disturbances in spermatogenesis, and indeed it is, if conducted on well-fixed tissue and by a pathologist with a clear understanding of spermatogenesis, the cell associations that make up the spermatogenic cycle, and the dynamics of the overall process (Lanning et al., 2002). If these requirements are not met, important lesions may be missed, especially in short-term studies of 2–4 weeks. This can be critical for human safety, since in the case of pharmaceutical development, initial clinical trials are often based on the results from such short-term studies (ICH, 2009).

### 3.3.1. Importance of Fixation

Fixation using conventional 10% neutral buffered formalin (NBF) causes severe shrinkage of the Sertoli and germ cells within the tubules of the testis. This seriously compromises the pathologist's ability to detect subtle changes such as tubular vacuolation, shape changes in the head of the elongating spermatids, spermatid retention, and displacement of germ cells from their normal position within the seminiferous epithelium. Fixation of testes with Bouin's or modified Davidson's fixative overcomes this problem, and should be used for all studies if possible, or at least for studies of  $\leq 13$  weeks (Latendresse

et al., 2002). Modified Davidson's fixative is generally preferred over Bouin's due to occupational safety concerns and slightly better overall morphologic appearance of the testis, but may have pale PAS staining of the acrosome (Lattendresse et al., 2002). The epididymis and accessory sex organs are best fixed in conventional NBF, although they can be fixed in modified Davidson's fixative along with the testis for convenience (Creasy, 2002).

Testes need to be fixed whole to maintain the architectural integrity of the seminiferous tubules and prevent disruption of the delicate germ cell-Sertoli cell junctions. This is especially important in rodents, which have limited connective tissue support within the testicular parenchyma. The testes should be fixed for at least 48 h, and they can then be transferred and stored in NBF and routinely processed (Creasy, 2002). Bouin's fixed testes should be transferred to 70% alcohol after 24–48 h fixation and washed thoroughly before processing or stored in 70% alcohol (Creasy, 2002).

Fixation of testes for immunohistochemistry (IHC) may require different fixatives and shorter fixation times, depending on the antigen being stained and antigen retrieval techniques employed. Trials are recommended to optimize for each antigen. Fixation of testes for electron microscopy and/or embedding in plastic (epoxy resin or glycol methacrylate resin) requires special fixation to provide optimal morphology. In the case of electron microscopy, perfusion fixation is essential if detailed ultrastructural evaluation is the goal. Successful perfusion of the testis can be challenging and following specific published methodology relating to testicular perfusion is recommended (Creasy, 2002). Perfusion fixation can also be used for glycol methacrylate embedding, although immersion fixation provides acceptable results. Surprisingly, NBF provides good results with this water-soluble embedding medium, and fixation is not improved when the fixative is perfused (Creasy, 2002).

### 3.3.2. Importance of Sampling

Sampling of the testis should always incorporate part of the rete testis so that this can be evaluated for changes. In rodents, the testes can be sampled to provide a transverse or longitudinal section, or one of each type can be taken from

each testis. The advantage of a transverse section is that all the tubules appear as regular cross-sections containing a single spermatogenic stage, and if the sample is taken from the anterior third of the testis, it will contain a portion of the rete testis. A longitudinal section taken through the region where the rete exits will provide a greater area of testicular tissue and rete for evaluation, but the tubular profiles will be much less regular and will often contain more than one spermatogenic stage. Another advantage of a longitudinal section is that it will allow examination of the lower frontal pole of the testis, which can be a specific site for certain ischemic lesions (Chattani, 1996). In large animals, the size of the testis may preclude obtaining an entire cross-section of testis unless using oversized slides. The section should at least contain a portion of the rete testis and also incorporate peripheral as well as the central regions of the tubule-containing lobules. Since the matrix of Sertoli cells and germ cells that constitutes the seminiferous epithelium is delicate and easily disrupted, it is important that the testes are handled gently at necropsy. Care should be taken to keep the capsule intact and not puncture or nick it when removing the epididymides. It is *not* necessary to puncture the capsule prior to immersion in fixative, even with nonrodents since this often causes more damage than benefit.

Sampling of the epididymis should include all regions (initial segment, head, body, tail, and junction with the vas deferens). This is best achieved by taking a longitudinal section through the entire organ. Lesions are often region-specific in the epididymis and sperm density varies significantly depending on species and location, so consistent and complete sampling is important. The efferent ducts can be an important target for toxicity, but in most cases, they are not routinely sampled. In rodents, they are long and tortuous and embedded in the epididymal fat pad between the head of the epididymis and the testis and are difficult to see and sample. In nonrodents, the efferent ducts are much shorter and embedded in the head of the epididymis, so they are generally present in routine sections. If the morphologic profile of testicular toxicity suggests efferent duct involvement, it may be necessary to prospectively sample and examine the efferent ducts.

Sampling the accessory sex organs is relatively straightforward, but species-specific anatomy should be considered (see [Table 9.3](#)).

### **3.3.3. Stage-Aware Evaluation of Spermatogenesis**

Whenever a pathologist examines a testis with the intent to identify changes in spermatogenesis, it needs to be done with an awareness of the stages of spermatogenesis. Failure to do this will result in important changes being missed. A stage-aware evaluation should not be considered a “special” evaluation; it should be the routine way that any toxicologic pathologist examines a testis. The only requirements are that the testes have been fixed appropriately as described above and that the pathologist has appropriate training and understanding of spermatogenesis. While a full knowledge of the cellular associations in each of the different stages of the spermatogenic cycle in each of the species routinely evaluated may be helpful for detailed or specialized assessments, in routine practice, most changes can be readily identified as long as the pathologist can recognize the basic cell types and associations as described above (see [Section 2.4](#)). Having this level of knowledge allows detection of relatively subtle changes in any routine regulatory study using conventional H&E sections.

If there is a suspicion that a drug or chemical belongs to a class of known testicular toxicants, then a more detailed stage-aware evaluation may be requested. In these situations, it is recommended that the testes be evaluated by a pathologist with expertise in the male reproductive system.

The value of examining the testis in a stage-aware manner is that it allows recognition of when a cell that should be present is in fact missing, or, conversely, is present when it should not be. This can be surprisingly difficult to see unless the observer is familiar with the correct number of layers of cells and their general appearance in the different phases of the cycle ([Figures 9.19 and 9.20](#)). Another advantage of examining the testis with a knowledge of stages and cellular associations is that it enables recognition of stage-specific cell degeneration or depletion ([Figure 9.20B and C](#)) or stage-specific Sertoli cell vacuolation. Cell- and/or stage-specificity of changes is only likely to be seen

in short-term studies ( $\leq 4$  weeks duration). Many testicular toxicants show cell and/or stage-specific changes at the earliest time points, but as the affected tubule continues through consecutive stages of the spermatogenic cycle and the repeat dosing regimen continually damages more tubules in the sensitive stage, the appearance of stage-specificity is lost.

Stage-aware evaluation is a qualitative evaluation using the pathologist’s knowledge of the normal cellular associations and basic patterns to recognize when something is abnormal. There is no cell counting or quantification involved in the procedure. If quantification of spermatogenesis is required, testicular spermatid head count and/or epididymal sperm counts are conducted. PAS-stained sections of testis can be used to visualize the acrosome and may be helpful to further characterize findings. While PAS-stained sections are sometimes quoted as a requirement for stage-aware evaluation of the testis, initial evaluation is best performed with H&E-stained sections. PAS-staining is often not optimized for testis within a given laboratory and when optimized typically, the hematoxylin counterstain is relatively light compared to routine H&E-stained sections. While this allows for good visualization of the acrosome, the lack of eosin and light hematoxylin does not allow for easy identification of degenerative changes in germ cells. As such, it is best to rely on H&E for initial assessment and utilize PAS staining on an as needed basis.

### **3.3.4. Nomenclature and Grading of Lesions**

As with any organ or tissue, using consistent nomenclature and severity grading for findings is important (See *Nomenclature and Diagnostic Resources in Anatomic Toxicologic Pathology*, Vol 1, Chap 25). Internationally (Europe, Great Britain, Japan, and North American Societies of Toxicologic Pathology) accepted standardized nomenclature is available for nonproliferative and proliferative lesions of the male reproductive tract in rodents ([Creasy et al., 2012](#)), dogs ([Woicke et al., 2021](#)), minipigs ([Skydsgaard et al., 2021](#)), NHPs ([Colman et al., 2021](#)), and rabbits ([Bradley et al., 2021](#)).

There is an added degree of complexity with respect to nomenclature and grading of changes in the testis because many of the early toxicant-induced disturbances in spermatogenesis may



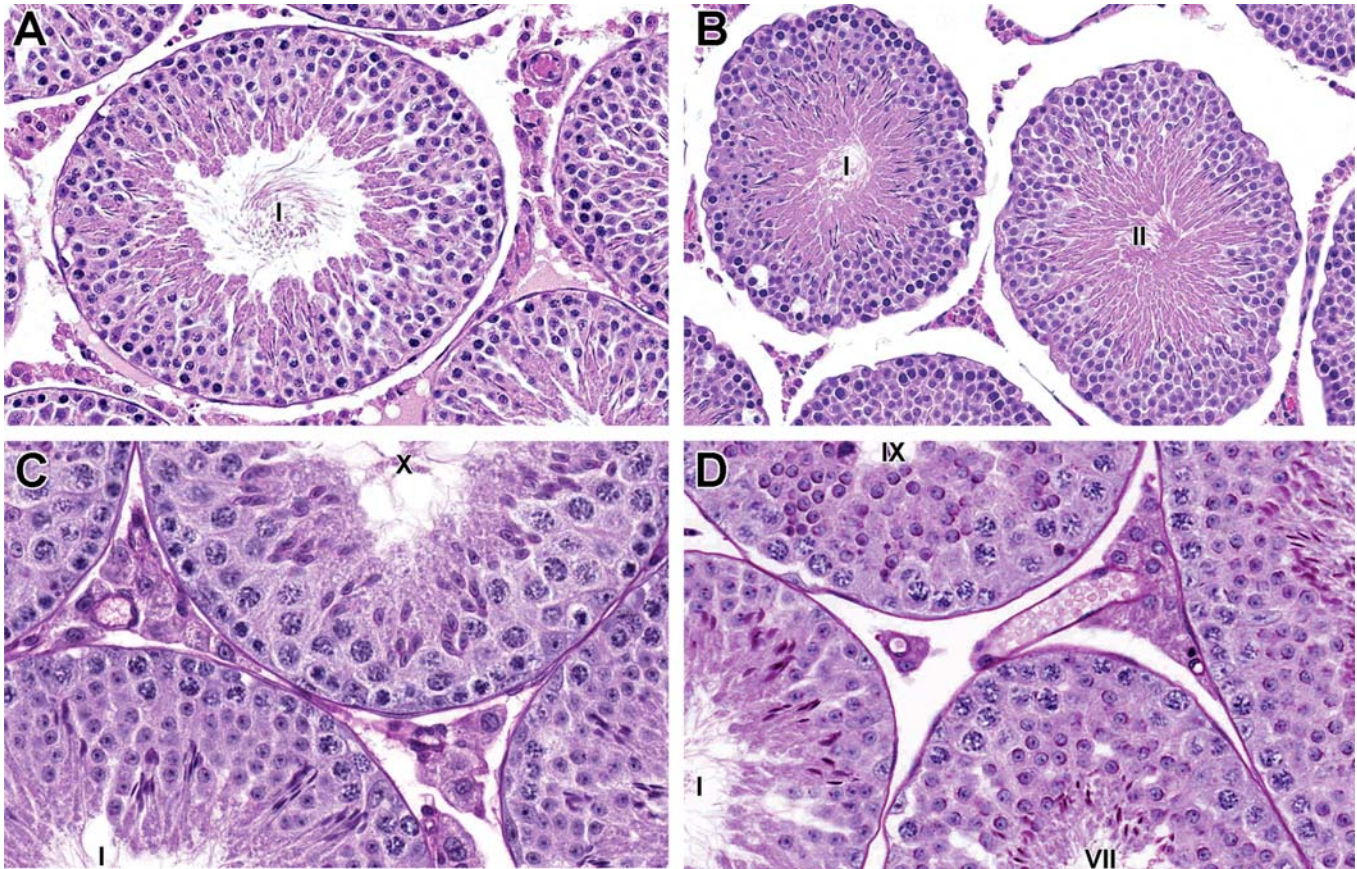


**FIGURE 9.19** (A) Normal stage I tubule from control rat. (B) Stage I tubule (left) and stage II tubule (right) after 2 days of dosing with a testicular toxicant that kills stage I pachytene spermatocytes. The stage I tubule shows swelling and early apoptosis of its pachytene spermatocytes. The stage II tubule shows complete absence of all pachytene spermatocytes (which were killed when the tubule was in stage I on day 1 of dosing). Rat, H&E,  $\times 20$ . (C) Testis from a control mouse showing normal cellular associations in a stage I and stage X tubule. (D) 14 days' dosing with a spermatogonial toxicant. The stage I tubule is missing its spermatogonia and its pachytene spermatocytes. The stage IX tubule is missing spermatogonia and leptotene spermatocytes. Notice that the stage VII tubule still has its pachytene spermatocytes but is missing its preleptotene spermatocytes. If dosing was continued, the "front" of germ cell depletion would continue to move through the stages and cell types. Mouse, PAS,  $\times 40$ . Reproduced from Haschek WM, Rousseaux CG, Wallig MA, editors: *Haschek and Rousseaux's handbook of toxicologic pathology*, ed 3, 2013, Academic Press, Figure 59.16, p. 2543, with permission.

only affect 1 cell type or only affect one or a few stages of the spermatogenic cycle. The nomenclature system for the male reproductive system in rodents (Creasy et al., 2012) recommends using cell- and stage-specific terminology when such changes are seen. Cell- and stage-specific changes are most likely to occur in short-duration studies ( $\leq 4$  weeks of dosing), since the longer the study duration, the more cell types and the more stages are likely to be affected. In the latter situation, nonspecific terminology (such as tubular degeneration/atrophy) is more appropriate. It is often

important to capture the cell- and stage-specificity of a finding because it can provide important mechanistic information or important information for risk assessment. For example, a finding of "degeneration, round spermatids and pachytene spermatocytes, stage VII/VIII" in rats indicates that reduced testosterone is the probable cause of the degeneration, especially if the change was associated with reductions in accessory sex organ weight. Alternatively, if the change only involved elongating spermatids (e.g., "degeneration and depletion, elongating spermatids"), this would



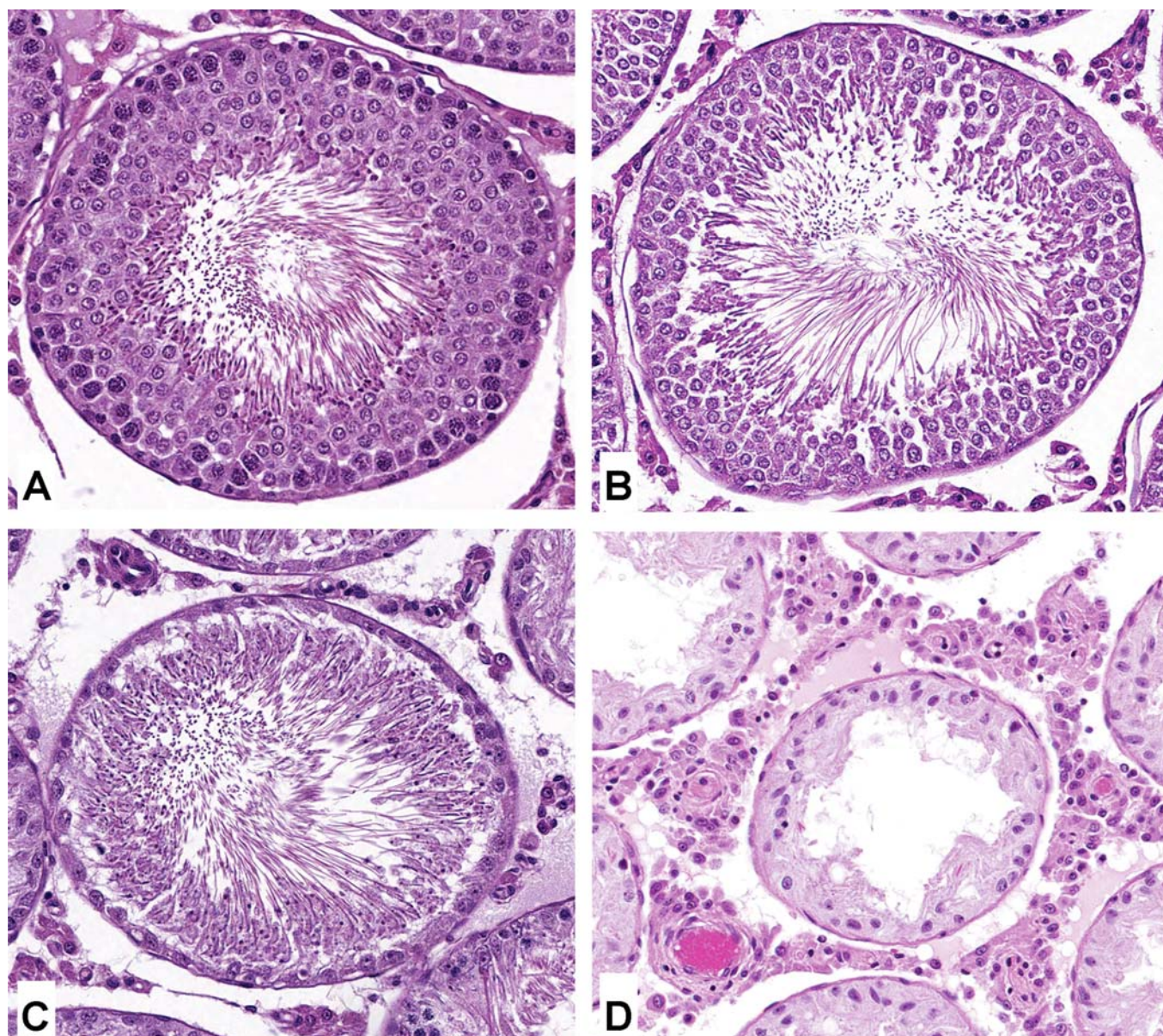


**FIGURE 9.20** Germ cell maturation depletion in the testis of rats due to pharmacologically induced spermatogonial mitotic inhibition. (A) Normal stage VII-VIII tubule. (B) Stage VII-VIII tubule with loss of spermatogonia, preleptotene spermatocytes, and pachytene spermatocytes after 4 weeks of dosing. (C) Stage VII-VIII tubule with loss of spermatogonia, preleptotene spermatocytes, pachytene spermatocytes, and round spermatids after 6 weeks of dosing. (D) After 8 weeks of dosing, there is complete tubular atrophy with no germ cells present. With a detailed stage aware evaluation of spermatogenesis, early changes of germ cell depletion can be detected in shorter term studies before the findings progress to complete atrophy. Rat, H&E,  $\times 20$ .

signify that the toxicity is limited to the final stages of spermatid development, which would suggest it is likely to be a rapidly reversible change with only transient effects on fertility (although this would need to be tested).

Epididymal lesions can be region-specific, and if this is the case, the nomenclature should reflect

the anatomic location because the information can have important mechanistic implications. Reductions in sperm content can even be region-specific depending on whether the reduction in sperm output from the testis occurred within the past few days of dosing (low sperm in the head, normal sperm in the tail) or occurred



over the previous 1–2 weeks of dosing (low sperm throughout the epididymis).

#### 3.3.4.1. SEVERITY GRADING

Grading the severity of disturbances in testicular spermatogenesis can present a challenge. Severity grading for nonspecific testicular changes such as tubular degeneration/atrophy is generally not difficult and can be based on the proportion of affected tubules (e.g., grade 1 (minimal) is <10% of tubules affected) (Creasy, 2008). However, severity grading for cell- and stage-specific changes needs to take into account the number of cells affected as well as the number of tubules affected. For example, the subtle but important change of spermatid retention (retention of mature, step 19 spermatids typically in stage IX–XI to XII tubules) generally only affects a very small proportion of the total tubular profiles even in its most severe form, because there are only a limited number of tubular profiles observed in those stages at a given time. For spermatid retention, minimal (grade 1) severity may be just detectable above control levels, mild (grade 2) severity may be consistently present in a high proportion (>50%) of stage IX–XII tubules, and moderate (grade 3) severity may be readily detectable spermatid retention, even at low magnification (Creasy, 2008). For additional guidance for severity grading of cell- and/or stage-specific findings, see Creasy (2008).

### 3.4. Special Techniques

(See *Special Techniques in Toxicologic Pathology*, Vol 1, Chap 11)

#### 3.4.1. Immunohistochemistry

The testis lends itself to IHC as well as any other tissue, although it should be noted that standard protocols using tissues fixed in NBF may require optimization for testes fixed in Bouin's or modified Davidson's fixative.

Immunohistochemical staining methods can be used to highlight dividing cells (predominantly spermatogonia in the adult) and apoptotic cells as well as specific cell types such as spermatogonia, Sertoli cells, Leydig cells, and/or interstitial macrophages (Angelopoulou et al., 2008; D'Andrea et al., 2010; Gilibili et al., 2014; Picut et al., 2014; Sandlow et al., 1997). These

techniques are generally best employed in a prospective manner to characterize specific findings rather than in routine studies as a screening endpoint.

#### 3.4.2. Flow Cytometry

A quantitative analysis of germ cell populations in spermatogenesis can be achieved using flow cytometric analysis (Aslam et al., 2002; Geisinger and Rodríguez-Casuriaga, 2017; Rotgers et al., 2015). For this method, the testis is mechanically dissociated and suspended in buffer and the cells are stained with a fluorescent DNA probe and separated into different fractions based on DNA content and ploidy. The different fractions are presented as a percentage of the total cells counted. This can provide a quantitative snapshot of the differential depletion of germ cell populations. While it is possible to quantify a change based on DNA content and ploidy, stage-specific information is lost because the entire testis is digested and turned into a single-cell suspension. Although the literature contains a few reports utilizing this method, it is recommended that the method be approached cautiously, based on the significant amount of work needed, the low throughput, and the restricted type of information generated.

#### 3.4.3. Electron Microscopy

Electron microscopy can be performed on tissues from the male reproductive tract and/or on sperm (Borg et al., 2009; Creasy, 2002; Moretti et al., 2016). When evaluating the testis, perfusion fixation is essential for ultrastructural studies (Creasy, 2002). Interpretation of testis ultrastructure is difficult even in ideally fixed tissue, and minimizing fixation artifacts is essential for the detection of subtle toxicologically induced changes. For ultrastructural studies, a formalin–glutaraldehyde mixture (Karnovsky's fixative) or 5% glutaraldehyde is recommended as the primary fixative. This should be perfused until the testis is firm. The tissue can then be diced and postfixed in 1% osmium tetroxide or a mixture of potassium ferrocyanide and osmium tetroxide, which improves contrast of all cell types but particularly the Leydig cells. If difficulties are encountered with the perfusion technique, it may be necessary to employ a vasodilator (0.1% procaine) or heparin in the saline wash prior to perfusing the fixative, or to



heparinize the animal for 15 min prior to perfusion. Whole body perfusion via the heart, or local perfusion via the testicular or iliac artery, may be used.

Compared with most tissues, the ultrastructure of the testis is extremely complex. Each tubule has four generations of germ cells undergoing continuous maturational changes. Spermiogenesis is particularly confusing, as the elongating spermatid may be sectioned through any number of possible orientations, either in the longitudinal or the transverse plane. Sertoli cells also have complex spatial relationships with one another and with the various populations of germ cells. Their shape, subcellular composition, and organization change markedly during the different stages of the spermatogenic cycle. Plane-of-section and sampling issues make it difficult to find and identify specific stages of spermatogenesis where early lesion could be identified.

In view of the difficulties outlined here, ultrastructural examination of the testis is not recommended as a routine method to detect toxic changes. However, it is a valuable tool for detailed investigation of an early lesion, particularly if mechanistic explanations are sought. Interpretation of any apparent changes is aided by exhaustive examination of control material.

#### **3.4.4. Laser Capture**

After examining the testis, questions are frequently generated about what biochemical or molecular changes might be occurring in the cells to produce the lesion that is seen. The problem is that because any given cell type is a small minority of the cells in the testis, simply homogenizing the tissue will dilute out the cell of interest and make that approach useless. One potential solution to this problem is laser capture microdissection to selectively collect specific stages of seminiferous tubules or interstitium (Sluka et al., 2002, 2008). This can serve as a powerful tool but is labor intensive with various methodologic challenges and still mostly employed for research purposes (Catlin et al., 2014).

#### **3.4.5. In Vitro Methods**

Given the anatomic complexity of the testis, in vitro models of testicular function and/or toxicity are challenging to develop. In vitro methods for isolating and assessing Leydig cells

are available and can serve as a method to answer investigative and mechanistic questions regarding steroidogenesis (Bilinska et al., 2009; Browning et al., 1983; Brun et al., 1991; Klinefelter and Ewing, 1989). In vitro methods to recapitulate seminiferous tubular function is considerably more challenging. A variety of single, coculture, and three-dimensional approaches have been described, but are generally still used for research purposes only (Baert et al., 2020; Parks et al., 2013; Pendergraft et al., 2017; Richer et al., 2020; Yin et al., 2017).

### **4. RESPONSE TO INJURY**

#### **4.1. Organ Weight Changes**

In routine general toxicity and male fertility studies, changes in the weight of the testes, epididymides, prostate, and/or seminal vesicles provide an important indicator of potential effects in the male reproductive system. Basic guidance on the evaluation of these organ weight changes is provided in Table 9.5. When assessing the weight of the testis and epididymis, it is important to use absolute weight or weight relative to brain weight rather than relative to body weight. The size and weight of testis and epididymis are dependent on spermatogenesis and sperm content and, like the brain, testis and epididymis size is maintained despite body weight loss. In studies with body weight loss, testis weight (relative to body weight) will increase compared with concurrent controls. A decrease in absolute testis weight generally reflects a loss of germ cell content, although organ weight changes are generally less sensitive than microscopic assessment. Depending on the magnitude and duration of the change, there may be a corresponding decrease in epididymal weight since sperm content is responsible for approximately 50% of its weight. An increase in the weights of testis or epididymis generally indicates increased fluid content. In the testis, this is usually due to increased tubular fluid and is accompanied by obvious tubular dilation. It is most likely due to blockage of the efferent ducts, while in the epididymis, interstitial edema, inflammation, and/or sperm granuloma may be the cause.

In the rat, decreased weight of the seminal vesicles and prostate is a relatively sensitive indicator of reduced androgen status; it is more sensitive than morphological evaluation of atrophic changes, and less variable than measuring hormone levels. Indeed, these weights are the best integrative indicator of androgen status currently available. Most of the weight change is due to a reduction in the stored secretion, and therefore it is important that this is captured when the tissues are weighed, that is, weigh the tissues with their stored secretions. The combined weight of the seminal vesicles, coagulating gland, and prostate can be used, or each organ can be weighed separately. In practice (and when allowed by the protocol), it is just as sensitive and much easier to lift the aggregate tissue mass by the bladder, cut the urethra immediately below the prostate, place the whole unit (bladder, prostate, seminal vesicles) intact on the balance, and then trim off the bladder. It is easy and fast and aids in retention of the accessory sex gland fluid.

In endocrine-disruptor screening studies, the ventral prostate is sometimes dissected and weighed separately since it is the most androgen-sensitive portion of the gland (Banerjee et al., 2000; Gray et al., 2005). Increased weight and secretory content of the accessory organs can occur if androgens are administered (Banerjee et al., 1994). Hyperprolactinemia has also been reported to cause enlargement of accessory sex organs in rodents (Coppenolle et al., 2001).

Changes in the weights of accessory sex organs are not as sensitive a parameter in the nonrodent because of the interanimal variation, smaller group sizes, and the fact that comparatively little secretion is stored in these organs; however, decreases in weight can be observed with decreased androgenic signaling.

## 4.2. Morphologic Changes (Nonproliferative)

The most common appearance of the testis following dosing with any testicular toxicant is varying degrees of germ cell degeneration, depletion, and/or disorganization of the germ cell layers within the seminiferous epithelium. This reflects the fact that the germ cells are

exquisitely sensitive to any disturbance of their support, be it mechanical, biochemical, nutritive, or regulatory. So, whether a toxicant acts through the Sertoli cell to disrupt a biochemical pathway that regulates or supplies energy to the germ cells or acts on the Leydig cells to decrease testosterone levels, or even on the vasculature to cause anoxia, it will be the germ cells that are most affected and show evidence of cell degeneration, death, and/or depletion.

Since different types of injury can cause a similar morphologic response in the testis, how can the pathologist gain insight into how and where the toxicant is acting? The answer is to look at the earliest morphological changes and concentrate on the *pattern* of toxicity (see Section 5 below). Table 9.6 provides a rapid reference guide on specific features to look for and how they can be interpreted. This may mean looking at the cell-specificity or stage-specificity of the early changes, as well as the character of the morphological changes (germ cell degeneration vs. germ cell depletion vs. tubular vacuolation or necrosis). It means taking into consideration the effects on the rest of the reproductive tissues (epididymis and accessory sex organs, and sperm endpoints if available). This kind of detailed morphologic examination of early changes relies heavily on the pathologist's knowledge of spermatogenesis and the ability to detect when a particular stage of the spermatogenic cycle is abnormal. This can be surprisingly subtle even when there are multiple cell types missing (Figures 9.19 and 9.20).

### 4.2.1. Germ Cell Degeneration

In other organ systems, the term "degeneration" suggests a potentially reversible effect on the target cell; however, in the testis, it is the recommended terminology that is applied to germ cells undergoing the irreversible effect of cell death (apoptosis) (Creasy et al., 2012). In the testis, apoptosis provides the important physiologic function of limiting the size of the germ cell population to numbers that can be supported adequately (Aitken and Baker, 2013; Kerr, 1992). The Sertoli cell regulates this function utilizing the FAS gene system (Lee et al., 1997). Germ cells express Fas, a transmembrane receptor protein that, when bound by Fas ligand (FasL) secreted by the Sertoli cell, transmits an apoptotic signal within the cell. All chemically

**TABLE 9.6** Rapid Reference Guide to Evaluation and Interpretation of Histopathologic Findings in the Male Reproductive Tract

Finding/observation	What to look for	Possible causes
Testicular germ cell loss	Is a specific cell type(s) affected? Does the germ cell loss fit into a pattern of maturation depletion, or is it nonspecific? Is it focal or diffuse, is it partial or generalized?	The pattern of the germ cell loss will provide valuable clues as to the likely mechanism of injury, but this will also be very much influenced by the duration of the study (see main text for detail). The pathogenesis of germ cell loss is best investigated in a short time-course study.
Loss of elongate and elongating spermatids	Degeneration of step 7 spermatids and pachytene spermatocytes in stage VII tubules.	Disruption of testosterone secretion, which may be caused by direct effects on the Leydig cells or endocrine-mediated effects. Direct effects on elongating spermatids.
Degeneration/apoptosis of germ cells	Is a specific cell type affected? Are the dying cells restricted to a specific tubular stage? Are the affected cells forming multinucleated cells?	The cause may be direct toxicity to the affected germ cell but may also be mediated through a stage-specific disturbance to the Sertoli cell. Apoptotic cells are rapidly removed. Multinucleate aggregates suggest a slow, nonspecific degenerative process.
Germ cell exfoliation	Presence of exfoliated germ cells in the rete and epididymal lumens.	Disruption of Sertoli/germ cell junctions leading to loss of adhesion. Disruption of Sertoli cell cytoskeletal fibers leading to sloughing of apical Sertoli cell cytoplasm and attached germ cells.
Macro/microtubular vacuolation (in the absence of severe germ cell injury/loss)	Is this located in the basal Sertoli cell cytoplasm, or scattered as large vacuoles throughout tubule? Look for accompanying or additional focal germ cell loss (suggesting focal Sertoli cell damage).	Disturbance of Sertoli cell function leading to vacuolation of organelles or disturbance of fluid balance. <i>Vacuolation should not be confused with osmotic induced fixation artifact.</i>
Necrosis and disorganization of tubular contents (including Sertoli cells)	Evidence of acute inflammatory infiltrate around affected tubules.	Disturbance in hemodynamics or damage to the vascular endothelium leading to ischemic necrosis.
Spermatid retention	Alteration in epididymal sperm parameters (morphology, motility and count) and possible increase in HRS. Are ASO weights reduced?	Reduced accessory sex organ weights → disturbance in testosterone secretion. No change in ASO weights implies disturbance in Sertoli cell function or in spermatid development.
Dilated seminiferous tubule lumens	Blockage of efferent ducts or epididymal duct if a diffuse pattern in rodents. Blockage at the level of the rete if segmental pattern in nonrodents. Evidence of pressure-induced germ cell loss.	Increased seminiferous tubule fluid due to obstruction of outflow, decreased emptying of tubules, decreased resorption of fluid by rete/epididymis, or increased production of fluid by Sertoli cell.

ASO, accessory sex organs; HRS, homogenization resistant spermatids.

Modified from Haschek WM, Rousseaux CG, Wallig MA, editors: Haschek and Rousseaux's handbook of toxicologic pathology, ed 3, 2013, Academic Press, Table 59.7, p. 2540, with permission.



induced germ cell death investigated so far also appears to occur through the process of apoptosis. This is true for both direct germ cell toxicity, as occurs with radiation, and indirect germ cell death resulting from Sertoli cell injury (Embree-Ku et al., 2002; Murphy and Richburg, 2014; Shaha et al., 2010). It is even true for death that appears pyknotic, such as the spermatocyte death induced by glycol ethers in rats (Ku et al., 1995). The precise mechanism triggering apoptosis appears to be different in each case. With Sertoli cell toxicants, there is upregulation of Fas and FasL, but with germ cell toxicants, there is only upregulation of Fas. Spermatogonia are particularly prone to apoptosis associated with the administration of cytotoxic agents as they are the only mitotically active class of germ cells and reside outside of the blood–testis barrier (Meistrich, 1986). Although DNA laddering electrophoresis might indicate that germ cell death occurs by apoptosis, for the bench pathologist looking at dying germ cells microscopically, the only dying cells that fit the classic morphologic appearance of apoptosis (DNA fragmentation and clumping at the periphery of the nucleus within an eosinophilic cytoplasm) are spermatogonia. These can often be seen undergoing normal attrition, particularly at the outside of stage XII tubules.

#### 4.2.2. Germ Cell Depletion

Once germ cells undergo apoptosis, they are rapidly phagocytized by the Sertoli cell, and all evidence of their previous existence disappears. Apoptosis or loss of spermatogonia is subtle and difficult to detect as there are relatively few spermatogonia present. With time, the germ cell depletion becomes more obvious as the more numerous mature cells begin to drop out due to the lack of precursors (Figure 9.20). This pattern of germ cell loss is often referred to as “maturation depletion” and the extent of the finding will vary with the original cell type affected and the length of dosing and/or off-dose period. In the case of a spermatogonial toxicant, with continued dosing, successive layers of more mature germ cells will continue to be lost and the lesion progresses to diffuse tubular atrophy. If the germ cell depletion affects more mature cell types, such as round spermatids, the lesion never progresses to full tubular atrophy as spermatogonia and spermatocytes are unaffected

and present. As such, whenever a diagnosis of germ cell degeneration or depletion is used, it is critical to clearly specify the cell(s) affected. This cell specificity can then be used in the context of the total duration of spermatogenesis for the species tested along with the study duration to understand the potential for progression and/or reversibility. When germ cell depletion occurs with a patchy, multifocal distribution, and is accompanied by disorganization and/or degeneration of the remaining germ cell layers, the term “degeneration/atrophy” might be more appropriate (Creasy et al., 2012).

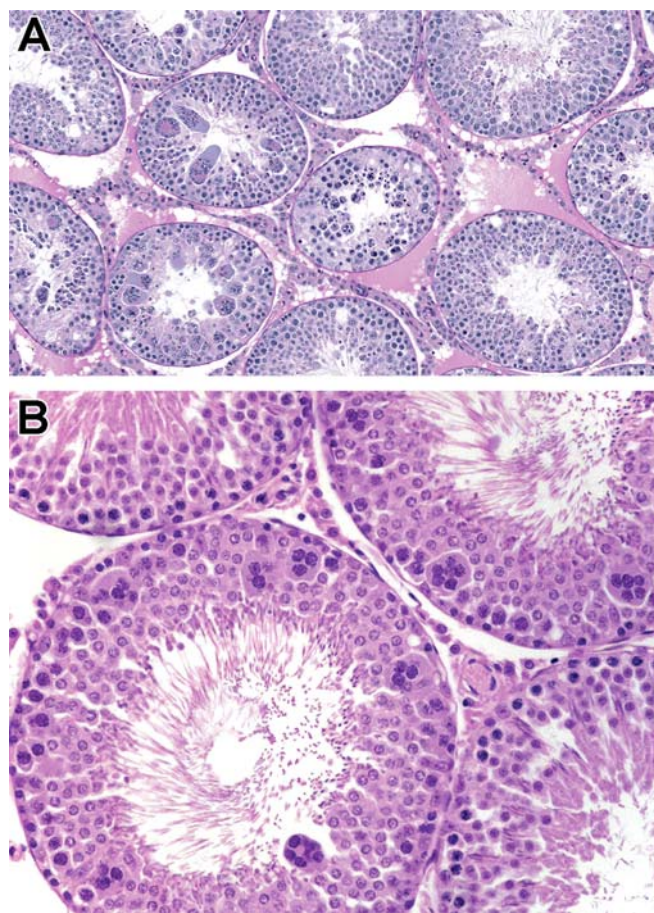


**FIGURE 9.21** (A) Nonspecific tubular degeneration/atrophy. Some tubules contain multinucleated degenerate germ cells; others are partially or totally depleted of germ cells. Rat, H&E,  $\times 10$ . (B) Stage-specific (stage VII) multinucleated pachytene spermatocytes. Rat, H&E,  $\times 20$ . Reproduced from Haschek WM, Rousseaux CG, Wallig MA, editors: *Haschek and Rousseaux's handbook of toxicologic pathology*, ed 3, 2013, Academic Press, Figure 59.19, p. 2552, with permission.



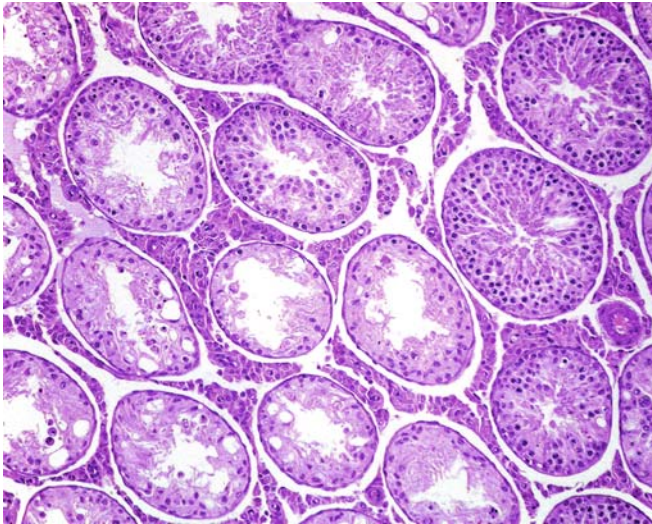


**FIGURE 9.22** Tubular degeneration/atrophy. Mixture of degenerating and depleted germ cells with no cell- or stage-specificity, accompanied by vacuoles within or between Sertoli cells and typically caused by injury to the Sertoli cell. This may be seen as an occasional background finding. Rat, H&E,  $\times 10$ . Reproduced from Haschek WM, Rousseaux CG, Wallig MA, editors: *Haschek and Rousseaux's handbook of toxicologic pathology*, ed 3, 2013, Academic Press, Figure 59.20, p. 2553, with permission.

#### 4.2.3. Tubular Degeneration/Atrophy, Testis

Tubular degeneration/atrophy is a nonspecific term that can be used to describe any situation where there is a mixture of tubules containing degenerating germ cells, partial loss of germ cells, disorganization of germ cell layers, and/or tubules lined only by Sertoli cells (Creasy et al., 2012). It is a commonly observed pattern seen in longer duration repeated-dose studies with testicular toxicants (Figures 9.21A and 9.22). Tubular degeneration/atrophy can be used as a combined term or separated into two diagnoses with either degeneration or atrophy used (Creasy et al., 2012). In many cases, the combined term of tubular degeneration/atrophy is appropriate for diagnosis of nonspecific tubular changes, but when one feature prevails, it may be helpful to use the individual terms. This is especially important with different lengths of dosing or recovery arms where degeneration may be the primary feature at the earlier timepoints with atrophy at the later timepoints (Figure 9.23). Using the combined term may mask the progression in these cases.

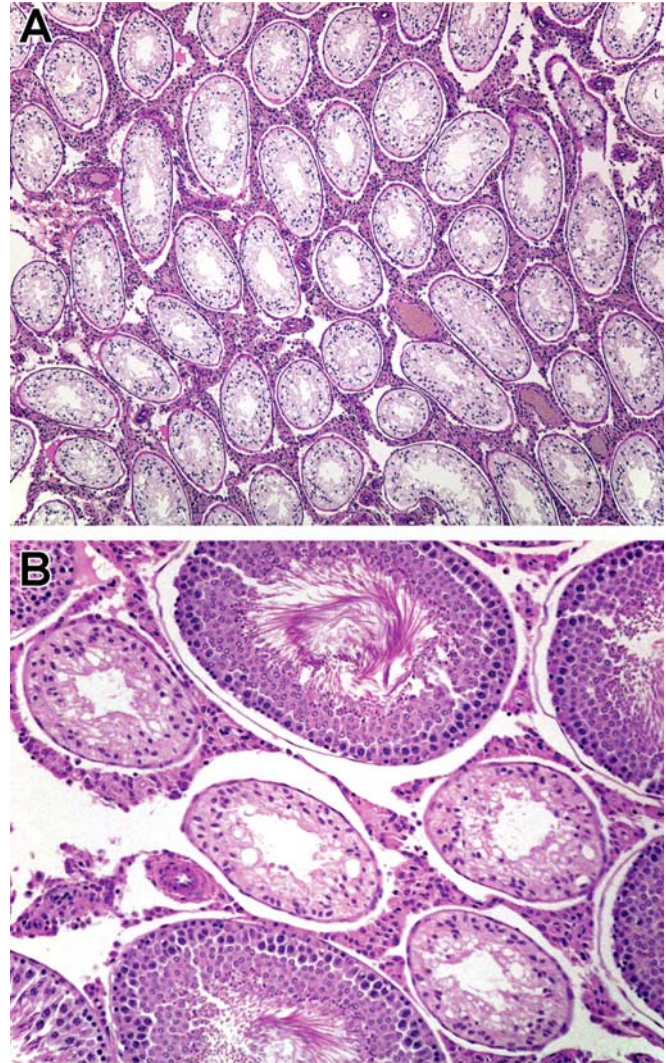


**FIGURE 9.23** (A) Tubular atrophy. Contracted tubules, totally depleted of germ cells and lined only by Sertoli cells. Rat, H&E,  $\times 4$ . (B) Occasional atrophic tubules. One to five atrophic tubular profiles per section of testis are frequently seen as a background finding in rat testes, and probably represent focal segmental loss of spermatogenesis. Rat, H&E,  $\times 10$ . Reproduced from Haschek WM, Rousseaux CG, Wallig MA, editors: *Haschek and Rousseaux's handbook of toxicologic pathology*, ed 3, 2013, Academic Press, Figure 59.21, p. 2553, with permission.

#### 4.2.4. Multinucleated Giant Cells

In cases of testicular toxicity, one of the most easily identified and common manifestations of degeneration is that of the “multinucleated giant cell” (Figure 9.21B). These generally comprise round spermatids or occasionally pachytene spermatocytes that have fused together into one large cell (Vidal and Whitney, 2014). The



multinucleate germ cells are believed to form when the cytoplasmic bridges between adjacent cells open and allow fusion of the cytoplasm. Multinucleate giant cells appear to be a relatively slow form of germ cell death, since the nuclear and cytoplasmic characteristics often retain normal staining and morphology, are TUNEL negative (Luo et al., 2013), and elicit very little response from the surrounding Sertoli cell. They can be seen as an occasional focal or diffuse background finding in rodents and more commonly in dogs (Figure 9.21A), but when a dose-related increase is seen in number and incidence, they are a good indication of toxicity (Vidal and Whitney, 2014). They can also be seen as a cell- and stage-specific change (Figure 9.21B).

#### 4.2.5. Tubular Necrosis, Testis

Tubular necrosis differs from tubular degeneration/atrophy in the fact that it involves coagulative necrosis (rather than apoptosis) of the germ cells and generally involves disruption and necrosis of the Sertoli cells lining the tubule (Figure 9.24A). If there is significant disruption of the Sertoli cells, the blood–testis barrier will be breached, resulting in an inflammatory infiltrate around and invading the affected tubule. There are very few other cases where toxicant-induced testicular injury gives rise to an inflammatory response. Tubular necrosis is a relatively uncommon finding, and most often occurs in response to ischemic injury from vascular effects (see necrosis/inflammation, vascular/perivascular below). Necrosis of large areas, or of the entire testis (testicular necrosis), can be seen following torsion or infarction of the testis (Figure 9.24B).

#### 4.2.6. Tubular Dilatation, Testis

Enlarged testes containing seminiferous tubules with dilated lumens and thinned seminiferous epithelium (Figure 9.25A) can be seen as incidental lesions (Creasy, 2012) but can also be chemically induced (see Section 5 below) (Vidal and Whitney, 2014). Diffuse tubular dilatation is related to outflow obstruction at the level of the efferent ducts and is typically observed in the rodent due to species-specific anatomy of the efferent ducts (see Section 2.5). Since the tubular dilatation is secondary, it can be either unilateral or bilateral. In short-term studies, testicular weight will increase as intratubular fluid increases, but over time, back-

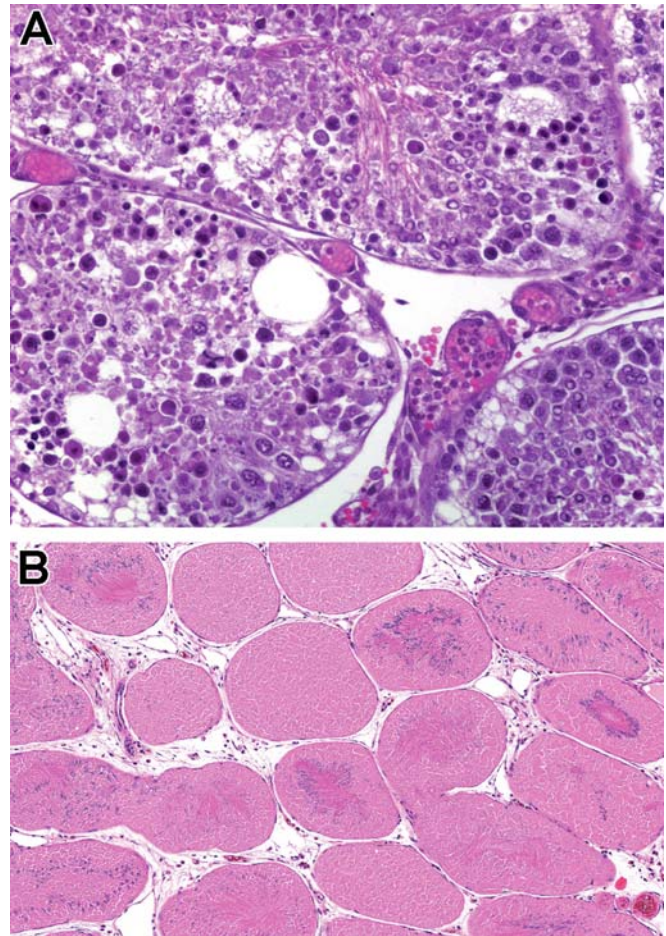


**FIGURE 9.24** (A) Tubular necrosis. This is an uncommon change in the testis that is usually caused by anoxia/ischemia. It is characterized by a coagulative necrosis of the germ cells with severe disruption of the organization of the germ cells. Death of the Sertoli cells, or disruption of the tight junctions between them, often causes breakdown of the blood–testis barrier leading to stimulation of a neutrophilic inflammatory response. Note the accumulation of neutrophils in the congested interstitial blood vessels. Rat, H&E,  $\times 20$ . (B) Testicular necrosis. Diffuse coagulative necrosis of all tubular elements caused by ischemia. Rat, H&E,  $\times 4$ . Reproduced from Haschek WM, Rousseaux CG, Wallig MA, editors: *Haschek and Rousseaux's handbook of toxicologic pathology*, ed 3, 2013, Academic Press, Figure 59.22, p. 2554, with permission.

pressure atrophy of the seminiferous tubules can progress to total tubular atrophy leading to a decrease in testicular weight (Figure 9.25B).

#### 4.2.7. Tubular Vacuolation

Tubular vacuolation consists of small or large clear spaces within the seminiferous epithelium and can occur as microvesicular vacuolation in



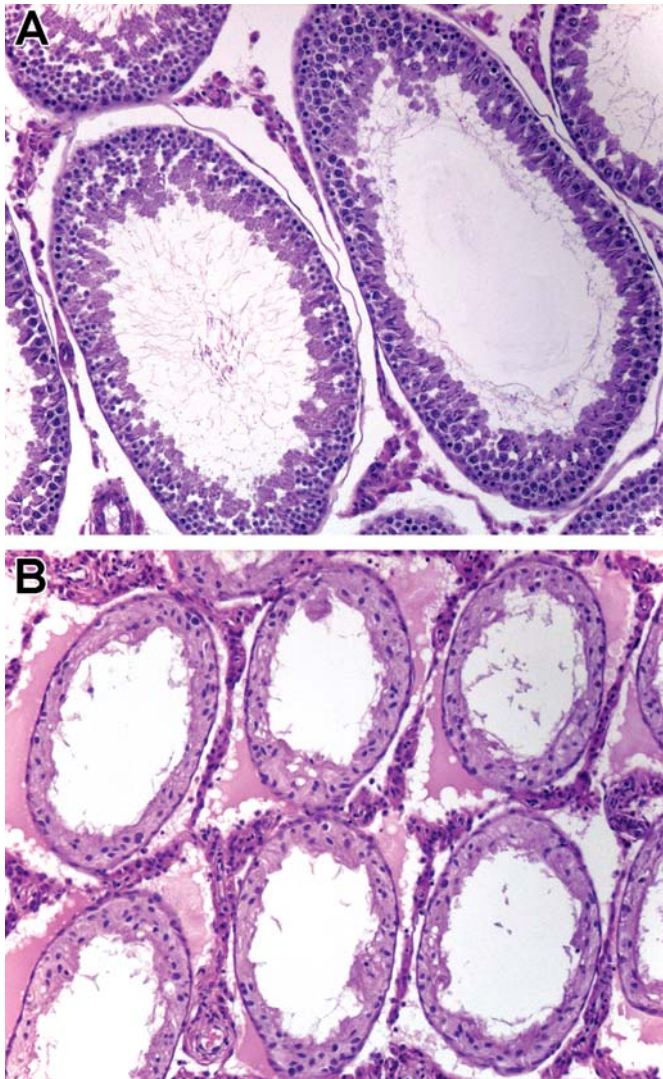


**FIGURE 9.25** (A) Tubular dilation. Tubules with dilated lumens caused by increased fluid content. The seminiferous epithelium is thinned but the normal layers of germ cells are present. In rats, the increased fluid content is frequently caused by obstruction of the efferent ducts. Rat, H&E,  $\times 10$ . (B) Tubular atrophy with dilated tubular lumens. This is frequently the sequel to prolonged tubular dilation and is caused by pressure atrophy from the increased fluid pressure on the epithelium. There is also edema in the interstitial space. Compare the dilated lumens with the contracted lumens in [Figure 9.23A](#). Rat, H&E,  $\times 10$ . Reproduced from Haschek WM, Rousseaux CG, Wallig MA, editors: *Haschek and Rousseaux's handbook of toxicologic pathology*, ed 3, 2013, Academic Press, Figure 59.22, p. 2554, with permission.

the basal Sertoli cell cytoplasm ([Figure 9.26A](#)) or as larger discrete vacuoles part way up the seminiferous epithelium ([Figure 9.26B](#)). Larger vacuoles can displace the germ cells lying adluminal

to it. With routine H&E-stained sections, it is usually difficult to ascertain whether the vacuoles are intra- or intercellular, but intracellular basal vacuoles typically represent expansion of cytoplasmic organelles (SER), phospholipidosis, or intracellular edema. These are generally an early toxicant-induced change associated with Sertoli cell disturbance and may progress to tubular degeneration/atrophy with continued dosing. Tubular vacuolation is only recommended to be used as a stand-alone diagnosis when it occurs as a primary feature in absence of other changes ([Creasy et al., 2012](#)). The appearance of tubular vacuolation can also be present when there is germ cell loss with gaps present between Sertoli cells or as a fixation/processing artifact and vacuolation should not be diagnosed in these cases. Occasional large vacuoles can be seen in normal testes, but they are generally few in number ([Figure 9.26D](#)).

#### 4.2.8. Spermatid Retention

In rats, step 19 mature spermatids should be released from the luminal Sertoli cell cytoplasm during Stage VIII of the spermatogenic cycle. If spermiation fails, then step 19 spermatids fail to be released and are still seen at the tubular lumen in stage IX, X, and XI tubules ([Figure 9.27](#)). This can occur due to disturbances in Sertoli cell processes, reduced testosterone levels, or abnormal spermatid development ([Carr et al., 2011](#); [O'Donnell, 2014](#); [Saito, 2000](#)). By the time the tubule reaches stage XII, the spermatid heads have generally been pulled down into the basal Sertoli cell cytoplasm where they are phagocytized. By Stage XIII, they have generally disappeared. Therefore, this subtle lesion will only be seen in a relatively small proportion of tubules within an affected testis. Although morphologically subtle, the finding is generally associated with significant changes in sperm parameters (particularly motility and morphology) and, potentially, fertility. If there is significant spermatid retention, testicular spermatid head count should increase while epididymal sperm count decreases.

While spermatid retention can be a regularly observed change in the rat, it is uncommon as a diffuse change in other species. In the dog, the appearance of spermatid retention can be observed as a focal change near the rete testis due to Sertoli cell phagocytosis of sperm in



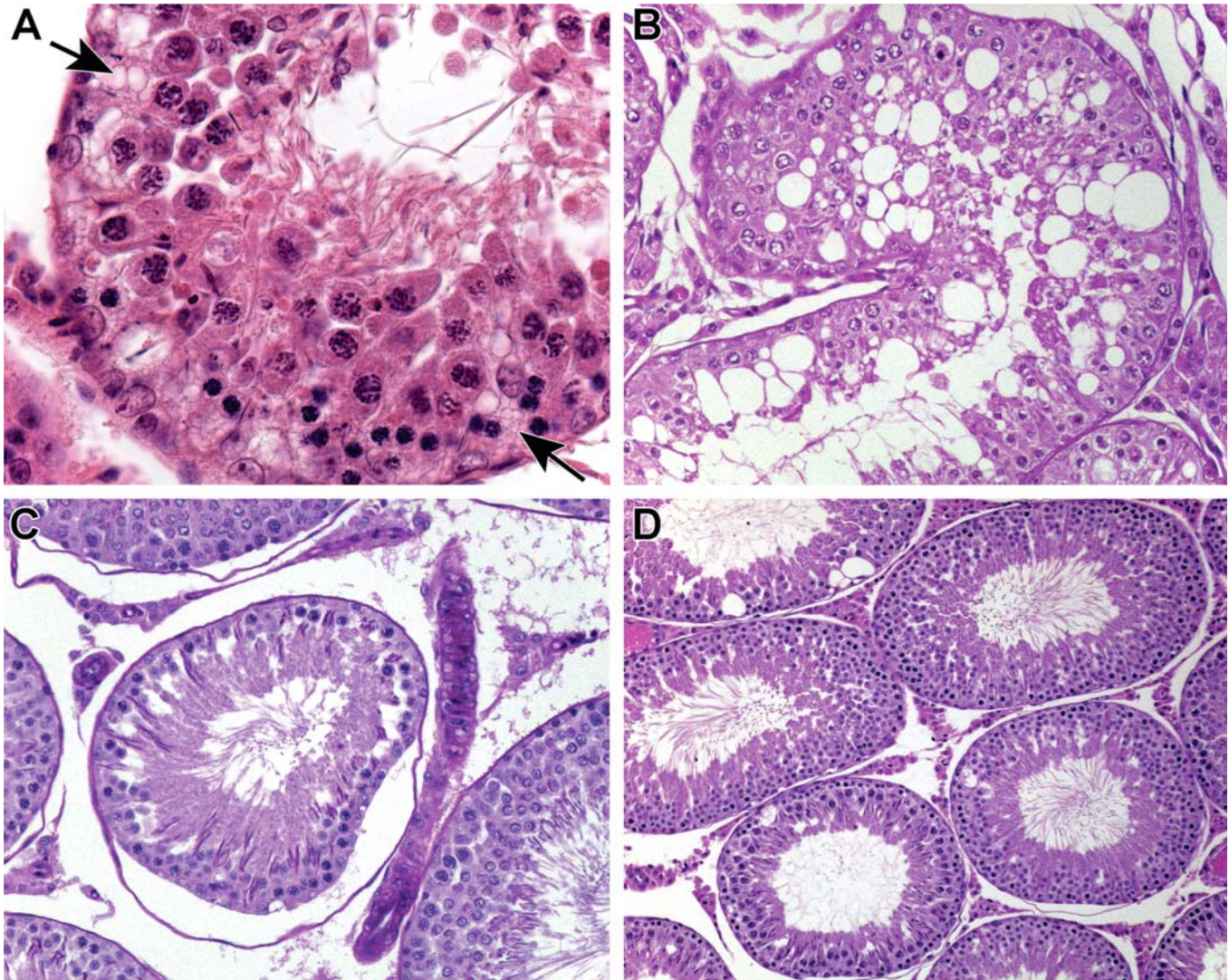


**FIGURE 9.26** (A) Tubular vacuolation. Microvacuolation of the basal Sertoli cell cytoplasm (arrowed) with displacement of the overlying germ cells. Note that the cytology of the germ cells appears mostly normal, suggesting that the primary change is in the Sertoli cell. This was caused by a drug that produced phospholipidosis in multiple tissues including the testis (Sertoli cell) and epididymis. Rat, H&E,  $\times 40$ . (B) Tubular vacuolation in dog testes. The vacuolation is macrovesicular and may be within or between Sertoli cells. Dog, H&E,  $\times 20$ . (C) Vacuolation due to loss of space-occupying germ cells. These vacuoles are due to the substantial loss of round spermatids and not a primary degenerative change in the Sertoli cells. Rat, H&E,  $\times 20$ . (D) Occasional vacuoles in the tubules of normal rat testis is a common background finding but an increase in the number of these vacuoles can be caused by test article-administration. Rat, H&E,  $\times 10$ . Reproduced from Haschek WM, Rousseaux CG, Wallig MA, editors: *Haschek and Rousseaux's handbook of toxicologic pathology*, ed 3, 2013, Academic Press, Figure 59.24, p. 2555, with permission.

seminiferous tubules with outflow obstruction and sperm stasis (Sato et al., 2012).

#### 4.2.9. Leydig Cell Atrophy, Apoptosis, or Necrosis

Leydig cells undergo atrophy in response to decreased LH stimulation (Figure 9.28) (Keeney et al., 1988). Atrophic Leydig cells have

decreased cell size due to reduced amounts of smooth endoplasmic reticulum and have decreased steroidogenic activity. If this leads to a reduction in testosterone production, there will be a secondary decreased size and weight of androgen-dependent tissues (epididymis and accessory sex glands) along with the species-specific seminiferous tubular changes.



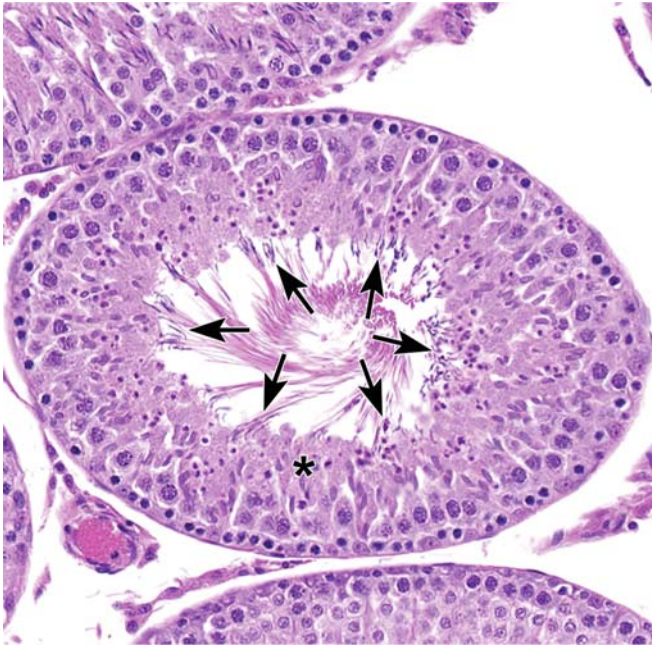


**FIGURE 9.27** Spermatid retention in a stage XI tubule. Note the presence of mature step 19 spermatids (arrows) at the luminal surface with tails extending into the lumen overlaying a newly elongating layer of spermatids (asterisk). There should never be two layers of elongating/elongated spermatids present. Rat, H&E,  $\times 20$ .

Decreased LH support of Leydig cells can occur with GnRH antagonists, as well as from androgen, estrogen, and progesterone receptor agonists (O'Connor et al., 2002). It is important to consider the species differences in hormonal regulation as formestane, an aromatase inhibitor, induced Leydig cell atrophy in rats but hypertrophy/hyperplasia in dogs (Juniewicz et al., 1988; Walker and Nogués, 1994). Due to the variability in size of Leydig cells, effects of fixation on their normal appearance, and difficulty in discerning Leydig cells from interstitial macrophages, it can be quite difficult to evaluate Leydig cell size by qualitative examination unless the effect is marked. Image analysis combined with immunohistochemical markers can be used to further characterize alterations in size/volume, although these are best attempted as prospective endpoints.

Degenerative changes to the Leydig cells are not common. The alkylating agent ethane dimethyl sulfonate causes necrosis and loss of Leydig cells following a single administration in rats (Bartlett et al., 1986; Molenaar et al., 1986), leading to decreases in testosterone and

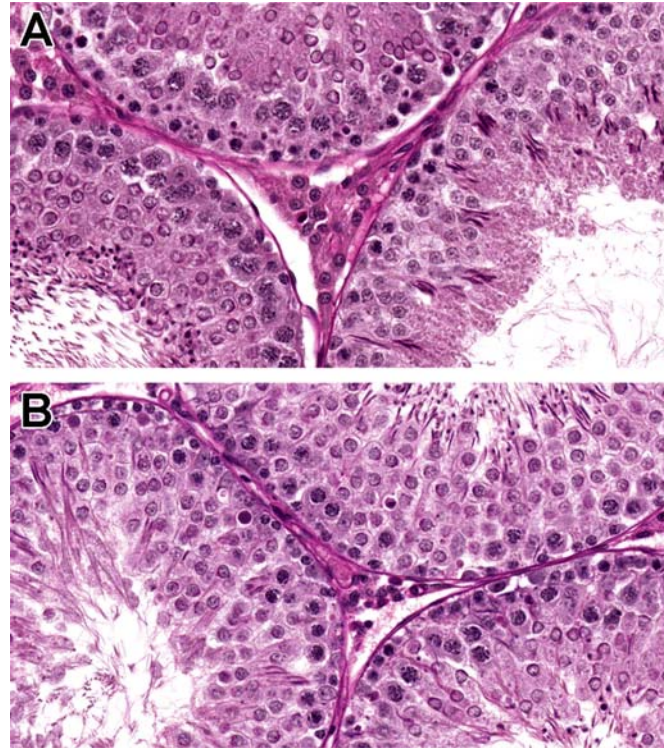


**FIGURE 9.28** Leydig cell atrophy caused by a gonadotropin releasing hormone (GnRH) antagonist. (A) Normal Leydig cells forming a cluster around a capillary. (B) Atrophic Leydig cells. Rat, PAS,  $\times 40$ . Reproduced from Haschek WM, Rousseaux CG, Wallig MA, editors: *Haschek and Rousseaux's handbook of toxicologic pathology*, ed 3, 2013, Academic Press, Figure 59.26, p. 2557, with permission.

a subsequent increase in gonadotrophins. Glucocorticoids as well as triptolide (active compound from a Chinese herb) have been reported to cause apoptosis of Leydig cells in rats (Andric et al., 2013; Gao et al., 2002; Lv et al., 2021).

#### **4.2.10. Necrosis/Inflammation, Vascular/Perivascular**

Necrosis with inflammation can occur within or around testicular and/or epididymal arteries/arterioles. This may be observed as isolated vascular effects or can cause ischemic coagulative necrosis of the seminiferous tubules and interstitial components of the testis with subsequent inflammation, fibrosis, and complete tubular atrophy (Vidal and Whitney, 2014). Depending on the extent of the vascular damage, these changes can be unilateral or bilateral, and may be present in the testis,



epididymis, and/or surrounding tissues. Spontaneous vascular findings can occasionally be observed in all species and need to be carefully considered in context of findings in other vascular beds and historical control data (Clemo et al., 2003; Creasy, 2012; Dincer et al., 2018; Snyder et al., 1995). Focal ischemic necrosis has been reported with high doses of human chorionic gonadotropin (hCG) due to local production of vasoactive prostaglandins (Chatani, 2006). Cadmium causes endothelial necrosis within the testis and epididymis leading to necrosis (Gunn et al., 1963). Less severe vascular effects due to vasoactive compounds such as serotonin, histamine, and epinephrine may also be observed (Vidal and Whitney, 2014).

#### 4.2.11. Cell Debris, Lumen, Epididymis

The presence of cells and cell debris admixed with sperm in the lumen of the epididymis generally reflects sloughing of germ cells from the

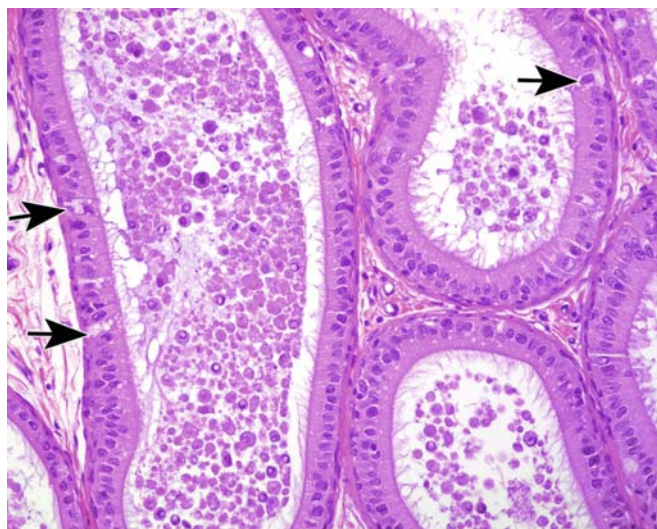


**FIGURE 9.29** Intraluminal cell debris/germ cells in the epididymis of a rat. The presence of sloughed germ cells and cell debris in the rat epididymis is often very sensitive indicator of testicular damage. The normal adult rat epididymis contains very few sloughed germ cells. The mouse, dog, minipig, and NHP have a low number as a normal background finding. In rats, increased numbers of clear cells (arrows) often accompany increased debris. Rat, H&E,  $\times 20$ . Reproduced from Haschek WM, Rousseaux CG, Wallig MA, editors: *Haschek and Rousseaux's handbook of toxicologic pathology*, ed 3, 2013, Academic Press, Figure 59.27, p. 2557, with permission.

testis (Figure 9.29). In the mature rat, there are normally very few sloughed cells, making this a very sensitive indicator of spermatogenic disturbance in the testis (Foley, 2001). Compared to the rat, sloughed cells are seen more frequently in the normal mouse, dog, minipig, and NHP (Creasy, 2012), but the level is still generally low and increases secondary to degenerative changes in the seminiferous tubules. Germ cell debris is also common in pubertal animals of any species, which reflects the higher background level of germ cell degeneration and exfoliation during the first wave of spermatogenesis. In rare cases, the sloughed cells seen in peripubertal epididymal lumens may also represent exfoliated epididymal cells (Hermo et al., 1992). Thus, while the vast majority of test article-related round cells in the epididymis of an animal treated with a testis-toxicant are exfoliated germ cells, be aware that in a peripubertal animal a test article-related increase in round cells can also be of epididymal epithelial origin as has been observed with administration of gossypol (de Andrade et al., 2006; Romualdo et al., 2002).

#### 4.2.12. Decreased Sperm, Lumen, Epididymis

Decreased sperm within the lumen of the epididymis can be qualitatively assessed during microscopic evaluation. Decreases in sperm content within the epididymis occur secondary to disruptions in spermatogenesis but can also be present as a feature of immaturity/peripuberty. It is important to consider the age, species, and location within the epididymis as relative levels of sperm content can differ normally. For example, sperm concentration is low in the head and proximal body of the dog epididymis and should not be mistaken for a test article-related effect (Creasy, 2012). With long standing decreases in luminal sperm, cribriform change can occur where the lumen of the epididymis can contract leading to numerous infoldings of the epithelium (Creasy et al., 2012).

#### 4.2.13. Single Cell Necrosis/Apoptosis, Epididymis

Single cell necrosis/apoptosis occurs within the epithelium of the epididymis due to decreased androgenic support and can be seen as an early response to decreased testosterone

levels, decreased conversion of testosterone to DHT, or AR antagonism (Chapin and Creasy, 2012; De Grava Kempinas and Klinefelter, 2014). Since epithelial apoptosis starts in the head of the epididymis and progresses distally in a wave-like fashion over time (Ezer and Robaire, 2002; Robaire and Fan, 1998), it is important to collect and evaluate all segments of the epididymis. With chronic androgen deprivation, the epididymal epithelium becomes atrophic and the apoptosis is no longer evident (De Grava Kempinas and Klinefelter, 2014).

#### **4.2.14. Vacuolation, Epithelium, Epididymis**

Epithelial vacuolation within the epididymis can be observed as an artifact, spontaneous change, or test article-related effect (Creasy, 2012; De Grava Kempinas and Klinefelter, 2014). It can be seen in specific segments of the epididymis and careful evaluation is critical to determine a difference from concurrent controls. Drugs that cause phospholipidosis can occasionally cause vacuolation in the epididymal epithelium (Rudmann et al., 2004).

#### **4.2.15. Sperm Granuloma, Epididymis**

Sperm granulomas can occur as an occasional spontaneous finding or as a result of xenobiotic exposure and can occur anywhere from the testis to the vas deferens. Epididymal sperm granulomas can occur due to local outflow obstruction, as seen with ligation of the vas deferens (Flickinger and Howards, 2002) or with any epithelial damage and/or breach of the barrier function (Kim et al., 2012). It is important to document the location within the male reproductive tract as sperm granulomas will occur in specific regions as either a function of the species anatomy or effect of the compound, and the location of the effect can give insight as to the underlying pathogenesis. For example, sperm granulomas present in the efferent ducts and head of the epididymis may be related to alterations in fluid resorption while those in the tail and vas deferens are often caused by decreased smooth muscle concentration. Sperm granulomas have been seen with 2-methylimidazole in the efferent ducts and head of the epididymis (Tani et al., 2005), with high doses of L-cysteine in the body and tail of the epididymis (Sawamoto et al., 2003), with methyl chloride in the tail (Chapin et al., 1984b), and with guanethidine at the

junction of the tail and vas deferens (Evans et al., 1972).

#### **4.2.16. Atrophy: Prostate or Seminal Vesicles**

This change is characterized by decreased secretion and reduced size of the epithelial lining of the prostatic acini or seminal vesicular epithelium. In sexually mature animals, this finding is pathognomonic of decreased androgen stimulation, which can be due to low testosterone, low conversion of testosterone to DHT, or interference with the AR in the affected tissue. As with Leydig cell atrophy, subtle changes can be difficult to recognize by qualitative morphologic evaluation. In rodents, organ weight is usually a much more sensitive endpoint (Creasy, 2008), but there can be considerable variability in non-rodents due to the large interanimal variability and small numbers of animals in each group (Dorso et al., 2008). The age/sexual maturity status of the animal should always be before diagnosing atrophy in the accessory sex glands as decreased size and secretory content are a feature of immaturity (Vidal et al., 2021). Atrophy of the accessory sex organs is a common age-related finding in rodents (Creasy, 2012).

#### **4.2.17. Inflammation and Metaplasia, Prostate or Seminal Vesicles**

Varying degrees of inflammatory cells, from minor infiltrates of interstitial lymphocytes to chronic inflammation, can be present within the prostate as a commonly observed spontaneous change (Creasy, 2012). Increased incidence and/or severity of inflammation in the prostate can occur as a xenobiotic-induced change and has been reported with estrogens and other compounds that increase serum prolactin (Robinette, 1988; Tangbanluekal and Robinette, 1993). Estrogens also cause squamous metaplasia of the epithelium and stromal proliferation within the prostate, seminal vesicles, and/or coagulating gland (Andersson and Tisell, 1982; Habenicht and el Etreby, 1988; Rhodes et al., 2000).

### **4.3. Morphologic Changes (Proliferative)**

The most commonly observed nonneoplastic or neoplastic proliferative lesions in the rodent testis are Leydig cell hyperplasia and Leydig

cell tumors, rete testis hyperplasia, and mesothelial tumors. Other testicular tumors (Sertoli tumors, seminomas, etc.) may occur, but they are seen only occasionally in nonrodent species used in toxicity studies, where the lifespan is normally restricted. Accepted nomenclature and diagnostic criteria are available for nonproliferative and proliferative lesions of the male reproductive tract in rodents (D Creasy et al., 2012), dogs (Woicke et al., 2021), minipigs (Skydsgaard et al., 2021), NHPs (Colman et al., 2021), and rabbits (Bradley et al., 2021). General references include the World Health Organization's *Histologic Classification of Tumors of the Genital System of Domestic Animals* (Kennedy et al., 1998), the chapter on tumors of the genital system in the textbook *Tumors of Domestic Animals* (Agnew and MacLachlan, 2016), and/or the current literature. There are very few proliferative lesions in the epididymis in all species. In the accessory sex glands, reactive hyperplasia of the prostatic epithelium or, less commonly, the seminal vesicle epithelium often accompanies inflammatory lesions associated with urogenital infections in rodents, but tumors in the accessory sex organs are uncommon except in some transgenic mouse strains.

### 4.3.1. Proliferative Lesions of the Testis

#### 4.3.1.1. LEYDIG CELL HYPERPLASIA AND TUMORS

Leydig (interstitial) cell hyperplasia can occur as a focal or diffuse lesion. Diffuse Leydig cell hyperplasia is generally a physiological response to hormone imbalance and may accompany severe atrophy of the seminiferous tubules as a compensatory response to decreased spermatogenesis (Cook et al., 1999). Diffuse hyperplasia (and tumors) can also be seen in response to estrogen or 5 $\alpha$ -reductase inhibitor administration in mice (Figure 9.30C) (Creasy et al., 2012) or in a chronic study of the GnRH-agonist buserelin in Wistar rats (Donaubauer et al., 1987). The Leydig cells are generally increased in size as well as number. Care must be taken when distinguishing real, diffuse hyperplasia from the impression of higher density of Leydig cell volume caused by shrinkage of atrophic tubules.

In rodents, focal Leydig cell hyperplasia and Leydig cell adenomas form a continuum of change, making it difficult to separate hyperplasia and adenoma (Figure 9.30A and B). In the absence of any significant morphological

differences in cellular appearance, a size that is equal to or greater than the diameter of three seminiferous tubules is generally used as the main but arbitrary classification criterion in rodents (Creasy et al., 2012). The spontaneous incidence of Leydig cell adenomas in rodents is species- and strain-specific and increases with age, but they are more common in the rat (up to 100% in aged F344 rats and generally 4%–7% in Sprague Dawley and Wistar rats) than in mice (Amador et al., 1985; Cook et al., 1999). In mice, the incidence is generally lower (B6C3F1 < 1%, CD-1 2%) (Cook et al., 1999). Leydig cell tumors have been reported in NHPs (Cline et al., 2012), rabbits (Reineking et al., 2019), and aged beagle dogs (James and Heywood, 1979), and while not reported in minipig breeds used in toxicology (Skydsgaard et al., 2021), they have been reported rarely in domestic swine.

Prolonged disruption of the pituitary–gonadal hormone axis in rodents is very likely to result in Leydig cell tumors (Cook et al., 1999). In the rat, focal or diffuse Leydig cell hyperplasia and Leydig cell tumors (Figure 9.30A and B) can be readily induced by a wide range of chemically diverse drugs and chemicals, including exogenous gonadotropins, dopamine agonists, antiandrogens, GnRH analogs, calcium channel antagonists, peroxisome proliferators, and histamine receptor antagonists (Alison et al., 1994). The proposed mechanism of action for these various classes of compounds is through interference with Leydig cell control mechanisms at a variety of points along the hypothalamic–pituitary–testicular axis (Alison et al., 1994). A major impetus for Leydig cell tumorigenesis in the rat is considered to be high circulating levels of LH (Steinbach et al., 2015). Interestingly, a significant number of Leydig cell tumorigens have no effect on circulating levels of LH but do alter intratesticular testosterone (and other hormones), thereby affecting the paracrine feedback control of Leydig cell proliferation, presumably through local growth factors (Cook et al., 1999).

In contrast, the chemical induction of Leydig cell tumors in the mouse is less common and is generally associated with high circulating levels of estrogen or administration of estrogenic compounds such as diethylstilbestrol (Figure 9.30C) (Cook et al., 1999). In general, the range of chemicals producing Leydig cell



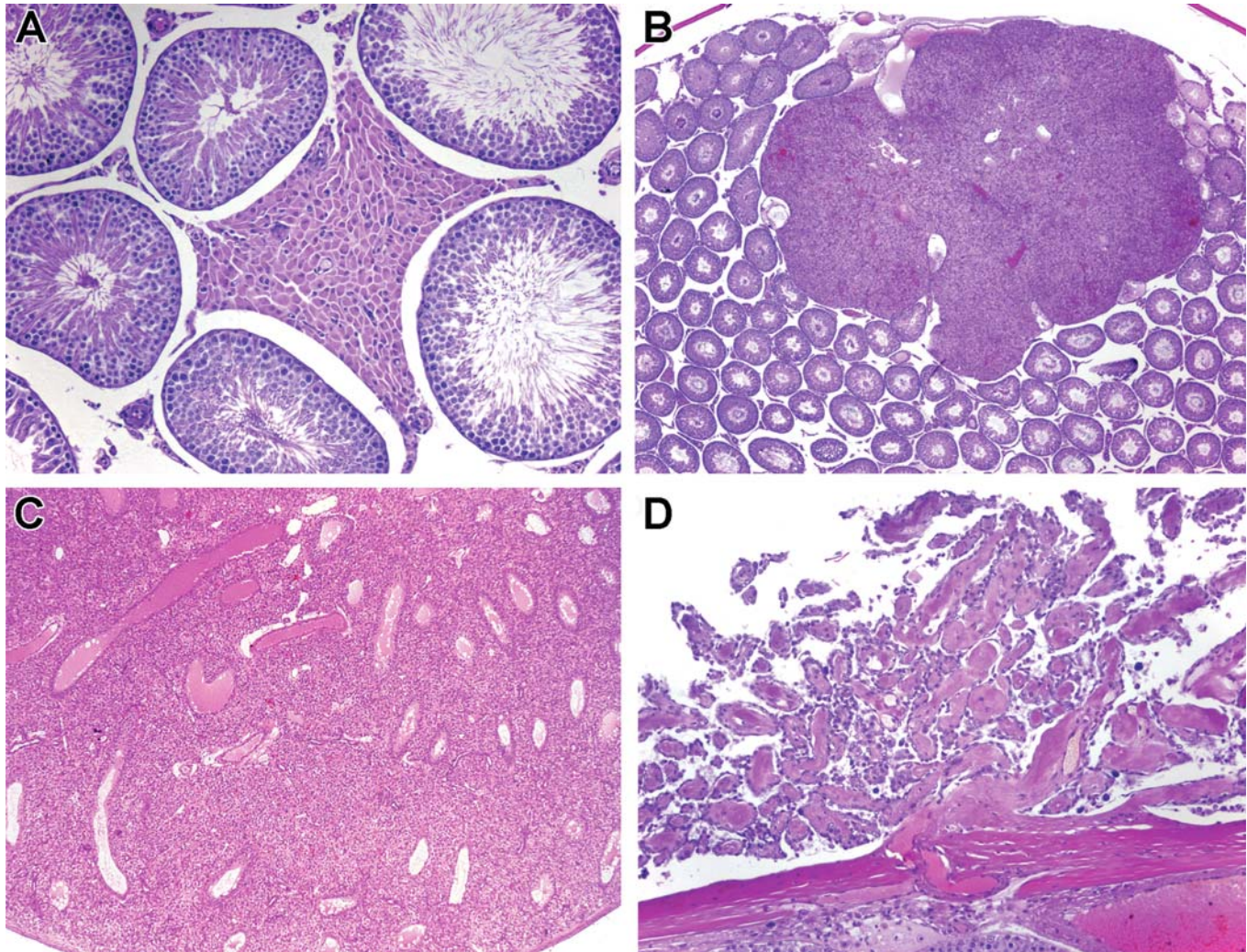


**FIGURE 9.30** (A, B) The continuum between Leydig cell hyperplasia and adenoma makes diagnosis difficult. Size is the most common criterion used. Aggregates of Leydig cells less than the diameter of three seminiferous tubules is recommended as a criterion for hyperplasia. (A) This aggregate is on the border of adenoma and hyperplasia. Rat, H&E,  $\times 10$ . (B) Leydig cell adenoma with growth between tubules. Rat, H&E,  $\times 2$ . (C) Diffuse Leydig cell hyperplasia in a mouse administered a selective estrogen receptor modulator (SERM). Estrogen causes Leydig cell hyperplasia in mice but not rats. Mouse, H&E,  $\times 4$ . (D) Mesothelioma of the tunica vaginalis, rat. The tumor often grows by extension to involve the epididymis. Rat, H&E,  $\times 10$ . *Reproduced from Haschek WM, Rousseaux CG, Wallig MA, editors: Haschek and Rousseaux's handbook of toxicologic pathology, ed 3, 2013, Academic Press, Figure 59.28, p. 2559, with permission.*

tumors in the rat is ineffective in mice. Furthermore, estrogen administration to the rat appears to be inhibitory to the development of spontaneous and chemically induced Leydig cell tumors, although in at least one case (ammonium perfluorooctanoate), the major detectable hormonal change leading to Leydig cell tumors is an increase in plasma estradiol levels (Biegel et al., 1995).

Aromatase inhibitors formestane and letrozole reduce plasma estradiol levels by inhibiting the conversion of testosterone to estrogen. In the dog, but not in rats, this results in Leydig cell hypertrophy and hyperplasia (Walker and Nogués, 1994). This is thought to be due to the differential sensitivity of the pituitary feedback mechanism to estrogens and androgens in the different species. The aromatization of



testosterone plays a significant role in the control of gonadotropins in dogs, NHPs, and man, whereas in rats, testosterone and DHT are the main regulatory molecules.

The testicular tumor profile and the physiology of Leydig cell tumorigenesis in rodents and humans appear to be very different, and it has therefore been argued that chemical induction of Leydig cell tumors in the rat is a species-specific effect and that nongenotoxic compounds that induce Leydig cell tumors in rats likely have low relevance to humans (Cook et al., 1999; Steinbach et al., 2015). Nevertheless, claims of species specificity need to be supported by careful investigations into the mechanism of hormonal disruption.

#### 4.3.1.2. MESOTHELIOMA: TUNICA VAGINALIS

Mesothelial tumors of the tunica vaginalis of the testis, the mesothelial layer that covers the tunica albuginea, occur most frequently in the Fischer 344 rat and are also occasionally seen in other rat strains (Figure 9.30D) (Creasy, 2012). They readily extend along the parietal mesothelial surface and can affect the epididymis and also other peritoneal mesothelial-lined surfaces. On the basis of their readiness to extend by local invasion, all are considered malignant. Their incidence has been increased by exposure to a number of chemicals, including acrylamide, bromochloroacetic acid, potassium bromate, o-nitrotoluene, and vinylidene chloride. Relationships between concurrent Leydig cell tumors and mesotheliomas of the tunica vaginalis in the rat have been proposed based on physical pressure or mechanical stress and subsequent release of growth factors, or based on age-related hormonal imbalances (Maronpot et al., 2009). As with Leydig cell tumors, chemical induction of mesothelioma of the tunica vaginalis is considered of uncertain relevance to man.

#### 4.3.1.3. RETE TESTIS HYPERPLASIA AND TUMORS

Proliferative lesions of the rete testis epithelium (hyperplasia, adenoma, and carcinoma) are seen as age-related findings in the mouse and, rarely, the rat (Figure 9.31) (Creasy, 2012). Rete testis hyperplasia can occasionally progress to adenoma (Figure 9.31B) or carcinoma. Rete testis proliferative lesions can also be induced in mice treated prenatally with diethylstilbestrol (Bullock et al., 1988) or in rats treated with

cadmium chloride (Rehm and Waalkes, 1988). Rete testis hyperplasia is uncommonly observed in the dog (Woicke et al., 2021).

#### 4.3.1.4. OTHER TUMORS OF THE TESTIS

Most other tumors of the testis are uncommon and rarely seen in laboratory animals; they will be mentioned only briefly here. Tumors arising from the germ cells (seminomas) are the most

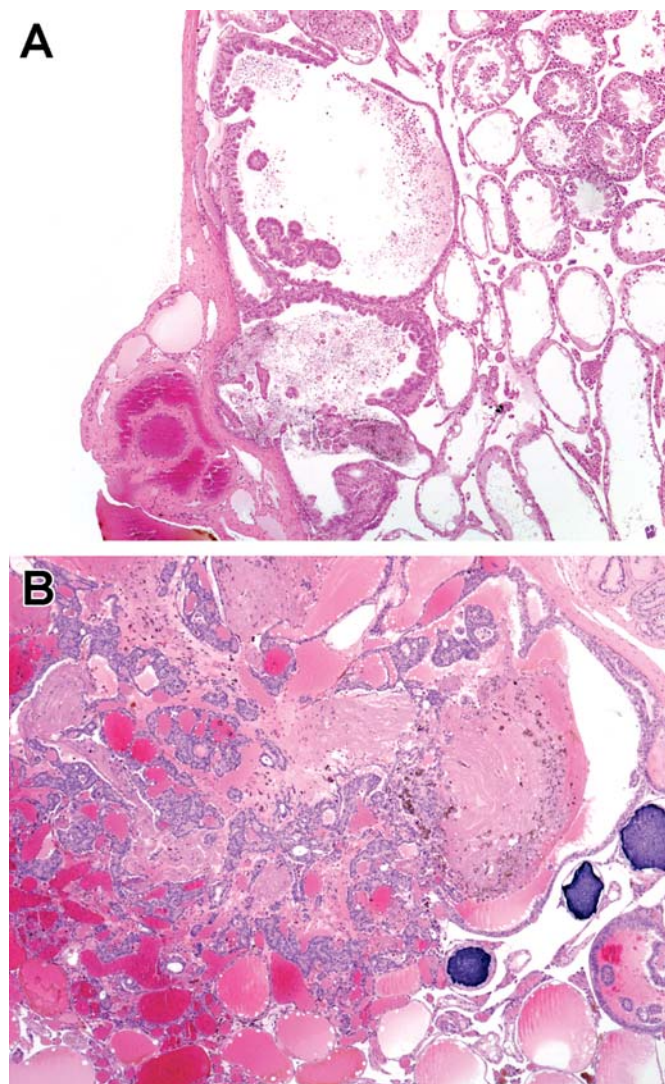


**FIGURE 9.31** (A) Rete testis hyperplasia, mouse. This is often seen in aging mice. Mouse, H&E,  $\times 4$ . (B) Rete testis adenoma, mouse. This is occasionally seen in aged mice. Note the dilation and atrophy of the remaining seminiferous tubules resulting from the obstructive tumor. Mouse, H&E,  $\times 4$ . Reproduced from Haschek WM, Rousseaux CG, Wallig MA, editors: *Haschek and Rousseaux's handbook of toxicologic pathology*, ed 3, 2013, Academic Press, Figure 59.29, p. 2560, with permission.

common type of tumor in man and are rarely seen in rodents but do occur in aging dogs. Sertoli cell tumors are more common than seminomas in laboratory species and can be seen occasionally in rodents as well as older dogs. Granulosa cell tumors, which arise from the gonadal stroma, have been seen rarely in male rats and occasionally in male mice (Mitsumori and Elwell, 1988). The neoplastic cell is reminiscent of ovarian granulosa cells and forms dense sheets of small basophilic cells, often replacing the entire testis. Tumors derived from embryonic tissue, such as teratoma, choriocarcinoma, and yolk sac carcinoma, are very rare and only occasionally reported in the literature (Creasy et al., 2012). In rabbits, testicular granular cell tumors, Leydig cell tumors, Sertoli cell tumors, and seminomas have been reported (Reineking et al., 2019).

#### **4.3.2. Proliferative Lesions of the Epididymis**

Proliferative lesions of the epididymis are almost nonexistent. Diffuse epididymal hyperplasia and hypertrophy were noted in NHPs administered recombinant human epidermal growth factor for 2 weeks (Reindel et al., 2001), but this is otherwise a very uncommon finding (Colman et al., 2021). Rather than epithelial proliferation, the epididymis more commonly exhibits cribriform change, where the epithelium folds in on itself and forms pseudoglandular structures lined by partially compressed epithelium (Goedken et al., 2008). Cribriform change is sometimes considered a hyperplastic lesion (De Grava Kempinas and Klinefelter, 2014), but it is generally associated with collapse and infolding of the ductal lumen. Cribriform change may be secondary to decreased ductal lumen fluid and/or sperm and has been associated with testicular toxicity in the rat and dog (Foley, 2001).

The only primary tumors that have been described in the epididymis are ectopic Leydig cell adenomas and histiocytic sarcomas; both occur in the mouse, but they are rare (Creasy et al., 2012). Since Leydig cells are not normally found in the epididymis, the occurrence of Leydig cell adenomas is unexplained and IHC is recommended to aid in definitive diagnosis, but there are a number of reports describing these tumors in mice (Creasy et al., 2012;

Mitsumori and Elwell, 1988; Mitsumori et al., 1989). The epididymis can also be a primary site for the development of histiocytic sarcoma in mice (Creasy et al., 2012).

#### **4.3.3. Proliferative Lesions of the Accessory Sex Organs**

In contrast to man, where hyperplasia and neoplasia of the prostate are extremely common, spontaneous neoplasia of the prostate in other species is rare. Reactive (reparative) hyperplasia of the prostatic epithelium commonly accompanies inflammatory lesions resulting from urogenital infections (Creasy et al., 2012). This is particularly common in mice, and generally located in the dorsolateral lobes of the prostate (Creasy et al., 2012). In more severe urogenital infections, the seminal vesicle epithelium may also respond. Hyperplasia of the accessory sex glands is not often seen as a response to inflammation in the dog or the NHP (Colman et al., 2021). Diffuse hyperplasia of the prostate or seminal vesicles unrelated to inflammation is uncommonly observed in the minipig (Skydsgaard et al., 2021). Prostatic hyperplasia is a common finding in mature beagle dogs and may be accompanied by dilated, cystic acini, but only in dogs older than those routinely included in toxicity studies (Lowseth et al., 1990).

Atypical (focal) hyperplasia in the absence of inflammation is most commonly seen in the ventral prostate of rats and mice, but can also be seen in the dorsolateral prostate, the coagulating gland, or seminal vesicle (Creasy et al., 2012). The diagnosis of atypical hyperplasia in the rodent prostate is mainly based on the occurrence of focal, multilayered normal epithelium in a few adjacent acini of otherwise normal glands without architectural disturbance. There appears to be a morphologic continuum between atypical hyperplasia and benign adenoma of the prostate (Creasy et al., 2012).

Adenomas and adenocarcinomas of the ventral prostate and seminal vesicles are occasionally seen as a background finding in rodents, more commonly in some of the transgenic mouse strains (Creasy et al., 2012). Dorsolateral prostatic adenomas appear to be rare as spontaneous lesions but have been chemically induced in rodents (Creasy et al., 2012). Experimental



models of prostate carcinogenesis have been developed in the rat using N-nitrosobis(2-hydroxypropyl)amine, N-methylnitrosourea (MNU), and 3,2'-dimethyl-4-aminobiphenyl (DMAB) (Bosland, 1992). Invasive carcinomas of prostate and seminal vesicles can be induced when these carcinogens are coadministered with high doses of testosterone (Bosland, 1992). Prostate carcinoma has also been induced by testosterone plus estradiol administration to a strain of rat (Noble rat) that has a genetic susceptibility to prostate cancer (Bosland, 1992). Transgenic mouse models such as Transgenic Adenocarcinoma of Mouse Prostate (TRAMP) have also been developed to study human prostate cancer.

In macaques, basal cell hyperplasia of the prostate is a common finding, and basal cell adenomas of the prostate have been reported, typically in older animals (Colman et al., 2021; McEntee et al., 1996). Basal cell hyperplasia is a focal lesion generally noted in the cranial lobe, likely represents a precursor lesion to adenoma, and it is considered similar morphologically to benign basal cell lesions in the human prostate (Colman et al., 2021). Also in macaques, there are individual case reports of prostate carcinoma (Hubbard et al., 1985), seminal vesicle adenoma (Kaspereit et al., 2007), and viral-associated squamous cell papillomas and carcinomas of the penis and/or prepuce (Harari et al., 2013; Ostrow et al., 1990).

#### 4.4. Recovery and Reversibility of Injury

Assessing the reversibility of effects on the male reproductive system after test article withdrawal is an important consideration in characterizing the hazard and understanding the potential risk posed to humans. Due to the kinetics of spermatogenesis, off-dose periods can often be longer than typically used for other organ systems and the potential for complete recovery is largely dependent on the site and the severity of the toxic insult. This puts additional importance on identifying the primary cell of toxicity and the pathogenesis of the lesion.

Following germ cell-specific damage or depletion (in the absence of significant Sertoli cell damage), the chances of regeneration of the entire germ cell population and recovery of functional spermatogenesis are good. Although many of the germ cell types are sensitive to

physical and chemical disturbances, the renewing stem cell spermatogonial population is relatively resistant. This has been well illustrated using varying doses of radiation (Clifton and Bremner, 1983; Meistrich et al., 1978; Oakberg, 1959). The order of cell sensitivity to increasing doses of radiation shows that although the generations of differentiating spermatogonia are very sensitive to radiation, primitive stem cell spermatogonia require a much larger dose to cause death.

Typical repeated dose toxicity studies employ recovery periods of 2–4 weeks, but when considering the total duration of spermatogenesis, this is an inadequate recovery period. In fact, it is common for the degree of germ cell depletion to appear more severe at the end of the recovery period than at the end of the dosing period. This can easily be misinterpreted as progression or irreversibility of the lesion, but is predictable due to the progression of maturation depletion through the later (and more numerous) round and elongating spermatid population (Vidal and Whitney, 2014). For example, if spermatogonia are the target cell in a 14-day study with a mitotic inhibitor, the only cells that will be missing at the end of the dosing period will be spermatogonia and early spermatocytes. This will be detectable but will be a relatively subtle lesion (Figures 9.19 and 9.20). If the animals complete a 4-week recovery period, the gap of missing cells will be spermatocytes and round spermatids as a result of “maturation depletion” caused by the loss of their precursor cells. Although spermatogonia and early spermatocytes may have recovered, the overall severity of the germ cell depletion will appear greater, and the weight and size of the testes will appear much less at the end of recovery than at the end of dosing. However, if the recovery period is extended to 8 weeks, full recovery will likely be evident, or, at least, significant evidence of recovery.

When choosing the duration of a recovery period, it is common to use at least one full duration of spermatogenesis for the species tested (Table 9.2) (FDA, 2018). This approach works well for minimal to mild testicular toxicity like maturation depletion of specific cell types described above. This is assuming that the compound and/or metabolites are rapidly cleared from the testis and circulation. Compounds with long half-lives or tissue

accumulation would require that the off-dose period be increased to account for the additional time for compound/metabolite clearance.

When severe testicular effects are present, one full duration of spermatogenesis is not typically sufficient for recovery and recommendations include extending the recovery to 2× the total duration of spermatogenesis (FDA, 2018). However, this may not be sufficient either. In humans, the total duration of spermatogenesis is 64 days, but following administration of various cancer chemotherapeutic agents or radiation, recovery from significant testicular toxicity is gradual and can take years (Clifton and Bremner, 1983; Meistrich, 2013; Roeser et al., 1978). Even with experimental hormonal contraceptive agents in men where treatment is meant to be easily reversible, recovery is often 4–5 months with full recovery in most all men by 1 year (Liu et al., 2006). Multiple variables can influence time to recovery, but it is important to note that stem cell spermatogonia are very slow to divide and the timing of division and replacement of new spermatogonia is not considered a part of the 64-day duration of spermatogenesis. With time, stem cell spermatogonia proliferate to a point where enough critical mass of spermatogonia is present to differentiate and spermatogenesis can begin. In addition, the kinetics of the compound and/or metabolite(s) need to be considered when planning for recovery length. Not all severe testicular toxicities will recover as some may have permanently damaged stem cell spermatogonia and/or Sertoli cells, but considerable time is required to determine this and lack of full reversibility in one to two total durations of spermatogenesis does not necessarily mean that a finding is irreversible.

When evaluating moderate to severe testicular effects in nonclinical species, this presents a problem as the length of recovery required to truly assess reversibility is often not logistically practical. In addition, rats have been shown to have an androgen-mediated block to stem cell spermatogonial proliferation (Meistrich and Shetty, 2003). In rats with xenobiotic- or radiation-induced tubular atrophy, hormonal agents, such as GnRH analogs or exogenous testosterone, have been used to suppress the HPG-axis and decrease intratesticular androgen production. Use of these agents has been shown to hasten recovery of effects that would have been otherwise considered irreversible (Abuelhija et al., 2012; Blanchard et al., 1998; Meistrich

et al., 1999, 2003; Shetty et al., 2000, 2002; Udagawa et al., 2006). It is unclear if blocks to spermatogonial proliferation exist in other species. Due to these issues, it is recommended to approach recovery times in nonclinical toxicity studies carefully as the choice of species, length of dosing, severity of the findings, endpoints measured, and kinetics of the compound all play a role in whether reversibility can be determined. Prior to attempting to assess reversibility in nonclinical species, it is often useful to first characterize the testicular effects by determining the cell types affected across a range of doses and/or timepoints. Once this information is determined, it can be used to select doses and a clinically relevant length of dosing that produce clear testicular effects, but not complete atrophy, to assess reversibility. This stepwise approach is preferred to placing a recovery period on the highest dose of the next planned study of longer duration. These longer studies can often produce more dramatic toxicity that would be harder to assess reversibility and may not be as clinically relevant.

While many of the challenges related to reversibility of toxic effects in the male reproductive system involve effects on spermatogenesis, additional effects may need evaluation and further characterization. Changes related to suppression of the HPG axis, which include species specific spermatogenic disruption and atrophy of the epididymis and accessory sex organs, are typically readily reversible with the reestablishment of normal hormone balance (Ramaswamy and Weinbauer, 2014). Effects on the epididymis that result in granulomatous inflammation and sperm granulomas are generally progressive and irreversible (La et al., 2012). In addition, the presence of persistent inflammation in close proximity to viable sperm may carry an additional risk of leukotriene-induced genotoxic damage to the sperm, as seen with methyl chloride (Chellman et al., 1986).

#### 4.5. Immaturity and Peripuberty as Confounding Factors for Identifying Toxicity

The onset of spermatogenesis marks the beginning of the peripubertal period (Vidal et al., 2021). The peripubertal period continues until spermatogenesis is complete (mature spermatids are formed) across the majority of seminiferous tubules, there is full sperm storage in the

tail of the epididymis, and accessory sex glands are fully developed (Vidal et al., 2021). Animals that are not fully sexually mature may show histologic features in the testis that can represent normal peripubertal findings but be confused with toxicant-induced lesions. It is critical that the study pathologist be aware of the age of the animals at necropsy and consider this as part of the weight of evidence in assessing the overall status of sexual maturity. If an animal is immature and at a stage where spermatogenesis has not started or has only barely started, then testicular toxicity, however severe, will go undetected. If spermatogenesis is progressing but the animal is peripubertal, then the testes will likely contain significant numbers of degenerating germ cells and have partially depleted seminiferous tubules which will be difficult to distinguish from a degenerative response to a testicular toxicant (Table 9.7). This presents a real risk of producing a false-positive result if a greater proportion of the peripubertal animals are in the high-dose group. For guidance on documentation of sexual maturity in nonclinical studies, the reader is referred to Vidal et al. (2021).

In rodents, sensitivity to detect lesions is high due to the relatively minimal interanimal

variability in timing of sexual maturation and microscopic appearance of testis and epididymis, as well as the relatively large group numbers in studies. However, in the dog, cynomolgus macaque, and minipig, there can be considerable variation between individual animals in timing of sexual development and microscopic appearance (Picut et al., 2018). This interanimal variation, coupled with small group numbers, warrants special consideration on the part of the pathologist in the microscopic assessment of the male reproductive tract in large species. A review of male reproductive tract development in the rat, NHP, minipig, dog, rabbit, and mouse can be found in Picut et al. (2018).

#### 4.5.1. Rodents

Rats are able to sire a litter from around 8 weeks of age, but the testis and epididymis do not appear morphologically “normal” and fully mature microscopically until around 10 weeks of age (Ojeda and Skinner, 2006). Rats aged 8–9 weeks often have low numbers of elongating spermatids in the testes with occasional evidence of degenerating cells. In addition, the epididymis contains increased numbers of degenerating germ cells and has

**TABLE 9.7** Distinguishing Immaturity from Testicular Toxicity in Nonrodents

Maturity status	Testicular degeneration/ multinucleate germ cells	Epididymal expansion	Epididymal sperm content	Epididymal germ cell debris
Immature; normal	None	Contracted	None	Infrequent
Peripubertal; normal	Few-frequent	Partial expansion	Few in head, limited in tail	Few-frequent
Mature; normal	Infrequent	Expanded	Distal body and tail full	Infrequent
Mature with testicular degeneration	Increased—frequent	Expanded, but may contract with severe reductions in sperm	Variable depending on the severity of the testicular change	Increased-frequent
Mature with hypospermatogenesis	Infrequent	Expanded	Usually normal but may be low in severe hypospermatogenesis	Infrequent

Modified from Haschek WM, Rousseaux CG, Wallig MA, editors: Haschek and Rousseaux's handbook of toxicologic pathology, ed 3, 2013, Academic Press, Table 59.12, p. 2568, with permission. From Vidal JD, Colman K, Bhaskaran M, et al.: Scientific and regulatory policy committee best practices: documentation of sexual maturity by microscopic evaluation in nonclinical safety studies, Toxicol. Pathol. 49:977–989, 2021.



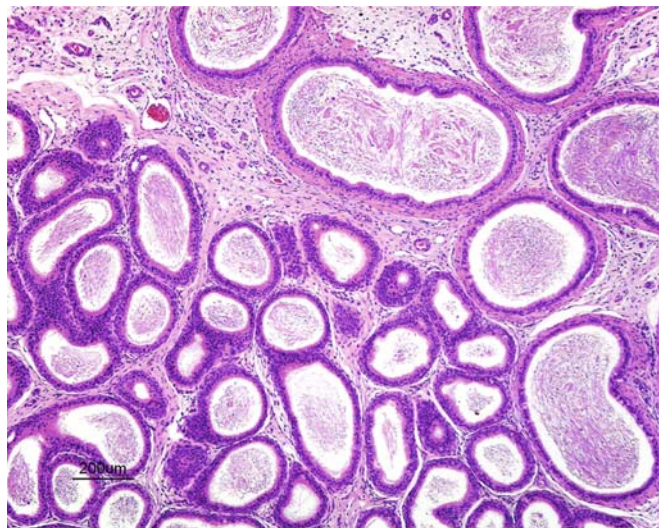


**FIGURE 9.32** Low sperm content in the epididymis of a 9-week-old rat. Peripubertal rats less than 10 weeks of age, commonly used in short-term studies, can have low numbers of sperm in the tail of the epididymis which can be mistaken as a test article-related change. Rat, H&E,  $\times 4$ . Reproduced from Haschek WM, Rousseaux CG, Wallig MA, editors: *Haschek and Rousseaux's handbook of toxicologic pathology*, ed 3, 2013, Academic Press, Figure 59.30, p. 2565, with permission.

relatively few sperm in the tail of the epididymis (Figure 9.32). Sloughed germ cells or debris in the epididymis can be seen in peripubertal rodents but are rare in the adult, so this can be a sensitive indicator of testicular toxicity in the adult. These features can be mistaken as evidence of testicular toxicity and reduced spermatogenesis if, by chance, there is a higher incidence in the high-dose group. A similar situation exists in 5- to 6-week-old mice. To overcome this problem, rats should be at least 10 weeks of age by the end of the study and mice should be at least 8 weeks old. In the event of early deaths, the assessment of peripubertal animals can be aided by the use of age-matched control animals (Catlin et al., 2018).

#### 4.5.2. Dogs

The use of immature and peripubertal dogs presents the most common cause of confusion to pathologists when evaluating testicular toxicity. Dogs may be 5–6 months of age at the start of a study, even though sexual maturity occurs at 7–12 months of age, but this can vary with animal source (Woicke et al., 2021). At 5–

6 months of age, spermatogonial proliferation and fluid secretion begins in the dog. This results in gradual lumen formation and progressive expansion of the tubules as secretion increases. In dogs of this age, it is common to see tubular (Sertoli cell) vacuoles accompanying the start of lumen formation (Creasy, 2012). These are likely fluid-filled vacuoles related to the initiation of fluid production by the Sertoli cell and should not be considered abnormal (Figure 9.33B and C). Dogs vary in the age they reach sexual maturity; at 7 months of age, one dog may have testes that appear fully mature with expanded epididymal ducts filled with sperm. Conversely, 75% of male dogs 6–7 months old may have testes with spontaneous focal degeneration and/or atrophy, partially depleted seminiferous tubules and frequent degenerating (swollen or multinucleated) germ cells and epididymides that have contracted ducts containing large numbers of sloughed degenerate germ cells and no sperm (Figures 9.33 and 9.34) (Creasy, 2012; Goedken et al., 2008; Kawakami et al., 1991).

Most dogs have normal appearing testes with significant sperm content in the tail of the epididymis by 10–11 months of age (Taha et al., 1981). With this degree of variability, small group sizes, and the fact that maturing and peripubertal testes are indistinguishable from testes undergoing toxicant induced degeneration, there is a risk that immaturity/peripuberty will mask a toxicant-induced lesion or that it will be mistaken for testicular toxicity. At the very least, it will add an additional layer of complexity to the evaluation of a tissue that is already difficult to evaluate.

The variation in age of maturation is reflected by dramatic differences in testicular weight and testicular size from animals that are the same age and same body weight. Prostatic development cannot be used as an indicator of sexual maturity in the dog because this tissue often develops at a different rate from the testis (Creasy, 2012), presumably due to differential development/expression of ARs between the two organs. It should also be borne in mind that size of dog and age of sexual maturation vary with the source (supplier) of the dogs.

The best way to avoid confusion and avoid the possibility of missing an important toxicant-induced lesion is to use dogs that are adults by

the end, or preferably, at the start of the study (*at least* 10 months of age, but ideally 11–12 months of age). For a juvenile study in the dog, dosing should be continued until the dogs are at least 10 months of age to avoid misinterpretation of changes in the developing testis.

If faced with having to evaluate dogs that are less than 10 months of age and the testes are showing varying degrees of degenerating germ cells and depleted seminiferous tubules, the pathologist needs to identify whether the testes were mature and are now undergoing degeneration or whether the testes are showing normal degenerative changes associated with the first wave of spermatogenesis. The best way is to examine the epididymis for sperm content and expansion of the distal epididymal duct (see [Table 9.7](#)). If sperm are not present in the distal body or tail of the epididymis and the ducts profiles appear contracted and contain degenerating germ cells, it is likely that the animal is still peripubertal and is not producing sufficient fluid or sperm to fill the epididymal ducts. If sperm are present in the distal body and tail of the epididymis, it indicates that spermatogenesis has been functioning to produce sperm within the last 2–4 weeks (based on the transit time for sperm and the fact that sperm is stored in the tail of the epididymis) ([Creasy, 2012](#); [Halpern et al., 2016](#)). If this epididymal appearance is seen with significant testicular germ cell depletion and degeneration, the possibility of testicular toxicity should be considered, especially if there are also significant numbers of sloughed germ cells in the epididymis. Depending on the animal age, length of dosing, and considering a weight of evidence approach, if sperm are not present in the epididymis, but the caudal duct profiles are expanded and contain degenerating germ cells, and this is combined with a testis that shows germ cell degeneration and depletion, it is possible that testicular toxicity has been progressing for some time and that any sperm present at the beginning of the study have already left the epididymis and not been replaced. The evaluation is not easy, which is why immature or peripubertal animals should not be used to assess testicular toxicity. If any doubt exists, the study should be repeated in older animals. For more

information on findings and sexual maturation in the male dog, see [Woicke et al. \(2021\)](#).

#### 4.5.3. Nonhuman Primates

The majority of studies undertaken in NHPs utilize animals that are immature or are a mixture of immature, peripubertal, and/or mature. As with dogs, the animals mature over a relatively wide age range. There are numerous references regarding the age and body weight of male NHPs in relation to attainment of sexual maturity, and most put the minimum age at around 4.5–5 years and a body weight of approximately 5 kg ([Haruyama et al., 2012](#); [Ku et al., 2010](#); [Mirsky et al., 2016](#); [Smedley et al., 2002](#)). [Smedley et al. \(2002\)](#) showed that NHPs need to be a minimum of 5 years 5 months and weigh 5.3 kg for a 90% probability of sexual maturity. Animals that were 3.7–4.3 kg in body weight only had a 20.5%–50.8% probability of being sexually mature. In studies where sexually mature NHPs are needed, minimal criteria can be based on age and body weight, but these are not reliable criteria of sexual maturity ([Vidal et al., 2021](#)). Male cynomolgus macaques 5 years of age or 5 kg or greater can still range in maturation status from peripubertal to mature ([Haruyama et al., 2012](#)). Additional measurements and endpoints, such as sperm evaluation and testicular volume, are generally needed to gain a high degree of confidence that the animals are sexually mature ([Dreef et al., 2007](#)). Criteria of sexual maturity may include bodyweight >5.0 kg, age >4–5 years, testicular volume >10 mL (cross-section diameter ~2.2 cm), and proof of sperm in the ejaculate ([Dreef et al., 2007](#)). Serum testosterone >15–20 nmol/L has been suggested ([Dreef et al., 2007](#)); however, pronounced diurnal variations in hormones generally preclude their usefulness in the assessment of sexual maturity ([Steiner et al., 1980](#)). Proof of sperm in the ejaculate appears to be a more robust metric for sexual maturity than body weight and age, and it is important to consider that age of sexual maturity for NHPs may differ depending on origin (Mauritius vs. mainland Asia) ([Luetjens and Weinbauer, 2012](#)). It should be borne in mind that studies conducted with immature or mixed maturity status animals greatly hinders the detection of testicular toxicants.



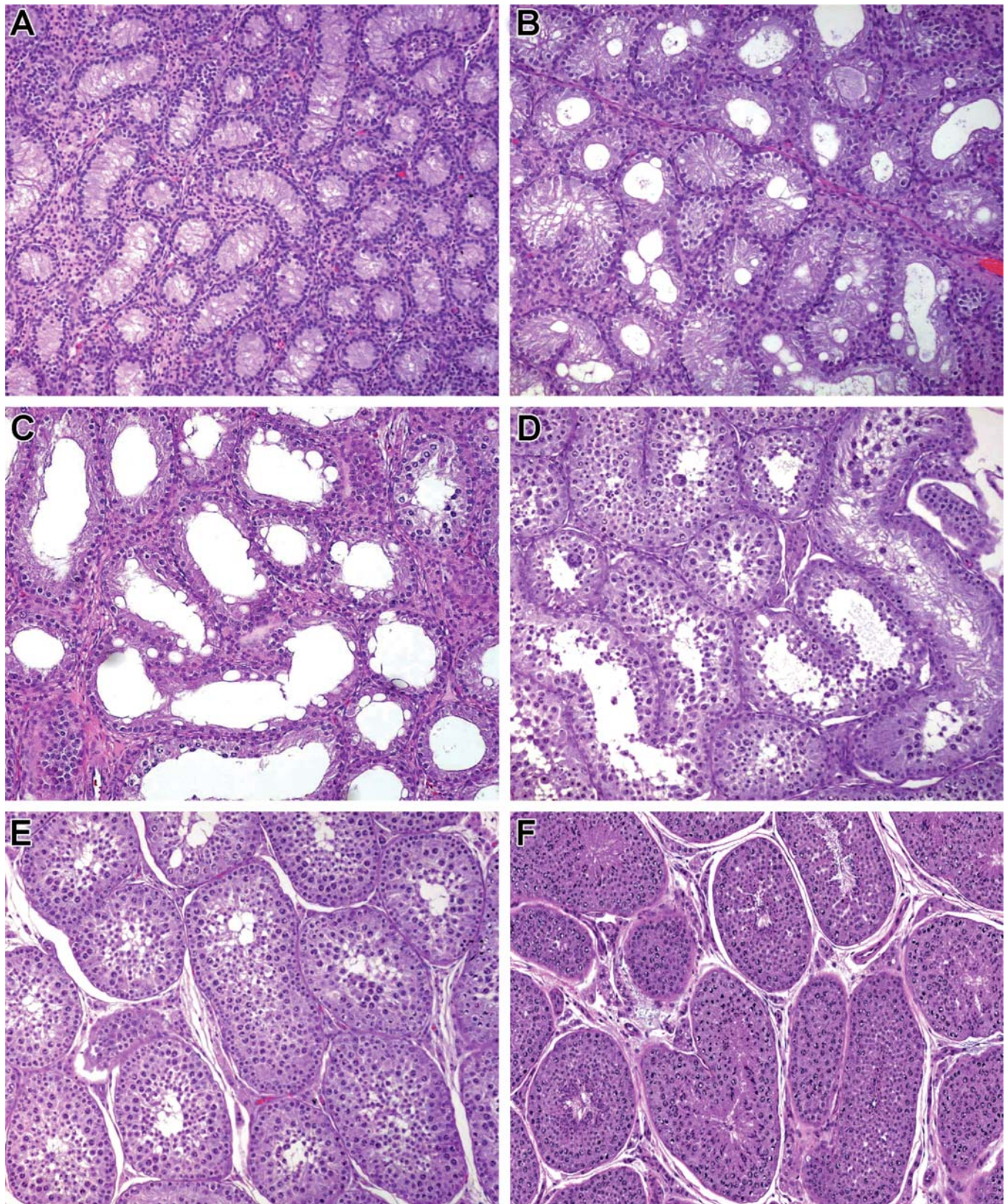


**FIGURE 9.33** (A) Immature testis from a 5- to 6-month-old dog. Tubules are contracted with no lumen and lined by Sertoli cells and spermatogonia. Dog, H&E,  $\times 10$ . (B) Immature testis from a 5- to 6-month-old dog that has just started fluid secretion. Fluid filled vacuoles are present in the epithelium and a lumen is beginning to develop. Dog,



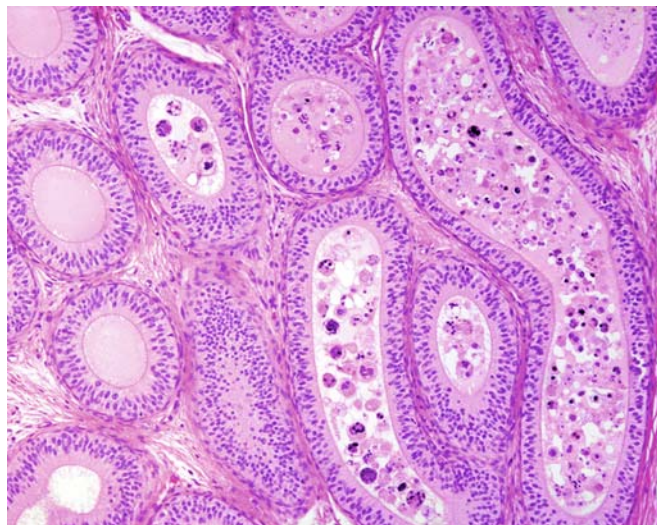


**FIGURE 9.34** Epididymis from a 6- to 7-month-old dog with intraluminal cell debris/sloughed germ cells but no sperm. Dog, H&E,  $\times 10$ . Reproduced from Haschek WM, Rousseaux CG, Wallig MA, editors: *Haschek and Rousseaux's handbook of toxicologic pathology*, ed 3, 2013, Academic Press, Figure 59.32, p. 2567, with permission.

#### 4.5.4. Minipigs

Use of the Göttingen minipig as a preclinical species is becoming more common. Mature sexual behavior is reported to commence at 3–4 months of age in Göttingen boars. Based on histology and morphometry, testicular and epididymal sexual maturity is reported at 4.5 months in minipigs, but accessory sex gland weights (prostate and bulbourethral gland) continue to increase until 6 months of age (Kangawa et al., 2016b). In general, 5–6 months of age may be considered fully sexually mature for minipigs and the use of animals this age at the start of a study will best enable the detection of toxicity (Creasy, 2012; Skydsgaard et al., 2021). Seminiferous tubules demonstrate varying stages of development in peripubertal animals, with some tubules containing sloughed germ

cells or multinucleated cells (Skydsgaard et al., 2021). Additional growth and development of the prominent Leydig cell population in pigs continues through puberty (Franca et al., 2005; Franca et al., 2000) and as a result there can be considerable variability in the number and size of the Leydig cells in peripubertal/young adult minipigs. The epididymis of peripubertal animals may contain small amounts of sperm along with germ cell debris and round giant cells (Skydsgaard et al., 2021). The regularity and efficiency of spermatogenesis will continue increasing with age, and there may be variability in pigs that have recently attained maturity at a given age.

### 4.6. Background Pathology as a Confounding Factor for Identifying Reproductive Toxicity

In addition to immaturity, background pathology can cause significant problems for detecting toxicity. This is rarely a problem when examining rodents, because they have relatively few background lesions and group sizes are large enough to be able to distinguish between test article-related changes and background changes. In all species, and especially nonrodents, a knowledge of the expected range of background microscopic changes is essential so that toxicant-induced changes can be distinguished from incidental background findings. A review of background lesions in the rat, mouse, dog, NHP, and minipig can be found in Creasy (2012).

#### 4.6.1. Rodents

Spermatogenesis is very efficient and consistently normal between animals. Even though there may be an occasional animal that shows degenerative testicular changes, the incidence is low and the group sizes large enough that

H&E,  $\times 10$ . (C) Immature testis from a 6- to 7-month-old dog. The lumen has started to expand and spermatogonial proliferation is beginning with occasional spermatocytes formed. Dog, H&E,  $\times 10$ . (D) Immature testis from a 7- to 8-month-old dog. Spermatogenesis is proceeding at different rates in different tubules, and there are numerous apoptotic and multinucleate germ cells in this first wave of spermatogenesis. Dog, H&E,  $\times 10$ . (E) Immature testis from a 7- to 9-month-old dog. Spermatogenesis has proceeded to produce round spermatids, but there are no elongating spermatids. Dog, H&E,  $\times 10$ . (F) Mature testis from 10- to 12-month-old dog. The tubules are fully expanded with all germ cell types present and a full complement of mature spermatids. Dog, H&E,  $\times 10$ . Reproduced from Haschek WM, Rousseaux CG, Wallig MA, editors: *Haschek and Rousseaux's handbook of toxicologic pathology*, ed 3, 2013, Academic Press, Figure 59.31, p. 2566, with permission.

distinguishing them from test article-induced changes is generally not a problem. A low incidence of unilateral or bilateral severe, diffuse tubular degeneration/atrophy is occasionally seen as a background finding in young adult rats and mice (Creasy, 2012; Li et al., 2014; Xie et al., 2014). When unilateral, the finding is likely associated with obstruction of the efferent ducts. Although the incidence of background findings in rodent testes is generally low, background changes in rat testes include occasional (up to 5) contracted, atrophic tubular profiles containing only Sertoli cells (not to be mistaken for tubuli recti adjacent to the rete testis or in a lateral subcapsular position), occasional tubular vacuoles, occasional degenerating (with eosinophilic cytoplasm or forming multinucleated cells) germ cells, occasional tubular dilation that may be associated with a dilated rete, and very low numbers of tubules with a very low number ( $\leq 3$ ) of retained spermatids (Creasy, 2008, 2012). In the mouse, occasional large, dense residual bodies can be seen in control animals at the luminal surface in postrelease (stage VIII-IX) tubules. They are large, may be increased in number, and can be seen at the luminal surface in other stages of the spermatogenic cycle (Creasy, 2012).

#### 4.6.2. Dogs

Background pathology in dogs presents much more of a problem than in rodents. Spermatogenesis in the beagle dog is relatively inefficient compared to the rodent or NHP, and it is very common to see tubules with partial depletion of one or more generations of germ cells (hypospermatogenesis) or focal areas, often with a lobular or wedge-shaped distribution, of undeveloped tubules (tubular hypoplasia) (Woicke et al., 2021). Hypospermatogenesis and tubular hypoplasia both have an approximate incidence of 30% in normal dogs (Creasy, 2012). Almost all dogs will have a few tubules with the degenerative changes of scattered multinucleated giant cells (representing degenerating spermatocytes or spermatids) and swollen spermatocytes (large cells considered to be germ cells arrested during meiosis) (Figure 9.35) (Woicke et al., 2021). The incidence and severity of these lesions seem to vary with the cohort of dogs, suggesting a possible genetic component, but the high incidence of the findings combined with small

group sizes make these changes problematic for distinguishing them from testicular toxicity (Goedken et al., 2008; Rehm, 2000).

The typical characteristics of hypospermatogenesis in the dog are the absence of one or more generations of germ cells (e.g., pachytene spermatocytes and round spermatids) combined with the presence of earlier (spermatogonia) and later (elongating spermatids) germ cells in the tubule. Characteristically, there are very few actively degenerating germ cells associated with this lesion, and the pattern suggests failure of spermatogonial division over two to three cycles in this part of the tubule (Creasy, 2012). Hypospermatogenesis can be distinguished from immaturity in that mature testes will have many tubules with a layer of elongated spermatids overlying missing or partially depleted layers of round spermatids and/or pachytene spermatocytes (Creasy, 2012). When distinguishing this background finding from toxicity, hypospermatogenesis can appear similar to “maturation depletion” as seen with spermatogonial toxicants, but the background finding is present in tubules in a segmental, patchy distribution rather than the more widespread, diffuse manner and more uniform population of cells seen with toxicity (Woicke et al., 2021). A cautionary note is that hypospermatogenesis can also be caused or exacerbated by test article-exposure (likely a low or intermittent level of germ cell depletion); thus, if the incidence and/or severity of this common background finding appears to be dose-related, a relationship to treatment should be considered. The difference between immaturity, hypospermatogenesis, and tubular degeneration/atrophy is subtle, but it is extremely important for the interpretation of a study and for distinguishing test article-related testicular toxicity from either background degenerative changes or peripubertal degenerative changes. Table 9.7 lists the main features and a recommended approach for addressing this issue.

Another finding common in dogs is tubular hypoplasia. The characteristics of this lesion are contracted tubules lined only by Sertoli cells. This is different from atrophic tubules, which are usually lined by Sertoli cells with vacuolated cytoplasm and evidence of residual germ cells or debris. Hypoplastic tubules generally form



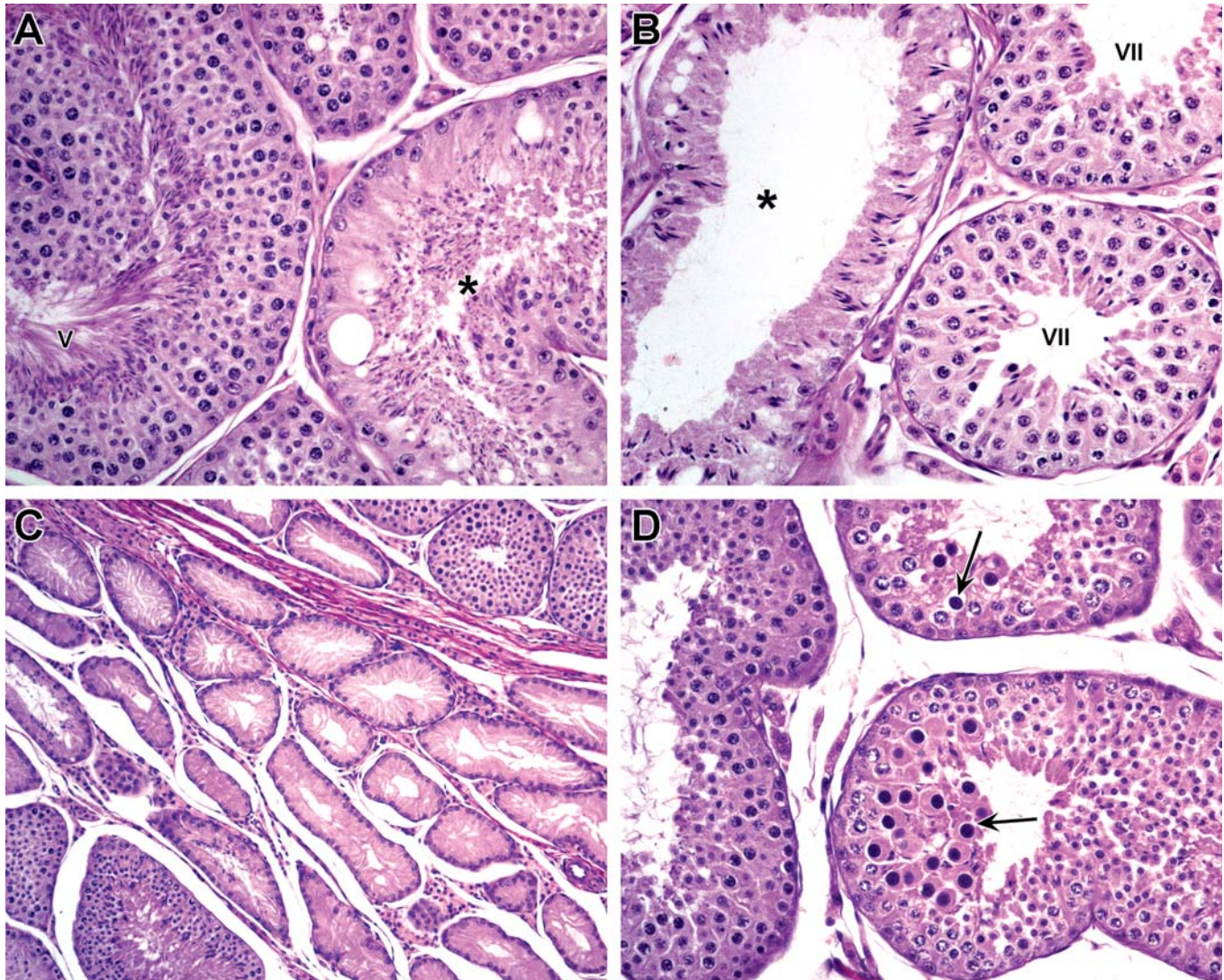


**FIGURE 9.35** (A, B) Segmental hypospermatogenesis in dog testes is characterized by the partial depletion of one or more layers of germ cells with no accompanying germ cell degeneration. (A) The depleted tubule (\*) is in the same stage as the adjacent tubule (stage V). Although it still has its normal luminal layer of elongating spermatids, it is missing the underlying round spermatids, pachytene spermatocytes, and preleptotene spermatocytes. (B) The depleted tubule (\*) is in the same stage as the adjacent tubule (stage VII). It has its normal layer of luminal elongating spermatids but is missing the underlying layers of pachytene spermatocytes and zygotene spermatocytes. Dog, H&E,  $\times 20$ . (C) Segmental tubular hypoplasia in the dog testis. This is a common background finding in dog testes, and typically forms a wedge shape of contracted tubules lined only by Sertoli cells and surrounded by otherwise normal tubules. The affected tubules appear to have never supported spermatogenesis, thus the term tubular hypoplasia. Dog, H&E,  $\times 10$ . (D) Swollen spermatocytes (arrows) are a common background finding in dog testes. They are generally larger in size and have densely staining nuclei with a tightly packed chromatin pattern. They appear to be secondary spermatocytes that did not complete their second meiotic division during stage VIII but survived into later stages. Dog, H&E,  $\times 20$ . *Reproduced from Haschek WM, Rousseaux CG, Wallig MA, editors: Haschek and Rousseaux's handbook of toxicologic pathology, ed 3, 2013, Academic Press, Figure 59.33, p. 2570, with permission.*



a focal or segmental, wedge-shaped area that is often subcapsular. The segmental/lobular distribution of tubular hypoplasia suggest that the affected tubular profiles may belong to a single, coiled seminiferous tubule that was never populated with germ cells (Creasy, 2012).

Distinguishing testicular toxicity from background pathology and immaturity is difficult, and ultimately comes down to a weight-of-evidence approach. This is where having multiple measures of the same thing can be most helpful (organ weights, sperm measures, histology). Since hypospermatogenesis can be exacerbated by chemical exposure, an important part of that evidence is the background incidence and severity of hypospermatogenesis in the laboratory conducting the study. This calls for consistent grading and recording of the main background changes so that the historical control database is an accurate reflection of these changes.

#### 4.6.3. Nonhuman Primates

Relatively few studies employ mature NHPs, so pathologists often have limited experience reviewing sexually mature NHPs. Common microscopic background findings in NHPs (Figure 9.36) include increased hypospermatogenesis and tubular dilatation in the testes, decreased sperm and cellular debris in the epididymis, inflammatory cell infiltrates in the epididymis and prostate, and corpora amylacea in the seminal vesicles (Colman et al., 2021; Vidal et al., 2022). Hypospermatogenesis, attributed to transient failure of spermatogenesis in a segment of a tubular profile, is seen as the absence of one or more generations (spermatocytes, round spermatids, and/or elongate spermatids) of germ cells. It affects scattered tubular profiles, and has no stage or cell specificity, and is not accompanied by germ cell debris in the epididymis (Colman et al., 2021; Vidal et al., 2022). A diffuse pattern of hypospermatogenesis can be observed in peripubertal to early adult animals and likely reflects a lack of full maturity (Vidal et al., 2022). Focal tubular dilatation with thinning of the seminiferous epithelium is quite commonly seen. The dilatation arises from outflow obstruction at the level of the rete testis and may be observed with or without increased stromal collagen (Pereira Bacares et al., 2017; Vidal et al., 2022).

#### 4.6.4. Minipigs

Tubular hypoplasia/atrophy is a very common background change in adult minipig testes (Figure 9.37C). Reports of incidence vary from approximately 24% to >70% of untreated pigs (Helke et al., 2016; Thuilliez et al., 2014). The features can vary from decreased numbers of spermatocytes and/or spermatids (hypospermatogenesis, not diagnosed separately) to a complete absence of germ cells, with contracted tubular profiles lined only by Sertoli cells (Skydsgaard et al., 2021). Tubular hypoplasia/atrophy also may be seen as vacuolation, decreased numbers of spermatogonia, and/or increased numbers of multinucleated or rounded germ cells in the lumen (Skydsgaard et al., 2021). Thus, in minipigs, these background degenerative-appearing tubules, tubules with hypospermatogenesis, and atrophic-appearing tubules are lumped diagnostically under the term “tubular hypoplasia/atrophy” (Skydsgaard et al., 2021). In most cases (approximately 60% of affected animals), the number of tubules affected is small (minimal severity) and the affected tubules are scattered throughout the testis, but in some cases, a large proportion or the majority of tubules are affected and they may be clumped multifocally. Tubular hypoplasia/atrophy in the testis may be accompanied by decreased sperm, or, if severe, an absence of sperm, and increased multinucleated germ cells and debris in the epididymis (Creasy, 2012). The change is generally bilateral, and the tubular contracture often makes the Leydig cells more prominent, which can be confused with an increase in the number of Leydig cells surrounding the affected tubules. If the incidence or severity appears to show a dose relationship, it makes it very difficult to distinguish this common developmental background finding of hypoplasia/atrophy from a test article-related effect. Since this background finding of tubular hypoplasia/atrophy can resemble toxicant-induced tubular degeneration/atrophy, a useful criterion is that toxicity may be associated with a significant number of apoptotic germ cells, depending on the length of dosing. Active germ cell death (apoptosis) is often a good indicator of ongoing toxicity and is less commonly associated with a longstanding background lesion.



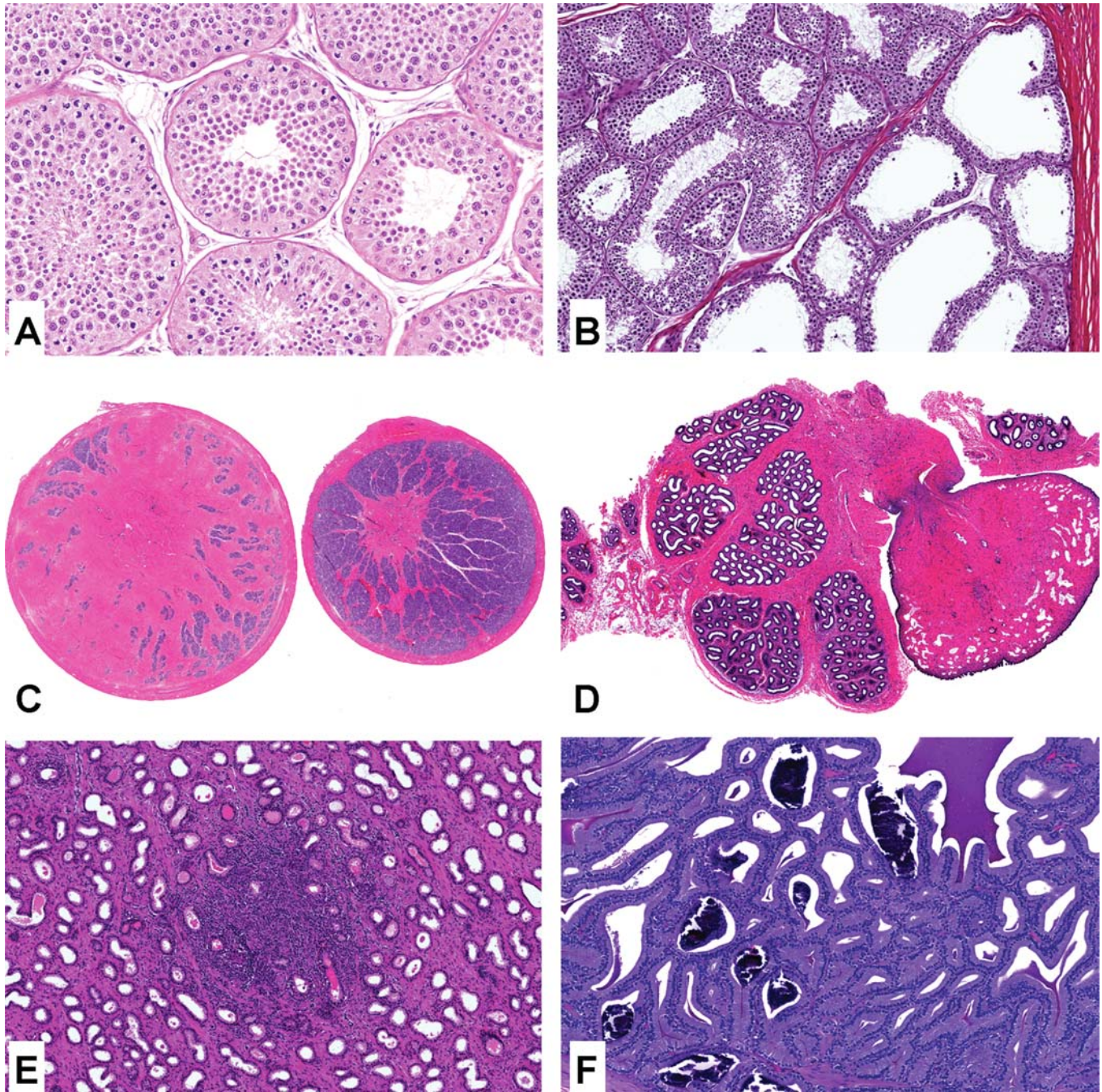


**FIGURE 9.36** Common spontaneous findings in nonhuman primates (NHP). (A) Hypospermatogenesis consists of random loss of various germ cell types. The tubule in the center has decreased numbers of pachytene spermatocytes while the tubule to the right has decreased numbers of round spermatids. NHP, H&E,  $\times 20$ . (B) Segmental dilatation of seminiferous tubules is commonly observed in NHPs. There is often compressive atrophy of the seminiferous epithelium with varying amounts of sperm stasis and/or surrounding inflammation. NHP, H&E,  $\times 20$ . (C) Right and left testes from an immature NHP with increased stromal collagen. NHP, H&E,  $\times 0.9$ . (D) Embryologic remnant attached via a pedunculated stalk to the epididymis. NHP, H&E,  $\times 1.7$ . (E) Prostate with a focal area of mononuclear cell infiltration. NHP, H&E,  $\times 5.0$ . (F) In mature NHPs, the seminal vesicles often have numerous corpora amylacea. NHP, H&E,  $\times 15$ .



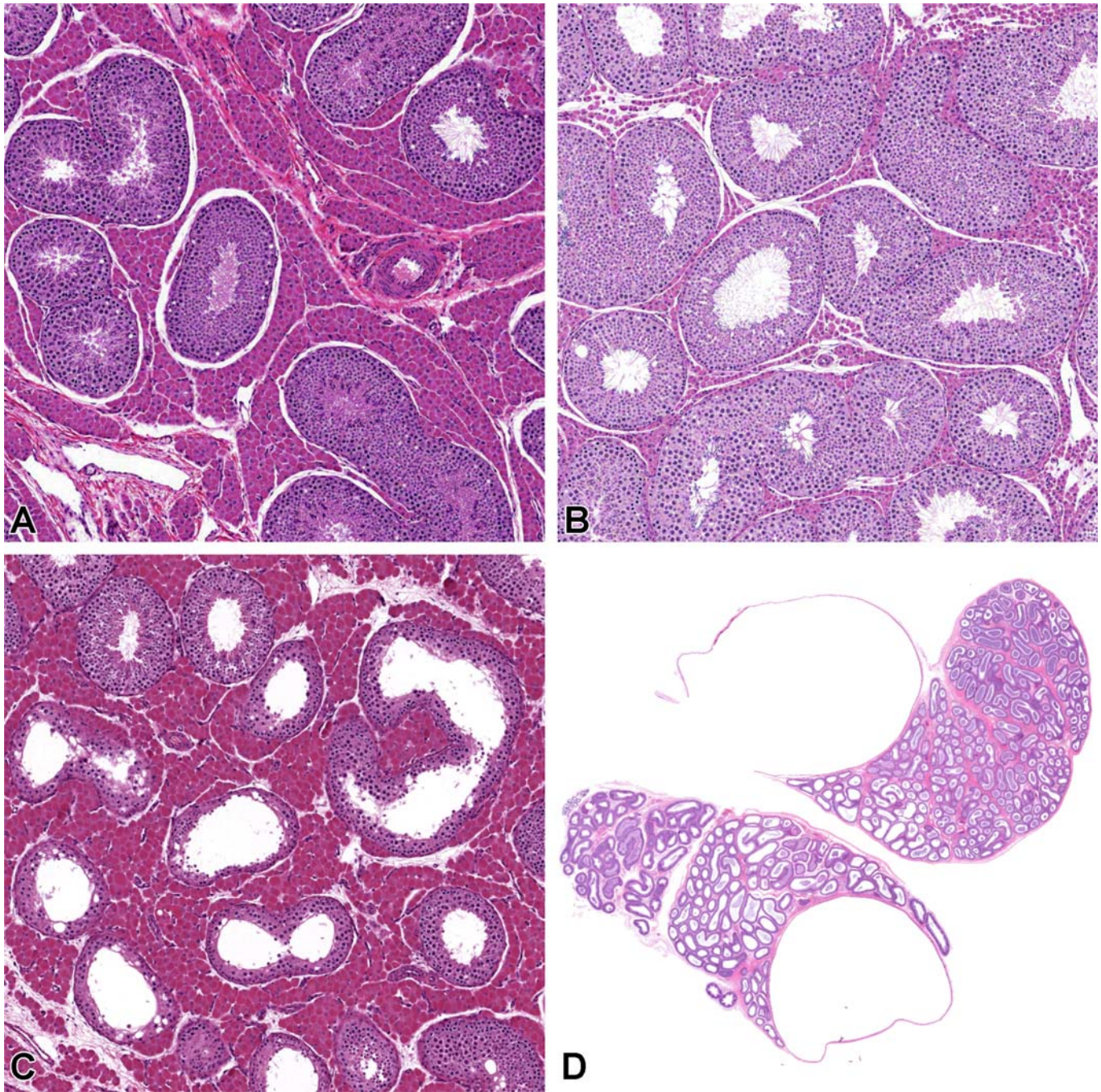


**FIGURE 9.37** Spontaneous findings are often present in the male reproductive system of minipigs. (A) Normal sexually mature minipig with active spermatogenesis and abundant Leydig cells. Minipig, H&E,  $\times 10$ . (B) Late peripubertal control minipig with active spermatogenesis, but less prominent, incompletely developed Leydig cells. Minipig, H&E,  $\times 10$ . (C) Sexually mature minipig with tubular hypoplasia/atrophy. This spontaneous change can be present at a high incidence and/or severity and can complicate the microscopic assessment of the testis due to the similarities with testicular toxicity. Minipig, H&E,  $\times 10$ . (D) Bilateral cysts in the head of the epididymis. These common embryologic remnants can be unilateral or bilateral and are often observed at necropsy. Minipig, H&E,  $\times 0.5$ .



One final consideration when evaluating pig testes is the wide variation in the density and size of the Leydig cell population between individual animals and depending on sexual maturation status (Figure 9.37A and B). Since many short-term studies in minipigs use animals that are generally examined at an age where they are undergoing sexual maturity or have only just attained sexual maturity, there may be considerable background variation between individuals in histology of the reproductive tract, including the size of the Leydig cell compartment and the efficiency of spermatogenesis. Thus, any determination of toxicity should be carefully considered, and differences should not necessarily be interpreted as test article-related findings. In addition, embryonic remnants are commonly observed as cysts in the head of the epididymis (Figure 9.37D).

#### 4.7. Stress and Body Weight Loss as a Confounding Factor for Identifying Reproductive Toxicity

Reproductive success is tied to food availability, adequate metabolic reserves, and suitable environmental conditions. In general, activation of the hypothalamic–pituitary–adrenal axis by stress results in suppression of the hypothalamic–pituitary–gonadal axis. Many of the neurotransmitters involved in energy homeostasis, such as leptin, ghrelin, cholecystokinin, and vasoactive intestinal peptide, as well as mediators of the stress response, such as corticotropin-releasing hormone, arginine-vasopressin, glucocorticoids, and  $\beta$  endorphins, are also major regulators of the GnRH neurons in the hypothalamus, and these will decrease reproductive capability in times of low food availability and/or stress (Everds et al., 2013). In nonclinical studies, decreased food intake, decreased body weight, and nonspecific stress are common consequences of dosing animals near the maximum tolerated dose, and therefore effects on reproductive parameters are relatively common.

GnRH suppression will result in reduced testosterone secretion from the Leydig cells and reduced plasma testosterone levels, and this largely dictates any morphological changes seen in the reproductive tissues. In rodents, the

most sensitive endpoint is a decrease in the weight of the accessory sex organs (prostate and seminal vesicles) (Chapin and Creasy, 2012). Epididymal weight may also be decreased, but testis weight is generally unaffected except in mice (Chapin et al., 1993a, 1993b). There are generally no detectable histopathological changes in any of the tissues. Exceptions include minimal tubular degeneration in the testes of mice and focal to multifocal tubular degeneration in the testes of rats subjected to repeated immobilization in restraint tubes.

Dogs and NHPs are generally less susceptible to the effects of stress and body weight decrease, and few changes are seen. In dogs, prostate weights may be decreased with severe stress or body weight loss, but the interanimal variability in prostate weights is high, making detection difficult (Chapin and Creasy, 2012). Dogs generally have no microscopic findings associated with stress in the testis or epididymis, but can have atrophy of the prostatic epithelium, including apoptosis of the acinar epithelium of the prostate gland in early stages of reduced testosterone, and loss of apical secretory granules in the acinar epithelium can be seen after prolonged reduced testosterone (Chapin and Creasy, 2012). In the dog, increased apoptosis in the prostate can provide a sensitive marker of early, reduced androgen tone (Everds et al., 2013).

It is becoming common practice to house NHPs in social groupings during nonclinical safety assessment studies, but introduction of individuals to one another naturally leads to a ranking of dominant and subordinate individuals. High-ranking males will be those animals with the highest body weight, and they will also maintain the highest testosterone levels, while the low-weight NHPs will generally be the subordinate animals and will have low testosterone levels, decreased testicular size, testis weights, and spermatogenesis associated with stress (Everds et al., 2013). Transient reductions in testicular size of 45% from baseline in subordinate males has been reported following introduction to social groupings (Niehoff et al., 2010) and this should be considered when randomizing animals.

## 5. MECHANISMS AND PATTERNS OF TOXICITY

There have been numerous in-depth discussions of mechanisms of specific toxicants in recent years (Boekelheide, 2005; Creasy and Chapin, 2015). Instead of duplicating these in detail here, a relatively high-level overview of nitroaromatics will be provided as a case example of the complexity of molecular and biochemical assessment of testicular toxicity. Additionally, a more detailed discussion on the morphologic patterns that may be observed by the toxicologic pathologist and the impact of developmental exposure on the male reproductive system will also be provided.

### 5.1. Molecular and Biochemical

When investigating the potential mechanism of action of testicular toxicity, it is important to consider the complexity and interdependency of cell types within the testis. Often early microscopic lesions can give initial clues to the potential underlying mechanism or at least cell type affected. While this is critical to the evaluation, it must be noted that the microscopic findings initially observed by the pathologist may or may not be the target cell type affected by experimental treatment. For example, a toxicant causing cell-specific death in the spermatocyte population may well be mediated through disturbances of cellular processes in the Sertoli cell that are critical to spermatocyte survival. Any mechanistic investigations into events leading up to cell death would benefit from looking not only at the spermatocytes but also at the cells required to keep the spermatocytes alive—the Sertoli cells.

The testis is sensitive to multiple nitroaromatics, including nitrofurantoin, nitrofurazone, nitroimidazoles, di- and trinitrotoluene, and 1,3-dinitrobenzene (DNB) (Chapin et al., 1997; Heindel et al., 1997; Hess et al., 1988; Matsuyama et al., 2011; NTP, 2002). The first morphologically identifiable effects produced by DNB are ultrastructural vacuolation in the Sertoli cells and, in fixed tissue sections, the appearance of space between the Sertoli cells and germ cells,

interpreted as retraction of Sertoli cells from the germ cells (Blackburn et al., 1988). The Sertoli cells catabolize DNB in vitro, creating more polar metabolites through the reactive nitrosonitrobenzene, which produces a similar type of germ cell loss when applied to the cultures and appears more potent than the parent DNB (Brown and Miller, 1991). This led to defining the Sertoli cell as the target of DNB's toxicity, and its site of metabolism. Another important aspect of the toxicity caused by DNB is the role of the glutathione detoxification pathway in determining species sensitivity to DNB. The hamster is resistant to testicular toxicity when exposed to the same blood levels or cumulative exposure of DNB that are toxic to the rat (Obasaju et al., 1991). This is despite the fact that mitochondrial preparations of hamster testicular tubular mitochondria are more efficient in catabolizing DNB to its active metabolite. However, cellular levels of glutathione and ATP are depleted more rapidly in rat mitochondria than in hamster, resulting in oxidative stress within the Sertoli cell of the rat but not the hamster. This has been proposed as the most likely cause of the differential species sensitivity (Jacobson and Miller, 1998).

In the case of DNB, toxicogenomics has led to several interesting insights, not least of which is the complexity of the response to a toxic insult (Matsuyama et al., 2011). First, as expected, there are numerous significant gene expression changes that occur before any lesion is visible in the tissue. The earliest gene reductions were those enriched in pachytene spermatocytes, which were the site of the first visible change by light microscopy (spermatocyte apoptosis), even though the initial ultrastructural changes were seen in the Sertoli cell. Those authors found that the genes coding for the cell-cell adhesion molecules were all significantly increased at times when cells were beginning to be sloughed from the testis before there were any observable lesions. In this situation, we are left considering how to relate an upregulated Sertoli adhesion gene to the release and death and sloughing of germ cells. The most likely possibility is that this increase responds to an earlier effect on the function of those adhesions. Adhesions malfunctioning because of an

oxidative damage-induced change in intracellular signaling will not be revealed by evaluation of gene expression. This demonstrates the need for additional biochemical assays which evaluate the function of subcellular components. To obtain a full and balanced picture of the events in lesion development will require relating biochemical, genomic, and structural changes to each other over time.

## 5.2. Morphologic Patterns of Response to Different Types of Injury

Complete understanding of any mechanism of testicular toxicity is rare and the information is difficult to generate. As discussed in [Sections 2.3 and 2.4](#), the complexity of cell–cell signaling in the testis is such that morphologic injury, even of a specific cell type within a specific stage of spermatogenesis, often are secondary to either disturbed cell signaling in a different cell type or endocrine changes.

Nevertheless, broad categories can be useful to better understand the nature of the changes seen. The terms “Sertoli cell toxicants” versus “germ cell toxicants” and “hormonally mediated toxicants” are commonly used to distinguish between different manifestations of toxicity within the testis ([Creasy, 2001](#); [Vidal and Whitney, 2014](#)). This classification is based largely on the cell type that shows the earliest morphological changes, along with the characteristics of the lesion as it progresses with time ([Table 9.8](#)). Toxicants can also be classified into broad categories based on their overall pattern of morphologic change. This allows the design of additional biochemical or molecular investigations and can provide useful information for risk assessment or MOA evaluation. There are a number of different patterns of change that the pathologist can recognize, but these depend on whether the lesion is very early in its development or has been developing for some time, or whether it has reached its end stage (see [Tables 9.9–9.11](#) for a summary of the major features of the different patterns). If an end-stage or advanced stage of a lesion is present in the high-dose group of a study, it is often possible to see the early stages of lesion development in the lower-dose groups, because in many

cases, lower exposure levels take longer to begin exerting their effects. When considering a time-course study to identify early changes, the duration of dosing will depend on the toxicant and the dose level, and the speed of onset of the lesion. Changes can be seen within hours of a single dose for some toxicants but can take weeks to develop for others.

The following patterns of change are based largely on the responses seen in the rat, which is an ideal species for detecting subtle changes due to the high efficiency of spermatogenesis and low incidence of spontaneous findings. The same broad principles apply across species, but it is much more difficult to identify specific changes in nonrodents due to the higher incidence of spontaneous changes and small group sizes.

### 5.2.1. Patterns of Changes Associated with Sertoli Cell Injury

When the Sertoli cell is the primary site of morphological damage, the pattern of subsequent germ cell death and depletion is frequently multifocal and affects numerous or all different germ cell types when examined in a repeat-dose study ([Table 9.9](#)) ([Vidal and Whitney, 2014](#)). However, if the earliest signs of the lesion are examined, it is common to see stage- and cell-specificity associated with the germ cell death ([Murphy and Richburg, 2014](#)). For example, DNB is a Sertoli cell toxicant that produces Sertoli cell vacuolation in stages VII and XI within 24 h of dosing, which is followed by apoptosis of late pachytene spermatocytes in stages VI–XIII 24–48 h after dosing ([Foster et al., 1986](#); [Hess et al., 1988](#)). With repeat dosing and examination at a later time point, this stage- and cell-specificity would no longer be present as the lesion expands through more cells and more stages.

#### 5.2.1.1. FOCAL GERM CELL LOSS

Each Sertoli cell supports a specific cohort of germ cells as they develop through spermatogenesis. If that Sertoli cell suffers significant injury, all of the germ cells it supports will likely die and disappear. In the earliest stages of lesion development, this leads to an appearance of focal loss or “dropout” of germ cells from that one



**TABLE 9.8** Site/Cell-Specific Histopathologic Changes Associated With Male Reproductive Toxicants

Reporter/target cell	Toxicant	Effect
Leydig cell	Ethane dimethane sulphonate	Leydig cell necrosis with secondary germ cell death and depletion and atrophy of accessory sex organs
	Lansoprazole (Prevacid)	Inhibition of testosterone synthesis and increased plasma clearance of testosterone resulting in Leydig cell hyperplasia and tumors in rats
Sertoli cell	2,5-Hexanedione, phthalate esters	Sertoli cell vacuolation with subsequent death or exfoliation of germ cells
	Carbendazim, colchicine	Disruption of apical Sertoli cell cytoskeleton resulting in shedding of germ cells and Sertoli cell cytoplasm
Spermatogonia	Busulphan, cyclophosphamide	Spermatogonial death with subsequent maturation depletion of later germ cells
Spermatocytes	Glycol ethers, nitroaromatics	Stage-specific death of pachytene spermatocytes, mediated through disturbances in Sertoli cell
Round spermatids	Ethyl methane sulfonate, methyl chloride	Damages the round spermatid and leads to depletion and abnormalities in the elongating spermatid head shape
Elongating spermatid	Dibromoacetic acid	Retention and phagocytosis of step 19 spermatids, abnormalities in the released sperm
Testicular blood vessels	Cadmium chloride	Damages endothelium of testicular blood vessels causing ischemic necrosis of all testicular cell types
Epididymis	Phosphodiesterase 4 inhibitors, $\alpha$ -chlorohydrin	Inhibition of fluid reabsorption in efferent ducts resulting in sperm granulomas and secondary testicular atrophy
	Methyl chloride	Epithelial degeneration resulting in sperm granulomas
Epididymal sperm	Ornidazole, $\alpha$ -chlorohydrin	Inhibition of glycolysis resulting in loss of sperm motility
Vas deferens	Guanethidine	Inhibition of ejaculation due to adrenergic receptor blockade, resulting in rupture at vas epididymal junction and sperm granulomas
Prostate and seminal vesicles	Flutamide	Androgen receptor blockade resulting in secretory inhibition and atrophy
	Finasteride	Inhibition of metabolism of testosterone to dihydrotestosterone resulting in secretory inhibition and atrophy

From Chapin RE, Creasy DM: Assessment of circulating hormones in regulatory toxicity studies II. Male reproductive hormones, *Toxicol. Pathol.* 40:1063–1078, 2012; Rouquié D, Friry-Santini C, Schorsch F, et al.: Standard and Molecular NOAELs for rat testicular toxicity induced by flutamide, *Toxicol. Sci.* 109:59–65, 2009; Carr TL, Ciurlionis R, Milicic I, et al.: Role of cytochrome P450c17 $\alpha$  in dibromoacetic acid-induced testicular toxicity in rats, *Arch. Toxicol.* 85:513–523, 2011; Chapin RE, White RD, Morgan KT, et al.: Studies of lesions induced in the testis and epididymis of F-344 rats by inhaled methyl chloride, *Toxicol. Appl. Pharmacol.* 76:328–343, 1984b; De Grava Kempinas W, and Klinefelter GR: Interpreting histopathology in the epididymis, *Spermatogenesis* 4:e979114, 2014; Fort FL, Miyajima H, Ando T, et al.: Mechanism for species-specific induction of Leydig cell tumors in rats by lansoprazole, *Fundam. Appl. Toxicol.* 26:191–202, 1995; Gunn SA, Gould TC, Anderson WA: The selective injurious response of testicular and epididymal blood vessels to cadmium and its prevention by zinc, *Am. J. Pathol.* 42:685–702, 1963; Heuser A, Mecklenburg L, Ockert D, et al.: Selective inhibition of PDE4 in Wistar rats can lead to dilatation in testis, efferent ducts, and epididymis and subsequent formation of sperm granulomas, *Toxicol. Pathol.* 41:615–627, 2013; Johnson KJ: Testicular histopathology associated with disruption of the Sertoli cell cytoskeleton, *Spermatogenesis* 4:e979106, 2014; Kim SH, Lee IC, Lim JH, et al.: Spermatotoxic effects of  $\alpha$ -chlorohydrin in rats, *Lab. Res.* 28:11–16, 2012; Vidal JD, Whitney KM: Morphologic manifestations of testicular and epididymal toxicity, *Spermatogenesis* 4:e979099, 2014; Yang ZW, Kong LS, Guo Y, et al.: Histological changes of the testis and epididymis in adult rats as a result of Leydig cell destruction after ethane dimethane sulfonate treatment: a morphometric study, *Asian J. Androl.* 8:289–299, 2006. Reproduced from Haschek WM, Rousseaux CG, Wallig MA, editors: Haschek and Rousseaux's handbook of toxicologic pathology, ed 3, 2013, Academic Press, Table 59.13, p. 2573, with permission.

**TABLE 9.9** Patterns of Histopathologic Change Associated with Testicular Sertoli and Germ Cell Injury

Injury	Pattern of change		
	Testis	Epididymis	Prostate/seminal vesicles
Sertoli cell injury (early)	Foamy vacuolation in basal Sertoli cell cytoplasm or solitary large discrete vacuoles. Focal drop out of germ cells. Spermatid retention. Disorganization of germ cell layers.	Sloughed testicular germ cells present in lumen (initially confined to head, later in the tail).	Normal
Sertoli cell injury (later/late)	Partial/patchy loss of germ cells. Progressive diffuse degeneration of germ cells (without cell- or stage-specificity). Sloughing of germ cells into lumen.	Larger numbers of sloughed germ cells. Decreased sperm content.	Normal
Germ cell injury (early)	Degeneration or depletion of a specific germ cell population(s) with remaining germ cell layers appearing normal (cell- and stage-specific).	Normal	Normal
Germ cell injury (later/late)	Progressive depletion of more mature germ cell layers (maturation depletion).	Decreased sperm content, but not until the maturation depletion has reached mature spermatids.	Normal

From Johnson KJ: Testicular histopathology associated with disruption of the Sertoli cell cytoskeleton, *Spermatogenesis* 4:e979106, 2014; Vidal JD, and Whitney KM: Morphologic manifestations of testicular and epididymal toxicity, *Spermatogenesis* 4:e979099, 2014. Reproduced from Haschek WM, Rousseaux CG, Wallig MA, editors: *Haschek and Rousseaux's handbook of toxicologic pathology*, ed 3, 2013, Academic Press, Table 59.14, p. 2577, with permission.

Sertoli cell, or a patchy partial loss of germ cells from multiple Sertoli cells in affected tubules (Figure 9.38) (Murphy and Richburg, 2014; Vidal and Whitney, 2014). As the degree of damage progresses and more Sertoli cells become injured, a more generalized germ cell degeneration and depletion will develop, leading to a final end-stage lesion of severe tubular degeneration/atrophy (Figures 9.23). Since different testicular toxicants can produce a similar end-stage lesion (severe tubular degeneration/atrophy), it is important to study the earlier changes to gain any insight into pathogenesis.

#### 5.2.1.2. VACUOLATION

Early evidence of Sertoli cell injury can also be reflected by macro- or microvesicular vacuolation of scattered Sertoli cells (Figure 9.26) (Murphy and Richburg, 2014; Vidal and Whitney, 2014).

Microvacuolation is generally present in the basal Sertoli cell cytoplasm and represents swelling and coalescence of membrane-bound organelles such as endoplasmic reticulum or vesicles. This may be accompanied by disorganization or displacement of the regular layering of germ cells. Although there may be degeneration of germ cells, it is generally infrequent or develops subsequent to the vacuolation of the Sertoli cells. Macrovesicular vacuolation also occurs with some testicular toxicants, such as 2,5-hexanedione (Chapin et al., 1983). This change is characterized by solitary or multiple large vacuoles at the base or part way up the tubular epithelium (Figure 9.26B). As an early change, this type of vacuolation can be observed prior to any detectable germ cell degeneration. Vacuolation can also occur spontaneously or as a fixation artifact.

**TABLE 9.10** Patterns of Histopathologic Change Associated with Epididymal Efferent Duct Obstruction and Testicular Anoxia/Ischemia

Injury or lesion	Testis	Epididymis	Prostate/seminal vesicles
Efferent duct obstruction/ disturbed fluid reabsorption	Mixture of tubular dilation and severe tubular atrophy. Frequently unilateral. Dilated testes are increased in weight. Rete testis may be dilated. Atrophic tubules frequently have patent or slightly dilated lumens. Interstitial edema may be present. Incidence of affected testes often sporadic with poor dose relationship.	Sperm stasis and granulomatous inflammation in the efferent ducts. Epithelial apoptosis of the initial segment. Epididymis associated with testis that has dilated tubules may or may not have sperm content. No sperm and generally no sloughed germ cells in epididymis of atrophic testis.	Normal
Anoxia/ischemia (testis)	Initial anoxia causes increased apoptosis of spermatogonia and early spermatocytes. Early ischemia causes separation of germ cells (similar to autolysis). Later progresses to necrosis (coagulative) of germ cells and Sertoli cells. Generally associated with an interstitial inflammatory response to necrotic tubules. Affected tubules often become mineralized and may proceed to fibrosis. May affect individual tubules or affect focal areas.	Sloughed testicular germ cells and reduced sperm	Normal

From Hess RA: *Disruption of estrogen receptor signaling and similar pathways in the efferent ductules and initial segments of the epididymis*, *Spermatogenesis* 4:e979103, 2014; Vidal JD, Whitney KM: *Morphologic manifestations of testicular and epididymal toxicity*, *Spermatogenesis* 4:e979099, 2014. Modified from Haschek WM, Rousseaux CG, Wallig MA, editors: *Haschek and Rousseaux's handbook of toxicologic pathology*, ed 3, 2013, Academic Press, Table 59.15, p. 2583, with permission.

#### 5.2.1.3. ALTERED SPERMATION

Spermiation is tightly regulated by Sertoli cells and requires mature spermatids to be located at the edge of the tubular lumen for release while simultaneously removing the residual bodies (O'Donnell, 2014). Early manifestation of Sertoli cell toxicity may include retained spermatids and/or residual bodies (Johnson, 2014; O'Donnell, 2014; Vidal and Whitney, 2014).

#### 5.2.1.4. GERM CELL EXFOLIATION

When immature germ cells (spermatocytes and round spermatids) are admixed with sperm in the epididymis, they have been prematurely released from the seminiferous epithelium

(Figure 9.39) (Johnson, 2014; Vidal and Whitney, 2014). In most cases, the exfoliated germ cells retain relatively normal nuclear and cytoplasmic characteristics, suggesting that they have lost contact with their Sertoli cell processes and been shed into the tubular lumen. Since the rat epididymis contains negligible round germ cells when there is normal spermatogenesis, this can be a very sensitive and very early indicator of spermatogenic disturbance, and often is easier to see than the testicular change that is causing it. Care should be taken not to confuse apocrine cytoplasmic blebs, originating from the normal process of apocrine secretion by the efferent duct or epididymal epithelium, with sloughed



**TABLE 9.11** Patterns of Histopathologic Change Associated with Androgen Imbalance in Rodents

Type of androgen imbalance	Pattern of change		
	Testis	Epididymis	Prostate/seminal vesicles
Decreased testosterone (early/mild)	Degeneration of occasional pachytene spermatocytes and round spermatids in stage VII/VIII tubules. Spermatid retention. Leydig cell atrophy (if severe testosterone reduction).	Apoptosis of ductal epithelium (most prominent in the initial segment).	Decreased weight. May see increased epithelial apoptosis
Decreased testosterone (late/severe)	Progressive degeneration and depletion of elongating spermatids. Leydig cell tumors (rat).	Reduced sperm content, reduced weight, ductal atrophy.	Reduced weight, reduced secretion, atrophy
Androgen agonist	Same effects as with decreased testosterone due to effects on hypothalamic pituitary feedback. Inverse dose relationship with most severe disruption of spermatogenesis at low doses and less severe effects at high dose.	Reduced sperm content, reduced weight, ductal atrophy.	Increased weight, increased secretion, enlargement.
Androgen antagonist	Leydig cell hyperplasia (early) and/or Leydig cell tumors (late) (rat).	Normal or slightly reduced weight.	Reduced weight, reduced secretion, atrophy.
Reduced dihydrotestosterone (5 $\alpha$ -reductase inhibitor)	Normal (rat). Leydig cell hyperplasia and tumors (mouse).	Normal or slightly reduced weight.	Reduced weight, reduced secretion, atrophy.
Estrogen agonist	Progressive degeneration and depletion of elongating spermatids. Leydig cell hyperplasia and tumors (mouse).	Apoptosis of ductal epithelium (most prominent in the initial segment). Reduced sperm content, reduced weight, ductal atrophy.	Reduced weight, reduced secretion, atrophy.

From Chapin RE, Creasy DM: *Assessment of circulating hormones in regulatory toxicity studies II. Male reproductive hormones*, *Toxicol. Pathol.* 40:1063–1078, 2012; Ramaswamy S, Weinbauer GF: *Endocrine control of spermatogenesis: role of FSH and LH/testosterone*, *Spermatogenesis* 4:e996025, 2014; Vidal JD, Whitney KM: *Morphologic manifestations of testicular and epididymal toxicity*, *Spermatogenesis* 4:e979099, 2014. Reproduced from Haschek WM, Rousseaux CG, Wallig MA, editors: *Haschek and Rousseaux's handbook of toxicologic pathology*, ed 3, 2013, Academic Press, Table 59.16, p. 2584, with permission.

testicular germ cells (De Grava Kempinas and Klinefelter, 2014; Hughes and Berger, 2015).

The Sertoli cell supports and moves the germ cells up and down within the seminiferous epithelium by utilizing a well-developed cytoskeleton of microtubules and intermediate filaments. The germ cells share a variety of specialized junctions with the Sertoli cell, some of them unique to the testis, that hold the germ cells in place within the Sertoli cell cytoplasmic

processes. If those junctions are broken or there is retraction of the cytoplasmic processes, the germ cells can be “cast loose” and shed into the lumen (Johnson, 2014). This can be a very prominent change with some Sertoli cell toxicants, such as the phthalate esters, where retraction of the cytoplasmic processes that support and separate the germ cells has been shown as an early change (Figure 9.39). Microtubule inhibitors, such as colchicine and carbendazim, cause

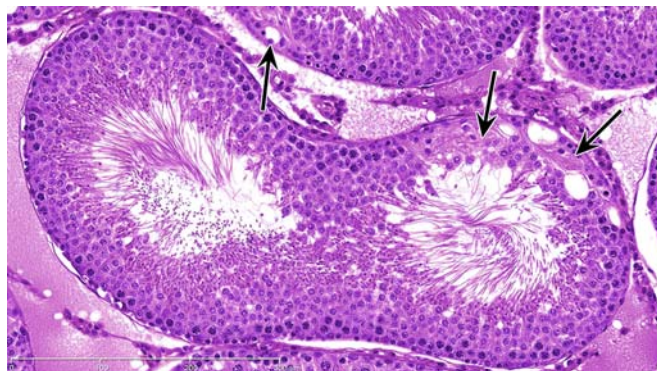


**FIGURE 9.38** Patchy partial loss of germ cells affecting multiple Sertoli cells (arrows). This is a typical early pattern of change that occurs when toxicity is mediated through the Sertoli cell. Rat, H&E,  $\times 20$ . Reproduced from Haschek WM, Rousseaux CG, Wallig MA, editors: *Haschek and Rousseaux's handbook of toxicologic pathology*, ed 3, 2013, Academic Press, Figure 59.35, p. 2578, with permission.

shedding of the germ cells in sheets that are still attached to the apical cytoplasm of the Sertoli cell (Nakai and Hess, 1994; Russell et al., 1981). This appears as sloughing of the apical third of the Sertoli cell and cytoplasm and germ cells, presumably due to disruption/dissolution of the cytoskeletal microtubules.

#### 5.2.1.5. TUBULAR CONTRACTION AND DECREASED SEMINIFEROUS TUBULAR FLUID

The Sertoli cells continuously secrete STF into the tubular lumen. This transports the sperm out of the tubule and into the rete and the efferent ducts and is responsible for the patency of the tubular lumens. The size of the tubular lumen is directly related to the amount of fluid within the lumen, so if secretion is decreased the tubule will contract, and if secretion increases, or its exit from the testis is blocked, the tubule will dilate. Reduced secretion of STF has been demonstrated as an early event with a number of Sertoli cell toxicants, including the phthalate esters and 2,5-hexanedione exposure (Gray and Gangolli, 1986; Richburg et al., 1994). Although qualitative microscopic evaluation is not very sensitive for detecting tubular contraction, particularly when there is differential shrinkage of tubules due to fixation artifact, the volume of STF can be measured. This measured experimentally in rodents by ligating the efferent ducts of one testis and comparing the weight difference between

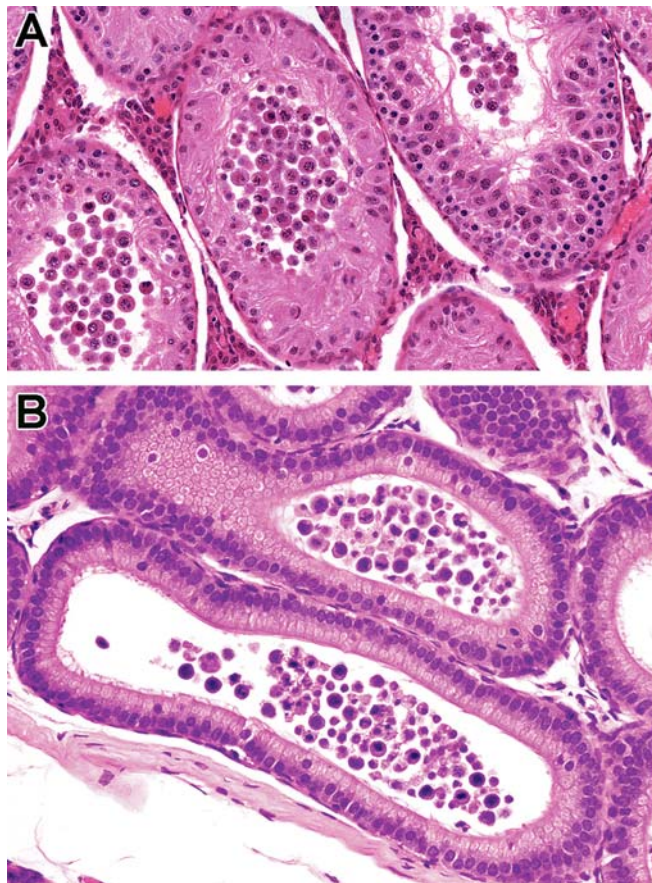


**FIGURE 9.39** Sloughed germ cells in (A) the testis and (B) the epididymis of a rat dosed with di-n-pentyl phthalate. The toxicity appears to cause loss of contact between germ cells and Sertoli cell processes. Rat, H&E,  $\times 20$ . Reproduced from Haschek WM, Rousseaux CG, Wallig MA, editors: *Haschek and Rousseaux's handbook of toxicologic pathology*, ed 3, 2013, Academic Press, Figure 59.36, p. 2579, with permission.

the ligated testis and the contralateral unligated testis after  $\geq 15$  h. Decreased fluid content will also be reflected by a decrease in the weight of the testis; therefore, if there is a significant weight loss in the testis and no obvious germ cell loss, a disturbance in STF should be considered.

#### 5.2.2. Patterns of Change Associated with Germ Cell-specific Toxicity

When germ cells are the primary cell type damaged, the changes are often cell- and stage-specific (Table 9.9). If the testes are examined early in lesion development, it is possible to identify apoptotic germ cells in the presence of normal-appearing Sertoli cells (Vidal and

Whitney, 2014). More often, the testes are examined after repeat dosing, and since apoptotic cells are rapidly eliminated, the most characteristic feature of germ cell toxicity is a stage- and cell-specific depletion, which is commonly referred to as “maturation depletion.” The number of cell types depleted will depend on the cell type that has died as well as the duration of the dosing regimen. Germ cell-specific toxicity is commonly observed with agents targeting either mitotic or meiotic division. As an example, if a toxicant kills spermatocytes during meiotic division, and this occurs on day 1 of dosing, within a few days most (but perhaps not all) of the apoptotic cells will have been phagocytized and the tubule will have progressed to the maturation phase (stages I-III), minus its round spermatid population. On days 2-3, tubules that were at the end of the elongation phase (XII-XIII) on Day 1 enter the meiotic division phase, the dividing spermatocytes will become susceptible to toxicity and die, and the process is repeated. If the testes are examined after 2 weeks of continuous dosing (one complete cycle of spermatogenesis), the initial loss of dividing spermatocytes 2 weeks previously will have progressed to the absence of all round spermatids and loss of elongating spermatids up to those in the meiotic division phase (step 14). Other examples of maturation depletion over time are illustrated in Figures 9.20 and 9.40, and understanding these patterns of germ cell depletion are important to allow for identification of direct germ cell toxicity.

A feature of maturation depletion is that the effect becomes more obvious as the later developmental stages of germ cells (e.g., spermatids) are lost. This is because there are theoretically four spermatids for every primary spermatocyte, two spermatocytes for every B spermatogonium, and 32 B spermatogonia for every type A1 spermatogonium that enters spermatogenesis (Figure 9.14). The progressive expansion of the germ cell population means that a compound which targets early spermatogonia will be very difficult to identify in conventional H&E sections during the first 2 weeks of dosing, because very few cells will be lost. By 4 weeks after the onset of dosing, depletion will have reached the much more numerous pachytene spermatocyte population and be more obvious, and by 6 weeks after the start of dosing, it will

be very obvious because a large proportion of the round spermatids will be missing, in addition to all the earlier cell types. In addition, as the more numerous mature germ cell layers are lost, testicular weight starts to decrease.

Another important aspect of the dynamics of this progressive maturation depletion is the appearance of the testes at the end of dosing versus the end of recovery. At the end of dosing, maturation depletion may only have caused the loss of spermatogonia and few pachytene spermatocytes and be difficult to identify (Figures 9.19 and 9.20), but following an additional 2- or 4-week recovery period, the progressive depletion of the spermatid population with decreased testicular weights will make the severity of germ cell loss appear much more severe. In these situations, it is important to note which cells are missing at the end of dosing (spermatogonia and certain stages of spermatocytes) versus which cells are missing at the end of recovery (e.g., round and elongating spermatids), but with recovery of spermatogonia and early spermatocytes. Failure to do this will result in an erroneous conclusion that the damage is getting worse rather than recovering.

Degeneration and malformation of elongating spermatids is a form of germ cell-specific toxicity that is occasionally seen, but this pattern may have overlapping features with Sertoli cell toxicity (O'Donnell, 2014; Vidal and Whitney, 2014). To recognize this, the pathologist needs to have a good knowledge of the normal shape changes that the elongating spermatid head goes through as it develops. A head malformation where the head loses its long delicate curvature and becomes shortened, clubbed, and condensed is most easily recognized in rats during early spermatid elongation (Figure 9.41). There may also be abnormal tail formation and retraction of the cytoplasmic coating around the developing flagellum of the tail, but this may be difficult to identify in routine sections. These changes are usually accompanied by the presence of cell debris in the head of the epididymis, which appears to consist of prematurely shed heads and tails of malformed elongating spermatids. It is possible that these deformed elongating spermatids are due to disturbances in the formation of the acrosome earlier in spermiogenesis. This has been described in the case of carbendazim (Nakai et al., 1997).



## Pattern of cell depletion with daily dosing of a spermatocyte toxicant

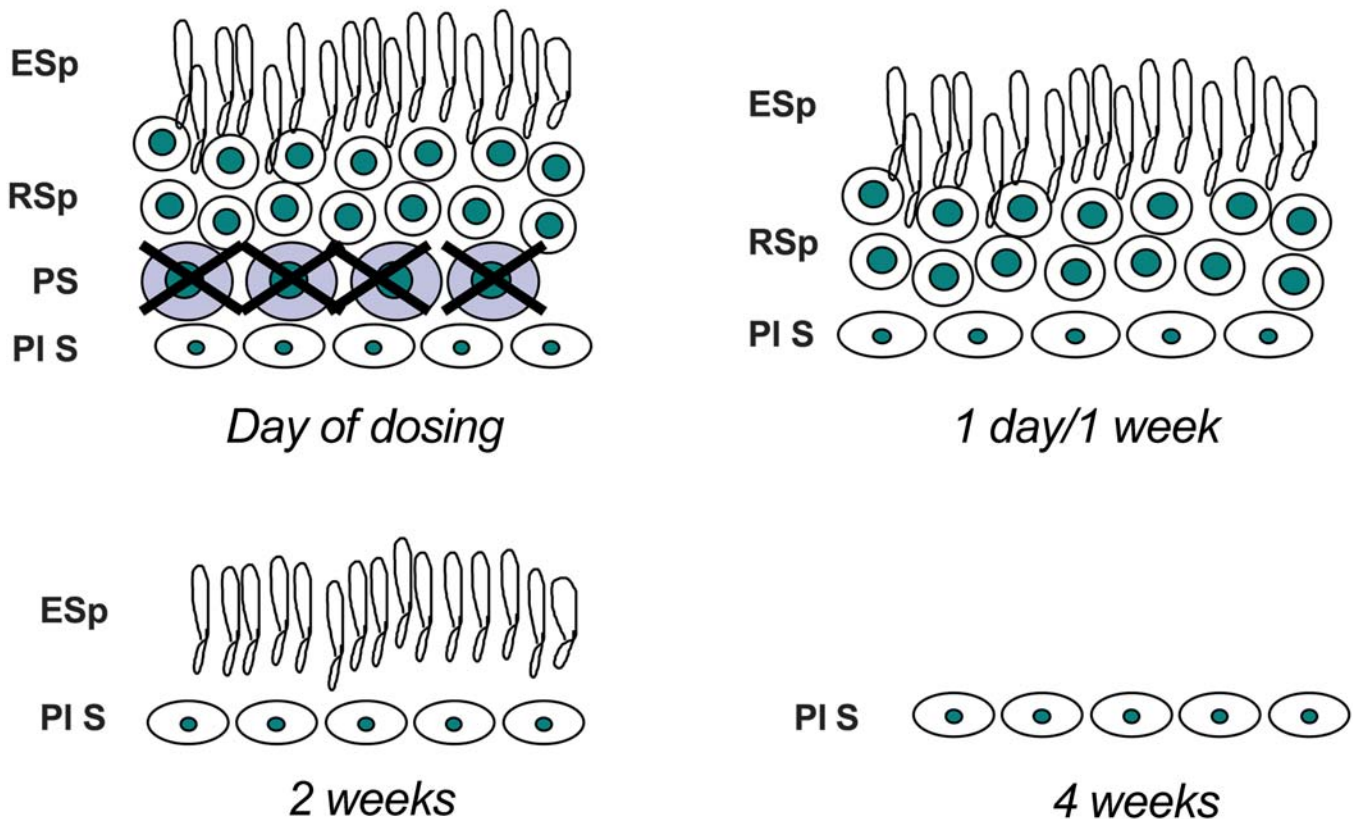


**FIGURE 9.40** Typical progression of maturation depletion that occurs following germ cell-specific toxicity in the rat. A Stage VII tubule is illustrated. On day 1, it contains preleptotene spermatocytes (PI S), pachytene spermatocytes (PS), round spermatids (RSp) and elongating spermatids (ESp). On the day of dosing, the toxicant causes apoptosis of the pachytene spermatocytes. If that stage is examined the following day or after a week of dosing, the pachytene spermatocytes will be missing but the other cell types will appear normal. If the same stage tubule is examined after 2 weeks of dosing (i.e., one complete spermatogenic cycle), pachytene spermatocytes will be missing (because they are still being killed by the toxicant) and round spermatids will be missing because their precursor cell was killed 2 weeks earlier, but preleptotene and elongating spermatids will still be present. After 4 weeks of dosing, the elongating spermatids will also be depleted, leaving the end-stage lesion of tubules containing preleptotene spermatocytes but with all subsequent cell types missing. *Modified from Haschek WM, Rousseaux CG, Wallig MA, editors: Handbook of toxicologic pathology, ed 2, 2002, Academic Press, Figure 20, p. 826, with permission.*

Germ cell toxicity has been described for a number of toxicants; the best documented is probably ethylene glycol monomethyl ether (EGME) or its active metabolite methoxy acetic acid (MAA) (Chapin et al., 1984a; Foster et al., 1984). At low doses, this chemical causes very specific death of stage I–V pachytene spermatocytes and stage XI–XIV pachytene and dividing spermatocytes within hours of dosing. Although

pachytene spermatocytes are the primary cell type affected, it is important to note that small vacuoles at the ultrastructural level in Sertoli cells have been reported, which resolved by 24 h after a single administration (Creasy et al., 1986) along with early changes in Sertoli cell enzymes, receptors, and/or kinases (Syed and Hecht, 1998; Wang et al., 2000). As the dose level increases, pachytene spermatocytes in all stages

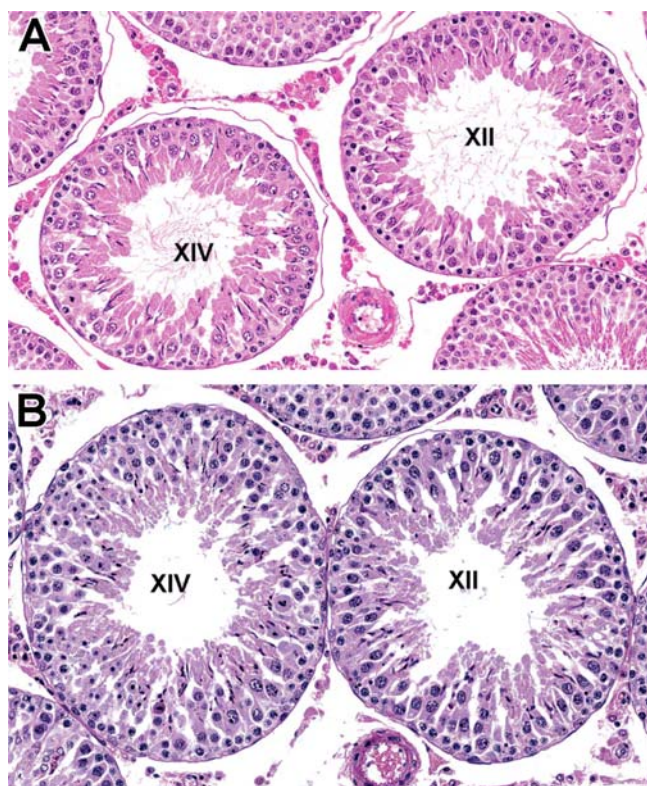


**FIGURE 9.41** Degeneration of elongating spermatids. This can be recognized by malformation of the shape of the head of elongating spermatids. To recognize this change, it is essential to know the normal shape of elongating spermatids in the different spermatogenic stages. (A) Normal stage XII and XIV tubules. (B) Stage XII and XIV tubules containing elongating (step 12 and 14) spermatids with condensed and clubbed heads. Rat, H&E,  $\times 20$ . Reproduced from Haschek WM, Rousseaux CG, Wallig MA, editors: *Haschek and Rousseaux's handbook of toxicologic pathology*, ed 3, 2013, Academic Press, Figure 59.38, p. 2582, with permission.

become susceptible, and at even higher doses, the toxicity expands into the spermatid population and the prepachytene spermatocyte population. This loss of cell- and stage-specificity as the dose level increases is a common phenomenon.

### 5.2.3. Patterns of Change Associated with Anoxia or Ischemia

The seminiferous epithelium is unique because there are no capillaries within the epithelium and all oxygen and nutrients need to travel from the interstitial capillaries into the interstitial fluid and be transported through the Sertoli cells to reach the germ cells sequestered within the Sertoli cell processes. As a result, the tubules

normally operate at relatively lower oxygen levels (Free et al., 1976). Effects of ischemia due to experimental testicular torsion are well described as a model for clinical testicular torsion in humans (Bergh et al., 2001; Oh et al., 2004; Turner et al., 2004; Turner and Brown, 1993). The most sensitive cells to the injurious effects of reduced oxygen tension appear to be the spermatogonia and early spermatocytes, which undergo an increased rate of apoptosis (Bergh et al., 2001). Reduction in testicular blood flow was also accompanied by increased numbers of leukocytes in the blood vessels, with some migrating out into the interstitial space. The extent of damage depends on the duration of the ischemia, but effects can be observed in germ cells, Sertoli cells, Leydig cells, and throughout the epididymis (Table 9.10). The effects often increase following reperfusion due to the generation of reactive oxygen species (ROS) by the leukocytes that infiltrate the ischemic tissue during the torsion phase (Reyes et al., 2012).

A particular pattern of ischemic necrosis is seen with reductions in blood flow produced by some kinds of toxicants. The change has been best described with GnRH agonists and following a subcutaneous injection of very large doses of hCG to the rat (Blanchard et al., 1998; Chatani, 1996, 2006; van Vliet et al., 1988). The lesion is characterized by a focal area of coagulative necrosis, associated with a leukocytic infiltrate, and located specifically in the frontal lower pole of the testis. The mechanism of the hCG-induced necrosis is due to stimulation of the Leydig cells by hCG to synthesize prostaglandins which cause prolonged ( $>12$  h) contraction and cessation of blood flow in the intratesticular arteries in the frontal lower pole of the testis, resulting in tubular necrosis in this part of the testis (Figure 9.42). Although the testicular arteries in the remainder of the testis initially showed the same contraction and reduced blood flow, they recovered much more rapidly and the reduced blood flow did not cause necrosis of the adjacent parenchyma.

### 5.2.4. Patterns of Change Associated with Altered Endocrine Support

Recognition of toxicity mediated by decreased endocrine support of the male reproductive system requires an integrated evaluation of the



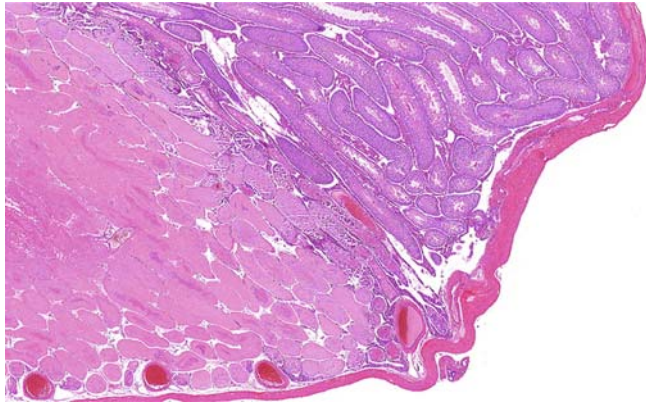


**FIGURE 9.42** Focal ischemic necrosis of the lower frontal pole of the testis. This has been described following ischemia induced by human chorionic gonadotropin (hCG). Rat, H&E,  $\times 2$ . Reproduced from Haschek WM, Rousseaux CG, Wallig MA, editors: *Haschek and Rousseaux's handbook of toxicologic pathology*, ed 3, 2013, Academic Press, Figure 59.39, p. 2583, with permission.

entire reproductive tract, because changes can be present in the testis, epididymis, accessory sex organs, mammary gland, and/or pituitary (Table 9.11). There are a number of different mechanisms including decreased GnRH/gonadotropin production, decreased androgen production, AR agonism/antagonism, and/or inhibition of 5- $\alpha$ -reductase (Chapin and Creasy, 2012; Creasy, 2008; Ramaswamy and Weinbauer, 2014; Vidal and Whitney, 2014).

LH stimulates the production of testosterone, and high levels of intratesticular testosterone are required to maintain spermatogenesis (much greater than in systemic circulation) (Coviello et al., 2004; Roth et al., 2010; Zirkin et al., 1989). The role of FSH varies across species. In rodents, FSH is not required to maintain fertility but plays a key role during pubertal development, while in NHPs, FSH plays a more prominent role in supporting spermatogenesis in the adult (Akhtar et al., 1982; Luetjens et al., 2005; McLachlan et al., 2002; Ramaswamy and Weinbauer, 2014). As a result, gonadotropin deficiency leads to different effects across species. In rats, there is a loss of postmeiotic germ cells due to decreases in intratesticular testosterone levels, but spermatogenesis is not completely halted (see below). This is in contrast with the dog, pig, and NHP, in which GnRH analogs or vaccines and other centrally mediated

reductions in GnRH produce significant tubular atrophy (Einarsson et al., 2009; Losco et al., 2007; Noritake et al., 2011; Ramaswamy and Weinbauer, 2014). In NHPs, tubular atrophy begins as a reduction in the number of B spermatogonia and progresses with time with maturation depletion (Zhengwei et al., 1998). These testicular changes are generally readily reversible once the endocrine support is resumed (Ramaswamy and Weinbauer, 2014).

The effects of testosterone withdrawal have been most fully described in the rat, following ethane dimethane sulfonate administration, which causes Leydig cell necrosis and reduces testosterone to castrate levels (Kerr et al., 1993; Molenaar et al., 1986; Yang et al., 2006). The earliest changes are seen 4 days after destruction of the Leydig cells and comprise a cell-specific and stage-specific apoptosis of occasional pachytene spermatocytes and round spermatids in stage VII and VIII tubules (Figure 9.43A). At later times, spermatocytes, and particularly elongating spermatids in later stages (IX–XIV), show degeneration (Figure 9.43B). This reflects the fact that these cells have passed through stages VII–VIII in the absence of testosterone, undergoing lethal damage in the process. However, degeneration is delayed to a later time when they undergo a critical event, which relies on their previous exposure to testosterone. The end-stage lesion for severe testosterone insufficiency in the rat, which is seen after about 2 weeks of treatment, is a slight reduction in the numbers of mid and late pachytene spermatocytes and round spermatids, but an almost complete loss of elongating and maturation phase spermatids (Figure 9.43B). This is accompanied by marked shrinkage of the tubule, which is partly due to a loss of germ cells but is also caused by a reduction in the secretion of androgen-dependent STF by the Sertoli cell. Testosterone withdrawal also leads to abnormal retention and phagocytosis of step 19 spermatids at stages IX–XII. Although spermatid retention appears to be a common finding with treatments that disturb testosterone levels, it is not unique to this class of compound.

Any morphologic changes in the Leydig cell will depend on the nature of the hormonal disturbance and the species. Increased LH stimulation of rodent Leydig cells will result in hypertrophy of the cell due to an increased volume of



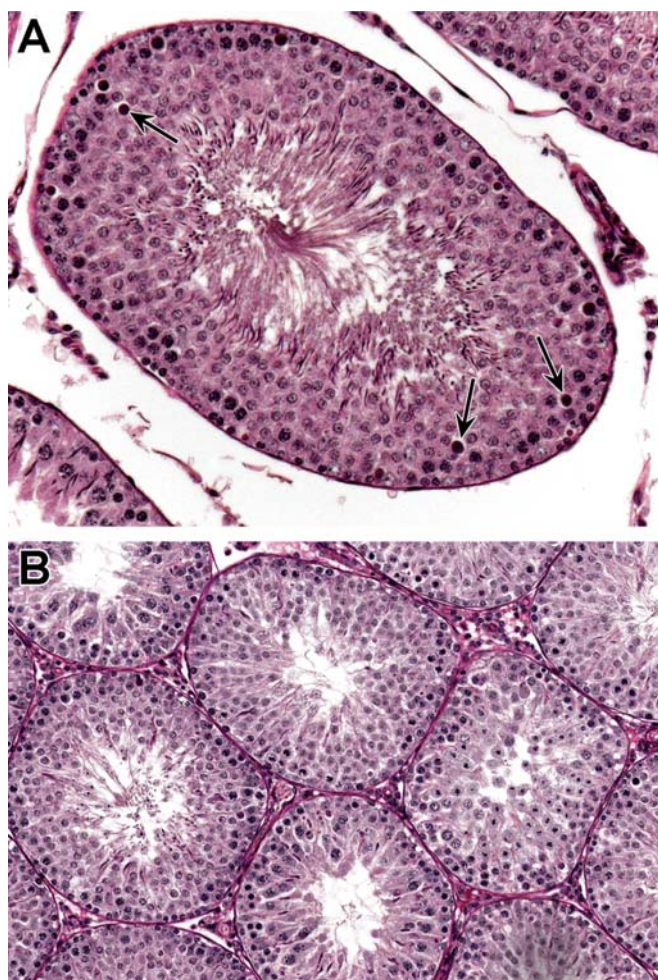


**FIGURE 9.43** Characteristic changes caused by low testosterone in the rat. (A) Stage VII tubule with occasional apoptotic round spermatids and pachytene spermatocytes (arrows). This can be the only testicular change seen following mild decreases in testosterone. Rat, H&E,  $\times 20$ . (B) Generalized depletion of elongating spermatids and contraction of tubular lumens. This is the end-stage lesion in the rat after marked reductions in testosterone. Rat, H&E,  $\times 10$ . Reproduced from Haschek WM, Rousseaux CG, Wallig MA, editors: *Haschek and Rousseaux's handbook of toxicologic pathology*, ed 3, 2013, Academic Press, Figure 59.40, p. 2585, with permission.

smooth endoplasmic reticulum and, if prolonged, may also lead to diffuse hyperplasia of the cell population and/or tumors (Prentice and Meikle, 1995). Increased LH may be a result of increased GnRH signaling, AR antagonism, decreased testosterone synthesis, and/or increased testosterone clearance. Conversely, reduced stimulation of the Leydig cell by LH will lead to a reduction in the size of the cells

and the volume of endoplasmic reticulum (Figure 9.28). In the dog, Leydig cell response is more variable, and Leydig cell vacuolation and hypertrophy is frequently seen accompanying decreased testosterone production (Figure 9.44D and E) (Losco et al., 2007).

Administration of exogenous androgens or AR agonists has an interesting inverse dose-response relationship with regard to its effect on testicular spermatogenesis. Administration of testosterone will inhibit LH production from the pituitary, resulting in inhibition of Leydig cell steroidogenesis and decreased intratesticular testosterone levels. Since spermatogenesis requires very high local testosterone concentrations to progress normally, spermatogenesis will decline in response to the locally reduced steroidogenesis. The higher the administered dose of testosterone, the more it is able to compensate for the decrease in testicular steroidogenesis, and the less effect it has on spermatogenesis (O'Donnell et al., 1994). The net result is that the lower the dose of testosterone administered, the more severe the degenerative effect on spermatogenesis (Figure 9.44A–C). The opposite is true for the effect on accessory sex organs, where the increased circulating levels of administered testosterone will be directly metabolized to DHT within the prostate and seminal vesicles and result in enlargement and increased weight of these tissues.

AR antagonists (e.g., flutamide) generally have no detectable histopathologic effect on spermatogenesis, but they cause Leydig cell hyperplasia through their stimulatory effect on LH levels (AR blockade in the central nervous system [CNS] leads to increased LH synthesis and release, which produces the Leydig cell hyperplasia) (Friry-Santini et al., 2007; Rouquié et al., 2009). 5 $\alpha$ -reductase inhibitors (e.g., finasteride) have no detectable effect on spermatogenesis (Rhoden et al., 2002). However, both cause marked atrophy of the accessory sex organs and the epididymis, which are dependent on DHT for their activity and interaction of the androgen with the AR. In the mouse, finasteride does produce Leydig cell hyperplasia and tumors (Prahalada et al., 1994) with Leydig cell hyperplasia occurring in rats only with chronic dosing and high exposure levels (PROPECIA, 2021). Decreased testosterone due to decreased production and/or increased clearance has



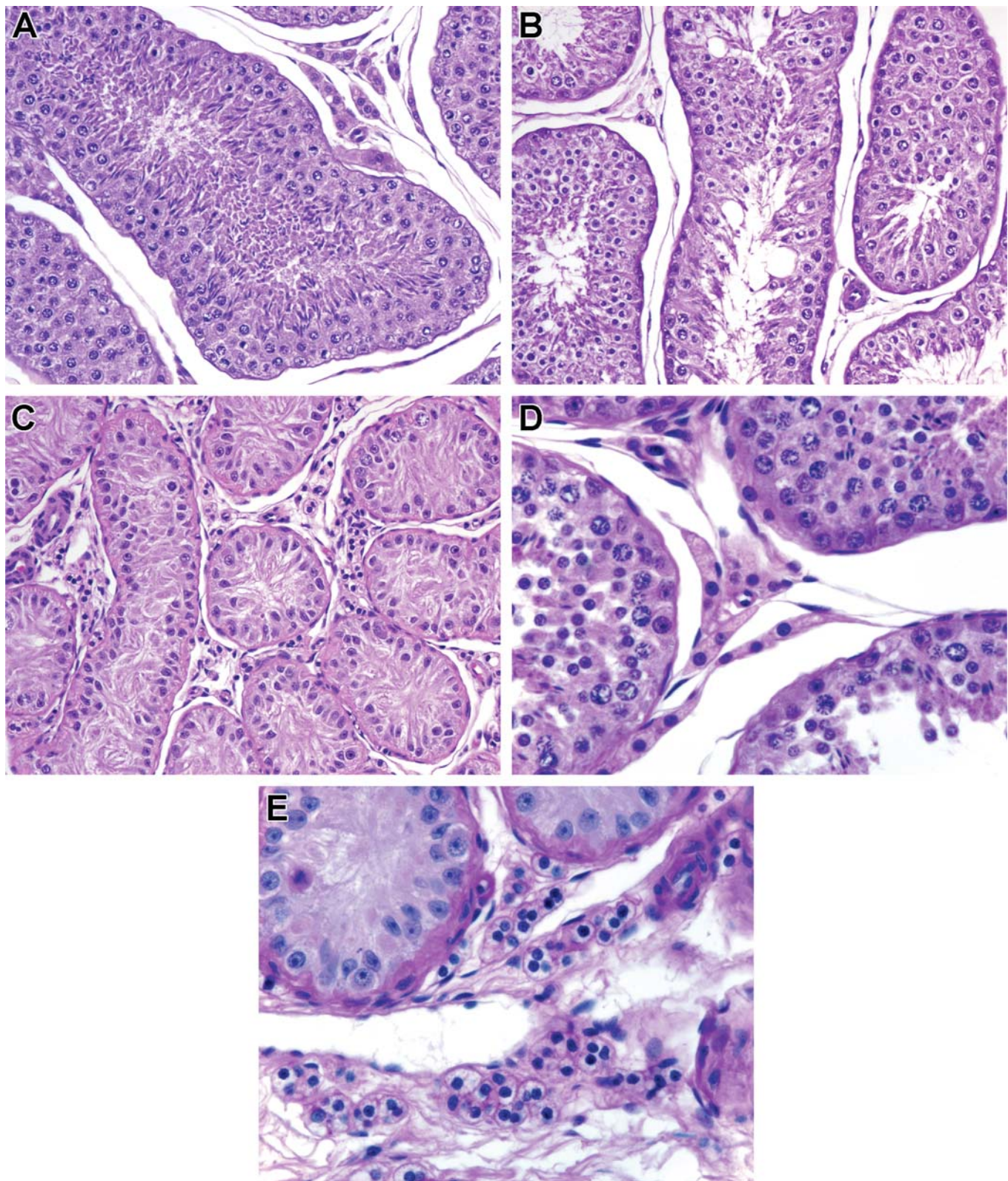


**FIGURE 9.44** (A–C) Effects of reduced testosterone in the dog. (A) Normal spermatogenesis. (B) Nonspecific patchy degeneration and depletion of germ cells after dosing with a high dose of testosterone (which causes a mild reduction in intratesticular testosterone). Dog, H&E,  $\times 20$ . (C) Complete loss of spermatogenesis and contraction of



been shown to cause elevations in LH and Leydig cell tumors in rats (Coulson et al., 2003; Fort et al., 1995).

In general, the epididymis and especially the accessory sex organs are much more sensitive than the testis to reduced androgen status, and rapidly respond with weight loss and epithelial atrophy (Figures 9.45–9.47) (Ward et al., 1989). Withdrawal of androgen results in a wave of apoptosis that starts in the initial segment of the epididymis and moves down the rest of the epididymis with time (Figure 9.45) (Fan and Robaire, 1998; Robaire and Fan, 1998). This wave in apoptosis is transient and begins within the first day and progresses over the course of approximately 1 week. As a result, the timing of sampling can impact the detection of this finding. In the prostate and seminal vesicles, there is epithelial apoptosis and epithelial atrophy (thinning) and decreased secretory content which is roughly proportional to the degree of hormone loss.

#### 5.2.5. Pattern of Change Associated with Disturbance of Fluid Production, Reabsorption, or Efferent Duct Obstruction

Patency of the seminiferous tubule lumen and the movement of sperm out of the testis and into the efferent ducts rely on the secretion of STF into the tubular lumen by the Sertoli cell. The production of STF is continuous, as is the reabsorption of most of the fluid in the efferent ducts.

Testosterone is a major regulator of STF and interstitial fluid production and decreases in testosterone lead to reductions in STF and interstitial fluid (Sharpe et al., 1994). Fluid content is a significant component of testis weight, and so if a decrease in absolute testis weight is seen in the absence of any significant germ cell loss, a decrease in STF and/or interstitial fluid can be a possible cause. Decreased STF has been observed with potassium channel blockers (Setchell et al., 1998).

In short-term studies, an increase in absolute testis weight almost always reflects an increase

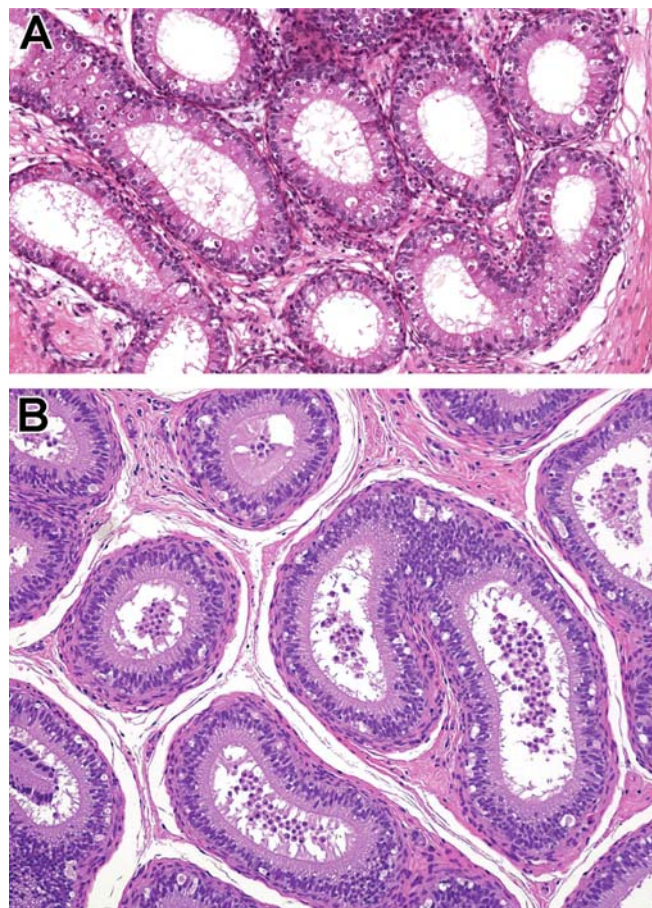


**FIGURE 9.45** Apoptosis of the initial segment of the epididymis often accompanies significant reductions in androgenic activity. (A) Rat, H&E, ×20. (B) Dog, H&E, ×20. Reproduced from Haschek WM, Rousseaux CG, Wallig MA, editors: *Haschek and Rousseaux's handbook of toxicologic pathology*, ed 3, 2013, Academic Press, Figure 59.42, p. 2587, with permission.

in tubular fluid content and is generally accompanied by an increase in the diameter of the tubular lumen (Table 9.10). Although increased fluid secretion by the Sertoli cell is a possible cause, there are no reports of this as a known chemically induced change. Another possibility is reduced emptying of the seminiferous tubules or relaxation of the encompassing peritubular cells. Endothelin antagonists cause increased

tubules after dosing with a low dose of testosterone (which causes a severe reduction in intratesticular testosterone). Dog, H&E, ×20. (D, E) Leydig cell hypertrophy and vacuolation can occur in the dog associated with low testosterone levels. (D) Normal Leydig cells. (E) Leydig cell hypertrophy and vacuolation from a dog with low testosterone secretion. Dog, H&E, ×40. Reproduced from Haschek WM, Rousseaux CG, Wallig MA, editors: *Haschek and Rousseaux's handbook of toxicologic pathology*, ed 3, 2013, Academic Press, Figure 59.41, p. 2586, with permission.



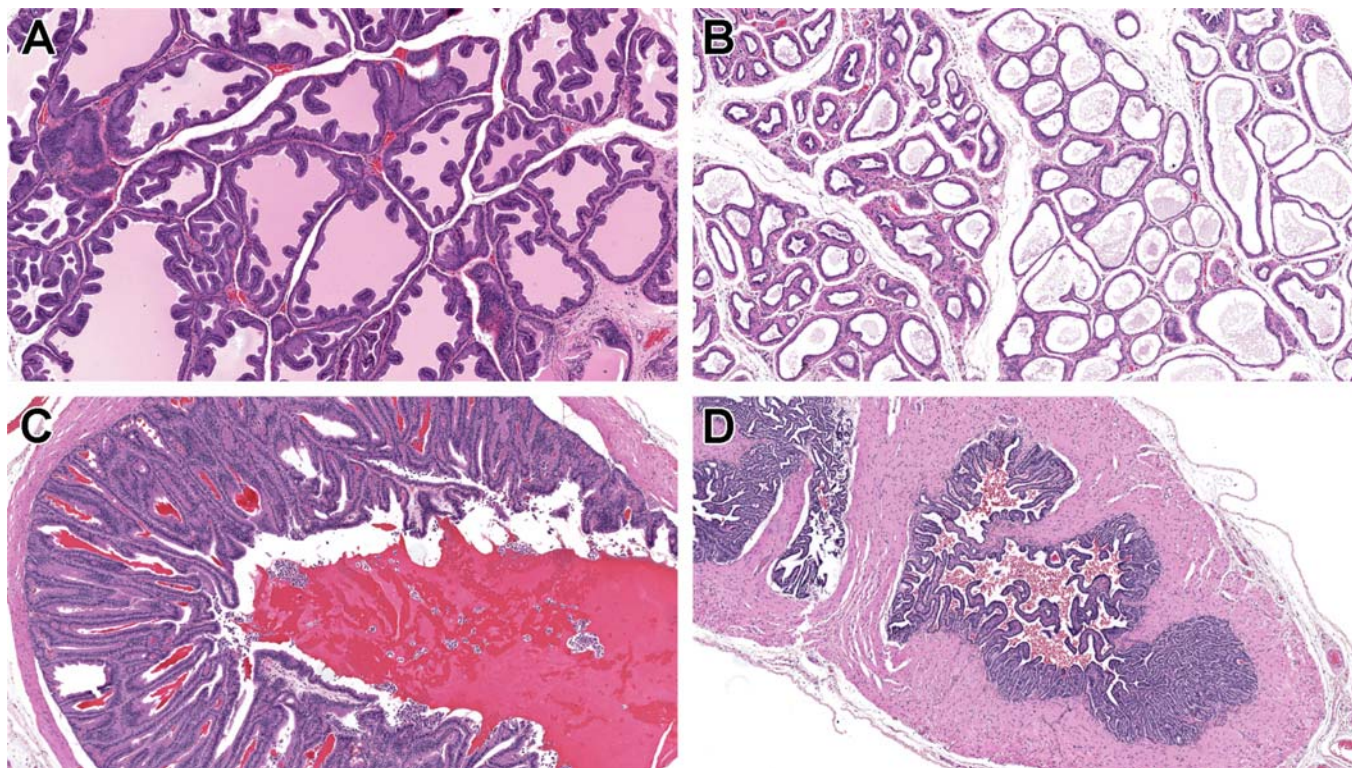


**FIGURE 9.46** Decreased weight of the accessory sex organs is a sensitive indicator of reduced androgenic activity. When there is a marked reduction in organ weight, morphological evidence of atrophy can also be seen. (A) Normal ventral prostate. Rat, H&E,  $\times 5$ . (B) Gonadotropin releasing hormone (GnRH) treatment, ventral prostate. Rat, H&E,  $\times 5$ . (C) Normal seminal vesicles. Rat, H&E,  $\times 4$ . (D) GnRH treatment, seminal vesicles. Rat, H&E,  $\times 5$ . Reproduced from Haschek WM, Rousseaux CG, Wallig MA, editors: *Haschek and Rousseaux's handbook of toxicologic pathology*, ed 3, 2013, Academic Press, Figure 59.43, p. 2588, with permission.

testis weight and tubular dilation (Figure 9.48), and endothelin-1 has been suggested as a mediator of tubular contraction in the rat (Piner et al., 2002). The most common cause of increased fluid in the testis of rodents is obstruction of outflow in the efferent ducts. It is important to identify and elucidate the efferent duct as a target site because an effect on it often leads to severe testicular tubular atrophy, which may otherwise be considered a primary testicular lesion caused by the drug. If the efferent ducts become blocked or the secretion rate of STF exceeds the reabsorption rate, pressure build-up of fluid in the seminiferous tubules will cause severe damage to the testis. The sequence of changes that occurs has been demonstrated using a number of models; the simplest is efferent duct ligation.

When the efferent ducts are ligated, there is a rapid (within hours) build-up of fluid within the testis that causes an increase in tubular luminal diameter, thinning of the tubular

epithelium, and an increase in testicular size and weight (Figure 9.49A) (Nykänen and Korman, 1978). This reaches a peak 16–24 h after the ligation and is then followed by a gradual shrinkage of testicular size and testis weight, due to the progressive degeneration and death of the germ cells from the tubules. By 28 days after ligation, the testis has lost 50% of its original weight and the tubules are severely atrophic, having lost all of their organization and most of their germ cells (Smith, 1962). The end-stage appearance of the testis following this type of injury is tubules lined only by Sertoli cells and occasional spermatogonia, generally having a slightly dilated (rather than collapsed) lumen, possibly accompanied by a dilated rete testis and interstitial edema (Figure 9.49B). The severity of the dilation and atrophy can be modified by ligating only a proportion of the proximal ducts, thereby leaving the common duct and some of the proximal ducts patent.



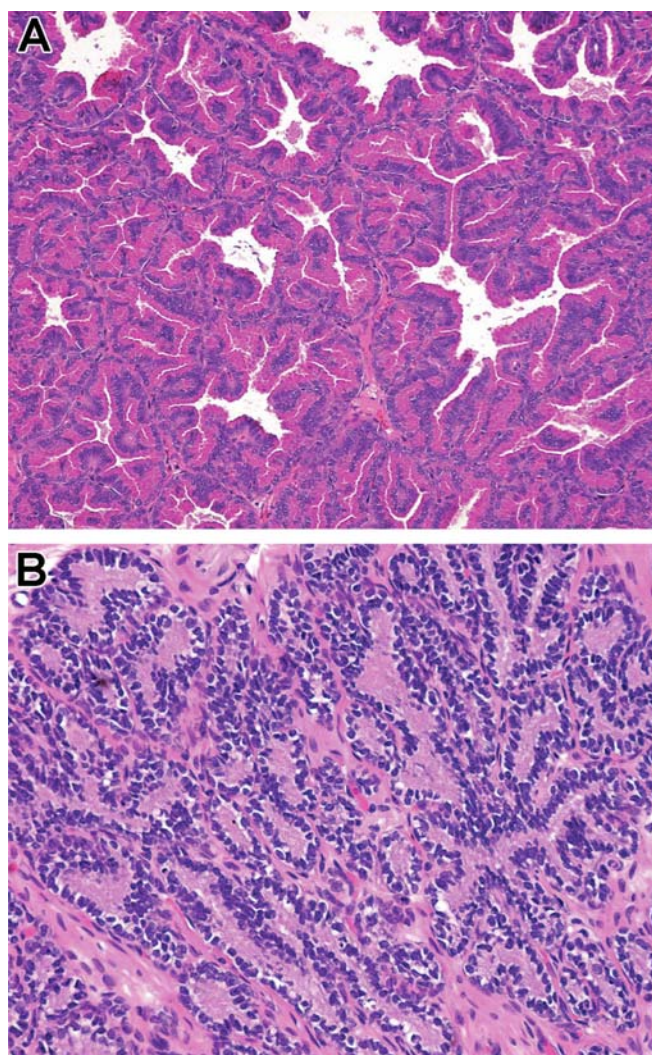


**FIGURE 9.47** Dog prostate is also sensitive to decreased androgenic activity. (A) Normal mature prostate. Dog, H&E,  $\times 10$ . (B) Mature prostate after antiandrogen administration demonstrating diffuse epithelial atrophy and decreased cytoplasmic secretory content. Dog, H&E,  $\times 10$ . Reproduced from Haschek WM, Rousseaux CG, Wallig MA, editors: *Haschek and Rousseaux's handbook of toxicologic pathology*, ed 3, 2013, Academic Press, Figure 59.44, p. 2589, with permission.

Although efferent duct obstruction and granulomas can be seen as a background incidental lesion in rats (Creasy, 2012), they can also be caused by a chemically induced disturbance of fluid reabsorption (Hess and Nakai, 2000; Heuser et al., 2013; La et al., 2012). It is important to recognize and distinguish tubular dilation and tubular degeneration/atrophy due to efferent duct blockage from other types of testicular

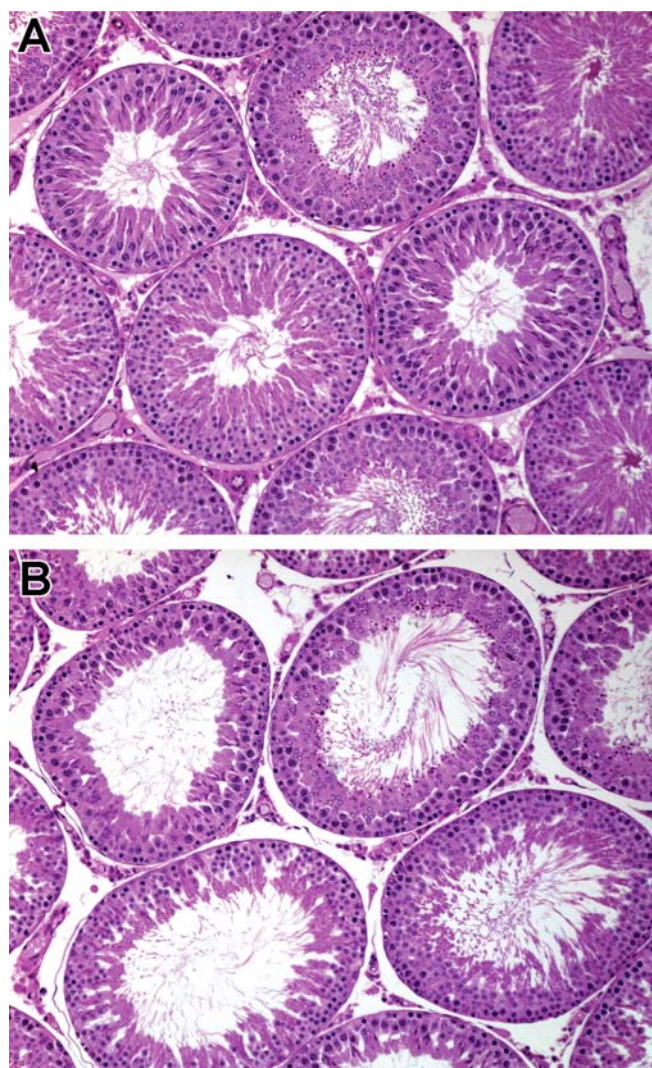


**FIGURE 9.48** Tubular dilation produced by an endothelin antagonist in the rat. (A) Normal testis. Rat, H&E,  $\times 10$ . (B) Treated group, testis. Note that there is no germ cell degeneration or depletion. Rat, H&E,  $\times 10$ . Reproduced from Haschek WM, Rousseaux CG, Wallig MA, editors: *Haschek and Rousseaux's handbook of toxicologic pathology*, ed 3, 2013, Academic Press, Figure 59.45, p. 2589, with permission.

toxicity, because the testicular damage is secondary to build-up of fluid pressure rather than a primary effect on spermatogenesis. Hallmarks of this type of toxicity include the phenomena that the lesions are frequently unilateral, some animals may have one dilated and one normal testis, others may have one atrophic and one normal testis and yet others may have one dilated and one atrophic testis. Another feature is that atrophic tubules often have a patent or



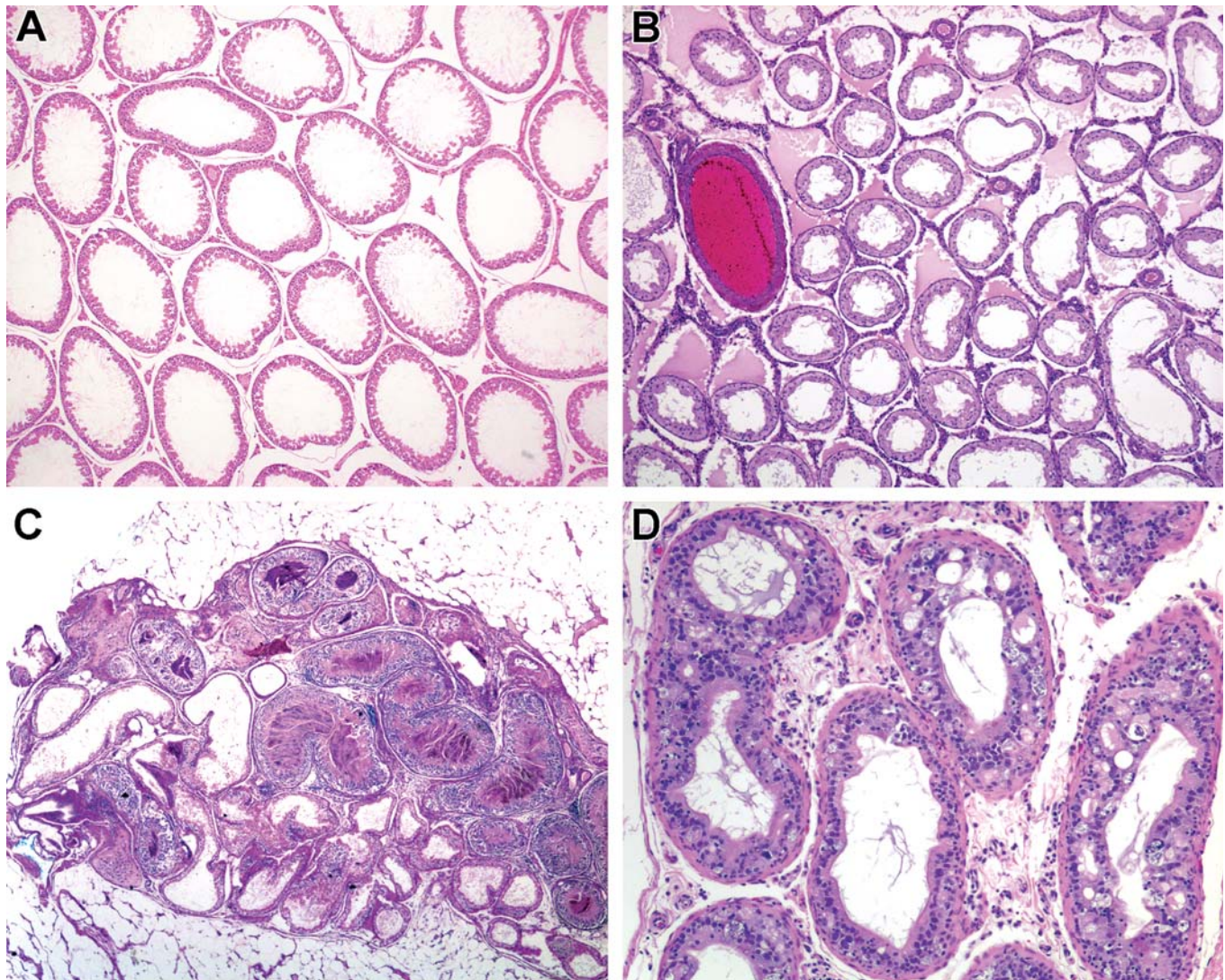


**FIGURE 9.49** Testicular and epididymal changes secondary to efferent duct blockage in the rat. (A) Diffuse tubular dilation (this is the early change) H&E,  $\times 4$ . (B) Diffuse tubular atrophy with dilated lumens and interstitial edema (this is a progression from tubular dilation). H&E,  $\times 4$ . (C) Efferent duct obstruction caused by sperm stasis and granulomatous inflammation. H&E,  $\times 2$ . (D) Absence of sperm and cribriform change within the epididymis may accompany efferent duct obstruction. H&E,  $\times 20$ . Reproduced from Haschek WM, Rousseaux CG, Wallig MA, editors: *Haschek and Rousseaux's handbook of toxicologic pathology*, ed 3, 2013, Academic Press, Figure 59.46, p. 2591, with permission.

slightly dilated lumen (rather than collapsed lumen) and the rete testis may be dilated. Due to the fact that the testicular lesion (initially dilation followed by atrophy) will only develop when there are enough efferent ducts obstructed to cause sufficient backpressure to the testis, the incidence may be sporadic and not show a strong dose relationship (La et al., 2012). In addition, apoptosis in the epithelium of the initial segment

of the epididymis can be seen when the efferent ducts are obstructed (Figure 9.49D) (Kim and Breton, 2020; Robaire and Fan, 1998). This spectrum of changes described here are rodent specific due to the anatomy of the efferent ducts (see Section 2.5). Sperm granulomas in the efferent ducts of others species are unlikely to cause obstructive effects in the testis due to the parallel array of efferent ducts (Foley et al., 1995).



### 5.3. Mechanisms of Developmental Toxicity

(See *New Frontiers in Endocrine Disruptor Research*, Vol 3, Chap 12)

#### 5.3.1. Effects via Estrogen Receptors

Methoxychlor is an insecticide whose metabolite displays both estrogenic and antiandrogenic activity in vitro and in vivo. If treatment is administered at weaning, methoxychlor will induce several effects in male rat offspring, including a delay in puberty (lack of preputial separation) and reduced accessory sex gland size (Gray et al., 1989). Interestingly, no effects on circulating levels of LH or testosterone were noted in the presence of delayed puberty (Gray et al., 1999a).

Methoxychlor is metabolized extensively to HPTE (2,2-bis [p-phenylhydroxyphenyl]- 1,1,1-trichloroethane), which displays interactions with estrogen receptor  $\alpha$ , estrogen receptor  $\beta$ , and the AR (Gaido et al., 2000; Maness et al., 1998). The lack of effect of methoxychlor on LH (estradiol tends to decrease and antiandrogens [such as flutamide] to increase these levels) makes it difficult to determine which of these receptor interactions is responsible for biological activity. The lack of an effect on LH is perhaps suggestive that, rather than working through the pituitary, the agent may have a direct effect on the reproductive tract.

#### 5.3.2. Effects via the Androgen Receptor

In rats, in utero exposure to antiandrogens such as flutamide causes a spectrum of changes in male offspring including decreased AGD, nipple retention, hypospadias, cryptorchidism, and decreased development of the accessory sex organs (McIntyre et al., 2001). Vinclozolin is a well-characterized fungicide with AR antagonism (Gray et al., 1994, 1999b; Kavlock and Cummings, 2005). The effects of vinclozolin and its metabolites on male reproductive function and development are well documented and related to their ability to interact with AR and disturb androgen-dependent gene expression. A wide variety of antiandrogenic male effects are noted following exposure to vinclozolin during pregnancy in rats, including a female-like anogenital distance (AGD), retained nipples, cleft phallus with hypospadias, suprainguinal

ectopic testes, vaginal pouch, epididymal granulomas and agenesis, small or absent accessory sex glands, and delays in preputial separation. Even though many of these endpoints (reduced AGD, retained nipples, effects on accessory sex gland weight, hypospadias, epididymal agenesis) are believed to be elicited by interference at the level of the AR, statistically significant changes are seen with a wide variety of effective dose levels, and many do not exhibit an obvious dose-response threshold, suggesting that additional mechanisms are at work.

#### 5.3.3. 5 $\alpha$ -Reductase Inhibition

Finasteride is a drug developed to inhibit the enzyme 5 $\alpha$ -reductase, which normally converts testosterone to the more active DHT (Steiner, 1993). The drug has principally been used to combat androgen-dependent prostate cancer, but has more recently received attention through its prescription use for hair loss in adult men (Ekman, 1999). Because DHT plays such a significant role in the development of the male reproductive tract, it is not surprising that inhibition of the enzyme responsible for its biosynthesis will produce profound effects on those male reproductive tissues dependent on it: the prostate and external genitalia. In the rodent, treatment of the dam with finasteride at a dose of 25 mg/kg/day results in significant feminization of the external genitalia in male offspring (Imperato-McGinley et al., 1992). There is no further feminization of the genitalia at doses up to 300 mg/kg/day. There is also a significant decrease in prostate size at 25 and 50 mg/kg/day, with no further decrease at higher doses. Furthermore, external genital abnormalities can be produced in male macaque fetuses when dams are exposed to a low oral dose (2 mg/kg/day) of finasteride (Prahalada et al., 1997). These studies clearly demonstrate the dependency of both prostate and male external genital differentiation on DHT. However, unlike AR blockade with flutamide, finasteride did not totally abolish prostate differentiation or completely feminize the external genitalia, despite increasingly higher dose levels. These results suggest that testosterone can compensate for DHT to some degree at the level of the AR. Wolffian differentiation, however, was not affected by the inhibition of DHT, demonstrating its testosterone dependency, but seminal vesicle

growth was impaired. AR blockade can inhibit testicular descent more effectively than inhibition of 5 $\alpha$ -reductase activity.

#### **5.3.4. Steroid Biosynthesis Inhibition**

Ketoconazole is an orally active fungicide that elicits its action by the inhibition of cytochrome P450-mediated sterol metabolism in fungi (Van Tyle, 1984). It also has broad activity against many cytochrome P450 enzymes, including those involved in P450-mediated steroidogenesis in both humans and experimental animals (Ayub and Levell, 1989; Kan et al., 1985). Effects on Leydig cell function have been demonstrated in Leydig cells in vitro (Sikka et al., 1985). Due to its effects on ovarian and uterine steroid responses in the dam, it is more difficult to separate out the role of decreased fetal testicular testosterone production on male reproductive development from the possible roles of adrenal hormones. That is, treatment of pregnant dams with ketoconazole is more likely to affect the ability to maintain pregnancy due to effects on ovarian progesterone synthesis, resulting in abortion and litter loss, thus precluding the observation of marked effects on the pups.

#### **5.3.5. Other Potential Mechanisms: The Example of Di-n-butyl Phthalate**

Di-n-butyl phthalate (DBP) is a plasticizer and solvent and is known to target the rat testis of adults, juveniles, and embryos. DBP and other phthalates have been shown to be potent developmental reproductive toxicants when administered during late gestation, specifically during the masculinization programming window of embryonic day (E)15.5–18.5 in the rat (van den Driesche et al., 2017; Welsh et al., 2008). Based on its range of effects on the developing male reproductive tract, it has been proposed as an animal model for testicular dysgenesis syndrome (TDS). TDS comprises a hypothesis that testicular cancer, foci of malformed seminiferous tubules (dysgenesis), poor sperm quality, cryptorchidism, hypospadias, and decreased AGD in men all share a common origin in fetal life (Fisher et al., 2003; Sharpe and Skakkebaek, 2008; Skakkebaek et al., 2016). Numerous studies have demonstrated that in utero phthalate exposure during late gestation produces a “phthalate syndrome” in the male offspring including gross abnormalities of decreased AGD, retained

nipples, delayed preputial separation, cryptorchidism, hypospadias, epididymal and testicular malformations, and decreased sperm count (Foster, 2006). With the exception of testicular germ cell cancer, which is rare in rats, phthalate exposure in utero in rats otherwise recapitulates other hallmarks of TDS syndrome in humans (Johnson et al., 2012).

In addition to studies showing its gross developmental effects on the male reproductive system, it is one of the few developmental toxicants that has been studied in detail for its histopathologic effects on testicular and epididymal development (Barlow and Foster, 2003). In rats, maternal administration of DBP during late gestation results in a marked reduction in Leydig cell hormone (testosterone and insulin-like factor 3) production, reduced numbers of Sertoli cells, occurrence of multinucleated gonocytes (with two to four nuclei), abnormal persistence of gonocytes in postnatal life beyond the normal 10 days of age, and focal dysgenesis lesions (Figure 9.50A) (Barlow and Foster, 2003; Barlow et al., 2004; Mylchreest et al., 2002; Willson, 2021). These focal dysgenesis lesions are composed of focal, multifocal, or extensive malformed, anastomosing seminiferous tubules that contain immature-appearing Sertoli cells and lack spermatogenesis. These tubules are typically lined by thickened, hyalinized basement membranes and surrounded by large aggregates of fetal-like, spindloid Leydig cells (Barlow and Foster, 2003; Barlow et al., 2004; Lara et al., 2017; Willson, 2021). In addition, there is an increased incidence of epididymal malformations, including decreased coiling of the duct and partial or complete agenesis (Figure 9.50B) (Barlow and Foster, 2003; Barlow et al., 2004; Mylchreest et al., 2002).

Abnormal fetal Leydig cell aggregation toward the center of the testis has been demonstrated at E17.5 in rats, two days after initiating exposure to DBP at the start of the masculinization programming window (Lara et al., 2017). These abnormal aggregations of fetal-like Leydig cells, which may have been diagnosed as Leydig cell adenomas in some studies, persist throughout life (Barlow et al., 2004). Seminiferous cord formation occurs between E13.5 and 14.5 in the rat, even when DBP exposure is initiated via the dam at E13.5 (Lara et al., 2017). DBP exposure appears to then cause rupture of the

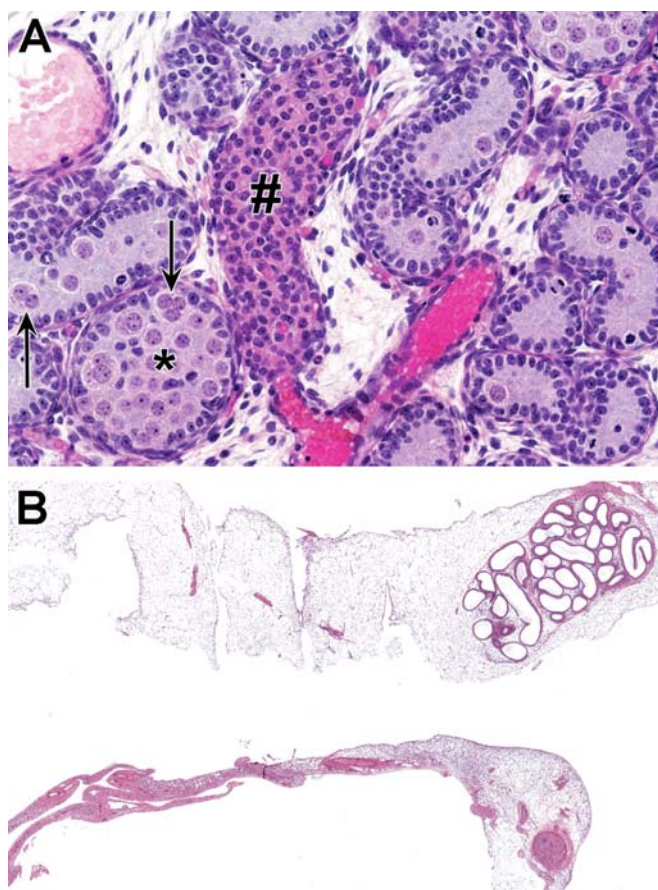


**FIGURE 9.50** Developmental toxicity of dibutyl phthalate (exposed in utero from gestation day 12) on the testis and epididymis of the rat. (A) Postnatal day 2 testis showing enlarged Leydig cell aggregates (#), multinucleate gonocytes, and occasional tubules with increased numbers of gonocytes (\*) (compare with Figure 9.1). Rat, H&E,  $\times 20$ . (B) Epididymal aplasia and hypoplasia at PND 49 following exposure in utero and up to PND 14. Rat, H&E  $\times 1.3$ . Reproduced from Haschek WM, Rousseaux CG, Wallig MA, editors: *Haschek and Rousseaux's handbook of toxicologic pathology*, ed 3, 2013, Academic Press, Figure 59.47, p. 2594, with permission.

cords at E18.5, with scattering of the peritubular myoid cells, Sertoli cells, and gonocytes in the interstitium (Lara et al., 2017). This rupture of seminiferous cords in utero may explain the occasional presence of ectopic cells (Sertoli cells and gonocytes in the interstitium and Leydig cells inside seminiferous tubules) and may be the origin of dysgenetic lesions, which first appear in early postnatal life and then persist throughout life (Lara et al., 2017).

Many of the effects of DBP on the developing male reproductive system are thought to result

from inhibition of testosterone synthesis in the fetal testes during a critical window in sexual development, but some may have mechanistic origins other than inhibition of testosterone. Other studies have indicated that neither DBP nor its metabolite monobutyl phthalate (MBP) interact directly with the AR. Thus, DBP probably represents a group of chemicals that markedly affect the androgen status of the fetus and disrupt reproductive development via a nonreceptor-mediated mechanism. The developmental effects, for example, cryptorchidism, appear to be due to the inhibition of testosterone and insulin-like factor 3 from the fetal Leydig cells (Foster, 2006). Also, alterations in seminiferous tubule development and increased incidence of multinucleated gonocytes have been observed in the testes of perinatal mice after DBP administration, despite the absence of testosterone inhibition (Gaido et al., 2007). Although germ cell tumors in rats are rare, the presence of multinucleated gonocytes in rodents exposed to DBP suggests abnormal germ cell differentiation. Impaired in utero germ cell differentiation is proposed to lead to impaired spermatogenesis in adult men and the development of the precursor lesion, germ cell neoplasia in situ, as well as testicular germ cell tumor (Skakkebaek et al., 2016).

## 6. CONCLUSION

Test article-related effects on the male reproductive system can have a profound effect on pharmaceutical and chemical development. The male reproductive system has several unique features that differ from other organ systems, including hormonal regulation; age-related changes during puberty; complex histology and timing of spermatogenesis; pronounced species differences; and evaluation occurring in the context of both repeated-dose general toxicology studies and stand-alone DART studies. This requires the pathologist to integrate toxicology and pathology endpoints with reproductive endocrinology, organ development, and comparative biology. This chapter provides an overview of the normal structure and function of the male reproductive system, details common methods for evaluation, describes patterns of spontaneous and induced injury, and reviews current



regulatory and translational issues in order to provide a guide for both new and experienced pathologists tasked with evaluating this complicated organ system.

## Acknowledgments

The authors acknowledge previous authors of this chapter, Drs. Dianne Creasy and Robert Chapin, and David Sabio for illustration support.

## REFERENCES

- Abe K, Takano H, Ito T: Microvasculature of the mouse epididymis, with special reference to fenestrated capillaries localized in the initial segment, *Anat. Rec.* 209:209–218, 1984.
- Abuelhija M, Weng CC, Shetty G, et al.: Differences in radiation sensitivity of recovery of spermatogenesis between rat strains, *Toxicol. Sci.* 126:545–553, 2012.
- Agnew DW, MacLachlan NJ: Tumors of the genital systems. In *Tumors in domestic animals*, 2016, pp 689–722.
- Aitken RJ, Baker MA: Causes and consequences of apoptosis in spermatozoa; contributions to infertility and impacts on development, *Int. J. Dev. Biol.* 57:265–272, 2013.
- Akhtar FB, Wickings EJ, Zaidi P, et al.: Pituitary and testicular functions in sexually mature rhesus monkeys under high-dose LRH-agonist treatment, *Acta Endocrinol.* 101:113–118, 1982.
- Alison RH, Capen CC, Prentice DE: Neoplastic lesions of questionable significance to humans, *Toxicol. Pathol.* 22:179–186, 1994.
- Amador A, Steger RW, Bartke A, et al.: Testicular LH receptors during aging in Fisher 344 rats, *J. Androl.* 6:61–64, 1985.
- Amann RP, Howards SS: Daily spermatozoal production and epididymal spermatozoal reserves of the human male, *J. Urol.* 124:211–215, 1980.
- Amann RP, Johnson L, Thompson Jr DL, et al.: Daily spermatozoal production, epididymal spermatozoal reserves and transit time of spermatozoa through the epididymis of the rhesus monkey, *Biol. Reprod.* 15:586–592, 1976.
- Andersson H, Tisell L-E: Morphology of rat prostatic lobes and seminal vesicles after long-term estrogen treatment, *Acta Pathol. Microbiol. Scand. Sect. A Pathol.* 90A:441–448, 1982.
- Andric SA, Kojic Z, Bjelic MM, et al.: The opposite roles of glucocorticoid and  $\alpha$ 1-adrenergic receptors in stress triggered apoptosis of rat Leydig cells, *Am. J. Physiol. Endocrinol. Metabol.* 304:E51–E59, 2013.
- Angelopoulou R, Balla M, Lavranos G, et al.: Sertoli cell proliferation in the fetal and neonatal rat testis: a continuous phenomenon? *Acta Histochem.* 110:341–347, 2008.
- Aoki VW, Liu L, Carrell DT: A novel mechanism of protamine expression deregulation highlighted by abnormal protamine transcript retention in infertile human males with sperm protamine deficiency, *Mol. Hum. Reprod.* 12:41–50, 2006.
- Ariyaratne HBS, Chamindrani Mendis-Handagama SML: Changes in the testis interstitium of Sprague Dawley rats from birth to sexual Maturity, *Biol. Reprod.* 62:680–690, 2000.
- Aslam H, Schneiders A, Perret M, et al.: Quantitative assessment of testicular germ cell production and kinematic and morphometric parameters of ejaculated spermatozoa in the grey mouse lemur, *Microcebus murinus*, *Reproduction* 123:323–332, 2002.
- Ayub M, Levell MJ: Inhibition of human adrenal steroidogenic enzymes in vitro by imidazole drugs including ketoconazole, *J. Steroid Biochem.* 32:515–524, 1989.
- Azzouni F, Godoy A, Li Y, et al.: The 5 alpha-reductase isozyme family: a review of basic biology and their role in human diseases, *Adv. Urol.*, 2012, <https://doi.org/10.1155/2012/530121>.
- Badia E, Briz MD, Pinart E, et al.: Structural and ultrastructural features of boar bulbourethral glands, *Tissue Cell* 38:7–18, 2006.
- Baert Y, Ruetschle I, Cools W, et al.: A multi-organ-chip co-culture of liver and testis equivalents: a first step toward a systemic male reprotoxicity model, *Hum. Reprod.* 35:1029–1044, 2020.
- Banerjee PP, Banerjee S, Dorsey R, et al.: Age- and lobe-specific responses of the brown Norway rat prostate to androgen, *Biol. Reprod.* 51:675–684, 1994.
- Banerjee S, Banerjee PP, Brown TR: Castration-induced apoptotic cell death in the Brown Norway rat prostate decreases as a function of age, *Endocrinology* 141:821–832, 2000.
- Barlow NJ, Foster PM: Pathogenesis of male reproductive tract lesions from gestation through adulthood following in utero exposure to Di(n-butyl) phthalate, *Toxicol. Pathol.* 31:397–410, 2003.
- Barlow NJ, McIntyre BS, Foster PMD: Male reproductive tract lesions at 6, 12, and 18 Months of age following in utero exposure to di(n-butyl) phthalate, *Toxicol. Pathol.* 32:79–90, 2004.
- Barsoum I, Yao HH: The road to maleness: from testis to Wolffian duct, *Trends Endocrinol. Metabol.* 17:223–228, 2006.
- Bartlett JMS, Kerr JB, Sharpe RM: The effect of selective destruction and regeneration of rat leydig cells on the intratesticular distribution of testosterone and morphology of the seminiferous epithelium, *J. Androl.* 7:240–253, 1986.
- Beil RE, Hart RC: Cowper's gland secretion in rat semen coagulation, II. Identification of the potentiating factor secreted by the coagulating glands, *Biol. Reprod.* 8:613–617, 1973.
- Beltramo M, Dardente H, Cayla X, et al.: Cellular mechanisms and integrative timing of neuroendocrine control of GnRH secretion by kisspeptin, *Mol. Cell. Endocrinol.* 382:387–399, 2014.
- Bergh A, Collin O, Lissbrant E: Effects of acute graded reductions in testicular blood flow on testicular morphology in the adult rat, *Biol. Reprod.* 64:13–20, 2001.

- Bernanke J, Köhler HR: The impact of environmental chemicals on wildlife vertebrates, *Rev. Environ. Contam. Toxicol.* 198:1–47, 2009.
- Biegel LB, Liu RC, Hurtt ME, et al.: Effects of ammonium perfluorooctanoate on Leydig cell function: in vitro, in vivo, and ex vivo studies, *Toxicol. Appl. Pharmacol.* 134: 18–25, 1995.
- Bilinska B, Kotula-Balak M, Sadowska J: Morphology and function of human Leydig cells in vitro. Immunocytochemical and radioimmunological analyses, *Eur. J. Histochem.* 53, 2009.
- Blackburn DM, Gray AJ, Lloyd SC, et al.: A comparison of the effects of the three isomers of dinitrobenzene on the testis in the rat, *Toxicol. Appl. Pharmacol.* 92:54–64, 1988.
- Blanchard KT, Lee J, Boekelheide K: Leuprolide, a gonadotropin-releasing hormone agonist, reestablishes spermatogenesis after 2,5-hexanedione-induced irreversible testicular injury in the rat, resulting in normalized stem cell factor expression, *Endocrinology* 139:236–244, 1998.
- Boekelheide K: Mechanisms of toxic damage to spermatogenesis, *J. Natl. Cancer Inst. Monogr.*, 2005:6–8, 2005.
- Bohmer T, Hansson V: Androgen-dependent accumulation of carnitine by rat epididymis after injection of [3H]butyrobetaine in vivo, *Mol. Cell. Endocrinol.* 3:103–115, 1975.
- Bonneau M, Carrié-Lemoine J, Prunier A, et al.: Age-related changes in plasma LH and testosterone concentration profiles and fat 5 $\alpha$ -androstenone content in the young boar, *Anim. Reprod. Sci.* 15:241–258, 1987.
- Borg CL, Wolski KM, Gibbs GM, et al.: Phenotyping male infertility in the mouse: how to get the most out of a 'non-performer', *Hum. Reprod. Update* 16:205–224, 2009.
- Bosland MC: Animal models for the study of prostate carcinogenesis, *J. Cell. Biochem. Suppl.* 16h:89–98, 1992.
- Bradley AE, Wancket LM, Rinke M, et al.: International harmonization of nomenclature and diagnostic criteria (INHAND): nonproliferative and proliferative lesions of the rabbit, *J. Toxicol. Pathol.* 34:183s–292s, 2021.
- Bremner WJ, Millar MR, Sharpe RM, et al.: Immunohistochemical localization of androgen receptors in the rat testis: evidence for stage-dependent expression and regulation by androgens, *Endocrinology* 135:1227–1234, 1994.
- Brown CD, Miller MG: Effect of culture age on 1,3-dinitrobenzene metabolism and indicators of cellular toxicity in rat testicular cells, *Toxicol. Vitro* 5:269–275, 1991.
- Browning JY, Heindel JJ, Grotjan Jr HE: Primary culture of purified Leydig cells isolated from adult rat testes, *Endocrinology* 112:543–549, 1983.
- Brun HP, Leonard JF, Moronvalle V, et al.: Pig Leydig cell culture: a useful in vitro test for evaluating the testicular toxicity of compounds, *Toxicol. Appl. Pharmacol.* 108:307–320, 1991.
- Bullock BC, Newbold RR, McLachlan JA: Lesions of testis and epididymis associated with prenatal diethylstilbestrol exposure, *Environ. Health Perspect.* 77:29–31, 1988.
- Campion SN, Carvallo FR, Chapin RE, et al.: Comparative assessment of the timing of sexual maturation in male Wistar Han and Sprague-Dawley rats, *Reprod. Toxicol.* 38: 16–24, 2013.
- Capel B: The battle of the sexes, *Mech. Dev.* 92:89–103, 2000.
- Cappone GD, Potter D, Hurtt ME, et al.: Sensitivity of male reproductive endpoints in nonhuman primate toxicity studies: a statistical power analysis, *Reprod. Toxicol.* 41:67–72, 2013.
- Carr TL, Ciurlionis R, Milicic I, et al.: Role of cytochrome P450c17 $\alpha$  in dibromoacetic acid-induced testicular toxicity in rats, *Arch. Toxicol.* 85:513–523, 2011.
- Carreau S, Hess RA: Oestrogens and spermatogenesis, *Philos. Trans. R. Soc. Lond. B Biol. Sci.* 365:1517–1535, 2010.
- Catlin NR, Huse SM, Boekelheide K: The stage-specific testicular germ cell apoptotic response to low-dose X-irradiation and 2,5-hexanedione combined exposure. I: validation of the laser capture microdissection method for qRT-PCR array application, *Toxicol. Pathol.* 42:1221–1228, 2014.
- Catlin NR, Willson CJ, Creasy DM, et al.: Differentiating between testicular toxicity and sexual immaturity in orthophthalaldehyde inhalation toxicity studies in rats and mice, *Toxicol. Pathol.* 46:753–763, 2018.
- Chapin R, Gulati D, Hope E, et al.: Reproductive toxicology. Nitrofurantoin, *Environ. Health Perspect.* 105(Suppl 1):329–330, 1997.
- Chapin R, Weinbauer G, Thibodeau MS, et al.: Summary of the HESI consortium studies exploring circulating inhibin B as a potential biomarker of testis damage in the rat, *Birth Defects Res. Part B Dev. Reproductive Toxicol.* 98:110–118, 2013.
- Chapin RE, Creasy DM: Assessment of circulating hormones in regulatory toxicity studies II. Male reproductive hormones, *Toxicol. Pathol.* 40:1063–1078, 2012.
- Chapin RE, Dutton SL, Ross MD, et al.: The effects of ethylene glycol monomethyl ether on testicular histology in F344 rats, *J. Androl.* 5:369–380, 1984a.
- Chapin RE, Gulati DK, Barnes LH, et al.: The effects of feed restriction on reproductive function in Sprague-Dawley rats, *Fund. Appl. Toxicol.* 20:23–29, 1993a.
- Chapin RE, Gulati DK, Fail PA, et al.: The effects of feed restriction on reproductive function in Swiss CD-1 mice, *Fund. Appl. Toxicol.* 20:15–22, 1993b.
- Chapin RE, Morgan KT, Bus JS: The morphogenesis of testicular degeneration induced in rats by orally administered 2,5-hexanedione, *Exp. Mol. Pathol.* 38:149–169, 1983.
- Chapin RE, White RD, Morgan KT, et al.: Studies of lesions induced in the testis and epididymis of F-344 rats by inhaled methyl chloride, *Toxicol. Appl. Pharmacol.* 76:328–343, 1984b.
- Chatani F: Testicular focal necrosis induced by hCG in rats time-course and age- and strain-differences, *J. Toxicol. Pathol.* 9:369–379, 1996.
- Chatani F: Possible mechanism for testicular focal necrosis induced by hCG in rats, *J. Toxicol. Sci.* 31:291–303, 2006.

- Chellman GJ, Bus JS, Working PK: Role of epididymal inflammation in the induction of dominant lethal mutations in Fischer 344 rat sperm by methyl chloride, *Proc. Natl. Acad. Sci. U. S. A.* 83:8087–8091, 1986.
- Cheng CY, Mruk DD: A local autocrine axis in the testes that regulates spermatogenesis, *Nat. Rev. Endocrinol.* 6:380–395, 2010.
- Cheng CY, Mruk DD: The blood-testis barrier and its implications for male contraception, *Pharmacol. Rev.* 64:16–64, 2012.
- Chiao YB, Van Thiel DH: Characterization of rat testicular alcohol dehydrogenase, *Alcohol Alcohol* 21:9–15, 1986.
- Chubb C, Desjardins C: Vasculature of the mouse, rat, and rabbit testis-epididymis, *Am. J. Anat.* 165:357–372, 1982.
- Clemo FAS, Evering WE, Snyder PW, et al.: Differentiating spontaneous from drug-induced vascular injury in the dog, *Toxicol. Pathol.* 31:25–31, 2003.
- Clermont Y: Kinetics of spermatogenesis in mammals: seminiferous epithelium cycle and spermatogonial renewal, *Physiol. Rev.* 52:198–236, 1972.
- Clifton DK, Bremner WJ: The effect of testicular x-irradiation on spermatogenesis in man. A comparison with the mouse, *J. Androl.* 4:387–392, 1983.
- Cline JM, Brignolo L, Ford EW: Chapter 10 - urogenital system. In Abee CR, Mansfield K, Tardif S, et al., editors: *Nonhuman primates in biomedical research*, Second Edition, Boston, 2012, Academic Press, pp 483–562.
- Colman K, Andrews RN, Atkins H, et al.: International harmonization of nomenclature and diagnostic criteria (INHAND): non-proliferative and proliferative lesions of the non-human primate (*M. fascicularis*), *J. Toxicol. Pathol.* 34:1s–182s, 2021.
- Cook JC, Klinefelter GR, Hardisty JF, et al.: Rodent leydig cell tumorigenesis: a review of the physiology, pathology, mechanisms, and relevance to humans, *Crit. Rev. Toxicol.* 29:169–261, 1999.
- Cooke PS, Nanjappa MK, Ko C, et al.: Estrogens in male physiology, *Physiol. Rev.* 97:995–1043, 2017.
- Coppenolle FV, Slomianny C, Carpentier F, et al.: Effects of hyperprolactinemia on rat prostate growth: evidence of androgeno-dependence, *Am. J. Physiol. Endocrinol. Metabol.* 280:E120–E129, 2001.
- Coquelin A, Desjardins C: Luteinizing hormone and testosterone secretion in young and old male mice, *Am. J. Physiol.* 243:E257–E263, 1982.
- Coulson M, Gibson GG, Plant N, et al.: Lansoprazole increases testosterone metabolism and clearance in male Sprague-Dawley rats: implications for Leydig cell carcinogenesis, *Toxicol. Appl. Pharmacol.* 192:154–163, 2003.
- Coviello AD, Bremner WJ, Matsumoto AM, et al.: Intra-testicular testosterone concentrations comparable with serum levels are not sufficient to maintain normal sperm production in men receiving a hormonal contraceptive regimen, *J. Androl.* 25:931–938, 2004.
- Creasy D: *Endocrine disruption: a guidance document for histologic evaluation of endocrine and reproductive tests. Part 2: male reproductive system. Organization of economic cooperation and development*, 2008.
- Creasy D: Chapter 9 - Reproduction of the rat, mouse, dog, non-human primate and minipig. In McInnes EF, editor: *Background lesions in laboratory animals*, Saint Louis, 2012, W.B. Saunders, pp 101–122.
- Creasy D, Bube A, deRijk E, et al.: Proliferative and non-proliferative lesions of the rat and mouse male reproductive system, *Toxicol. Pathol.* 40:40S–121S, 2012.
- Creasy DM: Pathogenesis of male reproductive toxicity, *Toxicol. Pathol.* 29:64–76, 2001.
- Creasy DM: Histopathology of the male reproductive system I: techniques, *Curr. Protoc. Toxicol.* 16, 2002, <https://doi.org/10.1002/0471140856.tx1603s12>. PMID: 20963755.
- Creasy DM, Beech LM, Gray TJ, et al.: An ultrastructural study of ethylene glycol monomethyl ether-induced spermatocyte injury in the rat, *Exp. Mol. Pathol.* 45:311–322, 1986.
- Creasy DM, Chapin RE: Testicular and epididymal toxicity: pathogenesis and potential mechanisms of toxicity, *Spermatogenesis* 4, 2015.
- Czoty PW, Gould RW, Nader MA: Relationship between social rank and cortisol and testosterone concentrations in male cynomolgus monkeys (*Macaca fascicularis*), *J. Neuroendocrinol.* 21:68–76, 2009.
- D'Agata R, Vicari E, Aliffi A, et al.: Direct evidence in men for a role of endogenous oestrogens on gonadotrophin release, *Acta Endocrinol.* 97:145–149, 1981.
- D'Andrea MR, Alicknavitch M, Nagele RG, et al.: Simultaneous PCNA and TUNEL labeling for testicular toxicity evaluation suggests that detection of apoptosis may be more sensitive than proliferation, *Biotech. Histochem.* 85:195–204, 2010.
- de Andrade SF, Oliva SU, Klinefelter GR, et al.: Epididymis-specific pathologic disorders in rats exposed to gossypol from weaning through puberty, *Toxicol. Pathol.* 34:730–737, 2006.
- De Grava Kempinas W, Klinefelter GR: Interpreting histopathology in the epididymis, *Spermatogenesis* 4:e979114, 2014.
- de Kretser DM, Buzzard JJ, Okuma Y, et al.: The role of activin, follistatin and inhibin in testicular physiology, *Mol. Cell. Endocrinol.* 225:57–64, 2004.
- de Kretser DM, Meinhardt A, Meehan T, et al.: The roles of inhibin and related peptides in gonadal function, *Mol. Cell. Endocrinol.* 161:43–46, 2000.
- de Rooij DG: The nature and dynamics of spermatogonial stem cells, *Development* 144:3022–3030, 2017.
- DePalatis L, Moore J, Falvo RE: Plasma concentrations of testosterone and LH in the male dog, *J. Reprod. Fertil.* 52: 201–207, 1978.
- Dere E, Spade DJ, Hall SJ, et al.: Identification of sperm mRNA biomarkers associated with testis injury during preclinical testing of pharmaceutical compounds, *Toxicol. Appl. Pharmacol.* 320:1–7, 2017.



- Dincer Z, Piccicuto V, Walker UJ, et al.: Spontaneous and Drug-induced arteritis/polyarteritis in the Göttingen minipig—review, *Toxicol. Pathol.* 46:121–130, 2018.
- Donaubauer HH, Kramer M, Krieg K, et al.: Investigations of the carcinogenicity of the LH-RH analog buserelin (HOE 766) in rats using the subcutaneous route of administration, *Fund. Appl. Toxicol.* 9:738–752, 1987.
- Dorso L, Chanut F, Howroyd P, et al.: Variability in weight and histological appearance of the prostate of Beagle dogs used in toxicology studies, *Toxicol. Pathol.* 36:917–925, 2008.
- Dostal LA, Juneau P, Rothwell CE: Repeated analysis of semen parameters in beagle dogs during a 2-year study with the HMG-CoA reductase inhibitor, atorvastatin, *Toxicol. Sci.* 61: 128–134, 2001.
- Dreef HC, van Esch E, Rijk EPCT D: Spermatogenesis in the cynomolgus monkey (*Macaca fascicularis*): a practical guide for routine morphological staging, *Toxicol. Pathol.* 35:395–404, 2007.
- Dyce KM, Sack WO, Wensing CJG: *Textbook of veterinary anatomy*, Philadelphia, 1987, Saunders, pp 162–204.
- Dym M: The fine structure of monkey sertoli cells in the transitional zone at the junction of the seminiferous tubules with the tubuli recti, *Am. J. Anat.* 140:1–25, 1974.
- Dym M: The mammalian rete testis—a morphological examination, *Anat. Rec.* 186:493–523, 1976.
- Dym M, Fawcett DW: The blood-testis barrier in the rat and the physiological compartmentation of the seminiferous epithelium, *Biol. Reprod.* 3:308–326, 1970.
- Einarsson S, Andersson K, Wallgren M, et al.: Short- and long-term effects of immunization against gonadotropin-releasing hormone, using Improvac, on sexual maturity, reproductive organs and sperm morphology in male pigs, *Theriogenology* 71:302–310, 2009.
- Ekman P: Finasteride in the treatment of benign prostatic hypertrophy: an update. New indications for finasteride therapy, *Scand. J. Urol. Nephrol. Suppl.* 203:15–20, 1999.
- Ellis GB, Desjardins C: Male rats secrete luteinizing hormone and testosterone episodically, *Endocrinology* 110:1618–1627, 1982.
- Embree-Ku M, Venturini D, Boekelheide K: Fas is involved in the p53-dependent apoptotic response to ionizing radiation in mouse Testis1, *Biol. Reprod.* 66:1456–1461, 2002.
- EPA U: OPPTS 870.3800, reproduction and fertility effects: in health effects test guidelines, 1998. <https://www.regulations.gov/document/EPA-HQ-OPPT-2009-0156-0018>. (Accessed 22 February 2024).
- Evans B, Gannon BJ, Heath JW, et al.: Long-lasting damage to the internal male genital organs and their adrenergic innervation in rats following chronic treatment with the antihypertensive drug guanethidine, *Fertil. Steril.* 23:657–667, 1972.
- Everds NE, Snyder PW, Bailey KL, et al.: Interpreting stress responses during routine toxicity studies: a review of the biology, impact, and assessment, *Toxicol. Pathol.* 41:560–614, 2013.
- Ezer N, Robaire B: Androgenic regulation of the structure and functions of the epididymis. In Robaire B, Hinton B, editors: *The epididymis: from molecules to clinical practice*, New York, 2002, Kluwer Academic/Plenum Publishers, pp 297–316.
- Fan X, Robaire B: Orchidectomy induces a wave of apoptotic cell death in the epididymis, *Endocrinology* 139:2128–2136, 1998.
- Fawcett DW, Neaves WB, Flores MN: Comparative observations on intertubular lymphatics and the organization of the interstitial tissue of the mammalian testis, *Biol. Reprod.* 9:500–532, 1973.
- FDA: *Testicular toxicity: evaluation during drug development guidance for industry*, 2018.
- Fisher JS, Macpherson S, Marchetti N, et al.: Human 'testicular dysgenesis syndrome': a possible model using in-utero exposure of the rat to dibutyl phthalate, *Hum. Reprod.* 18: 1383–1394, 2003.
- Flickinger CJ, Howards SS: Consequences of obstruction on the epididymis. In Robaire B, Hinton B, editors: *The epididymis: from molecules to clinical practice*, New York, 2002, Kluwer Academic/Plenum Publishers, pp 503–522.
- Foley GL: Overview of male reproductive pathology, *Toxicol. Pathol.* 29:49–63, 2001.
- Foley GL, Bassily N, Hess RA: Intratubular spermatoc granu-  
lomas of the canine efferent ductules, *Toxicol. Pathol.* 23: 731–734, 1995.
- Foot RH, Swierstra EE, Hunt WL: Spermatogenesis in the dog, *Anat. Rec.* 173:341–351, 1972.
- Forkert PG, Lash LH, Nadeau V, et al.: Metabolism and toxicity of trichloroethylene in epididymis and testis, *Toxicol. Appl. Pharmacol.* 182:244–254, 2002.
- Fort FL, Miyajima H, Ando T, et al.: Mechanism for species-specific induction of Leydig cell tumors in rats by lansoprazole, *Fund. Appl. Toxicol.* 26:191–202, 1995.
- Foster P, Sheard C, Lloyd S: 1,3-Dinitrobenzene: a sertoli cell toxicant? In Stefanini M, Conti M, Geremia R, et al., editors: *Molecular and cellular endocrinology of the testis*, Netherlands, 1986, Excerpta Medica, pp 281–288.
- Foster PM: Disruption of reproductive development in male rat offspring following in utero exposure to phthalate esters, *Int. J. Androl.* 29:140–147, 2006.
- Foster PM, Creasy DM, Foster JR, et al.: Testicular toxicity produced by ethylene glycol monomethyl and monoethyl ethers in the rat, *Environ. Health Perspect.* 57:207–217, 1984.
- Foster PM, Harris MW: Changes in androgen-mediated reproductive development in male rat offspring following exposure to a single oral dose of flutamide at different gestational ages, *Toxicol. Sci.* 85:1024–1032, 2005.
- Foster WG, Maharaj-Briceño S, Cyr DG: Dioxin-induced changes in epididymal sperm count and spermatogenesis, *Environ. Health Perspect.* 118:458–464, 2010.
- Fouquet JP, Dadoune JP: Renewal of spermatogonia in the monkey (*Macaca fascicularis*), *Biol. Reprod.* 35:199–207, 1986.
- Franca LR, Auharek SA, Hess RA, et al.: Blood-tissue barriers: morphofunctional and immunological aspects of the blood-

- testis and blood-epididymal barriers, *Adv. Exp. Med. Biol.* 763:237–259, 2012.
- Franca LR, Avelar GF, Almeida FF: Spermatogenesis and sperm transit through the epididymis in mammals with emphasis on pigs, *Theriogenology* 63:300–318, 2005.
- Franca LR, Silva Jr VA, Chiarini-Garcia H, et al.: Cell proliferation and hormonal changes during postnatal development of the testis in the pig, *Biol. Reprod.* 63:1629–1636, 2000.
- Frank J, Confino E, Friberg J, et al.: Effect of ejaculation frequency on sperm quality, *Arch. Androl.* 16:203–207, 1986.
- Free MJ, Schluntz GA, Jaffe RA: Respiratory gas tensions in tissues and fluids of the male rat reproductive tract, *Biol. Reprod.* 14:481–488, 1976.
- Friry-Santini C, Rouquié D, Kennel P, et al.: Correlation between protein accumulation profiles and conventional toxicological findings using a model antiandrogenic compound, flutamide, *Toxicol. Sci.* 97:81–93, 2007.
- Fukushima T, Taki K, Ise R, et al.: MicroRNAs expression in the ethylene glycol monomethyl ether-induced testicular lesion, *J. Toxicol. Sci.* 36:601–611, 2011.
- Gaido KW, Hensley JB, Liu D, et al.: Fetal mouse phthalate exposure shows that Gonocyte multinucleation is not associated with decreased testicular testosterone, *Toxicol. Sci.* 97:491–503, 2007.
- Gaido KW, Maness SC, McDonnell DP, et al.: Interaction of methoxychlor and related compounds with estrogen receptor alpha and beta, and androgen receptor: structure-activity studies, *Mol. Pharmacol.* 58:852–858, 2000.
- Gao H-B, Tong M-H, Hu Y-Q, et al.: Glucocorticoid induces apoptosis in rat Leydig cells, *Endocrinology* 143:130–138, 2002.
- García-Galiano D, Pinilla L, Tena-Sempere M: Sex steroids and the control of the Kiss1 system: developmental roles and major regulatory actions, *J. Neuroendocrinol.* 24:22–33, 2012.
- Geisinger A, Rodríguez-Casuriaga R: Flow cytometry for the isolation and characterization of rodent meiocytes, *Methods Mol. Biol.* 1471:217–230, 2017.
- Gilbert SF: *Developmental biology*, Eighth Edition 2006, Sinauer Associates Inc, pp 529–554.
- Gilibili RR, Vogl AW, Chang TKH, et al.: Localization of Cytochrome P450 and related enzymes in adult rat testis and downregulation by estradiol and bisphenol A, *Toxicol. Sci.* 140:26–39, 2014.
- Goedken MJ, Kerlin RL, Morton D: Spontaneous and age-related testicular findings in Beagle dogs, *Toxicol. Pathol.* 36:465–471, 2008.
- Gondos B, Berndtson WE: Postnatal and pubertal development. In Russell LD, Griswold MD, editors: *The Sertoli cell*, Clearwater, 1993, Cache River Press, pp 115–154.
- Granborg JR, Handler AM, Janfelt C: Mass spectrometry imaging in drug distribution and drug metabolism studies – principles, applications and perspectives, *TrAC, Trends Anal. Chem.* 146:116482, 2022.
- Gray Jr LE, Furr J, Ostby JS: Hershberger assay to investigate the effects of endocrine-disrupting compounds with androgenic or antiandrogenic activity in castrate-immature male rats, *Curr. Protoc. Toxicol.*, 2005, <https://doi.org/10.1002/0471140856.tx1609s26>.
- Gray Jr LE, Ostby J, Cooper RL, et al.: The estrogenic and antiandrogenic pesticide methoxychlor alters the reproductive tract and behavior without affecting pituitary size or LH and prolactin secretion in male rats, *Toxicol. Ind. Health* 15:37–47, 1999a.
- Gray Jr LE, Ostby J, Ferrell J, et al.: A dose-response analysis of methoxychlor-induced alterations of reproductive development and function in the rat, *Fund. Appl. Toxicol.* 12:92–108, 1989.
- Gray Jr LE, Ostby J, Monosson E, et al.: Environmental antiandrogens: low doses of the fungicide vinclozolin alter sexual differentiation of the male rat, *Toxicol. Ind. Health* 15:48–64, 1999b.
- Gray Jr LE, Ostby JS, Kelce WR: Developmental effects of an environmental antiandrogen: the fungicide vinclozolin alters sex differentiation of the male rat, *Toxicol. Appl. Pharmacol.* 129:46–52, 1994.
- Gray TJ, Gangolli SD: Aspects of the testicular toxicity of phthalate esters, *Environ. Health Perspect.* 65:229–235, 1986.
- Greer WE, Roussel JD, Austin CR: Prevention of coagulation in monkey semen by surgery, *J. Reprod. Fertil.* 15:153–155, 1968.
- Gu N-H, Zhao W-L, Wang G-S, et al.: Comparative analysis of mammalian sperm ultrastructure reveals relationships between sperm morphology, mitochondrial functions and motility, *Reprod. Biol. Endocrinol.* 17(66), 2019, <https://doi.org/10.1186/s12958-019-0510-y>.
- Gunn SA, Gould TC, Anderson WA: The selective injurious response of testicular and epididymal blood vessels to cadmium and its prevention by zinc, *Am. J. Pathol.* 42:685–702, 1963.
- Gurney JK, McGlynn KA, Stanley J, Merriman T, Signal V, Shaw C, Sarfati D: Risk factors for cryptorchidism, *Nat. Rev. Urol.* 14(9):534–548, 2017.
- Habenicht UF, el Etreby MF: The periurethral zone of the prostate of the cynomolgus monkey is the most sensitive prostate part for an estrogenic stimulus, *Prostate* 13:305–316, 1988.
- Hadley MA, Dym M: Immunocytochemistry of extracellular matrix in the lamina propria of the rat testis: electron microscopic Localization, *Biol. Reprod.* 37:1283–1289, 1987.
- Hales DB: Testicular macrophage modulation of Leydig cell steroidogenesis, *J. Reprod. Immunol.* 57:3–18, 2002.
- Halpern WG, Ameri M, Bowman CJ, et al.: Scientific and regulatory policy committee points to consider review, *Toxicol. Pathol.* 44:789–809, 2016.
- Hannema SE, Hughes IA: Regulation of Wolffian duct development, *Horm. Res.* 67:142–151, 2007.
- Harari A, Wood CE, Van Doorslaer K, et al.: Condylomatous genital lesions in cynomolgus macaques from Mauritius, *Toxicol. Pathol.* 41:893–901, 2013.

- Harneit S, Paust HJ, Mukhopadhyay AK, et al.: Localization of endothelin-1 and endothelin-receptors A and B in human epididymis, *Mol. Hum. Reprod.* 3:579–584, 1997.
- Harrison RG: Functional importance of the vascularization of the testis and epididymis for the maintenance of normal spermatogenesis, *Fertil. Steril.* 3:366–375, 1952.
- Haruyama E, Suda M, Ayukawa Y, et al.: Testicular development in cynomolgus monkeys, *Toxicol. Pathol.* 40:935–942, 2012.
- Heindel J, George J, Fail P, et al.: Reproductive toxicology. Nitrofurazone, *Environ. Health Perspect.* 105(Suppl 1):331–333, 1997.
- Helke KL, Nelson KN, Sargeant AM, et al.: Background pathological changes in minipigs: a comparison of the incidence and nature among different breeds and populations of minipigs, *Toxicol. Pathol.* 44:325–337, 2016.
- Hermo L, Barin K, Robaire B: Structural differentiation of the epithelial cells of the testicular excurrent duct system of rats during postnatal development, *Anat. Rec.* 233:205–228, 1992.
- Hermo L, Robaire B: Epididymal cell types and their functions. In Robaire B, Hinton B, editors: *The epididymis: from molecules to clinical practice*, New York, 2002, Kluwer Academic/Plenum Publishers, pp 81–102.
- Hess RA: Oestrogen in fluid transport and reabsorption in efferent ducts of the male reproductive tract, *Rev. Reprod.* 5: 84–92, 2000.
- Hess RA: The efferent ductules: structure and functions. In Robaire B, Hinton B, editors: *The epididymis: from molecules to clinical practice*, New York, 2002, Kluwer Academic/Plenum Publishers, pp 49–80.
- Hess RA: Disruption of estrogen receptor signaling and similar pathways in the efferent ductules and initial segments of the epididymis, *Spermatogenesis* 4:e979103, 2014.
- Hess RA, Cooke PS, Bunick D, et al.: Adult testicular enlargement induced by neonatal hypothyroidism is accompanied by increased Sertoli and germ cell numbers, *Endocrinol* 132:2607–2613, 1993.
- Hess RA, Fernandes SA, Gomes GR, et al.: Estrogen and its receptors in efferent ductules and epididymis, *J. Androl.* 32: 600–613, 2011.
- Hess RA, Hermo L, Testis R: Structure, cell biology and site for stem cell transplantation. In Skinner MK, editor: *Encyclopedia of reproduction*, Second Edition, Oxford, 2018, Academic Press, pp 263–269.
- Hess RA, Linder RE, Strader LF, et al.: Acute effects and long-term sequelae of 1,3-dinitrobenzene on male reproduction in the rat. II. Quantitative and qualitative histopathology of the testis, *J. Androl.* 9:327–342, 1988.
- Hess RA, Nakai M: Histopathology of the male reproductive system induced by the fungicide benomyl, *Histol. Histopathol.* 15:207–224, 2000.
- Hess RA: Renato de Franca L: Spermatogenesis and cycle of the seminiferous epithelium, *Adv. Exp. Med. Biol.* 636:1–15, 2008.
- Heuser A, Mecklenburg L, Ockert D, et al.: Selective inhibition of PDE4 in Wistar rats can lead to dilatation in testis, efferent ducts, and epididymis and subsequent formation of sperm granulomas, *Toxicol. Pathol.* 41:615–627, 2013.
- Holtz W, Foote RH: The anatomy of the reproductive system in male Dutch rabbits (*Oryctolagus cuniculus*) with special emphasis on the accessory sex glands, *J. Morphol.* 158:1–20, 1978.
- Howroyd PC, Peter B: de Rijk E: Review of Sexual Maturity in the Minipig, *Toxicol. Pathol.* 44:607–611, 2016.
- Hubbard GB, Eason RL, Wood DH: Prostatic carcinoma in a rhesus monkey (*Macaca mulatta*), *Vet. Pathol.* 22:88–90, 1985.
- Hughes J, Berger T: Development of apical blebbing in the boar epididymis, *PLoS One* 10:e0126848, 2015.
- Huhtaniemi I: Mechanisms in endocrinology: hormonal regulation of spermatogenesis: mutant mice challenging old paradigms, *Eur. J. Endocrinol.* 179:R143–R150, 2018.
- Huleihel M, Lunenfeld E: Regulation of spermatogenesis by paracrine/autocrine testicular factors, *Asian J. Androl.* 6: 259–268, 2004.
- Hutson JM, Nation T, Balic A, et al.: The role of the gubernaculum in the descent and undescend of the testis, *Ther. Adv. Urol.* 1:115–121, 2009.
- ICH: International Conference on Harmonisation of Technical Requirements for Registration of Pharmaceuticals for Human Use M3(R2): Guidance on nonclinical safety studies for the conduct of human clinical trials and marketing authorization for pharmaceuticals, 2009. [https://database.ich.org/sites/default/files/M3\\_R2\\_Guideline.pdf](https://database.ich.org/sites/default/files/M3_R2_Guideline.pdf) Last accessed February 22, 2024.
- ICH: International Conference on Harmonisation of Technical Requirements for Registration of Pharmaceuticals for Human Use: *International conference on harmonization of technical requirements for registration of pharmaceuticals for human use. ICH harmonised tripartite guideline. Preclinical Safety Evaluation of Biotechnology-derived Pharmaceuticals.* S6(R1), [https://database.ich.org/sites/default/files/S6\\_R1\\_Guideline\\_0.pdf](https://database.ich.org/sites/default/files/S6_R1_Guideline_0.pdf). (Accessed 22 February 2024).
- ICH: International Council for Harmonisation of Technical Requirements for Pharmaceuticals for Human Use: *ICH harmonised guideline detection of reproductive and developmental toxicity for human pharmaceuticals* S5(R3), 2020. [https://database.ich.org/sites/default/files/S5-R3\\_Step4\\_Guideline\\_2020\\_0218.pdf](https://database.ich.org/sites/default/files/S5-R3_Step4_Guideline_2020_0218.pdf). (Accessed 22 February 2024).
- Ilio KY, Hess RA: Localization and activity of Na<sup>+</sup>,K<sup>+</sup>-ATPase in the ductuli efferentes of the rat, *Anat. Rec.* 234:190–200, 1992.
- Ilio KY, Hess RA: Structure and function of the ductuli efferentes: a review, *Microsc. Res. Tech.* 29:432–467, 1994.
- Imperato-McGinley J, Binienda Z, Gedney J, et al.: Nipple differentiation in fetal male rats treated with an inhibitor of the enzyme 5 alpha-reductase: definition of a selective role for dihydrotestosterone, *Endocrinology* 118:132–137, 1986.
- Imperato-McGinley J, Sanchez RS, Spencer JR, et al.: Comparison of the effects of the 5 alpha-reductase inhibitor



- finasteride and the antiandrogen flutamide on prostate and genital differentiation: dose-response studies, *Endocrinology* 131:1149–1156, 1992.
- Jacobson CF, Miller MG: Species difference in 1,3-dinitrobenzene testicular toxicity: in vitro correlation with glutathione status, *Reprod. Toxicol.* 12:49–56, 1998.
- Jahnukainen K, Chrysis D, Hou M, et al.: Increased apoptosis occurring during the first wave of spermatogenesis is stage-specific and primarily affects midpachytene spermatocytes in the rat Testis1, *Biol. Reprod.* 70:290–296, 2004.
- James RW, Heywood R: Age-related variations in the testes and prostate of beagle dogs, *Toxicology* 12:273–279, 1979.
- Jarow JP, Fang X, Hammad TA: Variability of semen parameters with time in placebo treated men, *J. Urol.* 189:1825–1829, 2013.
- Johnson KJ: Testicular histopathology associated with disruption of the Sertoli cell cytoskeleton, *Spermatogenesis* 4:e979106, 2014.
- Johnson KJ, Heger NE, Boekelheide K: Of mice and men (and rats): phthalate-induced fetal testis endocrine disruption is species-dependent, *Toxicol. Sci.* 129:235–248, 2012.
- Joseph A, Shur BD, Hess RA: Estrogen, efferent ductules, and the epididymis, *Biol. Reprod.* 84:207–217, 2011.
- Juniewicz PE, Oesterling JE, Walters JR, et al.: Aromatase inhibition in the dog. I effect on serum LH, serum testosterone concentrations, testicular secretions and spermatogenesis, *J. Urol.* 139:827–831, 1988.
- Junker Walker U, Nogués V: Changes induced by treatment with aromatase inhibitors in testicular Leydig cells of rats and dogs, *Exp. Toxicol. Pathol.* 46:211–213, 1994.
- Kan PB, Hirst MA, Feldman D: Inhibition of steroidogenic cytochrome P-450 enzymes in rat testis by ketoconazole and related imidazole anti-fungal drugs, *J. Steroid Biochem.* 23:1023–1029, 1985.
- Kangawa A, Otake M, Enya S, et al.: Spermatogenesis in the microminipig, *Toxicol. Pathol.* 44:974–986, 2016a.
- Kangawa A, Otake M, Enya S, et al.: Histological development of male reproductive organs in microminipigs, *Toxicol. Pathol.* 44:1105–1122, 2016b.
- Karhumaa P, Kaunisto K, Parkkila S, et al.: Expression of the transmembrane carbonic anhydrases, CA IX and CA XII, in the human male excurrent ducts, *Mol. Hum. Reprod.* 7:611–616, 2001.
- Kaspereit J, Friderichs-Gromoll S, Buse E, et al.: Spontaneous neoplasms observed in cynomolgus monkeys (*Macaca fascicularis*) during a 15-year period, *Exp. Toxicol. Pathol.* 59:163–169, 2007.
- Kavlock R, Cummings A: Mode of action: inhibition of androgen receptor function—vinclozolin-induced malformations in reproductive development, *Crit. Rev. Toxicol.* 35:721–726, 2005.
- Kawakami E, Tsutsui T, Ogasa A: Histological observations of the reproductive organs of the male dog from birth to sexual maturity, *J. Vet. Med. Sci.* 53:241–248, 1991.
- Keeney DS, Mendis-Handagama SMLC, Zirkin BR, et al.: Effect of long term deprivation of luteinizing hormone on leydig cell volume, leydig cell number, and steroidogenic capacity of the rat testis, *Endocrinol* 123:2906–2915, 1988.
- Kennedy PC, Cullen JM, Edwards JF, et al.: Histological classification of tumors of the genital system of domestic animals. In Washington, 1998, Armed Forces Institute of Pathology, pp 17–18. *World health organization international histological classification of tumors of domestic animals. Second series*, vol 4. Washington, 1998, Armed Forces Institute of Pathology, pp 17–18.
- Kerr JB: Spontaneous degeneration of germ cells in normal rat testis: assessment of cell types and frequency during the spermatogenic cycle, *Reproduction* 95:825–830, 1992.
- Kerr JB, Millar M, Maddocks S, et al.: Stage-Dependent changes in spermatogenesis and sertoli cells in relation to the onset of spermatogenic failure following withdrawal of testosterone, *Anat. Rec.* 235:547–559, 1993.
- Kholkute SD, Gopalkrishnan K, Puri CP: Variations in seminal parameters over a 12-month period in captive bonnet monkeys, *Primates* 41:393–405, 2000.
- Kim B, Breton S: Androgens are essential for epithelial cell recovery after efferent duct ligation in the initial segment of the mouse epididymis, *Biol. Reprod.* 102:76–83, 2020.
- Kim SH, Lee IC, Lim JH, et al.: Spermatotoxic effects of  $\alpha$ -chlorohydrin in rats, *Lab. Res.* 28:11–16, 2012.
- Klein DM, Cherrington NJ: Organic and inorganic transporters of the testis: a review, *Spermatogenesis* 4:e979653, 2014.
- Klein DM, Harding MC, Crowther MK, et al.: Localization of nucleoside transporters in rat epididymis, *J. Biochem. Mol. Toxicol.* 31:e21911, 2017.
- Klinefelter GR, Ewing LL: Maintenance of testosterone production by purified adult rat Leydig cells for 3 days in vitro, *In Vitro Cell. Dev. Biol.* 25:283–288, 1989.
- Klonisch T, Fowler PA, Hombach-Klonisch S: Molecular and genetic regulation of testis descent and external genitalia development, *Dev. Biol.* 270(1–18), 2004.
- Knoblaugh SE, True L, Tretiakova M, et al.: 18 - male reproductive system. In Treuting PM, Dintzis SM, Montine KS, editors: *Comparative anatomy and histology*, Second Edition, San Diego, 2018, Academic Press, pp 335–363.
- Koopman P, Gubbay J, Vivian N, et al.: Male development of chromosomally female mice transgenic for Sry, *Nature* 351:117–121, 1991.
- Ku WW, Pagliusi F, Foley G, et al.: A simple orchidometric method for the preliminary assessment of maturity status in male cynomolgus monkeys (*Macaca fascicularis*) used for nonclinical safety studies, *J. Pharmacol. Toxicol. Methods* 61:32–37, 2010.
- Ku WW, Wine RN, Chae BY, et al.: Spermatocyte toxicity of 2-methoxyethanol (ME) in rats and Guinea pigs: evidence for the induction of apoptosis, *Toxicol. Appl. Pharmacol.* 134:100–110, 1995.
- Kumar A, Raut S, Balasinor NH: Endocrine regulation of sperm release, *Reprod. Fertil. Dev.* 30:1595–1603, 2018.
- Kumar TR, Wang Y, Lu N, Matzuk MM: Follicle stimulating hormone is required for ovarian follicle maturation but not male fertility, *Nat. Genet.* 15(2):201–204, 1997.

- La DK, Creasy DM, Hess RA, et al.: Efferent duct toxicity with secondary testicular changes in rats following administration of a novel leukotriene a4 hydrolase inhibitor, *Toxicol. Pathol.* 40:705–714, 2012.
- Lagarigue M, Becker M, Lavigne R, et al.: Revisiting rat spermatogenesis with MALDI imaging at 20-microm resolution, *Mol. Cell. Proteomics* 10, 2011.
- Lanning LL, Creasy DM, Chapin RE, et al.: Recommended approaches for the evaluation of testicular and epididymal toxicity, *Toxicol. Pathol.* 30:507–520, 2002.
- Lapwood KR, Florcruz SV: Luteinizing hormone and testosterone secretory profiles of boars: effects of stage of sexual maturation, *Theriogenology* 10:293–306, 1978.
- Lara NLM, van den Driesche S, Macpherson S, et al.: Dibutyl phthalate induced testicular dysgenesis originates after seminiferous cord formation in rats, *Sci. Rep.* 7:2521, 2017.
- Latendresse JR, Warbritton AR, Jonassen H, et al.: Fixation of testes and eyes using a modified Davidson's fluid: comparison with Bouin's fluid and conventional Davidson's fluid, *Toxicol. Pathol.* 30:524–533, 2002.
- Laurent MR, Hammond GL, Blokland M, et al.: Sex hormone-binding globulin regulation of androgen bioactivity in vivo: validation of the free hormone hypothesis, *Sci. Rep.* 6:35539, 2016.
- Leblond CP, Clermont Y: Definition of the stages of the cycle of the seminiferous epithelium in the rat, *Ann. NY Acad. Sci.* 55:548–573, 1952.
- Lee C, Holland JM: Anatomy, histology, and ultrastructure (correlation with function), prostate, rat. In Jones TC, Mohr U, Hunt RD, editors: *Genital system*, Berlin, Heidelberg, 1987, Springer, pp 239–251.
- Lee J, Richburg JH, Younkin SC, et al.: The Fas system is a key regulator of germ cell apoptosis in the testis, *Endocrinology* 138:2081–2088, 1997.
- Lee KH, Hess RA, Bahr JM, et al.: Estrogen receptor alpha has a functional role in the mouse rete testis and efferent ductules, *Biol. Reprod.* 63:1873–1880, 2000.
- Lejeune H, Habert R, Saez JM: Origin, proliferation and differentiation of Leydig cells, *J. Mol. Endocrinol.* 20:1–25, 1998.
- Levine H, Jørgensen N, Martino-Andrade A, et al.: Temporal trends in sperm count: a systematic review and meta-regression analysis, *Hum. Reprod. Update* 23:646–659, 2017.
- Lewis RW, Kim JC, Irani D, et al.: The prostate of the nonhuman primate: normal anatomy and pathology, *Prostate* 2:51–70, 1981.
- Li J, Zhu WJ, Xie BG: A retrospective analysis of pathological changes of testicular tissue in normal adult rats, *Andrologia* 46:633–636, 2014.
- Lilja H, Oldbring J, Rannevik G, et al.: Seminal vesicle-secreted proteins and their reactions during gelation and liquefaction of human semen, *J. Clin. Invest.* 80:281–285, 1987.
- Liu PY, Swerdloff RS, Christenson PD, et al.: Rate, extent, and modifiers of spermatogenic recovery after hormonal male contraception: an integrated analysis, *Lancet (London, England)* 367:1412–1420, 2006.
- Losco PE, Leach MW, Sinha D, et al.: Administration of an antagonist of neurokinin receptors 1, 2, and 3 results in reproductive tract changes in beagle dogs, but not rats, *Toxicol. Pathol.* 35:310–322, 2007.
- Lowseth LA, Gerlach RF, Gillett NA, et al.: Age-related changes in the prostate and testes of the beagle dog, *Vet. Pathol.* 27:347–353, 1990.
- Luetjens CM, Weinbauer GF: Functional assessment of sexual maturity in male macaques (*Macaca fascicularis*), *Regul. Toxicol. Pharmacol.* 63:391–400, 2012.
- Luetjens CM, Weinbauer GF, Wistuba J: Primate spermatogenesis: new insights into comparative testicular organisation, spermatogenic efficiency and endocrine control, *Biol. Rev. Camb. Phil. Soc.* 80:475–488, 2005.
- Luo L, Li Y, Yang Y, et al.: Multinucleated cells are involved in normal development and apoptosis in mouse testes, *Mol. Med. Rep.* 8:865–870, 2013.
- Lv L, Chang Y, Li Y, et al.: Triptolide induces leydig cell apoptosis by disrupting mitochondrial dynamics in rats, *Front. Pharmacol.* 12, 2021.
- Maddocks S, Sharpe RM: The route of secretion of inhibin from the rat testis, *J. Endocrinol.* 120:R5–R8, 1989.
- Maekawa M, Kamimura K, Nagano T: Peritubular myoid cells in the testis: their structure and function, *Arch. Histol. Cytol.* 59:1–13, 1996.
- Maness SC, McDonnell DP, Gaido KW: Inhibition of androgen receptor-dependent transcriptional activity by DDT isomers and methoxychlor in HepG2 human hepatoma cells, *Toxicol. Appl. Pharmacol.* 151:135–142, 1998.
- Mangelsdorf I, Buschmann J, Orthen B: Some aspects relating to the evaluation of the effects of chemicals on male fertility, *Regul. Toxicol. Pharmacol.* 37:356–369, 2003.
- Mann U, Shiff B, Patel P: Reasons for worldwide decline in male fertility, *Curr. Opin. Urol.* 30:296–301, 2020.
- Maronpot RR, Zeiger E, McConnell EE, et al.: Induction of tunica vaginalis mesotheliomas in rats by xenobiotics, *Crit. Rev. Toxicol.* 39:512–537, 2009.
- Marty MS, Chapin RE, Parks LG, et al.: Development and maturation of the male reproductive system, *Birth Defects Res. Part B Dev. Reprod. Toxicol.* 68:125–136, 2003.
- Matsuyama T, Niino N, Kiyosawa N, et al.: Toxicogenomic investigation on rat testicular toxicity elicited by 1,3-dinitrobenzene, *Toxicology* 290:169–177, 2011.
- Mayorga-Torres BJM, Camargo M, Agarwal A, et al.: Influence of ejaculation frequency on seminal parameters, *Reprod. Biol. Endocrinol. RB Elektron.* 13, 2015.
- McEntee MF, Epstein JL, Syring R, et al.: Characterization of prostatic basal cell hyperplasia and neoplasia in aged macaques: comparative pathology in human and nonhuman primates, *Prostate* 29:51–59, 1996.
- McIntyre BS, Barlow NJ, Foster PM: Androgen-mediated development in male rat offspring exposed to flutamide in utero: permanence and correlation of early postnatal changes in anogenital distance and nipple retention with malformations in androgen-dependent tissues, *Toxicol. Sci.* 62:236–249, 2001.

- McLachlan RI, O'Donnell L, Meachem SJ, et al.: Identification of specific sites of hormonal regulation in spermatogenesis in rats, monkeys, and man, *Recent Prog. Horm. Res.* 57:149–179, 2002.
- McNeilly AS: Diagnostic applications for inhibin and activins, *Mol. Cell. Endocrinol.* 359:121–125, 2012.
- Meistrich ML: Critical components of testicular function and sensitivity to Disruption1, *Biol. Reprod.* 34:17–28, 1986.
- Meistrich ML: Evaluation of reproductive toxicity by testicular sperm head counts, *J. Am. Coll. Toxicol.* 8:551–567, 1989.
- Meistrich ML: Effects of chemotherapy and radiotherapy on spermatogenesis in humans, *Fertil. Steril.* 100:1180–1186, 2013.
- Meistrich ML, Hughes TH, Bruce WR: Alteration of epididymal sperm transport and maturation in mice by oestrogen and testosterone, *Nature* 258:145–147, 1975.
- Meistrich ML, Hunter NR, Suzuki N, et al.: Gradual regeneration of mouse testicular stem cells after exposure to ionizing radiation, *Radiat. Res.* 74:349–362, 1978.
- Meistrich ML, Shetty G: Inhibition of spermatogonial differentiation by testosterone, *J. Androl.* 24:135–148, 2003.
- Meistrich ML, Wilson G, Huhtaniemi I: Hormonal treatment after cytotoxic therapy stimulates recovery of spermatogenesis, *Cancer Res.* 59:3557–3560, 1999.
- Meistrich ML, Wilson G, Porter KL, et al.: Restoration of spermatogenesis in dibromochloropropane (DBCP)-treated rats by hormone suppression, *Toxicol. Sci.* 76:418–426, 2003.
- Messiha FS: Subcellular fractionation of alcohol and aldehyde dehydrogenase in the rat testicles, *Prog. Biochem. Pharmacol.* 18:155–166, 1981.
- Messiha FS: Subcellular distribution of oxidoreductases in genital organs of the male rat, *Neurobehav. Toxicol. Teratol.* 5: 241–245, 1983.
- Meyer JK, Fitzsimmons D, Hastings TF, et al.: Methods for the prediction of breeding success in male cynomolgus monkeys (*Macaca fascicularis*) used for reproductive toxicology studies, *J. Am. Assoc. Lab. Anim. Sci.* 45:31–36, 2006.
- Mialot JP, Thibier M, Toubanc JE, et al.: Plasma concentration of luteinizing hormone, testosterone, dehydroepiandrosterone, androstenedione between birth and one year in the male dog: longitudinal study and hCG stimulation, *Andrologia* 20:145–154, 1988.
- Miller SR, Cherrington NJ: Transepithelial transport across the blood-testis barrier, *Reproduction (Cambridge, England)* 156: R187–R194, 2018.
- Mirsky ML, Portugal S, Pisharath H, et al.: Utility of orchidometric parameters for assessing sexual maturation in male cynomolgus macaques (*Macaca fascicularis*), *Comp. Med.* 66:480–488, 2016.
- Mital P, Hinton BT, Dufour JM: The blood-testis and blood-epididymis barriers are more than just their tight junctions, *Biol. Reprod.* 84:851–858, 2011.
- Mitsumori K, Elwell MR: Proliferative lesions in the male reproductive system of F344 rats and B6C3F1 mice: incidence and classification, *Environ. Health Perspect.* 77:11–21, 1988.
- Mitsumori K, Talley FA, Elwell MR: Epididymal interstitial (leydig) cell tumors in B6C3F1 mice, *Vet. Pathol.* 26:65–69, 1989.
- Molenaar R, Rooij DGD, Rommerts FFG, et al.: Repopulation of leydig cells in mature rats after selective destruction of the existent leydig cells with ethylene dimethane sulfonate is dependent on luteinizing hormone and not follicle-stimulating hormone, *Endocrinology* 118:2546–2554, 1986.
- Moretti E, Sutura G, Collodel G: The importance of transmission electron microscopy analysis of spermatozoa: diagnostic applications and basic research, *Syst. Biol. Reprod. Med.* 62:171–183, 2016.
- Mruk DD, Cheng CY: The mammalian blood-testis barrier: its biology and regulation, *Endocr. Rev.* 36:564–591, 2015.
- Mubiru J, Hubbard G, Dick E, et al.: Nonhuman primates as models for studies of prostate specific antigen and prostatic diseases, *Prostate* 68:1546–1554, 2008.
- Murphy CJ, Richburg JH: Implications of Sertoli cell induced germ cell apoptosis to testicular pathology, *Spermatogenesis* 4:e979110, 2014.
- Mylchreest E, Sar M, Wallace DG, et al.: Fetal testosterone insufficiency and abnormal proliferation of Leydig cells and gonocytes in rats exposed to di(n-butyl) phthalate, *Reprod. Toxicol.* 16:19–28, 2002.
- Nakai M, Hess RA: Morphological changes in the rat Sertoli cell induced by the microtubule poison carbendazim, *Tissue Cell* 26:917–927, 1994.
- Nakai M, Hess RA, Matsuo F, et al.: Further observations on carbendazim-induced abnormalities of spermatid morphology in rats, *Tissue Cell* 29:477–485, 1997.
- Nakata H, Omotehara T, Itoh M, et al.: Three-dimensional structure of testis cords in mice and rats, *Andrology* 9: 1911–1922, 2021.
- Nakata H, Wakayama T, Sonomura T, et al.: Three-dimensional structure of seminiferous tubules in the adult mouse, *J. Anat.* 227:686–694, 2015.
- Nath D, White JR, Bratslavsky G, et al.: Identification, histological characterization, and dissection of mouse prostate lobes for in vitro 3D spheroid culture models, *J. Vis. Exp.*, 2018, <https://doi.org/10.3791/58397>.
- Niehoff MO, Bergmann M, Weinbauer GF: Effects of social housing of sexually mature male cynomolgus monkeys during general and reproductive toxicity evaluation, *Reprod. Toxicol.* 29:57–67, 2010.
- Niemi M, Sharpe RM, Brown WR: Macrophages in the interstitial tissue of the rat testis, *Cell Tissue Res.* 243:337–344, 1986.
- NTP: Toxicology and carcinogenesis studies of p-nitrotoluene (CAS no. 99-99-0) in F344/N rats and B6C3F(1) mice (feed studies), *Natl. Toxicol. Program Tech. Rep. Ser.*, 2002:1–277, 2002.
- Noritake K, Suzuki J, Matsuoka T, et al.: Testicular toxicity induced by a triple neurokinin receptor antagonist in male dogs, *Reprod. Toxicol.* 31:440–446, 2011.
- Nykänen M: Fine structure of the transitional zone of the rat seminiferous tubule, *Cell Tissue Res.* 198:441–454, 1979.



- Nykänen M, Kormano M: Early effects of efferent duct ligation on the rat rete testis, *Int. J. Androl.* 1:225–234, 1978.
- O'Connor JC, Cook JC, Marty MS, et al.: Evaluation of tier I screening approaches for detecting endocrine-active compounds (EACs), *Crit. Rev. Toxicol.* 32:521–549, 2002.
- O'Donnell L: Mechanisms of spermiogenesis and spermiation and how they are disturbed, *Spermatogenesis* 4:e979623, 2014.
- O'Donnell L, McLachlan RI, Wreford NG, et al.: Testosterone promotes the conversion of round spermatids between stages VII and VIII of the rat spermatogenic cycle, *Endocrinology* 135:2608–2614, 1994.
- O'Donnell L, Meachem SJ, Stanton PG, et al.: Chapter 21 - endocrine regulation of spermatogenesis. In Neill JD, editor: *Knobil and Neill's physiology of reproduction*, Third Edition, St Louis, 2006, Academic Press, pp 1017–1069.
- O'Donnell L, Robertson KM, Jones ME, et al.: Estrogen and spermatogenesis, *Endocr. Rev.* 22:289–318, 2001.
- O'Shaughnessy P: Chapter 14 - testicular development. In Plant TM, Zeleznik AJ, editors: *Knobil and Neill's physiology of reproduction*, Fourth Edition, San Diego, 2015, Academic Press, pp 567–594.
- Oakberg EF: A description of spermiogenesis in the mouse and its use in analysis of the cycle of the seminiferous epithelium and germ cell renewal, *Am. J. Anat.* 99:391–413, 1956.
- Oakberg EF: Initial depletion and subsequent recovery of spermatogonia of the mouse after 20 r of gamma rays and 100, 300, and 600 r of x-rays, *Radiat. Res.* 11:700–719, 1959.
- Obasaju MF, Katz DF, Miller MG: Species differences in susceptibility to 1,3-dinitrobenzene-induced testicular toxicity and methemoglobinemia, *Fund. Appl. Toxicol.* 16: 257–266, 1991.
- Oduwale OO, Huhtaniemi IT, Misrahi M: The roles of luteinizing hormone, follicle-stimulating hormone and testosterone in spermatogenesis and folliculogenesis revisited, *Int. J. Mol. Sci.* 22, 2021.
- Oduwale OO, Peltoketo H, Huhtaniemi IT: Role of follicle-stimulating hormone in spermatogenesis, *Front. Endocrinol.* 9, 2018.
- OECD: *Test No. 422: combined repeated dose toxicity study with the reproduction/developmental toxicity screening test*, 2016.
- Oh SJ, Kwak C, Baek M, et al.: Histologic and molecular changes in the ipsilateral and contralateral epididymides of the rat in response to unilateral testicular torsion followed by detorsion, *Fertil. Steril.* 81(Suppl 1):882–887, 2004.
- Ojeda SR, Skinner MK: Puberty in the rat. In *Knobil and Neill's physiology of reproduction*, 2006, Elsevier Inc., pp 2061–2126.
- Olar TT, Amann RP, Pickett BW: Relationships among testicular size, daily production and output of spermatozoa, and extragonadal spermatozoal reserves of the dog, *Biol. Reprod.* 29:1114–1120, 1983.
- Oliveira CA, Victor-Costa AB, Hess RA: Cellular and regional distributions of ubiquitin-proteasome and endocytotic pathway components in the epithelium of rat efferent ductules and initial segment of the epididymis, *J. Androl.* 30:590–601, 2009.
- Oliveira P, Alves M: Sertoli. In *Cell metabolism and spermatogenesis*, 2015, Springer, pp 41–56.
- Omotehara T, Nakata H, Itoh M: Three-dimensional analysis of mesonephric tubules remodeling into efferent tubules in the male mouse embryo, *Dev. Dynam.* 251:513–524, 2022.
- Orth JM: Proliferation of sertoli cells in fetal and postnatal rats: a quantitative autoradiographic study, *Anat. Rec.* 203: 485–492, 1982.
- Orth JM, Gunsalus GL, Lamperti AA: Evidence from Sertoli cell-depleted rats indicates that spermatid number in adults depends on numbers of Sertoli cells produced during perinatal development, *Endocrinology* 122:787–794, 1988.
- Ostrow RS, McGlennen RC, Shaver MK, et al.: A rhesus monkey model for sexual transmission of a papillomavirus isolated from a squamous cell carcinoma, *Proc. Natl. Acad. Sci. U. S. A.* 87:8170–8174, 1990.
- Padda J, Khalid K, Moosa A, et al.: Role of kisspeptin on hypothalamic-pituitary-gonadal pathology and its effect on reproduction, *Cureus* 13:e17600, 2021.
- Parker RM: Reproductive toxicity testing—methodology. In Hood RD, editor: *Developmental and reproductive toxicology*, 2012, CRC Press, pp 184–228.
- Parks SL, Beyer BK, Breslin W, et al.: In vitro testicular toxicity models: opportunities for advancement via biomedical engineering techniques, *ALTEX* 30:353–377, 2013.
- Penberthy KK, Lysiak JJ, Ravichandran KS: Rethinking phagocytes: clues from the retina and testes, *Trends Cell Biol.* 28:317–327, 2018.
- Pendergraft SS, Sadri-Ardekani H, Atala A, et al.: Three-dimensional testicular organoid: a novel tool for the study of human spermatogenesis and gonadotoxicity in vitro, *Biol. Reprod.* 96:720–732, 2017.
- Pereira Bacares ME, Vemireddi V, Creasy D: Testicular fibrous hypoplasia in cynomolgus monkeys (*Macaca fascicularis*): an incidental, congenital lesion, *Toxicol. Pathol.* 45:536–543, 2017.
- Perey B, Clermont Y, Leblond CP: The wave of the seminiferous epithelium in the rat, *Am. J. Anat.* 108:47–77, 1961.
- Pholpramool C, White RW, Setchell BP: Influence of androgens on inositol secretion and sperm transport in the epididymis of rats, *J. Reprod. Fertil.* 66:547–553, 1982.
- Picut CA, Remick AK: Impact of age on the male reproductive system from the pathologist's perspective, *Toxicol. Pathol.* 45:195–205, 2016.
- Picut CA, Remick AK, de Rijk EP, et al.: Postnatal development of the testis in the rat: morphologic study and correlation of morphology to neuroendocrine parameters, *Toxicol. Pathol.* 43:326–342, 2015.
- Picut CA, Remick AK, de Rijk EPCT, et al.: Postnatal development of the testis in the rat, *Toxicol. Pathol.* 43:326–342, 2014.
- Picut CA, Ziejewski MK, Stanislaus D: Comparative aspects of pre- and postnatal development of the male reproductive system, *Birth Defects Res.* 110:190–227, 2018.

- Piner J, Sutherland M, Millar M, et al.: Changes in vascular dynamics of the adult rat testis leading to transient accumulation of seminiferous tubule fluid after administration of a novel 5-hydroxytryptamine (5-HT) agonist, *Reprod. Toxicol.* 16:141–150, 2002.
- Prahalada S, Majka JA, Soper KA, et al.: Leydig cell hyperplasia and adenomas in mice treated with finasteride, a 5  $\alpha$ -reductase inhibitor: a possible mechanism, *Fund. Appl. Toxicol.* 22:211–219, 1994.
- Prahalada S, Tarantal AF, Harris GS, et al.: Effects of finasteride, a type 2 5- $\alpha$  reductase inhibitor, on fetal development in the rhesus monkey (*Macaca mulatta*), *Teratology* 55:119–131, 1997.
- Prentice DE, Meikle AW: A review of drug-induced Leydig cell hyperplasia and neoplasia in the rat and some comparisons with man, *Hum. Exp. Toxicol.* 14:562–572, 1995.
- Prins GS, Lindgren M: Chapter 18 - accessory sex glands in the male. In Plant TM, Zeleznik AJ, editors: *Knobil and Neill's physiology of reproduction*, Fourth Edition, San Diego, 2015, Academic Press, pp 773–804.
- PROPECIA®: PROPECIA® finasteride tablets, USP film-coated tablets 1 mg type II 5 $\alpha$ -reductase inhibitor. In Inc MC, editor: *Product monograph*. [https://pdf.hres.ca/dpd\\_pm/00060786.PDF](https://pdf.hres.ca/dpd_pm/00060786.PDF). (Accessed 24 February 2024).
- Purvis K, Clausen OPF, Olsen A, et al.: Prolactin and leydig cell responsiveness to LH/hCG in the rat, *Arch. Androl.* 3: 219–230, 1979.
- Ramaswamy S, Weinbauer GF: Endocrine control of spermatogenesis: role of FSH and LH/testosterone, *Spermatogenesis* 4:e996025, 2014.
- Reader SC, Shingles C, Stonard MD: Acute testicular toxicity of 1,3-dinitrobenzene and ethylene glycol monomethyl ether in the rat: evaluation of biochemical effect markers and hormonal responses, *Fund. Appl. Toxicol.* 16:61–70, 1991.
- Redmon JB, Thomas W, Ma W, et al.: Semen parameters in fertile US men: the study for future families, *Andrology* 1: 806–814, 2013.
- Regaud C: Etudes sur la structure des tubes seminiferes et sur la spermatogenese chez les mammiferes, *Arch. Anat. Microsc.* 4:101–155, 1901.
- Rehm S: Spontaneous testicular lesions in purpose-bred beagle dogs, *Toxicol. Pathol.* 28:782–787, 2000.
- Rehm S, Waalkes MP: Mixed Sertoli-Leydig cell tumor and rete testis adenocarcinoma in rats treated with CdCl<sub>2</sub>, *Vet. Pathol.* 25:163–166, 1988.
- Reid BL, Cleland KW: The structure and function of the epididymis. I. the histology of the rat epididymis, *Aust. J. Zool.* 5:223–246, 1957.
- Reindel JF, Gough AW, Pilcher GD, et al.: Systemic proliferative changes and clinical signs in cynomolgus monkeys administered a recombinant derivative of human epidermal growth factor, *Toxicol. Pathol.* 29:159–173, 2001.
- Reineking W, Seehusen F, Lehmbecker A, et al.: Predominance of granular cell tumours among testicular tumours of rabbits (*Oryctolagus cuniculi* f. dom.), *J. Comp. Pathol.* 173: 24–29, 2019.
- Reyes JG, Farias JG, Henríquez-Olavarrieta S, et al.: The hypoxic testicle: physiology and pathophysiology, *Oxid. Med. Cell. Longev.* 2012:929285, 2012.
- Rhoden EL, Gobbi D, Menti E, et al.: Effects of the chronic use of finasteride on testicular weight and spermatogenesis in Wistar rats, *BJU Int.* 89:961–963, 2002.
- Rhodes L, Ding VD, Kemp RK, et al.: Estradiol causes a dose-dependent stimulation of prostate growth in castrated beagle dogs, *Prostate* 44:8–18, 2000.
- Richburg JH, Redenbach DM, Boekelheide K: Seminiferous tubule fluid secretion is a Sertoli cell microtubule-dependent process inhibited by 2,5-hexanedione exposure, *Toxicol. Appl. Pharmacol.* 128:302–309, 1994.
- Richer G, Baert Y, Goossens E: In-vitro spermatogenesis through testis modelling: toward the generation of testicular organoids, *Andrologia* 8:879–891, 2020.
- Risbridger GP, Cancilla B: Role of activins in the male reproductive tract, *Rev. Reprod.* 5:99–104, 2000.
- Robaire B, Fan X: Regulation of apoptotic cell death in the rat epididymis, *J. Reprod. Fertil. Suppl.* 53:211–214, 1998.
- Robaire B, Hales BF: Regulation of epididymal glutathione S-transferases: effects of orchidectomy and androgen replacement, *Biol. Reprod.* 26:559–565, 1982.
- Robaire B, Hamzeh M: Androgen action in the epididymis, *J. Androl.* 32:592–599, 2011.
- Robaire B, Hermo L: Efferent ducts, epididymis, and vas deferens: structure, functions, and their regulation. In Knobil E, Neill J, editors: *The physiology of reproduction*, New York, 1988, Raven Press, pp 999–1080.
- Robaire B, Hinton BT, Orgebin-Crist M-C: The epididymis. In Neill JD, editor: *Knobil and Neill's physiology of reproduction*, St. Louis, MO, 2006, Elsevier, Inc., pp 1071–1148.
- Robinette CL: Sex-hormone-induced inflammation and fibromuscular proliferation in the rat lateral prostate, *Prostate* 12:271–286, 1988.
- Roeser HP, Stocks AE, Smith AJ: Testicular damage due to cytotoxic drugs and recovery after cessation of therapy, *Aust. N. Z. J. Med.* 8:250–254, 1978.
- Romualdo GS, Klinefelter GR, de K: Postweaning exposure to gossypol results in epididymis-specific effects throughout puberty and adulthood in rats, *J. Androl.* 23:220–228, 2002.
- Roosen-Runge EC, Giesel Jr LO: Quantitative studies on spermatogenesis in the albino rat, *Am. J. Anat.* 87:1–30, 1950.
- Rotgers E, Cisneros-Montalvo S, Jahnukainen K, et al.: A detailed protocol for a rapid analysis of testicular cell populations using flow cytometry, *Andrologia* 3:947–955, 2015.
- Roth MY, Lin K, Amory JK, et al.: Serum LH correlates highly with intratesticular steroid levels in normal men, *J. Androl.* 31:138–145, 2010.
- Rouquié D, Friry-Santini C, Schorsch F, et al.: Standard and Molecular NOAELs for rat testicular toxicity induced by flutamide, *Toxicol. Sci.* 109:59–65, 2009.
- Rudmann DG, McNerney ME, VanderEide SL, et al.: Epididymal and systemic phospholipidosis in rats and dogs

- treated with the dopamine D3 selective antagonist PNU-177864, *Toxicol. Pathol.* 32:326–332, 2004.
- Rudolph LM, Bentley GE, Calandra RS, et al.: Peripheral and central mechanisms involved in the hormonal control of male and female reproduction, *J. Neuroendocrinol.* 28, 2016.
- Russell L: Movement of spermatocytes from the basal to the adluminal compartment of the rat testis, *Am. J. Anat.* 148: 313–328, 1977.
- Russell LD, Malone JP, MacCurdy DS: Effect of the microtubule disrupting agents, colchicine and vinblastine, on seminiferous tubule structure in the rat, *Tissue Cell* 13:349–367, 1981.
- Russell LD, Saxena NK, Turner TT: Cytoskeletal involvement in spermiation and sperm transport, *Tissue Cell* 21:361–379, 1989.
- Russell LD, Ettlin RA, Sinha Hakim AP, Clegg ED, et al.: *Histological and histopathological evaluation of the testis*, Clearwater, Florida, 1990, Cache River Press, pp 1–286.
- Saito K: Spermiation failure is a major contributor to early spermatogenic suppression caused by hormone withdrawal in adult rats, *Endocrinology* 141:2779–2785, 2000.
- Sakurai K, Mikamoto K, Shirai M, et al.: MicroRNA profiling in ethylene glycol monomethyl ether-induced monkey testicular toxicity model, *J. Toxicol. Sci.* 40:375–382, 2015.
- Sandlow JL, Feng HL, Sandra A: Localization and expression of the c-kit receptor protein in human and rodent testis and sperm, *Urology* 49:494–500, 1997.
- Sato J, Doi T, Wako Y, et al.: Histopathology of incidental findings in beagles used in toxicity studies, *J. Toxicol. Pathol.* 25:103–134, 2012.
- Sawamoto O, Yamate J, Kuwamura M, et al.: Development of Sperm granulomas in the epididymides of L-cysteine-treated rats, *Toxicol. Pathol.* 31:281–289, 2003.
- Schwartz CL, Christiansen S, Vinggaard AM, et al.: Anogenital distance as a toxicological or clinical marker for fetal androgen action and risk for reproductive disorders, *Arch. Toxicol.* 93:253–272, 2019.
- Seed J, Chapin RE, Clegg ED, et al.: Methods for assessing sperm motility, morphology, and counts in the rat, rabbit, and dog: a consensus report, *Reprod. Toxicol.* 10:237–244, 1996.
- Sellers RS, Morton D, Michael B, et al.: Society of toxicologic pathology position paper: organ weight recommendations for toxicology studies, *Toxicol. Pathol.* 35:751–755, 2007.
- Semet M, Paci M, Saïas-Magnan J, et al.: The impact of drugs on male fertility: a review, *Andrology* 5:640–663, 2017.
- Setchell BP: Spermatogenesis and spermatozoa. In Austin CR, Short RV, editors: *Reproduction in mammals book 1: germ cells fertilisation*, New York, NY, 1982, Cambridge University Press, pp 63–101.
- Setchell BP, Ploen L, Ritzen EM: Reduction in fluid secretion by rat testis by drugs that block potassium channels, *J. Reprod. Fertil.* 112:87–94, 1998.
- Shaha C, Tripathi R, Mishra DP: Male germ cell apoptosis: regulation and biology, *Philos. Trans. R. Soc. Lond. B Biol. Sci.* 365:1501–1515, 2010.
- Sharpe R, Kerr J, McKinnell C, et al.: Temporal relationship between androgen-dependent changes in the volume of seminiferous tubule fluid, lumen size and seminiferous tubule protein secretion in rats, *J. Reprod. Fertil.* 101:193–198, 1994.
- Sharpe RM: Androgens and the masculinization programming window: human-rodent differences, *Biochem. Soc. Trans.* 48:1725–1735, 2020.
- Sharpe RM, McKinnell C, Kivlin C, et al.: Proliferation and functional maturation of Sertoli cells, and their relevance to disorders of testis function in adulthood, *Reproduction* 125: 769–784, 2003.
- Sharpe RM, Skakkebaek NE: Testicular dysgenesis syndrome: mechanistic insights and potential new downstream effects, *Fertil. Steril.* 89:e33–e38, 2008.
- Shetty G, Wilson G, Hardy MP, et al.: Inhibition of recovery of spermatogenesis in irradiated rats by different androgens, *Endocrinology* 143:3385–3396, 2002.
- Shetty G, Wilson G, Huhtaniemi I, et al.: Gonadotropin-releasing hormone analogs stimulate and testosterone inhibits the recovery of spermatogenesis in irradiated rats, *Endocrinology* 141:1735–1745, 2000.
- Shing JC, Schaefer K, Grosskurth SE, et al.: Small RNA sequencing to discover circulating microRNA biomarkers of testicular toxicity in dogs, *Int. J. Toxicol.* 40:26–39, 2021.
- Sikka SC, Swerdloff RS, Rajfer J: In vitro inhibition of testosterone biosynthesis by ketoconazole, *Endocrinology* 116: 1920–1925, 1985.
- Skakkebaek NE, Rajpert-De Meyts E, Buck Louis GM, et al.: Male reproductive disorders and fertility trends: influences of environment and genetic susceptibility, *Physiol. Rev.* 96: 55–97, 2016.
- Skonieczna J, Madej JP, Bedziński R: Accessory genital glands in the New Zealand white rabbit: a morphometrical and histological study, *J. Vet. Res.* 63:251–257, 2019.
- Skydsgaard M, Dincer Z, Haschek WM, et al.: International harmonization of nomenclature and diagnostic criteria (INHAND): nonproliferative and proliferative lesions of the minipig, *Toxicol. Pathol.* 49:110–228, 2021.
- Sluka P, O'Donnell L, McLachlan RI, et al.: Application of laser-capture microdissection to analysis of gene expression in the testis, *Prog. Histochem. Cytochem.* 42:173–201, 2008.
- Sluka P, O'Donnell L, Stanton PG: Stage-specific expression of genes associated with rat spermatogenesis: characterization by laser-capture microdissection and real-time polymerase chain Reaction1, *Biol. Reprod.* 67:820–828, 2002.
- Smedley JV, Bailey SA, Perry RW, et al.: Methods for predicting sexual maturity in male cynomolgus macaques on the basis of age, body weight, and histologic evaluation of the testes, *Contemp. Top. Lab. Anim. Sci.* 41:18–20, 2002.
- Smith G: The effects of ligation of the vasa efferentia and vasectomy on testicular function in the adult rat, *J. Endocrinol.* 23:285–299, 1962.



- Smith LB, Walker WH: Chapter 16 - hormone signaling in the testis. In Plant TM, Zeleznik AJ, editors: *Knobil and Neill's physiology of reproduction*, Fourth Edition, San Diego, 2015, Academic Press, pp 637–690.
- Snyder PW, Kazacos EA, Scott-Moncrieff JC, et al.: Pathologic features of naturally occurring juvenile polyarteritis in beagle dogs, *Vet. Pathol.* 32:337–345, 1995.
- Soares JM, Avelar GF, Franca LR: The seminiferous epithelium cycle and its duration in different breeds of dog (*Canis familiaris*), *J. Anat.* 215:462–471, 2009.
- Sofikitis N, Giotitis N, Tsounapi P, et al.: Hormonal regulation of spermatogenesis and spermiogenesis, *J. Steroid Biochem. Mol. Biol.* 109:323–330, 2008.
- Steger K, Wilhelm J, Konrad L, et al.: Both protamine-1 to protamine-2 mRNA ratio and Bcl2 mRNA content in testicular spermatids and ejaculated spermatozoa discriminate between fertile and infertile men, *Human Reprod.* 23: 11–16, 2007.
- Steinbach TJ, Maronpot RR, Hardisty JF: Human relevance of rodent Leydig cell tumors. In *Hamilton and Hardy's industrial toxicology*, 2015, pp 1189–1196.
- Steinberger A, Steinberger E: Replication pattern of Sertoli cells in maturing rat testis in vivo and in organ culture, *Biol. Reprod.* 4:84–87, 1971.
- Steiner JF: Finasteride: a 5 alpha-reductase inhibitor, *Clin. Pharm.* 12:15–23, 1993.
- Steiner RA, Peterson AP, Yu JY, et al.: Ultradian luteinizing hormone and testosterone rhythms in the adult male monkey, *Macaca fascicularis*, *Endocrinology* 107:1489–1493, 1980.
- Stermer AR, Reyes G, Hall SJ, et al.: Small RNAs in rat sperm are a predictive and sensitive biomarker of exposure to the testicular toxicant ethylene glycol monomethyl ether, *Toxicol. Sci.* 169:399–408, 2019.
- Stoffel MH, Friess AE: The junctions between efferent ductules and epididymal duct in the boar, *Andrologia* 29:283–285, 1997.
- Su L, Mruk DD, Cheng CY: Drug transporters, the blood-testis barrier, and spermatogenesis, *J. Endocrinol.* 208:207–223, 2011.
- Suárez-Quian CA, Martínez-García F, Nistal M, et al.: Androgen receptor distribution in adult human testis, *J. Clin. Endocrinol. Metab.* 84:350–358, 1999.
- Swan SH, Elkin EP, Fenster L: The question of declining sperm density revisited: an analysis of 101 studies published 1934–1996, *Environ. Health Perspect.* 108:961–966, 2000.
- Swierstra EE, Foote RH: Cytology and kinetics of spermatogenesis in the rabbit, *J. Reprod. Fertil.* 5:309–322, 1963.
- Syed V, Hecht NB: Rat pachytene spermatocytes down-regulate a polo-like kinase and up-regulate a thiol-specific antioxidant protein, whereas sertoli cells down-regulate a phosphodiesterase and up-regulate an oxidative stress protein after exposure to methoxyethanol and methoxyacetic acid, *Endocrinology* 139:3503–3511, 1998.
- Taberner E, Navratil N, Jasmin B, et al.: Pubertal age based on testicular and epididymal histology in Gottingen minipigs, *Theriogenology* 86:2091–2095, 2016.
- Taha MA, Noakes DE, Allen WE: Some aspects of reproductive function in the male Beagle at puberty, *J. Small Anim. Pract.* 22:663–667, 1981.
- Tangbanluekal L, Robinette CL: Prolactin mediates estradiol-induced inflammation in the lateral prostate of Wistar rats, *Endocrinology* 132:2407–2416, 1993.
- Tani Y, Foster PM, Sills RC, et al.: Epididymal sperm granuloma induced by chronic administration of 2-methylimidazole in B6C3F1 mice, *Toxicol. Pathol.* 33:313–319, 2005.
- Terasawa E: The mechanism underlying the pubertal increase in pulsatile GnRH release in primates, *J. Neuroendocrinol.* 34:e13119, 2022.
- Thuilliez C, Tortoreau A, Perron-Lepage M-F, et al.: Spontaneous testicular tubular hypoplasia/atrophy in the Gottingen minipig: a retrospective study, *Toxicol. Pathol.* 42: 1024–1031, 2014.
- Torres JM, Ortega E: Differential regulation of steroid 5alpha-reductase isozymes expression by androgens in the adult rat brain, *Faseb. J.* 17:1428–1433, 2003.
- Turner KJ, Morley M, Atanassova N, et al.: Effect of chronic administration of an aromatase inhibitor to adult male rats on pituitary and testicular function and fertility, *J. Endocrinol.* 164:225–238, 2000.
- Turner TT: On the epididymis and its role in the development of the fertile ejaculate, *J. Androl.* 16:292–298, 1995.
- Turner TT, Bang HJ, Lysiak JL: The molecular pathology of experimental testicular torsion suggests adjunct therapy to surgical repair, *J. Urol.* 172:2574–2578, 2004.
- Turner TT, Brown KJ: Spermatogenic cord torsion: loss of spermatogenesis despite return of blood flow, *Biol. Reprod.* 49: 401–407, 1993.
- Turner TT, Jones CE, Howards SS, et al.: On the androgen microenvironment of maturing spermatozoa, *Endocrinology* 115:1925–1932, 1984.
- Turner TT, Reich GW: Influence of proteins in rat cauda epididymal lumen fluid on cauda sperm motility, *Gamete Res.* 18:267–278, 1987.
- Udagawa K, Ogawa T, Watanabe T, et al.: Testosterone administration promotes regeneration of chemically impaired spermatogenesis in rats, *Int. J. Urol.* 13:1103–1108, 2006.
- Usselman MC, Cone RA: rat sperm are mechanically immobilized in the caudal epididymis by “immobilin,” a high molecular weight glycoprotein, *Biol. Reprod.* 29:1241–1253, 1983.
- van den Driesche S, Kilcoyne KR, Wagner I, et al.: Experimentally induced testicular dysgenesis syndrome originates in the masculinization programming window, *JCI Insight* 2:e91204, 2017.
- Van Tyle JH: Ketoconazole. Mechanism of action, spectrum of activity, pharmacokinetics, drug interactions, adverse reactions and therapeutic use, *Pharmacotherapy* 4:343–373, 1984.

- van Vliet J, Rommerts FFG, de Rooij DG, et al.: Reduction of testicular blood flow and focal degeneration of tissue in the rat after administration of human chorionic gonadotrophin, *J. Endocrinol.* 117(1):51–57, 1988.
- Vergouwens RP, Huiskamp R, Bas RJ, et al.: Postnatal development of testicular cell populations in mice, *J. Reprod. Fertil.* 99:479–485, 1993.
- Vidal JD, Bhaskaran M, Carsillo M, et al.: Spontaneous findings in the reproductive system of sexually mature male cynomolgus macaques, *Toxicol. Pathol.* 50:660–678, 2022.
- Vidal JD, Colman K, Bhaskaran M, et al.: Scientific and regulatory policy committee best practices: documentation of sexual maturity by microscopic evaluation in nonclinical safety studies, *Toxicol. Pathol.* 49:977–989, 2021.
- Vidal JD, Whitney KM: Morphologic manifestations of testicular and epididymal toxicity, *Spermatogenesis* 4:e979099, 2014.
- Virtanen HE, Jørgensen N, Toppari J: Semen quality in the 21(st) century, *Nat. Rev. Urol.* 14:120–130, 2017.
- Vogl AW, Vaid KS, Guttman JA: The Sertoli cell cytoskeleton, *Adv. Exp. Med. Biol.* 636:186–211, 2008.
- Walker WH: Androgen actions in the testis and the regulation of spermatogenesis, *Adv. Exp. Med. Biol.* 1288:175–203, 2021.
- Wang W, Wine RN, Chapin RE: Rat Testicular Src: normal distribution and involvement in ethylene glycol monomethyl ether-induced apoptosis, *Toxicol. Appl. Pharmacol.* 163:125–134, 2000.
- Ward JA, Furr BJ, Valcaccia B, et al.: Prolonged suppression of rat testis function by a depot formulation of Zoladex, a GnRH agonist, *J. Androl.* 10:478–486, 1989.
- Weber JE, Russell LD, Wong V, et al.: Three-dimensional reconstruction of a rat stage V Sertoli cell: II. Morphometry of Sertoli–Sertoli and Sertoli–germ-cell relationships, *Am. J. Anat.* 167:163–179, 1983.
- Welsh M, Saunders PT, Fisker M, et al.: Identification in rats of a programming window for reproductive tract masculinization, disruption of which leads to hypospadias and cryptorchidism, *J. Clin. Invest.* 118:1479–1490, 2008.
- Whitney KM: Testicular histopathology in juvenile rat toxicity studies, *Syst. Biol. Reprod. Med.* 58:51–56, 2012.
- Wijayarathna R, de Kretser DM: Activins in reproductive biology and beyond, *Hum. Reprod. Update* 22:342–357, 2016.
- Williams J, Gladen BC, Schrader SM, et al.: Semen analysis and fertility assessment in rabbits: statistical power and design considerations for toxicology studies, *Fund. Appl. Toxicol.* 15:651–665, 1990.
- Willson CJ: Phthalate toxicity in rats and its relation to testicular dysgenesis syndrome in humans, *Toxicol. Pathol.* 49:1416–1424, 2021.
- Wilson CA, Davies DC: The control of sexual differentiation of the reproductive system and brain, *Reproduction* 133:331–359, 2007.
- Wing TY, Christensen AK: Morphometric studies on rat seminiferous tubules, *Am. J. Anat.* 165:13–25, 1982.
- Winter M, Falvo RE, Schanbacher BD, et al.: Regulation of gonadotropin secretion in the male dog. Role of estradiol, *J. Androl.* 4:319–323, 1983.
- Wistuba J, Schrod A, Greve B, et al.: Organization of seminiferous epithelium in primates: relationship to spermatogenic efficiency, phylogeny, and mating system, *Biol. Reprod.* 69:582–591, 2003.
- Woicke J, Al-Haddawi MM, Bienvenu JG, et al.: International harmonization of nomenclature and diagnostic criteria (INHAND): nonproliferative and proliferative lesions of the dog, *Toxicol. Pathol.* 49:5–109, 2021.
- Wu S, Yan M, Ge R, et al.: Crosstalk between Sertoli and germ cells in male fertility, *Trend Mol Med* 26:215–231, 2020.
- Xie BG, Li J, Zhu WJ: Pathological changes of testicular tissue in normal adult mice: a retrospective analysis, *Exp. Ther. Med.* 7:654–656, 2014.
- Yang ZW, Kong LS, Guo Y, et al.: Histological changes of the testis and epididymis in adult rats as a result of Leydig cell destruction after ethane dimethane sulfonate treatment: a morphometric study, *Asian J. Androl.* 8:289–299, 2006.
- Yin L, Wei H, Liang S, et al.: From the Cover: an animal-free in vitro three-dimensional testicular cell coculture model for evaluating male reproductive toxicants, *Toxicol. Sci.* 159:307–326, 2017.
- Yuan X, Jonker MJ, de Wilde J, et al.: Finding maximal transcriptome differences between reprotoxic and non-reprotoxic phthalate responses in rat testis, *J. Appl. Toxicol.* 31:421–430, 2011.
- Yuan Y-D, Ulrich RG, Carlson RG: Histology and ultrastructure, glands of the ductus deferens (ampullary gland), rat. In Jones TC, Mohr U, Hunt RD, editors: *Genital system*, Berlin, Heidelberg, 1987, Springer, pp 229–234.
- Zhengwei Y, Wreford NG, Schlatt S, et al.: Acute and specific impairment of spermatogonial development by GnRH antagonist-induced gonadotrophin withdrawal in the adult macaque (*Macaca fascicularis*), *J. Reprod. Fertil.* 112:139–147, 1998.
- Zirkin BR, Santulli R, Awoniyi CA, et al.: Maintenance of advanced spermatogenic cells in the adult rat testis: quantitative relationship to testosterone concentration within the testis, *Endocrinology* 124:3043–3049, 1989.

This page intentionally left blank



# Female Reproductive System

Daniel G. Rudmann<sup>1,3</sup>, Justin D. Vidal<sup>1</sup>, Eric van Esch<sup>2</sup>

<sup>1</sup>Charles River Laboratories, Ashland, OH, United States, <sup>2</sup>InSight Pathology BV, Oss, the Netherlands, <sup>3</sup>Moderna Therapeutics, Cambridge, MA, United States

## OUTLINE

<b>1. Introduction</b>	<b>743</b>	<b>5. Mechanisms of Toxicity in the Female Reproductive System</b>	<b>783</b>
<b>2. Structure, Function, and Cell Biology</b>	<b>746</b>	5.1. Stress and Negative Energy Balance	784
2.1. The Ovary	747	5.2. Hyperprolactinemia	788
2.2. The Histology of the Rat Ovary during Prepubertal and Pubertal Development	750	5.3. Altered Activity of Sex Steroid Enzymes and Cholesterol Metabolism	791
2.3. The Histology of the Rat Female Reproductive Tract during the Estrous Cycle	751	5.4. Targeted Cancer Therapies	791
2.4. The Histology of the Dog Female Reproductive Tract during the Estrous Cycle	756	5.5. Modulation of Central Nervous System Biology	792
2.5. The Histology of the Cynomolgus Macaque Female Reproductive Tract during the Menstrual Cycle	759	5.6. Toxicity Induced by Constituents of the HPO Axis and Modulators of Nuclear Hormone Receptors	793
2.6. The Histology of the Minipig Female Reproductive Tract during the Estrous Cycle	765	5.7. Toxicity due to Vaginal Irritation	796
2.7. The Histology of the Rabbit Female Reproductive Tract during the Estrous Cycle	770	5.8. Study, Interpretative, and Regulatory Issues in Female Reproductive Safety Assessment	796
2.8. The Endocrinology of the Estrous and Menstrual Cycles	770	<b>6. Carcinogenesis in the Female Reproductive System</b>	<b>797</b>
2.9. Hormonal Events during a Given Reproductive Cycle	770	6.1. Ovary	798
2.10. Regulation of Hormonal Secretion	773	6.2. Uterus	804
<b>3. Evaluation of Female Reproductive System Toxicity</b>	<b>775</b>	6.3. Vagina and Cervix	808
3.1. Spontaneous Changes in the Female Reproductive System	778	6.4. Clitoral Glands	809
<b>4. Responses to Injury</b>	<b>779</b>	<b>7. Conclusion</b>	<b>810</b>
		<b>References</b>	<b>811</b>

## 1. INTRODUCTION

During the COVID-19 pandemic, observational reports of menstrual cycle irregularities

linked to COVID-19 infection or vaccination received considerable attention and raised concerns by the public. The firestorm of news articles and potential impact on public health

(i.e., people electing to not become vaccinated) underscores the importance that public opinion has on reproductive health and safety (NIH, 2023). While there were no nonclinical data suggesting female reproductive system toxicity for the vaccines (Bowman et al., 2021; Dube et al., 2022), a recent retrospective evaluation of clinical data demonstrated lengthening of the female menstrual cycle after vaccination or infection (Edelman et al., 2022). This both highlights the need for comprehensive female reproductive assessment but also the challenge of modeling potential effects of xenobiotics in humans. The toxicologic pathologist is well positioned to partner with the toxicologist and endocrinologist to respond to these and many other unique challenges of female reproductive system human safety assessment.

While animal studies benefit from standardization in the laboratory, there are also numerous study design, environmental and genetic factors which may influence animal model responses and these need to be considered in data interpretation (see, *The Role of Pathology in Evaluation of Reproductive, Developmental, and Juvenile Toxicity*, Vol 1, Chap 7). There are important species-specific physiologic and anatomic differences between animal model species and women that can significantly influence the interpretation of the data at hand (Laffan et al., 2018; Vidal et al., 2018). The different outcomes of reproductive senescence or menopause in animals compared with women need to be considered

for the accurate interpretations of study data (Vidal, 2017). Effects at maximally tolerated doses may include alterations of normal female cyclicity because of general toxicity (e.g., decreased food consumption and stress) and these may mask or complicate interpretations regarding primary test article-related toxicity (Everds et al., 2013). For nonrodent studies, young, pre- or peripubescent animals may be used, limiting the ability to evaluate toxicologic effects on the reproductive system (Vidal, 2017). Even when sexually mature nonrodent adults are included, their estrous cycles are long, and consequently, to detect a significant change in female reproductive function, many animals and a long test period may be required. Finally, the normal variation of reproductive tissue organ weights and histology due to the formation and regression of follicles and corpora lutea (CL) in the ovary and the cyclic variation in trophic factors during the estrous/menstrual cycle may make detection and interpretation of reproductive tissue changes difficult. All of these will be discussed in detail later in this chapter.

Table 10.1 summarizes several assumptions the Environmental Protection Agency (EPA) published for female reproductive system human safety assessment (EPA, 1996). These assumptions for the most part hold true for the Food and Drug Administration (FDA) as well; however, there can be variability between the agencies as well as specific divisions within these government regulatory groups. Probably

**TABLE 10.1** Selected Assumptions Made by Regulators with Respect to Female Reproductive System Human Safety Assessment

Assumptions
An agent that produces an adverse reproductive effect in experimental animals is assumed to pose a potential threat to humans.
Effects of xenobiotics on female reproductive processes are assumed similar to humans unless demonstrated otherwise. For developmental outcomes, the specific effects in humans are not necessarily the same as those seen in the experimental species.
In the absence of information to determine the most appropriate experimental species, data from the most sensitive species should be used.
In the absence of information to the contrary, an agent that affects reproductive function in one sex is assumed to adversely affect reproductive function in the other sex <sup>a</sup> .
A nonlinear dose–response curve is assumed for reproductive toxicity <sup>a</sup>

<sup>a</sup> Not an assumption considered in adversity evaluation in drug development.  
Adapted from Environmental Protection Agency (EPA) Guidelines for Reproductive Toxicity Risk Assessment, published on October 31, 1996, Federal Register 61(212):56274–56322.

the most important difference between these agencies is their perspective: the EPA considers female reproductive toxicity due to unintended exposure to xenobiotics without any potential benefit, while the FDA's perspective is based on an intentional exposure with potential benefit and some risk. In either case, it is imperative that the toxicologic pathologist partners with the toxicologist in communicating with regulatory groups to ensure that their scientific approach to evaluating female reproductive effects is acceptable. Later in the chapter, the issue of assigning adversity to individual or groups of findings will be discussed in more detail (Patrick and Troth, 2019) (see also *Assigning Adversity to Toxicological Outcomes*, Vol 2, Chap 15).

The burden of proof that any or all these assumptions do not apply to an individual study or body of data lies with the toxicologic pathologist and the scientific team. In our experience, the two most common scenarios that occur in conflict with these assumptions are (1) when a toxicologic effect is species-specific or sex-specific, or (2) when sensitivity to the toxicity is different (greater or lesser) in the test animal than women because of some species-specific differences. For these situations, a weight of evidence argument is needed, and it is recommended that the appropriate subject matter experts are identified who can review the data and make recommendations for experiments or other approaches that could provide weight of evidence for a species-specific female reproductive effect. If a strong case is not made, the above assumptions may be applied in the safety assessment review and limit the opportunity for drug, agrichemical, or medical device development. Specific examples of these scenarios will be described later in this chapter.

The gold standard for evaluation of female reproductive system toxicity in general toxicology studies is the assessment of the test article-effects on organ weight, gross, and histologic changes in reproductive tissues in two animal models, generally using a nonrodent and rodent species. Regulatory guidance that describe reproductive system evaluation are available (FDA, 2021; ICH, 2009; ICH, 2011; ICH, 2020; OECD, 2008). For drug development, toxicologic pathologists are key contributors to the analysis of the data from these repeat-dose toxicology studies, which may last to a lifetime

in rodents (2 years) and 1 year in a nonrodent species (the nonhuman primate (NHP) or cynomolgus macaque, minipig, or Beagle dog). The recommended female reproductive endpoints for these studies are outlined in detail by several excellent multiauthor publications sponsored by the Society of Toxicologic Pathology and summarized in Table 10.2 (Bregman et al., 2003; Cline et al., 2001; Hutt et al., 2022; Michael et al., 2007; OECD, 2008; Van Esch et al., 2008b). It is important to note that xenobiotic-induced changes observed in the male reproductive tract (see *Male Reproductive Tract*, Vol 5, Chap 9) may provide important data which indicate the need for a targeted evaluation of the female reproductive tract.

In some cases, the toxicologic pathologist may also examine treatment effects as a component of the analysis done for development and reproductive toxicology (DART) studies, usually completed in rats and rabbits, and it is important for the toxicologic pathologist to be familiar with the regulations related to DART studies as well as the designs of the studies themselves (see *The Role of Pathology in Evaluation of Reproductive, Developmental, and Juvenile Toxicity*, Vol 1, Chap 7). For either general toxicology or DART studies, if there are treatment-related alterations, it is common practice to complete follow-on studies (second tier) that assess the reversibility of the changes, or alterations in reproductive hormone concentrations, or studies that help define the pathogenesis of the effects, such as classic pharmacology or endocrinology experimental designs. Some of these will be described later in this chapter. For the toxicologic

**TABLE 10.2** Recommended Female Reproductive System Endpoints for Standard Toxicology Studies

#### Recommendations

Organ weights: ovary (studies  $\leq 6$  months in rodents,  $\leq 12$  months in nonrodents); pituitary (all but mouse); uterus (case by case)

Gross pathology: examination of full reproductive tract

Histopathology: ovary, uterus, cervix, vagina, mammary gland, pituitary, adrenal

*Reproduced from Haschek WM, Rousseaux CG, Wallig MA, editors: Haschek and Rousseaux's handbook of toxicologic pathology, ed 3, 2013, Academic Press, Table 60.2, p. 2601, with permission.*



pathologist employed in the chemical, agricultural, or environmental toxicology areas, additional specialized studies may be required which necessitate a pathologist's expertise. While describing these studies is beyond the scope of this chapter, the reader is referred to specific regulatory guidance (FDA, 2021; ICH, 2020) (see also *Agricultural and Bulk Chemicals*, Vol 2, Chap 12).

It is important that toxicologic pathologists across the globe use similar scientific tools and techniques and speak the same scientific language when studying and reporting effects in the female reproductive system. Several excellent manuscripts have detailed approaches to staging the estrous/menstrual cycle of rodent and nonrodent species and the utility of morphometric analyses of ovarian follicle development to aid in deciphering treatment effects (Bartelmez, 1951; Buse et al., 2008; Carboni et al., 2021; Chandra and Adler, 2008; Chandra et al., 2010; Cline et al., 2001; de Rijk et al., 2014; Goldman et al., 2007; Koering, 1969; Li and Davis, 2007; Long and Evans, 1922; Picut et al., 2008, 2014, 2015). There is also an ongoing effort by INHAND (International Harmonisation of Nomenclature and Diagnoses) to produce a common global diagnostic language for female reproductive system changes and the reader should consult these documents that are now complete for the rodent, NHP, rabbit, dog, and minipig (Bradley et al., 2021; Colman et al., 2021; Dixon et al., 2014; Woicke et al., 2021; Skydsgaard et al., 2021). These manuscripts and updates on published terms can be found on the Society of Toxicologic Pathology (<http://www.toxpath.org>) and goRENI (<https://www.goreni.org>) web sites. Moreover, there are continuing education symposia and training programs in reproductive toxicologic pathology offered by groups like the Davis-Thompson Foundation, American College of Veterinary Pathologists (ACVP), Society of Toxicologic Pathologists (STP), European Society of Toxicologic Pathologists (ESTP), European College of Veterinary Pathologists (ECVP), British Society of Toxicologic Pathology (BSTP), and European Society for Veterinary Pathology (ESVP), among others. These efforts from the toxicologic pathology community will facilitate better comparisons of effects across studies and laboratories globally, as well as a more consistent

dialog with regulatory organizations. Finally, with the ongoing interrogation of the rat, dog, and cynomolgus macaque genome and metabolome (see *Toxicogenomics: A Primer for Toxicologic Pathologists*, Vol 1, Chap 15), there is ample opportunity to use molecular biologic, systems biology, and informatics tools to predict potential treatment effects or decipher the pathogenesis of observed effects. Useful public databases for molecular biology and informatics evaluations will be described in this chapter. More recently, deep learning-based artificial intelligence and novel in vitro 2D and 3D in vitro systems such as MPSs (multiphysiological systems) have emerged as additional modeling, diagnostic and image analysis tools for the pathologist (see *Alternative Models in Biomedical Research: In Silico, In Vitro, Ex Vivo, and Nontraditional In Vivo Approaches*, Vol 1, Chap 24) (Rudmann, 2019; Stokar-Regenscheit et al., 2024).

## 2. STRUCTURE, FUNCTION, AND CELL BIOLOGY

Before a toxicologic pathologist can effectively complete an accurate, thorough evaluation and safety assessment of female reproductive study data, he or she needs to be very familiar with normal anatomy and histology as well as the endocrinology associated with the different species used in nonclinical studies. The estrous cycle progresses in waves; for example, in the rat, it takes approximately 60 days for a primordial follicle to develop to a tertiary or antral follicle and ovulate. Most of these follicles however undergo atresia before ovulation. There are also several key species differences especially in the characteristics of the estrous/menstrual cycle. These are described for the rat, Beagle dog, rabbit, minipigs, and cynomolgus macaque later in this section. A summary of the differences in sexual development and reproductive cycle characteristics between the rat, Beagle dog, minipig, rabbit, and cynomolgus macaque is given in Table 10.3.

This section will summarize some of the more pertinent information from numerous sources, focusing on the normal reproductive system of the virgin, adult female in a specific nonclinical

**TABLE 10.3** Differences Between Sexual Development and Reproductive Cycle Characteristics

	SD rat	Beagle dog	Cynomolgus macaque	Minipig	Rabbit
Sexual maturity	~8 w	~1.5 y	~4 y	4–8 m	~6 m
Senescence (S) or menopause (M)	>4 m (S)	No	>20 y (M)	No	>6 y (S)
Cycle length	4–5 d	3.5–13 m	28 d	17–22 d	3–12 d
Seasonal/Social influence	No	No	Yes	Yes	No

w, weeks; m, months; y, years; d, days

Reproduced from Haschek WM, Rousseaux CG, Wallig MA, editors: *Haschek and Rousseaux's handbook of toxicologic pathology*, ed 3, 2013, Academic Press, Table 60.3, p. 2602, with permission.

animal model system. The embryologic and prepubescent development of the female reproductive system will not be described except as it pertains to the female rat pubertal assay, and in cases where it is critical to add perspective to comparative mammalian physiology and endocrinology. Occasionally pathologists will be asked to evaluate placenta in a targeted manner. Although this chapter will not elaborate on this subject, there are several outstanding publications on the normal histologic appearance of the placenta (Charest et al., 2018; de Rijk et al., 2002; Van Esch et al., 2008b; Furukawa et al., 2014; Woods et al., 2018) (also see *Embryo, Fetus and Placenta*, Vol 5, Chap 11). The focus of the description will be for the rat (Sprague–Dawley [SD] and Wistar strains), Beagle dog, minipig, rabbit, and cynomolgus macaque, which are by far the most common species used in toxicology, DART studies and toxicology models for dermal and medical device testing (see *Animal and Alternative Models in Toxicologic Research*, Vol 1, Part 3. Chaps. 16–20; *Biomedical Materials and Devices*, Vol 2, Chap 11).

The ovary is the most dynamic and complicated female reproductive organ with several common characteristics between species. For this reason, we describe the ovary in general first and then add species-specific differences in our detail of the reproductive cycles of the rat, Beagle dog, minipigs, rabbit, and cynomolgus macaque. For each of these estrous/menstrual cycle descriptions, we first highlight some of the species-specific characteristics of the female reproductive tract. Then, stage by stage, we describe the histologic changes in these tissues. It is important to note that we do not include the mammary gland in our descriptions because it is covered by a separate chapter in this book

(*Mammary Gland*, Vol 5, Chap 8). However, the mammary gland should be considered part of female reproductive tract assessment when studying a test article's potential to modulate the homeostasis of the female reproductive system (Rudmann et al., 2012). Descriptions of the clitoral glands are reserved for the neoplasia section of this chapter since these structures are generally only examined in the lifetime carcinogenicity bioassay in rodents.

## 2.1. The Ovary

The surface of the ovary is covered by a single layer of mesothelium (germinal epithelium). Depending on its location, this specialized peritoneal mesothelium may be squamous, cuboidal, or columnar. Beneath the mesothelium is a thin layer of connective tissue called the tunica albuginea or lamina propria. The parenchyma below the tunica albuginea can be divided into two poorly demarcated zones. The outer zone, or cortex, contains the oocytes, follicles, corpora lutea, interstitial glands, and other glandular structures embedded in a highly cellular compact stroma (Figure 10.1). The inner zone, or medulla, contains larger blood and lymph vessels, interstitial glands, and rudimentary epithelial structures, such as rete ovarii and medullary cords, in loosely arranged connective tissue. Nerves and blood vessels enter the ovarian parenchyma at the center of the median pole or hilus.

In healthy sexually mature animals, follicles in different stages of development are present. Most of these will undergo atresia sometime during maturation. The primordial follicle (Figure 10.2) is often located immediately beneath the tunica albuginea. It is the least developed follicle and consists of an oocyte

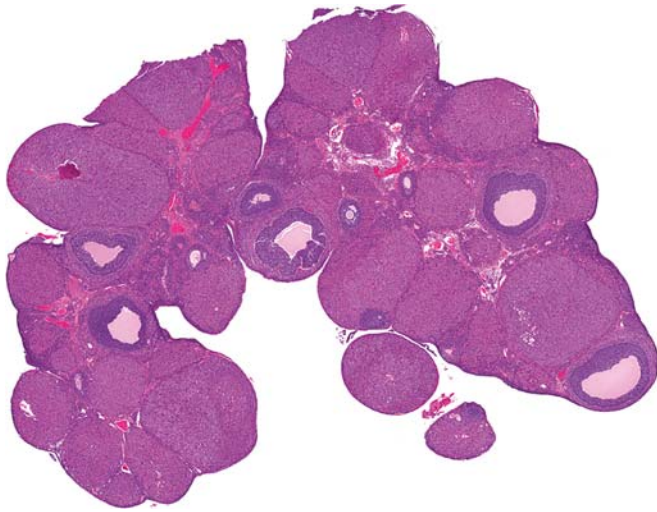


**FIGURE 10.1** Ovary, rat, normal ovary. Numerous corpora lutea and follicles give the ovary a grape cluster-like appearance. 15 $\times$ , H&E. Reproduced from Haschek WM, Rousseaux CG, Wallig MA, editors: *Haschek and Rousseaux's handbook of toxicologic pathology*, ed 3, 2013, Academic Press, Figure 60.1, p. 2603, with permission.

surrounded by a single layer of squamous epithelial (follicular, pregranulosa) cells (the primordial follicle type 1, see [Carboni et al., 2021](#)). It represents the resting stage of the oocyte and is present during fetal life. During this resting stage, the squamous pregranulosa cells surrounding the oocyte of primordial and early primary follicles fail to stain with the antibody against proliferating cell nuclear antigen PCNA ([Picut et al., 2008](#)) consistent with their dormant state. The first stage of follicular growth is the recruitment and development of a cohort of primordial follicles into primary follicles. As the oocyte develops, it rapidly increases in size from approximately 15–100  $\mu\text{m}$  in diameter, concomitant with a transformation of follicular cells surrounding the oocyte, from flattened to cuboidal/columnar (the primordial follicle type 2). The next phase of follicular growth consists of proliferation and further differentiation of the single layer of follicular cells into multiple layers of granulosa cells and the formation of the zona pellucida, a glycoprotein coat surrounding the oocyte. The follicle is now designated as a secondary or growing follicle ([Figure 10.2](#)). This stage is characterized by a two to five cell thick layer of granulosa cells without a clear antrum. Immunohistochemistry using an antibody against PCNA now show

positive stained nuclei in the granulosa cells, evidence they potentially can start to proliferate ([Picut et al., 2008](#)). As the follicle continues to grow, multiple fluid-filled intercellular spaces appear (vesicular follicles). When these spaces become confluent, they form a single large space called the antrum: this follicular stage is called a tertiary or antral follicle. At this stage, the oocyte with attached granulosa cells becomes eccentrically located in the follicle; the mass of granulosa cells enclosing the oocyte projects into the antrum forming a hillock called the cumulus oophorus ([Figure 10.2](#)). The granulosa cells surrounding the oocyte are called the corona radiata and the fluid in the antrum, the liquor folliculi. The term “Graafian follicle” or preovulatory follicle is used to denote a large tertiary follicle during preovulatory growth. During all stages of follicular development, the granulosa cell layer is avascular.

During follicular development, the stromal cells encapsulating the follicle also undergo morphological changes. The elongated fibroblast-like stromal cells which form concentric layers around the developing follicle are called thecal cells ([Figure 10.2](#)). Since the granulosa cells of a follicle are avascular, they rely on the vasculature of the theca. At later stages of follicular development, the theca is further divided into the theca interna and theca externa. Cells in the theca interna become polygonal in shape, with vacuolated cytoplasm and vesicular nuclei. These cells further enlarge as proestrus approaches and are believed to be the major site of sex steroid production. Thecal cells are not capable of producing estrogens but do produce androgens in response to LH, which are converted into estrogen by follicle-stimulating hormone (FSH)-induced aromatase in the neighboring granulosa cells of the growing follicles ([Young and McNeilly, 2010](#)). The cells of the theca externa maintain their fibroblast-like morphology. The theca externa contains contractile elements that are believed to assist in the process of ovulation.

Degeneration of the follicle, known as atresia, is a complex hormonally driven process that occurs most commonly with 200- to 400- $\mu\text{m}$  diameter follicles. There are clear indications that preantral follicles undergo atresia via enhanced granulosa cell autophagy, while antral follicles undergo atresia via granulosa cell



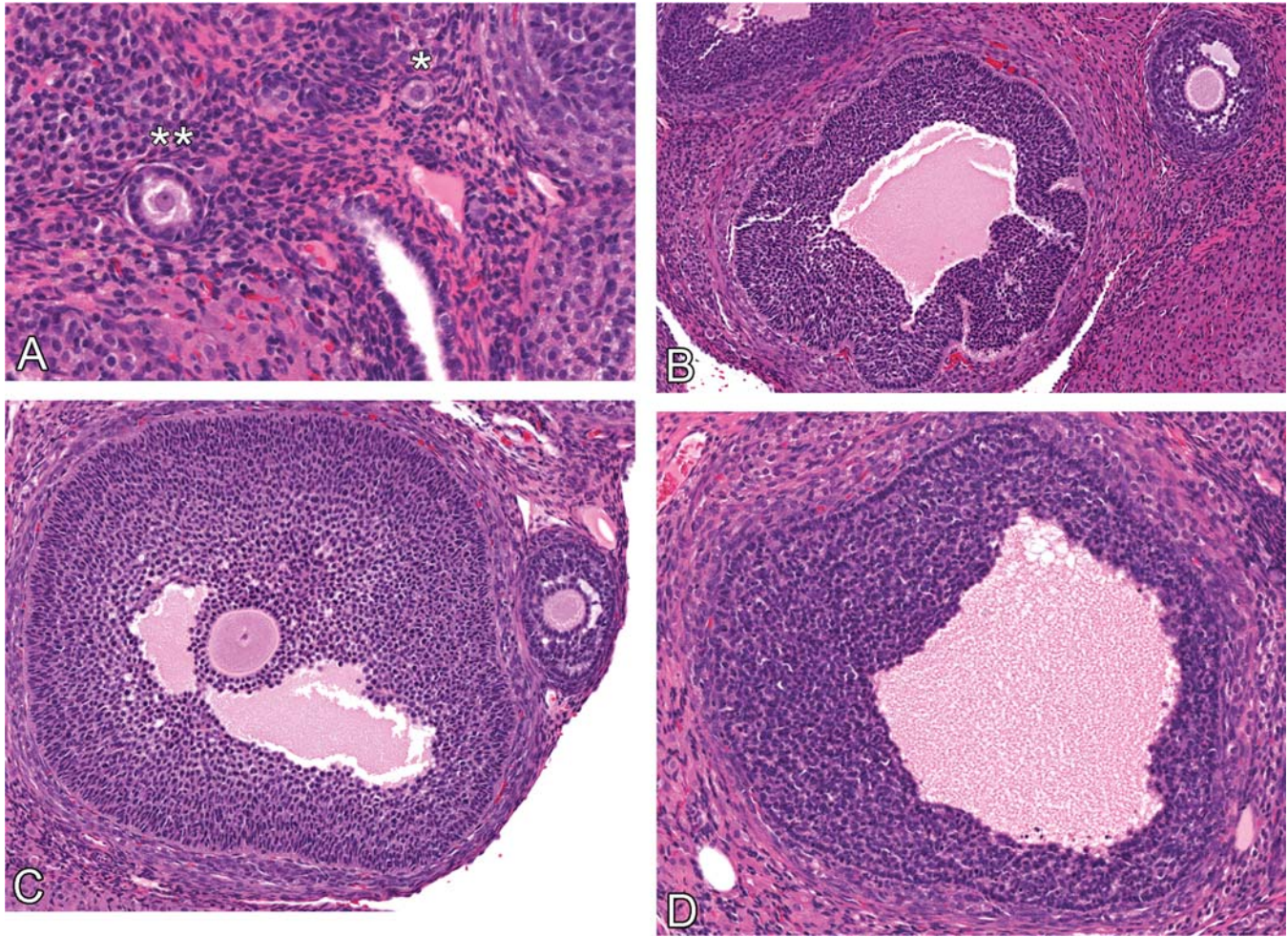


**FIGURE 10.2** Ovary, rat, normal follicle maturation. (A) Primordial (\*) and primary (\*\*) follicles. (B) Tertiary follicle (left) and small antral follicle (right). (C) A large and small antral follicle with (D) central oocytes, and an atretic tertiary follicle with apoptotic granulosa cells. (A) 100 $\times$ , (B) 5, and (C and D) 75 $\times$ . H&E. Reproduced from Haschek WM, Rousseaux CG, Wallig MA, editors: *Haschek and Rousseaux's handbook of toxicologic pathology*, ed 3, 2013, Academic Press, Figure 60.2, p. 2604, with permission.

apoptosis (Meng et al., 2018). Nevertheless, atresia of preantral follicles is not as conspicuous as that of vesicular and tertiary follicles, due to their relatively small size. In the antral follicle, the earliest noticeable changes, including nuclear pyknosis and karyorrhexis, frequently occur in, but are not limited to, the granulosa cells immediately adjacent to the lumen in tertiary follicles and just external to the corona radiata of vesicular follicles. In the tertiary follicle, apoptotic cells slough from their attachment, resulting in a greatly reduced cumulus oophorus; this sloughing allows the ovum, covered by the zona pellucida, to float in the follicular liquor. The zona pellucida and ovum

also undergo degeneration and granulosa cells undergo apoptosis. There is no inflammatory response during the process of atresia.

As mentioned previously, only a limited number of developed follicles reach the stage of preovulatory follicles and ovulate. After ovulation, both the thecal cells and the retained granulosa cells luteinize and become the luteal cells of the newly formed corpus luteum (Figure 10.3). Histologically, luteinization is characterized by both hyperplasia and hypertrophy of luteal cells, and by vascular proliferation. This often results in a corpus luteum larger than the mature follicle. Corpora luteal changes are observed in the cytoplasm and include an initial increased basophilia,



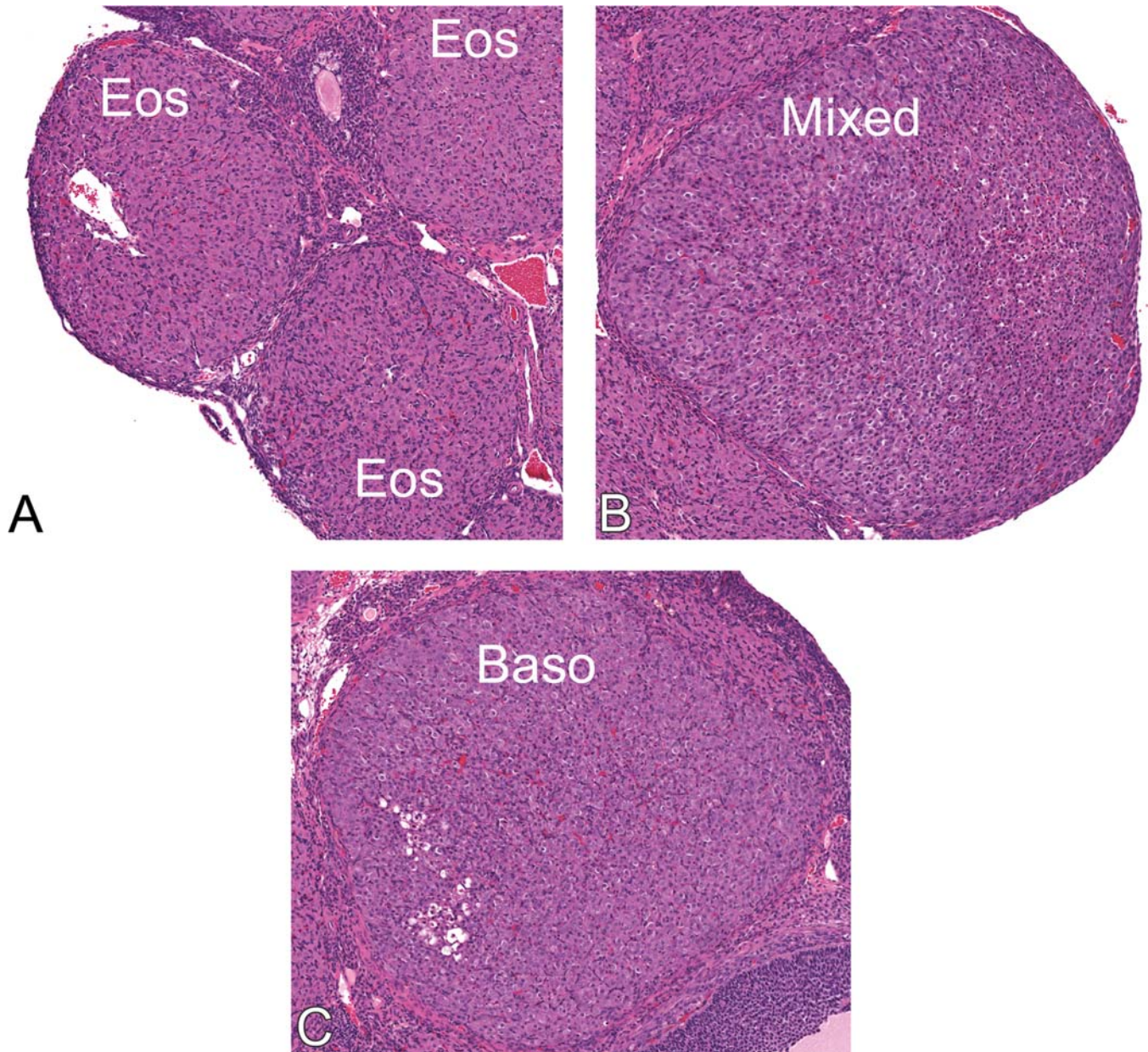


**FIGURE 10.3** Ovary, rat, corpora lutea (CL) types. (A) Normal eosinophilic (Eos) CL, (B) mixed eosinophilic and basophilic CL, and (C) basophilic (Baso) CL. 50 $\times$ , H&E. Reproduced from Haschek WM, Rousseaux CG, Wallig MA, editors: *Haschek and Rousseaux's handbook of toxicologic pathology*, ed 3, 2013, Academic Press, Figure 60.3, p. 2605, with permission.

an appearance reflecting the active synthetic state of the cells. As steroidogenesis declines, the CL develops a mixed eosinophilic appearance. Finally, the luteal cytoplasm in the CL turns eosinophilic and vacuolated, reflecting a rapid decrease of steroidogenesis. The changes in the CL are coordinated with the estrous cycle and described in more detail in [Section 2.3](#) below.

## 2.2. The Histology of the Rat Ovary during Prepubertal and Pubertal Development

The Endocrine Disrupter Screening Program (EDSP) test guidelines first released in 2009 by the US EPA included a female pubertal assay as part of the risk assessment paradigm for endocrine-active chemicals. Recent updates on

the entire program for Tier 1 and 2 testing (described later in the chapter) were published (EPA, 2023). The pubertal assay requires administration of a test article by oral gavage to female rats from postnatal day (PND) 22 through PND 42 or 43, followed by the evaluation of multiple endpoints including reproductive tissue histology. This period of female rat development includes the onset of estrus (PND 29–38) and vaginal patency (~PND 33). Because the toxicologic pathologist may be required to assess the histologic features of the reproductive tract from rats used in this assay, we include a brief outline of the normal histology of the peripubertal reproductive tract.

At PND 20–21, early antral follicles are present (Figure 10.4A) and the ovary has atresia of secondary and tertiary follicles (early to mid-stage) (Figure 10.4B), which progress to confluent expanses of apoptotic granulosa cells by PND 22 (Figure 10.4C). By PND 27–28, there is a dramatic increase in necrotic ova within the ovarian medulla (Figure 10.4D–E). Also, the outer cortex with larger antral follicles is clearly distinguished from the center of the medulla, which contains atretic follicles (Figure 10.4E). CL first appear between PND 28 and 38, and the numbers of necrotic ova and atretic follicles are decreased (Figure 10.4F). By PND 38, rats have several ovulatory follicles and 3–6 CL per section of ovary. At PND 43, 4–10 CL are present and atretic follicles are in lower numbers (one to four per section) (Figure 10.4G) (Picut et al., 2015).

### 2.3. The Histology of the Rat Female Reproductive Tract during the Estrous Cycle

For any toxicologic pathologist, a strong understanding of the normal histologic changes that occur in the rat reproductive tract during the estrous cycle is fundamental (Dixon et al., 2014; Taketa, 2022). Toxicology studies using the sexually mature female rat are probably the first and best opportunity for a pathologist to assess the potential reproductive effects of test articles in woman. Table 10.4 lists what we consider are the best distinguishing characteristics of each stage. The most useful histologic criteria for differentiating roughly among the various stages of estrous occur in the vagina

(Figure 10.5); however, definitive staging of the estrous cycle requires the evaluation of the morphologic characteristics of the ovary and uterus. Note that the most common rat strains used (SD and Wistar) have a similar estrous cycle, and our descriptions of the cycle will be limited to the SD and Wistar. The information provided below will be a compilation of our personal experience, the literature (Westwood, 2008; Sato et al., 2016; Taketa, 2022), and the results from a detailed estrous cycle study completed at Eli Lilly in the late 1990s with the Crl: CD (SD) IGS BR SD rat.

The cycle of the SD and Wistar rat is usually 4 days in length; however, occasionally rats will have 5-day cycles or will switch between 4- and 5-day cycles. As mentioned above, the vagina is very helpful for female reproductive tract staging; however, in young rats, there is a higher degree of cycle abnormalities such as two consecutive days of vaginal estrus and therefore the vaginal morphology may appear to be slightly different from the ovary and uterus. When available, vaginal cytology can be correlated with the histopathology. In the end, the ovary is the main driver of the cycle, and it is important to not overinterpret slight differences across the organs. Note that histologic samples of rat vagina should be collected from the anterior vagina since the posterior third of the vaginal mucosa is always covered by a thick, cornified stratified epithelium as it transitions to vulva. Also, trimming and sectioning should be standardized for all species to prevent bias, especially in the case of the ovary (Figure 10.6) (Kittel et al., 2004; Van Esch et al., 2008b).

A high level of proficiency in female reproductive tract staging can be attained quickly with a little practice at recognizing the cyclical changes in the ovary, uterus, and vagina of the young, sexually mature female rat. While Table 10.4 is an excellent quick reference, it is important to understand the details of tissue changes for each stage of the rat estrous cycle. Note that while we will not describe histologic changes in the cervix, generally cervical changes, albeit with a slight delay, mirror vaginal changes during the rat estrous cycle.

In the rat, the paired ovaries, suspended from the dorsal abdominal wall by the mesovarium, are globose. During each estrous cycle, several follicles and corpora lutea may develop. These



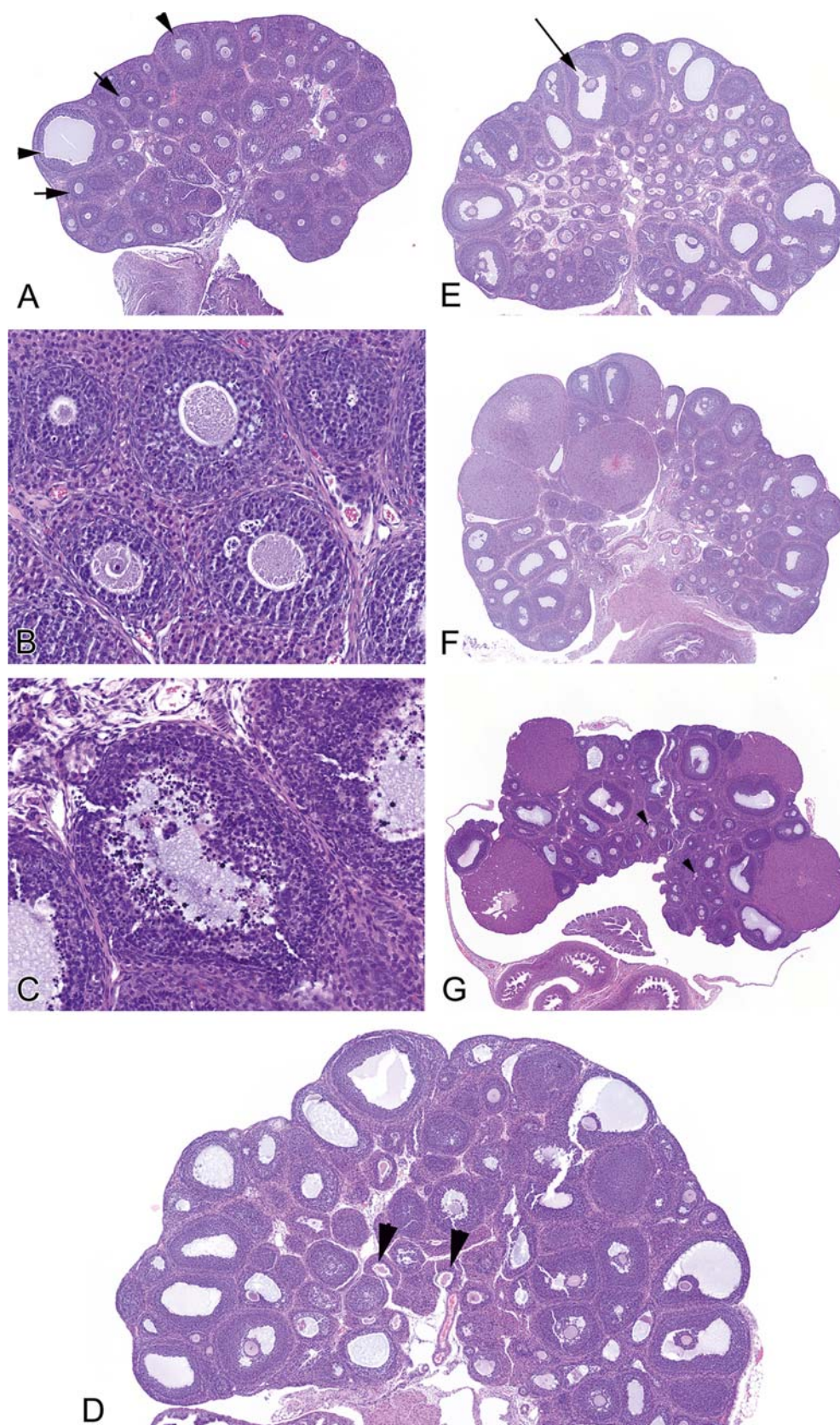


**FIGURE 10.4** Ovary, rat. (A) Post natal day (PND) 21. Early antral follicles are present (arrowheads). (B) PND 21, atresia of secondary and tertiary follicles (early to mid-stage). (C) PND 22, confluent expanses of apoptotic granulosa cells. (D) PND 26, necrotic oocytes (arrowheads). (E) PND 28, necrotic oocytes within the ovarian medulla; large antral follicles (arrow) are clearly distinguished from the center of the medulla which contains atretic follicles. (F) PND 37, corpora lutea (CL) present and numbers of apoptotic ova and atretic follicles are decreased. (G) PND 43, several ovulatory follicles and CL present; fewer atretic follicles (arrowheads). (A, E, F) 25 $\times$ , (B, C) 200 $\times$ , (D) 50 $\times$ , (G) 12.5 $\times$ . H&E. *Courtesy of Drs Cathy Picut and Amara Remick (Picut et al., 2015). Reproduced from Haschek WM, Rousseaux CG, Wallig MA, editors: Haschek and Rousseaux's handbook of toxicologic pathology, ed 3, 2013, Academic Press, Figure 60.4, p. 2606, with permission.*

**TABLE 10.4** Key Vaginal Histologic Criteria for the Rat Estrous Cycle

Stage	Histology
Proestrus	Mucified cuboidal epithelium overlying a cornified layer
Estrus	Stratified epithelium with keratin loosely associated or sloughed into lumen
Metestrus	Intraepithelial and stromal leukocytes; complete loss of stratum corneum
Diestrus	Thinner epithelium, less frequent leukocytes (early); thicker epithelium, mitoses (late)

*Adapted from Westwood FR: The female rat reproductive cycle: a practical histological guide to staging, Toxicol. Pathol. 36:375–384, 2008; Reproduced from Haschek WM, Rousseaux CG, Wallig MA, editors: Haschek and Rousseaux's handbook of toxicologic pathology, ed 3, 2013, Academic Press, Table 60.4, p. 2608, with permission.*

follicles and/or corpora lutea often protrude from the ovarian surface, thus giving rise to the grape-like appearance of the ovary at necropsy. Within the stroma in between the developing follicles and corpora lutea, the follicular theca interna from atretic follicles persists as the interstitial gland, which often contains degenerated zona pellucida in the center. The interstitial gland is endocrinologically active producing weak androgens and eventually breaks up into small groups of cells that are scattered in the medulla.

The rat has a duplex uterus with two long and straight uterine horns and separate uterine bodies joined externally at their cervical ends. Grossly the rat has a single cervix but with two independent cervical canals. The uterus is composed of an innermost mucosa, the endometrium, a middle muscular layer, the myometrium, and an outer serosal layer, the perimetrium (Figure 10.7). The endometrium is composed of a surface epithelium, endometrial glands, and the lamina propria. A single layer of columnar epithelial cells lines the luminal surface and endometrial glands. The lamina propria is composed of abundant small stromal cells, migrating lymphocytes and polymorphonuclear leukocytes, and vascular spaces within a framework of connective tissue. The myometrium is composed of inner circularly and outer

longitudinally arranged bundles of smooth muscle cells. The perimetrium is composed of a single layer of mesothelial cells which overlies a thin layer of connective tissue. Recently, the NTP started to implement an extended longitudinal sectioning protocol for the residual uterus and cervix tissue (Elmore et al., 2020) next to the commonly used midway transverse sections through both uterine horns and longitudinal sections through the body of the cervix. This sectioning protocol, when well executed, results in 10–20× more uterine tissue for microscopic examination, making the probability to detect changes and lesions much higher. Although this method requires more laboratory resources for trimming and sectioning and makes it difficult to compare the results with previously collected historical control datasets, it can be of benefit when potential uterine toxicity is expected or when the evaluation of transverse sections results in equivocal findings. Using this method, Hobbie and Dixon (2020) reviewed transverse and longitudinal section of the uterine tract, taken from three reproductive and developmental toxicity studies in SD rats, for cystic endometrial hyperplasia (CEH). Although for CEH there was not much difference between transverse and longitudinal sections, the authors concluded that longitudinal uterine sections allowed better appreciation of CEH as a typically diffuse lesion and decreased the likelihood of missing CEH lesions. For focal lesions, the longitudinal approach may increase the sensitivity for lesion identification.

The vagina consists of an inner layer, the mucosa, a middle layer, the muscularis, and an outer layer, the adventitia (Figure 10.8). The mucosa is composed of a stratified squamous epithelium and its underlying lamina propria. The muscularis is composed of smooth muscle fibers arranged circularly in the inner layer and longitudinally in the outer layer. The adventitia is composed of a thin layer of connective tissue.

On the day of estrus, the sexually mature rat ovary usually has three to occasionally four sets of corpora lutea. The smaller basophilic CL contain spindle-shaped basophilic cells filling the previous (follicular) lumen are from the most recent ovulation event. The CLs from the last cycle are eosinophilic with degenerative changes. There may also be smaller less distinct eosinophilic corpora lutea present from the



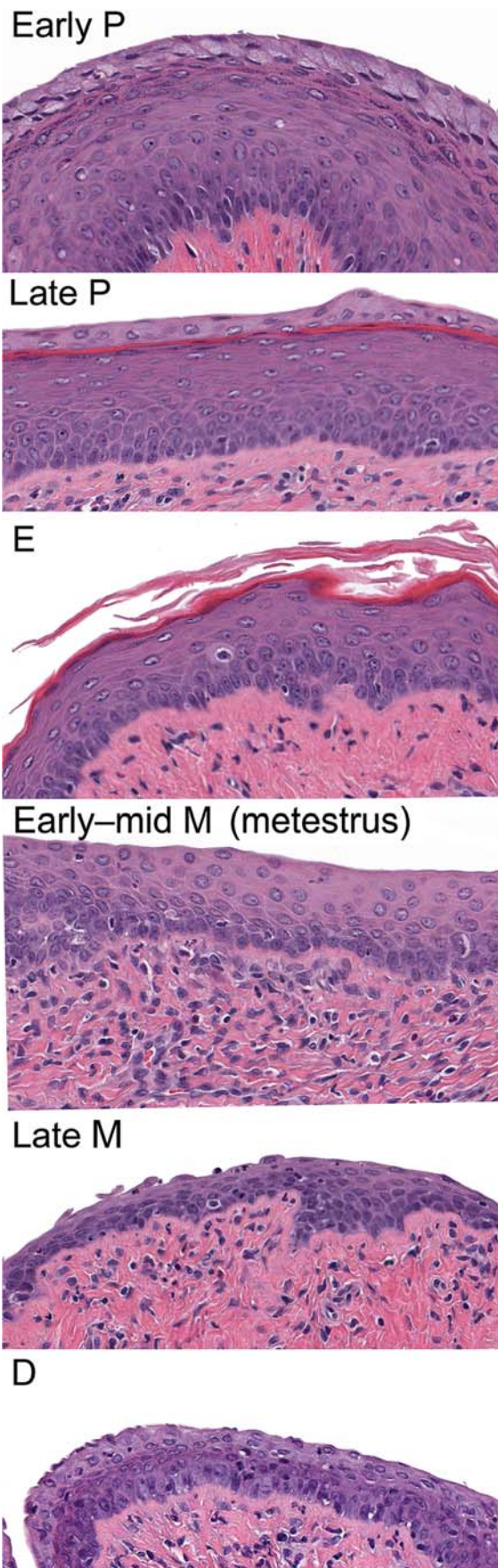


**FIGURE 10.5** Vagina, rat, changes with estrous cycle. Proestrus: Early in proestrus (Early P), the vagina is lined by four to eight layers of plump epithelial cells that have a mucoid character to their cytoplasm. Later in proestrus (Late P) the vaginal epithelium is thicker (up to 10 layers) and overlain by a thin layer of cornified cells. Estrus (E):



previous cycles and/or old shrunken CL remaining from several cycles ago (Figure 10.9). Dependent on section, one may observe an ovulatory fossa with hemorrhage, mitotic activity, and luteinizing granulosa cells, and the oviducts (if present) may have ova and/or cumulus oophorus cells. The uterus, initially lined by hypertrophic and high columnar surface epithelium, undergoes extensive apoptosis. Apoptosis is noted in *both* the luminal and glandular epithelium, and there is stromal edema and granulocytic infiltrates (Figure 10.9). The uterine epithelial cells are crowded and tall, and the uterine myometrium is thick. The vagina is approximately six to ten layers thick and has a superficial layer of strongly eosinophilic cornified epithelium that later is sloughed into the vaginal lumen when estrus progresses. Early on the day of estrus, there may be mucous layer remnants from proestrus sloughed into the lumen and by late on the day of estrus very little cornified debris may be left (Figures 10.5 and 10.8).

On the day of metestrus, three sets of corpora lutea are present: basophilic CL, occasionally with a central fluid-filled lumen; degenerating eosinophilic CL from the previous cycle; and old, shrunken CL from past cycles (Figure 10.10). The vagina has a noncornified epithelium that is four to six layers in thickness, with intraepithelial and luminal leukocytes (Figure 10.5). The uterus still has apoptosis but *only* in the luminal epithelial cells and often contains mitotic figures (Figure 10.6). The uterine epithelial cells lining both the lumen and the glands are low columnar and more distinct. The uterine myometrium is thinner (Figure 10.10).

On the day of diestrus, there are three sets of corpora lutea: eosinophilic CL from the current cycle, eosinophilic CL with signs of luteolysis, and old corpora lutea from past cycles. The CL

of the current cycle has luteal cells that are larger with very prominent nucleoli, some containing vacuoles (lipid droplets) in their cytoplasm (Figure 10.10). The vagina is thinner, only three or 4 cell layers thick, noncornified, and has variable amounts of intraepithelial leukocytes. Mitoses may be observed in the basal layer (Figure 10.5). The superficial layer may show mild cytoplasmic mucin accumulation. The uterus is generally quiescent, with occasional mitoses, a low columnar to cuboidal superficial lining and glandular epithelium, and a thinner myometrium (Figure 10.10).

On the day of proestrus, the ovary has mixed basophilic/eosinophilic and mature, eosinophilic corpora lutea from the previous cycles which show degenerative changes and old shrunken CL. Different patterns of luteolysis have been reported in different rat strains although the basic patterns are similar. In SD rats, luteolysis is usually characterized by the presence of scattered degenerating luteal cells, while in the Wistar rat, a clear central area of degeneration and apoptosis of luteal cell is more common and is surrounded by a rim of luteal cells showing vacuolar degeneration (Sato et al., 2014). These normal degenerative CL changes are sometimes misdiagnosed by pathologists as lesions. Large preovulatory follicles are often present in the ovary at this stage of the estrous cycle (Figure 10.11). Interstitial glands will be the most prominent during proestrus. The uterus has a dilated lumen, stromal edema, a hypertrophied myometrium, and mitoses in luminal and glandular epithelial cells (Figure 10.11). Eosinophils in the stroma are most prominent in this stage. Uterine weights are often increased during proestrus and uteri appear larger at necropsy because of intraluminal fluid. Early in proestrus, the vagina is lined by four to eight layers of plump epithelial cells,

There is no superficial vacuolated layer, the epithelium is approximately six to eight layers thick and has characteristic plaques of cornified epithelium. Metestrus: The vagina has a noncornified epithelium that is four to six layers in thickness with intraepithelial and luminal leukocytes (Early-mid M). At the end of metestrus (Late M), the epithelium is thinner. Diestrus (D): The vaginal epithelium is thin, only three or 4 cell layers thick, noncornified and superficially pale staining, and has prominent intraepithelial leukocytes. Later in diestrus, the epithelium is thickened, and leukocytes are less frequent. 80×, H&E. Reproduced from Haschek WM, Rousseaux CG, Wallig MA, editors: *Haschek and Rousseaux's handbook of toxicologic pathology*, ed 3, 2013, Academic Press, Figure 60.5, p. 2609, with permission.

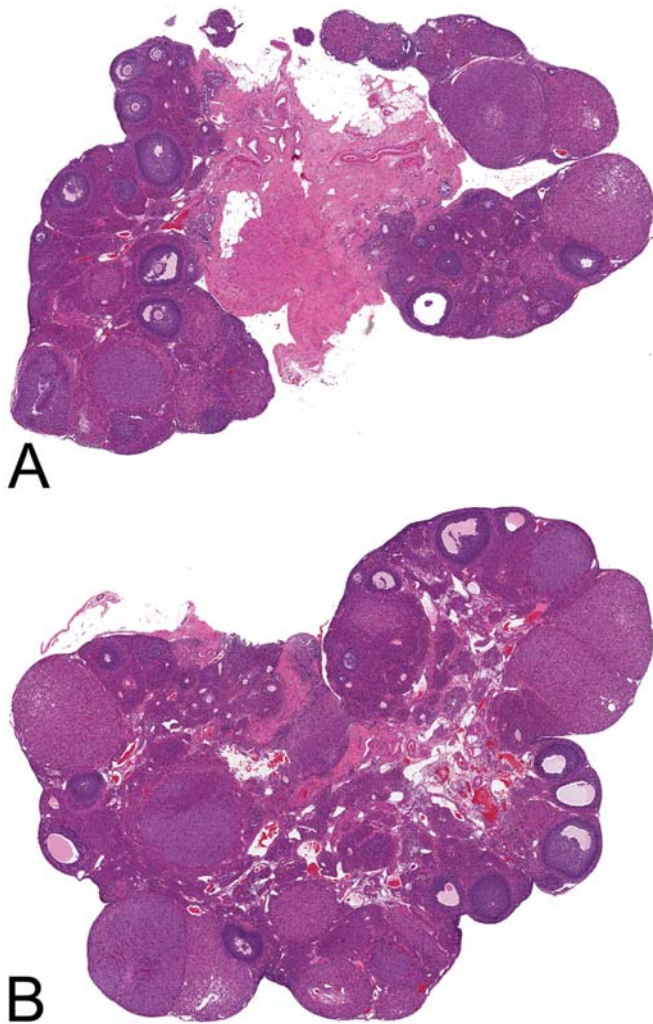


**FIGURE 10.6** Ovary, rat, effects of section. Because the section was not optimally processed, the top ovary (A) compared to the bottom (B) appears to have a lower number of follicles and CL. 15 $\times$ , H&E. Reproduced from Haschek WM, Rousseaux CG, Wallig MA, editors: *Haschek and Rousseaux's handbook of toxicologic pathology*, ed 3, 2013, Academic Press, Figure 60.6, p. 2610, with permission.

and the superficial layer has a mucoid character which is histochemically PAS and Alcian-blue positive for mucopolysaccharides. Later in proestrus, the vaginal epithelium is thicker (up to 10 layers) and characterized by an eosinophilic band of keratinized epithelium (stratum corneum) that developed in between the stratum granulosum and mucoid layer ([Figure 10.5](#)).

SD rats start entering senescence as early as 4 months of age, which alters the cycle, usually prolonging the portions of the cycle under estradiol influence (so called “persistent estrus”) ([Shirai et al., 2015](#); [Westwood, 2008](#)). Wistar

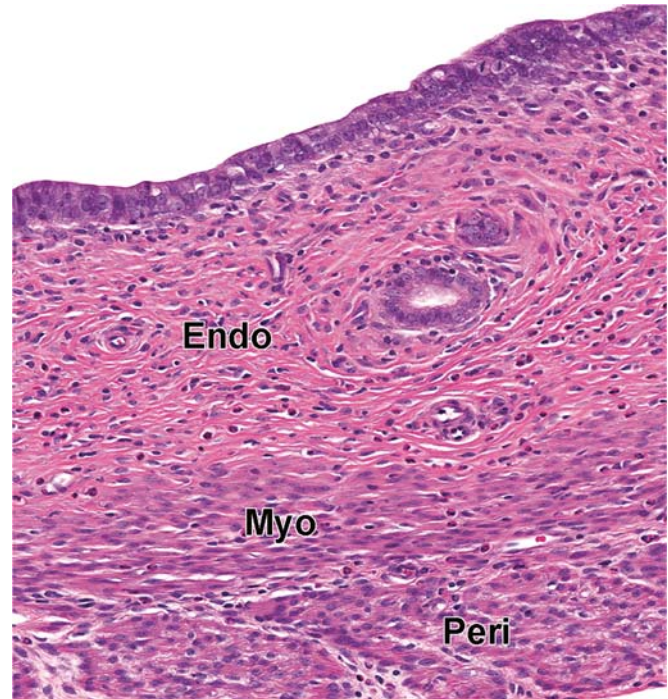


**FIGURE 10.7** Uterus, rat, normal. The uterus is composed of an innermost mucosa (Endo), the endometrium; a middle muscular layer, the myometrium (Myo); and an outer serosal layer, the perimetrium (Peri). 60 $\times$ , H&E. Reproduced from Haschek WM, Rousseaux CG, Wallig MA, editors: *Haschek and Rousseaux's handbook of toxicologic pathology*, ed 3, 2013, Academic Press, Figure 60.7, p. 2610, with permission.

rats tend to reach reproductive senescence at a relatively later age between 6 and 8 months and are often reported to have a pattern consistent with repetitive pseudopregnancy, although persistent estrus can also be observed ([Mitchard and Klein, 2016](#)). Older female rats can also enter a persistent diestrus state.

#### 2.4. The Histology of the Dog Female Reproductive Tract during the Estrous Cycle

The estrous cycle of the dog is very different from the rat. It is markedly longer, more variable in phase length (3.5–13 months), and has a normal “anestrus” phase ([Chandra and Adler, 2008](#); [Chandra et al., 2010](#)). Evaluating the reproductive tract in dog toxicology studies can be challenging because young, peripubertal dogs are often used in toxicology studies and numbers



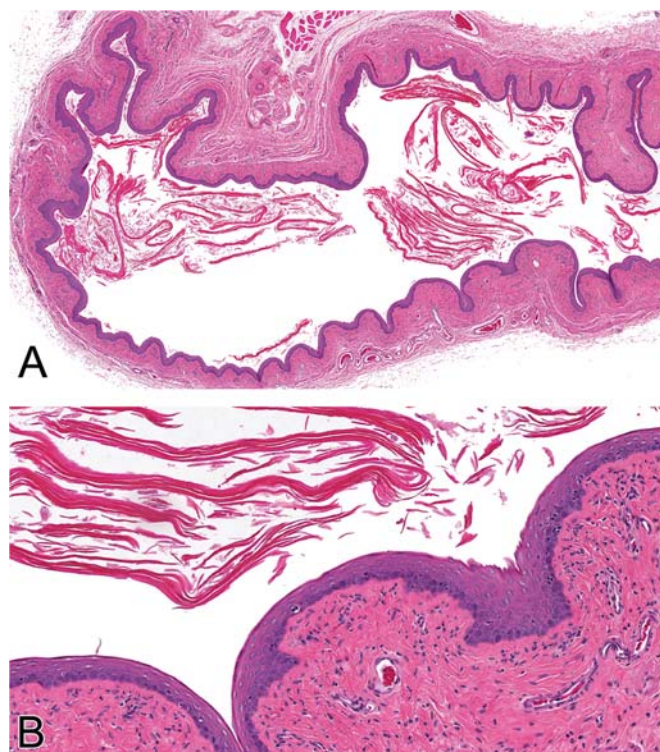


**FIGURE 10.8** Vagina, rat, estrus. Cornified material is sloughed into the vaginal lumen. (A) 12 $\times$ , (B) 60 $\times$ . H&E. Reproduced from Haschek WM, Rousseaux CG, Wallig MA, editors: *Haschek and Rousseaux's handbook of toxicologic pathology*, ed 3, 2013, Academic Press, Figure 60.8, p. 2611, with permission.

in test groups are small (generally three or four) (Figure 10.12). An accurate phasing of the dog estrous cycle will assist in assessing test article effects on the reproductive events in the female dog (bitch) reproductive tract.

Dog ovaries are irregularly ellipsoid. Several follicles and corpora lutea may develop during each cycle, and polyovular follicles (follicles with two or more oocytes) commonly occur in young bitches (Pavan-Carreira and Pires, 2008). Like the rat, the follicles and corpora lutea often protrude from the ovarian surface, thus giving rise to the grape-like appearance of the ovary. Dog ovaries also have interstitial glands or granulosa cell cords derived from atretic follicles and stromal cells. Granulosa cells of canine follicles begin to luteinize with extensive infoldings of the granulosa lining prior to ovulation (Rehm et al., 2007). It is important to note that the infolded luteinized preovulatory follicles in the dog are normal but can often be misinterpreted as abnormal. Unique to dogs at all phases of

the reproductive cycle are the presence of invaginated cord-like proliferations of the surface epithelium that extend through the tunica albuginea into the superficial cortex. These structures have been termed subsurface epithelial structures (SEs) and are most easily observed during anestrus (Figure 10.13). The SEs are hormonally responsive (e.g., estrogen and progesterone) and commonly become cystic in aged dogs (see Section 5.6). Their functional significance is not known. The dog has a bicornuate uterus with a short body and long and straight uterine horns. The two separate uterine horns open into one common cervical canal.

Proestrus and estrus phases together account for 1–3 weeks of the estrous cycle in dogs (Rehm et al., 2007; Sato et al., 2016). At estrus, the ovary has large preovulatory follicles with luteinization of the granulosa cell layers (Figure 10.14). The uterus has myometrial hypertrophy, stromal cell proliferation, and stromal congestion, edema, and hemorrhage (Figure 10.15). The surface and glandular epithelium are increased in height, and there are numerous mitotic figures. The vagina is the thickest during estrus, and heavily cornified (Figure 10.15). The stroma and smooth muscle are hypertrophied, and there is both stromal congestion and edema.

Metestrus or diestrus is up to 100 days in length in the dog. At metestrus, the ovary has new corpora lutea (Figure 10.14). Luminal glands are proliferative and straight and abruptly become tortuous toward the basement membrane (Figure 10.15). Often the glandular lumina contain pink secretions and the stromal edema and congestion are markedly decreased. The upper gland and luminal epithelial cells progressively develop more foamy cytoplasm because of the influence of progesterone. The vagina becomes much thinner (three or 4 cell layers) and loses its cornification (Figure 10.15). Because of the long life of the corporal lutea, pseudocyesis (false or pseudopregnancy) with or without clinical signs (e.g., nesting behavior) is relatively common in the dog. During diestrus, dog mammary glands will demonstrate alveolar lobular hyperplasia and increased secretions which could be interpreted as a treatment-related effect in a toxicology study. Also, the uterus can develop a hyperplastic endometrium and may have implantation-like areas



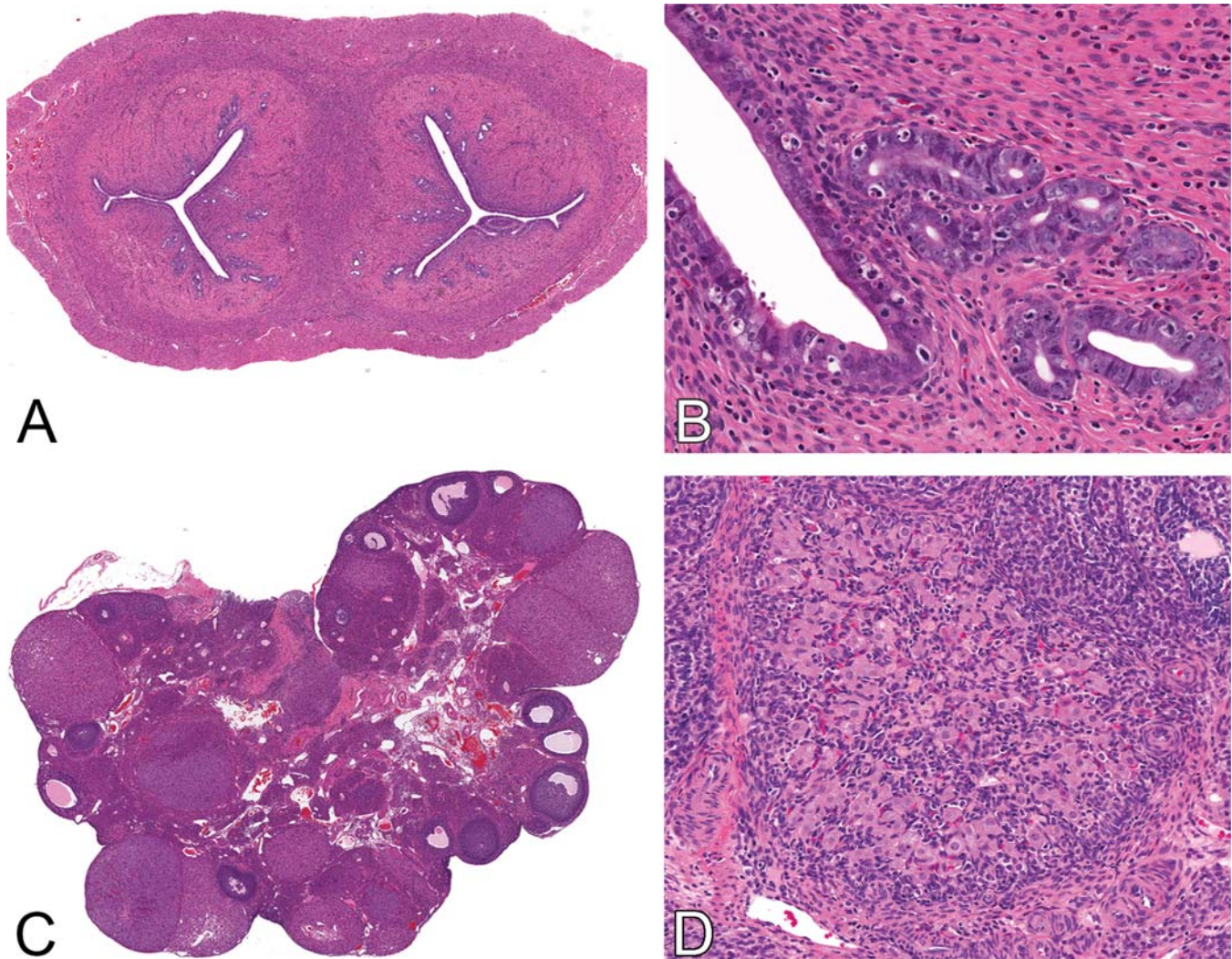


**FIGURE 10.9** Ovary and uterus, rat, estrus. (A) The uterus has a thick endometrium and myometrium. (B) There is apoptosis of both luminal and glandular epithelial cells with endometrial inflammatory cell infiltrates. (C) The ovary has three to four sets of corpora lutea. (D) The new, small basophilic CL are from the most recent ovulation event, CLs from the previous cycle are now eosinophilic with early degenerative changes, and corpora lutea present from the previous cycles show more pronounced degenerative changes and are shrunken (A) 12 $\times$ , (B) 120 $\times$ , (C) 10 $\times$ , (D, 150 $\times$ ). H&E. Reproduced from Haschek WM, Rousseaux CG, Wallig MA, editors: *Haschek and Rousseaux's handbook of toxicologic pathology*, ed 3, 2013, Academic Press, Figure 60.12, p. 2612, with permission.

without the fetal contribution (Figure 10.16) (Sato, 2011; Koguchi et al., 1995).

Anestrus is the most variable period in the dog, and its length is partially dependent on the breed. This stage can range from 1 to 6 months in length in the laboratory Beagle. During anestrus, the ovary appears quiescent with one or two sets of old CLs (Figure 10.14) and no evidence of follicular development. The uterine surface and glandular epithelium are lined by low columnar cells with basally

situated nuclei, and the vagina epithelium is three or 4 cell layers thick and noncornified (Figure 10.15).

At proestrus, there is a gradual increase in ovarian follicular development, and large antral follicles with thick granulosa cell layers are evident (Figure 10.14). If animals are old enough, there may be old CL composed of small foci of vacuolated cells and macrophages with intracytoplasmic lipofuscin. During proestrus, the uterine mucosa becomes more vascular and

edematous with occasional small focal areas of erythrocyte extravasation in the zona compacta. The surface and glandular epithelium increases in height, and numerous mitotic figures are present (Figure 10.15). The vaginal mucosa becomes thicker and cornified (Figure 10.15). The stroma and smooth muscle also start to thicken, and there is both stromal congestion and edema.

## 2.5. The Histology of the Cynomolgus Macaque Female Reproductive Tract during the Menstrual Cycle

The cynomolgus macaque (referred to as NHP) reaches sexual maturity at approximately 4–5 years and has a menstrual cycle (and endocrinology) that is very similar to the human, with a cycle length of approximately 30 days (Weinbauer et al., 2008; Van Esch et al., 2008a, 2008b). However, as was the case for the dog, assessment of the female reproductive system can be challenging because the numbers of animals used in toxicology studies are small (usually three or four) and animals are often pre- or peripubertal. The attention given to the NHP as an animal model has heightened because of the large influx of biologics and gene and cell-based therapies now in nonclinical development (see *Nucleic Acid Pharmaceutical Agents*, Vol 2, Chap 7, *Vaccines*, Vol 2, Chap 9, and *Stem Cell and Other Cell Therapies*, Vol 2, Chap 10). Many of these agents are not amenable to study in rodents, and the cynomolgus macaque has become a key animal model of human relevance. As a result, the use of sexually mature cynomolgus macaque is now more common, and it is important for the toxicologic pathologist to be familiar with this model system. Other nonrodent animal models like the minipig and nonanimal model in vitro systems (NAMs) are also emerging as potential alternatives to the NHP in response to 3Rs (refine, reduce, replace) initiatives. Recently the NHP supply chain has become challenging for the pharmaceutical and biotechnology industry because of the impact of the COVID pandemic, issues with Cambodian suppliers, and the political antagonism with China (FDA, 2022).

The cynomolgus macaque ovaries are amygdaloid in shape and found in the pelvic cavity. The ovary has multiple primary follicles that develop with each cycle, but usually only one follicle will become the preovulatory follicle, resulting in a single protrusion from one ovarian surface. Degenerating primary oocytes are likely the origin of calcified foci found in the ovarian cortex of cynomolgus macaques. The calcified areas may be multiple and/or bilateral (Buse et al., 2008).

In the sexually mature cynomolgus macaque, the cervix has a stratified squamous exocervix, squamocolumnar junction (SCJ) and transformation zone (the region where the columnar epithelium has been replaced by metaplastic squamous epithelium), and glandular endocervix with prominent colliculi. The stratified squamous epithelium of the exocervix changes to tall columnar glandular epithelium at the SCJ. In contrast, the cervical mucosa is atrophic in the sexually immature cynomolgus macaque and the SCJ is present within the endocervix and not distinct. The cervical epithelium in macaques is highly responsive to estrogens. Estrogen stimulation results in marked keratinization of the exocervical epithelium, thickening of the stratified squamous epithelium near the SCJ, and squamous metaplasia and hypertrophy of the endocervical glands (Wood, 2008).

The menstrual cycle of the cynomolgus macaque is divided into four major phases: the follicular (or proliferative) phase, the luteal (or secretory) phase, the menstrual phase, and the regenerative phase (Figures 10.17–10.19). For a detailed description of these phases, the reader is referred to the review by van Esch and colleagues (2008a). Descriptions of the menstrual cycle in the cynomolgus macaque may differ and a periovulatory phase may be included to address the variability around the time of ovulation and/or the regenerative phase may not be included. Cynomolgus macaque endometrial changes are like those of women, with menstrual discharge toward the end of each reproductive cycle. The follicular or proliferative stage follows menses. During the follicular (proliferative) phase, the endometrium has straight proliferative glands and prominent stromal edema due to the rising concentrations of estradiol. By day



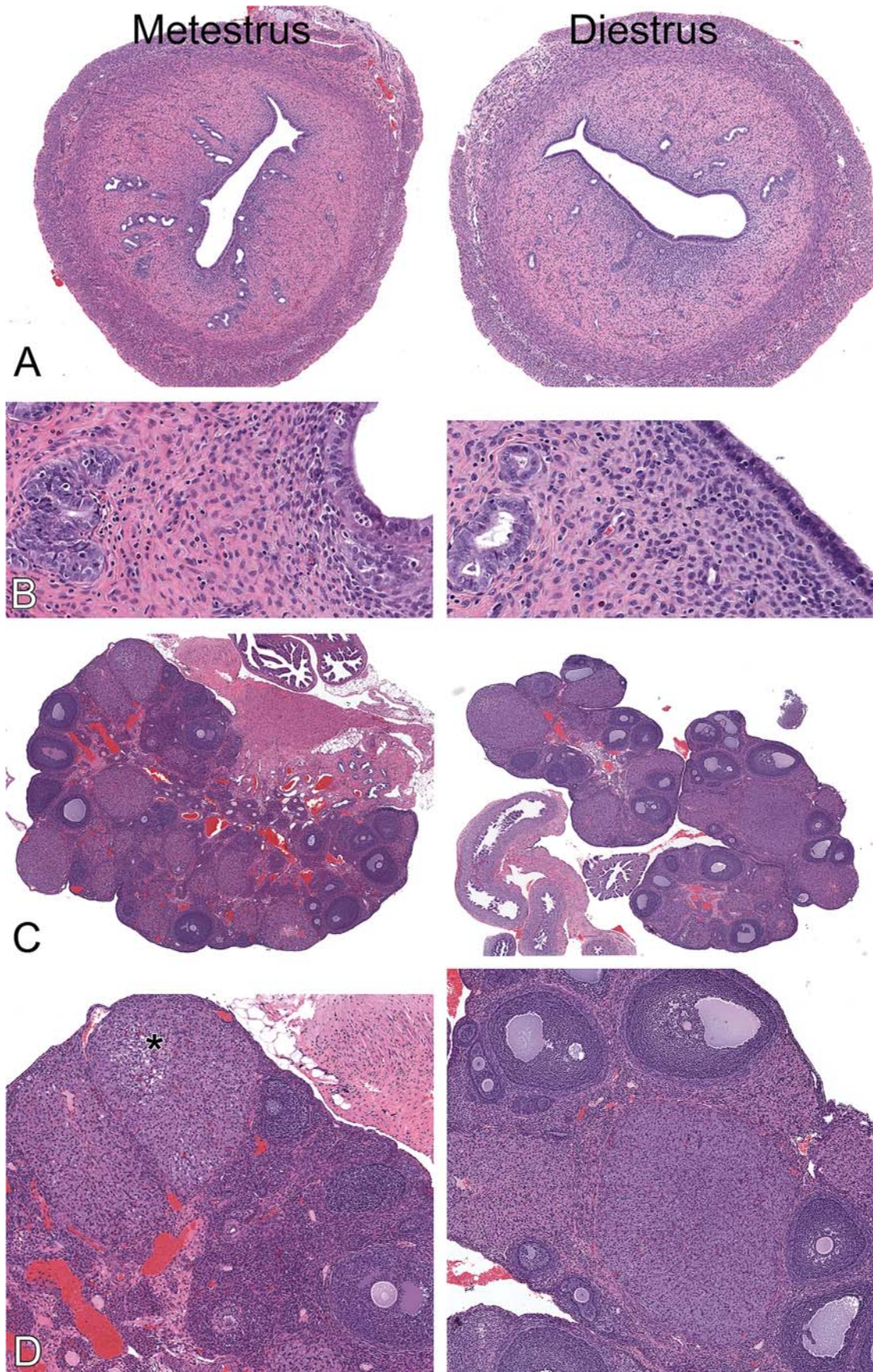


**FIGURE 10.10** Uterus and ovary, rat, metestrus (A–D left) and early diestrus (A–D right). Metestrus: the uterus (A, B left) has apoptotic cells but only in the luminal epithelial cells; uterine epithelial cells lining both the lumen and the glands are



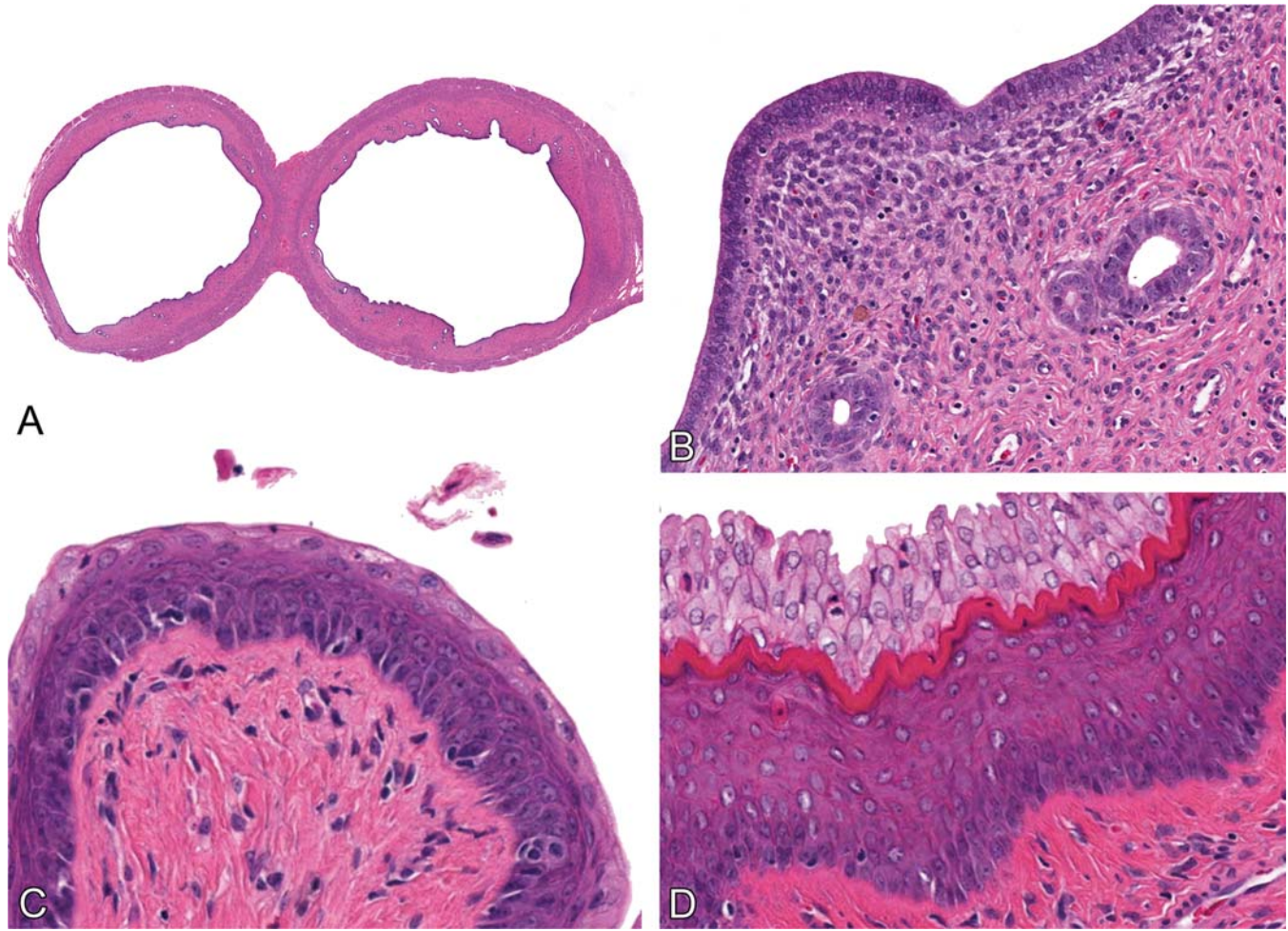


**FIGURE 10.11** Uterus and vagina, rat, proestrus. (A) Uterus: dilated lumen. (B) Uterus: stromal edema, hypertrophied myometrium, and mitoses in luminal and glandular epithelial cells can be seen. Eosinophils in the stroma are most prominent in this stage (not shown). (C) Vagina: in early proestrus the vagina is lined by 4 to 8 layers of plump epithelial cells that have a mucoid character to their cytoplasm. (D) Vagina: later in proestrus the vaginal epithelium thickens (up to 10 layers) and is overlain by a thin layer of cornified cells and a thicker layer of mucoid cells. (A) 10 $\times$ , (B) 80 $\times$ , (C, D) 125 $\times$ . H&E. Reproduced from Haschek WM, Rousseaux CG, Wallig MA, editors: *Haschek and Rousseaux's handbook of toxicologic pathology*, ed 3, 2013, Academic Press, Figure 60.11, p. 2616, with permission.

shorter and more distinct, and the uterine myometrium is thinner. In the metestrus ovary (C, D left), three sets of corpora lutea are present (C), with a partially filled basophilic CL with luteolytic changes (\*), an eosinophilic CL from a previous cycle, and old, shrunken CL from past cycles (D). Early diestrus: the uterus (A, B right) is quiescent with a short columnar lining and glandular epithelium with a thinner myometrium. In the early diestrus ovary (C, D right), there are three sets of corpora lutea (C) with a eosinophilic CL with luteolysis (D on left), a filled basophilic CL (D center), and old corpora lutea from past cycles (D on right). (A) 20 $\times$ , (B) 120 $\times$ , (C) 15 $\times$ , (D) 30 $\times$ , H&E. Reproduced from Haschek WM, Rousseaux CG, Wallig MA, editors: *Haschek and Rousseaux's handbook of toxicologic pathology*, ed 3, 2013, Academic Press, Figure 60.10, p. 2614, with permission.



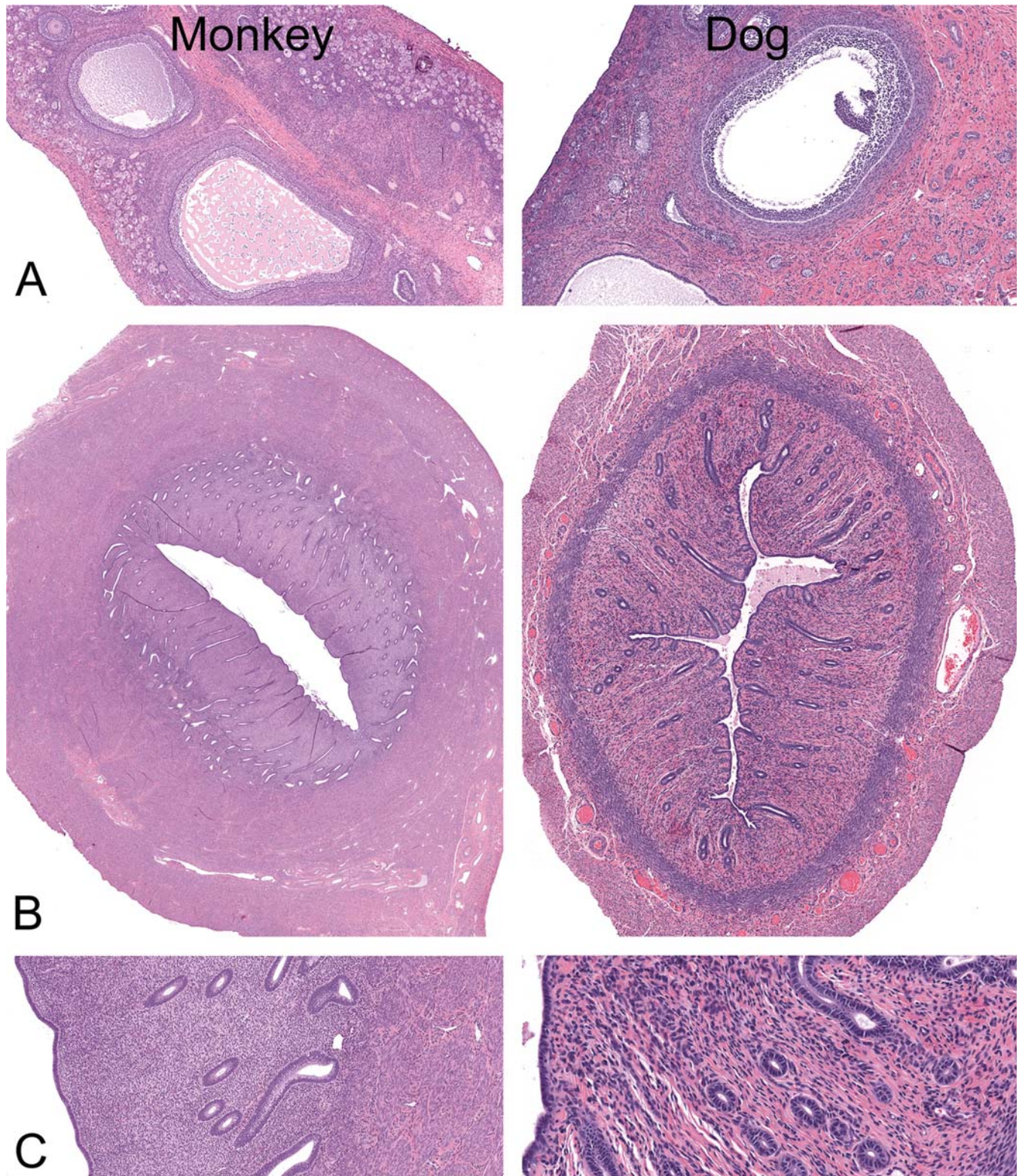


**FIGURE 10.12** Ovary and uterus, cynomolgus macaque and dog. Immature. Ovaries and uteri are small grossly (not shown). (A) Ovary: there are no corpora lutea or antral follicles; tertiary follicles are present (50 $\times$ ). (B, C) Uterus: The uterine endometrium and myometrium are thin and endometrial glands are quiescent (6 $\times$  and 20 $\times$ ). H&E. Reproduced from Haschek WM, Rousseaux CG, Wallig MA, editors: *Haschek and Rousseaux's handbook of toxicologic pathology*, ed 3, 2013, Academic Press, Figure 60.12, p. 2617, with permission.



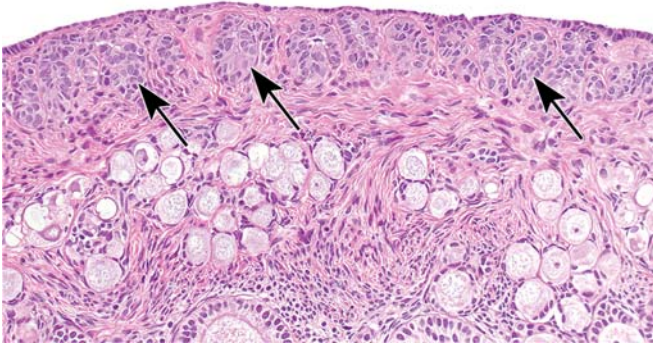


**FIGURE 10.13** Ovary, dog. Subsurface epithelial structures (SES, arrow) most easily observed during anestrus. 64 $\times$ , H&E.

6–8, the dominant ovarian follicle can be identified and will ovulate following the LH surge at the end of the proliferative phase (Figure 10.17).

Following ovulation, the secretory or luteal phase occurs; the hallmark of ovulation is the appearance of subnuclear vacuoles (Figure 10.17C). This phase lasts approximately 13–14 days and is marked by endometrial glands secreting a glycogen-rich material. The glands become coiled and saccular, giving a saw-tooth appearance. While in humans, subnuclear vacuoles and an increased saccular appearance of the glands are key characteristics of the secretory phase endometrium, these features can be more variable in the cynomolgus macaque and may begin to occur at the end of the proliferative phase. The spiral arteries become coiled and are often more prominent. Implantation typically occurs on day 21–23. If pregnancy is not established, the spiral arteries constrict with declining progesterone concentrations of the regressing corpus luteum, there is massive apoptosis of endometrial glands, stromal breakdown, and

stages of estrus. Anestrus (A): The ovary appears quiescent with one or two sets of old CL. Proestrus (P): there is a gradual increase in ovarian follicular development and large antral follicles with thick granulosa cell layers are evident. Estrus (E): The ovary has large preovulatory follicles with luteinization of the granulosa cells. Diestrus (D): The ovary has new corpora lutea. 10 $\times$ , H&E. Courtesy of Dr Sundeep Chandra. Reproduced from Haschek WM, Rousseaux CG, Wallig MA, editors: *Haschek and Rousseaux's handbook of toxicologic pathology*, ed 3, 2013, Academic Press, Figure 60.13, p. 2618, with permission.

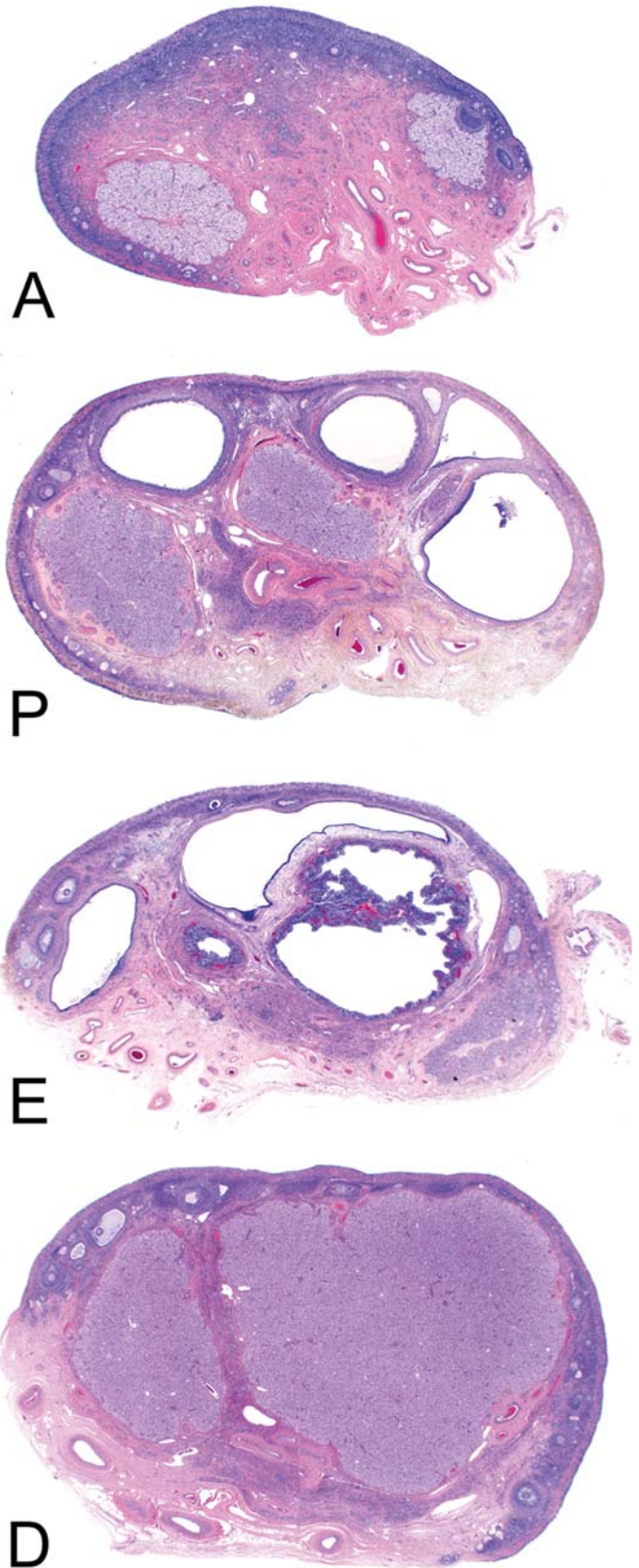


**FIGURE 10.14** Ovary, dog, estrous cycle. Typical morphologic features of the ovary during different



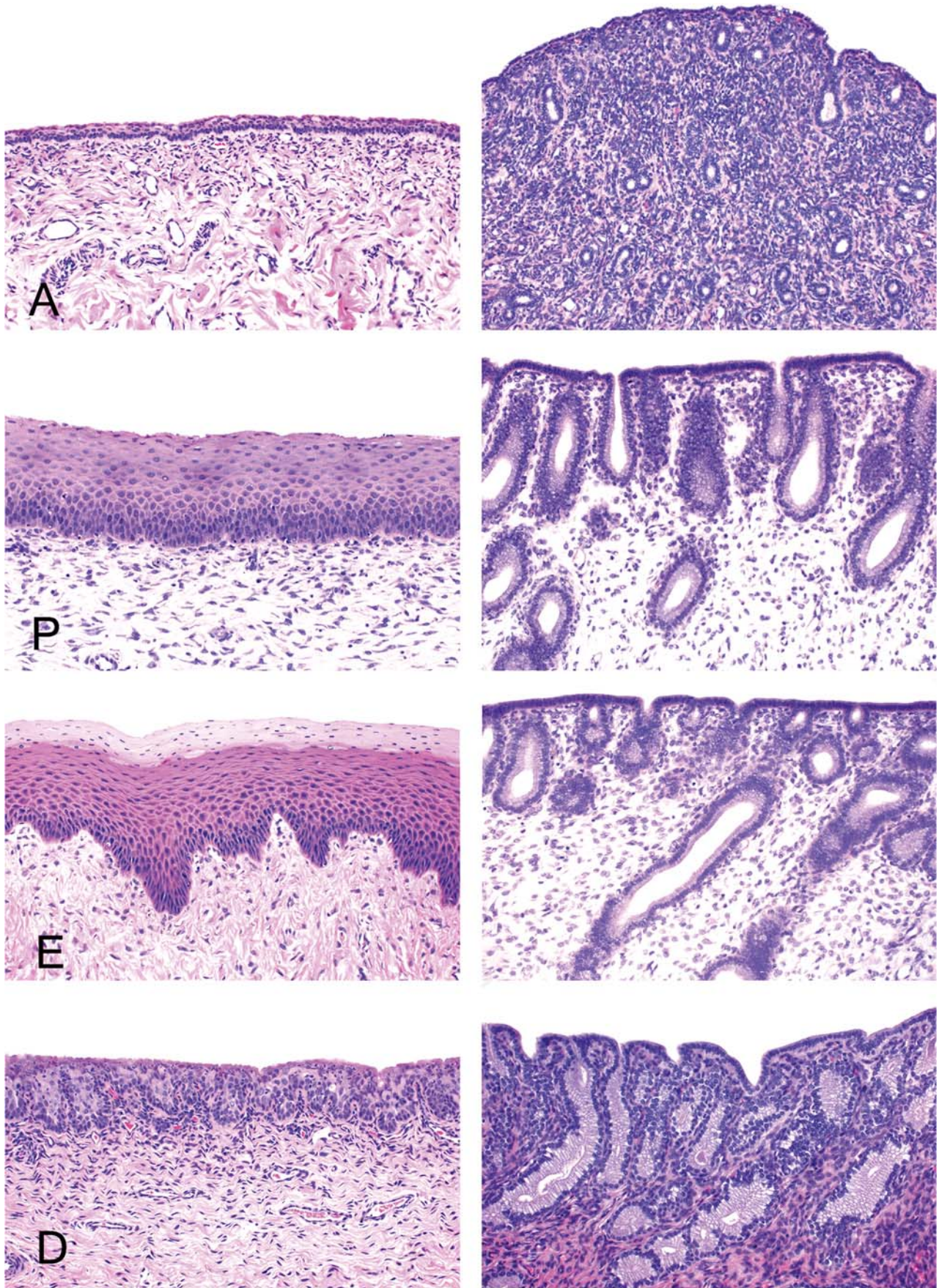


**FIGURE 10.15** Uterus (right) and vagina (left), dog. Vaginal changes as described in [Figure 10.11](#) In anestrus (A), the uterine surface and glandular epithelium are lined by low columnar cells with basally situated nuclei and the vaginal epithelium is thin and underlying stroma compact. In proestrus (P), the uterine mucosa becomes more



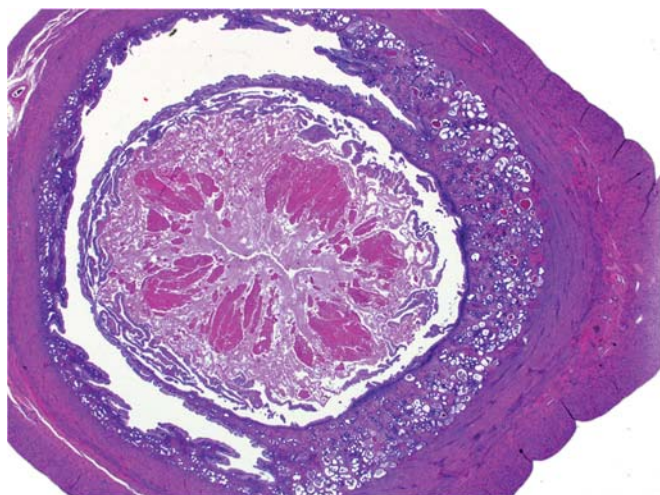


**FIGURE 10.16** Uterus, dog. In pseudopregnancy, the uterus develops a hyperplastic endometrium that has implantation-like areas without the fetal contribution. 4×, H&E.

hemorrhage (Figure 10.17D), and menses occurs over an approximately 3–5-day period. The myometrium of the postpartum uterus of macaques may have prominent hyalinized myometrial arteries that should not be confused with a toxicologic finding. Cervical intraepithelial neoplasia, endometriosis, ectopic growth of endometrial tissue outside the uterus (endometriosis), adenomyosis (extension of endometrium into the subjacent myometrium), and vascular hyalinization of uterine vessels are reported across the primate order as spontaneous findings (Figure 10.20). Because mostly young animals are used in toxicity studies, the incidence of neoplastic findings and endometriosis is extremely low.

## 2.6. The Histology of the Minipig Female Reproductive Tract during the Estrous Cycle

The use of the Göttingen, Yucatan, Bama, and Trolle miniature pigs (minipigs or micropig) has expanded in the last few decades because of dermal and medical device toxicity testing (see *Animal Models in Toxicologic Research: Pig*, Vol 1, Chap 20). There are several publications on spontaneous or experimentally induced female reproductive changes in any species of minipig, and detailed descriptions of the histologic and hormonal changes that occur in the minipig during the estrous cycle (McInnes, 2011; Jeppesen and Skydsgaard, 2015; Peter et al., 2016).

The female reproductive system of the minipig is like that of domestic swine; the uterus is bicornuate with tortuous fallopian tubes. However, unlike humans and cynomolgus macaques, the minipig does not menstruate; instead, the process of renewal of the endometrial epithelium is, like in the rodent, regulated via epithelial proliferation and apoptosis. Another feature of the minipig not observed in the human or cynomolgus reproductive tract is the presence of the pulvini cervicales, solid mucosal folds, and protrusions throughout the length of the porcine cervix (Lorenzen et al., 2015). Although the length of the cycle and the hormonal fluctuations in man and pigs are quite similar, it is important to know that the estrous cycle in pigs begins and ends with ovulation/estrous, while the menstrual cycle in women and macaques begin and ends with the start of menses, with the ovulation in the middle of the cycle (Lorenzen et al., 2015).

vascular and edematous with occasional small focal areas of erythrocyte extravasation in the zona compacta. The surface and glandular epithelium increases in height and numerous mitotic figures are present. The vagina becomes thicker and cornified. The stroma and smooth muscle also start to thicken and there is both stromal congestion and edema. In estrus (E), the uterus has myometrial hypertrophy, stromal cell proliferation, and stromal congestion, edema, and hemorrhage. The surface and glandular epithelium are increased in height and there are numerous mitotic figures. The vagina is thick and heavily cornified. In diestrus (D), luminal glands are proliferative and straight but abruptly become tortuous toward the basement membrane. The glandular lumina may contain pink secretions; stromal edema and congestion are decreased. The upper gland and luminal epithelial cells progressively develop more foamy cytoplasm because of the influence of progesterone. The vagina is much thinner (three or 4 cell layers) and loses its cornification. 50×, H&E. Courtesy of Dr Sundeep Chandra. Reproduced from Haschek WM, Rousseaux CG, Wallig MA, editors: *Haschek and Rousseaux's handbook of toxicologic pathology*, ed 3, 2013, Academic Press, Figure 60.14, p. 2620, with permission.

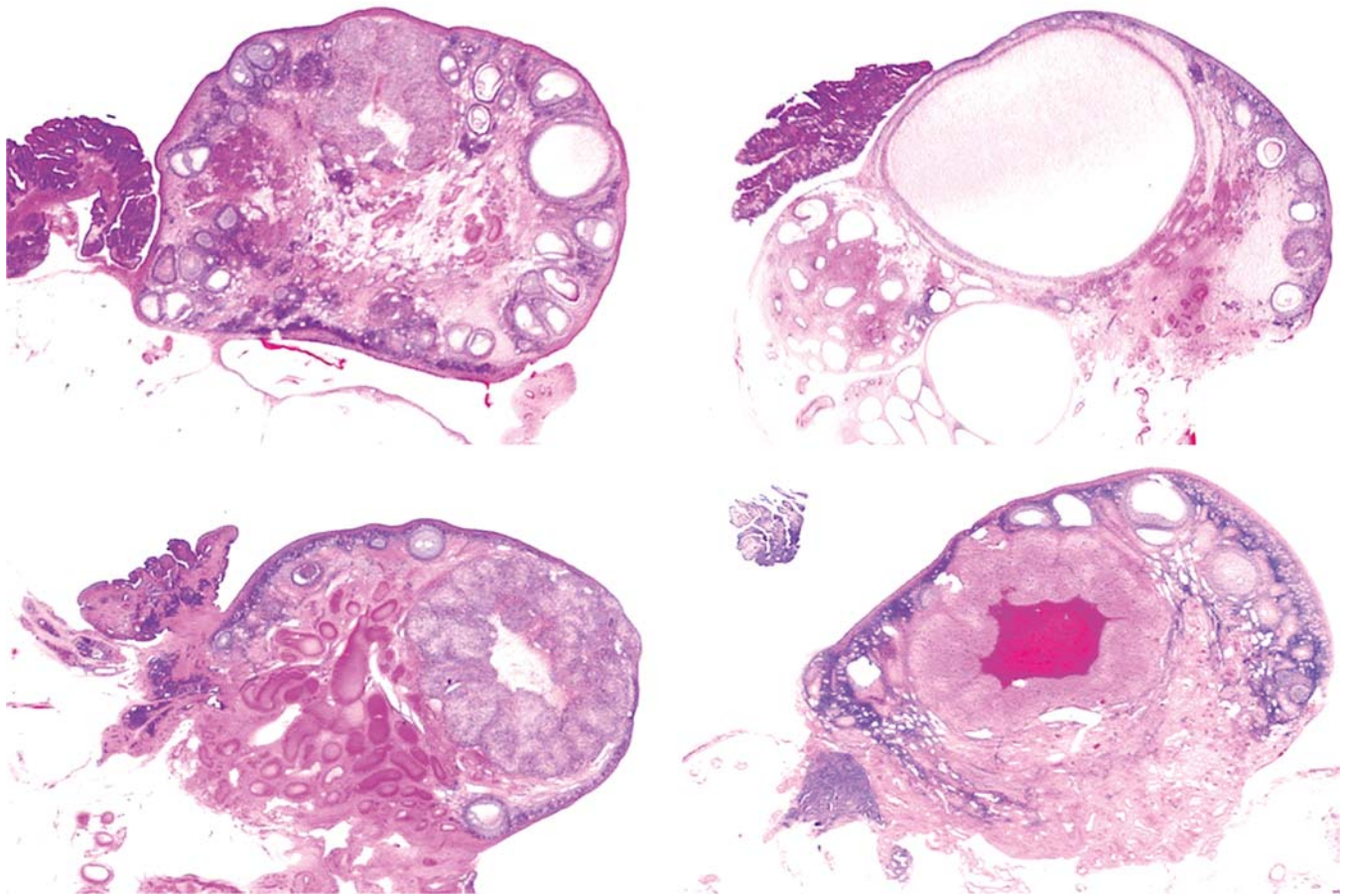


**FIGURE 10.17** Ovary, cynomolgus macaque. Ovarian histology during the menstrual cycle of cynomolgus macaques. Clockwise from upper left, the ovaries shown are from the early follicular phase (developing follicles and the corpus luteum of the prior cycle); late follicular phase (dominant follicle); ovulation (corpus hemorrhagicum); and late luteal phase (corpus luteum). 10 $\times$ , H&E. Courtesy of Dr Mark Cline. Reproduced from Haschek WM, Rousseaux CG, Wallig MA, editors: *Haschek and Rousseaux's handbook of toxicologic pathology*, ed 3, 2013, Academic Press, Figure 60.15, p. 2622, with permission.

Minipigs generally become mature between 4 and 8 months of age, which is a major difference to the 4–5 years in the cynomolgus macaque. For Göttingen minipigs, the age range of sexual maturity was determined to be between 3.7 and 6.5 month (Peter et al., 2016), when in the presence of a boar. When no boar was present, they reached maturity by 7.7 months of age (Howroyd et al., 2016). Yucatan minipigs become sexually mature between 4 and 4.8 month of age. In-life progesterone analysis has been reported in the literature as a method to determine sexual maturity of individual animals (Peter et al., 2016). In Figure 10.21, the morphologic changes in the uterus and vagina during the

normal estrous cycle are shown. As in other species, the estrous cycle is a very dynamic process with gradual hormonally driven morphologic changes.

The estrous cycle in the mature minipigs has a duration ranging from 17 to 22 days (Peter et al., 2016) and is divided into four phases; proestrus (follicular phase), estrus, (ovulatory phase) metestrus (early and mid-secretory phase), and diestrus (late secretory phase). The first day of estrus is designated as Day 0 of the cycle. The proestrus phase starts about 2 days before ovulation (Day-2). During the proestrus phase, dominant follicles mature to Graafian follicles which is the most recognizable feature



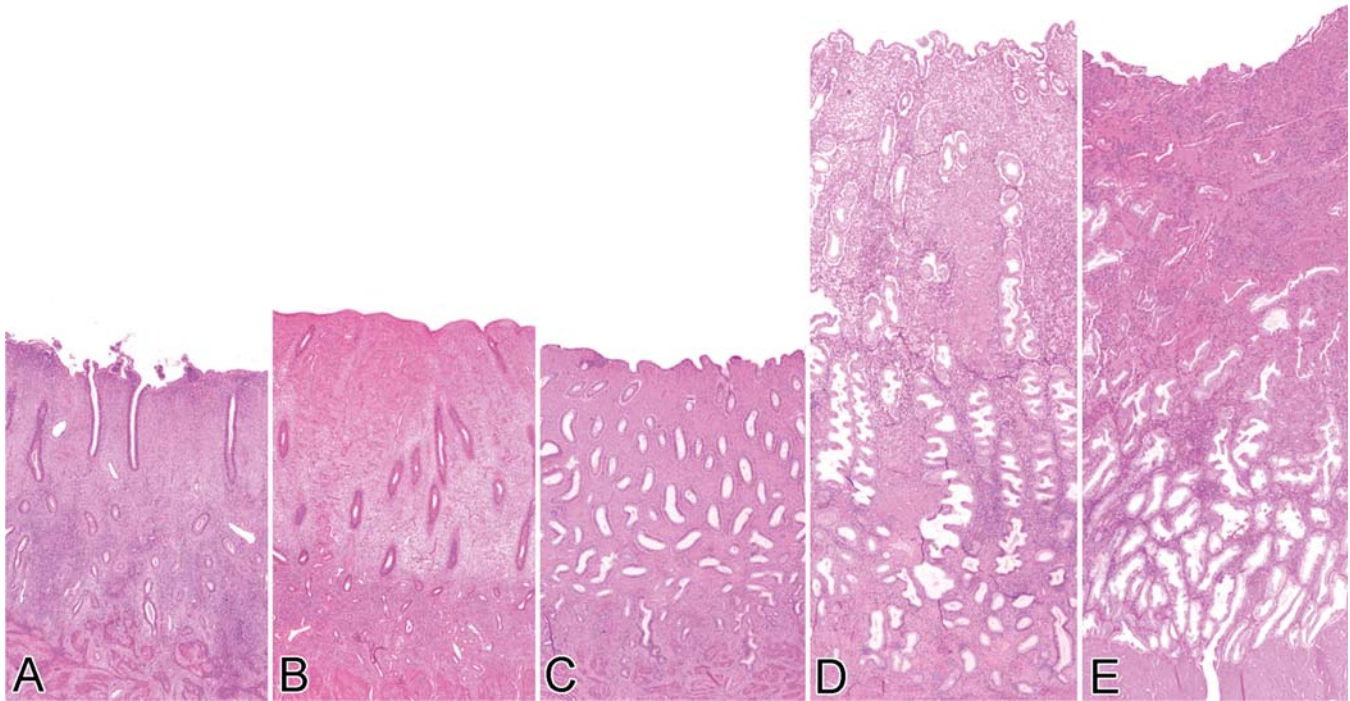


**FIGURE 10.18** Uterus, cynomolgus macaque. Uterine histology across the menstrual cycle of cynomolgus macaques. Stages shown from left to right are: (A) regenerative phase; (B) follicular phase; (C) periovulatory/early luteal phase; (D) luteal phase; and (E) early menstrual phase. For descriptions of each stage, see the text. 25 $\times$ , H&E. Courtesy of Dr Mark Cline. Reproduced from Haschek WM, Rousseaux CG, Wallig MA, editors: *Haschek and Rousseaux's handbook of toxicologic pathology*, ed 3, 2013, Academic Press, Figure 60.16, p. 2623, with permission.

of the proestrus phase. In minipigs, Graafian follicles can have a diameter of 5–8 mm and are visible at gross inspection as small cysts on the surface of the ovary. The wall of the Graafian follicle is lined by a layer of five to eight granulosa cells. Increasing FSH concentrations drive the rapid growth of the dominant follicles as well as the rising estradiol concentrations rise which peak on Day-2 (Lorenzen et al., 2015). Remaining tertiary follicles become atretic and there are regressing corpora lutea from the previous cycle. In the uterus, this phase is characterized by the presence of many apoptotic cells and mitoses within the surface epithelium and glands. The epithelium lining the endometrial glands consists of low columnar epithelial cells, that in the superficial layer of the endometrium may be ciliated. The nuclei of the epithelial cells are mostly small and round to oval. At the time of ovulation, there is an increase in mitotic activity in the uterine epithelium and glands. The sudden rise of LH and elevating

estrogen concentration during the estrous phase results in the release of the oocyte. The LH peak also initiates the postovulatory follicle to be transformed into a corpus luteum that produces progesterone. After ovulation, the large but collapsed follicles often fill with blood prior to developing into corpora lutea. Once the CL are formed, the progesterone concentration rises for several days and causes the epithelium lining the endometrial glands to increase in height and become clearer due to the accumulation of PAS-positive secretory material. Progesterone inhibits cell division and maturation but promotes secretion by the endometrial glands. The number of apoptotic cells in the glands and the number of mitotic figures rapidly decrease. With prior estrogen priming, the endometrial stromal cells change from the small inactive form with fusiform nuclei to large cells with ovoid nuclei. The myometrial cells become hypertrophic with prominent myofibrils. During the mid-luteal phase (around cycle Day 10), the ovary



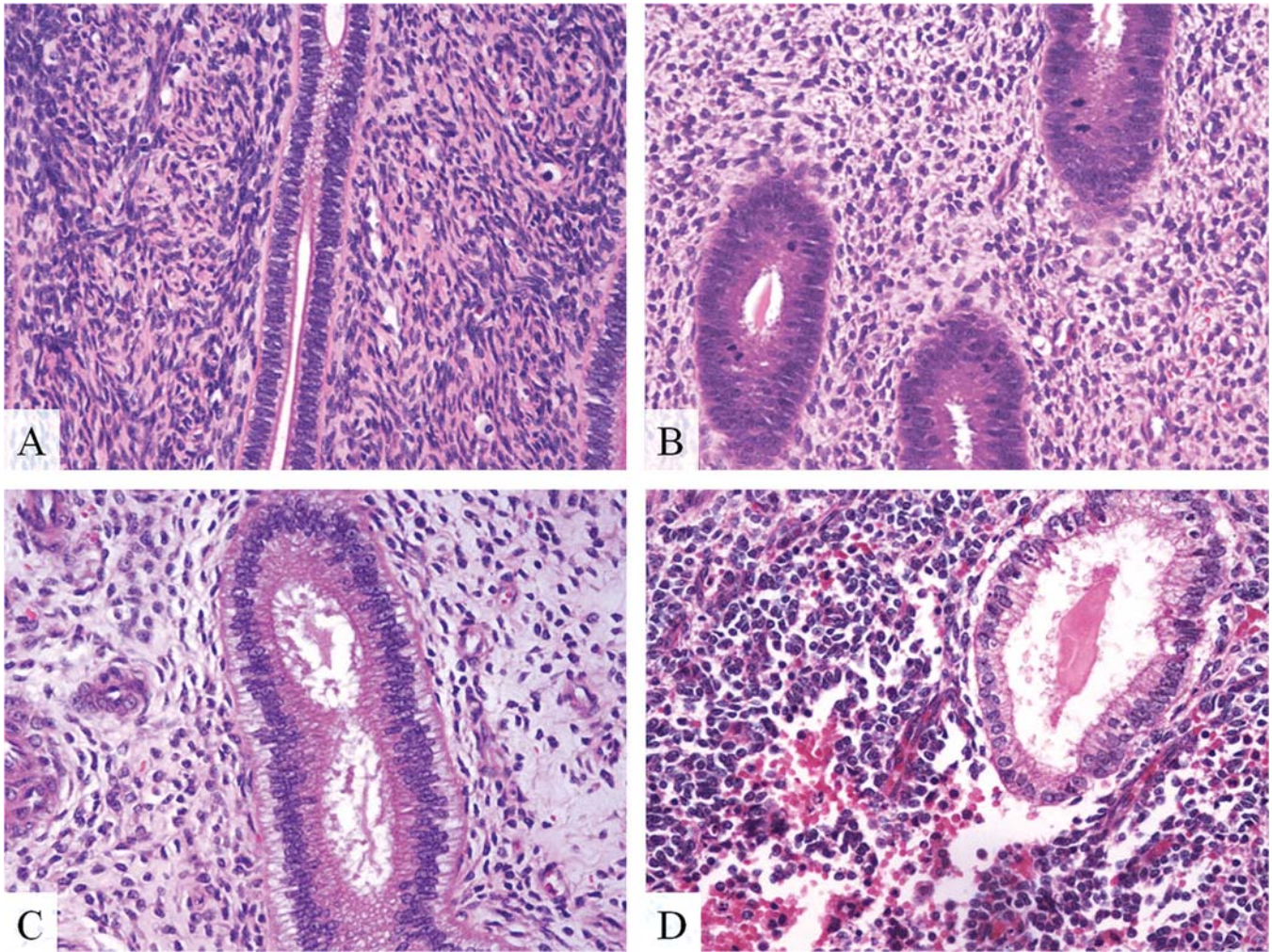


**FIGURE 10.19** Uterus, cynomolgus macaque. Uterine histology of cynomolgus macaques. (A) Quiescent/atrophic; (B) follicular phase (note mitoses and pseudostratification); (C) luteal phase (subnuclear vacuolation); (D) menstrual phase (hemorrhage, apoptosis). 100 $\times$ , H&E. *Courtesy of Dr Mark Cline. Reproduced from Haschek WM, Rousseaux CG, Wallig MA, editors: Haschek and Rousseaux's handbook of toxicologic pathology, ed 3, 2013, Academic Press, Figure 60.17, p. 2624, with permission.*

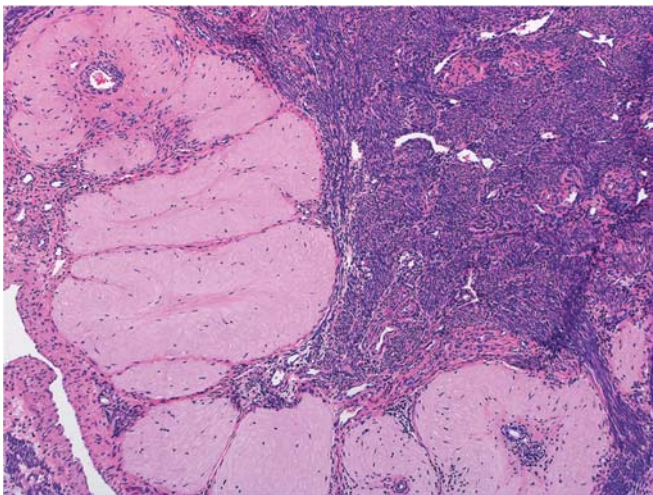


**FIGURE 10.20** Spontaneous findings in the cynomolgus macaque uterus: vascular hyalinization characterized by homogenous and eosinophilic material expanding vascular walls within the myometrium. 64 $\times$ , H&E.

is characterized by the presence of large mature corpora lutea, and the progesterone concentration reaches its peak ([de Rijk et al., 2014](#); [Lorenzen et al., 2015](#)). At that time, the epithelial cells lining the endometrial glands also reach their maximum height and have a clear cytoplasm and glands contain large amounts of secretory material. During this phase, lymphocytes become more abundant within the endometrial stroma.

The corpora lutea start to degenerate during the late luteal phase and the progesterone concentration declines. Within the uterus, the epithelial cells lining the glands decrease in height, while their nuclei become rounder and smaller. The cytoplasm of the cells remains somewhat clear. Granulosa cells produce estradiol-17 $\beta$  which rapidly increases and reaches its



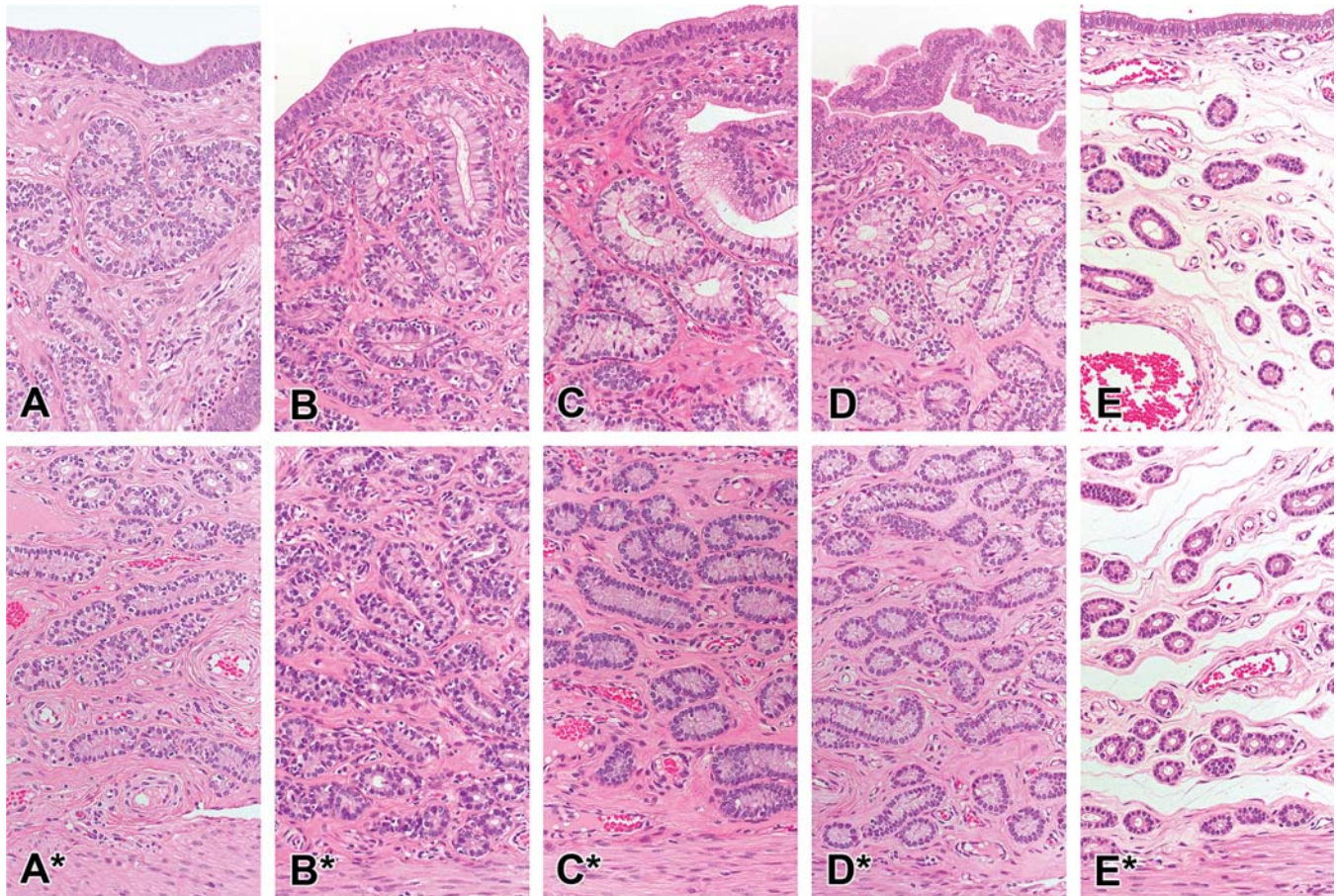


**FIGURE 10.21** Uterine endometrium in minipigs during the different phases of the estrous cycle. Upper image: morphologic characteristics of elements in zone I and II, lower image (\*): morphologic characteristics of elements in zone III, H&E, 64 $\times$ . (A & A\*) Follicular phase: The height of the luminal epithelium varies from cuboidal in early follicular phase to medium-sized columnar in the late follicular phase with numerous apoptotic bodies and cells in mitosis. There is pseudostratification of the oval-shaped nuclei in the surface epithelium and a tendency toward pseudostratification in the upper glandular epithelium. Among the epithelial cells lining the upper part of the glands there are many ciliated cells. Just underneath the luminal epithelium, a layer of eosinophilic granulocytes is present. (B & B\*) Ovulation phase: The height of the luminal epithelium is medium to high columnar in zone I and II and low columnar in zone III with apoptotic bodies and few mitotic cells. There is pseudostratification of the round to oval nuclei in the surface epithelium and a tendency toward pseudostratification in the upper glandular epithelium. Mainly in the upper part of the glands in zone II, ciliated glandular epithelial cells are present. There are many intraepithelial endometrial lymphocytes. (C & C\*) Early luteal phase: There is hypertrophic, medium to high columnar luminal and glandular epithelium with less nuclear pseudostratification. The glandular epithelial cells in zone II have rarified cytoplasm suggesting secretory activity and apoptotic bodies and mitoses are rare. In the glandular epithelium, round to slight oval nuclei are located in the basal part of the cells. Nucleoli are more indistinct in this phase. The ciliated cells and endometrial lymphocytes are reduced in number. (D & D\*) Mid luteal phase: The height of the luminal epithelium is medium columnar in zone I and II and low columnar in zone III. The nuclear pseudostratification has almost disappeared and round nuclei are located in the basal part of the cells. Nucleoli remain indistinct. In zone II the epithelial cells have rarefied cytoplasm, suggesting secretory activity, and apoptotic bodies and mitoses are rare. (E & E\*) Late luteal phase: The surface and glandular epithelium are low columnar to cuboidal small epithelial cells with most small round nuclei with compact chromatin. There is no nuclear pseudostratification, cytoplasmic rarefaction, or apoptotic bodies and mitosis. There is no clear difference between the cell volume and characteristics of epithelial cells lining the glands in zone II and zone III. The endometrial stroma is edematous.



maximum just before ovulation. The granulosa cells in the minipig from the growing follicles also produce inhibin, a hormone that negatively regulates pituitary FSH release. The publications by [de Rijk et al., \(2014\)](#) and [Kangawa et al., \(2017\)](#) describe the cyclic-related morphologic events in more detail.

The most well-described common spontaneous histopathologic findings in various strains of minipigs used in toxicology studies are mineral deposits, cystic follicles, and luteinized unruptured follicles in the ovaries, squamous metaplasia of the oviduct epithelium, endometrial hyperplasia, and inflammatory infiltrates in the uterus ([Helke et al., 2016](#); [McInnes, 2011](#); [Skydsgaard et al., 2021](#)). Generally, minipigs used for toxicology studies are young (approximately 3 months of age at study start), so uterine histologic findings are unlikely to be encountered in minipigs used for toxicologic research.

### 2.7. The Histology of the Rabbit Female Reproductive Tract during the Estrous Cycle

Female rabbits are induced ovulators, and it is normal for nonmated rabbits to lack corpora lutea regardless of age ([Bradley et al., 2021](#)). Repeated waves of follicular development and atresia occur with mating behavior evident every 4–6 days. Occasionally, corpora lutea will be present in group housed females due to repeated mounting behavior and subsequent stimulation of ovulation. This lack of spontaneous ovulation and formation of corpora lutea precludes accurate assessment of sexual maturity based on ovarian histology. The rabbit has abundant interstitial gland development that occupies most of the ovarian stroma. Spontaneous lesions are uncommon except for various cysts which can be blood filled. In absence of regular ovulation, changes in the uterus, cervix, and vagina are generally limited. The rabbit vagina is unique, and the proximal two-thirds is lined by a tall columnar epithelium with mucous filled cytoplasm, which is morphologically like the cervix ([Barberini et al., 1991](#)). The

distal one-third of the vagina has a stratified squamous epithelium.

### 2.8. The Endocrinology of the Estrous and Menstrual Cycles

While a strong fundamental understanding of the anatomy and histology of the female reproductive system is critical for the toxicologic pathologist, the ability to interpret the gross and microscopic changes requires an understanding of the corresponding cellular and endocrinological connections between structure and function ([Davis et al., 2001](#); [Dixon et al., 2014](#); [Putti and Varano, 1979](#)). Following input from the cerebral cortex, the hypothalamus secretes gonadotropin-releasing hormone (GnRH) into the hypophyseal portal circulation, which stimulates the anterior lobe of the pituitary to release the gonadotropins FSH and luteinizing hormone (LH) into systemic circulation ([Aiyer and Fink, 1977](#)). After gonadotropin stimulation, the ovary synthesizes and releases sex steroid hormones ([Levine, 2015](#)). The concentrations of circulating sex steroid hormones in turn affect the activity of the hypothalamus and pituitary in the regulation of reproductive function in either a stimulatory (positive) or an inhibitory (negative) manner, depending on the stage of the cycle ([Figure 10.22](#)). In addition to steroidogenesis, ovarian tissues can synthesize many growth hormones and cytokines. Ovarian hormones and growth factors exert stimulatory and inhibitory effects both locally (e.g., adjacent follicles) and systemically. In nonrodents and women, the adrenal cortex also produces sex hormones; therefore, the adrenal cortex should also be considered when there is the potential for endocrine mediated toxicity (see *Endocrine System*, Vol 4, Chap 7).

### 2.9. Hormonal Events during a Given Reproductive Cycle

Between puberty and senescence, the reproductive cycle is manifested by changes of the reproductive organs as described in the previous section. The cyclic changes within the ovary are

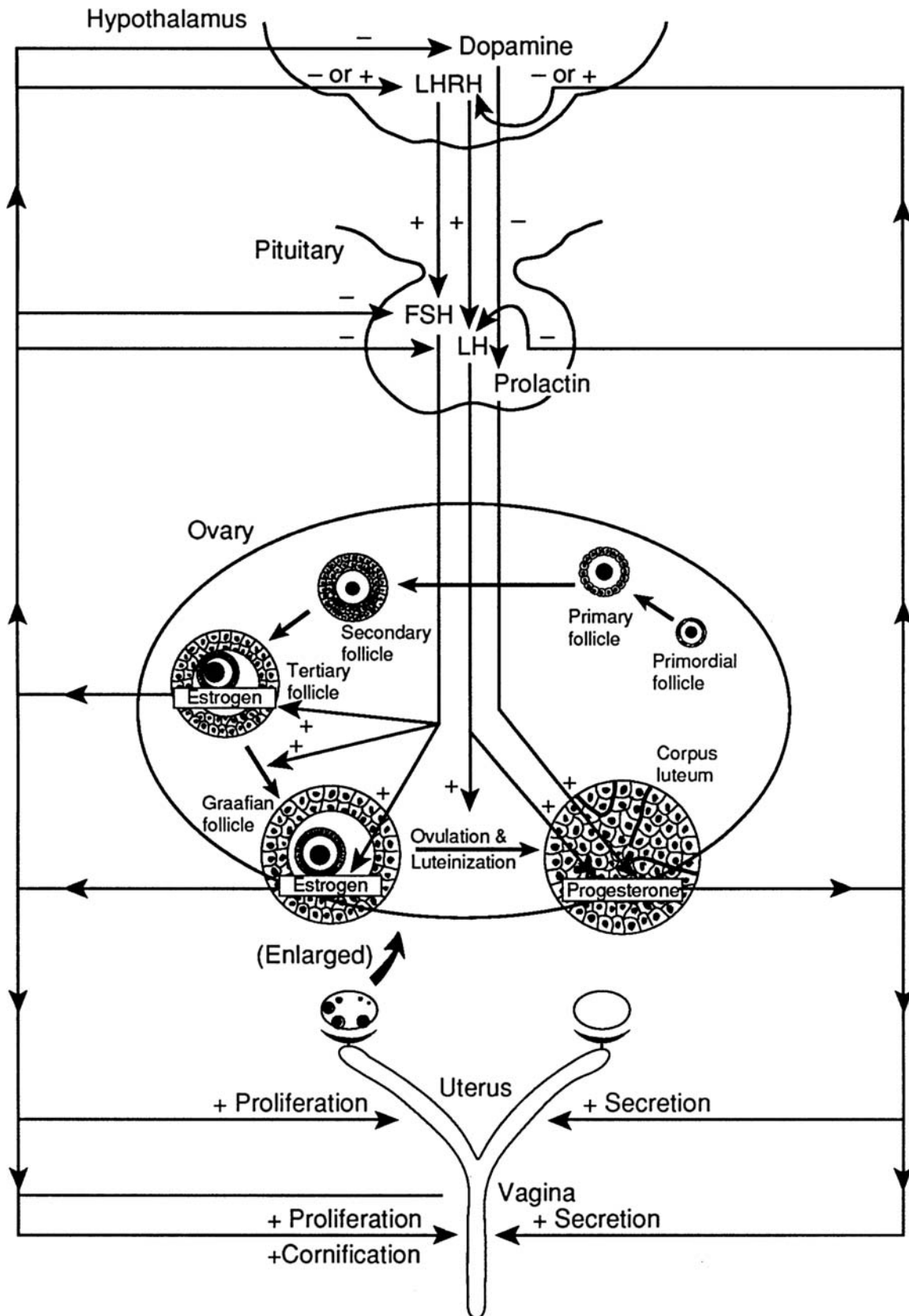


**FIGURE 10.22** Schematic drawing of hormonal regulation of reproduction (+, stimulatory; -, inhibitory). FSH = follicular stimulating hormone; LH = luteinizing hormone; LHRH= luteinizing hormone-releasing hormone receptor. Reproduced from Haschek WM, Rousseaux CG, Wallig MA, editors: *Handbook of toxicologic pathology*, ed 2, 2002, Academic Press, Figure 9, p. 863, with permission.

mainly regulated by FSH and LH, whereas the cyclic changes of the uterus and vagina are dependent on ovarian sex steroids. [Figure 10.22](#) provides a relational diagram for the hypothalamic–pituitary–ovarian (HPO) axis.

Each cycle begins with follicular growth and maturation, followed by ovulation, and the subsequent formation and regression of the corpus luteum. Although the recruitment and growth of a primordial follicle to the stage of an early tertiary follicle occurs spontaneously and does not require hormonal stimulation in mammals, the presence of FSH and LH is necessary for continued tertiary follicular maturation to the stage of a preovulatory follicle. It takes approximately 60 days for a primordial follicle to develop into a preovulatory follicle in the adult rat, compared to 150 days in human, 100 days in the pig, and 215 days in the cynomolgus macaque. Selection of follicles to continue to the preovulatory stage depends on follicles having granulosa cells able to express the necessary gonadotropin receptors at the time of elevated gonadotropin concentrations. Most follicles undergo atresia and do not reach the preovulatory stage.

FSH and LH are glycoprotein hormones secreted from the anterior pituitary. In polyestrous nonseasonal breeding animals such as the rat, FSH and LH concentrations increase shortly after the end of the preceding cycle. FSH stimulates the proliferation of granulosa cells and induces receptors for LH on these cells. LH stimulates thecal cells to secrete androgens, which serves as a precursor for estrogen synthesis by granulosa cells through the catalytic function of aromatase.

The estradiol secreted from growing follicles promotes cell proliferation and maturation in both the uterus and the vagina. Under the influence of estradiol, the stromal fibroblasts and epithelial cells of the endometrium proliferate and increase in size. Estradiol also promotes the synthesis of actomyosin and glycogen in smooth muscle cells, resulting in hypertrophy of the myometrium. In addition, estradiol primes the uterus for its response to progesterone by upregulating progesterone receptors. Polymorphonuclear leukocyte migration in the uterus,

associated with intercellular edema and hyperemia, is also attributed to the effect of estrogen ([Zheng et al., 1988](#)). In the vagina, estrogen not only stimulates cell proliferation but also induces epithelial cornification. In the rodent vagina, when estrogen is present, progesterone induces epithelial cell mucification by increased production and intracytoplasmic accumulation of sialic acid.

In the mature preovulatory follicle, a surge of LH results in ovulation with subsequent formation of the CL. The newly formed corpus luteum incorporates both granulosa and thecal cells and is capable of secreting progesterone for only a certain period. Continued function of the corpus luteum requires stimulation by luteotrophic hormones such as LH and prolactin. Prolactin secretion in rats is stimulated by cervical stimulation and without it the corpus luteum produces very limited amounts of progesterone. The ovarian steroid hormones, including estrogens, progestins, and androgens, exert their influence on the uterus and vagina, through the circulatory system. In humans but not cynomolgus macaques, corpora lutea secrete estrogen as well as progesterone.

In primates, dogs, and (mini)pigs, ovulation occurs spontaneously. In the rat and mouse, ovulation is also spontaneous and coincides with the preovulatory LH surge that is under photoperiod control. In rabbits and other induced ovulators, the LH surge does not occur until cervical neurons are stimulated by mating or other means to activate the release of GnRH.

In the newly formed corpus luteum, initial progesterone secretory activity seems to be autonomous and, in most species, does not require luteotrophic factors. For continued function, luteotrophic hormones from the pituitary are required; LH is considered the most important luteotrophic factor in most species. However, in rats, prolactin has been identified as the luteotrophic factor, whereas in rabbits, estrogen is the only known luteotrophic factor.

The functional life of the corpus luteum in nonpregnant animals varies among animal species. In the rat, it functions only for the first 2 days after formation. If cervical stimulation takes place, prolactin continues to be secreted



by the pituitary gland and the functional life of corpora lutea is prolonged with continued progesterone secretion. If implantation does not take place, the life of corpora lutea is terminated 12–14 days after formation (Smith and Neill, 1976).

In dogs, luteinization of the preovulatory follicles is accompanied by progesterone secretion prior to ovulation. This is most likely due to the long interval between the LH surge and ovulation. The life span of a corpus luteum in the dogs exceeds more than 80 days. The corpus luteum stays functionally active for approximately 60 days and is not affected by mating or implantation, and both LH and prolactin are required for their maintenance. Due to the long luteal lifespan in dogs, pseudopregnancy is common but not always clinically apparent. The life span of the corpus luteum in the pigs is approximately 16 days (de Rijk et al., 2014).

In NHPs and pigs, the corpus luteum has a defined functional lifespan of about 14–16 (NHP) and 16 days (pigs) (de Rijk et al., 2014) that is unaffected by mating or mechanical stimulation of the cervix. A continuous low concentration of LH is required to maintain the corpus luteum. If pregnancy occurs, the embryonic trophoblast secretes chorionic gonadotropin as early as 8–9 days after fertilization, thus maintaining the corpus luteum throughout early pregnancy. If not, prostaglandin F (2- $\alpha$ ), produced by the endometrium promotes luteolysis.

## 2.10. Regulation of Hormonal Secretion

As indicated earlier, the regulation of hormonal secretion in mammals is complex and involves many modulators that exert positive (stimulatory) or negative (inhibitory) feedback control. Readers are referred to a standard textbook of endocrinology for a complete discussion.

LH and FSH secretion by gonadotrophs in the anterior pituitary are initiated by a rhythmic pulsatile secretion of GnRH from the hypothalamus into hypothalamic-hypophyseal portal vasculature. GnRH is assumed to be the only GnRH responsible for the release of both LH and FSH; other hormones may specifically

control the release of FSH (Namwanje and Brown, 2016). The pulsatile release of GnRH is essential for normal LH and FSH secretion from the pituitary. The continuous presence of GnRH will at first stimulate and later desensitize secretion of LH and FSH due to a downregulation of receptors.

Each LH peak is preceded by an GnRH peak, but not every GnRH peak is followed by an LH peak. When GnRH release is not followed by LH release, the pulse may serve as a self-priming signal by increasing the number of GnRH receptors in the pituitary; this requires the presence of a small amount of estrogen in the serum.

Ovarian hormones modulate both the amplitude and/or frequency of GnRH pulses. Experimental data suggest that estradiol suppresses LH pulse amplitude but not the frequency, while progesterone primarily suppresses frequency. At the beginning of a reproductive cycle, the secretion of LH is inhibited by estrogen secreted from growing follicles. This negative feedback control affects LH release but not LH synthesis, which enables the pituitary to accumulate enough LH for the preovulatory surge.

Like their effect on LH secretion, ovarian steroids also affect FSH secretion, and this effect depends on the stage of the cycle and the hormonal status of the animal. During late estrus through early proestrus, estradiol has an inhibitory effect on FSH secretion. This inhibition is potentiated by the presence of progesterone. However, this negative feedback changes just prior to the preovulatory surge of LH. Estradiol is the dominant force, acting directly on the hypothalamus, whereas progesterone potentiates the effect by stimulating FSH synthesis. The secretion of FSH is inhibited by the peptide hormone, inhibin B, which is produced by the granulosa cells of growing follicles.

When follicles approach their final stage of maturity, the output of steroid hormones increases prior to ovulation. As concentrations of these hormones reach a certain concentration, their effects on the regulation of GnRH secretion also change from inhibitory to stimulatory. This is the basis of the preovulatory surge of GnRH and subsequent LH and FSH secretion. The

preovulatory surge of GnRH induces a cascade of events within the hypothalamus that is necessary for normal ovulation to proceed. The mechanism responsible for this may involve estrogen, which augments the number of pituitary binding sites for GnRH, increases the responses of the pituitary to hormone binding, and directly promotes GnRH secretion from the hypothalamus. An alternative possibility is that estradiol affects norepinephrine activity, which in turn stimulates GnRH secretion. Estradiol may also contribute by inducing and maintaining GnRH receptors in conjunction with GnRH in the pituitary. The effect of progesterone on GnRH secretion is less clear but is believed to be like that of estrogen.

Neurons controlling the secretion of GnRH also receive innervation, capable of either stimulation or inhibition, from other neural sites. Accordingly, the reproductive cycle adjusts to changes in light cycle, seasonal variation, and other physical (cervical stimulation) or olfactory (pheromone) stimuli. GnRH has been found in extrahypothalamic neurons in different regions of the limbic system of the cerebrum and has been implicated in the regulation of reproductive behavior.

Factors involved in termination of the gonadotropin surge may include downregulation of GnRH receptor numbers and subsequent loss of sensitivity of the pituitary gonadotrophs. During the luteal phase in women, estrogen acts in concert with progesterone to inhibit LH synthesis and release.

Unlike the LH release, prolactin secretion is normally inhibited by the presence of dopamine from the hypothalamus. At the height of prolactin secretion, the concentration of dopamine is lowest and that of thyroid-releasing hormone (TRH) is highest, indicating that TRH may also play a role in the release of prolactin. Estradiol stimulates prolactin release prior to ovulation by acting through the pituitary to decrease the dopamine inhibitory effect.

Several growth factors have been identified in the ovary. These factors are large protein molecules with molecular weights of several to tens of thousands. The interaction between these factors and gonadotropins is believed to be vital for normal follicular growth and luteinization.

Although the precise mechanisms of action need to be investigated, the participation of these molecules in reproductive function has been postulated as follows. Epidermal growth factor and insulin-like growth factor may assist in the induction of granulosa and thecal cell proliferation and are regarded as initiation factors. Insulin-like growth factor may also be required for continuation of cellular proliferation. Epidermal growth factor has been localized to oocytes, pregranulosa cells, and ovarian stroma. The granulosa cell is believed to be a major source of insulin-like growth factor. A growth factor from thecal cells, transforming growth factor alpha, may also contribute to both the initiation and maintenance of ovarian cellular proliferation. Vascular proliferation during follicular growth and corpus luteum formation is attributed, in part, to an angiogenic factor including fibroblastic growth factor and vascular endothelial growth factor (VEGF). Transforming growth factor beta, also produced by thecal cells, may inhibit cell proliferation and promote differentiation and transformation of granulosa cells to luteal cells during luteinization ([Adashi and Reshick, 1986](#)). TGF- $\beta$ 1 has also been localized in areas of corpora lutea. Growth factor secretion by ovarian cells has been reported to vary depending on the stage of estrous and the stage of follicular development. These factors may also be involved in the regulation of cyclic changes that occur in the remainder of the reproductive tract. Many other cytokines are reported to be both locally produced by ovarian structures as well as having regulatory effects on follicular development, atresia, and luteal function. An example of one such cytokine interaction is tumor necrosis factor alpha (TNF- $\alpha$ ), which has been reported to play an interactive role with Fas ligand in the induction of atresia ([Skinner and Coffey, 1988](#)). If a xenobiotic is designed to modify the response or secretion of these cytokines or alter the underlying downstream cellular signaling pathways, alterations in ovarian function and/or morphology may result.

Control of the female reproductive cycle is complex and comprises a cascade of events emanating from the hypothalamus and extending to the pituitary, ovary, uterus, and vagina, with stimulatory or inhibitory regulation by the

ovarian steroids. Any disruption in this cascade of hormonal events may result in functional and structural alterations. If a xenobiotic has a direct effect on a single steroid pathway, the biological response in the animal model may be relatively straightforward. However, xenobiotics may have multiple effects on steroid synthesis pathways or may alter differentially, based on end organ, the response of the nuclear hormone receptors for the steroids. Ovarian steroid nuclear hormone receptors are complicated receptors that are influenced by tissue and binding pocket specific corepressor or costimulating proteins. Pharmaceutical companies have taken advantage of this characteristic of steroid receptors and designed therapeutics with the advantageous properties of a hormone while eliminating or minimizing the unwanted effects of the hormone. A classic example of this type of therapeutic is the selective estrogen receptor modulator (SERM).

### 3. EVALUATION OF FEMALE REPRODUCTIVE SYSTEM TOXICITY

Once a toxicologic pathologist becomes engaged in the study of a xenobiotic's potential effects on the female reproductive system, it is important to take advantage of the various bioinformatics toxicology data sources available. These databases and tools are constantly being invented or improved, are usually open to the public, and are often accessible via the Internet. One database is maintained by the EPA. Formerly referred as ACTor, the computational data can be downloaded at the EPA's website ([EPA, 2024](#)). The EPA houses 500 public sources of over 500,000 environmental chemicals and 40 years of rat reproductive toxicity data for hundreds of chemicals.

A comparable digital data warehouse of nonclinical data submitted to the FDA is built based on the output of the SEND initiative. SEND supports automated creation of tables and graphs and allows data categorization and mining, thus facilitating collaborative interindustry efforts to interrogate information across boundaries ([Choudhary et al., 2018](#)).

As discussed previously, organ weight and histologic assessment of reproductive tissues in

routine general toxicology studies constitute the gold standard for reproductive toxicity safety assessment. However, the toxicologic pathologist has additional endpoints in the standard toxicology study that can assist in data analysis and interpretation. Changes in food consumption, body weight, and/or clinical signs may indicate perturbation of the female reproductive system. Examples include precocious behavior (estrogenic), increased weight/muscle gain or aggressive behavior (androgenic), disrupted menses (progestogenic), or gynecomastia (prolactinogenic). In addition, monitoring of estrous or menstrual cyclicity with daily vaginal swabs is a powerful tool for assessing effects in the female reproductive system and may be added to general toxicity studies for cause.

Recommendations for the evaluation of the female reproductive system were listed earlier, in [Table 10.2](#), by species and study length. As is always the case for organ weights and gross necropsy, the skill of the prosector is critical, or unwanted systematic error may be introduced into a study data set. For example, variable inclusion of bursa, fat, and/or oviducts may alter ovarian weights. For organ weights, data should be recorded in absolute terms and calculated relative to body weight and brain weight so that the appropriate rigor can be applied to understanding the effects of body weight losses or gains on the interpretation of results ([Michael et al., 2007](#)). Understanding of the sexual maturity status and impact of the cycle is also important when assessing reproductive organ weights ([Vidal, 2017](#); [Vidal et al., 2021](#)). Finally, especially in the case of nonrodent studies, it is important to have a data set of control ranges for reproductive tissue organ weights from the study laboratory from which the data originate to enable study data analysis and interpretation ([Michael et al., 2007](#)).

When assessing the female reproductive system microscopically, it is important for the study pathologist to be aware of the sexual maturity status, age, and the estrous/menstrual cycle stage of each animal ([Vidal, 2017](#)). This "stage-aware" assessment allows the pathologist to rapidly detect changes in the female reproductive system. In addition to the descriptions earlier in this chapter, several excellent references describe reproductive staging for rodents, dogs, minipigs, and cynomolgus macaques ([de](#)



Rijk et al., 2014; Li and Davis, 2007; Westwood, 2008; Sato et al., 2016; van Esch et al., 2008a; Rehm et al., 2007). In some laboratories, histologic staging is accompanied by vaginal smear collection at necropsy; however, in our experience, postmortem vaginal smear collection provides no clear advantage to histologic staging unless it is used as an antemortem method for monitoring effects on estrous cycle in a time course fashion using the animal as its own control.

There are numerous specialized techniques, animal models, and study designs that may be helpful when general toxicology findings determine that there is a treatment-related effect on the female reproductive system. Techniques include morphometry and machine learning (see *Digital Pathology and Tissue Image Analysis*, Vol 1, Chap 11), immunohistochemistry, and other molecular pathology techniques such as in situ hybridization and laser capture microdissection followed by quantitative PCR (see *Special Techniques in Toxicologic Pathology*, Vol 1, Chap 10). Genetically engineered mice (GEM) (CRISPR, gene knockout or knockins, transgenics) and ovariectomized or hypophysectomized rodents or nonrodents may help in the testing of specific hypotheses (see *Special Techniques in Toxicologic Pathology*, Vol 1, Chap 11; *Digital Pathology and Tissue Image Analysis*, Vol 1, Chap 12). Study designs such as hormone studies allow the measurement of effects on the HPO axis. It is important to emphasize that these second-tier approaches must be used in a fit-for-purpose manner and designed in partnership with subject matter experts (Halpern et al., 2016). Morphometric and machine learning procedures can be effective ancillary methods in assessing female reproductive effects, especially for the ovary and uterus. If direct effects on the ovarian follicle numbers or maturation synchrony are anticipated or suggested based on histology and organ weight data, ovarian follicle morphometric methods may be a useful adjunct for data analysis. This procedure allows a quantifiable assessment of effects on specific follicular stages, and the methods are summarized in detail in an STP position paper (Regan et al., 2005). Recently deep machine learning methods have been developed to differentiate and quantify ovarian follicles in mice and rats (Sonigo et al., 2018; Carboni et al., 2021).

Machine learning methods are emerging as potential adjunctive diagnostic aids (i.e., decision support) for the toxicologic pathologist. For example, feature-based machine learning using a tool such as the open source QuPath (QuPath | Quantitative Pathology & Bioimage Analysis, accessed Dec 12, 2021) or deep learning approaches using convolutional neural networks can be used to assess uterine endometrial and myometrial changes such as atrophy and hypertrophy, and in combination with immunohistochemistry for the assessment of changes in pituitary gonadotroph numbers or to help estimate the proliferative index of uterine endometrial or myometrial compartments. Deep learning machine learning methods can also be developed as screening decision support tools for lesion detection (Rudmann et al., 2021).

Immunohistochemistry and in situ hybridization itself can be powerful tools for diagnostic targeted approaches for investigating female reproductive toxicity. Reproductive hormones in almost all cases bind nuclear hormone receptors that in an inactive state localize to the cytoplasm, but, when activated, upregulate and migrate readily to the nucleus. Antibodies for these receptors are well characterized and are useful in multiple species. Therefore, the toxicologic pathologist can examine the pattern (intensity and localization) of expression of these receptors to predict the reproductive hormone pathophysiology at the reproductive end organ of interest. Published examples representing the screening approach include the characterization of glutamate and P38 receptors in rats, dogs, cynomolgus macaques, and/or humans (Radi and Khan, 2006). In situ hybridization can be especially useful to test for germ cell integration in the ovary in gene therapy safety assessment (Hutt et al., 2022) (also see *Stem Cell and Other Cell Therapies*, Vol 2, Chap 10). In general, we do not recommend that immunohistochemistry or in situ hybridization be used for general screening of potential hormone-mediated effects on reproductive end organs.

In some cases, because of the indicated target, disruption of normal HPO function is expected and an assessment of treatment-related reproductive hormone concentration changes may be considered as an addition in standard toxicology studies or as a follow-on study after reproductive system changes are identified (Andersson et al.,

2013; Halpern et al., 2016). In either situation, the study design for hormone collection and the reproductive hormone analysis is complicated and requires careful planning regarding animal selection, randomization and handling, room light cycles and caging design, and plasma/serum collection procedures (time of day and method). For example, several hormones (LH, prolactin) may be markedly altered with the stress associated with standard euthanasia and blood collection; therefore, vascular ports or cannulas are preferred. Also, significant differences in hormone concentrations may not be identified with single time-point collections. These hormones are secreted in a pulsatile manner, and one must demonstrate caution and be consistent when selecting time points to assess treatment effects on hormones.

The toxicologic pathologist may, based on the data at hand, choose to investigate effects on the HPO axis using a more diagnostic or targeted approach. A diagnostic approach may be justified if an observed toxicity has a well-characterized link to an effect on the HPO axis. An example of the diagnostic approach would be the measurement of prolactin in cases where hyperprolactinemia is suspected as the etiology of mammary gland lobular hyperplasia. A second approach is the targeted approach where, based on knowledge concerning the intended effect or anticipated off-target effects of the test article, a specific subset of HPO axis biomarkers is evaluated. We recommend that the diagnostic or targeted approach be used only in special cases. Because of the complicated interplay within the HPO axis and the uncertainty regarding the mechanism of test article effects, we have found that a screening approach that measures a select panel of hormones in carefully designed prospective studies is a better strategy.

Apart from the alternative mouse bioassay (i.e., TgRasH2) for carcinogenicity, GEM have not been extensively used in a toxicology setting. However, since the early 1990s, the manipulation of the genome of the mouse has been a common approach for research biologists to decipher the function of a gene product in an animal model. This chapter will not detail the phenotypes of these GEM. However, there are excellent databases available on the Internet that provide a summary of GEM phenotypes (The Mouse Phenome database at <http://phenome.jax.org/>, and

MGI at <http://www.informatics.jax.org/phenotypes.shtml>). There are also protein (<http://www.proteinatlas.org/>) and mRNA expression data bases (<http://www.informatics.jax.org/expression.shtml>) online that allow the toxicologic pathologist to compare the expression of a target across mammalian species virtually. It is recommended that the toxicologic pathologist becomes familiar with these technologies and some of these databases as well as partner with a bioinformatics scientist early and often to harness the power of these data sets.

If a toxicologic effect from a test compound on the female reproductive tissue is suspected to be related to a specific gene product, a GEM study can be designed to test whether loss of the gene target alters the toxicologic phenotype in the animal. An example of the value of mutant animals is observed with the Staggerer mutation in mice which effects RAR-related orphan receptor alpha (ROR $\alpha$ ) function and results in a phenotype characterized by irregular estrous cycles and early senescence (Guastavino and Larson, 1992; Steinmayr et al., 1998). As mentioned above, the major limitations to this approach are the cost and availability of the GEM, the possibility for compensation by closely related gene products, and the reality that the toxicologic effect observed in a rat, dog, or cynomolgus macaque may not be manifested in the wild-type mouse (usually C57BL/6) of the GEM or even be reflective of human reproductive physiology. While the generation of inducible knockout animals is possible, unless these animals are available "off the shelf" or are already carefully described in the published literature, these models are not generally amenable to the development timelines for toxicologic pathologists. Recent gene editing CRISPR technology has accelerated the development timeline for GEM models and extended applications in other mammalian and nonmammalian systems (see *Genetically Engineered Animal Models in Toxicologic Research*, Vol 1, Chap 23). Gene editing does not require the generations of breeding necessary for homologous recombination and is not dependent on transgene integration and expression. However, like any novel technology, limitations are likely to evolve in scaling the method for safety assessment.

Other approaches to understanding female reproductive toxicity include the use of various

animal models and pharmacological tool compounds. The goal of these studies is to determine whether the effects on the female reproductive tract observed in standard toxicology studies are due to hypothalamic/pituitary and/or gonadal effects. Animal models include sexually immature, hypophysectomized or ovariectomized rats, mice, and cynomolgus macaques. There are numerous tool compounds available commercially, such as estradiol and other ovarian sex hormones that can be used to simulate ovarian estrogens/hormones in ovariectomized animals; pentobarbital, which can block neurogenic stimulus for the LH surge; ovine LH, a good exogenous source of LH for use in pentobarbital blocked animals; pregnant mare serum (PMS), which can replace hypothalamic/pituitary signals in hypophysectomized animals; and various gonadotropin or sex hormone receptor agonists or antagonists for use in these animal models to test hypotheses regarding mechanisms of female reproductive toxicity. While a description of all these models is beyond the scope of this chapter, we provide here an example which utilizes the tool compound flutamide and a rodent animal model for hypothesis-testing.

In this case, a mammary gland alteration initially diagnosed as hyperplasia was observed in female rats given a SERM in GLP studies conducted prior to clinical testing (Rudmann et al., 2005). In the initial female reproductive system evaluation, ovarian follicular dilation and follicular granulosa cell hyperplasia, and mammary gland hypertrophy and hyperplasia in female rats, were described. It was known from earlier investigations that the estrogen receptor (ER)-mediated negative feedback on gonadotropin release was blocked by the SERM, resulting in sustained LH secretion, ovarian follicle stimulation, and increased ovarian estrogen production. It was hypothesized that the “hyperplasia” observed in female mammary glands represented a conversion of the normal female rat (tubuloalveolar) mammary gland to a male phenotype (lobuloalveolar). Based on the male-like morphologic appearance of the mammary glands, it was suspected that the tonic LH ovarian stimulation resulted in overproduction of ovarian androgens and resulted in the SERM-induced mammary gland alterations. Increased androgens were measured in the affected rats and the development of the

histologic changes was blocked using a tool compound, the androgen receptor antagonist flutamide. This work enabled safe progression of the compound into clinical testing.

There is a great advantage to the consistent use of terminology when annotating histologic alterations of the female reproductive tissue. The efforts of a global group of pathologists (INHAND) to provide a uniform descriptive nomenclature for the rodent and nonrodent female reproductive system have been completed. The reader is referred to the full INHAND publications for rodent and nonrodents published as open access manuscripts in the journals, *Toxicologic Pathology* and *Journal of Toxicologic Pathology* and are available on the STP website, [toxpath.org](http://toxpath.org).

In applying the recommended diagnostic terminology, we recommend that the simplest descriptive terms and grading scales be used in GLP studies for the initial characterization of test article-related effects. Grading criteria should be defined in the protocol and report. More detailed diagnostic terms and descriptions should be reserved for targeted or mechanistic studies. The text of the toxicology report is also an excellent place for more complicated descriptions and interpretations when they add value to the risk assessment.

### 3.1. Spontaneous Changes in the Female Reproductive System (Table 10.5, Figures 10.24–10.27)

No matter the mechanism of female reproductive system toxicity, an understanding of the spontaneous changes observed in the female reproductive tract is required for a consistent and accurate evaluation of test article effects in the nonclinical animal model. In Table 10.5, we list some of the most common spontaneous findings in the rat, mouse, dog, rabbit, minipig, and cynomolgus macaque by tissue and stage of the cycle, based on our own experience and that reported in the literature (Bradley et al., 2021; Brix et al., 2005; Chamanza et al., 2010; Cline et al., 2008; Colman et al., 2021; Dixon et al., 2014; Greaves, 2012; Woicke et al., 2021; Chamanza et al., 2022). Note that we limited our list to changes expected to occur in toxicology studies. Therefore, changes reported in older Beagle



**TABLE 10.5** Reported Spontaneous Changes or Conditions in the Female Reproductive Tract of Nonclinical Animal Species in General Toxicology Studies

Species	Ovary
Rat	Luteal, follicular, or parovarian cysts (Figure 10.24)
Beagle dog	Corporal lutea, persistent
Cynomolgus macaque	Cortical mineralization; cysts, paraovarian/follicular/rete ovarii; hyperplasia, ovarian surface epithelium
Minipig	Mineralization
Rabbit	Atrophy, bursal cyst
Species	Uterus
Rat	Squamous metaplasia (Figure 10.25), cystic endometrial hyperplasia (Figure 10.26), glandular neutrophilic infiltrates, endometrial glandular polyps (Figures 10.26 and 10.27)
Beagle dog	Segmental cystic hyperplasia
Cynomolgus macaque	Endometrial polyps, ectopic ovary, uterine hemorrhage, adenomyosis, endometriosis
Minipig	Glandular cystic hyperplasia, adenosis
Rabbit	Cyst NOS, epithelial/granular cell hyperplasia
Species	Vagina/cervix
Rat	Squamous metaplasia
Beagle dog	Inflammation (usually neutrophilic)
Cynomolgus macaque	Squamous metaplasia of endocervical glands
Minipig	None
Rabbit	Atrophy, cyst NOS

Modified from Haschek WM, Rousseaux CG, Wallig MA, editors: *Haschek and Rousseaux's handbook of toxicologic pathology*, ed 3, 2013, Academic Press, Table 60.7, p. 2629, with permission.

dogs (>8 years) are not listed. Also, it is important to understand the age and sexual maturity status of each animal evaluated, since Beagle dogs, minipigs, and cynomolgus macaques used in toxicology studies are often sexually immature or peripubertal (Peter et al., 2016; Vidal, 2017). Readers are recommended to follow recent STP Best Practices in documentation of sexual maturity in nonclinical toxicity studies (Mecklenburg et al., 2019; Vidal et al., 2021).

#### 4. RESPONSES TO INJURY

Female reproductive system toxicity can be manifested by changes in multiple parameters, including physiologic (changes in behavior, menses, lactation, fertility), biochemical (HPO axis disruption), and morphologic (end-organ nonproliferative and proliferative lesions). Specific patterns and mechanisms will be described in detail in Section 5; however, a brief overview of key concepts will be provided here.

The basic responses of the reproductive system to insult are often comparable among different species of laboratory animals because of the similarity of reproductive function control, but species-specific responses are important to consider and will be detailed where appropriate. As described earlier, pituitary gland and reproductive end-organ growth and development are dependent on numerous trophic biomolecules produced by the pituitary, ovary, and, in the non-rodent, the adrenal gland. These trophic agents modulate cell growth, metabolism, and differentiation within the varied compartments of the ovary, uterus, vagina/cervix, mammary gland, and clitoral glands. It is not only the systemic and local concentrations but also the ratio and timing of these agents that are important determiners for the tissue response. Therefore, it is not surprising that a major mode of response to injury in the female reproductive system is that of disturbances of growth: atrophy, hypertrophy/hyperplasia, metaplasia, dysplasia, and neoplasia.

Atrophy (Figure 10.23) and hypertrophy/hyperplasia (Figures 10.26 and 10.32) may result

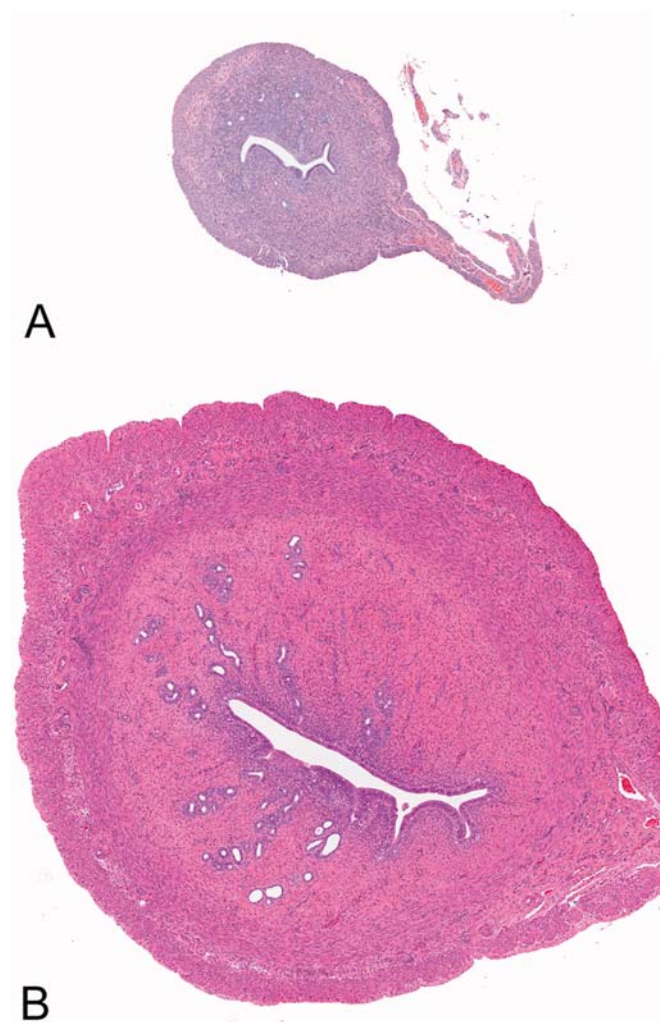


**FIGURE 10.23** Uterus, rat. (A) Uterine atrophy (markedly thin endometrium and myometrium) in ovariectomized rat in comparison to (B) the ovary-intact rat uterus (A, B 20 $\times$ ). H&E. Reproduced from Haschek WM, Rousseaux CG, Wallig MA, editors: Haschek and Rousseaux's handbook of toxicologic pathology, ed 3, 2013, Academic Press, Figure 60.20, p. 2631, with permission.

from increases or decreases in cell proliferation or apoptosis, both important and normal physiologic processes in the cycling female reproductive tract. As discussed in [Sections 2.7–2.9](#), on endocrinology, hormones produced by the hypothalamus, pituitary, ovary, and, in nonrodents, the adrenal gland modulate the balance between cell proliferation and apoptosis in the reproductive tract.

For example, estradiol normally induces proliferation within the endometrium and induces keratinization within the vagina as part of the

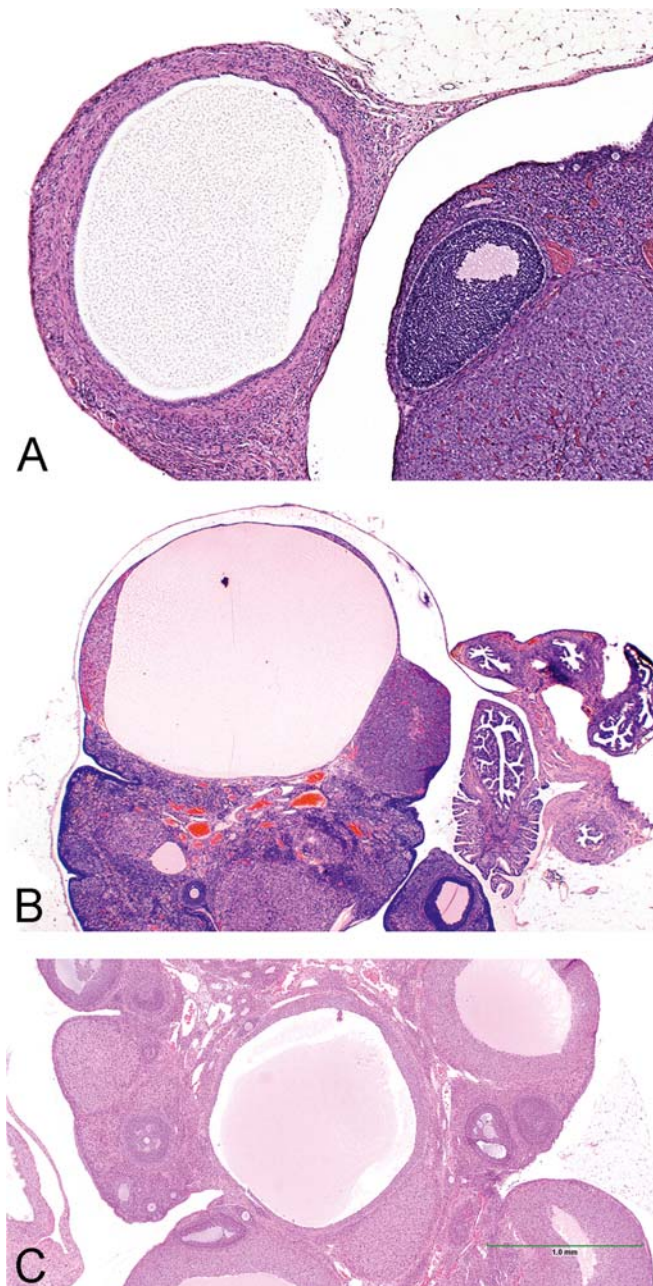


**FIGURE 10.24** Ovary, rat. (A) Parovarian cyst (note muscular wall), (B) luteinized follicular cyst, and (C) luteal cyst. The parovarian cyst lies outside the ovarian parenchyma. The follicular cyst is lined by an attenuated luteinized granulosa cell layer. The luteal cysts are characterized by CL with a central fluid filled space. (A, C) 30 $\times$ , (B) 5 $\times$ . H&E. Courtesy of National Toxicology Program (NTP). (A and B) Reproduced from Haschek WM, Rousseaux CG, Wallig MA, editors: Haschek and Rousseaux's handbook of toxicologic pathology, ed 3, 2013, Academic Press, Figure 60.21, p. 2631, with permission. (C) Courtesy of NTP.



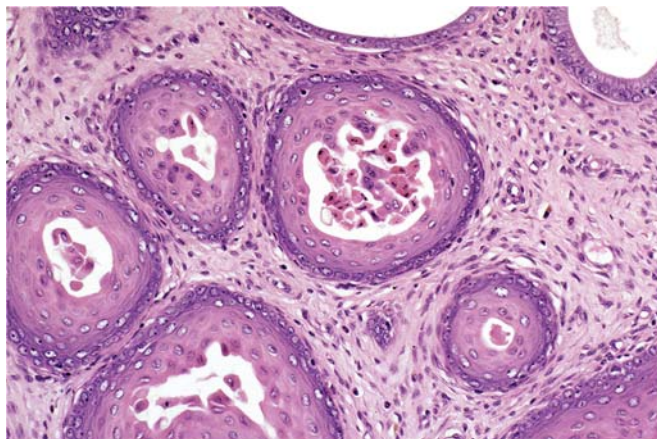


**FIGURE 10.25** Uterus, rat. Squamous metaplasia of endometrial glands. Glands are lined by a squamous epithelium and lumina are filled with keratinized debris. 66 $\times$ , H&E. *Courtesy of NTP. Reproduced from Haschek WM, Rousseaux CG, Wallig MA, editors: Haschek and Rousseaux's handbook of toxicologic pathology, ed 3, 2013, Academic Press, Figure 60.22, p. 2633, with permission.*

normal estrous cycle. However, when the balance of trophic factors becomes altered in toxicity, the toxicologic pathologist should expect to observe disturbances of growth as an outcome of an altered homeostasis between proliferation and apoptosis. Too little estradiol leads to atrophy of the uterus and vagina, while too much can lead to endometrial hyperplasia of the uterus and/or squamous metaplasia of the vagina.

The trophic hormones are tumor promoters and potential nongenotoxic carcinogens due, in part, to their effects on cell proliferation in the reproductive tract of animals and women (Capen, 2004). Therefore, the incidence of spontaneous tumors in the reproductive tract may increase if the HPO axis is modified or a toxicant has a direct hormone-like effect. The toxicologic pathologist should recognize the potential for shifts in the incidence of spontaneous tumors from hormone-responsive tissues (pituitary, mammary gland, vagina, uterus, cervix, ovary, and clitoral gland) in animal model systems. For example, rats treated with certain SERMs in lifetime bioassays have an increased incidence of granulosa cell tumors because of hypersecretion of FSH, but a decreased incidence of mammary gland neoplasms due to antiestrogenic effects of the SERM on the mammary gland epithelium (Long et al., 2001). Of course, a toxicant may also produce neoplasms through a genotoxic

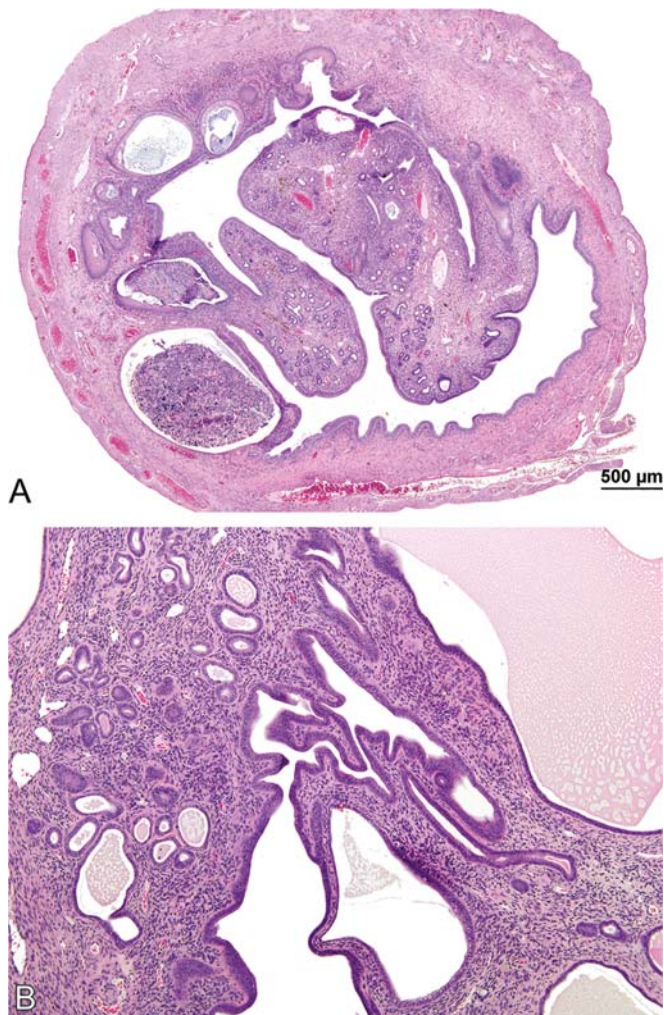


**FIGURE 10.26** Uterus, rat and mouse. (A) Rat, cystic endometrial hyperplasia and glandular polyp. (B) Mouse, cystic endometrial hyperplasia. In (A) the endometrial mucosa is extended into the uterine lumen (glandular polyp); in (A) and (B) endometrial gland profiles are distended and lined by a hypertrophic epithelium (hyperplasia). Focally there is squamous metaplasia, and sometimes glands contain fluid and cellular debris. (A) 3.2 $\times$ , (B) 10 $\times$ . H&E. *Courtesy of NTP. Reproduced from Haschek WM, Rousseaux CG, Wallig MA, editors: Haschek and Rousseaux's handbook of toxicologic pathology, ed 3, 2013, Academic Press, Figure 60.23, p. 2633, with permission.*

pathogenesis. This is a rare observation in pharmaceutical toxicology, because in almost all cases, genotoxic compounds do not advance to lifetime bioassay studies. A discussion of specific neoplasms is presented later in this chapter.

The predictable endocrine profiles during estrous and menstrual cycles in healthy adult



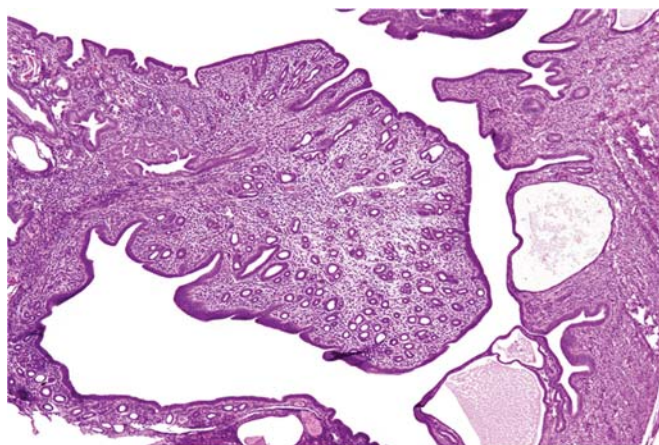


**FIGURE 10.27** Uterus, rat. Glandular polyp. A discrete focal extension of normal appearing stromal connective tissue and glandular profiles underlying a normal superficial epithelium extend into the uterine lumen. Adjacent endometrial glands are dilated, and fluid filled. 13.2 $\times$ , H&E. Courtesy of NTP. Reproduced from Haschek WM, Rousseaux CG, Wallig MA, editors: *Haschek and Rousseaux's handbook of toxicologic pathology*, ed 3, 2013, Academic Press, Figure 60.24, p. 2634, with permission.

animals and women induce the reproductive tissues follow a specific pattern manifested by coordinated morphologic and functional changes. Toxicity may alter estrous or menstrual cycle length or cause changes in female reproductive tissues. These changes may be more difficult for the toxicologic pathologist to recognize without specific study designs assessing cycle length due to several factors, including the long, variable estrous cycle in the Beagle dog; the small number of nonrodents per group used in toxicology studies (generally three or four); and the use of peripubertal nonrodents. However, for rodent studies, the number of animals and study designs offer an opportunity for the pathologist to recognize toxicity-mediated lack of coordination between the expected morphologic appearance of the uterus, vagina, and ovary for any specific stage of the cycle.

Angiogenesis is a key process in the normal cycling of the ovary. Normal development of the CL requires cyclic changes in blood vessels. Toxicity that results in the modulation of angiogenesis pathways (e.g., VEGF inhibitors) may result in partial or complete failure of CL formation as well as secondary changes in the uterus

and vagina (atrophy) due to alterations in ovarian hormone production, a consequence of an interruption in ovarian cycling (Brown et al., 2005; Hall et al., 2016; Ryan et al., 1999).

Direct toxicity of components of the female reproductive tract is less common; however, there are some specific examples of degenerative, inflammatory, and immune-mediated processes that result in injury to the reproductive tract. These include those secondary to intravaginal test article administration and degeneration and necrosis of ovarian follicles secondary to chemical toxicants or radiation that target rapidly dividing cell populations (Baker, 1978) (see also *Radiation and Other Physical Agents*, Vol 3, Chap 14). Historically, the chemical 7,12-dimethylbenz[a]anthracene (DMBA) is an example of an important toxicant in the ovary and now is used commonly in reproductive system research. DMBA causes follicular degeneration in primary, secondary, and tertiary follicles by perturbing gap junctions, damaging DNA, and altering gene expression. Studies in the pig also have shown that DMBA desynchronizes the nuclear and cytoplasmic maturation of pig oocytes (Song et al., 2017).

Locally applied test articles in the vagina are usually unevenly distributed on the vaginal mucosa and different areas of the vagina may be affected at different times so that the stages of inflammation may differ in the same animal (Goette and Odom, 1980). The vaginal inflammatory response is like that of other squamous epithelial surfaces in the body, and may include intracellular and intracellular edema, polymorphonuclear leukocyte infiltration, and microabscess formation. As the lesion progresses, erosion and ulceration may follow. Repair and recovery are accomplished by the process of regeneration with accelerated cell proliferation in the stratum germinativum. The number of cell layers increases in the stratum germinativum (acanthosis). This may result in premature migration of epithelial cells with retained nuclei into the stratum corneum (parakeratosis) or an increase in the thickness of the stratum corneum (hyperkeratosis). Once the stratum corneum is formed, the inflammatory response is likely to subside. Cornification of the vaginal epithelium appears to take place only when the epithelium has reached a certain thickness. If the rate of regeneration does not exceed the rate of loss

induced by the irritant, the epithelium will not become cornified and inflammation will continue if treatment with the irritant continues. In this case, the inflammatory process becomes chronic and mononuclear cells become the major component of the exudate.

Delayed hypersensitivity responses can also be observed in the vagina after sensitization by either dermal or vaginal exposure (Newman et al., 1983). Since perivascular accumulations of lymphocytes is the hallmark of the lesion, histological examination is necessary to demonstrate the nature of the inflammatory reaction. When a nonirritating sensitizer is administered, the inflammatory reaction is usually limited to lymphocytic infiltration. In the case of an irritating sensitizer, the inflammatory response may include neutrophils and eosinophils in the response reaction; however, perivascular lymphocytic cuffing is always present. Such vascular cuffs consist of multiple layers of lymphocytes surrounding vessels of the lamina propria, muscularis, and mesometrial attachment.

Medical devices are used uncommonly for urogenital conditions, and their safety evaluation are usually adapted from those completed for predicate devices (see *Biomedical Materials and Devices*, Vol 2, Chap 11). However, this does not minimize the importance of medical device safety assessment for the female reproductive system. In an FDA review of data concerning the vaginal safety of transvaginal surgical mesh, the agency determined the risk: benefit of the medical device was not justified which resulted in its Type III (high risk) reclassification and withdrawal in 2019 (Mao et al., 2021).

## 5. MECHANISMS OF TOXICITY IN THE FEMALE REPRODUCTIVE SYSTEM

For reproductive end-organ effects, changes are either categorized as being secondary to endocrine disruption or as reflective of direct tissue toxicity, or possibly a combination of the two. In our experience, morphologic and functional effects on female reproductive system end organs are most often secondary to HPO axis disruption rather than direct end-organ

toxicity; however, this observation is biased by the large efforts in hormone modulator therapeutic approaches that have been made by the pharmaceutical industry over the past several decades. Direct mechanistic or mixed direct and HPO modulatory mechanisms may be more common because of the emergence of new cellular targets.

Probably underappreciated in the assessment of female reproductive toxicity is that clinical pathology data also may contribute to the interpretation of patterns of endocrine disruption. For example, increases in estrogens or progestins may be accompanied by increases or decreases, respectively, in total serum cholesterol. Androgens increase total cholesterol and hematocrit. As emphasized later, clinical pathology parameters such as the leukogram and alkaline phosphatase activity are very helpful in assessing the level of “stress” in the animal.

In Table 10.6, we list several considerations and recommendations when evaluating the mechanism of toxicity for a female reproductive change. Some of these have been discussed earlier; however, they are presented together in this table because as a group they are very important when completing a human safety assessment.

Mechanisms of toxicity in the female reproductive tract can be classified into three broad categories: (1) direct disruption of the HPO axis; (2) indirect disruption of the HPO axis; and (3) direct organ specific pathology. Table 10.7 presents an overview of the types of HPO disruption, a possible cause, and the easiest to recognize and most consistent histologic change(s) observed. The causes are based on our experience and literature reports and are limited mostly to patterns in the rat because of the paucity of published data in nonrodent species. The toxicologic pathologist should be warned that often things are not this straightforward, as test articles can produce a mixed HPO phenotype based on the biology of nuclear hormone receptors and their tissue-specific cofactors (discussed below).

It can be difficult to differentiate direct versus indirect effects of xenobiotics on specific cell populations in the female reproductive system. While, in our experience, direct organ toxicity is an uncommon cause of female reproductive toxicity, there are examples of xenobiotics that

**TABLE 10.6** Considerations for the Toxicologic Pathologist When Evaluating Female Reproductive Toxicities**Safety assessment considerations**

Detection of female reproductive effects in the rat can be complicated by age-related senescence that can begin as early as 4 months of age.

Dogs and nonhuman primates used in toxicology studies are often immature or pubescent, which will limit the ability to assess female reproductive toxicity.

The variation in histological background changes for the female reproductive tract of all species is such that small changes in the incidence or severity of these changes should be interpreted with caution. Spontaneous lesions may mimic test article-related effects.

In rats, the vagina, uterus, and mammary gland are generally more sensitive as indicators of treatment-related effects in shorter-term studies (<30 days) than the ovary.

Treatments that have a weak effect on the female reproductive tract may only cause limited changes. Therefore, the assessment of the ovary, uterus, and vagina as a unit is critical.

Organ weights for the ovary and uterus may be somewhat variable and small increases (<20%) in mean weights should be interpreted with caution in all nonclinical species.

Xenobiotics, especially those that interact directly with nuclear hormone receptors, may have mixed agonist/antagonist tissue effects in the female reproductive system (e.g., selective estrogen receptor modulators).

*Reproduced from Haschek WM, Rousseaux CG, Wallig MA, editors: Haschek and Rousseaux's handbook of toxicologic pathology, ed 3, 2013, Academic Press, Table 60.8, p. 2636, with permission.*

target cell populations in the reproductive tract resulting in specific organ-dependent effects. As will be mentioned later, xenobiotics that pharmacologically target rapidly dividing cell populations may impact negatively on ovarian follicular development resulting in atresia.

Another approach to categorizing the mechanism(s) of female reproductive toxicity is by considering what is known by a compound class perspective. In [Table 10.8](#), we list several classes of compounds that modulate a biological target or pathway and the histologic changes that may be observed. The examples listed include those cited in the literature and unpublished observations. These classes of compounds include sex hormone receptor ligands, other nuclear hormone receptor ligands, and centrally active neurohormone receptor agents.

While the above approaches to categorizing female reproductive toxicity are useful, there are innumerable possible causes for female reproductive toxicity. Yet it is our experience that several recurring mechanisms are frequent enough to merit a focused discussion. We recommend that the toxicologic pathologist be familiar with the mechanisms and toxicologic outcomes detailed below.

## 5.1. Stress and Negative Energy Balance

As mentioned briefly earlier in the chapter, in our experience, a pattern of female reproductive changes that may be observed in toxicology studies is secondary to the effects of stress and reduced food consumption, both common outcomes of administering high doses of test articles to young, rapidly growing animals used in safety assessment studies ([Everds et al., 2013](#)). Because reproduction is not an essential process for survival of an animal, when animals enter a negative energy balance, gonadotropin production is reduced and reproductive cycling can be prolonged or delayed, eventually resulting in atrophy of the female reproductive tissues ([Figures 10.28–10.30](#)). Stress by itself induces excessive secretion of epinephrine, acutely, and glucocorticoids, chronically which can depress the frequency and amplitude of LH secretion and interfere with the reproductive cycle. The toxicologic pathologist needs to be familiar with female reproductive gross, organ weight, and histologic changes associated with this common pattern of toxicity, as well as the changes observed in clinical pathology data (i.e., stress leukogram), and nonreproductive



**TABLE 10.7** Patterns of Toxicity in the Female Rat Reproductive System Based on Effects on the Hypothalamic–Pituitary–Ovarian (HPO) Axis in Relative Order of Frequency

Primary and secondary hormonal effect	Most common cause	Most characteristic histologic change(s)
↓ GnRH and ↓ LH/FSH, ↓ ovarian steroid hormones	Stress and negative energy balance	Ovarian, vaginal and uterine atrophy
↑ PRL or ↓ dopamine, ↑ P4	Central inhibition of pituitary dopamine release; dopamine receptor antagonism	Mammary gland lobular hyperplasia and lactogenesis, persistent vaginal/uterine diestrus
↑ P4, ↓ GnRH and LH/FSH	Progesterone receptor agonism	Vaginal hypertrophy and hyperplasia with mucification
↓ P4 or PR blockade	Progesterone receptor antagonism and increased E2: P4 ratio	Persistent vaginal/uterine estrus
<sup>a</sup> ↑ E2, ↓ GnRH and LH/FSH	Estrogen receptor agonism	Vaginal and uterine epithelial hyperplasia and squamous metaplasia
ER blockade, ↑ GnRH and LH/FSH, ↑ E2 and T	Selective estrogen receptor antagonists (e.g., raloxifene)	Ovarian granulosa cell hyperplasia, mammary gland masculinization
↑ GnRH, ↑ LH/FSH, ↑ E2/P4/androgens	Gonadotropin receptor agonism	Uterine endometrial cystic hyperplasia
↑ Androgens	Androgen receptor agonism	Vaginal mucification, uterine hypertrophy/hyperplasia; mammary gland

<sup>a</sup> In rodents, exogenous administration of estrogens or ER agonists can cause hyperprolactinemia and persistent diestrus.

E2, estradiol; ER, estrogen receptor; FSH, follicle-stimulating hormone; GnRH, luteinizing hormone-releasing hormone; LH, luteinizing hormone; P4, progesterone; PR, progesterone receptor; PRL, prolactin; T, testosterone.

Reproduced from Haschek WM, Rousseaux CG, Wallig MA, editors: *Haschek and Rousseaux's handbook of toxicologic pathology*, ed 3, 2013, Academic Press, Table 60.9, p. 2637, with permission.

tissue histology (i.e., decreased lymphoid cellularity in the thymus, decreased hematopoietic cellularity in the bone marrow, and adrenal cortical hypertrophy). The organ weight, gross, and histologic changes associated with this common pattern of nonspecific toxicity are listed in [Table 10.9](#).

It is important to note that ovarian atrophy (i.e., decreased number of corpora lutea and antral follicles) ([Figure 10.29](#)) is difficult to assess in short-term rat studies ( $\leq 14$  days) because the follicular development from primordial to early tertiary stage does not require hormonal stimulation. Also, while expected to decrease with atrophy, the corpora lutea number can be highly variable because they may have been formed

prior to dosing and may not be obviously reduced in number if there is a treatment effect. These studies also may have fewer animals than definitive studies because they are used for compound screening or dose setting for later studies. Alterations in the vagina and uterus may also be difficult to interpret. Morphologic changes in the vagina are easiest to identify because the uterine epithelium that lines the luminal and endometrial glands is only a single cell layer that can undergo limited morphological changes under the influence of estrogen, androgens, and progesterone. In contrast, the vaginal epithelium from the anterior two-thirds of the vagina, owing to its multilayered structure and high turnover rate, undergoes a variety of

**TABLE 10.8** Nonclinical Toxicology Female Rat Histologic Findings Associated with Modulation of Specific Mammalian Targets or Pathways

Compound class	Proposed mechanism	Reported histologic findings
Selective estrogen receptor modulators (SERM)	LH/FSH hypersecretion due to hypothalamic ER antagonism	Ovarian follicular cysts <sup>a</sup> and granulosa cell hyperplasia/neoplasia; diffuse endometrial hyperplasia
Estrogen receptor-alpha or beta agonists	Central and end-organ ER agonism, prolactin hypersecretion	Increased tertiary ovarian follicles, decreased number CLs; vaginal squamous metaplasia, uterine cystic glandular hyperplasia and vaginal and cervical increased mucification; mammary gland lobular hyperplasia
Androgen agonists	Tissue-specific AR agonism	Ovarian follicular cysts, decreased number CLs, interstitial gland atrophy; diffuse endometrial and myometrial hyperplasia; vaginal increased mucification
Dopamine or opioid receptor antagonists	Prolactin hypersecretion	Mammary gland lobular hyperplasia, CL hypertrophy, vaginal and cervical increased mucification,
Progesterone receptor antagonists	Progesterone receptor antagonism (E2/P4 ratio decreased)	Increased ovarian weights, ovarian follicular cysts, all rats in estrus
Progesterone receptor modulators	Mixed progesterone agonist and antagonist activity	Dyssynchronous endometrium (cystic dilatation of endometrial glands, distortion of gland architecture, abortive secretory differentiation, occasional squamous metaplasia of the uterine endometrial epithelium)
Histamine 3 antagonist	Increase in TRH and prolactin hypersecretion; interference in steroidogenesis	Decreased number CLs, follicular cysts, uterine and vaginal atrophy, mammary gland lobular hyperplasia
Mitogen activated kinase inhibitors	Angiogenesis inhibition; StAR inhibition	Ovarian follicular and luteal cysts and hemorrhage, endometrial atrophy
Growth hormone secretagogues, receptor agonists	Prolactin hypersecretion	Decreased number CL (basophilic), uterine atrophy, vaginal increased mucification

(Continued)

**TABLE 10.8** Nonclinical Toxicology Female Rat Histologic Findings Associated with Modulation of Specific Mammalian Targets or Pathways—cont'd

Compound class	Proposed mechanism	Reported histologic findings
Retinoid activated receptor gamma antagonists	Unknown; RAR gamma highly expressed in rat uterus and ovary	Vaginal estrus without uterine/ovarian estrus morphology
Peroxisome proliferator activated receptor agonists (Long et al., 2009)	Direct PPAR-mediated ovarian aromatase cytochrome P450 and estrogen synthesis inhibition	Decreased number CLs, increased number atretic follicles, ovarian follicular cysts, decreased uterine and ovarian weights, cystic endometrial hyperplasia

<sup>a</sup> Also reported in nonrodent.

Modified from Haschek WM, Rousseaux CG, Wallig MA, editors: Haschek and Rousseaux's handbook of toxicologic pathology, ed 3, 2013, Academic Press, Table 60.10, p. 2638, with permission.

**TABLE 10.9** Organ Weight, and Gross and Histologic Changes That may be Associated with Stress and Negative Energy Balance in Female Animals

Organ weight: decreased thymic, ovarian, uterine weights; increased adrenal weights

Gross pathology: Small thymus, decreased visceral fat, large adrenal, reddened gastric/duodenal mucosa

Histopathology: Bone marrow decreased cellularity, thymic lymphocyte decreased cellularity, adrenal cortical hypertrophy, pancreatic zymogen granule depletion, erosion/ulceration of gastric or duodenal mucosa, ovarian/uterine/vaginal/cervical atrophy

Reproduced from Haschek WM, Rousseaux CG, Wallig MA, editors: Haschek and Rousseaux's handbook of toxicologic pathology, ed 3, 2013, Academic Press, Table 60.11, p. 2639, with permission.

changes and is a very sensitive indicator of the hormonal status of the animal. The morphology of the ovarian interstitial glands also changes rapidly with negative energy balance. In a quiescent ovary, normally prominent, large polygonal cells with round nuclei and a moderate amount of deeply acidophilic foamy cytoplasm (Figure 10.30) become small, spindle-shaped cells with dark elongated nuclei and a small amount of lightly acidophilic or basophilic cytoplasm. As mentioned previously, the toxicologic pathologist should consider the female reproductive system as a unit and all tissues endpoints when evaluating potential individual tissue effects.

During the in-life portion of toxicity studies, it is not uncommon to observe accommodation to the stress and food consumption effects that occur acutely. In these studies, there may be a mixed phenotype at necropsy whereby the histologic pattern of past cycle cessation is combined with a pattern of normal cycling. The

toxicologic pathologist should closely evaluate the food consumption and clinical signs in individual animals to appropriately interpret these types of changes in the female reproductive system.

Differentiating findings from stress or negative energy balance and primary test article related effects can be challenging (Everds et al., 2013). It is important that the toxicologic pathologist closely examines the dose-response of the cycle disruption relative to the effects on animal food consumption, clinical signs, and thymic weights and histology—the latter, in our experience, being the most sensitive indicator of previous or ongoing stress in animals. If cycle disruption is only observed at doses that produce decreased food consumption or significant clinical signs or changes indicative of stress, it may not be possible to assess whether there are primary effects on the female reproductive system. However, if this pattern of cycle disruption is



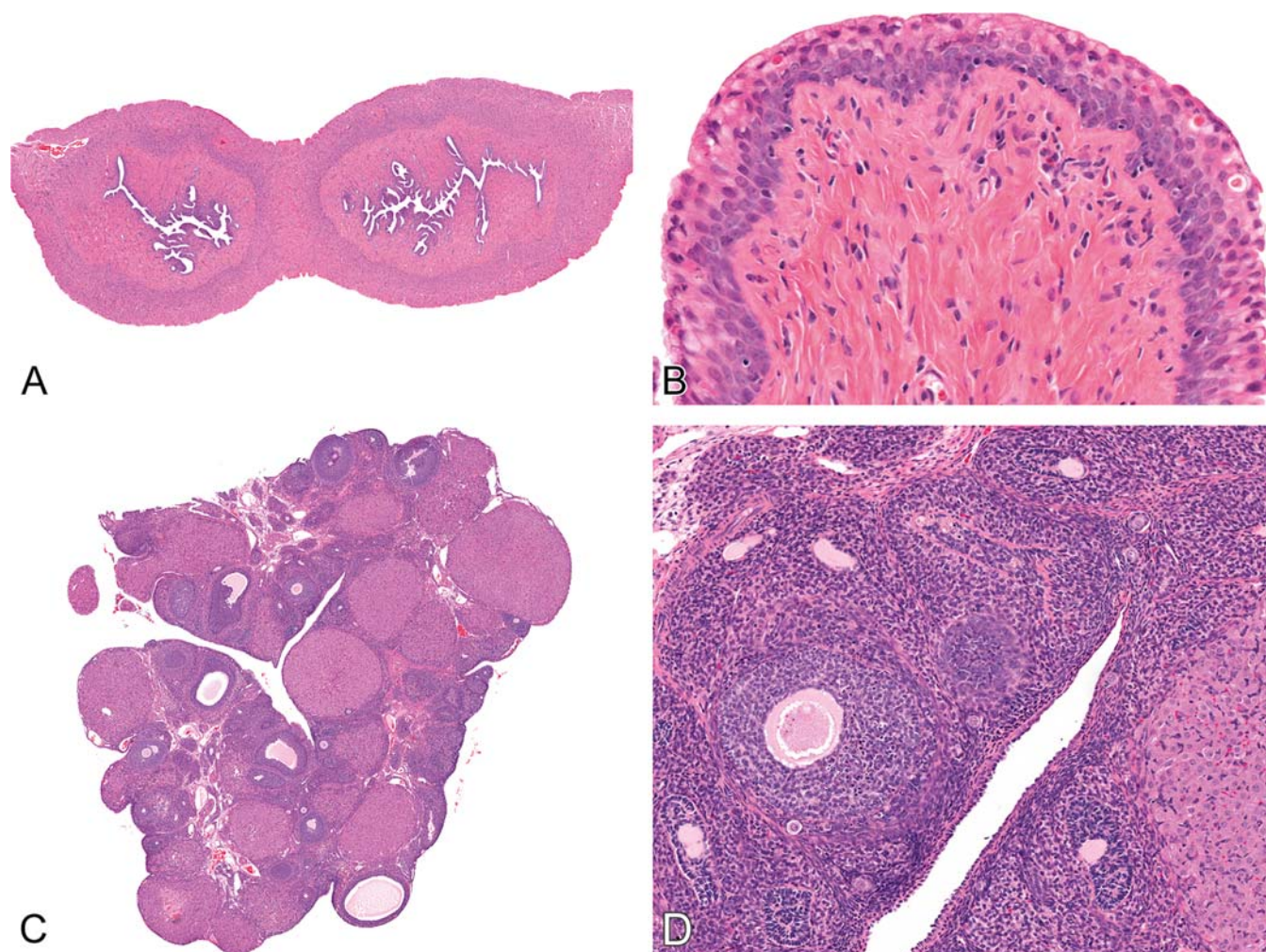


**FIGURE 10.28** Uterus, vagina, and ovary, rat. Late pseudopregnancy in a rat. (A) The uterine mucosa has mild endometrial hyperplasia. (B) The vaginal mucosa is thin (two or three layers thick) and the superficial epithelial cells have prominent, mucoid cytoplasm. (C) The ovary only has eosinophilic and involuted CL from prior cycles. (D) The follicles are undergoing atresia. (A) 10 $\times$ , (B) 100 $\times$ , (C) 10 $\times$ , (D) 50 $\times$ . H&E. Reproduced from Haschek WM, Rousseaux CG, Wallig MA, editors: *Haschek and Rousseaux's handbook of toxicologic pathology*, ed 3, 2013, Academic Press, Figure 60.25, p. 2635, with permission.

observed at doses that cause very little or no changes in food consumption or clinical signs, a primary effect of the test article should be considered.

In group housed NHPs, there is a strong social influence on reproductive function. In established social hierarchies, the dominant animals cycle regularly, while the subordinate animals have a high incidence of anovulatory cycles and/or luteal phase defects (Adams et al., 1985; Cline et al., 2008). It is important to consider the influence of social hierarchy due to housing and timing of randomization when assessing the female reproductive system in NHPs.

## 5.2. Hyperprolactinemia

Another common female reproductive toxicity pattern that toxicologic pathologists will likely experience is that which is manifested by hyperprolactinemia in rats (Ben-Jonathan et al., 2008; Rehm et al., 2007). Female rats are especially sensitive to the effects of hyperprolactinemia, and there are several classes of test articles that induce a hyperprolactinemia phenotype in animals. The most common mechanism of hyperprolactinemia is the excessive prolactin secretion that occurs when dopamine is depleted or antagonized by compounds such as reserpine



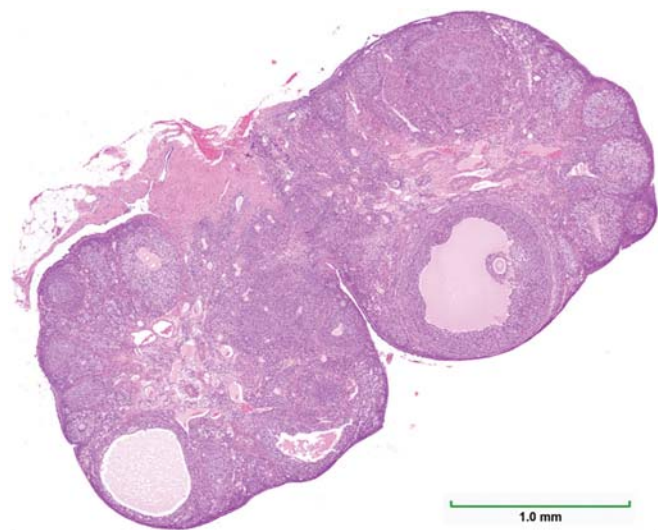


**FIGURE 10.29** Ovary, rat. Decreased number, corpora lutea. Corpora lutea are decreased in number and those remaining are atretic. Interstitial cells are prominent. There is a large degenerate antral follicle and cystic tertiary follicle.

or phencyclidine hydrochloride. The constellation of changes associated with hyperprolactinemia is outlined in [Table 10.10](#), with the most classic and easily recognized change being that of mammary gland lobular hyperplasia from increased prolactin and vaginal mucification due to the increased progesterone production from the hypertrophic corpora lutea ([Figure 10.31](#)).

It is important to note that the histologic manifestations of xenobiotic-induced hyperprolactinemia may change with the chronicity of the study. In our experience, the mammary gland and vaginal changes are most easily recognized in shorter-term studies. For example, the structure–activity relationship (SAR) of a group of compounds which have a propensity to increase prolactin can be assessed using the mammary gland and vagina in 4-to-7-day repeat-dose studies in rats (personal observation by DGR). In longer-term studies, in animals, the reproductive cycle is perturbed and there are histologic changes indicative of prolactin's effect of extending the lifespan of the ovarian corpora lutea (increased size of ovarian corpora lutea) and the effects of increased progesterone on the uterus and vagina (endometrial hypertrophy/hyperplasia, and vaginal mucification) ([Table 10.10](#)).

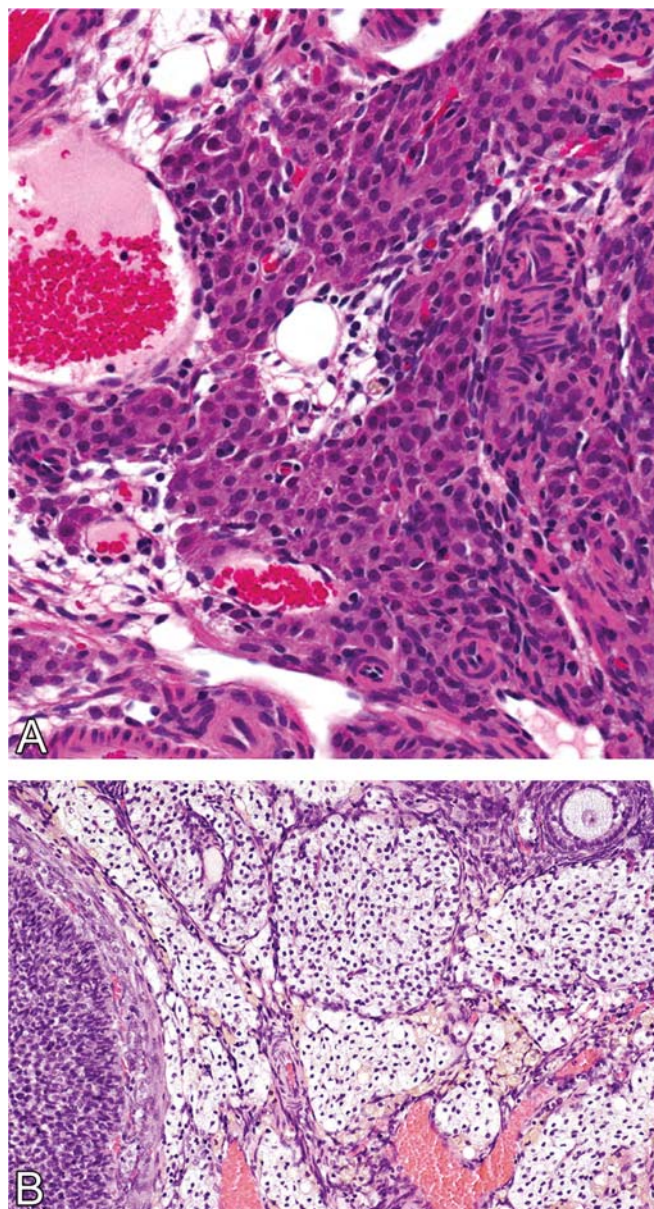


**FIGURE 10.30** Ovary, rat. Interstitial glands, (A) normal or (B) hypertrophied. (A) 50 $\times$ , (B) 10 $\times$ , H&E. Courtesy of NTP. Reproduced from Haschek WM, Rousseaux CG, Wallig MA, editors: *Haschek and Rousseaux's handbook of toxicologic pathology*, ed 3, 2013, Academic Press, Figure 60.27, p. 2640, with permission.

While the most common mechanism of hyperprolactinemia in the rat is pharmacologic alterations of the dopamine regulatory pathway for pituitary prolactin production, other possible mechanisms can occur. Opioid receptor biology is also important in prolactin homeostasis. Nonspecific antagonists of opioid receptors



**TABLE 10.10** Histologic Changes Associated with Hyperprolactinemia in the Female Rat

Mammary gland: lobuloalveolar hyperplasia with secretions

Ovary: corpora lutea hypertrophy

Uterus: morphology consistent with diestrus

Vagina/cervix: increased mucification

*Reproduced from Haschek WM, Rousseaux CG, Wallig MA, editors: Haschek and Rousseaux's handbook of toxicologic pathology, ed 3, 2013, Academic Press, Table 60.12, p. 2640, with permission.*

(e.g., naloxone) suppress prolactin secretion, and natural opioids or synthetic agonists increase prolactin release. Rats given growth hormone develop a prolactogenic phenotype (Ikeda et al., 1997). Increases in the estrogenic stimulation due to a variety of xenobiotics (e.g., phytoestrogens) can result in hyperprolactinemia.

There are important rat and human species differences regarding prolactin. For instance, prolactin is luteotrophic in rats but not in humans, and, as discussed earlier, the luteotrophic effects of hyperprolactinemia in rats result

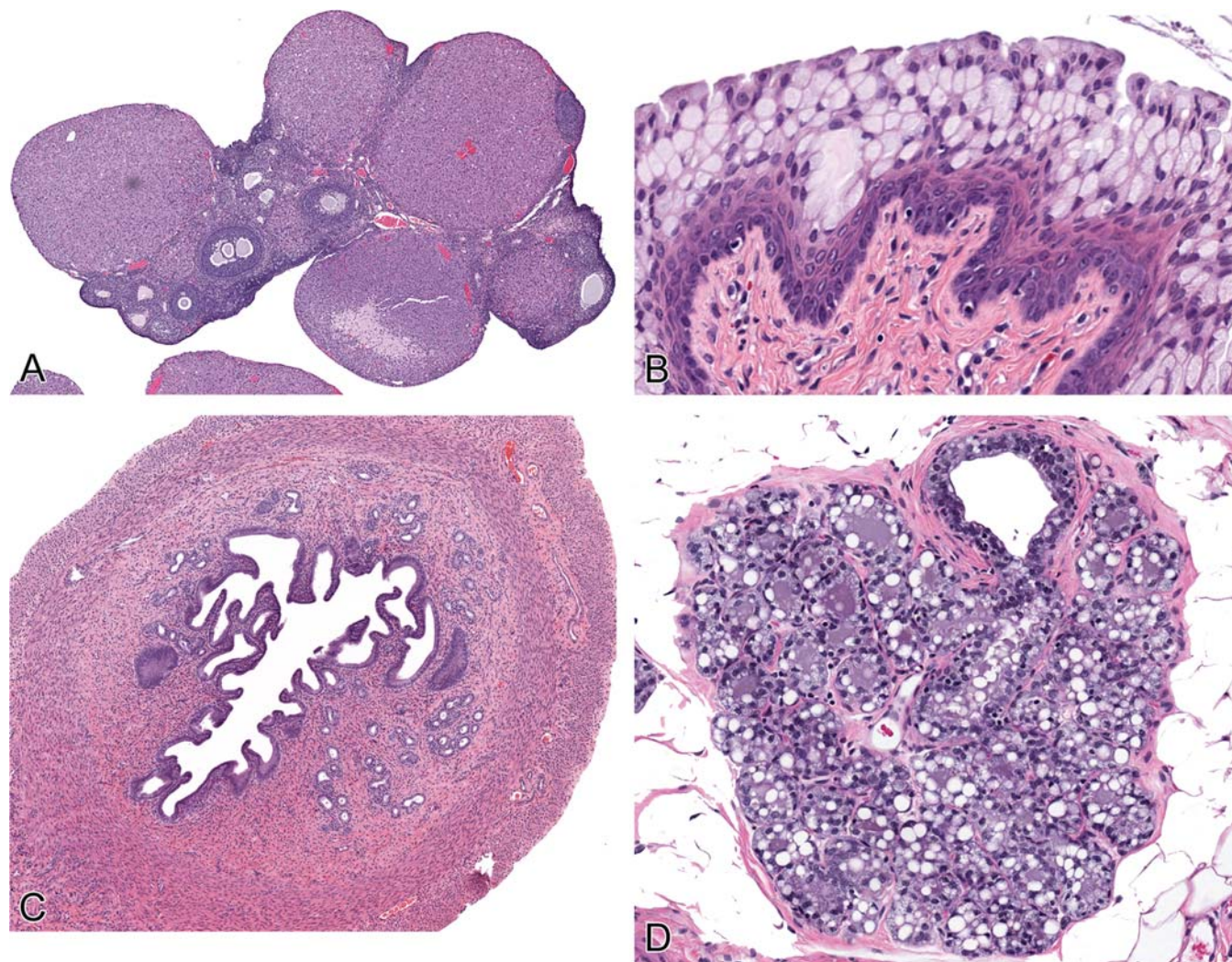


**FIGURE 10.31** Mammary gland, vagina, and ovary, rat. Selected female reproductive changes in hyperprolactinemia. (A) Ovary: corpora lutea (CL) hypertrophy. (B) Vaginal diestrus with mucification secondary to prolonged CL progesterone production. (C) Uterus: Endometrial folding (diffuse endometrial hypertrophy/hyperplasia) secondary to prolonged CL progesterone production. (D) Mammary gland lobuloalveolar hyperplasia and increased secretions. (A, C) 2 $\times$ , (B) 200 $\times$ , (D) 50 $\times$ . *Reproduced from Haschek WM, Rousseaux CG, Wallig MA, editors: Haschek and Rousseaux's handbook of toxicologic pathology, ed 3, 2013, Academic Press, Figure 60.28, p. 2641, with permission.*



in specific uterine (hyperplasia/hypertrophy) and vaginal (mucification) changes would not be expected in women. Also, rats are markedly more sensitive than women to prolactin increases secondary to estrogen-mediated inhibition of dopamine secretion, and prolactin control is more central (hypothalamic) in rats than in women, where peripheral regulation of prolactin is more important. Likewise, extra pituitary production of prolactin is not important in the nonpregnant rat, while in women, prolactin is produced in mammary gland, the myometrium, and in lymphocytes and adipocytes in both pregnancy and nonpregnancy. While the spectrum of changes observed in rodents due to prolactin regulation of corpus luteum life span does not occur in humans, hyperprolactinemia may still occur and induce changes such as galactorrhea, amenorrhea, and/or infertility.

The dogma has been that the effects of hyperprolactinemia in rats are species-specific, but there is some controversy as to the significance of the hyperprolactinemic rodent phenotype when assessing the human safety of xenobiotics (Harvey et al., 2008; Harvey, 2011). Prolactin is considered a nongenotoxic carcinogen in rodents, and xenobiotics such as dopamine receptor antagonists, for example, aripiprazole, that cause hyperprolactinemia in rodent models are associated with an increased incidence of mammary gland tumors in 2-year carcinogenicity bioassays (Amerio et al., 2015). A retrospective analysis of complex cancer data sets suggests that prolactin may also have an important contributory role in the pathogenesis of human breast cancer (Harvey, 2011). Therefore, as is the case with the safety assessment of all xenobiotics, the potential risk to the exposed population must always be placed in perspective regarding the benefit to that group.

### 5.3. Altered Activity of Sex Steroid Enzymes and Cholesterol Metabolism

Sex steroid synthesis is a complicated multi-step process that requires the activity of numerous substrates and enzymes. In our experience, female reproductive toxicity due to test article effects on the enzymatic machinery

involved in sex steroid synthesis is probably the third most common mechanism of toxicity a toxicologic pathologist may observe in nonclinical animal models. It is important that the metabolic fate of a test article is well understood, and the drug disposition scientist is an important partner in this assessment. If a chemical structure, by its metabolism, alters the homeostasis of sex steroid enzymatic activity, female reproductive changes are likely to be observed. Some compounds like ketoconazole inhibit multiple steroidogenesis enzymes (Cummings et al., 1997). Other compounds may inhibit a single enzyme.

The most classic example of this mechanism is the inhibition of the cytochrome P450 enzyme, aromatase, which is necessary for the synthesis of estrogens (Brodie et al., 1987; Mirsky et al., 2011; Shirai et al., 2009; Toda et al., 2003). The inhibition of this enzyme became a major therapeutic breakthrough for diseases like estrogen-responsive breast cancers. Dioxin and dioxin-like compounds which are common environmental contaminants produce numerous changes via the aryl hydrocarbon receptor (AhR) in the female reproductive system, including modulation of the incidence of inflammation and growth disturbances (ovarian and uterine atrophy, hyperplasia, metaplasia, and neoplasia) (Mattison and Thorgeirsson, 1979; Mattison, 1980). The mechanism in part for the effects of these compounds appears related to induction of cytochrome P450s, namely 1A1 and 1B1, resulting in an antiestrogenic pattern. Other examples of potential target enzymes and some compounds that alter their activity are listed in Table 10.11.

All sex hormone synthesis requires a pool of cholesterol substrate; therefore, test article effects on cholesterol absorption, synthesis, or metabolism may also have an important downstream impact on sex steroid homeostasis.

### 5.4. Targeted Cancer Therapies

Cancer remains the scourge of modern medicine, and efforts to control this complicated disease continue to be a major focus of biotechnology and pharmaceutical companies globally. Historically, the primary focus of chemotherapy was to interfere generically with cells that were undergoing high rates of proliferation, using the

**TABLE 10.11** Effects of Inhibiting Steroid Metabolic Enzymes on the Female Reproductive Tract

Target enzyme	Example compounds	Pattern of effect
Aromatase	Exemestane, anastrozole	Antiestrogen
3 beta-hydroxysteroid dehydrogenase	Troglitazone, trilostane	Antiprogesterone
17 beta-hydroxysteroid dehydrogenase type 1	Various estrone and estrogen derivatives	Antiestrogen
11 beta-hydroxysteroid dehydrogenase	PF-877423, carbenoxolone	Hypercortisolemia

Modified from Haschek WM, Rousseaux CG, Wallig MA, editors: Haschek and Rousseaux's handbook of toxicologic pathology, ed 3, 2013, Academic Press, Table 60.13, p. 2643, with permission.

so-called cytotoxic chemotherapeutics such as alkylating agents. As a result, toxicity was expected in any noncancer cell that had high turnover, such as those present in the bone marrow, gastrointestinal tract, hair follicle, and ovary (Sato et al., 2009; Sakurada et al., 2009; Hao et al., 2019; Rosendahl et al., 2010). Maturation of the ovarian follicle depends on active proliferation of granulosa cells, and xenobiotics or radiation that targets a tumor because of its rapid cell turnover can cause direct damage to the oocyte or disrupt granulosa cell proliferation, thus interfering with reproductive function. In addition to oocyte injury, these xenobiotics and radiation may interfere with granulosa cell proliferation, thecal cell differentiation, and active steroidogenesis. For example, cadmium induces necrosis of preovulatory follicles and damages the microcirculation in the uterus of the rat (Peereboom-Stegeman and Jongstra-Spaapen, 1979). Ionizing radiation damages primordial and primary oocytes (Lee et al., 2000). The result of these processes is a reduction in the total number of oocytes and follicles and an absence of corpora lutea in the ovary. This may result in permanent hormonal imbalance due to the loss of negative feedback control from ovarian steroid hormones. If the insult occurs early in life, neoplasms may develop in the remaining hyperstimulated ovarian components.

Cytotoxic agents are now more commonly part of the payload for a targeted therapeutic which concentrates at the cancer site. Therapies that target specific pathways important for cancer survival that are selectively expressed or overexpressed by a cancer cell, or therapies that modulate the immune response or the surveillance of

a cancer are now the primary focus of the pharmaceutical industry. Major approaches used in the past several decades for cancer chemotherapy have involved targeting inflammatory pathways, growth factors, the immune response and surveillance for the tumor, the tumor cell cycle and the tumor microenvironment, the latter focused on vascular neogenesis and integrity. The structural changes within the female reproductive tract during the estrous/menstrual cycle involve a cascade of events that are highly dependent on cell turnover and angiogenesis; therefore, it is not a surprise that the female reproductive tract is a common target for unwanted toxicologic effects associated with the development of novel chemotherapeutics. For this reason, we consider these mechanisms to be important potential causes of female reproductive toxicity. Table 10.12 lists several chemotherapeutics and associated patterns of toxicities in the female reproductive system. For the budding area of gene therapy for cancer and other medical conditions, a unique safety concern is the potential for germ cell integration into the oocyte.

### 5.5. Modulation of Central Nervous System Biology

Many drugs and chemicals may have a modulatory effect on the central nervous system and the hypothalamus and influence the regulation of gonadotropin secretion (Steger et al., 1981). There is an ongoing effort in the pharmaceutical industry to design more effective drugs with better side-effect profiles for the treatment of important neurological disorders like schizophrenia, Parkinson's disease, Alzheimer's

**TABLE 10.12** Chemotherapeutic Mechanisms of Female Reproductive System Toxicity

Inhibitory Target	Mechanism	Primary effect
VEGF (Ryan et al., 1999)	Antiangiogenesis	Inhibition of corpora lutea formation
Tyrosine receptor kinase (e.g., VEGFR, KIT, FLT3, PDGF, PDGFR) (Hall et al., 2016)	Antiangiogenesis	Decreased number of corpora lutea, increased follicular atresia; uterine endometrial atrophy, pericyte depletion and hemorrhage- corpus luteum
FGF receptors (Yu et al., 2020)	Altered Ca:P metabolism	Metastatic mineralization
Cox-2 (Diao et al., 2007)	Prostaglandin inhibition	Impaired ovulation
Cell cycle checkpoint inhibition (Xu et al., 2020)	Inhibition of rapidly dividing cell populations	Ovarian granulosa cell apoptosis and increased follicle atresia
CREB-binding protein (CBP) and EP300/E1A-binding protein (p300) (Katavolos et al., 2020)	Acid receptor signaling, and germ cell differentiation	Decreased number of corpora lutea

*Modified from Haschek WM, Rousseaux CG, Wallig MA, editors: Haschek and Rousseaux's handbook of toxicologic pathology, ed 3, 2013, Academic Press, Table 60.14, p. 2644, with permission.*

disease, depression, and anxiety. As the size of the older segment of the population increases, attention to these disorders and their treatment will only increase. For this reason, the toxicologic pathologist should anticipate the potential for female reproductive system toxicities when studying drugs targeted at the central nervous system.

This is especially the case for test articles that modulate cannabinoid (CB), dopamine, or opioid pathway physiology (Vuong et al., 2010). There are several well-studied drugs that affect these pathways and produce female reproductive toxicity in animal models. For example, narcotics such as morphine in rats reduce both serum LH and FSH and block the proestrus surge of GnRH and subsequent ovulation by decreasing the activity of norepinephrine neurons and the storage of hypothalamic norepinephrine. Also in rats, opioid peptides such as beta-endorphin suppress both the amplitude and frequency of the LH pulse and the preovulatory surge of LH, presumably by lowering norepinephrine concentration in the hypothalamus and decreasing the rate of dopamine turnover. Cocaine stimulates LH secretion in rats at low doses, inhibits LH secretion at high doses, and blocks the uptake of dopamine, the latter

increasing the secretion of prolactin. Marijuana, containing tetrahydrocannabinol as its principal psychoactive ingredient, depresses LH, FSH, and prolactin secretion at the level of the hypothalamus in rats.

Central nervous system toxicants like heavy metals also may produce multiple adverse effects on reproductive function. Inorganic mercury has been reported to block follicular growth and result in anestrus in laboratory rodents, possibly by altering both pituitary gonadotropin and ovarian steroid secretions (Lamperti and Nieuwenhuis, 1976). In rats treated with lead, atrophy of the ovary, reduction of serum progesterone concentration and alteration of uterine hormonal receptors have been observed (Kimmel et al., 1980). These toxicities may result from different effects along the hypothalamic-pituitary-ovarian-endometrial axis. Other metals with the potential to affect reproductive function include manganese, tin, and cadmium.

## 5.6. Toxicity Induced by Constituents of the HPO Axis and Modulators of Nuclear Hormone Receptors

Many naturally occurring and synthetic sex steroid hormones were developed as



contraceptives, fertility drugs, and therapeutic agents for the treatment of cancer in the latter half of the 20th century. These include both agonists and antagonists of gonadotropins (FSH and LH), androgens, estrogen, and progesterone (Butterstein et al., 1997; Clark and Markaverich, 1981; Far et al., 2007; Grunert et al., 1987). When sex steroid hormones are given in large nonphysiological quantities in animal toxicity studies, the result is the inhibition of gonadotropin secretion and atrophy of the ovary. However, organs at the bottom of the cascade of control may respond dramatically to the stimulation provided by the massive exogenous doses of these steroids and undergo a high degree of hyperplasia and hypertrophy (Schwartz et al., 1969; Seaman, 1985). Depending on the type of test article and species used for testing, the changes in these organs will be consistent with what is expected for estrogen, progesterone, or a combination of these two steroids. A summary of the types of test articles and histologic changes that one will observe with an estrogen, progesterone, or mixed stimulus is listed in Table 10.13.

With administration of these various naturally occurring and synthetic sex steroid hormones, the ovary eventually develops atrophy (i.e., decreased number of corpora lutea and antral follicles) due to the negative feedback of the exogenous sex steroid hormones. However, in dogs and rabbits given estrogenic test articles, ovarian atrophy is accompanied by papillary

proliferation of the ovarian surface epithelium (SES). In dogs, there can be metastatic implantation of these epithelial cells onto the capsule of the spleen, kidney, and other abdominal viscera. Since continued growth of these cells is estrogen-dependent, they undergo degeneration, necrosis, and mineralization once these estrogenic compounds are removed (Schwartz et al., 1969). The regression of the canine proliferations has posed the question of whether they are true neoplasms since they are not autonomous in growth. Similar regression of granulosa cell "tumors" and hyperplasia following withdrawal of SERM treatment have been described in the literature in rats (Long et al., 2001).

Another important species difference occurs in dogs, which are very sensitive to stimulation by progestins (Nelson and Kelly, 1976). In dogs, estrogens and some progestins can cause papillary proliferation of the surface epithelium of the atrophic ovary with occasional thecal-luteal cell hyperplasia. The uterus may become uniformly enlarged and the endometrium is lined by hypertrophic epithelial cells with abundant foamy cytoplasm. Endometrial glands may become hyperplastic and cystic, and exudate may accumulate in glandular lumens. The uterine lumen is often filled with mucoid material, which may lead to endometritis and pyometra due to superimposed bacterial infection. Cystic glands may also be present in the vagina.

In the latter few decades, a more targeted approach has been attempted for hormone

**TABLE 10.13** Summary of Uterine and Vaginal/Cervical Histologic Changes for Test Articles that have Estrogen, Progesterone, or Mixed Effects

Hormone pattern	Observation		
	Endometrial hyperplasia	Uterine squamous metaplasia	Vaginal and cervical mucosa
Estrogen dominant	Cystic with leukocytic infiltrates	Present	Hyperplasia
Progesterone or androgen dominant	Noncystic with foamy cytoplasm	Not present	Atrophy with increased mucification
Mixed	Cystic with large cytoplasmic vacuoles	Present	Hyperplasia with increased mucification

*Reproduced from Haschek WM, Rousseaux CG, Wallig MA, editors: Haschek and Rousseaux's handbook of toxicologic pathology, ed 3, 2013, Academic Press, Table 60.15, p. 2645, with permission.*

therapies by focusing on nuclear hormone receptor physiology and taking advantage of tissue-specific responses that are influenced by the presence of coregulatory proteins. Most of the effort in this area has been focused on tissue-specific modulation of the ER, with the objective of maximizing the positive outcome of ER agonism for bone, metabolic, and peri/postmenopausal symptoms while minimizing the risk for hypothalamic, breast, or uterus ER stimulation. These therapeutics pose an interesting challenge to the toxicologic pathologist because they often produce a mixed female reproductive histologic phenotype due to their disparate effects on ERs in different tissues and species of animals. Similar modulators have been developed or are in development for several other classes of sex nuclear hormone receptors, including the progesterone and androgen receptors, and produce other complicated phenotypes. It is important for the toxicologic pathologist to understand the potential for these mixed phenotypes. Data that may help in the interpretation of the changes and their relevance to human risk assessment include the properties of the test article for the target receptor across species, as well as some of the peculiarities of rodents with regard to endocrine physiology as discussed earlier.

SERMs are one class of compounds that in nonclinical animal models may cause upregulation of gonadotropin secretion and abnormally elevated concentrations of circulating gonadotropins that are unresponsive to negative feedback from ovarian steroid hormones (Carthew et al., 1996; Carthew et al., 2000; Long et al., 2001; Rudmann et al., 2005). This is due to the SERM acting as an antagonist at the hypothalamic ER. The ovary will be hyperactive in these animals and have morphologic changes including follicular cysts (Figure 10.24B) and granulosa cell hyperplasia (Figure 10.32); however, for most SERMs, despite the increased production of ovarian sex hormones, including estrogens, progestins, and androgens, the histologic changes in the uterus, vagina, and mammary gland will reflect a lack of estrogenic stimulation because of the SERMs' antagonist activity at the level of the ER in these tissues. Tamoxifen is a SERM with a slightly different pattern in neonatal and adult mice, whereby this SERM acts as an

ER agonist at the uterus in mice and rats (Carthew et al., 1996; Carthew et al., 2000; Karlsson et al., 1998). These types of observations again underscore the complexity of cross-species comparisons for toxicologic responses of the female reproductive system.

The changes induced by (synthetic) progesterone receptor modulators (PRMs or SPRMs) developed for the treatment of fibroids, endometriosis, and heavy or irregular menstrual bleeding can be very challenging to interpret. PRMs are synthetic (non-)steroidal compounds with tissue-dependent selective mixed progesterone agonistic and antagonistic effects. Some examples of PRMs are Ulipristal acetate, Telapristone acetate, Mifepriston, and Asoprisnil. Selective antagonism of the progesterone receptor in premenopausal women might result in a unique pattern characterized by cystically dilated endometrial glands with low proliferative activity and nonphysiological secretory changes in cynomolgus macaques (Ioffe et al., 2009; Williams et al., 2012). In women, the specific spectrum of morphological changes due to PRM's is described as progesterone receptor modulator associated endometrial changes or PAEC (Mutter et al., 2008). The PRM-associated simultaneous presence of low mitotic activity and apoptotic bodies in the glandular epithelium of dilated glands indicates the activation of apoptotic cell death to counteract cell proliferation (Mutter et al., 2008; McAvey et al., 2021). Long-term treatment with these compounds in women can result in confusing endometrial changes that differ from the changes normally observed during the menstrual cycle (Chabbert-Buffet et al., 2007); these histopathologic changes might easily be misinterpreted as disordered proliferative or hyperplastic endometrium (Ioffe et al., 2009; Williams et al., 2012). Although there are no clear signs of an increased incidence in atypical hyperplasia and endometrial carcinoma in PRM users, the long-term net effect of the induced epithelial cell proliferation still is unknown and the endometrial safety of long-term PRM therapy remains a concern (Critchley and Chodankar, 2020). For that reason, it is important the toxicologic pathologist evaluating tissues from animals treated with this compound class also is aware of the spectrum of changes induced by selective progesterone

receptor modulators (SPRMs), not least because the changes induced in macaques are more or less similar to those described in women (Brenner et al., 2010; Chwalisz et al., 2006; Pohl et al., 2013; Taketa et al., 2018). In a 39-week study in the cynomolgus macaque, ulipristal acetate induced cystic dilatation of endometrial glands, some distortion of gland architecture, and abortive secretory differentiation, occasionally associated with squamous metaplasia of the uterine endometrial epithelium (Pohl et al., 2013). For these induced morphologic endometrial changes that do not match any of the normal cyclic related morphologic events, the term dyssynchronous endometrium is proposed (Colman et al., 2021).

There are many other examples of agents that increase gonadotropin concentrations. These include direct analogs of GnRH (e.g., Lupron) which are used for the treatment of prostatic cancer and as male contraceptive agents, and human chorionic gonadotropin (HCG) used for the treatment of infertility in women. In rats, administration of these exogenous gonadotropins results in the continuous stimulation of the growth and maturation of follicles resulting in increased numbers of antral follicles as well as numbers and size of corpora lutea. The uterus and vagina will have the expected estrogen-mediated hyperplasia and hypertrophy. As discussed earlier, compounds such as reserpine or phencyclidine hydrochloride that elevate prolactin will prolong the functional life of the corpus luteum in rats resulting in hypertrophied and increased numbers of CLs and interruption of the normal reproductive cycle.

### 5.7. Toxicity due to Vaginal Irritation

Animals such as rats, rabbits, sheep, dogs, guinea pigs, and cynomolgus macaques have been used in the testing of vaginal formulations (Eckstein et al., 1969; Hussain and Ahsan, 2005; Kaminsky et al., 1985; Weiss et al., 2019). The macaque is considered an appropriate animal model for prediction of irritation in women because of the stratified epithelial configuration; however, the cynomolgus macaque vagina is keratinized, while the vagina in women is nonkeratinized. The rabbit is believed to be a more sensitive animal model

for testing the potential for irritation. The response in the rabbit is exaggerated because of it has a nonkeratinized, columnar mucus secreting epithelium (Kaminsky et al., 1985). The guinea pig has been used to test the delayed hypersensitivity potential of compounds developed for vaginal application.

A potential problem encountered during irritation studies that require repeated daily dosing is the induction of pseudopregnancy in rodent species since pseudopregnancy can be induced by mechanical stimulation of the cervix (Figure 10.28). To increase the retention time of the test material in the vagina, it is necessary to deposit the formulation adjacent to the cervix. If the animal struggles during dosing, the cervix may be stimulated and pseudopregnancy induced. Once pseudopregnancy is induced, the vaginal epithelium atrophies, mimicking the progesterone-excessive response. Since the inactive epithelium is much thinner, the response to irritation is exaggerated.

### 5.8. Study, Interpretative, and Regulatory Issues in Female Reproductive Safety Assessment

Several challenges inherent to the use of animal models exist for the pathologist. Already discussed previously was the use of immature and peripubertal nonrodents in general toxicology studies and the differences in reproductive tissue histology and estrous/menstrual cycle between women and the main animal species used in general toxicology studies (rats, dogs, minipigs, and NHPs).

Circulating biomarkers of toxicity are important in animal models as they afford an excellent method to monitor for adverse events in clinical trials or the general human population (see *Biomarkers: Discovery, Qualification and Application*, Vol 1 Chap 14). Unfortunately for acute or subacute injury in the female reproductive tract, methods to monitor direct reproductive organ toxicity are lacking for animal models. Primary injury to the ovarian follicle will not result in correlative changes in standard serum chemistry, hematological or hormonal endpoints until it disrupts the antral follicle and the hormone producing granulosa cells, corpora lutea, and luteal cells. If the female reproductive organ



toxicity is secondary to HPO disruption, monitoring of hormone concentrations is a logical approach for establishing translational biomarkers for clinical studies. However, hormone measurements are subject to considerable variability related to collection methods and the cyclic nature of these hormones (Foster, 2017). Monitoring the cycle with daily vaginal cytology is often the best in-life assessment of effects on the female reproductive system in nonclinical toxicity testing. Given these limitations, evaluating animal recovery from female reproductive toxicity is important considering this challenge for monitoring toxicity and implications on fertility. However, when assessing recovery, it is important to consider the age of the animals as reproductive senescence in rodents can limit the assessment of recovery.

Assigning adversity in general toxicology studies is covered elsewhere in detail (see *Assigning Adversity to Toxicologic Outcomes*, Vol 2, Chap 15), and the principles are the same for the female reproductive tract. If the pathology findings indicate a likelihood of loss of function of the affected organ, the finding is considered adverse because it impacts the animal's ability to thrive in the context of the study (Patrick and Troth, 2019). Examples of adverse findings for the female reproductive tract would be induced ovarian follicular degeneration/necrosis or atrophy (decreased reproductive potential).

Regulatory reviewers of pathology data are usually not pathologists. The reviewers depend on the pathologist for a well-written interpretive report that is based on a comprehensive examination of the data (see *Preparation of the Anatomic Pathology Report for Toxicity Studies*, Vol 2, Chap 13). Pathology peer review provides additional context for the reviewer in that it delivers a consultative summary of a second pathologist's data evaluation and interpretation (see *Pathology Peer Review*, Vol 1, Chap 26). It is always prudent to describe proactively any unusual findings in the female reproductive tract that, while possibly spontaneous or related to the animal model, could create doubt in the reviewer's mind when evaluating the study reports. This is especially the case if a spontaneous finding occurs in high dose groups at a greater incidence than the control groups. Literature references and data

from laboratory historical reference ranges are also helpful benchmarks for the reviewer. Importantly the use of standard nomenclature (e.g., INHAND) across all studies for a given xenobiotic will help prevent questions. Examples of female reproductive study findings that could create questions include organ weight and microscopic findings associated with pseudopregnancy and senescence in rats (Figure 10.28), pseudopregnancy in dogs, and the immature or peripubertal status of nonrodents (Figure 10.12).

## 6. CARCINOGENESIS IN THE FEMALE REPRODUCTIVE SYSTEM

Cervical, uterine, and ovarian cancers are important causes of morbidity and mortality in women. Unfortunately, animal models used in standard toxicology study designs are imperfect systems to study female reproductive cancers. For example, while the rat and mouse are advantageous models to use for practical reasons, as discussed earlier, neither species is a good model of the human menstrual cycle. NHPs, while like women in endometrial physiology, rarely develop spontaneous neoplasms during a study due to the relatively young ages of animals in nonclinical toxicity testing. Laboratory Beagle dogs and minipigs are also young adults in most nonclinical experimental designs. For NHPs, Beagle dogs, and minipigs, the reader is referred to the recently published INHAND manuscripts ([www.toxpath.org](http://www.toxpath.org)) as well as other publications detailing findings in older animals. Certain inbred rat strains (BDII) have a higher incidence of endometrial cancer, but as is the case for genetically engineered animal models, these strains are not useful for general toxicology studies (Deerberg and Kaspareit, 1987).

Carcinogenesis in the female reproductive tract is presented on an organ-by-organ basis. In some cases, tumor relevance is presented for species other than the rodent. Hyperplastic changes are not specifically discussed except when important for differentiation morphologically from neoplasms. The peer-reviewed literature and publicly available information (i.e., drug labels) on xenobiotic-induced female reproductive tumors is rather limited. The ongoing

efforts by the EPA (ToxRef DB) and FDA (SEND) are helping increase the knowledge base. Toxicologic pathologists are strongly encouraged to share any findings related to female reproductive system neoplasia in the public domain.

A summary of carcinogens and the tumors they are associated with for each tissue is presented in Tables 10.14–10.16 (Carthew et al., 2000; Greenman et al., 1984; Jones et al., 1987; Mori, 1965; Owen et al., 1972; Picut et al., 2003; Schardein et al., 1970; Symenoides, 1954). As discussed previously, the reader is referred to the full INHAND publications and updates for rodent and nonrodents which are available on the STP ([www.toxpath.org](http://www.toxpath.org)) and goRENI (<https://www.goreni.org>) web sites. Publications are in the journals *Toxicologic Pathology* and *Journal of Toxicologic Pathology*.

### 6.1. Ovary (Figures 10.32–10.42)

The susceptibility to tumor induction in the ovary depends on the strain, species, and age of

the animal at the time of exposure. Gonadotropins are potent growth factors, and when their normal homeostasis is disrupted, they can act as nongenotoxic carcinogens in the ovary (Fowler, 1979; Gibson et al., 1967; Greenman et al., 1984). Types of ovarian hyperplastic changes and neoplasms, with very recently updated INHAND terminology (see [www.toxpath.org](http://www.toxpath.org) and <https://www.goreni.org>) in parenthesis, include: granulosa cell hyperplasia and tumors (tumor, sex cord stromal, granulosa cell, benign or malignant), rete ovarii hyperplasia and adenoma, luteoma (tumor, sex cord stromal, luteinized, benign), thecoma (tumor, sex cord stromal, theca cell, benign or malignant), cystadenoma and adenocarcinoma (mouse), tubulostromal adenoma and carcinoma, yolk sac carcinoma, choriocarcinoma, embryonal carcinoma, dysgerminoma, sex cord stromal tumors (tumor, sex cord stromal, mixed, benign or malignant), Sertoli cell tumor (tumor, sex cord stromal, Sertoli cell, benign or malignant) teratomas, and leiomyoma in the mesovarium (Dixon et al., 2014).

**TABLE 10.14** Selected Carcinogenic Agents Affecting the Ovary in Laboratory Animals

Tumor type	Agent	Species
Granulosa cell or thecal cell tumors, luteoma, benign	Benzo[a]pyrene	Mouse
	Iodine-131	Hamster
	Progestins	Mouse
	Radiation	Mouse
	7,12 or 7,8,12- Dimethylbenz[a]anthracene	Mouse
Granulosa cell tumors and/or adenoma, tubulostromal	SERMs	Rat
	SERMs	Mouse
Adenoma, tubulostromal	Radiation	Mouse
Sertoli cell tumor	N-Ethyl-N-nitrosourea	Rat
Fibroma	Mibolerone (an androgen)	Dog
Leiomyoma, mesovarium	Soterenol and Mesuprine HCl	Rat

Reproduced from Haschek WM, Rousseaux CG, Wallig MA, editors: *Haschek and Rousseaux's handbook of toxicologic pathology*, ed 3, 2013, Academic Press, Table 60.16, p. 2647, with permission.

**TABLE 10.15** Selected Carcinogenic Agents Affecting the Uterus in Laboratory Animals

Tumor type	Agent	Species
Adenocarcinoma	Diaminozide	Mouse
	Estrogens	Rabbit
	Intrauterine devices	Rat
	Methylcholanthrene	Mouse
	<i>N,N</i> -Dimethyl- <i>N</i> -nitrosourea	Hamster
	3-Amino-9-ethylcarbazole	Mouse
	4-Methyl- <i>N'</i> -nitro- <i>N</i> -nitrosoguanidine	Mouse
	4-Nitroguaninoline-1-oxide	Mouse
	4,4-Thiodianiline	Mouse
	Tamoxifen (SERM)	Rat, mouse
Deciduosa sarcoma	Estrogen and progesterone combination	Rabbit
Fibrosarcoma	2-Acetylaminofluorene	Rat
Leiomyoma/leiomyosarcoma	Medroxalol (an antihypertensive agent)	Mouse
Papillary mesothelioma	Estrogens	Rabbit, dog
Squamous cell carcinoma	Intrauterine devices	Rat
	7,12-Dimethylbenz[a]anthracene	Mouse

*Reproduced from Haschek WM, Rousseaux CG, Wallig MA, editors: Haschek and Rousseaux's handbook of toxicologic pathology, ed 3, 2013, Academic Press, Table 60.17, p. 2648, with permission.*

**TABLE 10.16** Selected Carcinogenic Agents Affecting the Vagina in Mice

Basal cell carcinoma, squamous cell carcinoma	Benzo[a]pyrene
	Estrogens
	Methylcholanthrene
	Phenylmercuric acetate
	Polyethylene glycol
	Quinine sulfate
	7,12-Dimethylbenz[a]anthracene
	8-Hydroxyquinoline

*Reproduced from Haschek WM, Rousseaux CG, Wallig MA, editors: Haschek and Rousseaux's handbook of toxicologic pathology, ed 3, 2013, Academic Press, Table 60.18, p. 2648, with permission.*

Estrogen and progesterone, produced by the growing follicle and corpus luteum, are the main factors involved in the negative feedback control of gonadotropin secretion. When the negative feedback control of gonadotropin secretion is impaired, serum gonadotropin concentrations may be elevated. Constant stimulation of ovarian tissue by gonadotropins may result in hyperplastic and neoplastic lesions. For example, chronic ovarian stimulation in rats treated with SERMs that antagonize hypothalamic ER receptors and cause chronic gonadotropin hypersecretion result in granulosa cell hyperplasia and tumors (Long et al., 2001). Radiation and compounds such as DMBA damage oocytes, resulting in loss of negative feedback on the HPO axis, pituitary hypersecretion of LH/FSH, and stimulation of the remaining oocytes that are damaged by the genotoxic insults of



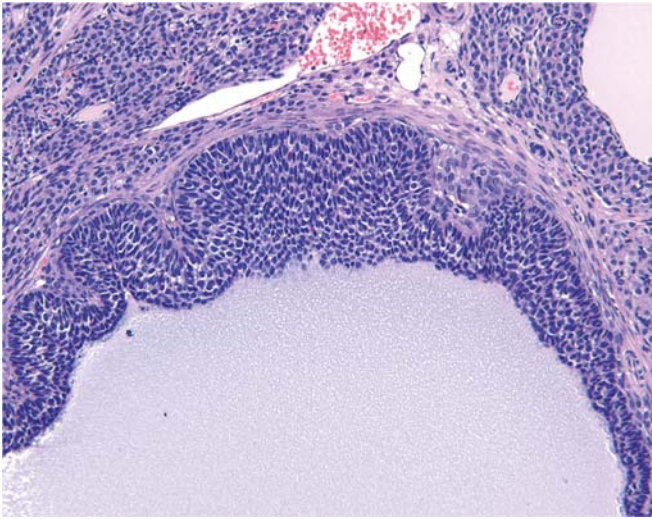


**FIGURE 10.32** Ovary, rat. Granulosa cell hyperplasia. The follicular granulosa cell layer is thickened and undulating. 50 $\times$ , H&E. Courtesy of Dr Gerald Long. Reproduced from Haschek WM, Rousseaux CG, Wallig MA, editors: *Haschek and Rousseaux's handbook of toxicologic pathology*, ed 3, 2013, Academic Press, Figure 60.30, p. 2646, with permission.

radiation or DMBA (Song et al., 2017). There may be confusion in distinguishing histologically between a chronic hyperplastic and a neoplastic response in the ovary. Chronic stimulation by estrogenic compounds is reported to induce ovarian neoplasia in rats and dogs; however, in both species, the proliferative lesions regress, suggesting that the lesions may represent hyperplastic responses rather than true neoplasms (Jabara, 1962).

**Adenoma, tubulostromal (Figure 10.33):** The tubulostromal (previously tubular) adenoma is the most important ovarian tumor in mice (Dixon et al., 2014). These tumors vary greatly in size, and generally appear as round, firm, tan masses in mouse ovaries. They are uncommon in rats, rare in other species, and not observed in the ovaries of women. Development of these tumors has been studied in mice following radiation and increases in tubulostromal adenoma incidence occur because of various endocrine perturbations associated with exposure to xenobiotics, senescence, or inherited genic deletion. The ovarian surface epithelium becomes columnar and thickened, and invaginating folds are

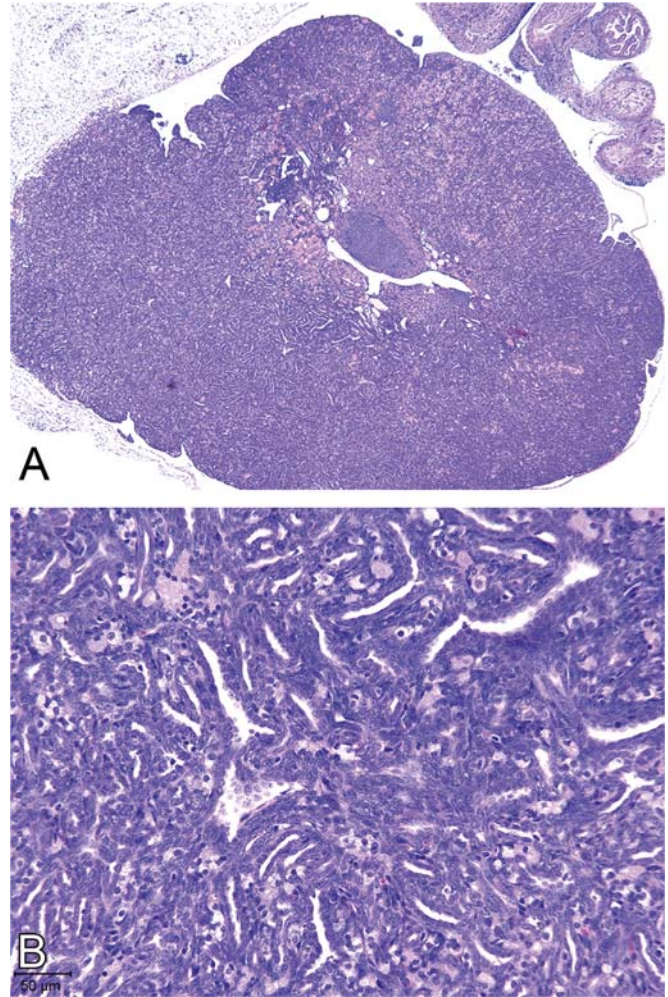


**FIGURE 10.33** Ovary, mouse. Adenoma, tubulostromal. (A) The adenoma replaces the normal architecture of the ovary. (B) Tubular profiles are lined by a thickened, invaginated columnar epithelium with down growth of the germinal epithelium and formation of numerous ramifying crypts. (A) 2.5 $\times$ , (B) 25 $\times$ , H&E. Courtesy of Dr. David Gregory Hall. Reproduced from Haschek WM, Rousseaux CG, Wallig MA, editors: *Haschek and Rousseaux's handbook of toxicologic pathology*, ed 3, 2013, Academic Press, Figure 60.33, p. 2650, with permission.

formed from the downgrowth of the germinal epithelium with subsequent formation of numerous ramifying crypts. Continuous expansion and proliferation of these tubular down growths may form a large tumor mass that eventually occupies the entire ovary. Histologically, the tumor may appear as papillary, solid, or cystic. The tubules are lined by cuboidal epithelium resembling germinal



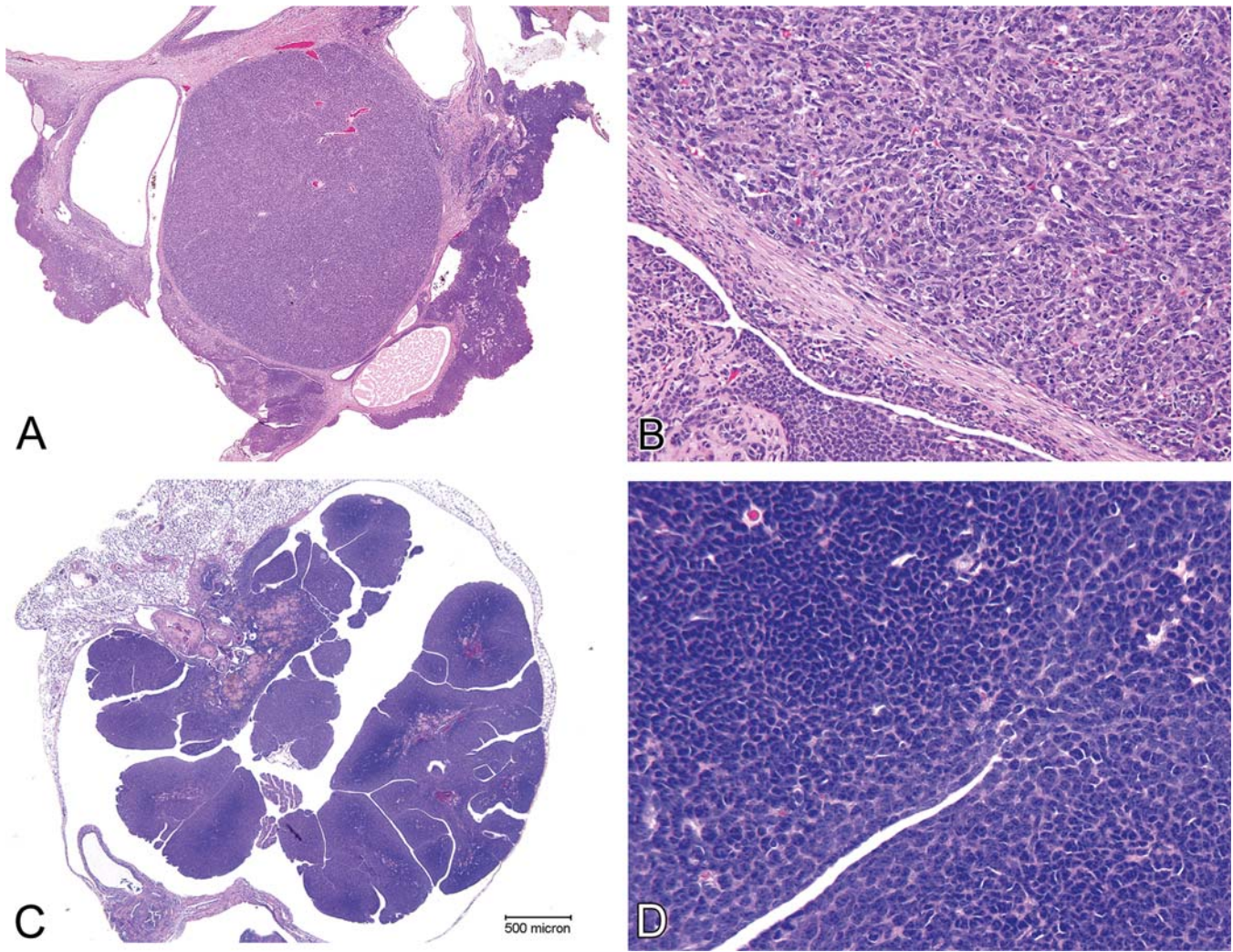


**FIGURE 10.34** Ovary, rat (A and B) and mouse (C and D). Granulosa cell tumor, malignant (INHAND: tumor, sex cord stromal, granulosa cell, malignant). (A, rat; C, mouse) The ovarian parenchyma is effaced by dense sheets and nests of neoplastic cells. (B, rat; D, mouse) The granulosa cells are round to spindle-shaped, have high nuclear to cytoplasmic ratios, and have variable degrees of atypia. (A) 0.5 $\times$ , (B) 10 $\times$ . H&E. Courtesy of NTP (A, B) or Dr. David Gregory Hall (C, D). Reproduced from Haschek WM, Rousseaux CG, Wallig MA, editors: *Haschek and Rousseaux's handbook of toxicologic pathology*, ed 3, 2013, Academic Press, Figure 60.31, p. 2649, with permission.

epithelium. Between these tubular structures, lipid-laden cells resembling granulosa or luteal cells may occur and constitute a major component of these neoplasms. Depending on the mouse strain, the incidence of spontaneous cases varies from less than 1% (Balb/c) to nearly 100% (C57B1-Wv/Wv). The latter strain lacks oocytes at birth.

*Tumor, sex cord stromal, granulosa cell (tumor, granulosa cell), benign or malignant (Figure 10.34):* Granulosa cell tumors are the most common spontaneous ovarian

tumors in Fischer F344 and SD rats (Dixon et al., 2014). In mice, the incidence of granulosa cell tumors varies markedly between the various strains. Granulosa cell tumors may secrete estrogen. The distinction between benign and malignant granulosa cell tumors is based on the degree of atypia, infiltrative growth pattern, presence of metastasis, and areas of necrosis and hemorrhage indicative of a high growth rate. Granulosa cell tumors have been induced in rodents with treatment of SERMs.



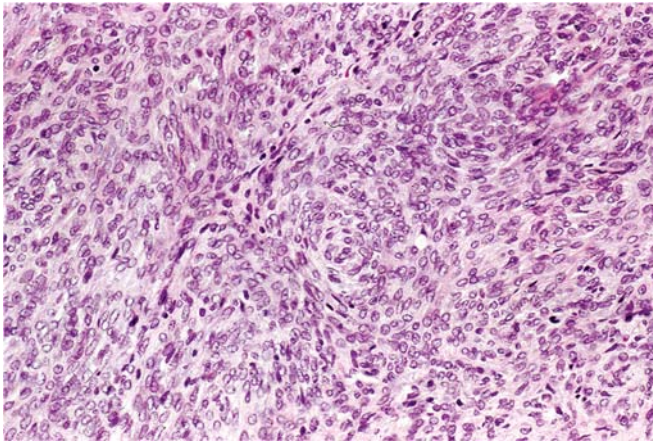


**FIGURE 10.35** Ovary, rat. Thecoma (INHAND: tumor, sex cord stromal, theca cell). Note that the large polygonal cells have thecal cell differentiation with abundant eosinophilic/amphophilic cytoplasm and round nuclei with well-dispersed chromatin. 66×, H&E. Courtesy of NTP. Reproduced from Haschek WM, Rousseaux CG, Wallig MA, editors: *Haschek and Rousseaux's handbook of toxicologic pathology*, ed 3, 2013, Academic Press, Figure 60.32, p. 2650, with permission.

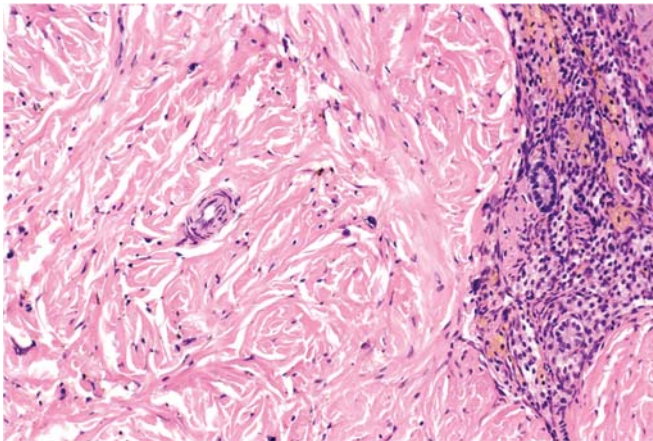


**FIGURE 10.36** Ovary, rat. Fibroma. The tumor is composed of dense fibrous tissue with collagen deposition and low cellularity. 50×, H&E. Courtesy of NTP. Reproduced from Haschek WM, Rousseaux CG, Wallig MA, editors: *Haschek and Rousseaux's handbook of toxicologic pathology*, ed 3, 2013, Academic Press, Figure 60.35, p. 2652, with permission.

*Tumor, sex cord stromal, luteinized (luteoma):*

Luteomas appear to arise in atrophic ovaries where sex cord stromal elements have undergone diffuse luteinization. The luteoma consists of large polygonal cells with abundant eosinophilic cytoplasm and

round nuclei with well-dispersed chromatin. Within areas of neoplastic luteal proliferation, progressive change from large cells to smaller cells with compact and dark-staining nuclei may occur. When the neoplasm consists of large numbers of these small cells, they are identified as granulosa cell tumors. Spontaneous occurrence of these tumors is believed to be uncommon in rats and mice. However, in certain inbred strains of mice, the incidence may be higher than 60%.

**Fibroma (Figure 10.36):** Fibromas may arise from the ovarian parenchyma after prolonged treatment with an androgen in dogs (Greaves, 2012). These tumors appear to arise from the ovarian medulla or from the hilar region that lies between the blood vessels and cortex. Grossly, the tumor appears as a pale, tan-to-white, very firm nodule up to 1.5 cm in diameter. These unencapsulated tumors grow by expansion and are often poorly delineated from the adjacent compressed tissue. Histologically, small neoplasms are composed of dense fibrous tissue with relatively uniform cellularity, while larger tumors often have a central area of dense collagen deposition with a relatively low cellularity. Spontaneous cases of this tumor have not been reported.

**Hyperplasia, sex cord stromal, Sertoli cell (sertoliform hyperplasia) and tumor, sex cord stromal, Sertoli cell (Sertoli cell tumor), benign or malignant (Figure 10.37):** The development of ovarian tumors composed of cells resembling Sertoli cells is poorly understood yet reported in many species (Dixon et al., 2014). These tumors in rats are lobulated, solid, white-yellow masses with occasional fluid-filled cysts. They are often unilateral and may become large (up to 5 cm in diameter). Intraperitoneal dissemination with growth on the peritoneal surface is occasionally observed. Histologically, Sertoli cell tumors are characterized by proliferation of tubular or cystic structures lined by large, elongated, or polyhedral cells with basally situated nuclei and abundant cytoplasm. Nests of less-differentiated mesenchymal cells may also be found. Spontaneous occurrence of



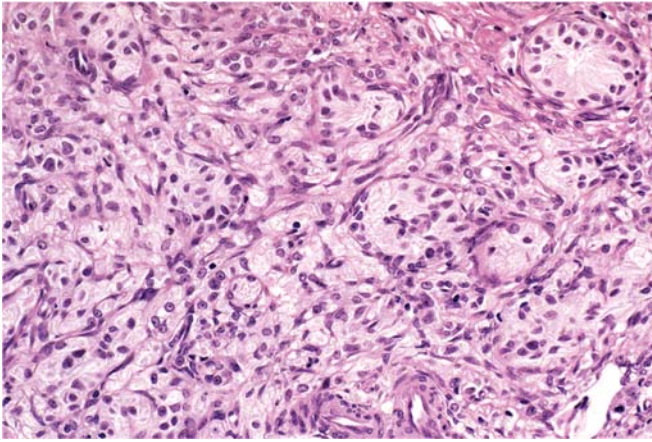


**FIGURE 10.37** Ovary, rat. Sertoliiform hyperplasia. Cells are large, elongated, or polyhedral with basally situated nuclei and abundant cytoplasm. Cells sometimes form tubular-like structures. 80 $\times$ , H&E. *Courtesy of NTP. Reproduced from Haschek WM, Rousseaux CG, Wallig MA, editors: Haschek and Rousseaux's handbook of toxicologic pathology, ed 3, 2013, Academic Press, Figure 60.34, p. 2651, with permission.*

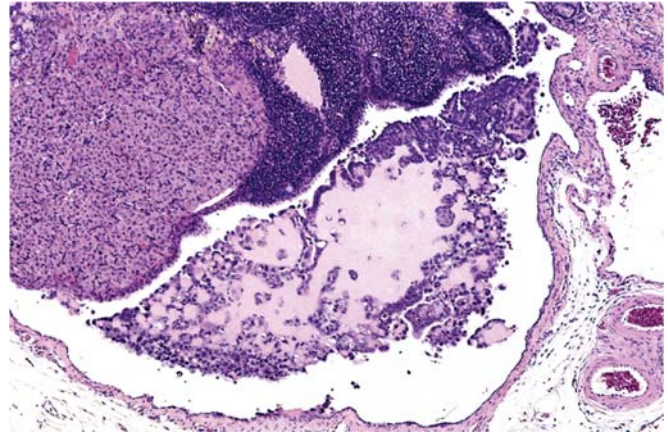


**FIGURE 10.39** Ovary, rat. Yolk sac carcinoma. The tumor is arranged in nests and cords in an abundant eosinophilic matrix. Cylindriform parietal cells form papillary and tubular patterns. 20 $\times$  8, H&E. *Courtesy of NTP. Reproduced from Haschek WM, Rousseaux CG, Wallig MA, editors: Haschek and Rousseaux's handbook of toxicologic pathology, ed 3, 2013, Academic Press, Figure 60.37, p. 2652, with permission.*

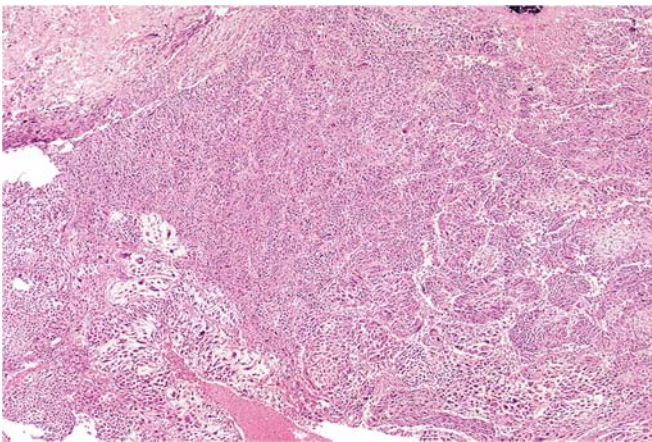


**FIGURE 10.38** Ovary, rat. Choriocarcinoma. The tumor is composed of nests of cytotrophoblasts and giant cells overlying a scant fibrous stroma. 10 $\times$ , H&E. *Courtesy of NTP. Reproduced from Haschek WM, Rousseaux CG, Wallig MA, editors: Haschek and Rousseaux's handbook of toxicologic pathology, ed 3, 2013, Academic Press, Figure 60.36, p. 2652, with permission.*

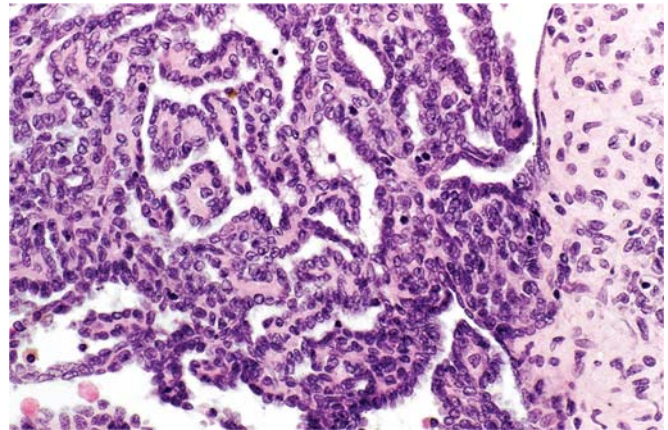


**FIGURE 10.40** Ovary, rat. Cystadenoma. Well-differentiated cuboidal epithelial cells form single layers of papillary structures overlying a thin fibrous connective tissue stalk. 100 $\times$ , H&E. *Courtesy of NTP. Reproduced from Haschek WM, Rousseaux CG, Wallig MA, editors: Haschek and Rousseaux's handbook of toxicologic pathology, ed 3, 2013, Academic Press, Figure 60.38, p. 2653, with permission.*

this tumor is rare in rats and mice. Some authors argue that Sertoli cell tumors are a subtype of granulosa cell tumors; however, both tumor types are likely sex cord stromal tumors with differing degrees of differentiation. The biological activity of Sertoli cell tumors tends to be more

aggressive. This category includes sertoliiform tubular adenomas, which have been previously described as occurring primarily in SD rats. These tumors are composed of irregular tubules of pale vacuolated cells with indistinct cell boundaries which may give a syncytial



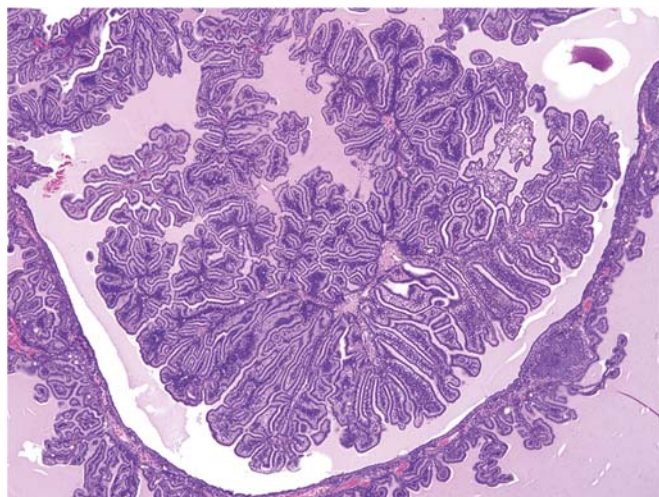


**FIGURE 10.41** Ovary, mouse. Cystadenoma. Well-differentiated cuboidal epithelial cells form single layers of papillary structures. 4 $\times$ , H&E. *Courtesy of NTP. Reproduced from Haschek WM, Rousseaux CG, Wallig MA, editors: Haschek and Rousseaux's handbook of toxicologic pathology, ed 3, 2013, Academic Press, Figure 60.39, p. 2653, with permission.*

appearance. These cells often have intracytoplasmic hyaline-like PAS-positive inclusions. This variant differs from the other Sertoli cell type tumors in that the tubular cells lack basal nuclei and vertically oriented cytoplasm.

*Leiomyoma, mesovarium:* Grossly, leiomyomas appear as circumscribed, tan, firm and rounded nodules that vary from a few millimeters to a few centimeters in size; they are located closely opposed to the ovary and may extend into the hilar region of the ovary (Gopinath and Gibson, 1987; Nelson et al., 1972). The neoplastic cells are typical smooth muscle cells arranged in a whorling pattern or forming interwoven bundles with a crisscrossing pattern. Beta-adrenoreceptor agonists induce these tumors in the rat (Jack et al., 1983). Spontaneous occurrence of this tumor has not been described.

Other uncommon or rare tumors include teratoma, tumor sex cord stromal, theca cell (thecoma) (Figure 10.35), choriocarcinoma (Figure 10.38), yolk sac carcinoma (Figure 10.39), papillary and nonpapillary cystadenoma (Figures 10.40–41), and adenocarcinoma (Figure 10.42).

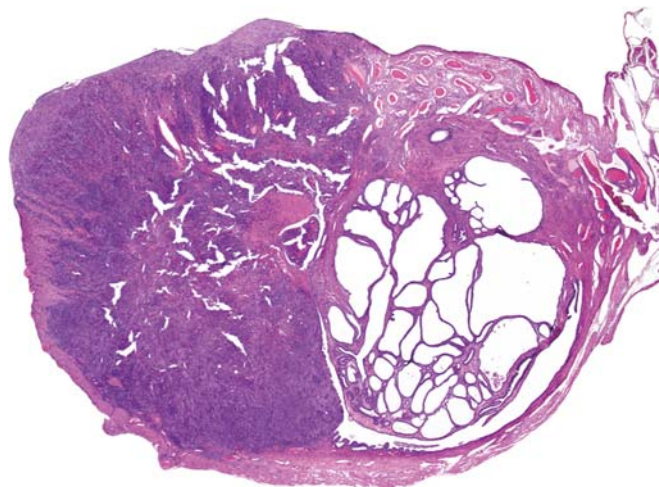


**FIGURE 10.42** Ovary, rat. Adenocarcinoma. Poorly differentiated epithelial cells form sheets and line cystic structures. 2.5 $\times$ , H&E. *Courtesy of NTP. Reproduced from Haschek WM, Rousseaux CG, Wallig MA, editors: Haschek and Rousseaux's handbook of toxicologic pathology, ed 3, 2013, Academic Press, Figure 60.40, p. 2653, with permission.*

## 6.2. Uterus (Figures 10.43–10.50)

Endometrial cancer has long been associated with estrogen or estrogen analog treatment as well as with SERMs like tamoxifen that have ER agonist activity in the uterus (Grunert et al., 1987; Meissner et al., 1957; Owen et al., 1972). The uterus is an estrogen-dependent organ, and endometrial cells proliferate after estrogen stimulation. Early neoplastic growth requires the continuous presence of estrogen. However, once neoplastic growth is established, continuing proliferation or transformation may result in the tumor becoming estrogen independent. Many other compounds are also capable of inducing neoplasms in the uterus (Table 10.15). In some studies, compounds were introduced into the uterine cavity by mechanical means such as a string impregnated with the test compound. The physical presence of a foreign body in the uterine cavity and its effect on the endometrial cells has not been ruled out as a major factor in tumor induction in such cases. The types of neoplasms induced in the uterus include adenocarcinoma, deciduosarcoma, fibrosarcoma, leiomyoma/leiomyosarcoma, papillary mesothelioma, and squamous cell carcinoma.

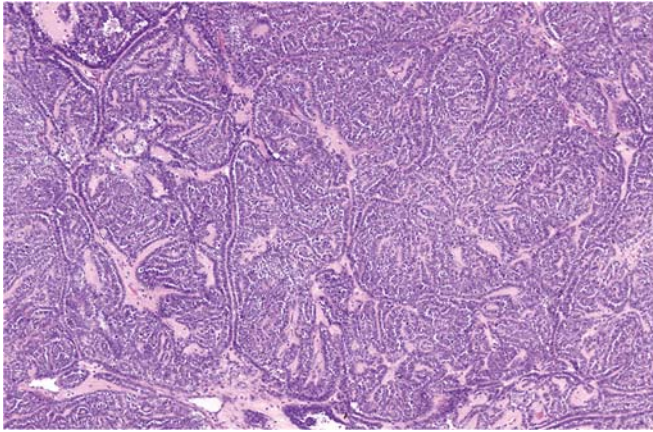


**FIGURE 10.43** Uterus, rat. Adenocarcinoma. The tumor is characterized by large epithelial cells with eosinophilic or amphophilic cytoplasm and large vesicular nuclei with prominent nucleoli. The cells are arranged in acini, glandular structures, or solid cords. In areas of anaplasia (not shown), the cells may be smaller with basophilic cytoplasm and a high mitotic index. 10 $\times$ , H&E. Courtesy of NTP. Reproduced from Haschek WM, Rousseaux CG, Wallig MA, editors: *Haschek and Rousseaux's handbook of toxicologic pathology*, ed 3, 2013, Academic Press, Figure 60.42, p. 2654, with permission.

**Adenoma and adenocarcinoma (Figure 10.43):**

Adenocarcinomas of the uterus often present as discrete growths involving the entire thickness of the uterine wall. Areas of necrosis and cystic dilatation are often found in the tumor. Histologically, the tumors are composed of large epithelial cells with eosinophilic or amphophilic cytoplasm and large vesicular nuclei with prominent nucleoli. The cells may be arranged in acini, glandular structures, or solid cords. In areas of anaplasia, the cells are smaller with basophilic cytoplasm and a high mitotic index. The term carcinoma, adenosquamous, is used to describe a uniformly well-differentiated adenocarcinoma limited to the endometrium with a zone of squamous epithelial metaplasia.

Spontaneous adenocarcinomas are rare in rats and occur sporadically in most other species with incidence increasing with age. In rabbits, the incidence may approach 60% in animals over 4 years of age (Green, 1958).

**Decidualization, focal and decidual reaction (Figure 10.44):** Decidual reactions have been

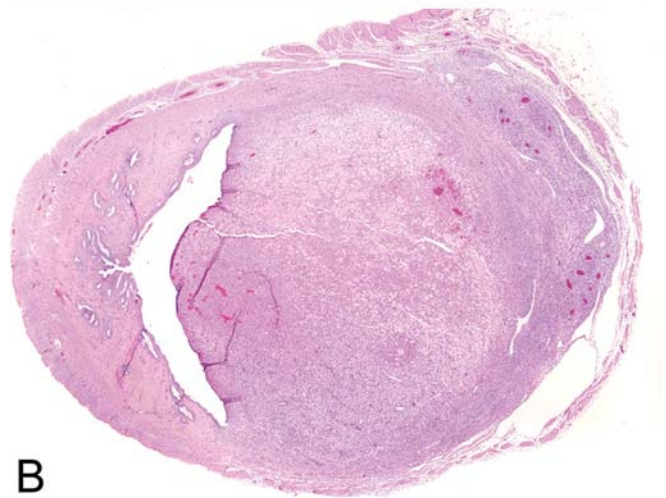


**FIGURE 10.44** Uterus, rat. (A) Decidual reaction (2.5 $\times$  [inset shows higher magnification of polygonal epithelial cells, 32 $\times$ ]). The uterine lumen is filled with eosinophilic fluid and cell debris. It overlies an endometrial stroma that is expanded focally by sheets of large, rounded stromal cells with large nuclei, prominent nucleoli, and abundant eosinophilic cytoplasm. (B) Decidual reaction (previously called deciduoma) (4 $\times$ ). The uterine lumen is compressed by an expansile mass composed of decidual-like cells. H&E. Courtesy of NTP. Reproduced from Haschek WM, Rousseaux CG, Wallig MA, editors: *Haschek and Rousseaux's handbook of toxicologic pathology*, ed 3, 2013, Academic Press, Figure 60.43, p. 2654, with permission.

reported as deciduomas in rats and other laboratory species. Although initially reported as tumors, most current literature regards them as an exaggerated uterine response (e.g., endometrial irritation due to bacterial infection), hence the name decidual reaction (Karbe, 1999).



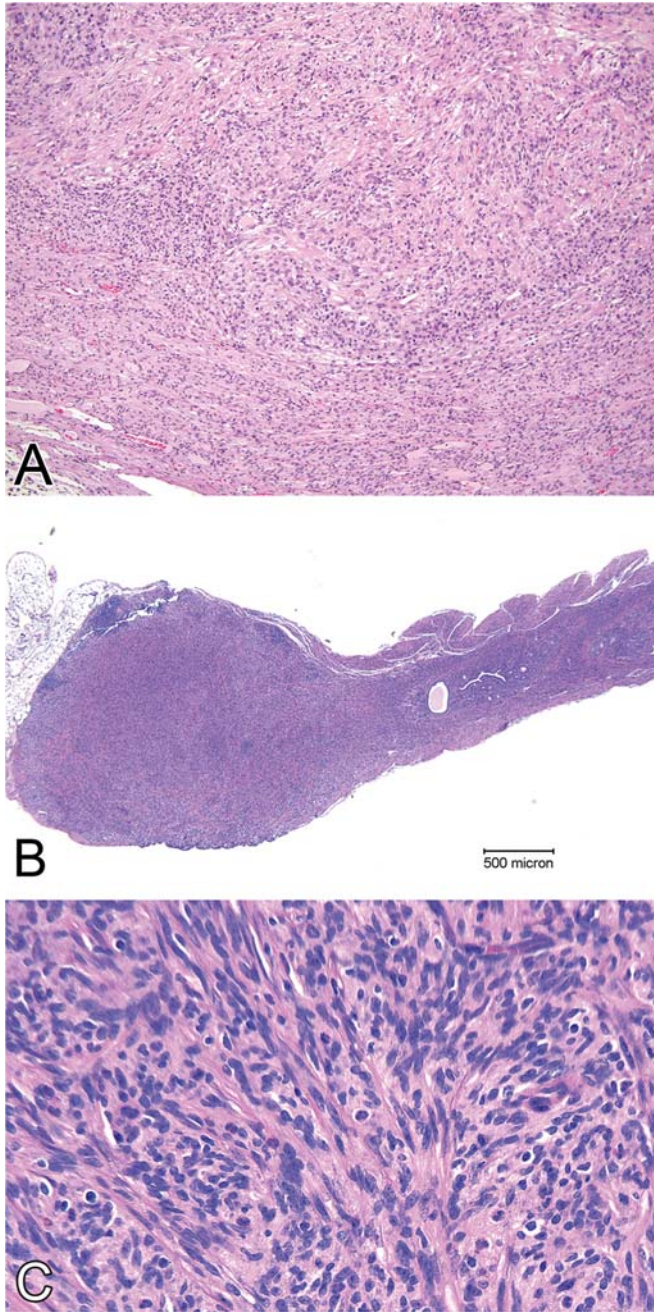


**FIGURE 10.45** Uterus, rat (A) and mouse (B). (A) Leiomyosarcoma. The neoplasm is characterized by interlacing bundles of pleomorphic smooth muscle cells. (B) Leiomyoma. The neoplasm is well circumscribed and expansile. (C) Leiomyoma. Higher magnification of (B) 10 $\times$  (A), 2.5 $\times$  (B), 20 $\times$  (C) H&E. Courtesy of NTP (A) or Dr. David Gregory Hall (B, C). Reproduced from Haschek WM, Rousseaux CG, Wallig MA, editors: *Haschek and Rousseaux's handbook of toxicologic pathology*, ed 3, 2013, Academic Press, Figure 60.44, p. 2655, with permission.

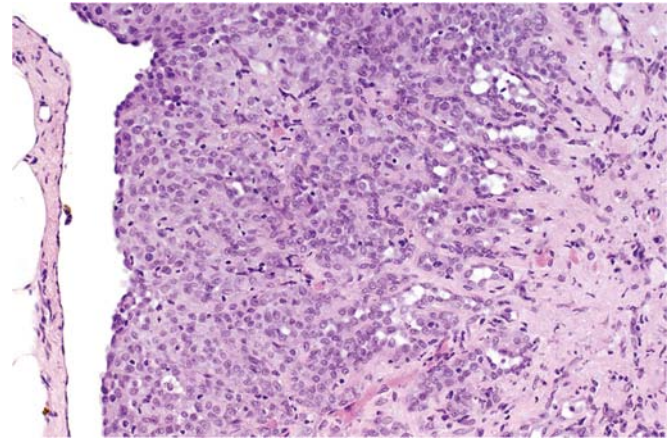


**FIGURE 10.46** Uterus, rat. Mesothelioma. The mesovarium is expanded by sheets, nests, and cords of monomorphic, polygonal cells with round nuclei and moderate amounts of eosinophilic cytoplasm. 50 $\times$ , H&E. Courtesy of NTP. Reproduced from Haschek WM, Rousseaux CG, Wallig MA, editors: *Haschek and Rousseaux's handbook of toxicologic pathology*, ed 3, 2013, Academic Press, Figure 60.45, p. 2655, with permission.

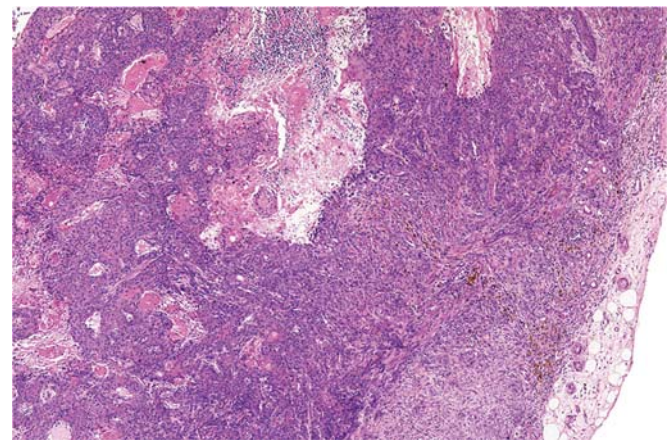


**FIGURE 10.47** Uterus, rat. Squamous cell carcinoma. The uterus is effaced by nests and sheets of epithelial cells with squamous differentiation occasionally surrounding keratin pearls. 13.2 $\times$ , H&E. Courtesy of NTP. Reproduced from Haschek WM, Rousseaux CG, Wallig MA, editors: *Haschek and Rousseaux's handbook of toxicologic pathology*, ed 3, 2013, Academic Press, Figure 60.46, p. 2656, with permission.

**Deciduosisarcoma:** Observed in rabbits, deciduosarcomas are soft, yellowish-reddish-gray, irregular spherical masses originating from the uterus. A necrotic center is a common finding in larger tumors. These tumors usually arise from



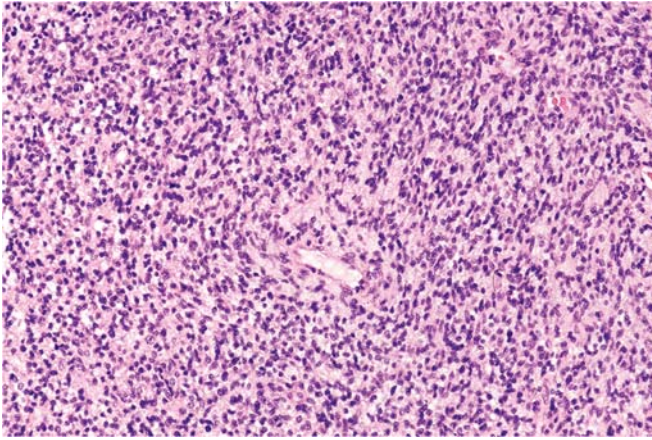


**FIGURE 10.48** Uterus, rat. Stromal sarcoma. The neoplasm is highly cellular and organized in sheets of uniform spindle cells with abundant eosinophilic cytoplasm. 40 $\times$ , H&E. *Courtesy of NTP. Reproduced from Haschek WM, Rousseaux CG, Wallig MA, editors: Haschek and Rousseaux's handbook of toxicologic pathology, ed 3, 2013, Academic Press, Figure 60.47, p. 2656, with permission.*

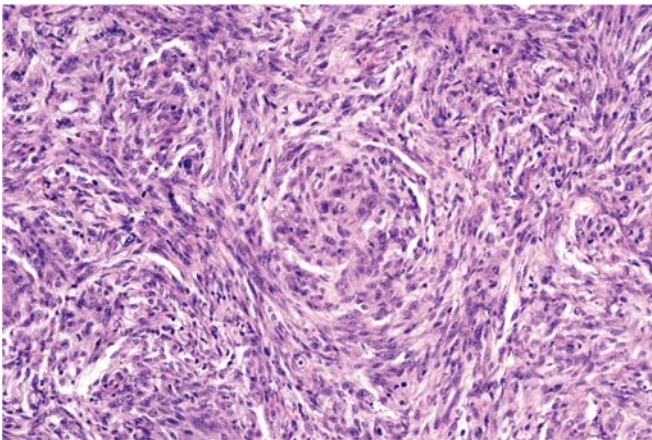


**FIGURE 10.49** Uterus, rat. Pleiomorphic fibrosarcoma (previously named malignant fibrous histiocytoma). The endometrium is expanded by a pleomorphic spindle cell population that is arranged in sheets and whorls. Multinucleated cells are common, although not demonstrated in this photomicrograph. 50 $\times$ , H&E. *Courtesy of NTP. Reproduced from Haschek WM, Rousseaux CG, Wallig MA, editors: Haschek and Rousseaux's handbook of toxicologic pathology, ed 3, 2013, Academic Press, Figure 60.48, p. 2656, with permission.*

the endometrium and are often multiple. Large tumors seem to form by coalescence of several smaller tumors. Focal invasion into the myometrium and metastasis by

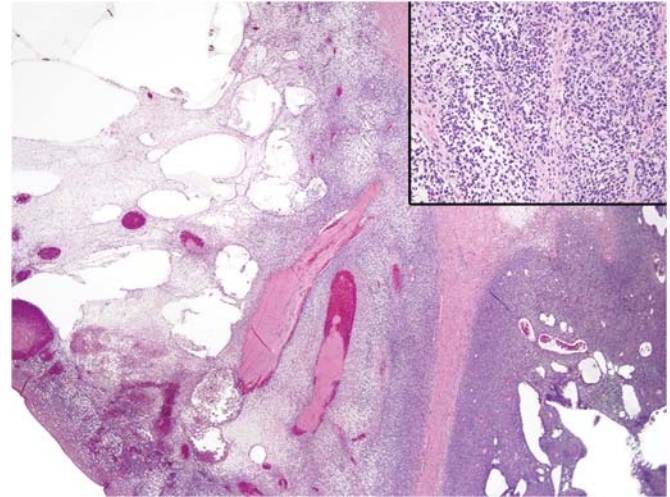


**FIGURE 10.50** Uterus, rat. Schwannoma, benign. The neoplasm is characterized by a spindle cell population forming the classic Antoni type A and B orientations. 2 $\times$  (inset Antoni type B, 20 $\times$ ), H&E. *Courtesy of NTP. Reproduced from Haschek WM, Rousseaux CG, Wallig MA, editors: Haschek and Rousseaux's handbook of toxicologic pathology, ed 3, 2013, Academic Press, Figure 60.49, p. 2657, with permission.*

way of lymphatic channels may be observed. Histologically, the tumor is composed of sheets of large pleomorphic polygonal cells. These cells are packed closely together but retain distinct cellular borders. The nuclei are generally small and round with multiple nucleoli. The cytoplasm may vary in stainability depending on the amount and distribution of glycogen. There are no reported cases of spontaneous occurrence of this tumor in animals (see [Zook et al., 1987](#)).

**Leiomyoma and leiomyosarcoma (Figure 10.45):** Grossly, tumors of smooth muscle cells are firm grayish pink nodules. They can arise from any location in the myometrium. Histologically, leiomyomas are composed of interlacing bundles of smooth muscle cells with long slender vesicular nuclei that are blunted at both ends. In leiomyosarcomas, areas of malignancy are characterized by the presence of a high mitotic index, irregular shape, and size of the nuclei, cellular pleomorphism, invasive growth, and metastasis. These tumors also occur spontaneously in rats, with incidences of 1%–11% for leiomyoma and 1%–3% for

leiomyosarcoma depending on the strain (see Solleveld, 1987).

**Fibroids:** These tumors are benign growths in the uterus of women which may occur in as many as 70% of women (Stewart et al., 2017). Fibroids are described by their location in the uterus (myometrial, submucosal, subserosal, or pedunculated) and appear to be estrogen-sensitive (many regress in postmenopausal women) and are likely smooth muscle in origin. Rats and mice are not useful as models of fibroid pathogenesis; however, potbellied pigs have a high incidence of spontaneous uterine smooth muscle tumors which resemble fibroids (Mozzachio et al., 2004).

**Mesothelioma and mesothelioma, papillary (Figure 10.46):** Mesothelioma and papillary mesothelioma appear as markedly thickened areas of the perimetrium and, when papillary, with extensive and complex papillary outgrowths. Although the surface epithelium appears healthy, the underlying tissue may degenerate and become relatively acellular, and may be accompanied by inflammatory changes. Metastasis occurs by direct implantation of sloughed tissue on the peritoneal surface and abdominal organs. These neoplasms are difficult to differentiate from cystadenocarcinomas and spontaneous occurrence of these tumors in nonclinical species is rare (Dixon et al., 2014).

Other less common tumors include squamous cell carcinoma (Figure 10.47), stromal sarcoma (Figure 10.48), pleomorphic fibrosarcoma (previously named malignant fibrous histiocytoma) (Figure 10.49), and schwannoma (Figure 10.50).

### 6.3. Vagina and Cervix (Figures 10.51 and 10.52)

A diverse group of chemicals, which includes chemically inert materials such as urea and propylene glycol, can induce vaginal neoplasms in laboratory animals (Table 10.16). The mechanism of tumor induction is not understood, but the prolonged exposure may induce irritation that stimulates epithelial cell proliferation (Fishman et al., 1941). Extended proliferation has been postulated to progress to uncontrolled

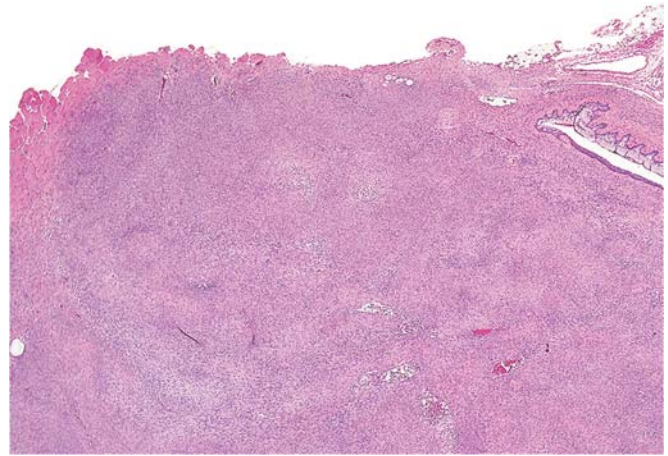


**FIGURE 10.51** Vagina, rat. Leiomyosarcoma. The neoplasm is unencapsulated and effaces and expands the vaginal subepithelial stroma. 2×, H&E. Courtesy of NTP. Reproduced from Haschek WM, Rousseaux CG, Wallig MA, editors: Haschek and Rousseaux's handbook of toxicologic pathology, ed 3, 2013, Academic Press, Figure 60.50, p. 2657, with permission.

neoplastic growth through a transitional stage characterized by epithelial dysplasia. Basal cell carcinomas, leiomyosarcomas (Figure 10.51), squamous cell papillomas and carcinomas, and granular cell tumors (Figure 10.52) have been induced in mice and rats. In older rats, spontaneous granular cell tumors are relatively common in the vagina and cervix. The incidence of these tumors in mice is increased with estrogenic treatments (Highman et al., 1980) and reduced in rats treated with aromatase inhibitors suggesting that estrogen is important in their development (Markovitz and Sahota, 2000).

**Basal cell carcinoma:** The basal cell carcinoma is composed of compact groups of small, darkly staining cells, with hyperchromatic nuclei and scant cytoplasm; intercellular bridges between cells are not observed.

**Squamous cell carcinoma:** Squamous cell carcinoma usually occurs in the vagina or cervix (rarely uterus). In humans, it is associated with the human papillomavirus (Barel et al., 2022). All grades of malignancy may be found in squamous cell carcinomas, ranging from slow-growing well-differentiated tumors to fast-growing anaplastic tumors with nuclear pleomorphism and numerous mitotic figures. In mucin-secreting tumors, the



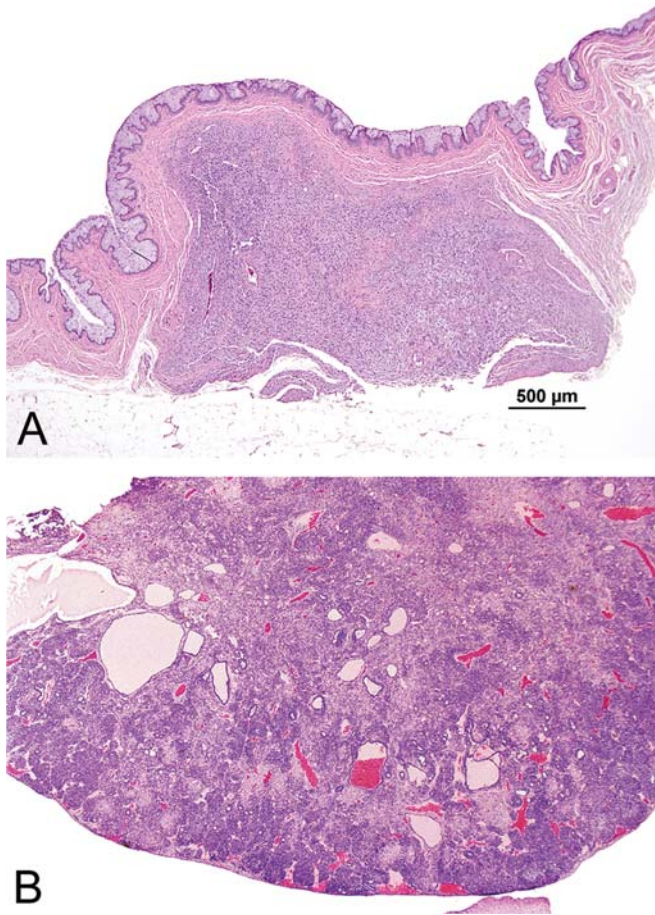


**FIGURE 10.52** (A) Vagina, rat. Granular cell tumor, benign. The tumor is composed of an unencapsulated sheet of cells that expands the vaginal stroma. 4×, H&E. (B) Ovary, rat. Granular cell tumor, malignant. The neoplasm is invasive and forms solid sheets of cells that are pleomorphic. 5×, H&E. Courtesy of NTP. Reproduced from Haschek WM, Rousseaux CG, Wallig MA, editors: *Haschek and Rousseaux's handbook of toxicologic pathology*, ed 3, 2013, Academic Press, Figure 60.51, p. 2657, with permission.

neoplastic epithelial cells are distended with basophilic mucin and most often are located on the surface of the epithelium away from the basal layer. As discussed earlier, vaginal epithelial cells become hypertrophic with large amounts of cytoplasmic mucoid material only when they are under sex steroid hormone stimulation. Acute inflammation of the luminal surface may accompany the neoplastic growth. The occurrence of this type of tumor is accelerated in mice with overexpression of KRAS and conditional

knockout of the *Arid1a* gene (Wang et al., 2021).

The incidence of natural occurrence of these vaginal tumors is believed to be very low in all species of animals.

#### 6.4. Clitoral Glands (Figures 10.53–10.55)

Clitoral glands (also called preputial glands) are found in multiple species. They are usually examined in 2-year carcinogenicity rat and mouse studies but can be observed in rectal or vaginal sections from dog studies (Figure 10.53) (Rudmann et al., 2012). They are paired modified sebaceous glands located in the inguinal region adjacent to the vagina that can be confused with carcinomas by the untrained eye. The glands produce material secreted into a large duct that empties into the clitoral fossa. The growth and secretory activity of clitoral glands is regulated primarily by testosterone and the pituitary hormones, adrenocorticotrophic hormone, growth hormone, and prolactin. Administration of testosterone, but not estrogens, causes hypertrophy and hyperplasia of clitoral gland acinar cells. In rats but not mice, large intracytoplasmic eosinophilic granules are a prominent feature in normal glands. These granules contain pheromones (aliphatic

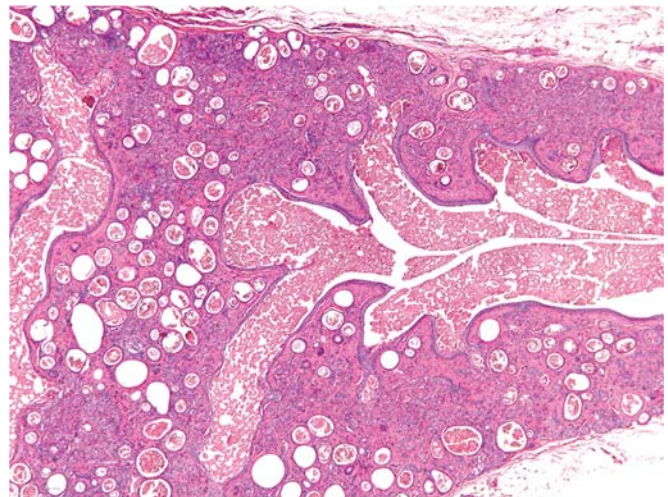


**FIGURE 10.53** Preputial gland, rat. Normal. 5×, H&E. Courtesy of NTP. Reproduced from Haschek WM, Rousseaux CG, Wallig MA, editors: *Haschek and Rousseaux's handbook of toxicologic pathology*, ed 3, 2013, Academic Press, Figure 60.52, p. 2658, with permission.



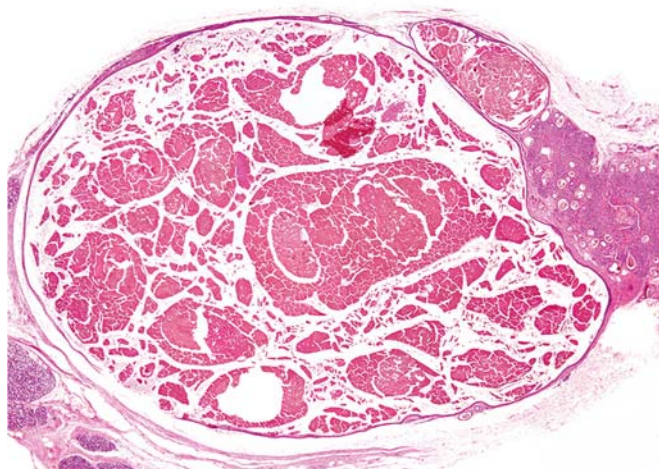


**FIGURE 10.54** Preputial gland, rat. Cyst. The large cyst is filled with keratin debris. 2.5×, H&E. Courtesy of NTP. Reproduced from Haschek WM, Rousseaux CG, Wallig MA, editors: *Haschek and Rousseaux's handbook of toxicologic pathology*, ed 3, 2013, Academic Press, Figure 60.53, p. 2658, with permission.

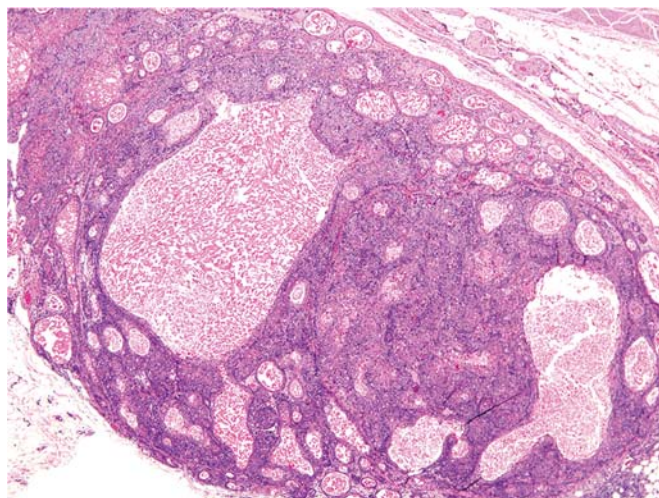


**FIGURE 10.55** Preputial gland, rat. Adenoma. The neoplasm compresses the adjacent glandular parenchyma and is composed of nests of monotonous epithelial cells with abundant eosinophilic cytoplasm. 2.5×, H&E. Courtesy of NTP. Reproduced from Haschek WM, Rousseaux CG, Wallig MA, editors: *Haschek and Rousseaux's handbook of toxicologic pathology*, ed 3, 2013, Academic Press, Figure 60.54, p. 2658, with permission.

alcohols) and  $\beta$ -glucuronidase. The degenerative, inflammatory, vascular, and other nonneoplastic changes observed in clitoral glands are comparable to those observed in the mammary gland (see *Mammary Gland*, Vol 5, [Chap 8](#)). The

most common spontaneous lesion observed in these glands is cystic dilation of the duct ([Figure 10.54](#)). The dilated duct usually contains keratin-like material with accompanying inflammatory cell infiltrates. Tumors are often not large enough to be recognized at gross necropsy and may be missed in studies where the gland is not a standard protocol tissue. Neoplasms in the clitoral gland include adenoma ([Figure 10.55](#)), adenocarcinoma, squamous cell papilloma or carcinoma, and malignant basal cell tumor. They may be incidental findings but can be induced by chemical carcinogens such as 1,2-dimethylhydrazine ([Turusov, 1980](#)).

## 7. CONCLUSION

The female reproductive system is a dynamic and complicated, hormone-dependent group of tissues. It is important for the pathologist to interpret potential test article-related effects in the context of those observed for all the reproductive and specific endocrine tissues (pituitary and adrenal gland). The toxicologic pathologist should be involved in the design of in vivo experiments, ensure the consistent evaluation and interpretation of study-related findings, and provide the appropriate translation for the patient population in support of veterinary and human safety assessment (see *Risk Assessment*, Vol 2, Chap 16). The rat, mouse, Beagle dog, cynomolgus macaque, and more recently, the minipig are species used in female reproductive assessments in standard toxicology studies. They each have advantages and disadvantages in modeling the human response. The tool kit for female reproductive system assessment is becoming more modernized with the availability of novel animal models using gene editing (CRISPR or similar) and computer-based methods such as deep learning. The patterns of toxicity may be complicated and represent a combination of direct xenobiotic-mediated toxicity and alterations in HPO axis function. The toxicologic pathologist is well positioned to partner with scientists that represent other disciplines to characterize mechanistically these patterns of toxicity. The purpose remains to improve the quality of life for humans and veterinary species while limiting risk to their reproductive potential.

## REFERENCES

- Adams MR, Kaplan JR, Koritnik DR: Psychosocial influences on ovarian endocrine and ovulatory function in *Macaca fascicularis*, *Physiol. Behav.* 35:935–940, 1985.
- Adashi EY, Reshick CE: Antagonistic interactions of transforming growth factors in the regulation of granulosa cell differentiation, *Endocrinology* 119:1879–1881, 1986.
- Aiyer MS, Fink G: The role of sex steroid hormones in modulating the responsiveness of the anterior pituitary gland to luteinizing hormone releasing factor in the female rat, *J. Endocrinol.* 62:553–572, 1974.
- Amerio A, Gálvez JF, Odone A, et al.: Carcinogenicity of psychotropic drugs: a systematic review of US Food and Drug Administration–required preclinical in vivo studies, *Aust. N Z J. Psychiatry* 49:686–696, 2015.
- Andersson H, Rehm S, Stanislaus D, et al.: Scientific and regulatory policy committee (SRPC) paper: assessment of circulating hormones in nonclinical toxicity studies III. female reproductive hormones, *Toxicol. Pathol.* 41:921–934, 2013.
- Baker TG: Effect of ionizing radiation on mammalian oogenesis: a model of chemical effects, *Environ. Health Perspect.* 24:31–37, 1978.
- Barberini F, Correr S, De Santis F, et al.: The epithelium of the rabbit vagina: a microtopographical study by light, transmission and scanning electron microscopy, *Arch. Histol. Cytol.* 54:365–378, 1991.
- Barel SK, Biswas P, Kaium MA, et al.: A comprehensive discussion in vaginal cancer based on mechanisms, treatments, risk factors, and prevention, *Front. Oncol.* 12:883805, 2022.
- Bartelmez GW: *Cyclic changes in the endometrium of the rhesus macaque (Macaca mulatta)* (vol 34). 1951, Contributions to Embryology Carnegie Institute, pp 99–146.
- Ben-Jonathan N, LaPensee CR, LaPensee EW: What can we learn from rodents about prolactin in humans, *Endocr. Rev.* 29:1–41, 2008.
- Bowman CJ, Bouressam M, Campion SN, et al.: Lack of effects on female fertility and prenatal and postnatal offspring development in rats with BNT162b2, a mRNA-based COVID-19 vaccine, *Reprod. Toxicol.* 103:28–35, 2021.
- Bradley AE, Wancket LM, Rinke M, et al.: International harmonization of nomenclature and diagnostic criteria (INHAND): nonproliferative and proliferative lesions of the rabbit, *J. Toxicol. Pathol.* 34:183S–292S, 2021.
- Bregman CL, Adler RR, Morton DG, et al.: Recommended tissue list for histopathologic examination in repeat-dose toxicity and carcinogenicity studies: a proposal of the Society of Toxicologic Pathology (STP), *Toxicol. Pathol.* 31:252–253, 2003.
- Brenner RM, Slayden OD, Nath A, et al.: Intrauterine administration of CDB-2914 (Ulipristal) suppresses the endometrium of rhesus macaques, *Contraception* 81(4):336–342, 2010.
- Brix AE, Nyska A, Haseman JK, et al.: Incidences of selected lesions in control female Harlan Sprague-Dawley rats from two-year studies performed by the National Toxicology Program, *Toxicol. Pathol.* 33:477–483, 2005.
- Brodie AHM, Coombes RG, Dowsett M: Basic and clinical studies with the aromatase inhibitor 4-hydroxyandrostenedione, *J. Steroid Biochem.* 27:899–903, 1987.
- Brown AP, Courtney CL, King LM, et al.: Cartilage dysplasia and tissue mineralization in the rat following administration of a FGF receptor tyrosine kinase inhibitor, *Toxicol. Pathol.* 33:449–455, 2005.
- Buse E, Martina Zöller M, Van Esch E: The macaque ovary, with special reference to the cynomolgus macaque (*Macaca fascicularis*), *Toxicol. Pathol.* 36:24S–66S, 2008.
- Butterstein GM, Mann DR, Gould K, et al.: Prolonged inhibition of normal ovarian cycles in the rat and cynomolgus macaques following a single s.c. injection of danazol, *Hum. Reprod.* 12:1409–1415, 1997.
- Capen CC: Mechanisms of hormone-mediated carcinogenesis of the ovary, *Toxicol. Pathol.* 32:1–5, 2004.
- Carboni E, Marxfeld H, Tuoken H, et al.: A workflow for the performance of the differential ovarian follicle count using deep neuronal networks, *Toxicol. Pathol.* 49(4):843–850, 2021.
- Carthew P, Edwards RE, Nolan BM, et al.: Tamoxifen associated uterine pathology in rodents: relevance to women, *Carcinogenesis* 17:1577–1582, 1996.
- Carthew P, Edwards RE, Nolan BM, et al.: Tamoxifen induces endometrial and vaginal cancer in rats in the absence of endometrial hyperplasia, *Carcinogenesis* 21:793–797, 2000.
- Chabbert-Buffet N, Kairis AP, Bouchard P: Effects of the progesterone receptor modulator VA2914 in a continuous low dose on the hypothalamic-pituitary-ovarian axis and endometrium in normal women: a prospective, randomized, placebo-controlled trial, *J. Clin. Endocrinol. Metab.* 92:3582–3589, 2007.
- Chamanza R, Marxfeld HA, Blanco AI, et al.: Incidences and range of spontaneous findings in control cynomolgus macaques (*Macaca fascicularis*) used in toxicity studies, *Toxicol. Pathol.* 38:642–657, 2010.
- Chamanza R, Naylor SW, Gregori M, et al.: The influence of geographical origin, age, sex, and animal husbandry on the spontaneous histopathology of laboratory cynomolgus macaques (*Macaca fascicularis*): a contemporary global and multisite review of historical control data, *Toxicol. Pathol.* 50:607–627, 2022.
- Chandra SA, Adler RR: Frequency of different estrous stages in purpose-bred beagles: a retrospective study, *Toxicol. Pathol.* 36:944–949, 2008.
- Chandra SA, Cline JM, Adler RR: Cyclic morphological changes in the beagle mammary gland, *Toxicol. Pathol.* 38:969–983, 2010.
- Charest PL, Vrolyk V, Herst P, et al.: Histomorphologic analysis of the late-term rat fetus and placenta, *Toxicol. Pathol.* 46(2):158–168, 2018.
- Choudhary S, Walker A, Funk K, et al.: The standard for the exchange of nonclinical data (SEND): challenges and promises, *Toxicol. Pathol.* 46(8):1006–1013, 2018.



- Chwalisz K, Garg R, Brenner R, et al.: Role of nonhuman primate models in the discovery and clinical development of selective progesterone receptor modulators (SPRMs), *Reprod. Biol. Endocrinol.* 4(Suppl 1):S8, 2006.
- Clark JH, Markaverich BM: The agonistic-antagonistic properties of clomiphene: a review, *Pharmacol. Ther.* 15:467–519, 1981.
- Cline JM, Söderqvist G, Register TC, et al.: Assessment of hormonally active agents in the reproductive tract of female nonhuman primates, *Toxicol. Pathol.* 29:84–90, 2001.
- Cline JM, Wood CE, Vidal JD, et al.: Selected background findings and interpretation of common lesions in the female reproductive system of macaques, *Toxicol. Pathol.* 36(Suppl.):142S–163S, 2008.
- Colman K, Andrews RN, Atkins H, et al.: International harmonization of nomenclature and diagnostic criteria (INHAND): non-proliferative and proliferative lesions of the non-human primate (*M. fascicularis*), *J. Toxicol. Pathol.* 4(3 Suppl):1S–182S, 2021.
- Critchley HOD, Chodankar RR: 90 years of progesterone: selective progesterone receptor modulators in gynaecological therapies, *J. Mol. Endocrinol.* 65:T15–T33, 2020.
- Cummings AM, Hedge JL, Laskey J: Ketoconazole impairs early pregnancy and the decidual cell response via alterations in ovarian function, *Fund. Appl. Toxicol.* 40:238–246, 1997.
- Davis BJ, Travlos G, McShane T: Reproductive endocrinology and toxicological pathology over the life span of the female rodent, *Toxicol. Pathol.* 29:77–83, 2001.
- Deerberg F, Kaspereit J: Endometrial carcinoma in BDII/Han rats: model of a spontaneous hormone-dependent tumor, *J. Natl. Cancer Inst.* 78:1245–1251, 1987.
- de Rijk E, van den Brink H, Lensen J, et al.: Estrous cycle-dependent morphology in the reproductive organs of the female Göttingen Minipig, *Toxicol. Pathol.* 42(8):1197–1211, 2014.
- de Rijk E, van Esch E, Flik G: Pregnancy dating in the rat: placental morphology and maternal blood parameters, *Toxicol. Pathol.* 30(2):271–282, 2002.
- Diao H, Zhu H, Ma H, et al.: Rat ovulation, implantation and decidualization are severely compromised by COX-2 inhibitors, *Front. Biosci.* 12:3333–3342, 2007.
- Dixon D, Alison R, Bach U, et al.: Nonproliferative and proliferative lesions of the rat and mouse female reproductive system, *J. Toxicol. Pathol.* 27(3–4 Suppl):1S–107S, 2014.
- Dube C, Paris-Robidas S, Primakova I, et al.: Lack of effects on female fertility or pre- and postnatal development of offspring in rats after exposure to AS03-adjuvanted recombinant plant-derived virus-like particle vaccine candidate for COVID-19, *Repro. Toxicol.* 107:69–80, 2022.
- Eckstein P, Jackson MC, Millman N, et al.: Comparison of vaginal tolerance tests of spermicidal preparations in rabbits and macaques, *J. Reprod. Fertil.* 20:85–93, 1969.
- Edelman A, Boniface ER, Benhar E, et al.: Association between menstrual cycle length and coronavirus disease 2019 (COVID-19) vaccination: a U.S. cohort, *Obstet. Gynecol.* 139(4):481–489, 2022 Jan 5.
- Elmore SA, Blystone C, Lubeck BA, et al.: The assessment of longitudinal sections of rat female reproductive tissues for NTP 2-year toxicity and carcinogenicity studies, *Toxicol. Pathol.* 48(6):747–755, 2020.
- Environmental Protection Agency (EPA), 2023. EDSP test guidelines and guidance document US EPA, <https://www.epa.gov/test-guidelines-pesticides-and-toxic-substances/edsp-test-guidelines-and-guidance-document>, updated August 10, 2023; accessed 12 February 2024.
- Environmental Protection Agency (EPA), 2024. Downloadable computational toxicology data. <https://www.epa.gov/comptox-tools/downloadable-computational-toxicology-data#actor> updated December 13, 2023; accessed February 10, 2024.
- EPA (Environmental Protection Agency).1996 Guidelines for reproductive toxicity risk assessment, published on October 31, 1996, Fed. Regist. 61(212): 56274–56322.
- Everds NE, Snyder PW, Bailey KL, et al.: Interpreting stress responses during routine toxicity studies: a review of the biology, impact, and assessment, *Toxicol. Pathol.* 41(4):560–614, 2013.
- FDA: Food and drug administration. S5(R3) detection of reproductive and developmental toxicity for human pharmaceuticals, Silver Spring, MD, 2021, Center for Drug Evaluation and Research. <https://www.federalregister.gov/documents/2021/05/12/2021-10017/s5r3-detection-of-reproductive-and-developmental-toxicity-for-human-pharmaceuticals-international>. (Accessed 12 February 2024). updated May 12 2021.
- FDA: Food and drug administration. Nonclinical considerations for mitigating nonhuman primate supply constraints arising from the COVID-19 pandemic, Silver Spring, MD, 2022, Center for Drug Evaluation and Research. <https://www.federalregister.gov/documents/2022/02/24/2022-03915/nonclinical-considerations-for-mitigating-nonhuman-primate-supply-constraints-arising-from-the>. (Accessed 12 February 2024). published Feb 24 2022.
- Furukawa S, Kuroda Y, Sugiyama A: A comparison of the histological structure of the placenta in experimental animals, *J. Toxicol. Pathol.* 27:11–18, 2014.
- Far HRM, Ågren G, Lindqvist AS, et al.: Administration of the anabolic androgenic steroid nandrolone decanoate to female rats causes alterations in the morphology of their uterus and a reduction in reproductive capacity, *Eur. J. Obstet. Gynecol. Reprod. Biol.* 131:189–197, 2007.
- Fishman M, Shear MJ, Friedman HF, et al.: Studies in carcinogenesis. XVII. Local effect of repeated application of 3,4-benzpyrene and of human smegma to the vagina and cervix of mice, *J. Natl. Cancer Inst.* 2:361–367, 1941.
- Foster PMD: Influence of study design on developmental and reproductive toxicology study outcomes, *Toxicol. Pathol.* 45: 107–113, 2017.
- Fowler EH: Progesterone and synthetic progestins: their biological activity and role in neoplasia. In Kellen JA, Hilf R,

- editors: *Influence of hormones in tumor development*, Boca Raton, FL, 1979, CRC Press, pp 45–84.
- Gibson JP, Newberne JW, Kuhn WL, et al.: Comparative chronic toxicity of three oral estrogens in rats, *Toxicol. Appl. Pharmacol.* 11:489–510, 1967.
- Goette DK, Odom RB: Vaginal medications as a cause for varied widespread dermatitides, *Cutis* 26:406–409, 1980.
- Goldman JM, Murr AS, Cooper RL: The rodent estrous cycle: characterization of vaginal cytology and its utility in toxicological studies, *Birth Defects Res. B* 80:84–97, 2007.
- Gopinath C, Gibson WA: Mesovarian leiomyomas in the rat, *Environ. Health Perspect.* 73:107–113, 1987.
- Greaves P: Female genital tract. In *Histopathology of preclinical toxicity studies*, 4th ed., New York, NY, 2012, Academic Press, pp 717–779.
- Green HSN: Adenocarcinoma of uterine fundus in rabbit, *Ann. NY Acad. Sci.* 75:535–542, 1958.
- Greenman DL, Highman B, Kodell RL, et al.: Neoplastic and nonneoplastic responses to chronic feeding of diethylstilbestrol in C3H mice, *J. Toxicol. Environ. Health* 14:551–567, 1984.
- Grunert G, Neumann G, Porcia M, et al.: The estrogenic responses to clomiphene in the different cell types of the rat uterus: morphometrical evaluation, *Biol. Reprod.* 37:527–538, 1987.
- Guastavino JM, Larsson K: The staggerer gene curtails the reproductive life span of females, *Behav. Genet.* 22:101–112, 1992.
- Hall AP, Ashton S, Horner J, et al.: PDGRF inhibition results in pericyte depletion and hemorrhage into the corpus luteum of the rat ovary, *Toxicol. Pathol.* 44:98–111, 2016.
- Halpern WG, Ameri M, Bowman CJ, et al.: Scientific and regulatory policy committee points to consider review: inclusion of reproductive and pathology endpoints for assessment of reproductive and developmental toxicity in pharmaceutical drug development, *Toxicol. Pathol.* 44(6): 789–809, 2016.
- Hao X, Anastácio A, Liu K, et al.: Ovarian follicle depletion induced by chemotherapy and the investigational stages of potential fertility protective treatments-A review, *Int. J. Mol. Sci.* 20:4720, 2019.
- Harvey PW: Prolactin-induced mammary tumorigenesis is not a rodent-specific response, *Toxicol. Pathol.* 39:1020–1022, 2011.
- Harvey PW, Everett DJ, Springall CJ: Adverse effects of prolactin in rodents and humans: breast and prostate cancer, *J. Psychopharmacol.* 22:20–27, 2008.
- Helke KL, Nelson KN, Sargeant AM, et al.: Pigs in toxicology: breed differences in metabolism and background findings, *Toxicol. Pathol.* 44(4):575–590, 2016.
- Highman B, Greenman DL, Norvell MJ, et al.: Neoplastic and preneoplastic lesions induced in female C3H mice by diets containing diethylstilbestrol or 17 beta-estradiol, *J. Environ. Pathol. Toxicol. Oncol.* 4:81–95, 1980.
- Hobbie KR, Dixon D: Evaluation of cystic endometrial hyperplasia and the normal estrous cycle in longitudinal sections of uterus from female Harlan Sprague-Dawley rats, *Toxicol. Pathol.* 48(5):616–632, 2020.
- Howroyd PC, Peter B, de Rijk E: Review of sexual maturity in the minipig, *Toxicol. Pathol.* 44:607–611, 2016.
- Hussain A, Ahsan F: The vagina as a route for systemic drug delivery, *J. Contr. Release* 103:301–313, 2005.
- Hutt JA, Assaf BT, Bolon B, et al.: Scientific and Regulatory Policy Committee Points to Consider: nonclinical research and development of in vivo gene therapy products, emphasizing adeno-associated virus vectors, *Toxicol. Pathol.* 50(1):1–29, 2022.
- Ikedo A, Matsumoto Y, Chang K, et al.: Different female reproductive phenotypes determined by human growth hormone (hGH) concentrations in hGH-transgenic rats, *Biol. Reprod.* 56:847–851, 1997.
- International Conference on Harmonisation (ICH) of Technical Requirements for Registration of Pharmaceuticals for Human Use: *ICH harmonised tripartite guideline. Preclinical safety evaluation of biotechnology-derived pharmaceuticals S6(R1)*, 2011. [https://database.ich.org/sites/default/files/S6\\_R1\\_Guideline\\_0.pdf](https://database.ich.org/sites/default/files/S6_R1_Guideline_0.pdf). (Accessed 12 February 2024).
- International Conference on Harmonisation (ICH) of Technical Requirements for Registration of Pharmaceuticals for Human Use. *ICH Harmonised Tripartite Guideline: Guidance on nonclinical safety studies for the conduct of human clinical trials and marketing authorization for pharmaceuticals M3(R2)*, 2009. [https://database.ich.org/sites/default/files/M3\\_R2\\_Guideline.pdf](https://database.ich.org/sites/default/files/M3_R2_Guideline.pdf). (Accessed 12 February 2024). adopted June 11, 2009.
- International Council for Harmonisation (ICH) of Technical Requirements for Pharmaceuticals for Human Use. *ICH Harmonised Guideline. Detection of reproductive and developmental toxicity for human pharmaceuticals (2020)* [https://database.ich.org/sites/default/files/S5-R3\\_Step4\\_Guideline\\_2020\\_0218.pdf](https://database.ich.org/sites/default/files/S5-R3_Step4_Guideline_2020_0218.pdf), adopted 18 February 2020. accessed February 12 2024.
- Ioffe OB, Zaino RJ, Mutter GL: Endometrial changes from short-term therapy with CDB-4124, a selective progesterone receptor modulator, *Mod. Pathol.* 22(3):450–459, 2009.
- Jabara AG: Induction of canine ovarian tumours by diethylstilboestrol and progesterone, *Aust. J. Exp. Biol. Med. Sci.* 40: 139–152, 1962.
- Jack D, Poynter D, Spurling NW: Beta-adrenoceptor stimulants and mesovarian leiomyomas in the rat, *Toxicology* 27: 315–320, 1983.
- Jeppesen G, Skydsgaard M: Spontaneous background pathology in Göttingen minipigs, *Toxicol. Pathol.* 43(2):257–266, 2015.
- Jones TC, Mohr U, Hunt RD: In Jones TC, Mohr U, Hunt RD, editors: *Genital system in: monographs on pathology of laboratory animals*, Berlin, Germany, 1987, Springer-Verlag.
- Kaminsky M, Szivos MM, Brown KR, et al.: Comparison of the sensitivity of the vaginal mucous membranes of the albino rabbit and laboratory rat to nonoxynol-9, *Food Chem. Toxicol.* 23:705–708, 1985.

- Kangawa A, Otake M, Enya S, et al.: Normal developmental and estrous cycle-dependent histological features of the female reproductive organs in microminipigs, *Toxicol. Pathol.* 45(4):551–573, 2017.
- Karbe E: “Mesenchymal tumor” or “decidual-like reaction”? *Toxicol. Pathol.* 27:354–362, 1999.
- Karlsson S, Iatropoulos MJ, Williams GM, et al.: The proliferation in uterine compartments of intact rats of two different strains exposed to high doses of tamoxifen or toremifene, *Toxicol. Pathol.* 26:759–768, 1998.
- Katavolos P, Cain G, Farman C, et al.: Preclinical safety assessment of a highly selective and potent dual small-molecule inhibitor of CBP/P300 in rats and dogs, *Toxicol. Pathol.* 48(3):465–480, 2020.
- Kimmel CA, Grant LD, Sloan CS, et al.: Chronic low-level lead toxicity in the rat. I. Maternal toxicity and perinatal effects, *Toxicol. Appl. Pharmacol.* 56:28–41, 1980.
- Kittel B, Ruehl-Fehlert C, Morawietz G, et al.: Revised guides for organ sampling and trimming in rats and mice – Part 2. A joint publication of the RITA and NACAD groups, *Exp. Toxicol. Pathol.* 55:413–431, 2004.
- Koering MJ: Cyclic changes in ovarian morphology during the menstrual cycle in *Macaca mulatta*, *Am. J. Anat.* 16:73–101, 1969.
- Koguchi A, Nomura K, Fujiwara T, et al.: Maternal placenta-like endometrial hyperplasia in a beagle dog (Canine deciduoma), *Exp. Anim.* 44:251–253, 1995.
- Laffan SB, Posobiec LM, Uhl JE, et al.: Species comparison of postnatal development of the female reproductive system, *Birth Defects Res.* 110:163–189, 2018.
- Lamperti A, Niewenhuis R: The effects of mercury on the structure and function of the hypothalamo-pituitary axis in the hamster, *Cell Tissue Res.* 170:315–324, 1976.
- Lee JL, Park HH, Do BR, et al.: Natural and radiation-induced degeneration of primordial and primary follicles in mouse ovary, *Anim. Reprod. Sci.* 59:109–117, 2000.
- Levine J: Chapter 26 - neuroendocrine control of the ovarian cycle of the rat. In Plant TM, Zeleznik AJ, editors: *Knobil and neill's physiology of reproduction*, Fourth Edition, 2015, Academic Press, pp 1199–1257.
- Li S, Davis B: Evaluating rodent vaginal and uterine histology in toxicity studies, *Birth Defects Res. B* 80:246–252, 2007.
- Long GG, Reynolds VL, Dochterman LW, et al.: Neoplastic and non-neoplastic changes in F-344 rats treated with naveglitazar,  $\gamma/\delta$ -dominant PPAR  $\gamma/\delta$  agonist, *Toxicol. Pathol.*, 2009:741–753, 2009.
- Long JA, Evans HM: The oestrous cycle in the rat and its associated phenomena, *Memoirs Univ. Calif.* 6:1–148, 1922.
- Long GG, Cohen IR, Gries CL, et al.: Proliferative lesions of ovarian granulosa cells and reversible hormonal changes induced in rats by a selective estrogen receptor modulator, *Toxicol. Pathol.* 29:403–410, 2001.
- Lorenzen E, Follmann F, Jungersen G, et al.: A review of the human vs. porcine female genital tract and associated immune system in the perspective of using minipigs as a model of human genital Chlamydia infection, *Vet. Res.* 46:116, 2015.
- Mao J, Chughtai B, Ibrahim S, et al.: FDA safety communication on the use of transvaginal mesh in pelvic organ prolapse repair surgery: the impact of social determinants of health, *Female Pelvic Med. Reconstr. Surg.* 27:e133–e138, 2021.
- Markovitz JE, Sahota PS: Aromatase inhibitors prevent spontaneous granular cell tumors in the distal female reproductive tract of Sprague-Dawley rats, *Toxicol. Pathol.* 47:4–10, 2000.
- Mattison DR: Morphology of oocyte and follicle destruction by polycyclic aromatic hydrocarbons in mice, *Toxicol. Appl. Pharmacol.* 53:249–259, 1980.
- Mattison DR, Thorgeirsson SS: Ovarian aryl hydrocarbon hydroxylase activity and primordial oocyte toxicity of polycyclic aromatic hydrocarbons in mice, *Cancer Res.* 39:3471–3475, 1979.
- McAvey B, Kuokkanen S, Zhu L, et al.: The selective progesterone receptor modulator, telapristone acetate, is a mixed antagonist/agonist in the human and mouse endometrium and inhibits pregnancy in mice, *F S Sci.* 2:59–70, 2021.
- McInnes EF: Minipigs. In McInnes EF, editor: *Background lesions in laboratory animals: a color atlas*, 2011, Saunders/Elsevier Ltd, pp 81–85.
- Mecklenburg L, Luetjens CM, Weinbauer GF: Toxicologic Pathology Forum\*: opinion on sexual maturity and fertility assessment in long-tailed macaques (*Macaca fascicularis*) in nonclinical safety studies, *Toxicol. Pathol.* 47(4):444–460, 2019.
- Meissner WA, Sommers SC, Sherman G: Endometrial hyperplasia, endometrial carcinoma, and endometriosis produced experimentally by estrogen, *Cancer* 10:500–509, 1957.
- Meng L, Jan SZ, Hamer G, et al.: Preantral follicular atresia occurs mainly through autophagy, while antral follicles degenerate mostly through apoptosis, *Biol. Reprod.* 99:853–863, 2018.
- Michael B, Yano B, Sellers RS, et al.: Guidelines and a survey of current practices evaluation of organ weights for rodent and non-rodent toxicity studies: a review of regulatory guidelines, *Toxicol. Pathol.* 35:742, 2007.
- Mirsky ML, Sivaraman L, Houle C, et al.: Histologic and cytologic detection of endocrine and reproductive tract effects of exemestane in female rats treated for up to twenty-eight days, *Toxicol. Pathol.* 39:589–605, 2011.
- Mitchard TL, Klein S: Reproductive senescence, fertility and reproductive tumour profile in ageing female Han Wistar rats, *Exp. Toxicol. Pathol.* 68:143–147, 2016.
- Mori K: Induction of pulmonary and uterine cancers, and leukemia in mice by injection of 4-nitroquinoline 1-oxide, *GANN* 56:513–518, 1965.
- Mozzachio K, Linder K, Dixon D: Uterine smooth muscle tumors in potbellied pigs (*Sus scrofa*) resemble human fibroids: a potential animal model, *Toxicol. Pathol.* 32:402–407, 2004.
- Mutter GL, Bergeron C, Deligdisch L, et al.: The spectrum of endometrial pathology induced by progesterone receptor modulators, *Mod. Pathol.* 21(5):591–598, 2008.



- Namwanje M, Brown CW: Activins and inhibins: roles in development, physiology, and disease, *Cold Spring Harbor Perspect. Biol.* 8:a021881, 2016.
- Nelson LW, Kelly WA: Progesterone related gross and microscopic changes in female Beagles, *Vet. Pathol.* 13:143–156, 1976.
- Nelson LW, Kelly WA, Weikel JHJ: Mesovarial leiomyomas in rats in a chronic toxicity study of mesuprine hydrochloride, *Toxicol. Appl. Pharmacol.* 23:731–737, 1972.
- Newman EA, Buehler EV, Parker RD: Delayed type hypersensitivity in the vagina and skin of the Guinea pig, *Toxicol. Appl. Pharmacol.* 3:521–527, 1983.
- NIH: COVID-19 vaccines and the menstrual cycle, 2023, NIH COVID-19 Research. <https://covid19.nih.gov/news-and-stories/covid-19-vaccines-and-menstrual-cycle>. (Accessed 12 February 2024). updated May 2023.
- OECD. Organisation for Economic Co-operation and Development: *OECD guidelines for the testing of chemicals. Doc 407. Repeated dose 28-day oral toxicity study in rodents*, 2008. <https://www.oecd-ilibrary.org/docserver/9789264070684-en.pdf?expires=1707772517&id=id&accname=guest&checksum=BD7CA6F1DE414003D7430A64435E9319>. (Accessed 12 February 2024). adopted October 3, 2008.
- Owen NV, Pierce EC, Anderson RC: Papillomatous growths on internal genitalia of bitches administered the synthetic estrogen trans-4,4-dime, *Toxicol. Appl. Pharmacol.* 21:582–585, 1972.
- Patrick DJ, Troth SP: Toxicologic pathology forum\*: commentary on “opinion on designation of adverse and nonadverse histopathological findings in toxicity studies: the pathologist’s dilemma”, *Toxicol. Pathol.* 47(5):574–576, 2019.
- Pavan-Carreira R, Pires MA: Multioocyte follicles in domestic dogs: a survey of frequency of occurrence, *Theriogenology* 69(8):977–982, 2008.
- Peereboom-Stegeman JH, Jongstra-Spaapen EJ: The effect of a single sublethal administration of cadmium chloride on the microcirculation in the uterus of the rat, *Toxicology* 13: 199–213, 1979.
- Peter B, De Rijk EP, Zeltner A, et al.: Sexual maturation in the female Göttingen minipig, *Toxicol. Pathol.* 44(3):482–485, 2016.
- Picut CA, Aoyama H, Holder JW, et al.: Bromoethane, chloroethane and ethylene oxide induced uterine neoplasms in B6C3F1 mice from 2-year NTP inhalation bioassays: pathology and incidence data revisited, *Exp. Toxicol. Pathol.* 55:1–9, 2003.
- Picut CA, Dixon D, Simons ML, et al.: Postnatal ovary development in the rat: morphologic study and correlation of morphology to neuroendocrine parameters, *Toxicol. Pathol.* 43:343–353, 2015.
- Picut CA, Remick AK, Asakawa MG, et al.: Histologic features of prepubertal and pubertal reproductive development in female Sprague-Dawley rats, *Toxicol. Pathol.* 42:403–413, 2014.
- Picut CA, Swanson CL, Scully KL, et al.: Ovarian follicle counts using proliferating cell nuclear antigen (PCNA) and semi-automated image analysis in rats, *Toxicol. Pathol.* 36(5):674–679, 2008.
- Pohl O, Williams AR, Bergeron C, et al.: A 39-week oral toxicity study of ulipristal acetate in cynomolgus macaques, *Regul. Toxicol. Pharmacol.* 66(1):6–12, 2013 Jun.
- Putti R, Varano L: Histological and histochemical modifications of the uterine and vaginal mucosa of the mouse during the oestrus cycle, *Basic Appl. Histochem.* 23:25–37, 1979.
- Radi ZA, Khan NK: Comparative expression and distribution of *c-fos*, estrogen receptor  $\alpha$  (ER- $\alpha$ ), and p38 $\alpha$  in the uterus of rats, macaques, and humans, *Toxicol. Pathol.* 34:327–335, 2006.
- Regan KS, Cline JM, Davis B, et al.: STP position paper: ovarian follicular counting in the assessment of rodent reproductive toxicity, *Toxicol. Pathol.* 33:409–412, 2005.
- Rehm S, Stanislaus DJ, Wier PJ: Identification of drug-induced hyper- or hypoprolactinemia in the female rat based on general and reproductive toxicity study parameters, *Birth Defects Res. B Dev. Reprod. Toxicol.* 80:253–257, 2007.
- Rosendahl M, Andersen CY, la Cour Freiesleben N, et al.: Dynamics and mechanisms of chemotherapy-induced ovarian follicular depletion in women of fertile age, *Fertil. Steril.* 94:156–166, 2010.
- Rudmann DG: The emergence of multiphysiological systems (organs-on-a-chip) as paradigm-changing tools for toxicologic pathology, *Toxicol. Pathol.* 47:4–10, 2019.
- Rudmann DG, Albrechtsen J, Doolan C, et al.: Using deep learning artificial intelligence algorithms to verify N-nitroso-N-methylurea and urethane positive control proliferative changes in Tg-RasH2 mouse carcinogenicity studies, *Toxicol. Pathol.* 49(4):938–949, 2021.
- Rudmann DG, Cardiff R, Chouinard L, et al.: Proliferative and non-proliferative lesions of the rat and mouse mammary, Zymbal’s, preputial, and clitoral glands, *Toxicol. Pathol.* 40: 7S–39S, 2012.
- Rudmann DG, Cohen IR, Robbins MR, et al.: Androgen dependent mammary gland virilism in rats given the selective estrogen receptor modulator LY2066948 hydrochloride, *Toxicol. Pathol.* 33:711–719, 2005.
- Ryan AM, Bates-Eppler D, Hagler KE, et al.: Preclinical safety evaluation of rhuMABVEGF, an antiangiogenic humanized monoclonal antibody, *Toxicol. Pathol.* 27:78–86, 1999.
- Sakurada Y, Kudo S, Iwasaki S, et al.: Collaborative work on evaluation of ovarian toxicity 5) Two- or four-week repeated-dose studies and fertility study of busulfan in female rats, *J. Toxicol. Sci.* 34:SP65–SP72, 2009.
- Sato J, Hashimoto S, Doi T, et al.: Histological characteristics of the regression of corpora lutea in Wistar Hannover rats: the comparisons with Sprague-Dawley rats, *J. Toxicol. Pathol.* 27(2):107–113, 2014, <https://doi.org/10.1293/tox.2013-0054>.
- Sato J, Nasu M, Tsuchitani M: Comparative histopathology of the estrous or menstrual cycle in laboratory animals, *J. Toxicol. Pathol.* 29(3):155–162, 2016.
- Sato M, Shiozawa K, Uesugi T, et al.: Collaborative work on evaluation of ovarian toxicity 7) Effects of 2- or 4- week

- repeated dose studies and fertility study of cyclophosphamide in female rats, *J. Toxicol. Sci.* 34:SP83–SP89, 2009.
- Sato Y: Pseudo-placentational endometrial hyperplasia in a dog, *J. Vet. Diagn. Invest.* 23(5):1071–1074, 2011.
- Schardein JL, Kaump DH, Woosley ET, Jellema MM: Long-term toxicologic and tumorigenesis studies on an oral contraceptive agent in albino rats, *Toxicol. Appl. Pharmacol.* 16:10–23, 1970.
- Schwartz E, Tornaben JA, Boxill GC: Effects of chronic oral administration of a long-acting estrogen, quinestrol, to dogs, *Toxicol. Appl. Pharmacol.* 14:487–494, 1969.
- Seaman WJ: Canine ovarian fibroma associated with prolonged exposure to mibolerone, *Toxicol. Pathol.* 13:177–180, 1985.
- Shirai M, Sakurai K, Saitoh W, et al.: Collaborative work on evaluation of ovarian toxicity 8) Two- or four-week repeated-dose studies and fertility study of Anastrozole in female rats, *J. Toxicol. Sci.* 34:SP91–SP99, 2009.
- Shirai N, Houle C, Mirsky ML: Using histopathologic evidence to differentiate reproductive senescence from xenobiotic effects in middle-aged female Sprague-Dawley rats, *Toxicol. Pathol.* 43:1158–1161, 2015.
- Skinner MK, Coffey Jr RJ: Regulation of ovarian cell growth through the local production of transforming growth factor- $\alpha$  by theca cells, *Endocrinology* 123:2632–2638, 1988.
- Skydsgaard M, Dincer Z, Haschek WM, et al.: International harmonization of nomenclature and diagnostic criteria (INHAND): nonproliferative and proliferative lesions of the minipig, *Toxicol. Pathol.* 49:110–228, 2021.
- Smith MS, Neill JD: Termination at midpregnancy of the two daily surges of plasma prolactin initiated by mating in the rat, *Endocrinology* 98:696–701, 1976.
- Solleveld HA: Leiomyoma and leiomyosarcoma, uterus, rat. In Jones TC, Mohr UHRD, editors: *Monographs on pathology of laboratory animals, genital system*, 1987, pp 116–120.
- Song ZQ, Li X, Wang YK, et al.: DMBA acts on cumulus cells to desynchronize nuclear and cytoplasmic maturation of pig oocytes, *Sci. Rep.* 7:1687, 2017.
- Sonigo C, Jankowski S, Yoo O, et al.: High-throughput ovarian follicle counting by an innovative deep learning approach, *Sci. Rep.* 8(1):13499, 2018.
- Steger RW, Silverman AY, Johns A, et al.: Interactions of cocaine and delta 9-tetrahydrocannabinol with the hypothalamic-hypophyseal axis of the female rat, *Fertil. Steril.* 35:567–572, 1981.
- Steinmayr M, André E, Conquet F, et al.: *Staggerer* phenotype in retinoid-related orphan receptor  $\alpha$ -deficient mice, *Proc. Natl. Acad. Sci. U.S.A.* 95:3960–3965, 1998.
- Stewart EA, Cookson CL, Gandolfo RA, et al.: Epidemiology of uterine fibroids: a systematic review, *BJOG* 124:1501–1512, 2017.
- Stokar-Regenscheit N, Bell L, Berridge B, et al.: Complex in vitro model characterization for context of use in toxicologic pathology: use cases by collaborative teams of biologists, bioengineers, and pathologists, *Toxicol. Pathol.*, 2024, <https://doi.org/10.1177/0192623324125381>.
- Symenoides A: Tumors induced by 2-acetyl-aminofluorene in virgin and breeding females of five strains of rats and in their offspring, *J. Natl. Cancer Inst.* 15:539–549, 1954.
- Taketa Y: Luteal toxicity evaluation in rats, *J. Toxicol. Pathol.* 35:7–17, 2022.
- Taketa Y, Horie K, Tetsuya G, et al.: Histopathologic characterization of mifepristone-induced ovarian toxicity in cynomolgus macaques, *Toxicol. Pathol.* 46(3):283–289, 2018.
- Toda K, Okada T, Miyauchi C, et al.: Fenofibrate, a ligand for PPAR $\alpha$ , inhibits aromatase cytochrome P450 expression in the ovary of mouse, *J. Lipid Res.* 44:265–270, 2003.
- Turusov VS: Morphology and histogenesis of anal region and clitoral gland tumors induced in mice by 1,2-dimethylhydrazine, *J. Natl. Cancer Inst.* 64:1161–1167, 1980.
- Van Esch E, Cline JM, Buse E, et al.: The macaque endometrium, with special reference to the cynomolgus macaque (*Macaca fascicularis*), *Toxicol. Pathol.* 36:67S–100S, 2008a.
- Van Esch E, de Rijk EPCT, Buse E, et al.: Recommendations for routine sampling, trimming, and paraffin-embedding of female reproductive organs, mammary gland, and placenta in the cynomolgus macaque, *Toxicol. Pathol.* 36(Suppl.):164S–170S, 2008b.
- Vidal J, Wood C, Colman K, et al.: Reproductive system and mammary gland. In Sahota PS, Popp JA, Hardisty JF, Gopinath C, Bouchard P, editors: *Toxicologic pathology: nonclinical safety assessment*, 2nd ed., 2018, Taylor & Francis, pp 889–1020.
- Vidal JD: The impact of age on the female reproductive system, *Toxicol. Pathol.* 45(1):206–215, 2017.
- Vidal JD, Colman K, Bhaskaran M, et al.: Scientific and Regulatory Policy Committee Best Practices\*: documentation of sexual maturity by microscopic evaluation in nonclinical safety studies, *Toxicol. Pathol.* 9(5):977–989, 2021.
- Vuong C, Van Uum SHM, O'Dell LE, et al.: The effects of opioids and opioid analogs on animal and human endocrine systems, *Endocr. Rev.* 31(1):98–132, 2010.
- Wang X, Praca MSL, Wendel JRH, et al.: Vaginal squamous cell carcinoma develops in mice with conditional Arid1a loss and gain of oncogenic Kras driven by progesterone receptor Cre, *Am. J. Pathol.* 191:1281–1291, 2021, <https://doi.org/10.1016/J.AJPATH.2021.03.013>.
- Weinbauer GF, Nieho M, Niehaus N, et al.: Physiology and endocrinology of the ovarian cycle in macaques, *Toxicol. Pathol.* 36:7S–23S, 2008.
- Weiss H, Martell B, Ginger D, et al.: Pharmacokinetics and tolerability of a novel 17 $\beta$ -estradiol and progesterone intravaginal ring in sheep, *J. Pharmaceut. Sci.* 108:2677–2684, 2019.
- Westwood FR: The female rat reproductive cycle: a practical histological guide to staging, *Toxicol. Pathol.* 36:375–384, 2008.
- Williams A, Bergeron C, Barlow D, et al.: Endometrial morphology after treatment of uterine fibroids with the selective progesterone receptor modulator, ulipristal acetate, *Int. J. Gynecol. Pathol.* 31:556–569, 2012.
- Woicek J, Al-Haddawi MM, Bienvenu J, et al.: International harmonization of nomenclature and diagnostic criteria

- (INHAND): nonproliferative and proliferative lesions of the dog, *Toxicol. Pathol.* 49(1):5–109, 2021.
- Wood CE: Morphologic and immunohistochemical features of the cynomolgus macaque cervix, *Toxicol. Pathol.* 36:119S–129S, 2008.
- Woods L, Perez-Garcia V, Hemberger M: Regulation of placental development and its impact on fetal growth-new insights from mouse models, *Front. Endocrinol.* 27(9):570, 2018.
- Xu J, Wang Y, Kauffman AE, et al.: A tiered female ovarian toxicity screening identifies toxic effects of checkpoint kinase 1 inhibitors on murine growing follicles, *Toxicol. Sci.* 177:405–419, 2020.
- Young JM, McNeilly AS: Theca: the forgotten cell of the ovarian follicle, *Reproduction* 140(4):489–504, 2010.
- Yu P, Knippel A, Onidi M, et al.: A novel monovalent FGFR1 antagonist: preclinical safety profiles in rodents and non-human primates, *Toxicol. Appl. Sci.* 406:115215, 2020.
- Zheng Y, Zhou ZZ, Lyttle CR, et al.: Immunohistochemical characterization of the estrogen-stimulated leukocyte influx in the immature rat uterus, *J. Leukoc. Biol.* 44:27–32, 1988.
- Zook BC, Spiro I, Hertz R: Malignant neoplasms of decidual origin (deciduomas) induced by estrogen-progestin-releasing intravaginal devices in rabbits, *Am. J. Pathol.* 128: 315–327, 1987.



This page intentionally left blank

# Embryo, Fetus, and Placenta

Brad Bolon<sup>1</sup>, Susan A. Elmore<sup>2</sup>, Wendy Halpern<sup>3</sup>, Colin G. Rousseaux<sup>4</sup>

<sup>1</sup>GEMpath, Inc., Longmont, CO, United States, <sup>2</sup>ElmorePathology, LLC, Chapel Hill, NC, United States, <sup>3</sup>Genentech (a Member of the Roche Group), South San Francisco, CA, United States, <sup>4</sup>University of Ottawa, Faculty of Medicine, Ottawa, ON, Canada

## OUTLINE

<b>1. Introduction</b>	<b>820</b>	<b>7. Mechanisms of Developmental Toxicity</b>	<b>876</b>
<b>2. Fundamentals of Developmental Toxicologic Pathology</b>	<b>821</b>	7.1. Excessive Cell Death	876
2.1. Basic Principles	821	7.2. Dysregulated Autophagy	877
2.2. Critical Phases of Development	821	7.3. Interference with Programmed Cell Death (Apoptosis)	877
2.3. Incidence of Congenital Defects	823	7.4. Reduced Cell Proliferation	878
<b>3. Structure, Function, and Cell Biology—Embryo and Fetus</b>	<b>823</b>	7.5. Failed Cellular Interactions	879
3.1. Fertilization to Blastocyst Formation	824	7.6. Impeded Morphogenetic Movements	879
3.2. Implantation	826	7.7. Reduced Biosynthesis of Essential Components	880
3.3. Gastrulation	827	7.8. Inhibition of Angiogenesis	881
3.4. Organogenesis	829	7.9. Endocrine Disruption	881
3.5. Histogenesis and Functional Maturation	832	7.10. Oxidative Stress	882
<b>4. Structure, Function, and Cell Biology—Placenta</b>	<b>833</b>	7.11. Mechanical Disruption	882
4.1. Structure	833	7.12. Intracellular pH Alterations	883
4.2. Cell Biology and Function	835	<b>8. Developmental Toxicity Issues in Product Development</b>	<b>883</b>
<b>5. Evaluation of Toxicity</b>	<b>838</b>	8.1. Biological Factors that Modify Developmental Toxicity	883
5.1. Toxicity Testing	839	8.2. Study Design Considerations	889
5.2. Key Endpoints in Developmental Toxicity Testing	841	<b>9. Regulatory Considerations</b>	<b>902</b>
<b>6. Responses to Injury</b>	<b>847</b>	9.1. Managing Risk	902
6.1. Death	848	<b>10. Conclusion</b>	<b>904</b>
6.2. Malformations	848	<b>Glossary</b>	<b>905</b>
6.3. Deformations	868	<b>Acknowledgments</b>	<b>908</b>
6.4. Intrauterine Growth Restriction	870	<b>References</b>	<b>908</b>
6.5. In-Life Functional Alterations	871		
6.6. Congenital Neoplasia	872		

## 1. INTRODUCTION

Scientists have investigated mechanisms of **embryogenesis** (i.e., the process of embryonic formation and development) for decades by using exogenous chemicals and other agents to explore biochemical, functional, and structural outcomes of disrupting normal developmental processes (DeSesso, 2019; Ujházy et al., 2012). In the first half of the 20th century, **congenital** (i.e., present from birth) defects in all species were generally believed to arise from genetic or infectious causes. The thalidomide tragedy of the late 1950s and early 1960s affecting approximately 10,000 European children showed that assumption to be incorrect (Vargesson, 2015). This unanticipated iatrogenic episode sensitized the biomedical community and the public to the potential hazards of exposing the developing conceptus to **teratogens** (i.e., agents that cause birth defects).

In retrospect, the fact that chemical imbalances and exogenous chemicals were able to alter in utero development should not have been surprising. **Birth defects**—traditionally structural but more recently functional and biochemical as well—are abnormalities that are evident at birth, usually due to inherited genetic damage or a malign environmental influence. Many syndromes induced by **xenobiotics** (i.e., exogenous agents, especially synthetic chemicals) have been identified during the last century. For example, ocular malformations are produced in many species, including humans, by a deficiency or excess of vitamin A (Maden, 2001; Padmanabhan et al., 1981; Palludan, 1961). In like manner, human malformations have been linked to gestational exposures with enzyme inhibitors (e.g., aminopterin (Shaw, 1972)); hormones (e.g., diethylstilbestrol [DES] (Titus-Ernstoff et al., 2010)) and testosterone (Larkins et al., 2016); ethanol (Kotch and Sulik, 1992); and metals (e.g., lead (Thomason et al., 2019)). In utero xenobiotic exposure may induce structural defects (macroscopic or microscopic) (Wilson and Fraser, 1977a), functional deficits (Lowndes and Reuhl, 1997; Spyker, 1975), or both depending on the timing of exposure.

Humans and animals are potentially exposed to numerous agents during critical periods of development, and many of these agents have the capacity to act as teratogens (ACOG, 2021; Gupta, 2022; Hood, 1997; 2012; Scialli, 1992; Shepard and Lemire, 2010). Key classes of

developmental toxicants include chemicals in the workplace (e.g., heavy metals [see *Metals*, Vol 3, Chap 10 and solvents) or in the environment (e.g., *Agrochemicals*, Vol 3, Chap 11 and *New Frontiers in Endocrine Disruptor Research*, Vol 3, Chap 12); various drug classes (e.g., cytotoxic and/or genotoxic cancer chemotherapies) (Briggs et al., 2017); metabolic byproducts (e.g., ammonia and bilirubin); mycotoxins (*Mycotoxins*, Vol 3, Chap 6) and phycotoxins (*Phycotoxins*, Vol 3, Chap 5); and radioactive materials (*Radiation and Physical Agents*, Vol 3, Chap 14). Therefore, in recent years, safety assessment for new products intended for purposeful administration to patients or to which humans might be exposed often evaluates not only conventional endpoints of developmental toxicity but may explore fundamental mechanisms that determine normal development as well as initiate and drive abnormal development (*The Role of Pathology in Evaluation of Reproductive, Developmental, and Juvenile Toxicity*, Vol 1, Chap 7).

Toxicologic pathology evaluation for animal toxicity studies typically involves two main scenarios. In conventional developmental and reproductive toxicity (DART) studies, morphologic evaluations of dams, conceptuses, and placentas at necropsy generally are performed by well-trained and experienced technical staff, and the assessment is limited to macroscopic observations of external and internal structural abnormalities, including both visceral and skeletal assessments. This task typically is performed in the absence of dedicated pathologist support. In contrast, investigational studies to characterize mechanisms of developmental toxicity often include microscopic endpoints, including routine stains, and can also include various special stains or molecular procedures. Toxicologic pathologists are typically integral members of the research teams that perform such investigations, and determine whether such investigations are necessary.

This chapter describes normal developmental events and processes in selected vertebrate species, details essential methods to assess whether such processes have been disrupted by teratogens, reviews common mechanisms and responses to developmental injury, and discusses important regulatory considerations and guidance for minimizing developmental toxicity to the embryo and fetus. Additional details on developmental toxicology principles, practices,



and data interpretation may be obtained from the scientific literature as well as many excellent reference books (Ferretti et al., 2006; Gilbert-Barness, 1999, 2007; Gupta, 2022; Hansen and Abbott, 2008; Hood, 1997, 2012; Kimmel and Buelke-Sam, 1994; Koren, 2001; Schardein, 2000; Shepard and Lemire, 2010; Slikker and Chang, 1998; Szabo, 1989; Wilson, 1973; Wilson and Fraser, 1977a, b).

## 2. FUNDAMENTALS OF DEVELOPMENTAL TOXICOLOGIC PATHOLOGY

In the strict sense, developmental toxicology investigates the effects, causes, and mechanisms responsible for functional and/or structural abnormalities that occur during any developmental period. Teratology is the branch of developmental toxicology that investigates the manifestations, causes, and mechanisms of birth defects that involve injury during gestation to the **conceptus** (i.e., the embryo or fetus together with its placenta). Juvenile toxicology is the branch of developmental toxicology that assesses comparable attributes in developing animals after birth (Rao et al., 2021). Developmental toxicologic pathology typically emphasizes evaluation of the offspring (embryo, fetus, or juvenile) rather than the placenta, but the placenta should not be ignored in performing such examinations. The conceptus as a whole and its individual elements are considered here based on their status as transient organs susceptible to xenobiotic-induced damage.

### 2.1. Basic Principles

Embryonic and fetal periods of development usually are defined by their relationship to **organogenesis**, which is the stage during which organ **anlagen** (i.e., the rudimentary primordia of organs) first differentiate. Embryogenesis begins prior to and encompasses organogenesis, while the fetal period is that portion of gestation following the conclusion of organogenesis in which the initiated organs expand to assume their adult forms and approximate positions. The fetal period covers most of gestation in species with long gestations (e.g., humans). In contrast, embryogenesis occupies the bulk of gestation in species with short gestations (e.g.,

rodents), such that some events which occur in utero for humans take place some days after birth in rodents. For example, the majority of brain development that corresponds to the third trimester of the human fetus actually occurs during the first postnatal week of life in rats and mice, ending at approximately postnatal day (PND) 7 (Bolon and Ward, 2015a; Clancy et al., 2007a). Whether developmental events in other organs of human versus rodent fetuses conform to this timing often is not completely characterized or is not known.

Developmental toxicologic pathologists must know the fundamental principles of teratology (Brent et al., 2006; Wilson, 1973; Wilson and Fraser, 1977a; Wolpert et al., 2019). These principles are conceptually similar to those that govern toxicity in adult animals. Six basic tenets were originally proposed by Wilson:

1. Interactions between the genotype of an embryo or fetus and many environmental factors will influence the onset and degree of teratogenicity;
2. The stage of development during which an embryo or fetus is exposed determines its susceptibility to teratogenic agents;
3. Teratogens induce abnormal development according to specific mechanisms;
4. Physical properties of developmental toxicants determine their access to the embryo or fetus;
5. Death, malformation, intrauterine growth retardation, and postnatal functional abnormalities can all be manifestations of teratogenesis; and
6. Expressions of developmental toxicity tend to be dose-related, ranging from slight defects or weight decrements to major malformations or death.

The effects of xenobiotic exposure vary among species and among individuals in a given litter. Maternal toxicity should be examined as one component of developmental toxicity evaluations.

### 2.2. Critical Phases of Development

Developmental processes occur in specific locations and at particular times. In many cases, the success of developmental processes is affected by the integrity of previous developmental events. The sequence and timing of events generally is consistent for individuals of a given species, and the overall pattern is conserved across mammalian species even though the timing varies among species depending on the length of gestation and the lifespan.

Critical periods for structural development typically occur prior to birth, although some organs do not complete their differentiation until after birth (e.g., hippocampus and cerebellum in rodents). In contrast, both functional and molecular development continues to evolve throughout the neonatal and juvenile periods, not achieving full maturity until after puberty. Taken together, these principles indicate that some structure, function, and/or biochemical pathway will still be differentiating any time a pregnant individual or her newly born or juvenile offspring are exposed to a xenobiotic agent.

The critical period of intrauterine development is that time during its differentiation and growth when the conceptus has the greatest sensitivity to noxious influences. Critical periods begin during early organogenesis when various organs are undergoing their initial formation (Figure 11.1). Rolling critical periods for structural development of individual organs

continue, while cell division and differentiation as well as organ morphogenesis proceed rapidly and taper off as their final configuration nears completion.

Each organ and system has its own critical period or periods. Distinct regions in complex structures (e.g., the central nervous system [CNS]) typically have their own critical periods. Some (e.g., hippocampus, olfactory bulb) may have more than one such peak of sensitivity (Rodier, 1980). Accordingly, a xenobiotic exposure during a particular stage of development is likely to produce lesions in those organs and systems having critical periods that overlap with the time of exposure. For example, in mice, gross defects of the brain are produced by exposures at approximately embryonic day (E) 7 to E8, while cleft palate develops if the exposure occurs at about E11. Since the timing of principal developmental events and critical periods of organ differentiation (DeSesso, 2006)

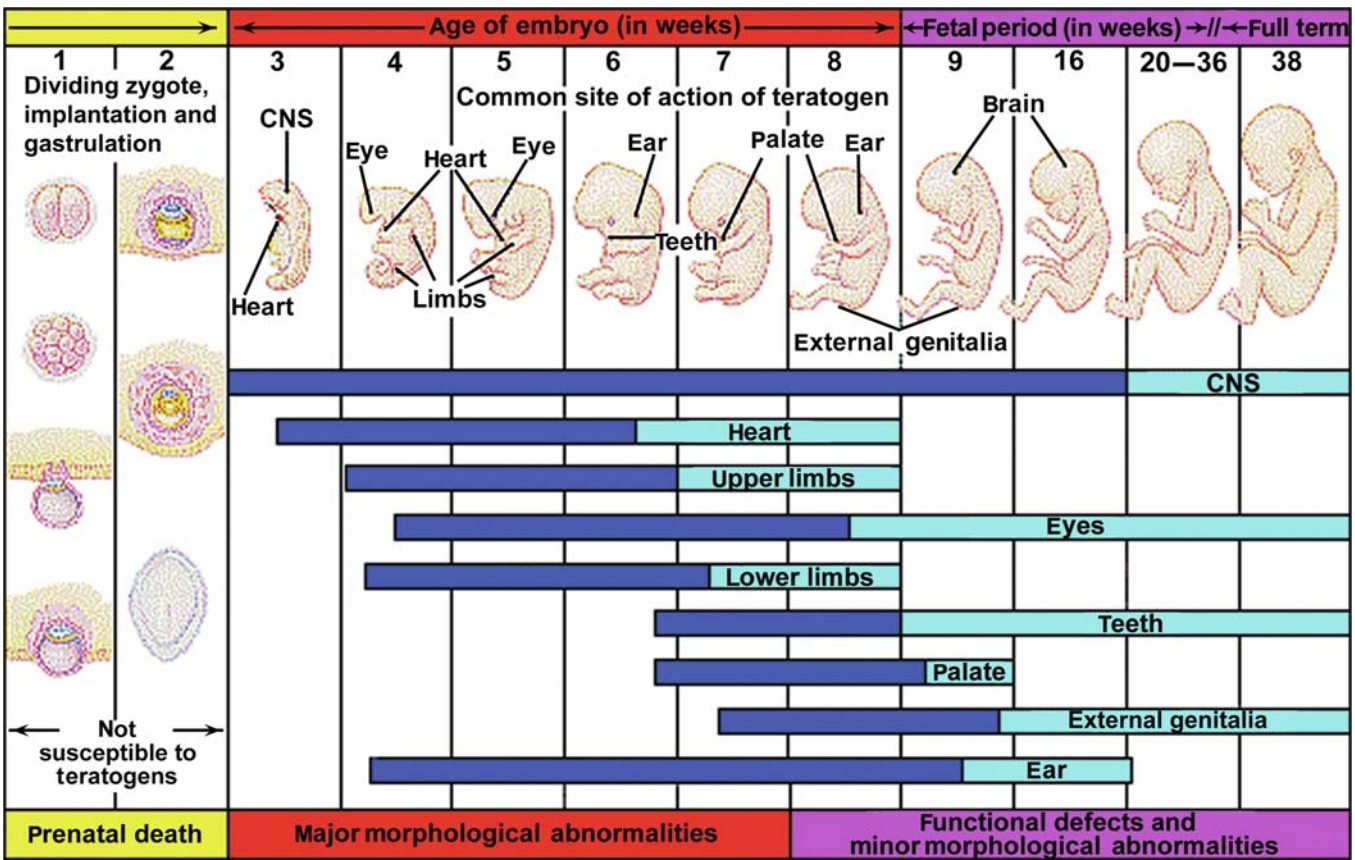


**FIGURE 11.1** Schematic diagram of the critical periods of human development. Reproduced from Haschek WM, Rousseaux CG, Wallig MA, editors: *Handbook of toxicologic pathology*, ed 2, 2002, Academic Press, Figure 3, p. 902, with permission., as adapted from the “Embryology” education web site maintained by Dr. Mark Hill, University of New South Wales, Sydney, Australia ([https://embryology.med.unsw.edu.au/embryology/index.php/Foundations\\_Practical\\_-\\_Critical\\_Periods](https://embryology.med.unsw.edu.au/embryology/index.php/Foundations_Practical_-_Critical_Periods)).

are known in relevant animal species and humans, hypotheses about the cause and timing of a specific birth defect often can be made. A **malformation** (i.e., a congenital structural defect resulting from intrinsic [internal] tissue damage) cannot result from xenobiotic exposure if the organ or tissue was completely developed at the time of exposure. Therefore, gross malformations tend to follow exposures early in development. However, a **deformation** (i.e., a gross **anomaly** [abnormality] arising from ineffective repair of a developmental injury caused by an external force) can occur even in a normally developing or fully formed organ as long as the tissues remain soft and readily malleable to the influence of mechanical forces. Finally, congenital neoplasms initiated by transplacental exposure to mutagenic carcinogens during gestation may not become apparent for extended periods after birth.

### 2.3. Incidence of Congenital Defects

The frequency of abnormal development (structural, functional, and/or biochemical) is quite high in humans (CDC, 2006; Mai et al., 2019). In developed countries, the incidence of major malformation is 2%–4% of human births per year, although the total incidence of human morphologic abnormalities is estimated to range as high as 8% of births if subtle structural defects diagnosed later in life are included. About 4% of overt structural birth defects in humans are thought to arise from maternal exposure to teratogens (Feldkamp et al., 2017).

The incidences of various developmental abnormalities in animals range from 2% to 12%, depending on the species and degree of inbreeding (Szabo, 1989). Morphologic anomalies in laboratory animals have been well characterized, especially in those species commonly used for teratology studies (particularly mice, rats, and rabbits) (Bailey and Balcombe, 2005; Palmer, 1972; Shepard and Lemire, 2010). Major spontaneous structural malformations incompatible with postnatal life (e.g., cardiac septal defects, neural tube defects [NTDs], organ agenesis) occur at a frequency of less than 1% in most mouse strains, although certain strains exhibit higher incidences. Minor structural anomalies that do not prevent postnatal survival are detected at higher incidences in mice, ranging from 1% to 5% for such lesions as sternebral asymmetry and unossified phalanges and up

to 35% for common variants such as renal pelvic cavitation and supernumerary or wavy ribs. Malformation clusters can occur in animal colonies, more often in laboratory strains of inbred mice compared to rats. The incidences of spontaneously occurring developmental anomalies often may be obtained from animal suppliers. Such data may reveal minor variations in the spectrum of developmental defects among vendors, knowledge of which is useful in determining the significance of pathologic findings noted in developmental toxicity studies.

### 3. STRUCTURE, FUNCTION, AND CELL BIOLOGY—EMBRYO AND FETUS

In one sense, the embryo/fetus may be viewed as a transient organ that develops during pregnancy. In a more important sense, the embryo/fetus is not an organ at all but rather a complex organism tethered to a maternal host for the time needed to develop its own set of appropriately formed and functioning organs. The extensive evolution of the mammalian embryo from a single cell at conception to a complex multicellular embryo that experiences constant remodeling throughout all of prenatal and some of postnatal life indicates that development must be understood as a 4-dimensional process (i.e., structures morphing in three dimensions of space [length, width, height] as well as one dimension in time). Some mental recalibration is needed when performing structural evaluations for embryos and fetuses relative to juvenile and adult animals because organ contours and locations evolve progressively throughout gestation.

The general processes involved in the normal development of placental mammals including humans are well characterized (Figure 11.2 and Table 11.1). Starting with fertilization, morphologic development (i.e., **morphogenesis**) of the embryo and fetus proceeds via a series of cell expansions and ordered rearrangements that occur in a stereotypical fashion.

This process of ordered conceptus development is guided by many factors. Genetic programming, including faithful transcription and translation, is essential to the ultimate differentiation pathway that a cell follows. Accurate intercellular communication is also critical to normal development and occurs via several mechanisms: direct cell-to-cell contact, **morphogen** gradients (i.e., nonuniform



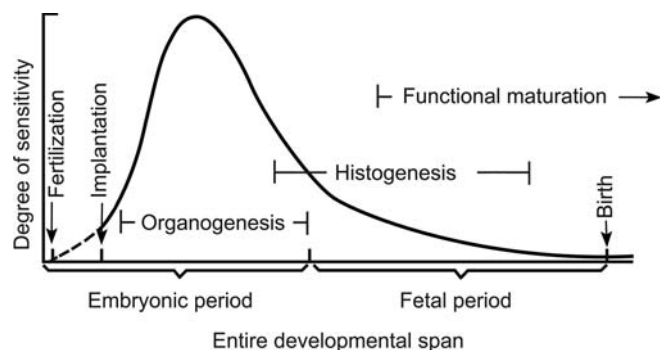


**FIGURE 11.2** Sensitivity of the developing mammalian embryo and fetus to xenobiotic insults during gestation. Reproduced from Haschek WM, Rousseaux CG, Wallig MA, editors: *Handbook of toxicologic pathology*, ed 2, 2002, Academic Press, Figure 1, p. 897, with permission.

distribution of differentiation-regulating chemical signals within tissues), and tissue **induction** (i.e., control exerted by one group of cells to guide the differentiation of another group of cells). Cell populations respond to their genetic predispositions as well as their internal and external chemical milieus by following one or more functional outcomes—cell shape changes, movements, etc.—that will promote ordered formation and growth of the organism. An understanding of these processes is essential before alterations caused by prenatal exposure to teratogens can be understood. Many superb books and papers may be consulted to obtain a more detailed consideration of developmental anatomy (Chen et al., 2017; Cochard, 2002; Crawford et al., 2010; DeSesso, 2006; Drews, 1995; Fletcher and Weber, 2013; Hill, 2014; McGeady et al., 2006; Elmore et al., 2019; Elmore et al., 2022; Moore et al., 2020; Noden and de LaHunta, 1985; O’Rahilly and Müller, 1994; R.R. O’Rahilly and Müller, 2006; Parker and Picut, 2016; Paxinos et al., 1994; Paxinos et al., 2007; Petiet et al., 2008; Ruffins and Jacobs, 2009; Rugh, 1990; Savolainen et al., 2009; Schambra, 2008; Schambra et al., 1992; Schoenwolf, 2008; Steding, 2009; Sulik and Bream, 2013; Swartley et al., 2016; Theiler, 1989); developmental biochemical and molecular biology (Barry, 2002; Edelman, 1988; Lewandowski, 2014; Paxinos et al., 2008; Sharpe and Mason, 2008); and developmental physiology (Behringer et al., 2014; Bolon, 2015; Hanson and Gluckman, 2014; Hood, 1997, 2012).

### 3.1. Fertilization to Blastocyst Formation

In mammals, fertilization (or conception) involves a series of changes in ejaculated sperm (i.e., capacitation and the acrosomal reaction) leading to their ability to fuse with the plasma membrane of the oocyte. Following penetration of a single sperm with delivery of its nucleic acid payload, changes occur in the *zona pellucida* (the glycoprotein layer that envelops the plasma membrane of the mammalian oocyte and that prevents entry of any additional sperm [the “zona reaction”]). These processes are followed by completion of the second meiotic division leading to formation of the female pronucleus and release of the second polar body. The sperm nucleus enlarges to form the male pronucleus. Both pronuclei then merge to form the nucleus, which restores a diploid chromosome number to the **zygote** (i.e., the one-celled embryo) (E0.5 of Figure 11.3).

The zygote divides repeatedly to produce a **morula**, a solid sphere of **totipotent** embryonic stem cells (E2.5 of Figure 11.3). Over time, differentiation of the stem cells leads to two distinct lineages that are distributed to different portions of the embryo, thus producing polarity. Fluid accumulates in a cavity (the **blastocoel**) at one pole of the morula, thereby forming a thin-walled sphere of undifferentiated cells termed the **blastula**. Shortly thereafter, a small plate of **pluripotent** (i.e., partially differentiated) stem cells termed the **inner cell mass** (ICM) forms at one pole of the embryo (visible as the crescent of cells along the right wall of the embryo at E3.5 of Figure 11.3); this initial differentiation event denotes the transition from blastula to **blastocyst** (i.e., a cavitated, polarized embryo). The ICM will become the embryo, while the **trophoblast** (the thin outer wall of cells surrounding the blastocoel) will evolve into the placenta. In placental mammals, the blastocyst is the developmental stage that implants in the endometrium of the uterine wall.

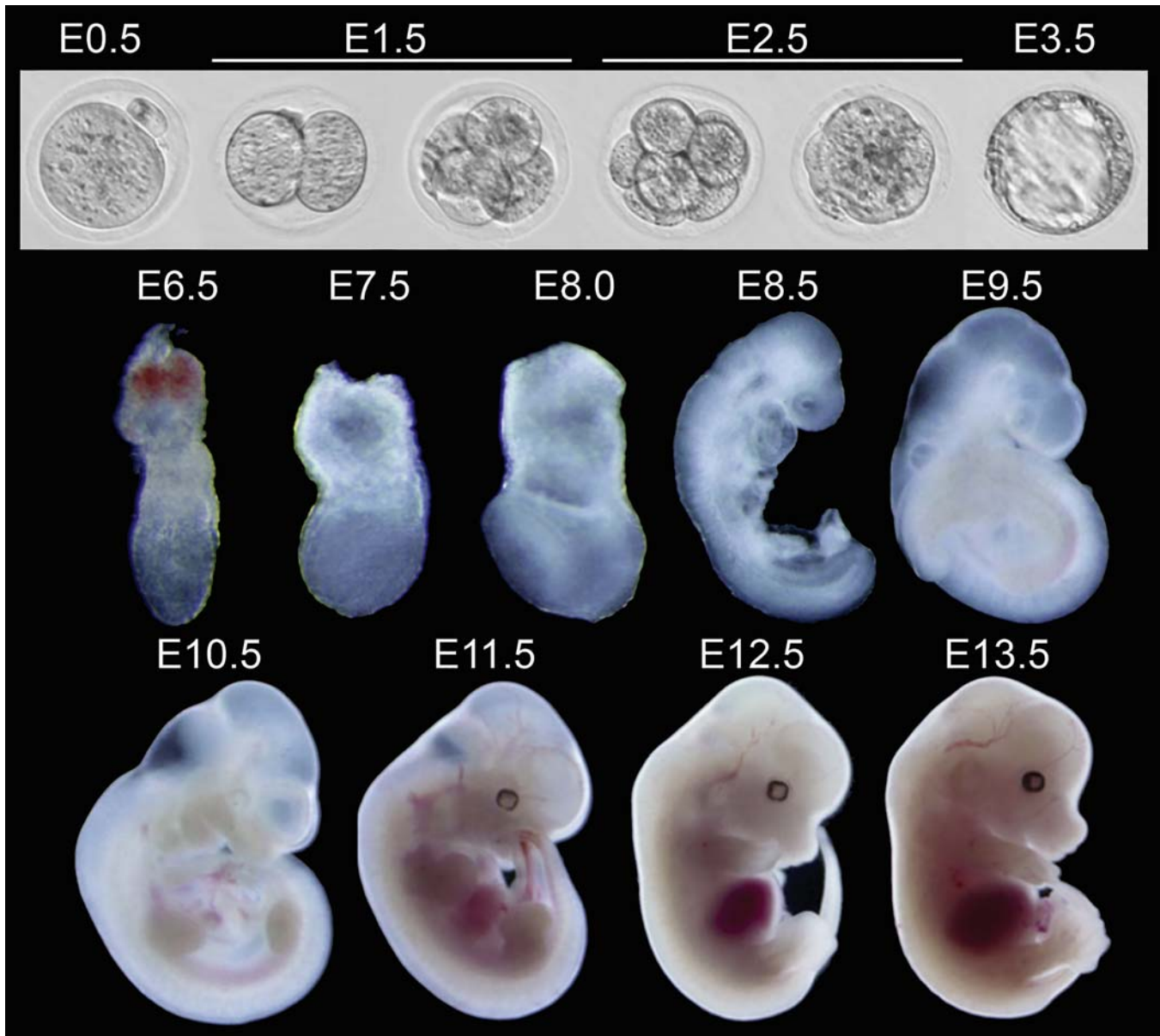
These early developmental stages are relatively resistant to toxic insults because of the totipotent nature of most embryonic stem cells during this period. Toxicant-induced damage that can severely injure the stem cells of the morula and ICM will typically lead to embryonic loss prior to implantation, while less serious injuries permit the surviving stem cells to

TABLE 11.1 Timing of Developmental Landmarks in Selected Vertebrates<sup>a</sup>

Species		Length of Gestation	2-cell	8-cell	Morula	Blastocyst	Implantation	Gastrula	Neurula	10-somite	Embryo-genesis Completed
Zebrafish	<i>Danio rerio</i>	60 h	0.75 h	1.25	2 h	5 h	N/A	8 h	10 h	12 h	48 h
Frog	<i>Xenopus laevis</i>	4	3.5 h	5.5 h	6 h	7 h	N/A	13 h	20 h	~30 h	~15
Chick	<i>Gallus gallus</i>	21	3 h	4 h	5 h	10 h	N/A	18 h	24 h	36 h	10
Mouse	<i>Mus musculus</i>	19	1	2	3	3.5	5.5	6.5	7.5	8.5	15
Rat	<i>Rattus norvegicus</i>	22	2	3.2	3.5	5	6	8.5	9	10.5	16.5
Guinea pig	<i>Cavia porcellus</i>	65	1	3.5	4	4.8	6	12	14	15	~27
Rabbit	<i>Oryctolagus cuniculus</i>	32	2	2.5	3	3.5	7	7	8	9	17
Ferret	<i>Mustela putorius</i>	42	2	4	5	6	13	13	14	15	20
Cat	<i>Felis domesticus</i>	63	3	3.5	4	5	12	12	13	14	28
Dog	<i>Canis domesticus</i>	63	4	6	7	8	16	16	17	18	40
Pig	<i>Sus scrofa</i>	115	1	2.5	4	5	14	9	14	15	33
Sheep	<i>Ovis aries</i>	145	1	2.5	4	6	16	10	15	16	35
Cow	<i>Bos taurus</i>	282	1	3	6	8	30	14	19	21	40
Horse	<i>Equus caballus</i>	336	1	3	4	6	35	14	18	19	45
Rhesus monkey	<i>Macaca mulatta</i>	165	1	2	4	5	8	16	20	23	47
Human	<i>Homo sapiens</i>	267	1	2	3	5	9	13	16	25	58

<sup>a</sup> Times are estimated mean values in hours (h) or days postconception.

Reproduced from Haschek and Rousseaux: Handbook of toxicologic pathology, ed 3, 2013, Table 62.1 p. 2706 with permission.



**FIGURE 11.3** Composite image of embryonic mouse developmental stages from conception (single-celled zygote at embryonic day [E] 0.5, at far left of upper row) through preimplantation (E1.5 to E3.5, rest of upper row) and during early postimplantation (E6.5) through midgestation (E13.5). *Reproduced by permission of the copyright holder: Dr. Yi Zhang, Harvard Medical School and the Howard Hughes Medical Institute.*

replenish their full complement with either no effect or a modest developmental delay. While these outcomes are the norm, in some cases, comparatively mild insults at the morula or blastocyst stages have been linked to embryonic loss.

### 3.2. Implantation

In mammals, adherence of the blastocyst to the endometrium is followed by invasion of the uterine wall in a process termed **implantation**.

The events at this stage are dictated principally by interaction between the embryo-derived trophoblasts (i.e., outer wall of the blastocyst) and the maternal-derived endometrium.

Implantation occurs through several sequential steps. The first step ("hatching") involves ejection of the zona pellucida by the blastocyst. This expulsion is mediated by proteases within the blastocyst wall and present in the uterine fluid as well as by tension resulting from progressive expansion of the blastocoel. The second step ("apposition") occurs when the



blastocyst wall comes to rest on the endometrial surface but connections have not yet been established. This event usually takes place in an endometrial crypt as a means of increasing the contact area involved in this initial connection. The third step (“adhesion”) is characterized by the initial penetration of processes from trophoblasts forming the blastocyst wall widely into the endometrium. The ICM is located randomly with respect to the endometrium during apposition but then rotates to position itself nearest the endometrial surface (i.e., the nutritional source) during adhesion. The final step (“invasion”) results from progressive entry of proliferating trophoblast cells deeply into the uterine wall.

Implantation is coordinated by a complex communication network that involves many receptor-mediated pathways. Principal signaling cascades are mediated by integrins and proteoglycans. For example, proteoglycans expressed on trophoblast cells anchor to proteoglycan receptors present on endometrial cells. Expression of these molecules is restricted to the “implantation window,” which is the short period following ovulation during which the uterine wall is primed to facilitate adhesion and invasion of a developing embryo.

The endometrial reaction that takes place during the implantation window varies among species, but the major alterations include decidualization of the endometrial lining and the formation of tortuous glands. The **decidua** results from endometrial modification (tissues and vascular remodeling) to form polyhedral cells that are capable of nourishing the embryo until the definitive placenta (i.e., fully mature organ [described below]) is formed. Decidualization and the subsequent formation of the definitive placenta are regulated by mediators released from the blastocyst, although additional support is provided by progesterone produced by the *corpora lutea* in the ovary. The decidua and endometrial glands will regress in the absence of implantation, either by degeneration or by detachment and expulsion in those species capable of menstruation (i.e., primates).

The expansion of the uterine lining near the time of implantation is a maternal response designed to support embryonic survival and growth until the definitive placenta can be formed. The decidual cells accumulate glycogen and lipids, presumably to serve as a nutrient store for the growing embryo. The uterine glands secrete fluid that serves several purposes. First, the fluid is a source of

nourishment as it contains albumin in abundance as well as important diffusible micronutrients (e.g., fat-soluble vitamins). Second, the fluid carries many molecules that facilitate implantation (e.g., integrins and other adhesion molecules, matrix proteins like fibronectin and laminin) and prevent blastocyst rejection (e.g., hormones like prolactin and relaxin). Third, the fluid contains factors (e.g., fibroblast growth factors [FGFs] 1 and 2, steroids) to promote blastocyst survival and growth after implantation has been achieved.

### 3.3. Gastrulation

In mammalian embryos, the process of gastrulation begins shortly after implantation (Figure 11.4). This process marks the transition from a radially symmetrical, spherical, preimplantation embryo to a bilaterally symmetrical, planar embryo. The first event during gastrulation is differentiation of the monomorphic elements of the ICM into a bilaminar plate-shaped embryo consisting of an epiblast (which will give rise to the embryonic germ layers [ectoderm, mesoderm, and endoderm] as well as certain extraembryonic ectoderm and mesoderm) and a hypoblast (which serves as the origin of the yolk sac (YS) endoderm and some extraembryonic mesoderm). The primitive streak forms as a linear thickening in the epiblast, with a primitive node and pit at its cranial end. The cells associated with this transient streak produce numerous signaling molecules that direct craniocaudal (anteroposterior) and dorsoventral spatial patterning of embryonic tissues (Sheng et al., 2021). Next the prechordal plate, the site of the future mouth, arises in the hypoblast just rostral to the primitive node. A similar area, the cloacal membrane, arises caudal to the primitive streak and gives rise to the anus. The trilaminar embryo is formed when cells from the epiblast migrate inward and spread away from the primitive streak, thereby giving rise to the mesoderm and endoderm. The notochordal process, progenitor of the notochord (i.e., primitive cartilaginous column defining the body axis), is derived from cells migrating cranially from the primitive node and pit.

The sensitivity of the embryo to teratogens is still relatively low during gastrulation. Toxicant exposures at this developmental stage typically do not induce structural defects. Instead, the usual expression of a toxic insult during this

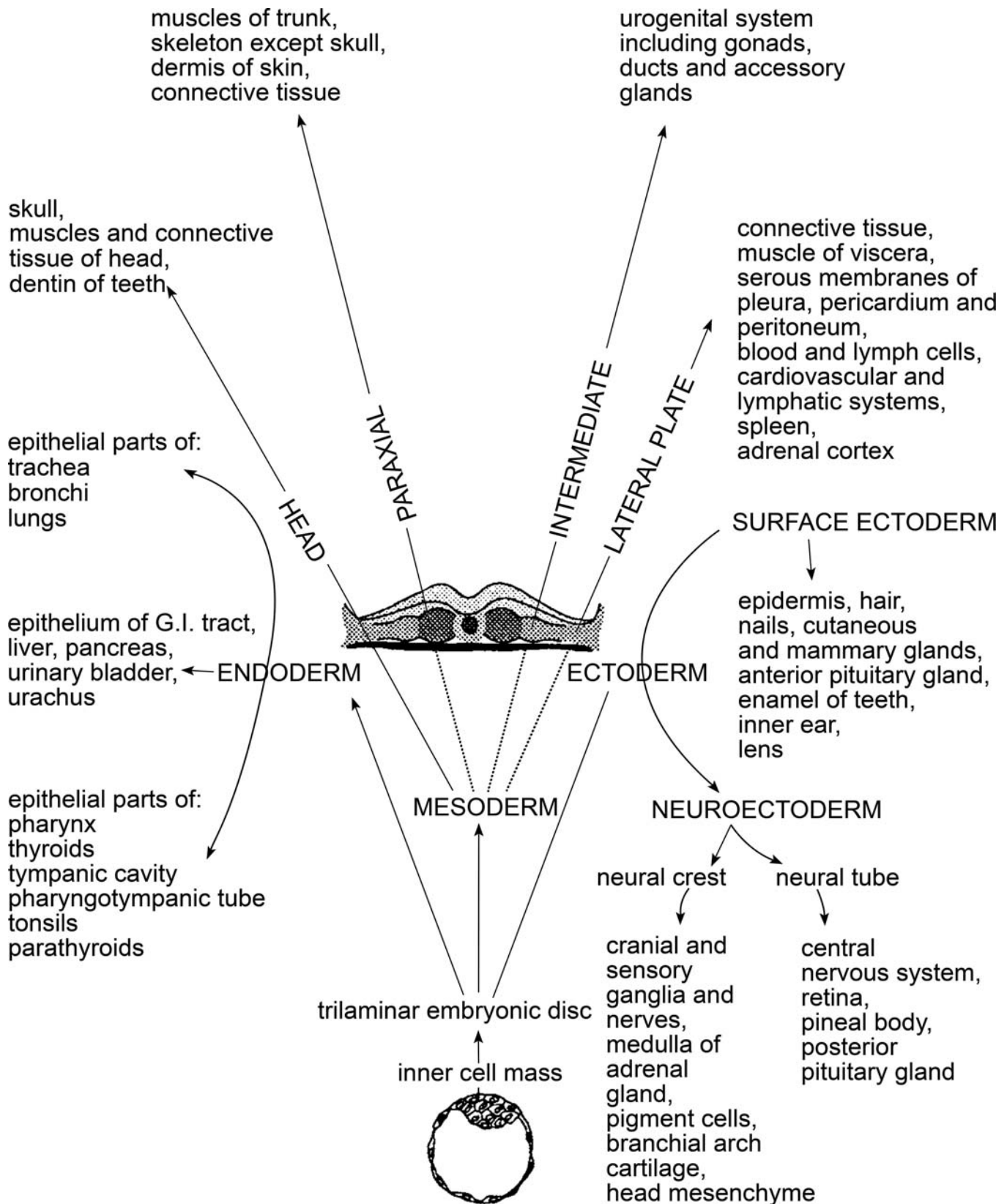


**FIGURE 11.4** Schematic diagram showing the origin and derivatives of the three embryonic germ layers. Reproduced from Haschek WM, Rousseaux CG, Wallig MA, editors: *Fundamentals of toxicologic pathology*, ed 2, 2010, Academic Press, Figure 2, p. 636, with permission.

stage is embryonic death and resorption. This outcome occurs because embryonic cells at this stage are pluripotent rather than totipotent, so the loss of a few critical components can thwart development of certain tissues that are necessary for long-term survival.

### 3.4. Organogenesis

Organ initiation is the most intricate stage of embryonic development. The period of organogenesis results in initial specification of all organs in the embryo. Accordingly, cell and tissue interactions are critical determinants during this phase. The complexity of this developmental stage means that interference by exogenous toxicants can produce devastating effects on the growing organism, usually in the form of major malformations (i.e., congenital birth defects). This section briefly describes the primary cell and tissue interactions that drive organogenesis in mammalian embryos. Further details may be obtained in other publications (Barry, 2002; DeSesso, 2006; Kaufman and Bard, 1999; McGeady et al., 2006; Rossant and Tam, 2002; Sadler, 2009).

#### 3.4.1. Induction

Induction is a key mechanism by which ordered development occurs in the embryo. During induction, one population of cells (the inducing tissue) directs another population of cells (the responding tissue) to differentiate. Primary induction involves establishing the basic embryonic body plan (mainly the body axis and neural tube), while secondary induction results in a “cascade” of serial cell and tissue interactions during development of a given organ. If the inducing tissue is absent at the necessary stage of organogenesis, the responding tissue usually will form improperly or fail to form at all.

The genesis of the eye is a good example of both primary and secondary induction. Primary induction of the neuroectoderm (i.e., the anlage of the CNS) results from the promoting activity of the primitive streak, via the influences of the notochord and paraxial mesoderm. Subsequent secondary induction of the forebrain neuroectoderm under the influence of the adjacent mesenchyme leads to formation of an outward extension, the optic vesicle. This evagination ultimately develops a central invagination to form the optic cup, which then launches a series of secondary inductive events leading to final

anatomic patterning of the eye. The optic vesicle (i.e., eye primordium) induces overlying surface ectoderm to thicken and form the lens placode. The lens placode invaginates into the optic vesicle (which transitions into the optic cup) and then loses its connectivity with the surface ectoderm to produce the lens vesicle (lens primordium). Finally, the lens vesicle induces the reconstituted surface epithelium to differentiate as the cornea.

Induction is mediated through direct cell-to-cell contact, via diffusible substances (termed morphogens [described in more detail below] because they dictate morphologic organization of the embryo), or via the extracellular matrix (ECM). The proper stage-dependent expression of multiple cell adhesion molecules (CAMs), substrate adhesion molecules (SAMs), and cell junction molecules (CJMs) is vital for determining the mammalian body form. These molecules serve distinct functions. For instance, CAMs define the position of an embryonic cell relative to other cells within a “collective” destined to differentiate into a specific structure. In contrast, CJMs enable communication among cells within a collective, while SAMs (particularly with respect to their relationship to integrins) influence the patterns of gene and protein expression in specific cells and groups of cells within a collective. These molecules and others work together to define and modulate the intermediate and final patterns of tissue development.

#### 3.4.2. Morphogenetic Movements

Stereotypical movements are a characteristic response of induced embryonic cells. Cells are specified for a particular fate during gastrulation and then migrate widely to reach their final location. The cumulative effect of these morphogenetic movements is the production of a multilayered embryo with head, trunk, and tail sections initially and an appropriate complement of properly sized and positioned organs ultimately. Direct cell-to-cell contact affects the direction of cell movements by contact inhibition of migration and by eliciting surface changes in cell membranes.

The ECM plays an essential role in controlling cell migration. The ECM directs morphogenetic movements via the arrangement of collagen fibers as scaffolding (i.e., attachment sites) and the precise constellation of glycosaminoglycans (GAGs) and other proteins as molecular guideposts. For example, hyaluronic acid may aid



cell movement through the ECM, and gradients of SAMs, such as fibronectin and laminin, may provide positional information for migrating cells. It is likely that these forms of regulation apply to cell collectives (designated by their CAM signatures) behaving as a group, rather than to individual cells; each cell passes positional information to other cells in the collective via various communication molecules. As differentiation progresses, these collectives may subdivide into “sub-collectives” to form smaller structures within a larger organ.

Cell movements during development typically occur in a stepwise fashion. Narrow processes extend from cells in a particular direction under the guidance of cell-anchored CAMs and soluble morphogens, after which the tip of the process attaches to the nearby ECM. The cytoskeleton within the cell process then contracts to transfer the cell soma toward the tip of the process. Subsequent cycles of cell movement recapitulate these same steps independently in every cell within the collective. Morphogenetic movements thus depend on the integrity of cytoskeletal structure and function, especially such contractile molecules as actin and tubulin. Multicell coordination leading to harmonized movement of all cells in a collective is mediated by the function of many communication molecules, particularly the CJs. Gap junctions allow passage of macromolecules between adjacent cells (Levin, 2007), while tight junctions serve the same role for very small molecules. The CAMs are also essential to such coordinated movement, especially desmosomes that act as anchor points for the cytoskeleton.

As cells reach their final positions and differentiate, they lose their ability for further movement. Therefore, cell collectives that have entered terminal differentiation become more selective in their molecular repertoires, adopting a modest array of tissue-specific proteins. For example, cells that express L-CAM have committed to life as mesenchymal cells and can no longer alter their genetic programming to become epithelial cells. The final morphology of cells, tissues, and organs depends upon orderly and appropriate decisions with respect to when and where specific cells choose to cease migration.

### 3.4.3. Morphogen Gradients

Vigorous debate continues regarding the signal(s) responsible for morphogenetic movements by various cell collectives. The “regulator

hypothesis” (sometimes called the morphoregulator hypothesis) posits that multiple morphogens mediate such movements during development by directly participating in intercellular signaling (Edelman, 1984). In particular, molecular events at cell surfaces that fluctuate in space and time control major developmental events such as cell movement, differentiation, division, and death. An alternative “signal-neutral hypothesis” proposes that multiple morphogens act instead through simple mechanochemical events between adhesion molecules on the cell surface and cytoskeletal elements inside the cell (Edelman, 1992). By this latter model, physical and chemical interactions for some morphogens change the thresholds for signaling pathways mediated by other morphogens. These hypotheses are not mutually exclusive.

Morphogens are molecular signals that specify positional and directional information needed by growing cells. The usual framework for morphogen activity is that one cell collective secretes the morphogen, which then diffuses outward in a radial or parabolic fashion through other groups of cells. Subsequently, target cells (or their processes) from another collective migrate up the morphogen gradient to reach and interact with the cells located where the concentration of the morphogen is optimal. In many instances, a specific site directs the morphogen gradients at a given location; a well-known example is the apical epidermal ridge (AER), a zone at the tips of the limb primordia that specifies polarity in the developing limb buds. Morphogens are presumed to act via modifications of the extracellular microenvironment, likely by interactions at the level of integrins and SAMs.

Many different chemicals serve as morphogens during specific times of gestation. During normal development, such chemicals are produced by cells in the embryo. For example, endogenous retinoids have potent effects on development, seemingly by their ability to react with retinoic acid receptors (RARs) and retinoid X receptors (RXRs) within the cell nucleus. Abnormal expression of retinoids or their receptors, or gestational exposure to an exogenous retinoid-like xenobiotic (e.g., isotretinoin (Draghici et al., 2021), vitamin A supplements), induces major malformations affecting multiple organ systems (especially the CNS, heart, and skeleton).

Retinoids can act as morphogens indirectly by inducing expression of the sonic hedgehog (*SHH*) gene, which encodes a signaling protein that controls dorsal-ventral patterning of axial structures like the neural tube and somites (Helms et al., 1997), cranial-caudal patterning of the limbs (Helms et al., 1994), and cell specification of certain pluripotent stem cells (Kondo et al., 2005). Some molecules that serve as morphogens during development also function in other fashions during adulthood. Catecholamine (e.g., dopamine) and indoleamine (e.g., serotonin) neurotransmitters (Lauder, 1988) are important examples of this principle, and agents that disrupt neurotransmitter signaling during pregnancy can induce malformations (Shuey et al., 1992). In general, most cell collectives appear to be specified by multiple morphogens.

#### 3.4.4. Selective Cell Regulation

Cell responses to endogenous and exogenous chemicals in their microenvironment differ according to the cell type and stage of development. The regulator hypothesis provides a reasonable model for growth and induction of various cell collectives. This hypothesis is based on four premises (described below) and incorporates the principles of morphogenetic movements and morphogen gradients as discussed above to explain the structural and functional blueprints established by the developing embryo.

The first premise is that the cells in a collective induce cells of other collectives by epigenetic means. In other words, external signals produced by one group of cells will alter gene expression in other cell groups. Such inductive interactions occur in a context set by CAMs, CJMs, and SAMs. The network formed by these signaling pathways acts by directing all cells in a given collective to follow one among several potential primary processes, such as cell division, cell migration, or programmed cell death (PCD). The message may be delivered by chemical or physical means. For example, SAMs may act via concentration gradients (chemical) or changes in the viscosity of GAGs in the ECM that envelops the cell (physical). The epigenetic influence may occur between cell collectives that are either adjacent to each other or separated by some distance. Chemical means of epigenetic signaling may be used over short or long distances, while physical means are most relevant for nearby cell populations.

The second premise is that morphoregulatory genes are the essential elements that link epigenetic mechanochemical events to gene expression in a particular cell collective. Morphoregulatory genes like *SHH* and *Hox* (homeobox) are not critical for cell survival but rather are needed for appropriate pattern formation. Two other gene classes control the activities of morphoregulatory elements: historegulatory genes and selector genes. Historegulatory genes control the structural genes that specify the general characteristics and cellular functions necessary for the correct differentiation of cells and tissues. These structural genes make up the largest class of genes, and they are required for cell survival. Selector genes, by affecting the actions of historegulatory genes, restrict the sequence of events needed to complete differentiation to certain sites and/or developmental stages. Switch genes dictate the determination between alternative developmental phenotypes that might be adopted by a particular organ or system by turning other genes on or off at various times and for different lengths of time.

The third premise of the regulator hypothesis is that cells from a given collective will function in harmony as they respond to the epigenetic information provided by other cell collectives. Examples of cell collectives that provide such epigenetic signals include the left-right organizer, which determines body axis asymmetry (Hamada, 2020), and the primitive (Hensen's) node (alternatively: primitive knot), which acts together with the primitive streak to define rostro-caudal (anterior-posterior) patterning during gastrulation (Gilbert, 2013; Rossant and Tam, 2002). In this scenario, all cells for a given collective receive a common input from another cell collective, often via the expression pattern of cell type-specific CAMs. The incoming signal causes all cells that receive it to initiate a common internal reaction, such as generation of secondary messengers, which ultimately alters gene expression within the targeted cells. The CJMs link adjacent cells within a collective, which permits consistent action of all cells at the same point in time. The outcome of coordinated activity across cells is that historegulatory genes, morphoregulatory genes, selector genes, and switch genes act together to correctly specify the production and activity of morphoregulatory molecules, which ultimately drives stage-appropriate differentiation.

The fourth premise is that interactions of historegulatory and morphoregulatory genes in series provide the epigenetic basis of pattern formation in organogenesis. Specific gene expression signatures control spatial and temporal sequences of mitosis, migration, and mortality in particular cell collectives. In other words, the preceding space- and time-dependent relationships of a cell collective control the later events in which the collective participates as the cell and tissue patterns are organized. The position of a cell collective in space and time is probably of greater importance than the exact profile of expressed genes in defining the ultimate patterns for differentiation of tissues, organs, and systems.

In summary, groups of cells react to external signals in accordance with both their particular location in space and the precise time during development. A unique CAM signature specifies cells that belong to a given collective, while functions and movements of that collective are modulated by SAM variations. Finally, networks of cells in a given collective are connected by divergent CJM constellations that allow all the cells to act together as one.

#### **3.4.5. Programmed Cell Death**

PCD (or apoptosis) is an evolutionarily conserved process in which certain embryonic cells die physiologically (rather than pathologically) as a means of shaping solid structures (e.g., the digits, long bones, or palate) or hollowing tubular structures (e.g., blood vessels and the neural tube) (Compagnucci et al., 2021; Penalzoza et al., 2006). Apoptosis can form an organ by eliminating unneeded cells without inducing tissue remodeling (e.g., digit separation) or by inducing cell and tissue reorganization (e.g., cardiac and craniofacial morphogenesis). At each site, apoptosis is driven by a predetermined gene expression pattern that causes individual cells to degenerate and die. In normal embryos, this prearranged genetic profile is invoked only in those cells which fail to achieve the optimal cell collective-specific connections and functions; in this regard, apoptosis is an expected physiological response to eliminate transient cell types during morphogenesis (morphogenetic cell death) and tissue differentiation (histogenetic cell death). A more detailed discussion of apoptosis in terms of its structural appearance and molecular causes can be found in other publications (*Morphologic Manifestations of Toxic Cell Injury*, Vol 1, Chap 6) as well as several

reviews directed to toxicologic pathology practice (Elmore, 2007; Elmore et al., 2016; Santagostino et al., 2021).

Certain developmental toxicants are known to induce aberrant apoptosis, which can occur via several distinct mechanisms. The chief of these are changes in CAM, CJM, and/or SAM expression as well as perturbations in intracellular signaling including morphogen production. Xenobiotic-induced apoptosis resulting from interference in any of these processes often leads to extreme or failed apoptosis, which in turn contributes to such adverse outcomes as inappropriate cell and tissue differentiation, inadequate or excessive growth, structural malformations, and functional deficits. Apoptosis to prune injured embryonic cells has been proposed as a means for minimizing teratogenic effects following teratogen exposure (Torchinsky et al., 2005).

#### **3.5. Histogenesis and Functional Maturation**

As development proceeds, stem cells progressively follow certain cell- and tissue-specific fates, thus limiting the cell lineages that they may generate. Differentiation restricts developmental plasticity. Final cell fate determinations occur as organogenesis is ending and are associated with the expression of certain structural genes. Expression of these genes differs among various cell collectives and probably alters not only the cell structure but also the function of DNA control elements, locking the control elements so that only specific DNA segments can be expressed going forward.

Therefore, as development proceeds, totipotent stem cells (which can express all genes and so can become any cell at need) evolve to pluripotent stem cells (which can develop into many but not all cell types), then to oligopotent stem cells (which can form only a few cell types), and finally to terminally differentiated cells. The increased cell specialization restricts the ability of more differentiated cells with respect to such major developmental processes as cell division and migration, and instead diverts the mature elements into performing their specific functions. This process of cell maturation into fully functional tissues and organs is termed **histogenesis** (Figure 11.4).

Histogenesis is promoted by many biochemical changes. Perhaps the most critical is an increase in



protein synthesis, especially of tertiary (i.e., tissue-specific) molecules that define the identity and function of a given cell and tissue. The need for more protein is accompanied by the expansion of the endoplasmic reticulum (ER) and Golgi apparatus, which serve respectively to manufacture and package proteins. This rise in protein synthesis may be regulated at either the transcriptional or translational level and is often mediated by internalization of CAMs or ligand-receptor complexes. In this fashion, the epigenetic information detected at the cell surface is transferred from the extracellular environment to the cell control machinery. These maturation messages appear to pass from cell to cell in a collective through the cell type-specific CJs.

The time of functional maturation of cells depends on the organ system in question (Table 11.1). The majority of organs and systems become functionally competent during gestation, but histogenesis continues in others well into the postnatal period (e.g., central nervous, reproductive, and skeletal systems). Some structures (particularly many brain regions, such as the cerebellum, hippocampus, and olfactory bulb) exhibit many peaks of histogenesis at various periods of prenatal and postnatal development (PPND), involving distinct cell collectives during each peak.

Histogenesis continues throughout postnatal life at the cytoarchitectural level (e.g., synapse formation and plasticity in the brain) and in the functional sense (e.g., clonal selection for antigen recognition and antibody production by various immune cells). Indeed, cell division and histogenesis continue in some “terminally differentiated” organs (e.g., the cerebral cortex) until puberty, and beyond. Toxicant-induced disruption of such maturation processes during postnatal life usually induces minimal if any malformations, instead eliciting functional deficits. Well-known examples of “functional teratogenesis” include subtle behavioral or immunological aberrations, many of which may be detected using neurotoxicology (Bolon et al., 2021; Li et al., 2017; Lowndes and Reuhl, 1997; van de Bor, 2019) or immunotoxicology (DeWitt et al., 2012; Dietert, 2014) tests. Examples in children include cognitive deficits associated with maternal consumption of alcohol (Mattson et al., 2019) or cocaine (Mayes, 2002) and an increased incidence of asthma associated with early exposure to high levels of air pollution (Nadeau et al., 2010) or multiple rounds of

antibiotic therapy (Raciborski et al., 2012). Such effects may not impact an affected individual’s survival but may diminish the chance to thrive.

## 4. STRUCTURE, FUNCTION, AND CELL BIOLOGY—PLACENTA

In contrast to the embryo/fetus, the placenta is a transient but true organ formed in utero to sustain the developing embryo and fetus. Tissues of the placenta are the first differentiated elements formed by a newly implanted blastocyst. The placenta serves as an interface for moving nutrients and waste products between embryonic and maternal circulations, thereby providing a permissive environment that supports embryonic growth. Other roles of the placenta include hormone production to control maternal hemodynamic and metabolic activities that sustain pregnancy as well as to provide a physical barrier to possible immunogenic stimuli. The structure and molecular expression of the placenta evolves extensively during gestation to meet the embryo’s shifting metabolic needs (Elmore et al., 2022; Georgiades et al., 2002).

### 4.1. Structure

The organization of the placenta has been well characterized (Benirschke, 2011; Cross, 1998; Cross et al., 2003; Elmore et al., 2022; Furukawa et al., 2014; Georgiades et al., 2002; Maltepe et al., 2010; Rossant and Cross, 2001; Wooding and Burton, 2008). Placental structure may be defined based on its gross appearance as well as its histological arrangement.

Macroscopically, placentas (alternatively placentae) of major domestic and laboratory animals exhibit four basic arrangements based on the extent of the surface contact between the embryonic and maternal tissues (Figure 11.5). Common species employed in developmental toxicity testing (rodents, rabbits, nonhuman primates [NHPs]) exhibit macroscopic features similar to those of humans. The four main macroscopic arrangements are:

- *Diffuse*—the maternal-derived tissue contacts the entire surface of the embryo-derived chorion—typical of horses and pigs;
- *Cotyledonary*—the maternal-derived tissue forms flattened plaques (known as caruncles) separated

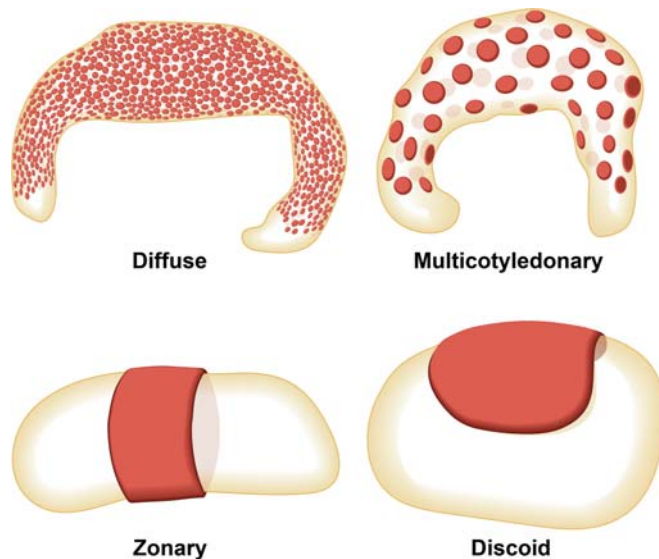


**FIGURE 11.5** Schematic diagram showing the macroscopic patterns of placental organization based on the extent of the surface contact between the embryonic and maternal tissues. The *diffuse* pattern is typical of horses and pigs; the *cotyledonary* arrangement is characteristic of ruminants; the *zonary* form is found in carnivores; and the *discoid* variant is observed in rodents, rabbits, and primates (including humans). Crafted by Mr. Timothy Vojt, Columbus, OH.

by intervening expanses of smooth and relatively avascular chorion—typical of ruminants;

- **Zonary**—the maternal-derived tissue forms a band that encircles the chorionic sac—typical of carnivores; and
- **Discoid**—the maternal-derived tissue produces a single (discoid) or sometimes double (bidiscoid), roughly circular cap that covers one pole of the chorionic sac—typical of rodents, rabbits, and primates (including humans).

The pattern appropriate to a given species should be considered when recording gross placental malformations.

Microscopically, placentas of major domestic and laboratory animals possess one of four basic arrangements. The structures are distinguished based on the cell layers comprising the interface between the embryonic membranes and uterine wall (Figure 11.6). These four patterns are:

- **Epitheliochorial**—all 3 cell layers (endothelium, connective tissue, and either epithelium [maternal] or trophoblast [embryo])—are maintained for the maternal and embryonic sides—typical of horses and pigs;

- **Synepitheliochorial**—all 3 cell layers are retained on the embryonic side, while the maternal side contains an additional multinucleate trophoblast type that attenuates the maternal epithelial layer—seen in ruminants;
- **Endotheliochorial**—all 3 cell layers are retained on the embryonic side, while only the endothelium remains after implantation on the maternal side—typical of carnivores;
- **Hemochorial**—all 3 cell layers are retained on the embryonic side, while all three maternal cell layers are eroded, allowing direct contact between maternal blood and embryonic tissue—typical of rodents, rabbits, and primates (including humans).

A minor difference among hemochorial species is the number of trophoblast layers on the embryonic side. Primates have one trophoblast layer (hemomonochorial), rabbits have two layers (hemodichorial), and rodents possess three layers (hemotrichorial). In recent years, the synepitheliochorial (or syndesmochorial) type has been grouped with the epitheliochorial arrangement (Furukawa et al., 2014).

Placentas also may be categorized based on the organization of the embryonic membranes. For example, in rodents two arrangements are present at different times during gestation. The *choriovitelline* placenta, colloquially termed the “yolk sac placenta,” develops when the YS membrane directly contacts the uterine wall soon after implantation. The YS (specifically its visceral wall) is the first functional placenta in the mouse and remains the only source of gas and nutrient exchange until midgestation (about E12 in the mouse). Gases are transferred across the YS by simple diffusion while macromolecules are taken up by phagocytosis (a process known as **histiotrophic nutrition**) (Georgiades et al., 2002; Zohn and Sarkar, 2010). The *chorioallantoic* or “definitive” placenta begins to develop at approximately E10.5 and is fully formed by E12.5 in the mouse. This mature placental arrangement brings maternal and embryonic circulations into close apposition to permit direct diffusion of materials to and from the embryo, a process known as **hemotrophic nutrition**. The switch from histiotrophic to hemotrophic nutrition is essential to meet the increasing metabolic needs of the growing embryo and fetus. Failure to properly form the choriovitelline placenta results in early embryonic death

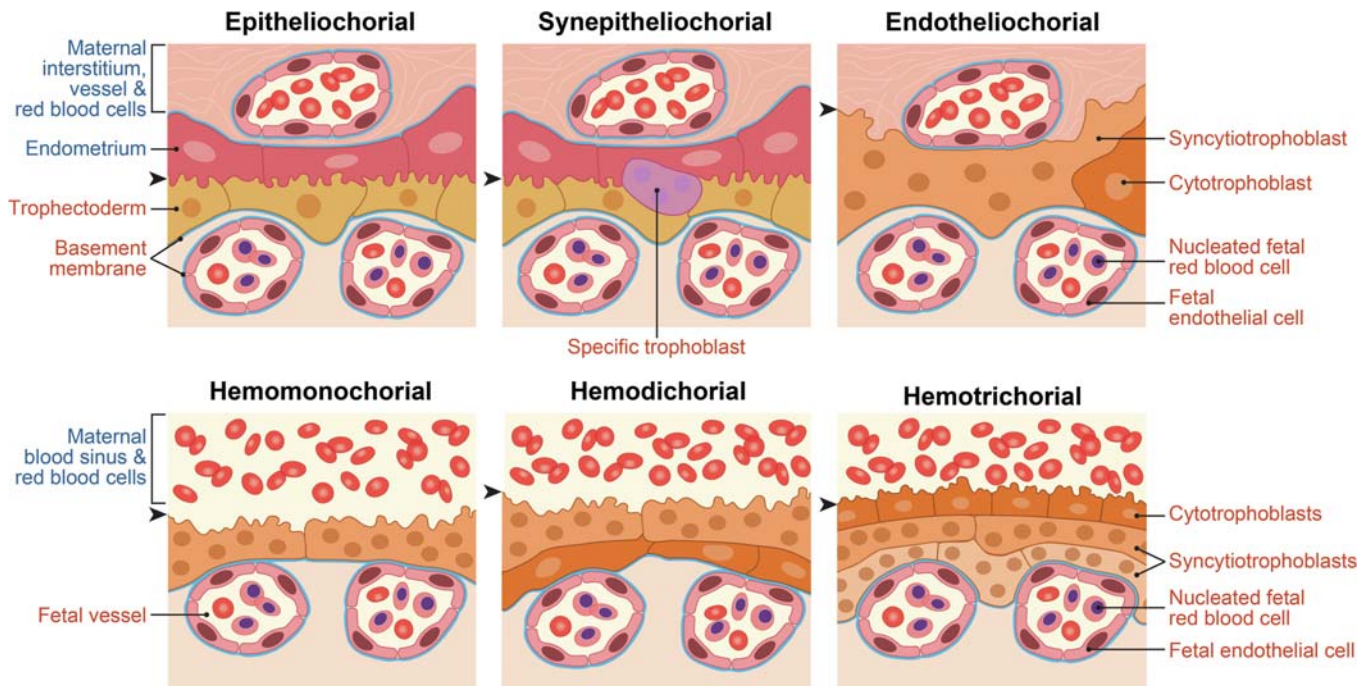


**FIGURE 11.6** Schematic diagram showing the microscopic patterns of placental organization based on the cell layers forming the interface between the embryonic membranes and uterine wall. The *epitheliochorial* pattern (where all 3 cell layers comprising the embryonic and maternal sides remain intact) is typical of horses and pigs. The *synepitheliochorial* variety (where all 3 cell layers are retained on the embryonic side while the maternal side possesses an additional trophoblast type and attenuated epithelial cell layer) is found in ruminants. The *endotheliochorial* arrangement (where 2 cell layers on the maternal side are absent) is observed in carnivores. The *hemochorial* pattern (where all three maternal cell layers are missing) is characteristic of rodents, rabbits, and primates (including humans). A minor difference among hemochorial species is the number of trophoblast layers present on the embryonic side: primates possess one (hemomonochorial), rabbits retain two (hemodichorial), and rodents have three (hemotrichorial) trophoblast cell layers. *Crafted by Mr. Timothy Vojt, Columbus, OH.*

in rodents (before E10 in mice), while inappropriate organization of the chorioallantoic placenta will cause embryonic death later in gestation (after E12.5 in mice) (Bolon and Ward, 2015b).

## 4.2. Cell Biology and Function

The initial placenta forms from the trophoblast (outer blastocoel wall) with a small contribution of somatic mesoderm (a derivative of the embryonic endoderm) that lines the inner surface of the blastocoel. The trophoblast represents the first fully differentiated cell lineage in the conceptus and is divided into various phenotypes that serve different roles depending on time during gestation (Elmore et al., 2022).

### 4.2.1. Placental Histology

The placenta consists of readily discernible embryonic and maternal components. The microscopic structure evolves during gestation,

leading to shifts in the complexity of placental layering and cellular composition. The nature and timing of these shifts also depends on the length of gestation for a given species (Table 11.1).

The initial microscopic structure of placenta is as a simple layer of trophoblast surrounding the embryo when it initially implants in the uterine wall. This trophoblast layer separates the embryo (ICM and blastocoel) from the maternal tissue.

Shortly thereafter, the YS gains ascendancy as the first placenta stage capable of transferring materials between the embryonic and maternal compartments. The amnion is a thin protective membrane that envelops and conforms to the embryo. The YS develops outside the amnion as a translucent, fluid-filled, well-vascularized pouch that appears in tissue sections as a thin, undulating membrane encircling the embryo. In sections, the YS forms as cuboidal epithelium resting on a thin layer of mesoderm. Aggregates of hematopoietic stem cells (“blood islands”)



form in the YS mesoderm early during gestation. These foci act as the source of erythrocytes (RBCs) in early pregnancy.

Later in gestation, the definitive placenta arises as a means of vastly increasing the surface area between embryonic and maternal tissues, thereby providing an expanded interface for nutrient and waste exchange. At the microscopic level, the placenta at this stage is arranged in layers that can be identified based on their locations and distinctive cytoarchitectural features (Figure 11.7); the arrangement of these layers depends to some degree on the macroscopic structure of the embryo–maternal vascular interface (i.e., epitheliochorial, synepitheliochorial, endotheliochorial, hemochorial [Figure 11.6]). Placental layering is understood most easily by working from the flat chorionic plate that

anchors the umbilical attachment outward to the surface that contacts the decidua. The inner domain is a network of intermingled embryonic and maternal vessels arranged as a dense, spongy labyrinth (as in rodents) or narrow, columnar villi (as in primates).

The rodent (mouse and rat) placenta is widely used as a model for understanding fundamental placental structure based on its many similarities to the human placenta and the rapid pace of its structural evolution during the abbreviated rodent gestational period (Elmore et al., 2022; Furukawa et al., 2019). This section briefly describes some key cytoarchitectural features of placenta using the mouse as a model. At the cytoarchitectural level, polar trophoblast cells form a cap over the ICM that differentiates into a boundary layer of spongiotrophoblast.

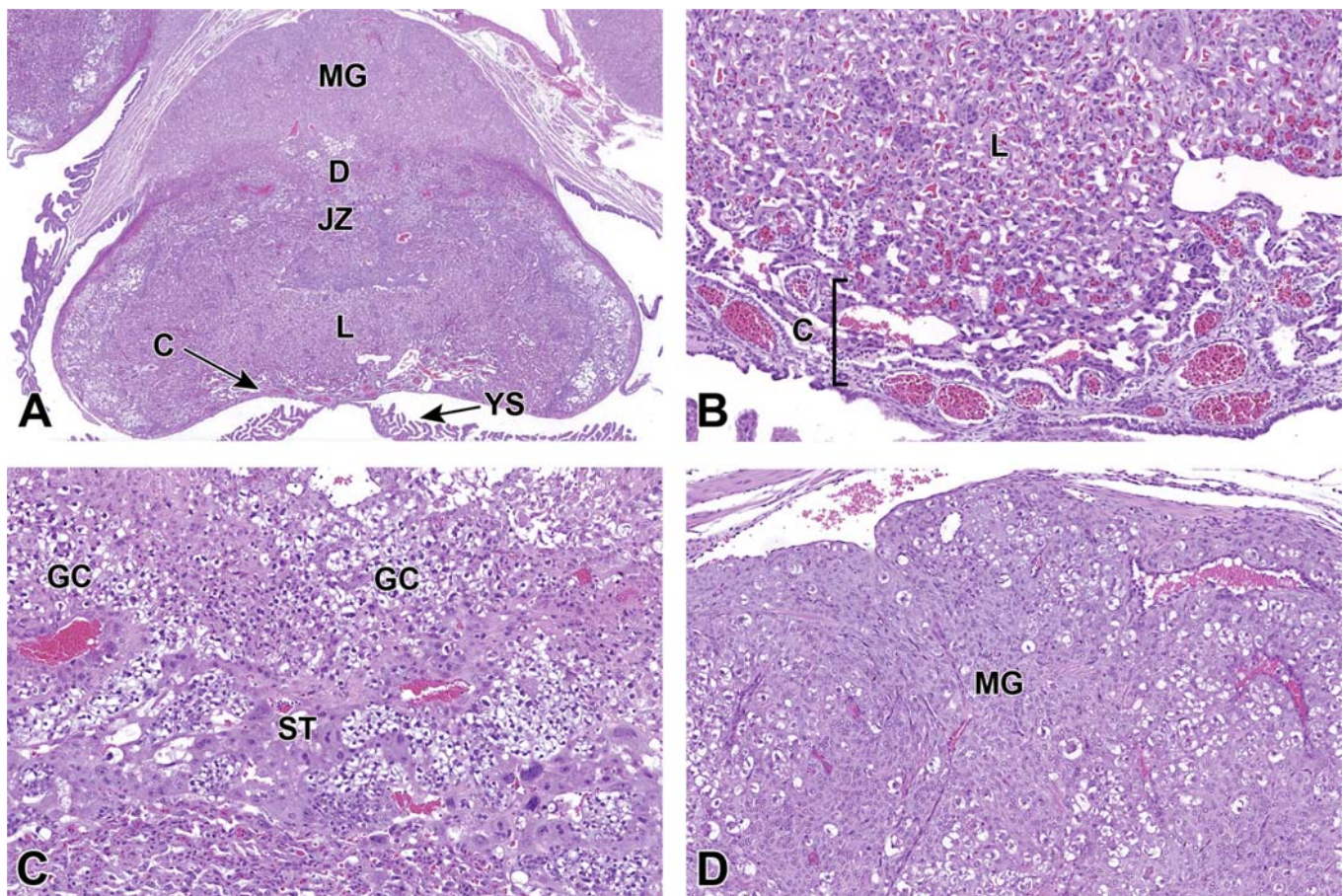


**FIGURE 11.7** Representative images of a definitive placenta cross-section at E15.5. The placenta has reached its peak weight and is beginning its regression in preparation for birth. Panel A: Low magnification of a placenta cross-section highlighting the maternal decidua (D), junctional zone (JZ), labyrinth (L), and chorionic plate (C). The metrial gland (MG) and yolk sac (YS) are also present. Panel B: Higher magnification of the labyrinth and chorionic plate. Panel C: Higher magnification of the junctional zone highlighting glycogen cells (GC) and spongiotrophoblast (ST) cells. Panel D: High magnification of the metrial gland. *Reproduced from Elmore SA et al.: Histology atlas of the developing mouse placenta, Toxicol. Pathol. 50:60–117, 2002.*



The mural trophoblast that encloses the blastocoel differentiates into an outer interrupted layer of trophoblast giant cells (TGCs) overlying a syncytial layer of syncytiotrophoblast and a monolayer of cytotrophoblast. The syncytiotrophoblast and cytotrophoblast together form the labyrinthine or villar trophoblast. Various trophoblast phenotypes exhibit unique gene expression patterns (Bolon and Ward, 2015a). In rodents, the metrial gland (or mesometrial triangle) is a transient, pregnancy-specific, maternal-derived modification of the mesometrial uterus that is characterized by extensive maternal arterial beds, intimate interactions with trophoblast, and a dense population of uterine natural killer (uNK) cells (alternatively granulated metrial gland [GMG] cells) (Picut et al., 2009). More details regarding microscopic features of the placenta for many species have been published elsewhere (Avagliano et al., 2016; Benirschke, 2011; Elmore et al., 2022;

Furukawa et al., 2014, 2019; Wooding and Burton, 2008).

In all types of placentas, the trophoblast is intimately associated with embryonic blood vessels lined by endothelium. Maternal blood vessels lack endothelium in hemochorial placentas. Embryonic blood vessels contain nucleated (“primitive”) RBCs early in gestation but contain an increasing proportion of nonnucleated (“definitive” [adult-type]) RBCs as gestation continues (Figure 11.8). Maternal blood vessels contain nonnucleated RBCs throughout gestation.

#### 4.2.2. Maternal Endpoints of Developmental Toxicity

In addition to nutrient transfer, various trophoblast lineages have important local and systemic regulatory roles during pregnancy. Both spongiotrophoblast cells and TGCs secrete hormones, including luteotropic molecules to

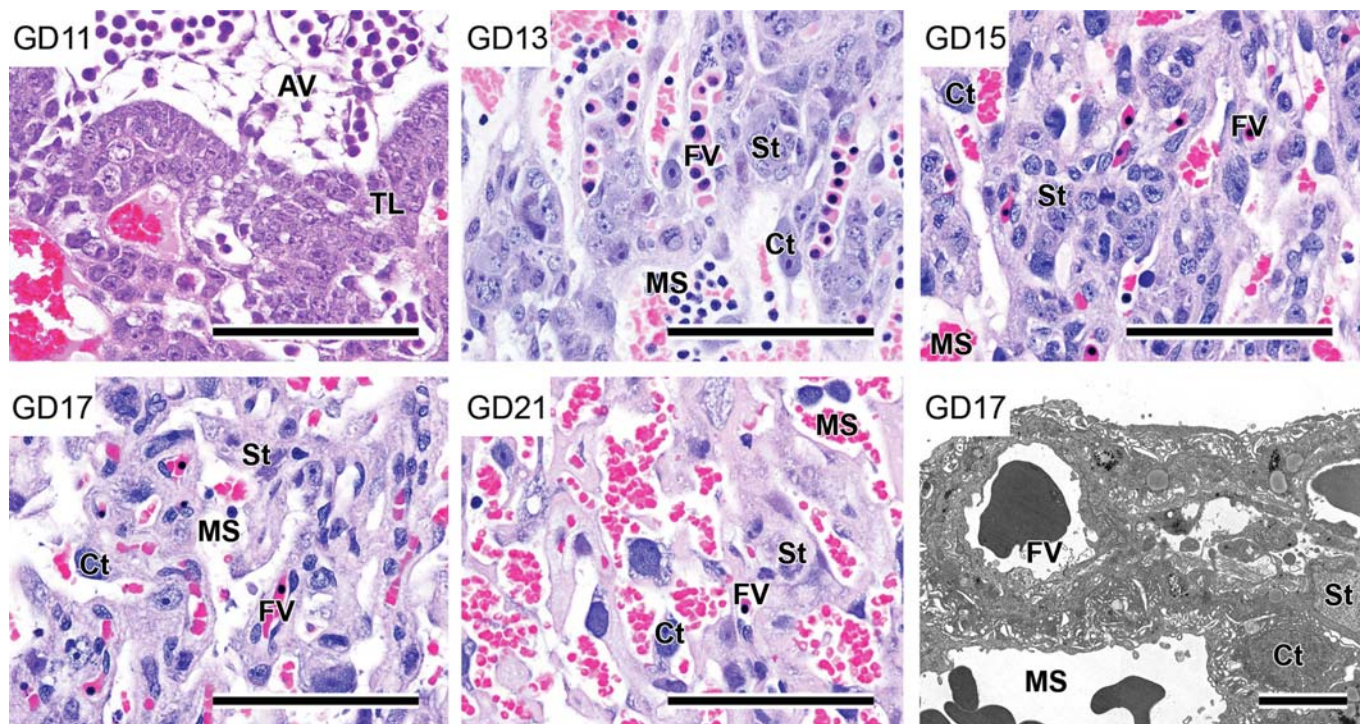


**FIGURE 11.8** Morphology of trophoblastic septa in the labyrinth zone of the rat placenta evolves over time as gestation progresses. Light microscopy: HE stain, bar = 100  $\mu$ m. Transmission electron microscopy (lower right panel), bar = 15  $\mu$ m. AV, allantoic vessel; Ct, cytotrophoblast; FV, fetal vessel (with nucleated red blood cells [RBCs]); GD, gestational day; MS, maternal sinusoid (with non-nucleated RBCs); St, syncytiotrophoblast; TL, trophoblast layers. Reproduced with minor adaptations to the figure legend from Furukawa S et al.: *Morphology and physiology of rat placenta for toxicological evaluation*, J. Toxicol. Pathol. 32:1–17, 2019, under a Creative Commons License (CC-BY-NC-ND 4.0).

maintain pregnancy as well as lactogenic factors to promote mammary gland development and milk generation to sustain the neonate. TGCs also produce numerous vasoactive molecules including angiogenic factors, anticoagulants, and vasodilators; these actions enhance the proximity of the maternal and embryonic circulations, thereby promoting blood flow toward the placenta that ensures a sufficient nutrient supply for the embryo. The maternal decidual cells also secrete many cytokines, growth factors, and hormones that modulate placental function.

The placental structure serves as an effective barrier to a maternal immune attack against the embryo. Shortly after implantation, the maternal decidua limits excessive penetration by embryonic cells and maternal immunoglobulins (Wang et al., 2004). This blockade results from both the dense character of the decidual reaction, which provides a physical barrier, but also by the generation of chemical inhibitors of tissue proteases. Infiltrating uNK cells, a lineage of bone marrow-derived large granular leukocytes that collect in the decidua during early and midgestation (Elmore et al., 2022), are thought to modulate the success of implantation (Ashkar and Croy, 1999) as well as regulate local angiogenic and immunological reactions (Croy et al., 2003, 2010; Erlebacher, 2014; Zhang et al., 2011).

Several structural adaptations in placental organization are designed to increase the physiological efficiency of gas, nutrient, and waste transfer. For example, branching morphogenesis in the labyrinth of rodents and villi in primates involves extension of embryonic capillaries into trophoblast columns, thus increasing the amount of vascular surface available for exchange. The trophoblast layers become attenuated as gestation advances, while the individual trophoblast cells develop adaptations (e.g., microvilli, invaginations) that increase the surface area available for exchange. Moreover, the countercurrent direction of blood flow in maternal and embryonic blood vessels ensures that the gradients for nutrient and waste exchange between the two circulations always favor the transfer of oxygen and nutrients into embryonic capillaries and the removal of waste products into maternal sinusoids (Adamson et al., 2002).

## 5. EVALUATION OF TOXICITY

The toxicologic pathology aspects of developmental toxicity testing are usually performed using various *in vivo* test systems. The goal is to determine the extent to which substances can interfere with normal development and cause adverse effects in the offspring. The four main adverse effects that may be experienced by the developing organism are death, altered growth, malformations, and functional deficiencies. Basic aspects of developmental biology at the cellular and molecular levels have utilized invertebrates, such as fruit flies (*Drosophila melanogaster*) and worms (*Caenorhabditis elegans*); nonmammalian vertebrates, including zebrafish (*Danio rerio*) and birds (e.g., chick [*Gallus gallus*] and quail [*Coturnix japonica*]); and many mammalian species (see *In Silico, In Vitro, Ex Vivo, and Non-Traditional In Vivo Approaches in Toxicologic Research*, Vol 1, Chap 24). The test species used in routine developmental toxicity testing are generally mammals. For substances known to be teratogenic in humans, concordance of developmental toxicity outcomes among test species and humans depends on the chemical properties of the agents, and no single species is completely accurate in predicting the human response (Table 11.2).

This section briefly reviews the main principles of developmental toxicity testing and delineates the factors that make various mammalian species the subjects of choice for such analyses. This presentation emphasizes general considerations of study design and interpretation to supplement the more comprehensive technical discussion provided in the chapter on DART testing (see *The Role of Pathology in Evaluation of Reproductive, Developmental, and Juvenile Toxicity*, Vol 1, Chap 7). Additional details on pathology evaluation of embryos, fetuses, neonates, and placentas for various species may be found in the scientific literature and many reference books (Altshuler, 1997; Behringer et al., 2014; Bolon, 2015; Bui, 2006; Croy et al., 2014; Wigglesworth and Singer, 1998). Indeed, **dysmorphology** (i.e., the study of congenital structural malformations) in the clinical setting remains the foundation for efforts to identify new human teratogens when performing postmarketing



**TABLE 11.2** Comparative Teratological Outcomes of Known Human Teratogens in Common Mammalian Test Species

Substance Class	Rodents				Nonrodents			
	Mouse	Rat	Hamster	Guinea Pig	Rabbit	Dog	Pig	Primate
Antibiotics (aminoglycosides)	±	+		±	—			—
Antibiotics (tetracyclines)	±	±		+	—	—		
Anticancer alkylating agents	+	+			+			+
Anticancer antimetabolites	±	+	+	+	±	±	+	±
Anticoagulants (coumarins)	—	+			—			
Anticonvulsant diones	+	±						±
Anticonvulsant hydantoins	+	+	—		+	—		+
Antihormones (thyroid)	+	±		+	±			
Hormones (androgenic)		+	+	+	+	+	+	+
Polychlorinated biphenyls	—	—		—	—	+	±	±
Vitamin A analogs	+	+	+	+	+	+	+	+

**RESULTS**

Positive (+[i.e., predicts human response])	5	7	3	5	4	3	3	4
Variable (±)	3	3	0	1	2	1	1	3
Negative (—)	2	1	1	1	4	2	0	1
Concordance with human response	50%	64%	75%	71%	40%	50%	75%	50%

Key: + = positive response, ± = variable response, — = negative response, empty cell = not reported.

Adapted from Table 1b of Bailey J, Balcombe JP.: *The future of teratology research is in vitro*, *Biog. Amines* 19:97–145, 2005, with permission.

assessments of recently approved therapeutic products (Epstein, 1995; Jones and Carey, 2011).

## 5.1. Toxicity Testing

Multiple models and study designs are used to assess developmental toxicity for new products. The current section briefly describes routine in vitro (and ex vivo) and in vivo animal models and key design parameters employed for this purpose.

### 5.1.1. In Vitro and Ex Vivo Assays

In vitro and ex vivo models examine toxic responses in cells and tissues in isolation from systemic factors (e.g., absorption, circulation, excretion). The absence of these factors means that even the best in vitro and ex vivo models

are not fully equivalent to responses that might occur in vivo. That said, in vitro and ex vivo models have several advantages for mechanistic toxicology investigations. First, assays may be prepared from isolated cells or pieces of most major organs (brain, liver, placenta, etc.) or from entire developing organisms (e.g., eggs or larvae). Second, substances may be applied directly to specimens at known concentrations. Third, the cost of performing these assays is often substantially lower than comparable in vivo studies. These short-term assays are not meant to substitute for in vivo testing in pregnant mammals but rather are utilized in mechanistic investigations (Daston, 2011) and to prioritize chemicals with little existing data for further in vivo developmental toxicity testing. These short-term assays are used for evaluating mechanisms of toxicity due to the ability to observe

developmental events over time and the elimination of confounding maternal influences. These techniques are particularly popular as indicators of accumulating developmental toxicants in polluted water.

In vitro systems currently employed for developmental toxicity testing may explore the effects of substances in isolated cells and tissues or in whole organisms. Specimens used for evaluating embryonic injury include cell and tissue (e.g., micromass) cultures; mini-organs (e.g., embryoid bodies, organoids, and sometimes microphysiological systems); eggs or larvae of several invertebrate or nonmammalian species including hydras (*Hydra attenuata*), nematodes (*C. elegans*), fruit flies (*D. melanogaster*), small fish (e.g., medaka [*Oryzias* spp.] or zebrafish [*D. rerio*]), African clawed frogs (*Xenopus laevis*), and birds (e.g., chickens and quail); rodent whole embryo cultures; and stem cells (see *In Silico, In Vitro, Ex Vivo, and Non-Traditional In Vivo Approaches in Toxicologic Research*, Vol 1, Chap 24). In the future, synthetic embryos derived wholly by combining various cultured stem cell types may be adapted for toxicity testing (Amadei et al., 2022). Three in vitro models—the mouse embryonic stem cell assay (mESC), rat limb micromass assay (rLMM), and rodent whole embryo culture assay (rWEC)—have been validated for developmental toxicity testing by the European Center for the Validation of Alternative methods (ECVAM). These three assays are highly accurate (70% for rLMM, 78% for mESC, 80% for rWEC) in predicting developmental toxicity (Luz and Tokar, 2018) and correctly identify non-teratogens about 85% of the time. The mESC and the zebrafish embryotoxicity test are reported to better correlate with in vivo developmental toxicity outcomes compared to the rWEC assay for at least some chemicals (de Jong et al., 2011).

In vitro and ex vivo tests also can be used to examine placental toxicity (Göhner et al., 2014). Recently proposed models include primary trophoblast cultures, immortal cell lines, and tissue explants. Ex vivo evaluation of perfused human placenta seems to be a representative and highly informative method for toxicity testing that offers better insights into various drug transporters, xenobiotic metabolic pathways, and tissue binding.

These short-term screens (especially those using invertebrates or isolated cells and tissues) have several advantages over in vivo testing. The major benefits include their rapidity, low cost, and reduced utilization of sentient beings. Unfortunately, these short-term assays also have several significant disadvantages. The main problems are lack of specificity, inability to model pharmacokinetic (PK) events, and uncertain applicability to intact organisms (Neubert et al., 1985). When considered together, these attributes often preclude a definitive interpretation of data from in vitro and ex vivo tests. The relevance of such models may be improved using data from physiologically based pharmacokinetic (PBPK) modeling (see *ADME Principles in Small Molecule Drug Discovery and Development*, Vol 1, Chap 3) to define more appropriate exposure levels and by employing model systems (e.g., rodent whole embryo culture) that undergo biologically equivalent developmental events that closely resemble those that occur in the target species.

### 5.1.2. In Vivo Studies in Animals

The conventional strategy for developmental toxicity safety assessment is to examine the ability of a substance to adversely impact development of the intact organism in vivo. In general, the study design includes prenatal exposure throughout the entire period of organogenesis. Program designs commonly test the product in one rodent and one nonrodent species, most often the rat and the rabbit unless other species (e.g., NHP) are deemed more relevant. Decisions regarding relevance are based on comparisons of species-specific developmental parameters (Table 11.1) in combination with empirical evidence (e.g., PK data).

As in any risk assessment, the route of exposure by which the substance is delivered should parallel the likely route of human exposure. This requirement is especially true in developmental toxicity testing because the effects of some xenobiotics depend on their route of administration.

Several designs may be used for developmental exposures of offspring. Traditional embryofetal development (EFD) studies for safety assessment expose the conceptus by treating the dam (i.e., pregnant animal) during organogenesis or from the beginning of organogenesis

until just before parturition. This approach evaluates maternal reproductive endpoints (number of implantation sites, number of viable implantations, etc.) and macroscopic embryonic features (e.g., major internal and external malformations). Abbreviated exposure periods may be used if the intent of the *in vivo* study is to examine the mechanism of a particular defect. In such cases, exposure often is limited to the time during gestation that represents the critical period of development for a particular organ anlage (Bolon et al., 1994; O'Leary-Moore et al., 2010).

Adequate assessment of developmental toxicity to address certain questions may necessitate exposure of offspring after birth. For example, developmental neurotoxicity testing for chemicals requires continuous treatment from the time of neurulation (i.e., the time at the start of organogenesis when the neural tube is forming as the primordium of the CNS) through weaning because certain structures (e.g., cerebellum, hippocampus) and processes (e.g., myelination) as well as most cognitive, motor, and sensory functions do not form until well after birth (Bolon et al., 2021). In such instances, assessments of developmental toxicity include both structural and functional endpoints (Li et al., 2017, 2018).

Additional study designs that test both reproductive and developmental capabilities may initiate exposure before mating (in either males or females, or both) and continue through late gestation and lactation (ICH, 2020a). In some instances, PPND studies span several generations (typically two or three) to evaluate the potential for "heirloom" developmental toxicity arising from toxicant-induced injury affecting parental gametes. Combined DART studies are performed because it is often difficult to distinguish the effects mediated through parental toxicity versus those from direct developmental toxicity to developing offspring. The rationale for such all-in-one designs is to broaden the likelihood of detecting both developmental and reproductive hazards while reducing the cost, effort, and time required for conducting and analyzing such studies. These approaches assess adverse events that manifest as prenatal and/or postnatal abnormalities, and they typically encompass a greater range of anatomic and functional endpoints.

More detailed consideration of various design options for EFD and PPND studies can be obtained in *The Role of Pathology in Evaluation of Reproductive, Developmental, and Juvenile Toxicity*, Vol 1, Chap 7.

## 5.2. Key Endpoints in Developmental Toxicity Testing

Developmental toxicity testing is intended to examine the potential of substances to impact the health and survival of offspring. Accordingly, depending on the study design, the evaluation will focus on examining effects in embryos, fetuses, neonates, and/or juveniles. Nonetheless, additional examination of the placenta and maternal reproductive attributes is necessary since these entities directly impact developmental success in the developing progeny.

### 5.2.1. Maternal Endpoints of Developmental Toxicity

Standard EFD protocols often use top dose levels that induce minimal overt maternal toxicity (ICH, 2020a). The developmental effects of this toxicity are often difficult to interpret (Beyer et al., 2011; Rogers et al., 2005). Major fetal malformations like NTDs; open eyes; rib defects (fused, missing, or supernumerary bones); sternal abnormalities (disorganized or fused segments); and vertebral anomalies (e.g., altered fusion or segmental arrangement of arches or bodies) often occur at maternally toxic doses, while these malformations are absent at doses that are distinctly nontoxic for the mother (Khera, 1984). In all species, embryo-fetal lethality increases with maternal dose. A visible developmental toxic finding may be considered to be of potential human relevance by regulatory agencies even if it is mediated via maternal pharmacological effects or occurs at doses causing signs of maternal toxicity unless mechanistic and/or other convincing evidence to the contrary is provided (Danielsson, 2013).

Appropriate nutrition is essential to prevent spurious results in developmental toxicity studies. Feed restriction in pregnant rats and rabbits has been shown to reduce fetal body weight and cause minor changes in skeletal development such as altered ossification of



metacarpals, metatarsals, sternebra, or caudal vertebrae (Cappon et al., 2005; Fleeman et al., 2005). These changes occur in the absence of external visceral malformations in the fetus (Cappon et al., 2005; Fleeman et al., 2005).

The initial endpoints examined in developmental toxicity studies are related to the health of the mother. The rationale for this approach is that in-life measurements of the dam throughout the course of gestation provide information regarding the health of the gestating offspring. Importantly, many in-life measurements (e.g., gentle palpation, intermittent body weights) may be repeated without harm to the dam or the progeny.

Multiple endpoints for assessing maternal reproductive health provide data regarding the health status of the progeny. Key in-life measurements of maternal health generally include clinical signs, food and water consumption, and maternal weight gain during pregnancy. Essential parameters to quantify at necropsy are the terminal body weight of the dam, target organ weights (including the uterus), and in some cases microscopic analysis of selected target organs; an important consideration is to also measure either the total weight of the gravid uterus or the maternal carcass weight after uterine removal to avoid bias due to different litter sizes. In addition, the number of total implantation sites and viable implantation sites should be determined. Sites may be counted in fresh tissue, or implantation sites may be highlighted using ammonium sulfide staining (Narotsky et al., 1997) (see *The Role of Pathology in Evaluation of Reproductive, Developmental, and Juvenile Toxicity*, Vol 1, Chap 7); fresh tissue may be processed for microscopic evaluation, while ammonium sulfide staining precludes microscopic analysis. When treatment is begun prior to mating, fertility endpoints (e.g., time to conception) are often useful. If parturition is included in the study design, changes in the timing and duration of birth as well as the number of live offspring can be informative. Care must be taken when considering the relevance of maternal data because these endpoints are relatively crude measures of developmental toxicity. In some instances, maternal parameters (e.g., weight gain over time in pregnant rabbits) can vary greatly for reasons unrelated to treatment.

### 5.2.2. Progeny Endpoints of Developmental Toxicity

Many endpoints that may be objectively measured at necropsy will directly reflect the developmental health of the litter as a whole, and of the individual conceptuses within the litter. Important parameters to measure in all developmental toxicity studies include several measures of litter size—the total number of conceptuses, the numbers of viable and dead conceptuses, and the number of resorptions (abnormal implantation sites)—and the incidences of gross structural malformations and incidental variations. Other suitable endpoints incorporated in some cases include histopathological examination and (after birth) clinical signs and symptoms (e.g., abnormal skin coloration, inability to suckle) as well as simple behavioral tests (Bolon and Omer, 1989; Crawley, 2007; Rogers et al., 1997).

#### 5.2.2.1. MACROSCOPIC EVALUATION OF MORPHOLOGIC EFFECTS

The numbers of dead fetuses and resorptions give information regarding a substance's ability to induce prenatal mortality. These two macroscopic endpoints are increased by exposure to many developmental toxicants. In isolated near-term fetuses and neonates, the quality of intra-uterine growth may be ascertained by measuring body dimensions (typically the crown-to-rump length) and total body weights, and the sex ratio can be determined using the anogenital distance (AGD) (Bolon et al., 2017). At necropsy or in preserved fetuses, the kinds and incidences of external defects are recorded (Figure 11.9). In developmental toxicity tests that include collection of parturition and lactation data, additional endpoints to acquire for neonates (or juveniles) include numbers of perinatal deaths, structural malformations, birth weights, and progressive weight gain over time. A critical issue in necropsy planning for developmental toxicity studies is that dams often cannibalize malformed, functionally defective, and nonviable offspring shortly after delivering during the dark cycle (i.e., when a technician is not available to collect them), so evaluation for developmental toxicity may be more accurate if a necropsy is performed to obtain near-term fetuses.

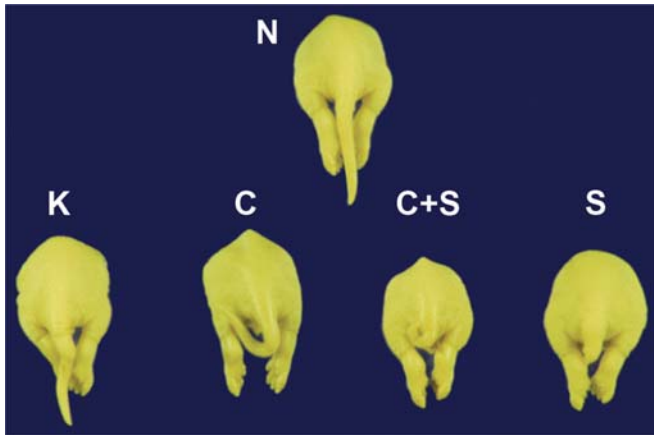


**FIGURE 11.9** Minor skeletal defects—kinking (K), curling (C), and shortening (S)—affect the tails of near-term (gestational day [GD] 17.5) mouse fetuses following maternal inhalation of methanol throughout organogenesis (GD 6 to GD 15). In contrast, the sham-exposed control has a straight (i.e., structurally normal [N]) tail. Processing: Fixation by immersion in Bouin's solution.

The *Chernoff-Kavlock test* has been suggested as a less labor-intensive alternative to routine EFD studies (Chernoff and Kavlock, 1982). This protocol involves administration of minimally toxic doses of a substance to pregnant rodents during organogenesis, with measurements of changes in maternal weight during the treatment period, the proportion of pregnant survivors at term that produce a viable litter, average litter size, pup weights at birth, and average neonatal survival and body weight gains from PNDs 1 to 3. Reduced survival and/or growth at PND 3 are interpreted to indicate prenatal toxicity. Therefore, this test has the advantage of being a relatively rapid and simple in vivo screen. Extending the postnatal observation period may increase the sensitivity of the test.

Some macroscopic structural parameters require special postnecropsy processing of near-term fetuses or neonates. Gross examination of internal organs may be performed by making multiple, parallel free-hand cross sections (Wilson's technique (Barrow and Taylor, 1969; Leroy and Jocteur-Monrozier, 2013; Newbigging et al., 2015; Wilson, 1972; Ziejewski et al., 2015)) through the heads and bodies of near-term fetuses or neonates that have been fixed in Bouin's solution, Davidson's solution, or modified Davidson's solution. The object of the

Wilson's technique is to detect altered shapes, sizes, and positions of expected organs as well as to recognize adventitious (unnatural) or missing organs. Appropriate formation of skeletal morphology may be assessed by skeletal double staining of unfixed fetuses or sometimes neonates with Alcian blue (to highlight cartilage) and alizarin red S (to demonstrate bone) (Menegola et al., 2001; Trueman and Stewart, 2014). The output of skeletal double staining is to detect changes in the shapes and sizes of bone profiles that are indicative of malformations or developmental delays (Yasuda and Yuki, 1997) (Figure 11.10). These techniques are somewhat time-consuming and require considerable technical expertise on the part of the prosection personnel.

#### 5.2.2.2. MICROSCOPIC EVALUATION OF MORPHOLOGIC EFFECTS

Fixed conceptuses may be processed for histopathologic examination. Conventional fixatives include Bouin's solution, Davidson's solution, and modified Davidson's solution (i.e., combinations of aldehydes, acids, and alcohol that penetrate well and can decalcify skeletal tissues) as well as 4% methanol-free formaldehyde ("paraformaldehyde") and neutral buffered 10% formalin (4% formaldehyde with methanol as a stabilizer). Bouin's solution typically is not used as a fixative for placenta as this agent disrupts erythrocytes. Larger specimens with thick skin will need to be incised to permit fixative to reach viscera. Histological processing times should be evaluated in each laboratory to ensure that tissue dehydration and paraffin infiltration are sufficient to ensure good section quality (Bolon et al., 2015; Kaufman, 1992).

As with adult organs, evaluation of developing animals starts with low magnification scanning of the entire section. This practice is especially important in developing animals (embryos, fetuses, and neonates) as the shapes, sizes, and locations of multiple organs may be examined simultaneously. The differentiation of possible toxicant-related changes from normal tissue features will require some practice due to the constantly evolving organ contours and cellular compositions throughout gestation and, in certain organs (e.g., bone marrow, brain, lymphoid organs), the early postnatal period. An important consideration is to detect new or missing organs. Successful diagnosis and

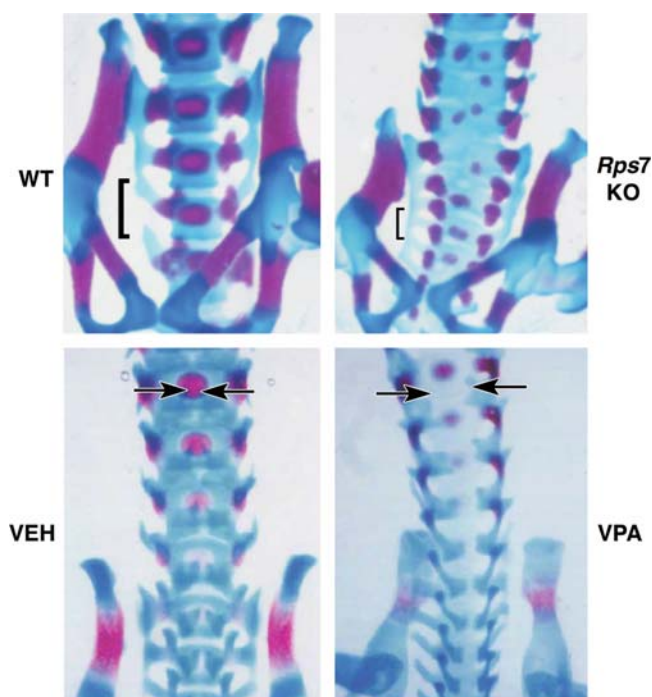


**FIGURE 11.10** Axial patterning defects in the vertebral column of near-term (gestational day [GD] 18) mouse fetuses are highlighted using double staining with Alcian blue (for cartilage) and Alizarin red (for bone) to compare the position, shape, and differentiation state (as revealed by the distinct double staining patterns). Top row: Relative to age-matched wild-type (WT) controls, fetuses with a null mutation (knockout [KO]) of the ribosomal protein S7 (*Rps7*) exhibited widespread disorganization of the ossification centers (i.e., red foci not aligned along the midaxial plane) in the lumbar and sacral regions as well as abnormal fusion of several sacral vertebrae (brackets). Bottom Row: Compared to age-matched vehicle-treated (VEH) controls, fetuses exposed to valproic acid (VPA) on GD 9 had *spina bifida occulta* as revealed by the greater distance between the margins of the vertebral arches (at arrow tips). (Top row) Reproduced from Watkins-Chow D et al.: Mutation of the diamond-blackfan anemia gene *Rps7* in mouse results in morphological and neuroanatomical phenotypes, *PLoS Genet* 9:e1003094, 2013; (Bottom row) Reproduced from Ehlers K et al.: Valproic acid-induced *spina bifida*: a mouse model, *Teratology* 45:145–154, 1992, by permission of John Wiley and Sons.

interpretation require comparison of potential findings to structures in concurrent control animals and, if available, a developmental anatomy atlas (e.g., Ashwell and Paxinos, 2008; Baldock et al., 2016; Bellairs and Osmond, 2005; Cochard, 2002; EMAP, 2013; Kaufman,

1992; Menegola et al., 2001; Saber, 2013; Steding, 2009; Theiler, 1989; Yasuda and Yuki, 1997). Several considerations dictate the choice of appropriate concurrent controls. These factors are especially important during early embryogenesis in species like invertebrates, nonmammalian vertebrates, and rodents where key developmental milestones evolve over a very short time span. Where feasible, the preferred approach is to compare developmental stage-matched conceptuses based on external macroscopic features that occur at known points during gestation; this option accounts for differences between “developmental stage” (as determined using anatomic criteria) and “developmental age” (based on the time after conception). In mice, animals in the same litter (i.e., having the same developmental age) differ in developmental stage by 10–24 h between the oldest and youngest embryos (Flaherty and Richtsmeier, 2018; Kaufman, 1999; Thiel et al., 1993). This inconsistency in timing should be considered in performing midgestation morphologic evaluations in rodents to ensure that structural differences between control and toxicant-exposed embryos represent treatment effects and not normal biological variation.

#### 5.2.2.3. IN-LIFE OBSERVATIONS OF DEVELOPING ANIMALS

For most test species, embryonic and neonatal animals exhibit a narrow spectrum of behaviors and physiological effects that may be visible in life or at necropsy. Examples include breathing, movement when stimulated (by light touch), and suffusion of the skin as blood circulates. These attributes may be assessed rapidly and reliably at necropsy. Routine clinical pathology analysis performed on blood samples may provide evidence of altered organ function especially for bone marrow, the immune system, kidney, and liver (*Clinical Pathology in Nonclinical Toxicity Testing*, Vol 1, Chap 10). In small species such as rodents, clinical pathology samples may need to be expanded (e.g., by adding physiological saline) or pooled (i.e., by combining specimens from several individuals from the same treatment group) to obtain enough material for analysis (Boyd et al., 2015).

Altricial animals (e.g., mice, rats, rabbits, carnivores, primates) are not capable of self-care immediately after birth, and thus will



demonstrate progressively greater behavioral and cognitive abilities over time. The times at which developmental landmarks (e.g., eye opening, sexual maturity, tooth eruption) and stereotypical behaviors are acquired are fairly consistent for a particular altricial species (Bolon and Omer, 1989). Similar behavioral evaluations may be performed for juveniles using functional observational batteries (Gad and Gad, 2003; Gauvin and Baird, 2008; Mathiasen and Moser, 2018; Moser, 2000; Zhong et al., 2017). Other functional characteristics including cardiac electrophysiology or noninvasive imaging (*In Vivo Small Animal Imaging*, Vol 1, Chap 13) and pulmonary function (*Respiratory Tract*, Vol 4, Chap 4) may be examined if warranted in juveniles but typically are not evaluated for developmental toxicity safety assessment.

Apparently healthy newborns may have morphologically invisible deficits leading to immunological, metabolic, and neurological abnormalities following gestational exposure to a teratogenic insult (Capitanio et al., 2022; Madden et al., 2020; Mattson et al., 2019). Several brain regions and the retina also undergo extensive postnatal differentiation in rodents, while the basic structural organization of these organs is essentially complete in NHP at term birth. Neural connections needed to establish vision require stimulation, which begins at birth in NHP and pigs but is delayed in species born with closed eyes such as rodents, rabbits, and dogs. Mammals are born with the elements of an immune system but have passive immunity during the initial postnatal period (DeWitt et al., 2012). In rodents, rabbits, and NHP, maternal immunoglobulin is actively transported across the placenta to provide the offspring with some immunity starting at birth, but in dogs, horses, pigs, and ruminants, limited or no placental transfer of immunoglobulin takes place. Juvenile animal studies have been designed to address subtle functional changes related to toxicity or delayed development as a means of assessing risk posed to pediatric populations by new therapies (De Schaepdrijver et al., 2019).

#### 5.2.2.4. IN SILICO ANALYSIS

Attempts to predict developmental toxicity in silico using the chemical structure of the test article or similar attributes have met with

variable success (Bal-Price et al., 2018; Mathiesen et al., 2021). Our ability to devise broadly relevant predictive models is hampered by several considerations. The first is the lack of uniform, reliable structure–activity relationship (SAR) data regarding the extent of developmental toxicity induced by substances, including prototypical agents used as the basis for generating new mathematical models. Combined with this lack of concrete data, the current level of mechanistic understanding is low with respect to normal developmental events and the ways in which particular classes of toxicants can perturb them.

**5.2.2.4.1. QUANTITATIVE MODELING** One approach to predicting toxicity of substances in the absence of experimental data is quantitative SAR (QSAR) analysis (Valerio, 2009). Published studies typically have compared relative toxicities among closely related compounds within a chemical class, such as phenols, glycol ethers, or retinoids. In some instances, the significant SAR are not the presence of a common chemical backbone but rather the presence of a particular moiety that influences the molecule's physicochemical properties. An example of this latter category is weak acids, which have many different structures but share a common side chain.

An alternative approach to quantitative analysis of developmental toxicity is adverse outcome pathway (AOP) modeling. This approach applies data from in vitro assays with known biological pathway information to produce an integrated computational analysis linking molecular-initiating events (MIEs) with a series of key events (KEs) that combine predictably to produce a biological response (Myden et al., 2022; Perkins et al., 2019). The initial step is to produce a qualitative AOP model around which a quantitative AOP model can be generated (see *In Silico, In Vitro, Ex Vivo, and Non-Traditional In Vivo Approaches in Toxicologic Research*, Vol 1, Chap 24).

Species-specific PK differences related to placental structure and function play an important role in determining developmental toxicity (Grigsby, 2016; Nau, 1986). Some research groups have developed detailed PBPK models to predict embryonic and fetal drug exposure. These PBPK models appear to be a promising in silico tool for predicting exposure of the

conceptus. These models often focus on the last stages of gestation, so knowledge regarding early developmental time points as well as specific data for placental biology (e.g., transporter composition) and permeability are urgently needed (Bouazza et al., 2019).

Integration of ex vivo data from human perfused placenta preparations in a placental PBPK model represents a promising approach for predicting fetal exposure to xenobiotics (De Sousa Mendes et al., 2016). Ex vivo perfusion of human placental cotyledons is the reference method for studying the transfer of substances from maternal circulation to the embryonic compartment because the processes are thought to mimic those that are active in functional placental tissue. In vitro models using primary trophoblastic cells, immortal cell lines, and tissue explants of placental origin have been advanced as tools for translational science. Recently, in silico methods have been advanced as complementary tools to validate experimental data on placental transfer, offering an attractive alternative for high-throughput screening of potential fetotoxicity at the early stages of drug design (Giaginis et al., 2011).

**5.2.2.4.2. ARTIFICIAL INTELLIGENCE** The introduction of artificial intelligence (AI) to accelerate and assist drug development has resulted in cheaper and more efficient processes, ultimately boosting the success rates of clinical trials. Use of AI technology can enhance success in drug development, particularly in improving QSAR models, novel target detection, rational drug design, biomarker identification, and effective patient stratification (Hessler and Baringhaus, 2018; Zhong et al., 2018). This approach can be used for many purposes, including developmental toxicity assessment (Ciallella and Zhu, 2019; Zhang et al., 2020).

### **5.2.3. Differentiating Developmental Toxicity from Maternal Toxicity**

A key question when trying to identify and characterize hazards and manage risk is to define whether a toxicant-associated developmental defect results from direct damage to the embryo (a primary effect) or is the indirect sequel to some maternal disturbance (a secondary effect). This

question has received considerable attention as maternal toxicity can influence the outcome of in vivo testing for developmental toxicity. However, developmental toxicity that arises as a secondary consequence to obvious maternal toxicity typically is not considered helpful for human risk assessment (see *The Role of Pathology in Evaluation of Reproductive, Developmental, and Juvenile Toxicity*, Vol 1, Chap 7).

The concern arises from difficulties in selecting the range of doses over which dams should be exposed in toxicity testing. Mild embryoletality and nonspecific fetotoxicity are common occurrences for doses at which dams exhibit clinical signs of overt toxicity. This fact suggests that such developmental defects are likely of questionable significance in efforts to extrapolate such developmental effects to lower doses and other species.

The potential for maternal toxicity to induce secondary developmental toxicity renders the task of using experimental animal data to predict human hazards, and to manage the risk associated with them, much more challenging. The conceptus nestled in its maternal support system represents a special situation in toxicologic risk assessment. Because the viability of the conceptus depends intimately on the health of the dam, unintended factors that disturb the maternal environment may produce adverse outcomes affecting some or many processes required for the offspring's conception, differentiation, and growth. Of course, the reverse is also true. The maternal organism offers a degree (and often a large one) of protection against at least some environmental perturbations. However, in other cases, damage to developing offspring may be substantial while maternal health is less affected, as has been demonstrated for perinatal neurotoxicity seen with transplacental transfer of methylmercury to the fetus (Minamata disease; Sakamoto et al., 2018) or lactational exposure to high levels of 2,3,7,8-tetrachlorodibenzo-p-dioxin (Tai et al., 2013). Lesions of the maternal-derived placenta in the absence of effects on maternal homeostasis have been linked to developmental toxicity for some agents (Khera, 1992).

Developmental defects arising indirectly from maternal toxicity differ from direct toxic effects on the conceptus primarily in their origin rather

than the end result. The number of possible mechanisms by which maternally mediated effects indirectly induce embryonic and fetal injury is probably much lower than the number of direct-acting (i.e., embryotoxic) mechanisms, and the range of embryonic or fetal consequences to maternal damage is also likely to be more limited.

Several hypotheses have been offered to explain this phenomenon. One prospect is that disrupted maternal support of the conceptus (e.g., by anemia or reduced placental circulation) leads to hypoxia in tissues of the conceptus (Webster and Abela, 2007). A second possibility is that an endogenous toxicant produced by xenobiotic-damaged maternal tissues (e.g., acidosis leading to a precipitous drop in the pH of embryonic tissues) crosses the placenta and damages the differentiating embryo. A third risk is that chemically induced damage in maternal metabolic pathways will produce an increase in maternal core body (and therefore uterine) temperature—in other words, hyperthermia (or fever) (Nelson et al., 1999). Finally, modification of maternal metabolism can lessen or intensify the effects of a substance (e.g., by activation of a nontoxic prodrug or production of a more toxic or longer-lasting metabolite). Maternal toxicity can promote developmental toxicity by several means, so it is probable that the spectrum of potential maternally controlled developmental abnormalities in the offspring will be quite broad.

The kinds of developmental defects that result indirectly from maternal toxicity, their incidence, and their significance are still subjects of considerable debate. Litters exposed to xenobiotics following maternal exposure may exhibit a constellation of adverse events including structural malformations, functional alterations, and deaths. These effects may result directly from primary embryo and/or fetal toxicity, indirectly as a consequence of maternal toxicity, or from some combination of the two.

Historical practice in the analysis of developmental toxicity data sets has been to ignore the potential that maternally mediated effects to the conceptus have the potential to impact the study outcome. However, the reverse situation can occur in which effects on the conceptus that appear only at maternally toxic doses are

automatically interpreted as secondary consequences of maternal toxicity. In a regulatory setting, study interpretation must consider both maternal toxicity and any identified developmental effects to distinguish, where possible, evidence of primary embryonic (and/or placental) damage versus secondary effects directly related to and only seen with maternal stress. Our experience suggests that decisions regarding the origin of adverse developmental outcomes (i.e., primary embryonic/fetal toxicity vs. secondary responses to maternal dysfunction) will be made on a case-by-case basis (see *The Role of Pathology in Evaluation of Reproductive, Developmental, and Juvenile Toxicity*, Vol 1, Chap 7), and that any effects on embryonic development will be viewed askance regardless of their cause.

## 6. RESPONSES TO INJURY

The conceptus represents a pair of unique transient organs—embryo/fetus and placenta—that just happen to be passengers together abiding in the maternal host. The embryo in particular exhibits unique responses to injury, especially during the earlier stages of gestation, in large part due to its lesser degree of cellular differentiation and its tolerance for low-oxygen conditions. Both these factors permit more ready repair of damage that would decimate the more differentiated and oxygen-dependent tissues of older animals. Nonetheless, the fundamental responses of the embryo/fetus and placenta to toxicant-induced damage are similar to the well-recognized reactions that occur in the tissues of toxicant-treated adult animals. Indeed, this equivalency was the underpinning for early efforts to predict developmental toxicity via the extrapolation of adult toxicity data.

As seen in other tissues, the conceptus (and neonate) responds to toxicant-induced injury by initiating mechanisms that either sustain the damaged cells until they can be repaired or ameliorate the damage when severely injured cells degenerate and die. The basic manifestation of toxicity in the conceptus is cell death (*Morphologic Manifestations of Toxic Cell Injury*, Vol 1, Chap 6), the ramifications of which range from none or slight (in early embryos with totipotent



or pluripotent stem cells) to major structural malformations, growth retardation, or in utero death. Cytotoxic agents include not only chemicals but also many infectious pathogens (especially bacteria and viruses) and physical agents (e.g., heat, ionizing radiation—see *Radiation and Physical Agents*, Vol 2 Chap 31). However, unlike adults, the conceptus seldom mounts an inflammatory response to necrosis (or other insults) until the latter half of gestation when the immune system has begun to show signs of maturity.

The plasticity of the early embryo (based on its large complement of totipotent and pluripotent stem cells) allows compensatory growth to completely restore many tissue defects after nonlethal exposure that would induce lethality or major malformations in older embryos (Kojima et al., 2014; Snow and Tam, 1979). That said, the compensation often necessitates a delay in repair so that a sufficient mass of new cells can be produced to patch sizable defects. This restorative capability may cause difficulties in interpreting data derived from some models (e.g., rodent whole embryo cultures) because statistically significant growth retardation in some cases is likely to represent a developmental delay (i.e., a slowed developmental pace ultimately culminating in a structure or function that is within normal limits albeit later in life than usual) rather than a genuine reflection of teratogenic activity per se. To be sure, attempts at repair following developmental toxicant exposure may result in deformations, which are congenital anomalies arising from an external force (as opposed to malformations, which are defects produced by internal injury). Deformations are generally seen later in fetal life and are caused by lack of movement. An example of a deformation is arthrogryposis.

### 6.1. Death

Death of developing conceptuses is a common event in human pregnancies, a process termed “terathanasia” or “teratothanasia” (Table 11.3) (Giagounidis et al., 1997). Traditional estimates of spontaneous embryonic loss held that at least 75% of all human conceptuses are lost during the first 6 weeks of development (Boklage, 1990), while more recent analyses suggest that

human embryonic and fetal loss under natural conditions is approximately 10%–40% before implantation and 40%–60% from conception to birth (Jarvis, 2016). Chromosomal anomalies are responsible for many instances of human embryonic attrition, especially in conceptuses lost early during gestation (Blue et al., 2019). Genetic mutations or broader chromosomal damage cause many malformations in fetuses that survive until term (El-Attar et al., 2021). Therefore, a general principle of developmental toxicologic pathology is that structural abnormalities in conceptuses are usually fatal. The most common lethal defects that occur during early gestation are NTDs, cardiovascular malformations, and multisystemic anomalies that cannot be linked to preexisting chromosomal damage. However, mortality does not stop with birth. About 8% of human infants with major congenital malformations die during the neonatal and juvenile periods (Boyle et al., 2018; Lozano et al., 2012).

### 6.2. Malformations

Overt embryonic and fetal malformations provide the most spectacular evidence of developmental disaster and as such have caused curiosity and dread for millennia. The modern science of teratology began to facilitate investigations of the biological basis of developmental defects and then expanded to encompass testing for other developmental damage including toxicity. The reason for this expanded focus is that many xenobiotics are **teratogens** (i.e., substances capable of inducing malformations).

Teratogens often affect multiple species and induce a similar spectrum of effects across species. Examples of toxic agents that generate malformations in both humans and laboratory animals include recreational (e.g., cocaine, ethanol, nicotine) and therapeutic (e.g., anticonvulsants, antineoplastics, immune suppressants) drugs as well as many environmental contaminants (e.g., heavy metals, plant toxins, solvents). Indeed, some xenobiotics are so effective as teratogens, and their spectrum of defects so reproducible, that they constitute preferred agents for investigating teratogenic mechanisms (e.g., ethanol [“alcohol”], retinoic acid, and valproic acid).

**TABLE 11.3** Estimated Outcomes of 100 Human Pregnancies versus Time From Conception<sup>a</sup>

Time from Conception	Live Births During Interval (Number)	Survival to Term (%)	Death During Interval (%)	Last Time for Induction of Selected Malformations
<i>PREIMPLANTATION</i>				
0–6 days	0	25	54.55	
<i>POSTIMPLANTATION</i>				
7–13 days	0	55	24.66	
14–20 days	0	73	8.18	
3–5 weeks	0	79.5	7.56	Day 23 <i>cyclopia</i> ; <i>sirenomelia</i>  Day 26 <i>anencephaly</i>  Day 28 <i>meningomyelocele</i>  Day 34 transposition of great vessels (of the heart)
6–9 weeks	0	96.00	6.52	Day 36 cleft lip; limb reduction defects  Week 6 diaphragmatic hernia; <i>rectal atresia</i> ; ventricular septal defect; <i>syndactyly</i>  Week 9 <i>palatoschisis</i>
10–13 weeks	0	92.00	4.42	Week 10 <i>omphalocele</i>
14–17 weeks	0	96.26	1.33	Week 12 <i>hypospadias</i>
18–21 weeks	0.01	97.56	0.85	
22–25 weeks	0.04	98.39	0.31	
26–29 weeks	0.24	98.69	0.30	
30–33 weeks	0.66	98.98	0.30	
34–37 weeks	9.72	99.26	0.34	
38+ weeks	14.33	99.32	0.68	CNS cell depletion

<sup>a</sup> Reprinted from Beckman DA, Brent RL: *Mechanism of known environmental teratogens: drugs and chemicals*, Clin. Perinatol. 13:649–687, 1986 with permission.

Reproduced from Haschek WM, Rousseaux CG, Wallig MA, editors: *Handbook of toxicologic pathology*, ed 2, 2002, Academic Press, Table III, p. 907, with permission.

Malformations have been reported in essentially all organs and systems of multiple vertebrate species. This section briefly describes

some of the more common anomalies observed in human obstetrical practice and animal developmental toxicity experiments.

### 6.2.1. Central Nervous System

#### 6.2.1.1. DYSRAPHISM

**Dysraphism** is the generic term for incomplete fusion of the neural tube (i.e., a “neural tube defect” [NTD]). Variants of this lesion are typically defined based on the affected site. Common forms are **cranioschisis** (nonfusion of the cranial portion), as exemplified in anencephaly, exencephaly, and encephalocele (Figure 11.11), as well as **rachischisis** (nonfusion of the caudal region) leading to *spina bifida* and meningocele. Rarely the entire neural tube remains open, a condition called **craniorachischisis**.

If the head is affected, the development of the pituitary gland is often rudimentary. These structural defects are associated with functional abnormalities, which may lead to secondary hypoplasia of endocrine tissues (i.e., adrenal, gonadal, and thyroid) that require pituitary releasing factors for their own maturation.

**6.2.1.1.1. ANENCEPHALY** **Anencephaly** (“no brain”) is more common in humans than in domestic animals. The usual appearance is the absence of neural tissue rostral to the brainstem (Figure 11.11). The prevalence varies considerably depending on the locale. Areas with heightened prevalence typically have populations with genetic predispositions or who live in regions with substantial environmental pollution (Campbell et al., 1986).

The pathogenesis for anencephaly is failed elevation and/or fusion of the neural folds. The shreds of exposed tissue in anencephalic brains develop an abnormal vascular supply that results in secondary neural destruction, so that only an angiomatous mass termed the “*area cerebral vasculosa*” remains at birth. The brain defect does not prevent the optic vesicles from developing normally, but the optic nerves may or may not be present.

**6.2.1.1.2. EXENCEPHALY** **Exencephaly** (Figure 11.11) is seen more frequently in laboratory animals than its counterpart anencephaly. In exencephaly, the brain protrudes through the missing skull; a typical presentation involves the cerebral cortex capping the forehead and a disorganized mass of midbrain at the crown of the skull. Erosion of the exposed brain tissue is less extensive in exencephaly relative to anencephaly. It has been proposed that exencephaly



**FIGURE 11.11** Neural tube defects (NTD) represent a continuum of cephalic dysraphism. Relative to an aged-matched control littermate (N), near-term mouse fetuses (gestational day [GD] 17.5) exhibit a spectrum of neural tube and craniofacial defects following maternal inhalation of methanol during neurulation (i.e., the period of neural tube closure, or GD7 to GD9 in the mouse). The mildest NTD variant is encephalocele (E), in which meningeal-covered cerebral cortex protrudes through a small opening in the frontal region as a consequence of incomplete anterior neuropore closure. Severe defects arising from complete failure of the anterior neuropore to close include exencephaly (X), in which the exposed cerebrum and midbrain form a tattered cap on the dorsal cranium, and anencephaly (A), where the brain and upper head are absent. The fetus marked by H has holoprosencephaly, or failure of the primary forebrain vesicle to divide into paired secondary vesicles. Craniofacial defects associated with NTD also reflect abnormal closure of the anterior neuropore. Mild effects (relative to the narrow inverted-T conformation of the N [control] fetus) usually present as hypognathism of the maxillae (upper jaw), indicated by the triangular oral openings for the E and X fetuses in the top row. Marked effects include clefting of the nose (X fetuses of the lower row), aplasia of the cranium (the A and all X fetuses), and aplasia of craniofacial bones (maxillae and mandibles [lower jaws], most prominent in the H fetus) and eyes. *Reproduced from Bolon B et al.: Methanol-induced neural tube defects in mice: pathogenesis during neurulation, Teratology 49:497–517, 1994, with permission.*

develops in animal species with short gestations, while anencephaly is more common for species with extended gestations due to the corrosive



effects of amniotic fluid over time. However, this explanation is not the only factor as anencephaly can be observed in rodents (Figure 11.11).

Numerous experimental agents can cause exencephaly in rodents, especially mice (Campbell et al., 1986). Some examples include conditions that reduce metabolism, like hypoglycemia; physical agents, such as X-irradiation; and many toxicants. Class effects are obvious for substances that work by similar mechanisms, like disrupting signals that control tissue interactions (e.g., hypervitaminosis A and retinoid drugs), inhibiting cell proliferation (e.g., colchicine and vincristine), or producing general cytotoxicity (e.g., cyclophosphamide, inorganic arsenate). Most substances that induce exencephaly act by preventing neural tube closure, but some cytotoxic agents can cause the recently fused neural tube to reopen. The occurrence of exencephaly depends heavily on genetic factors in some species, especially rodents. For example, in mice certain inbred strains (e.g., SELH/Bc) spontaneously develop this change at a fairly high rate. The incidence can be increased by xenobiotic exposure.

**Encephalocele** is the extension of brain tissue (usually the cerebral cortex and the overlying meninges) through a small opening in the calvarium (upper skull). These lesions typically present as small round nodules on the midline, often in the frontal region (Figure 11.11). The masses may be covered by skin, or the brain tissue may be exposed. In general, the neural tissue is fairly well differentiated. In mice, both encephalocele and exencephaly occur together in litters exposed to various xenobiotics, suggesting that they represent different expressions of the basic neural tube closure defect. Encephaloceles usually are much less common than exencephaly in animal models of NTD.

**6.2.1.1.3. HOLOPROSENCEPHALY** **Holoprosencephaly** (formerly designated arhinencephaly) stems from the failed partitioning of the prosencephalon (the primary forebrain vesicle) into the two portions of the telencephalon (the secondary brain vesicles from which the cerebral cortex arises bilaterally). The resulting single lobed brain with a single telencephalic ventricle is called a **holosphere**. The olfactory bulbs and tracts are absent.

The defect typically produces malformations in both the brain and the craniofacial skeleton

(Figure 11.11). A common variant is a reduction in the distance between the two eyes, or even their fusion into a single globe located at the midline (i.e., cyclopia). The condition can be mild or severe, but in most instances, individuals are so deformed that they die before birth. In less severe cases, the brain and craniofacial development is nearly normal, and deformities may be limited to the nose and upper lip.

The proposed pathogenesis is aberrant or absent activation of the forebrain-specific complement of *Hox* genes, resulting in dysregulation of *Shh* gene expression that controls patterning of distal structures. Expression of these genes specifies the position of many neural structures along the longitudinal neuraxis. Many substances can induce this lesion, including infections, metabolic disturbances (e.g., gestational diabetes), and toxicants. Perhaps the best-known animal model for xenobiotic-induced holoprosencephaly is maternal ethanol ingestion. All environmental causes are associated with elevated levels of reactive oxygen species (ROS), suggesting that oxidative stress may have a role in mediating the teratogenic effects.

**6.2.1.1.4. ACRANIA** **Acrania** (lack of the calvarium) is the skeletal defect that accompanies anencephaly and exencephaly. Associated skeletal reductions or loss affect the petrous temporal bone, sphenoid bone, and internal ear. The bones of the skull base usually develop normally. However, the cerebellum, pons, and cranial nerves are usually malformed. The pathogenesis may involve loss-of-function mutations in the *hedgehog acyltransferase (Hhat)* gene, and involvement of this pathway may explain why acrania may develop in combination with holoprosencephaly (Dennis et al., 2012).

**6.2.1.1.5. SPINA BIFIDA** *Spina bifida* is an NTD of the caudal axial skeleton resulting from failure of the neural arches of the vertebra to unite. This finding has been reported in all species. The prevalence varies widely depending on the country. This divergence in incidence raises questions regarding potential environmental, genetic, metabolic (e.g., diabetes and obesity), and nutritional influences as etiologies for the lesion in humans. Administration of some drugs has been linked to a heightened incidence of *spina bifida*, including carbamazepine

and valproate. Offspring of rodents given excess vitamin A or an antineoplastic drug (e.g., actinomycin D and vincristine) often have *spina bifida* and other spinal cord malformations; rabbits respond similarly to these agents and also to methyl salicylate. The risk of developing this defect decreases if folic acid levels are maintained by dietary supplementation prior to conception.

The degree of *spina bifida* is variable. **Myeloschisis**, the most severe form, appears as an area of open neural plate with no covering tissue (i.e., overlying meninges, vertebrae, epaxial muscles, and skin are all absent) (Figure 11.12). Degeneration of the exposed neural tissue results in paralysis of the hind limbs (paraplegia). Severe *spina bifida* may occur in conjunction with other CNS malformations at the cranial end of the neural tube, such as hydrocephalus and cerebellar malformations.

The intermediate form, termed *spina bifida cystica* (due to the bulging cyst-like sac characterizing these defects), encompasses the entities called **myelomeningocele** and **meningocele**. The former condition features the herniation of both the meninges and neural tissues through the vertebral defect, while the latter is distinguished by protrusion of the meninges but not the spinal cord through the osseous defect. Both usually present as a small, fluctuating mass located on or just beneath the skin surface near the base of the vertebral column. The spinal



**FIGURE 11.12** *Spina bifida* in a neonatal dog. The skin and vertebral column in the lumbar and sacral regions have failed to close. Courtesy of Dr. Wayne Crowell, Department of Pathology, College of Veterinary Medicine, University of Georgia, Athens, GA.

cord is abnormal by definition in myelomeningocele and may be structurally altered in meningocele even though it remains in situ.

The least severe form is *spina bifida occulta*, which is not an NTD in the strict sense and is most commonly asymptomatic. The only indication of its presence may be a sacral skin dimple or abnormally arranged tuft of hair. It is characterized by a gap in one or more vertebral arches with no protrusion of spinal cord or meninges outside the vertebral canal and no break in the skin covering the area.

**Arthrogryposis** (multiple joint contractures) is commonly seen in severe forms of *spina bifida*. The pathogenesis for joint contracture is spinal cord dysgenesis leading to reduced or absent motor activity.

#### 6.2.1.2. HYDROCEPHALUS

Hydrocephalus results from abnormal accumulation of cerebrospinal fluid (CSF) in the ventricular system, usually in conjunction with pronounced ventricular dilatation. Increased fluid pressure in the lateral ventricle leads to bulging of the uncalcified skull (Figure 11.13)



**FIGURE 11.13** Foal with markedly rounded skull due to congenital hydrocephalus. Reproduced from Haschek WM, Rousseaux CG, Wallig MA, editors: *Fundamentals of toxicologic pathology*, ed 2, 2010, Academic Press, Figure 20.5, p. 652, with permission.

and compresses the adjacent brain tissue, which usually is thinner than normal but still exhibits its normal anatomic features (distinct cortical layers, white matter tracts, etc.). Extreme cases lead to degeneration and loss of the ependymal epithelium with CSF dissection into the neuropil, especially along the white matter tracts. Morphologically, this lesion must be differentiated from hydranencephaly.

Two forms of hydrocephalus have been described, which have distinct pathogeneses. Obstructing CSF circulation within the ventricular system produces the common “non-communicating” form. The typical reasons for this blockade are space-occupying lesions that occlude the mesencephalic aqueduct (of Sylvius) or atresia of the median aperture (of Magendie) and the lateral apertures (of Luschka) in the roof of the fourth ventricle. The less frequent “communicating” form results from CSF overproduction by the choroid plexus, or rarely as a consequence of arachnoid granulation defects that prevent removal of CSF. Hydrocephalus can arise during development or at any time during later life where CSF flow is impeded.

#### 6.2.1.3. HYDRANENCEPHALY

**Hydranencephaly** is characterized by the absence of the cerebral hemispheres with replacement of their normal location by a membranous sac filled with CSF. This finding is considered to be an extreme variant of **porencephaly** (in which a localized brain cyst collects CSF). This condition is distinct from hydrocephalus, in which the dilated CSF-containing spaces are bordered by attenuated but visible brain tissue.

Many etiologies have been reported to cause this lesion in animals. The list includes nutritional conditions, such as deficiencies of vitamin A, B<sub>2</sub>, B<sub>6</sub>, or B<sub>12</sub>; physical agents, like ionizing radiation; many toxicants, such as ethylenethiourea and several metals (lead nitrate, mercuric mercury, and tellurium); and vascular infections. Mice are a common test species for investigating this defect.

#### 6.2.1.4. MICROCEPHALY

**Microcephaly** (“small brain”) is a primary defect in brain development leading to secondary skull involvement. Both the brain and calvarium are diminished in size. Pure cases

of microcephaly, in which brain size is decreased but the calvarium is unaffected, are rare.

The cerebral hemispheres of microcephalic brains, and particularly the frontal lobes, are reduced in size and have a simplified pattern of gyri. **Microgyria** or **macrogyria** (reduced or increased size, respectively, of cerebral gyri [brain folds]), often with marked asymmetries, are common findings in the cerebrum. Microscopic evaluation reveals fewer large neurons with corresponding increases in undifferentiated neuroblasts and abnormal spindle-shaped cells in the cerebral cortex. Microcephaly has been linked to cognitive deficits, microphthalmia, and cleft palate, and occasional defects may arise in the appendicular skeleton as well.

Microcephaly may be modeled in rats using many different agents. Examples include multiple antineoplastic drugs (e.g., busulfan, 5-fluorouracil, and vincristine); at least one auxin (indole-3-acetic acid); and methylazoxymethanol (MAM), to name a few. Other etiologies that have been linked to microcephaly include excessive alcohol consumption, hyperthermia, and radiation. In humans, many infections during the first trimester cause microcephaly. Known etiologies include viruses like flavivirus (Zika), herpesvirus (chickenpox and cytomegalovirus), and rubivirus (rubella) as well as protozoa (*Toxoplasma gondii*).

#### 6.2.1.5. DYSPLASIA

In teratology, **dysplasia** represents a morphologic anomaly arising from altered cell constitution and/or tissue organization within an organ (Hennekam et al., 2013). This definition for dysplasia is analogous to its usage in oncology, where the term means the presence of abnormal cells within a tissue.

In any organ, this change can occur as a localized or diffuse change. The functional impact may be negligible (especially for focal lesions), or function may deteriorate over time as widespread tissue disorganization prevents physiological maturation throughout the juvenile and adult periods of life. Dysplasias typically arise from genetic, metabolic, or teratogenic events including chemical exposure and radiation. In the nervous system, a frequent presentation is abnormal regional organization of the cerebellum (Figure 11.14), cerebral cortex, and/or hippocampus characterized by altered density



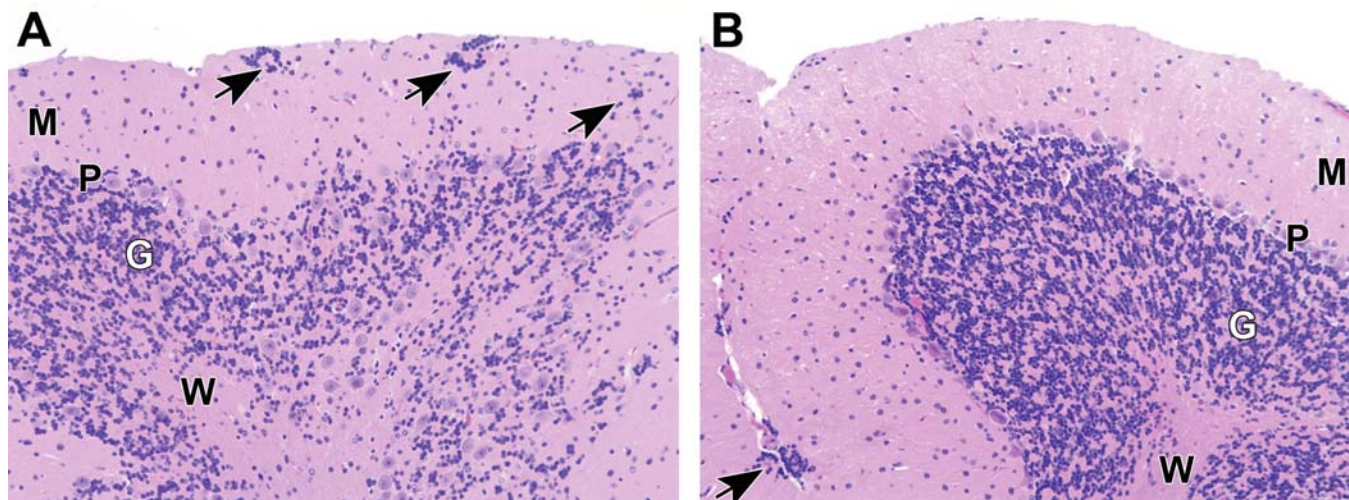


**FIGURE 11.14** Neuronal heterotopia (Panel A) in the cerebellum of an adult, neurologically normal mouse following whole body irradiation on postnatal day (P) 1 to ablate bone marrow prior to introduction of non-murine stem cells. The key findings are increased cellularity of the myelin-rich molecular layer (M) and deep white matter (W); diffuse disarray and intermingling of the Purkinje cell (P) and granule cell (G) layers; and many intra-parenchymal nests of retained external granule cells (arrows), which serve as the precursors to the (“internal”) granule cell layer. In contrast, a nonirradiated adult mouse (Panel B) exhibits regular organization of the neuronal layers, low cellularity of myelin-rich regions, and one incidental focus (arrow) of external granule cells beneath the meninges. *Reproduced from Bolon B: Nervous system. In Haschek WM, Rousseaux CG, Wallig MA, editors: Haschek and Rousseaux’s handbook of toxicologic pathology (Vol. 3), ed 3, 2013, Academic Press, Figure 52.30, p. 2061, with permission.*

or location of one or more cell types. The proposed mechanism is disrupted cell production and/or migration resulting from exposure during an organ’s critical period of development. In conventional product development programs, neural dysplasia occurs as a procedure-related effect in rodents following whole body irradiation shortly after birth to permit engraftment of cell-based test articles.

### 6.2.2. Craniofacial Structures

#### 6.2.2.1. ANOPHTHALMIA AND MICROPHTHALMIA

**Anophthalmia** is the complete absence of all optic structures: the globe, optic nerves, optic foramen, and optic chiasm. **Microphthalmia** represents hypoplasia. Both lesions may be either unilateral or bilateral. Anophthalmia often occurs with other defects of the musculoskeletal, cardiovascular, and central nervous systems and may occur concurrently with microphthalmia, while microphthalmia is often accompanied by anomalies of other eye-associated structures. The extent of ocular malformation depends on the timing of the developmental arrest. The ocular blood supply may be reduced or missing;

indeed, attenuation of the hyaloid artery to the rodent eye may result in microphthalmia. Other examples of linked lesions include congenital cataract; coloboma (a gap in the iris, lens, or retina); pupillary obstruction; corneal scarring; and extraocular muscle imbalance. The correlation of microphthalmia with facial and cardiovascular defects suggests that this is an anomaly of the first branchial arch.

Several mechanisms have been defined leading to anophthalmia or microphthalmia. Anophthalmia is a consequence of unsuccessful optic vesicle extension and subsequent lack of lens placode induction. This circumstance may represent a primary anomaly (i.e., abortive vesicle formation) or a secondary effect (e.g., suppressed forebrain growth with later failure of eye development). Another mechanism is the destruction of a previously formed optic vesicle. Genetic, environmental, and toxic causes have been reported for several species. Many teratogens induce these lesions in rodents including antineoplastic drugs like actinomycin D, chlorambucil, and methylhydrazine as well as X-irradiation.

#### 6.2.2.2. CYCLOPIA

This malformation typically coexists with holoprosencephaly. **Cyclopia** may present as complete ocular fusion (one eye) in a single orbit or as two eyes in a single orbit (Figure 11.15). Ocular defects associated with cyclopia include colobomas, abnormal optic nerves, and an absent or attenuated optic chiasm. Cyclopia occurs when the rostral (anterior) portion of the notochord and adjacent mesoderm are deficient in mass. This shortage leads to aberrant induction of forebrain tissues followed by severe derangement of midline facial development.

Cyclopia is uncommon in humans. A well-recognized cyclops syndrome occurs as outbreaks in sheep or cattle that graze on hellebore (*Veratrum californicum*) at day 13.5 of gestation due to the steroidal alkaloids cyclopamine,



**FIGURE 11.15** Cyclopia with holoprosencephaly in a fetal pig. Courtesy of Dr. John King, College of Veterinary Medicine, Cornell University, Ithaca, NY; Reproduced from Haschek WM, Rousseaux CG, Wallig MA, editors: *Fundamentals of toxicologic pathology*, ed 2, 2010, Academic Press, Figure 20.8, p. 654, with permission.

cycloposine, and jervine. Cyclopia–holoprosencephaly can be induced in rodent embryos by maternal exposure to X-irradiation or certain xenobiotics (e.g., cyclophosphamide and vincristine) during early neurulation.

#### 6.2.2.3. AGNATHIA AND MICROGNATHIA

**Agnathia** is the total absence of the maxilla or mandible and is extremely rare in mammals. This condition is a common feature of agnathia–otocephaly complex, a rare, lethal malformation of the head. Cardinal features include marked mandibular hypoplasia or agenesis combined with microstomia (reduced size of the oral aperture) and **aglossia** (absence of the tongue) or **hypoglossia** (shortening of the tongue). **Otocephaly** is characterized by close approach (**melotia**) or midline fusion (**synotia**) of the ears in the rostral (anterior) neck region. This condition may accompany cyclopia and/or holoprosencephaly (Figure 11.11); hence, it may be seen in ruminant fetuses exposed to *V. californicum*. These findings result from disrupted development of the first branchial arch.

**Micrognathia** is hypoplasia of the maxilla and/or mandible and occurs more frequently than agnathia. Maxillary micrognathia is an expression of reduced formation of premaxillary tissue during development. Mandibular micrognathia may occur with cleft palate, **glossoptosis** (downward displacement of the tongue), microcephaly, and microphthalmia. Genetic as well as teratogenic causes including antineoplastic agents like actinomycin D, colchicine, and vincristine cause agnathia and micrognathia as well as other jaw anomalies in mice.

#### 6.2.2.4. CLEFT LIP AND CLEFT PALATE

**Palatoschisis**, or cleft palate, is an important developmental anomaly of mammals as the neonate cannot nurse properly with an incomplete palate (Figure 11.16). Moreover, a cleft palate usually results in inhalation of milk and aspiration pneumonia. Cleft palate may be accompanied by cleft lip (**cheiloschisis**). Cleft palate occurs when one or both palatal shelves (the palate primordia) do not rotate from their original position on either side of the tongue to assume their final horizontal position above the tongue, where fusion of the two shelves forms the palate. The cause may be multifactorial, including genetic, infectious, and





**FIGURE 11.16** Cleft palate (palatoschisis) in a near-term Simmental cross calf. *Reproduced from the SAC VS (Scottish Agricultural College Veterinary Services) Disease Surveillance Report: Outbreaks of idiopathic haemorrhagic diathesis syndrome in young calves, Vet. Rec. 165: 39–42, 2009, with permission.*

environmental factors including toxicant exposure. Common xenobiotics associated with these conditions include alcohol, smoking, dioxin, estrogen, and retinoic acid. Of children with both cleft lip and cleft palate, 28% have diverse malformations in other organ systems as well (Milerad et al., 1997). The prevalence of palatoschisis in animals may be greater than thought at present since not all animals that die during or after birth undergo a complete necropsy examination. Cleft palate is commonly bilateral, indicating that neither palatal shelf was elevated. However, in some instances, only one shelf failed to assume its expected position, or interference by a protruding tissue mass (e.g., caudal misplacement of the prolabium [the central part of the upper lip]) prevents the palatal shelves from fusing.

Cleft palate is an excellent model system for demonstrating mechanisms that lead to the formation of developmental defects. Reorientation and fusion of the palatal shelves must occur and are especially time-dependent. Correct spatiotemporal positioning during palate formation depends on the appropriate expressions of many molecules and the correct pattern of PCD and palatal growth. The final process of palatal shelf fusion with elimination of the medial edge epithelium requires the generation of intercellular junctions, activation or appearance of intracellular contractile elements,

synthesis of GAGs, and genesis of the nerve and vascular supplies for the tissues. Simultaneously, the tongue must descend so that it does not obstruct reorienting palatal shelves.

Obviously, with such an intricate embryological process, interference with proper palate formation can occur in many ways. Particular influences include several genetic factors, exposure to xenobiotics, or an interaction between the two. The mouse is a common model species for investigations of cleft palate as it is particularly sensitive to any substance that may decrease growth of the palatine shelves. Teratogens that induce cleft palate include decreased maternal nutrition, hormones (especially corticosteroids), hypoxia, and virtually all cytotoxic xenobiotics.

### 6.2.3. Cardiovascular System

#### 6.2.3.1. ATRIAL SEPTAL DEFECTS

Although not fatal, **atrial septal defects** (ASDs) occur during fetal development and account for a substantial fraction of all human heart defects. Generally, small ASDs are hemodynamically insignificant and may therefore go undetected. The incidence of ASDs in domestic animals is probably similar to that in humans. Experimental induction of ASDs is not a commonly reported teratogenic effect but has been included for preclinical development of implantable ASD closure devices.

Four types of clinically significant ASDs have been described. First, defects of the oval fossa (the location of the *ostium secundum* in the interatrial septum) account for most ASDs in humans, exhibiting a female: male predilection of 3:1. This ASD is also the most common variant in dogs and cats. The lesion is characterized by a patent *foramen ovale* with a short or fenestrated primary septum, occurring with or without defective development of the secondary septum. The second form is the *sinus venosus* type, a relatively uncommon condition featuring a high ASD. It results from abnormal absorption of the *sinus venosus* into the right atrium or from altered formation of the *septum secundum*. Third, a persistent *ostium primum* results from incomplete fusion of the primary septum and the endocardial cushions, with resultant anomalies in the atrioventricular (AV) valves. Finally, the least common type of ASD stems from complete absence of the interatrial septum resulting from failed development of both primary and secondary septa.



Many other cardiac malformations have been associated with ASDs in humans. Examples include anomalies of the left AV valve (alternatively the mitral or bicuspid valve), atresia of the right AV (tricuspid) valve, common ventricle, coarctation (narrowing) of the aorta, noncyanotic patent *ductus arteriosus*, pulmonary stenosis or atresia, tetralogy of Fallot, transposition of the great vessels, and ventricular septal defects (VSDs). The etiology of ASDs is unclear but may involve genetic mutations, certain medical conditions (e.g., maternal diabetes or lupus), some medications (e.g., antiseizure and mood-stabilizing products), and environmental or life-style factors (e.g., use of alcohol, cocaine, or tobacco).

#### 6.2.3.2. VENTRICULAR SEPTAL DEFECTS

These malformations occur more commonly than ASDs. VSDs are classified according to their location in the septum as either membranous or muscular. In some cases, absence of both septal parts coexists with other cardiovascular anomalies (e.g., aortic hypoplasia, transposition of the large vessels). Generally, VSDs result from incomplete fusion of the AV endocardial cushions with the ventricular muscular septum and conus ridges. Some VSDs close spontaneously. This type of defect is also common in cattle and, to a lesser extent, other domestic species (Figure 11.17).

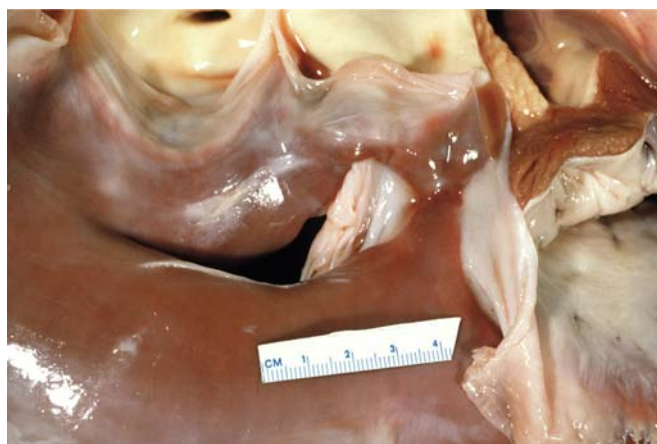


**FIGURE 11.17** Ventricular septal defect in the subvalvular region of a horse heart. *Reproduced from Haschek WM, Rousseaux CG, Wallig MA, editors: Fundamentals of toxicologic pathology, ed 2, 2010, Academic Press, Figure 20.10, p. 655, with permission.*

The etiology of VSDs is still unclear, but genetic and environmental factors may play a role. In humans, approximately 4% are thought to stem from a chromosomal or genetic defect. VSDs may be concentrated in families with trisomy 13, 18, or 21. The literature shows that maternal diseases like diabetes mellitus and infections (especially those inducing fever) also may play a role. Experimental treatments that delay closure of the cardiac septa can induce VSDs. Etiologies include hypoxia; nutritional deficiencies (e.g., folic acid or vitamin A) or excesses (copper); and various chemicals (e.g., griseofulvin in cats, trypan blue and salicylate in rats, thalidomide in rabbits, and several anti-neoplastic agents in many laboratory animals).

#### 6.2.3.3. RIGHT ATRIOVENTRICULAR (TRICUSPID) VALVE ANOMALIES

**Atresia** (congenital absence) of the right AV valve has been linked to defective development of the right ventricle, certain ASDs (patent *foramen ovale* or fenestration of the primary septum), hypoplasia of the left ventricle, hyperplasia of the left AV (mitral) valve, and an atretic or hypoplastic pulmonary artery. These defects are classified into type I defects (normal orientation of the great vessels) and type II defects (transposition of the great vessels).

**Ebstein's anomaly** is a rare cardiac malformation in humans. The exact cause is unknown, but genetic and environmental factors are believed to play a role. Maternal exposure to benzodiazapines or lithium carbonate may increase the risk. This anomaly occurs due to improper development of the right AV (tricuspid) valve; the valve ring is correctly placed, but the valve orifice is displaced into the right ventricle, resulting in a decreased ventricular volume. The posterior and septal leaflets of the valve have an abnormally low attachment. Since excavation of the endocardial outgrowths is incomplete, the upper parts of the posterior and medial cusps remain attached to the wall. Patent *foramen ovale* and fenestration of the primary septum commonly occur with Ebstein's anomaly in humans.

Experimental investigation of valve anomalies and prosthetics in animals usually is restricted to assessing how cardiac valves are formed (Kheradvar et al., 2017). Drug-induced valvulopathies reported in adult humans are induced by

numerous chemicals including anorexigens (appetite suppressants), dopamine agonists, ergot alkaloids, and some recreational drugs (Elangbam, 2010). Valvulopathy as a teratogenic effect has been described for some antiepileptic drugs and has been suggested for ibuprofen (Lynch and Abel, 2015).

#### 6.2.3.4. TRANSPOSITION OF THE GREAT VESSELS

**Great vessel transposition** results from an abnormal spatial arrangement of any of the large blood vessels: aorta, cranial (superior) and/or caudal (inferior) *vena cavae*, pulmonary artery, or pulmonary vein. The outcomes may range from a change in blood pressure to interruption of the normal right-to-left circulation, depending on the exact location and extent of the malpositioning. Regardless of which great vessel is affected, survival requires the presence of additional cardiac anomalies, such as septal defects and persistent *ductus arteriosus*, which allow mixing of the two parallel circulations. This disorder appears to be more prevalent in human male infants, but in animals it is not recognized as a sex-linked trait.

Great vessel transposition is one of the four cardiovascular defects that comprise the **tetralogy of Fallot**. In this defect, the aorta is shifted to the right from its usual position over the left ventricle, coming to rest over a VSD (the second defect). Accordingly, the aorta delivers a mix of oxygenated (left ventricle) and poorly oxygenated (right ventricle) blood to the body. The other two defects are narrowing of the pulmonary valve (which is located between the right ventricle and the pulmonary trunk serving the lung) and right ventricular hypertrophy. Surgical intervention is required to correct the defects in order to avoid heart failure.

The pathogenesis by which transposition of the aorta and pulmonary trunk takes place is still largely unknown. Hypotheses include lack of spiral twisting of the great vessels around each other, abnormal division of the *truncus arteriosus*, and anomalous cardiac looping. The latter possibility has been confirmed in mice exposed to retinoic acid, where altered looping has been linked to hypoplasia of the conotruncal ridges and aorticopulmonary septum, with subsequent delayed fusion of the AV cushions. Great vessel transposition accompanies numerous other

cardiac anomalies in rats exposed to X-rays (100–200 rad). Studies in mice with targeted mutations of perlecan, a heparan sulfate proteoglycan, have shown complete transposition of large arteries in nearly 75% of embryos, thus showing the importance of proper ECM function for vessel development.

#### 6.2.4. Respiratory System

Total absence of the lungs, bronchi, and vascular structures—pulmonary **agenesis** (or **aplasia**)—is usually unilateral. Although the main etiology is unknown, genetic mutations, viral infections, and vitamin A deficiency in early pregnancy may all result in developmental failure of the primitive lung bud. In rodents, it typically affects the left lung. Aplastic lungs have absent pulmonary and vascular structures with either rudimentary bronchi or abrupt termination at the distal trachea. This condition is likely caused by failed interactions between endodermal components of the tracheobronchial buds and the surrounding mesenchyme.

**Pulmonary hypoplasia** is a more frequent anomaly. The lung parenchyma resembles fetal lung tissue in that there are underinflated alveoli. Primary hypoplasia may be caused by viral infections, genetic disorders like trisomy 21, or nitrofen administration. Secondary lung hypoplasia has been associated in humans with congenital diaphragmatic hernia (which increases intrathoracic pressure on lung tissue); **oligohydramnios** (abnormally reduced amounts of amniotic fluid [usually due to bilateral renal agenesis], loss of which restricts thoracic wall movement); and thanatophoric dwarfism (where abnormal skeletal contours alter the thoracic cavity shape and size).

#### 6.2.5. Gastrointestinal System

##### 6.2.5.1. APLASIA/HYPOPLASIA OF THE CAUDAL ENTERIC GANGLIA

Digestive tract motility is profoundly affected by defective development of the enteric nervous system (ENS). The ganglia that comprise the ENS are seeded by migration of neural crest cells during gestation. This developmental event is controlled, at least in part, by the glial-derived neurotrophic factor (*Gdnf*) signaling pathway. Mice engineered to have null mutations of *Gdnf* or in either one of the two proteins that contribute to its complex receptor, GDNF

receptor  $\alpha$ -1 (*Gfra1*) and the RET tyrosine kinase receptor (*Ret*), do not form enteric ganglia in the caudal portion of their intestines; these animals also lack kidneys. In humans, the condition is termed **congenital aganglionic megacolon** (Hirschsprung disease) and in the US occurs in approximately 1 per 5000 births and has a male predisposition. The most accepted pathophysiology for this condition is a defect in the craniocaudal migration of neuroblasts originating from the neural crest, which results in a lack of neural crest-derived cells at the distal end of the colon. Mutations in several genes have been identified in patients with Hirschsprung disease. A similar defect is characteristic of lethal white foal syndrome (LWFS) in overo American Paint horses as well as some mutant mouse models. Consumption of cocaine, opiates, and selective serotonin reuptake inhibitors (SSRIs) has been suggested to alter neurotransmitter gradients necessary for appropriate differentiation of ENS neurons (Rao and Gershon, 2018).

#### 6.2.5.2. DIAPHRAGMATIC HERNIA

**Diaphragmatic hernia** may arise by several mechanisms, and the severity may range from a thinned area of the diaphragm to its complete absence. It may or may not occur together with other birth defects. Mechanisms of diaphragmatic herniation include failed or delayed fusion of the pleuroperitoneal membranes with the *septum transversum* and the dorsal mesentery of the esophagus, premature relocation of the intestines from the extraembryonic coelom to the abdominal cavity, and weak or abnormal diaphragmatic musculature. Most herniation sites are located in the dorsolateral portion of the diaphragm, thereby leaving room for part or all of the abdominal viscera to enter the thorax. Diaphragmatic hernias are predominantly located on the left side.

Various pharmacological, surgical, and transgenic manipulations can elicit this lesion in experimental animals (Chiu, 2014). Nitrofen exposure as well as deficiencies of vitamin A and zinc all can induce diaphragmatic hernias in rodents. The same effect occurs in pigs exposed to methallibure, a nonsteroidal pituitary gonadotropin inhibitor. At least 18 transgenic mouse models with phenotypic similarities to human congenital diaphragmatic hernia have been identified (Nakamura et al.,

2020). In utero surgical models in nonrodents (e.g., fetal lambs) are used to assess life-size interventions designed to treat the condition in human infants.

#### 6.2.5.3. UMBILICAL HERNIA, OMPHALOCELE, AND GASTROSCHISIS

This trio of related abdominal wall malformations occurs with some frequency in humans, and collectively they are common in laboratory animals. **Umbilical hernia** is relatively minor, as one or several loops of intestine are displaced through the abdominal musculature but remain covered by subcutaneous tissue and skin. **Omphalocele** is a more significant lesion in which a variable portion of the intestines and occasionally other organs protrude through the umbilical and supraumbilical portion of the abdominal wall while remaining covered by peritoneum. This lesion is due to underdevelopment and closure defects of the abdominal wall muscles and in humans is commonly associated with additional chromosomal abnormalities or serious malformations in other organs, particularly affecting the heart but often also the urinary tract, limbs, digestive system, and/or vertebral column (Figure 11.18).



**FIGURE 11.18** Omphalocele in a chick embryo model of gastroschisis, induced by surgical intervention to open the umbilical cord to permit exposure to the disruptive effects of amniotic fluid. Reproduced from the Tarrio Gandara CA et al.: Chicken embryo as an experimental model for the study of gastroschisis, Acta Cir. Bras. 23:247–252, 2008, with permission.



**Gastroschisis** is the most severe form of abdominal wall malformation, presenting as eventration of abdominal contents without a membranous covering. This lesion occurs as a hole, typically on the right side of the umbilical ring with an intact umbilical cord on the left side. The intestines may be swollen, inflamed, thickened, and twisted. Other concomitant lesions may be shorter intestines, slow intra-uterine growth, prematurity, or heart abnormalities. Several hypotheses have been proposed as the pathogenesis for this lesion, but the exact mechanism is not known. The latest proposal is that a midline defect of the primordial umbilical ring prevents the normal attachment of the umbilical cord (Chuaire Noack, 2021). The amnio-ectodermal junction is either not intact on the right side or it later separates, allowing evisceration of the digestive tract and other abdominal organs.

Both genetic and environmental factors have been proposed to induce this defect. Maternal exposure to xenobiotics is a frequent cause of abdominal wall defects in laboratory animals. The combination of protein-zinc deficiencies and carbon monoxide exposure during gestation in pregnant CD-1 mice has also been shown to cause this congenital defect. Many antineoplastic drugs can produce this malformation in rodents, while corticosteroid administration can cause this lesion in rabbits.

### 6.2.6. Urinary System

#### 6.2.6.1. RENAL AGENESIS

Bilateral **renal agenesis** is rare in humans, most often affecting males. In contrast, unilateral renal agenesis is a relatively common finding at postmortem. In the unilateral condition, one kidney is absent or present as a small, barely recognizable remnant and the remaining kidney is functional but may be deformed. Common anomalies include altered orientation (ectopia or rotation), hydronephrosis, polycystic disease, or urolithiasis (calculi in the renal pelvis). Genital defects are another frequent finding in affected individuals, especially in females.

Renal agenesis represents a defect occurring at the earliest stages of organogenesis. Several mechanisms have been proposed, all involving lesions of the ureteric bud. This bud is an outgrowth from the mesonephric kidney (i.e.,

the precursor to the metanephric or adult kidney). If the bud fails to form, degenerates, or is unable to establish contact with the metanephric blastema (i.e., the mesoderm that will develop into the nephrons), then induction of the adult kidney cannot occur.

The primary molecular mechanism for ureteric bud deficits is abnormal signaling between the metanephric mesoderm, which expresses the morphogen *Gdnf*, and the ureteric bud, which harbors the *Gdnf* receptor (a heterodimeric complex formed by *Gfra1* and *Ret*). Mice lacking any of these molecules do not form kidneys, as the ureteric bud has no gradient to follow as it seeks its target. These animals also develop aplasia of the caudal enteric ganglia (Hirschsprung disease).

Several xenobiotics can induce renal agenesis. Examples include hypervitaminosis A and chlorambucil in rodents, methyl chloride in ferrets, and thalidomide in rabbits. These agents have not been linked to enteric ganglion lesions, suggesting that the mechanism of action is not associated with disruption of *Gdnf*-mediated signaling.

#### 6.2.6.2. RENAL DYSPLASIA

**Renal dysplasia** affects males more than females as a consequence of unilateral or bilateral alterations in organ differentiation and/or organization. This finding features primitive mesenchymal tissue or primitive ectodermal tissue resembling metanephric ducts intermingled with nests of metaplastic cartilage. Interstitial tissue may be expanded by fibrosis or amorphous hyaline material. Bilateral dysplasia is associated with neonatal death or chronic renal failure. Dysplasia is frequently associated with obstructive uropathy characterized by posterior urethral valves and ureteropelvic junction blockage.

Renal dysplasia occurs as a congenital defect in several animal species. In dogs, the condition is common in many breeds as a familial (genetic) syndrome. In pigs, the disease may be idiopathic or associated with vitamin A deficiency. In rodents, renal dysplasia has a genetic basis in some strains but is induced by exposure to teratogens during prenatal or early postnatal periods. In mice, decreased cyclooxygenase-2 (COX-2) activity produced by targeted gene

deletion or pharmacological inhibition cause cystic renal dysplasia. The extent of the dysplasia is greater for gene defects compared to administration of COX-2 inhibitors. Classical nonsteroidal antiinflammatory drugs (NSAIDs, such as diclofenac and naproxen) induce more severe dysplasia compared to the highly selective COX-2 inhibitor (i.e., coxib) NSAIDs (Olliges et al., 2011).

#### 6.2.6.3. RENAL HYPOPLASIA

**Renal hypoplasia** presents as an abnormally small kidney without dysplasia and can be either bilateral or unilateral. Structural organization is normal, but the nephron number is reduced. Other conditions sometimes associated with renal hypoplasia include prenatal hydronephrosis and vesicoureteral reflux. In rodents, this abnormality may result in chronic renal disease and also anemia given that the kidneys are a major source of erythropoietin in adults. Studies in humans and mice have implicated parallel and interacting signaling pathways including GDNF/Ret, FGF, hedgehog (HH), and paired box 2 (PAX2) in the pathogenesis.

#### 6.2.6.4. HYDRONEPHROSIS

**Hydronephrosis** is enlargement of the renal pelvis in one or both kidneys. This finding occurs in all age groups and may develop in conjunction with **hydroureter** (i.e., dilated ureter [see below]). As in adults, hydronephrosis results from either intrinsic or extrinsic obstruction of urinary outflow, commonly at the level of the renal pelvis or ureter. Examples of intrinsic obstructions include renal calculi, renal cysts, posterior urethral valves, lower urinary tract dysfunction due to nerve damage ("neurogenic bladder"), and tumors. Extrinsic causes include pregnancy, peripelvic renal cysts, retrocaval (misplaced) ureter, retroperitoneal fibrosis, and trauma. The duration and severity of the obstruction determine the extent of lost kidney function. Additional renal defects may develop in individuals with hydronephrosis, including agenesis or hypoplasia of the contralateral kidney, cystic kidney, and **hypospadias**.

During normal development, one or both ureters may experience transient closure, and if urine secretion by the kidney commences before the reopening of the ureters, the proximal ureter and renal pelvis will be distended. Certain

anatomic features predispose to this condition, such as normal flexion and narrowing of the ureter at the ureteropelvic junction. This arrangement can cause fixation of the ureter against the renal pelvis with persistent obstruction to urine flow, especially when combined with aberrant vascular formation at the renal hilus. Such dilation is often observed in near-term rodent fetuses during teratology studies (Figure 11.19), but the

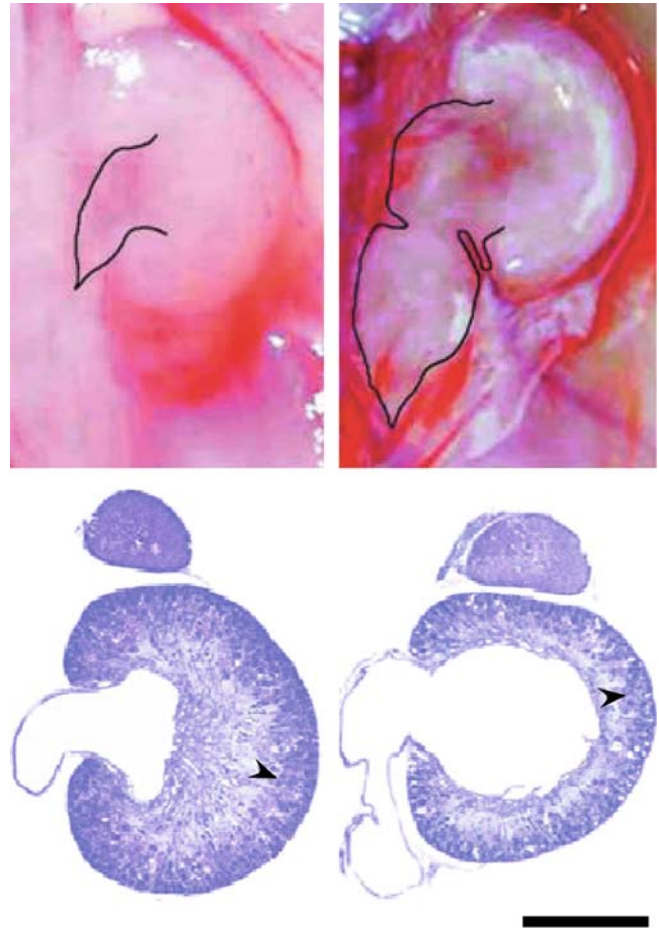


**FIGURE 11.19** Hydronephrosis in near-term (gestational day [GD] 21.5) fetal Sprague-Dawley rats, showing the difference between the mild physiological dilation in saline-treated control rats (left side) and the marked renal expansion (right side) in age-matched animals delivered from dams that had been exposed to adriamycin (2.2 mg/kg given on GD8 to GD9 by intraperitoneal injection). The lines (upper panel) indicate the borders of the ureters, while arrowheads show the corticomedullary boundary. Bar = 1 mm. Reproduced from the Gonçalves A et al.: Adriamycin-induced fetal hydronephrosis, *Int. Braz. J. Urol.* 30:508–513, 2004, with permission.

distension appears to be transient since the incidence in adult animals is much lower than expected based on the number of affected fetuses. Permanent hydronephrosis will result if the obstruction is not reversed.

Several substances can reproducibly induce hydronephrosis in various animal species. Agents with this activity in rodents include aspirin, cadmium, dioxin, ethylenethiourea, methotrexate, rubidomycin, and hypervitaminosis A. Trypan blue and hypovitaminosis A can cause this lesion in pigs.

#### 6.2.6.5. HYDROURETER

This lesion, characterized by dilatation of the ureter, is a common abnormality in rodents and is usually a consequence of urinary tract outflow obstruction. The blocked ureter dilates, elongates, bends, and becomes tortuous. **Hydroureter** generally occurs in conjunction with hydronephrosis due to urine reflux into the renal pelvis. Other lesions have been linked to hydroureter including ureteral duplication, ectopia, **ureterocele** (i.e., distal ureter dilation), and ureterovesical strictures. Unilateral renal agenesis and renal dysplasia have also been associated with this ureter defect.

The most frequent cause of hydroureter is urethral valve obstruction. Some cases may be the result of unduly prolonged preservation of the ureteric membrane; this change also has been proposed as a mechanism for hydronephrosis (Figure 11.19). Fetal mice and rats often have ureter obstruction following in utero X-irradiation. The obstruction frequently permits the onset of hydroureter and hydronephrosis.

#### 6.2.6.6. HYPOSPADIAS

**Hypospadias** is a common urogenital anomaly and is thought to involve both genetic susceptibility and environmental exposure to endocrine disrupters. It presents in males as three related anomalies. The first and most common appearance is a urethral defect with an abnormally placed external urethral orifice, where the opening is located somewhere along the underside of the penis rather than at the tip. In more than 50% of cases, the shift in meatus position is confined to the ventral surface of the glans, with the remainder opening on the shaft or in the perineal region. The second anomaly is a preputial defect, and the third is an

abnormal ventral curvature of the penis (termed a **chordee**). The penis may be reduced in size as well.

Hypospadias is thought to arise from either failure of formation of the urethral plate, incomplete fusion of the urethral folds, or failed canalization of the glandular plate. The molecular mechanism is posited to be insufficient production of androgens or androgen insensitivity, thereby resulting in a partially feminized phenotype. This premise is logical given the apparent connection between exposure of male fetuses to estrogenic chemicals in utero and the induction of this lesion. Differences in human and mouse hypospadias arise from divergence in developmental mechanisms for the penile urethra. Adult mice treated perinatally with DES possess an abnormal urethral meatus, hypoplasia of the expandable vascular beds (corporea cavernosa urethra) in the penis, malformed external and internal prepuces, and/or ventral tethering of the penis to the inner surface of the external prepuce.

#### 6.2.7. Reproductive System

##### 6.2.7.1. CRYPTORCHIDISM

Failure of one or both testes to descend from their original inguinal position into the scrotum is called **cryptorchidism**. It is the most common genital defect observed in many species, including humans. The condition is usually unilateral but may be bilateral. The term should not be used for those laboratory animal species (e.g., rodents) in which the wide inguinal rings permit position-dependent movement of the testes between the scrotum and abdominal cavity into adulthood.

Cryptorchidism exhibits a range of severities. Approximately 90% of human cases exhibit retention of the testes in the inguinal canal. The remainder are true instances of ectopia related to aberrant migration (e.g., into the contralateral inguinal canal, perineal region, or even the subcutis) or nonmigration (e.g., continued presence in the abdominal cavity, which is the most extreme variant). The persistence of an abdominal testis leads to impaired fertility and increases the risk of testicular cancer (typically seminoma), which suggests the likely concordance between abnormal cell differentiation and proliferation during



embryonic development and a later resurgence of such aberrant cellular processes during neoplastic transformation. Prepubertal treatment to correct cryptorchidism reduces the risk of testicular cancer. Other complications associated with cryptorchidism include testicular torsion, inguinal hernia, and trauma from pressure against the pubic bone.

The causes of undescended testes are not known. Mechanical explanations include abnormal fibrous bands that tether the testis in an abnormal position and aberrant genesis of either the *gubernaculum* (i.e., scrotal ligament, which anchors the testis to the ventral [inferior] wall of the scrotum) or the *tunica vaginalis* (i.e., the peritoneal extension that forms the serosal lining of the testis), and congenital inguinal hernia. MIEs responsible for this defect likely involve a deficiency of gonadotropic hormones. For example, a putative AOP identified in rats is reduced levels of insulin-like hormone 3 (Insl3), which is necessary for appropriate gubernaculum development late in gestation. Dibutyl phthalate exposure specifically between E15.5–18.5 in rats yields cryptorchidism, seemingly due to reduced Insl3 expression and subsequent agenesis of the gubernaculum (reviewed in [Palermo et al., 2021](#)).

Risk factors for cryptorchidism include premature birth, low birth weight, family history of cryptorchidism, conditions that restrict fetal growth, maternal prenatal use of alcohol and/or cigarettes, nutritional deficiencies, and maternal exposure to certain pesticides (e.g., organochlorine pesticides with antiandrogenic effects). Rodents and pigs have been shown to develop this defect when vitamin A levels are low. Treatment with benzhydrylpiperazines or sodium arsenate can result in undescended testes in rodents.

#### 6.2.7.2. INTERSEX (PSEUDOHERMAPHRODITISM)

Sexual ambiguity, often referred to as **intersex**, is a reasonably frequent occurrence in humans and various laboratory animal species. This condition occurs when an individual has a single chromosomal and gonadal sex but possesses external genitalia that combine features of both males and females. The phenotypic sex of developing mammals is defined by three main factors: the genotype, gonadal development, and the genesis of accessory genital organs

([Figure 11.20](#)). Female pseudohermaphrodites have ovaries but also have secondary sexual characteristics or external genitalia resembling those of a male, while male pseudohermaphrodites carry testes but have secondary sexual characteristics or external genitalia resembling those of a female.

**Genotypic sex** depends on the expression of several genes. Genotypic sex is determined at fertilization as either male (XY) or female (XX), except in rare instances where an abnormal number of sex chromosomes are transferred (e.g., XXY, XYY, or XO). In contrast, **phenotypic sex** depends on expression of the *SRY* (*sex-determining region of the Y chromosome*) gene; production of the SRY protein results in differentiation as a male, while a lack of SRY leads to



**FIGURE 11.20** Male pseudohermaphroditism in a dog. Reproduced from Haschek WM, Rousseaux CG, Wallig MA, editors: *Fundamentals of toxicologic pathology*, ed 2, 2010, Academic Press, Figure 20.11, p. 658, with permission.

a female offspring. If the SRY protein is mutated so that it cannot bind to DNA, sex reversal to a female phenotype will occur.

While numerical and structural aberrations of the sex chromosomes may produce intersex individuals, they are not the only cause of this condition. Gonadal development, and in particular the hormone complement, plays a critical ancillary role in determining phenotypic sex. Androgens induce male characteristics, while estrogens produce female attributes. Several conditions produce pseudohermaphrodites, which are individuals in whom genotype and gonad development do not agree with the phenotype as expressed in external genital structure and secondary sex traits.

Hyposecretion of appropriate gonadal hormones (androgens or progestins for male fetuses, estrogens for females), defective receptors for these hormones, or gestational exposure to xenobiotics with endocrine-disrupting activities (see “Endocrine Disruption” subsection below) can produce pseudohermaphrodites. For example, androgenic agents or progestin can convert a fetus with a female genotype and female gonads into a female pseudohermaphrodite having male genitalia and secondary sex characteristics. The degree of prenatal masculinization varies with the potency of the androgen or progestin and the timing of exposure. Adrenal or ovarian androgen-producing tumors may also result in masculinization of a female fetus. Congenital adrenal cortical hyperplasia arises from an inherited defect in 21-hydroxylase, the enzyme needed for cortisol production. With this condition, excessive quantities of adrenal androgens will be produced to compensate for the decreased cortisol production. In females, adrenal hyperplasia results in masculinization with anomalous development of genital organs.

Similarly, several causes can convert a fetus with a male genotype and male gonads into a male pseudohermaphrodite having female genitalia and female secondary sex characteristics. Examples include cytogenetic abnormalities, defects in testosterone biosynthesis, defects in androgen action, and teratogens. As an example, individuals with tissue receptors for androgens that are reduced or absent will have partial to complete androgen resistance. With complete resistance, the individual will have testes, but the genital ducts and external genitalia will be

female organs; secondary sex characteristics may or may not be present. The most extreme example is an individual with complete testicular feminization where the individuals are born with female genitalia and a vagina that ends blindly (i.e., with no cervix or uterus). The testes may be located within the labia or within the abdomen.

### 6.2.8. Skeletal System

#### 6.2.8.1. DIGIT ANOMALIES

Malformations of the digits (fingers or toes) are relatively common in both humans and laboratory animals. Such defects may be an isolated anomaly or part of a more generalized genetic abnormality. Multiple different digit abnormalities may occur. The common pathogenesis is abnormal remodeling of the AER during initial specification of the digital rays during the process of limb organogenesis. The type of lesion that develops depends on the manner in which limb differentiation is disrupted.

**Ectrodactyly**, the absence of part or all of at least one digit on a hand or foot, results from interference in normal mesenchymal condensation of digital rays. The lesion often presents as a combination of **adactyly** (missing digits) and **brachydactyly** (short digits) affecting central digits (Figures 11.21 and 11.22) although digits away from the limb axis also may be affected (Figure 11.22). The hands usually exhibit more severe deformities. This typical pathogenesis is a genetic defect, and the most frequent mode of inheritance is autosomal dominant with reduced penetrance. Possible mechanisms include failed intercellular interactions or cytotoxicity of critical stem cells. The most common type of ectrodactyly in humans is the split hand/foot malformation, where the middle digits (II and III) are absent while the outer digits (I on one side with IV and V on the other) that border the cleft may be normal or fused. All four hands and feet may be affected, and several related congenital anomalies may occur including cleft lip and/or palate as well as ectodermal dysplasia and obstructive uropathy. Ectrodactyly is easily induced in rodents following cadmium or acetazolamide administration. Missing digits are seen in primates following thalidomide exposure during the period of initial limb growth and patterning (gestational weeks 4–8). The chemotherapy

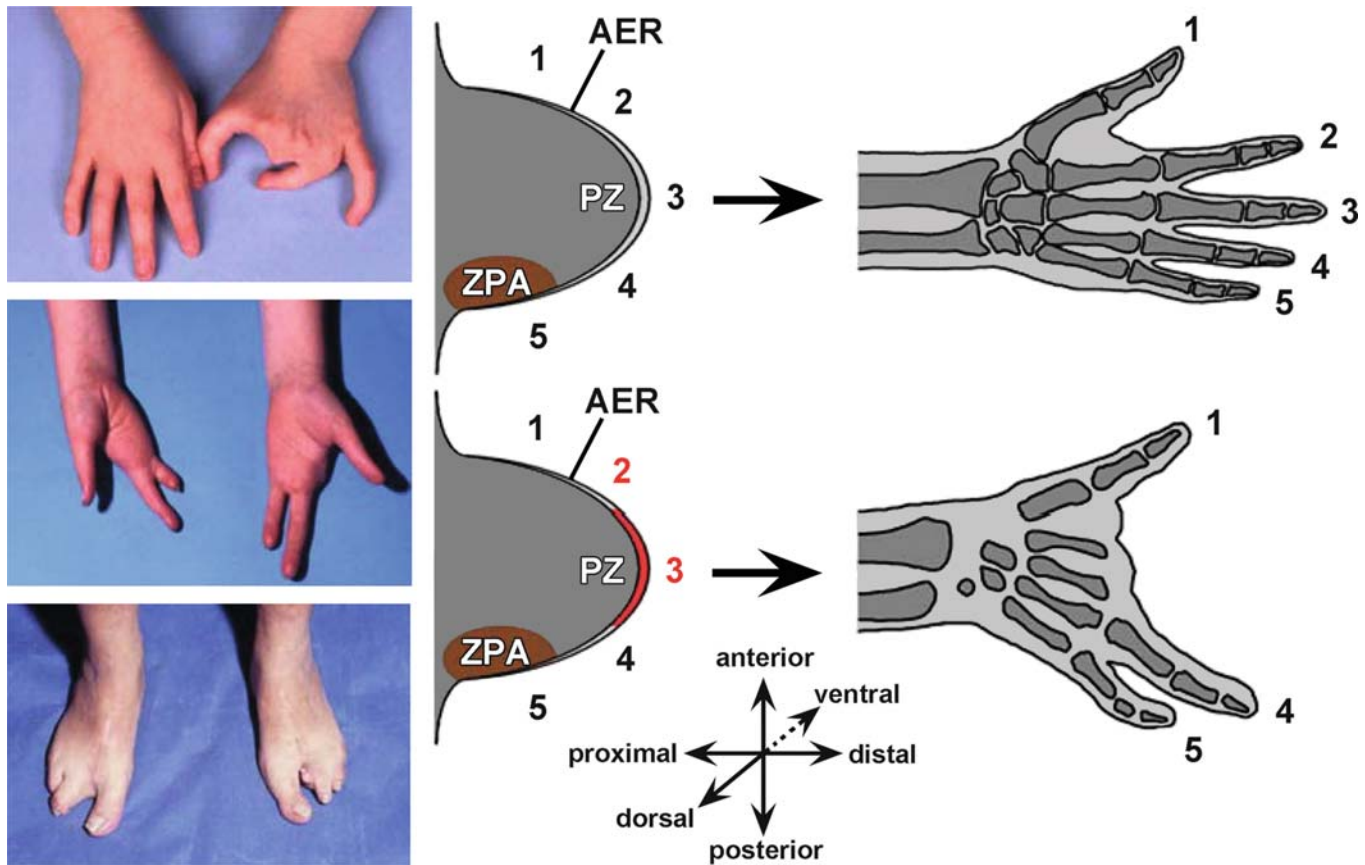


**FIGURE 11.21** The ectrodactyly phenotype (shown here in photographs of the hands and feet in affected humans) results from failed differentiation of the apical epidermal ridge (AER). Relative to the normal progression (upper row of schematic diagrams) from limb bud (left diagram) to fully formed limb (right diagram), ectrodactyly affecting the middle digits arises when the median AER (red zone) does not maintain its normal molecular signature and cellular activities, thereby leading to the absence of the central digit rays (right). The numbers denote the positions (future for the bud, actual for the formed hand) of digits 1–5. Other abbreviations: PZ, progress zone; ZPA, zone of polarizing activity. Reproduced from Duijf PH et al.: *Pathogenesis of split-hand/split-foot malformation*, Hum. Mol. Genet. 12 (Spec No 1):R51–60, 2003, with permission.

drug busulfan has also been associated with ectrodactyly in humans when exposure occurs at around day 41 of gestation.

**Polydactyly**, the presence of extra digits, is a common anomaly in mammalian species, including humans (Figure 11.22). In most instances, only a single extra digit is present. The first and fifth digits are most commonly duplicated in humans. **Preaxial polydactyly** is duplication or splitting of the thumb; **central polydactyly** is duplication of the index, middle and ring fingers; and **postaxial polydactyly** is duplication of the small finger. Two mechanisms have been proposed to explain these lesions. The first is a failure of PCD, thereby leading to inappropriate pruning of the digital blastema (i.e.,

the undifferentiated bed of cells from which a mature structure arises). The second is formation of a supernumerary digital blastema as a consequence of alterations in the composition, configuration, and quantity of ECM. This condition may occur because of an autosomal dominant mutation in a single gene, mutations in several genes, or from environmental causes. Many teratogens induce polydactyly in mice, including nutritional deficiencies (reduced folic acid); physical damage (X-irradiation); and numerous toxicants including bromodeoxyuridine (BrdU), cyclophosphamide, cytosine arabinoside, and thalidomide.

**Syndactyly** is the presence of webbed or fused digits. The defect may be bilateral or



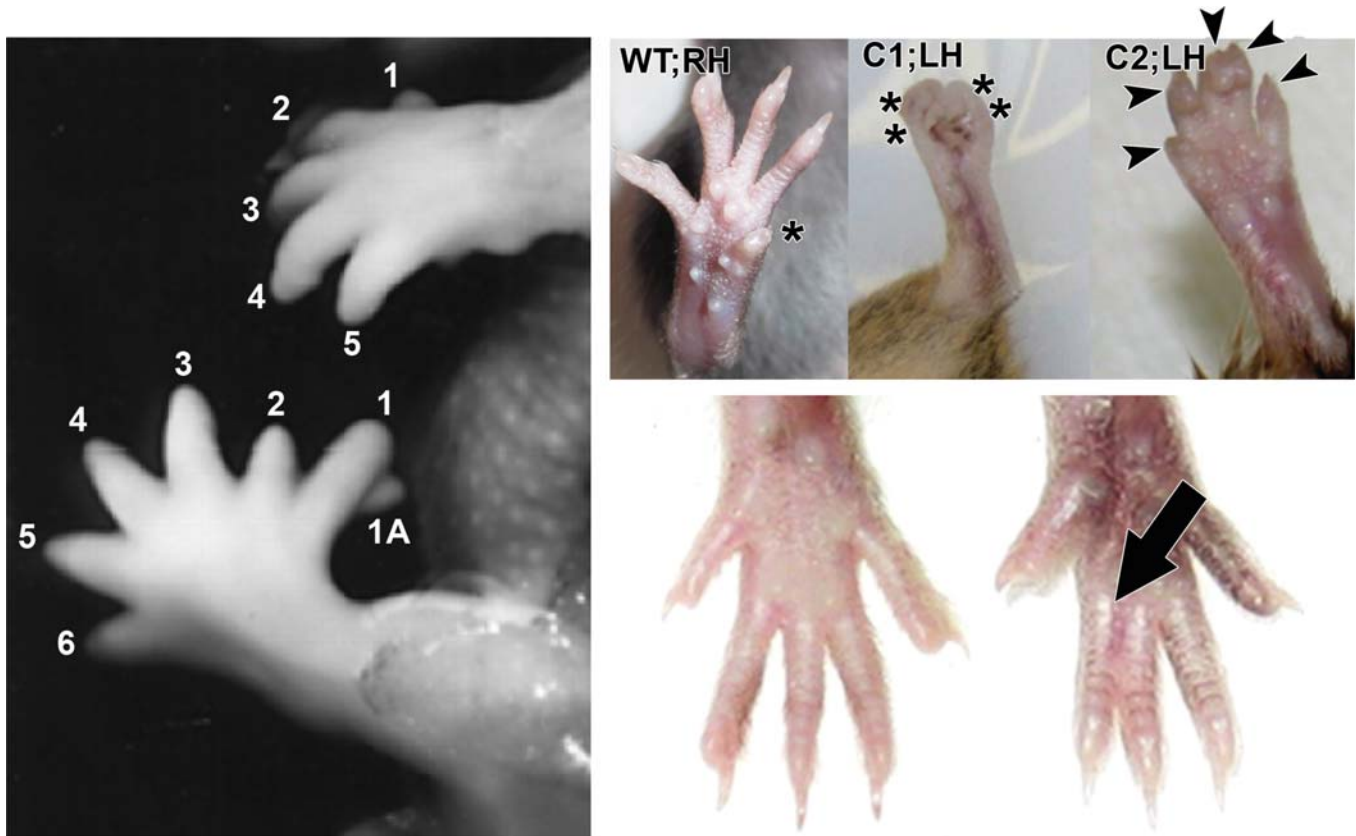


**FIGURE 11.22** Common developmental defects of digits observed in mutant or toxicant-exposed animals include adactyly (missing digits [asterisks]), brachydactyly (short digits [arrowheads]), polydactyly (too many digits), and syndactyly (fused digits [arrow]). In some cases, extra appendages (1A [left image]) that grow from existing digits is a manifestation of polydactyly. C, chimera; LH, left hind paw; RH, right hind paw; WT, wild-type. Reproduced from multiple papers: left panel, from Sinawat S et al.: Fetal abnormalities produced after preimplantation exposure of mouse embryos to ammonium chloride, Hum. Reprod. 18:2157–2165, 2003, by permission of Oxford University Press; upper right panel, from Liu W et al.: Deletion of *Porcn* in mice leads to multiple developmental defects and models human focal dermal hypoplasia (Goltz syndrome), PLoS ONE 7:e32331, 2012; lower right panel, from Kalcheva N et al.: Gap junction remodeling and cardiac arrhythmogenesis in a murine model of oculodentodigital dysplasia, Proc. Natl. Acad. Sci. USA 104:20512–20516, 2007; © 2007 by the U.S. National Academy of Sciences.

unilateral, symmetrical or asymmetrical, affecting fingers and/or toes, and is a moderately common congenital defect in multiple species including rodents and humans (Figure 11.22). The anomaly may occur as an isolated entity or may be a component of more than 300 malformation syndromes. In humans, at least nine different forms of syndactyly with additional subtypes have been reported. **Zygodactyly**, fusion of the long (digit III) and ring (digit IV) fingers, is the most common form of syndactyly. Skin connections, or webbing, is normally present between the digits in utero and in humans usually will disappear prior to gestational day 56. Most types are inherited as autosomal

dominant. The mechanism is reduced or failed differentiation between two digits, typically due to interference with PCD that is required to separate the digital rays. In most cases, the fusion consists of soft tissue, such as cutaneous webbing. The fusion may be partial or complete, cutaneous or osseous, involve only the phalanges, or may extend farther up to the metacarpal/metatarsal or carpal/tarsal levels. Syndactyly often occurs with other limb anomalies, such as **brachydactyly** and **ectrodactyly**. The lesion is often linked to **amniotic band syndrome** (i.e., ischemia-related deformations that arise when limbs are ensnared in fibrous bands formed following amniotic damage). This defect

has been induced in laboratory animals using many toxicants, including hydroxyurea and methylnitrosourea in mice, busulfan in rats, and methotrexate in rabbits.

#### 6.2.8.2. REDUCTION DEFORMITIES OF THE LIMBS

A reduction deformity is the congenital absence or shortening of a limb or part of a limb. These defects may be unilateral or bilateral and may involve the upper and/or lower limbs, depending on the cause. Such lesions may occur together with malformations of other skeletal regions as well as additional birth defects including abdominal wall (e.g., gastroschisis, omphalocele) and heart defects. The cause is not always known but may involve in utero exposure to chemicals (including alcohol and possibly tobacco smoke), some medications, and viruses.

**Amelia** is the complete absence of an entire limb. This term can be expanded to **tetra-amelia** for the absence of all four limbs or **meromelia** for the partial absence of a limb or limbs. These defects may affect any limb and may occur in isolation or with congenital malformations in additional organ systems. For example, amelia often is associated with defects in the remaining limbs (e.g., *talipes equinovarus* [club foot]) as well as cleft lip and/or cleft palate and scoliosis (curvature of the spine from side to side). Causes include autosomal recessive mutations or the use of teratogenic drugs such as thalidomide during early pregnancy at the critical period when the limb buds are forming.

**Hemimelia** is the absence of a long bone, in a limb, thereby resulting in shortening of the appendage. Complete hemimelia denotes the absence of the entire bone, while partial hemimelia indicates that only part of the bone is missing. Tibial hemimelia occurs when the tibia is shortened or missing, while fibular hemimelia is the term for a shortened or missing fibula. The right side is more often affected than the left. This anomaly is one of the most common reduction malformations, typically involving the distal forearm and hand. Proposed causes include environmental influences, vascular dysgenesis, and viral infections. These defects have been described in human infants after gestational exposure to such agents as amantadine and thalidomide. Maternal treatment with

the chemotherapy drug chlorambucil has been shown to result in fibular hemimelia in rats.

**Phocomelia** ("seal limbs") is defined as undeveloped limbs and absent pelvic bones although other limb abnormalities may occur. This extremely rare defect is typically characterized by greater shortening of the upper extremities with relatively more development of distal regions (hands, feet, and digits) (Figure 11.23). Abnormalities of chromosome 8 represent the most common genetic cause for this anomaly. The classic teratogenic etiology is maternal use



**FIGURE 11.23** Phocomelia affecting the forelimb of a CD-1 mouse fetus from a dam treated on gestational day 10.5 with all-trans retinoic acid (200 mg/kg). Reproduced from Haschek WM, Rousseaux CG, Wallig MA, editors: *Fundamentals of toxicologic pathology*, ed 2, 2010, Academic Press, Figure 20.13, p. 659, with permission.

of thalidomide during pregnancy (as an anti-nausea agent to combat morning sickness); this agent induced phocomelia in thousands of human infants following exposure during the critical period of limb organogenesis (gestational days 35–50). The same lesion occurs in some NHP species and also in rabbits, but not in rodents. Phocomelia has also been seen in rabbits given hydroxyurea, and in mice given retinoic acid.

The pathogenesis for limb reduction anomalies involves interference with regional specification of cell populations in the proximal limb bud. Potential mechanisms are disrupted regional interactions between ectoderm and mesoderm, altered morphogen production, failed morphogenetic movements, or disturbed inductive processes. The reduction or absence of proximal structures coupled with the fairly normal appearance of distal features, as in phocomelia, indicates that limb bud damage induced by toxicants does not thwart limb differentiation. Instead, compensatory processes attempt to repair or bypass reductions in cell mass so that surviving structures can attempt to continue their developmental program.

### 6.3. Deformations

As noted above, a **deformation** is a gross defect arising from damage to developing tissue associated with application of an external influence. Deformations are generally caused by lack of fetal movement produced by mechanical force (e.g., friction related to decreased amniotic fluid or physical constraint imposed by an amniotic band), functional deficit (e.g., neuromuscular disorders), or primary structural defect (e.g., *spina bifida*). Deformations tend to occur later in development and affect entire regions rather than specific organs. Examples include arthrogryposis, craniofacial asymmetry, intestinal atresia resulting from serosal fibrosis, and *talipes*.

#### 6.3.1. Arthrogryposis

This defect, also termed **arthrogryposis multiplex congenita**, comprises a number of nonprogressive clinical syndromes that are characterized by skeletal muscle weakness and persistent flexure or contracture of two or more joints in two different body regions that result

from abnormal fibrosis of the muscle tissue. Other sequelae include shortened ligaments and fibrous ankylosis of the joints along with reduced amounts of connective tissue under the skin. This defect is the most common limb deformity in animals and is often accompanied by lesions of the appendicular skeleton ([Figure 11.24](#)).

Arthrogryposis is not a separate disease entity but is a descriptive diagnosis for more than 300 individual diseases with varying etiologies. Three main categories have been defined. **Amyloplasia**, the most common form, is characterized by a generalized lack of muscular development and growth with severe contracture and deformity involving most joints. **Distal arthrogryposis** exhibits similar joint and muscle changes that are mainly localized to the hands and feet. **Syndromic arthrogryposis** also affects the internal organs along with the joints and muscles.

Although usually classified as a skeletal deformity, this defect typically arises from insufficient limb movement rather than from a primary failure in skeletal development. Mechanical compression resulting from increased pressure and/or reduced fetal mobility (e.g., from intra-uterine crowding) can be one cause. Other common causes are gestational diseases of the developing CNS, connective tissue, or skeletal muscles. For example, the absence of neural input (usually due to CNS lesions in the motor neurons or motor tracts in the spinal cord) thwarts skeletal muscle activity, which causes denervation hypoplasia and atrophy, and eventually arthrogryposis. Arthrogryposis is more severe if mobility of the fetus is restricted early (i.e., is present for a longer period of time) during gestation.

Arthrogryposis has been linked to infectious and noninfectious etiologies as well as many toxicants. In humans, the defect has been associated with nutritional and vascular disorders, neurogenic and myogenic damage, maternal diseases such as *myasthenia gravis* and diabetes, and mechanical factors such as multiple pregnancy and amniotic bands. Livestock often develop the lesion following maternal ingestion of many toxic plants, including members of the genera *Astragalus*, *Lathyrus*, *Lupinus*, *Oxytropis*, *Senecio*, *Sophora*, *Thermopsis*, and *Veratrum* (calves, foals, lambs, pigs). Methallibure (a





**FIGURE 11.24** Arthrogryposis in an Angus calf is indicated by abnormal angling of all four limbs. The altered orientation results from permanent fixation of multiple joints in a contracted position. In cattle, this finding is a common end-stage lesion produced by several etiologic agents, including genetic defects; microbial infections (e.g., the RNA virus that causes bluetongue); and maternal ingestion of some plant-derived teratogens (e.g., lupine [*Lupinus* sp.], poison hemlock [*Conium maculatum*]) between gestational days 40–75. This congenital malformation often is accompanied by other skeletal defects—especially cleft palate as well as excessive vertebral column deviations like kyphosis (dorsal or ventral displacement) and scoliosis (lateral curvature)—and soft tissue changes, like atrophy of the limb musculature and loss of the motor neurons in the spinal cord that control these muscles. Courtesy of Dr. David Steffen, Veterinary Diagnostic Center, University of Nebraska, Lincoln, NE.

gonadotropin inhibitor used to control estrus cycling) and tobacco have caused this problem in pigs. Toxicant-induced arthrogryposis in rodents is rare, although Zika virus has induced this lesion in mice and tubocurarine has been shown to cause this lesion in rats, presumably by inducing fetal paralysis.

### 6.3.2. Talipes

*Talipes* is a congenital hind limb defect where one or both of a neonate's feet or paws are rotated relative to the expected position (i.e., clubfoot). The general category involves multiple misorientations depending on which portion of the foot ultimately contacts the ground. Simple rotations include *talipes calcaneous*, where the foot is rotated up so that only the heel contacts the ground; *talipes equinus*, where the heel is elevated so that only the toes touch down; *talipes valgus*, where the foot is turned out so that the medial side contacts the

ground; *talipes varus*, where the foot is turned in so that the lateral side touches the ground; and *talipes cavus*, where the toes and heel contact the surface, but the plantar region is elevated. When present, talipes is often bilateral and may be one defect in a developmental syndrome also affecting other skeletal regions (commonly the hips, knees, and sometimes elbows) or other systems (e.g., NTDs, renal agenesis).

The pathogenesis of this defect is not known with certainty. Altered movement in utero has been proposed, possibly as a consequence of connective tissue or neurological abnormalities. Gestational exposure to certain neuroactive medications (e.g., opioids, selective serotonin reuptake inhibitors, and some but not all antihistamines) and antiviral agents has been proposed as a possible explanation, presumably as a result of altered CNS differentiation and not aberrant limb innervation (Werler et al., 2014). Assisted reproductive technologies have been linked to

a modestly higher risk for *talipes*, possibly as a consequence of placental manipulation (e.g., chorionic villus sampling or early amniocentesis). Tobacco smoke as well as high-level consumption of alcohol and coffee (presumably caffeine) also appear to enhance the risk that offspring will develop *talipes* (Werler et al., 2015).

#### 6.4. Intrauterine Growth Restriction

Individuals with **intrauterine growth restriction** (IUGR) are not born prematurely but are born with a small size given the length of their gestation (Figure 11.25). This condition is strictly defined as less than 10% of predicted fetal weight for gestational age although the reduction may be closer to 5% when corrected for factors such as maternal weight and high-altitude location. Perinatal morbidity and mortality may result if undiagnosed and untreated. Historically, IUGR has been categorized as symmetric, with equally poor growth of the head, abdomen, and long bones (entire body proportionally small), or asymmetric, where the head and long bones are unaffected compared with the abdomen and viscera. Current thinking is that IUGR represents a continuum where asymmetric growth occurs

in the early stages of gestation, while symmetric growth occurs in the late stages.

Maternal chronic hypertension with inadequate maternal-fetal circulation is the most common cause of IUGR. Placental insufficiency is the most common cause for asymmetric IUGR. A poorly functioning placenta restricts nutrient supply to the fetus, thereby impeding normal fetal growth. Fetal exposures to certain drugs (e.g., aminopterin and busulfan), X-irradiation, and hypoxia cause IUGR even though placental structure is apparently normal.

IUGR often occurs in conjunction with congenital malformations as a result of two pathogenic mechanisms: growth retardation due to a congenital malformation, or growth retardation and congenital malformations developing as distinct manifestations of a common independent etiologic factor. Common examples of concurrent defects affect the CNS (hydrocephalus, macrocephaly, microcephaly, *spina bifida*); heart (VSD); kidney (agenesis); and limbs (arthrogryposis, fractures secondary to osteogenesis imperfecta). The severity of these defects often is inversely correlated with the fetal body weight. Bilateral ligation of the uterine arteries in rats and mice is one of the most common experimental animal models currently used to mimic human fetal growth restriction. Animal models of IUGR



**FIGURE 11.25** Intrauterine growth retardation occurs in fetal mice lacking one allele of both *Gata4* (a zinc finger transcription factor) and *Tbx5* (a T-box transcription factor), but not in littermates missing an allele for only one of the genes. The scale bar represents 1 mm. Reproduced from Maitra M et al.: *Interaction of Gata4 and Gata6 with Tbx5 is critical for normal cardiac development*, Dev. Biol. 326:368–377, 2009, by permission.

also have been produced using dietary manipulation, heat, hypoxia, and treatment with glucocorticoids (Andersen et al., 2018). Experimental IUGR is investigated most often using rats, but other species including mice, guinea pigs, rabbits, pigs, and sheep have been studied.

### 6.5. In-Life Functional Alterations

Developmental events induced by toxicant exposure during gestation may not be apparent until after birth. Examples of altered function include abnormal cell reactivity (e.g., by immune or reproductive elements), metabolic errors, and neurobehavioral deficits. Subtle (microscopic or ultrastructural) morphologic defects may accompany the functional deficiencies, but in many instances, the functional deficits occur in the absence of structural changes. Often these functional effects result from depleted cell numbers due to inadequate repair of the primary injury or insufficient compensation by related systems.

**Abnormal cell reactivity** in various organ systems during the perinatal period is a common developmental toxicity outcome. The **ontogeny** (i.e., an organism's individual developmental history) of immune system differentiation is commonly impacted by xenobiotic exposures in utero (Table 11.4). The major functional deficits resulting from toxicant exposures during gestation (or early lactation) are improper immunosuppression and immunostimulation, either of which can initiate inflammatory diseases (especially allergic or autoimmune) or neoplasia later in life. Interference with postnatal reproductive functions can follow intrauterine exposure to many substances, including antineoplastic drugs (e.g., busulfan, procarbazine); hormones (e.g., DES); pesticides (e.g., chlordecone, dichlorodiphenyltrichloroethane [DDT]); and certain polycyclic aromatic hydrocarbon carcinogens (e.g., benzo[ $\alpha$ ]pyrene, dimethylbenz[ $\alpha$ ]anthracene [DMBA]).

**Errors of metabolism** arising from genetic mutations or xenobiotic exposures often induce developmental dysfunction. Most congenital metabolic disorders involve absent or ineffective enzyme activity. Inborn errors of metabolism can manifest in utero, in newborns, in children, during adolescence, or in adults; most genetically based “inborn” errors are not expressed until after birth. An environmentally caused disease—termed a **phenocopy** because its lesions

**TABLE 11.4** Developmental Immunotoxics<sup>a</sup>

#### *Alkylating agents*

Busulfan

Cyclophosphamide

#### *Heavy metals*

Methylmercury

Lead acetate

#### *Hormones*

Cortisone

Diethylstilbestrol

Epinephrine

Estrogen

Testosterone

#### *Organochlorines*

Polychlorinated biphenyls

2,3,7,8-Tetrachlorodibenzo-*p*-dioxin

#### *Pesticides*

Carbofuran

Chlordane

Diazinon

#### *Nutrition*

Protein deficiency

#### *Irradiation*

X-rays

#### *Carcinogens*

Benzo[*a*]pyrene

7,12-Dimethylbenz[*a*]anthracene

Methylcholanthrene

Urethane

<sup>a</sup> Roberts DW, and Chapman JR: Concepts essential to the assessment of toxicity to the developing immune system, In Kimmel C.A., and Buelke-Sam J., editors: *Developmental toxicology*, New York, 1981, Raven, pp. 167–189. Reproduced by permission of Taylor & Francis Group.  
Reproduced from Haschek WM, Rousseaux CG, Wallig MA, editors: *Handbook of toxicologic pathology*, ed 2, 2002, Academic Press, Table V, p. 911, with permission.

mimic those of a known genetic ailment—may mirror such congenital genetic conditions. For example, cattle exhibit similar morphologic



lesions when afflicted with  $\alpha$ -mannosidosis (genetic cause) or locoism (i.e., locoweed toxicity). However, accumulation of  $\alpha$ -mannoside in these two conditions results from distinct mechanisms: the inherited disorder arises from the complete absence of functional  $\alpha$ -mannosidase protein, while the environmental phenocopy follows  $\alpha$ -mannosidase inhibition after ingestion of the indolizidine alkaloid swainsonine. The existence of phenocopies highlights the difficulty in determining the etiology of defects.

Many substances produce developmental deficits typified by **neurobehavioral abnormalities**. The anticonvulsant drugs diphenylhydantoin and trimethadione cause mental deficiency and delayed speech in addition to more obvious structural alterations, such as impaired growth and various other malformations. Similarly, maternal exposure to high alcohol levels during critical prenatal and postnatal periods of CNS development leads to variable (but often severe) and permanent mental dysfunction characterized by hypotonia, hyperactivity, incoordination, and learning disabilities in addition to reduced growth and the well-recognized physiognomy of fetal alcohol syndrome. Behavioral and neurological deficits, often including profound cognitive disabilities, also occur after prenatal and early postnatal exposure to such common environmental pollutants as lead and methyl mercury. The developing brain is especially sensitive to organic mercury as it is lipophilic and exhibits a high affinity for cysteine residues that are commonly found in essential proteins of neurons. Methyl mercury poisoning ("Minamata disease") also induces major sensory and peripheral motor disturbances arising from damage to the somatosensory cortex rather than damage to the peripheral nervous system.

### 6.6. Congenital Neoplasia

**Congenital neoplasia** is defined as a tumor that is present at birth or shortly after birth (during the first 3 months of life). Common entities include embryonal tumors, such as neuroblastoma or pulmonary blastoma, and brain tumors (mostly gliomas); the kinds of neoplasm vary among species (Rice et al., 1989). Congenital tumors are, by definition, indicators of

abnormal embryogenesis; these tumors represent only 1.5%–2% of pediatric tumors. Embryonic and fetal cells are inherently susceptible to mutagenic teratogens like carcinogenic chemicals and radiation due to their high intrinsic rates of proliferation and undifferentiated cell characteristics (Donovan, 1999). However, an individual's genetic makeup and metabolic pathways (or absence thereof) will influence the in utero expression of a xenobiotic's carcinogenic potential.

Most cancers in infants have inherited gene alterations that drive uncontrolled cell growth. The most frequent childhood tumors are extracranial teratomas, neuroblastomas, soft tissue tumors, CNS tumors, leukemia, renal tumors, and hepatic tumors. These neoplasms arise from committed stem cells for specific cell lineages such as leukocytes (leukemia, lymphoma) or mesenchyme (osteosarcoma, rhabdomyosarcoma), although some may be derived from multiple lineages, including nephroblastoma (Wilm's tumor) and neuroblastoma. Neonatal tumors also occur in other mammalian species, but the incidence in animals is seldom known.

While it is accepted that carcinogenesis involves DNA alterations following initiation, promotion may involve effects on gene expression secondary to disruption of other cellular processes such as signal transduction pathways, selective enhancement of cell proliferation, and inhibition of apoptosis (see *Carcinogenesis: Mechanisms and Evaluation*, Vol 1, Chap 8). The early stages of gestation are considered to be the period when the fetus is most sensitive to carcinogens due to the high rate of cell division and undifferentiated characteristics of the cells, which readily fix toxicant-induced mutations in cells that survive the initial insult (Anderson et al., 2000; Donovan, 1999).

**Transplacental carcinogens** may act directly without prior metabolism or require enzymatic bioactivation to reactive intermediates (Tables 11.5 and 11.6). The long latent period required for neoplastic transformation has been used to support the argument that many if not all cancers that arise during the period from birth to young adulthood are induced by a prenatal initiation event. The classic example is the induction of vaginal clear cell adenocarcinoma following maternal exposure to DES during the first trimester. Although this tumor

TABLE 11.5 Selected Direct-Acting Transplacental Carcinogens<sup>a</sup>

Compound	Species	Principal Target Organs
<i>ALKYLNITROSOUREAS</i>		
Methylnitrosourea	Rat	Nervous system
Ethylnitrosourea	Mouse	Lung, liver
	Mouse	Nervous system
	Rat	Nervous system
	Syrian hamster	Nervous system
	Rabbit	Kidney
	Rabbit	Nervous system
	Patas monkey	Connective tissues
<i>n</i> -Propylnitrosourea	Rat	Nervous system
<i>OTHER ACYLALKYLNITROSAMINES</i>		
Ethylnitrosobiuret	Rat	Nervous system
Methylnitrosourethane	Rat	Nervous system, kidney, liver
<i>SULFATE AND SULFONATE ESTERS</i>		
Dimethyl sulfate	Rat	Nervous system
Diethyl sulfate	Rat	Nervous system
Methyl methanesulfonate	Rat	Nervous system
Propane sulfone	Rat	Nervous system
<i>MISCELLANEOUS</i>		
Ethylurea and sodium nitrite	Rat	Nervous system
	Syrian hamster	Nervous system
	Rabbit	Kidney
Methylazoxymethanol	Rat	Nervous system, kidney, intestine

<sup>a</sup> Rice JM: *Effects of prenatal exposure to chemical carcinogens and methods for their detection*, In Kimmel C.A., and Buelke-Sam J., editors: *Developmental toxicology*, New York, 1981, Raven, pp. 191–212. Reproduced by permission of Taylor & Francis Group.

Modified from Haschek WM, Rousseaux CG, Wallig MA, editors: *Handbook of toxicologic pathology*, ed 2, 2002, Academic Press, Table VI, p. 911, with permission.

does not occur in childhood, there is an increased risk of its development later in life. Animal experiments have shown that tumors can be initiated in utero and that promotion can occur after birth by treatment with tumor promoters. This fact emphasizes the prolonged latency of some transplacentally initiated tumors

and the importance of subsequent postnatal exposure to promoting agents.

**Direct-acting carcinogens** are the most potent known transplacental carcinogens. These substances cause molecular damage without the need for prior biotransformation, usually reacting with intracellular receptors or with

**TABLE 11.6** Selected Metabolism-Dependent Transplacental Carcinogens Other than Aliphatic Nitrogen-Containing Compounds<sup>a</sup>

Compound	Species	Principal Target Organs
<b>POLYNUCLEAR AROMATIC HYDROCARBONS</b>		
Benzo[ <i>a</i> ]pyrene	Mouse	Lung, skin <sup>b</sup>
Methylcholanthrene	Mouse	Lung
7,12-Dimethylbenz[ <i>a</i> ]-anthracene	Rat	Nervous system, kidney
	Mouse	Lung, skin <sup>b</sup> liver, ovary
<b>HETEROAROMATIC COMPOUNDS AND AROMATIC AMINES</b>		
3-Hydroxyxanthine		
Furylfuramide (AF-2)	Rat	Liver, mammary gland
4-Nitroquinoline-oxide	Mouse	Lung
<i>o</i> -Aminoazotoluene	Mouse	Lung
4-Dimethylaminoazobenzene	Mouse	Liver
<i>o</i> -Toluidine	Mouse	Liver, lung
3,3-Dichlorobenzidine	Mouse	Liver, lung
	Mouse	Liver, lung
<b>NATURAL PRODUCTS OF PLANT AND FUNGAL ORIGIN</b>		
Aflatoxin		
Cycasin	Rat	Liver
Safrole	Rat	Nervous system, intestine
	Mouse	Kidney
<b>MISCELLANEOUS COMPOUNDS</b>		
Ethyl carbamate	Mouse	Lung, skin, <sup>b</sup> liver, ovary
Vinyl chloride	Rat	Blood vessels, kidney, Zymbal's gland

<sup>a</sup> Modified from Rice JM: *Effects of prenatal exposure to chemical carcinogens and methods for their detection*. In Kimmel CA, Buelke-Sam J, editors: *Developmental toxicology*, New York, 1981, Raven, pp. 191–212, with permission.

<sup>b</sup> Skin tumorigenesis in mice occurred during postnatal topical application of a promoter (croton oil or phorbol ester).

Reproduced from Haschek WM, Rousseaux CG, Wallig MA, editors: *Handbook of toxicologic pathology*, ed 2, 2002, Academic Press, Table VII, p. 913, with permission.



target molecules such as DNA or glutathione. Alterations to the DNA may become fixed due to rapid cell cycling, thereby inducing a heritable predisposition to carcinogenesis. For this reason, all prenatal stages of development are susceptible to the action of these agents. Other examples of direct-acting transplacental carcinogens include DMBA, ethylnitrosourea, and methylnitrosourea, all of which form covalent adducts that induce point mutations in replicating DNA strands. Accordingly, it is not surprising that these chemicals have been shown to increase the incidences of tumors in F<sub>1</sub> and F<sub>2</sub> generations of exposed mice and rats.

In contrast, **metabolism-dependent transplacental carcinogens** are relatively less carcinogenic due to required conversion of a parent molecule to the reactive carcinogen. Although the required enzymes for metabolic conversion are present at low levels in the fetus, the intrinsic susceptibility of rapidly dividing fetal cells can compensate for this deficiency. Agents of this type tend to pose a greater hazard late in gestation when fetal cells typically begin their terminal differentiation and first assume their adult functions. For example, nitrosamines are metabolized to reactive alkylating intermediates in the mammalian fetus via the mixed-function oxidase (MFO) system, which first becomes functional just before birth in rodents. The MFOs are enzyme complexes, such as cytochromes P450 (CYP450), that oxidize both endogenous substrates and toxic compounds, rendering them more susceptible to metabolism and excretion. Based on their intracellular location, MFOs are sometimes referred to as microsomal enzymes.

Maternal enzymes activate some metabolism-dependent transplacental carcinogens, but this role is seldom of significance, for two reasons. First, circulating concentrations in maternal blood are usually insufficient to initiate and promote carcinogenesis in the fetus unless the metabolite is quite stable and can accumulate in fetal tissues via a mechanism like “ion trapping” (Carney et al., 2004). More importantly, reactive intermediates bind to maternal tissues before they can cross the placenta.

The effects of most transplacental carcinogens manifest during the postnatal period. Therefore, in most instances, developmental toxicants act as either a teratogen, resulting in structural or

physiological changes in a developing embryo or fetus, or transplacental carcinogens that result in neoplasia, but not both. This division is reasonable as most known teratogens do not act by causing mutations but rather function via mechanisms such as endocrine disruption, oxidative stress, vascular disruption, and neural crest cell disruption to initiate a cascade of altered developmental events. Indeed, the genetic causes of malformations are likely to reflect chromosomal abnormalities rather than chemically induced mutations, while the genomes of animals exposed to transplacental carcinogens will exhibit numerous aberrations at the DNA level. That said, it is not uncommon to see cancers in individuals displaying defective development (Table 11.5), indicating that at least a few substances can cause congenital malformations and cancers by a common molecular mechanism. For example, certain developmental toxicants, such as DES, induce both carcinogenesis (cervical/vaginal clear cell adenocarcinoma) and teratogenesis (reproductive tract abnormalities). It is probable that a permanent change to nuclear DNA is responsible for both the congenital defects and the tumors.

The nature of the abnormal developmental response—teratogenesis only, or both teratogenesis and transplacental carcinogenesis—has been postulated to depend on differences in xenobiotic availability. Exposure during the early stages of development is thought to engender malformations while contact throughout gestation is considered more likely to produce a mixture of teratogenic and carcinogenic effects. The presence of an agent during late gestation or the early postnatal period of development is likely to initiate a carcinogenic rather than a teratogenic reaction in most species, although it is still possible to observe gross malformations in certain organs of species that have not completed histogenesis by the time of birth (e.g., rodent cerebellum).

An environmental insult later during childhood may serve as the catalyst required to promote tumor development in cells that were initiated during gestation. For example, increased hormonal levels at puberty are thought to stimulate tumors in the dysgenic epithelial tissues of the mammary gland and reproductive tract of young women (usually between 15 and 30 years of age) exposed in utero to DES (Lagiu,

2006; Ma, 2009; Zamora-León, 2021). Enhanced vulnerability to DES-related vaginal clear cell adenocarcinoma may occur for nearly 6 decades after initial in utero exposure (Herbst and Anderson, 1990; Huo et al., 2017). The same carcinogen that provided the initiation event during the fetal period may also drive postnatal promotion.

## 7. MECHANISMS OF DEVELOPMENTAL TOXICITY

The pathogeneses and etiologies responsible for birth defects are quite complex, and many mechanisms have been proposed to explain the generation of toxicant-induced morphological defects. Some defects arise from cellular responses to damage, while others reflect actual biochemical and molecular elements that are thought to invoke the cellular reactions. The most important hypotheses are listed here. As the fundamental processes responsible for developmental toxicity are comparable to those that occur in adults, additional details might be gleaned from *Biochemical and Molecular Basis of Toxicity*, Vol 1, Chap 2.

It is often difficult to determine the precise cause of a developmental defect. This problem reflects the multiple potential etiologies of specific lesions due to gestational damage. A particular developmental anomaly can be induced via multiple pathways. In other words, different mechanisms of abnormal development often produce a common lesion. This quandary highlights the limited repertoire of pathologic responses to injury (whether genetic, toxic, or otherwise) that can be expressed by the conceptus.

### 7.1. Excessive Cell Death

Cell populations with a high proliferative rate, or those beginning to differentiate, are the most susceptible to cytotoxicity. This sensitivity results from the presence of more euchromatin and the lack of compact heterochromatin. The architecture of euchromatin and its reduced level of condensation provide a greater amount of active (or “exposed”) genome, thus yielding greater access to many genes. Such active DNA is

vulnerable to damage by foreign substances that can form adducts via covalent bonding to nucleotides. The exposed DNA can also be subject to nucleotide substitutions in which native bases are replaced by analogs that distort annealing between the complementary strands. If left in place, such modified bases can engender point mutations during DNA propagation; in many instances, such irreparable damage results in gene inactivation, which is often fatal to the affected cell. Another potential point at which toxicants can inflict damage is by altering energy metabolism as the internal nutritional requirements of rapidly dividing cells in the G<sub>1</sub> phase may be higher than those of resting (G<sub>0</sub>) cells that are common in differentiated tissues of adult animals.

Excessive cytotoxicity is a proven cause of abnormal embryonic development (Table 11.7). For example, cell loss confined to a local area impacts such key processes as limb formation and neural tube closure. Administration of supplemental folate to pregnant women has been shown to reduce the incidences of such defects, indicating that folate deficiency (Imbard et al., 2013) or folate antagonism (van Gelder et al., 2010) are likely mechanisms responsible for such outcomes. The pattern of death may encompass large cell groups (i.e., necrosis) or be limited to isolated cells (i.e., single-cell death or apoptosis). Early and excessive cell attrition may leave too few cells to initiate critical inductive events at specific stages of development. The lack of positional information associated with this loss will produce incorrect spatiotemporal relationships that can prevent expansion of a given target cell population—including all future cell collectives that cannot be induced without the help of the affected target cells. Thus, small deficits resulting from excessive cell death at early points in gestation can cascade into additional deficits affecting many more cell populations later in development. Limb reduction defects, which are sometimes seen after cyclophosphamide cytotoxicity, are thought to develop via this pathogenesis.

The regenerative capacity of embryonic tissues in compensating for cell death is also vital in defining the extent of toxicant-induced injury. This premise is exemplified by studies with 2-amino-1,3,4-thiadiazole (aminothiadiazole),

**TABLE 11.7** Selected Agents Producing Cytotoxicity in Organ Anlagen Followed by Malformation of that Organ<sup>a</sup>

Agent	Species
Actinomycin D	Chick
6-Aminonicotinamide	Rat
Aminopterin	Chick
Aminothiadiazole	Rat
5-Azacytidine	Mouse
5-Azaauridine	Mouse
Busulfan	Rat
Colchicine	Hamster
Cyclophosphamide	Rat
Cytosine arabinoside	Rat
Dinitrophenol	Chick
Ethylnitrosourea	Rat
5-Fluorodeoxyuridine	Mouse, rat
5-Fluorouracil	Chick, mouse
5-Fluoro-2-deoxycytidine	Mouse
Hadacidin	Rat
6-Mercaptopurine	Rat
Methylnitrosourea	Rat
Methylbenzantracene	Rat
Mitomycin C	Chick
Nitrogen mustard	Chick, mouse
Urethane	Mouse
Vincristine	Hamster
Vinblastine	Hamster

<sup>a</sup> Modified from Scott WJ, Jr.: *Cell death and reduced proliferative rate*, In Wilson JG, Fraser FC, editors: *Handbook of teratology*, New York, 1977, Plenum, pp. 81–98, by permission. Reproduced from Haschek WM, Rousseaux CG, Wallig MA, editors: *Handbook of toxicologic pathology*, ed 2, 2002, Academic Press, Table IV, p. 908, with permission.

a nicotinamide antagonist. This substance causes less severe limb defects if exposure is timed so that digit primordia have sufficient time to restore their cell numbers and orientations before stem cells lose their pluripotent potential.

## 7.2. Dysregulated Autophagy

Damaged cells in the developing conceptus may undergo autophagy (self-deletion), and this process is crucial for maintaining health of the conceptus starting prior to implantation (Tan et al., 2020). An imbalance in the protective (for mild stress) versus destructive (for severe stress) aspects of autophagy during development may lead to excess or insufficient autophagy, either of which may cause embryonic loss. Extensive oxidative stress leading to autophagy of trophoblasts has been proposed as a common pathway responsible for tissue degeneration and disrupted circulation of the placenta. Dysregulated autophagy also alters placental expression of ATP-binding cassette (ABC) transporters (Shahnawaz et al., 2021), which are involved in protecting the embryo from xenobiotics (Joshi et al., 2016). Teratogens that have been implicated as causes of dysregulated autophagy during pregnancy include elevated glucose levels, which have been reported with heart malformations; PIKfyve (phosphoinositide kinase, FYVE-type zinc finger-containing) inhibitors, which are linked to embryonic stem cell damage; and Zika virus, which induces placental damage.

## 7.3. Interference with Programmed Cell Death (Apoptosis)

Embryonic tissue and organ sculpting by the space- and time-specific activation of PCD or apoptosis is a normal developmental phenomenon that controls the elimination of transitory organs and tissues as well as participates in tissue remodeling. The physiologic process of cell death is under tight genetic control with activation sometimes being regulated by local environmental factors. PCD shapes an organ by inducing tissue reorganization or by removing cells that are suboptimally integrated and/or no longer needed. Many organs use PCD including the brain (to remove abnormal and superfluous neurons); digits (to eliminate interdigital tissue to attain the right degree of separation and appropriate size; Figure 11.26); heart (to shape the outflow tract, cardiac valves, and coronary vasculature); and hollow organs (to create cavities in solid organ primordia). The process involves



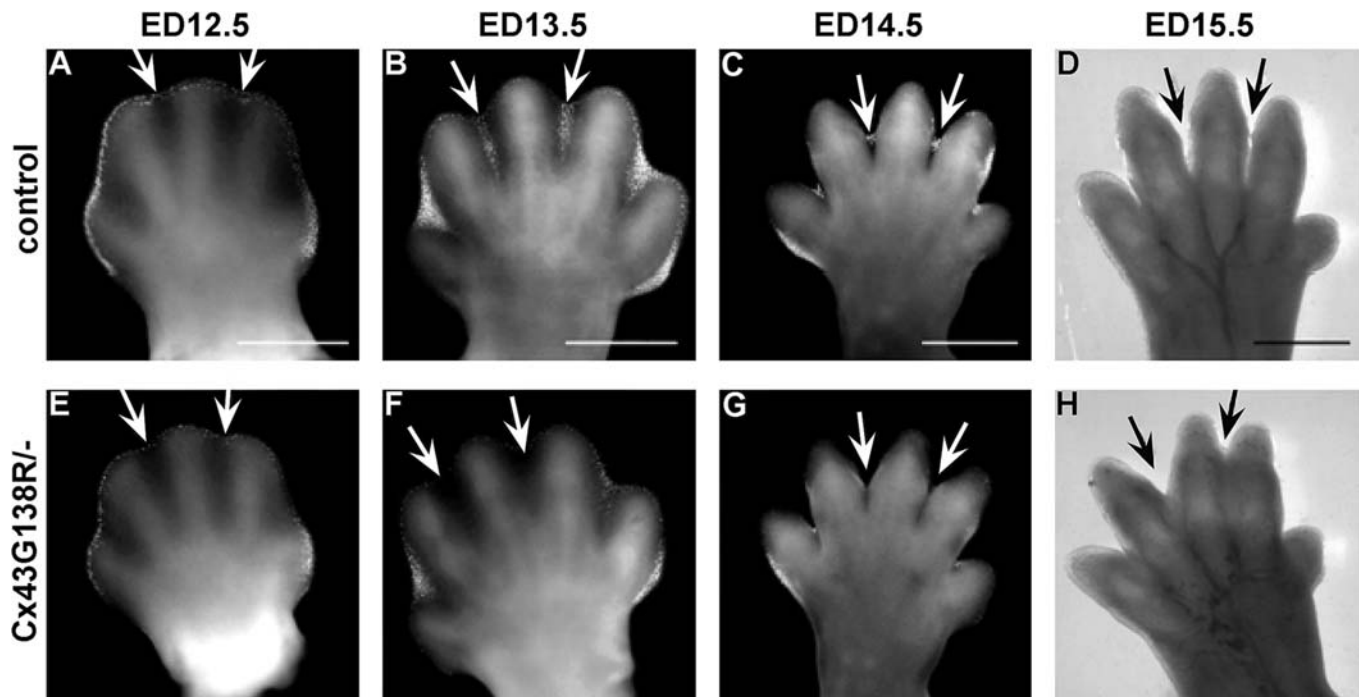


**FIGURE 11.26** Paw development in the developing mouse depends on timely programmed cell death at the proper sites. In control animals (top row), the limb bud at gestational day (GD) 12.5 (panel A) is defined by a rise in apoptosis in the soft tissues of the interdigital rays (arrows), which progresses over time (panels B, C) to yield complete separation of the digits by GD 15.5 (panel D). In contrast, stage-matched littermates with a point mutation in connexin-43 (a constituent of gap junctions) have reduced apoptosis (panels E, F, G) that results in a variable degree of syndactyly (persistent fusion of digits). Scale bars: 500  $\mu$ m. *Reproduced with modified labeling from Dobrowolski RM et al.: Loss of connexin43-mediated gap junctional coupling in the mesenchyme of limb buds leads to altered expression of morphogens in mice, Hum. Mol. Genet. 18:2899–2911, 2009, by permission.*

selective elimination of cells that do not complete their developmental program, and it is an active undertaking designed to prune exuberant cell numbers during histogenesis and organogenesis.

Signals that can initiate PCD usually are chemical messages, such as hormones or growth factors. Interference with these signaling pathways by chemicals, drugs, physical agents, or viral infections may prevent timely cell death and lead to supernumerary cells or structures. For example, necrotic mesodermal cells in rat embryos release apical ectodermal maintenance factor following acetylsalicylic acid (aspirin) exposure. This molecule prevents PCD in the apical ectodermal ridge, thereby producing pups with polydactyly. Brain development is particularly susceptible to the maternal exposure of certain drugs during gestation such as general anesthetics, antiepileptics, barbiturates, benzodiazepines, and ketamine. As an example, maternal consumption of alcohol has been shown to result

in widespread apoptotic death of neurons and oligodendroglia in the developing brain when administered to animals, including NHPs. Alcohol also induces PCD in cranial ectodermal, mesodermal, and neural crest cells in developing embryos, which explains the link between brain functional deficits and structural defects and the craniofacial features that develop during fetal alcohol syndrome.

#### 7.4. Reduced Cell Proliferation

Diminished rates of cell division may occur following exposure to toxicant doses that are lower than the doses that induce overt cytotoxicity. The diminished cell numbers may cause growth suppression of one or more organs. Growth suppression can have dramatic effects that resonate throughout development since a critical mass of one tissue is often essential to induce many secondary structures. For example,

if dental anlagen are not of sufficient mass, teeth will fail to develop, and their supporting bony structures will be smaller than normal.

The growth of various tissues occurs at dissimilar rates, so reduced proliferation of tissues during histogenesis can result in different degrees of abnormal growth depending on the affected organs. This loss of developmental synchrony is a striking characteristic of hypovitaminosis A in pigs, where piglets are born blind because premature closure of the cranial sutures leads to smaller optic foramina and compression of the optic tracts as they exit the cranium. Similarly, corticosteroids reduce palatal shelf size, resulting in cleft palate formation in mice.

### 7.5. Failed Cellular Interactions

During development, progenitor cells differentiate into specialized cell types to form organs and tissues. To do this, cells use different signaling pathways to modulate the expression of key transcription factors. Genetic factors, exogenous agents, or both can cause unsuccessful or ineffective cell signaling pathways in divergent cell populations, and this effect may induce various functional and nonfunctional embryonic conditions. For example, abnormal cerebellar development in the *weaver (wv)* mouse mutant (gene symbol: *wv*) results from a genetically programmed decrease in numbers of radial glia processes needed to guide the migration of granule cells from the brain surface through the molecular layer to the granule cell layer. Similarly, a genetic defect in cattle produces anophthalmia or microphthalmia via reduced or absent contact between the optic cup and overlying ectoderm, thereby preventing induction of the lens placode. Antineoplastic agents including actinomycin D, chlorambucil, and methylhydrazine as well as ionizing radiation also incite these ocular lesions by the same mechanisms. Hypovitaminosis A disrupts the spatial orientation among cells in mesenchymal condensations by changing cell adhesion expression, which leads to altered shapes of cartilage models and their bony successors.

### 7.6. Impeded Morphogenetic Movements

During embryonic development, the normal rearrangement of tissues leads to germ layer

positioning, patterning, and organ morphogenesis. These feats are accomplished by highly coordinated and cooperative migration of cells. Abnormal cellular migration produced by several mechanisms is involved in many diseases and congenital disorders. Common mechanistic factors include decreased cell mobility; abnormal quantity or quality of the ECM, especially through altered SAMs; aberrant quality of cell adhesion interactions as mediated through anomalous patterns of CAMs, SAMs, or CJMs; and disruption of cytoskeletal microtubules or microfilaments. Accordingly, altered perception of critical positional information and/or inability to follow the signals seem to be primary themes responsible for such defects.

The ECM is composed of GAGs such as chondroitin, chondroitin sulfate, heparin, heparin sulfate, hyaluronic acid, and keratin sulfate as well as abundant collagen. These molecules and other SAMs interact with the integrins on cell membranes, allowing adhesion and ultimately directed motion among tissues in defined planes. The ECM content of these elements varies at different stages of development. High levels of hyaluronic acid during early morphogenesis encourage cell migration by increasing cell proliferation, inhibiting aggregation, and increasing the fluidity of the ECM. During later differentiation, hyaluronic acid levels decrease as cells begin to aggregate and chondroitin sulfate production is increased. Similarly, concentrations of fibronectin vary across gestation.

BrdU, a synthetic nucleoside analogue, and 6-diazo-5-exo-L-norleucine (DON), a glutamine antagonist, produce limb defects and cleft palates. As these teratogens can inhibit the synthesis of chondroitin sulfate, toxicant-induced enhancement of pro-migratory ECM elements has been proposed as a possible mechanism for inducing these major malformations.

Diminished cell adhesion can also result in malformations. Cortisone disrupts the synthesis of GAGs and collagen, resulting in reduced production and sulfation of ECM constituents. The decreased adhesive qualities of the ECM may contribute to the inability of the palatine shelves to fuse. In addition, cell surface receptors may be altered, thereby thwarting recognition and induction of certain cell collectives.

Microtubules and microfilaments are essential contractile elements of all cells. Function of these

elements can be affected by disrupting the synthesis and turnover of tubulin, changing the number and arrangement of microtubule organizing centers, altering the phosphorylation of tubulin-associated proteins, and perturbing tubulin polymerization. Certain antineoplastic agents incite developmental toxicity in this fashion: colchicine and vincristine distort microtubule structures, while cytochalasin B inactivates microfilaments. The actions of these cytoskeletal components can also be impacted by indirect means. Calcium ( $\text{Ca}^{++}$ ) is required for appropriate microtubular and microfilamentous function; therefore, treatment with ethylenediaminetetraacetic acid (EDTA) induces heart malformations by reducing the movement of pioneer cells through the cardiac jelly. The defects arise by the ability of EDTA to chelate  $\text{Ca}^{++}$ , which paralyzes the migrating cells during this critical period of cardiogenesis.

### 7.7. Reduced Biosynthesis of Essential Components

Altered production of many molecules can profoundly affect normal growth and development. In this regard, the usual change is decreased molecular synthesis. All the major molecules required to support rapidly expanding tissues—nucleic acids (DNA and RNA), proteins of all kinds, and energy storage molecules (e.g., the complementary molecules adenosine di- and triphosphate [ADP and ATP, respectively] as well as the native and phosphorylated forms of nicotinamide adenine dinucleotide [NAD and  $\text{NADP}^+$ , respectively])—are subject to such perturbations following xenobiotic exposure during development.

Inhibition of DNA synthesis is not teratogenic per se. However, cytotoxicity is a common outcome of reduced DNA synthesis, and the resulting cell loss can engender teratogenic effects at future stages of embryogenesis. Important factors in the outcome of such inhibition are the time available for cellular repair, which can be minimal in the rapidly dividing cell collectives characteristic of the embryo, and the degree of cell death. Cytosine arabinoside and hydroxyurea both inhibit enzymes required for DNA synthesis, the former by repressing DNA polymerase and the latter by suppressing ribonucleoside

diphosphate reductase. Cytosine arabinoside elicits more prolonged depression of DNA synthesis, which allows less time for repair before the next cycle of cell division and heightens the likelihood of anomalous development.

A primary reduction in RNA synthesis may inhibit DNA synthesis since RNA primers are required for some DNA replication. However, decreased RNA synthesis more typically interferes with protein production, thereby depriving metabolically active cells of essential building blocks needed for growth. Several antineoplastic agents such as actinomycin D, chromomycin  $\text{A}_3$ , and daunomycin act in this manner. The degree of RNA depletion correlates well with their cytotoxic potential and potency as teratogens.

Inhibition of protein synthesis occurs by several mechanisms. For example, failure to assemble ribosome complexes prevents protein translation. This outcome explains the developmental toxicity of chloramphenicol, an antibiotic that stops mRNA from binding to ribosomes. This nonattachment precludes translation of mRNA and therefore foils protein synthesis. Another instance is misreading of mRNA, which results in the release of defective proteins; this outcome is produced by exposure to the antibiotics kanamycin or streptomycin. A similar aberration is premature termination and release of peptide chains, which is a consequence of puromycin administration. Finally, the inability to perform posttranslational modification can foil the manufacture of functional proteins, which may secondarily impact many cell activities (including nucleic acid synthesis). An example of this effect is altered phosphorylation of glucose, which is observed following tetracycline administration. In general, protein synthesis inhibitors often produce little cytotoxicity, but they nonetheless are efficient agents for inducing embryo lethality or growth retardation.

Abnormal energy metabolism is generally a critical blow to developing organisms. Inadequate reserves of ATP and  $\text{NAD}/\text{NADP}^+$  can have serious effects on biosynthesis by altering the efficiency of glycolysis and electron transport during critical periods of organogenesis. As adequate energy stores are an absolute requirement for many aspects of cellular function, especially in rapidly dividing cells, it is not surprising that agents which block the synthesis of ATP and/or  $\text{NADP}^+$  can have



disastrous effects on the developing embryo. A well-known example of this mechanism is 6-aminonicotinamide (6-AN), an inhibitor of 6-phosphogluconate dehydrogenase that inhibits turnover of energy storage molecules. In turn, altered energy storage alters proteoglycan production and produces limb defects in chicken embryos. Similarly, the teratogenic effects of organophosphate and methylcarbamate insecticides in the developing chicken may lie not only in their ability to inhibit acetylcholinesterase but also in their ability to reduce cellular NAD pools. Interventions that inhibit mitochondrial electron transport, such as cyanide, dinitrophenol, and hypoxia, can incite cell death. If sufficiently severe, cell loss can be followed by embryonic or fetal death.

### 7.8. Inhibition of Angiogenesis

Consistent circulation of blood is essential for normal development of the embryo, fetus, and placenta. As the embryo grows, blood vessels form first by **vasculogenesis** (i.e., differentiation of angioblasts into endothelial cells that drive de novo formation of an interconnected vascular network) and subsequently by **angiogenesis** (i.e., formation of new blood vessels from preexisting vessels). In certain types of vessels, smooth muscle cells are recruited to stabilize the vessel wall and regulate intraluminal pressure.

Certain substances induce teratogenic effects by their antiangiogenic activity. For example, some thalidomide metabolites inhibit vascular formation and thereby engender limb malformations by altering FGF-mediated pathways in the apical ectodermal ridge and mesenchyme (Therapontos et al., 2009; Vargesson, 2015). Certain inhibitors of mammalian target of rapamycin (mTOR, a serine/threonine kinase) and many tyrosine kinase inhibitors reduce proliferation in human vascular endothelial cell (HUVEC) cultures and also function in vivo to elicit such embryotoxic effects as lethality and various malformations (typically affecting the heart and/or skeleton) (Beedie et al., 2016). These small molecule agents appear to impact vascular growth through interference with mTOR or platelet-derived growth factor (PDGF) and/or vascular endothelial growth factor (VEGF) signaling pathways.

### 7.9. Endocrine Disruption

Exogenous substances that act as endocrine disruptors induce a number of toxic effects, of which developmental toxicity is among the most pervasive and substantial (see *New Frontiers in Endocrine Disruptor Research*, Vol 3, Chap 12). Endocrine-disrupting chemicals (EDCs) mimic or interfere with the function of one or more endocrine organs by either acting as an agonist or antagonist in place of the native molecule or by interfering with the hormone's synthesis, secretion, transport, binding, action, or elimination. In this way, exogenous endocrine disruptors alter systemic hormonal signals essential for the proper molecular, cellular, and structural development of body organs during gestation as well as their functional maturation and performance during postnatal life. The primary concern with respect to EDCs has centered on their potential for impairing reproductive system development, behavior, and/or fertility as a consequence of aberrant endocrine pathways in the gonads. For example, the feminization of male alligators and "super-feminization" of their female swamp mates in central Florida's Lake Apopka has been attributed to a large pesticide spill that occurred in 1980, leading to accumulation and persistence of chemical residues in fat. Perinatal exposure of rats to antiandrogenic compounds such as vinclozolin and di(2-ethylhexyl) phthalate (DEHP) have been shown to inhibit fetal testicular testosterone production and result in newborns with a variety of lesions including reduced AGD, retained nipples, cleft phallus with hypospadias, undescended testes, a vaginal pouch, epididymal agenesis, and small to absent accessory sex glands as adults. Additional lesions following exposure to DEHP included hepatocellular carcinomas and pancreatic acinar adenomas whereas additional lesions following exposure to vinclozolin resulted in prostate disease, kidney disease, immune system abnormalities, tumor development (e.g., breast), and blood abnormalities including hypercholesterolemia.

Many chemicals have been implicated as endocrine disruptors. Bisphenol A (used in production of polycarbonate plastics and resins, such as beverage and food containers) and phthalates (utilized as "plasticizers" to make plastics more durable) have garnered particular interest in recent years based on evidence that

their presence alters pregnancy outcomes (Filardi et al., 2020). Other EDCs include PCBs, organochlorine pesticides, and flame retardants. Many experiments investigate a single EDC, but in recent years, studies performed with EDC mixtures (which mirror the “real world” situation) have shown the potential for additive or synergistic effects. Mechanisms by which EDCs may mediate their effects include altering the methylation pattern in the fetal epigenome (Bommarito et al., 2017), disrupting the maternal and neonatal inflammasome (Kelley et al., 2019), and interference with signaling pathways for various thyroid hormones (Patrick, 2009).

Although experimental animal models have confirmed the negative impact of endocrine disrupting chemicals, there are fewer definitive studies in humans. That said, developmental EDC exposures have been postulated to impact both pregnant women (e.g., gestational diabetes, immune dysfunction, preeclampsia) and the conceptus (e.g., IUGR, premature delivery, reproductive tract malformations). Adverse effects of EDCs persist into juvenile development (e.g., altered puberty and neurobehavioral function) and adulthood (Meeker, 2012), perhaps contributing to the precipitous rise of metabolic diseases (e.g., type II diabetes, obesity) in many developed nations. In utero exposure to the synthetic estrogen DES is a known cause of breast and cervical/vaginal clear cell adenocarcinomas in young women.

### 7.10. Oxidative Stress

Excessive quantities of ROS in tissues of the developing embryo can induce severe or even lethal injury (Fantel, 1996; Ornoy, 2007). Many substances appear to increase oxidative stress in developing conceptuses. The situations associated with this effect include physiological states such as hyperglycemia (i.e., diabetes) and hypoxia as well as exposure to teratogens including alcohol, cocaine, ionizing radiation, and tobacco smoke. Exposure to teratogens may decrease the activities of antioxidant enzymes and also deplete cellular levels of antioxidant molecules including vitamin C and vitamin E in embryonic and YS tissues. The extent of such reductions appears to be greater in malformed compared to morphologically normal conceptuses.

Antioxidant systems in the embryo/fetus and placenta are relatively weak throughout

gestation, but this feebleness is especially pronounced at early stages of embryogenesis. Many antioxidants effectively mitigate the adverse outcomes induced by oxidative stress in test animals and seemingly in pregnant women. Carotenoids, folic acid, and vitamins C and E have been suggested to be effective antioxidant supplements with potential clinical applications.

### 7.11. Mechanical Disruption

Damage by agents that physically impact cytoarchitectural and/or tissue development can profoundly impact the viability of the conceptus. Amniotic band syndrome (also called constriction ring syndrome), in which digits or limbs are entangled and constricted by amnion-derived fibrous tissue, is a classic example of this mechanism. Mechanical disruptions may sever interactions among neighboring cells, impede morphogenetic movements, and decrease proliferation and growth through pressure-induced ischemia and necrosis. Changes in the local ionic balance can provoke fluid buildup within cells and fluid-filled organs (e.g., brain, eye) that alters the integrity of these structures. For example, in the chick embryo, both dimethyl sulfoxide (DMSO) and hypoxia precipitate increases in CSF volume that raise the pressure within the brain ventricles and spinal cord central canal. Over time, distension can exceed the elastic limits of the ependymal lining, thereby permitting escape of the CSF into the adjacent neuropil. This mechanism is thought to explain such congenital defects as hydrocephalus and **syringomyelia** (i.e., formation of a fluid-filled cyst in the spinal cord).

Altered pressure is also thought to contribute to the genesis of VSDs, which are the most common congenital cardiac anomalies. Substances that interfere with aortic arch development can change the blood flow patterns in the heart tube. Over time, distorted flow dynamics increases the intraluminal pressure within the reorganizing heart, thereby preventing normal cardiac partitioning—and particularly the complete closure of the ventricular septum. A number of xenobiotics have been implicated in VSDs induced by this mechanism including alcohol, lithium, retinoic acid, thalidomide, and trimethadione. The constant pressure overload in the ventricles is commonly

accompanied by defects in the atrial septum and/or one or more major cardiac vessels, including patent ductus arteriosus, tetralogy of Fallot (of which VSD is an integral component), or transposition of the great vessels. Other etiologies can also induce these changes including infections (e.g., rubella) and maternal diseases (e.g., diabetes mellitus).

Excessive mechanical constraint has been linked to many instances of gross malformation in external structures. Examples include malpositioning, reduction, or amputation of the limbs as well as failed closure of the abdomen, neural tube, palate, or philtrum (middle portion of the upper lip). Abnormalities of placental structure (e.g., umbilical cord bands) or function (e.g., oligohydramnios) have been linked to these outcomes. In like manner, aberrations of uterine structure (e.g., malformations) or function (prolonged severe contractions) have been associated with such lesions. In all these cases, the putative pathogenesis is an extrinsic increase in the mechanical pressure applied to the surface of the developing embryo or fetus.

Heightened pressure may disrupt development by mechanisms other than direct trauma to the conceptus. A common pathway for such changes seems to be insufficient circulation to the rapidly evolving tissues. For example, vascular occlusion by tissue compression (e.g., from intense uterine contractions) will decrease organ perfusion. Alternatively, early embryonic trauma through overzealous manual pregnancy testing of cattle can cause atresia coli in calves. The presumed pathogenesis of such lesions is hypoperfusion, cell hypoxia, eventual endothelial cell loss, and necrosis, with eventual repair by fibrosis. Developmental toxicants such as misoprostol (a synthetic prostaglandin E<sub>1</sub> analog) and phenytoin as well as certain placental manipulations (e.g., chorionic villous sampling) have been shown to induce leg defects in human infants by vascular disruption in limbs that had first formed normally. The spectrum of such defects is broad, ranging from digit fusion or truncation to arthrogryposis to constriction rings.

### 7.12. Intracellular pH Alterations

The hydrogen (H<sup>+</sup>) ion concentration in developing cells has been implicated as a common pathogenesis for many developmental toxicants

(Carney et al., 2004). Very small changes in pH have been shown to significantly affect various embryonic systems. Fetal metabolism results in the consistent production of carbonic and organic acids, but extracellular pH is kept within normal range. Intracellular pH is normally lower than extracellular pH due to lower concentrations of bicarbonate [HCO<sub>3</sub><sup>-</sup>]; maintaining this pH within the appropriate dynamic range plays a critical role in membrane transport and other cellular processes. Teratogen-induced decreases in intracellular pH interfere with many processes, including such critical functions as proliferation, internal signaling, enzyme activity, and cytoskeletal protein polymerization. Thus, it is not surprising that toxicant-induced alterations in fetal pH can produce developmental defects. Substances implicated as modifiers of intracellular pH in embryonic cells include anti-convulsants (e.g., diphenylhydantoin, sodium valproate); carbon dioxide (which is converted in the body to bicarbonate); and carbonic anhydrase inhibitors (e.g., acetazolamide). These substances have been associated with many types of malformations including NTDs and postaxial right forelimb ectrodactyly.

## 8. DEVELOPMENTAL TOXICITY ISSUES IN PRODUCT DEVELOPMENT

The impact of xenobiotic exposure on the developing organism depends on many interrelated factors, and these elements must be addressed when assessing the risk of developmental toxicity for new products in development. This section briefly reviews these factors as well as key design considerations for developmental toxicity studies. Additional details may be garnered from *The Role of Pathology in Evaluation of Reproductive, Developmental, and Juvenile Toxicity*, Vol 1, Chap 7.

### 8.1. Biological Factors that Modify Developmental Toxicity

Intrinsic parameters of both the progeny and the parents may influence the onset and progression of developmental toxicity. Some of these factors are common to progeny and parents while others are specific to progeny or parents.



### 8.1.1. Conceptus

#### 8.1.1.1. GENETIC BACKGROUND

Species differences in expression of defective development following xenobiotic exposure have been clearly shown experimentally. The classic example is thalidomide, which is highly teratogenic in humans and certain NHPs but does not readily cause malformations in rodent and chicken embryos. In like manner, glucocorticoids are teratogenic in mice but not in rats. Species differences in teratogenic responses are probably a manifestation of many species-specific factors.

Embryo development requires complex orchestrated events that are finely regulated at the molecular and cellular level. The most important parameters for dictating the teratogenic potential of a substance in any species are thought to be its PK properties—including the individual rate of transplacental transfer—and differences in the distribution and/or sensitivity of the xenobiotic's receptors and target cells. The key means for controlling these response factors are the embryo's complement of genes. Genetic technologies, including gene editing and single-cell RNA analysis, allows assessment of embryonic gene expression with increased precision, providing insights into complex processes.

The responses of individuals in outbred species (e.g., humans, CD-1 mice [a common mouse stock for developmental toxicity testing]) are specified chiefly by the individual's own allelic complement. In species with multiple highly inbred strains (especially mice), individuals for a given strain tend to react in a comparable fashion. This similarity arises because the lack of genetic diversity in a highly inbred strain produces more uniform, reproducible, and stable gene complements than are found in outbred strains. In contrast, distinct inbred strains may respond in divergent fashions to toxicants depending on how much concordance exists among their gene complements.

The divergence among strains for a species may represent intrinsic differences, such as unique patterns of protein expression or timing for developmental events, or they can result from extrinsic differences that are defined by specific maternal biotransformation rates or products. For example, cortisone induces a higher incidence of cleft palate in A/J mice than occurs in either CBA or C57BL/6J mice.

The greater vulnerability of the A/J strain appears to reflect a genetically determined increase in numbers of glucocorticoid receptors in the developing maxillary processes as well as the slightly later timing of palatal shelf elevation in this strain. Furthermore, A/J dams metabolize cortisone differently than do CBA dams, thus producing a greater exposure in the A/J embryos.

The importance of the embryonic genotype in determining the response of the conceptus to xenobiotics is readily apparent in the discordant defective development that may occur between dizygotic human twins exposed to a teratogen. This discordance also manifests itself in the rodent since offspring in a single litter are rarely all affected in the same manner or to the same degree following in utero teratogen exposure. However, such within-litter discordance may arise from other causes. Examples include variations in maternal blood supply to offspring at various locations in the uterine horns and the impact of a sibling's metabolic profile (e.g., hormone production) on nearby conceptuses.

#### 8.1.1.2. MULTIFACTORIAL/THRESHOLD CONCEPT

The foundation of the multifactorial/threshold ("multiple hit") concept is that a vulnerable conceptus must be genetically predisposed to develop a malformation before the action of a teratogen results in manifestation of the defect (Fraser, 1976). In other words, some defects do not occur unless two or more factors occur together that permit damage to manifest. The sum of genetic and environmental factors constitutes an individual's level of risk, or threshold, for the defect; thus, this concept explains the inheritance of traits that do not follow the usual Mendelian patterns of inheritance. In humans, examples of multifactorial malformations include certain cardiac anomalies, cleft lip and cleft palate, congenital hip dislocation, hypertrophic pyloric stenosis, *spina bifida*, and *talipes*. Approximately 50% of all developmental malformations may involve multifactorial inheritance, with or without the need for additional teratogen-induced damage.

Each organ system exhibits a threshold for abnormal organogenesis. Damage below the threshold does not alter the normal developmental program, while damage exceeding the threshold will result in a malformation. If the

genetically determined pathway that specifies the normal progression of developmental events is close to the threshold, then only minor noxious stimuli may be capable of inducing an abnormality. A corollary concept is that a higher number of predisposing genes will reduce the severity of the teratogenic insult required to exceed the threshold. In fact, most, if not all, individuals are likely to have one or more "weak points" in their genetically programmed developmental plans that are especially vulnerable to influences that produce abnormal development. The absence of major defects in most individuals speaks to the resiliency of genetic and molecular controls in the conceptus.

As with human epidemiological data, cleft palate in rodents is a classic example of the multifactorial concept in an experimental animal system. The palatal processes of susceptible A/J mice elevate and fuse later in gestation than do those of the resistant C57BL/6J strain (Diewert, 1982). Late palatine closure predisposes an individual to having a cleft palate, so the threshold required for a teratogenic insult (e.g., cortisone) to induce cleft palate is lower in A/J mice.

#### 8.1.1.3. EMBRYONIC AND FETAL PHARMACOKINETICS

**8.1.1.3.1. METABOLISM** Variability exists among species with respect to the stage in which metabolic systems begin to develop and mature. In general, conceptuses of species with longer gestations (e.g., humans) develop greater metabolic capabilities in utero, while those of species with short gestations (e.g., rodents) typically show little enzyme activity until close to or after birth and thus are incapable of extensive in utero metabolism. For a particular species, metabolic pathways are much less developed in embryos than they are in fetuses and neonates. Similarly, metabolic pathways of conceptuses and neonates are less proficient than are the corresponding activities in the dam. In terms of in utero exposure to foreign substances, maternal metabolism (biotransformation and excretion) plays a significant and possibly determining role in embryonic and fetal exposure.

Nonetheless, the biotransforming capability of the embryo (and in some instances the placenta) during organogenesis may be substantial, at least

in species with longer in utero terms. In fact, some enzymes have essential functions as hormonal or biological response modifiers of metabolism. For example, human fetal adrenal glands and liver possess a large complement of enzymes as early as 6–8 weeks of gestation. Important examples include some isoforms of CYP450, cytochrome *b*<sub>5</sub>, NADPH-cytochrome C reductase, NADPH-cytochrome P-450 reductase, and NADH-cytochrome C reductase. These enzymes are capable of affecting many biotransformation reactions (e.g., aromatic and sidechain hydroxylations, *N*-demethylation, nitroreduction, and, to a limited extent, glucuronic acid conjugation), so a human fetus can metabolize many foreign substances to which it is exposed. Nonetheless, this embryonic capacity is likely to be too low to have much impact on blood and tissue concentrations of most xenobiotics compared to the metabolizing capabilities of the mother.

Human fetal hepatic enzyme activities are approximately the same as those found in the adult on a body weight basis. Therefore, fetal drug metabolism is capable of making either toxic or nontoxic metabolites from xenobiotics that cross the placenta. Since these metabolites are water-soluble, they may accumulate in the fetal compartment due to its relatively higher water content. Fortunately, detoxification reactions tend to predominate over activating reactions in fetal tissues. Thus, fetal metabolism usually serves to protect the fetus.

Fetal renal excretion also aids elimination of xenobiotics. During the latter stages of gestation, the glomerular filtration rate increases, resulting in a concomitant increase in the fetal renal drug clearance.

**8.1.1.3.2. ENZYME INDUCTION** Drug metabolizing enzymes catalyze the biotransformation of xenobiotics. Prenatal exposure to some known enzyme-inducing agents does increase enzyme activity in laboratory rodents. Both 3-methylcholanthrene (3-MC) and phenobarbital induce effects in conceptuses that are similar to those seen in mature animals. Again, the balance with respect to risk and benefit regarding whether enzyme-mediated metabolism will result in detoxification versus bioactivation depends on the xenobiotic in question. This issue

is discussed in more detail in *Biochemical and Molecular Basis of Toxicity*, Vol 1, Chap 2.

In mouse models of teratogenicity, the ability to respond to xenobiotics that induce phase I and phase II metabolic reactions depends on the strain. In phase I reactions, a polar reactive group is introduced into a molecule, thus rendering it a suitable substrate for phase II enzymes. Phase I reactions are more likely to form reactive intermediates as the products are generally potent electrophiles. In phase II reactions, conjugating enzymes will typically add endogenous hydrophilic groups, thereby resulting in an increase in xenobiotic water solubility and a more easily excreted product. For example, aryl hydrocarbon hydroxylase (AHH), which metabolizes benzo[a]pyrene, can be induced in C57BL/6J mice by maternal exposure to phenobarbital. Subsequent maternal exposure to benzo[a]pyrene results in embryonic malformations. In contrast, AHH activity cannot be induced in DBA mice, so benzo[a]pyrene is not teratogenic in this strain after similar pretreatment of dams with phenobarbital.

**8.1.1.3.3. TISSUE ACCUMULATION** Preferential sequestration of some teratogens in embryonic or fetal tissues occurs in some species, resulting in higher toxicant concentrations in the offspring than occur in the maternal blood. Lead is transported via maternal blood and modifies calcium transport through the placental syncytiotrophoblast where pinocytosis allows transport into fetal blood. Once in fetal blood, lead can accumulate in tissues and bind to mineralizing bone. Methyl mercury is retained in the fetus (where it affects neural development) because it cannot be converted to inorganic mercury, which is more readily eliminated. Indeed, fetal sequestration of methyl mercury is so complete that women are cautioned against eating large marine fish and shellfish (in which methyl mercury is bioconcentrated) during pregnancy because of the risk for developing fetal methyl mercury toxicity. Thalidomide is sequestered in embryos of sensitive species (e.g., rabbit) because embryonic enzymes hydrolyze the parent drug to hydrophilic metabolites that cannot readily cross cell membranes. As noted above, many mammalian teratogens are weak acids and so tend to concentrate in embryonic and fetal tissues, which are more basic than maternal plasma.

## **8.1.2. Mother**

### **8.1.2.1. MATERNAL PHYSIOLOGIC STATUS**

Alterations in maternal homeostasis must be severe to affect the conceptus since the needs of the growing organism are usually met even at the expense of the mother. Some exceptions do exist, however, due to known congenital malformations in humans that are related to various maternal metabolic and nutritional imbalances. Examples include diabetes (e.g., limb defects, macrosomia, microcephaly, several NTDs [anencephaly, holoprosencephaly, *spina bifida*], sacral agenesis); malnutrition (e.g., spontaneous abortion, stillbirths, NTDs, neonatal deaths); phenylketonuria (e.g., cardiac defects, cognitive deficits, microcephaly); thyroid disorders (e.g., hypothyroidism leading to cognitive deficits and deafness); and virilizing tumors (e.g., male pseudohermaphroditism due to androgen-secreting ovarian sex cord-stromal tumors, luteomas, or adrenocortical tumors).

### **8.1.2.2. MATERNAL PHARMACOKINETICS**

Maternal physiologic changes that occur during pregnancy can have a profound effect on the PK of many xenobiotics. These changes take place in multiple organs.

Absorption from the gut is altered during pregnancy because of increased gastric emptying time and reduced intestinal motility. Progesterone causes smooth muscle relaxation that can slow digestion in the stomach as well as the small and large intestines by about 30%–50%. The gall bladder is also affected by delayed gastric emptying. Uterine expansion as gestation progresses can also compress or sometimes block parts of the digestive tract. These changes increase the residence times in both the stomach and intestines, with the effect on the amount of uptake depending upon whether a given xenobiotic is more readily absorbed via the stomach or the intestine. Conversely, the absorption of substances from the gut may be decreased by emesis, which is a common response in some species during some portions of gestation (e.g., women with “morning sickness”).

Absorption of inhaled substances is also influenced by pregnancy. The pulmonary tidal volume increases during pregnancy by 30%–50% due to improved displacement of the rib cage, which permits greater lung expansion



needed to dispel higher carbon dioxide levels associated with the enhanced metabolism necessary to support the conceptus. Increased circulating progesterone levels will also increase tidal volume due to the bronchodilator effect of altered smooth muscle tone in airways (LoMauro and Aliverti, 2015). Taken together, these changes result in increased uptake of inhaled xenobiotics.

Drug distribution is impacted by plasma protein levels as well as cardiovascular dynamics. Progressive gestational decrease in plasma albumin concentration may affect binding of xenobiotics. Reduced plasma protein capacity for chemical binding during pregnancy leads to higher unbound circulating levels of substances, which favors higher distribution into tissues. This shift may be significant for substances, including many current drugs, whose efficacy and toxicity are related to unbound concentrations in plasma. With respect to cardiovascular physiology, the volume of distribution (Vd) markedly increases during pregnancy because of increased cardiac output, higher plasma volume, increased total body water, and greater body fat. This rise in Vd for hydrophilic drugs leads to decreases in the initial plasma concentrations of absorbed xenobiotics.

Maternal hepatic enzyme activities are enhanced during pregnancy, probably because of the growing need to metabolize fetal wastes. Progesterone, which is increased during pregnancy, functions to induce enzymes needed in the metabolism of some xenobiotics. Alternatively, drug metabolism may be reduced, at least for certain xenobiotics, because of competitive enzyme inhibition by steroid hormones. These counterbalancing trends are complicated. As an example, estrogen decreases the efficiency of some metabolic pathways by competing with xenobiotics for metabolizing enzymes. It is likely that effects of steroids and other hormones depend on the timing of gestational exposures as well as physicochemical characteristics of a given xenobiotic. Metabolic efficiency for a species depends on the strain-specific genetic background. For example, SJL/J mice (resistant strain) and C57BL/6J mice (sensitive strain) differ in their ability to metabolize 5-fluorouracil by the pyrimidine reductase pathway.

Maternal excretion of substances also is altered during pregnancy. Renal elimination of water-

soluble substances is more rapid (20%–65%) because blood flow to the kidney and the glomerular filtration rate increases by up to 50%. The increase in glomerular filtration rate is most likely secondary to vasodilation of afferent and efferent arterioles.

### 8.1.3. *Father*

#### 8.1.3.1. DIRECT TOXIC EFFECTS ON SPERM

Xenobiotics may accumulate in the epididymis, prostate, and/or seminal vesicles and have a profound effect on sperm morphology with or without eliciting sperm functional deficits. **Teratospermia** (or **teratozoospermia**) is the production of myriad structurally abnormal sperm which are often functionally deficient as well. Direct actions of xenobiotics on sperm including dioxins, fracking chemicals, some pesticides, and various air pollutants alter their cytoarchitecture and/or their function. The aberrant functional attributes are reported more frequently, and likely are of greater consequence. Examples of functional deficits include altered sperm motility, reduced ribosomal activity (often with decreased RNA content), and impaired protein synthesis. Paternal exposure to some toxicants (e.g., cigarette smoke, pesticides) has been linked to increased incidences of such congenital malformations as heart and orofacial clefts as well as certain childhood cancers (Oldereid et al., 2018; Ueker et al., 2016). Mechanistic pathways responsible for toxicant-induced sperm damage include oxidative stress and endocrine disruption.

#### 8.1.3.2. ABNORMALITIES IN SEMINAL FLUID

Xenobiotics dissolved in the seminal fluid, including halogen-containing hydrocarbon pesticides and heavy metals like barium, cadmium, lead, and uranium, induce secondary morphological abnormalities in sperm, impair sperm motility, and reduce sperm viability. Chemicals bound to the spermatozoa may result in delivery of substances directly into the ova. Dissolved toxicants may also have some influence on the uterus by directly injuring endometrial tissue, disrupting the immunological balance that maintains fetal-maternal tolerance, and/or impacting more distant maternal functions following systemic uptake. Subsequent adverse effects on the timing of implantation,

the number and distribution of implantation sites, and the success of placentation are possible, and some xenobiotics delivered in semen theoretically may be directly toxic to the developing embryo (Table 11.8).

8.1.4. Placenta

8.1.4.1. PLACENTAL BIOLOGY

8.1.4.1.1. BARRIER PROPERTIES The placenta serves as the first major physical barrier between the conceptus and any xenobiotics within the surrounding “external” environment (i.e., the maternal circulation) (Al-Enazy et al., 2017). Placental structure evolves over time in mammals. The initial form is composed of the maternal endometrial (or “decidual”) reaction to the newly implanted conceptus. This reaction is characterized by both morphological and functional changes of the endometrial stromal cells and is apparent anatomically as endometrial thickening around the gestational sac (cavity of fluid that surrounds the implanted embryo). The placental contribution derived from the embryo’s extraembryonic membranes builds over time, transitioning from the simple trophoblast lining of the blastocyst through the primitive choriovitelline (YS) variant to the fully functional chorioallantoic placenta later in gestation. Over time, the placenta becomes responsible for many vital gestational functions, besides oxygen and nutrient uptake as well as waste removal, including hormone production (peptides and steroids), immunosurveillance, and metabolism of endogenous and xenobiotic materials.

The rates at which xenobiotics are transported across the placenta play a great part in determining whether or not toxic levels of a substance can reach and accumulate in the conceptus. Major factors affecting xenobiotic passage across any membrane barrier—lipid solubility, molecular size, ionic charge, concentration gradients, potential to form complexes with other molecules, and the availability of carrier molecules—also apply to the placental membranes. Absorption may occur via either passive (simple) diffusion or via carrier-mediated membrane transporters; the most common mechanism is passive diffusion, which depends on properties such as the concentration gradient, membrane thickness and surface area, and temperature as well as the molecular weight, lipophilicity, and polarity of the substance. In general, passive diffusion is facilitated by movement along a gradient (i.e., from higher to lower concentration), increased membrane surface area, decreased membrane thickness, lower molecular weight (less than 500 Da), higher temperature, nonpolar molecular structure (since polar molecules require polar protein channels to pass via facilitated diffusion), and increased lipid solubility. Steric hindrance, the process by which the shape and/or size of a molecule may interfere with molecular binding sites, may occasionally play a part in reducing transport across the placenta. Binding of xenobiotics by plasma proteins is also frequently a major influence as it decreases the amount of the freely diffusible form that is available for transplacental transport.

TABLE 11.8 Some Agents Suspected of Paternally Induced Developmental Toxicity

Anesthetic Gases	Ionizing Radiation
Caffeine	Lead
Chlorambucil	Methyl methanesulfonate
Cyclophosphamide	Opiates (e.g., methadone)
Ethanol	Urethane
Ethylnitrosourea	Vinyl chloride

Reproduced from Haschek WM, Rousseaux CG, Wallig MA, editors: *Fundamentals of toxicologic pathology*, ed 2, 2002, Academic Press, Table II, p. 905, with permission.

8.1.4.1.2. PHYSIOLOGICAL PROPERTIES Since most drugs cross the placenta by passive diffusion, thinning of the placental membrane leading to substantial attenuation of the cytotrophoblast layer enhances the rate at which both drugs and nutrients are transferred from the maternal circulation to the conceptus. The rate of transfer for most small molecules into the fetus is also correlated with the rate of placental blood flow. However, if a substance’s permeability is a rate-limiting step in its transfer (e.g., for hydrophobic agents), physiological changes in the placenta over the course of gestation may cause significant shifts in fetal exposure. Some substances may alter placental blood flow through their pharmacological activity. For example, epinephrine, 5-

hydroxytryptamine, and vasopressin decrease placental blood flow, while prostaglandin E<sub>2</sub> increases it.

Drug transporter proteins offer another protective mechanism from the embryotoxic effects of xenobiotics (Al-Enazy et al., 2017). In human placental tissues, membrane-localized transport proteins specific for particular materials are numerous including ABC (ATP-binding cassette), organic anion, organic cation, serotonin, and noradrenaline variants (see *Biochemical and Molecular Basis of Toxicity*, Vol 1, Chap 2). Both embryonic syncytiotrophoblast and embryonic capillary endothelium express many drug transporters. Phospho-glycoprotein (P-gp, also known as multidrug resistance protein 1 [MDR1]) and breast cancer resistance protein (BCRP) are expressed predominantly in placental syncytiotrophoblasts where they actively extrude many xenobiotics. However, near the end of gestation P-gp expression declines, which make the fetus more susceptible to teratogens. Many animal studies have underscored the importance of placental drug transporters as protective mechanisms. Mouse fetuses that lack placental P-gp have greater susceptibility to the teratogenic effects of the antiparasitic drug ivermectin and exhibit increased drug concentration when dams are given digoxin, paclitaxel, or saquinavir.

#### 8.1.4.2. PLACENTAL PHARMACOKINETICS

**8.1.4.2.1. TRANSFER** The teratogenic actions of developmental toxicants are influenced by the physical properties of both the substance and the placental membranes. Transfer of substances may occur by passive diffusion, facilitated diffusion, active transport, and pinocytosis. Given sufficient time, most xenobiotics will reach the embryo. The likelihood of transfer is greatest during organogenesis, especially during the early stages before the placental tissues have matured (Griffiths and Campbell, 2015). Effects on the conceptus may be due to direct pharmacological activity or alterations in intracellular conditions (e.g., by accumulation of weak acids). One notable exception to this is for Fc-containing proteins, where active placental transportation to the fetus increases during gestation, and is greatest in humans during the third trimester, after completion of organogenesis (DeSesso et al., 2012).

**8.1.4.2.2. METABOLISM** The placenta serves to regulate embryonic and fetal exposure to many substances via expression of a diverse repertoire of xenobiotic-metabolizing enzymes. These enzymes protect the embryo by mediating the conjugation, hydrolysis, oxidation, or reduction of xenobiotics. The numbers and quantities of these enzymes depend on maternal age and health status as well as the time during gestation. Some developmental toxicants, such as the polyaromatic hydrocarbon 3-methylcholanthrene (3-MC), require enzyme-mediated metabolic conversion to reactive intermediates to produce their effect (transplacental liver and lung carcinogenesis in the case of 3-MC). Placental enzymes as well as maternal and embryonic enzymes contribute to this conversion.

**8.1.4.2.3. SEQUESTRATION** A generalized decrease in nutrient transport has been observed when xenobiotics such as cadmium and the azo dye trypan blue bind to placental tissue. The placenta does not appear to act as a sink for xenobiotics, but sequestration of certain substances is possible and can impact its function. For example, cortisone exposure decreases glucose transport, methyl mercury inhibits amino acid transport, and trypan blue affects enzyme function.

The pH of the conceptus with respect to the dam changes over the course of gestation. During organogenesis, blood and tissues of rodent embryos are more basic (i.e., possess a higher pH) than maternal blood, so weakly acidic drugs tend to accumulate in the early embryo. Later in gestation, fetal blood becomes relatively more acidic than maternal blood, leading to “ion trapping” of basic compounds in the fetal circulation and tissues where they are unable to recross the placenta. This trapping results in a higher level of nonionized drug in the maternal circulation and a net transfer to the fetus over a long period.

## 8.2. Study Design Considerations

Careful consideration must be given to the experimental objectives in designing developmental toxicity studies (which are intended to examine the viability, structure, growth, and/or function of developing offspring) as opposed to reproductive toxicity studies (which assess



adverse effects on fertility and sexual function in adult males and females) and juvenile toxicity studies (which examine structural and functional integrity following exposures during postnatal development) (see *The Role of Pathology in Evaluation of Reproductive, Developmental, and Juvenile Toxicity*, Vol 1, Chap 7 and *Experimental Design and Statistical Analysis for Toxicologic Pathologists*, Vol 1, Chap 16). Developmental toxicity studies have evaluated the effects of numerous substances in many species, and the outcomes and species differences for a selection of them are listed in [Table 11.9](#).

### 8.2.1. Hazard Identification and Dose–Response Analysis

The first two steps in the risk assessment evaluation for the developmental toxicity potential of any substance are hazard identification and the dose–response evaluation. These steps are difficult to separate as hazard should always be evaluated in the context of the exposure dose, duration, route, and timing. The goal of developmental toxicity tests is to determine whether or not any evidence shows that the substance impacts the developing animal. A detailed description of hazard identification and risk assessment may be found in *Risk Assessment*, Vol 2, Chap 16. Regulatory guidance regarding key design considerations for developmental toxicity testing is listed in [Table 11.11](#).

#### 8.2.1.1. DEFAULT ASSUMPTIONS

Extrapolation to humans of developmental toxicity data derived from animals is a complex process. A number of general default assumptions can be made to guide the risk assessment process.

The first assumption is that a substance which produces an adverse developmental effect in experimental animal studies will pose a potential hazard to humans following sufficient exposure during a susceptible stage of development. This supposition has been confirmed for many developmental toxicants, including ethanol and retinoids ([Table 11.9](#)). Apparent departures from this assumption do not automatically indicate substantial differences in teratogen sensitivity among species. The most glaring example of this discordance is the thalidomide syndrome. Early developmental toxicity tests for

thalidomide in rodents were relatively superficial and thus did not predict the severe embryotoxicity that occurred in humans ([Vargesson, 2015](#)). Subsequently, more comprehensive developmental toxicity testing confirmed that animal embryos (rabbits and rodents) are sensitive to thalidomide as well ([Botting, 2015](#)).

The second assumption is that all four manifestations of developmental toxicity—death, structural malformations, growth alterations, and functional deficits—should be considered in defining whether or not a substance is a potential developmental hazard. The premise is readily confirmed for substances that significantly decrease the number of viable implantation sites, increase the incidences of birth defects or perinatal death, or lessen progeny birth weight or postnatal weight gain. These macroscopically detectable endpoints offer objective (visible or easily quantified) measurements of developmental injury, and the range of interindividual variation for these parameters is fairly narrow under normal circumstances. The assumption is also readily established for permanent functional abnormalities (e.g., cognitive defects in animals and humans with fetal alcohol syndrome) but may be harder to prove for cases in which the functional deficit is hard to detect or is transient.

The third assumption is that the types of developmental effects seen in animal studies are not necessarily the same as those that may be induced in humans. This assumption is necessary because it is difficult to choose a priori which species may be the most suitable in terms of predicting the specific categories of developmental toxicity that might occur in humans. The fact that various species respond to a given compound in dissimilar ways may stem from any of several species-specific differences. The principal factors intrinsic to the test species are thought to include the timing of critical developmental events and processes ([Table 11.1](#)): variations in spatial and/or temporal developmental patterns; and inherent inconsistencies in the anatomic, biochemical/molecular, and physiological traits of the conceptus (embryo/fetus, placenta, or both). Additional parameters unique to the substance or study design may also play a role. These factors include variations in the dose, duration, route, and timing of exposure; unique kinetic and/or metabolic disposition of the substance

**TABLE 11.9** Examples of Specific Congenital Defects With Known Etiologic Agents in Mammals

System	Defect	Etiology	Species
Central nervous/ axial skeleton	Anencephaly/exencephaly	Colchicine	Mouse
		Injected inorganic arsenic	Mouse, rat, hamster
		Ethyl nitrosourea	Rat
		Methylhydrazine	Rabbit
		Retinoic acid	Hamster
		Thalidomide	Rabbit
	Auditory nerve hypoplasia	Quinine	Human
	Cerebellar hypoplasia	Triamcinolone acetonide	Baboon, monkey
	Encephalocele	Ionizing radiation	Mouse
		Hydroxyurea	Mouse
	Hydrocephalus	Ionizing radiation	Mouse, rat
		Vitamin A deficiency	Rat, rabbit, pig
	Iniencephaly	Streptonigran	Rat
	Microcephaly	Hyperthermia	Guinea pig, rabbit
		Methyl nitrosourea	Rat
		X-rays	Rat
	Spina bifida	Actinomycin D	Mouse
		7,12-Dimethyl-benz[ <i>a</i> ]anthracene	Rat
		Thalidomide	Baboon, monkey
Craniofacial	Agnathia/micrognathia	Injected inorganic arsenic	Mouse
		Pyrimethamine	Rat
		Retinoids	Hamster, monkey
	Anophthalmia/ microphthalmia	Ethyl nitrosourea	Rat
		Glycol ethers	Mouse
	Cataracts	Mirex	Rat
	Cleft face	Ochratoxin A	Mouse
	Cheiloschisis/palatoschisis	Dioxin (TCDD)	Mouse
		Diphenylhydantoin	Mouse
		Glucocorticoids	Mouse
		Griseofulvin	Cat
	Cyclopia	<i>Veratrum californicum</i>	Ruminants
	Microtia and/or synotia	<i>Veratrum californicum</i>	Mouse
	Nasal defects	Griseofulvin	Cat
	Open eye	Methyl salicylate	Mouse
	Retinal defects	X-rays	Rodents

(Continued)

**TABLE 11.9** Examples of Specific Congenital Defects With Known Etiologic Agents in Mammals—cont'd

System	Defect	Etiology	Species
Cardiovascular	Atrial septal defects	Alcohol	Human
		Dextroamphetamine sulfate	Mouse
	Dextrocardia	Actinomycin D	Rat
	Great vessel and vena cava anomalies	Valproic acid	Rat
	Tricuspid valve anomalies	Methyl chloride	Mouse
	Various defects	Diethylene glycol dimethyl ether	Mouse
		Alcohol	Human
		Dextroamphetamine sulfate	Mouse
	Ventricular septal defects	Thalidomide	Rabbit
Respiratory	Lung agenesis	Vitamin A deficiency	Rat, pig
	Lung hypoplasia	L-Asparaginase	Rabbit
Gastrointestinal	Absent gallbladder	Nitromifene	Dog
		Retinoic acid	Hamster
	Anal atresia	Colchicine	Mouse
	Diaphragmatic hernia	Nitrofen	Mouse, rat
	Esophageal/duodenal atresia	Thalidomide	Human
	Gastroschisis	Vincristine	Mouse
		6-Azaauridine	Rat
	Omphalocele	Actinomycin D	Mouse, rabbit
		Hyperthermia	Rat
Urogenital	Cryptorchidism	Cadmium	Rat
		Vitamin A deficiency	Rat, pig
	Hydronephrosis	Bradykinin	Mouse
	Hydroureter	Vitamin A excess	Rat
	Hypospadias	Chlorambucil	Rat
	Intersexuality	Androstenedione	Rat
		<i>Prunus serotina</i>	Pig
	Ovarian hypoplasia	Diethylstilbestrol	Mouse, rat
	Renal agenesis	Chlorambucil	Rat
		Injected sodium arsenate	Rat
		Thalidomide	Human

(Continued)



**TABLE 11.9** Examples of Specific Congenital Defects With Known Etiologic Agents in Mammals—cont'd

System	Defect	Etiology	Species
Musculoskeletal	Arthrogryposis	Anagryne	Cow, pig, sheep
		<i>Nicotiana glauca</i>	Pig
		Sudan grass	Horse
	Digit malformations	Cyclophosphamide	Human
		Ethylenethiourea	Rat
	Limb reduction defects	Acetazolamide	Mouse, rat
		Caffeine	Mouse
		Hydroxyurea	Rabbit
		<i>N</i> -Methyl- <i>N</i> -nitro- <i>N</i> -nitrosoguanidine	Mouse
		Thalidomide	Rabbit, monkey, human
	Muscular dystrophy	Vitamin E deficiency	Rat, rabbit
	Polydactyly	Cytosine arabinoside	Mouse
	Rib and/or vertebral defects	Ethylene glycol	Mouse, rat
		Injected sodium arsenate	Mouse, rat
		Hydroxyurea	Rabbit
	Tail shortened and/or malformed	Colchicine	Rabbit
		T-2 toxin	Mouse

Reproduced from Haschek WM, Rousseaux CG, Wallig MA, editors: *Fundamentals of toxicologic pathology*, ed 2, 2002, Academic Press, Table IX, p. 917–918, with permission.

and its metabolites; and species-specific differences in the mechanisms of pharmacologic action and toxicity.

The fourth assumption is that the most appropriate animal species will be used to obtain data for estimating human risk. Ideally, translation of animal data to human risk assessment is based on direct evidence, such as comparable PK and pharmacodynamic (PD) profiles or similar reactivity of the target cells or molecules in animal and human tissues. In the absence of such direct evidence, the most sensitive animal species is presumed to be the most appropriate for predicting human risk. This supposition is supported by epidemiological (in human) and experimental (in animal) observations showing that, relative to the most sensitive animal species, humans are as sensitive or more so to the great majority of human developmental toxicants (Shepard and Lemire, 2010).

The fifth and final assumption is that developmental toxicants will generally follow a dose-response curve that includes a distinct threshold. This idea is based on the known capacity of the developing organism to either repair or compensate for a certain amount of damage at the cellular, tissue, and organ levels. The multipotency of various stem cell populations in embryos, fetuses, and (to some extent) infants and juveniles supports this premise as several overlapping or sequential insults at the molecular or cellular levels may be required to induce an effect on the whole organism during a given developmental period.

#### 8.2.1.2. SPECIES SELECTION

Animal models for developmental toxicity testing are chosen based on several factors (Downes, 2018; Ross et al., 2015; Stanton, 1978;

Stanton and Spear, 1990). First, the route of administration to the dam (or pup) ideally should be the same as the route that will be experienced by humans. This approach may be impractical if the organ size in developing animals is too small to accommodate the administration device and volume of test article (e.g., intraocular injections). In such cases, the substances may be delivered systemically in developmental toxicity studies (regardless of species chosen) in an attempt to obtain any exposure data. Second, PK and biotransformation events in the animal model should be comparable to the responses that occur in humans. Third, administration to the animal model should span the entire period of gestational development in humans; in some species (e.g., altricial rodents like mice and rats), exposure will need to encompass most of gestation as well as one or more weeks of postnatal growth. Finally, outcome measures being tested in the animals should conform to relevant endpoints in the clinical literature. Examples include the ability to assess developmental landmarks and progressive acquisition of functional capabilities (e.g., immune system responses, motor and sensory behaviors).

In general, EFD studies are performed with a rodent species (rats or mice) and a nonrodent species (typically rabbits). On occasion, alternative species may be chosen based on species-specific physiological parameters and/or the ability of the substance to interact with the intended cellular target; options include guinea pigs, hamsters, dogs, minipigs, or NHPs. Genetically engineered animals or immunodeficient animals may be necessary for certain purposes (e.g., engraftment of cell xenografts, simultaneous evaluation of efficacy and toxicity); in most cases, the model of choice is an inbred mouse strain. Alternative nonmammalian models such as fish or frogs are used increasingly for some purposes, such as screening contaminated water for toxic levels of environmental pollutants (see *Animal Models in Toxicologic Research: Nonmammalian*, Vol 1, Chap 22).

Nonetheless, no single animal species has clearly distinguished itself as being more advantageous in detecting human teratogens over any other. Mice and rats successfully model human responses, as do rabbits and NHPs, but to a lesser degree (Bailey and Balcombe, 2005). Rabbits are

less likely than other animal species to exhibit outcomes in concordance with human responses (Bailey and Balcombe, 2005; Theunissen et al., 2016). NHPs offer a higher level of predictivity, although NHP studies offer less statistical power since each dam carries only a single offspring per pregnancy. The mouse and rat produce the greatest number of concordant responses with respect to developmental toxicity, but these species also are responsible for the highest number of nonconcordant responses. For this reason, safety decisions are founded on an integrated assessment of all developmental toxicity (and reproductive toxicity) data in combination with a substance's known PK, PD, and metabolic characteristics. Mean positive and negative predictabilities are 60% and 54%, respectively, across the six common test species: mice, rats, hamsters, rabbits, dogs, and NHPs (Bailey and Balcombe, 2005).

**8.2.1.2.1. RODENTS** Mice and rats are particularly useful as the initial mammalian test species for most conventional developmental toxicity screens due to their small size, short gestation, large litter size, ease in breeding, ready availability, and relatively lower cost (*Animal Models in Toxicologic Research: Rodents*, Vol 1, Chap 17). Rats have the further advantage of producing larger conceptuses, thereby enabling easier evaluation. Data are available (both in online databases and from vendors) for rates of spontaneous anomalies in numerous strains and species of rodents. Many inbred mice have a high incidence of strain-specific malformations. For example, CBA/J, C57BL/6J, A/J, Ch, and JCl:ICh mouse strains exhibit an elevated incidence of ectrodactyly (i.e., absence of all or part of at least one digit) following exposure to acetazolamide on E9 or E10.

Other mouse strains have low incidences of spontaneous defects and are quite impervious to developing them under the influence of teratogens. This phenomenon means that pairing sensitive and resistant strains of inbred mice in a single study can provide a powerful platform for investigating the influences of genotype and specific molecular mechanisms on the genesis of certain developmental defects, and particularly the potential actions of toxicants in promoting them.

A number of rodent physiological traits must be compared to those of humans. For example, the length of rodent gestation is less than 10% of human gestation (Table 11.1). The definitive rodent placenta and the human placenta are both hemochorial organs, characterized by a limited cellular barrier in which the embryonic trophoblast is in direct contact with maternal blood. In rodents, the embryonic blood supply in the labyrinth is hemotrichorial, separated from the maternal circulation by three layers of embryo-derived cells (syncytiotrophoblast I and II, cytotrophoblasts), but no maternal layers. Humans have a hemomonochorial structure with a single layer of trophoblast cells separating the embryonic and maternal circulations. Moreover, the rodent conceptus derives its nutrition from the YS placenta before the definitive placenta is formed, similar to humans where the YS is the main nutritional supply line to the embryo prior to establishment of the intervillous circulation of the placenta. The YS regresses in both rodents and humans once the mature placenta becomes functional. Importantly, variations among rodents, humans, and other test animals should be considered as xenobiotic exposures in rodents may give different results than those acquired using nonrodent test animals.

Finally, effects of developmental exposure on the functional maturity of certain systems (e.g., the CNS) must be simulated in rodents by extending treatment into the postnatal period. This adjustment is required because some organs (e.g., cerebellum and hippocampus regions of the brain) complete a portion or all of their differentiation after birth in rodents but before birth in humans (Clancy et al., 2013, 2007b). As an approximation, brain development in mice and rats at PND 7 is comparable to that of a full-term human infant (Bolon et al., 2021).

Some institutions use alternative rodent species for teratology studies. In this regard, the golden (Syrian) hamster (*Mesocricetus auratus*) is a model of choice. Like other rodents, this species has a 4-day estrous cycle and produces litters averaging 8 to 10 pups. However, the gestation length of the golden hamster is the shortest known for a placental mammal (16 days, vs. 18–20 days for various mouse strains and 20–22 days for rat strains). Similar considerations apply to interpretation of

developmental data from hamster experiments as pertain to developmental toxicity studies performed in mice and rats.

**8.2.1.2.2. RABBITS** Rabbits (as lagomorphs and not rodents) are the nonrodent species of choice for developmental toxicity testing (Foote and Carney, 2000). Factors favoring this choice include their large size (which provides ample samples for analysis), accuracy in timing the start of conception (since ovulation is induced by copulation, occurring about 10 h after mating), and large number of progeny (ranging from 4 to 12) (*Animal Models in Toxicologic Research: Rabbits*, Vol 1, Chap 18). The length of gestation is usually 31–32 days (range, 28–35). Some strains produce a spectrum of malformations similar to those of humans when exposed to substances during gestation (e.g., thalidomide (Vargesson, 2015)), but in general, rabbits do not appear to be superior to other animal models in predicting the human response to most developmental toxicants. Rabbits are prone to acute hypersensitivity reactions to xenoprotein test articles, so studies performed in this species may lead to occasional death of the dam or loss of whole litters due to nonspecific innate immune reactions rather than pharmacologic effects.

**8.2.1.2.3. NONHUMAN PRIMATES** In certain instances, the preferred nonrodent species might be an NHP. A number of species have been employed for this purpose, notably cynomolgus (*Macaca fascicularis*) and rhesus (*Macaca mulatta*) monkeys, and less often common marmosets (*Callithrix jacchus*). Biological factors that favor this choice include close similarities relative to humans in terms of genetics, maternal kinetics and metabolism of xenobiotics, placental structure, and reproductive physiology—especially anatomic and temporal aspects of early embryogenesis and organogenesis (Hendrickx and Cukierski, 1987; Hendrickx et al., 2000). However, despite these resemblances, these animals are avoided when possible due to their scarcity, high cost, long gestation, monoparous pregnancy (i.e., tendency to produce a single conceptus per pregnancy), and sentience (*Animal Models in Toxicologic Research: Nonhuman Primate*, Vol 1, Chap 21).

These factors (and especially “litter” size) substantially limit sizes in treatment groups



(typically 12–20 per cohort) and routinely result in a data set in which interactions between the test article and sex cannot be reliably assessed due to the low and unequal numbers of male and female progeny. Another complicating aspect of developmental toxicity testing with NHPs is that their sensitivity to xenobiotic-induced teratogenicity may differ from that of humans. An example is methotrexate, a folic acid analog, which has been shown to induce skeletal defects (chiefly in the limbs and skull) in humans but produces little or no embryotoxicity in monkeys. In contrast, antiretroviral medications have been shown to induce NTDs in cynomolgus monkey conceptuses but have not been linked to an increased risk of NTDs in human conceptuses based on extensive post-marketing pharmacovigilance data. Finally, NHPs are commonly not used due to their cognitive abilities leading to a need for substantial environmental enrichment and socialization activities.

**8.2.1.2.4. OTHER MAMMALIAN SPECIES** Other mammals including ferrets (Gad, 2000; McLain et al., 1985), guinea pigs (Rocca and Wehner, 2009; Schneider et al., 2013), dogs (Holson et al., 2015), and swine (Bode et al., 2010; Gad, 2000) are occasionally used in developmental toxicity studies. Characteristics such as size, cost, handling difficulties, long gestation periods, lack of a historical database, and the absence of obvious predictive superiority limit their use.

**8.2.1.2.5. NONMAMMALIAN SPECIES** Several non-mammalian vertebrate species are employed for developmental toxicity screening, and wild nonmammalian vertebrates (e.g., fish, frogs, birds) may be used as sentinel species for toxic levels of environmental pollutants (Hamlin and Guillette, 2010). Biological advantages in utilizing these species include their fecundity, small size, fairly short developmental period, ability to directly expose eggs or larvae to the substance of interest, and the minute quantity of substance needed to dose all animals in the study. As noted above, these alternative screens typically are used in mechanistic investigations and to prioritize chemicals for further testing by providing preliminary data on the toxicity of chemicals that have little or no existing data.

In the strict sense, such assays are not equivalent to *in vivo* screening as maternal PK processes and placental transfer can play no role in these test systems.

Chicken or quail embryos (i.e., fertilized eggs) provide a low-cost, readily available model with a short developmental period (21 days in chickens and 16.5 days in quail at the optimal temperature) and relatively robust historical database (Bardai et al., 2011; Stark and Ross, 2019). Bird embryos also have a fairly high sensitivity to many exogenous agents.

Embryos of aquatic species including frogs (the FETAX [frog embryo teratogenesis assay *Xenopus*] test) and zebrafish (the FET [Fish Embryo Acute Toxicity] assay (von Hellfeld et al., 2020)) have gained acceptance as screens for developmental toxicants in polluted wetland habitats. Key advantages of these methods are that multiple embryos can be exposed simultaneously in a single container (thus providing a large sample size), while the translucence nature of the fertilized eggs, the very rapid pace of embryogenesis, and the well-known progression of developmental events permits easy recognition of any abnormalities that might arise.

**8.2.1.2.6. HUMAN EPIDEMIOLOGICAL STUDIES** Epidemiological studies in humans provide two lines of evidence indicating whether or not a substance might pose a risk of developmental toxicity. The first way uses such data in an attempt to identify new teratogens based on increased incidences of structural and/or functional abnormalities in exposed individuals. Importantly, nearly 50 human teratogens were identified initially in humans based on environmental, occupational, or therapeutic exposure data (Bailey and Balcombe, 2005; Schardein and Keller, 1989). The second approach is to compare the human epidemiological data with results from animal studies to assess whether or not the spectrum of defects seen in test animals under laboratory conditions (i.e., repeated exposure to high doses for extended periods during development) is recapitulated in humans. Animal data provide insight regarding potential toxicant-induced developmental effects, but their relevance must be assessed on a case-by-case basis in drawing

inferences with respect to possible human outcomes.

Epidemiological studies have proven quite useful in clarifying the status of putative development toxicants. Examples of human developmental toxicants identified in this manner include pharmaceutical agents (e.g., anticonvulsants, antineoplastic agents, thalidomide); environmental and lifestyle pollutants (e.g., maternal alcohol abuse, heavy smoking, metals); and viral infections (e.g., rubella, zika).

However, human epidemiological studies have serious limitations as well with respect to hazard identification and risk assessment. One limitation is the nature of the answers that can be obtained. Epidemiological studies can provide evidence for an association between a given defect and exposure to a particular substance, if confounding variables and bias are adequately controlled (Lash et al., 2021). However, these data are restricted by the inability to recognize and limit all variables and thus cannot prove causality. In addition, epidemiological studies for developmental toxicity have poor sensitivity; potent toxicants or a higher incidence of a normally rare anomaly can be detected reliably while subtle increases in common incidental defects cannot be discerned against the normal background of fetal abnormalities. Furthermore, the study population generally must be large to allow an effect to be discerned, and such extensive populations of exposed and control individuals may be difficult to find. Finally, accurate exposure data for women at various stages of pregnancy are challenging to obtain, if they can be gathered at all.

A modest rise in the incidence of a birth defect in human epidemiological studies may be interpreted as evidence of developmental toxicity if the anomaly is relatively common in the baseline population. An example of this phenomenon is the antinausea combination of doxylamine (an antihistamine) and pyridoxine (vitamin B<sub>6</sub>), which is specifically indicated for use by pregnant women to ameliorate morning sickness. This product was marketed in the US as Bendectin and later withdrawn (in 1983) after low exposures were tentatively linked to several fetal malformations, although an opinion by the U.S. Food and Drug Administration (FDA) stated that the withdrawal of Bendectin was not based on a lack of safety (FDA,

1999). This treatment remained available as Debendox in the UK and Diclectin in Canada and was eventually reintroduced in the US (in 2013) as Diclegis when the purported link to malformations was not confirmed in later epidemiological and metaanalysis assessments.

#### 8.2.1.3. DOSE SELECTION

The choices of dose levels and the dosing regimen (i.e., duration, frequency, and route of administration) are important study design considerations. Information guiding such decisions should include prior experimental observations and published data that define the pharmacology, PK, and toxicity (e.g., dose range-finding and repeat-dose toxicity studies) of the substance. Guidance on dose selection may be found in the International Council for Harmonisation (ICH) 5(R3) guideline on reproductive and developmental toxicity for human pharmaceuticals (ICH, 2020a).

Evidence of a dose–response is critical for identification of developmental toxicants. This is especially true because considerable fluctuations in the incidences of sporadic malformations, common variants, and prenatal deaths can occur in mammalian test species even in the absence of treatment. In general, clear-cut dose relationships that lead to a rise in adverse events, like gross malformations or deaths, are readily accepted as true indices of developmental toxicity, but the presence of dose-related increases in incidental structural variants that have no functional relevance should also be considered to be potentially related to product exposure. Where available, human dose–response data (e.g., from epidemiological meta-analyses) should be assessed along with the animal data when drawing conclusions about the dose–response relationship.

Several different standards may be used for examining the biological implications of small molecule (i.e., chemical or drug) doses used in developmental toxicity studies. One conventional approach is to define the No Observable Adverse Effect Level (NOAEL) or the Lowest Observable Adverse Effect Level (LOAEL) using data inspection and statistical analysis. The benchmark dose (BMD) calculation has been proposed as an improvement over, or supplement to, the use of the NOAEL in making risk assessment decisions (Sand et al., 2008; Travis

et al., 2005). Using the BMD approach, mathematical modeling is employed to derive a BMD value, which is defined as the lower confidence limit on a dose that produces a particular preselected level of response (e.g., 1%, 5%, or 10%). Calculation of a reference dose (RfD) or reference concentration (RfC) also has been proposed as a better means for low-dose extrapolation to explore exposure thresholds below which developmental toxicity will not occur. These values represent estimates of the daily exposure to humans that is predicted to be without appreciable risk of inducing harmful effects during development. The RfD or RfC are derived by dividing the NOAEL, or the BMD, for the most sensitive developmental toxicity outcome by an uncertainty factor (the value of which is variable). A drawback of this approach is that these two numbers do not predict the risk at exposure levels that exceed the RfD or RfC.

Biologic test articles (e.g., recombinant proteins) that are active in test animals may not exhibit increasing activity or toxicity once the available targets or receptors have been saturated, and often the toxicity profile is limited to “exaggerated pharmacology” (i.e., toxicity that is directly related to excessive activity of the intended pharmacologic effect). Especially in cases where the desired human exposure also achieves this saturable pharmacology, and where the biopharmaceutical is highly specific in activity, dose ranging provides limited benefit. In addition, human-specific test articles that do not demonstrate pharmacologic cross-reactivity and relevance with animal species used for toxicity testing typically require little or no nonclinical developmental toxicity testing as such studies would be unlikely to inform human developmental risk assessment.

#### 8.2.1.4. EXPERIMENTAL UNIT AND GROUP SIZE

The experimental unit in developmental toxicity studies depends on the design (see *Experimental Design and Statistical Analysis for Toxicologic Pathologists*, Vol 1, Chap 16). For in vitro and ex vivo studies where isolated specimens are exposed to a substance directly, the individual sample (cell culture, micromass, whole embryo, etc.) serves as the experimental unit. For in vivo studies where a pregnant female is exposed to a substance during gestation, lactation, or both, the full litter represents

the experimental unit because all conceptuses for that dam are exposed to a similar degree (Lazic and Essioux, 2013). Litter-specific (“intra-litter”) effects are often responsible for adverse events among siblings even though other litters exposed to the same treatment are unaffected. Therefore, assuming a mean litter size of 8 conceptuses, the sample size for a treatment group in a standard rodent developmental toxicity study is 10 litters, and not 80 pups; sample sizes for studies in which functional testing is included often are increased to 20 litters per treatment group due to the inherent variability in functional responses of individual animals. Macroscopic structural effects are typically examined in 50%–100% of fetuses during EFD studies using such techniques as the Wilson’s technique and skeletal double staining. In contrast, functional evaluation (e.g., neurobehavioral testing for PPND studies) often is limited to one or two randomly chosen neonates (1 male and 1 female) due to the laborious, low-throughput methods available for this purpose.

If each pup in a treatment group is considered to be an experimental unit, the chance of obtaining false positive results is significantly higher as the confounding role of intralitter effects will be ignored in the analysis. For example, a dose group comprised of one affected litter with 10 malformed fetuses (rodent or rabbit) and nine normal litters is of considerably less concern than a dose group of 10 litters in which five litters contained two defective fetuses each. The total number of abnormal fetuses is the same (10), but the likelihood of a genuine treatment-related potential for inducing developmental toxicity is much greater in the latter case, where 50% of litters are impacted.

With regard to developmental toxicity data, biological relevance is as important as statistical significance in assessing human risk (Ciallella et al., 2022; EPA, 1991). A substance that causes a minor depression in birth weight or an increase in the incidence of one or more potentially incidental developmental variants (e.g., dilated renal pelvises, enlarged cerebral ventricles, and/or supernumerary or wavy ribs) is more difficult to assess for potential hazard to the target species than a substance that induces a distinct pattern of major malformations. A higher incidence of embryonic lethality may mask a concomitant rise in teratogenicity, which is a crucial



consideration as many teratogenic effects are not the cause of in utero mortality. Therefore, embryonic lethality should be considered an important endpoint of developmental toxicity in its own right. The evaluator must exercise sound scientific judgment regarding the relevance of such calculations rather than blindly accepting the results of statistical analyses when deciding whether or not a particular developmental toxicity test is positive or negative.

#### 8.2.1.5. EXPOSURE TIMING

The stage of embryonic or fetal development must be considered before attempting to define the correlation between dose and the consequences of abnormal development. Low doses do not necessarily cause functional deficits and high doses do not always lead to embryonic or fetal death. The outcome also depends on the stage of development at which the substance is administered and the mechanism by which it acts.

During early development, moderate exposures to xenobiotics may induce death or may elicit few visible changes. These divergent outcomes result from the considerable range of fates open to embryonic stem cells (i.e., totipotent or pluripotent) prior to the start of organogenesis. Once organogenesis starts, similar or lesser concentrations of a substance may produce prominent morphological defects. This change in the pattern of alterations occurs because the death of partially committed stem cells tends to produce cell losses and/or functional abnormalities that can no longer be fully reversed by the surviving members of the targeted cell population or compensated for by other partly differentiated cell collectives. For instance, the mycotoxins citrinin and T-2 toxin cause embryonic lethality with little or no abnormal development following exposure in early gestation.

Toward the end of organogenesis, gross malformations are less likely and tend to require larger doses than those that would prove to be teratogenic if given during the critical period for an organ's initial formation. Thus, later in embryogenesis, xenobiotic exposures are more likely to cause microscopic defects, intrauterine growth retardation, and/or functional deficits rather than overt malformations. Once the fetal period begins (i.e., when organs have first formed but now must differentiate and expand),

very large doses likely will be required to induce functional changes in most organ systems. Of course, exceptions to these rules do exist.

Transplacental carcinogenesis depends on the nature of the carcinogen. Current thinking is that neoplasms can be induced by exposure to very small concentrations during organogenesis, or to moderate concentrations after organogenesis. Such modest insults induce MIEs that over time lead to cancer formation rather than inciting severe damage that leads to immediate death of the developing cells.

#### 8.2.1.6. PHARMACOKINETICS

As is the case with other toxic effects, developmental toxicity is strongly impacted by PK parameters. The influence of such factors is complicated by the fact that two different organisms are involved, mother and conceptus, both of which have separate and often distinct PK profiles. Maternal uptake, transplacental passage into and away from the embryo, and maternal elimination are critical parameters that govern the access of xenobiotics to the offspring. Biotransformation (metabolism) also plays an essential role in defining the extent of developmental toxicity. In this regard, the fully mature maternal metabolic pathways are of greater importance in dictating the effect of xenobiotics, as enzyme systems in the embryo and fetus usually are incompletely differentiated and/or incapable of high-throughput chemical conversion. Some toxicants may be sequestered in embryonic tissues due to the altered conditions (e.g., different pH, lower oxygen tension, reduced glucose stores) relative to those in the dam.

The PK characteristics of pregnant and lactating animals follow the same principles that operate in other adult animals with the exception that some parameters are amplified (e.g., fluid volumes, uterine blood flow) or reduced (e.g., erythrocyte numbers, serum protein levels) during part or all of gestation. In most instances, the exact influence of physiological alterations during pregnancy on a given agent's PK profile is unknown, which renders extrapolation from animal models to humans in this setting more difficult. This problem is augmented by the usual paucity of information regarding a substance's PD (i.e., the manner in which toxic injury is expressed). Therefore, in

most cases, risk assessment as applied to developmental toxicity must place considerable reliance on arbitrary safety factors.

For most substances, adverse effects in the conceptus vary with the gestational state and/or among species due to changes in the degree of embryonic exposure (i.e., resulting from shifts over time in the PK of the substance in the mother and/or embryo) or to changes in the susceptibility of the embryo to the substance (Abduljalil et al., 2012). Interspecies differences with respect to the teratogenicity of substances can result from differing PK processes that determine the crucial concentration-time relationships in the embryo. Maternal absorption as well as distribution of substances does not usually show great interspecies differences. The first-pass effect after oral application is often more pronounced in animals than humans (e.g., valproic acid, 13-cis-retinoic acid), although in some cases the reverse occurs (e.g., hydrolysis of valpromide). Existing differences can be adjusted by appropriate choice of the route of administration as well as measurements for circulating and tissue levels of the substance. The distribution of substances during pregnancy appears to follow a two-compartment model (Ochiai et al., 2021).

Many variables determine the placental transfer of drugs. Among these, the type of placenta, developmental stage, and properties of the drug are among the most important. Even closely related drugs (e.g., retinoids) may differ substantially in regard to placental transfer. Maternal protein binding is an important determinant of placental transfer since only the free (unbound) substance in maternal plasma can equilibrate with the embryo; this parameter differs greatly across species. For example, the free fraction of valproic acid in plasma is approximately fivefold higher in mouse and hamster compared to NHP and humans. Animals usually have a higher rate of xenobiotic elimination relative to humans. Therefore, drastic drug level fluctuations may be present during developmental toxicity testing in animals, but not to the same degree in human therapy. Therefore, testing in animals must investigate if toxicity is associated with the peak concentration (such as for valproic acid and possibly caffeine) or the total area under the concentration (AUC) time curve (such as for cyclophosphamide and possibly retinoids)

(Mihaly and Morgan, 1983; Nau, 1986). Metabolism involves CYP450 isoenzymes that may increase or reduce activity of the substance in question. Tissue levels of these enzymes often rise or fall as gestation progresses, especially during the third trimester (Sheffield et al., 2014).

#### 8.2.1.7. REPOSITORIES FOR DEVELOPMENTAL TOXICITY DATA

Traditional developmental toxicology investigations relied heavily on prospective animal experiments and human epidemiological studies to ask and answer questions regarding the safety of novel substances. At present, these conventional approaches are increasingly supplemented and occasionally even supplanted by databases that allow in silico prospecting to identify and characterize developmental toxicants. Selected databases for developmental toxicants are listed in Table 11.10.

The original databases were print catalogs of animal and human teratogens, which were republished at intermittent intervals (often spanning many years). In recent years, the growing power of bioinformatics has permitted assembly of regularly maintained and expanded electronic registries. Moreover, these databases have shifted away from single product repositories to either disease-specific databases that capture data in parallel for multiple products or to adverse event reporting systems (AERSs) for pregnancy and/or lactation endpoints that can be searched across a range of diseases and many products.

Information housed in these repositories encompasses the impact of teratogens including biological, chemical, and physical agents on all aspects of animal and human reproduction (e.g., fertility, in utero and neonatal viability, lactation, and the impact of paternal exposures). The substances covered by such databases include industrial and environmental chemicals; prescription, over-the-counter, and recreational drugs; food additives and other nutritional constituents; and occasionally biological (e.g., viral) and physical (e.g., heat, radiation) agents. Some databases focus on empirical studies (in vitro, ex vivo, and/or in vivo; short-term, long-term, or multi-generational), while others emphasize human clinical experiences or comprehensive reviews of the existing literature. In some databases, the information is subjected

**TABLE 11.10** Annotated List of Selected Databases for Developmental and Reproductive Toxicants

1. Society for Birth Defects Research and Prevention (formerly The Teratology Society) Resources for Scientists/Professionals is a clearinghouse for numerous teratology resources including other databases, developmental biology courses, journals, government agencies, scientific societies, and relevant web sites. <https://www.birthdefectsresearch.org/resources-for-scientists-professionals.asp> (last accessed May 24, 2024).
2. REPROTOX (Reproductive Hazard Information, Environmental Impact of Human Reproduction and Development) was developed in the 1980s, and is updated regularly. It lists the impact of the physical and chemical environment on human reproduction and development. It covers many aspects of reproduction including fertility, lactation, and male exposures while considering the reproductive influence of industrial and environmental chemicals; prescription, over-the-counter, and recreational drugs; and nutritional agents. <https://www.reprottox.org/> (last accessed May 24, 2024).
3. TERIS (Teratogen Information System) provides current information on teratogenic effects of >700 drugs and environmental agents. Agent synopses and reproductive risk ratings are derived from a comprehensive literature review and sponsor-provided data summaries. It also provides agent summaries by domestic, international, generic, and proprietary names. <https://deohs.washington.edu/teris/> (last accessed May 24, 2024).
4. REPRORISK is a subscription-based CD-ROM collection of reproductive risk information databases compiled for professionals, especially physicians. It classifies the reproductive risks of drugs, chemicals, and physical and environmental agents on males, females, and unborn children. It includes the REPROTEXT and REPROTOX Systems, Shepard's *Catalog of Teratogenic Agents*, and the TERIS Teratogen Information System. The database includes entries for acute and chronic exposure to over 600 industrial chemicals and physical agents, with descriptions of potential carcinogenic, genetic, and reproductive effects. <https://www.environmental-expert.com/software/reprorisk-system-evaluations-of-reproductive-effects-of-drugs-and-chemicals-134960> (last accessed May 24, 2024).
5. TOXNET Toxicology Data Network, National Library of Medicine (NLM) contains databases on toxicology, hazardous chemicals, environmental health, and toxic releases. <https://www.nlm.nih.gov/toxnet/index.html> (last accessed May 24, 2024).
6. OTIS (Organization of Teratology Information Specialists) manages the MotherToBaby web site through which it provides bilingual (English and Spanish) fact sheets for various exposures of concern including medications, herbal products, infections and vaccines, maternal medical conditions, illicit substances and other exposures (e.g., alcohol). MotherToBaby California (formerly CTIS, the California Teratogen Information Services Pregnancy Health Information Line) has been merged into the same web site. <https://mothertobaby.org/fact-sheets/> (last accessed May 24, 2024).
7. ORPHANET is a database dedicated to information on rare diseases and orphan drugs. There is information on > 1150 rare diseases, each with text (written by an expert) with links to current research, diagnostic laboratories, support groups, outpatient clinics, and orphan drugs. <https://www.orphanet/> (last accessed May 24, 2024).
8. North American AED (Antiepileptic Drug) Pregnancy Registry contains information about the uses and risks of old and new AEDs. Available information includes an AED registry; flyers/fact sheets in English, Spanish, and French; patient cards; slides; and updates. <https://www.epilepsy.com/tools-resources> (last accessed July 4, 2024).
9. RepDose (Repeated-Dose Toxicity) is a database that contains peer-reviewed and confidential repeated-dose toxicity studies in rodents with subacute to chronic exposure durations. It currently contains about 650 chemicals and 2500 studies. <https://repdose.item.fraunhofer.de/> (last accessed May 24, 2024).
10. FeDTex (Reproductive and Developmental Toxicity) is a database (currently under construction) on reproductive toxicity with a focus on one- and two-generation studies. Parameters and effects describing maternal toxicity, reproductive performance, and developmental toxicity are documented according to affected generation, developmental stage, and sex. The database can be used both for risk assessment and for structure–activity relationship (SAR) analyses. <http://www.cefic-lri.org/lri-toolbox/fedtex> (last accessed May 24, 2024).



to rigorous peer review before the entry is finalized. As a group, these registries contain data on approximately 1000 chemicals drawn from hundreds of studies and several hundred thousand literature citations, making such databases an invaluable starting point for research programs and risk assessments in developmental toxicologic pathology.

## 9. REGULATORY CONSIDERATIONS

Risk characterization and management for developmental toxicity must evaluate the degree of toxicity, the extent of possible exposure, and the timing during which exposure might occur. The complexity of the developing conceptus, its complex and ever-evolving interactions with the maternal system and (in typical animal species) its siblings, and the multiple endpoints examined in the course of developmental toxicity testing often result in large and intricate data sets. In many instances, these data are difficult to interpret, not least because of the large variation in biological responsiveness within and among litters. Therefore, developmental toxicity data must be analyzed and interpreted by scientists with a broad background in developmental biology (animal and human) as well as ample practical experience in toxicology.

This convention is important because decisions regarding a substance's potential for inducing developmental toxicity are seldom obvious. Instead, the more common scenario requires a weight-of-evidence approach in which all available data—and the reliability of those data—are considered in terms of both quality and quantity (completeness) in arriving at a conclusion. This approach is likely to change in the future as the latest advances in biologically based dose-response modeling show considerable promise for translating our growing knowledge of normal developmental pathways and toxic mechanisms in animal test species into more accurate estimates of risk to the human population.

### 9.1. Managing Risk

Regulatory expectations for pathology endpoints from developmental toxicity studies that include fetal evaluations are described in published guidelines for medicinal products

(ICH, 2020a) and for environmental/agricultural and toxic chemicals (CFR, 1999; EPA, 1998a; OECD, 2018b). Additional guidance is available for developing medicinal products, including generic (ICH, 2009a) and product-specific (ICH, 2009b, 2011, 2018) guidelines as well as guidance for pediatric medicines (ICH, 2020b). Study design recommendations for assessing developmental toxicity are similar across these guidelines and reflect the body of accumulated knowledge to address concerns of this type (Table 11.11). For example, the expectation that two species will be evaluated for teratogenic potential is based on the knowledge that there are different outcomes and sensitivities among species given the same substance (Theunissen et al., 2016, 2017). A more comprehensive list of regulatory guidance for developmental, juvenile, and reproductive toxicity studies is given in *The Role of Pathology in Evaluation of Reproductive, Developmental, and Juvenile Toxicity*, Vol 1, Chap 7.

Extensive experience with EFD studies in rodents and in rabbits over decades has produced sufficient data to support relatively clear regulatory expectations for studies in these species. In general, group sizes for conventional EFD studies will include at least 20 litters per group for rodents (rat, mouse, hamster) and 12–16 litters or more for rabbits. The dosing period should begin at or near implantation (6 days postcoitus for rodents and rabbits) and should minimally include the entire period of major organogenesis (i.e., through E14 for hamsters, E15 for mice and rats, and E19 for rabbits). Some guidance recommends that dosing continues throughout gestation until the day prior to cesarean delivery (OECD, 2018b). In rodents, fetuses typically are removed 1–3 days prior to expected parturition while rabbit fetuses are obtained on E29 (i.e., approximately a week before expected natural parturition on E35).

For both rabbits and rodents, the external examination of all pups or kits in each litter is included as an endpoint in all major regulatory guidelines. Determination of sex using external landmarks, which can be confirmed with internal exam, as well as measurement of AGD and total body weight are typical endpoints as is opening the mouth to confirm closure of the palate. With the head as a notable exception, each fetus can be processed by both microdissection to

**TABLE 11.11** Selected Core Guidance Documents for Developmental Toxicity and Related Studies

Entity	Document No.	Title	References
<b>EPA</b>	<b>870.3700</b>	<b>Prenatal developmental toxicity study</b>	<a href="#">ICH (2020a)</a>
EPA	870.6300	Developmental neurotoxicity study	<a href="#">EPA (1998b)</a>
EPA	Series 890	Endocrine disruptor screening program test guidelines	<a href="#">EPA (n.d.)</a>
FDA	None	Reproductive and developmental toxicities—integrating study results to assess concerns	<a href="#">FDA (2011)</a>
ICH	<b>S5(R3)</b>	<b>Detection of reproductive and developmental toxicity for human pharmaceuticals</b>	<a href="#">ICH (2020a)</a>
OECD	150	Revised guidance Document 150 on standardized test guidelines for evaluating chemicals for endocrine disruption	<a href="#">OECD (2018a)</a>
<b>OECD</b>	<b>414</b>	<b>Prenatal developmental toxicity study</b>	<a href="#">OECD (2018a)</a>
OECD	421	Reproduction/developmental toxicity screening test	<a href="#">OECD (2016a)</a>
OECD	422	Combined repeated dose toxicity study with the reproduction/developmental toxicity screening test	<a href="#">OECD (2016b)</a>
OECD	426	Developmental neurotoxicity study	<a href="#">OECD (2007)</a>
OECD	443	Extended one-generation reproductive toxicity study	<a href="#">OECD (2018c)</a>

**Bolded** guidance documents include fetal assessments, nonbolded entries incorporate preweaning endpoints but have no scheduled fetal assessments

*EPA*, U.S. Environmental Protection Agency; *FDA*, U.S. Food and Drug Administration; *ICH*, International Council for Harmonisation of Technical Requirements for Pharmaceuticals for Human Use; *OECD*, Organisation for Economic Co-operation and Development.

identify soft tissue malformations and variations as well skeletal double staining (Alcian blue and Alizarin red S) to assess skeletal malformations and variations. To evaluate cranial structures, the head is carefully removed from approximately half of the fetuses in a litter and sectioned to permit examination of the cranial soft tissues, while heads of the remaining fetuses are left attached to be stained with the rest of the skeleton. For rodent studies, it is generally acceptable to divide the litter in half such that 50% of the fetuses are allocated to soft tissue endpoints and 50% to skeletal endpoints ([EPA, 1998a](#); [OECD, 2018b](#)). However, when feasible, 100% of fetuses should be processed to examine both soft tissue and skeletal endpoints ([ICH, 2020a](#)).

In general, regulatory guidance for fetal examinations during routine developmental toxicity studies focuses on external, soft tissue and skeletal assessments but does not include histopathology endpoints. The nonclinical study team must decide if histopathologic evaluation will

contribute meaningfully to study interpretation; based on an industry survey, it is rare for pathology of fetuses to be routinely included in safety studies ([Halpern et al., 2016](#)). All major guidelines for developmental toxicity studies with fetal evaluations do recommend that a gross evaluation of maternal tissues be performed at the time of cesarean section ([EPA, 1998a](#); [ICH, 2020a](#); [OECD, 2018b](#)); abnormal tissues may be preserved for histopathologic examination, and often tissues from at least 1 normal/control dam are collected in parallel as a “within-study” comparator. The placenta, which is composed of both maternal and fetal elements, represents a “gray” area. The ICH guidance recommends gross assessment of placentas and includes placental weight as an optional assessment ([ICH, 2020a](#)), but none of the current regulatory guidelines for developmental toxicity studies specify histopathologic evaluation of the placenta as an expected endpoint. When grossly abnormal and associated with adverse

fetal outcomes, microscopic evaluation of the placenta may be warranted.

Traditional approaches to evaluating EFD in rodents and rabbits for small molecules (chemicals and drugs) are not always possible or relevant for other product classes, especially highly selective and specific biopharmaceuticals. Testing options for these products are discussed in some detail in the ICH S6(R1) guidance on biotechnology-derived pharmaceuticals (ICH, 2011). In some cases, as with infectious disease targets, little or no value may be gained by conducting EFD studies. Likewise, for anticancer pharmaceuticals, assessment of developmental toxicity is usually not required for clinical testing since patients with advanced cancer typically will not be pregnant. The EFD data would be expected for registration, but in some instances, the hazard might be inferred from existing data without the need to actually conduct EFD studies (e.g., molecules that are mutagenic, or that have a well-established mechanism of action that is expected to cause fetal harm) (ICH, 2009b).

Additional types of developmental toxicity testing may be appropriate for certain substances. For instance, guidance for safety assessment of agrochemicals highlights the need for evaluation of developmental neurotoxicity using qualitative and quantitative morphological methods as well as neurobehavioral testing (EPA, 1998b; Garman et al., 2016; Li et al., 2017; OECD, 2007). Similarly, screening programs for endocrine disruption by environmental chemicals are designed to integrate data from multiple in vitro and in vivo assays (EPA, 2009; OECD, 2018a). Therefore, further DART testing may be necessary in assessing product safety, not all of which include fetal assessments.

In situations where NHP is the relevant model for use in DART studies, a combined EFD and PPND study (termed a “PPND, enhanced design” or “ePPND” study) can be considered. This study design has been well established especially for monoclonal antibodies that have the highest fetal exposures in the second half or last trimester of gestation (i.e., after most organogenesis has been completed). In ePPND studies, the immature skeleton of offspring is evaluated early in the postnatal period via radiography, while soft tissue anomalies are

investigated at the time of necropsy, usually 3–6 months after birth. In addition to these modified skeletal and soft tissue endpoints, the “EFD” component of these studies includes an assessment of pregnancy outcomes, neonatal birth weights, and neonatal external examinations. The design for ePPND studies in macaques is discussed in *The Role of Pathology in Evaluation of Reproductive, Developmental, and Juvenile Toxicity*, Vol 1, Chap 7.

International agreements (e.g., the Convention on International Trade in Endangered Species [CITES]), transportation limitations (e.g., air shipments of live wild animals), and more recently the prioritization of animal models for vaccine development to address the SARS-COV-2 pandemic have substantially reduced availability of NHPs for nonclinical safety testing. Recent FDA guidance related to this situation highlights potential animal alternatives to NHP use and specifically refers to the challenges of DART testing. In general, DART testing in NHP should be reserved for programs where the NHP is the only relevant test species. This paradigm would generally exclude most small molecules (chemicals and drugs) as well as biopharmaceuticals that cross-react with their pharmacologic ortholog targets in rodents or rabbits. For hazard identification specific to a given mechanism of action, a study using a rodent-specific surrogate molecule might be considered for developmental toxicity testing even if the NHP is relevant with the clinical candidate. Finally, in some cases where the mechanism of action and potential risk of fetal harm are well-characterized, a weight-of-evidence argument could be made to inform the risk assessment. These measures to reduce NHP use during the pandemic have expanded our experience with these alternative approaches for DART (and general toxicity) testing.

## 10. CONCLUSION

Developmental toxicity studies, including the pathology endpoints that comprise a part of the analysis, are essential elements for hazard identification and characterization that are needed to assess potential developmental risks posed by novel xenobiotics. The developing embryo or fetus with its rapidly dividing cells and



replicating DNA is often the biological system that is most sensitive to xenobiotic exposure. The complexity of developmental processes makes risk assessment for developmental toxicants challenging, especially because a mechanistic understanding of toxicity requires a deep understanding of many biological processes for which data are currently lacking. Many factors help produce a constantly changing spectrum of functional and structural manifestations of developmental toxicity, including tissue-specific critical periods of organogenesis; the intricate relationship between the spatial and temporal expression of various genes (especially those for morphogens and their signaling pathways); and interactions between the genotype and various metabolic processes and the toxicant. To date, research in this field has predominantly attempted to identify new hazards and develop new methods for evaluating prenatal toxicity. However, the explosion in our understanding of cellular and molecular mechanisms of teratogenesis that has accompanied the rise of bioengineering, coupled with the advent of powerful new bioinformatic and computing platforms, should permit scientists and regulators to improve their predictive capabilities, thereby allowing society to avoid, reduce, or even reverse the consequences of developmental toxicity.

## GLOSSARY

**Ablepharia** Reduction or absence of the eyelids with continuous skin covering the eyes  
**Abrachia** Absence of the arms (forelimbs)  
**Acampsia** Rigidity or inflexibility of a joint [**Arthrogryposis**]  
**Acardia** Absence of the heart  
**Acaudia, Acaudate** Without a tail [**Anury**]  
**Acephaly** Agenesis of the head [alternatively **Acephalia**]  
**Acheiria** Congenital absence of one or both hands (forepaws)  
**Achondroplasia** Inadequate bone formation [skeletal **Dysplasia**] resulting in short limbs and other defects, due to abnormal cartilage resulting from a defect in fibroblast growth factor receptors  
**Acorea** Absence of the pupil of the eye  
**Acrania** Partial or complete absence of the cranium  
**Acystia** Absence of the urinary bladder  
**Adactyly** Absence of digits  
**Agensis** Lack of development of an organ [**Aplasia**]  
**Aglossia** Absence of the tongue  
**Agnathia** Absence of the lower jaw (mandible)  
**Agyria** Small brain lacking the normal convolutions of the cerebral cortex [**Lissencephaly**]  
**Altricial** Animals (e.g., mice, rats, rabbits, carnivores, primates) that are not capable of self-care immediately after birth  
**Amastia** Absence of the mammae (breasts)

**Amelia** Absence of a limb or limbs (see also **Ectromelia**, **Phocomelia**)  
**Ametria** Absence of the uterus  
**Amniotic band syndrome** Ischemia-related defects that occur when limbs or digits are constricted by amnion-derived fibrous bands  
**Anasarca** Generalized edema  
**Anencephaly** Absence of the cranial vault with the brain missing or greatly reduced  
**Anephrogenesis** Absence of kidney(s)  
**Angiogenesis** Formation of new blood vessels from preexisting vessels  
**Aniridia** Absence of the iris  
**Anisomelia** Inequality between paired limbs  
**Ankyloglossia** Partial or complete adhesion of the tongue to the floor of the mouth  
**Ankylosis** Abnormal fixation of a joint; implies bone fusion  
**Anlage** (plural: **Anlagen**) The initial group of embryonic cells from which an organ develops (i.e., the primordium of an organ)  
**Anodontia** Absence of some or all of the teeth  
**Anomaly** See **Birth Defect**  
**Anonchia** Absence of some or all of the nails  
**Anophthalmia** Absent or vestigial eye(s)  
**Anorchism** Uni- or bilateral absence of the testes [alternatively **Anorchia**]  
**Anostosis** Defective development of bone, specifically failure to ossify  
**Anotia** Absence of the external ear(s) (i.e., pinnae, auricles)  
**Anovarium** Absence of the ovaries [alternatively **Anovaria**]  
**Anury** See **Acaudia**  
**Aphakia** Absence of the eye lens  
**Aphalangia** Absence of a digit or of one or more phalanges  
**Aplasia** See **Agenesis**  
**Apodia** Absence of one or both of the feet (paws)  
**Aprosopia** Partial or complete absence of the face  
**Arachnodactyly** Abnormal length and slenderness of the digits—"spider-like"  
**Arrhinia** Absence of the nose  
**Arthrogryposis** Persistent flexure or contracture of a joint  
**Arthrogryposis multiplex congenita** Syndrome distinguished by congenital fixation of the joints and muscle hypoplasia  
**Asplenia** Absence of the spleen  
**Astomia** Absence of the opening of the mouth  
**Atelectasis** Incomplete expansion of a fetal lung or a portion of the lung at birth  
**Athelia** Absence of the nipple(s)  
**Athymism** Absence of the thymus gland [alternatively **Athymia**]  
**Atresia** Congenital absence of a normally patent lumen or closure of a normal body opening  
**Atresia ani** Agenesis or closure of the anal opening [**Imperforate anus**]  
**Atrial septal defect** Postnatal communication between the atria  
**Bifid tongue** Cleft tongue  
**Bipartite** Division of what is normally a single structure into two parts; usually refers to areas of skeletal ossification  
**Birth defect** A **congenital** abnormality (customarily anatomic but more recently functional and biochemical as well) that is evident at birth, usually as a consequence of inherited genetic damage or a malign environmental influence  
**Blastema** The primary undifferentiated cells from which a tissue is produced  
**Blastocoel** The fluid-filled cavity that forms at one pole of the morula as it is evolving into the **Blastocyst**  
**Blastocyst** A **Blastula** in which stem cell differentiation has produced a layered **Inner cell mass** at one pole and a **Blastocoel** at the other  
**Blastula** A free-floating embryo with a monolayered wall surrounding a **Blastocoel**  
**Brachydactyly** Abnormal shortness of digits

- Brachygnathia** Abnormal shortness of the mandible
- Brachyury** Abnormally short tail
- Buphthalmos** Enlargement and distension of the fibrous coats of the eye; often a consequence of congenital glaucoma [alternatively **Buphthalmia**, **Buphthalmus**]
- Camptodactyly** Permanent flexion of one or more digits [alternatively **Camptodactylia**]
- Carpal Flexure** Abnormal flexion of the fetal carpus (wrist); most often seen in the rabbit; may be transient or permanent
- Celoschisis** Congenital fissure of the abdominal wall
- Celosomia** Fissure or absence of the sternum, with visceral herniation
- Cephalocele** Protrusion of part of the brain through the cranium
- Cheiloschisis** See **Cleft lip**
- Cleft Face** Clefting due to incomplete fusion of the embryonic facial primordia
- Cleft Lip** Cleft or defects in the upper lip [**Hare lip**]
- Cleft Palate** Fissure or cleft in the bony palate [**Palatoschisis**]
- Clinodactyly** Permanent lateral or medial deviation of one or more fingers
- Club Foot** See **Talipes**
- Coarctation** A stricture or stenosis usually of the aorta
- Coloboma** Fissure due to incomplete development of the eye
- Conceptus** Everything that develops from the fertilized egg including the embryo/fetus and the extraembryonic membranes (i.e., placenta)
- Congenital** Present from birth
- Craniorachischisis** Fissure of the skull and vertebral column due to nonclosure of the entire neural tube
- Cranioschisis** Congenital cranial fissure due to nonclosure of the rostral neural tube
- Craniostenosis** Premature cessation of cranial growth because of craniosynostosis
- Craniosynostosis** Premature ossification of cranial sutures
- Cryptorchidism** Failure of one or both testes to enter the scrotum [alternatively **Cryptorchism**]
- Cyclopia** Fusion of the orbits into a single orbit, with the nose absent or present as a tubular appendage (proboscis) above the orbit
- Decidua** Modified endometrium in which tissue and vascular remodeling takes place to support implantation and maintenance of the embryo
- Deformation** A congenital anomaly arising from ineffective regeneration of a developmental injury caused by an external force (contrast to **Malformation**)
- Delayed ossification** Incomplete mineralization of an otherwise normal ossification center
- Developmental delay** Transient deferral in the attainment of one or more anatomic (e.g., weight gain) or functional (e.g., behavioral) attributes
- Dextrocardia** Abnormal displacement of the heart to the right
- Diaphragmatic hernia** Protrusion of abdominal viscera through a defect in the diaphragm
- Dicephalus** Conjoined twins with two heads and one body
- Diplomyelia** Complete or incomplete doubling of the spinal cord, due to a longitudinal fissure
- Diplopagus** Symmetrically duplicated conjoined twins with largely complete bodies that may share some internal organs
- Diprosopus** A fetus with partial duplication of the face
- Dysarthrosis** Malformation of a joint
- Dysgenesis** Defective development; typically used to imply that development was abnormal from the time the structure was first starting to form
- Dysmorphology** The study of congenital structural malformations (birth defects)
- Dysplasia** Abnormal cell composition and tissue organization that occurs during development
- Dysraphism** Failure of fusion, especially of the neural folds [alternatively **Dysraphia**]
- Dystocia** Prolonged, abnormal, or difficult delivery
- Ectoderm** The outermost **Germ layer** from which superficial structures such as the central nervous system and skin arise
- Ectopia** Displacement or malposition
- Ectopia cordis** Displacement of the heart outside of the thoracic cavity
- Ectopic kidney** Abnormal position of one or both kidneys
- Ectopic pregnancy** Pregnancy occurring outside the uterine cavity
- Ectrodactyly** Absence of all or only part of one or more digits
- Ectromelia** Hypoplasia or absence of one or more limbs
- Ectropion** Abnormal eversion of the margin of the eyelid
- Embryogenesis** The development period during which embryonic formation takes place
- Encephalocele** Herniation of part of the brain, encased in meninges, through an opening in the skull (see also **Encephalomeningocele** and **Meningoencephalocele**)
- Endocardial cushion defect** Heart defects resulting from incomplete fusion of the embryonic endocardial cushions
- Endoderm** The innermost **Germ layer** from which internal structures such as the digestive tract, lower respiratory tract, and associated structures arise
- Entropion** Abnormal inversion of the margin of the eyelid
- Epispadias** Absence of the upper wall of the urethra; more common in males, where it opens on the dorsal surface of the penis
- Eventration** Protrusion of bowels through the abdominal wall
- Exencephaly** Defective development of the cranium resulting in extrusion of the brain through the defective skull
- Exomphalos** See **Omphalocele** [**Umbilical hernia**]
- Exophthalmos** Abnormal protrusion of the eyeball [**Exophthalmus**]
- Exostosis** Abnormal bony growth projecting outward from the surface of a bone
- Exstrophy** Congenital eversion of a hollow organ, e.g., of the bladder
- Fetal wastage** Postimplantation death of embryo or fetus
- Fetus** The developing mammal from the completion of major organogenesis to birth
- Gastroschisis** Fissure of the abdominal wall, not involving the umbilicus and usually involving protrusion of viscera
- Gastrula** An implanted embryo in which the third germ layer (i.e., **Mesoderm**) has formed
- Gastrulation** The developmental stage during which the **Inner cell mass** of an implanted embryo transforms into a trilaminar **Gastrula**
- Germ layer** A group of stem cells that differentiate into particular embryonic organs and tissues
- Gonadal dysgenesis** General term for various abnormalities of gonadal development (e.g., gonadal aplasia, hermaphroditism, "streak gonads")
- Hamartoma** A benign nodular or tumor-like mass resulting from faulty embryonal development of cells and tissues natural to the part
- Hemimelia** Absence of all or part of the distal half of a limb
- Hemivertebra** Incomplete development of one side of a vertebra
- Hermaphrodite** An individual with both male and female gonadal tissue (see also **Pseudohermaphrodite**)
- Heterotopia** The development of a normal tissue in an abnormal location
- Histogenesis** The process of stem cells differentiating into specific cells, tissues, and organs
- Holocardius** A grossly defective monozygotic twin whose circulation is dependent upon the heart of a more perfect twin
- Holoprosencephaly** Failure of division of the prosencephalon (the unified primordial cerebral vesicle) resulting in a deficit in midline

- facial development, with **Hypotelorism**; **Cyclopia** occurs in the severe form, whereas in the mildest form a single central incisor tooth may be present
- Hydramnion, hydramnios** See **Polyhydramnios**
- Hydranencephaly** Complete or almost complete replacement of the cerebral hemispheres by a large cavity filled with cerebrospinal fluid
- Hydrocele** A collection of fluid in the tunica vaginalis of the testis or along the spermatic cord
- Hydrocephalus** Marked dilation of the cerebral ventricles with excessive fluid, usually accompanied by vaulted or dome-shaped head (see also **Hydranencephaly**)
- Hydronephrosis** Distension of the pelvis and calyces of the kidney with fluid, as a result of obstruction of urinary outflow
- Hydroureter** Distension of the ureter with urine because of obstruction of the ureter
- Hypermastia** Presence of one or more supernumerary mammary glands [**Polymastia**]
- Hypertelorism** Abnormally great distance between paired parts or organs, e.g., between the eyes
- Hypoglossia** Shortened and/or malformed tongue
- Hypospadias** Anomaly in which the urethra opens on the underside of the penis or on the perineum in males or into the vagina in females
- Hypotelorism** Abnormally lessened distance between paired parts or organs (e.g., between the eyes)
- Ichthyosis** Developmental skin disorders characterized by excessive or abnormal keratinization, with dryness and scaling
- Implantation** Adherence of the **Blastocyst** to the uterine wall
- In utero** In the uterus (i.e., during gestation)
- Induction** The embryonic process in which one group of cells (the inducing tissue) guides the development of another group of cells
- Iniiencephaly** An anomaly of the brain and neck characterized by an occipital bone defect, *spina bifida* of the cervical vertebrae, and fixed retroflexion of the head on the cervical spine
- Inner cell mass (ICM)** A crescentic mass of embryonic stem cells that forms at one pole of the **Blastocyst**
- Intersex** Condition in which structural attributes of both genders are evident
- Kyphosis** Abnormal dorsal convexity in the curvature of the thoracic spine (humpback, hunchback)
- Lissencephaly** See **Agyria**
- Lordosis** Abnormal anterior convexity in the curvature of the spine (swayback)
- Macroglossia** Abnormally large tongue, often protruding
- Macrogyria** Increased size of cerebral gyri (surface folds)
- Macrophthalmia** Abnormally large eye(s)
- Malformation** A congenital body defect characterized by abnormal shape, size, or structure that results from exuberant tissue injury
- Malformation** A permanent deviation that generally is incompatible with or severely detrimental to normal postnatal survival or development; a morphologic defect of an organ, or large region of the body, resulting from an intrinsically abnormal development process. A major malformation is one that has medical, surgical or cosmetic significance.
- Melotia** Displacement of the ears leading to their close approach on the rostral neck
- Meningocele** Herniation of the meninges through a defect in the cranium [**cranial m.**] or spinal column [**spinal m.**]
- Meningoencephalocele** Herniation of meninges and brain tissue through a defect in the cranium (see also **Encephalocele** and **Encephalomeningocele**)
- Meningomyelocele** Herniation of meninges and spinal cord through a defect in the spinal column [**Myelomeningocele**]
- Meromelia** Absence of part of a limb
- Mesoderm** The middle **Germ layer** from which internal tissue such as bone, cartilage, muscle, and associated connective tissues (including dermis) arise
- Micrencephaly** Having an abnormally small brain
- Microcephaly** Abnormally small head [alternatively **Microcephalia**; **microcephalus**]
- Microglossia** Tongue hypoplasia
- Micrognathia** Abnormally small jaw (usually the mandible)
- Microgyria** Reduced size of cerebral gyri (surface folds)
- Micromelia** Having abnormally small or short limb(s)
- Microphthalmos** Abnormal smallness of one or both eyes [alternatively **Microphthalmia**]
- Microstomia** Hypoplasia of the mouth
- Microtia** Hypoplasia of the pinna, with an absent or atretic external auditory meatus
- Misaligned sternbrae** When the two ossification centers of each sternbra are not aligned in the transverse plane
- Morphogen** A chemical substance whose nonuniform localization directs the pattern of tissue development
- Morphogenesis** The entire course of structural development
- Morula** Early embryos comprised of a solid ball of essentially totipotent cells
- Myelocele** Herniation of spinal cord through a vertebral defect
- Myelomeningocele** See **Meningomyelocele**
- Myeloschisis** Cleft spinal cord caused by failure of neural tube closure
- Neural tube defect** Any malformation (anencephaly, exencephaly, *spina bifida*, *craniorachischisis*, etc.) resulting from failure of the neural tube to close and fuse during embryonic development
- Neurula** An early embryo at the stage where neural tube (central nervous system) formation is beginning
- Nevus** A circumscribed skin malformation, usually hyperpigmented or with abnormal vascularization
- Oligodactyly** having fewer than the normal number of digits
- Oligohydramnios** Abnormally reduced quantity of amniotic fluid
- Oligopotent** A partially differentiated state in which the cell can form only a few cell lineages
- Omphalocele** Herniation of intestine covered with peritoneum and amnion through a defect in the abdominal wall at the umbilicus [**Exomphalos**, **Umbilical hernia**]
- Ontogeny** An organism's individual developmental history from conception to maturity
- Organogenesis** The developmental period during which organs first form in the embryo
- Otocephaly** Close approach or fusion (**Synotia**) of the ears on the front of the neck
- Overriding aorta** Displacement of the aorta to the right, so that it appears to arise from both ventricles
- Pagus** Combining form (suffix) indicating conjoined twins (e.g., **Diplopagus**)
- Palatine rugae alteration** Misaligned or otherwise abnormal palatal ridges
- Patent ductus arteriosus** An open communication between the pulmonary trunk and aorta persisting postnatally
- Patent foramen ovale** Failure of adequate postnatal closure of the *foramen ovale*, an **Atrial septal defect** allowing interchange of blood between the atria; primary atrial septal defects are larger than a patent *foramen ovale*
- Phenocopy** A non-genetic disease with lesions that mimic those induced by a genetic defect
- Phocomelia** Absence of the proximal part of a limb(s), leaving the distal part attached to the trunk by a small, irregularly shaped bone
- Plagiocephaly** An asymmetrical condition of the cranium, resulting from premature closure of the cranial sutures on one side causing deformation



**Pluripotent** A partially differentiated state in which the cell can form many but not all cell lineages

**Polydactyly** Supernumerary digits

**Polyhydramnios** Abnormally increased quantity of amniotic fluid

**Polymastia** See **Hypermastia**

**Porencephaly** Localized expansion of the brain associated with a cavity filled with cerebrospinal fluid

**Precocial** Animals (e.g., guinea pigs) that are capable of substantial self-care immediately after birth

**Proboscis** A cylindrical protuberance of the face usually associated with holoprosencephaly

**Pseudohermaphroditism** Partial masculinization or partial feminization, with gonadal tissue of only one sex present

**Ptoxis** Drooping of the upper eyelid because of abnormal muscle or nerve development

**Rachischisis** Congenital fissure of the vertebral column due to non-closure of the caudal neural tube

**Resorption** A conceptus that died after implantation and is being, or has been, removed (reabsorbed)

**Runt** Normally developed fetus or newborn significantly smaller than the rest of the litter

**Scoliosis** Lateral deviation of the vertebral column

**Sirenomelia** Having fused lower limbs [**Symmelia**]

**Situs inversus** Lateral transposition of the viscera

**Spina bifida (S.B.)** Localized defective closure of the vertebral arches, through which the spinal cord and/or meninges may protrude; a neural tube defect

**Spina bifida aperta** S.B. in which the neural tissue is exposed

**Spina bifida cystica** S.B. with intact skin and no herniation

**Spina bifida occulta** S.B. with herniation of a cystic swelling containing the meninges (**Meningocele**), spinal cord (**Myelocele**), or both (**Myelomeningocele**)

**Stillbirth** Birth of a dead fetus

**Sympodia** Fusion of the feet

**Syndactyly** Webbing or fusion between adjacent digits

**Synotia** Displacement of the ears leading to their fusion on the rostral neck

**Syringomyelia** Development of a fluid-filled cyst (termed a syrinx) in the spinal cord

**Talipes** Congenital deformity of the foot, which is twisted out of shape or position [**Clubfoot**]

**Teratogen** A substance (e.g., chemical, heat, infectious agent, radiation) that causes abnormal development (especially structural **Malformations**) of the embryo or fetus

**Teratogenicity** The ability to cause defective development

**Tetralogy of Fallot** A combination of cardiac defects consisting of pulmonary or infundibular stenosis, **Ventricular septal defect**, overriding aorta, and right ventricular hypertrophy

**Totipotent** An undifferentiated state in which the cell can form all cell lineages

**Tracheoesophageal fistula** Abnormal connection between the trachea and esophagus

**Trophoblast** Extraembryonic cells forming the wall of the **Blastocoel** that will differentiate into the placenta

**Umbilical hernia** See **Omphalocele**

**Vasculogenesis** Differentiation of precursor cells (termed angioblasts) into endothelial cells that participate in de novo formation of new blood vessels

**Ventricular septal defect** Persistent communication between the ventricles

**Wavy ribs** Extra bends in one or more ribs

**Xenobiotic** An agent (especially a synthetic chemical) that is foreign to the body

**Zygote** The one-celled embryo formed by fusion of the oocyte (female gamete) and sperm (male gamete)

The glossary was adapted in part, with modifications, from the following sources:

- EPA (U.S. Environmental Protection Agency). "Standard Evaluation Procedure, Developmental Toxicity Studies." Health Effects Division, Office of Pesticide Programs, 1993, Washington, DC
- Keller, K. Unpublished glossary
- Makris SL, Solomon HM, Clark R et al: Terminology of developmental abnormalities in common laboratory mammals (version 2). *Birth Defects Res. B Dev. Reprod. Toxicol.* 86:227–327, 2009
- MARTA (Middle Atlantic Reproduction and Teratology Association) Committee: Glossary of fetal anomalies. In Hood R, editor: *Handbook of developmental toxicology*, Boca Raton, FL, 1997, CRC Press, pp. 697–711
- Moore KL, Persaud TVN: *The developing human*, ed 6, Philadelphia, 1998, W. B. Saunders
- O'Rahilly R, Müller F: *Human embryology and teratology*, ed 2, New York, 1996, Wiley-Liss
- Schardein, J. L. Unpublished glossary
- Wise LD, Beck SL, Beltrame D et al.: Terminology of developmental abnormalities in common laboratory mammals (version 1), *Teratology* 55:249–292, 1997
- Wise LD, Beck SL, Beltrame D et al.: *Dorland's illustrated medical dictionary*, ed 28, Philadelphia, 1983, W. B. Saunders
- Wise LD, Beck SL, Beltrame D et al.: *Stedman's medical dictionary*, ed 26, Baltimore, 1995, Williams & Wilkins

## Acknowledgments

The authors thank Ms. Beth Mahler for her assistance in optimizing the hues and resolution of images, and Mr. Tim Vojt for his superb schematic diagrams.

## REFERENCES

- Abduljalil K, Furness P, Johnson TN, et al.: Anatomical, physiological and metabolic changes with gestational age during normal pregnancy: a database for parameters required in physiologically based pharmacokinetic modelling, *Clin. Pharmacokinet.* 51:365–396, 2012.
- ACOG: Reducing prenatal exposure to toxic environmental agents: ACOG Committee Opinion Number 832, *Obstet. Gynecol.* 138:e40–e54, 2021.
- Adamson SL, Lu Y, Whiteley KJ, et al.: Interactions between trophoblast cells and the maternal and fetal circulation in the mouse placenta, *Dev. Biol.* 250:358–373, 2002.
- Al-Enazy S, Ali S, Albekairi N, et al.: Placental control of drug delivery, *Adv. Drug Deliv. Rev.* 116:63–72, 2017.
- Altshuler G: Pathology of the placenta. In Gilbert-Barnes E, editor: *Potter's pathology of the fetus and infant*, St. Louis, 1997, Mosby, pp 241–279.
- Amadei G, Handford CE, Qiu C, et al.: Synthetic embryos complete gastrulation to neurulation and organogenesis, *Nature* 60:143–153, 2022.

- Andersen MD, Alstrup AKO, Duvald CS, et al.: Animal models of fetal medicine and obstetrics. In Bartholomew I, editor: *Experimental animal models of human diseases an effective therapeutic strategy*, 2018, IntechOpen, <https://doi.org/10.5772/intechopen.74038>.
- Anderson LM, Diwan BA, Fear NT, et al.: Critical windows of exposure for children's health: cancer in human epidemiological studies and neoplasms in experimental animal models, *Environ. Health Perspect.* 108(Suppl 3):573–594, 2000.
- Ashkar AA, Croy BA: Interferon- $\gamma$  contributes to the normalcy of murine pregnancy, *Biol. Reprod.* 61:493–502, 1999.
- Ashwell KWS, Paxinos G: *Atlas of the developing rat nervous system*, ed 3rd San Diego, 2008, Academic Press (Elsevier).
- Avagliano L, Massa V, Bulfamante GP: *Histology of human placenta*, 2016, Semantic Scholar. <https://api.semanticscholar.org/CorpusID:35915698>. (Accessed 24 May 2024).
- Bailey J, Balcombe JP: The future of teratology research is *in vitro*, *Biog. Amines* 19:97–145, 2005.
- Bal-Price A, Pistollato F, Sachana M, et al.: Strategies to improve the regulatory assessment of developmental neurotoxicity (DNT) using *in vitro* methods, *Toxicol. Appl. Pharmacol.* 354:7–18, 2018.
- Baldock R, Bard JB, Davidson DR, et al.: *Kaufman's atlas of mouse development supplement: with coronal sections*, San Diego, 2016, Academic Press (Elsevier).
- Bardai GK, Hales BF, Sunahara GI: Developmental toxicity of glyceryl trinitrate in quail embryos, *Birth Defects Res. A Clin. Mol. Teratol.* 91:230–240, 2011.
- Barrow MV, Taylor WJ: A rapid method for detecting malformations in rat fetuses, *J. Morphol.* 127:291–305, 1969.
- Barry JM: *Molecular embryology: how molecules give birth to animals*, Boca Raton, 2002, CRC Press (Taylor & Francis).
- Beckman DA, Brent RL: Mechanism of known environmental teratogens: drugs and chemicals, *Clin. Perinatol.* 13:649–687, 1986.
- Beedie SL, Mahony C, Walker HM, et al.: Shared mechanism of teratogenicity of anti-angiogenic drugs identified in the chicken embryo model, *Sci. Rep.* 6:30038, 2016.
- Behringer R, Gertsenstein M, Nagy KV, et al.: *Manipulating the mouse embryo: a laboratory manual*, ed 4th Cold Spring Harbor, NY, 2014, Cold Spring Harbor Laboratory Press.
- Bellairs R, Osmond M: *Atlas of chick development*, ed 2nd, San Diego, 2005, Academic Press.
- Benirschke K: *Comparative placentation*, 2011. <http://placentation.ucsd.edu/>. (Accessed 24 May 2024).
- Beyer BK, Chernoff N, Danielsson BR, et al.: ILSI/HESI maternal toxicity workshop summary: maternal toxicity and its impact on study design and data interpretation, *Birth Defects Res. B Dev. Reprod. Toxicol.* 92:36–51, 2011.
- Blue NR, Page JM, Silver RM: Genetic abnormalities and pregnancy loss, *Semin. Perinatol.* 43:66–73, 2019.
- Bode G, Clausing P, Gervais F, et al.: The utility of the minipig as an animal model in regulatory toxicology, *J. Pharmacol. Toxicol. Methods* 62:196–220, 2010.
- Boklage CE: Survival probability of human conceptions from fertilization to term, *Int. J. Fertil.* 35:75, 1990, 79–80, 81–94.
- Bolon B: *Pathology of the developing mouse: a systematic approach*, Boca Raton, FL, 2015, CRC Press (Taylor & Francis).
- Bolon B, Dostal LA, Garman RH: Neuropathology evaluation in juvenile toxicity studies in rodents: comparison of developmental neurotoxicity studies for chemicals with juvenile animal studies for pediatric pharmaceuticals, *Toxicol. Pathol.* 49:1405–1415, 2021.
- Bolon B, Duryea D, Foley JF: Histotechnological processing of developing mice. In Bolon B, editor: *Pathology of the developing mouse: a systematic approach*, Boca Raton, FL, 2015, CRC Press (Taylor & Francis), pp 195–210.
- Bolon B, Newbigging S, Boyd KL: Pathology evaluation of developmental phenotypes in neonatal and juvenile mice, *Curr. Protoc. Mol. Biol.* 7:191–219, 2017.
- Bolon B, Omer VES: Behavioral and developmental effects in suckling mice following maternal exposure to the mycotoxin secalonic acid D, *Pharmacol., Biochem. Behav.* 34:229–236, 1989.
- Bolon B, Ward JM: Anatomy and physiology of the developing mouse and placenta. In Bolon B, editor: *Pathology of the developing mouse: a systematic approach*, Boca Raton, FL, 2015a, CRC Press (Taylor & Francis), pp 39–98.
- Bolon B, Ward JM: Pathology of the placenta. In Bolon B, editor: *Pathology of the developing mouse: a systematic approach*, Boca Raton, FL, 2015b, CRC Press (Taylor & Francis), pp 355–376.
- Bolon B, Welsch F, Morgan KT: Methanol-induced neural tube defects in mice: pathogenesis during neurulation, *Teratology* 49:497–517, 1994.
- Bommarito PA, Martin E, Fry RC: Effects of prenatal exposure to endocrine disruptors and toxic metals on the fetal epigenome, *Epigenomics* 9:333–350, 2017.
- Botting J: The history of thalidomide. In Botting J, editor: *Animals and medicine: the contribution of animal experiments to the control of disease*, Cambridge, UK, 2015, Open Book Publishers.
- Bouazza N, Foissac F, Hirt D, et al.: Methodological approaches to evaluate fetal drug exposure, *Curr. Pharmaceut. Des.* 25:496–504, 2019.
- Boyd KL, Bolon B, Bounous DI: Clinical pathology analysis in developing mice. In Bolon B, editor: *Pathology of the developing mouse: a systematic approach*, Boca Raton, FL, 2015, CRC Press (Taylor & Francis), pp 175–193.
- Boyle B, Addor M-C, Arriola L, et al.: Estimating Global Burden of Disease due to congenital anomaly: an analysis of European data, *Arch. Dis. Child. Fetal Neonatal Ed.* 103: F22–F28, 2018.
- Brent RL, Fawcett L, Beckman DA: Principles of teratology. In Evans MI, Johnson MP, Yaron Y, et al., editors: *Prenatal diagnosis*, New York, 2006, McGraw-Hill, pp 79–112.
- Briggs GG, Freeman RK, Towers CV, et al.: *Drugs in pregnancy and lactation*, ed 11th, Philadelphia, 2017, Wolters Kluwer.
- Bui T-H: Syndrome: an approach to fetal dysmorphology. In Evans MI, Johnson MP, Yaron Y, et al., editors: *Prenatal diagnosis*, New York, 2006, McGraw-Hill, pp 57–62.

- Campbell LR, Dayton DH, Sohal GS: Neural tube defects: a review of human and animal studies on the etiology of neural tube defects, *Teratology* 34:171–187, 1986.
- Capitanio JP, Del Rosso LA, Gee N, et al.: Adverse bio-behavioral effects in infants resulting from pregnant rhesus macaques' exposure to wildfire smoke, *Nat. Commun.* 13: 1774, 2022.
- Cappon GD, Fleeman TL, Chapin RE, et al.: Effects of feed restriction during organogenesis on embryo-fetal development in rabbit, *Birth Defects Res. B Dev. Reprod. Toxicol.* 74:424–430, 2005.
- Carney EW, Scialli AR, Watson RE, et al.: Mechanisms regulating toxicant disposition to the embryo during early pregnancy: an interspecies comparison, *Birth Defects Res. C Embryo Today* 72:345–360, 2004.
- CDC: *Improved national prevalence estimates for 18 selected major birth defects—United States, 1999–2001*, 2006. <https://www.cdc.gov/mmwr/preview/mmwrhtml/mm5451a2.htm>. (Accessed 24 May 2024).
- CFR: Title 40—Protection of Environment: Chapter I—Environmental protection agency. Subchapter R—Toxic substances control act (continued). Part 798—Health effects testing guidelines. Subpart E—Specific organ/tissue toxicity. Section 798.4900—Developmental toxicity study, 1999. <https://www.govinfo.gov/app/details/CFR-2009-title40-vol31/CFR-2009-title40-vol31-sec798-4900>. (Accessed 24 May 2024).
- Chen VS, Morrison JP, Southwell MF, et al.: Histology atlas of the developing prenatal and postnatal mouse central nervous system, with emphasis on prenatal days E7.5 to E18.5, *Toxicol. Pathol.* 45:705–744, 2017.
- Chernoff N, Kavlock RJ: An *in vivo* teratology screen utilizing pregnant mice, *J. Toxicol. Environ. Health* 10:541–550, 1982.
- Chiu PP: New insights into congenital diaphragmatic hernia – a surgeon's introduction to CDH animal models, *Front. Pediatr.* 2(36), 2014.
- Chuaire Noack L: New clues to understand gastroschisis. Embryology, pathogenesis and epidemiology, *Colomb. Méd.* 52:e4004227, 2021.
- Ciallella HL, Russo DP, Sharma S, et al.: Predicting prenatal developmental toxicity based on the combination of chemical structures and biological data, *Environ. Sci. Technol.* 56:5984–5998, 2022.
- Ciallella HL, Zhu H: Advancing computational toxicology in the big data era by artificial intelligence: data-driven and mechanism-driven modeling for chemical toxicity, *Chem. Res. Toxicol.* 32:536–547, 2019.
- Clancy B, Charvet CJ, Darlington RB, et al.: *Translating time (across developing mammalian brains)*, 2013. <http://translatingtime.net/>. (Accessed 24 May 2024).
- Clancy B, Finlay BL, Darlington RB, et al.: Extrapolating brain development from experimental species to humans, *Neurotoxicology* 28:931–937, 2007a.
- Clancy B, Kersh B, Hyde J, et al.: Web-based method for translating neurodevelopment from laboratory species to humans, *Neuroinformatics* 5:79–94, 2007b.
- Cochard LR: *Netter's atlas of human embryology* teterboro, NJ, 2002, Icon Learning Systems.
- Compagnucci C, Martinus K, Griffin J, et al.: Programmed cell death not as sledgehammer but as chisel: apoptosis in normal and abnormal craniofacial patterning and development, *Front. Cell Dev. Biol.* 9:717404, 2021.
- Crawford LW, Foley JF, Elmore SA: Histology atlas of the developing mouse hepatobiliary system with emphasis on embryonic days 9.5–18.5, *Toxicol. Pathol.* 38:872–906, 2010.
- Crawley JN: *What's wrong with my mouse? Behavioral phenotyping of transgenic and knockout mice*, ed 2nd New York, 2007, Wiley-Liss.
- Cross JC: Formation of the placenta and extraembryonic membranes, *Ann. N.Y. Acad. Sci.* 857:23–32, 1998.
- Cross JC, Simmons DG, Watson ED: Chorioallantoic morphogenesis and formation of the placental villous tree, *Ann. N. Y. Acad. Sci.* 995:84–93, 2003.
- Croy BA, He H, Esadeg S, et al.: Uterine natural killer cells: insights into their cellular and molecular biology from mouse modelling, *Reproduction* 126:149–160, 2003.
- Croy BA, Yamada AT, DeMayo FJ, et al.: *The guide to investigation of mouse pregnancy*, London, 2014, Academic Press (Elsevier).
- Croy BA, Zhang J, Tayade C, et al.: Analysis of uterine natural killer cells in mice, *Methods Mol. Biol.* 612:465–503, 2010.
- Danielsson BR: Maternal toxicity, *Methods Mol. Biol.* 947:311–325, 2013.
- Daston GP: Laboratory models and their role in assessing teratogenesis, *Am. J. Med. Genet. C Semin. Med. Genet.* 157: 183–187, 2011.
- de Jong E, Barenys M, Hermesen SA, et al.: Comparison of the mouse embryonic stem cell test, the rat whole embryo culture and the zebrafish embryotoxicity test as alternative methods for developmental toxicity testing of six 1,2,4-triazoles, *Toxicol. Appl. Pharmacol.* 253:103–111, 2011.
- De Schaeppdrijver LM, Annaert PPJ, Chen CL: Ontogeny of ADME processes during postnatal development in man and preclinical species: a comprehensive review, *Drug Metabol. Dispos.* 47:295, 2019.
- De Sousa Mendes M, Hirt D, Vinot C, et al.: Prediction of human fetal pharmacokinetics using *ex vivo* human placenta perfusion studies and physiologically based models, *Br. J. Clin. Pharmacol.* 81:646–657, 2016.
- Dennis JF, Kurosaka H, Iulianella A, et al.: Mutations in *Hedgehog acyltransferase* (Hhat) perturb Hedgehog signaling, resulting in severe acrania-holoprosencephaly-agnathia craniofacial defects, *PLoS Genet.* 8:e1002927, 2012.
- DeSesso JM: Comparative features of vertebrate embryology. In Hood RD, editor: *Developmental and reproductive toxicology: a practical approach*, Boca Raton, FL, 2006, CRC Press, pp 147–197.
- DeSesso JM: The arrogance of teratology: a brief chronology of attitudes throughout history, *Birth Defects Res.* 111:123–141, 2019.



- DeSesso JM, Williams AL, Ahuja A, et al.: The placenta, transfer of immunoglobulins, and safety assessment of biopharmaceuticals in pregnancy, *Crit. Rev. Toxicol.* 42:185–210, 2012.
- DeWitt JC, Peden-Adams MM, Keil DE, et al.: Current status of developmental immunotoxicity: early-life patterns and testing, *Toxicol. Pathol.* 40:230–236, 2012.
- Dietert RR: Developmental immunotoxicity, perinatal programming, and noncommunicable diseases: focus on human studies, *Adv. Met. Med.* 2014:867805, 2014.
- Diewert VM: A comparative study of craniofacial growth during secondary palate development in four strains of mice, *J. Craniofac. Genet. Dev. Biol.* 2:247–263, 1982.
- Donovan PJ: Cell sensitivity to transplacental carcinogenesis by *N*-ethyl-*N*-nitrosourea is greatest in early post-implantation development, *Mutat. Res.* 427:59–63, 1999.
- Downes NJ: Consideration of the development of the gastrointestinal tract in the choice of species for regulatory juvenile studies, *Birth Defects Res.* 110:56–62, 2018.
- Draghici C-C, Miulescu R-G, Petca R-C, et al.: Teratogenic effect of isotretinoin in both fertile females and males (Review), *Exp. Ther. Med.* 21:534, 2021.
- Draws U: *Color atlas of embryology*, New York, 1995, Thieme Medical Publishers.
- Edelman GM: Cell adhesion and morphogenesis: the regulator hypothesis, *Proc. Natl. Acad. Sci. U. S. A.* 81:1460–1464, 1984.
- Edelman GM: *Topobiology: an introduction to molecular embryology*, New York, 1988, Basic Books.
- Edelman GM: Morphoregulation, *Dev. Dynam.* 193:2–10, 1992.
- El-Attar LM, Bahashwan AA, Bakhsh AD, et al.: The prevalence and patterns of chromosome abnormalities in newborns with major congenital anomalies: a retrospective study from Saudi Arabia, *Intractable Rare Dis. Res.* 10:81–87, 2021.
- Elangbam CS: Drug-induced valvulopathy: an update, *Toxicol. Pathol.* 38:837–848, 2010.
- Elmore S: Apoptosis: a review of programmed cell death, *Toxicol. Pathol.* 35:495–516, 2007.
- Elmore SA, Cochran Z, Bolon B, et al.: Histology atlas of the developing mouse placenta, *Toxicol. Pathol.* 50:60–117, 2022.
- Elmore SA, Dixon D, Hailey JR, et al.: Recommendations from the INHAND apoptosis/necrosis working group, *Toxicol. Pathol.* 44:173–188, 2016.
- Elmore SA, Kavari SL, Hoenerhoff MJ, et al.: Histology atlas of the developing mouse urinary system with emphasis on prenatal days E10.5–E18.5, *Toxicol. Pathol.* 47:865–886, 2019.
- EMAP: *EMAP: e-Mouse Atlas*, v3.5, 2013. <http://www.emouseatlas.org/emap/home.html>. (Accessed 24 May 2024).
- EPA: *Guidelines for developmental toxicity risk assessment*, 1991. <https://www.epa.gov/risk/guidelines-developmental-toxicity-risk-assessment>. (Accessed 24 May 2024).
- EPA: Health Effects Test Guidelines: OPPTS 870.3700: prenatal developmental toxicity study, 1998a. <https://www.epa.gov/test-guidelines-pesticides-and-toxic-substances/series-870-health-effects-test-guidelines>. (Accessed 24 May 2024).
- EPA: Health Effects Test Guidelines: OPPTS 870.6300: developmental neurotoxicity study, 1998b. <https://www.epa.gov/test-guidelines-pesticides-and-toxic-substances/series-870-health-effects-test-guidelines>. (Accessed 24 May 2024). Listed under “Group E – Neurotoxicity Test Guidelines”.
- EPA: Endocrine disruptor screening program Tier 1 battery of assays, 2009. <https://www.epa.gov/endocrine-disruption/endocrine-disruptor-screening-program-tier-1-battery-assays>. (Accessed 24 May 2024).
- EPA: Series 890 – endocrine disruptor screening program test guidelines, <https://www.epa.gov/test-guidelines-pesticides-and-toxic-substances/series-890-endocrine-disruptor-screening-program> (last accessed May 24, 2024).
- Epstein CJ: The new dysmorphology: application of insights from basic developmental biology to the understanding of human birth defects, *Proc. Natl. Acad. Sci. U. S. A.* 92:8566–8573, 1995.
- Erlebacher A: Leukocyte population dynamics and functions at the maternal–fetal interface. In Croy BA, Yamada AT, DeMayo FJ, et al., editors: *The guide to investigation of mouse pregnancy*, London, 2014, Academic Press (Elsevier), pp 227–242.
- Fantel AG: Reactive oxygen species in developmental toxicity: review and hypothesis, *Teratology* 53:196–217, 1996.
- FDA: *Determination that Bendectin was not withdrawn from sale for reasons of safety or effectiveness*, 1999. <https://www.govinfo.gov/content/pkg/FR-1999-08-09/pdf/99-20362.pdf>. (Accessed 24 May 2024).
- FDA: *Reproductive and developmental toxicities — integrating study results to assess concerns*, 2011. <https://www.fda.gov/regulatory-information/search-fda-guidance-documents/reproductive-and-developmental-toxicities-integrating-study-results-assess-concerns>. (Accessed 24 May 2024).
- Feldkamp ML, Carey JC, Byrne JLB, et al.: Etiology and clinical presentation of birth defects: population based study, *BMJ* 357:j2249, 2017.
- Ferretti P, Copp C, Tickle C, et al.: *Embryos, genes and birth defects*, ed 2nd, Chichester, England, 2006, John Wiley & Sons, Ltd.
- Filardi T, Panimolle F, Lenzi A, et al.: Bisphenol A and phthalates in diet: an emerging link with pregnancy complications, *Nutrients* 12, 2020.
- Flaherty K, Richtsmeier JT: It's about time: ossification center formation in C57BL/6 mice from E12–E16, *J. Dev. Biol.* 6(31), 2018.
- Fleeman TL, Cappon GD, Chapin RE, et al.: The effects of feed restriction during organogenesis on embryo-fetal development in the rat, *Birth Defects Res. B Dev. Reprod. Toxicol.* 74:442–449, 2005.
- Fletcher TJ, Weber AF: *Veterinary developmental anatomy (veterinary embryology)*, 2013. <http://vanat.cvm.umn.edu/vanatpdf/EmbryoLectNotes.pdf>. (Accessed 24 May 2024).
- Footo RH, Carney EW: The rabbit as a model for reproductive and developmental toxicity studies, *Reprod. Toxicol.* 14:477–493, 2000.

- Fraser FC: The multifactorial/threshold concept—uses and misuses, *Teratology* 14:267–280, 1976.
- Furukawa S, Kuroda Y, Sugiyama A: A comparison of the histological structure of the placenta in experimental animals, *J. Toxicol. Pathol.* 27:11–18, 2014.
- Furukawa S, Tsuji N, Sugiyama A: Morphology and physiology of rat placenta for toxicological evaluation, *J. Toxicol. Pathol.* 32:1–17, 2019.
- Gad SC: Pigs and ferrets as models in toxicology and biological safety assessment, *Int. J. Toxicol.* 19:149–168, 2000.
- Gad SC, Gad SE: A functional observational battery for use in canine toxicity studies: development and validation, *Int. J. Toxicol.* 22:415–422, 2003.
- Garman RH, Li AA, Kaufmann W, et al.: Recommended methods for brain processing and quantitative analysis in rodent developmental neurotoxicity studies, *Toxicol. Pathol.* 44:14–42, 2016.
- Gauvin DV, Baird TJ: A functional observational battery in non-human primates for regulatory-required neuro-behavioral assessments, *J. Pharmacol. Toxicol. Methods* 58: 88–93, 2008.
- Georgiades P, Ferguson-Smith AC, Burton GJ: Comparative developmental anatomy of the murine and human definitive placentae, *Placenta* 23:3–19, 2002.
- Giaginis C, Tsantili-Kakoulidou A, Theocharis S: Assessing drug transport across the human placental barrier: from *in vivo* and *in vitro* measurements to the *ex vivo* perfusion method and *in silico* techniques, *Curr. Pharmaceut. Biotechnol.* 12:804–813, 2011.
- Giagounidis AA, Giagounidis AY, Giagounidis AS, et al.: Terathanasia or teratothanasia? *Lancet* 350:1712, 1997.
- Gilbert-Barness E: *Potter's atlas of fetal and infant pathology*, St Louis, MO, 1999, Mosby.
- Gilbert-Barness E: *Potter's pathology of the fetus. Infant and child*, Philadelphia, PA, 2007, Mosby (Elsevier).
- Gilbert SF: *Developmental biology*, ed 10th, Sunderland, MA, 2013, Sinauer Associates, Inc.
- Göhner C, Svensson-Arvelund J, Pfarrer C, et al.: The placenta in toxicology. Part IV: battery of toxicological test systems based on human placenta, *Toxicol. Pathol.* 42:345–351, 2014.
- Griffiths SK, Campbell JP: Placental structure, function and drug transfer, *Cont. Educ. Anaesth. Crit. Care Pain* 15:84–89, 2015.
- Grigsby PL: Animal models to study placental development and function throughout normal and dysfunctional human pregnancy, *Semin. Reprod. Med.* 34:11–16, 2016.
- Gupta RC, editor: *Developmental and reproductive toxicology*, San Diego, 2022, Elsevier.
- Halpern WG, Ameri M, Bowman CJ, et al.: Scientific and regulatory policy committee points to consider review: inclusion of reproductive and pathology end points for assessment of reproductive and developmental toxicity in pharmaceutical drug development, *Toxicol. Pathol.* 44:789–809, 2016.
- Hamada H: Molecular and cellular basis of left-right asymmetry in vertebrates, *Proc. Jpn. Acad. Ser. B Phys. Biol. Sci.* 96:273–296, 2020.
- Hamlin HJ, Guillelte Jr LJ: Birth defects in wildlife: the role of environmental contaminants as inducers of reproductive and developmental dysfunction, *Syst. Biol. Reprod. Med.* 56: 113–121, 2010.
- Hansen DK, Abbott BD: *Developmental toxicology*, ed 3rd 2008, CRC Press (Taylor & Francis).
- Hanson MA, Gluckman PD: Early developmental conditioning of later health and disease: physiology or pathophysiology? *Physiol. Rev.* 94:1027–1076, 2014.
- Helms J, Thaller C, Eichele G: Relationship between retinoic acid and sonic hedgehog, two polarizing signals in the chick wing bud, *Development* 120:3267–3274, 1994.
- Helms JA, Kim CH, Hu D, et al.: Sonic hedgehog participates in craniofacial morphogenesis and is down-regulated by teratogenic doses of retinoic acid, *Dev. Biol.* 187:25–35, 1997.
- Hendrickx AG, Cukierski MA: Reproductive and developmental toxicology in nonhuman primates, *Prog. Clin. Biol. Res.* 235:73–88, 1987.
- Hendrickx AG, Makori N, Peterson P: Nonhuman primates: their role in assessing developmental effects of immunomodulatory agents, *Hum. Exp. Toxicol.* 19:219–225, 2000.
- Hennekam RC, Biesecker LG, Allanson JE, et al.: Elements of morphology: general terms for congenital anomalies, *Am. J. Med. Genet.* 161A:2726–2733, 2013.
- Herbst AL, Anderson D: Clear cell adenocarcinoma of the vagina and cervix secondary to intrauterine exposure to diethylstilbestrol, *Semin. Surg. Oncol.* 6:343–346, 1990.
- Hessler G, Baringhaus K-H: Artificial intelligence in drug design, *Molecules* 23, 2018.
- Hill MA: *Embryology*, 2014. [https://embryology.med.unsw.edu.au/embryology/index.php?title=Main\\_Page](https://embryology.med.unsw.edu.au/embryology/index.php?title=Main_Page). (Accessed 24 May 2024).
- Holson JF, Stump DG, Pearce LB, et al.: Absence of developmental toxicity in a canine model after infusion of a hemoglobin-based oxygen carrier: implications for risk assessment, *Reprod. Toxicol.* 52:101–107, 2015.
- Hood RD, editor: *Handbook of developmental toxicology*, Boca Raton, FL, 1997, CRC Press.
- Hood RD, editor: *Developmental and reproductive toxicology: a practical approach*, London, 2012, Informa Healthcare.
- Huo D, Anderson D, Palmer JR, et al.: Incidence rates and risks of diethylstilbestrol-related clear-cell adenocarcinoma of the vagina and cervix: update after 40-year follow-up, *Gynecol. Oncol.* 146:566–571, 2017.
- ICH: M3(R2): guidance on nonclinical safety studies for the conduct of human clinical trials and marketing authorization for pharmaceuticals, 2009a. [https://database.ich.org/sites/default/files/M3\\_R2\\_Guideline.pdf](https://database.ich.org/sites/default/files/M3_R2_Guideline.pdf). (Accessed 24 May 2024).
- ICH: S9: nonclinical evaluation for anticancer pharmaceuticals, 2009b. [https://database.ich.org/sites/default/files/S9\\_Guideline.pdf](https://database.ich.org/sites/default/files/S9_Guideline.pdf). (Accessed 24 May 2024).
- ICH: S6(R1): preclinical safety evaluation of biotechnology-derived pharmaceuticals, 2011. [https://database.ich.org/sites/default/files/S6\\_R1\\_Guideline\\_0.pdf](https://database.ich.org/sites/default/files/S6_R1_Guideline_0.pdf). (Accessed 24 May 2024).

- ICH: S9: *nonclinical evaluation for anticancer pharmaceuticals: questions and answers guidance for industry*, 2018. [https://database.ich.org/sites/default/files/S9\\_Q%26As\\_Q%26As.pdf](https://database.ich.org/sites/default/files/S9_Q%26As_Q%26As.pdf). (Accessed 24 May 2024).
- ICH: S5(R3): *detection of reproductive and developmental toxicity for human pharmaceuticals*, 2020a. [https://database.ich.org/sites/default/files/S5-R3\\_Step4\\_Guideline\\_2020\\_0218\\_1.pdf](https://database.ich.org/sites/default/files/S5-R3_Step4_Guideline_2020_0218_1.pdf). (Accessed 24 May 2024).
- ICH: S11: *nonclinical safety testing in support of development of paediatric medicines*, 2020b. [https://database.ich.org/sites/default/files/S11\\_Step4\\_FinalGuideline\\_2020\\_0310.pdf](https://database.ich.org/sites/default/files/S11_Step4_FinalGuideline_2020_0310.pdf). (Accessed 24 May 2024).
- Imbard A, Benoist JF, Blom HJ: Neural tube defects, folic acid and methylation, *Int. J. Environ. Res. Publ. Health* 10:4352–4389, 2013.
- Jarvis GE: Early embryo mortality in natural human reproduction: what the data say, *F1000Res* 5:2765, 2016.
- Jones KL, Carey JC: The importance of dysmorphology in the identification of new human teratogens, *Am. J. Med. Genet. C Semin. Med. Genet.* 157C:188–194, 2011.
- Joshi AA, Vaidya SS, St-Pierre MV, et al.: Placental ABC transporters: biological impact and pharmaceutical significance, *Pharm. Res. (N. Y.)* 33:2847–2878, 2016.
- Kaufman MH: *The atlas of mouse development*, ed 2nd, San Diego, 1992, Academic Press.
- Kaufman MH: *The anatomical basis of mouse development*, San Diego, Calif, 1999, Academic.
- Kaufman MH, Bard JBL: *The anatomical basis of mouse development*, San Diego, 1999, Academic Press.
- Kelley AS, Banker M, Goodrich JM, et al.: Early pregnancy exposure to endocrine disrupting chemical mixtures are associated with inflammatory changes in maternal and neonatal circulation, *Sci. Rep.* 9:5422, 2019.
- Khera KS: Maternal toxicity—a possible factor in fetal malformations in mice, *Teratology* 29:411–416, 1984.
- Khera KS: A morphologic basis postulated for valproic acid's embryotoxic action in rats, *Teratog. Carcinog. Mutagen.* 12: 277–289, 1992.
- Kheradvar A, Zareian R, Kawauchi S, et al.: Animal models for heart valve research and development, *Drug Discov. Today Dis. Model.* 24:55–62, 2017.
- Kimmel CA, Buelke-Sam J, editors: *Developmental toxicology*, New York, 1994, Raven Press.
- Kojima Y, Tam OH, Tam PPL: Timing of developmental events in the early mouse embryo, *Semin. Cell Dev. Biol.* 34:65–75, 2014.
- Kondo T, Johnson SA, Yoder MC, et al.: Sonic hedgehog and retinoic acid synergistically promote sensory fate specification from bone marrow-derived pluripotent stem cells, *Proc. Natl. Acad. Sci. U. S. A.* 102:4789–4794, 2005.
- Koren G: *Maternal-fetal toxicology: a clinician's guide*, ed 3rd New York, NY, 2001, Marcel Dekker.
- Kotch LE, Sulik KK: Experimental fetal alcohol syndrome: proposed pathogenic basis for a variety of associated facial and brain anomalies, *Am. J. Med. Genet.* 44:168–176, 1992.
- Lagiou P: Intrauterine exposures, pregnancy estrogens and breast cancer risk: where do we currently stand? *Breast Cancer Res.* 8:112, 2006.
- Larkins CE, Enriquez AB, Cohn MJ: Spatiotemporal dynamics of androgen signaling underlie sexual differentiation and congenital malformations of the urethra and vagina, *Proc. Natl. Acad. Sci. U. S. A.* 113:E7510–E7517, 2016.
- Lash TL, VanderWeele TJ, Haneause S, et al.: *Modern epidemiology*, ed 4th 2021, Wolters Kluwer Health.
- Lauder JM: Neurotransmitters as morphogens, *Prog. Brain Res.* 73:365–387, 1988.
- Lazic SE, Essioux L: Improving basic and translational science by accounting for litter-to-litter variation in animal models, *BMC Neurosci.* 14(37), 2013.
- Leroy M, Jocteur-Monrozier A: Fetal soft tissue examinations by microdissection. In Barrow P, editor: *Teratogenicity testing*, Totowa, NJ, 2013, Humana Press, pp 243–253.
- Levin M: Gap junctional communication in morphogenesis, *Prog. Biophys. Mol. Biol.* 94:186–206, 2007.
- Lewandowski M: *Mouse molecular embryology: methods and protocols*, New York, 2014, Humana Press (Springer).
- Li AA, Garman RH, Sheets LP, et al.: Regulatory testing for developmental neurotoxicology. In McQueen CA, editor: *Comprehensive toxicology*, Oxford, 2018, Elsevier Ltd., pp 183–215.
- Li AA, Sheets LP, Raffaele K, et al.: Recommendations for harmonization of data collection and analysis of developmental neurotoxicity endpoints in regulatory guideline studies: proceedings of workshops presented at Society of Toxicology and joint Teratology Society and Neurobehavioral Teratology Society meetings, *Neurotoxicol. Teratol.* 63:24–45, 2017.
- LoMauro A, Aliverti A: Respiratory physiology of pregnancy. Physiology masterclass, *Breathe* 11:297–301, 2015.
- Lowndes HE, Reuhl KR: *Nervous system and behavioral toxicology* (vol 11). New York, 1997, Elsevier.
- Lozano R, Naghavi M, Foreman K, et al.: Global and regional mortality from 235 causes of death for 20 age groups in 1990 and 2010: a systematic analysis for the Global Burden of Disease Study 2010, *Lancet* 380:2095–2128, 2012.
- Luz AL, Tokar EJ: Pluripotent stem cells in developmental toxicity testing: a review of methodological advances, *Toxicol. Sci.* 165:31–39, 2018.
- Lynch TA, Abel DE: Teratogens and congenital heart disease, *J. Diagn. Med. Sonogr.* 31:301–305, 2015.
- Ma L: Endocrine disruptors in female reproductive tract development and carcinogenesis, *Trends Endocrinol. Metabol.* 20:357–363, 2009.
- Madden JC, Enoch SJ, Paini A, et al.: A review of *in silico* tools as alternatives to animal testing: principles, resources and applications, *Altern. Lab. Anim.* 48:146–172, 2020.
- Maden M: Vitamin A and the developing embryo, *Postgrad. Med.* 77:489–491, 2001.
- Mai CT, Isenburg JL, Canfield MA, et al.: National population-based estimates for major birth defects, 2010–2014, *Birth Defects Res.* 111:1420–1435, 2019.



- Maltepe E, Bakardjiev AI, Fisher SJ: The placenta: transcriptional, epigenetic, and physiological integration during development, *J. Clin. Invest.* 120:1016–1025, 2010.
- Mathiasen JR, Moser VC: The Irwin test and functional observational battery (FOB) for assessing the effects of compounds on behavior, physiology, and safety pharmacology in rodents, *Curr. Protoc. Pharmacol.* 83:e43, 2018.
- Mathiesen L, Buerki-Thurnherr T, Pastuschek J, et al.: Fetal exposure to environmental chemicals; insights from placental perfusion studies, *Placenta* 106:58–66, 2021.
- Mattson SN, Bernes GA, Doyle LR: Fetal alcohol spectrum disorders: a review of the neurobehavioral deficits associated with prenatal alcohol exposure, *Alcohol Clin. Exp. Res.* 43:1046–1062, 2019.
- Mayes LC: A behavioral teratogenic model of the impact of prenatal cocaine exposure on arousal regulatory systems, *Neurotoxicol. Teratol.* 24:385–395, 2002.
- McGeady TA, Quinn PJ, FitzPatrick ES, et al.: *Veterinary embryology*, Oxford, 2006, Blackwell Publishing.
- McLain DE, Harper SM, Roe DA, et al.: Congenital malformations and variations in reproductive performance in the ferret: effects of maternal age, color and parity, *Lab. Anim. Sci.* 35:251–255, 1985.
- Meeker JD: Exposure to environmental endocrine disruptors and child development, *Arch. Pediatr. Adolesc. Med.* 166:E1–E7, 2012.
- Menegola E, Broccia ML, Giavini E: Atlas of rat fetal skeleton double stained for bone and cartilage, *Teratology* 64:125–133, 2001.
- Mihaly GW, Morgan DJ: Placental drug transfer: effects of gestational age and species, *Pharmacol. Ther.* 23:253–266, 1983.
- Milerad J, Larson O, Hagberg C, et al.: Associated malformations in infants with cleft lip and palate: a prospective, population-based study, *Pediatrics* 100:180–186, 1997.
- Moore KL, Persaud TVN, Torchia MG: *The developing human: clinically oriented embryology*, ed 11th, Edinburgh, 2020, Elsevier.
- Moser VC: The functional observational battery in adult and developing rats, *Neurotoxicology* 21:989–996, 2000.
- Myden A, Hill E, Fowkes A: Using adverse outcome pathways to contextualise (Q)SAR predictions for reproductive toxicity - a case study with aromatase inhibition, *Reprod. Toxicol.* 108:43–55, 2022.
- Nadeau K, McDonald-Hyman C, Noth EM, et al.: Ambient air pollution impairs regulatory T-cell function in asthma, *J. Allergy Clin. Immunol.* 126:845–852 e810, 2010.
- Nakamura H, Doi T, Puri P, et al.: Transgenic animal models of congenital diaphragmatic hernia: a comprehensive overview of candidate genes and signaling pathways, *Pediatr. Surg. Int.* 36:991–997, 2020.
- Narotsky MG, Brownie CF, Kavlock RJ: Critical period of carbon tetrachloride-induced pregnancy loss in Fischer-344 rats, with insights into the detection of resorption sites by ammonium sulfide staining, *Teratology* 56:252–261, 1997.
- Nau H: Species differences in pharmacokinetics and drug teratogenesis, *Environ. Health Perspect.* 70:113–129, 1986.
- Nelson BK, Snyder DL, Shaw PB: Developmental toxicity interactions of salicylic acid and radiofrequency radiation or 2-methoxyethanol in rats, *Reprod. Toxicol.* 13:137–145, 1999.
- Neubert D, Blankenburg G, Lewandowski C, et al.: Misinterpretation of results and creation of “artifacts” in studies on developmental toxicity using systems simpler than *in vivo* systems. In Lash JW, Saxen L, editors: *Developmental mechanisms: normal and abnormal*, New York, 1985, Alan R. Liss, pp 241–266.
- Newbigging S, Ward JM, Bolon B: Necropsy sampling and data collection for studying the anatomy, histology, and pathology of mouse development. In Bolon B, editor: *Pathology of the developing mouse: a systematic approach*, Boca Raton, FL, 2015, CRC Press (Taylor & Francis), pp 133–173.
- Noden DM, de LaHunta A: *The embryology of domestic animals: developmental mechanisms and malformations*, Baltimore, 1985, Williams & Wilkins.
- O’Leary-Moore SK, Parnell SE, Godin EA, et al.: Magnetic resonance microscopy-based analyses of the brains of normal and ethanol-exposed fetal mice, *Birth Defects Res. A Clin. Mol. Teratol.* 88:953–964, 2010.
- O’Rahilly R, Müller F: *The embryonic human brain: an atlas of developmental stages*, New York, 1994, Wiley-Liss.
- O’Rahilly RR, Müller F: *The embryonic human brain: an atlas of developmental stages*, ed 3rd, Wilmington, DE, 2006, Wiley-Liss.
- Ochiai W, Kitaoka S, Kawamura T, et al.: Maternal and fetal pharmacokinetic analysis of cannabidiol during pregnancy in mice, *Drug Metabol. Dispos.* 49:337–343, 2021.
- OECD: Test No. 426: developmental neurotoxicity study, 2007. [http://www.oecd-ilibrary.org/environment/test-no-426-developmental-neurotoxicity-study\\_9789264067394-en](http://www.oecd-ilibrary.org/environment/test-no-426-developmental-neurotoxicity-study_9789264067394-en). (Accessed 24 May 2024).
- OECD: Test No. 421: reproduction/developmental toxicity screening test, 2016a. [https://www.oecd-ilibrary.org/environment/test-no-421-reproduction-developmental-toxicity-screening-test\\_9789264264380-en](https://www.oecd-ilibrary.org/environment/test-no-421-reproduction-developmental-toxicity-screening-test_9789264264380-en). (Accessed 24 May 2024).
- OECD: Test No. 422: combined repeated dose toxicity study with the reproduction/developmental toxicity screening test, 2016b. [https://www.oecd-ilibrary.org/environment/test-no-422-combined-repeated-dose-toxicity-study-with-the-reproduction-developmental-toxicity-screening-test\\_9789264264403-en](https://www.oecd-ilibrary.org/environment/test-no-422-combined-repeated-dose-toxicity-study-with-the-reproduction-developmental-toxicity-screening-test_9789264264403-en). (Accessed 24 May 2024).
- OECD: Revised guidance document 150 on standardised test guidelines for evaluating chemicals for endocrine disruption, 2018a. <https://www.oecd.org/chemicalsafety/guidance-document-on-standardised-test-guidelines-for-evaluating-chemicals-for-endocrine-disruption-2nd-edition-9789264304741-en.htm>. (Accessed 24 May 2024).
- OECD: Test No. 414: prenatal developmental toxicity study, 2018b. [https://www.oecd-ilibrary.org/environment/test-no-414-prenatal-development-toxicity-study\\_9789264070820-en](https://www.oecd-ilibrary.org/environment/test-no-414-prenatal-development-toxicity-study_9789264070820-en). (Accessed 24 May 2024).

- OECD: *Test No. 443: extended one-generation reproductive toxicity study*, 2018c. [http://www.oecd-ilibrary.org/environment/test-no-443-extended-one-generation-reproductive-toxicity-study\\_9789264185371-en](http://www.oecd-ilibrary.org/environment/test-no-443-extended-one-generation-reproductive-toxicity-study_9789264185371-en). (Accessed 24 May 2024).
- Oldereid NB, Wennerholm U-B, Pinborg A, et al.: The effect of paternal factors on perinatal and paediatric outcomes: a systematic review and meta-analysis, *Hum. Reprod. Update* 24:320–389, 2018.
- Olliges A, Wimmer S, Nusing RM: Defects in mouse nephrogenesis induced by selective and non-selective cyclooxygenase-2 inhibitors, *Br. J. Pharmacol.* 163:927–936, 2011.
- Ornoy A: Embryonic oxidative stress as a mechanism of teratogenesis with special emphasis on diabetic embryopathy, *Reprod. Toxicol.* 24:31–41, 2007.
- Padmanabhan R, Singh G, Singh S: Malformations of the eye resulting from maternal hypervitaminosis A during gestation in the rat, *Acta Anat.* 110:291–298, 1981.
- Palermo CM, Foreman JE, Wikoff DS, et al.: Development of a putative adverse outcome pathway network for male rat reproductive tract abnormalities with specific considerations for the androgen sensitive window of development, *Curr. Res. Toxicol.* 2:254–271, 2021.
- Palludan B: The teratogenic effects of vitamin A deficiency in swine, *Acta Vet. Scand.* 2:32–59, 1961.
- Palmer AK: Sporadic malformations in laboratory animals and their influence on drug testing. In Klingberg MA, Abramovici A, Chemke J, editors: *Drugs and fetal development*, New York, 1972, Plenum Press, pp 45–60.
- Parker GA, Picut CA: *Atlas of histology of the juvenile rat*, San Diego, 2016, Academic Press (Elsevier).
- Patrick L: Thyroid disruption: mechanism and clinical implications in human health, *Altern. Med. Rev.* 14:326–346, 2009.
- Paxinos G, Ashwell KWS, Törk I: *Atlas of the developing rat nervous system*, ed 2nd San Diego, 1994, Academic Press.
- Paxinos G, Halliday G, Watson C, et al.: *Atlas of the developing mouse brain at E17.5, P0, and P6*, San Diego, 2007, Academic Press (Elsevier).
- Paxinos G, Watson C, Carrive P, et al.: *Chemoarchitectonic atlas of the rat brain*, ed 2nd, San Diego, 2008, Academic Press (Elsevier).
- Penaloza C, Lin L, Lockshin RA, et al.: Cell death in development: shaping the embryo, *Histochem. Cell Biol.* 126:149–158, 2006.
- Perkins EJ, Ashauer R, Burgoon L, et al.: Building and applying quantitative adverse outcome pathway models for chemical hazard and risk assessment, *Environ. Toxicol. Chem.* 38:1850–1865, 2019.
- Petiet AE, Kaufman MH, Goddeeris MM, et al.: High-resolution magnetic resonance histology of the embryonic and neonatal mouse: a 4D atlas and morphologic database, *Proc. Natl. Acad. Sci. U.S.A.* 105:12331–12336, 2008.
- Picut CA, Swanson CL, Parker RF, et al.: The metrial gland in the rat and its similarities to granular cell tumors, *Toxicol. Pathol.* 37:474–480, 2009.
- Raciborski F, Tomaszewska A, Komorowski J, et al.: The relationship between antibiotic therapy in early childhood and the symptoms of allergy in children aged 6–8 years—the questionnaire study results, *Int. J. Occup. Med. Environ. Health* 25:470–480, 2012.
- Rao DB, Hoberman AM, Brown PC, et al.: Regulatory perspectives on juvenile animal toxicologic pathology, *Toxicol. Pathol.* 49:1393–1404, 2021.
- Rao M, Gershon MD: Enteric nervous system development: what could possibly go wrong? *Nat. Rev. Neurosci.* 19:552–565, 2018.
- Rice JM: Effects of prenatal exposure to chemical carcinogens and methods for their detection. In Kimmel CA, Buelke-Sam J, editors: *Developmental toxicology*, New York, 1981, Raven, pp 191–212.
- Rice JM, Rehm S, Donovan PJ, et al.: Comparative transplacental carcinogenesis by directly acting and metabolism-dependent alkylating agents in rodents and nonhuman primates, *IARC Sci. Publ.*, 1989:17–34, 1989.
- Roberts DW, Chapman JR: Concepts essential to the assessment of toxicity to the developing immune system. In Kimmel CA, Buelke-Sam J, editors: *Developmental toxicology*, New York, 1981, Raven, pp 167–189.
- Rocca MS, Wehner NG: The guinea pig as an animal model for developmental and reproductive toxicology studies, *Birth Defects Res. B Dev. Reprod. Toxicol.* 86:92–97, 2009.
- Rodier PM: Chronology of neuron development: animal studies and their clinical implications, *Dev. Med. Child Neurol.* 22:525–545, 1980.
- Rogers DC, Fisher EM, Brown SD, et al.: Behavioral and functional analysis of mouse phenotype: SHIRPA, a proposed protocol for comprehensive phenotype assessment, *Mamm. Genome* 8:711–713, 1997.
- Rogers JM, Chernoff N, Keen CL, et al.: Evaluation and interpretation of maternal toxicity in Segment II studies: issues, some answers, and data needs, *Toxicol. Appl. Pharmacol.* 207:367–374, 2005.
- Ross EJ, Graham DL, Money KM, et al.: Developmental consequences of fetal exposure to drugs: what we know and what we still must learn, *Neuropsychopharmacology* 40: 61–87, 2015.
- Rossant J, Cross JC: Placental development: lessons from mouse mutants, *Nat. Rev. Genet.* 2:538–548, 2001.
- Rossant J, Tam PPL: *Mouse development: patterning, morphogenesis, organogenesis*, San Diego, 2002, Academic Press.
- Ruffins S, Jacobs R: *Caltech  $\mu$ MRI atlas of mouse development*, 2009. <https://sectional-anatomy.org/mouse-embryo/>. (Accessed 24 May 2024).
- Rugh R: *The mouse. Its reproduction and development*, Oxford, 1990, Oxford University Press.
- Saber ASM: *Atlas of veterinary teratology: developmental abnormalities* Saarbrücken, Germany, 2013, Lambert Academic Publishers (OmniScriptum GmbH).
- Sadler TW: *Langman's medical embryology*, ed 11th, Philadelphia, 2009, Lippincott Williams & Wilkins.
- Sakamoto M, Tatsuta N, Izumo K, et al.: Health impacts and biomarkers of prenatal exposure to methylmercury: lessons from Minamata, Japan, *Toxics* 6(45), 2018.

- Sand S, Victorin K, Filipsson AF: The current state of knowledge on the use of the benchmark dose concept in risk assessment, *J. Appl. Toxicol.* 28:405–421, 2008.
- Santagostino SF, Assenmacher CA, Tarrant JC, et al.: Mechanisms of regulated cell death: current perspectives, *Vet. Pathol.* 58:596–623, 2021.
- Savolainen SM, Foley JF, Elmore SA: Histology atlas of the developing mouse heart with emphasis on E11.5 to E18.5, *Toxicol. Pathol.* 37:395–414, 2009.
- Schambra U: *Prenatal mouse brain atlas*, New York, 2008, Springer.
- Schambra UB, Lauder JM, Silver J: *Atlas of the prenatal mouse brain*, San Diego, 1992, Academic Press.
- Schardein JL: *Chemically induced birth defects*, ed 3rd, New York, 2000, Marcel Dekker.
- Schardein JL, Keller KA: Potential human developmental toxicants and the role of animal testing in their identification and characterization, *Crit. Rev. Toxicol.* 19:251–339, 1989.
- Schneider S, Hofmann T, Stinchcombe S, et al.: Species differences in developmental toxicity of epoxiconazole and its relevance to humans, *Birth Defects Res. B Dev. Reprod. Toxicol.* 98:230–246, 2013.
- Schoenwolf GC: *Atlas of descriptive embryology*, ed 7th San Francisco, 2008, Pearson Benjamin Cummings.
- Scialli AR: *A clinical guide to reproductive and developmental toxicology*, Boca Raton, FL, 1992, CRC Press.
- Scott Jr WJ: Cell death and reduced proliferative rate. In Wilson JG, Fraser FC, editors: *Handbook of teratology*, New York, 1977, Plenum, pp 81–98.
- Shahnawaz S, Nawaz US, Zaugg J, et al.: Dysregulated autophagy leads to oxidative stress and aberrant expression of ABC transporters in women with early miscarriage, *Anti-oxidants* 10, 2021.
- Sharpe P, Mason I: *Molecular embryology: methods and protocols*, ed 2nd, New York, 2008, Humana Press (Springer).
- Shaw EB: Fetal damage due to maternal aminopterin ingestion. Follow-up at age 9 years, *Am. J. Dis. Child.* 124:93–94, 1972.
- Sheffield JS, Siegel D, Mirochnick M, et al.: Designing drug trials: considerations for pregnant women, *Clin. Infect. Dis.* 59(Suppl 7):S437–S444, 2014.
- Sheng G, Martinez Arias A, Sutherland A: The primitive streak and cellular principles of building an amniote body through gastrulation, *Science* 374:abg1727, 2021.
- Shepard TH, Lemire RJ: *Catalog of teratogenic agents*, ed 13th, Baltimore, MD, 2010, Johns Hopkins University Press.
- Shuey DL, Sadler TW, Lauder JM: Serotonin as a regulator of craniofacial morphogenesis: site specific malformations following exposure to serotonin uptake inhibitors, *Teratology* 46:367–378, 1992.
- Slikker WJ, Chang LW: *Handbook of developmental neurotoxicology*, San Diego, 1998, Academic Press.
- Snow MH, Tam PPL: Is compensatory growth a complicating factor in mouse teratology? *Nature* 279:555–557, 1979.
- Spyker JM: Behavioral teratology and toxicology. In Weiss B, V GL, editors: *Behavioral toxicology*, New York, 1975, Plenum Press, pp 311–344.
- Stanton HC: Factors to consider when selecting animal models for postnatal teratology studies, *J. Environ. Pathol. Toxicol.* 2: 201–210, 1978.
- Stanton ME, Spear LP: Workshop on the qualitative and quantitative comparability of human and animal developmental neurotoxicity, work Group I report: comparability of measures of developmental neurotoxicity in humans and laboratory animals, *Neurotoxicol. Teratol.* 12:261–267, 1990.
- Stark MR, Ross MM: The chicken embryo as a model in developmental toxicology, *Methods Mol. Biol.* 1965:155–171, 2019.
- Steding G: *The anatomy of the human embryo: a scanning electron-microscopic atlas*, Basel, 2009, Karger.
- Sulik KK, Bream PRJ: *Embryo images: normal and abnormal mammalian development*, 2013. [http://www.med.unc.edu/embryo\\_images/](http://www.med.unc.edu/embryo_images/). (Accessed 24 May 2024).
- Swartley OM, Foley JF, Livingston 3rd DP, et al.: Histology atlas of the developing mouse hepatobiliary hemolymphatic vascular system with emphasis on embryonic days 11.5–18.5 and early postnatal development, *Toxicol. Pathol.* 44:705–725, 2016.
- Szabo KT: *Congenital malformations in laboratory and farm animals*, San Diego, 1989, Academic Press.
- Tai PT, Nishijo M, Anh NT, et al.: Dioxin exposure in breast milk and infant neurodevelopment in Vietnam, *Occup. Environ. Med.* 70:656–662, 2013.
- Tan HX, Yang SL, Li MQ, et al.: Autophagy suppression of trophoblast cells induces pregnancy loss by activating decidual NK cytotoxicity and inhibiting trophoblast invasion, *Cell Commun. Signal.* 18(73), 2020.
- Theiler K: *The house mouse: atlas of embryonic development*, New York, 1989, Springer-Verlag.
- Therapontos C, Erskine L, Gardner ER, et al.: Thalidomide induces limb defects by preventing angiogenic outgrowth during early limb formation, *Proc. Natl. Acad. Sci. U. S. A.* 106:8573–8578, 2009.
- Theunissen PT, Beken S, Beyer B, et al.: Comparing rat and rabbit embryo-fetal developmental toxicity data for 379 pharmaceuticals: on systemic dose and developmental effects, *Crit. Rev. Toxicol.* 47:402–414, 2017.
- Theunissen PT, Beken S, Beyer BK, et al.: Comparison of rat and rabbit embryo-fetal developmental toxicity data for 379 pharmaceuticals: on the nature and severity of developmental effects, *Crit. Rev. Toxicol.* 46:900–910, 2016.
- Thiel R, Chahoud I, Jürgens M, et al.: Time-dependent differences in the development of somites of four different mouse strains, *Teratog. Carcinog. Mutagen.* 13:247–257, 1993.
- Thomason ME, Hect JL, Rauh VA, et al.: Prenatal lead exposure impacts cross-hemispheric and long-range connectivity in the human fetal brain, *Neuroimage* 191:186–192, 2019.
- Titus-Ernstoff L, Troisi R, Hatch EE, et al.: Birth defects in the sons and daughters of women who were exposed *in utero* to diethylstilbestrol (DES), *Int. J. Androl.* 33:377–384, 2010.



- Torchinsky A, Fein A, Toder V: Teratogen-induced apoptotic cell death: does the apoptotic machinery act as a protector of embryos exposed to teratogens? *Birth Defects Res. C Embryo Today* 75:353–361, 2005.
- Travis KZ, Pate I, Welsh ZK: The role of the benchmark dose in a regulatory context, *Regul. Toxicol. Pharmacol.* 43:280–291, 2005.
- Trueman D, Stewart J: An automated technique for double staining mouse fetal and neonatal skeletal specimens to differentiate bone and cartilage, *Biotech. Histochem.* 89:315–319, 2014.
- Ueker ME, Silva VM, Moi GP, et al.: Parenteral exposure to pesticides and occurrence of congenital malformations: hospital-based case-control study, *BMC Pediatr.* 16:125, 2016.
- Ujházy E, Mach M, Navarová J, et al.: Teratology – past, present and future, *Interdiscipl. Toxicol.* 5:163–168, 2012.
- Valerio Jr LG: *In silico* toxicology for the pharmaceutical sciences, *Toxicol. Appl. Pharmacol.* 241:356–370, 2009.
- van de Bor M: Fetal toxicology, *Handb. Clin. Neurol.* 162:31–55, 2019.
- van Gelder MM, van Rooij IA, Miller RK, et al.: Teratogenic mechanisms of medical drugs, *Hum. Reprod. Update* 16:378–394, 2010.
- Vargesson N: Thalidomide-induced teratogenesis: history and mechanisms, *Birth Defects Res. C Embryo Today* 105:140–156, 2015.
- von Hellfeld R, Brotzmann K, Baumann L, et al.: Adverse effects in the fish embryo acute toxicity (FET) test: a catalogue of unspecific morphological changes versus more specific effects in zebrafish (*Danio rerio*) embryos, *Environ. Sci. Eur.* 32:122, 2020.
- Wang X, Matsumoto H, Zhao X, et al.: Embryonic signals direct the formation of tight junctional permeability barrier in the decidualizing stroma during embryo implantation, *J. Cell Sci.* 117:53–62, 2004.
- Webster WS, Abela D: The effect of hypoxia in development, *Birth Defects Res. C Embryo Today* 81:215–228, 2007.
- Werler MM, Yazdy MM, Kasser JR, et al.: Medication use in pregnancy in relation to the risk of isolated clubfoot in offspring, *Am. J. Epidemiol.* 180:86–93, 2014.
- Werler MM, Yazdy MM, Kasser JR, et al.: Maternal cigarette, alcohol, and coffee consumption in relation to risk of clubfoot, *Paediatr. Perinat. Epidemiol.* 29:3–10, 2015.
- Wigglesworth JS, Singer DB: *Textbook of fetal and perinatal pathology*, ed 2nd 1998, Wiley-Blackwell.
- Wilson IG: Methods of administering agents and detecting malformations in experimental animals. In Wilson IG, Wilson JG, editors: *Teratology: principles and techniques*, Chicago, 1972, University of Chicago Press, pp 262–277.
- Wilson JG: *Environment and birth defects*, New York, 1973, Academic Press.
- Wilson JG, Fraser FC, editors: *Handbook of teratology*. General Principles and Etiology, vol. 1. New York, 1977a, Plenum Publishing.
- Wilson JG, Fraser FC, editors: *Handbook of teratology*. Mechanisms and Pathogenesis, vol. 2. New York, 1977b, Plenum Publishing.
- Wolpert L, Tickle C, Arias AM: Oxford. In *Principles of development*, ed 6th, 2019, Oxford University Press.
- Wooding P, Burton G: *Comparative placentation. Structures, functions and evolution*, Berlin, 2008, Springer-Verlag.
- Yasuda M, Yuki T: *Color atlas of fetal skeleton of the mouse, rat, and rabbit*, Osaka, Japan, 1997, Ace Art Company.
- Zamora-León P: Are the effects of DES over? A tragic lesson from the past, *Int. J. Environ. Res. Publ. Health* 18, 2021.
- Zhang H, Mao J, Qi H-Z, et al.: In silico prediction of drug-induced developmental toxicity by using machine learning approaches, *Mol. Divers.* 24:1281–1290, 2020.
- Zhang J, Chen Z, Smith GN, et al.: Natural killer cell-triggered vascular transformation: maternal care before birth? *Cell. Mol. Immunol.* 8:1–11, 2011.
- Zhong F, Xing J, Li X, et al.: Artificial intelligence in drug design, *Sci. China Life Sci.* 61:1191–1204, 2018.
- Zhong M, Shoemaker C, Fuller A, et al.: Development of a functional observational battery in the minipig for regulatory neurotoxicity assessments, *Int. J. Toxicol.* 36:113–123, 2017.
- Ziejewski MK, Solomon HM, Rendemonti J, et al.: Comparison of a modified mid-coronal sectioning technique and Wilson's technique when conducting eye and brain examinations in rabbit teratology studies, *Birth Defects Res. B Dev. Reprod. Toxicol.* 104:23–34, 2015.
- Zohn IE, Sarkar AA: The visceral yolk sac endoderm provides for absorption of nutrients to the embryo during neurulation, *Birth Defects Res. A Clin. Mol. Teratol.* 88:593–600, 2010.

This page intentionally left blank

# Index

Authors and editors participated in index generation.

'Note: Page numbers followed by "f" indicate figures and "t" indicate tables.'

## A

- Absorption, 217, 878  
distribution, metabolism, and excretion (ADME), 114–115  
percutaneous, 520–521  
Acanthosis, 553  
Accessory sex organs. *See also* Male reproductive system  
anatomy and function, 652–655, 655t  
ampullary gland, 652, 655t  
bulbourethral glands, 655, 655t  
coagulating gland, 653–654, 655t  
preputial gland, 655, 655t  
prostate, 653–654, 655t  
seminal vesicles, 654–655, 655t, 699f  
microscopic findings  
coagulating gland, 684, 688  
prostate, 660, 661t, 675, 684, 688–689, 699f, 701, 707t, 715, 716f, 717f  
seminal vesicles, 660, 661t, 675, 684–685, 688–689, 707t, 715, 716f  
organ weights, 660, 661t, 675, 701  
Acetylcholine, 294–295  
Acid-base balance, 106–107  
Acinus, pulmonary. 258. *See also* Alveolus, Respiratory system  
Acrania, 842f, 843  
Activins, 593, 657  
Acute phase proteins, 440–441  
Acute respiratory distress syndrome (ARDS), 306–308, 308f  
Adactyly, 856, 858f  
Adaptive immune system, 438–441, 443–444, 467t, 491  
Adenocarcinoma, 228–229, 614, 688–689, 798  
Adenoma, 613, 688–689, 798. *See also* individual organ systems  
fibroadenoma. 613–614. *See also* Mammary gland  
mammary gland. *See* Mammary gland  
sebaceous cell, 557  
tubulostromal, ovary, 793–794  
Adenomyoepithelioma, 614. *See also* Mammary gland  
Adenomyosis, 758  
Adjuvants, 474–475  
Adnexa. *See* Integument  
Adrenal gland, 772–773  
insufficiency, 494  
Adrenocorticotrophic hormone (ACTH), 512, 573  
Adverse event reporting systems (AERS), 892  
Adverse outcome pathway (AOP), 837  
Adversity, 419–420, 476  
practices and regulatory considerations, 497–499  
African clawed frog (*Xenopus laevis*), 832  
Agency for Toxic Substances and Disease Registry (ATSDR), 601  
Agenesis (developmental), 847, 850, 852–854, 884t  
Aggregate reticulocyte. *See* Reticulocyte  
Aging, 199, 572  
age-related changes in rats, 611  
age-related immune responses, 464  
age-related kidney findings, 116  
Agnathia, 847, 883t  
Ah receptor (AhR), 575  
Air-liquid interface (ALI), 280–281  
Airways. *See also* Respiratory system  
fixation, optimal, 270–271  
hyperresponsiveness, 296  
mucous cells, 252–253  
Albumin, 117, 120  
Albuminuria, 120  
Allergies, 438  
Alopecia, 574  
Alpha-2 $\mu$ -globulin nephropathy, 183–185, 184f–185f, 185t  
Alpha-melanocyte-stimulating hormone ( $\alpha$ -MSH), 512, 573  
Alveolus, Respiratory system, 258–259  
alveolar macrophages (AMs), 236  
diffuse alveolar damage (DAD), 306  
ducts, 258  
epithelium, 259–260, 259f  
type I cells, 260  
type II cells, 260  
phospholipidosis, 302  
sacs, 258  
Amelia, 859  
Amino acids, 106  
toxicity, 186  
transport, 105–106  
Amniotic band syndrome, 858, 860, 874.  
*See also* Deformations  
Amphotericin B, 153, 188  
Ampullary gland. *See* Accessory sex organs  
Amyloidosis, 73–74, 151  
Amyoplasia, 860  
Anaphylaxis, 466  
Androgen-binding protein (ABP), 657  
Androgen receptors (ARs), 594, 637  
agonists, 713, 780t. *See also* Androgens  
antagonists, 713–715  
effects via, 719  
Androgens, 522, 593, 632–633, 651–652, 658, 686, 742, 765, 776  
Anemia  
causes  
blood loss, 379  
chronic disease, 382  
hemolysin toxins, 411–412  
immune-mediated, 386–387, 413, 417–418  
iron deficiency, 408–409  
types  
aplastic anemia, 385, 393  
autoimmune hemolytic anemia (AIHA), 413  
Heinz body, 409, 410t  
hemolytic, 373, 378, 411–413  
immune-mediated hemolytic anemia (IMHA), 386–387  
megaloblastic, 385  
non-regenerative, 373, 411  
pancytopenia (aplastic), 372, 385  
pure red cell aplasia, 382–383, 417–418  
regenerative, 373  
sideroblastic, 386, 411  
Anencephaly, 842, 842f, 878, 883t. *See also* Acrania  
Anergy, 443  
Anestrus. *See* Estrous cycle  
Angiogenesis, 775, 873  
Angiopoietin (Ang), 344–345  
Angiotensin converting enzyme (ACE)  
ACE 2, 277–278  
inhibitors, 30–31, 91  
Angiotensin II (Ang II), 64–65, 91, 132–133  
Animal Models of Diabetic Complication Consortium (AMDCC), 201–202  
Anogenital distance (AGD). *See* Male reproductive system  
Anoikis, 148  
Anophthalmia, 846, 883t  
Anoxia, patterns of change associated with, 711, 712f  
Antiandrogens, 609, 615, 719  
Antibiotics, 172–174, 182



- Antibodies, 441, 443  
 therapeutic candidates, lung injury  
 induced by, 286–287
- Antibody-dependent cellular cytotoxicity  
 (ADCC), 443
- Antibody-dependent enhancement (ADE),  
 274–275
- Antibody-drug conjugates (ADCs), 137, 178,  
 286–287
- Antidiuretic hormone (ADH), 100–101
- Antidrug antibodies (ADAs), 129, 168–169,  
 287, 401–402, 467–468  
 in animals and human patients, 168–169
- Antigen, 298, 441  
 antigen-specific  
 derangement process, 495  
 effects, 468–469  
 toxicity, 472, 473t  
 presentation, 441, 442f  
 recognition, 441, 442f
- Antigen-presenting cells (APCs), 359,  
 440–441, 511
- Anti-Müllerian hormone (AMH), 630
- Antioxidant systems, 874
- Antisense oligonucleotides (ASOs), 78, 120,  
 169–171, 170f, 572
- Antral follicle, 741–743
- Aorta-gonad-mesonephros (AGM), 345,  
 446–447
- Aplasia, 90, 842f, 850  
 caudal enteric ganglia, 850–852  
 red blood cells, 393
- Apocrine glands, 516–517
- Apoptosis, 147, 220, 403–404, 443, 447, 550,  
 552, 574–575, 583, 585, 588, 677,  
 681–682, 749, 824, 869–870, 870f.  
*See also* Programmed cell death  
 (PCD)
- Arginine-vasopressin, 701
- Aromatase, 659, 784
- Arrhythmias, 26–27, 51, 56
- Arthrogryposis, 840, 844, 860–862, 861f, 875,  
 885t
- Artificial intelligence (AI), 21–22, 146, 838
- Aryl hydrocarbon hydroxylase (AHH), 522,  
 878
- Aryl hydrocarbon receptor (AhR), 312, 399,  
 593–594, 784
- Aspartate transaminase (AST), 491–493
- Aspiration exposures, 263–264
- Asthma, 296–298  
 allergic, 299f, 300f  
 atopic, 297–298  
 occupational, 298
- Atherosclerosis, acceleration by toxic  
 agents, 73–74
- Atopic dermatitis, 541
- ATP binding cassette (ABC), 56–57,  
 103–104, 881
- Atresia, 742–743, 849, 860, 875, 884t
- Atrial natriuretic peptides (ANPs), 6
- Atrial septal defects (ASD), 25, 848–849,  
 884t
- Atrial thrombosis, 22, 48–49
- Atrioventricular (AV) valves, 3, 848–850.  
*See also* Valvulopathy
- Atrophy, 479–482, 579, 611, 684, 772–773
- adnexa, 552
- epidermis, 550
- testis, 677–678
- Atypical hyperplasia  
 kidney, 193  
 mammary gland, 688
- Autoantibodies, 129
- Autocrine regulation of testicular function,  
 659
- Autoimmune disease, 438  
 auto-reactive lymphocytes, 443  
 hemolysis, 386, 412. *See also* Hemolysis  
 renal disorders, biologic-induced, 168  
 thrombocytopenia, 413–414
- Automated image analysis, 146, 370
- Autophagy, 869
- Autoradiography, 221, 281
- ## B
- BALT. *See* Bronchus-associated lymphoid  
 tissue (BALT)
- Basal cell(s)  
 locations  
 adnexal changes, 552  
 nasal cavity, 242f, 244–245  
 respiratory epithelium, 249, 253t,  
 255–256  
 skin, 550  
 proliferation  
 adenoma, 560  
 carcinoma  
 female reproductive system, 801  
 skin, 689  
 hyperplasia (prostate), 689
- Basic fibroblast growth factor (bFGF), 68,  
 92–93
- BCRP. *See* Breast cancer resistance protein  
 (BCRP)
- Blood pressure, measurements, 17–18
- Bisphenol A (BPA), 597f, 599
- Bleomycin, 33, 273, 291t, 307, 309, 321, 400
- Blood urea nitrogen (BUN), 113, 493–494.  
*See also* Kidney, Urea nitrogen
- Blood vessels, 2, 59–60, 218, 247. *See also*  
 Vascular system
- anatomy and physiology, 60–72, 60f,  
 61f  
 age-related lesions, 70–71  
 arteriovenous anastomoses, 635  
 background findings, 70–71  
 circulation and tissue perfusion, 8–9, 63  
 endothelial cells, 61–63, 65–66  
 extracellular components, 61–62  
 innervation, 64  
 metabolism, 63–64  
 pericytes and veil cells, 62  
 smooth muscle cells (SMCs), 62  
 vasoactive substances, responses to,  
 64–65  
 evaluation of toxicity, 66–72  
 biomarkers of injury, 72  
 functional assessment, 63–67  
 in vitro methods, 67–69  
 morphologic evaluation, 60–61, 60f, 61f,  
 69  
 responses to injury, 73–79  
 aneurysms, 76
- atherosclerosis, acceleration by toxic  
 agents, 73–74
- calcification, 75–76, 75f
- immune complex formation, 78,  
 150–152, 468f. *See also* Immune  
 complex disease
- inflammation, 70–71, 77–78  
 Beagle pain syndrome (idiopathic  
 necrotizing polyarteritis), 70  
 immune-mediated, 77–78  
 polyarteritis nodosa, 71
- mediolysis, 77
- microangiopathy, 77. *See also* Thrombotic  
 microangiopathy (TMA)
- necrosis  
 fibrinoid, 77  
 hemorrhagic, 76–77
- proliferation  
 intimal, 74–75  
 medial, 74  
 regeneration and repair, 78–79
- toxicity, 70, 77  
 organ-specific vascular toxicity, 79–81
- Bone marrow, 360, 362, 439t, 449, 464,  
 484–486
- anatomy and physiology, 346–347, 349,  
 379–380  
 iron overload, 383f  
 microenvironment, 418  
 stromal cells, 371
- cellularity changes, 379–386, 380f, 381f,  
 388f, 486
- clonal hemopathies, 385–386
- decreased hematopoietic cellularity, 381f
- myelodysplastic syndromes (MDS), 373,  
 385, 387–389
- myelofibrosis, 386
- necrosis, 382–383, 384f
- nonproliferative bone marrow lesions,  
 380–386
- stromal cell hyperplasia, 384f
- evaluation of, 362–366  
 cytology, 364–366  
 histopathology, 362–364  
 myeloid to erythroid (M:E) ratio,  
 484–485  
 quantitative bone marrow assessment,  
 365–366  
 toxicity, 393, 399–400
- Bone morphogenetic protein (BMP),  
 344–345
- Bouin's fixative/solution, 673, 835
- Brachydactyly, 856–858, 858f
- Bradycardia, 14–15
- Breast cancer resistance protein (BCRP),  
 56–57, 103–104, 881
- Brain natriuretic peptide (BNP), 25
- Bromodeoxyuridine (BrdU), 192–193, 221,  
 281, 857, 871
- Bronchi, 248–257, 260–261  
 centriacinar regions (in laboratory rat and  
 rhesus monkey), 252f  
 inflammation (bronchitis), 274–275
- Bronchioles, 248–257, 250f  
 centriacinar region (in laboratory rat and  
 rhesus monkey), 252f  
 inflammation (bronchiolitis), 274–275

Bronchoalveolar lavage (BAL), 261, 265  
 Bronchus-associated lymphoid tissues (BALT), 246, 257, 456–457  
 Brush cells (conducting airways), 256–257  
 Bulbourethral glands. *See* Accessory sex organs  
 Bullous pemphigoid, 513, 519

## C

Cadmium, 175, 312, 784–785  
 CAKUT (congenital anomalies of kidney and urinary tract), 90  
 Calcinosis circumscripta (integument), 551, 552f.  
 Calcitonin gene-related peptides (CGRPs), 93–94, 247  
 Calcium, 101, 218, 871–872  
 Calcium channel blockers, 416  
 Cap cells (mammary gland), 580–581  
 Carbon nanotubes, 326–327  
 Carcinogenicity, 218, 223–226, 579, 595–597, 599, 603–605, 615–616, 791–803  
 Cardiomyopathy, 29  
   drug-induced  
     alcoholic, 29  
     anticancer chemotherapy, 29–34  
     antimicrobial agents, 29  
   variants  
     congestive, 37  
     dilated, 29  
     hypertrophic, 23–24  
     rodent progressive cardiomyopathy, 21–22, 58  
 Cardiotoxicity  
   atherosclerosis, acceleration by toxic agents, 73–74  
   drug interactions, 55–57, 327  
   issues in drug development, 57–59  
 CARPA (compliment activation-related pseudoallergy), 472  
 CAR-T cell (chimeric antigen receptor T-cell) therapy, 34, 171–172  
 Cell adhesion molecules (CAMs), 344–345, 444, 456, 594–595, 821  
 Cervix, 739t, 745, 747, 753, 759, 764, 773t, 780t, 781t, 784t, 788t, 790–791, 802  
   regional specification in primates (endocervix and exocervix), 753  
 Chemokines, 110, 187, 440–441  
 Chernoff-Kavlock test, 835  
 Chloracne, 561t, 575, 575f  
 Chloramphenicol, 386, 400  
 Choriocarcinoma, 687–688, 792, 797  
 Chronic obstructive pulmonary disease (COPD), 272, 297  
 Chronic progressive nephropathy (CPN), 116, 130f, 132–133, 197–198, 214  
 Cisplatin, 33, 153–154, 176–177, 200  
 Clear cell renal cell carcinoma (ccRCC), 139  
 Cleft palate. *See* Palatoschisis  
 Clitoral glands, 803–804, 803f, 804f. *See also* Female reproductive system  
 Clonogenic assay, 371  
 Club cells, 249, 253–255, 296

Clubfoot. *See* Talipes  
 Clustered regularly interspaced short palindromic repeats. *See* CRISPR  
 Clusterin, 124  
 Coagulating gland. *See* Accessory sex organs  
 Coagulation  
   coagulopathy, 19  
   complement system, 168–169, 401–402, 443  
   disseminated intravascular coagulation (DIC), 416–417  
   hemostasis, 369  
 Colchicine, 400, 707–708  
 Colony-forming units (CFUs), 352, 371.  
   *See also* Hematopoiesis  
 Complement activation-related pseudoallergy (CARPA), 472  
 Complement system. *See* Coagulation  
 Complete blood count (CBC).  
   *See* Hematology  
 Computed tomography (CT), 14, 532  
 Conceptus, 876–878  
 Confocal microscopy, 271, 532–533  
 Congenital aganglionic megacolon, 850–851  
 Congenital anomalies of kidney and urinary tract (CAKUT), 90  
 Congenital neoplasia, 864–868, 865t  
 Connective tissue growth factor (CTGF), 157  
 Constriction ring syndrome. *See* Amniotic band syndrome  
 Contact dermatitis, 506, 524, 539, 540, 567, 571  
 Convention on International Trade in Endangered Species (CITES), 896  
 Coronavirus disease 2019. *See* COVID-19 (coronavirus disease 2019)  
 Corpora amylacea (mammary gland), 583  
 Corpora lutea (CL), 588, 738, 742f, 744f, 746f, 750f, 752f, 761, 766, 774f, 780, 782, 784f, 788. *See also* Ovary  
 Corticotropin releasing hormone (CRH), 701  
 Costimulatory molecules, 441  
 COVID-19 (coronavirus disease 2019), 238, 273, 277–278, 279t, 286, 737–738  
 Craniofacial malformations, 846–848  
 Creatinine, 117, 119. *See also* Kidney, Renal system  
 Creatinine clearance, 101–102  
 Cribriform change (epididymis), 683, 688  
 CRISPR, 591–592, 769  
 Critical periods (of development), 813–815, 814f  
 Cryptorchidism, 719, 721, 854–855, 884t  
 Crystalluria, 189  
 Cyclooxygenase (COX), 110–111, 403  
   COX-1, 110–111, 415–416  
   COX-2, 110–111, 852–853  
 Cyclophosphamide, 32, 223, 321  
 Cyclopia, 843, 847, 847f, 883t  
 Cyclosporine, 188, 490  
 Cynomolgus monkeys (*Macaca fascicularis*), 610–611, 739–741, 755–758, 887–888. *See also* Nonhuman primate

Cystic endometrial hyperplasia (CEH), 747–748  
 Cytochromes P450 (CYP450), 107, 288, 296, 319, 399, 522, 615–616, 665, 784, 867  
 Cytokine release syndrome (CRS), 34, 171–172, 474–475  
 Cytokines, 109–110, 440–441  
   proinflammatory, 494, 635  
 Cytotrophoblast, 828–829. *See also* Placenta

## D

Danger-associated molecular patterns (DAMPs), 536, 539f, 541, 543, 544f, 567  
 Decay accelerating factor (DAF), 386  
 Decidua, 819, 828f, 830, 880  
 Decidual reaction, 798  
 Deciduosa sarcoma, 799  
 Deep learning approaches, 21, 146, 769  
 Defensins, 440–441  
 Deformations (in embryonic development), 815, 840, 858, 860–862, 861f  
 Degmacyte, 409  
 Demarcation membrane system (DMS), 357  
 Dendritic cells (DCs), 92–93, 260, 349–351, 359, 440–441, 512–513, 536, 538–541, 542f  
 Dendritic epidermal T cells (DETCs), 541–542  
 Deoxynivalenol, 181  
 Deoxyribonucleic acid (DNA), 342–343  
   adducts, 230–231  
   synthesis, 399–400  
   repair enzyme, 603  
 Dermis, 508, 509f, 512–515, 514f. *See also* Integument  
   irritancy potential, 524  
   neoplasms, 558  
   nonproliferative lesions, 550–553  
 Desmosomes (in cutaneous barrier formation), 508, 510–511, 514f, 551  
 Developmental and reproductive toxicology (DART), 464, 597–598, 629–630, 739–740, 812, 830–831  
 Developmental delay, 840  
 Developmental landmarks, 817t, 837, 886, 894  
 Developmental stages, 815–825, 817t, 818f  
   gastrulation, 819–821  
   histogenesis and functional maturation, 816f, 820f, 824–825  
   implantation, 818–819  
   organogenesis, 813, 821–824. *See also* Morphogen gradients  
 Developmental toxicity. *See also* Female reproductive system, Male reproductive system  
   basic principles, 813  
   critical periods of development, 813–815, 814f  
   evaluation of toxicity, 833–839  
   fertility assessment, 663–664, 834  
   in vitro/ex vivo assays, 831–832  
   maternal endpoints, 833–834  
   progeny endpoints, 834–838

- Developmental toxicity (*Continued*)  
 in-life observations, 836–837  
 in silico analysis, 837–838  
 morphologic evaluation, 665, 834–836  
 mechanisms of toxicity, 868–875  
 paternal effects, 879–880, 880t  
 pharmacokinetics  
 embryonic and fetal, 877–878, 881  
 maternal, 878–879  
 repositories for developmental toxicity  
 data, 892–894, 893t  
 responses to injury, 839–868  
 congenital neoplasia, 864–868, 865t, 866t  
 death, 840  
 deformations, 815, 840, 858, 860–862  
 functional alterations, 863–864  
 intrauterine growth restriction (IUGR),  
 839–840, 862–863, 862f, 872, 891  
 malformations, 815, 840–860, 869t  
 toxicity, 664–665  
 issues in product development, 875–894  
 differentiating embryonic from  
 maternal toxicity, 838–839  
 regulatory considerations, 894–896,  
 895t  
 species selection, 885–889  
 risk assessment, 832, 838, 882, 885, 889,  
 890, 892  
 risk management, 894–896, 895t  
 thresholds, 876–877, 885
- Diabetes mellitus, 409, 494
- Diestrus. *See* Estrous cycle
- Diethylstilbestrol (DES), 685–686, 812, 854,  
 863–864, 867–868, 874
- Diffuse alveolar damage (DAD), 306, 309
- Digestive system, 110–111  
 congenital defects of, 850–852  
 aplasia of caudal enteric ganglia,  
 850–851  
 diaphragmatic hernia, 851, 884t  
 gastroschisis, omphalocele, and  
 umbilical hernia, 851–852, 851f, 884t  
 reflux, gavage-related, 268–270, 269f
- Dihydrotestosterone (DHT), 630, 658–659
- Dimethylbenz(a)anthracene (DMBA),  
 553–555, 603, 775
- Dimethylnitrosamine (DMN), 49, 198
- Direct-acting carcinogens, 865–867
- Disseminated intravascular coagulation  
 (DIC), 416–417. *See also* Coagulation
- Dog, 530, 585–588, 603, 605–606, 611,  
 614–615, 631, 632t, 692–694,  
 696–698, 701, 753–755, 766
- Dose response analysis, 231, 882–894
- Doxorubicin, 31–32, 52–53, 552
- Draize scale, 524, 525t. *See also* Integument
- Drug development, 199–206  
 adversity, 202–206, 419–420  
 nonclinical to clinical translation, 59, 419  
 regulatory considerations, 205–206,  
 419–421, 891–896
- Drug-drug interactions, 56, 87–88
- Ductus arteriosus, 19, 849, 850, 875
- Dyserythropoiesis, 387–388. *See also*  
 Hematopoiesis
- Dysgenesis, 720–721, 844, 859, 898
- Dysmorphogenesis, 610
- Dysmorphology, 830–831
- Dysplasia, 228, 387–388, 609, 845–846, 846f,  
 852–854. *See also* Heterotopia,  
 neuronal
- Dysraphism, 842–844, 842f, 883t  
 acrania, 842f, 843  
 anencephaly, 842, 842f  
 encephalocele, 842f, 843  
 exencephaly, 842–843, 842f  
 holoprosencephaly, 842f, 843, 847f  
 meningocele, 844  
 rachischisis (spina bifida), 842f, 843–844,  
 844f
- Dysrhythmia, 33
- ## E
- Eccentrocyte, 409–410
- Echinocyte, 411–412
- Echocardiography, 14, 49
- Ectopia, 854
- Ectrodactyly, 856–859, 857f, 858f
- Elastosis, 545
- Electrocardiograms (ECGs), 11, 14–17
- Electrolytes, control of, 100–101
- Electron microscopy, 230, 534, 673–674
- Embryo, 814f, 815–825, 817t, 818f. *See also*  
 Developmental toxicity
- Embryo fetal development (EFD), 832–833,  
 886, 890, 894–896. *See also*  
 Developmental toxicity
- Embryo lethality (embryolethality), 833,  
 838, 872, 890–891
- Embryogenesis, 464, 630, 812, 814f
- Embryonic stem cells (ESC), 16, 816, 824,  
 840, 864  
 embryonic stem cell assay (mESC), 832
- Encephalitozoon cuniculi, 135–137
- Encephalocele, 842f, 843
- Endocapillary proliferation, 151
- Endocardium, 4, 7–8, 48–49. *See also* Heart  
 endocardiosis, 70–71  
 fibrosis, 48–49  
 inflammation (endocarditis), 43
- Endocrine Disrupter Screening Program  
 (EDSP), 744–745
- Endocrine disruption, 595, 598–599,  
 603–604, 609–610, 616, 665, 777,  
 873–874
- Endocrine modifiers of development,  
 591–595
- Endocrine system, 494, 591–592  
 endocrinology of estrous and menstrual  
 cycles, 763, 764f
- Endometriosis, 759, 789
- Endometrium, 747  
 endometrial reaction, 819  
 neoplasia, 796–800
- Endomitosis, 356–357
- Endothelium, 16, 60–64, 89–90, 94–95, 289,  
 301  
 effects of damage on blood vessel activity,  
 65–66  
 permeability, 63  
 precursor cells, 349
- Endothelial nitric oxide synthases (eNOS),  
 111
- Endothelin (ET), 102, 111–112, 188, 647  
 antagonists, 716
- Environmental Protection Agency (EPA),  
 498–499, 596–597, 630, 738
- Environmental tobacco smoke (ETS), 314
- Eosinophilic crystalline pneumonia,  
 266–267, 267f
- Epicardium, 50. *See also* Heart  
 calcification, 23  
 hemorrhage, 50
- Epidermal growth factor (EGF), 89–90, 519,  
 592t, 594, 767  
 EGF receptor (EGFR) inhibitors, 506, 594
- Epidermis. *See also* Integument  
 nonproliferative lesions, 550–552  
 proliferative lesions, 555–557
- Epididymis, 645–652, 651t, 653f, 654f,  
 659–663, 665, 682–684, 686–688, 715.  
*See also* Male reproductive system
- evaluation  
 fixation and sampling, 669  
 organ weights, 661t  
 sperm count, microscopic assessment,  
 662t  
 metabolism, 665  
 microscopic findings, 672–673, 705t, 706t,  
 707t  
 nonproliferative lesions, 682–684, 692f  
 proliferative lesions, 686f, 687–688  
 organ weights, 674
- Epithelial–mesenchymal interactions,  
 593–594
- Epithelial mesenchymal transition (EMT),  
 89–90
- Equilibrative nucleoside transporters  
 (ENTs), 103–104
- Eryptosis, 406
- Erythrocytes, 338, 354–355, 378, 385–386,  
 391–392, 406–407, 466, 469–472.  
*See also* Hematology, Hematopoiesis,  
 Red blood cells (RBCs)
- anatomy and physiology, 337–338,  
 391–392  
 erythropoietin (EPO), 102, 344–345,  
 352–353  
 hemoglobin. *See* Hemoglobin  
 life cycles of blood cells, 352–360, 355t
- cytological findings  
 macrocytosis, 386–387  
 megalocytosis, 402  
 microcytosis, 393  
 ringed sideroblast, 411  
 schistocytes, 409–410  
 siderocyte, 393, 411  
 spherocyte, 378  
 spherocytinocyte, 411–412
- mechanisms of injury  
 hemolysin toxins, 411–412  
 immune-mediated, 386–387  
 nonimmune injury, 404–412, 405–406  
 responses, 406–407  
 anemia. *See* Anemia



- erythrophagocytosis, 413–414  
hemolysis. *See* Hemolysis
- Erythropoiesis, 186–187, 352–358, 391f.  
*See also* Erythrocytes, Hematopoiesis  
developmental phases, 344–345, 344t  
dyserythropoiesis, 387–388  
erythropoietic islands, 351f, 352, 363  
extramedullary hematopoiesis (EMH), 357, 389, 391–392, 391f  
impact of stress, 354–355  
normal erythrocyte lifespan in selected mammalian species, 352–360, 355t.  
*See also* Red blood cells (RBCs)
- Erythropoietin (EPO), 102, 344–345
- E-selectin, 72
- Esthesioneuroblastoma, 293
- Estradiol, 263–264, 658, 765, 770–771
- Estrogen, 198–199, 417, 521  
in developmental toxicity, 848, 863t, 874  
in females, 631, 659  
in males, 742, 751, 753, 761, 766–768, 772, 779, 788t, 790, 793, 793t, 795, 798, 802
- Estrogen receptors (ER), 585–588, 592t, 779t, 780t  
effects via, 719  
mediated negative feedback, 772
- Estrous cycle, 608. *See also* Female reproductive system, Menstrual cycle, Ovary, Uterus, Vagina  
development, 740–741  
endocrinology of, 764–769, 765f  
histology, site-specific effects  
mammary gland, 581, 583–584, 588, 589f, 615  
reproductive tract  
dog, 750–753  
minipig, 759–764  
primate, 755–758  
rabbit, 764  
rat, 745–750, 747t
- stages, 745, 747t  
anestrus, 588, 589f, 750–752, 757, 758, 787  
diestrus, 582, 585–588, 589f, 747t, 748f, 749–750, 757f, 758f, 760, 779t, 784f  
estrus, 581–582, 585, 589f, 745, 747, 747t, 748f, 749–751, 751f, 752f, 757f, 758f, 760, 767, 779t, 780t, 781t  
metestrus, 747t, 748f, 751, 754f, 760  
proestrus, 582, 585, 742, 747t, 748f, 749–752, 755f, 757f, 758f, 760–761, 767
- Ethylendiaminetetraacetic acid (EDTA), 365, 871–872
- European Center for the Validation of Alternative Methods (ECVAM), 832
- European Committee for Proprietary Medicinal Products (EU CPMP), 498–499
- European Medicines Agency (EMA), 487, 523
- Ex vivo assays, 13, 15, 139–140, 285–286, 831–832, 838
- Exencephaly, 842–843, 842f
- Extracellular matrix (ECM), 94–95, 259, 600, 821–823, 850, 871
- Extramedullary hematopoiesis (EMH), 357, 389, 391–392, 391f. *See also* Hematopoiesis
- ## F
- Fanconi syndrome, 106
- Fat-associated lymphoid cluster (FALC), 462
- Federal Hazardous Substances Act (FHSA), 524
- Female reproductive system. *See also* Cervix, Ovary, Uterus, Vagina  
anatomy and physiology, 740–764  
development, 744–745  
endocrinology, 764–769, 765f  
species differences, 741t, 745–764, 766–767  
spontaneous changes, 771–772, 772t  
evaluation of toxicity, 739, 739t, 769–772, 778t. *See also* Estrous cycle, Menstrual cycle  
mechanisms of toxicity, 777–790  
responses to injury, 772–777, 779t, 780t–781t, 788t  
safety assessment, 738–739, 738t, 739t, 778t, 790–791
- Ferrochelatase, 411
- Fetus, 813, 814f. *See also* Developmental toxicity, Embryo
- Fibroadenomas, 595, 613–614. *See also* Mammary gland
- Fibroblast growth factors (FGFs), 344–345, 819  
FGF2, 68, 92–93  
FGF receptor 3 (FGFR3), 228
- Fibroblastic reticular cells (FRCs), 454–455
- Fibroids (uterine), 799–800
- Fibrosis, 48–49, 222–223, 309–312, 611
- Fibrous osteodystrophy, 418
- Fine particle dose (FPD), 263
- Fine particle fraction (FPF), 263
- Fluorometric microculture cytotoxicity assays (FMCA), 371
- FMS-like tyrosine kinase 3 (FLT3), 349–351
- Focal segmental glomerulosclerosis (FSGS), 149
- Folate, 385–386  
deficiency, 868  
folate receptor 1 (FOLR1), 278–279, 287
- Follicles, lymphoid, 439t–440t, 447, 450–458, 455f, 461f, 486. *See also* Germinal centers
- Follicles, ovarian, 741–744, 742f, 743f, 746f, 750f, 751–753, 752f, 756f, 757f, 760–761, 760f, 764, 766–767, 776, 779, 780t–781t, 782f, 784f, 786, 788, 790
- Follicle-stimulating hormone (FSH), 631, 655, 656f, 657, 666–667, 715, 742, 765–766
- Food and Drug Administration (FDA), 121–122, 274, 476, 523, 738–739
- Frog embryo teratogenesis assay *Xenopus* (FETAX), 888
- ## G
- GalNAc (N-acetylgalactosamine), 169–171
- GALT. *See* Gut-associated lymphoid tissue
- Gas exchange (respiratory), 237, 257–261
- Gastric reflux (gavage-related), 268–270, 269f
- Gastrointestinal (GI) system. *See* Digestive system
- Gastroschisis, 851–852, 851f, 884t
- Gastrulation, 819–821, 820f, 823
- Gelatinous marrow transformation (GMT), 382
- Genotypic sex, 855–856
- Gentamicin, 172–173, 200
- Germinal centers (GC), lymphoid organs, 439t–440t, 442f, 451–454, 455f, 457f, 461f. *See also* Follicles, lymphoid
- Gestation, length in various species, 817t
- Gestational day (GD), 89–90, 446–447, 631
- Gestational week (GW), 89–90
- Globin, 345, 356, 394t–398t, 409–412, 476
- Globose basal cells (GBCs), 244–245
- Globule leukocytes, 266
- Glomerular. *See also* Glomerulus, Kidney, Renal system  
glomerular basement membrane (GBM), 94–95, 166–167  
glomerular capillary hydraulic pressure (GCHP), 167  
glomerular endothelial cell injury, 164–166, 165f  
glomerular epithelial protein-1 (GLEPP-1), 164  
glomerular filtration, 157–159, 166  
glomerular filtration rate (GFR), 100–101, 114
- Glomerulus, 94–95, 148–149, 149f. *See also* Glomerular, Kidney, Renal system  
anatomy, 94–95  
injury, 148–149, 168, 177  
fibrosis (glomerulosclerosis), 150, 202  
inflammation (glomerulonephritis), 151–153, 169–171  
mechanisms of injury, 167–168  
microscopic findings, 133, 148–149, 202–204  
age-related changes, 96f  
endothelial cell injury, 164–166  
podocyte injury, 150, 160–164  
perturbation of renal hemodynamics, 167  
ultrastructure, 95f
- Glomeruloid bodies, 129–132
- Glucocorticoids, 444, 472, 522, 682, 701
- Glutathione (GSH), 105, 159, 307, 403, 523
- Glutathione S transferases (GSTs), 117, 121, 523
- Gonadotropin-releasing hormone (GnRH), 655–658, 656f, 764, 766–768, 799  
analogs, 685, 690, 711–713, 716f  
suppression, 682, 682f, 701
- Gonocytes, 631, 633, 720–721
- Granular cell tumors, vagina and cervix, 800–802

Granulocytes, 358, 366, 379–380, 404–406, 449. *See also* Granulopoiesis, Hematopoiesis, Leukocytes

classes

- basophils, 440–441
- eosinophils, 440–441
- granulocyte/monocyte progenitor (GMP), 349–351
- neutrophils, 401–402, 440–441. *See also* Neutrophils

granulopoiesis, 358, 363

toxic responses

- agranulocytosis, 413–415
- granulocytopenia (neutropenia), 380, 400–401, 412
- nuclear hypersegmentation, 399, 401

Granulopoiesis, 358, 363

Granulosa cells, ovary, 742–743, 746f, 757f, 761–762, 764, 766–768

tumors, 775, 792t, 795–796

Growth factors, 520, 593–594. *See also*

- Activins, Inhibins, Insulin-like growth factor (IGF), Platelet-derived growth factor (PDGF), Transforming growth factor (TGF), Vascular endothelial growth factor (VEGF)

epithelial, 89–90, 518, 594, 767. *See also*

- Epidermal growth factor (EGF)

fibroblastic, 68, 344–345, 519, 819. *See also*

- Fibroblast growth factor (FGF)

hemopoietic, 413–414

receptors, 228, 610

Gut-associated lymphoid tissues (GALT), 246, 456–458, 457f

## H

Hair follicles, 507t, 509f, 513–518, 516f, 517f, 531, 552, 553f, 556, 558, 561t

Hapten, 412, 415, 468–469

Heart. *See also* Endocardium, Epicardium, Myocardium

anatomy and physiology, 3–11

- cardiac cycle, 8–10
- conduction system, 4, 6–7
- contractility, 48–49
- electrical activity, 9–10
- innervation, 10
- metabolism, 10
- output, 16
- valves, 8. *See also* Valvulopathy

evaluation of toxicity, 11–25

- bioactivity screening, 12, 57
- biomarkers, 24–25
- ex vivo preparations, 13, 15
- functional testing, 12–18. *See also* Electrocardiogram
- in vitro preparations, 15–16
- in vivo assessments, 13–18
- mass changes as response to toxicity, 28–29
- organoids, 16
- pathology, 18–24
- troponins, 24–25, 59
- weight, 4, 28–29

microscopic findings, 29–34, 40–42

background findings, 22–24

- contraction bands, 40f
- fibrosis, 42f
- lipofuscinosis, 37
- myofibrillar degeneration, 35–37
- necrosis, 34–35, 38–43
- phospholipidosis, 37–38
- rodent progressive cardiomyopathy, 58
- schwannoma, endocardial, 49
- vacuolar degeneration, 35

mechanisms of toxicity, 26–27, 50–57

responses, 25–50. *See also* Cardiomyopathy

- age-related lesions, 22–24
- arrhythmias, 14–15, 26–28
- artifacts, 22–24
- background alterations, 22–24
- functional changes, 26–28
- hypersensitivity, 43–48
- hypertrophy, 28
- malformations, 848–850, 849f, 884t
- toxicity, 29–34, 44–47t, 48–50, 55–59, 199–202. *See also* Cardiotoxicity
- attrition, cardiac-related, 57–58
- atherosclerosis, acceleration by toxic agents, 73–74
- catecholamine-related, 43
- dysfunction as manifestation of toxicity, 26–28, 27t
- issues in drug development, 57–59
- toxicant interactions, 56–57

Heat shock proteins, 110

Heavy metals, 153–154, 174–175, 195–196

Hemangioblasts, 344–345

Hematology, 360, 366–369, 367t–368t, 387, 466. *See also* Peripheral blood cells

analyzers (Advia, Sysmex), 368–370, 368t–369t

biomarkers, 369–371

complete blood count (CBC), 360–362, 484–485

hematocrit (HCT), 486

hemoglobin (Hgb). *See* Hemoglobin

mean corpuscular volume (MCV), 378

packed cell volume (PCV), 342

white cell differential, 368–369

Hematopoiesis, 60, 337–338, 347–360, 350f, 362, 372, 379, 410–402, 495. *See also*

- Erythropoiesis, Granulopoiesis, Lymphopoiesis, Megakaryopoiesis, Myelopoiesis, Thrombopoiesis

anatomy and physiology, 344–360

- bone marrow, 346–347
- colony-forming units, 303–304, 352, 358
- erythroblastic islands, 351f, 352, 363
- growth factors, 413–414
- hematopoietic niches, 347–349
- lineages, 350f
- life cycles, 352–360
- life spans, species comparison, 374t–375t
- ontogenesis, 340–345, 344t
- stem cells, 345, 349–351
- stimulating factors, 102, 344–345, 359

cell types

- granular hemocytes (invertebrates), 343

- hematopoietic stem cells (HSCs), 340, 349–351, 379
- hemogenic endothelial cells, 345
- multipotent progenitors (MPPs), 349–351

developmental stages

- adult (definitive), 343–344
- embryonic (primitive), 344

Hematopoietic niches, 347–349

Hematotoxicity, 338, 400, 419, 421

animal models, 371–372

cell targets

- circulating cells, 404–412. *See also* Erythrocytes, Leukocytes, Peripheral blood cells progenitor cells, 392–404

evaluation of toxicity, 360–372, 361t

- blood, 366–371
- functional testing, 370
- hematology analysis, 366–367, 368t–369t
- in vitro techniques, 371
- morphological evaluation

  - bone marrow cytology, 364–366, 364t
  - histopathology, 362–364

responses to injury, 361t, 372–392, 376t–377t

- cell lysis (hemolysis), 378, 406
- extravascular, 378
- intravascular, 378
- decreased cellularity, 387f, 388f
- idiosyncratic reactions, 415
- redistribution and sequestration, 373

mechanisms, 392–419, 394t–398t

- altered cell function, 415–417
- bone marrow failure/myelosuppression, 372, 393, 417–418
- decreased cell lifespan, 418–419
- DNA damage (dividing cells), 399–400
- immune-mediated injury, 412–415
- inhibited protein synthesis (maturing pool), 400–404
- indirect injury, 417–419
- nonimmune (direct) injury, 392–404, 394t–398t, 404–412
- oxidative injury, 402–404, 407–408

responses to injury, 361t, 372–392

- altered cell size, 386–387, 401
- blood, 373–379
- bone marrow, 379–386
- secondary hematopoietic organs, 389–392
- myeloproliferative lesions, 386–389
- myelosuppression, 393
- myelotoxicity, 399–400
- secondary hematopoietic organs, changes, 389–392, 391f
- toxicity, 372, 412–415
- classes of hematotoxic agents, 394t–398t
- regulatory considerations, 419–421

Hemimelia, 859

Hemoglobin (Hgb), 106, 185–186, 340–342, 354, 406–412, 486

Hemolymph, 340–342

Hemolysis, 378, 406

- Hemolytic uremic syndrome (HUS), 164, 166, 417
- Hemophilia, 263–264
- Hemosiderin, 342, 479–482, 585
- Heterotopia, neuronal, 846f, 898
- Hexachloro-1,3-butadiene, 178–179
- 2,5-Hexanedione, 705–706
- High endothelial vessels (HEVs), 444
- Histiocytic sarcoma, 496–497, 498f
- Hormones, 579, 582–583, 585, 590–595, 604, 666–667
- elaboration of hormones and regulatory peptides, 102
  - events during a reproductive cycle, 765–766
  - immune responses to, 464–465
  - influence on renal carcinogenesis, 198–199
  - regulation of male reproductive function, 655–659
  - toxicant effects mediated by, 703
- Human immunodeficiency virus (HIV), 160–162
- Human-induced pluripotent stem cells (hiPSCs). *See* Induced pluripotent stem cells
- Human leukocyte antigen (HLA), 124–125, 447–449
- Hyaline droplet nephropathy, 183–185
- Hyaline glomerulopathy, 148–149
- Hydrocephalus, 844–845, 844f, 862, 874, 883t
- Hydronephrosis, 201, 223, 853–854, 853f, 884t
- Hydroureter, 853–854, 853f, 884t
- Hyperplasia, epidermis, 553
- Hypersensitivity, 43–48, 48t, 56, 77–78, 321–322, 413, 467–468, 473t, 495, 566–567, 776
- Hypertension, 32, 202
- Hyperthyroidism, 28–29
- Hypospadias, 853–854, 884t
- Hypospermatogenesis, 696, 698
- Hypotension, 32–33
- Hypothalamic-pituitary-gonadal (HPG) axis, 606
- Hypothalamic-pituitary-ovarian (HPO) axis, 765
- Hypoxia, 186–188, 186f
- Hypoxia-inducible factors (HIF), 33, 132–133, 348–349, 353
- I**
- ICANS (immune cell-associated neurotoxicity syndrome), 494
- Immune cells, 343, 366, 438, 488. *See also* Immune system, Leukocytes
- anatomy and physiology
  - anti-tumor effects, 472–473
  - biomarkers, 490
  - circulating immune cell, 445–446
  - influence of skin microbiome on, 549–550
  - resident immune cell, 445–446
  - turnover, 281
- cell types
- antigen-presenting cells (APCs), 440–441
    - Langerhans cells, 512–513
    - M (microfold) cell, 442f, 457–458. *See also* Gut-associated lymphoid tissue (GALT)
  - dendritic cell (DC), 440–441, 537–539. *See also* Integument
    - follicular DC, 453–454. *See also* Integument
    - interdigitating DC, 447
  - lymphocytes. *See also* Lymphocytes
    - B cell, 441, 450f
    - intraepithelial lymphocytes (IELs), 457–458
    - large unstained cells (LUC), 368–369
    - mucosa-associated invariant T cell (MAIT cell), 540
    - natural killer (NK) cell, 440–441, 461–462
    - regulatory (Treg) cell, 494–495
    - T cell, 441, 442f, 448f
    - uterine NK (uNK) cells, 828–829
  - macrophages
    - alveolar, 236
    - intravascular, 260
    - sinusoidal (Kupffer cell), 445–446
  - mast cell, 215, 349–351, 440–441
  - mononuclear cells, 493–494
  - neutrophils, 295, 401–402, 440–441. *See also* Granulocytes
  - neuroendocrine cell, 447
  - plasma cells, 444
  - reticular cell, 449–450
- Immune checkpoint inhibitors (ICIs), 33–34, 178, 287, 472–473, 475
- Immune competency, 445–446
- Immune complex disease (ICD), 78, 323, 413, 468f, 495
- Immune deficiencies, 475–476
- Immune system, 438, 441–445, 469–472, 479
- anatomy and physiology, 444–462
    - adaptive immune system, 438–441, 443–444, 467t, 491
    - aging, impact of, 463–466, 463t
    - bone marrow, 449
    - compartments, 439t–440t
    - elimination and exclusion, 441–443
    - immune-privileged organs, 462
    - immune-specific components, 461–462
    - immunological memory, 443–444
    - innate immune system, 440–441, 467t
    - isotype switching, 444
  - lymph nodes, 453–456. *See also* Lymph nodes
  - lymphocyte trafficking, 444
  - mucosa-associated lymphoid tissue, 456–458. *See also* Mucosa-associated lymphoid tissue (MALT)
  - neuroendocrine system impact, 445f, 452–453, 464–465
  - spleen, 449–452. *See also* Spleen
  - tertiary lymphoid structures (TLSs), 458–461. *See also* Tertiary lymphoid structures (TLS)
- thymus, 446–449. *See also* Thymus
- tolerance, 443, 461
- transcription factors, 441
- evaluation, 476–490, 477t–478t
- clinical pathology, 487–490
  - functional evaluation, 438–444, 488. *See also* TDAR (T cell-dependent antibody response)
  - immunophenotyping, 483, 487–490, 489t
  - microscopic evaluation, 483–487
    - enhanced histopathology, 483
  - organ weights, 482–483
  - recommended sampling practices and regulatory considerations, 497–499
  - toxicity testing, 479, 480t–481t
    - interpretation of changes, 476, 477t–478t
- mechanisms of toxicity, 466–476, 469f, 470t–471t, 480t–481t
- antigen-independent toxicity, 469–472
  - antigen-specific toxicity, 472
  - autoimmunity, 495
  - drug-related toxicity, 472–475
  - exaggerated pharmacology, 466–467
  - hypersensitivity, 412, 473t, 495
  - immune derangements, 475–476
  - immunomodulation, 466–476, 474f
  - immunosuppression and immunostimulation, 310–311, 322, 466, 473–476, 490–495
  - stress (and other hormones), 463t, 464–466, 465f
- responses, 412–415, 438, 464–476
- acute phase proteins, 440–441
  - bone marrow stromal injury, 418
  - death, 217, 220, 484
  - decreased cell lifespan, 418–419
  - decreased cellularity (depletion), 465
  - findings in non-immune tissues, 491–495, 492t–493t
  - proliferation, 495–497
  - recoverability, 467–469, 475
  - toxicity, 466, 476, 479, 490
- Immunogenicity, 323, 467–468, 863t
- Immunoglobulin (Ig), 444
- IgA, 243, 445–446
  - IgE, 358, 472
  - IgG, 444
- Induced pluripotent stem cells (iPSCs), 12, 16
- human iPSCs (hiPSCs), 68, 143, 280
- Infusion site reaction (for integument), 401–402, 468–469, 506
- Inhibins, 593–594, 645, 656f, 657, 667
- Innate immune system, 440–441, 467t
- Insulin-like growth factor (IGF), 63–64, 89–90, 520, 554, 592t, 594, 632–633, 767
- Integrated Risk Information System (IRIS), 604–605
- Integrins, 255–256, 352
- Integument
- anatomy and physiology, 506–522
  - adnexa, 509f, 515–518, 516f, 517f, 518f
  - biochemistry, 520



Integument (*Continued*)

- dermal-epidermal junction, 507–510, 513–515, 514f
  - epithelial elements, 461, 508–511, 509f, 515, 518, 535, 541, 545, 554, 574–576
  - function, 521–522
  - immune elements, 359, 453–454, 511–513, 536–541
  - melanocytes, 511–512, 545
  - metabolism, 522–523
  - microbiome, 511, 549–550
  - neural elements, 512
  - percutaneous absorption, 520–522
  - species differences, 506, 508, 507t
  - subcutis, 515
  - vasculature, 513
  - evaluation of toxicity, 523–535
    - animal models, 528–529
      - carcinogenicity, 527, 553
    - Draize scale, 524, 525t
    - in vitro model systems, 545
    - irritancy assessment, 524
    - minipig dermal toxicity assessment, 506, 507t, 518–519, 519f
    - phototoxicity testing, 524–527, 526t
    - sample collection, 506, 528–531
    - special techniques
      - molecular profiling, 531
      - morphological, 531–534, 550–554
    - wound healing, 543–549, 544f, 546t
  - mechanisms of toxicity, 559–576, 560t–561t
    - altered pigmentation, 561t, 574
    - direct effects, 559, 562–565, 560t–561t
    - immune-mediated effects, 560t, 565–568
    - photoaging, 551, 569, 572
    - photosensitivity, 568–570, 569f, 570f
    - thermal injury, 548, 560t, 562–563, 563f
  - responses to injury, 536–559
    - nonproliferative, 550–553
      - alopecia, 574–575
      - altered pigmentation, 573–574
      - atrophy, 517, 550, 552
      - calcinosis, 551, 552f
      - edema, 550–551
      - elastosis, 551–552
      - erosion/ulcer, 550
      - hyperkeratosis, 551
      - immune-mediated, 506, 525, 565–568
      - inflammation, 538, 539–540, 543, 545, 552–554, 560t–561t, 565f, 565–567, 570f, 572
      - infusion site reaction, 401–402, 468–469, 506
      - metaplasia, 576
      - necrosis, 550, 552, 760–763
    - proliferative, 553–557
      - dermal, 559
      - epithelial, 553–559, 561–562
      - melanocytic, 511–512, 554
  - toxicity, 523–535, 559–576, 559–568
    - cosmetics testing, 523
- Interferon (IFN), 32–33, 399
- Interleukin(s), 296, 344–345, 635
- International Council for Harmonisation (ICH), 498–499, 523, 525, 597, 889
- International Harmonization of Nomenclature and Diagnostic Criteria (INHAND), 71, 266, 362–363, 479, 550, 610–611, 740
- Intersex. *See* Pseudohermaphroditism
- Intrauterine growth restriction (IUGR), 839–840, 862–863, 862f, 872, 891
- Involution, 447, 449, 582–583
- Ion trapping, 867, 881
- Ionizing radiation, 167, 784–785, 845, 846f, 864
- Ionocytes (conducting airways), 256–257
- Iron. *See also* Hemoglobin
  - deficiency, 417. *See also* Anemia
  - in hemoglobin, oxidation of, 408–409
  - iron-sulfur (FeS) clusters, 353–354
  - stores, 382
  - toxicity, 181
- Ischemia reperfusion injury (IRI), 148, 200

## J

- Juvenile animal studies, 837
- Juvenile toxicology, 813
- Juxtaglomerular apparatus (JGA), 93–94, 94f, 97–98

## K

- Keratins, 216, 255–256, 532
- Keratoacanthoma, 551
- Kidney, 78, 81, 87–88. *See also* Renal system
  - anatomy and physiology, 89–113. *See also* Glomerular, Glomerulus, Renal tubules
  - age-dependent characteristics, 114–116
  - anatomy, 91–100
  - development, 89–91
  - function, 100–109, 113–116, 147–148
  - spontaneous findings, 129–137, 130f, 136f
  - species comparisons, 98–100
- evaluation of toxicity, 113–146
  - animal models, 99–100, 110–111, 199–202, 203t–204t
  - biomarkers, 116–127, 117t–119t
    - kidney injury molecule-1 (KIM-1), 122–123
    - neutrophil gelatinase-associated lipocalin (NGAL), 123–124
  - in vitro techniques, 139–145, 141t
  - morphologic evaluation, 129–137, 145–146
    - scoring schemes, 145
    - suggested descriptive nomenclature, 128t, 138t
  - proteinuria and albuminuria, 120
  - in vitro methods, 139–145
- mechanisms of toxicity, 157–199
  - endothelial injury, 163–166
  - glomerular injury, 160–168
  - interstitial injury, 168–172
  - tubular injury, 172–188
- responses to injury, 147–157, 158f, 168–172, 189–191, 382
  - amyloidosis, 151
  - apoptosis, 147–148, 148t, 154

- degeneration, 147, 153
- end-stage disease, 132–133
- fibrosis, interstitial, 157
- glomerulosclerosis, 149–150
- glomerulopathy, 148–149, 160–162
- hydronephrosis, 201, 223. *See also* Hydronephrosis
- hyperplasia, 222–223
- hypertrophy, 116
- inflammation
  - glomerular, 150–153, 165
  - interstitial, 157, 164, 200
  - pelvis, 188
  - renal papillary necrosis (RPN), 125–126
- ischemia, 186–188, 192f
- malformations, 852–854, 853f, 884t
- mesangiolysis, 164–166
- mesangioproliferative disease, 164–166
- necrosis
  - papillary, 125–126, 158f
  - tubular, 91, 153, 156
- neoplasia, 191–199
- nephropathy
  - alpha<sub>2</sub> $\mu$ -globulin, 183–185, 184f–185f, 185t, 197f
  - chronic progressive (CPN), 116, 130f, 132–133, 197–198, 214
  - diabetic, 109–110
  - hyaline droplet, 183–185
  - melamine, 182, 224–225
  - membranous, 150–151
  - obstructive, 182
  - retrograde, 156
- nephrosis, 200
- proximal convoluted tubule injury, 142–143, 153–154, 186–187
- podocyte injury, 149–150, 160–162
- tubular dilation, 154–155
- vacuolation, tubular, 154
- toxicity. *See also* Nephrotoxicity
  - causes, 108, 113, 148t, 157–159, 160t, 169–191
    - antibiotics, 172–174, 182
    - antineoplastic agents, 176–178
    - antisense oligonucleotides, 169–171
    - ethylene glycol, 182, 183f
    - heavy metals, 174–176, 195–196
    - melamine, 182, 224–225
    - NSAIDs, 189–191, 190f
    - therapeutic antibodies, 168–169
  - classifications, 159–160, 160t, 162t–163t, 164t
  - issues in drug development, 199–206
    - acute kidney injury (AKI), 199–201
    - chronic kidney injury (CKI), 201–202, 204t–205t
  - target sites, 188–191
- KIM-1 (kidney injury molecule-1), 121–123

## L

- Lactation, 578, 582–583
- Laminin, 255–256, 821–822
- Large unstained cells (LUC), 368–369
- Larynx, 247–248, 270

- anatomy, species differences, 247–248  
responses to injury, 290–293, 291t
- Lead, 176, 417, 786  
toxicity, 401
- Leukogram  
inflammatory, 379, 413–414  
left shift, 373
- Leukemia, 230, 388–389. *See also*  
Lymphoma  
leukemogenesis, 389  
leukemoid reaction, 379–380
- Leukocytes, 444, 455–456. *See also*  
Granulocytes, Immune cells, Large  
unstained cells, Lymphocytes, Mast  
cells, Monocytes, Neutrophils  
anatomy and physiology  
cell life cycles, 352–360  
redistribution, sequestration and  
demargination/margination, 373–378  
responses  
nonproliferative  
infiltration, 472, 473t  
inflammation, 379  
leukopenia, 379  
myelodysplasia, 385  
proliferative  
leukemia, 230, 388–389  
myelodysplastic syndrome (MDS),  
373, 387–389  
myeloproliferative lesions, 386–389
- Leydig (interstitial) cell hyperplasia, focal,  
685. *See also* Male reproductive  
system
- Limbs, reduction deformities of, 859–860,  
859f
- Lipid nanoparticles (LNP), 171
- Lipofuscin, 37, 479–482
- Liver, 80–81, 264, 461–462, 461f
- Lower urinary tract, 213, 227  
anatomy and physiology, 213–217, 216f,  
217f. *See also* Kidney  
ureters, 214  
urethra, 215  
urinary bladder, 214–215  
evaluation of toxicity, 217–221  
functional, 217–218  
morphologic evaluation, 218–219  
urinalysis, 219–221. *See also* Urinalysis  
mechanisms of toxicity, 230–231  
responses to injury, 221–230  
calcification, 227  
diverticula, 227  
hypertrophy, 226  
hyperplasia and metaplasia, 226–227  
inflammation, 221–222  
inclusions, 227  
neoplasia, 223–225, 228–230  
toxicity  
issues in drug and chemical  
development, 231–232
- Lung, 79–80, 262. *See also* Airways,  
Alveolus, Respiratory system,  
Respiratory system  
anatomy and physiology, 257–261  
background findings, 266–268  
lung cell types, 249–257, 260, 277–278,  
301  
species differences, 237t, 248–249,  
253t  
evaluation of toxicity  
biomarkers, 284–285  
bronchoalveolar lavage, 265  
imaging, non-invasive, 281–287  
in vitro methods, 264, 280–281  
morphologic evaluation, 270, 277–278  
patterns of injury, 288–290, 289f, 291f,  
293, 295–316  
sampling approaches, 271  
weights, 270  
fixation, optimal, 270–271
- Luteinizing hormone (LH), 586, 635, 655,  
656f, 657–658, 666–667, 681–682,  
685, 712–713, 715, 719, 764, 765f
- Luteoma, 792t, 796. *See also* Ovary
- Lymph nodes, 439t, 453–456, 455f, 464,  
486–487, 496  
anatomy, 446–456, 454f, 458, 459t–460t,  
460f  
function, 439t–440t, 456  
reactive lymph nodes, 455–456
- Lymphatic vessels, 260–261, 445–446, 458,  
580, 635
- Lymphocytes, 215, 349–351, 360, 442f, 444,  
448f, 450f, 466, 484, 486. *See also*  
Immune cells, Leukocytes,  
Lymphoma
- Lymphoid system. *See also* Lymph nodes,  
Marginal zone, Mucosa-associated  
lymphoid tissue (MALT),  
Periarteriolar lymphocyte sheath,  
Serosa-associated lymphoid tissue,  
Tertiary lymphoid structures  
cells, 389, 469–472. *See also* Immune cells  
functions, 439t–440t  
effector reactions, 441–443  
immunological memory, 443–444  
organs, 439t–440t, 458–461, 479–482,  
495  
primary, 486. *See also* Bone Marrow,  
Thymus  
secondary, 495–496. *See also* Bronchus-  
associated lymphoid tissues (BALT),  
Gut-associated lymphoid tissues  
(GALT), Lymph nodes, Mucosa-  
associated lymphoid tissue (MALT),  
Spleen  
tertiary, 458–461. *See also* Serosa-  
associated lymphoid cluster (SALC),  
Tertiary lymphoid structures (TLSs)  
organ-specific immune components,  
461–462
- Lymphoma, 230, 363–364, 496. *See also*  
Leukemia, Lymphocyte
- Lymphopoiesis, 344, 359–360, 449. *See also*  
Hematopoiesis
- ## M
- Machine learning (ML), 21–22, 146, 769
- Macrocytosis, 386–387. *See also*  
Erythrocytes
- Macrophages, 7, 216, 260, 301, 349–351, 366,  
407, 440–441. *See also* Immune Cell,  
Leukocytes, Monocytes
- Magnetic resonance imaging (MRI), 14, 283,  
531
- Major histocompatibility complex (MHC),  
56, 441, 124–125, 539
- Male reproductive system. *See also*  
Accessory sex organs, Epididymis,  
Testis  
anatomy and physiology  
development, 630–634, 690–695,  
691t  
hormonal regulation, 632t, 655–659,  
656f  
species comparisons, 636f, 649f, 650f,  
691–695  
incidental findings, 695–701, 699f,  
700f  
spermatogenesis and spermatogenic  
cycle, 639f, 642–645, 644f, 645f,  
646–647f, 648f, 649f, 650f, 651t, 670,  
671f, 672f  
structure and function of  
accessory sex organs, 652–655  
epididymis, 647–648, 651–652, 651t,  
653f, 654f  
testis, 634–647, 649f, 651t  
evaluation of toxicity, 659–674  
biomarkers, 665–668  
fertility, 663–665  
morphologic evaluation, 670–673  
anogenital distance (AGD), 664, 719,  
834  
fixation and sampling, 668–669  
spermatogenesis  
semen analysis, 662, 666  
sperm counts, 660–661, 662t,  
663  
staging, 643, 645, 645f, 649f, 650f,  
670  
weight changes, 660, 661t, 674–675,  
701  
mechanisms of toxicity, 702–721, 704t, 705t,  
706t  
altered hormone levels, 707t, 711–715,  
713f, 714f  
germ cell toxicity, 671f, 672f,  
708–711  
ischemia, 711  
responses to injury, 674–689, 674t, 677f,  
678f, 679f, 680f, 681f, 682f, 683f, 686f,  
687f, 697f, 703–721. *See also* Accessory  
sex organs, Epididymis, Testis  
multinucleated germ cells, 676t, 677f,  
678–679, 692, 695–696, 698,  
720–721  
immaturity as a confounding factor,  
690–695, 691t, 694f  
recovery and reversibility of injury,  
689–690
- Malformations, 814–815, 840–860,  
869t
- MALT. *See* Mucosa-associated lymphoid  
tissue (MALT)

- Mammary gland, 578  
 anatomy and physiology, 579–597,  
 609–610  
 breast cancer resistance protein (BCRP),  
 56–57, 103–104, 881  
 development, 579–583, 580f, 581f, 584f,  
 586f, 587f, 593–595, 596f  
 hormonal influences, 578–579, 581, 582f,  
 583, 591–592, 591f. *See also* Prolactin  
 lactation, 578, 582–583, 582f, 586f, 596–597  
 structure, 578, 580–581, 580f, 581f, 582f,  
 585–587, 586f, 587f, 589f, 596f, 611  
 sex differences, 585, 587f  
 species differences, 579, 583–591, 584f,  
 586f  
 evaluation of toxicity, 597–609, 619–623  
 animal models, 592f, 600–604  
 biomarkers, 607–609  
 function, 595–597, 604–605,  
 609–610  
 in vitro techniques, 600  
 morphologic evaluation, 585, 588,  
 606–607, 608t, 610–615  
 interpretation, nuances of, 580f, 588,  
 596, 598, 603, 615  
 sample collection, 598, 598f  
 whole mount preparations, 602f, 607,  
 608t, 616–623  
 mechanisms of toxicity, 615–616, 779t,  
 780t  
 responses to injury, 609–615  
 nonproliferative  
 fibrosis, 585, 602f, 611, 615  
 galactoceles, 585  
 proliferative, 581–582, 585, 588, 594, 606,  
 612–614  
 nonneoplastic  
 altered development, 605f, 609  
 atypical hyperplasia, 688  
 hyperplasia, 580f, 584, 592f,  
 595–597, 609, 611–613,  
 612f, 615, 784t  
 neoplastic  
 adenoma, 596, 613  
 adenomyoepithelioma, 614  
 carcinoma, 555–558, 595–596, 613f,  
 614f  
 carcinoma in situ, 595–596  
 fibroadenoma, 601, 613–614, 613f  
 toxicity, 597–609  
 Marginal zone (MZ, spleen), 450–453, 451f  
 Mast cells, 215, 349–351, 440–441  
 Maternal endpoints of developmental  
 toxicity, 596–597, 829–830, 833–834,  
 867, 878–879  
 differentiating developmental toxicity  
 from, 838–839  
 Matrix metalloproteinases (MMPs), 63–64,  
 112, 594–595  
 Maximum tolerated dose (MTD), 121–122,  
 371, 599  
 Megakaryocyte growth and development  
 factor (MGDF), 413–414  
 Megakaryocytes (MKs), 344–345, 363,  
 365–366, 486  
 Megakaryopoiesis, 349–351, 356–358, 356f,  
 402. *See also* Hematopoiesis  
 Melamine, 182, 224–225  
 Menstrual cycle, 588, 738. *See also* Estrous  
 cycle, Female reproductive system,  
 Vagina  
 endocrinology, 764–769, 765f  
 histology, 753, 756f, 757, 759, 760f, 761f, 762f  
 Mesenchymal stem cells (MSCs), 349  
 Mesothelioma, 286–287, 326, 687, 800  
 Metaplasia, 226–227, 227f, 684  
 Metestrus. *See* Estrous cycle  
 Methemoglobin, 408–409, 420  
 Metrial gland, 828f, 829. *See* Placenta  
 Microangiopathy, 77. *See also* Thrombotic  
 microangiopathy (TMA)  
 Microbiome, 327–328, 490, 521, 541–543,  
 549  
 Microcephaly, 845, 847, 862, 878, 883t  
 Microphysiological systems (MPSs),  
 142–143, 371  
 MicroRNAs (miRNAs), 113, 668  
 Minipigs, 518–519, 632, 632t, 635, 636f, 649f,  
 655t, 683f, 691, 695, 759–760  
 common spontaneous lesions, 134, 135f,  
 698, 700f  
 dermal toxicity assessment, 518–519  
 miRNA. *See* MicroRNAs  
 Monkeys. *See* Menstrual cycle.  
*See also* Nonhuman primate  
 Monocytes, 401–402, 496–497. *See also*  
 Immune cell, Leukocytes,  
 Macrophages, Myelopoiesis  
 mononuclear cells, 301  
 mononuclear phagocyte system (MPS),  
 441  
 Morphogen gradients, 815, 822–824, 852,  
 860  
 Mouse/mice, 272, 276–277, 580, 582, 603,  
 631–633, 635, 643, 645, 765, 770,  
 886–887  
 common spontaneous findings, 134–137,  
 315–317, 31f  
 Meromelia, 859  
 Mucosa-associated lymphoid tissue  
 (MALT), 257, 438, 439t, 456–458,  
 457f, 486–487. *See also* Serosa-  
 associated lymphoid cluster  
 airway-associated  
 bronchus-associated (BALT), 257,  
 456–457  
 larynx-associated (LALT), 456–457  
 nasal-associated (NALT), 246, 456–457,  
 457f, 459t–460t  
 conjunctiva-associated (CALT), 456–457  
 duct-associated (DALT [lacrimal and  
 salivary glands]), 456–458  
 gut-associated (GALT), 246, 456–458,  
 457f  
 Myelodysplastic syndromes (MDS), 373,  
 385, 387–389  
 Myeloid to erythroid (M:E) ratio, 484–485  
 Myelopoiesis, 344, 358–360, 402, 487–488.  
*See also* Bone marrow, Hematopoiesis  
 Myocardium. *See also* Heart  
 anatomy, 3–6  
 metabolism, 10  
 responses to injury  
 calcification, 23  
 myofibrillar degeneration and lysis,  
 35–37  
 necrosis, 38, 42–43, 44t–47t  
 Myoglobin, 24–25, 185–186, 200
- ## N
- N-Acetyl-b-(D)-glucosaminidase (NAG),  
 117  
 N-acetylgalactosamine (GalNAc),  
 169–171  
 Nanofibers, 326–327  
 Nanoparticles, 171, 325–326  
 Nasal cavity, 237–247. *See also* Respiratory  
 system  
 anatomy and physiology, 239–247, 242f,  
 268–270  
 epithelium, regional specialization,  
 240–246, 242f  
 nasal-associated lymphoid tissue  
 (NALT), 246–247, 457f,  
 459t–460t  
 species differences, 239, 240f  
 responses to injury, 290–293, 291t  
 Nasopharynx, 238, 247  
 anatomy and physiology, 238, 246–250,  
 270, 456–457  
 responses to injury, 290–293, 291t  
 National Toxicology Program (NTP), 48–49,  
 137, 596–597  
 Neoplasia. *See under individual organ system*  
 Nephroblastoma, 129–132, 135–137, 139  
 Nephrotoxicity, 154–157, 163, 159–169,  
 172–177, 180, 189–192, 205–206.  
*See also* Kidney  
 classification of lesions, 159–160,  
 160t–162t  
 classification of nephrotoxicants, 154–155,  
 159–160, 160t  
 mechanisms of injury, 160  
 Neural tube defects (NTDs).  
*See* Dysraphism  
 Neutropenia, 400–401  
 Neutrophil gelatinase-associated lipocalin  
 (NGAL), 72, 121–124  
 Neutrophils, 295, 401–402, 440–441. *See also*  
 Granulocytes, Leukocytes  
 function testing, 370  
 NGAL. *See* Neutrophil gelatinase-  
 associated lipocalin (NGAL)  
 Nitric oxide (NO), 111, 307, 402  
 Nonhuman primates (NHPs), 224, 277, 585,  
 594, 604, 701, 739, 755–758, 765–766,  
 791, 825–826, 887–888. *See also*  
 Menstrual cycle  
 common spontaneous findings, 133–134,  
 694–695, 698, 699f  
 Nonsteroidal anti-inflammatory drugs  
 (NSAIDs), 110, 182, 189–191,  
 412–413, 852–853  
 Nose. *See* Nasal cavity  
 NSAIDs. *See* Nonsteroidal anti-  
 inflammatory drugs (NSAIDs)
- ## O
- Oligonucleotides. *See* Antisense  
 oligonucleotides  
 Omphalocele, 851–852, 851f, 884t



- Ontogenesis, 340–345, 344t. *See also*  
Hematopoiesis, Ontogeny
- Ontogeny (in development), 89, 863
- Opioid peptides, 786
- Optical imaging, 281–283, 532
- Organic anion transporters (OATs), 103–104
- Organic anion transporting polypeptides (OATPs), 103–104
- Organic cation transporters (OCTs), 103–104
- Organic cation/carnitine transporters (OCTNs), 103–104
- Organisation for Economic Co-operation and Development (OECD), 498–499, 523, 596–597
- Organogenesis, 813, 821–824. *See also*  
Morphogen gradients
- Ovary. *See also* Female reproductive system  
anatomy and physiology, 741–744  
hormones, 764–769, 765f  
follicle-stimulating hormone (FSH), 742, 764, 765f, 766–768. *See also* Follicle-stimulating hormone  
gonadotropin-releasing hormone (GnRH), 764, 766–768. *See also* Gonadotropin-releasing hormone  
luteinizing hormone (LH), 742, 757, 761, 764, 765f. *See also* Luteinizing hormone  
prolactin, 765f, 766–768. *See also* Prolactin
- processes  
luteinization, 743–744, 751, 757f, 767–768  
ovulation, 760–764, 766  
species differences, 766–767
- structures  
corpora lutea (CL), 588, 738, 742f, 744f, 746f, 750f, 752f, 761, 766  
follicles, 741–744, 742f, 743f, 746f, 749, 750f, 751–753, 752f, 756f, 757f, 760–761, 760f, 764, 766–767  
granulosa cells, 742–743, 746f, 757f, 761–762, 764, 766–768  
oocytes, 741–742
- evaluation of toxicity  
biomarkers, 771, 779t, 790–791  
follicle morphometric methods, 770  
in vitro techniques, 740, 753  
morphologic evaluation, 769–770  
effects of section plane, 750f  
spontaneous changes, 772–773, 773t
- mechanisms of toxicity, 777–791, 779t, 780t–781t, 784t, 786t, 787t
- responses to injury  
nonproliferative. *See also* Corpora lutea, Follicles, ovarian  
atrophy, 779, 779t, 780t, 787–788, 791  
degeneration, 776, 788, 791  
squamous metaplasia, 764, 785  
proliferative, 791, 794f, 796f, 797f, 798f  
choriocarcinoma, 688, 792, 797f, 798
- granulosa cell tumor, 688, 775, 792t, 795–797, 795f  
luteoma, 792t, 796  
thecoma, 792, 796f, 798  
toxicity, 777–798, 779t, 780t–781t, 786t, 787t, 792t
- Oxidative stress, 177, 196, 403–404, 407–408, 874
- Oxygen (O<sub>2</sub>), 10–11, 402  
hemoglobin dissociation curve, 340–342. *See also* Hemoglobin
- Ozone, 297f, 318–319
- ## P
- Palatoschisis, 847–848, 848f, 883t
- Pappenheimer body, 411
- Parathyroid hormone-related protein (PTHrP), 592t, 593
- Paroxysmal nocturnal hemoglobinuria, 386
- Pathogen-associated molecular patterns (PAMPs), 536, 538, 539f, 541, 543, 544f
- Pattern recognition receptors (PRRs), 511
- PDGF. *See* Platelet-derived growth factor (PDGF)
- Percutaneous absorption, 520–522
- Perfluorooctanoic acid (PFOA), 605
- Periarteriolar lymphocyte sheath (PALS, of spleen), 439t, 449–452, 451f, 485
- Pericytes (near blood vessels), 61–62
- Periodic acid-Schiff (PAS), 20, 95–96, 252–253, 641
- Peripheral bloodcells, 404–406. *See also*  
Erythrocytes, Leukocytes  
evaluation of, 366–371. *See also*  
Hematology  
emerging technologies and biomarkers, 369–371  
routine hematology, 366–369, 367t–368t
- responses  
anemia. *See* Anemia  
changes in, 373–379, 374t–377t, 379. *See also* Leukogram  
redistribution, sequestration  
and demargination/margination, 373–378
- Peroxisome proliferator activated receptor (PPAR), 415–416, 781t
- Peyer's patches (PPs). *See* Mucosa-associated lymphoid tissue (MALT). *See also* gut-associated (GALT)
- P-glycoprotein (Pgp), 103–104, 881
- Pharynx, 247–248. *See also* Respiratory system
- Phocomelia, 859–860, 859f
- Phospholipidosis, 37–38, 39f, 154, 302–303, 302f
- Photosafety, 568–571. *See also* Phototoxicity
- Phototoxicity, 570. *See also* Integument  
evaluation for, 524–527, 525t  
photoactivation (of chemicals), 568, 570–571  
photoaging, 572  
photoallergy, 525, 561t  
photocarcinogenicity, 525, 571  
photogenotoxicity, 571
- photoirritancy, 526, 569  
photosensitivity, 568–570
- Phylogenesis (Phylogeny), 340–345, 341t. *See also* Ontogenesis  
hematopoietic organs, 343–344  
hemostatic systems, 342  
immunologic systems, 342–343  
respiratory systems, 340–342
- Pigmentation (integument), 511–512, 568–569  
disorders, 561t, 573–574  
plucked hair testing, 531
- Pituitary hormones, 579, 655, 657, 659, 713
- Placenta  
anatomy and physiology, 825–829, 880–881. *See also* Metrial gland  
anatomy, 825–829, 826f, 827f, 828f, 829f  
developmental evolution, 826–829, 826f, 827f, 829f  
species variations, 826–827, 826f, 827f  
countercurrent blood flow, 830  
metabolism, 877, 881  
pharmacokinetics, 881  
uterine natural killer (uNK) cells, 829–830
- evaluation of toxicity  
in vitro techniques, 831–832  
morphologic evaluation, 835  
mechanisms of toxicity, 869, 873  
toxicity, species differences, 831t
- Plasma cells, 444
- Platelet-derived growth factor (PDGF), 34, 64–65, 92–93, 356–357, 873
- Platelets (PLTs), 301, 344–345, 338, 366, 401–402, 452  
anatomy and physiology, 356, 369–370, 407–408. *See also* Platelet-derived growth factor (PDGF),  
Thrombopoiesis  
reticulated platelets, 367, 369–370
- evaluation of toxicity  
biomarkers, 367–370  
function, 370  
in vitro techniques, 371  
morphologic evaluation, 367  
mechanisms of toxicity, 392–393  
responses to injury  
thrombocytopenia, 380, 400–401, 412–414  
drug-induced, 413  
immune-mediated, 413–414
- Podocyte injury, 149–150, 160–162
- Polycyclic aromatic hydrocarbons, 107–108
- Polydactyly, 857, 858f
- Preputial gland. *See* Accessory sex organs
- Proestrus. *See* Estrous cycle
- Progesterone, 522, 576, 751, 757, 760–762, 766–768, 779, 779t, 780t, 783, 784f, 787–789, 788t, 793t
- Progesterone receptor(s), 594, 780t  
modulators (PRMs), 788–789
- Programmed cell death (PCD), 823–824. *See also* Apoptosis  
interference with, 869–870

Progressive cardiomyopathy (PCM) in rodents, 21–22, 58  
 Prolactin, 584–586, 592t, 594–595, 610, 613, 656f, 658, 684, 765f, 766–768, 771, 779t, 780t, 782–785, 784t, 787, 803  
 Proliferating cell nuclear antigen (PCNA), 20, 281, 558, 606–607, 741–742  
 Prostacyclin (PGI<sub>2</sub>), 102, 415–416  
 Prostaglandin E<sub>2</sub> (PGE<sub>2</sub>), 102, 359–360  
 Prostaglandins (PGs), 98, 102–103, 359–360, 522  
 Prostate. *See* Accessory sex organs  
 Proto-oncogenes, 109  
 Proton pump inhibitors (PPIs), 87–88  
 Pseudoallergy, 472  
 Pseudocyesis, 753–755  
 Pseudohermaphroditism, 855–856, 855f, 884t  
 Pseudopregnancy, 766, 789–790  
 Pubertal assay, 744–745. *See also* Female reproductive system, Ovary  
 Puberty, 449–450, 464, 578, 583, 585, 629–630, 765  
 Pulmonary system. *See* Lung, Respiratory system

## Q

QT prolongation, 15  
 Quantitative analysis  
   bone marrow, 365–366  
   heart, 20–21  
   lung, 281  
   morphometry, 21, 606  
 Quantitative polymerase chain reaction (qPCR), 274–275  
 Quantitative structure-activity relationship (QSAR), 837–838

## R

Rabbits, 524, 575, 739–740, 763, 887, 894–895  
 Rachischisis. *See* Dysraphism  
 Rats, 575, 674–675, 691–692, 719, 783–784, 886–887. *See also* Sprague Dawley (SD) rats  
   histology during the estrous cycle, 745–753  
   histology of ovary throughout development, 744–745  
   mammary gland whole mounts, 616–623  
 Reactive oxygen species (ROS), 159, 167, 187, 196, 317, 343, 402–405, 406t, 711, 843  
 Red blood cells (RBCs), 60, 338. *See also* Erythrocytes, Hematology, Hematopoiesis  
 Reflux, gastric (gavage-related), 268–270, 269f  
 Regenerative anemia. *See* Anemia.  
   *See* Hematology  
 Renal system. *See also* Glomerulus, Kidney, Lower urinary tract  
   anatomy and physiology, 91–100, 109–113  
   function, 91–94, 157  
   acid-base regulation, 106–107  
   calcium-phosphate regulation, 101

electrolyte regulation, 100–101  
 growth factors, regional effects of, 109  
 hormone production, 102  
 metabolism, 101–108, 108t, 157–159  
 transporter systems, 103–106, 103t  
 microscopic anatomy, 94–98  
 variations by species, 90t, 98–100, 99t, 100f  
 evaluation of toxicity  
   biomarkers, 116–117  
   function, 100–109  
   in vitro techniques, 139–145  
   morphologic evaluation, 129  
   toxicity testing, 137–139, 138t  
 mechanisms of toxicity  
   altered clearance, 108–109  
   altered hemodynamics, 167  
   altered transport systems, 180–181  
   direct toxicity, 160, 178–179, 179t, 189–191  
   immune-mediated injury, 168  
   neoplastic transformation, 191t–195t  
     exacerbation by chronic progressive nephropathy, 197–198  
     hormonal responsiveness, 198–199  
     impact of oxidative stress, 196  
 responses to injury. *See also* Glomerulus, Podocyte injury  
   cyst, 139  
   developmental defects, 90, 852–853  
   fibrosis, 157  
   necrosis, renal papillary (RPN), 125–126  
   neoplasia, 113, 129–132, 139, 191–199  
   phospholipidosis, 154  
   repair, 217  
   toxicity, 108–109  
 Renal tubules. *See also* Kidney, Renal system  
   anatomy and physiology, 95–98, 97f, 123–124, 186–187  
 responses to injury  
   atrophy, 188  
   degeneration and necrosis, 153–154, 153f, 156, 200, 204–205  
   dilation and cysts, 154–155, 155f  
   hypertrophy, 107–108  
   proliferation, 199  
   regeneration, 124  
   vacuolation, 154  
   toxicity, 204–205  
 Respiratory syncytial virus (RSV), 273–275  
 Respiratory system, 33, 236, 850. *See also* Airways, Alveolus, respiratory, Lung, Larynx, Nasal cavity, Pharynx  
   anatomy and physiology, 237–261  
   anatomy  
     nose, 237–247. *See also* Nasal Cavity  
     pharynx and larynx, 247–248. *See also* Larynx, Pharynx  
     lower respiratory tract, 248–261, 270–271, 272f. *See also* Club cells, Ionocytes  
   background findings, 266–270  
   function, 264–265  
   gas exchange, 257–261  
   metabolism, 319–321

evaluation of toxicity, 261–287  
   animal models, 272–278, 279t  
   biochemical evaluation, 265–266  
   bronchoalveolar lavage (BAL), 261, 265, 267  
   functional testing, 370  
   imaging, 281–287  
   in vitro systems, 264, 278–281  
   morphological evaluation, 266, 270–271  
   target expression analysis, 261, 278–279, 283  
 mechanisms of toxicity, 272, 317–328, 318t  
 immune-mediated damage, 321–322. *See also* Asthma, allergic  
   metabolic activation, 319–321, 320f  
   particle-related physical damage, 324–327  
 pathogens  
   influenza, 276–277  
   COVID-19. *See* COVID-19  
   RSV. *See* Respiratory syncytial virus (RSV)  
   SARS-CoV-2. *See* COVID-19  
 responses to injury, 287–317. *See also* Acute respiratory distress syndrome (ARDS), Asthma, Diffuse alveolar damage (DAD)  
   alveolar proteinosis, 303–304  
   asthma, 296–298. *See also* Asthma  
   chronic obstructive pulmonary disease (COPD), 272, 297  
   edema, 79–80, 304–307, 305f, 306f  
   emphysema, 312–314, 313f  
   factors affecting host response, 287–288  
   fibrosis, 272, 309–312, 310f  
   hyperactive airways, 296  
   inflammation, 307–309  
   neoplasia, 298, 314–317, 316f, 317f  
   phospholipidosis, 302–303, 303f  
   regeneration and repair, 288–289  
 toxicity  
   exposure methods, 261–264  
   patterns induced by airborne toxicants, 288  
     inhaled materials, 322–327  
     nose, larynx, and pharynx, 290–293  
     lower respiratory tract, 294–298, 301–317  
     toxicant interactions, 327  
 Reticulocytes, 354–355. *See also* Erythrocytes, Hematology  
   reticulocytopenia, 383–385  
   reticulocytosis, 413–414  
 Retinoblastoma (Rb) gene, 139, 228  
 Retinoic acid/Retinoids, 770, 823  
   retinoid receptors, 440–441, 770, 781t, 822  
 Rhesus macaque (*Macaca mulatta*), 277, 887–888. *See also* Nonhuman primate  
 Ribonucleic acid (RNA), 342–343, 872  
 Rodents, 21–22, 530, 579, 583, 585, 599, 603–605, 611, 613, 660–661, 685, 691–692, 695–696, 739–740, 886–887, 894–895

## S

- SARS-CoV-2 (severe acute respiratory syndrome coronavirus 2).  
*See* COVID-19
- Scanning electron microscopy (SEM), 7, 216–217, 271, 534
- Schwannoma, 49, 800
- Selective estrogen receptor modulators (SERMs), 686f, 769, 772, 775, 778t, 780t, 788–789, 793t
- Selective progesterone receptor modulators (SPRMs), 788–789
- Selective serotonin reuptake inhibitors (SSRIs), 416, 850–851
- Self-tolerance, 443
- Seminal vesicles. *See* Accessory sex organs
- Seminiferous tubules. *See* Spermatozoa, Spermatogenesis, Testis
- SEND (Standardization for Exchange of Nonclinical Data), 483–484, 767
- Serosa-associated lymphoid cluster (SALC), 462. *See also* Lymphoid system, Mucosa-associated lymphoid tissues (MALT)
- Sertoli cells. *See* Testis
- Severe acute respiratory syndrome coronavirus 2 (SARS-CoV-2).  
*See* COVID-19
- Single cell necrosis, 147–148, 204–205, 611, 683–684. *See also* Apoptosis
- Skeleton, congenital defects, 835, 856–860.  
 axial skeleton defects (skull and vertebrae), 835f, 836f. *See also* Dysraphism  
 digit anomalies, 857f, 858f, 870f. *See also* Adactyly, Brachidactyly, Ectrodactyly, Polydactyly, Syndactyly  
 limb defects, 859f. *See* Amelia, Hemimelia, Meromelia, Phocomelia, Tetramelia
- Skin. *See* Integument
- Small cell lung cancer (SCLC), 314–315
- Smooth muscle, 7, 60, 219  
 smooth muscle actin (SMA), 219  
 smooth muscle myosin (SMM), 219
- Spermatozoa. *See also* Spermatogenesis, Testis  
 anatomy and physiology  
 morphologic features, 644f, 645f, 646f, 648f, 649f, 650f, 652f  
 production, 640–652. *See* Spermatogenesis  
 species comparison, 649f, 650f, 651t  
 structure, 639f  
 spermatids, 641–642, 642f, 644f  
 spermatocytes, 641, 642f, 644f  
 spermatogonia, 640, 642f, 644f, 675–677, 689  
 evaluation of toxicity, 660–663, 662t, 666  
 staging, 643, 644f, 645f, 650f  
 stage-aware evaluation, 670. *See also* Spermatogenesis  
 mechanisms of toxicity, 668  
 responses to injury, 879–880  
 altered maturation, 609  
 decreased numbers, 683  
 degeneration, 709–710  
 granuloma, 684  
 spermatid retention, 680, 682  
 toxicity, 879
- Spermatogenesis, 631, 633–635, 640, 641–642, 645f, 695–696. *See also* Spermatozoa, Testis  
 anatomy and physiology  
 spermatogenic cycle, 634–635, 642–645, 644f, 645f, 646–647f, 648f, 649f, 650f, 651t  
 spermiation, 639–641, 706  
 evaluation of toxicity, 659–660  
 sperm counts, 660–661, 662t, 663  
 staging, 643, 644f, 645, 645f, 649f, 650f, 670  
 mechanisms of toxicity, 668  
 responses to injury, 609–615  
 toxicity, 615–616
- Spina bifida. *See* Dysraphism
- Spleen, 438, 439t–440t, 449–452, 450f–451f, 482, 486–487. *See also* Immune system  
 anatomy, 450–452  
 development, 449–450  
 functions (compartment-specific), 439t–440t, 452–453  
 weight, 482–483
- Sprague Dawley (SD) rats, 116–117, 601, 740–741
- Standardization for Exchange of Nonclinical Data (SEND). *See* SEND
- Stem cell factor (SCF), 344–345
- Stem cells. *See* under individual organ systems
- Steroids, 521–522, 607–609  
 steroid hormone-binding globulin (SHBG), 658
- Structure-activity relationship (SAR), 781–782, 837
- Study design  
 developmental toxicity, 881–894  
 topical dermatologic testing, 527–528
- Subcutis, 515. *See also* Integument
- Syncytiotrophoblast, 829, 829f, 878, 887.  
*See also* Placenta
- Syndactyly, 857, 858f, 870f
- Syringomyelia, 874
- Systemic lupus erythematosus (SLE), 110–111, 540

## T

- Talipes, 859–862, 876
- Tamm-Horsfall protein, 97
- Target liability assessment (TLA), 278–281
- Target safety assessment (TSA), 278–279
- T cell-dependent antibody response.  
*See* TDAR (T cell-dependent antibody response)
- T cells, 363–364, 441–443. *See also* Immune cells, Leukocytes, Lymphocytes  
 memory cells, 444  
 resident cells, 540
- TDAR (T cell-dependent antibody response), 488. *See also* Immune system
- Teratology, 812–813, 831t, 840, 841t, 845.  
*See also* Developmental toxicity
- Teratothanasia, 840
- Tertiary lymphoid structures (TLSs), 438, 458–461, 461f. *See also* Immune system, Lymphoid
- Testis. *See also* Spermatozoa, Spermatogenesis  
 anatomy and physiology  
 anatomy, 634–652  
 interstitial (Leydig) cells, 631–632, 635, 636f  
 seminiferous tubules, 633–635, 637, 638f, 643, 646f–647f, 648f, 649f  
 Sertoli cells, 631, 637–640, 658–659, 707–708  
 spermatogonia, 640, 642f, 644f, 675–677, 689. *See also* Spermatozoa  
 testicular macrophages, 635  
 blood-testis barrier, 632t, 633, 637, 640  
 descent, 632–633, 632t  
 hormonal regulation of, 632t, 655–659, 656f. *See also* Follicle-stimulating hormone (FSH), Gonadotropin-releasing hormone (GnRH), Luteinizing hormone (LH)  
 spermatogenesis. *See* Spermatogenesis  
 evaluation of toxicity, 660–663, 666  
 biochemical / molecular evaluation, 665–668  
 morphological evaluation, 660–663, 661t, 662t, 703–718  
 mechanisms of toxicity, 703–718  
 hormone imbalances, 707t, 711–715, 713f, 714f, 719–720  
 ischemia, 706t, 711  
 responses to injury  
 nonproliferative lesions  
 interstitial (Leydig) cells  
 abnormal fetal aggregation, 720–721  
 atrophy, 681–682  
 necrosis, 682–683  
 seminiferous tubules, 675–681, 676t, 703–715  
 altered spermiation, 706  
 contraction, 708  
 decreased fluid production, 708  
 degeneration/atrophy, 675–677, 676t, 696, 698, 711f  
 dilatation, tubule, 679  
 germ cell depletion, 670–672, 671f, 672f, 675, 677, 703–705, 704t, 705t, 708–709, 710f  
 germ cell exfoliation, 703–708  
 multinucleated germ cells, 676t, 677f, 678–679, 692, 695–696, 698  
 necrosis, 679  
 obstruction, 716–718  
 spermatid retention, 680, 682f



- Testis (*Continued*)  
     vacuolation, 679–680, 705  
     Sertoli cell injury, 703–708, 705t  
     proliferative lesions, 684–688, 686f  
     interstitial (Leydig) cell hyperplasia  
         and tumors, 685–687, 686f  
     Sertoli cell hyperplasia, 688  
     mesothelioma, 686f, 687  
     teratoma, 688  
     testicular dysgenesis syndrome (TDS),  
         720  
 Testosterone, 576, 658–659, 712–713,  
     715–716  
 Tetraamelia, 859  
 Thecoma, 792–793  
 Thelarche, 579  
 Thrombocytopenia, 380, 400–401, 412–414.  
     *See also* Platelets  
 Thrombopoiesis, 356–358, 356f, 402. *See also*  
     Hematopoiesis  
 Thrombopoietin (TPO), 344–345  
 Thrombotic microangiopathy (TMA),  
     152–153, 417  
 Thrombotic thrombocytopenic purpura  
     (TTP), 164–166, 417  
 Thymus, 439t, 443, 446f, 484, 485f, 495–496  
     anatomy and physiology, 446–449  
     weight, 482  
     thymoma, 495–496, 496f  
 Tolerance, immune, 443, 461  
 Toxic epidermal necrolysis (TEN).  
     *See* Integument  
 Toxicogenomics, 668, 702–703  
 Trachea, 248–257, 250f. *See also* Respiratory  
     system  
 Transforming growth factors (TGF)  
     TGF alpha (TGF $\alpha$ ), 554  
     TGF beta (TGF $\beta$ ), 19, 50, 573, 657, 767  
 Transgenic Adenocarcinoma of Mouse  
     Prostate (TRAMP), 688–689  
 Transgenic mouse models, 372, 592–592,  
     689  
 Translational immunology, 541–543  
 Transmission electron microscopy (TEM),  
     20, 216–217, 271, 533  
 Transplacental carcinogenesis, 864–868,  
     865t, 866t, 881, 891  
 Transvaginal surgical mesh, 776  
 Trefoil factor, 3, 124  
 Trophoblast, 816, 826–830, 827f, 829f.  
     *See also* Placenta  
 Trophoblast giant cells (TGCs), 829–830.  
     *See also* Placenta  
 Troponins, 24–25, 59  
 Tuft cells (conducting airways), 256–257  
 Tumor necrosis factor (TNF), 311, 635, 767
- ## U
- Ultraviolet (UV) radiation, 536, 542, 573  
 Urea nitrogen (UN), 117, 119. *See also* Blood  
     urea nitrogen, Kidney  
 Uric acid/Urates, 182, 219–229  
 Urinalysis, 182, 183f, 189, 219–221  
 Urinary beta2-microglobulin, 124–125  
 Urinary bladder, 201, 213–215, 224. *See also*  
     Lower urinary tract  
 Urine, 13–214. *See also* Kidney, Renal  
     system, Lower urinary tract,  
     Urinalysis  
     composition, 217–219  
     markers, 117, 120–123  
     pH, 218  
 Uterus, 778t. *See also* Female reproductive  
     system, Estrous cycle, Menstrual  
     cycle, Placenta anatomy and  
     physiology, 747, 749, 750f, 751–769,  
     752f, 754f, 755f, 756f, 758f, 759f, 761f,  
     762f, 763f, 765f, 766  
     evaluation of toxicity  
     morphological methods, 745, 770  
     sampling, 739t, 747  
     responses to injury, 789–790  
     atrophy, 774f, 775, 781t, 787t  
     endometriosis, 759, 773t, 789  
     hyperplasia, 762, 764, 773t, 775f, 779t,  
     780t, 781t, 782f, 783, 784, 784f, 788–790,  
     788t  
     proliferative changes, 773t, 776f, 793t,  
     798–802, 799f, 800f, 801f  
     spontaneous changes, 773t  
     squamous metaplasia, 775f, 779t, 780t,  
     788t, 790  
     vascular damage, 786  
     uterine natural killer (uNK) cells, 829–830
- ## V
- Vaccine-associated enhanced respiratory  
     disease (VAERD), 273–274  
 Vagina, 739t, 745, 766. *See also* Estrous cycle,  
     Female reproductive tract, Menstrual  
     cycle morphology, 745, 747–755, 760,  
     764
- estrous cycle, histomorphology, 747t,  
     748f, 751f, 755f, 758f  
 responses, 783, 784t, 788–790,  
     800–802  
     delayed hypersensitivity, 777  
     irritation, 790  
     mucification, 766, 779t, 780t, 783, 784f,  
     784t, 785, 788t  
     neoplasia, 793t, 802f, 803f  
     pseudopregnancy, 751, 759f, 767, 782f,  
     790–791  
     squamous metaplasia, 773t, 775, 779t,  
     780t  
     toxicity, 773t, 774–775, 776, 778t, 779  
 Valvulopathy, 49–50. *See also* Heart  
 Vascular endothelial growth factor (VEGF),  
     20, 89–90, 344–345, 541, 767, 873.  
     *See also* Blood vessel, Growth factors  
     influences on expression, 64–65  
     VEGF receptor (VEGFR), 34, 402  
 Vascular system, 60. *See also* Blood vessel,  
     Heart  
     function, 64–67  
     regulation of activity, 65–66  
     responses  
         altered lumen size, 32–33, 74  
         inflammation, 77–78  
     toxicity, 66, 71–72  
 Vehicle, percutaneous absorption, 521  
 Von Hippel-Lindau (VHL), 139  
 Von Willebrand's  
     disease, 263–264  
     factor (vWF), 72, 164, 356
- ## W
- Wilms tumor, 139  
     Wilms tumor 1 gene (WT1), 139  
     Wilms tumor protein-1 (WT-1), 164  
 Wilson's technique (for embryo evaluation),  
     835
- ## X
- Xenograft, 139
- ## Y
- Yolk sac (YS), 819, 826–828. *See also* Placenta  
     carcinoma, 687–688, 792–793
- ## Z
- Zebrafish (*Danio rerio*), 372, 830

# Haschek and Rousseaux's Handbook of **TOXICOLOGIC PATHOLOGY**

**FOURTH EDITION**

**VOLUME 5**

## Toxicologic Pathology of Organ Systems

### Editors

**WANDA M. HASCHEK**, University of Illinois at Urbana Champaign, Urbana, IL, USA

**COLIN G. ROUSSEAU**, University of Ottawa, Ottawa, Ontario, Canada

**MATTHEW A. WALLIG**, University of Illinois at Urbana Champaign, Urbana, IL, USA

**BRAD BOLON**, GEMpath, Inc., Longmont, CO, USA

### Associate Editors

**JEFFREY I. EVERITT**, Duke University School of Medicine, Durham, North Carolina, USA

**KAREN S. REGAN**, Regan Path/Tox Services, Inc., Kewadin, MI, USA

### Illustrations Editor

**BETH W. MAHLER**, Experimental Pathology Laboratories, Inc./NIEHS, Research Triangle Park, NC, USA

*Haschek and Rousseaux's Handbook of Toxicologic Pathology* is a key reference on the integration of structural and functional changes in tissues associated with the response to many toxicant classes including pharmaceuticals, biologics, innovative therapeutic products (cell and gene therapies as well as gene editing), vaccines, chemicals (both natural and manmade), metals, toxins, and physical agents such as radiation. Volumes 4 and 5 of the Fourth Edition, both titled "Toxicologic Pathology of Organ Systems", provide comprehensive coverage of the basic biology as well as key principles and procedures for evaluating toxicant-induced injury to essential organs and systems,

Volume 5 addresses the following systems, cardiovascular, renal, lower urinary, respiratory, hematopoietic, immune, integumentary, mammary, and male and female reproductive, as well as the embryo, fetus, and placenta. The topics covered in Volume 5 of the Haschek and Rousseaux's Handbook of Toxicologic Pathology are an essential part of the most authoritative reference on toxicologic pathology for pathologists, toxicologists, research scientists, and regulators studying and making decisions regarding various toxicants. This volume also is an essential reference for educators in this arena.

### KEY FEATURES

- Completely revised and extensively expanded chapters on systems toxicologic pathology
- High-quality and trusted content in collaborative work written by leading international authorities in all areas of toxicologic pathology
- Hundreds of full-color images in both the print and electronic versions of the book to highlight difficult concepts with clear illustrations



**ACADEMIC PRESS**

An imprint of Elsevier

[elsevier.com/books-and-journals](http://elsevier.com/books-and-journals)

ISBN 978-0-12-821045-1



9 780128 210451